Machine Learning in Mobile Computing: Methods and Applications

Lead Guest Editor: Wenqing Wu
Guest Editors: Song Jiang, Wei Liu, and Xuyun Zhang

Machine Learning in Mobile Computing: Methods and Applications

Machine Learning in Mobile Computing: Methods and Applications

Lead Guest Editor: Wenqing Wu
Guest Editors: Song Jiang, Wei Liu, and Xuyun Zhang

Contents

Contents

Contents

Contents

Contents

WILEY | Hindawi

Retraction

Retracted: Holographic Projection Technology in the Field of Digital Media Art

Wireless Communications and Mobile Computing

This article has been retracted by Hindawi following an investigation undertaken by the publisher [1]. This investigation has uncovered evidence of one or more of the following indicators of systematic manipulation of the publication process:

1. Discrepancies in scope
2. Discrepancies in the description of the research reported
3. Discrepancies between the availability of data and the research described
4. Inappropriate citations
5. Incoherent, meaningless and/or irrelevant content included in the article
6. Peer-review manipulation

The presence of these indicators undermines our confidence in the integrity of the article's content and we cannot, therefore, vouch for its reliability. Please note that this notice is intended solely to alert readers that the content of this article is unreliable. We have not investigated whether authors were aware of or involved in the systematic manipulation of the publication process.

Wiley and Hindawi regrets that the usual quality checks did not identify these issues before publication and have since put additional measures in place to safeguard research integrity.

We wish to credit our own Research Integrity and Research Publishing teams and anonymous and named external researchers and research integrity experts for contributing to this investigation.

The corresponding author, as the representative of all authors, has been given the opportunity to register their agreement or disagreement to this retraction. We have kept a record of any response received.

References

[1] Y. Liu, S. Wu, Q. Xu, and H. Liu, "Holographic Projection Technology in the Field of Digital Media Art," *Wireless Communications and Mobile Computing*, vol. 2021, Article ID 9997037, 12 pages, 2021.

Retraction

Retracted: Student Physical Fitness Test System and Test Data Analysis System Based on Computer Vision

Wireless Communications and Mobile Computing

This article has been retracted by Hindawi following an investigation undertaken by the publisher [1]. This investigation has uncovered evidence of one or more of the following indicators of systematic manipulation of the publication process:

(1) Discrepancies in scope

(2) Discrepancies in the description of the research reported

(3) Discrepancies between the availability of data and the research described

(4) Inappropriate citations

(5) Incoherent, meaningless and/or irrelevant content included in the article

(6) Peer-review manipulation

The presence of these indicators undermines our confidence in the integrity of the article's content and we cannot, therefore, vouch for its reliability. Please note that this notice is intended solely to alert readers that the content of this article is unreliable. We have not investigated whether authors were aware of or involved in the systematic manipulation of the publication process.

In addition, our investigation has also shown that one or more of the following human-subject reporting requirements has not been met in this article: ethical approval by an Institutional Review Board (IRB) committee or equivalent, patient/participant consent to participate, and/or agreement to publish patient/participant details (where relevant).

Wiley and Hindawi regrets that the usual quality checks did not identify these issues before publication and have since put additional measures in place to safeguard research integrity.

We wish to credit our own Research Integrity and Research Publishing teams and anonymous and named external researchers and research integrity experts for contributing to this investigation.

The corresponding author, as the representative of all authors, has been given the opportunity to register their agreement or disagreement to this retraction. We have kept a record of any response received.

References

[1] L. Wang and S. Chen, "Student Physical Fitness Test System and Test Data Analysis System Based on Computer Vision," *Wireless Communications and Mobile Computing*, vol. 2021, Article ID 5589065, 8 pages, 2021.

WILEY | Hindawi

Retraction

Retracted: Application of Fuzzy Decision Tree Algorithm Based on Mobile Computing in Sports Fitness Member Management

Wireless Communications and Mobile Computing

This article has been retracted by Hindawi following an investigation undertaken by the publisher [1]. This investigation has uncovered evidence of one or more of the following indicators of systematic manipulation of the publication process:

1. Discrepancies in scope
2. Discrepancies in the description of the research reported
3. Discrepancies between the availability of data and the research described
4. Inappropriate citations
5. Incoherent, meaningless and/or irrelevant content included in the article
6. Peer-review manipulation

The presence of these indicators undermines our confidence in the integrity of the article's content and we cannot, therefore, vouch for its reliability. Please note that this notice is intended solely to alert readers that the content of this article is unreliable. We have not investigated whether authors were aware of or involved in the systematic manipulation of the publication process.

Wiley and Hindawi regrets that the usual quality checks did not identify these issues before publication and have since put additional measures in place to safeguard research integrity.

We wish to credit our own Research Integrity and Research Publishing teams and anonymous and named external researchers and research integrity experts for contributing to this investigation.

The corresponding author, as the representative of all authors, has been given the opportunity to register their agreement or disagreement to this retraction. We have kept a record of any response received.

References

[1] Z. Gu and C. He, "Application of Fuzzy Decision Tree Algorithm Based on Mobile Computing in Sports Fitness Member Management," *Wireless Communications and Mobile Computing*, vol. 2021, Article ID 4632722, 10 pages, 2021.

WILEY | Hindawi

Retraction

Retracted: Monitoring System of Key Technical Features of Male Tennis Players Based on Internet of Things Security Technology

Wireless Communications and Mobile Computing

This article has been retracted by Hindawi following an investigation undertaken by the publisher [1]. This investigation has uncovered evidence of one or more of the following indicators of systematic manipulation of the publication process:

(1) Discrepancies in scope

(2) Discrepancies in the description of the research reported

(3) Discrepancies between the availability of data and the research described

(4) Inappropriate citations

(5) Incoherent, meaningless and/or irrelevant content included in the article

(6) Peer-review manipulation

The presence of these indicators undermines our confidence in the integrity of the article's content and we cannot, therefore, vouch for its reliability. Please note that this notice is intended solely to alert readers that the content of this article is unreliable. We have not investigated whether authors were aware of or involved in the systematic manipulation of the publication process.

Wiley and Hindawi regrets that the usual quality checks did not identify these issues before publication and have since put additional measures in place to safeguard research integrity.

We wish to credit our own Research Integrity and Research Publishing teams and anonymous and named external researchers and research integrity experts for contributing to this investigation.

The corresponding author, as the representative of all authors, has been given the opportunity to register their agreement or disagreement to this retraction. We have kept a record of any response received.

References

[1] G. Wu, "Monitoring System of Key Technical Features of Male Tennis Players Based on Internet of Things Security Technology," *Wireless Communications and Mobile Computing*, vol. 2021, Article ID 4076863, 6 pages, 2021.

WILEY | Hindawi

Retraction

Retracted: An Analysis of the Effectiveness of Machine Learning Theory in the Evaluation of Education and Teaching

Wireless Communications and Mobile Computing

This article has been retracted by Hindawi following an investigation undertaken by the publisher [1]. This investigation has uncovered evidence of one or more of the following indicators of systematic manipulation of the publication process:

(1) Discrepancies in scope

(2) Discrepancies in the description of the research reported

(3) Discrepancies between the availability of data and the research described

(4) Inappropriate citations

(5) Incoherent, meaningless and/or irrelevant content included in the article

(6) Peer-review manipulation

The presence of these indicators undermines our confidence in the integrity of the article's content and we cannot, therefore, vouch for its reliability. Please note that this notice is intended solely to alert readers that the content of this article is unreliable. We have not investigated whether authors were aware of or involved in the systematic manipulation of the publication process.

In addition, our investigation has also shown that one or more of the following human-subject reporting requirements has not been met in this article: ethical approval by an Institutional Review Board (IRB) committee or equivalent, patient/participant consent to participate, and/or agreement to publish patient/participant details (where relevant).

Wiley and Hindawi regrets that the usual quality checks did not identify these issues before publication and have since put additional measures in place to safeguard research integrity.

We wish to credit our own Research Integrity and Research Publishing teams and anonymous and named external researchers and research integrity experts for contributing to this investigation.

The corresponding author, as the representative of all authors, has been given the opportunity to register their agreement or disagreement to this retraction. We have kept a record of any response received.

References

[1] B. Wu and C. Zheng, "An Analysis of the Effectiveness of Machine Learning Theory in the Evaluation of Education and Teaching," *Wireless Communications and Mobile Computing*, vol. 2021, Article ID 4456222, 10 pages, 2021.

WILEY | Hindawi

Retraction

Retracted: Dynamic Index Optimal Investment Strategy Based on Stochastic Differential Equations in Financial Market Options

Wireless Communications and Mobile Computing

This article has been retracted by Hindawi following an investigation undertaken by the publisher [1]. This investigation has uncovered evidence of one or more of the following indicators of systematic manipulation of the publication process:

(1) Discrepancies in scope
(2) Discrepancies in the description of the research reported
(3) Discrepancies between the availability of data and the research described
(4) Inappropriate citations
(5) Incoherent, meaningless and/or irrelevant content included in the article
(6) Peer-review manipulation

The presence of these indicators undermines our confidence in the integrity of the article's content and we cannot, therefore, vouch for its reliability. Please note that this notice is intended solely to alert readers that the content of this article is unreliable. We have not investigated whether authors were aware of or involved in the systematic manipulation of the publication process.

Wiley and Hindawi regrets that the usual quality checks did not identify these issues before publication and have since put additional measures in place to safeguard research integrity.

We wish to credit our own Research Integrity and Research Publishing teams and anonymous and named external researchers and research integrity experts for contributing to this investigation.

The corresponding author, as the representative of all authors, has been given the opportunity to register their agreement or disagreement to this retraction. We have kept a record of any response received.

References

[1] J. Zhang, "Dynamic Index Optimal Investment Strategy Based on Stochastic Differential Equations in Financial Market Options," *Wireless Communications and Mobile Computing*, vol. 2021, Article ID 5545956, 9 pages, 2021.

WILEY | Hindawi

Research Article

Prediction of Mineralization Prospects Based on Geological Semantic Model and Mobile Computer Machine Learning

Zhengzhen An,[1] Yue Zhao,[1,2] Yanfei Zhang,[1,3] and Xuguang Li [ID][3]

[1]Mining College of Liaoning Technical University, Fuxin, 123000 Liaoning, China
[2]Institute of Innovation and Development for Fuxin Transition, Liaoning Technical University, Fuxin, 123000 Liaoning, China
[3]Shenyang Geological Survey Center, China Geological Survey, Shenyang, 110034 Liaoning, China

Correspondence should be addressed to Xuguang Li; lixuguang@mail.cgs.gov.cn

Mineral resources are indispensable in the development of human society and are the foundation of national economic development. As the prospecting target shifts from outcrop ore to concealed ore, from shallow to deep, the difficulty of prospecting becomes more and more difficult. Therefore, the prediction of mineralization prospects is of great significance. This paper is aimed at completing the prediction of mineralization prospects by constructing geological semantic models and using mobile computer learning to improve the accuracy of prediction of mineralization prospects and expanding the application of semantic mobile computing. We use five different semantic relations to build a semantic knowledge library, realize semantic retrieval, complete information extraction of geological text data, and study mineral profiles. Through the distributed database of mobile computing, the association rules and random forest algorithm are used to describe the characteristics of minerals and the ore-controlling elements, find the association rules, and finally combine the geological and mineral data of the area and use the random forest algorithm to realize the prospect of mineralization district forecast. The geological semantic model constructed in the article uses the knowledge library for associative search to achieve an accuracy rate of 87.9% and a recall rate of 96.5%. The retrieval effect is much higher than that of traditional keyword retrieval methods. The maximum value of the posterior result of the mineralization prospect is 0.9027, the average value is 0.0421, and the standard deviation is 0.1069. The picture is brighter, and the probability of mineralization is higher.

1. Introduction

Contemporary mineral resource evaluation is the modeling and evaluation process of complex high-dimensional nonlinear systems. Mineralization prediction is based on the guidance of scientific prediction theory, applying geological and mineralization theories and mathematical statistics to comprehensively study geology, geophysics, geochemistry, and remote sensing. We analyze mineralization geological conditions, summarize mineralization rules, establish comprehensive information mineralization prediction model, delineate and evaluate mineralization prospects, provide scientific basis for regional prospecting work deployment, and overall plan mineral resources development.

With the rapid development of computer technology, the digitization of geological information has become more and more popular, prompting the application of mathematical methods, mobile computing, and machine learning in mineralization prediction more and more. The prediction of mineralization prospects is the use of modeling and mobile calculation methods to continuously excavate information, such as geophysical and geochemical prospecting, focusing on the research of the information extraction process, and can truly understand the singularity of the enrichment and loss of elements in the mineralization process law, advanced and precise. We applying the learning method of the geological semantic model deterioration mobile computing machine to the prediction of mineral resources, aim to analyze how to efficiently use geological and mineral information under complex geological conditions, and realize the automation, intelligence, and accuracy of the prediction process of mineralization prospects.

Lombardo et al. introduced a novel, semantic-based geological mapping method, and its application fields are the production of comprehensive geological maps of large administrative areas. Many methods for expressing geological knowledge through UML patterns and ontology have existed for more than ten years. These methods generate resources related to specific fields, such as lithology. They developed a conceptual model aimed at establishing digital codes for several areas of geological knowledge to support source interoperability. They used the term library designed to classify the elements of the geological map of the Alps in western Italy and the Apennines (Piedmont region) in the north. The digitally coded knowledge base is a group of merged ontology, called ontology. The encoding process identifies the semantically encoded objects, that is, geological units, and collects relevant information about these objects from authoritative resources (such as GeoSciML) (preferred to the application of SCHE). However, their conceptual model design is not applicable to applications in other regions [1]. Lamperti et al. effectively calibrate the agent-based model (ABM) to real data which is an open challenge. They combined machine learning and intelligent iterative sampling to clearly solve the problem of parameter space exploration and calibration of ABMs. This method "learns" a fast surrogate metamodel through a limited number of ABM evaluations and approximates the nonlinear relationship between ABM input (initial conditions and parameters) and output. The performance is evaluated according to the asset pricing model of Brock and Hommes (1998) and the "island" endogenous growth model (Fagiolo and Dosi, 2003). The results show that the machine learning agent obtained using the proposed iterative learning process provides a fairly accurate real model agent and greatly reduces the calculation time required for large-scale parameter space exploration and calibration. However, they have no specific settings in parameter design [2]. Lalomov et al.'s research established the heterogeneity of placer gold, reflecting the multistage history of the development of placer gold clusters and the diversity of bedrock mineralization formed by placer gold deposits. In the placer structure, three epochs are divided, reflecting the post-Palaeozoic development history of the Ural fold belt: (1) Mesozoic-Early Cenozoic quasiplain action, regional weathering crust formation, disintegration of primary gold sources, linear erosion-tectonics. The depression was formed, which accumulated material from the displaced weathering crust. (2) Primary mineral sources and intermediate gold deposits in the Pliocene-Quaternary orogenic tectonic activation and erosion stage. (3) Modern topography, water network, and alluvial deposits, the formation of placer. In terms of morphology, chemical composition, and internal structure of grains, five types of primary placer gold have been identified, three of which reflect the structure of the primary mineral source and have been almost completely eroded; the fourth records the quasiplanation stage and erosion traces of superficial changes in the development area of structural depressions. The fifth type has the typomorphic characteristics of near provenance gold, which is characterized by the mineralization exposed in the final stage of the morphological and structural development of the tectonic-magmatic Ural belt. Reconstructing the development stage of the Wagland Placer Group, it is possible to assess the potential of the existing placer and determine the prospect of economic primary mineralization. However, his research found diversity but did not fundamentally show the characteristics of its heterogeneity [3].

The innovations of this article are as follows: (1) fully construct a brand-new geological semantic model and complete the search of mining areas in combination with geological information; (2) use a mobile computing machine learning algorithm, mainly using a rule algorithm and a random forest algorithm, which is very good used in model construction; and (3) use five different semantic relations to construct a semantic knowledge base, realize semantic retrieval, complete information extraction of geological text data, and study mineral profiles.

2. Prediction Method of Mineralization Prospect Based on Geological Semantic Model and Mobile Computer Machine Learning

2.1. Mobile Computing. Mobile computing is a new technology that has emerged with the development of the Internet, mobile communications, distributed computing, databases, and other technologies [4, 5]. Through mobile computer technology, computers and other intelligent terminal information devices can transmit data wirelessly, share resources, and provide customers with useful, accurate, and timely information at any time [6]. As a result, people's life and working methods have undergone great changes. Mobile information technology is an interacademic and extensive new technology. This is currently a hot field of computer technology research. In addition to network infrastructure, e-commerce, and software technical indicators, mobile computing is considered one of the important technologies that will have a broad impact on the future [7, 8]. As a hotspot and emerging computing model, it is of great significance to study the problems, but there are also great challenges.

The computer environment is different from the previous distributed computer environment. In the traditional distributed computing environment, the location of the central computer is stable, the address information of the central computer is known, and each node maintains an uninterrupted connection through a fixed network, assuming that the network communication is symmetrical. In mobile computer systems, these assumptions no longer apply [9, 10]. The entire environment of mobile computers is a distributed computer system composed of fixed nodes and mobile nodes. In this system, the user's location is not restricted by fixed equipment. The terminal can move freely and maintain the connection with each node of mobile communication through the network. This computing mode, which is not restricted by fixed networks and restricted by fixed hosts, provides great convenience for people to access information [11, 12].

Traditional distributed computer research is based on wired networks and fixed central computers. The search of

the distributed database must be carried out under the conditions of fixed network connection, peer-to-peer communication cost, and fixed central computer node [2, 13]. However, with the development of mobile computers and the popularity of portable devices, many computer nodes may create network connections in free loops, and the above assumptions are no longer valid [14, 15]. Therefore, the concept of mobile computers and mobile databases was born, which became the new research direction of the international database community. Due to the characteristics and characteristics of the mobile computer environment, the distributed database and C/S (client/server) database in the database field cannot effectively support the mobile computer environment [16, 17]. To fully support portability, the computer needs to be improved or redesigned and upgraded to a new mobile database.

2.2. Semantic Technology. At present, the main semantic modeling technologies include semantic modeling technology based on semantic research and ontology-based semantic modeling technology. This article adopts a semantic modeling method based on logical relationships. The two technologies are introduced separately [18, 19].

The basic idea of the semantic web was first proposed by Tim Berners-Lee in 1998 who then formally proposed the concept of the semantic web at the XML2000 conference in 2000. The status of the semantic web was formally established when the W3C established the "Semantic Web Activity" organization in 2001 [20, 21]. The goal of the semantic network is to convert the information on the web page into the meaning of words that can be read by the computer system, so that smart devices can independently retrieve and access the information on the network effectively, thereby completing the application and higher-level internet semantics knowledge application. Through the operation and processing of the semantic grammar form, the standardization of the semantic content is determined, and the operability at the semantic level is realized. In simple terms, semantics is used to implement a logical architecture [22, 23].

Ontology-based semantic modeling methods are also based on the semantic web, to better solve the sharing and reuse of information on the semantic level. Ontology or ontology is originally a philosophical concept, used to study the essence of the objective world and is a systematic explanation and explanation of objective existence. The application of semantic modeling methods in the field of artificial intelligence can clearly indicate the standardization and specification of all shared conceptual models. Ontology-based modeling includes the following five basic modeling primitives: class, relationship, function, axiom, and instance.

The logical relationship-based method defines a nested data model for expressing data relationships and a set of SQL-like description languages for describing the logical relationship between data. In the process of semantic analysis, the Chase method is used to continuously compare the data. We track the existing constraint relationships until the largest semantic set is generated, so as to obtain complete semantic information.

2.3. Machine Learning. Random forest (RF) is a general data extraction method in the field of machine learning. This is a typical multiclass algorithm. Decision tree is the main classification method of random forest algorithm. The essence of a decision tree is actually a tree composed of many nodes. The basic principle of the random forest algorithm is to use technical sampling to form a new random sampling training group and then use an autonomous data set to model the decision tree, form a random forest, and vote for the classification result.

The random forest algorithm combines the initial sampling method based on the decision tree algorithm theory, collects multiple independent tree classifiers, and sorts and predicts the final result through a voting strategy. The random forest algorithm has the characteristics of theoretically easy to understand, low adaptability parameters, and strong antinoise function. The most important thing is that it has high classification efficiency in practical applications and is not easy to cause overload. Because there is no need to understand the excellent random performance and the performance of historical samples, it is widely used in many fields. Therefore, many researchers have conducted extensive research and applications on random forests.

The random forest algorithm has excellent antinoise ability and outlier ability. The random forest algorithm does not need to preprocess the classification object, so it simplifies the preprocessing procedure of related data. The random forest algorithm has excellent performance in many aspects, but it still has shortcomings. For example, when selecting features, the random forest algorithm will randomly select from the data set, and the parameter selection of the random forest algorithm is manually set. These functions do not show the error that increases the classification result. From the perspective of practical applications, it is necessary to further enhance the ability of the random forest algorithm to output high-quality features, optimize parameter selection, further reduce the generalization error of the random forest model, and improve the accuracy of the random forest algorithm classification [24].

3. Prediction Model of Mineralization Prospect Based on Geological Semantic Model and Mobile Computer Machine Learning

3.1. Geological Semantic Model

3.1.1. Construction of Semantic Model of Geological Data. This paper mainly constructs a geological semantic model based on the meaning of the semantic model and proposes a four-element combination, which are a collection of geological data concepts, a collection of geological relations, a collection of geological attributes, and a collection of examples, which are represented by GDO, GDR, GDP, and GDI [25]. According to the research status of geological ontology, according to the types of geological work and the application of geological data, in order to realize the functions of compilation, analysis, reflection, restoration, and intelligent advancement of geological data, various classification systems have been classified into many subcategories.

3.1.2. Semantic Relationship of Geological Semantic Model Application. The geological semantic model constructed in this paper is mainly applied to five kinds of semantic relations, namely the following: (1) subordinate relation: mainly the concept level problem in the model and the subordination relation; (2) equivalence relation: the concept of the same level or the equivalence relation; (3) cross-relationship: that is, there are some identical conceptual relationships between two different geological concepts; (4) concept instance relationship: used to more clearly illustrate the relationship between various concepts and corresponding cases; and (5) spatial relationship: mainly refers to the inclusion, the facts of the positional relationship of the phase relationship, such as cutting off, connecting, and integrating.

3.1.3. Semantic Retrieval. First of all, we need to collect geological data and build a basic dictionary of geology and mineral resources in order to achieve semantic retrieval. There are two main sources of data: one is the professional knowledge in the geological field; the other is the mining of geological data through mobile computer learning technology [26].

Here, the user's needs are an entity. Through data preprocessing, the user only needs to enter understandable keywords and information to obtain intelligent, accurate, and user-friendly data results, which have undergone data fusion and data preprocessing. And other related processes achieve the semantic conversion of data information, to meet the needs of users.

3.1.4. Functions Realized by Geological Semantic Model. Functions realized by geological semantic model are as follows: (1) Coarse-grained geological information knowledge serves geological text clustering. When the user retrieves the relevant geological information, the relevant conditions and grouping results will be automatically saved, which is conducive to the user's second search; (2) comprehensive semantic retrieval of geological data and geological literature information. Semantic retrieval includes text and tables, which requires solving these two data fusion problems in the process of establishing a database; (3) display and obtain content information based on complete text; (4) the comprehensive problem of spatial data and nonspatial data. It can solve the nonspatial data problem of the system and complete the visual representation of spatial data; (5) association analysis: research on geology not only is limited to geological knowledge but also includes related information such as authors, units, projects, and mineral resources and conducts correlation analysis.

3.2. Prediction of Mineralization Prospects Based on Geological Semantic Model and Mobile Computer Machine Learning

3.2.1. Right of Evidence Law. The weight of evidence method is to use a certain ore-controlling mineralization geological condition or prospecting information sign as a predictive factor in the mineralization prediction. The predictive factor is the evidence factor, and the weight value is used to quantitatively measure the importance of each evidence factor to the mineralization. Then, each evidence factor is assigned a binary value according to the two states of the evidence factor "existence" and "nonexistence." The most important and critical step in the calculation of mineralization prediction using the weight of evidence method is to determine the weight of evidence for these evidence factors and the importance of mineralization. The model of the right of evidence is

$$\mathrm{EVI}(F|B_1 B_2 \cdots B_n) = Q_O + Q_1 + \cdots + Q_n. \tag{1}$$

In the formula, F is the event to be predicted, $B_1 B_2 \cdots B_n$ is the predictor, Q is the prior probability of the predicted event F, and $Q_1, Q_2, \cdots Q_n$ is the corresponding weight value. The weight value is divided into positive full $Q+$ and negative right $Q-$ two kinds.

According to the existence or nonexistence of each evidence factor, the corresponding weight value is calculated. $Q+$ represents the weight value of the existing state, and $Q-$ represents the weight value of the nonexistent state. The calculation of mineralization prediction based on the weight of evidence method is roughly divided into three steps: first, calculate the probability of occurrence of deposits (points) in the study area according to the principle of probability theory; secondly, calculate the corresponding weight values according to the two states of each factor; and finally, all the evidence factors involved in the prediction are integrated to calculate the posterior probability value.

To apply the weight of evidence method, the research area must be divided into cells first. The number of deposit points in the research area is set as F. From the principle of probability theory, it can be obtained that any cell in the research area can be selected. This cell contains the deposit points the probability: $L(F) = F/N$. $L(F)$ is the prior probability of the study area, into the form of chance.

$$I(F) = \frac{L(F)}{[1 - L(F)]}. \tag{2}$$

The probability of mineral occurrence in the presence of evidence factor B is obtained as

$$L(F|B) = L(B \cap F)/L(B) = N(B \cap F)/F. \tag{3}$$

From Equation (3), it can be obtained that the posterior probability of the occurrence of a mining point in the presence of the evidence factor B is

$$L(F|B) = \frac{L(B|F)}{L(B)} \times L(F). \tag{4}$$

From Equation (4), it can be concluded that the posterior probability can actually be understood as the conditional probability of the existence of the mine in the presence of the evidence factor B. In the same way, the posterior probability when factor B does not exist is

$$L(F|\bar{B}) = \frac{L(\bar{B}|F)}{L(\bar{B})} \times L(F). \tag{5}$$

3.2.2. Definition and Calculation of Weight. The importance of each evidence factor to mineralization is quantitatively analyzed by the weight value of the evidence factor. If the weight of evidence method is used to carry out mineralization prediction, then it is necessary to calculate the weight value of each evidence factor to the mineralization, and the formula is as follows:

$$Q^+ = \ln \frac{L(B|F)}{L(B|\bar{F})}, \tag{6}$$

$$Q^- = \ln \frac{L(\bar{B}|F)}{L(\bar{B}|\bar{F})}. \tag{7}$$

In the above formula, $Q+$ and $Q-$, respectively, represent the weight values of the evidence factor in the "existence" and "nonexistence" states in the weight of evidence model. In (6), $Q+$ represents the weight value in the state of existence, and in (7), $Q-$ represents the size of the weight value in the absence of state.

3.2.3. Comprehensive Multiple Evidence Factors. In the actual mineralization prediction, due to the complexity of the mineralization and the accuracy of the prediction results, we need to use multiple predictive factors. At this time, we need to comprehensively calculate multiple evidence factors and calculate the posterior probability of multiple evidence factors. The method and steps are the same as when calculating one evidence factor in the previous section. For example, in a certain mineralization prediction, there are n factors related to mineralization, which are represented as 1, 2,…,n. According to the calculation steps in the previous section, the posterior probability of occurrence or nonoccurrence of deposit point F under the existence of these n evidence factors can be obtained as

$$L(F|B_1 B_2 \cdots B_n) = \frac{L(B_1 B_2 \cdots B_n|F)}{L(B_1 B_2 \cdots B_n)} L(F), \tag{8}$$

$$L(\bar{F}|B_1 B_2 \cdots B_n) = \frac{L(B_1 B_2 \cdots B_n|\bar{F})}{L(B_1 B_2 \cdots B_n)} L(\bar{F}). \tag{9}$$

The posterior probability is converted to the probability form to get

$$I(F|B_1 B_2 \cdots B_n) = \frac{L(B_1 B_2 \cdots B_n|F)}{L(B_1 B_2 \cdots B_n|\bar{F})} I(F). \tag{10}$$

Assuming that the evidence factors are conditionally independent, the probability of the occurrence of the evidence factors under the condition of the existence of the mine F can be obtained as

$$L(B_1, B_2, \cdots, B_n|F) = L(B_1|F)L(B_2|F) \cdots L(B_n|F). \tag{11}$$

In the same way, it can be obtained that when the mine point F does not exist, the probability of occurrence of the evidence factor is

$$L(B_1, B_2, \cdots, B_n|\bar{F}) = L(B_1|\bar{F})L(B_2|\bar{F}) \cdots L(B_n|\bar{F}). \tag{12}$$

From the above two formulas, the probability formula can be obtained, which can be expressed as

$$I(F|B_1 B_2 \cdots B_n) = \frac{L(B_1|F)L(B_2|F) \cdots L(B_n|F)}{L(B_1|\bar{F})L(B_2|\bar{F}) \cdots L(B_n|\bar{F})} \times I(F). \tag{13}$$

The logarithmic transformation of the above formula obtains the posterior probability of the occurrence of the deposit point F under the condition of the existence of n evidence factors as

$$\text{EVI}(F|B_1 B_2 \cdots B_n) = \text{EVI}(F) + Q_1^+ + Q_2^+ + \cdots Q_n^+. \tag{14}$$

According to the mathematical symbol of sum, the above formula can be simplified to

$$\text{EVI}(F|B_1 B_2 \cdots B_n) = \text{EVI}(F) + \sum_{j=1}^{n} Q_j^k, \tag{15}$$

$$Q_j^k = \begin{cases} Q^+ \\ Q^-. \end{cases} \tag{16}$$

The weight when the evidence factor exists is $Q+$, and the weight when the evidence factor does not exist is $Q-$. The formula as a posterior probability is expressed as follows:

$$L\left(F|B_1^k \cap B_2^k \cdots B_n^k\right) = \frac{\exp\left\lfloor \text{EVI}\left(F|B_1^k \cap B_2^k \cdots B_n^k\right)\right\rfloor}{1 + \exp\left[\text{EVI}\left(F|B_1^k \cap B_2^k \cdots B_n^k\right)\right]}. \tag{17}$$

Fuzzy weight calculation formula is as follows.

$$S_{\lambda B(x)} = \ln \frac{L\left[\lambda_{B(x)}|F\right]}{L\left[\lambda_{B(x)}|\bar{F}\right]} = \ln \frac{\lambda_{B(x)} L(B_1|F) + \left[1 - \lambda_{B(x)}\right] L(B_2|F)}{\lambda_{B(x)} L(B_1|\bar{F}) + \left[1 - \lambda_{B(x)}\right] L(B_2|\bar{F})}. \tag{18}$$

Among them, the membership function can be calculated from the following linear relationship.

$$\lambda_B(x) = \frac{V - \min_{x \in B_2} V}{\max_{x \in B_2} V - \min_{x \in B_2} V}. \tag{19}$$

Fuzzy weights can explain the importance of various forms of uncertain factors, while ordinary weight of evidence can only explain the importance of the existence or nonexistence of uncertain factors, so fuzzy weights can be more comprehensive explain the importance of the factor. According to the calculation steps of the ordinary weight of evidence method, we can get the posterior probability of

the fuzzy weight of evidence method as

$$\mathrm{EVI}\left(F \Big| B_1^k \cap B_2^k \cdots B_n^k \right) = \mathrm{EVI}(F) + \sum_{j=1}^{n} Q_j^k. \qquad (20)$$

In the above formula, $B_1^k, B_2^k, \cdots B_n^k$ represent the evidence factors of n different states and Q_j^k the corresponding weight values of these factors in different states. Since the calculation of the weight value of the fuzzy weight of evidence first needs to calculate the two extreme sets and remove these two extreme combinations, then it should correspond to a smaller subset, so formula (20) only needs to satisfy the condition of independence in a smaller range. Therefore, the conditional independence required to apply the fuzzy weight of evidence method is weaker than that of the ordinary weight of evidence. This also shows that the fuzzy weight of evidence method reduces the overall error of the posterior probability. Then it can be said that compared with ordinary evidence rights methods, to a certain extent, fuzzy evidence rights avoid conditional independence.

4. Prediction and Analysis of Mineralization Prospects Based on Geological Semantic Model and Mobile Computer Learning

4.1. Comparison of Experimental Results of Geological Semantic Model. In the process of semantic retrieval, the geological semantic model established in this paper can not only use keywords but also use related search and thesaurus retrieval, which improves the accuracy and comprehensiveness of the search. Hierarchy excavates the rules and knowledge of keywords, supplements, and expands related knowledge searches. It can be seen from Table 1 that using the thesaurus and knowledge map to search is more accurate and comprehensive than keyword retrieval. The knowledge map finds a large number of materials, and the accuracy rate reaches 87.9%. The rate reached 96.5%.

We have adopted three fusion methods: PCA fusion, IHS fusion, and wavelet fusion, respectively, fusion processing of R, G, and B multispectral data, to maximize the role of the data. From Figure 1, we can see that the wavelet transform method is superior to other fusion methods in terms of spectral information retention and peak signal-to-noise ratio for the statistical calculation of the amount of information after fusion, so this time, the wavelet transform method is used for fusion processing.

4.2. Spectral Characteristics of Rock and Mineral Alteration. Different information such as minerals, rocks, or alteration and mineralization have different characteristic absorption spectrum and characteristic reflection spectrum characteristics, so that different geological bodies or geological phenomena are directly reflected as different spectrum curves on remote sensing images. With the improvement of spectral resolution, the spectral characteristics of rock minerals have become a favorable tool for remote sensing mineralization information extraction, and they play an increasingly

important role in the process of detailed exploration and mineralization prediction.

The ions and groups corresponding to the spectral characteristics of various rock minerals are shown in Table 2. The spectral characteristics within the range of $1.3 \sim 2.5\,\mu m$ are mainly affected by carbonate ions, hydroxide ions, and possible water molecules in the minerals. The absorption band of CO_3^{2-} is the strongest at $2.35\,\mu m$, corresponding to the 8th band of ASTER, which can be used to detect the presence of carbonate minerals. The absorption band of OH- is stronger at $1.4\,\mu m$ and $2.2\,\mu m$. Since $1.4\,\mu m$ is not within the spectral range of the ASTER data, the absorption characteristics of the 6th band corresponding to OH- at $2.2\,\mu m$ and $2.3\,\mu m$ are often used in the ASTER data to identify minerals.

The altered minerals formed by cyanide rock formation include chlorite, carbonated minerals, albite, and epidote. The related minerals include Au, Cu, Pb, Zn, Fe, and other metal minerals. According to the analysis results of the mineral spectrum characteristics, the 6 bands (Band1, Band2, Band3, Band5, Band8, and Band9) of the ASTER data are combined to extract the green rock formation alteration information [27]. The negative high value of the 8th band and the positive high value of the 9th band are used as the criterion of the alteration information eigenvector. It can be seen from the eigenvector matrix of Figure 2 that the main contribution of the fifth principal component (PC5) comes from Band8 (-0.63562) and Band9 (0.66101), satisfying the judgment criterion. Therefore, the highlight area of the PC5 image is the area with strong chlorite and carbonate alteration.

It can be seen from Figure 3 that each element has a higher extreme value, and the second and third highest values have a large change gradient, and the standard deviation and coefficient of variation are also large. Based on the statistics of the characteristic value of each element in the study area, the content distribution histogram and the content logarithmic distribution histogram of each element are, respectively, analyzed. The results show that due to the existence of extremely high and extremely low values, whether each element is difficult for the original value or the logarithmic value to obey the normal distribution, the iterative processing method is used to deal with the extreme outliers of the element data.

4.3. Statistical Analysis of the Weight Coefficient of the Evidence Layer. We set 7 evidence layer numbers, all of which belong to the element anomaly distribution map. The letters indicate the meaning: (a) Ag element, (b) Au element, (c) Cr element, (d) Cu element, (e) Mo element, (f) Ni, and (g) Pb.

It can be seen from Figure 4 that all the layers we set meet the conditional test. We, respectively, estimated the positive and negative weight coefficients, variances, partial variances, etc. of these evidence layers. The estimation results are shown in Figure 4.

We conducted regression analysis on the abnormal distribution of nine types of elements with different iteration times. In the process of parameter optimization using

TABLE 1: Comparative verification and analysis of semantic retrieval experiments.

Search method	Number of obtained materials	Find accuracy, %	Find comprehensive rate, %
Keyword search	265	78.5	46.7
Semantic retrieval (thesauri)	412	90.6	82.1
Semantic retrieval (knowledge illustrated book)	456	87.9	96.5
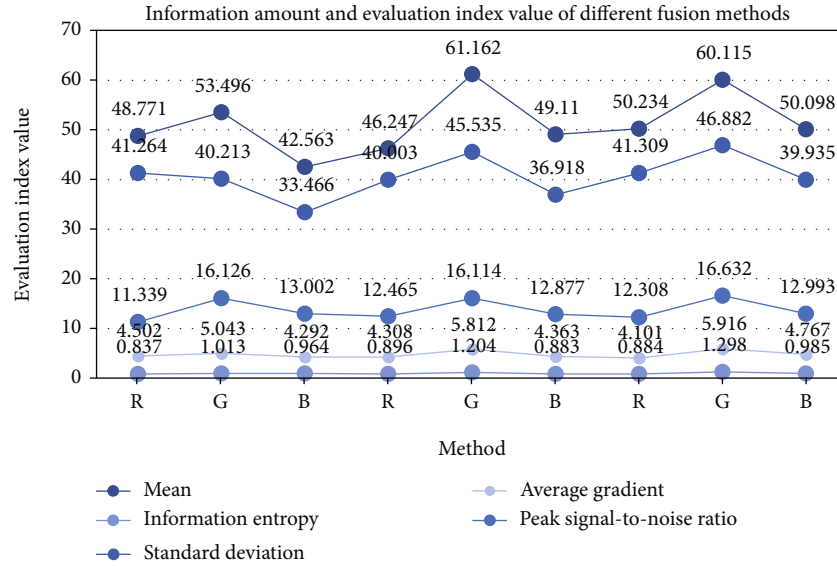
FIGURE 1: Information amount and evaluation index value of different fusion methods.

TABLE 2: Ion and group absorption bands corresponding to the characteristics of rock mineral reflection spectrum.

Ion or group	Characteristic absorption band center	Corresponding ASTER band	Typical minerals
Iron ion Fe^{2+}	0.45, 0.52, 0.55, 1.0~1.1	Band1 (0.52~0.60)	Lepidocrocite
Iron ion Fe^{3+}	0.49, 0.70, 0.87	Band2 (0.61~0.69)	Goethite, hematite, jarosite
		Band3 (0.76~0.86)	
Hydroxyl(OH-)Al-OH, Mg-OH	1.4, 2.2, 2.3	Band6 (2.185~2.225)	Kaolinite, pyrophyllite, muscovite, talc, serpentine
		Band7 (2.225~2.285)	
Carbonate ion $CO^{3\sim}$	1.9, 2.0, 2.16, 2.35, 2.55	Band6 (2.185~2.225)	Calcite, dolomite
		Band7 (2.225~2.285)	
		Band8 (2.295~2.285)	

conjugate gradient, we tested the predictions of 30, 50, 80, and 100 search iterations, respectively. The effect, the calculation result of the regression coefficient, is shown in Figure 5. It can be seen from Figure 5 that when the parameter optimization is iterated to 80 and 100 times, the regression coefficient is very close and basically reached a stable state.

In order to compare the evidence-weighted model, the logistic regression model, and the constrained Boltzmann machine model for the mineralization prediction effect, the Youden index is also defined as the sum of the TP rate and the FP rate minus 1, the threshold increment interval is defined, and three types are calculated, respectively. The model predicts the Youden index of the metallogenic unit,

and the threshold corresponding to the maximum Youden index is used as the threshold for the corresponding model to determine the metallogenic unit. After obtaining the corresponding judgment threshold, the AUC value and the standard deviation SEAUC value of the three models were calculated using formulas (3) and (5), and the significance level $\alpha = 0.05$ was set to calculate the corresponding ZAUC value. The results are shown in Figure 6.

4.4. Experimental Prediction Results of Mineralization Prospects. Figure 7 shows the typical linear and circular fault trace characteristics in the study area and nearby areas. The intrusive body in Figure 7(a) is the Cenozoic Eocene strata; the left side in Figure 7(b) is the Mesozoic Triassic intrusion
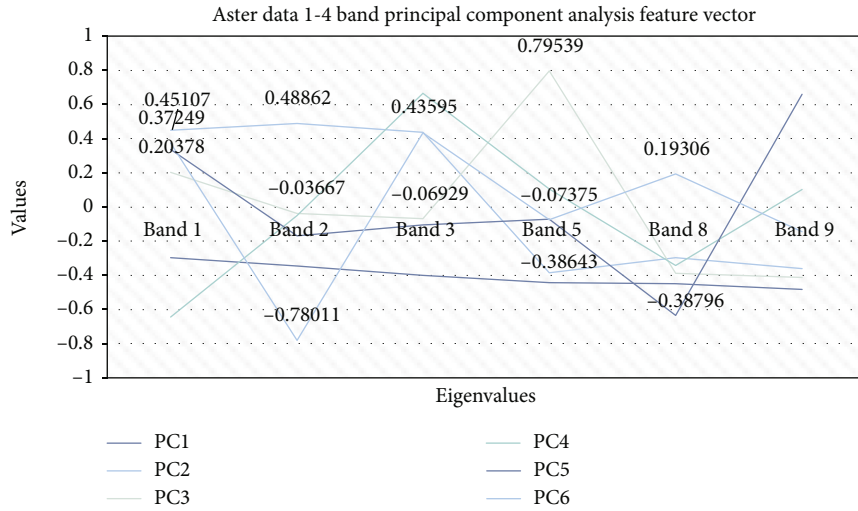
FIGURE 2: ASTER data 1-4 band principal component analysis feature vector.
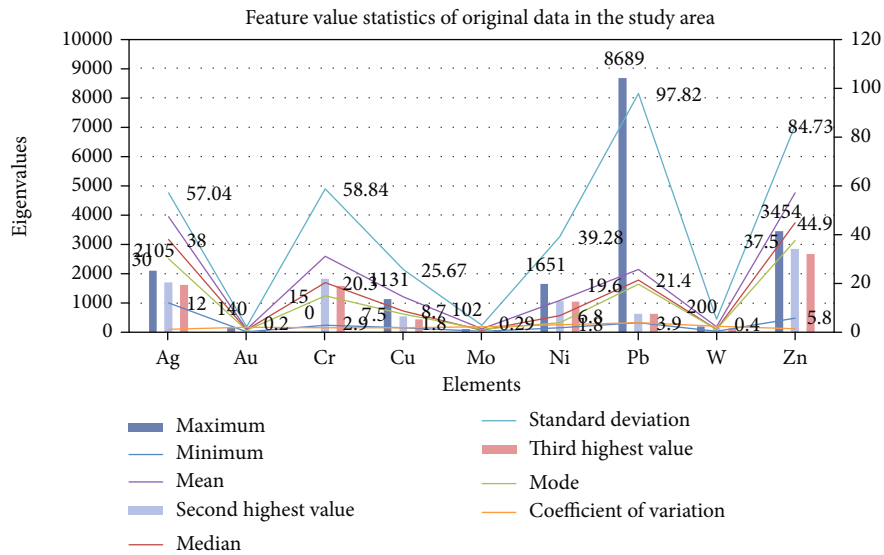
FIGURE 3: Feature value statistics of original data in the study area.
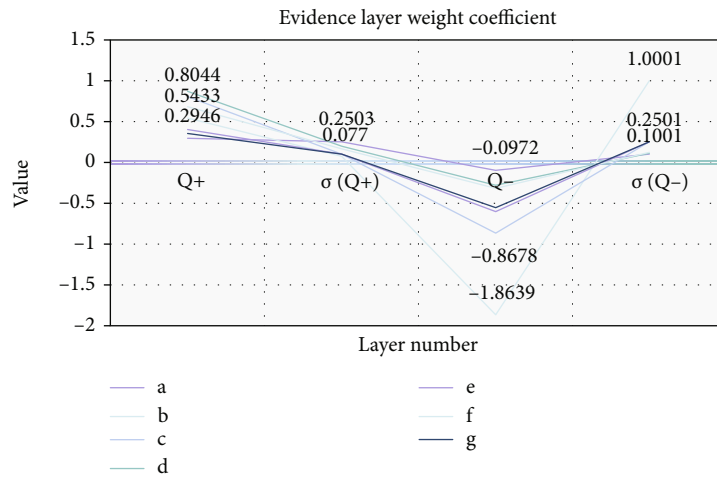
FIGURE 4: Evidence layer weight coefficient.
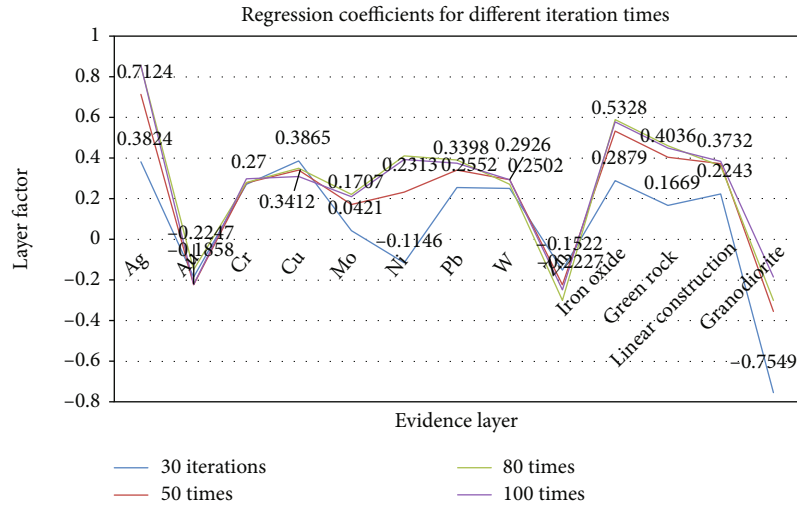
FIGURE 5: Regression coefficients for different iteration times.
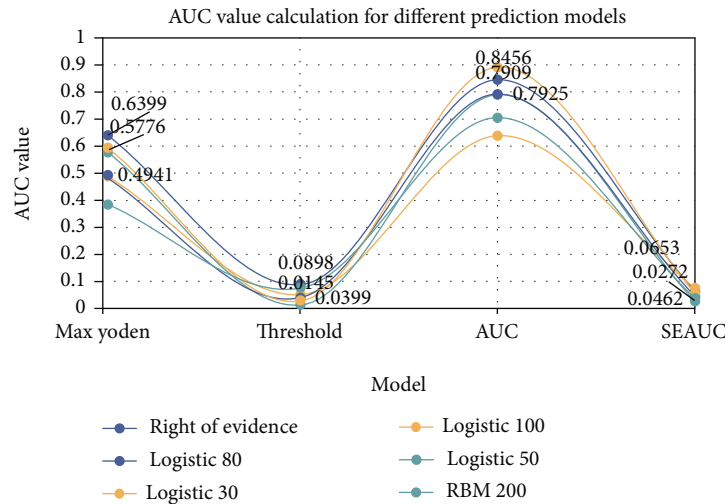
FIGURE 6: AUC value calculation for different prediction models.

body, and the right side is the fold formed during the Jurassic-Cretaceous period; Figure 7(c) is the fault divided into many triangular fault cliffs form fault triangles; Figure 7(d) shows the fractured fracture zone accompanying the formation of large faults, mostly small parallel fractures; Figure 7(e) shows the interruption and loss of the Upper Cretaceous (Ks2c) strata; Figures 7(e) and 7(f) are the displacement of the Jurassic stratum, and there are faults.

From the slope of the broken line in Figure 8, it can be seen that the ring structure within the range of 0-0.5 km contains 50% of the mine points, and the formation of minerals in this area is mainly affected by the ring structure; the secondary faults within the range of 1-1.5 km include the number of mine points has risen sharply, including nearly 43% of the mine points, and the large-scale faults have always been at a value of 0, indicating that the secondary faults in this range play a major role in controlling the formation of the deposit; within the

range of 1.5-3 km, the secondary faults have a major control effect on the formation of the deposit. The rate of increase in the number of ore points contained in the fault exceeds the ring structure, indicating that the formation of ore bodies in this range is mainly controlled by secondary faults; and the influence of large faults on the formation of ore deposits is in the range of 4-6 km and 8-10 km. In general, the relationship between the structure of the study area and the known ore sites reflects the characteristics of the structure controlling the location of the deposit.

Based on the optimized weight of evidence algorithm module, the seven weight of evidence factors are superimposed and analyzed, and the final result of the posterior probability of mineralization in the study area is shown in Figure 9. The minimum is 0, the maximum is 0.902722; the mean is 0.042112, and the standard deviation is 0.106953. The picture is brighter, and the probability of mineralization is higher.

(a)   (b)   (c)

(d)   (e)   (f)
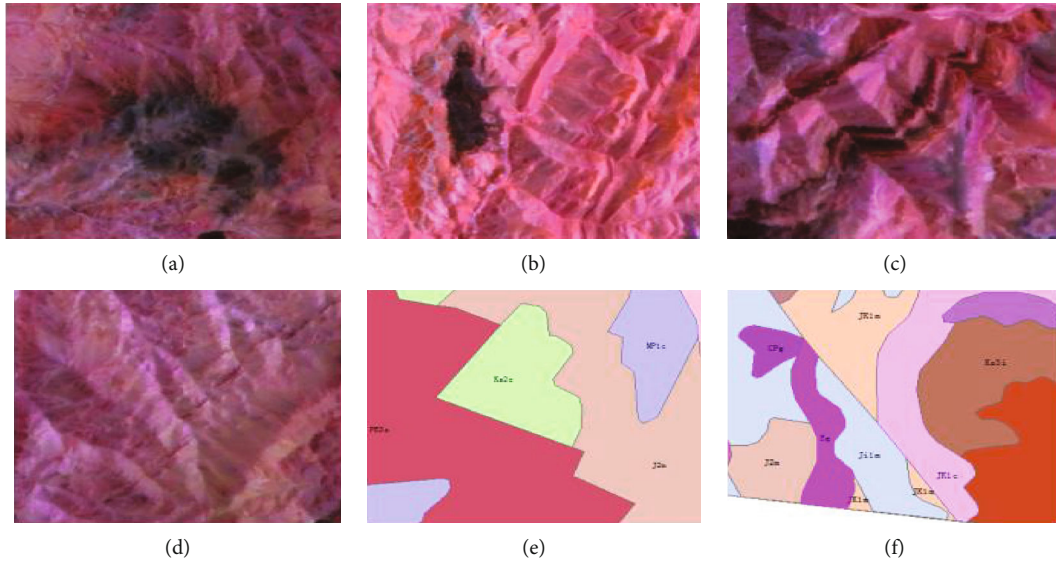
FIGURE 7: Characteristic map of linear and circular fault tracks (the picture from Baidu Gallery). (a) Semicircular intrusion body. (b) Intrusion + folds. (c) Fault triangle. (d) Broken shear zone. (e) Disruption and lack of formation. (f) Displacement of faults in the same stratum.
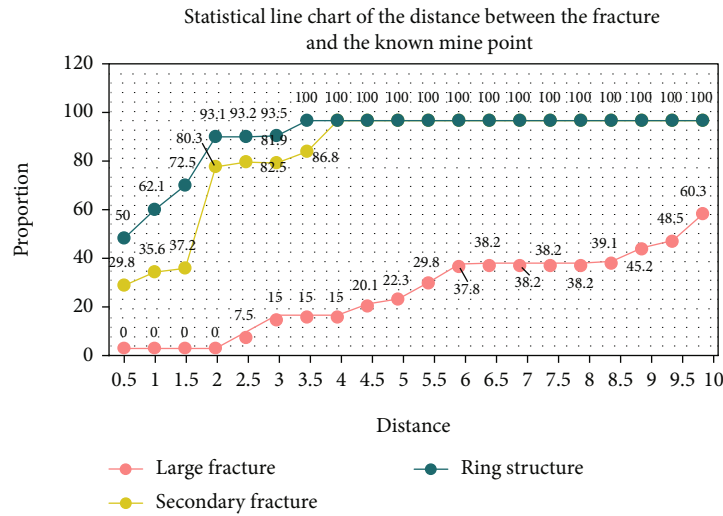
FIGURE 8: Statistical line chart of the distance between the fracture and the known mine point.
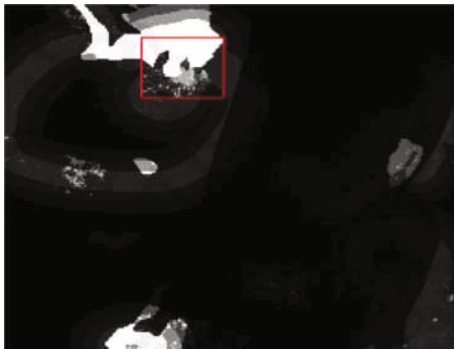
FIGURE 9: Result map of the posterior probability of mineralization in the study area (the picture from Baidu Gallery).

5. Conclusions

This article is mainly based on the study of geological semantic model and mobile computing machine learning to predict the mineralization prospects, constructs the geological semantic model, uses the rule algorithm and random forest algorithm in machine learning, and completes the collection and preprocessing of geological information which achieved a high recall rate and precision rate. We analyzed the geological conditions of mineralization, summarized the rules of mineralization, established a prediction model of mineralization prospects based on geological semantic model and mobile computer learning, and realized the prediction of prospects of mineralization, which is conducive to the deployment of prospecting work and the development

and utilization of mineral resources overall planning. The innovation of this paper is to fully construct a brand-new geological semantic model, complete the search of the mining area in combination with geological information, and use the mobile computing machine learning algorithm, mainly using the rule algorithm and the random forest algorithm, which are well applied to the model construction. The shortcomings of this article are the limitations of working conditions and the influence of the number of studies. It is hoped that it can be more perfect in the future research work to improve the accuracy of the research results.

Data Availability

No data were used to support this study.

Conflicts of Interest

The authors declare that they have no conflicts of interest.

Acknowledgments

References

[1] V. Lombardo, F. Piana, and D. Mimmo, "Semantics-informed geological maps: conceptual modeling and knowledge encoding," *Computers & Geosciences*, vol. 116, pp. 12–22, 2018.

[2] F. Lamperti, A. Roventini, and A. Sani, "Agent-based model calibration using machine learning surrogates," *Journal of Economic Dynamics & Control*, vol. 90, pp. 366–389, 2018.

[3] A. V. Lalomov, V. A. Naumov, A. V. Grigorieva, and L. O. Magazina, "Evolution of the Vagran gold-bearing placer cluster (northern Urals) and prospects for revealing bedrock mineralization," *Geology of Ore Deposits*, vol. 62, no. 5, pp. 407–418, 2020.

[4] Y. Lei, Z. Zhu, and Q. Li, "An ontological metamodeling framework for semantic simulation model engineering," *Journal of Systems Engineering and Electronics*, vol. 31, no. 3, pp. 527–538, 2020.

[5] L. Lalicic and A. Dickinger, "An assessment of user-driven innovativeness in a mobile computing travel platform," *Technological Forecasting and Social Change*, vol. 144, pp. 233–241, 2019.

[6] H. Gao and Y. Yin, "Editorial: ACM/Springer mobile networks & applications-special issue on mobile computing and software engineering," *Mobile Networks and Applications*, vol. 25, no. 2, pp. 672-673, 2020.

[7] L. YIN, Y. GUO, H. ZHANG, W. HUANG, and B. FANG, "Threat-based declassification and endorsement for mobile computing [J]," *Chinese Journal of Electronics*, vol. 28, no. 5, pp. 1041–1052, 2019.

[8] S. K. Singh and D. P. Vidyarthi, "A heuristic channel allocation model with multi lending in mobile computing network," *International Journal of Wireless and Mobile Computing*, vol. 16, no. 4, pp. 322–339, 2019.

[9] C. Z. Lu, G. S. Zeng, and Y. J. Xie, "Bigraph specification of software architecture and evolution analysis in mobile computing environment," *Future Generation Computer Systems*, vol. 108, pp. 662–676, 2020.

[10] T. Yang, Z. Jiang, R. Sun, N. Cheng, and H. Feng, "Maritime search and rescue based on group mobile computing for unmanned aerial vehicles and unmanned surface vehicles," *IEEE Transactions on Industrial Informatics*, vol. 16, no. 12, pp. 7700–7708, 2020.

[11] B. Liao, Y. Ali, S. Nazir, L. He, and H. U. Khan, "Security analysis of IoT devices by using mobile computing: a systematic literature review," *IEEE Access*, vol. 8, pp. 120331–120350, 2020.

[12] C. Helma, T. Cramer, S. Kramer, and L. De Raedt, "Data mining and machine learning techniques for the identification of mutagenicity inducing substructures and structure activity relationships of noncongeneric compounds," *Journal of Chemical Information and Computer Sciences*, vol. 35, no. 4, pp. 1402–1411, 2018.

[13] N. Zimmerman, A. A. Presto, S. P. N. Kumar et al., "A machine learning calibration model using random forests to improve sensor performance for lower-cost air quality monitoring," *Atmospheric Measurement Techniques*, vol. 11, no. 1, pp. 291–313, 2018.

[14] I. Goodfellow, P. Mcdaniel, and N. Papernot, "Making machine learning robust against adversarial inputs," *Communications of the ACM*, vol. 61, no. 7, pp. 56–66, 2018.

[15] S. L. Benjamin, "Inverse molecular design using machine learning: generative models for matter engineering," *Science*, vol. 361, no. 6400, pp. 360–365, 2018.

[16] V. L. Kornienko, G. A. Kolyagin, G. V. Kornienko, and T. A. Kenova, "The prospects of the in situ and ex situ use of aqueous solutions of hydrogen peroxide electrogenerated from oxygen," *Russian Journal of Electrochemistry*, vol. 56, no. 5, pp. 405–417, 2020.

[17] R. Ghezelbash, A. Maghsoudi, M. Daviran, and H. Yilmaz, "Incorporation of principal component analysis, geostatistical interpolation approaches and frequency-space-based models for portraying the Cu-Au geochemical prospects in the Feizabad district, NW Iran," *Geochemistry*, vol. 79, no. 2, pp. 323–336, 2019.

[18] L. I. ZhenZhen, Key Laboratory of Mineral Resources, Institute of Geology and Geophysics, Chinese Academy of Sciences, Beijing 100029, China, Institutions of Earth Science, Chinese Academy of Sciences, Beijing 100029, China et al., "Basic characteristics, research progresses and prospects of Sn-Ag-base metal metallogenic system," *Acta Petrologica Sinica*, vol. 35, no. 7, pp. 1979–1998, 2019.

[19] B. Mishra, K. L. Pruseth, P. Hazarika, and S. S. Chinnasamy, "Nature and source of the ore-forming fluids associated with orogenic gold deposits in the Dharwar Craton," *Geoscience Frontiers*, vol. 9, no. 3, pp. 715–726, 2018.

[20] F. D. Wang, L. I. Yun-Ping, and Y. H. Jia, "Metallogenic regularity and prospecting direction of gold deposits in Qinghai, China," *Journal of Earth Sciences & Environment*, vol. 40, no. 2, pp. 162–175, 2018.

[21] G. Song, K. Qin, and G. Li, "Basic characteristics and research progresses of intermediate sulfidation type epithermal gold poly-metallic deposits, and prospects," *Acta Petrologica Sinica*, vol. 34, no. 3, pp. 748–762, 2018.

[22] A. A. Gasanov, A. V. Naumov, O. V. Yurasova, I. M. Petrov, and T. E. Litvinova, "Certain tendencies in the rare-earth-

element world market and prospects of Russia," *Russian Journal of Non-Ferrous Metals*, vol. 59, no. 5, pp. 502–511, 2018.

[23] J. F. Hernández, "machine learning and statistical techniques. An application to the prediction of insolvency in Spanish non-life insurance companies," *The International Journal of Digital Accounting Research*, vol. 5, no. 9, pp. 1–45, 2020.

[24] Y. Chen, W. Zheng, W. Li, and Y. Huang, "Large group activity security risk assessment and risk early warning based on random forest algorithm," *Pattern Recognition Letters*, vol. 144, pp. 1–5, 2021.

[25] R. S. Bhadoria and N. S. Chaudhari, "Pragmatic sensory data semantics with service-oriented computing," *Journal of Organizational and End User Computing*, vol. 31, no. 2, pp. 22–36, 2019.

[26] Q. Wang and P. Lu, "Research on application of artificial intelligence in computer network technology," *International Journal of Pattern Recognition and Artificial Intelligence*, vol. 33, no. 5, p. 1959015, 2019.

[27] P. Shan, X. Lai, and X. Liu, "Correlational analytical characterization of energy dissipation-liberation and acoustic emission during coal and rock fracture inducing by underground coal excavation," *Energies*, vol. 12, no. 12, p. 2382, 2019.

WILEY | Hindawi

Retraction

Retracted: An Analysis of the Effectiveness of Machine Learning Theory in the Evaluation of Education and Teaching

Wireless Communications and Mobile Computing

This article has been retracted by Hindawi following an investigation undertaken by the publisher [1]. This investigation has uncovered evidence of one or more of the following indicators of systematic manipulation of the publication process:

(1) Discrepancies in scope

(2) Discrepancies in the description of the research reported

(3) Discrepancies between the availability of data and the research described

(4) Inappropriate citations

(5) Incoherent, meaningless and/or irrelevant content included in the article

(6) Peer-review manipulation

The presence of these indicators undermines our confidence in the integrity of the article's content and we cannot, therefore, vouch for its reliability. Please note that this notice is intended solely to alert readers that the content of this article is unreliable. We have not investigated whether authors were aware of or involved in the systematic manipulation of the publication process.

In addition, our investigation has also shown that one or more of the following human-subject reporting requirements has not been met in this article: ethical approval by an Institutional Review Board (IRB) committee or equivalent, patient/participant consent to participate, and/or agreement to publish patient/participant details (where relevant).

Wiley and Hindawi regrets that the usual quality checks did not identify these issues before publication and have since put additional measures in place to safeguard research integrity.

We wish to credit our own Research Integrity and Research Publishing teams and anonymous and named external researchers and research integrity experts for contributing to this investigation.

The corresponding author, as the representative of all authors, has been given the opportunity to register their agreement or disagreement to this retraction. We have kept a record of any response received.

References

[1] B. Wu and C. Zheng, "An Analysis of the Effectiveness of Machine Learning Theory in the Evaluation of Education and Teaching," *Wireless Communications and Mobile Computing*, vol. 2021, Article ID 4456222, 10 pages, 2021.

WILEY | Hindawi

Research Article

An Analysis of the Effectiveness of Machine Learning Theory in the Evaluation of Education and Teaching

Bo Wu[1,2] and Changlong Zheng [iD][1]

[1]*Faculty of Education, Northeast Normal University, Changchun, 130021 Jilin, China*
[2]*High School Attached to Northeast Normal University, Changchun, 130021 Jilin, China*

Correspondence should be addressed to Changlong Zheng; wub257@nenu.edu.cn

Artificial intelligence was first proposed in the 1950s, when it was only a forward-looking concept. If machines can have the same learning ability as human beings and the computing power of computers themselves, this concept has been placed high hopes. Until about 2010, with the explosion of data volume and the improvement of computer performance, machine learning has become a leader in breaking through the bottleneck of artificial intelligence. Research on machine learning in education and teaching has attracted much attention. From the above research status, we can see that in the current period of the vigorous development of machine learning, many applications are still not perfect and ordinary education and teaching evaluation is difficult to meet people's requirements, so how to gradually improve its effectiveness is a significant goal with research significance and practical interests. However, in the environment of colleges and universities, prediction information and evaluation methods have important application value and development space in education and teaching. In this context, according to the theory of machine science, the effectiveness of several conventional prediction and evaluation methods is analyzed. In this paper, machine learning theory is used to study college students' performance prediction and credit evaluation, as well as teaching quality evaluation and comprehensive ability evaluation in colleges and universities. Questionnaire survey is used to investigate and analyze the results. The effectiveness of machine theory in teaching is analyzed. It is found that machine learning has great advantages in education and teaching evaluation. It builds models in complex computing environment and is not affected by human factors; the effectiveness of prediction and evaluation is significant.

1. Introduction

Nowadays, with the development and popularization of mobile products, people's demand for content information products is increasingly urgent. In contrast, the increase of internal capacity has brought unprecedented pressure on editors and reviewers. Fortunately, with the rapid development of machine learning, also with the research and progress of machine learning theory, part of the work can be done by machine instead of humans, and the advantages brought by the application in all walks of life are gradually reflected.

Since China implemented the national policy of opening to the outside world, with the globalization of economy, the diversification of convenient information and ideas, and the invasion trend of various foreign cultures, people are easy

to lose the ability of independent judgment of right and wrong thinking and lack of cultural identity with China's socialist mainstream ideology [1, 2]. In the National Congress, the Communist Party of China (CPC) clearly stated that the fundamental task of "cultivating people and moral education" is not only the general direction of China's education but also the fundamental task of China's education. At the 2016 National Conference on Ideological and Political Work in Colleges and Universities, comrade Xi Jinping, the vice president of the state, pointed out that colleges and universities should clarify the importance of ideological and political education and put forward suggestions on how to do well in education and teaching in colleges and universities. According to the 13th five-year plan for the development of national education issued by the State Council in 2017, it is

necessary to cultivate high-quality talents with all-round development of morality, intelligence, sports, and beauty and train socialist builders and successors. The report of the 19th National Congress of the Communist Party of China in 2018 also stressed that education should be built as the basis for the great rejuvenation of the Chinese nation [3]. It can be seen that only by firmly grasping the leading power of ideological work in the field of education can we adhere to the goal that education must serve the socialist modernization. This is also the realistic background of this paper, that is, how to popularize the effectiveness of machine science theory in education evaluation.

The new era calls for new talents, the society needs high-quality talents, and education needs the cultivation of talents. In order to adapt to the environment of education in the new era, the traditional teaching concept, content, and method are undergoing a great change. The traditional teaching [4] has been unable to meet the needs of the current social environment for the overall ability of students, and it is an important component of the education reform that cannot be ignored. After years of continuous research and exploration, on the whole, the traditional teaching mode in China has not made substantial and fundamental progress, and many reforms are still in the form and on the surface. The whole teaching activity focuses on classroom teaching. Classroom teaching activity is mainly based on teachers' teaching and students' passive acceptance. It does not fully mobilize students' enthusiasm and initiative, it is not good to cultivate students' habits and abilities of active learning, and it is almost certain to form students' own personality and perfection. It also makes the classroom the main place to stifle students' innovative spirit and sense of responsibility.

Examination is the main form to test students' learning and teaching effect. Through the above discussion, we can know that it is an important part of education evaluation to evaluate students' learning effect accurately and objectively through examination results. The objectivity of examination results is not only related to the objectivity of students' learning level and ability evaluation but also to the objectivity of teachers' teaching ability and teaching effect evaluation. There are many objective factors that affect the test results, such as test paper quality, invigilation, grading, and students' ability level. The examination paper is composed of many questions. The quality of the examination paper is closely related to the quality of the examination paper. For example, in an exam, students' scores are generally low, because of the difficulty of the exam paper, students feel depressed, because of the exam, and so they can learn negatively. Or because the difficulty of the test paper is too small, the test results of students are generally on the high side, which will make students have self-expansion and pride. These factors will lead to the evaluation result of students' learning effect being not objective. However, students play an important role in the teaching management and evaluation of teachers. Students can use evaluation methods to reflect the situation of teachers' classroom teaching. Teachers can use students' evaluation of teaching results to reflect their own teaching effect and improvement. The school can also understand the individual teaching situation and the overall teaching level of teachers

through the analysis of students' teaching evaluation data, so as to put forward corresponding training plans and effective education management measures. Since the implementation of student evaluation, it has become a routine work of teaching management in colleges and universities. In view of this problem, this paper investigates the teaching evaluation of students at home and abroad and finds that it is necessary to analyze the teaching ability in more detail in the information feedback of teachers. A large number of student evaluation data have been accumulated, which can provide more information for teachers' teaching ability. Based on this idea, this paper puts forward how to make full use of the evaluation data of students and make more effective use of machine theory to evaluate and diagnose teachers' classroom teaching ability.

Therefore, the main research work of this paper is as follows: it analyzes the education of existing evaluation methods, focuses on the analysis and research of some related problems of evaluation methods, discusses how to apply them to the comprehensive evaluation decision-making problems, and analyzes the characteristics and limitations of the methods. This paper discusses the support vector machine and neural network technology and their application in the comprehensive evaluation, especially the learning algorithm of support vector machine [5] and neural network [6]. Based on the comprehensive evaluation of students' test scores, the paper analyzes the factors that affect the quality of test papers and uses the theory of machine science to predict the scores. In this paper, the comprehensive evaluation of students' academic examination results is taken as the research object, the comprehensive evaluation and prediction based on machine learning theory are discussed, and the effectiveness of the evaluation and prediction is simulated and analyzed.

2. Conventional Machine Learning Theory

2.1. Concept of Machine Learning. Machine learning [7] is an interdisciplinary subject, involving probability theory [8], statistics [9], approximation theory [10], convex analysis [11], computational complexity theory [12], etc. Machine learning is to study how to improve the performance of the system through the use of intelligent computing and experience. The corresponding algorithm model is generated by experience, and the generation process of algorithm model is actually the process of machine automatic learning. It is these learning algorithms that machine learning studies. The generation of learning algorithm includes the process of simulating human thinking learning, the process of reasoning incomplete information, the process of constructing new things discovery, and the process of processing current big data trend. At present, machine learning algorithms are mainly divided into supervised learning algorithm, unsupervised learning algorithm, and semisupervised learning algorithm. Among them, supervised learning is generally divided into regression algorithm and classification algorithm. Regression is a method of using continuous functions to correspond to input and output variables. Classification is the matching of input variables and discrete categories.

Unsupervised learning means that we do not know in advance what the output will be. For example, we can extract a special structure from the data by clustering. There is no label or only one label in unsupervised learning. Semisupervised learning is a learning method combining supervised learning with unsupervised learning. In the process of machine learning, there are both marked data and unmarked data. Using semisupervised learning can improve the efficiency and accuracy of learning.

2.2. Support Vector Machine. Support vector machine (SVM) [5] is a binary classification algorithm supporting linear and nonlinear classification. After evolution, it now supports multivariate classification and is widely used in regression and classification. SVM was proposed by Vapnik et al. in 1963. It solves the problems encountered in traditional methods and can solve nonlinear, small sample, and high-dimensional problems well. Practical tests show that this method performs well in these aspects and has become an indispensable part of the machine learning field.

SVM can be simply described as the classification of sample data, and the real decision function is to solve. First, the maximum classification interval is found, then the optimal classification hyperplane is determined, and the classification problem is transformed into a quadratic programming problem. By using the Lagrangian optimization method, the element problem is transformed into a dual problem and then into a convex quadratic programming problem. In this process, if the sample points are linear and indivisible, relaxation variables must be introduced to solve the optimization problem. If the sample is nonlinear, the kernel function is used to solve the problem.

Since the birth of support vector machine (SVM), it has swept the field of machine learning with its good classification performance. Since the 1990s, it has developed rapidly and derived a series of improved and extended algorithms, including C-SVC, least squares support vector machine, support vector regression, support vector clustering, and semisupervised support vector machine. This paper uses C-SVC, which is an extension of standard support vector machine. The optimization of C-SVC is as follows:

$$
\begin{cases}
\min\ L(w, \xi) = \dfrac{1}{2} w^t w + \dfrac{c}{2} \sum_{j=1}^{h} \xi_j^2 \\
\text{s.t}\ \ y_y^{t+1} = w^t \Phi\left(x_{j,d}^t\right) + b + \xi^2.
\end{cases}
\tag{1}
$$

In this formula, ξ^2 is a nonnegative relaxation variable; $c/2$ is the given regularization parameter.

The optimization problem of multiclassification SVM is transformed into the solution of visualization equation, and the final classification function is as follows:

$$
y_i^{t+1} = \sum_{j,q=1}^{h} \alpha_g K\left(x_{j,d}^t + x_{q,d}^t\right) + b,
\tag{2}
$$

where $x_{j,d}^t + x_{q,d}^t$ is the kernel function. The function of kernel is to map the nonlinear problems in low-dimensional space to high-dimensional space and transform them into linear problems. At present, the commonly used kernel function types are as follows:

(1) Linear kernel function

(2) Polynomial kernel function

(3) Gaussian radial basis kernel function

(4) Sigmoid kernel function

At this time, C-SVC is a multilayer perceptron including the hidden layer, and the algorithm automatically determines the number of nodes in the hidden layer. Support vector machine is an introduction to machine learning theory. For the same data, SVM with different kernel functions can get different classification accuracy.

To sum up, SVM has good generalization ability in nonlinear classification, function approximation, pattern recognition, and other applications and gets rid of the long-term constraints of building learning machine from the perspective of bionics. Compared with analytic hierarchy process (AHP) [13], logistic regression analysis [14], and BP neural network [15], support vector machine (SVM) has a more solid mathematical theoretical basis and can effectively solve the problem of constructing high-dimensional data model with limited samples.

2.3. AHP. Analytic hierarchy process (AHP) is a decision-making analysis method put forward by Soary of University of Pittsburgh in the 1970s [16]. Because decision-making itself is an evaluation behavior, AHP has been widely used in the field of evaluation. This section mainly introduces the application of AHP in education evaluation.

(1) The Basic Idea of AHP. The process of establishing evaluation model by AHP is actually a program structure of evaluation. Through qualitative analysis, the relationship between the factors reflecting the value of the evaluated object is established, and the hierarchical structure chart reflecting the relationship between these factors is established. Using the hierarchy chart of logical judgment and establishment, the importance of two factors is compared under the direct upper factor, and the comparison matrix is established. When the eigenvector corresponding to the maximum eigenvalue of the comparison matrix is converted into the weight (standard) vector, the value of the standard vector component is a quantitative value, indicating the importance of the factor relative to other factors under the same upper factor.

For the object that can be quantitatively evaluated by linear method, the quantitative value obtained by AHP method can be used as the weight of each evaluation index that affects the evaluation result, and the comprehensive evaluation result value of the evaluated object can be easily obtained.

(2) The Main Steps of Establishing AHP Model [17]. Analytic hierarchy process (AHP) reflects the basic characteristics of people's evaluation and decision-making thinking: decomposition, judgment, and comprehensive thinking process. The main steps of applying AHP method to evaluation and decision are shown in Figure 1.

Step 1. The first step is to analyze the factors (i.e., evaluation indexes) that affect the value of the evaluated object and determine the value objectives (i.e., evaluation objectives) of the evaluated object.

Step 2. According to the evaluation objectives, analyze whether the factors affecting the value of the evaluated object are hierarchical and linear. If so, construct a hierarchical diagram that reflects this relationship and move on to the next step.

Step 3. Compare the factors at the same level with the same dominant factors as the evaluation criteria, establish a comparison matrix (some data are also called judgment matrix), and determine its relative importance according to the evaluation scale. The establishment of contrast matrix is the key step of evaluation decision. The evaluation scale used to establish the comparison matrix is shown in Table 1.

Step 4. Through a certain calculation, determine the relative importance of each factor in this level relative to a factor in the previous level, i.e., single ranking of the levels.

Step 5. Verify the consistency of the comparison matrix to ensure the reliability of the results. If there is any inconsistency, go back to Step 3 and modify the contrast matrix again. If it is an acceptable consistency matrix, continue.

Step 6. After calculating the relative importance of the factors in each layer relative to the factors in the previous layer, the comprehensive importance of the factors in the current layer to the whole of the previous layer can be calculated from top to bottom, that is, the overall arrangement of the layers.

Step 7. Check the consistency of the overall sorting results of the hierarchy. If there are any inconsistencies, go back to Step 3 and change it to a comparison matrix. If they are consistent, the sorting results are accepted. Then, get the effectiveness analysis of education evaluation.

2.4. BP Neural Network. The BP neural network is a multi-layer feedforward network [18]. The typical network structure includes input layer, hidden layer, and output layer, where x_i is the input layer, z_j is the output of the hidden layer node, c_t is the output of the output layer node, c_t is the target signal, and i is the input layer node of the hidden layer node. Among them, the connection weight of the hidden layer node j to the output layer node is w_{ij}, and the thresholds of the hidden layer node and the output layer node are, respectively, according to the weight of V_{ij}, θ_j, and γ_i. In practical application, the BP neural network can establish multiple hidden
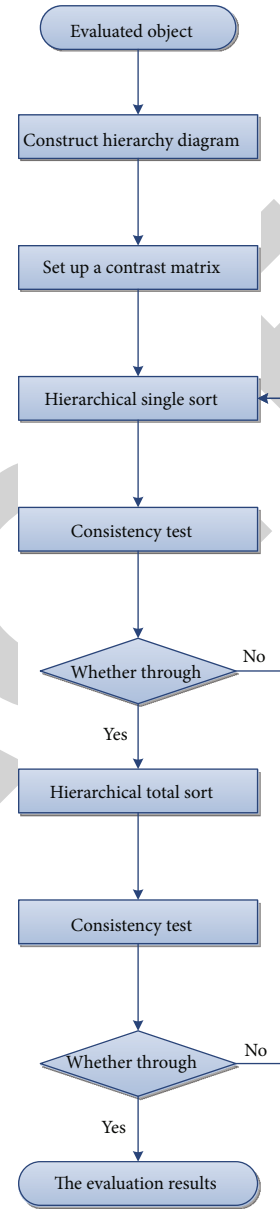
Figure 1: Using AHP to make evaluation decision.

layers according to the needs of the problem. The neural network is an explanation of a learning ability in machine learning, and then, it is applied to the effective analysis of education and teaching.

In the structure of BP neural network, each layer is completely interconnected, and there is no interconnection between the elements of the same layer. When an input mode is given in the network, it is transmitted from the input layer unit to the hidden layer unit and then processed by the hidden layer unit to the output layer unit, resulting in an output response. If the error output response and the expected output do not meet the requirements, the error connection path will be followed one by one, and the correct connection weight and threshold of each layer will reduce the error, modify the connection weight and threshold, and then use a new connection weight and threshold to calculate the input

TABLE 1: Factor comparison judgment scale.

Comparison results	Value
For the upper level factor H, A_i and A_j are equally important.	2
For the upper level factor H, A_i is more important than A_j.	4
For the upper level factor H, A_i is significantly more important than A_j.	6
For the upper level factor H, A_i is much more important than A_j.	8
For the upper level factor H, A_i is extremely important than A_j.	10
For the upper level factor H, between two adjacent judgment scales.	1, 3, 5, 7

mode to generate an output response compared with the expected output, through iterative calculation, until the error is less than the given value.

The BP learning algorithm is a learning algorithm with tutor [19]. The BP learning algorithm is divided into two stages: input forward calculation and error back propagation. Taking the three-layer BP neural network as an example, it is assumed that the activation functions of neurons in the output layer and hidden layer can be found in the network $f(u) = 1/(1 + e^{-n})$. There are p neurons in the hidden layer. The whole learning process can be divided into the following steps, as shown in Figure 2.

3. Effective Evaluation Method of Machine Theory in Education Evaluation

3.1. Prediction of College Students' Performance. The BP neural network is a multilayer feedforward network. The basic principle of comprehensive evaluation [20] is to take the information describing the characteristics of the evaluation object as the input vector of the neural network and the value representing the corresponding comprehensive evaluation as the output of the neural network. Then, enough samples are used to train the network, and different output values of different input vectors are obtained. If the error between the output value and the expected value exceeds the specified error range, adjust the weight of the neural network according to the error according to a certain method, the connection between each layer and the value of the hidden layer and the output layer nodes, until the system error is acceptable, and the weight and Fujian price value will not change anymore. In this way, the weights and thresholds held by the neural network are the correct internal representation of the neural network through adaptive learning. The trained neural network can be used as an effective tool for qualitative and quantitative evaluation of the target system outside the sample model.

Therefore, the basic idea of applying the BP neural network to the comprehensive evaluation of examination results is to use four evaluation indexes to evaluate the quality of examination papers (reliability, effectiveness, difficulty, and differentiation degree) and the original points (that is, the
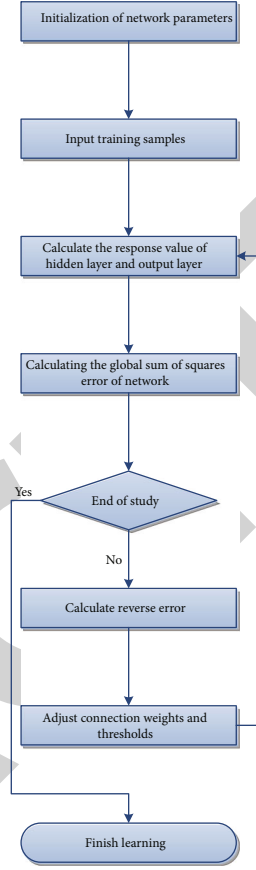
FIGURE 2: Flowchart of BP model training.

scores of students' examination papers) to form the input vector of BP neural network and use value (that is, the quantitative value of learning effect) to form the output vector of the BP neural network. The quantitative value of physical fitness is also output as a vector. Design a reasonable network structure and training samples, input the training samples into the network operation, until the comprehensive evaluation model test results need the system error of the network model, and it can meet the specified requirements.

3.2. Credit Evaluation of College Students. With the rapid development of the times, especially the rapid progress of the market economy, China's overall economic level has been greatly improved. In view of the frequent occurrence of lack of credit in society, this paper adopts the establishment of citizen credit files based on machine learning theory. As the main force of social development, college students began to establish credit files on the basis of machine learning theory in the first year of university, which has been the starting point of the construction of college students' credit files since the student era. At present, the problem of college students' lack of credit often occurs, which is not only the objective cause of college students' lack of credit awareness but also the impact of social environment. The establishment of credit files based on machine learning theory can not only effectively improve the credit awareness of college students but also improve the ideological and moral level of college

students, which is conducive to the harmonious development of society. The author believes that the reasons for college students' dishonesty are closely related to their credit awareness. In order to prevent this kind of phenomenon, it is the best choice to establish college students' credit files. As a group with high comprehensive quality, they should build credit files based on machine learning theory. College students shoulder the important task of social development, so as to cultivate their comprehensive quality, let them better display themselves after entering the society, improve their credit awareness, and choose to build credit files based on machine learning theory, which is undoubtedly the best choice. In this paper, the author uses the experience of domestic and foreign countries for reference to establish credit files and, on the basis of in-depth analysis and discussion of relevant research, establishes the machine learning theory of credit files in the academic field, which can help China to better establish credit files for college students to assess their credibility.

Under the condition of a large population, the construction of college students' credit files can better establish a social credit system. In view of the frequent occurrence of social credit crisis, it is necessary to establish and improve the credit mechanism documents. For the commercial credit system of social development, the credit file system should be gradually established from the college students' credit files. It is necessary to use the system in the future university credit documents and improve the credit documents and settings, which can better guide the university to implement the credit system. It is not only of high education quality, the credit of the evaluation is divided into credits to improve the education of students' credit and responsibility, but also of strong sense of social responsibility, which is of guiding significance for the development of the credit system.

3.3. Evaluation of Teaching Quality in Colleges and Universities. There is less research on teachers' teaching ability; Professor Sun said, "the research on how to form the limited literature research university teachers' teaching ability and teaching ability is the least, and the teaching ability to improve teaching ability is more important." This is a good summary of the existing research on the teaching ability of university teachers, but we still need to see the efforts of researchers. The existing teaching ability of university teachers is mainly to decompose the teachers' ability from the perspective of teachers. For example, from the perspective of the general law of teaching activities, Zhou Yuanyuan thinks that the structural teaching ability of teachers includes the ability to organize and monitor teaching, the ability to communicate with teachers or other students, the ability to use modern technology and information, and the ability to conduct teaching research and lifelong learning. Tian Jinmei et al. constructed a conceptual model of teachers' teaching ability, including teaching ability, knowledge promotion ability, training ability, and method and tool application ability [21], by studying the current situation of teachers' teaching ability at home and abroad and combining with many factors such as teachers' living environment.

The structure of teachers' teaching ability ignores the main body of students in teaching. For example, Dean Dong of Higher Education Research Institute of Yunnan University said, "the students of Yunnan University are not the purpose of education, but the service object. On the premise that targeted teachers understand the needs of students, combined with the existing structure of teachers' ability, paying attention to teacher development can help teachers develop professional skills and form a harmonious relationship between teachers and students."

The structure of teachers' teaching ability is stipulated in teachers' standard, including basic methods of teaching major [22], teaching plan and preparation [23], teaching management, teaching evaluation [24], and teaching methods and strategies. According to this standard, the corresponding evaluation scale of teachers' teaching quality is established, that is, the scale is the evaluation of students' using school. This is the expectation of teaching managers of teachers' teaching ability structure. Students' behavior in teachers is based on the scale of compatibility, in which a certain gap of students' and teachers' ability is worrisome. This study uses the machine theory to analyze the teaching evaluation data of students, and from the perspective of students to rename and explain the factors mined, it also evaluates from the perspective of teachers, to make a scientific and rigorous teaching evaluation, from which we can infer the teaching quality of the school.

3.4. Evaluation of Comprehensive Ability of Colleges and Universities. At present, scholars have not formed a unified understanding of "university comprehensive ability" [25]. Some scholars believe that from a macro perspective, the composition of the comprehensive ability of colleges and universities can be divided into two aspects: hard power and soft power, which is the result of the synergy of hard power and soft power. The expression of hard power is the sum of components in material form, mainly including human (teacher resources, student status, etc.), financial (economic status, etc.), material (fixed assets), and other hard indicators that can be measured and quantified. Soft power refers to the level of school management (school vitality and school efficiency), school characteristics (school tradition and social prestige), school spirit and cohesion, and other nonmeasurable or hard to quantify soft indicators. "Comprehensive ability of colleges and universities," in a broad and narrow sense, refers to the comprehensive ability of regional higher education relative to a country or a region [26]. It is the influence of strength, resources, competitiveness, and innovation of colleges and universities, including the democratic political environment, sustained economic development, harmonious cultural atmosphere, good higher education foundation, development potential, colleges and universities and many other people, commodity content, information, resource power, and top professors, standardized management, advanced equipment, excellent core competitiveness and creativity research, the impact of talent training quality, the transformation of scientific research results, and the degree of internationalization on economic and social development; in a narrow sense, it refers to colleges and universities with
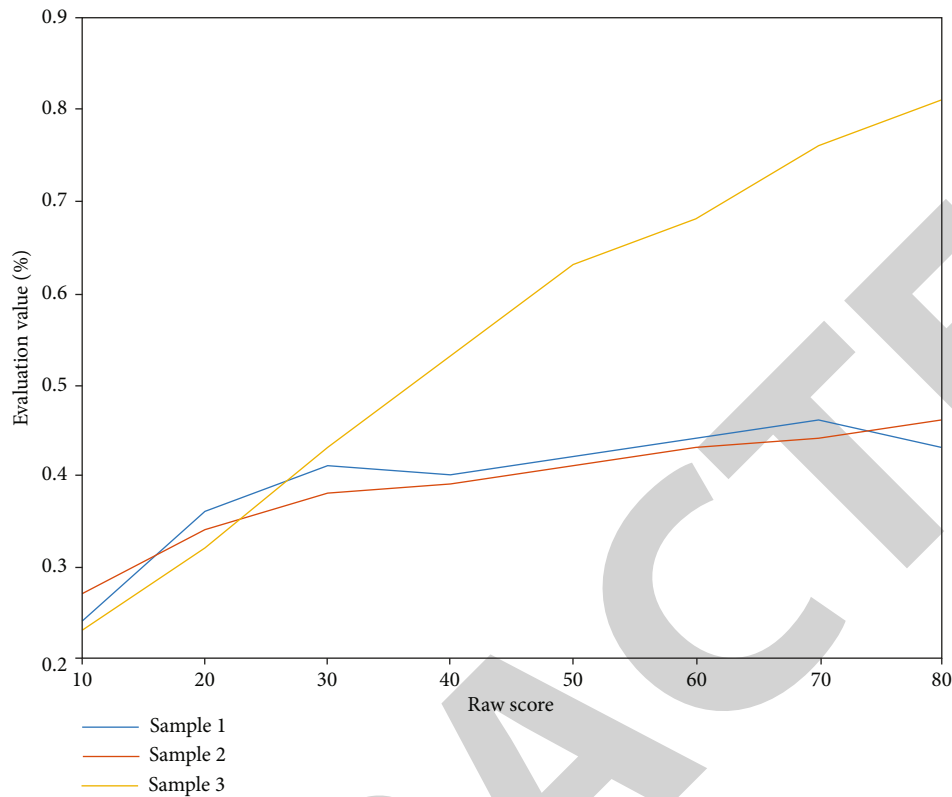
FIGURE 3: Comparison of simulation results and curves.

operation intensity and operation level, including the principles and guiding ideology of the school, the quality of teachers and students, education funds, infrastructure, professional construction, scientific research efficiency, management level, and the reputation of the school. Combined with these two aspects, this paper mainly studies the overall strength of Guangxi institutions of higher learning from a general point of view, which is to cultivate talents, scientific research, and social services and support these functions to achieve the required education philosophy, education funds, teaching staff, science construction, infrastructure, organizational management, and other conditions [27, 28]. They are the core factors of comprehensive ability evaluation in colleges and universities.

The core of the comprehensive strength evaluation of regional colleges and universities is to establish a scientific, systematic, and operable evaluation index system. It itself is a very complex system engineering, which not only requires researchers to study the development logic of the university itself based on the university and in-depth but also the university to break through and master the macro external environmental factors affecting the comprehensive strength of the university, such as the university, social politics, economy, and culture. Therefore, using the theory and method of machine science to study the comprehensive strength of colleges and universities and its influencing factors and on this basis to build a scientific evaluation index system, this system is used as an evaluation standard to conduct research on the comprehensive ability of other schools.

4. Results and Discussion

4.1. Analysis of the Results of College Room Performance Prediction. In order to verify the influence of machine learning theory in the evaluation of education and teaching, this paper takes the results of the "data structure" course of college students' school in the past three years as an example to form three groups of test samples, using the evaluation model of machine learning theory, through simulation calculation as shown in Figure 3.

Figure 3 shows the comparison curve of simulation results of three groups of samples. It can be seen from the figure that the original scores of each group of samples increase with the increase of evaluation value, which is consistent with the original scores and evaluation values of qualitative relationship between people's understanding, indicating that the model established in this paper is reasonable to a certain extent. However, according to people's understanding, under the same original score, the evaluation value of three groups of samples should also show an upward trend, that is, the evaluation value of sample 2 should be greater than the evaluation value of sample 1 and less than the evaluation value of sample 3. However, Figure 3 does not reflect this trend well, which shows that the model established in this paper still has shortcomings. The main reason is that the accuracy of the training samples used to establish the evaluation model is not enough. The existence of certain errors also leads to the defects of this model.

4.2. Analysis of Credit Evaluation Results of College Students. In order to verify the influence of machine learning theory on
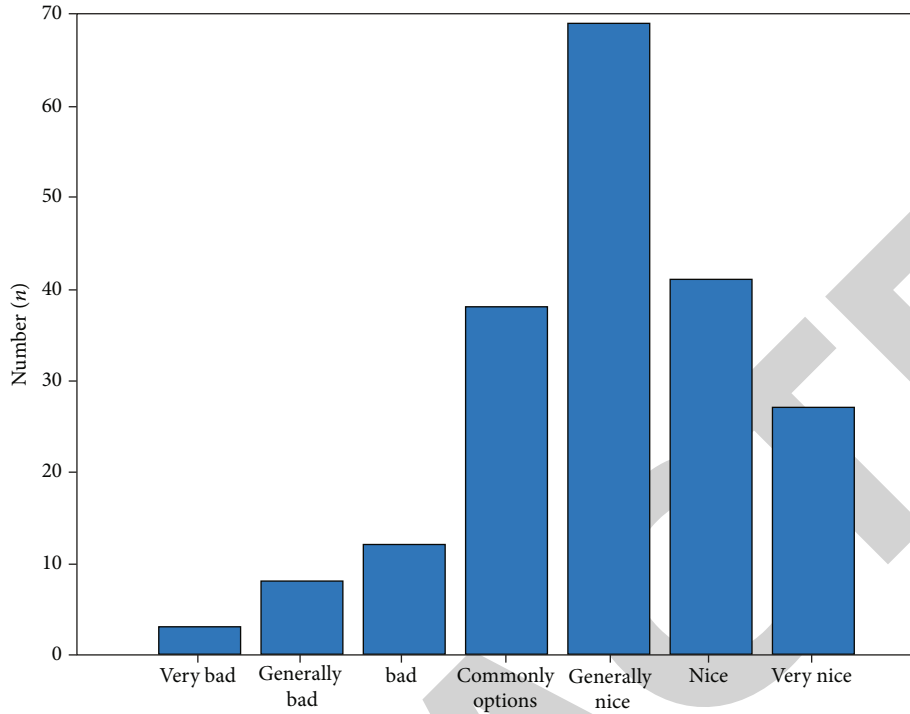
FIGURE 4: Credit conditions.

education credit evaluation, 201 college students are selected for questionnaire survey, as shown in Figure 4.

In the survey results of college students' credit status, 38.26% of the students think that the overall credit status of college students is good and needs to be evaluated, and the credit evaluation based on machine science theory has great advantages; 22.68% of the students think that the overall credit status of college students is good and should be properly supervised; 14.36% of the students think that the overall credit status of college students is good and does not need to be evaluated. Through the above data analysis, we can see that most students are optimistic about the overall credit status of college students. It shows that some learning education does not link credit with credits, which leads to some students not paying enough attention to credit. However, some students think that the credit status of college students is not very good, so colleges and universities need to evaluate college students in time to improve their credit awareness.

4.3. Analysis of Teaching Quality Evaluation Results in Colleges and Universities. The data used in this paper is from the teaching evaluation data of 20 teachers in a department of Changchun University of Technology. A total of 80 students participated in the scoring, and a total of 1300 records were obtained. In order to interpret the teaching ability of teachers from the perspective of students, it is also hoped that the samples can keep stable. Therefore, the average value of the original data is taken as the overall summary of students' evaluation of teachers as shown in Figure 5.

From the ideological data in the figure, it can be seen from the evaluation results that the main factors determining the basic teaching skills are teachers' sufficient preparation
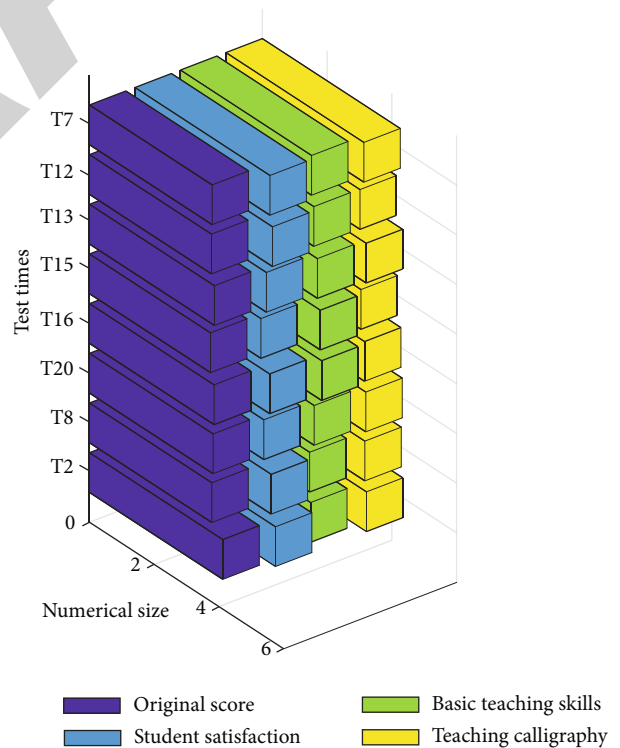
FIGURE 5: New summary results.

for lessons and serious investment in teaching, and other indicators have no direct impact on the basic teaching skills. These factors indicate that these factors should be emphasized in the evaluation of teaching.

TABLE 2: Ranking of universities in Guangxi.

Colleges and universities/ranking system	Ranking of online universities							
	2012	2013	2014	2015	2016	2017	2018	2019
Guangxi University	178	139	188	78	65	183	155	178
Guangxi Normal University	319	210	203	198	157	178	89	53
Guangxi Medical University	115	102	74	135	173	120	67	85
Guangxi University for Nationalities	332	309	298	314	243	267	210	289
Guilin University of Electronic Science and Technology	374	365	385	342	339	376	392	332
Guilin Institute of Technology	259	240	254	232	324	206	214	229
Guangxi College of Traditional Chinese Medicine	429	416	447	438	356	439	448	410
Guangxi Normal University	539	512	534	552	574	502	498	488

4.4. Analysis of Comprehensive Ability Evaluation Results of Colleges and Universities. By analyzing the comprehensive ability of colleges and universities and its influencing factors and combining the comprehensive ability evaluation system of colleges and universities with the principles and methods of construction, we take Guangxi colleges and universities as an example and use the theory of machine science to evaluate the comprehensive ability of colleges and universities, and the content is shown in Table 2:

According to the ranking results of Guangxi and 8 normal universities planned for key construction, the national key universities rank only Guangxi University, while other universities rank below the average level in the country, ranking in 300 ordinary universities, which shows that Guangxi university education is not high. At the same time, from the ranking of Guangxi universities, some are on the rise and some are on the decline. These can reflect the quality of higher education. The position and stability of the rankings reflect whether the quality and development level of higher education in the region is lower or higher than the national average.

5. Conclusion

It is very important to accurately express the results for various aspects of prediction and evaluation and various factors mentioned in this paper. No matter which learning machine predicts any problem, colleagues need to establish a model from the cause to the result, which mainly uses the existing information and problems related to such information to make reasonable inference, so as to deduce the results. For example, the credit detection of college students mentioned in this paper, some of which are known, can be used for the simulation training of the machine learning system. As proposed in this paper, the use of machine learning system can avoid the uncertain factors of human evaluation. It is not only the respect for teachers but also the affirmation of their teaching level to evaluate and evaluate the education level fairly and reasonably according to the various indicators of teaching quality. This paper also finds that this method can be used in the intelligent learning algorithm to predict a wider range, such as population prediction and risk prediction. This method plays an important role in the future evaluation and prediction to promote the development of the education industry and build the infrastructure for the future development of the education industry.

Data Availability

No data were used to support this study.

Conflicts of Interest

The authors declare that they have no conflicts of interest.

References

[1] O. A. Maiga, X. Hu, T. M. Mekongcho, and S. K. Coulibaly, "Effects of economic globalization, foreign capital influx on export in ECOWAS," *Nephron Clinical Practice*, vol. 18, no. 4, pp. 23–29, 2018.

[2] R. Scully and J. Larner, "A successful defence: the 2016 National Assembly for Wales election," *Parliamentary Affairs*, vol. 70, no. 3, pp. 507–529, 2017.

[3] T. Kveder and B. Bozic, "10th national congress of the Portuguese society of clinical chemistry, genetics and laboratory medicine," *Clinical Chemistry & Laboratory Medicine*, vol. 56, no. 11, 2018.

[4] V. Balliu, "Modern teaching versus traditional teaching- Albanian teachers between challenges and choices," *Ejms European Journal of Multidisciplinary Studies Articles*, vol. 4, no. 4, p. 20, 2017.

[5] X. Zhang, J. Wang, and K. Zhang, "Short-term electric load forecasting based on singular spectrum analysis and support vector machine optimized by cuckoo search algorithm," *Electric Power Systems Research*, vol. 146, no. 2, pp. 270–285, 2017.

[6] C. Bergmeir and J. M. Benítez, "Rsnns: neural networks in r using the Stuttgart neural network simulator (snns)," *Carpathian Journal of Electronic & Computer Engineering*, vol. 46, no. 2, 2017.

[7] S. Liu, X. Wang, M. Liu, and J. Zhu, "Towards better analysis of machine learning models: a visual analytics perspective," *Visual Informatics*, vol. 1, no. 1, pp. 48–56, 2017.

[8] G. Gallavotti, "Lucio Russo: probability theory and current interests," *Mathematics & Mechanics of Complex Systems*, vol. 4, no. 3-4, pp. 461–469, 2017.

[9] M. Sobel and B. Mishra, "Communications in statistics: theory and methods," *Communications in Statistics*, vol. 27, no. 9, pp. 2307–2323, 2018.

WILEY | Hindawi

Research Article

Influencing Factors of e-Commerce Enterprise Development Based on Mobile Computing Big Data Analysis

Yixue Zhu[1] **and Boyue Chai** [2]

[1]*Yancheng Teachers University, Yancheng, 224007 Jiangsu, China*
[2]*Hebei University of Engineering, Handan, 056038 Hebei, China*

Correspondence should be addressed to Boyue Chai; chaiboyue@hebeu.edu.cn

With the development of increasingly advanced information technology and electronic technology, especially with regard to physical information systems, cloud computing systems, and social services, big data will be widely visible, creating benefits for people and at the same time facing huge challenges. In addition, with the advent of the era of big data, the scale of data sets is getting larger and larger. Traditional data analysis methods can no longer solve the problem of large-scale data sets, and the hidden information behind big data is digging out, especially in the field of e-commerce. We have become a key factor in competition among enterprises. We use a support vector machine method based on parallel computing to analyze the data. First, the training samples are divided into several working subsets through the SOM self-organizing neural network classification method. Compared with the ever-increasing progress of information technology and electronic equipment, especially the related physical information system finally merges the training results of each working set, so as to quickly deal with the problem of massive data prediction and analysis. This paper proposes that big data has the flexibility of expansion and quality assessment system, so it is meaningful to replace the double-sidedness of quality assessment with big data. Finally, considering the excellent performance of parallel support vector machines in data mining and analysis, we apply this method to the big data analysis of e-commerce. The research results show that parallel support vector machines can solve the problem of processing large-scale data sets. The emergence of data dirty problems has increased the effective rate by at least 70%.

1. Introduction

1.1. Background. With the continuous improvement of information technology, the data model has become highly complex, and the scale of data has also grown rapidly. The whole society has entered the era of big data. In recent years, my country's e-commerce has developed vigorously and on a large scale, and it has become the world's largest Internet market. At the same time, with the development of information technologies such as cloud computing and the Internet of Things, rapidly expanding data has brought mankind into the era of big data. It has become possible to use big data technology to analyze the development of the regional e-commerce industry chain and provide corresponding guidance. Due to differences in the economic development status of different regions, the construction of e-commerce infra-structure, and the online shopping habits of local residents, the differences in the level of regional e-commerce development have been created. The rapid rise of big data has become a link to the ternary world. With the development of big data, the role of e-commerce in the network economy is becoming more and more important, and vigorously developing e-commerce has become the primary task of all countries and regions.

1.2. Significance. E-Commerce is one of the hottest topics nowadays, and it is also one of the fields with the most development potential. Countries around the world have listed e-commerce companies as strategic industries for development. At the same time, due to the rapid development of the network economy, big data will also become a strategic decision for countries to seize development, and the control

and use of data will become the core competitiveness of the future society. Regional e-commerce development research based on big data analysis will enhance the development of e-commerce in the region and better promote governments, enterprises, and other institutions to obtain benefits from big data, so as to lay the cornerstone of the big data industry and improve service capabilities and operation efficiency, etc. The development of e-commerce will inevitably have a huge impact on the organizational structure of traditional enterprises and cause changes in corporate management. The positive significance of e-commerce to the development of small- and medium-sized enterprises is very significant, and the development of e-commerce activities has become an urgent need for small- and medium-sized enterprises. e-Commerce breaks through time and geographical restrictions, creating good conditions for small- and medium-sized enterprises and large enterprises to compete on an equal basis. Especially when information technology is widely popularized and the transfer of technological achievements is accelerated, small- and medium-sized enterprises can use e-commerce to put new products on the market faster than large enterprises.

1.3. Related Work. With the vigorous development of e-commerce in China, more and more enterprises in China have begun to use the powerful capabilities of e-commerce to create new profit growth points, which has enabled many scholars and professionals to carry out in-depth theoretical and practical explorations. But referring to the current research, we found that the research on the factors affecting the profit of e-commerce companies is nonsystematic, unilateral, or inclined to management. Yang pointed out that this article integrates the e-commerce situation, corporate financial model, corporate performance, and other elements into the same overall framework; analyzes the internal connections between different elements; and then perfects related corporate financial management theories. With reference to relevant research results at home and abroad, the influencing factors of financial processing procedures and financial management models of e-commerce enterprises are deeply studied. In addition, a financial management model that is suitable for e-commerce companies and conforms to the characteristics of e-commerce companies has been constructed, but so far, my country's e-commerce economy still lags behind foreign countries in some aspects [1]. Yuen pointed out that this article is based on the Innovation Diffusion Theory (IDT) and analyzed the customer's intention to use self-pickup as the last mile delivery method. It is assumed that innovative characteristics are the key factors that affect customers' willingness to use self-service pickup services. Demographic characteristics were also tested. The survey data was collected from 164 consumers in Singapore and analyzed using hierarchical regression analysis. The results show that among the five key characteristics of innovation, relative advantages, compatibility, and trialability have a positive impact on customers' willingness to use self-service pickup services. The study also found that the first step to improve customer willingness is to integrate self-collection into consumers' lifestyles, values, and needs.

In addition, the marketing method of self-service pickup service should have obvious advantages over other last-mile delivery methods, but for some customers, door-to-door delivery is more satisfactory [2]. Tawalbeh pointed out that mobile devices are increasingly becoming an indispensable part of people's daily lives, facilitating various useful tasks. Mobile cloud computing combines mobile and cloud computing to expand its functions and advantages and overcome its limitations, such as limited memory, CPU power, and battery life. Big data analysis technology can extract value from data with four Vs: quantity, variety, speed, and authenticity. This article discusses the role of online healthcare and mobile cloud computing and big data analysis in its implementation. With the adoption of cloud computing in healthcare, the motivation and development of network healthcare applications and systems have also been revealed. Describe a cloudlet-based mobile cloud computing infrastructure for medical big data applications. The technology, tools, and applications of big data analysis are reviewed, but network delays still exist in the process of remote surgery [3]. In recent years, more and more IT industries have begun to pay attention to the impact of IT applications on the sustainable development of the environment, including companies such as IBM and HP. Simon Mingay defined green IT and believed that IT organizations should not only understand green IT in terms of energy efficiency. But his research does not consider the application of green industry in other areas, which has limitations [4]. Hegmin-Younger et al. made a comparative study on the overall mean imputation method, group mean imputation method, thermal card method, and regression imputation method when analyzing the relationship between college students' performance before and after enrollment. It embodies the content of big data to meet the green challenge. But his research did not introduce specific algorithms [5]. In the research, someone defined a knowledge base of preattack results to realize the causal association method of association analysis. Experiments show that this method can dig out the essential connections between independent alarm information, but the result of the scene construction is very dependent on the expert knowledge base. The completeness and correctness of the knowledge base construction greatly affect the results of the association analysis [6]. With the rapid development of the Internet, IP data services have been rapidly popularized. IP data services are uncertain and unpredictable, and WDM networks use fixed-size wavelengths as the smallest granularity to allocate bandwidth to services. However, due to the diversity of services, it is difficult for WDM networks to adapt to service requests of different granularities, resulting in low spectrum utilization [7].

1.4. Main Content. The main purpose of this paper is to use big data information technology to analyze the influencing factors of the development of e-commerce enterprises, analyze the evaluation results, and combine the development of the domestic economic environment to propose targeted and construction to promote the development of e-commerce industry. Sexual opinions have contributed to the development of the domestic economy. First, the big

data preprocessing technology and methods are introduced in detail. Generally speaking, the data we use are often incomplete and inconsistent and are greatly affected by noise. Data cleaning is the use of various cleaning techniques to remove "dirty data" and obtain "clean" consistent collection of data. The next step is to conduct experiments on the research of big data quality evaluation standards and analyze it through big data prediction in the field of e-commerce. From the perspective of data availability, it can be evaluated from two aspects: accessibility and timeliness. Finally, the use of parallel support vector machines to analyze big data in the field of e-commerce has certain theoretical and practical significance for solving the problems of big data quality evaluation and predictive analysis in the field of e-commerce. From the point of view of the time to predict data, the parallel support vector machine only takes about one-seventh of the time of the traditional support vector machine, which shows the advantages of the parallel support vector machine in processing large-scale data sets. It is more effective than traditional support vector machines. The experimental results show that the parallel support vector machine has a good effect in predicting and analyzing data, both in accuracy and efficiency.

2. Big Data Preprocessing Technology Method

2.1. Data Cleaning. Generally, the data we use often has incomplete information and inconsistencies and is greatly affected by noise. Data cleaning is the use of various cleaning techniques to remove "dirty data" and obtain "clean" consistent collection data [6, 7]. Data cleaning is divided into the following categories:

(1) Cleaning of duplicate data

Delete the duplication in the data volume to ensure the speed and accuracy of data generation. There are two or more instances of the same object, and the data focus is returned as repeated data. Usually, in order to see the meaning of repetition, it is necessary to compare each example one by one, and then determine a common example. Statistical methods are usually used to test the numeric attributes of cells, and the attributes of different attributes and even the default values of different numeric attributes are based. In this way, information of anomalous nature can be determined, and the amount of duplicate data can be determined and avoided [8, 9].

(2) Missing data cleaning

In many fields, missing data is a complex and difficult to avoid problem. Due to improper operation, confidentiality of information, or unreliability of data sources, the contents of the data set are incomplete and incomplete. In data mining, the lack of data will cause many problems [10]. For example, if the wrong model is applied to the grassroots system, there will be serious differences in the evaluation and implementation of the effectiveness of resource management rules and the accuracy of export rules. Many modern methods can be used to clean fluids. Clothing can be divided into two categories:

(1) *Ignore Incomplete Data*. Incomplete data is ignored, and its characteristics and examples can be deleted. Its advantage is that when the data is too small, too small to collect complete data, the data will be very effective. Its drawback is that when a large amount of incomplete data is in the subset, a smaller number can be obtained after deleting from the file, which can only increase the representativeness of the model and greatly reduce the reliability of the model [11, 12]

(2) *Missing Value Interpolation Method*. Because the neglect method is likely to delete useful information, after being ignored, useful information may also be deleted to complete incomplete data. How will it make up for these missing values? Replace the value with the value closest to the data, and obtain the obtainable value of the quantity and quality of the data. The supplement will provide potentially valuable data, more information about the sample than the method used by the despised person, and will not lead to deviation of the data analysis results, making the designed model extremely unreliable [13]

(3) *Noisy Data Processing*. Usually, we assume that the data set is data mining without interference. However, in real life, due to various reasons, in the process of data collection, a large amount of noise data is often generated, which we call "outliers." If the data range is not reasonable, it may be difficult to ensure the quality of input and output in the data mining process, resulting in inaccurate results. So there are usually two ways to process voice control data. The first is fractal technology. The preliminary data is divided into different containers, and the data is smoothly displayed with corresponding values, including measuring two wide and deep containers. The second method is to use the group method for outlier analysis [14, 15]

2.2. Data Integration. In the context of big data, data sources are often diverse, and data integration is to store data in different databases into a unified data store. Obviously, it is not feasible to forcibly merge two databases of different designs. This often leads to redundancy and inconsistency of data sets. Therefore, how to match the patterns and objects of multiple data sources is the main problem solved by data integration [16]. The following problems are mainly solved in data integration:

(1) *Mode Integration*. Integrate metadata from different data sources [17]

(2) *Entity Recognition Problem*. Matching equivalent entities from different databases [18]

(3) *Data Redundancy*. The same entity will have its corresponding attribute representation in different databases [19]

(4) *Data Value Conflict.* In the real world, metadata is very different, because there are big differences between different ratios and different codes. For example, the size attribute is based on the metric system in one system and the British system in another system [20]

2.3. Data Transformation.
Finding the characteristic representation of data is the core of data transformation. Through dimensional transformation or transformation, the number of effective variables is compressed, or the invariant of the data is found, and the data is transformed into a data suitable for various mining modes through methods such as normalization, switching, and projection form [21]. Commonly used transformation methods include the following:

(1) *Function Transformation.* Use some mathematical functions to map each attribute value

(2) *Normalize the Data.* Make the data scaled proportionally, and it is easy to reduce the scope [22]. In order to avoid excessive reliance on individual categories and algorithms and correct imbalances, some factors may need to be considered

2.4. Data Protocol.
In today's information age, with the increasing scale of data sets, higher requirements are placed on data mining technology. However, the analysis and mining of massive data not only increase the complexity of the technology but also greatly extend the mining time, which is a huge challenge for data mining research. In response to this type of problem, the technology of data entry completion can be used to replace a large amount of original data; although its scale is much smaller than the data itself, it also retains the integrity and exclusivity of the original data. For complex and huge data sets, the data reduction step is essential. It can not only effectively reduce mining complexity and mining time but also has good and reliable mining quality [23]. Data reduction techniques mainly include dimension reduction, data compression, discretization, data cube technology, data block reduction, and concept hierarchy generation methods.

3. Big Data Quality Evaluation Standard Research Experiment

First, let us briefly introduce the self-organizing competitive neural network (SOM). The SOM artificial neural network will simulate the function of the human brain neural network. The network consists of an input layer and an output layer. The input neurons are a one-dimensional matrix that receives the input signals of the network. The output layer is arranged by neurons in a certain way into a two-dimensional node matrix. The number of neurons is from the corresponding number. The vector based on the signals received in the network and the neurons from the network stand in a specific way in an X-ray matrix X-ray node target. When the network receives a signal, the neurons in their input layer are connected to the neurons in the output layer.

The network initialization assigns small random numbers to the weight vectors of the output layer and normalizes them to obtain $w(j = 1, 2, \cdots, m)$, establish the initial winning field $N(0)$, and the initial learning rate η value. m is the number of neurons in the output layer [24].

$$\frac{1}{2}\eta = \sqrt{\frac{N + w_i(a)}{m)}}. \tag{1}$$

An input pattern is randomly selected from the training set and normalized to obtain $X(i = 1, 2, \cdots, n)$, where n is the number of neurons in the input layer.

$$\eta = N_j \left[x_m - w_{ij}(t)\right]. \tag{2}$$

Calculate the dot product of X and w, and find the winning node j with the largest dot product. If the input mode is not normalized, the Euclidean distance should be calculated according to equation (2), and the winning node with the smallest distance should be found from it.

$$d_j = \left\|X_t - W_j\right\| = \sqrt{\sum_{j=1}^{m} \left[X_i - W_j\right]^2}. \tag{3}$$

Let j be the center to determine the weight adjustment domain at time t. Generally, the initial domain $N(0)$ is large, and $N(t)$ shrinks with the training time during the training process.

$$j \in N_j^*(t). \tag{4}$$

Adjust the weights of all nodes in the winning field $N(t)$

$$w_{ij}(t + 1) = w_{ij}(t) + a(t, N). \tag{5}$$

Before introducing structural risk minimization, first introduce the following concept: Suppose VC-dimension h is finite, then the following formula holds with probability $\geq 1 - \eta$:

$$R(a) \leq R_{\text{emp}}(a) + \forall a \in \wedge, \tag{6}$$

where η is a small integer:

$$\varepsilon = 4\left[\left(\ln \frac{2\int}{h} + 1\right) - \ln\left(\ln\left(\frac{\eta}{4}\right)\right)\right] / \int. \tag{7}$$

For the linearly separable training set, its samples all meet the following conditions:

$$y_i((w \cdot x_i) + b) - 1 \geq 0. \tag{8}$$

Then, looking for the optimal classification surface of the training set Ω is to satisfy the condition of equation (3) to solve the hyperplane equation that minimizes $\|w\|$ [25]. This is a typical constrained optimization problem, so after

TABLE 1: The basic information of 7 numerical variables in the data set.

Statistical magnitude	Collection	Original cost	Price	Discount	Has evaluation
Least value	0	1	1	0.05	0
Lower quartile	186	22	15	0.42	52
Median	524	57	29	0.7	124
Mean	2095	141	71	0.6914	686
Upper quartile	1538	180	94	1.00	318.00
Maximum	900	2380	1850	11.00	5459.7
Missing value	0	8	8.00	0.00	8
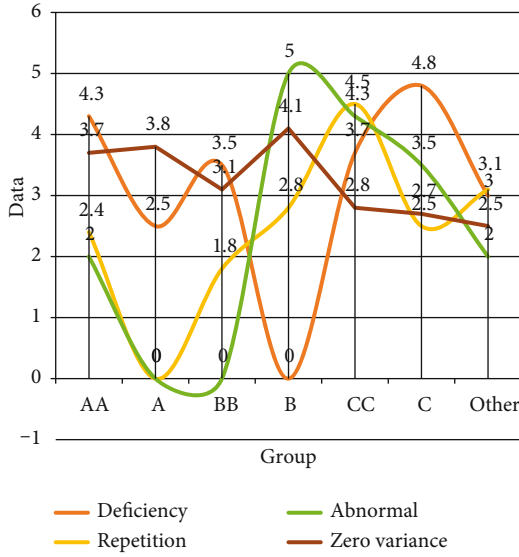
FIGURE 1: The frequency of missing values for only four variables.

transforming the problem of minimization into a problem of minimizing equivalently, equation (9) can be obtained:

$$\min \frac{1}{2}\|w\|^2. \tag{9}$$

Generally, to solve the convex quadratic optimization problem of equation (9), it can be solved by converting it into its dual problem by Lagrange optimization method, as shown in equation (10).

$$\max \sum_{i=1}^{N} a_i - \frac{1}{2}\sum_{i=1}^{N}\sum_{i=1}^{N} y_i y_j a_i a_j (x_i \cdot x_j). \tag{10}$$

i in equation (10) is the Lagrange multiplier corresponding to the constraint condition [26, 27]. We can know that the edge hyperplane is only related to a few samples on its plane. These samples are what we call the support vector; that is to say, the Lagrange multiplier k corresponding to the support vector Xk must be greater than 0, and X must be the following conditions:

$$1 - y_i((w \cdot x_i) + b) = 0. \tag{11}$$

From equation (11), we find b in the classification function:

$$b = y_k - W \cdot X_k = y_k - \sum_{a_{j>0}} a_j y_j (X_j, X_k). \tag{12}$$

In this way, we can get the expression of the classification function $f(x)$:

$$f(x) = \text{sgn}\left[(W \cdot X) + y_k - \sum_{a_j>0} a_j y_j (X_j, X_k)\right]. \tag{13}$$

Since it is not necessary to ensure that the training samples are classified correctly in all cases, sometimes we need to weigh the empirical risk and generalization ability. This is the approximate linear separability problem [28]. This kind of problem can be obtained by adding a relaxation factor § to the original problem, and formula (14) can be obtained:

$$\min_{w,b,\xi} = \frac{1}{2}\|w\|^2 + C\sum_{i=1}^{N}\xi_i. \tag{14}$$

The nonlinear separability situation means that there is no hyperplane for a training set that can directly separate the two types of samples. To solve this kind of problem, a nonlinear transformation function, that is, a kernel function can generally be used to map the training sample data to a high-dimensional space to make it linearly separable [29]. The optimization problem after introducing the kernel function can be expressed as:

$$\sum_{i=1}^{N} y_i a_i = 0. \tag{15}$$

4. Big Data Predictive Analysis in the Field of e-Commerce

4.1. e-Commerce Mobile Computing. The data used in the experiment in this article comes from the "searching glasses sales ranking 100 pages of baby data" provided by a data provider. The purpose of this experiment is to use the support vector machine parallel method to predict the sales of glasses. Although before doing the experiment, we hope that the larger the amount of experimental data, the better, but

because the data acquisition is really difficult, in the end, we only obtained about 5,000 data. Some of these 5000 data have certain problems. We need to analyze the entire data set through the following data processing and quality evaluation. First of all, let us take a look at the situation of the collected data. There are 5,000 pieces of data collected and 7 variables in total. Two of the seven variables are text variables: credit and commercial name; the other five variables are numerical variables: collection, original price, price, discount, and postage; therefore, we first analyze the seven numerical variables in the data set that makes a summary, as shown in Table 1:

We know that some of the product names in the product name are repeated, and the highest frequency reached 5, indicating that the data we have taken may be repeated, and we need to delete the repeated values; from the perspective of credit, the main points are there are six types of "AA, A, BB, B, CC, C," so we need to convert the data to facilitate our next analysis. In summary, we know that the data set contains at least missing, duplicate, outlier, and zero variance phenomena, so we need to clean the data to get a high-quality data set that can be used for analysis.

As shown in Figure 1, when we know that there are missing values among the 7 variables, the frequency of missing values for only four variables is 0, especially for the description score, service score, and shipping score as high as 24 missing values. The maximum and minimum values of the variable of the main credit ratio are both 8, which means that all the data of the variable is 8, which means that the variable has zero variance and is invalid information and the description points, service points, and shipping points. The highest value of is greater than 5, and the minimum is basically above 4.4, but according to the rules, we know that the score is between 0 and 5, indicating that the sampling information is not accurate, and some data has abnormal values. Therefore, data cleaning must be necessary for the data, and the "dirty data" can be filtered out before the following analysis can be carried out. In the next step, we will perform a summary analysis on the two text variables.

This section is to provide data preprocessing and quality evaluation for the following data analysis work. First, we preprocess the 5000 "glasses" data we have collected and finally get 3953 data that can be used for quality evaluation. Next, the quality of this part of the data is evaluated. Each quality dimension has its corresponding quality element, and the quality element corresponds to its index. The purpose of establishing an evaluation baseline is to compare the data set with the quality dimension after data preprocessing to see if it meets the evaluation baseline. If it meets the evaluation baseline, it can be used for data analysis. Otherwise, data collection must be performed again. The specific process is shown in Figure 2.

In the process of data preprocessing, each step is to process the data set into a data set that can be used for parallel SVM predictive analysis. For example, in the data cleaning process, we cleaned the "Taobao" data set for missing values, duplicate values, outliers, and zero variance; in the data transformation process, we processed the data in the "credit" dimension numerically; data specification in the link, we
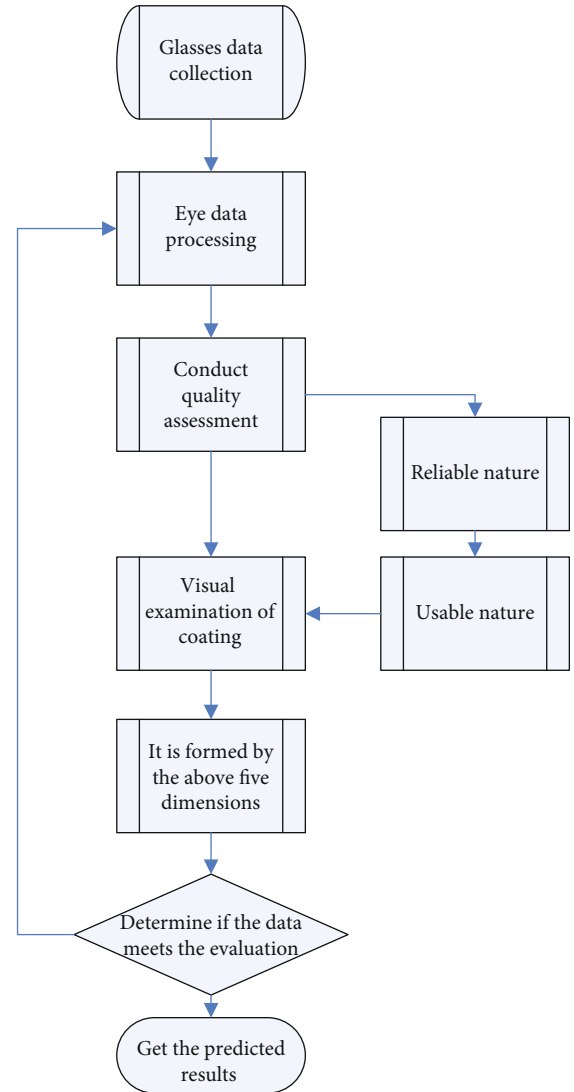
FIGURE 2: Glasses data quality evaluation and predictive analysis process.

TABLE 2: The basic situation of two textual variables in the data set.

Product name	Frequency	Credit	Frequency
Bow	24	Star	1372
Sun glasses	21	4 drill	519
Spectacle frame	20	3 blue crown	438
Polariscope	18	5 drill	418
Buy frames	17	1 blue crown	322
Authentic sunglasses	17	2 blue crown	328
(Other)	20	(Other)	1598

made a correlation analysis and deleted the dimension that has a lower correlation with the "30 glasses volume" dimension. In the end, we get 1598 data with a dimension size of 7. This part of the data can be used in the following data quality evaluation, as shown in Table 2.
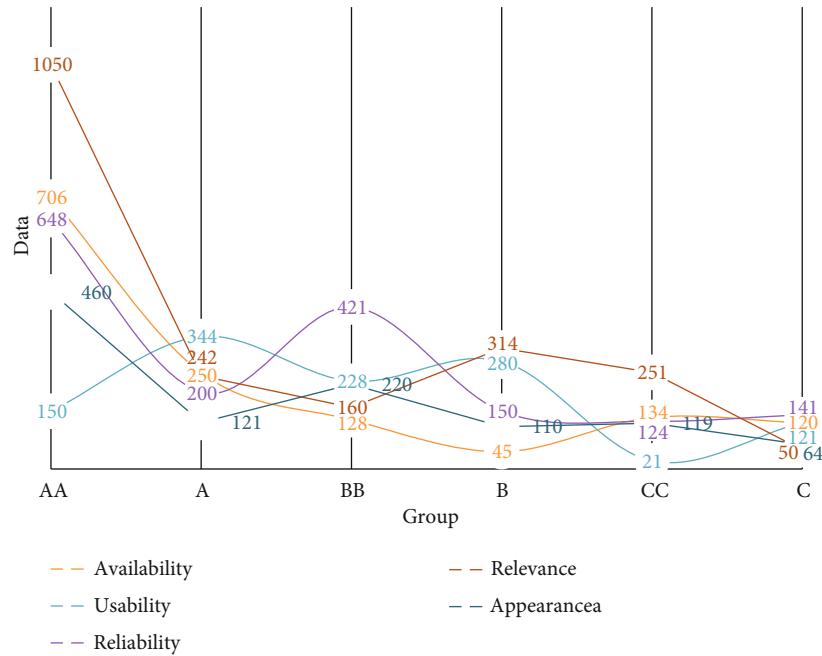
FIGURE 3: Further numerization is carried out according to the level of credit.

TABLE 3: The shows that the data has good timeliness.

	Construction stage	Cost management content	Calculation basis
Investment decision stage	Project proposal, feasibility study, and preparation design task book	Prepare investment estimates	Investment estimation indicators, previous similar project cost data
Design phase	Initial design	Preparation of the overall design budget	Preliminary design drawings, relevant budgetary quotas, or budgetary indicators
Bidding stage	Bidding	Compile the block price (mark bottom) to determine the contract price	Construction drawings, consumption quota, and relevant funding standards
Construction stage	Contract/project implementation	Control cost, stage settlement	Control according to the contract price
Completion acceptance stage	Completion acceptance	Completion settlement/final accounts	Completion settlement (final accounts) and other documents

Here is a point to explain, because the data we collect comes from this e-commerce platform; the method of data integration is not used in the data processing process. However, this method is also indispensable when analyzing other e-commerce big data. For example, when we need to analyze the sales of "iPhone X" mobile phones on these two e-commerce platforms in a certain quarter, we must use data integration technology. Integrate data from two different platforms for analysis.

As shown in Figure 3, the frequency of "AA" credits is the largest, namely, 1050, followed by the frequency of "BB" credits reaching 421, followed by "A" and "B"; the lowest frequency is "CC" and "C." From the distribution point of view, the credit distribution of the sampled data is relatively uniform. Therefore, the digitization is further carried out according to the level of credit, the value of high credit is high, and the value of low credit is low, and the final digitization result is as above.

4.2. Forecast and Analysis of the Development of e-Commerce Enterprises. In this section, we evaluate the quality of the "clean" data obtained after data preprocessing. The method of quality evaluation is to compare the data to be evaluated with the evaluation baseline formed by the five dimensions of availability, usability, reliability, relevance, and appearance quality. From the perspective of data availability, it can be evaluated from two aspects: accessibility and timeliness. Accessibility usually refers to the difficulty for users to obtain data. This data is the sales data of a certain product. It is an open that the data can generally be obtained through Internet search or data providers, so the data accessibility is relatively high; timeliness usually refers to whether the data can be quickly obtained during the collection process, and the data is for the current task. Whether it is the latest data, after communicating with the "glasses" data supplier, it shows that the data has good timeliness, as shown in Table 3.
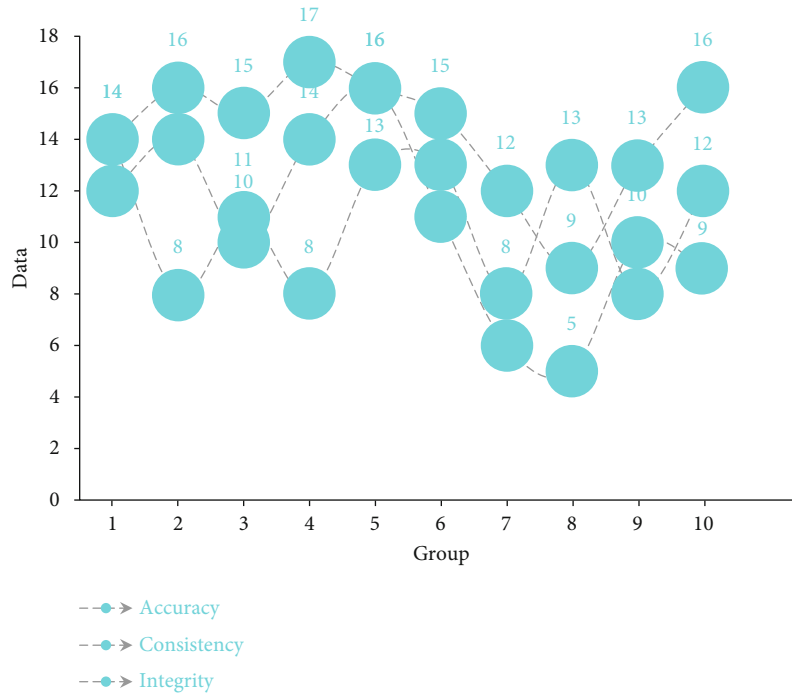
FIGURE 4: From the reliability point of view generally data.
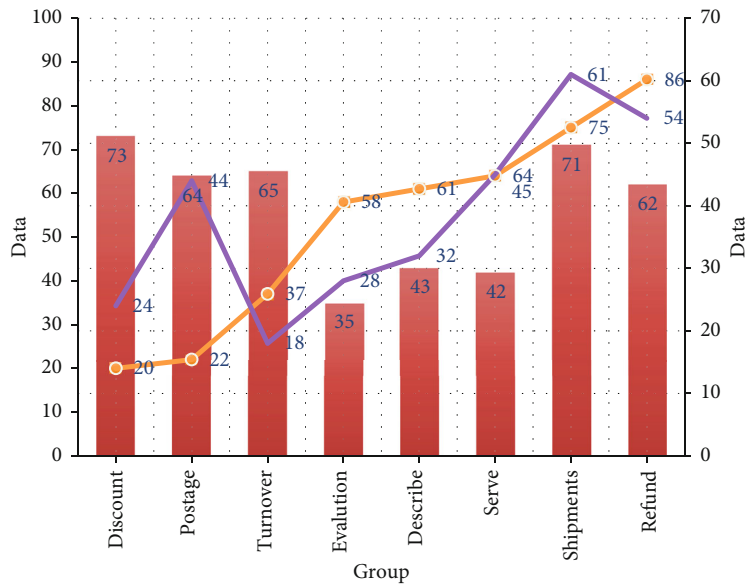
FIGURE 5: Relevance refers to whether the data is relevant to the task at hand.

As shown in Figure 4, from a reliability perspective, reliability generally refers to how much we can trust this part of the data. We searched the top 10 eyewear shops in the data set on the Internet and found that by comparing some of the data, the data is basically consistent with the real data, which shows that the data set is very reliable. From a usability perspective, we can see progress in three areas: accuracy, consistency, and completeness. Accuracy means that the real data and complete information next to the data are free of incompleteness and omissions. For the study of these two

indicators, we use data cleaning in data preprocessing to eliminate duplicate data, missing data, and abnormal data, and irrelevant data is processed, and the "clean" data obtained meets these two indicators; consistency usually indicates whether the logical relationship between data and data is clear. Our research found that the data dimensions in the "glasses" data set are in addition to "credit." The data of the dimensions are all expressed in numerical values. In order to facilitate the data prediction and analysis in this section, we use the data transformation in the data
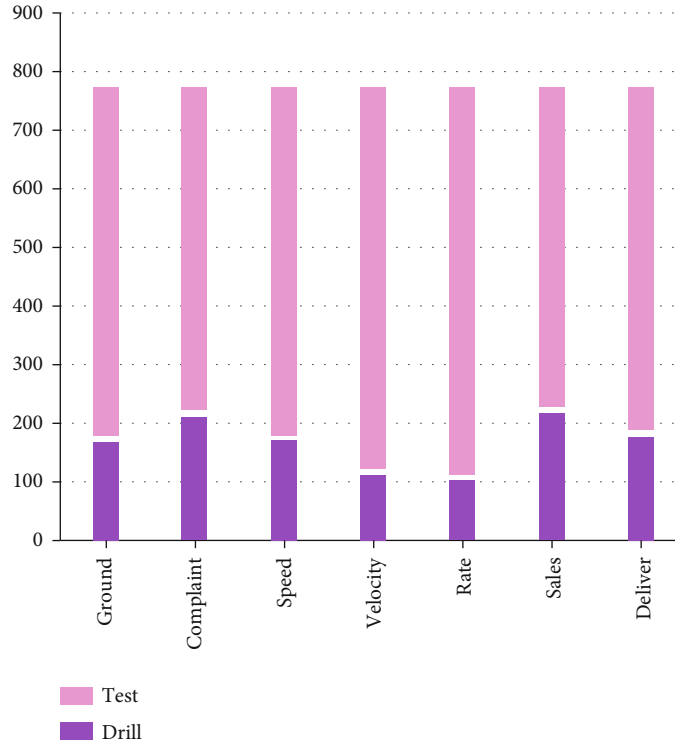
FIGURE 6: Glasses data quality evaluation and predictive analysis process.

TABLE 4: Kernel parameter P and penalty parameter C are used as training.

	Parameter	Search	Punishment	Optimal	Scope	Comprehensive
Parallel	1.5	2.5	4.5	-1.5	6.0	4.5
SVM	2.5	3.0	2.0	7.5	4.0	2.5
LIBSVM	7.5	6.0	4.5	5.0	5.0	10.0

preprocessing to numerically process the data expressed in Chinese characters in the dimension "credit" to ensure the data consistency.

As shown in Figure 5, from the perspective of relevance, relevance refers to whether the data is suitable for the current task. The purpose of this experiment is to predict the "30-day sales of search glasses," so in order to make the prediction results more accurately, we conducted a correlation analysis on the data set through the data specification in the data preprocessing. Through correlation analysis, we selected the dimensions related to sales volume for analysis, while other dimensions were deleted. The remaining dimensions are "evaluated, discount rate, postage, 30-day transaction volume, service points, delivery Goods points, description points, and the refund rate in the past 30 days"; from the analysis of appearance quality, it is used as an additional attribute to improve user satisfaction. It usually indicates whether the data can be clearly understood by people. From the data we get from the description point of view, it includes "collection, reputation, page views," etc., which are all easy-to-understand terms, and the content of the data is also very clear, all expressed by numerical values, so the data has a high appearance quality. After data quality

evaluation, we finally got a total of 3953 useful data with a dimension of 8.

As shown in Figure 6, the sales volume of glasses can be predicted by analyzing the dimensions related to the "30-day trading volume of search glasses." We divide the experimental process into two steps. The first step is to use the training algorithm to get the training model, that is, to find the hyperplane that classifies the data. The second step is to judge whether the training model is accurate by predicting the test set in the data set, so as to verify whether the training algorithm is effective. In the data set of the experiment, the data is divided into two parts: the training set and the test set. The first 70% (2767) data are used as the training set data, and the last 30% (1186) data are used as the test set data.

This experiment was carried out on a PC (2.40 GHz CPU, 16 GB memory), the experiment platform was MATLAB 2017b, and the experiment environment was the LIBSVM toolbox. All experiments use Gaussian kernels, and the kernel parameters and penalty parameters are determined by grid search. The grid search range of the kernel parameter P and the penalty parameter C is between -10 and 10, and the step size is 0.5. Take each job, the kernel
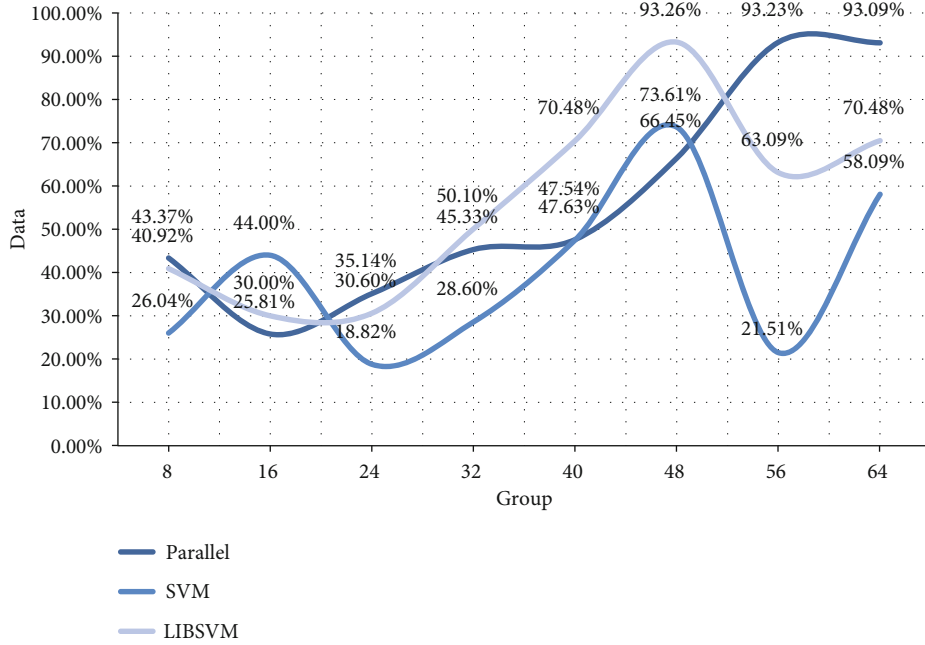
FIGURE 7: Computers will first go through the SOM algorithm.

	FPPL	CNG	FL	SVM
■ 1	45%	35%	25%	93%
■ 2	28%	48%	93%	24.00%
■ 3	51%	73%	42%	20%
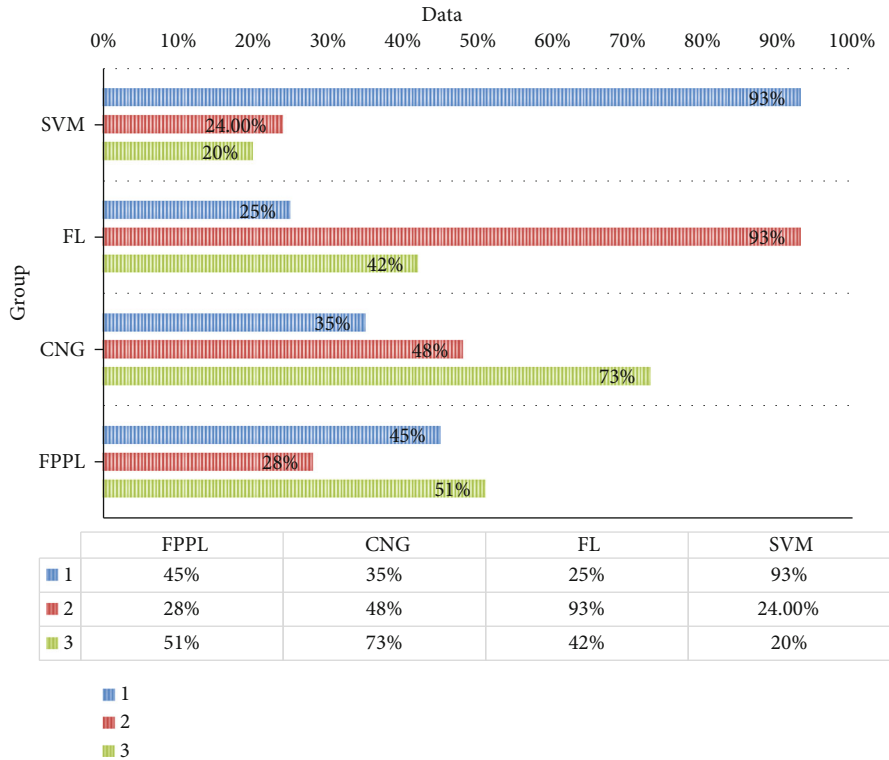
FIGURE 8: Through the comparison of the above two groups of experiments.

function parameter P and the penalty parameter C with the highest corresponding accuracy on the subset are used as the optimal parameters for training, as shown in Table 4.

Before doing the parallel SVM prediction model, we first use the SOM self-organizing neural classification algorithm to group the 2767 data in the training set and set the maxi-

mum number of cycles T to 64. According to the SOM self-organizing neural classification algorithm, we get 64 sets of data, according to parallel algorithm, assign these 64 groups of data to a computing core of parallel operation and run the SVM fitting algorithm to find the support vector, and get each support vector subset SV. The support vector subsets

are combined to obtain the support vector set SV, and the SVM fitting algorithm is used for it, and the grid search method is used to select the optimal kernel parameter P and the penalty parameter C. After that, we use the obtained optimal kernel parameter P and penalty parameter C to train the entire support vector set SV to obtain the prediction model of the parallel SVM. Finally, the model is used to predict 1186 data on the test set, and the prediction result is obtained.

In order to verify the efficiency and accuracy of the support vector machine parallel algorithm, we also used traditional SVM to perform prediction experiments on this data set. The experimental configuration all adopts the default configuration of LIBSVM, and the experimental results are as follows:

As shown in Figure 7, when performing parallel prediction, we found that the computer's memory usage has increased significantly. This is because when the parallel algorithm is executed, the computer first allocates 64 sets of data obtained through the SOM algorithm to the computer's 64 operation core, and fitting at the same time, the whole running time is 106 seconds. We first used the obtained prediction model to predict 2767 data on the training set with a prediction accuracy of 93.26%; then, we predicted 1186 data on the test set with a prediction accuracy of 70.48%.

When using traditional SVM for predictive analysis, the computer's memory occupancy has almost no change. This is because the serial algorithm used by traditional SVM does not occupy too much computer cores, and the entire system runs for 779 seconds. Similarly, we first use the prediction model obtained by traditional SVM to predict 2767 data on the training set with a prediction accuracy of 93.09%; then, we predict 1187 data on the test set with a prediction accuracy of 58.09%.

As shown in Figure 8, through the comparison of the above two sets of experiments, it is found that the prediction accuracy of the two sets of experiments on the training set is about 93%, which can show that the prediction models of parallel SVM and traditional SVM are accurate. From the comparison of prediction accuracy, the accuracy of the parallel SVM is much higher than that of the traditional SVM. This may be because the parallel SVM extracts a large number of useful support vectors during the execution process and deletes the support that has no influence or side effects on the classification results. Vector thus ensures that the classifier has good generalization performance, and from the time of predicting data, parallel SVM only takes about one-seventh of the time of traditional SVM, which shows that parallel SVM is in processing large-scale data sets. It is more efficient than traditional SVM. The experimental results show that the parallel SVM plays an excellent role in predicting and analyzing the data, both in terms of accuracy and efficiency.

5. Conclusions

With the development of information technology, big data has become popular in all industries, and the great value of big data has been widely recognized. Bad data leads to inefficiency and often leads to serious wrong decisions, and the quality of existing big data does not even have a standard. High-quality data is important for analyzing and using big data and ensuring its value. How to ensure the quality of big data and how to ensure the information and knowledge behind the data have become an important issue in the industry and the scientific community. In addition, in order to analyze the big data in the field of e-commerce, this topic uses support vector machines for research. Although there are many documents on big data research at present, there are still few studies on the quality evaluation of big data, and the research level of this article is limited. There are many shortcomings. In terms of quality standards and evaluation processes, they should be measured according to the standards of authoritative experts. Especially people like big data are still in the cutting-edge technology of the continuous cognitive process. As time progresses, the amount of data will inevitably become larger and more complex, the dimensions and indicators will inevitably have errors, and the evaluation system will not be able to adapt to the future development of data, but I believe that these issues will continue to be studied in the future has been solved.

Data Availability

No data were used to support this study.

Conflicts of Interest

The authors declare that they have no conflicts of interest.

References

[1] J. Xu, Z. Luo, H. He, and Y. Zhou, "Research on the spatial characteristics and influence factors of the development of e-commerce in China's county areas," *Shanghai Urban Planning*, no. 2, pp. 90–97, 2017.

[2] N. Wang and X. Wang, "The mobile online shopping behavior execution intent prediction model based on situational big data," *Computer Age*, vol. 322, no. 4, pp. 30–33, 2019.

[3] H. Yuhua, "Distributed big data's group behavior pattern mining algorithm," *Yulin Normal College Journal*, vol. 40, no. 2, pp. 151–157, 2019.

[4] J. Wu, S. Guo, H. Huang, W. Liu, and Y. Xiang, "Information and communications technologies for sustainable development goals: state-of-the-art, needs and perspectives," *IEEE Communications Surveys & Tutorials*, vol. 20, no. 3, pp. 2389–2406, 2018.

[5] J. Wu, S. Guo, J. Li, and D. Zeng, "Big data meet green challenges: big data toward green applications," *IEEE Systems Journal*, vol. 10, no. 3, pp. 888–900, 2016.

[6] R. Atat, L. Liu, J. Wu, G. Li, C. Ye, and Y. Yang, "Big data meet cyber-physical systems: a panoramic survey," *IEEE Access*, vol. 6, pp. 73603–73636, 2018.

[7] H. Song, J. Bai, Y. Yi, J. Wu, and L. Liu, "Artificial intelligence enabled Internet of Things: network architecture and spectrum access," *IEEE Computational Intelligence Magazine*, vol. 15, no. 1, pp. 44–51, 2020.

[8] Z. Miao, "The design and implementation of the mobile terminal precision marketing system based on big data analysis," *Electronic Design Engineering*, vol. 26, no. 21, pp. 71–76, 2018.

[9] D. Xiaomei, J. Wang, and Z. Lihong, "Mobile big data analysis algorithms based on deep learning and spark computing," *Journal of Changsha University*, vol. 34, pp. 13–18, 2020.

[10] C. Haixuan, "Heterogeneous real-time computing architecture analysis based on mobile Internet big data," *Automation Technology and Applications*, vol. 39, pp. 48–51, 2020.

[11] L. He, "Health data management and analysis system research based on edge computing," *Electronic Design Engineering*, vol. 28, pp. 60–64, 2020.

[12] W. Wu, Z. Long, and S. Chao, "MEC-based indoor positioning of big data applications," *Telecommunications Science*, vol. 35, no. S2, pp. 207–211, 2019.

[13] Z. Tianxuan, "Spatial distribution statistics of urban population based on mobile communication big data," *Computer and Modernization*, vol. 273, pp. 49–53, 2018.

[14] J. Peng, Y. Wang, and C. Fudong, "Power mobile Internet of Things information security terminal architecture based on big data analytics," *Electrical*, no. 1, pp. 63–66, 2017.

[15] L. Guofeng, "Research based on mobile Internet big data analytics platform," *Consumer Guide*, no. 19, pp. 43-44, 2017.

[16] J. Wang and S. Sai, "Build a big data analytics system based on the whole process of purchasing," *Digital Design*, vol. 6, no. 3, pp. 12–14, 2017.

[17] X. Wei, "Cloud-based big data mining system building analysis," *Chinese and foreign entrepreneurs*, vol. 673, no. 11, pp. 116–116, 2020.

[18] H. Cong, "Study on the route tracking of urban rail trains based on big data analysis," *Modern Electronics*, vol. 41, no. 508, pp. 110–115, 2018.

[19] S. Lin, T. Jin, Y. Cheng, and Y. Jin, "Wireless big data analytics user QoE perceived improvement strategy," *Communications Technology*, vol. 51, no. 10, pp. 2418–2422, 2018.

[20] Y. Cheng and G. Wu, "Empirical study of intelligent bracelet big data analysis system based on"T-in-One"ecological chain," *Software*, vol. 39, pp. 30–33, 2018.

[21] L. Zexin, "Smart city systems based on big data," *Communications World*, vol. 26, no. 1, pp. 79-80, 2019.

[22] S. Wen, "To analyze the application of big data analysis in the optimization of mobile communication networks," *Global Markets*, no. 17, pp. 180–180, 2017.

[23] Z. X. Lu, "Power mobile Internet of Things (IoT) information security terminal architecture analysis based on big data," *Electronic Design Engineering*, vol. 28, pp. 159–163, 2020.

[24] Y. Smelting and L. Yangwu, "Research based on the ocean aquatic big data price analysis and prediction system," *Wireless Connected Technology*, vol. 17, pp. 44-45, 2020.

[25] C. Long and H. Danxuan, "Big data processing and analytics systems based on the hadoop framework," *Fujian Computer*, vol. 34, no. 5, pp. 120-121, 2018.

[26] O'Jianlin, "Hadoop-based commercial bank big data platform research and implementation," *China Financial Computer*, no. 1, pp. 50–53, 2019.

[27] S. Wang, Z. Bao, and L. Chenxuan, "Spark-based big data analytics technology," *Computer Systems Network and Telecommunications*, vol. 1, no. 2, pp. 254–258, 2019.

[28] W. Yang, S. Xiaoxing, H. Luo, and Y. Xuan, "Based on operator big data public opinion innovation application research," *Jiangsu Communications*, vol. 33, no. 1, pp. 70–72, 2017.

[29] Y. Wang, "Based on the innovative analysis of enterprise financial management in the era of big data," *Tax*, vol. 12, 2018.

WILEY | Hindawi

Research Article

Open Platform for Intelligent R&D and Technology Innovation Management Service Based on Edge Computing

Bing Xie (ID)

General Manager's Office, Jiangsu Shenyuhuhang Technology Development Co. Ltd., Nanjing 210001, Jiangsu, China

Correspondence should be addressed to Bing Xie; 201601015117@stu.zjsru.edu.cn

The rapid development of mobile Internet and Internet of Things makes the future network face higher speed, lower delay, and higher reliability. Because this edge computing becomes the most likely network architecture to realize the vision of intelligent R&D and technological innovation, it has attracted wide attention. Edge computing can meet the high computing needs of mobile devices with limited resources by using computing-intensive tasks from the mobile device open platform to nearby edge computing servers. This paper mainly studies the open platform of intelligent R&D and technology innovation management service based on edge computing, which can study the characteristics of edge computing more. The characteristics of edge computing will have a certain impact on the open platform strategy. This paper mainly uses the edge computing algorithm, model, edge computing time-to-time optimization open platform policy, platform function investigation experiment, platform module analysis, and other methods to study the open platform of intelligent R&D and technology innovation management service based on edge computing. This can better meet the actual application and improve the effect of the open platform which can better meet the different needs of the open platform. The results show that the number of users in the useful task open platform increases by 27.4% in the open platform of intelligent R&D and technology innovation management services based on edge computing. The platform can also meet the simulation of different scenes well, and the edge algorithm has some advantages in comparison with other algorithms.

1. Introduction

In November 2016, many technology companies led by Huawei jointly initiated the edge computing industry alliance, elaborating the functional design of the framework. Meanwhile, the International Electrotechnical Commission also issued a white paper on the intelligent application of the vertical industry, which introduced the important value of edge computing for vertical industries such as manufacturing. All kinds of signs show that the cooperation of all parties in "government, industry, university and research" is promoting development and application of edge computing in various industries.

Edge computing has been widely used in the commercial field. Among them, Internet enterprises hope to extend the existing cloud service capabilities to the edge network with the help of their own advantages in the service industry, improving the technical position of the enterprise in the consumer Internet of Things and industrial Internet by strengthening the relevant performance of the access side network. Cisco, as the initiator of the concept of fog computing, has planned the overall framework of edge computing from its own aspects, including publishing edge side dedicated network hardware equipment for intelligent manufacturing or Internet of Things scenarios, building the IOS application framework by using software definition and other technologies to restructure edge side capabilities. Microsoft released edge products such as "Azure IOT edge," and for Azure, cloud services enhance the ability of streaming data analysis; Amazon released "AWS Greengrass" edge side software, which seamlessly extends AWS cloud services to devices.

When edge devices are collecting and preprocessing data, if the current scene is a real-time system, the delay effect of the module for the subsequent data analysis needs to be considered. A data analysis system can be divided into

the delay-sensitive type and the delay-tolerant type. For the data analysis system with tolerable delay, the delay increase to a certain extent does not seriously affect the performance of such data analysis. Shi et al. believe that the popularity of Internet of Things and the success of enriching cloud services have promoted the emergence of a new computing paradigm called edge computing, which requires processing data on the edge of the network. Edge computing may solve the problems of response time requirements, battery life limit, bandwidth saving cost, and data security and privacy. This paper introduces several cases from the cloud open platform to the smart home and city and implements edge computing by collaborative edge. It puts forward challenges and opportunities in edge computing, but it lacks specific data [1]. Vallati et al. believe that the future smart R&D and technology innovation cellular network is expected to play an important role in the support of the Internet of Things because of its ubiquitous coverage, plug and play configuration, and embedded security. However, in addition to connectivity, the Internet of Things also needs to be calculated and stored near sensors and actuators to support time critical and opportunistic applications. Mobile edge computing is a new paradigm, which is in a standardized state. It is expected to enrich the future broadband communication network. With edge computing, traditional networks will enhance their capabilities by placing cloud computing functions in wireless access networks and in edge computing services near end users. This distributed computing and storage infrastructure will enable applications and services to be deployed on the edge of the network, enabling operators to provide virtualized environments for enterprise customers and industries to achieve near end applications and services, but they lack necessary experimental data [2]. Since the concept of bitcoin was put forward by Satoshi Nakamoto and then put into practice, Li et al. believe that bitcoin has completely changed the world economy in many ways by introducing scattered point-to-point transactions. These transactions do not require intermediary elements between traders, namely, banks; users can access their resources directly, while maintaining a comfortable Internet environment, but they lack numerical analysis content [3]. Shi and Dustdar believe that research on the adoption of intelligent R&D and technological innovation usually evaluates the functions users use when using these innovations. In this study, we identify internal factors that affect intelligent R&D and technological innovation defined by a medical information system, namely, electronic health records, and evaluate the results of the adoption of individuals and groups using the system. The multistatistical techniques such as communication, participation process, and innovation decision-making form, which are modeled by a structural equation, can effectively promote the adoption of intelligent R&D and technological innovation for reference, but some of the discussions are not accurate [4].

The innovation of this paper is to study the open platform of intelligent R&D and technology innovation management service based on edge computing by using the edge computing algorithm, model, edge computing open platform policy, platform function investigation experiment, platform module analysis, etc., and it analyzes all aspects of the open platform mode of management services and the overall system frame The research on frame design and special construction has certain scalability.

2. Edge Calculation Algorithm

2.1. Edge Calculation. Edge calculation, which is the core idea of the paper, is used to sink computing, storage, and network services to the network edge. On the basis of not changing the original network architecture, a series of devices near the network edge are used for auxiliary computing, and the data open platform originally needed to be transmitted to the cloud computing platform to the place closer to the terminal for local processing can achieve the purpose of quick response and reduce the service response delay. In edge computing, edge computing equipment is usually an existing network device such as a switch, router, and gateway on the edge of the network or a private edge computing server connected by it [5, 6]. In addition, because edge computing is to make up for the deficiency of cloud computing, the combination of cloud computing and me can give full play to their advantages and provide better service quality for users. It is necessary to study a new cloud edge computing network architecture based on edge computing technology. It is necessary to consider that the computing capacity and storage capacity of edge computing equipment are usually limited, and a single cloud edge computing device is usually limited in computing capacity and storage capacity. Edge computing equipment may not be able to process a large amount of data in effective time; however, there are many edge devices in the network. Therefore, it is proposed to group multiple edge computing devices based on the idea of distributed computing to form a distributed mobile edge network [7, 8]. When the user needs to process the service, the service opening platform can be represented in the mobile edge network as shown in Figure 1.

2.2. Edge Local Calculation Model

2.2.1. Local CPU Execution. When the task open platform policy determines that an edge calculation is performed on the local CPU, the edge calculation does not need to be uploaded through [9]. The delay is the total time before the task plus the execution time of the task. The symbol t and symbol f are, respectively, the execution time and waiting time of task i, and h is the computing capacity of the local CPU. Then, the task execution time can be expressed as

$$t = \frac{f_i}{h}. \tag{1}$$

Suppose that after the decision of open platform policy, one edge calculation in the M edge calculation is performed on the local CPU, and two edge computations need to be performed on the edge computing server by open platform
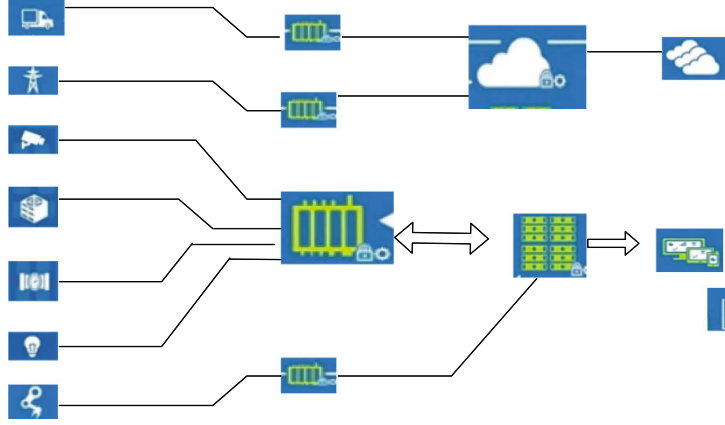
Figure 1: Internet edge computing (http://alturl.com/ga3ct).

to meet the following requirements:

$$M_1 + M_2 = M. \tag{2}$$

Let i and j denote the task label and execution order executed on the local CPU and the task label and execution order executed on the edge computing server from the open platform, respectively [10]. Then, we can get the waiting time of task t as follows:

$$t = \sum_{j=1}^{i-1} t. \tag{3}$$

2.2.2. Cloud Computing Model. The data of edge computing needs to be sent to the edge computing server through the transmitting device of the mobile device [11, 12]. Here, we assume that the Tu unit can only upload one edge computing data to the edge computing server at the same time. If the transmission power of the Tu unit is expressed as H(a), then the transmission rate can be expressed as

$$H(a) = r \log_2 \left(1 + \frac{g(a)^\theta}{Mr} \right). \tag{4}$$

For a given task open platform strategy, we can get the task set and execution order from the open platform to the edge computing server. For edge computing, the following two conditions need to be met before it can be executed by the edge computing server [13]. Firstly, the data of the edge computing has been uploaded to the task queue of the edge computing server; secondly, the edge computing server is idle and can execute a new edge computation. For the j-th task among all the tasks that need to be executed on the edge computing server from the open platform, if the symbol a and the symbol h, respectively, indicate the completion time of any upload and the completion time of execution, then we can get

$$t^j = \sum_{k \le j} \frac{a}{h}. \tag{5}$$

For the task completion time, it is not only related to the upload completion time of edge computing but also related to whether the previous upload edge computation is finished [14].

2.2.3. Load Model of Edge Computing. The energy consumption and time required for edge computing to be executed on the local CPU and edge computing server are obtained. Next, we use these data to construct an edge computing load model [14]. The load can meet the personalized needs of different users and flexibly adjust the factors concerned. According to the above analysis, the time t needed to complete all edge calculation is as follows:

$$t = \max \{t_1, t_2\}. \tag{6}$$

The energy required to complete all tasks f can be expressed as

$$f = f_1 + f_2, \tag{7}$$

$$N_1 + N_2 = N. \tag{8}$$

We assume that the overall load of the system is expressed as follows:

$$H = \lambda t + \lambda f. \tag{9}$$

The coefficients t and f, respectively, represent the weight of edge calculation delay and energy consumption in an open platform decision. The two coefficients satisfy the above relationship [15, 16].

2.3. Edge Computing Model Cloud. The computing and storage capacity of edge computing equipment is usually limited, and a single edge computing device may not be able to process a large amount of data in effective time; however, there are many edge devices in the network, so it is proposed to combine multiple edge computing devices based on the idea of distributed computing to form a distributed mobile edge network. When users need to process services, they can open the service platform to the mobile edge network [17]. In the meantime, the edge computation submitted by users is

divided into multiple subtasks first, then each subtask is reasonably opened to each computing node in the mobile edge network for parallel computing, and the results are returned to the user, thus greatly reducing the transmission pressure of the backbone network, reducing the computing pressure of the cloud center, and reducing the service response delay [18]. At the same time, because of the different computing capacities and link communication speeds of each edge computing device, it is very important to study an open platform strategy for edge computing suitable for a distributed cloud edge computing network considering the computing capacity and communication resources of the equipment. The edge computing model cloud is shown in Figure 2.

Low latency is one of the most important characteristics of edge computing, which solves the problem of high transmission latency when data is transmitted to remote cloud servers for storage and processing [19]. Mobile devices get high quality and low delay data service by connecting the edge computing open platform to the nearby edge computing server, which avoids the problems of poor user experience caused by the lack of performance of mobile devices and the high transmission delay of cloud computing [20–22].

2.4. Time Delay Optimization Open Platform for Edge Computing. The assigned subtasks are opened to each edge computing device to obtain the minimum delay. In the edge computing architecture, subtasks of the open platform on each edge computing device can be expressed as r. Therefore, the subtasks on K edge computing devices can form a k-dimensional vector G. Assuming that the total task is received by the edge computing device w, the total service delay t can be expressed as follows:

$$f(G) = \max \left\{ \frac{r}{c} + w \right\}. \tag{10}$$

The solution of the task allocation coefficient f can be transformed into the solution of vector g, so it is modeled as the following optimization problem:

$$\sum_{i=1}^{k} G(i) = r. \tag{11}$$

I is the search space of feasible solution g, which is expressed as follows:

$$I = \prod_{i=1}^{k} [r_{\min}, r_{\max}]. \tag{12}$$

The fitness value of each dimension value is calculated by optimizing the objective function $T(g)$. The fitness value is used to evaluate the quality of dimension values and to calculate the edge calculation radius and the number of edge calculation results of each dimension value. The edge calculation radius and the number of edge calculation results s of

each dimension value G is calculated as follows:

$$S = A \times \frac{t_{\min} + \varepsilon}{\sum_{i=1}^{N} (t(G) - t_{\min}) + \varepsilon}. \tag{13}$$

The edge calculation results are generated by the calculated edge calculation results s and the edge radius a. When edge calculation occurs, a position offset will be generated within the radius of the edge calculation. The offset is added to z dimensions randomly selected from dimension value g, thus generating new edge calculation results. The selected z dimensions are calculated as follows:

$$z = \text{round}(d * S(0, 1)). \tag{14}$$

The selected A dimensions form a set G. Therefore, the k-th dimension of the result of the edge calculation in the set G is expressed as follows:

$$G = A \times S(-1, 1). \tag{15}$$

3. Experiments on Intelligent R&D and Technology Innovation Management

3.1. Functions of Intelligent R&D and Technological Innovation Service Platform. The intelligent R&D and technological innovation service platform is an organization system which is aimed at supporting industrial development and takes enterprises, especially small- and medium-sized enterprises, as its goal. It provides public services for common needs of enterprise intelligent R&D and technological innovation by effectively integrating advantageous resources such as universities, scientific research institutes, science and technology intermediary service institutions, and backbone enterprises. The concept of intelligent R&D and technological innovation service platform shows that the participants of the organizational system are diverse, so the intelligent R&D and technological innovation service platform has the characteristics of openness. The purpose of intelligent R&D and the technological innovation service platform is to serve for a theme of intelligent R&D and technological innovation, so it has the characteristics of service. The articles of association, decision-making procedures, technical cooperation and exchange, benefit distribution, and operation of the intelligent R&D and technological innovation service platform focus on the public service of intelligent R&D and technological innovation of social industry and strive to provide conditional resource services, technological R&D services, and technological innovation services for enterprises. The function of achievement transformation service and talent training service. Intelligent R&D and technology innovation service platform can achieve strong integration of research institutions in the industry; combine relevant industries, universities, and research institutes in the region; avoid vicious competition in scientific research projects of research institutes; avoid repeated investment among production enterprises; and ensure good relations among technology development subjects, technology application
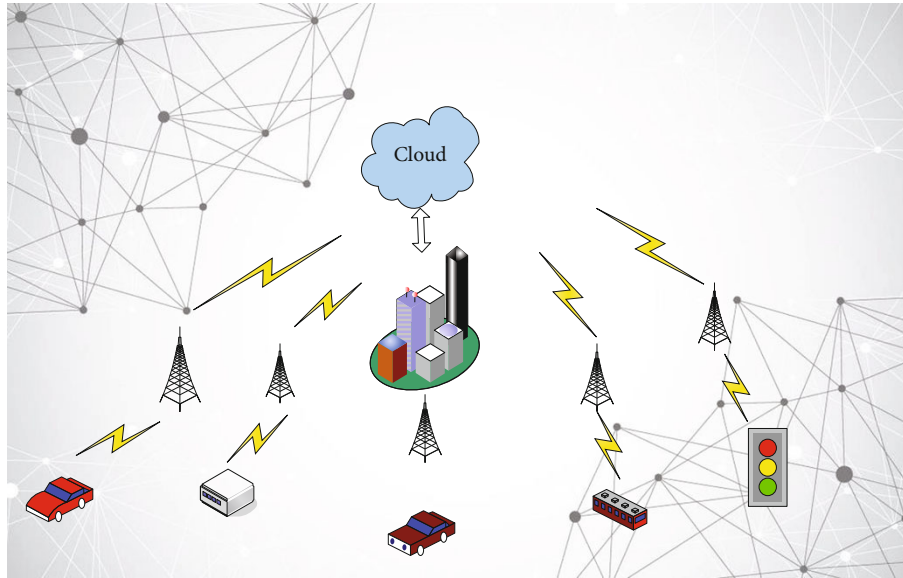
Figure 2: Edge computing model cloud (http://alturl.com/f6i9y).

subjects, and technology development and application subjects.

3.2. *Functional Requirements and Expandability Investigation of Service Platform Construction.* It is mainly designed around the functional requirements and scalability of service management platform construction. The first is to investigate the basic information and the cognition of the service management platform website. If you know nothing about it, the questionnaire you fill in will be regarded as invalid. The second is to understand the use of similar websites, expectations of the service management platform, participation motivation, usage habits, and interaction with the platform. The last is to understand the evaluation of the investigated objects on the current platform websites. In view of the fact that the first choice of website service users is the company's internal staff, the scope of this questionnaire is limited to the company's internal staff, who are the initial seed level users. A total of 60 questionnaires were distributed, of which 50 were valid. The basic information of the staff is shown in Table 1.

Node machine management module includes five submodules, including node machine basic information management, node machine status view, node machine log management, node machine power management, and node machine user management, as shown in Table 2.

3.3. *Platform User Management Module.* First, when the system initializes the service management platform, a default user will be automatically established with the administrator's permission. After the user logs in, you can select user management operation and establish, modify, or delete users. When a new user is established, the corresponding access rights to the user need to be assigned. Its access rights can involve each node machine. To simplify operations, the system will have default permissions: administrators and visitors. Administrators will have all access rights, including

managing operations on other administrator accounts. Visitors only have to modify their access password and view information on node machines (no user information for viewing node machines). Therefore, the corresponding user records will include basic information such as username, password, name, access rights, and the time of establishment of users. In addition to the statistical information such as the last visit, access times, and other statistics, a definition derived table will be included. The table associates the user with the node machine. The associated node machine is the machine that the user can access and operate as shown in Figure 3.

3.4. *Innovation-Driven Development Strategy and Technological Innovation.* Technology effectiveness refers to the continuous and in-depth research on technology effectiveness since the high-tech innovation expenditure is brought about by the high-tech innovation when the output is not reduced or the input is not added. The data envelopment analysis method establishes the evaluation model of the technical effectiveness of the discipline, observes the input data of many colleges and universities in the students and disciplines, and draws the corresponding technical effectiveness conclusion. Because the efficiency of technological innovation is a relative index, it is difficult to obtain an absolute value in the real technological economic activities, which reflects the efficiency of technological innovation comprehensively. This index of relative technological and economic activities mainly depends on the change of the input and output of scientific and technological innovation activities. Resource allocation plays an important role in the improvement of technological innovation efficiency. The concept of relative economic efficiency is given, and then, the relationship between the relative technological innovation efficiency and the relative price allocation efficiency is analyzed in depth. If the output level of one enterprise is higher than that of another enterprise, the efficiency

TABLE 1: Platform questionnaire survey personnel.

	Number	Proportion
Gender		
Man	20	40
Woman	30	60
Age		
10-19	10	20
20-29	30	60
30-40	10	20

TABLE 2: Node machine management module.

Serial number	User level
1	Node machine information management
2	Node machine state management
3	Node machine log management
4	Node electromechanical node source management
5	Node machine user administration

of technological innovation is relatively high when the input level is the same. If the income is higher than that of the other enterprise, the efficiency of technological innovation is higher.

4. Open Platform for Intelligent R&D and Technology Innovation Management Service

4.1. *Platform Module Analysis.* The platform module is mainly used to manage the basic information of each node machine that can be managed (with functions). The basic information includes the address of the node machine management port, the physical address of the network card of the node machine, and the username and password with access rights. It will also include the supported version, firmware version, and related gateway information in the node machine and will also include the information about the increase time and modification time of the node machine. After the first visit to the function module, the basic information of the managed node machine saved in the sweet management system will be displayed. Meanwhile, the operation of adding, modifying, and deleting can be performed as shown in Table 3.

According to Table 3, node machines (that is, managed servers) have management modules. Before being managed, they should be known by the management platform. Therefore, users with management authority must log in to the system and perform the new node machine function. The basic information of connecting the node machine includes the address of the node machine, and the connection username of the node machine is also the username and password that are recorded. In the user login function, users should fill in their own username and password on the login page to perform the login operation. After receiving the login request, the server will query the database to verify whether the data is correct. If it is correct, the software will enter the main interface of the program. If it is wrong, the user will be prompted according to the specific situation. The common errors are that the username does not exist and the user password is incorrect. The flow chart of user login is shown in Figure 4.

In the process of software development of an intelligent R&D value-added service system, in addition to the requirement analysis of platform functions, we should also find out the actual business process of software. Clear and concise software business processes can help developers to better build the overall software architecture. The following establishes the software business process according to the results of the requirement analysis.

4.2. *Simulation of Technical Innovation Management Service Platform.* In the simulation experiment, we do many different experiments on each scheme. In each experiment, the number of mobile users n is $n = 20$ and 60, and we assume that the MEC server can serve up to 30 users at the same time. For each n, we repeat the experiment 100 times and then select the average as the final result as shown in Table 4.

Table 4 shows the situation that the number of users in the useful task open platform in different schemes is shown under different user numbers. When all users do not have an open platform and only perform locally, the concept of a useful task open platform is meaningless. It can be seen that under different users, the proposed multiuser distributed task open platform algorithm can always have the most users in the beneficial task open platform state, which increases 27.4% of the users in the beneficial task open platform status than all the tasks executed on the cloud. When $n \leq 30$, the number of users in the platform is the same, while when $n > 30$, although the number of users in the beneficial task open platform state in IWD is greater than CC, it is still slightly smaller than TCO. This is because the only difference between the two is that TCO considers the computing limitations of MEC servers.

4.3. *Reliability and Validity of Intelligent R&D and Technological Innovation Capability.* The reliability analysis results of the technical innovation ability of high-tech enterprises show that the overall reliability of the technical innovation capability scale is 0.775, of which the reliability of the technical R&D capability is 0.822, the reliability of the production and manufacturing capacity is 0.935, and the reliability of the innovation marketing ability is 0.821, which is in conformity with the requirements as shown in Table 5.

Further reliability and validity analysis, extraction of relevant factors, and the number of factors extracted in reliability and validity can be seen from Table 5. The results show that the total variance of the original variables is explained by the factors, and the factors reflect most of the information of the original variables, with good reliability and validity. According to the corresponding items and factors, we can judge that they are the manufacturing capacity factor, innovation marketing capacity factor, and technology R&D capacity factor. The results of reliability and validity show that the measurement items contained in the factor are consistent with the assumption. Therefore, we can draw the
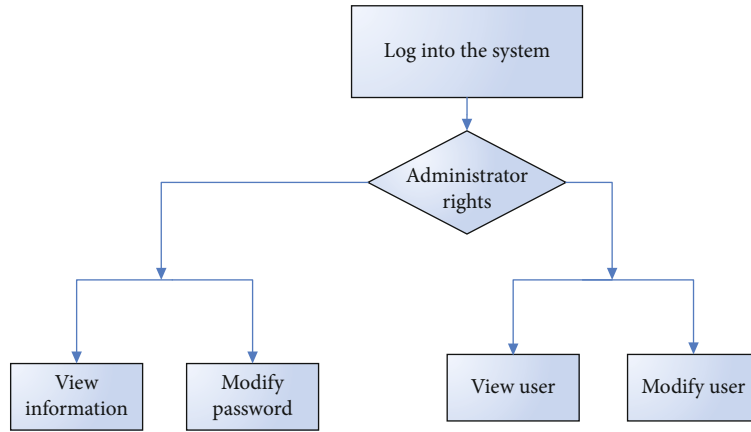
FIGURE 3: Platform user management module.

TABLE 3: Permission definition table.

User level	Administrator	Visitor	Normal user
1	Reject	With	Reject
2	User	Read only	User
3	Read only	With	With
4	With	Reject	User

FIGURE 4: Platform user login.

TABLE 4: Number of users in beneficial task platform.

Number of users	Phase task	Queuing delay	Execution on cloud
20	10	12	21
30	8	11	23
40	12	16	12
50	15	15	23
60	13	17	15

TABLE 5: Reliability analysis of technological innovation capability of high-tech enterprises.

Variable dimension	Reliability and validity	Cronbach's alpha
Technology R&D capability	0.822	0.765
Manufacturing capacity	0.935	0.531
Innovative marketing ability	0.821	0.912

conclusion that the technological innovation ability of high-tech enterprises can be composed of three dimensions: technological R&D ability, manufacturing ability, and marketing innovation ability. It is reasonable and feasible to measure this variable by the items of the assumption scale, and the validity of the measurement meets the research requirements, as shown in Figure 5.

In order to meet the personalized needs of different mobile users, four kinds of typical mobile edge computing are selected. Different tasks have different requirements for delay, and the amount of calculation and data of different tasks is also different. The specific parameters are shown in Figure 6.

It is not feasible to test some ideas of mobile edge computing in real scenes. Therefore, we need a simulation tool to adapt to multiple scenarios. CloudSim, a famous simulation tool in cloud computing, does not pay attention to some problems in mobile edge computing, such as the management of mobile devices and the management of network connection between mobile devices and cloud servers.

The task open platform service has a broad development platform because of mobile edge computing. Through the task open platform, mobile devices with limited resources can implement some delay-sensitive applications and computing-intensive applications on the server not far away. Relying on the computing, storage, and other resources that the server is far larger than the mobile device, they can provide users with various services, which not only has broad market application prospects from the perspective of operators but also has broad market application prospects from
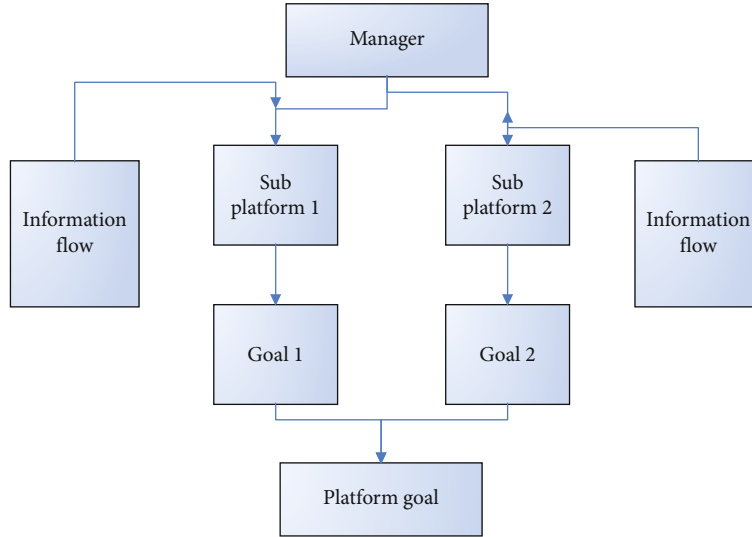
FIGURE 5: Platform collaborative management.
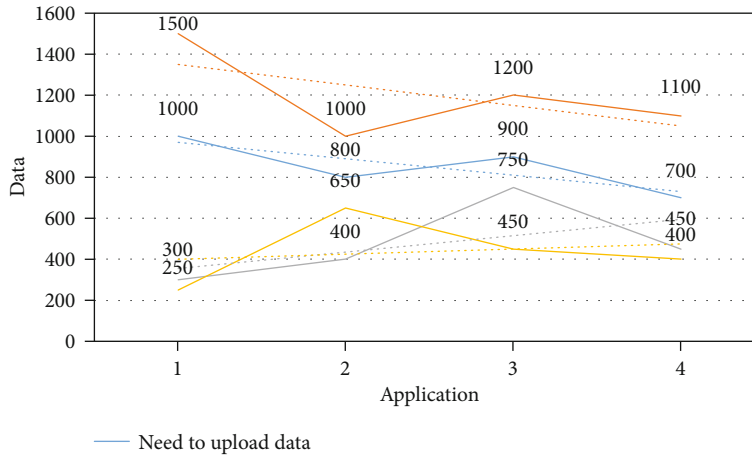
FIGURE 6: Parameter selection for different applications.

the perspective of mobile users It also solves the problem of limited equipment resources and has obvious performance improvement.

The rapid increase of intelligent networking equipment and explosive growth of Internet traffic have promoted the continuous development of the mobile communication network. Now, it has gradually moved towards the era of intelligent R&D and technological innovation. The rapid development of mobile communication in turn also leads to the emergence of various emerging applications, and the requirements for the network are also higher and higher. In order to meet the higher requirements of the network in the future intelligent R&D and technology innovation era, such as ultrahigh bandwidth and ultralow delay, mobile edge computing is the new network architecture which is most likely to realize the next generation network vision. By reducing some services to the range closer to users, a traditional wireless access network also has the conditions of service localization, close range, and multiple deployments. Due to being closer to users, the service servicing under this

network architecture can provide computing, storage, and delivery services for users nearby, greatly improving the user experience.

5. Conclusion

This paper uses the edge computing algorithm, model, edge computing time-to-time optimization open platform policy, platform function investigation experiments, platform module analysis, and other methods to study the edge computing based intelligent R&D and technology innovation management service open platform and edge data processing technology with edge computing as the core which can be produced and is widely promoted. Edge computing is defined as a distributed open platform which integrates the core capabilities of the network, computing, storage, and application near the source of objects or data. In fact, edge computing is a new ecological mode. By gathering five kinds of resources, such as the network, computing, storage, application, and intelligence on the edge of the network, the

network service performance and open network control capability are improved, thus stimulating a new mode and new business form similar to mobile Internet. Edge computing is the key technology to solve the problem of network delay in intelligent R&D and technological innovation. In recent years, it has been tried in the emerging fields such as the Internet of vehicles and Internet of Things. The problems in the above cloud computing can be solved by edge computing technology. The near intelligent service provided by edge computing technology can meet the key requirements of agile connection, data optimization, application intelligence, security, and privacy protection. An intelligent and flexible network is built on the edge of the network, which complements with the centralized cloud computing platform.

Data Availability

The data that support the findings of this study are available from the corresponding author upon reasonable request.

Conflicts of Interest

The author declared no potential conflicts of interest with respect to the research, authorship, and/or publication of this article.

References

[1] W. Shi, J. Cao, Q. Zhang, Y. Li, and L. Xu, "Edge computing: vision and challenges," *Internet of Things Journal, IEEE*, vol. 3, no. 5, pp. 637–646, 2016.

[2] C. Vallati, A. Virdis, E. Mingozzi, and G. Stea, "Mobile-edge computing come home connecting things in future smart homes using LTE device-to-device communications," *IEEE Consumer Electronics Magazine*, vol. 5, no. 4, pp. 77–83, 2016.

[3] Z. Li, W. M. Wang, G. Liu, L. Liu, J. He, and G. Q. Huang, "Toward open manufacturing," *Industrial Management & Data Systems*, vol. 118, no. 1, pp. 303–320, 2018.

[4] W. Shi and S. Dustdar, "The promise of edge computing," *Computer*, vol. 49, no. 5, pp. 78–81, 2016.

[5] M. Satyanarayanan, "The emergence of edge computing," *Computer*, vol. 50, no. 1, pp. 30–39, 2017.

[6] Y. Wang, M. Sheng, X. Wang, L. Wang, and J. Li, "Mobile-edge computing: partial computation offloading using dynamic voltage scaling," *IEEE Transactions on Communications*, vol. 64, no. 10, pp. 4268–4282, 2016.

[7] T. Taleb, K. Samdanis, B. Mada, H. Flinck, S. Dutta, and D. Sabella, "On multi-access edge computing: a survey of the emerging 5G network edge cloud architecture and orchestration," *IEEE Communications Surveys & Tutorials*, vol. 19, no. 3, pp. 1657–1681, 2017.

[8] Y. Mao, J. Zhang, S. H. Song, and K. B. Letaief, "Stochastic joint radio and computational resource management for multi-user mobile-edge computing systems," *IEEE Transactions on Wireless Communications*, vol. 16, no. 9, pp. 5994–6009, 2017.

[9] D. Sabella, A. Vaillant, P. Kuure, U. Rauschenbach, and F. Giust, "Mobile-edge computing architecture: the role of MEC in the internet of things," *IEEE Consumer Electronics Magazine*, vol. 5, no. 4, pp. 84–91, 2016.

[10] K. Zhang, Y. Mao, S. Leng, Y. He, and Y. Zhang, "Mobile-edge computing for vehicular networks: a promising network paradigm with predictive off-loading," *IEEE Vehicular Technology Magazine*, vol. 12, no. 2, pp. 36–44, 2017.

[11] P. Corcoran and S. K. Datta, "Mobile-edge computing and the internet of things for consumers: extending cloud computing and services to the edge of the network," *IEEE Consumer Electronics Magazine*, vol. 5, no. 4, pp. 73-74, 2016.

[12] L. He, K. Ota, and M. Dong, "Learning IoT in edge: deep learning for the internet of things with edge computing," *IEEE Network*, vol. 32, no. 1, pp. 96–101, 2018.

[13] G. Ananthanarayanan, P. Bahl, P. Bodik et al., "Real-time video analytics: the killer app for edge computing," *Computer*, vol. 50, no. 10, pp. 58–67, 2017.

[14] S. Nastic, T. Rausch, O. Scekic et al., "A serverless real-time data analytics platform for edge computing," *IEEE Internet Computing*, vol. 21, no. 4, pp. 64–71, 2017.

[15] R. Wang, J. Yan, D. Wu, H. Wang, and Q. Yang, "Knowledge-centric edge computing based on virtualized D2D communication systems," *IEEE Communications Magazine*, vol. 56, no. 5, pp. 32–38, 2018.

[16] X. Chen, Q. Shi, L. Yang, and J. Xu, "ThriftyEdge: resource-efficient edge computing for intelligent IoT applications," *IEEE Network*, vol. 32, no. 1, pp. 61–65, 2018.

[17] E. Ahmed, A. Ahmed, I. Yaqoob et al., "Bringing computation closer toward the user network: is edge computing the solution?," *IEEE Communications Magazine*, vol. 55, no. 11, pp. 138–144, 2017.

[18] G. Qun, G. Jing, and W. Yao, "Fiscal subsidiaries, agency problem and technical innovation–based on R&D heterogeneity," *Soft Science*, vol. 30, no. 7, pp. 70–73, 2016.

[19] G. Perez, S. Popadiuk, and A. Cesar, "Internal factors that favor the adoption of technological innovation defined by information systems: a study of the electronic health record," *Rai Revista De Administrao E Inovao*, vol. 14, no. 1, pp. 67–78, 2016.

[20] Y. Zhang, H. Huang, L. X. Yang, Y. Xiang, and M. Li, "Serious challenges and potential solutions for the industrial internet of things with edge intelligence," *IEEE Network*, vol. 33, no. 5, pp. 41–45, 2019.

[21] Z. Lv, D. Chen, R. Lou, and Q. Wang, "Intelligent edge computing based on machine learning for smart city," *Future Generation Computer Systems*, vol. 115, pp. 90–99, 2021.

[22] X. Li, H. Jianmin, B. Hou, and P. Zhang, "Exploring the innovation modes and evolution of the cloud-based service using the activity theory on the basis of big data," *Cluster Computing*, vol. 21, no. 1, pp. 907–922, 2018.

WILEY | Hindawi

Research Article

Study on Spectrum Allocation and Optimization of Wireless Communication Networks Based on SFOA

Yu Zhang[1,2] and Jianying Li [1]

[1]*Northwestern Polytechnical University, Xi'an, 710072 Shaanxi, China*
[2]*Guangdong Mechanical & Electrical Polytechnic Guangzhou 510515, China*

Correspondence should be addressed to Jianying Li; zyu_2015160528@mail.nwpu.edu.cn

Wireless communication network spectrum is a limited resource. With the rapid increase of mobile communication services in recent years, traditional spectrum allocation methods are only based on a fixed spectrum allocation strategy, which often results in uneven and wasteful resource allocation. Therefore, spectrum allocation and the optimization problem need to be solved urgently. The application of semantic mobile computing in the Internet of Things and the research of emerging bionic models provide new ideas for this problem. In order to solve the problem of spectrum optimization and allocation, this paper proposes an optimization algorithm that simulates fisherman fishing to reasonably arrange the allocation and optimization of wireless network spectrum. This paper selects SFOA and the other two algorithms, designs experimental functions to perform calculations separately, obtains relevant data indicators, and uses comparative analysis to analyze. The analysis shows that in terms of performance, the success rate of SFOA is higher than that of PSO, and the success rate of the two function calculations has reached 100%. In the signal-to-noise ratio analysis, when the signal-to-noise ratio is -4 dB, the throughput of GPSO reaches the maximum value of 0.17, the throughput of PSO reaches the maximum value of 0.56, and the throughput of SFOA reaches 1, which shows that SFOA is adopted. The stability and accuracy of the algorithm are higher than the other two algorithms, and in the case of high signal-to-noise ratio, the advantages of the SFOA algorithm are also more obvious. This shows that the use of this algorithm will be very helpful for spectrum allocation and optimization. Because SFOA has high stability and accuracy, through reasonable adjustment and improvement, it can make good use of spectrum allocation and optimization. Chinese wireless communication network and the development of Internet of Things technology are of great significance.

1. Introduction

Wireless communication uses electromagnetic wave signals to propagate and exchange information in space. It is not restricted by the geographical environment. When the application environment changes, wireless communication only needs slight adjustments to quickly adapt to the new environment. The wireless communication network system has been implemented in many countries. Using the radio frequency identification technology in the Internet of Things, combined with the reasonable allocation and optimization of the spectrum, can minimize interference to other users. Mobile computing refers to the existence of movable devices, users, or programs in a distributed system, and the corresponding computing mode needs to support the mobility of these entities; in a narrow sense, mobile computing refers to the following: users carry mobile devices to access information services through public facilities, regardless of their what physical location is it or what kind of movement behavior it has. Mobile computing technology has developed rapidly in recent years, and the technology has become quite mature. For smart phones, mobile technology not only provides rich content, but also has powerful functions that can be expanded infinitely and the upgradeability of hardware, which enables it to truly realize the integration of communications, computers, and the Internet.

In this regard, many scholars at home and abroad have conducted a lot of related research. Bertini et al. believe that heuristic evaluation is very popular in desktop and web interfaces, whether it is used in actual design or as a research topic. Compared with full user research, heuristic evaluation may be cost-effective. Therefore, in the case of limited resource input, this evaluation can detect large usage defects before the resources are fully developed, and these defects may appear on both mobile computing and traditional interfaces. But usability evaluation will also bring some specific problems, involving screen space, user attention, and background factors. The authors introduced an improved heuristic method suitable for mobile computing evaluation in their research, which was systematically derived from a large amount of literature and verified by certain experience. These methods can provide a good foundation for heuristic evaluation in mobile computing. The study not only introduced the practical use of heuristic evaluation, but also analyzed its application prospects. However, the study lacked a large amount of relevant data, and its credibility was not strong [1]. Ma et al. introduced that their research optimizes power and spectrum allocation at the same time to improve the communication quality of the demand side in the smart grid, thereby further reducing the cost of utility companies. First, the authors model the electricity bill based on the adjustment error caused by the direct load control in the smart grid. Then, according to the confidence level of the frequency band and the highest cost of the utility company, the subbands are allocated to different data aggregator units. An algorithm is designed to optimize the transmission power of the repeater and optimize the spectrum allocation to reduce the cost of the utility company. The simulation results show that the packet loss rate and cost of public utility companies can be greatly reduced. This research compares with other solutions by designing its own scheme, and the consideration is more comprehensive, but there is a lack of discussion on how to realize spectrum data sharing [2, 3]. Sohul et al. believe that wireless communication plays a vital role in national security and disaster relief and is widely used by emergency personnel such as police officers, firefighters, and ambulances. In an emergency, the first discoverer of the accident must always keep in touch with the remote service center for effective cooperation and coordination. However, in many emergency situations, the existing public safety services cannot meet the needs of users, which usually results in excessive traffic load. Therefore, increasing network capacity is one of the main problems at present, and spectrum sharing is a key solution. Through the spectrum sharing partnership between public safety service organizations and commercial networks, users can access the licensed public safety spectrum when needed to realize data sharing. In the study, the authors introduced different measures taken for the next generation of public safety networks. The authors also have an outlook on public safety systems that can be quickly deployed and reconfigured to meet the demand for critical communication infrastructure and discuss the value of spectrum sharing. In their research, the authors discussed the value of spectrum sharing in wireless communication and gave a very detailed introduction to

its application. However, they failed to design a specific model for simulation experiments. It is difficult to predict the problems and problems that may occur in practical applications [4, 5].

This article is aimed at studying the optimization and allocation of wireless network communication spectrum. First, it summarizes the research results of some scholars at home and abroad and then introduces semantic mobile computing and its working principles, the basic principles of the SFOA algorithm model, and spectrum allocation and optimization. And comb and then design an experiment based on SFOA, compare with other algorithms, conduct in-depth analysis of performance, operating speed, throughput, system benefits, etc., and then analyze the practical application of mobile computing in the Internet of Things. Finally, a brief summary of this article is made, and the shortcomings of this article are put forward. The innovation of this paper is to combine the current new bionic method SFOA algorithm for spectrum allocation and optimization analysis and design an experimental model that simulates fisherman fishing, which has profound significance for the reasonable utilization of wireless network spectrum resources in reality.

2. Research Method of Spectrum Allocation and Optimization of Wireless Communication Network Based on SFOA

2.1. Semantic Mobile Computing. Mobile computing is a new technology that has emerged with the development of honeycomb technology, wireless WLAN, wireless Internet, and GPS positioning technology. Mobile computing enables mobile terminal equipment to achieve network access, resource transmission, and information sharing in a wireless network environment. Its role is to provide customers with accurate, useful and immediate information anywhere, at any time, which has made a huge difference to people's lives [1]. Mobile computing is an extension of distributed computing, enabling computers or other devices to transmit data without a fixed physical device connected and to transmit this information to users in need. In this mode, users use portable computing devices to access information networks through wireless communication interfaces without being affected by changes in geographic locations [6, 7].

Mobile computing technology is to implement a mobile system for transaction and data processing in an environment with limited resources, intermittent connections, and lightweight computing. Due to the power limit of mobile devices, network instability caused by frequent movement, poor network performance, etc., frequent network disconnections occur under mobile computing. Therefore, it is necessary to maintain a normal user environment with intermittent connections. Critical transactions will not be undone due to disconnection [8]. The communication bandwidth, battery power, storage capacity, and processing capabilities of mobile devices are all limited. These restrictions require applications in mobile computing systems to use less memory, improve operating efficiency, and comprehensively use caching, multithreading, and other technologies to optimize processing.

Process and improve efficiency in query processing, transaction management, storage management, etc.

2.1.1. Mobile Computing Working Mode.

The working mode of mobile computing is shown in Figure 1, which includes three types of computing units: a mobile support node (MSS) with a wireless communication module, communicating with mobile devices, a fixed host (MS) without a wireless communication module, and a mobile terminal (MC). The mobile terminal is linked with the mobile support node core through the wireless network and finally enters the fixed network. Relative to the low credibility of the wireless network unit, the fixed network is called the credible part. In this working mode, MC can access a fixed network or other MC from any wireless network via MSS and enables MC to move freely in the wireless network while still maintaining the network connection between MC and MSS [9, 10].

2.1.2. Semantic Cache.

Mobile computing involves the problem of semantic caching. Cache technology has been applied in many fields. Caching technology has different meanings in different fields. In a traditional computing environment, caching technology refers to storing some commonly used data on high-speed devices, thereby improving processing performance. The caching technology in the mobile computing environment saves part of the server's data on the mobile client, thereby reducing network traffic [11]. Although their meanings are not exactly the same, their purpose is to improve data access performance, and mobile devices can effectively increase the cache hit rate by selecting a suitable cache replacement algorithm, thereby further improving computing efficiency.

Cache is divided into traditional cache and semantic cache. The comparison between the two is shown in Table 1. The traditional cache has low cache efficiency, high network cost, and low data processing efficiency. The cache mode used is generally divided into a page cache mode and a tuple cache mode. The semantic cache is a cache mode established based on the semantic correlation between customer query sentences. The query results are produced by mining the semantic information in the query words, and the query results and description information are cached to make the cache utilization more effective. The semantic cache first decomposes the query through the local system and then performs the trial query and the remaining query to obtain the result, and then, the server processes and exports and finally obtains the final result [12].

2.2. Description of Fisherman's Fishing Method SFOA.

SFOA, also known as the optimization algorithm for simulating fisherman fishing, is a new type of bionic algorithm. The algorithm is simple in principle, involves fewer parameters, and is easy to operate. It provides a new idea for solving the allocation and optimization of the wireless communication network spectrum. How much fisherman fishes each time depends on where he casts the net, and the choice of where to cast the net is determined by the density of the fish [11]. This algorithm is a search method that simulates the fishing behavior of a fisherman based on the fishing behavior of the fisherman. Figure 2 is a real scene of the fisherman fishing.

The fishermen's fishing habits are as follows: initially, each fisherman randomly chooses a location to fish; the fisherman always randomly casts a fishing net around his location to try to understand the density of the fish around him and move within the maximum radius of the net, each time moving to a place with greater fish density than its current location; the fisherman always reports the fish density of his location to other teammates in a timely manner; when there is no better within the radius of the net, when the fisherman shrinks the net radius in order to accurately obtain the point with a higher density of fish nearby, and when the fisherman cannot find a better density point in the area of his maximum casting net radius, he will leave the current casting area and look for other casting points [13].

2.3. Wireless Communication.

Wireless communication gets rid of the shackles of fixed location of wired communication equipment, can communicate anytime and anywhere, and is favored by users. At the same time, the continuous emergence of wireless communication services has also promoted the progress of wireless communication technology. With the continuous emergence of new technologies and the continuous expansion of wireless applications, the demand for wireless spectrum resources in communication systems is growing rapidly [14]. However, the available wireless spectrum resources are very limited, and the available wireless spectrum resources are increasingly scarce, which seriously hinders the development of communication technology. Therefore, allocation and optimization issues are very important.

2.3.1. Spectrum Allocation Problem.

The problem of spectrum allocation in wireless communication networks is to effectively reuse frequency resources for communication nodes or communication links and reduce network interference. The problem of spectrum resource allocation stems from the mobile phone network. The carrier frequency is effectively allocated to the base station to avoid various interference. Therefore, the problem of spectrum allocation is also called the problem of frequency allocation [15, 16].

From the point of view of the allocation mode, the spectrum allocation technology can be divided into static spectrum allocation and dynamic spectrum allocation. Static spectrum allocation assigns fixed spectrum resources to specific users, and users cannot flexibly adjust according to their own needs. The advantage of this technology is that the allocation strategy is simple, but the spectrum utilization rate is low [17, 18]. The dynamic spectrum allocation technology dynamically schedules spectrum resources among users according to network requirements, which can effectively meet the spectrum needs of different users, improve network capacity and spectrum utilization, and achieve better user performance experience. According to the spectrum access method, it can generally be divided into fully restricted spectrum allocation and partial restricted spectrum allocation; according to the network structure
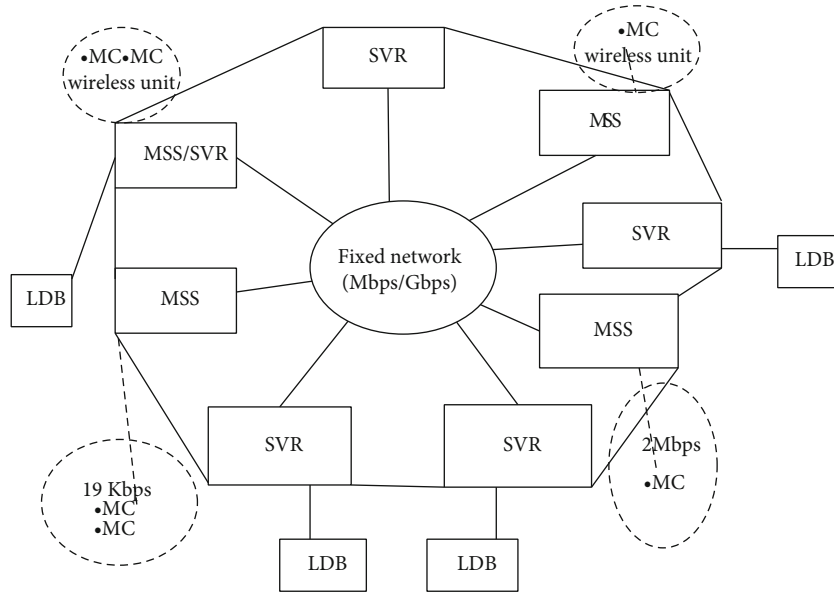
FIGURE 1: Model of mobile computing.

TABLE 1: Comparison between traditional cache and semantic cache.

Index	Traditional cache	Semantic cache	Description
Cache efficiency	Low	High	Contains historical query results with cache items as the granularity
Network cost	High	Low	Only transfer the remaining query data
Query processing efficiency	Low	High	Able to process in parallel
Adaptability	Bad	Good	More query results can be obtained in a disconnected environment

FIGURE 2: Fisherman fishing sketches (pictures from Baidu Picture).

classification, it can generally be divided into centralized spectrum allocation and distributed spectrum allocation; classified by cooperation method, it generally can be divided into for cooperative spectrum allocation and noncooperative spectrum allocation [19].

The principles of the spectrum allocation algorithm are as follows: to ensure the flexibility of the algorithm, and the time complexity should be low; to improve the overall performance of the network system, such as increasing the network capacity, reducing the network load, etc., and reducing the network signaling overhead (referring to the number of communication handshake) and computational complexity; must consider the application requirements in the system, network structure characteristics, cooperation forms, and other issues [20].

In the distribution, some interference problems will appear, mainly caused by stations working on the same channel or adjacent channels. Generally speaking, cochannel interference is the main source of interference and a key issue in spectrum allocation, while adjacent channel interference is the interference caused by modulated radio frequency signals entering adjacent channels. At present, this distribution technology has been applied in mobile cellular networks, wireless local area networks, and satellite
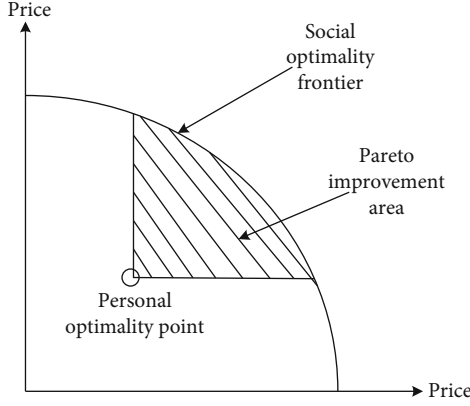
FIGURE 3: Relation between social and personal optimality.

communication networks. According to the different frequency allocation methods, similar channel allocation principles are adopted in the above applications, and one or more frequency points are allocated to the station to meet the communication needs and reduce network interference [21, 22].

On the issue of spectrum allocation, graph theory coloring models, auction bidding models, and interference temperature models are generally used. Here is an introduction to the interference temperature model. This model is used to manage and quantify the interference between wireless communication users. The main content is to monitor the power of the receiving end of the communication process. When using this model, the CU device operating in the licensed frequency band can monitor the interference situation at its location in real time and select the spectrum and configure the transmit power according to the interference situation [23]. The interference temperature threshold T_i refers to the maximum value of interference that can be tolerated in a certain frequency band in a certain area. The interference temperature is defined as follows:

$$T_i(f_c, A) = \frac{M_i(f_c, A)}{kA}. \tag{1}$$

Among them, f_c is the frequency center of the spectrum, A is the bandwidth of the spectrum, T_i is the noise temperature, and k is the Boltzmann constant [24].

2.3.2. Spectrum Optimization Problem.
For the spectrum optimization problem, game theory is mainly used. Game theory is a series of models and analysis tools used to study the interactive decision-making process of decision makers with contradictory goals, including the set of participants, the behavior of each participant, the preferences of the participants, the order of the game, and the benefits of the participants [25].

In the game, K is often used to represent a game. The income of participant z is represented by P_z, and P_{z1} is a multivariate function about the strategies of each participant. Therefore, the game K with n participants can be expressed as

$$K = \{T_1, \cdots, T_n; P_1, \cdots, P_n\}. \tag{2}$$

Among them, the strategy combination is

$$t^* = (t_1^*, \cdots, t_n^*). \tag{3}$$

If for any strategy $t_i \in T_i$, we have

$$P_z(t^*) \geq P_z(t_1^*, \cdots, t_{z-1}^*, t_z, t_{z+1}^*, \cdots, t_n^*). \tag{4}$$

It is said that the strategy combination is a Nash equilibrium of game K, which is called individual optimal. The combination of strategies in this state is stable. In addition, there is also a social optimum. As shown in Figure 3, it shows the relationship between personal optimal and social optimal [26].

3. SFOA-Based Wireless Communication Network Allocation and Optimization Experiment

3.1. Experiment Object.
This experiment selects three algorithms of SFOA, PSO, and GPSO for comparative analysis. The SFOA aspect has been introduced before, so I will not repeat it here. PSO is also a kind of bionic algorithm model. Its principle is that each bird in the flock will constantly compare its own position and then adjust its speed and position through the bird closest to the food in the flock, thereby searching for food. GPSO, also known as gradient particle swarm optimization algorithm, has the shortcomings of slow convergence speed and easy to fall into local optimum [27, 28].

3.2. SFOA Experimental Procedure.
The specific content of the algorithm is as follows:

Suppose a finite closed area is

$$M = M_1 \times M_2 \times \cdots \times M_k. \tag{5}$$

The fisherman's status is

$$Y = (y_1, y_2, \cdots, y_k) \in M. \tag{6}$$

$f(y)$ is the continuous objective function on M, that is, the density distribution function of the fish.

First, there are x fishermen randomly distributed in M, and the initial position of fisherman a is

$$S_0^{(a)} = \left(y_{01}^{(a)}, y_{02}^{(a)}, \cdots, y_{0n}^{(a)}\right). \tag{7}$$

The fisherman a casts the fishnets on the four sides of the initial position $S_0^{(a)}$, namely, up and down, front, back, left, and right and then gets the fishnet point set with the point $S_0^{(a)}$ as the center:

$$\beta_0^{(a)} = \left\{ Y^{(a)} = \left(w_1^{(a)}, w_2^{(a)}, \cdots, w_n^{(a)}\right) \middle| w_j^{(a)} \right.$$
$$\left. \in \left\{ y_{0j}^{(a)} - l_j^{(-)}, y_{0j}^{(a)}, y_{0j}^{(a)} + l_j^{(+)} \right\}, j = 1, 2, \cdots, n \right\}. \tag{8}$$

When $y_{0j}^{(a)} = d_j$, we have $l_j^{(-)} = 0$, and $l_j^{(+)} < f_j - y_{oj}^{(a)}$. When $y_{0j}^{(a)} = f_j$, we get $l_j^{(-)} < y_{0j}^{(a)} - d_j$. And when $y_{0j}^{(a)} \neq d_j$ and $y_{0j}^{(a)} \neq f_j$, we get $l_j^{(-)} < y_{0j}^{(a)} - d_j$ and $l_j^{(+)} < f_j - y_{oj}^{(a)}$, where $a = 1, 2, \cdots, k$ and $j = 1, 2, \cdots, n$.

In this area, there are three search methods, divided into mobile search, narrow search, and accelerated search.

3.2.1. Mobile Search. If the relationship between the initial position and the new position is

$$f\left(Y_0^{(a)}\right) = \max_{Y^{(a)} \in \beta_0^{(a)}} f\left(Y^{(a)}\right) > f\left(S_0^{(i)}\right), Y_0^{(a)} \neq S_0^{(a)}, a = 1, 2, \cdots, k. \tag{9}$$

Then, fisherman a moves from the current location to the new location

$$S_1^{(a)} = Y_0^{(a)}. \tag{10}$$

And repeat the previous method with $S_1^{(a)}$ as the new center in order to search for point $S_2^{(a)}$ where the density of fish is greater than that of point $S_1^{(a)}$. After a limited number of movements, the position of fisherman a is $S_0^{(a)}, S_1^{(a)}, S_2^{(a)}, \cdots, S_n^{(a)}$.

3.2.2. Shrink Search. Assuming that after a finite number of state changes, the position of fisherman a is

$$S_t^{(a)} = \left(y_{t1}^{(a)}, y_{t2}^{(a)}, \cdots, y_{tn}^{(a)}\right). \tag{11}$$

If the initial position and the new position meet,

$$\max_{Y^{(a)} \in \beta_0^{(a)}} f\left(Y^{(a)}\right) \leq f\left(S_0^{(i)}\right). \tag{12}$$

Among them, we have

$$\beta_t^{(a)} = \left\{ Y_t^{(a)} = \left(w_1^{(a)}, w_2^{(a)}, \cdots, w_n^{(a)}\right) | w_j^{(a)} \right.$$
$$\left. \in \left\{ y_{tj}^{(a)} - l_j^{(-)}, y_{tj}^{(a)}, y_{tj}^{(a)} + l_j^{(+)} \right\}, j = 1, 2, \cdots, n \right\}, \tag{13}$$
$$a = 1, 2, \cdots, k.$$

Then, the current position of fisherman a is still $S_t^{(a)}$, and the net is cast once again around the current position $S_t^{(a)}$. At this time, another fishnet point set that is centered at $S_t^{(a)}$ is

$$\beta_{t+1}^{(a)} = \left\{ Y_{t+1}^{(a)} = \left(w_1^{(a)}, w_2^{(a)}, \cdots, w_n^{(a)}\right) | w_j^{(a)} \right.$$
$$\left. \in \left\{ y_{tj}^{(a)} - l_j^{(-)}, y_{tj}^{(a)}, y_{tj}^{(a)} + l_j^{(+)} \right\}, j = 1, 2, \cdots, n \right\}. \tag{14}$$

Among them, $l_j^{(-)} = \lambda l_j^{(-)}$, $l_j^{(+)} = \lambda l_j^{(+)}$, $0 < \lambda < 1$, and λ is the shrinkage coefficient.

3.2.3. Speedup Search. Suppose that after a limited number of position changes, the position of fisherman a remains unchanged, and

$$f\left(S_t^{(a)}\right) - \max \left\{ f(Y) \mid Y \in \beta_t^{(a)}, Y \neq S_t^{(a)} \right\} < e,$$
$$f\left(S_t^{(a)}\right) < \max \left\{ f\left(S_t^{(a)}\right), a = 1, 2, \cdots, k \right\},$$
$$\beta_t^{(a)} = \left\{ Y_t^{(a)} = \left(w_1^{(a)}, w_2^{(a)}, \cdots, w_n^{(a)}\right) | w_j^{(a)} \right.$$
$$\left. \in \left\{ y_{tj}^{(a)} - l_j^{(-)}, y_{tj}^{(a)}, y_{tj}^{(a)} + l_j^{(+)} \right\}, j = 1, 2, \cdots, n \right\}, \tag{15}$$
$$a = 1, 2, \cdots, k.$$

Among them, $e > 0$ is a self-defined smaller constant, and then, fisherman a accelerates to move out of the local fishing area, so as not to fall into the local optimum.

3.2.4. Experimental Function. This experiment selects three functions f_1, f_2, and f_3 and uses the above three algorithms to calculate and analyze various experimental indicators: optimal solution, worst solution, average solution, standard deviation, number of successes, and average time-consuming. The optimal solution refers to the best situation that can achieve the goal, and the worst solution is the opposite. The average solution represents the general case. The standard deviation is used to detect the degree of distribution. The number of successes is used to indicate the accuracy and accuracy of the algorithm. The time is used to measure the running speed.

(1) $f_1(x) = (x_1^2 - x_2^2)^{0.89}[\tan(x_1^4/x_2 - 5x_1^2 + 0.5)], -50 \leq x_1 \leq 50, -50 \leq x_2 \leq 50$

(2) $f_2(x) = \sqrt{(x_1 x_2 - x_1^2)}(\cos x_1/5x_2 - 100x_1)], -50 \leq x_1 \leq 50, -50 \leq x_2 \leq 50$

(3) $f_3(x) = \sin[2x_2^5 - 5(x_1 - 7x_1^9)] - 3\sqrt{x_1^2 + x_1^2}, -50 \leq x_1 \leq 50, -50 \leq x_2 \leq 50$

4. SFOA-Based Wireless Communication Network Spectrum Allocation and Optimization Research Analysis

4.1. SFOA and Other Algorithm Performance Analysis. In order to compare the performance of SFOA and other algorithms, this paper selects five indicators for evaluation and analysis: optimal solution, worst solution, average time-consuming, average solution, and success rate. In order to reduce the influence of randomness on the results of this experiment and make the comparison more reasonable, each algorithm must be run 100 times independently. The experimental data are recorded in Tables 2 and 3, and the running time is recorded in Table 4.

As shown in Table 2, SFOA and PSO algorithms are used to calculate the function f_1. The worst solution and optimal solution of the two are relatively close, but from the perspective of operating speed, the average time of SFOA is shorter, and its operating speed is higher than that of PSO. Both methods have a 100% operation success rate, which can

TABLE 2: Experimental comparison results.

	Function	SFOA	PSO
	f_1	3.6738839402812837e-16	4.5987453450717516e-03
Worst solution	x_1	1.0082782276343545	1.0000027638792636
	x_2	1.0097487234612278	1.0000076437264872
	f_1	1.2637632476348764e-07	2.3784792384892744e-12
Best solution	x_1	1.0000063272636327	0.9999999999993272
	x_2	1.0000083742637863	0.9999999999993627
Average time	f_1	1.6372632636371863e-09	2.3787264378648972
Average value	f_1	1.836278	1.361728
Success rate	f_1	100%	100%

TABLE 3: Experimental comparison results.

	Function	SFOA	PSO
	f_2	6.6376246328796438e-02	4.0037678263879126
Worst solution	x_1	1.3762986398723898	1.0000000007436482
	x_2	1.7233823829083482	-12.3727647836478386
	f_2	1.2578647865874654e-07	2.0093487724893274e-11
Best solution	x_1	-6.2637263782638213	8.9274389372489327
	x_2	1.2743894598375758	3.3627361726334232
Average time	f_2	4.3762863872687326e-07	4.8327928798217388e-02
Average value	f_2	1.293774	10.7483974
Success rate	f_2	100%	90%

TABLE 4: Performance contrast between two algorithms.

Function	Algorithm	Average value of function	Success times	Average working time
f_1	SFOA	3.473826292748262e-022	100	4.123
	PSO	4.382749823729834e-012	100	4.334
f_2	SFOA	1.124683629426498e-018	100	0.892
	PSO	1.578497598437894e-015	100	1.783
f_3	SFOA	9.000000000033443e-002	100	0.829
	PSO	9.000000472867823e-001	100	2.412

indicate that the two algorithms have strong stability when calculating the function. Therefore, in order to avoid randomness, these two methods are used to calculate the function f_2.

It can be seen from Table 3 that the SFOA algorithm is generally better than the PSO algorithm. From the perspective of the optimal solution and the worst solution, the stability of SFOA is better than that of PSO. The success rate of SFOA algorithm operation is 100%, while PSO is only 90%. It can be seen that SFOA is not easy to fall into local extreme values, and its accuracy and stability are both better than PSO, and the retrieval quality is also the highest.

From the perspective of running time, as shown in Table 4, when calculating functions f_1, f_2, and f_3, the average time used by SFOA is lower than PSO, and the number of runs in this experiment reaches 100 times, which can effec-

tively avoid chance and randomness. It can be seen that the average operating speed of SFOA is higher than that of PSO, and the convergence speed of SFOA is faster than that of PSO. It can be seen from the above that the SFOA algorithm is generally better than the PSO algorithm in terms of optimization accuracy.

4.2. System Throughput and Signal-to-Noise Ratio Change Analysis. The signal-to-noise ratio is an important technical indicator used to measure the reliability of the communication quality of a communication system. It is often used to detect the number of information bits correctly transmitted by a system in a unit time, that is, the value of the throughput. This experiment limits the signal-to-noise ratio to between -16 and 4 dB and compares the system throughput of the three algorithms with different signal-to-noise ratios.
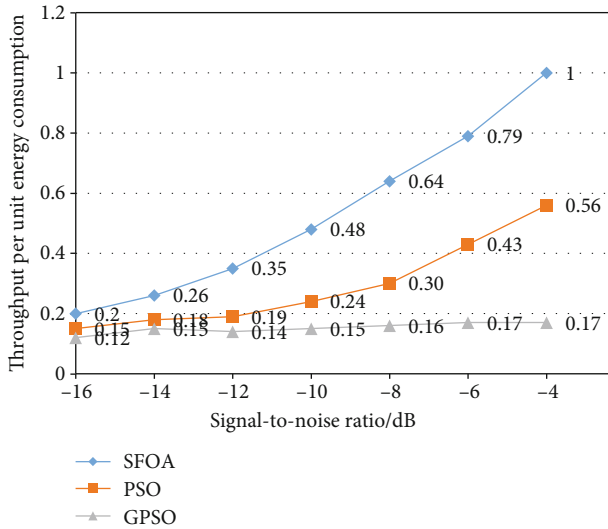
FIGURE 4: The relationship between normal throughput energy ratio and signal-to-noise ratio.

PSO	0.3	0.35	0.45	0.65	0.82	0.87	0.88
SFOA	0.25	0.5	0.7	0.8	0.85	0.87	0.88
GPSO	0.15	0.3	0.35	0.5	0.7	0.75	0.8

Signal-to-noise ratio/dB
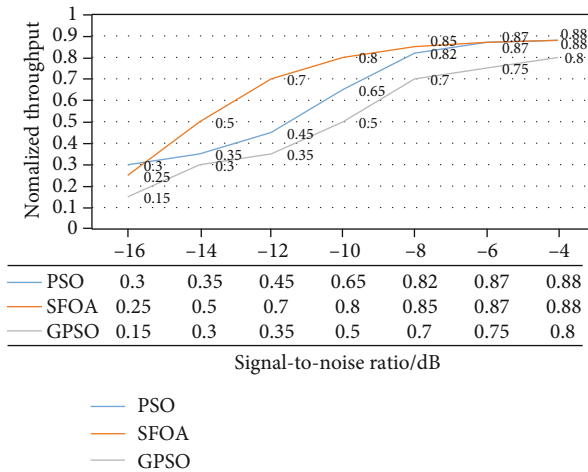
FIGURE 5: The relationship between throughput and signal-to-noise ratio under different algorithms.

As shown in Figure 4, in the range of signal-to-noise ratio of -16 to 4, the throughput per unit energy consumption of SFOA is significantly higher than the throughput of the other two algorithms. Among them, the throughput of PSO is moderate, and the throughput of GPSO is the lowest. When the signal-to-noise ratio reaches -4 dB, the throughput of GPSO reaches the maximum of 0.17, the throughput of PSO reaches the maximum of 0.56, and the throughput of SFOA reaches 1. It can be seen that the SFOA algorithm is significantly better than the other two algorithms.

As shown in Figure 5, it can be seen that under different signal-to-noise ratios, different algorithms have different throughputs. When the signal-to-noise ratio is -16 dB, the throughput of PSO is the highest at 0.3, while the throughput of GPSO is the lowest at 0.15, and when the signal-to-noise ratio is -14, the algorithm with the highest throughput is SFOA, which is 0.5. When the signal-to-noise ratio is -4 dB, the throughput of PSO and SFOA is the highest, both

being 0.88. It can be seen that in the case of low signal-to-noise ratio, the throughput of the PSO algorithm is the best. When the signal-to-noise ratio is higher than -8 dB, the throughput of PSO and SFOA is close, while the throughput of GPSO is always worse than the two algorithms.

4.3. Changes in the Number of Users. Assuming that the user needs to continuously send information to its neighboring nodes at every moment, the user may be allocated multiple channels, and a certain channel may also be allocated to multiple conflict-free users. Therefore, this paper also analyzes the changes in the allocation performance of the spectrum under different algorithms with the increase of different users.

Figure 6(a) shows the situation when the number of primary users increases, and Figure 6(b) shows the situation when the number of cognitive users increases. It can be seen that as the number of users increases, the throughput decreases, that is, the spectrum allocation performance gradually decreases. But at the same time, it can be seen that as the number of users increases, the advantages between different algorithms are gradually becoming apparent. When the number of primary users increases, the advantages of SFOA and PSO algorithms gradually become greater than GPSO. When the number of cognitive users increases, the advantage of the SFOA algorithm is significantly higher than the other two algorithms at first, but when the number of cognitive users reaches 60, the advantage of the PSO algorithm begins to increase again.

As shown in Figure 7, when the number of users changes, the system benefits will also change. As the number of users increases, various spectrums among users will compete with each other, thereby increasing the interference effect on system benefits. It can be seen that the three algorithms will all be affected by the interference frequency after the number of users increases. Among them, the SFOA decreases the most slowly, and even when the number of users reaches 40, the system revenue rebounds. The performance of the system revenue brought by the GPSO algorithm first decreases, then increases, and finally begins to decrease all the time. PSO maintains the same downward trend as SFOA, but the decline is higher than that of the SFOA algorithm.

The SFOA algorithm, as shown in Table 5, can always get a better optimal solution than the other two algorithms. In terms of average net loss, the SFOA algorithm has the lowest loss of 0.1248, while the GPSO algorithm has a loss of 0.1294. In terms of standard deviation, SFOA is only 0.0019, indicating that the algorithm is more accurate.

4.4. Semantic Mobile Computing in the Internet of Things Application Analysis. The application scenario of semantic mobile computing in the Internet of Things is for mobile RFID terminals, collecting data in a wireless network communication environment, and transmitting tags to the server through wireless communication. During the use of the mobile terminal, the collected information can be processed and transmitted at any time according to the change of the network communication access point, so that real-time
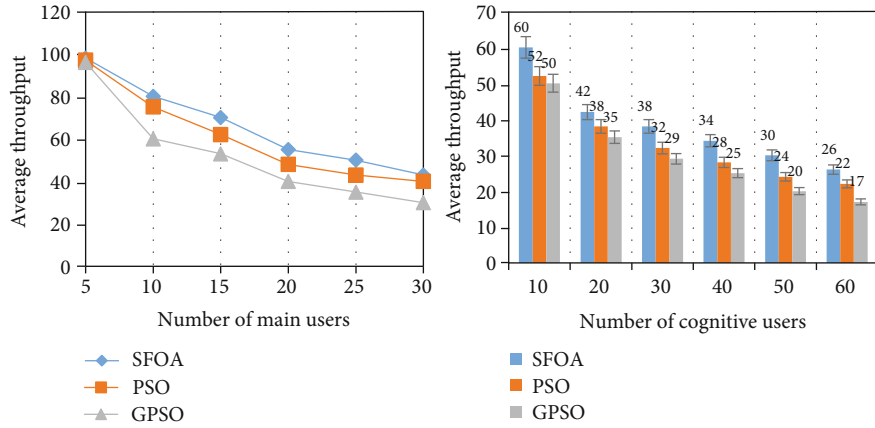
Figure 6: The curve of spectrum allocation performance as users increase.
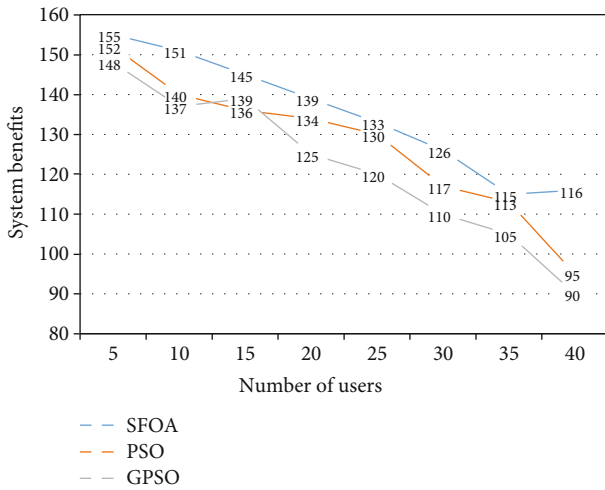
Figure 7: System benefits when the number of users changes.

Table 5: Net loss comparison.

	SFOA	PSO	GPSO
Average net loss	0.1248	0.1287	0.1294
Difference with initial net loss	0.0143	0.0139	0.0134
Standard deviation	0.0019	0.0021	0.0029
Reducing percentage	11.51%	10.52%	9.32%

communication can be realized between the mobile terminal and the wireless network. The consistency of the receiving nodes of the two is relatively high, so that users can obtain satisfactory information about the Internet of Things and use this mobile computing to achieve various operations.

Currently, wireless network communication technology is highly developed, and the integration and application of technologies such as RFID in the Internet of Things to mobile terminals have become a development trend. Semantic mobile computing provides the possibility for this trend. Due to the characteristics of RFID technology, the information in wireless network communication can guarantee its own security. At the same time, we also need to pay attention to information security issues that may occur in infor-

mation transmission to ensure the normal transmission of information and the user's information security. Through mobile computing, various businesses and activities in the Internet of Things can be effectively carried out, providing a good environment for its stable operation and making the information communication in the Internet of Things more reliable and effective.

Not only the mobile communication system, but also in the Internet of Things, a management and maintenance platform is also needed to realize the management and maintenance of the Internet of Things, so as to ensure that the information itself and the process of transmission remain safe and reliable. Therefore, the relevant organizational structure and the working mechanism can be applied to the Internet of Things. Due to the wide application of the Internet of Things technology, it can use its own sensor technology and RFID tags to effectively control various information. Therefore, the combination of wireless network communication technology and Internet of Things technology, plus semantic mobile computing, can effectively promote information and the rapid development of technology.

5. Conclusion

Starting from the spectrum allocation and optimization of wireless networks, this paper summarizes and draws on the research results of some scholars, comprehensively introduces and studies concepts such as semantic mobile computing, spectrum allocation, and optimization, and proposes the use of SFOA algorithms to solve wireless network spectrum, the method of allocation and optimization, and in-depth analysis of this algorithm and multiple algorithms in terms of performance, operating speed, throughput, and system benefits. Due to the high stability and accuracy of SFOA, through reasonable adjustment and improvement, it can make good use of spectrum allocation and optimization, which is of great significance to the development of my country's wireless communication network and the development of Internet of Things technology. This article also has some shortcomings, such as the following: it did not further improve the SFOA algorithm theoretically, but only compared it with the other two algorithms in

several aspects; the indicators selected in the analysis part are relatively simple, without considering the impossibility. Control factors: for the feature that the SFOA algorithm can converge to the global optimal solution, there is a lack of theoretical derivation in mathematics. In response to these problems, it will be further improved in the following research to strengthen the knowledge and understanding of this field and efforts to achieve reasonable optimization and allocation of spectrum resources.

Data Availability

The data that support the findings of this study are available from the corresponding author upon reasonable request.

Conflicts of Interest

The authors declare that they have no conflicts of interest.

References

[1] E. Bertini, T. Catarci, A. J. Dix, S. Gabrielli, and G. Santucci, "Appropriating heuristic evaluation methods for mobile computing," *International Journal of Mobile Human Computer Interaction*, vol. 1, no. 1, pp. 20–41, 2017.

[2] K. Ma, P. Liu, J. Yang, X. Wei, and C. Dou, "Spectrum allocation and power optimization for demand-side cooperative and cognitive communications in smart grid," *IEEE Transactions on Industrial Informatics*, vol. 15, no. 3, pp. 1830–1839, 2019.

[3] B. Han, J. Li, J. Su, and J. Cao, "Self-supported cooperative networking for emergency services in multi-hop wireless networks," *IEEE Journal on Selected Areas in Communications*, vol. 30, no. 2, pp. 450–457, 2012.

[4] M. M. Sohul, M. Yao, X. Ma, E. Y. Imana, V. Marojevic, and J. H. Reed, "Next generation public safety networks: a spectrum sharing approach," *IEEE Communications Magazine*, vol. 54, no. 3, pp. 30–36, 2016.

[5] I. Butun, P. Österberg, and H. Song, "Security of the Internet of Things: vulnerabilities, attacks, and countermeasures," *IEEE Communications Surveys & Tutorials*, vol. 22, no. 1, pp. 616–644, 2020.

[6] E. Baccarelli, N. Cordeschi, A. Mei, M. Panella, M. Shojafar, and J. Stefa, "Energy-efficient dynamic traffic offloading and reconfiguration of networked data centers for big data stream mobile computing: review, challenges, and a case study," *Computers & Chemical Engineering*, vol. 30, no. 2, pp. 54–61, 2016.

[7] M. R. Hossen, M. M. Rahman, K. T. Ahmed, and M. S. Miah, "Spectrum allocation management in cognitive femtocell networks for 5G wireless communication," *Iosr Journal of Electronics & Communication Engineering*, vol. 11, no. 6, pp. 14–23, 2016.

[8] S. Lee and R. Zhang, "Cognitive wireless powered network: spectrum sharing models and throughput maximization," *IEEE Transactions on Cognitive Communications & Networking*, vol. 1, no. 3, pp. 335–346, 2015.

[9] T. Haustein, S. Stanczak, A. Wolisz et al., "Cognitive wireless communications - a paradigm shift in dealing with radio resources as a prerequisite for the wireless network of the future - an overview on the topic of cognitive wireless technologies," *Frequenz*, vol. 70, no. 7-8, pp. 281–288, 2016.

[10] Z. H. Yuan, C. Chen, X. Cheng, G. C. Lv, L. Q. Yang, and Y. Jin, "Correlated channel model-based secure communications in dual-hop wireless communication networks," *Frontiers of Information Technology & Electronic Engineering*, vol. 18, no. 6, pp. 796–807, 2017.

[11] F. Yao, H. Wu, Y. Chen, Y. Liu, and T. Liang, "Cluster-based collaborative spectrum sensing for energy harvesting cognitive wireless communication network," *IEEE Access*, vol. 5, no. 99, pp. 9266–9276, 2017.

[12] L. Jun, "A synthetic research on the multimedia data encryption based mobile computing security enhancement model and multi-channel mobile human computer interaction framework," *Multimedia Tools and Applications*, vol. 76, no. 16, pp. 16963–16987, 2017.

[13] A. Imran, V. Quimno, and M. Hussain, "Current landscape and potential of mobile computing research in the least developed countries," *The Electronic Journal of Information Systems in Developing Countries*, vol. 74, no. 1, pp. 1–25, 2016.

[14] Y. Shu, K. G. Shin, H. Tian, Y. Zhang, and Y. Ye, "Proceedings of the annual international conference on mobile computing and networking, MOBICOM," *Wireless Networks*, vol. 3, no. 5, pp. 512–524, 2016.

[15] L. Ying-Fen, "Numerical analysis of optimization of scheduling based on fisher fishing algorithm," *International Journal of Hybrid Information Technology*, vol. 9, no. 6, pp. 245–252, 2016.

[16] Y. Zhang, Y. Shen, H. Wang, Y. Zhang, and X. Jiang, "On secure wireless communications for service oriented computing," *IEEE Transactions on Services Computing*, vol. 11, no. 2, pp. 318–328, 2018.

[17] H. S. Dhillon, H. Huang, and H. Viswanathan, "Wide-area wireless communication challenges for the Internet of Things," *IEEE Communications Magazine*, vol. 55, no. 2, pp. 168–174, 2017.

[18] W. Hong, Z. H. Jiang, C. Yu et al., "Multibeam antenna technologies for 5G wireless communications," *IEEE Transactions on Antennas & Propagation*, vol. 65, no. 12, pp. 6231–6249, 2017.

[19] L. Kong, M. K. Khan, F. Wu, G. Chen, and P. Zeng, "Millimeter-wave wireless communications for IoT-cloud supported autonomous vehicles: overview, design, and challenges," *IEEE Communications Magazine*, vol. 55, no. 1, pp. 62–68, 2017.

[20] A. Ghazal, Y. Yuan, C. X. Wang et al., "A non-stationary IMT-advanced MIMO channel model for high-mobility wireless communication systems," *IEEE Transactions on Wireless Communications*, vol. 16, no. 4, pp. 2057–2068, 2017.

[21] J. M. Romero-Jerez and F. J. Lopez-Martinez, "A new framework for the performance analysis of wireless communications under Hoyt (Nakagami-q) fading," *IEEE Transactions on Information Theory*, vol. 63, no. 3, pp. 1693–1702, 2017.

[22] G. I. Tsiropoulos, O. A. Dobre, M. H. Ahmed, and K. E. Baddour, "Radio resource allocation techniques for efficient spectrum access in cognitive radio networks," *IEEE Communications Surveys & Tutorials*, vol. 18, no. 1, pp. 824–847, 2016.

[23] Y. Liu, L. Lu, G. Y. Li, Q. Cui, and W. Han, "Joint user association and spectrum allocation for small cell networks with wireless backhauls," *IEEE Wireless Communications Letters*, vol. 5, no. 5, pp. 496–499, 2016.

[24] M. K. Hasan, A. F. Ismail, S. Islam, W. Hashim, and B. Pandey, "Dynamic spectrum allocation scheme for heterogeneous

network," *Wireless Personal Communications*, vol. 95, no. 2, pp. 299–315, 2017.

[25] A. F. Ismail, M. K. Hasan, N. I. Othman, and W. Hashim, "Assessment of dynamic spectrum allocation technique in heterogeneous network," *International Journal of Future Generation Communication and Networking*, vol. 10, no. 3, pp. 41–48, 2017.

[26] Y. Xiong, X. Fan, and S. Liu, "Fairness enhanced dynamic routing and spectrum allocation in elastic optical networks," *IET Communications*, vol. 10, no. 9, pp. 1012–1020, 2016.

[27] F. Li, K. Y. Lam, M. Jia, K. Zhao, X. Li, and L. Wang, "Spectrum optimization for satellite communication systems with heterogeneous user preferences," *IEEE Systems Journal*, vol. 14, no. 2, pp. 2187–2191, 2020.

[28] C. M. Baronio and A. Barth, "Correction to "The Amide I Spectrum of Proteins Optimization of Transition Dipole Coupling Parameters Using Density Functional Theory Calculations"," *The Journal of Physical Chemistry B*, vol. 124, no. 13, pp. 2730–2730, 2020.

WILEY | Hindawi

Research Article

Designation and Multiobjective Optimization of a New Six-DOF Haptic Device Based on Genetic Algorithm

Baoyu Shi [1,2] **and Hongtao Wu**[1]

[1]*College of Mechanical and Electrical Engineering, Nanjing University of Aeronautics and Astronautics, Nanjing 210016, China*
[2]*College of Mechanical Engineering, Anhui University of Technology, Ma'anshan 234001, China*

Correspondence should be addressed to Baoyu Shi; sytb@ahut.edu.cn

This paper focuses on designation and multiobjective optimization of a new haptic device. A new six-DOF hybrid haptic device has been designed combining series mechanism 3PRPaR and parallel mechanism ROBO_003.3PRPaR which is the positioning mechanism and ROBO_003 which is the directional mechanism. Screw theory was carried out to analyze the DOF of ROBO_003, aiming at the requirement performances of working space, stiffness, reverse drive, and output capacity of haptic device. Forward kinematics and inverse kinematics of the positioning mechanism were analyzed. To ensure the force transmission performance and compact structure, the evaluating indicator is dexterity and volume. Generalized coordinates as constraint condition, length of moving rod, and dexterity were chosen as the objective function. The parameters were optimized based on multiobjective optimization of the genetic algorithm. The paretooptimal solution set of the objective function was received. The results showed that the most suitable parameters are 0.502 rad. The optimized dexterity is 69% higher than the unoptimized, and the rod length is reduced by 6%.The research of this paper provides a theoretical basis for the designation of new haptic device.

1. Introduction

With the development of virtual reality technology, the importance of haptic device is becoming increasingly prominent. As an indispensable part of the interactive exploration system, haptic device can realize the movement and force transmission information between human and virtual environment, reproduce the contact between human and environment, and enhance the telepresence of virtual reality. Haptic devices are divided into finger type, arm type, and whole body type. Immersion has developed a finger type haptic device called CyberGrasp [1], which can make operators feel the size and shape of virtual object. Its disadvantage is that it can only control the movement of operators' whole finger, but cannot give force feedback to a single joint of the finger. Rutgers University of America has developed a built-in multifinger force feedback glove Master II-ND [2], which can measure the posture and feedback force of the haptic device simultaneously. It has the advantages of small mass,

large dynamic range, and small friction. The disadvantage of Master II-ND is that it is installed on the palm, the palm cannot hold tightly, and the finger's range of motion is limited. Among the arm type force feedback devices, the phantom force feedback device of sensable company is more representative [3]. The whole body force feedback equipment is usually bulky and inconvenient to operate. Haptic devices are divided into series structure and parallel structure according to robot configuration [4]. The series structure force feedback equipment which is widely used is phantom series products of sensable technology company [5]. Haption Virtuose introduced by literature [6] was developed by the Haption company of France. It is also a 6-DOF series force feedback device, which can be operated in the range of human multi arm movement. Parallel mechanism has a closed chain structure, which has higher structural stiffness, greater bearing capacity, and higher positioning accuracy [7]. The characteristics make parallel mechanisms meet the requirements of haptic device. The 6-DOF hybrid haptic

device introduced in literature [8] was developed by Niigata University of Japan, and 3-DOF in moving directions is provided by delta mechanism. It has a compact structure and is suitable for operation on desktop platform [8], but it has a small stiffness. If the feedback force is large, it may cause small deformation of the mechanism which can affect the accuracy of position detection. Therefore, it is necessary to adopt the mechanism with higher structural stiffness. At present, most of the research on haptic devices are based on surgical or medical robot, which has a certain specificity in the designation of mechanism (including the number of degrees of freedom, the shape, and size of workspace). For example, high feedback force or torque is not needed in surgical robot. Therefore, the output capacity may be insufficient in other applications. Therefore, the existing structure and hardware need to be improved to enhance its versatility.

Better performance can be obtained by optimizing the parameters of mechanism. The construction of reasonable kinematic index is an important basis to evaluate the kinematic performance of mechanism. In the structural optimization design of parallel mechanism, Jacobian matrix condition number is used as the evaluation index of mechanism design performance in literature [9]. The singular value of Jacobian matrix is used as the performance index to optimize the structure of parallel mechanism in literature [10]. Carbon used the binary method to optimize the workspace volume of reachable mechanism in literature [11].

The dimension synthesis of mechanism is based on the performance index to optimize the size and other parameters of the mechanism [12]. Many literatures focus on the intelligent optimization algorithm. Zhang et al. used the differential evolution algorithm to optimize the stiffness and reachable workspace of 3-UPU in literature [13]. Cui and others optimized the workspace and dexterity of 3-ups-s based on Isight in literature [14]. ZHANG et al. used the genetic algorithm to optimize the global condition number and workspace of spherical mechanism [15].

This paper is aimed at the problems of the existing haptic devices, such as low structural stiffness, limited output capacity, and application simplification, and a 6-DOF haptic device with large output capability was designed for general operation object. The 6-DOF haptic device satisfies high structural stiffness and is a universal haptic device. Combined with screw theory, Based on the analysis of its positioning mechanism and orientation mechanism, taking the generalized coordinates θ and β as constraints, the length ρ and dexterity Q_D of the moving rod as objective functions, the size, volume, and dexterity of the mechanism were optimized in the multiobjective optimization method based on the genetic algorithm. The minimum workspace and the optimal dexterity were obtained, which provide a theoretical basis for the design of universal haptic device with better performance.

The following content is structured as follows. The designation and kinematic analysis of the haptic device is in Section 2. Section 3 discusses the workspace analysis of the haptic device. Section 4 is structural parameter optimization of the haptic device. Section 5 is multiobjective optimization of GA. Section 6 is results and discussion. Section 7 concludes this paper.

2. Designation and Kinematic Analysis of the Haptic Device

2.1. Mechanism Designation. The structure of haptic device can be divided into series connection, parallel connection, and hybrid connection. Series mechanism belongs to the open chain structure, and the parallel mechanism contains at least two independent kinematic chains between the end and the base. Series mechanism belongs to the open chain structure, and there are at least two independent kinematic chains between the end and the base of the parallel mechanism. The hybrid mechanism includes series mechanism and parallel mechanism. The advantage of series mechanism is that it has a large working space, but its actuator is installed at the joint of each connecting rod. It increases the motion inertia of the mechanism, which is not conducive to the reverse drive and affects the output ability of the series mechanism. The actuator of the parallel mechanism is installed on the base, which reduces the motion inertia. It has a high structural stiffness and can transfer large force or torque. However, the parallel mechanism is not suitable for force feedback because of its small workspace and insufficient speed output capability. In view of the advantages and disadvantages of the series mechanism and parallel mechanism, a new type of haptic device was designed by using the hybrid structure of the series and parallel mechanism, which is convenient for real-time control of haptic device.

2.1.1. The Designation of the Positioning Mechanism. Generally speaking, the workspace of haptic device is smaller than that of the virtual simulation environment. When mapping the operation space, if the workspace is inconsistent, there will be problems in the mapping of displacement scale factor and reachable workspace. To eliminate these situations, the workspace of the haptic device should be a regular cube space, which can correspond to the real or virtual three-dimensional space. Meanwhile, the structure of the whole mechanism should be kept as compact as possible. In order to achieve fast motion, the moving parts of the haptic device need a small inertia.

If there is no force sensor at the end effector, the haptic device needs to be structurally isotropic [16], which ensure good control of forces in all directions. On the contrary, if a force sensor is used, the inertia at the end effector and the size of the haptic device will be increased, and the cost will also be increased. Therefore, it is better to choose the mechanism with isotropic configuration in the workspace. A fully isotropic 3-DOF mechanism was described in literature [17]. The movement direction of the branch chain is perpendicular to the length direction of the rod, which needs to increase the structure size to increase the bending capacity and the motion inertia; so, it is not suitable for haptic device. An improved translational mechanism 3PRPaR was described in literature [18] as shown in Figure 1.

The direction of the moving pair of the mechanism is consistent with the direction of the rod length, and the force transmission direction is also along the direction of the rod length; so, it has high stiffness [19], which can achieve large output of feedback force. At the same time, because the
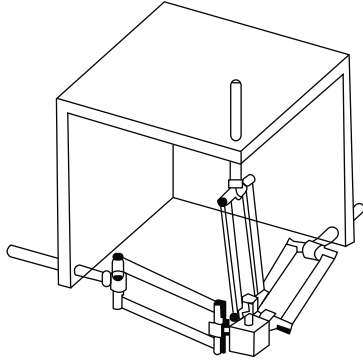
FIGURE 1: 3PRPaR.
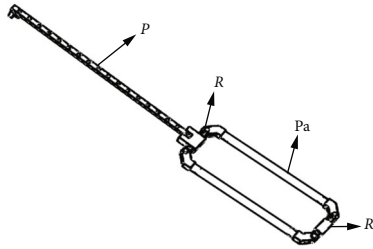
FIGURE 2: PRPaR.

FIGURE 3: 3PRPaR.

FIGURE 4: Triplanar.

FIGURE 5: ROBO_003.

mobile joints are installed perpendicular to each other, they have an isotropic configuration in their workspace. In addition, the workspace of the mechanism is approximately a regular cube; therefore, the mechanism is suitable for the positioning mechanism of haptic device [20]. The branch chain structure of 3PRPaR and schematic diagram of three branch chain combination structures are shown as Figures 2 and 3.

Three branch chains of 3PRPaR can move along X, Y, and Z directions; so, the positioning mechanism has three degrees of freedom.

2.1.2. The Designation of the Directional Mechanism and the Analysis of DOF

(1) A 6-DOF parallel mechanism Triplanar (Figure 4) was described in literature [21]. Triplanar is driven by three planar motors with two degrees of freedom. The design concept of ROBO_003 comes from Triplanar but has its own obvious characteristics (Figure 5). Three planar motors with two degrees of freedom in Triplanar are replaced by three turntables rotating around the fixed axis in ROBO_003. It is equivalent to limiting the two degrees of freedom motion of three planar motors to a single degree of freedom motion along a fixed circle
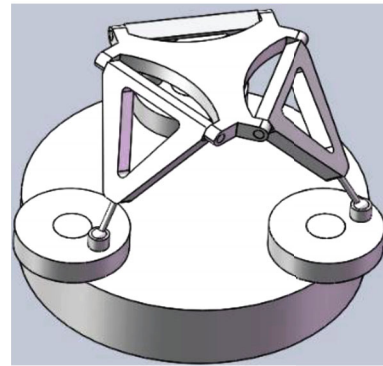
(2) Analysis of freedom degree of directional mechanism based on screw theory

Plüc kerHomogeneous coordinates [22]:

$$
\begin{aligned}
S &= \begin{bmatrix} s \\ s_0 \end{bmatrix} = \begin{bmatrix} s \\ r \times s + hs \end{bmatrix}, \\
S &= [l\, m\, n\, p\, q\, r]^T, \\
l^2 &+ m^2 + n^2 = 1, \\
lp &+ mq + nr = 0,
\end{aligned}
\tag{1}
$$

when S is a motion screw: $S = \begin{bmatrix} \omega \\ v \end{bmatrix}$, to get a branch chain $P_1G_1Q_1$ in ROBO_003. Motion screw of each joint in the branch chain is shown in Figure 6.

In the branch chain $P_1G_1Q_1$, P_1 is the rotating pair, G_1 is the spherical pair, and Q_1 is the rotating pair. Five screws in the branch chain are shown in Figure 6 as follows:

$$s_1 = (0\,0\,1\,;\,0\,0\,0),$$

$$s_2 = (1\,0\,0\,;\,0\,0\text{-}b),$$

$$s_3 = (0\,1\,0\,;\,0\,0\,a),$$ (2)

$$s_4 = (0\,0\,1\,;\,b\text{-}a\,0),$$

$$s_5 = (d\,e\,f\,;\,g\,h\,i).$$

The motion screw of $P_1 G_1 Q_1$ in the parallel robot ROBO_003 can be set as $S = (s_1\,s_2\,s_3\,s_4\,s_5)$. It can be expressed as the matrix:

$$S = \begin{bmatrix} 0 & 1 & 0 & 0 & d \\ 0 & 0 & 1 & 0 & e \\ 1 & 0 & 0 & 1 & f \\ 0 & 0 & 0 & b & g \\ 0 & 0 & 0 & -a & h \\ 0 & -b & a & 0 & i \end{bmatrix},$$ (3)

$$S^T E S^r = 0^{[22]}.$$

S^T is the transpose matrix of S, E is the unit matrix, and S^r is the unit force screw of terminal constraint.

Let $\Re = S^T E$, and the problem of solving S^r can be transformed into the problem of solving the following homogeneous linear equation.

$$\Re x = 0\,;\,x = S^r, S^r = [x_1 x_2 x_3\,;\,x_4 x_5 x_6].$$ (4)

It was calculated by MATLAB:

$$x_1 = 1\,;\quad x_2 = b/a\,;\quad x_3 = \frac{g + (b/a)h}{ae - bd - i}\,;$$

$$x_4 = \frac{bg + (b^2/a)h}{ae - bd - i}\,;\quad x_5 = -\frac{ag + bh}{ae - bd - i}\,;\quad x_6 = 0.$$ (5)

According to equation (5), it can be concluded that

$$x_1 \cdot x_4 + x_2 \cdot x_5 + x_3 \cdot x_6 = 0.$$ (6)

The S^r is a line vector. The constraints of the other two branched chains of ROBO_003 on the moving platform are force vectors. It is proved that the three force vectors are linear independent. Therefore, the three branches restrict the three degrees of freedom of the moving platform. For the spatial mechanism, only three degrees of freedom of rotation are unconstrained. Therefore, ROBO_003 is a pure rotating mechanism with three degrees of freedom. Its moving platform can rotate along the x, y, and z axis, respectively.

The movement and rotation of the haptic device are decoupled. The assembly diagram of the haptic device is shown in Figure 7.

2.2. Kinematic Analysis of the Haptic Device. It is necessary to analyze the kinematics of the haptic device and establish the mapping relationship between the joint space and the opera-
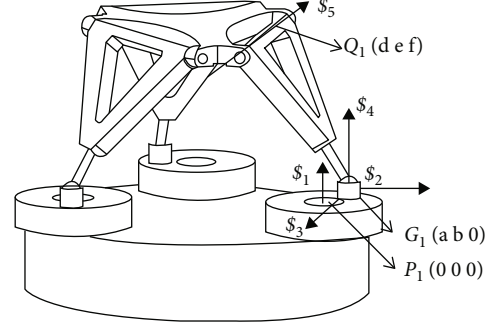
Figure 6: Screw of the branch chain in ROBO_003.

Positioning mechanism   Directional mechanism
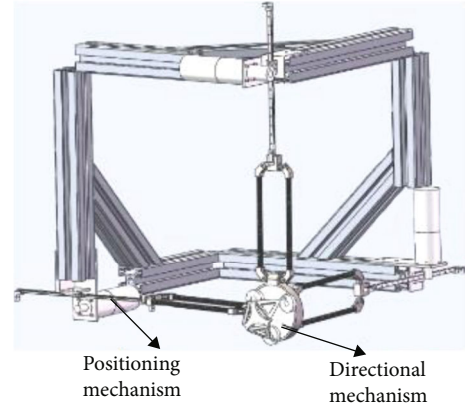
Figure 7: Assembly diagram of the haptic device.

tion space of the haptic device. Deduce the position of the end effector in the space by detecting the position change of its joint and then transfer the position information of the haptic device to the slave and carry out the inverse kinematics. Control the movement of the slave joints to make the slave reach the target position.

2.2.1. Kinematic Analysis of the Positioning Mechanism

(1) Inverse Kinematic Analysis. 3PRPaR consists of three branch chains (Figure 3), and the prismatic pair of the three branch chains is perpendicular to each other. Point O is defined as the origin of fixed coordinate system and P as the origin of the moving platform coordinate system. Point P coincides with point O at initial moment. The X axis, Y axis, and Z axis point to the origin along the prismatic pair, respectively. As shown in Figure 7, the three branch chains are spatially symmetric. So, we only need to analyze the kinematics of a branch chain. In order to simplify the calculation, the parallelogram joint in each branch chain is replaced by an equivalent branch chain composed of a connecting rod and two universal joints. A_{i1} ($i = 1,2,3$) is driving slider of linear motion pair as shown in Figure 8.

Given generalized coordinates β_{i1}, β_{i2}, θ_{i1}, θ_{i2}, and β_{i1} are the angles that rotate around the axis z_{i1}, β_{i2} is the angle that rotate around the axis z_{i5}, θ_{i1} is the angle that rotate around the axis z_{i3}, and θ_{i2} is the angle that rotate around the axis
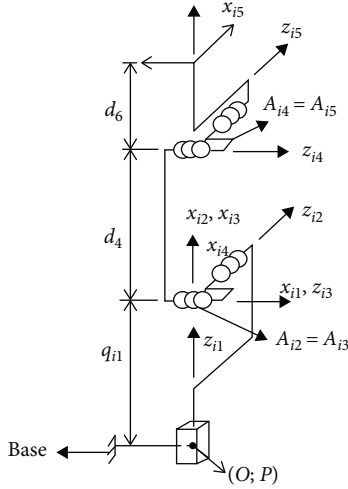
FIGURE 8: Equivalent kinematic chain of the single chain.

z_{i4}.(i is the ith branch chain): $\beta_{i1} = -\beta_{i2}$, $\theta_{i1} = -\theta_{i2}$. The end position of the first branch chain can be expressed as

$$\begin{bmatrix} x_1 \\ y_1 \\ z_1 \end{bmatrix} = \begin{bmatrix} q_{11} + d_4 \cos(\beta_1) \cos(\theta_1) + d_6 \\ -d_4 \sin(\beta_1) \\ -d_4 \cos(\beta_1) \sin(\theta_1) \end{bmatrix}. \qquad (7)$$

The end positions of branched chain 2 and branched chain 3 can also be expressed as

$$\begin{bmatrix} x_2 \\ y_2 \\ z_2 \end{bmatrix} = \begin{bmatrix} d_4 \cos(\beta_2) \sin(\theta_2) \\ q_{21} + d_4 \cos(\beta_2) \cos(\theta_2) + d_6 \\ d_4 \sin(\beta_2) \end{bmatrix}. \qquad (8)$$

$$\begin{bmatrix} x_3 \\ y_3 \\ z_3 \end{bmatrix} = \begin{bmatrix} d_4 \sin(\beta_3) \\ d_4 \cos(\beta_3) \sin(\theta_3) \\ q_{31} + d_4 \cos(\beta_3) \cos(\theta_3) + d_6 \end{bmatrix}. \qquad (9)$$

The ends of the three branch chains are connected together, so that

$$\begin{bmatrix} x \\ y \\ z \end{bmatrix} = \begin{bmatrix} x_1 \\ y_1 \\ z_1 \end{bmatrix} = \begin{bmatrix} x_2 \\ y_2 \\ z_2 \end{bmatrix} = \begin{bmatrix} x_3 \\ y_3 \\ z_3 \end{bmatrix}. \qquad (10)$$

Equation (10) square is as follows:

$$\begin{bmatrix} x^2 \\ y^2 \\ z^2 \end{bmatrix} = \begin{bmatrix} (q_{11} + d_4 \cos(\beta_1) \cos(\theta_1) + d_6)^2 \\ (-d_4 \sin(\beta_1))^2 \\ (-d_4 \cos(\beta_1) \sin(\theta_1))^2 \end{bmatrix}. \qquad (11)$$

Each line of equation (11) is added and simplified:

$$(x - q_{11} - d_6)^2 + y^2 + z^2 - d_4^2 = 0. \qquad (12)$$

Similarly, it was added and simplified the lines of equation (8) and (9), respectively:

$$x^2 + (y - q_{21} - d_6)^2 + z^2 - d_4^2 = 0; \quad x^2 + y^2 + (z - q_{31} - d_6)^2 - d_4^2 = 0. \qquad (13)$$

To solve q_{i1}, expand each lines of equation (13) and simplified:

$$\begin{aligned} &q_{i1}^2 + c_{i1} q_{i1} + c_{i0} = 0, (i = 1, 2, 3); \quad c_{11} = 2d_6 - 2x; \\ &c_{10} = -d_4^2 + d_6^2 - 2xd_6 + x^2 + y^2 + z^2; \quad c_{21} = 2d_6 - 2y \\ &c_{20} = -d_4^2 + d_6^2 - 2yd_6 + x^2 + y^2 + z^2 \quad c_{31} = 2d_6 - 2z \\ &c_{30} = -d_4^2 + d_6^2 - 2zd_6 + x^2 + y^2 + z^2. \end{aligned} \qquad (14)$$

Solve $q_{i1}^2 + c_{i1} q_{i1} + c_{i0} = 0$, $(i = 1, 2, 3)$ and get

$$q_{i1} = \frac{-c_{i1} \pm \sqrt{c_{i1}^2 - 4c_{i0}}}{2} (i = 1, 2, 3). \qquad (15)$$

"$\pm$" means two different working patterns, as shown in Figures 9 and 10.

In Figure 9, branch chain 1 has crossed the singular boundary point, and the travel has exceeded the limit displacement range of the guide rail. Therefore, the displacement can be used to determine the unique solution of the inverse kinematic solution. After the variables of each driving joint are calculated, the variable value of the passive joint can be obtained according to the geometric relationship.

$$\begin{aligned} \theta_1 &= a \tan 2(-z, x - q_{11} - d_6); \\ \theta_2 &= a \tan 2(x, y - q_{21} - d_6); \\ \theta_3 &= a \tan 2(y, z - q_{31} - d_6), \end{aligned}$$

$$\begin{aligned} \beta_1 &= a \tan 2\left(-y, \frac{x - q_{11} - d_6}{\cos(\theta_1)}\right); \\ \beta_2 &= a \tan 2\left(z, \frac{y - q_{21} - d_6}{\cos(\theta_2)}\right) \\ \beta_3 &= a \tan 2\left(x, \frac{z - q_{31} - d_6}{\cos(\theta_3)}\right). \end{aligned} \qquad (16)$$

(2) Forward Kinematic Analysis. Equation (10) can be written as follows:

$$
\begin{bmatrix}
x^2 + y^2 + z^2 + 2c_1 x + 2c_2 z + c_1^2 + c_2^2 - d_4^2 \\
x^2 + y^2 + z^2 + 2c_3 x + 2c_4 y + 2c_5 z + c_3^2 + c_4^2 + c_5^2 - d_4^2 \\
x^2 + y^2 + z^2 + 2c_6 x + 2c_7 y + 2c_8 z + c_6^2 + c_7^2 + c_8^2 - d_4^2
\end{bmatrix}
=
\begin{bmatrix} 0 \\ 0 \\ 0 \end{bmatrix},
$$

(17)

$$
\begin{aligned}
&c_1 = -d_6, c_2 = -q_{11}, c_3 = -q_{21}, \\
&c_4 = -d_6, c_4 = -d_6, c_5 = 0, \\
&c_6 = -d_6, c_7 = -q_{31}, c_8 = 0.
\end{aligned}
$$

(18)

Solve equations (17), and we get the forward kinematic model of $3PRR_aR$:

$$ x = c_9 z + c_{10}, $$

$$ y = c_{11} z + c_{12}, $$

$$ z = \frac{-c_{14} \pm \sqrt{c_{14}^2 - 4c_{13} c_{15}}}{2c_{13}}, $$

$$ c_9 = \frac{-(c_2 - c_5) c_7}{(c_1 c_4 + c_1 c_7 - c_3 c_7 - c_4 c_6)}; $$

$$ c_{10} = \frac{-\left(c_1^2 + c_2^2 - c_3^2 - c_4^2 - c_5^2\right) c_4}{(c_1 c_4 + c_1 c_7 - c_3 c_7 - c_4 c_6)}; $$

$$ c_{11} = \frac{(c_2 - c_8)(c_1 - c_6)}{(c_1 c_4 + c_1 c_7 - c_3 c_7 - c_4 c_6)}, $$

$$ c_{12} = \frac{-\left(c_1^2 + c_2^2 - c_6^2 - c_7^2 - c_8^2\right)(c_1 - c_3)}{(c_1 c_4 + c_1 c_7 - c_3 c_7 - c_4 c_6)}; $$

$$ c_{13} = c_9^2 + c_{11}^2 + 1; $$

$$ c_{14} = 2(c_9 c_{10} + c_{11} c_{12} + c_1 c_9 - c_2), $$

$$ c_{15} = c_{10}^2 + c_{12}^2 + 2c_1 c_{10} + c_1^2 + c_2^2 - d_4^2. $$

(19)

3. Workspace Analysis of the Haptic Device

The workspace of haptic device should be cube, which is convenient to establish the spatial mapping relationship between master hand and slave hand in the teleoperation system.

3.1. Monte Carlo Method. The Monte Carlo method is a numerical calculation method based on statistical theory and probability theory [23]. The basic idea is to use random number to solve the problem with definite law. When it is used to solve the problem of robot workspace, the joint variables can be used as input, and the space position of the end of the manipulator can be obtained through the forward
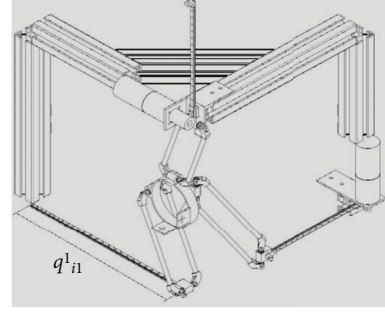
Figure 9: Working pattern 1.
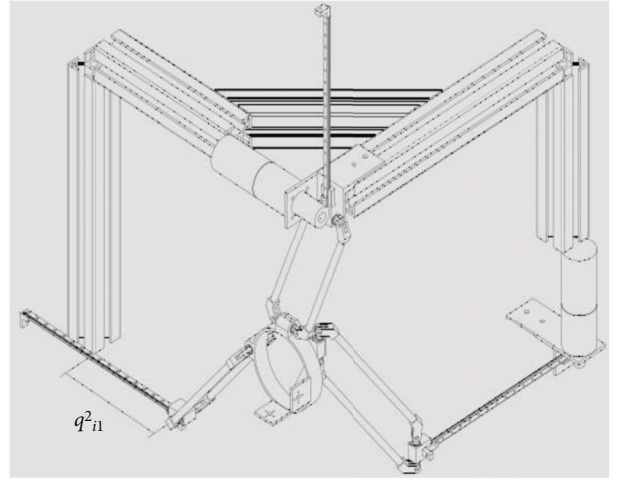
Figure 10: Working pattern 2.
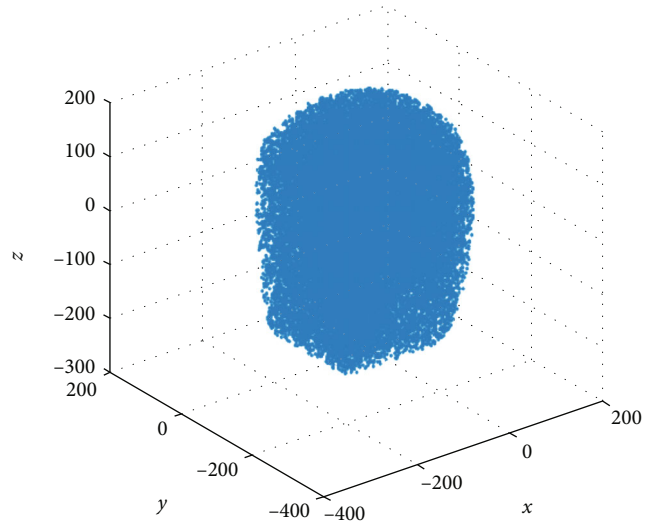
Figure 11: Workspace of the haptic device.

kinematic calculation of the robot. When the number of joint variables is enough, the set of corresponding end space positions will approximately constitute the workspace of the robot.
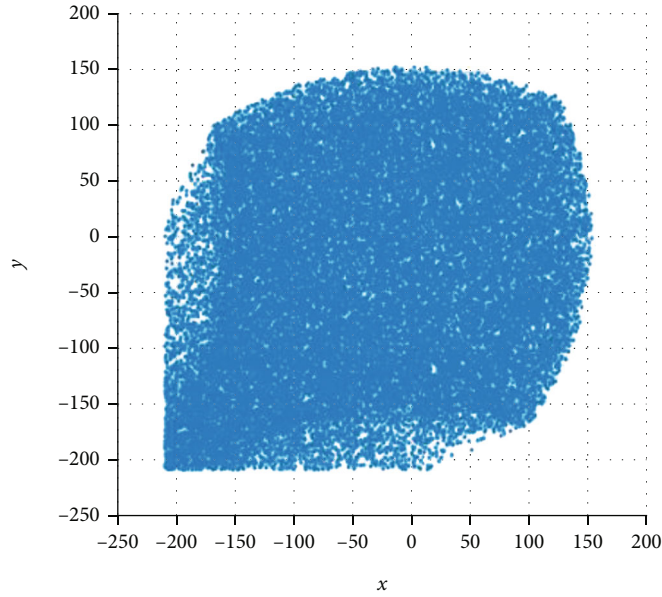
FIGURE 12: X-Y view.

The steps are as follows:

(1) Determine the range of motion of each joint

(2) The forward kinematics of the mobile mechanism is analyzed

(3) By randomly selecting an input for each joint, the random variables of each joint can be obtained by the following formula: $\theta_i = \theta_{i-\min} + (\theta_{i-\max} - \theta_{i-\min}) \times \mathrm{rand}\,()$

$\theta_{i-\max}$ is the maximum input angle of the ith joint.
$\theta_{i-\min}$ is the minimum input angle of the ith joint.
Rand is the function that generates random numbers

(4) The randomly generated joint variables are brought into the kinematic equation to calculate the position of the operation end in the operation space

(5) Repeat the above steps to get the set of spatial positions of the operation end, which is the approximate solution of the workspace. The more groups of joint variables are taken, the closer the result is to the actual workspace

Follow the above steps. The workspace of the positioning mechanism is calculated by MATLAB as shown in Figures 11–14.

It contains a square in Figure 14. So, in the workspace of 3PRPaR, it contains a cube. It meets the design requirements of the haptic device.

4. Parameter Optimization and Evaluation Index of the Haptic Device

The objective of haptic device optimization is to optimize the size of the mechanism [24]. First of all, the workspace should
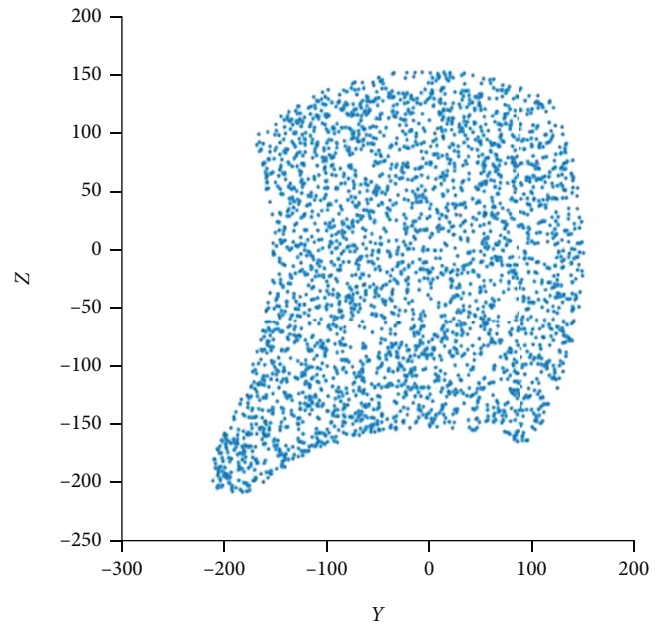
FIGURE 13: $X = 0$ slice diagram.

meet the preset requirements, so that the size of the whole mechanism is as small as possible. At the same time, the transfer coefficient of the mechanism should be limited in a certain range to ensure the stiffness and reverse driving performance of the mechanism. Therefore, it is necessary to select appropriate evaluation indexes. The main evaluation indexes of the haptic device are dexterity and operation space volume.

4.1. Dexterity. Dexterity is an important index to measure the transmission accuracy of input and output motion or force of robot [25]. When the robot structure is in or near the singular
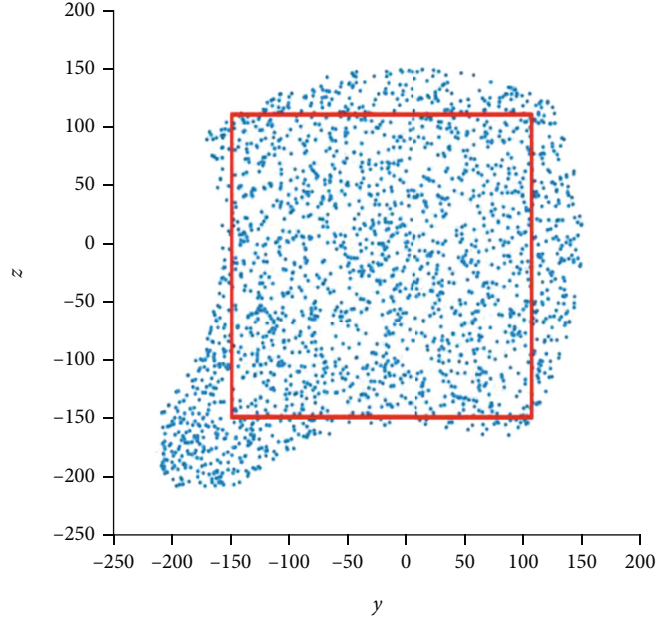
FIGURE 14: $Y = 0$ slice diagram.

configuration, the transfer relationship between input motion and output motion will be distorted. The minimum condition number, minimum singular value, and operability based on Jacobian matrix can reflect the degree of motion distortion to a certain extent.

The minimum condition number is as follows:

$$k(J) = \|J\| \|J^{-1}\|. \tag{20}$$

$\|\cdot\|$ is the arbitrary matrix norm; when using Frobenius norm, the above formula can be expressed as

$$k_F(J) = \sqrt{\frac{1}{n} tr(JJ^T)} \sqrt{\frac{1}{n} tr(JJ^T)^{-1}}. \tag{21}$$

When $k_F(J) = 1$, the mechanism is in isotropic configuration and has the best performance of motion and force transmission. The main axis direction of operating ellipsoid is defined by eigenvalues of $(JJ^T)^{-1}$. Square root of eigenvalue ξ_1, ξ_2, ξ_3 is the length of the spindle. The length of the spindle of operating ellipsoid is directly related to the operating performance of the mechanism. The shorter the length is, the greater the structural stiffness along this direction is. That is, the actuator only needs to output a small force to offset the effect of the external force. Define the velocity transfer coefficients along the three principal axes that are $\psi_1 = 1/\xi_1, \psi_2 = 1/\xi_2, \psi_3 = 1/\xi_3$ respectively. In order to ensure good force transmission performance and speed transmission performance, ψ_i needs to be limited to a certain range. Let $\psi_{min} \leq \psi_i \leq \psi_{max}$ and $\psi_{min} = 1/\psi_{max}$ and get $1/\psi_{max} \leq \psi_i \leq \psi_{max}$.

As shown in Figure 15, the workspace of the haptic device contains a cube. Point Q_1 and point Q_2 are two vertices on the diagonal of the cube. When the haptic
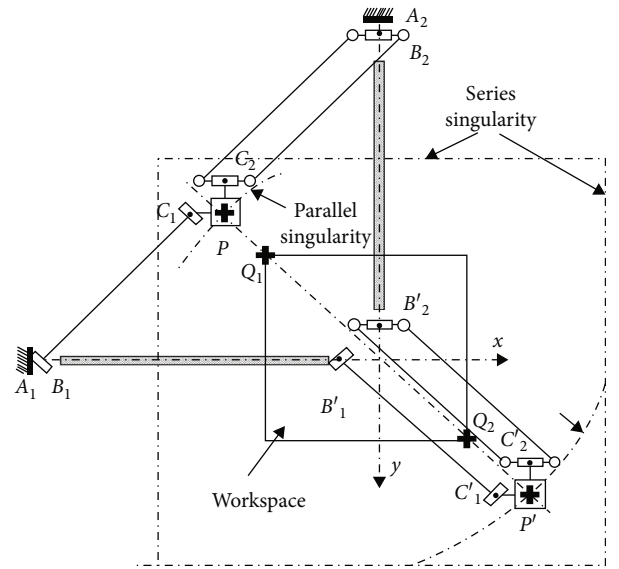
FIGURE 15: Singular configuration of the haptic device.

device is in singular configuration, point Q_1 and pointQ_2 are two points closest to the end of the haptic device. According to interval analysis theory [26], if the condition can be satisfied with $1/\psi_{max} \leq \psi_i \leq \psi_{max}$ at points Q_1 and Q_2, ψ_i can satisfy this condition in the whole workspace.

As shown in Figures 16 and 17, $\rho_i(i = 1, 2, 3)$ is the length of the moving rod. When the moving platform of the haptic device is at point Q_1, $\rho_1 = \rho_2 = \rho_3 = \rho_{min}$, when the moving platform of the haptic device is at point Q_2, $\rho_1 = \rho_2 = \rho_3 = \rho_{max}$.
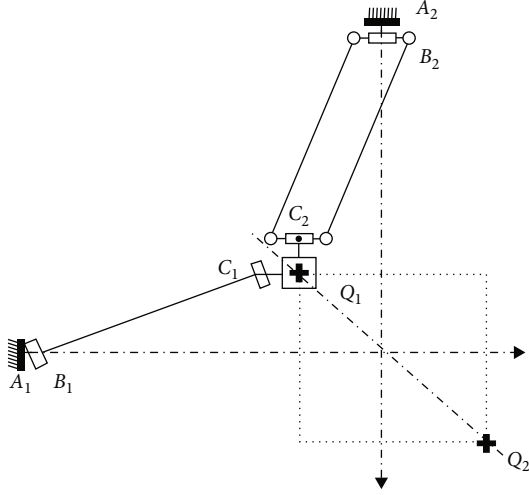
FIGURE 16: Configuration of Q_1.
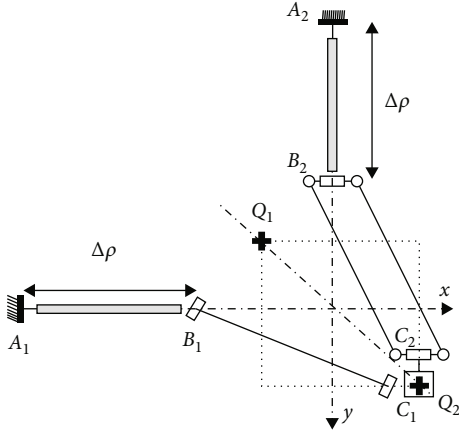
FIGURE 17: Configuration of Q_2.

As shown in Figure 18, the length of parallelogram connecting rod is L. The distance from the end of the connecting rod to the center of the moving platform is e. Let $\rho_{\min} = 0$, and the coordinate of point P along Z axis can be expressed as $Z = -\sin(\beta_1)L$ or $Z = -\sin(\theta_1)\cos(\beta_2)L$. In the axis $Q_1 Q_2$, $\beta_1 = \beta_2 = \beta_3 = \beta$, $\theta_1 = \theta_2 = \theta_3 = \theta$. The relationship between β and θ can be expressed as $\beta = -\arctan(\sin(\theta))$. By substituting the haptic device kinematic equation, we get the following results:

$$J^{-1} = \begin{pmatrix} 1 & -\tan(\theta) & -\tan(\theta) \\ -\tan(\theta) & 1 & 1 \\ -\tan(\theta) & -\tan(\theta) & 1 \end{pmatrix},$$

$$\xi_1 = |2\tan(\theta) - 1|, \xi_2 = \xi_3 = |\tan(\theta) + 1|\psi_1$$
$$= \frac{1}{|2\tan(\theta) - 1|}, \psi_2 = \psi_3 = \frac{1}{|\tan(\theta) + 1|}. \tag{22}$$
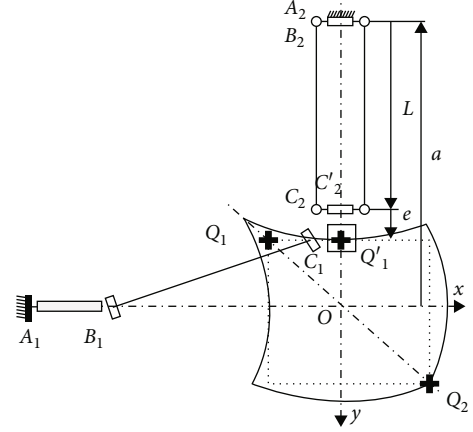
FIGURE 18: Calculation diagram of the single chain.

Solve the equation:

$$\frac{1}{\psi_{\max}} \leq \frac{1}{|\tan(\theta) + 1|} \leq \psi_{\max}, \frac{1}{\psi_{\max}} \leq \frac{1}{|2\tan(\theta) - 1|} \leq \psi_{\max}. \tag{23}$$

Q_D is the dexterity.

$$Q_D = \sqrt{\frac{1}{(1 + \tan(\theta))^4(\tan(\theta) - 1)^2}}. \tag{24}$$

4.2. Workspace Volume. As shown in Figure 18, $a = OA_1 = OA_2 = OA_3$. when point P coincides with point Q_1',

$$OA_2 = OQ_1' + Q_1'C_2' + C_2'A_2. \tag{25}$$

For $\rho_2 = 0$, $C_2A_2 = C_2B_2 = L$, $Q_1'C_2 = PC_2 - e$, and $OQ_1' = q_1$, we get

$$a = q_1 + e + L. \tag{26}$$

q_1 can be obtained by formula (13); so, a can be obtained by $e, L, \psi_{\max}$. Project $A_2P = A_2B_2 + B_2C_2 + C_2P$ onto the Y axis gets:

$$\rho = q_1 + a + \cos(\theta)\cos(\beta)L + e + 37, \tag{27}$$

$$q_1 = \sin(\beta)L ; a = q_1 + e + L ;$$
$$L = \left(\frac{100}{\sin(\beta)} + 153.5\right)mm ; e = 51mm. \tag{28}$$

ρ determines the volume of the workspace. Its length is determined by θ, β.
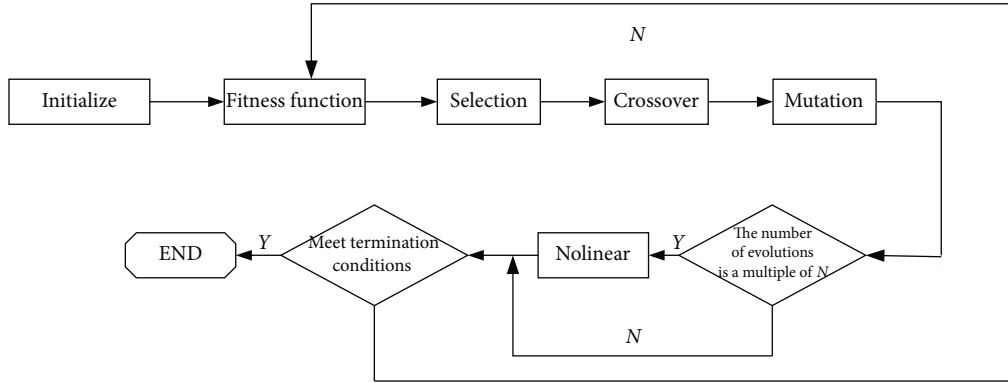
FIGURE 19: Flow chart of the genetic algorithm.
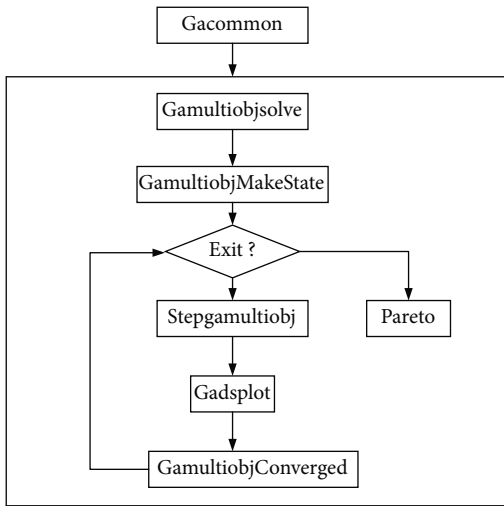
FIGURE 20: Organization chart of the gamultiobj function.
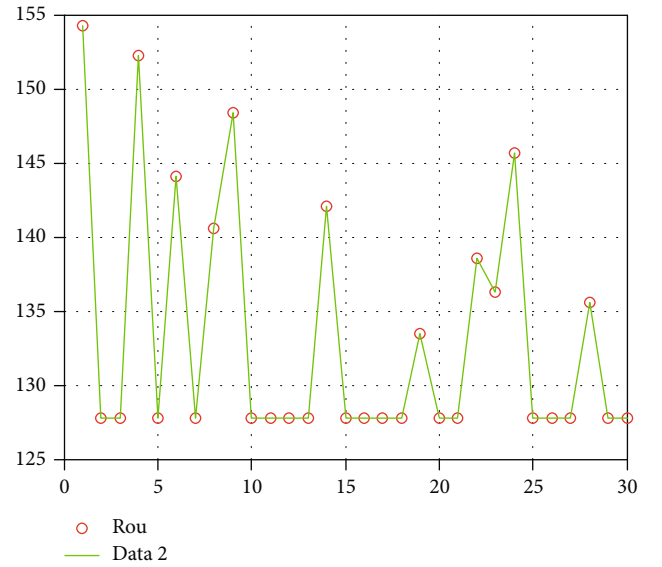
FIGURE 21: Optimization curve of rod length ρ.

In summary,

$$\rho = q_1 + a + \cos{(\theta)} \cos{(\beta)}L + e, \qquad (29)$$

$$Q_D = \sqrt{\frac{1}{(1 + \tan{(\theta)})^4 (\tan{(\theta)} - 1)^2}}, \qquad (30)$$

$$\theta = -\arcsin{(\tan{(\beta)})}, \beta \in \left[0 \frac{\pi}{4}\right]. \qquad (31)$$

5. Multiobjective Optimization of the Genetic Algorithm

GA (genetic algorithm) is a kind of evolutionary algorithm. The basic principle is to encode the problem parameters as chromosomes and to exchange the information of chromosomes in the population by means of iterative operation such as selection, crossover, and mutation, so as to generate the chromosomes that meet the optimization objectives [27]. In the genetic algorithm, chromosomes correspond to data or array, which is represented
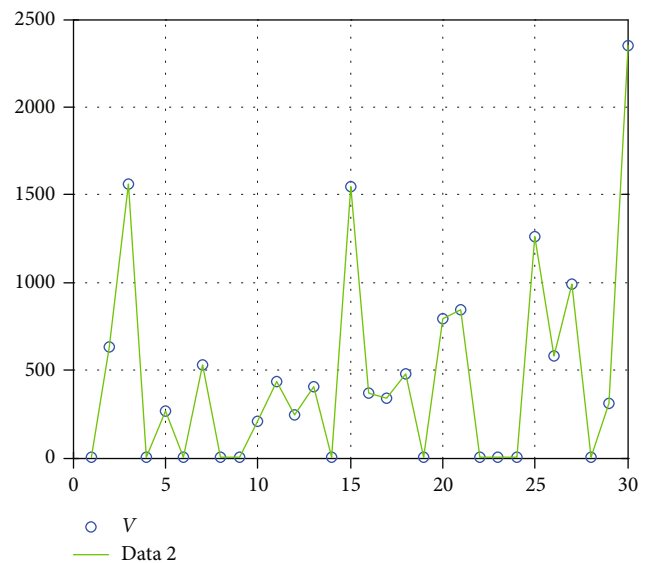
FIGURE 22: Optimal volume.
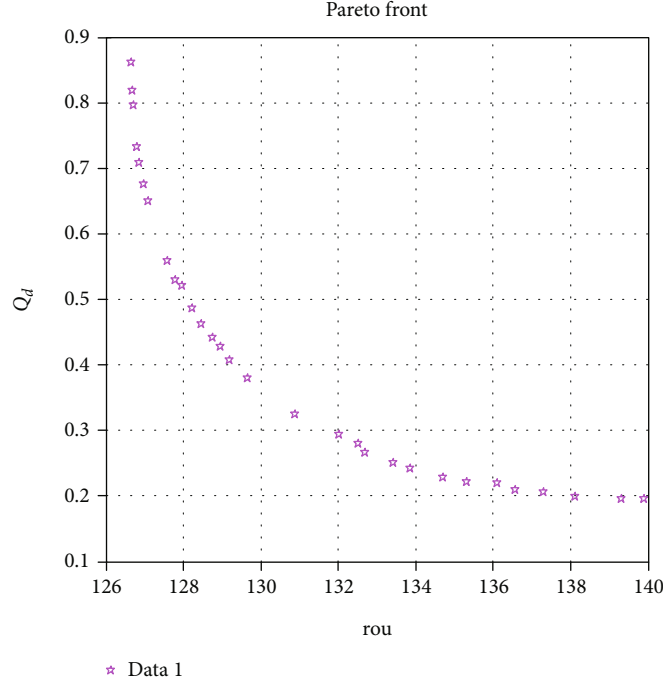
FIGURE 23: ρ corresponds to the dexterity after optimization.

by one-dimensional string structure data. A string of genes is a chromosome which is called individuals. A certain number of individuals form a population, and the number of individuals in population is called population size. Each individual's adaptability to the environment is called fitness. Flow chart of the genetic algorithm is shown in Figure 19.

5.1. Paretooptimal Solution of Multiobjective Optimization.
The problem of multiobjective optimization can be described as follows:

$$\min [f_1(x), f_2(x), \cdots, f_m(x)],$$
$$s.t. \begin{cases} lb \leq x \leq ub, \\ Aeq * x = beq, \\ A * x \leq b. \end{cases} \quad (32)$$

$f_i(x)$ is the objective function to be optimized, x ($lb \leq x \leq ub$): variables to be optimized.

$Aeq * x = beq$ is the linear equality constraint of x, $A * x \leq b$: linear inequality constraints.

$lb \leq x \leq ub$ is the range of x.

5.1.1. Gamultiobj Function.
The gamultiobj function is an improved multiobjective optimization algorithm based on NSGA (a variant of NSGA). The emergence of the gamultiobj function provides a good way to solve the multiobjective optimization problem in the MATLAB platform. Organization chart of multiobjective optimization function gamultiobj based on GA is shown in Figure 20. In this paper, the length ρ and dexterity Q_D are taken as the objective functions, and the

TABLE 1

Paretofraction	Population size	Generations	StallGenLimit	TolFun
0.4	100	200	200	1e-100

TABLE 2

	Values			
	(θ)rad	(β)rad	(ρ)mm	Q_D
Unoptimized	-1.0000	0.500000	135.000000	0.2213
Optimized	-1.270261	0.321750	134.247156	0.2452
	-1.570771	0.784929	127.828284	0.5246
	-1.460782	0.391701	144.055299	0.0015
	-0.580130	0.502304	126.297573	0.7158
	-1.170757	0.785391	133.496546	0.2445
	-0.770781	0.785163	137.519930	0.2001
	-1.370783	0.425692	128.797083	0.4209
	-0.970779	0.534215	130.797173	0.3262

independent variables are θ, β. The best matching value between the volume space suitable for the optimal dexterity is shown in Figures 21–23.

Objective functions are as follows:

$$f(1) = \min \rho = (2 \sin (\beta) + \cos (\theta) \cos (\beta) + 1)L + 51,$$

$$f(2) = \min Q_D = \sqrt{\frac{1}{(1 + \tan (\theta))^4 (\tan (\theta) - 1)^2}}.$$

$$(33)$$
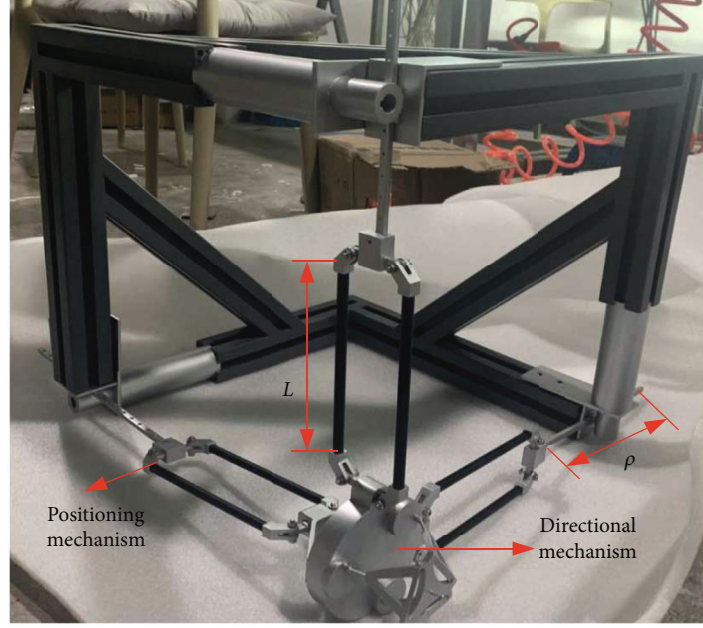
FIGURE 24: Assembled haptic device.

Constraints are as follows:

$$\frac{-\pi}{2} \le \theta \le 0 \; ; 0 \le \beta \le \frac{\pi}{4} \; ; L = \frac{100}{\sin (\beta)} + 153.5 \left(0 \le \beta \le \frac{\pi}{4}\right).$$

(34)

The parameters of multiobjective optimization algorithm are shown in Table 1:

As shown in Figure 23, $\rho_{\min} = 126.3$mm.

It is calculated by equations (28), (29), and (31): $\beta = 0.502$ rad, $\theta = -\arcsin (\tan (\beta)) = -0.581$rad

$$L = \frac{100}{\sin (\beta)} + 153.5 = \frac{100}{0.481} + 153.5 = 361.7\text{mm}.$$

(35)

Paretooptimal solutions (8 groups selected) are shown in Table 2.

Based on the results of parameter optimization, and considering the processing and assembly technology, select the fourth group of parameters in Table 2. Assembled haptic device is shown in Figure 24.

6. Results and Discussion

According to the characteristics of series and parallel mechanisms, a new six-DOF hybrid haptic device was designed combining series mechanism 3PRPaR and parallel mechanism ROBO_003. The DOF of 3PRPaR is 3. In this paper, the freedom form of parallel mechanism ROBO_003 was analyzed based on screw theory. It can be concluded from equations (5) and (6) that the DOF of the moving platform of ROBO_003 is 3, and the DOF form is rotation. That is, moving plat-

form of ROBO_003 rotates around X, Y, and Z axes, respectively. The kinematics of 3PRPaR was analyzed in this paper. The workspace of the haptic device was analyzed in the Monte Carlo method. As shown in Figures 11–14, the workspace of 3PRPaR contains a cube, and it meets the design requirements of the haptic device. The workspace corresponds to the length and volume of the haptic device. In order to make the length and the volume meet the requirements, the optimization indices are selected to optimize the haptic device. Multiobjective optimization algorithm based on GA was selected. θ, β was selected as independent variables, Length of moving rod ρ and dexterityQ_D was selected as objective functions. The optimal angle θ, β is -0.581 rad and 0.502 rad obtained, and $L = 361.7$mm. The optimal length ρ and optimal dexterity $Q_D$of the haptic device were obtained. The fourth data is selected from 8 paretooptimal solutions in Table 2. The optimal length is $\rho_{\min} = 126.3mm$, and the optimal dexterity is $Q_D = 0.7158$ .Minimum ρ means minimum volume, and minimum volume and optimal dexterity mean optimal performance of the haptic device. The optimized dexterity is 69% higher than unoptimized, and the rod length is reduced by 6%.It can be concluded in Figure 23 that $\rho$and Q_D are approximately inversely proportional. The larger the volume is, the worse the dexterity of the haptic device.

The requirements of the haptic device are tracking performance and force feedback performance, which are determined by the appropriate volume and dexterity. When the rod length is determined, the performance of haptic device is determined by the maximum volume and optimal dexterity of the haptic device. In this paper, the multiobjective optimization algorithm based on the genetic algorithm was used to optimize the relevant parameters to obtain the optimal results. It provides a theoretical basis for the designation of haptic devices.

7. Conclusion

A new six-DOF hybrid haptic device was presented in this paper. Screw theory was carried out to analyze the DOF of ROBO_003.The workspace of the haptic device is determined in the Monte Carlo method. Based on the genetic algorithm, the parameters of the mechanism are optimized according to the dexterity index and volume evaluation index, and the results showed that the optimal parameters were obtained. The results meet the designation requirements of the haptic device. As an indispensable part of virtual reality interaction, haptic device has become a hot spot in the research field of robot technology. Haptic devices are applied to teleoperation robots which are widely used in underwater, space, and land dangerous places. In the future, there will be more mathematical theories applied in the theory of mechanism, kinematics, and dynamics. It has great application and research value.

Data Availability

No data were used to support this study.

Disclosure

Conflicts of Interest

The authors declare that they have no conflicts of interest.

Acknowledgments

References

[1] G. Burdea and P. Coiffet, "Virtual reality technology," *Presence: Teleoperators and Virtual Environments*, vol. 12, no. 6, pp. 663-664, 2003.

[2] D. Lee, T. W. Seo, and J. Kim, "Optimal design and workspace analysis of a mobile welding robot with a 3P3R serial manipulator," *Robotics & Autonomous Systems*, vol. 59, no. 10, pp. 813–826, 2011.

[3] Y. Tanaka, T. Kikuchi, and A. Kaneko, "Dynamic force display in virtual world by fluid power glove," in *Proceedings of the JFPS International Symposium on Fluid Power*, pp. 187–192, Tokyo, 1999.

[4] S. Hesse, "Recovery of gait and other motor functions after stroke: Novel physical and pharmacological treatment strategies," *Restorative Neurology and Neuroscience*, vol. 22, no. 3-5, pp. 359–369, 2004.

[5] D. Feygin and F. Tendick, *A critical study of the mechanical and electrical properties of the phantom haptic interface and improvements for High performance control*, Department of Electrical Engineering and Computer Science, University of California, Berkeley, CA 94720, USA, 1999.

[6] S. Grange, F. Conti, and P. Helmer, "The delta and omega haptic device," Institute of Systems Robotiques Ecole Polytechnique Federale of Lausanne, 2002.

[7] H. Zhen, "Research on basic theory of parallelrobot mechanism," *Robot Technology and Application*, vol. 6, pp. 11–14, 2001.

[8] Y. Tsumaki, H. Naruse, D. N. Nenchev, and M. Uchiyama, "Design of a compact 6-DOF haptic interface," in *Proceedings. 1998 IEEE International Conference on Robotics and Automation (Cat. No.98CH36146)*, pp. 2580–2585, Leuven, Belgium, May 1998.

[9] C. M. Gosselin and J. Angeles, "A global performance index for the kinematic optimization of robotic manipulators," *ASME Journal of Mechanical Design*, vol. 113, no. 3, pp. 220–226, 1991.

[10] X. L. Chen, D. Y. Jiang, L. L. Chen, and Q. Wang, "Kinematics performance analysis and optimal design of redundantactuation parallel mechanism," *Transactions of the Chinese Society for Agricultural Machinery*, vol. 47, no. 6, pp. 340–347, 2016.

[11] G. Carbone, E. Ottaviano, and M. Ceccarelli, "An optimum design procedure for both serial and parallel manipulators," *Proceedings of the Institution of Mechanical Engineers Part C-Journal of Mechanical Engineering Science*, vol. 221, no. 7, pp. 829–843, 2007.

[12] X. Liu, C. Wu, and J. Wang, "A new approach for singularity analysis and closeness measurement to singularities of parallel manipulators," *ASME Journal of Mechanisms Robotics*, vol. 4, no. 4, article 041001, 2012.

[13] D. Zhang and B. Wei, "Interactions and optimizations analysis between stiffness and workspace of 3-UPU robotic mechanism," *Measurement Science Review*, vol. 17, no. 2, pp. 83–92, 2017.

[14] G. Cui, H. Zhou, N. Wang, and H. Q. Zhang, "Multi-objective optimization of 3-UPS-S parallel mechanism based on isight," *Transactions of The Chinese Society of Agricultural Machinery*, vol. 44, no. 9, pp. 261–266, 2013.

[15] X. Zhang and C. A. Nelson, "Multiple-criteria kinematic optimization for the design of spherical serial mechanisms using genetic algorithms," *Journal of Mechanical Design*, vol. 133, no. 1, pp. 819–827, 2011.

[16] H. S. Kim and L. W. Tsai, "Evaluation of a Cartesian manipulator," in *Advances in Robot Kinematic*, J. Lenarčič and F. Thomas, Eds., pp. 21–38, Kluwer, Norwell, MA, USA, 2002.

[17] M. Carricato and V. Parenti-Castelli, "Singularity-free fully-isotropic translational parallel mechanisms," *International Journal of Robotics Research*, vol. 21, no. 2, pp. 161–174, 2002.

[18] F. Majou, P. Wenger, and D. Chablat, "Design of a 3 axis parallel machine tool for high speed machining: the Orthoglide," in *4ème Conférence Internationale Sur La Conception Et La Fabrication Intégrées En Mécanique*, pp. 1–10, 2007, http://arxiv.org/abs/0705.1271.

[19] A. Pashkevich, A. Klimchik, D. Chablat, and P. Wenger, "Stiffness analysis of multi-chain parallel robotic systems," *Intelligent Manufacturing Systems*, vol. 3, no. 3, pp. 75–82, 2009.

[20] D. Chablat, P. Wenger, and J. Merlet, "Workspace analysis of the Orthoglide using interval analysis," in *Advances in Robot*

Kinematics, J. Lenarčič and F. Thomas, Eds., pp. 397–406, Springer Netherlands, 2002.

[21] R. Featherstone, "The calculation of robot dynamics-using articulated-body inertias," *The-International Journal of Robotics Research*, vol. 2, no. 1, pp. 13–30, 1983.

[22] J. Zhao and F. Zhijing, *Analysis theory of robot mechanism degree of freedom*, Science Press, Beijing, 2009.

[23] J. Rastegar and B. Fardanesh, "Manipulation workspace analysis using the Monte Carlo Method," *Mechanism & Machine Theory*, vol. 25, no. 2, pp. 233–239, 1990.

[24] Z. Wang, S. Ji, Y. Wan et al., "Optimal Design of Parallel Robots for the Prescribed Regular Dexterous Workspace," in *2007 IEEE International Conference on Automation and Logistics*, pp. 563–568, Jinan, China, August 2007.

[25] Y. Wang and W. Hongtao, *Design and Research of a Six-Degree-of-Freedom Haptic Device*, Nanjing University of Aeronautics and Astronautics, College of Mechanical and Electrical Engineering, 2016.

[26] J. A. Persson, X. Feng, D. Wappling, and J. Ölvander, "A framework for multidisciplinary optimization of a balancing mechanism for an industrial robot," *Journal of Robotics*, vol. 2015, Article ID 389769, 8 pages, 2015.

[27] F. Sérgio Lobato and J. Valder Steffen, "Multi-objective optimization firefly algorithm applied to (Bio) chemical engineering system design," *American Journal of Applied Mathematics and Statistics*, vol. 1, no. 6, pp. 110–116, 2013.

WILEY | Hindawi

Research Article

Role of Internet of Things Technology in Promoting the Circulation Industry in the Transformation of a Resource-Based Economy

Dongqing Zhu,[1,2] **Ting Li** [iD],[3] **Can Zhang,**[3] **Ying Ren,**[2] **Huan Wang,**[2] **and Xia Duan**[2]

[1]*School of Economics, Yunnan University of Finance and Economics, Kunming, 650221 Yunnan, China*
[2]*Lancang-Mekong International Vocational Institute, Yunnan Minzu University, Kunming, 650504 Yunnan, China*
[3]*School of Logistics, Yunnan University of Finance and Economics, Kunming, 650221 Yunnan, China*

Correspondence should be addressed to Ting Li; holly@ynufe.edu.cn

In recent years, the business scale of my country's circulation industry has continued to expand, and the output value has continued to increase. The leading role in guiding the transformation of the industrial economy has become more and more important. Based on this, this article discusses the research on the promotion of the Internet of Things technology to the circulation industry in the transformation of the resource-based economy. The application of RFID technology and wireless sensor technology in the Internet of Things in the circulation industry can greatly improve work efficiency and information transmission accuracy. This article establishes the circulation industry based on the principles of science, system, safety, and relative independence. The evaluation index system analyzes the role of the circulation industry in the transformation of the resource-based economy in terms of circulation scale, circulation structure, circulation efficiency, circulation innovation, etc., and uses the analytic hierarchy process and entropy method to analyze the collected data. With the support of RFID technology, the output value of the circulation industry in Province Y has reached 140.508 billion yuan in 2019, accounting for about 27% of the tertiary industry, and the number of employees in the circulation industry has also increased to 57.88%, which is a strong boost to the economy of Province Y. It has a greater contribution to the total economic volume. The research of this article has realized the economic transformation of resource-based cities in the circulation industry and has a certain reference effect for the transformation and upgrading of similar cities.

1. Introduction

Resource-based cities played a huge role in the initial stage of my country's development. However, due to limited resources, traditional resource-based cities had to undergo economic transformation and thus develop into a new economy. The application of Internet of Things technology in the circulation industry can effectively promote the development of the circulation industry and solve the problems faced by the circulation industry from the source.

The circulation industry can effectively increase social employment, stimulate residents' consumption, and optimize the industrial structure. As the proportion of the circulation industry in economic growth continues to rise, the main body is becoming more and more diversified, the development of the circulation industry has received more and more attention, and its contribution to economic development has gradually increased. The development status of the circulation industry directly affects the development of other industries. The development of the circulation industry is fast, and the development of industry and agriculture is fast; on the contrary, the development of the circulation industry is slow, and the development of industry and agriculture is slow. It can be said that the circulation industry is the vanguard of economic development, the propellant of economic development, and the source of sustained economic development.

As more and more resource-based cities have the need for transformation, there are more and more researches on it. Taking Huainan, a typical coal resource city, as an example, Zhang et al. constructed a multidimensional index system of "economic, social and ecological." The entropy weight method, the coupled coordinated development model, and the gray correlation coefficient method are used to investigate the development of the system from 2002 to 2016. It analyzes the coordinated development of Huainan's multidimensional relations from a macro perspective. The results show that the ecological subsystem has the largest weight, and the overall development level is U-shaped, which first decreases and then increases, which has a significant impact on the comprehensive development level. The ternary coupling system is generally on the rise, and the absolute level of coupling is relatively low. As the pressure on the ecosystem increases, the development of the ecosystem will restrict economic and social development and offset the level of coordinated development. Economic development and economic vitality have a positive impact on social and ecological development, while social development has a greater impact on the ecological subsystem. The improvement of environmental status has a supporting effect on economic and social development. In the process of Huainan's transformation, it is necessary to maintain stable and rapid economic development, increase investment in social development and environmental pollution control, pay attention to ecological support capabilities, and avoid restricting social and economic development. But his research experiment did not carry out more experimental parameter settings [1]. Yongshi and Mingxing aim to conduct an empirical study on the correlation between the distribution industry in Fujian Province and regional economic growth. The results show that the circulation industry has a positive correlation with regional economic growth, and the circulation industry is the main reason for regional economic growth. Further study the dynamic mechanism of the circulation industry to promote regional economic growth and found that the circulation industry has the correlation effect, diffusion effect, and spillover effect on the regional economic growth, and it is the leading industry and basic industry of the regional economy. However, his correlation study considered fewer factors and did not consider multiple factors [2]. Ni et al. integrate fog computing into the Internet of Things, extending computing, storage, and network resources to the edge of the network. Unfortunately, it faces various security and privacy risks, which brings serious concerns to users. In this review, they reviewed the architecture and characteristics of fog computing and studied the key roles of fog nodes, including real-time services, instantaneous storage, data distribution, and decentralized computing. They also studied fog-assisted IoT applications based on different roles of fog nodes. Then, they raised the security and privacy threats of IoT applications. However, the combined application of the Internet of Things and fog computing has yet to be resolved [3].

The innovations of this article are (1) in-depth thinking about the development bottleneck of resource-based cities and innovatively put forward the idea of using the develop-

ment of the circulation industry in economic transformation; (2) ingeniously integrating the Internet of Things RFID and infinite sensor technology. In the process of application in the circulation industry, it has solved the technical support problems in the circulation industry.

2. Internet of Things Technology Promotes the Research Method of the Circulation Industry in the Transformation of the Resource-Based Economy

2.1. Internet of Things

2.1.1. RFID. The RFID system is generally composed of three parts: an electronic tag, a reader, and an information processing system [4]. Tag: also called a transponder, the tag is equipped with an antenna and a chip. The antenna is mainly used to communicate with the radio frequency antenna, and the chip is mainly used to store the ID sequence that uniquely identifies the product information [5, 6]. According to the internal power supply, it is mainly divided into two types: active and passive. Active tags obtain energy from their own power sources, and their identification distance is much longer than passive tags, but the price and power consumption will be relatively much higher. Reader: the reader can identify the information stored in the tag without contact and send it to the information system for data processing [7, 8]. Antenna: the electronic tag and the reader are equipped with an antenna. The antenna mainly realizes the radio frequency signal propagation between the two and establishes a wireless communication connection between the two.

The working principle of RFID technology: first, after the reader receives the read instruction, it sends the signal to the antenna and then interrogates the tag through the antenna, and finally, the antenna transmits the obtained tag data to the information processing system for processing [9, 10].

2.1.2. Technical Application. Because RFID identification technology can realize the functions of wireless noncontact identification, multitag identification, and information networkability, it gradually replaces several other identification technologies [11]. Several developed countries in the United States, Japan, and South Korea have widely applied radio frequency identification technology to logistics management, traffic management, industrial automation, retail, and other related fields [12]. In our country, due to its high cost and limited research and development technology, the application of radio frequency identification technology is currently mainly concentrated in the field of intelligent transportation and the second-generation ID card of residents. However, due to the gradual expansion of production scale and the increasingly sophisticated integrated circuit technology, the production cost of radio frequency identification technology will also continue to decline, which can gradually expand the application of RFID in my country [13]. The following briefly introduces several main application areas of RFID technology.

(1) Traffic Management. Mainly used for car entry and exit registration, no parking fees, thereby avoiding traffic jams due to parking during peak periods and improving the efficiency and capacity of transportation.

(2) Food Safety. The use of RFID electronic tags can record the entire process information of food raw materials, production, processing, circulation, and sales in time, so as to ensure the safety of all aspects of food [14, 15]. The specific process is the producer uses the radio frequency identification technology to mark the agricultural products, and then the distributors and sellers scan the code to record the product flow, so that the agricultural product manufacturer can track the sales of each bottle of pesticide through the background management system [16, 17]. At the same time, consumers can also scan the code to enter the client to trace the specific production information of the product.

(3) Library Management. The library collects and recognizes readers' various certificate information by installing different readers on self-service borrowing and returning equipment and realizes the function of readers' self-service borrowing and returning [18, 19]; by installing RFID at the entrance of each library, the security door of the tag reader can not only automatically identify the effective information carried by the reader and ensure the safety of mobile personnel but also effectively identify whether the book carried by the reader has a borrowing record, so as to ensure the safety of the book; in addition to this, the application of RFID technology in the library can also realize the functions of visual navigation of books, book positioning, and automatic inventory of books, which greatly improves the efficiency of book borrowing, return, and sorting, while also ensuring the security of library management [20, 21].

(4) Logistics Management. With the increasing expansion of the online shopping industry, enterprises' demand for logistics is also increasing. Large-scale quantities of goods and complex supply chains are undoubtedly a big problem for traditional logistics management. It not only consumes a lot of labor to manually count the goods but also greatly reduces work efficiency and cannot guarantee data processing [22, 23]. The application of RFID technology in the logistics management system can not only accurately process the entry and exit of goods and inventory data in universities but also monitor all the information of the goods in real-time, thereby reducing labor costs and improving the accuracy and efficiency of data processing bring greater benefits [24–26]. Figure 1 is a diagram of the application of RFID technology to product circulation mode.

2.2. Resource-Based Economic Transformation. Resource-based economic development cities refer to cities developed based on local resources. Resource-based cities are closely related to resource reserves and even the rise and fall of cities. It can generally be classified according to two types of methods. First, it is classified according to resource storage. The reserves of specific resources have an absolute advantage, and their mining volume accounts for more than 50% of the total industrial output value, which is called depletion. Second, it is divided according to the proportion of urban employed population [27]. 40% of the urban population is engaged in specific resource development, processing, management, and other activities, which can be called a resource city.

Chinese resource-based cities are mainly distributed in the central and western regions and the northeastern region, for example, Inner Mongolia, Guizhou, Gansu, Shanxi, Xinjiang, Jilin, Heilongjiang, and Liaoning. Since it takes a long time for these cities to export resources, most cities face the same problem, that is, how to convert depleted resources [28]. It must be emphasized that some cities are constantly increasing resources, funds, and development, and their development and prosperity depend on convenient transportation systems, advanced technology, strong economic strength, and high-level information. Therefore, such a city cannot be said to be a resource-based city like Japan. Japan is an island country with limited resources, and the steel and automobile industries are very competitive countries. Shanghai Baosteel is also a self-produced steel company based on large amounts of Australian iron ore and high-quality internal carbon fiber. These are not actual cities based on mineral resources. The resource-based cities we want to investigate refer to regions rich in resources, but if the mining time is long, the resources will almost be exhausted, but the comparative advantages of other regions cannot be used. Such exhausted urban resources have long relied on their own resource advantages, which have gradually formed a stable development model. When resources are exhausted, its development will inevitably face serious problems. Therefore, these cities must complete economic transformation and change before resources are exhausted.

2.3. Circulation Industry

2.3.1. Connotation of the Circulation Industry. Before analyzing the connotation of the circulation industry, it is necessary to analyze the meaning of circulation and industry, respectively. The concept of circulation has three levels: the first level is circulation in a broad sense, that is, the continuous transfer process of matter. The second level is the circulation from the perspective of economics. It mainly refers to the circulation of commodities. It is generally defined as the exchange of commodities with currency as the medium. It includes the three behaviors and processes of commodity "purchase," "transfer," and "sell." The third level is based on the existence of social division of labor. Commodities transfer from the field of production to the field of consumption, and finally reach the series of processes experienced by consumers. This does not include the circulation of tangible goods, currency, services, etc. The circulation discussed in this article is defined as the circulation under the second-level economics perspective, that is, the circulation of tangible goods, services, funds, etc. [29, 30]. An industry is defined as the collection of interrelationships in the same market between a group of companies that produce similar products (or services) and their substitutes (or services). This article adopts the definition of this industry.
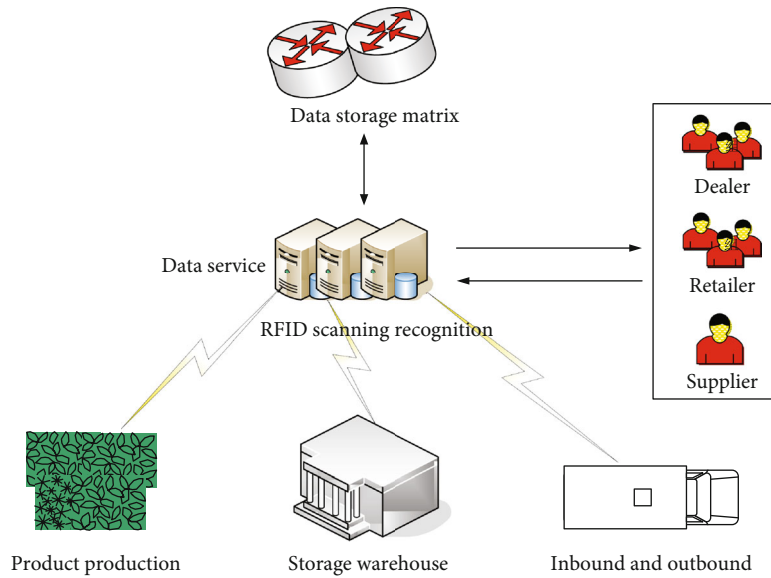
Figure 1: RFID technology applied to product circulation pattern diagram.

The definition of the connotation of the circulation industry must be based on circulation and industry as a constraint. The circulation industry is the carrier that carries the transfer process and exchange function and is a collection of enterprise groups that provide services for tangible goods, services, and funds. Therefore, according to the classification of the three industries, the circulation industry belongs to the tertiary industry. To be precise, the circulation industry belongs to the service industry. The circulation industry specifically includes the wholesale industry, retail industry, accommodation and catering industry, and logistics industry. The wholesale industry and retail industry are the main parts of the circulation industry, and the extension part of the circulation industry is the logistics industry. Generally, in the formulation of government policies, it is generally not considered the accommodation industry and the catering industry are two types of life service industries.

2.3.2. Related Theories about the Development of the Circulation Industry. The development of the circulation industry is driven by a variety of factors, and many theories of economics are involved in the development process. This chapter selects the theory of division of labor, the theory of transaction costs, the theory of industrial organization and industrial structure, and its relevance to the development of the circulation industry. Make a brief analysis and provide theoretical support for subsequent research work.

(1) The Theory of Division of Labor. The division of labor divides the process into several parts, and each part is completed by a different person. This concept includes social division of labor, factory or manufacturing division of labor, and natural division of labor. As early as the 17th century, classical economics advocated free trade and believed that exchange was the result of specialized division of labor, and foreign trade was the true source of wealth. Adam Smith (1776) advocated free trade and believed that the

division of labor resulted from the ability of exchange, and exchange made various specialized production possible. In short, the division of labor is to constantly weigh the high efficiency brought about by the division of labor and the increase in coordination costs, and the increase in coordination costs provides space for the generation and development of the circulation industry. Circulators will first be formed in a better location and then continuously improve transaction efficiency and expand the scope of the market, thereby promoting social division of labor. Therefore, the social division of labor is the basic condition for the formation of the circulation industry, and the circulation industry will in turn promote the continuous deepening of the social division of labor and form a benign interaction and coordinated development.

(2) Theory of Industrial Organization. The founders of industrial organization theory, Marshall, Chamberlain, etc., based on price theory, expounded the basic principles of industrial organization theory, namely, the relationship and contradiction between competition and monopoly among enterprises in the industry. The New Austrian School put forward an extreme liberalism theory, advocating full competition in the free market and denying antimonopoly and regulatory policies. The theory of industrial organization believes that the nature of an industrial market competition and economies of scale determine the level of industrial economic benefits. It can be seen that the circulation industry organization has played a certain role in promoting the development of the circulation industry.

(3) Industrial Structure Theory. Industrial structure refers to the configuration and composition of various factors of production among various industrial sectors. Industrial structure theory is an economic theory that studies the law of industrial structure evolution, and its ideas originated from William Petty's discussion of the phenomenon of

resource flow between industries. Then, Clark, Hoffman, Kuzkintz, and others analyzed the internal change law of each industry and the change trend of the economic promotion effect and believed that the continuous optimization of the industrial structure can promote economic development.

The circulation industry is the foundation and leading industry of the national economy, and its status and role are becoming more and more obvious. Under the guidance of industrial policy theory, research the current situation of the circulation industry in a certain province, analyze the environmental factors that affect the development of the circulation industry, and make targeted suggestions.

2.3.3. Current Problems in the Circulation Industry. At present, the development of the circulation industry is not perfect, and there are some problems that need to be solved: (1) the development of the circulation scale is lagging: the development scale of the circulation industry is very large, and its contribution to the regional economy is high, but the circulation scale is developing in the regional economy as a whole. It is relatively slow and does not play its due role; (2) the degree of circulation organization is not high: at present, the circulation industry operators are mainly self-employed and some small wholesale retailers. Generally, they have not formed large-scale, and there is no unified standard and plan. The overall level of specialization is not high; 3) there are few modern circulation formats: most of them maintain the traditional circulation form, there is no complete product information system, the quality of the product cannot be guaranteed, and the communication efficiency between users and merchants is extremely low, which affects commercial circulation; (4) the low degree of information circulation: for commodity information and commodity accounting, most of them use visual and manual accounting methods, lack of information communication, and insufficient information about commodities; (5) the circulation infrastructure is backward: in most areas, the circulation infrastructure has not been constructed, the transportation is backward, the network density is low, there is no advanced technology and financial support, and the overall circulation service level is not high.

3. Model of the Role of Internet of Things Technology in Promoting the Circulation Industry in the Transformation of a Resource-Based Economy

This chapter mainly aims to build an evaluation index system for the development level of the circulation industry in Province Y to objectively evaluate the circulation industry in Province Y from the perspectives of circulation scale, circulation structure, efficiency, contribution, and innovation value, and adopt the RFID technology in the Internet of Things. It is to understand its promotion and effects on the circulation industry in the transformation of the resource-based economy, so as to provide reference and

guidance for other cities in the transformation and development of the resource-based economy.

3.1. Principles of Establishing an Evaluation Index System. Whether the design of the evaluation index system is reasonable is directly related to the quality of the evaluation. Therefore, when establishing an evaluation index system based on the development level of the circulation industry, the following basic principles need to be considered: (1) scientific principles. The established indicator system can truly reflect the development of the circulation industry in the region. By analyzing the development level of the circulation industry in Province Y, specific development level indicators can be obtained. (2) System principles. When designing the index system, in terms of the macroeconomic market environment of economic development and the particularity of the development of the circulation industry, not only the specific political, economic, and cultural history but also the region must be investigated in detail. (3) Functional principle. The functions of data collection and data processing need to be fully considered. During the data collection period, the relevant data collected by the questionnaire survey and related service departments are classified as receiving the indicator data of this chapter. In the data processing stage, the index data needs to be arranged in the form of recognizable and executable index data to realize the established index system. (4) The principle of relative independence. It shows that there is often duplication of information among indicators of the development of the circulation industry. Therefore, when selecting indicators, in order to improve the scientificity and accuracy of the evaluation, it is necessary to fully consider the relative independence of the indicators. (5) Target directionality. In order to measure and evaluate the development level of the circulation sector, on the one hand, a detailed analysis of the development of the circulation sector is needed.

3.2. Construction of the Index System. Table 1 shows the indicator system for measuring the development level of the circulation industry. On the one hand, the construction of the indicator system should consider the real situation in Province Y. On the other hand, it is also based on the basic indicators, selecting indicators with regional characteristics for data acquisition, processing, and analysis.

3.3. Model Construction

3.3.1. Empirical Analysis Method. Empirical evaluation of the development level of the circulation industry is a comprehensive, dynamic, and comprehensive process. This article first selects the multiplicative synthesis normalization method. The purpose of this method is to multiply each weight by normalization to obtain the combined weight. The calculation formula is

$$E_j = \begin{cases} \dfrac{\chi_{ij} \cdot \delta_{ij}}{\sum_{i=1}^{n} \chi_{ij} \cdot \delta_{ij}} \end{cases} (j = 1, 2, \cdots, m). \qquad (1)$$

TABLE 1: Index system for measuring the development level of circulation industry.

First-level index	Secondary measure	Index code	Index unit
Circulation scale	Added value of circulation industry	X1	100 million yuan
	The total retail sales of social consumer goods	X2	100 million yuan
	Number of employees in the circulation industry	X3	People
	Cargo transportation turnover	X4	Whole society cargo transportation volume/transport mileage
Circulation structure	Employee ratio in the circulation industry	X5	Number of employees in the circulation industry/number of employees in the tertiary industry
	Retail sales ratio of foreign-funded enterprises in the circulation industry	X6	Retail sales of foreign-funded enterprises above designated size/total retail sales
	Ratio of total retail sales above designated size	X7	Net operating income/ending balance of total assets
	Turnover rate of total assets	X8	Net operating income/ending balance of total assets
Circulation efficiency	Batch to retail ratio of wholesale and retail enterprises above designated size	X9	Wholesale sales/retail sales above designated size
	Profit margin of wholesale and retail income above the limit	X10	Total sales profit/total income of wholesale and retail businesses above designated size
	Economic contribution rate of the circulation industry	X11	Value added of the circulation industry/gross regional product
Circulation contribution	Employment contribution rate of the circulation industry	X12	Employees in the circulation industry/employees in the whole society
	Tax contribution rate of the circulation industry	X13	Total tax revenue of the circulation industry/total tax revenue of the whole society
Circulation innovation	Information management level	X14	Commodity online transaction value/circulation industry added value
	Logistics distribution degree	X15	Increase in commodity transportation/increase in circulation industry

Among them, the subjective weight is χ_{ij}, the objective weight is δ_{ij}, and the equation on the left is the comprehensive weight.

3.3.2. AHP. Then, we use the analytic hierarchy process to quantify the indicators to solve more complex logic and decision-making problems. First, judge the matrix according to the column normalization method:

$$c_{ij} = \begin{cases} c_{ij} \\ \sum_{k=1}^{n} c_{kj} \end{cases} (i, j = 1, 2, \cdots, n). \tag{2}$$

Assign c_{ij} values to the criterion layer.

After normalization by line addition:

$$E_i = \sum_{i=1}^{n} c_{ij} (i, j = 1, 2, \cdots, n). \tag{3}$$

The equation on the left is the weight ratio between two objects.

Normalize the vector:

$$E = [E1, E2, \cdots, En]^T. \tag{4}$$

The largest characteristic root is calculated as:

$$\vartheta_{\max} = \sum_{i=1}^{n} \frac{(BM)_i}{nM_i}, \tag{5}$$

where I is each vector component.

Multiply the rank normalization formula to get objective weight:

$$E_j = \frac{\chi_{ij} \cdot \delta_{ij}}{\sum_{i=1}^{n} \chi_{ij} \cdot \delta_{ij}} (j = 1, 2, \cdots, m). \tag{6}$$

3.3.3. Entropy Method. The entropy method is usually used to determine the objective weight value. Generally, the entropy value is the smaller, the greater the degree of indicator variation and the greater the weight.

Data standardization:

$$Q_{ij} = \frac{Y_{ij}}{\sum_{i=1}^{n} Y_{ij}}. \tag{7}$$

Among them, Y_{ij} refers to the value of the j-th evaluation index in the i-th year, and n is the index value.

Calculate the information entropy of the data:

$$R_j = -\ln{(n)}^{-1} \sum_{i=1}^{n} q_{ij} \ln q_i. \qquad (8)$$

Among them,

$$q_{ij} = \frac{\gamma_{ij}}{\sum_{i=1}^{n} \gamma_{ij}}. \qquad (9)$$

If $q_{ij} = 0$, define

$$\lim q_{ij} \ln q_{ij} = 0. \qquad (10)$$

Calculate the weight value of each indicator:

$$E_i = \frac{1-R_i}{l-\sum R_i} \, (i = 1, 2, \cdots, l). \qquad (11)$$

In the formula, R_{ij} represents the number of evaluation indexes for the jth item in the i-th year.

Composite index:

$$T = \sum_{i=1}^{5} B_i \times Q_i. \qquad (12)$$

In the formula, B_i is the index value, and Q_i is the corresponding index weight. The larger the T value, the higher the development level of the circulation industry. The larger the comprehensive index value, the higher the development level of the circulation industry.

3.4. Data Source and Preprocessing. In order to evaluate the development of the circulation industry of resource-based cities in the economic transformation, this paper selects Y Province as the research sample and organizes statistical data to compare and analyze the promotion and effects brought by the Internet of Things technology. Data is reviewed repeatedly, and empirical analysis is performed after data processing.

4. Role of Internet of Things Technology in Promoting the Circulation Industry in the Transformation of a Resource-Based Economy

4.1. Necessity of Economic Transformation of Resource-Based Cities. Resource-based cities have played an important role in the process of national economic development. However, as the amount of resource extraction increases year by year, cities with resource-based economic development must also face the results of economic transformation. Resource-based industries need to go through the following stages: exploration period-mining period-stable production period-decline period, and then resource-based cities will either face a period of exhaustion and decline, or choose to transform and develop. The same is true for the urban economic development process. After the prosperity period, there will inevitably be a period of recession or transformation and revitalization.

Figure 2 shows the life cycle theory of resource-based cities. Therefore, in summary, if resource-based economic cities want to further promote the development of the city, they must carry out economic transformation. From the perspective of Internet of Things technology, it is feasible and practical to conduct research on the circulation industry.

4.2. Current Status of the Distribution Industry in Province Y. The scale of the circulation industry in Province Y is shown in Figure 3, showing an expanding form. In recent years, with the steady increase in the disposable income of urban and rural residents in Y Province, the consumption demand of residents has continued to expand, and the circulation industry has also developed rapidly. The added value of the circulation industry in Province Y increased from 36.65 billion yuan in 2010 to 108.935 billion yuan in 2016, breaking through the 100 billion mark, with an average annual growth rate of about 19.96%. In 2020, it will develop rapidly, and the circulation industry will increase throughout the year. The value was 193.582 billion yuan, an increase of 7.81% over the previous year. Among them, the total retail sales of consumer goods increased from 338.76 billion to 171.515 billion yuan, with an average annual growth rate of 17.65%; the transportation and postal storage industry increased from 2.885 billion yuan to 21.877 billion yuan, with an average annual growth rate of 22.89%.

It can be seen from Figure 4 that the degree of organization of circulation in Province Y has increased. The added value of the wholesale and retail industry in Province Y has increased from 29.666 billion yuan in 2010 to 139.867 billion yuan in 2020, with an average annual growth rate of 17.17%. At the same time, the number of corporate enterprises above the designated size in the wholesale and retail industry continues to grow. In 2020, the added value of the accommodation and catering industry above the designated size is 4.337 billion yuan, with an average annual growth rate of 20.69%. The growth trend of the commodity trading market of more than 100 million yuan in Province Y is obvious, and the wholesale transaction volume accounts for 82.54% of the total transaction volume. From this, it can be seen that the wholesale of Province Y takes up a large proportion, and the retail terminal needs to continue to develop. At the same time, in order to improve the degree of organization of circulation, the Y provincial government has increased its support for circulation organizations such as circulation cooperative organizations, supply and marketing cooperatives, large agricultural product circulation enterprises, and circulation associations. A total of 46 large agricultural product circulation enterprises and 79 supply and marketing organizations have been built. The professional level of cooperative organizations, circulation
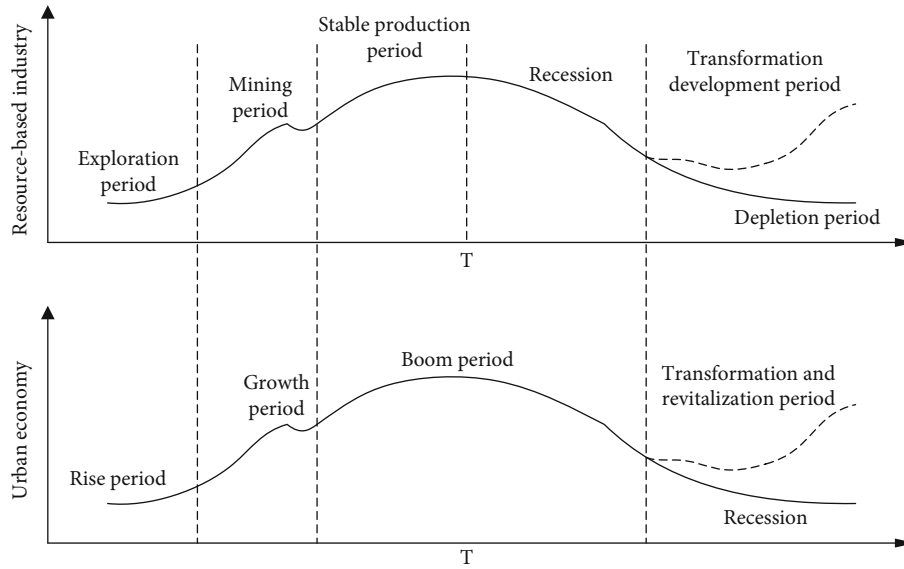
Figure 2: Resource-based city life cycle diagram.
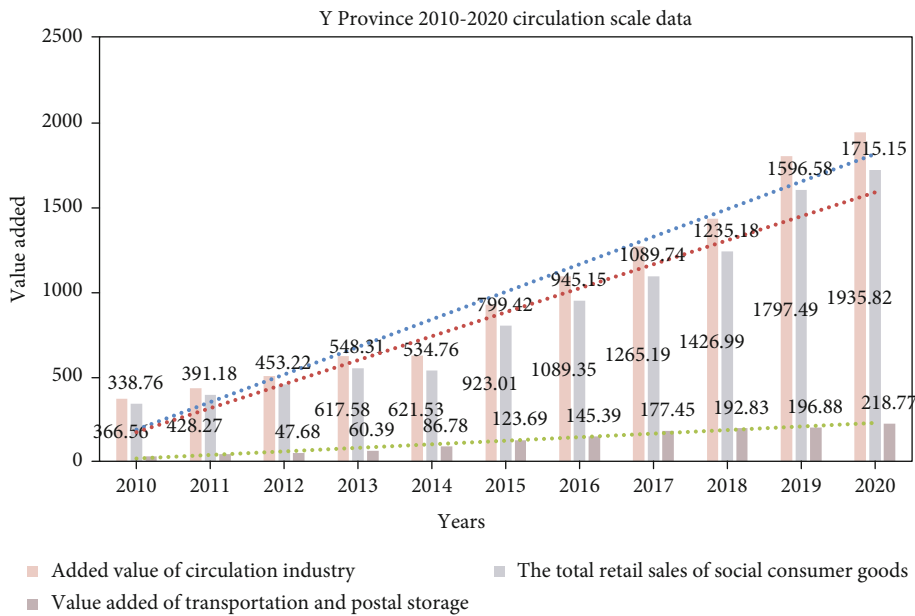
Figure 3: Y Province 2010-2020 circulation scale data.

cooperative organizations, and circulation associations has been continuously strengthened, thus, accelerating the process of circulation organization.

It can be seen from Table 2 that the opening of circulation in Province Y has accelerated, and the development of circulation foreign-funded enterprises has been relatively rapid. Due to the relatively backward economy in Province Y, few local companies can develop and grow independently. In order to promote the development of the circulation industry, the local government actively introduces foreign-funded enterprises with various preferential policies, and the number of foreign-invested circulation enterprises is rapidly increasing. It is specifically embodied in first, the

increase in investment projects and investment amount. According to preliminary statistics from the Hunan Department of Commerce, for the whole year of 2020, the number of newly approved foreign-invested wholesale and retail contract projects in Y Province will exceed 100, and the contractual use of foreign capital will exceed 10 billion. The second is the preemption of circulation formats. 38% of large-scale comprehensive supermarkets and large-scale logistics markets in Y Province are foreign investment. Large-scale foreign investment has accelerated the development of circulation enterprises in Province Y and improved the overall level of the local circulation industry. At the same time, it has also intensified competition in the circulation market.
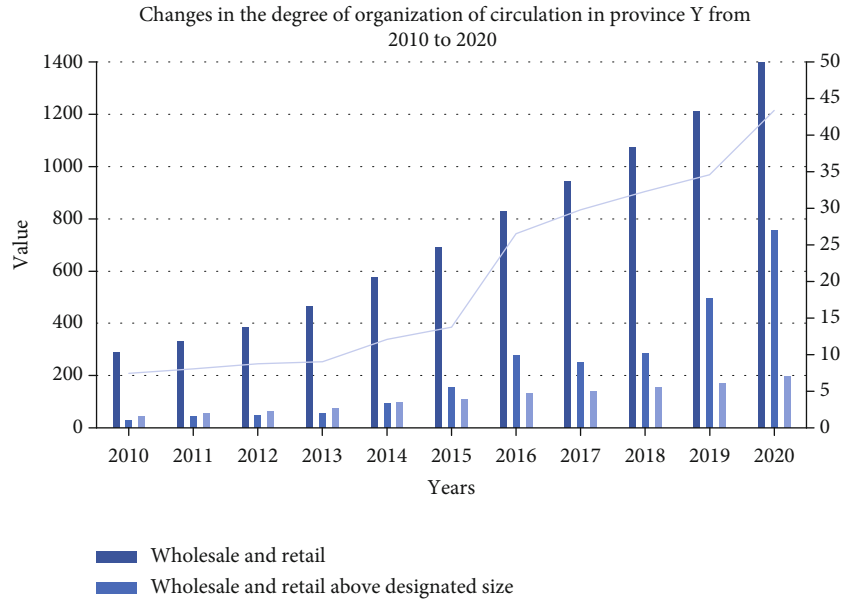
Figure 4: Changes in the degree of organization of circulation in Province Y from 2010 to 2020.

Table 2: New batch of foreign investment sales in wholesale and retail industries.

Years	Foreign-funded enterprises above designated size (units)	Contract items above quota (a)	Foreign investment (100 million yuan)
2010	17	33	105.36
2015	28	66	357.23
2020	43	108	598.51
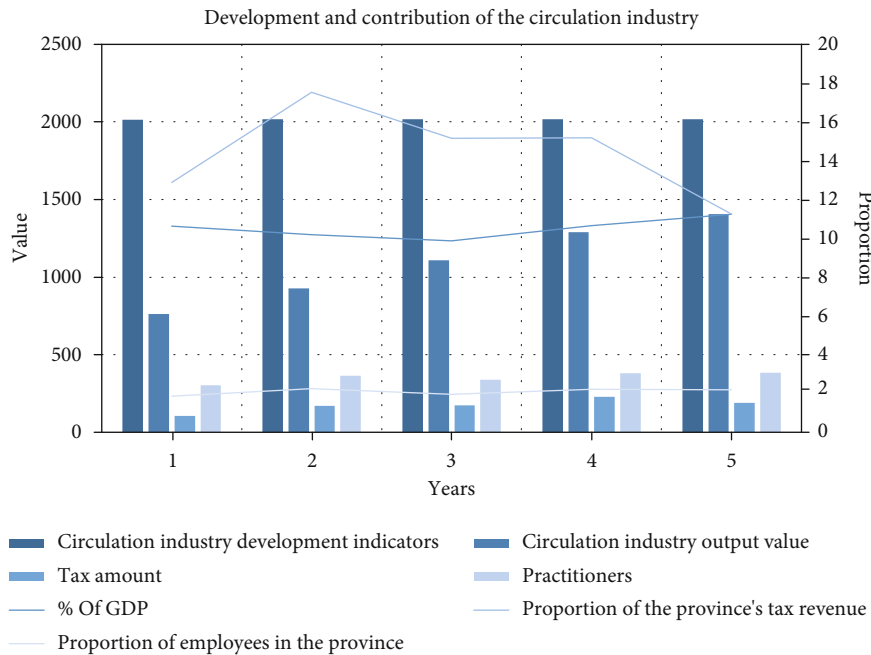
Figure 5: Development and contribution of the circulation industry.

4.3. Role of RFID Technology in Promoting the Circulation Industry in the Transformation of a Resource-Based Economy. The contribution rate of the circulation industry in docking production and consumption, expanding effective demand, and improving people's quality of life is gradually increasing, as shown in Figure 5. In the past five years,
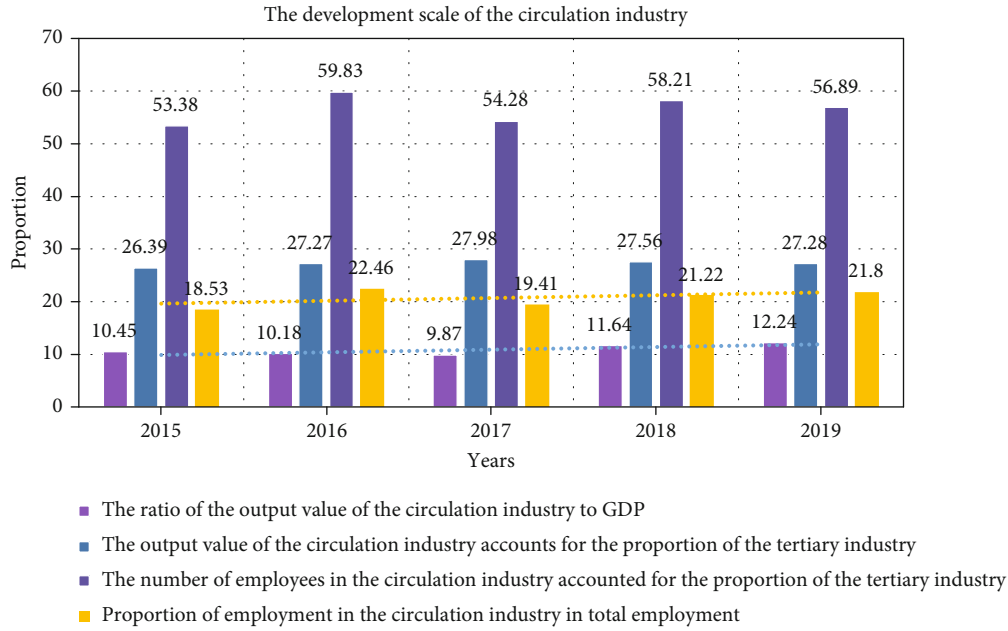
Figure 6: The development scale of the circulation industry.

Table 3: Comprehensive evaluation index data for urbanization.

Area	A	B	C	D	E	F	G
X1	53.56	84.22	59.13	64.11	46.88	55.53	51.19
X2	0.38	0.46	0.51	0.55	0.22	0.29	0.33
X3	53.27	42.56	50.17	53.78	50.73	42.25	58.78
X4	41.85	56.73	48.52	45.59	48.33	59.29	37.48
X5	1194.50	2398.94	958.73	1361.71	4754.11	8931.78	1225.53
X6	0.86	1.27	0.94	0.98	0.86	0.98	0.87
X7	22455.61	24000.42	21429.87	23238.75	22813.15	23249.61	23714.23
X8	21.91	69.87	32.53	38.81	22.26	14.31	12.26

various indicators of the development of the circulation industry have shown a significant growth trend. The output value of the industry has increased from 76.233 billion yuan at the beginning to 140.508 billion yuan in 2019. The tax revenue has doubled, showing the impact on the economy of Province Y. Strong pulling action. In terms of the number of employees, in 2015 it was 3.0299 million, accounting for 1.85% of the province's employment; in 2019, it was 3.846 million, accounting for 2.08% of the province's employment. The overall trend is increasing, highlighting the employment absorption of the circulation industry. "Reservoir" functions. Although the output value of the circulation industry has grown rapidly, the share of the circulation industry in GDP has not risen significantly. After 2015, the output value of the circulation industry accounted for about 27% of the tertiary industry, indicating that the circulation industry in Province Y has strong stability, but insufficient growth momentum, it is necessary to find growth points that promote the sustainable development of the circulation industry.

In Figure 6, from the analysis of the proportion of the output value of the circulation industry in the tertiary indus-

try and GDP, it can be concluded that the proportion has been increasing, but the growth rate of each year has not changed much. From the analysis of the proportion of employment in the circulation industry, the number of employees is increasing, and the proportion has gradually increased, from 54.37% and 19.52% in 2015 to 57.88% and 21.80% in 2019. This shows that the circulation industry in Y Province is the main channel to absorb social employment.

Table 3 shows the evaluation of the eight urbanization indicators in the A-G area. It can be seen from the table that with the support of Internet of Things technology, the circulation industry in the resource-based economic transformation of Province Y has not only obtained good economic benefits but also promoted the improvement of the level of urbanization in the region and increased. The per capita income of residents has expanded the number of employees in the circulation industry.

It can be seen from Figure 7 that, first, from the perspective of the share component of Y Province, the share component of the tertiary industry is involved in the study, so all sectors are growth sectors. It shows that the overall
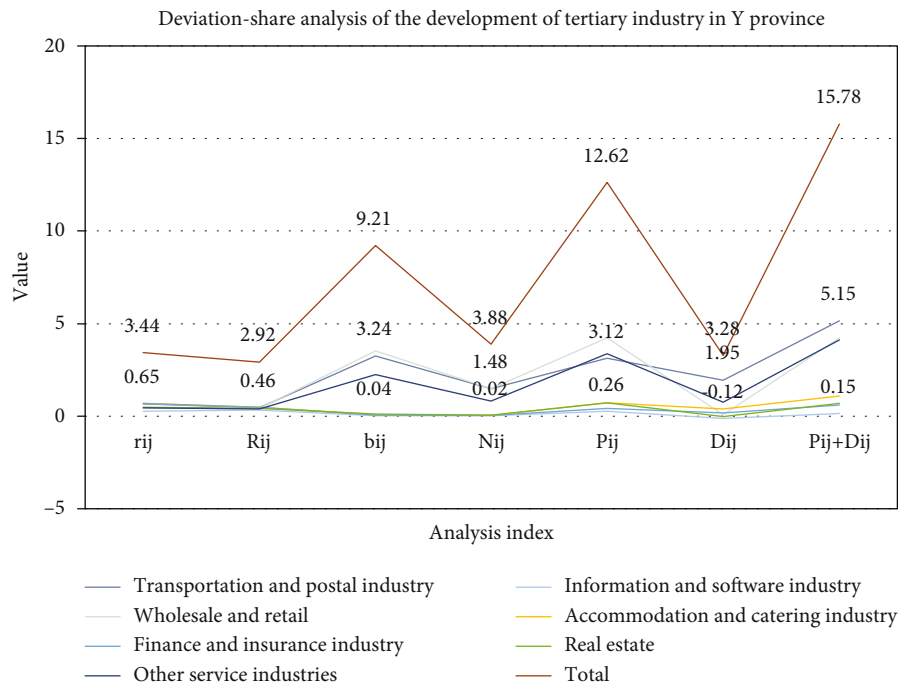
Figure 7: Deviation-share analysis of the development of tertiary industry in Y Province.

development speed of the tertiary industry in Y Province is higher than the average level, and the output value of the tertiary industry in Y Province has increased by 158 million yuan due to the advantage of share weight. Second, from the perspective of structural deviation, the value of the tertiary industry in Y Province is greater than the average level, of which wholesale and retail industries account for the largest proportion, followed by other service industries, transportation and postal industries, accommodation and catering industries, and real estate industries., Finance and insurance, information and software industries, indicating that these sectors have a good production base, and the existing economic structure has a greater contribution to the total economic volume.

5. Conclusion

This article mainly studies the role of Internet of Things technology in promoting the circulation industry in the transformation of a resource-based economy. The traditional circulation industry has problems such as lagging development in scale, low degree of organization, few modern circulation formats, and low degree of informatization. Most of the resource-based cities have relatively backward infrastructure and it is difficult to solve these problems. However, the RFID technology and infinite sensor technology in the Internet of Things can solve the above problems well and have a good promotion effect in terms of circulation scale, circulation structure, efficiency, contribution, etc., and can fundamentally improve the efficiency of the circulation industry and information accuracy. The research in this article is based on a combination of theoretical research and empirical research and a combination of qual-

itative research and quantitative research. The disadvantage of this article is that there are still limitations in the selection of resource-based cities, and the representativeness is not strong. However, the experimental results of this article have certain reference and reference for other resource-based cities to prepare for economic transformation.

Data Availability

The data that support the findings of this study are available from the corresponding author upon reasonable request.

Conflicts of Interest

The authors declare that they have no conflicts of interest.

References

[1] Q. Zhang, L. G. Zheng, H. Liu, and H. Cheng, "Analysis on the coordinated development of ecology-economy-society in coal resource cities: a case study of Huainan, China," *The journal of applied ecology*, vol. 30, no. 12, pp. 4313–4322, 2019.

[2] H. Yongshi and X. Mingxing, "The impact of circulation industry on regional economic growth: an empirical study on Fujian Province," *Beijing Jiaotong Daxue Xuebao/journal of Beijing Jiaotong University*, vol. 14, no. 2, pp. 92–100, 2019.

[3] J. Ni, K. Zhang, X. Lin, and X. Shen, "Securing fog computing for internet of things applications: challenges and solutions," *IEEE Communications Surveys & Tutorials*, vol. 20, no. 1, pp. 601–628, 2018.

[4] Y. Kikuchi, M. Nakai, Y. Kanematsu et al., "Application of technology assessments to co-learning for regional transformation: a case study of biomass energy systems in

Tanegashima," *Sustainability Science*, vol. 15, no. 5, pp. 1473–1494, 2020.

[5] Q. Xu, "Sharing Economy: a new economic revolution to step into an era of ecological civilization," *Contemporary social sciences*, vol. 10, no. 2, pp. 17–52, 2018.

[6] M. Song, X. Zhao, Y. Shang, and B. Chen, "Realization of green transition based on the anti-driving mechanism: an analysis of environmental regulation from the perspective of resource dependence in China," *The Science of the Total Environment*, vol. 698, p. 134317, 2020.

[7] A. Abadías Llamas, N. J. Bartie, M. Heibeck, M. Stelter, and M. A. Reuter, "Simulation-based exergy analysis of large circular economy systems: zinc production coupled to CdTe photovoltaic module life cycle," *Journal of Sustainable Metallurgy*, vol. 6, no. 1, pp. 34–67, 2020.

[8] A. Sarkar and P. Chouhan, "Dynamic simulation of urban expansion based on cellular automata and Markov chain model: a case study in Siliguri Metropolitan Area, West Bengal," *Modeling Earth Systems and Environment*, vol. 5, no. 4, pp. 1723–1732, 2019.

[9] C. Zhuo and F. Deng, "How does China's Western Development Strategy affect regional green economic efficiency?," *The Science of the Total Environment*, vol. 707, p. 135939, 2020.

[10] B. Y. Sun and X. H. Yang, "The input and output relationship of water resource in Jilin from 2004 to 2017," *Thermal Science*, vol. 24, no. 4, pp. 2337–2345, 2020.

[11] S. Kivel, "Political geographies of health care: governmentality of population health in the constitution and transformation of state spatiality," *Nordia Geographical Publications*, vol. 47, no. 2, pp. 1–102, 2018.

[12] L. A. Seybert, S. C. Nelson, and P. J. Katzenstein, "Protean Power," in *Slumdog Versus Superman: Uncertainty, Innovation, and the Circulation of Power in the Global Film Industry*, Cambridge University Press, 2018.

[13] D. Perez-Estevez, J. Doval-Gandoy, and J. M. Guerrero, "AC-voltage harmonic control for stand-alone and weak-grid-tied converter," *IEEE Transactions on Industry Applications*, vol. 56, no. 1, pp. 403–421, 2020.

[14] S. J. Greene, R. J. Mentz, M. Fiuzat et al., "Reassessing the role of surrogate end points in drug development for heart failure," *Circulation*, vol. 138, no. 10, pp. 1039–1053, 2018.

[15] J. H. Pikul and H. Ning, "Powering the internet of things," *Joule*, vol. 2, no. 6, pp. 1036–1038, 2018.

[16] M. Chernyshev, S. Zeadally, Z. Baig, and A. Woodward, "Internet of things forensics: the need, process models, and open issues," *IT Professional*, vol. 20, no. 3, pp. 40–49, 2018.

[17] T. Qiu, R. Qiao, and D. O. Wu, "EABS: an event-aware backpressure scheduling scheme for emergency internet of things," *IEEE Transactions on Mobile Computing*, vol. 17, no. 1, pp. 72–84, 2018.

[18] H. Li, K. Ota, and M. Dong, "Learning IoT in edge: deep learning for the internet of things with edge computing," *IEEE Network*, vol. 32, no. 1, pp. 96–101, 2018.

[19] L. Hu, H. Wen, B. Wu et al., "Cooperative jamming for physical layer security enhancement in internet of things," *IEEE Internet of Things Journal*, vol. 5, no. 1, pp. 219–228, 2018.

[20] N. Ansari and X. Sun, "Mobile edge computing empowers internet of things," *IEICE Transactions on Communications*, vol. 101, no. 3, pp. 604–619, 2018.

[21] G. Yang, Q. Zhang, and Y. C. Liang, "Cooperative ambient backscatter communications for green internet-of-things," *IEEE Internet of Things Journal*, vol. 5, no. 2, pp. 1116–1130, 2018.

[22] R. Ranjan, O. Rana, S. Nepal et al., "The Next Grand Challenges: Integrating the Internet of Things and Data Science," *IEEE Cloud Computing*, vol. 5, no. 3, pp. 12–26, 2018.

[23] T. Listyorini and R. Rahim, "A prototype fire detection implemented using the internet of things and fuzzy logic," *World Transactions on Engineering and Technology Education*, vol. 16, no. 1, pp. 42–46, 2018.

[24] H. F. Atlam, A. Alenezi, R. K. Hussein et al., "Validation of an adaptive risk-based access control model for the internet of things," *International Journal of Computer Network and Information Security*, vol. 1, no. 1, pp. 26–35, 2018.

[25] M. Papert and A. Pflaum, "Development of an ecosystem model for the realization of internet of things (IoT) services in supply chain management," *Electronic Markets*, vol. 27, no. 3, pp. 1–15, 2018.

[26] L. Yin, W. Pan, J. Kuang, and M. Zhuang, "Application of bootstrap-DEA with fuzzy computing in performance evaluation of forklift leasing supplier," *in IEEE Access*, 2019.

[27] "Energy efficiency optimization with SWIPT in MIMO broadcast channels for internet of things," *IEEE Internet of Things Journal*, vol. 99, p. 1, 2018.

[28] Z. Cui, Y. Cao, X. Cai et al., "Optimal LEACH protocol with modified bat algorithm for big data sensing systems in internet of things," *Journal of Parallel and Distributed Computing*, vol. 132, pp. 217–229, 2018.

[29] J. Chen, X. Wang, and Z. Chu, "Capacity sharing, product differentiation and welfare," *Economic Research-Ekonomska Istraživanja*, vol. 33, no. 1, pp. 107–123, 2020.

[30] W. Wu, S. An, C. H. Wu, S. B. Tsai, and K. Yang, "An empirical study on green environmental system certification affects financing cost of high energy consumption enterprises-taking metallurgical enterprises as an example," *Journal of Cleaner Production*, vol. 2020, 2020.

Research Article

Design and Implementation of 3D Film and Television Scene Production Algorithm Based on the Internet of Things

Ruiying Kuang

Xiangtan University, Xiangtan, 411105 Hunan, China

Correspondence should be addressed to Ruiying Kuang; kuangruiying@xtu.edu.cn

Film and television itself is a product of culture and innovation, combining digital technology, creative thinking, and artistic design. In the rapid development of 3D film and television, the situation of scene design and production has also become an important role. In a typical environment, the main scene plays the role of film and television and coherent plot. This thesis mainly analyzes the design and implementation of a 3D movie scene production algorithm based on the Internet of Things and also makes 3D movie scenes through the algorithm of Internet of Things technology. This article also analyzes the traditional 3D scene-making algorithm, which is mainly composed of a plane mapping part, a basic primitive generation part, a collision detection and positioning part, and a terrain generation part. Among them, the plane mapping technology provides the function of using plane mapping to simulate 3D objects. The basic primitive generation part uses the OpenGl function to draw 3D primitives and paste the BMP format image on each surface of the stereo primitives, so that the 3D model can be represented by a plane texture; collision detection is a key part of mechanical physics, which can detect games of the physical edge of the object in the middle; the terrain generation part uses the converted gray height value as the corresponding grid terrain height and uses planar mapping technology to capture the image of the entire terrain, that is, paste and generate a terrain map. The results show that a characteristic of the algorithm of the Internet of Things technology is that the 3D scene is completely mapped. This avoids the trouble of using 3DMAX and other tools to create 3D models and also reduces the difficulty of creating 3D scenes and makes the execution efficient, which is better than directly importing 3D models, runs faster, and runs very smoothly. The Internet of Things is an important development trend in the Internet information age and can be used to produce 3D film and television scenes to reduce development difficulty and cost and has a variety of research and development value and practical value. In the analysis part, this article also introduces the algorithms used in the scene production and passes the tests of 4 different files in 4 different frames and also found that more than 83% of people feel that the use of Internet of Things algorithms in the production of 3D movie scenes has improved production efficiency.

1. Introduction

1.1. Background of Topic Selection. In recent years, China's digital technology and Internet multimedia technology have developed rapidly, and the shooting, production, and transmission of 3D film and television have achieved unprecedented progress and results. Among them, the combination of digital technology and traditional art design challenged many ways of expressing traditional art design and gradually formed a new form of art creation, namely, traditional digital art. In the production of 3D film and television scenes, it has a wide range of application prospects and strong development momentum. From the perspective of the architec-

tural design of the main 3D film and television scenes we studied, with the rapid development of the domestic film and television industry, the concept of the Internet of Things has become more and more important and irreplaceable. The creation of 3D film and television in my country is still in its infancy. In terms of film and television scene design, China still has room for further research on the artistic features and technical methods of the main scene design.

1.2. Significance of the Research. 3D film and television scenes are usually the second visual level of the works on the screen, because they are the settings of character performances and fictional spaces. Successful 3D movies need

good scenes to improve their artistic quality. Therefore, the design of the scene requires both high aesthetics and strict rationality. A good main scene structure and design can enhance the beauty of the film and television, enhance the personality of the character, and improve the emotional resonance with the audience. Appropriate design of the main scene can also establish the style of the entire film and television production. Therefore, in 3D film and television, the main scene must be the main "character" that explains the storyline. This shows the importance of scene production. The scene produced by the Internet of Things algorithm can achieve low development difficulty, low cost, safety, and reliability and has a variety of research and development value and practical value.

1.3. Related Work of 3D Film and Television Scene Production. With the continuous development of the Internet of Things technology, we should calm down while creating, sum up the experience of previous production, and study its theories, so that the production of 3D animation scenes can be more systematic, and the creation and appreciation issues can be closely linked, so that technology and art can be more perfectly combined. Pikul and Ning said that all history is modern history. It can be said that all historical dramas are modern film and television, and the success of historical dramas lies in the modernization of historical themes and historical culture [1]. In this sense, as the indoor scene design of the place for characters in film and television, the traditional indoor design style in historical drama should be guided by the aesthetic value of modern people. And the essence of traditional national culture should be used in modern design technology. Showing it make the past serve the present and develop innovatively. However, the view that history is all modern history is wrong. Yang et al. believe that making film and television is a very complicated process. This is a labor-intensive process that requires a team to complete, which is the crystallization of collective wisdom [2]. There are many ways to make movies, such as handmade movies and cut-out methods. However, through the Internet of Things technology, the production of film and television scenes can be very simple, safe, reliable, and efficient. Liu et al. believe that another important reason for studying 3D movie scenes is its wide application in live action movies [3]. In current movies and TV movies, more and more digital technologies are used to create various virtual scenes and special effects to produce movies and TV images. This effect can achieve visual effects, which is impossible to achieve in actual shooting. However, the actual shooting can be done through the Internet of Things technology.

1.4. Innovation Points of This Research

(1) 3D film and television scene production adopts the algorithm of Internet of Things technology, which can make the scene production process very intelligent, safe, and reliable

(2) Compared with traditional algorithms, the algorithm of the Internet of Things technology is more intelligent, convenient, safe, and reliable

2. Design and Implementation Method of 3D Film and Television Scene Production Algorithm Based on the Internet of Things

2.1. IoT Architecture. Internet of Things applications are widely used, but because applications cover different industries and different scenarios, they have different functions and structural characteristics [4]. Currently, there is no uniformly recognized standard for the structure of IoT applications [5]. Experts, technicians, and production personnel usually accept the "three-tier structure" of IoT applications [6]. This structure divides the Internet of Things application into three layers, which are the application layer, the network layer, and the perception layer. The "three-layer structure" of the Internet of Things application is shown in Figure 1.

2.2. Concept of Scenes in Film and Television. Film and television scenes are usually specific environmental spaces that can tell stories, shape characters, expand the plot, and promote the development of film and television [7]. In addition to modeling characters in film and television, it usually refers to scenes in film and television. Modeling design of all things changes over time, including living environment, furniture, social environment, natural environment, and historical environment where the role is located [8]. Stage design requires a high degree of creativity and strong artistry. The movie scene can be divided into two parts: scene and background. The so-called scene is the active scene or natural landscape that the character can pass through, and the background is the scene behind the character and the atmosphere, such as the scene. To display each lens image, there must be a scene [9]. It is impossible for the character to appear in every frame of the cartoon, but the scene always occupies the main screen or the auxiliary screen. Animated films and TV scenes are usually based on scripts at the beginning of design, providing background design to develop plot and character creation space [10]. The content of the scene is very extensive, as long as there are various entities in the space related to the object, from minor characters to fixed or uncorrected scenes; they are all called scenes [11].

2.3. Style of the 3D Scene. The content determines the format. The title, content, and theme of the script and the aesthetic inclination of the creator determine the style of the scene.

2.3.1. Realistic Style. Realism is a relatively true reflection of time and space, and a faithful recording and reproduction of objective reality. In traditional two-dimensional animation or three-dimensional animation, realistic style scenes are the most common scene styles, which refer to the use of design methods from modeling styles, natural materials, viewing angles, light and shadow relationships, color laws, etc. In terms of processing, it follows the basic historical nature and natural laws, conforms to the physical characteristics of objects at a certain time, specific environment, and specific light conditions, and conforms to human traditional
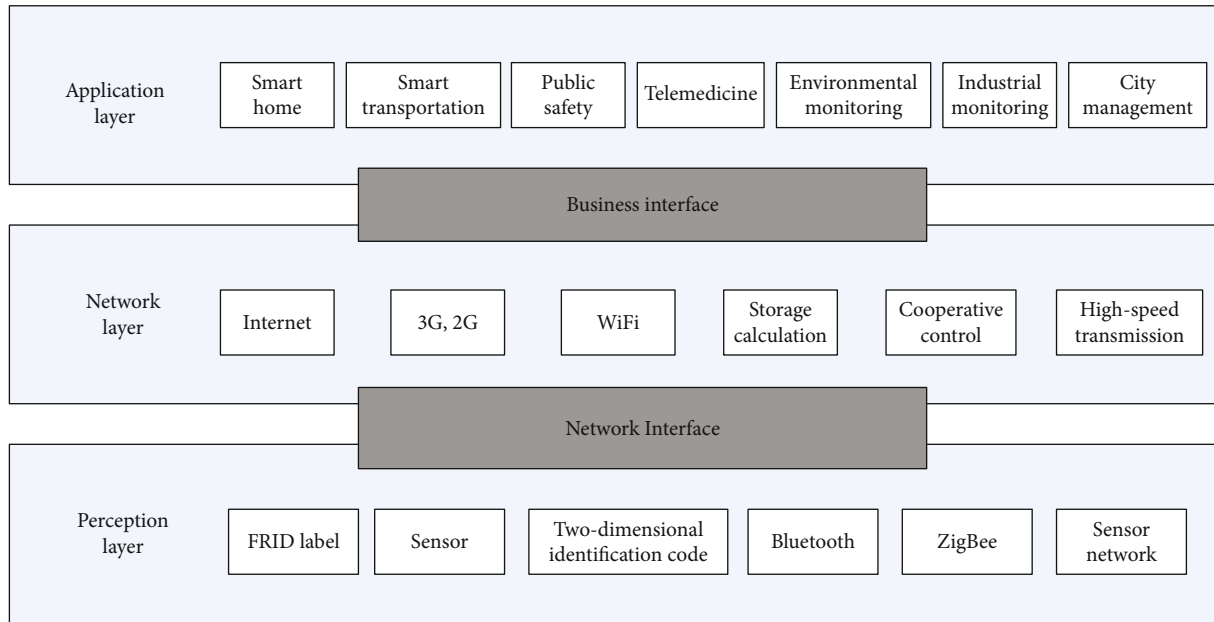
FIGURE 1: Secure Internet of Things architecture.

psychological and physiological habits [12]. 3D animation scenes have a strong sense of reality and serve the appreciation habits of audiences of all ages. It not only has a real sense of light but also a real texture. The rich images make people feel excited [13].

2.3.2. Decorative Style. Any artistic style with regularity and order can be called a decorative style. The decoration style has regular beauty, order beauty, universal beauty, and formal beauty. This style is to carry out a specific artistic and organic generalization, standardization, and processing of a large number of natural shapes and complex colors of the original life form in order to realize the beauty of form [14].

2.3.3. Comic Style. Comic style is also a commonly used modeling form in 3D animation scene design. Comic books and TV animation works are usually adapted from comics, and their modeling usually shows universality, simplicity, and exaggeration [15].

2.3.4. Fantasy Style. Fantasy refers to unreality, unconventional vision and imagination, unconventional thoughts and fantasy that exceed people's daily life, and conventional vision and imagination. According to the needs of the plot, most fantasy-style movies and TV shows use unconventional imagination in the scenes and props, adopt bold and exaggerated methods, and adopt new, bold, and transcending human psychology when using colors [16]. Selective color processing provides viewers with a brand-new visual experience and produces powerful emotional and peculiar effects in people's vision and psychology, while the space-time effects have an illusion that surpasses the conventional human imagination.

2.4. Scene Design Ideas. The stage design of a movie must first closely follow the script, understand the director's expression style and intentions, and conform to the histori-

cal background of the story. Secondly, when designing movie scenes, we must also ensure the unity of film art style, that is, the unity of tones between the scene and the characters, as well as the unity of consciousness and technology of the creative team [17]. The design of movie scenes requires a rich imagination, a process of thinking and creativity. Collect data during the design process, reprocess and recreate materials with the help of imagination, and create new designs. Imagination mainly uses collective thinking and comprehensive thinking such as similarity, correlation, and contrast [18]. Combinatorial thinking is mainly to combine unrelated things or certain parts of things to form a new way of thinking. Combinatorial thinking is the most common method of designing scenes and drawing characters in film and television.

2.5. Key Technologies of the Internet of Things

2.5.1. Radio Frequency Identification Technology. Radio frequency identification technology is a noncontact automatic identification system that can automatically detect targets and receive related data through radio frequency signals. The system mainly includes electronic tags, readers, and computer networks [19]. An electronic tag is composed of a chip and an antenna and is mainly associated with an object used to identify it. The electronic tag has a unique electronic code for storing related object information.

2.5.2. Global Positioning System. The Global Positioning System is a technical application that combines satellites and communications. GPS is not affected by weather and time and can quickly and accurately obtain 3D position, speed, and time information of an object and has the characteristics of high precision, high efficiency, and automation [20]. GPS is an integral part of the Internet of Things system.
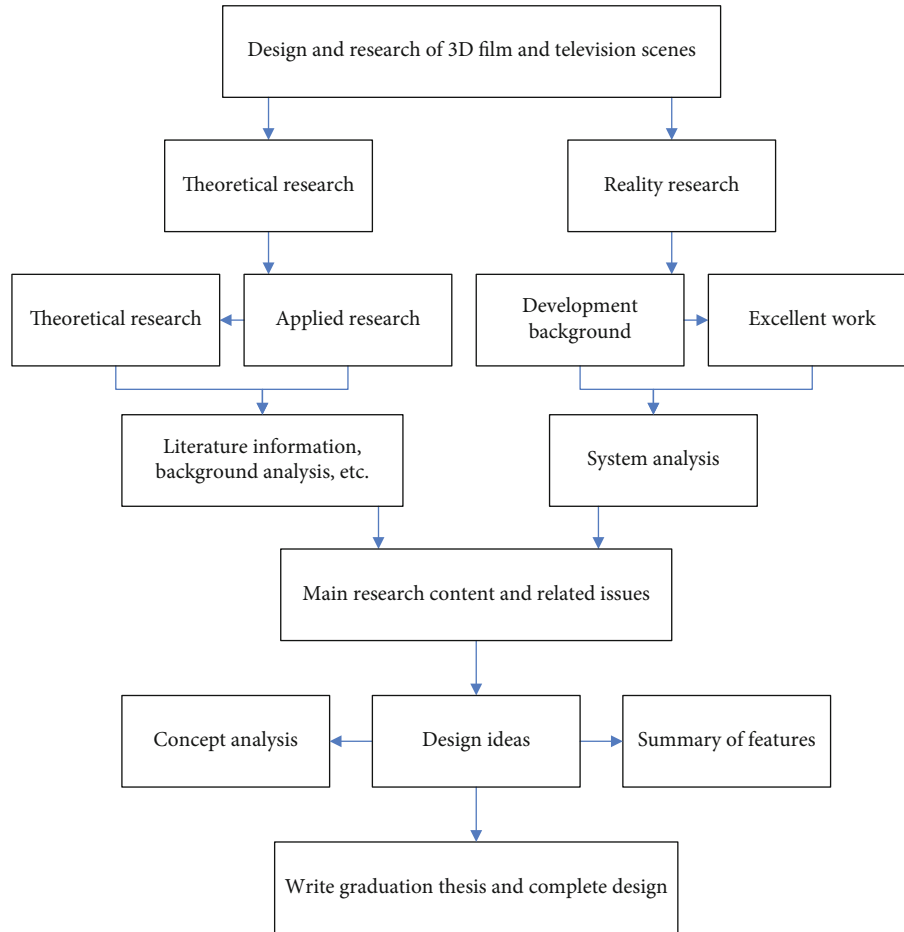
Figure 2: Design flow chart.

2.5.3. Data Analysis and Processing Technology. At the architecture level of the Internet of Things, the type and amount of information sent from the perception layer to the application layer are gradually increasing, doubling the amount of data that needs to be processed and analyzed. For the Internet of Things, how to effectively mine, classify, and apply a large amount of information is a difficult problem. Data analysis and processing functions are the key to the effective application of the Internet of Things, and the emergence of cloud computing makes these possibilities possible [21]. Cloud computing can process hundreds or billions of information in a few seconds. It provides a quick way to process large amounts of information collected from IoT systems.

2.6. Overview of the Design of the Scene. Through the generation of 3D movie scenes, users will feel the visual experience brought by movie scenes, understand the importance of the main scene in creating movies, and be familiar with movie scenes and the art theory of creating the main scene and the main scene. Exploring how to create a scene, 3D technology has improved the audience's awareness of the film and television scene and allowed them to experience the artistry of the scene itself [19].

The following is the flow chart of the thesis design, researches the relevant background under the premise of multianalysis, and completes the thesis according to the rules of scene art construction. The design flow chart of the scene is shown in Figure 2.

2.7. Description of Traditional 3D Scene-Making Algorithm

2.7.1. Plane Texture Part. Usually, landscapes such as stones, trees, and grass are added to the 3D scene. This is a real 3D object used to give it a 3D feel when viewed in the scene. In order to make the imported objects look 3D rather than flat, you can create a scene with a flat map and then replace the 3D scene with a flat map to ensure that the front of the flat map always faces the player's field [20]. This ensures that no matter what the player is doing, the front of the scene always faces the player's field of vision. This rotating plane mapping technology provides the function of using plane mapping to simulate 3D objects.

2.7.2. Basic Graphic Element Production Part. When creating a 3D scene, importing the model created in 3D MAX will greatly reduce the speed of the game. Therefore, consider another way to add a model created using basic primitives. Therefore, the 3D scene is decomposed into basic primitives, such as cuboid and triangular vertebrae. When creating primitives, use the OpenGl function to draw 3D primitives

and paste the BMP format image on each surface of the stereo primitives so that the 3D model can be represented by a plane texture [22].

2.7.3. Collision Detection and Positioning Part. Collision detection is a key part of mechanical physics, which can detect the physical edges of objects in the game. If two 3D objects collide, this technique prevents the objects from passing through each other. This ensures that when an entity hits a wall, collision detection determines its position and interaction so that the entity does not pass through the wall or hit the wall. The solid and the wall are based on two features [23]. When creating 3D basic primitives to simulate the real world and prevent characters from roaming in the game, collision detection is added to each primitive. Create a graphic element and add a check box of appropriate size to this graphic element. When using primitives to build large 3D scenes, collision detection is not difficult because it adds collision detection to the basic primitives.

2.7.4. Terrain Generation Part. The terrain generation part uses contour line generation technology. In the first step, use white to represent the high position and black to represent the low position. In this way, you can use the grayscale map to display the terrain. The second step is to convert the black and white of the grayscale image into a terrain height value. The third step is to split the entire scene map into a grid map, use the converted gray height value as the corresponding grid terrain height, and use planar mapping technology to capture the image of the entire terrain, that is, paste and generate the terrain map.

2.8. Functions of 3D Film and Television Scene Design. The functions of 3D film and television scene design are embodied in the following three aspects.

2.8.1. Set the Emotional Tone of the Work. In 3D film and television, scene design needs to provide ideas expressed in work. Designers should start from the overall picture, grasp the theme of the entire film and television, and make a keen observation of life. Make adjustments and designs to use the completed experience. Bright colors are used as the main tone for creating interesting and relaxing rhythms; warm colors are used to create a warm and peaceful atmosphere; gray is used to express painful and depressed emotions and to understand the unique lifestyle, the creation of true touches and the establishment of the emotional tone of the work.

2.8.2. Character Characteristics. Characters and scenes are interdependent in 3D movies and TV. The design of the scene must be logically structured in order to provide space for performance and mental activity for the characters and through suggestive and symbolic arrangements to shape the character of the character. Creators can enhance the image of characters in film and television by making the audience feel the setting of the psychological space of the scene and infer the characters' interests, hobbies, lifestyle, and other personalities and make them more vivid and rich. 3D film and television scene design can easily identify the

identity, psychology, and personality of the character and achieve the goal, usually focusing on the characteristics. It is the most obvious sky, landscape, architecture, flower, and tree style in history. Rely on the landscape to provide the owner, and borrow the landscape to express emotions.

2.8.3. The Development of the Storyline. Scene design serves the plot of the story, and the development of 3D film and television is inseparable from the interpretation of the plot. The design of the activity space and the role scene must be based on the narrative and accurately describe the environmental characteristics of the story. Show the background and local style, combine the narrative function and the metaphor function, and establish the space-time relationship. By changing the scene factors (such as time, location, and environment), the design provides suitable opportunities for role-playing. The scene factors are suitable not only for the theme but also for the dramatic style that promotes the development of the story.

2.9. Performance Analysis of Algorithm Production. The principle of performance analysis of algorithm production based on the Internet of Things is shown in Figure 3. Data security requirements are the key integration of the entire algorithm; all selected data structures must require data reliability and stability and be able to maintain a stable working condition for a long time. Typical time requirements are mainly to limit the waiting time for information query. If the client sends a query request, the corresponding performance of the server is extremely slow, and it is impossible to quickly find a query that meets the requirements. The operating efficiency of the system will be very low.

3. Experiments Based on the Design and Implementation of the 3D Film and Television Scene Production Algorithm of the Internet of Things

3.1. Production of the 3D Scene of "Fantasy Variations." By studying the artistic rules of the main stages of fantasy style, this chapter focuses on the process of completing the scene production. It is mainly divided into two processes: one is to make models of mountains, castles, and trees, and the other is to use tents to roam and switch between seasons. Modeling and virtual tour development are inseparable from software support. The main software used in this theme is 3D modeling software and image editing software. Combining the functions of this theme, the specific production process is shown in Figure 4.

3.2. Internet of Things Algorithms. In terms of Internet of Things technology, in order to ensure the security of the Internet of Things system, we need to further improve the data encryption of the terminals in the system. On the basis of existing algorithms, the focus will be on whether the Internet of Things is suitable for embedded systems and whether it is more effective. The security encryption algorithm that can be applied to the Internet of Things environment will be researched and tested.
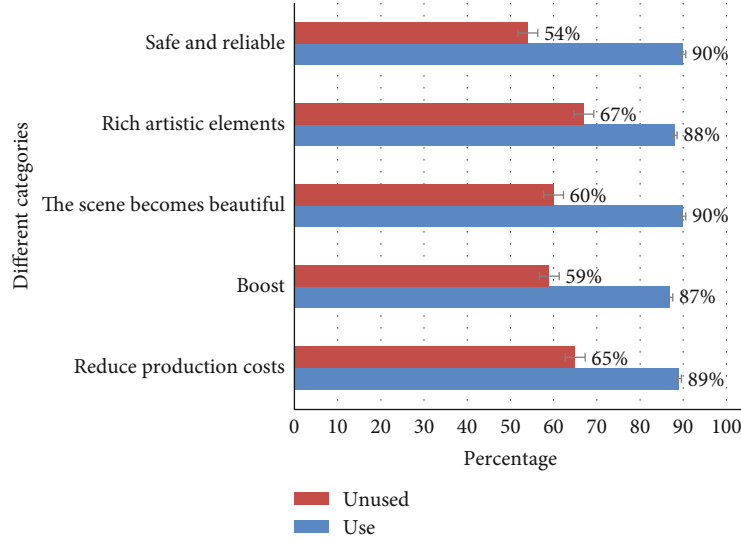
FIGURE 3: Is there an analysis of film and television scenes made using IoT algorithms.

The Advanced Encryption Standard algorithm is a symmetric, block encryption algorithm; the algorithm uses a multiround replacement mode.

(1) Arrange the plaintext and the key into the state matrix with 128 bits in units of words

$$\{H_{0,0}, H_{0,1}, H_{0,2}, H_{0,3}, \cdots, H_{3,3}\},$$
$$\{G_{0,0}, G_{0,1}, G_{0,2}, G_{0,3}, \cdots, G_{3,3}\} \tag{1}$$

(2) XOR the key and ciphertext as shown in

$$\begin{bmatrix} H_{0,0} & H_{0,1} & H_{0,2} & H_{0,3} \\ H_{1,0} & H_{1,1} & H_{1,2} & H_{1,3} \\ H_{2,0} & H_{2,1} & H_{2,2} & H_{2,3} \\ H_{3,0} & H_{3,1} & H_{3,2} & H_{3,3} \end{bmatrix} \oplus \begin{bmatrix} G_0 & G_4 & G_8 & G_{12} \\ G_1 & G_5 & G_9 & G_{13} \\ G_2 & G_6 & G_{10} & G_{14} \\ G_3 & G_7 & G_{11} & G_{15} \end{bmatrix}$$
$$= \begin{bmatrix} H'_{0,0} & H'_{0,1} & H'_{0,2} & H'_{0,3} \\ H'_{1,0} & H'_{1,1} & H'_{1,2} & H'_{1,3} \\ H'_{2,0} & H'_{2,1} & H'_{2,2} & H'_{2,3} \\ H'_{3,0} & H'_{3,1} & H'_{3,2} & H'_{3,3} \end{bmatrix} \tag{2}$$

(3) H-box byte transformation, including multiplication inverse and radiation process

In order to improve the efficiency of the algorithm, the creator of the AES algorithm made the H-box through a nonlinear algorithm. The user can quickly obtain the corre-sponding replacement data by using the table look-up method to improve the calculation speed. The H-box operation is shown in

$$\begin{bmatrix} H_0 \\ H_1 \\ H_2 \\ H_3 \\ H_4 \\ H_5 \\ H_6 \\ H_7 \end{bmatrix} = \begin{bmatrix} 1 & 0 & 0 & 0 & 1 & 1 & 1 & 1 \\ 1 & 1 & 0 & 0 & 0 & 1 & 1 & 1 \\ 1 & 1 & 1 & 0 & 0 & 0 & 1 & 1 \\ 1 & 1 & 1 & 1 & 0 & 0 & 0 & 1 \\ 1 & 1 & 1 & 1 & 1 & 0 & 0 & 0 \\ 0 & 1 & 1 & 1 & 1 & 1 & 0 & 0 \\ 0 & 0 & 1 & 1 & 1 & 1 & 1 & 0 \\ 0 & 0 & 0 & 1 & 1 & 1 & 1 & 1 \end{bmatrix} \begin{bmatrix} H'_0 \\ H'_1 \\ H'_2 \\ H'_3 \\ H'_4 \\ H'_5 \\ H'_6 \\ H'_7 \end{bmatrix} + \begin{bmatrix} 1 \\ 1 \\ 0 \\ 0 \\ 0 \\ 1 \\ 1 \\ 0 \end{bmatrix} \tag{3}$$

(4) Column transformation: multiply each column of the state matrix by a fixed polynomial $f(y)$. Because of the AES algorithm, mod $(y^4 + 1)$ modulus transformation is performed. The definition of $f(y)$ is shown in

$$f(y) = 03y^2 + 01y + 02 \tag{4}$$

The inverse column transformation multiplies each column of the state matrix by the polynomial $g(y)$ to perform mod $(y^4 + 1)$ modular transformation. The definition of $g(y)$ is shown in

$$g(y) = oBy^3 + 0Dy^2 + 09y + 0E. \tag{5}$$

The column transformation has the characteristics of

$$g(y) = f^{-1}(y) \bmod (y^4 + 1). \tag{6}$$
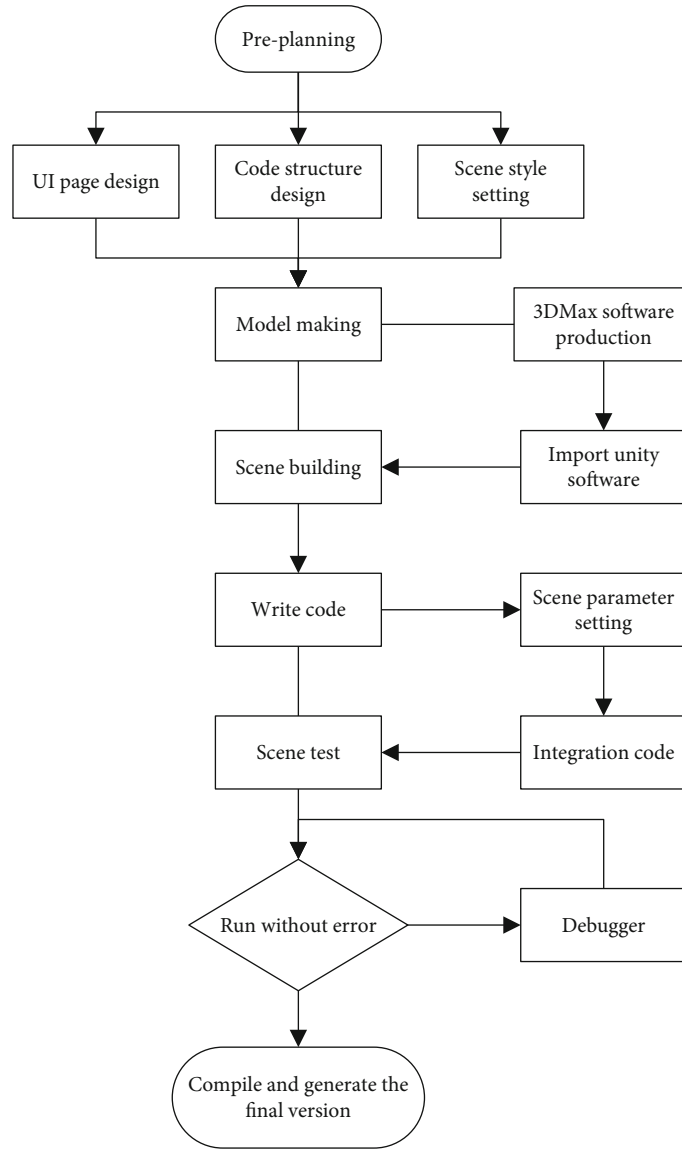
Figure 4: Production flow chart.

The specific transformation process of column transformation and inverse column transformation is shown in

$$
\begin{bmatrix} 02 & 03 & 01 & 01 \\ 01 & 02 & 03 & 01 \\ 01 & 01 & 02 & 03 \\ 03 & 01 & 01 & 02 \end{bmatrix} \begin{bmatrix} H_{0,0} & H_{0,1} & H_{0,2} & H_{0,3} \\ H_{1,0} & H_{1,1} & H_{1,2} & H_{1,3} \\ H_{2,0} & H_{2,1} & H_{2,2} & H_{2,3} \\ H_{3,0} & H_{3,1} & H_{3,2} & H_{3,3} \end{bmatrix}
$$

$$
= \begin{bmatrix} H'_{0,0} & H'_{0,1} & H'_{0,2} & H'_{0,3} \\ H'_{1,0} & H'_{1,1} & H'_{1,2} & H'_{1,3} \\ H'_{2,0} & H'_{2,1} & H'_{2,2} & H'_{2,3} \\ H'_{3,0} & H'_{3,1} & H'_{3,2} & H'_{3,3} \end{bmatrix}.
$$

(7)

Correspondingly,

$$
\begin{bmatrix} 0E & 0B & 0D & 09 \\ 09 & 0E & 0B & 0D \\ 0D & 09 & 0E & 0B \\ 0B & 0D & 09 & 0E \end{bmatrix} \begin{bmatrix} 02 & 03 & 01 & 01 \\ 01 & 02 & 03 & 01 \\ 01 & 01 & 02 & 03 \\ 03 & 01 & 01 & 02 \end{bmatrix} = \begin{bmatrix} 1 & 0 & 0 & 0 \\ 0 & 1 & 0 & 0 \\ 0 & 0 & 1 & 0 \\ 0 & 0 & 0 & 1 \end{bmatrix}.
$$

(8)

3.3. Singular Value Decomposition.

Singular value decomposition is one of the commonly used methods in mathematical statistics. It is widely used in infinite minimum cube problems, matrix order estimation, norm correlation analysis, and other problem solving. In the information retrieval problem, a special form of unique value decomposition is used to retrieve information, because the matrix that

TABLE 1: Introduction to 4 test scenarios.

Serial number	Scene file name	Original scene size	Total texture size	Number of texture files	The total size of scene files and textures	Total number of frames	Animation characteristics	Remarks
1	s1.max	18.2 MB	5.33 MB	32	23.6 MB	124	Have	People, houses
2	s2.max	18.1 MB	757 kB	3	18.8 MB	101	Have	Furniture
3	s3.max	51.1 MB	817 kB	5	51.9 MB	100	Have	Teapot
4	s4.max	151 MB	817 kB	5	152 MB	100	Have	Teapot

TABLE 2: Split data statistics table of s1.max file under different split granularities.

Split granularity	Number of subscene file blocks	Average size of subscene files (MB)	Average size of subscene texture (MB)	Average number of textures in subscene	Average size of subscene and texture files (MB)	Split processing delay (s)
25 frames	25	3.468	5.246	31.4	8.784	993
50 frames	13	3.562	5.244	31.385	8.898	411
75 frames	7	3.866	5.250	31.429	9.124	259
100 frames	3	4.62	5.237	31.333	9.83	147

requires unique value decomposition is usually a sparse high-order matrix.

Lemma 1. *Suppose A is a nondifferent real matrix of order n, then there must be orthogonal matrices P and Q such that*

$$P'AQ = \begin{bmatrix} a_1 & & & \\ & a_2 & & \\ & & \cdots & \\ & & & a_n \end{bmatrix}, \qquad (9)$$

$a_i > 0$, and a_i^2 is the characteristic value of $A^T A$: $i = 1, 2, \cdots, n$.

Theorem 2. *The $m \times n$ real matrix A with rank r must have a decomposition formula:*

$$A = U \begin{bmatrix} a_1 & & & \\ & a_2 & & \\ & & \cdots & \\ & & & a_r \end{bmatrix} V^T, \qquad (10)$$

where U and V are orthogonal matrices, and $a_i > 0$; $i = 1, 2, \cdots, n$.

Without loss of generality, suppose A is a sparse matrix with m rows and n columns, where $m >> n$, and rank $(A) = r$ is known. The singular value decomposition of A can be defined as

$$A = U \sum V^T. \qquad (11)$$

Theorem 3. *Suppose the singular value decomposition of A is given by equation (11), and there are*

$$a_1 \ge a_2 \ge a_3 \ge . \cdots \ge a_r \ge a_{r+1} = .. \cdots = a_n = 0. \qquad (12)$$

$R(A)$ and $N(A)$, respectively, represent the representation area of A and the null space of A, then

(1) Phase

$$\begin{aligned} \text{rank } (A) &= r, \\ N(A) &= span\{v_{r+1}, \cdots, v_n\}, \\ R(A) &= span\{u_1, \cdots, u_r\}, \\ U &= [u_1, u_2, \cdots, u_m], \\ V &= [v_1, v_2, \cdots, v_n] \end{aligned} \qquad (13)$$

(2) Connect and decompose

$$A = \sum_{i=1}^{r} u_i \cdot a_i \cdot v_i^T \qquad (14)$$

(3) Normative

$$\begin{aligned} \|A\|_F^2 &= a_1^2 + \cdots \cdots + a_r^2, \\ \|A\|_2^2 &= a_1 \end{aligned} \qquad (15)$$

TABLE 3: Split data statistics table of s2.max file under different split granularities.

Split granularity	Number of subscene file blocks	Average size of subscene files (MB)	Average size of subscene texture (MB)	Average number of textures in subscene	Average size of subscene and texture files (MB)	Split processing delay (s)
25 frames	21	3.548	0.280	1.286	3.833	92
50 frames	11	4.020	0.316	1.364	4.335	63
75 frames	6	4.178	0.333	1.333	4.5	46
100 frames	3	5.373	0.250	1.333	5.647	46

TABLE 4: Split data statistics table of s3.max file under different split granularities.

Split granularity	Number of subscene file blocks	Average size of subscene files (MB)	Average size of subscene texture (MB)	Average number of textures in subscene	Average size of subscene and texture files (MB)	Split processing delay (s)
25 frames	20	7.307	0.325	3.05	7.630	139
50 frames	11	7.799	0.345	3.182	8.143	95
75 frames	5	9.218	0.378	3.4	9.596	83
100 frames	2	12.255	0.536	4	12.79	80

TABLE 5: Split data statistics table of s4.max file under different split granularities.

Split granularity	Number of subscene file blocks	Average size of subscene files (MB)	Average size of subscene texture (MB)	Average number of textures in subscene	Average size of subscene and texture files (MB)	Split processing delay (s)
25 frames	20	28.49	0.325	3.05	28.835	1377
50 frames	10	30.58	0.352	3.2	30.95	851
75 frames	5	36.28	0.378	3.4	36.68	662
100 frames	2	48.85	0.536	4	49.4	518

4. Design and Implementation of 3D Movie Scene Production Algorithm Based on the Internet of Things

4.1. Scene Production Algorithm Data Test Analysis. In order to test the effect of the script on the separation of scene files, under the assumption that the scene files can be separated, based on the 3D output as a test case and the separation processing time delay and separation processing, 4 scenes were selected. Render correctly before and after separation. Perform statistical analysis on the scene file size and the number of textures in the subscene. Table 1 briefly introduces these four situations.

In order to test the splitting effect of scene files and textures in different split granularities, 4 different situations with split granularity of 25 frames, 50 frames, 75 frames, and 100 frames are, respectively, given. The split data statistics of scene files s1.max, s2.max, s3.max, and s4.max are shown in Tables 2–5, respectively.

The split data statistics table of the s1.max file under different split granularities is shown in Table 2.

The split data statistics table of the s2.max file under different split granularities is shown in Table 3.

The split data statistics table of the s3.max file under different split granularities is shown in Table 4.

The split data statistics table of the s4.max file under different split granularities is shown in Table 5.

From the data in Tables 2–5, it can be concluded that the greater the separation, the less times the script processes the internal scene model, texture, and film data and stores them when the separation process is complete. Therefore, the overall processing delay of script separation is relatively small. Details are shown in Figure 5.

4.2. Design of the Main Scene of "Fantasy Variations." In the process of making the main scene of the "fantasy change," first, based on a large amount of materials, the overall plan of the plan was drawn, and then, the castle, trees, lakes, waterfalls, etc., were modeled according to the main fantasy style. Tune. Finally, the individual is placed in the whole for fine-tuning.

4.3. Film and Television Scenes Based on Internet of Things Algorithm. In the 300 questionnaires, we know the film and television scenes produced using the Internet of Things algorithm. Most people believe that the use of Internet of Things technology can significantly reduce production costs, increase production speed, make scenes more beautiful, and enrich artistic elements and make them safer and more reliable. The specific situation is shown in Figure 3.
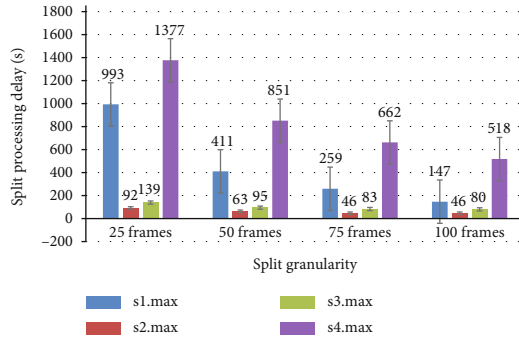
Figure 5: Four different files are processed in four different frames in total processing delay.
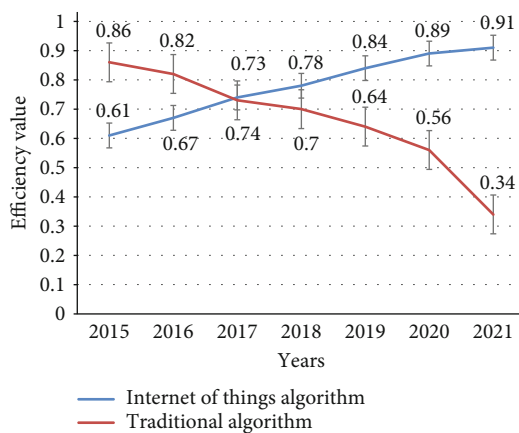
Figure 6: The efficiency of different algorithms for making 3D film and television scenes.

4.4. Efficiency Analysis of IoT Algorithms and Traditional Algorithms. With the development of the times, the Internet of Things technology has become more and more popular with everyone. We have used Internet of Things algorithms in the production of 3D film and television scenes. During 2015-2021, the efficiency change trends of different algorithms for making 3D film and television scenes are as follows, as shown in Figure 6.

It can be seen from the figure that the Internet of Things technology is becoming more and more popular with everyone, because the use of the Internet of Things technology can make most items intelligent, more convenient, and efficient. The traditional method is relatively inefficient, so it is gradually replaced by the Internet of Things.

5. Conclusion

3D film and television scenes occupy a very important position in film and television and incorporate knowledge of painting, architecture, lighting, perspective, and other disciplines. 3D movie scenes have greatly changed the way traditional scenes are created. This makes us must carefully study the design of 3D animation scenes. However, at present, my country's research on film and television scenes has not attracted people's attention. Background or role, even some

film and television professionals do not pay enough attention to film and television scenes. With the continuous development of the Internet of Things technology, we should calm down while creating, sum up the experience of previous production, and study its theories, so that the production of 3D animation scenes can be more systematic, and the creation and appreciation issues can be closely linked, so that technology and art can be more perfectly combined. I hope this article can play a role in inspiring others to contribute to other practical 3D movies dedicated to theoretical research and practical creation. The following conclusions can also be drawn. Firstly, the use of Internet of Things technology when creating traditional film and television scenes can use 3D lighting, textures, and other methods to display richer artistic elements in the scene design. Excellent model and reasonable stage layout are also very important. Therefore, the use of Internet of Things technology can make up for the single shortcomings of traditional production methods. Secondly, the main stage of designing with the Internet of Things technology is not a simple technical copy but requires us to effectively create a second time according to the artistic law of fantasy style, in order to accurately process various parameters and use appropriate materials and textures. Create excellent works with a more artistic atmosphere. Thirdly, when the Internet of Things technology is widely used in film and television art, it must be effectively combined with film and television art and must not conflict with it. It is believed that this emerging Internet of Things art will achieve greater growth in the field of 3D film and television in the near future.

Data Availability

No data were used to support this study.

Conflicts of Interest

The authors declare that they have no conflicts of interest.

Acknowledgments

References

[1] J. H. Pikul and H. Ning, "Powering the internet of things," *Joule*, vol. 2, no. 6, pp. 1036–1038, 2018.

[2] W. Yang, M. Wang, J. Zhang et al., "Narrowband wireless access for low-power massive internet of things: a bandwidth perspective," *IEEE Wireless Communications*, vol. 24, no. 3, pp. 138–145, 2017.

[3] Z. Liu, X. Huang, Z. Hu, M. Khurram Khan, seo, and L. Zhou, "On emerging family of elliptic curves to secure internet of things: ECC comes of age," *IEEE Transactions on Dependable and Secure Computing*, vol. 14, no. 3, pp. 1–248, 2016.

[4] S. Mumtaz, A. Alsohaily, Z. Pang, A. Rayes, K. F. Tsang, and J. Rodriguez, "Massive internet of things for industrial applications: addressing wireless IIoT connectivity challenges and ecosystem fragmentation," *IEEE Industrial Electronics Magazine*, vol. 11, no. 1, pp. 28–33, 2017.

[5] S. Sicari, C. Cappiello, F. de Pellegrini, D. Miorandi, and A. Coen-Porisini, "A security-and quality-aware system architecture for internet of things," *Information Systems Frontiers*, vol. 18, no. 4, pp. 665–677, 2016.

[6] J. C. Balda, A. Mantooth, R. Blum, and P. Tenti, "Cybersecurity and power electronics: addressing the security vulnerabilities of the internet of things," *IEEE Power Electronics Magazine*, vol. 4, no. 4, pp. 37–43, 2017.

[7] I. Azimi, A. M. Rahmani, P. Liljeberg, and H. Tenhunen, "Internet of things for remote elderly monitoring: a study from user-centered perspective," *Journal of Ambient Intelligence and Humanized Computing*, vol. 8, no. 2, pp. 273–289, 2017.

[8] N. Abuzainab, W. Saad, C. S. Hong, and H. V. Poor, "Cognitive hierarchy theory for distributed resource allocation in the internet of things," *IEEE Transactions on Wireless Communications*, vol. 16, no. 12, pp. 7687–7702, 2017.

[9] K. Kaur, S. Garg, G. S. Aujla, N. Kumar, J. J. P. C. Rodrigues, and M. Guizani, "Edge computing in the industrial internet of things environment: software-defined-networks-based edge-cloud interplay," *IEEE Communications Magazine*, vol. 56, no. 2, pp. 44–51, 2018.

[10] Y. Chen, J. Zhou, and M. Guo, "A context-aware search system for internet of things based on hierarchical context model," *Telecommunication Systems*, vol. 62, no. 1, pp. 77–91, 2016.

[11] O. Iova, P. Picco, T. Istomin, and C. Kiraly, "RPL: the routing standard for the internet of things... or is it?," *IEEE Communications Magazine*, vol. 54, no. 12, pp. 16–22, 2016.

[12] B. R. Ray, M. U. Chowdhury, and J. H. Abawajy, "Secure object tracking protocol for the internet of things," *IEEE Internet of Things Journal*, vol. 3, no. 4, pp. 544–553, 2016.

[13] F. Al-Turjman and M. Gunay, "CAR approach for the internet of things," *Canadian Journal of Electrical & Computer Engineering*, vol. 39, no. 1, pp. 11–18, 2016.

[14] C. Kolias, A. Stavrou, J. Voas, R. Kuhn, and I. Bojanova, "Learning internet-of-things security "hands-on"," *IEEE Security & Privacy*, vol. 14, no. 1, pp. 37–46, 2016.

[15] C. Chang, S. Narayana Srirama, and R. Buyya, "Indie fog: an efficient fog-computing infrastructure for the internet of things," *Computer*, vol. 50, no. 9, pp. 92–98, 2017.

[16] C. González García, D. Meana-Llorián, B. C. Pelayo G-Bustelo, J. M. Cueva Lovelle, and N. Garcia-Fernandez, "Midgar: detection of people through computer vision in the internet of things scenarios to improve the security in smart cities, smart towns, and smart homes," *Future Generation Computer Systems*, vol. 76, pp. 301–313, 2017.

[17] S. Mayer, J. Hodges, D. Yu, M. Kritzler, and F. Michahelles, "An open semantic framework for the industrial internet of things," *IEEE Intelligent Systems*, vol. 32, no. 1, pp. 96–101, 2017.

[18] X. Lin, J. Bergman, F. Gunnarsson et al., "Positioning for the internet of things: a 3GPP perspective," *IEEE Communications Magazine*, vol. 55, no. 12, pp. 179–185, 2017.

[19] T. Listyorini and R. Rahim, "A prototype fire detection implemented using the internet of things and fuzzy logic," *World Transactions on Engineering and Technology Education*, vol. 16, no. 1, pp. 42–46, 2018.

[20] X. Luo, Y. Lv, M. Zhou, W. Wang, and W. Zhao, "A Laguerre neural network-based ADP learning scheme with its application to tracking control in the internet of things," *Personal & Ubiquitous Computing*, vol. 20, no. 3, pp. 361–372, 2016.

[21] V. P. Kafle, Y. Fukushima, and H. Harai, "Internet of things standardization in ITU and prospective networking technologies," *IEEE Communications Magazine*, vol. 54, no. 9, pp. 43–49, 2016.

[22] F. Wu, L. Xu, S. Kumari, and X. Li, "A privacy-preserving and provable user authentication scheme for wireless sensor networks based on internet of things security," *Journal of Ambient Intelligence & Humanized Computing*, vol. 8, no. 1, pp. 101–116, 2017.

[23] T. Qiu, R. Qiao, M. Han, A. K. Sangaiah, and I. Lee, "A lifetime-enhanced data collecting scheme for the internet of things," *IEEE Communications Magazine*, vol. 55, no. 11, pp. 132–137, 2017.

WILEY | Hindawi

Research Article

Impact of High-Tech Image Formats Based on Full-Frame Sensors on Visual Experience and Film-Television Production

Jie Liu [ORCID]

Henan Police College, Zhengzhou, 450046 Henan, China

Correspondence should be addressed to Jie Liu; 5961@hnp.edu.cn

Today, the application of high-tech image format technology in contemporary visual experience and film and television production has become infinitely mature. In the era of the combination of modern technology and the Internet, virtual numbers connect the past with the future, merge reality, and myth and even synchronize the world between primitive and modern. This article adopts experimental analysis and comparative analysis, setting the experimental group and the reference group aim to use high-tech image formats from the perspective of a full-frame sensor to basically realize a perspective screen and a three-dimensional screen for observers in indoor scenes. In addition, the process of reconstructing a 3D model using high-precision geometric information and realistic color information is also described. The experimental results show that the sharpness threshold cannot be too small; otherwise, part of the clear image is misjudged as a blurred image. If the threshold is too large, the missed detection of the blurred image will increase. Combined with the subjective evaluation of the image, when the threshold is 0.8, the experimental result is close subjective evaluation, and the missed detection rate is 2.41%. This shows that the ASODVS three-dimensional digital scene constructed in this article can meet the needs of real-time image processing; it can effectively evaluate the clarity of realistic analog images. It shows that controlling the size of the y coordinate value can affect the user's visual experience. The smaller the y value in a certain range, the clearer the result can be.

1. Introduction

Computer-based 3D reconstruction technology is an emerging application technology, which has huge growth potential and practical value. It can be widely used in urban planning, medical investigation, construction site, geographic research, bone remodeling, cultural relic investigation, crime investigation, and data collection. The reconstruction of 3D models with high-precision geometric information and realistic color information has always been the focus of research in computer interaction, intelligence, scanning molds, graphic drawing, and map drawing. The 3D model reconstruction technology can be applied to different objects. The purpose of the 3D reconstruction of specific objects is to obtain information such as the 3D shape, curved surface, and actual color of the object. 3D scene reconstruction is mainly used to capture the distribution, shape, and actual color of objects in the scene, for example, the reconstruction of cultural and histori-

cal sites, the reconstruction of urban scenes, the reconstruction of urban landscapes, natural environment map modeling, and underground scene modeling. 3D scene reconstruction plays an important role in intelligent robot distance sensors, reshaping crime scenes, virtual displays, and many other fields. Its main purpose is to objectively reproduce real scenes and display them on mobile and client displays.

Based on data acquisition methods, commonly used 3D scene reconstruction methods can be divided into passive and active. When performing 3D reconstruction of scenes based on laser scanning, the calculation is complicated, and the reconstruction process cannot be fully automated. Generally, commercial 3D laser scanners are expensive and complicated to operate, which limits its application to a certain extent. The method of reconstructing the scene based on active vision has the characteristics of low cost and high efficiency and is regarded as the most effective method of 3D reconstruction of the scene.

Existing passive 3D reconstruction scenes require a lot of computing resources for point matching and stereo measurement, and there are some "unconditional" calculation problems. Although the obtained model has texture information, the accuracy of the model is low, and depth information is lacking. Existing laser scanners must perform functions such as recording and combining 3D point data during reconstruction. In order to obtain point cloud data with color information, it is usually necessary to have a one-to-one correspondence between the three-dimensional coordinates and the color information of the spatial points. The existing data input methods are relatively strict, and some methods require prior knowledge of known scenes.

In the early years, Yu used a sequence of images taken by a normal camera to reconstruct the scene. He proposed a factorization method to solve the geometric information of the scene when the object is far away and the problem of calculating camera movement. However, the parallel projection reconstruction method cannot fully restore the realism of the scene when it is applied to the real scene [1]. Zajdel et al. used a multicamera imaging method to capture eight camera video images distributed along the vertical axis, and used GPS and inertial navigation to assist position and motion estimation, and perform 3D urban scene modeling, but this only applies to formal and regular urban scenes. In this imaging method, the precise installation of the camera and the seamless stitching of multiple images have become obstacles to the realization of advanced eye technology [2]. In the field of fisheye lens imaging, Lhuillier has made improvements based on the image capture of common cameras in the home. He used the principle of light reflection and refraction and used multiple cameras to scan and shoot a scene in 360 degrees. For the first time, he made a true 3D reconstruction of the target scene, but his research did not simplify the calculation process and could not solve the problem of obtaining all point cloud data and color information corresponding to the scene from the same sensor at the same time [3].

The innovation of this article is related to: (1) The new ASODVS scanning program is used. The program can simplify most of the calculation work in the experimental design of this article. The input data is loaded in an orderly manner according to the order set by the experimenter. In the process from the field to the cloud, the cloud to the mobile terminal, the data will not be lost or scattered, but ordered in a matrix form. Therefore, the collected two sets of lattice data can be automatically matched according to a certain order, which greatly reduces the amount of calculation and manual operation on the machine side, and greatly improves the efficiency. (2) This article directly simulates the picture observed by the human eye when building the scene, which greatly improves the requirements and standards of the experiment. It also enables the experimenter to produce an immersive observation experience similar to the 3D movie version. The platform construction, parameter setting, and algorithm optimization have successfully completed the process of indoor 3D scene reconstruction [4].

2. Impact of the High-Tech Image Format of the Full-Frame Sensor on the Visual Experience and Film and Television Production

2.1. Design and Hardware Composition of ASODVS. As shown in Figure 1, the four coordinate systems composed of four devices required for the experiment cannot form a single topological structure in space. Therefore, we need to pair and calibrate different coordinate systems, and only after conversion can we meet the needs of the measurement and reconstruction platform [5]. The objects in the global coordinate system are finally displayed after the transformation of 4 coordinate systems [6]. Formula (1) is a formula linking the relationship between coordinate systems [7]. This formula converts the dot matrix data put into the matrix very well [8].

$$x \begin{bmatrix} v \\ w \\ 1 \end{bmatrix} = \begin{bmatrix} f_v & -f_v \cot \theta & v_0 \\ 0 & f_w/\sin \theta & w_0 \\ 0 & 0 & 1 \end{bmatrix} \begin{bmatrix} f & 0 & 0 & 0 \\ 0 & f & 0 & 0 \\ 0 & 0 & 1 & 0 \end{bmatrix} \begin{bmatrix} T & r \\ 0_3^R & 1 \end{bmatrix} \begin{bmatrix} x_P \\ y_p \\ z_p \\ 1 \end{bmatrix}. \tag{1}$$

In terms of hardware composition, the moving surface laser generator and the ODVS rear-view sensor form the ASODVS. The overall structure of the system is shown in Figure 2. The four main modules are directional vision sensor, moving surface laser generator, drive unit, and operation unit. Among them, the omnidirectional vision sensor is mainly composed of a hyperboloid mirror, a common condenser, and an imaging chip, which can simultaneously obtain a 180-degree platform panorama in the positive direction and a platform panorama with the same angle in the negative direction [9]. The experimental field of vision has been greatly expanded [9] as shown in Figure 2. The moving surface laser generator consists of four green line laser generators [10], which can emit 360-degree laser lines in the horizontal direction. The driver model is M542 (4.2 A, 50 V), and the motion controller model is TC4510. The end controller used by the experimenter is actually operated by software, from laser emission, recovery of lattice data [10], uploading to the cloud, data matching, data calculation, and making modeling files to forming an operable panel, all in one go [11, 12].

Establish a coordinate system with the single viewpoint on as the origin, let axis x'' be aligned with the optical axis of the mirror, let $W = [x, y, z]^t$ be a point in space, $p'' = [p'', q'']^t$ is the projection of point W on the sensor plane, and $p' = [p', q']^t$ is the pixel point of point W on the image plane. The process of displaying point W is projecting point W onto point A in the mirror by transforming the projection matrix [13], and point A is focused on the optical center point C of the camera after reflection and intersects the sensor plane at point $p'' = [p'', q'']^t$ and point $p' = [p', q']^t$. After affine transformation, point $p' = [p', q']^t$ on the image plane is obtained. The aforementioned single-view mirror camera imaging model describes the spatial points up to the mirror
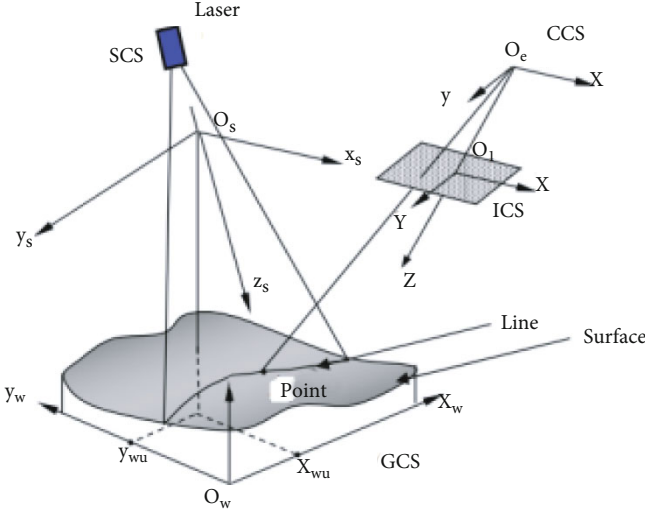
FIGURE 1: Four coordinate systems and their associations (from https://www.ixueshu.com/search/index.html).

point [14, 15], from the angle of the mirror to the point in the imaging plane, and then to the point in the image plane to form the pixels in the image Point process.

Among them, the conversion relationship from the cata-dioptric mirror to the sensor plane is shown in formula (2):

$$\lambda p'' = \lambda \begin{pmatrix} X''^T \\ Y'' \end{pmatrix} = \lambda \begin{pmatrix} h\left(\|u''\|\right)u'' \\ g\|u''\| \end{pmatrix} = P \cdot W, \lambda > 0.$$

(2)

In the formula, $W \in R^4$ represents the second coordinate of the space point Q, q is the projection interaction matrix $q = [R \mid T] \in R^{3\times4}$, T is the rotation matrix $T \in T^{3\times3}$ from the space point to the catadioptric mirror point [16], and R is the translation matrix from the space point to the catadioptric mirror point $R \in R^{3\times1}$.

The formula for converting from the sensor plane to the image plane is as follows [17]. The formula is referring to a extremely truly fact that we can collect the matrix into the collection B, and after calculating then, let the answer be added with p.

:

$$u'' = Bu' + p.$$ (3)

Use a function to replace the functions g and h in formula (2), that is, use the function f to connect the two-dimensional lattice and the three-dimensional space to obtain the formula (4):

$$\lambda p'' = \lambda \begin{bmatrix} u'' \\ f\left(\|u''\|\right) \end{bmatrix} = \lambda \begin{bmatrix} Bu' + p \\ f\left(\|Bu' + p\|\right) \end{bmatrix} = P \cdot w, \lambda > 0.$$

(4)

Since the error will be introduced into the actual processing and assembly of the omnidirectional vision sensor, it can be assumed that the ODVS conforms to the ideal model [18], replacing the nonideal model with some errors in the simplified model conversion type, and formula (5) can be obtained:

$$\lambda p'' = \lambda \begin{bmatrix} u'' \\ f\left(\|u''\|\right) \end{bmatrix} = \lambda \begin{bmatrix} Au' + p \\ f\left(\|Au' + p\|\right) \end{bmatrix} = P \cdot W, \lambda > 0.$$

(5)

Formula (5) can be used to establish the correspondence between any pixel on the imaging plane and the angle of incidence Table 1 [19]:

2.2. Moving Surface Laser Transmitter. In the design of 3D perception and information reconstruction system based on active vision, the effective projection of the light source plays a vital role in the structure and accuracy of the point cloud data. In order to adapt to the function of ODVS that can simultaneously shoot 360-degree panoramic images of the scene, the mobile surface laser generator must project a laser light source that can cover 360 degrees in the horizontal direction of the scene. It can move up and down in the vertical direction to complete the scan of the scene [20]. Based on this design goal, the following article will first introduce the principle of laser ranging and then explain the specific design of the moving surface laser generator in ASODVS and the assembly method of the moving surface laser light source [21].

Commonly used laser ranging principles are triangle ranging method, time-of-flight method, and phase method [20]. The triangulation method is a method of measuring the distance between the target point and the known end point of a fixed reference line, as shown in Figure 3. The three lines in the figure meet the requirements of the triangular distance measurement method. Its included angle can be geometrically calculated to obtain ranging information. The laser scanning system using this method is mainly composed of a laser generator and a CCD camera, which form a spatial plane triangle with the target point, as shown in Figure 3. The emitted light, incident light, and baseline all come from the scanner angle sensor. Its included angle can complete geometric calculations to obtain 3D information.

The time-of-flight method and phase ranging method, as the distance measurement principle, and the transmitting and receiving devices of the laser rangefinder must be laser receivers and transmitters, which belong to point-to-point measurement; while the receiver of the triangulation method is a CCD imaging chip. The CCD imaging chip can obtain planar image information, so that the laser of the triangulation method can use a line laser light source or a surface laser light source. This method not only improves the scanning efficiency of the laser but also effectively reduces the complexity of the system.

The line laser generator is an important part of the moving surface laser generator. Laser light sources of different power levels have different effects on the user's personal
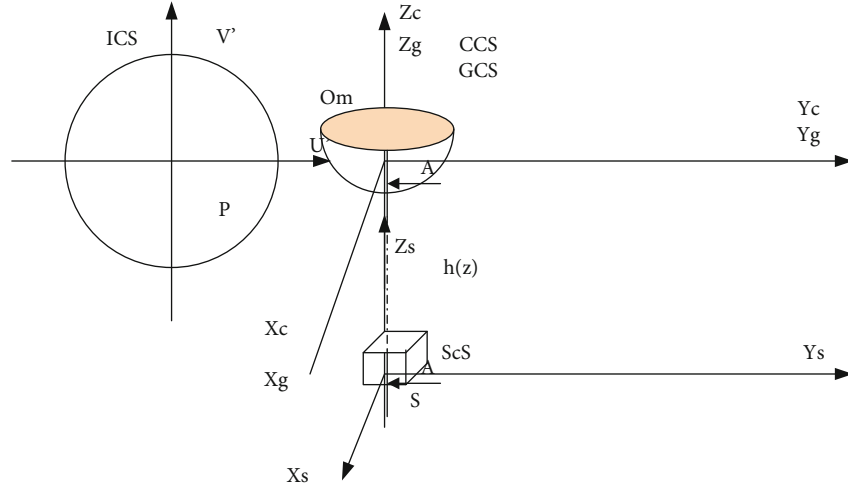
FIGURE 2: Relationship among the various coordinate systems.

TABLE 1: ODVS's calibration result.

Calibration object	a_0	a_2	a_4	A		t	Center point
ODVS	-106.597	0.0021	-0.001	$\begin{bmatrix} 1.01 & -5.21e-006 \\ -6.07e-006 & 1 \end{bmatrix}$		$\begin{bmatrix} 49.463 \\ -14.692 \end{bmatrix}$	$\begin{bmatrix} 590.541 \\ 374.691 \end{bmatrix}$
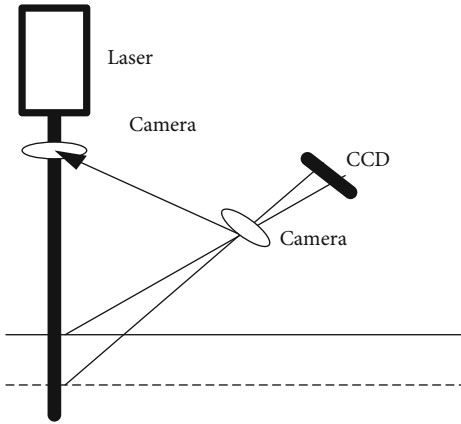
FIGURE 3: Triangular ranging method.

safety. For this reason, this article analyzes the selection and precautions of laser emission power. Under normal circumstances, the greater the laser power, the wider the emission range, but high-power laser generators usually have safety hazards [21]. Laser manufacturers use class I to class IV to indicate the degree of laser damage to the human body from low to high. Class I lasers are not harmful to the human body and are mainly used in laser printers and some experimental equipment. The class II laser has a certain degree of damage to the eyes and can be used for aiming equipment or distance measuring equipment. Class III is a medium-power laser transmitter, which can be divided into two levels: class IIIA and class IIIB. The laser power of class A is in the range of 1 milliwatt to 5 milliwatts and can emit continuous laser waves. Class B laser power ranges from 5 to 500 milliwatts

[22]. It can be used for laser scanners and stereo photography. Eyes must be protected when using class IIIB lasers, and the eyes cannot look directly at the laser light source. Class IV lasers are high-power lasers that can be used in surgery, cutting, and other fields [23].

When designing the hardware, the ODVS and the moving surface laser generator are fixed on the same axis. The ideal assembly situation is that the axis line of the single viewpoint Om of the ODVS and the scanning planes of the 360° laser emitted by the moving surface laser generator are perpendicular to each other. To achieve this goal, we used a hollow cylinder to calibrate ASODVS during assembly. The specific method is as follows: (1) put the ASODVS into the hollow cylinder vertically so that the axis of the ASODVS coincides with the axis of the hollow cylinder, (2) constantly change the distance between the moving surface laser generator and the viewpoint Om of the ODVS, and (3) observe the panoramic sequence images obtained from ODVS.

2.3. Application of ASODVS. If the aperture produced by the projection of the moving surface laser generator in the panoramic sequence image is a series of perfect circles centered on the panoramic image, then the ASODVS configuration is over; otherwise, fine tuning is required to make the ASODVS meet the ideal design requirements. In addition to the observation method, you can also save the panoramic image with laser information generated in the above process and use the algorithm to analyze the image to determine whether the ASODVS has reached the assembly requirements [24, 25].

Figure 4 is the flow chart of the entire system:
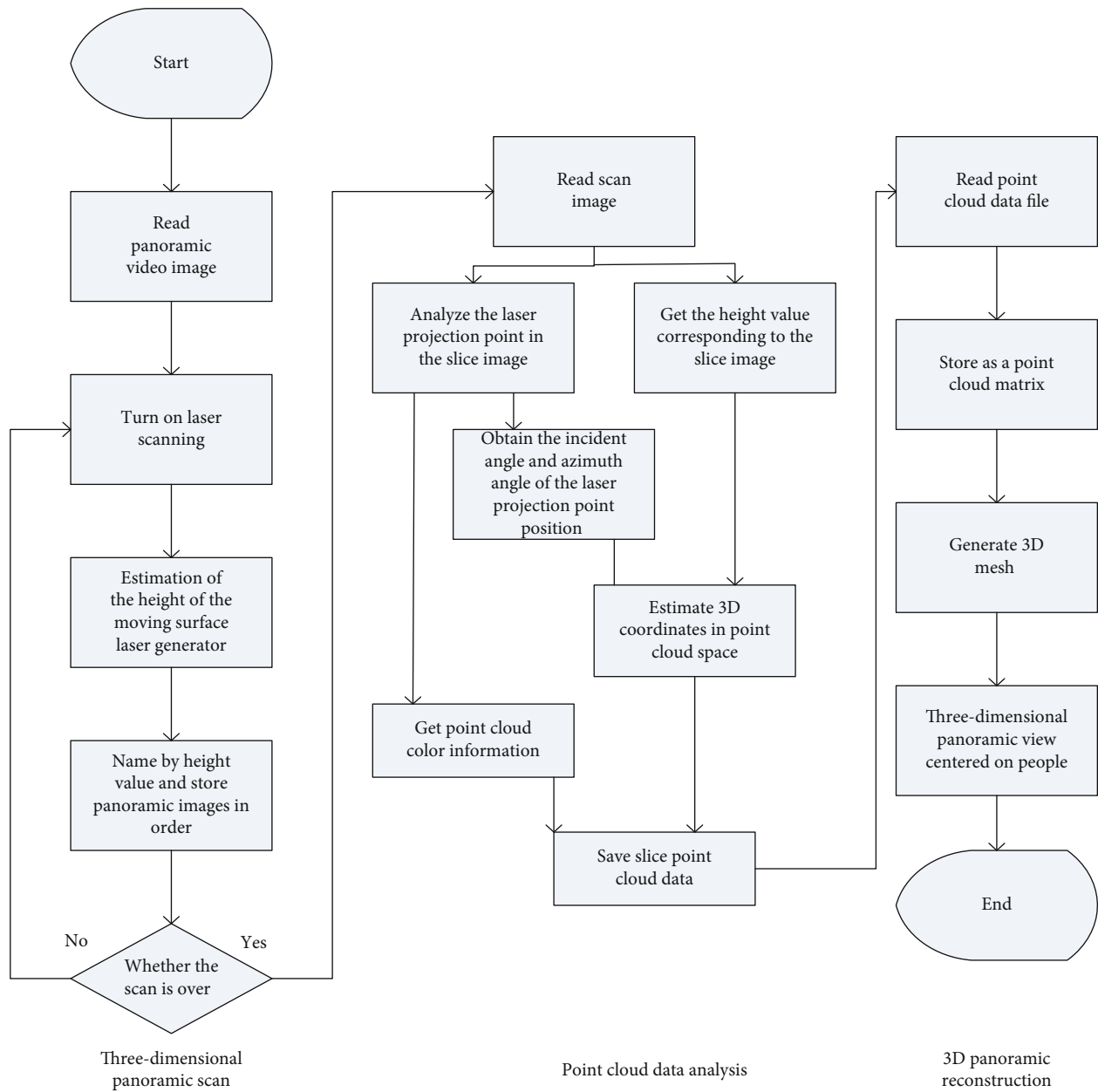
Figure 4: System flow chart.

When SODVS calculates the three-dimensional coordinates of a space point, it first needs to analyze the laser point in the panoramic image. The analysis algorithm of the laser point includes the algorithm based on the HIS color model, the algorithm based on the interframe difference algorithm, and the three-frame difference algorithm. The sampling speed of ASODVS is also closely related. ASODVS inevitably has some errors in the calculation of the three-dimensional coordinates of the space point. The maximum error of the distance from the point cloud to the single viewpoint in the statistical space is within 3%. In most cases, the laser generator, the measured object, and the camera are in different spatial positions, which is why the four coordinate systems mentioned above cannot form a coincident, parallel, or vertical relationship. Since the four coordinate systems cannot form a simple rela-

tionship, the registration and conversion between coordinate systems is a necessary step in the process of measurement and reconstruction. Objects in the world coordinate system pass through the camera coordinate system, the ideal image coordinate system, and the real image coordinate system and finally are imaged in the digital image coordinate system.

3. Experimental Research on the Impact of High-Tech Image Formats of Full-Frame Sensors on Visual Experience and Film and Television Production

ASODVS can scan the indoor scene volume and realize the reconstruction of the scene, which is the main software

platform used in this experiment. It mainly elaborates the method of acquiring and modeling indoor scene 3D information. With the research and development of computer three-dimensional graphics, the point-based three-dimensional model has attracted the attention of many researchers. Therefore, a relatively simple point model method was chosen.

The 3D mesh model is obtained by processing the point cloud data. Generally, it is necessary to construct the topological structure of the 3D point cloud in order to perform neighborhood operations on each point. On this basis, some algorithms can be used to obtain the corresponding 3D mesh model.. The 3D mesh model is the mainstream method of 3D modeling at present. It contains the topological relationship between points and can better reflect the geometric information of the surface of the object. Based on the above considerations, this work uses a 3D point cloud model and a mesh model to reconstruct the 3D internal scene. And because of the classification of the three-dimensional point cloud data obtained based on ASODVS, the system can better meet the real-time requirements without constructing a topological structure.

3.1. Preparing. The ODVS in this article uses a 1280×720 pixel USB CMOS camera module and is connected to the microprocessor through a USB interface. The configuration of the microprocessor is as follows: CPU is Pentium 4, memory 2G, discrete graphics card, and 512 M video memory, operating system is Windows 7, and a self-developed 3D panoramic point cloud data acquisition software based on ASODVS is installed in the system. The software is composed of Java and Java3D implementation. We have placed a number of colored obstacles in the indoor scene, and the obstacles are arranged in an irregular manner. In addition to ordinary flat objects, indoor scenes also include curved surfaces and door-shaped parts to increase the richness of the scene.

3.2. Experiment Method. In this paper, an experiment was conducted in a scene of about 25 square meters arranged in the lobby of a certain teaching building of a university, and an indoor scene was built with a full-scale sensor for data collection [26]. Before acquiring the point cloud data, first place the ASODVS and place it in the center of the scene. The azimuth angle of the omnidirectional vision sensor $\beta = 0$ is aligned with the true north direction in the space. At this time, the projection point of the single viewpoint Om on the plane of the ground is the origin (0,0,0) of the three-dimensional world coordinate system. In order to make the contour features of the reconstructed model more obvious, we placed a number of colored obstacles in the indoor scene, and the obstacles are arranged in an irregular manner. In addition to ordinary flat objects, indoor scenes also include curved surfaces and door-shaped parts to increase the richness of the scene.

Use ASODVS software to edit algorithm calculations, use different parameters, observe the effect of modeling on the display, and evaluate the impact of different image formats on the visual experience under different parameters.

In the 3D display and drawing of the scene, due to the three characteristics of immersion, interaction, and imagination of the experimental effect, virtual reality technology is adopted. This technology is realized by integrating multiple technologies, such as graphics, digital image processing, and three-dimensional modeling. This technology enables people to observe and experience realistic environmental scenes and interact with them.

3.3. Experiment Procedure. Before acquiring the point cloud data, first place the ASODVS and place it in the center of the scene. The sharpness evaluation method is not only an important link to measure the quality of a digital image but also the basis for realizing the automatic focus of a digital imaging system, and it is also an important means of judging the imaging quality of a digital imaging device. The good link of the evaluation system is related to the quality and efficiency of data collection, eliminates the influence of subjective factors in the evaluation process of different people, ensures the consistency of evaluation standards, and facilitates comparison and optimization between different algorithms, so that subjective evaluation is objective and objective. The evaluation is consistent and has high application value. Based on this, this article studies a class of document image sharpness evaluation problems collected by high-speed scanners.

The azimuth of the omnidirectional vision sensor = 0 is aligned with the true north direction in the space. At this time, the projection point of the single viewpoint Om on the plane of the ground is the origin (0,0,0) of the three-dimensional world coordinate system.

Figures 5(a)–(c) are the actual images and point cloud models at different angles in different scenes. The red line in the figure represents the scene ground profile. In addition to reading the point cloud data and displaying it in real time, the software system can also perform operations such as rotation, translation, enlargement, and reduction on the obtained model through the keyboard and mouse, as shown in Figure 6.

Compared with Figure 5, it is found that the scanned point cloud data model can basically reflect the edge contour of the scene and can express the distribution, shape, and color information of the objects in the scene. This article refers to the method of displaying Figure 5 as "object-centric model display," which means that the entire scene is treated as an object from the outside.

In this paper, an experiment was conducted on the method of establishing a grid model of an ordered point cloud. From the steps of the algorithm, it is known that the points on each scan slice need to be connected with their neighboring points in the specific implementation. In this paper, the geometric shape of the line (line) in Java3D is used to connect the point cloud data to construct a grid. The grid model established by this method does not need to perform normal vector calculation and topological structure establishment operations and generates point cloud data in real time. Since there are several ways to connect quadrilateral meshes into triangular meshes, two triangular mesh models of indoor scenes can be obtained.

(a) Arc part

(b) Gate part

(c) Color obstacle part
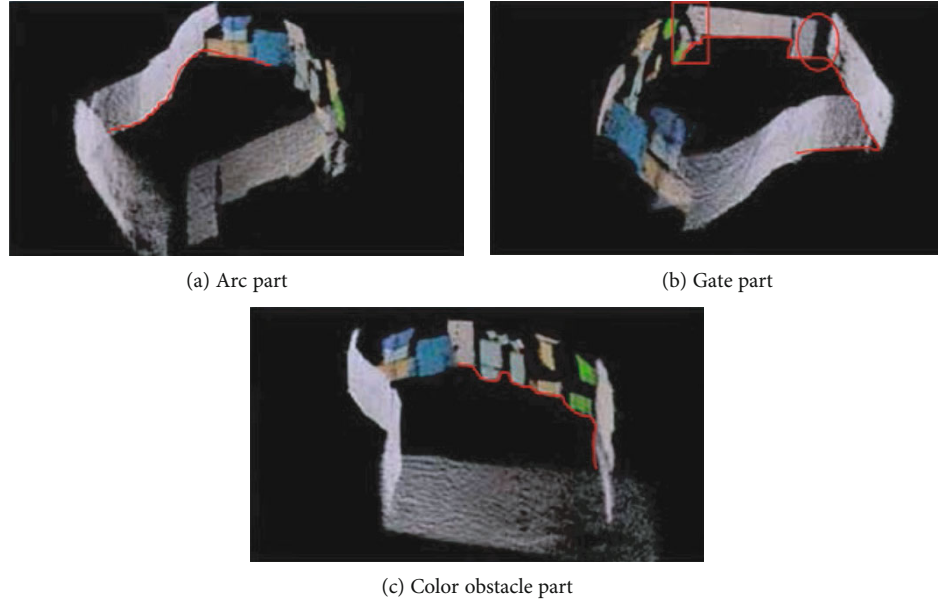
FIGURE 5: 3D point cloud model (from: https://xueshu.baidu.com/usercenter/paper/show?paperid=2719cddff42797aee6fdf9704d1f203d&site=xueshu_se).
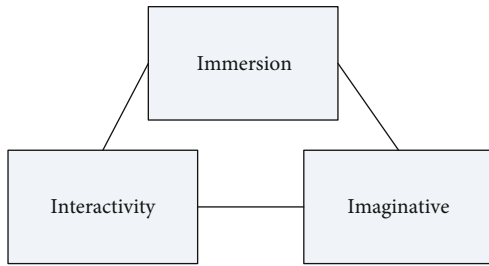
FIGURE 6: Virtual display technology.

Virtual reality technology must have the three characteristics of immersion, interactivity, and imagination, and the relationship is shown in Figure 6. Immersiveness refers to making the observer feel immersed in the scene and environment. Computer-related technology is used to simulate and approximate the three-dimensional scene realistically. In some cases, it needs the help of specific equipment such as 3D glasses and helmets to achieve this. Interactivity means that the observer can operate and interact with the observed scene environment through a computer keyboard, mouse, and other equipment. Imagination means that the observer can have a sense of reality in the virtual environment and feel this virtual space. This article refers to the characteristics of virtual reality technology, namely, immersion, interactivity, and imagination when designing the observer-centered 3D panorama rendering. Since the applied active panoramic stereo vision sensor has the characteristics of a single viewpoint, the single viewpoint is used as the origin to establish a spatial coordinate system when data acquisition and reconstruction of indoor scenes are carried out. Therefore, when displaying, you can start from the characteristics of single viewpoint and combine the characteristics of human vision that are rendered in 3D panorama centered on the observer.

According to the principle of ergonomics, the right viewpoint image can be calculated by using the perspective view as the left viewpoint image, and vice versa, if the above generated perspective view is used as the central eye image, left and right viewpoint images need to be generated to realize the generation of a stereo image pair. This article adopts the first method, which takes the abovementioned perspective view result as the left view point, and then constructs the disparity map by obtaining the right view point perspective view to realize stereo display.

Taking the single viewpoint Om (0,0,0) of ASODVS as the coordinates of the left eye viewpoint, applying formula (6) can calculate the coordinates of the space P point in the right eye viewpoint, where A is the distance between the two eyes and the distance between the two eyes of women. The distance is 55-65 mm, the distance between male eyes is 58-68 mm, and $A = 60$ mm is used in formula (6).

$$\begin{cases} H_l = H_r \\ R_l = \sqrt{A^2 + R_r^2 + 2 \times A \times R_r \times \cos \beta_r} \\ \beta_l = \arcsin \left(\dfrac{R_l}{R_r} \times \sin \beta_r \right). \end{cases} \quad (6)$$

According to the previous description of the perspective drawing with the observer as the center, we first need to determine the initial azimuth angle corresponding to the viewpoint. Through the spatial relationship between the left and right viewpoints, when the initial azimuth angle corresponding to the left viewpoint is known, we need to determine the initial azimuth angle corresponding to the left viewpoint. Calculate the initial azimuth corresponding to the right viewpoint. The observer-centered stereo map drawing algorithm is specifically described as follows:

(a)

(b)

FIGURE 7: Operation of 3D point cloud model (data *B*) (from https://xueshu.baidu.com/usercenter/paper/show?paperid=2719cddff42797aee6 fdf9704d1f203d&site=xueshu_se).

Step 1. Determine the respective initial azimuth angles of the left and right viewpoints and read the minimum incident angle $\alpha_{\min}$ and the maximum incident angle $\alpha_{\max}$.

Step 2. $\alpha = \alpha_{\min}$.

Step 3. Perform perspective view display calculation for the point cloud data to be displayed corresponding to the left and right viewpoints and obtain two perspective display matrices PL1 and PR1. The calculation method will not be repeated.

Step 4. Judge whether to display the grid, if the judgment result is yes, then construct the grid model, otherwise, continue.

Step 5. Determine whether $\alpha \geq \alpha_{\max}$ is established, if the result is not established, go to step 3, if the result is established, continue.

Step 6. Assign the color value *R* of the point cloud matrix PL1 calculated in step 3 to the *R* in the corresponding PR1.

Step 7. End, get a new matrix PS of size 120×300.

Based on the perspective display drawing of the indoor scene model, through the red and blue stereo display technology, the 3D stereo display output rendering of the indoor scene can be obtained, which is similar to the perspective display drawing. It is also possible to perform a perspective transformation on the basis of a stereoscopic display to realize a stereoscopic display of a panoramic scene. Observation with the aid of red and blue 3D glasses can achieve 3D stereoscopic display of indoor scenes. The stereoscopic display in this article can achieve a certain 3D effect, but it cannot completely simulate the fine stereoscopic effects such as movies.

4. Impact of High-Tech Image Formats of Full-Frame Sensors on Visual Experience and Film and Television Production

4.1. Actual Results after Using Different Parameters. In order to better test the impact of high-tech image formats on visual experience and film and television production, we designed the experimental group (*A*) and the control group (*B* and *C*), respectively, using different lattice data parameter settings, using the ASODVS experimental device. The software conducts simulation analysis and obtains the scene pictures of the other two groups of reference groups.

As shown in Figure 7(b), the point cloud data in the red box is missing, and this part of the missing has a certain shape; so, it can be judged that the laser line is blocked. By analyzing the shape of each part of the scene, it can be known that this part of the loss is caused by the shielding of the line laser by the support rod of the device itself.

As shown in Figures 7 and 8 above, the resulting 3D modeling diagrams show varying degrees of model loss and sharp reduction due to missing data and parameter settings beyond the range, which is not in line with experimental expectations.

4.2. Parameter Comparison. In order to explore the impact of different lattice parameters on the clarity of 3D modeling, we set a total of five sets of 3D point cloud data as shown in Table 2:

Two rows of data represent a point, the first row is the three-dimensional space coordinates (*x*, *y*, *z*) of the point, and the second row is the color value (*r*, *g*, *b*) of the point. The *rbg* color mode is a color standard in the industry. It obtains a variety of colors by changing the three color channels of red (*R*), green (*G*), and blue (*B*) and their superpositions. Yes, *RGB* is the color representing the three channels of red, green, and blue. This standard includes almost all the colors that human vision can perceive, and it is one of the most widely used color systems at present.

All six attribute values are saved when stored in one class. It is worth noting that due to the limitation of the size of the site space when selecting the points, the laser line emitted by ASODVS is located on the horizontal plane; so, it is impossible to calculate the three-dimensional coordinates of the spatial points on the horizontal plane. In other words, the *z* coordinate in the collected point cloud data cannot be set. Therefore, the value of the *z* coordinate in the five sets of three-dimensional point cloud data we selected is set to 30 unchanged.

After putting the set data into the matrix calculation and comparison, make a statistical graph according to the software clarity score statistics as shown in Figure 9. The 3D

(a)   (b)

FIGURE 8: Operation of 3D point cloud model (data C) (from https://xueshu.baidu.com/usercenter/paper/show?paperid=2719cddff42797aee 6fdf9704d1f203d&site=xueshu_se).

TABLE 2: 3D point cloud data parameter setting.

Type	$x(r)$	$y(g)$	$z(b)$	Clarity point
Data 1	252.78	11.13	30.0	0.779844
	0.5490196078431474	0.5491196078631383	0.6470588236294119	
Data 2	252.87	12.77	30.0	0.659842
	0.6470588234296118	0.6470589235274112	0.7690176078441379	
Data 3	252.78	14.37	30.0	0.485497
	0.6470788235294118	0.6970588235294118	0.7497196078431373	
Data 4	252.78	15.97	30.0	0.171234
	0.516078431372549	0.5382352941176471	0.6731960784313725	
Data 5	252.78	17.57	30.0	0.021564
	0.5872352941176471	0.5676274509803921	0.6789235294117647	

Software clarity point
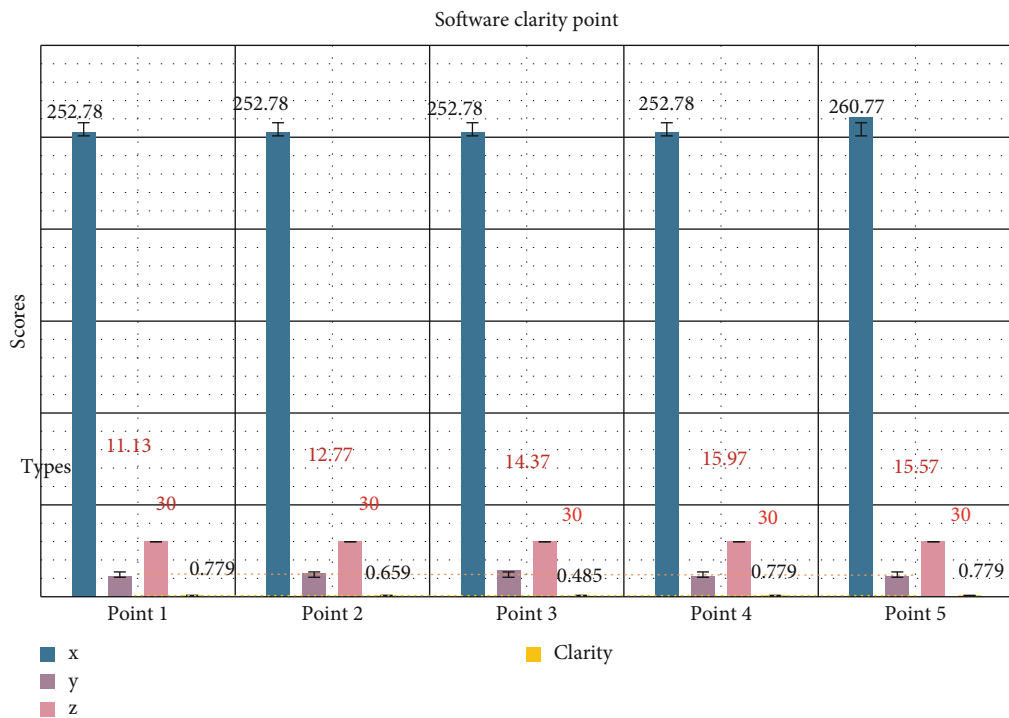
FIGURE 9: Software clarity point.

The relationship between Y coordinate and visual
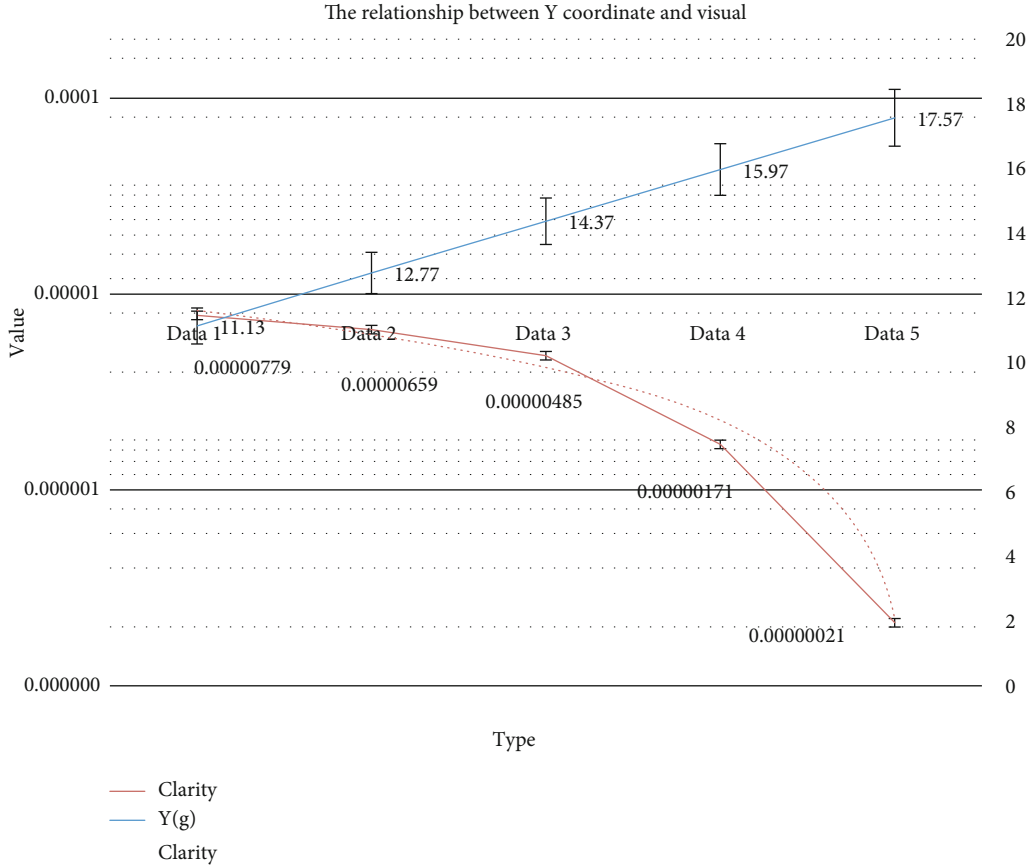
FIGURE 10: The relationship between y coordinate and visual.

point cloud data obtained by ASODVS is saved in a text file. Some examples of point cloud data are as follows:

252.76, 11.12, 30.0,
0.5490196078431373, 0.5490196078431373, 0.6470588235294118
252.86, 12.72, 30.0.
0.6470588235294118, 0.6470588235294118, 0.7490196078431373
252.77, 14.31, 30.0.
0.6470588235294118, 0.6470588235294118, 0.7490196078431373
:

It can be seen from the statistical graph that the sharpness data is closely related to the y value when the z coordinate does not change in the lattice coordinates. When z remains 30.00 and x changes from 252.78 to 260.77, the sharpness data of the produced model remains 0.779.

When z remains 30.00 and x changes from 252.78 to 260.77, the sharpness data of the produced model remains 0.779. Therefore, when using the dot matrix model set by ASODVS, the abscissa (x) of the collected data points has no effect on the sharpness. The 3D point cloud model of the scene does not show these horizontal planes of the scene. The reason for this problem is that the laser line emitted by ASODVS is located on the horizontal plane; so, it is impossible to calculate the three-dimensional coordinates of the spa-

TABLE 3: Clarity test result.

Quantity	Threshold	Detection amount	Subjective evaluation	Missed
	0.50	742		0
4000	0.80	322	267	6
	0.90	104		144

tial points on the horizontal plane. This problem can be solved by improving the hardware of ASODVS.

4.3. Relationship between the y Coordinate of 3D Point Cloud Data and the Clarity of Visual Experience. Based on the above research results, we ignore the two parts of coordinate x and coordinate z when collecting data and focus on analyzing the impact of the y coordinate in the five sets of data on the clarity of the visual experience.

After rearranging the data, make a statistical graph based on the software clarity score again, as shown in Figure 10.

Analyzing Figure 10, it can be seen that when the y coordinate increases linearly from 11.13 to 17.57, the sharpness decreases from 0.779 (very high sharpness) to 0.021. The definition evaluation score range used in this article is 0-0.2 ambiguous, 0.2-0.4 can be seen clearly, 0.4-0.6 is clearly visible, 0.6-0.8 is very clear, and 0.8-1 is ultra-high definition.

Performance comparison with the state-of-the-art general purpose NR quality metrics
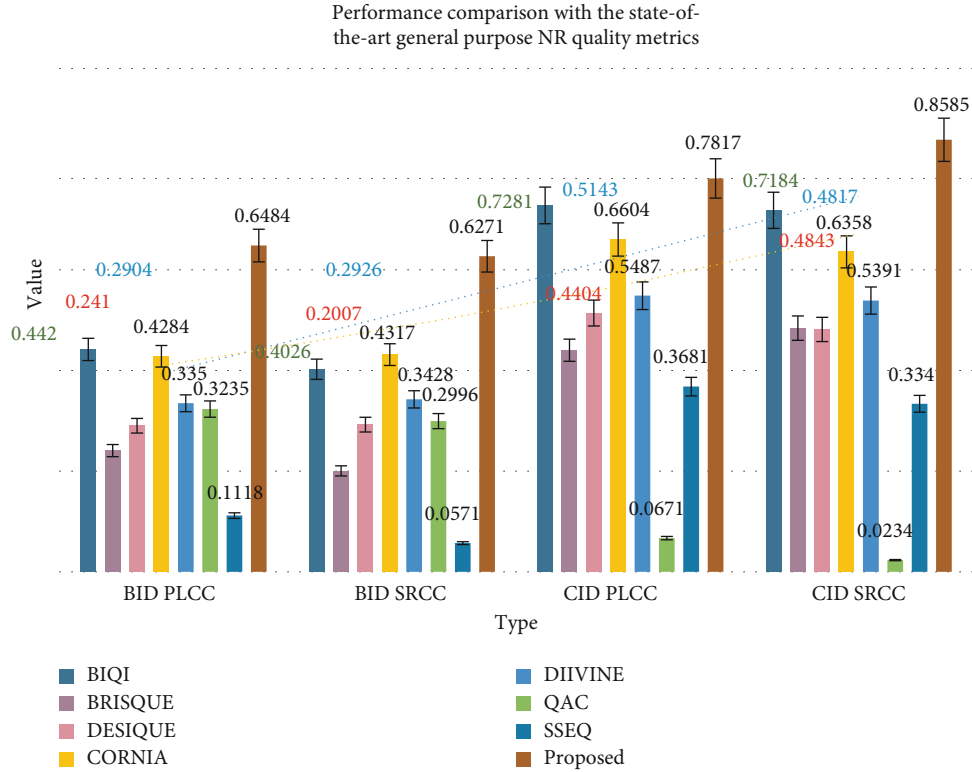
FIGURE 11: Performance comparison with the state-of-the-art general purpose NR quality metrics.

This shows that changing the value of the y coordinate within a certain range can control the decrease of the visual clarity experience of 3D modeling. It is worth mentioning that in the data of data 1, the clarity has reached an astonishing 0.779, which basically simulates human vision to display the 3D reconstruction results of the scene. Through the combination of object-centered and observer-centered display technologies, the inside and outside panorama of the scene is better integrated and displayed, and the observer can experience and appreciate the three-dimensional digital scene from multiple angles and omnidirectional under the secondary parameters.

In order to test the effectiveness of the evaluation algorithm, we evaluated 4000 onsite document images. The image was scanned using Belllink's copi8000, 100 dpi, and 256-level grayscale, which contained 267 fuzzy images. The experiment has obtained relatively ideal results. To detect blurred images as an example, different threshold parameters can be selected to evaluate the sharpness of the image. The experimental results are shown in Table 3. The sharpness evaluation is as follows:

As shown in Table 3, the experimental results show that the sharpness threshold cannot be too small; otherwise, part of the clear image is misjudged as a blurred image. If the threshold is too large, the missed detection of the blurred image will increase. Combined with the subjective evaluation of the image, when the threshold is at 0.8, the experimental result is close to the subjective evaluation, and the missed detection rate is 2.41%. This shows that the ASODVS 3D digital scene constructed in this paper can meet the needs of

real-time image processing; it can effectively evaluate the clarity of realistic analog images.

In order to further illustrate the superiority of the method proposed in this article, this article compared with other general quality assessment methods without reference, including BIQI, BRISQUE, DESIQUE, CORNIA, DIIVINE, QAC and SSEQ. Plot the test data in Figure 11.

It can be seen from Figure 11 that the overall performance of the methods related to BID and CID camera image databases in this chapter is better than these unreferenced conventional quality evaluation methods. In the BID database, when the PLCC evaluation index is used, the BIQI fuzzy score of the universal nonreference treatment evaluation method is 0.442, while the fuzzy score of the picture processed by the ASODVS three-dimensional modeling software rises to 0.6483.

5. Conclusions

Experimental research shows that the ASODVS designed in this paper can quickly obtain the three-dimensional coordinate data and color data of the surface of all measured objects in the panoramic range at one time and can obtain the three-dimensional point cloud model and grid model of the scene based on this information. When displaying the reconstruction results of the scene, the observer-centered method is adopted, so that the observer can experience the scene immersively. Experiments show that the sharpness is only related to the abscissa y of the dot matrix in the parameter setting. When the y coordinate increases from 11.13 to

17.57, the sharpness decreases from the highest 0.779 to 0.021; so, the y coordinate should be reduced as much as possible within the range to increase visual experience and immersion. The characteristics and innovations of this article are when using ASODVS to reconstruct the indoor scene in 3D, only need to start the software system and start the scanning thread to scan the scene, the program operation is simple, and the degree of automation is high. When collecting point cloud data, ASODVS always takes the single viewpoint Om as the coordinate origin. Therefore, there is no point cloud overlap, density difference, and data redundancy, and no more complicated calculation steps, such as point cloud data recording, are required. The disadvantage of this paper is that the depth measurement accuracy of space object points is not high. An ultra-high-definition imaging chip can be used to collect images to solve this problem. And the direction of the laser light source emitted by the current moving surface laser generator is parallel to the horizontal plane; so, it is impossible to effectively obtain the data (i.e., the z coordinate) that is also on the horizontal plane (such as the desktop). The projection direction of the laser light source can be changed so that the scanning of the three-dimensional laser can cover the entire vertical field of view, as well as the 3D reconstruction of the point cloud data obtained directly from ASODVS in this article, and the density of the point cloud data in the scene has nothing to do with the surface shape, which also affects the storage and modeling efficiency of the point cloud data to a certain extent. Future research will be based on the surface shape of the reconstructed object, intelligently identify the plane and complex surface of the reconstructed object, and select a suitable texture mapping and appropriate triangular mesh model to be accurate, true, fast, complete, and realistic. Simplicity and reliability have achieved simultaneous development.

Data Availability

No data were used to support this study.

Conflicts of Interest

The author declares that there are no conflicts of interest regarding the publication of this article.

References

[1] L. Yu and B. Pan, "Full-frame, high-speed 3D shape and deformation measurements using stereo- digital image correlation and a single color high-speed camera," *Optics & Lasers in Engineering*, vol. 95, no. 8, pp. 17–25, 2017.

[2] R. Zajdel, K. Sośnica, M. Drożdżewski, G. Bury, and D. Strugarek, "Impact of network constraining on the terrestrial reference frame realization based on SLR observations to LAGEOS," *Journal of Geodesy*, vol. 93, no. 11, pp. 2293–2313, 2019.

[3] T. Xie, K. Wang, R. Li, and X. Tang, "Visual robot relocalization based on multi-task CNN and image-similarity strategy," *Sensors*, vol. 20, no. 23, p. 6943, 2020.

[4] S. Kabir and C. Smith, "optimization of CMOS image sensor utilizing variable temporal multisampling partial transfer technique to achieve full-frame high dynamic range with superior low light and stop motion capability," *Journal of Electronic Imaging*, vol. 27, no. 2, pp. 1–4, 2018.

[5] S. Kabir, C. Smith, F. Armstrong et al., "Optimization of CMOS image sensor utilizing variable temporal multisampling partial transfer technique to achieve full-frame high dynamic range with superior low light and stop motion capability," *Electronic Imaging*, vol. 2017, no. 11, pp. 52–63, 2017.

[6] L. Shen, X. Feng, Y. Zhang, M. Shi, D. Zhu, and Z. Wang, "Stroboscope based synchronization of full frame CCD sensors," *Sensors*, vol. 17, no. 4, pp. 799–802, 2017.

[7] X. Ren, P. W. Connolly, A. Halimi et al., "High-resolution depth profiling using a range-gated CMOS SPAD quanta image sensor," *Optics Express*, vol. 26, no. 5, pp. 5541–5557, 2018.

[8] D. Kim, M. Song, B. Choe, and S. Y. Kim, "A multi-resolution mode CMOS image sensor with a novel two-step single-slope ADC for intelligent surveillance systems," *Sensors*, vol. 17, no. 7, pp. 1497–1499, 2017.

[9] S. R. Soomro, E. Ulusoy, and H. Urey, "Decoupling of real and digital content in projection-based augmented reality systems using time multiplexed image capture," *Journal of Imaging ence & Technology*, vol. 61, no. 1, p. 10406, 2017.

[10] M. A. Mazhar, C. Russell, M. Amiri, and N. A. Riza, "CAOS line camera," *Applied Optics*, vol. 58, no. 33, pp. 9154–9162, 2019.

[11] T. G. Vaikhanskaya, L. N. Sivitskaya, T. V. Kurushko et al., "Non-compaction cardiomyopathy. Part II: limitations of imaging techniques and genetic screening, clinical observations," *Russian Journal of Cardiology*, vol. 25, no. 12, pp. 3873–3875, 2020.

[12] S. Zhang, H. Li, Q. Yao et al., "A unique two-photon fluorescent probe based on ICT mechanism for imaging palladium in living cells and mice," *Chinese Chemical Letters*, vol. 31, no. 11, pp. 2913–2916, 2020.

[13] D. Lee, "Thermal imaging drones," *Law and order*, vol. 64, no. 5, pp. 20–22, 2016.

[14] U. S. Hort G. Kocaolu et al., "Gastrointestinal stromal tumor of the ileum mimicking adnexal mass," *Ege Tıp Dergisi*, vol. 59, no. 3, pp. 232–234, 2020.

[15] S. A. Korotkih, E. V. Sabadash, I. D. Medvinskiy et al., "Diagnostics of early signs of ocular pathology in patients with HIV/tuberculosis co-infection," *Vestnik Oftalmologii*, vol. 135, no. 5, pp. 61–65, 2019.

[16] V. S. Bereznitskiy and S. A. Alexandrova, "Multimodal diagnosis of right ventricular hamartoma," *Vestnik Rentgenologii i Radiologii*, vol. 101, no. 6, pp. 354–357, 2021.

[17] V. I. Kuplevatskiy, M. A. Cherkashin, D. A. Roshchin, N. A. Berezina, and N. A. Vorob'ev, "Prostate biopsy under magnetic resonance imaging guidance," *Vestnik Rentgenologii i Radiologii*, vol. 97, no. 1, pp. 48–55, 2016.

[18] K. J. GH, N. S. van den Berg, J. de Jong et al., "Multimodal hybrid imaging agents for sentinel node mapping as a means to (re)connect nuclear medicine to advances made in robot-assisted surgery," *European Journal of Nuclear Medicine and Molecular Imaging*, vol. 43, no. 7, pp. 1278–1287, 2016.

[19] J. Lyon, "MacArthur winner adapts high-tech medicine to third world," *JAMA*, vol. 317, no. 7, pp. 683–685, 2017.

[20] K. Danilovskiy, V. Glinskikh, and O. Nechaev, "Evaluation of the BKS LWD tool spatial resolution based on the numerical simulation results," *Interexpo GEO-Siberia*, vol. 2, no. 3, pp. 89–94, 2019.

[21] C. Fergo, J. Burcharth, H. C. Pommergaard, N. Kildebro, and J. Rosenberg, "Three-dimensional laparoscopy vs 2-dimensional laparoscopy with high- definition technology for abdominal surgery: a systematic review," *American Journal of Surgery*, vol. 213, no. 1, pp. 159–170, 2017.

[22] D. Ahlberg, V. Tassion, and A. Teixeira, "Sharpness of the phase transition for continuum percolation in R^2," *Probability Theory and Related Fields*, vol. 2, pp. 1–57, 2016.

[23] S. Ziesche, "Sharpness of the phase transition and lower bounds for the critical intensity in continuum percolation on R~d," *Annales de L'institut Henri Poincare*, vol. 54, no. 2, pp. 866–878, 2018.

[24] J. Uthayakumar, M. Elhoseny, and K. Shankar, "Highly Reliable and Low-Complexity Image Compression Scheme using Neighborhood Correlation Sequence Algorithm in WSN," *IEEE Transactions on Reliability*, vol. 69, no. 4, pp. 1398–1423, 2020.

[25] K. Geetha, V. Anitha, M. Elhoseny, S. Kathiresan, P. Shamsolmoali, and M. M. Selim, "An evolutionary lion optimization algorithm-based image compression technique for biomedical applications," *Expert Systems*, vol. 38, no. 1, article e12508, 2020.

[26] W. Elsayed, M. Elhoseny, S. Sabbeh, and A. Riad, "Self-maintenance model for wireless sensor networks," *Computers & Electrical Engineering*, vol. 70, pp. 799–812, 2018.

WILEY | Hindawi

Research Article

Automatic Recognition Algorithm of Information Architecture Reliability Based on Energy Internet Network Topology

Guowen Ren,[1] **Minrong Wu** **,**[2] **and Miao Yu**[3]

[1]*New Energy Research Institute, Chinese Society for Urban Studies, Beijing 100835, China*
[2]*State Grid Ningxia Electric Power Co., Ltd., Ningxia 750001, China*
[3]*Business School, China University of Political Science and Law, Beijing 102249, China*

Correspondence should be addressed to Minrong Wu; 90102332@ncepu.edu.cn

As a type of energy network, the scale of the power network is constantly expanding, and its structure has become more and more complicated. Correspondingly, the risks to the energy network are even less likely to be discovered, which will undoubtedly cause great troubles for the safe operation of the network. The traditional manual inspection method can no longer meet the requirements of huge and complex energy networks. Therefore, this paper proposes the algorithm, a research on the automatic identification of reliability of information architecture based on the topology of the energy Internet network. Abstract the server, storage, and other devices in the Energy Internet as network nodes, divide them according to service modules, and use Bayes estimation to evaluate and judge the impact of these nodes on the system function, so as to find the nodes with hidden risks. The results show that, compared with the traditional manual inspection method, the method proposed in this paper can efficiently and accurately find the nodes with risks and can help optimize the topology of the energy Internet network.

1. Introduction

Electric energy is one of the important energy sources for industrial development, and it is also the driving force for the sustainable development of social and economic development. The intelligent development of the power grid has also become the focus of research in various countries and regions [1]. However, with the increase in power demand, the power network has formed a huge interconnection network and has become more and more complex [2]. In the future, the power grid should provide safer, more reliable, clean, and high-quality power sources to meet the various power needs of society. Due to the huge size and complexity of the energy internet, there are likely to be risks and hidden dangers, and the operational reliability of the energy internet is directly related to the social production and operation order [3, 4]. If the energy internet fails, it is not only inefficient to rely on manual identification but it is also likely to be missed. Therefore, the research on the reliability identification of the information architecture of the energy internet will have a strong practical significance for the research and construction of the energy internet.

With the advancement of the smart grid, the addition of a large number of electronic devices and the introduction of new information technologies have brought many uncertainties and operational risks to the power network information system. In response to this problem, many experts and scholars have conducted research. In [5], the author pointed out that the traditional 10 kV AC distribution network uses a large number of distributed energy and DC loads, which reduces the reliability of power supply and greatly increases the number of converters. In the study, the author proposed an AC/DC hybrid distribution network structure to ensure the reliability of the power supply. In [6], the author discusses potential network attacks and their adverse effects on power grid operation and proposes a general SCADA network attack process. In addition, the main challenges and strategies for protecting the smart grid from cyberattacks are also

discussed. In [7], and the author proposed a social mobilization inspection system based on blockchain technology for external damage to the power grid, which helped to improve the detection level of power grid damage. In [8], according to the failure mechanism, failure type, and evolution characteristics of components in the relay protection system of intelligent substation, the author divides the factors that affect the operation status of equipment into long-term degradation failure and short-term impact failure. The single-configuration and dual-configuration risk assessment models of the relay protection system are established, and the degradation shock model is described based on the gamma distribution. In [9], the authors modeled and simulated the time-domain protection relays during the transmission of the power grid and used backup transient programs to simulate various failure scenarios. In [10], based on the hierarchical idea, the author used Markov chain and fault tree analysis to analyze the reliability of the wide-area measurement system and studied the importance of the wide-area communication components. In [11], the author proposes a high-voltage DC grid protection strategy to suppress DC fault current and prevent overcurrent in the branch of the modular multilevel converter. The strategy is based on the coordination of half-bridge modular multilevel converters and hybrid DC circuit breakers. In [12], in order to improve the reliability of the microgrid system, the author adopted a nonlinear signal transformation called "mathematical morphology" to introduce an intelligent differential protection scheme for the microgrid system. By considering various operating conditions such as microgrid topology (radial/-grid) and microgrid operation mode (island/grid connection), many fault and no-fault conditions are simulated. In [13], the authors compared the performance of protection coordination (time setting and area selection interlock) and digital modular protection when deployed to grid-connected battery storage systems. The comparison between these protection management methods is based on their structure, function, and responsiveness to achieve a specific response. The above research has played a good role in protecting the power network. However, these methods have some shortcomings. First of all, substations, etc. tend to be networked, and the form of information sharing has brought a fundamental change to the relay protection structure model and also brought new problems to the reliability evaluation of relay protection. Second, the management of the huge power grid needs improvement, such as providing services through modular thinking, which can improve the efficiency of existing methods. Third, the reliability identification of the system is one of the important factors to ensure the smooth progress of the work. The reliability of existing research on large and complex systems is still insufficient, and there are many loopholes in the manual detection method of operation and maintenance personnel.

The energy network has the characteristics of large number and complicated structure. In the study of reliability identification, the topology of the energy internet network can be applied. The use of the characteristics of the network topology has yielded many good results. In [14], the author used the network topology for time series data measurement of the distribution network, basically projecting the actual voltage phasor pattern into the signal library related to the possible topological transition of a given distribution network. In [15], the author used the network topology to detect the essential proteins in the protein-protein interaction network, which effectively improved the prediction accuracy of essential proteins and was of great significance for understanding the cellular process. In [16], the author applied the network topology to key infrastructures such as the Internet and solved the problem that traditional packet-switched networks often suffer from long-term communication when network congestion occurs. In [17], the author applied the network topology to improve the computing network performance of the IHEP data center in China and improved the development efficiency, effectively responding to the problems of large storage resources and structural responsibility. In [18], the author integrated the network topology index into the study of the impact of the aquifer of the river characteristics. The results show that the network density index is a more powerful measurement standard and provides an improved accounting network topology in concept and function. This method has influence on the convection system. In [19], the author applied the network topology to the brains of patients with severe motor function and found that this method is helpful to help patients recover. It may take the role of compensation in the early stage of the disease, and the compensation gradually weakens later. When evaluating recovery, it is beneficial to consider changes in global and local parameters. In [20], the author applied network topology to the modeling of random processes at the boundary layer of complex systems to evaluate the service quality requirements of the NGN concept telecommunication network. In [21], the author uses the network topology for chaotic image encryption, so that multimedia information, images, etc. can be safely transmitted through unsecured channels such as social networks. In [22], the author applied the network topology to the study of food trade, and the insights obtained can be used to understand how to maintain fair access to resources in the world under climate change. In [23], the author's network topology is used for power network vulnerability analysis and provides the best attack strategy based on network congestion and maximum damage. Think of congestion as a cascading propagation mechanism and compare the reward functions based on increased congestion and immediate power outages. In [24], the author applied network topology to moving target tracking in a nonline-of-sight environment and extracted range estimates from received signal strength and time-of-arrival measurements to help a priori knowledge gained during target movement. In [25], the author used the network topology for the exploration of forming materials to rationalize the physical and mechanical properties. The above research shows that the network topology has great advantages in dealing with complex problems and can deal with problems with network structure. Therefore, it is considered to use the network topology to study the automatic identification algorithm of the reliability of energy information architecture.

This paper proposes an automatic recognition algorithm for the reliability of information architecture based on the

energy Internet network topology. It solves the complexity and hugeness of the Energy Internet, and traditional manual inspection methods cannot meet the requirements of risk identification. This paper first abstracts devices such as servers, storage, and switches of the energy Internet as network nodes and abstracts the links between these devices to obtain network topology information. The obtained network topology is used to measure the distance, and an automatic reliability identification method is given. Through experiments, the method proposed in this paper can efficiently and accurately identify the risk nodes in the network, which provides practical reference for relevant maintenance personnel. In the experiment, the influence of noise on energy network performance evaluation was also considered. The Internet of energy continues to expand in scale, and the research in this paper provides a reference for the construction of related information systems.

2. Automatic Recognition Method of Information Architecture Reliability Based on Energy Internet Network Topology

2.1. Energy Internet Network Topology Model

2.1.1. Topological Composition of Energy Internet.
Relying on the national backbone network, the Energy Internet connects several energy local area networks and other self-organized energy networks to realize on-demand energy allocation and intelligent management of power generation, transmission, distribution, and power supply. The energy local area network is composed of energy routers, distributed power generation equipment, energy storage equipment, and controllable load equipment. The energy local area network can work on-grid or off-grid to operate independently, that is, it is highly autonomous in the domain and interconnected between domains. The intelligent energy sensors in each energy local area network continuously collect various information such as power generation equipment, energy storage equipment, and loads in the energy local area network, and make energy control decisions based on the scheduling instructions of the upper-level transmission dispatching system. Then send control commands to the energy router for execution to achieve a high degree of integration of information flow and energy flow.

2.1.2. National and Regional Networks.
First, construct a fully connected faction network with N nodes to realize the interconnection of the national backbone network. This avoids the collapse of a large-scale energy network caused by a certain transmission line interruption under the deliberate attack of the energy internet and at the same time realizes the remote transmission of energy and on-demand scheduling. Each node here is a large-scale energy router, and the lower layer can be connected to the regional-level energy network as well as large-scale power generation equipment.

Second, the regional energy network serves the energy supply of the region internally and connects to other regions and backbone networks externally. Not only can it be directly connected to large and medium-sized power generation and storage facilities and directly provide energy for large enterprises and defense departments but also can realize energy transmission and distribution.

The basic model framework of the energy internet is as follows: (1) the interconnection of the backbone network improves the robustness of the energy internet and the freedom of energy scheduling at the global level. (2) The construction of regional hierarchical topologies facilitates efficient management of the energy internet and ensures critical load power supply and improves power supply reliability in the event of a serious power grid failure. (3) The "long side" within the hierarchical structure establishes and solves the special power needs of some regions, ensuring the normal operation of key facilities and important industries.

2.2. Overall Plan for Automatic Risk Identification

2.2.1. Basic Requirements for Safe and Stable Operation of Power Systems.
In order to ensure the safe and stable operation of the power system, the basic requirements are as follows:

(a) In order to ensure the stability, frequency, and voltage level of the normal operation of the power system, the system should have sufficient static stability reserves, active and reactive power reserve capacity, and necessary adjustment means. At normal load fluctuations and when regulating active and reactive power flows, no sudden oscillations should occur

(b) The power grid structure is the basis for the safe and stable operation of the power system. In the planning and design, we should look at the overall situation and look forward to the overall consideration, rationally arrange the grid structure, strengthen the backbone network, and meet the following requirements: (1) it can adapt to the needs of development and changes and tide changes under various operating modes and has certain flexibility. (2) If any component is disconnected without failure, it should be able to maintain the stable operation of the power system and not cause other components to exceed the accident overload regulations. (3) It should have greater antidisturbance capability and meet the relevant requirements specified in this guideline. (4) Realize the principle of layering and zoning

(c) When the power system is damaged for any reason, predetermined measures must be taken to prevent the system from collapsing. Avoid long-term large-scale power outages and catastrophic power outages for the most important users. The load loss should be minimized as much as possible, and the system should resume normal operation as soon as possible

2.2.2. Basic Idea of Automatic Reliability Identification Scheme.
The composition of the energy information system includes multiple service modules, such as application-level service modules and storage-level service modules. Each service module of the information system needs to provide

services to users or other constituent modules through a network link. At the same time, some service modules also usually need to access one or more other support service modules through a network link to provide external services. If the service node in the service module fails, other users or modules that need to access the service node will not be able to access the service node via the network. This also means that the network link from the user or other nodes to the abnormal node is not available. At this time, if the other nodes in the service module are in a normal operating state, and the user can access other normally operating nodes through other links, the work of the module will not be affected by a faulty node. Correspondingly, the network may fail to access the node because of a certain faulty node, then, this is a single point of failure.

In this paper, the service cluster is divided according to the functional characteristics of the energy network. After that, according to the topology structure of the energy internet network, the network link set through which all service cluster access relationships pass through is found. By calculating whether there is an available link in each link set when a single node device fails, it is determined whether the single node device is a single hidden point.

2.2.3. Reliability Assessment of the Module.

The reliability of the module is the basis for evaluating the reliability of the system. The Bayesian estimation and correction method are used here. Unlike the general parameter estimation method, Bayes estimation does not assume that the parameter to be determined in the model formula is a fixed value constant, but instead sets it as a variable related to time t. Considering the randomness of the actual failure data, it is more scientific to set the parameter as a variable. Common parameter estimation methods only use overall information and sample information to estimate parameters. The concept of prior information was first proposed by Bayes. It combines the overall information of the failure data with the sample information of the real data to establish the concept of posterior information, obtains the prior distribution through the statistical characteristics of the failure data, and then speculates draw out the parameters in the model formula.

The prior distribution of the distribution function $F(x)$ of the population sample X is $DP(\alpha, P_0)$, $F_0(x) = P_0(X \le x)$. Where $DP(\alpha, P_0)$ is called the Dirichlet distribution subject to the parameter α, and α is a positive real number. If there is $p \sim Dir(\alpha)$, the probability density function of $p = (p_1, \cdots, p_m)$ is needed, and the formula is as follows:

$$\pi(p) = \frac{\Gamma\left(\sum_{j=1}^{m} \alpha_j\right)}{\prod\limits_{j=1}^{m} \Gamma(\alpha_j)} p_1^{\alpha_1 - 1} \cdots p_m^{\alpha_m - 1}, p_j \ge 0. \tag{1}$$

In the above formula, $p_1 + p_2 + \cdots + p_m = 1$. The Bayesian estimation formula for the distribution function $F(x)$ of the total failure sample is as follows:

$$\widehat{F}(x) = \sum_{i=1}^{h} \widehat{p}_i = \frac{\alpha}{\alpha + n} F_0(x) + \frac{1}{\alpha + n} \sum_{i=1}^{n} F_0(x \mid B_i). \tag{2}$$

2.3. Reliability Identification Based on Energy Internet Network Topology

2.3.1. Energy Network Topology Structure Ranging Method.
Reasonable topology structure can realize state detection and reduce the probability of accidents, so as to quickly and accurately deal with and restore to normal state. At the same time, the distribution network is a kind of network with many nodes and complex structure. Due to daily maintenance, changes, construction, etc., there is a lack of real-time status monitoring and feedback in the distribution network. This also leads to possible errors in the actual network topology. In the network topology, the line length between two nodes can be measured by the signal transmission function of power line carrier communication, and the most important is the time of arrival (ToA) measurement. Serious errors will inevitably affect the reliability and stability of the power system. Therefore, the ToA problem is a parameter estimation of the cumulative exponential signal.

2.3.2. Reliability Identification Method.
In this paper, the automatic identification of the reliability of the information architecture can be understood as the risk identification of the energy network. The main steps of this process are as follows: topology mapping and node initialization, definition of clusters, definition of access relationships between clusters, finding the set of access relationship links, and calculating the state value of nodes.

(1) Topology mapping and node initialization

Map the network topology diagram of the energy information system to the network connection diagram. In the network connection diagram, each node object contains three data attributes: node type, directly connected node set, and node status value. Among them, the node type storage area 0 or 1 is used to indicate whether the node belongs to a terminal node or a network node. A set of connected nodes stores a set of adjacent node objects directly connected to the node. The node status value storage area "+" or "-" is used to indicate whether the node status is normal or abnormal.

(2) Definition of cluster

Based on the architecture of the energy system, according to the principle of functional similarity, the nodes are divided into clusters. When a node is individually classified under a certain type of function, the single node is still regarded as a cluster. Number all clusters.

(3) Definition of access relationship between clusters

If there is an access relationship between the two clusters, R is used to indicate this access relationship, and the access relationship will be numbered in order from 1 to j. Relation$_j$ represents the j-th cluster access relationship. The node set included in Relation$_j$ mainly has two parts, one part is the source node set. The other part is the collection of destination cluster nodes.

(4) Find out the collection of links to visit
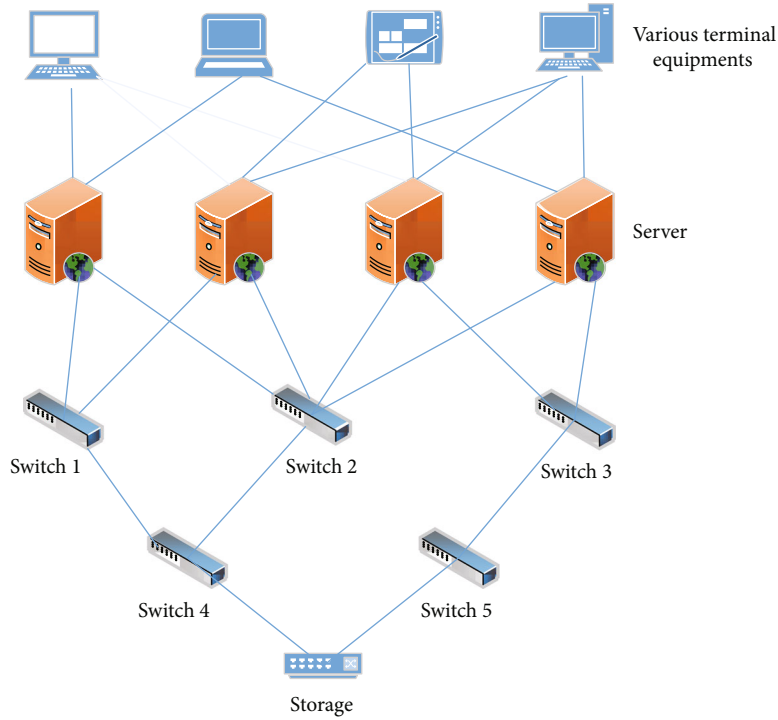
FIGURE 1: Energy network topology.
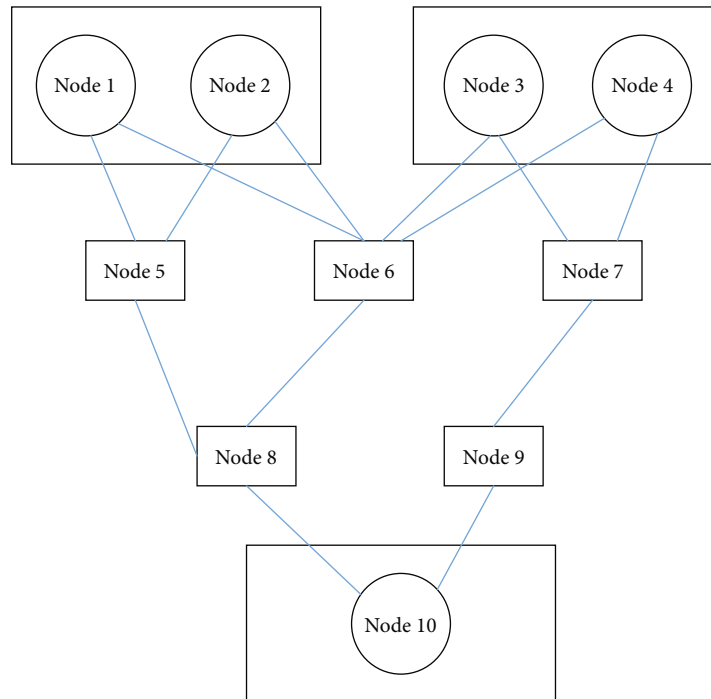
FIGURE 2: Topology map.

Since each node records neighbor node information, this information is similar to the next hop information in network routing. Therefore, it starts from a terminal node and transmits hop by hop through neighbor network nodes. Finally, it will reach another terminal node to form a network link with the terminal node as the head/tail node and several network nodes as intermediate nodes. In this step, computer traversal calculations can be used to obtain network links

from all end nodes to all other reachable end nodes. After calculating all network links, according to the terminal node information in the cluster access relationship, it is found that all cluster access relationships need to pass through the network link set. Let $\text{Relation}C_j$ denote the j-th cluster access relation network link set, and number the k network links in the set from 1 to k in sequence. That is, Link_{j-k} is used to denote the k-th network link in the j-th cluster access relationship.

(5) Calculate the state value of the node

Calculate the system function availability status value of each node in the system when a single node fails. To calculate the functional availability status value of each node, we first need to initialize and reset all node status values. Set the state value of the node to "-", and set the state value of the remaining $n - 1$ nodes to "+". Then calculate the state value of the link Link_{j-k}, the state value of the network link set contained in the $\text{Relation}C_j$, and the availability state value in turn. Therefore, assuming that there are n nodes in the energy internet, a total of n calculations are required.

3. Experiment of Automatic Recognition of Information Architecture Reliability

This paper abstracts the power network and uses the network topology of the energy Internet information system to describe the interrelationships among various devices in the energy Internet. Forming the link between the devices, the devices of the energy Internet topology include devices such as switches, gateways, storage, and servers. The energy Internet topology is shown in Figure 1.

By using the energy Internet network topology structure information, the function availability status value of the information system network topology node is calculated to find hidden risks in the network, so as to help relevant personnel adjust the system architecture. One of the important methods for automatically identifying the reliability of information architecture is the distance measurement between nodes in the network. Here, in order to facilitate the identification and research of energy network topology, the signal transmission function of power line carrier communication is used for measurement. This method is expressed as the measurement of time of arrival.

4. Results and Discussion of Automatic Identification of Information Architecture Reliability Based on Energy Internet Network Topology

4.1. Function Availability State Value Calculation. According to the existing topology structure diagram of the Energy Internet, after removing various terminal devices in the network, the network topology diagram is mapped, and the mapping result is shown in Figure 2.

TABLE 1: State value results.

Node	1	2	3	4	5	6	7	8	9	10
Link set 1	+	+	+	+	+	+	+	—	+	—
Link set 2	+	+	+	+	+	+	+	+	+	—
Link set 3	+	+	+	+	+	+	+	+	+	+
Functional availability	+	+	+	+	+	+	+	—	+	—

TABLE 2: Comparison of fit before and after.

	Model 1	Model 2	Model 3
Original	19.157	5.834	5.942
Modified	25.9	7.386	7.784
Increase	35.2%	26.6%	30.1%

TABLE 3: The obtained power channel model.

Path number	1	2	3	4	5	6
Length	198	213	228	236	251	483
Weight coefficient	0.49	0.262	-0.13	0.07	-0.026	-0.01
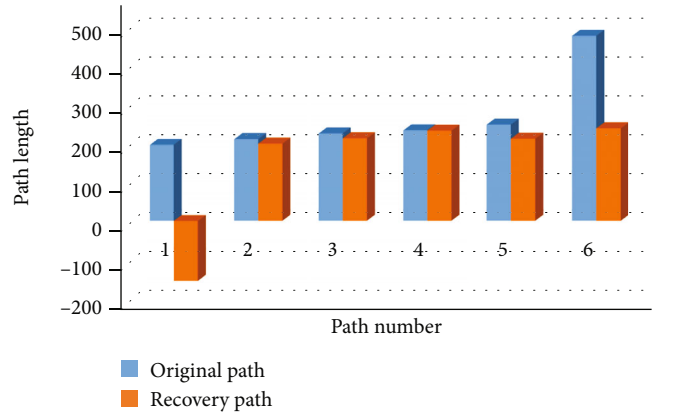
FIGURE 3: Channel estimation results when the signal-to-noise ratio is 60 dB.

As shown in the figure above, there are 3 link sets. According to the reliability identification method proposed above, the access relationship link set is found, and the state value of the node is calculated. The final results are shown in Table 1.

As can be seen from Table 1, in the bottom column of functional availability, the representation form of node 8 and node 10 is "-", indicating that these two nodes are potential risk nodes. According to the analysis of the topology diagram, when node 8 fails, nodes 1 and 2 in the cluster cannot access storage node 10, and the entire function of the cluster will be abnormal due to the inaccessibility of storage. Therefore, node 8 is indeed a hidden risk node, consistent with the calculation results. The storage nodes represented by node 10 are grouped into a cluster. Obviously, they are a single hidden risk node. In the process of calculating the availability of functions, node 8 and node 10 affect the access between clusters. Taking into account the reliability risks that exist here,
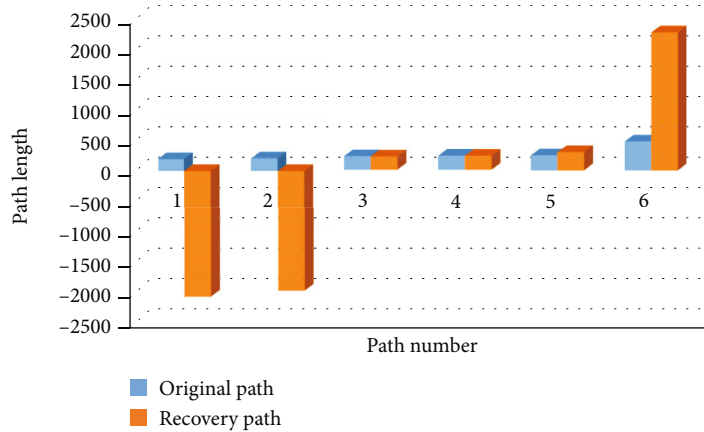
FIGURE 4: Channel estimation results when the signal-to-noise ratio is 30 dB.

certain adjustments can be made, such as adjusting network connections and adding spare device nodes, to the dangers posed by the presence of a single node.

4.2. Validation of Bayesian Estimate Revision Validity. To date, the reliability assessment of information system architecture has not yet had a commonly used method. There are many factors that will affect the reliability of the module, and the same factor will affect the different modules differently. Therefore, the module reliability evaluation model with the highest fitting degree corresponding to each module is also different. First, verify that the Bayesian estimate is revised so that each model's ability to estimate and predict module failure data is improved. Compare the fits of the three different models before and after, as shown in Table 2.

It can be seen from Table 2 that the prediction ability of the module has been improved in different degrees after combining with the Bayesian estimation and correction, and the corresponding improvement of the fitting degree of the three is 35.2%, 26.6%, and 30.1%, respectively. The analysis found that before the correction, the difference was mainly due to the model mismatch caused by the difference in the statistical characteristics of the module data. The candidate model correction based on Bayes estimation effectively avoids the inaccurate model fitting caused by the deviation of the parameter estimation.

4.3. ToA-Based Ranging Performance Evaluation. In the experiment, a power line channel model obtained is shown in Table 3. This is a power line channel model with 6 diameters, and the length and strength of each diameter are indicated in the table. It can be seen from the channel model that between the two points of channel transmission, there are 6 channels from the direct path to the reflected path, and the shortest path has a maximum weight of 0.49, which can be considered as a direct path. As the path becomes longer and the weight gradually decreases, other paths are complex reflection paths. The channel model will be used to estimate the time of arrival between two points. These reflection paths appear as multipaths that are continuously reflected between nodes other than the two points measured in the network. These numerical relationships are not

directly controlled by ToA, but may be affected by the location of other nodes in the network. Therefore, in terms of measuring ToA between two points only, it is only necessary to measure the first diameter, which is the shortest straight diameter. However, in order to measure the overall topology of the network, ToA needs to be measured between any two points. Knowing the reflection path between every two nodes may be helpful for a more detailed and thorough understanding of the overall situation, so it is also very helpful to piggy-back the value of the reflection path.

Add 60 dB and 30 dB noise to the channel and observe the recovery of each channel. The channel estimation results under different signal-to-noise ratios are shown in Figures 3 and 4.

It can be seen from Figures 3 and 4 that although the signal-to-noise ratio of 60 dB is already high, it still makes the estimation error. The presence of noise will affect the channel estimation results, mainly manifested in the emergence of negative value paths, as well as the misalignment and loss of paths. The accuracy of the method can be increased by discarding negative-value paths, but this reduces the total number of estimated paths, thereby reducing the sum of the number of reflected paths and the number of direct paths. The direct path is actually reserved by low errors, and high errors are mainly concentrated on the reflection path. In order to ensure the accuracy of measuring the direct path between two points, the accuracy of the reflection path is also required but not necessary, so it is necessary to verify the sensitivity of the direct path to noise. If the direct path is not sensitive to noise, the correct direct path can still be measured to provide correct information for the layer-by-layer reconstruction of the network. The inaccuracy of the information of the reflection path makes it necessary to discard them.

4.4. Comparison of Recognition Accuracy. In order to further explore the recognition accuracy level of the method proposed in this paper on the reliability identification of information architecture, here, we count the changes in the accuracy rate of the manual inspection method and the method proposed in this paper as the scale of the energy Internet continues to increase. As we all know, with the
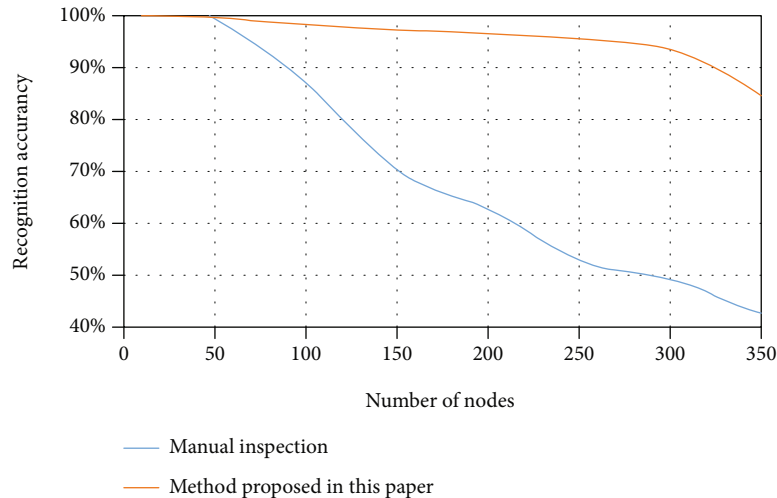
FIGURE 5: Change in recognition accuracy of different methods with network size.

increase of energy Internet nodes, the network has become more complex, and the determination of potential risks and faults on related nodes has become particularly difficult. The recognition rate of different methods on the expanding energy network is shown in Figure 5.

As can be seen from Figure 5, when the number of nodes is less than 50, the recognition accuracy of the proposed method and the manual inspection method is almost at the same level, and the difference is not very large. When the number of nodes in the network is higher than 50, the difference between the two methods starts to become obvious. The inspection accuracy of the proposed method is much higher than that of the manual inspection method. However, when the number of nodes is higher than 300, the recognition rate of risk-risk nodes with more methods mentioned in this paper shows a significant downward trend. The analysis found that this is because as the number of network nodes continues to increase, the topology of the energy Internet becomes extremely complex, which exceeds the reasonable number of network nodes in the method designed in this paper, resulting in a decrease in accuracy. Therefore, in the follow-up research, improving the recognition accuracy of the method in the larger and more complex network is one of the key research directions.

5. Conclusion

The energy internet is constantly developing and growing, and its complexity and scale are changing accordingly. Based on the actual situation, this paper solves the problem of automatic identification of the reliability of related information architecture and proposes a research on the automatic identification of information architecture reliability based on the energy Internet network topology. This effectively solves the problem that the traditional manual method is seriously insufficient in inspection efficiency and accuracy. In the future, the energy internet in different countries and regions will evolve with different topological characteristics. The research in this article will provide a reference for practical problems in related fields.

Data Availability

This article does not cover data research. No data were used to support this study.

Conflicts of Interest

The authors declare that they have no conflicts of interest.

Acknowledgments

References

[1] I. Yildiz and H. Caliskan, "Energetic and exergetic carbon dioxide equivalents and prices of the energy sources for buildings in Turkey," *Environmental Progress & Sustainable Energy*, vol. 37, no. 2, pp. 912–925, 2018.

[2] S. Z. Stefanov and P. P. Wang, "Taming the dragon-king of a day-ahead smart grid blackout," *New Mathematics & Natural Computation*, vol. 14, no. 1, pp. 11–20, 2018.

[3] N. Ferraz Junior, A. Silva, A. Guelfi, and S. T. Kofuji, "Iot6sec: reliability model for internet of things security focused on anomalous measurements identification with energy analysis," *Wireless Networks*, vol. 25, no. 4, pp. 1533–1556, 2019.

[4] Z. Song, J. Zhang, X. Xiao, and D. Niu, "Multi-energy combined peak dispatching system synthetic benefit evaluation based on variable weight theory and matter-element extension model," *International Journal of Energy Sector Management*, vol. 13, no. 3, pp. 713–725, 2019.

[5] X. Xu, N. Tai, Y. Hu, W. Wang, F. Zheng, and W. He, "Reliability calculation of ac/dc hybrid distribution network with a solid-state transformer," *The Journal of Engineering*, vol. 2019, no. 16, pp. 3067–3071, 2019.

[6] L. A. Kumar, "Protecting power grid automation systems," *Electrical India*, vol. 59, no. 6, pp. 52–54, 2019, 56, 58-60.

[7] H. E. Bing, L. I. Ren-De, S. S. Wang, and L. Jian-Guo, "A social mobilized inspection system against external damage of power

grid based on block chain technology," *Journal of Physics Conference Series*, vol. 1453, article 012104, 2020.

[8] F. Xiao, Z. Wang, Z. Zhang, X. Yin, and H. Li, "Study on maintenance strategy of relay protection system based on condition monitoring," *Power System Protection & Control*, vol. 46, no. 6, pp. 74–83, 2018.

[9] J. P. G. Ribeiro and F. V. Lopes, "Modelling and simulation of a time-domain line protection relay," *The Journal of Engineering*, vol. 2018, no. 15, pp. 861–865, 2018.

[10] W. Zhang, J. Xu, Y. Li, and X. Zou, "Detecting essential proteins based on network topology, gene expression data, and gene ontology information," *IEEE/ACM Transactions on Computational Biology and Bioinformatics*, vol. 15, no. 1, pp. 109–116, 2018.

[11] S. Wang, C. Li, O. D. Adeuyi, G. Li, C. E. Ugalde-Loo, and J. Liang, "Coordination of mmcs with hybrid dc circuit breakers for hvdc grid protection," *IEEE Transactions on Power Delivery*, vol. 34, no. 1, pp. 11–22, 2019.

[12] M. Mishra, R. R. Panigrahi, and P. K. Rout, "A combined mathematical morphology and extreme learning machine techniques based approach to micro-grid protection," *Ain Shams Engineering Journal*, vol. 10, no. 2, pp. 307–318, 2019.

[13] S. A. Saleh, C. Richard, X. F. St Onge, J. Meng, and E. Castillo-Guerra, "Comparing the performance of protection coordination and digital modular protection for grid-connected battery storage systems," *IEEE Transactions on Industry Applications*, vol. 55, no. 3, pp. 2440–2454, 2019.

[14] G. Cavraro and R. Arghandeh, "Power distribution network topology detection with time-series signature verification method," *IEEE Transactions on Power Systems*, vol. 33, no. 4, pp. 3500–3509, 2018.

[15] Z. H. Dai, Z. P. Wang, and Y. J. Jiao, "Reliability evaluation of the communication network in wide-area protection," *IEEE Transactions on Power Delivery*, vol. 26, no. 4, pp. 2523–2530, 2011.

[16] Y. Hu and M. Koibuchi, "Optimizing slot utilization and network topology for communication pattern on circuit-switched parallel computing systems," *IEICE Transactions on Information and Systems*, vol. E102.D, no. 2, pp. 247–260, 2019.

[17] A. Nechaevskiy, G. Ososkov, D. Pryahina, V. Trofimov, and W. Li, "Simulation approach for improving the computing network topology and performance of the China IHEP Data Center," *The European Physical Journal Conferences*, vol. 214, no. 5, article 08018, 2019.

[18] E. L. Heasley, N. J. Clifford, and J. D. A. Millington, "Integrating network topology metrics into studies of catchment-level effects on river characteristics," *Hydrology and Earth System Sciences*, vol. 23, no. 5, pp. 2305–2319, 2019.

[19] R. Chen, C. Li, and M. Su, "A study on the brain network topology attributes in stroke patients under severe motion function," *Chinese Journal of Rehabilitation Medicine*, vol. 34, no. 1, pp. 52–58, 2019.

[20] T. V. Azarnova, S. A. Barkalov, and V. V. Ukhlova, "Estimation of time characteristics of systems with network topology and stochastic processes of functioning," *Journal of Physics Conference*, vol. 1203, no. 1, article 012055, 2019.

[21] R. Vidhya and M. Brindha, "A novel conditional butterfly network topology based chaotic image encryption," *Journal of Information Security and Applications*, vol. 52, p. 102484, 2020.

[22] A. G. Dolfing, J. R. F. W. Leuven, and B. J. Dermody, "The effects of network topology, climate variability and shocks on the evolution and resilience of a food trade network," *PLoS One*, vol. 14, no. 3, article e0213378, 2019.

[23] C. Caro-Ruiz, A. S. al-Sumaiti, S. Rivera, and E. Mojica-Nava, "A mdp-based vulnerability analysis of power networks considering network topology and transmission capacity," *IEEE Access*, vol. 8, no. 1, pp. 2032–2041, 2020.

[24] S. Tomic, M. Beko, R. Dinis, and P. Montezuma, "Estimating directional data from network topology for improving tracking performance," *Journal of Sensor and Actuator Networks*, vol. 8, no. 2, p. 30, 2019.

[25] M. Formanek and F. Martelli, "Probing the network topology in network-forming materials: the case of water," *AIP Advances*, vol. 10, no. 5, article 055205, 2020.

WILEY | Hindawi

Research Article

Design and Implementation of a Rural Social Security System Based on Deep Learning

Yan Zhao [ID]

School of Economics and Management, Inner Mongolia Normal University, Hohhot, 010022 Inner Mongolia, China

Correspondence should be addressed to Yan Zhao; zhaoyan@imnu.edu.cn

After the reform and opening up, my country's economic level and total national strength have achieved unprecedented growth. The building of a well-off society in an all-round way is moving towards a harmonious society. The development of social security is also an important part of the development and improvement of a socialist harmonious society. This article is aimed at designing a rural social security system based on deep learning algorithms, using sample collection and statistical analysis methods, collecting samples, simplifying the algorithm, and establishing a new rural social security system. The data collected by the system shows that the proportion of farmers who choose very satisfied, satisfied, average, dissatisfied, and very dissatisfied with the satisfaction of the new rural insurance is 8.94%, 45.53%, 34.96%, 8.13%, and 2.44%. It can be seen that the proportion of farmers who choose to be satisfied is the largest, and more than 10.0% of farmers choose to be dissatisfied or very dissatisfied. Investigate the factors that farmers worry about participating in the new rural insurance, and the questionnaire options can also be set to multiple choices. The survey results show that 29.27% of the farmers think that the individual payment for participating in the new rural insurance is higher; 26.02% of the farmers believe that they do not understand the new rural insurance system; 9.76% of the farmers believe that it is unnecessary to pay for the new rural insurance; 22.76% of farmers choose to rely on themselves or their children in the future; 27.64% of farmers think that the system is unstable. It has basically realized the design of a brand new rural social security system starting from the deep learning of semantic computing.

1. Introduction

The rural social security system (the new rural endowment insurance system is a personal endowment insurance account in which the state establishes a lifetime record for each new rural insurance participant; individual payment, collective subsidies, and other economic organizations, social welfare organizations, and individual subsidies for the insured person's payment, and the local government's subsidy for the insured person's payment, all are credited to the personal account) is an indispensable system of people's livelihood security proposed based on our country's social status quo. Nowadays, most countries and regions are facing the problem of aging population. The issue of aging has increasingly become a hot issue of concern to various countries. At this stage, my country has become one of the countries with the largest aging population. Data shows that my country's aging population will reach its peak in the middle of this century, and my country's aging

problem will be extremely important. Through comparison between the urban and rural areas, the problem of rural population aging is even more serious. Therefore, solving the problem of the aging of the rural population is an important step in solving the problem of the aging of the population in our country. For a long time, my country's dual economy has caused the rural economy to lag far behind the urban areas. For example, rural areas are at a disadvantage compared with urban areas in terms of pension insurance. Nowadays, the majority of rural residents are not fully guaranteed for the elderly, and the concept of raising children and preventing the elderly is still deeply ingrained in many rural areas. With the continuous development of the national economy, the outflow of agricultural laborers and the development of family planning have resulted in the labor force being less than the elderly population. These undoubtedly increase the burden of agricultural pensions. Therefore, there is an urgent need to solve the problem of agricultural pensions. No matter from a theoretical level

or a practical point of view, it is imperative to solve the problem of rural old age security. In theory, the establishment of a modern old age security system in the vast rural areas can better enhance farmers' awareness of old age security and enrich my country's overall old age security system. From a practical point of view, it can effectively solve the current problem of providing services for the elderly in the vast rural areas of our country. At the same time, solving the problem of rural endowment insurance is an important way to develop the rural economy, build a new socialist countryside, and build a harmonious society. It is the only way to realize the Chinese people's pension in rural areas.

Deep learning is an important part of the field of artificial intelligence research. Machine learning allows computers to learn. Without the participation of machine learning, artificial intelligence will become insufficient. Therefore, machine learning is essential to the field of artificial intelligence. Through learning algorithms, machine learning enables the machine to learn the internal laws of the data from a large amount of data input from abroad so that it can identify and judge. The development of machine learning has experienced two major development stages of shallow learning and deep learning in history. Generally, deep learning can be understood as an important development of artificial neural networks. The artificial neural network (the artificial neural network is a research hotspot that has emerged in the field of artificial intelligence since the 1980s; it abstracts the human brain neuron network from the perspective of information processing, establishes a certain simple model, and composes different networks according to different connection methods; in engineering and academia, it is often abbreviated as the neural network or quasi-neural network; the aneural network is a computing model, which is composed of a large number of nodes (or neurons) connected to each other; each node represents a specific output function, called an activation function; each connection between two nodes represents a weighted value for the signal passing through the connection, which is called a weight, which is equivalent to the memory of an artificial neural network; the output of the network varies according to the connection method of the network, the weight value, and the activation function; the network itself is usually an approximation of a certain algorithm or function in nature, or it may be an expression of a logic strategy) simulates the neural network of the human brain to remove features and model it, learn from the knowledge imported from the external environment, and have the recognition and judgment capabilities similar to the animal brain. The artificial neural network is an important part of intelligence, and it provides an effective way to solve complex problems and control intelligence. Artificial neural networks are also an important research direction in the field of machine learning. Based on the deep learning method, this paper has determined the research goal, simplified the complex algorithm and designed the software, and realized the design and realization of the rural social security system. Deep learning applications include speech recognition, automatic machine translation, instant visual translation (photograph translation), and self-driving cars, which involve the intelligent direction of semantic computing.

In 1986, Wu et al. published an article on the application of the backpropagation algorithm, which is still in use today. But their algorithm is complex and general, and they did not design a more concise and simplified formula [1]. In 1998, Chen and Smys developed the LeNet5 convolutional neural network model. The network model contains 2 convergence layers, 2 concentrated layers, and 2 fully connected layers. This method uses local connection and weight distribution methods, which not only extracts features from the data but also reduces a large number of weight parameters. However, due to the limitation of computing resources at that time, even training a small neural network took a long time. Compared with other classification models in the same period (such as supporting carrier machines), it has no major advantages. In addition, when using the backpropagation algorithm on the traditional neural network, it is easy to deal with the problem of the disappearance of the step size [2]. In 2006, Zhong et al. published an article on deep neural networks in *Science* and proposed the idea of deep learning algorithms, which promoted the development of artificial neural networks and the application of deep learning methods in the field of image recognition. However, their research focuses on image recognition rather than optimization algorithms, and the proposed algorithm is still not easy to understand and not easy to operate [3].

The innovations of this article are as follows. (1) Under the general trend of vigorous development of intelligence, pioneeringly combine the concept of deep learning, a semantic computing aspect, with the rural social security system and consider rural society from a new perspective. Under the background of rural households' livelihood transformation, that is, under the separation of production and life of rural households, starting from the perspective of rural households, constructing rural household decision-making models to provide theoretical support for the improvement of a rural social security system is beneficial to rural economic development and rural stability. Sustainable development of the social security system guarantees this basic livelihood issue. (2) The algorithm that simplifies the training process of the convolutional neural network and the gradient descent method is studied. Compared with the traditional complex algorithm, it is more concise, and it is convenient to establish a model related to the actual problem. (3) The output efficiency of the system is maintained at a very high level. At the same time, a series of relevant government policies have been added to the algorithm to strictly ensure the standardization and efficiency of the system.

2. Design and Implementation Method of a Rural Social Security System Based on Deep Learning

2.1. Rural Social Security. The security system in which the state and social organizations provide financial and material assistance to all farmers in accordance with the law is called agricultural social security [4]. Its purpose is to narrow the gap between rich and poor among members of society, gradually improve the material life of farmers, and ensure social

security [5]. Fair and stable, realize social stability and economic development in rural areas, provide a good environment for rural development, promote healthy and sustainable development in rural areas, and accelerate agricultural modernization [6]. My country's rural social security system includes the following parts: rural social security, rural social welfare, rural social assistance, and rural preferential treatment. Agricultural social insurance covers a wide range of fields, such as family planning insurance, occupational injury insurance, medical insurance, and pension insurance [7]. However, the aging of the rural population in our country is extremely serious, the population is relatively dense, and farmers are unable to carry out their daily lives due to medical treatment, which increase the burden on farmers [8]. Therefore, my country's current agricultural social security system mainly includes aging and medical care, with the focus on the construction of the rural social pension and cooperative medical system [9]. Agricultural cultural relics insurance refers to the provision of pensions to farmers who have reached the retirement age in accordance with relevant laws and regulations of our country [10]. The purpose is to ensure the basic livelihood of retired farmers. The pension fund is jointly funded and established by the state, enterprises, and individuals [11]. Rural cooperative medical care is an interactive medical insurance system supported by the government. It is jointly funded by rural economic organizations and rural groups to reduce rural poverty caused by diseases and protect the health of rural residents [12].

Rural social assistance refers to a system in which the state and social groups provide material assistance to farmers who cannot guarantee their daily lives due to special reasons [13]. The system is aimed at maintaining income loss or income that cannot meet the minimum living needs of farmers [14]. At present, my country's rural social assistance focuses on disaster relief and rural livelihood systems [15]. The target of disaster relief is natural disaster farmers, and the target of the minimum agricultural security system is poor farmers who have not yet solved their clothing deficiencies [16]. The prosperity of rural society is a public welfare activity, which is a guarantee provided to certain special farmer groups, such as the elderly and the disabled [17], as well as vulnerable groups in rural areas. Its main purpose is to provide financial and material assistance to the elderly who cannot take care of themselves and the elderly without children in rural areas to ensure their basic living standards [18]. At the same time, they provide mental and physical support to the elderly, widows, and disabled in rural areas [19]. Help improve the living standards of rural residents [20]. In recent years, the per capita income and consumption levels of Chinese farmers have undergone earth-shaking changes [21]. At the same time, the original level of social welfare has been unable to meet their current needs [22]. Former farmers pay more attention to their living standards, such as food, clothing, housing, and transportation [23]. Now, they have begun to pay attention to their spiritual consumption needs [24]. However, rural social welfare security requires higher capital investment from state finance, which is extremely difficult for a developing country with a large population, so social welfare in rural areas cannot be realized in the short term [25].

2.2. Convolutional Neural Network.

In the field of deep learning, the most widely used convergent neural network (also known as convergent network) is a neural network specifically designed to process data with a similar grid structure. Compact neural networks perform well in many application areas, such as time series data (which can be thought of as a one-dimensional grid formed regularly over time) and image data (which can be regarded as a two-dimensional grid of pixels) [26–27]. A trainable multilayer network structure is composed of multiple single-layer convolutional neural networks. In convergent network terminology, the first parameter of convergence is usually called the input (that is, the data to be processed), the second parameter is called the kernel function (can be regarded as the processing function), and the output is called the feature map. In a traditional neural network, the output of a neuron is related to the weight of the input node and its connection, but the weight will not be reused according to the calculation rules of the calculation type; that is, when multiplied by an element, the input will not be used again. Parameter sharing exists in the feature map. Each feature map in level 2 will detect the same feature map in level 1. The same idea is expressed as a network with bound weights (i.e., weight distribution). The specific weight sharing is shown in Figure 1.

A typical plane in a convergent neural network includes three stages. In the first stage, the layer computes multiple convergences in parallel to generate a set of linear activation responses. In the second stage, each linear activation response will pass through a nonlinear activation function. This phase is sometimes called the detection phase. In the third stage, the concentrated function provided by the cohesive neural network is again used to optimize its output. The centralized function is responsible for processing the element's output from the adhesive layer to replace the network output at this location. The use of centralized functions can be considered a sufficiently powerful additional function before: the functions obtained through this level of learning must have a small amount of variable translation requirements. When this assumption is true, concentration can significantly improve the statistical performance of the network [28].

2.3. Simplification of the Algorithm.

The training of convolutional neural networks can be mainly classified into two algorithms, the gradient descent method and the backpropagation method. This part will simplify the algorithm of the gradient descent method.

The whole process takes the pixel data of the picture as input and extracts different features through several convolutional layers. Each convolutional layer is followed by a pooling layer to reduce the number of parameters, and finally, the fully connected layer is used to calculate the loss function, as shown in

$$Z = W^T X, \tag{1}$$

$$h(x) = g(z). \tag{2}$$

Among them, X refers to the pixel data matrix of the image and W^T refers to the transposition of the weight
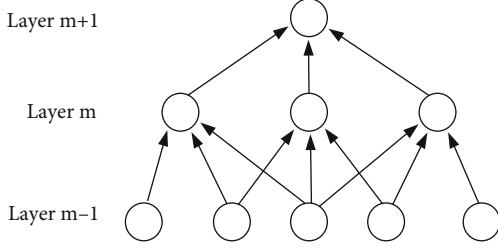
FIGURE 1: Weight sharing.

parameter matrix, which is the same as the input dimension, which contains a bias vector and the parameter weight of each data feature. The two are multiplied and then passed through. The activation function of g is used as the output of this layer, g can be an activation function such as sigmoid function or ReLU, and the output obtained can be used as the neuron input value of the next layer of the network, until the output result of the last layer is compared with the actual result. Construct a loss function, as shown in

$$C(h, X, Y) = \cos t(h(x), Y) = \frac{1}{2}(h(x) - y)^2. \quad (3)$$

Among them, X represents the input, $h(x)$ represents the output value after the last layer is activated, and Y represents the actual output of the input data sample. The cost function is a loss function, generally a square loss function. The $C(h, X, Y)$ obtained by the equation is the error value between the result and the label. When the error value continues to decrease, it means that the neural network model makes smaller and smaller errors. Based on the above requirements, it is possible to obtain the partial derivative of the weight of the equation and use the partial derivative to continuously update the weight parameter, which is the principle of the gradient descent method. Equation (4) is the partial derivative formula of this parameter:

$$\frac{\partial C(\theta)}{\partial \theta} = \lim_{\delta\theta \longrightarrow 0} \frac{C(\theta + \delta\theta)}{\delta\theta} = -\frac{1}{m}\sum_{i=1}^{m}(y^i - h_\theta(x^i))x^j, \quad (4)$$

where θ represents each weight parameter, and the obtained partial derivative is used as the adjusted value of the weight parameter, as described in

$$\theta^{k+1} = \theta^k - \eta\frac{\partial C(\theta^k)}{\partial \theta^k}. \quad (5)$$

Since there are so many weight parameters in the network, the calculation of partial derivatives for each parameter will lead to a huge amount of calculation, and the use of the back-propagation method can solve the problem of a large amount of calculation. The basic idea of the algorithm is that the residual of the latter layer is formed by the residual of the previous layer. Therefore, the residual of the previous layer can be

obtained by finding the residual of the last layer, as shown in

$$\delta_i^{(nl)} = \frac{\partial C}{\partial z_i^{(nl)}} = \left(a_i^{(nl)} - y_i\right) \cdot f'\left(z_i^{(nl)}\right). \quad (6)$$

It can be seen that the residual value of the neuron is actually the partial derivative of the weighted input of the loss value to this layer of the neuron. Then, for the number of layers l, the residual value should be as shown in Equation (7) below:

$$\delta^l = \left(W^{l+1}\right)^T \delta^{(l+1)} * g'\left(z^l\right). \quad (7)$$

Derive the following partial derivatives of the weight parameters (in the quality evaluation process, in order to be able to express the extent to which the relevant inspection items meet the specified requirements with data, according to the amount of work occupied by each item and the degree of importance of affecting the overall ability, the proportion of each item is divided (value)) and bias vectors in each neuron, as shown in

$$\frac{\partial C}{\partial w_{ij}^{(l)}} = a_j^{(l-1)}\delta_i^{(l)}, \quad (8)$$

$$\frac{\partial C}{\partial b_i^{(l)}} = \delta_i^l. \quad (9)$$

According to the above two formulas, multiply the learning rate to update each weight parameter and bias vector until the error value of the loss function is small enough.

In actual research and application, what we need to get is the distribution of observation data v defined by RBM, that is, the marginal distribution of common probability distributions, also called probability function distributions, as shown in Equation (10) (marginal distribution refers to the probability distribution of only part of the multidimensional random variables in probability theory and statistics):

$$P(v, \theta) = \frac{1}{Z(\theta)}\sum_h e^{-E(v,h|\theta)}. \quad (10)$$

The offset a_i of the visible layer unit is expressed as

$$\frac{\partial \log P(v\,|\,\theta)}{\partial a_i} = \langle v_i\rangle_{\text{data}} - \langle v_i\rangle_{\text{model}}. \quad (11)$$

The partial derivative of the bias b_j of the hidden layer unit is expressed as

$$\frac{\partial \log P(v\,|\,\theta)}{\partial b_i} = \langle h_i\rangle_{\text{data}} - \langle h_i\rangle_{\text{model}}. \quad (12)$$

In summary, we have completed the algorithm optimization of the gradient descent method of the convolutional neural network.

3. Design and Implementation Method Experiment of a Rural Social Security System Based on Deep Learning

3.1. System Requirement Analysis

3.1.1. Functional Requirement Analysis. The main function of this research system is to complete the storage of income and expenditure, business processing, and generation of various files of the municipal, county, district, and township and rural social endowment insurance funds. (One is the livelihood status of farmers, from the perspective of farmers' arable land area, income sources, main expenditures, and difficulties faced in production and life. The second is to investigate the implementation status of the rural social insurance system from the perspectives of farmers' participation in the new rural social pension insurance and new rural cooperative medical insurance, payment levels, and policy satisfaction. Third, the evaluation of the implementation effect of the rural minimum living security system is carried out from the perspectives of farmers' satisfaction with the system, the minimum living security standard, and the effect of poverty reduction.) With municipal management as the center, a central database is established to supervise, manage, and analyze data. Take county-level management as the main body, and carry out the management of various businesses and townships as auxiliary management. Most business operations can be carried out when the conditions are ripe.

The city bureau network version of this system mainly completes the business module design including township (village) management, personnel participation management, insurance relationship change management, payment management, account management, benefit distribution management, system connection management, financial management, financial subsidy management, and comprehensive query management, as well as information publicity, statistical reports, and system maintenance. No matter what kind of software the server is running on, the outlets can use the above Win7 operating system. The city level can operate the data of the city. Each county and city can only use and operate the data of the county and city. Each town can only use and operate the data of the county and city and can use and manipulate the data of the township.

3.1.2. Analysis of Nonfunctional Requirements. Since the proposal and final application of this topic provide a usable army equipment management system for specific units, it is necessary to consider how to build a stable, easy-to-maintain, expandable, and highly supportive system based on actual usage (concurrent number of troops of the equipment management system).

The construction of the server-side environment is one of the research contents of this topic. As a server, the machine is required to have enough loads for multiple users to access the required hardware configuration at the same time and have enough hard disk space to store data, and the machine is required to be equipped with the software interface system required by the operating system. In addition, it is necessary to combine the existing network conditions of the internal network, comprehensively consider factors such as stability, concurrency, security, and ease of use, and conduct reasonable selection, configuration, testing, evaluation, and evaluation of web services, databases, and operating systems. Trial deployment gets a strong operating, stable performance server-side environment construction plan.

3.2. The Data Flow of the System. Next, we design the data flow of the system.

The data flow diagram illustrates the information flow and data conversion from input to output. It is the logical process of data flow and processing in software and is the analysis of flow, storage, transmission, processing, and information. When designing a flowchart, only the basic operating logic of the system should be considered, not how to implement these functions in detail. The data processing of agricultural social insurance activities is basically divided into 7 parts. First, participate in the insurance and create file information based on the declared initial personal information. Then, pay the fee, and based on the file information, generate the payment information according to the declared payment details. Follow up payment account opening, according to the declared account opening personnel list, and based on the existing payment information, generate the issuance standard. According to the designated issuance time period, on the basis of the existing issuance standards, the issuance information is generated. According to the declared list of final insurance personnel, the final insurance information is generated by referring to the issuance information and payment information. According to the transfer-out application, the transfer-out information is generated on the basis of the existing file information, and the file information is modified. Finally, according to the surrender application, refer to the payment information to generate surrender information.

3.3. System Business Design. This system meets the needs of the daily work of the new rural social endowment insurance management (the survey adopts a random sampling method; the survey content mainly covers three aspects: first, the production and living conditions of farmers, from the perspective of farmland area, income sources, main expenditures, and difficulties faced by farmers in production and life; the second is to investigate the implementation status of the rural social insurance system from the perspectives of farmers' participation in the new rural social endowment insurance and new rural cooperative medical insurance, payment levels, and policy satisfaction; and third, the evaluation of the implementation effect of the rural minimum living security system is carried out from the perspectives of farmers' satisfaction with the system, the minimum living security standard, and the effect of poverty reduction), with complete functions, easy operation, and practical management software. Through investigation, I learned about the business related to the daily work of the rural social pension insurance management department. The business of the system consists of the following parts. Next, we will introduce several important business processes in the system design of this article.

The business flowchart of insurance registration is shown in Figure 2.
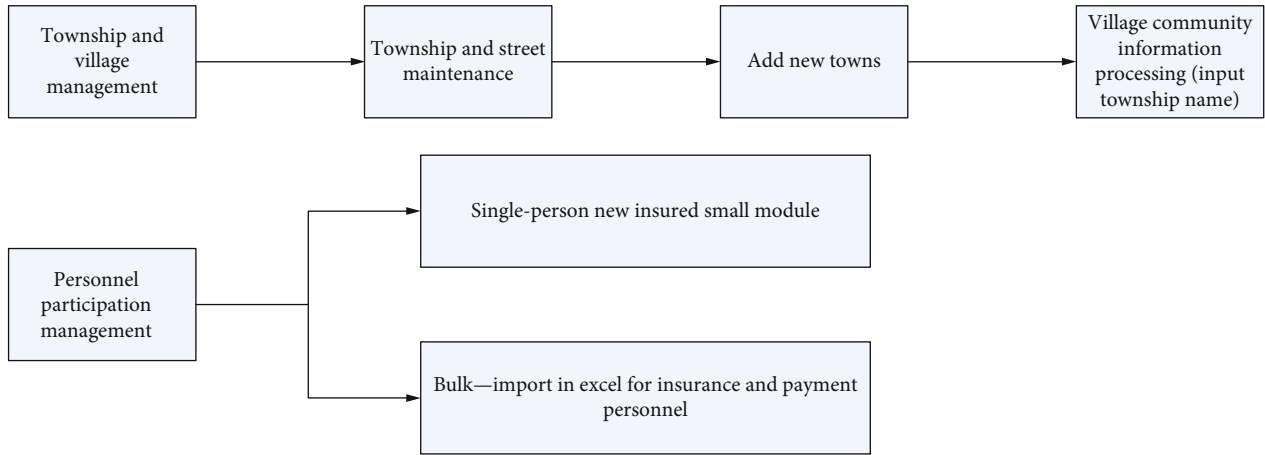
Figure 2: Business flow processes of insured registration.
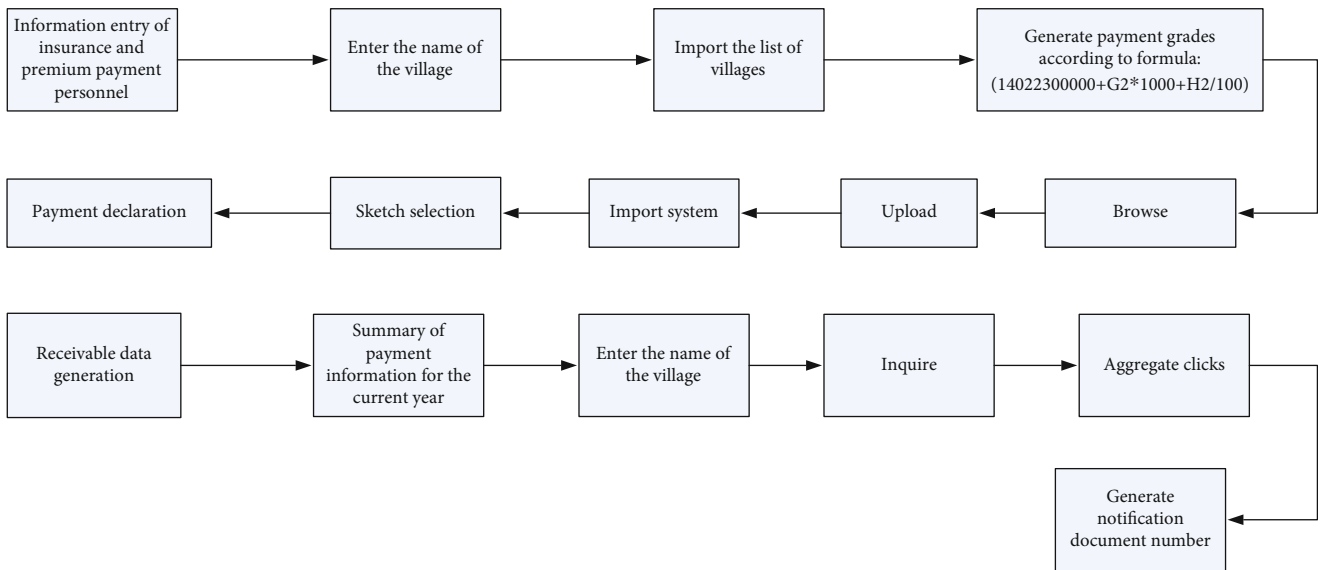
Figure 3: Business flow processes of pay insured fees.

The business flowchart of insurance premium payment is shown in Figure 3.

The flowchart of the payment of benefits is shown in Figure 4.

The above is the basic business flowchart of the system design of this article.

4. Experimental Results of the Design and Implementation of the Rural Social Security System Based on Deep Learning

4.1. Survey Content and Sample Analysis. The survey adopts a random sampling method. The survey content mainly covers three aspects. First, the production and living conditions of farmers, from the perspective of farmland area, income sources, main expenditures, and difficulties faced by farmers in production and life. The second is to investigate the imple-mentation status of the rural social insurance system from the perspectives of farmers' participation in the new rural social endowment insurance and new rural cooperative medical insurance, payment levels, and policy satisfaction. Third, the evaluation of the implementation effect of the rural minimum living security system is carried out from the perspectives of farmers' satisfaction with the system, the minimum living security standard, and the effect of poverty reduction. The samples involved 2 counties and cities, 7 towns, and 17 villages, and a total of 192 valid samples were collected. The sample distribution is shown in Table 1.

In the survey sample, males accounted for 61.4%, and females accounted for 38.6%; illiterate accounted for 16.6% (more left-behind elderly in the survey area), 41.5% of the education level is only elementary school, 31.1% of the education level is junior high school, and the education level is high school (middle school). Those with a college degree or above accounted for 6.2%; those with a college degree or
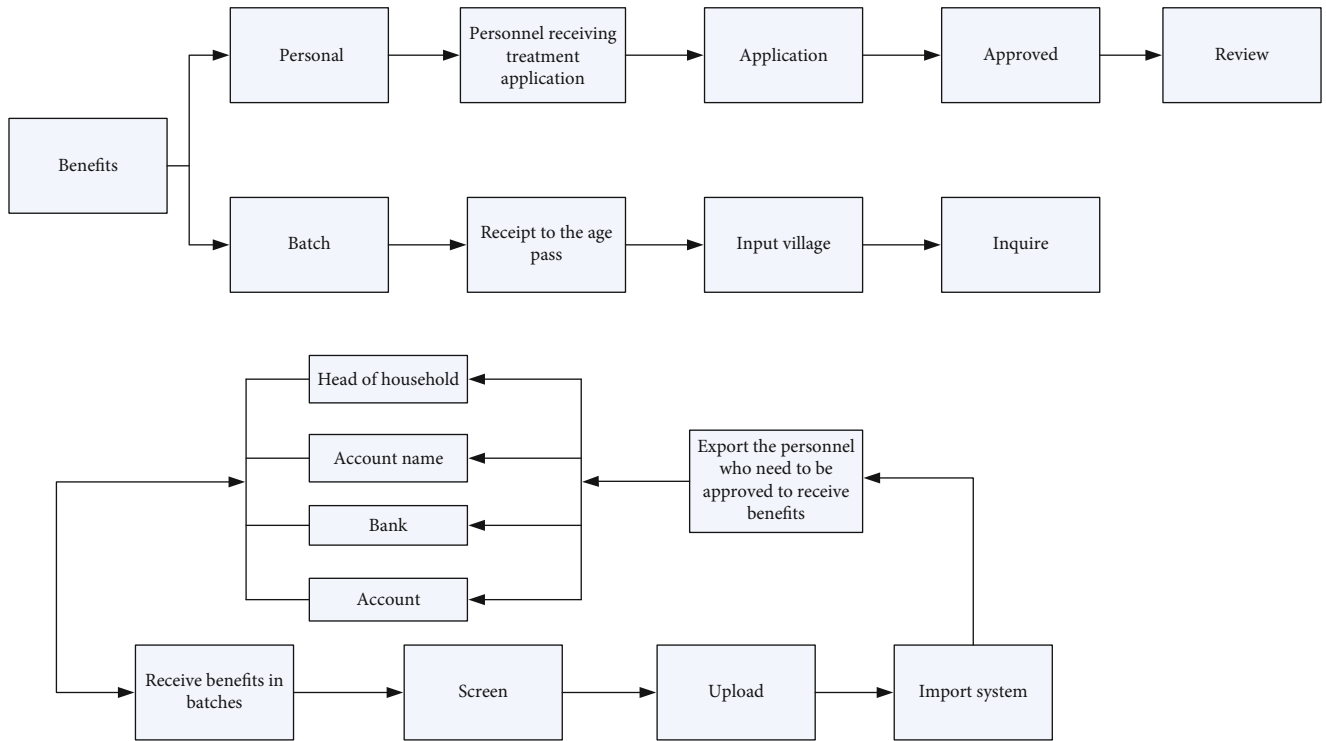
Figure 4: Business flow processes of benefit distribution.

above accounted for 4.1%; those aged 18-29 accounted for 5.2%, those aged 30-44 accounted for 24.0%, those aged 45-59 accounted for 38.0%, those aged 60-74 accounted for 28.1%, and those aged 75 or above accounted for 4.7%; 18.8% of households had 3 persons or less, 23.4% had 4 persons, 25.0% had 5 persons, 22.4% had 6 people, and 10.4% had 7 or more people; people with financial resources of 0 accounted for 2.6%, 1 person accounted for 16.1%, 2 people accounted for 36.5%, 3 people accounted for 30.2%, 4 people accounted for 9.9%, and those with 5 or more people accounted for 4.7%; 28.1% indicated those with capable relatives at home, 71.9% indicated those with no capable relatives, 17.7% indicated those with college students at home, and 82.3% indicated those without college students. Accounting for 49.0%, 51.0% indicated those who did not go out to work; 3.3% of the cultivated land area was less than 1 mu, and 11.5% accounted for 1-2 acres (including 1, less than 2) and 2-3 acres (including 2, less than 3). Accounting for 46.5%, 3-4 acres (including 3, less than 4) accounted for 23.0%, 4-5 acres (including 4, less than 5) accounted for 14.8%, and 5 acres and above accounted for 24.6%.

Among them, the composition of the income sources of statistical farmers is shown in Table 2.

Due to the fragility characteristics of farmers, there are many life pressures, including irresistible natural risks, lack of production materials and technological limitations, people's livelihood issues closely related to life, and systemic risks from changes in national policies. Figure 5 shows the life and production pressure of the survey sample farmers.

From the specific survey data, in the survey sample population, 12.26% of the farmers feel that the pressure on production and life is very high, 40.47% of the farmers feel that

Table 1: Survey sample distribution table.

	Town	Village	Residents
County seat A	a	1	11
	b	2	28
	c	2	25
	d	2	23
	e	2	24
County seat B	a	4	38
	b	4	43

Table 2: The composition of income sources of survey sample farmers.

Income type	The proportion (%)
Agricultural income	23.23
Self-employed income	2.94
Income from migrant workers	58.07
Transfer income	4.76
Other income	13.00

the pressure on production and life is relatively high, 37.48% of the farmers feel that the pressure on production and life is average, and 8.97% of the farmers feel that the pressure on production and life is very small, and the number of farmers who choose not to be pressured is 0. It can be seen that the farmers in the survey area feel that the pressure on production and life is very high, and the relatively large samples account for 51.76% of the total sample.

FIGURE 5: Investigate the life and production pressure of sample farmers.

4.2. Farmers' Risk Aversion Methods. In the survey data, a large number of the rural surplus labor force in the survey sample source areas a and b transferred to the cities. For the sample farmers surveyed, 51% of the farmers did not receive a more stable, flexible, and higher income than those engaged in agricultural production. There are migrant workers in the family. This kind of higher income through the process of migrant workers is one of the main ways for farmers to prevent risks; the rural social security system is gradually improved in the survey area, and farmers pass on part of the risk to the society by participating in social insurance. At present, the participation rate of rural households is relatively high. The participation rate of the new rural cooperative medical system in the survey sample is as high as 98.57%, and the participation rate of the new rural social endowment insurance reaches 85.66%. At the same time, a small number of rural households whose income is lower than the local minimum living standard also receive subsistence allowances and will avoid falling into extreme poverty; the surveyed farmers are generally not well-educated. Even if the cost of education continues to rise, farmers are paying more and more attention to their children's education, especially their children's higher education. 23.8% of the survey sample farmer households have college students; with the in-depth development of the rural market economy, the number of farmers engaged in business activities such as self-employed businesses has gradually increased. The survey sample has 20 farmers' families engaged in large-scale business activities such as vegetables and fruits through contracted land, and 18 of the farmer households are engaged in self-employed business activities, accounting for 19.79% of the sample population; farmers participating in commercial insurance are also gradually increasing, accounting for 35.21% of the sample population. Farmers have participated in agricultural insurance and other commercial insurance, as shown in Table 3.

TABLE 3: Investigate the risk aversion portfolio of sample farmers.

	Rate (%)	Motivation
Shift labor	51	Get higher income
Self-employed	35.21	
Investment education	23.9	Reserve human capital
Bank savings	39.1	Prevent risks
Pension	85.66	Pass on risk
Medical insurance	98.57	
Business insurance	27.97	

Join the satisfaction evaluation system (satisfaction evaluation is based on whether the service recipient's needs are met as an objective evaluation scale, and it is a method of final quality evaluation), as shown in Table 4.

The same as farmers' satisfaction with the new rural cooperative medical system, the survey of farmers' satisfaction with the new rural insurance (pension insurance is an important part of the social security system, and it is one of the most important types of insurance in the five major types of social insurance; the purpose of endowment insurance is to protect the basic living needs of the elderly and provide them with a stable and reliable source of life) shows that the percentages of farmers choosing very satisfied, satisfied, average, dissatisfied, and very dissatisfied are 8.94%, 45.53%, 34.96%, 8.13%, and 2.44%, respectively; it can be seen that the proportion of farmers who choose to be satisfied is the largest, and more than 10.0% of farmers choose to be dissatisfied or very dissatisfied. Investigate the factors that farmers worry about participating in the new rural insurance, and the questionnaire options can also be set to multiple choices. The survey results show that 29.27% of the farmers think that the individual payment for participating in the new rural insurance is higher; 26.02% of the farmers believe that they do not understand

TABLE 4: Satisfaction of rural households' social insurance system.

	Very satisfied	Satisfied	Generally satisfied	Dissatisfied	Very dissatisfied
NCMS	16.26	35.77	40.65	6.50	0.81
New rural insurance	8.94	45.53	34.96	8.13	2.44

NCMS: new cooperative medical system.
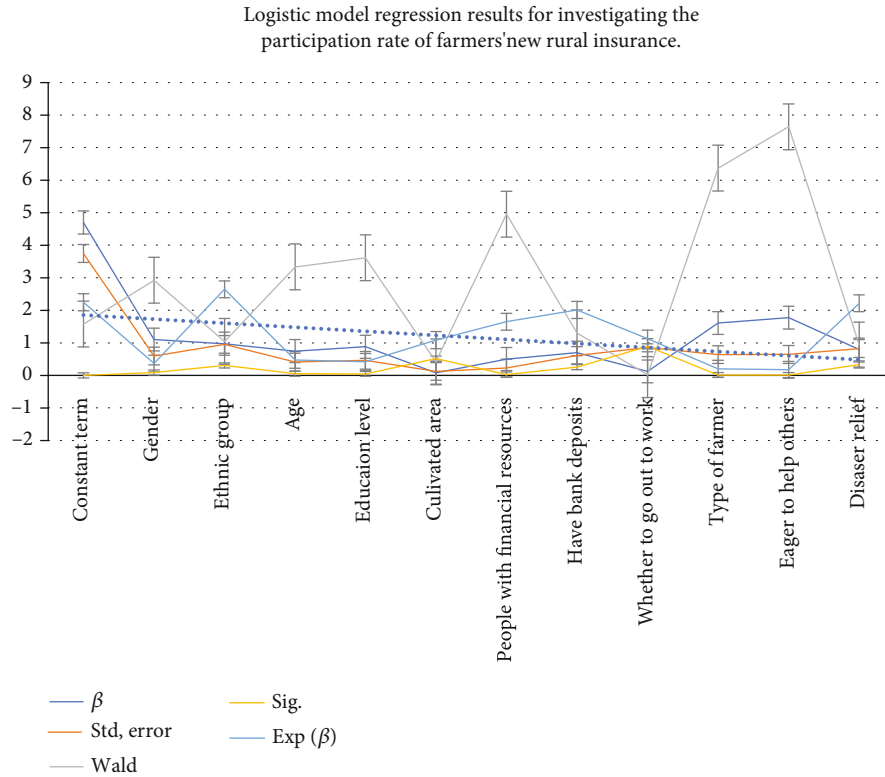
FIGURE 6: Logistic model regression results for investigating the participation rate of farmers' new rural insurance.

the new rural insurance system; 9.76% of the farmers believe that it is unnecessary to pay for the new rural insurance; 22.76% of farmers choose to rely on themselves or their children in the future; 27.64% of farmers think that the system is unstable.

4.3. Use the Logistic Model Established by the Gradient Descent Method Based on Deep Learning to Analyze the Regression Results. According to the content of the questionnaire survey, the factors that affect farmers' participation in the new rural insurance are summarized into individual characteristics of farmers, family resource endowments, and social environmental factors. Among them, the individual characteristics of farmer households include four variables: gender, ethnicity, age, and educational level; family resource endowment factors include the following: arable land area, number of households with financial resources, whether the family has bank deposits, whether the family has migrant workers, and the main income of the household (source type: agriculture, work, and business); social environmental factors include the following: whether relatives and friends give help when encountering difficulties and encountering natural

disasters and whether they receive government assistance in times of difficulty. Using SPSS 19.0 statistical software, the logistic regression model established above was used to estimate the factors affecting the farmers participating in the new rural insurance in the dependent variable survey area, as shown in Figure 6.

From the overall model estimation results, the chi-squared test value of the model is 29.633 (the chi-squared test is a very versatile method of hypothesis testing; its application in the statistical inference of classified data includes the following: the chi-squared test comparing two rates or two constituent ratios and comparing multiple rates or multiple constituent ratios and the chi-squared test and correlation analysis of classification data), and its corresponding Sig value is 0.002 (Sig is a significant index, where generally greater than 0.05 indicates that the difference is not significant, less than 0.05 indicates that the difference is significant, and less than 0.01 indicates that the difference is extremely significant), which has reached significance, indicating that the overall estimation effect of the regression model is better. However, in terms of the effect of explaining the dependent variable for a single independent variable, the independent
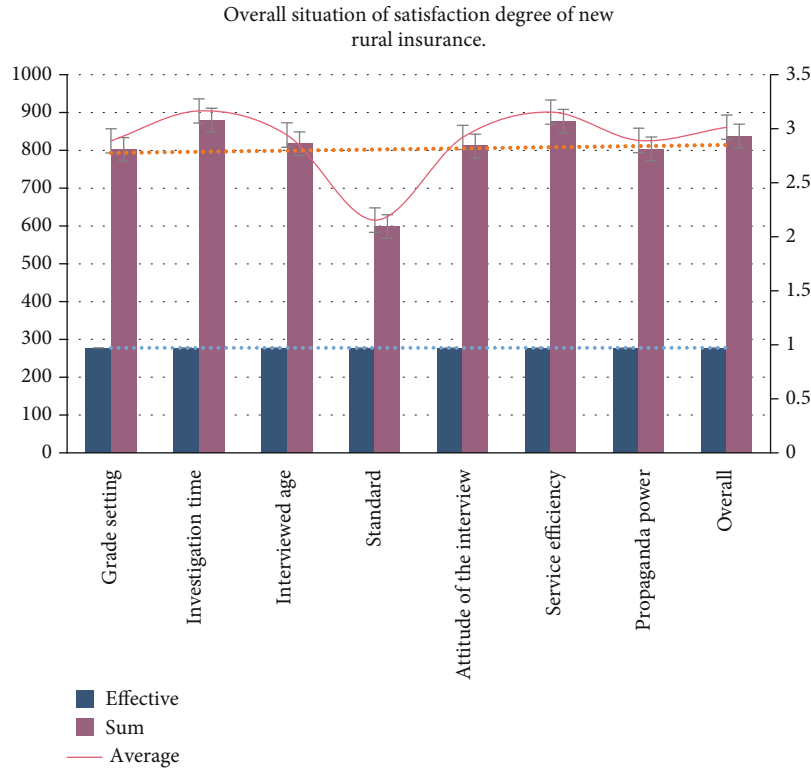
FIGURE 7: Overall situation of the satisfaction degree of new rural insurance.

variables in the research question are only X_3, X_4, X_6, X_9, and X_{10}. These variables are statistically significant, and the other 6 independent variables are statistically significant. The above is not significant.

From the regression model, gender and ethnicity have no significant effect on the new rural insurance participation rate of farmers in the survey area, age has a positive effect on the insurance participation rate, the education level has a negative effect on the insurance participation rate, and family resource factors have economic sources. The number of people has a positive impact on the participation rate of the new rural insurance, and whether or not they receive assistance when encountering difficulties such as natural disasters has no significant impact on the participation rate.

Finally, we have done satisfaction statistics on the rural social security system designed in this article. In the overall analysis of satisfaction with the new system, the questionnaire uses a 5-level Likert scale, with a total of 1, 2, 3, 4, and 5 ratings, which are very dissatisfied, dissatisfied, fair, satisfied, and very satisfied. The lowest score is 1 point, and the highest score is 5 points. The higher the score, the higher the satisfaction level, and vice versa. Use SPSS 24.0 software (SPSS (Statistical Product and Service Solutions) software) (initially, the full name of the software was "Statistical Software Package for Social Sciences," but with the expansion of SPSS product services and the increase in service depth, SPSS officially changed its English name to "Statistical Product and Service Solutions" in 2000, which marks that major adjustments are being made to the strategic direction of SPSS; SPSS is the general term for a series of software products and

related services for statistical analysis operations, data mining, predictive analysis, and decision support tasks launched by IBM; there are Windows and Mac OS X versions) to analyze the average satisfaction data of the recovered new system. The specific distribution is shown in Figure 7.

It can be seen from the figure that the overall satisfaction rate of this questionnaire is relatively qualified, reaching an average of 2.5 for general satisfaction. Among them, the average satisfaction of the grade setting, receiving age, payment method, and service efficiency is slightly less. Higher than average, it shows that some rural residents are quite satisfied with these tasks, but the proportion is not too large. It shows that the design of the rural social security system based on deep learning designed in this paper is relatively successful.

5. Conclusions

The research design shows that the design of the rural social security system based on deep learning proposed in this article is more powerful in statistical data, better in data retention, and more timely in response to the system than other current rural social security systems. The statistical capacity is also more powerful. This article uses the sample collection method and statistical analysis method, collects samples, simplifies the algorithm, and establishes a new rural social security system. The data collected by the system shows that the proportion of farmers who choose very satisfied, satisfied, average, dissatisfied, and very dissatisfied with the satisfaction of the new rural insurance is 8.94%, 45.53%, 34.96%, 8.13%, and 2.44%. It can be seen that the proportion of

farmers who choose to be satisfied is the largest, and more than 10.0% of farmers choose to be dissatisfied or very dissatisfied. Investigate the factors that farmers worry about participating in the new rural insurance, and the questionnaire options can also be set to multiple choices. The survey results show that 29.27% of the farmers think that the individual payment for participating in the new rural insurance is higher; 26.02% of the farmers believe that they do not understand the new rural insurance system; 9.76% of the farmers believe that it is unnecessary to pay for the new rural insurance; 22.76% of farmers choose to rely on themselves or their children in the future; 27.64% of farmers think that the system is unstable. The data collected by the system designed in this paper is very accurate, the sample size is large enough, and the automatic analysis of the system is also very fast. The shortcomings of this article are as follows: the preliminary work is very complicated and cumbersome, and the part related to semantic calculation is relatively obscure and cannot be widely applied to other system designs. Due to the limitation of conditions, this paper only selected two counties and cities in the north for data collection and did not comprehensively consider the development trend of rural areas in the north and south of my country. This system cannot be used in rural social security throughout the country. In the simplification and refinement of the future system, we can comprehensively select rural areas in different situations in my country's southern, northern, and even western regions for larger data analysis so that the rural social security system based on deep learning can be representative across the country.

Data Availability

No data were used to support this study.

Conflicts of Interest

The author declares no conflict of interest.

Acknowledgments

References

[1] T. Wu, S. Wen, S. Liu et al., "Detecting spamming activities in Twitter based on deep-learning technique," *Concurrency and Computation: Practice and Experience*, vol. 29, no. 19, pp. 14–17, 2017.

[2] J. Chen and S. Smys, "Social multimedia security and suspicious activity detection in SDN using hybrid deep learning technique," *Journal of Information Technology and Digital World*, vol. 2, no. 2, pp. 108–115, 2020.

[3] M. Zhong, Y. Zhou, and G. Chen, "A security log analysis scheme using deep learning algorithm for IDSs in social network," *Security and Communication Networks*, vol. 2021, no. 4, 2021.

[4] K. Huang, Q. Li, and G. Zhu, "Electric tower fault detection method based on deep learning," *IPPTA: Quarterly Journal of Indian Pulp and Paper Technical Association*, vol. 30, no. 8, pp. 733–737, 2018.

[5] R. Greiner, L. Fernandes, F. McCartney, and J. Durante, "Reasons why some irrigation water users fail to comply with water use regulations: a case study from Queensland, Australia," *Land Use Policy*, vol. 51, no. 9, pp. 26–40, 2016.

[6] C. Kumar, T. S. Bharati, and S. Prakash, "Online social network security: a comparative review using machine learning and deep learning," *Neural Processing Letters*, vol. 53, no. 1, pp. 843–861, 2021.

[7] D. Osabe, Y. Litsuka, and A. Higashi, "Solutions to social problems leveraging image analysis technology based on machine learning," *Fujitsu Scientific & Technical Journal*, vol. 53, no. 3, pp. 32–38, 2017.

[8] C. Zhou, F. Li, W. Cao, C. Wang, and Y. Wu, "Design and implementation of a novel obstacle avoidance scheme based on combination of CNN-based deep learning method and liDAR-based image processing approach," *Journal of Intelligent and Fuzzy Systems*, vol. 35, no. 2, 2018.

[9] A. Dayal, N. Paluru, L. R. Cenkeramaddi, J. Soumya, and P. K. Yalavarthy, "Design and implementation of deep learning based contactless authentication system using hand gestures," *Electronics*, vol. 10, no. 2, pp. 182–184, 2021.

[10] M. Saber and E. M. Elkenawy, "Design and implementation of accurate frequency estimator depend on deep learning," *International Journal of Engineering & Technology*, vol. 9, no. 2, 2020.

[11] W. Qian and Y. Ge, "The implementation of leisure tourism enterprise management system based on deep learning," *International Journal of Systems Assurance Engineering and Management*, vol. 2, no. 9, pp. 45–51, 2021.

[12] A. T. Q. Al-Aqbi, R. R. K. Al-Taie, and S. K. Ibrahim, "Design and implementation of online examination system based on MSVS and SQL for university students in Iraq," *Webology*, vol. 18, no. 1, pp. 416–430, 2021.

[13] C. Wang, L. Zheng, B. Li, and Z. Li, "Design and implementation of EtherCAT Master based on Loongson," *Procedia Computer Science*, vol. 183, no. 2, pp. 462–470, 2021.

[14] O. Akanbi and O. Abegunde, "Design and implementation of mobile information system for Federal Road Safety Corps (FRSC) of Nigeria," *International Journal of Sensor Networks and Data Communications*, vol. 9, no. 1, 2021.

[15] S. Dario Alessandro et al., "Mobile-edge computing architecture: the role of MEC in the Internet of Things," *IEEE Consumer Electronics Magazine*, vol. 5, no. 4, pp. 84–91, 2016.

[16] P. Corcoran and S. K. Datta, "Mobile-edge computing and the Internet of Things for consumers: extending cloud computing and services to the edge of the network," *IEEE Consumer Electronics Magazine*, vol. 5, no. 4, pp. 73-74, 2016.

[17] Z. Tian, D. Liu, W. Chen, W. Wang, S. Pan, and N. Guo, "Analysis and optimization of asymmetric wireless power transfer in concrete," *Wireless Communications and Mobile Computing*, vol. 2020, no. 3, 2020.

[18] V. Pande, C. Marlecha, and S. Kayte, "A review-fog computing and its role in the Internet of Things," *International Journal of Engineering Research and Applications*, vol. 6, no. 10, pp. 2248–96227, 2016.

[19] X. Sun and N. Ansari, "EdgeIoT: mobile edge computing for the Internet of Things," *IEEE Communications Magazine*, vol. 54, no. 12, pp. 22–29, 2016.

[20] H. Ning, Y. Li, F. Shi, and L. T. Yang, "Heterogeneous edge computing open platforms and tools for Internet of Things," *Future Generation Computer Systems*, vol. 106, no. 11, pp. 67–76, 2020.

[21] D. Thanh, K. Younghan, and L. Hyukjoon, "A location-based interactive model of Internet of Things and cloud (IoT-cloud) for mobile cloud computing applications," *Sensors*, vol. 17, no. 3, pp. 489–491, 2017.

[22] N. Ansari and X. Sun, "Mobile edge computing empowers Internet of Things," *IEICE Transactions on Communications*, vol. 101, no. 3, pp. 604–619, 2018.

[23] A. Kamilaris and A. Pitsillides, "Mobile phone computing and the Internet of Things: a survey," *IEEE Internet of Things Journal*, vol. 3, no. 6, pp. 885–898, 2017.

[24] O. Fragou and A. Mavroudi, "Exploring Internet of Things, mobile computing and ubiquitous computing in computer science education: a systematic mapping study," *International Journal of Technology in Education and Science*, vol. 4, no. 1, pp. 72–85, 2020.

[25] X. Lyu, H. Tian, L. Jiang et al., "Selective offloading in mobile edge computing for the green Internet of Things," *IEEE Network*, vol. 32, no. 1, pp. 54–60, 2018.

[26] P. Botu, "Strong semantic computing," *Procedia Computer Science*, vol. 123, no. 7, pp. 98–103, 2018, Conversations with the following people helped me develop some aspects of this paper: Riccardo Sanz, Jack Copeland, John Barker, Kevin O\Regan and Gadi Pinkus.

[27] L. Fabisiak, "Web service usability analysis based on user preferences," *Journal of Organizational and End User Computing*, vol. 30, no. 4, pp. 1–13, 2018.

[28] T. Grubljesic, P. S. Coelho, and J. Jaklic, "The shift to socio-organizational drivers of business intelligence and analytics acceptance," *Journal of Organizational and End User Computing*, vol. 31, no. 2, pp. 37–64, 2019.

WILEY | Hindawi

Research Article

Simulation Training of E-Sports Players Based on Wireless Sensor Network

Feng Qian (ORCID)

Department of Physical Education, Suzhou University of Science and Technology, Suzhou, 215009 Jiangsu, China

Correspondence should be addressed to Feng Qian; qianfeng@mail.usts.edu.cn

The application of wireless sensors in sports competitions is becoming more and more common. This research mainly discusses the simulation training of e-sports players based on a wireless sensor network. Under the same experimental conditions, in order to avoid mutual influence and interference between the hand grip test and continuous endurance load, the exercise experiment for each subject was repeated twice. At the same time, the EMG signal collection and reaction time test during the endurance load are performed. All tests are data records before and after 40 minutes of the DOTA game competition. Before the start of each experimental test, the experimental equipment is calibrated and the parameters of the required indicators are set; the software was opened to run and checked whether it is normal; before the measurement, let the subjects perform simple preparation activities, train the subjects, and understand and be familiar with the action essentials required by the test to reduce the error. The original surface EMG signal recorded directly uses the built-in signal processing function in the MR-XP 1.08 master edition software to perform full-wave rectification and smoothing. Processing of original EMG data: firstly, the EMG signal during endurance contraction is intercepted. In order to exclude individual differences in sEMG indicators of different subjects, the starting point is the first rise of each subject to 60% MVC or 25% MVC. The arrival time is the end point. In e-sports, the reaction speed when the prompt is effective is significantly faster than when the prompt is invalid ($p < 0.05$). At this time, the time interval between the cue prompt and the target stimulus is 500 ms. This study is helpful to improve the athletes' technical and tactical level.

1. Introduction

The wireless sensor network is a highly application-related network. For different application requirements, the hardware structure of the wireless sensor network node is not the same, but its core components are basically the same. In certain environments, certain nodes require higher energy, stronger communication distance and processing capabilities, and even include GPS positioning functions.

A scientific training plan is an important part of high-level training and a prerequisite for coaches to achieve their training goals. The introduction of information technology into the work of formulating scientific training plans can not only reduce the time spent on statistics by coaches and improve work efficiency but also quickly grasp and complete systematic and detailed information in time.

Shen et al. studied the reliability and applicability of active and continuous smart phone authentication using motion sensor behavior in various operating scenarios and systematically evaluated the uniqueness and durability of the behavior. Although they provide accurate and fine-grained representations of user touch actions, their research process lacks data [1]. Yurtman and Barshan proposed a novel noniterative direction estimation method based on the physical and geometric characteristics of acceleration,

angular velocity, and magnetic field vector to estimate the direction of the motion sensor unit. They obtain the orientation of the sensor unit according to the rotation quaternion transformation between the sensor unit frames. They evaluate the proposed method by incorporating it into the activity identification scheme for daily and sports activities. Although their scheme needs to accurately estimate the direction of the sensor unit to achieve the invariance of the direction the unit is worn on the body, the research process lacks experimental data. Signature recognition is to identify the owner of the signature, and verification is the process of finding the authenticity of the signature. Although both are important in the field of forensic science, verification is even more important for banks and credit card companies [2]. Behera et al. proposed a method to analyze 3D signatures captured using leap motion sensors. They extended the original 2D function from the original signature to 3D and applied a well-known classifier for identification and verification. Although they used the leap motion interface to create a large data set containing more than 2,000 signatures registered by 100 volunteers, their research method is still not new enough [3]. Motion sensor technology and automatic fall detection systems have become reliable and low-cost solutions for falls. Yu et al. has developed a fall detection system based on the hidden Markov model (HMM), which can use a single motion sensor to automatically detect falls for actual home monitoring scenarios. They proposed a new representation for the acceleration signal in HMM to avoid feature engineering. The HMM classifier is trained to detect falls based on the acceleration signal data collected from the motion sensor. Although they collect data sets from experiments that simulate falls and normal activities, the research process lacks theoretical foundation [4].

This research mainly discusses the simulation training of e-sports players based on a wireless sensor network. Under the same experimental conditions, in order to avoid mutual influence and interference between the hand grip test and continuous endurance load, the exercise experiment for each subject was repeated twice. The first test is for grip strength and finger flexibility, and the second test is done after two days of rest. At the same time, the EMG signal collection and reaction time test during endurance load are performed. All tests are data records before and after 40 minutes of the DOTA game competition. Before the start of each experimental test, the experimental equipment is calibrated and the parameters of the required indicators are set; the software was opened to run and checked whether it is normal; before the measurement, let the subjects perform simple preparation activities, train the subjects, and understand and be familiar with the action essentials required by the test to reduce the error. The original surface EMG signal recorded directly uses the built-in signal processing function in the MR-XP 1.08 Master Edition software to perform full-wave rectification, smoothing, calculation, and analysis of the original signal. The processing of the original EMG data is as follows: first, intercept the EMG signal during endurance contraction, in order to exclude the individual differences in sEMG indicators of different subjects, with

each subject's first rise to 60% MVC or 25% MVC as the starting point; the arrival time is the end point. This research helps to improve the technical and tactical level of athletes.

2. Simulation Training of E-Sports Players Based on Wireless Sensor Network

2.1. Related Technologies of Wireless Sensor Network

2.1.1. Wireless Sensor Network. A wireless sensor network is a multihop self-organizing network system formed by deploying a large number of sensor nodes in a certain area through wireless network communication. Its purpose is to cooperate and sense, collect, process, and transmit the sensing objects in the network coverage area. [5–7]. The schematic diagram of the wireless sensor network structure is shown in Figure 1.

2.1.2. Target Tracking Technology. Target tracking can be divided into active active and passive passive according to the sensor type. In practical applications, passive passive multitarget tracking is more practical. Active active target tracking refers to obtaining the position information of the monitored target at any time through the cooperation of sensor nodes in the network when the target is actively carrying the transmitter. This method requires the cooperation of the tracked target to a certain extent. Active active target tracking is basically divided into two types based on ranging and nonranging. In practical applications, the monitored target generally does not actively carry active devices, and the main purpose of people deploying wireless sensor networks is to monitor some unknown things, so passive passive target tracking is more important [8]. Compared with single-target tracking, multitarget tracking is more complicated, faces greater difficulties, and involves more technologies. The basic idea of multitarget tracking is to divide the entire tracking process into three stages. In order to eliminate ambiguity, it is necessary to introduce methods such as source separation and target classification. The third stage is single-target tracking when the target is separated. At present, the research on multitarget tracking technology is a hot topic in the world. The main research content includes sensor node task allocation, data fusion, multitarget identification, and saving network resources. It is necessary to make breakthroughs in target detection and classification, state estimation, and key technologies such as forecasting and data association [9].

2.1.3. Target Activity Trajectory Mining Technology. The trajectory of the target refers to the path formed after the target has been active in the wireless sensor network for a period of time. Trajectory mining is a technology that obtains the true path by analyzing the sensor data triggered by the target within the time interval. At present, the target activity trajectory mining technology has become one of the research hotspots in the field of data mining and WSN target tracking. There are many methods for trajectory mining, which are mainly divided into three types: mining based on the overall trajectory, mining based on local trajectory similarity, and
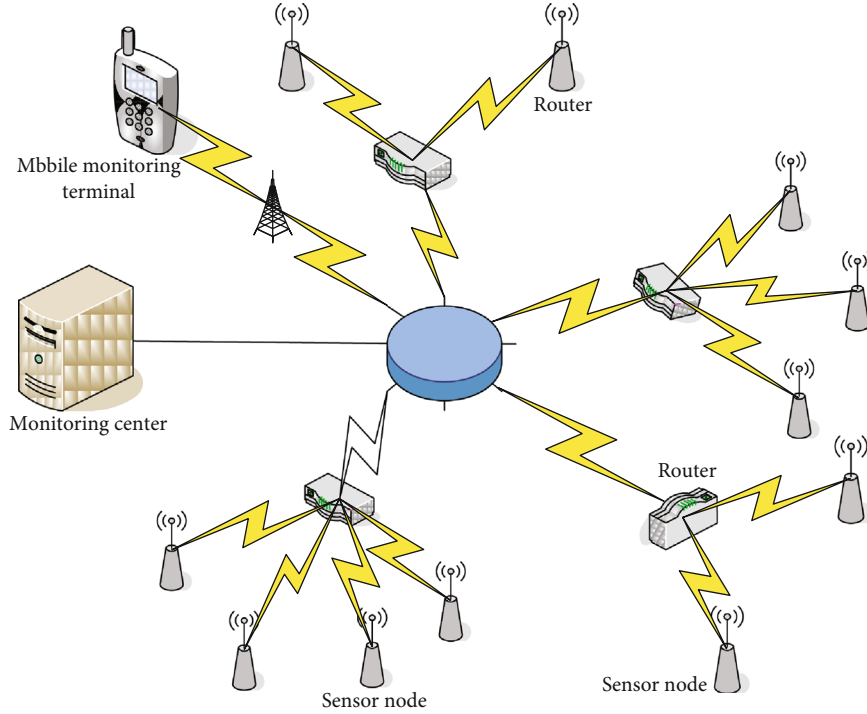
Figure 1: Schematic diagram of the wireless sensor network structure.

mining based on time and space information. The main goal is to realize the prediction and estimation and cluster analysis of target trajectories to form a reliable trajectory pattern library, while the trajectory mining method based on time and space information is more. To be flexible, it can not only well achieve the goals of the above two methods but also the mining method is flexible and suitable for a variety of applications.

2.2. Wireless Sensor Network Algorithm

2.2.1. LEACH Algorithm.
In the initialization phase of a cycle, the system will randomly generate a random value from 0 to 1 and compare this value with the threshold $T(n)$. If the value is between $T(n)$ and 1, then the node is a normal node; otherwise, this node is the cluster head node [10]. $T(n)$ is calculated using the following method [11, 12]:

$$T(n) = \begin{cases} \dfrac{P}{1 - P \times (r \bmod (1/P))}, & n \in G, \\ 0, & \text{if } n \notin G, \end{cases} \quad (1)$$

where P represents the ratio of the cluster head node to all nodes in the network. The value of P changes with different networks and is not fixed. r represents the number of cycles currently in progress, and G represents the set of nodes that have not been selected as cluster head nodes in the past $1/P$ cycles. The generating formula of $T(n)$ ensures that every node in $1/P$ cycles can become the cluster head node [13, 14].

2.2.2. The Cluster Head Selection of LEACH Algorithm.
The work efficiency of wireless sensor networks is related to many factors, such as the internal energy consumption of network nodes, the distribution of nodes, and the distance between nodes. For a wireless sensor network, the LEACH algorithm actually has an optimal range for the number of clusters that should be divided. In the process of constructing a cluster, we should try to ensure that the number of cluster heads is within this optimal position. In this way, the working efficiency of the entire wireless sensor network is improved. The energy consumption of each node in the entire network was analyzed. The energy consumed by the cluster head includes data transmission, data fusion, and data reporting. We assume that the total energy consumption of the cluster head node in each cycle is [15]

$$E_{\text{CH}} = lE_{\text{elec}} \frac{N}{k} + lE_{\text{DA}} \frac{N}{k} + l\varepsilon d_{\text{toCH}}^4. \quad (2)$$

Assuming that in a cycle, the cluster head node and the ordinary nodes in the cluster communicate with each other, and the energy required to be consumed is expressed as [16, 17]

$$E_{\text{non-CH}} = lH_{\text{elec}} + lH_{\text{friss-amp}} d_{\text{toCH}}^2. \quad (3)$$

Here, we believe that the entire wireless sensor network divides all nodes into S clusters according to the node distribution area k, so the area occupied by each cluster can be expressed as S/k. At the same time, it is assumed that the density function of the node distribution within this cluster can mean $P(x, y)$; then, the distance

between each node and the cluster head node is expressed as d_{toCH}, and the mathematical expectation of d_{toCH}, d_{toCH} can be expressed by the following formula [18]:

$$E\left[d_{\text{toCH}}^2\right] = \iint \left(x^2 + y^2\right)\rho(x, y)dxdy = \iint r^2 \rho(r, \theta)rdrd\theta. \quad (4)$$

Here, we regard the area of one of the clusters as a circular area with a radius of $R = S/\sqrt{\pi k}$. At the same time, the density distribution function is a constant of $\rho(r, \theta)$ with respect to r and θ. Then, the distance between each node and the cluster head node, d_{toCH}, can be expressed as [19, 20]:

$$E\left[d_{\text{toCH}}^2\right] = \rho \int_{\theta=0}^{2\pi} \int_{r=0}^{S/\sqrt{\pi k}} drd\theta = \frac{\rho}{2\pi}\frac{S^4}{k^2}. \quad (5)$$

Assuming that in the circular area, all sensor nodes are evenly distributed; according to the mathematical principle, there is d_{toCH}; then, the mathematical expectation of the distance between a node and the cluster head node can be expressed as [21]

$$E\left[d_{\text{toCH}}^2\right] = \frac{1}{2\pi}\frac{S^2}{k}. \quad (6)$$

That is,

$$E_{\text{non-CH}} = lH_{\text{elec}} + lH_{\text{friss-amp}}\frac{1}{2\pi}\frac{S}{k}. \quad (7)$$

Then, the energy consumed by ordinary nodes in the cluster can be expressed as [22, 23]

$$E_{\text{cluster}} = E_{\text{CH}} + \frac{N}{k}E_{\text{non-CH}}. \quad (8)$$

Then, in the wireless sensor network, the total energy consumed by a single-cluster head node in a cycle is [24]

$$E_{\text{round}} = kE_{\text{cluster}} = I\left(NE_{\text{elec}} + NE_{\text{DA}} + k\varepsilon_{\text{two-ray-amp}}d_{\text{toBS}}^4 + N\varepsilon_{\text{friss-amp}}\frac{1}{2\pi}\frac{S^2}{k}\right), \quad (9)$$

where d_{toCH} represents the number of clusters in the wireless sensor network, and d_{toCH} represents the average distance from the cluster head node to the network transmission base station. Take the derivative of k in this formula and set the value of the partial derivative function to 0. In a wireless sensor network, the optimal number of clusters should be [25, 26]

$$k = \sqrt{\frac{N}{2\pi}}\sqrt{\frac{\varepsilon_{\text{feiss-amp}}S}{\varepsilon_{\text{two-ray-amp}}d_{\text{toBS}}^2}}. \quad (10)$$

According to this formula, for a wireless sensor network within a specific range, we can more accurately calculate the number of optimal clusters that should be divided [27].

2.2.3. LEACH Algorithm Energy Consumption Model.

When the distance between two nodes in the wireless sensor network is d, and they transmit data to each other, the length of the message transmitted is l bit; then, the energy consumed by the information node can be expressed as

$$E_{\text{tx}}(l, d) = E_{\text{tx-elec}}(l) + E_{\text{tx-amp}}(l, d) = \begin{cases} lE_{\text{elec}} + le_{fs}d^2, & d < d_0, \\ lE_{\text{elec}} + le_{fs}d^2, & d < d_0. \end{cases} \quad (11)$$

The energy consumed by the receiving information node can be expressed as

$$E_{\text{tx}}(l) = E_{\text{tx-elec}}(l) = lE_{\text{elec}}. \quad (12)$$

In the above formula, E_{elec} represents the energy consumed in the process of node sending unit data and node receiving unit data. In the above model, the two are equal in value. The monitoring area of each sensor node is πR^2, and the probability that each sensor can monitor the entire area is

$$p = \frac{\pi R^2}{S}. \quad (13)$$

Then, the coverage probability of n nodes is

$$P(A + A + \cdots + A) = 1 - (1 - p)^n. \quad (14)$$

The number of randomly distributed sensor nodes is [28]

$$n = \log_{(1-\pi R^2)/S}^{1-p} = \lg\frac{1-p}{(1-\pi R^2)/S}. \quad (15)$$

3. Experimental Design of Simulation Training for E-Sports Players

3.1. Subjects.
Select 15 boys in the professional e-sports class of a college, aged between 20 and 24 years old (average age: 22.7 ± 2.8 years old), height: 174.6 ± 3.2 cm, weight: 65.7 ± 9.6 kg, and engaged in DOTA special training 1-4 years (average age: 2.2 ± 1.3 years). He was in good physical health, had no strenuous exercise 24 hours before the experiment, had not used a computer for a long time, in good mental state, not lacking sleep, and no malaise and other bad states. The subjects used the right hand to operate the mouse during the game. Before the experiment, the subjects were briefly explained with the subjects of the experiment procedures, experimental requirements, etc., so that the subjects understood the basic procedures of the experiment and signed the informed consent form voluntarily.

3.2. Experimental Instruments and Methods.
Under the same experimental conditions, in order to avoid mutual influence and interference between the hand grip test and continuous endurance load, the exercise experiment for each subject was repeated twice. The first test is for grip strength and

finger flexibility, and the second test is done after two days of rest. At the same time, the EMG signal collection and reaction time test during endurance load are performed. All tests are data records before and after 40 minutes of the DOTA game competition. Before the start of each experimental test, the experimental equipment is calibrated and the parameters of the required indicators are set; the software to run was opened and checked whether it is normal; before the measurement, let the subjects perform simple preparation activities, train the subjects, and understand and be familiar with the action essentials required by the test to reduce the error.

3.2.1. Grip Strength Test. Before the test, adjust the grip distance according to the size of the testee's hand and bend the second joint of the middle finger by 90 degrees to fully exert force. During the test, the subject is required to stand upright, with the two feet naturally separated by about one foot distance, the arms are naturally drooped, the palms are inward, the display window of the grip meter is facing outwards, and then the inner and outer grips are fully held. The instrument displays the maximum grip strength and maintains it. Do not touch the dynamometer with your body or clothing.

3.2.2. Finger Flexibility Test. In the experiment, considering that the familiarity of each subject with tweezers is different, and it takes too long to insert a complete hole in the experiment plate and it takes too long to test 3 times in a row, the subject's patience will affect the accuracy of the data, in order to avoid these situations The error caused by this experiment requires the subject to directly insert the metal rod from the first hole in the upper left corner by hand. The start and end of the experiment were manually pressed by the tester.

3.2.3. Response Time Test. First, press the simple response button (the experiment will present a stimulus), instruct the subject to look at the stimulus light source light, and pay attention to waiting for the signal to be sent. The preparation signal light below the light turns on first. When the stimulus light is on, press the red button at the fastest speed. The timing of the display window is stopped, waiting for the next signal to be sent; there are 5 signals in total. Each time a stimulus is presented, the number of responses is displayed during the test, and when the response is wrong, the number of errors is displayed. At the end of the experiment, the average response time and the number of errors are displayed.

3.2.4. Test Method of EMG Signal and Acquisition of Original EMG Signal. The surface EMG collection using the surface EMG telemetry system is shown in Figure 2. The sampling frequency is 1000 Hz, the preamplifier gain value is 1000, the input impedance > 100 Mohm, the common mode rejection ratio > 100 dB, the channel sampling bandwidth is 10-500 Hz, and the sensitivity is 1 V.

3.3. Processing and Analysis of Surface EMG. The original surface EMG signal recorded directly uses the built-in signal processing function in the MR-XP 1.08 Master Edition software to perform full-wave rectification, smoothing, calculation, and analysis of the original signal. The processing of
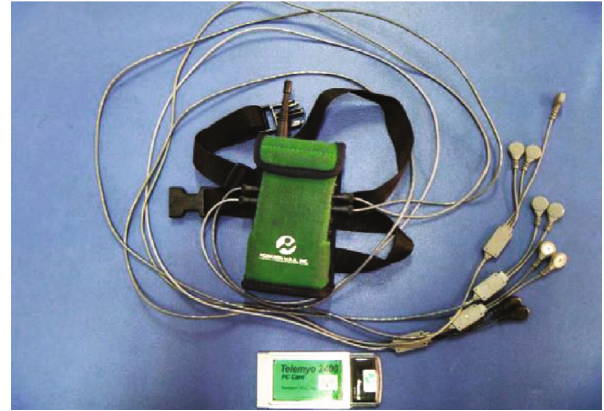
Figure 2: Surface EMG telemetry system.

Table 1: The relationship between packet loss rate and communication distance.

Communication distance (m)	Number of packets sent	Number of received packets	Packet loss rate (%)
10	53645	53450	0.36%
15	62850	62511	0.54%
20	63224	62635	0.93%
25	55628	49275	11.42%
30	58605	44978	23.25%
35	63542	30665	51.74%
40	65826	1527	97.68%

the original EMG data is as follows: first, intercept the EMG signal during endurance contraction, in order to exclude the individual differences in sEMG indicators of different subjects, with each subject's first rise to 60% MVC or 25% MVC as the starting point; the arrival time is the end point.

3.4. Statistical Processing. Statistical analysis was performed with SPSS 13.0 statistical software. The significance test of the difference was performed by one-way analysis of variance, the difference between the two groups was tested by LSD-t, and the statistics of simulation training results of e-sports players were performed by a group t-test. $p < 0.05$ is considered to be significant and statistically significant.

4. Results and Discussion

Select the serial port baud rate of 57600 bps, after writing the test data to the node, send it through the CC2420 radiofrequency, and send the data received by the receiving end to the PC serial port, and receive the data through the serial port tool. The data sent, received data, and communication distance are measured in the experiment. The relationship is shown in Table 1. When the communication distance between nodes is about 20 m, the communication can be roughly regarded as reliable. When the node communication distance increases to more than 30 m, the node packet loss rate increases rapidly. When it approaches 40 m, the network is almost interrupted.
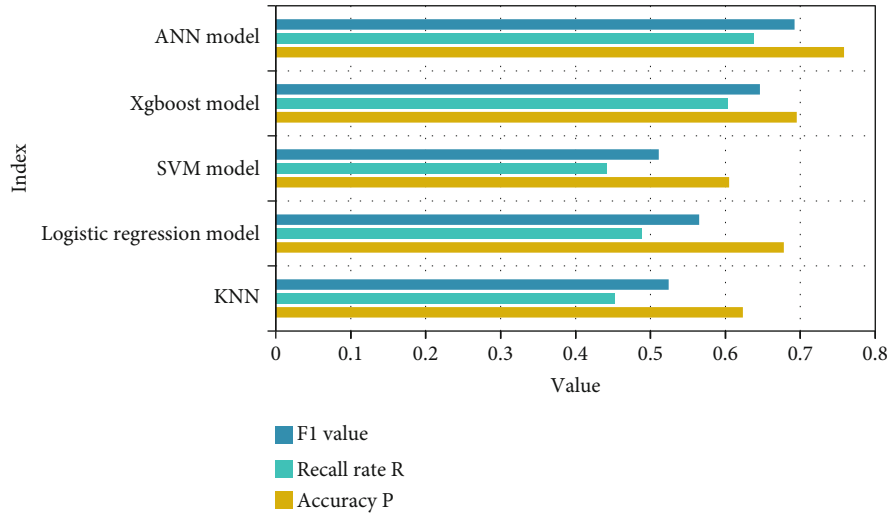
Figure 3: Comparison of performance indicators of each model.
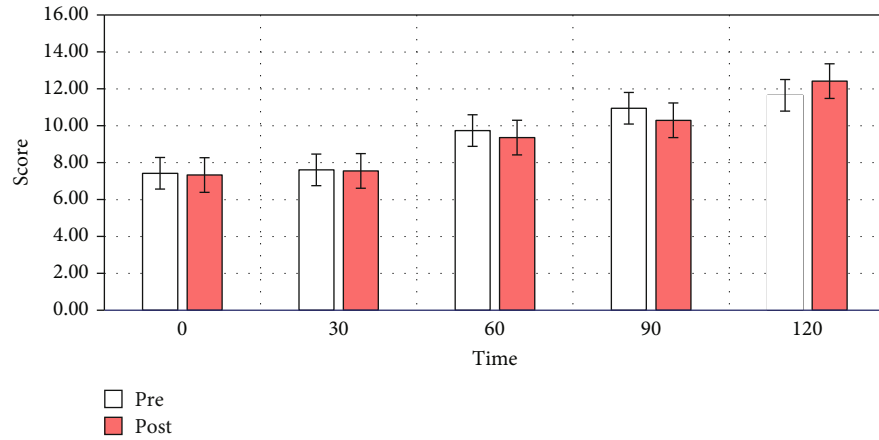
Figure 4: Changes in endurance load time and subjective fatigue feeling of flexor superficial muscle (FDS).

The performance index comparison of each model is shown in Figure 3. Using traditional one-hot encoding (one-hot) input data, combined with traditional machine learning algorithms (excluding neural network models), the integrated tree regression algorithm represented by XGBoost performs the most eye-catching, not only the accuracy rate is as high as 0.788 but also the calculation is the fastest speed, only 1.67 hours. In contrast to other highly explanatory algorithms, the logistic regression algorithm has the highest accuracy rate of only 0.690, and it takes 4.17 hours. The KNN algorithm is not ideal because of its simplicity. It can be seen from the figure that the related time consumption is a concern. Due to the parallel and multithreading of the algorithm itself, the speed of XGBoost is the fastest among all models, and it processes about 80 W of data in about 1.5 hours.

Figure 4 shows the changes in the endurance load time and subjective fatigue of the finger superficial flexor muscles (FDS). With the extension of the mouse click duration, the subject's subjective fatigue score gradually increased. When the endurance contracted for 30 seconds after exercise, there

was no significant change; when contracted to 60 s, compared with before exercise, the subjective fatigue feeling was significantly increased compared with before exercise ($p < 0.05$). At 90s, the subjective fatigue feeling was higher than before exercise. The difference is significant ($p < 0.01$), and at 120 s, there is a significant increase compared to before exercise ($p < 0.05$).

The selection of e-sports athletes is also different from the selection of traditional competitive sports. E-sports players often do not need excellent physical conditions, and they pay more attention to the eye-hand coordination ability, reaction speed, and thinking ability of the players during the selection. E-sports is a new type of sports under the conditions of the times and technological development, and it has a broader development prospect and future. The amplitude values of the surface EMG signal of the extensor muscle at each time point of 25% MVC endurance contraction are shown in Table 2. The amplitude value of the surface EMG signal before exercise gradually increases with time; 30 s after exercise is slightly lower than the amplitude value at the beginning of exercise, and after 60 s, the amplitude value

TABLE 2: 25% MVC endurance contraction at each time point of the amplitude of the surface EMG signal of the extensor muscle.

	0	30s	60s	90s	120s
Before exercise	48.52 ± 16.0	65.55 ± 19.12	72.12 ± 26.20	74.95 ± 25.74	83.77 ± 36.07
After exercise	65.68 ± 34.4	64.62 ± 20.74	72.73 ± 22.67	94.91 ± 51.55	109.7 ± 56.6
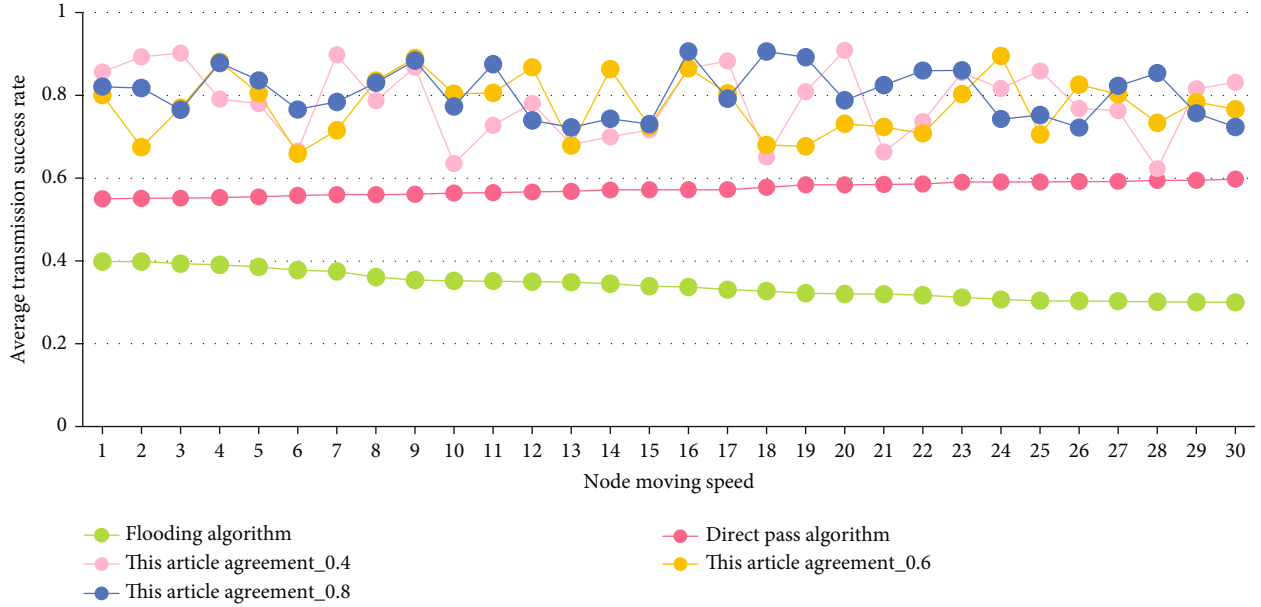
FIGURE 5: The effect of node moving speed on the average transmission success rate.
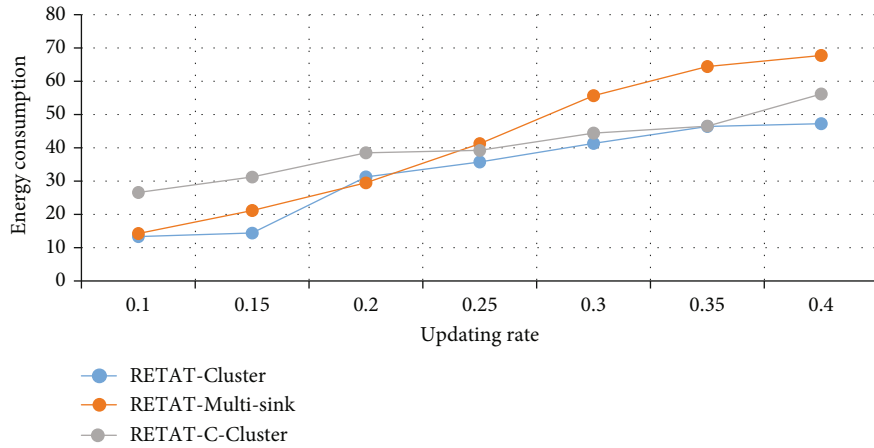
FIGURE 6: Energy consumption of three transmission task allocation strategies under different network update ratios.

gradually increases with the continuation of time, and at 120 s and before exercise, compared with a significant increase ($p < 0.05$).

The influence of node moving speed on the average transmission success rate is shown in Figure 5. With the increase of the node's moving speed, the average information transmission success rate of the protocol and the direct delivery algorithm in this paper has been continuously improved, while the average information transmission success rate of the flooding algorithm has gradually decreased. This is because in the protocol and direct deliv-

ery algorithm in this article, as the speed of the node increases, the communication opportunities between nodes and between nodes and base stations are increased, and the information needs to be forwarded. The node has more opportunities to choose a suitable relay node. To forward the message, however, in the flooding algorithm, the nodes move too fast, which leads to the increase of communication conflicts and reduces the performance of the network. In addition, we can see from the figure that the initial importance still affects the average success rate of information transmission.
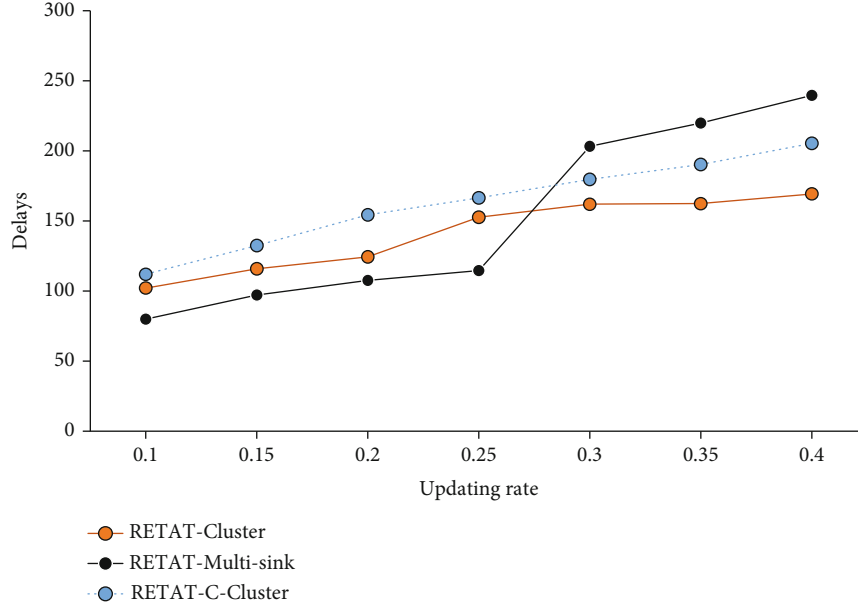
FIGURE 7: Delay of transmission task allocation under different network update frequencies.

TABLE 3: Analysis of the difference in response time of clue prompts.

Sample book	Effective reminder	Invalid prompt	Difference	t	df	p
ESports player	580.53 ± 70.70	615.02 ± 98.70	-34.98	-2.568	29	0.015
Traditional athletes	672.02 ± 79.96	725.28 ± 110.64	-53.26	-3.453	29	0.002
Ordinary college students	654.86 ± 100.78	717.38 ± 97.78	-62.52	-3.329	29	0.002

The energy consumption of the three transmission task allocation strategies under different network update ratios is shown in Figure 6. It can be seen that as the network update rate increases, the energy consumption of the three transmission task distribution increases significantly as the network update rate increases. Since the network update in RETAT-C-cluster has to be aggregated to the only sink after long distances and multiple hops, which increases the communication load of the network, in most cases, the energy consumption of the RETAT-C-cluster of the three strategies is directly higher than the other two distributed transmission task allocation methods. As the network update rate is greater than 25%, the energy consumption of RETAT-multisink increases rapidly, surpassing RETAT-C-cluster and RETAT-cluster to become the highest energy consumption of the three strategies. Because of the high network update rate, the exchange of global views between multiple sinks in RETAT-multisink and the operation of ensuring the consistency of the global view all lead to a rapid increase in energy consumption.

The delay of transmission task allocation under different network update frequencies is shown in Figure 7. With the increase of the network update rate, the delays of the three kinds of transmission tasks are all on the rise. In the current network simulation parameter environment, statistics found that when the network update rate is lower than 25%, the delays of both RETAT-cluster and RETAT-multisink are less than RETAT-C-cluster. This is because when there are a small amount of updates in the network, the first two are processed locally without affecting the reliability of the mission target, and the entire network is not required to be updated, so the delay is low. When the network update rate exceeds 25%, the delay of RETAT-multisink increases rapidly and is higher than that of RETAT-C-cluster, which is caused by the operation to ensure the consistency of the global view under the high update rate.

E-sports is an adversarial competitive sports event, which requires players from both sides to arrive at the designated venue and compete in skill and physical stamina under fair and just referee supervision and competition rules. However, traditional online games are only used for game entertainment on dedicated servers provided by network operators, without the performance of the spirit of sports competition. When there are 3 distracting stimuli, the response time is the dependent variable, and the effective prompt and invalid prompt are the independent variables. Table 3 shows the results of the matched sample 1 test of e-sports athletes, traditional athletic athletes, and ordinary college students. In the three groups of participants, the response speed when the prompt is effective is significantly faster than when the prompt is invalid ($p < 0.05$). At this time, the time interval between the prompt and the target stimulus is 500 ms, which shows that in the three groups of participants the facilitating effect of attention appeared in the time interval of 500 ms.

5. Conclusion

This research mainly discusses the simulation training of e-sports players based on a wireless sensor network. Under the same experimental conditions, in order to avoid mutual influence and interference between the hand grip test and continuous endurance load, the exercise experiment for each subject was repeated twice. The EMG signal collection and reaction time test during endurance load are performed. All tests are data records before and after 40 minutes of the DOTA game competition. Before the start of each experimental test, the experimental equipment is calibrated and the parameters of the required indicators are set; the software to run was opened and check whether it is normal; before the measurement, let the subjects perform simple preparation activities, train the subjects, and understand and be familiar with the action essentials required by the test to reduce the error. The original surface EMG signal recorded directly uses the built-in signal processing function in the MR-XP 1.08 Master Edition software to perform full-wave rectification, smoothing, calculation, and analysis of the original signal. The processing of the original EMG data is as follows: first, intercept the EMG signal during endurance contraction, in order to exclude the individual differences in sEMG indicators of different subjects, with each subject's first rise to 60% MVC or 25% MVC as the starting point. This research helps to improve the technical and tactical level of athletes.

Data Availability

No data were used to support this study.

Conflicts of Interest

There are no potential competing interests in our paper.

Authors' Contributions

The author has seen the manuscript and approved to submit to your journal.

Acknowledgments

References

[1] C. Shen, Y. Li, Y. Chen, X. Guan, and R. A. Maxion, "Performance analysis of multi-motion sensor behavior for active smartphone authentication," *IEEE Transactions on Information Forensics & Security*, vol. 13, no. 1, pp. 48–62, 2018.

[2] A. Yurtman and B. Barshan, "Novel noniterative orientation estimation for wearable motion sensor units acquiring accelerometer, gyroscope, and magnetometer measurements," *IEEE Transactions on Instrumentation and Measurement*, vol. 69, no. 6, pp. 3206–3215, 2020.

[3] S. K. Behera, D. P. Dogra, and P. P. Roy, "Analysis of 3D signatures recorded using leap motion sensor," *Multimedia Tools and Applications*, vol. 77, no. 11, pp. 14029–14054, 2018.

[4] S. Yu, H. Chen, and R. A. Brown, "Hidden Markov model-based fall detection with motion sensor orientation calibration: a case for real-life home monitoring," *IEEE Journal of Biomedical and Health Informatics*, vol. 22, no. 6, pp. 1847–1853, 2018.

[5] M. Hirata, R. Watanabe, Y. Koyano et al., "Using a motion sensor-equipped smartphone to facilitate CT-guided puncture," *Cardiovascular & Interventional Radiology*, vol. 40, no. 4, 2017.

[6] J. K. Min, E. J. Cheon, J. M. Kim, S. C. Lee, and K. Choi, "Comparison of the 6-DOF motion sensor and stain gauge data for ice load estimation on IBRV ARAON," *Journal of the Society of Naval Architects of Korea*, vol. 53, no. 6, pp. 529–535, 2016.

[7] I. Butun, P. Österberg, and H. Song, "Security of the internet of things: vulnerabilities, attacks, and countermeasures," *IEEE Communications Surveys & Tutorials*, vol. 22, no. 1, pp. 616–644, 2020.

[8] M. Elhoseny, "Multi-object detection and tracking (MODT) machine learning model for real-time video surveillance systems," *Circuits, Systems, and Signal Processing*, vol. 39, pp. 611–630, 2020.

[9] I. I. Duma and S. Giurgiu, "Circadian activity and nest use of *Dryomys nitedula* as revealed by infrared motion sensor cameras," *Folia Zoologica*, vol. 61, no. 1, pp. 49–53, 2012.

[10] Z. Hong, R. Wang, and X. Li, "A clustering-tree topology control based on the energy forecast for heterogeneous wireless sensor networks," *IEEE/CAA Journal of Automatica Sinica*, vol. 3, no. 1, pp. 70–79, 2016.

[11] L.-B. Huang, W. Xu, C. Zhao et al., "Multifunctional water drop energy harvesting and human motion sensor based on flexible dual-mode nanogenerator incorporated with polymer nanotubes," *ACS Applied Materials And Interfaces*, vol. 12, no. 21, pp. 24030–24038, 2020.

[12] D. Ebrahimi and C. Assi, "On the interaction between scheduling and compressive data gathering in wireless sensor networks," *IEEE Transactions on Wireless Communications*, vol. 15, no. 4, pp. 2845–2858, 2016.

[13] J. M. Pak, C. K. Ahn, P. Shi, Y. S. Shmaliy, and M. T. Lim, "Distributed hybrid particle/FIR filtering for mitigating NLOS effects in TOA-based localization using wireless sensor networks," *IEEE Transactions on Industrial Electronics*, vol. 64, no. 6, pp. 5182–5191, 2017.

[14] F. Deniz, H. Bagci, I. Korpeoglu, and A. Yazıcı, "An adaptive, energy-aware and distributed fault-tolerant topology-control algorithm for heterogeneous wireless sensor networks," *Ad Hoc Networks*, vol. 44, no. 7, pp. 104–117, 2016.

[15] W. Liu, X. Zhou, S. Durrani, H. Mehrpouyan, and S. D. Blostein, "Energy harvesting wireless sensor networks: delay analysis considering energy costs of sensing and transmission," *IEEE Transactions on Wireless Communications*, vol. 15, no. 7, pp. 4635–4650, 2016.

[16] T. A. Donaldson, "Inline calibration of motion sensor," *Journal of Chinese Pharmaceutical Sciences*, vol. 48, no. 23, pp. 2022–2025, 2016.

[17] G. Marin, F. Dominio, and P. Zanuttigh, "Hand gesture recognition with jointly calibrated leap motion and depth sensor," *Multimedia Tools and Applications*, vol. 75, no. 22, pp. 14991–15015, 2016.

[18] H. Jin, Q. Chen, Z. Chen, Y. Hu, and J. Zhang, "Multi-Leap-Motion sensor based demonstration for robotic refine tabletop object manipulation task," *Caai Transactions on Intelligence Technology*, vol. 1, no. 1, pp. 104–113, 2016.

[19] Z. Wei, W. Zhang, and W. Liu, "Attitude theory and experimental research of micro-aircraft based on MEMS sensor," *Piezoelectrics & Acoustooptics*, vol. 40, no. 4, pp. 516–520, 2018.

[20] D. Laurijssen, S. Truijen, W. Saeys, W. Daems, and J. Steckel, "An ultrasonic six degrees-of-freedom pose estimation sensor," *IEEE Sensors Journal*, vol. 17, no. 1, pp. 151–159, 2016.

[21] K. F. Chiang and H. H. Wang, "Nurses' experiences of using a smart mobile device application to assist home care for patients with chronic disease: a qualitative study," *Journal of Clinical Nursing*, vol. 25, no. 13-14, pp. 2008–2017, 2016.

[22] D. Korpi, J. Tamminen, M. Turunen et al., "Full-duplex mobile device - pushing the limits," *IEEE Communications Magazine*, vol. 54, no. 9, pp. 80–87, 2016.

[23] L. Zhou, "Mobile device-to-device video distribution," *ACM Transactions on Multimedia Computing Communications and Applications*, vol. 12, no. 3, pp. 1–23, 2016.

[24] E. Noei, M. D. Syer, Y. Zou, A. E. Hassan, and I. Keivanloo, "A study of the relation of mobile device attributes with the user-perceived quality of android apps," *Empirical Software Engineering*, vol. 22, no. 6, pp. 3088–3116, 2017.

[25] Y. Zou and G. Wang, "Intercept behavior analysis of industrial wireless sensor networks in the presence of eavesdropping attack," *IEEE Transactions on Industrial Informatics*, vol. 12, no. 2, pp. 780–787, 2016.

[26] J. Jiang et al., "Geographic multipath routing based on geospatial division in duty-cycled underwater wireless sensor networks," *Journal of Network & Computer Applications*, vol. 59, no. 1, pp. 4–13, 2016.

[27] Z. Xu, L. Chen, C. Chen, and X. Guan, "Joint clustering and routing design for reliable and efficient data collection in large-scale wireless sensor networks," *IEEE Internet of Things Journal*, vol. 3, no. 4, pp. 520–532, 2016.

[28] S. Kumari, X. Li, F. Wu, A. K. Das, H. Arshad, and M. K. Khan, "A user friendly mutual authentication and key agreement scheme for wireless sensor networks using chaotic maps," *Future Generation Computer Systems*, vol. 63, no. 10, pp. 56–75, 2016.

WILEY | Hindawi

Research Article

Problems and Countermeasures in the Process of Applying Multimedia Technology in Basketball Teaching

Bixia Yan (ORCID)

Faculty of General Education, Chongqing Vocational and Technical University of Mechatronics, Bishan, 402760 Chongqing, China

Correspondence should be addressed to Bixia Yan; 171445003@cqvie.edu.cn

Nowadays, there are few researches on using multimedia animation technology to assist basketball tactics teaching and training in college physical education. The research of multimedia animation assisting basketball tactics teaching can help promote the current teaching mode, teaching environment, and teaching methods. From the perspective of the development trend of modern education and the benefits of multimedia technology in physical education teaching, this article demonstrates the inevitability of applying multimedia technology in college basketball teaching and demonstrates the feasibility of implementing multimedia physical education in colleges and universities from the three aspects of multimedia teaching environment, teacher teaching ability analyzes the factors that affect the effect of multimedia-assisted teaching. Students' acceptance characteristics of the multimedia environment are obtained. Relevant research results and suggestions on the use of multimedia animation in basketball tactics teaching will be submitted. Research shows the ability and student's learning ability. It analyzes the effects of multimedia-assisted teaching in basketball tactics. In this article, at 84% of teachers feel that multimedia-assisted teaching is better. However, some objective factors restrict teachers' use of multimedia-assisted teaching methods. Among them, poor production technology and inconvenient use are the main factors that teachers think affect the application of multimedia-assisted teaching methods in actual teaching, and these influencing factors are difficult to eliminate in a short time.

1. Introduction

Multimedia network teaching can achieve a wider range of information resource sharing because of its wide coverage. Teachers can also use various forms of teaching methods to enrich and invigorate the classroom, which also helps improve the effect of teaching applications. Multimedia network teaching is more important to support collaborative learning. Through mutual cooperation and communication, students will have a deeper understanding of the content of learning, a broader learning mindset, more diverse learning methods, more efficient intelligence training, and higher learning efficiency. Therefore, the subject research provides practical guidance for improving the application effect of basketball teaching.

The development of multimedia network teaching abroad is relatively mature, and many countries have widely used network teaching. And many scholars have learned it. For example, Salski et al. analyzed the application of multi-

media technology in basketball teaching, training, and learning from different perspectives. It is generally believed that multimedia technology can help teachers and students communicate effectively and improve teaching. In quality and effect, it enhances the intuitive teaching effect, stimulates students' interest in learning, helps students understand and master basketball techniques and tactics, and can improve learning efficiency [1]. Wahab expands the cooperation space between multimedia technology and college basketball leagues, improves the more user friendly operation efficiency of multimedia technology, strengthens the linkage with the audience of the college basketball league, reasonably formulates the game schedule, and realizes multimedia technology and wonderful college basketball mutual benefit and win-win of the league [2].

In my country, Li et al. has carried out computer training for teachers at all levels. In terms of training teachers' multimedia teaching abilities, various forms have been adopted, such as centralized school district training (inviting experts

with profound multimedia teaching theories and computer operator teachers for tutoring), school-based training (group training in schools), and individual tutoring (teach multimedia teaching skills in one-to-one form) [3]. Haiqing allows the computer program to play the role of the "midwife" and continuously asks students new and challenging questions in the ongoing dialogue and hardly provides any answers to the students, thereby enhancing students' thinking ability and improving thinking method [4]. Ying et al. uses computer animation production technology to produce multimedia-assisted teaching virtual animations in accordance with the actual requirements of teaching and understand the technical difficulty of making sports-assisted teaching animations. In the process of using multimedia animation to assist teaching, I explore the problems in the process of teaching implementation in combination with different teaching methods and study the effect of sports multimedia virtual animation-assisted teaching [5].

This article selects the two contents of the basic cooperation of basketball tactics, the screen and the exchange of defense, and designs the multimedia teaching courseware. Through the teaching experiment and the students' evaluation of the teaching effect, the effect of the application of multimedia-assisted teaching in the basketball tactics cooperation is analyzed. The majority of sports workers design and produce multimedia teaching courseware to provide references. In order to improve teaching conditions and give full play to the potential of multimedia-assisted teaching, multimedia technology combined with flexible and diverse teaching organization forms is used, and the use scientific, intuitive, visualized, and interesting sports teaching mobilizes students' interest in learning, stimulates their enthusiasm for learning, cultivates students' sports ability, promotes the overall development of students' basketball skills and tactics, and lays the foundation for lifelong physical exercise.

2. Problems and Countermeasures in the Process of Applying Multimedia Technology to Basketball Teaching

2.1. Problems Existing in the Process of Applying Multimedia Technology to Basketball Teaching

2.1.1. The Quality of Teachers Using Multimedia Network Technology in Teaching is Generally Not High

(1) Relatively lagging in thought

Although the leaders of the school attach great importance to the classroom teaching application of multimedia network technology, the deep-rooted influence of the traditional teaching mode of our country for thousands of years on many teachers of the school, especially the old teachers, resulted in them having insufficient knowledge of multimedia network technology, and the production of courseware is not enough. It is so handy, and it takes a lot of effort. Therefore, some teachers are resistant to the teaching methods of multimedia and network technology. Moreover, there are not many corresponding encouragement policies in schools.

The new classroom teaching methods put forward higher requirements for teachers. For them, who have a relatively stable working environment and have formed their own teaching habits, they have greatly increased their workload and brought them a sense of psychological insecurity. Therefore, they tend to be more inclined to impart knowledge in accordance with traditional teaching methods [6, 7]. In addition, most students report that they are accustomed to the traditional exam-oriented education and are not very comfortable with the new teaching methods. In addition, the individual subjective consciousness is not strong, which makes independent learning more difficult.

(2) Improper role positioning

For example, in the teaching process of multimedia chemistry class, teachers just blindly let students learn on the Internet without monitoring, allowing students to discuss the reactions between various compounds, completely out of the subject of chemistry class. The teaching order is disordered, the teaching theme is not clear, and the learning effect is not obvious. Not only the advantages of learning under the multimedia network technology are not reflected, but also the traditional teaching tasks cannot be effectively completed, let alone the emotional exchange between teachers and students [8, 9].

(3) Attach importance to human-computer interaction and ignore interpersonal interaction

In the multimedia network teaching environment, teachers often pay more attention to the interaction between teachers and students and computers, and the direct interaction between people has become indirect. Some teachers have no emotional interaction design in the teaching process, rarely move around in the classroom, rarely write on the blackboard, click the mouse on the main console to explain, and lack the attention to students and emotional communication, making the classroom atmosphere very dull [10, 11]. Many students also report that they feel that they are learning in a mechanical environment, transforming into learning robots, lonely, confused, and confused and dull, leading to loss of interest and confidence in learning.

2.1.2. Students Have Deviations in Learning Using Multimedia Network Technology. Multimedia network classroom teaching provides a wealth of learning resources, which also requires students to have a strong ability to learn independently, and the level of students in this school is quite different and there are certain difficulties [12, 13]. Students who have a good knowledge base and know how to learn believe that personalized learning and freedom allow them to arrange their time more reasonably, and they will obtain more information per unit of time, while students with a poor foundation and weaker self-discipline do not have a teacher. In the case of supervision and guidance, they often focus on the rich pictures, learning is easy to fatigue, the attention is easy to be distracted, and the focus and goals of learning are not clear. Facing a large amount of information, they do not know how to choose and cannot give feedback on

their own learning in time. Not to be able to supervise their own preview and review will ultimately affect the learning effect.

2.1.3. The Management of Multimedia Network Technology in Schools Is Relatively Lagging Behind

(1) Ignore computer network maintenance due to insufficient funds

Although the school leaders want to increase investment in multimedia networks, because the school has just moved to a new campus, large-scale enrollment and new construction of the campus have to be carried out, resulting in relatively insufficient investment in teaching funds; on the other hand, the speed of computer updates very fast, it will be obsolete if it is not updated for three years, and the investment in network technology and multimedia is huge. It takes at least 100,000 to build a fully functional multimedia classroom, and the investment in network construction is even greater [14, 15]. In addition, the school has a serious shortage of full-time personnel for equipment maintenance. It is often one person doing three people's work. In addition, there is not enough sense of responsibility and the technical level is not high. It often appears that the teaching software is out of date and has not been updated, and failures cannot be timely. Over time, the resolved phenomenon has consumed the patience of teachers and students and also affected the teaching progress.

(2) Inadequate feedback and monitoring using multimedia network teaching

Quality supervision and scientific management are important measures to ensure teaching quality and improve teaching effectiveness. For example, although the school's research on the network teaching model is in full swing, the corresponding teaching monitoring, evaluation, and feedback mechanisms have not been implemented into a system. Due to the lack of interactive initiative of teachers in the teaching process, the monitoring of students' learning seems weak [16, 17]. Some even think that as long as they provide support, students will definitely use it, but the actual situation is that students' learning arbitrariness becomes greater, and their self-control and awareness of autonomy are weakened.

2.2. Countermeasures in the Process of Applying Multimedia Technology to Basketball Teaching.

The biggest difference between multimedia-assisted teaching and traditional teaching methods is that the teaching media used in teaching activities is different. It uses multimedia computers and some external output devices as communication media and spreads in the form of text, graphics, images, sound, video, etc. In terms of teaching information, teaching resources are obtained from digital publications, networks, self-developed production, and other forms. The changes in teaching methods have changed the status and role of teachers in teaching and students' learning styles. Therefore, in multimedia-assisted teaching, the teaching of middle school teachers and the learning of students must adapt to the new teaching methods [18, 19]. According to the characteristics of multimedia-assisted teaching, the implementation of multimedia-assisted teaching must meet three conditions, namely, the computer teaching environment must meet the needs of multimedia teaching, teachers must have multimedia teaching capabilities, and students must have the ability to learn in a multimedia teaching environment.

(1) The social environment of multimedia teaching

With the strengthening of my country's comprehensive national strength, education investment continues to grow, and campus networking and digital construction have begun to take shape, providing economic conditions and material foundations for the application of multimedia technology in teaching [20, 21]. The country's continuous high investment in education has made great progress in the construction of campus networks. At present, all universities in our country have basically completed broadband campus networks that can better transmit multimedia information, which provides for the high-tech construction of education and the upgrading and transformation of education. A solid economic foundation and a good environment make it possible for multimedia technology to be widely used in teaching [22, 23].

(2) Multimedia hardware environment construction

The demonstration multimedia teaching environment has changed the traditional simple chalk and blackboard teaching methods. It uses a variety of media to stimulate students' senses, which is conducive to students' acceptance of knowledge and strengthening memory. However, in this form of multimedia teaching environment, students are still in passive status, the teacher demonstrates that students watch, lack of student participation, is not conducive to exerting the initiative of students in learning and developing students' personality [24, 25]. Therefore, schools with a better campus network can build a sports multimedia teaching environment into a shared type.

(3) Teachers must have multimedia-assisted teaching capabilities

Only with good hardware cannot be considered that multimedia sports teaching can proceed smoothly and guarantee the quality of teaching. Teachers play a leading role in teaching practice. The basis of multimedia technology is computer technology. The teacher's computer application ability directly affects the effect of multimedia teaching. If teachers lack modern high-tech literacy, the use of multimedia teaching is still empty talk. Due to the relationship between history and disciplines, the computer level of the physical education teachers in our country was generally low in the past, which became a bottleneck in the application of multimedia technology in the field of physical education. Now with the popularization of computer education and the continuing education of teachers, teachers' computer skills have generally improved. Those who can use computers and the Internet proficiently or more proficiently account for the vast

majority of physical education teachers. They are proficient in computer operations and capable of multimedia teaching. Therefore, the implementation of multimedia-assisted teaching in the field of sports has the guarantee of qualified teachers.

2.3. Countermeasures to Improve the Application of Multimedia Network Technology in Classroom Teaching

(1) Leaders should look at the application value of multimedia network technology from the long-term development of teaching

From a long-term perspective, the correct understanding of Gao teachers should be improved. First of all, the school can set up a special group led by the teaching department and specifically responsible for each teaching and research group and organize teachers to learn advanced and systematic education and teaching concepts in the way of assembly concentration or subject grouping. For example, the relevant theories of multimedia network teaching (including cognitivism, behaviorism, constructivism, and multimedia learning cognitive theories), as well as advanced teaching design theories and methods, are collected, printed, and bound into a book and distributed to various subject groups. Organize teachers to study seriously and let them realize the advantages of online teaching different from traditional teaching.

(2) Teachers should understand multimedia network technology from the reform of teaching methods and means

Multimedia network teaching is a new teaching method under the background of the new era. It mainly displays teaching content intuitively and vividly through images, sounds, and text, which greatly stimulates interest in learning, activates students' thinking, and improves the efficiency and efficiency of learning (positivity). In the multimedia network technology teaching environment, education and teaching activities are carried out. As long as the teacher carefully prepares the courseware, that is, or the web page, before class, effective teaching can be carried out. In this environment, teachers can not only use multimedia to strengthen teaching but also the content is systematic, scientific, intuitive, and interesting.

3. Basketball Teaching Experiment under Multimedia Technology

3.1. Selection of Teaching Experiment Objects.
The choice of experiment subjects not only needs to study and master basic basketball skills such as passing, playing, throwing, and moving but also students who have little understanding of the basics of basketball tactics and rarely learn basketball knowledge independently in their spare time. This experiment chooses Northwest Normal University's two female classes in the second-year "University Sports" basketball option as the experimental subjects: one class was used as the experimental group (32 students), and the other class (35 people) was used as the control group.

3.2. Experimental Method.
According to the research design, the experimental subjects were randomly grouped and taught. In order to ensure the objectivity of the teaching experiment, in addition to the method of random grouping, in the teaching experiment process, I personally take charge of the whole process of basketball tactics teaching for the general group and the experimental group and pay attention to the design of the content of the teaching plan to ensure the tactical explanation Consistent with the tactical practice form, the tactical teaching of the general group is mainly based on traditional teaching methods, while the tactical teaching of the experimental group is a combination of traditional teaching methods and multimedia-assisted teaching methods. In basketball tactics teaching, multimedia animation methods are only used as teaching aids, and the use of multimedia occupies a relatively small proportion of the classroom time and is only used when necessary. The only different influencing factor for the two groups of students during the teaching experiment is the use of multimedia-assisted teaching animation. Aiming at the problems in tactical teaching, the ordinary group mainly solves the problems through traditional teaching methods, while the experimental group solves the problems through the combination of traditional teaching methods and multimedia auxiliary methods.

3.3. Questionnaire Survey Method.
Relevant basketball teaching experts, teachers, and students are invited to evaluate the made teaching animation courseware and survey expert teachers and students in the form of questionnaires. Student questionnaires are distributed in class to ensure the questionnaire recovery rate. A total of 112 questionnaires were distributed, including 100 student questionnaires, with a recovery rate of 98% and an efficiency of 90%, and 10 expert and teacher questionnaires, including 6 associate professors, 4 lecturers, and 2 teaching assistants. 20 questionnaires were recovered, the recovery rate was 80%, and the effective rate was 90%.

4. Research and Analysis of Basketball Teaching Experiment under Multimedia Technology

4.1. There Is a Certain Feasibility of Multimedia Animation to Assist Basketball Tactics Teaching.
This paper studies the nature of the learner's learning process under the condition of multimedia assistance. Through the study of the interaction between the learner and the multimedia environment during the learning process, the three essential characteristics of the learning process in the learner's interaction with the multimedia prototype were proven. The learner believes that the multimedia environment is necessary; the execution of intellectual ability under the interaction with the multimedia system, the exploration, and the search for the motivation of learning are helpful to learning. The experimental results are shown in Figure 1.

It can be seen from Figure 1 that students have greater consistency in their choice of multimedia animation-assisted teaching methods. 93% of students like this assisted teaching method, but 6% of students dislike this assisted
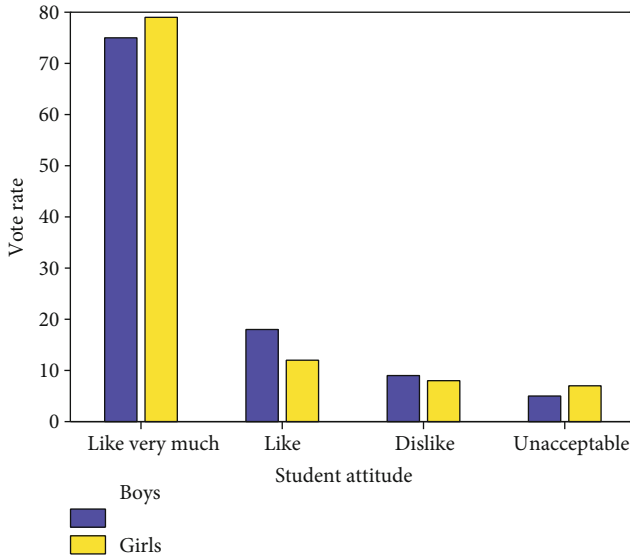
Figure 1: Students' attitudes towards animation-assisted teaching method.

Table 1: Multimedia usage survey of experimental group.

	Frequently used	Not often used	Rarely use	Never used
Test group 1	0	3	7	8
Test group 2	1	2	5	10

understanding of multimedia courseware-assisted teaching, and teachers subjectively accept multimedia-assisted teaching methods and are willing to improve current teaching methods and methods when conditions permit. In actual teaching, 84% of teachers feel that multimedia-assisted teaching is better. However, some objective factors restrict teachers' use of multimedia-assisted teaching methods. Among them, poor production technology and inconvenient use are the main factors that teachers think affect the application of multimedia-assisted teaching methods in actual teaching, and these influencing factors are difficult to eliminate in a short time.

teaching method. There are two main reasons for the attitude of 6% of the students: this teaching method is quite different from the traditional teaching method, and it is difficult for them to accept it in a short time; they are more accustomed to traditional tactical expression methods, and it is difficult to change their concepts. Although this group of students is a minority, in teaching, it is necessary to adopt the principle of differentiated treatment for this group of students. On the one hand, appropriate methods to change students' understanding of multimedia animation-assisted teaching were adopted, and on the other hand, traditional tactical teaching methods and forms are appropriately combined, to take care of this part of the students. Generally speaking, students still agree with the aid of multimedia animation methods and are subjectively easy to accept. After the students' interest in learning is stimulated, their learning attention will increase accordingly, which will help learn tactical knowledge and content. In basketball tactics teaching, the teaching of tactical knowledge should be carried out when students' attention is relatively concentrated in order to achieve better teaching results.

Although students have a strong tendency to use multimedia technology, in the current realistic basketball teaching, the application of multimedia-assisted teaching methods is not satisfactory. The survey shows that in the past learning process of students, only 30% of the teachers have used the video format to teach. Fewer people use multimedia animation technology to assist tactical teaching in basketball teaching. The survey results are shown in Table 1 and Figure 2.

From Figure 2, we can see that the proportion of students who have received multimedia-assisted teaching in the past is very small, and most students focus on the two options of seldom or not using multimedia-assisted teaching. This reflects the current application status of multimedia technology in college physical education from one aspect. According to the teacher survey questionnaire, teachers have a certain

4.2. Screening Coordination Evaluation Results. In order to further analyze the influence of multimedia-assisted teaching on the teaching effect of shielding cooperation, the results of statistical analysis of the seven connotative features of shielding cooperation are shown in Figure 3.

Through analysis, it is concluded that the experimental group and the control group have significant differences in the scores of the three connotative characteristics of the time, space, and cooperation of the screen cooperation, which shows that the application of multimedia-assisted teaching in the screen cooperation teaching is helpful to help students understand the timing, location, and location of cooperation. There are significant effects in terms of moving routes and overall structure of tactical coordination. There is no difference in the scores of the four connotative features of covering coordination, regularity, adaptability, effectiveness, and technical action, indicating that the application of multimedia-assisted teaching has little effect on the regularity, adaptability, effectiveness, and movement technique of covering coordination. The grasp of the rules, the response to the situation on the field, and the formation of technical movements must be accumulated in a lot of practice and competition.

In order to further analyze the impact of different teaching methods on the exchange defense teaching effect, the statistical analysis results of the connotative characteristic scores of the 7 exchange defense cooperations are shown in Figure 4. The average time characteristic score of the exchange cooperation is 3.52 in the experimental group. The control group was 3.26.

Through analysis, it is found that the experimental group and the control group have significant differences in the scores of the two scoring indicators of exchange defense cooperation and cooperation. This shows that the application of multimedia-assisted teaching in exchange defense cooperation teaching can help students understand the movement route of exchange defense cooperation. The overall structure
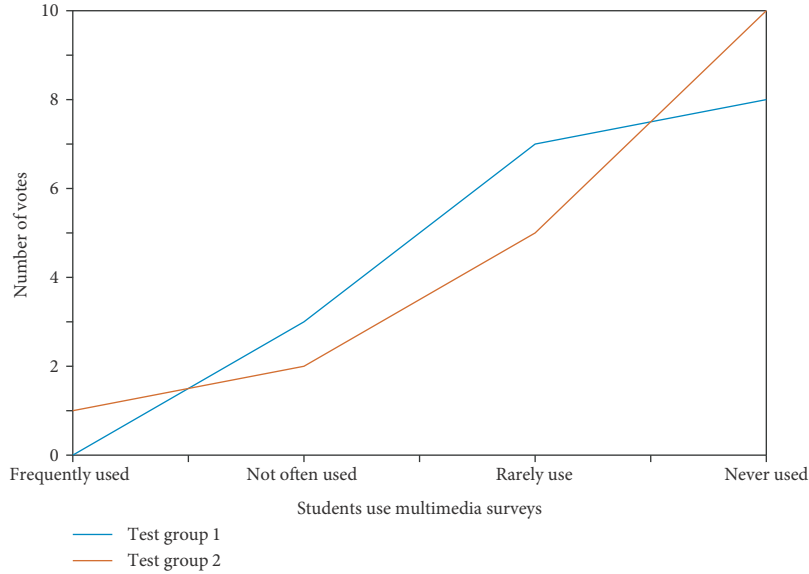
FIGURE 2: Multimedia usage survey of experimental group.
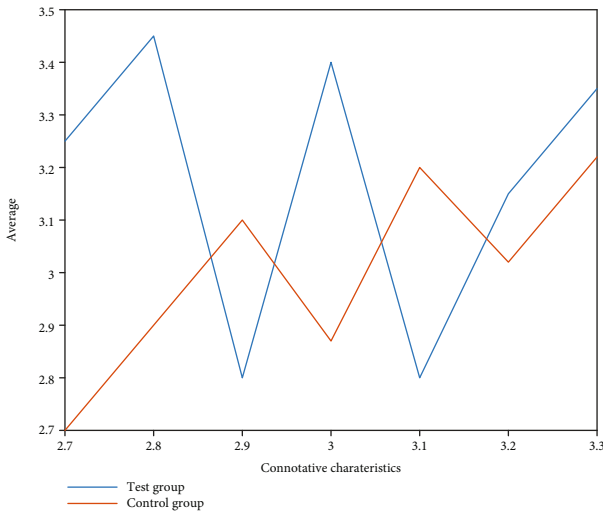
FIGURE 3: Screening coordination scoring checklist.

FIGURE 4: Single test result of the exchange defense coordination score.

of the coordination and the interaction between the players have significant effects; while the timeliness, adaptability, regularity, effectiveness, and technical movement learning of the exchange defense coordination have no significant difference compared with the conventional teaching methods, indicating that the application multimedia-assisted teaching has little effect on the timeliness, adaptability, regularity, effectiveness, and technical movements of exchange defense coordination. The analysis suggests that there is no significant difference in temporal characteristics because the exchange of defense coordination is a passive behavior of the defender based on the cooperation of the offensive player. The timing of the player's coordination, movement speed, and rhythm changes are affected by the timing of the offensive player's behavior, the influence of characteristics has little to do with the teaching methods adopted, and there is no signifi-

cant difference in the adaptability, regularity, effectiveness, and technical movements of exchange defensive cooperation. This is because students' grasp of the rules, adaptability to the field situation, and technical movements in the formation, and so on need to accumulate in a lot of practice and competition.

5. Conclusions

The application of multimedia-assisted teaching in basketball tactics basic coordination teaching has a positive effect on students' understanding of the overall structure of tactical coordination, timing, movement routes, and interaction among players, while the formation of coordination

techniques and on-the-spot adaptability have no significant effect. This is because the learning of basic basketball tactics is a process of thinking and physical exercises. In the basic teaching of basketball tactics, multimedia-assisted teaching should be combined with traditional teaching methods to give full play to the advantages of multimedia technology to help students understand tactics, establish the concept of tactical coordination, and form a preliminary awareness of tactical coordination, combined with traditional teaching methods, after a lot of practice and competition to be further strengthened, in practice and competition to further improve, through knowledge-practice-reunderstanding—the continuous cycle of "re-practice" process deepens, consolidates, and improves, and finally forms tactical awareness.

Most students believe that the use of multimedia-assisted teaching can intuitively express the teaching content in the form of text, graphics, images, videos, animations, etc., which can stimulate learning interest, improve learning enthusiasm, help understand the teaching content, and use multimedia-assisted teaching methods. It can speed up the mastery of the basic cooperation of basketball tactics, and the teaching effect of the basic cooperation of basketball tactics with the aid of multimedia teaching methods is satisfactory. It can be seen that multimedia-assisted teaching is a teaching method recognized and welcomed by students.

Traditional teaching methods and multimedia animation-assisted teaching methods have their own strengths. Traditional basketball tactics teaching methods are difficult to explain a relatively complex new tactic in a short time and enable students to form a clearer tactical appearance and concept; it is not easy to demonstrate tactical cooperation and control the classroom process, but it can provide various effective practice methods that can help students master tactics; and under the aid of multimedia animation, students generally reflect better learning results, and teachers control easier the classroom process.

Data Availability

No data were used to support this study.

Conflicts of Interest

The author declares that they have no conflicts of interest.

References

[1] B. Salski, J. Cuper, P. Kopyt, and P. Samczynski, "Radar cross-section of sport balls in 0.8 – 40 GHz range," *IEEE Sensors Journal*, vol. 18, pp. 7467–7475, 2018.

[2] N. A. Wahab, "The use of multimedia in increasing perceived knowledge and awareness of cyber-bullying among adolescents: a pilot study," *Procedia-Social and Behavioral Sciences*, vol. 176, no. 3, pp. 745–749, 2015.

[3] Z. Li, X. Wang, and H. Yu, "Application of multimedia technology in network course teaching," *Modern Computer (Professional Edition)*, no. 24, pp. 80–83, 2018.

[4] D. Haiqing, "Analysis of the function of multimedia in the teaching of basketball special technology," *Wireless Internet Technology*, no. 15, pp. 69-70, 2015.

[5] Y. Xu, T. Ye, T. Yue, J. Wu, and P. Zhao, "The application of multimedia technology in teaching anatomy of anesthesiology," *China Continuing Medical Education*, vol. 9, no. 4, pp. 40–42, 2017.

[6] J. Xinxin and L. Jia, "The importance of multimedia application in junior high school English teaching," *Journal of Jiamusi Education Institute*, no. 7, p. 294, 2016.

[7] S. Wenxia, "Study on application of multimedia technology in physics teaching in senior high school," *Wireless Internet Technology*, no. 21, pp. 98-99, 2015.

[8] Y. Lin, "On the application of multimedia Technology in computer teaching in secondary vocational schools," *Science & Education Wenhui*, no. 10, pp. 108-109, 2017.

[9] W. Jinsong, "Application of multimedia technology in orthopedics teaching," *China Continuing Medical Education*, vol. 8, no. 2, pp. 24–26, 2016.

[10] D. Hongyun, "On the application of hierarchical teaching method in basketball teaching in higher vocational colleges," *Journal of Jiamusi Education College*, no. 7, pp. 346-347, 2016.

[11] J. Wang and Y. Fengxian, *The Application of Multimedia to High School English Teaching——Take No. 6 Junior High School as an example*, no. 48, 2017Charming China, 2017.

[12] H. Sheng, "On the application of multimedia technology in physical education teaching in primary and middle schools," *Sports Science and Technology Literature Bulletin*, vol. 27, no. 6, pp. 98-99, 2019.

[13] L. Huyi, "A study on strategies of optimizing college basketball teaching based on flipped classroom," *Journal of Heihe University*, vol. 10, no. 2, pp. 116-117, 2019.

[14] J. Dongsheng, "Application of sports education model in basketball teaching in higher vocational colleges," *Journal of Xiangyang Vocational and Technical College*, vol. 18, no. 4, pp. 56–58, 2019.

[15] Z. Lichao, "An experimental research on TBL learning method in basketball teaching of medical specialty%"TBL" experimental research on basketball teaching of medical specialty," *Sports Products (Academic Edition)*, vol. 35, no. 8, pp. 58–60, 2016.

[16] C. Jin, "On the teaching mode of \"plate concentration\" in basketball teaching in higher vocational colleges%\"plate concentration\" in basketball teaching in higher vocational colleges," *Sports Science and Technology*, vol. 39, no. 5, p. 143, 2018.

[17] J. Yuguang, "Reflections on the teaching evaluation of public basketball course," *Sports Excellence (Academic Edition)*, vol. 38, no. 2, pp. 22-23, 2019.

[18] S. Lin, "Secondary vocational school basketball teaching present situation and countermeasure analysis," *Education Teaching Forum*, no. 26, pp. 228–230, 2017.

[19] Y. Yue, H. He, and Y. Hu, "Strategy of the application of flipped classroom in basketball teaching in universities: a case study of Anhui University of Chinese Medicine," *Journal of Hefei University of Technology (Social Science Edition)*, vol. 31, no. 4, pp. 121–124, 2017.

[20] S. Kuo, "Research on new method of basketball teaching and training in higher vocational colleges," *Heilongjiang Science*, vol. 8, no. 7, pp. 122-123, 2017.

[21] B. Yu, "The application of sports game method in basketball teaching in high school," *Heilongjiang Science*, vol. 8, no. 13, pp. 58-59, 2017.

[22] B. Xiaojing and H. Yu, "Influential factors and strategies of junior high school basketball teaching," *Sports Science and Technology Literature Bulletin*, vol. 25, no. 5, p. 68, 2017.

[23] J. Guangyuan, "Research on basketball teaching reform in higher vocational colleges under the background of sunshine sports," *Journal of Liaoning Teachers College (Natural Science Edition)*, vol. 18, no. 4, pp. 79-80, 2016.

[24] L. Wang, "Analysis of the common basketball teaching mode of training and improvement strategy," *Hubei Sports Science and Technology*, no. 2, pp. 128–130, 2016.

[25] Z. Xie, "Design of basketball teaching in higher vocational colleges under the guidance of cooperative learning theory," *Journal of Jiamusi Education College*, no. 12, pp. 284-285, 2016.

WILEY | Hindawi

Research Article

Soccer-Assisted Training Robot Based on Image Recognition Omnidirectional Movement

Bin Tan (ID)

College of Physical Education, Hunan Institute of Science and Technology, Yueyang, 414000 Hunan, China

Correspondence should be addressed to Bin Tan; gjxshqfwzx@nwu.edu.cn

With the continuous emergence and innovation of computer technology, mobile robots are a relatively hot topic in the field of artificial intelligence. It is an important research area of more and more scholars. The core of mobile robots is to be able to realize real-time perception of the surrounding environment and self-positioning and to conduct self-navigation through this information. It is the key to the robot's autonomous movement and has strategic research significance. Among them, the goal recognition ability of the soccer robot vision system is the basis of robot path planning, motion control, and collaborative task completion. The main recognition task in the vision system is the omnidirectional vision system. Therefore, how to improve the accuracy of target recognition and the light adaptive ability of the robot omnidirectional vision system is the key issue of this paper. Completed the system construction and program debugging of the omnidirectional mobile robot platform, and tested its omnidirectional mobile function, positioning and map construction capabilities in the corridor and indoor environment, global navigation function in the indoor environment, and local obstacle avoidance function. How to use the local visual information of the robot more perfectly to obtain more available information, so that the "eyes" of the robot can be greatly improved by relying on image recognition technology, so that the robot can obtain more accurate environmental information by itself has always been domestic and foreign one of the goals of the joint efforts of scholars. Research shows that the standard error of the experimental group's shooting and dribbling test scores before and the experimental group's shooting and dribbling test results after the standard error level is 0.004, which is less than 0.05, which proves the use of soccer-assisted robot-assisted training. On the one hand, we tested the positioning and navigation functions of the omnidirectional mobile robot, and on the other hand, we verified the feasibility of positioning and navigation algorithms and multisensor fusion algorithms.

1. Introduction

In order to further improve the robot's load capacity, movement flexibility, and for adaptability to small spaces, various types of omnidirectional mobile robots have emerged. The most important is the omnidirectional vision system, which collects images through hardware devices such as omnidirectional cameras and image capture cards to establish a model of the real environment, thereby controlling the robot to recognize the ball, goal, and other robots and providing information for the decision-making system. Therefore, the research on omnidirectional vision has become the focus and difficulty of the research on the vision system of the medium-sized soccer robot. Target recognition has long occupied a very important position in the field of pattern rec-

ognition. It is one of the most advanced research directions in computer vision. Through target recognition, computers can have perception and recognition capabilities similar to those of humans. Therefore, more and more scholars are concerned in related fields.

The world's first autonomously mobile robot, Shakey, was successfully developed. The robot was developed by the Stanford International Research Institute in the United States and possesses a certain degree of intelligence. For the first time, human beings successfully applied artificial intelligence under the conditions of the development to a mobile robot entity. Computer technology has been developing rapidly, and at the same time, microelectromechanical technology and sensor technology have also been greatly improved. Related researchers have begun to gradually apply

multisensor technology to the research of mobile robots. Cho et al. applies the extended Kalman filter to the SLAM problem. The algorithm breaks through the linear assumption of the system and extends to the nonlinear system, and it is still widely used [1]. Wang et al. proposed a nonlinear filtering algorithm based on SIS and really began to study particle filtering algorithms. This algorithm is based on the idea of Monte Carlo and expresses the probability of each group of particles, which is applicable to all nonlinear systems [2]. Wang et al. proposed the FastSLAM algorithm based on particle filtering, which can establish a more accurate map in a large-scale environment with few landmarks [3].

In recent years, our country has increased its investment in the research of mobile robots and made great progress. Although color contains more and richer information than grayscale images, it also brings new difficulties. An important aspect is that color images are easily affected by ambient lighting conditions. The study of the relationship between color and lighting, the disclosure of its inherent stable relationship, and the development of powerful algorithms and technologies in lighting changes are among the most urgent research areas today. Jia et al. proposed the idea of using evolutionary strategy in the study of SLAM algorithm based on monocular vision to improve the RBPF-SLAM algorithm and verified the reliability of the algorithm [4]. Yang et al. improved the RBPF-SLAM algorithm and then proposed a data association technology based on global constraints, which robustly reduces the probability of mismatch [5]. Ammar et al. introduced the fixed-level model of route planning and solved it using fast forward method and gave the result of route model calculation and visual interface [6].

The purpose of the image enhancement recognition algorithm in this article is to remove the unfriendly effects of uneven lighting on the color image, enhance the contrast and clarity of the image, and highlight the color features of the target object in the image, so as to better further feature extraction and target recognition. According to the experimental results, the average score and the highest score of the experimental group were higher than those of the control group, and the data were better than those of the control group. If the learning time is the same, the learning effect of the experimental group will definitely be much better than that of the control group, which also proves from the side football assist robot has a broader development prospect.

2. Soccer-Assisted Training Robot Based on Image Recognition Omnidirectional Movement

2.1. Deep Learning. In deep learning, by studying the inherent laws and representation levels of massive data samples, the simple features at the bottom are combined to form more abstract and advanced composite features, and the distributed representation of data features is realized. The dominant neural network is a typical representative of the principle of deep artificial intelligence in neuroscience. As a powerful deep learning technology tool, it has become an important part of the deep learning algorithm driven by the wave of

artificial intelligence [7, 8]. Deep learning is the process of learning features. The principle is to describe the characteristics of the model by learning the inherent characteristics and abstraction levels of the original data and then fine-tune the test data.

2.1.1. Deep Learning Framework. With the rapid development of deep learning technology, researchers are no longer satisfied with the basic theoretical analysis, and the requirements for practical applications are getting higher and higher, and the idea of creating a large-scale deep learning framework is being proposed [9]. The in-depth learning framework can contain basic algorithm modules and provide a solid foundation for the subsequent rapid construction of required models or training, coordination, testing, and development of existing models.

2.1.2. Deep Learning Model. After the concept of deep learning was proposed, more and more models appeared, such as deep belief network, convolutional neural network, and recurrent neural network.

(1) Deep Belief Neural Network. Deep belief network is a probabilistic generative model. Unlike traditional neural network models, training data is generated with the greatest probability by observing the joint distribution of data and labels. We can use DBN not only for feature selection and classification but also for data generation [10, 11]. The more common DBN neural network structure is shown in Figure 1.

In Figure 1, there are connections between neurons in the upper and lower layers of the DBN neural network structure, but there is no connection between neurons in the same layer. The neural unit in the optical layer is mainly used to receive input, and the neural unit in the hidden layer is mainly used to capture the high-order data correlation displayed in the optical layer.

(2) Convolutional Neural Network. Convolutional neural network is a feedforward neural network that uses convolution kernel operations instead of general matrix multiplication operations. It has the characteristics of sparse interaction and parameter sharing. In traditional neural networks, any pair of input and output neurons will interact to form a densely connected structure, while in convolutional neural networks, each output neuron will only exist with neurons in a specific area of the previous layer connect weights to achieve the characteristics of sparse interaction [12, 13].

Because of the progressive characteristics of its network structure, the extraction of image features also gradually changes from low-level simple texture features to high-level complex structure features, and the final combination is a feature map [14]. Image features extracted based on this characterization learning method often have good stability, so convolutional neural networks have huge advantages in processing two-dimensional image data.
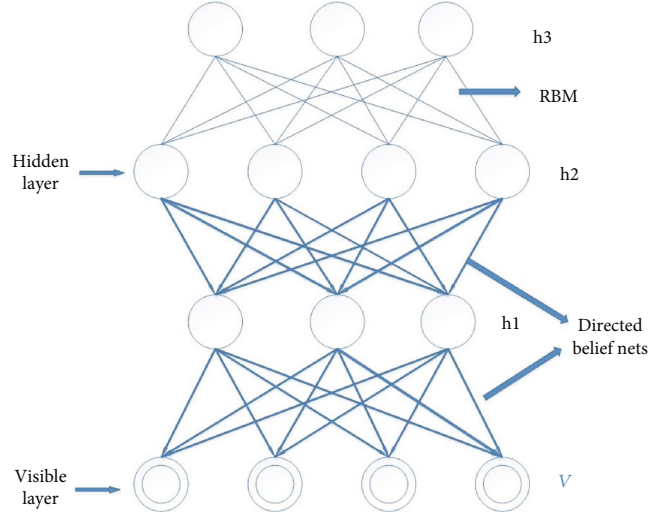
Figure 1: DBN structure diagram.

Table 1: System function test table.

Functional module	Function name	Test steps	Test results
Mobile function module	Forward function module	Robot forward test	Testing successfully
	Back function module	Robot back test	Testing successfully
	Left turn function module	Robot turning left test	Testing successfully
	Right turn function module	Robot turning right test	Testing successfully
Obstacle recognition module	Identify the football module	Take the pickup football test	Testing successfully
	Recognizer module	Take a turn test	Testing successfully
	Identify the wall module	Take a turn test	Testing successfully
	Identify the goal module	Take a shot test	Testing successfully
Pick and dribble function module	Ball pickup function module	Take the pickup football test	Testing successfully
	Dribble function module	Take a shot test	Testing successfully

2.2. Image Recognition Classifier Algorithm.

Sparse representation classifier is a very important feature encoding classifier and also a nondictionary learning classifier model. The SRC model is widely used in computer vision fields such as face recognition, object recognition, and scene understanding. The mathematical representation of the SRC model is given below in detail. We assume that there are a total of C categories in the image data set. The dimension of each image sample is m, and there are a total of n training samples for the i-th category. For a test image sample $Z \in R\, m$ from the i-th category, intuitionally, z can be approximated by a linear combination of samples in Y, namely

$$Z = \sum_{j=1}^{n} a_i = Y_i a_i. \tag{1}$$

Y is the dictionary in the model. It can be seen that the original sample is directly used as a dictionary in the SRC model, instead of retraining a dictionary. If we use y to represent the test sample z, then z can be expressed as

$$Z = Y\alpha. \tag{2}$$

Table 2: Data analysis chart of test scores before shooting and dribbling.

Scores	C dribble test score	E dribble test score	C shot test score	E shot test score
Number of surveys	11	11	11	11
Average value	62.84	63.42	62.77	63.92
Standard deviation	7.467	7.523	7.847	7.962
Standard error of the mean	1.375	1.378	1.42	1.423

In the actual SRC model, Y and Z are known, and the coding coefficient α is unknown. We can solve the sparsest solution by imposing the L-norm minimization restriction on the linear representation system, so formula (2) can turn into the following optimization problem:

$$\alpha = \text{argmin} |a| s.t. \tag{3}$$

Further, if only k column vectors are selected from Y to represent Z, then it will be equivalent to the following
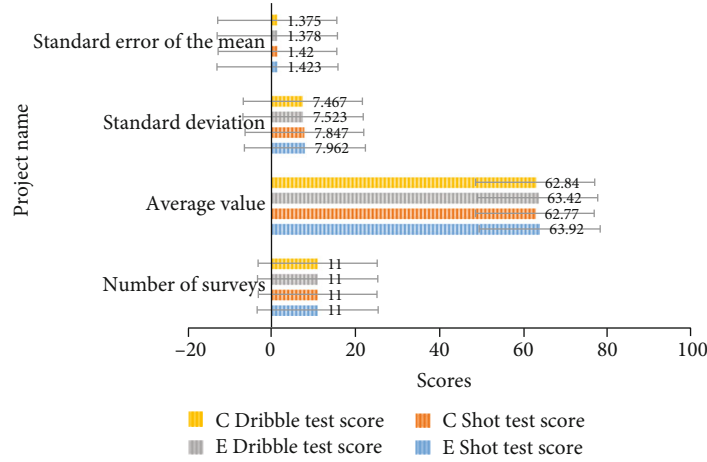
Figure 2: Data analysis chart of test scores before shooting and dribbling.

Table 3: Analysis chart of the pretest scores and back-side scores of the shooting and dribble control groups.

Serial numbers	1	2	3	4	5	6	7	8	9	10	11
Preshot score	67	71	76	62	65	55	74	57	63	67	62
Postshot score	69	70	76	64	66	58	77	61	60	66	60
Predribble score	60	67	68	62	57	58	71	57	65	60	59
Postdribble score	65	66	70	64	60	56	70	61	67	62	60

Table 4: Analysis chart of the pretest scores and back scores of the shooting and dribble experimental groups.

Serial numbers	1	2	3	4	5	6	7	8	9	10	11
Preshot score $\pm$ 4	63	72	75	64	66	56	75	58	61	67	61
Postshot score $\pm$ 3	69	76	77	65	67	59	79	60	61	68	62
Predribble score $\pm$ 2	58	65	67	61	58	59	70	58	67	58	57
Postdribble score $\pm$ 2	62	66	69	63	62	56	69	60	68	65	63

$$\alpha = L(\alpha, \varphi) = \mathrm{argmin}|y - Xa|. \tag{6}$$

It can be seen from the above algorithm (6) that when solving the sparse coding coefficient α, the dictionary based on is X, that is, the original training image samples, and these initial samples are not used to train a new criterion based on a new criterion dictionary. In addition, the SRC algorithm uses the size of the reconstruction residual of each category to determine the label of the test sample, and most feature coding classifiers also use the size of the reconstruction error to predict the category, so most feature coding classifiers are based on reconstruction methods.

Figure 3: Analysis chart of the pretest scores and back-side scores of the shooting and dribble control groups.

optimization problem:

$$Z = Y\alpha + s. \tag{4}$$

Because of the presence of noise, the sparse solutions of problems (3) and (4) can be approximated by solving the following optimization problems:

$$\alpha = \mathrm{argmin}|a| * |y - Xa|. \tag{5}$$

Furthermore, according to the Lagrangian multiplier theory, the above two optimization problems are equivalent to the following unconstrained minimization problems:

2.3. Image Enhancement Algorithm for Omnidirectional Vision System. There are many factors that make the image not clear enough. The images collected by the camera are converted from analog to digital, and line transmission will cause noise pollution. Uneven changes in indoor and outdoor lighting will cause excessive concentration of grayscale images, which affects image quality. The shallowest degree indicates that there is noise in the image, which will affect the representation of image details; the more serious degree indicates that the image is blurred, and even the rough outline of the object is difficult to see [15, 16]. Therefore, before processing and analyzing the collected images, we can improve the image quality in a targeted manner, that is, image improvement. Image enhancement processing is to highlight the interesting part of the image, reduce or delete the uninteresting part, thereby improving useful information, obtaining an image that is more in line with human visual acceptance or transforming it into a more suitable
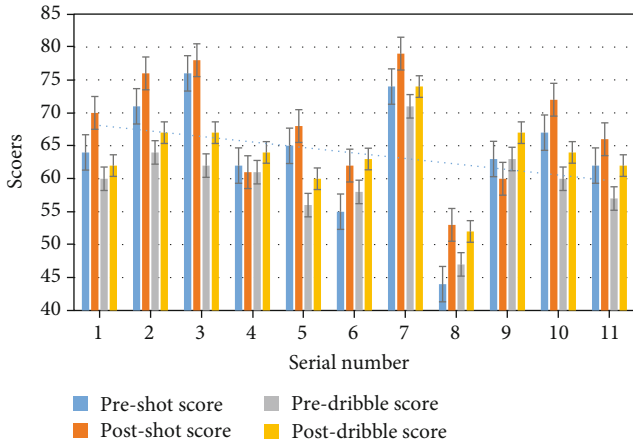
FIGURE 4: Analysis chart of the pretest scores and back scores of the shooting and dribble experimental groups.

TABLE 5: Football match training effect analysis chart.

	Experimental class	Control class
The average score	75 ± 15	63 ± 13
Highest score	90 ± 18	77 ± 16
Lowest score	68 ± 11	56 ± 13
High score	26 ± 16	16 ± 8
Low score	36 ± 14	36 ± 11
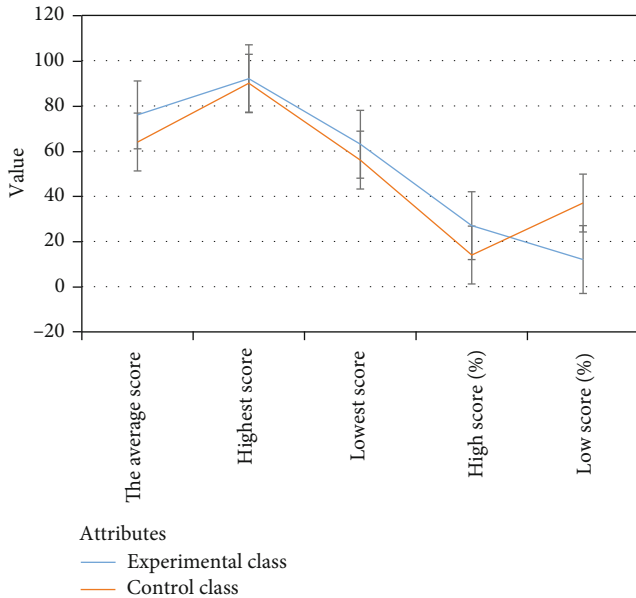
FIGURE 5: Football match training effect analysis chart.

machine for processing and analysis Image. There are many image enhancement methods, and they have a wide range of applications.

2.3.1. Selection of Color Space for Image Enhancement. Color space, also known as color coordinate system, is a method of expressing colors with numbers. The color space is usually a three-dimensional model, and colors can be defined by hue, saturation, and lightness. It is the basis of image processing, analysis, and understanding. The purpose of image enhancement is to remove the effect of changing or uneven lighting on the image color. RGB color space is closely related to hardware devices. It is not completely equivalent to the difference in color perception. It is rarely used to process pictures under variable lighting conditions. Therefore, people often convert it into other color spaces that are more consistent with visual characteristics and more stable [17, 18]. Compared with the normalized YUV color space, the HSI color space has independent brightness components, but the HSI color space is the space most suitable for human visual characteristics and is more suitable for images based on the color perception characteristics of the human visual system processing, and the effect of changing lighting response on the color space is mainly concentrated in the brightness of the brightness component.

2.3.2. Selection of Color Space for Target Recognition. The task of target recognition is to separate the orange ball from other colors, such as green, white, and black, and to improve the accuracy of target recognition. Because the RGB color space is not suitable for images with changing illumination, the feature quantity that is more suitable for identifying the target orange ball is mainly selected from the two color spaces of HSI and YUV. HSI color space and YUV color space are two color spaces that are often used in football robot vision systems, and neither of them is specifically for identifying a certain color or a few colors. The two color spaces are merged, and several components that have a better aggregation effect on the orange sphere are extracted from the six components and combined together. Since this paper inputs the color feature quantity into the support vector machine for target recognition, in order to reduce the complexity of the algorithm, only two components are selected from these six components to form a new color model [19, 20]. The separability criterion of the distance between classes within a class is widely used because of its intuitiveness, clear concept, and convenient calculation. However, it is calculated directly based on the distance between various types of samples, without considering their probability distributions, and cannot clearly calculate various overlapping problems, which leads to the final selection of the optimal feature subset when the classification decision is made. Not necessarily optimal. Therefore, the intraclass divergence matrix is introduced as the criterion.

2.4. Robot Rapid Target Acquisition and Distance Measurement. In the autonomous robot soccer game, the robot is a highly intelligent body that collects information from sensors, performs data fusion, and then makes behavior decisions, and then controls the robot to move according to the planned behavior strategy. Many robots complete competition tasks through mutual cooperation. It can be said that it is a microcosm of robot society. As we all know, about 80% of the external world information that people perceive is obtained through visual means [21]. Similarly, in order to

TABLE 6: Comparison of recognition speed and accuracy of different algorithms.

Algorithm	Number of test frames	Average frame time (ms)	Accuracy (%)
Traditional threshold segmentation	80	38	91
Unimproved RHT algorithm	80	22.2	94
Based on Gabor filter + SVM	80	55	93.4
Edge detection segmentation method	80	41	94
Improved BP algorithm	80	32.1	96.6
Improved RHT algorithm	80	5.6	8.3
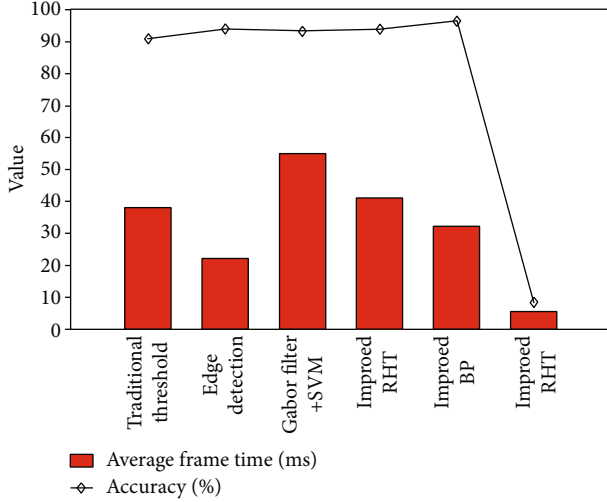
FIGURE 6: Comparison of recognition speed and accuracy of different algorithms.

make intelligent robots reachable, providing robots with human vision functions is extremely important for the development of intelligent robots. Especially for the quadruped robot football game, vision is its only source of information. Unlike the human eye, the quadruped robot has a very narrow viewing angle, and the amount of information that can be received at the same time is very small.

From the human point of view, it is very simple to understand the surrounding scene correctly, but it is a great challenge for the machine. Therefore, although computer vision has made significant progress in recent years, a large number of technologies and algorithms have been studied and widely used in various fields. However, machine vision technology is still at a very immature stage, and there are still many problems, especially in the following aspects: the 3D scene is projected into a 2D image, and the depth and invisible parts of the information are lost, so the images displayed in different 3D shape image planes. The object will produce the same image. At the same time, the images of the same object taken from different angles will also be very different [22]. Many factors are in the real scene, such as shape, color, lighting conditions, camera, and noise. The image of the object will affect the image and bring difficulties and errors to the recognition of the target object. The amount of information in images is very high, especially color images, which have become a major obstacle to fast image processing. At the same time, the huge amount of data requires huge storage space and will increase the system load.

2.5. Image Color Model. In order to use colors correctly, a color model is also needed. A color can be described by a basic quantity, so to establish a color model is to establish a coordinate system, in which each spatial point represents a certain color.

The most commonly used color model for hardware devices is the RGB model, and the most commonly used color model for color processing is the HSI model, where H represents hue, S represents saturation, and I represents density, corresponding to imaging brightness and image grayscale [23]. These two color models are also the most common models in image technology [24].

Since people's sensitivity to brightness is obviously stronger than that of color shades, in order to better color processing and recognition, robot vision systems often use HSI color space, which is more suitable for the characteristics of the human eye than RGB color space. A large number of algorithms in image processing and computer vision can be conveniently used in the HSI color space. They can be processed separately and are independent of each other.

The formula for transforming from space to space widely used in the visual processing of soccer robots is as follows:

$$H = \cos^{-1} \frac{1/2[(R - B) + (R - G)]}{\sqrt{(R - G)^2 + (R - B)(G - B)}}, \tag{7}$$

$$S = 1 - \frac{\min(R, G, B)}{I}, \tag{8}$$

$$I = \frac{(R + G + B)}{3}. \tag{9}$$

Among them, the value range of H is $[0°, 180°]$. When $G < B$,

$$H = \begin{cases} H, G \geq B \\ 360° - H, G < B \end{cases}. \tag{10}$$

The formula for converting from HSI to RGB has different formulas according to the different sectors of the color circle:

When $0° \leq H \leq 120°$,

$$R = 1/\sqrt{3}\left[1 + \frac{S \cos(H)}{\cos(60° - H)}\right], B = 1/\sqrt{3}(1 - S), G = \sqrt{3}I - R - B. \tag{11}$$

TABLE 7: Comparison of recognition speed and accuracy of two algorithms.

Algorithm	Number of frames	10	20	30	40	50	60
Unimproved RHT algorithm	Time-consuming (ms)	22.02	21.71	21.75	21.77	21.92	21.86
	Accuracy (%)	93.2	93.2	93.6	92.6	93.1	93.4
Improved RHT algorithm	Time-consuming (ms)	5.21	5.77	6.22	5.97	5.11	5.34
	Accuracy (%)	98.6	98.8	97.3	97.8	98.1	98.7
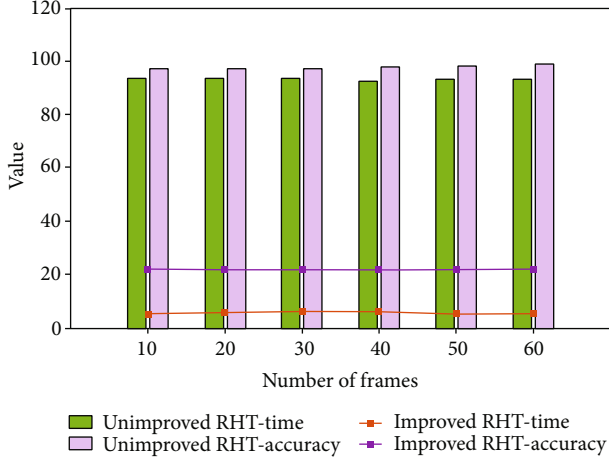
FIGURE 7: Comparison of recognition speed and accuracy of two algorithms.

When $120° \leq H \leq 240°$,

$$R = 1/\sqrt{3}\left[1 + \frac{S\cos(H-120°)}{\cos(180°-H)}\right], B = 1/\sqrt{3}(1-S), G = \sqrt{3}I - R - B. \tag{12}$$

When $240° \leq H \leq 360°$,

$$R = 1/\sqrt{3}\left[1 + \frac{S\cos(H-240°)}{\cos(300°-H)}\right], B = 1/\sqrt{3}(1-S), G = \sqrt{3}I - R - B. \tag{13}$$

3. Experimental Football Aided Training Robot Based on Image Recognition and Omnidirectional Movement

3.1. Test Subject.
In this study, we used an omnidirectional football-assisted training robot. This experiment selects two novice football players with similar technical level from a college from our province Sports Institute, and they are divided into experimental group and control group. The football players in the experimental group use football-assisted robot training when training, and the football players in the control group use the method of training. A commonly used training method, the experiment duration is 3 months, and every member of the team is tested for shooting and dribbling every half month. A total of 22 football players participated in this experiment. The tests of these football players are the main source of data.

3.2. Mean Shift Segmentation Based on Confidence.
In low-level image visual processing, combining image segmentation algorithms with edge detection algorithms can improve the quality of segmented images. Combine the edge confidence map into a color image segmenter based on the Mean Shift program. This method can recover areas with weak signals but strong boundaries, so that it can provide more accurate input data for high-level interpretation.

Using the $\rho\eta$ chart in the confidence edge detection, the weight assigned to each pixel (i, j) can be defined as

$$w_{ij} = a_{ij} * \rho_{ij} + (1 - a_{ij}) * \eta_{ij}. \tag{14}$$

a_{ij} is any value in [0,1]; this parameter is used to control the mixed information of ρ and η, so this parameter is called a mixed parameter. When $\rho < 0.02$, the weight is 0. When the pixel is closer to the edge, these weights are smaller, which further strengthens the Mean Shift filtering effect.

3.3. Material Handling.
Production materials include five categories: text, graphics, audio, animation, and video. Text material is the simplest material. When using text in multimedia, we should focus on the accuracy, simplicity, and functionality of the content. The sound material is generally selected from the existing sound material library and collected from the microphone through the sound card in the computer. The more commonly used method of image material collection is the use of digital camera collection. Flash animation material is currently the most popular two-dimensional animation technology. Video material is a combination of one or more of text, graphic images, sound, and animation.

3.4. Experiment Procedure.
Because of its unique characteristics, surveillance cameras make it possible to extract some basic attribute information of the surrounding environment from remote sensing images. These basic information include the location of obstacles, the height of obstacles, and the area of obstacles. The shadow has obvious spectral characteristics in the surveillance camera and has a lower gray value, and the gray value has a strong consistency.

The 22 novice football players we selected were randomly divided into two teams with 11 people in each team. In them, the football players in the experimental group were trained with a football-assisted robot-assisted training method, and the football players in the control group were trained by using common training methods. Before the start of the experiment, we conducted shooting and dribbling tests and scores on these novice football players. After one and a half

months, we conducted the second shooting and dribble test and scored. At the end of the experiment, we conducted the shooting and dribble tests and conducted the score again. Score. And analyze and get a conclusion.

3.5. Gather Data. In order to obtain accurate data to compare and analyze the feasibility and effectiveness of this experiment, this paper uses the Cora dataset and the IMB dataset. The statistical data used in this article has a different unit dimension for each index data. After calculating the data in the previous steps, we can get the similarity between users and select several users closest to user u_a interests and preferences to form set N_a. Then, calculate the user u_a score on j according to the user's score on the unrated item j in the set N_a. The prediction formula is shown in formula (8)

$$p_{a,i} = \frac{\sum_{b \in N_a} \mathrm{sim}_{u_a,u_b} r_{b,i}}{\sum_{b \in N_a} |\mathrm{sim}_{u_a,u_b}|}, \tag{15}$$

where $p_{a,i}$ is the predicted score of user a for the unrated i item. In the recommendation system, users scoring preferences are sometimes different. For example, some users are accustomed to giving higher ratings to items, while some are accustomed to giving lower ratings. In order to reduce the difference between users scoring preferences and improve the accuracy of scoring predictions, the average rating $\bar{r}$ of the user is introduced, and the specific form is shown in formula (9)

$$p_{a,i} = \overline{r_a} + \frac{\sum_{b \in N_a} \mathrm{sim}_{u_a,u_b} (r_{b,i} - \overline{r_b})}{\sum_{b \in N_a} |\mathrm{sim}_{u_a,u_b}|}. \tag{16}$$

4. Soccer-Assisted Training Robot Based on Image Recognition Omnidirectional Movement

4.1. System Function Test Analysis. The function test of the system mainly includes main functions such as forward, backward, left turn, right turn, automatically bypass obstacles, and recognize football. The results are shown in Table 1.

In the process of testing the monitoring effect, technical tests such as background sampling and encoding are carried out using specific video formats, and the server and other hardware are repeatedly tested until satisfactory test results are obtained. It can be seen from the table that the system is basically designed and tested successfully after analyzing the required functions.

4.2. Shot and Dribble Test Data Analysis

4.2.1. Pretest Score Data Analysis. The data obtained through shooting and dribbling tests and scoring can calculate the mean, standard deviation, and standard error of the pretest scores of the experimental group and the control group. At the same time, independent samples drawn at the same time, the individual and overall variance scores are not equal waiting for data is also an important condition for the beginning

of the experiment, and the results are shown in Table 2 and Figure 2.

The control group's shooting and dribble pretest scores are tested by independent samples from the experimental group's shooting and dribble pretest scores. The standard error of the mean is 0.003 < 0.05, and the mean and standard deviation of the scores are similar; that is, there is no significant difference in results, which shows that there is no significant difference between the shooting and dribbling skills of the experimental class and the control class before the start of the experiment, which meets the preconditions for the start of the experiment.

4.2.2. Data Analysis of Pretest Scores and Posttest Scores of the Control Group. In order to have a deeper and more accurate understanding of the improvement of football training brought by the omnidirectional football-assisted training robot, we analyzed the data of the pretest and posttest results of the control group and drawn a line chart, as shown in Table 3 and Figure 3. At the same time, the pretest scores of the control class and the posttest scores of the control class are tested in pairs, and data such as the mean, standard deviation, and standard error of the mean are obtained.

It can be seen from Table 3 and Figure 3 that there is not much change between the pretest and posttest results of the shooting and dribble tests of the control group. At the same time, the pretest scores of the shooting and dribbling tests of the control group are tested in pairs with the posttest scores of the shooting and dribbling tests of the control group. The standard error value of the mean is 0.262. The value is greater than 0.05, indicating the control group shooting and dribbling that there is no significant difference between the pretest results of the test and the posttest results of the control group's shooting and dribbling tests, which also shows that the traditional football training model has little effect on improving the training effect of athletes.

4.2.3. Data Analysis of Pretest Scores and Posttest Scores of the Experimental Group. We analyzed the data of the pretest scores and posttest scores of the experimental group and drew an area chart, as shown in Table 4 and Figure 4. At the same time, the pretest scores of the control class and the posttest scores of the control class are tested in pairs, and data such as the mean, standard deviation, and standard error of the mean are obtained.

It can be seen from Table 4 and Figure 4 that the pretest and posttest scores of the experimental group's shooting and dribble tests have significantly increased. At the same time, the pretest scores of the shooting and dribble tests of the experimental group are tested in pairs with the posttest scores of the shooting and dribbling tests of the experimental group. The standard error value of the mean is 0.004, which is less than 0.05, indicating that the experimental group's shooting and dribbling the pretest scores of the test are significantly different from the posttest scores of the experimental group's shooting and dribbling tests, which also proves the effectiveness of the football-assisted robot-assisted training method.

4.3. Training Effect of Football Match. We analyze the data of all the athletes after training to test and score the football match and draw an area chart, as shown in Table 5 and Figure 5. Reduce the difference between the teacher's scoring preference, improve the accuracy of scoring prediction, and compare the average score of the experimental group and the control group to get a conclusion.

It can be clearly seen in Table 5 and Figure 5 that the experimental group is relative to the control group. The average and highest scores of the experimental group are higher than those of the control group, and all data are better than those of the control group. If the learning efficiency is the same, the learning time of the experimental group must be longer than the control group, which also proves the use of football assistance robot-assisted training method makes the athletes' training effect better. It also proves from the side that football-assisted robots have broader development prospects.

4.4. Soccer Robot Target Image Recognition Algorithm. Simulate the construction of the football robot game environment in the laboratory, and change the lighting situation in the laboratory by adjusting the curtains and light tubes in the laboratory, so as to collect the field images under different lighting required for algorithm verification. At the same time, in order to verify the effectiveness of the proposed algorithm, a dynamic test of 80 frames was carried out on the algorithm. The improved RHT algorithm was compared with traditional threshold method, edge detection algorithm, and improved BP neural network algorithm. The experimental results are shown in Table 6 and Figure 6.

From the data trend in the chart, it can be seen that the traditional threshold method and edge detection method have reached more than 90% in recognition accuracy, but the recognition speed is slow; based on the method of Gabor filter + SVM, the recognition accuracy rate reaches 93.4%. However, the same recognition speed is slow and cannot meet the real-time requirements of soccer robot matches, and the improved BP neural network algorithm mentioned above has achieved certain improvements in both the real-time performance of the algorithm and the recognition accuracy. The frame takes 32.1 ms, and the recognition accuracy is more than 96%. The improved RHT algorithm greatly improves the recognition speed while ensuring that the recognition accuracy rate is not reduced. The average time per frame is 5.6 ms, which meets the real-time requirements of the football robot game.

To further illustrate that the improved RHT algorithm has improved recognition speed and accuracy, a detailed comparison is made with the unimproved RHT algorithm. Comparative experiments were carried out at the 10th, 20th, 30th, 40th, 50th, and 60th frames of the collected video images. The experimental results are shown in Table 7 and Figure 7.

According to the data analysis in the chart, it can be seen that the improved RHT algorithm has higher recognition accuracy than the unimproved RHT algorithm, and at the same time, the running time of the algorithm is shorter. This is because the improved RHT algorithm improves the performance of RHT by limiting the radius range, reducing the effective calculation area of the picture, and calculating using the image gradient, which greatly improves the real-time performance of the algorithm. Therefore, the improved RHT algorithm is more suitable and applied in soccer robot games with high real-time requirements.

5. Conclusions

In recent years, robot vision systems have always been a hot and difficult point in computer vision research and digital image processing. The medium-sized football game provides a typical test environment for the research of machine vision-related technology. Expand the application scope of image processing and recognition technology, and enrich the theory of image processing and recognition technology. This dissertation conducts an in-depth study on how to improve the adaptability and target recognition rate of the robot's all-view system under changing lighting conditions. Recreate the filtered wave factor, and then perform an antagonist transformation to finally obtain an improved image. This method has strong adaptability and high stability and is suitable for image preprocessing in competitions. This paper studies the adaptive target recognition problem of the mid-size vision system of soccer robots and has achieved some results. However, due to the complexity of robot vision problems and the limited research time, many of the above issues should be further studied.

For a long time, people have been doing many explorations to understand the world through automatic perception similar to human vision. These explorations are very active in the research fields of computer vision, mechanical imaging, and robot vision. As automation and the latest equipment, intelligent robots can enter the network world and play more and more roles. This has important practical significance for mankind to open up new industries and improve production and living standards. With the continuous development and progress of the system, the structure of the system, the search, and tracking algorithms for target recognition are becoming more and more perfect.

Correspondingly, the hardware and software systems of the omnidirectional mobile robot are designed, the working principles of the main hardware units used on the platform are introduced, and the communication methods between the modules are designed; the software in the program of this document has also been analyzed and tested. After simulation analysis and experimental testing, the module driver in the system is normal, and the communication between the modules is normal and stable, indicating that the system module driver and the communication between them are complete and feasible. The omnidirectional robot positioning and navigation system designed and researched in this field is appropriately designed, has integrated and feasible functions, and can achieve the original design goal.

Data Availability

No data were used to support this study.

Conflicts of Interest

The authors declare that they have no conflicts of interest.

Acknowledgments

References

[1] H. Cho, E. K. Kim, E. Jang, and S. Kim, "Improved positioning method for magnetic encoder type AGV using extended Kalman filter and encoder compensation method," *International Journal of Control Automation & Systems*, vol. 15, no. 4, pp. 1844–1856, 2017.

[2] Y. Wang, J. Yue, Y. Dong, and Z. Hu, "Review on kernel based target tracking for autonomous driving," *Journal of Information Processing*, vol. 24, no. 1, pp. 49–63, 2016.

[3] S. Wang, D. Bi, H. Ruan, and S. Chen, "Cognitive structure adaptive particle filter for radar manoeuvring target tracking," *IET Radar, Sonar & Navigation*, vol. 13, no. 1, pp. 23–30, 2019.

[4] B. Jia, R. Liu, and M. Zhu, "Real-time obstacle detection with motion features using monocular vision," *The Visual Computer*, vol. 31, no. 3, pp. 281–293, 2015.

[5] M. Yang, Y. Wu, and Y. Jia, "A hybrid data association framework for robust online multi-object tracking," *IEEE Transactions on Image Processing*, vol. 26, no. 12, pp. 5667–5679, 2017.

[6] A. Ammar, H. Bennaceur, I. Châari, A. Koubâa, and M. Alajlan, "Relaxed Dijkstra and A with linear complexity for robot path planning problems in large-scale grid environments," *Soft Computing*, vol. 20, no. 10, pp. 4149–4171, 2016.

[7] X. Hao, G. Zhang, and S. Ma, "Deep learning," *International Journal of Semantic Computing*, vol. 10, no. 3, pp. 417–439, 2016.

[8] G. Litjens, T. Kooi, B. E. Bejnordi et al., "A survey on deep learning in medical image analysis," *Medical Image Analysis*, vol. 42, no. 9, pp. 60–88, 2017.

[9] L. Nie, M. Wang, L. Zhang, S. Yan, B. Zhang, and T. S. Chua, "Disease inference from health-related questions via sparse deep learning," *IEEE Transactions on Knowledge & Data Engineering*, vol. 27, no. 8, pp. 2107–2119, 2015.

[10] Y. Jayasimha and R. V. S. Reddy, "A robust face emotion recognition approach through optimized SIFT features and adaptive deep belief neural network," *Intelligent decision technologies*, vol. 13, no. 3, pp. 379–390, 2019.

[11] P. T. Sheeba and S. Murugan, "Hybrid features-enabled dragon deep belief neural network for activity recognition," *The imaging science journal*, vol. 66, no. 6, pp. 355–371, 2018.

[12] N. Tajbakhsh, J. Y. Shin, S. R. Gurudu et al., "Convolutional neural networks for medical image analysis: full training or fine tuning?," *IEEE Transactions on Medical Imaging*, vol. 35, no. 5, pp. 1299–1312, 2016.

[13] Y. Li, X. du, F. Wan, X. Wang, and H. Yu, "Rotating machinery fault diagnosis based on convolutional neural network and infrared thermal imaging," *Chinese Journal of Aeronautics*, vol. 33, no. 2, pp. 427–438, 2020.

[14] R. N. Ruliputra and S. Darma, "Control system of hexacopter using color histogram footprint and convolutional neural network," *AIP Conference Proceedings*, vol. 1862, no. 1, pp. 1–6, 2017.

[15] S. Kumar, M. Pant, and A. K. Ray, "DE-IE: differential evolution for color image enhancement," *International Journal of System Assurance Engineering and Management*, vol. 9, no. 3, pp. 577–588, 2018.

[16] P. K. Mahapatra, S. Ganguli, and A. Kumar, "A hybrid particle swarm optimization and artificial immune system algorithm for image enhancement," *Soft Computing*, vol. 19, no. 8, pp. 2101–2109, 2015.

[17] A. Das and M. Bhattacharya, "FPGA based embedded system for medical image enhancement technique used in mask mode radiography," *International Journal of Computing & Information Technology*, vol. 7, no. 1, pp. 9–17, 2015.

[18] J. W. Kim, Y. D. Jung, D. S. Lee, and D. H. Shim, "Landing control on a mobile platform for multi-copters using an omnidirectional image sensor," *Journal of Intelligent & Robotic Systems*, vol. 84, no. 1-4, pp. 529–541, 2016.

[19] P. Tian and H. Duan, "A discriminant method of single-optical-axis omnidirectional vision system," *Multimedia Tools and Applications*, vol. 78, no. 1, pp. 1117–1130, 2019.

[20] Luyang Li, Yun-Hui Liu, Kai Wang, and Mu Fang, "Estimating position of mobile robots from omnidirectional vision using an adaptive algorithm," *IEEE Transactions on Cybernetics*, vol. 45, no. 8, pp. 1633–1646, 2015.

[21] K. Ni, M. Xu, Q. Zhou, H. Dong, X. Li, and G. Wu, "Implementation of a data processing platform for real-time distance measurement with dual-comb lasers," *Proceedings of SPIE The International Society for Optical Engineering*, vol. 9623, no. 9, pp. 372–374, 2015.

[22] W. Pan, J. Zhao, Q. Chen, and D. Zhang, "Simultaneous and rapid measurement of main compositions in black tea infusion using a developed spectroscopy system combined with multivariate calibration," *Food Analytical Methods*, vol. 8, no. 3, pp. 749–757, 2015.

[23] B. Chen, L. Kuang, and W. He, "Framework design and material processing of gymnastics teaching network courseware," PREPRINT (Version 1) available at Research Square, 2020.

[24] S. Hua, K. Han, Z. Xu, M. Xu, H. Ye, and C. Q. Zhou, "Image processing technology based on Internet of Things in intelligent pig breeding," *Mathematical Problems in Engineering*, vol. 2021, Article ID 5583355, 9 pages, 2021.

WILEY | Hindawi

Research Article

Social Group Behavior Analysis Model Integrating Multitask Learning and Convolutional Neural Network

Chuan Zhou [ID],[1,2] **Suying Gui,**[1,3] **Gaoming Zhang** [ID],[2] **Qirui Zhang,**[3] **Xudong Wang,**[4] **and Jianqing Wei**[2]

[1]*School of Microelectronics, Tianjin University, Tianjin 300072, China*
[2]*The Second Institute of China Aerospace Science and Technology Corporation, Beijing 100039, China*
[3]*Polytechnic Institute, Zhejiang University, Hangzhou, 310015 Zhejiang, China*
[4]*Institute of Information Engineering, Chinese Academy of Sciences, Beijing 100195, China*

Correspondence should be addressed to Chuan Zhou; zhouchuan@tju.edu.cn

Social group behavior analysis has always been the key research direction of sociologists and psychologists. With the rapid development of the Internet of Things and the proposal of deep learning theory, convolutional neural networks are also used in social group research. In the process of social development, group incidents continue to increase, and there are more and more studies on social group behavior analysis. Although the research content and research methods are also richer, the research that combines the Internet of Things, convolutional neural network, and group behavior is more. This article will specifically propose a social group behavior analysis model that combines multitask learning and convolutional neural networks. This paper deeply learns the research of convolutional neural network and group behavior-related theories, makes full use of the advantages of convolutional neural network algorithm and multitask learning mode, and builds a social group behavior analysis model based on multitask learning and convolutional neural network. The experimental results on different data sets are analyzed. The results show that the accuracy rate of the experimental algorithm of convolutional neural network is as high as 95.10%, and it is better than other algorithms in time complexity, which is very suitable for social group behavior analysis.

1. Introduction

In recent years, with the development of the economy, the adjustment of economic structure, and the acceleration of urbanization, various social collective actions have also increased, and their development has become more and more complex, which has had a huge impact on the construction of today's society and moral culture. Various group theories are becoming more and more abundant and perfect, exploring and explaining group processes or group dynamics and discussions of related issues. As an object of study, the group integrates multitask learning and convolutional neural networks and allows for more group behavior characteristics to be fully considered under the Internet's big data.

Multitask learning and convolutional neural network are both promising fields, and they are the development exten-

sion of deep learning. The role of multitask learning is to extract feature information to help improve learning more accurately. Its biggest characteristic is parallel transfer learning, which is different from the traditional progressive and procedural learning methods. In multitask learning, multitask learning is also called parallel migration learning because information is shared between tasks and is transferred between different tasks. It can realize the sharing and transmission of information between tasks. Convolutional neural network has the same characteristics as it; that is, it can classify the network data information by translation. It has the representation learning ability of artificial intelligence. At the same time, it can also be called "translation invariant artificial neural network."

In this paper, Mishkin et al. systematically studied the impact of a series of recent developments in the structure

and learning methods of convolutional neural networks (CNN) on object classification (ILSVRC). The evaluation tested the impact of the following architecture choices: nonlinearity (ReLU, ELU, max-out, comparability of batch standardization), pool variables (random, maximum, average, mixed), network width, classifier design (convolution, fully connected, SPP), image preprocessing, and learning parameters: learning rate, batch size, data cleanliness, etc. The performance gain of the proposed modification is first tested individually and then tested in combination. When all the modifications are introduced, the sum of individual returns is greater than the observed improvement, but the "deficit" is small, which indicates that their returns are independent. They show that the use of 128×128 pixel images is sufficient to make a qualitative conclusion on the best network structure of the full-size Caffe and VGG network. The result is an order of magnitude faster than the standard. However, CNN is not good at feature understanding [1]. Guo et al. have extensively studied traditional artificial methods and intelligence-based methods, which extract effective features from vibration data to perform high-precision classification and diagnosis of various mechanical faults, such as support vector machines and backpropagation neural networks. He researched and proposed a new layered learning rate adaptive deep convolutional neural network based on an improved algorithm and studied its application in bearing fault diagnosis and determining its severity. In order to test the effectiveness of the proposed method, experiments were carried out on the bearing failure data samples obtained from the test bench. This method has achieved satisfactory performance in both fault pattern recognition and fault size evaluation. However, the problem of maximizing accuracy under overly complex situations has not yet been solved [2]. Yan et al., in recent years, head pose estimation (HPE) based on low-resolution monitoring data has received increasing attention. However, the monocular and multiview HPE methods still have poor results under target motion, because when a person moves, the facial appearance will be distorted due to changes in the camera's perspective and scale. To this end, they proposed a new multitask learning- (MTL-) based framework FEGA-MTL, which is used to classify the head posture of people moving freely in an environment monitored by multiple large-field surveillance cameras. After FEGA-MTL divides the surveillance scene into dense and uniform spatial grids, it also learns the head pose classifier of a specific area and divides the grid into areas with similar facial features. In the learning phase, FEGA-MTL uses two pictures as a guide to perform a priori modeling of (1) the meshing based on camera geometry and (2) the similarity between head pose classes to obtain the optimal scene division and related pose classifiers. However, it has not been able to completely solve the problems arising from the movement of the target [3].

The innovations of this article are as follows: (1) This article uses a combination of quantitative and qualitative methods, which is well reflected in the fourth part of this article, the convolutional neural network model; (2) This article uses a combination of theoretical analysis and empirical research. This method uses experimental data to explain the

problem while establishing the model for analysis. This method runs through this article.

2. Method of Social Group Behavior Analysis Model Integrating Multitask Learning and Convolutional Neural Network

2.1. Multitask Learning Theory. Multitask learning and applications are also very promising. In machine learning, the useful information of historical data is used to analyze future data [1]. Usually, a lot of labeled data is needed for the next purpose for excellent training. The deep learning model is a typical model of machine learning. Because the model is a neural network with multiple levels and multiple parameters, it usually requires millions of data samples to obtain the correct parameters, and a lot of manual operations are usually required to label the data, so this data requirement cannot be met. Under the background of such data problems, the solution of MTL is to extract the feature information that can be used in other related tasks, so as to make up for the sparse data [2].

MTL research topics include multiple useful information, so that every student can get the correct goal [3]. Assume that all work (at least part) is related. Based on this, experimental and theoretical, I understand that learning multiple tasks at the same time is more effective than individual learning. According to the nature of the work, MTL can be divided into multiple levels of monitoring learning, multitasking nonmonitoring learning, multitasking nonmonitoring learning, multitasking and semimonitoring learning distribution, multitasking learning distribution, other learning, and other settings. One job and multiple jobs learn multiple perspectives [4, 5].

Based on this parameter, MTSL uses model parameters to learn various tasks in relation to each other. Five different operation modes include low-rank method, task clustering method, task relationship learning method, dirty method, and multilevel method [6]. Specifically, because it is assumed that the tasks are related, the parameter matrix W is likely to be of low rank, which may be due to the low motivation of the W class. The purpose of the combination method is to divide the operations into multiple groups, on the premise that all operations of each complex have the same or similar parameter models. The way to learn working relationships is to learn working relationships directly from data. The premise of the dirty method is that the parameter table W can be decomposed into two subtables. Here, each matrix is normalized with various types [7]. The multilevel method is a popular form of the dirty method, which decomposes the parameter list into more than 3 component lists to simulate the complex relationship between all tasks.

2.2. Convolutional Neural Network Structure. Convolutional neural network is a typical algorithm in the deep learning module. It uses the convolution calculation method in mathematical calculations and a neural feedforward network with a deep convolution structure [8, 9]. Therefore, it is also called "translation invariant artificial neural network" [10]. Since the beginning of the 21st century, with the advancement of

deep learning theory and the continuous improvement of computer equipment, collective neural networks have developed rapidly and are widely used in computer vision, language processing, and other fields [11]. The main neural network is composed of input layer, hidden layer, and output layer. The hidden layer includes various convolutional layers and pooling layers [12, 13].

2.2.1. Input Layer. Its input layer is capable of multidimensional processing of input information [14]. A one-dimensional input layer can usually accept one to two-dimensional values, such as time or spectral data collection; a two-dimensional neural network can receive two- to three-dimensional arrays, and so on, to receive input of multidimensional data information. Aggregate neural networks are widely used in the field of computer vision, so three-dimensional input data needs to be introduced in many studies, that is, the level of two-dimensional pixel and RGB channel structure [15].

The input layer expression of convolution neural network is as follows:

$$x_{ij}^l = \sum_{a=0}^{m-1} \sum_{b=0}^{m-1} \omega_{ab} y_{(i+a)(j+b)}^{l-1}. \tag{1}$$

2.2.2. Convolutional Layer. The effect of the aggregation layer is to draw characteristics from the enter data [16]. Each factor of the core assembly homologous the same weight quotient and departure as the neural supply network. Each neuron cell in the assembly layer is linked to many nerve cells neighboring to the front floor layer. The size of this area varies according to the size of the core [17]. It is called "receptive field" in the literature, which depends on the receiving area of visual cortex cells. When fusing the core work, periodically scan the input characteristics, multiply the matrix elements, summarize the possibility of entering the acceptance field, and apply deviations.

$$Z^{l+1}(i, j) \left[Z^l \otimes \omega^{l+1} \right](i, j) + b \sum_{k=1}^{k_l} \sum_{x=1}^{f} \sum_{y=1}^{f} \left[Z_k^l(s_0 j \right.$$
$$\left. + x, s_0 j + y) \omega_k^{l+1}(x, y) \right] + b, \tag{2}$$

$$(i, j) \in \{0, 1, \cdots, L_{l+1}\} \ L_{l+1} = \frac{L_l + 2p - f}{s_0} + 1. \tag{3}$$

The sum of the formulas is equal to the analysis of the relationship, cross-correlation [18]. b is the amount of deviation, Z^l and Z^{l+1} represent the total of the input and output of the $l + 1$ level (also referred to as a feature map), L_{l+1} and Z_{l+1} are the same total size as the length and width of the feature map. Corresponding to the pixels in the feature map $Z(i, j)$, K is the number of channels in the feature map. f, s_0, and p are the parameters of the entire layer, corresponding to the size of the connection core, the length of the connection step, and the number of filling layers.

Especially when the size of the convolution kernel is $f = 1$, the step size is $s_0 = 1$, and the filling unit of the convolution

kernel is not included. The interconnection calculation of the convolutional layer is the same as matrix multiplication, and the matching layer is fully connected to the network as follows:

$$Z^{l+1} = \sum_{k=1}^{k_l} \sum_{i=1}^{L} \sum_{j=1}^{L} \left(Z_{i,j,k}^l \omega_k^{l+1} \right) + b = \omega_{l+1}^T Z_{l+1} b, L^{l+1} = L. \tag{4}$$

The convolutional layer parameters include the size of the convolution kernel, the stepping, and the size of the overlay layer. These are the size of the output map of the aggregation layer and the hyperparameters of the convolutional neural network. The combined kernel size can be determined to be any value smaller than the input image size. The larger the interconnected core, the more complex the exportable entry function.

The folding layer embody activation functions to give assistance to express sophisticated properties [11], and its representation is as follows:

$$A_{i,j,k}^l = f \left(Z_{i,j,k}^l \right). \tag{5}$$

After exporting the aggregate level features to the aggregate level, the output feature matching is moved to a concentrated level, the function is selected, and the information is filtered. The pooling layer contains the default pooling function [19]. The function of this function is to use the mapping of adjacent regions to create statistics. The steps of selecting the pooling area are the same as the mapping characteristics of the convolution kernel and are controlled by the concentration, step length, and filling.

Lp pool is a type of pooling model which is aroused by the hierarchical construction in the sense of sight cerebral cortex, and its form is as follows:

$$A_k^l(i, j) = \left[\sum_{x=1}^{f} \sum_{y=1}^{f} A_k^l(s_0 i + x, s_0 j + y)^p \right]^{1/p}. \tag{6}$$

In the formula, the step size s_0 and pixel (i, j) have the same meaning as the convolutional layer, and p is a prespecified parameter. When $p = 1$, Lp pooling takes the average value in the pooling area, which is called mean pooling; at that time, Lp pooling takes the maximum value in the area, which is called maximum pooling.

Random pooling and blending pooling are all development of the concept of pooled Lp. Random pooling stochastic chooses values within the pooling range on the basis of a specially appointed probability distribution, so that the specific nonmaximum signal stimulus enters the next stage of construction. Pooling concentration may be indicating a linear combination of maximum and average pooling.

$$A_k^l = \lambda L_1 \left(A_k^l \right) + L_\infty \left(A_k^l \right), \lambda \in [0, 1]. \tag{7}$$

According to research, compared with average pooling and maximum pooling, mixed pooling and random pooling have a normalization function, which is beneficial to avoid overconfiguration of the group neural network.
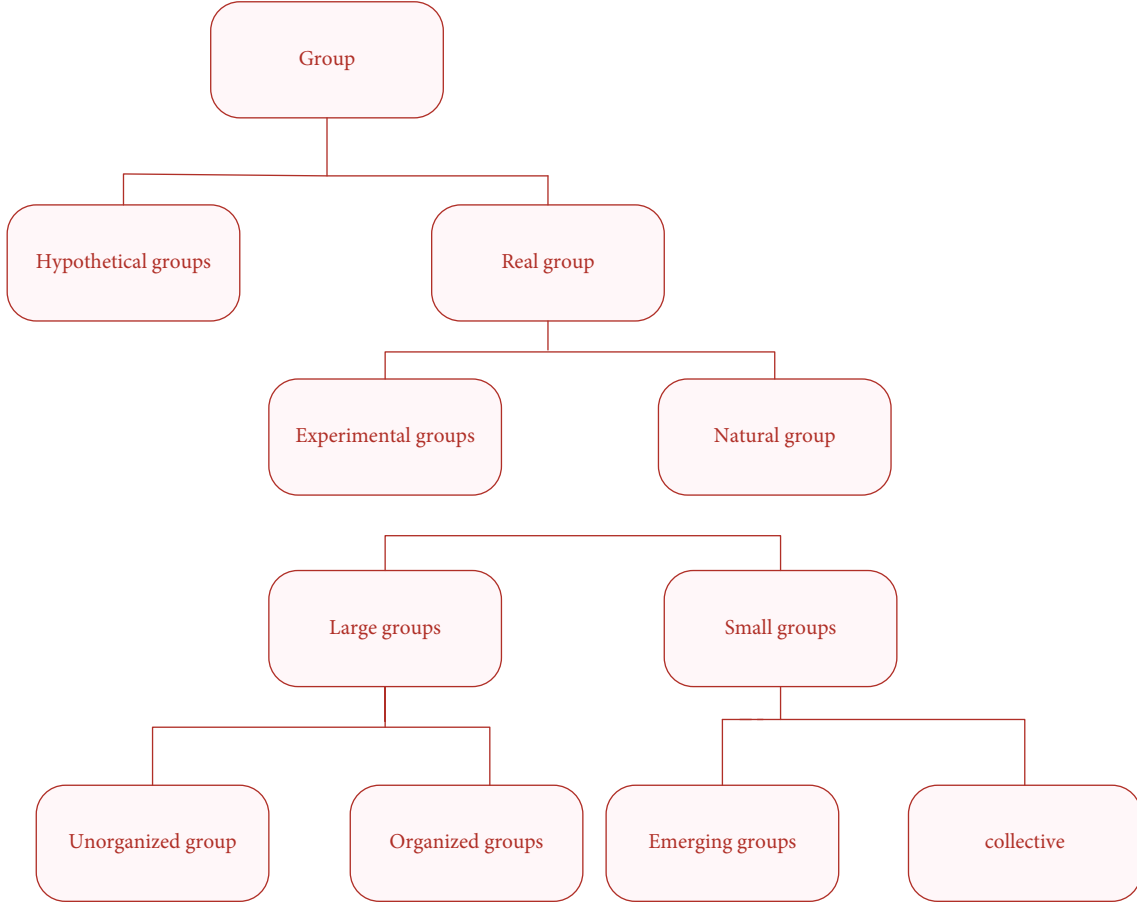
FIGURE 1: Structure of group theory.

2.2.3. Output Layer. In a convolutional neural network, the upper end of the output layer is generally a fully connected layer, which is the same as the traditional neural network algorithm. In the process of image classification, it is generally necessary to use mathematical logic functions or use normalization methods to add complete classification labels; in the field of object recognition, the design of the output layer is very different, which can be divided into coordinates, dimensions, etc.; in semantics segmentation, only pixel classification is required [20].

The output layer expression of convolution neural network is as follows:

$$y_{ij}^l = \sigma\left(x_{ij}^l\right). \tag{8}$$

If the input is represented by $x_1, x_2, \cdots x_n$, the detailed calculation process of convolution neural network is as follows:

$$\left\{\begin{array}{c} o_i^{(l)} = x_i, l = 1 \\ O_i^{(C)} = \left(\omega_{ij}^{(l)}\right) * o_i^{(l-1)} + \left(b_i^{(l)}\right) \\ O_i^l = \sigma\left(o_i^l\right), 2 \le l \le n \end{array}\right\}. \tag{9}$$

2.3. Sociological Theory of Group Behavior. Sociologists and social psychologists have conducted in-depth research on group behavior very early and have reached systematic conclusions as shown in Figure 1. The French sociologist Gustave Le Pen proposed the infection theory in 1896. Regarding a group as an individual with a collective will, the ability to stimulate an individual group is incompatible; that is to say, gaining power from a simple person, infection, rapid spread of new ideas, and similar infections are three factors. It spreads between people and is easy to get infected. According to Mr. Rupe, in a group, people's thinking can easily be reduced to low-level activities. It is easy to accept the actions and attitudes of other people in the group and passively imitate [21].

In abnormal action theory, this theory was considered by the participants to be a group action caused by the participants' violation of social rules and the belief that there was no normal action and was praised by the participants. At the same time, as a member of a group, individual abnormal behavior can avoid severe punishment. Such a social environment provides a destructive environment for action, and many people will inevitably gather together to produce the same reaction, leading to an explosive increase in collective action [22].

In emergency theory, this theory believes that the actions of a group are generated for the purpose of discovering rules.

Someone guides their actions and unifies the actions of the entire group. Such rules are not general social rules, but they will be temporarily overwhelmed when the masses become emotional. These rules will guide people to deal with unexpected situations at the time. This theory denies the infection theory and believes that group actions occur based on the knowledge of participants. People recognize the code of conduct in emergency situations and replace the expansion of feelings with common sense [11].

In convergence theory, this theory believes that people in this group will see things the same and have the same tendency to act. This tendency also contacts [23]. In social comparative theory, this theory is the main benchmark for others to evaluate and verify their own abilities and opinions. This is a simple concept and an overall relationship of use within a group. Actions between social groups are more scientific.

3. Experiment on Social Group Behavior Analysis Model Integrating Multitask Learning and Convolutional Neural Network

3.1. Construction of a Social Group Behavior Analysis Model Based on Convolutional Neural Networks. The linear convolutional layer and the multilayer MLP receptor together form a mlpconv layer, and only a part of the input information in the range domain is needed to obtain the corresponding feature vector [24]. The process of acquiring the feature information of the target by the mlpconv layer is to use a large number of nonlinear activation functions to perform algorithmic calculations, to integrate the feature information and output it into a feature map, and then to perform the next feature input cycle process and then uses function mapping until it enters the next level.

One of the biggest advantages of convolutional neural network is that it has local characteristics. It can effectively separate in a complex background to obtain effective feature information of the target, and it can automatically complete multitask learning and deep learning goals and respond to background changes. The same is true for aggressive goals.

When training the plug-in network model, the weights of the mlpconv full neural network model including a single layer are first divided, and then, the entire neural network is trained. The entire PV update process ends. Then, connect to the second layer of mlpconv. The entrance of the second layer of mlpconv is the exit of the first layer of mlpconv. First, initialize the weights of the second layer of mlpconv and then train the entire neural network. After the entire training process is completed, lpconv will be notified of the second layer weight. When adding a new mlpconv level, perform weighted initialization, comprehensive neural network training, and weight update according to the above procedures.

In addition, the combination of convolution calculation and BN technology can make the nonlinear unit generate a relatively stable distribution, thereby achieving the combined effect. Add the BN operation to the nested mlpconv layer, and the calculation method of the feature map in the model

is as follows:

$$f^1_{i,j,k_1} = \max\left(\text{BN}\left(W^{1^T}_{k_1} x_{i,j} + b_{k_1}\right), 0\right), \tag{10}$$

$$f^2_{i,j,k_2} = \max\left(\text{BN}\left(W^{2^T}_{k_2} f^1_{i,j} + b_{k_2}\right), 0\right), \tag{11}$$

$$f^n_{i,j,k_n} = \max\left(\text{BN}\left(W^{n^T}_{k_n} f^{n-1}_{i,j} + b_{k_n}\right), 0\right). \tag{12}$$

In formulas (10)–(12), BN (g) is the BN layer, the position of the pixel in the feature map is represented (i, j), the input $x_{i,j}$ blocks with the pixel as the center (i, j), etc., are the channel numbers in the feature map, and n is the number of MLP layers. Figure 2 is a flow chart of a convolutional neural network.

3.2. Pooling Model Design

3.2.1. Classic Pooling Model. The most commonly used in classic pooling models is average pooling and maximum pooling models. Average pooling is to take the average value on the calculation result of the algorithm and use it as the feature value in the subsampling; the maximum pooling is to take the maximum value to complete the pooling process.

The algorithmic expressions of average pooling and maximum pooling are as follows:

$$S_{ij} = \frac{1}{c^2}\left(\sum_{i=1}^{c}\sum_{j=1}^{c} F_{ij}\right) + b_2, \tag{13}$$

$$S_{ij} = \max_{i=1,j=1}^{c}\left(F_{ij}\right) + b_2. \tag{14}$$

In the above formula, F is the feature map matrix, the pooling area range is c∗c, the offset is b2, and the final subsampling feature map is S.

3.2.2. Improved Intermediate Model. The classic pooling model has several disadvantages. For example, it cannot best extract the features of the target, and the use of the maximum value instead of the feature value will also have a certain weakening effect, which is not conducive to improving the accuracy of the model. Therefore, in view of the shortcomings of the classic pooling model, two improved models are proposed, namely, the maximum two-mean pooling method and the median pooling method.

The formula of the maximum two-mean pooling method is as follows:

$$S_{ij} = \frac{1}{2}\sum_{i=1,j=1}^{c} M2\left(F_{ij}\right) + b_2. \tag{15}$$

This formula can extract the two largest values from the pooling domain for summing.

The formula of the median pooling method is as follows:

$$S_{ij} = \frac{T}{2} + b_2, \tag{16}$$
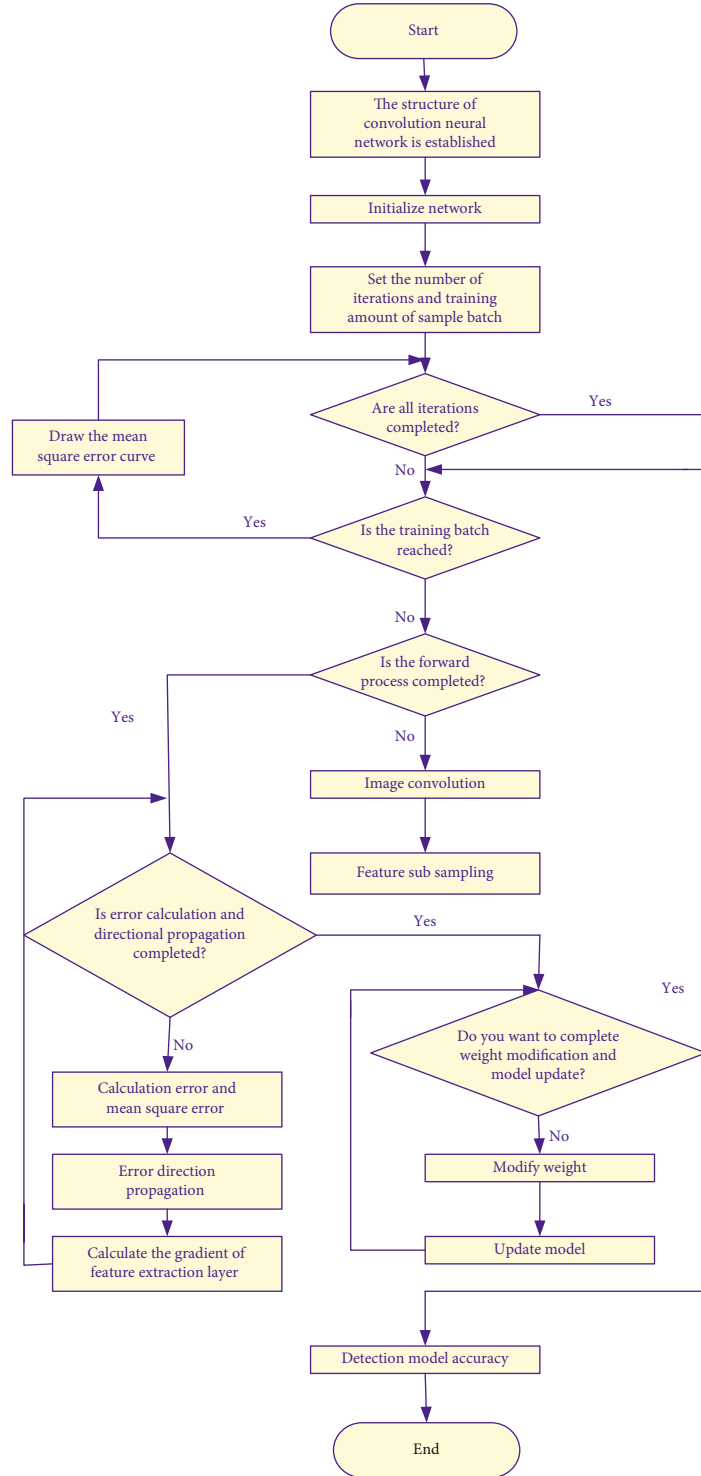
FIGURE 2: Flow chart of convolution neural network.

$$T = \frac{1}{c^2}\left(\sum_{i=1}^{c}\sum_{j=1}^{c}F_{ij}\right) + \max_{i=1,j=1}^{c}\left(F_{ij}\right). \qquad (17)$$

This algorithm is a compromise algorithm, which can minimize the damage of model accuracy and reduce errors. It is suitable for general image algorithms.

3.2.3. Dynamic Adaptive Pooling Model. The purpose of optimizing output characteristics is to improve output pooling. In the whole process of learning neural network union, various feature maps and concentrated areas will be created. This is a feature that is difficult to focus on patterns and patterns, and it is difficult to achieve a satisfactory result [25].

In order to be further optimized on the traditional pooling model, this paper proposes a dynamic adaptive pooling model based on the maximum pooling algorithm. The advantage of this model is that compared with the traditional pooling model, it is more flexible and can make dynamic adjustments according to different feature values and different pooling content to adapt to the pooling model and optimize the pooling process. If there is only one pooling value in the existing pooling area, then this value is the maximum value, which can indicate its characteristics; if all the eigenvalues in the pooling area are the same, the maximum value is still taken as the eigenvalue. Therefore, after understanding the calculation process of the maximum pooling algorithm, a corresponding mathematical function model can be made.

Set as the pooling factor, the dynamic adaptive pooling algorithm function can be expressed as follows:

$$S_{ij} = \mu \max_{i=1, j=1} \left(F_{ij} \right) + b_2. \quad (18)$$

This type is a basic expression of the possibility of adaptive algorithms. The essence is to use the pooling coefficient m to optimize the maximum concentration algorithm. Through optimized performance, functions can be expressed more accurately. Other parameters are set according to the parameters of the maximum pooling model.

$$\mu = \rho \frac{a(v_{\max} - a)}{v_{\max}^2} + \theta. \quad (19)$$

In formula (14), a represents the average value of all elements except the maximum value, which $V_{\max}$ is the maximum value, θ represents the correction error term, and ρ represents the characteristic coefficient. The specific mathematical formula is as follows:

$$\rho = \frac{c}{1 + \left(n_{epo} - 1 \right) c^{n_{epo}^2 + 1}}, \quad (20)$$

where n_{epo} is the number of iterations during training.

According to the maximum pooling to improve and optimize the dynamic adaptation pooling, the input part of the maximum pooling model is the core of the two-dimensional item feature table and correlation. Use 4 different convolution kernels, such as matrices with weights $A = \begin{bmatrix} 1 & 0 \\ 0 & 0 \end{bmatrix}$, $B = \begin{bmatrix} 0 & 1 \\ 0 & 0 \end{bmatrix}$, $C = \begin{bmatrix} 0 & 0 \\ 1 & 0 \end{bmatrix}$, and $D = \begin{bmatrix} 0 & 0 \\ 0 & 1 \end{bmatrix}$, to convolve the input feature maps to obtain the convolution results corresponding to 4 different values in the pooling domain.

TABLE 1: Model parameter design.

Parameter	Value
Learning rate	0.001
Learning strategy	"inv"
Energy	0.75
γ	0.01
Maximum number of iterations	2000000
Impulse	0.9
Weight attenuation	0.05
Optimization mode	Adam

TABLE 2: AUC and EER are frame and pixel level comparisons on ped1 (UCSD data set).

Algorithm	Ped1 (frame)		Ped1 (pixel)		Ped2 (frame)	
	EER/%	AUC	EER/%	AUC	EER/%	AUC
TCP	8	0.967	38	0.632	18	0.817
AMDN	17	0.922	40.2	0.662	18	0.918
Motion energy	23	0.811	56	0.590	22	0.913
ST-CNN	24.5	0.861	38.6	0.881	25.6	0.853
Ours	7.6	0.961	35.3	0.686	16.3	0.932
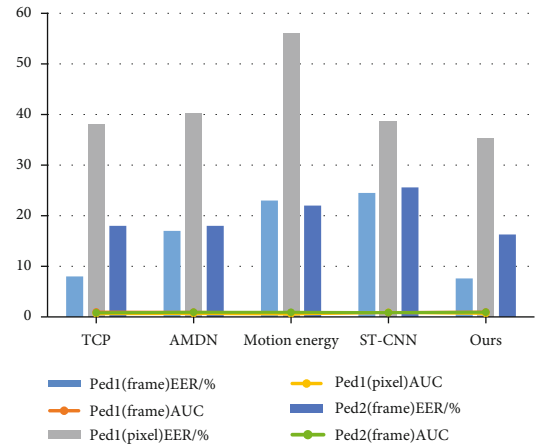
FIGURE 3: AUC and EER are frame and pixel level comparisons on ped1 (UCSD data set).

4. Social Group Behavior Analysis Model Integrating Multitask Learning and Convolutional Neural Network

4.1. Social Group Behavior Model Based on Multitask Learning and Convolutional Neural Network. This experiment was carried out in the MATLAB environment. Related procedures include the process of data acquisition system, data processing process based on a complete neural network, and data classification process.

Model data parameters are shown in Table 1.

In 3.0 GHz CPU, 64-bit Windows 7 software operating system, MATLAB2016a, and Open CV were selected as the development tools, and then, the simulation experiment
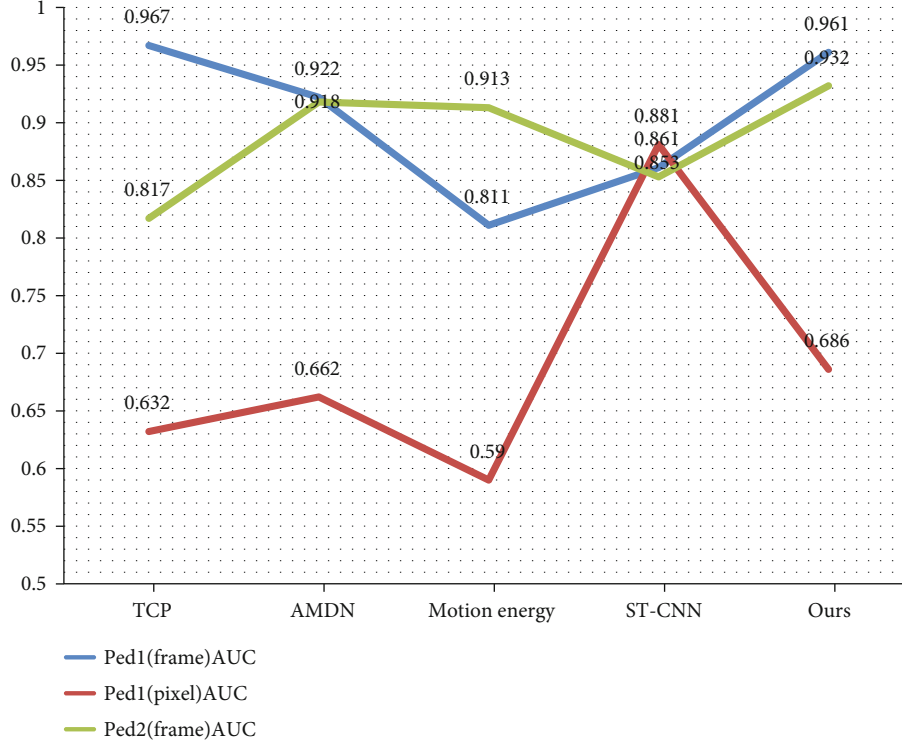
Figure 4: AUC comparison of five algorithms on data subset.

Table 3: AUC and EER for frame and pixel level comparisons on UMN data sets.

| Algorithm | Frame-level | | |
	EER/%	AUC	Time/s
TCP	3.3	0.987	0.33
Motion energy	4.2	0.988	0.08
ST-CNN	3.8	0.997	0.48
Commotion	3.2	0.987	0.35
Ours	3.2	0.991	0.22

was carried out. In order to achieve the purpose of verifying the effectiveness of the algorithm, the reference data sets commonly used in the recognition investigation of multiple actions are selected in this article, namely, the UCSD data set and the UMN data set. These two data sets cover all extractable group behavior actions. In the simulation experiment, a quantitative evaluation method is used, and the evaluation indicators select AUC, EER, and calculation time parameters.

4.1.1. Experimental Results on the UCSD Data Set. The USCD data set was produced by the University of California, San Diego. The data set is collected through the camera as the medium.

The camera is selected to be able to observe the sidewalk at a specified height, mainly to collect social group behaviors that occur under natural conditions. In this paper, we choose TCP model, AMDN model, energy motion model, spatial neural network model, chaos model,
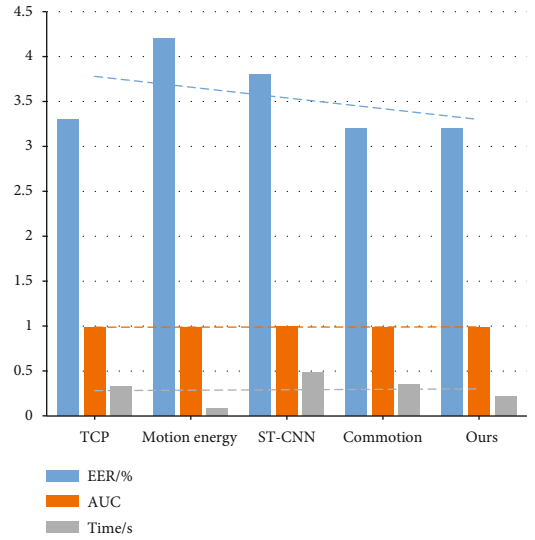
Figure 5: AUC and EER for frame and pixel level comparisons on UMN data sets.

Table 4: The relationship between the number of prototypes and accuracy.

Number of prototypes	Accuracy	Precision	Recall	F1	TNR
50	98.6	98.6	98.6	98.6	99.7
100	99.1	99.1	99.1	99.1	99.9
150	98.6	98.7	98.6	98.6	99.7
200	98.6	98.6	98.6	98.6	99.7
250	98.1	98.1	98.1	98.1	99.6

TABLE 5: Comparison of deep learning method and nondeep learning method on classified data sets.

		Accuracy	Precision	Recall	F1	TNR
Nondeep learning method	LapRLS	0.635	0.534	0.548	0.667	0.917
	KSRC	0.831	0.792	0.853	0.814	0.954
	mSRC	0.877	0.844	0.923	0.872	0.963
	MCMI-AB	0.618	0.595	0.574	0.564	0.898
	mcSVM	0.684	0.698	0.578	0.577	0.922
	ESRC	0.801	0.731	0.885	0.778	0.941
Deep learning methods	CNN + SVM	0.969	0.969	0.969	0.969	0.993
	CNN + mi-SVM	0.988	0.989	0.988	0.988	0.998
	CNN + MI-SVM	0.982	0.982	0.982	0.982	0.996
	K-means	0.991	0.991	0.991	0.991	0.998
	Random	0.976	0.976	0.976	0.975	0.995
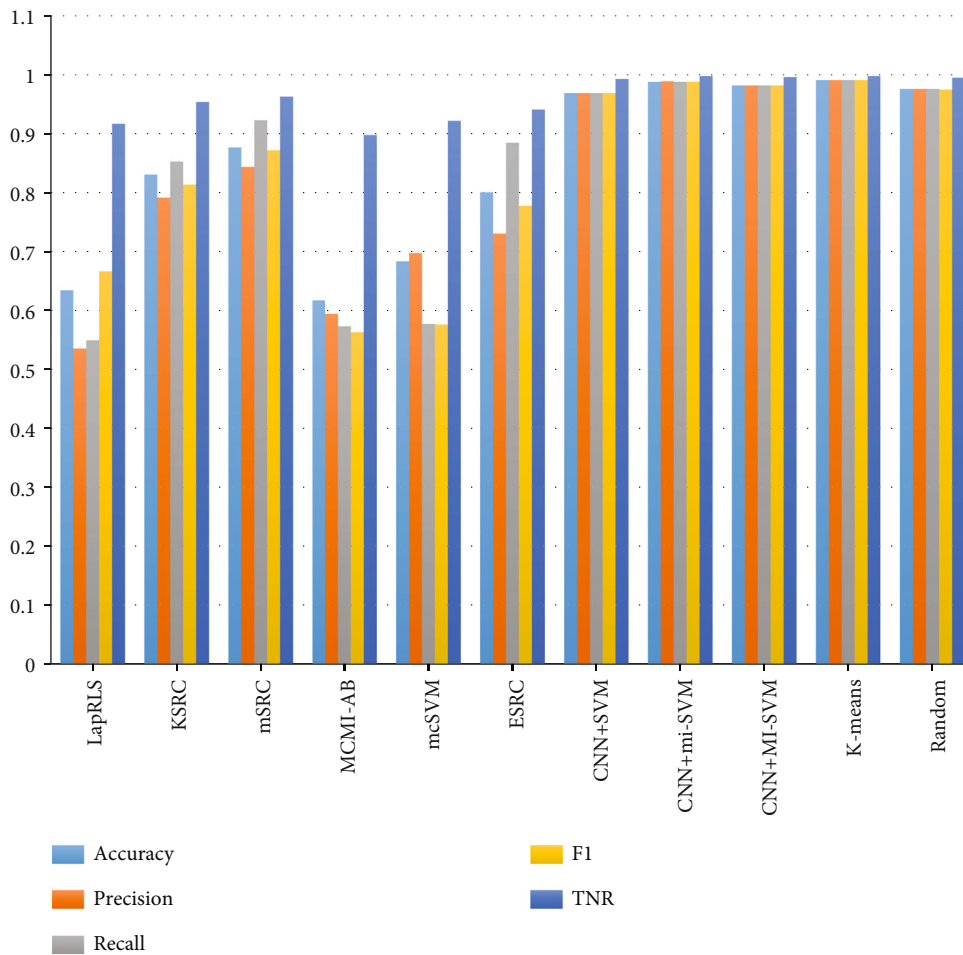
FIGURE 6: Comparison of different algorithms in data classification.

and other algorithms to achieve a better recognition rate in the above database. The source of the total data is divided into ped1 and ped2. These two subdata sets store 100 scene videos. Each video is subdivided into approximately 200 frames of video clips with a pixel resolution of 160 ∗ 249 and 250 ∗ 368 pixel.

The effectiveness of the algorithm needs to be verified through the UCSDped1 and UCSDped2 data sets. It can be seen from Table 2 that on the UCSDped1 data set, when frame-level metrics are used, the EER of the ST-CNN algorithm used in this paper is 24.5% and 38.6%, and the AUC values are 0.861 and 0.881; when pixel-level metrics are used,
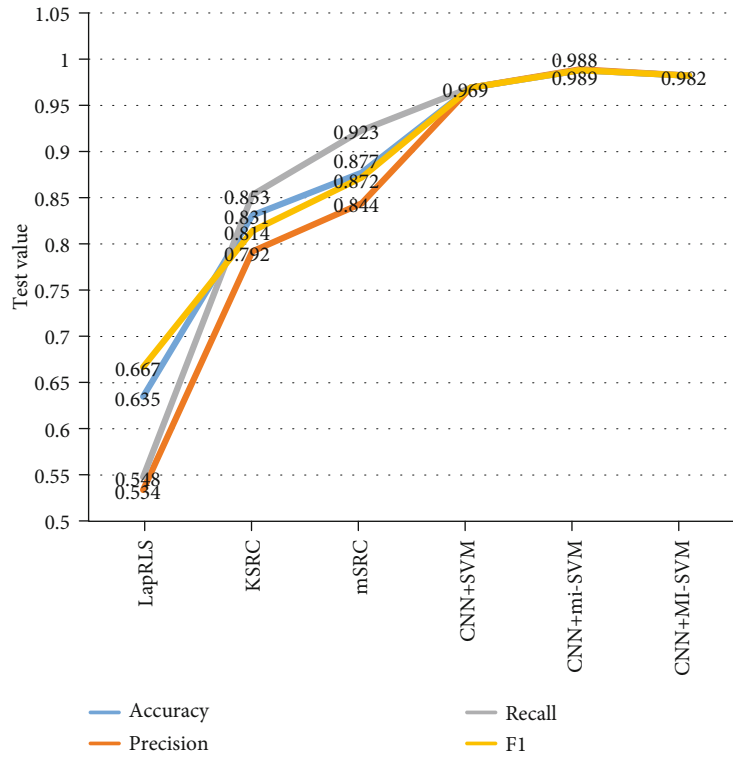
FIGURE 7: Line chart of comparison of deep learning method and nondeep learning method on classified data sets.
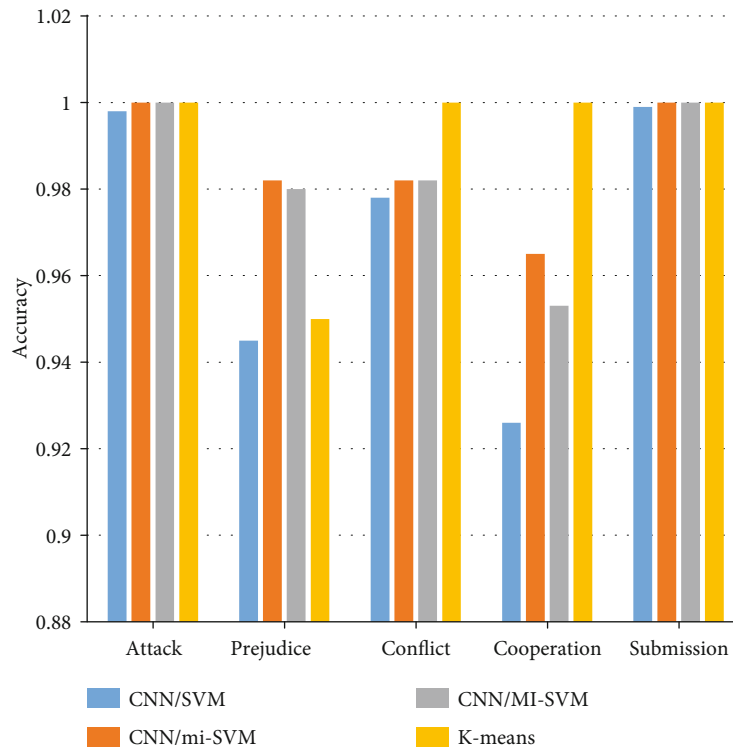
FIGURE 8: Accuracy comparison of five social group behaviors using CNN algorithm.
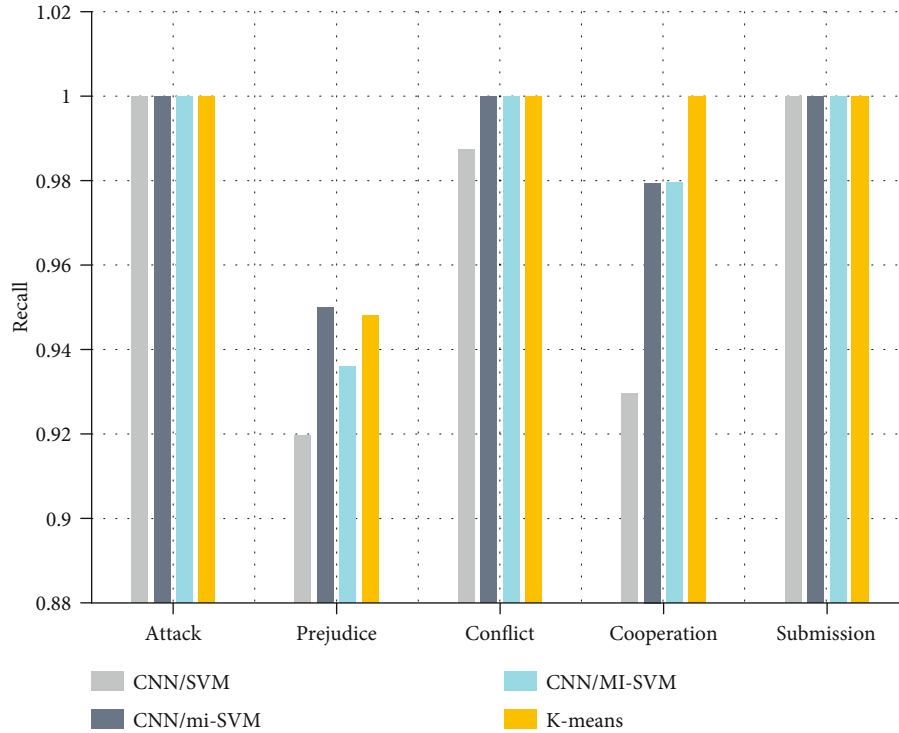
FIGURE 9: Comparison of recall rate data of CNN algorithm in social group behavior analysis.

the EER index of CNN is 25.6%, and the AUC evaluation index is 0.853.

It can be seen from Figures 3 and 4 that in the UCSDped1 data set, if framework-level metrics are used, the EER of the paper's algorithm will decrease, and the AUC evaluation will be greatly improved. When using pixel level measurement, the EER and AUC values show that the index improvement effect is not good, but it is still higher than the other two index algorithms. In the UCSDped2 data set, the frame-level measurement scale is used for testing. The algorithm in this paper is good for EEA and AUC scores, and the AUC score is increased to 0.11.

4.1.2. Experimental Results on UMN Data Set. In addition, the UMN data set has also been experimentally verified. Data set is used in the first half and the second half. In this data set, framework-level metric EEA and AUC evaluation indicators are used to evaluate the performance of the algorithm. The verification results are shown in Table 3.

As can be seen from Figure 5, the results of the algorithm performance test using the EER and AUC evaluation indicators below the framework level of the UMN data set are as follows. The algorithm of this paper has the same performance as the existing algorithm of AUC rate index and other algorithms with higher performance than EEA index. The algorithm time spent has been improved.

4.1.3. The Effect of Adjusting the Number of Prototypes on the Results. The research method used in this article needs to verify the influence of the number of prototypes on the effect of group behavior division. The relationship between the num-

ber of prototypes and accuracy is shown in Table 4. The number of prototypes in the experiment is set to 80, 100, 150, 200, and 250; it can be seen from Table 4 that the number of experiments is 100, which has the highest accuracy. Therefore, in the subsequent experiments, the number is set to 100.

4.2. Group Behavior Recognition Model Fusing Multitask Learning and Convolutional Neural Network. We compare and test the algorithm proposed in this paper and related methods in five aspects: accuracy, accuracy, recall, F1 value, and TNR. As shown in Table 5, they are all methods of manually extracting features, as shown in Table 5. The data shows that the highest accuracy index of traditional nondeep learning methods is 87.7%, which is much lower than the accuracy of deep learning methods. In the deep learning method, CNN combined with multitask learning methods are used, and the accuracy values are greater than 95%.

It can be clearly seen from Figures 6 and 7 that compared to traditional learning methods, the fusion multitask learning method and convolutional neural network learning method used in this paper have achieved better results. The algorithms in the table are all for target monitoring, and for the target recognition operation, the training mode adopts the fully supervised form of multitask learning. From the data results, the results of the new algorithm are all above 0.95, and the effect is very good.

We divide social group behaviors into five types of behaviors: aggression, prejudice, conflict, cooperation, and obedience. The following three graphs are the comparison diagrams of the classification data effects of the five types of group behaviors on various indicators. As shown in
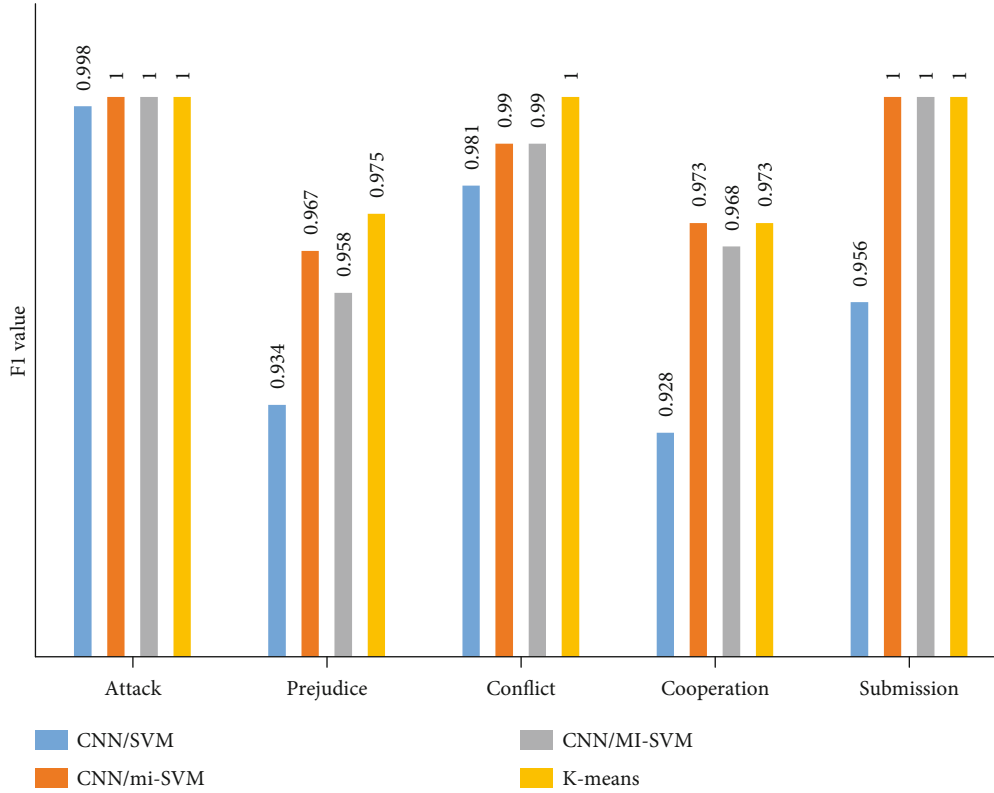
FIGURE 10: Comparison of F1 values of different group behaviors in four algorithms.

Figure 8, the accuracy of the five behaviors in each test method is greater than 85%. Among them, the accuracy of the attack behavior and the compliant behavior using the CNN combination method is higher, reaching more than 95%.

As can be seen in the above two figures, using the CNN joint method, the recall rate and F1 value of the observation results of the five group behaviors are clearly contrasted. In Figure 9, the recall rate of each method of attack and obedience has reached 100%, but the overall recall rate of biased behavior is very low, of which CNN/SVM is only 92%. In Figure 10, the F1 values of prejudice, conflict, and cooperation are continuously improved by using four methods. The conflict is extremely obvious. The F1 value of CNN/SVM is 0.981, and the value of CNN/mi-SVM and CNN/MI-SVM is 0.981. The values are the same; both are 0.985, and the F1 value of K-means reaches 100%. It can be seen that the algorithm used in this paper has achieved good results in the study of social group behavior.

It can be seen from Table 6 that the overall accuracy of the recognition of group behaviors integrated with deep learning is very high, and the corresponding reaction behaviors can be fully made in the process of cross-experiment.

Table 6 shows the comparison between the traditional neural network model, the MVP model, and the convolutional neural network model in terms of testing algorithm accuracy and cross-validation accuracy. Comparing the accuracy of the experimental algorithms of the three models, it can be seen that the experimental accuracy of the convolutional neural network method is as high as 92.10%, which is

TABLE 6: Accuracy comparison of three common behavior recognition models.

Machine learning algorithm	Test set accuracy (%)	Cross-validation accuracy (%)
Traditional neural network	52.12	65.82
MVP	58.19	75.54
Convolution neural network	92.10	84.5

much higher than the other two experimental methods. Therefore, modeling based on convolutional neural network is more suitable for multifeature-based modeling. Through the model analysis of group behavior. The cross-validation accuracy is also significantly higher than traditional neural networks and MVP, reaching 84.5%.

5. Conclusion

This paper mainly studies the social group behavior analysis model that combines multitask learning and convolutional neural network and consults a large number of references and in-depth study of convolutional neural network, multitask learning, and group theory-related content. This paper constructs a social group behavior analysis model and a dynamic adaptive pooling model based on convolutional neural networks and makes full use of the advantages of convolutional neural network algorithms to analyze social group

behaviors. Combining multitask learning and convolutional neural networks can already extract the deep-level features of foreground moving targets, and the improved convolutional neural network reduces the acquisition of redundant information.

The innovation of this paper is that it adopts a combination of quantitative and qualitative methods, which is well reflected in the convolutional neural network model in the fourth part of this paper. The method of combining theoretical analysis and empirical research is used to establish model analysis. While using experimental data to explain the problem, this method runs through this article. The complete convolutional neural network of this experiment can obtain effective feature information of social group targets and avoid the collection of redundant information. The experiments of UCSD and UMN show that the convolutional neural network algorithm can optimize the calculation time and learning time to the greatest extent, which is very suitable for social group behavior analysis. The innovation of this paper is to combine multitask learning and convolutional neural networks with group behavior research in the field of psychology, which shows the development and application of the Internet of Things in behavior research cognition.

The disadvantage of this article is that due to the limitations of actual conditions, the number of samples collected is small, and the sample results need to be more standardized; the convolutional neural network itself has the defects of translation invariance and back propagation, which has a certain impact on the data parameters.

Data Availability

No data were used to support this study.

Conflicts of Interest

The authors declare that they have no conflicts of interest.

Acknowledgments

References

[1] D. Mishkin, N. Sergievskiy, and J. Matas, "Systematic evaluation of convolution neural network advances on the Imagenet," *Computer vision and image understanding*, vol. 161, pp. 11–19, 2017.

[2] X. Guo, L. Chen, and C. Shen, "Hierarchical adaptive deep convolution neural network and its application to bearing fault diagnosis," *Measurement*, vol. 93, pp. 490–502, 2016.

[3] Y. Yan, E. Ricci, R. Subramanian, G. Liu, O. Lanz, and N. Sebe, "A multi-task learning framework for head pose estimation under target motion," *IEEE Transactions on Pattern Analysis and Machine Intelligence*, vol. 38, no. 6, pp. 1070–1083, 2016.

[4] Z. Liu, X. Yu, Y. Gao, S. Chen, X. Ji, and D. Wang, "CU partition mode decision for HEVC hardwired intra encoder using

convolution neural network," *IEEE Transactions on Image Processing*, vol. 25, no. 11, pp. 5088–5103, 2016.

[5] Y. Tang and X. Wu, "Scene text detection and segmentation based on cascaded convolution neural networks," *IEEE Transactions on Image Processing*, vol. 26, no. 3, pp. 1509–1520, 2017.

[6] K. H. Cha, L. M. Hadjiiski, R. K. Samala et al., "Bladder cancer segmentation in CT for treatment response assessment: application of deep-learning convolution neural network-a pilot study," *Tomography a Journal for Imaging Research*, vol. 2, no. 4, pp. 421–429, 2016.

[7] Y.-x. Li, Y.-y. Pu, D. Xu, W.-h. Qian, and L.-p. Wang, "Image aesthetic quality evaluation using convolution neural network embedded learning," *Optoelectronics Letters*, vol. 13, no. 6, pp. 471–475, 2017.

[8] R. Mena-Yedra, J. Casas, and R. Gavaldà, "Assessing spatio-temporal correlations from data for short-term traffic prediction using multi-task learning," *Transportation Research Procedia*, vol. 34, pp. 155–162, 2018.

[9] X. Zhu, H.-I. Suk, S.-W. Lee, and D. Shen, "Subspace regularized sparse multitask learning for multiclass neurodegenerative disease identification," *IEEE Transactions on Biomedical Engineering*, vol. 63, no. 3, pp. 607–618, 2016.

[10] X. Lu, X. Li, and L. Mou, "Semi-supervised multitask learning for scene recognition," *IEEE Transactions on Cybernetics*, vol. 45, no. 9, pp. 1967–1976, 2017.

[11] R. Mogan, R. Fischer, and J. A. Bulbulia, "To be in synchrony or not? A meta-analysis of synchrony's effects on behavior, perception, cognition and affect," *Journal of Experimental Social Psychology*, vol. 72, pp. 13–20, 2017.

[12] J. Yu, B. Zhang, Z. Kuang, D. Lin, and J. Fan, "iPrivacy: image privacy protection by identifying sensitive objects via deep multi-task learning," *IEEE Transactions on Information Forensics & Security*, vol. 12, no. 5, pp. 1005–1016, 2017.

[13] Z. Zhang, Y. Xie, W. Zhang, Y. Tang, and Q. Tian, "Tensor multi-task learning for person re-identification," *IEEE Transactions on Image Processing*, vol. 29, pp. 2463–2477, 2020.

[14] A.-A. Liu, N. Xu, W.-Z. Nie, Y.-T. Su, and Y.-D. Zhang, "Multi-domain and multi-task learning for human action recognition," *IEEE Transactions on Image Processing*, vol. 28, no. 2, pp. 853–867, 2019.

[15] Z. Wen, K. Li, Z. Huang, C.-H. Lee, and J. Tao, "Improving deep neural network based speech synthesis through contextual feature parametrization and multi-task learning," *Journal of Signal Processing Systems*, vol. 90, no. 7, pp. 1025–1037, 2018.

[16] H. D. Vargas Cardona, M. A. Alvarez, and A. A. Orozco, "Multi-task learning for subthalamic nucleus identification in deep brain stimulation," *International Journal of Machine Learning & Cybernetics*, vol. 9, no. 7, pp. 1181–1192, 2018.

[17] A. A. Sandel, J. A. Miller, J. C. Mitani, C. L. Nunn, S. K. Patterson, and L. Z. Garamszegi, "Assessing sources of error in comparative analyses of primate behavior: intraspecific variation in group size and the social brain hypothesis," *Journal of Human Evolution*, vol. 94, pp. 126–133, 2016.

[18] G. Robert, "Animated images in the analysis of zebrafish behavior," *Current Zoology*, vol. 63, no. 1, pp. 35–44, 2017.

[19] F. C. Mace, "Tony Nevin: the embrace of translational work by a basic scientist," *Journal of the Experimental Analysis of Behavior*, vol. 109, no. 1, pp. 56–65, 2018.

[20] A. T. Stull, L. Fiorella, and R. E. Mayer, "An eye-tracking analysis of instructor presence in video lectures," *Computers in Human Behavior*, vol. 88, pp. 263–272, 2018.

[21] M. Sutter, D. Glätzle-Rützler, L. Balafoutas, and S. Czermak, "Cancelling out early age gender differences in competition: an analysis of policy interventions," *Experimental Economics*, vol. 19, no. 2, pp. 412–432, 2016.

[22] J. M. Garcia, J. R. Sirard, N. L. Deutsch, and A. Weltman, "The influence of friends and psychosocial factors on physical activity and screen time behavior in adolescents: a mixed-methods analysis," *Journal of Behavioral Medicine*, vol. 39, no. 4, pp. 610–623, 2016.

[23] A. Rana, M. Hamid, and Y. Qin, "Understanding the joint behavior of temperature and precipitation for climate change impact studies," *Theoretical and Applied Climatology*, vol. 129, no. 1, pp. 321–339, 2016.

[24] M. L. Chang, "On the relationship between intragroup conflict and social capital in teams: a longitudinal investigation in Taiwan," *Journal of Organizational Behavior*, vol. 38, no. 1, pp. 3–27, 2017.

[25] I. Tung and S. S. Lee, "Latent trajectories of adolescent antisocial behavior: serotonin transporter linked polymorphic region (5-HTTLPR) genotype influences sensitivity to perceived parental support," *Development and Psychopathology*, vol. 29, no. 1, pp. 185–201, 2016.

WILEY | Hindawi

Research Article

Design of Children's Product Packaging Preference Based on Big Data Machine Learning

Yuan Gao [ORCID]

College of Fine Arts and Design, Suzhou University, Suzhou, 234000 Anhui, China

Correspondence should be addressed to Yuan Gao; goumiao429@ahszu.edu.cn

Children's product packaging is also gaining more and more attention from the society as the hope of the future of the homeland and the most interested groups of the society. However, the current packaging design for children's products is uneven and lacks a good user experience. Therefore, the packaging design of children's products needs to be improved urgently. Therefore, this article uses big data and machine learning technology to first investigate the packaging preferences of children's products, and on this basis, designs a product packaging style that is more in line with the current children's preferences and needs, which provides a reference for subsequent related research. In order to find out the preference of children's product packaging under big data machine learning, this article uses the literature method, questionnaire survey method, interview method, experimental method, and other research methods to conduct research on the basis of previous research. The results of the study show that the packaging preferences of children and parents for children's products are mainly affected by the color, type, and material. Children's products of different colors have different attractiveness to children of different ages, and the difference can reach more than 20%. Parents' children's products are mainly affected by the materials and uses of the products, and products that are useful for children's education and growth are more favored by parents. This shows that if companies want to increase the sales of children's products, they need to consider the ideas of children and parents at the same time to achieve their goals.

1. Introduction

In recent years, with the development of the society, the number of children's products has been increasing in the consumer market and competition is intensifying. As an important visual element of packaging, modeling plays an important role in the design of packaging for children's products [1]. By investigating the current situation of children's product packaging in the domestic and foreign markets, it is analyzed and found that children's product packaging has a trend of simplification. In response to this situation, the application of bionic elements to the packaging of children's products for redesign has not only met children's psychological needs but also played a certain degree of interest. In this context, this article combines the bionic design theory to design the packaging of children's products [2]. Use literature research method, design practice method, case investigation method, and induction verification method for analysis and research. This article combs the consumption

characteristics of children and parents and analyzes the relationship between bionic elements and the packaging of children's products. According to the theory of the bionic design, this article is dedicated to summarizing the methods and principles of the bionic design [3].

The problems of modern children's product packaging design have long gone beyond pure sex and physicality. The psychological effects, humanities, and cultural connotations implicit in packaging have long been radiated from the inside out [4]. Packaging is a combination with sociology and aesthetics and has a trend of scientific life and folklore development. The beauty embodied in the packaging of children's products not only represents new culture, new information, and new vitality but also embodies the public welfare and contemporary flavor of the product packaging culture. Relatively speaking, under the influence of the commercial atmosphere of chasing interests and reputation in modern society, packaging of children's products has gradually become a means for businesses to invest and make profits. Therefore,

potential product safety hazards have appeared in the packaging design of children's products. How to make good use of the role of various elements in product packaging design to promote children's physical and mental development and eliminate potential safety issues as much as possible has gradually become a modern packaging design for children's products, an important task [5].

Among the foreign children's product packaging, the current situation of children's product packaging design is relatively comprehensive compared with domestic development. Kent MP takes advantage of this color rule, starting from the colors of children's preferences, choosing colors with strong contrast, high brightness, and brightness as the main colors of children's product packaging, increasing the popularity of products, and promoting sales [6]. Signal LN believes that the most innovative and attractive products can be designed through the rich, vivid, and interesting expressions displayed by the graphics. The graphics can directly express the information of the product and will increase the interest of the packaging [7]. In China, Li Yibin proposed that more attention should be paid to the design function of packaging. Continuously developing, creating, and innovating design concepts and ideas, while accurately conveying product packaging information, can not only guide new consumption concepts but also continuously acquire, inspire, and use new ideas, which will subtly influence the development of children's minds [8]. Yang Xianyi explored and analyzed the art design from different perspectives such as design history, morphology, and aesthetics. He examined and evaluated the influence and significance of the design from multiple angles and all rounds. However, he did not discuss the specific methods of design in detail. The research in this paper provides directions [9]. Zhao Tingting studied the "color," "function," and "texture" of different organisms and found relevant design elements that can be applied to food packaging and to better imitate and apply natural elements in food packaging. Make food closer to nature. From the imitation of food packaging, summing up consumers' aesthetic concepts, it points out the development direction of food packaging and bionics [10]. The problems faced by the packaging design of children's products in China are mainly ignoring the thoughts of children's inner world, not observing things from their perspectives and extracting them for use in the design.

Through the research on the market of children's food packaging and the collection of relevant literature, this paper finds that there are relatively few studies on the design of children's food packaging. Many academic papers and monographs have carried out research on the colors and graphics of children's food packaging. Although the research on children's food packaging design has provided a lot of specific academic theoretical knowledge, it has not made a design performance for children's food packaging and proposed a detailed and systematic methodology. Taking the design system of design methodology as the starting point, combined with relevant theoretical knowledge of the design, aesthetics, etc., an in-depth design analysis of children's food packaging shapes was carried out and practical operability and detailed design techniques and principles were summa-

rized and summarized for children's food The design of the packaging shape provides a reference.

2. Preference Design Methods for Children's Product Packaging

2.1. Children's Products. With the rapid development of the times, packaging has gradually become a bridge between goods and consumers. The design embodied in packaging is no longer satisfied with its most basic functions and people's consumption in food, clothing, housing, and transportation is gradually increasing. The ground is based on the user experience [11, 12]. Due to the rapid development of high technology, people have been unable to obtain the slowly missing emotional needs and user experience from the pure "you design and I use" product design concept. In short, its packaging can no longer provide consumers with real user experience and psychological satisfaction. Nowadays, packaging designed based on user experience is increasingly attracting more consumers to buy for the experience. The humanistic thinking brought about by design concepts that are easily accepted by society and enterprises can pave the way for the product packaging design that emphasizes the emotional market in the future. As people's consumption consciousness strengthens and they pursue spiritual needs, a design trend that focuses on aesthetics and uses feedback information from experience to design more humane products has gradually emerged. This design trend can allow people to find their own emotional outlet and enhance the user experience that they obtain when using the product [13].

At the same time, as the society pays more and more attention to the special group of children, the packaging of children's products has followed that people's attention to the packaging of children's products has also increased. Children's physical and mental development is very important; they have their own unique ability to perceive things and ways of communication [14, 15]. Therefore, compared to other types of product packages, designers need to make specific plans for packaging designs for children's products. On the basis of children's user experience, use their feedback information to make targeted and planned improvements and then implement them and get some real and very helpful feedback information from users to further improve the design of product packaging to attract more children, satisfy their curiosity to a greater extent, bring unforgettable experiences, make them have fun, develop their intelligence, and satisfy their physical and psychological needs [16].

Although color is one of the powerful design languages that directly attract children's attention, at the same time, graphics also play an indispensable role. Graphics also make up a large proportion of the packaging of children's products and are also part of the designer's focus on the design. Graphics can directly represent product information, adding interest and personality to the package [17]. Through the rich, vivid, and interesting expressions shown by the graphics, the most novel and attractive products are designed. We investigated the packaging design of some popular children's products, as shown in Figure 1.

(a)

(b)

(c)

(d)

(e)

(f)

FIGURE 1: Popular children's product packaging.

In addition to the two design languages of color and graphics, designers are also good at using the packaging structure. The packaging structure of children's products plays an obvious auxiliary role in improving user experience and increasing interest. Children are more sensitive than rational when choosing their favorite products. In addition to bright colors and interesting patterns, the cute and ingenious structure is also one of the powerful weapons that can attract their attention.

2.2. Big Data. The development of the big data industry is closely related to big data and its applications. Although it originated from industry practice, academic research on the "big data industry" lags far behind the development of practice [18]. From a domestic perspective, the current research on the big data industry is mainly based on government industrial policies and plans, industrial development suggestions, comparisons of domestic and foreign big data industries, and industrial development influencing factors. There is a lack of appropriate theoretical perspectives on the internal big data industry. Research on constituent elements and governance mechanisms; from a foreign perspective, although there are not many related studies, scholars have begun to discuss the big data industry from the perspective

of business ecology. Big data is generally achieved through the following methods.

$$m_a = \sum_{b=1}^{n} \lambda_{ab} \vartheta_{ab}. \tag{1}$$

Among them, m_{ab} is the individual's contribution to the overall degree of ordering and λ_{ab} is the weight of each order parameter. Therefore,

$$y(kT + t_i) = \frac{1}{\alpha(z)} \sum_{j=1}^{r} \beta_{ij}(z)\bar{u}(kT + t_{j-1}) + v(kT + t_i), \tag{2}$$

which can be transformed into

$$\alpha(z) = 1 + \alpha_1 z^{-1} + \alpha_2 z^{-2} + \cdots + \alpha_n z^{-n}, \tag{3}$$

$$\beta_{ij}(z) = \beta_{ij}^0 + \beta_{ij}^1 z^{-1} + \beta_{ij}^2 z^{-2} + \cdots + \beta_{ij}^n z^{-n}. \tag{4}$$

Its function $s(kT + t_{i-1})i = 1, 2, \cdots, r - 1$ is to move the sampling signal $s(kT + t_{i-1})$ in time backward by 1 nonuniform sampling interval, and a new transfer function model is proposed:
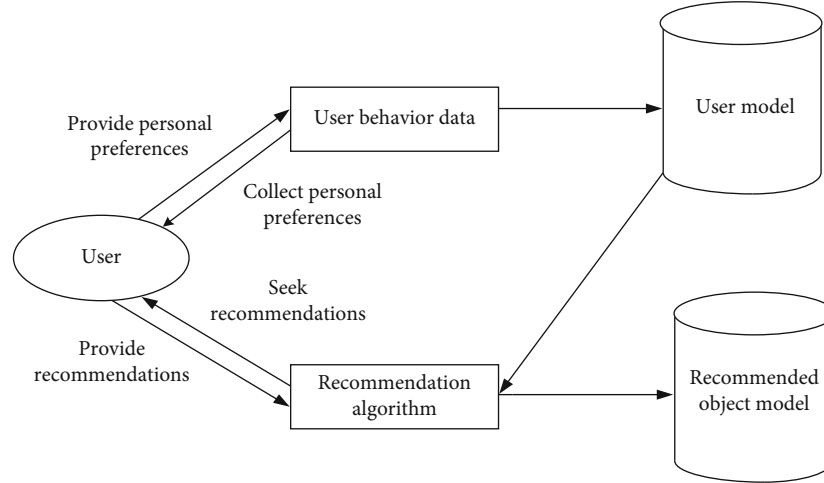
FIGURE 2: Recommendation algorithm composition.

$$y(kT + t_t) = \frac{B_i(\delta)}{A_i(\delta)} \bar{u}(kT + t_i) + v(kT + t_i). \qquad (5)$$

Big data ecology can be divided into three levels: microlevel core value chain, mesolevel extended value chain, and macrolevel big data ecology [19]. Among them, the core value chain is centered on the data value chain, including direct data suppliers and data value distribution channels; the extended value chain is centered on the core value chain, consisting of providers, data markets, data suppliers' suppliers, complementary data products, service providers, and direct data end users. The macrolevel big data ecosystem mainly refers to some related organizations in the periphery, such as government agencies, regulatory agencies, investors, venture capital & incubators, industry associations, academics and research institutions, standardization organizations, start-ups, and entrepreneur groups, as well as various other competitors, stakeholders, and peripheral members. The recommendation algorithm through big data is shown in Figure 2.

For the big data ecology, the diversity of members is crucial [20]. Diversity is an ecological concept. Various organisms in the ecology play different important roles in the environment. Many complete food chains and complex food webs have been formed between species and species and between organisms and the environment. The circle constitutes a virtuous circle of material and energy flow. Once the food chain is broken, the function will not be able to perform normally. Similar to the natural ecology, diversity is also indispensable to the big data business ecology: first, the diversity of members plays a buffer role for its response to environmental uncertainty; second, the value creation of diversity on the big data business ecology is of great benefit. For example, in order to build a data-centric business ecosystem, Alibaba has successively invested or acquired many Internet companies with a large amount of high-quality data, such as Sina Weibo and Didi Chuxing. This has played a huge role in the creation of ecological value; third, diversity

is a prerequisite for self-organization of the big data business ecology [21].

2.3. Machine Learning. The research object of machine learning is how to make machines have the same judgment ability and intelligence as humans. Its goal is to use various data to train machines. By improving algorithms and data structures, the machine can continuously improve its own analysis and prediction capabilities [22, 23].

The so-called machine learning is based on a lot of past and post experience for predicting problems. This type of prediction includes classification and regression problems. It is committed to solve the problem of using a lot of experience to improve the performance of the entire predictive system, so that it can successfully complete the task and meet the target requirements. Due to the huge amount of calculation required for machine learning, it is unrealistic and impractical to rely solely on people to calculate, so the help of computers is needed [24]. In computer systems, what people call "experience" is actually a set of disorganized data. What machine learning needs to do is to use algorithms to generate models from the appealed experience and then use the generative models to achieve what needs to be done.

Among the machine learning algorithms, the most widely used judgment methods are the omission method, crossvalidation method, and self-service method. The retention method is to divide the dataset into two mutually exclusive subsets, which can be combined into a whole. The two sets are divided into two parts: the verification set and the learning set. The two sets must maintain the consistency of the data distribution to prevent the introduction of additional errors and cause unnecessary errors in the final result. When the omission method is used, it needs to be used multiple times, and then, the average value of the multiple results is taken as the final result [25].

For a machine learning algorithm, in order to verify the pros and cons of the algorithm, and whether the algorithm can successfully solve people's problems, it must pass the evaluation and test of the model. Support vector machines

can be divided into linear support vector machines and nonlinear support vector machines. The advantage of linear classification advantage is that no sample data is required. The formula is as follows:

$$f(x) = xw^t + b. \tag{6}$$

w and b are obtained based on training data. For nonlinear classification, part of the support vector (sample data) is required, namely,

$$w = \sum_{i=1}^{n} a_i y_i x_i. \tag{7}$$

Therefore, the expression of the nonlinear vector machine is

$$f(x) = \sum_{i=1}^{n} a_i y_i K(x_i, x) + b. \tag{8}$$

In the formula, x_i is the training data i, y_i is the label value of the training data i, and a_i is the Langera day multiplier of the training data i. The kernel function is

$$K(x_1, x_2) = \exp\left(-\frac{\|x_1 - x_2\|^2}{2\sigma^2}\right). \tag{9}$$

a, σ, and b are the values generated in the training data. The σ adjustment can match different dimensions. The smaller the value of σ, the higher the dimension. Under normal circumstances, the overall sample will be classified into two categories—one is classified correctly and the other is classified incorrectly. We call the ratio of the number of samples judged to be positive examples as negative examples to the total number of samples as the "model error rate". Once a certain point is misclassified a lot of times, the weight assigned to it will be high accordingly. Estimate a constant value and minimize the loss function, and then,

$$f(x) = ag\min_c \sum_{i=1}^{n} L(y_i, c). \tag{10}$$

The value of the negative gradient of the current model loss function is used as the residual estimation value.

$$r_{mi} = -\left[\frac{\partial L(y_i, f(x_i))}{\partial f(x_i)}\right]_{f(x)=f_{m-1}(x)}. \tag{11}$$

The advance search method is used to estimate the value of the leaf node area to minimize the loss function.

$$f_m(x) = f_{m-1}(x) + \sum_{i=1}^{i} c_{mi} I(x \in R_{mi}). \tag{12}$$

Finally, we get the model that we need

$$\bar{f}(x) = f_M(x) = \sum_{m=1}^{M} \sum_{i=1}^{I} c_{mi} I(x \in R_{mi}). \tag{13}$$

2.4. Design Features of Children's Products. For children, it is a very pleasurable thing to get a children's food packaging design that makes them "satisfied." Children often have corresponding dependence or emotional sustenance on some emotional and interesting small toys or small packages with interesting structures around them. Directly speaking, the psychological development of children may be affected by the quality of children's products. Designers must treat this issue with caution. By consulting relevant materials, investigating and researching small target users with meticulous and cautious methods, and testing the product many times before it can be put on the market, these are the necessary design processes for the design of children's products, as is the emotional design process for children's product packaging. Therefore, its products must have the following characteristics:

(1) It can improve children's enthusiasm for life. Innocent and lively, richly imaginative, and curious beyond ordinary people are the nature of children, and their inner world is very colorful. Every word, every graphic, and even a color block on the packaging of children's products can cause emotional changes and increase their concentration and curiosity. As children grow older, their emotional and cognitive abilities will change significantly. Designers need to pay attention not to bring negative emotions into the packaging design of children's products, let alone use adult thinking to guess children's psychological nature. Only a packaging design for children's products that is full of emotional design factors can enhance children's curiosity to explore the unknown and allow them to face life positively

Not only in the packaging design of children's products but in the entire children's products, fun is one of the indispensable features. "Education and fun" is highly praised by children's education. Therefore, the packaging design of children's products should be colorful, in fun and attractive in appearance, and can transmit knowledge.

(2) Simpler outer packaging structure compared with the complicated structure of the outer packaging structure, children's product packaging with a simple appearance structure will be very popular with children. They can easily explore the method of opening the package and can quickly and easily reconcile the packaging. The packaging generates interaction and enters a state of happily enjoying the food. The simple structure of children's product packaging can help them improve their judgment and self-confidence and obtain a very good user experience

from it, which can also be further improved emotionally

In summary, designers should have a correct and in-depth understanding of children's emotional cognition and aesthetics, start with their operational capabilities and creativity, and combine the development trend of children's product packaging in the future society and carry out a system from the perspective of children analysis and design, combined with user experience feedback information to design children's product packaging with rich emotions and good user experience.

3. Children's Product Packaging Preference Design Experiment

3.1. Research Purpose. Under the circumstances of much concern, the society and the packaging of children's products have also given certain expectations. Based on ensuring the safety of children's products, it is expected that children's product packaging can incorporate more elements to improve the quality and quality of children's lives. Based on user experience, conduct in-depth research on the design of children's product packaging and try to design children's product packaging that is more suitable for children's lives and actual needs and express the potential emotional expression contained in the design language of children's product packaging design. A detailed investigation and analysis have also been carried out to provide a strong theoretical basis for this article.

3.2. Research Objects. Currently, the direct audience for children's product packages is children. However, due to the peculiarities of the children in this group, most buyers are parents or elders of the child. Therefore, the user research objects of children's product packaging should not be limited to children, but also their family members, especially their parents.

Through the in-depth investigation and analysis of children's product packaging in the early stage, we are deeply aware of the current situation of the use and demand of children's product packaging by children and their families, the latest survey results of users' purchasing needs. Through the content of the questionnaire, it is possible to analyze the problems existing in the packaging of children's products and the trend of user demand. The content of the questionnaire roughly includes how users choose children's product packaging and their expectations for future children's product packaging design.

3.3. Determine the Evaluation Weight. The index weight is a numerical index indicating the importance and function of the index. In the indicator system of the evaluation plan, the weight of each indicator is different. Even if the indicator level is the same, the weight is different. Index weight is also called weight and is usually represented by a. It is a number greater than zero but less than 1, and the sum of the weights of all first-level indicators must be equal to 1, that is, satisfying the conditions $0 < a < 1$ and $\sum a - 1$.

3.4. Statistics. All data analyses in this article use SPSS19.0, the statistical test uses the two-sided test, significance is defined as 0.05, and $p < 0.05$ is considered significant. The statistical results are displayed as mean ± standard deviation ($x \pm$ SD). When the test data obeys the normal distribution, the double t-test is used for comparison within the group and the independent sample t-test is used for comparison between the groups. If the regular distribution is not sufficient, two independent samples and two related samples will be used for inspection.

4. Analysis of the Preference Design of Children's Product Packaging

4.1. Children's Color Preferences. The use of appropriate colors in children's packaging can accurately convey the information of the product and prompt consumers to buy the product in the end. Through the investigation of children, the age and color hobbies of children based on the investigation and research are shown in Table 1.

It can be seen in Table 1 that children in early childhood like bright colors, especially colors with strong contrast and some children's love for bright colors can continue until elementary school. Among preschoolers, the three favorite colors of boys are blue, yellow, and orange and those suitable for girls are yellow, orange, and red. After entering school age after six years old, the colors that boys and girls like gradually have their own personalities. School-age boys like orange, yellow, and light-blue. Girls like very light green and orange. Therefore, when using product packaging colors, it is necessary to conduct research on consumer groups and design color packaging suitable for this group of people. In order to verify the correctness of the results, we surveyed 200 children and obtained relevant data, as shown in Figure 3.

It can be seen in Figure 3 that the results of the experiment are basically consistent with the data and the true validity of the data can be determined. Consumers of children's products are mainly children's parents, but their personalities and environments are different, and their consumption habits are also different. Therefore, we have made statistics on the purchase of children's products by parents, as shown in Table 2.

In Table 2, we can see that when parents buy products for children, the main reason is that they feel that the products are good for children's development, followed by children who want to buy and go shopping in the mall. This shows that contemporary young parents also tend to consume more rationally.

4.2. Children Choose Preferences. We have carried out statistics on children's preferences on toys and show children's preferences for different toys through the difference of educational toys. The specific toy choices are shown in Table 3:

We collect statistics on children's preferences for these five types of toys at different ages and quantify their preferences for easy comparison. The results are shown in Figure 4.

TABLE 1: Children's color preference.

Age ranking	Gender	1	2	3	4	5
Early childhood (2–6 years old)	Male	Blue	Yellow	Orange	Powder	—
	Female	Yellow	Orange	Red	Purple	Yellow-green
School age (6–12 years old)	Male	Orange	Yellow	Blue-green	Yellow-green	White
	Female	Light green	Orange	Yellow	Canary	White
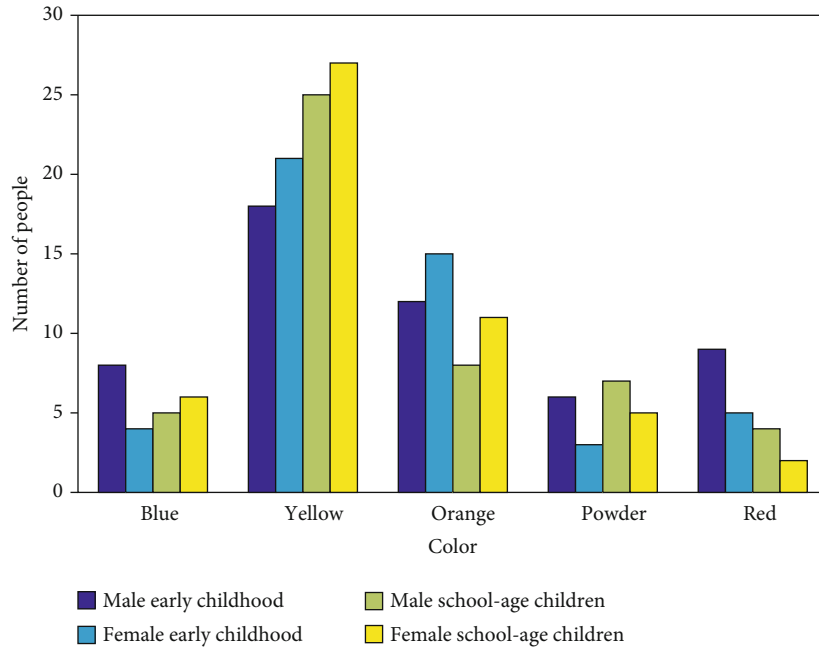
FIGURE 3: Trends in children's product selection.

TABLE 2: Parents' purchase of children's products.

Options	Proportion (%)
Child requirements	15.92
Feel good for development	50.03
Other children playing	3.81
Children birthday	8.8
Holidays	6.6
Introduction	1.01
Advertising	1.05
Random to see	12.4

TABLE 3: Preference materials for the selection of educational toys.

Toy number	Class concept	Specific toys
1	Building class	Building blocks
2	Puzzles	Animal jigsaw
3	Pairing	Number letter
4	Rubik's cube	Rubik's cube
5	Labyrinth	Planar magnet maze

In Figure 4, we can see that children of different grades have different preferences for toys. On the whole, preschool-age children prefer educational toys and maze toys, while school-age children prefer construction toys. This is also due to the nature of the children. We combine colors and types of toys to investigate their attractiveness to children. The attractiveness to children is shown in Figure 5.

It can be seen in Figure 5 that children's preference for red toys is higher than other colors and yellow toys are the least attractive to children and the gap between the two is more than 30%. This shows that, for children, the production of products according to different colors can well grasp the preferences of children and increase the sales volume of the company. Of course, the way parents and children think is not the same. If companies want to increase sales, they must not only target children but also understand the parents' thoughts. Therefore, we have also conducted relevant surveys on parents' preferences for children's products, as shown in Figure 6.

In Figure 6, we can see that there is a certain difference between parents and children's preferences for colors and materials. When companies produce children's products, they need to conduct related investigations on the
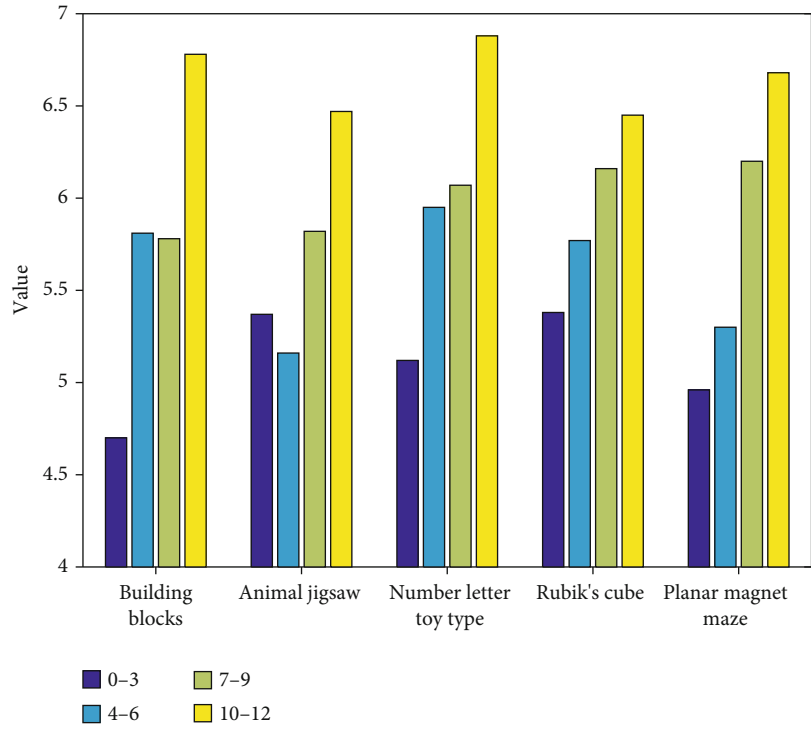
Figure 4: Children's preferences for toys of different ages.
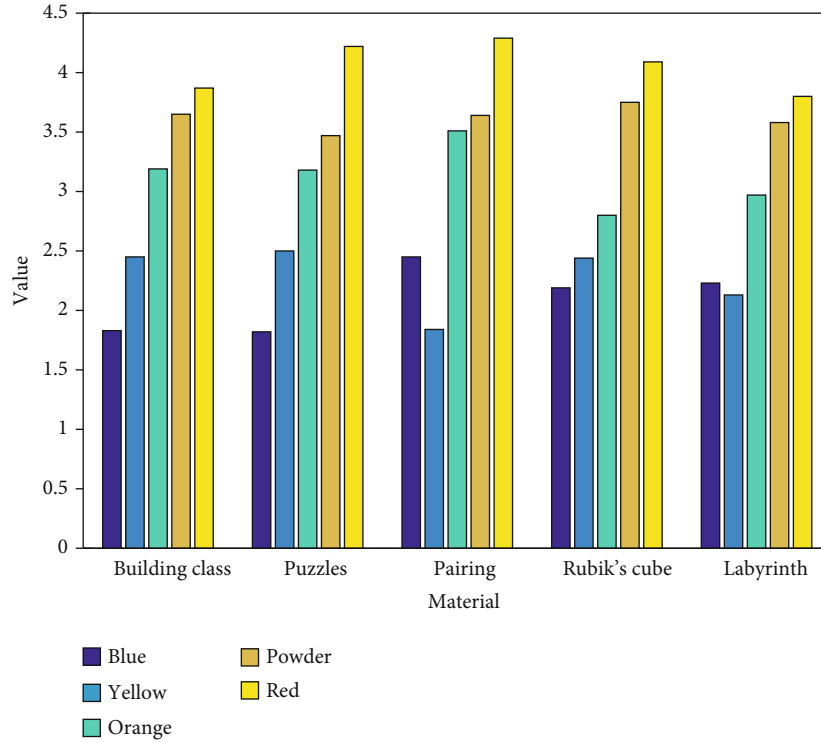
Figure 5: Male children's preference for different colors of toys.
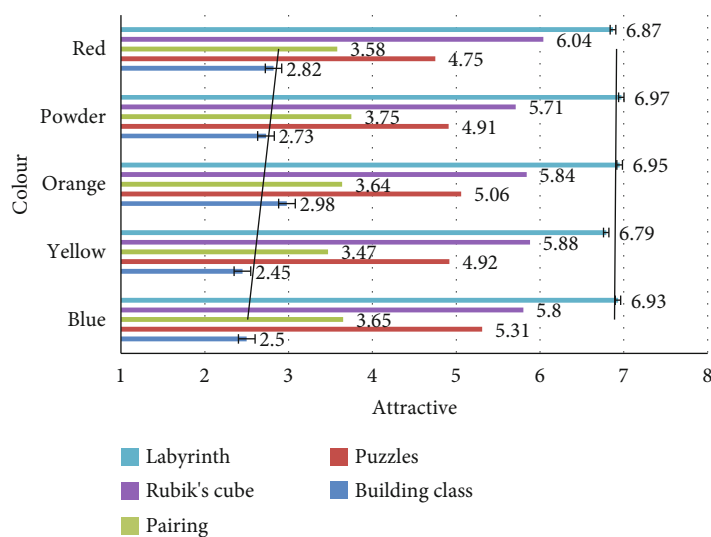
FIGURE 6: Parents' preference for children's products.

preferences of parents and children to clarify the target customers of their products, good to increase product sales.

5. Conclusion

Modern children's product packaging design is a comprehensive design subject art, and it is no longer a simple packaging design application. Related aspects include surface modeling art, material art, text, and graphic design art. The psychological effects and humanity and cultural implications of the packaging itself radiate from within the product itself. This article takes child consumers as the main target and starts from how the emotional design of children's product packaging can more successfully enhance the user experience. Transform the current children's product packaging that lacks emotional color and interactivity into an emotional packaging design for the purpose of satisfying children's user experience. There are also some shortcomings in the research of this paper. In the research, there is not too much attention to the application of green packaging in the emotional design of children's products and there is a problem of low attention to the packaging of children's green products. The user experience design in children's product packaging has not been fully developed, and some entry points are still very vague. It is necessary to increase the study and work in the future and work hard to research and propose better solutions.

Data Availability

The data that support the findings of this study are available from the corresponding author upon reasonable request.

Conflicts of Interest

The author declares that they have no conflicts of interest.

References

[1] Z. Wang, Q. Ma, H. Bai, Q. Zhang, Y. Cai, and Q. Lv, "Migration regularity of six preservatives from wooden children's products to saliva and sweat based on microstructure-related migration models," *Ecotoxicology and Environmental Safety*, vol. 173, pp. 149–155, 2019.

[2] S. K. Murnen, C. Greenfield, A. Younger, and H. Boyd, "Boys act and girls appear: a content analysis of gender stereotypes associated with characters in children's popular culture," *Sex Roles*, vol. 74, no. 1-2, pp. 78–91, 2016.

[3] D. Y. Kim, S. H. Chun, Y. Jung et al., "Phthalate plasticizers in children's products and estimation of exposure: importance of migration rate," *International Journal of Environmental Research and Public Health*, vol. 17, no. 22, pp. 8582–8584, 2020.

[4] M. Li, R. Li, Z. Wang, Q. Zhang, H. Bai, and Q. Lv, "Optimization of headspace for GC-MS analysis of fragrance allergens in wooden children's products using response surface methodology," *Separation Science Plus*, vol. 2, no. 1, pp. 26–37, 2019.

[5] A. R. Popa, "Advertisements for children's products in women's magazines: traits of the discourse," *Gender Studies*, vol. 17, no. 1, pp. 94–104, 2018.

[6] L. Rosana, H. Silva, and R. M. Gomes, "Evaluation of the presence of allergens in children's products available for sale in a big city," *Anais Brasileiros de Dermatologia*, vol. 93, no. 3, pp. 457–459, 2018.

[7] C. H. Basch, A. Kecojevic, V. Cadorett, and C. E. Basch, "Advertisements for children's entertainment products in a

popular parenting magazine: sedentary or active?," *Health Promotion Perspectives*, vol. 7, no. 1, pp. 47–49, 2017.

[8]   M. A. Silva, L. C. Milagres, A. P. Castro et al., "O consumo de produtos ultraprocessados está associado ao melhor nível socioecocômico das famílias das crianças," *Ciencia & Saude Coletiva*, vol. 24, no. 11, pp. 4053–4060, 2019.

[9]   L. A. Fletcher, T. Pham, M. Herriman, B. Kiely, R. Milanaik, and G. A. Rosner, "Peanut-containing products in children's hospitals: putting pediatric patients at risk," *Journal of Allergy and Clinical Immunology*, vol. 137, no. 2, pp. 78–85, 2016.

[10] J. L. Pomeranz and J. L. Harris, "Children's fruit "juice" drinks and FDA regulations: opportunities to increase transparency and support public health," *American Journal of Public Health*, vol. 110, no. 6, pp. e1–e10, 2020.

[11] G. Gary, G. Justine, and F. Brenda, "Approaches to children's exposure assessment: case study with diethylhexylphthalate (DEHP)," *International Journal of Environmental Research & Public Health*, vol. 13, no. 7, pp. 670–673, 2016.

[12] Z. Mchome, S. Yousefzadeh, A. Bailey, and H. Haisma, ""When I breastfeed, it feels as if my soul leaves the body": maternal capabilities for healthy child growth in rural Southeastern Tanzania," *International Journal of Environmental Research and Public Health*, vol. 17, no. 17, pp. 6215–6522, 2020.

[13] S. Demiral, "Considering discourse with children through animations," *International Journal of Pedagogy Innovation and New Technologies*, vol. 7, no. 2, pp. 47–57, 2020.

[14] A. Z. Teixeira, "Sodium content and food additives in major brands of Brazilian children's foods," *Ciencia & saude coletiva*, vol. 23, no. 12, pp. 4065–4075, 2018.

[15] A. Anwar, P. M. Abruzzo, S. Pasha et al., "Advanced glycation endproducts, dityrosine and arginine transporter dysfunction in autism - a source of biomarkers for clinical diagnosis," *Molecular Autism*, vol. 9, no. 1, pp. 3–10, 2018.

[16] W. L. Yuan, N. Rigal, S. Monnery-Patris et al., "Early determinants of food liking among 5y-old children: a longitudinal study from the EDEN mother-child cohort," *International Journal of Behavioral Nutrition & Physical Activity*, vol. 13, no. 1, pp. 20–25, 2016.

[17] S. Beckwith, "Feeding the baby products supply chain," *Inbound logistics*, vol. 39, no. 6, pp. 67–70, 2019.

[18] S. I. Lee and C. H. Kim, "A study of consideration of children's furniture design elements," *Journal of the Korea furniture Society*, vol. 28, no. 3, pp. 185–197, 2017.

[19] S. H. Min, "Study on recognition and consumption behavior of quality-certified children's preferred foods of nursery directors and parents in Jecheon area," *Korean Journal of Food and Cookery Science*, vol. 33, no. 3, pp. 353–362, 2017.

[20] F. Bellisle, P. Hébel, A. Salmon-Legagneur, and F. Vieux, "Breakfast consumption in French children, adolescents, and adults: a nationally representative cross-sectional survey examined in the context of the International Breakfast Research Initiative," *Nutrients*, vol. 10, no. 8, pp. 1056–1059, 2018.

[21] S. M. Ng, J. C. Agwu, and K. Dwan, "A systematic review and meta-analysis of synacthen tests for assessing hypothalamic-pituitary-adrenal insufficiency in children," *Archives of Disease in Childhood*, vol. 101, no. 9, pp. 847–853, 2016.

[22] J. Gómez-Paredes, A. Alsamawi, E. Yamasue et al., "Consuming childhoods: an assessment of child labor's role in Indian production and global consumption," *Journal of Industrial Ecology*, vol. 20, no. 3, pp. 611–622, 2016.

[23] F. P. Perera, K. Wheelock, Y. Wang et al., "Combined effects of prenatal exposure to polycyclic aromatic hydrocarbons and material hardship on child ADHD behavior problems," *Environmental Research*, vol. 160, pp. 506–513, 2018.

[24] C. Mei-Ju, "Board games play matters: a rethinking on children's aesthetic experience and interpersonal understanding," *Eurasia Journal of Mathematics Science & Technology Education*, vol. 13, no. 6, pp. 2405–2421, 2017.

[25] V. R. Kuchma, L. M. Sukhareva, M. I. Stepanova, P. I. Chramtsov, I. E. Aleksandrova, and S. B. Sokolova, "Scientific bases and technologies of security hygienic safety of children in the digital school," *Gigiena i Sanitariia*, vol. 98, no. 12, pp. 1385–1391, 2019.

WILEY | Hindawi

Research Article

Consumer Decision-Making Power Based on BP Neural Network and Fuzzy Mathematical Model

Weijie Li ⓘ

School of Economics & Management, Ankang University, Ankang, 725000 Shaanxi, China

Correspondence should be addressed to Weijie Li; liweijie@aku.edu.cn

In real life, because of the uncertainty of risk, incomplete information, perceived cost, and other factors, there are irrational behaviors in the decision-making power of consumers, so it is of great practical significance to study the decision-making power of consumers in the choice of countermeasures and personalized product recommendation. The purpose of this paper is to analyze the decision-making power of consumers based on the BP neural network and fuzzy mathematical model. First, the basic theory of artificial neural network and the concepts of set theory and fuzzy reasoning of fuzzy mathematics are described. Second, the behavior prediction model with the equal emphasis on rationality and irrationality and the integration of artificial neural network and fuzzy mathematics are constructed. The comments of a certain mobile phone are selected as the experimental objects to analyze the decision-making reasoning and prediction of individual consumers in the network and the decision-making reasoning of group consumers in the network, the experimental results show that through Mamdani reasoning, behavioral intention = 5.72. Through the fuzzy set processing, it is finally determined that the consumer's purchase intention is close to the VT mode, which is "very inclined." In the first method, the user's recognition rate of product C1 is 82%, and in the second method, the user's recognition rate is 55%. The comparison of the two methods is in line with the expectation. The first method extracts the user's emotion and evaluation information from the comments, fully considers the personalized needs of consumers, and is closer to the prediction results of the system.

1. Introduction

With the rapid development of e-commerce, many consumers begin to choose to consume online. Because of the virtual, interactive, convenient, and word-of-mouth communication of online consumption, the role of irrational factors is more prominent. At the same time, people's ability in learning, thinking, and action is limited. Psychology and emotion play a great role in purchase intention and behavior. Therefore, it is necessary to fully consider the irrational emotion in the prediction of online consumers' decision-making power. Online consumers often describe their opinions and feelings about the purchased goods or services through online comments, and emotion is the irrational performance. Therefore, we can fully consider the irrational factors of online consumers by mining the emotional information contained in online reviews, so as to better predict the decision-making power of consumers. Both model control technology

and artificial neural network belong to artificial intelligence technology. For the latter, learning operation can be carried out, but fuzzy information cannot be described. Therefore, it is necessary to integrate the two and, then, build a corresponding system, so that it can not only master the learning ability but also process the fuzzy information.

At present, the emotional analysis of consumers is just in its infancy, and it is rare to predict the behavior of online consumers by using massive online comments to calculate the emotional and product cognition information of consumers. The combination of emotion calculation and decision-making power prediction of online consumers, supplemented by fuzzy sets and fuzzy reasoning, will produce more important theoretical guidance and application value for the formulation of marketing strategies of merchants. At the same time, the discussion of online consumer group behavior will lead the research of group behavior in an e-commerce environment. The prediction results are of great

practical significance for the selection of countermeasures and recommendation of personalized products in network marketing and personalized marketing.

In this paper, based on the evaluation system of the decision-making power of online consumers, the fuzzy processing is carried out, and the degree is divided into seven categories from weak to strong. The calculation method based on the dimension of the behavior prediction model is given, and the trial calculation is carried out. According to the behavior prediction model of both rationality and irrationality, the fuzzy reasoning rule base is established with the subjective attitude of online consumers and the subjective norms of online consumption as the antecedent and the decision-making power of consumers as the consequent, which realizes the reasoning and prediction of the decision-making power of consumers. At last, it calculates and analyzes the two cases from the perspectives of network individual behavior and network group behavior and gives the comparison of two cases whether to consider irrational emotional factors. At the same time, it selects experts to evaluate the predicted results, tries to obtain a large number of data information of group consumers from different perspectives, and makes purchase decision-making reasoning, This paper attempts to further explore the group buying behavior of online consumers.

The main structure of this article is introduced as follows. The first part introduces the background and significance of the topic, as well as the work and organizational structure of this article. The second part introduces related work, as well as the concepts of set theory and fuzzy reasoning in fuzzy mathematics, as well as the more popular rational behavior theory in the field of behavior prediction. The third part takes mobile phone reviews as the experimental object to conduct data collection and experimental steps; the fourth part realizes the prediction of decision-making power, discusses the possibility of approximate reasoning of online group buying behavior, and gives examples to verify the rationality of the prediction algorithm. The fifth part is a summary of the full-text work.

2. Proposed Method

2.1. Related Work.
Portfolio management includes deciding which assets to include in the portfolio based on the objectives of investors and changing market and economic conditions. The always difficult selection process involves determining which assets to purchase, how many assets to purchase. Chen proposed a new meme neural fuzzy system (MNFS-FPM) for financial portfolio management, which simulates the thinking process of rational investors and generates the optimal portfolio from a group of assets according to the selected investment style. The system is mainly composed of two modules: General self-organizing fuzzy neural network (GenSoFNN-Yager) to realize Yager reasoning, which is used to predict the expected return of each asset; memory algorithm of simplex local search (MA-NM/SMD) is used to determine the optimal investment weight distribution of each asset in the portfolio. The experimental results of the Dow Jones Industrial Average (DJIA) stock show that the

system proposed in this paper has better performance than the existing statistical mean variance analysis and capital asset pricing model (CAPM) [1].

The future web business model involves a virtual environment, in which entities interact to sell or purchase information products. This environment is called the information market (IMS). The intelligent agent is used in IMS to represent the buyer or information provider (seller). Daniela Šálková focuses on the decisions made by the buyer in the procurement negotiations with the seller. A kind of reasoning mechanism based on fuzzy logic is put forward. The knowledge of the buyer negotiation process is modeled by a fuzzy set. They propose a fuzzy reasoning machine to deal with the decisions made by the buyer at each stage of the negotiation process. The results of the proposed reasoning method indicate whether the buyer should accept or reject the seller's offer. Their findings are very promising for the efficiency of automated transactions by intelligent agents [2].

The policy of purchasing chips is decided by the notebook computers and computers of the original equipment manufacturers (OEMs) through similarity standards and probability rules. Sax's research aims to establish an expert system for predicting the purchase behavior of the semiconductor market. Similarity criteria and probability rules are extracted from the OEM information sequence of the quarterly list of the semiconductor market. Through the statistical methods of data collection and data mining, the rules of OEM purchasing behavior data are analyzed and extracted and transformed into fuzzy sets. In addition to the information from the nature of the market, they also created an inference expert system. Their analysis of similar products shows that when purchasing similar products, there are mainly two categories of OEM that use probability rules for one-year recovery information processing, with an average score of about 95% per quarter [3].

2.2. Basic Theory of Artificial Neural Network

2.2.1. Artificial Neural Network.
Artificial neural network (ANN) is an adaptive nonlinear dynamic system formed by standardized neuron connection. At present, it has been deeply explored in the world. Through the connection of many simple artificial neurons, the ability of a biological neural network is simulated [4]. From other neurons or the external environment, obtain the consultation, and simply operate on it, and output the results to other artificial neurons and the external environment [5]. Under the influence of input information, the neural network will enter into the corresponding state. Because of the dynamic characteristics of neurons and their connections with each other, this excitation mode will automatically change into a new equilibrium state. In this way, this kind of neural network can define the corresponding mode transformation and realize the mapping relationship [6].

Because in the network, the corresponding connection mode of an artificial neuron is different, that is to say, a variety of artificial neural network modes are formed. Among them, the most widely used and representative model is the BP network, which is an error back propagation network

[7]. In practice, BP neural network model is widely used, which consists of input, output, and hidden layer. As far as the transfer function is concerned, most of them are based on the application of the sigmoid function, which can approach all continuous functions and has good nonlinear mapping ability. In addition, the related parameters, including the network learning coefficient, can be set according to the specific situation, so the flexibility is more prominent. Therefore, in many areas, the role of this model is particularly prominent. Relying on this technology, a nonlinear evaluation model can be constructed, which can properly solve the randomness of weight definition, and better ensure the accuracy and scientificity of evaluation results and activities [8, 9].

2.2.2. Classification of Artificial Neural Network.
According to the topological structure of the network, the artificial neural network can be classified into prefeedback grid [10].

(1) *Feedforward Network.* Input the information flow from the input layer, and then transmit it to the lower layer. After the standardized network processing, output it from the output layer. In this process, there is no feedback flow. The whole structure of neurons arrangement is input layer, hidden layer, and output layer. For neural networks, they are usually multilayer feedforward networks [11]

(2) *Feedback Network.* It can combine the connection weight, set the output from the corresponding layer as the input, and feed back to the previous layer or the same layer, which is called feedback network. According to the classification of learning strategies, it can be divided into the following categories, namely, the most appropriate application network, association, supervision, and unsupervised learning [12]

2.2.3. Operation Process and Sample Classification of Artificial Neural Network.
As far as the operation of the artificial neural network is concerned, it involves two stages, one is the recall stage, and the other is the learning process [13].

(1) The learning process is the process that the network learns the rules in the sample according to the learning algorithm, so as to adjust the network weight. There are three kinds of learning algorithms: association, supervised, and unsupervised. All algorithms are often obtained by deriving the energy function. In essence, this process is the process of minimizing energy function. Therefore, the learning effect of the network can be reasonably measured through the energy function [14, 15]

(2) Recall process is a process that combines the use of a recall algorithm. The network uses input information to make the output information clear. It can be divided into three categories: association, supervision, and unsupervised recall. During the operation of artificial neural network, the learning information is generally sampled, which can be divided into the following three categories: training samples in the

learning process, the network will often use the training samples, so as to adjust the weighted value of the network [16]. It can be divided into association, supervision, and unsupervised training samples. When the test samples complete the learning process and evaluate the network learning effect, they will use the test samples, which have the same type as the training samples. After the learning process, the samples to be pushed can use the network to calculate the target samples, which is different from the test samples

2.3. Fuzzy Mathematics

2.3.1. Fuzzy Phenomenon.
The concept of the fuzzy phenomenon is a kind of phenomenon that the boundary division is not strict and cannot be described with an accurate scale. No matter in human society or in nature, there are a lot of fuzzy phenomena. The concept embodied in this phenomenon is the fuzzy concept. In terms of humanities, life sciences, etc., there are often the most concentrated fuzzy concepts [17, 18]. For example, the phenomenon of rain, people's description of rainfall, often for heavy rain, drizzle, and so on [19]. However, the standard of heavy rain and drizzle is often hard to say, and there is no clear boundary, so it is considered as a fuzzy division. In addition, as for the characteristics of the same person, it can accurately describe the level of education, gender, etc., and all people have a clear gender, culture, etc. At the same time, there are many people's characteristics, which cannot be clearly described. For example [20], the human health status expressed by poor, good, etc. belongs to qualitative estimation, which belongs to a subjective judgment carried out by people themselves. In terms of daily life, there are relatively many such cases [21, 22]. Fuzzy mathematics, a mathematical subject, is to explore and deal with fuzzy phenomena from the perspective of self-quantity. Classical sets are difficult to describe fuzzy concepts accurately, because it is difficult to distinguish them in a single way. For its conceptual level, it is not absolute 1 and 0. Therefore, if we want to describe fuzzy concepts or phenomena quantitatively, we need to expand the classical set [23].

2.3.2. Fuzzy Sets.
For a common set A, any element X in the space, either $x \in A$ or $x \notin A$, must be one of them. This feature can be represented by a function:

$$A(x) = \begin{cases} 1 \ x \in A, \\ 0 \ x \notin A. \end{cases} \tag{1}$$

$A(x)$ is the characteristic function of set A. In this paper, the characteristic function is extended to the fuzzy set, and only two values of 0 and 1 are taken in the general set.

Definition 1. Sets x as the whole field. If a is a function with value [0,1] on X, then a is called fuzzy set.

For example, if five students are graded on the stability degree of their personalities, they are graded on the basis of

the percentage system and, then, divided by 100, a mapping from the domain $x = \{x1, X2, X3, x4, X5\}$ to the [0,1] closed interval is given.

$$
\begin{aligned}
X_1 85, \text{ is } A(x_1) &= 0.85, \\
X_2 75, A(x_2) &= 0.75, \\
X_3 98, A(x_3) &= 0.98, \\
X_4 30, A(x_4) &= 0.30, \\
X_5 60, A(x_5) &= 0.60.
\end{aligned}
\tag{2}
$$

In this way, a fuzzy subset $A = (0.85, 0.75, 0.98, 0.30, 0.60)$ is determined.

Define 2 if A the first mock exam on any X, and $A\lambda = \{x | x \in X, A(x \geq \lambda)$ for any $0 \leq \lambda \leq 1$, $A\lambda$ is A cut set. $A\lambda$ is a normal set rather than a fuzzy set. Because the boundary of the fuzzy set is fuzzy, if we want to transform a fuzzy concept into mathematical language, we need to select different confidence level $\lambda(0 \leq \lambda \leq 1)$ to determine its membership relationship [24]. λ cut set is the method of transforming the fuzzy set into the common set. Fuzzy set A is a set with wandering boundary, which increases with the decrease of λ value, that is, when $\lambda_1 < \lambda_2$, there is $A\lambda_1 \cap A\lambda_2$.

Definition 2. Definition of fuzzy set operation. If A and B are two fuzzy sets on X, their sum set, intersection set and A's remainder set are all fuzzy sets, and their membership functions are defined as follows:

$$
\begin{aligned}
(A \vee B)(x) &= \max(A(x), B(x)), \\
(A \wedge B)(x) &= \min(A(x), B(x)), \\
A^C(x) &= 1 - (A(x).
\end{aligned}
\tag{3}
$$

The sum and intersection operations of fuzzy sets can be extended to any number of fuzzy sets [25].

2.3.3. Fuzzy Comprehensive Evaluation. A comprehensive evaluation is to make a general evaluation of the things or objects restricted by many factors, which is a common problem in daily life and scientific research work, such as product quality evaluation, scientific and technological achievements appraisal, and evaluation of a crop planting adaptability, all belong to the comprehensive evaluation problem. Due to the fuzziness and subjectivity in the evaluation of things from many aspects, the comprehensive evaluation with the fuzzy mathematics method will make the results as objective as possible and achieve better practical results [26].

The mathematical model of fuzzy comprehensive evaluation can be divided into one level model and multilevel model. Generally, it can be concluded into the following steps:

(1) Establish the factor set $U = \{u_1, u_2, \cdots, u_n\}$. Factors are all kinds of attributes or performance of the object. In different situations, they are also called parameter indexes or quality indexes. They can com-

prehensively reflect the quality of the object, so they can be used to evaluate the object [27]

(2) Establish evaluation set $V = \{v_1, v_2, \cdots, v_n\}$. For example, for the evaluation of industrial products, the evaluation set is the set of grades, and the evaluation set is the set of adaptability

(3) To establish a single factor evaluation is to establish a fuzzy mapping from u to F (V):

$$
f : U \longrightarrow F(V), \forall u_i \in U.
\tag{4}
$$

The fuzzy relation can be induced by F, and the fuzzy matrix can be obtained

$$
R = \begin{bmatrix}
r_{11} r_{12} \cdots r_{1m} \\
r_{21} r_{22} \cdots r_{2m} \\
\cdots \cdots \cdots \cdots \\
r_{n1} r_{n2} \cdots r_{nm}
\end{bmatrix}.
\tag{5}
$$

R is called a single factor evaluation matrix, so (U, V, R) constitutes a comprehensive evaluation model.

(4) *Comprehensive Evaluation.* Due to the different emphasis on each factor in U, each factor needs to be given different weights, which can be expressed as a fuzzy subset $A = (a_1, a_2, \cdots, a_n)$

After R and A are calculated, the comprehensive evaluation model is $B = A \circ R$. Note $B = (b_1, b_2, \cdots, b_m)$, which is a fuzzy subset of V, where

$$
b_j = \bigvee_{i=1}^{n} (a_i \wedge r_{ij}) (j = 1, 2, \cdots, m).
\tag{6}
$$

If the result is $\sum_{j=1}^{m} b_j \neq 1$, the result will be normalized.

From the above four steps of a fuzzy comprehensive evaluation, it can be seen that the establishment of single factor evaluation matrix R and the determination of weight distribution a are two key tasks, but at the same time, there is no unified format to follow, which can generally be obtained by statistical experiments or expert scoring methods [28, 29].

2.3.4. Semantic Fuzziness of Online Comments. Online reviews mainly include two categories: cognitive words and emotional words. Cognitive and emotional words are very broad concepts with fuzzy attributes. Taking emotion as an example, the current emotional semantic analysis is still in its infancy, and the classification of emotion is relatively rough, which is only based on the dual tendency analysis of "yes" and "no." Emotion has uncertainty, which makes it difficult to deal with it by simple quantitative means, so we choose the method of fuzzy set to build the semantic fuzzy system of multi sentiment analysis [30].

The emotional words and cognitive words in online reviews are fuzzified, and the positive and negative degree
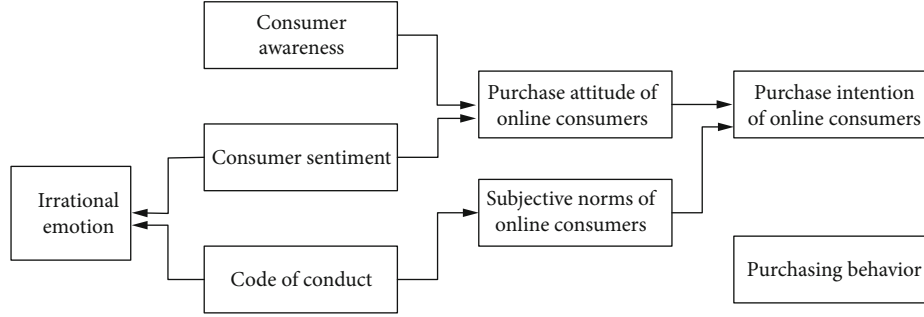
Figure 1: Theoretical framework of behavior prediction.

measures are, respectively, divided into levels: each level corresponds to a fuzzy membership function, s (less), m (medium), l (large), V (very), and Z (none) without polarity, as shown in the formula.

$$P(w) = P_w(x, \sigma_w, c_w) = \exp\left[\frac{-(x - c_w)^2}{2\sigma_w^2}\right]. \qquad (7)$$

Among them, w represents the emotion level of vocabulary, $w \in \{-VL, -L, -M, -S, Z, +S, +M, +L, +VL\}$, σ_w, c_w are the expectation and standard deviation of Gaussian membership function of a corresponding level, $x \in [-a, a]$ represents the emotion value of consumers, and a is a real number greater than zero (representing the boundary of emotion domain).

(5) The construction of consumer decision-making power model with rational and irrational consideration

Based on the current theoretical development and the redefinition of the connotation and extension of the constituent variables of the existing models in the field of online purchase, a prediction model of online purchase behavior with rational and irrational consideration is proposed as shown in Figure 1. This kind of network irrational emotion is mostly expressed through network comments on the evaluation of the network products or services after purchase and will directly affect the purchase attitude of other network consumers, and then affect their purchase behavior.

2.4. Fusion of Artificial Neural Network and Fuzzy Mathematics. According to the form and function of connecting the two, the combined form of the model can be summarized as follows:

Series type: as for the system, the two are connected through the application of series mode, i.e., output and input correspondence. Neural network and fuzzy system can be used as input and output, respectively, and vice versa.

Parallel type: in terms of the system, the two are connected through the use of parallel mode, i.e., the input is the same. As far as neural networks are concerned, learning data can be used to describe the range of network characteristics as a workspace. In addition, it is necessary to use the

Table 1: Mamdani reasoning.

Attitude	Norm	Behavior intention
1.88	0.72	5.72

fuzzy function to calculate the output value in the extreme and boundary region.

Network learning type: the fuzzy system is the system. Combining with the neural network system, i.e., control rules, the output and input information of this process can be combined to carry out adaptive adjustment. On the contrary, the connection of neurons can be adjusted through the use of fuzzy logic.

Structural equivalence: the equivalent structural neural network can be used to represent the fuzzy system. For neural network, all parameters and nodes have a very clear meaning. It is not a black box structure, but it does not cover the obvious dividing line in the combination.

3. Experiments

3.1. Data Acquisition. The corpus in this case comes from https://taobao.com. In order to predict the decision-making power of network consumers, we choose two products C1 and C2 (Note: C1 Samsung i9103, C2 Samsung i9105, two Samsung phones have similar function and performance). More than 190 evaluation records were downloaded through the web statement collection tool "network spirit". The repeated and worthless comments were removed, and 188 effective comments were finally selected as the comment set A. Select a user who has browsed a mobile phone but has not purchased it. In the same way, 98 effective comments are finally selected and set as comment set B.

In other words, the values of "attitude" and "norm" are used as forward language changes, and the constructed rules are used to infer the subsequent parts. According to the comprehensive emotion fuzzy calculation algorithm, combined with example calculations in the previous chapter, we will evaluate the attitudes corresponding to the B set and the subjective criteria corresponding to the A set as the reason for the fuzzy calculation.

3.2. Research Object. This paper focuses on the decision-making power of online consumers. The measurement of behavioral intention is mostly based on the measurement table. In the development process of the measurement table,
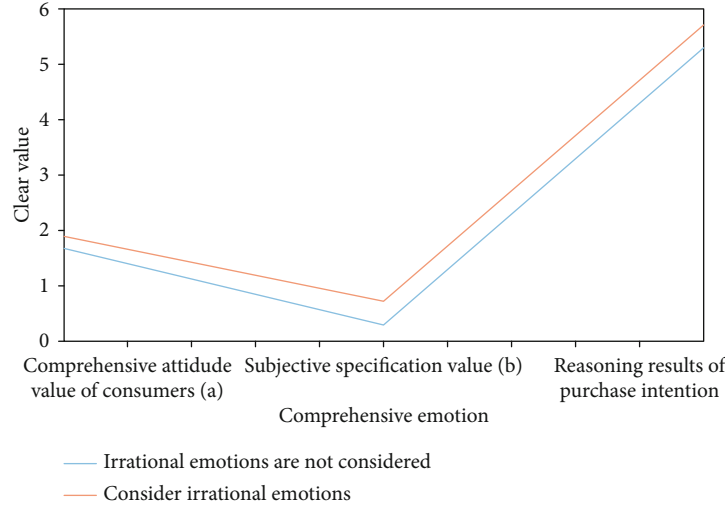
FIGURE 2: Fuzzy inference results of individual behavior intention.

different levels of scales will be used to measure the decision-making power of consumers, and the table will be adjusted appropriately according to the actual situation. However, due to the uncertain psychological variables such as emotion, cognition, and attitude, which cause the decision-making power of online consumers, it is difficult to clearly describe the fuzzy attribute of purchase behavior, so the fuzzy set method can be used to classify. The decision-making power of online consumers is divided into seven levels from weak to strong. The degree of decision-making power of all online consumers is between the extreme tendency and the extreme nontendency.

3.3. Calculation Method. Based on the consumer information behavior model in consumer behavior, Mamdani-type fuzzy inference is used to formulate fuzzy inference rules under different weights. The principle is that attitude variables dominate, and subjective normative variables play a secondary role. $R_c(A_1, A_2) = \int \vee (\mu_{A_1}(u_1) \wedge \mu_{A_2}(u_2), 1 - \mu_{A_1}(u_1))/(u_1, u_2)$ is used to determine the compound relationship of rules in the case of two antecedents. In this fuzzy reasoning system, some basic attributes are set as follows: "and" calculation and fuzzy implication adopt minimum operation and "or" calculation and fuzzy rule synthesis adopt maximum operation.

4. Discussion

4.1. Reasoning and Prediction of Decision-Making Power of Individual Consumers on the Internet. According to the steps of the experiment, we get the comprehensive emotion value and the upper norm value under the condition of considering irrational emotion, i.e., attitude = 1.88 and norm = 0.72. According to this, we can directly deduce the "behavior intention" value of the consumer. The reasoning is shown in Table 1. We can get behavior intention = 5.72 through Mamdani reasoning, and we can get behavior intention = 5.72 through fuzzy set processing. Finally, it is determined that the consumer's purchase intention for the product is close to the VT mode, which is "very inclined." Each line of

the reasoning process diagram is represented as a reasoning rule. Each rule antecedent is small, then mapped to the reasoning consequent, and then, all the reasoning consequent is large. Finally, the aggregate output membership function is obtained, and the behavior intention value is finally obtained by using the centroid method.

In the same way, we skip the consideration step of irrational emotion factors in the comprehensive emotion fuzzy calculation method which takes both rational and irrational into account. The purpose of neglecting this step is to try to conduct behavioral intention reasoning without considering irrational emotion factors, so as to make an effective comparison between them. Based on the same comment set and the same reasoning method, the clear values of the two methods are finally obtained as shown in Figure 2.

Through fuzzy set processing, it is finally determined that without considering irrational emotional factors, it can be seen that considering irrational emotional factors has a significant impact on online shopping consumer behavior intentions, and consumers' decision-making power on products is close to the PT model. The consumers are more affected by the positive irrational emotion, and their shopping behavior intention mode deviates to a certain extent, so they are inclined consumers.

4.2. Reasoning and Prediction of Decision-Making Power of Consumers in Network Groups. For product C1, we further select 51 more representative online consumers, whose oral characteristics of online comments are obvious, shopping time and scope are more extensive, and they can represent online shopping groups. Considering the comprehensive emotional factors of each consumer, the same method is used to calculate, and relevant statistics are carried out to get their purchase tendency for the product. For C2, we also select a certain amount of potential network consumption and use the same method to get their purchase tendency for this product, as shown in Figure 3.

By comparison, it can be seen that the group buying intention of C1 products is close to the VT mode, indicating
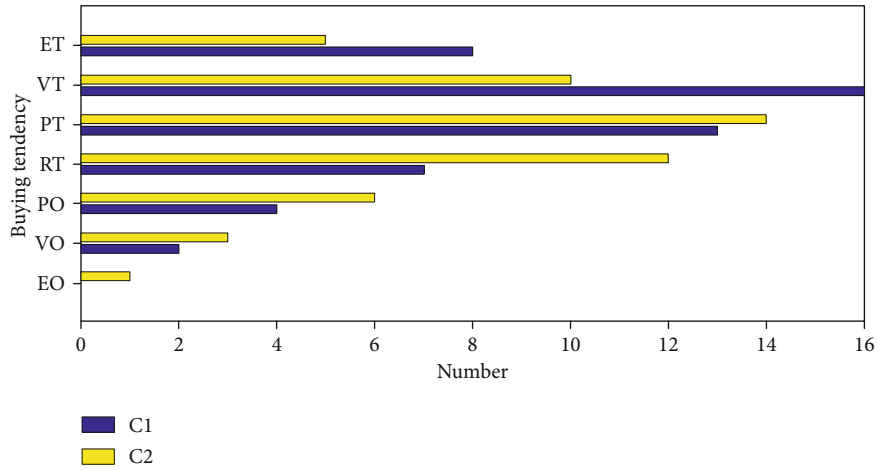
FIGURE 3: Distribution of online group purchase intention patterns.
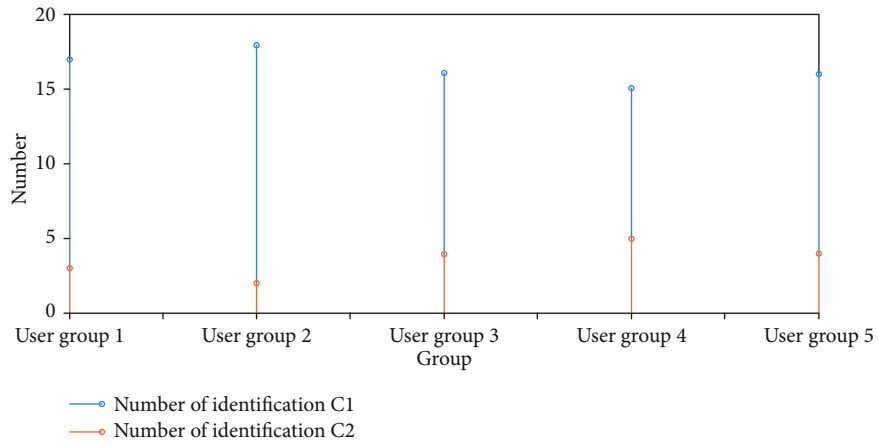
FIGURE 4: Statistical results of user group identity.

that the group buying intention of C2 products is close to the RT mode, and that the group buying intention of C1 products is relatively average. As a similar product, C1 shows a higher purchase intention than C2, indicating that C1 produces more various purchase factors and is a more attractive commodity. Therefore, most buyers prefer C1 when they choose between C1 and C2.

For the results of this fuzzy inference prediction, five groups of users who are familiar with this kind of mobile phone products participated in the evaluation process of the system prediction effect, each group of 20 people, each of them made a click choice according to their own needs and understanding of the product. The evaluation of these five user groups is equivalent to the experts of the industry, and the experts' guidance for consumers through evaluation is equivalent to fuzzy prediction, which shows the intelligence. If the user group agrees with the predicted result, it indicates that the prediction is successful; otherwise, it indicates failure. The statistical result is shown in Figure 4.

The number of identification here indicates that the prediction results of the system are consistent with the opinions of experts, while the number of disagreement indicates that the prediction results are inconsistent with the opinions of

TABLE 2: Statistical results of user group identification.

User group	Number of identification C1	Number of identification C2
User group 1	10	10
User group 2	12	8
User group 3	9	11
User group 4	13	7
User group 5	11	9

experts. In the absence of online comment data from Internet users, online shopping malls generally take sales volume and user rating as their opinions, which is reasonable and ignores the emotional needs of consumers. In order to simulate this traditional method, five groups of experts were asked to take the product sales volume, average level of play, and the number of user comments as the basis. Similarly, five-user groups click on two products, respectively, 20 people in each group, 20 times in total. The statistical results are shown in Table 2.

In Figure 5, the user's recognition of product C1 reaches 82%, while in Table 2, the user's recognition is 55%. The comparison of the two methods fully conforms to the
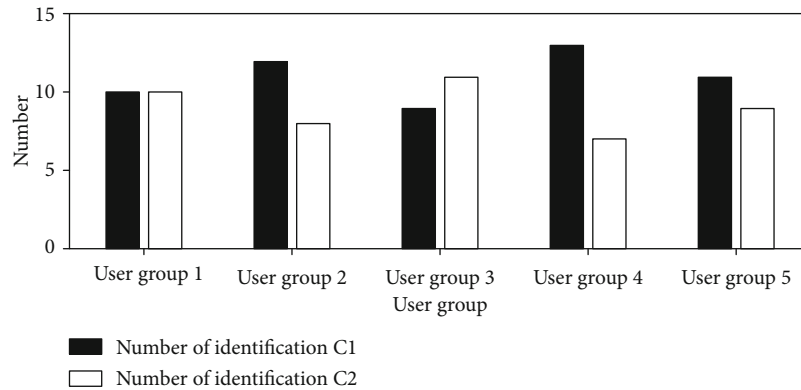
FIGURE 5: Statistical results of user group identification.

expectation in advance. The first method digs out the user's emotion and evaluation information from the comments, fully considers the personalized needs of the consumers, so it is closer to the prediction results of the system. The second method essentially recommends from the attention degree of the products and the overall quality of the products, less considers the comment information of the consumers. Therefore, there is a deviation from the predicted results.

5. Conclusions

This paper extracts consumers' online comments, uses the fuzzy attributes of natural language, calculates consumers' cognitive and emotional information with semantic fuzzy, fully considers the irrational emotional factors in online shopping, and innovatively expands rational behavior. Model and propose reasonable and irrational behavior prediction models. At the same time, the fuzzy semantic modeling is used to transfer and transform the membership function of emotional words, and a comprehensive emotional calculation method of combining rationality and irrationality is put forward innovatively. The fuzzy reasoning rules are constructed based on the subjective attitude and behavior norms of consumers in the extended model. Realize the reasoning of online buyers' purchase intention.

Finally, through case-based reasoning calculation, the distribution of three comprehensive emotional degrees of individuals and group products is calculated, and it is concluded that the comprehensive emotional degree of the group approximately obeys the normal distribution, and the average is in a more rational level. Furthermore, the reasoning of individual behavior of online consumers verifies the significant influence of considering irrational emotional factors on online shopping behavior intention. At last, the object is extended to the network purchasing group to realize the approximate reasoning of consumer group behavior. In the method in this paper, the user's recognition rate of product C1 is 82%. The method in this paper extracts the user's emotion and evaluation information from the comments, fully considers the individual needs of consumers, and is closer to the system's prediction results.

There are two main innovations in this paper. One is to make full use of the fuzzy semantic resources in online

reviews, to fully consider the irrational emotions, to put forward a behavior prediction model combining rationality and irrationality, and to give a comprehensive emotion calculation method combining the two. The second is to use the fuzzy inference system to predict the individual consumption behavior of the network and to explore the group consumption behavior of the network, which greatly enriches the traditional theory and research methods of network consumption prediction.

Data Availability

Data studies are not covered in the article.

Conflicts of Interest

The authors declare that they have no conflicts of interest.

References

[1] Y. Chen, W. Wei, and F. Liu, "CES utility function based consumer optimal decision making in heat-power market," *Dianli Xitong Zidonghua/Automation of Electric Power Systems*, vol. 42, no. 13, pp. 118–126, 2018.

[2] D. Šálková and A. Hes, "Gluten-free food-the influence of selected qualitative characteristics on consumer decision making of coeliacs in hospitality establishments," *Czech Journal of Food Sciences*, vol. 33, no. 6, pp. 513–517, 2015.

[3] J. K. Sax, "Biotechnology and consumer decision-making," *Seton Hall Law Review*, vol. 47, no. 2, p. 433, 2017.

[4] D. O'Rourke and A. Ringer, "The impact of sustainability information on consumer decision making," *Journal of Industrial Ecology*, vol. 20, no. 4, pp. 882–892, 2016.

[5] F. Rothenfluh, E. Germeni, and P. J. Schulz, "Consumer decision-making based on review websites: are there differences between choosing a hotel and choosing a physician?," *Journal of Medical Internet Research*, vol. 18, no. 6, article e129, 2016.

[6] A. Kumar, A. Vohra, and H. K. Dangi, "Consumer decision-making styles and post purchase behaviour of poor for Fast Moving Consumer Goods," *International Journal of Consumer Studies*, vol. 41, no. 2, pp. 121–137, 2017.

[7] E. B. H. Treichler and D. William, "Beyond shared decision-making: collaboration in the age of recovery from serious

mental illness," *The American Journal of Orthopsychiatry*, vol. 87, no. 5, pp. 567–574, 2017.

[8] Y. Joshi and Z. Rahman, "Predictors of young consumer's green purchase behaviour," *Management of Environmental Quality An International Journal*, vol. 27, no. 4, pp. 452–472, 2016.

[9] A. Hortaçsu, S. A. Madanizadeh, and S. L. Puller, "Power to choose? An analysis of consumer inertia in the residential electricity market," *Nber Working Papers*, vol. 9, no. 4, pp. 192–226, 2017.

[10] R. Babcock, "Medical decision-making for minors: using care ethics to empower adolescents and amend the current power imbalances," *Asian Bioethics Review*, vol. 8, no. 1, pp. 4–19, 2016.

[11] M. Zubatsky, "Relationship power in health care: science of behavior change, decision making, and clinician self-care," *Family Medicine*, vol. 50, no. 1, pp. 70-71, 2018.

[12] Y. Bao, C. Feng, and T. Xu, "Online security and stability comprehensive auxiliary decision-making of power system," *Automation of Electric Power Systems*, vol. 39, no. 1, pp. 104–110, 2015.

[13] T. Zhu, J. Ding, and X. Zheng, "A comprehensive decision-making method for power network planning schemes based on the combination of the improved TOPSIS method with Delphi-entropy weight method," *Power System Protection & Control*, vol. 46, no. 12, pp. 91–99, 2018.

[14] S. L. Lima, O. R. Saavedra, and V. Miranda, "A two-level framework to fault diagnosis and decision making for power transformers," *IEEE Transactions on Power Delivery*, vol. 30, no. 1, pp. 497–504, 2015.

[15] J. Sousa, O. R. Saavedra, and S. L. Lima, "Decision-making in emergency operation for power transformers with regard to risks and interruptible load contracts," *IEEE Transactions on Power Delivery*, vol. 33, pp. 1556–1564, 2017.

[16] P. P. Zubcsek, Z. Katona, and M. Sarvary, "Predicting mobile advertising response using consumer co-location networks," *Journal of Marketing*, vol. 81, no. 4, pp. 109–126, 2017.

[17] Y. Liu, H. Li, X. Xu, V. Kostakos, and J. Heikkilä, "Modeling consumer switching behavior in social network games by exploring consumer cognitive dissonance and change experience," *Industrial Management & Data Systems*, vol. 116, no. 4, pp. 801–820, 2016.

[18] S. Ding, S. Qu, Y. Xi, and S. Wan, "Stimulus-driven and concept-driven analysis for image caption generation," *Neurocomputing*, vol. 398, 2020.

[19] W. H. Allen, A. Rubaai, and R. Chawla, "Fuzzy neural network-based health monitoring for HVAC system variable-air-volume unit," *IEEE Transactions on Industry Applications*, vol. 52, no. 3, pp. 2513–2524, 2016.

[20] J.-Y. Yeh and C.-H. Chen, "A machine learning approach to predict the success of crowdfunding fintech project," *Journal of Enterprise Information Management*, 2019.

[21] M. Billah and S. Waheed, "Predicting closing stock price using artificial neural network and adaptive neuro fuzzy inference system (ANFIS): the case of the dhaka stock exchange," *International Journal of Computer Applications*, vol. 129, no. 11, pp. 1–5, 2015.

[22] S.-Y. Chen, C.-Y. Lee, C. H. Wu, and Y. H. Hung, "Intelligent motion control of voice coil motor using PID-based fuzzy neural network with optimized membership function," *Engineering Computations*, vol. 33, no. 8, pp. 2302–2319, 2016.

[23] M.-L. Zhou, J.-A. Zhang, and Y. Zhao, "Hybrid control for piezoelectric micro positioning platform based on BP neural network and expert fuzzy control," *Control & Decision*, vol. 33, no. 1, pp. 95–100, 2018.

[24] Y. Zhang and Q. Gao, "Comprehensive prediction model of water quality based on grey model and fuzzy neural network," *Chinese Journal of Environmental Engineering*, vol. 9, no. 2, pp. 537–545, 2015.

[25] M. Elhoseny, G.-B. Bian, S. K. Lakshmanaprabu, K. Shankar, A. K. Singh, and W. Wu, "Effective features to classify ovarian cancer data in internet of medical things," *Computer Networks*, vol. 159, pp. 147–156, 2019.

[26] Y. Deng, Z. Ren, Y. Kong, F. Bao, and Q. Dai, "A hierarchical fused fuzzy deep neural network for data classification," *IEEE Transactions on Fuzzy Systems*, vol. 25, pp. 1006–1012, 2017.

[27] S. Azali and M. Sheikhan, "Intelligent control of photovoltaic system using BPSO-GSA-optimized neural network and fuzzy-based PID for maximum power point tracking," *Applied Intelligence*, vol. 44, no. 1, pp. 88–110, 2016.

[28] Z. Lv, S. Zhang, and W. Xiu, "Solving the security problem of intelligent transportation system with deep learning," *IEEE Transactions on Intelligent Transportation Systems*, vol. 22, pp. 4281–4290, 2021.

[29] X. Xu, D. Cao, Y. Zhou, and J. Gao, "Application of neural network algorithm in fault diagnosis of mechanical intelligence," *Mechanical Systems and Signal Processing*, vol. 141, article 106625, 2020.

[30] S. K. Paul, A. Azeem, and A. K. Ghosh, "Application of adaptive neuro-fuzzy inference system and artificial neural network in inventory level forecasting," *International Journal of Business Information Systems*, vol. 18, no. 3, pp. 268–284, 2015.

WILEY | Hindawi

Research Article

Research on Query Optimization of Classic Art Database Based on Artificial Intelligence and Edge Computing

Xiang Dong [1] **and Lijia Zeng** [2]

[1]*School of Architecture and Design, Jiangxi University of Science and Technology, Ganzhou, 341000 Jiangxi, China*
[2]*Department of Art and Design, Dong-Eui University, Busanjin-gu, 47340 Busan, Republic of Korea*

Correspondence should be addressed to Xiang Dong; 9120010035@jxust.edu.cn

With the changes and development of the social era, my country's classic art is slowly being lost. In order to more effectively inherit and preserve classic art, the collection and sorting of classic art data through modern information technology has become a top priority. Database storage is a good way. However, as the amount of data grows, the requirements for computing processing power and query speed for massive amounts of data and information are also increasing day by day. Faced with this problem, this article is aimed at studying the optimization of database queries through effective algorithms to improve the efficiency of data query. Based on the traditional database query optimization algorithm, this article improves on the traditional algorithm and proposes a semi-join query optimization algorithm, which reduces the number of connection cards and the number of columns and uses the number of blocks that participate in the semi-link algorithm connection and preconnection preview and selection. And other functions reduce the size of the participating block, and the connection sent between sites reduces the cost of sending between networks. The graph data query optimization algorithm is used to optimize the graph data query in the database to reduce the extra task overhead and improve the system performance. The experimental results of this paper show that through the data query optimization algorithm of this paper, the additional task overhead is reduced by 19%, the system performance is increased by 22%, and the data query efficiency is increased by 31%.

1. Introduction

Classic art has been carrying the prosperity and replacement of the Chinese nation since ancient times and is a cultural treasure handed down by the Chinese nation. However, as the diversified development of art and the acceleration of the modernization process, coupled with the slowdown of modern attention to it, some classic art and works that have been handed down for a long time are disappearing continuously. This urgently requires us to keep up with the changes of the times, systematically collect and organize data, and establish relevant databases. To show the classic art of the Chinese clan in a new situation can better pass on the classic art. Building a database to protect relevant data more effectively is a necessary trend for modern information technology to be used in various fields. Due to the large and complex data volume of classical art inherited by China for

thousands of years and a large number of data and query operation user groups, a wide range of data queries will bring great challenges to the performance of the database and the processing cost of the database query operation. It has become a huge problem that needs to be solved urgently, and optimizing database query operations has become very important and meaningful.

In order to conduct research in the field of artificial intelligence, Pigozzi et al. made a key overview of the existence and application of the concept of "preference" in artificial intelligence. Preference is the core concept of decision-making, and it has been extensively studied in disciplines such as economics, operations research, decision analysis, psychology, and philosophy. However, in recent years, in various fields from recommendation systems to automatic planning and from nonmonotonic reasoning to computational social choice and algorithmic decision theory, it has also become

an important subject of computer science research and application, especially in the field of artificial intelligence. The survey basically covers the basic knowledge of preference modeling, the use of preference in reasoning and argumentation, the problem of compact representation of preferences, preference learning, and the use of nontraditional preference models based on extended logical language. But the concept he put forward is too advanced for modern technology to be effectively implemented [1, 2]. In order to meet the urgent needs of customers, database vendors have been pushing advanced analysis techniques into the database. Most major DBMSs use user-defined aggregation (UDA) (a data-driven operator) to implement analysis techniques in parallel. In statistical algorithms, most of the work is performed by iterative transitions in larger states. UDA alone is not enough to implement statistical algorithms and cannot be naively partitioned due to data dependence. Generally, this type of statistical algorithm first needs to be preprocessed to establish a large state and needs to be postprocessed after statistical inference. Li et al. proposed General Iterative State Transition (GIST), a new database operator for parallel iterative state transitions on large states. GIST receives the state constructed by UDA and then performs several rounds of transitions on the state until convergence. The final UDA performs postprocessing and result extraction. Li et al. believe that the combination of UDA and GIST (UDA-GIST) unifies data parallel and state parallel processing in a single system and can effectively implement statistical algorithms. However, the general iterative state transition operator they proposed may cause errors in the data during the iteration process, thereby affecting the result of the operation [3]. Moreau et al. introduced the ClusterXplain method, which is a way to help users better understand their query results. These results are constructed using a clustering algorithm and described using a personal vocabulary. They proposed a clear and vague version of this method, with the goal of finding what the elements of a cluster have in common and distinguishing them from the elements of other clusters. The data that Moreau et al. consider to characterize each answer cluster is not limited to the attributes used in the query, thus revealing unexpected relevance to users. They use natural language terms to provide users with characterization to describe the obtained clusters. But his method is too simple to meet the needs of users [4].

This article uses a distributed database to manage data. The innovations of this article are as follows: (1) Commonly used distributed query optimization techniques such as semi-join and direct join algorithms still have certain defects and room for improvement, based on the basis of query optimization technology. Making some query optimization improvements can effectively reduce database query response time and improve query efficiency. (2) Based on artificial intelligence, deep learning methods are used to determine the mapping relationship between system states and behaviors. This avoids many calculations in the augmented learning process and provides a quick solution. It is possible to send as much data as possible while reducing the loss of data packets while reducing power consumption.

2. Based on Artificial Intelligence Database Query Optimization Algorithm

2.1. Artificial Intelligence.
Artificial intelligence is an emerging technological science, which researches and develops theories, methods, technologies, and application systems for simulating and expanding human intelligence [5]. Artificial intelligence is a branch of computer science that attempts to create a new type of intelligent machine that can understand the essence of intelligence and can react in the same way as human intelligence [6, 7]. Research areas include robotics, language recognition, image recognition, natural language processing, and expert systems [8–10]. Since the birth of artificial intelligence, theory and technology have become more and more mature, and its scope is also expanding. The technological products that artificial intelligence will bring in the future can become "containers" of human wisdom. It can simulate the information processing of human consciousness and thought, not only limited to logical thinking, but also imaginative and inspirational thinking can be considered to promote the pioneering development of artificial intelligence [11]. The main content of artificial intelligence research includes knowledge representation, automatic methods of reasoning and retrieval, machine learning and knowledge acquisition, knowledge processing systems, natural language understanding, computer vision, intelligent robots, and automatic programming [6, 12]. The focus of artificial intelligence is to enable computers to perform tasks that must be completed by human advanced intellectual activities [9, 13].

2.2. Edge Computing.
Edge computing refers to the "sinking" of cloud computing functions at the network edge, which is a new computer model used with network edge devices [14]. The "end" of edge computing is the data source generated by the end of the network terminal [15, 16]. For the resources between the data paths in the cloud data center, the basic idea is to perform computer work on the computer resources near the data source. Edge computing and cloud computing are complementary to each other [17, 18]. Portable computing chip is a computing chip. The traditional wireless access network is located between the wireless access point and the wired network, which can provide end users with higher bandwidth and waiting for data service, which can save time and reduce bandwidth, data service requirements for network search [19, 20].

2.3. Deep Learning Algorithms Based on Artificial Intelligence

2.3.1. Adaptive Grouping Algorithm.
In the cognitive network, users access and send data according to the state of the channel. When the channel status is better, more data streams will be transmitted on it. Therefore, the amount of data sent on the channel will maintain a continuous and steady trend. On the other hand, a channel with a more general state will only be accessed by users when other channels are occupied, and its traffic value will show indirectness and hopping. According to the above two characteristics, the data stream is divided into two groups [21, 22]. Using adaptive grouping (AG) method to group different channel traffics,

data with similar characteristics can be grouped together. The algorithm is as follows:

$$\bar{s}^t = \frac{1}{R} \sum_{n=1}^{R} s_n^t. \tag{1}$$

Calculate the average value of the traffic on t communication channels, respectively, where t is the data on the t-th communication channel and R is the number of data on the communication channel. Calculate the variance of the traffic data on each communication channel separately and use the variance to express the volatility of the data:

$$\phi_t^2 = \frac{1}{R} \sum_{n=1}^{R} \left(s_n^t - s^t \right)^2. \tag{2}$$

According to the variance, each data stream is grouped, and the volatility is used to indicate the stability and fluctuation of the data stream. Calculate the mean variance of t data streams and use this as the threshold for grouping.

$$\bar{\phi}^2 = \frac{1}{R} \sum_{m=1}^{t} \phi_t^2. \tag{3}$$

2.3.2. Deep Learning Algorithm. When it comes to wireless data transmission, full consideration will be given to packet loss, power consumption, and system performance. In an actual wireless network, the logical assumption is that the environmental information is unknown; that is, the retransmission node cannot know in advance that environmental conditions may occur. Therefore, the system model modeled as MDP uses the amplification method of deep learning algorithms to train relay nodes to learn environmental state transition information and guide node operations [23, 24]. The strategy selection method has been improved to obtain better state behavior data to allow for the balance between exploration and use when retrieving state behavior. In addition, based on behavioral data from learning enhancements, deep learning methods are used to establish a mapping relationship between situations and behaviors to achieve the goal of rapid resolution.

$$\pi^*(e_n, v_n) = \max \sum_{e_n+1} T_{e_n e_n+1}^{v_n} (c^{\pi}(e_n + 1)), \tag{4}$$

where the T value in the learning algorithm is the evaluation value of the state and behavior, and the goal is to maximize the utility of the system.

When the scale of the system is large, how to realize the exploration and utilization of the strategy is the key issue in the deep learning algorithm. How to effectively choose behavior will directly affect the convergence speed of the algorithm and the performance of the system. This article introduces the behavior evaluation based on behavior and increases the index value to select the behavior that maximizes revenue, namely,

$$\text{Index}(e_n, v) = \ell \sqrt{\frac{2\text{In}}{P_n(m)} \min \left\{ \frac{1}{6}, c_n(m) \right\}}, \tag{5}$$

where $P_n(m)$ represents the number of times the e_n behavior is selected after m behavior selections, ℓ is a constant greater than 0, and $c_n(m)$ represents the deviation factor to reflect the volatility of the value.

2.4. Query Optimization Based on Semi-Join Algorithm

2.4.1. Cost Function. Query optimization refers to the implementation of specific optimization measures to minimize the total time and cost of the query. There are generally two basic types: one is to optimize the query response time during the query process and the other is to optimize the execution cost during the query process. Optimizing the query response means that the processing time from the delivery of the query statement to the feedback of the query result to the user should be as short as possible. The focus of cost-based optimization is to minimize the use of system resources in the query process.

The cost of a distributed execution strategy can be expressed as the total time it takes to complete the query or as the response time from the start of the query to the completion of the query. The formula for calculating the total time spent is as follows:

$$D_{\text{tt}} = D_{\text{CPU}} \times \text{its} + D_E \times E_S + D_{\text{MSG}} \times \text{msgs} + D_R \times \text{bts}, \tag{6}$$

where D_{tt} represents the total time taken to complete the query, D_{CPU} is the instruction execution time of the query command CPU, and D_E is the time spent reading and writing database data on the local disk during query execution.

When the response time becomes the main consideration performance index of the optimization program, it is necessary to comprehensively consider the problems of local processing and parallel communication. The general response time calculation method is as follows:

$$D_{Rt} = D_{\text{CPU}} \times \text{seq\_its} + D_E \times \text{seq\_}E_S + D_{\text{MSG}} \times \text{seq\_msgs} + D_R \times \text{seq\_bts}, \tag{7}$$

where seq represents the maximum number required to complete the query serially.

The selection factor is also an important statistic in the database. Its value is a real number between 0 and 1. The expression of the selection factor TK connected by the relations M and N is as follows:

$$TK(M, N) = \frac{T(M) \infty T(N)}{T(M) \times T(N)}, \tag{8}$$

where $T(M)$ represents the cardinality of the range and $T(N)$ represents the number of tuples contained.

For the intermediate results generated by the calculation query, in order to simplify the calculation amount, two simple assumptions are often made on the database, and all the

attributes in the relationship are distributed and uniform with independent attribute values.

Operation result formula is as follows:

$$T(\rho_K(M)) = TK_N(K) \times T(M). \tag{9}$$

The cardinality formula of the relations M and N is as follows:

$$T((M \times N)) = T(M) \times T(N). \tag{10}$$

The first step of query optimization is to generate the search space of the query execution plan. The second step is to select the search strategy to calculate the cost of the equivalent execution plan in the search space one by one, and select the best execution under the current search strategy from the calculated results plan.

2.4.2. Semi-Join Algorithm Query Optimization. Whether it is a central database system or a distributed database system, selection, viewing, and connection are the three most commonly used functions. There is no difference between central database and distributed database options and views, which are executed at the local site. Considering the physical distribution of the sites in the distributed database system and the subdivision characteristics of the relationship, the connection operation on it is very complicated. When the two relational objects associated with the connection operation are located on different sites, in order to complete the connection operation, data transmission between the sites is inevitable. When the two relational objects associated with the connection operation are located on different sites, in order to complete the connection operation, data transmission between the sites is inevitable. In order to reduce communication costs, the intuitive idea is to avoid unnecessary tuple transmission on the network. Especially in the wide area network, the communication cost accounts for a large part of the query cost, and the semi-join algorithm is optimized based on the idea of reducing the amount of data transmission.

The semi-join operation is derived from the projection and the connection operation. The projection operation realizes the reduction of the cardinality of the connection attribute, and the connection operation realizes the reduction of the number of tuples of the left connection relationship. Its definition and operation process semi-join (semi-join) is a reduction operation on the attribute column of the full join result. Assume that the relations M and N have the same attribute join-attr, namely,

$$
\begin{aligned}
M \infty N &= \pi_M(M \infty N) = M \infty \pi_{\text{join-attr}}(N), \\
N \infty M &= \pi_N(N \infty M) = N \infty \pi_{\text{join-attr}}(M),
\end{aligned} \tag{11}
$$

where $M \infty N$ or $N \infty M$ is the description of the semi-join operation of the relations M and N.

The semi-join operation can be understood as using another relation to reduce the number of tuples of its own relationship, and the semi-join operation does not satisfy the commutative law; that is, $M \infty N \neq N \infty M$. When per-
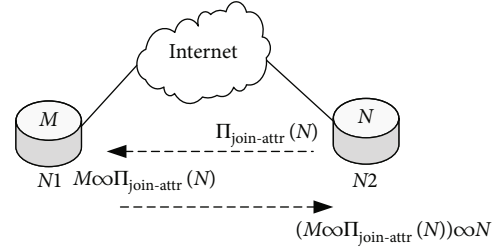
FIGURE 1: Flow chart of semi-join algorithm optimization.

forming a semi-join operation, the site information and fragmentation statistics of the database system are used to select $M \infty N$ or $N \infty M$.

The execution process of the semi-join operation includes the projection operation and the connection operation of the connection relationship. The execution process is shown in Figure 1. The execution steps of the semi-connection are shown in Figure 2.

2.4.3. Cost Estimation of Semi-Join Algorithm. It can be seen from the execution process of the semi-connection that compared to the full connection, the semi-connection has one more data transmission process than the full connection, but in most cases, the total amount of data transmitted by the semi-connection is much less than that of the full connection. At this time, the use of a semi-connected algorithm can reduce the communication cost. The estimated cost of the semi-join operation is as follows:

$$D_{\text{join-attr}} = b_0 + b_1 \times S(\text{join-attr}) \times T(M). \tag{12}$$

The case where the semi-join operation is applicable is that only a small number of tuples in the relation M participate in the connection with the relation N. At this time, the semi-join algorithm can be used to reduce the number of tuples in the relation M. When there are many connection relations, there are many types of semi-connections. At this time, it is necessary to calculate the communication cost of all semi-connection forms, select the semi-connection scheme with the least cost from them, and select the site with the least data transmission cost as the connection operation site.

2.5. Graph Data Query Optimization Algorithm

2.5.1. PageRank Hyperlink Analysis Algorithm. Traditional databases have natural advantages in processing phenotypic data, but there are many difficulties in processing graph data. In terms of query optimization, it is mainly divided into two levels: system-level optimization and application-level optimization. The PageRank algorithm uses a well-known random walk model to model the behavior of a web browser: any web browser may take two possible actions when browsing a web page. The first action is click on a hyperlink in the current webpage to jump to another webpage. The second action is to close the current webpage directly and then randomly open a new webpage in the browser to continue browsing [25, 26].
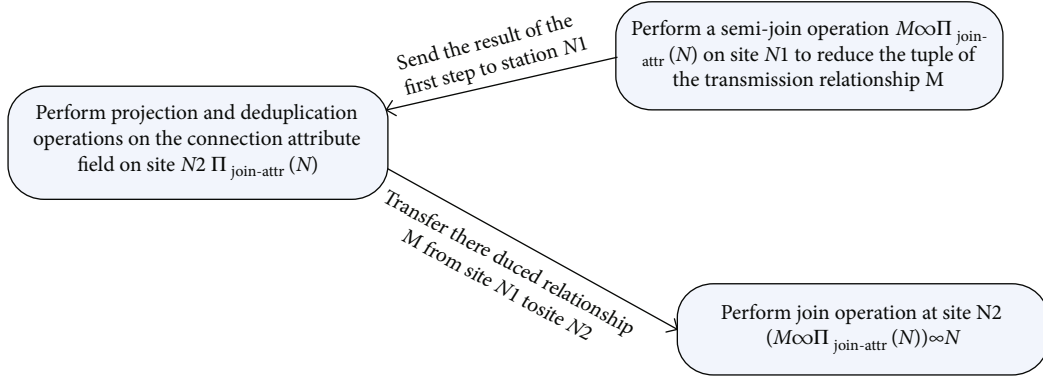
FIGURE 2: Diagram of the execution steps of the semi-connected algorithm.
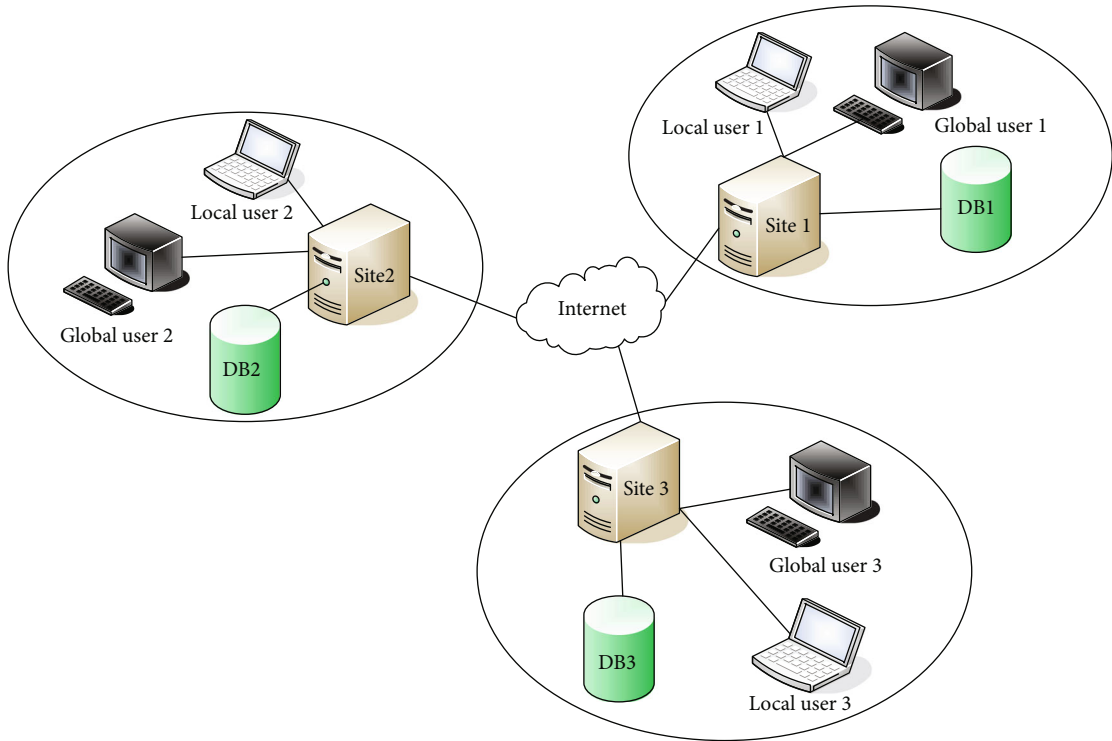
FIGURE 3: Physical structure diagram of distributed database system.

According to this random walk model, the PageRank algorithm calculates the score expression as follows:

$$GE\left(g_j\right) = \frac{1-a}{M} + a \times \sum_{g_i \in N\left(g_j\right)} \frac{GE(g_i)}{K(g_i)}, \quad (13)$$

where g_i and g_j represent each webpage, M represents the number of all webpages in the Internet, a represents the retention coefficient, $GE(g_j)$ represents the score of the webpage g_j, $N(g_j)$ represents the collection of all webpages constituting (g_j), and $K(g_j)$ represents the number of hyperlinks derived from the webpage g_j.

During the execution of the PageRank algorithm, these web pages converge slowly and require more iterations, but for most web pages, only a few generations are needed to converge to a stable score. Therefore, it is obviously not an efficient way to repeat the calculation of the entire graph for a few unconverged nodes.

Therefore, we can optimize it and only consider webpage nodes that have not yet converged in the calculation process, namely,

$$F^{t+1} = SF^t, \quad (14)$$

where the score value of each web page node is recorded in the vector F. If a distinction is made between currently converged nodes and unconverged nodes, the expression is as follows:

$$F_x^{t+1} = S_x^t \times F_x^t + S_y^t \times F_y^t, \qquad (15)$$

where F_x^t represents the set of nodes that have converged in the t-th iteration and F_x^{t+1} represents those nodes that have not converged in the t-th iteration. The matrix block S_x^t represents the connection mode from the set of unconverged nodes to the set of unconverged nodes in the graph, and some new nodes will converge in this round of iterations. Therefore, the dimension of the vector F_x will continue to shrink, and the amount of calculation for the entire algorithm will also become smaller.

3. Distributed Database Query Optimization Operation Experiment

3.1. Distributed Database. A distributed database is physically composed of multiple databases connected to each other and distributed in different physical locations [27], which can manage the data stored in each physical location independently of other physical locations, and is logically managed by the database management system. Since the data has been scattered in different physical locations, the database can be easily expanded, and distributed databases can be easily accessed from different networks [24, 28]. Compared with centralized databases, this database is more secure. The physical independence of distributed databases often triggers queries in distributed systems that span multiple sites. This includes subquery site allocation, timeline settings, and multisite query results. Issues such as merging routing make the query function of a distributed database much more complicated than that of a central database [29, 30]. The physical structure diagram of the distributed database system is shown in Figure 3.

Figure 3 shows the physical structure of a typical DDBS. Computers or servers located at various physical sites and database systems deployed on them are the basic units of distributed database systems. The sites, databases, and local users on the site are controlled by computers or servers on the site. Different site network communication links communicate, and the network can be a local area network or a wide area network.

3.2. Database Query Steps. Figure 4 is the work flow chart of the research on data query optimization in this paper. To generate the final physical query plan, the combined cost of each query operation is calculated, and the physical query plan with the smallest combined cost is selected as the final query plan, which requires every query operation to be an estimated cost is given in advance, so the establishment of the query operation cost estimation model is crucial to the correctness of the final query plan selection. The acquisition process of statistics is carried out in the preprocessing stage of the operation of the entity-based inferior data management system. It is not in the query compilation stage and does not take up the actual query time. The physical query plan is generated in the query compilation process, so we have to consider it as the time efficiency of the optimal physical query plan selection algorithm.
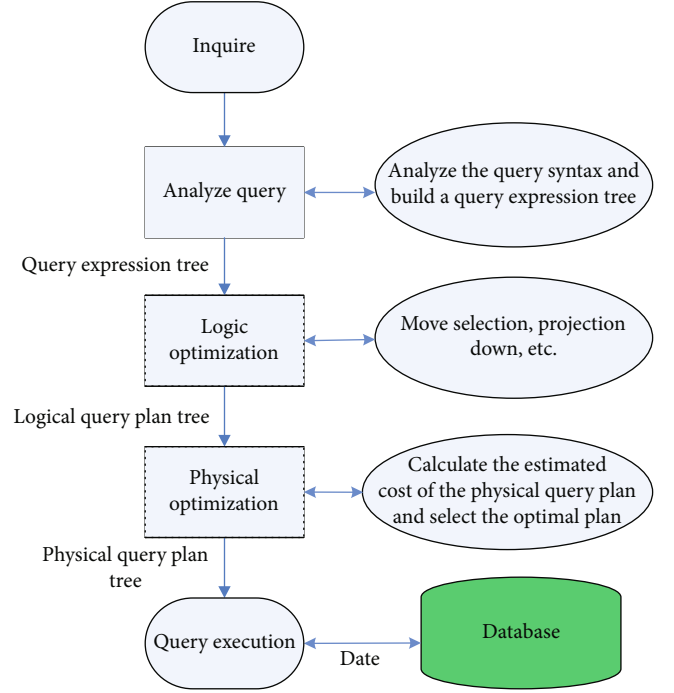
FIGURE 4: Data query optimization research work flow chart.

TABLE 1: Simulation parameter design.

Parameter	Value/description
Signal-to-noise ratio threshold (dB)	SNR $= [-1.25, -0.36, 0.79]$
Vibration length (s)	$F_d = 18$
Arrival rate	$\lambda = [0.1, 0.3, \cdots, 0.9]$
Bit error rate constraint	BER $= 10^{-3}$
Learning factor	$\theta = 0.19$
Discount factor	$\delta \in (0, 1)$

4. Database Query Optimization Algorithm Based on Artificial Intelligence

4.1. Deep Learning Algorithm Based on Artificial Intelligence. Use detailed learning methods to get the best behavior information, save it in the search panel, and then use this information to monitor SAE web training. The input part of training is the saved learned system state, and the output label part is the behavior in that state. There are many states involved in the system. It is more difficult to find an optimal decision for each state. So, use the method in this article to compare performance. The simulation parameter settings are shown in Table 1.

Figure 5 shows the average comparison of system power consumption using different data arrival rates and different algorithms. The figure shows that the RS method is relatively stable. Because the RS method is not affected by system status information, the data arrival rate basically does not affect the choice of RS transmission mode, but will greatly affect the functions of the other three methods. When the amount of data in the system is large, the pressure in the buffer becomes
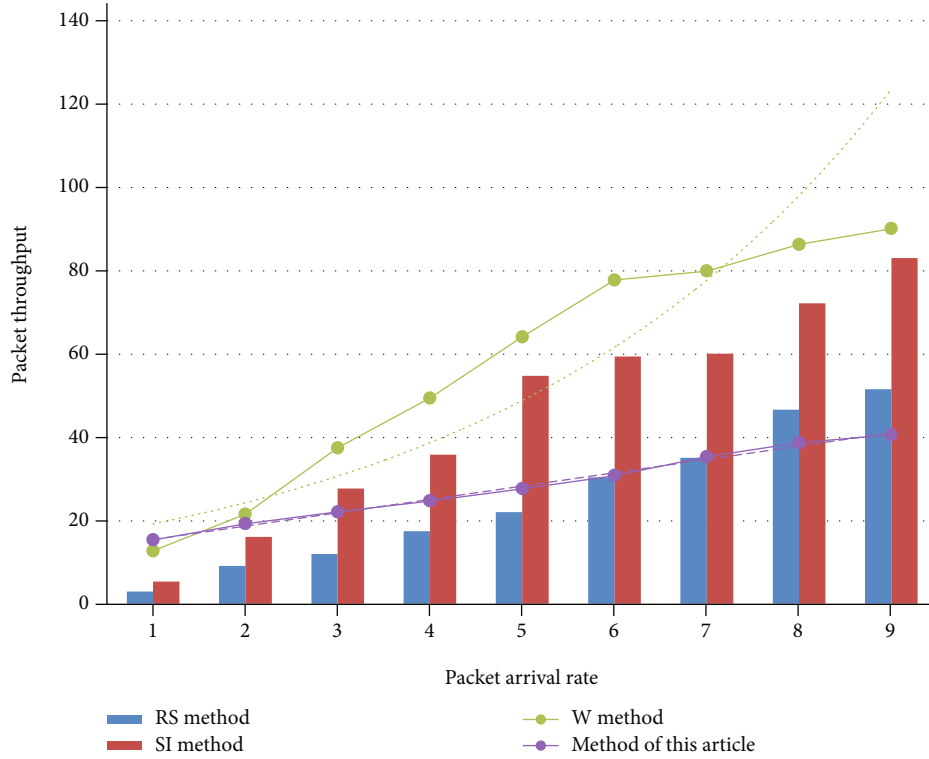
FIGURE 5: Energy consumption comparison chart.

TABLE 2: TPCH operation result graph.

Statement number	2G data before improvement	Improved 2G data	5G data before improvement	Improved 5G data
1	6.84	3.25	20.52	9.46
2	18.46	8.48	69.34	33.06
3	20.35	9.37	76.78	37.28
4	9.25	4.92	31.45	14.12
5	4.18	2.01	41.62	17.91

greater, and the relay node sends more data to reduce the pressure in the buffer and finally chooses a better transmission method to increase power consumption. The energy consumption of the three methods first showed a trend of rapid growth and then showed a moderate increase. The more data in the buffer, the more power is consumed, and the faster the power curve grows. Due to the limited cache space, when the amount of data reaches the maximum cache strength, the cache pressure will not increase, and eventually, the power consumption will stabilize.

4.2. Query Optimization Analysis Based on Semi-Join Algorithm. According to the proposed improved semi-connected algorithm, it is applied to the GreatDDB database system. In order to analyze the performance of the improved semi-connected algorithm in the database system, the performance test of the GreatDDB distributed database system with semi-connected algorithm and without semi-connected algorithm is compared. Analyze the improvement effect of the algorithm through the time taken by the system

TABLE 3: Data query improvement rate after improved algorithm.

Statement number	2G data promotion rate	5G data promotion rate
1	52.49%	53.90%
2	54.06%	52.32%
3	53.96%	51.45%
4	46.81%	55.10%
5	51.91%	56.97%

to execute the TPC-H sentence before and after the improvement of the algorithm. Execute 5 different TPCH statements in the GreatDDB environment to analyze the optimization results of the algorithm before and after the improvement.

It can be seen from Table 2 and Table 3 that the execution speed of the improved connection algorithm is significantly higher than that of the previous connection algorithm, and it takes less time to execute the same TPCH test statement; that is, it can return results faster. Improve when the amount
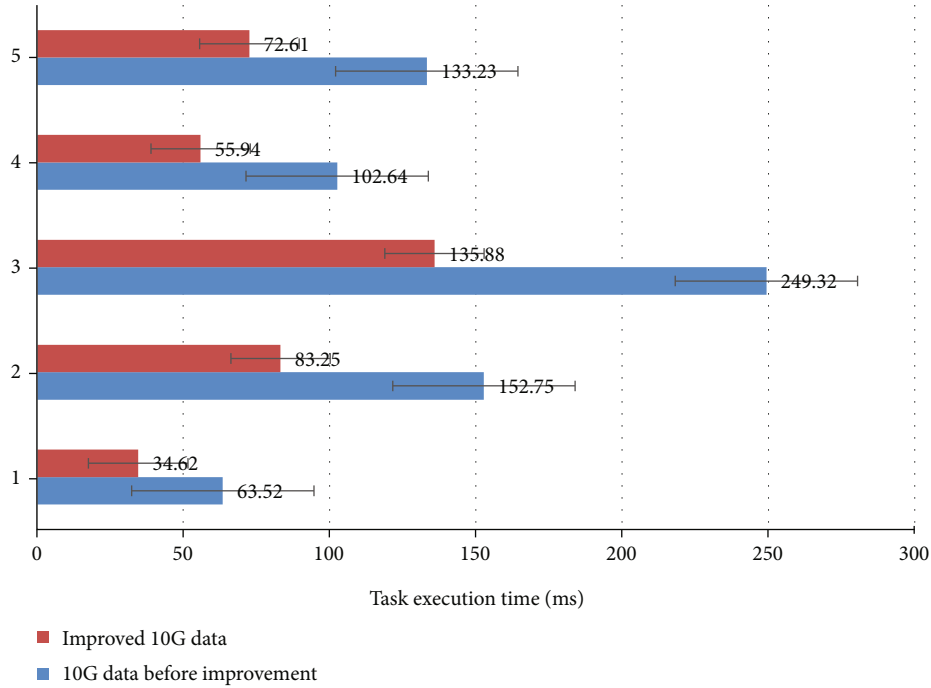
FIGURE 6: Test result comparison chart.

of data is large. The optimization effect of the latter algorithm is more obvious, because when the amount of data is large, more connection operations are involved, which shows that the connection algorithm does have practical significance in the case of multitable connection. Table 2 shows the time improvement ratio of the improved algorithm when executing test sentences. It can be seen that the improved algorithm runs better and the network transmission cost is reduced more obviously.

Figure 6 is a comparison chart of 10G data size data results, using the improved algorithm and the unimproved algorithm to execute sentences in the same amount of time. This is mainly because the statement only involves the selection and projection operations of a table, and these operations can be executed at the local site where the table line item is involved; the statement does not involve the connection operation between multiple tables, so there is no intersite table due to the data transmission cost incurred by the connection. The improved algorithm is optimized based on the multitable connection. Since only a single table is involved, the connection algorithm is not called during query execution. Therefore, when the parameter use_update_GreatDDB is equal to 0 or 1, and the amount of data is the same, there is not much difference in the time spent using improved and unimproved connection algorithms for query operations.

4.3. Graph Data Query Optimization Analysis. Perform a query experiment of graph pattern matching on the US patents data set. Construct 6 different graph pattern types (triangle, diamond, cross, hexagon, double diamond, and octagon, respectively) and then use the MATCH clause to describe and query. We choose Neo4j as the comparison object. There is no table in Neo4j, but the structure of the graph (nodes,

TABLE 4: Connection summary diagram.

Connection relationship	Number of tuples	Number of connection attribute value sets	Tuple length
RE	15	10	8
TU	40	50	5

edges, attributes, etc.) is directly stored. The Neo4j database system is completely implemented in Java language, supports standard ACID features, and also provides a query language for users to use. Among them, the description method of graph mode is very similar to the MATCH clause introduced in this article. We repeated the same experiment on Neo4j and GraphLab to compare the gap in query performance between GraphView and graph databases.

Table 4 is the statistical data table of the relationship in the graph data query. In order to implement the PageRank algorithm described above, the performance comparison and analysis of the two will be shown later.

For each graph mode, we have tested multiple sets of data. From the final result shown in Figure 7, we can see that the advantages of the graph data query optimization algorithm in this article are very obvious. The method in this paper automatically converts the graph mode equivalently, and the generated execution plan is less expensive, but in Neo4j, there is no such optimization technology. It is executed completely according to the user's input. The specific graph traversal sequence is in the database and the user. The input order in the query statement is completely the same, but because the user's input only gives a description of the graph mode, its order may not be the best performance in terms of execution efficiency, so the query performance of Neo4j is good or bad. Guarantee the best. GraphLab is a
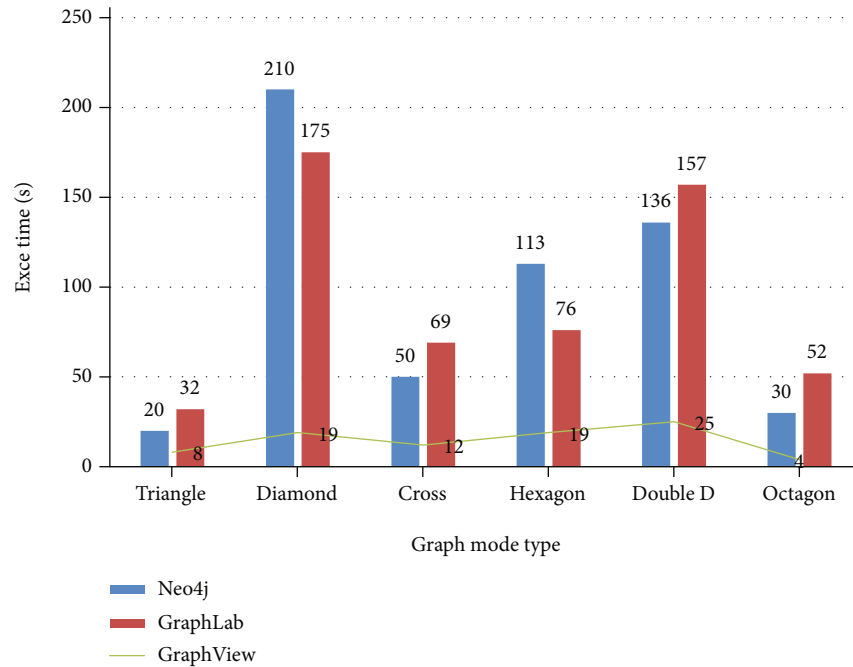
FIGURE 7: System performance comparison chart.

100	200	300	400	500	600	700	800	900	1000
73.2	125.5	163.4	219.3	241.4	333.9	362.7	437.2	479.1	541.3
107.2	167.4	201.4	229.8	295.7	326.1	389.4	418.2	483.4	660.6

FIGURE 8: Concurrent query graph for key value.

graph computing platform that supports parallel processing. It uses a node-oriented iterative computing model. It is not a graph database itself and is not responsible for storing and managing data. Graph data used in calculations is directly read from disk. The method in this paper has more prominent performance advantages when processing graph queries.

Since the algorithm designed in this article will automatically make the structure of the memory dimension table the

same as that of the dimension table in the database, there is no need to worry about the problem of data out of synchronization, and the maximum number of connections to the database is set to 1000. Now simulate multiple network users to query the value in the "ID" attribute at the same time. Because of the limitation of the experimental equipment and the experimental environment, in order to reduce the experimental error as much as possible, the number of concurrent tests for each item will be tested 50 times to find the average value. The result is shown in Figure 8. From the figure, it can be seen that the memory SQL of the query time consumption basically increases linearly with the number of concurrent user accesses; the time consumption of database SQL queries will reach more than twice the time consumption of memory SQL queries after the number of concurrent user accesses reaches 120 or more. It is proved that the algorithm designed in this paper has achieved the expected effect on the concurrent query optimization of the key value in the relational database dimension table.

5. Conclusions

This article optimizes database queries based on artificial intelligence and edge computing and uses query optimization algorithms to optimize database performance and improve query efficiency. This paper proposes a database query optimization solution for the problems in the database query data processing process, which reduces the network transmission cost to reduce the cost in the query process and optimize the data query response time. This article introduces the mechanism for implementing this optimization technique in detail and focuses on analyzing the performance advantages of this technique on storage sites. Finally, we tested and evaluated different data sets through a series of detailed experiments. The implementation results show that the query optimization algorithm shown in this article can better reflect the effectiveness and efficiency by comparing with other query optimization methods and has obvious advantages. However, this article has not invested too much research on logical query optimization, and further research is still needed.

Data Availability

The data that support the findings of this study are available from the corresponding author upon reasonable request.

Conflicts of Interest

The authors declared no potential conflicts of interest with respect to the research, authorship, and/or publication of this article.

Acknowledgments

References

[1] G. Pigozzi, A. Tsoukias, and P. Viappiani, "Preferences in artificial intelligence," *Annals of Mathematics and Artificial Intelligence*, vol. 77, no. 3-4, article 9475, pp. 361–401, 2016.

[2] L. Fabisiak, "Web service usability analysis based on user preferences," *Journal of Organizational and End User Computing*, vol. 30, no. 4, pp. 1–13, 2018.

[3] K. Li, X. Zhou, D. Z. Wang, C. Grant, A. Dobra, and C. Dudley, "In-database batch and query-time inference over probabilistic graphical models using UDA–GIST," *VLDB Journal*, vol. 26, no. 2, pp. 177–201, 2017.

[4] A. Moreau, O. Pivert, and G. Smits, "Linguistically characterizing clusters of database query answers," *Fuzzy Sets and Systems*, vol. 366, pp. 18–33, 2019.

[5] D. Hassabis, D. Kumaran, C. Summerfield, and M. Botvinick, "Neuroscience-inspired artificial intelligence," *Neuron*, vol. 95, no. 2, pp. 245–258, 2017.

[6] H. Lu, Y. Li, M. Chen, H. Kim, and S. Serikawa, "Brain intelligence: go beyond artificial intelligence," *Mobile Networks and Applications*, vol. 23, no. 2, pp. 368–375, 2018.

[7] Q. Wang and P. Lu, "Research on application of artificial intelligence in computer network technology," *International Journal of Pattern Recognition and Artificial Intelligence*, vol. 33, no. 5, article 1959015, 2019.

[8] S. Jha and E. J. Topol, "Adapting to artificial intelligence: radiologists and pathologists as information specialists," *JAMA*, vol. 316, no. 22, pp. 2353-2354, 2016.

[9] L. D. Raedt, K. Kersting, S. Natarajan, and D. Poole, "Statistical relational artificial intelligence: logic, probability, and computation," *Synthesis Lectures on Artificial Intelligence and Machine Learning*, vol. 10, no. 2, pp. 1–189, 2016.

[10] F. Zhong, J. Xing, X. Li et al., "Artificial intelligence in drug design," *Science China Life Sciences*, vol. 61, no. 10, pp. 1191–1204, 2018.

[11] N. J. Nilsson, "Artificial intelligence: a modern approach," *Applied Mechanics & Materials*, vol. 263, no. 5, pp. 2829–2833, 2003.

[12] J. Davies, "Program good ethics into artificial intelligence," *Nature*, vol. 538, no. 7625, pp. 291–291, 2016.

[13] S. Makridakis, "The forthcoming artificial intelligence (AI) revolution: its impact on society and firms," *Futures*, vol. 90, pp. 46–60, 2017.

[14] Z. Lv, D. Chen, R. Lou, and Q. Wang, "Intelligent edge computing based on machine learning for smart city," *Future Generation Computer Systems*, vol. 115, pp. 90–99, 2021.

[15] I. E. Gordon, L. S. Rothman, C. Hill et al., "The HITRAN2016 molecular spectroscopic database," *Journal of Quantitative Spectroscopy & Radiative Transfer*, vol. 130, no. 11, pp. 4–50, 2017.

[16] S. H. Yoon, S. M. Ha, S. Kwon et al., "Introducing EzBioCloud: a taxonomically united database of 16S rRNA gene sequences and whole-genome assemblies," *International Journal of Systematic and Evolutionary Microbiology*, vol. 67, no. 5, pp. 1613–1617, 2017.

[17] J. Klimešová, J. Danihelka, J. Chrtek, F. de Bello, and T. Herben, "CLO-PLA: a database of clonal and bud-bank traits of the central European flora," *Ecology*, vol. 98, no. 4, pp. 1179–1179, 2017.

[18] K. Corder, S. J. Sharp, A. J. Atkin et al., "Age-related patterns of vigorous-intensity physical activity in youth: the International

Children's Accelerometry Database," *Preventive Medicine Reports*, vol. 4, no. C, pp. 17–22, 2016.

[19] M. Gleeson, A. Hannigan, R. Jamali et al., "Using electronic medical records to determine prevalence and treatment of mental disorders in primary care: a database study," *Journal of Chromatography A*, vol. 33, no. 1, pp. 3–12, 2016.

[20] G. Wernet, C. Bauer, B. Steubing, J. Reinhard, E. Moreno-Ruiz, and B. Weidema, "The ecoinvent database version 3 (part I): overview and methodology," *The International Journal of Life Cycle Assessment*, vol. 21, no. 9, pp. 1218–1230, 2016.

[21] J. Xiao, K. A. Ehinger, J. Hays, A. Torralba, and A. Oliva, "SUN database: exploring a large collection of scene categories," *International Journal of Computer Vision*, vol. 119, no. 1, pp. 3–22, 2016.

[22] J. Gartner, D. B. Larson, and G. D. Allen, "Religious commitment and mental health: a review of the empirical literature," *Journal of Psychology & Theology*, vol. 19, no. 1, pp. 6–25, 2018.

[23] A. R. Bradlow and D. B. Pisoni, "Recognition of spoken words by native and non-native listeners: talker-, listener-, and item-related factors," *Journal of the Acoustical Society of America*, vol. 106, no. 4, pp. 2074–2085, 1999.

[24] W. Shi, J. Cao, Q. Zhang, Y. Li, and L. Xu, "Edge computing: vision and challenges," *IEEE Internet of Things Journal*, vol. 3, no. 5, pp. 637–646, 2016.

[25] J. H. Thrall, X. Li, Q. Li et al., "Artificial intelligence and machine learning in radiology: opportunities, challenges, pitfalls, and criteria for success," *Journal of the American College of Radiology*, vol. 15, no. 3, pp. 504–508, 2018.

[26] Z. Xiong, Y. Zhang, D. Niyato, P. Wang, and Z. Han, "When mobile blockchain meets edge computing," *IEEE Communications Magazine*, vol. 56, no. 8, pp. 33–39, 2018.

[27] S. Nastic, T. Rausch, O. Scekic et al., "A serverless real-time data analytics platform for edge computing," *IEEE Internet Computing*, vol. 21, no. 4, pp. 64–71, 2017.

[28] Z. Li, W. M. Wang, G. Liu, L. Liu, J. He, and G. Q. Huang, "Toward open manufacturing," *Industrial Management & Data Systems*, vol. 118, no. 1, pp. 303–320, 2018.

[29] M. Satyanarayanan, "The emergence of edge computing," *Computer*, vol. 50, no. 1, pp. 30–39, 2017.

[30] Y. Wang, M. Sheng, X. Wang, L. Wang, and J. Li, "Mobile-edge computing: partial computation offloading using dynamic voltage scaling," *IEEE Transactions on Communications*, vol. 64, no. 10, pp. 1–4282, 2016.

WILEY | Hindawi

Research Article

Segmented Cantilever and Array Configurations for Wider Frequency Band and Higher Power Generation in Piezoelectric Vibration Energy Harvester

Aicheng Zou [ID],[1,2] **Jiefeng Li,**[1] **Xingguo Han,**[2] **and Qunying Wang**[2]

[1]*State Key Laboratory of Mechanics and Control of Mechanical Structures, Nanjing University of Aeronautics and Astronautics, Nanjing 210016, China*
[2]*College of Mechanical Engineering, Guilin University of Aerospace Technology, Guilin 541004, China*

Correspondence should be addressed to Aicheng Zou; zouaicheng@guat.edu.cn

This letter reports a piezoelectric vibration energy harvester which energy conversion efficiency is significantly improved by arraying piezoelectric sheets on cantilever beams, and the operation frequency band is widened by applying two-segment cantilever beams. A prototype is developed and tested. In this case, two group piezoelectric arrays are combined on the cantilever beams with the optimum load resistance. The total output power remains above 6.54 mW within the operation frequency band ranges from 27.5 Hz to 37.5 Hz when the generator is under an acceleration of 0.7 g and reaches two power peaks: 20.5 mW at 29.2 Hz and 12.95 mW at 35.4 Hz.

1. Introduction

With the rapid development of the applications of wireless sensor networks, particular in some low-power conditions, wireless sensors with the function of converting the energy in the environment into electric energy are much desired. In recent years, vibration energy harvester (VEH) based on piezoelectric has attracted extensive attention of researchers [1–4]. Traditional VEHs are designed to work only in resonant mode so that they must be designed for specific environments, which results in narrow frequency band since environmental vibration is usually broadband and time-varying. In addition, the performance of VEHs declines drastically when the ambient vibration frequency deviates from their resonant frequency which poses a big challenge for energy collection [5]. Therefore, VEHs that with high efficiency of energy conversion and that can respond to low-frequency vibrations with a time-variant frequency broadband operation range are considered as the very promising solutions [6].

The contributions of this manuscript are as follows:

(i) Designing a two-segment cantilever beam piezoelectric vibration energy harvester (C-VEH) based on array arrangement of piezoelectric patches on the beam for improving the energy harvesting efficiency and working frequency bandwidth of the piezoelectric energy harvesting structure

(ii) Establishing the electromechanical conversion analysis model and its control equation under the influence of load coupling of piezoelectric composite cantilever vibration energy harvester and deducting the mathematical models of its output voltage and output power for analyzing the performance of piezoelectric vibration energy acquisition structure accurately

(iii) Analyzing the energy harvesting performance of C-VEH experimentally and compared with the traditional nonarray piezoelectric cantilever vibration energy harvester (T-VEH)

The rest of the manuscript is organized as follows: In Section 2, related works are discussed followed by the proposed

two-segment cantilever beam piezoelectric vibration energy harvester based on array arrangement of piezoelectric patches on the beam explanation in Section 3. Section 4 discusses the electromechanical conversion analysis model of piezoelectric composite cantilever energy harvester and its control equation with load coupling and the mathematical models of its output voltage and output power. Section 5 simulates and analyzes the C-VEH. Section 6 discusses the experimental analysis and summarizes a comparative assessment, and the manuscript is concluded in Section 6.4.

2. Related Works

Researchers have proposed several methods to improve the energy conversion efficiency and expand the band of the operation frequency of VEHs. One of the approaches is frequency tuning, such as mechanical tuning [7–11], circuit tuning, and magnetic tuning [12–15]. This strategy allows VEHs to adjust their resonant frequency according to the environmental vibration frequency. However, this would increase the complexity or consume extra energy of the VEHs. For instance, Eichhorn et al. [7] proposed a piezoelectric energy harvesting structure of cantilever beam with additional mechanical mass, which changes the resonant frequency of the structure by applying pressure or tensile force to the cantilever beam. Fan et al. [15] designed a vibration energy harvester composed of piezoelectric, stopper, and magnet. The system can tune the vibration energy harvester to a lower working frequency range by changing the gap between mass and magnets, so as to improve the efficiency of energy collection. Another approach is to use multimodal energy capture technology that has different resonant frequencies, including generator arrays [16–19] and coupled vibration [20–25]. Although coupled vibration is easy to achieve, the maximum output power of the VEH would be consequently reduced. Nabavi and Zhang [16] proposed a piezoelectric MEMS harvester with symmetrical and double clamping structure, which has multimode and nonlinear characteristics and effectively broadens the working bandwidth. Hu and Xu [20] proposed a broadband multimass and multispring piezoelectric vibration energy harvester based on folded asymmetric gap cantilever beam, which can make each stage of pure bending form multiple resonance modes. The working frequency band of the structure is widened effectively. Recently, nonlinear vibration energy harvesting approaches, for instance, the nonlinear magnetic coupling [26–32] and piecewise-linear structure [33–36], have attracted the interest of investigators. Although energy conversion efficiency of the unit volume material is decreased, operation frequency band of the VEH could be widened. The new piezoelectric structure which can broaden the frequency band and increase the efficiency of energy capture is the aim that researchers have been exploring, and it attracts a lot of researchers.

3. Description of the C-VEH Model Design

This letter reports a high-efficiency and broadband vibration energy harvester based on the structure of two-segment can-tilever beams with piezoelectric array configuration structure (C-VEH), as shown in Figure 1. Figure 1(a) is the model of the C-VEH, and Figure 1(b) is the proposed C-VEH design which includes the side view and top view of the structure. The proposed C-VEH consists of primary cantilever beam (the 1st), secondary cantilever beam (the 2nd), and two suspended masses M1 and M2. The left end of the 1st is fixed to the base of the structure, and the mass M1 is suspended from the right end of the 1st. The right end of the 2nd is fixed to M1, and the mass M2 is then suspended to the left end of the 2nd. There are two piezoelectric sheets of the same size attached on the upper surface of each cantilever beam. The base of the structure is fixed on the excitation platform.

The operation frequency band of the C-VEH is widened by applying two-segment cantilever beams. The structure of two-segment cantilever beams has two close resonant frequencies, which responds to ambient low-frequency vibration. To improve the energy capture efficiency, the piezoelectric arrays isolated by gaps are installed on the cantilever beams and electrically independent from each other.

4. Theoretical Analysis

4.1. The Governing Equation. For the vibration energy harvester of piezoelectric composite cantilever beam (VEH) shown in Figure 2, the traditional method is to use lumped parameter for modeling. The system is equivalent to the lumped parameter model composed of mass, stiffness, damping, and piezoelectric (as shown in Figure 3), in which the mass (M) is on the spring with stiffness K, the damper with coefficient (η), and the piezoelectric element with piezoelectric coefficient Θ, the electric field is along the thickness direction of the piezoelectric layer, and the piezoelectric layer works in d_{31} mode.

The main limitation of the model is that it assumes the motion characteristics of the piezoelectric cantilever are independent of the load, that is, it belongs to the state of no-load coupling. But the actual situation is due to the physical characteristics of the piezoelectric structure; system vibration leads to the electricity generated by the piezoelectric layer, and after the load consumption, it will have an impact on the stiffness of the piezoelectric layer itself, which is reflected by the piezoelectric circuit coupling.

Therefore, considering the load coupling effect, the traditional lumped parameter model is improved to predict the dynamic characteristics of VEH more accurately. The equivalent model of the system is shown in Figure 4. The lumped parameters in the equivalent model include equivalent mass (M_{eq}), equivalent stiffness (K_{eq}), system damping (η), equivalent current source ($\Theta\dot{z}(t)$), and equivalent capacitance (C_{eq}) (the upper and lower piezoelectric parts are connected in series), the external circuit includes rectifier bridge, rectifier capacitor (C_o), and load (R). The piezoelectric part is the link between the load part and the vibration part, which is equivalent to two parts equivalent current source ($\Theta\dot{z}(t)$) and equivalent capacitance (C_{eq}).

The control equation of the equivalent model of VEH under the influence of load coupling shown in Figure 4 is as
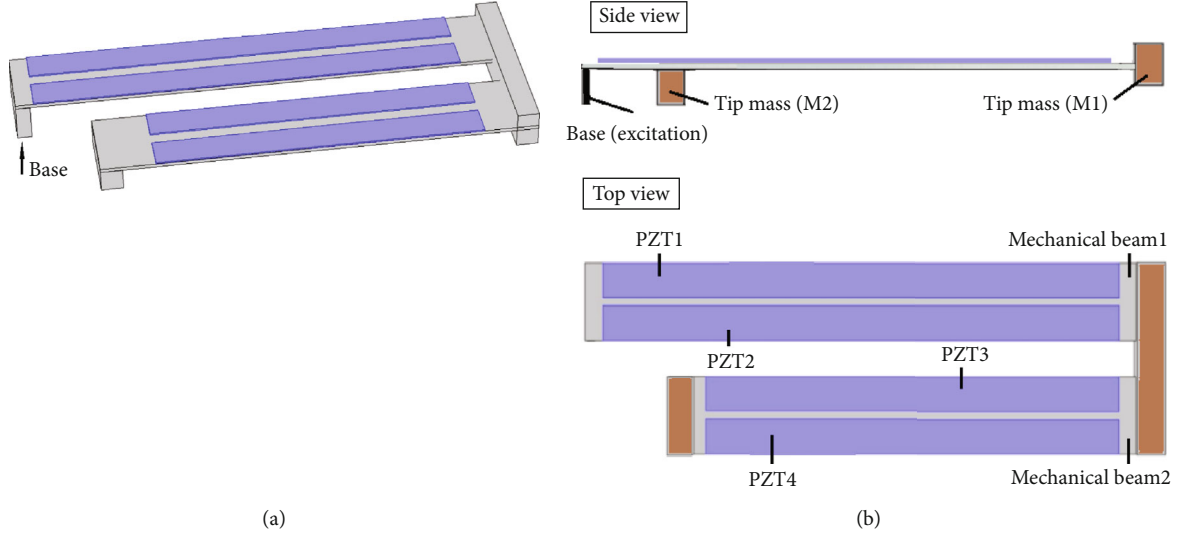
FIGURE 1: Structure of C-VEH: (a) mode of C-VEH; (b) the proposed C-VEH design.
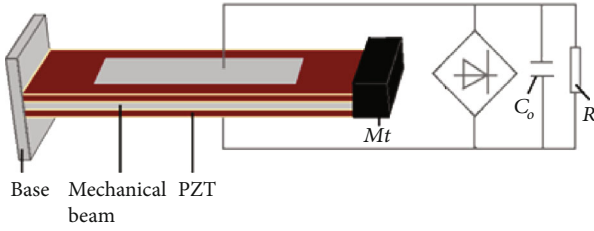
FIGURE 2: Structure diagram of energy harvester of piezoelectric composite cantilever.
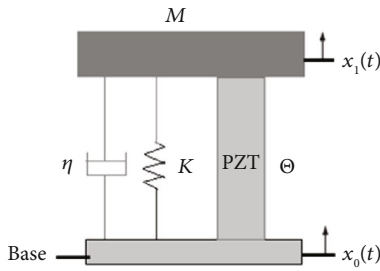
FIGURE 3: The traditional lumped parameter mode.
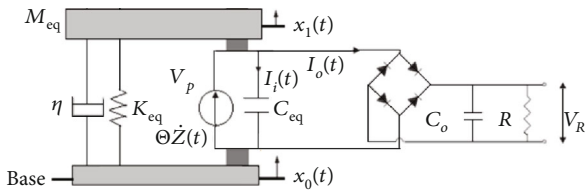
FIGURE 4: VEH equivalent analysis model with load coupling influence.

follows [37]:

$$M_{eq} * \ddot{x}_1(t) + \eta * [\dot{x}_1(t) - \dot{x}_0(t)] + K_{eq} * [x_1(t) - x_0(t)] = 0,$$

(1)

$$\Theta * \dot{z}(t) = I_i(t) + I_o(t),$$

(2)

where

$$z(t) = x_1(t) - x_0(t),$$
$$I_i(t) = C_{eq} * \dot{v}_P(t),$$
$$I_o(t) = \frac{V_R}{R} + C_o * v_R(t).$$

(3)

Equations (1) and (2) are the governing equation of the system considering the influence of load coupling, and $z(t)$ is the displacement of the cantilever beam relative to the base. Combined with the motion boundary conditions of the system, the vibration displacement, output voltage, and output power of VEH can be further solved.

4.2. Output Voltage and Vibration Displacement Response. The excitation source of the system is a sine function, and the vibration displacement response of the cantilever beam can also be regarded as a sine function. It is obvious that $z(t)$, $v_P(t)$, and $v_R(t)$ in equation (2) are also sine functions. By integrating the two sides of equation (2), we can get the following:

$$\int_a^b \Theta * \dot{z}(t)dt = \int_a^b C_{eq} * \dot{v}_P(t)dt + \int_a^b C_o * v_R(t)dt + \int_a^b \frac{V_R}{R}dt.$$

(4)

According to the method, [37] can solve equation (4), that is, let $b - a = T/2$ (T is the period of sine function) in equation (4), and $z(t)$, $v_P(t)$, and $v_R(t)$ be the minimum

and maximum at the points a and b, respectively. Let $z(t) = Z_0 \sin \omega t$, $v_P(t) = V_P \sin \omega t$, and $v_R = V_R \sin \omega t$, and after the system is stable, $\int_a^b C_{eq} * \dot{v}_P(t)dt = 0$, $V_P = V_R$. From equation (2), it can be concluded that

$$2\Theta Z_0 = 2C_{eq}V_R + \frac{T}{2}\frac{V_R}{R}. \tag{5}$$

Since $\omega = 2\pi/T$, so

$$V_R = \frac{R\omega\Theta}{C_{eq}\omega R + \pi/2}Z_0. \tag{6}$$

Equation (6) reflects the relationship between the amplitude of vibration displacement response and the amplitude of output voltage. By solving Z_0, V_R can be obtained, and then, the power of the load can be obtained.

4.3. Amplitude of Vibration Displacement Response. Let $x_0(t) = X_0 e^{j\omega t}$, $x_1(t) = X_1 e^{j\omega t}$, and $z(t) = Z_0 e^{j\omega t} = X_1 e^{j\omega t} - X_0 e^{j\omega t}$, where X_0, X_1, and Z_0 are the amplitudes of the response of the excitation source and the cantilever beam, respectively. By substituting them into equation (1), we can get the following results:

$$M_{eq} * \left(-\omega^2 X_0 e^{j\omega t}\right) + \eta * \left[jwX_1 e^{j\omega t} - jwX_0 e^{j\omega t}\right] + K_{eq} * \left[X_1 e^{j\omega t} - X_0 e^{j\omega t}\right] = 0. \tag{7}$$

By solving equation (7), the following results can be obtained:

$$Z_0 = \frac{\omega^2 M_{eq}}{j\omega\eta + K_{eq} - \omega^2 M_{eq}}X_0. \tag{8}$$

In equation (8), X_0 and Z_0 are the amplitude of vibration displacement response of excitation source and cantilever beam, respectively. Let

$$\omega = \sqrt{\frac{k_{eq}}{M_{eq}}}, \xi = \frac{\eta}{2\sqrt{K_{eq}M_{eq}}}, \Delta = \frac{\omega}{\omega_n}. \tag{9}$$

By substituting (9) into equation (8), we can get the following results:

$$Z_0 = \frac{\Delta^2}{1 - \Delta^2 + 2j\xi\Delta}X_0. \tag{10}$$

4.4. Output Voltage and Power. Substituting equation (10) into equation (6), the output voltage of the load can be obtained. That is,

$$V_R = \frac{R\omega\Theta}{C_{eq}\omega R + \pi/2} \times \frac{\Delta^2}{1 - \Delta^2 + 2j\xi\Delta}X_0. \tag{11}$$

TABLE 1: The parameters of VEH.

Object	Parameters	Value
	Material	Aluminum
	$l \times b \times t_m$ (mm)	$80 \times 20 \times 0.5$
Elastic layer	ρ_p (kg/m³)	2700
	E_m (GPa)	70
	Material	PZT-51
	$l \times b \times t_m$ (mm)	$80 \times 20 \times 0.2$
Piezoelectric layer	ρ_m (kg/m³)	7500
	E_P (GPa)	56
	ε_{33}^s (10^{-8} F/m)	3.01
	e_{31} (10^{-3} N/Vm)	8.4

The output power of the system is as follows::

$$\begin{aligned}P = \frac{V_R^2}{R} &= \left[\left[R\omega\Theta/\left(C_{eq}\omega R + \frac{\pi}{2}\right)\right]\right.\\ &\quad \left.\times \left[X_0\Delta^2/\left(1 - \Delta^2 + 2j\xi\Delta\right)\right]\right]^2/R\\ &= R \times \left[\frac{\Delta\omega_n\Theta}{C_{eq}\Delta\omega_n R + \frac{\pi}{2}} \times \frac{\Delta^2}{1 - \Delta^2 + 2j\xi\Delta}X_0\right]^2.\end{aligned} \tag{12}$$

Equation (12) is the amplitude expression of the output power of the system with the influence of load coupling and simple harmonic vibration excitation, which reflects the power generation capacity of VEH and can be used as the basis for the structural optimization design of the system. It can be seen that P is not only related to the geometry and material parameters of the system but also related to the external environmental conditions (frequency ω and amplitude X_0 of the excitation signal, frequency ratio Δ (ratio of the excitation frequency to the first natural frequency of the system), and load R), in which the frequency ratio is $\Delta = \omega/\omega_n$. Therefore, when the system structure size and the amplitude of the excitation signal are determined, the power generation of the piezoelectric composite cantilever vibration energy harvester is essentially related to the ω and R. Equation (12) can be rewritten as follows:

$$P = f(\omega, R). \tag{13}$$

According to equation (13), the optimal matching resistance of the system can be obtained when other structural factors and the frequency of the excitation signal are determined, that is, the R^{opt} obtained by solving equation (14). The optimal excitation frequency of the system can also be obtained when the load is determined, that is, get ω^{opt} obtained by solving equation (15).

$$\frac{\partial}{\partial R}f(\omega, R)|_{\omega} = 0, \tag{14}$$

$$\frac{\partial}{\partial \omega}f(\omega, R)|_R = 0. \tag{15}$$
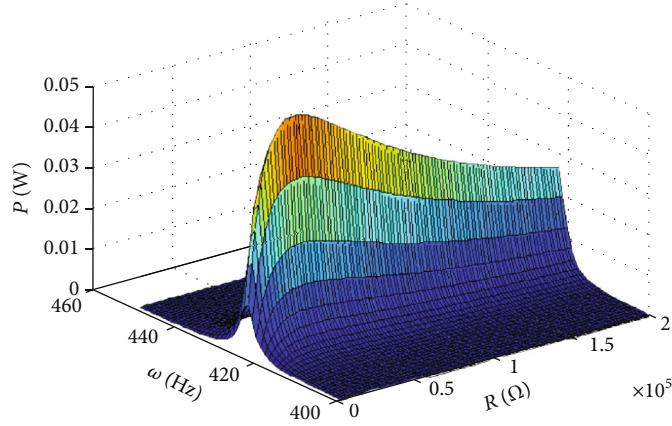
FIGURE 5: $P—(\omega, R)$.

TABLE 2: Parameters of the C-VEH Investigated in this letter.

		Primary cantilever beam	Secondary cantilever beam
Piezoelectric layer (PZT)	Dimension ($l \times w \times t$) (mm)	$60 \times 5 \times 0.2$ (PZT1, PZT2)	$45 \times 5 \times 0.2$ (PZT3, PZT4)
	Material	Ceramic PZT-5H (Lead zirconate titanate)	
	Density (10^3 kg/m^3)	7.5	
	Young's modulus (GPa)	66	
Mechanical beam	Dimension ($l \times w \times t$) (mm)	$70 \times 11 \times 0.6$	$60 \times 11 \times 0.6$
	Material	Aluminum	
	Density (10^3 kg/m^3)	2.7	
	Young's modulus (GPa)	60	
Proof mass	Material	Fe (iron)	
	Weight (g)	5.06 (M1)	2.89 (M2)

4.5. Numerical Calculation. A vibration energy harvesting structure (VEH) is constructed, in which the middle is an elastic layer, and the upper and lower surfaces of the elastic layer are covered with piezoelectric layers. The parameters of VEH are shown in Table 1.

The first-order natural frequency of the system is estimated to be about 420 Hz. The optimal load $R^{opt} = 0.28 \times 10^5 \, \Omega$ can be calculated from equation (14). Therefore, according to equation (13), the influence of frequency (ω) and load (R) of excitation signal on VEH output power is numerically analyzed by MATLAB. The frequency scanning range of excitation signal is 400~460 Hz, and the scanning range of load is $0 \sim 2 \times 10^5 \, \Omega$. The results are shown in Figure 5, and it can be seen that when R is fixed, P first increases and then decreases with the increase of ω. When $\omega^{opt} = \omega_n$, the output power reaches the peak. When ω is fixed, P first increases and then decreases with the increase of R, and there is an optimal load $R^{opt} = 0.28 \times 105 \Omega$ to maximize the output power.

5. Finite Element Simulation Analysis

A C-VEH is developed using the aluminum sheet and the Lead zirconate titanate (PZT-5H). The resonant frequencies of the proposed C-VEH are closely related to the length,

thickness, and weight of the cantilever beams, which are around 30 Hz, and the band of the resonant frequencies is about 6 Hz. The length of primary cantilever beam ($l = 70$ mm) is selected in accordance with the specific application situation of the structure, and the dimensions of the other parts of the C-VEH are designed to achieve the requirements of resonant frequencies and band, respectively, as shown in Table 2.

The vibration modes and the resonant frequencies of the C-VEH are analyzed via finite element simulation (by COMSOL Multiphysics®). The material and size of piezoelectric structure are shown in Table 2. The setting of the COMSOL software is as follows: damping ratio is 0.01 and scanning frequency range is 20 Hz-40 Hz. The results of the first two resonant modes shown in Figure 6(a) demonstrate the displacement of the beams, two peaks appear at the first two open circuit resonant frequencies (28.01 Hz and 34.02 Hz, respectively) of C-VEH, and operating frequency bandwidth of which is 6.01 Hz. In the first resonant mode (Figure 6(b)), the deformations of the free ends of the 1st beam and the 2nd beam are significant, and the largest stresses occurs at the left end of the 1st beam and right end of the 2nd beam. Figure 6(c) shows that the left end of the 2nd beam has a significant deformation while the 1st beam has deformed in the second mode as well. Also, noticed that
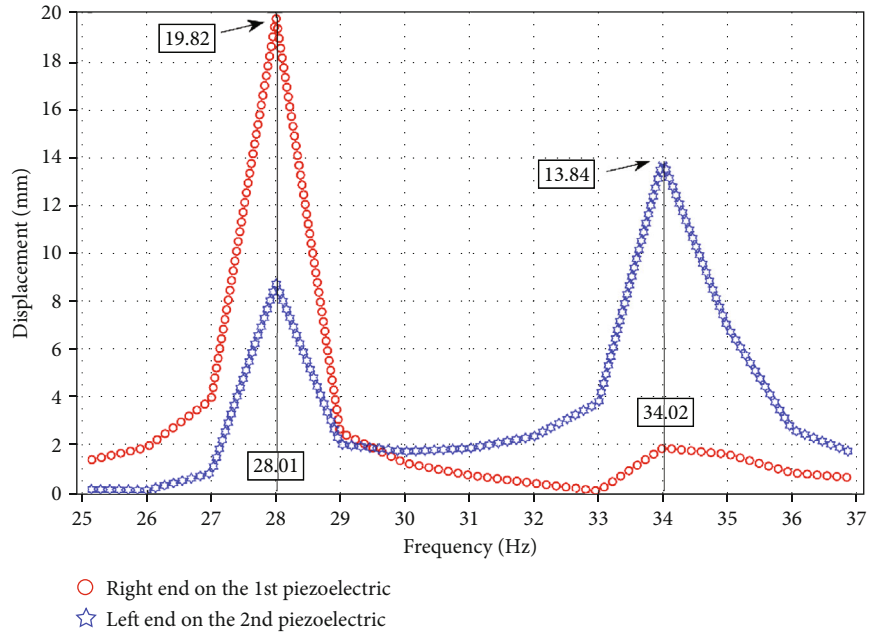
(a)
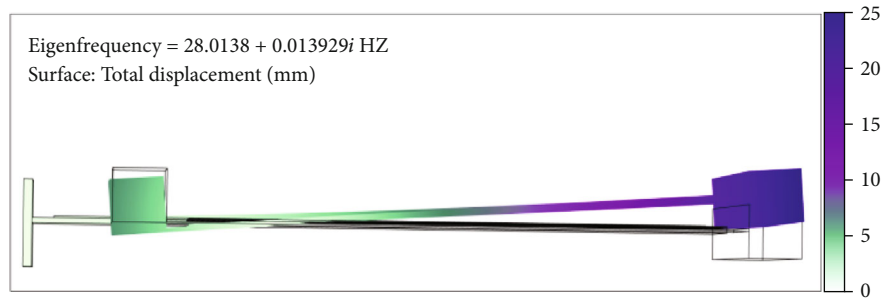
(b)
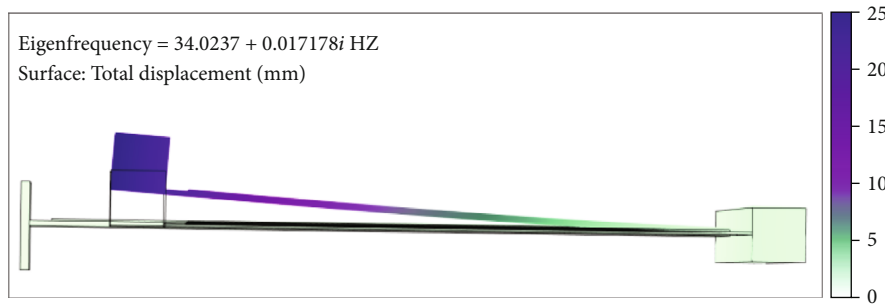
(c)

FIGURE 6: The simulation results of the first two resonant modes of the C-VEH structure: (a) displacement; (b) the first resonant mode; (c) the second resonant mode.

the C-VEH is continuously operating effectively at the frequencies that between the two modes.

6. Experimental Analysis

6.1. Experimental Scheme. A prototype device with the design parameters as shown in Table 2 is constructed to evaluate its power generation capability. As shown in Figure 7, upper face of each beam is bonded with two separated piezoelectric sheets. Four piezoelectric sheets connected in parallel and are equipped with electric terminal numbered #1, #2, #3, and #4, respectively, and another common ground terminal (#0). The electric terminals (#1, #2, #3, and #4) are individually connected to the terminal of load resistors R1, R2, R3, and R4, respectively. The experimental platform (Figure 7) consists of a signal generator (AFG3210C, Tektronix), a power amplifier (YE5871A), a shaker (YE5871), an external resistor box, an accelerometer (Model752A13, Endevco), and a
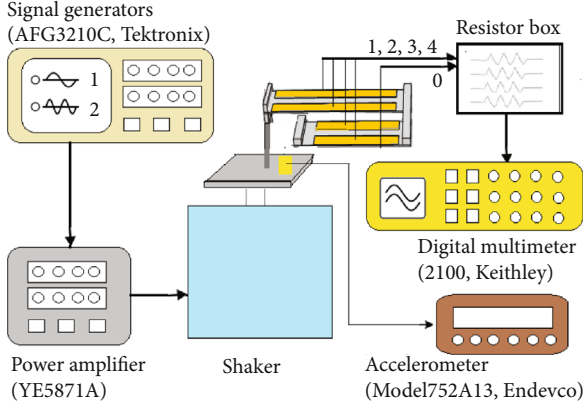
FIGURE 7: Schematic of the experimental setup.

FIGURE 9: The output power of the C-VEH versus the excitation frequency at each optimum load resistance, acceleration = 0.7 g.

FIGURE 8: The output power of the C-VEH versus the load resistance at each resonant frequency, acceleration = 0.7 g.

digital multimeter (2100, Keithley). The C-VEH is assembled on a shaker with a reference accelerometer measuring the acceleration. The signal generator produces the sinusoidal signal that is intensified by a power amplifier to drive the shaker. The root mean square of output voltage (V_{rms}) of the C-VEH is measured by the digital multimeter. The total output power of the C-VEH can be calculated by the following:

$$P_{tol} = \sum_i^n P_i = \sum_i^n \frac{V_{rms(i)}^2}{R_i}, \qquad (16)$$

where P_{tol}, P_i, and $V_{rms(i)}$ are the total output power, the output power of the ith piezoelectric sheet, and the output root mean square voltage of the ith piezoelectric sheet, respectively.

6.2. Optimal Load Resistance.

6.2. Optimal Load Resistance. Experiments are carried out to determine the optimum load resistance of each C-VEH piezoelectric in the case of resonance since the output power of piezoelectric vibration energy harvester is closely related to load resistance. It can be seen from equation (13) that when other parameters are determined, the output power of the piezoelectric vibration energy collector is related to the excitation frequency and load. The reason for the existence of the optimal load is that the piezoelectric structure can be equivalent to a current source with internal resistance. According to the circuit principle, the change of the load has a significant impact on its output power, and there is an optimal load to maximize its output power. According to equation (14), the optimal matching load (R^{opt}) of the structure can be calculated theoretically. When measuring the (R^{opt}) of the structure, first, sweep the excitation frequency from 10 Hz to 200 Hz (step size is 0.2 Hz); the maximum output power is obtained when the C-VEH closed-loop resonance frequency is 29.2 Hz and 35.4 Hz, and the error is less than 5% compared with the simulation results. Then, the optimal matching load of PZT1/PZT2 is measured. The experimental method is to set the excitation frequency at 29.2 Hz; connect the external load to PZT1/PZT2, and take the measuring points in logarithmic manner within the range of load resistance $1 \times 10^3 \sim 1 \times 10^6$. The optimal matching load of PZT1/PZT2 is roughly between $1 \times 10^4 \sim 1 \times 10^5$ pairs, and in this range, twenty resistance points are measured, and the optimal matching load is in the range of 15 KΩ-22 KΩ. Finally, the excitation frequency is set at 35.4 Hz, and the optimal matching load of PZT3/PZT4 is in the range of 50 KΩ-70 KΩ. The experimental results are shown in Figure 8, which exhibit the optimum load resistance range of PZT1/PZT2 and PZT3/PZT4 (15 KΩ-22 KΩ
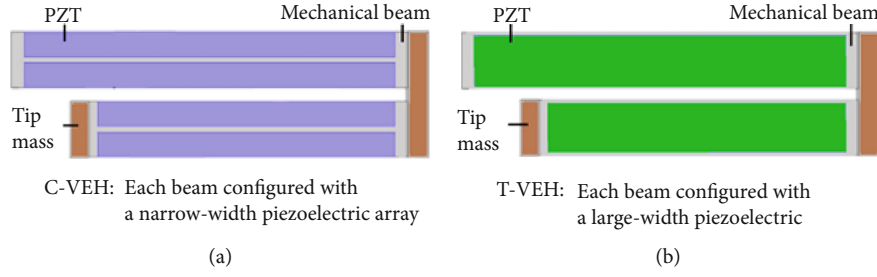
Figure 10: The C-VEH and T-VEH design.
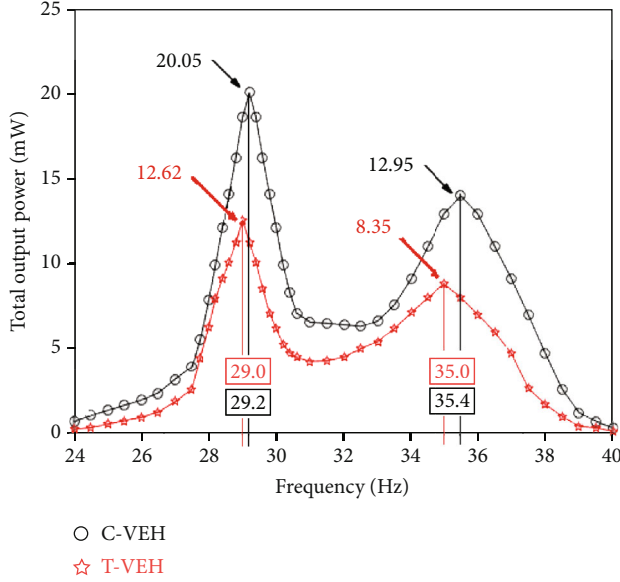
Figure 11: The total output power of C-VEH and T-VEH changing with the excitation frequency under their optimal load resistance, acceleration = 0.7 g.

at the first resonant frequency of 29.2 Hz and 50 KΩ-70 KΩ at the second resonant frequency of 35.4 Hz, respectively).

6.3. Output Power.
The output power of the prototype is tested with each electric terminal in parallel and connecting to the optimum load resistance. It can be seen from equations (14) and (15) that when other parameters are determined, the output power of the piezoelectric vibration energy harvester is related to the excitation frequency after matching the optimal load, and when the system is in the resonant frequency region, it can obtain larger output power. According to the results of the previous optimal matching load experiment, in the process of the experiment, PZT1/PZT2 is connected with a load of 20 KΩ, and PZT3/PZT4 is connected with a load of 60 KΩ. Then, apply excitation signal to the system (the amplitude is 0.5 mm, the frequency scanning range is 20 Hz-40 Hz and the step is 0.5 Hz, and the acceleration is 0.7 g) and measure the output power of PZT1/PZT2 and PZT3/PZT4.

The corresponding relationship between the output power and the excitation frequency is shown in Figure 9. The C-VEH achieves two total output power (P_{tol}) peaks (20.5 mW and 12.95 mW) at frequencies of 29.2 Hz and

35.4 Hz. When the excitation frequency is lower than 29.2 Hz or higher than 35.4 Hz, P_{tol} decreases sharply. As the excitation frequency sweeping from 27.5 Hz to 37.5 Hz, P_{tol} keeps above 6.48 mW, which is about the half of the peak power outputs. The half-peak-power frequency bands of the designed structure are 27.8-30.6 Hz and 30.6-37.4 Hz, respectively.

6.4. Discussion.
For comparison between the proposed C-VEH of narrow-width piezoelectric arrays (Figure 10(a)) and a traditional large-width piezoelectric structure named T-VEH shown in Figure 10(b), experiment on a T-VEH with the width of piezoelectric sheet on its primary beam is the sum of the widths of the two piezoelectric sheets on C-VEH primary beam and the width of the piezoelectric sheet on its secondary beam is the sum of the widths of those on the C-VEH secondary beam is conducted. Firstly, the optimal matching resistance of PZT on the primary beam and secondary beams of T-VEH is measured, and the results are 8 KΩ-15 KΩ and 25 KΩ-30 KΩ. Then, the primary beam is matched with a load of 10 KΩ, and the secondary beam is matched with a load of 30 KΩ. And then, apply excitation signals to the two systems, respectively (the amplitude is 0.5 mm, the frequency scanning range is 20 Hz-40 Hz and the step is 0.5 Hz, and the acceleration is 0.7 g), and measure the corresponding situation of the total output power with the excitation frequency. The results are in Figure 11, which shows the comparison of total output powers between C-VEH and T-VEH with respect to the excitation frequency and under their optimal load resistance. For T-VEH, two total output power peaks (12.62 mW and 8.35 mW) occur at the first two resonant frequencies (29.0 Hz and 35.0 Hz), the corresponding optimum load resistance are 10 KΩ and 30 KΩ, respectively, and the half peak power bands are 28.0 Hz-30.6 Hz and 30.8 Hz-37.2, respectively. For C-VEH, two total output power peaks (20.05 mW and 12.95 mW) occur at the first two resonant frequencies (29.2 Hz and 35.4 Hz), the corresponding optimum load resistance are 20 KΩ and 60 KΩ, respectively, and the half peak power bands are 27.8 Hz-30.6 Hz and 30.6 Hz-37.4, respectively. Table 3 shows the comparison of experimental results of the T-VEH and C-VEH. By 1/2-width configuring the piezoelectric sheets, the first two resonant frequencies of both structures almost remain the same, the optimal matching resistance increases, the total output power increases, and the two harmonic response peaks increase by 58.88% and 55.09%, respectively. That is to say, narrow-width

TABLE 3: Comparison of experimental results of the C-VEH and the T-VEH.

	Acceleration (g)	Half peak band 1			Half peak band 2			Optimum load resistance (KΩ) of 1st, 2nd
		Frequency band (Hz)	Center frequency (Hz)	Total output power peak (mW)	Frequency band (Hz)	Center frequency (Hz)	Total output power peak (mW)	
T-VEH	0.7	3.0	29.0	12.62	6.8	35.0	8.35	10 KΩ, 30 KΩ
C-VEH	0.7	2.8	29.2	20.05	6.8	35.4	12.95	20 KΩ, 60 KΩ

piezoelectric array configuration on the beams displays better power generation capability.

7. Conclusion

In summary, a vibration energy harvester based on the structure of two-segment cantilever beam with piezoelectric array configuration for low-frequency vibration energy harvesting has been studied in this letter, which energy conversion efficiency is significantly improved by arraying piezoelectric sheets on cantilever beams, and the operation frequency band is widened by applying two-segment cantilever beams. Our investigation provides a way to improve the energy conversion efficiency and broaden the operation frequency band of piezoelectric vibration energy harvesting structures. The follow-up work is to theoretically discuss and explain why the harvested power by T-VEH is less than C-VEH, that is to say, why energy conversion efficiency is significantly improved by arraying piezoelectric sheets on cantilever beams, and design efficient energy storage circuits.

Data Availability

There is no data available for this article.

Conflicts of Interest

The authors declare that they have no conflicts of interest.

Acknowledgments

References

[1] J. W. Matiko, N. J. Grabham, S. P. Beeby, and M. J. Tudor, "Review of the application of energy harvesting in buildings," *Measurement Science and Technology*, vol. 25, no. 1, article 012002, 2014.

[2] J. Abdelkefi, M. Scanlon, E. McDowell, and M. R. Hajj, "Performance enhancement of piezoelectric energy harvesters from wake galloping," *Applied Physics Letters*, vol. 103, no. 3, article 033903, 2013.

[3] L. Tang and J. Wang, "Modeling and analysis of cantilever piezoelectric energy harvester with a new-type dynamic magnifier," *Acta Mechanica*, vol. 229, no. 11, pp. 4643–4662, 2018.

[4] Z. Xie, C. K. Kwuimy, T. Wang, X. Ding, and W. Huang, "Theoretical analysis of an impact-bistable piezoelectric energy harvester," *The European Physical Journal Plus*, vol. 134, 2019.

[5] A. Marin, J. Turner, D. S. Ha, and S. Priya, "Broadband electromagnetic vibration energy harvesting system for powering wireless sensor nodes," *Smart Materials and Structures*, vol. 22, no. 7, article 075008, 2013.

[6] L. J. Gong, Q. S. Pan, W. Li, G. Y. Yan, Y. B. Liu, and Z. H. Feng, "Harvesting vibration energy using two modal vibrations of a folded piezoelectric device," *Applied Physics Letters*, vol. 107, article 033904, 2015.

[7] C. Eichhorn, F. Goldschmidtboeing, and P. Woias, "Bidirectional frequency tuning of a piezoelectric energy converter based on a cantilever beam," *Journal of Micromechanics and Microengineering*, vol. 19, no. 9, article 094006, 2009.

[8] W. G. Li, S. Y. He, and S. D. Yu, "Improving power density of a cantilever piezoelectric power harvester through a curved L-shaped proof mass," *IEEE Transactions on Industrial Electronics*, vol. 57, no. 3, 2010.

[9] D. Shen, J.-H. Park, J. Ajitsaria, S.-Y. Choe, H. C. Wikle, and D.-J. Kim, "The design, fabrication and evaluation of a MEMS PZT cantilever with an integrated Si proof mass for vibration energy harvesting," *Journal of Micromechanics and Microengineering*, vol. 18, no. 5, 2008.

[10] D. J. Morris, J. M. Youngsman, and M. J. Anderson, "A resonant frequency tunable, extensional mode piezoelectric vibration harvesting mechanism," *Smart Materials and Structures*, vol. 17, no. 6, article 065021, 2008.

[11] Q. C. Guan, B. Ju, J. W. Xu, Y. B. Liu, and Z. H. Feng, "Improved strain distribution of cantilever piezoelectric energy harvesting devices using H-shaped proof masses," *Journal of Intelligent Material Systems and Structures*, vol. 24, pp. 1059–1066, 2013.

[12] D. Huang, S. Zhou, and G. Litak, "Theoretical analysis of multi-stable energy harvesters with high-order stiffness terms," *Communications in Nonlinear Science and Numerical Simulation*, vol. 69, pp. 270–286, 2019.

[13] T. C. Yuan, J. Yang, and L. Q. Chen, "A harmonic balance approach with alternating frequency/time domain progress for piezoelectric mechanical systems," *Mechanical Systems and Signal Processing*, vol. 120, pp. 274–289, 2019.

[14] C. Wang, Q. Zhang, and W. Wang, "Low-frequency wideband vibration energy harvesting by using frequency up-conversion

and quin-stable nonlinearity," *Journal of Sound and Vibration*, vol. 399, pp. 169–181, 2017.

[15] K. Fan, Q. Tan, H. Liu, Y. Zhang, and M. Cai, "Improved energy harvesting from low-frequency small vibrations through a monostable piezoelectric energy harvester," *Mechanical Systems and Signal Processing*, vol. 117, pp. 594–608, 2019.

[16] S. Nabavi and L. Zhang, "Nonlinear multi-mode wideband piezoelectric MEMS vibration energy harvester," *IEEE Sensors Journal*, vol. 19, no. 13, pp. 4837–4848, 2019.

[17] Y. J. Wang, T. Y. Chuang, and C. Lee, "Resonant frequency self-tunable piezoelectric cantilevers for energy harvesting and disturbing torque absorbing," *Sensors and Actuators A: Physical*, vol. 285, pp. 25–34, 2019.

[18] J. Wang, S. Zhou, Z. Zhang, and D. Yurchenko, "High-performance piezoelectric wind energy harvester with Y-shaped attachments," *Energy Conversion and Management*, vol. 181, pp. 645–652, 2019.

[19] Z. Wu and Q. Xu, "Design and testing of a novel bidirectional energy harvester with single piezoelectric stack," *Mechanical Systems and Signal Processing*, vol. 122, pp. 139–151, 2019.

[20] Y. Hu and Y. Xu, "A wideband vibration energy harvester based on a folded asymmetric gapped cantilever," *Applied Physics Letters*, vol. 104, no. 5, article 053902, 2014.

[21] G. Sebald, H. Kuwano, D. Guyomar, B. Ducharne, and S. Mater, "Experimental Duffing oscillator for broadband piezoelectric energy harvesting," *Smart materials and structures*, vol. 20, no. 10, p. 102001, 2011.

[22] I. H. Kim, H. J. Jung, B. M. Lee, and S. J. Jang, "Broadband energy-harvesting using a two degree-of-freedom vibrating body," *Applied Physics Letters*, vol. 98, no. 21, p. 214102, 2011.

[23] A. Abdelkefi, F. Najar, A. H. Nayfeh, and S. Ben Ayed, "An energy harvester using piezoelectric cantilever beams undergoing coupled bending–torsion vibrations," *Smart Materials and Structures*, vol. 20, no. 11, p. 115007, 2011.

[24] A. Hajati and S. G. Kim, "Ultra-wide bandwidth piezoelectric energy harvesting," *Applied Physics Letters*, vol. 99, no. 8, article 083105, 2011.

[25] M. A. Karami and D. J. Inman, "Parametric study of zigzag microstructure for vibrational energy harvesting," *Journal of Microelectromechanical Systems*, vol. 21, no. 1, pp. 145–160, 2012.

[26] K. Fan, J. Chang, W. Pedrycz, Z. Liu, and Y. Zhu, "A nonlinear piezoelectric energy harvester for various mechanical motions," *Applied Physics Letters*, vol. 106, no. 22, p. 223902, 2015.

[27] H. Hu, L. Dai, H. Chen, S. Jiang, H. Wang, and V. Laude, "Two methods to broaden the bandwidth of a nonlinear piezoelectric bimorph power harvester," *Journal of Vibration and Acoustics*, vol. 139, no. 3, article 031008, 2017.

[28] X. Rui, Y. Li, Y. Liu, X. Zheng, and Z. Zeng, "Experimental study and parameter optimization of a magnetic coupled piezoelectric energy harvester," *Applied Sciences*, vol. 8, no. 12, p. 2609, 2018.

[29] B. Zhang, J. Yu, L. Elmaimouni, and X. Zhang, "Magneto-electric effect on guided waves in functionally graded piezoelectric–piezomagnetic fan-shaped cylindrical structures," *Materials*, vol. 11, no. 11, p. 2174, 2018.

[30] S. Sun and P. W. Tse, "Modeling of a horizontal asymmetric U-shaped vibration-based piezoelectric energy harvester (U-VPEH)," *Mechanical Systems and Signal Processing*, vol. 114, pp. 467–485, 2019.

[31] L. R. Alcala-Jimenez, T. P. Jensen, A. Lei, and E. V. Thomsen, "Increased mechanical robustness of piezoelectric magnetoelastic vibrational energy harvesters," *Microelectronic Engineering*, vol. 207, pp. 19–26, 2019.

[32] V. Apicella, C. S. Clemente, D. Davino, D. Leone, and C. Visone, "Magneto-mechanical optimization and analysis of a magnetostrictive cantilever beam for energy harvesting," *Journal of Magnetism and Magnetic Materials*, vol. 475, pp. 401–407, 2019.

[33] L. Zhao, S. C. Conlon, and F. Semperlotti, "Broadband energy harvesting using acoustic black hole structural tailoring," *Smart Materials and Structures*, vol. 23, no. 6, article 065021, 2014.

[34] S. Leadenham and A. Erturk, "Nonlinear M-shaped broadband piezoelectric energy harvester for very low base accelerations: primary and secondary resonances," *Smart Materials and Structures*, vol. 24, no. 5, article 055021, 2015.

[35] R. L. Harne, A. Sun, and K. W. Wang, "Leveraging nonlinear saturation-based phenomena in an L-shaped vibration energy harvesting system," *Journal of Sound and Vibration*, vol. 363, pp. 517–531, 2016.

[36] Y. Qin, T. Wei, Y. Zhao, and H. Chen, "Simulation and experiment on bridge-shaped nonlinear piezoelectric vibration energy harvester," *Smart Materials and Structures*, vol. 28, no. 4, article 045015, 2019.

[37] Y. C. Shu and I. C. Lien, "Analysis of power output for piezoelectric energy harvesting systems," *Smart Materials and Structures*, vol. 15, p. 1502, 2006.

WILEY | Hindawi

Research Article

Research on Intelligent Algorithm of Identity Authentication Based on Facial Features

Bin Yuan,[1] Changqing Du [iD],[1] Zhongyuan Wang,[2] and Rong Zhu[2]

[1]*School of Information Engineering, Qujing Normal University, Qujing, 655000 Yunnan, China*
[2]*NERCMS, School of Computer, Wuhan University, Wuhan, 430072 Hubei, China*

Correspondence should be addressed to Changqing Du; ducq@mail.qjnu.edu.cn

Identity recognition is a research hotspot in the information age. Nowadays, more and more occasions require identity recognition, especially in smart home. Identity recognition of the head of the household can avoid many troubles, such as home identification and network information authentication. Nowadays, in smart home identification, especially based on face recognition, system authentication is basically through feature matching. Although this method is convenient and quick to use, it lacks intelligence. Nowadays, for the make-up, facelift, posture, and other differences, the accuracy of the system is greatly reduced. In this paper, the face recognition method is used for identity authentication. Firstly, the AdaBoost learning algorithm is used to construct the face detection and eye detection classifier to realize the detection and localization of the face and eyes. Secondly, the two-dimensional discrete wavelet transform is used to extract facial features and construct a personal face dynamic feature database. Finally, an improved elastic template matching algorithm is used to establish an intelligent classification method for dynamic face elasticity models. The simulation shows that the proposed method can intelligently adapt to various environments without reducing the accuracy.

1. Introduction

With the rapid development of computer and network technology, the influence of the Internet has penetrated into various fields of social life. More and more enterprises, institutions, and government agencies rely on information networks to carry out related business activities such as e-commerce and e-government. At the same time, however, the security of networks and information systems has become a research hotspot in the industry. As the first barrier to network security and information system security, identity authentication technology has received more and more attention in the information security era. Traditional identity authentication methods mainly rely on identity identification items such as keys, certificates, and cards and identity identification knowledge such as user name and password. Once identity identification items and identification knowledge are stolen or forgotten, their identity is easy to be impersonated by others. With the development of cyber fraud and attack technology, higher requirements are placed on the

accuracy, security, and reliability of the identity authentication method. Traditional identity authentication methods can no longer meet this requirement, and some human biometric features such as fingerprints, irises, sounds, and facial images provide a reliable solution for identity authentication because of their uniqueness and lifetime invariance.

Biometric technology is primarily a technique for identity authentication through measurable biological characteristics such as body or behavior. The so-called biometrics is the only physiological characteristics or behaviors that can be measured or automatically recognized and authenticated. Biological characteristics are divided into two categories: physical characteristics and behavioral characteristics. Physical characteristics include the fingerprints, palm shape, retina, iris, human body odor, face shape, blood vessels of the hand, and DNA; behavioral characteristics include signature, speech, and walking gait. Some scholars classify retinal recognition, iris recognition, and fingerprint recognition as advanced biometrics; classify palm recognition, face recognition, speech recognition, and signature recognition as

secondary biometrics; classify vascular texture recognition, human odor recognition and DNA recognition as "profound" biometrics. Compared with traditional identity authentication technology, biometric technology has the characteristics of portability, security, uniqueness, stability, extensiveness, convenience, collectability, and acceptability.

Face recognition technology is one of the most important biometric identity authentication technologies. Among various biometric authentication technologies, the market share of face recognition technology is second only to fingerprint recognition technology, and it has broad application prospects in the fields of public security, justice, finance, customs, and military. Compared with other biometric authentication technologies, face recognition has the advantages of being intuitive and convenient, noninterfering to users, and no special requirements on hardware [1–3].

The earliest research on face recognition dates back to the 1950s in the field of psychology, dating back to the 1960s in engineering. Other earlier studies include Darwin's research on emotional facial expression and Galton's research on facial features [4].

Earlier research on face recognition mainly focused on two aspects: extraction of face geometric features and template matching methods. The method of extracting the geometric features of the face includes the normalized interpoint distance and ratio of the face component and some feature points of the face, such as the two-dimensional topography composed of the corners of the eyes, the corners of the mouth, and the tip of the nose. The template matching method mainly uses the autocorrelation of the calculation template and the image gray scale to realize the recognition function.

Since the 1990s, face recognition has made significant progress and many new methods have emerged. At present, there are two main research directions: the research method based on the whole and the method based on the local feature analysis. The method based on the whole considers the overall properties of the model, including the eigenface method, the SVD decomposition method, the face density line method, the elasticity map matching method, the hidden Markov model method, and the neural network method. The method based on local feature analysis is to form the recognition feature vector together with the relative ratio of the face reference point and other shape parameters or class parameters describing the facial feature. The recognition based on the whole not only retains the topological relationship between the face components but also retains the information of each component itself. The recognition based on the local is to design a specific recognition algorithm by extracting the local contour and gray information. Local recognition is more intuitive than global recognition. It extracts and utilizes the most useful features, such as the location of key points and the shape analysis of components. For face recognition based on the whole face, because the whole face image is taken as a pattern, illumination, visual angle, and face size will have a great impact on face recognition. Therefore, how to effectively remove these disturbances is the key. For face recognition methods based on local analysis, the difficulty lies in how to build a good model to express the recognition components. In recent years, a trend is to combine global recognition with local feature analysis. For example, Kezheng et al. proposed a global and local weighted fusion feature extraction algorithm. Experiments show that this method has high robustness in the recognition of 3D face [5].

In recent years, on the basis of careful research on feature face technology, domestic scholars have tried to combine feature extraction method based on feature face with various back-end classifiers and proposed various improved versions or extended algorithms. The main research contents include linear/nonlinear discriminant analysis [6], Bayesian probability model [7], support vector machine (SVM) [8], artificial neural network (NN) [9], and intra/intraclass dual subspace analysis method [10].

Generally speaking, face recognition technology has made unprecedented development in recent years and has been applied in practice, but there are still many unsolved problems [11]. Because its recognition accuracy is not as good as fingerprint and iris recognition, the current identity authentication system based on biometric is mostly based on fingerprint and iris recognition. In the last two years, some new face recognition technologies have emerged, including 3D face scan data, high resolution still images, multiple still images for face recognition, multimodal face recognition, multialgorithm fusion, and preprocessing algorithms for correcting illumination and pose changes. These new technologies provide the possibility of improving the performance of automatic face recognition. Therefore, the research and improvement of face recognition technology can not only promote the development of biometric technology but also lay a good foundation for the application of a more accurate and reliable identity authentication system based on face features.

In this paper, the face recognition method is used for identity authentication. Firstly, the face detection and eye detection classifier are constructed by using the AdaBoost learning algorithm [12] to realize the detection and localization of face and eyes. Then, the face features are extracted by Gabor filter [13], and the personal face dynamic feature database is constructed. Finally, the improved elastic template matching algorithm is used to establish the intelligent classification algorithm of the dynamic face elasticity model to realize identity recognition. The specific contributions of this paper can be expressed as follows:

(1) Using the AdaBoost learning algorithm to construct the face detection and eye detection classifier to realize the detection and localization of face and eyes

(2) For the time-consuming problem of convolution operation of Gabor kernel function, this paper uses two-dimensional discrete wavelet transform to extract facial features and construct a personal face dynamic feature database

(3) Using the improved elastic template matching algorithm to establish an intelligent classification algorithm for dynamic face elasticity model to realize identity recognition

2. Proposed Method

2.1. Face Localization and Normalization Processing

2.1.1. Face Detection and Eye Location. AdaBoost algorithm is proposed by Freund and Schapire on the basis of a boosting algorithm to solve the problem of how to train weak classifiers into strong classifiers [14]. For a boosting algorithm, there are two problems: (1) how to adjust the training set so that the weak classifier can be trained on the training set and (2) how to combine the weak classifiers to form a strong classifier. The AdaBoost algorithm makes corresponding adjustments to these two problems: using weighted selected training data instead of randomly selected training data, so that the focus of training will be focused on more difficult to separate training data when weak classifiers are combined, and using weighted voting mechanism instead of average voting mechanism. The weak classifier with good classification effect has larger weight, while the classifier with poor classification effect has smaller weight.

The starting point of the AdaBoost learning algorithm is to improve the classification performance of weak classifiers. It uses a large number of weak classifiers with general classification ability to synthesize a strong classifier by weighted voting method. It is proved theoretically that the error rate of strong classifiers tends to zero when the number of simple classifiers tends to infinity as long as the classification ability of each simple classifier is slightly better than that of random guessing.

Viola and others applied the AdaBoost algorithm to face detection [15]. The basic idea is to train the same classifier (weak classifier) for different training sets and then combine the classifiers from these different training sets to form a final strong classifier. The weak classifier is constructed as follows: a rectangular feature j corresponds to a weak classifier h_j. For a candidate input window x, if the value of the matrix feature on x is $f_j(x)$, the weak classifier classification function is expressed as follows:

$$h_j(x) = \begin{cases} 1, & p_j f_j(x) \geq p_j \theta_j, \\ 0, & \text{others}, \end{cases} \tag{1}$$

where $p_j = \pm 1$ is used to control the direction of inequality and θ_j represents a threshold.

It is worth mentioning here that the AdaBoost training learning algorithm uses a similar Haar wavelet basis function holding feature and introduces the concept of an integral graph. Using the integral graph, each image can be detected and all the training sample images can be calculated by calculating the corresponding integral graph, so as to obtain its rectangular eigenvalue, and only needs to calculate once.

The training and learning algorithms of AdaBoost are as follows.

Given a training sample set: $(x_1, y_1), (x_2, y_2), \cdots, (x_n, y_n)$, x_i is an image sample and $y_i = 0, 1$ is the category label of the sample, corresponding to the nonface image and the face image, respectively, where $i = 1, 2, \cdots, n$, n is the total number of training samples. Initialize the weights of the two types of samples of $y_i = 0, 1$ to $w_{1,i} = 1/2m, 1/2l$, where m and l are the number of two types of samples, respectively. Suppose the number of weak classifiers to be trained is T, where T is also the number of features to be selected.

Let $t = 1, 2, \cdots, T$ execute the following loop:

(1) Normalized weights:

$$w_{t,i} \longleftarrow \frac{w_{t,i}}{\sum_{j=1}^{n} w_{t,j}}. \tag{2}$$

Let w_t be the probability distribution, that is, $\sum_{i=1}^{n} w_{t,i} = 1$

(2) For each feature j, a weak classifier h_j that only utilizes the feature is trained. The training error of the weak classifier h_j can be expressed as a function of the weight w_t:

$$\varepsilon_j = \sum_{i=1}^{n} w_{t,i} |h_j(x_i) - y_i| \tag{3}$$

(3) A weak classifier with the smallest training error is selected from the weak classifiers corresponding to all the features. This classifier is denoted as h_t with a training error of ε_t

(4) Adjust the weights according to this best weak classifier:

$$w_{t+1,i} = w_{t,i} \beta_t^{1-e_i}, \tag{4}$$

Where $e_i = 0$ means x_i is correctly classified, $e_i = 1$ means x_i is incorrectly classified; $\beta_t = \varepsilon_t / (1 - \varepsilon_t)$, since ε_t is always less than 0.5, $\beta_t < 1$. When the weights are updated each round, the weights of the correctly classified samples are reduced, while the weights of the misclassified samples remain unchanged.

The final strong classifier consists of weak classifiers corresponding to T features:

$$C(x) = \begin{cases} 1, & \sum_{t=1}^{T} \alpha_t h_t(x) \geq \frac{1}{2} \sum_{t=1}^{T} \alpha_t \\ 0, & \text{others}, \end{cases} \tag{5}$$

where $\alpha_t = \log(1/\beta_t)$, at each round of training t, the algorithm selects the rectangular features that are most advantageous for classification from all of the features.

In formula (5), as the number of weak classifiers $h_j(x)$ increases, the resulting strong classifier $H(x)$ becomes more and more complex. Some simple strong classifiers are highly efficient and can be used to exclude most nonface areas and detect almost all possible face areas. In order to improve the overall detection performance but reduce the calculation time, multiple classifiers can be cascaded in series in order from simple to complex. The entire face detection process forms a decision tree, as shown in Figure 1. Simple classifiers at the cascaded front end of the classifier initially exclude most of the nonface windows by a small amount of
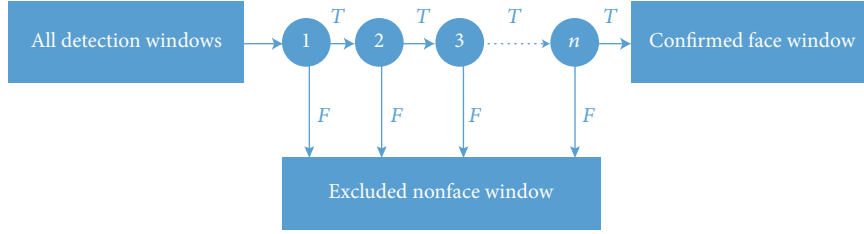
FIGURE 1: Classifier cascade diagram.

processing, while the latter complex classifiers further exclude suspected nonface windows by more computation, reducing the false positive rate of detection. For each level of classifier, if the output of the classifier is 1, it is considered that the detection window may be a face area, and the detection window is input to the next level of classifier for further judgment; otherwise, the detection window is excluded as a nonface area at the level. In training each classifier, the number of stages is increased until the desired final detection rate and false positive rate are achieved.

After detecting the face, it is necessary to further detect and locate the position coordinates of the eye as a benchmark for geometric normalization. Using a method similar to face detection, using eye images and noneye images as training samples, a human eye detection cascade classifier is trained, and the AdaBoost learning algorithm is applied to human eye detection to accurately locate the human eye [16–18].

According to the prior knowledge of the face model, we only need to detect the eye in the upper part of the detected face area. This saves the time of detecting the eye, improves the speed of eye detection, and reduces the probability of detecting errors, thereby improving the accuracy of eye detection.

2.1.2. Normalized Processing. In order to reduce the influence of partial illumination and attitude changes on the quality of captured face images, the accuracy of subsequent feature extraction and matching is improved, and the performance of the entire authentication system is improved. In order to detect the face image that has been detected, this paper proposes a standardized processing method for the system. The main process consists of the following steps:

(1) The angle θ of the rotation of the face image is calculated based on the positioned eye coordinates, and the image is rotated by the method of .

$$[x', y', 1] = [x, y, 1] \begin{bmatrix} \cos\theta & \sin\theta & 0 \\ -\sin\theta & \cos\theta & 0 \\ 0 & 0 & 1 \end{bmatrix} \quad (6)$$

(2) The center points of two faces are E_l and E_r, the O is the center of $\overline{E_l E_r}$, and $d = |\overline{E_l E_r}|$. After cropping, in the $2d \times 2d$ face image, it is guaranteed that O is fixed at $(0.5d, d)$. This ensures the consistency of the posi-

tion of the face and embodies the translation invariance of the face in the image plane

(3) Use the bilinear interpolation algorithm to reduce or enlarge the image to obtain a uniform size calibration image I_e. The size of the calibration image used in this paper is 128×128 pixels; then, the zoom factor is $\beta = 64/d$, where $d = |\overline{E_l E_r}|$

(4) Using formula (7), histogram equalization is applied to face images

$$s_k = T(r_k) = \sum_{j=0}^{k} \frac{n_j}{N}, 0 \le r_k \le 1, 0 \le s_k \le 1, k = 0, 1, \cdots, L-1, \quad (7)$$

where L is a gray scale series, N is the total number of pixels, n_k is the total number of pixels in level k gray, r_k is the grayscale of the original image $f(x, y)$ at point (x, y), s_k is the gray level of $g(x, y)$ in (x, y) after histogram equalization, and $T(r_k)$ is a transformation function and satisfies the following conditions:

(1) s_k is monotonically increasing function in $0 \le r_k \le 1$ interval and satisfies $0 \le T(r_k) \le 1$

(2) In $0 \le s_k \le 1$ interval, the inverse transformation $r_k = T^{-1}(s_k)$ exists and is monotonically increasing function

(3) Calculate the mean and mean square error of face contour gray and use formula (8) to grayscale transform the face image

$$I'(i, j) = \frac{\sigma'}{\sigma} (I(i, j) - \mu) + \mu', \quad (8)$$

where $I(i, j)$ is a gray value distribution matrix; μ and σ are the gray mean and variance of the image, respectively; and $I'(i, j)$ is the gray distribution matrix of the transformed image and usually takes the parameters: $\mu' = 0$ and $\sigma' = 1$

2.2. Face Image Processing. Facial image processing is the process of extracting facial features. Gabor function is often used to extract facial features. However, convolution operation between image and Gabor kernel function is a time-consuming process. Although convolution operation can be

implemented by fast Fourier transform, there is a computational burden when the feature points of the transform are selected more frequently. In this paper, two-dimensional discrete wavelet transform is used to extract face features. For wavelet transform, it can depict various kinds of signals with different frequency components, especially for the signal with catastrophic nature. The extracted features belong to low-level features. Compared with other parts of the face image, the extracted feature points are the key points of the face features, which belong to the region with obvious changes.

2.2.1. Two-Dimensional Discrete Wavelet Transform. In order to remove the redundant information after the specific wavelet transform, the scale factor and translation factor can be discretized. Now, we define the two-order wavelet space:

$$s = \frac{1}{2^j}, u = k, v = l, \quad \text{and} \quad j, k, l \in Z. \tag{9}$$

The corresponding two-order wavelet function and scaling function coefficient can be calculated by

$$c_m = \langle f(x), \psi_m(x) \rangle = 2^{j/2} \int_{-\infty}^{\infty} f(x)\psi(2^j x - k) dx. \tag{10}$$

The corresponding inverse wavelet transform function is

$$f(x) = \sum_{m=0}^{\infty} c_m \overline{\psi_m}(x). \tag{11}$$

In this way, a continuous sequence of functions can be represented by a single infinite sequence, such as the Fourier sequence. According to formula (10) and (11), we can deduce the formula of discrete wavelet transform. At the same time, the two-order scaling function in the scale space can be expressed as

$$\psi_m(x) = \sqrt{s}\psi(sx - k), \tag{12}$$

where m is a function of j and k.

2.2.2. Resolution Image Analysis. Before performing multiresolution analysis on image function $f(x, y)$, you need to understand the closed-scale subspace $V_n \subset V_{n-1} \subset \cdots \subset V_1 \subset V_0$. Let A_j be an approximation operator, and the image is roughly expressed as $A_j f$ at the j layer resolution. A_0 is the function itself, and $A_j f$ belongs to space V_j. The scale factor at the j layer is $s = 1/2^j$. In practice, $j = 0, 1, \cdots, n$ is specified, where n layer is the roughest representation of the image, where the scaling function is $s = 1/2^n$. Here, the differential operator D_j is introduced, so that $D_j f$ represents the difference between the approximate image in the j layer $A_j f$ and the $(j-1)$ layer $A_{j-1} f$. In an approximate representation of the difference between $A_j f$ and $A_{j-1} f$ in a two-dimensional analysis, Mallat first proves that it can be represented by three components:

$$D_j f = A_{j-1} f - A_j f, j = 1, 2, K, n. \tag{13}$$

So the function $f(x, y)$ multidimensional analysis can be expressed as

$$\begin{aligned} f(x, y) &= A_1 f + D_{1,1} f + D_{1,2} f + D_{1,3} f \\ &= A_2 f + D_{2,1} f + D_{2,2} f + D_{2,3} f + D_{1,1} f + D_{1,2} f + D_{1,3} f \\ &= A_n f + \sum_{j=1}^{n} \left[D_{j,1} f + D_{j,2} f + D_{j,3} f \right], \end{aligned} \tag{14}$$

where the approximation $A_j f(x, y)$ and the difference $D_{j,p} f(x, y)$, $p = 1, 2, 3$ can be completely represented by the two-dimensional scaling function $\Phi(x, y)$ and the wavelet function $\Psi(x, y)$:

$$\begin{aligned} A_j f(x, y) &= \sum_{k=-\infty}^{+\infty} \sum_{l=-\infty}^{+\infty} \alpha_{j,k,l} \Phi_{j,k,l}(x, y), \\ D_{j,p} f(x, y) &= \sum_{k=-\infty}^{+\infty} \sum_{l=-\infty}^{+\infty} d_{j,k,l} \Psi_{j,k,l}(x, y). \end{aligned} \tag{15}$$

Assuming that x and y are not correlated, the two-dimensional scaling function $\Phi(x, y)$ and the wavelet function $\Psi(x, y)$ are independent, so that the following formula can be derived:

$$\begin{aligned} \Phi(x, y) &= \phi(x)\phi(y), \\ \Psi_1(x, y) &= \phi(x)\psi(y), \\ \Psi_2(x, y) &= \psi(x)\phi(y), \\ \Psi_3(x, y) &= \psi(x)\psi(y). \end{aligned} \tag{16}$$

Among them, the one-dimensional scaling function and the one-dimensional wavelet function are $\phi(x)$ and $\psi(x)$, respectively. It can be clearly seen that the details of the two-dimensional image function $f(x, y)$ in the x-axis and y-axis, and diagonal directions are represented by Ψ_1, Ψ_2, and Ψ_3, so this is called wavelet pyramid decomposition of a two-dimensional image.

A series of image sets that are progressively reduced in resolution in a pyramid shape form a so-called image pyramid decomposition [19–21]. In general, the top of the pyramid is a low-resolution approximation, while the bottom is a high-resolution representation of the image to be processed, and as the pyramid moves from bottom to top, its size and resolution are reduced. Each decomposition of discrete wavelet can form three high-frequency subband images and one low-frequency subband image. The three high-frequency subband images provide image information in vertical, horizontal, and diagonal directions, respectively. The low-frequency subband image provides a low-resolution image.

2.2.3. Normalized Eigenvector. According to the analysis in the previous section, the three differential components $D_{j,p} f$ (x, y), $p = 1, 2, 3$ can be used to represent the points in the j layer. In the case of point-to-point matching, in order to go about the correlation between the image matching process

and the image gradation, normalization must be used [22]. Therefore define the following feature vector:

$$B_j(x, y) = \left[B_{j,1}(x, y) \, B_{j,2}(x, y) \quad B_{j,3}(x, y) \right], \tag{17}$$

where $B_{j,p} = D_{j,p}(x, y)/|A_j(x, y)|$, $p = 1, 2, 3$.

2.2.4. Discrete Wavelet Face Template. According to the above analysis, after the image is decomposed by wavelet, a certain point on a certain decomposition layer can be represented by $B_j(x, y)$. Now, we use it in face recognition, assuming that in the face image domain, N is the neighborhood of the key feature point $p_f = (x_f, y_f)$ of the face, which satisfies the following relationship:

$$N\left(p_f\right) = \left\{ I(x, y) \middle| \left\| (x, y) - \left(x_{p_f}, y_{p_f} \right) \right\| < \varsigma \right\}, \tag{18}$$

where ς is defined as the size of the neighborhood.

After the wavelet transform, the neighborhood of the key points in the j layer is defined as

$$N_j\left(p_f\right) = \left\{ I\left(x_j, y_j\right) \middle| \left\| \left(x_j, y_j\right) - \left(x_{p_f}/2^j, y_{p_f}/2^j \right) \right\| < \varsigma/2^j \right\}. \tag{19}$$

Define the following variables on this neighborhood:

$$
\begin{aligned}
A_j &= \left[A_{j,1}, A_{j,2}, A_{j,3} \right]^T, \\
A_{j,p} &= \sum_{N_j} \frac{1}{1 + \sqrt{\left(\left(x_j - x_{p_f}\right)/2^j \right)^2 + \left(\left(y_j - y_{p_f}\right)/2^j \right)^2}} B^2_{j,p}\left(x_j, y_j\right), p = 1, 2, 3
\end{aligned}
\tag{20}
$$

Therefore, the key point p_f of the image field can be represented by the following vector:

$$\mathrm{Jet} = \mathrm{Jet}\left(p_f\right) = \left[A_1\left(p_f\right), A_2\left(p_f\right), \cdots, A_J\left(p_f\right), \right]^T. \tag{21}$$

According to the previous definition, we can define the following face attribute map $C = \{N, A, E, J\}$, where

(1) Node set: $N = \{p_i | i = 1, 2, K, N\}$

(2) Undirected arc set: $A = \{(p_i, p_j) | i, j = 1, 2, K, N\}$

(3) Set of characteristic functions: $J = \{\mathrm{Jet}(p_i) | i = 1, 2, K, N\}$

(4) Euclidean distance function: $E = \{E_{i,j} | E_{i,j} = E_{p_i, p_j}, i, j = 1, 2, 3, K, N\}$

where p_i represents the key feature point of the face image.

2.3. Face Recognition

2.3.1. Face Elastic Template. The face elastic template is a property map (FBG) containing multiple (M) facial expressions, which is defined as follows:

$$\mathrm{FBG} = \left\{ N^B, A^B, J^B, E^B \right\}, \tag{22}$$

where

$$
\begin{aligned}
N^B &= \left\{ p_i^B \mid p_i^B = \frac{1}{M} \sum_{m=0}^{M} \sum_{i=1}^{N} p_i^{Bm} \right\}, \\
A^B &= \left\{ \left(p_i^B, p_j^B \right) \mid i, j = 1, K, N \right\}, \\
J^B &= \left\{ J_j^B \mid J_i^B = J\left(p_i^{Bm} \right), m = 1, K, M, i = 1, K, N \right\}, \\
E^B &= \left\{ E_{i,j}^B \mid E\left(p_i^B, p_j^B \right) = \frac{1}{M} \sum_{m=0}^{M} E\left(p_i^{Bm}, p_j^{Bm} \right), i, j = 1, K, N \right\}.
\end{aligned}
\tag{23}
$$

2.3.2. Matching Strategy. Aiming at the matching between face elastic template and face image, this paper adopts rough matching and fine matching combined with matching strategy for face recognition matching [23–25].

(1) Rough Match. In order to improve the matching speed, this paper adopts the strategy of combining the rough and the fine, and the specific steps of the rough matching strategy are as follows:

(1) Global search: in this paper, the face elasticity template is first set to a rigid model ($\lambda = \infty$), which is fixed and cannot be deformed. Then, the image is moved in groups of 4 pixels on the face image, and the similarity between the average map and the corresponding point of the face image is calculated. Iteratively calculates the similarity of the evaluations to search, find the optimal position of each pixel to stop the search, and take the optimal position as the next input. In this step, it is possible to achieve an effect of concentrating the points in the feature relationship diagram of the test image in the vicinity of the corresponding points in the elastic template [26]

Compressing the face elastic template map into an average graph is the key to the global search step, which helps to reduce the amount of calculation.

(2) Local adjustment: after a global search, the use of flexible templates does not require averaging but changes based on location and scale. After locating the key points of the face to be recognized in the global search, four different pixel offsets are selected as the new positions for exhaustive search. So that the Jet value of each node of the face image to be recognized is the most similar to the average Jet value of the corresponding node of the reference face image, and the angle-independent similar function is still used here

(2) Fine Match. First, the definition uses the following functions to find the optimal solution for comparison:

$$S(C, \text{FBG}) = \frac{1}{N} \sum_{i=1}^{N} \max_{m} \left(S\left(J_i^C, J_i^{Bm}\right) \right) - \frac{\lambda}{E} \sum_{e=1}^{E} \left(\frac{\overrightarrow{\Delta}_e^C - \overrightarrow{\Delta}_e^B}{\overrightarrow{\Delta}_e^B} \right),$$

(24)

where $S(J, J') = (\sum_j A_j \cdot A'_j) / \left(\sqrt{\sum_j A_j^2 \sum_j A_j'^2} \right)$

In this paper, the rough matching strategy is used to determine the key points of the face image, but this is not enough for the matching of face recognition. In order to more accurately locate the specific location of the key points of the face, this paper introduces a genetic algorithm to improve the matching precision of the key feature points of the face and achieve the effect of accurately locating the specific position of the key points of the face. The idea of genetic algorithm is an optimization algorithm based on the biological law of "natural selection, survival of the fittest" in the biological world. The specific algorithm process is as follows:

(1) Gene chain code: the biological information of the organism is determined by the chromosome of the biological genetic gene. In this paper, the sequence of feature points consisting of key feature points of the face is used as the gene coding, and each feature point is represented by coordinates

(2) Fitness: each gene chromosome corresponds to the optimal solution of a problem, and fitness refers to the degree of similarity between the optimal solution and the problem. In this paper, the similarity between the key feature points of the face and the face elastic template is studied, and the individual with the highest fitness value is reserved according to the principle of eliminating the fittest

(3) Cross: this paper adopts two-point intersection method, selects two different individuals to cross, and uses the roulette model to ensure that the probability that the individual is selected is proportional to its fitness value. Then, the two random positions in the sequence of feature point sequences in the randomly selected two individuals are exchanged coordinates to complete the intersection process

(4) Variation: variation is an individual gene mutation and is a means to expand the diversity of the population. In the optimization algorithm, using mutation in the optimal solution interval for traversal search. In this paper, the mutation operator is aimed at the sequence of feature points, randomly selects a position in the sequence string, randomly selects coordinate values in the neighborhood of the position, and mutates into a new individual

2.3.3. Face Recognition. After the appellate process is implemented, the facial feature graph is successfully extracted from the face image to be recognized. This paper only needs to compare the successfully extracted facial feature graph with the dynamic facial feature database constructed in this paper to realize face recognition. In this paper, the average value of the sum of Jet comparisons between the corresponding points of different feature graphs is used as the similarity function between feature graphs. The calculation formula is as follows:

$$S_G\left(G^I, G^M\right) = \frac{1}{N'} \sum_n S_\alpha\left(J_{n'}^I, J_n^M\right),$$

(25)

where G^I is a facial feature attribute graph in face database, G^M is the feature graph of face image to be recognized, and N' represents the total number of nodes.

The value of similarity function is sorted. If the maximum value of all the values is obviously too large, it shows that the face is in the face database. Otherwise, the face is not in the database.

3. Experiments

In the experimental simulation work of this paper, the computer hardware configuration is as follows:

(1) Processor: Intel i5 2.50 GHz

(2) Memory: 4GB

(3) Operating system: Windows 7 64-bit Ultimate

(4) The simulation software is MATLAB 2014B

The simulation images are simulated by using star photos and ORL face database.

4. Discussion

In order to illustrate the method of this paper, this paper uses a picture to simulate the face detection effect of the AdaBoost learning algorithm. Figure 2 shows the simulation result of the AdaBoost learning algorithm for detecting a human face. Firstly, face detection is performed on the original image (Figure 2(a)). After detecting the face, the image is clipped to get Figure 2(b). The results show that the AdaBoost learning algorithm can accurately find the face and cut it. Then, in order to reduce the impact of partial illumination and pose changes on the quality of the collected face images, we improve the accuracy of subsequent feature extraction and matching, and then improve the performance of the entire authentication system. After processing, Figure 2(c) is obtained. Compared with Figure 2(b), it can be clearly seen that the result of the gradation normalization is more clear. Features such as the eyebrows, eyes, and mouth are easier to identify than the surrounding area.

In order to solve the time-consuming problem of the original elastic template method using Gabor function to extract face features, this paper uses two-dimensional

(a) The original image   (b) Crop image   (c) Grayscale normalization
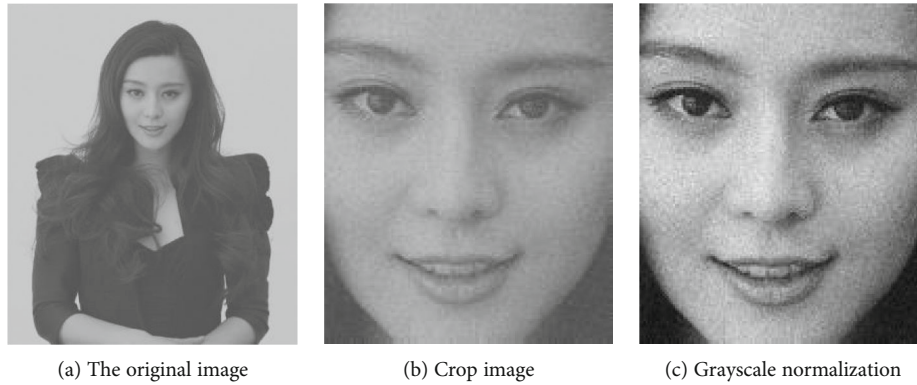
FIGURE 2: AdaBoost learning algorithm face detection effect diagram.

(a) Rough matching strategy   (b) Fine matching strategy
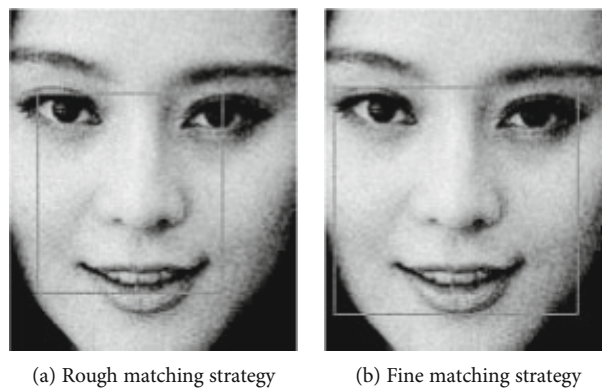
FIGURE 3: Matching strategy effect graph in this paper.

(a) Traditional elastic template method   (b) Improved elastic template method
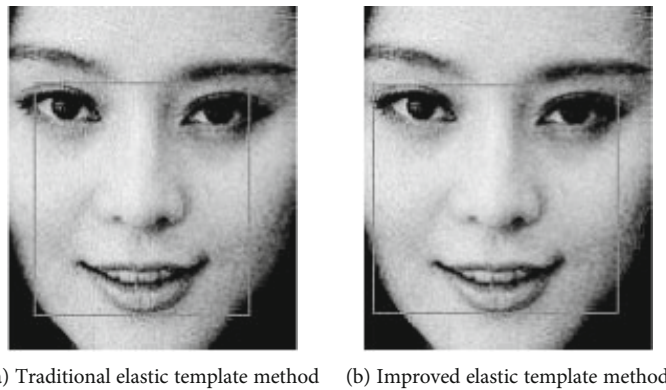
FIGURE 4: Matching strategy effect contrast graph.

discrete wavelet transform to extract face features. In the matching strategy, rough matching and fine matching are used to superimpose. Figure 3 shows the effect of rough matching and fine matching. It can be seen from Figure 3(a) that the rough matching strategy is not accurate for the location of the key points (eyes, mouths) of the face. In the feature selection, the left eye is slightly deviated, but the right eye positioning deviation is about half, and the lip positioning does not include the lower lip. Figure 3(a) is obtained after fine matching strategy. It can be seen that the

problem of inaccurate location after rough matching strategy has been greatly improved. The left eye is almost accurate positioning, the right eye is only a little bit biased, and the whole face feature is almost captured.

In order to better illustrate the superiority and effectiveness of the matching strategy in this paper, this paper compares it with the traditional elastic template method matching strategy, as shown in Figure 4. It can be seen that in the accuracy of feature point calibration, the traditional elastic template method has deviations in the positioning of

TABLE 1: Performance comparison of different face recognition methods.

Method	Correct recognition rate (%)
Feature face method	90.5
Hidden Markov method	87
Traditional elastic template matching	96
Dynamic connection matching	92
The method of this paper	97.3

TABLE 2: Comparison of face recognition performance under different conditions.

Category	Condition	Correct recognition rate (%)
Light	Sunny day	92.9
	Rainy day	90.9
	Dark	88.3
Postures	Head-up	93.5
	Look-up	91.3
	Look-down	91.1
Make-up	No make-up	93.1
	Light make-up	91.7
	Heavy make-up	89.5

the left and right eyes, which is not accurate enough compared to the improved elastic template method; this can be concluded: In this paper, the improvement of the traditional elastic template method has improved the problem that the traditional elastic template method is not accurate enough.

In this paper, different face recognition methods such as eigenface method, hidden Markov method, traditional elastic template matching method, and dynamic connection matching method are compared with the method designed in this paper. The comparison results are shown in Table 1. The number of categories used in the experiment was 40, and 10 images in the ORL face database per person with different expressions, poses, and illumination effects were simulated. Among them, the first five of 40 people (200 in total) were taken out for training, and the last five (200 in total) were used for testing. The test results of other methods in Table 1 are from the literature, and the comparison results are shown in Table 1:

It can be seen from Table 1 that the proposed method, elastic template matching method, and dynamic connection matching method are face recognition methods that use the gray information and geometric features of the face to elastically match, which are less affected by illumination and the recognition rate is higher. However, the feature face method only uses gray information and does not use geometric structure features for elastic matching, which is greatly affected by illumination and has a low recognition rate.

In order to prove that the intelligent algorithm based on facial features designed in this paper can effectively improve the inaccuracy of face recognition caused by different light, posture, make-up, and other problems in reality, this paper uses 20 males and 20 females as performance tests; they are between 20 and 29 years old. They were given different light, postures, make-up, and other simulation tests, and the results are shown in Table 2:

The histogram is as follows.

Figure 5 is a histogram of face recognition performance comparison under different conditions, in which conditions one, two, and three correspond to the conditional order in Table 2. It can be seen from Figure 5 and Table 2 that the accuracy of face recognition is different under the three environments, and the accuracy rate is reduced in the comparison of ORL face database simulation under three environments. First of all, for different light, this paper uses three kinds of light environment tests, such as sunny day, rainy day, and dark weather, corresponding to conditions 1,

FIGURE 5: Comparison of face recognition performance under different conditions.

2, and 3 in the histogram. It can be seen that the light has an influence on the accuracy of the face recognition of the system. Among them, the light of the sunny day is the best, the accuracy rate is the highest, and the accuracy rate is 92.9%; the rainy day is second, and the accuracy rate is 90.9; and under the dark condition, although there is light, the light is the worst, the accuracy of face recognition is the worst, and the accuracy rate is 88.3%.

For posture, this paper uses three conditions of head-up, look-up, and look-down to test, corresponding to conditions 1, 2, and 3 in the histogram. It can be seen that the best accuracy rate of face recognition of the three postures is head-up, the accuracy rate is 93.5%, and the difference between the accuracy of look-down and look-up is only 0.2%.

Make-up is indispensable for modern women, so in the context of smart homes, face recognition testing about make-up is an indispensable part. In this paper, no make-up, light make-up, and heavy make-up three conditions were tested, corresponding to conditions 1, 2, and 3 in the histogram. It can be seen that for the simulation of the method designed in this paper, the face recognition accuracy of nonmake-up is the best, and the accuracy rate is 93.1%, followed by light make-up, the accuracy rate is 91.7%, the accuracy of heavy make-up is the lowest, and the accuracy rate is 89.5%.

In summary, it can be explained that different light, postures, and make-up have an influence on the accuracy of face recognition in this design method, but the most influential is that under the condition of darkness, the accuracy rate is 88.3%. This accuracy is acceptable in practice and can be improved by increasing the intensity of night light. This shows that the method designed in this paper can also achieve a good face recognition effect in practice and can be applied to practice. Similarly, the intelligent algorithm based on facial features designed for identity authentication in smart home is an algorithm with good performance.

5. Conclusions

With the development of science and technology, more and more occasions need identity recognition, which makes identity recognition become the research hotspot of today's era. People cannot meet the needs of today's society by traditional authentication methods, such as identification items such as keys, certificates, and cards and identification knowledge such as user names and passwords. More and more research is focused on biometric identification technology, which provides a reliable solution for identity authentication through some biological characteristics such as the fingerprint, iris, voice, and face. This paper studies the problem that the authentication of the smart home identification system is basically based on feature matching and lacks intelligence. Especially for today make-up, facelift and posture problems will greatly reduce the system resolution accuracy proposed solutions. Firstly, the AdaBoost learning algorithm is used to construct the face detection and eye detection classifier, which realizes the detection and localization of face and eyes, and proposes a standardized processing method. It effectively reduces the influence of part of illumination and posture changes on the quality of the collected face images and improves the accuracy of subsequent feature extraction and matching; secondly, it uses two-dimensional discrete wavelet transform to extract face features and constructs a dynamic feature library of individual faces; finally, the improved elastic template matching algorithm is used to build an intelligent classification method of the dynamic face elastic model. The matching strategy in the elastic template matching algorithm is combined with rough matching and fine matching. The simulation shows that the proposed method can intelligently adapt to various environments without reducing the accuracy. The research and improvement of face recognition technology can not only promote the development of biometric technology but also lay a good foundation for the application of more accurate and reliable identity authentication system based on face features.

Data Availability

None.

Conflicts of Interest

The authors declare that they have no conflicts of interest.

References

[1] J. Zhang and University D, *Study on Library Access Control System Based on Face Recognition Technology*, Modern Electronics Technique, 2016.

[2] C. Xie, *Face Recognition Technology in Accesss Control System*, Modern Architecture Electric, 2017.

[3] J. Xiao, *Application Status and Prospects of Face Recognition in Suspects Hunting*, Forensic Science & Technology, 2016.

[4] F. Galton, "Personal identification and description," *Journal of the Royal Anthropological Institute of Great Britain and Ireland*, vol. 18, no. 973, pp. 177–191, 1889.

[5] K. Lin, S. Xu, A. Li, and D. Wu, "Multiple information fusion face recognition using key feature points," *Journal of Harbin University of Science and Technology*, vol. 22, no. 3, pp. 19–24, 2017.

[6] S. Chen, H. Zhao, and S. Zhu, "A novel Gabor feature based null space algorithm for face recognition," *Journal of Xiamen University*, vol. 55, no. 1, pp. 108–113, 2016.

[7] J. J. Lv, J. S. Huang, X. D. Zhou, X. Zhou, and Y. Feng, "Latent face model for across-media face recognition," *Neurocomputing*, vol. 216, pp. 735–745, 2016.

[8] J. Olivares-Mercado, K. Toscano-Medina, G. Sánchez-Pérez, M. Nakano-Miyatake, and H. Pérez-Meana, "Modifications to the eigenphases method for face recognition based on SVM," *Ingeniería Investigación Y Tecnología*, vol. 17, no. 1, pp. 119–129, 2016.

[9] P. S. Aulestia, J. S. Talahua, V. H. Andaluz, and M. E. Benalcázar, "Real-time face detection using artificial neural networks," in *Artificial Neural Networks and Machine Learning – ICANN 2017*, Springer, 2017.

[10] Y. Chu, T. Ahmad, G. Bebis, and L. Zhao, "Low-resolution face recognition with single sample per person," *Signal Processing*, vol. 141, pp. 144–157, 2017.

[11] W. Wang, R. Wang, Z. Huang, S. Shan, and X. Chen, "Discriminant analysis on Riemannian manifold of Gaussian distributions for face recognition with image sets," *IEEE Transactions on Image Processing*, vol. 99, p. 1, 2017.

[12] H. Min and X. Luo, "Calibration of soft sensor by using just-in-time modeling and AdaBoost learning method," *Chinese Journal of Chemical Engineering*, vol. 24, no. 8, pp. 1038–1046, 2016.

[13] L. He, J. Li, A. Plaza, and Y. Li, "Discriminative low-rank Gabor filtering for spectral-spatial hyperspectral image classification," *IEEE Transactions on Geoscience & Remote Sensing*, vol. 55, no. 3, pp. 1381–1395, 2017.

[14] R. E. Schapire and Y. Singer, "Improved boosting using confidence-rated predictions," *Machine Learning*, vol. 37, no. 3, pp. 297–336, 1999.

[15] P. Viola and M. J. Jones, "Fast and robust classification using asymmetric AdaBoost and a detector cascade," *Advances in Neural Information Processing System*, pp. 1311–1318, 2001.

[16] P. L. Hou, D. Wang, and X. Li, *Application of Human Eye Detection in Robot Arm*, Electronics Quality, 2017.

[17] N. Alioua, A. Amine, and M. Rziza, "Driver's fatigue detection based on yawning extraction," *International Journal of Vehicular Technology*, vol. 2014, no. 1, Article ID 678786, p. 7, 2014.

[18] H. Xia, L. Zhang, W. U. Xiaotian, and K. P. Q. Zhang, "Improved and implementation of Adaboost eye location method," *Journal of Dalian Jiaotong University*, 2017.

[19] X. Liu, X. Yang, and C. N. Center, *Research on Image Registration Algorithm Based on Normalized Mutual Information and Pyramid Decomposition Optimization*, Microcomputer Applications, 2016.

[20] A. Kolesnikov and C. H. Lampert, "Deep probabilistic modeling of natural images using a pyramid decomposition," 2016, https://arxiv.org/abs/1612.08185.

[21] X. Liu, Q. Sang, and C. Sun, "Stereo image quality evaluation method based on steerable pyramid decomposition," *Chinese Journal of Quantum Electronics*, vol. 34, no. 6, p. 672, 2017.

[22] W. Guo and H. Lin, "Study on data normalization processing based on Hadoop platform," *Journal of Air Force Early Warning Academy*, 2016.

[23] Q. Wang, J. Ning, Y. Cao, and W. Han, "Matching technologies of UAV remote sensing image based on SIFT," *Journal of Jilin University*, 2017.

[24] S. Yang, B. Xiao, L. Yan, Y. Xia, M. Fu, and Y. Liu, "Robust scene matching method based on sparse representation and iterative correction," *Image and Vision Computing*, vol. 60, pp. 115–123, 2016.

[25] L. I. Xiang, H. U. Yixin, Z. H. Hong, and Z. H. Jiangshui, "Positioning correction algorithm of vector road aided inertial navigation based on the rough/fine matching method," *Acta Geodaetica et Cartographica Sinica*, vol. 46, article 1034, 2017.

[26] S. Liu, Y. Peng, X. Ben, W. Yang, and G. Qiu, "A novel label learning algorithm for face recognition," *Signal Processing*, vol. 124, pp. 141–146, 2016.

WILEY | Hindawi

Research Article

Blockchain Equity System Transaction Method and System Research Based on Machine Learning and Big Data Algorithm

Kanghua Peng [iD]

Guangdong Engineering Polytechnic, Information Engineering Institute, Guangzhou, 510520 Guangdong, China

Correspondence should be addressed to Kanghua Peng; pengkanghua@gdep.edu.cn

With the development of machine learning and big data, traditional equity trading system methods can no longer meet the current trading needs, and there are still problems such as low operating efficiency and serious homogeneity. Blockchain technology has the characteristics of decentralization and can also complete transactions through smart contracts, innovating the way of equity system transactions. The purpose of this paper is to build an equity trading system in combination with blockchain in the context of machine learning and big data and provide innovative trading methods, so as to provide reference and reference significance for the construction of my country's equity market. This article uses literature data method, comparative analysis method, factor analysis method, and other methods to carry out research, in-depth study of machine learning and big data, blockchain-related concepts, system composition, application situation, etc., and discusses the allocation of equity trading market The functions of resources, risk diversification, risk transfer, price determination, etc., have built a blockchain equity trading system, designed a consensus mechanism, block generation protocol, block verification, decentralization, and smart contract platform, and finally conducted a national equity transaction the background of the market is analyzed, and the experimental results, simulation indicators, transaction time, transmission consumption, and other content of the system constructed in this article are analyzed. In the single-node test, the CPU usage of the PoW consensus mechanism algorithm reached 100%, but the improved PBFT consensus mechanism was only 16%, which saved a lot of computing power and improved computing performance.

1. Introduction

After the emergence of Bitcoin in 2009, blockchain technology has slowly entered people's field of vision. Blockchain technology has the characteristics of decentralization, transparency, reliability, etc., so it has attracted the attention of experts and researchers. As an application of blockchain technology, Ethereum provides a decentralized application platform. The application of blockchain technology initially developed from the financial field to other fields. In recent years, many fields have gradually tried to use blockchain technology, which has promoted the research and development of blockchain technology.

In recent years, the state has actively promoted the construction of a multilevel capital market and vigorously developed the over-the-counter market. Because the traditional equity trading system method can no longer meet the current trading needs, there are problems such as low operating effi-

ciency and serious homogeneity, so there is a blockchain stock system trading method and system. In January 2013, the country established a share transfer system for SMEs, and the over-the-counter market entered a stage of rapid growth. At the same time, as an important part of the multilevel capital market system, the equity market promotes regional economic development, provides funds for small and medium-sized enterprises, and enhances the company's image. However, in the process of vigorous development of the equity market, some problems have been exposed, such as qualitative, redundant construction, and low efficiency. The equity trading market plays an important role in the country's economic development and provides strong economic support.

Boehm et al.'s growing demand for customized machine learning (ML) algorithms and the growing amount of data that need to utilize distributed data parallel frameworks (such as Map Reduce or Spark) pose a major challenge to the

productivity of data scientists. They solved these challenges through declarative ML: (1) increased the productivity of data scientists because they were able to express custom algorithms in familiar domain-specific languages, including linear algebra primitives and statistical functions; (2) in distributed computers to run these ML algorithms transparently, the data parallel framework applies cost-based compilation techniques to generate efficient, low-level execution plans, which include single-node and large-scale distributed operations in memory. He described the end-to-end system ML on apache spark, including an in-depth understanding of various optimizers and runtime technologies and performance characteristics. They also shared the lessons learned from porting system ML to spark and declarative ML. Finally, system ML is open source, which allows the database community to use it as a testing platform for further research. However, his system contains too many mathematical algorithms and functions, so it does not have much practical performance [1]. Obermeyer and Emanuel proposed a deep learning-based traffic flow time series prediction model, deep TFP, which makes full use of the effectiveness of time series function analysis sequence data and deep learning to extract traffic flow features. Accurate and timely prediction of future traffic flow is an urgent need for personal travel, public transportation, and transportation planning. In recent years, with the explosive growth of traffic data, various traffic flow prediction methods based on big data analysis have been proposed. He proposed deep TFP, which uses a time series function that considers the temporal and spatial correlation of traffic data to predict and track changes in traffic flow. Deep TFP uses deep learning to extract the characteristics of traffic data as the basis of the time series function. The performance of the model is verified through comparative experiments. However, his experimental model is difficult to provide timely predictions for the processing of real-time traffic data [2]. The purpose of Hamzah et al.'s research is to study the motivation of risk transfer in debt and equity contracts based on criticizing the similarities between sukuk and bonds. He uses a theoretical and mathematical model to study whether there is a motivation for risk-taking: debt contracts and equity contracts. Based on this theoretical model, it believes that the risk transfer behavior only exists in the debt contract, because the debt will naturally produce risk transfer behavior when the transaction occurs. In contrast, stock contracts, by their very nature, involve the sharing of transaction risks and returns and are therefore considered undesirable risk transfer behavior. Nevertheless, previous researchers found that equity financing may also bring motivation for risk transfer. Even so, he believes that the amount of capital provided and the underlying assets must be considered, especially in the case of default. Through mathematical modeling, this element of equity financing can make risk transfer unattractive. However, his research model is only a theoretical model. There are many factors that need to be considered in actual operation, and the author did not take them into consideration [3].

The main innovations of this paper are (1) using literature analysis, comparative analysis, and other methods to describe and analyze the equity trading system, through the comparison of different system models, highlight the feasibility and effectiveness of the framework of this paper; (2) the combination of theoretical analysis and empirical research not only analyzes the shortcomings of the traditional equity trading system and explains possible countermeasures but also collects data and analyzes through data comparison.

2. Blockchain Equity System Transaction Methods and System Research Methods Based on Machine Learning and Big Data Algorithms

2.1. Machine Learning

2.1.1. Overview of Machine Learning. Machine learning is a field of computer science. There is no clear program design method for the computer to learn [4]. Its purpose is to allow the computer to simulate the human learning process, use existing knowledge (data) to form an independent knowledge system, and solve future problems. At the same time, the data is updated and improved through the knowledge system produced by machine learning [5, 6].

The mathematical description of the basic model of machine learning is as follows: the data generator H generates m samples $(x_1, y_1), (x_2, y_2), (x_3, y_3) \cdots (x_n, y_n)$, assuming that the probability distributions of x and y of the observation samples are consistent, and generates independent observation samples of the same distribution $G(x|y)$. Machine learning is to find the most suitable learning function $\{g(x, w)\}$ from a series of learning functions based on observation samples $g(x, w_0)$. Therefore, when predicting and evaluating the observed samples, the predicted risk $T(w)$ of x and y is the smallest:

$$T(w) = \int K(y, g(x, w)) dG(x, y). \tag{1}$$

Among them, w is the general parameter of the learning function, $K(y, g(x, w)$ is the error function between the predicted value y and the actual value y when using the predictive learning machine $g(x, w)$ [7]. It is called the risk function. The form of the risk function varies with learning problems. General machine learning problems are divided into pattern recognition problems, regression evaluation problems, and probability evaluation problems. The risk functions corresponding to these three problems are as follows [8]:

Pattern recognition problem:

$$K(y, g(x, w)) = \begin{cases} 0, y = g(x, w), \\ 1, y \neq g(x, w). \end{cases} \tag{2}$$

Regression estimation problem:

$$K(y, g(x, w)) = (y - g(x, w))^2. \tag{3}$$

Probability density problem:

$$K(\sigma(x, w)) = -\ln \sigma(x, w). \tag{4}$$

2.1.2. Gemini Support Vector Machine.
The traditional vector machine SVM realizes SRM by constructing a pair of parallel classification hyperplanes [9]. Different from traditional SVM, TWSVM looks for a pair of nonparallel classification hyperplanes, which are a positive hyperplane $\varpi_1^T \gamma(x_i) + b_1 = 0$ and a negative hyperplane $\varpi_2^T \gamma(x_i) + b_2 = 0$. The positive sample points are located near the positive hyperplane, while the negative sample points are far away from the positive hyperplane, and vice versa [10]. We assume that the positive sample with the label +1 is a matrix $X_1 \in i^{m_1 \times n}$, and the negative sample with the label -1 is a matrix $X_2 \in i^{m_2 \times n}$, so that the optimization problem can be expressed as a formula:

$$\begin{cases} \min_{\varpi_1, b_1, \psi} \dfrac{1}{2} \|\gamma(X_1)\varpi_1 + e_1 b_1\|^2 + c e_2^T \psi_1, \\ s.t. -(\gamma(X_2)\varpi_1 + e_2 b_1) + \psi_1 \geq e_2, \psi_1 \geq 0, \end{cases} \tag{5}$$

and,

$$\begin{cases} \min_{\varpi_1, b_1, \psi} \dfrac{1}{2} \|\gamma(X_2)\varpi_2 + e_2 b_2\|^2 + c e_1^T \psi_2, \\ s.t. -(\gamma(X_1)\varpi_2 + e_1 b_2) + \psi_2 \geq e_1, \psi_2 \geq 0, \end{cases} \tag{6}$$

where $c > 0$, ψ_1, ψ_2 is the relaxation vector. In order to obtain the corresponding dual problem, TWSVM assumes that the matrix $J^T J$ sum $H^T H$ is a nonsingular matrix [11], where $J = \gamma(X_1) + e_1$, $H = \gamma(X_2) + e_2$. Under the constraint of this condition, the corresponding dual problem can be expressed as a formula:

$$\begin{cases} \max_{\beta} e_2^T \beta - \dfrac{1}{2} \beta^T H (J^T J)^{-1} H^T \beta, \\ s.t. 0 \leq \beta \leq c, \end{cases} \tag{7}$$

and,

$$\begin{cases} \max_{\beta} e_2^T \chi - \dfrac{1}{2} \chi^T J (H^T H) J^T \chi, \\ s.t. 0 \leq \chi \leq c, \end{cases} \tag{8}$$

where $\beta \in R^{m_2}$, $\chi \in R^{m_1}$ is the Lagrange multiplier.

When $J^T J$ or $H^T H$ is a singular matrix, the corresponding dual problem cannot be expressed in the form of the above two formulas. In order to make the formula hold when $J^T J$ and $H^T H$ are singular matrixes, replace the $(J^T J)^{-1}$ sum $(H^T H)^{-1}$ with the $(J^T J + \varphi I)^{-1}$ sum $(H^T H + \varphi I)^{-1}$, respectively, where $\varphi > 0$ I is the identity matrix. After replacement,

it can be expressed as the following formula:

$$\begin{cases} \max_{\beta} e_2^T \beta - \dfrac{1}{2} \beta^T H (J^T J + \varphi I)^{-1} H^T \beta, \\ s.t. 0 \leq \beta \leq c, \end{cases} \tag{9}$$

And,

$$\begin{cases} \max_{\beta} e_1^T \chi - \dfrac{1}{2} \chi^T J (H^T H + \varphi I)^{-1} J^T \chi, \\ s.t. 0 \leq \chi \leq c. \end{cases} \tag{10}$$

By solving the two dual problems of the above formula, a pair of nonparallel hyperplanes can finally be constructed.

$$\begin{cases} \begin{bmatrix} \varpi_1 \\ b_1 \end{bmatrix} = -(J^T J + \varphi I)^{-1} H^T \beta, \\ \begin{bmatrix} \varpi_2 \\ b_2 \end{bmatrix} = (H^T H + \varphi I)^{-1} J^T \chi. \end{cases} \tag{11}$$

It should be noted that, strictly speaking, the solution formula is only an approximate solution to the original problem. In classification prediction, the unknown sample is closer to the positive (negative) hyperplane than the negative (positive) hyperplane, and the sample is marked as the positive (negative) [12, 13].

In short, the difference between SVM and TWSVM is that SVM separates the positive and negative samples by a maximum interval classification hyperplane, while TWSVM separates the positive and negative samples by a pair of nonparallel hyperplanes [14]. In TWSVM, the decision planes of the two types of samples are based on the other type of samples as constraints, so that the two types of samples are closer to the type of decision plane, and at the same time far away from the nontype of decision plane. The samples are classified by judging the distance between the sample points and the positive and negative decision planes [15].

When dealing with nonlinear problems, the Gemini Support Vector Machine is the same as the ordinary support vector machine, which recognizes linear separation by mapping data samples from the low-dimensional input space to the high-dimensional space [16, 17]. The experiment in this chapter uses the RBF kernel function. The RBF kernel function parameter v and penalty coefficient c affect the prediction performance of the model. Therefore, it is very important to choose the right combination of parameters.

2.2. Blockchain Technology.
With the advent of Bitcoin, a decentralized and highly reliable transaction system based on electronic virtual currency—a system associated with blockchain technology—has slowly emerged. The emergence of Bitcoin has received widespread attention in the financial and computer fields, and research scholars have also begun to further study blockchain technology [18, 19].

2.2.1. Related Concepts of Ethereum. Ethereum is a distributed computer platform based on the public chain, providing a distributed virtual machine that can run a complete scripting language. Ethereum is composed of smart contract layer, incentive layer, consensus layer, network level, and data level [20]. The data layer includes the most basic data structure and account encryption algorithm of the Ethernet core part of the Ethernet, especially the data transmission verification mechanism of each node of the Ethernet. Ethereum adopts a consensus mechanism based on consensus-level verification work [21, 22]. This is mainly used to induce nodes to independently mine and maintain Ethereum. The data layer, network layer, consensus level, and incentive level are also the basic content of the blockchain structure [23].

(1) Data Layer. The data layer merges the data structure of the block with the content related to data encryption. The block is divided into two parts: the block header and the block body. All transaction-related information is contained in the main body [24].

The network layer needs to include the implementation of the P2P network, message delivery mechanism, and data verification. The network layer is a network guarantee for the interaction between Ethernet nodes [25]. Ethernet uses P2P networks to solve the decentralization and other characteristics of Ethernet. Because the P2P network uses flags, the status of each node is the same, and there is no central server. Each node is equivalent to the routing, verification, and sending functions of the Ethernet system. P2P network architecture is the foundation of Ethernet distributed network.

(2) Consensus Layer and Incentive Layer. In a centralized decentralized system, the method for each node to reach a consensus is the main content, and Ethereum also faces the inevitable problems of a distributed system. Ethereum uses a consensus mechanism based on work evidence to enable systems with decentralized decision-making power to reach consensus. Each node solves mathematical problems through the competition of computer power and rewards the first node who solves the problem, thereby promoting the competition of the overall computing power of the network.

Based on the PoW negotiation mechanism, the total computing power of the nodes in the network must be large enough to avoid the concentration of computing power. Therefore, in order to make full use of the total computing power of the entire network, it is necessary to rely on an incentive mechanism that promotes the utilization of the entire network to confirm that the decentralization of Ethernet is safe and reliable.

2.2.2. Smart Contract. Blockchain technology simplifies the value transfer process through its network architecture and the virtual electronic currency it realizes. In the blockchain, a transaction is divided into the following three steps: (1) A sends a message to the blockchain network, and a transaction is defined in the message; (2) B accepts the transaction through broadcast, indicating that B accepts the transaction;

(3) participants in the blockchain network verify the legality of the transaction and complete the transaction. To be sure, this transaction model defines a process in which the owner of a certain currency in the blockchain has changed. But when sending or accepting transactions, the value in the message can also be conveyed, just like the electronic envelope, the electronic currency may be contained in the electronic envelope and transmitted through the network, but it can also transmit some other information to achieve additional utility.

A typical transaction can be regarded as a simple "script," this script is equivalent to a set of instructions. The instruction sets allow nodes in the blockchain to execute transactions. However, when the script changes and contains information other than transactions, then users can use this script to implement complex "transactions." A smart contract is a convenient, verifiable, and executable computer agreement with the terms of a commercial agreement. This concept is not a new concept nor is it proposed by the blockchain. What the blockchain realizes is the decentralization of smart contracts. In other words, smart contracts are built in public databases without central supervision and execution. Participants can automatically execute the content of the contract without the supervision of a third party. Smart procurement is also the basis of blockchain decentralized applications.

In Ethereum, a smart contract is a collection of code and data and is stored in the Ethereum blockchain with the address of the smart contract account. Smart contracts are transmitted on the network in the form of messages, and smart contracts in Ethereum are stored in transactions. EVM judges whether it is a contract type transaction by whether a transaction contains a code. EVM implements the execution of the contract by executing the binary bytecode in the contract. In the Ethereum smart contract, it is defined that the application binary interface (ABI) is strongly typed, and the ABI will be formed and persisted during the compilation of the smart contract. Here, ABI is similar to the regulations in the actual contract, which must be obtained every time the contract is called. The first four bytes of a function call data specify the function to be called. The account uses the smart contract ABI to call the method in the contract.

2.3. Equity Trading Market

2.3.1. Overview of the Equity Market. The positioning of my country's equity trading market has become increasingly clear with the practice of various regional equity markets and the continuous release of relevant policies. From the perspective of policy analysis, the positioning of my country's equity trading market is mainly divided into three aspects: first, the equity trading market is an extension of our multi-level capital market, an important part of my country's capital market system, and it belongs to the private equity market; second, it serves as a platform for small, medium, and microenterprises in provincial administrative regions to cultivate and regulate small, medium, and microenterprises; third, it is a comprehensive platform for local governments to

support and promote the development of small, medium, and microenterprises in the region.

2.3.2. Functions of the Equity Trading Market. The equity trading market does not exist independently. It is an important part of my country's capital market. The main functions of the capital market are basic functions such as the optimal allocation of resources, the dispersion of risks, the transfer of risks, and the determination of prices. It also has a unique function as the foundation of the capital market: to cultivate small, medium, and microenterprises and regulate their development as an incubator; to strengthen the function of local governments to guide and support the development of small, medium, and microenterprises in the region.

The equity trading market is an extension of the capital market's function, which is manifested in the following aspects: (1) optimal allocation of resources: The equity trading market is an important part of the multilevel capital market. The basic function is to adjust the function of funds and transfer the surplus of funds in the market. The fund is transferred to the party lacking funds, but it is biased to serve small, medium, and microenterprises and provide more financing channels for small, medium, and microenterprises; on the other hand, it also provides a new investment platform for institutional investors to make it from small, medium, and microenterprises. (2) Risk diversification and risk transfer: when institutional investors invest in small, medium, and microenterprises, they often face greater investment risks because they face market risks and the moral hazard of major shareholders. The equity trading market provides institutional investors with more investment opportunities, so that it can effectively reduce the risks faced by institutional investors. In the early stages of development, small and medium-sized and microenterprises, especially those in the industry in the introduction and growth stages, have a large demand for funds and often face higher financial risks. The regional equity trading market provides them with equity and convertible bonds. The way in which financing transfers its risk. (3) Determine the price: SMEs can increase their credit by putting stocks into the market by SMEs, thereby expanding financing channels, providing a new evaluation platform, and reducing financing costs.

The unique functions of the equity trading market are (1) the incubator function for cultivating small, medium, and microenterprises and standardizing their development: The equity trading market can carry out professional corporate governance and investment and financing training courses through its own capital market's professional attributes, thereby improving the performance of listed companies. Professional management capabilities and a sound internal control system have laid a solid foundation for its rapid development. (2) Strengthen the ability of local governments to guide and support the development of small, medium, and microenterprises in the region. Since the establishment of China's capital market is to serve state-owned enterprises, and the capital market's characteristics of "dislike the poor and love the rich", a huge number of small, medium, and microenterprises obtain a very small proportion of resources from the capital market. The guidance and support of local governments can effectively reduce the difficulty of financing small and medium-sized enterprises in the capital market and also help local governments develop business clusters with local characteristics, thereby driving the development of local economy and social people's livelihood.

In addition to the above functions of the equity trading market, the equity trading market is also a comprehensive functional market for local governments to promote the development of small, medium, and microenterprises in the region. In this market, local governments can directly introduce targeted preferential policies to attract banks, brokerages, insurance, and VC/PE markets. Participants actively participate in the development of local enterprises. At the same time, the market can also guide equity investment institutions and bond investment institutions to cooperate for high-growth enterprises to introduce comprehensive financing plans for the long-term development of enterprises.

3. Blockchain Equity Trading System Design Model Based on Machine Learning and Big Data Algorithms

Based on the background of machine learning and big data algorithms, this paper designs a blockchain equity trading system model, adopts the Ethereum PBFT consensus mechanism, and through the decentralized smart contract design, it improves computing time and efficiency and reduces the communication overhead. In addition, the implementation process is given in this article, and the experiment is verified.

3.1. Problem Assumptions and Definitions

3.1.1. Problem Assumption. The mechanism proposed in this paper is based on the alliance chain scenario and has the following assumptions: (1) there are n nodes, $\{M_1, M_2, \cdots, M_n\}$, each node is independent of each other, and there is no centralized platform. During the operation of the system, nodes will not be dynamically added or removed. (2) To establish a link between nodes, the verification method provided by Ethernet is required. Verification is considered safe, and malicious nodes cannot pretend to be connected to other nodes in the network. (3) After the node is disconnected, the system tries to reconnect to the node, but the connection fails after the limit time is exceeded, which is an error node.

The generation of a block of the blockchain is jointly decided by all preselected nodes (the preselected nodes participate in the consensus process), and other access nodes can participate in the transaction, but the process is not involved.

3.1.2. Algorithm Definition. The PBFT mechanism has the following definitions:

Definition 1. We set Quorum as a set group, and there is an intersection between the two. The set of system nodes is set to $\nabla = \{W_1, W_2, W_3, \cdots, W_n\}$, and $W_i \subseteq I$ if the formula is satisfied, W is called a quorum.

$$\forall W_i, W_j \in \nabla \quad \text{and} \quad W_i \cap W_j \neq \varphi. \tag{12}$$

Quorum has the following properties: (1) any two quorums have at least one common and correct node. (2) There must be a quorum without errors. Among them, this article defines a $2g + 1$ node as a quorum, which can ensure that there is at least $g + 1$ node in a quorum without errors, where g is the maximum number of error nodes in the system.

Definition 2. The PBFT organization will perform segmentation calculations for the execution process and mark it as b. There are master nodes in the view, the node set is N, the number of master nodes is recorded as q, and the other nodes are called backup nodes. When copying, each node is represented by an integer in order $\{0, 1, \cdots, N - 1\}$, which satisfies

$$q = b \bmod N. \tag{13}$$

Here, b is the number of projections. When the master node in the group fails, the next numbered node will become the master node, and the view number will be modified accordingly.

Definition 3. Certificate (certificate), this article specifies the type of message sent in the system matching process. This message is called a certificate. The request is an information type $\{REPLY, m, b, i\}$. According to the certificate type, m means block or block fragment, b means project number, and i means node number.

3.2. System Design

3.2.1. Description of Consensus Mechanism. In a system with M nodes, the master node q is responsible for generating a block, and after all nodes negotiate and verify the block, they reach a consensus on the block. In order to tolerate Byzantine errors, there must be at least four nodes in the system designed in this paper. Each node adopts the same sequence during initialization. Each node establishes internode communication according to the IP address in the configuration file. After the communication is established, it will send the corresponding public key to other nodes, and the other nodes will complete the verification through the private key signature, and the verification will indicate that a valid connection is established between nodes. During the negotiation process, for a message node, there are three states: preprepare, prepare, and commit, which are represented by $PP_i^{\{v,m,n\}}$, $P_i^{\{v,m,n\}}$, and $C_i^{\{v,m,n\}}$, respectively, where v represents the number of the view, m is the certificate message, and n is the number of the node that sends the certificate message. i is the number of the current node.

In the consensus algorithm, when a certificate is generated, the state of the node is first judged, and the method of the current state will be executed, and at the same time, it will enter the next state, where the preprepare state needs to judge the master node, and only the master node can execute it. When a certificate has passed the three-state condition judgment, it is considered that the content of the certificate has reached a consensus among nodes.

As can be seen from the above, the experiment uses role-based access control (RBAC) and discretionary access control (DAC).

3.2.2. Block Generation Protocol. In the blockchain, transactions are sent in blocks and are permanently recorded in the blockchain. This article uses the Ethereum transaction verification protocol. After the same node confirms the validity of the transaction, the transaction is recorded in batches in the block, and the block is sent. The transaction on this block will be verified by other nodes on the network, and added to the blockchain, the transaction is considered to be executed. When a transaction occurs, the master node writes the transaction into the block and transmits the block. If all the network nodes agree on the block, try to add the block to the blockchain. The whole process is inconsistent. The order of the blocks is guaranteed by the block number and partition value of the block record. If the transaction list is empty, the node monitors the timing and system time of the best block in the blockchain. When the time exceeds t, an empty block will be created and added to the blockchain. There may be network delays in the sending process. The longest time for a block to be added to the blockchain after reaching consensus is Δt. Here, t must satisfy $t > \Delta t$. In this way, when a blank block is created, all transactions will be completed through the network. If an empty block is added to the blockchain, the master node will stop the creation of the block and reset the block after waiting for the transaction to arrive.

3.2.3. Block Verification. The verification process of the block is mainly based on the verification of the block header information. This article combines the block structure in Ethereum to perform the block verification. First, check ParentHash to determine whether the newly generated block points to the BestBlock of the blockchain in this node. When a block does not show the BestBlock of the current blockchain, the block will be added to the list first and another block will be added to the list. The thread surrounds to determine if there is a block that shows the BestBlock of the current blockchain in the list. If there is, it executes the block verification process and tries to add it to the blockchain. When the block points to the BestBlock of the current blockchain, the transactions in the block are first verified. The transactions in the block are sorted according to the time sequence of the transaction execution. According to this order, the Merkle tree can be generated, and the rootHash of the Merkle tree is compared with the root hash of the transaction tree of the new block is verified. The verification will verify each transaction and then generate a copy of the Repository object, where the repository contains the local database data of the node, and the next operation is performed in the copy. Because the state tree verification needs to modify the repository state, the operation in the copy can be rolled back. When the number of transactions in the block, the state tree, and the receipt tree roothash verification are all passed, the copy is submitted, and the block is added to the blockchain. Transaction verification is the core content of the entire blockchain verification. Here, we define the status

transaction function as ω, the transaction is Y, and the execution of the transaction will change the local state database. Here, if the database status is defined as U, then, there is

$$U' = \omega(U, Y). \tag{14}$$

Among them, U' is the changed state, a transaction valid judgment needs to meet the following conditions:

$$u(Y) \neq \omega \wedge U[u(Y)] \neq \omega \wedge Y_n = U[u(Y)]_{\text{nonce}} \wedge v_0 \leq U[u(Y)]_{\text{balance}}. \tag{15}$$

Among them, $u(Y)$ is the initiator of a transaction, which Y_n and v_0 are the nonce and transaction amount in the transaction, nonce is the number of transactions in each account, used to ensure the orderliness of the transaction, and recorded in the account information. When a transaction fails, the local warehouse must implement the rollback function. Here, we define the state $U0$ as the rollback state. Then, there is

$$U_0 = U, \text{ except : } \begin{cases} U_0[u(Y)]_{\text{balance}} = U[u(Y)]_{\text{balance}} - c, \\ U_0[u(Y)]_{\text{nonce}} = U[u(Y)]_{\text{nonce}} + 1. \end{cases} \tag{16}$$

Among them, c is the cost of executing this transaction. Next, the operation of adding the block to the blockchain will be executed, and after the successful addition, the state of the block being generated will be set to empty. Changes in these two states will trigger the next block generation process.

3.3. Implementation of Decentralized System Platform

3.3.1. Ethereum Interface Development. Since Ethereum only provides the Json-RPC call interface, it is necessary to write a Web Service interface for Ethereum to realize the interaction process with the web server. The interface management information is shown in Table 1.

In the smart contract module, it is also necessary to open the Web Service interface and open the web server to call the relevant interface of the smart contract.

3.4. Implementation of Smart Contract. The global variable taskMapping is defined in the smart contract to store all transactions. The structure describes the parameter information of the contract, taskId is used to distinguish tasks, and taskSender and taskReceiver are the account addresses of the task initiator and recipient, respectively. Used for bounty transactions, the amount is the value of the bounty, and state is the current state of the character. The event changeTask is to perform corresponding operations according to the triggered parameters each time it is triggered, including the modification of the task status and the bounty transaction process. Through this smart contract, the decentralization of the task release platform is realized.

4. Blockchain Equity System Transaction Method and System Research Analysis Based on Machine Learning and Big Data Algorithm

4.1. Background Research on the National Equity Exchange Market. Through a certain webpage, you can get the data of the national equity trading centers and show in the form of tables that the development level and overall scale of the Chinese equity trading centers have large regional differences, but the data obtained is still only the data of some provinces in the country. As shown in Table 2, the regional equity trading centers in eastern China are relatively active, especially in Shanghai, Shenzhen (Qianhai), and Zhejiang. These three equity trading centers have relatively more indicators such as the number of listed companies, total shares, and total assets than the central and western regions. This regional difference is directly proportional to the level of economic development and financial development to a certain extent. In particular, it can be seen from the distribution of the number of listed companies in Figure 1 that this trend is more obvious. For example, Shanghai, Shenzhen (Qianhai), Zhejiang, Wuhan, Beijing, and Liaoning equity trading centers in the east are relatively active.

It can be seen from Figure 1 that in terms of the number of listed equity trading platforms, the activity of regional equity trading centers is roughly proportional to the level of economic development and financial development, especially the top transactions. Most of the centers are located in the eastern coastal areas, but there are still equity trading centers such as Guangxi, Xinjiang, Chengdu (Sichuan-Tibet), and Chongqing, and the number of listed companies is relatively large.

The regional differences in the performance of regional equity trading centers are mainly due to the existence of thousands of small, medium, and microenterprises in the eastern coastal area. The huge base number has given birth to a large number of listed companies, and because the financial industry in this region is relatively developed, it can provide enterprises with financial services such as good corporate planning, listing training, and listing counseling, so the number of listings is relatively large. However, due to the limited number of enterprises and imperfect financial supporting services in the central and western regions, the number of listed companies in the equity trading center is limited and the transaction volume is relatively insufficient.

We divided the industries into three categories, namely, industry, agriculture, and service industries, and made specific subdivisions. We selected Y city as the data collection point and collected the number and proportion of the industry distribution. The results are shown in Table 3. From the perspective of industry distribution, at this stage, Guizhou stock exchange center listed companies basically cover industry, agriculture, and service industries, accounting for 80% of the total and emerging industries such as information technology and financial services account for a relatively low proportion.

TABLE 1: Blockchain management interface information.

Name	Parameters and description
AccountInfo	The parameter is the account address, used to query account related information
BlockNum	Used to query the number of current blockchain blocks
BlockInfo	The parameter is the block number, which is used to query the information of the block
ActiveNode	Return the reliable node considered by the current node
Balance	The parameter is the account address. Return the account balance
BatchTransactions	The parameters are the account address and the corresponding account amount. Used for system initialization account amount
BatchAccounts	The parameter is the account address, used to initialize the account

TABLE 2: National equity exchange center data.

Exchange	Number of listed companies	Total number of shares (ten thousand shares)	Total assets (ten thousand yuan)	Total net assets (ten thousand yuan)	Total operating income (ten thousand yuan)
Shanghai equity custody center	8353	77185	2318728.96	1006714.32	845103.31
Qianhai equity exchange center	7588	0.00	8944099.28	3959800.11	1028475.09
Zhejiang equity exchange center	3093	16353	417248.66	164218.83	152012.29
Gansu equity exchange center	2244	16000	464167.32	302259.12	32529.56
Wuhan equity custody center	2154	0.00	43316.71	19912.26	18383.01
Guangzhou equity exchange center	1870	3300	62396.12	47492.84	6138.67
Beijing equity exchange center	1765	0.00	404534.95	259568.38	128411.28
Strait equity exchange center	1465	0.00	130682.83	55944.22	487825.15
Liaoning equity exchange center	1128	0.00	1874387.19	307181.09	301953.34
Guangxi Beibu gulf equity center	735	0.00	2051062.88	975735.54	20322.86
Qilu equity exchange center	630	6636.15	792448.28	197742.58	268369.11
Tianjin equity exchange center	528	5463	2902140.41	1425672.28	761876.04
Xinjiang equity exchange center	510	0.00	794447.95	624536.68	24811.05
Shaanxi equity exchange center	407	0.00	2874714.24	548469.71	2580821.85
Chengdu (Sichuan-Tibet) center	338	0.00	7091.92	4893.71	56.08
Jiangsu equity exchange center	281	0.00	1449275.06	754236.32	71365.69
Chongqing share transfer center	255	14450	1317880.58	300509.70	561124.37

4.2. Performance Analysis of Blockchain Equity Trading System. Figure 2 shows the number of features selected by each method, the time it takes to select features, and the accuracy and accuracy of the selected feature subsets in the prediction of the test set and the time-limited training set. It can be seen from the experimental results in Figure 2 that the accuracy and accuracy of the support vector machine model without feature selection are the worst among many

Distribution map of the number of listing on national
equity trading plaiforms
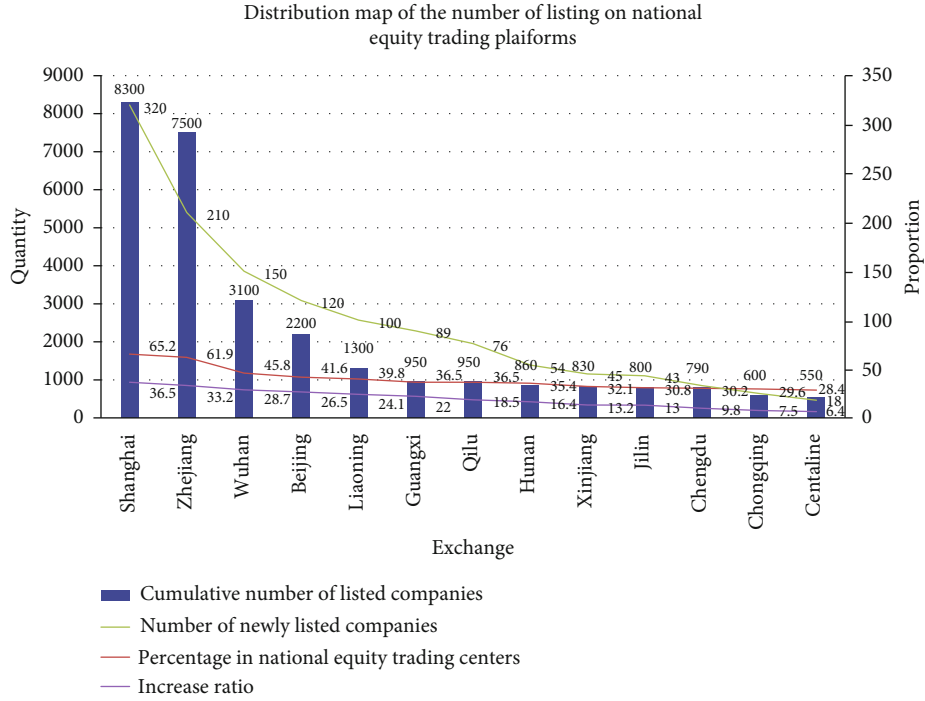
FIGURE 1: Distribution map of the number of listings on national equity trading platforms.

TABLE 3: Industry distribution of listed companies.

—	Industry category	Quantity	Proportion
	Manufacturing	274	23%
Industry	Construction and real estate development	188	16%
	Mining industry	38	6%
	Transportation, storage, and post	32	5.8%
Agriculture	Agriculture, forestry, animal husbandry, and fishery	201	17%
	Information transmission, software, and information technology services	39	3%
	Business and tourism services	132	11.5%
	Wholesale and retail	157	13%
Service industry	Science technology and technical services	31	3.8%
	Financial industry	24	2.8%
	Accommodation and meals	14	2.2%
	Culture and entertainment industry	17	2.5%
	Other	10	2.0%
—	Total	1184	100%

methods, and the training time is also the highest. The feature selection process of the PCA-SVM model is very fast, but its accuracy and accuracy are not as good as the GA-SIM model and DFS-BPSO-SVM model.

It can be seen from Figure 3 that under the basic transaction input vector, the Gaussian radial kernel function performs best, and all indicators perform the highest. The polynomial kernel function has the highest accuracy, but its accuracy, recall rate, and F-measure performance are far inferior to the Gaussian radial kernel western number and linear kernel function. The performance of the sigmoid ker-

nel function is the worst, and the performance of all four evaluation indicators is far inferior to other types of kernel functions. Therefore, at the end of this article, we choose to use the Gaussian radial kernel function to build a dynamic model under the basic market transaction input vector system.

Figure 4 shows the usage rate of the five types of consensus mechanism algorithms on the CPU. It can be seen from Figure 4 that in the single-node test, the CPU usage rate of the PoW consensus mechanism algorithm reached 100%, but the improved PBFT consensus mechanism was only
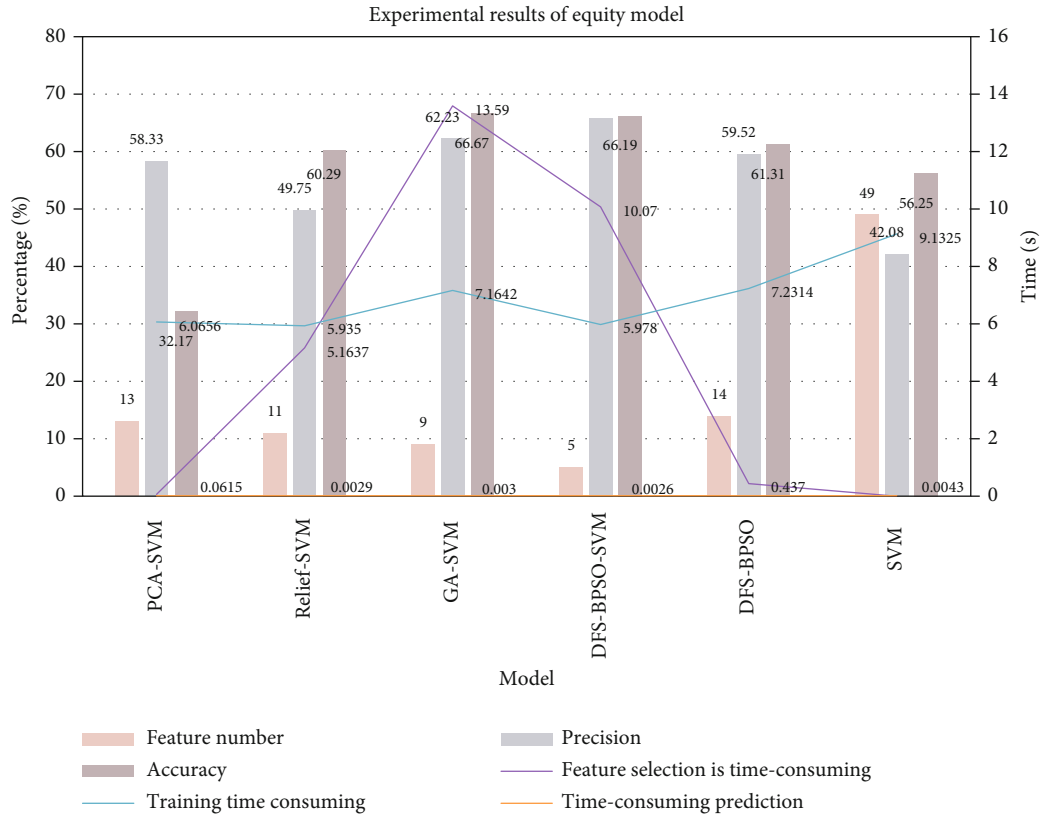
Figure 2: Experimental results of equity trading model.
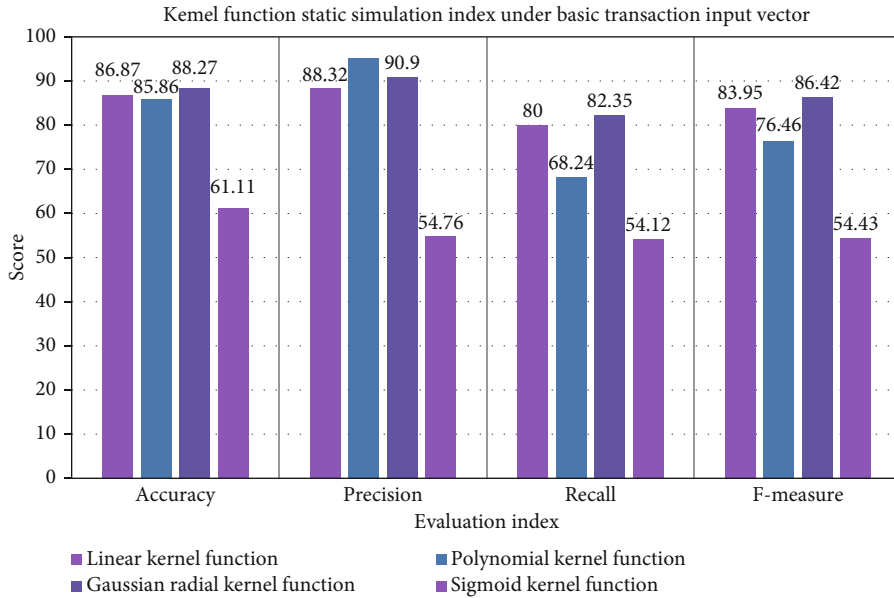
Figure 3: Kernel function static simulation index under basic transaction input vector.

16%, which resulted in a large energy saving and reduced computing power, improved computing performance, and the CPU can also run more stable.

Finally, it is experimentally verified that the improved PBFT mechanism can reduce the data transmission when

the node has an error, and the result is shown in Figure 5. This paper uses the PBFT mechanism and the improved PBFT mechanism to test, respectively. In a complete process of deleting the certificate, the test result of the certificate transmission network overhead is shown in Figure 5. Among
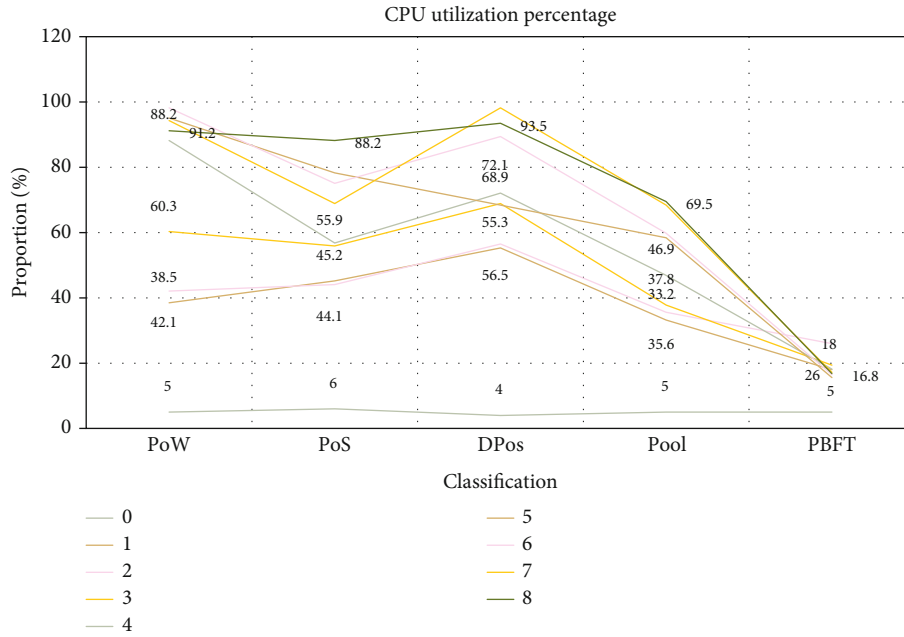
FIGURE 4: CPU usage.
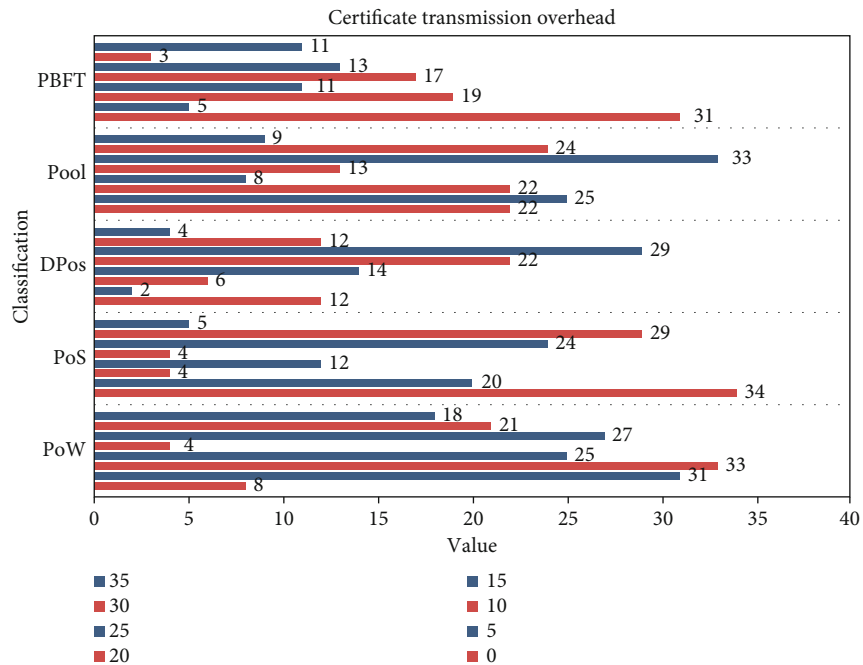
FIGURE 5: Certificate transmission overhead.

them, the abscissa in the figure is the number of certificates that need to be cleared for a checkpoint. In the figure, it is represented by blockcount, and the ordinate represents the transmission consumption, that is, the number of block hashes that need to be transmitted for each checkpoint execution. As can be seen from the figure, the Ethereum certificate delivery overhead using the PBFT consensus mechanism will increase in proportion to the number of blocks contained in the certificate. This is because each cleanup request needs

to transmit the hash value of the block, so the more blocks, the more hash values passed, and the larger the certificate size, which causes a certain network overhead. However, the improved PBFT consensus mechanism is adopted, and there is no certificate transmission, so it is zero.

Figure 6 shows the transmission consumption and overhead required in view switching when an error occurs in the master node. It can be seen from Figure 6 that in the PBFT negotiation mechanism, increasing the maximum number
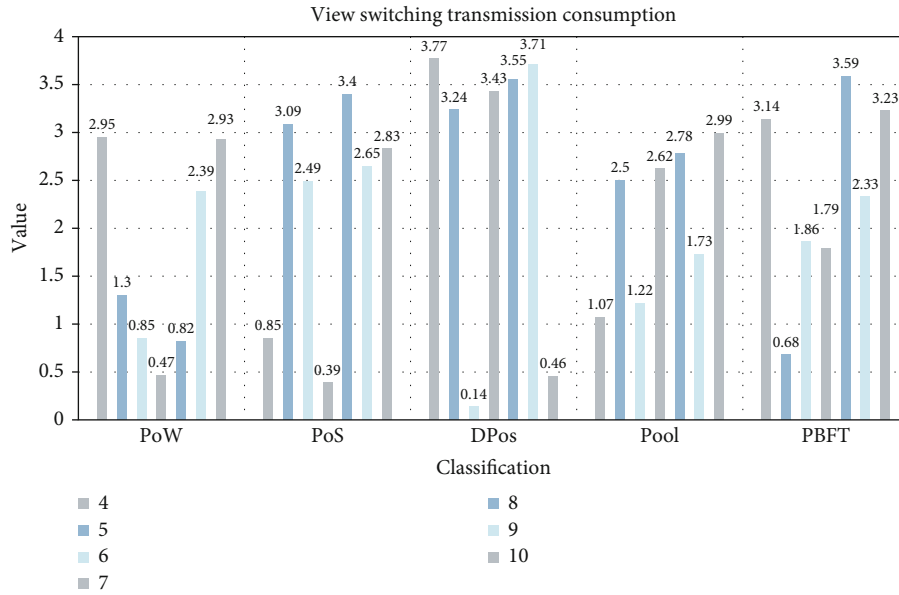
FIGURE 6: View switching transmission consumption.
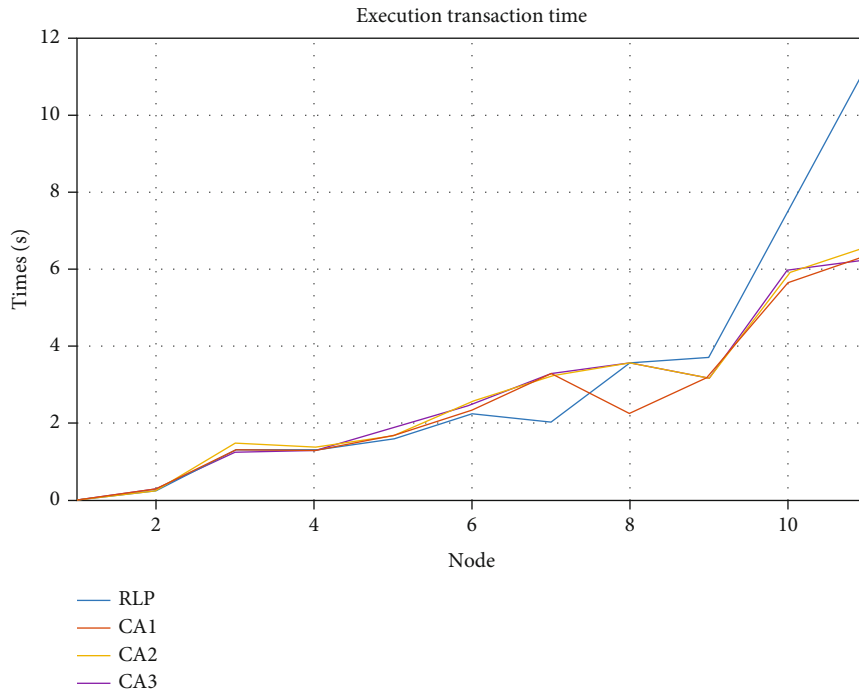
FIGURE 7: Execution transaction time.

of resistances for node errors will increase the cost, while in the improved PBFT consensus mechanism, this part of the cost is zero. This also shows that compared with the PBFT consensus mechanism, the improved PBFT consensus mechanism will increase the overall cost to a certain extent.

This article separately stores 400 accounts in Ethereum's existing RLP encoding method and adds the clustered account classification to the Merkle Patricia tree for testing. This article performs batch transaction execution according to the transaction information in the sample and repeats

the experiment 50 times. Take the average value, and the experimental results are shown in Figure 7. In the figure, CA1 is the K-means clustering algorithm that uses the degree of relevance to select the initial value, and CA2 is the K-means clustering algorithm that uses random sampling to select the initial value. From the figure, it can be seen that the batch transaction execution time is based on the two clustering results. Similarly, so the two clustering results are considered to be similar. For accounts inserted in RLP codes, using the algorithm of two account modifications in one

transaction in Ethereum, the time consumption is significantly higher than the execution time of the related account processing, and the execution time of the related account processing is 70% of the RLP encoding processing. Therefore, by optimizing the account storage structure, the performance of the state tree in Ethereum is improved.

5. Conclusion

This article mainly researches the blockchain equity system trading methods and systems based on machine learning and big data algorithms. In the context of machine learning and big data algorithms, the construction of the blockchain equity trading system has innovated the way of equity trading, improved transaction efficiency, and increased operating efficiency. Taking into account the heterogeneity of nodes and access control strategies, when nodes are added or deleted, data distribution may be uneven, and data accuracy may also be affected. Therefore, there is room for further improvement in the scheme proposed in this article. The innovations of this article are the combination of qualitative analysis and quantitative analysis and the combination of theoretical analysis and empirical analysis, which fully and accurately illustrate the comprehensiveness of the system constructed in this article, overcome the shortcomings of traditional trading methods, and provide new trading methods. The methods have broken through the shackles of the equity trading market and promoted the construction of a new equity market. The disadvantage of this article is that the amount of data in the experimental model is less, and more in-depth research and more detailed analysis are needed. It is hoped that the research in this article can provide effective reference and theoretical support for the construction of the equity market.

Data Availability

Data Availability. No data were used to support this study.

Conflicts of Interest

The authors declare that they have no conflicts of interest.

Acknowledgments

References

[1] M. Boehm, M. W. Dusenberry, D. Eriksson et al., "SystemML," *Proceedings of the VLDB Endowment*, vol. 9, no. 13, pp. 1425–1436, 2016.

[2] Z. Obermeyer and E. J. Emanuel, "Predicting the future-big data, machine learning, and clinical medicine," *The New England Journal of Medicine*, vol. 375, no. 13, pp. 1216–1219, 2016.

[3] S. R. Hamzah, N. Ishak, and A. F. N. Rasedee, "Risk shifting elimination and risk sharing exposure in equity-based financing – a theoretical exposition," *Managerial Finance*, vol. 44, no. 10, pp. 1210–1226, 2018.

[4] A. Buczak and E. Guven, "A survey of data mining and machine learning methods for cyber security intrusion detection," *IEEE Communications Surveys & Tutorials*, vol. 18, no. 2, pp. 1153–1176, 2017.

[5] C. Helma, T. Cramer, S. Kramer, and L. De Raedt, "Data mining and machine learning techniques for the identification of mutagenicity inducing substructures and structure activity relationships of noncongeneric compounds," *J Chem Inf Comput*, vol. 35, no. 4, pp. 1402–1411, 2018.

[6] S. Mullainathan and Z. Obermeyer, "Does machine learning automate moral hazard and error?," *The American Economic Review*, vol. 107, no. 5, pp. 476–480, 2017.

[7] M.-D. Yu, M. Hiller, J. Delvaux, R. Sowell, S. Devadas, and I. Verbauwhede, "A lockdown technique to prevent machine learning on PUFs for lightweight authentication," *IEEE Transactions on Multi-Scale Computing Systems*, vol. 2, no. 3, pp. 146–159, 2017.

[8] Y. Chen, T. Chen, Z. Xu, N. Sun, and O. Temam, "DianNao family," *Communications of the ACM*, vol. 59, no. 11, pp. 105–112, 2016.

[9] E. Hesamifard, H. Takabi, M. Ghasemi, and R. N Wright, "Privacy-preserving machine learning as a service," *Proceedings on Privacy Enhancing Technologies*, vol. 2018, no. 3, pp. 123–142, 2018.

[10] J. Cai, J. Luo, S. Wang, and S. Yang, "Feature selection in machine learning: a new perspective," *NEUROCOMPUTING*, vol. 300, pp. 70–79, 2018.

[11] D. Assouline, N. Mohajeri, and J. L. Scartezzini, "Quantifying rooftop photovoltaic solar energy potential: a machine learning approach," *Solar Energy*, vol. 141, pp. 278–296, 2017.

[12] D. Sacha, M. Sedlmair, L. Zhang et al., "What you see is what you can change: human-centered machine learning by interactive visualization," *Neuro computing*, vol. 268, pp. 164–175, 2017.

[13] M. Zaharia, R. S. Xin, P. Wendell et al., "Apache spark: a unified engine for big data processing," *Communications of the ACM*, vol. 59, no. 11, pp. 56–65, 2016.

[14] E. D. Siew, R. K. Basu, H. Wunsch et al., "Optimizing administrative datasets to examine acute kidney injury in the era of big data: workgroup statement from the 15thADQI consensus conference," *Canadian Journal of Kidney Health and Disease*, vol. 3, no. 1, p. 98, 2016.

[15] S. Athey, "Beyond prediction: using big data for policy problems," *Science*, vol. 355, no. 6324, pp. 483–485, 2017.

[16] M. Chen, Y. Ma, J. Song, C.-F. Lai, and B. Hu, "Smart clothing: connecting human with clouds and big data for sustainable health monitoring," *Mobile Networks & Applications*, vol. 21, no. 5, pp. 825–845, 2016.

[17] S. Underwood, "Blockchain beyond bitcoin," *Communications of the ACM*, vol. 59, no. 11, pp. 15–17, 2016.

[18] D. Kraft, "Difficulty control for blockchain-based consensus systems," *Peer-to-Peer Networking and Applications*, vol. 9, no. 2, pp. 397–413, 2016.

[19] J. Kang, R. Yu, X. Huang, S. Maharjan, Y. Zhang, and E. Hossain, "Enabling localized peer-to-peer electricity trading

among plug-in hybrid electric vehicles using consortium blockchains," *IEEE Transactions on Industrial Informatics*, vol. 13, no. 6, pp. 3154–3164, 2017.

[20] H. J. Kim, "Study on equity of taxation for non-residential property by analysis of actual transaction price," *journal of the korean data & information science sociaty*, vol. 27, no. 3, pp. 639–651, 2016.

[21] L. Xu and X. Yu, "Thorny roses: the motivations and economic consequences of holding equity stakes in financial institutions for China's listed nonfinancial firms," *China Journal of Accounting Research*, vol. 10, no. 2, pp. 105–125, 2017.

[22] B. Grdoi, E. Skreli, and D. Imami, "Determinants of sustainable relationships in the Albanian apple production sector," *International Journal on Food System Dynamics*, vol. 7, no. 1, pp. 50–65, 2016.

[23] B. E. James and J. B. Mcguire, "Transactional-institutional fit: corporate governance of R&D investment in different institutional contexts," *Journal of Business Research*, vol. 69, no. 9, pp. 3478–3486, 2016.

[24] F. Baetje and L. Menkhoff, "Equity premium prediction: are economic and technical indicators unstable?," *International Journal of Forecasting*, vol. 32, no. 4, pp. 1193–1207, 2016.

[25] V. Jha, "Timing equity quant positions with short-horizon alphas," *The Journal of Trading*, vol. 11, no. 3, pp. 53–59, 2016.

WILEY | Hindawi

Research Article

Application of Mathematical Economic Model in Financial System in Manufacturing Industry

Boqi Tang [ID]

School of Economics & Management, Ankang University, Ankang, 725000 Shaanxi, China

Correspondence should be addressed to Boqi Tang; tangboqi@aku.edu.cn

In the field of economic research, most of the sample data is not obtained based on controllable experiments but generated during the normal operation of the economic system. Therefore, the change of an economic variable is usually not caused by a single change of a cause variable. It is the result of a combination of multiple factors. Therefore, it is necessary to study the application of mathematical intelligent computing in computer intelligent manufacturing system. The purpose of this paper is to explore the application of mathematical intelligent computing in computer intelligent manufacturing system. For this reason, this paper uses the furnace temperature control model to carry out simulation experiment. In this simulation experiment, three algorithms of mathematical intelligent computing are mainly used, including BPES intelligent computing method, genetic algorithm, and MARS algorithm. The research results show that the superparameter optimization based on MARS has high efficiency, and the best result, the worst result, the average result, the variance, and the average time of multiple independent runs are controlled below 0.03 s. In this experiment, when the hidden layer node is 9, the prediction error value is the smallest, and the model simulation curve is basically consistent with the measured curve trend. In the simulation experiment of this paper, these three algorithms have shown good results in their respective links.

1. Introduction

Using economic principles to study the causal relationship between two economic variables is an important part of economics knowledge, and it is also an ability that economists should possess. There are a large number of simple causal relationships among various economic variables. The combination of some causal relationships constitutes a causal chain, and various causal chains can develop various complex causal relationships. However, due to the lack of specific technical guidelines for the development of smart manufacturing from digital manufacturing to the development of smart manufacturing, the progress of my country's smart manufacturing application promotion is slow, and there is still a big gap compared with industrialized countries. In this context, my country announced the "Made in China 2025" plan, which advocates innovation-driven intelligent transformation and accelerates the transition from manufacturing to creation.

Intelligent computing technology is to describe the problem object through a specific mathematical model, making it an operable, programmable, computable, and visualized subject. Mathematical intelligent computing technology is an interdisciplinary subject, including computer science, intelligent technology, neuroscience, physics, mathematics, physiology, and psychology [1]. Today, intelligent computing technology has been widely used in interdisciplinary fields, such as neuroinformatic, bioinformatics, and cheminformatics [2]. The advancement of this technology will further promote the development of interdisciplinary subjects such as neuroinformatic, bioinformatics, and cheminformatics. Secondly, the detailed research and further development of the latter will also greatly promote the development of intelligent computing technology [3].

In the current field of intelligent computing, many experts have conducted in-depth research on it. Kusiak proposed a network model and solved the traveling salesman problem. He successfully introduced the concept of "calcu-
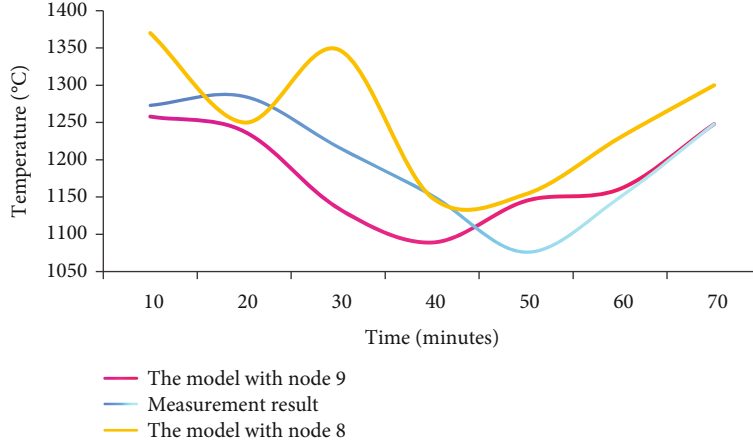
Figure 1: Genetic algorithm for furnace temperature prediction curve.

lated energy function" into the study of neural networks and provided a basis for determining the stability of the network [4]. Thoben et al. proposed a parallel distributed processing theory and at the same time proposed a multilayer network back propagation learning algorithm called BP algorithm [5]. On the basis of observing the activities and behaviors of the herd, Rehman et al. use the information sharing of individuals in the group to make the movement of the entire group produce an evolutionary process from disorder to order in the problem-solving space and obtain solutions [6]. Sprock and Mcginnis pointed out that only through proper design and implementation of intelligent manufacturing system technology can the huge potential value be fully utilized [7]. Nagorny et al. pointed out that the intelligent manufacturing system is a system composed of computers, storage, and network resources. The overall analysis of the intelligent manufacturing system mainly comes from the software control level [8]. Lu and Ju proposed a new technology that describes the intelligent manufacturing system of small cars, which can completely change the implementation of manufacturing and supply chain management and prove the effectiveness of the method and evaluate it through case studies [9].

2. Principles of Mathematical Intelligent Computing and Intelligent Manufacturing System

2.1. The Principle of Mathematical Intelligent Computing. There are many different kinds of algorithms in mathematical intelligent computing. Typical intelligent algorithms include neural network, fuzzy logic, genetic algorithm, ant colony optimization algorithm, particle swarm optimization algorithm, immune algorithm, distribution estimation algorithm, memetic algorithm, and simulated annealing algorithm.

The first is neural network, and now, more is BP neural network, which is a widely used multilayer feedforward neural network. The training of BP neural network mainly depends on error back propagation [10]. Back propagation can adjust network weights and thresholds and solve many

nonlinear problems. The learning process of BP neural network is mainly divided into two stages: forward propagation and backward propagation. The first stage is the forward propagation process. The formula of forward propagation process of BP neural network is shown in the following formula.

$$I_h = \sum_n \omega_{hi} Y_i + b_h. \tag{1}$$

In this formula, I represent the input of neurons in the hidden layer and Y represents the output of neurons in output layer. ω represents the weight coefficient, B represents the vector of hidden layer neurons, and H and I represent the corresponding neurons.

At the beginning of training, multiple sample data sets are input into the network at the same time for processing and finally reach the output layer to output the results. Compare the output value of each set of input samples with the corresponding expected output value to calculate the total error of all samples [11]. If the error does not reach the ideal level or the number of iterations is insufficient, the second stage is back propagation. The original connection path will feed back information, so the network will readjust the connection weight and threshold of each neuron [12]. Then, the output error is adjusted to the minimum, so that the output value of the network is as close as possible to the value given by the actual sample. The most common BP neural structure has an input layer, hidden layer, and output layer, and the calculation formulas of each layer are shown in Figures 1–3.

$$Y_h = f(I_h),$$
$$I_j = \sum_n \omega_{hi} Y_h + b_j, \tag{2}$$
$$Y_j = f(I_j),$$

in which f stands for activation function, which is to judge whether a neuron is activated by receiving all the weighted sums of inputs. I represent the input of neurons in hidden
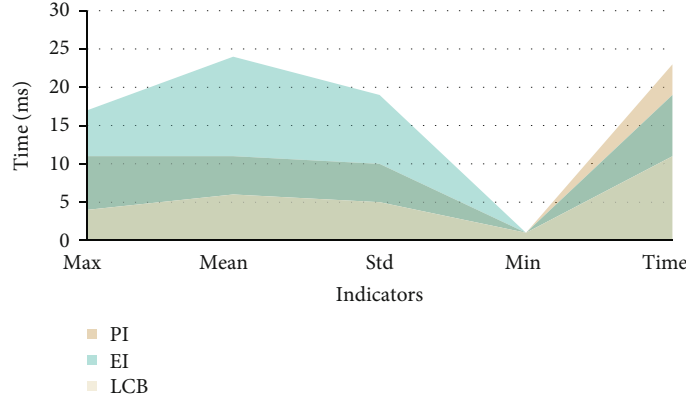
FIGURE 2: Changes in the efficiency of model simulation experiments.
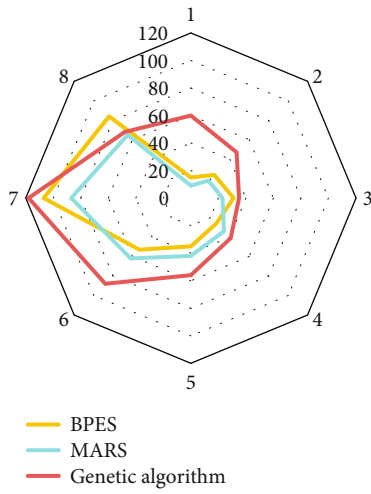
FIGURE 3: Comparison of the application range of intelligent computing.

layer, and y represents the output of neurons in output layer. ω represents the weight coefficient, B represents the vector of hidden layer neurons, and H and I represent the corresponding neurons.

The input layer is used for data input, the hidden layer is used for processing data, and the output layer is used for outputting results. If the network has an input signal, the input signal is first sent to the hidden layer node and then sent to the output layer node of the next hidden layer [13]. When the signal reaches the output layer, the algorithm will correct the weights and thresholds, and the calculation process is shown in Formulas (3) and (4).

$$W_K(K + 1) = W_K(K) + \delta_K^P t_t^p, \qquad (3)$$

$$\theta_k(k + 1) = \theta_k(k) + \delta_K^P t_t^p. \qquad (4)$$

W denotes weight, θ denotes threshold, k denotes any neuron in output layer, p denotes sample, and δ denotes error.

In this process, the propagation of the input signal is carried out layer by layer. BP neural network has at least one hidden layer, but it is difficult to determine the number of

nodes [14]. In the actual network construction process, we mainly use the trial and error method to determine the optimal number of nodes, and the signals are sent layer by layer until the output layer is sent, so BP neural network is a parallel multilayer feedforward network.

Secondly, we will introduce the genetic algorithm in mathematical intelligent computing, which is an algorithm developed according to the biological evolution process and can find the optimal solution by simulating the natural evolution process. Genetic algorithm is a global optimization algorithm with random search. The basic principle of genetic algorithm is to simulate the evolution law of genetic selection and survival of the fittest [15]. The parameters solved in the problem are encoded as chromosomes. Through many iterations, selection, mutation, intersection, and so on, we use genetic manipulation to create and retain excellent individuals to ensure that individuals have the best adaptability. Genetic algorithm has three important operations: chromosome coding and decoding, design of fitting function and genetic manipulation, and parameter adjustment of genetic function [16]. Chromosome coding and decoding solve this problem. The process of constructing chromosomes in a specific order is called coding, and the process of decompiling the optimal single chromosome output by genetic algorithm to solve the problem is called decoding. Today, common coding techniques include binary coding and real coding. Among them, binary coding is a relatively simple and easy-to-use method, which follows the minimum character set coding principle of genetic algorithm [17]. Binary coding is the main choice for coding in genetic algorithm toolbox of MATLAB. The genetic algorithm is shown in the following formula:

$$\begin{cases} \max f(X), \\ X \epsilon R, \\ R \subset U. \end{cases} \qquad (5)$$

X is a decision variable, $\max f(x)$ is an objective function, u is a basic space, and r is a subset of u. The solution x satisfying the constraint conditions is called feasible

solution, and the set r represents the set composed of all solutions satisfying the constraint conditions, which is called feasible solution set.

The main parameters of genetic algorithm are population size, crossing probability, mutation probability, evolutionary algebra, and population initialization method. These parameters determine whether the population will mature prematurely [18]. If the parameter value is too small, it will cause the inbred lines to produce pathological genes. If it is too large, the algorithm will be inefficient. Therefore, the commonly used population size should be between 100 and 200. The execution of genetic algorithm does not depend on the characteristics of the optimization problem itself, and the optimization result can be completed by simple genetic operation. Genetic algorithm searches possible feature strings in space to find good matching strings [19]. In order to perform this search, the algorithm uses only the fitting values related to the inspected points in the search space. No matter how complex the problem itself is, genetic algorithm performs its search by performing the same crossover and accidental mutation operations. In practice, genetic algorithm can search complex and highly nonlinear multidimensional space quickly and effectively.

2.2. Principle and Function of Intelligent Manufacturing System. Intelligent manufacturing system applies mathematical intelligent calculation method to carry out intelligent perception, intelligent reasoning, intelligent decision-making, and intelligent control in the manufacturing process, thus greatly improving the automation and flexibility of the whole manufacturing system [20]. Intelligent manufacturing is the integration of intelligence and manufacturing technology, which uses intelligent technology to solve manufacturing problems. It refers to the representation and learning of manufacturing activity knowledge; the perception and analysis of product life cycle design, processing, assembly, and other linked information; and the realization of intelligent decision-making and execution, manufacturing system, manufacturing equipment knowledge reasoning, dynamic sensing, independent decision-making, and other functions [21]. Intelligent manufacturing is a manufacturing activity, including all links of the whole product life cycle, including some main links: intelligent design, intelligent processing, and intelligent assembly.

Intelligent manufacturing can be divided into three different levels: manufacturing object or product intelligence, manufacturing process intelligence, and manufacturing tool intelligence. Knowledge base/knowledge engineering, dynamic sensing, and independent decision-making constitute the three cores of intelligent manufacturing. Intelligent manufacturing is a higher development stage based on digital manufacturing. Its realization cannot be separated from the foundation of digital manufacturing [22]. Therefore, digital manufacturing technology includes product data management technology, virtual manufacturing technology, rapid prototyping technology, computer-aided inspection technology, and digital manufacturing technology. Control technology is the basic technology of intelligent manufacturing. However, the intelli-

gent manufacturing process focuses on knowledge and reasoning, while the digital manufacturing process focuses on data and information processing. There are essential differences between them. Digital manufacturing system deals with data, but intelligent manufacturing system deals with objects [23]. The processing method of digital manufacturing system mainly stays at the data processing level, while the processing method of intelligent manufacturing system is based on the new generation of artificial intelligence. The mathematical method of digital manufacturing system modeling is a classical mathematical (arithmetic) method. The mathematical method of intelligent manufacturing system modeling is nonclassical mathematics (intelligent mathematics). The performance of digital manufacturing system is declining in use, while intelligent manufacturing system is self-optimizing, and its performance will decline in use. Intelligent manufacturing system has fault tolerance. When the environment is abnormal or abused, the digital manufacturing system will not work normally. Intelligent manufacturing is the result of continuous integration, development, and application of intelligent manufacturing technology. Data mining, machine learning, expert system, neural network, computer vision, Internet of Things, and other intelligent methods are integrated with manufacturing technology to form knowledge representation and modeling technology [24]. Knowledge base construction search technology, heterogeneous knowledge transfer and sharing technology, real-time positioning technology, wireless sensor technology, dynamic navigation technology, autonomous reasoning technology, autonomous compensation technology, autonomous early warning technology, and other types of intelligent manufacturing technologies play an important role in intelligent manufacturing.

The key functions of intelligent manufacturing system are as follows: (1) intelligent perception. Manufacturing equipment of intelligent manufacturing system has the ability to identify unique conditions and environment and supports intelligent analysis and decision-making by identifying and analyzing unique working conditions in real time; (2) intelligent decision. Intelligent manufacturing system has the ability of sensing analysis, making decisions, making decisions, and collecting information. Strong knowledge base is an important element to support intelligent decision; (3) intelligent learning. Intelligent manufacturing system can perform data analysis and mining based on manufacturing operation data or user usage data, so as to continuously improve knowledge base through learning; (4) intelligent diagnosis. Intelligent manufacturing system can automatically diagnose and predict faults based on real-time monitoring of operational data, so as to carry out intelligent troubleshooting and repair; and (5) intelligent optimization. Intelligent manufacturing system can adaptively adjust the organizational structure and operation mode according to the perceived information, so the system performance and efficiency are always the best.

The application models in intelligent manufacturing system can be divided into two types in depth. The first is the traditional shallow learning model, and the second is the deep learning model. The key feature of the shallow model is to use artificial experience to extract the features of samples,

but the focus of the model is mainly on complete classification or prediction. Assuming that there is no error in the application of the model, the quality of functions will become the bottleneck affecting the performance of the whole system [25]. Therefore, R&D teams usually spend a lot of time looking for better functions, which requires R&D personnel to have a deep understanding of the problems to be solved. In order to reach this level, it is usually necessary to repeatedly explore even years of sharpening. Therefore, the function of manually designing samples is not an extensible method [26]. The essence of deep learning is to build a machine learning model with many hidden layers and a large amount of training data, so as to learn more useful functions and ultimately improve the accuracy of classification or prediction. Different from traditional shallow learning, deep learning has the following differences: emphasizing the depth of model structure. There are usually 5, 6, or even 10 hidden nodes. Clearly emphasize the importance of feature learning, that is, the feature transformation of each layer transforms the feature representation of samples in the original space into a new feature space, which is beneficial to classification and prediction. Compared with the way of constructing features by artificial features, deep learning with the features of big data can better explain the rich interior of data. Therefore, in the next few years, more and more examples will use deep learning models with big data instead of traditional shallow models.

Combining mathematical intelligent computing with manufacturing system, various intelligent manufacturing technologies are formed, such as intelligent CAD/CAM technology (ICAD/ICAM), intelligent computer aided process planning technology (ICAPP), intelligent numerical control technology (INC), intelligent database technology (IDB), and intelligent computer integrated manufacturing system (ICIMS). The combination of intelligent methods and manufacturing system models and technologies is very flexible. It can be combined through the commonness of disciplines, levels, and methods, such as knowledge-based digital product/process design, knowledge-based virtual enterprise, illusory virtual technology, and agent-based manufacturing technology. In addition, remote network manufacturing technology, smart grid technology, intelligent Internet of Things technology, intelligent cloud computing technology, intelligent mass data processing technology, and so on have also appeared.

3. General Database Construction Experiment

3.1. Experiment Preparation

3.1.1. Determine Different Mathematical Intelligent Calculation Methods. For big data, the data can be processed and utilized based on intelligent algorithms (such as deep learning) to actively predict output and control all aspects of production. In the absence of data, production can be completed through independent learning. Therefore, different intelligent computing methods are compared to better study them. The situation of multiple algorithms is shown in Table 1.

TABLE 1: The situation of multiple intelligent calculation methods.

	The first algorithm	The second algorithm	The third algorithm
Algorithm	BPES	Genetic algorithm	MARS

3.1.2. Construction of BPES Intelligent Calculation Method. The application of BP neural network in deterministic expert system is called neural network expert system (BPES). According to the rules in the rule base, BPNN is generated, and CF value is used as network weight. Then, BPNN trains and learns according to the training data to form BPES. BPES system extracts IF-THEN rules from knowledge base and generates graphics according to the rules. Deterministic values are used as connection values between nodes of a graph. The specific algorithm is as follows: initialization: rule record parameter $I = 0$, graph record number $k = 0$, rule number in knowledge base KD is m, if it is greater than 0, $m > 0$. Put the first rule r into the knowledge base KD, and then, place d. Otherwise, it ends; select a new rule. Exit if $I = M$, otherwise, determine whether k is the predecessor or successor of R. If so, please increase r to d, otherwise, create a new subgraph. When constructing a BPES intelligent computing method, an empirical formula is needed, as shown in the following formula:

$$h = a + \sqrt{(m + n)}, \tag{6}$$

where a is an adjustment constant between 1 and 10, h is the number of hidden layer nodes, m is the number of input layer nodes, and n is the number of output layer nodes.

The BP algorithm is divided into two steps, namely, forward propagation and backward propagation. Forward propagation passes through all hidden layers and then transmits to the output layer. In the process of layer-by-layer processing, the state of neurons in each layer only affects the state of neurons in the next layer. At the output layer, the current output is compared with the expected output, and if the current output is not equal to the expected output, the BP process is entered. Back propagation used is to transmit the error signal back according to the original forward propagation path and modify the weight coefficient of each neuron in each hidden layer in order to minimize the error signal. In back propagation, an error function is needed, as shown in the following equation:

$$e = \frac{1}{2} \sum_{i=1}^{M} (X_i - Y_i)^2, \tag{7}$$

in which e represents error, X_i represents sample, and Y_i represents expected output. This learning process should be performed for any given sample and expected output until all input and output requirements are met.

3.1.3. The Construction of Genetic Intelligence Algorithm. Genetic algorithm needs to design fitness function. It can be used to evaluate personal strengths and weaknesses and

often changes from the objective function of optimization problems. If the standard function is a maximization problem, it can be used as a direct fitting function. Objective function is a minimization problem, which needs to be transformed into fitness function. Typical methods include converting opposites or each other. The process of optimization calculation using genetic algorithm is as follows: Step 1: determine the solution space and single phenotype X of the problem, and establish an optimization model; Step 2: when executing genetic algorithm, it is necessary to determine the search space and genotype X of individuals in the population. Therefore, the corresponding relationship between x and z should be made clear; Step 3: different mapping relationships will affect, depending on whether genetic algorithm can find the best solution. Therefore, it is necessary to determine the transformation rules from objective function to individual fitness function; Step 4: design gene operator; and Step 5: determine the operation parameters of genetic algorithm: m, h, p, c, and m. In the construction of genetic algorithm, covariance matrix is needed, and the specific formulas are shown in (8), (9), and (10).

$$\sigma_x^2 = \frac{1}{N} \sum_{i=1}^{N} (x_i - \mu_x)^2, \tag{8}$$

$$\sigma_y^2 = \frac{1}{N} \sum_{i=1}^{N} \left(y_i - \mu_y\right)^2, \tag{9}$$

$$\sigma_{xy} = \frac{1}{N} \sum_{i=1}^{N} (x_i - \mu_x)\left(y_i - \mu_y\right), \tag{10}$$

in which σ_x, σ_y, and σ_{xy} represent covariance, μ_x and μ_y represent average value, and x_i and y_i represent sample data.

3.1.4. Construction of MARS Intelligent Algorithm. The basic idea of MARS is to partition the entire data area first and then fit the data by fitting a spline function to each truncated area. The modeling process is usually divided into three steps. The first step is the forwarding process. The forward process is a weighted combination process of different basis functions, giving different basis functions different weights. The transmission process is basically the process of dividing the data area and selecting nodes. Each time a node is selected, a smaller area is divided and a pair of spline functions are generated. The second step is the backward trimming process. The forward process will produce many truncated spline function groups, and the model obtained at this time is overfitting. At present, some basic functions have been deleted and the model complexity has been reduced to prevent overfitting. The third step is model selection. Different models will be generated during the pruning process. People need to find the best model according to certain conditions.

3.2. Experiment Content. After obtaining the input feature vectors and corresponding labels of various algorithms, a network design is needed, including network type, topology, hyperparameters, and optimization algorithm. In order

TABLE 2: Parameter settings.

Parameter	Number of hidden neurons	Initial learning rate	Regularization coefficient
Interval	[10, -625]	[0.00000001, 1.0]	[0.00000001, 1.0]

to ensure the independence of design and verification, network design and optimization are based on the cross-validation set in the data set, network training is based on the training set, and the final network test is based on the test set.

The model used in this paper is the furnace temperature control model, which has many links, including power data processing, heating furnace predictive control, and superparameter optimization. BPES intelligent computing method, genetic algorithm, and MARS algorithm are applied to this model. BPES intelligent calculation method is mainly used in power data processing, genetic algorithm is mainly used in predictive control of heating furnace, and MARS algorithm is mainly used in superparameter optimization. The details are as follows:

3.2.1. Application Process of BPES Intelligent Calculation Method in Power Data Processing. The power data processing process has many complicated processes, and it is more difficult to operate stably for a long time. Over the years, operators have often managed power data based on years of experience, and accumulating such experience requires long-term operating experience and extensive knowledge. Therefore, a neural network is used based on the deterministic expert system. The training and learning expert system are used to supplement the knowledge base of the power 0 data fault diagnosis system and improve the learning ability and diagnosis accuracy of the system.

The application process is as follows: initial training: according to the generated network diagram, the training is carried out according to the BP algorithm. When the error is met or the number of training times is reached, the training ends; learning process: the network is fully connected, and the initial weight of the new connection is set to -1; retraining: train a fully connected network, and the training encounters errors or reaches the end of the training time.

3.2.2. Parameter Setting of MARS in Hyperparameter Optimization. In the Internet age, methods and technologies for handling large amounts of data are particularly important. Multivariate adaptive regression spline is a regression method that can handle high-dimensional data. The experimental parameters are set as follows. The initial random number of points is set to $2d + 1$. d is the dimension of the optimization problem. Due to the optimization of functions, the number of iterations set in the experiment is 500. For the hyperparameter optimization of the machine learning model, the number of iterations set in the experiment is 100. In the hyperparameter optimization based on MARS, the adaptive sampling method used is CAND.
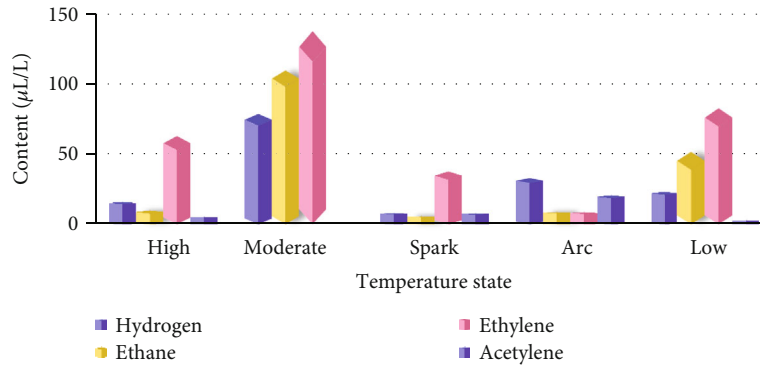
FIGURE 4: Comparison of transformer sample data.

4. Digital Intelligent Computing Application Results

4.1. Analysis on Application Effect of Mathematical Intelligent Calculation in Computer Intelligent Manufacturing System. Based on the above configuration, the experiment of MARS for hyperparameter optimization mainly optimizes the following hyperparameters. That is, the size of hidden layer neurons, the type of optimization algorithm (solver), the type of activation function, the initial learning rate, and the regularization coefficient. The parameters are shown in Table 2.

As shown in Table 2, the number of hidden layer neurons is set to [10-625], and the initial learning rate and regularization coefficient are both set to [0.00000001, 1.0]. This ensures that MARS can have a good effect comparison when applied to hyperparameter optimization. If the parameters change after optimization, the application effect of MARS can be evaluated. If the parameters are not set in advance, there is no good standard for proceeding.

The BPES intelligent calculation method is applied to power data processing. More than 1,000 rules have been obtained from the actual data of the power supply design laboratory, of which more than 600 are related to transformer failures as shown in Figure 4.

4.2. Analysis on the Efficiency of Mathematical Intelligent Computing in Computer Intelligent Manufacturing System. Use MARS to screen and sort on hyperparameter optimization. Min, Max, Mean, Std, and time, respectively, represent the best result, worst result, average result, variance, and multiple times when various data-driven optimization algorithms perform multiple minimums on the same optimization problem. In the average time of independent operation, GP-PI, GP-EI, and GP-LCB represent optimization based on the acquisition functions PI, EI, and LCB, respectively. It is very important to observe its work efficiency, because hyperparameter optimization is to find a set of suitable hyperparameters in a limited time.

As shown in Figure 2, the efficiency of hyperparameter optimization based on MARS is very high. The best results, worst results, average results, variance, and average time of multiple independent runs are all controlled below 0.03 s. Of course, this is also related to the lack of sample data. The computational complexity of the data-driven hyperpara-

meter optimization algorithm involves two main aspects. On the one hand, it comes from functional evaluation, involving the training and testing of machine learning models. Another aspect is the establishment and update of regression models.

The era of big data puts forward higher requirements on intelligent computing technology. With the in-depth research and development of deep models such as deep learning, the widespread use of GPUs and other computing devices, and the rapid development of distributed parallel algorithms, intelligent computing technologies for big data have now been applied to speech recognition, facial recognition, image recognition, search engine, and other fields. A horizontal comparison of three intelligent computing technology application fields: MARS, genetic algorithm, and BPES, was performed.

As shown in Figure 3, the application interval similarity of MARS, genetic algorithm, and BPES is above 67%. Not only that, the application of BPES intelligent computing technology is more extensive than the other two groups, but in general, the three groups of algorithms. There are many intersections in the application. This shows that the three sets of algorithms have good optimization performance and play an important role in many fields.

5. Conclusions

(1) With the rapid development of economics, people are not only concerned about the qualitative economic relationship in practical problems but also more concerned about the quantitative relationship between various economic variables, so as to maximize their own benefits with better decisions. The requirements for digital intelligence in various fields are getting higher and higher, and the application scope of intelligent manufacturing systems is expanding, it is urgent to solve this problem. And mathematical intelligent computing technology plays an important role in integrating data and improving efficiency. Through the research on the application of mathematical intelligent calculation in computer intelligent manufacturing system, it is found that mathematical intelligent calculation has significant application effects in many fields

(2) The purpose of this article is to explore the application research of mathematical intelligent calculation in the computer intelligent manufacturing system; construct BPES, genetic algorithm, and MARS intelligent calculation methods; and carry out the in-power data processing, heating furnace predictive control, and hyperparameter optimization. In application, to measure the application effect of BPES, genetic algorithm, and MARS, it is found that the application effect of mathematical intelligent calculation is very good, and the effect is significant in big data processing and temperature prediction

Data Availability

The data used to support the finding of the article are available upon the author's reasonable request.

Conflicts of Interest

The author declares that there are no conflicts of interest.

References

[1] P. Verma, S. K. Sood, and S. Kalra, "Smart computing-based student performance evaluation framework for engineering education," *Computer Applications in Engineering Education*, vol. 25, no. 6, pp. 977–991, 2017.

[2] S. Vijaykumar, S. G. Saravanakumar, and M. Balamurugan, "Unique sense: smart computing prototype for industry 4.0 revolution with IOT and Bigdata implementation model," *Indian Journal of Ence & Technology*, vol. 8, no. 35, pp. 1–4, 2015.

[3] H. J. Jung, F. Shang, E. S. El-Alfy, Q. Shi, C. Y. Yeun, and C. Leung, "Editorial note: smart computing with innovative multimedia technologies and applications," *Multimedia Tools and Applications*, vol. 76, no. 4, article 4445, pp. 5785-5786, 2017.

[4] A. Kusiak, "Smart manufacturing must embrace big data," *Nature*, vol. 544, no. 7648, pp. 23–25, 2017.

[5] K. D. Thoben, S. Wiesner, T. Wuest, BIBA – Bremer Institut für Produktion und Logistik GmbH, the University of Bremen, Faculty of Production Engineering, University of Bremen, Bremen, Germany, and Industrial and Management Systems Engineering, ""Industrie 4.0" and smart manufacturing – a review of research issues and application examples," *International Journal of Automation Technology*, vol. 11, no. 1, pp. 4–16, 2017.

[6] A. U. Rehman, D. S. Necsulescu, and J. Sasiadek, "Robotic based fire detection in smart manufacturing facilities," *IFAC Papers OnLine*, vol. 48, no. 3, pp. 1640–1645, 2015.

[7] T. Sprock and L. F. Mcginnis, "A conceptual model for operational control in smart manufacturing systems," *IFAC Papers OnLine*, vol. 48, no. 3, pp. 1865–1869, 2015.

[8] K. Nagorny, P. Lima-Monteiro, J. Barata, and A. W. Colombo, "Big data analysis in smart manufacturing: a review," *International Journal of Communications Network & System Ences*, vol. 10, no. 3, pp. 31–58, 2017.

[9] Y. Lu and F. Ju, "Smart manufacturing systems based on cyber-physical manufacturing services (CPMS)," *Ifac Papersonline*, vol. 50, no. 1, pp. 15883–15889, 2017.

[10] F. Lopez, M. Saez, Y. Shao et al., "Categorization of anomalies in smart manufacturing systems to support the selection of detection mechanisms," *IEEE Robotics & Automation Letters*, vol. 2, no. 4, pp. 1885–1892, 2017.

[11] J. Herwan, S. Kano, R. Oleg, H. Sawada, and M. Watanabe, "Comparing vibration sensor positions in CNC turning for a feasible application in smart manufacturing system," *International Journal of Automation Technology*, vol. 12, no. 3, pp. 282–289, 2018.

[12] K. S. Wong and M. H. Kim, "Privacy protection for data-driven smart manufacturing systems," *International Journal of Web Services Research*, vol. 14, no. 3, pp. 17–32, 2017.

[13] Y. T. Lee, S. Kumaraguru, S. Jain et al., "A classification scheme for smart manufacturing systems' performance metrics," *Smart Sustain Manuf Syst*, vol. 1, no. 1, pp. 52–74, 2017.

[14] C. Cimini, R. Pinto, and S. Cavalieri, "The business transformation towards smart manufacturing: a literature overview about reference models and research agenda," *Ifac Papersonline*, vol. 50, no. 1, pp. 14952–14957, 2017.

[15] F. B. Lunelli and I. Cecconello, "Definition and application of a maturity model for smart manufacturing, from the perspective of Industry 4.0," *Scientia cum Industria*, vol. 7, no. 2, pp. 126–134, 2019.

[16] N. Anwer, B. Eynard, L. Qiao, and P. Maropoulos, "Editorial for the special issue on 'smart manufacturing and digital factory'," *Proceedings of the Institution of Mechanical Engineers Part B Journal of Engineering Manufacture*, vol. 233, no. 5, pp. 1341–1341, 2019.

[17] Y. Liu, X. S. Zhang, L. Zhang, F. Tao, and L. H. Wang, "A multi-agent architecture for scheduling in platform-based smart manufacturing systems," *Frontiers of Information Technology & Electronic Engineering*, vol. 20, no. 11, pp. 1465–1492, 2019.

[18] H. S. Sim, "A study on the development and effect of smart manufacturing system in PCB line," *Journal of Information Processing Systems*, vol. 15, no. 1, pp. 181–188, 2019.

[19] S. Mittal, M. A. Khan, D. Romero, and T. Wuest, "Smart manufacturing: characteristics, technologies and enabling factors," *Proceedings of the Institution of Mechanical Engineers Part B Journal of Engineering Manufacture*, vol. 233, no. 5, pp. 1342–1361, 2019.

[20] F. Tao, Q. Qi, L. Wang, and A. Y. C. Nee, "Digital twins and cyber-physical systems toward smart manufacturing and Industry 4.0: correlation and comparison," *Engineering*, vol. 5, no. 4, pp. 653–661, 2019.

[21] M. Shahin, F. Chen, H. Bouzary, and K. Krishnaiyer, "Integration of Lean practices and Industry 4.0 technologies: smart manufacturing for next-generation enterprises," *The International Journal of Advanced Manufacturing Technology*, vol. 107, no. 5-6, pp. 2927–2936, 2020.

[22] B. C. Menezes, J. D. Kelly, A. G. Leal, and G. C. le Roux, "Predictive, prescriptive and detective analytics for smart manufacturing in the information age," *IFAC-Papers Online*, vol. 52, no. 1, pp. 568–573, 2019.

[23] L. Wang, G. Wu, and L. Gao, "Thematic issue on "advanced intelligent scheduling algorithms for smart manufacturing systems"," *Memetic Computing*, vol. 11, no. 4, pp. 333-334, 2019.

[24] K. T. Park, D. Lee, and S. D. Noh, "Operation procedures of a work-center-level digital twin for sustainable and smart manufacturing.," *International Journal of Precision Engineering and Manufacturing-Green Technology*, vol. 7, no. 3, pp. 791–814, 2020.

[25] S. W. Pickl, B. Tao, T. W. Liao, and F. Tao, "Editorial for the special issue on "Intelligent computing and system towards smart manufacturing"," *Journal of Ambient Intelligence and Humanized Computing*, vol. 10, no. 3, pp. 825–827, 2019.

[26] J. Tan, L. Daxin, L. Zhenyu, and J. Cheng, "Study on the key technology approaches from digital manufacturing to intelligent manufacturing," *Engineering Science in China*, vol. 19, no. 3, pp. 39–44, 2017.

WILEY | Hindawi

Research Article

Art Effect of Photographic Darkroom Stunt Simulation Based on Mobile Computing to Synthesize Images across Image Moving Selected Regions

Wen Liu [ID], Feng Qiu, and Xi Zeng

School of Art & Design, Wuhan Institute of Technology, Wuhan, 430205 Hubei, China

Correspondence should be addressed to Wen Liu; 09091401@wit.edu.cn

Prior to the advent of digital image processing technology, image composition primarily used human vision to identify colors and artificially convert them. However, manually synthesizing and transforming graphics images will not only consume a lot of manpower, time, and energy but also due to manual limitations in the process of synthesizing and coloring the pictures, the resulting pictures cannot meet people's needs. In order to improve the speed and quality of image synthesis, and to synthesize the pictures people need more quickly and accurately, this article synthesizes the image based on the movement calculation across the selected area of the image and analyzes the photographic darkroom special effects of the synthesized image to simulate the artistic effect. Using case analysis method, literature analysis method, and other methods, the database was collected and a model of photographic darkroom stunt simulation artistic effect recognition was built. The results of the study found that the composite image based on the movement calculation across the selected area of the image is better than the composite image of other algorithms, and the quality of hue and saturation is more than 30% higher than other synthesis methods. It should be verified by experiments. The results are significantly different. This shows that the composite image based on moving calculation across the selected area of the image can achieve good results in the photographic darkroom stunt simulation artistic effect.

1. Introduction

Which are the basic information of society, are a bridge between 3D objects and 2D information. It allows people to simply build three-dimensional shapes in their consciousness through images. Images are mainly divided into analog images and digital images. The images that can often be seen in life are analog images, such as books, advertisements, televisions, and pictures [1, 2]. Digital image is a form of functional expression that converts analog images into information that can be processed by a computer. The analog images obtained by various devices such as cameras and scanners can be processed into digital information. The form of the digital information of an image is usually a two-dimensional function, where the parameter domain of the function is the coordinate of the pixel of the image, and the value domain is the value of the image pixel, which often represents its color information [3].

As an important branch of information fusion, image fusion integrates the disciplines of sensor technology, signal processing, image processing, and artificial intelligence and is an effective way to accurately obtain image information. Multifocus image fusion is the focus of research in the field of multisource image fusion, overcoming the problem of single images in terms of spectral, shape, and spatial resolution [4–6]. Among them, pixel-level fusion information is less lost, and more detailed information is acquired, which has become the mainstream direction of multifocus image fusion research. However, pixel-level fusion requires high registration accuracy, and a large amount of image details need to be processed in the fusion process, and the real-time performance is poor. With the continuous improvement of information technology, various image fusion technologies will be widely used in various fields. In the continuous application and research process, it will also continue to develop and improve. Detailed research on the basic theory, methods,

and applications of image fusion technology proves to have very important practical significance for the development of the national economy, defense construction, and follow-up work of image processing [7, 8].

For the research of synthetic images, experts at home and abroad have also done long-term research. Image synthesis is first carried out in the analysis and processing of remote sensing images. Since then, the fusion of infrared images and visible light images has gradually become a new research hotspot [9]. Abroad, MChandana et al. proposed a multifocus medical image fusion method based on wavelet transform and conducted experiments on CT, MRI, and X-ray photographs. Experiments show that it has ideal performance. HZMa et al. proposed a new multifocus image fusion method, which considers the energy of low-frequency coefficients instead of focusing on the fusion rules of high-frequency coefficients. The simulation results prove the feasibility of this method. However, image fusion based on wavelet transform has two main shortcomings: lack of translation invariance of various scales and poor direction selectivity [10]. In order to make the image effect more natural and the visual effect more realistic, Cohen may propose a color-coordinated color migration algorithm. The algorithm uses a suitable palette to perform color migration on the reference image, and the color of the image is balanced and coordinated by changing the foreground or background hue [11]. In China, Xiang Shiming et al. proposed a pyramid model of color migration. The idea of this algorithm is to realize the offset between the reference image and the corresponding subblock information of the target image through comparison, so as to achieve the purpose of color offset between images [12]. In addition, Teng Shenghua et al. proposed a color migration algorithm by analyzing the extended nature of color from local to global and solving the Laplace equation [13]. When performing color migration on text images, Ru Chao proposed a color migration algorithm for text images, such as unclear text borders and weak text edge fonts. By using the guided filtering enhancement algorithm on the original image and the reference image to increase the proportion of the text in the image, and then using the color shift algorithm to calculate the color shift coefficient of the enhanced source image and the reference image, the color shift effect of the text image is obvious to improve [14]. Su Xinjun proposed color migration based on texture similarity. Through the principal component analysis of the texture features extracted from the image, the feature texture space is constructed, and the image is segmented on this basis. The region formed after segmentation establishes the mapping relationship between texture information and color information and realizes the color shift. The diffusion problem of color shift at the boundary [15].

This article is based on existing group photos and manages the group photo image set. The image registration process slows down the calculation due to the inaccuracies in the initial matching point pairs. This paper proposes a feature matching method based on disparity constraint and cluster analysis. The cluster analysis is introduced into the feature point image registration method, and this stage is improved. Real-time and accuracy of registration results.

The feature point detection and edge detection are used to mark the feature points in the photo, and different methods are used to synthesize the characteristic area and the noncharacteristic area, which not only achieves the effect of feature synthesis but also shortens the synthesis time.

2. Synthetic Image Method

2.1. Image Registration. Normally, the original image cannot be directly used in the vision system, so preprocessing becomes an indispensable process in image fusion. Commonly used preprocessing methods in image fusion include image grayscale transformation, size transformation, and image registration. In image fusion processing, especially pixel-level image fusion processing, the fusion quality drops sharply due to slight differences in pixel positions and pixel gray level noise contamination. This is important for the overall performance of the image fusion system as a whole. Therefore, image registration has become an indispensable preprocessing step in image fusion [16–18].

Image registration can be understood as the process of matching (corresponding, overlapping, etc.) images of the same scene obtained by one or more sensors (usually different types of sensors) under different time and space conditions, that is, establishing feature correspondence. Make the spatial positions of the same target information in different images overlap as much as possible. It can usually be regarded as a key step in the preprocessing stage of technology such as image fusion and target recognition. At the same time, it has been widely used in medical image processing [19]. Among them, the feature point matching method is the key direction, which mainly includes feature point detection and matching, transformation model estimation, image resampling, and transformation. Among them, feature point detection and matching is the most difficult and research hotspot in registration technology. These two links are related to the real-time and accuracy of image registration [20].

As the basic carrier of recorded information, images play a huge role in daily life production. Various image processing and applications are gradually being valued by researchers in various fields. For example, the colorization of medical images can be realized by a variety of algorithms based on color shift, which improves the accuracy of diagnosis and treatment and the efficiency of image segmentation; the color shift of multilevel region matching can realize the natural transition color of the video; structural texture decomposition uses color shifts to perform detailed processing on fabric images. Color shifts based on texture similarity can achieve better texture fusion and achieve the desired objectives for better results in 3D reconstruction [21].

According to the different multisource image acquisition channels, multisource images can be roughly divided into multisensor image sources, remote sensing image sources, and similar sensor image sources (including multifocus images, multiexposure images, and time series images). The system functions of the image sources are different, and it is impossible to establish a general fusion scheme and quality evaluation mode. Because of this, scholars in the field of image fusion are still looking for a general theoretical

framework. Therefore, it is difficult to classify image fusion technology uniformly and clearly [22]. As far as pixel-level image fusion is concerned, the existing algorithms are mainly based on image fusion in the transform domain and image fusion in the space domain. Image fusion based on the transform domain first needs to transform the multisource images and, then, complete the fusion at the pixel level, while the image fusion based on the spatial domain is usually directly fused at the pixel level of the image. The two pixel-level image fusion methods are not independent of each other. In fact, according to different purposes and different images, various methods are usually used in combination [23, 24].

2.2. Image Embedding.

Clustering usually means splitting a particular set into multiple classes. This increases the correlation within the class and makes the correlation between the classes uncorrelated or low. Clustering uses "correlation" as a measurement. For example, in zoology, animals are divided into viviparous and oviparous animals according to the way they reproduce their offspring. This is a simple clustering method based on certain characteristics. To put it simply, clustering is based on a certain classification standard, and the data is summarized and classified according to the classification standard, so that the objects within the class have greater relevance, and the objects outside the class have greater differences [25]. Clustering is usually divided into three steps. First, select the features of the object, extract them, and describe the correlation between the objects according to the extracted features. In group image coding, the correlation between images is determined by the distance between the images. Description: second, select the appropriate clustering algorithm and cluster the given objects to get the clustering results; third, test the clustering results [26].

After the reference image is determined, a series of transformations need to be performed on it to generate a transformed image. The transformed image has a stronger correlation with the reference image, and better coding efficiency can be obtained. Then, use the model obtained after screening to perform perspective transformation and photometric transformation on the reference image to obtain the final transformed image. The formula is

$$P(f_1, \cdots, f_n) = P\left(f_1 \middle| f_{n(i)}\right), \tag{1}$$

where $f(i)$ refers to the neighborhood node of the ith node in the image. The test photo and output portrait can be expressed as

$$P(I_s, I_p) = P\left(I_s^1, \cdots I_s^n, I_p^1, \cdots I_p^n\right),$$
$$\varepsilon \prod_{(i,j)} \psi\left(I_s^i, I_s^j\right) \prod_k \phi\left(I_s^i, I_p^i\right). \tag{2}$$

The formula (i, j) represents that i and j are two adjacent positions. According to the Markov weight field model, the relationship between the photo block and the corresponding weight is shown in the following formula:

$$P\left(I_p^1, \cdots, I_p^n, w^1, \cdots, w^n\right) \varepsilon \prod_{i=1}^n \varphi \prod_{(i,j)} \varphi\left(w^i, w^j\right). \tag{3}$$

Among them, similar to the MRF algorithm

$$\phi = \left(I_p^i, w^i\right) = \exp\left\{-\frac{\left\|I_p^i - \sum_{k=1}^k w_k^i I_{pk}^i\right\|^2}{2\sigma_d^2}\right\},$$

$$\varphi\left(w^i, w^j\right) = \exp\left\{-\frac{\left\|\sum_{k=1}^k w_k^j o_k^{ji}\right\|^2}{2\sigma_s^2}\right\}. \tag{4}$$

Similarly, i and j are two adjacent image blocks, which o_k^{ij} represent the pixel vector on the ith block in the overlapping area when the ith block and the jth block overlap.

2.3. Image Color Processing.

With the advent of the Internet information age, all kinds of information are transmitted to the Internet at all times, and the number of pictures that can be obtained has increased significantly. With the acquisition of massive picture information, more and more channels are available for obtaining pictures. Many, convenience has also been significantly improved [27]. As the basic carrier of recorded information, images play a huge role in daily life production. The various processing and applications of images are gradually being valued by researchers in various fields. For example, colorization of medical images can be achieved by a variety of algorithms based on color transitions. This improves the accuracy of diagnosis and treatment and the efficiency of image segmentation. Color transitions with multilevel region matching allow you to achieve natural transition colors in your video. By structural texture decomposition. The color migration can be used for deep processing of cloth images; and the color migration based on texture similarity can achieve better texture fusion, so that it can get better results in three-dimensional reconstruction and achieve the desired purpose [28]. It plays an important role in life, health, security control, satellite, industry, entertainment, and commerce. Since most of the obtained original images are meaningless, in order to meet different needs, people need to process the colors of the obtained images.

With the rapid development of image processing technology in recent years, color migration is an important research issue in the field of image processing. It still has very important application value in image segmentation and texture style changes. Color migration is currently widely used in various fields. For example, in various styles of picture apps, the seasonal information expressed by the image can be easily changed through color migration, and the rendering of the scene and the production of special effects can be achieved through color migration [29]. In the field of remote sensing, continuously collected images cannot maintain color consistency due to light temperature and other reasons. Through color migration, the collected pictures can be unified, so that the stitched panoramic image has a natural transition. In terms of image texture style, color migration can
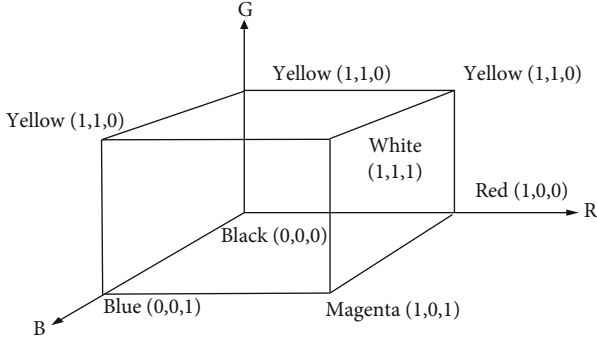
Figure 1: Color RGB color space.

make the transition and fusion of texture more natural; in terms of the expression style after image stitching, a consistent effect can be obtained. With the development of virtual reality technology, color migration will also have important application value in this field. Because users need to get a high degree of natural feedback in the simulation environment, in the 3D real-time modeling, the required scene can be quickly changed through color migration, making the constructed scene more natural, and the virtual reality and color scenes are enhanced. All aspects have significant significance [30].

Color is a color that is perceived through light, brain, and life experience. Color space is the basis for studying the color migration of pictures. This article briefly introduces the RGB color space. As shown in Figure 1, the RGB color space obtains different colors through different coordinate values of R, G, and B, that is, by comparing red, green, and yellow. The coordinate value of each color produces the corresponding color value. But in fact, the superposition of the three primary colors cannot produce all the colors. The colors contained in the RGB space are located in the area as shown in the figure, and the corresponding coordinate points are different colors. The diagonal line means that the three components of the point have the same value, which means that the image based on the diagonal line color is a grayscale image without color.

Color is expressed mainly through hue, saturation and intensity. Color conversion as formula

$$H = \begin{cases} \theta & B \le G, \\ 360 - \theta & B > G. \end{cases} \tag{5}$$

Here,

$$\theta = \arccos \left\{ \frac{1/2[(R-G) + [R-B]]}{(R-G)^2 + (R-G)(G-B)^{1/2}} \right\}. \tag{6}$$

The saturation is as follows:

$$S = 1 - \frac{3}{(R+G+B)} [\min (R, GB)]. \tag{7}$$

Intensity component is as the following:

$$I = \frac{1}{3} (R + G + B). \tag{8}$$

Perform brightness regulation processing on the image, and determine the mapping relationship between the input image color area to which the pixel belongs and the reference image color area by calculating the matching similarity between the reference image pixel point and the input image color area, and get A one-to-one mapping relationship between the reference color area of each image and the input area.

$$l_{ref(n)} = \frac{\sigma_{in}^l}{\sigma_{ref(n)}^l} * \left(l_{ref(n)} - \mu_{ref(n)}^l \right) = \mu_{ref(n)}^l,$$

$$f(in_i, ref_i(n)) = \frac{1}{p_{ref}^i} * \left| \mu_{ref_i(n)} - \mu_{in_i} \right|. \tag{9}$$

Because the color migration based on the optimal transmission theory does not depend on the color space, and the theory does not require a single point-to-one mapping in color matching mapping. When the image is relatively large, it stores more pixels and more color values. Optimal transmission between the reference image and the shape image will consume a lot of time. Therefore, it can be performed by clustering the image colors. Processing to improve the efficiency of transmission matching. The algorithm flow chart is shown in Figure 2:

The key to color migration is to choose a suitable and superior color matching mapping relationship. When various algorithms establish color mapping, they consider the direct transmission between colors. When there are more color pixels in the image, the time complexity of the algorithm processing will increase [31]. After clustering the image colors, when matching, it is easy to cause unnatural color transitions and other phenomena. Therefore, the algorithm in this chapter proposes a color matching strategy based on the optimal transmission theory on this basis and considers that when the color difference of different reference images changes greatly, it is hoped that the color change of the target image is not very obvious, so that it can be independent the purpose of finding a variety of different reference images to obtain colorful result pictures [32, 33].

3. Image Synthesis Experiment

3.1. Subjects. In this paper, we process the images selected for image features to resemble the color distribution between the images, reducing the color noise caused by discrete optimal transmission multimapping and increasing the number of reference images. The phenomenon can be reduced. It can be adjusted sensitively to changes. In order to normalize the color of the image, the similarity of the color distribution between the images needs to be measured. Use relative entropy to measure the similarity between two color distributions. The selected image is shown in Figure 3:

FIGURE 2: Image color migration process.

FIGURE 3: Selected picture.

tion of the cluster center points through each iteration. This paper takes the cluster centers obtained by the K-means algorithm and their proportions in the color space as the new cluster center. Reclassify the pixel to the cluster to which the closest center point belongs, recalculate the updated cluster center, and the number of pixels contained in each cluster, and perform the above operations on all points in the cluster until the center point of the cluster class obtained after a certain iteration is consistent with the center point of the last cluster class, or the maximum number of iterations is reached. Stop the iteration at this time and save the clustering results, otherwise repeat the operation.

3.4. Statistics. All data analysis in this article uses SPSS19.0, statistical test uses two-sided test, significance is defined as 0.05, and $p < 0.05$ is considered significant. The statistical results are displayed as mean ± standard deviation ($x \pm$ SD). When the test data complies with the normal distribution, the double T-test is used as the comparison within the group, and the independent sample P test is used as the comparison between the groups. If the regular distribution is not sufficient, two independent samples and two related samples will be used for inspection.

4. Experimental Analysis of the Artistic Effect of Image Synthesis

4.1. Image Processing. We first perform relevant processing on the selected pictures, use MATLABR2010a version software to write programs, process moving pictures and non-moving pictures, and compare different experimental results. The results are shown in Figures 4 and 5.

From the picture, we can see that in the traditional method of detecting moving targets, when the target and background colors are similar, problems such as incomplete

3.2. Image Preprocessing. Because the color migration based on the optimal transmission theory does not depend on the color space, the theory does not require a single point-to-one mapping in color matching mapping. When the image is relatively large, it stores more pixels and more color values. Optimal transmission between the reference image and the shape image takes a lot of time. Therefore, it can be done by clustering the colors of the image, processing to improve the efficiency of transmission matching. When the image is large, the stored color information value is large, and the mapping and matching between pixels will consume a lot of time. Therefore, clustering the image colors can simplify the optimal transmission and mapping and matching between image colors and time.

3.3. Image Clustering. First, randomly select the initial cluster points of a given number of clusters, and update the informa-

(a)

(b)

(c)

FIGURE 4: Traditional filter processing.

(a)

(b)

(c)
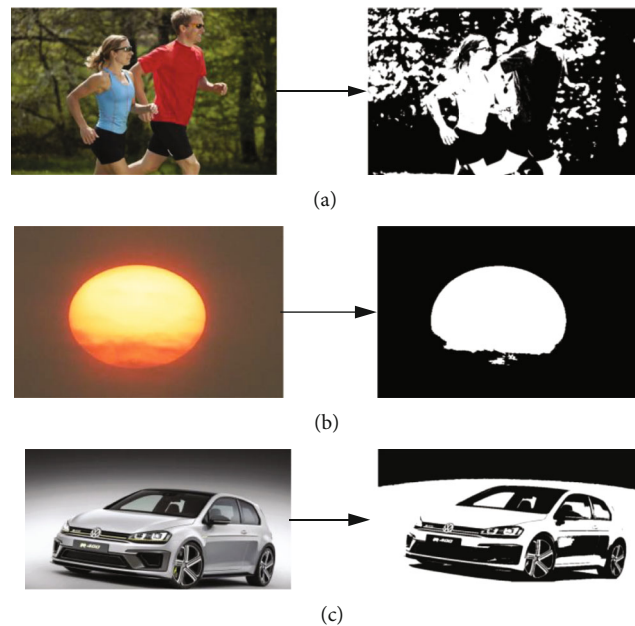
FIGURE 5: Using the algorithm of this article.

detection of the target, discontinuous contour or even no detection of the target will occur, as shown in the detection result in Figure 4. The improved method significantly improves this problem, makes the detected contour of the moving target clearer than the traditional method, and enriches the internal content of the contour. It can extract the moving target better and completely and segment the target area more accurately. In the traditional algorithm and the algorithm in this paper, the image parameters are shown in Tables 1 and 2:

Through comparative analysis, the most similar image set selected by the optimal insertion image set selection method is consistent with the subjective judgment of the human eye. The optimal insertion image set selection is shown in the table. Moreover, the cosine similarity between the most similar image set and the subsimilar image set generally has a big difference. Therefore, the optimal insertion image set selection method based on the packet model is suitable for selecting the image set with the highest similarity for the insertion image in the group image.

TABLE 1: Image parameters of traditional algorithms.

Insert picture	The most similar image set selected by the algorithm	Cosine similarity	The most similar image set selected by the algorithm	Cosine similarity	Subjectively judged set of most similar images
A	Corner	0.7713	Sculpture	0.6441	Corner
B	Defense	0.7197	Xidian	0.3025	Defense
C	Sculpture	0.6331	Corner	0.4965	Sculpture

TABLE 2: Image parameters of the algorithm in this paper.

Insert picture	The most similar image set selected by the algorithm	Cosine similarity	The most similar image set selected by the algorithm	Cosine similarity	Subjectively judged set of most similar images
A	Corner	0.9213	Sculpture	0.8341	Corner
B	Defense	1.0197	Xidian	0.5139	Defense
C	Sculpture	0.8246	Corner	0.6532	Sculpture

(a)

(b)

FIGURE 6: Synthetic picture effect.

TABLE 3: Differences in image parameters.

	A	B
Sculpture	40.75	90.38
Defense	85.50	87.95
Patheon	69.20	91.71

It can be seen from the table that when only one image is inserted, the coding structure generated by the new coding structure adjustment method for image insertion selects a reference image for the inserted image, and uses the selected reference image to encode the inserted image. The efficiency is better than the node-based structural adjustment method.

4.3. Different Filtered Synthetic Picture Artistic Effects. We compare the parameters of pictures synthesized by different methods. Different image synthesis algorithms are prone to synthesis errors and inaccurate synthesis when facing unclear image edges. Through comparison, we can find the best synthesis method, and improve the artistic effect of the image. The details are shown in Table 4.

From the table, we can see that the quality of the composite image is different in different algorithms. From the table, we can see that in terms of image parameters, whether it is hue, saturation, etc., the image quality of the method used in this article is all. The parameters are higher than other methods, which shows that the method used in this article can have certain advantages in image synthesis. In order to verify the superiority of the method in this paper, we have performed multiple statistics on the relevant parameters and calculated the error between them, as shown in Figure 7:

From Figure 7, we can see that the errors between the data used in this experiment are all less than 0.05, which proves that the experimental data is within the error and there is no significant difference, so it can be used. This shows that the image synthesis method used in this article is better than other image synthesis methods.

4.2. Image Synthesis. Regularization processing is mainly used in the field of image restoration. Because regularization usually repairs jump edges in image restoration, and the optimal transmission mapping obtained based on the discrete optimal transmission, the color transfer is irregular in the performance of the color result image density. We can use the regularization of the pixel area to perform denoising processing on the obtained optimal transmission mapping result to improve the quality of the result of the color shifted picture. As shown in Figure 6, we combine Figures 6(a) and 6(b).

From this figure, you can see that the distances between the inserted and referenced images in the two image sets are quite different. This is because the inserted image and the corresponding image of the node in the image are completely different. The A image set is compared to the nodes in the B image. The corresponding image difference is small, so the distance difference to the reference image is small. The parameters between the two figures are shown in Table 3.

TABLE 4: Image synthesis under different algorithms.

	Tone	Saturation	Brightness	Transparency	Pixel
Group image synthesis	2.02	2.16	2.36	2.28	2.44
Multi-focus image synthesis	2.03	2.46	2.47	2.23	2.04
High dynamic image synthesis	2.06	2.09	2.5	2.14	1.82
Fast processing of image synthesis	2.03	2.31	2.24	2.22	2.12
Move composition across images	4.94	5.29	4.9	5.16	5.11
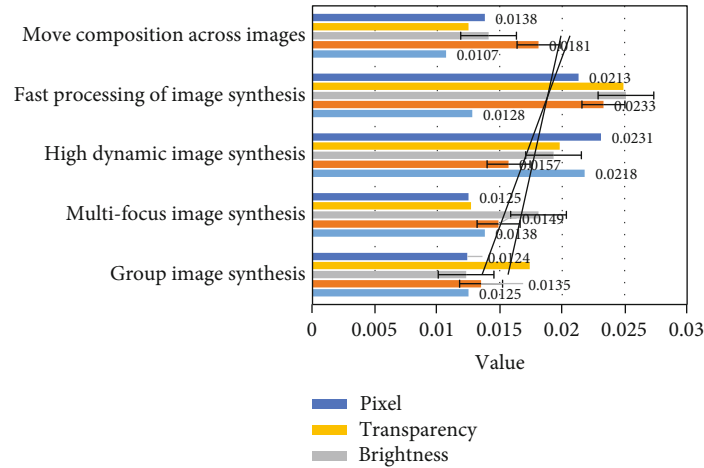
FIGURE 7: Parameter difference value.

5. Conclusion

Graphic image composition is an important method in information processing, pattern recognition, and artificial intelligence. Composite images also have many application areas such as cultural relic restoration, styling, 3D texture fitting, and graphic search. Image color is not only used in traditional application areas, such as changing the color to make it richer and fuller, and coloring pictures and videos such as black and white fading. In emerging computer fields such as artificial intelligence, image retrieval, and art, 3D reconstruction still plays an important role. This paper has done an in-depth study on the color migration between color images and the color migration of grayscale images in the composite image, and the color transformation of video images is also studied. Because the information contained in the grayscale image is less than the information contained in the color image, the coloring of the grayscale image is researched, even if the algorithm results show a good grayscale image color migration result, and there is no in the running time. But for the coloring of grayscale images, the richness of colors is still a problem that needs to be solved. The evaluation method of image synthesis still relies on subjective methods. Different subjective evaluation standards may result in different evaluation results. With the development of algorithms such as machine learning, image migration algorithms can obtain the desired color migration more objectively result.

Data Availability

Data sharing not applicable to this article as no datasets were generated or analyzed during the current study.

Conflicts of Interest

The authors declare that they have no conflicts of interest.

References

[1] S. B. Liu, J. H. Wang, R. Y. Yuan, W. X. Zhao, L. Li, and Q. H. Wang, "Real-time and ultrahigh accuracy image synthesis algorithm for full field of view imaging system," *Scientific Reports*, vol. 10, no. 1, pp. 12389–12392, 2020.

[2] W. Jiang and X. Luo, "Research on unsupervised coloring method of Chinese painting based on an improved generative adversarial network," *World Scientific Research Journal*, vol. 5, no. 11, pp. 168–176, 2019.

[3] H. Yang, W. Kim, K. Kim, Y. J. Park, H. J. Han, and J. H. Ryu, "An increased remote sensing observation by goci daily composite image," *Journal of Marine Science and Technology*, vol. 24, no. 6, pp. 1161–1170, 2016.

[4] A. Takeda, K. Yoshimura, and S. H. Saar, "The Hinode/XRT full-Sun image corrections and the improved synoptic composite image archive," *Solar Physics*, vol. 291, no. 1, pp. 317–333, 2016.

[5] S. K, M. Elhoseny, L. S K et al., "Optimal feature level fusion based ANFIS classifier for brain MRI image classification,"

Concurrency and Computation: Practice and Experience, vol. 32, no. 1, p. 24887, 2020.

[6] J. Uthayakumar, M. Elhoseny, and K. Shankar, "Highly reliable and low-complexity image compression scheme using neighborhood correlation sequence algorithm in WSN," *IEEE Transactions on Reliability*, vol. 69, no. 4, pp. 1398–1423, 2020.

[7] D. Shuang and J. Wenxiao, "DWI manifestations and DCE-MRI quantitative analysis of the activity evolution of brain parenchymal tuberculosis after treatment," *Chinese Journal of Medical Computer Imaging*, vol. 26, no. 4, pp. 301–305, 2020.

[8] Z. Lv, D. Chen, R. Lou, and H. Song, "Industrial security solution for virtual reality," *IEEE Internet of Things Journal*, vol. 99, 2021.

[9] S. Wan, Y. Zhao, T. Wang, Z. Gu, Q. H. Abbasi, and K. K. R. Choo, "Multi-dimensional data indexing and range query processing via Voronoi diagram for internet of things," *Future Generation Computer Systems*, vol. 91, pp. 382–391, 2019.

[10] Y. Zhou, J. Peng, and C. Chen, "Extreme learning machine with composite kernels for hyperspectral image classification," *IEEE Journal of Selected Topics in Applied Earth Observations & Remote Sensing*, vol. 8, no. 6, pp. 2351–2360, 2017.

[11] S. Yang and S. Yuda, "Application of close-range photogrammetry combined with unsupervised image cluster classification method in road paving pothole judgment," *Pavement Engineering*, vol. 17, no. 3, pp. 59–66, 2019.

[12] Y. Kang, F. Wang, Z. Zhang, N. Li, and F. Lv, "Edge detection of composite insulators hydrophobic image based on improved canny operator," *Energy & Power Engineering*, vol. 5, no. 4, pp. 593–596, 2016.

[13] M. Mingming, X. Lin, C. Zhijie et al., "CT imaging on development of the fetal spinal canal of T12 vertebrae," *Anatomy and Clinics*, vol. 22, no. 3, pp. 177–180, 2017.

[14] H. Zhu, Y. Bin, D. Wei, L. Mo, and Y. Zhengxu, "Preoperative three-dimensional image measurement combined with laser navigator-assisted puncture for transforaminal approach percutaneous endoscopic discectomy," *Journal of Spine Surgery*, vol. 17, no. 1, pp. 17–23, 2019.

[15] S. Tao, "One-dimensional line pattern detection system based on image and laser interference technology," *China Metrology*, vol. 45, no. 437, pp. 96–98, 2017.

[16] Z. Lu, H. Lu, X. Lin, C. Huang, and Y. Qiu, "A new method for measuring the internal deviation of pedicle screws using X-ray imaging data," *Journal of Spine Surgery*, vol. 17, no. 4, pp. 262–266, 2019.

[17] S. Wan, Y. Xia, L. Qi, Y. H. Yang, and M. Atiquzzaman, "Automated colorization of a grayscale image with seed points propagation," *IEEE Transactions on Multimedia*, vol. 22, no. 7, pp. 1756–1768, 2020.

[18] M. Elhoseny and K. Shankar, "Optimal bilateral filter and convolutional neural network based denoising method of medical image measurements," *Measurement*, vol. 143, pp. 125–135, 2019.

[19] L. Shuxin, R. Cheng, and L.-m. Sheng, "Application of improved canny operator in the evaluation of industrial image clarity," *Journal of Chongqing Normal University: Natural Science Edition*, vol. 34, no. 2, pp. 86–90, 2017.

[20] Srinivasa K G, Sowmya BJ, A. Shikhar, R. Utkarsha, and A. Singh, "Data analytics assisted internet of things towards building intelligent healthcare monitoring systems," *Journal of Organizational and End User Computing*, vol. 30, no. 4, pp. 83–103, 2018.

[21] Y. Yang, L. Wei, and G. Wang, "3D imaging model to measure the best passage of S1 sacroiliac joint screw and its clinical application," *Chinese Journal of Traumatology and Orthopedics*, vol. 21, no. 2, pp. 138–143, 2019.

[22] S. Kamiya, S. Iwano, H. Umakoshi et al., "Computer-aided volumetric measurement of partial solid lung cancer based on CT: solid component size prediction prognosis," *International Journal of Medical Radiology*, vol. 41, no. 4, pp. 113-114, 2018.

[23] R. E. Jung, P. Grohmann, I. Sailer et al., "Evaluation of a one-piece ceramic implant used for single-tooth replacement and three-unit fixed partial dentures: a prospective cohort clinical trial," *Clinical Oral Implants Research*, vol. 27, no. 7, pp. 751–761, 2016.

[24] S. S. Francisco, A. D. J. Soares, and R. D. Murrer, "Evaluation of elementary education teachers' knowledge on avulsion and tooth replantation," *RSBO*, vol. 12, no. 1, p. 32, 2016.

[25] A. A. Kamenskikh, T. N. Ustjugova, and A. G. Kuchumov, "Comparative analysis of mechanical behavior of the tooth pair contacting with different mouthguard configurations," *IOP Conference Series: Materials Science and Engineering*, vol. 511, no. 1, pp. 3–12, 2019.

[26] P. Toti, S. Marconcini, G. Enrica, G. Pedretti, A. Barone, and U. Covani, "The influence of prosthesis design on the outcomes of tooth-implants immediately placed and loaded by means of one-piece titanium restoration," *Journal of Oral Implantology*, vol. 44, no. 2, pp. 87–93, 2017.

[27] S. Schnutenhaus and R. G. Luthardt, "Ceramic implants and potential advantages of a one-piece design," *Implantologie*, vol. 25, no. 2, pp. 163–173, 2017.

[28] D. R. Lekhadia, G. Hegde, and K. Sindhuja, "A modified three-piece base arch for en masse retraction and intrusion in a class II division 1 subdivision case," *International Journal of Orthodontic Rehabilitation*, vol. 8, no. 2, p. 81, 2017.

[29] Z. C. Muñoz, A. D. Caballero, E. E. Gómez, Y. R. Gómez, and L. T. Carrillo, "Soft tissues and bone healing response in impacted third molar osteotomies," *Revista Odontológica Mexicana*, vol. 21, no. 1, pp. e29–e32, 2017.

[30] S. A. Basheer, R. J. Govind, A. Daniel, and A. Rao, "Comparative study of piezoelectric and rotary osteotomy technique for third molar impaction," *Journal of Contemporary Dental Practice*, vol. 18, no. 1, p. 60, 2017.

[31] J. Hartlev, T. Klit Pedersen, and S. E. Nørholt, "Cone beam computed tomography evaluation of tooth injury after segmental Le Fort I osteotomy," *International Journal of Oral and Maxillofacial Surgery*, vol. 48, no. 1, pp. 84–89, 2019.

[32] B. Wang, X. Sun, P. . Feng, C. . Yan, and X. . Jia, "Solution and verification of cutter position for machining split equal-base circle bevel gear," *Mathematical Problems in Engineering*, vol. 2019, Article ID 8024701, 14 pages, 2019.

[33] B. M. Andreasi, M. A. Lopez, L. Confalone, R. M. Gaudio, L. Lombardo, and D. Lauritano, "Clinical outcome of a two-piece implant system with an internal hexagonal connection: a prospective study," *Journal of Biological Regulators and Homeostatic Agents*, vol. 30, 2 Suppl 1, pp. 7–12, 2016.

WILEY | Hindawi

Research Article

Workflow Scheduling Based on Mobile Cloud Computing Machine Learning

Fanghai Gong [ID]

Guangdong Lingnan Institute of Technology, Guangzhou, 510663 Guangdong, China

Correspondence should be addressed to Fanghai Gong; 1311410609@st.usst.edu.cn

In recent years, cloud workflow task scheduling has always been an important research topic in the business world. Cloud workflow task scheduling means that the workflow tasks submitted by users are allocated to appropriate computing resources for execution, and the corresponding fees are paid in real time according to the usage of resources. For most ordinary users, they are mainly concerned with the two service quality indicators of workflow task completion time and execution cost. Therefore, how cloud service providers design a scheduling algorithm to optimize task completion time and cost is a very important issue. This paper proposes research on workflow scheduling based on mobile cloud computing machine learning, and this paper conducts research by using literature research methods, experimental analysis methods, and other methods. This article has deeply studied mobile cloud computing, machine learning, task scheduling, and other related theories, and a workflow task scheduling system model was established based on mobile cloud computing machine learning from different algorithms used in processing task completion time, task service costs, task scheduling, and resource usage The situation and the influence of different tasks on the experimental results are analyzed in many aspects. The algorithm in this paper speeds up the scheduling time by about 7% under a different number of tasks and reduces the scheduling cost by about 2% compared with other algorithms. The algorithm in this paper has been obviously optimized in time scheduling and task scheduling.

1. Introduction

With the widespread popularization and application of Internet technology, as well as the rapid growth of information, the data that scientific research and business need to face and process has become increasingly large and complex, far exceeding the computing power of the existing IT infrastructures. In order to solve the problem of large-scale and massive processing, the concept of cloud computing is proposed. Cloud computing is a new resource delivery and service provision model. Cloud computing service providers can transfer various software and hardware resources to the cloud computing environment to provide users with abundant computing resources and computing services, such as large-scale scientific computing services and data storage services. At this point, users only need to dynamically select the appropriate resources according to their own needs and pay a certain fee to the cloud service provider, avoiding the need for users to buy large-scale software and hardware equipment

(saving resource investment costs) or to develop specific applications for time overhead.

In recent years, the application range of cloud computing has become wider and wider, covering all aspects of our lives. With the continuous improvement of cloud computing processing task capability, people's requirements for hardware have gradually changed from pure device functionality to service quality claim. For example, service cost, time, flexibility, security, scalability, and reliability are all factors that need to be considered in cloud computing. This is also the main reason why cloud computing has become a research hotspot today.

According to Tawalbeh et al., mobile devices are increasingly becoming an indispensable part of people's daily lives and are conducive to performing various useful tasks. Mobile cloud computing integrates mobile and cloud computing to expand its functions and benefits, overcoming their limitations, such as limited memory, CPU power, and battery life. Big data analysis technology can extract values from data. Data has four aspects: volume, change, speed, and accuracy.

Tawalbeh et al. discussed online healthcare and the role of mobile cloud computing and big data analysis in its implementation. With the application of cloud computing in the field of healthcare, the development and momentum of networked medical applications and systems have also emerged. They reviewed the techniques, tools, and applications of big data analysis. Finally, the research results of using big data and mobile cloud computing technology to design networked medical systems are summarized. The prospects for networked medical care are put forward. However, their research results did not actually solve the application problems in related fields, and there are still many problems in actual operations [1]. Buczak and Guven introduced a centralized literature review of machine learning (ML) and data mining (DM) methods for network analysis to support intrusion detection. A short tutorial description of each ML/DM method is provided. Based on the number of citations or the relevance of emerging methods, they identified, read, and summarized papers that represent each method. Since data is very important in ML/DM methods, they introduced some well-known network data sets for ML/DM. Then, they discussed the complexity of ML/DM algorithms, discussed the challenges of using ML/DM algorithms in network security, and put forward some suggestions on when to use a given method. However, they did not innovate in this area nor did they combine with other applications to explore practical applications [2]. According to Masdari et al., workflow scheduling is a prominent problem in cloud computing. Its goal is to complete the execution of the workflow by considering the service quality requirements of the workflow (such as deadlines and budget constraints). Aiming at the simple and scientific workflow scheduling problem in cloud computing, many latest workflow scheduling schemes have been proposed in the literature, and they have conducted a comprehensive review and analysis of these schemes. They clarified the goals of scheduling schemes in cloud computing, and they classified the proposed schemes according to the type of scheduling algorithm applied in each scheme. In addition, each program is explained and a comprehensive comparison is made to highlight their goals, characteristics, and limitations. Finally, the conclusions and future research directions are put forward. However, their research plan only considers a single effect, and they did not conduct a combined study of multiple goals [3, 4].

The innovations of this article are as follows: (1) We combined qualitative research with quantitative research and fully analyzed the research data. (2) We combined theoretical research with empirical research based on mobile cloud computing and machine learning theory, and then we investigated based on the specific situation of workflow task scheduling.

2. Research Method of Workflow Scheduling Based on Mobile Cloud Computing Machine Learning

2.1. Cloud Computing

2.1.1. Cloud Computing Overview. Cloud computing is developed on the basis of utility computing, distributed comput-

ing, and virtualization. It can integrate different software and hardware resources into a large "resource pool" through virtualization technology [5], and users can use the Internet Visit as the "resource pool" and then purchase these computing resources according to their own needs [6]. At present, there is no unified definition of cloud computing. Many research scholars and institutions have defined cloud computing according to their own understanding.

According to the National Institute of Standards and Technology (NIST), cloud computing is defined as a kind of computing resource (including networks, servers, storage, applications, and services) that can be obtained through the Internet in a convenient and on-demand manner. These resources come from a configurable and shared resource pool [7], and they only need very little management effort from the users and enable users to quickly configure and release related computing resources without interacting with cloud providers [8]. In summary, cloud computing can also be called grid computing; it can complete the processing of tens of thousands of items of data in a short period of time (a few seconds), so as to achieve powerful network services, and through a system composed of multiple servers, it can process and analyze these small programs to get the results and return them to the user.

2.1.2. Features of Cloud Computing. The concept of cloud computing is constantly changing with the development of technology. However, regardless of the future development of cloud computing, cloud computing will have the following major characteristics:

(1) Virtualization [9]: cloud computing can integrate many different hardware physical resources into a large virtual resource pool through virtualization technology, which can be managed uniformly by cloud computing. Users can purchase various services through the Internet and then use various terminal devices anytime and anywhere, without knowing the specific location of the resources used [10]

(2) High scalability: cloud computing can realize the scalability of IT resource utilization. Users can dynamically purchase resources from cloud service providers according to their own needs. When users do not need redundant computing resources, they can also release them in time [11]. Cloud service provider Yi can provide more virtualized resources to meet the needs of different users to obtain more users

(3) Transparency and pooling of resources: the transparency of resources is aimed at users. Users do not need to understand the internal structure of cloud computing resources [12], but only need to pay attention to whether their own needs are met. Pooling is for cloud providers. In the cloud computing environment, the cloud provider virtualizes all resources into a "virtual resource pool," and then it performs unified management and scheduling of virtual resources [13] and provides corresponding services according to the different requirements of users
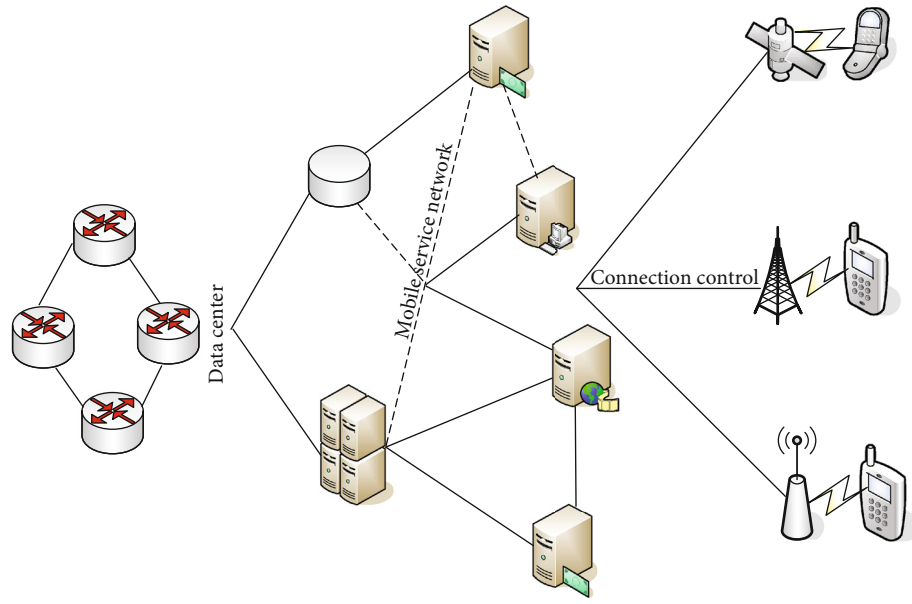
FIGURE 1: Mobile cloud computing structure.

(4) The scale is huge: the scale of cloud computing is quite large. For example, Google's cloud computing platform is built with more than 1 million servers. Companies such as IBM, Microsoft, and Amazon are also building cloud computing platforms through spectacular physical computer clusters [14, 15] and providing users with super computing capabilities and storage capabilities

(5) Pay on-demand: users can pay corresponding fees based on the resources used, which is the same as the payment method for public infrastructure such as electricity, water, and natural gas

(6) Reliable automatic management: the cloud computing data center is in an unsupervised state, realizing high-reliability automated management [16]. The data can be backed up in time, and the failed nodes can be automatically detected and eliminated without affecting the normal operation of the system, thereby avoiding server overload, reducing the waste of resources, and ensuring that cloud computing can provide users with stable, safe, and sustainable service [17]

2.1.3. Cloud Computing Classification. There are many forms of cloud computing. According to the scope of services provided by cloud computing, it can be divided into the public cloud, the private cloud, and the hybrid cloud.

The public cloud is a platform for several enterprises and public users. Cloud service providers usually provide users and enterprises with related services through the Internet, such as storage, computing, and other types of services [18]. Enterprises or users do not need to build and manage software and hardware platforms by themselves, but they only

need to pay on-demand to easily obtain cloud services. The private cloud is the opposite of the public cloud. It is mainly for enterprise users. It is a cloud computing platform independently built by enterprises or organizations, and it only provides resources and services for internal users of enterprises or organizations [19]. And compared with public clouds, private clouds are more secure. The hybrid cloud is formed by the integration of the public cloud and the private cloud. This is the development direction of cloud computing in recent years. For some enterprises, considering the security of data, they are more willing to store data in a private cloud. At the same time, they want to obtain public cloud computing resources [20, 21]. Therefore, the hybrid cloud is adopted by more and more enterprises. Because the hybrid cloud makes full use of the advantages of both public and private clouds, it maximizes enterprise benefits. Figure 1 shows the structure of mobile cloud computing.

2.2. Neural Network. A neural network is a commonly used method in artificial intelligence, which mainly imitates the working principle of a human neural network to process information. A neural network is an arithmetic model composed of a large number of nodes, and each layer of nodes is connected with each other. The output of each node of the neural network needs a transformation function to limit it. In addition, the nodes between two adjacent layers are connected by a variable called weight, which is equivalent to the memory of a human neural network [22, 23].

A neural network has a strong information synthesis capability, it can process qualitative and quantitative information at the same time, it can coordinate well this relationship, and it is suitable for processing complex nonlinear and uncertain objects. The design of a neural network has strong plasticity, so it can realize self-learning, self-organization, and self-adaptation, and it can conveniently deal with

uncertain systems. Since the information in the neural network is distributed and stored in the neurons of the neural network, it has strong robustness and fault tolerance. Each neuron of the neural network is structurally parallel, which can increase the calculation speed during design.

2.3. Workflow Scheduling. Workflow is a business process that is automatically executed according to a series of defined rules. Documents and tasks are transferred between different actors and completed by multiple participants. In the process of workflow execution, the workflow management system executes and manages the workflow through computer technology and coordinates the information interaction between members or jobs [24].

The traditional workflow system allows users to build visual applications without complicated and time-consuming programming. However, the disadvantage of the workflow system is that it cannot easily access the software components, which prevents the workflow system from being widely used [25]. It happens that cloud computing provides a service for accessing resource pools and software and hardware, and therefore, the workflow system has been well developed. Among them, the cloud workflow task scheduling algorithm is one of the core technologies of the cloud workflow system. The quality of its scheduling strategy will directly affect the performance of the cloud workflow system.

With the continuous development of cloud computing, distributed workflow systems have gradually evolved to the direction of cloud computing workflow systems [26]. This is a brand-new application mode produced by the workflow management system in the cloud computing environment, which is referred to as the cloud workflow for short. The cloud workflow management system uniformly manages the computation or storage of resources and realizes the orderly and efficient execution of cloud workflow task scheduling [27], thereby realizing the automation of business processes.

The cloud workflow has the following characteristics:

(1) Transparency: in the cloud computing environment, all resources are virtualized. The operating environment, operating system, and implementation language of all services in the cloud can be the same or different. The user does not need to know the internal implementation structure of the service used, let alone where the resource used is located

(2) Scalability: cloud resources have the characteristics of on-demand allocation, and users can purchase the resources they need through the Internet anytime, anywhere. Users can also release redundant resources to reduce the cost of renting resources [28]. This dynamic resource management method enables efficient execution of workflow tasks. In addition, this scalability not only enables users to adapt to computing resources but also enables cloud service providers to maximize their use of resources and maximize their own benefits

(3) Real-time monitoring: in the cloud computing environment, the monitoring management module can realize resource load balancing, fault monitoring, and node scale control by monitoring the running status of cloud workflow tasks [29]

In addition to some of the above features, the cloud workflow also includes its strong security features, and it can implement flexible out-of-office and overtime management strategies, which are in line with the flexible task configuration requirements required by the cloud workflow. All in all, the cloud workflow is an optimized solution for cloud computing systems that require flexible configuration, automatic task scheduling, optimized management of resources, and computing process. The cloud workflow can not only compress the cost of cloud computing but also improve the quality of cloud services. Therefore, the cloud workflow is bound to receive more and more attention, and it will develop rapidly, thereby promoting the development of the entire cloud computing industry.

3. Workflow Scheduling Research System Model Based on Mobile Cloud Computing Machine Learning

3.1. Research Goals of Workflow Scheduling Based on Cloud Computing. For the goal optimization problem of cloud workflow task scheduling, most of them pay attention to the following QOS indicators:

(1) Execution time: it represents the time required for the completion of cloud workflow tasks, and it is the most important goal in the scheduling strategy. For users, if the submitted cloud workflow tasks have an urgent need for completion time, they only need to map them to computing resources with good performance, which can greatly reduce the execution time of cloud workflow tasks

(2) Execution cost: this is the cost incurred from the use of service resources after the execution of a cloud workflow task, including bandwidth transmission costs and calculation costs. The execution cost of a cloud workflow task is related to the performance of the resources it uses, that is to say, if the user wants to submit the workflow task to be completed quickly, the task can be assigned to a virtual resource with strong processing capabilities for execution, and at the same time, users need to pay more for it

(3) Reliability: in some fields such as aerospace and aviation, the reliability of the execution of workflow tasks is very high, because a data uncertainty may bring unexpected disasters. However, it is difficult to maintain the reliability of data in the cloud computing environment, because some abnormalities may occur in the processing of the task, or the task cannot be

executed due to problems in the underlying software and hardware

(4) Security: cloud computing is cross-domain, and the virtual resources used by users may be distributed in different regions. When the cloud workflow tasks submitted by users are executed on virtual machine resources in different regions, tasks with dependencies will have data that is transmitted on the network. At this time, some network hackers may steal the user's data and cause the leakage of some important data of the user. Therefore, cloud workflow tasks need to ensure data security during the execution process and meet the security requirements of users in the cloud computing environment

In the cloud computing environment, the workflow tasks submitted by users will be assigned to each virtual resource for execution, and then the scheduling results will be fed back to the user. Therefore, this section first establishes a cloud workflow task model and a virtual resource model.

3.2. Workflow Task Scheduling System Model Based on Mobile Cloud Computing Machine Learning

3.2.1. Cloud Computing Workflow Task Model. The cloud workflow task in the cloud computing environment is composed of interdependent tasks. This paper uses an undirected cyclic graph (DAG) to describe them. Use $H = (Y, R, V)$ to describe cloud workflow tasks; the meaning of each attribute and related definitions are expressed as follows: $Y = (y_1, y_2, y_3, \cdots, y_i)$ represents a cloud workflow task set, where y_i is the ith task $(i = 1, 2, \cdots, n)$. $y_i = \{y_{id}, y_{length}\}$ represents different attributes of the task, where y_{id} represents the number of the task y_i and the length of the task y_{length}. $R = (r_{ij} \mid r_{ij})$ represents the edge of task y_i to task y_j, task y_i is the predecessor task of task y_j, task y_j is the successor task of task y_i, and task y_j must be executed after all of its predecessor tasks are completed. $V = \{v(y_i, y_j) \mid v(y_i, y_j)\}$ represents the communication time between task y_i and task y_j. The following interdependent tasks are represented as follows:

(a) Predecessor task set

$$\mathrm{Pre}(y_i) = \left\{ y_j \middle| r_{ji} \in R \right\}. \tag{1}$$

(b) Successor task set

$$\mathrm{Suc}(y_i) = \left\{ y_j \middle| r_{ij} \in R \right\}. \tag{2}$$

(c) Best precursor

$$\mathrm{ZPre}(y_i) = y_j \middle| \mathrm{Est}\left(y_j\right) + v\left(y_j, y_i\right) \geq \mathrm{Est}(y_k, y_i), \tag{3}$$

$$y_j, y_i \in \mathrm{Pre}(y_i), \quad j \neq k. \tag{4}$$

3.2.2. Resource Model. Cloud resources are composed of a series of heterogeneous virtual machine resources. The heterogeneity of virtual machines means that the computing power, memory, computing service unit price of different virtual machines, and the service unit price of communication bandwidth are different. Therefore, remember $B_i B_j (B_1, B_2, B_3, \cdots, B_m)$ as the set of virtual machines in the cloud computing data center, $B_i = (B_{id}, B_{pe}, B_{mips}, B_{ram})$ represents the different attributes of virtual machines, B_{id} represents the number of the virtual machine resource B_i in the data center, B_{pe} represents the number of cores of the virtual machine B_i, B_{mips} represents the computing power of the virtual machine B_i, B_{ram} represents the memory size of the virtual machine B_i, and $\mathrm{price}(B_i)$ represents the task in the virtual machine B_i. The service unit price is calculated above, where c_{wij} represents the communication bandwidth between the virtual machine B_i and the virtual machine BB_j and $\mathrm{tr}(b_i, b_j)$ represents the service unit price of the communication between the virtual machine B_i and the virtual machine B_j.

In order to facilitate the study of subsequent algorithms, the following assumptions are made for the model: (1) A virtual machine can only perform one task in a period of time, and virtual resources cannot be preempted when a task is being performed. (2) There are two dependent relationships, and the communication time of a task in the same virtual machine is 0. (3) The communication bandwidth between a virtual machine and another virtual machine is 1, that is, the communication time between tasks is equal to the amount of data transfer between tasks. (4) For tasks and tasks, the data transmission between virtual machines can be completed concurrently. (5) The communication of tasks between virtual machines does not affect the execution of tasks on virtual machines.

3.2.3. Scheduling Algorithm for Task Migration. The HEFT algorithm is used to find the earliest completion time of each cloud workflow task, the latest completion time is defined as the global latest completion time, and then makespan is used to replace the global latest completion time. For the convenience of the subsequent algorithm description, the following definitions are given.

Definition 1. Task execution time refers to the execution time allocated to the virtual machine resource b_k for the cloud workflow task y_i, which is recorded as follows:

$$e(y_i, b_k) = \frac{y_{length}}{b_{mips}}. \tag{5}$$

Definition 2. The earliest start time Est refers to the earliest start time of the cloud computing workflow task y_i scheduled
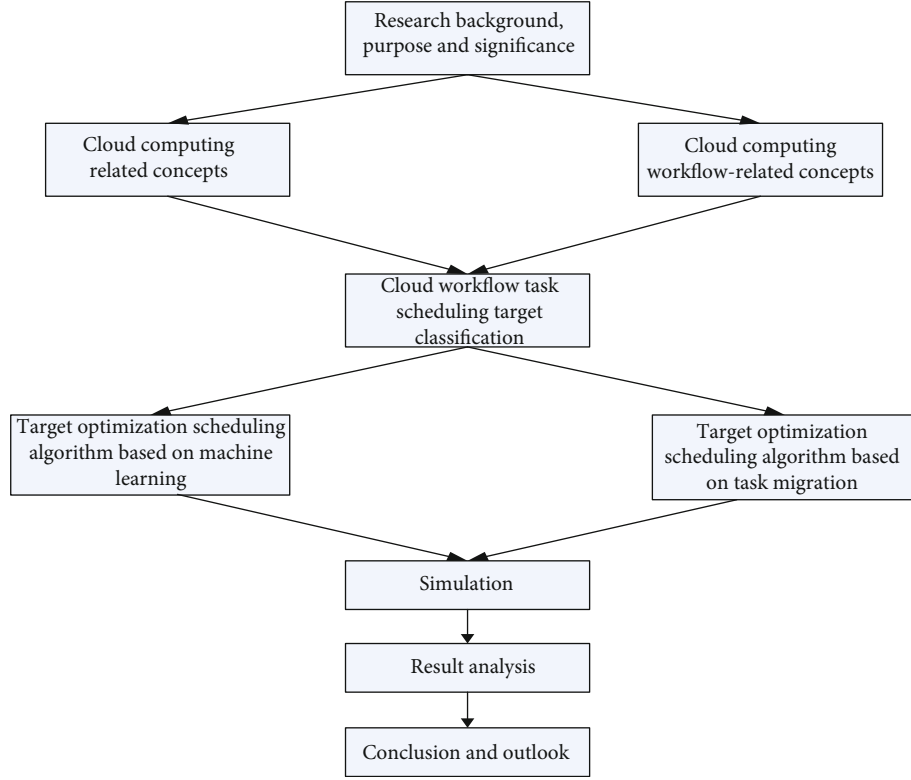
Figure 2: The research framework of this article.

to the virtual machine resource b_k. The calculation formula is as follows:

$$\text{Est}(y_i, b_k) = \begin{cases} 0, & \text{Pre}(y_i) = 0, \\ \max\left\{\text{ava}(b_k), \max\left\{\text{Aft}\left(y_j\right) + v\left(y_j, y_i\right)\right\}\right\}, & \text{Pre}(y_i) \neq 0,\ y_j \in \text{Pre}(y_i). \end{cases} \tag{6}$$

Among them, $\text{ava}(bk)$ represents the earliest available time of the virtual machine.

Definition 3. The earliest completion time Eft, that is, the earliest completion time of a cloud computing workflow task on a virtual machine, is recorded as follows:

$$\text{Eft}(y_i, b_k) = \text{Est}(y_i, b_k) + e(y_i, b_k). \tag{7}$$

Definition 4. Actual start time (Ast)/actual completion time (Aft) refers to the actual start time/actual completion time of the task on the assigned virtual machine.

Definition 5. The total time to complete a cloud computing workflow task makespan, that is, the longest time to complete a cloud computing workflow from the beginning of the task to the end of the task, is denoted as follows:

$$\text{Mak} = \max\left\{\text{Eft}(y_i)\right\}. \tag{8}$$

Definition 6. The latest completion time Lft, that is, the latest completion time of a cloud workflow task on a virtual machine, is denoted as follows:

$$\text{Lft}(y_i, b_k) = \begin{cases} \text{makespan}, & \text{Suc}(y_i) = 0, \\ \min\left\{\text{Lst}\left(y_j\right) - v\left(y_i, y_j\right)\right\}, & \text{Suc}(y_i) \neq 0,\ y_j \in \text{Suc}(y_i). \end{cases} \tag{9}$$
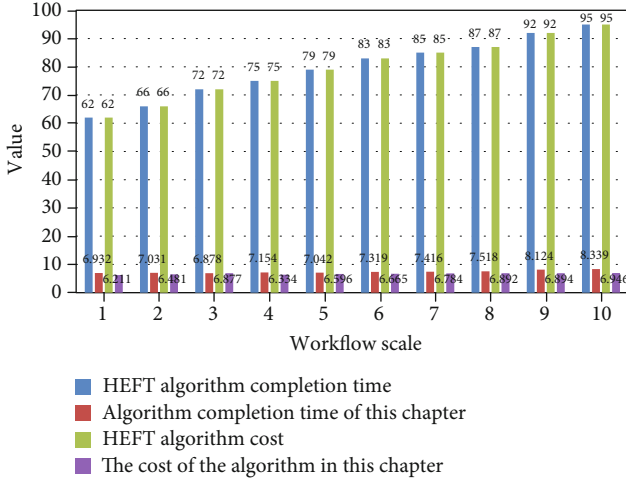
FIGURE 3: 10 simulation effects with 9 tasks assigned to 3 virtual machines.

FIGURE 5: Heterogeneous computing overhead of DAG tasks.

FIGURE 4: Comparison of task completion time of five algorithms under a different number of tasks.
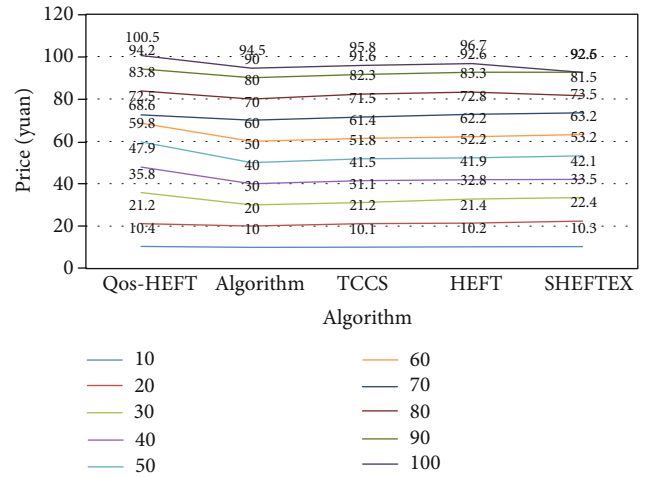
FIGURE 6: Task total service cost.

Definition 7. The latest start time Lst, that is, the latest start time of the cloud workflow task on the virtual machine, is recorded as follows:

$$\text{Lst}(y_i, b_k) = \text{Lft}(y_i, b_k) - e(y_i, b_k). \tag{10}$$

Definition 8. Critical Path (CP), the longest path of the cloud workflow from the starting task to the ending task, is defined as the critical path of the cloud workflow.

Definition 9. Critical tasks refer to the tasks on the critical path. For cloud workflow tasks, if the task satisfies

$$\text{Eft}(y_i) = \max \{\text{Eft}(y_i)\}, \tag{11}$$

then y_i is the key task, and right again $y_q \in \text{Pre}(y_i)$, if the task y_q satisfies $\text{Eft}(y_q) + v(y_q, y_i) = \max_{y_q \in \text{Pre}(y_i)} \{\text{Eft}(y_q) + v(y_q,$

$y_i)\}$, then y_q is the key task. This way, we get all the key tasks on the critical path in turn.

Definition 10. Execution cost refers to the sum of the cost of cloud workflow tasks mapped to virtual machine resources and the communication cost of all predecessor tasks and tasks:

$$\text{Cos}(y_i) = \sum_{y_j \in \text{Pre}(y_i)} \left(v\left(y_j, y_i\right) * \text{tr}(b_c, b_k) + e\left(y_{i,b_k}\right) * \text{Pri}(b_k)\right),$$

$$\tag{12}$$

where b_c is the virtual machine allocated by the predecessor task y_j. The completion time and economic cost of task y_i are related to the processing performance of resource b_k and the communication time between tasks.

When migrating noncritical tasks, you need to find a suitable idle time period [Ds, Df] on other virtual machines with low execution costs. First, determine whether the idle time

TABLE 1: Details of algorithm task scheduling in this article.

| Task | Data transmission before task execution | | | | | | Task performance | | |
	Parent task	Subtasks	Source resource	Target resource	Transmission time	Resources	Starting time	Operation hours	Complete time
1	—	—	—	—	—	—	15.8	12.6	32.8
2	1-1	1-3	3	3	0.0	3	17.8	14.0	31.8
3	1-1	1-2	3	1	0.0	1	17.8	15.3	33.2
4	1-2	1-4	1	3	0.0	3	33.1	12.5	45.5
5	1-3	1-4	3	3	0.0	3	33.1	12.5	45.5
6	1-6	1-4	3	3	0.0	3	45.5	9.4	54.9
7	1-7	1-4	3	1	0.0	1	45.5	7.5	52.9
8	2-2	—	—	—	—	4	0.0	13.2	13.2
9	2-1	—	—	—	—	2	0.0	14.5	14.5
10	2-3	2-1	2	4	0.0	4	14.5	19.8	34.3
11	2-1	2-5	2	2	0.0	2	14.5	9.4	23.9
12	2-2	2-4	4	2	0.0	2	23.9	4.6	28.5
13	2-4	2-6	2	4	0.0	4	34.3	16.2	50.4
14	2-3	2-7	4	2	0.0	2	36.3	15.8	50.1
15	3-3	3-5	2	4	0.0	4	58.4	13.7	72.1
16	3-1	3-6	4	2	0.0	2	58.4	13.8	72.2
17	3-2	3-4	4	3	14.2	3	68.6	5.2	73.8
18	3-1	3-7	4	1	8.4	1	66.0	9.3	75.3

period can execute the task to be migrated, and then determine after the task is migrated whether it will affect the completion time of the subsequent tasks; if the idle time period $[Ds, Df]$ can execute the task to be migrated and does not affect the completion time of the subsequent tasks, then the task will be migrated. That is, for a given cloud workflow task $y_i \in Y$, if $\text{Suc}(y_i) \neq 0$, the migration condition (10), condition (11), and condition (12) are met, and the task can be migrated; if $Succ(y\_i) = 0$, only condition (10) and condition (11) can migrate, where b_k is its newly allocated virtual machine, b_p is its previously allocated virtual machine, and $\text{cost}'_{\text{sum}}$ is the cost of all tasks after task y_i migrates from virtual machine b_k to virtual machine b_p.

$$\max \left\{ \max \left\{ \text{Aft}\left(y_j\right) + v\left(y_j, y_i\right), F_s \right\} + e(y_i, b_k) \right\} \leq F_f, \tag{13}$$

$$\text{Cost}'_{\text{sum}} < \text{Cost}_{\text{sum}}, \tag{14}$$

$$\text{Aft}(y_i, b_k) + v(y_i, y_c) \leq \min \left\{ \text{Aet}(y_c) \right\}, \quad y_c \in \text{Suc}(y_i). \tag{15}$$

When the current noncritical tasks have migrated, provide more free time for migration for the tasks to be migrated later, and move the current noncritical tasks to the latest completion time of the assigned virtual machine. If the current noncritical task does not meet the migration conditions, it will also be moved to the latest completion time of the allocated virtual machine.

The ranku(ti) value of the task is determined by the HEFT algorithm, then the priority of the task is determined, then the cloud workflow tasks with high priority are scheduled to the virtual machine with the minimum completion time in turn, and finally the total of the cloud workflow tasks is obtained. Completion time ismakespan, and total completion cost iscostsum. We define makespan as the global latest completion time. And according to the abovementioned knowledge, the total completion time of cloud workflow tasks is determined by the critical path, that is, determined by all the key tasks on the critical path. The cost optimization scheduling algorithm based on task migration is mainly for reasonably migrating some noncritical tasks to virtual machine resources with low execution cost under the premise of ensuring that the total completion time of the task remains unchanged, so as to optimize the total service cost. Figure 2 shows the research framework of this article.

4. Workflow Scheduling Based on Mobile Cloud Computing Machine Learning

4.1. Cloud Computing Workflow Task Scheduling Experiment Results. Nine DAG workflow tasks are randomly generated and assigned to 3 virtual machines for simulation, and then the results of 10 simulation experiments of the algorithm in this section and the HEFT algorithm are compared as shown in Figure 3. It can be seen that the algorithm in this section does not increase cloud work. In the case of the total completion time of the flow task, the algorithm in this section can save costs more effectively than the HEFT algorithm. This is mainly because the algorithm in this section migrates some noncritical tasks to low execution costs while ensuring that

TABLE 2: Details of resource usage in the algorithm scheduling process of this article.

Resources	Previous task completion time	Idle time	Task	Starting time	Operation hours	Complete time	Resource utilization
1	0.0	17.8	1-2	17.8	15.3	33.1	
2	33.2	12.5	1-7	45.6	7.4	52.9	
3	52.9	0.0	1-5	52.9	2.0	54.9	45.0
4	54.9	11.1	3-7	66.0	9.3	75.3	
5	0.0	0.0	2-1	0.0	15.5	14.5	
6	14.5	0.0	2-5	14.5	9.4	23.9	
7	23.9	0.0	2-4	23.9	4.6	28.5	
8	28.6	5.8	2-7	34.3	15.8	52.1	88.2
9	50.2	0.0	3-3	50.2	8.3	58.4	
10	58.4	0.0	3-6	58.4	13.8	72.3	
11	0.0	0.0	1-1	0.0	17.6	17.8	
12	17.8	0.0	1-3	17.8	14.0	31.8	
13	31.8	1.3	1-4	33.2	12.5	45.5	78.1
14	45.6	0.0	1-6	45.6	9.5	54.9	
15	54.9	13.7	3-4	68.6	5.3	73.8	
16	0.0	0.0	2-2	0.0	13.2	13.2	
17	13.2	1.3	2-3	14.5	19.8	34.3	93.0
18	34.3	0.0	2-6	34.4	16.2	52.4	

the total completion time of cloud workflow tasks is not affected. It executes on virtual machine resources. The worst-case cost of the algorithm in this section is the same as the cost of the HEFT algorithm.

4.2. Comparison of Task Completion Time. Compare the algorithms in this section with the HEFT, QOS-HEFF, and TCCS algorithms. Among them, the QOS-HEFF algorithm is an improved algorithm for the HEFT algorithm according to user preferences (time and cost). This section evaluates the performance of this section's cloud workflow task scheduling algorithm through two indicators: cloud workflow task completion time and total service cost. This experiment uses five types of cloud workflows: 10, 20, 30, 40, and 50 tasks. The number of layers is set to 4, 6, 8, 10, 12, and 10 of each type of cloud workflow task that is randomly generated and then assigned to 3 virtual machines for simulation experiments, and each cloud work is recorded. The average values of the completion time and cost of the flow task and the experimental results are shown below.

It can be seen from Figure 4 that when the cloud workflow task scale is small, the task completion time of the algorithm in this section is slightly lower than the TCCS and HEFT algorithms, but far lower than the QOS-HEFT algorithm. As the cloud workflow task scale increased, the difference in completion time between the algorithm in this section and the TCCS, HEFT, and QOS-HEFT algorithms is becoming more and more obvious. This is mainly because the algorithm in this section reasonably copies the predecessor tasks of the current task and reduces the communication time between tasks. Thus, the current task is completed early, and the total completion time of the cloud workflow tasks is ultimately reduced.

TABLE 3: Energy consumption composition of cloud data center.

Energy consumption composition	Composition ratio
Computing equipment	46%
Cooling equipment	32%
Power system	5%
Lighting system	5%
Other devices	12%

4.3. Task Cost Comparison. Assuming that the v_{mips} of virtual machines V1, V2, and V3 are 600, 700, and 800 Mbits/s, respectively, the corresponding virtual machine service prices are 0.02, 0.05, and 0.09 yuan/sec, and the communication bandwidth service price is 0.03 yuan/sec. It can be seen from Figure 5 that by determining the rank (ti) of each task, the priority order of the cloud workflow task scheduling is determined as T2, T1, T5, T3, T4, T6, T7, T9, and T8. First, the cloud workflow task is prescheduled through the HEFT algorithm, and the total completion time of the cloud workflow task is madepan = 61.75 seconds, the total cost spent is costsum = 6.8569 yuan, and makespan is defined as the global latest completion time.

The total service cost refers to the cost of completing all tasks. As shown in Figure 6, the algorithm in this section requires the least cost to complete all tasks, which is significantly better than the TCCS and QOS-HEFT algorithms. The performance of the HEFT algorithm is the worst. This is because the algorithm in this section takes into account the communication cost between tasks. The replication stage reasonably replicates the precursor tasks to reduce the execution cost, then goes through the recopying stage to further
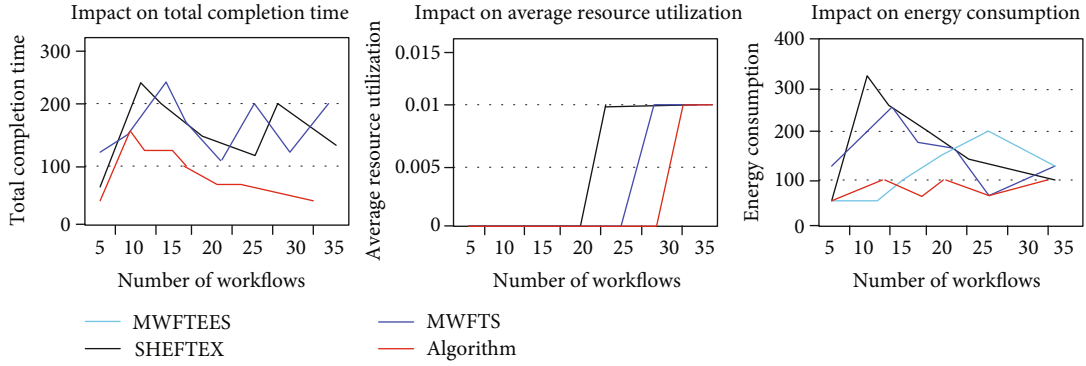
FIGURE 7: Data intensive: the influence of the number of workflows on experimental results.
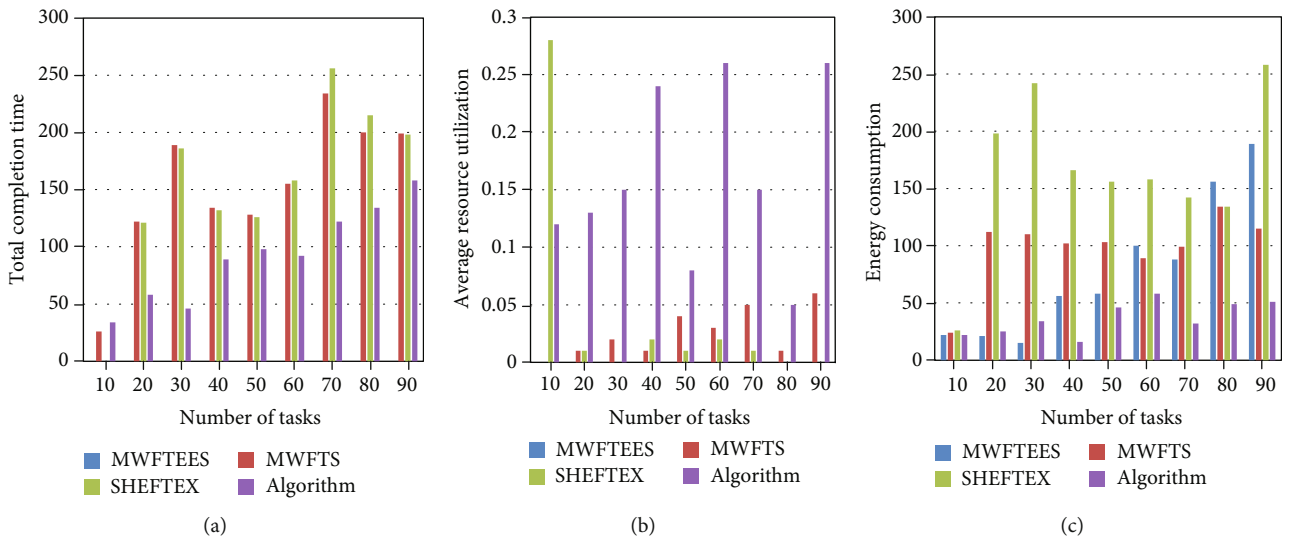
FIGURE 8: The influence of the number of tasks in each workflow on the experimental results.

reduce the execution cost, and finally optimizes the overall service cost by deleting redundant tasks.

4.4. Task Scheduling and Resource Usage.
According to the algorithm in this paper, for the tasks of the three workflows, first, the time weight of the task is calculated according to the average execution time of the task, the average transmission time of the task in the resource, the task entry time, and the task exit time; then the tasks are sorted into the task execution sequence; and then appropriate resources are assigned to the task for execution. The execution scheduling results of the tasks are shown in Table 1:

The scheduling algorithm in this article is based on the task execution sequence. For each task in the sequence, first traverse all resources, then determine the idle time period in the resource, whether the task is satisfied, and if it is satisfied, it will be scheduled; otherwise, the running time will be selected.

It can be seen from Table 2 that in the process of the scheduling algorithm, resource 1 generates a total of 3 idle time periods, resource 2 generates a total of 1 idle time period, resource 3 generates a total of 2 idle time periods, and resource 4 generates a total of 2 idle time periods. The

resource utilization rates of the 4 resources are 45.0%, 88.2%, 78.1%, and 93.0%, respectively, and the average resource utilization rate is 74.1%.

4.5. Influence of the Number of Workflows and Tasks on the Experimental Results.
The current development trend of cloud data centers is towards high-density and large-scale models, and its energy consumption is mainly concentrated on computer equipment, refrigeration equipment, and power systems. Many companies and researchers have investigated the energy consumption rate of various types of machines in data centers. It can be seen from Table 3 that other machinery and equipment account for about 22%, and the energy consumption of the computing machine as the processor accounts for 46% of the total energy consumption. Therefore, computer equipment has become an important factor in data center energy consumption.

Figure 7 shows that for data-intensive workflows, as the number of workflows increases, the total completion time of the tasks of the four algorithms does not change much, while the average resource utilization rate has increased but the growth is slower, and the maximum value of the resource utilization rate is always small and does not exceed 0.15. This

is also due to the fact that the data transmission time of the data-intensive workflow is much longer than the task execution time, which results in an excessively long period of resource idle time.

MWFTS is a task scheduling algorithm based on multiple workflows, and on this basis, the MWFTEES energy-saving strategy is proposed. The SHEFTEX algorithm is mainly used to deal with resource idleness that easily occurs in the workflow process. Through the comparison of the data in Figure 8, it can be found that whether it is the total completion time of the task or the average utilization of resources, the performance of the algorithm in this paper is far better or slightly better than the MWFTS algorithm, the MWFTEES algorithm, and the SHEFTEX algorithm in terms of scheduling; in the system energy consumption above, the energy-saving effect of the algorithm in this paper is obviously better than the other three algorithms. From this set of experiments, we can fully see the superiority of the algorithm in this paper for task scheduling based on multiple workflows.

Figure 8 shows the comparison between the SHEFTEX algorithm, the MWFTS algorithm, and the MWFTEES algorithm, and the experimental results of this algorithm from the three aspects of the total completion time of workflow tasks, the average utilization of resources, and system energy consumption. It can be seen from graphical comparison that for data-intensive workflows, the total task completion time and the average resource utilization change of the SHEFTEX algorithm and the MWFTS algorithm are basically the same; but the resource utilization is very small, not exceeding 0.3. This is also due to the fact that the data transmission time of the data-intensive workflow is much longer than the task execution time, which results in an excessively long period of resource idle time. In terms of energy consumption, the algorithm in this paper is better than the other three algorithms.

This paper defines the standard deviation of the total number of tasks running on a virtual machine as a load factor. If a large number of tasks are allocated on some virtual machines and some are idle, the load of the system is unbalanced. A 10-layer DAG workflow model is used for experiments; Gaussian random is used to set virtual machine and task parameters, and 20 virtual machines are configured. The average processing capacity of the virtual machine is 1200, and the standard deviation is 150; the average of the task length is 15000, the standard deviation is 200, and the number of tasks is 100~400. The experimental results are shown in Figure 9. As can be seen from the data in Figure 9, the algorithm in this paper achieves simple load balancing.

According to the random search function of the algorithm, the results of multiple simulation experiments are selected, and the results are shown in Figure 10. Because the number of LIGO operations is increased from 30 to 150, and the overall average and variance of the solution are compared, the algorithm proposed in this article has specific advantages. The reason for this phenomenon is that the algorithm proposed in this paper improves the grid coordinate adaptation system and dynamically adapts to changes based on network distribution, so that the algorithm takes into account a certain degree of time and cost.
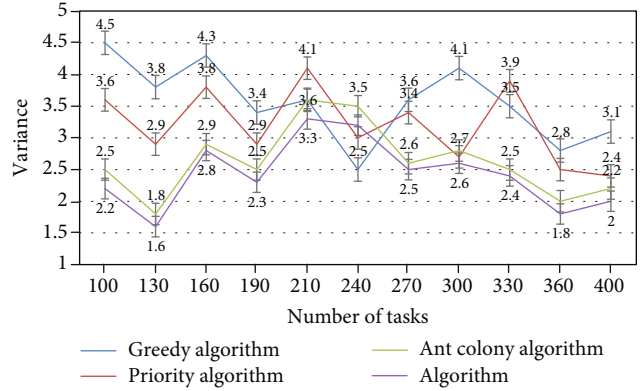
FIGURE 9: The influence of load balancing factor on the algorithm model of this paper.
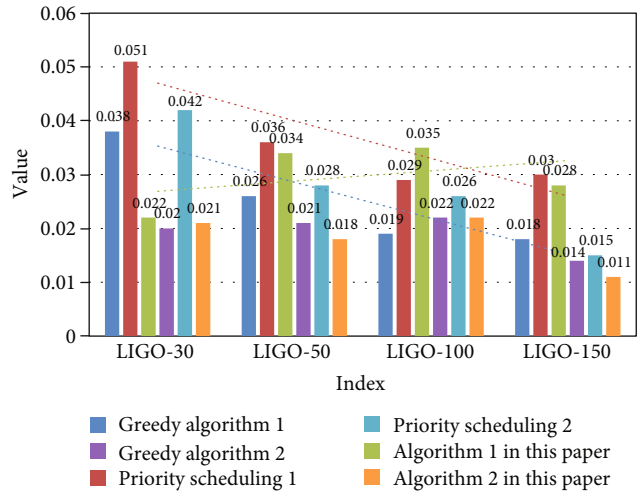
FIGURE 10: Mean and variance of various algorithms.
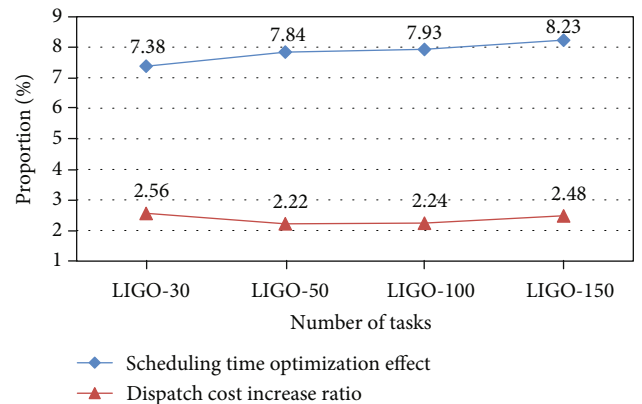
FIGURE 11: Comparison chart of scheduling time optimization effect and cost increase.

4.6. Task Scheduling Optimization Effect of the Algorithm. Figure 11 shows that the algorithm in this paper is 7.38%, 7.84%, 7.93%, and 8.23% faster in scheduling time. Moreover, as the workload increases, the effect of the algorithm in this
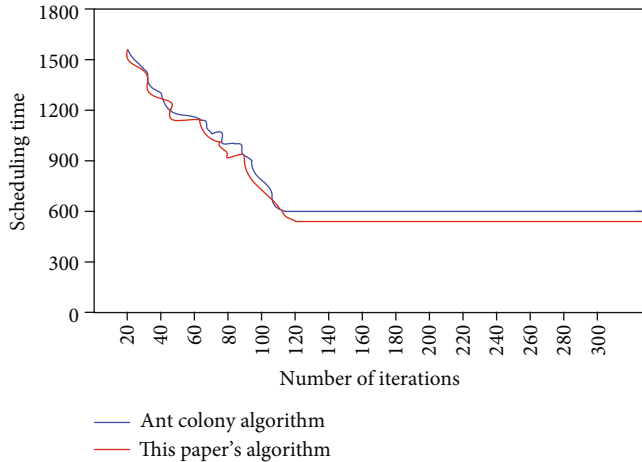
FIGURE 12: Convergence speed comparison.

paper to optimize the time will be more obvious. Compared with the HEFT algorithm, this algorithm only increases the service overhead by 2.56%, 2.22%, 2.24%, and 2.48%. Experimental results show that by adding a small amount of cost, the scheduling time can be greatly optimized. This is especially important in time-sensitive mission planning.

In this paper, the number of LIGO tasks is set to 150, and the time to plan to obtain the optimal solution is used as an indicator. As shown in Figure 12, the ant colony algorithm will iterate about 90 times for convergence, but the algorithm in this paper will converge about 105 times for iteration. Therefore, the experimental results show that the ant colony algorithm is slightly better than the algorithm proposed in this paper in terms of convergence speed. From the perspective of scheduling time, the final scheduling time of the ant colony algorithm is about 640 s, but the algorithm scheduling time of this article is about 588 s. Therefore, the algorithm in this paper is better than the ant colony algorithm in terms of time scheduling. It can be seen that task aggregation plays a better role in work scheduling.

5. Conclusion

This article is mainly about the research of workflow scheduling based on mobile cloud computing machine learning. Unlike previous research, this article adds new concepts and uses new applications of machine learning based on this research, and considers the cost and time dual-objective optimization problem. The algorithm in this paper is better than other algorithms on the whole, and has obvious improvements in time scheduling and task scheduling, in shortening the total completion time of the entire workflow task, and in saving the cost of task service. The innovation of this paper is to conduct a large number of simulation experiments, combining theory with empirical research and analysis, highlighting the focus of this paper. In the future, we will consider the next step of multiworkflow task scheduling, expanding the application of mobile computing and machine learning, and hope that there will be better breakthroughs.

Data Availability

No data were used to support this study.

Conflicts of Interest

The authors declare no conflicts of interest.

References

[1] L. A. Tawalbeh, R. Mehmood, E. Benkhlifa, and H. Song, "Mobile cloud computing model and big data analysis for healthcare applications," *IEEE Access*, vol. 4, no. 99, pp. 6171–6180, 2016.

[2] A. Buczak and E. Guven, "A survey of data mining and machine learning methods for cyber security intrusion detection," *IEEE Communications Surveys & Tutorials*, vol. 18, no. 2, pp. 1153–1176, 2016.

[3] M. Masdari, S. ValiKardan, Z. Shahi, and S. I. Azar, "Towards workflow scheduling in cloud computing: a comprehensive analysis," *Journal of Network & Computer Applications*, vol. 66, pp. 64–82, 2016.

[4] Z. Lv and H. Song, "Mobile internet of things under data physical fusion technology," *IEEE Internet of Things Journal*, vol. 7, no. 5, pp. 4616–4624, 2020.

[5] L. Yang, Z. Han, Z. Huang, J. Ma, Han et al., "A remotely keyed file encryption scheme under mobile cloud computing," *Journal of Network and Computer Applications*, vol. 106, pp. 90–99, 2018.

[6] X. Jin, Y. Liu, W. Fan, F. Wu, and B. Tang, "Energy-efficient resource management in mobile cloud computing," *IEICE Transactions on Communications*, vol. 101, no. 4, pp. 1010–1020, 2018.

[7] N. Parajuli, A. Alsadoon, P. Prasad, R. S. Ali, and O. H. Alsadoon, "A recent review and a taxonomy for multimedia application in mobile cloud computing based energy efficient transmission," *Multimedia Tools and Applications*, vol. 79, no. 41-42, article 9516, pp. 31567–31594, 2020.

[8] Z. Almusaylim and N. Z. Jhanjhi, "Comprehensive review: privacy protection of user in location-aware services of mobile cloud computing," *Wireless Personal Communications*, vol. 111, no. 1, article 6872, pp. 541–564, 2020.

[9] Q. Jiang, V. Leung, H. Tang, and H. S. Xi, "Adaptive scheduling of stochastic task sequence for energy-efficient mobile cloud computing," *IEEE Systems Journal*, vol. 13, no. 3, pp. 3022–3025, 2019.

[10] S. Misra, B. E. Wolfinger, M. P. Achuthananda, T. Chakraborty, S. N. Das, and S. Das, "Auction-based optimal task offloading in mobile cloud computing," *IEEE Systems Journal*, vol. 13, no. 3, pp. 2978–2985, 2019.

[11] D. Facchinetti, G. Psaila, and P. Scandurra, "Mobile cloud computing for indoor emergency response: the IPSOS assistant case study," *Journal of Reliable Intelligent Environments*, vol. 5, no. 3, pp. 173–191, 2019.

[12] Y. Zhang, A. Wu, and D. Zheng, "Efficient and privacy-aware attribute-based data sharing in mobile cloud computing," *Journal of Ambient Intelligence and Humanized Computing*, vol. 9, no. 4, pp. 1039–1048, 2018.

[13] H. S. Lee and J. W. Lee, "Task offloading in heterogeneous mobile cloud computing: modeling, analysis, and cloudlet deployment," *IEEE Access*, vol. 6, no. 99, pp. 14908–14925, 2018.

[14] R. U. Amin, I. Inayat, B. Shahzad, K. Saleem, and L. Aijun, "An empirical study on acceptance of secure healthcare service in Malaysia, Pakistan, and Saudi Arabia: a mobile cloud computing perspective," *Annals of Telecommunications*, vol. 72, no. 5-6, pp. 253–264, 2017.

[15] A. Tharwat, H. Mahdi, M. Elhoseny, and A. E. Hassanien, "Recognizing human activity in mobile crowdsensing environment using optimized k-NN algorithm," *Expert Systems with Applications*, vol. 107, pp. 32–44, 2018.

[16] Y. Ding, G. Xu, C. Wu, L. Hu, Y. Zhai, and J. Zhao, "Explore virtual machine deployment to mobile cloud computing for multi-tenancy and energy conservation in wireless network," *Cluster Computing*, vol. 20, no. 4, article 1054, pp. 3263–3274, 2017.

[17] Z. Lv and L. Qiao, "Optimization of collaborative resource allocation for mobile edge computing," *Computer Communications*, vol. 161, pp. 19–27, 2020.

[18] N. Jean, M. Burke, M. Xie, W. M. Davis, D. B. Lobell, and S. Ermon, "Combining satellite imagery and machine learning to predict poverty," *Science*, vol. 353, no. 6301, pp. 790–794, 2016.

[19] N. D. Sidiropoulos, L. de Lathauwer, X. Fu, K. Huang, E. E. Papalexakis, and C. Faloutsos, "Tensor decomposition for signal processing and machine learning," *IEEE Transactions on Signal Processing*, vol. 65, no. 13, pp. 3551–3582, 2017.

[20] Y. Li, M. Chen, W. Dai, and M. Qiu, "Energy optimization with dynamic task scheduling mobile cloud computing," *IEEE Systems Journal*, vol. 11, no. 1, pp. 96–105, 2017.

[21] M. Elhoseny and K. Shankar, "Reliable data transmission model for mobile ad hoc network using signcryption technique," *IEEE Transactions on Reliability*, vol. 69, no. 3, pp. 1077–1086, 2020.

[22] C. Stergiou and K. E. Psannis, "Recent advances delivered by mobile cloud computing and internet of things for big data applications: a survey," *International Journal of Network Management*, vol. 27, no. 3, article e1930, pp. 1–12, 2017.

[23] C. Helma, T. Cramer, S. Kramer, and L. de Raedt, "Data mining and machine learning techniques for the identification of mutagenicity inducing substructures and structure activity relationships of noncongeneric compounds," *Journal of chemical information and computer sciences*, vol. 44, no. 4, pp. 1402–1411, 2004.

[24] Z. Zhu, G. Zhang, M. Li, and X. Liu, "Evolutionary multi-objective workflow scheduling in cloud," *IEEE Transactions on Parallel & Distributed Systems*, vol. 27, no. 5, pp. 1344–1357, 2016.

[25] H. Xu, B. Yang, W. Qi, and E. Ahene, "A multi-objective optimization approach to workflow scheduling in clouds considering fault recovery," *KSII Transactions on Internet and Information Systems (TIIS)*, vol. 10, no. 3, pp. 976–995, 2016.

[26] K. Sathish and A. RamaMohan Reddy, "Workflow scheduling in grid computing environment using a hybrid GAACO approach," *Journal of the Institution of Engineers*, vol. 98, no. 1, pp. 121–128, 2017.

[27] S. Shukla, A. Kumar, S. Saxena, and S. Kumar, "An evolutionary study of multi-objective workflow scheduling in cloud computing," *International Journal of Computer Applications*, vol. 133, no. 14, pp. 14–18, 2016.

[28] B. Lin, W. Guo, N. Xiong, G. Chen, A. V. Vasilakos, and H. Zhang, "A pretreatment workflow scheduling approach for big data applications in multi-cloud environments," *IEEE Transactions on Network & Service Management*, vol. 13, no. 3, pp. 581–594, 2016.

[29] A. Deldari, M. Naghibzadeh, and S. Abrishami, "CCA: a deadline-constrained workflow scheduling algorithm for multicore resources on the cloud," *The Journal of Supercomputing*, vol. 73, no. 2, pp. 756–781, 2017.

WILEY | Hindawi

Research Article

Ultrasonic Image Diagnosis of Liver and Spleen Injury Based on a Double-Channel Convolutional Neural Network

Maorui He,[1] Rui Zhang [ID],[1] Shuni Liu,[2] Yansong Tan [ID],[3] and Yang Zeng[3]

[1]The Ninth People's Hospital of Chongqing, Chongqing 400700, China
[2]The Department of Ultrasound Medicine, Chongqing Emergency Medical Center, Chongqing City 400014, China
[3]School of Artificial Intelligence and Big Data, Chongqing College of Electronic Engineering, Chongqing 401331, China

Correspondence should be addressed to Rui Zhang; 35613817@qq.com

Automatic and accurate diagnosis of liver and spleen injury in ultrasonic images is of great significance for the development of automatic clinical diagnosis. In order to realize more accurate ultrasonic image diagnosis of liver and spleen injury, an algorithm of ultrasonic image classification diagnosis of liver and spleen injury based on double-channel convolutional neural network was proposed. Firstly, the anisotropic diffusion denoising model is used to realize data preprocessing of ultrasonic images of the liver and spleen to improve the image quality of ultrasonic images. Secondly, the external edge of the lesion location was detected to obtain the characteristics of the external edge. Then, the rotation invariant local binary mode feature of the extracted image is taken as the inner texture feature of the image. Finally, the external edge feature and internal texture feature are used as two input channels of the convolutional neural network, respectively, to classify and identify ultrasonic images of liver and spleen injury. The experimental results show that the proposed method diagnoses liver and spleen injury more accurately.

1. Introduction

Ultrasound imaging technology is widely used in clinical medicine due to its nonradiation damage and noninvasive features, such as the observation and diagnosis of the liver, gallbladder, spleen, kidney, and other vital organs of the human body. For sensitive groups such as pregnant women and children, the application of ultrasound imaging technology is particularly important [1].

Liver and spleen injury is classified into 6 levels, according to the American Association for the Surgery of Trauma (AAST) [2] classification method, which are shown in Table 1.

It is the key to provide reasonable treatment for liver and spleen injury complicated with many injuries, complicated injuries, and dangerous conditions. At present, texture features commonly used in image recognition have been successfully applied in the real world, including spatial gray scale independent matrix [3], Fourier energy spectrum [4], gray scale difference statistics [5], and laws texture energy measurement [6]. The image characteristics extracted by M-band wavelet transform and fractal characteristics are adopted to

represent liver diseases [7]. His study proved that fractal feature vectors could provide better classification performance than other features, and could also distinguish normal and abnormal liver. Convolutional neural network (CNN) has a significant effect in image recognition, image segmentation, and other image processing applications [8]. Hijazi et al. [9] proposed that CNN has the superiority as follows.

(1) CNN-based detection and feature extraction have good robustness for image degradation of image quality due to changes in camera focal length, ambient light intensity, photo pose, image obscuration, image displacement, etc.

(2) The calculation amount of CNN-based feature extraction algorithm is relatively low, because for different input images, the convolution parameters of each layer network are the same

CNN is widely recognized in general image processing, so it is gradually applied in medical image recognition and classification. In literature [10], CNN is used to identify

Table 1: The AAST liver trauma grading system.

Classification	Detail description
Level I	Hematoma: subcapsular, <10% surface area Laceration: capsular tear, <1 cm parenchymal depth
Level II	Hematoma: subcapsular, 10-50% surface area Hematoma: intraparenchymal, <10 cm diameter Laceration: capsular tear 1-3 cm parenchymal depth, <10 cm length
Level III	Hematoma: subcapsular, >50% surface area of ruptured subcapsular or parenchymal hematoma Hematoma: intraparenchymal, >10 cm Laceration: capsular tear, >3 cm parenchymal depth Vascular injury with active bleeding contained within liver parenchyma
Level IV	Laceration: parenchymal disruption involving 25-75% hepatic lobe or involves 1-3 Couinaud segments Vascular injury with active bleeding breaching the liver parenchyma into the peritoneum
Level V	Laceration: parenchymal disruption involving >75% of hepatic lobe Vascular: juxtahepatic venous injuries (retrohepatic vena cava/central major hepatic veins)
Level VI	Hepatic avulsion: this vascular injury is rarely seen on imaging due to its high mortality rate; no case could be featured as a result

pathological images of breast cancer. Literature [11] applied CNN to the pulmonary nodule identification system. Literature [12] applied CNN to the lymph node recognition system. From these literatures, we can find that CNN has made impressive application in medical diagnosis. In order to identify the damage of liver and spleen ultrasound images, CNN will be used as an identification network in this paper. Before using CNN, we analyzed CNN model, and its training methods have the disadvantages as follows.

(1) Images were collected from different medical institutions for algorithm training, so the image scale in the data set changed too much

(2) The amount of training image data is not enough, so the ideal CNN network cannot be obtained by independent training

It is very necessary to improve the image quality and carry out transfer learning training to the existing convolutional neural network; thus, the network can extract the features in medical images.

In order to achieve more accurate ultrasound image diagnosis of liver and spleen injury, this paper proposes a classification and diagnosis algorithm for ultrasound images of liver and spleen injury based on a double-channel convolutional neural network. An algorithm based on dual channel convolution neural network is designed to recognize and diagnose ultrasound images of liver and spleen injury. To increase the signal-to-noise ratio of ultrasound image, the anisotropic diffusion denoising model is used to preprocess the ultrasound image of the liver and spleen. In order to obtain the outer edge feature, this paper detects the outer edge of the lesion location. Then, the rotation invariant local binary mode feature of the extracted image is taken as the internal texture feature of the image. In the process of neural network recognition, the recognition ability of neural network is enhanced by adding key features. Because the clinicians of ultrasound image usually take the lost external edge features and internal texture features as the important basis

for diagnosis, so these two points are used as the two input channels of the network in this paper. In the experimental part, the clinical medical ultrasound image is used as a data set and compared with other recognition algorithms to further verify the effectiveness and accuracy of this algorithm.

2. The Basic Theory

2.1. Convolutional Neural Network. A typical convolutional neural network consists of four layers: input layer, convolution layer, downsampling layer, and output layer. It is a kind of network structure with the characteristics of self-supervised learning. It optimizes the network structure through reverse conduction and then updates the optimal parameters of each layer of the network. In the convolution layer processing, the mapping relationship of multiple characteristics can be obtained, and each feature mapping corresponds to one characteristic extraction. Each neuron in the neural network is connected with the upper and lower layers. In the process of convolution calculation, each neuron shares a set of weights to complete feature extraction. The weights of different feature graphs are different, and each feature graph has its own weights. In the training phase, the method of updating weights by reverse conduction makes the CNN recognition results more accurate. The convolution layer calculation equation can be expressed as follows:

$$x_j^l = f\left(\sum_{i \in M_j} x_j^{l-1} * k_{ij}^l + b_j^l\right), \tag{1}$$

where b_j is the offset, and each input map contains an offset. M_j is a collection of input maps. k_{ij} is the convolution kernel for convolution processing.

The image resolution is reduced and the amount of characteristic maps remains the same by pooling the feature map on the downsampling layer. After convolution operation of convolution layer, the dimension of image features is reduced. At the same time, convolution operation makes

the robustness of image displacement, scale, and distortion further improved. The convolution layer is followed by the downsampling layer, and the downsampling formula can be expressed as follows:

$$x_j^l = f\left(\beta_j^l d\left(x_j^{l-1}\right) + b_j^l\right), \tag{2}$$

where the downsampling function is represented by d. b_j is the offset and β_j is the weight coefficient of downsampling.

2.2. GoogLeNet Neural Networks. Among the current popular CNN network, GoogLeNet was confirmed to perform well in image classification [13]. GoogLeNet was the classification champion of ILSVRC in 2014, and its top 5 error rate was 6.7%. In the GoogLeNet structure, the author designs a 22-layer network and proposes a new structure, namely, perception layer. The perception layer is a combination of filters, which is composed of internal network filters and convolution filters with different sizes each other. The internal network filter is linked to the 3 by 3 pixel or 5 by 5 pixel filter. Then, the feedback is sent to the pool and connection layer. The size of each filter layer is different, so the characteristics of input layer with different resolution are processed. Despite its depth, GoogLeNet has 12 times fewer parameters than AlexNet; thus, the training speed is faster and the efficiency is better.

Despite GoogLeNet has an impressive recognition effect on natural images, it cannot be directly applied to liver and spleen ultrasonic images. Due to the large difference between the image content and the original training samples, the network could not converge and could not achieve the ideal result of classification and recognition. Thus, the preprocessed liver and spleen ultrasound image samples are input into the pretrained network, and then, the parameters are fine tuned by transfer learning method. The fine tuning makes the network more sensitive to the content of liver and spleen images, and then carries out feature extraction and classification recognition for liver and spleen ultrasound images.

3. Algorithm Implementation

3.1. Image Preprocessing. Liver and spleen ultrasound images are obtained by using ultrasonic signals reflected when ultrasound encounters human tissues. Limited by the imaging mechanism of medical ultrasound images, the noise interference of liver and spleen ultrasound images is serious, mainly manifested as additive thermal noise and multiplicative speckle noise. Thermal noise is caused by the heating of imaging equipment and can be avoided by cooling imaging equipment and other physical means. Speckle noise is the light and dark granular speckle caused by the long interference and the canceling interference generated by the reflected ultrasound, which cannot be eliminated by adjusting the physical equipment. Therefore, the ultrasonic image denoising of the liver and spleen needs to be realized by preprocessing.

By combining the diffusion equation and image features [14], the anisotropic diffusion method can retain or even enhance the image edge information while smoothing the image. The noise distribution and strength of liver and spleen ultrasonic images are different in different tissue parts of the human body, so the denoising model should implement isotropic diffusion denoising in homogeneous regions and anisotropic diffusion denoising in heterogeneous regions, so as to avoid reducing the quality of ultrasonic images. Therefore, the EEAD [15] model based on edge enhancement is adopted in this paper to denoise the image. In this model, the diffusion velocity is determined by the image gradient. The filtering diffusion direction is decomposed into two parts that are the normal direction and the tangent direction. The diffusion equation is as follows:

$$\begin{cases} \dfrac{\partial I}{\partial t} = \operatorname{div}\left(c(\|\nabla I\|)\nabla I\right) = f_1 I_{nn} + f_2 I_t, \\[2mm] f_1 = \dfrac{1}{1 + a|v_n|^2 + b|v_{nn}|^2}, \\[2mm] f_2 = \dfrac{1}{\sqrt{1 + a|v_n|^2 + b|v_{nn}|^2}}, \\[2mm] v = G_t \cdot I, \end{cases} \tag{3}$$

where I is the original image, t is a time iteration parameter, $c(\|\nabla I\|)$ is a margin stop function also known as flow diffusion coefficient, and ∇ is a gradient operator. The subscripts t and n are the first-order partial derivatives of the image in the direction of unit tangent and normal vector. The subscripts tt and nn stand for second-order partial derivatives of the image in the direction of unit tangent and normal vector. f_1 is the diffusion coefficient in the normal direction, f_2 is the diffusion coefficient in the tangent direction. a is the retention coefficient of edge and local details when anisotropic diffusion is controlled for denoising, b is the retention coefficient of ultrasonic echo bright bar when anisotropic diffusion is controlled for denoising, G_t is Gaussian smoothing function, and v is the smoothed image.

In order to maintain useful information in ultrasonic images, mean square error (MSE) is used as an objective quantitative standard for image quality, and set the parameters $f_1 < f_2$, $f_1 \longrightarrow 0$, and $f_2 \longrightarrow 0$.

3.2. Extract Texture Features. Compared with other feature extraction methods, uniform local binary pattern (ULBP) has the characteristics of simple calculation and good robustness [16]. ULBP can be used as shallow image features to accurately describe texture features in ultrasonic images. The local binary pattern encoding of pixels in image (x_c, y_c) is defined as follows:

$$\mathrm{BPR}(x_c, y_c) = \sum_{p=0}^{P} S\left(n_p - n_c\right) \times 2^p, \tag{4}$$

where $S(\cdot)$ is defined as follows:

$$S(x) = \begin{cases} 1, & |x| \geq T_{\text{LBP}}, \\ 0, & |x| < T_{\text{LBP}}, \end{cases} \tag{5}$$

where n_c is the pixel value of the neighborhood center point (x_c, y_c). On the circle of radius R, n_P is the value of the pth pixel on the circle. In order to enhance the robustness of LBP in describing the smooth region of the image, T_{LBP} is set as a small and positive value.

The local binary mode with rotation invariance can be calculated as follows. First, the LBP code of any pixel is calculated, and then, the LBP translation code of the minimum value is obtained by rotating it to the right. The minimum LBP translation code of each pixel in the image is calculated. Finally, the histogram of local binary mode translation value is used as the shallow texture characteristic value of the input image.

For the ultrasound images of the liver and spleen to be processed, the images are input into GoogLeNet as input information, and the output is the depth features of the images. For the shallow texture features of the image, ULBP is used as the texture feature extraction method. In order to integrate the two characteristics of deep layer and shallow layer, they are normalized, respectively. After normalization processing, the high and low level image features are as follows:

$$\widehat{F}_{\text{high}} = \frac{F_{\text{high}} - F_{\text{high}}^{\min}}{F_{\text{high}}^{\max} - F_{\text{high}}^{\min}}, \tag{6}$$

$$\widehat{F}_{\text{low}} = \frac{F_{\text{low}} - F_{\text{low}}^{\min}}{F_{\text{low}}^{\max} - F_{\text{low}}^{\min}}, \tag{7}$$

$$F_{\text{low}} = \{F_{\text{high}}, F_{\text{low}}\}, \tag{8}$$

where $\widehat{F}_{\text{high}}$ is the depth characteristics F_{high} after a normalized value. $\widehat{F}_{\text{high}}^{\min}$ and $\widehat{F}_{\text{high}}^{\max}$ are the minimum and maximum values of the prenormalized depth eigenvectors, respectively. $\widehat{F}_{\text{low}}$ is the normalized value. F_{low} represents the unnormalized value. $F_{\text{low}}^{\min}$ expressed the minimum value of the unnormalized characteristic vector. $F_{\text{high}}^{\min}$ is maximum value of the unnormalized characteristic vector, while F is the fused characteristic, which is used for ultrasonic image recognition and classification.

3.3. Segment Edge Information. Among the numerous image edge detection methods for image edge detection, the common edge detection operators are Sobel, Log, Prewitt, and Roberts. The implementation of these algorithms is relatively simple and the detection is fast, but they are vulnerable to noise interference. If it is applied to remote sensing image edge detection, there will be many interference edges, edge discontinuity, or loss of road details.

Canny edge detection method based on optimization idea can make up for the shortcomings of other gradient operators, and is considered to be the most successful and widely

used gray edge detection method [17]. Canny method is mainly implemented in four steps.

(1) Smooth image denoising. The Gaussian function g (x, y) is used to convolute the image $d(x, y)$ to get the smooth image $s(x, y)$:

$$G(x, y) = \frac{1}{\sqrt{2\pi}\sigma} \exp\left(\frac{-(x^2 + y^2)}{2\sigma^2}\right), \tag{9}$$

$$s(x, y) = d(x, y) \times G(x, y), \tag{10}$$

where σ is the smoothing scale parameter.

(2) The gradient amplitude and direction are calculated. The appropriate gradient operator is selected to calculate the gradient size and direction of each pixel after noise reduction

(3) Nonmaximum suppression (NMS). In order to locate the edge points accurately, the gradient value of each pixel is suppressed by nonmaximum method. In the neighborhood of the current pixel, the gradient amplitude of the point is compared. If the gradient amplitude is greater than the gray value of two adjacent pixels along the gradient direction, then the point is judged to be a possible edge point. Otherwise, the point is judged as nonedge point

(4) High and low threshold detection and edge connection. Through the above steps, the edge is only rough. Then, the false edge points are removed by high and low threshold detection. The points smaller than the low threshold are excluded, and the points larger than the high threshold are determined as edge points. If it is between the two, it will be marked as weak edge point, and then judge whether the weak edge point is connected with the edge point. If the weak edge point is connected with the edge point, the point is recorded as the edge point

The amplitude and direction of the gradient are calculated by using Canny algorithm with the traditional template of size (2×2). However, it is greatly affected by the noise and cannot accurately detect the edge. Therefore, on this basis, this paper adopts Sobel edge detection operator to calculate the first partial derivative from the four directions of horizontal, vertical, 45°, and 135°, respectively. Good results are achieved in the experiment. The template is shown in Figure 1.

3.4. Classification of Ultrasound Images of Liver and Spleen Injury with Double-Channel CNN. In the structure of convolutional neural network, the first layer is the input layer, namely, the input image. The feature extracted from the first convolution layer behind the input layer is the feature graph of the first layer. Since the first layer feature map is the basis of subsequent feature map and feature used for classification, the first convolution layer is very important to the degree of image understanding. In the convolution layer, the size of the convolution kernel determines the size of the granularity

−1	−2	−1
0	0	0
1	2	1

(a) Directions of horizontal

−1	0	1
−2	0	2
−1	0	1

(b) Directions of vertical

−2	−1	0
−1	0	1
0	1	2

(c) Directions of 45°

0	1	2
−1	0	1
−2	−1	0
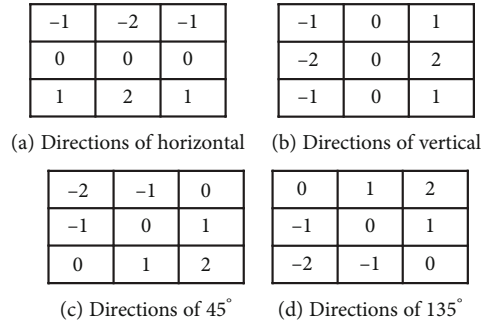
(d) Directions of 135°

FIGURE 1: Gradient direction template diagram of four directions.

of the network recognition image. If the size of the convolution kernel is too large, some details of the edge contour of the feature will be lost; if the size of the convolution kernel is too small, the ability of the convolution operation to transform the feature will be reduced, and the feature cannot be extracted effectively. Therefore, the size of the convolution kernel is very important to the effect of network feature extraction.

The deep features extracted by convolutional neural network are combined by the shallow features, so the loss of the first layer features will lead to the failure of subsequent networks to obtain effective deep features. In traditional convolutional neural networks, only one input channel is usually designed. Moreover, the kernel size of the first convolution layer is set to a fixed value, so the initial image recognition granularity of this neural network is fixed. However, for different kinds of images to be processed, the original features generally do not exist in a fixed size. Therefore, the design of a single convolutional kernel will lead to the loss of features of other scales of the original image; that is, the single-channel convolutional neural network cannot adequately extract the eigenvalues of the original image.

Aiming at the problem of insufficient feature extraction in traditional single-channel convolutional neural network, a dual-channel convolutional neural network for ultrasonic image diagnosis is proposed in this paper. The network consists of two relatively independent network structures. Each network is composed of an input layer, a convolution layer, a pooling layer, and a full connection layer. In the input layer, external edge features and internal texture features are taken as input information of the dual channel convolutional neural network, respectively. In the first layer of the convolution layer, the size of the convolution kernel is set according to the characteristics, respectively, so the two networks usually use the convolution check of different sizes to extract the two input layers. Compared with the maximum pooling method, the dynamic K-max pooling method can not only retain a number of important features of the image but also improve the training efficiency of the network structure. Therefore, the K-max pooling method is chosen in this paper. After the pooling layer, the two channels are connected to one full connection layer for a full connection mapping, and then, the two full connection layers are combined together through one full connection layer, followed by the Softmax classifier to classify the extracted characteristics.

In clinical diagnosis, the external edge information and internal texture information of the liver and spleen are often used as the important basis for doctors' diagnosis. Therefore, the external edge feature and internal texture feature are, respectively, taken as the two input channels of the convolutional neural network in this paper. Then, combined with the dynamic K-max pooling method, this paper proposed an ultrasonic image classification algorithm for liver and spleen injury with the double-channel CNN.

4. Experimental Results and Analysis

All the experiments in this paper are implemented under the framework of Python 3 and tensor flow. The CPU of the computer is Intel Core i7 processor. GPU is used to improve the computing speed. The GPU model is GTX965M, and the GPU memory is 8G.

4.1. Experimental Data. In this study, the data set we used was obtained by SAMSUNGRS80A color Doppler ultrasonography, with a total of 1200 images. These instrumental images clearly show the morphology, internal structure, and surrounding tissue of liver and spleen injury. Figure 2 is an example of liver ultrasound image, and Figure 3 is an example of spleen ultrasound image.

In the process of algorithm training, the ultrasonic image data is first divided into two sample sets of training and testing, and then, the neural network training is used to reach the acceptable range of error. In this experiment, MATLAB neural network toolbox was used to classify the level of ultrasonic image injury of the liver and spleen. The edge information and texture information are input, and the six levels of damage are output. 1200 images were selected for the experiment, including 600 images as training data and 600 images as test data.

According to AAST diagnostic criteria shown in Figure 4, the liver and spleen morphological injuries were classified into levels I to VI. However, level VI injury is rarely seen on imaging due to its high mortality rate, and no case could be featured as a result. Therefore, the experimental data in this paper only includes 5 levels.

4.2. Comparative Experiment. The feasibility of the two-channel convolution recognition algorithm proposed in this paper is verified at first. For the same experimental data set,
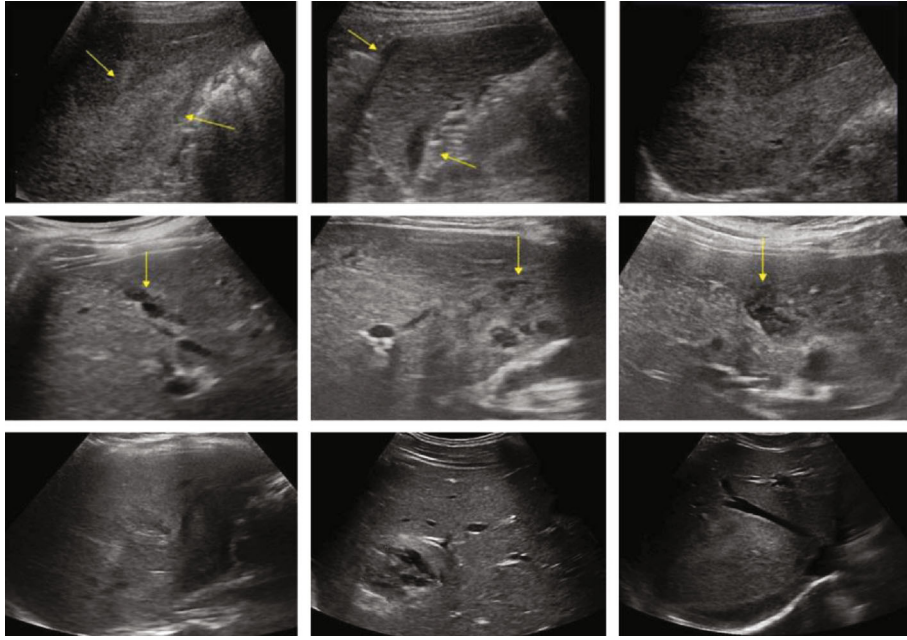
FIGURE 2: Ultrasound image of the liver.
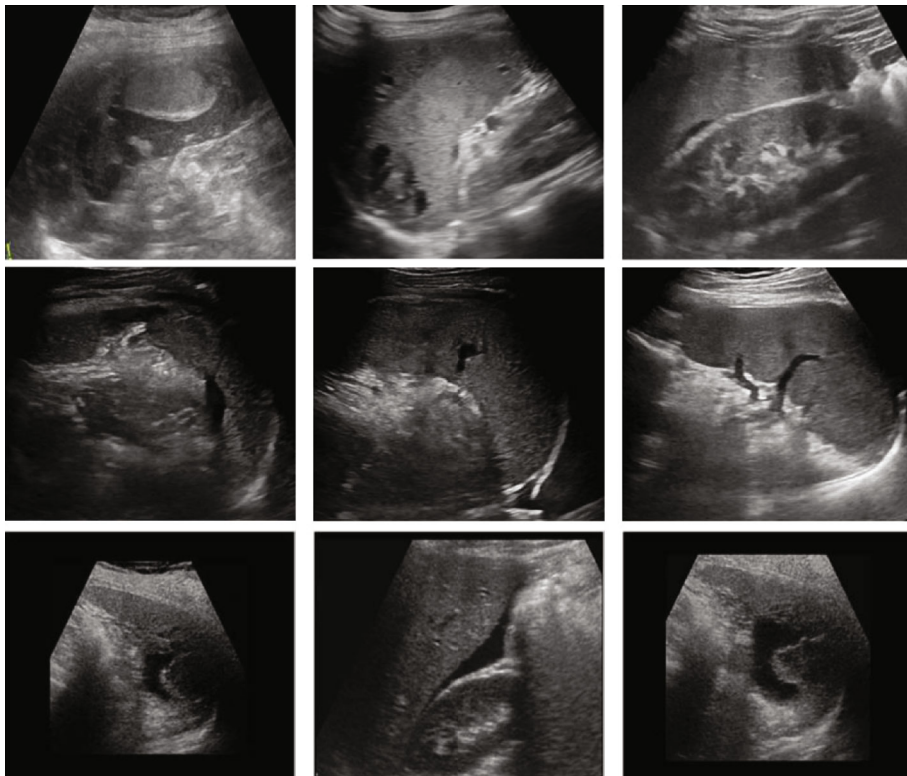
FIGURE 3: Ultrasound image of the spleen.

a single channel network and a multichannel network were used for comparative experiments. The feasibility of the proposed algorithm is verified by comparing the networks designed with different parameters. At the same time, according to the identification results of various parameters, the most appropriate network parameters are selected as the recommended parameters of the algorithm in this paper. In order to further verify the performance comparison between the algorithm in this paper and other algorithms, a comparative experiment of different algorithms will be carried out.
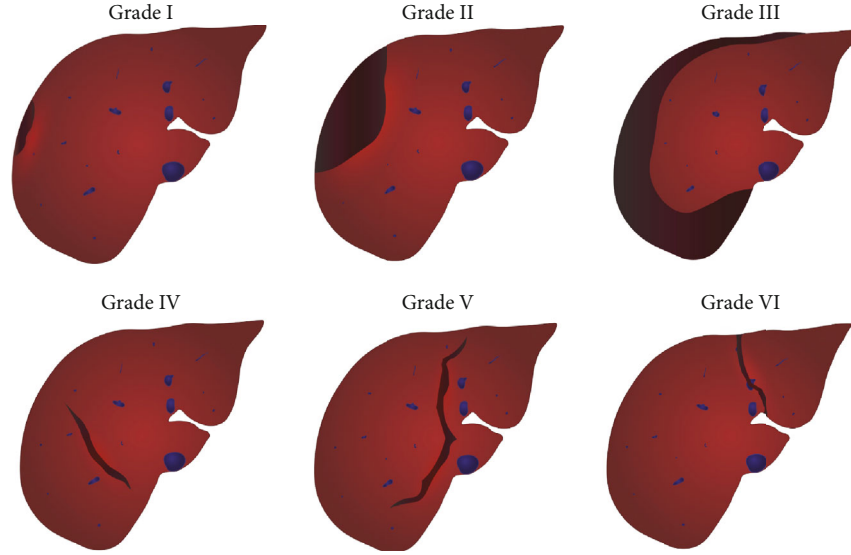
FIGURE 4: The schematic diagram of liver injury.

TABLE 2: The recognition results of the double-channel and single-channel CNN.

Model structure	Level I	Level II	Level III	Level IV	Level V
Single-channel CNN A (3 ∗ 3)	81.25	81.74	82.36	80.74	80.53
Single-channel CNN A (5 ∗ 5)	83.84	83.17	83.48	84.25	85.3
Single-channel CNN A (7 ∗ 7)	82.36	81.76	82.82	82.85	80.94
Single-channel CNN B (3 ∗ 3)	80.13	80.62	81.24	79.62	79.41
Single-channel CNN B (5 ∗ 5)	81.35	80.75	81.81	81.84	79.93
Single-channel CNN B (7 ∗ 7)	82.62	81.95	82.26	83.03	84.08
Double-channel CNN (5 ∗ 5 and 7 ∗ 7)	**94.96**	**93.33**	**94.63**	**94.82**	**92.40**

TABLE 3: The recognition results of different algorithms.

Algorithms	Level I	Level II	Level III	Level IV	Level V
Literature [18]	86.33	82.52	83.52	84.25	87.36
Literature [19]	88.42	83.41	86.28	87.13	82.74
Literature [20]	92.41	91.92	93.49	91.31	90.37
Proposed method	**94.96**	**93.33**	**94.63**	**94.82**	**92.40**

The most appropriate parameters are selected as the premise, and then compared with other algorithms, so as to analyze the advantages of the algorithm in this paper.

4.2.1. Validation of Proposed Double-Channel CNN Algorithm. In the convolutional layer of convolutional neural network, the effect of feature extraction of convolutional check with different sizes is different. In general, different sizes of convolutional kernels are set according to their characteristics when designing convolutional neural networks. After setting the appropriate size of the convolution kernel, the convolution layer can extract more sufficient and effective eigenvalues. Only when the feature extraction is sufficiently effective, can it provide effective guarantee for the subsequent output layer. In order to analyze the algorithm recognition rate of the proposed algorithm under different convolutional kernel sizes,

the convolutional kernel size of the single-channel convolutional neural network was first set, and the feature extraction effect was observed. In the single-channel convolutional neural network A, 3 ∗ 3, 5 ∗ 5, and 7 ∗ 7 are, respectively, set as the convolutional kernel in order to extract the texture information of the damaged site. In the single-channel convolutional neural network B, 3 ∗ 3, 5 ∗ 5, and 7 ∗ 7 are, respectively, set as convolutional cores in order to extract the edge information of the damaged site. The recognition results of single-channel convolutional neural network are shown in Table 2. It can be seen from Table 2 that in single-channel convolutional neural network A, the recognition result of 5 ∗ 5 convolutional kernel is higher; that is, its extraction of texture features is more effective. In single-channel convolutional neural network B, the recognition result of 7 ∗ 7 convolutional kernel is higher; that is, its extraction of edge information is better.

When setting the parameters of the two-channel convolutional neural network proposed in this paper, 5 ∗ 5 convolutional kernel is selected as the convolutional kernel of the texture information input channel, and 7 ∗ 7 convolutional kernel is selected as the convolutional kernel of the edge information input channel. The results of the two-channel convolutional neural network in this paper are shown in the last column of Table 2. By comparing with single-

channel convolutional neural network, it can be seen that the two-channel convolutional neural network algorithm proposed in this paper has a higher recognition rate.

4.2.2. Comparison Experiment. In order to compare the recognition performance of the algorithm presented in this paper, the damage recognition algorithms with excellent performance in recent years are selected for comparative experiments under the same experimental data. According to the experimental results above, the convolutional kernel size of the two-channel convolutional neural network designed in this paper is set as $5 * 5$ and $7 * 7$. The damage recognition results of different algorithms are shown in Table 3.

Literature [18] proposed a method using multifractal dimension and back propagation neural network. Literature [19] used the deep learning framework to distinguish the unique types of acquired lesions and nodules of the breast through ultrasound imaging. Literature [20] proposed a stacked deep polynomial network (S-DPN) algorithm to improve the representation performance of the original DPN, and the S-DPN algorithm was applied to the texture feature learning of ultrasonic tumor classification in small data sets. Compared with other methods, the recognition rate of this algorithm is higher. This is because the proposed algorithm uses anisotropic diffusion denoising model to preprocess the data of ultrasonic images of the liver and spleen, which improves the image quality. Then, the external edge feature and the internal texture feature are taken as the double-input channels of the convolutional neural network, respectively, which makes the extracted features more abundant and conducive to recognition, so the recognition rate is higher. Based on the above results, it can be seen that the double-channel convolutional neural network can learn more features by using the two input channels of texture information and edge information of damaged images. Compared with other damage identification algorithms, double-channel CNN has higher accuracy in damage identification.

5. Conclusion and Future Work

In order to realize more accurate ultrasonic image diagnosis of liver and spleen injury, a double-channel convolutional neural network based algorithm for ultrasonic image classification diagnosis of liver and spleen injury is proposed. To improve the image quality of ultrasonic images, the anisotropic diffusion denoising model is first used to realize data preprocessing of ultrasonic images of the liver and spleen. The location of the lesion was detected with the outer edge to obtain the characteristics of the outer edge. Then, the rotation invariant local binary mode feature of the extracted image is taken as the inner texture feature of the image. In the process of convolutional neural network recognition, external edge features and internal texture features are used as double-input channels, respectively, so as to realize the effective use of the learning and recognition ability of convolutional neural network. The experiment results show that the method of this paper can accurately diagnose liver and spleen injury.

In the future work, we will systematically analyze the time-consuming situation of each module algorithm, and put forward improvement measures to improve the overall efficiency of the algorithm.

Data Availability

The labeled datasets used to support the findings of this study are available from the corresponding authors upon request.

Conflicts of Interest

The authors declare no competing interests.

Acknowledgments

References

[1] R. Goel and A. Jain, "Improved detection of kidney stone in ultrasound images using segmentation techniques," *Advances in Data and Information Sciences*, vol. 94, pp. 623–641, 2020.

[2] S. Hapugoda, C. Hacking, F. Gaillard, and A. Dixon, "AAST liver trauma grading system: a pictorial essay," European Congress of Radiology-2017 ASM, 2017.

[3] O. Aiadi and M. L. Kherfi, "Image classification using texture features and support vector machine (SVM)," 2019.

[4] X. Hu and A. Ensor, "Fourier spectrum image texture analysis," in *2018 International Conference on Image and Vision Computing New Zealand (IVCNZ)*, pp. 1–6, Auckland, New Zealand, 2018.

[5] C. P. Loizou, C. S. Pattichis, M. Pantziaris, E. Kyriacou, and A. Nicolaides, "Texture feature variability in ultrasound video of the atherosclerotic carotid plaque," *IEEE Journal of Translational Engineering in Health and Medicine*, vol. 5, pp. 1–9, 2017.

[6] S. Dash and U. R. Jena, "Gaussian pyramid based laws' mask descriptor for texture classification," in *2017 International Conference on Wireless Communications, Signal Processing and Networking (WiSPNET)*, pp. 654–658, Chennai, India, 2017.

[7] L. Dandan, M. Huanhuan, L. Xiang, J. Yu, J. Jing, and S. Yi, "Classification of diffuse liver diseases based on ultrasound images with multimodal features," in *2019 IEEE International Instrumentation and Measurement Technology Conference (I2MTC)*, pp. 1–5, Auckland, New Zealand, 2019.

[8] L. D. Nguyen, D. Lin, Z. Lin, and J. Cao, "Deep CNNs for microscopic image classification by exploiting transfer learning and feature concatenation," in *2018 IEEE International Symposium on Circuits and Systems (ISCAS)*, pp. 1–5, Florence, Italy, 2018.

[9] S. Hijazi, R. Kumar, and C. Rowen, *Using convolutional neural networks for image recognition*, Cadence Design Systems, Inc, San Jose, CA, USA, 2015.

[10] S. Mejbri, C. Franchet, I. A. Reshma, J. Mothe, P. Brousset, and E. Faure, "Deep analysis of CNN settings for new cancer whole-slide histological images segmentation: the case of small training sets," in *6th International Conference on BioImaging*

(BIOIMAGING 2019), pp. 120–128, Prague, Czech Republic, 2019.

[11] H. Lee, H. Lee, M. Park, and J. Kim, "Contextual convolutional neural networks for lung nodule classification using Gaussian-weighted average image patches," in *Medical Imaging 2017: Computer-Aided Diagnosis*, vol. 10134, p. 1013423, California, United States, 2017.

[12] O. A. Debats, G. J. S. Litjens, and H. J. Huisman, "Lymph node detection in MR lymphography: false positive reduction using multi-view convolutional neural networks," *PeerJ*, vol. 7, article e8052, 2019.

[13] P. Ballester and R. M. Araujo, "On the performance of GoogLeNet and AlexNet applied to sketches," in *Proceedings of the AAAI Conference on Artificial Intelligence*, Phoenix, Arizona, USA, 2016.

[14] Yongjian Yu and S. T. Acton, "Speckle reducing anisotropic diffusion," *IEEE Transactions on Image Processing*, vol. 11, no. 11, pp. 1260–1270, 2002.

[15] S. J. Fu, Q. Q. Ruan, W. Q. Wang, and Y. Li, "Adaptive anisotropic diffusion for ultrasonic image denoising and edge enhancement," *International Journal of Information Technology*, vol. 2, no. 4, pp. 284–292, 2005.

[16] T. Ojala, M. Pietikainen, and T. Maenpaa, "Multiresolution gray-scale and rotation invariant texture classification with local binary patterns," *IEEE Transactions on Pattern Analysis and Machine Intelligence*, vol. 24, no. 7, pp. 971–987, 2002.

[17] J. Canny, "A computational approach to edge detection," *IEEE Transactionson Pattern Analysis and Machine Intelligence*, vol. PAMI-8, no. 6, pp. 679–698, 1986.

[18] M. A. Mohammed, B. Al-Khateeb, A. N. Rashid, D. A. Ibrahim, M. K. Abd Ghani, and S. A. Mostafa, "Neural network and multi-fractal dimension features for breast cancer classification from ultrasound images," *Computers and Electrical Engineering*, vol. 70, pp. 871–882, 2018.

[19] S. Han, H. K. Kang, J. Y. Jeong et al., "A deep learning framework for supporting the classification of breast lesions in ultrasound images," *Physics in Medicine and Biology*, vol. 62, no. 19, pp. 7714–7728, 2017.

[20] J. Shi, S. C. Zhou, X. Liu, Q. Zhang, M. H. Lu, and T. F. Wang, "Stacked deep polynomial network based representation learning for tumor classification with small ultrasound image dataset," *Neurocomputing*, vol. 194, pp. 87–94, 2016.

WILEY | Hindawi

Retraction

Retracted: Application of Fuzzy Decision Tree Algorithm Based on Mobile Computing in Sports Fitness Member Management

Wireless Communications and Mobile Computing

This article has been retracted by Hindawi following an investigation undertaken by the publisher [1]. This investigation has uncovered evidence of one or more of the following indicators of systematic manipulation of the publication process:

1. Discrepancies in scope
2. Discrepancies in the description of the research reported
3. Discrepancies between the availability of data and the research described
4. Inappropriate citations
5. Incoherent, meaningless and/or irrelevant content included in the article
6. Peer-review manipulation

The presence of these indicators undermines our confidence in the integrity of the article's content and we cannot, therefore, vouch for its reliability. Please note that this notice is intended solely to alert readers that the content of this article is unreliable. We have not investigated whether authors were aware of or involved in the systematic manipulation of the publication process.

Wiley and Hindawi regrets that the usual quality checks did not identify these issues before publication and have since put additional measures in place to safeguard research integrity.

We wish to credit our own Research Integrity and Research Publishing teams and anonymous and named external researchers and research integrity experts for contributing to this investigation.

The corresponding author, as the representative of all authors, has been given the opportunity to register their agreement or disagreement to this retraction. We have kept a record of any response received.

References

[1] Z. Gu and C. He, "Application of Fuzzy Decision Tree Algorithm Based on Mobile Computing in Sports Fitness Member Management," *Wireless Communications and Mobile Computing*, vol. 2021, Article ID 4632722, 10 pages, 2021.

Research Article

Application of Fuzzy Decision Tree Algorithm Based on Mobile Computing in Sports Fitness Member Management

Zhu Gu[1] and Chaohu He [1] [2]

[1]*School of Physical Education, Hunan International Economics University, Changsha, 410205 Hunan, China*
[2]*School of Physical Education, Kunming University, Kunming, 650214 Yunnan, China*

Correspondence should be addressed to Chaohu He; holy921@163.com

After the reform and the opening, the economy of our country has developed rapidly, and the living conditions of the people have become better and better. As a result, they have a lot of time to pay attention to their health, which has promoted the rapid development of the sports and fitness industry in my country. In response to the increasing development of the sports and fitness sector of my country, the current state of the administration of members of the sports fitness industry does not keep pace with the development of the sports and fitness industry of my country. Based on this, this article uses a fuzzy decision tree algorithm to establish a decision tree based on the characteristics of customer data and loses existing customers. Analyzing the situation is of strategic significance for improving the competitiveness of the club. This article selects the 7 most commonly used data sets from the UCI data set as the initial experimental data for model training in three different formats and then uses the data of a specific club member to conduct experiments, using these data files as training samples to construct a vague analysis of the decision tree to overturn the customer to analyze the main factors of customer change. Experiments show that the fuzzy decision tree ID3 algorithm based on mobile computing has the highest accuracy in the Iris data set, reaching 97.8%, and the accuracy rate in the Wine data set is the smallest, only 65.2%. The mobile computing-based fuzzy decision tree ID3 algorithm proposed in this paper obtained the highest correct rate (86.32%). This shows that, compared to traditional analysis methods, the blurred decision tree obtained for churn client analysis has the advantages of high classification accuracy and is understandable so that ideal classification accuracy can be achieved when the tree is small.

1. Introduction

With the rapid development of information, more and more data information will inevitably be created. This data not only has a particularly large amount of data but also contains a large amount of potentially valuable information. Gym clubs are increasingly facing the question of how to effectively manage and how to effectively use the useful data you need from these large amounts of data. Use the right methods to gather relevant data and information, be able to identify customer characteristics in the database in a timely manner, analyze key drivers of customer change to reduce customer turnover, and provide helpful information to managers in decision support.

The decision tree induction learning algorithm represented by the ID3 algorithm is feasible when solving classification problems, but this algorithm does not take into account the ambiguity of customer data, so there are some limitations in expressing and understanding customer characteristics. The fuzzy decision algorithm ID3 based on the theory of fuzzy mathematics is a fuzzy extension of the classical ID3 algorithm. Because it can deal with the uncertainty associated with human thought and emotion, it extends the scope of the ID3 algorithm, creating decision trees is more logical, and sorting speed Faster, can provide decision support for various areas. Then, how to effectively use business intelligence technology to make strategic decisions requires companies to analyze these customer data. Traditional

analysis methods have great limitations in solving enterprise customer relationship management, which makes the results of analysis and prediction unsatisfactory.

In the past ten years, scholars at home and abroad have conducted a large number of pioneering and fruitful researches on the application of fuzzy decision tree algorithm in management and have accumulated rich research results and research experience. Chiu et al. tried to apply the fuzzy decision tree that combines the advantages of fuzzy theory and fuzzy tree into this field by analyzing the problems in the management of high school teachers. It briefly introduces the construction principle of fuzzy decision and the algorithm of fuzzy ID3 decision tree and applies it to the management of teachers in colleges and universities. Therefore, a preliminary analysis of the reasons for the loss of high school teachers is carried out. The research of several high schools shows that the results obtained by this method are in line with the facts and therefore provide a theoretical basis for high schools to solve the problem of faculty management. However, his research did not clearly put forward the relevant data on the loss of high school teachers [1]. In Yumi's business management, it is very important to analyze the crisis of customer confiscation to improve competitiveness, which is an important branch of business intelligence. Compared with decision trees, based on the advantages of fuzzy decision trees in solving the ambiguity of customer data, genetic algorithms are used to optimize two important parameters in the fuzzy decision trees. Then, a method based on optimized fuzzy decision-making to analyze the crisis of customer forfeiture is proposed. The experimental results show that the method is feasible and effective. It provides new ideas for analyzing and predicting customer confiscation crises and helps managers make better decisions in business strategies. However, the overall research lacks data support and needs more data support its conclusion [2]. Jang and Kim can identify different types of soil through these characteristics. Good soil classification is very important for better use of soil. The opinions of experts may be very different. It is not easy for experts to manually classify soil. In addition, different types of soil cannot be defined deterministically. In order to explore alternative methods to solve this problem, the application of using an automatic program to generate a soil classifier from data using a fuzzy decision tree induction algorithm is studied. In order to compare the results obtained by the fuzzy decision tree classifier, we used two well-known classifier generation methods: the classic decision tree induction algorithm C4.5 and the fuzzy rule induction algorithm named FURIA. The experimental results lack more data support. As a result, the results obtained by the fuzzy decision tree classifier are still doubtful [3, 4].

Based on the analysis of the fuzziness of customer data characteristics, this paper compares the two inductive learning algorithms of decision trees and fuzzy decision trees and then uses mobile computing to optimize two important parameters involved in the establishment of fuzzy decision trees. And use the optimized fuzzy decision tree for customer churn analysis. According to the relevant data elements of member management, the spatial data of the sample area is selected, and the ID3 algorithm in the decision tree algorithm

is combined with the fuzzy algorithm based on mobile computing to realize the program establishment of the sample area, and the classification model of the decision tree in the member management is established, and through the established classification prediction model, whether users will be lost was analyzed and predicted, and the correctness of the three schemes was evaluated at the same time.

2. Application of Fuzzy Decision Tree Algorithm in the Management of Sports Fitness Members

2.1. Decision Tree Model Design and Algorithm

2.1.1. Decision Tree Construction. In the process of building a decision tree, we must first have data samples. This is the database for the construction. People do feature tests and sort this data through the test features to form a tree structure with nodes and branches. This is the basic idea of the decision tree. The decision tree sort algorithm is performed from top to bottom. Characteristics with good classification results are selected at each node to classify the samples. The process continues to execute, and finally, all training sets are classified by this tree, or all attributes have been used [5, 6]. To build a decision tree, first, select the best test attribute, and then, use the selected attribute to divide the sample set, and at the same time, build the next level of nodes. In the end, the result of the division is only the same sample. This division is pure.

The following description is for the general process of constructing a decision tree: a sample set and an empty tree form the initial state. For a node, use the test attribute of this node to divide the node; if all the samples of the node are contained in the same category, a leaf node with the imprint of this category will be created, and the creation will stop; otherwise, use the best measurement to calculate each possible division of each set; if a test is the best category selected as the node in the test, a child node with as many outputs as the number of outputs different from the division will be established; when marking the boundary between the parent and the child, the output result of this classification is used, and finally, the sample set is divided into the child nodes. As the current node, the child node will stop the classification when it cannot be classified again [7–9].

2.1.2. Simplification of Decision Tree. The data of a decision tree is quite complex, so it is difficult for users to understand, so the meaning of this decision tree is not so important. Therefore, if there are fewer branches and leaves that constitute a decision tree, the classification process is relatively simple, and the space for storing data is relatively small, so when constructing the tree, pay attention to as simple as possible, and do not build the tree's branches and leaves too large [10–12]. Therefore, the decision tree needs to be simplified. For decision trees, a technique that effectively targets noise is called pruning technique. This technique enables people to better understand and simplify a tree. The decision tree is relatively simple and good, but the pruning technology is not a panacea. If there is too little data and we still use the pruning technology, the information of the tree will be

seriously insufficient. Therefore, pruning technology is not an absolute technology. It can achieve better results when it is applied at an appropriate time. Of course, it is necessary to prevent it from being applied when it is not needed.

2.1.3. Prepruning. Before a tree is built, pruning the tree data as soon as possible to stop the growth of the tree. Regarding the prepruning method, when to stop is a key issue. There are many methods to study the prepruning and choose the appropriate time. A more concise method is to specify the height of a tree, choose to stop the growth of the tree when it reaches this height, and no longer continue to test the data with attributes [13, 14]. This method is a double-edged sword. Sometimes checking the height of the tree can have good results, but stopping the growth of the tree too early will cause incomplete data classification, which will cause the results to be inaccurate. Set an appropriate feature value for the data attribute. When categorizing data, when the attribute value of a node is this operating value, the tree does not stop growing and does not split. This method can avoid data fragmentation very well and also avoid data conflicts caused by excessive data classification.

Set a limit value, which can be called a threshold. This value means the number of nodes. As the tree continues to grow, when reaching a certain node, the number of nodes is less than this value; then, the growth of the tree can be forcibly stopped [15, 16]. This method is also an important means to limit the excessive growth of the tree, but its application is limited to the small amount of data; processing with this method will affect the accuracy of the results. When building a tree, it will affect the performance of the model. A tree that is too large will affect the speed of the model, and a tree that is too small will not be able to fully classify the data. Therefore, there must be a value for the benefit of the model, and the growth will stop when the benefit value is less than the limit value as the tree grows.

2.1.4. Postpruning

(1) REP (Reduced Error Pruning) Method. For pruning, every point on the decision tree may be processed. Because the construction of the decision tree is from top to bottom, the coordinated pruning process is also such a sequential process. This method does not deal with each node one by one. It is an abstract and concise way of thinking. The decision tree T is divided into many subtrees S, and the number of subtrees is regarded as leaf nodes, so that a simple tree is formed first [17, 18]. It has S leaf nodes. For a leaf node, it covers N samples, and there are E errors. Then, the misjudgment rate of the subtree is estimated as:

$$p = \frac{\sum_{i=1}^{S} E_i + 0.5S}{\sum_{i=1}^{S} N_i}. \tag{1}$$

We assume that the misjudgment of each sample in the subtree obeys a binomial distribution, where N represents the number of all samples contained in the subtree. Therefore, before pruning, the expected number of misjudgments is:

$$E = N * p. \tag{2}$$

If the error rate caused by the classification of the new tree is very low and the properties of the subtrees in the construction of the number of subtrees S are different, replace S with leaf nodes. This process is done continuously, and finally, the number of children of the decision tree T is replaced by leaf nodes. This processing method will get the ideal tree [7, 19]. The advantage of this method is that a decision tree with higher accuracy can be obtained, and the tree will not be too large.

(2) PEP (Pessimistic Error Pruning) Method. Assuming that the initial decision tree is T and a certain child node has a branch of number $n(t)$, there are $e(t)$ misclassifications in the results of these cases, and the error rate of the data set is:

$$r(t) = \frac{e(t)}{n(t)}. \tag{3}$$

The error rate is biased, because the training data is used to generate the tree while also pruning the tree, so the degree of pruning of this method is not accurate enough. In order to improve the evaluation of this method for accuracy, the error rate can be corrected to:

$$r'(t) = \frac{[e(t) + 1]}{n(t)}. \tag{4}$$

The number of children $T(t)$ of tree T is set to S; the number of leaves in this tree is $L(S)$; then, the classification error of $T(t)$ is:

$$r'(T_1) = \frac{\sum_S [e(s) + 1/2]}{\sum_s n(s)} = \frac{\sum e(s) + (L(s)/2)}{\sum n(s)}. \tag{5}$$

When the samples in the training set conflict, this result will be invalid. The PEP method introduces a continuous correction mechanism in the error estimation. This correction method has a better effect on the situation where the data is more troublesome. If the data simply introduces this mechanism, the result will be inaccurate [20, 21]. If the classification method is applied to classify the data of all sample sets, then:

$$e'(T_1) + SE\left[e'(T_1)\right] = \frac{1}{2}\left[L(T_1) + \sqrt{L(T_1)}\right]. \tag{6}$$

If the leaf node for correcting classification errors in subtree T_1 is large enough, pruning it.

2.1.5. Performance Evaluation of Decision Tree. For decision trees, high complexity does not mean accuracy. In this sense, accuracy is not related to the complexity of the tree. Of course, complexity is not an evaluation criterion for accuracy. For a decision tree, people usually have many evaluation criteria as follows:

According to this rule, unknown data is processed. Such a process can help people discover unknown knowledge information. The accuracy of the information obtained from the data can determine the accuracy of staff decision-making. Even if a model is accurately classified, its understanding is complex and cannot be considered a good method. A good classification model can present a classification method with a description that is easy for people to understand and uncomplicated [22, 23]. For decision-makers, a concise model description is more conducive to understanding and more conducive to widespread application. The amount of data that a model can bear is also a factor in whether people use this model. When the amount of data is very large, a good model can still show good accuracy, and this model is worth applying.

2.2. Classical Decision Tree Algorithm

2.2.1. ID3 Algorithm. The ID3 algorithm is characterized by first calculating the information entropy of the attributes of the sample set and selecting the optimal attributes for splitting by comparing these values. Use this attribute to divide the nodes to form a decision tree [24, 25]. If the element included in member management Y is $\{x_1, x_2, \cdots, x_n\}$, and the occurrence probability of each element is $\{p_1, p_2, \cdots, p_n\}$, respectively, then the entropy of member management Y is defined as follows:

$$\text{info}(Y) = -\sum_{i=1}^{n} p_i \log_2 p_i. \tag{7}$$

The probability that an instance can be classified into category i is:

$$p(c_i) = \frac{c_i}{|Y|}. \tag{8}$$

At this time, the entropy of member management Y is:

$$\text{info}(Y) = -\sum_{i=1}^{n} p(c_i) \log_2 p(c_i). \tag{9}$$

If the attribute A is selected as the splitting attribute, the value is $\{a_1, a_2, \cdots, a_m\}$, and the data set is divided into m class through A, where the conditional information entropy is expressed as:

$$\text{Info}(Y \mid A) = -\sum_{i=1}^{n} \sum_{j=1}^{m} p(c_i, a_j) \log_2 p(c_i, a_j),$$

$$\text{Info}(Y \mid A) \sum_{j=1}^{m} p(a_j) \sum_{i=1}^{n} p(c_i \mid a_j) \log_2 p(c_i \mid a_j). \tag{10}$$

Then, the information gain brought by attribute A is:

$$\text{Gain}(X, A) = \text{Info}(X) - \text{Info}(X \mid A). \tag{11}$$

When building a decision model through the ID3 algorithm, it is necessary to traverse each decision attribute and use the attribute with the largest information gain to divide the data set, so the decision tree obtained in this way is more accurate. The ID3 algorithm is shown in Algorithm 1.

2.2.2. C4.5 Algorithm. In order to calculate the efficiency of member management, the definition of its split information is as follows [26, 27]:

$$\text{Split}(Y, A) = -\sum_{i=1}^{m} p(a_1) \log_2 p(a_1),$$

$$\text{Split}(Y, A) = -\sum_{i=1}^{m} \frac{n_i}{n} \log_2 \frac{n_i}{n}. \tag{12}$$

Split information represents the information generated by dividing data set Y into subsets according to the value of decision attribute A, so there is a definition of membership management efficiency:

$$\text{GainRatio}(Y, A) = \frac{\text{Gain}(Y, A)}{\text{Split}(Y, A)}. \tag{13}$$

2.2.3. Comparison and Analysis of Decision Tree Algorithms. There are many decision tree algorithms. There are many differences in the scalability, execution speed, comprehensibility of the results, and accuracy of classification and prediction. A summary comparison of these algorithms is shown in Table 1.

3. Experimental Design of Fuzzy Decision Tree Algorithm in Sports Fitness Member Management

3.1. Model Realization. In order to complete the comparative experiment of the three decision tree schemes and realize a fuzzy decision model, it has the functions of data importing, data fuzzification, generating decision tree model, model testing, and instructions for use. The main business flowchart of the sports fitness membership management model is shown in Figure 1.

3.2. Test Subject. In order to obtain accurate and reliable experimental results to complete the analysis of the algorithm, we must first select the appropriate experimental data set. This article selects the 7 most commonly used data sets from the UCI data set as the initial experimental data to conduct model training on three different schemes. The specific description of the data set used is shown in Table 2. After training, apply the model to the analysis of customer churn and then use the data of a certain club to conduct experiments. Customer data consists mainly of basic information, geographic distribution information, and service information. Use statistical sampling to extract 1500 records from customer data in a given year. The characteristics of the customer in the database include customer age, residential area, profitability, period of service, and type of contract, and customers are divided into YES (churn) and NO (no churn) two

```
BuildID3(Y, T)
Input:
X: Training samples;
T: Root node, initially empty;
Output:
T: Decision tree root node
Begin
   Create node T with Y
   if Y all belong to the same class C
      return T
   end if
   if Y is empty or less than the given threshold
      return T
   end if
   Let n be the number of candidates attributes in node T
   for i=1:n
      Calculate Gain (Y, A) and find the attribute A that maximize the value
   end for
   Use A to divide Y into k subsets
   for i=1:k
      T. add(BuildID3(Y_i, T_i))
   end for
End
```

Algorithm 1: ID3 algorithm diagram.

Table 1: Comparison of typical decision tree algorithms.

	Attribute selection metrics	Dealing with continuous attributes	Pruning method	Do you need an independent test sample	Decision tree structure
ID3	Information gain rate	Discretization	Misclassification	Yes	Polytree
C4.5	Information gain rate	Presort	Misclassification	No	Polytree
CART	CINI coefficient	Presort	MDL	No	Binary tree
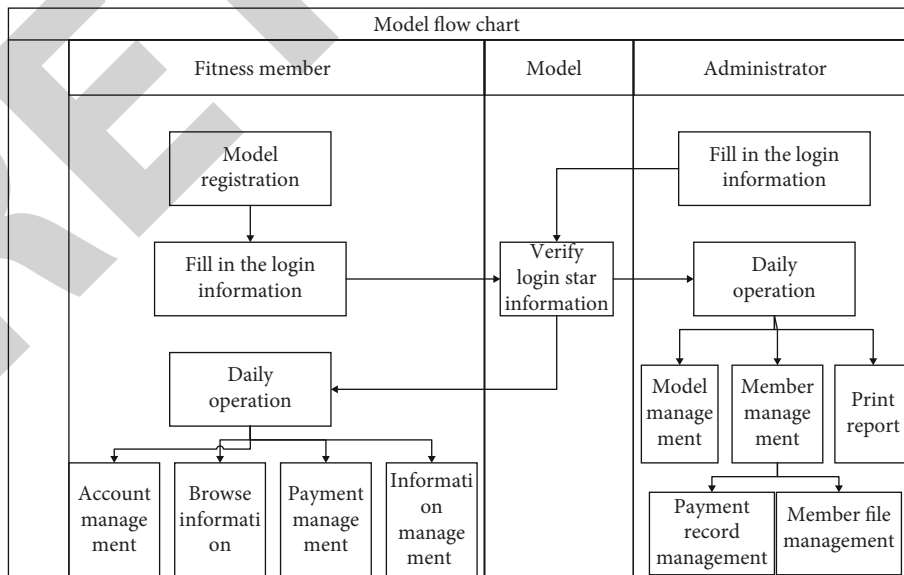
Figure 1: The main business flow chart of the sports fitness membership management model.

Table 2: Data set introduction.

S.no	Data sets	Instances	Number of classes (k)	Number of features (d)	Size of class
1	Iris	150	3	4	50, 50, 50
2	Wine	178	3	13	59, 74, 48
3	Glass	214	5	9	29, 76, 70, 17, 22
4	Diabetes	768	2	8	268, 500
5	Heartstatlog	270	2	13	150, 120
6	Ionosphere	351	2	34	126, 225
7	Sonar	208	2	60	97, 111
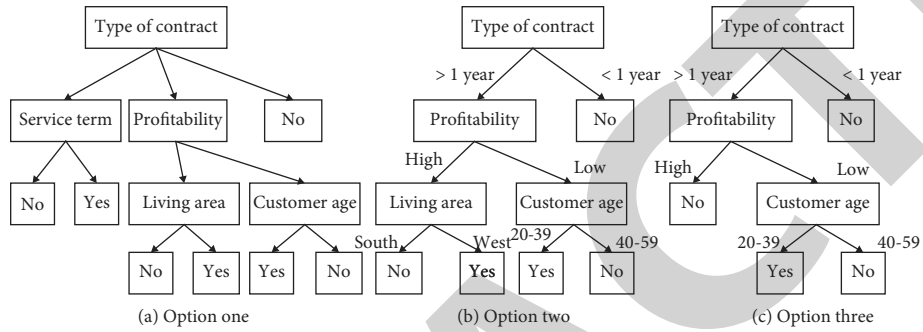
Figure 2: Decision tree built by three options.
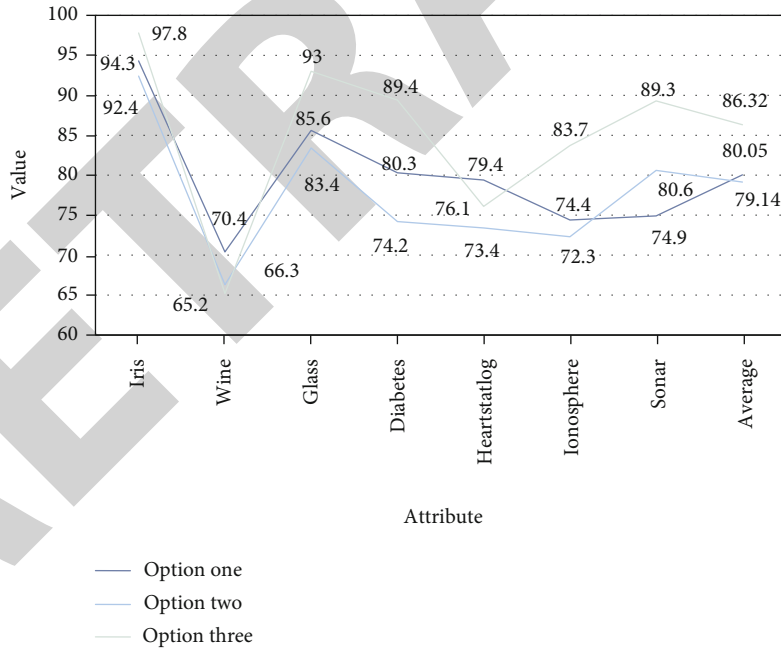
Figure 3: Comparison diagram of classification accuracy of three schemes.

types. Use these data files as training samples to create a vague decision tree for customer analysis and analyze the key factors of customer change [28].

3.3. Experiment Procedure. The experiment compared the three schemes. The first plan is to use the traditional decision tree ID3 algorithm to build a decision tree; the second plan is to use the fuzzy decision tree ID3 algorithm to build a deci-

sion tree, and the third plan is to build a decision tree based on the fuzzy decision tree ID3 algorithm of mobile computing. Figure 2 shows the decision tree established by the three schemes.

3.4. Statistical Processing. Statistical analysis was performed with the SPSS 13.0 statistical software. The significance test of the difference was performed by one-way analysis of
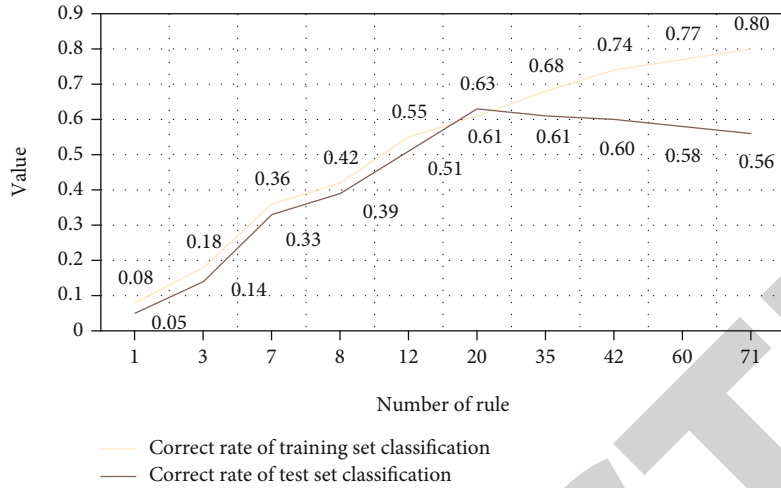
FIGURE 4: Schematic diagram of comparison of classification accuracy of training and test data sets under different rules of a decision tree.
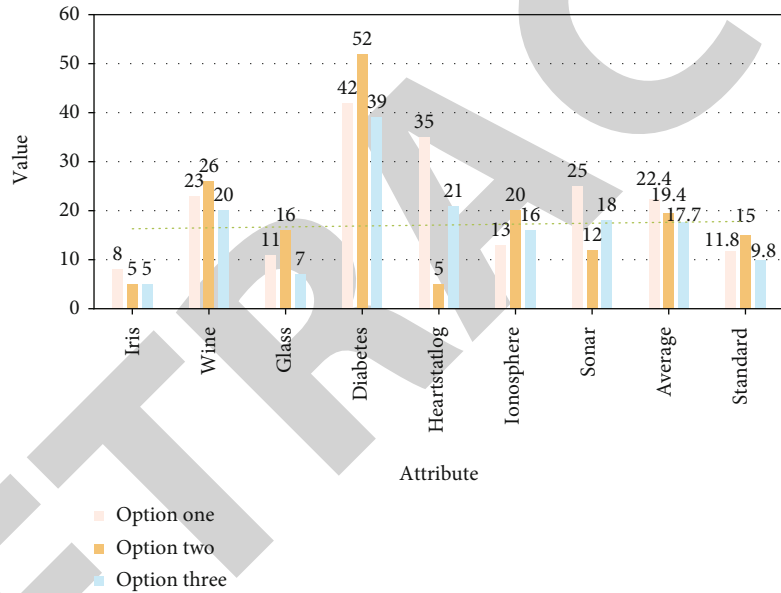
FIGURE 5: Comparison of the number of classification rules generated by the three schemes.

variance, the difference between the two groups was tested by LSD-t, and the statistics of the results of the application of the fuzzy decision tree algorithm in the management of sports and fitness members were performed by the group t test. $P < 0.05$ is considered to be significant and statistically significant.

4. Fuzzy Decision Tree Algorithm in the Management of Sports Fitness Members

4.1. Data Set Training Results

4.1.1. Correct Rate Comparison. By applying three different decision tree schemes to the seven preprocessed data sets, the correct rates of different algorithms in the classification of each data set can be obtained as shown in Figure 3.

It can be seen from Figure 3 that the fuzzy decision tree ID3 algorithm based on mobile computing has the highest accuracy in the Iris data set, reaching 97.8%, and the accuracy rate in the Wine data set is the smallest, only 65.2%; the fuzzy decision tree ID3 algorithm is in the Iris data set; the accuracy rate is the highest, reaching 94.3%, and the accuracy rate in the Wine data set is the smallest, only 66.3%; the traditional decision tree ID3 algorithm has the highest accuracy rate in the Iris data set, reaching 92.4%, and the accuracy rate in the Wine data set is the smallest, only 70.4%. The mobile computing-based fuzzy decision tree ID3 algorithm proposed in this paper achieved the highest accuracy rate (86.32%), which shows that the fuzzy decision tree ID3 algorithm based on mobile computing can produce high accuracy when dealing with continuous attributes.

4.1.2. Rule Number Comparison. Figure 4 shows the classification accuracy of training and testing under the same scheme with different numbers of rules.

TABLE 3: Data table of the effect of authenticity on accuracy.

Correct rate (%)	0.50	0.56	0.64	0.70	0.76	0.82	0.88	0.94	0.96	0.98
Option one	86	87	87	87	89	90	94	89	85	79
Option two	86	87	87	87	90	92	95	90	85	80
Option three	86	87	87	87	92	98	91	88	87	83
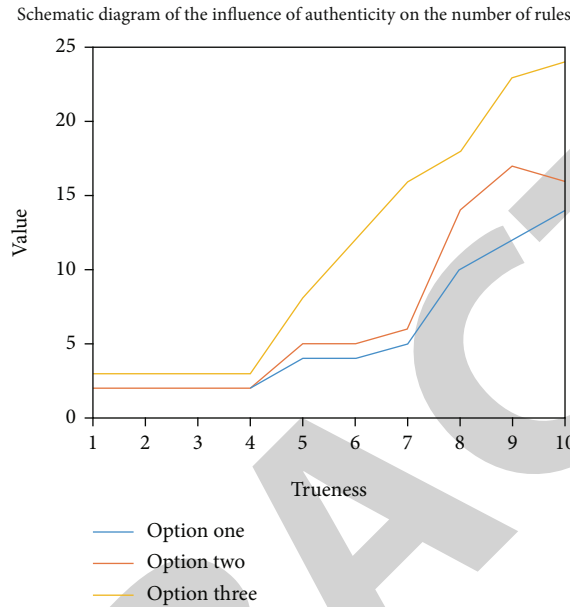
FIGURE 6: Schematic diagram of the influence of authenticity on the number of rules.
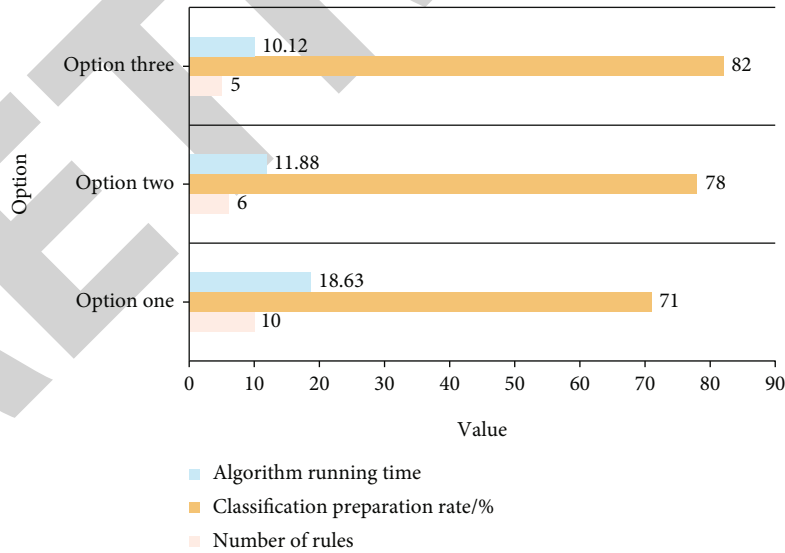
FIGURE 7: Comparison chart of the efficiency of the three algorithms.

As can be seen in Figure 4, too many rules tend to cause overfitting, which means that the classification effect on the training set will be better, but the prediction accuracy of the test set will decrease. It shows that the model can reasonably describe the volume expansion of the soil-soil mixture at low constraint pressure, the compression of the volume under high constraint pressure, and the increase of the maximum strength of the soil-rock mixture with the increase of the constraint pressure, which confirms that the model simulates a soil-rock mixture.

It can be seen from Figure 5 that the fuzzy decision tree ID3 algorithm based on mobile computing produces the least

number of rules in each data set, indicating that its overall decision-making efficiency is higher than the traditional decision tree ID3 algorithm and the fuzzy decision tree ID3 algorithm. The fuzzy decision tree ID3 algorithm of mobile computing is more applicable than the other two schemes.

4.1.3. Authenticity Analysis. The degree of realism has a very close relationship with the scale of the decision tree. It is very important for the fuzzy decision tree algorithm to choose an appropriate degree of realism for different schemes. The results are shown in Table 3.

It can be seen from Table 3 that for fuzzy decision trees, as the degree of reality increases, the accuracy of classification first increases and then decreases, and the fuzzy decision tree ID3 algorithm based on mobile computing achieves the maximum accuracy around 0.82, and fuzzy decision-making the tree ID3 algorithm and the traditional decision tree ID3 algorithm achieve the maximum correct rate at 0.88, which shows that the fuzzy decision tree ID3 algorithm and the traditional decision tree algorithm need to obtain the maximum correct rate when the number of rules generated is more, and the efficiency is lower. Fuzzy decision tree ID3 algorithm is based on mobile computing.

It can be seen from Figure 6 that as the degree of reality increases, the number of rules generated by the model increases. This is because the greater the degree of truth, the more recursive times of each branch, so the scale of the spanning tree is the larger, the more rules can be obtained.

4.2. Application in the Management of Sports Fitness Members. After the training, the model is applied to the analysis of customer churn, and experiments are conducted with the data of a certain club member. The results are shown in Figure 7.

It can be seen from Figure 7 that the customer churn analysis model constructed by the fuzzy decision tree optimized by the genetic algorithm not only has fewer rules but also has obvious advantages in classification accuracy. This advantage can help club managers to provide targeted services to those customers with high churn rates in future marketing. At the same time, the running time of scheme 3 is short, which is particularly important in the analysis of the company's massive customer data.

5. Conclusions

Based on the analysis of the importance of the process of establishing the fuzzy decision tree, this paper uses mobile computing to optimize these two parameters, which provides a basis for the value of the parameters when the fuzzy decision tree solves specific problems. At the same time, the optimized fuzzy decision tree is used for the analysis and prediction of the customer churn crisis in sports and fitness, and the experiment is carried out with the customer data of a club. The experimental results show that the optimized fuzzy decision tree is used in customer churn crisis analysis, and the generated decision tree has fewer rules, simpler structure, and higher classification accuracy. These advantages can more effectively provide managers with a new research idea

and analysis method for the retention research of sports and fitness customers. The disadvantages of this research are that in this paper; when the decision tree algorithm is analyzed experimentally, the client data of a particular association is selected. In order to make the research more universal, the scope can be increased accordingly. At the same time, the fuzzy decision model designed in this document only supports one fuzzy decision algorithm, and more mainstream algorithms can be added. In addition, other algorithms related to data mining can be added to become a complete data mining tool.

Data Availability

No data were used to support this study.

Conflicts of Interest

There are no potential competing interests in our paper.

Authors' Contributions

All authors have seen the manuscript and approved to submit to your journal.

Acknowledgments

References

[1] W. Chiu, D. Won, and J. S. Bae, "Internal marketing, organizational commitment, and job performance in sport and leisure services," *Sport, Business and Management: An International Journal*, vol. 10, no. 2, pp. 105–123, 2019.

[2] J.-H. Yumi and Seo, "Communication competence exercise participation type fitness applications interpersonal relation self-disclosure% sports club," *Journal of Exercise Rehabilitation*, vol. 14, no. 6, pp. 934–938, 2018.

[3] W. Y. Jang and J. K. Kim, "The relationship among relationship marketing, customer trust, customer loyalty and repurchase intention focused on fitness center," *Korean Journal of Sports Science*, vol. 26, no. 6, pp. 783–800, 2017.

[4] A. Liu, Y. Xiao, H. Lu, S. B. Tsai, and W. Song, "A fuzzy three-stage multi-attribute decision-making approach based on customer needs for sustainable supplier selection," *Journal of Cleaner Production*, vol. 239, article 118043, 2019.

[5] Z. Lv and L. Qiao, "Optimization of collaborative resource allocation for mobile edge computing," *Computer Communications*, vol. 161, pp. 19–27, 2020.

[6] R. L. Sonza and G. M. Tumibay, "Decision tree algorithm in identifying specific interventions for gender and development issues," *Journal of Computer and Communications*, vol. 8, no. 2, pp. 17–26, 2020.

[7] P. Nancy, S. Muthurajkumar, S. Ganapathy, S. V. N. Santhosh Kumar, M. Selvi, and K. Arputharaj, "Intrusion detection using dynamic feature selection and fuzzy temporal decision tree classification for wireless sensor networks," *IET Communications*, vol. 14, no. 5, pp. 888–895, 2020.

WILEY | Hindawi

Research Article

Hotel Management Evaluation Index System Based on Data Mining and Deep Neural Network

Peilin Chen (ORCID)

China University of Labor Relations, Beijing 100048, China

Correspondence should be addressed to Peilin Chen; dr.peilin.chen@culr.edu.cn

In recent years, with the increase in computing power, the sharp drop in costs, and the successful use of data management technology, a large amount of data has been rapidly spread and stored in various fields of the company. How can we passively find active data and form active knowledge from these big data information, know how to use equipment to quickly and accurately obtain high-quality information, use the obtained information to guide users in decision-making, and provide more economic and social benefits? This paper focuses on the study of the classifier model based on BP neural network, and the combination of BP neural network model and other optimization algorithms, including genetic algorithm (GA), particle swarm algorithm (PSO), Adaboost algorithm, GA, and PSO have global search performance. It is mostly used to optimize the weight threshold of the network and the number of hidden layer nodes. The Adaboost algorithm builds an enhanced classifier based on the idea of integration. At present, data mining technology has moved from the laboratory research stage to the commercialization stage. The use of widely owned knowledge and information as analysis tools can be used in many fields: such as financial analysis, engineering design, scientific research, management, and production control. At the end of this paper, the improved Adaboost_BP classifier is used, and the result proves that the efficiency of hotel management has increased by at least 75%.

1. Introduction

With the development of information technology, people's ability to produce and collect data has been greatly improved. Correspondingly, the ability of data analysis and knowledge acquisition is relatively lagging. From data collection, database creation, and data management to advanced data analysis technology, data mining (data mining) technology emerges and develops accordingly. Data mining is a nontrivial process of identifying effective, novel, useful, and understandable patterns from data sets or databases. Classification mining is one of the important applications of data mining. The classification ability is realized by constructing a classifier. Its construction methods include statistical methods, machine learning methods, and artificial neural network methods. The pattern that the neural network can recognize is determined by the network topology, connection weights, and node thresholds. Therefore, the optimization methods for neural network models are mainly divided into

optimizing the network topology and optimizing the weight threshold of the network.

Wang Li uses artificial neural network mapping rules and data mining methods to perform data mining on GIS alumni results and uses SQL Server data mining services to define closing plan results and various courses, professional GIS courses and closing plan results, and for professional closing plans Data mining model. B. Grade applies the effect of data mining to the design of the GIS vocational education plan. The results show that the learning outcomes of geographic information system (GIS) graduates are more affected by professional courses and computer courses. The performance of GIS graduates is affected by remote testing. Digital imaging, the design and development of GIS courses, and other hands-on courses have a greater impact. In the new round of vocational education and training courses review, computer courses, digital imaging with remote sensing functions, and hands-on time for GIS design and development courses have been added. However, the system can only be copied

by a single machine, and data cannot be shared at any time [1]. Mengjie believes that with the use of the Internet, online teaching has changed the traditional teaching methods, making the network fast and convenient without being restricted by time and space, reducing teaching costs, and improving teaching quality. Network (neural network) and data mining technology (data mining) completed the recommendation of online training courses. The online course recommendation mechanism he researched and proposed can be divided into two parts: preprocessing online course recommendation and processing online course recommendation. The course recommendation mechanism is applied to online learning recommended by online homeschools, to verify the feasibility and applicability of the study. However, this mechanism has not been widely promoted, and it will take some time to implement it [2]. Xinping takes data mining neural network classification algorithm as the main research object, adopts classification application experiment and bibliographic research methods, and chooses three artificial neural network algorithms, namely, neural network algorithm VM, data mining algorithm, and ELM algorithm. After comparing the experimental results, it can be seen that different data mining classification algorithms have their own different advantages. In the sorting experiment of corn seeds and red wine, the ELM algorithm used in the neural network has the best sorting results, its accuracy is more than 83%, and the modeling time is the shortest. He believes that the only choice is to combine specific data volume conditions. The data mining classification algorithm can effectively improve the accuracy and efficiency of data mining. However, the experimental data is too small to effectively explain the experimental results, and continuous improvement is needed [3].

The empirical analysis of this article is to apply the classifier model based on BP neural network to the field of financial analysis and establish a financial crisis early warning model for listed companies. Through the data preparation phase, the classifier modeling phase, the mining phase, and the interpretation and analysis phase, the data mining method is applied to the financial early warning system to build a classifier suitable for financial early warning, and through a single BP classifier, Adaboost_BP classifier and the comparison of the classification results of the test samples of the improved Adaboost_BP classifier show that the data using the improved version of the classifier has improved the work efficiency by nearly 75%, which further verifies the effectiveness of the Adaboost algorithm and the improved algorithm.

2. Constructing Classifiers and Data Mining Techniques and Methods

Methods for cataloging catalogers include statistical methods, machine learning, neural network methods, and so on. Statistical methods include Bayesian classification algorithms and nonparametric methods (such as evidence-based learning), in which relevant knowledge is used as the target or basis. Among them, machine learning includes the decision tree method and rule induction method, and then, in the case of reflecting the production rules, it is basically

reverse. The application of long-distance network model is very advanced. In addition, there are rough set (Rough Set) methods, support vector machines (SVM), etc. [4, 5].

2.1. Bayesian Classification Algorithms. The Bayesian classification algorithm is a classification method of statistics. This algorithm is used for statistics. This algorithm is carried out with probability statistics. Generally, the selection algorithm of Bayesian classification can match the selection tree and neural network category and can be used in large databases. The method used is simple, high, and fast in a specific category [6].

2.2. Nonparametric Methods. From the question of extrapolation, we know the exact form of the distribution (especially when the normal distribution is assumed), and we only need to make an estimate or assume that it is an unknown parameter. But we usually know little or nothing about the distribution form of the two (such as asymmetric mode or uneven asymmetry). At this time, statistical extrapolation that does not rely on (or at least not) the cumulative distribution is usually called a nonparametric method [7, 8].

2.3. Decision Tree Analysis Method. Decision tree analysis is a possible comparison with probability and graph theory. Decision tree is a risk-centric approach to make decisions in order to obtain the best algorithm. The trees on the plane are horizontal, centered on 0, centered on zero, and centered on zero. The decision tree includes the root (decision node), other internal nodes (program nodes, stage nodes), leaves (target nodes), branches (line segments, probability), probability factors, and cost-benefit factors [9].

2.4. Rule Induction. The basic idea of induction is to list a few special situations, analyze a few limited special situations, and finally determine the overall situation of the relationship. However, it is not an easy task to generalize practical problems, and there are often no certain rules in the process of induction.

To build a catalog, you need a training memory containing test subject data. The training area includes a set of databases or metadata, and each satisfactory carrier is composed of features or features. In addition, the training model can also represent elements. The form of a specific sample can be $(v1, v2, \cdots, vn)$, where v represents the field value and c represents the category [10, 11].

3. Research Experiment on Optimization Method of BP Neural Network Classifier

Starting the network, the number of nodes in the network input module is specified by the system output (X, Y), the number of nodes specified with or without the system, and the system-based entry system (m [12]). This analogy illustrates the connection between the original input layer of the input layer and the energy wave that it carries.

$$x = \frac{-b \pm \sqrt{b^2 - 4ij}}{2a}. \tag{1}$$

Includes implicit deduction of output, the input quantity X is displayed, and the numerical value between the input value and the hidden value corresponds, and H [13] is calculated from the input value.

$$H = f\left(\sum x_{ij} - a^2\right). \tag{2}$$

In the formula, the number of hidden layer nodes; f is the hidden layer activation function, which has many expressions, and the commonly used activation functions are as follows [14]. Step function:

$$y = \varphi(x)1 - f. \tag{3}$$

Piecewise linear function [15]:

$$y = \varphi(x) + 0.5(1 + x). \tag{4}$$

The most commonly used sigmoid function is the formula [16, 17], and there is also a commonly used hyperbolic tangent symmetric function, such as the formula

$$\varphi(x) = \frac{1}{1 + \exp(-ax)}. \tag{5}$$

The parameter of the controllable slope:

$$\varphi(x) = \tanh(0.5). \tag{6}$$

The output layer output calculation. According to the hidden layer output H, connect the weight jk and the threshold b, and calculate the BP network output O [18].

$$ok = \sum_{n=i} HJ - BK. \tag{7}$$

Error calculation, according to the network prediction output O and the expected output Y, the network prediction error e is calculated [19].

$$ek = Yk - Ok. \tag{8}$$

The weight is updated. Update the network connection weight ij, jk according to the network prediction error e [20, 21].

$$w_{jk} = w_{ij} + H_j(1 - H_j)\left(w_{jkek}\right). \tag{9}$$

Initialization has randomly given the input layer to the hidden layer connection weight ij and the hidden layer to the output layer connection weight jk, as well as the hidden layer threshold j, and the output layer threshold k

$$E = \frac{1}{2}\sum_k (Z_t - y_t)^2. \tag{10}$$

If the average error of the system is greater than the allowable error value, the new connection weight and threshold are calculated [22], the calculation formula is as follows:

$$e_t = (Z_t - y_t) \pm (1 - y_t)^2. \tag{11}$$

The greater the learning rate n, the greater the amount of weight change, which can speed up the network training process [23, 24]. However, the result may produce oscillations. In order to increase the learning rate without causing oscillations, a momentum term is added to the formula, namely,

$$(x + a)^n = \sum_{k=0}^{n} x^k a^{n-k}. \tag{12}$$

σ is the variable of the jth hidden layer node, which is a standardized constant, or base width [25]. The output of the kth node in the output layer of the network is a linear combination of the outputs of the hidden layer nodes

$$y_k = \sum_j W_{jk} n_j. \tag{13}$$

After the clustering is completed, start training the neural network NNm used to calculate the membership of the fuzzy rules and calculate the membership of each output. The training samples of each neural network are composed of multiple inputs and j outputs [26, 27]. It is defined as follows: if a sample in the original training sample set is clustered into the ith group, the output part corresponding to the sample is

$$\frac{1}{e} = \frac{1}{n}\sum_{i-1}^{n} \frac{(y_n - y_i)}{y_i}. \tag{14}$$

Note that although the neural network gets one-tenth of the training, the following network will use the characteristics of the Seamer function to correctly apply the rules to all other functions [28]. It is also because the Sigmoid function cannot completely take 1/0 value, so it is replaced by 0.9/0.1, which can speed up the training speed of the network [29, 30]. After deciding on the training samples, you can train the network.

$$y = \sum_j u_j + g_j. \tag{15}$$

4. GA Optimized BP Neural Network Model

4.1. Principle of GA Algorithm. A genetic algorithm is a parallel way to optimize and compare nature's genetic mechanism through biological evolution. It introduces the biological evolutionary principle of "survival of the fittest and survival of the fittest" in nature into the coded serial group formed by optimized parameters. The role of selection media, as well as the selection of genes, nonpatents, and mutations, ensures that well-trained individuals are preserved and cultivation fails of people died, and new groups were given information from the previous and first generations. Repeat the test until the conditions are met.

	Technological innovation	Energy conservation
2006	51	65
2007	40	72
2008	60	77
2009	72	89
2010	83	98
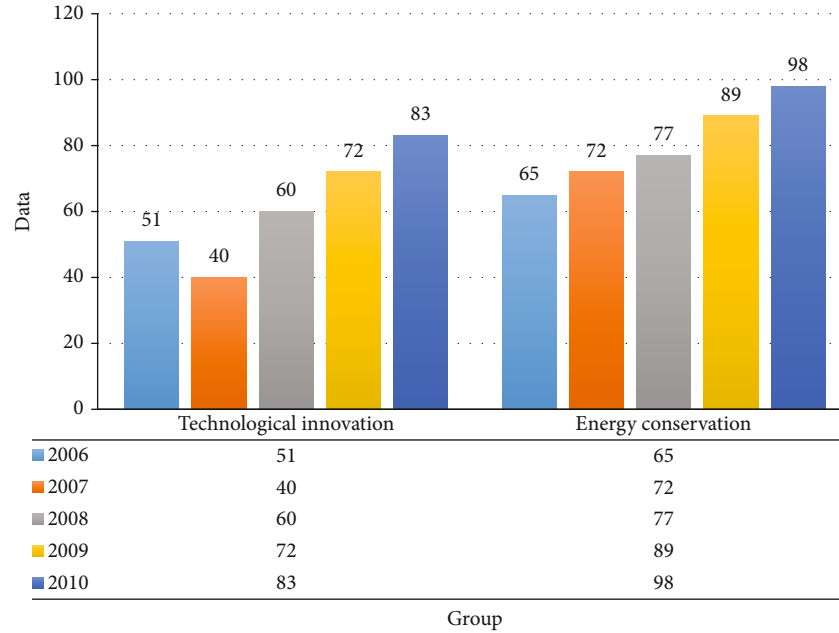
Figure 1: The new group inherits information from the previous generation.

As shown in Figure 1, GA adjusts and optimizes the BP neural network. It will be discovered in part of the interaction between genetic algorithms and neural networks and finally reached the best communication and critical value and used this as a benchmark for tpp network simulation and prediction. If GA does not optimize the neural network, it will be a genetic algorithm that enables it to optimize the initial weights and thresholds of the neural network. The optimization of the neural network connected with the genetic algorithm includes the main population improvement, adaptive function, selection operation, abnormal operation, and crossover operation.

The basis of the genetic algorithm is as follows: genome coding method, function, genetic manipulation, and surgical parameters. This genetic coding technology is a coding technology for individuals. Now includes binary or mathematical formulas. Binary is to use code to repeat and effectively adjust the period. Function refers to the function of calculating the personal fitness value based on the calculation of the evolution result and the calculation of the function that can be selected.

The genetic algorithm is an optimization method for ordinary neural networks. If the neural function of BP is considered to be a predictable function, then when the genetic algorithm optimizes the neural network, it is like a parameter. The optimized network predictive ability is generally better than the network before optimization. However, the algorithm is limited. It can only enhance the data accuracy of the existing neural network, but not enough to optimize the current neural network with high neural errors. In particular, there are some prediction errors because of the small sample size and uneven distribution as shown in Table 1.

4.2. PSO Optimized BP Neural Network Model. Similar to the genetic algorithm, the particle swarm optimization (genetic algorithms) optimization algorithm can also be divided into

Table 1: The appropriate neural network structure sample data.

	Mexico	Careful	Bolivia
Brazil	Belgium	Observe	Chile
Argentina	Romania	Topic	Paraguay
Spain	Austria	Manage	Peru
Factor	Cubic	Diffuse	Glass

optimized network initial weight threshold and optimized network structure, which is consistent with the previous article. This section mainly discusses the PSO optimization of the initial weight and threshold of the BP network algorithm. PSO is a swarm intelligence optimization algorithm in the field of intelligent computing. The PSO algorithm studies the behavior of predators. The easiest and most effective way for any bird to find food is to find the area closest to them.

The PSO algorithm first initializes a group of particles in the solvable space, and each particle represents a potential optimal solution of the optimization problem, which is represented by the three characteristics of position, speed, and fitness value. The fitness value indicates the pros and cons of the solution and is calculated by the fitness function.

As shown in Figure 2, the algorithm for optimizing particles is an algorithm based on the theory of collective intelligence, which guides the search for particles through information about the particles. Compared with the GA algorithm, PSO includes a search strategy based on time tracking, but it uses fast and replacement models to avoid complex genetic behaviors.

Generally speaking, PSO searches for the optimal solution faster than GA, as shown in Table 2.

Project the individual's body into a network full of energy to form a neural network. Please enter the training sample of the corresponding neural network. Optimizing Internet

	Power	Ability	Capacity
West coast	52%	40%	60%
Midwest	40%	16%	34%
South	34%	30%	15%
Northeast	17%	50%	51%
Canada	62%	36%	48%

Group
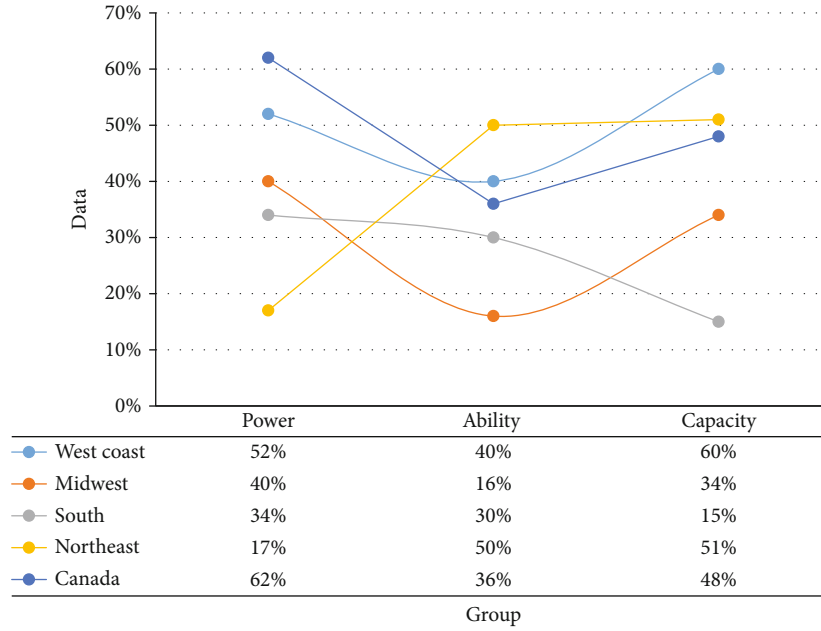
FIGURE 2: Optimization algorithm based on swarm intelligence theory.

TABLE 2: The speed of PSO to find the optimal solution.

	Operate	Cross	Variation	Process	Parameter	Inheritance	Algorithm
Ascertain	1.48	2.51	1.23	1.24	2.58	1.28	1.51
Confirm	3.15	2.51	1.21	1.21	4.12	1.24	2.41
Ensure	1.41	6.21	2.15	4.51	1.21	6.21	4.12

rights is a process of trial and error. In order to ensure that there are more storage rooms, the sample space on the trained neural network is often divided into two parts as training rooms or test fields. When measuring the source code, a sampling survey is used to ensure that the test results of each exercise are different.

The diagonal points listed in the training documents will also be calculated, and then, their respective adaptation periods will be set so that individual workers can act.

4.3. Adaboost_BP Neural Network Model. Different from the GA and PSO optimization algorithms discussed in the previous two sections, the Adaboost algorithm enhances the classification effect of the BP classifier through iteration and combination. Boosting algorithm is a typical ensemble learning algorithm based on resampling technology and is used to better solve classification problems. Therefore, Boosting has been well developed and widely used in solving classification problems. Its core idea is when training new classifiers, which pay more attention to the training books that are difficult to classify correctly. In 1995, Freund and Schapire proposed the Adaboost algorithm, which is easy to practically apply, which is an improvement to the Boosting algorithm. It is mostly used and the problem of two classifications.

On the basis of the single BP classifier in the previous section, a BP classifier is regarded as a "weak classifier," and multiple weak classifiers are integrated through the Adaboost

algorithm. A strengthened classifier composed of 2 to 20 weak classifiers of a single BP neural network was trained sequentially.

As shown in Figure 3, the first view is to combine the output of different "weak" categories to generate effective categories. We assume that BP is a weak cataloging unit. We have trained a large number of methods to measure input and built a powerful classic format composed of weak recurrent neural networks in Adaboost to improve the accuracy and reliability of the category. Adaboost is a very high-precision classifier, suitable for two-classification problems and multi-classification problems. One disadvantage of this type of ensemble algorithm is that it is sensitive to noise; in addition, when there are too many wild points in the training data, it is easy to cause serious overtraining, which is manifested as a sharp expansion of weights on a small number of samples, which ultimately leads to the effectiveness of the classifier.

Through self-organizing neural network to obtain data, independent organizations organize learning data based on part of their own creation of the organizational model in order to obtain data with salient features, such as classification by feature, a neural network. Just like neurons in the human brain, each cell is unique. The interaction between humans and humans allows people to test the data gaps of these signals connected to false neural networks through adjustments. However, the research on neural networks is becoming more and more intense. Cannot give the best
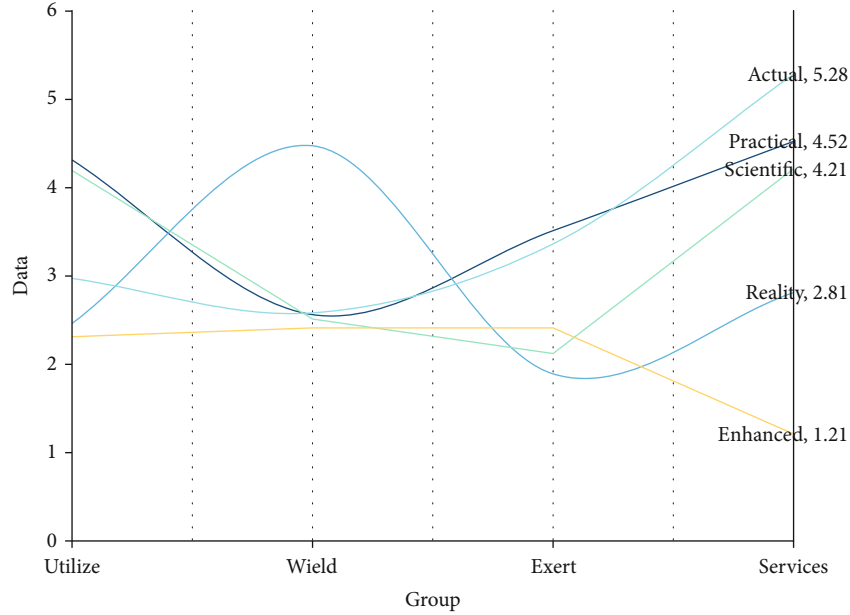
FIGURE 3: The many outfield points in the training data.

TABLE 3: The ones used to generate the enhancement.

	Expansion of weight	Samples number
GreenDevelopment	In order to improve the classification accuracy and accuracy	The strong classifier is composed of several weak classifiers of BP neural network
Dichotomous problem	Such integration algorithms	This can lead to severe overtraining
RepetitionTrain	There are two types of samples in general	Although the overall classification error meets the target requirements
WeakClassifier	This algorithm can take the misdivision rates of positive and negative samples into consideration	Increase the weight of the positive sample set The other came second
Implement unit	Repeatedly trained BP neural network to predict sample output	The importance of each weak classifier to the positive sample

explanation for the results obtained from the download. The data acquisition system based on the opaque neural network is not so easy to lose the results, which increases the stability of the system, as shown in Table 3.

For the neural network model, it can only improve its fit as much as possible, but it is impossible to achieve 100% accuracy. All errors and errors are inevitable. The classification accuracy rate is the most important indicator to measure the classifier. For the financial crisis early warning model, the classification accuracy rate needs to consider two situations. One is that when the financial situation is actually healthy, it is predicted to be in crisis. The second is that it is predicted to be healthy when there is a financial crisis. The former generally does not have a large impact on the company and the enterprise and is beneficial and harmless, but the latter is relatively risky and loses its early warning function for management decision-makers and delays the opportunity for crisis management. We define the former as the first type of error and the latter as the second type of error. When evaluating a financial early warning model, it is necessary to consider both the overall misclassification rate and minimize the second type of error. When the error rate of the second category
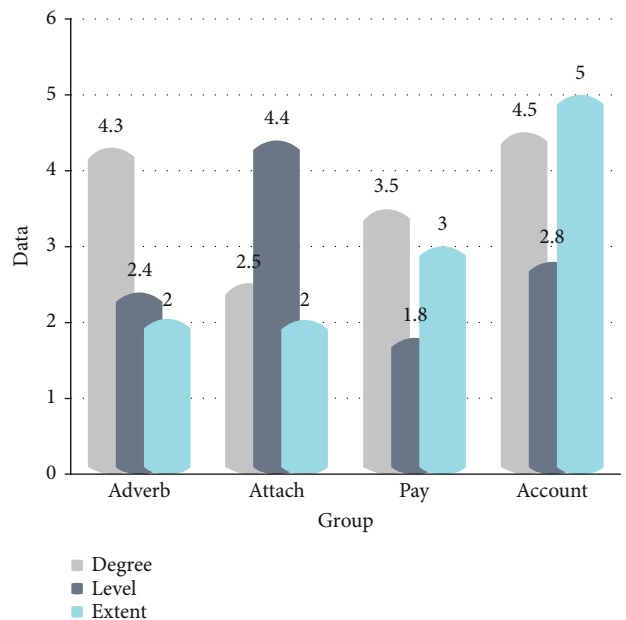
FIGURE 4: Neural network as a weak classifier unit.
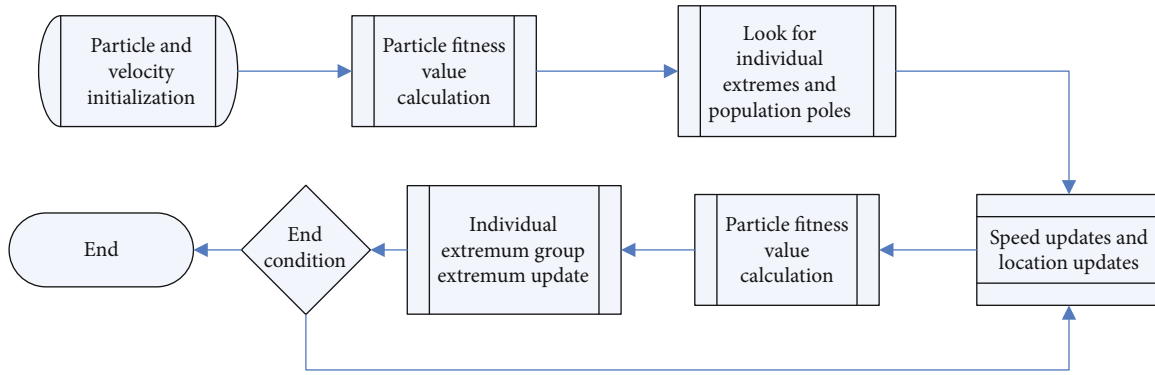
FIGURE 5: The idea of the algorithm is to merge multiple.

	Neural	Network	Sample	Authority	Chary	Mold
Output	0.43	0.25	0.35	0.5	0.35	0.45
Result	0.24	0.44	0.18	0.44	0.18	0.28
Layout	0.2	0.21	0.24	0.23	0.14	0.5
Plan	0.43	0.25	0.35	0.25	0.35	0.45
Hierarchy	0.24	0.44	0.18	0.44	0.18	0.28

Group
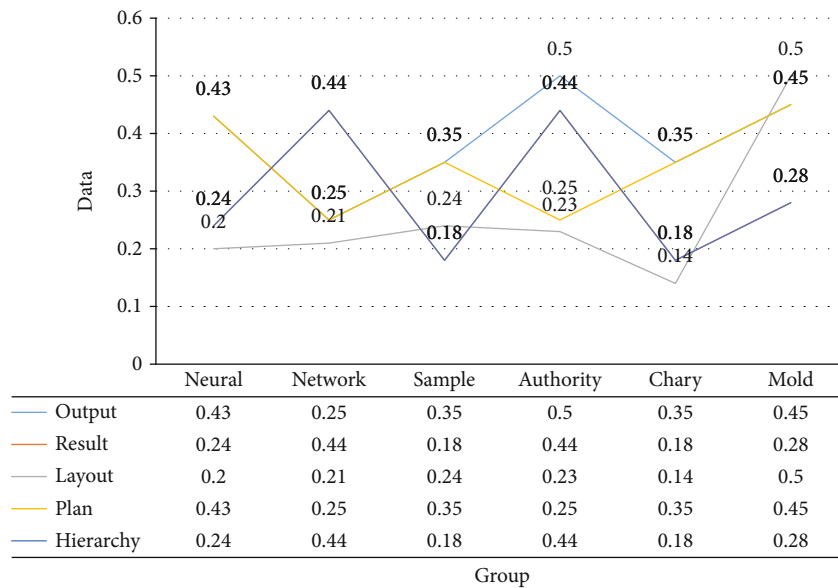
FIGURE 6: The dichotomy problem of two types in the sample.

is 0, it means that no company or enterprise in crisis has been misjudged. This is the classification result that the early warning model strives to achieve.

In this round of testing, the relationship between the number of weak classifiers and the error rate is shown in Figure 4. From the test results, the classification error rate of the strong classifier integrated with 12 weak classifiers is the smallest.

After 12 sets of tests on a strong classifier with 20 BP neural networks, the average classification error rate is 0.1236, which is 1.46 percentage points lower than that of a single BP classifier, which has a certain optimization effect. The classification error rate of the first type is 0.07518, and the classification error rate of the second type is 0.1437. It shows that the integrated strong classifier optimizes the classification ability of the samples of financially normal companies, but there is no significant change in the classification ability of the samples of financial crisis companies, but the overall classification ability has been improved to a certain extent, and the optimization effect has been achieved. The second type of classification error rate has not increased significantly because of the following reasons: first, the financial data char-

acteristics of the financially normal companies are relatively high, and it is easier to extract the characteristics of the indicator data, while most of the companies in the financial crisis have different characteristics. It has its own characteristics and is not easy to extract. The second is the uneven distribution of the number of companies in the financial crisis. For example, there are more ST companies in the manufacturing industry than in other industries. The third is that the second type of error rate of the BP classifier is inherently high. If the samples of crisis companies are not fully trained, it will be difficult to improve the classification accuracy. Therefore, the ability to classify a sample of companies in the financial crisis has not been significantly improved.

As shown in Figure 5, from the above data, the average error rate of the first type is 0.1020, the error rate of the second type is 0.0872, and the overall error rate is 0.0922. This is an increase of 2.14 percentage points over the classifier before the improvement. It shows that by improving the algorithm to increase the emphasis on the samples of financial crisis companies and adaptively adjusting the weight of the misjudgment samples, it can significantly improve the classification error of the second category, the comparison curve

	Restaurant	Mandatory	Manual	Labour
■ Manager	2	2	3	5
■ Michelin	2.4	4.4	1.8	2.8
■ Guide	4.3	2.5	3.5	4.5

Group

■ Manager
■ Michelin
■ Guide
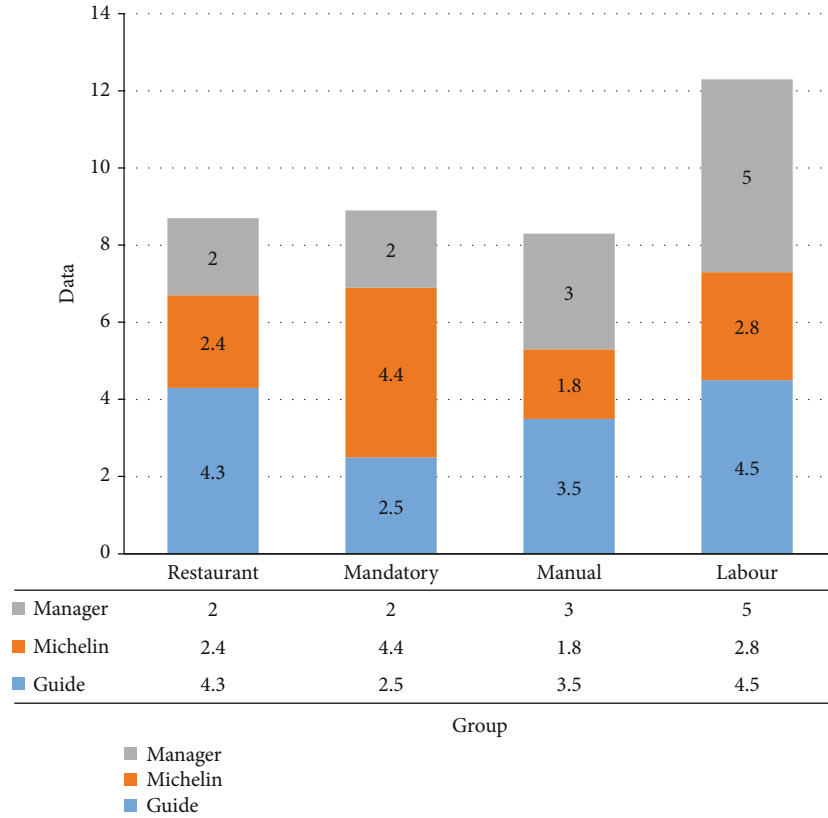
FIGURE 7: The financial crisis of a company is not a sudden event.

TABLE 4: First determine the degree of attention to the classification.

Years	Least value	Middle value	Peak value
2006	2866.21	1423.91	0.73
2007	3411.15	3230.44	1.24
2008	5724.24	1466.43	-4.43
2009	1384.51	4220.83	-6.17

graph of the error rate of the first type, and the error rate of the second type in the 10 sets of tests.

First, take out the various characteristics. When these attributes are higher than the threshold, you will be calculated in the higher dimensions corresponding to the numbered data in the random forest. This information will also be filtered out, using the ant algorithm to filter attributes. First, the parameters are initialized, and an action is accidentally generated at the beginning of the iteration. When the action starts to look for, it will choose one at random. Each action should be calculated according to each specific situation, until the result is satisfied. The system will stop the search and redistribute a pheromone to create a complete action again, reproduce the offspring to complete the iteration, and get the best results.

As shown in Figure 6, for a two-category problem, we generally give priority to one of the two types in the sample, followed by the other. The weight update rule of the standard Adaboost algorithm only updates the weight of a sample based on whether it is misclassified and does not focus on

training a certain type of sample. In the actual situation, although the overall classification error meets the target requirements, for one category, the error may be higher. If this type of misjudgment brings a higher risk, it is not suitable for practical problems. In response to this problem, this paper proposes a sample adaptive weighting algorithm based on the degree of importance.

For this reason, the algorithm can compare the errors in the positive and wrong samples with the matching algorithm, so that it can be classified into the structure of the sample. First, determine the importance of the classification accuracy of the positive and negative sample classes and divide the boundary of the weight distribution according to the degree ratio. If the detection rate of positive samples is highly concerned, it means that the FNR value is required to be relatively small. If the value of positive samples can be added, each weak sample will be given the power to strengthen the ability to group positron infections.

It can be seen from the previous experiment that the second type of error is smaller than the first type of error. In other words, the number of companies that are in the financial crisis is judged to be normal is more than that of companies that are financially normal. The cost of the first type of error is much higher than that of the second type of error. The risk of misjudgment is very high. According to the sample adaptive weighting algorithm based on the degree of importance proposed in Chapter 3, the FNR and FPR indicators can be, respectively, corresponded to the probability of two types of errors.
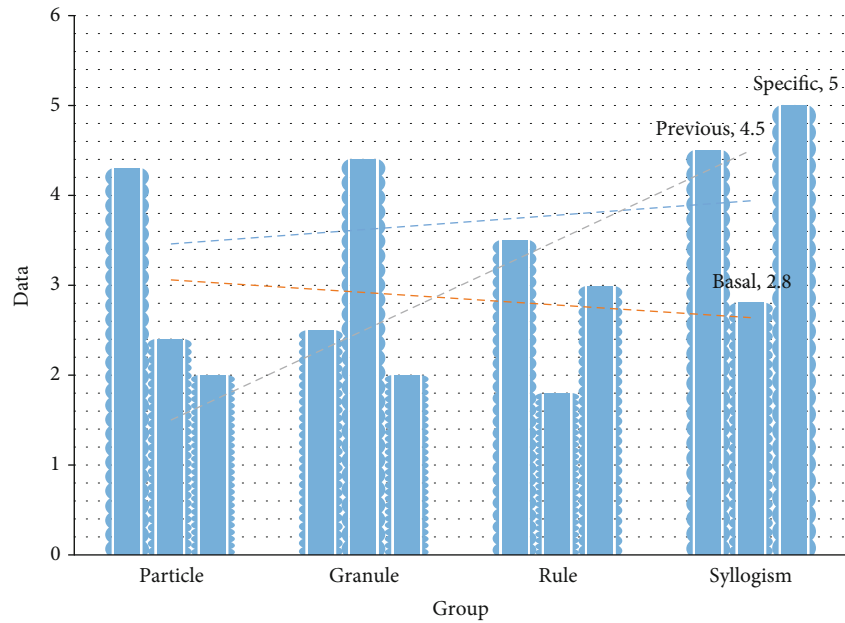
FIGURE 8: The overall classification error meets the target requirements.

As shown in Figure 7, the financial crisis of the hotel is not a sudden event, but a continuous process, from the time of the crisis to the completion of the hotel's bankruptcy and liquidation, at a moment of the financial crisis. In the past, through statistical particle analysis, main component analysis, factor analysis, chronology, etc., methods for studying and predicting corporate financial crises have been continuously developed. Among them, statistical analysis has always been a good way to study and predict whether a company will have a financial crisis. The application of artificial neural networks to hotel financial early warning is a research direction in recent years. This paper applies the BP classifier to the classification and mining of financial data, establishes a hotel financial early warning model, and improves the algorithm to improve the accuracy of the BP category, as shown in Table 4.

The hotel financial early warning system provides scientific decision-making knowledge support for decision-makers by comprehensively evaluating and predicting indicators of financial status, trends, and company changes. The indicators for evaluating financial crises include a series of indicators. If all indicators are evaluated and integrated, the model is too complicated and not conducive to the accuracy of the forecast. Therefore, firstly, you need to screen the indicators and select the ones that have a greater impact on the identification of the category.

This paper selects 30 financial indicator variables from the six aspects of hotel solvency, per share indicators, earnings quality, profitability, operating capacity, and capital structure, as well as various indicators. The 30 major indicators also include subindices of the current period, the same period last year, or year-on-year growth rate. In this article, mathematical statistics are used to screen indicator variables, so first of all 90 financial data variables are included in the scope of investigation.

Data digitization is a processing method of digitizing data to selected data. Between [0,1], the difference in the amount of data has been corrected, and the original data must be converted to avoid making higher and different estimates, because the indicators are the single digits are different. There are two main ways of collecting data: minimum and medium deviations and functional formulas.

As shown in Figure 8, the initial power of the network determines the initial location of the network error by selecting the corresponding source code, so its impact is to greatly shorten the duration of network training and improve the pertinence of training. Then, in order to define the neural network, it automatically sets the right threshold of the hotel company and the threshold value [-1, 1]. It is also possible to adopt a trial method and use the weight and threshold that are the most initialized with the weight threshold with the smallest one-time error. In this paper, the single BP classifier uses the random initial value method in matlab.

Determining the number of hidden neurons is the key issue. This is a fairly traditional method. The number of subconscious neurons is equal to the input vector; this means that when the vector value is too high, the number of hidden units does not get enough accuracy and speed. In order to promote adaptation to climate change, a new and better method has been adopted. The basic principle is to train small neurons, which automatically increase the number of neurons on the network by constantly checking the output. In each cycle, the input quantity is equivalent to the total value and may lead to a new neuron layer input quantity, so the error rate of the new network is studied. This process will be repeated in a repeated manner until the specified error or maximum potential nerve cell is reached. The structure of the RBF neural network, as discovered here, is not related to the initial value.

5. Conclusions

This research mainly involves researching data-based neural network methods, including permuting neural networks. The application of neural network to extract data was not recognized from the beginning, mainly because of its too large scale, too complicated structure, and too long learning time. It is also important to increase the resilience of acoustic data and improve training algorithms, especially in improving network-based algorithms and tampering rules, which makes neural networks more and more popular for collecting a wide range of user data. At present, the feedforward BP neural network is the most widely used network. This article mainly studies the method of constructing data mining classifier based on BP neural network, and the combination with a variety of optimization algorithms, and analyzes through actual cases. The constructed BP classifier is applied to the hotel management problem—evaluation index system. The evaluation index system helps the hotel management decision-making level to avoid and diversify risks early and effectively. Based on the theories of data mining and deep neural network, this paper studies the combination of the Adaboost algorithm and neural network and establishes a new indicator system through the significance test. When selecting indicators, it draws on the empirical research of domestic scholars. The selected 30 indicators more comprehensively express the financial situation of a hotel. There is certain relevance among these indicators. In order to include as much information as possible, this article includes 30 indicators into the early warning system. The research content of this article is still relatively simple. The main result is the application of BP neural network to the classifier., which uses the Adaboost algorithm to improve the BP classifier, proposes and verifies the optimization algorithm, and introduces the constructed BP classifier into the hotel management evaluation system. However, in the intersection of data mining, neural networks, and financial early warning, there are still many aspects that need to be studied in depth. I hope that this model can be further optimized and perfected in the follow-up research and exploration, and it can truly serve every business enterprise and firm. The supported system functions make my greatest contribution.

Data Availability

No data were used to support this study.

Conflicts of Interest

The authors declare that they have no conflicts of interest.

Acknowledgments

References

[1] L. Wang, J. Haitao, and D. Jiusheng, "Research on GIS professional curriculum system based on data mining," *Surveying and Spatial Geographic Information*, vol. 41, no. 1, pp. 18–21, 2018.

[2] L. Mengjie, "Research on the learning recommendation system based on data mining," *Information and Computer Theoretical Edition*, vol. 405, no. 11, pp. 123-124+127, 2018.

[3] Y. Xinping, "Comparison and thinking of data mining classification algorithms based on neural network," *Microcomputer Applications*, vol. 303, no. 7, pp. 98–100, 2018.

[4] W. Xuandong, A. Wang, Q. Jun et al., "Screening of core genes in pediatric hepatoblastoma based on omics data mining and co-expression network model," *Chinese Physician Journal*, vol. 23, no. 2, pp. 240–244, 2021.

[5] W. Jianbing, "Research on 4G customer recognition system model based on data mining," *Computer Programming Skills and Maintenance*, no. 1, pp. 37–39, 2017.

[6] J. Cheng and Z. Wanhe, "Research on data mining based on neural network," *Information System Engineering*, vol. 323, no. 11, pp. 15-16, 2020.

[7] J. Qiyan and L. Wang, "Financial abnormal data monitoring and analysis algorithm based on data mining and neural network," *Electronic Design Engineering*, vol. 433, no. 11, pp. 20–23+28, 2020.

[8] "Research on data mining of hospital management system based on CAPSO-BPNN," *Modern Scientific Instruments*, no. 3, pp. 192–194, 2019.

[9] L. You, X. Zheng, and J. Xue, "Research and implementation of second-hand commercial vehicle valuation model and application system based on neural network algorithm," *Operations and Management*, vol. 425, no. 11, pp. 65–72, 2019.

[10] L. Yanpeng, L. Zhu, and Z. Yongzhang, "Experimental research on big data mining and intelligent prediction of prospecting target area-application of convolutional neural network model," *Tectonics and Metallogenesis*, vol. 44, no. 2, pp. 192–202, 2020.

[11] D. Guoyong and C. Jinkuan, "Research on university student academic performance modeling based on educational data mining," *Heilongjiang Higher Education Research*, vol. 310, no. 2, pp. 81–86, 2020.

[12] Z. Wanzhen, C. Di, X. Yunfeng et al., "A review of recommender system research," *Journal of Hebei University of Science and Technology*, vol. 41, no. 1, pp. 76–87, 2020.

[13] Z. Deng and L. Bin, "Research on application hotspots of data mining—based on Kaggle competition data," *Journal of Library Science Research*, no. 6, pp. 2–9, 2019.

[14] F. Xu and C. Hui, "Analysis and implementation of business data mining based on neural network," *Science and Technology Vision*, no. 11, pp. 240-241, 2019.

[15] M. Dong, J. Tao, Y. Wanchen, S. Weihang, and X. Bin, "Application research of BP neural network and decision tree technology in data mining," *Economic Research Guide*, no. 20, pp. 186–190, 2018.

[16] Z. Liman, Z. Xiangxian, L. Zhongmei, and L. Heng, "Research on the evaluation of information dissemination power of think tank WeChat public platform based on BP neural network," *Information Theory and Practice*, vol. 41, no. 10, pp. 93–99, 2018.

[17] W. Kuang and X. Wu, *Research on the evaluation index system of health communication effect based on WeChat public account*, International Press, 2019.

[18] C. Weimin, S. Liang, and C. Xie, "Research on training effect evaluation index system based on learning map," *China Electric Power Education*, vol. 385, no. 3, pp. 28–30, 2020.

[19] K. Elbaz, S. L. Shen, Y. Tan, and W. C. Cheng, "Investigation into performance of deep excavation in sand covered karst: a case report," *Soils and Foundations-Tokyo*, vol. 58, no. 4, pp. 1042–1058, 2018.

[20] C. Ying, M. Wu, and L. Li, "Research on online learning evaluation index system based on ability," *Southern Vocational Education Journal*, vol. 58, no. 4, pp. 74–79, 2020.

[21] L. Pei, "Research on the evaluation index system of computer network technology practice teaching quality based on big data," *Network Security Technology and Application*, no. 5, pp. 99-100, 2020.

[22] C. Ruirui and L. Zhao, "Research on the index system of learning performance evaluation based on the network learning environment," *Computer Knowledge and Technology*, vol. 15, no. 25, pp. 148-149+152, 2019.

[23] W. Lu, Z. Chengling, and L. Wan, "Research on the construction of the quality evaluation index system of online open courses based on grounded theory—taking the national excellent resource sharing course as an example," *China Distance Education*, no. 11, pp. 70–76, 2017.

[24] F. Hu and C. Chaoqun, "Research on the evaluation index system of students' professional ability based on big data," *Software Engineering*, vol. 252, no. 6, pp. 59–63, 2020.

[25] L. Feng and Y. Zhiheng, "Research on the evaluation index system of university scientific research performance based on DEA," *Jiangsu Science and Technology Information*, vol. 621, no. 36, pp. 31–34, 2019.

[26] F. Yang and Q. Yang, "Research on the construction of the national library service quality evaluation index system based on the LibQUAL+TM system," *Library Science*, vol. 41, no. 5, pp. 23–29, 2019.

[27] Z. Yang, P. Jinjing, and Z. Xufeng, "Research on the comprehensive evaluation index system of academic journals based on ranking space," *Journal of Information*, vol. 38, no. 12, pp. 184–190, 2019.

[28] L. Kenan and Y. Meiling, "Research on the teaching effect evaluation index system of the problem-based teaching model based on the analytic hierarchy process," *Contemporary Educational Practice and Teaching Research*, no. 7, pp. 56-57, 2018.

[29] X. Wang and Z. Shulin, "Research on the evaluation index system of sustainable tourism development based on analytic hierarchy process—a case study of the ancient town of Zouma in Chongqing," *Journal of Hebei Vocational College of Tourism*, vol. 22, no. 1, pp. 16–19, 2017.

[30] K. Liang, "Research on the evaluation index system of online courses based on learning analysis," *Software Guide. Educational Technology*, vol. 16, no. 7, pp. 41–43, 2017.

Research Article

Multivariate Time Series Data Clustering Method Based on Dynamic Time Warping and Affinity Propagation

Xiaoji Wan [1,2] **Hailin Li** [1] **Liping Zhang,** [1] **and Yenchun Jim Wu** [3,4]

[1]*School of Business Administration, Huaqiao University, Quanzhou 362021, Fujian*
[2]*Oriental Enterprise Management Research Center, Huaqiao University, Quanzhou 362021, Fujian*
[3]*Graduate Institute of Global Business and Strategy, National Taiwan Normal University, Taipei 106, Taiwan*
[4]*Leisure & Recreation Administration Department, Ming Chuan University, Taipei 111, Taiwan*

Correspondence should be addressed to Yenchun Jim Wu; wuyenchun@gmail.com

In view of the importance of various components and asynchronous shapes of multivariate time series, a clustering method based on dynamic time warping and affinity propagation is proposed. From the two perspectives of the global and local properties information of multivariate time series, the relationship between the data objects is described. It uses dynamic time warping to measure the similarity between original time series data and obtain the similarity between the corresponding components. Moreover, it also uses the affinity propagation to cluster based on the similarity matrices and, respectively, establishes the correlation matrices for various components and the whole information of multivariate time series. In addition, we further put forward the synthetical correlation matrix to better reflect the relationship between multivariate time series data. Again the affinity propagation algorithm is applied to clustering the synthetical correlation matrix, which realizes the clustering analysis of the original multivariate time series data. Numerical experimental results demonstrate that the efficiency of the proposed method is superior to the traditional ones.

1. Introduction

Time series is a kind of time-dependent and high-dimensional data type, which can be divided into univariate time series (UTS) and multivariate time series (MTS) in terms of the variable type. With the rapid development of society and economy, such time-axis-sorted data widely exist in finance [1], economy [2], engineering [3], wireless communication [4], and other fields. Owing to the high dimensionality of variable attributes, MTS brings extremely difficulties to clustering, classification, prediction, pattern discovery, visualization, and other mining tasks. Therefore, the research on MTS mining has gained growing interests from scholars. In particular, MTS clustering is the most concerned issue in the field of data mining, from which the feature pattern or data classification of MTS are easily found [5].

In fact, the current academic research on the clustering of time series mainly focuses on the UTS data. Generally, they concentrate on the clustering for the whole time series class,

subseries, time points, etc. [6–8]. The traditional time series clustering methods involve model-based clustering [9, 10], feature-based clustering [11, 12], segmentation-based clustering [13], and distance-based clustering [14, 15]. However, since MTS data have the characteristics of high dimensionality, uncertainly, and dynamics [16], the above methods cannot be effectively adapted to MTS clustering. To reduce the high dimensionality of MTS attributes, both principal component analysis (PCA) [17] and wavelet analysis [18] are commonly adopted to conduct the clustering analysis for MTS. However, most clustering algorithms [18–21] cannot solve nonspherical distribution of MTS data well. In the process of clustering, due to the lengths of most MTSs are different, it is necessary to use the dynamic time warping (DTW) [22–26] to measure the similarity between their corresponding component attributes. But the importance of component attributes has not yet received due attention. To further analyze the features of component attributes, Li et al. [27] apply the affinity propagation (AP) algorithm

[28, 29] to adaptively cluster the component attributes which addressed the shortcomings of other traditional methods in a certain extent. However, their calculation process for the comprehensive relationship matrix is still complex. The quality and efficiency of MTS clustering need to be further improved.

To better solve the asynchronous correlation of different time points in MTS clustering, this paper proposes a simple and high-quality clustering method DTW_AP based on the DTW and AP. DTW is used to measure the similarity of both the component attributes and the overall MTS data. After that, from the perspective of local characteristics and global information, we quickly construct the comprehensive correlation matrix of MTS data. Based on this matrix, we further use the AP algorithm to achieve MTS clustering. Numerical experimental results indicate that the proposed method can achieve better clustering results compared with other traditional methods.

The proposed method possesses some advantages that the current MTS clustering research does not have. These advantages are as follows: (1) The similarity among the components of the MTS data is considered during the clustering process. The accurate of MTS clustering is ensured. (2) With a thorough consideration of the complicated relationships between the local component attributes and the overall information, it retains the multipath nature of MTS information.

The rest of this paper is organized as follows. "Preliminaries" introduces some related theoretical methods, such as the DTW and AP algorithms. In "Multivariate Time Series Clustering," the detailed construction process of the novel method is described. In "Numerical Experiment," the comparison analysis among the clustering methods is fulfilled in the experimental evaluation. Finally, the conclusions and future work are drawn in "Conclusions."

2. Preliminaries

2.1. Dynamic Time Warping. Euclidean distance is a common and efficient distance measurement method of time series which can be denoted as

$$d(x, y) = \sqrt{\sum_{i=1}^{L} \|x_i - y_i\|^2}, \qquad (1)$$

where $X = \{x_1, x_2, \cdots, x_n\}$ and $Y = \{y_1, y_2, \cdots, y_m\}$ are two MTSs, and the dimension of x_i is p, $x_i = (x_i^1, x_i^2, \cdots x_i^p)$, $n = m = L$.

From (1), we know that the Euclidean distance usually needs to be measured by two time series with equal length at the same time point. That is, we regard the square difference between x_i and y_i at the same time point as the contribution of the Euclidean distance. Obviously, its characteristics with equal sequence length, equal time matching, and being sensitive to abnormal data make it impossible to obtain satisfactory results when measuring the similarity between time series data.

Compared with the Euclidean distance, dynamic time warping (DTW) [22–26] is a distance measurement method, in which it firstly calculates the distance matrix D between

time series data and then uses the dynamic programming method to construct the cost matrix R. Finally, based on the matrix R, an optimal bending path W is found so that

$$\text{DTW}(X, Y) = \min_W \sum_{k=1}^{K} \|w_k\|^2, \qquad (2)$$

where $w_k \in W$, K is the number of elements in the optimal bending path W, and $\max(n, m) \le K \le m + n - 1$. In addition, $w_k = (i_k, j_k)$ indicates that the path element consists of the ith data point in X and the jth data point in Y.

According to the dynamic programming method, the cumulative cost matrix R can be figured out as follows:

$$R(i, j) = D(i, j) + \min\{R(i, j - 1), R(i - 1, j), R(i - 1, j - 1)\}, \qquad (3)$$

where $R(0, 0) = 0$, $R(i, 0) = \infty$, and $R(0, j) = \infty$.

Obviously, the cumulative distance is $R(n, m)$, that is, $\text{DTW}(X, Y) = R(n, m)$. Meanwhile, a corresponding dynamic bending path W is also found.

Using DTW to measure the distance of time series data not only matches the data points with the same shape but also measures the similarity between time series data with unequal length. In addition, it can also better solve certain sensitive problems caused by the abnormal data points in the Euclidean distance [22, 23]. However, since the time and space complexity of DTW is higher than that of the Euclidean distance, it will result in poor efficiency when directly applying DTW to measure the similarity between high-dimensional time series data. To solve this problem, many improved methods are proposed by scholars. Salvador and Chan [30] presented a fastDTW based on the search range limitation and data abstraction. On the basis of the penalty coefficient, Li and Du [31] proposed an improved DTW algorithm (γ_DTW) to effectively measure the similarity among an asynchronous approximation of the morphology. To promote the quality of DTW, Li [32] designed a novel DTW with time weight in measuring the distance between time series.

In this paper, to reduce the impact of high dimensionality of variable attributes on the clustering, we will utilize the traditional DTW method to measure the similarity among each component of MTS.

2.2. Affinity Propagation. The classical Kmeans algorithm randomly chooses the initial center points, and certain local optimal solutions are easily obtained. To avoid this problem, Frey proposed the affinity propagation (AP) clustering method [33] based on the graph theory. Compared with other algorithms, AP clustering does not limit the number of clusters and does not choose the initial points randomly. It takes each data point as the potential representative point of the candidate class, which effectively reduces the influence of the selection of original clustering centers on the clustering results. In addition, it also has no symmetry requirement for the similarity matrix, and the speed of dealing with multiclass data is also faster. Therefore, AP clustering algorithm can solve non-Euclidean space problems caused by asymmetry

or trigonometric inequalities or large-scale sparse matrix computing issues [28, 34]. Owing to the important functions, AP algorithm is employed to the various research fields, and its performance and efficiency are also improved [35–37]. For instance, Li et al. [35] proposed a new AP algorithm, the adjustable preference affinity propagation (APAP) algorithm, in which the initial value of each element preference $p(k)$ is independently determined on the basis of the data distribution and is automatically adjusted during the iteration process. Experiments verify its better performance comparing with the standard AP algorithm.

As a type of clustering algorithm depending on the information exchange between data points, AP algorithm can locate the optimal set of representative points when the cluster error function is minimized. Each representative point is from a certain point in original data set, and the sum of cumulative information volume between it and other data points reaches the maximum. In this algorithm, there exist two kinds of information between any two data points i and k. They are called the responsibility degree $r(i, k)$ and the availability degree $a(i, k)$, respectively. $r(i, k)$ refers to the information exchanged from the data point i to the candidate representative data point k, which reflects the representative degree of data point k to data point i. And $a(i, k)$ denotes the effectiveness degree in which data point i chooses data point k as its cluster center, which indicates the information transmitted from the candidate cluster center k to data point i.

Given a data set $X = \{x_1, x_2, \cdots, x_n\}$, the detailed process of AP clustering algorithm is described as follows.

During the AP clustering process, the purpose of setting the matrices r and a to zero matrix in S1 is to choose each point in data set as the original cluster center. After initializing, each element in the matrices r and a is needed to be updated from S2 to S4. Specifically, to avoid the possible vibration, a damping coefficient λ is introduced to S4. S5 is the condition for the end of algorithm. The corresponding cluster center of each object and the final cluster set can be obtained in S6 and S7, respectively.

In the process of calculation, it is worth noting that the number of iterative cycles is affected by the damping coefficient λ. Generally, they change in opposite directions with each other. When the damping coefficient λ is large, the number of iterative cycles is small, otherwise the opposite. Gui and Yang [38] found that when the range of λ is [0.5, 1], the stability of AP algorithm can be extremely improved. To reduce the probability of the appearance of fluctuations, we take the value of λ to be 0.9 as suggested by Frey and Dueck [33].

3. Multivariate Time Series Clustering

Compared with univariate time series (UTS), multivariate time series (MTS) has high-dimensional attribute variables, which makes it necessary to consider their approximation in clustering. However, to achieve the MTS clustering, some traditional clustering methods usually regard MTS data as the complete data object and select certain appropriate distance measurement methods to calculate their similarity.

Due to the high dimensionality of attribute variables in MTS, the distance measurement method will affect the clustering quality of MTS. To this end, this paper proposes a MTS clustering method based on DTW and AP from the view of univariate attribute series of MTS data.

Given a MTS data set $X = \{X_1, X_2, \cdots, X_N\}$, where $X_i = \{X_i^1, X_i^2, \cdots, X_i^m\}$ is the ith MTS, X_i^p refers to the pth attribute sequence of the ith MTS, and $p = 1, \cdots, m$. DTW is used to measure the following similarity distance between two MTSs X_i and X_j:

$$S_{ij}^0 = -\text{DTW}(X_i, X_j). \tag{4}$$

Obviously, the bending path $W = \{\omega_1, \omega_2, \cdots, \omega_K\}$ measured by the minimum bending distance S_{ij}^0 will be obtained, where $\omega_k = (i_k, j_k)$.

Since each dimension of the MTS X_i can be viewed as the UTS, we can compute the similarity between any two MTSs from the data bending path W provided by (4). That is, under the same attribute of different MTS, we can calculate the following similarity of UTS by using the DTW.

$$\begin{aligned} S_{ij}^p &= S\left(X_i^p, X_j^p\right) \\ &= -\sum_{k=1}^{K} \left(X_i^p(i_k) - X_j^p(j_k)\right)^2. \end{aligned} \tag{5}$$

From (5), we can construct the similarity matrix S^p of the UTS data set under each attribute component.

This paper employs the AP algorithm to cluster the similarity matrices S^0 and S^p constructed by formulas (4) and (5). The clustering results C^j can reflect the relationship R^j among MTSs under the overall information environment and local component. Furthermore, we obtain the relation matrices R^j by the transformation formula $R^j = C2R(C^j)$. Notice that $C^p = AP(S^p)$ and $C^o = AP(S^0)$ and the element of the relation matrix R^j only include 0 or 1. If two data objects in the final clustering result point to the same representative object, then their relationship is denoted to be 1, otherwise 0.

Based on the above relationship R^j, we design the following comprehensive relationship matrix R.

$$R = R^0 * \sum_{j=1}^{m} R^j. \tag{6}$$

Regarding the matrix as the similarity matrix, we will further obtain the clustering results by means of AP algorithm. A new clustering algorithm $C = \text{DTW\_AP}(X)$ constructed by DTW and AP is described as follows.

Compared with the traditional clustering methods with Euclidean distance, $\text{DTW\_AP}(X)$ has better clustering effects. In fact, DTW can measure the similarity of time series with different lengths while not being sensitive to sudden change or outlier of time series. In addition, DTW also can fulfill the asynchronous similarity comparison. Meanwhile,

AP clustering $C = \text{AP}(S)$
Input: similarity matrix S between data points, the maximum iteration number cot, damping coefficient λ.
Output: cluster set C.
S1: initialize the responsibility matrix r and the availability matrix a to be $n * n$ zero matrix.
S2: Update the responsibility matrix r.
$$r(i,k) = \begin{cases} s(i,k) - \max_{k' \neq k}\{a(i,k') + s(i,k')\}, i \neq k \\ s(k,k) - \max_{k' \neq k}\{a(k,k') + s(k,k')\}, i = k. \end{cases}$$
S3: update the availability matrix a.
$$a(i,k) = \begin{cases} \min\{0, r(k,k) + \sum_{i' \notin \{i,k\}}\max[0, r(i',k)]\}, i \neq k \\ \sum_{i' \neq k}\max[0, r(i',k)], i = k. \end{cases}$$
S4: introduce the damping coefficient $\lambda(0 < \lambda < 1)$ to reduce the possible vibration when updating information. Apply the weighted sum of λ times of the last iteration update value and $1 - \lambda$ times of the current information update value to assign each information. That is
$$\begin{cases} r_{t+1}(i,k) = \lambda \times r_t(i,k) - (1-\lambda) \times r_{t+1}(i,k) \\ a_{t+1}(i,k) = \lambda \times a_t(i,k) - (1-\lambda) \times a_{t+1}(i,k). \end{cases}$$
S5: repeat steps S2 to S4. Stop the algorithm when the clustering results tend to be stable or achieve the preset iterative number cot.
S6: construct the matrix g by adding the matrices r and a and further find the corresponding column k where the value of each row i is the maximum. k is the cluster center of object i.
S7: assign the objects with the same cluster center to the same cluster and obtain the finally cluster set C.

ALGORITHM 1

Input: MTS data set $X = \{X_1, X_2, \cdots, X_N\}$, where each time series has m-dimensional attribute.
Output: representative object set C of MTS.
S1: obtain the corresponding similarity matrix S_{ij}^0 and optimal bending path W according to the formulas (2) and (4).
S2: based on the optimal bending path W and formula (5), calculate the similarity S_{ij}^p between two MTSs X_i and X_j under the different component attribute.
S3: repeat steps S1 to S2, calculate the similarity between the corresponding component sequences of all MTSs under the different dimensional condition, and further achieve the corresponding similarity matrices $S^1, S^2, \cdots, S^m$. Herein, m is the attribute dimension of MTS.
S4: use the AP algorithm to cluster each similarity matrix and then achieve the clustering results C^p and C^0 under the different component attribute and the perspective of overall MTS, respectively.
S5: transform the clustering results C^p and C^0 to the relation matrix, that is, $R^j = C2R(C^p)$ and $R^0 = C2R(C^0)$. Meanwhile, calculate the synthetic relation matrix R from (6).
S6: employ the AP algorithm to cluster the comprehensive relation matrix R and finally obtain the clustering result C of MTS.

ALGORITHM 2

this paper applies the AP algorithm to cluster the component attribute of MTS. The influence of each component on the clustering is considered in a comprehensive manner. The application of the AP algorithm not only avoids the limitation of the clustering results achieved by the representative point of the initial class but also has no requirement for the symmetry of similarity matrix. When processing the multi-class data, once the operation speed is faster, its performance will be better.

With the help of the effectiveness evaluation, we find that the algorithm proposed by this paper has significantly higher clustering accuracy than other algorithms. Meanwhile, it also achieves the purpose of high accuracy for the high-dimensional data, which proves its component steps to be effective and meaningful. In this paper, the AP clustering algorithm is used twice. The first time is to cluster each com-

ponent and the overall of MTS. The last time is to cluster the comprehensive relationship matrix R. Thus, the achieved clustering results will be more accurate. In addition, it is more universal for MTS with missing data or different length to use DTW as the distance measurement, which can be widely adopted in practical application.

In the method DTW_AP, the AP algorithm solves the problem that the traditional methods are only suitable for data clustering with spherical distribution. Moreover, the application of DTW in the clustering process enhances the clustering effect of asynchronous morphological similarity. In addition, this paper mainly focuses on the effect of each component attribute sequence on the clustering result and achieves MTS clustering under the local component attribute sequence and the overall information environment.

4. Numerical Experiment

To verify the performance of the proposed method, we choose an effective evaluation index and compare it to several other MTS clustering methods when processing various MTS data sets. In the experiments, the computer is Lenovo T420. The CPU is Intel Core i7-2640M, the computer main frequency is 2.8 GHz, and the memory is 4.0 GB. The operation system is Windows 7 (64 bit). The programming environment is MATLAB R2012b.

4.1. Effectiveness Evaluation Index. Due to the existence of different application requirement, the quality of clustering has no uniform standards for a long time. Therefore, it must rely on certain indicators to evaluate the effectiveness of algorithm. The evaluation methods of clustering validity are divided into external effectiveness and internal effectiveness. The former is to judge the validity of clustering results based on the known correct results. By comparing the known correct clustering results with the experimental clustering results, we can get the degree of similarity, which is the accuracy. The latter is a completely opposite method to the former, which usually uses the self-characteristics of original data set to evaluate the results based on the unknown standard clustering results. Since the measurement is labeled by the known clustering results, this paper chooses the former as the valuation index.

Suppose Pre is the external index of measuring the clustering effect and algorithm quality. Label is the correct result, while idx is the experimental result. n is the total number of points in the data set. The evaluation index Pre of clustering validity between Label and idx is defined as

$$\text{Pre} = \frac{\sum \text{Label(idx)} == \text{Label}}{n}. \tag{7}$$

Given that the class label clustered by the AP algorithm is the coordinate of clustering center points in Pre, we only need to figure out the class label value of experimental results. For example, if the class label of data 1 is 5, and the value of data 5 in the real result is also 5, then data 1 should be clustered into the cluster of data 5. Obviously, this clustering proves to be true and records as 1. Similarly, the correct matching is marked by 1, otherwise 0. Obviously, the cumulative sum divided by the value of Pre is between 0 and 1. The closer the value is to 1, the more accurate the clustering result is.

4.2. Clustering Analysis. To demonstrate the performance of the proposed method, ten MTS data sets from the UCR and UCI are selected. They mainly come from the fields of industrial engineering, medical and health, gestures behavior, language pronunciation, and so on. The detailed information of these data sets are shown in Table 1.

As shown in Table 1, the former five MTS data sets have different lengths. For instance, the time dimension of data set AD is from 4 to 93. The last five MTS data sets with the same industry have 6 variables, and their time dimension is 15. However, they contain different numbers of categories and data volume.

TABLE 1: Experimental data sets of MTS.

ID	Name	Variables	Length	Classes	Volume
1	ASL	22	[45-136]	95	1425
2	AD	13	[4-93]	10	2200
3	CMUS16	62	[127-580]	2	29
4	ECG	2	[39-152]	2	100
5	JV	12	[7-29]	9	370
6	LP1	6	15	4	50
7	LP2	6	15	5	30
8	LP3	6	15	4	30
9	LP4	6	15	3	75
10	LP5	6	15	5	100

The traditional clustering methods of time series usually use the feature representation and similarity measurement to process data and further achieve time series clustering based on the designed specific distance measurement method and the classical clustering method. To demonstrate the clustering performance of the method DTW_AP, PCA_AP [19] based on PCA and AP, Kmeans based on the distance measurement, and OAP based on AP clustering for the original data [33] are selected to be compared with it. In addition, our experiment also compares DTW_AP with the permutation distribution clustering (PDC) [20] and the component attributes based affinity propagation clustering for multivariate time series data (cACM) [27]. Different methods are adopted to carry out the clustering analysis on ten different data sets. The experimental results are displayed in Table 2, where the best experimental result in PCA_AP is from the former $P/2$ main ingredient, P represents the attribute dimension of the MTS data set. The bias parameter Pr affecting the number of clustering and the damping factor λ affecting the algorithm convergence in AP clustering algorithm are set to be the median of the similarity matrix and 0.9, respectively [33].

As shown in Table 2, we know that the mean value obtained by DTW_AP is higher than all other methods on ten different data sets. Meanwhile, the standard deviation (SD) value obtained by DTW_AP is also lower than that by OAP, PCA_AP, Kmeans, and PDC. Note that the SD value computed by cACM is lower than that by DTW_AP. However, its stability advantage is not extremely clear. In a word, compared with other MTS clustering methods, DTW_AP is more effective and feasible. Clearly, it is more superior to most traditional AP clustering algorithms based on the whole original data information.

We take the novel method as the benchmark and compare the clustering effect between this method and other traditional methods. The scatter diagrams of clustering results are shown in Figure 1. Obviously, if the data point in the figure is below the gray line, it will indicate that the novel method is better than the traditional method, otherwise the opposite. From the visual comparative analysis of clustering results in Figure 1, we observe that the method DTW_AP achieves better clustering results, compared with other traditional methods on most data sets. In fact, it is easy to find that

TABLE 2: Experimental clustering effectiveness results.

Method	1	2	3	4	5	6	7	8	9	10	Mean	SD
DTW_AP	0.76	1.00	0.93	0.72	0.95	0.80	0.73	0.83	0.89	0.64	0.83	0.12
cACM	0.76	0.99	0.79	0.73	0.95	0.84	0.73	0.83	0.88	0.64	0.81	0.11
OAP	0.51	0.98	0.93	0.81	0.92	0.74	0.73	0.67	0.88	0.57	0.77	0.16
PCA_AP	0.10	0.86	0.72	0.83	0.16	0.64	0.70	0.67	0.76	0.66	0.61	0.26
Kmeans	0.31	0.48	0.59	0.67	0.67	0.52	0.67	0.57	0.77	0.41	0.56	0.14
PDC	0.08	0.10	0.59	0.68	0.31	0.50	0.60	0.67	0.68	0.38	0.46	0.23

(a)

(b)

(c)

(d)

(e)
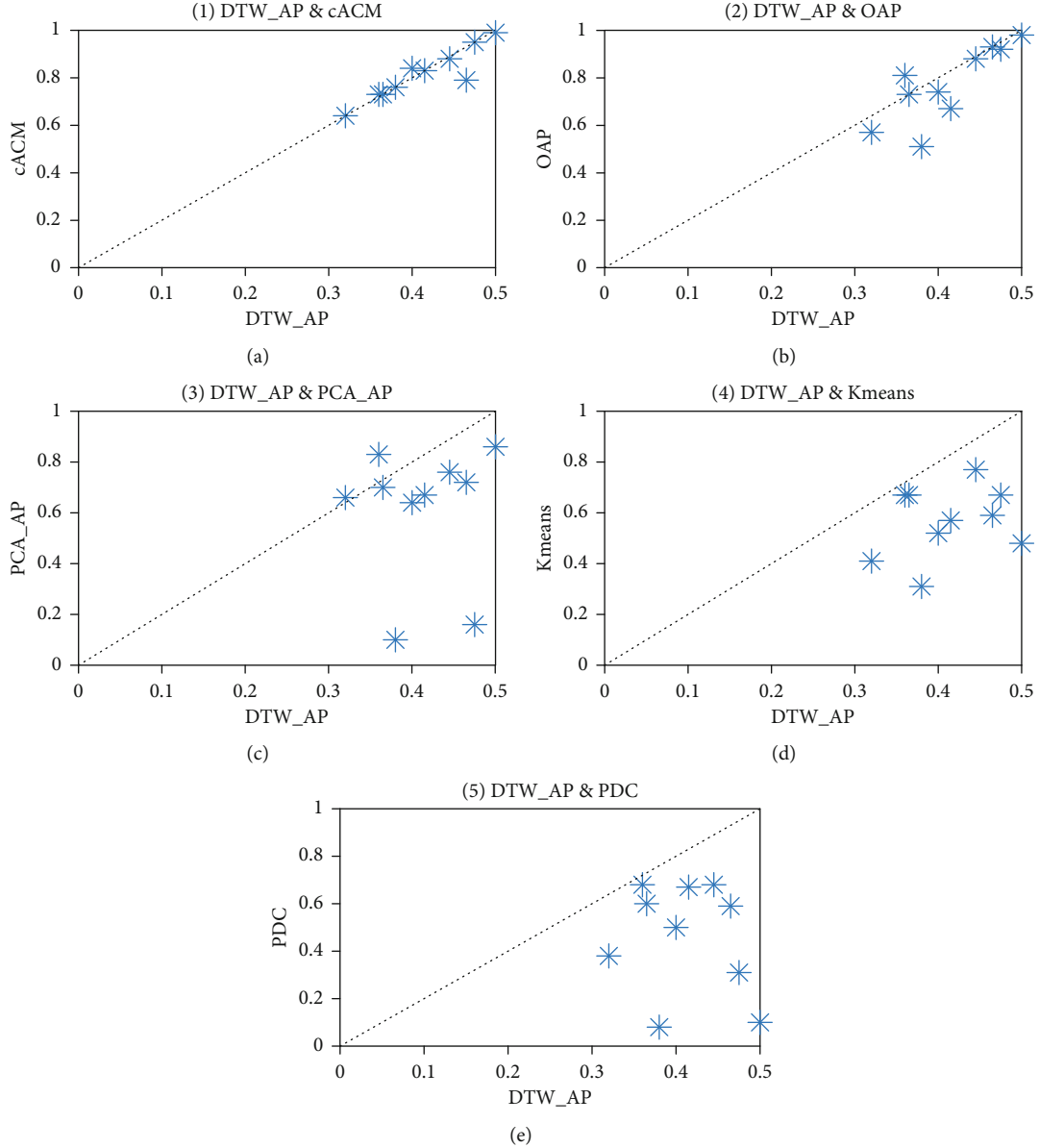
FIGURE 1: Visual comparison of clustering experimental results of different data.

most discrete points in Figure 1 are below the gray line except Figure 1(a), which proves that the novel method has stronger advantages. However, Figure 1(a) generally fluctuates near the gray line, and there is one discrete point deviating from the gray line downward. To a certain extent, it also shows that the clustering quality of the novel method is better. In particular, from the visual comparison analysis of different methods on all data sets in Figure 2, we find that the ranking of clustering quality is roughly DTW_AP>cACM>OAP>PCA_AP>Kmeans>PDC. Meanwhile, based on
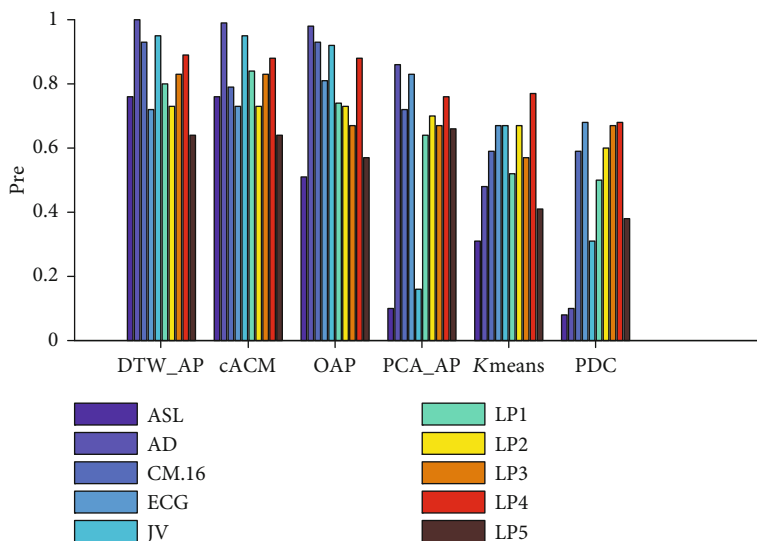
FIGURE 2: Visualization of clustering results of all data sets by different methods.

the average effect and the variance stability of clustering results in Table 2, it also indicates that the clustering performance of DTW_AP is better than other traditional methods.

5. Conclusions

In this paper, a new MTS clustering method is proposed on the basis of DTW and AP. DTW is used to calculate the similarity between the whole information of MTS and parse out the similarity between the component attributes. Meanwhile, the AP algorithm is utilized to construct the clustering relationship between each component attribute and the whole sequence. After that, certain MTS relationship matrices are further presented based on the component attributes and global information. The numerical experimental results indicate that the novel method can achieve better clustering performance when comparing with other traditional clustering methods of time series. However, during the clustering process, the operation using the AP algorithm to cluster the UTS of each component attribute is time-consuming. Therefore, further work should consider improving the time efficiency of the proposed method.

Data Availability

The datasets analyzed in this study are available from the corresponding author upon reasonable request.

Conflicts of Interest

The authors declare that they have no conflicts of interests.

Acknowledgments

References

[1] R. Chandra and S. Chand, "Evaluation of co-evolutionary neural network architectures for time series prediction with mobile application in finance," *Applied Soft Computing*, vol. 49, pp. 462–473, 2016.

[2] R. A. Davis and L. Song, "Noncausal vector AR processes with application to economic time series," *Journal of Econometrics*, vol. 216, no. 1, pp. 246–267, 2020.

[3] D. Yang, Z. Dong, L. Lim, and L. Liu, "Analyzing big time series data in solar engineering using features and PCA," *Solar Energy*, vol. 153, pp. 317–328, 2017.

[4] K. Cao, T. Hu, Z. Li, G. Zhao, and X. Qian, "Deep multi-task learning model for time series prediction in wireless communication," *Physical Communication*, vol. 44, article 101251, 2021.

[5] Q. Yang and X. Wu, "10 challenging problems in data mining research," *International Journal of Information Technology and Decision Making*, vol. 5, no. 4, pp. 597–604, 2006.

[6] E. Keogh, J. Lin, and A. Fu, "Hot sax: efficiently finding the most unusual time series subsequence," in *Fifth IEEE International Conference on Data Mining (ICDM'05)*, pp. 226–233, Houston, TX, USA, 2006.

[7] D. Ye, Y. Wu, and M. Goh, "Hub firm transformation and industry cluster upgrading: innovation network perspective," *Management Decision*, vol. 58, no. 7, pp. 1425–1448, 2020.

[8] P. Esling and C. Agon, "Time-series data mining," *ACM Computing Surveys*, vol. 45, no. 1, pp. 1–34, 2012.

[9] C. Matias and V. Miele, "Statistical clustering of temporal networks through a dynamic stochastic block model," *Journal of the Royal Statistical Society*, vol. 60, no. 4, pp. 12–31, 2016.

[10] A. Cobo, E. R. Rocha, and M. A. Villamizar, "Innovative propensity with a fuzzy multicriteria approach," *Management Decision*, vol. 57, no. 11, pp. 2940–2957, 2019.

[11] M. S. Yang and Y. Nataliani, "A feature-reduction fuzzy clustering algorithm based on feature-weighted entropy," *IEEE Transactions on Fuzzy Systems*, vol. 26, no. 2, pp. 817–835, 2018.

[12] M. Caron, P. Bojanowski, A. Joulin, and M. Douze, "Deep clustering for unsupervised learning of visual features," in *Proceedings of the European Conference on Computer Vision (ECCV)*, pp. 139–156, Munich, Germany, 2018.

[13] S. Bhati, S. Nayak, K. Murty, and N. Dehak, "Unsupervised acoustic segmentation and clustering using siamese network embeddings," in *Interspeech 2019*, pp. 2668–2672, Graz, Austria, 2019.

[14] C. Liu, J. Liu, D. Peng, and C. Wu, "A general multiobjective clustering approach based on multiple distance measures," *IEEE Access*, vol. 6, pp. 41706–41719, 2018.

[15] H. Li, Y. J. Wu, and Y. Chen, "Time is money: dynamic-model-based time series data-mining for correlation analysis of commodity sales," *Journal of Computational and Applied Mathematics*, vol. 370, article 112659, 2020.

[16] B. T. Pentland, P. Liu, W. Kremser, and T. Haerem, "The dynamics of drift in digitized processes," *MIS Quarterly*, vol. 44, no. 1, pp. 19–47, 2020.

[17] H. Li, "Accurate and efficient classification based on common principal components analysis for multivariate time series," *Neurocomputing*, vol. 171, pp. 744–753, 2016.

[18] P. D'Urso and E. A. Maharaj, "Wavelets-based clustering of multivariate time series," *Fuzzy Sets and Systems*, vol. 193, no. 4, pp. 33–61, 2012.

[19] J. F. Barragan, C. H. Fontes, and M. Embirucu, "A wavelet-based clustering of multivariate time series using a multiscale SPCA approach," *Computers & Industrial Engineering*, vol. 95, no. 5, pp. 144–155, 2016.

[20] A. M. Brandmaier, "PDC: permutation distribution clustering," *Psychological Methods*, vol. 18, no. 1, pp. 71–86, 2015.

[21] H. Li, "Multivariate time series clustering based on common principal component analysis," *Neurocomputing*, vol. 349, pp. 239–247, 2019.

[22] H. Li, "On-line and dynamic time warping for time series data mining," *International Journal of Machine Learning and Cybernetics*, vol. 6, no. 1, pp. 145–153, 2015.

[23] E. Keogh and M. Pazzani, "Derivative dynamic time warping," in *Proceedings of the 2001 SIAM International Conference on Data Mining (SDM)*, pp. 1–11, Chicago, USA, 2001.

[24] T. Han, Q. Peng, Z. Zhu, Y. Shen, H. Huang, and N. N. Abid, "A pattern representation of stock time series based on DTW," *Physica A: Statistical Mechanics and its Applications*, vol. 550, article 124161, 2020.

[25] H. Li and M. Wei, "Fuzzy clustering based on feature weights for multivariate time series," *Knowledge-Based Systems*, vol. 197, article 105907, 2020.

[26] T. Górecki and M. Łuczak, "Non-isometric transforms in time series classification using DTW," *Knowledge-Based Systems*, vol. 61, pp. 98–108, 2014.

[27] H. Li, C. Wang, and X. Deng, "Multivariate time series clustering based on affinity propagation of component attributes," *Control and Decision*, vol. 33, no. 4, pp. 649–656, 2018.

[28] T. Wu, Y. Liang, R. Varela, C. Wu, G. Zhao, and X. Han, "Self-adaptive SVDD integrated with AP clustering for one-class classification," *Pattern Recognition Letters*, vol. 84, pp. 232–238, 2016.

[29] S. Basloom, N. Akkari, and G. Aldabbagh, "Reducing handoff delay in SDN-based 5g networks using AP clustering," *Procedia Computer Science*, vol. 163, pp. 198–208, 2019.

[30] S. Salvador and P. Chan, "FastDTW: toward accurate dynamic time warping in linear time and space," *Intelligent Data Analysis*, vol. 11, pp. 561–580, 2007.

[31] H. Li and T. Du, "Multivariate time-series clustering based on component relationship networks," *Expert Systems with Applications*, vol. 173, article 114649, 2021.

[32] H. Li, "Time works well: dynamic time warping based on time weighting for time series data mining," *Information Sciences*, vol. 547, pp. 592–608, 2021.

[33] B. J. Frey and D. Dueck, "Clustering by passing messages between data points," *Science*, vol. 315, no. 5814, pp. 972–976, 2007.

[34] Y. Liu, J. Liu, Y. Jin, F. Li, and T. Zheng, "An affinity propagation clustering based particle swarm optimizer for dynamic optimization," *Knowledge-Based Systems*, vol. 195, article 105711, 2020.

[35] P. Li, H. Ji, B. Wang, Z. Huang, and H. Li, "Adjustable preference affinity propagation clustering," *Pattern Recognition Letters*, vol. 85, pp. 72–78, 2017.

[36] K. Nabar and G. Kadambi, "Affinity propagation-driven distributed clustering approach to tackle greedy heuristics in mobile ad-hoc networks," *Computers & Electrical Engineering*, vol. 71, pp. 988–1011, 2017.

[37] Z. Geng, R. Zeng, Y. Han, Y. Zhong, and H. Fu, "Energy efficiency evaluation and energy saving based on DEA integrated affinity propagation clustering: case study of complex petrochemical industries," *Energy*, vol. 179, pp. 863–875, 2019.

[38] B. Gui and X. Yang, "Research on parameters of affinity propagation clustering," *Advanced Technologies, Embedded and Multimedia for Human-Centric Computing*, vol. 260, pp. 637–644, 2014.

WILEY | Hindawi

Research Article

Application of Deep Learning Algorithms in Determination of Trace Rare Earth Elements of Cerium Group in Rocks and Minerals

Sumin Ma[1,2] **and Wenhui Huang** [1,3]

[1]*School of Energy Resource, China University of Geosciences (Beijing), 100083 Beijing, China*
[2]*Key Laboratory of Marine Reservoir Evolution and Hydrocarbon Enrichment Mechanism, Ministry of Education, 100083 Beijing, China*
[3]*Beijing Key Laboratory of Unconventional Natural Gas Geological Evaluation and Development Engineering, 100083 Beijing, China*

Correspondence should be addressed to Wenhui Huang; huangwh@cugb.edu.cn

Since the breakthrough of deep learning in object classification in 2012, extraordinary achievements have been made in the field of target detection, but the high time and space complexity of the target detection network based on deep learning has hindered the technology from application in actual product. To solve this problem, first of all, this paper uses the MobileNet classification network to optimize the Faster R-CNN target detection network. The experimental results on the rare earth element detection data set show that the MobileNet classification network is not suitable for optimizing the Faster R-CNN network. After that, this paper proposes a classification network that combines VGG16 and MobileNet, and uses the fusion network to optimize the Faster R-CNN target detection network. The experimental results on the rare earth element detection data set show that the Faster R-CNN target detection network optimized by the fusion classification network has the advantages of using VGG16 and MobileNet's Faster R-CNN target detection network to detect rare earth elements. The innovation of this article is that the results on 5 time series data sets show that CDA-WR has better predictive performance than other ELM variant models. The effect of determining trace cerium elements in rocks and minerals is increased by more than 50%, based on deep learning. The algorithm studies the methods of target detection and recognition and integrates it into the intelligent robot used in this subject, giving the robot the ability to accurately detect the target object in real time.

1. Introduction

Adding trace amounts of cerium to steel for offshore platforms is expected to replace the more expensive titanium and vanadium elements and reduce costs. This is also in line with my country's resource characteristics (the properties and functions of cerium in the smelting, processing, and alloying of steel are relatively similar), cerium reserves are abundant, and the price is relatively low. It can be used to improve the quality of steel for offshore platform structures. Optimize the smelting, plastic processing, and heat treatment processes of rare earth steel with trace cerium, and it is expected that trace cerium will be used to improve the perfor-

mance of rare earth steel for offshore platforms. Compared with other alloying elements in steel, rare earth elements have a larger atomic radius, ranging from 0.161 nm to 0.204 nm, which is about 50% more than iron atoms (0.117 nm); this makes rare earth elements easy to lose their outer electrons. As cations are formed, their electronegativity is very low, which is only slightly higher than that of alkali metals and alkaline earth metals of the same period; this also makes rare earth elements exhibit extremely strong reactivity in molten steel, and they are not only easy to interact with molten steel. Oxygen, sulfur, and other nonmetallic elements combine to form high melting point rare earth compounds. At the same time, rare earth elements can interact with many low melting

point metals in steel, thereby reducing their harm to the mechanical properties of materials.

Shugui and Wang used the least squares regression algorithm to process the data by spectrophotometry with the same hair color and tribromide system to simultaneously identify rare earth cerium in geological samples and achieved satisfactory results. Discuss in the sample, determine the composition of the calibration sample group through the proposed method, determine the best factor and the GSD and GSR series of the national standard geological sample series, and the overall results are consistent with the recommended values. However, they took very few samples and cannot generalize [1]. Yan and Zhijie proposed an SSD deep learning algorithm to improve the performance of multiobject protocols. Three different sample projects were trained. Firstly, the SSD neural network algorithm detects the type of object and creates a delimiter around the location of the object in the image. Secondly, find the smallest rectangle around the object according to the contour feature of the object and calculate the position coordinates of the object in the image. Finally, complete the handle configuration design information to prevent the handle from colliding with other objects and causing the handle to fail, but the algorithm is not complete, and the actual effect is not ideal [2]. Jun et al. believe that as the demand for oil and natural gas resources continues to grow, it is necessary to strengthen technological innovation in oil and natural gas exploration. Therefore, more effective seismic data processing technology is needed. The increase in computer performance has led to an explosive growth in the field of deep learning. The exploration field has also been extensively developed. Deep learning is a machine learning method. Its development has experienced two waves, namely, BP algorithm and deep learning. The applications listed below were also created in these two waves. Deep learning is a type of supervised learning, which allows to learn more advanced abstract representations of data and automatically extract features from the data. But deep learning needs to be more intelligent, and they did not solve the problem of deep learning intelligence [3].

To study the effect of trace rare earth element cerium (ppm level) on the structure and properties of steel, the steel used for offshore platforms has higher requirements for impact toughness in addition to the conventional mechanical performance test. Denatured inclusions (sulfides) change the strip-shaped manganese sulfide into spherical or ellipsoidal rare earth sulfides, which is beneficial to improve the plastic toughness of steel. Study the influence and effect of the trace rare earth element cerium on the CCT curve, Ac1 and Ac3 points of the experimental steel, and use the end quenching experiment to determine the hardenability of the steel [4]. In microstructure organization analysis mechanical properties, analyze the influence of trace rare earth element cerium. The rare earth element cerium improves the seawater corrosion resistance of steel. Rare earth sulfide has a more positive electrode potential than manganese sulfide. Due to the reduced potential difference and the reduction of the galvanic effect, the presence of rare earth sulfide in the grain boundary is beneficial to improve the steel corrosion resistance of the substrate.
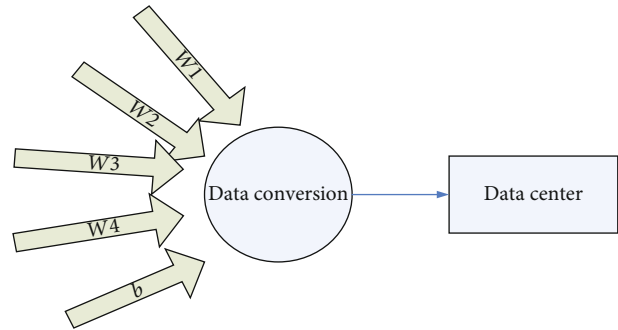
Figure 1: Neuron model.

The corrosion resistance of the high-strength steel used in seawater solution was analyzed [5].

2. Deep Learning Algorithms Are Measuring Rock and Mineral Methods

2.1. Traditional Target Detection Algorithm. Target detection is an important problem in computer vision, and many researchers have developed a large number of algorithms. The general flow of the traditional target detection algorithm is shown in Figure 1. The main flow is to first perform redundant window interception through a sliding window to ensure that the target is contained by at least one window. Due to the various sizes and aspect ratios of the target, the interception window also uses preselected windows of different sizes and aspect ratios for interception [6, 7]. With the intercepted image, it is necessary to perform preprocessing operations, including unifying the size, removing the mean value, eliminating irrelevant features, and reducing noise. Then, a series of images after processing and processing are used for feature extraction using artificially designed feature operators. Feature selection is the key to the problem of target detection, and the quality of features can often determine the performance of the final target detection algorithm to a large extent. Different tasks often require different requirements for features, so there is no universal and universal feature. Commonly used traditional feature extraction methods include shape, color, texture, edge, corner, and other visual features, as well as better performance of artificially designed feature operators, such as HOG features, SIFT features, LBP features, and Haar wavelet feature operators. After feature extraction, classifiers commonly used in machine learning, such as SVM and AdaBoost, are used for classification and regression, and finally, the detection results are generated.

The basic computing unit of artificial neural network is called perceptron, also known as neuron, which was first developed by Rosenblatt in 1957 [8, 9]. It is a simplified human neuron cell model. It is essentially a function. It accepts multiple real number input variables. Each variable has a weight value on the connection. The input variable is added to a bias term after weighted summation. As the input of the neuron, it passes through a linear activation function. The linear activation function finally produces an activation value [10]. The input value simulates the stimulation of nerve

cells, and the output value simulates the response of nerve cells. The neuron model is shown in Figure 1:

2.2. Deep Learning Algorithm.
When using deep learning in real life, the first thing to do is to optimize the network. The training process includes layer-by-layer training for unsupervised learning and network optimization for supervised learning. Through sampling and training the network, they found the inherent rules and used it to improve the user's network performance [11, 12]. To improve network performance, it must be achieved through specific learning steps. The three common learning steps that are commonly used are presented as follows:

2.2.1. Supervised Learning.
A common method of machine learning is supervised learning, which means that external monitoring methods are used in network learning to reward good learning, punish misleading learning, and always correct errors in the learning process. At the same time, the training pattern used in this learning method must be recognized as a pattern [13, 14]. In order to make training more appropriate, the training model should cover as many situations as possible. Supervised learning includes inputting samples into the network, obtaining network labels through step-by-step learning, then comparing the obtained network labels with the control group, and finally changing the network parameters according to the supervised learning criteria so that the network labels are similar to the sample labels [15, 16].

2.2.2. Unsupervised Learning.
Unsupervised learning is different from supervised learning. Unsupervised learning has no external monitoring function. The learning system is very smart. It will add to its own database and make statistics based on the data entered by the user, change the network label according to the internal changes in the database, and finally complete the upgrade of the network. This learning method is often used to learn labels and collect data [17, 18].

2.2.3. Reinforcement Learning.
Learning aid is an ongoing Markov decision-making process. In the process of online training, there are no formal results like supervised learning. After each online training course, only one evaluation function is provided. The network usage evaluation function evaluates learning outcomes. In addition to evaluation, network parameters must be adjusted according to the evaluation results, and finally, the entire network evaluation function is optimized [19, 20].

In the actual application of neural networks, it is necessary to choose appropriate learning methods for different application fields. The most important thing is that the three proposed learning methods have strong learning ability [21]. However, generally speaking, supervised learning algorithms are mainly used to optimize and adjust network parameters, and unsupervised learning algorithms are mainly used to classify multiple samples. Reinforcement learning algorithms are mainly used for intelligent control, analysis, and prediction.

3. Correlation Experiment of Rare Earth Elements of Cerium Group in Rocks and Minerals

The location of the rare earth element lanthanum and cerium in steel is very important. The segregation at grain boundaries or the amount of solid solution in the grain will have a great impact on the quality of steel. Therefore, it is necessary to explore the location of trace amounts of lanthanum and cerium. In the neuron model shown, X is the input variable of the neuron, representing a sample defined by four attribute values [22, 23]. W represents the corresponding weights of the four attribute values on the neuron, b is the bias term of the neuron, and the activation function used is the hard limiter. The function expression is as follows:

$$f(x) = \left\{ \begin{array}{cc} 1 & x > 0 \\ -1 & \text{otherwise} \end{array} \right\}. \tag{1}$$

The input value Z of the neuron is the weighted sum of the bias item plus the attribute value and the weight:

$$Z = \sum_{i=1}^{4} x_i y_{i+b}. \tag{2}$$

The neuron model can perform simple sorting and regression tasks, but cannot perform complex tasks [24, 25].

The activation function is an important part of the neuron, which is essentially a nonlinear function. It takes real numbers as input and produces real number outputs. Its main function is to improve the expressive ability of neurons and neural networks so that they can handle complex nonlinear problems. The first activation function used is a hard limiter, but it has many disadvantages. With the continuous development and improvement of artificial neural network theory, researchers have developed a variety of activation functions. Commonly used activation functions include sigmoid and hyperbolic tangent functions tanh and ReLU, Leaky ReLU, and maxout [26].

The sigmoid function accepts a real number and assigns it a number between [0, 1]. Its expression is as follows:

$$\varepsilon(x) = \frac{1}{1 + e^x} + b. \tag{3}$$

The double tangent function tanh accepts a real number and maps it to a number between [0,−1], and its expression is as follows:

$$\tanh(y) = \frac{e^x - e^{-x}}{e^x + e^{-x}} - \frac{1}{x}. \tag{4}$$

The powerful function of the deep learning system far exceeds the previous system. Based on the neural network and based on the huge network structure and huge data information, the number of hidden layers has increased [27, 28]. Due to its excellent learning ability and random distribution, the application fields of deep learning are
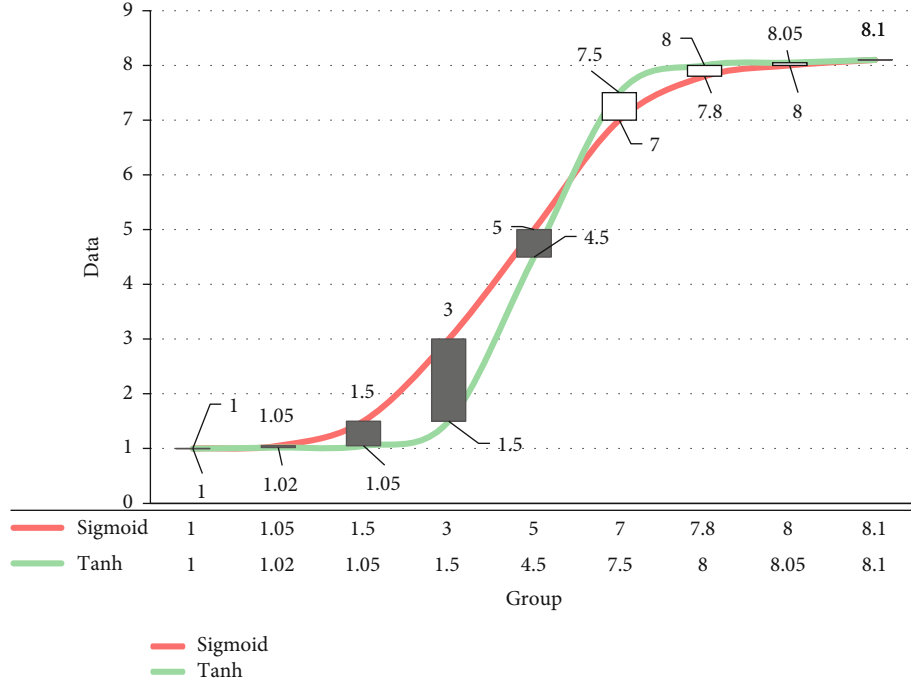
FIGURE 2: Sigmoid and tanh function images.

rapidly expanding. With the continuous expansion of deep learning research, deep learning algorithms for different fields are constantly being proposed. In order to make it easy to use, common deep learning algorithms and their respective application fields are given. Automated encoders and deep trust networks usually classify documents most effectively. For image classification, gravure network and convergent neural network are more suitable, but deep network is considered to be suitable for image recognition and classification, while convergent neural network is suitable for image recognition, and repetitive neural network is more suitable for speech recognition. For predictive analysis conducted in chronological order, the deep trust network can handle it well [29].

The curves corresponding to the two functions are shown in Figure 2. Their common feature is that the curve is symmetrical about a certain point, changes quickly near the symmetrical point, and smoothly changes away from the symmetrical point. These two activation functions have been widely used in early artificial neural networks, but there are problems in the back propagation process such as a large amount of calculation and vanishing gradient (vanishing gradient). These problems make the training efficiency of multilayer neural networks more efficient, low or no training at all. In response to these problems, new activation functions have been developed one after another [30] as shown in Figure 2.

ReLU (rectified linear unit) is an activation function developed by Vinod Nair et al. in 2010. Its function expression is as follows:

$$f(x) = \max\left(\cos x * e^x, \int_1^n \sqrt[3]{x+b}\right). \tag{5}$$

The output is 0 when $x < 0$, and x is output when $x > 0$. Compared with sigmoid and tanh functions, ReLU can greatly accelerate the convergence speed of neural network training using the backpropagation algorithm, and because it does not involve complex exponential calculations, it reduces the amount of calculation.

$$f(x) = \begin{Bmatrix} ae^x + b & x < 0 \\ \sqrt{e^x} & \text{else} \end{Bmatrix}. \tag{6}$$

Early artificial neural networks are mostly composed of fully connected layers; that is, any neuron in the current layer is connected to every neuron in the previous layer. The following figure shows a three-layer artificial neural network model constructed from fully connected layers:

$$Q_j = \sum Q_{ij} + a_j Z_k = \sum Q_{jk} x_j + a_k r_i. \tag{7}$$

The batch stochastic gradient descent algorithm first divides the training set into n batches; each batch contains a part of samples, and each update process uses only one batch of training data for parameter update. Mini-batch SGD is a generalization of the SGD algorithm. The original SGD is a special case of mini-batch SGD when $n = 1$; that is, only one sample is used for each training. The literature also proves the convergence of the SGD algorithm. The expression of mini-batch SGD algorithm is as follows:

$$\theta_i = \theta_{i+1} - \mu \bullet \varepsilon (\sin \alpha, \cos \beta). \tag{8}$$

In addition to the parameter update algorithms introduced above, algorithms such as RMSprop, Adam, Adamax, and

TABLE 1: Adding trace rare earth elements of cerium group to stainless steel.

Grade	After solution treatment (b)	After solution treatment (s)	80% cold processed (b)	80% cold processed (s)
Modification 201	803	380	1890	1652
W (Cu) = 1%	726	360	1703	1503
W (Cu) = 2%	692	344	1620	1096
W (Cu) = 3%	663	335	1517	1121
304	599	270	1415	1317
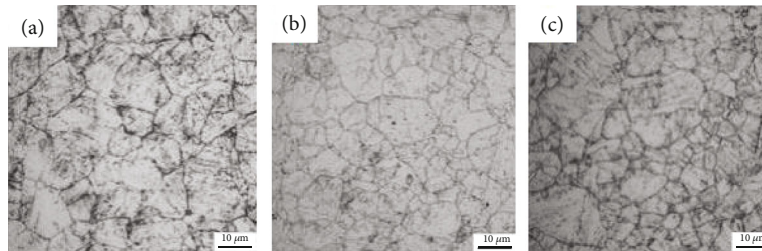
FIGURE 3: The optical morphology of original austenite of the three steels: (a) steel A, (b) steel B, and (c) steel C.

Nadam have been successively released. These algorithms ensure that deep learning models can be effectively trained. In summary, the matrix $f(x)$ required to complete the PCA dimensionality reduction goal is the matrix arranged in rows after unitizing the eigenvectors of the covariance matrix, where each row is an eigenvector of x. High-dimensional data uses the PCA algorithm to reduce the data to the Q dimension, and the value of Q needs to be determined by the percentage of the original information retained. Due to its special external electronic structure and very active chemical properties, rare earth elements will affect the thermodynamics, kinetics, crystallization process, and final electronic properties of the metallurgical steel grid during the solidification process. Compared with stainless steel without rare earth elements, the mechanical properties after adding rare earth elements have been significantly improved. The tensile strength is increased by more than 15%, the yield point is increased by about 5%, the impact strength is increased by more than 20%, and the hardness is reduced by more than 170 HV. In addition, rare earths added to stainless steel can also play a role in improving oxidation resistance and hot workability.

4. Experimental Analysis of Trace Rare Earth Elements in the Cerium Group

In order to ensure the stability of the structure after adding trace elements of the rare earth element of the cerium group to the stainless steel, a method of reducing the content of nickel and carbon and increasing the content of manganese and nitrogen is generally used. On the one hand, it stabilizes the structure of austenite. On the other hand, stainless steel has good cold forming properties, which can ultimately reduce material costs and processing costs. In recent years, in order to improve and improve the corrosion resistance and cold workability of 200 series stainless steel, expand its

application range, and achieve the purpose of replacing 304 in some application fields, the performance of 200 series stainless steel has been researched and improved mainly as shown in Table 1.

Adding copper elements and adding copper to stainless steel can greatly improve the corrosion resistance and can also increase the destructive power of the stainless steel laminate, improve the hardening effect that occurs during the cold forming process, and improve the cold forming efficiency. The research of adding copper to 201 modified stainless steel to make 204Cu stainless steel and replacing 304 stainless steel with this type of stainless steel is very successful. Due to the addition of copper to 204Cu, the work hardening rate is significantly reduced, and the cold resistance is better than 304.

Figures 3(a), 3(b), and 3(c) are the original austenite metallographic morphology diagrams of the three steel samples of A, B, and C, respectively. There are three statistics for each group of samples of A, B, and C. For the grain size data, the average size of the original austenite grains is shown in Tables 2 and 3. It can be seen from Tables 2 and 3 that the rare earth element cerium has no effect on the average size of the original austenite grains. The blank sample A, the sample B with cerium, and the sample C with cerium have no effect on the original austenite. The average size of the bulk crystal grains is basically the same. Although many documents report that the trace rare earth element cerium has the effect of refining crystal grains, the cerium added in this experiment formed a compound of cerium at about 10 ppm. Because the amount of cerium did not play a role in refining the crystal grains, it played a role in refining the crystal grains. The granular effect is still the fine-grained elements niobium, vanadium, and titanium. Marine engineering steel belongs to low-carbon microalloyed steel. Niobium, vanadium, and titanium are commonly used and effective elements for refining austenite grains in low-

Table 2: The different cooling speeds of the phase transition temperature.

Sample no.	A				B		
Organizational change	A $\longrightarrow$ P	A $\longrightarrow$ B	A $\longrightarrow$ M	Mf	A $\longrightarrow$ B	A $\longrightarrow$ M	Mf
40	669.5	431	—	295.6	—	—	—
50	630.8	438.2	—	267	—	—	—
60	—	478.1	—	259	450.3	436.3	275.2
70	—	478.2	458.3	256.6	439.7	425.7	284.2
80	—	486.7	466.9	266.4	413.1	401.9	249.4
186	—	460.8	443.9	250	430	420.8	276.8

Table 3: Test result statistics of the hardness of fracture surface.

Sample	1.5	3	4.5	6
A	34	36.5	39	41
	37.5	38	38	41
B	36.5	37.5	41	39.5
	38.5	42	42	40.5
C	40	43	41	37
	38	42.5	41.5	41

carbon microalloyed steels. Due to the high carbide stability of niobium and titanium, titanium is carbonized. The substance is slowly dissolved into the austenite when it is heated above 1000°C, and the titanium carbide particles effectively prevent the austenite grains from coarsening. The pinning effect of vanadium on the growth of austenite is inferior to that of niobium and titanium.

According to the thermal expansion curve and metallographic analysis, when the cooling rate reaches 70°C/s, the metallographic structure is bainite and martensite. Since the transformation point of bainite to martensite cannot be distinguished in the expansion curve, the martensite is observed as variable temperature martensite from the expansion curve. The phase transition amount on the thermal expansion curve is approximately proportional to the temperature change.

As shown in Table 2, the cooling rates of samples A and B at 40°C/s, 50°C/s, 60°C/s, 70°C/s, 80°C/s, and 186°C/s are combined with thermal expansion curve and gold CCT curve drawn by phase and hardness.

The line with triangles in the figure is sample A, the line with squares is sample B, and the dashed line is the transition line inferred from the experimental results. The pearlite transition zone combined with the slope of the thermal expansion curve of a-40 and a-50 in Figure 3 shows that at about 600°C, sample A has an obvious phase transition process at 50°C/s; it can be seen from b-40 at about 600°C that the turning line of sample B at 40°C/s curve is not obvious, and very little pearlite transformation occurs. The "nose tip area" of the pearlite transformation of sample B with the addition of element lanthanum and cerium shifted to the right, which improved the stability of the supercooled austenite.

As shown in Table 3, when the rare earth element is added in a few hundred ppm, when it is combined with sul-
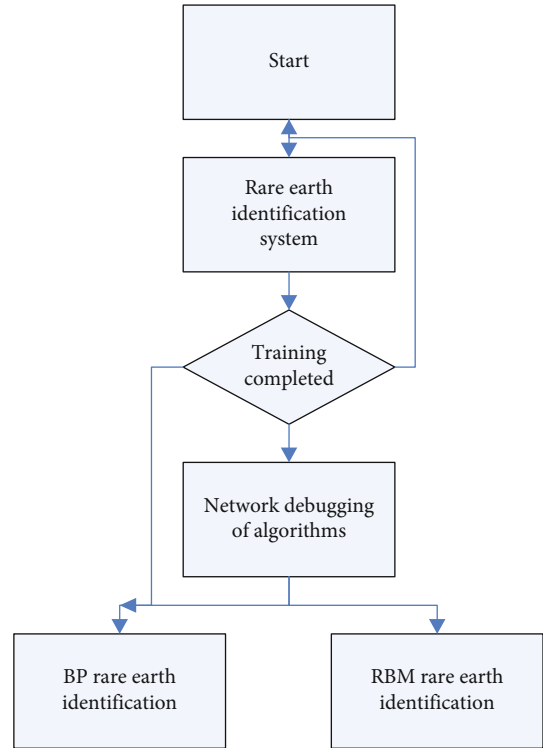
Figure 4: Test result statistics of the hardness of fracture surface.

fur, oxygen, etc., a part of it will dissolve in the matrix. When heated to austenitization, rare earth atoms will inevitably segregate to austenite grain boundaries. The segregation of rare earth atoms at the grain boundary inhibits the diffusion of carbon atoms to the grain boundary and delays the formation of cementite.

From Figure 4, we can see that when the training sample of the BP neural network increases, the learning ability and nonlinear mapping ability of the network decrease, which leads to the decline of the face recognition effect of the PCA-GA-BP algorithm. In order to overcome this shortcoming, this chapter replaces the BP neural network with the DBNs network with stronger learning ability to form the PCA-GA-DBNs network. The network first uses the PCA algorithm to process face images, reduces the amount of image data, and simplifies the network structure. During the corrosion process, the first part to be corroded is the
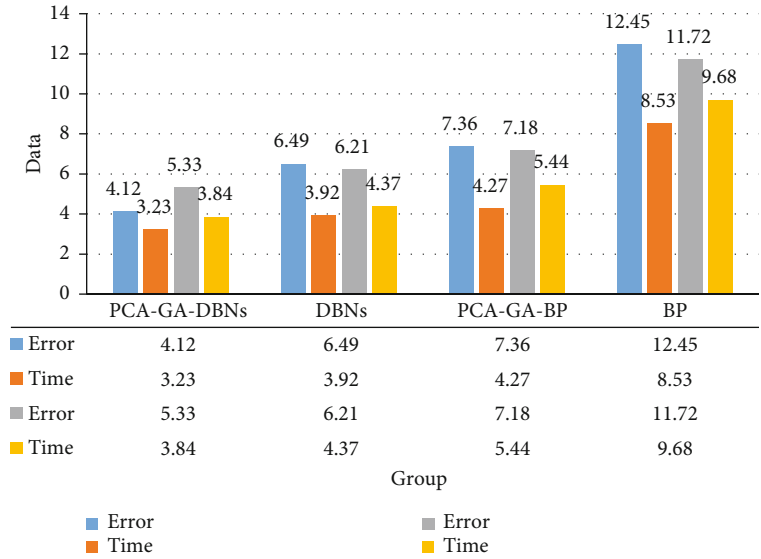
FIGURE 5: Recognition results of four comparison algorithms.

matrix around the elongated MnS inclusions, and as the corrosion progresses, a deep corrosion groove is formed on the periphery of the MnS. At the same time, the MnS inclusions themselves also appear a lot of dissolution. Increase the speed of corrosion pits to the surrounding development. In addition, MnS inclusions will be concentrated along the rolling direction during the rolling process, which seriously affects the mechanical properties of the experimental steel such as tensile strength and impact toughness.

It can be seen from Figure 5 that for all the test sets, the PCA-GA-DBNs network has the lowest average recognition error (4.61%), followed by the DBNs network (6.69%), PCA-GA-BP network (7.63%), and BP neural network (12.59%). And the recognition speed of the PCA-GA-DBNs network is significantly higher than other algorithms. The DBNs network is relatively close to the PCA-GA-BP network, and the BP neural network is the slowest. The PCA-GA-DBNs network not only has the highest recognition accuracy but also has good recognition stability. For stainless steel, the number, composition, shape, and distribution of nonmetallic inclusions directly affect corrosion resistance and mechanical properties. After adding rare earth elements to stainless steel, the composition and morphology of inclusions change, and the overall performance of the stainless steel is improved. Generally, there are two methods to determine the critical point from the extension curve: the peak method (extreme value method) and the tangent method. When using the peak method, the extreme point with a clear slope in the extension curve is used as the critical point. The advantage of this method is that it is easy to determine the critical point, but the critical point determined by this method is not the actual critical point, and the set transition start temperature is higher than the actual critical point. The final transition temperature is lower than the actual temperature. The tangent method takes the boundary point between the extension line of the straight part of the expansion curve

and the curve part as the critical point, which is closer to the actual starting temperature and ending temperature of the conversion. The sample inclusions are large composite rare earth inclusions composed of several smaller rare earth inclusions. The formation of such inclusions is due to the high adsorption of rare earth elements, which may lead to a high concentration of rare earth elements in the surrounding rare earth elements. Although this type of inclusion reduces the distribution of inclusions in the steel due to its larger size and uneven distribution and refines the steel to a certain extent, it has a significant impact on the performance of the tested steel. This experiment uses the tangent method.

From Figure 6, we can use BP network and RBM network to construct the PCA-GA-DBNs classifier and use it for face recognition. With the increase in the number of training samples, the recognition effect of each algorithm has been improved, but when the training sample is large, the face recognition accuracy of each algorithm has a small range of decline. Further analysis of the reasons can be obtained, GA algorithm in the case of a large number of training samples, the search range increases and the calculation amount increases sharply, its climbing ability is insufficient, and the defects that are prone to premature convergence are gradually revealed, thus slowing down the convergence speed of the network. This increases the probability of the network falling into the local optimum and affects the final face recognition result.

The main reason for the analysis is that the DBNs network is formed by superimposing multiple RBMs. The RBM is used to construct a classifier. During the training process, the data can be well connected from the hidden layer to the classification layer, and then, a good recognition effect can be obtained. For deep learning algorithms, different classifiers will get different recognition results. The main reason is that different classification algorithms have different training effects during network training, resulting in differences in

	RBM classifier			BP classifier		
Recognition time (s)	3.33	3.65	3.24	4.02	3.75	4.12
Training samples	29	20	16	27	22	13
Recognition error	4.33	3.87	4.97	4.87	4.28	5.43
	6.75	4.85	5.32	4.86	5.24	5.93

Number of samples

Recognition time (s) — Recognition error
Training samples —

FIGURE 6: The average recognition error of the two classifiers.
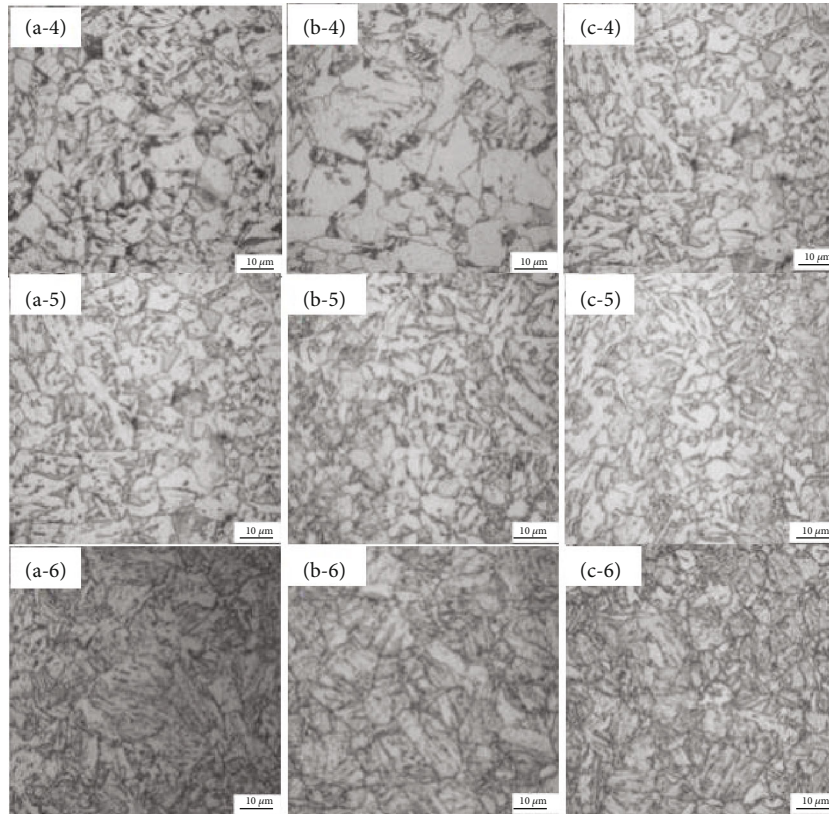
FIGURE 7: Microstructure normalizing (a-4), (b-4), and (c-4), subcritical quenching-tempering (a-5), (b-5), and (c-5), and quenching-tempering (a-6), (b-6), and (c-6).

classification capabilities between classification algorithms. But in general, after the classifier is fully trained, it can achieve better classification results.

Figures 7(a-4), 7(b-4), and 7(c-4) are the metallographic structures of the normalized state of the impact sample. The metallographic structure of the three is basically the

same in morphology and size, and they are all iron element body pearlite tissue. Figures 7(a-5), 7(b-5), and 7(c-5) are the subtemperature quenched and tempered structure, the metallographic structure of the three is ferrite+ tempered troostite, and the ferrite grains tend to be multilateral because the subtemperature quenching temperature is in the two-phase region of austenite and ferrite, partial austenitization, and the ferrite dissolved in the two-phase region has a cutting effect on the formed austenite grains and refines the austenite. The size of the tempered troostite is smaller than that of the tempered and tempered troostite. Figures 7(a-6), 7(b-6), and 7(c-6) in the quenched and tempered state are all tempered troostites. Under different heat treatment conditions, the metallographic structure of steel grades A, B, and C is basically the same. The addition of trace elements lanthanum and cerium does not change the structure of the steel, alters and changes the inclusions in the grain boundary, and improves the toughness.

Figure 7 shows the scanning morphology and energy spectrum of samples B and C. It has been determined by the nonaqueous electrolyte low-temperature electrolysis method that all lanthanum and cerium exist in the steel as inclusions. Observe the morphology of the inclusions modified by lanthanum and cerium. They are all round-shaped, and along with calcium, the elongated sulfides have been modified. (b-6) and (c-6) are the energy spectrum analysis of the inclusions. It can be inferred that the chemical composition of the inclusions is complex. Titanium can form TiC, TiN, and (TixV1-x) N phases, and niobium can also generate carbon and nitrogen of niobium. It is possible that inclusions formed by calcium, lanthanum, cerium, and aluminum combine with niobium and titanium to form composite inclusions.

5. Conclusions

With the steady growth of deep learning, artificial intelligence has gradually invaded people's lives. As an important subject in the field of deep learning and computer vision, object recognition has gradually become the research focus of researchers. This article focuses on deep learning algorithms and points out that most deep learning algorithms use the same feature map to predict the two positions of prediction and category prediction. The prediction of the category requires different contradictions in the features of the feature map. In-depth target-based target research shows that the location prediction and category prediction in the target task put forward different requirements for the feature map function. For location prediction, the function map must contain a lot of detailed information and location information, while for category prediction, the function map needs abstract semantics: function and variability. However, existing algorithms use the same feature map to predict the two tasks of position prediction and category prediction. Target detection algorithms will play a huge role in the era of artificial intelligence. This paper studies the existing target detection algorithm and proposes several improvements to the SSD300 algorithm, which improves the performance of the algorithm to a certain extent, but there are still many

problems that have not been solved. In the future, in-depth research will be conducted in the following areas. This article has improved the SSD network. The next step will try to apply the idea of separation of features to other target detection algorithm models based on deep learning and combine the characteristics of the algorithm to carry out targeted structural design for improvement.

Data Availability

No data were used to support this study.

Conflicts of Interest

The authors declare that they have no conflicts of interest.

References

[1] C. Shugui and Y. Wang, "Partial least squares-spectrophotometric determination of cerium group rare earth elements in geological samples," *Rock and Mineral Testing*, vol. 13, no. 4, pp. 249–253, 1994.

[2] L. Yan and F. Zhijie, "The application of SSD deep learning algorithm in manipulator grasping system," *Modular Machine Tool and Automated Processing Technology*, vol. 556, no. 6, pp. 72–75, 2020.

[3] G. Jun, Z. Xin, Z. Zikang, Y. Xinhao, and L. Shaoze, "Application of deep learning in oil and gas seismic exploration," *China Petroleum and Chemical Standards and Quality*, vol. 39, pp. 88–92, 2019.

[4] W. Wang, C. Tieyong, Y. Zheng, and L. Feibin, "Lecture 5: application of deep learning in saliency detection," *Military Communication Technology*, vol. 37, no. 2, pp. 92–97, 2016.

[5] Y. Tao and Z. Xi, "Application of deep learning technology in the teaching of mechanical engineering testing technology," *Education Modernization*, vol. 7, no. 19, pp. 181–184, 2020.

[6] G. Jiachen, G. Lei, and L. Lulu, "Application of object detection algorithm based on deep learning in cold rolling surface defect detection," *Metallurgical Automation*, vol. 43, pp. 25–28+33, 2019.

[7] Y. Shen, J. Yang, and Q. Shengchang, "Application of deep learning algorithm in intelligent equipment," *Equipment Machinery*, vol. 4, no. 7-9, p. 18, 2017.

[8] S. Huansheng, Z. Xiangqing, Z. Baofeng, and Y. Teng, "Vehicle target detection in complex scenes based on deep learning methods," *Application Research of Computers*, vol. 35, no. 4, pp. 316–319, 2018.

[9] W. Lu, "Application of deep learning in the field of high energy physics," *Physics*, vol. 46, no. 9, pp. 597–605, 2017.

[10] L. Xiaodong and N. Haoran, "Application of deep learning technology in disciplinary fusion research," *Frontiers of Data and Computing Development*, vol. 2, pp. 103–113, 2020.

[11] W. Shunzhi, "Research on the application of deep learning method based on GWS platform——taking a block of Daqing Oilfield as an example," *Information System Engineering*, vol. 313, no. 1, pp. 83-84+87, 2020.

[12] W. Hao, Y. Jiayong, F. Guangming, and W. Yu, "Application status and prospects of deep learning in geophysics," *Progress in Geophysics*, vol. 35, pp. 256–269, 2020.

[13] Y. Hong, L. Guoye, L. Yan, X. Rui, W. Qian, and W. Chengbin, "Research and application of deep learning in laboratory

medicine," *Chinese Journal of Laboratory Medicine*, vol. 42, no. 12, pp. 1063–1066, 2019.

[14] T. Chunxia, L. Wenhua, and L. Jing, "Analysis of rare earth elements," *Analysis Laboratory*, vol. 37, no. 2, pp. 222–248, 2018.

[15] T. Qinghua, "Plant physiological effects of rare earth elements," *Journal of Jilin Teachers College of Engineering and Technology*, vol. 32, no. 2, pp. 87-88, 2016.

[16] Z. Huaiwei, Z. Xinyao, L. Yang, T. Xiao, and L. Xingguo, "Progress in the application of rare earth elements in hydrogen storage materials," *Journal of the Chinese Rare Earth Society*, vol. 34, no. 1, pp. 1–10, 2016.

[17] T. Chunxia, "Application progress in the analysis of rare earth elements by mass spectrometry," *Analytical Laboratory*, vol. 35, no. 12, pp. 1477–1482, 2016.

[18] H. Zhi, H. Qun, Y. Hong, J. Xiaoping, and R. Yuansheng, "Effect of trace Sm addition on microstructure and mechanical properties of AZ61 magnesium alloys," *Rare Metal Materials and Engineering*, vol. 45, no. 9, pp. 2275–2281, 2016.

[19] X. Mingjie, M. Shengming, and L. Chengsheng, "The geochemical characteristics of trace and rare earth elements of the Zhaojikou lead-zinc deposit in Anhui and discussion on the genesis of the deposit," *Geology and Mineral Surveying*, vol. 3, no. 2, pp. 160–164, 2020.

[20] L. Kun, T. Chaoyang, L. Jinsong, C. Yingxiong, and L. Fei, "Sources of ore-forming materials from the Xionao lead-zinc deposit in Songtao, Qiandong: rare earth elements and carbon, oxygen, sulfur, and lead isotopic constraints," *Journal of Guilin University of Technology*, vol. 38, no. 3, pp. 365–376, 2018.

[21] L. Wu, L. Yibo, J. Wang, W. Liangying, Z. Nan, and W. Na, "Study on the pretreatment method for the determination of rare earth elements in manganese ore by high-pressure closed digestion-inductively coupled plasma mass spectrometry," *Rock and Mineral Testing*, vol. 37, no. 6, pp. 637–643, 2018.

[22] W. Zhonghua, S. Peishi, Z. Ping et al., "The strengthening effect of rare earth elements on the simultaneous desulfurization and denitrification of biological tower flue gas," *Environmental Engineering Journal*, vol. 10, no. 4, pp. 321–327, 2016.

[23] L. Zheng and Z. Jiayi, "The effect of different rare earth elements on the primary phase morphology of semi-solid aluminum alloy in chaotic convection," *Chinese Journal of Mechanical Engineering*, vol. 52, no. 16, pp. 77–85, 2016.

[24] F. Wang, G. He, S. Xiaoming, Y. Yang, and Z. Taiping, "Study on the carrier of rare earth elements in rare earth-rich deep-sea sediments in the Pacific," *Acta Petrologica Sinica*, vol. 32, no. 7, pp. 2057–2068, 2016.

[25] W. Peipei, L. Xiao, and S. Weijiao, "Determination of rare earth elements in geological samples by microwave digestion-inductively coupled plasma mass spectrometry," *Chinese Journal of Analysis Laboratory*, vol. 35, no. 2, pp. 235–240, 2016.

[26] G. Jiangfeng, Y. Duoxi, C. Jian, and C. Ping, "Geochemistry and geological genesis analysis of rare earth elements in the coal of Chongqing Longtan Formation," *Earth Science Frontiers*, vol. 23, no. 3, pp. 51–58, 2016.

[27] Y. Yang, L. Dexian, D. Wang et al., "Distribution characteristics and influencing factors of dissolved rare earth elements in surface water around ion-adsorbed rare earth mining areas," *Earth Science Frontier*, vol. 24, no. 5, pp. 172–181, 2017.

[28] L. Shiyou, C. Yingbin, Z. Guowei, W. Yanqing, and H. Ye, "Geochemical characteristics and significance of rare earth elements in the fourth member of Leikoupo Formation in West Sichuan Depression, Sichuan Basin," *Petroleum Geology & Experiment*, vol. 39, no. 1, pp. 94–98, 2017.

[29] J. Biao, G. Wu, C. Yuchuan et al., "Characteristics of trace rare earth elements in Shuangjianzishan silver polymetallic deposit in Balinzuoqi, Inner Mongolia and its genetic constraints," *Acta Geology*, vol. 92, no. 4, pp. 769–786, 2018.

[30] C. Xinxin, H. Song, and L. Zheng, "Influence of rare earth elements on the biological effects of sh_2 sweet corn seed germination," *Journal of the Chinese Rare Earth Society*, vol. 34, no. 2, pp. 229–234, 2016.

WILEY | Hindawi

Research Article

The Dominant Design of Disruptive Innovations in the 3rd-Party Online Payment in China

Lu Lu (ID),[1] **Yang Zhou** (ID),[2] **Chenxiao Wang** (ID),[1] and **Qingpu Zhang** (ID)[1]

[1]*School of Economic and Management, Harbin Institute of Technology, Harbin, 150001 Heilongjiang, China*
[2]*Business School, University of Shanghai for Science and Technology, Shanghai 200000, China*

Correspondence should be addressed to Qingpu Zhang; zzqp2000@hit.edu.cn

As a disruptive innovation on the traditional payment mode, the 3rd-party online payment has been involved in disruptive innovations featuring contextualized and modernized characteristics, but a theoretical summary is urgently needed for the dominant design of these disruptive innovations. Therefore, an in-depth case study is done with Alipay and PayPal as the subject, and it comes to elaborate four key aspects involved in the dominant design of disruptive innovations of the 3rd-party online payment. Namely, adopt new innovative derivations, create new product attributes, construct new business models, and process subsequent performance improvements. In addition, the factors that differ from the traditional disruptive innovations are also spotted, including two innovative driving forces, two new product features, and four business modes.

1. Introduction

In recent years, the demand of online payment in China is so vast that domestic and international online payment agencies compete for this "big cake." Interestingly, the world's largest online payment company PayPal Co. does not perform satisfyingly in China. On the contrary, the local inexperienced company Alipay Co. develops prosperously. Its market share has already surpassed the former incumbent China Union-Pay in Chinese online payment market. According to the statistics report of Analysys Co., titled "Shares of 3rd-party Payment Platforms in the Online Market Trading in the 1rd Quarter of 2020," by the end of the statistical period, the total online trading deals reached RMB 64.03355 trillion, among which the share of Alipay (belongs to Alipay Co.), Tencent Financial (belongs to Tencent Co.), and ChinaPay (belongs to China UnionPay) occupies 48.44%, 33.59% and 9.75%, respectively, and the share of PayPal China (belongs to PayPal Co.), however, has dropped to less than 1% [1].

Alipay Co. was no more than an unnoticeable private company at beginning. Finally, it replaced ChinaPay's incumbent position and obtained the largest share in the market of online payment. From this view, it conforms to the result of disruptive innovation proposed by Christensen, namely, the entrant company firstly focusing on a low-end market or an emerging market, gradually eroding the incumbent company's market share, and ultimately replacing their dominant position [2–7]. Is the development process of Alipay Co. indeed a disruptive innovation?

So far, the theory of disruptive innovation has been verified in many industries, such as hard disk drive industry, iron and steel industry [2], cellular phone industry [6], computer industry, retail industry, service industry, and manufacturing industry [3]. However, the existing researches focused mainly on the substantive products or the face-to-face services. The R&D, manufacturing, and marketing processes of these products or services were in a relatively stable environment. There is a lack of research on whether disruptive innovation theory is appropriate for virtual products and services in the emerging context. Meanwhile, the cases and data collected to construct or verify the theory mainly derived from companies in developed areas, e.g., the United States and Europe [8, 9]. The existing research on successful disruptive innovations does not apply to other companies in the volatile market [10]. To our knowledge, rare research explains why different companies' innovations in China turned into

different results, just like Alipay Co and PayPal Co. did. It is in need for further theoretical exploration on disruptive innovation issues in Chinese context.

The 3rd-party online payment companies suffer from more challenges in Chinese context. Firstly, technology changes rapidly, which makes the chance for technology innovation easier to fleet [11]. Secondly, information bursts drastically, which makes the concealed market demand easier to be submerged [12, 13]. Thirdly, trade virtualizes extensively, which facilitates the shift of valuable product attributes [12, 14–16]. Fourthly, Chinese online payment starts relatively late. The public awareness of online payment security is insufficient. The construction of credit system is not complete enough, causing the lack of constraints on the dishonest behaviors in online payment [17]. Fifthly, Chinese government takes regulation on the 3rd-party online payment to some extent. Only these 3rd-party payment companies which obtain the "3rd-party electronic payment license," issued by the central bank, can engage in the 3rd-party payment activities within the territory of China [18].

Chinese context is so special with general disruptive innovation theory or practice hardly explaining some cases in China perfectly. For example, the dilemma of PayPal Co. in China shows us that even the mature development mode that is verified to be successful in other places of the world may not be appropriate for Chinese context. What are the common characteristics of the successful disruptive innovations of the 3rd-party online payment in Chinese context?

Three disruptive innovation products of Alipay Co. were selected as successful cases, and three products of PayPal Co. were selected as control cases. Based on the cases, we found that the successful disruptive innovations of the 3rd-party online payment not only keep to the relative propositions of disruptive innovation theory but also adapt to Chinese context, while unsuccessful ones fail in doing so. These adaptations include the following: (1) adapt to the corresponding Chinese context when identifying the innovation derivations, (2) create new product attributes that highlight security and quickness, (3) construct new business models to fit the disruptive innovation products, and (4) process subsequent performance improvement. The empirical analysis of these assumptions constitutes the main content of this paper.

2. Theoretical Background

2.1. Corresponding Points of Disruptive Innovation Theory.
According to the disruptive innovation theory, innovations are divided into two classifications: disruptive and sustaining [2, 3]. The differences between these two kinds of innovations mainly concentrate on two aspects, technological change and customer segment, which is shown in Table 1.

Disruptive innovation derives from the incumbent's failure in dealing with the change of technology and market demand, as well as the entrant's venture on the derivations [2, 3]. According to the resource dependency theory, incumbent companies would always tend to allocate the limited resources to the customer segment that could bring them more profits [19]. Thus, they concentrate on the vaster and more profitable existing mainstream market and neglect the low-end market or new emerging market that seems less profitable at present. The more resources flow into mainstream market; the harder incumbent makes a shift to other markets. The entrant accurately utilizes incumbent's dilemma and provides products to the low-end market or emerging market. Some attributes of the product may be inferior to that of the mainstream products, but it has some attributes that low-end or emerging customers appreciate, such as cheapness, simplicity, and convenience. The mainstream customers generally do not want to use the disruptive products at beginning. So incumbents conclude that it is not a rational decision to allocate resources to the low-end market or emerging market and neglect the opportunity to invest in disruptive innovation. The entrant who implements disruptive innovations steadily improve in product performance until it meets the standards of performance demanded by the mainstream market. At that point, the incumbents' reaction to disruptive innovation is late and ineffective. The entrant finally displaces the dominant incumbents in the mainstream market.

In sum, sustaining innovations strengthen the dominance of the incumbent companies, whereas disruptive innovations enable entrant companies to replace incumbents over time. The latter, which is considered more significantly change the whole industry [2, 20], attracts more and more attention of researchers and practitioners [21].

2.2. Contextualization of Disruptive Innovation Theory.
Since Christensen firstly put forward the conception of disruptive innovation in 1997, disruptive innovation theory only has a more than 20-year-long development history. Christensen stated that there are two stages in the construction and development process of disruptive innovation theory, descriptive stage, and normative stage [22]. Each stage consists of three steps. Currently, researches on disruptive innovation mainly focused on the three steps in the descriptive stage—observation, categorization, and association. On the one hand, the constructs, frameworks, and models of the theory were constructed in some studies [2, 3, 5, 6, 8, 23]. On the other hand, anomalies are found and the constructs and hypotheses are refined by other studies [9, 24, 25].

However, those prior studies still remained in the descriptive stage. The development of theory needs to transit from descriptive stage to normative stage. The normative theory has more predictive power than the descriptive theory, for the reason that researchers building normative theory categorize different situations or circumstances in which managers might find themselves [22], and the circumstance-contingent predictive power of normative theory enables managers to know what they ought to do given their circumstance. Therefore, the further development of disruptive innovation theory tends to be contextualization [22].

This point of view is supported by the related theory in the research field of organizational management. Lawrence and Lorsch's contingency theory [26] stated that the best way to organize a company depended on the circumstances in which the company was operating. Context assimilation impedes us to understand what happens in the context different from the mainstream paradigm [27, 28]. Contextualize

TABLE 1: Differences between disruptive innovation and sustaining innovation.

	Disruptive innovation	Sustaining innovation
Technological change	(i) "Degeneration" along the existing trajectories, simplification of the existing technology, solution of the technology overload (ii) Escape from the existing technological trajectories, entrance into a new trajectory	(i) Incremental or radical improvement along the existing trajectories
Customer segment	(i) Low-end customers for whom mainstream technology was excess (ii) Noncustomers	(i) Mainstream customers who have not been satisfied by the antecedent technology

theory is helpful to identify the boundary conditions of a theory or to adjust the predictive power of a theory in the new context [29]. In addition, some researches on organizational behavior pointed that there are many special context factors in Chinese context which are very useful for understanding the Chinese organizational behavior [30].

Many local and international companies are waiting for the time to disrupt China's 3rd-part online payment market as this market is such profitable and attractive. However, the Chinese context is distinct. It is of great significance to study on the disruptive innovation of the 3rd-party online payment in Chinese context.

2.3. Dominant Design of Disruptive Innovation Theory. Utterback and Abernathy [31] first introduced the concept of Dominant design in 1975. If a dominant design wins the position on the market, then, the competitors and innovators must adhere to this dominant design if they hope to capture market share [32]. A dominant design can be a new technology, a new product or a set of key factors of different technological innovations from existing products. Dominant design may not be better than other designs, but it still can have dominating positions in the market. This may be due to network effects, technological superiority, appropriate business model, or strategic manipulation by business managers.

Before a dominant design achieves its status, companies will continuously explore its development modes. As a result, economy of scale cannot be realized during this period. After a dominant design comes out, earlier developing firms, with advantages in market shares, will soon resort to economy of scale, thus increasing the barriers to entry to and flow of the industry. That is the reason why earlier developing firms have advantages over latecomer firms [8]. As a dominant design is acknowledged only when it procures over 50% of the market sharer, it is often recognized after successfully achieving its dominance [20].

Disruptive innovation is a process of breaking the original market pattern and reconstruction of a new market structure [11]. However, before the new market is established, there will be a time when numerous disruptive innovative designs coexist. When brought to the market test, those inappropriate designs will be eliminated and a dominant design will come out. Then, the industry will continue its development under the guidance of the new dominant design [33]. The 3rd-party online payment in China is just experiencing a disruptive innovation process as above. Therefore, based on the existing theoretical framework of disruptive innova-

tion, this paper explores the dominant design of disruptive innovation in the 3rd-party online payment in China.

3. Method and Data

3.1. Research Design. Contextualization, as well as idealization, is the practical strategy of inductive reasoning, providing the logical thread when the theoretical conclusions are drawn from empirical data [34], from particulars to generalizations and from grounds to claims [35]. In contrast with idealization that is abstracted and idealized, contextualization is aimed at providing maximal access to the example and contextual detail to establish a sense of empirical authenticity [36]. Ketokivi and Mantere [34] suggested one kind of contextualization, theoretical contextualization, through which relevant propositions would be established with respect to a particular theory [34]. Namely, this method processes both explanation of the links between the empirical data and the concerns of a theory and inference based on the empirical data, which is quite applicable for our study. Meanwhile, in respect to the fact that there is few research on disruptive innovation of the 3rd-party online payment in China, this inductive method is suitable [37].

Following the process of theoretical contextualization, the specific phenomenon is analyzed based on the existing theory at first. Then, the new propositions are inducted and verified. Digging into the data of Alipay Co. and PayPal Co., we finally choose to focus on identifying the common characteristics in successful disruptive innovations of the 3rd-party online payment in Chinese context. We select a series of cases, each of which is used to confirm or deny the conclusion of any other case, which allows for theoretical replication in a multicase study [37]. The multicase study is more complex than the single-case study; therefore, it provides a more reliable result [11, 33].

3.2. Data Collection. Secondary data of Alipay Co. and PayPal Co. is collected, including related literatures, news on Internet, public performance reports, the statistical analysis reports from EnfoDesk Co., executives' blogs, and public lecture materials.

Secondary data is more suitable for this study for the reasons as follows. Firstly, the macrolevel research of management mainly relies on the secondary data and there are too numerous examples that use secondary data in organizational theory research to mention one by one [38]. The issue of disruptive innovation refers to the organizational level,

rather than the individual level. Secondly, secondary data allows for time span [38]. It needs a certain amount of time waiting for the reflection before judging out whether a potential disruptive innovation is successful or not. Some innovations may fail, while others may progress to spark an era of disruption when they reach a "good enough" point, through a relatively longer time horizon of experimentation and adaptation [39]. Disruptive innovation is a problem with time span on which secondary data has an obvious advantage. Thirdly, the disruptive innovation of the 3rd-party online payment is in a high-velocity environment. Limited by individual ability, the individuals can hardly form a clear and accurate understanding of the phenomena in this kind of environment [11], so that the first-hand data collected only by the method of questionnaires or interviews may be subjective to some extent. However, in the solution of this problem, secondary data is more objective.

We set up the research team of 4 experts who are engaged in disruptive innovation theory or practical research to analyze all of innovation activities of the two companies since they were established to now. According to the method of theoretical sampling, the successful cases are selected only if a company's market share turns up a significant increase after the advent of innovation. Finally, three disruptive innovation products of Alipay Co. are selected as the successful disruptive innovation cases. They are Alipay, Yu'ebao, and mobile wallet. And three products of PayPal Co. are selected as control cases. They are PayPal, PayPal China, and PayPal money market fund (PayPal MMF).

Different from confirmatory researches, there is a lack of normative framework for induction research [34, 40].Thus, we adopt the following method: from the numerous data, the "whole story" according to the time sequence of each case is extracted. Each case begins with the advent of the disruptive product and includes all events related to it mentioned in the data. Common characteristics are concluded through comparison within the successful cases. And the differences between successful cases and control cases are also concluded through comparison between two case groups. The variables that occur in each case are sorted out, and the tentative relationships are concluded. Then, we return to each case to verify whether these findings are valid. After repeated comparison and verification between data and hypotheses, a comparison between our findings and existing literatures is conducted, through which the "commons" and "exceptions" of disruptive innovation of the 3rd-party online payment in Chinese context are highlighted.

4. The Dominant Design of Disruptive Innovations

Existing findings declared that some disruptive innovations are facilitated by technology breakthrough, the occurred conditions of which are similar with the technology-oriented breakthrough innovation [2, 3, 23]. This kind of disruptive innovation usually occurs in the high-end market that is technology-oriented [5, 6, 23]. However, some other disruptive innovations are facilitated by the special target of customer segment. When there are customers who feel the

products in mainstream market providing them excess functions and charging them for these functions they never use or there are customers who want to pay for other functions that the existing products do not provide, companies target at these customers who consist of the special customer segment that is called "the niche market" [41, 42]. In the niche market, disruptive innovation gradually erodes to the mainstream market and finally disrupts it. This kind of disruptive innovation usually occurs in the low-end market or new market [2, 3]. In most cases, the occurred condition of disruptive innovation is mixed, based on both technology breakthrough and accurate target of the niche market.

The consistent conclusion of disruptive innovation has been reached among researches under the background of traditional industries: the disruptive innovation initially under-performs the mainstream one but is "typically cheaper, simpler, smaller, and frequently more convenient" [2, 5, 7]. Perceived safety is an important factor for consumers who purchase online service products [43]. Zhang et al. [44] analysis the disruptive innovations for microcredit mentioning efficiency and safety—the two new attributes of products. Based on a flexible business model, these new products have taken the lead in the market [44].

Disruptive innovation can be caused by a new technology or a solution and can be eventually accompanied by an alteration of the existing business model [45, 46]. Corporate decision-making, action, and value network will impact the driving force and effect of disruptive innovations [47]. It is only a one-side view to think that it means the end of disruptive innovation once the innovation is commercialized. Disruptive innovation is a process [22]. Every type of disruptive innovation put forward requires different business ecosystems to be practicable and disruptive [47]. Whether the suitable business model can be constructed at the subsequent stage of this process is also the key to the success of disruptive innovation. Disruptive innovations represent a process, and the products of disruptive innovations in the early period are less impressive than mainstream products. But constant improvements can be made to enable quick iterations of product attributes and business models for gradually taking the lead [2, 3].

Therefore, we propose the following propositions:

Proposition 1. *The successful disruptive innovations of the 3rd-party online payment are able to identify and utilize the innovation derivations in Chinese context.*

Proposition 2. *In China, the successful disruptive innovations of the 3rd-party online payment follow the new special product attributes.*

Proposition 3. *In China, the successful disruptive innovations of the 3rd-party online payment obtain sustaining profitability through constructing the suitable business model.*

Proposition 4. *In China, the successful disruptive innovation of the 3rd-party online payment obtains sustaining profit by the subsequent continuous improvement.*

5. Background Information of Each Case

5.1. Alipay. Alipay is a product of Alipay Co. launched on Oct. 18, 2003. At beginning, Alipay is only a payment mode for the e-commerce web sites, http://Taobao.com/ and http://Tmall.com/, playing a guarantee role between the seller and buyer. When the trade agreement is achieved, the buyer pays the bill using his Alipay account. However, in fact, the money does not directly go into the seller's account but is held by Alipay Co. momentarily. When the buyer receives the product, the buyer clicks the confirm button to transfer money from Alipay Co. to the seller's Alipay account provided that he is satisfied with the product. Otherwise, the buyer returns the product to the seller and asks for drawback the money from Alipay Co.

Before the advent of Alipay, the main payment modes in e-commerce are traditional post office remittance, pay on delivery, and online banking. These modes either make logistics lag behind capital or make capital lag behind logistics, which brings much more risks on either of the two parties. The 3rd-party online payment acts as a guarantor role in e-commerce, bearing the trade risks. It is of great contribution to the rapid development of e-commerce.

Alipay introduces several security measures to protect users' Alipay accounts such as digital certificate and authentication messages on cellphone. Meanwhile, it puts forward the slogan "you dare to use, I dare to compensate" to commitment that if the user happens to be stolen owing to the security problem, Alipay Co. would pay for the full loss. On the other hand, it no longer just stays to http://Taobao.com/ or http://Tmall.com/, but expanses its boundary. First, it cooperates with many other e-commerce sites, such as http://JD.com/ and http://DangDang.com/. Second, it provides payment service for public utilities, such as water electricity payment and ticket payment. Third, it provides cross-border payment service and bulk payment service.

5.2. Yu'ebao. Yu'ebao is a cooperation product of Alipay Co. and Tianhong Fund Co. launched on Jun. 17, 2013. The money in Yu'ebao accounts equals to buy the money market fund (MMF) of Tianhong Fund Co., and the profit is given to the users. However, different from traditional MMF, Yu'ebao does not charge any fees and gives daily profit. The user can use the money in Yu'ebao account to pay the bill directly or withdraw them to bank account. With Yu'ebao, there are no longer restrictions of the minimum purchase threshold and the fixed redemption date. More and more people are interested in Yu'ebao because of its profitability and flexibility. According to Souhu Net report, until the end of 2017, the total capital in Yu'ebao accounts approximated RMB 1.5 trillion and the user number had exceeded 600 million [48].

Yu'ebao account is bounded to Alipay account, which allows users to transfer the money between the two accounts freely. Alipay has a large number of users who are easy to accept Yu'ebao, which accelerates the extension of Yu'ebao. And the finance function of Yu'ebao also strengthens the user viscosity of Alipay and attracts more users to use Alipay. The two products promote each other and jointly enhance the overall competitiveness of Alipay Co.

5.3. Mobile Wallet. Mobile wallet is a mobile payment product of Alipay Co. Mobile payment refers to the new payment mode using mobile terminal to realize "paying online and experiencing offline (O2O)." Chinese virgin mobile payment market is so vast that attracts lots of companies competing for it. Many other companies launched their own mobile payment product, too: Tencent Holdings' TenPay wallet, Suning's Yifubao wallet, Baidu's Baidu wallet, etc. This intensified competition was called "the fight for the entrance of mobile payment" by Ma Yun the founder of Alipay Co.

In order to survive in this fight, Alipay Co. took several measures to improve the attributes of mobile wallet and implemented a new marketing model to commercialize the mobile wallet. Firstly, new functions such as "acoustic payment," "sweep-code payment," and "AA payment" were added to mobile wallet. Secondly, Alipay Co. decisively adopted a new marketing model to strengthen the fight for mobile payment market. It cooperated with the mobile APP Kuaidi Taxi and successively invested more than RMB 1 billion, giving subsidies to the tax drivers and passengers who use this APP and mobile wallet. Thanks to this marketing model, users knew and adopted mobile wallet in the shortest time. One professional visitor appraised it as "a disruptive marketing that is more powerful than any advertising." In just 3 months during the end of 2013 to the beginning of 2014, the user number of mobile wallet exceeds 170 million.

5.4. PayPal. PayPal is a 3rd-party online payment product of PayPal Co. It was launched in 1998 and was purchased by the famous American e-commerce company ebay Co. after which PayPal became the main payment mode on http://ebay.com/. Gradually, many other e-commerce companies cooperated with PayPal Co. one after another. As PayPal provides the payment transaction among 6 kinds of currency (USD, CAD, EUR, GBP, JPY, and AUD), it is widely used in international transactions. PayPal is commercialized by e-mail, which leads the user number becoming larger and larger, just like snowball rolling. PayPal quickly occupied the largest share of international online payment market thanks to this kind of marketing called "email virus marketing style."

However, PayPal is based on credit payment system directly. The user can only use his own credit card to transfer money to his PayPal account. So the people who do not have a credit card are unable to register PayPal accounts. On the other hand, when using PayPal in the e-commerce transactions, the buyer transfers the money directly into the seller's PayPal account. The money is received in real time. Theoretically, the seller can bring away the money without delivering the product to the buyer. So there still exists some security risk in PayPal.

When the user pays by PayPal, it does not charge any fee. But when the user receipts the money, it charges some handling fee, which makes up the main incomes of PayPal Co. The handling fee is the base fee (generally around 3%) plus 0.3 dollars. The maximum is limited within 5 dollars.

5.5. PayPal China. PayPal China is the product that PayPal Co. specially designed for Chinese users. It oriented to the

transactions by CNY, transferring CNY between PayPal China accounts and bank accounts. PayPal Co. not only adopted a free policy for the payers in China but also made an exception to accept transactions by CNY only, unlike in other places that generally adopted the multicurrency transaction. However, PayPal China still charge receivers a fee.

Since Sep. 1, 2010, the central bank, People's Bank of China, introduced "Non-financial payment services management method" to strengthen the management of nonfinancial institutions engaged in payment service. It stipulated that only the 3rd-party institutions that obtained the payment business license were allowed to engage in CNY payment service within Chinese territory. Unfortunately, PayPal China has not acquired the payment business license so far. Since then, PayPal China's shares in China's 3rd-party payment market decreased sharply. PayPal China had to find another way out. Finally, it turned to the international cross-border payment service although it is less attractive.

5.6. PayPal MMF. PayPal MMF is an open-end money market fund based on users' PayPal account balances, set up by PayPal Co. in United States in 1999. This fund mainly invests in the high-quality and short-term money market instruments denominated in dollars. The operation mode and the dividend distribution principle of PayPal MMF were similar with those of Yu'ebao, which attracted users to keep more money in their accounts. During 2005 to 2007, PayPal MMF scrambled a considerable portion of deposit money from the banks by virtue of its high customer profit, which incurs the discontent of banks. Under the pressure of the banks, the U.S. government started to implement the zero interest rate policy.

When the zero interest rate policy was unveiled in 2008, the short-term investment return rate of funds fell to 0.25% from 0.75%. The performance of all monetary funds including PayPal MMF is very low. Just before PayPal MMF closing, customers could only obtain a profit at the rate of 0.04% after deducting any fees. The scale of PayPal MMF shrank since it lost its profit advantage. According to the financial report of PayPal Co., before announcing the closure of PayPal MMF, PayPal Co. had actually already subsidized the fund for 2 years in order to maintain positive customer profit. The MMF became a burden that was getting too heavy for PayPal Co. to bear. In June 2011, PayPal Co. eventually chose to abandon PayPal MMF.

6. Case Analysis: Alipay and PayPal

Alipay, Yu'ebao, mobile wallet, PayPal, PayPal China, and PayPal MMF are all the disruptive explorations of the 3rd-party online payment. However, their performances in China are quite different. The former three perform actively, while the latter three perform unsatisfactorily in China. Summing up and comparing these cases, we draw some conclusions on common characteristics of successful disruptive innovations in Chinese online payment context. Here, we comprehensively summarized the specific hypotheses for each proposition.

6.1. New Innovative Driving Forces. The successful disruptive innovations of the 3rd-party online payment are able to identify and utilize the innovation derivations in Chinese context. Our data also confirmed these views. Firstly, in Chinese context, successful disruptive innovations of 3rd-party online payment are able to accurately and timely identify innovation derivations facilitated by technology change. The disruptiveness of Alipay reflects in that it establishes and develops along the online payment development trajectory. This process is shown from T_0 to P_a in Figure 1. The disruptiveness of Yu'ebao reflects in that it jumps from the online payment trajectory to online finance trajectory, which is shown from P_a to $P_a{}'$. The disruptiveness of mobile wallet reflects in that it jumps from the online payment trajectory to mobile payment trajectory, which is shown from P_b to $P_b{}'$. The customer number of Alipay Co. increases steadily thanks to these three disruptive innovation products, which conforms to the viewpoint of Sun et al. that disruptive innovation is able to break the S curve of innovation diffusion proposed by Rogers [49].

Secondly, successful disruptive innovations of the 3rd-party online payment are able to find out the incumbents whom they are going to disrupt and the niche markets which they are going to derive from. The incumbents and niche markets of each successful cases in our study are summed up as shown in Table 2. Moreover, the context factors facilitating these disruptive innovation derivations are also shown in Table 2.

In addition, we have some new findings. In Chinese context, disruptive innovation derivations of 3rd-party online payment also come from competitive basis change and government regulation.

There are three reasons causing the competitive basis change in Chinese online payment context. First, information is more and more symmetrical, allowing customer to access to all kinds of payment modes. When the number of available alternative payment modes that can also meet customer demand increases, customers' choice criterion transfers from the basic payment function to other product attributes. Second, the Internet security problems cannot be ignored. Since the advent of online payment, it is nothing new to read the news about hackers stealing customers' electronic accounts through Internet, which makes customers take security into consideration when choosing payment modes. Third, in China, due to the historical reasons of market development, the credit management system is imperfect. There is a lack of relevant law and policy constraints to regulate the dishonest activities in online trading. Customers feel insecure about the present payment modes and deeply demand for the new payment product with the "guarantee" attribute. Therefore, we come to the following hypothesis:

H1.1. The successful disruptive innovations of the 3rd-party online payment are able to identify and utilize the competitive basis change in Chinese context.

This finding is somewhat different from the perspective of Christensen on the relationship between disruptive innovation and competitive basis. Christensen stated that it is disruptive innovation that changes the criterion of customers' choice [2]; in other words, disruptive innovation facilitates
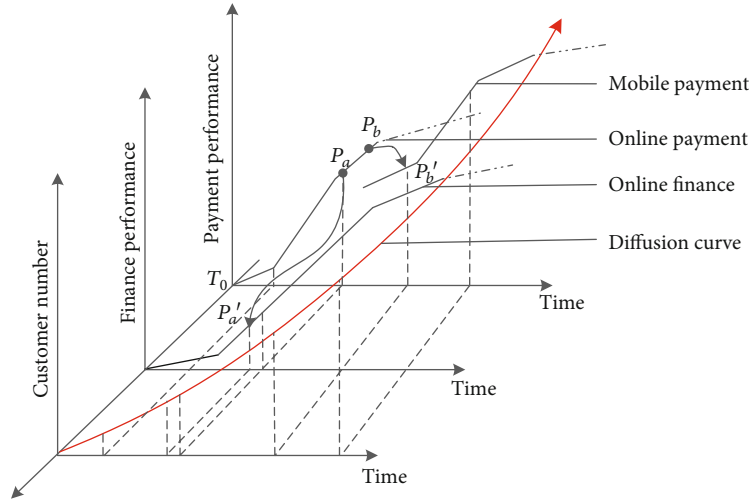
FIGURE 1: Technology change in each successful case.

TABLE 2: Related details of each successful case.

	Alipay	Yu'ebao	Mobile wallet
Incumbent	(i) Online bank payment (ii) Pay on delivery (iii) Post office remittance (iv) Bank transfer (v) Installment payment	(i) Financial products (ii) Fixed deposit (iii) Current deposit	(i) Online payment
Niche market	(i) The buyer who is worried that he pays the bill but cannot receive the product (ii) The seller who is worried that he sends the product but cannot receive the money (iii) The customer who is unsatisfied with problems of existing payment ways, e.g., security & inconvenience	(i) The customer who is unable to meet the constraints, e.g., minimum purchase amount & redemption period of financial products (ii) The customer who is unsatisfied with mobility of fixed deposit (iii) The customer who is unsatisfied with low returns of current deposit	(i) The new customer who would like to use mobile wallet (ii) The customer who is unsatisfied with inconvenience of online payment
Context factor	(i) Online payment technology (ii) Drastic information burst (iii) Extensive trade virtualization (iv) Underperforming credit management system (v) Specific government regulation	(i) Drastic information burst (ii) Extensive trade virtualization (iii) Specific government regulation	(i) Mobile payment technology (ii) Drastic information burst (iii) Extensive trade virtualization

the new competitive basis. However, our finding suggests that it is the competitive basis that could change on its own initiative and further facilitate disruptive innovation. The main reason why our finding is different from the existing ones is that the 3rd-party online payment we study on is in the emerging technology environment. Many new product attributes spring up with the emerging technology and become new competitive basis of product suppliers. Thus, suppliers are engaged in disruptive innovation based on the new competitive basis. For example, Internet security is a new product attribute of payment born with emerging online payment technology. These new attributes facilitate Alipay Co. to research and develop the disruptive product Alipay.

On the other hand, from the comparison of PayPal Co. and Alipay Co., we find that PayPal Co. (established in 1997) was established earlier than Alipay Co. (established in 2003). So, the online payment technology is no longer dis-

ruptive when Alipay Co. established. Why Alipay also show vivid disruptiveness? That is because of region segmentation owing to domestic regulation. Region segmentation, just like the high entry barrier set by the government, impedes companies to enter in without permit [50]. Chinese government has always been strictly supervising the financial market, so as to maintain the normal order of financial market and promote the construction of financial market system. People's Bank of China has launched the "Regulations for the Payment Services of Non-financial Institutions" on September 1, 2010, which stipulates that only the third-party payment institutions attaining business licenses can engage in RMB payment business in China. Therefore, many successful international 3rd-party online payment companies, such as PayPal, are unable to enter the Chinese market for the lack of this license, which greatly alleviates the fierce competition pressure in China's 3rd-party online payment market,

providing opportunities for local companies like Alipay to make disruptive innovations in China. This also explains why PayPal China was launched into the Chinese market, but its influence is far less than Alipay. Because in Chinese segment market Alipay Co. is the first to innovate in 3rd-party online payment, while PayPal Co. is just an entrant no long having the absolute advantage. In the meantime, since the 3rd-party online payment market in China is relatively independent from the international 3rd-party online payment market, innovatively introducing 3rd-party online payment technology into Chinese market also can effectively drive the disruptive innovation. Therefore, we put forward the following hypothesis:

H1.2. The successful disruptive innovations of the 3rd-party online payment are able to utilize the region segmentation in Chinese context.

Disruptive innovation is a relative phenomenon [22], which emphasizes the same innovation can be competency enhancing relative to one company and competency destroying relative to another. Our finding further develops this point of view, stating that the nondisruptive innovation in one market segmentation can still be disruptive in other untapped market segmentation caused by government regulation. It has a similar conclusion with the regulation theory. Regulation theory suggests that regulation shapes the competitive situation [9]. The competitiveness of online service innovation changes due to three reasons: basic competition, environment of competition, and competing strategy [43]. Therefore, the special competitive situation under different regulation in different areas offers motivations and abilities for entrants to conduct disruptive innovation.

6.2. New Product Attributes. Based on the analysis of Alipay, Yu'ebao, and mobile wallet, we find that the successful disruptive innovations of 3rd-party online payment all have some new product attributes in Chinese context. The new product attributes of the three successful disruptive innovation cases and the corresponding proof are summarized in Table 3.

As the summary of disruptive product attributes shown in Table 3, we find out two new attributes that Christensen did not mention: security and quickness.

The first is security. The products in online payment are the virtual currency. On the one hand, virtual trade involves credit problems. If there are no effective laws or institutional constraints to restraint the dishonest behaviors, people may choose not to conduct the virtual transaction. It also explains why PayPal Co. is prosperous in developed countries where the credit card payment system is relatively more perfect than in China. The credit system is not perfect enough at present, which makes it hard for the 3rd-party online payment companies to conduct innovations following the development mode of PayPal Co. On the other hand, virtual trading relies on the security of Internet. The thefts and frauds in online payment took place frequently in China or other countries. In such situation, it was in great need of a payment product that can guarantee the security. Thus, we put forward the following hypothesis:

H2.1. It highlights security among the competitive basis of the 3rd-party online payment disruptive innovation in Chinese context.

The second is quickness. In addition to the payment function of online payment product, people pay more and more attention to its quickness. The disruptiveness of Alipay reflects in that it makes the payment quicker than the laborious payment modes such as bank transfer. The disruptiveness of mobile wallet reflects in that it makes the payment further quicker than the online payment. The quickness of the 3rd-party online payment has become an important product attribute nowadays. Therefore, we put forward the following hypothesis:

H2.2. It highlights quickness among the competitive basis of the 3rd-party online payment disruptive innovation in Chinese context.

6.3. Suitable Business Models. Based on the analysis of Alipay and PayPal, we find that the business models including the profit mode, the operation mode, the marketing mode, and the incentive mode are very special in our cases. The details are summarized in Table 4.

Alipay, Yu'ebao, and mobile wallet all charge normal users for free, while PayPal and PayPal China do not. As "free" mode benefits users more, Alipay Co. wins more users than PayPal Co. It means that Alipay Co. dose not regard the transaction fee as a profit source. But it would like to profit from advertisement, data analysis service, and other ways after its market share is big enough. That is what the president of Alipay Co. Mr. MA Yun said "Make the market share big first. Everything will be well if the market share is big." We put forward the following hypothesis:

H3.1. The "free" mode gives more profit to customers in the subsequent stage of disruptive innovation.

Alipay Co. is the subsidiary company of Alibaba Co, the biggest B2B and B2C e-commence company in China. At beginning, the main purpose of Alipay Co. is to provide the payment service for the trades on Alibaba Co.'s e-commence sites. Alipay Co. obtains a strong customer base since it integrates to e-commence sites. Gradually, Alipay Co. wins a monopoly on payments of these sites.

Yu'ebao and mobile wallet all integrates to Alipay. In the process of their diffusion, Alipay provides them with a huge customer base, which makes them to be known and adopted by a large number of customers in a very short time. On the other side, when the performances of Yu'ebao and mobile wallet are improved, their influence rises. Then, they will in turn attract new customers who are in favor of the financial function and mobile payment function of Yu'ebao and mobile wallet to use Alipay. Finally, the user number of all the three products will rise. What is more important, Yu'ebao and mobile wallet increase the user viscosity of Alipay, which greatly enhances Alipay Co.'s competitiveness.

Comparing with Yu'ebao, PayPal MMF fails in constructing a suited business model, which facilitates its final failure. Yu'ebao inherits all payment functions of Alipay and gives customers a profit higher than the interest of current deposit interest. It allows customers to both pay and manage their money, which meet their composite demand,

TABLE 3: The abstract of disruptive products' attributes.

	Alipay	Mobile wallet	Yu'ebao
Simplicity	Online bank payment 　(i) Redundant operations between banks 　Alipay 　(i) Provide a unified platform 　(ii) Reduce operations of the banks & users 　(iii) Transfer money freely, Alipay-to-Alipay, bank-to Alipay, & Alipay-to-bank	Online payment 　(i) Pay on a computer in a certain place 　(ii) Enter redundant ID & password information 　Mobile wallet 　(i) A mobile phone bound to Alipay 　(ii) Enter a 6-letter password 　(iii) Pay through QR code & sound wave & phone number	Traditional financial products 　(i) Put collected money into profitable investment 　(ii) Allot the profit to customers proportionally, & earn the profit gap 　(iii) Set minimum purchase threshold 　(iv) Neglect the scattered customers 　(v) Bring companies few benefit increase management burden 　Yu'ebao 　(i) Target at the scattered customers 　(ii) Based on the low-cost internet platform 　(iii) Conceal minimum purchase threshold
Convenience	Post office remittance & bank transfer 　(i) Specific place & specific time 　Alipay 　(i) A device connected to Internet 　(ii) Pay anywhere and anytime	Traditional payment & online payment 　(i) Specific place or at least an internet device 　Mobile wallet 　(i) A connected mobile phone 　(ii) Pay anywhere and anyplace.	Money in Yu'ebao account can use to pay the bill and also can earn profit. 　(i) Payment function as it integrating to Alipay 　(ii) Financial function giving users some profit.
Cheapness	UnionPay 　(i) Charge a fee in interbank or across region payment 　Alipay 　(i) Charge normal users no fee	Similar to Alipay	Yu'ebao gives users more profit 　(i) Collect scattered money, & turn into a large funds cumulatively 　(ii) Negotiate with bank on the interest rates & obtaining a higher interest rate 　(iii) Allot profits to users proportionally 　(iv) Profit equivalent to long-term wholesale deposits
Security	Alipay is more secure than traditional payment 　(i) "3rd-party guarantor" 　(ii) Put forward the slogan of "you dare to buy I dare to compensate"	Traditional payment & online payment 　(i) Passwords are easily lost or stolen 　(ii) It is easy to make mistakes in operation (transfer to the wrong account) 　Mobile wallet 　(i) Specific transaction voucher 　(ii) Dechange 　(iii) Guarantee function	Traditional financial products 　(i) Fixed redemption period 　(ii) Response lag to depression of financial market 　Yu'ebao 　(i) Withdraw immediately, reducing the risk 　(ii) The scattered users' small account 　(iii) Random redemption behavior 　(iv) Low risk of mass redemption & capital shortage
Quickness	Post office remittance, bank transfer, etc. 　(i) Receive in several days or several hours 　Alipay 　(i) Receive & pay immediately	Traditional payment & online payment 　(i) Use complicated ID and password input 　(ii) On the account in a matter of hours or days 　Mobile wallet 　(i) On the account instantly	Traditional financial products 　(i) Redemption period is at least 1 month 　(ii) Fixed deposit 　(iii) Redemption period is at least 1 year 　Yu'ebao 　(i) Small amount: 2 hours 　(ii) Large amount withdraw: 1 work day

while PayPal MMF is relatively independent and has no function other than a fund. In addition, Yu'ebao also gives customers a perfect experience. The profit is calculated by compound rate every day. Customers can see the increase of money in their Yu'ebao account. It is indeed a mental stimulation giving rise to psychological satisfaction for customers, especially for the ones who are sensitive to financial profit. Therefore, we put forward the following hypothesis:

H3.2. The "integrating" mode gives more profit to customers in the subsequent stage of disruptive innovation.

The superiority of the "integrating" mode in disruptive innovation diffusion is also verified in some other industries. Sultan researched on the case of Microsoft Co. [24]. He stated, as is customary with Microsoft office, many of its products tend to integrate well with each other. The newest product SharePoint is not an exception to integrate to its famous product Microsoft office. By doing so, Microsoft Co. does not only popularize its new product quickly but also gives customers more conveniences by allowing them to save Office Word file to SharePoint.

Mobile wallet is Alipay Co.'s important product to contend in mobile payment market. However, this "blue ocean" also attracts the attention of other companies. Ma Yun called this battle "the layout war of mobile payment." In China, the most important competitors of mobile wallet are TenPay wallet. The two competitors both have strong parent

TABLE 4: Comparison of each case's business models.

	Fee (unit: dollar)	Integrating	Marketing	Incentive
Alipay	Free	Integrating to http://taobao.com/ & http://tmall.com/	Marketing through http://taobao.com/ Taking advantage of the powerful user base of http://taobao.com/	Credit incentive mode Charity incentive mode
Yu'ebao	Free Giving a profit	Integrating to Alipay	Marketing through Alipay Giving users more profit Engaging on the margins of policy Speculating through media	Member points reward Consumption bonus rewards
Mobile wallet	Free	Integrating to Alipay	Marketing through a taxi app	Consumption rewards Charity incentive mode
PayPal	Withdraw: free Payment: free Receipt: $(1.9\% \sim 2.9\%) * sum + 0.3$	Integrating to http://ebay.com/	Email virus marketing style	Discount coupon
PayPal MMF	Free Giving a profit	Integrating to PayPal	—	—
PayPal China	Withdraw: 35 Payment: free Receipt: $(2.9\% \sim 3.9\%) * sum + 0.3$	—	Marketing focus on cross-border payment	Discount coupon

TABLE 5: The continuous improvements of each successful case.

	Attribute	Items
Alipay	Security	Free SMS alerts; digital certificates; SMS verification; shield; fingerprint verification; security association with browser vendors & antivirus vendors
	Convenience	Fee for water, electricity, LPG, phone, internet, cable TV, education, traffic fine, and online game; ticket for train, film, and lottery; book for hospital and hotel; channel of charity donation; channel of student loan project
	Payment	Cooperation with 134 banks; quick payment; B2C payment; cross-border payment; large payment
Yu'ebao	Payment	Instant payment; quick transfer within 2 hours
	Profitability	Profit by day
Mobile wallet	Quickness	Bar code scanning; QR code scanning; phone number payment; sound wave payment
	Security	Advance compensation for stolen

company, Alibaba Co. and Tencent Co.; both have unique advantages in technology, mobile wallet's sound wave payment and TenPay wallet's QR code payment; both have large user bases, Alibaba's users and Tencent's users; and both are eager to occupy the leading position of the new mobile payment market. Since the advent of taxi app in 2013, mobile wallet and TenPay wallet, respectively, cooperate with two taxi apps Kuaidi and Didi. They totally took out billions of yuan to compensate the passengers and taxi drivers who use the taxi apps and pay by mobile wallet or TenPay wallet. The vigorous burning money activities are aimed at popularization of taxi apps superficially, but in fact, these are the disruptive marketing strategies of the two companies to cultivate their own mobile payment customer base. This "subsidizing" mode indeed turned to a good result. Mobile wallet survived in the battle. During that period, the payments completed by mobile wallet exceeded 2.78 billion times and RMB 900 billion in total. Since then, Alipay Co.

becomes the biggest mobile payment company in worldwide. Thus, we propose a hypothesis:

H3.3. The "subsidizing" mode enables disruptive innovation to occupy the market quickly.

In such an intensely competitive market of 3rd-party online payment, to maintain current market shares, Alipay has made each effort to enhance current users' loyalty and satisfaction, launching multiple incentive products and services. For example, Alipay has launched credit score and its auxiliary services. Alipay objectively calculates users' credit scores according to credit history, behavior no., performing ability, identity, and interpersonal connections. Alipay has raised the concept of "make credit equal to wealth," feeding back corresponding services with users' credit scores to users, such as enhancing Ant Credit Pay limit, deposit-free borrowing, cash loan, installment consumption, and pay later.

To a certain extent, Sesame Credit Score meets users' social respect needs. The credit score is a recognition of the
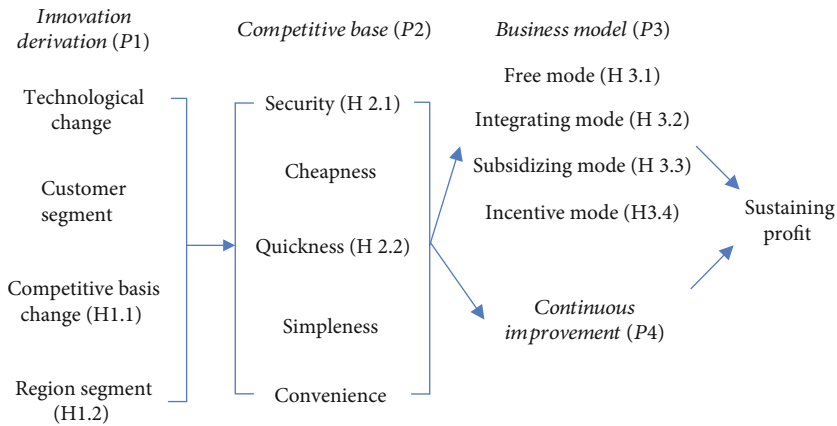
FIGURE 2: Characteristics of disruptive innovation of the 3rd-party online payment in China.

user's ability to perform credit. It not only enhances users' activity and users' stickiness but also reduces users' untrustworthy behavior. In another example, Alipay has also introduced features such as Yu'ebao. The profit of Yu'ebao is calculated at compound interest rate every day, and users can see the daily income of their Yu'ebao account. This is a psychological incentive that can significantly improve user satisfaction. Thus we, propose a hypothesis:

H3.4. The "incentive" mode enables disruptive innovation to maintain market share.

It should be noticed that the business model suited to disruptive innovation we proposed is different from the disruptive business model innovation on both the range of concept and the time innovation happens. Disruptive business model innovation generally refers to the entrant replaces the existing company's business model by a totally different model, through which it disrupts the incumbent [51]. The business model we proposed refers to the one improved or constructed to fit the disruptive innovation, no matter it is a disruptive technology innovation or a disruptive business model innovation. The business model can be either a disruptive one or a general one.

6.4. Continuous Improvement. The disruptive product usually underperforms on some product attributes at the beginning. To success in the end, it needs to improve its product attributes until they meet the "good enough" point. Alipay, Yu'ebao, and mobile wallet all implement the subsequent continuous improvement after advent. The details are shown in Table 5.

7. Conclusion

7.1. Findings. The point we focus on is the common characteristics in successful disruptive innovations of the 3rd-party online payment in China. The existing researches mainly focused on the traditional industries in the context of developed countries [8, 9] or focused on the theory descriptive stage [6, 22]. However, the situation of 3rd-party online payment in Chinese context is unprecedented and complicated, but inevitable to confront if someone wants to contend for this attractive market. Therefore, we conclude

some propositions and hypotheses, shown in Figure 2, to enrich the disruptive innovation theory in the special and important context.

Our findings confirm that some propositions in disruptive innovation theory are also valid to the 3rd-party online payment in Chinese context and propose that some new points should be added to the propositions, such as innovation derivation (P1), product attributes (P2), business model (P3), and continuous improvement (P4). Context factors of the 3rd-party online payment in China facilitate new derivations for disruptive innovation. We suggest that competitive basis change (H1.1) is not only a feature but also a driver of disruptive innovation. Moreover, disruptive innovation may also come from region segment (H1.2) causing by regulations. Under the derivations and context factors, the product attributes that customers' appreciations are no longer limited to cheapness, simplicity, and convenience. They also highlight security (H2.1) and quickness (H2.2).

In addition, we suggest that subsequent stages of disruptive innovation are also important. The suitable business model (P3) should be constructed. No matter the business model by itself is disruptive or not, it must fit the disruptive innovation. At the same time, continuous improvement (P4) should be done in order to gain the sustaining profit.

7.2. Implications. Our findings do not only confirm and enrich the disruptive innovation theory, but also give some suggestions for the emerging companies especially 3rd-party online payment when implementing disruptive innovation in China in the future.

First, companies could diversify through disruptive innovation. The single innovation diffusion curve is presented as an "S." It will always go into the low-growth stage unless it is disrupted or replaced. Gopalakrishnan and Bierly stated that sustaining innovation tends to strengthen company's competitiveness [52], while disruptive innovation tends to diversify by exploring new markets and changing the focus of the industry competition. Therefore, for the companies who are in the low-growth stage of sustaining innovation, it is not a bad choice to conduct the disruptive innovation. It can not only diversify the business scope so as to continue

the rapid-growth but also promote the mutual benefit among each business.

Second, a business model should suit to disruptive innovation. The profitability of the integration is far more important than that of innovation itself. From the cases of Alipay Co., the profit of its disruptive products is low, even negative, in quite a long time. However, Alipay Co. realizes overall profit and continuous user number increase by constructing suitable business models. It enlightens companies to have a long-term and overall sight. They should learn to pay more attention to construct suitable business models to realize overall profit as well as attaching importance to the disruptive innovation itself.

Third, the emerging technology such as data mining makes it possible to find out innovation opportunity in the information burst. The key reason why Alipay Co. is able to seize the "window of opportunity" of innovation every time refers to its large database and its ability of data mining. Ma Yun once stated that the development of Ali would go through three stages: guarantee-platform-data. No matter the 3rd-party payment or other industries, it would fail in the competition if it is unclear with the change of external environment. Therefore, it is necessary to dig into the knowledge behind the burst data, to identify the trend of disruptive technology and the change of market demand structure, and to adjust the business model and strategic sensitively in an effort to maintain competitive advantage.

8. Limitations

Our study focuses on the field of 3rd-party online payment. Although the industry of third-party online payment becomes mature, there are few studies on disruptive innovation of digital products or services. It still has its specificities. The findings concluded from 3rd-party online payment looks forward to be verified in general industry in the future research. In addition, the propositions and hypotheses are built on 6 cases of Alipay Co. and PayPal Co. Although they are outstanding enough to be representative, future studies could include more cases to find more universal conclusions.

Data Availability

No data were used to support this study.

Conflicts of Interest

The authors declare that they have no conflicts of interest.

Acknowledgments

References

[1] Analysys, "EnfoDesk analysis: shares of the 3rd-party payment platform in the online trading in the 1rd quarter of 2020," 2020, 2020, https://www.analysys.cn/article/detail/20019827.

[2] C. M. Christensen, *The Innovator's Dilemma: When New Technologies Cause Great Firms to Fail*, Harvard Business School Press, Boston, 1997.

[3] C. M. Christensen and M. E. Raynor, *The Innovator's Solution: Creating and Sustaining Successful Growth*, Harvard Business School Press, Boston, 2003.

[4] C. M. Christensen, R. M. Mcdonald, E. J. Altman, and J. Palmer, "Disruptive innovation: intellectual history and future paths," *Academy of Management Proceedings*, vol. 2017, no. 1, article 14218, 2017.

[5] S. Corsi and A. D. Minin, "Disruptive innovation ... in reverse: adding a geographical dimension to disruptive innovation theory," *Creativity and Innovation Management*, vol. 23, no. 1, pp. 76–90, 2014.

[6] V. Govindarajan and P. K. Kopalle, "The usefulness of measuring disruptiveness of innovations ex post in making ex ante predictions," *Journal of Product Innovation Management*, vol. 23, no. 1, pp. 12–18, 2006.

[7] G. J. Tellis, "Disruptive technology or visionary leadership?," *Journal of Product Innovation Management*, vol. 23, no. 1, pp. 34–38, 2006.

[8] C. M. Christensen, S. D. Anthony, and E. A. Roth, *Seeing What's Next*, Harvard Business School Press, Boston, 2004.

[9] S. Huesig, K. Timar, and C. Doblinger, "The influence of regulation and disruptive potential on incumbents' submarket entry decision and success in the context of a network industry," *Journal of Product Innovation Management*, vol. 31, no. 5, pp. 1039–1056, 2014.

[10] C. M. Christensen, M. Raynor, and R. Mcdonald, "What Is Disruptive Innovation?," *Harvard Business Review*, vol. 93, no. 12, pp. 44–53, 2015.

[11] L. J. III Bourgeois and K. M. Eisenhardt, "Strategic decision processes in high velocity environments: four cases in the microcomputer industry," *Management Science*, vol. 34, no. 7, pp. 816–835, 1988.

[12] R. Hoover, "From gutenberg to zuckerberg: disruptive innovation in the age of the internet," *Library Journal*, vol. 138, no. 20, p. 115, 2013.

[13] D. G. Sirmon, M. A. Hitt, and R. D. Ireland, "Managing firm resources in dynamic environments to create value: looking inside the black box," *Academy of Management Review*, vol. 32, no. 1, pp. 273–292, 2007.

[14] E. P. Morais, J. A. Pires, and R. M. Goncalves, "E-business maturity: constraints associated with their evolution," *Journal of Organizational Computing and Electronic Commerce*, vol. 22, no. 3, pp. 280–300, 2012.

[15] J. K. Ryan, D. Sun, and X. Y. Zhao, "Competition and coordination in online marketplaces," *Production and Operations Management*, vol. 21, no. 6, pp. 997–1014, 2012.

[16] R. Varadarajan, R. G. Srinivasan, M. S. Vadakkepatt et al., "Interactive technologies and retailing strategy: a review, conceptual framework and future research directions," *Journal of Interactive Marketing*, vol. 24, no. 2, pp. 96–110, 2010.

[17] G. Lao and S. Jiang, "Risk analysis of third-party online payment based on PEST model," in *International Conference on*

Management and Service Science, MASS 2009, IEEE Computer Society, pp. 1–5, Washington, D.C., 2009.

[18] People's Bank Of China, "Non-financial payment services management method," 2010, January 2014, http://www.gov.cn/flfg/2010-06/21/content_1632796.htm.

[19] R. Henderson, "The innovator's dilemma as a problem of organizational competence," *Journal of Product Innovation Management*, vol. 23, no. 1, pp. 5–11, 2006.

[20] Y. Chen, D. Luo, and W. Li, "Political connections, entry barriers, and firm performance," *Chinese Management Studie*, vol. 8, no. 3, pp. 473–486, 2014.

[21] S. Salomo, H. G. Gemunden, and R. Leifer, "Research on corporate radical innovation systems–a dynamic capabilities perspective: an introduction," *Journal of Engineering and Technology Management*, vol. 24, no. 1-2, pp. 1–10, 2007.

[22] C. M. Christensen, "The ongoing process of building a theory of disruption," *Journal of Product Innovation Management*, vol. 23, no. 1, pp. 39–55, 2006.

[23] S. R. Habtay, "A firm-level analysis on the relative difference between technology-driven and market-driven disruptive business model innovations," *Creativity and Innovation Management*, vol. 21, no. 3, pp. 290–303, 2012.

[24] N. Sultan, "Knowledge management in the age of cloud computing and Web 2.0: experiencing the power of disruptive innovations," *International Journal of Information Management*, vol. 33, no. 1, pp. 160–165, 2013.

[25] S. T. Walsh, "Roadmapping a disruptive technology: a case study: the emerging microsystems and top-down nanosystems industry," *Technological Forecasting and Social Change*, vol. 71, no. 1-2, pp. 161–185, 2004.

[26] P. R. Lawrence and J. W. Lorsch, "Differentiation and integration in complex organizations," *Administrative Science Quarterly*, vol. 12, no. 1, pp. 1–47, 1967.

[27] J. G. March, "Parochialism in the evolution of a research community: the case of organization studies," *Management and Organization Review*, vol. 1, no. 1, pp. 5–22, 2005.

[28] A. S. Tsui, "From homogenization to pluralism: international management research in the academy and beyond," *Academy of Management Journal*, vol. 50, no. 6, pp. 1353–1364, 2007.

[29] D. A. Whetten, "An examination of the interface between context and theory applied to the study of chinese organizations," *Management and Organization Review*, vol. 5, no. 1, pp. 29–56, 2009.

[30] P. B. Smith, "Chinese management theories: indigenous insights or lessons for the wider world," in *The Handbook of Chinese Organizational Behavior: Integrating Theory, Research and Practice*, X. Huang and M. H. Bond, Eds., pp. 502–510, Edward Elgar Pub, Northampton, Massachusetts, 2012.

[31] J. M. Utterback and W. J. Abernathy, "A dynamic model of process and product innovation," *Omega*, vol. 3, no. 6, pp. 639–656, 1975.

[32] J. M. Utterback, *Mastering the Dynamics of Innovation*, Harvard Business School Press, Boston, 1994.

[33] K. M. Eisenhardt, "Better stories and better constructs: the case for rigor and comparative logic," *Academy of Management Review*, vol. 16, no. 3, pp. 620–627, 1991.

[34] M. Ketokivi and S. Mantere, "Two strategies for inductive reasoning in organizational research," *Academy of Management Review*, vol. 35, no. 2, pp. 315–333, 2010.

[35] S. E. Toulmin, *The Uses of Argument (Updated Ed.)*, Cambridge University Press, Cambridge, 2003.

[36] S. D. N. Cook and J. S. Brown, "Bridging epistemologies: the generative dance between organizational knowledge and organizational knowing," *Organization Science*, vol. 10, no. 4, pp. 381–400, 1999.

[37] R. K. Yin, *Case Study Research: Design and Methods*, Sage, Beverly Hills, 1984.

[38] C. Zhou, "The use of secondary data in management research," in *Empirical Methods in Organization and Management Research, 2nd Edition*, X. Chen, S. Xu, and J. Fan, Eds., Peking University Press, Beijing, 2012.

[39] R. Adner, "When are technologies disruptive? A demand-based view of the emergence of competition," *Strategic Management Journal*, vol. 23, no. 8, pp. 667–688, 2002.

[40] K. M. Eisenhardt and L. J. III Bourgeois, "Politics of strategic decision making in high-velocity environments: toward a midrange theory," *Academy of Management Journal*, vol. 31, no. 4, pp. 737–770, 1988.

[41] M. T. Hannan and J. Freeman, "The population ecology of organizations," *American Journal of Sociology*, vol. 82, no. 5, pp. 929–964, 1977.

[42] H. R. Greve, "Marketing niche entry decisions: competition, learning, and strategy in Tokyo banking, 1894–1936," *Academy of Management Journal*, vol. 43, no. 5, pp. 816–836, 2000.

[43] Y. Zhou and Q. Zhang, "Disruptive online service innovation in the presence of competition among disruptors: the case of 3rd-party online payment," *International Journal of Services Technology and Management*, vol. 25, no. 3/4, pp. 384–403, 2019.

[44] W. Zhang, T. Daim, and Q. Zhang, "Understanding the disruptive business model innovation of E-business microcredit: a comparative case study in China," *Technology Analysis and Strategic Management*, vol. 30, no. 2, pp. 1–13, 2018.

[45] J. L. Bower and C. M. Christensen, "Disruptive technologies: catching the wave," *Harvard Business Review*, vol. 73, no. 1, pp. 43–53, 1995.

[46] T. Kyoseva, V. Poulkov, M. Mihaylov, and A. Mihovska, "Disruptive innovations as a driving force for the change of wireless telecommunication infrastructures," *Wireless Personal Communications*, vol. 78, no. 3, pp. 1683–1697, 2014.

[47] K. Ripley, "The role of business ecosystems in the building of disruptive innovations," in *Academy of Management Annual Meeting Proceedings*, p. 15200, Atlanta, Ga, 2017.

[48] SouhuNet, "Just now, Yu'ebao announced that the number of its users exceeded 600 million, enable customers to earn 170 billion," 2019, January 2019, https://www.sohu.com/a/287596237_100120495.

[49] J. Sun, R. Tan, and P. Jiang, "Model for roadmapping disruptive innovation based on technology evolution theory," *Journal of Mechanical Engineering*, vol. 48, no. 11, pp. 11–20, 2012.

[50] H. Chen, H. Liu, and H. Cheung, "Radical innovation, market forces, political and business relationships," *Chinese Management Studies*, vol. 8, no. 2, pp. 218–240, 2014.

[51] G. Simmons, M. Palmer, and Y. Truong, "Inscribing value on business model innovations: insights from industrial projects commercializing disruptive digital innovations," *Industrial Marketing Management*, vol. 42, no. 5, pp. 744–754, 2013.

[52] S. Gopalakrishnan and P. Bierly, "Analyzing innovation adoption using a knowledge-based approach," *Journal of Engineering and Technology Management*, vol. 18, no. 2, pp. 107–130, 2001.

WILEY | Hindawi

Research Article

Link Interference and Route Length Based Dynamic Channel Allocation Algorithm for Multichannel Wireless Mesh Networks

Zhengping Li [iD],[1] **Didi Zhang,**[2] **and Hao Shi**[3]

[1]*North China University of Technology, Beijing 100144, China*
[2]*Wireless Network RAN Research Department, Shanghai Huawei Technologies Co., Shanghai 200135, China*
[3]*The Ministry of Public Security of People's Republic of China the First Research Institute, Beijing 100048, China*

Correspondence should be addressed to Zhengping Li; lizp@ncut.edu.cn

In this paper, the theoretical analysis showed that the length of the route and the interference of links were the main factors that influence the throughput of the network. Then, a dynamic channel allocation algorithm base on the length of routes and the interference of links was proposed to enhance the system throughput. In the proposed algorithm, ant colony algorithm was used to collect the information of network, such as the length of routes and the interference of links. Then, the priority of link access channel was decided according to the collected information. The simulation results showed that the proposed algorithm could improve the whole network throughput obviously.

1. Introduction

Wireless mesh networks (WMNs), evolving from ad hoc network with comparative static characteristics, could be regarded as a wireless version of the Internet. WMN could also be involved into self-organizing network (SON) of mobile network to enhance the network performance. Compared with their wired counterparts, WMNs have a serious capacity limitation, and the interference is the primary factor that affects the capacity of the network. A multichannel WMN consists of a number of stationary wireless routers, where each route is equipped with multiple network interface cards. Usually, the number of radio interfaces is much more than the number of effective channel, which leads to the results that different and links among mesh routers and mesh clients to operate on the same channels. This case severely affects the network overall performance. Therefore, researchers had done great work with the purpose of improving the capacity of WMNs. [1, 2] proposed a centralized channel assignment concept called the first random channel assignment algorithm (FRCA). [3, 4] proposed a distributed channel allocation algorithm. [5, 6] proposed a traffic-aware channel assignment algorithm. [7] proposed

multiple channel allocation algorithm basing on the link priority determined by the information of link interference and link services. [8, 9] proposed an ant colony intelligence-based dynamic channel allocation algorithm (ACI-DCA), but the algorithm was just adept to single-hop networks, not adept to multihop networks. There are only a few algorithms involving the channel allocation problem in multihop networks. [10] came up with a cross-layer channel allocation algorithm (CLCA), which considered not only the interference of route but also the connectivity of network, and it transmitted packets on route with least interference to others. In this paper, route interference and route length-based dynamic channel allocation algorithm was proposed to combat the interference in wireless mesh networks [11, 12]. The proposed algorithm requires the information of the network topology and the interference of the link and route. This information could be collected with the ant colony-based intelligent algorithm [8]. Since CLCA studied a similar problem with the proposed algorithm, the comparison was done between CLCA and the proposed algorithm.

The rest of the paper was organized as follows. Section 2 described the ant colony algorithm. Section 3 described the mathematical derivation of the algorithm. Section 4

described the channel allocation algorithm. Section 5 showed the simulation results. Finally, in Section 6, a simple conclusion was given.

2. Ant Colony Intelligence Algorithm

Ant colony intelligence algorithm was developed by Dr. Eberhart and Kennedy. In this paper, the ant colony intelligence algorithm was modified to collect the information of the whole networks. The core idea of the ant colony intelligence algorithm was that the ant packet migrated through all the nodes in the networks as soon as possible and collect the information of the network. According to the information of the ant packet collected, some wise decisions were made to improve the performance of the network.

The ant packets were generated by the nodes in the network with a node selection algorithm. Each node generated a random number Z_i following uniform distribution between the interval $[a, b]$, and i denoted the node ID. That was $Z_i \sim U(a, b)$; $i = $ nodeID. If Z_i was smaller than a threshold number TH, this node would generate an ant packet. TH must be within the interval $[a, b]$ and could be used to control the number of ant packets in the networks. The larger of TH, the more of ant packets would be generated in the networks. After generating the ant packets, the packets would be forwarded in the networks as follows.

An ant packet started from node i and was passed to node i's neighbors. The ant packet was passed to the neighbor nodes which had been passed by ant packets with least times. If more than one neighbor node had the same least passing times, a neighbor node was randomly selected to passing the ant packet. According to the above rules, when the ant packets were transmitted in the network, they collected the information of the nodes, for example, service volume information, the interference links, and the hops of the route passed the link and some other important information. If two ant packets passed the same nodes, they could exchange the collected information through the buffer on the nodes. This process helped the ant packet passed nodes to know the whole network's information which was employed to make channel allocation.

3. Mathematical Analysis

According to the information of the network, let S denoted the whole network's throughput. i denoted the link ID and j represented the route of network, and it equaled to the integer from 1 to N, and n was the number of links in the networks. C denoted the total number of available channels. M was the number of routes in the networks.

  (i) $\tau(i)$ indicated the number of the channels occupied by link i

 (ii) $S(i)$ indicated the throughput of link i

(iii) I_i denoted the interference link set of link i

 (iv) g_i denoted the number of the interference links of link i

  (v) R_i represented the set of the route through link i

 (vi) α_i represented the number of elements in the set R_i

(vii) Q_i represented the set of links passed by route j

(viii) δ_{ij} indicated the number of channels occupied by the services of route j on link i

 (ix) G_j indicated the sum of the interference links of all the links passed by route j

  (x) Θ indicated the mean value of the interference links of the links in the network

 (xi) q_i indicated the channel accessing probability of link i

(xii) φ_j indicated the service success transmission probability of route j

(xiii) H_j indicated the number hops of route j

(xiv) $H_{\max}$ and $H_{\min}$ indicated the maximum and the minimum hops of route of the routes in the networks, respectively

 (xv) D_i indicated the mean number of hops of the routes passing link i

(xvi) F_i indicated the mean number of interference links of the routes passing link i

Supposing every link had enough services at time t, the number of available channels was not enough, so if link i did not occupy the idle channel, the channel would be occupied by other links in I_i (hypothesis ①).
So

$$S = \sum_{i=1}^{N} S(i). \tag{1}$$

Supposing each channel transmits one packet in per time unit. Then, the networks' throughput could also be denoted with the sum of the number of the occupied channels.

$$S = \sum_{i=1}^{N} \tau(i). \tag{2}$$

According to hypothesis ①, $\tau(i)$ could be denoted with I_i,

$$\tau(i) = f(I_i) = N - \sum_{k \in I_i} \tau(k). \tag{3}$$

According to equations (2) and (3),

$$S = C * N - \left\{ \sum_{k \in I_1} \tau(k) + \cdots + \sum_{k \in I_i} \tau(k) + \cdots + \sum_{k \in I_N} \tau(k) \right\}. \tag{4}$$

Let

$$S' = \sum_{k \in I_1} \tau(k) + \sum_{k \in I_2} \tau(k) + \cdots + \sum_{k \in I_i} \tau(k) + \cdots + \sum_{k \in I_N} \tau(k). \quad (5)$$

Then

$$S = C * N - S'. \quad (6)$$

S' was the total number of channels occupied by all the interference links of each link. Let the number of interference links of link i be g_i. So $\tau(i)$ would appear g_i times. Then S' could be reorganized as follows.

$$S' = \sum_{i=1}^{N} g_i \tau(i). \quad (7)$$

Supposing $g_1 \sim g_N$ was arranged in the order from small to large (hypothesis ②).

Extracting a $g_1 S$ from S', then

$$\begin{aligned} S' = g_1 S + (g_2 - g_1)(\tau(2) + \cdots + \tau(N)) \\ + (g_i - g_{i-1})(\tau(i) + \cdots \tau(N)) + \cdots + (g_n - g_{n-1})\tau(N). \end{aligned} \quad (8)$$

Since

$$(g_i - g_{i-1})(\tau(i) + \cdots + \tau(N)) = (g_i - g_{i-1})(S - \tau(1) - \cdots - \tau(i-1)). \quad (9)$$

Then equation (8) was simplified as

$$\begin{aligned} S' = g_1 S + (g_2 - g_1)(S - \tau(1)) + \cdots + (g_i - g_{i-1})(S - \tau(1) + \cdots \\ + \tau(i-1)) + \cdots + (g_N - g_{N-1})(S - \tau(1) - \cdots - \tau(N-1)). \end{aligned} \quad (10)$$

Extracting $(g_i - g_{i-1})S \, (2 \leq i \leq N)$

$$\begin{aligned} S' = [g_1 + (g_2 - g_1) + \cdots + (g_i - g_{i-1}) + \cdots + (g_N - g_{N-1})]S \\ - \{(g_2 - g_1)\tau(1) + \cdots + (g_i - g_{i-1})(\tau(1) + \cdots + \tau(i-1)) \\ + \cdots + (g_N - g_{N-1})(\tau(1) + \cdots + \tau(N-1))\}. \end{aligned} \quad (11)$$

Then equation (11) makes further simplifying

$$\begin{aligned} S' = g_N S - \{(g_2 - g_1)\tau(1) + \cdots + (g_i - g_{i-1})\tau(i) \\ + \cdots + (g_N - g_{N-1})\tau(N-1)\}. \end{aligned} \quad (12)$$

Then according to equations (6) and (12), the following formula could be gotten.

$$\begin{aligned} (1 + g_N)S = C * N + \{(g_N - g_1)\tau(1) + \cdots + (g_N - g_i)\tau(i) \\ + \cdots + (g_N - g_{N-1})\tau(N-1). \end{aligned} \quad (13)$$

Supposing the service would be successfully transmitted to the terminal (hypothesis ③).

Then

$$\tau(i) = \sum_{j \in R_i} \delta_{ij}. \quad (14)$$

According to equations (13) and (14), the following formula could be gotten.

$$\begin{aligned} (1 + g_N)S = C * N + \left\{ (g_N - g_1) \sum_{j \in R_1} \delta_{1j} \right. \\ \left. + \cdots + (g_N - g_i) \sum_{j \in R_i} \delta_{ij} + \cdots + (g_N - g_{N-1}) \sum_{j \in R_{N-1}} \delta_{ij}. \right. \end{aligned} \quad (15)$$

Links forward the services of the same route are equal, that was

$$\delta_{i_1 j} = \delta_{i_2 j} (i_1, i_2) \in Q_j. \quad (16)$$

According to equations (15) and (16), the following formula could be gotten.

$$\begin{aligned} (1 + g_N)S = C * N + \sum_{i \in Q_1} (g_N - g_i)\gamma_1 + \cdots + \sum_{i \in Q_j} (g_N - g_i)\gamma_j \\ + \cdots + \sum_{i \in Q_M} (g_N - g_i)\gamma_M. \end{aligned} \quad (17)$$

Since the number of element in the set Q_j was H_j. So equation (17) was simplified as follows.

$$\begin{aligned} (1 + g_N)S = C * N + \left(H_1 g_N - \sum_{i \in Q_1} g_i \right) \gamma_1 + \cdots \\ + \left(H_j g_N - \sum_{i \in Q_j} g_i \right) \gamma_j + \cdots + \left(H_M g_N - \sum_{i \in Q_M} g_i \right) \gamma_M. \end{aligned} \quad (18)$$

The above formula could be further simplified

$$(1 + g_N)S = C * N + g_N \sum_{j=1}^{M} H_j \gamma_j - \sum_{j=1}^{M} \sum_{i \in Q_j} g_i \gamma_j. \quad (19)$$

According to hypothesis ③, the following formula could be gotten.

$$S = \sum_{j=1}^{M} H_j \gamma_j. \tag{20}$$

According to equations (19) and (20), the following formula could be gotten.

$$S = C * N - \sum_{j=1}^{M} \sum_{i \in Q_j} g_i \gamma_j. \tag{21}$$

According to equation (21), the expectations of the throughput could be expression as follows.

$$E(S) = C * N - \sum_{j=1}^{M} \sum_{i \in Q_j} E(g_i) \gamma_j. \tag{22}$$

Since the nodes were uniformly distributed in the networks, the following formula would get:

$$\theta = E\left(g_j\right) = E(g_i) 1 \le i, j \le N. \tag{23}$$

Since H_j indicates the number of hops of route j.

$$\sum_{i \in Q_j} E(g_i) = L_j \theta \, 1 \le j \le M. \tag{24}$$

Then, according to equations (22) and (24), the following formula could be gotten.

$$E(S) = C * N - \theta * \sum_{j=1}^{M} H_j \gamma_j. \tag{25}$$

Since $G_j = \sum_{i \in Q_j} g_i$, the following formula could be gotten from equation (21).

$$S = C * N - \sum_{j=1}^{M} G_j \gamma_j. \tag{26}$$

Supposing the links and it interference links access channel with equal probability (hypothesis ④).

Then link i access channel probability could be denoted as follows.

$$q_i = \frac{1}{g_i}. \tag{27}$$

According to equation (27), the route j success transmission service probability could be denoted as follows.

$$\varphi_j = \prod_{i \in Q_j} q_i = \prod_{i \in Q_j} \frac{1}{g_i}. \tag{28}$$

According to equations (23) and (28), the expectations of the φ_j could be expressed as follows.

$$E\left(\varphi_j\right) = \prod_{i \in Q_j} \frac{1}{E(g_i)} = \prod_{i \in Q_j} \frac{1}{\theta}. \tag{29}$$

Since the number of element in the set Q_j was L_j. So equation (29) was simplified as follows.

$$E\left(\varphi_j\right) = \frac{1}{\theta^{L_j}}. \tag{30}$$

According to equation (30), the conclusion could be drawn that the shorter the route, the higher the service success transmission probability.

D_i indicated the mean number of hops that decided link i's priority, F_i indicated the mean number of interference links of the routes passing link i. So if the number of elements in the set R_i was one, then, the following formula could be gotten.

$$D_i = H_i i \in R_i, \tag{31}$$

$$F_i = G_i i \in R_i. \tag{32}$$

Supposing the link i was occupied by multiple routes, and α_i represented the number of elements in the set R_i. So, the following formula could be gotten.

$$D_i = \frac{\sum_{\beta \in R_i} H_\beta}{\alpha_i}, \tag{33}$$

$$F_i = \frac{\sum_{\beta \in R_i} G_\beta}{\alpha_i}. \tag{34}$$

When the network topology was fixed, $g_1 \sim g_N$, $H_1 \sim H_M$, N, M, and C were constant. From equation (25), conclusions could be drawn that the routes with smaller hops had a higher influence on whole network's throughput. From equation (26), the conclusion could be drawn that the routes with less interference links had a higher influence on the whole network's throughput. Since the shorter the route, the higher the service success transmission probability, the channel allocation algorithm should choose the links with shorter route access channel with higher priority, and let the links in route with lower interference access channel with larger probability, which was a benefit to improve the throughput of network.

4. The Principle of Channel Allocation

4.1. The Principle of Channel Allocation. According to the information of the network, such as the length of route, the interference of links, and the interference of the routes, links were assigned with different priority as follows:

(1) The smaller of D_i, the higher priority of link i. If $D_{x_1} = D_{x_2}$, it would be gotten that the link x_1 and the link x_2 had the same priority value. This was defined as primary priority value
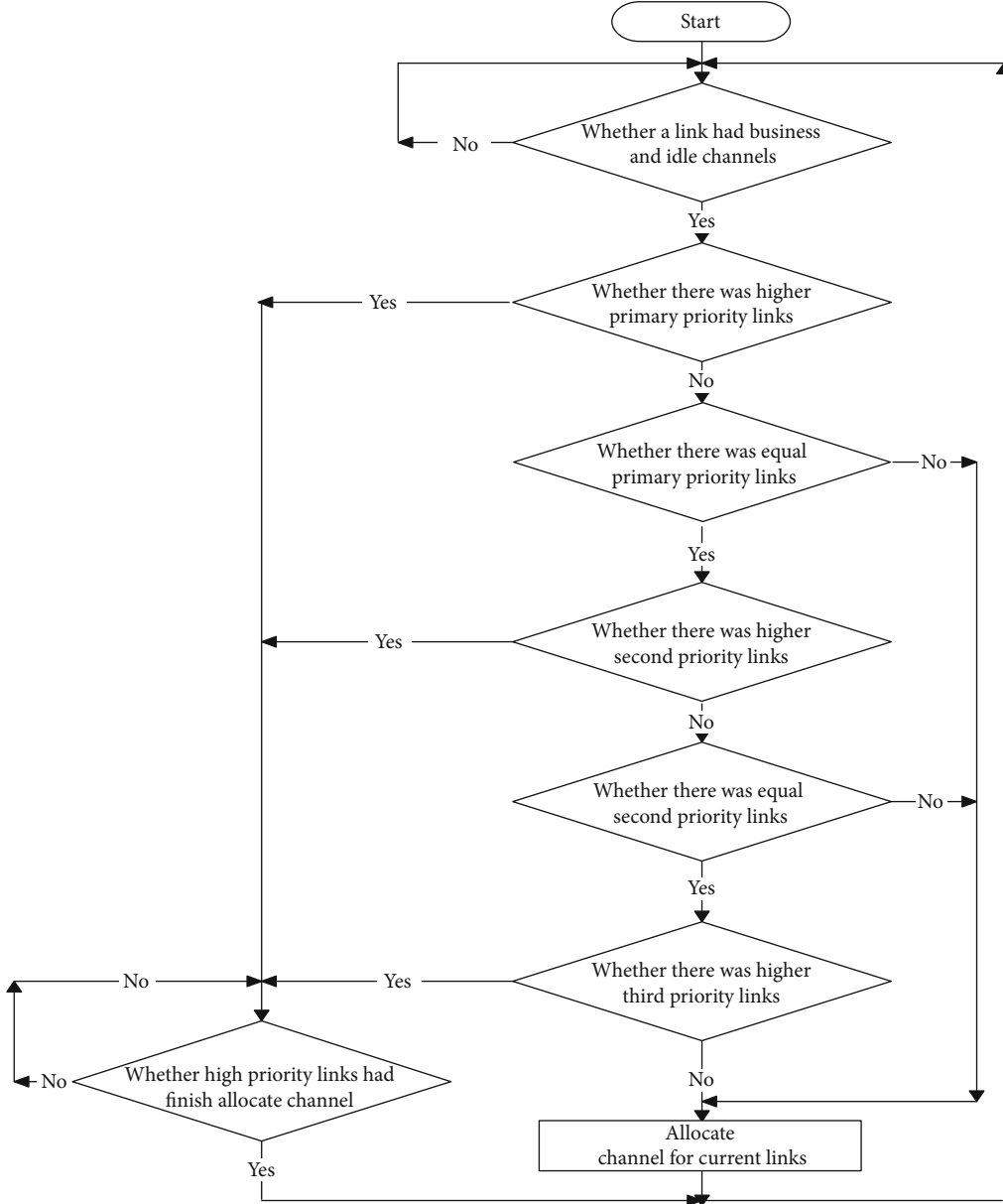
FIGURE 1: Channel allocation process of link.

(2) Among the links with the same primary priority value, the links with lesser interference links had a higher priority value. This was defined as the secondary priority value

(3) Among the links with the same primary and secondary priority value, the links with larger service had a higher priority value. This was defined as the third priority value

Considered the factors that the channel assigned with greedy algorithm which would cause the congestion in the network and increase the end-to-end delay, the routes with less interference links had a higher influence on the whole network's throughput, and the following algorithm was proposed to solve the problem. G_{max} and G_{min} denoted the maximum and the minimum value of the G_j, respectively, and H_{max} and H_{min} indicated the maximum and the minimum hops of the routes in the networks, respectively. Z_i indicated the set of the routes with hop i, and ∂_i indicated the element number of Z_i. IC_i indicated the idle channels for link i. Then defined two interference threshold $Td_1 = \sum_{i \in Z_{H_{min}+2}} G_i/\partial_{H_{min}+2}$, if the route with hops $H_{min} + 2$ was not existence then replace it with hops $H_{min} + 1$, in the same way, until the hops was H_{min} and $Td_2 = \sum_{i \in Z_{H_{min}+4}} G_i/\partial_{H_{min}+4}$ under assumption that $(H_{min} + 4 < H_{max})$, if the route with hops $H_{min} + 4$ was nonexistence then replace it with hops $H_{min} + 3$, in the same way, until the hops was H_{min}. A random value $Rd_{ij}(j \in IC_i)$ for each idle channel of link i was generated following the uniform distribution from 0 to 1 to determine

Table 1: The simulation parameters.

node_position	Node position, including horizontal and vertical coordinates, values are generated randomly.
network_range	The size of network, the upper limit of horizontal and vertical coordinates
node_number	The number of communication nodes in network
P2P_number	The number of P2P service
Server_number	The number of servers of FTP service
Client_number	The number of clients of each FTP server.
node_coverage	Indicates communication and interference radius of nodes.

whether link i access channel j ($j \in IC_i$). Pt_1 and Pt_2 were two channel access threshold values. Pt_1 and Pt_2 were gotten with the following formulas.

$$Pt_1 = \frac{G_{\max} - Td_2}{G_{\max} - G_{\min}}, \tag{35}$$

$$Pt_2 = \frac{G_{\max} - Td_1}{G_{\max} - G_{\min}}. \tag{36}$$

U_i indicated the number of available channels that could be occupied by link i, and $I_{q_{ij}}(x)$ was a indicative function of the set Rd_{ij}. So how many channels could be occupied by link i was shown as follows.

$$U_i = \begin{cases} \sum_{j \in I_i} I_{Rd_{ij}}\left(Rd_{ij} \le Pt_1\right) G_{\min} < F_i \le Td_1, \\ \sum_{j \in I_i} I_{Rd_{ij}}\left(Pt_1 < Rd_{ij} \le Pt_2\right) Td_1 < F_i \le Td_2, \\ \sum_{j \in I_i} I_{Rd_{ij}}\left(Pt_2 < Rd_{ij}\right) Td_2 < F_i \le G_{\max}. \end{cases} \tag{37}$$

4.2. The Process of Channel Allocation. At the beginning of the simulation, nodes in the network randomly generated a certain number of ant packets. The ant packets rambled in the network and collected information of the number of interference links, number of routes' hops, and the amount of service. Then, the nodes who got the information determined the priority of the link according to the collected information. The priority was updated upon the information updating by the ant packets. First, the priority values of the links were nearly zeros, links occupied idle channels if available, and there was no regulation for channel occupancy. Then, after a period of time, the link that had been passed by the ant packets would have updated priority values. Each link occupied channels according to the steps shown in Figure 1.

5. Result Analysis

5.1. Simulation Parameter. The important simulation parameters were shown in Table 1.

In the practical WMNs, the interference radius is usually longer than the communication radius. For simplicity in the simulation, supposed the interference radius is equal
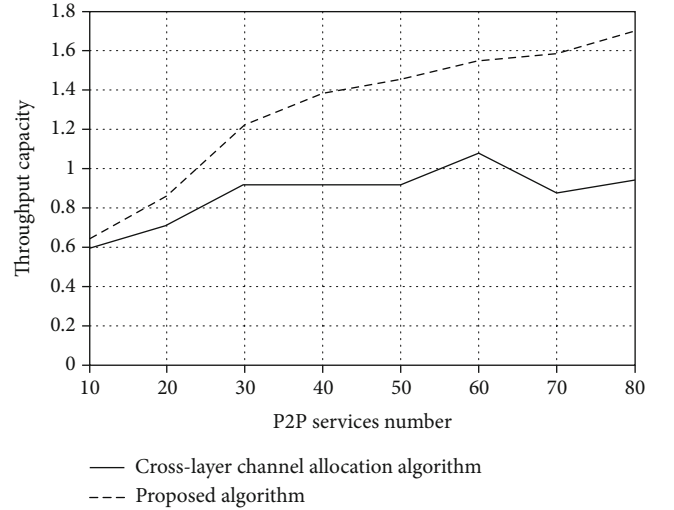
Figure 2: Relationship between P2P services number and throughput.

to the communication radius in the simulation. network_range was 500, node_coverage was 50, node_number was 100, and node_position was generated by function rand, multiplied by network_range, obtaining the horizontal and vertical coordinates. Calculating the Euclidean distance, distance $= \sqrt{(x1 - x2)^2 + (y1 - y2)^2}$, comparing with node_coverage, obtaining the neighbor relationship of nodes. According to the neighbor relationship of nodes, the links and the interference relationship among links were built. Randomly choose nodes as the peers of P2P services, servers, and clients of FTP services. Then, routes were established with the shortest path routing algorithm. In the simulation, the P2P services were transmitted at constant rate, and the FTP services were transmitted based on TCP.

5.2. Simulation Results. In order to validate the algorithm, we carried out simulation with Matlab. Randomly choose nodes as the peers of P2P services and FTP services. Then, routes were established with the shortest path routing algorithm. In the first scenario, the P2P services were transmitted at constant rate, the FTP services were transmitted based on TCP, and the pairs of nodes with P2P service were increased. As shown in Figure 2, the throughput of the proposed algorithm was higher than the CLCA algorithm. As Figure 3 shows the packet lost ratio of the proposed algorithm was lower than
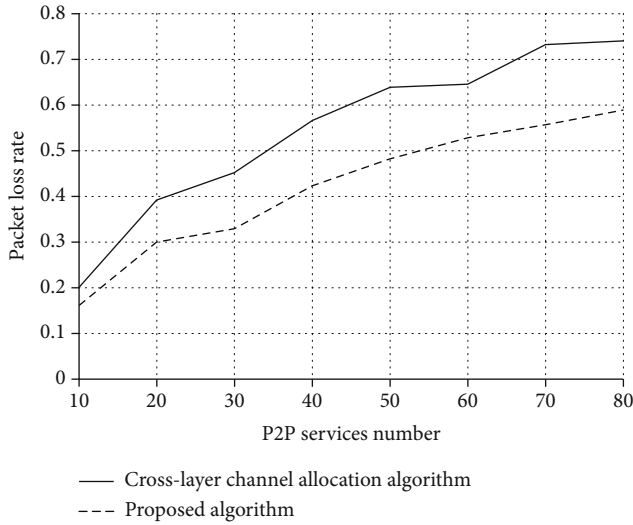
FIGURE 3: Relationship between P2P services number and packet loss rate.
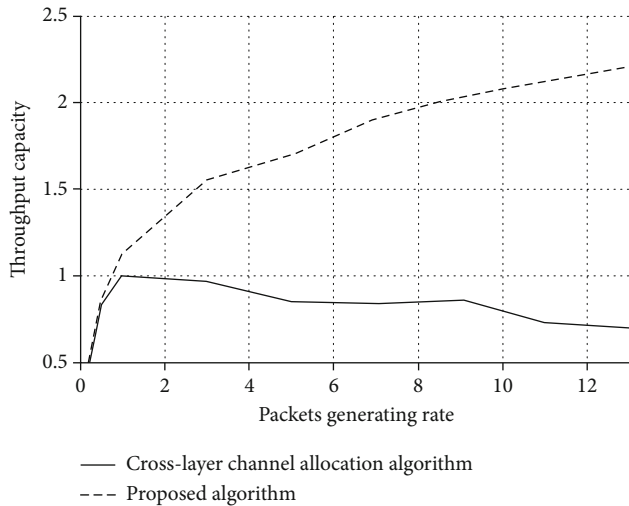
FIGURE 4: Relationship between packet generating rate and throughput.

the CLCA algorithm. Since, the short routes had a much higher packet successful transmit probability than the long routes, and the links with low interference accessed channel with high probability which was a benefit to reduce the interference of the network. Therefore, the proposed algorithm decreased interference and inclined the end-to-end delay.

In the second scenario, the nodes as the peers of P2P services are constant, the FTP services were transmitted based on TCP, and the P2P packet generating rate was 0.2 packet per simulation time and was gradually increased later. As the simulation results in Figure 4 shows that the throughput of the two algorithms increases rapidly with the packet generating rate, and the proposed algorithm increased faster than the CLCA algorithm. However, the throughput tended to decrease after reaching the peak point with the increase of the packet generating rate. Since, with the increase packet generating rate the congestion of the network is much more
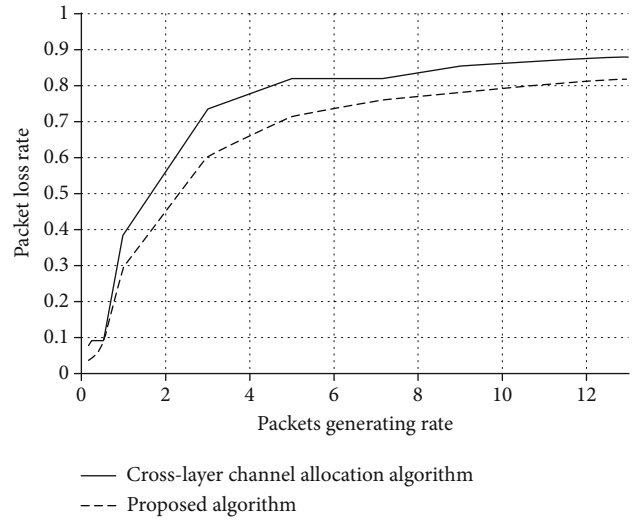
FIGURE 5: Relationship between packet rate and packet loss rate.

serious, which increase the end-to-end delay and much more packet data would be a loss. As shown in Figure 5, the packet loss ratio was increased with the packet generating rate, and the packet loss ratio of the proposed algorithm was lower than the cross-layer channel allocation algorithm.

6. Conclusion

In this paper, a dynamic channel allocation algorithm base on the length of routes and the interference of the links was proposed to reduce the effects of interference. In the algorithm, the links with the shorter route and less interference links had a higher priority to access channels, which was a benefit to reduce the packet loss ratio caused by end-to-end delay. The links with less interference links accessing channel with the higher probability, which was helpful to reduce the effects of interference and improved the throughput of the network. According to the mathematical analysis and the simulated results, the performance of the proposed algorithm was better than the CLCA algorithm.

With the high-speed development of the wireless communication, the future wireless networks would be layered and heterogeneous. How to allocation the channel in layered heterogeneous network would be investigated further.

Data Availability

The data that support the findings of this study are available from the corresponding author upon reasonable request.

Conflicts of Interest

The authors declared no potential conflicts of interest with respect to the research, authorship, and/or publication of this article.

Acknowledgments

References

[1] W. Si, S. Selvakennedy, and A. Y. Zomaya, "An overview of channel assignment methods for multi-radio multi-channel wireless mesh networks," *Journal of Parallel and Distributed Computing*, vol. 70, no. 5, pp. 505–524, 2010.

[2] S. Pollak, V. Wieser, and A. Tkac, "A channel assignment algorithm for wireless mesh networks with interference minimization," in *Wireless and Mobile Networking Conference (WMNC), 2012 5th Joint IFIP*, pp. 17–21, Bratislava, Slovakia, 2012.

[3] M. Ahmadi, Y. Zhuang, and J. Pan, "Distributed robust channel assignment for multi-radio cognitive radio networks," in *2012 IEEE Vehicular Technology Conference (VTC Fall)*, pp. 1–5, Quebec City, QC, Canada, 2012.

[4] W. L. W. Hong, F. Long, P. Xia, and S. H. G. Chan, "Distributed joint channel and routing assignment for multimedia wireless mesh networks," in *2012 IEEE International Conference on Multimedia and Expo*, pp. 404–409, Melbourne, VIC, Australia, 2012.

[5] S. Avallone, F. D'Elia, and G. Ventre, "A traffic-aware channel re-assignment algorithm for wireless mesh networks," in *2010 European Wireless Conference (EW),*, pp. 683–688, Lucca, Italy, 2010.

[6] S. Avallone, G. D. Stasi, and A. Kassler, "A traffic-aware channel and rate reassignment algorithm for wireless mesh networks," *IEEE Transactions on Mobile Computing*, vol. 12, no. 7, pp. 1335–1348, 2012.

[7] K. Yonggyu, J. Doyoung, K. Youngdoo, C. Sungchang, and M. Joongsoo, "Efficient interference-aware channel allocation in multi-radio wireless mesh networks," in *2012 14th International Conference on Advanced Communication Technology (ICACT)*, pp. 920–925, Poenix Park, PyeongChang, Korea(South), 2012.

[8] L. ZhengPing, S. Hao, and L. Wenkai, "Ant colony intelligence based cognitive wireless mesh network dynamic channel allocation algorithm," *ICIC Express Letters*, vol. 8, no. 10, pp. 2877–2883, 2014.

[9] B. Han, J. Li, J. Su, and J. Cao, "Self-supported cooperative networking for emergency services in multi-hop wireless networks," *IEEE Journal on Selected Areas in Communications*, vol. 30, no. 2, pp. 450–457, 2012.

[10] L. Yanbing and D. Guoping, "Cross-layer design for channel assignment with connectivity maintenance in wireless mesh networks," in *In 2011 International Conference on Mechatronic Science, Electric Engineering and Computer (MEC)*, pp. 1996–2000, Jilin, China, 2011.

[11] D. Jiang, Y. Xu, H. Yang, and Z. Lv, "Collaborative multi-hop routing in cognitive wireless networks," *Wireless Personal Communications*, vol. 86, no. 2, pp. 901–923, 2016.

[12] N. Zhang, N. Cheng, A. T. Gamage, K. Zhang, J. W. Mark, and X. Shen, "Cloud assisted HetNets toward 5G wireless networks," *IEEE Communications Magazine*, vol. 53, no. 6, pp. 59–65, 2015.

Research Article

Medical Monitoring and Management System of Mobile Thyroid Surgery Based on Internet of Things and Cloud Computing

Heng Kong [ID] [1] **and Jixin Chen** [2]

[1]*Department of Thyroid and Breast Surgery, Baoan Central Hospital of Shenzhen, The Fifth Affiliated Hospital of Shenzhen University, Shenzhen, 518102 Guangdong, China*
[2]*Department of General Surgery, Shenzhen University General Hospital, Shenzhen University Clinical Medical Academy, Shenzhen, 518000 Guangdong, China*

Correspondence should be addressed to Heng Kong; generaldoc@126.com

With the rapid development of the Internet of Things and cloud computing technologies, the Internet of Things technology based on comprehensive perception and interconnection and cloud computing based on virtualization, dynamic resources, and parallel computing have become the driving force for the innovation and development of informatization and intelligence. The cloud-based Internet of Things mobile medical is an ecosystem of health information and medical information, with the medical Internet of Things at its core and highly mobile and highly shared information. Therefore, in the context of in-depth research on mobile medical care, research on mobile postoperative thyroid monitoring and management systems based on the Internet of Things and cloud computing is a practical tool for promoting the development of mobile medical systems. *Monitoring and Management*. In this experiment, 48 cases of patients undergoing thyroid surgery were selected from a hospital. The experimental group was informed by the experiment that they need to be equipped with sensors. The control panel and GPS positioning module are used to obtain the exact position of the patient at the first time. The loading of the sensor is agreed by the patient and the patient's family. Afterward, the control group will not be processed. It will conduct functional tests and software performance tests on the mobile medical monitoring and management system and analyze the satisfaction of medical staff with the mobile medical monitoring and management system. Experiments have proved that the cloud computing medical monitoring and management system is used to obtain the exact location of the patient in the first time, and the response time needs to be shorter. The response time of the system increases with the increase of the number of sensors ($P < 0.05$), which shows that the mobile medical monitoring and management system is essential for medical care and medical care. Obtaining the exact position of the patient for the first time is of great importance for the successful rescue of the patient.

1. Introduction

With the continuous development of the Internet of Things, cloud computing, and smart hardware technologies, and the continuous popularization of mobile medical monitoring equipment, more people tend to use mobile smart terminals to obtain services. It can be seen from this that the products of the information age such as big data and cloud computing have had a large impact on the architecture of traditional medical systems. On this basis, the state proposed medical information as an important direction for the development of medical physique reform. With the trend and encouragement of national policies, more and more service providers can provide medical services, allowing increasingly people to access high-quality medical and health services.

With the development of modern society and economy, the quality of life has gradually improved. People have realized the importance of health and daily maintenance. People have gradually paid attention to physical exercise, improved dietary structure, and paid attention to daily health data. Patients no longer want to be limited to the traditional mode of registering a doctor. People hope that medical services can

be provided through multiple channels and multiple medical modes. Mobile medical monitoring can share the hospital's original information system with greater mobility and flexibility. The mobile application can simplify the work process and improve the overall work efficiency. Another advantage of mobile applications is that it can reduce medical errors and can effectively reduce information asymmetry in the implementation of nursing handover, improper time management, patient information collection errors, or patient care errors.

After half a century of exploration in the field of mobile medical monitoring at home and abroad, many achievements have been made in sensors, damage identification, safety assessment, and system integration. Edafe et al. reviewed the current wearable mobile medical monitoring system, focusing on textile and wireless sensor network-based devices. These monitoring systems are composed of various types of small physiological sensors, transmission modules, and processing capabilities. In addition, the wearable mobile medical monitoring system has the potential to change the medical model by providing inexpensive, wearable, and unobtrusive solutions for continuous medical health monitoring. It is hoped that the current survey can provide guidance for future research improvements and provide reference for current achievements and maturity. These systems can also be used as an effective method to identify the technical advantages and disadvantages of the current state of the art in wearable device solutions. However, the experimental results lack more data support so that the wearable mobile medical monitoring system cannot be convincing [1, 2]. von Ahnen et al. proposed a self-learning scheme for patient activity recognition. In this scheme, the patient only needs to carry an ordinary smartphone containing ordinary motion sensors. After collecting data in real-time through a smartphone, we use coordinate system transformation to preprocess the data to eliminate the influence of the phone's orientation. Then extract a set of robust and effective features from the preprocessed data. Since patients may inevitably perform various unpredictable activities without prior knowledge in the training data set, we propose a self-learning activity recognition scheme. This program determines whether there are prior training samples and labeled categories in the training pool. These samples match the unpredictable activity data well. However, because ordinary smartphones often forget to bring data, the data is not comprehensive. The self-learning activity recognition program does not immature [3]. Mchenry explained the research status of the medical monitoring systems from the aspects of mobile medical treatment, physiological index testing equipment, medical institution-level monitoring system, home monitoring system, etc. From the three aspects of health monitoring cloud platform, wearable medical equipment, and human sensor network, the research hotspots of medical monitoring system are analyzed. Pointed out the problems of the medical monitoring system based on the Internet of Things and predicted its future development. However, his research did not clearly propose how to solve the problem of the medical monitoring system, and the overall research lacks data support [4, 5].

This article is to study the medical monitoring and management system after mobile thyroid surgery. On the basis of summarizing the existing Internet of Things and cloud computing, a mobile medical monitoring and management system is established. The basic physiological parameters of patients after thyroid surgery are collected through sensors, and these basic parameters are collected. The normal parameters are preprocessed, then, this processed data is entered into the cloud computing platform via the wireless sensor network, and the game data is analyzed and processed on the cloud computing platform. Use cloud computing technology to compare stored medical records and medical information, find similar physiological parameters from large amounts of data to realize early warning of disease progression assess and monitor risks, and help users create a differentiated medical service mechanism.

2. Mobile Medical Monitoring and Management System Based on Internet of Things and Cloud Computing

2.1. Conceptual Design of Each Functional Sublayer of the System

2.1.1. Field Sensor Network. The design of the cloud computing system should fully consider the future development. It will be used as a basic platform for the deployment of related software, rather than a simple management system. The subsequent research and development upgrades of users or enterprises will be carried out on the basis of this platform. In the technical architecture, advanced application platforms and development platforms must be adopted, and each relevant application function system needs to realize the corresponding specific business functions [6, 7]. Service-oriented, component-oriented technical frameworks and concepts should be adopted between systems, which is conducive to future business formulation or reorganization and development, and at the same time, facilitates service management. The system must have a certain degree of self-adaptability to prepare for future changes in the environment and requirements. Scalability is mainly reflected in that the system should be easy to expand and upgrade, and the scalability of the system can be improved by adopting distributed design, modular design of the system structure [6, 8]. This system should fully consider the changes in user visits and network environment and make adjustments and optimizations in the physical architecture at the right time. Since this system is positioned as the basic platform of structural health monitoring, it must meet the requirements of system target changes. The schematic diagram of the overall system scheme is shown in Figure 1.

At present, the development direction of wireless sensors is to have both data collection and analysis functions. However, due to the limitation of power consumption of wireless sensors, its analysis and processing functions are relatively simple and inconvenient to upgrade. After constructing the structural health monitoring Internet of Things, the function of the sensor should be relatively simple, that is, to sense the monitored amount and transmit it upwards [9, 10]. There are
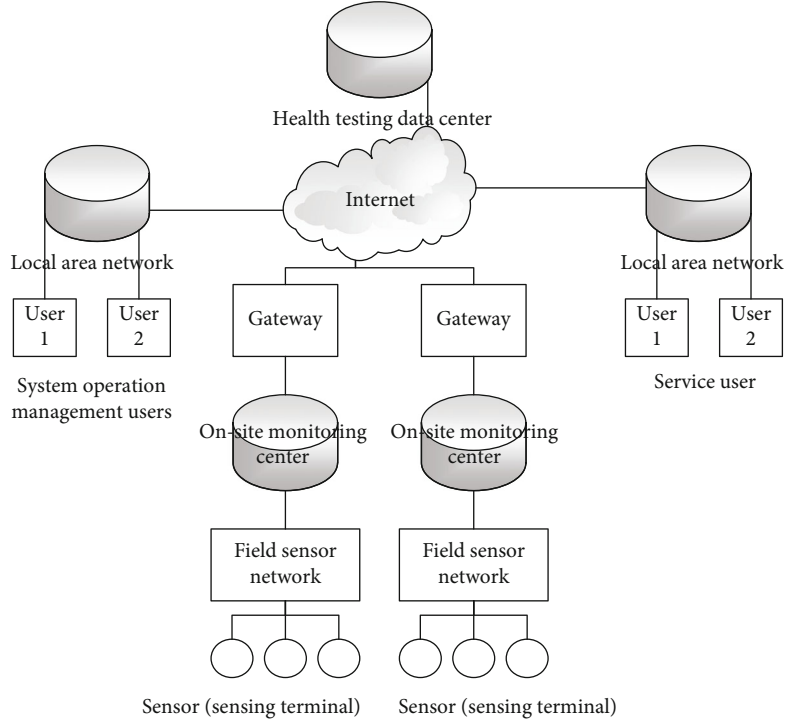
FIGURE 1: Schematic diagram of the overall system scheme.

a variety of short-range wired and wireless networking technologies, and different structures can use appropriate networking technologies to build on-site sensor networks according to specific design requirements, mainly considering the amount of monitoring, network coverage, network capacity, transmission rate, and security reliability and economy are required. No matter what kind of networking technology is adopted, the relevant information must eventually be gathered to the on-site monitoring center, so that the information can be transmitted to the data center; at the same time, the on-site monitoring center must also meet the control of each sensor node [11, 12]. At present, the typical networking technology of wireless sensor networks is ZigBee network. In terms of wired sensor networks, fieldbus is a more typical networking technology with more applications.

2.1.2. Management System Architecture Design. The cloud computing platform system application is composed of multiple functional parts. To facilitate the operation, management, and maintenance of the system, the solution has designed a complete and visualized management subsystem for the operation and maintenance personnel to ensure the normal operation of the system, and at the same time, it is convenient for users to connect and maintain use resources in the cloud [13, 14]. The economics of the system means that the revenue of the system is greater than the total cost of expenditure. Among them, the cloud platform system expenditure is mainly composed of operation and maintenance costs and investment costs for development, and the system application design should provide users with corre-

sponding economic benefits [15, 16]. In the process of system design and development, some open source software and technologies should be selected to reduce development costs. Practicability requirements meet the operability and user friendliness of the cloud platform system, provide users with convenient and reliable services, include whether the system platform can operate normally after the completion of the construction, and provide safety guarantees for real-time monitoring and safety assessment of the structure [17, 18]. System management users interact with the data center database server through the C/S mode, and external service users access the WEB server through the B/S mode to interact with the data center database server, as shown in Figure 2.

2.2. Vibration Signal Preprocessing

2.2.1. Eliminate Trend Items. Assuming that the sampled data received by the structural health monitoring cloud is a digital signal after calibration conversion, the calibration conversion is completed by the field data acquisition base station, and the deviation from the baseline contained in the signal is a trend item of the signal, which needs to be removed [18, 19]. It is a more common method to use the least square method to eliminate the trend item:

$$Y(t) = X(t) - Z(t). \tag{1}$$

In the formula, $X(t)$ is to read the sampled data, the polynomial function fits $X(t)$ to obtain the polynomial coefficient vector a of the trend term, and the estimated value $Z(t)$ of the polynomial trend term at each sampling point determined by
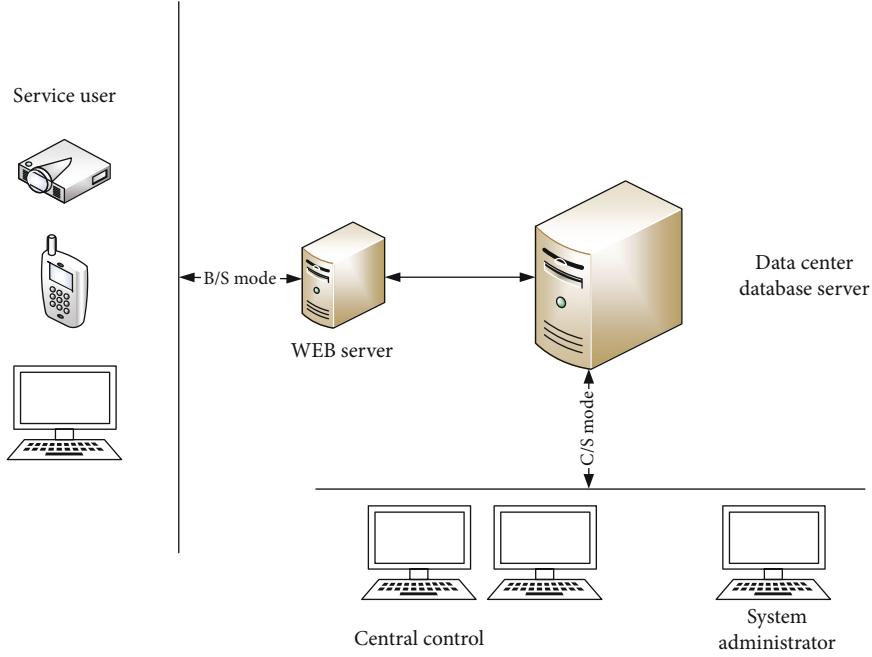
FIGURE 2: C/S and B/S hybrid architecture of medical monitoring management system.

a. In the processing flow, through coarse-grained correlation based on the analysis, it is obvious that the adjacent steps are flow-related and cannot be executed in parallel within the task.

2.2.2. Smoothing. The vibration signals collected by the health monitoring system are generally mixed with noise components and are affected by high-frequency component noise:

$$P(y_i|X_i) = \pi(X_i)^{y_i}[1 - \pi(X_i)]^{1-y_i}. \tag{2}$$

Here, $X_i = [x_{i1}, x_{i2}, \cdots, x_{in}]$ $i = 1, 2, \cdots, n$, the maximum likelihood function of n sample observations is

$$L(\beta|X, y) = \prod_{i=1}^{n} [\pi(X_i)]^{y_i}[1 - \pi(X_i)]^{1-y_i}. \tag{3}$$

The log-likelihood function is

$$l(\beta) = \sum_{i=1}^{n} \{y_i \ln [\pi(X_i)] + (1 - y_i)[1 - \pi(X_i)]\}. \tag{4}$$

Too many smoothing times will significantly reduce the peak value of the spectrum curve, make the body shape wider, and even lead to larger recognition errors.

2.2.3. Infinite Impulse Response IIR Digital Filter. The purpose of filtering time-domain method and frequency-domain methods is to achieve signal frequency selection, filter out designated frequency components, and retain the required frequency components [20]. The filtering expres-

sion of the IIR filter can be defined as the following difference equation:

$$y(n) = \sum_{k=0}^{M} a_k x(n - k) - \sum_{k=1}^{N} b_k y(n - k). \tag{5}$$

In the formula, $x(n)$ is the input time-domain signal sequence; $y(n)$ is the output time-domain signal sequence; a_k, b_k is the filter coefficient; M is the number of zeros of the filter system transfer function; N is the filter order. The IIR filter not only inputs the finite term of the original signal for calculation but also considers the output term before the filter. Clearly, the calculation and execution of the filter are realized through the loop body, and each loop outputs a filtered value. The output result of the previous loop needs to be used as the input of the subsequent loop, and the loop has relevance [21, 22].

2.2.4. Time-Frequency Domain Processing of Vibration Signals

(1) Time Domain Processing. The random vibration signal has no obvious regularity. Let $\{x(k)\}$ be the discrete data sequence of the random vibration signal, the length is N, and the sampling time step is Δt. The mean value of the random vibration signal is estimated as:

$$\mu_x = \frac{1}{N} \sum_{k=1}^{N} x(k). \tag{6}$$

For this kind of averaging, the original data segment can be divided into several subdata segments of equal length to

obtain the average value, respectively, and then the calculation results of the subdata segments are summed and averaged to obtain the average value estimate. The processes of averaging the data segments are not related and can be executed in parallel, and then the results of the parallel execution are summarized to obtain the final result. For the mean square estimate:

$$\psi_x^2 = \frac{1}{N} \sum_{k=1}^{N} x^2(k). \tag{7}$$

The calculation process is the same as the mean estimation. Variance estimation:

$$\sigma_x^2 = \frac{1}{N} \sum_{k=1}^{N} [x(k) - \mu_x]^2 = \psi_x^2 - \mu_x^2. \tag{8}$$

The calculation process can be decomposed into two unrelated subtasks to calculate the mean and mean square estimation. The parallelism of its task is embodied in that it can be decomposed into subtasks that can be executed in parallel, and its expression is

$$R_{xx}(k) = \frac{1}{N} \sum_{i=1}^{N-k} x(i)x(i+k). \tag{9}$$

It can be seen from Expression (9) that the calculations of the instantaneous function values of the autocorrelation function are not related and can be executed in parallel. Since the calculation of the autocorrelation function also takes the single-channel random vibration time-domain signal as the input, the effect of parallel calculation on the calculation efficiency is not considered here.

$$R_{xy}(k) = \frac{1}{N-k} \sum_{i=1}^{N-k} x(i)y(i+k). \tag{10}$$

The calculation of the cross-correlation function is also a two-level nested loop body calculation task, but its input signal is sampled data from two different channels, and the rest is the same as the calculation of the autocorrelation function [23].

In the structural health monitoring system, some physical quantities sometimes need to be acquired by transforming other physical quantities. For example, the speed signal or displacement signal can be obtained by the acceleration signal (twice) integration. The calculation and evaluation formula is

$$y(k) = \Delta t \sum_{i=1}^{k} \frac{x(i-1) + x(i)}{2}. \tag{11}$$

The calculation of the value of each discrete point of the signal after integration is not related and can be calculated in parallel. Since its input is a time series, parallelism here is

of little significance to distributed computing, and it can only be used to increase the running speed of the time-domain integral calculation within the node.

(2) Frequency Domain Processing. Ultrasound images have high requirements for edge detail and are nonstationary signals that cannot be met by traditional Fourier transform-based signal denoising methods. Ultrasonic speckle suppression and denoising methods can be broadly divided into spatial area local statistical filtering, anisotropic diffusion filtering, and wavelet transform-based filtering. The auto-power spectral density function is the Fourier transform of the autocorrelation function, namely,

$$S_{xx}(k) = \frac{1}{N} \sum_{n=0}^{N-1} R_{xx}(n)e^{-i2\pi kn/N}, \tag{12}$$

$$S_{xy}(k) = \frac{1}{N} \sum_{n=0}^{N-1} R_{xy}(n)e^{-i2\pi kn/N}. \tag{13}$$

The power spectral density function can be used as the input data of some specific modal parameter identification methods, namely,

$$H(k) = \frac{S_{xy}(k)}{S_{xx}(k)}, \tag{14}$$

$$C_{xy}(k) = \frac{|S_{xy}(k)|^2}{S_{xx}(k)S_{yy}(k)}. \tag{15}$$

In the formula, $S_{xx}(k)$ means self-power spectrum estimation of random vibration excitation signal; $S_{xy}(k)$ means cross-power spectrum estimation of random vibration excitation and response signal. The left is used for the coherence function to evaluate the quality of the frequency response function estimation result [24, 25].

3. Experimental Design of Mobile Medical Monitoring and Management System

3.1. Test Subject. In this trial, 48 patients undergoing thyroid surgery in a hospital from 2019 to 2020 were selected and randomly divided into two groups with 24 people in each group. The experimental group was informed by the experiments that it needed to be equipped with sensors and used the control panel and GPS positioning module for the first time. Obtain the exact location of the patient at a time, and load the sensor with the consent of the patient and the patient's family; the control group will not be processed. The general information of these 48 patients is presented in Table 1. For functional tests and software performance tests of the mobile medical monitoring and management system, and at the same time, analyzing the satisfaction of the medical staff with the mobile medical monitoring and management system, the research tool used in the questionnaire survey method is the questionnaire, which uses the Likert

TABLE 1: General information of the two groups of patients.

Group	Number of cases		Years	Course of disease	Years of education
	Male	Female			
Experiment group	16	8	43.27 ± 11.21	7 ± 5.5	8 ± 5.12
Control group	14	10	41.98 ± 14.02	9 ± 3.4	9 ± 4.57
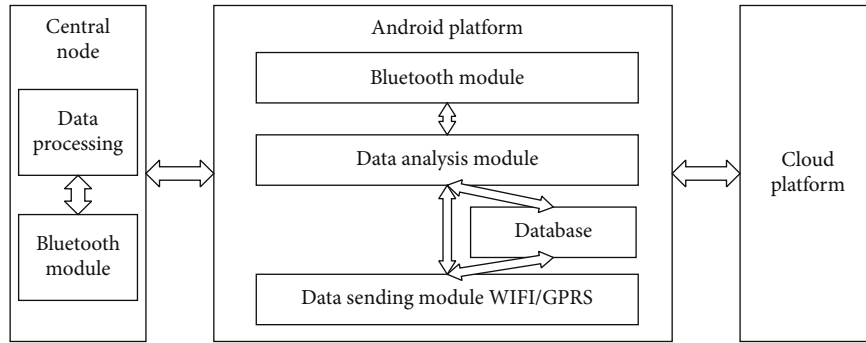
FIGURE 3: System structure frame diagram.

TABLE 2: System function test table.

Functional module	Function name	Test steps	Test results
Login/registration module	Login	Perform login operation	Successfully logged in
	Control panel	Manually control other module operations	Test success
	GPS positioning module	Manual GPS positioning operation	Test success
	Bluetooth module	Connection between central nodes	Test success
Main functions of the system	Data analysis module	Cloud platform for data analysis operations	Test success
	Data storage module	Database for data storage operations	Test success
	Data sending module	Cloud platform for data sending operations	Test success
	System home	Enter the system homepage operation	Test success
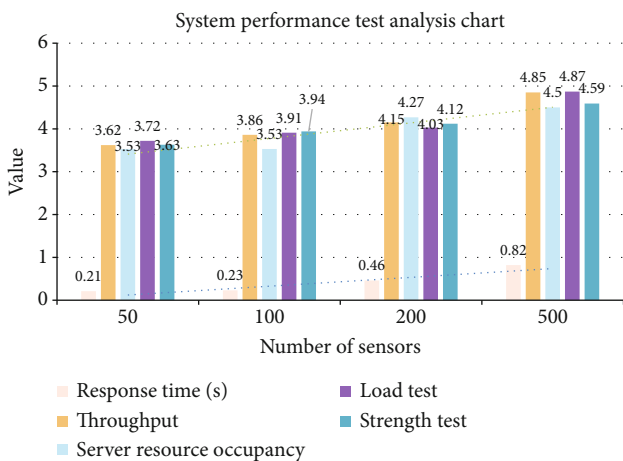
FIGURE 4: System performance test analysis chart.

five-level scoring method, the score ranges from 1 to 5, which, respectively, represent completely disagree with this view, disagree with this view, neither disagree nor agree, agree with it view, and I fully agree with that view, respec-

tively. The higher the price, the more you agree with the point of view.

3.2. Experimental Method

3.2.1. Cloud Computing Medical Monitoring and Management System.
In the daily work of thyroid postoperative care, the medical monitoring and management system uses the Internet of Things and cloud computing technology, and uses real-time monitoring procedures for the physiological indicators in the patient care process, and uploads and transmits information in time, and the members of the nursing team conduct real-time monitoring feedback, etc. Through the Internet of Things technology to implement all-weather monitoring of each patient and each hospital bed, to achieve a 24-hour uninterrupted effect, so that the nursing team members can know the patient's infusion situation at any time in the nurse station or mobile state and carry out timely replacement of infusion bottles and handling of accidental infusions improve the work efficiency of medical staff and bring better experience to patients [26, 27].

3.2.2. System Composition.
The medical monitoring and management system consists of monitoring instruments,

TABLE 3: Monitoring system energy consumption data sheet.

	Power consumption	Equipment cost	System standby time	Scope of action
Surveillance system	Medium	High	Long	Small
Medical monitoring and management system	Cheap	Cheap	Long	Wide

TABLE 4: Monitoring system transmission speed data table.

	Data transmission speed	Accuracy	Information processing capability	Helpful to medical staff	Anti-interference
Surveillance system	Slow	Medium	Medium	Medium	Medium
Medical monitoring and management system	Fast	Accurate	Power	Power	Power
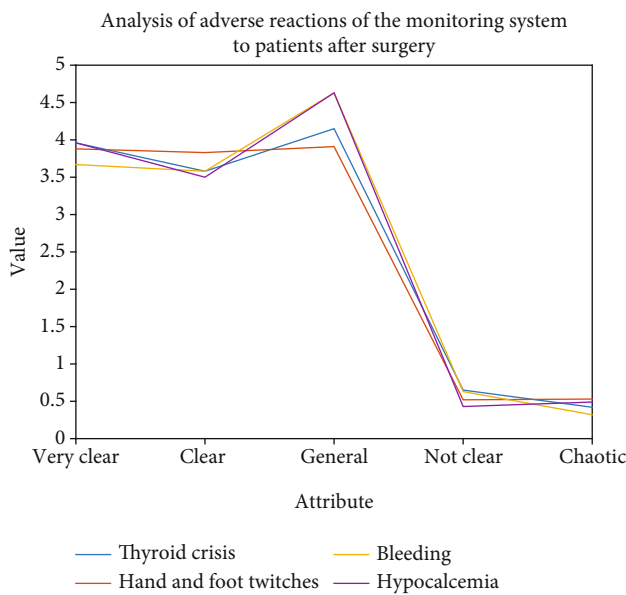
FIGURE 5: Analysis of adverse reactions of the monitoring system to patient surgery.

data receivers, and computer screen (with network interface), and its structural framework is shown in Figure 3. First, the monitoring instrument is used to collect data on various physiological indicators of the patient's body, and then the relevant information is uploaded and sent to the data receiver. Each bed in the room is equipped with a monitor and hung with a hook under the screen window. Each information bar is equipped with a data receiver, and the monitor will send data. In the cloud service layer, the data uploaded through the transmission layer is stored in a database cluster, and the data processing component analyzes the data according to related algorithms and organizes related health files or related medical records [28–30].

3.3. Establish Model Evaluation Index System. The evaluation index is a specific evaluation item determined according to some evaluation goals, which can reflect some basic characteristics of the evaluation object. The index is specific and measurable, and it is the observation point of the goal. Definite conclusions can be drawn through actual observation of the object. Generally speaking, the evaluation index system includes three levels of evaluation indexes: they are the relationship between gradual decomposition and refinement. Among them, the first-level evaluation indicators and the second-level evaluation indicators are relatively abstract and cannot be used as a direct basis for evaluation. The third-level evaluation indicators should be specific, measurable, and behavior-oriented, and can be used as a direct basis for evaluation [30, 31].

3.4. Statistical Processing. Statistical analysis was performed with SPSS 13.0 statistical software. The significance test was performed by one-way analysis of variance, the difference between the two groups was performed by LSD-t test, and the postoperative recovery of the thyroid was performed by group t test. $P < 0.05$ is considered significant and statistically significant.

4. Mobile Medical Monitoring and Management System

4.1. System Test

4.1.1. System Function Test. The functional of the system mainly includes eight functional modules including system login, control panel, GPS positioning module, Bluetooth module, data analysis module, data storage module, and data transmission module. The test results are shown in Table 2.

In the process of testing the monitoring effect, technical tests such as background sampling and encoding are carried out using specific video formats, and the server and other hardware are repeatedly tested until satisfactory test results are obtained. It can be seen from the table that the system is designed and tested successfully after analyzing the required functions.

4.1.2. System Performance Test. Here, we are mainly from five perspectives (response time, throughput, server resource occupancy, load test, and strength test) to carry out the performance test of the system, and the results are shown in Figure 4.

It can be seen from Figure 4 that the general response time is within 3 s, and the user will feel more satisfied.
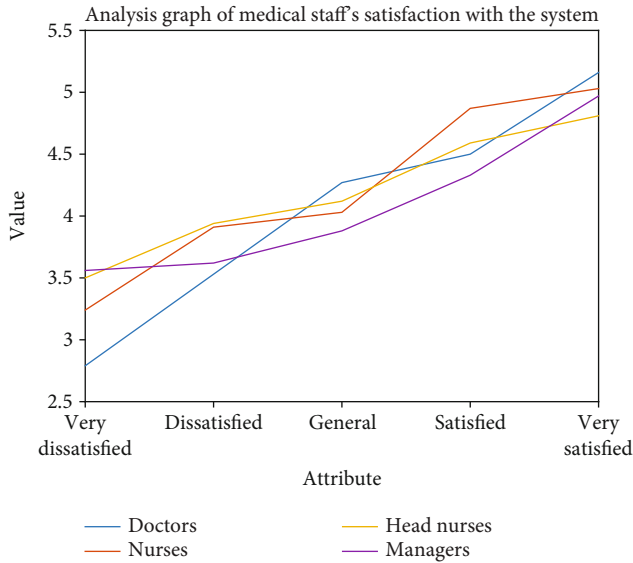
FIGURE 6: Analysis graph of medical staff's satisfaction with the system.

Between 3 s and 8 s, users can barely accept it, and users who are longer than 8 s may not accept it. Because the cloud computing medical monitoring and management system is used to obtain the exact location of the patient in the first time, the response time needs to be shorter, and the response of this system within the time increases as the number of sensors increases ($P < 0.05$), but it is always much less than 3 s; the throughput and server resource occupancy test scores do not rise much within 100 sensors; load test and strength test scores are at 200. The rise within the sensor is not large.

4.2. Based on Monitoring System

4.2.1. Analysis Based on the Energy Consumption of the Monitoring System.
Here, the energy consumption of cloud computing, medical monitoring management system, and general monitoring system is compared, and the results are shown in Table 3.

It can be seen from Table 3 that the power consumption of the general monitoring system is not too high, but the cloud computing, medical monitoring, and management system, data is transmitted by sensors, and the power consumption is less than that of the general monitoring system; the equipment cost is relative to the general there are also fewer monitoring systems; the standby time of the two monitoring systems is very long; and the cloud computing medical monitoring management system has a wider range of action than the general monitoring system.

4.2.2. Analysis Based on the Transmission Speed of the Monitoring System.
Here, we compare the energy consumption of the cloud computing medical monitoring and management system with the general monitoring system, and the results are shown in Table 4.

Table 4 shows that medical cloud computing monitoring and management system data uses visualization technology to visualize normal data, while the general tracking system

is propagated by image transmission, so medical computing and cloud computing management system is relevant to the general, and the monitoring system is faster in data transmission speed. The cloud computing medical monitoring and management system directly detects the patient's heart rate, blood pressure, and other physiological data in real-time. Compared to the general monitoring system, it can only read the patient image. To be precise, stronger in the ability to process information and more help to medical staff.

4.2.3. Analyze the Adverse Reactions of Patients after Surgery Based on the Monitoring System.
It can be seen from Figure 5 that the monitoring system can detect the adverse reactions of the patients based on the patient's physiological data. A total of 25% of patients have postoperative complications, including 8.33% of thyroid crisis, 8.33% of hand and foot convulsions, with 4.17% bleeding, and 4.17% hypocalcemia, for medical emergency and medical care, obtaining the exact location of the patient at the first time will bring a lot of time to the success of the rescue.

4.3. System Satisfaction Based on Medical Staff.
It can be seen from Figure 6 that doctors' satisfaction with cloud computing, medical monitoring, and management system increased from 2.79 to 5.16; nurses' satisfaction with cloud computing, medical monitoring, and management system increased from 3.24 to 5.03; head nurses' satisfaction with cloud computing, medical monitoring, and management system the degree of satisfaction increased from 3.50 to 4.81; the administrator's degree of satisfaction with the cloud computing medical monitoring and management system increased from 3.56 to 4.97, which shows that the medical staff are very satisfied with this system.

5. Conclusions

The research of mobile medical monitoring and management system started relatively late. At present, a complete monitoring system has been built on many large-scale structures at home and abroad to ensure the normal operation of the structure during service. The Internet of Things and cloud computing technologies, as new technologies developed in recent years, have high research and application value and can play a major role in promoting economic development and industrial upgrading. Analyzing the characteristics of the Internet of Things, cloud computing technology, and mobile medical monitoring, comparing it from three levels, and demonstrating the functional correspondence between their system architectures and the three common features: comprehensive perception, reliable transmission, and intelligent processing. Mobile medical monitoring is a specific application of the Internet of Things and cloud computing technology in the field of engineering monitoring. For medical emergency and medical care, obtaining the exact location of the patient for the first time is of great significance to the success of the rescue. This article implements the function of sending the location of the patient to the designated medical caregiver in the map service. It provides an effective way

for patients to get help as soon as they encounter emergencies.

Data Availability

The data underlying the results presented in the study are available within the manuscript.

Conflicts of Interest

The authors declare that they have no conflicts of interest.

Acknowledgments

References

[1] O. Edafe, E. Cochrane, and S. P. Balasubramanian, "Reoperation for bleeding after thyroid and parathyroid surgery: incidence, risk factors, prevention, and management," *World Journal of Surgery*, vol. 44, no. 4, pp. 1156–1162, 2020.

[2] K. G. Srinivasa, B. J. Sowmya, A. Shikhar, R. Utkarsha, and A. Singh, "Data analytics assisted internet of things towards building intelligent healthcare monitoring systems," *Journal of Organizational and End User Computing*, vol. 30, no. 4, pp. 83–103, 2018.

[3] T. von Ahnen, M. von Ahnen, S. Militz et al., "Compartment pressure monitoring after thyroid surgery: a possible method to detect a rebleeding," *World Journal of Surgery*, vol. 41, no. 9, pp. 2290–2297, 2017.

[4] B. C. Brajcich and C. R. Mchenry, "The utility of intraoperative nerve monitoring during thyroid surgery," *Journal of Surgical Research*, vol. 204, no. 1, pp. 29–33, 2016.

[5] H. Hamidi and M. Jahanshahifard, "The role of the internet of things in the improvement and expansion of business," *Journal of Organizational and End User Computing*, vol. 30, no. 3, pp. 24–44, 2018.

[6] I. H. Gardner, G. M. Doherty, and D. McAneny, "Intraoperative nerve monitoring during thyroid surgery," *Current Opinion in Endocrinology, Diabetes, and Obesity*, vol. 23, no. 5, pp. 394–399, 2016.

[7] R. Malik and D. Linos, "Intraoperative neuromonitoring in thyroid surgery: a systematic review," *World Journal of Surgery*, vol. 40, no. 8, pp. 2051–2058, 2016.

[8] K. V. Chávez, J. Ramírez, J. P. Pantoja, M. Sierra, D. Velázquez-Fernández, and M. F. Herrera, "Continuous intraoperative neural monitoring in thyroid surgery: a Mexican experience," *Updates in Surgery*, vol. 69, no. 4, pp. 505–508, 2017.

[9] A. Jansen, J. P. Berg, O. Klungsøyr, M. H. B. Müller, J. L. Lyche, and J. O. Aaseth, "The influence of persistent organic pollutants on thyroidal, reproductive and adrenal hormones after bariatric surgery," *Obesity Surgery*, vol. 30, no. 4, pp. 1368–1378, 2020.

[10] R. Schneider, G. Randolph, G. Dionigi et al., "Prospective study of vocal fold function after loss of the neuromonitoring signal in thyroid surgery: the International Neural Monitoring Study Group's POLT study," *The Laryngoscope*, vol. 126, no. 5, pp. 1260–1266, 2016.

[11] J. Scharpf and G. Randolph, "Intraoperative nerve monitoring for parathyroid surgery," in *Medical and Surgical Treatment of Parathyroid Diseases*, B. Stack Jr. and D. Bodenner, Eds., pp. 459–468, Springer, 2017.

[12] M. M. Chen, R. K. Orosco, G. C. Lim, and F. C. Holsinger, "Improved transoral dissection of the tongue base with a next-generation robotic surgical system," *The Laryngoscope*, vol. 128, no. 1, pp. 78–83, 2018.

[13] N. Komune, K. Matsushima, S. Matsuo, S. Safavi-Abbasi, N. Matsumoto, and A. L. Rhoton, "The accuracy of an electromagnetic navigation system in lateral skull base approaches," *The Laryngoscope*, vol. 127, no. 2, pp. 450–459, 2017.

[14] S. R. Chandra and Y. Wang, "Cloud things construction-the integration of internet of things and cloud computing," *Future Generation Computer Systems*, vol. 56, pp. 684–700, 2016.

[15] M. Díaz, C. Martín, and B. Rubio, "State-of-the-art, challenges, and open issues in the integration of Internet of things and cloud computing," *Journal of Network and Computer Applications*, vol. 67, pp. 99–117, 2016.

[16] M. Nazari Jahantigh, A. Masoud Rahmani, N. Jafari Navimirour, and A. Rezaee, "Integration of internet of things and cloud computing: a systematic survey," *IET Communications*, vol. 14, no. 2, pp. 165–176, 2020.

[17] A. Kobusińska, C. Leung, C. H. Hsu, S. Raghavendra, and V. Chang, "Emerging trends, issues and challenges in Internet of Things, Big Data and cloud computing," *Future Generation Computer Systems*, vol. 87, pp. 416–419, 2018.

[18] A. Celesti, O. Amft, and M. Villari, "Guest editorial special section on cloud computing, edge computing, internet of things, and big data analytics applications for healthcare industry 4.0," *IEEE Transactions on Industrial Informatics*, vol. 15, no. 1, pp. 454–456, 2019.

[19] J. Yang, C. Wang, Q. Zhao, B. Jiang, Z. Lv, and A. K. Sangaiah, "Marine surveying and mapping system based on Cloud Computing and Internet of Things," *Future Generation Computer Systems*, vol. 85, pp. 39–50, 2018.

[20] P. N. Mahalle, M. S. Pathan, and V. V. Kimbahune, "Special issue on internet of things, next generation networks, data mining, and cloud computing 2017- part II," *International Journal of Synthetic Emotions*, vol. 8, no. 2, pp. 76–76, 2017.

[21] J. Dizdarević, F. Carpio, A. Jukan, and X. Masip-Bruin, "A survey of communication protocols for internet of things and related challenges of fog and cloud computing integration," *ACM Computing Surveys*, vol. 51, no. 6, pp. 1–29, 2018.

[22] W. Rivera, *Sustainable Cloud and Energy Services||Cloud Computing and Internet of Things Integration: Architecture, Applications, Issues, and Challenges*, Springer, 2018.

[23] B. d. T. P. Gomes, L. C. M. Muniz, F. J. da Silva e Silva, L. E. T. Ríos, and M. Endler, "A comprehensive and scalable middleware for ambient assisted living based on cloud computing and internet of things," *Concurrency and Computation: Practice and Experience*, vol. 29, no. 11, article e4043, 2017.

[24] F. Wu, X. Li, L. Xu, A. K. Sangaiah, and J. J. P. C. Rodrigues, "Authentication protocol for distributed cloud computing: an explanation of the security situations for internet-of-things-

enabled devices," *IEEE Consumer Electronics Magazine*, vol. 7, no. 6, pp. 38–44, 2018.

[25] R. Deng, R. Lu, C. Lai, T. H. Luan, and H. Liang, "Optimal workload allocation in fog-cloud computing toward balanced delay and power consumption," *IEEE Internet of Things Journal*, vol. 3, no. 6, pp. 1171–1181, 2017.

[26] F. Xiao and W. Ding, "Divergence measure of Pythagorean fuzzy sets and its application in medical diagnosis," *Applied Soft Computing*, vol. 79, pp. 254–267, 2019.

[27] X. Li, H. Jianmin, B. Hou, and P. Zhang, "Exploring the innovation modes and evolution of the cloud-based service using the activity theory on the basis of big data," *Cluster Computing*, vol. 21, no. 1, pp. 907–922, 2018.

[28] Z. Lv and F. Piccialli, "The security of medical data on internet based on differential privacy technology," *ACM Transactions on Internet Technology (TOIT)*, vol. 21, no. 3, pp. 1–18, 2021.

[29] S. Wan, Z. Gu, and Q. Ni, "Cognitive computing and wireless communications on the edge for healthcare service robots," *Computer Communications*, vol. 149, pp. 99–106, 2020.

[30] S. Biswas, D. Devi, and M. Chakraborty, "A hybrid case based reasoning model for classification in internet of things (Iot) environment," *Journal of Organizational and End User Computing*, vol. 30, no. 4, pp. 104–122, 2018.

[31] M. Elhoseny, G.-B. Bian, S. K. Lakshmanaprabu, K. Shankar, A. K. Singh, and W. Wu, "Effective features to classify ovarian cancer data in internet of medical things," *Computer Networks*, vol. 159, pp. 147–156, 2019.

WILEY | Hindawi

Research Article

Intelligent Data Mining Based on Market Circulation of Production Factors

Hefang Sun [ORCID]

School of Marxism, Capital Normal University, Beijing 10010, China

Correspondence should be addressed to Hefang Sun; 2140301011@cnu.edu.cn

R&D investment is an important way to improve scientific and technological innovation capabilities. In an increasingly competitive market, the rapid changes in science and technology have brought new opportunities for enterprise development. However, if production factors cannot be rationally allocated, low allocation efficiency or low allocation efficiency is likely to occur. The phenomenon of excessive overflow of production factors makes the input factors unreasonable and causes the problem of lowering the economic output of enterprises. Therefore, this article analyzes the feasibility and timeliness of R&D investment from factors of production and enterprise output performance based on data mining. The problem is to optimize the rational allocation of future factors of production and provide assistance in achieving a combination of existing and new factors of production. For this test, we selected the companies listed in the Growth Enterprise Market and the survey period is from 2018 to 2020. The data is taken from the Guotaian database, some of which is obtained by manually reading the company's annual report, and a multiple regression analysis model is established and tested. The relationship between R&D investment, production factors, and corporate performance is obtained. The group regression method is used to test the impact of production factors on R&D. Whether input and corporate performance have a moderating effect, and the specific moderating and lagging effects of production factors are investigated. Experiments have proved that the nonstandardized coefficient of R&D investment intensity and operating gross profit margin is 0.714, and the T value of 9.296 is positive and significant. Each increase of enterprise R&D investment intensity by 1 will increase operating gross profit margin by 0.714. The coefficient of operating gross profit margin is much smaller than the coefficient of Tobin's Q value. This shows that the factor of production has a great influence on the relationship between R&D investment and corporate performance. It has the importance of being a specific practical guide for guiding GEM companies in my country with different elemental intensities to carry out R&D activities and improve corporate performance.

1. Introduction

In today's global economic integration, the concept of technological innovation has sounded the clarion call of the new industrial revolution one after another, and the scientific and technological capabilities of enterprises have become the touchstone of whether enterprises can survive. In recent years, Chinese companies are growing rapidly as a whole, but their growth point remains at the top of the total economic volume, and their capacity and quality development are not well coordinated. A series of common problems, such as low technical content and low market value of finished products, have become bottlenecks that limit the develop-

ment and growth of many companies, making them difficult to even break through.

In today's world, economic downward pressure is relatively high, companies want to create economic benefits in the downturn, and research and development activities may be another option for companies. As for the economic consequences that R&D investment will bring to enterprises, many scholars at home and abroad have also conducted fruitful research on this, but the research conclusions are inconsistent and there are big differences. As the main body of scientific and technological innovation, enterprises must proceed from their own perspective and demand resource allocation that meets their own conditions, and the ultimate goal of

the enterprise is to make profits and maximize the effectiveness of production factors in order to improve performance more effectively.

Kim and Yang proposed that it is a top priority to realize the transition from traditional agriculture to modern market agriculture as soon as possible in the construction of a new socialist countryside. Realizing market agriculture can improve China's agricultural core competitiveness, increase farmers' income, and contribute a lot. They also discussed the current situation and influencing factors of the flow of production factors in the process of implementing market-oriented agriculture in our country and discussed the means to promote the circulation of agricultural production factors. However, their research did not clearly propose how to realize the transition from traditional agriculture to modern market agriculture, and the overall research lacks data support [1]. Data mining is playing an increasingly important role in politics, economy, transportation, and life. There have been many cases of applying data mining to solve practical problems at home and abroad. Wang et al. proposed that thresholding the ensemble coherence is a common method to identify radar scatterers that are less affected by decorrelated noise. However, thresholding the consistency may result in the loss of information in areas that experience more complex deformed scenes. If differences in moderately coherent regions have similar behaviors, it is important to consider their spatial correlation for correct reasoning. Then, the information on the low-coherence area may be used in a similar way, while the coherence is used for thematic mapping applications, such as change detection. A method based on data mining and statistical procedures is proposed to reduce the influence of outliers in the results. Our method allows minimizing the outliers in the final results, while preserving the spatial and statistical correlation between the observations. The experimental results lack more data support so that data mining can alleviate the impact of outliers in the results is still doubtful [2]. Tao et al. collect data on IoT devices to achieve better decision-making, higher automation, higher efficiency, productivity, accuracy, and wealth creation. Data mining and other artificial intelligence methods will play a key role in creating a smarter IoT, despite the many challenges. The applicability of eight well-known data mining algorithms to IoT data is tested. Including the deep learning artificial neural network, which constructs a feedforward multilayer artificial neural network for modeling advanced data abstraction, their research data is insufficient, making the data mining results inaccurate [3].

This article will apply the data mining classification algorithm to the actual problems of the performance evaluation of the market-oriented enterprises of production factors. The data comes from the Guotaian database, or by consulting the GEM 2018-2020 annual report, applies the algorithm to the actual problems and improves the market. In this article, we add Tobin's Q value as an indicator to measure the market performance of a company's R&D investment and use Tobin's Q value to reflect its impact on the future of the company. At the same time, this article introduces the variables of factors of production, investigates the relationship between them in detail and in detail, and expands the research space for corpo-

rate performance in future scientific research activities and research ideas.

2. Intelligent Data Mining Market Circulation of Production Factors

2.1. Data Mining

(1) Data mining method

Data mining is different from ordinary information retrieval. Ordinary information retrieval is to directly obtain the required content through query commands, while data mining is to obtain effective information from the data through association rules and machine learning algorithms [4, 5]; the information obtained is indirect and abstract, and the hidden patterns used for evaluation are discovered through data mining. The general framework of data mining is shown in Figure 1.

The prediction task predicts the value of the target attribute based on the existing attributes, mainly regression tasks and classification tasks. The target variable predicted by the regression task is a continuous variable, and the target variable predicted by the classification task is a discrete variable. However, both of these are used to train the prediction model through the training set. The target variable of the training set is known; that is, the training set there is labeled data, so the generated model is a mapping of existing attributes and target attributes generated under supervision, which is a supervised learning method. Descriptive tasks generally summarize the potential association patterns in the data, mainly including cluster analysis, association analysis, and anomaly detection [6, 7].

(2) Data preprocessing

(a) Reasons for data preprocessing

The purpose of data preprocessing is to obtain reliable data for data mining tasks. There are many reasons for the low quality of data, such as equipment failure during the data collection stage, human error during data input, technical errors during data transmission, and the user's cover-up of information [8, 9]. Due to technical or confidential reasons, the data is incomplete data, which is reflected in the missing part of the attribute values of the data or the missing values of some important attributes. The imbalance of data is reflected in the imbalance of the data distribution, and the imbalance of the data will lead to the inaccuracy of the trained model [10].

(b) Data preprocessing method

Data cleaning is to remove the "dirty data" from the data. Smooth noise, general data will have random noise, and the data obtained by smooth processing is more realistic; the detection and deletion of outliers, generally speaking, the data of outliers has a lot of noise, which can be considered noise data. The training of the model is unfavorable,
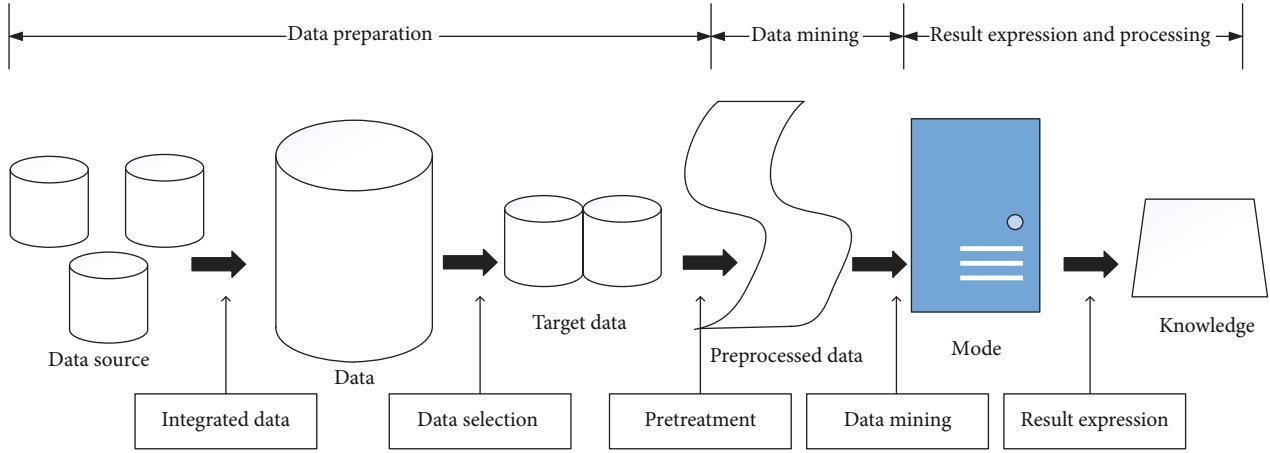
FIGURE 1: Data mining framework diagram.

TABLE 1: Confusion matrix of classification results.

Reality forecast result	Positive example	Counterexample
Positive example	TP (real positives)	FN (false counterexample)
Counterexample	FP (false positives)	TN (true counterexample)

and the general processing method is to delete it directly. Since data is generally collected in different systems, and these systems are generally independent, the data is also isolated data from each other [11, 12]. Data reduction is to reduce the scale of data, such as deleting irrelevant attributes, replacing words with numbers in the bag-of-words model, and discretizing continuous values. These processing will greatly reduce the scale of data and save calculation space and time.

2.2. Classification Algorithm Performance Evaluation. For the performance evaluation of the algorithm, in addition to the test set, the performance evaluation index of the algorithm is also required. For different tasks, there are different algorithm performance evaluation indicators to compare the effects of different algorithms or the same algorithm with different parameters [13, 14]. For the two-class classification problem, the category predicted by the classification algorithm and the true category of the sample can be combined to obtain the confusion matrix of the classification result, as shown in Table 1. Among them, TP represents the number of samples predicted by the classification algorithm to be positive and are actually positive examples, called true examples; FP represents the number of samples predicted by the classification algorithm to be positive but actually negative examples, called false positives; FN represents the classification algorithm the number of samples predicted to be negative examples but actually positive examples is called false negative examples; TN represents the number of samples predicted by the classification algorithm to be negative examples and actually is also a negative example, which becomes a true negative example [15, 16].

(1) Accuration (refers to the proportion of correctly classified samples to the total number of samples)

$$accuration = \frac{TP + TN}{TP + FP + FN + TN} \quad (1)$$

(2) Precision (refers to the proportion of the number of positive samples predicted to be correct to the total number of positive samples predicted)

$$precision = \frac{TP}{TP + FP} \quad (2)$$

(3) Recall (refers to the proportion of the number of positive samples that are correctly predicted to the total number of positive samples)

$$recall = \frac{TP}{TP + FN} \quad (3)$$

(4) F1 value

F1 value is proposed on the basis of precision rate and recall rate, and is defined as

$$F1 = \frac{2 \times precision \times recall}{precision \times recall}. \quad (4)$$

For a classification problem, the prediction accuracy and recall are usually mutually restricted, and the F1 value balances the influence of these two indicators

(5) ROC and AUC

For the predicted value, the larger the probability that the sample belongs to the positive sample, the same, the smaller the value, the greater the probability that the sample belongs to the negative sample. For practical applications, if we pay more attention to the accuracy rate, we can increase the

threshold; if we pay more attention to the recall rate, we can lower the threshold [17, 18]. The proportion of real positive cases predicted to be positive is consistent with the recall rate. The ordinate is the true rate, indicating the proportion of real negative cases predicted to be positive. The definitions are as follows:

$$FPR = \frac{FP}{FP + TN}, \tag{5}$$

$$TPR = \frac{TP}{TP + FN}. \tag{6}$$

AUC is the area included under ROC. When AUC is greater than 0.5, the classification algorithm is effective, and the larger the AUC, the stronger the generalization ability of the classification algorithm. When the AUC is less than or equal to 0.5, the classification algorithm is invalid [19].

2.3. Data Mining Classification Algorithm

(1) Naive Bayes

Bayes' theorem is defined as follows:

$$P(B|A) = \frac{P(A|B)P(B)}{P(A)}, \tag{7}$$

where $P(B|A)$ refers to the probability of event B occurring under the condition of event A and $P(B)$ and $P(A)$, respectively, represent the probability of event B occurring in event A, and event B is two independent events in event A [20].

Assume that there are t classified samples in the training sample T, and the sample attribute $X = \{x_1, x_2, \cdots, x_k\}$ belongs to the c class, where x_i represents the i attribute in the sample sign. According to Bayes' theorem,

$$P(c|X) = \frac{P(X|c)P(c)}{P(X)}, \tag{8}$$

where $P(c|X)$ is the conditional probability that the sample attribute X is the class label c; $P(X|c)$ is the conditional probability that the sample attribute is X under the c class; $P(C)$ is the proportion of each type of sample, which is obtained by counting the frequency of each type of sample; and $P(X)$ is a normalized evidence factor and has nothing to do with category [21, 22].

For the unknown sample X, we calculate the conditional probability of this sample for each category separately. The calculation of $P(X|c)$ is more difficult because the attributes of the unknown sample may not appear in the training set. According to the assumption that the attributes are independent of each other, there are

$$P(X|c) = \prod_{i=1}^{k} P(x_i|c). \tag{9}$$

So, the expression of the Bayesian classification algorithm can be written as

$$h(X) = \arg \max P(c) \prod_{i=1}^{k} P(x_i|c) \tag{10}$$

(2) Logistic regression

The Sigmoid function is similar to a step function. At the jumping point, it can be regarded as jumping from 0 to 1 in myopia, which meets the requirements of classification. At the same time, the differentiability of the function ensures that the solution is more convenient [23, 24]. The calculation formula of the Sigmoid function is

$$y = \frac{1}{1 - e^{-z}}. \tag{11}$$

Among them, z is a regression function; set the regression coefficient ω, and the input is X, then $z = \omega^T X$, into the above formula, we can get

$$y = \frac{1}{1 - e^{-(\omega^T X)}}. \tag{12}$$

Ultrasound images have high requirements for edge detail and are nonstationary signals that cannot be met by traditional Fourier transform-based signal denoising methods. Ultrasonic speckle suppression and denoising methods can be broadly divided into spatial area local statistical filtering, anisotropic diffusion filtering, and wavelet transform-based filtering.

$$\ln \frac{y}{1 - y} = \omega^T X. \tag{13}$$

If y is the probability that sample X belongs to a positive sample, $1 - y$ is the probability of a negative example, and $\ln (y/(1 - y))$ is the relative probability that sample X is a positive sample. Considering y as the posterior probability, estimate $P(y = 1|X)$, then Equation (13) can be something like

$$\ln \frac{P(y = 1|X)}{P(y = 0|X)} = \omega^T X. \tag{14}$$

Obviously,

$$P(y = 1|X) = \frac{e^{\omega^T X}}{1 + e^{\omega^T X}}, \tag{15}$$

$$P(y = 0|X) = \frac{1}{1 + e^{\omega^T X}}. \tag{16}$$

To estimate ω through the maximum likelihood method, we can get

$$L(\omega) = \sum_{i=1}^{m} y_i \ln P(y = 1|x_1) + (1 - y_1) \ln P(y = 0|x_1). \tag{17}$$

The loss function $J(\omega)$ is

$$J(\omega) = -\frac{1}{m} L(\omega). \tag{18}$$

This formula cannot be solved analytically, and the gradient descent algorithm can be used to approximate the solution to obtain the best regression parameter ω [25].

3. Experimental Design of Market-Oriented Circulation of Production Factors

3.1. Variable Selection

(1) Dependent variable: corporate performance

There are various indicators that reflect the performance of enterprise R&D input and output, including financial and nonfinancial. Nonfinancial indicators include upgrade of production process, number of patent applications, and update of knowledge and skills, considering that the measurability and availability of this type of data is difficult, so when combined with assumptions and samples, Choose financial indicators to measure R&D input and output. Tobin's Q value is also added as an indicator to measure the market performance of enterprise R&D investment. Regarding R&D investment as a dynamic and long-term process, it has given high weight to the development prospects of the company, and the Tobin Q value is used to reflect its impact on the future of the company.

(2) Independent variable: R&D investment

The R&D expenditure is divided into two parts: expense and capitalization. It includes the actual R&D investment of the enterprise in the year, the investment of personnel and equipment, and the investment of information and creativity. On a quantifiable basis, the current R&D investment amount is obtained. In order to avoid a large gap in the value of the sample's R&D investment due to the difference in company size, the R&D investment ratio is selected as an independent variable.

(3) Categorical variable: intensity of production factors

The factors of production are divided into three dimensions: labor, capital, and technology. Different measurement standards are used for the dimensional division of production factors, and the intensity division is completed according to corresponding indicators and methods. Capital-labor ratio and fixed asset ratio are selected to measure capital-labor intensity. The ratio of capital to labor can reflect the quotas between the two most basic factors of production; the ratio of fixed assets can indicate whether the company has idle fixed assets and the importance of fixed assets, and the two can be directly measured and complemented and analyzed, and the ratio obtained the larger the value, the more important the capital. The ratio of R&D expenses to product costs is cited to reflect how much R&D expenses are condensed in each unit cost; the ratio of R&D personnel to the number of employees reflects the personnel input of

the company in conducting R&D activities, combining the above two indicators to distinguish between technology and nontechnology type enterprise.

(4) Control variables

(a) Enterprise scale

Since the scale of listed companies has an impact on output effects, large-scale companies often have certain accumulated advantages, so company scale is a control variable that needs to be established. Since R&D investment not only has an impact on the value of fixed assets but also has a more important impact on the value of intangible assets. In addition, in the R&D investment intensity index, the operating income has been calculated as the denominator, so the total assets are taken as the natural logarithm.

(b) Asset-liability ratio

Since R&D activities are a corporate activity with high capital investment, and the sample selected companies listed on the Growth Enterprise Market, the sample has the characteristics of short business cycle, fast replacement, and large growth inertia. The specific situation of corporate debt management will eventually be reflected in business performance. Therefore, from the perspective of the relationship between corporate capital stock and technological innovation capabilities, the asset-liability ratio is used as a control variable to indicate the abundance of corporate funds. The relationship and meaning between the variables are shown in Table 2.

3.2. Test Subject.
This test selects companies listed on the Growth Enterprise Market, and the research period is from 2018 to 2020. The data comes from the Guotaian database, partly obtained by manually reading the company's annual report. Since the China Securities Regulatory Commission did not include the R&D investment data in the scope of mandatory disclosure by listed companies, the R&D investment data is not available in databases such as Guotaian. Therefore, such data is manually collected by reading the company's annual report. After strict screening of the sample data through the screening criteria, a total of 2942 sample data were obtained.

(i) Screening criteria

Financial data for the period 2018-2020 must be complete. If something is missing, the sample will not be used. If the data is complete, the subject should be representative. If your company's industry data is less than 5 (including 5), it will be deleted. Due to the peculiarities of the financial industry, data on listed companies in the financial industry have also been deleted.

3.3. Moderating Effect Test Method.
For companies, the relationship between R&D activities and corporate performance will also be affected by the company's own "personality." The exact same R&D management model is effective for some

Table 2: List of variable relations and meanings.

Variable type	Variable meaning	Variable value and method description
Dependent variable	Enterprise market performance	Market value/total assets at the end of the year
	Corporate financial performance	Main business income-main business cost/main business income
Independent variable	R&D investment intensity	R&D investment/operating income
	Capital labor ratio	Fixed assets/labor force
Categorical variables	Proportion of fixed assets	Net fixed assets/total assets
	Proportion of R&D expenses	R&D expenses/product production costs
	Proportion of R&D personnel	Number of R&D personnel/total number of employees
Control variable	Enterprise size	Natural logarithm of the company's total assets
	Assets and liabilities	Total liabilities/total assets

companies, but invalid for some companies. The "personality of an enterprise" can be expressed as the "foundation" of the enterprise, that is, the factors of production, specifically the number of laborers, the richness of assets, or the level of technology. When the independent variable is a continuous variable and the adjustment variable is a categorical variable, the adjustment effect can be tested by the group regression method; that is, after the adjustment variable M is grouped, X and Y are linear regressions; if there is a difference between the group regression coefficients, it proves that there is a moderating effect.

3.4. Model Building. We establish a multiple regression analysis model to test the relationship between R&D investment, production factors, and corporate performance. The establishment steps are as follows: put independent variables and control variables into the model and perform regression analysis to explore the relationship between R&D investment intensity and corporate performance and introduce adjustment variables, divide the samples into three groups in the three-dimensionality groups of production factors, and build the model as follows:

$$Y_i = a + bX_{1i} + cX_2 + \varepsilon. \tag{19}$$

Among them, Y_i represents the performance of different groups of enterprises, X_{1i} represents the R&D investment of different groups, X_2 represents the control variable, and ε is introduced as a random variable to represent other influencing factors not involved in this study to modify the hypothetical model established. If there are significant differences in the grouping regression under each dimension of production factors, it can be concluded that each dimension of production factors has a moderating effect on the relationship between R&D investment and enterprise performance. On this basis, the subsamples classified according to the various dimensions of the production factors are then used for regression comparison. By observing the significance of b in different groups, there are significant differences. It can further reflect the concrete manifestation of the relationship between production factors and R&D investment and enterprise performance.

3.5. Statistical Processing. Statistical analysis was carried out with SPSS 13.0 statistical software. The significance test of the difference was performed by one-way analysis of variance, the difference between the two groups was tested by LSD-t, and the statistics of intelligent data mining analysis results of the market-oriented circulation of production factors were performed by the group t-test. $P < 0.05$ is considered to be significant and statistically significant.

4. Market Circulation of Production Factors

4.1. Descriptive Statistical

(1) Overall situation analysis

Here, we first analyze the overall situation of GEM listed companies from 2018 to 2020 according to the intensity of R&D investment. The results are shown in Figures 2–4.

It can be seen from Figure 2 that during the three years from 2018 to 2020, the average R&D investment intensity of listed companies on the ChiNext is 6.9%, and the standard deviation is only 0.0675, indicating that this value can well represent the overall level. The R&D intensity of 2% is only the level at which the company can barely survive, and the R&D intensity of 5% is the level at which the company has a competitive advantage. This shows that the Growth Enterprise Market as a whole has innovative vitality. This is mainly because most of the companies listed on the ChiNext are high-tech companies or entrepreneurial companies, and they regard R&D activities as a necessary condition for maintaining innovation and competitiveness.

It can be seen from Figures 3 and 4 that the overall Tobin Q value of the sample varies between 0.6149 and 13.267, with an average of 3.5792 and a standard deviation of 2.67, indicating that there is a large gap in the market value of listed companies on the GEM. The operating gross profit margin values are relatively the same. The standard deviation is 0.167, the minimum is -0.03, the maximum is as high as 0.92, and the overall average is 0.366, maintaining a gross profit margin of about 38%. This shows that the GEM listed companies have continuous competitive advantages.

As can be seen from Figures 2–4, from the perspective of time span, the average value of R&D investment intensity has increased from 7.3% in 2018 to 6.73% in 2019 and 6.67% in
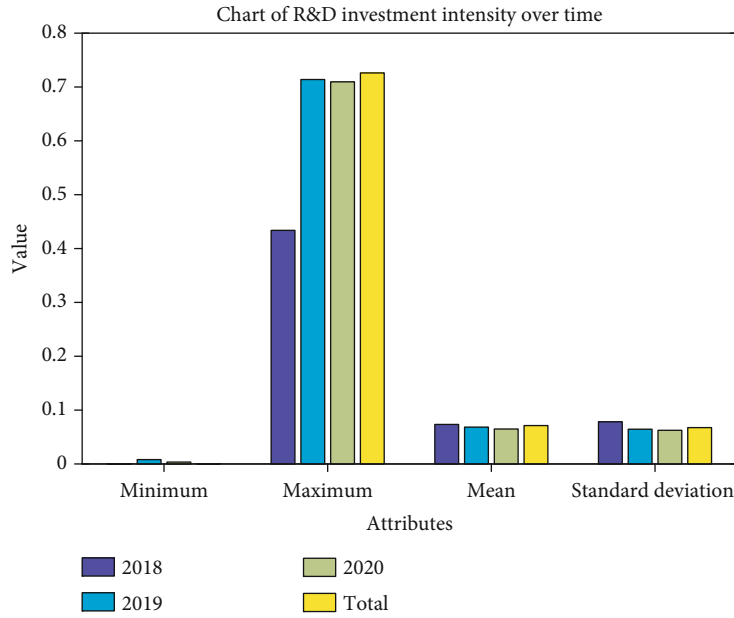
FIGURE 2: Chart of R&D investment intensity over time.
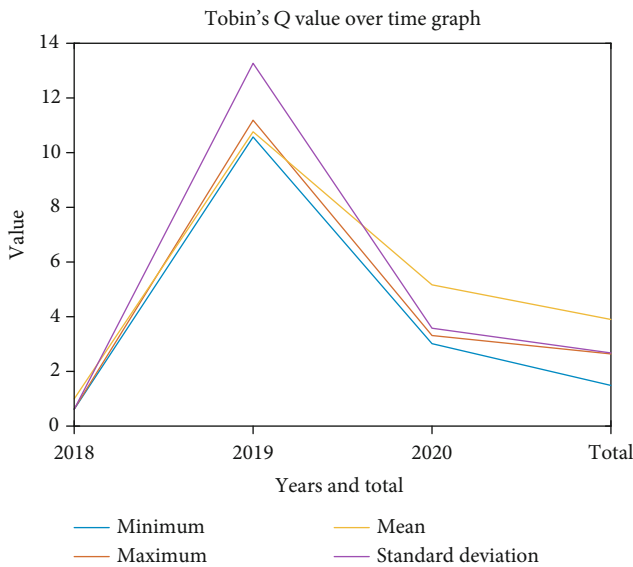
FIGURE 3: Tobin's Q value over time graph.

2020. Although there is a slight downward trend, compared with the 3.5% R&D investment intensity of main board listed companies, it still has a big advantage. Tobin's Q value has been significantly improved in three years. While growing, the gap in the market value has gradually widened, and the standard deviation has increased by 1.26 compared with the previous year. In comparison, the company's operating gross profit margin data has basically stabilized at 0.34 during 2018-2020, indicating that the company's short-term profit level has changed less.

(2) Analysis of each grouping situation

It can be seen from Table 3 that the R&D investment intensity of labor-, capital-, and technology-intensive industries are 4.32%, 4.49%, and 8.96%, respectively; Tobin's Q values are 3.613, 3.623, and 4.346, respectively; operating gross profit margins are 0.304, 0.347, and 0.358, respectively, indicating that under different production factor intensities, there is a difference between enterprise R&D investment and enterprise performance. The specific difference is reflected in a stepped difference. Technology-intensive industries far surpass other groups in terms of R&D investment and corporate performance. At the same time, capital-intensive industries are slightly higher than labor-intensive industries. The R&D intensity of technology-intensive samples, Tobin's Q value, and operating gross profit margin are the largest; capital-intensive industries have the smallest standard deviation of R&D intensity, indicating that the R&D intensity of enterprises in this type of industry remains at a relatively stable level; labor-intensive industries, the industry's operating gross profit margin standard deviation, is relatively lowest, indicating that the gross profit margin of this type of industry tends to be stable, but the overall profitability is weak.

4.2. Correlation. This paper uses SPSS 13.0 software to analyze the data and conducts correlation analysis before regression analysis. Correlation analysis is used to describe the degree of interdependence between variables. It can detect whether there is autocorrelation between explanatory variables in the model. The results of correlation analysis are shown in Table 4. The table lists the coefficients of the correlation between R&D investment intensity, corporate performance, and control variables. Based on the correlation analysis results in Table 4, the relationship between the explanatory variables and the explained variables in the model will be described separately.
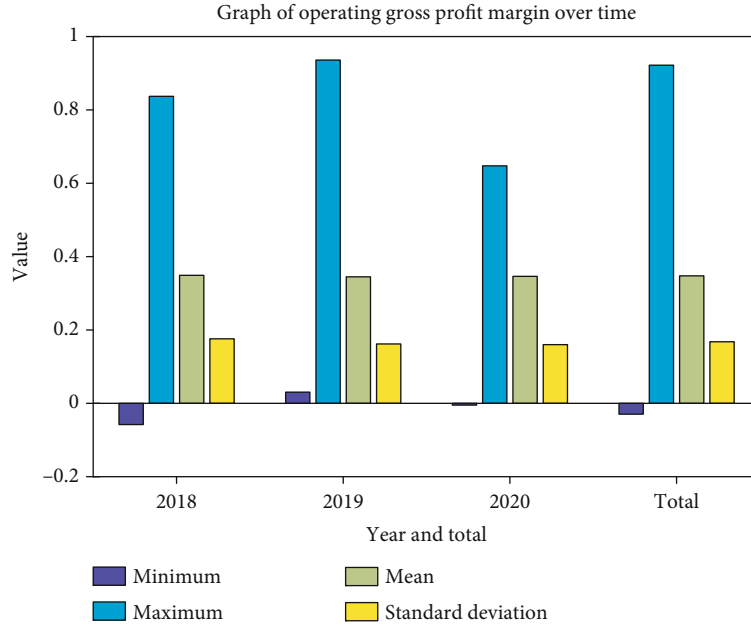
Figure 4: Graph of operating gross profit margin over time.

Table 3: Descriptive statistics grouped by the intensity of production factors from 2018 to 2020.

Intensity of production factors		N	Minimum	Maximum	Mean	Standard deviation
	R&D investment intensity	64	0.003	0.450	0.045	0.061
Labor intensity	Tobin's Q	64	0.976	9.736	3.613	1.838
	Operating gross profit margin	64	0.056	0.663	0.304	0.141
	R&D investment intensity	462	0.003	0.166	0.051	0.028
Capital intensity	Tobin's Q	462	0.619	19.544	3.623	2.514
	Operating gross profit margin	462	0.030	0.959	0.347	0.169
	R&D investment intensity	597	0.009	0.728	0.091	0.084
Technology intensity	Tobin's Q	597	0.844	18.105	4.346	2.298
	Operating gross profit margin	597	-0.060	0.980	0.358	0.182

Table 4: Correlation analysis data sheet.

	R&D investment intensity	Assets and liabilities	Enterprise size	Tobin's Q	Operating gross profit margin
R&D investment intensity	1	—	—	—	—
Assets and liabilities	-0.293	1	—	—	—
Enterprise size	-0.132	0.461	1	—	—
Tobin's Q	0.165	-0.216	-0.273	1	—
Operating gross profit margin	0.378	-0.413	-0.119	0.419	1

It can be seen from Table 4 that the correlation coefficients between the independent variable R&D investment intensity and the dependent variable Tobin's Q value and operating gross profit margin are 0.165 and 0.378, respectively, and the associated probability P value is less than the significance level of 0.01. There is a significant positive correlation between. Moreover, the operating margin coefficient is greater than Tobin's Q coefficient, indicating that the correlation between R&D investment and operating gross

profit margin is stronger than its correlation with Tobin's Q value, which indirectly proves that it is suitable for further analysis of different groups and variables. The difference exists. The two control variables of asset-liability ratio and enterprise scale are also analyzed here. It can be seen that the correlation coefficients between asset-liability ratio and Tobin's Q value and operating gross profit margin are, respectively -0.216 and -0.413, with a significance level of 0.001; enterprise size and the correlation coefficients between
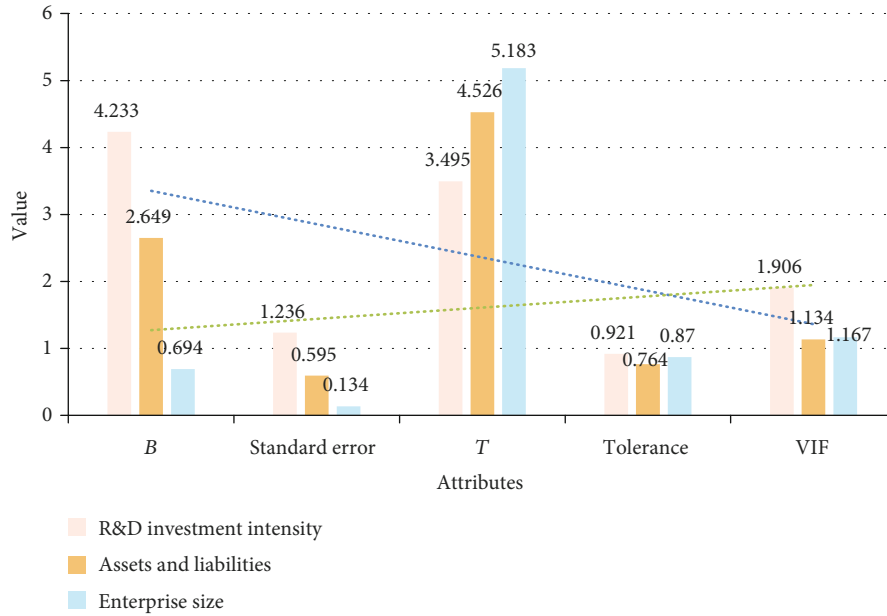
FIGURE 5: The regression result of R&D investment on Tobin's Q value.
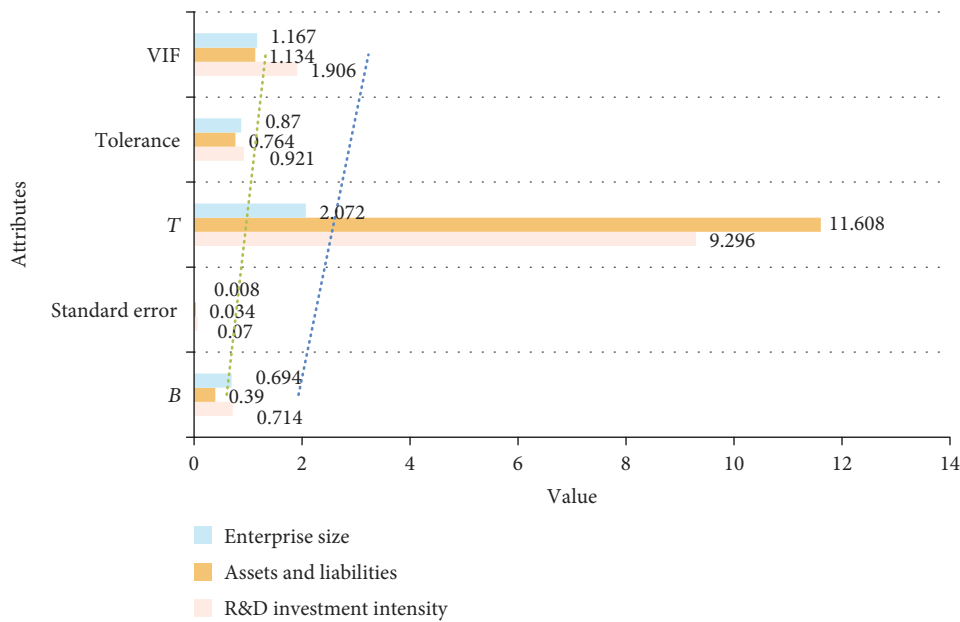
FIGURE 6: The regression result of R&D investment on operating gross profit margin.

Tobin's Q value and operating gross profit margin are -0.273 and -0.119, respectively, and the significance level is 0.001, indicating that in addition to the impact of R&D investment intensity on corporate performance, there are other variables that act in it.

4.3. Regression R&D Investment on Enterprise Performance

(1) The influence of R&D investment intensity on Tobin's Q value

The statistical performance of this model is significant, reaching 19.118, indicating that the regression model of R&D investment intensity and Tobin's Q value is overall significant in the regression analysis based on the full sample. 8.8% of the model is adjusted, indicating that the regression equation explains the 8.8% square difference of Tobin's Q value. According to the collinearity diagnosis result, it is found that the tolerances are 0.921, 0.764, and 0.870, respectively, and there are no small values; the variance expansion factor (VIF) is 1.906, 1.134, and 1.167, respectively, and there are no very large values, further explanation there is no problem of collinearity between variables in the equation. The nonstandardized coefficient of R&D investment intensity and Tobin's Q value is 4.233, T value is 3.459, the sign is positive, and it is lower than the significance level of 0.01, which means that for

each increase in R&D investment intensity of enterprises, Tobin's Q value will increase accordingly 4.233 shows that R&D investment is positively correlated with the company's market performance. The results are shown in Figure 5.

(2) The impact of R&D investment intensity on operating gross profit margin

The statistical performance of this model is significant, reaching 117.457, indicating that in the regression analysis of operating gross profit margin, the regression model of R&D investment intensity and operating gross profit margin is overall significant. The adjusted model is 22.5%, indicating that the regression equation explains 22.5% of the variation of operating gross profit margin. At the same time, the collinearity diagnosis result also shows that there is no collinearity problem among the explanatory variables in the equation. The nonstandardized coefficient of R&D investment intensity and operating gross profit margin is 0.714, and the T value of 9.296 is positive and significant, indicating that the R&D investment of an enterprise can directly promote the growth of operating gross profit margin and thus bring business performance to the enterprise. An increase of 1 will increase the operating gross profit margin by 0.714 accordingly. The coefficient of the operating gross profit margin is much smaller than the coefficient of Tobin's Q value, indicating that R&D investment has a greater effect on the market value of the company, which proves that R&D investment and corporate finance performance are positively correlated, and the results are shown in Figure 6.

5. .Conclusions

This article uses the 2018-2020 GEM listed companies as a sample, based on the perspective of production factors, to study the impact of R&D investment and corporate performance. The article divides the entire industry on the Growth Enterprise Market into labor-, capital-, and technology-intensive industries by calculating the corresponding production factor intensity indicators. Through the use of statistical software SPSS 13.0, descriptive statistical analysis, correlation analysis, and regression analysis were performed on the full sample and subsamples. At the same time, the group regression method was used to test whether production factors have a moderating effect on R&D investment and corporate performance. It also examines the specific adjustment and hysteresis effects of production factors in it. In the research of this article, the factors of production are divided into three parts: labor factors, capital factors, and technology factors. It is found that the factors of production have a significant impact on the relationship between R&D investment and corporate performance. This conclusion will guide my country's GEM in the future. Companies with different factor intensives carry out R&D activities to improve corporate performance, which has certain practical guiding significance.

Data Availability

This article is not supported by data.

Conflicts of Interest

The author declares that he/she has no conflicts of interest.

References

[1] W.-Y. Kim and K.-M. Yang, "regional upgrade plan for smart circulation of pedestrian - case study of district circulation including pedestrian -," *Journal of the Architectural Institute of Korea Planning & Design*, vol. 32, no. 11, pp. 39–46, 2016.

[2] L. Wang, R. Huang, and R. Wu, "Tropical cyclogenesis associated with four types of winter monsoon circulation over the South China Sea," *Atmospheric Science Letters*, vol. 17, no. 5, pp. 326–333, 2016.

[3] T. Gao, L. Li, T. Chen, L. Shi, Y. Yang, and G. Li, "DNA-oriented shaping of cell features for the detection of rare disseminated tumor cells," *Analytical Chemistry*, vol. 91, no. 1, pp. 1126–1132, 2018.

[4] Y. Wang, A. D'Ariano, J. Yin, L. Meng, T. Tang, and B. Ning, "Passenger demand oriented train scheduling and rolling stock circulation planning for an urban rail transit line," *Transportation Research Part B: Methodological*, vol. 118, pp. 193–227, 2018.

[5] C. Shiyin and M. A. Zhiyu, "Influencing factors of rural land internal circulation market in Guangdong province," *Asian Agricultural Research*, vol. 12, no. 4, pp. 32–37, 2021.

[6] E. Jernström, V. Karvonen, T. Kässi, A. Kraslawski, and J. Hallikas, "The main factors affecting the entry of SMEs into bio-based industry," *Journal of Cleaner Production*, vol. 141, pp. 1–10, 2017.

[7] M. Yang, X. Zhao, and T. Meng, "What are the driving factors of pesticide overuse in vegetable production? Evidence from Chinese farmers," *China Agricultural Economic Review*, vol. 11, no. 4, pp. 672–687, 2019.

[8] M. Wang and C. Feng, "Impacts of oriented technologies and economic factors on China's industrial climate mitigation," *Journal of Cleaner Production*, vol. 233, pp. 1016–1028, 2019.

[9] G. De Pietro, L. Gallo, R. J. Howlett, and L. C. Jain, "Smart innovation, systems and technologies," in *Intelligent Interactive Multimedia Systems and Services: Proceedings of 2018 Conference*, vol. 98, pp. 53–63, 2019.

[10] J. Chrząszcz, Ł. Skonieczny, G. Protaziuk, M. Kryszkiewicz, and H. Rybinski, "Studies in big data," in *Intelligent Methods and Big Data in Industrial Applications*, vol. 40 of Studies in Big Data, pp. 103–113, Springer International Publishing, Cham, 2019.

[11] H. S. Behera and D. P. Mohapatra, "Advances in intelligent systems and computing," in *Computational Intelligence in Data Mining—Volume 2: Proceedings of the International Conference on CIDM, 5-6 December 2015*, vol. 411, pp. 229–237, Cape Town, South Africa, 2016.

[12] A. Akay, A. Dragomir, and B. E. Erlandsson, "Assessing antidepressants using intelligent data monitoring and mining of online fora," *IEEE Journal of Biomedical & Health Informatics*, vol. 20, no. 4, pp. 977–986, 2016.

[13] H. AbouEisha, T. Amin, I. Chikalov, S. Hussain, and M. Moshkov, "Intelligent systems reference library," in *Extensions of Dynamic Programming for Combinatorial Optimization and Data Mining*, vol. 146 of Intelligent Systems Reference Library, pp. 85–104, Cham, 2019.

[14] Y. Y. Jo, S. W. Kim, S. W. Cho, D. H. Bae, and H. Oh, "High-performance data mining with intelligent SSD," *Cluster Computing*, vol. 20, no. 2, pp. 1155–1166, 2017.

[15] J. Mizera-Pietraszko, P. Pichappan, and L. Mohamed, "Advances in intelligent systems and computing," in *Lecture Notes in Real-Time Intelligent Systems*, vol. 756 of Advances in Intelligent Systems and Computing, pp. 332–341, Springer International Publishing, Cham, 2019.

[16] M. Nematollahi, R. Akbari, S. Nikeghbalian, and C. Salehnasab, "Classification models to predict survival of kidney transplant recipients using two intelligent techniques of data mining and logistic regression," *International Journal of Organ Transplantation Medicine*, vol. 8, no. 2, pp. 119–122, 2017.

[17] J. Zhang, S. O. Williams, and H. Wang, "Intelligent computing system based on pattern recognition and data mining algorithms," *Sustainable Computing: Informatics and Systems*, vol. 20, pp. 192–202, 2018.

[18] V. B. Aggarwal, V. Bhatnagar, and D. K. Mishra, "Advances in intelligent systems and computing," in *Big Data Analytics: Proceedings of CSI 2015*, vol. 654, pp. 717–726, New Delhi, India, 2018.

[19] H. S. Behera, J. Nayak, B. Naik, and D. Pelusi, "Advances in intelligent systems and computing," in *Computational Intelligence in Data Mining: Proceedings of the International Conference on CIDM 2017*, vol. 711, pp. 697–707, Beijing, China, 2019.

[20] R. Ghazali, M. M. Deris, N. M. Nawi, and J. H. Abawajy, "Advances in intelligent systems and computing," in *Recent Advances on Soft Computing and Data Mining*, vol. 700 of Advances in Intelligent Systems and Computing, pp. 318–329, Springer International Publishing, Cham, 2018.

[21] M. Alenezi and B. Qureshi, "Advances in intelligent systems and computing," in *5th International Symposium on Data Mining Applications*, vol. 753 of New Feature Extraction Approach Based on Adaptive Fuzzy Systems for Reliable Biometric Identification, pp. 210–222, Springer International Publishing, Cham, 2018.

[22] S. Koren, "How to compare and cluster every known genome in about an hour," *Neural Computation*, vol. 27, no. 7, pp. 1373–1404, 2016.

[23] H. Liu, Y. Wang, J. Liu, J. Yang, Y. Chen, and H. V. Poor, "Authenticating users through fine-grained channel information," *IEEE Transactions on Mobile Computing*, vol. 17, no. 2, pp. 251–264, 2018.

[24] S. M. Sombolestan, A. Rasooli, and S. Khodaygan, "Optimal path-planning for mobile robots to find a hidden target in an unknown environment based on machine learning," *Journal of Ambient Intelligence and Humanized Computing*, vol. 10, no. 5, pp. 1841–1850, 2019.

[25] I. Kavakiotis, O. Tsave, A. Salifoglou, N. Maglaveras, I. Vlahavas, and I. Chouvarda, "Machine learning and data mining methods in diabetes research," *Computational and Structural Biotechnology Journal*, vol. 15, no. C, pp. 104–116, 2017.

WILEY | Hindawi

Research Article

Impact of Enterprise Financing Constraints on Labor Income Share Based on Internet of Things Data Analysis Technology

Mengting Zhang🆔, Wei Xu, and Jun Zhang🆔

Business School, Wuxi Taihu University, Wuxi, 214064 Jiangsu, China

Correspondence should be addressed to Mengting Zhang; zhangmt@wxu.edu.cn

Although the Chinese economy has developed rapidly since the reform and opening up, the income distribution gap is widening year by year. The final social income distribution pattern is highly dependent on the primary distribution pattern. Therefore, the changing trend and influencing factors of labor income share have become the focus of academic research and the focus of government attention. Based on this, this article proposes enterprise financing based on Internet of Things data analysis technology. Studies on the impact of restraints on labor income shares will help further research on the impact of corporate financial restraints on future labor income shares. Based on the financial data reports published in the CCER database and the company's IPO prospectus and annual report, this paper discusses whether the company's key business products belong to the Internet of Things' key technology application categories. Take 226 IoT companies as the research objects of this article, and conduct a secondary screening. The final survey sample is used to investigate the impact of corporate funding constraints on labor income share. Tests have proved that among the 179 resource-based enterprises undergoing transformation, 109 enterprises have undergone intraindustry transformation, accounting for 48.23% of the overall sample and 60.89% of the sample of transformed enterprises. Downstream expansion makes the business industry expand. This shows that funding constraints have a negative impact on labor income share. This is primarily the result of the impact of the long-term debt-to-asset ratio on labor income share.

1. Introduction

The share of labor income in the primary distribution plays an important role in the economy and society that cannot be ignored. At the same time, during the new normal period of economic change, my country's economy emphasizes structural optimization and upgrades and advocates supply-side reforms. Adjusting and upgrading the industrial structure is becoming more and more important. Declining labor income shares affect consumer demand and threaten social harmony, stability, and sustainable development. Therefore, in the context of inconsistent understanding of the evolution trend of labor income share in existing research, and the increasingly important and urgent industrial structure transformation and upgrading, it is necessary to further examine the changing trend of labor income share in China and thor-

oughly study the impact of corporate financing constraints on labor income share path.

SMEs are the fundamental force for building a market economy and play an important role in the prosperity of the market economy. They are close to users, serve users, and generally operate in the most competitive areas of the market. A series of properties make it innovative in research and development. In this respect, it has the unparalleled innate advantage of large- and medium-sized businesses. The Ministry of Industry and Information Technology of China pointed out that the contribution rate of SMEs in national invention patents, enterprise innovation, and new product research and development can reach approximately 65%, 75%, and 80%, respectively. They are the main implementers of research, development, and innovation. In the main body and main force of my country's scientific and

technological progress, its R&D investment level is closely related to the speed of my country's economic development, overall innovation capability, and competitiveness [1, 2].

In the past ten years, scholars at home and abroad have conducted a lot of pioneering and fruitful research on the impact of corporate financing constraints on labor income share based on Internet of Things data analysis technology and accumulated rich research results and research experience. From the perspective of the influence of financialization on the market power of enterprises and the degree of labor market competition, Tian and Nie link financialization with the proportion of labor income through theoretical derivation and analyze whether the financialization of physical enterprises will affect labor income. In addition, he also used the empirical data of Chinese listed companies from 2008 to 2016 to conduct empirical tests. The results show that the increase in the degree of financialization has reduced the price increase and the rate of return. In addition, in the eastern region, during the period of capital and technology-intensive industries and monetary policy tightening, the degree of financialization has a greater negative impact on labor income. However, its overall research lacks data support, and more data is needed to support its conclusions [3]. Yin pointed out that the increase in the shareholding of institutional investors will have a greater impact on corporate governance. Therefore, the asymmetry of information and agency costs of listed companies can be improved. Based on Almeida's financing constraint model, it verifies the relationship between institutional investors and financing constraints from the perspective of heterogeneity. The results show that financing constraints are common in enterprises. In non-state-owned enterprises, stress-resistant institutional investors can significantly alleviate financing difficulties. The experimental results lack more data support so that the results obtained through Almeida's financing constraint model are irrelevant. However doubtful [4], Fang pointed out that in corporate debt financing, the combination of information asymmetry, agency issues, and transaction costs leads to the difference between the internal and external financing costs of the company, which leads to constraints on corporate debt financing. It uses models to study debt financing constraints and analyzes its impact on corporate investment behavior choices to help companies respond more reasonably to debt financing constraints, optimize investment behavior choices, fully enhance corporate value, and enhance competition between companies. However, the research did not clearly put forward the different factors between the internal and external financing costs of enterprises [5, 6].

This paper analyzes the effect of corporate financing constraints on labor income share through empirical analysis, reveals the impact of corporate financing constraints on primary income distribution, provides a better theoretical explanation and model basis for quantitative research on income distribution, and provides a new way to solve the problem of income disparity thoughts and enrich the theory of the primary distribution of labor income. In this paper, we qualitatively and quantitatively analyze the effects of corporate financial constraints on labor income shares and break down

fluctuations in labor income shares into interindustry effects and intraindustry effects. It is hoped that the government will be able to adopt relevant policies in developing constraints on corporate financing. Develop and innovate systems, take into account corporate funding constraints and increasing labor income shares, and reasonably adjust income distribution to provide a useful policy base.

2. Corporate Financing Constraints and Labor Income Share

2.1. IoT Data Analysis Technology. Entering the era of the Internet of Things, data on the Internet will explode at an unprecedented rate. To retrieve the information people need from massive data, some other related knowledge is needed, such as the popular statistical machine learning. Data mining, recommendation systems, etc. are all based on massive user data and modeling user data and then used to predict new users or give relevant recommendations to achieve the purpose of data commercialization; that is, use known data to obtain related business profits [7, 8].

Suppose that n sensors are deployed in the grid, and the surrounding environment is periodically monitored for data collection. The calculation IED node is located in the center of the area. At this time, the network can cover the entire monitoring area [9]. Let s_i denote the i sensor node, then the set of nodes is $S = \{s_i | 1 \le i \le n\}$, and the energy consumption of the node sending bit data to a position with a distance of d is as follows:

$$E_{Tx}(l, d) = \begin{cases} lE_{\text{elec}} + l\varepsilon_{fs}d^2, & d < d_0, \\ lE_{\text{elec}} + l\varepsilon_{mp}d^4, & d \ge d_0, \end{cases} \quad (1)$$

where E_{elec} represents the energy consumption of the transmitting circuit. If the transmission distance is less than the threshold d_0, the power amplification loss adopts the free space model; if the transmission distance is greater than or equal to the threshold d_0, the multipath attenuation model is adopted.

The collection of n sensing data sampled by nodes in the monitoring network in chronological order is denoted as follows:

$$TS = \{(t_1, \alpha_1), (t_2, \alpha_2), \cdots, (t_n, \alpha_n)\}, \quad (2)$$

where t represents the acquisition time and α' represents the predicted value corresponding to t.

In order to minimize the sum of squares of errors between the sampled data and the fitted curve, let

$$D = \sum_{i=1}^{n} d_i^2 = \sum_{i=1}^{n} [\alpha_i - (a + bt_i)]^2. \quad (3)$$

At the same time, in order to make the predicted data closer to the true value, D finds the second-order partial derivative of a and b. Solutions have to

$$\begin{cases} a = \bar{\alpha} - b\bar{t}, \\ b = \dfrac{\sum_{i=1}^{n} t_i \alpha_i - nt\bar{\alpha}}{\sum_{i=1}^{n} t_i^2 - n\bar{t}^2}. \end{cases} \quad (4)$$

The heuristic mathematical expression of CFS is as follows:

$$\text{Merits}(K) = \frac{k\bar{r}_{cf}}{\sqrt{k + k(k-1)\bar{r}_{ff}}}, \quad (5)$$

where Merits represents an evaluation score containing K feature subset S. The larger the value, the greater the correlation between the feature subset S and the classification result [4, 10].

Assuming that an information source continuously emits a series of uncertain source symbols, if these source symbols C have a value $C_1, C_2, \cdots, C_n$, the corresponding uncertainty probability is $P_1, P_2, \cdots, P_n$, and these source symbols are independent of each other [11, 12]. Then, the information entropy of these information source symbols can be defined as follows:

$$H(C) = -\sum_{i=1}^{n} P(C_i) \log_2 P(C_i), \quad (6)$$

where n is the sample set, class C_i means that n sample sets contain individual samples, and $H(C)$ means the degree of uncertainty of the source samples C divided into n classes [13, 14].

Assuming that a certain feature F in the sample set S has multiple values $\{F_1, F_2, \cdots, F_v\}$, the conditional entropy of dividing S under the precondition of a given feature F can be expressed as $H(C \mid F)$; then,

$$H(C \mid F) = -\sum_{i=1}^{m} \sum_{j=1}^{v} P(F_j) P(C_i \mid F_j) \log_2 P(C_i \mid F_j)$$
$$= \sum_{j=1}^{v} P(F_j) H(C \mid F = F_j), \quad (7)$$

where $H(C \mid F = F_j)$ represents the conditional entropy when the feature F takes the value F_j:

$$H(C \mid F = F_j) = -\sum_{i=1}^{m} P(C_i \mid F = F_j) \log_2 P(C_i \mid F = F_j)$$
$$= -\sum_{i=1}^{m} P_{ij} \log_2 P_{ij}. \quad (8)$$

Given the large-scale polymorphic and multidimensional properties of the Internet of Things perception data in real time, the storage, calculation, and analysis of the perception data at the bottom of the Internet of Things are not only fully utilized, increasing the number of intelligent heterogeneous network elements and intelligence in the perceptual layer of the Internet of Things. It can also reduce the network transmission consumption brought by the application layer of a large amount of sensing data uploading and solve the problem of large processing feedback delay at the application layer [15, 16]. After the IoT terminal device perceives the surrounding environment data, it needs to transmit these data. Therefore, it needs the support of the network layer. Through the connection of the network layer, the objects can be connected in series to form a mesh structure. In addition to transmission, the confidentiality and correctness of data transmission must be ensured, while stability and continuity are required. The higher-level requirement is to occupy less bandwidth, and the transmission process requires less energy consumption.

2.2. Corporate Financing Constraints. The investment decision of an enterprise is closely related to the financing situation. Asymmetric information will increase the cost of external financing of the enterprise. It is difficult for enterprises facing financing constraints to obtain the required funds from the outside, so they have to give up good investment opportunities. The financial market is the basic environment for the economic activities of enterprises, and its degree of development will undoubtedly affect the investment and financing behavior of enterprises [17, 18]. In the actual capital market, a single investor cannot understand the business situation of the company due to lack of information, and the cost of evaluating the company is very high. Therefore, investors with idle funds are not willing to invest their funds in companies and projects that they do not understand. The existence of information asymmetry is not conducive to corporate financing, so that the best investment opportunity is missed.

The R&D activities of enterprises have a strong demand for funds. It is necessary not only to ensure that there are sufficient funds to carry out activities but also to ensure that funds can be supplied in time to support the continued activities [19]. However, based on the various characteristics of R&D investment itself, such as information asymmetry between the supply and demand sides of funds caused by the confidentiality of R&D core information, the uncertainty of the income results caused by the long R&D cycle, and the low guarantee value of the limited collateral in R&D, all make it difficult for enterprises to obtain funds for R&D from the outside, or although they can obtain funds, the cost is relatively high, and the use of funds is also subject to greater restrictions.

If the company's capital liquidity is insufficient, it will cause the company to be unable to pay the initial fixed costs necessary for export, and this cost is an indispensable condition for the company to conduct foreign trade. Even for companies, they have higher labor productivity and expect that exports will bring certain profits to the company, but if the company's funds are not enough to pay the fixed costs in the early stage, then they will not be able to carry out export trade. Therefore, from this perspective, the financing constraints faced by enterprises will be limited to whether they can participate in export trade [19].

2.3. Labor Income Share. China has always been at the low end of the world's industrial chain. Many multinational

investment companies have transferred some industries to China in order to save costs in order to seek advantages in labor costs. For China, different industries transferred from developed countries to my country will also cause corresponding changes in my country's labor income share. If the transfer is capital-intensive industries, then the high wages in these industries will drive the increase in China's overall labor income share and increase the wage gap in my country with different skills; if the transfer is labor-intensive industries, it will inevitably lead to low-end industry competition intensified, thereby reducing the labor income share [20, 21].

Based on this model, this paper adds a set of control variables that may affect labor income shares. The mathematical expression of the model is as follows:

$$LS_{it} = C + \alpha \mathrm{Trade}_{it} + \gamma_i + \delta_t + \mu_{it}, \tag{9}$$

$$LS_{it} = C + \alpha \mathrm{Trade}_{it} + \theta X_{it} + \gamma_i + \delta_t + \mu_{it}. \tag{10}$$

In the formula, LS_{it} represents my country's labor income share as the explained variable of the regression equation. Trade_{it} represents the total amount of foreign trade, as the main explanatory variable of the model, because trade involves imports and exports. In order to further analyze the impact of imports and exports on the labor income share, this variable is specifically divided into import trade and export trade species [22, 23].

The elasticity of capital output is as follows:

$$e_{Kt} = \frac{\partial Y_t}{\partial K_t} \cdot \frac{K_t}{Y_t} = MP_{Kt}{}^{1-\sigma} \pi^\sigma \left(\Gamma_t^K\right)^{\sigma-1}. \tag{11}$$

The labor output elasticity is as follows:

$$e_{Lt} = \frac{\partial Y_t}{\partial L_t} \cdot \frac{L_t}{Y_t} = MP_{Lt}{}^{1-\sigma} (1-\pi)^\sigma \left(\Gamma_t^K\right)^{\sigma-1}. \tag{12}$$

In the process of industrial transfer, foreign direct investment is the most direct manifestation. There are also differences in propensity to consume between capitalists and workers. Workers and capital owners have different marginal propensity to consume. As the labor income share increases, workers' incomes generally increase, capital owners' profits decrease, and workers' consumption increases. The magnitude is greater than the decrease in capitalist consumption, total consumption increases, and income increases [24, 25]. The increase in the labor income share reduces the average propensity to save in the whole society, and the total amount of loanable funds for investment decreases, which has a restraining effect on investment. However, considering China's high public investment rate and overcapacity, China's high investment problem should not be a problem of total volume, but a problem of investment structure. The reduction of total investment and the optimization of investment structure can also promote rapid economic development. The increase in the income share is conducive to increasing the income of laborers and promoting private investment.

In terms of labor income share, the technology contribution of the capital-intensive sector is higher than the average contribution of the labor-intensive sector, the technological progress in my country is still the introduction of technology, and independent innovation is second. When industrialization develops to some extent, after developing countries acquire a certain amount of capital accumulation and technological research ability, the rate of capital accumulation tends to decrease to some extent, and the production efficiency of capital tends to be balanced. In the intensive industrial development that is heading, the current technological progress is dominated by independent R&D and innovation. The demand for human capital has increased, and the output efficiency of human capital has gradually improved. This is manifested as capital-saving technological progress, which leads to an increase in labor income [26, 27]. With the development of the economy, the labor income share is showing a pattern of changes, and my country is in a downward stage of declining labor income share.

3. Experimental Design of the Influence of Enterprise Financing Constraints on Labor Income Share

3.1. Data Sources. Based on the financial data report published by the CCER database and the company's IPO prospectus and annual report, this article will conduct a secondary screening based on whether the company's main business products belong to the Internet of Things key technology application classification and exclude those that do not meet the requirements of the Internet of Things technology concept and belong to ST or companies with missing data, finally got 226 IoT listed companies as the final research sample of this article.

3.2. Sample Index Selection. This paper selects dividend payment rate, interest guarantee multiple, and enterprise size as the main proxy variable indicators when judging the degree of corporate financing constraints. The maximum percentage of dividends in a company's net earnings per share is 100%, and the minimum is 0%. A low dividend payout ratio means that companies have to face higher external financing constraints. The data on the company's dividend per share and net income selected in this article are derived from the company's annual financial income statement and owner's equity statement. In this paper, based on the basic characteristics of my country's Internet of Things listed companies and considering the availability of index data, the independent variables of the binary logistic regression model are selected as return on equity (ROE), asset-liability ratio (LEV), working capital allocation ratio (WCAR), and cash flow ratio (CFR). It is measured by the ratio of accounts receivable to the total assets of the enterprise. It indicates the amount of commercial loans that a company can provide to other sellers as a supplier. It is also a key indicator that reflects the ability of enterprises to obtain financing in commercial credit. The value of this indicator is also inversely related to financing constraints.

3.3. Model Building. The system GMM estimation method sends the difference equations and levels as equations and uses more information than the first-order GMM to control intrinsic problems and improve the effectiveness of the estimation results. If the cash flow coefficient CF/K is significantly positive, it indicates that the investment scale of the company is positively correlated with the internal cash flow, and that the investment activity of the company faces the constraint of external financing. It reflects the reality. If the coefficients of the lagging variable of investment expenditures are all significantly positive, it means that there is obvious continuity of corporate investment behavior. At the same time, in order to prevent the overseas financing behavior of the enterprise after the foreign direct investment from forming a certain mitigation effect on the financing constraints of the enterprise, only the first foreign direct investment behavior of the enterprise is considered in this regression. In addition, in order to avoid the influence of endogeneity on the estimation results, the explanatory variable adopts a lagging approach.

3.4. Data Processing. In order to test the applicability of the regression model of each model variable and the multicollinearity of the independent variables, this paper uses STATA/SE12.0 software to perform the Pearson correlation test on the above three different regression model variables based on the specific data calculated by each indicator variable. Here, this article has carried out a transformation on the measurement of the comprehensive index of financing constraints, replaced the comprehensive index of financing constraints score A with score B, and used the probit model to conduct further robustness tests. And the logit model is still used for regression verification again.

4. Influence of Enterprise Financing Constraints on Labor Income Share

4.1. Analysis Based on the Regression Results of the Logit Model. The larger the KZ index value, the more severe the financing constraints the enterprise faces. The regression results based on the logit model are shown in Table 1.

It can be seen from Table 1 that the coefficient of cash dividend is -36.2548, which shows that companies with fewer dividend distributions face higher financing constraints. The smaller the company's dividend distribution, the more net profit will be reserved for own use in the profit distribution. This reflects that companies are facing a relatively high degree of financing constraints and need to use most of their net profits to meet the capital needs for corporate development. The coefficient of Tobin's Q is 0.522, which shows that companies with more growth opportunities face higher financing constraints. Companies with more growth opportunities generally need more capital to meet their development needs, and the higher the degree of financing constraints they face. The above coefficients all reject the null hypothesis that the coefficient is 0 at the 1% probability level, indicating that these five indicators are a good measure of the degree of financing constraints of Chinese enterprises.

TABLE 1: Regression results based on the logit model.

Evaluation coefficient	CF/A	DIV/A	C/A	LEV	Q
KZ	-13.9816	-36.2548	-5.5084	3.8642	0.5220
	(0.3729)	(1.0295)	(0.1534)	(0.1135)	(0.0180)

4.2. Analysis Based on Individual Indicators

4.2.1. Analysis Based on KZ Index. From 2011 to 2020, the KZ index of sample companies is shown in Figure 1.

From Figure 1, we can see that between 2011 and 2020, the sample company's KZ index rose from 1.22 in 2011 to 2.23 in 2020, an increase of 80.07% compared to 2011. This shows that the funding constraints companies are facing are becoming more and more stringent. It is serious. From 2013 to 2020, the KZ index is on a downward trend, gradually declining to 1.86 in 2011 and 1.66 in 2012. Compared to 2011, it is still up 50.86% and 36.29%, indicating that corporate funding constraints have not improved. From 2013 to 2017, the KZ index was still fluctuating. It went through a process of rising first and then falling. It increased from 1.67 in 2013 to 2.16 in 2015 and decreased to 1.57 in 2017, but it had increased by 76.98% and 29.02% respectively from 2011. The above analysis also further illustrates the current situation in which Chinese companies are widely affected by funding constraints.

4.2.2. Analysis Based on R&D Funding. My country's R&D funding investment is shown in Figure 2.

It can be seen from Figure 2 that the intensity of R&D investment in my country (the ratio of total R&D expenditure to gross domestic product) has also shown a trend of increasing year by year. In 2010, my country's R&D investment intensity was 1.37%; in 2020, the R&D investment intensity exceeded the 1.5% mark, reaching 1.66%; as of 2020, my country's R&D investment intensity was 2.13%. The main bodies of technological innovation in my country are mainly divided into enterprises, colleges and universities, and scientific research institutions. The overall R&D investment situation cannot accurately represent the research and development investment situation of each subject. Therefore, this article further discusses the R&D investment status of enterprises as one of the main technological innovation subjects.

4.2.3. Microenterprise R&D Investment. Figure 3 shows the R&D expenditures of microenterprises.

It can be seen from Figure 3 that, as the backbone of my country's technological innovation, microenterprises' total R&D expenditures have shown an increasing trend, but the proportion of R&D expenditures in the country has fluctuated slightly, reflecting the possibility of financing constraints from the side. This has had an impact on corporate R&D expenditures. In 2007, Chinese enterprises invested 268.1 billion yuan in R&D expenditures, accounting for 72.28% of the total R&D expenditures of the country, far exceeding the proportion of R&D expenditures of colleges and universities and
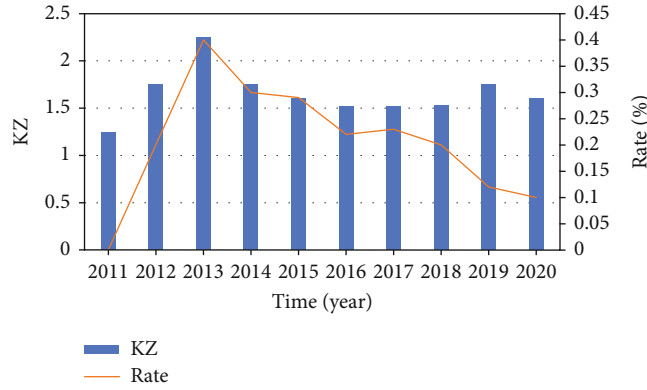
Figure 1: The KZ index of sample companies from 2011 to 2020.
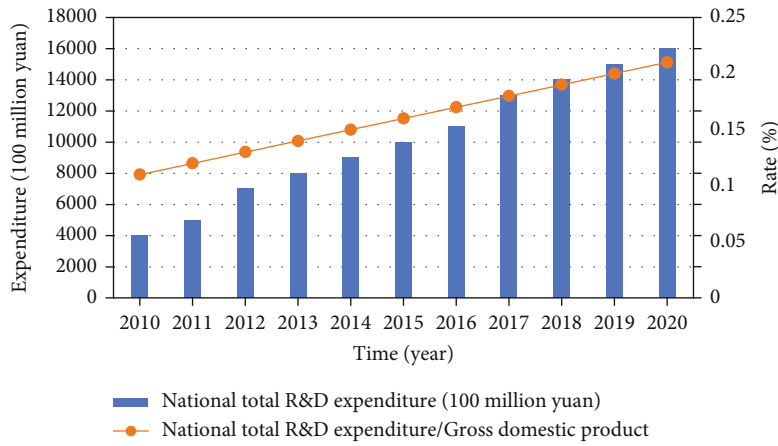
Figure 2: Our country's R&D funding input.
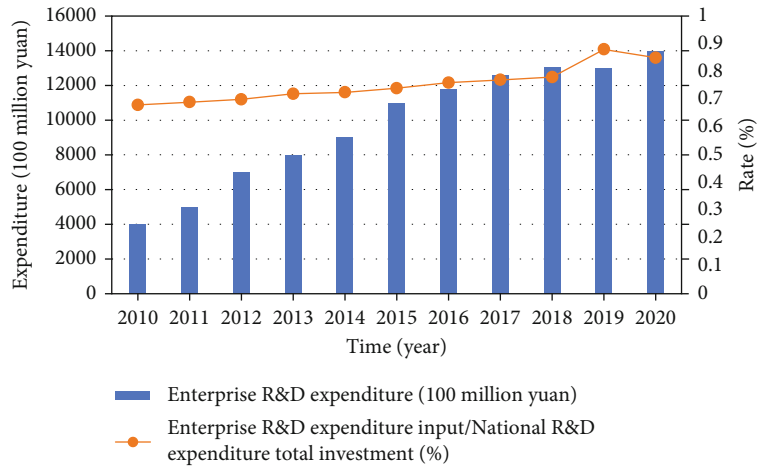
Figure 3: Microenterprise R&D expenditures.

professional scientific research institutions in the total R&D expenditures of the country, and it further proves the dominance of microenterprises in our country's technological innovation. From 2013 to 2014, the proportion of corporate R&D expenditures in the total R&D expenditures of the country increased significantly, from 73.42% in 2013 to

75.74% in 2014, an increase of 2.32%. In 2014, corporate R&D expenditures also broke through the trillion yuan mark, reaching 1.01 trillion yuan, accounting for 77.30% of the country's total R&D expenditures. But by 2015, the proportion of corporate R&D investment in the total R&D expenditure of the country has declined, to 76.79%. As of 2017, the

TABLE 2: Variable descriptive statistics.

Variable	Mean	Standard deviation	Minimum	Median
Total number of patent applications	101.2165	490.9228	1.0000	24.0000
Invention patent application	47.9385	290.2382	0.0000	9.0000
Utility model application	44.3933	211.3312	0.0000	10.0000
Design application	8.8846	41.6548	0.0000	0.0000
Financing constraints	1.7756	1.5451	-2.7538	1.8065
R&D	5.0603	5.4002	0.0000	3.8000
Credit market development	1.3645	0.4985	0.5372	1.2111
Stock market development	0.3103	0.3205	0.0299	0.1809
Company size	21.8286	1.2328	18.3308	216136

R&D expenditure of Chinese enterprises was 137 million yuan, accounting for 77.59% of the national R&D expenditure.

4.3. Analysis Based on Variable Descriptive Statistics. The descriptive statistics of the variables used in this paper are shown in Table 2. The minimum value of the total number of patent applications of the explained variable enterprises is 1, and the maximum value is 20,007. This shows that there are large differences in technological innovation capabilities between different companies. Some companies have strong innovation capabilities and can apply for more patents within a year, while some companies are obviously lacking in innovation capabilities and have almost no patent applications.

Based on the socialist market economy system with Chinese characteristics, state-owned enterprises enjoy the hidden protection of all aspects of the government, and at the same time, they undertake a heavier historical mission than private enterprises. On the one hand, the stable development of state-owned enterprises reflects the prosperity and stability of my country's economy and society to a certain extent. People may be extra conservative in their investment policies and tend to invest in projects that have shorter investment cycles and faster returns and can improve the current capital situation of the enterprise. On the other hand, in the process of my country's transition from a technological power to a technological power, state-owned enterprises have assumed the responsibility of playing a pioneering role. Even in the face of financing constraints, state-owned enterprises still have the motivation to devote themselves to higher technological content and stronger technological innovation activities. This article further explores the impact of financing constraints on the technological innovation activities of state-owned and non-state-owned enterprises. The specific regression results are shown in Table 3.

Technological innovation activities are closely related to the level of financing constraints. Companies with different levels of financing constraints have greater differences in technological innovation activities. Companies with high financing constraints have low investment in technological innovation, while companies with low financing constraints have higher investment in technological innovation. In order to more clearly illustrate the correlation between the degree of financing constraints and technological innovation activi-

TABLE 3: Specific regression results.

Parameter	Total number of patents	Patent	Practical	Exterior
Financing	-0.0155	-0.0041	-0.0207	-0.0084
	(0.0072)	(0.0081)	(0.0091)	(0.0147)
Constraints	0.0983	0.1114	0.1308	0.1769
	(0.0196)	(0.0220)	(0.0226)	(0.0388)
Company age	-0.0025	-0.0088	-0.0046	0.0210
	(0.0064)	(0.0070)	(0.0071)	(0.0100)
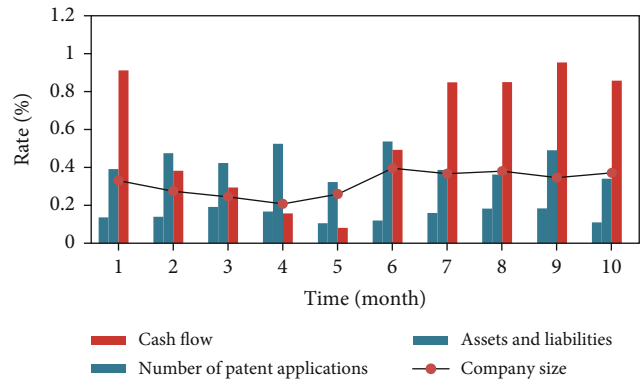
FIGURE 4: KW inspection result.

ties, this article continues to conduct a multisample bilateral test and KW rank sum test on the samples to analyze whether the innovation activities of enterprises with different financing constraints are significant. This can be seen from the inspection results in the third row to the fifth row. At the same time, the overall difference in asset-liability ratio and cash flow, the difference between the first two groups and the latter two groups, and the difference between groups have also passed the significance test, again confirming that the degree of financing constraints is positively correlated with the asset-liability ratio, and cash flow is negatively correlated. The KW inspection result is shown in Figure 4.

The result of variance decomposition is shown in Figure 5. It can be seen that the variance decomposition of technological innovation investment is basically stable after the fourth period. From the perspective of the variance
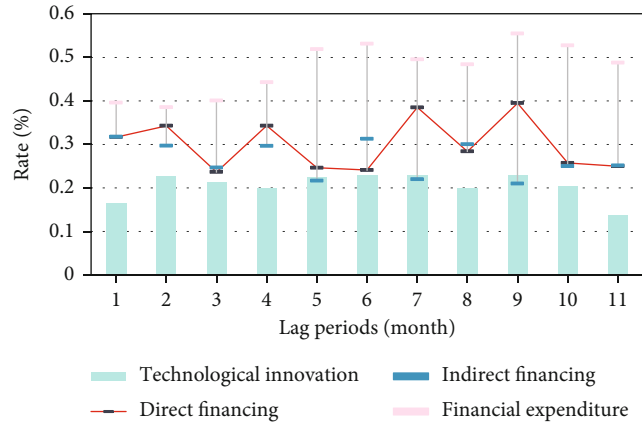
Figure 5: Variance decomposition result.
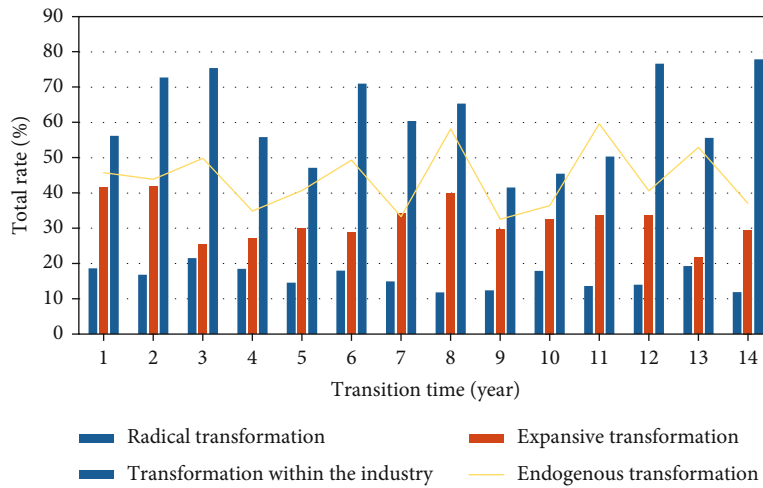
Figure 6: Resource-based enterprises account for the sample of transformed enterprises.

contribution rate of each variable, the fluctuation of technology innovation investment is mainly due to its own inertia, whether it is short term or long term. The variance contribution rate has always been dominant. The contribution rate reached 100% in the first period and then slowly declined. After the fourth period, it stabilized at 97.3%. The contribution of indirect financing to technological innovation investment volatility is relatively small, and it is basically stable at 0.4% after the fourth period, indicating that the impact of indirect financing on technological innovation changes is very weak. The variance contribution rate of direct financing is rising and stabilized at 2.2% after the fourth period, indicating that compared with the contribution of indirect financing, direct financing has a greater impact on technological innovation and can have a greater impact on technological innovation investment, mainly because the external financing channel for technological innovation in my country's strategic emerging industries is equity financing; that is, it is mainly affected by the direct financing market, while the indirect financing market with bank loans as the main method is not its main financing channel. The impact of technological innovation is relatively small. Fiscal science and technology expenditures have a small contribution to

technological innovation investment volatility, which shows that compared with the main external financing methods of enterprises, the policy guidance effect and financial support of fiscal science and technology expenditures are weak and can only be used as a supplement to the source of technological innovation funds. In general, the variance decomposition results show that the fluctuation of regional technological innovation investment mainly comes from its own inertia, followed by direct financing market, indirect financing market, and fiscal expenditures on science and technology.

There are a total of 226 listed resource-based companies studied in this article, of which 179 have undergone transformation, accounting for 79.20% of the overall sample, and 47 have not undergone transformation, accounting for 20.80% of the overall sample. This shows that, in the context of increasingly prominent resource environment, industrial structure reform, and fierce market competition, most companies are changing their original survival mode. Among the 179 resource-based enterprises that have undergone transformation, 109 of them have undergone intraindustry transformation, accounting for 48.23% of the overall sample and 60.89% of the sample of transformed enterprises. That is, most of them are keeping the main business unchanged.

Enterprise transformation chooses to expand upstream or downstream of the industry, which makes the enterprise industry expand. The sample of resource-based enterprises accounted for in transformation enterprises is shown in Figure 6.

5. Conclusions

This paper adopts the logit model to conduct empirical research on the impact of corporate financing constraints on labor income share after controlling the capital output ratio, technological progress, opening factors, and state-owned enterprise restructuring, and conducts a robustness test of the model; finally, adopts the decomposition method that measures the fluctuation of labor income share in China and decomposes the fluctuation of labor income share into interindustry effects and intraindustry effects. From the perspective of the fluctuation characteristics of labor income share, it examines the influence of industrial structure upgrading and changes in labor income share of various industries on the overall labor income share. Affected by the inherent characteristics of R&D investment and the limitations of SMEs, my country's SMEs have significant R&D input-cash flow sensitivity, and their R&D input level obviously depends on internal cash flow, and there are financing constraints. For non-state-owned enterprises and smaller enterprises, the degree of funding constraints they face is even more serious. The impact of funding constraints on labor income share is negative, primarily as a result of the impact of long-term debt-to-asset ratios on labor income share. This study still has some drawbacks, which are mainly reflected in the following: Many companies are not willing to disclose R&D input information, and it is difficult to obtain R&D input data. After screening, the sample size will be limited. Follow-up surveys should strive to increase the sample size to improve the universality of the survey results.

Data Availability

No data were used to support this study.

Conflicts of Interest

The authors declare that they have no conflicts of interest.

References

[1] I. Kitouni, D. Benmerzoug, and F. Lezzar, "Smart agricultural enterprise system based on integration of Internet of Things and agent technology," *Journal of Organizational and End User Computing*, vol. 30, no. 4, pp. 64–82, 2018.

[2] S. B. Tsai, "Using the DEMATEL model to explore the job satisfaction of research and development professionals in China's photovoltaic cell industry," *Renewable and Sustainable Energy Reviews*, vol. 2018, no. 81, pp. 62–68, 2018.

[3] X. Tian and P. Nie, "Econometric analysis of political connection affect corporate credit financing constraints based on fuzzy logic and SEM model," *Journal of Intelligent & Fuzzy Systems*, vol. 37, no. 1, pp. 441–454, 2019.

[4] Z. Yin, "Research on the relationship between China's supply-side structural reform and enterprise innovation–from the perspective of financing constraints," *World Scientific Research Journal*, vol. 6, no. 5, pp. 130–135, 2020.

[5] J. Fang, C. Liu, and C. Gao, "The impact of environmental regulation on firm exports: evidence from environmental information disclosure policy in China," *Environmental Science and Pollution Research International*, vol. 26, no. 36, pp. 37101–37113, 2019.

[6] S. B. Tsai and K. Wang, "Using a novel method to evaluate the performance of human resources in green logistics enterprises," *Ecological Chemistry and Engineering S*, vol. 26, no. 4, pp. 629–640, 2019.

[7] H. Agyei-Boapeah, "Easing financing and M&A investment constraints: the role of corporate industrial diversification," *Annals of Economics and Finance*, vol. 18, no. 2, pp. 277–290, 2017.

[8] F. Luo, "The impact of foreign direct investment on the labor income share of listed companies," *Modern Economy*, vol. 11, no. 2, pp. 541–560, 2020.

[9] Y. Liu and J. Wang, "Environmental pollution, environmental regulation, and labor income share," *Environmental Science and Pollution Research*, vol. 27, no. 36, pp. 45161–45174, 2020.

[10] N. Phaosathianphan, A. Leelasantitham, and H. K. Tang, "Understanding the adoption factors influence on the use of Intelligent Travel Assistant (ITA) for eco-tourists: an extension of the UTAUT," *International Journal of Innovation and Technology Management*, vol. 16, no. 8, article 1950060, 2019.

[11] M. Mehrabanpour, O. Faraji, R. Sajadpour, and M. Alipour, "Financial statement comparability and cash holdings: the mediating role of disclosure quality and financing constraints," *Journal of Financial Reporting and Accounting*, vol. 18, no. 3, pp. 615–637, 2020.

[12] P. Gonzalez-Gil, J. A. Martinez, and A. F. Skarmeta, "Lightweight data-security ontology for IoT," *Sensors*, vol. 20, no. 3, pp. 801–819, 2020.

[13] S. Yadav, S. Luthra, and D. Garg, "Modelling Internet of Things (IoT)-driven global sustainability in multi-tier agri-food supply chain under natural epidemic outbreaks," *Environmental Science and Pollution Research*, vol. 28, no. 13, pp. 16633–16654, 2021.

[14] W. Zhao, G. Wang, S. Atapattu, T. A. Tsiftsis, and X. Ma, "Performance analysis of large intelligent surface aided backscatter communication systems," *IEEE Wireless Communications Letters*, vol. 9, no. 7, pp. 962–966, 2020.

[15] Y. Wu, Y. Liu, S. H. Ahmed, J. Peng, and A. A. Abd el-Latif, "Dominant data set selection algorithms for electricity consumption time-series data analysis based on affine transformation," *IEEE Internet of Things Journal*, vol. 7, no. 5, pp. 4347–4360, 2020.

[16] B. Y. Ooi, Z. W. Kong, W. K. Lee, S. Y. Liew, and S. Shirmohammadi, "A collaborative IoT-gateway architecture for reliable and cost effective measurements," *IEEE Instrumentation and Measurement Magazine*, vol. 22, no. 6, pp. 11–17, 2019.

[17] M. Khan and D. H. Kim, "Service process modelling and performance analysis for composite context provisioning in IoT," *The International Arab Journal of Information Technology*, vol. 15, no. 1, pp. 141–147, 2018.

[18] C. Malathi and M. Nithyavelam, "IoT based access and analysis of wireless sensor node protocols with low power host

connectivity," *International Journal of Civil Engineering and Technology*, vol. 8, no. 12, pp. 89–95, 2017.

[19] J. A. Uqaili, S. Memon, H. M. Bilal et al., "Implementation of scalable and energy efficient WSN platform for IoT applications," *Indian Journal of Science and Technology*, vol. 13, no. 36, pp. 3725–3737, 2020.

[20] P. Sandner, A. Lange, and P. Schulden, "The role of the CFO of an industrial company: an analysis of the impact of blockchain technology," *Future Internet*, vol. 12, no. 8, pp. 128–131, 2020.

[21] L. Feng, J. Yu, F. Zhao, and H. Jiang, "A novel analysis of delay and power consumption for polling schemes in the IoT," *Tsinghua Science and Technology*, vol. 22, no. 4, pp. 368–378, 2017.

[22] Z. Qian and J. Gong, "Research on monitoring system of underground gas pipeline network based on Internet of Things and GIS," *Journal of Geomatics*, vol. 44, no. 1, pp. 111–114, 2019.

[23] Z. Meng, Z. Wu, C. Muvianto, and J. Gray, "A data-oriented M2M messaging mechanism for industrial IoT applications," *IEEE Internet of Things Journal*, vol. 4, no. 1, pp. 236–246, 2017.

[24] F. Conti, R. Schilling, P. D. Schiavone et al., "An IoT endpoint system-on-chip for secure and energy-efficient near-sensor analytics," *IEEE Transactions on Circuits and Systems I: Regular Papers*, vol. 64, no. 9, pp. 2481–2494, 2017.

[25] X. Yao, J. Wang, M. Shen, H. Kong, and H. Ning, "An improved clustering algorithm and its application in IoT data analysis," *Computer Networks*, vol. 159, no. AUG.4, pp. 63–72, 2019.

[26] A. Ait-Mlouk, F. Gharnati, and T. Agouti, "Application of big data analysis with decision tree for road accident," *Indian Journal of Science and Technology*, vol. 10, no. 29, pp. 1–10, 2017.

[27] W. Wu, S. An, C. H. Wu, S. B. Tsai, and K. Yang, "An empirical study on green environmental system certification affects financing cost of high energy consumption enterprises-taking metallurgical enterprises as an example," *Journal of Cleaner Production*, vol. 244, p. 118848, 2020.

Research Article

Big Data Credit Report in Credit Risk Management of Consumer Finance

Lu Gao[1] and Jian Xiao [2]

[1]School of Business, Shandong University, Weihai 264209, China
[2]School of Business, Beijing International Studies University, Beijing 100024, China

Correspondence should be addressed to Jian Xiao; xiaojian@bisu.edu.cn

Traditional consumer finance is a modern financial service method that provides consumer loans to consumers of all classes. With the gradual improvement of China's credit reporting system, big data credit reporting has effectively made up for the lack of traditional credit reporting and has been widely used in the consumer finance industry. In this context, the in-depth analysis of the specific application of big data credit reporting in the credit risk management of consumer finance and the strengthening of the research on the application of big data credit reporting in the credit risk management of consumer finance are urgently needed to be resolved in the economic and financial theoretical and practical circles' problem. This article mainly studies the research on credit risk management of consumer finance by big data. The experimental results of this paper show that the model has a good forecasting ability, can distinguish between normal loan customers and default loan customers, and is suitable for practical personal credit risk control business. The prediction accuracy of the default model of the fusion model is 97.14%, and the default rate corresponding to the actual business is 2.86%. By combining the risk items such as the blacklist and gray list in the Internet finance industry, the bad debt rate and illegal usury can be well controlled to meet industry supervision.

1. Introduction

Personal credit evaluation is an important evaluation standard in personal credit reporting, and it has gradually entered the stage of market-oriented development. However, for a long period of time, China has relied on the personal credit report of the personal credit center of the central bank as the standard, with the rise of big data.

There are many studies of personal credit risk assessment nationally and internationally, including studies of multi-source data, Internet data, and Internet behavior data, but few studies exist to assess credit risk for personal big data. In theory, this research can enrich and perfect the theoretical system of personal credit risk assessment [1, 2]. It will help implement China's inclusive financial strategy, lower the threshold for financial services, benefit more people, eradicate poverty, and achieve social equity. At the same time, it has a certain reference significance for the application of big data risk control in the industry [3, 4]. In terms of inter-

pretability, new big data algorithms can evaluate the importance of statistical indicators, and statistical indicators with the highest comprehensive ranking of statistical indicators have better interpretability. On the whole, some big data algorithms are excellent in accuracy and stability and can be used as a strategic reserve for my country's new generation of credit risk assessment models.

In theory, Morris and Shin decompose bank credit risk into bankruptcy and liquidity risk and define liquidity risk as the possibility of reverse bankruptcy caused by the bank's operation for free [5]. The "liquidity ratio" (that is, the ratio of cash to current liabilities) on the balance sheet has been shown to reduce liquidity risk, reduce excessive debt yields, and increase solvency uncertainty (a measure of portfolio volatility index). For the method in [6], Petrone and Latora believe that the interconnectedness of financial institutions will affect instability and credit crises. In order to quantify systemic risks, research shows that this mechanism is highly contagious; that is, the lower the correlation between

bankrupt banks, the greater the loss. This is in sharp contrast with the different advantages of standardized credit risk models adopted by banks and regulatory agencies. Therefore, this may depreciate the capital needed to overcome the crisis and lead to instability of the financial system [6]. And this mechanism has a negative impact on consumer finance. Aolin believes that joint loan guarantee agreements and mutual guarantee agreements between SMEs form the basis of the SME guarantee network. Therefore, a risk control plan is formulated according to the situation and importance of the company in the network. Use real-time mortgage data to determine the company's node location on the mortgage network (including Coriolis and near the company) to understand the protection mechanism and prevent systemic credit risks before the crisis [7].

The innovations of this paper are as follows: (1) Internet financial risk prevention strategies. From the unique perspective of big data, the actual business big data is applied to personal credit risk assessment, and method theory is derived to better provide services for Internet financial risk control. (2) Use the machine learning algorithm model to conveniently construct an individual credit risk assessment index system. XGBoost machine learning algorithm method application innovation and XGBoost in the processing of large amounts of data; its distributed, parallel computing; and GPU graphics card computing advantages significantly improve model training efficiency and can output feature importance scores, for noncorrelation. The index is filtered to facilitate the rapid establishment of a personal credit risk assessment index system.(3) Using the big data technology platform, the financial industry can establish a comprehensive risk view, and management and risk managers can understand the risk view of the financial industry from different dimensions and grasp the control status of its main risk points.

2. Proposed Method

2.1. Big Data Credit. Credit evaluation in the traditional sense is mainly based on the interbank financial lending relationship; that is, based on the historical economic data and behavior of the debtor, the overall credit level of the debtor is evaluated by a simple linear analysis. It can be seen that the advantage of this method of analyzing historical information based on the individual user is that the credibility of the data is often high, so the risk control is also relatively good [8]. In addition, due to the small dimensions of data collection, the time lag effect is obvious, and credit service products are relatively few [9, 10]. The emergence of big data has largely overturned this traditional credit reference model and concept. Big data credit can be regarded as "big data technology + traditional credit," which uses computer and Internet technology to support the model analysis and processing of data analysis and processing involved in credit information activities, which can more fully reflect the economic activities and the credit situation involved [11–13].

From the perspective of China's current credit information system, there are great differences in the sources, statistical calibers, and methods of processing credit information. From the perspective of foreign countries, it was originally only a financial product that provided online alternatives based on credit information. Later, it was the first to introduce big data technology in the industry, classify data sources, and use computers to perform simulation analysis to reduce credit risk. Control capacity has increased by about 40%, and credit information service efficiency has increased by nearly 90%.

2.2. Theory of Information Economics. Information economics is based on a society with a certain level of information technology development. Information economists believe that information is another important resource in the market in addition to labor and capital. Information is also an element of transaction costs. People who are in a strong position of information can obtain excess returns, while those who are weak in information pay excess costs, which will lead to a lack of fairness in market transactions, increase the cost of transactions, and ultimately reduce market efficiency [14, 15].

The personal credit information system can well solve the problem of adverse selection and moral hazard in information asymmetry, and it is an effective system that can transmit signals and punish unbelievers and encourage trustworthy people. The information sharing platform provided by the personal credit information system can allow the lender (such as a bank) to have a deep understanding of the credit status of the borrower before making a loan decision, effectively eliminating the problem of adverse selection, and after the loan, the penalty for personal credit information The existence of mechanisms can prevent the occurrence of moral hazard. From the perspective of the borrower, the borrower continuously improves its information in the personal credit information system and then improves its credit status by keeping promises, so that it can obtain a more favorable interest rate in future loans [16, 17]. In the long run, the establishment and improvement of the personal credit information system are beneficial not only to both borrowers and lenders on the micro level but also to the healthy development of the entire market economy on the macro level.

2.3. Credit and Credit. Credit information in English is "credit reporting" or "credit investigation," and its specific meaning is to collect credit data from nature. From this perspective, credit information is a series of activities with purposeful and directional information collection, processing, and evaluation [18, 19]. Literally, credit also means honesty and trust. It can be seen that credit often appears in the moral and ethical dimensions of economic life and is a relatively broad concept [20]. On a narrower level, credit specifically refers to the behavior of the goods or currency holder (creditor) to provide the borrower (debtor) with the goods or currency under the condition that the other party promises to repay, which is essentially a debt-debt relationship. Therefore, credit can be understood as the debtor's ability to repay, as well as credit and trust activities based on commodities or currencies [21, 22].

2.4. Construction and Optimization of Personal Credit Risk Assessment Index System Based on Big Data. With the continuous improvement of the personal credit system, personal
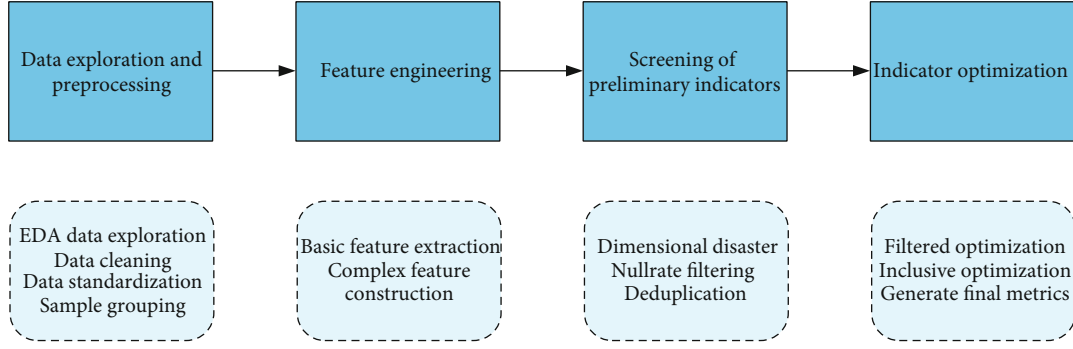
FIGURE 1: Steps to build a personal credit risk assessment indicator system.

credit behavior has gradually been recognized and become a necessary means to reflect personal morality and maintain social and economic order. It can be seen that personal credit risk assessment is of great significance for both commercial banks and residents. The construction of indicators requires high matching rate, high saturation, good timeliness, and multidimensional data. In this way, indicators are comparative and easy to understand, and it is easy to understand the actual situation of personal credit. The data studied in this project comes from the company's big data platform. The data of the big data platform comes from multiple sources, such as company APP product data, central bank credit data, Internet credit company credit data, and e-commerce company's online shopping data. Data are from three-party cooperative enterprises, Internet public data captured by crawlers, and data released by public inspection law. The data used in the research of this project are desensitized from multiple levels to ensure data security [23, 24]. The construction of a personal credit risk assessment indicator system requires engineering steps such as data exploration and preprocessing, feature engineering, preliminary screening of indicators, and optimization of indicators. The specific data flow diagram is shown in Figure 1.

2.5. Construction and Optimization of Personal Credit Risk Assessment Model Based on Big Data Index System. The main idea of logistic regression for classification is to establish a classification formula based on existing data to establish a regression formula for classification boundaries. The purpose of logistic regression is to find the best-fitting parameters of the nonlinear function sigmoid, which can be done by optimization algorithms [25, 26]. Among the optimization algorithms, the most commonly used is the gradient ascent algorithm. The gradient ascent algorithm can be simplified to a stochastic gradient ascent algorithm. The stochastic gradient ascent algorithm is equivalent to the gradient ascent algorithm, but it occupies less computing resources [27]. In addition, stochastic gradient ascent is an online algorithm that updates parameters when new data arrives without having to reread the entire data set of the batch operation. The advantage of logistic regression is that linear calculation is low in cost, easy to understand, and simple to implement. The disadvantage is that it is easy to underfit, and the classification accuracy may not be high. The applicable data types are numerical and nominal data.

The logistic regression model is a binary classification model, which can be expressed by a conditional probability distribution $p(y = 1 \mid x)$. The form is a parameterized logistic distribution. Assuming that the vector $x = (x_1, x_2, x_3, \cdots, x_n)$ has n independent variables, the condition rate $p(y = 1 \mid x) = p$ is the probability that the observed value occurs for x. Therefore, the logistic regression model can be expressed as follows:

$$p(y = 1|x) = \pi(x) = \frac{1}{1 + e^{-g(x)}}. \tag{1}$$

$f(x) = 1/(1 + e^{-g(x)})$ is called logistic function.

$$g(x) = w_0 + w_1 x_x + \cdots + w_n x_n. \tag{2}$$

The probability that y does not occur under x conditions is

$$p(y = 0|x) = 1 - p(y = 1|x) = 1 - \frac{1}{1 + e^{-g(x)}} = \frac{1}{1 + e^{g(x)}}. \tag{3}$$

The ratio of the probability of occurrence of y to the occurrence of y is

$$\frac{p(y = 1|x)}{p(y = 0|x)} = \frac{p}{1 - p} = e^{g(x)}. \tag{4}$$

This ratio is called the occurrence ratio of events (odds), and taking the log of odds gives

$$\ln\left(\frac{p}{1 - p}\right) = g(x) = w_0 + w_1 x_1 + \cdots + w_n x_n. \tag{5}$$

It can be seen that the dependent variable and the independent variable are nonlinear relationships, and the linear conversion can be performed by odds ratio of logarithmic occurrence.

Usually, the maximum likelihood estimation is used to find the parameters of the logistic model. The likelihood function is

$$L(w) = \prod_{1}^{n} (\pi(x_i))^{y_i} (1 - \pi(x_i))^{1-y_i}. \tag{6}$$

The basic idea of applying the logistic model to personal credit risk assessment is as follows: a sample of $(X_{i1}, X_{i2}, X_{i3}, \cdots, X_{in} : Y_i)(i = 1, 2, 3, \cdots, k)$ sample data of n groups of loan customers is given, where Y is a 0-1 variable and $Y_i = 1$ indicates that the ith customer is a bad credit customer.

The logistic equation is

$$P_i = \frac{\exp (\beta_0 + \beta_1 X_{i1} + \beta_2 X_{i2} + \beta_3 X_{i3} + \cdots + \beta_n X_{in})}{1 + (\beta_0 + \beta_1 X_{i1} + \beta_2 X_{i2} + \beta_3 X_{i3} + \cdots + \beta_n X_{in})}. \tag{7}$$

The above equation can be linearly changed to obtain

$$\operatorname{In}\left(\frac{P_i}{1 - P_i}\right) = \beta_0 + \beta_1 X_{i1} + \beta_2 X_{i2} + \beta_3 X_{i3} + \cdots + \beta_n X_{in}, \quad i = 1, 2, \cdots, n. \tag{8}$$

$Y_1, Y_2, Y_3 \cdots Y_n$ is an independent binary classification variable. Let $f_i(Y_i)$ represent the probability of $Y_i = 1$ or $Y_i = 0$; then, its likelihood function (LF) is

$$Inf(Y_1, \cdots, Y_n)_i = \sum_{1}^{n} [Y_i InP_i + (1 - Y_i)(\operatorname{In}(1 - P))]. \tag{9}$$

For ease of use, take the natural logarithms on both sides of formula (9), and obtain the log-likelihood function (LLF) as

$$\begin{aligned} Inf(Y_1, \cdots, Y_n) &= \sum_{1}^{n} [Y_i InP_i + (1 - Y_i)(1 - P_i)] \\ &= \sum_{1}^{n} [Y_i InP_i - Y_i \operatorname{In}(1 - P_i) + \operatorname{In}(1 - P_i)] \\ &= \sum_{1}^{n} \left[Y_i \operatorname{In}\left(\frac{P_i}{1 - P_i}\right) + \sum_{1}^{n} \operatorname{In}(1 - P_i) \right]. \end{aligned} \tag{10}$$

Putting formula (8) into formula (10), we get

$$\begin{aligned} Inf(Y_1, \cdots, Y_n) &= \sum_{i}^{n} Y_i (\beta_0 + \beta_1 X_{i1} + \beta_2 X_{i2} + \cdots + \beta_n X_{in}) \\ &\quad - \sum_{i}^{n} \operatorname{In}\left[1 + e^{(\beta_0 + \beta_1 X_{i1} + \beta_2 X_{i2} + \cdots + \beta_n X_{in})} \right], \\ &\quad i = 1, 2, 3, \cdots, n. \end{aligned} \tag{11}$$

Find the partial derivatives of β_i, and make their expressions 0, so you get the maximum likelihood estimator.

3. Experiments

3.1. Experimental Design

3.1.1. Index Selection. According to the foregoing theoretical analysis, we found from the basic information of individual users in a bank that the borrower's basic personal information and loan-related information will affect the borrower's credit limit. In view of the fact that all the borrowers' default records disclosed by the Renrendai platform are 0 times and the credit ratings are all grade A, select the total amount of the subject as the explanatory variable. The specific situation of each indicator is as follows:

(1) The total amount of the subject. The total amount of the target refers to the amount of the loan that the borrower wishes to post on the Renrendai platform. The minimum value is 5250 yuan, and the maximum value is 193,500 yuan, so the value range of the target total is 5250-193,500. This article uses the target total Act as a proxy for credit lines

(2) Age. Age refers to the actual age of the borrower. The youngest borrower is 22 years old, and the oldest borrower is 58 years old. The age range is 22-58

(3) Educational background. The borrower's education includes four levels: graduate or above, undergraduate, college, and high school or below. This variable is a nominal variable, so it needs to be quantified and converted to a dummy variable. Set "high school or below" as 1, "college" as 2, and "undergraduate" as 3, and the value of "graduate or above" is 4

(4) Marital status. Borrowers have three types of marital status: divorced, unmarried, and married. This variable is nominal, so it needs to be quantified and converted to a dummy variable. The value of "divorce" is 1, the value of "unmarried" is 2, and the value of "Married" is 3

3.1.2. Research Hypotheses. Based on the relevant research results of the existing literature, this paper proposes the following research hypotheses:

Hypothesis 1. In terms of the personal characteristics of the borrower, the older the borrower, the higher the credit limit; the higher the borrower's education, the higher the credit limit; the more stable the marriage status of the borrower, the higher the credit limit; the larger the credit limit, the higher the borrower's job position, the higher the credit limit; the longer the borrower's working time, the higher the credit limit; the more developed the province of the borrower's economy, the higher the credit limit.

Hypothesis 2. In terms of the financial characteristics of the borrower, the higher the borrower's income, the higher the credit limit; if the borrower owns real estate or car production, the higher the credit limit; if the borrower has the mortgage or car loan, the lower the credit limit.

TABLE 1: Regression results of credit line influencing factors.

Volume	Coefficient	Standard	t value	$p > \mid t \mid$	95% confidence interval	
Age	1098.593	219.4229	5.01	0.0000***	667.8678	1529.318
Education	9673.968	2870.089	3.37	0.001***	4040.01	15,307.93
Marital status	-711.139	2468.392	-0.29	0.773	-5556.569	4134.292
Company size	-25,407	3121.991	8.14	0.000***	31,535.39	19,278.52
Work position	4330.822	669.6249	6.47	0.000***	3016.355	5645.29
Operating hours	-470.134	1572.361	-0.3	0.765	-3556.663	2616.395
Work place	-324.846	1833.539	-0.18	0.859	-3924.066	3274.373
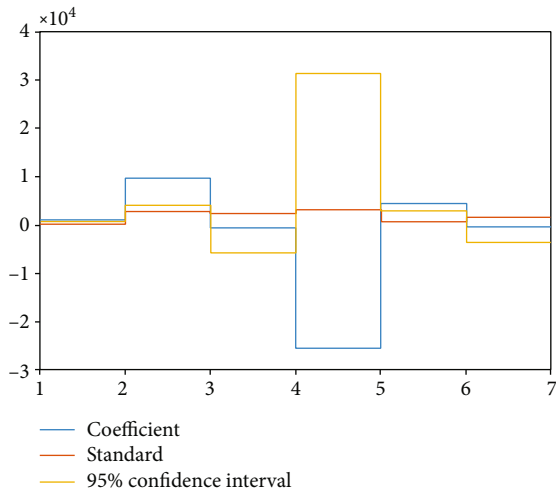
FIGURE 2: Regression results of credit line influencing factors.

FIGURE 3: Statistics of financial characteristics.

Hypothesis 3. In terms of the creditworthiness of the borrower, the more times the borrower successfully applies for a loan, the higher the credit limit obtained; the more the borrower pays off, the higher the credit limit.

Hypothesis 4. In terms of borrowing characteristics of borrowers, the higher the annual interest rate, the lower the credit line; the longer the repayment period, the lower the credit line.

3.1.3. Credit Report. The information in the personal credit report mainly includes six aspects: the results of the identity information verification by the Ministry of Public Security, basic personal information, bank credit transaction information, nonbank credit information, personal declarations and objections, and query historical information.

4. Discussion

4.1. Regression Results of Factors Affecting Credit Lines

4.1.1. Personal Characteristics. As shown in Table 1 and Figure 2, among the several variables representing personal characteristics, the three variables of marital status, working hours, and working place have no significant effect on the borrower's credit line. Age is statistically significant at a significant level of 1%, and the sign of the coefficient is positive, indicating that the age of the borrower has a positive impact on its credit limit. The older the borrower is, the larger the

amount of borrowing that can be obtained. Older borrowers tend to have richer social experience and richer asset accumulation, so the larger the amount of borrowing they can get.

4.2. Financial Characteristics. As shown in Figure 3, the experimental object of the survey is my country's multiple variables representing financial characteristics in 2014-2019; whether or not owning a real estate or car production has no significant effect on its credit line. When the borrower cannot repay on time, it is difficult to conduct mortgage auctions on the borrower's real estate and car properties, so whether or not owning the real estate or car properties has no obvious effect on the borrower's credit limit.

Housing loans and car loans are statistically significant at significant levels of 5% and 10%, respectively, and the signs of the coefficients are positive, indicating that housing loans and car loans have a positive impact on borrowers' credit lines. On the contrary, borrowers who have a home loan or car loan can also obtain a higher amount of borrowing because investors have very limited information about the borrower. If the borrower can obtain a house loan or car loan through bank inspection, it means good solvency, so the amount of borrowing that can be obtained may also be higher.

4.3. Empirical Analysis of Personal Credit Risk Assessment Based on Big Data Platform

4.3.1. Analysis of the Company's Personal Credit Risk Assessment Results. Using the above-built logistic regression

TABLE 2: Forecast results of personal credit risk model of personal credit business data.

Model name	Actual normal customers	Actual default customers	Predict the number of normal customers	Predicted default customers	Accuracy in predicting default customers
Logistic + XGBoost fusion model	22,470	6701	19,738	6509	97.14%
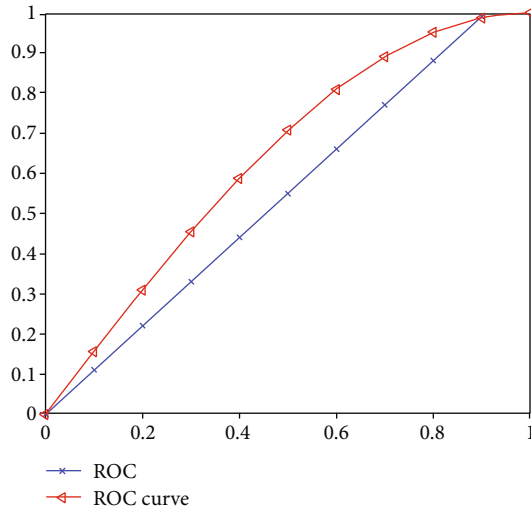
FIGURE 4: ROC curve of the fusion model.

+ XGBoost decision tree fusion model to make empirical predictions on the company's personal credit data, there were 29,171 loan customers, 22,470 normal customers, and 6,701 default customers.

As shown in Table 2, compared with the single model, the personal credit risk assessment model based on the fusion model in the company's big data business environment has higher classification accuracy, can well predict normal customers and default customers, and is suitable for practical individual's credit risk control business. These characteristics are highly interpretable and can be cross-validated with the industry's professional knowledge, which further promotes the improvement of personal credit business and facilitates the construction of a comprehensive personal credit risk assessment system in the Internet finance industry.

As shown in Figure 4, the AUC of this project fusion model is 0.93 and KS is 0.66; it shows that the predictive ability of the personal credit risk assessment model is good, and it can accurately distinguish between normal loan customers and default loan customers, which is suitable for practical personal credit risk control in business. The prediction accuracy of the default model of the fusion model is 97.14%, and the default rate corresponding to the actual business is 2.86%. The default rate of personal credit loans was well controlled, from the original default rate of 4% to 2.86%, and the default rate decreased by 1.14%.

5. Conclusions

Currently, most Chinese companies are facing many challenges in terms of data infrastructure system architecture and data analysis. In the context of big data and the Internet, big data credit reporting and consumer finance have developed rapidly. The prerequisite for the healthy development of the consumer finance industry is efficient and accurate credit risk management. In the context of the timeliness and comprehensiveness, this paper studies and analyzes the limitations of the classic credit risk rating system, avoids the limitations of traditional indicators when designing a personal big data risk rating system, and creates complete and logical personal credit rating data. In the context of system, after the index is created for the first time, the index may have relevance issues and unequal predictability. Therefore, the focus of research is to use effective feature selection methods to optimize indicators when creating indicators.

Data Availability

No data is available. The article does not touch on data.

Conflicts of Interest

The authors declare that they have no conflicts of interest.

References

[1] D. V. Kousenidis, A. C. Ladas, and C. I. Negkakis, "Aggregate accounting data and the prediction of credit risk," *International Journal of Accounting*, vol. 54, no. 1, article 1950001, 2019.

[2] T. Schmitt, A. Schmitt, R. Schäfer, and T. Guhr, "Credit risk: taking fluctuating asset correlations into account," *Journal of Credit Risk*, vol. 11, no. 3, pp. 73–94, 2016.

[3] Y. Sun, R. Mendoza-Arriaga, and V. Linetsky, "Marshall–Olkin distributions, subordinators, efficient simulation, and applications to credit risk," *Advances in Applied Probability*, vol. 49, no. 2, pp. 481–514, 2017.

[4] S. Wang, Y. Qi, and F. Bin, "Credit risk evaluation based on text analysis," *International Journal of Cognitive Informatics and Natural Intelligence*, vol. 10, no. 1, pp. 1–11, 2016.

[5] S. Morris and H. S. Shin, "Illiquidity component of credit risk," *Working Papers*, vol. 57, no. 4, pp. 1135–1148, 2016.

[6] D. Petrone and V. Latora, "A dynamic approach merging network theory and credit risk techniques to assess systemic risk in financial networks," *Scientific Reports*, vol. 8, no. 1, p. 5561, 2018.

[7] A. Leng, G. Xing, and W. Fan, "Credit risk transfer in SME loan guarantee networks," *Journal of Systems Science & Complexity*, vol. 30, no. 5, pp. 1084–1096, 2017.

[8] Y.-H. Yuan, S.-H. Tsao, J.-T. Chyou, and S.-B. Tsai, "An empirical study on effects of electronic word-of-mouth and internet risk avoidance on purchase intention: from the

perspective of big data," *Soft Computing*, vol. 2020, no. 24, pp. 5713–5728, 2020.

[9] Z. Zhang, J. He, and G. Gao, "Sparse multi-criteria optimization classifier for credit risk evaluation," *Soft Computing*, vol. 23, no. 1, pp. 1–14, 2017.

[10] M. Y. Kang and M. Ausloos, "An inverse problem study: credit risk ratings as a determinant of corporate governance and capital structure in emerging markets: evidence from Chinese listed companies," *Economies*, vol. 5, no. 4, p. 47, 2017.

[11] G. F. Amanollahi, "The influence of external factors on the credit risk in leasing industry," *Management Science Letters*, vol. 6, no. 3, pp. 251–258, 2016.

[12] W. Wu and D. G. McMillan, "Dynamic linkages in credit risk: modeling the time-varying correlation between the money and derivatives markets over the crisis period," *Journal of Risk*, vol. 16, no. 2, pp. 51–59, 2013.

[13] J. Skoglund and W. Chen, "The application of credit risk models to macroeconomic scenario analysis and stress testing," *Journal of Credit Risk*, vol. 12, no. 2, pp. 1–45, 2016.

[14] M. Punniyamoorthy and P. Sridevi, "Identification of a standard AI based technique for credit risk analysis," *Benchmarking An International Journal*, vol. 23, no. 5, pp. 1381–1390, 2016.

[15] J. Skoglund and W. Chen, "Rating momentum in the macroeconomic stress testing and scenario analysis of credit risk," *The Journal of Risk Model Validation*, vol. 11, no. 1, pp. 21–47, 2016.

[16] J. Eckert, K. Jakob, and M. Fischer, "A credit portfolio framework under dependent risk parameters: probability of default, loss given default and exposure at default," *Journal of Credit Risk*, vol. 12, no. 1, pp. 97–119, 2016.

[17] Z. Qing, J.-j. Yang, and W.-x. Wu, "Pricing vulnerable options with correlated credit risk under jump-diffusion processes when corporate liabilities are random," *Acta Mathematicae Applicatae Sinica*, vol. 35, no. 2, pp. 305–318, 2019.

[18] H. Altinbas and G. C. Akkaya, "Improving the performance of statistical learning methods with a combined meta-heuristic for consumer credit risk assessment," *Risk Management*, vol. 19, no. 4, pp. 255–280, 2017.

[19] S. Yamanaka, H. Nakagawa, and M. Sugihara, "Random thinning with credit quality vulnerability factor for better risk management of credit portfolio in a top-down framework," *Japan Journal of Industrial and Applied Mathematics*, vol. 33, no. 2, pp. 321–341, 2016.

[20] Y. Lee and S.-H. Poon, "Modeling the credit contagion channel and its consequences via the standard portfolio credit risk model," *Journal of Credit Risk*, vol. 10, no. 1, pp. 33–62, 2016.

[21] F. Kaposty, M. Löderbusch, and J. Maciag, "Stochastic loss given default and exposure at default in a structural model of portfolio credit risk," *Social Science Electronic Publishing*, vol. 13, no. 1, pp. 93–123, 2017.

[22] I. Basoglu, W. Hormann, and H. Sak, "Efficient simulations for a Bernoulli mixture model of portfolio credit risk," *Annals of Operations Research*, vol. 260, no. 1-2, pp. 113–128, 2018.

[23] L. Bo and A. Capponi, "Optimal investment in credit derivatives portfolio under contagion risk," *Mathematical Finance*, vol. 26, no. 4, pp. 785–834, 2016.

[24] J. Lee, D. H. Lee, and S.-G. Yun, "Systemic risk on trade credit systems: with the tangible interconnectedness," *Computational Economics*, vol. 51, no. 2, pp. 211–226, 2018.

[25] D. Froneberg, F. Kiesel, and D. Schiereck, "CDS and bank ownership structures: does the credit side show who advocates more risk?," *Journal of Risk Finance*, vol. 17, no. 2, pp. 169–193, 2016.

[26] F. Lin, S.-y. Xie, and J.-p. Yang, "Semi-analytical formula for pricing bilateral counterparty risk of CDS with correlated credit risks," *Acta Mathematicae Applicatae Sinica*, vol. 34, no. 2, pp. 209–236, 2018.

[27] M. Reddy, "Smart vehicular system based on the Internet of Things," *Journal of Organizational and End User Computing*, vol. 30, no. 3, pp. 45–62, 2018.

WILEY | Hindawi

Research Article

Design of Shock Wave Storage and Test System with Variable Parameters Based on the Sensor of Piezoelectric Circuit

Zhi Li (ID)

College of Mathematics and Information Engineering, Chongqing University of Education, Nan'an, 400065 Chongqing, China

Correspondence should be addressed to Zhi Li; lizhi@cque.edu.cn

With the wide application of science and technology in the field of weapons, shock wave is an important breakthrough point in weapon research, and the storage and testing system of shock wave is a breakthrough point that people pay most attention to at present. Shock wave data storage has the characteristics of large scale, complex structure, low cost efficiency, and strong timeliness. This paper mainly studies the design of shock wave storage test system with variable parameters based on numerical piezoelectric circuit sensor. Based on fluid dynamics simulation theory and numerical simulation method, the normal and concave-convex three-dimensional models of two pressure measuring devices are constructed by using the flow waveform of calculator, and then, the network is divided. The results show that, under the same inlet pressure, the larger the bulge or depression value, the greater the influence on the experimental results. The influence of disk is 10% higher than that of pen, and the change rate of relative difference is increased by 1.5% with the increase of concave-convex value. Finally, experiments are carried out in different environments to verify the reliability, survivability, and flexibility. The shock wave storage test system is optimized when the parameters of the digital voltage circuit sensor are variable.

1. Introduction

The research on the overpressure and impulse of shock wave can provide an important reference for the comparison of the impact damage strength of weapon equipment. At present, there are two kinds of shock wave sensors at home and abroad: piezoresistive sensor and piezoelectric sensor. The biggest disadvantage of piezoresistive sensor is that its silicon element is very sensitive to the light produced by explosion. Even if the light film is attached to the back of the polished silicon chip to reduce light transmission, the strong light generated by the explosion can cause system failure and reduce the reliability of the system. The shortcomings of piezoelectric sensors are as follows: high output obstacles lead to increase of rise time; low tuning frequency makes it impossible to achieve a good negative pressure curve; signal conversion and processing are more complex, requiring high insulation of cables and joints; electromagnetic waves generated in explosion environment are connected; and debris and vibration of mounting bracket can easily cause signal deviation and affect test results. With the development of IC, a

new sensor has been developed. The traditional position charge amplifier is placed on it, the signal is not easy to be interfered, and all high interference circuits are sealed, so that the signal can be transmitted for a long distance without affecting the signal quality, which is convenient to use. It is very suitable to use in the test of shock wave overpressure storage test.

With the continuous development of science and technology, testing plays an increasingly important role in scientific experiments, technical research, and mechanical testing. The more accurate the test is, the more feedback and guidance scientific research can be provided. At present, with the rapid development of sensor technology, sensor design, and dynamic calibration principle, the accuracy of sensor measurement results is improving. In a word, an accurate and reliable sensor is essential behind the formation of an automatic detection and control system. Modern electronic technology and computer provide perfect means for transforming and processing information. Great changes are taking place in the field of modern detection and control system. Various sensors are used to detect data and provide

information. Therefore, the sensor plays an important role. In the current shock wave overpressure test, pen sensor and disk sensor structures have been widely used, but the shape of the pressure sensor which should be placed in the explosion field is not important. In the test, because the fluidity of the forward shock wave is affected by the geometry of the sensor, the measurement accuracy of the peak value of the shock wave overpressure will inevitably be affected. Therefore, it is necessary to test the overpressure data of the shock wave under the extreme pressure environment. Under these circumstances, the urgent problems to be solved in the shock wave overpressure test include the selection of the sensor settings and the installation of the sensor and error correction of test results. Therefore, it is necessary to simulate and test the shape and structure of various commonly used shock wave testing devices to improve the accuracy of test results.

Robert et al. designed a set of integrated sensor storage test system, regulation circuit, and data acquisition circuit design. Based on the principle of storage test technology and the new ICP piezoelectric sensor, the explosion wave overpressure acquisition and storage test system are designed. The piezoelectric module is integrated with the built-in charge amplifier to output the amplified signal. Through the matching operation of OPAMP and max4638, the function of adjustable gain is realized. The corresponding analog voltage is filtered by a LC Π filter, and the amplified signal is filtered by a Sallen key second-order filter. Using FPGA to design digital logic control improves the stability and reliability of the test system and reduces the system volume. Under the same test conditions, the duration of shock wave overpressure is directly proportional to the test radius and inversely proportional to the shock wave size and shock wave. However, because they did not have a control group for comparison, the results obtained were not very convincing [1]. Couldrick et al. designed a system including a data storage medium and a shock wave generator. The data storage medium includes cell and multilayer. Each unit is configured to store information in it. In the same layer of a plurality of layers of a data storage medium, at least two units are arranged in a horizontal plane, and in different layers of a plurality of layers of a data storage medium, at least two units are arranged in a vertical plane. The shock wave generator is configured to generate a shock wave signal propagating through one of the multilayer layers of the data storage medium. When the shock wave signal passes through the target cell, the target cell in the layer stores information in response to the light beam emitted from the transmitter targeting the target unit. After the shock wave signal exits through the target unit, the target unit will retain the information. However, because the shock signal is not stable, the cell information stored in the experiment is not very accurate [2]. Tobin and Hargather propose a wireless passive pressure sensor based on a miniature flexible pressure-sensitive capacitor, which is specially designed to monitor the intracranial pressure (ICP) of patients with craniocerebral trauma. A flexible varistor capacitor is characterized by creatively utilizing PDMS wrinkles generated spontaneously in the process of PDMS etching to construct cavity structure to improve sensi-

tivity. In addition, the flexible reader coil for signal reading has been optimized to better couple the sensor in a sufficiently large detection range for ICP monitoring. In addition, because of its flexibility and thin thickness, flexible varistor can adapt to the bending morphology of the skull and dura. Compared with the previous reports, the sensor has lower resonance frequency, higher quality factor, and better sensitivity, but it is also more complex, and it is difficult to control when using [3].

The innovation of this paper lies in the three-dimensional modeling and simulation of the external flow field of the pen type and disc type shock wave overpressure testing device, further carries out simulation and comparative analysis on the influence of the concave-convex and angle installation modes on the flow field, and summarizes the comparison results [4, 5].

2. Shock Wave Storage Test Method Based on Variable Parameters

2.1. Formation Method of Explosion Shock Wave. The initial state of many substances contains huge energy. In some cases, the state of materials changes suddenly, and the rapid release process of internal energy is called explosion. Generally speaking, explosion refers to a kind of chemical reaction, in which one substance is converted into high-temperature and high-pressure gas, and the reaction time is very short, accompanied by high temperature of about 4000°C and tens of thousands of atmospheric pressure, shock wave. The thickness of the wave front is very thin, and the amplitude of the time field is less than 2 ns. If the strong shock wave lacks strong airflow, it will rapidly decompose into weak shock wave. When the explosion product moves a certain distance, the pressure will drop to atmospheric pressure when the explosion does not occur, and the explosion product is still far away [6]. The pressure is less than that of the atmosphere, resulting in negative pressure area. When the energy of the explosion is exhausted, the negative pressure time is over. The pressure rises slowly; the surrounding material shrinks and reaches equilibrium after several cycles. The damage effect of explosion shock wave depends on the pressure in front of the shock wave, that is, the maximum overpressure dynamic value of shock wave ΔU:

$$
\begin{aligned}
\Delta U &= 0.085 \frac{\sqrt[3]{E}}{T} + 0.28 \left(\frac{\sqrt[3]{E}}{T} \right)^2 + 0.8 \left(\frac{\sqrt[3]{E}}{T} \right)^3, \\
y_{it} &= \alpha_0 + D \max_{it} + \alpha_2 X_{it} + \mu_i + \eta_t + \alpha_{it}, \quad (1) \\
U_2 &= \begin{cases} s - p_1 - k x_2, \\ x - p_2 - k(1 - x_2). \end{cases}
\end{aligned}
$$

In the formula, E is the charge weight and t is the detonation distance [7].

2.2. Method for Estimating Shock Wave Parameters

2.2.1. Calculation Method of Maximum Overpressure Value of Shock Wave Produced by Air Explosion. At present, there

is no direct method to measure the specific impulse when evaluating the effect of shock wave. Generally, the method of numerical integration is used to measure the specific impulse based on the pressure signal curve. The specific impulse of explosion shock wave refers to the real statistical data of pressure and time when explosion occurs in the experimental pressure model [8, 9]. When air explosion occurs, the main factors related to overpressure peak value ΔU include explosion energy R_0, initial pressure P_0, initial air density ρ_0, and combustion distance t [10]. Therefore, the maximum value can be expressed as

$$\Delta A = G(R_0, P_0, \rho_0, t). \tag{2}$$

Through theoretical analysis and numerical calculation, the maximum value of shock wave overpressure can be expressed as a function in the form of charge weight and ignition distance of $\sqrt[3]{\tilde{E}}/t$ [11, 12]:

$$\Delta A = G\left(\frac{\sqrt[3]{\tilde{E}}}{t}\right). \tag{3}$$

The above function expansion is transformed into a power function form:

$$\Delta A = G\left(\frac{\sqrt[3]{\tilde{E}}}{t}\right) = S_O + \frac{S_1}{t} + \frac{S_2}{t^2} + \cdots,$$

$$C(k) = [\zeta_1 c_1(t) + \zeta_2 c_2(k) + \zeta_3 c_3(k)$$
$$+ \zeta_4 c_4(k) + \zeta_5 c_5(k) + \zeta_6 w_{ik}],$$
$$c_1(t) \geq 0, \tag{4}$$
$$c_2(k) \geq 0,$$
$$c_3(k) \geq 0,$$
$$c_4(k) \geq 0,$$
$$c_5(k) \geq 0,$$

where t is the propagation distance of shock wave and $\tilde{E}$ is the charge quantity:

$$\bar{t} = \frac{t}{\sqrt[3]{\tilde{E}}},$$

$$P(d_i, w_j) = P(d_i)P(w_j|d_i) ; P(w_j|d_i)$$
$$= \sum_{k=1}^{K} P(w_j|z_k)P(z_k|d_i), \tag{5}$$

$$\frac{\partial \pi_B^{LH}}{\partial p_2} = \frac{1 - p_2 + p_1}{2} - \frac{p_2 - c_2}{2} + \frac{k - p_2 + p_1}{2k}$$
$$- \frac{p_2 - c_2}{2k} - et\left[-\frac{1}{2} - \frac{1}{2k}\right] = 0.$$

The above formula is the proportional distance; S_0, S_1, S_2, etc. are determined by the test results [13, 14].

TABLE 1: Basic test parameters of the shock wave storage test system.

Item	Reliable	Accurate	Error	Stable	Multiple	Frequency
1	1.38	1.14	0.06	0.37	1.93	1.43
2	1.66	3.97	3.85	3.84	3.34	1.13
3	4.51	5.76	5.06	2.25	5.38	5.41
4	1.03	1	1.04	2.64	1.18	4.09

For the air explosion of naked TNT and spherical explosive, the maximum pressure has the following expression:

$$\Delta A = \frac{0.0086}{\bar{t}} + \frac{0.0035}{\bar{t}^2} + \frac{0.75}{\bar{t}^3},$$

$$\min w_k(t) = \left[\omega_1\left(\frac{d_k}{V}\right) + \omega_2\left(\frac{d_k}{V}\right) + \omega_3\left(\frac{T_k}{ND_K}\right) + \omega_1(P_K T_K)\right]. \tag{6}$$

2.3. Calculation Method of Action Time in Barotropic Zone. In the case of air explosion, the duration of positive pressure of shock wave is determined by energy R_0, initial pressure p_0, initial air density ρ_0, and ignition distance t. Therefore, it can be expressed as

$$\delta = G(R_0, P_0, \rho_0, t),$$

$$\wp_\kappa = \frac{2k}{k+1} + \left[\frac{1}{2} + \frac{1}{2k}\right]\left[\frac{c_2 - c_1}{3}\right]^2 + \frac{2(c_2 - c_1)}{3}, \tag{7}$$

$$y = \alpha W y + \beta_1 X - W \beta_2 X + \varepsilon.$$

It is also available.

$$\frac{\delta}{\sqrt[3]{\tilde{E}}} = G_1\left(\frac{t}{\sqrt[3]{\tilde{E}}}\right),$$
$$w_{ik} = \sum_{a}^{n} \tau_1 X_{ik} + \sum_{b}^{n} \tau_2 U(Y_{ik}) + B_{ik}. \tag{8}$$

2.4. Fluent Processing Method. Fluent is a special software for numerical simulation and analysis of fluid movement in and out of the complex geometry area and analysis of experimental simulation data. Fluent supports a wide range of network types, enabling users to solve problems smoothly under the premise of ensuring the accuracy of experimental data [15]. Fluent also provides a variety of physical models and the best numerical solutions, so that users can obtain satisfactory computing speed, stability, and accuracy. The process can monitor the simulation process and calculation results in real time through multiple operations [16]. It has a variety of display and storage modes, such as cloud, contour, vector, and animation. It can store results in the format supported by the processing software. It includes three basic functions: preprocessing, solver, and postprocessing.

(1) Preprocessing includes gambit, tgrid, and filters, which are used to model and process simulation objects; grid can import uploaded geometric patterns
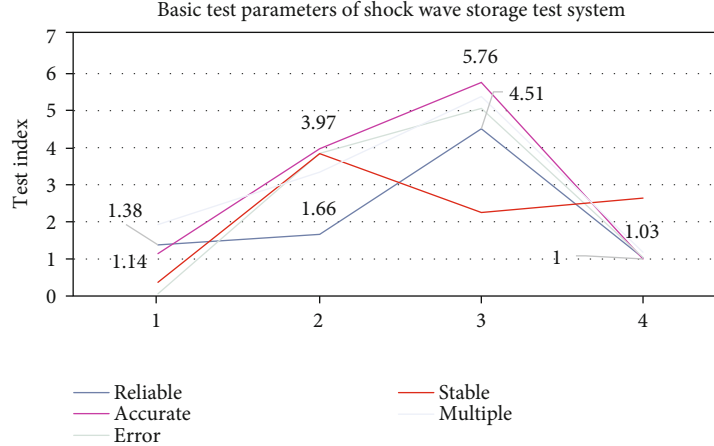
Figure 1: Basic test parameters of the shock wave storage test system.

on gambit software; filters are subsystems of another CAD or CAE and can read the network composed of them [17, 18]

(2) The solver is the basic part of fluent. After reading the grid file correctly, the tasks of setting boundary conditions, material selection, numerical solution, mesh optimization, and simple postprocessing can be easily completed

(3) The postprocessor flow software provides cloud, vector, contour, and animation to display the calculation results. It can also enlarge, translate, and rotate the data results and export the current results to other postprocessing software (such as tecpart) for editing [19, 20]

2.5. AD Conversion Method. AD inverter is an important part of the whole test system, which is related to the acquisition rate and accuracy of the signal. The principle of AD conversion is as follows: the first step of converting analog signal $F(t)$ into digital signal $F(n)$ is to sample $F(t)$ at fixed intervals [21, 22]. The sampling value f_s (NTS) is obtained. The TS parameter is the sampling period, and the reciprocal is the sampling frequency f_s. According to Nyquist sampling theorem, if the original signal is to be completely recovered from the sampled signal, $f_s \geq 2f_m$ must be satisfied [23]. The highest frequency of the signal is f_m, and f_s (NTS) is quantized into $F_q(nT_s)$ signal. Finally, digital signal $F(n)$ is received through a coding process to convert analog signal into digital signal [24, 25].

3. Shock Wave Storage Test System Design Experiment

3.1. Sensor Adaptation Circuit Design. In addition to the constant voltage and current circuit, the analog system also has a linear LDO power supply, which mainly generates 8 V constant voltage for multiple voltage stabilizing circuits and filter circuits and 1.65 V bias voltage for system use. In order to reduce power ripple, lp2985 is used as the main component

Table 2: Error test results of adaptation circuit.

Working parameters				Actual output		
Gain	Frequency (Sa·s^{-1})	Input voltage V_{PP} (V)	Sampling frequency (Sa·s^{-1})	Output voltage V_{PP} (V)	Gain	Error (%)
0.125	3 M	6 M	3 M	0.635	0.127	0.14
0.25	3 M	6 M	3 M	1.037	0.263	0.53
0.5	2 M	4 M	2 M	1.274	0.561	1.22
1	2 M	2 M	2 M	0.926	1.027	0.35

of linear power supply. The chip has a large dynamic range input and can achieve 8.5 V to 10 V power conversion, corresponding to peripheral resistance and capacitance.

3.1.1. Adjustable Amplifier Circuit. The output of ICP sensor is -8~+10 V AC signal, which is based on 10~15 V DC voltage. It is usually input to operational amplifier circuit after AC connection through a capacitor. The voltage sequence is designed by opa2340 and manufactured by TI company. It has the characteristics of single power supply, rail input and output, high swing speed, high input, and low output, and the former circuit is in high-strength state, and the last circuit is on low-intensity conditions, so that the front and back stage circuits can be isolated and stored.

3.1.2. Power Amplifier Circuit. In this paper, 10.5 V lithium battery is used as the power supply of the system. In order to meet the driving requirements of ICP piezoelectric sensor, a DC-DC boost power supply circuit and DC power supply circuit are designed. Using the tps670 power level chip and the corresponding resistance and capacitance design, the power supply can be converted from 10.5 V to 36 V, and the constant current can be realized by a constant current diode.

3.2. Physical Model of Shock Wave Overpressure Tester and Related External Flow Settings. The general steps to determine the calculation model are as follows:
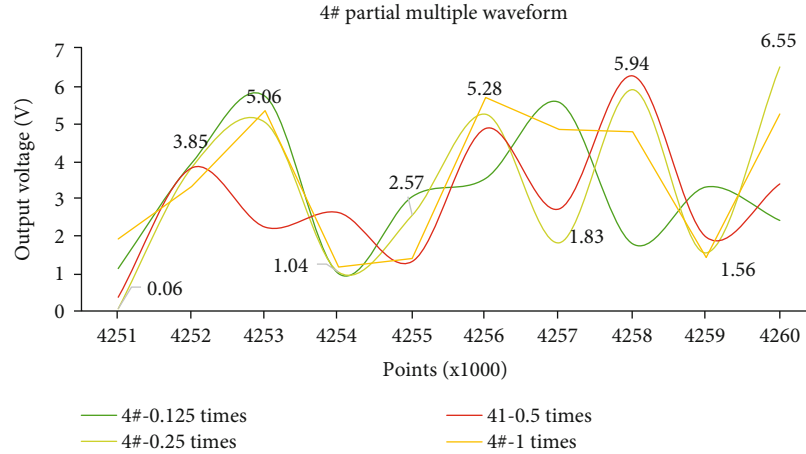
FIGURE 2: 4# partial multiple waveform.

(1) Create 3D geometry (cube, cone, cylinder, etc.), and divide and cut geometry according to actual structure

(2) Create mesh: divide the border of the geometric structure and the lines of the external area of the structure into isometric or nonisometric network, and then, create the line network as the face network

(3) Determine input and output constraints and solid walls, and store network files

According to the above steps, the external flow field of the disc and pen piezometers is formed as follows: the main body of the impact pipe is constructed, and the simplified cylinder model is determined according to the actual size of the low-pressure chamber (6500 mm). The length and radius are 60 mm; the structural model of the sensor is specified, and the cylindrical and conical models are moved to the actual installation position, and the impact pipe and sensor group are moved to the actual installation position. External flow entity modeling and related settings of shock wave overpressure storage and testing device are used.

3.3. Setting External Flow Problems. The external flow around the disc and pen gauges has been specially activated. After making the model with gambit software, the grid file is inserted into fluent solver for analysis. Since this is a three-dimensional problem, the three-dimensional and one-dimensional accuracy is selected to solve the problem. The decomposition steps are as follows:

(1) Mesh relevancy: check the mesh to ensure that the minimum mesh volume is not negative, otherwise the mesh will be reused; set the unit size to millimeter; smooth and swap the mesh

(2) Selection model calculation: coupling solver is usually used in high-speed aerodynamics; S-A turbulence model is selected for liquid air problems with wall conditions

(3) Material properties: when Mach number is greater than 0.5, it can be considered as compressed fluid.

TABLE 3: Flexibility and adjustable magnification of the designed adaptive.

Points	4#-0.125 times	4#-0.25 times	4#-0.5 times	4#-1 times
4251	1.14	0.06	0.37	1.93
4252	3.97	3.85	3.84	3.34
4253	5.76	5.06	2.25	5.38
4254	1	1.04	2.64	1.18

Considering its compressibility and thermophysical properties, the calculated viscosity can be adjusted by Saran's law and open energy equation

(4) Because it is related to the total pressure, static pressure, and other pressures, setting the working pressure to 0 is convenient for setting the limit and posttreatment conditions, and the influence of gravity is not considered

(5) Determine the boundary conditions: in this paper, the wall and shape structures of the impact pipe are the wall conditions. The pressure value of shock tube, the corresponding Mach number and pressure value, and the setting of flow element in the XY direction must be adjusted according to the actual situation

(6) Control parameters: when the convergence rate is slow and stable, increase the Coulomb number and increase the relaxation factor to improve the convergence rate

(7) Initialize the flow field and specify the number of iterations to start the iteration operation

3.4. Big Data Evaluation Test and Database Parameter Data Collection. With the introduction of big data theory and design, cloud computing, and related MapReduce and HBase kernel technology, Hadoop has been determined to be born from big data. Then, the Hadoop platform is used to verify the ability of processing and evaluating case test data based on the big data technology proposed in this paper.
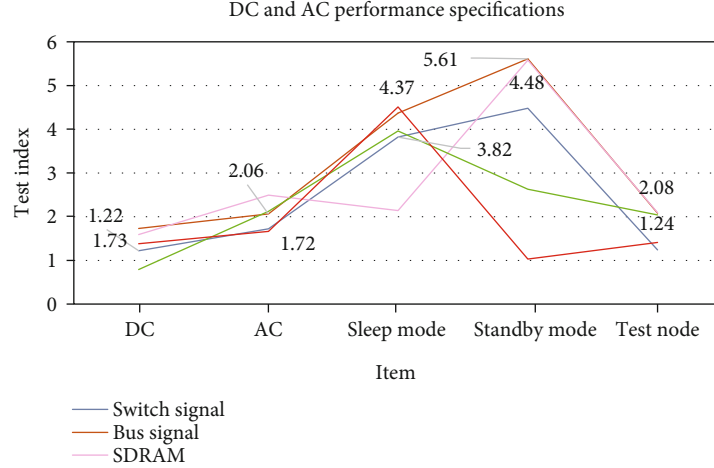
Figure 3: DC and AC performance specifications.

Table 4: Converted digital signal is mounted on the data line.

Item	Switch signal	Bus signal	SDRAM	FPGA	Power consumption
DC	1.22	1.73	1.59	0.79	1.38
AC	1.72	2.06	2.49	2.12	1.66
Sleep mode	3.82	4.37	2.14	3.96	4.51
Standby mode	4.48	5.61	5.58	2.63	1.03
Test node	1.24	2.08	2.09	2.04	1.41

4. Design and Analysis of Shock Wave Storage Test System

4.1. Performance Test and Analysis of Sensor Adapter Circuit. In order to test the reliability and accuracy of the adaptive circuit, the signal generator is used to debug the designed circuit system (in order to better test the system error, the original multiple is reduced to 0.125 times of the original setting). The basic test data is shown in Table 1 and Figure 1.

LabVIEW human-computer interaction interface is used to show the corresponding waveform change diagram of 4 × 10 (20 sets of devices) at 0.125 times, 0.25 times, 0.5 times, and 1 time. The amplitude of output voltage under different multiples can be read out at the software interface Δxy. Table 2 shows the test results of the 4 × 10 device, which shows that the error of the adaptive circuit is less than 2%. Compared with the traditional circuit, the system error is greatly reduced and the test accuracy is improved.

As shown in Figure 2, this paper designs a special power boost circuit, an adjustable amplification circuit, a bias circuit, and a filter circuit. In the natural environment, using the human-computer interface of the special software LabVIEW, the circuit parameters of the randomly selected 4 × 10 device are analyzed, and the waveform diagram of the 4 × 10 device at 0.125 times, 0.25 times, 0.5 times, and 1 time is given. As shown in Table 3, the results show that the error

is less than 2%, and the flexibility and adjustable magnification of the designed adaptive circuit are verified.

4.2. Realization of Free-Field Shock Wave

4.2.1. AD Circuit. This research mainly uses an AD converter to realize the key technology of free-field shock wave, its task is to realize the analog signal without distortion digitization, and conversion accuracy is the core of the design of AD circuit. However, many factors will affect its accuracy, such as bits, quantization error, reference voltage, component deviation and temperature, and sampling frequency. In order to ensure the test accuracy of the system, it is necessary to select a suitable analog-to-digital converter.

As shown in Figure 3, Ad7482 uses advanced technology to achieve extremely low integral nonlinear error and offset and gain error and has excellent DC and AC performance specifications. In addition, it also provides two power saving modes: sleep mode and standby mode. Even in the working mode, the power consumption is only 90 mw, which is suitable for the design of miniaturized test node, and its typical circuit design is adopted.

As shown in Table 4, when convst signal is in a low level, start sampling and analog-to-digital conversion, and then, the bus signal becomes high and keeps at a high level during conversion. Once the conversion is finished, the bus signal is reset to a low level, and the converted digital signal is mounted on the data line, which is convenient for FPGA to read or store in SDRAM.

4.2.2. Memory Circuit Test. As shown in Figure 4, the storage circuit caches the converted digital signal to the memory, which is convenient for data recovery. It is the key method to obtain the explosion environment signal. The core of the circuit is data memory, which transfers data from the AD converter to memory and from memory to the output interface. The power supply voltage of the storage circuit is 3.3 V. The memory chip adopts synchronous dynamic memory mt48lc8m, and the working interface mainly includes data bit, address bit, write/read control, and write/read clock. Dynamic memory also needs strict timing to realize the
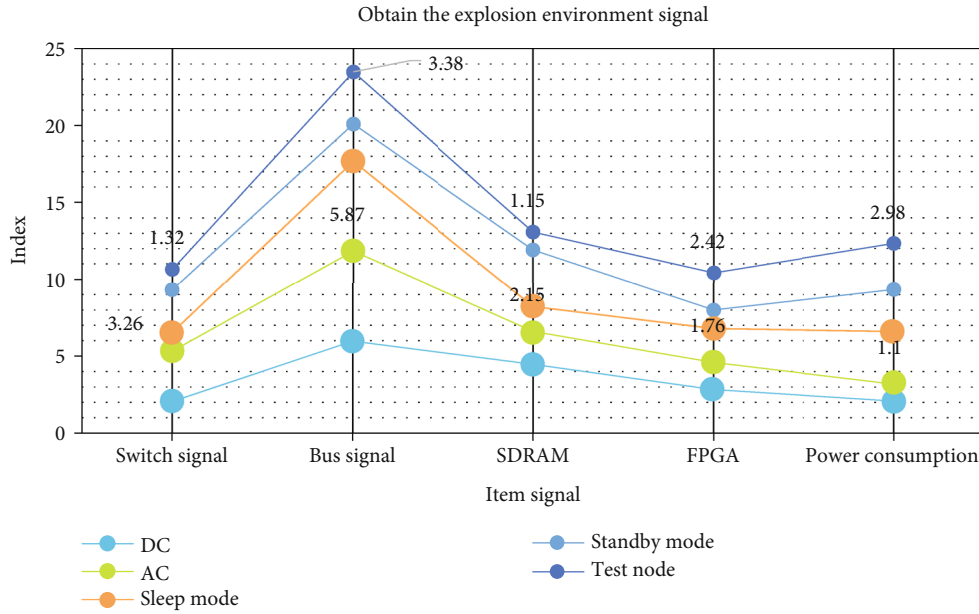
Figure 4: Obtain the explosion environment signal.

Table 5: Dynamic memory also needs strict timing to realize the functions.

Item	DC	AC	Sleep mode	Standby mode	Test node
Switch signal	2.05	3.26	1.22	2.8	1.32
Bus signal	5.97	5.87	5.83	2.43	3.38
SDRAM	4.46	2.15	1.62	3.69	1.15
FPGA	2.82	1.76	2.2	1.22	2.42
Power consumption	2.08	1.1	3.42	2.75	2.98

functions of writing, reading, and refreshing. As shown in Table 5, the system is implemented by FPGA, which is responsible for connecting the data bus of memory.

4.3. Pressure Time Curve Analysis. In this paper, the pressure time curve measured by the test device is directly read, and then, the value of shock wave overpressure is obtained. Taking two sets of devices as examples, their pressure time curves are shown in Figure 5.

As shown in Figure 5, it can be seen that before the arrival of shock wave overpressure, a lot of jitters are superimposed on the baseline of the test system. This is because the velocity of some fragments exceeds the velocity of shock wave in the pressure measuring area installed by the test device during explosion, and these fragments pass through the air at supersonic speed to form a projectile track shock wave; in response to the sensor, there are many small pressure disturbances overlapping on the time-varying curve of shock wave pressure.

4.4. Comparison and Analysis of External Flow Field Simulation Results of Two Kinds of Sensors. The disc type and pen type shape structures are simulated with multiple pressure values under different concave-convex heights and different deviation angles. The results are shown in Figure 3. The abscissa in the figure is the Mach number corresponding to the inlet pressure (calculated by using fluent modeling), and the ordinate is the measured pressure value. Different lines are used to represent the different heights and angles of the two structures, which is very good. It reflects the influence of different installation methods of the two structures on the test results. When the step pressure wave generated by the shock tube reaches the sharp corner of the windward surface of the disk, the shock wave below the disk plane flows through the disk plane according to the original propagation direction and passes through the sensor sensitive surface. The pressure change of the sensitive surface is very small. The shock wave above the disk plane reflects when it meets the rigid wall and forms an eddy current at the intersection of the vertical plane and inclined plane, the maximum pressure and density are 619394 pa, and a weak bow wave is formed at the sharp corner of the disk under the influence of the eddy current. With the propagation of shock wave, the eddy current range extends outward, and the shock wave propagates upward rapidly after passing through the disk plane of leeward surface. Under the influence of the shape structure, the vortex is formed. The pressure value decreases rapidly, and the minimum value reaches 25159 pa. In the simulation process, there is even negative pressure at the vortex, and there is flow separation phenomenon. From the pressure curve of the monitoring surface, it can be seen that the pressure change of the sensitive surface of the sensor is very small, close to the inlet pressure, indicating that the shock wave inflow is relatively stable. It can be seen from the same figure that the velocity of the incident flow and the reflected wave decreases sharply at the vertical plane of the configuration structure, and the minimum velocity is 0.55 mach. The maximum pressure changes in the flow field are at the windward side and leeward side of
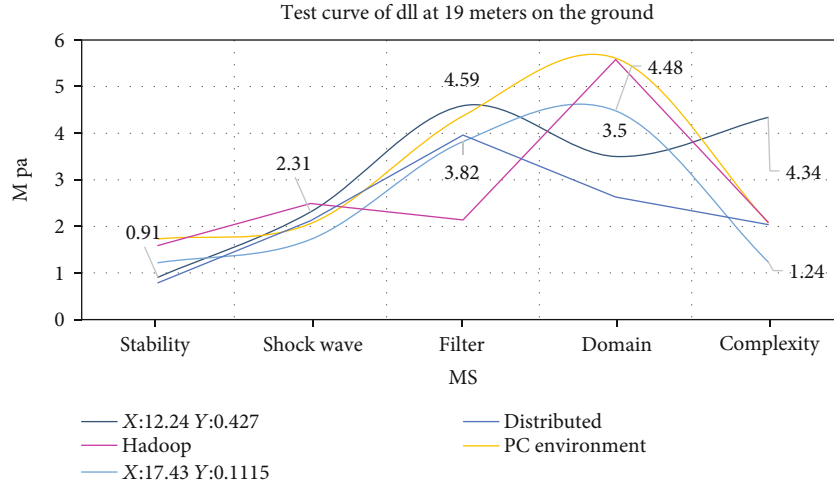
FIGURE 5: Test curve of d11 at 19 meters on the ground.
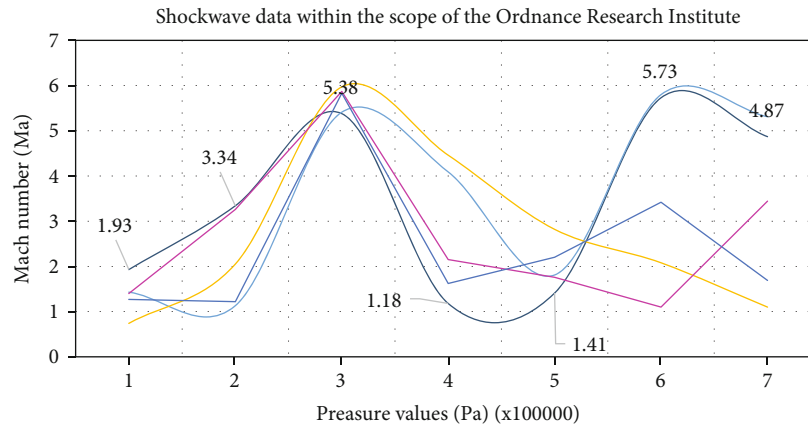
FIGURE 6: Histogram of comparison between the disc and pen bump.

TABLE 6: Two shape structures on the test results increase.

Num	Disc bump	Pen bump	PC environment	Hadoop	Distributed
1	1.93	1.43	0.74	1.4	1.27
2	3.34	1.13	2.05	3.26	1.22
3	5.38	5.41	5.97	5.87	5.83
4	1.18	4.09	4.46	2.15	1.62
5	1.41	1.81	2.82	1.76	2.2
6	5.73	5.8	2.08	1.1	3.42
7	4.87	5.31	1.1	3.44	1.69

the disk slope and the vertical pipe wall, respectively, and the pressure change is very small at the plane disk.

It can be seen from Figure 6 that when the two structures have the same protrusion height or depression depth, the influence of the two shape structures on the test results increases with the increase of the inlet pressure. For the same inlet pressure, the larger the bulge or depression value, the greater the impact on the results.

As shown in Table 6, the influence of the disk is greater than that of the pen type, and the change rate of the relative

difference increases with the increase of the concave-convex value. At the same angle deviation, the influence of the two shape structures on the test results increases with the increase of the inlet pressure. At the same inlet pressure, the larger the deviation angle, the greater the impact on the results. The influence of the disk is greater than that of the pen type, and with the increase of the angle value, the change rate of the relative difference also increases.

4.5. System Computing Performance Test. As shown in Figure 7, the data evaluation model algorithm designed in this paper has high accuracy, but it will generate more intermediate results and temporary matrix in the calculation and execution, and the time complexity reaches $O(n^2 \log(n))$, which is too much for an ordinary single machine environment processing platform, especially when the amount of data is large. By referring to a large number of data, the big data processing technology is introduced, as shown in Table 7.

The massive shock wave test data and calculation processing tasks are distributed on the cluster computer to solve the dilemma of a single machine mode, so as to improve the calculation efficiency and accuracy. Based on the measured
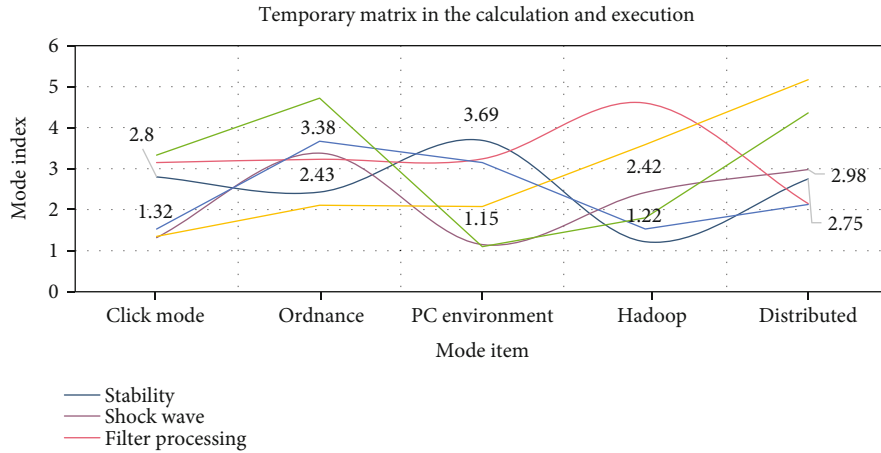
Figure 7: Temporary matrix in the calculation and execution.

Table 7: Big data processing technology is introduced.

Item	Shock wave	Filter processing	Domain analysis	Complexity	Temporary matrix
Click mode	1.32	3.15	1.35	1.53	3.33
Ordnance	3.38	3.23	2.11	3.67	4.72
PC environment	1.15	3.24	2.08	3.15	1.1
Hadoop	2.42	4.6	3.59	1.53	1.8
Distributed	2.98	2.15	5.17	2.13	4.36
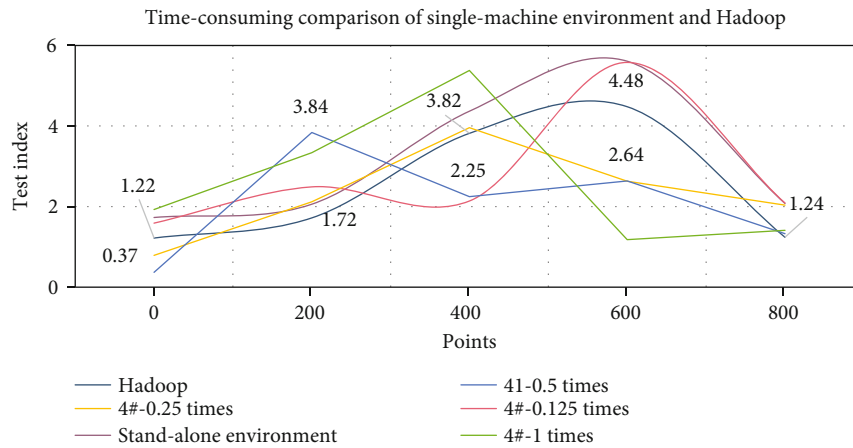
Figure 8: Time-consuming comparison of single-machine environment and Hadoop filtering.

Table 8: Hadoop needs more initialization preparation and intermediate.

Item	Click mode	Ordnance	PC environment	Hadoop	Distributed
Stability	0.91	1.22	1.73	1.59	0.79
Shock wave	2.31	1.72	2.06	2.49	2.12
Filter	4.59	3.82	4.37	2.14	3.96
Domain	3.5	4.48	5.61	5.58	2.63
Complexity	4.34	1.24	2.08	2.09	2.04

shock wave data in the range of Ordnance Research Institute, this part compares the time required for frequency domain decomposition and filtering processing under the traditional single PC environment and Hadoop distributed platform of the system.

As shown in Figure 8, through the above analysis, when the amount of data is small, Hadoop consumes more time because the MapReduce framework cannot open multiple nodes to process the calculation process, and the whole calculation is implemented on one node (equivalent to standalone mode).

As shown in Table 8, Hadoop needs more initialization preparation and intermediate result transmission time, so it consumes more time. When the amount of data reaches a certain scale, Hadoop will start the cluster node distributed processing the same computing process, and its advantages will naturally be highlighted.

5. Conclusions

In the destruction process of weapon warhead, explosion shock wave is one of the essential characteristic physical quantities, which can be measured accurately, which can provide some reference data for the research of weapon destructive power. However, in the actual shock wave test, the amount of test data increases rapidly, and the data structure and types are more and more. The traditional test procedures and data processing technology cannot meet the requirements of rapid testing and cannot meet the most valuable test evaluation results in sea level data. In the current research process, the accuracy and intelligence of the test need to be improved. In this paper, the basic technology and realization of free-field shock wave are completed. It includes AD circuit, storage and recording module, activation circuit, interface circuit, power management module, computer management system, and data processing system. We introduce the implementation of synchronization module and verify the errors of single and multiple synchronization units. Special circuit installation and protection structure are designed for the developed system structure, so as to avoid direct damage to test equipment due to bullet.

In this paper, a test method is studied. The rationality of overpressure value is tested by measuring the velocity of shock wave and directly measuring the overpressure time curve of shock wave. In the process of research and development of the test system, the wireless device complements the functions of flash data storage, gain amplification, frequency increase, retrigger, activation, and internal power generation adjustment, so as to effectively improve the system reliability, operation simplicity, and practicability. The dynamic characteristics of the test system are analyzed, and the performance index and operation index of the test system are verified by the actual explosion test.

In this paper, fluent fluid dynamics simulation software and impact tube are used to study the influence of the convexity and deflection angle of the sensor sensitive surface on the pen and disc test results. It focuses on the simulation of different convex angle, different convex height, depression depth, and installation error under different insertion angles.

The conclusion is that the two shape structures meet the safety requirements. Under the same conditions, the error measured by the pen structure is less than that of the disk structure, while the error caused by concave and convex installation is far greater than that caused by claim of disc structure. What is the reason for this? The simulation results of the broken line method are more intuitive. The results show that the influence of the two schematic structures on the test results increases with the installation angle or the concave-convex degree and increases with the increase of the concave-convex degree. The influence of the angle on the test results is that the pen structure has less influence on the test results than the disk structure, so the pen structure is used for dynamic calibration of the two structures under different installation conditions next. The experimental data and simulation results are compared and analyzed to verify the accuracy of the simulation results.

Data Availability

No data were used to support this study.

Conflicts of Interest

The authors declare that they have no conflicts of interest.

Acknowledgments

References

[1] M. Robert, B. Segui, C. Vergnes, P. Taourel, and J. Guiter, "Piezoelectric extracorporeal shockwave lithotripsy of distal ureteric calculi: assessment of shockwave focusing with unenhanced spiral computed tomography," *BJU International*, vol. 87, no. 4, pp. 316–321, 2015.

[2] J. S. Couldrick, S. L. Gai, J. F. Milthorpe, and K. Shankar, "Normal shock wave/turbulent boundary-layer interaction control using 'smart' piezoelectric actuators," in *Aeronautical Journal*, vol. 109, no. 1101pp. 577–583, 10.1017/s0001924000000919, 2016.

[3] J. D. Tobin and M. J. Hargather, "Quantitative schlieren measurement of explosively-driven shock wave density, temperature, and pressure profiles," *Propellants Explosives Pyrotechnics*, vol. 41, no. 6, pp. 1050–1059, 2016.

[4] M. Bai, Y. Zhao, B. Jiao, X. Zhai, and Y. Geng, "A novel easy-driving and easy-signal-processing electrostatic field sensor based on a piezoresistance and polyethylene terephthalate

lever," *Journal of Micromechanics & Microengineering*, vol. 27, no. 3, article 035002, 2016.

[5] C. Z. Peng and C. K. How, "Giant retroperitoneal abscess following extracorporeal shock wave lithotripsy," *Internal Medicine*, vol. 54, no. 24, pp. 3251-3252, 2015.

[6] S. M. Han and C. S. Huh, "Analysis of a piezoelectric generator under an elastic wave," *IEEE Transactions on Plasma Science*, vol. 45, no. 11, pp. 3001–3006, 2017.

[7] F. Castro, T. Pentiado, J. Blanco, R. Xavier, M. Sanches, and A. de Carvalho, "Crosstalk error analysis in IIDFC readout circuit for use in piezoresistive composite," *IEEE Sensors Journal*, vol. 18, no. 1, pp. 382–389, 2018.

[8] K. Winston, *June Heatwave Could Trigger Aliso Storage Withdrawals: California Official*, Platts Energy Trader, 2019.

[9] K. M. Thijs, J. Zwerver, F. J. G. Backx et al., "Effectiveness of shockwave treatment combined with eccentric training for patellar tendinopathy: a double-blinded randomized study," *Clinical Journal of Sport Medicine*, vol. 27, no. 2, pp. 89–96, 2017.

[10] S. Raghunathan and D. G. Mabey, "Passive shock-wave/boundary-layer control on a wall-mounted model," *AIAA Journal*, vol. 25, no. 2, pp. 275–278, 1987.

[11] L. Li, D. Qian, X. Zou, and X. Wang, "Underwater electrical wire explosion: shock wave from melting being overtaken by shock wave from vaporization," *Physics of Plasmas*, vol. 25, no. 5, article 053502, 2018.

[12] C. Sudhiesh Kumar and K. P. J. Reddy, "Experiments in hand-operated, hypersonic shock tunnel facility," *Shock Waves*, vol. 26, no. 6, pp. 845–849, 2016.

[13] J. S. Couldrick, S. L. Gai, J. F. Milthorpe, and K. Shankar, "Investigation of unswept normal shock wave/turbulent-boundary-layer interaction control," *Journal of Aircraft*, vol. 46, no. 5, pp. 1634–1641, 2015.

[14] G. Thomas, J. Y. Chapelon, and C. Lafon, "Finite element optimization of circular element used in lithotripsy and histotripsy piezoelectric transducers," *Journal of the Acoustical Society of America*, vol. 141, no. 5, pp. 3719–3719, 2017.

[15] J. L. Edwards, W. S. Hinman, and C. T. Johansen, "Extracting mole fraction measurements from the visualization of a shock reflection," *Journal of Visualization*, vol. 22, no. 1, pp. 35–49, 2019.

[16] M. V. Antipov, I. V. Yurtov, A. Utenkov et al., "Piezoelectric method for measuring the parameters of shock-induced ejecta," *Combustion Explosion and Shock Waves*, vol. 54, no. 5, pp. 599–605, 2018.

[17] S. Cooppan and B. Skews, "Three-dimensional shock wave diffraction off a discontinuous edge," *Shock Waves*, vol. 27, no. 2, pp. 131–142, 2017.

[18] G. Nath and S. Singh, "Corrigendum to: "Flow behind magnetogasdynamic exponential shock wave in self- gravitating gas" [Int. J. Non-Linear Mech. 88 (2017) 102-108]," *International Journal of Non-Linear Mechanics*, vol. 89, p. 132, 2017.

[19] C. Chelem Mayigue and R. Groll, "Computational magnetohydrodynamic modeling of hypersonic flows with resolved shock wave diffusion," *PAMM*, vol. 16, no. 1, pp. 621-622, 2016.

[20] W. Johanns, C. Jakobeit, L. Greiner, and J. Janssen, "Ultrasound-guided extracorporeal shock wave lithotripsy of pancreatic ductal stones: six years' experience," *Canadian Journal of Gastroenterology*, vol. 10, no. 7, pp. 471–475, 1996.

[21] A. M. Blokhin, D. L. Tkachev, and A. V. Yegitov, "Local solvability of the problem of the van Der Waals gas flow around an infinite plane wedge in the case of a weak shock wave," *Siberian Mathematical Journal*, vol. 59, no. 6, pp. 960–982, 2018.

[22] A. S. Savinykh, G. V. Garkushin, G. I. Kanel', and S. V. Razorenov, "Evaluation of viscosity of Bi–Pb melt (56.5%–43.5%) by the width of a weak shock wave," *High Temperature*, vol. 6, no. 5, pp. 685–688, 2018.

[23] M. H. Radfar, N. Simforoosh, M. Sotoudeh et al., "What is the impact of extracorporeal shock wave lithotripsy on semen parameters? A systematic review and meta-analysis," *Urologia Journal*, vol. 84, no. 1, pp. 28–34, 2017.

[24] R. Assaly-Kaddoum, F. Giuliano, S. Compagnie, J. Bernabé, and D. Behr-Roussel, "Additive pro-erectile effect of low intensity-shockwave therapy (Li-ESWT) delivered by Aries combined with sildenafil in spontaneously hypertensive rats (SHR)," *European Urology Supplements*, vol. 16, no. 3, pp. e1945–e1946, 2017.

[25] T. Mimura, Y. Igarashi, K. Ito et al., "Efficacy of combined endoscopic treatments and extracorporeal shock wave lithotripsy for pancreatic lithiasis," *Suizo*, vol. 30, no. 2, pp. 154–163, 2015.

WILEY | Hindawi

Research Article

An FPGA-Based Convolutional Neural Network Coprocessor

Changpei Qiu (ORCID), **Xin'an Wang** (ORCID), **Tianxia Zhao** (ORCID), **Qiuping Li** (ORCID), **Bo Wang, and Hu Wang**

The Key Laboratory of Integrated Microsystems, Peking University Shenzhen Graduate School, Shenzhen 518055, China

Correspondence should be addressed to Xin'an Wang; anxinwang@pku.edu.cn

In this paper, an FPGA-based convolutional neural network coprocessor is proposed. The coprocessor has a 1D convolutional computation unit PE in row stationary (RS) streaming mode and a 3D convolutional computation unit PE chain in pulsating array structure. The coprocessor can flexibly control the number of PE array openings according to the number of output channels of the convolutional layer. In this paper, we design a storage system with multilevel cache, and the global cache uses multiple broadcasts to distribute data to local caches and propose an image segmentation method that is compatible with the hardware architecture. The proposed coprocessor implements the convolutional and pooling layers of the VGG16 neural network model, in which the activation value, weight value, and bias value are quantized using 16-bit fixed-point quantization, with a peak computational performance of 316.0 GOP/s and an average computational performance of 62.54 GOP/s at a clock frequency of 200 MHz and a power consumption of about 9.25 W.

1. Introduction

Hardware acceleration of artificial neural networks (ANNs) has been a hot research topic since the 1990s [1, 2]. The most representative one is the implementation of a shallow artificial neural network gas pedal, ETANN, by Intel in 1989, which supports only a small amount of data [3, 4]. Convolutional neural networks have been proposed since 1989 and did not become a research hotspot until 2006, mainly due to the difficulty of hardware computing power at that time. The convolutional and fully connected layers in CNN are mainly multiplicative and additive operations with relatively single control process; however, the training and prediction process of CNN models generally requires hundreds of millions of multiplicative and additive operations [5, 6], of which 90% of the computations are concentrated in the convolutional layer [7]. To achieve high computational performance, it is often necessary to design highly parallel temporal and spatial architectures [8–10].

Temporal parallelism is mainly for CPUs and GPUs, which improve computational efficiency mainly by increasing frequency, multilevel cache, single instruction multiple data, single instruction multiple threads, etc. All Arithmetic Logic Units (ALUs) share controllers and memory. In these

computing platforms, the convolutional and fully connected layers are mapped into matrix multiplication to participate in the computation. CNN has high computational density, single task, and high data reuse and requires large-scale computational logic and storage bandwidth without complex control logic, so the CPU is not suitable for CNN computation. On the contrary, GPU has thousands of computational cores and is more suitable for CNN computation; however, the power consumption and area of GPU are large, and the energy efficiency ratio is low mainly deployed in the cloud. However, GPUs are not suitable for embedded applications, which are power sensitive. Spatial parallelism is mainly for ASICs and FPGAs, mainly through stream processing, local accumulation, proximity storage, etc. to improve data reuse and thus computational efficiency. FPGAs are highly programmable and configurable, with high energy efficiency and short development cycles, especially with tools such as High Level Synthesis and OpenCL, which accelerate the development of FPGAs.

Sankaradas et al. designed a coprocessor for CNN based on FPGA [11] with low precision data bit-width (20-bit fixed-point quantization for weights and 16-bit fixed-point quantization for feature map values), supporting only fixed size convolutional kernel size, frequent
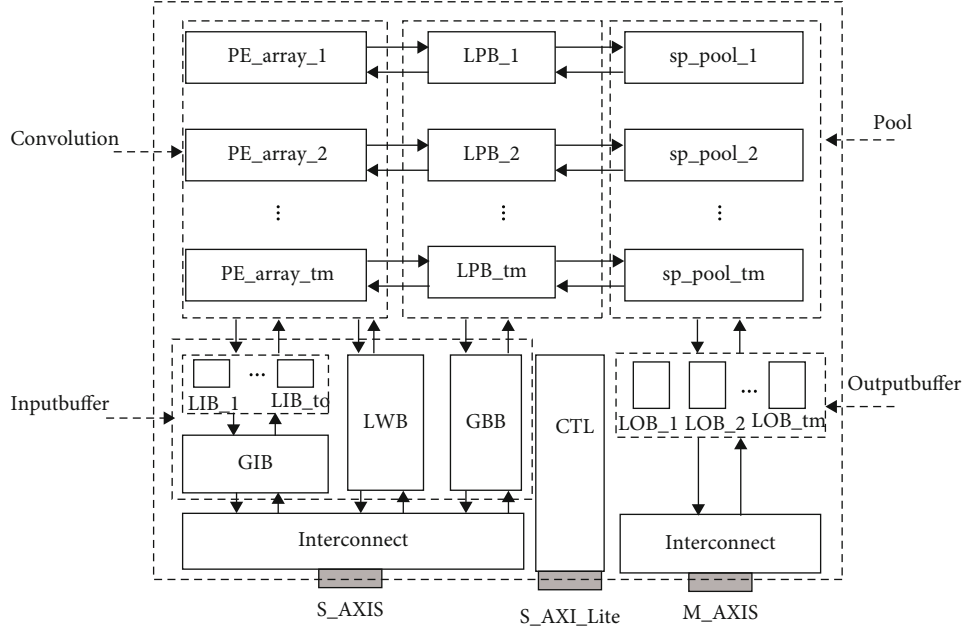
FIGURE 1: The schematic diagram of the overall architecture of the coprocessor.
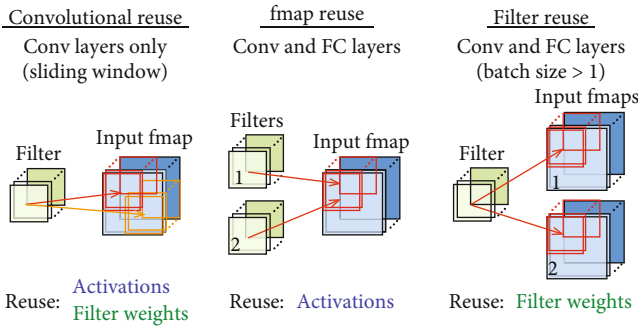
FIGURE 2: The form of data reuse in CNN.

accesses, high power consumption, and low computational efficiency because intermediate values need to be stored in DDR. Gokhale et al. designed the coprocessor nn-X for mobile embedded end [12, 13] with a peak computational performance of 200 GOP/s on Xilinx ZC706 platform. With the increasing complexity of CNN models, FPGA logic resources, and memory bandwidth, the design space of FPGAs is also expanding. In order to find the optimal gas pedal design solution, MIT proposed Eyeriss [14], a highly efficient and reconfigurable deep convolutional neural network accelerator chip. Eyeriss supports different sizes of input feature maps and convolutional kernel sizes, uses RLB (run-length-based) compression to reduce the average image data transfer bandwidth by a factor of 2, reduces the interaction between computational units and on-chip storage through data reuse and local accumulation, and reduces the interaction between data and DDR through hierarchical storage. This reduces power consumption.

In this paper, we analyze the convolutional neural network algorithm and design a high-performance and flexible FPGA-based convolutional neural network coprocessor by combining the hardware implementation and optimization with the characteristics of FPGA platform. The paper is organized in the following sections. Section 2 introduces the coprocessor architecture. Section 3 focuses on the design of each major module in the coprocessor. In Section 4, we perform FPGA hardware verification. Finally, Section 5 concludes.

2. Coprocessor Architecture

In this paper, we provide a coprocessor implementation for convolutional neural networks, which is aimed at accelerating the convolutional and pooling layers of convolutional neural networks on FPGAs and applying them to heterogeneous accelerated systems or embedded terminals. The design solution includes a controller, input buffer, output buffer, convolutional unit, and pooling unit. Figure 1 shows the schematic diagram of the overall architecture of the coprocessor. The input buffers include a global image buffer (GIB), tc local image buffers (LIBs), a global bias buffer (GBB), tm local weight buffers (LWBs), and tm local partial sum buffers (LPBs). The output buffers include tm local output buffers (LOBs); the convolution operation unit includes tm PE arrays; the pooling unit includes tm splice pools (referred to as sp_pool, a pooling unit containing image stitching function); tm and tc in the figure are given optimal values by theoretical analysis.

The main functions of each cell module in this architecture are as follows:

(1) The data I/O interface supports AXI4-Stream and AXI4-Lite bus protocols. The off-chip memory sends
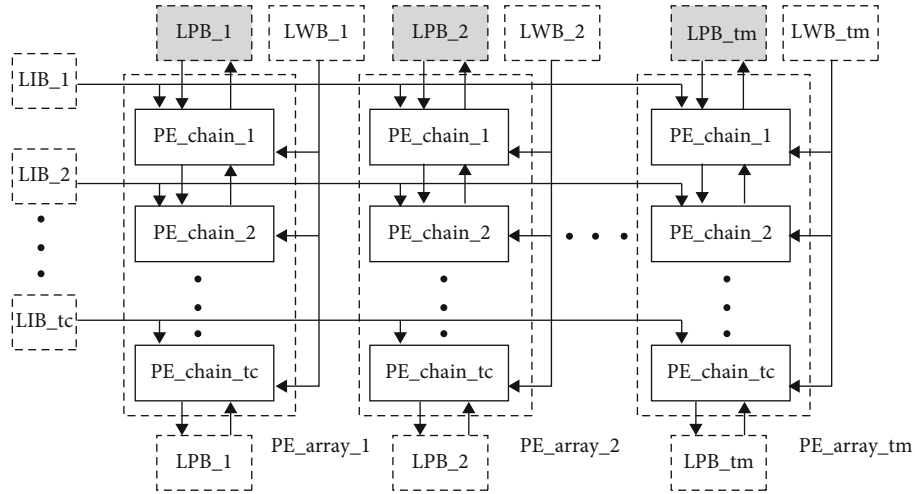
FIGURE 3: The schematic diagram of the proposed convolutional computation unit.
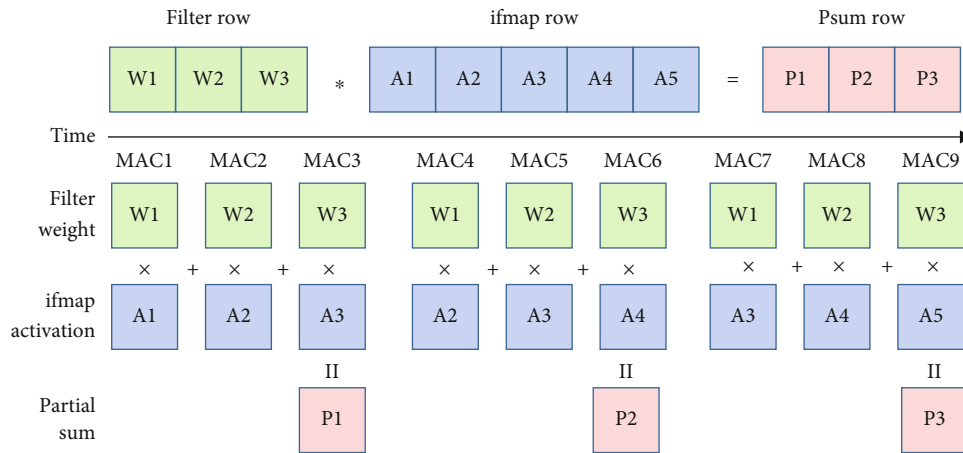
FIGURE 4: The schematic of the data flow of PE performing 1D convolution.
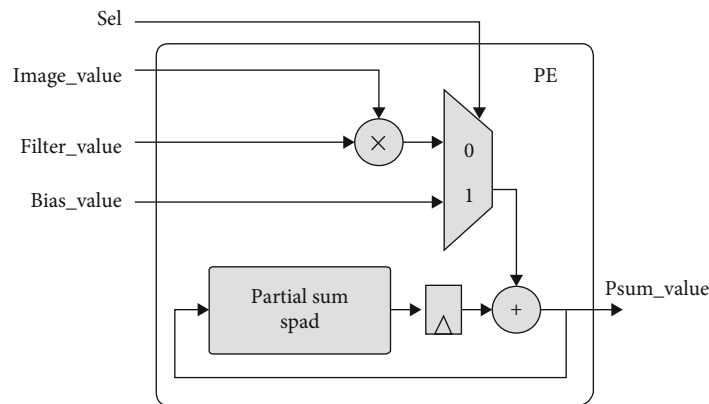
FIGURE 5: The schematic diagram of the PE unit.

data in bulk to the input buffer of the coprocessor through the AXI4-Stream Slave interface to provide feature map data, weight data, and bias data for the PE array

(2) The global controller communicates with external control signals through the AXI4-Lite bus interface. The global controller contains nine 32-bit instruction registers, which are used to store the parameters of

the convolutional layer as well as the enable signal and the end-of-computation signal

(3) GIB and GBB and tm LWBs all have an ID. After the data is input from the S_axis interface, only the buffer with the matching ID can receive the data

(4) GIB is distributing data to tc LIBs in the form of global broadcast, each LIB has its own ID, and only LIBs with matching IDs can receive data

(5) Each sp_pool can implement nonlinear activation, image stitching, and pooling. This design supports activation function ReLU and step size 2, size 2×2 maximum pooling

The FPGA development board used in this thesis is the ZYNQ-7000 ZC706 evaluation board, and the number of DSPs available and the size of on-chip storage is small compared to the mainstream chips. The amount of weight data in the fully connected layer is large, and there is no reusability. If the fully connected layer is executed in FPGA, only a small performance improvement can be obtained, but at the same time more computational and storage resources are occupied and the control logic is more complicated, which will directly affect the parallelism of the convolutional layer operation. Therefore, the coprocessor designed in this thesis is only responsible for the accelerated computation of the convolutional and pooling layers.

3. Design of Each Major Module in the Coprocessor

3.1. Convolutional Operation. Convolutional operations are the most central and computationally intensive operations in convolutional neural networks, so the efficiency of convolutional units directly affects the performance of the whole architecture. In fact, most of the hardware resources in the design solution are also allocated to the acceleration of convolutional operations. The basic operation of convolutional operation is matrix multiplication, and one convolutional operation consists of multiple multiplication and addition operations; in convolutional operation, the data is highly reusable, as shown in Figure 2.

3.1.1. Convolutional Reuse. A 3D convolutional kernel of size $k \times k \times C$ slides on a 3D feature of size fmap_size $\times$ fmap_size $\times$ C with a fixed step size. The same convolutional kernel convolves different receptive domains, and the filter weights are reused; the activations of two adjacent receptive domains overlap and are reused by different weights in one convolutional kernel.

3.1.2. fmap Reuse. M 3D convolutional kernels of size $k \times k \times C$ are slid over a 3D feature map of size fmap_size $\times$ fmap_size $\times$ C in a fixed step. When M convolution kernels convolve the same sensory domain, the activation values in that domain are reused.

3.1.3. Filter Reuse. A 3D convolutional kernel of size $k \times k \times C$ slides over N 3D feature maps of size fmap_size $\times$
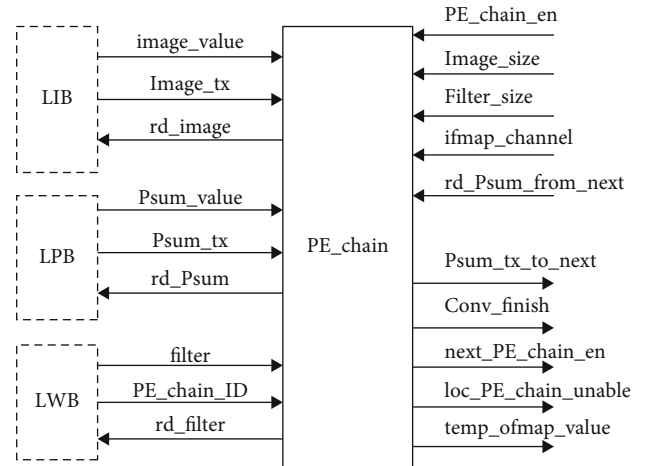
FIGURE 6: The schematic diagram of the I/O interface of the PE chain.

fmap_size $\times$ C with a fixed number of steps. The same convolutional kernel can convolve multiple sensory domains at the same location in the feature map, and the kernel weights are reused.

Although multiple multiplication and addition operations are required in a single iteration, the data demand is high, but in fact, since most of the data in the input feature subregion of the convolution operation can be reused, fully utilizing this feature can reduce the on-chip data cache capacity and off-chip storage bandwidth requirements.

3.2. Convolutional Cell Design. In this paper, in order to take full advantage of the data multiplexing form of the convolutional computation process and to fully consider the computational and storage resources of the FPGA, Figure 3 shows the schematic diagram of the proposed convolutional computation unit, which illustrates the data interaction between the computational unit and the memory.

The whole convolutional computation unit includes tm PE arrays, each PE array includes tc PE chains, each PE chain includes 3 PE, each PE contains a DSP, each PE can complete a one-dimensional convolution, each PE chain can complete a two-dimensional convolution, and multiple use of a PE chain or multiple PE chain parallel computation can achieve a three-dimensional convolution. As shown in Figure 3, first, there are tc LIBs corresponding to tc PE chains, and each LIB passes the image data to tm PE chains in the form of broadcast, realizing the feature map reuse form as shown in Figure 2. In addition, there are tm LWBs in the whole convolutional computation unit, and each LWB corresponds to one PE array, and the weights are passed to tc PE chains in the form of broadcast, realizing the convolutional reuse form shown in Figure 2. Finally, there are tm LPBs in the whole convolutional computation unit, each LPB stores the bias value (bias) from GBB for the first time and then stores the partial sum from PE chain; similarly, each LPB can output data to PE chain or to splice pool. Each LPB has two data input ports and two data output ports.
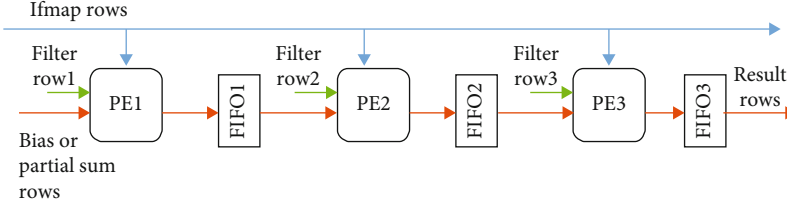
FIGURE 7: The schematic diagram of the proposed PE chain.
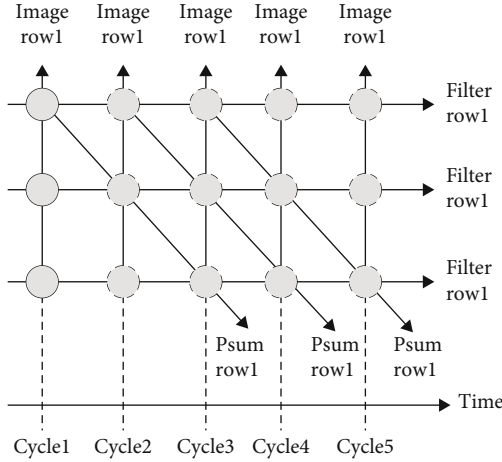
FIGURE 8: The space-time mapping (STM) of a PE chain.

3.3. PE. The most basic multiplication and addition unit PE in the convolution unit designed in this paper adopts the stream processing structure of RS, which can realize the one-dimensional convolution calculation. Assuming the size of the input feature map ifmap_size = 5 and the size of the convolution kernel $k = 3$, the data flow into PE is shown in Figure 4. The PE structure designed in this paper saves storage resources by reducing the Image Scratch Pad and Filter Scratch Pad compared to the PE structure of Eyeriss [10], which is certainly a good design in the case of storage constraints. Figure 5 shows the schematic diagram of the PE unit. Sel in the input signal is the selection control signal; Sel = 1 plus the bias value or the partial sum from the previous PE; Sel = 0 plus the product of the activation value and the weight value. This PE structure can be implemented in the FPGA with only one DSP example. In this paper, to avoid the logic overhead and control complexity associated with dynamic fixed-point quantization, both weights and activation values are quantized using a fixed-state 16-bit fixed-point quantization.

3.4. PE Chain. PE chain is the core of the entire convolutional computation unit. Without considering parallel computation, a PE chain can do all the computations of the convolutional layer in the neural network independently.

Figure 6 shows the schematic diagram of the I/O interface of the PE chain. When the PE chain detects an enable signal, it sends an activation request signal to the LIB, a partial sum signal to the LPB, and a weight request signal to the LWB; the LIB receives the request signal and sends a feature map value; the LPB sends a partial sum; the LWB sends a convolution

kernel. A channel counter is designed in PE chain. When a 2D feature map value is computed, the counter is incremented by one until the counter equals the computed channel, and all input feature map channels are computed. This marks the completion of the computation of all channels in a 3D tile (a large feature map divided into several smaller feature maps, each of which called a tile).

PE chain computational logic: if the size of the convolution kernel is k, then a PE chain consists of k PEs connected sequentially and expanded in space-time, which is a two-dimensional systolic array structure. In this design, only 3 × 3 convolutional kernels are supported, so a PE chain consists of 3 PEs, as shown in Figure 7, and each two PEs are connected by a FIFO (the last PE chain in a single PE array as shown in Figure 3 contains only two FIFOs, and the last FIFO is replaced by an LPB).

A PE chain can implement a 2D convolution, and a PE chain can fully implement a 3D convolution calculation without considering the computational speed (all 2D convolutions are executed serially by a PE chain). Assuming an input feature map of size ifmap_size = 5 and a convolution kernel of size $k = 3$, the space-time mapping (STM) of a PE chain is shown in Figure 8.

Each solid circle in the graph represents one PE, three PEs in total, and the computation process of each PE is expanded along the time axis to form a two-dimensional pulsating array structure. Each row of the feature map is passed to each PE simultaneously in the form of a broadcast. The data flow of Psum_row1 in the space-time mapping diagram of PE chain is shown in Figure 9, where the data flow of each PE is shown in Figure 4. The first row of the convolution kernel is given to PE1, the second row to PE2, and the third row to PE3, with three rows of input simultaneously, which requires that one convolution kernel must be taken from the LWB at a time. In each cycle, the PE computes a one-dimensional convolution, and the partial sum is temporarily stored in the FIFO. When the previous PE finishes computing a row, the next PE is opened, and the partial sum in the previous FIFO is read as bias into the current PE.

3.5. PE Array. PE array is an array of PE chain, and the whole convolutional computation unit is implemented by multiple PE arrays, utilizing two data reuse modes, such as convolutional reuse and feature map reuse shown in Figure 2, to achieve a high degree of parallelism in convolutional computation. Due to the limited on-chip storage, the input feature map must be segmented, and the segmentation strategy is related to the overall structure of the PE array, which also
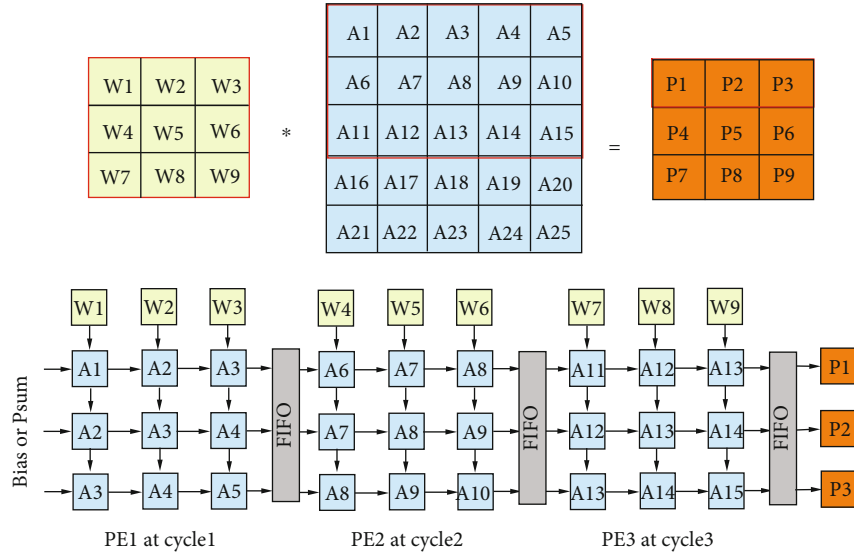
FIGURE 9: The data flow of Psum_row1 in the space-time mapping diagram of PE chain.
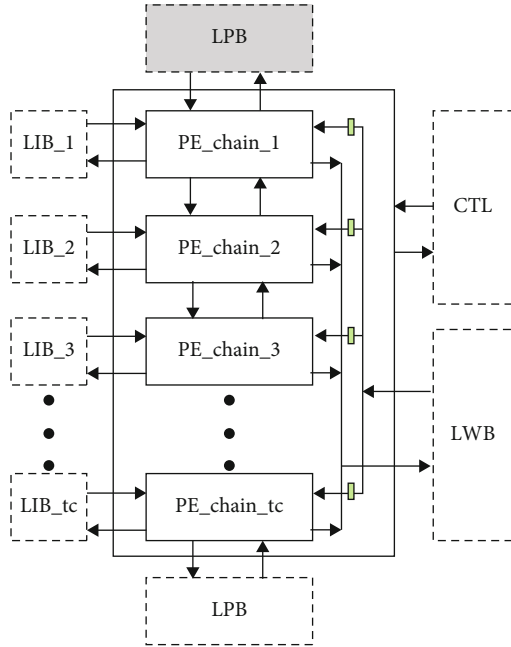
FIGURE 10: The overall structure of a single PE array.
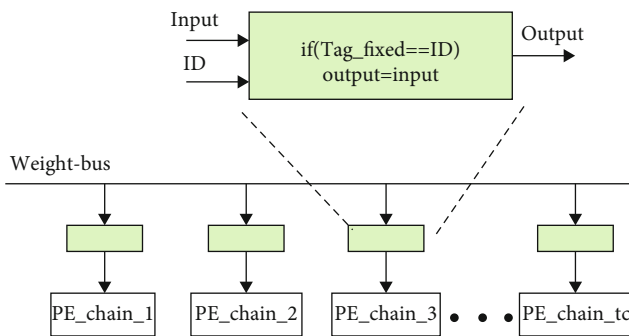
FIGURE 11: The schematic diagram of the proposed PE chain.

leads to the decision of computation modes for multiple PE arrays.

The overall structure of a single PE array is shown in Figure 10. The detailed I/O interfaces are omitted, and the directions indicated by the arrows in the figure only represent data interaction relationships.

A single PE array contains tc PE chains, and tc PE chains are connected in turn. When PE array receives the signal from each PE chain, it can easily control the opening and closing of each PE chain. The nth PE chain sends a signal to the nth-1st PE chain to request a partial sum. After the nth-1st PE chain receives the requested signal, it sends a signal to the next PE chain and at the same time reads its own FIFO3 and sends a partial sum. The tcth PE chain differs from the previous PE chain in that it contains only two FIFOs, and the third FIFO is replaced by the LPB, and the first PE chain sends a request signal to the LPB.

Data interaction between PE array and each buffer: each PE chain has its corresponding local image buffer (LIB), and all PE chains share a local weight buffer (LWB), as shown in Figure 11, and the LWB sends the weights to PE array in the form of broadcast, and only the PE chain with matching ID can receive them. chain can only receive them. The start of PE array is controlled by three signals, the signal from GIB and the signals from LPB and LWB, respectively.

3.6. Image Segmentation Strategy. For a PE array with a PE chain in each PE array, the entire convolutional computation unit has only one PE chain (with 3 DSPs), and all local caches alone require at least 53 Mb of storage space to satisfy the computation of all convolutional layers. For 4 PE arrays, each PE array contains 64 PE chains, i.e., the entire convolutional computation unit uses 256 PE chains (with 768 DSPs), and the local cache alone requires at least 255 Mb of storage space. The on-chip storage of FPGA chip resources is only 19.1 M, while the number of DSP is 900. Obviously, if the feature map is not divided, the on-chip storage is not enough and the computational unit cannot be fully utilized. In order
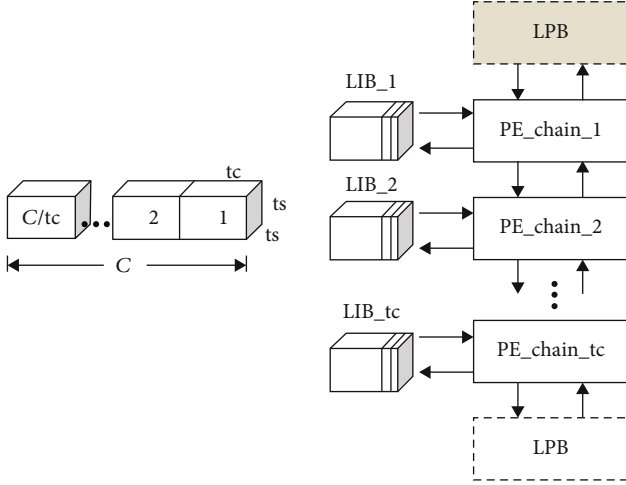
FIGURE 12: Correspondence of a 3D tile to a PE array.

to balance the allocation of on-chip storage and computational units, this paper adopts the strategy of splitting the feature map size. The smaller the size of the split feature map, the smaller the local storage occupation, and the larger the global cache can be allocated with limited storage resources, reducing the delay of data loading during each round of computation of computation units. Of course the trouble brought is the increase in the number of rounds of computation needed and the increase in the number of data loading from the global buffer. So the size of the partition needs to be adapted to the architecture of the hardware, taking into account both the parallelism of multiple PE arrays and the time delay of opening multiple PE chains in each PE array in turn.

In the hardware architecture design of this thesis, for the convenience of control, so that the size of each tile is equal, C should be divisible by tc. A tile ($\text{ts} \times \text{ts} \times C$) of depth C is decomposed into C/tc groups according to successive groups of tc 2D tile, and the 2D tile in each group is stored in the corresponding LIBs, which correspond to PE array, as shown in Figure 12. Each LIB stores 2D tile.

The actual simulation verifies that after PE chain is enabled, it needs to request feature map data, weight data, and partial sum data and then turn on the first PE, and the process takes five clock cycles. According to the calculation logic of PE chain, the previous PE needs to calculate one row of feature map data before the next PE can be turned on, and the process takes $3(\text{ts} - k + 1)$ clock cycles. The PE3 calculation of the previous PE chain produces the first partial sum to start the next PE chain, and the actual simulation verifies that the process takes seven clock cycles. It takes $\text{tc} \times [5 + 6(\text{ts} - k + 1) + 7]$ clock cycles from the first PE chain first enable to the second enable, while it takes $5 + \text{ts} \times 3(\text{ts} - k + 1)$ clock cycles for the first PE chain to finish computing the first 2D tile. tc and ts are bounded as follows:

$$5 + \text{ts} \times (\text{ts} - k + 1) < \text{tc} \times [5 + 6(\text{ts} - k + 1) + 7]. \quad (1)$$

When $k = 3$, the inequality is rewritten as follows:

$$0 < 6\text{tc} \times \text{ts} - 3\text{ts}^2 + 6\text{ts} - 5. \quad (2)$$

The constructor is as follows:

$$f(\text{ts}, \text{tc}) 6\text{tc} \times \text{ts} - 3\text{ts}^2 + 6\text{ts} - 5. \quad (3)$$

In order to minimize the interval time of PE chain, f (ts, tc) should be taken as the minimum value. To facilitate control, tc should be equal to 2^n, considering that there are only 900 DSPs in the FPGA and each PE chain contains 3 DSPs, the relationship between the number of DSPs used. When tc = 4 and ts = 9, the function $f(\text{ts}, \text{tc})$ is greater than 0 and smallest. The theoretical interval of the PE is 22 clock cycles.

The design of this thesis uses 64 PE arrays for parallel computation. When tc = 4, tm = 64, ts = 9, the local buffer occupies at most 5.5 Mb. This paper uses distributed RAM instantiation for memories with larger bit width (48 bits) or smaller space occupancy, such as FIFO, LPB, and LOB.

3.7. Computational Decision for Multiple PE Chains.

The convolutional computation unit uses 64 PE arrays, and each PE array contains 4 PE chains. The computation model used in this paper is as follows: the feature map values in each LIB are shared by 64 PE arrays, and each PE array has its own separate LWB, as shown in Figure 13.

The previous PE chain passes the computed partial sum to the next PE chain. Each tc 2D tile is computed as a small cycle (called a 2D_tile_cycle), and each 3D tile takes C/tc small cycles to compute, so the number of clocks (time$_{\text{tile}}$) needed to finish computing a 3D tile is as follows:

$$\text{time}_{\text{tile}} = \text{tc} \times [5 + 6(\text{ts} - k + 1) + 7] \times \frac{c}{\text{tc}}. \quad (4)$$

Each 3D tile is a large cycle (called a 3D_tile_cycle), and 64 PE arrays produce 64 output feature maps at the same time. The PE array designed in this paper contains 4 PE chains, and each PE chain corresponds to a channel of the input feature map, and when there are only three channels of the input feature map, the value stored in the fourth LIB is all 0 for the convenience of control.

This computational model has a great improvement for the utilization of computational units. According to the parameters of the neural network model of VGG16, the minimum number of output channels is 64, so it can ensure that all 64 PE arrays can be effectively computed when computing each layer of convolution. For neural networks with less than 64 output channels, we can flexibly control the number of PE array through the controller parameter configuration to reduce unnecessary power consumption.

3.8. Splice Pool.

The overall structure of splice pool is shown in Figure 14 (the clock signal and reset signal are omitted in the figure) and contains an internal Pool Buffer and a specially designed comparator. After PE array calculates a 3D tile, it sends a signal to splice pool, and splice pool detects
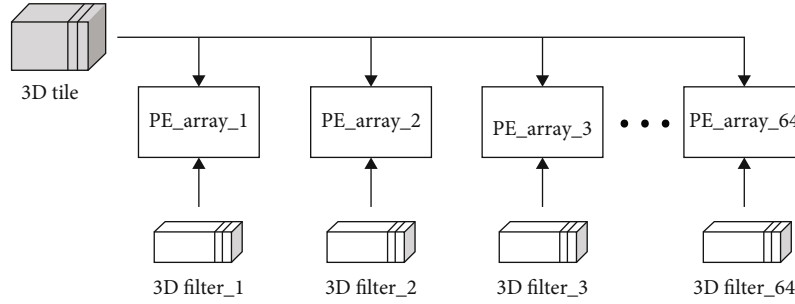
Figure 13: Convolutional unit computation model.
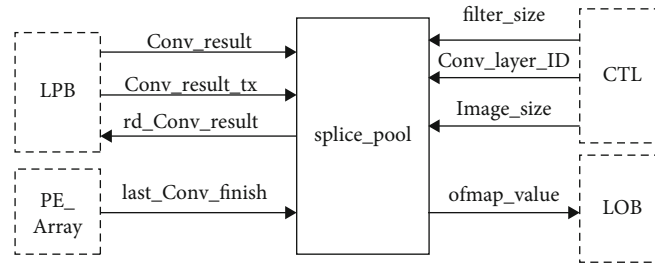
Figure 14: The overall structure of splice pool.
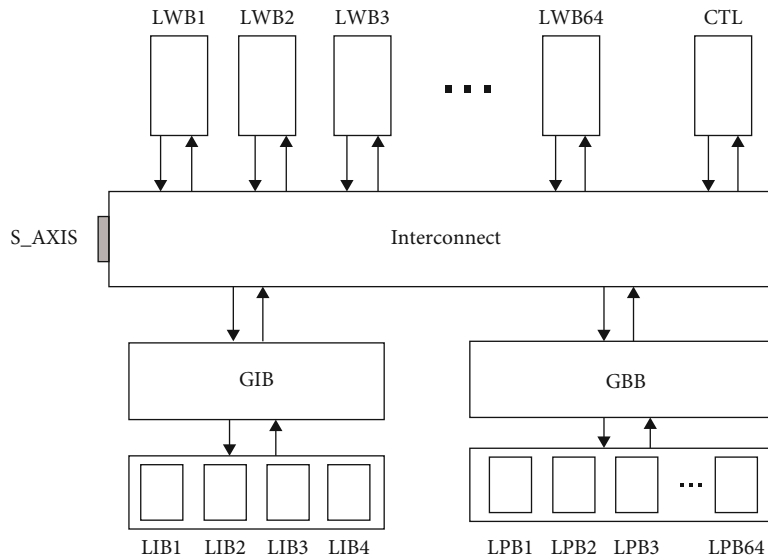
Figure 15: Data interaction of input buffers with the bus.

Table 1: Individual input buffer IDs.

Memory	GBB	LWB1	…	LWB64	GIB
ID	1	2		65	66

the signal and starts to enable it, delays one clock cycle to send a signal to request the convolution result, and after LPB receives the request signal, it sends a transmission signal and delays one clock cycle to send the convolution result. When an output tile is stored, splice pool stops enabling and enters the state of waiting for the next enable. When four

output tiles are spliced, the comparator is started and the ready pooling signal is sent to the LOB, and then, the pooling result is output every four clock cycles.

3.9. Memory System. The memory system mainly consists of input buffers and output buffers, both of which are connected to the DMA controller through the AXI4-Stream bus, and interacts with DDR3 by DMA. This avoids frequent data exchange with DDR3 memory and reduces access to memory power. The memory capacity configuration in the coprocessor is combined with the features of Block RAM and Distributed RAM (DistRAM) in FPGAs. The memory capacity
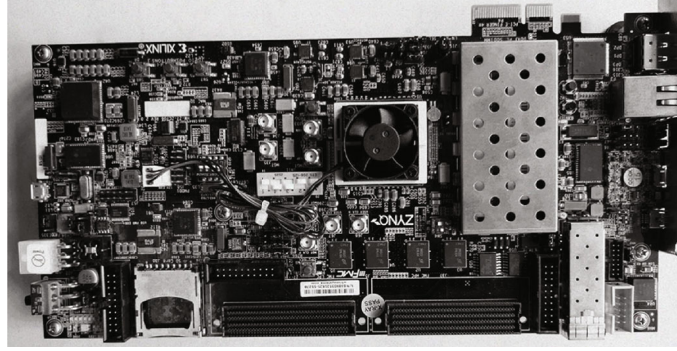
Figure 16: The ZC706 evaluation board.
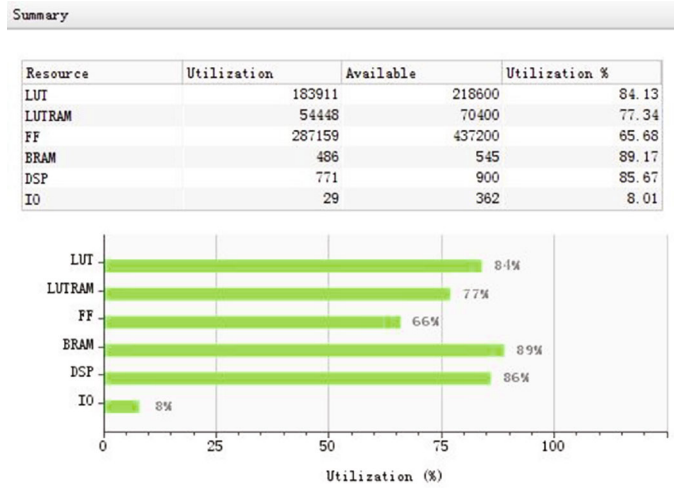
Figure 17: The resource utilization report.

Table 2: The performance statistics of the coprocessor computing VGG16.

Layer	Number of operations (Ops)	Number of clocks (clk_num)	Performance (GOP/s)	Power (W)
Model	9437184	21669	87.10	9.21
Conv1	176518656	471803	74.83	9.21
Conv2	3765731328	33739520	22.32	9.23
Conv3	1916338176	4287402	89.39	9.24
Conv4	3832676352	17419712	44.00	9.23
Conv5	1984167936	2440995	162.57	9.22
Conv6	3968335872	9996224	79.40	9.23
Conv7	3968335872	9996224	79.40	9.25
Conv8	2123366400	3468295	122.44	9.28
Conv9	4246732800	7790023	109.03	9.25
Conv10	4246732800	7790023	109.03	9.26
Conv11	1207959552	3621895	66.70	9.23
Conv12	1207959552	3621895	66.70	9.24
Conv13	1207959552	3621895	66.70	9.23

Table 3: The computational performance comparison results for different platforms.

Layer group	This work (GOP/s) VGG16	[15]	[16]	[17]
Conv_1	23.04	46.42	1578.8	45.15
Conv_2	52.97	80.44	1675.5	69.60
Conv_3	88.45	151.57	2177.1	103.51
Conv_4	111.47	147.91	2791.6	86.04
Conv_5	66.70	186.99	1003.5	36.27

configuration method in this design is flexible based on performance requirements and resource redundancy.

The input buffers include GIB, LIB, LWB, GBB, and LPB. The data interaction relationship is as follows Figure 15. Since all data needs to be input from the axis_S port, each memory connected to the interconnect logic is assigned an ID for efficient distribution, and only the memory with the matching ID can receive the current data. Table 1 shows the individual input buffer IDs. Considering that DDR reads and writes are usually in burst mode, the bandwidth utilization is higher when reading or writing batches of data sequentially and lower when random address reads and random address writes alternate frequently. Therefore, the data

TABLE 4: The computational performance of the coprocessor of this design compared with other FPGA processor.

Parameters	[18]	[13]	[19]	[17]	This work
Platform	Virtex5SX240t	ZynqXC7Z045	Virtex7VX485t	ZynqXC7Z045	ZynqXC7Z045
Frequency (MHz)	120	150	100	150	200
Quantification	48 bits	16 bits	32 bits	16 bits	16 bits
Power	14	8	18.61	9.63	9.30
Performance (GOP/s)	16	23.18	61.62	187.80	62.54

is stored in DDR in the order of the first layer (bias–filter–feature map), the second layer (bias–filter–feature map), and so on. Therefore, the order of ID change is 1,2,3 ......66, when data is loaded from off-chip memory into the input buffer before each layer of convolutional computation, and the order of ID change after that varies according to the configuration parameters of the controller.

The output buffer consists of tm local output buffer (LOB) with one LOB connected after each pooling unit. 64 LOBs are stored at the same time, and a signal is sent to the controller, and the host reads the output feature values sequentially through the M_axis port.

3.10. Global Controller. The global controller mainly consists of a lookup table and a register configuration unit, which completes the control of each module of the whole coprocessor. The configuration of the registers is done through the AXI4-Lite interface configuration, including nine 32-bit registers, each with corresponding address and description. The global controller starts the coprocessor when it detects an enable signal. In order to use as much DSP as possible for convolution calculation instead of for address or other intermediate parameters, this thesis unifies the parameters that may be used by each module in the controller for calculation and then sends them to each module on demand.

4. FPGA Hardware Verification

The coprocessor designed in this thesis focuses on the accelerated computation of the convolutional layer in the VGG16 neural network model. The coprocessor is verified in hardware based on the ZC706 evaluation board kit, as shown in Figure 16. The evaluation board contains a configurable dual-core ARM Cortex A9 processor and a 28 nm XC7Z045 FFG900-2-based FPGA chip with 54650 Slice (each Slice contains 4 LUTs and 8 flip-flops), 900 DSP cells, and 545 Block RAM cells.

The proposed coprocessor implements parallel computation of 64 PE arrays with the coprocessor resources as shown in Figure 17. 768 DSPs are used for the convolutional computation unit, 2 DSPs for the controller, and 1 DSP for the GIB. In the process of implementation and layout wiring, the "default" implementation strategy is selected, and the clock frequency can reach 200 MHz.

At the clock frequency of 200 MHz, the peak computation capacity of the coprocessor designed in this paper is 316.0 GOP/s. Due to the long loading time of the data, especially in the case of a relatively large number of 3D tiles, the interval time of PE array accumulates relatively large, resulting in a relatively low average computation capacity. Table 2 shows the performance statistics of the coprocessor computing VGG16. In the verification scheme, the ROM of the off-chip memory needs to be instantiated using Block RAM. Therefore, the verification can only have the storage capacity of GIB, so the convolutional layers with more parameter values and activation values cannot be verified. We can extrapolate the convolutional computation time and data loading time based on the verified convolutional layers and then infer the computational performance of the convolutional layers that cannot be verified directly. According to the actual test results in Table 2, it can be found that the total computational power consumption increases slightly with the number of accesses when all DSPs are involved in the computation. The main reason is that the DDR is not accessed during the test, and all data interactions take place between on-chip memory and registers and before registers and DSPs. The difference in the number of accesses results in a slight difference in the total power consumption.

Table 3 shows the computational performance comparison results for different platforms. The CPU is Intel Xeon E5-2690 CPU@2.90GH, the GPU is Nvidia K40 GPU, and the mGPU is Nvidia TK1 Mobile GPU development kit. The convolutional layers between the two pooling layers are called a conv group, and there are five groups. The weights of this design are not processed by any compression, while the paper [12] uses SVD compression, and the weight values are reduced to 36% of the original; nevertheless, the computational performance of the coprocessor designed in this paper is at the same level as the mGPU.

Table 4 shows the computational performance of the coprocessor of this design compared with other FPGA processor. The coprocessor designed in this paper mainly adopts two solutions to achieve higher clock frequency. First, reduce the fan-out, the signal fan-out from LIB broadcast output to 64 PE arrays is 64, and the design reduces the fan-out to 8 by adding intermediate flip-flops. Second, reduce the multiplication calculation except convolution calculation, put all the parameters involved in the controller to calculate uniformly, and then distribute to each module as needed. The computational performance of this design scheme is relatively high compared to the paper [14–16] and much worse compared to the paper [13]. On the one hand, it is because the paper [13] uses the SVD compression algorithm to reduce the amount of weight value to 36% of the original, and on the other hand, this design scheme in the cache read and write processes, we often start the computation process or the transfer operation between memories only after all the read and write processes are completed in order to

simplify the logic, which will cause the computation unit to hang, and the waiting time overhead at this time will become larger as the 2D_tile. The waiting time overhead becomes larger as the number of 2D_tile increases.

5. Conclusion

In this paper, an FPGA-based architecture for convolutional neural network coprocessor is proposed and fully validated, starting from the optimization methods of convolutional neural networks at the algorithmic and hardware acceleration levels. A one-dimensional convolutional computation unit PE with row stationary (RS) streaming mode is proposed to maximize the energy efficiency of convolutional computation by using RF-level data reuse and partial and local accumulation; a three-dimensional convolutional computation unit PE chain with pulsating array structure is proposed with the MIT Eyeriss structure. Each PE chain consists of three PEs connected in sequence, which can achieve the functions that require nine PEs in the Eyeriss structure. Multiple PE chains form a PE array in the form of pipeline processing, and the coprocessor can flexibly control the number of PE array openings according to the number of output channels of the convolutional layer to reduce invalid computation and reduce power consumption. A picture segmentation method is proposed that is compatible with the hardware architecture, and this segmentation method can make the PE chain run with the shortest interval between two runs. The performance evaluation results show a peak computational performance of 316.0 GOP/s and an average computational performance of 62.54 GOP/s at a clock frequency of 200 MHz, with a power consumption of around 9.25 W.

Data Availability

The data that support the findings of this study are available from the corresponding author upon reasonable request.

Conflicts of Interest

The authors declare that they have no conflicts of interest.

Acknowledgments

References

[1] J. Misra and I. Saha, "Artificial neural networks in hardware: a survey of two decades of progress[J]," *Neurocomputing*, vol. 74, no. 1-3, pp. 239–255, 2010.

[2] F. M. Dias, A. Antunes, and A. M. Mota, "Artificial neural networks: a review of commercial hardware[J]," *Engineering Applications of Artificial Intelligence*, vol. 17, no. 8, pp. 945–952, 2004.

[3] Y.-H. Chen, C.-P. Fan, and R. C.-H. Chang, "Prototype of low complexity CNN hardware accelerator with FPGA-based PYNQ platform for dual-mode biometrics recognition," in *2020 International SoC Design Conference (ISOCC)*, pp. 189-190, Yeosu, Korea (South), 2020.

[4] M. Holler, S. Tam, H. Castro, and R. Benson, "An electrically trainable artificial neural network (ETANN) with 10240 floating gate synapses," in *International Joint Conference on Neural Networks*, pp. 191–196, Washington, DC, USA, 1989.

[5] H. Srivastava and K. Sarawadekar, "A depthwise separable convolution architecture for CNN accelerator," in *2020 IEEE Applied Signal Processing Conference (ASPCON)*, pp. 1–5, Kolkata, India, 2020.

[6] N. Suda, V. Chandra, G. Dasika et al., "Throughput-optimized OpenCL-based FPGA accelerator for large-scale convolutional neural networks," in *Proceedings of the 2016 ACM/SIGDA International Symposium on Field-Programmable Gate Arrays*, pp. 16–25, New York, NY, USA, February 2016.

[7] J. Cong and B. Xiao, *Minimizing computation in convolutional neural networks[C]//International Conference on Artificial Neural Networks*, Springer, Cham, 2014.

[8] H. Kim and K. Choi, "Low power FPGA-SoC design techniques for CNN-based object detection accelerator," in *2019 IEEE 10th Annual Ubiquitous Computing, Electronics & Mobile Communication Conference (UEMCON)*, pp. 1130–1134, New York, NY, USA, 2019.

[9] V. Sze, Y. H. Chen, T. J. Yang, and J. S. Emer, "Efficient processing of deep neural networks: a tutorial and survey," *Proceedings of the IEEE*, vol. 105, no. 12, pp. 2295–2329, 2017.

[10] V. Sze, Y. H. Chen, J. Emer, A. Suleiman, and Z. Zhang, "Hardware for machine learning: challenges and opportunities," 2016, http://arxiv.org/abs/1612.07625.

[11] M. Sankaradas, V. Jakkula, S. Cadambi et al., "A massively parallel coprocessor for convolutional neural networks," in *2009 20th IEEE International Conference on Application-specific Systems, Architectures and Processors*, pp. 53–60, Boston, MA, USA, 2009.

[12] D. T. Kwadjo, J. M. Mbongue, and C. Bobda, "Performance exploration on pre-implemented CNN hardware accelerator on FPGA," in *2020 International Conference on Field-Programmable Technology (ICFPT)*, pp. 298-299, Maui, HI, USA, 2020.

[13] V. Gokhale, J. Jin, A. Dundar, B. Martini, and E. Culurciello, "A 240 g-ops/s mobile coprocessor for deep neural networks," in *Proceedings of the IEEE Conference on Computer Vision and Pattern Recognition Workshops*, pp. 682–687, Columbus, OH, USA, 2014.

[14] Y. H. Chen, T. Krishna, J. S. Emer, and V. Sze, "Eyeriss: an energy-efficient reconfigurable accelerator for deep convolutional neural networks[J]," *IEEE Journal of Solid-State Circuits*, vol. 52, no. 1, pp. 127–138, 2017.

[15] A. Krizhevsky, I. Sutskever, and G. E. Hinton, "Imagenet classification with deep convolutional neural networks," *Advances in Neural Information Processing Systems*, vol. 25, pp. 1097–1105, 2012.

[16] K. Simonyan and A. Zisserman, "Very deep convolutional networks for large-scale image recognition," 2014, http://arxiv.org/abs/1409.1556.

[17] C. Szegedy, W. Liu, Y. Jia et al., "Going deeper with convolutions," in *Proceedings of the IEEE conference on computer vision and pattern recognition*, pp. 1–9, Boston, MA, USA, 2015.

[18] S. Chakradhar, M. Sankaradas, V. Jakkula, and S. Cadambi, "A dynamically configurable coprocessor for convolutional neural networks," *ACM SIGARCH Computer Architecture News*, vol. 38, no. 3, pp. 247–257, 2010.

[19] C. Zhang, P. Li, G. Sun, Y. Guan, B. Xiao, and J. Cong, "Optimizing fpga-based accelerator design for deep convolutional neural networks," in *Proceedings of the 2015 ACM/SIGDA International Symposium on Field-Programmable Gate Array*, pp. 161–170, New York, NY, USA, 2015.

Research Article

Sports Dance Action Recognition System Oriented to Human Motion Monitoring and Sensing

Shasha Ni [ID] **and Dawei Yao**

College of Physical Education, Qiqihar University, Qiqihar, 161006 Heilongjiang, China

Correspondence should be addressed to Shasha Ni; nishasha@qqhru.edu.cn

Because of its high research value, action recognition has become a very popular research direction in recent years. However, the research on the combination of motion recognition technology and dance movements is still in its infancy. At the same time, due to the high complexity of dance movements and the problems of human body self-occlusion when performing dances, research on dance video action recognition has been caused. Progress is relatively slow. This article mainly introduces the research of sports dance action recognition system oriented to human motion monitoring and sensing, fully considers the abovementioned problems, and makes in-depth research and analysis on the current excellent action recognition research content in this field. This paper proposes a research method of sports dance movement recognition for human movement monitoring and sensing, including sports dance movement classification algorithm and sports dance movement preprocessing algorithm, which is used to conduct research experiments on sports dance movement recognition for human movement monitoring and sensing. The experimental results of this article show that the average recognition accuracy of the sports dance action recognition system for human motion monitoring and sensing is 92%, which can be used in daily sports dance training and competition.

1. Introduction

As a new sports project that has evolved and developed in recent centuries, sports dance combines a variety of artistic features, such as clothing, music, dance, and sports. In the existing sports dance training process, dancers usually watch videos repeatedly or seek corrective guidance from coaches to achieve the purpose of training. This not only consumes a lot of time and energy but also brings certain difficulties and challenges to learners.

Under the background of the continuous development of science and technology, human movement-oriented monitoring and sensing technology is gradually applied to sports dance and other fields, so that the majority of dance teaching workers, dancers, and dance learners who have strong needs in teaching and self-study can make accurate adjustments to the dance movements that are not standardized enough to ensure the accuracy of dance positions in training. Trainers can find their own rhythm and sense of rhythm through training and can also promote the further development of digital and basic dance training and other dance learning information.

Gorman et al. studied the relationship between the perception of human actions and the influence of social psychological resources. According to the resource and perception model, it tested and analyzed the common influence of subjective threats and buffer threats to social psychological resources. Two experiments tested whether social threats (i.e., rejection) and psychosocial resources affect the perception of human movement. The observer tries to recognize the movement of the person in the fuzzy point light display after being repelled or not repelled. In addition, the observer tries to measure trait resources (self-esteem plus social support) and manipulate self-affirmation. One of the studies shows that rejection will reduce the sensitivity of detecting human movement, but not for people with rich feature resources. Another study replicated this interaction between rejection phenomena and traits. These studies show that the basic visual skills for detecting human movements are affected by social threats and psychosocial resources. The correlation between the research elements is not strong, and the practicality is weak [1]. Geng et al.'s research found that in the real-time health monitoring, they believe that even

a subset of available radio frequency functions can provide acceptable classification rates, which can be achieved by making the proposed scheme easier to reduce computational costs. This research is a research on human motion recognition technology for firefighters, and it is not targeted [2]. Chinnadurai and Sridharan found that in recent years, the concept of deep learning has been used to research image processing and machine learning applications. In order to monitor a specific person, Chinnadurai and Sridharan applied a set of image processing steps in the motion area containing the moving object, applied convolutional neural network classifiers with different levels in the selected area, and learned tools in Google TensorFlow used. In the experiment, shaking videos and low-resolution videos were considered and the video dataset was checked. This research process is cumbersome [3].

The innovations of this paper are as follows: (1) propose a classification algorithm using support vector machine model (SVM) as an action recognition method; (2) propose the hardware design of a sports dance action recognition system; and (3) design a sports dance action and identify the software of the system.

2. Method of Sports Dance Movement Recognition Oriented to Human Motion Monitoring and Sensing

2.1. Sports Dance Movement Classification Algorithm. This article will use the support vector machine model (SVM) as the classification algorithm of the action recognition method. Support vector machine is a new type of machine learning method based on statistical learning theory and structural risk minimization criteria, and it is also a major achievement of machine learning research in recent years [4]. It finds the global optimal solution from the limited sample information. It not only has the descriptive ability to accurately describe the training sample but also has the learning ability to identify any test sample without error [5]. In this case [6, 7], using the $K(x, y)$ function that satisfies the Mercer condition as the inner product operation of the two sample features is equivalent to mapping the sample from the original feature space to a new feature space [8].

The following formula exists [9, 10]:

$$L(W, b, a) = \frac{1}{2}\left(W^T \cdot W\right) - \sum_{i=1}^{m} a_1\left[a_i\left(W^T \cdot x_i + b\right) - 1\right], \quad (1)$$

$L(W, b, a)$ with respect to W and b, and make them equal to zero [11].

$$\sum_{i=1}^{m} a_i y_i = 0, \quad a_i \geq 0, \ i = 1, 2, \cdots, m, \quad (2)$$

$$W = \sum_{i=1}^{m} a_i y_i x_i, \quad (3)$$

where a_i is under the constraint condition [12, 13]:

$$Q(a) = \sum_{i=1}^{m} a_i - \frac{1}{2}\sum_{i,j=1}^{m} a_i a_j y_i y_j\left(X_i^T X_j\right). \quad (4)$$

A dual problem has an optimal solution [14]. The solution of this optimization problem must satisfy the following condition:

$$a_i^*\left[y_i\left(W^T \cdot x_i + b\right) - 1\right] = 0, \quad i = 1, 2, \cdots, m. \quad (5)$$

The model is represented by the number of support vectors [15].

$$f^*(x) = \text{sgn}\left(\sum_{i=1}^{m} a_i^* y_i(x_i \cdot x) + b^*\right). \quad (6)$$

The function $K(x, y)$ from the original feature space to a new feature space [16] was used.

$$f^*(x) = \text{sgn}\left(\sum_{i=1}^{N} a_i^* y_i \cdot K(x_i, x) + b\right). \quad (7)$$

2.2. Sports Dance Movement Preprocessing Algorithm. Sports dance moves contain a lot of noise when recognizing and transforming, and these noises will affect the edge features of dance video images [17]. Therefore, we need to perform preprocessing operations on the dance dataset first [18]. The preprocessing operations in this paper include background subtraction and median filtering operations. Background subtraction is used to extract the foreground to separate the human action area, and the median filtering operation is used to filter out the noise in the image to reduce the impact on edge features [19, 20].

2.2.1. Background Subtraction. Regarding background subtraction, the Gaussian mixture model method is adopted, and the video image sequence is regarded as a combination of multiple single Gaussian models. The model maintains a multidistributed density function for each pixel in the image. The video image sequence is usually described as the pixel probability distribution function [21].

Assuming that the value of a certain pixel at time t is p_t, the probability of occurrence of p_t has the following formula:

$$P(p_t) = \sum_{i=1}^{K} \omega_{i,t} \cdot \eta\left(p_t, \mu_{i,t}, \sigma_{i,t}\right). \quad (8)$$

Among them, $\omega_{i,t}$ is the weight of the ith Gaussian distribution at time t, and $\eta(p_t, \mu_{i,t}, \sigma_{i,t})$ is the corresponding probability density function [22, 23]. The specific manifestation of $\eta(p_t, \mu_{i,t}, \sigma_{i,t})$ is

$$\eta\left(p_t, \mu_{i,t}, \sigma_{i,t}\right) = \frac{1}{\sqrt{2\pi|\sigma_{i,t}|}} e^{-(1/2)\left(p_t - \mu_{i,t}\right)^T \sigma_{i,t}^{-1}\left(p_t - \mu_{i,t}\right)}. \quad (9)$$

And their weights are assigned the same value [24].

Assuming that the value of a pixel in a newly input image is p_t, the following formula can be used to determine whether the pixel matches the established K Gaussian distribution:

$$\left| p_t - \mu_{i,t-1} \right| \leq 2.5 \sigma_{i,t-1}. \tag{10}$$

2.2.2. Median Filter. The specific process of median filtering is as follows:

(1) First, move the template in the image, and move the center of the template to coincide with the center pixel of the image [25]

(2) Get the gray value of all pixels under the template

(3) Sort the gray values of all pixels obtained from the template in an ascending order

(4) Calculate the median of all gray values after the arrangement [26]

The specific process is shown in Figure 1.

3. Experiment of Sports Dance Action Recognition System Oriented to Human Motion Monitoring and Sensing

3.1. Hardware Design of Sports Dance Action Recognition System

3.1.1. System Hardware Architecture. The data acquisition module is used to collect information related to the human body state in real time and provides three-axis acceleration and three-axis angular velocity data for the sports dance action recognition system [27]. It is the data basis of the sports dance action recognition system, so the performance of the entire wearable human body motion state perception system is observed. The pros and cons all depend on the design part of the data acquisition module.

The main composition of the hardware of this system is composed of two parts: data acquisition of sensors and Bluetooth radio frequency. The sensor part is mainly composed of six-axis sensor MPU6050 and air pressure temperature sensor BMP180. The Bluetooth chip uses TI's CC2541. MPU6050 and BMP180 are connected to CC2541 through I2C bus and transmit the collected data to the Bluetooth chip. The Bluetooth chip transmits the collected data through the ceramic antenna on the board.

3.1.2. Motion Sensor Chip MPU6050. The main function of the data acquisition module is to comprehensively collect the acceleration signal and angular velocity signal when the human body moves, so when choosing the sensor chip, give priority to the three-axis accelerometer and the three-axis gyroscope. Based on the above considerations, the sports dance action recognition system designed in this article chooses the MPU6050 motion sensor chip introduced by InvenSense. The MPU6050 motion sensor chip is the world's first integrated 6-axis motion processing chip. It integrates a 3-axis gyroscope and a 3-axis accelerator into a chip with only a millimeter package. It reduces the size of the space that

originally required two motion sensor chips to achieve and greatly reduces the space on the PCB circuit board.

3.1.3. Bluetooth 4.0 Wireless Module. The Bluetooth 4.0 wireless module is composed of the core chip TI's CC2541 and its related circuits.

3.2. Software Design of Sports Dance Action Recognition System

3.2.1. C# Development Language and Its Development Environment. The main content of this paper is to realize the recognition of sports dancers' human movements in a stable environment. Therefore, it is necessary to choose a stable and powerful development environment as the software platform. Due to the powerful functions of Microsoft Visual Studio 2010 and good human-computer interaction, we choose this development environment as the software development platform of this system.

3.2.2. Software Hierarchy and Functions. The human body motion recognition system software for sports dancers designed in this paper adopts a three-layer structure, namely, user layer, business logic layer, and device layer.

The user layer is responsible for displaying the results of the data to users in the form of charts, data, and graphs and accepting user settings and feedback information.

The business logic layer is designed to store, process, and analyze the three-axis acceleration and gyroscope data after receiving the data transmitted by the node.

The device layer is mainly responsible for wireless network interface and communication and works with the upper layer to maintain reasonable and effective network routing and to set the current network topology and protocol.

3.2.3. Using MATLAB's Engine Technology. MATLAB's engine function library is a collection of a series of programs provided by MATLAB, allowing users to call MATLAB in their own C language programs, using MATLAB as a calculation engine, and let it run in the background. Its task is to complete complex matrix operations and simplify the user programming task of the front desk. When the MATLAB engine is started, it is equivalent to starting another process in the background. The MATLAB engine function acts as a bridge between the user application and the MATLAB engine. It completes the exchange of data and the transmission of commands between the two. The three interface functions PutFullMatrixO, ExecuteO, and GetFullMatrix() are mainly used here. These three functions are the three member functions of MLAppClass, so we first need to add the COM application "MatlabApplication (version 7.7) Type Library" to instantiate the engine object, then use its interface for programming. Among the above three functions, PutFullMatrix and GetFullMatrix realize the functions of adding matrix to MATLAB Server and reading matrix from MATLAB Server, and Execute realizes the function of running script.

The specific function form is as follows: matlab. PutFullMatrix("P","Base",TrainIn,ImIn); matlab. GetFullMatrix("R", "Base",TrainOut,ImOut); matlab.

Specific process is shown in Table 1.
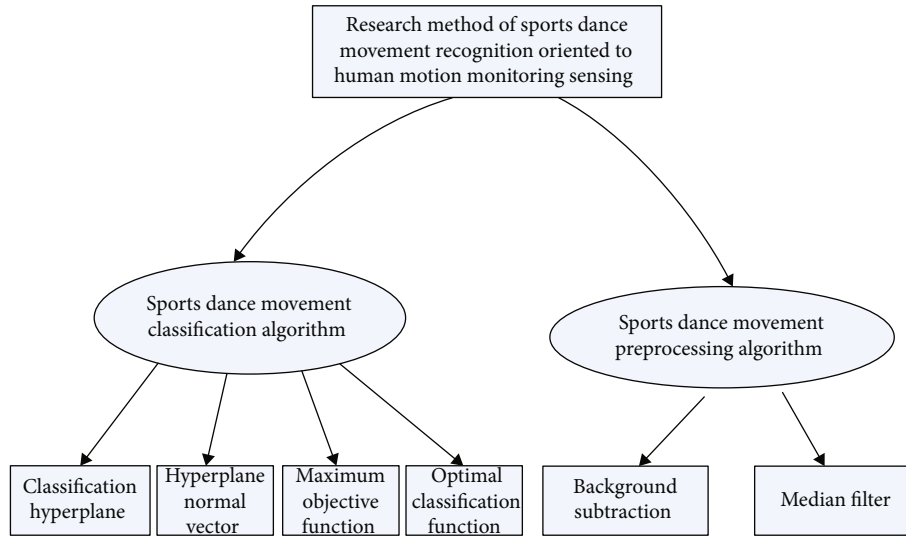
FIGURE 1: Part of the technical process of this method.

TABLE 1: Experimental steps.

Research and experiment of sports dance action recognition system oriented to human motion monitoring and sensing	3.1	Hardware design of sports dance action recognition system introduction to identification system	1	Introduction to identification system
			2	Power circuit design
			3	Reset circuit design
			4	Clock circuit design
			5	USB circuit design
			6	Design of adding meter interface circuit
	3.2	Software design of sports dance action recognition system	1	C# development language and its development environment
			2	Software hierarchy and function
			3	Using MATLAB's engine technology

4. Sports Dance Action Recognition for Human Motion Monitoring and Sensing

4.1. Preliminary Work Analysis of Action Recognition

(1) Before performing action recognition on sports dancers, first, classify and analyze the dance movements of sports dancers according to the relevant opinions of professionals. As shown in Table 2 and Figure 2, the average represents the evaluation of the importance of the indicator by professionals, and the coefficient of variation reflects the degree of dispersion of the evaluation of an indicator by professionals

It can be seen from the chart that among the secondary indicators, the coefficients of variation of "crossdance step," "lock step," "flicking," and "inhibition" are all greater than 0.40. Experts have disputes over these indicators. It is believed that "lock step" steps are mostly locked rotation. It is recom-

mended to adjust the name of the index to "lock turn" and move the item to the first-level index "rotation," while doing "crossdance step" and "flick step." The technical link of the index action is not based on mobile technology, but more includes reflexive action position and body rotation. In addition, the first-level index "linear movement" cannot accurately cover the above three second-level index types of actions, so consider adding a level. The indicator "connection category" and the "crossdance step category", "flicking category," and "inhibition category" are included under it, as the secondary indicators of the primary indicator "connection category."

(2) Ask the dancers about their willingness to apply the sports dance action recognition system to the training process, as shown in Table 3 and Figure 3

According to the data, 90.25% of the dancers are very willing to use the system, 7.75% do not care whether they use the system or not, and only 2.00% are reluctant to use

TABLE 2: Opinion statistics of professionals.

First-level indicator	Secondary indicators	Number	Average	Standard deviation	Coefficient of variation
Linear movement	Transition class	1	3.97	0.86	0.21
	Rotation	2	4.03	0.63	0.32
	Screw type	3	4.21	0.74	0.28
	Axis rotation	4	4.33	0.69	0.23
Rotating	Cross dance	5	3.86	0.61	0.19
	Detours	6	3.65	0.56	0.31
	Lock step class	7	4.07	0.47	0.26
	Flutes	8	3.76	0.58	0.19
Modeling	Inclined modeling class	9	3.89	0.62	0.22
	Hinge modeling class	10	4.11	0.51	0.18
	Sword step modeling	11	4.52	0.59	0.11
Unique dance steps	Tango walking class	12	4.28	0.38	0.14
	Vienna group transfer	13	4.47	0.32	0.16
	Foxtrot undulate	14	4.16	0.44	0.25
	Fast step and jump class	15	3.85	0.46	0.31
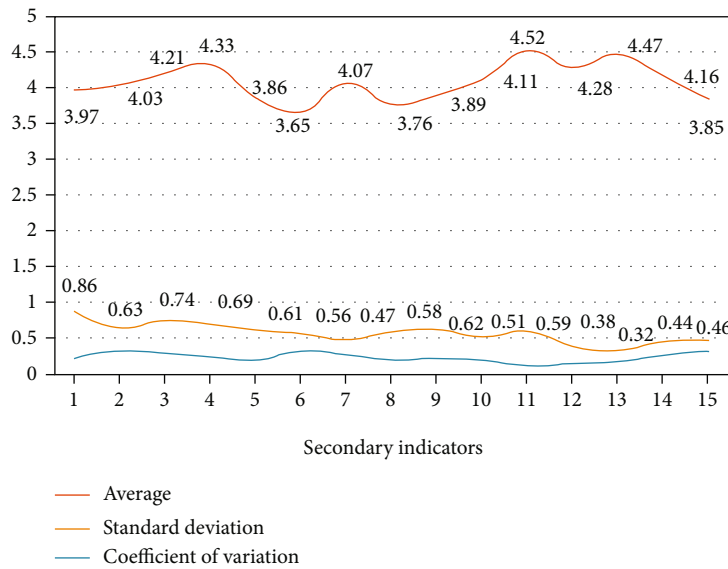
FIGURE 2: Classification of opinions statistics of professionals.

TABLE 3: Related wishes of dancers.

	Very willing	Indifferent	Not really
Male dancer	46.14%	4.56%	1.21%
Female dancer	44.11%	3.19%	0.79%
In total	90.25%	7.75%	2.00%

the system. Among them, the difference between male and female dancers is small.

4.2. Performance Analysis of Sports Dance Action Recognition

(1) Experiment with the algorithm [28] and three features of this paper in the four groups of dance combinations on the FolkDance dance dataset, and count and organize the relevant results, as shown in Table 4 and Figure 4

From the experimental results shown in the chart, it can be seen that the recognition rate of dance movements for each single feature in each group is still relatively low. It can be seen from the table that the action feature extraction method in this paper has the highest recognition and extraction rate for modeling actions and other unique dance steps, which are 55.47% and 56.19%, respectively; the recognition rate for linear movement dance steps is 49.76%; for rotating dance steps. The recognition extraction rate is 52.32%; the average recognition rate is about 53.44%.
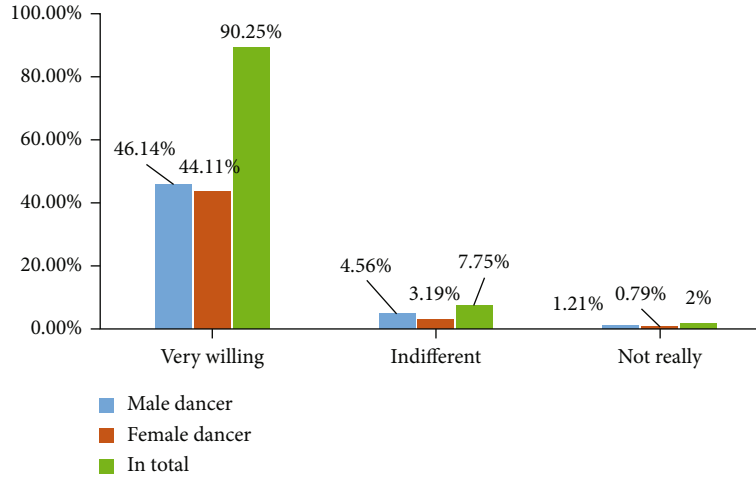
Figure 3: The willingness of dancers.

Table 4: Comparison of single feature on FolkDance dataset and experimental results of this method.

	Histogram features of directional gradient	Histogram characteristics of optical flow direction	Audio signature features	The method of this paper
Linear movement	46.71%	40.12%	34.61%	49.76%
Rotating	41.23%	38.16%	39.24%	52.32%
Modeling	39.51%	36.44%	36.12%	55.47%
Unique dance steps	36.45%	35.43%	33.09%	56.19%
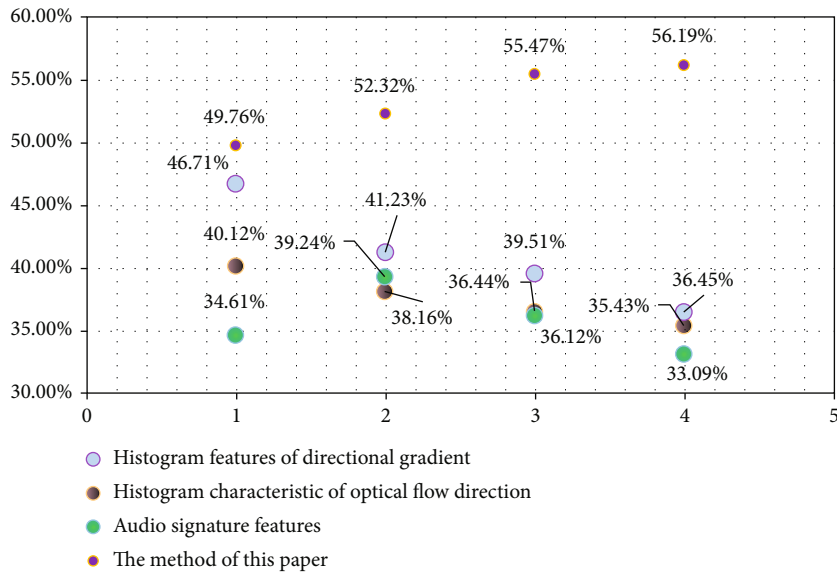
Figure 4: Comparison of a single feature on the FolkDance dataset and the experimental results of this method.

(2) In the experiment process, the effect of action recognition in the above database is observed. At the same time, the recognition effect of the combination of 3D-SIFT and optical flow is better than the combination of RGB and optical flow. The different feature recognition effects are shown in Table 5 and Figure 5

The recognition rate is the highest when the combination of human body regions is used, and the whole body region is directly recognized.

(3) Sports dance is a dance type with a larger opening and closing of movements, and dancers often fall

TABLE 5: Different feature recognition effects of different body regions.

| Body parts | Northeast Yangko | | | |
	RGB	SIFT	Flow	SIFT + flow
Upper body	10.6	23.4	32.3	46.2
Lower body	11.5	26.1	35.6	45.4
Upper body + lower body	21.4	24.3	41.4	55.3
Whole body	22.7	22.1	40.9	53.9
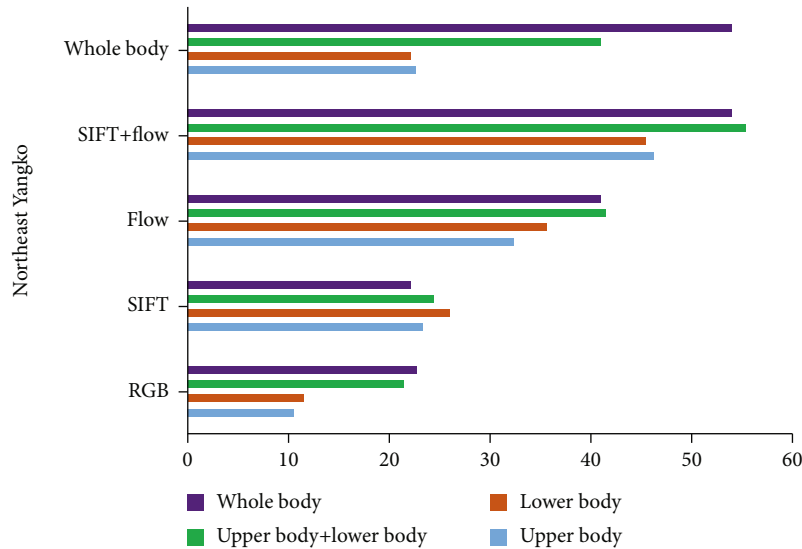
FIGURE 5: Different feature recognition effects extracted from different body regions.

TABLE 6: Results of different types of falls.

Falls	Total number of experiments	Correct recognition times	Correct rate	Number of false negatives	False-negative rate
Fall forward	25	23	92%	4	8%
Fall backward	25	23	92%	2	8%
Fall to the left	25	22	88%	3	12%
Fall to the right	25	24	96%	1	4%

down during training. A protective activation mechanism can be added to the recognition of sports dance movements. The system will automatically send a signal to the team doctor when the dancer falls or has a sports injury, so that the doctor can rush to treat the dancer in time. This article carried out related experiments, and the experimental results recorded the correct identification, underreporting, and false alarming of falls. Among them, correct recognition means correct recognition of the fall and its direction; false negative means that the experimenter did not recognize the fall behavior after the fall. We made a detailed record of the entire experiment process, and the experimental statistical results are shown in Table 6 and Figure 6

It can be seen from the chart that the accuracy of the algorithm proposed in this paper for the recognition of falling behaviors has reached more than 85%, and the average recog-

nition accuracy is 92%. There was very little underreporting during the whole experiment.

(4) This paper implements a GM-based recognition method on the segmented action pattern sets of CityU. For each set of experiments, we selected samples collected by 3 of the captured persons as the training set, and the other two samples are used as a test sample. The recognition accuracy rates of GM-based DTW and LCS on the segmented action pattern sets on the CityU and HDM05 datasets are shown in Table 7 and Figure 7

But it has the lowest recognition accuracy on the HDM05 dataset. This is because the HDM05 dataset has more significant time domains than the CityU dataset, through its own penalty mechanism, unlike DTW, which uses repeated E matching for longer samples in the middle frame, which is extremely easily brings overfitting problems.
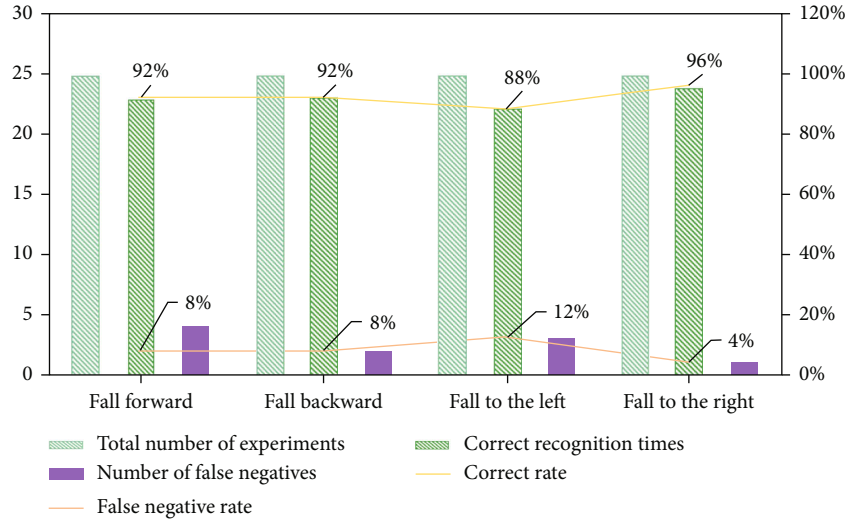
Figure 6: Results of different types of falls.

Table 7: Recognition accuracy based on GM.

		Team 1	Team 2	Team 3
CityU	DTW	93.26%	93.17%	93.21%
	LCS	91.12%	90.19%	91.07%
HDM05	DTW	95.34%	88.49%	89.14%
	LCS	97.47%	86.23%	86.24%
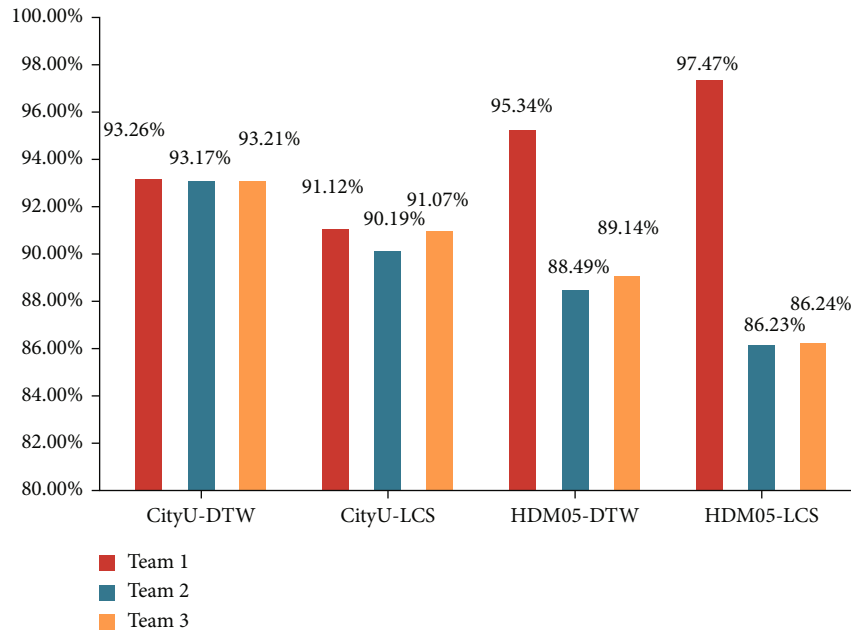
Figure 7: Recognition accuracy based on GM.

5. Conclusions

Sports dance is a sport which includes standard dance and Latin dance. It has gone through three stages: folk dance, standard dance, and competitive dance. Less than a century ago, it has triggered a global upsurge of sports dance and competitive sports dance. In the 1930s, it was introduced into China in the form of social dance. At present, four international dance sports organizations, including the world sports dance federation, the World Dance Federation, the Royal

Association of dance teachers, and the International Association of dance teachers, are committed to the development and popularization of dance sport in the world.

Motion capture technology is used to track the motion of some or all joints of the human body or animal through video devices, motion sensors, and other devices and measure the motion information of joints, so as to provide reference data for gait recognition and video production. This technology has been widely used in film and television production, interactive games, virtual reality, and personnel training. In order to better correct the movement of sports dancers and to have accurate training, the motion capture recognition technology is introduced into the design of sports dance action recognition system.

This paper designs the hardware part and software part of the system. The software part includes data acquisition, data processing, and auxiliary training. In the data acquisition part, the standard dance movements are input into the system, and the standard human dance posture database is established. The data processing part repairs the occluded joint points and restores the human skeleton structure. The auxiliary training part is divided into two parts, which are based on the joint point position and the joint angle. The system has the effect of assisting training. It mainly provides real suggestions for the trainer's training through data analysis, and the suggester can make reasonable adjustments based on the suggestions. The experimental results show that the system can effectively improve the dance level of trainers.

Data Availability

No data were used to support the study.

Disclosure

We confirm that the content of the manuscript has not been published or submitted for publication elsewhere.

Conflicts of Interest

There are no potential competing interests in our paper.

Authors' Contributions

All authors have seen the manuscript and approved its submission.

Acknowledgments

References

[1] J. L. Gorman, K. D. Harber, M. Shiffrar, and K. S. Quigley, "Ostracism, resources, and the perception of human motion," *European Journal of Social Psychology*, vol. 47, no. 1, pp. 53–71, 2017.

[2] Y. Geng, J. Chen, R. Fu, G. Bao, and K. Pahlavan, "Enlighten wearable physiological monitoring systems: on-body RF characteristics based human motion classification using a support vector machine," *IEEE Transactions on Mobile Computing*, vol. 15, no. 3, pp. 656–671, 2016.

[3] M. Chinnadurai and M. Sridharan, "Prediction of human motion detection in video surveillance environment using tensor flow," *International Journal of Advanced Science and Technology*, vol. 29, no. 5, pp. 2791–2798, 2020.

[4] M. Sun, Y. Jiang, Q. Liu, and X. Liu, "An auto-calibration approach to robust and secure usage of accelerometers for human motion analysis in FES therapies," *Computers, Materials & Continua*, vol. 60, no. 1, pp. 67–83, 2019.

[5] B. Ruscello, M. Esposito, G. Siligato et al., "Gender differences in instep soccer kicking biomechanics, investigated through a 3D human motion tracker system," *The Journal of Sports Medicine and Physical Fitness*, vol. 60, no. 8, pp. 1072–1080, 2020.

[6] J. Lin and X. Huang, "Application of clothing friction nano-power generators in human motion energy acquisition," *Nanomaterials and Energy*, vol. 9, no. 2, pp. 163–172, 2020.

[7] H. Mai, R. Mutlu, C. Tawk, G. Alici, and V. Sencadas, "Ultra-stretchable MWCNT-Ecoflex piezoresistive sensors for human motion detection applications," *Composites Science and Technology*, vol. 173, no. MAR.22, pp. 118–124, 2019.

[8] X. Zhou, M. Zhu, G. Pavlakos, S. Leonardos, K. G. Derpanis, and K. Daniilidis, "MonoCap: monocular human motion capture using a CNN coupled with a geometric prior," *IEEE Transactions on Pattern Analysis and Machine Intelligence*, vol. 41, no. 4, pp. 901–914, 2019.

[9] S. Park, H. Ryu, S. Lee, S. Lee, and J. Lee, "Learning predict-and-simulate policies from unorganized human motion data," *ACM Transactions on Graphics*, vol. 38, no. 6, pp. 1–11, 2019.

[10] W. Mrabti, H. Tairi, F. M. Nicolier, and B. Bellach, "Human motion tracking under indoor and outdoor surveillance system," *International Journal of Innovative Computing and Applications*, vol. 11, no. 4, pp. 181–192, 2020.

[11] J. S. Park, C. Park, and D. Manocha, "I-Planner: intention-aware motion planning using learning-based human motion prediction," *The International Journal of Robotics Research*, vol. 38, no. 1, pp. 23–39, 2019.

[12] P. B. Zhang and Y. S. Hung, "Articulated deformable structure approach to human motion segmentation and shape recovery from an image sequence," *IET Computer Vision*, vol. 13, no. 3, pp. 267–276, 2019.

[13] M. M. Rana and R. Bo, "IoT-based improved human motion estimations method under cyber attacks," *IEEE Internet of Things Journal*, vol. 6, no. 6, pp. 10934-10935, 2019.

[14] C. K. Chan and G. Cala, "Impact of number of attributes on the accuracy of human motion classification," *Journal of Engineering Science and Technology*, vol. 13, no. 7, pp. 1967–1978, 2018.

[15] Y. Lang, Q. Wang, Y. Yang, C. Hou, D. Huang, and W. Xiang, "Unsupervised domain adaptation for micro-Doppler human motion classification via feature fusion," *IEEE Geoscience and Remote Sensing Letters*, vol. 16, no. 3, pp. 392–396, 2019.

[16] P. Wang, H. Liu, L. Wang, and R. X. Gao, "Deep learning-based human motion recognition for predictive context-aware human-robot collaboration," *CIRP Annals - Manufacturing Technology*, vol. 67, no. 1, pp. 17–20, 2018.

[17] M. C. Sashikkumar, S. Selvam, N. Karthikeyan, J. Ramanamurthy, S. Venkatramanan, and C. Singaraja, "Remote sensing for recognition and monitoring of vegetation affected by soil properties," *Journal of the Geological Society of India*, vol. 90, no. 5, pp. 609–615, 2017.

[18] W. Kumne and S. Samanta, "Remote sensing and GIS application on forest resource mapping and monitoring in Bulolo district, Morobe province," *Journal of Geoscience and Environment Protection*, vol. 7, no. 2, pp. 37–48, 2019.

[19] G. Xia, H. Sun, B. Chen et al., "Nonlinear low-rank matrix completion for human motion recovery," *IEEE Transactions on Image Processing*, vol. 27, no. 6, pp. 3011–3024, 2018.

[20] L. Davaze, A. Rabatel, Y. Arnaud et al., "Monitoring glacier albedo as a proxy to derive summer and annual surface mass balances from optical remote-sensing data," *The Cryosphere*, vol. 12, no. 1, pp. 271–286, 2018.

[21] R. Li, Z. Liu, and J. Tan, "Human motion segmentation using collaborative representations of 3D skeletal sequences," *IET Computer Vision*, vol. 12, no. 4, pp. 434–442, 2018.

[22] D. H. Yoo, "Effects of dance sports and yoga program on body composition, physical fitness, blood lipids and liver function Indicator in the elderly," *Exercise Science*, vol. 29, no. 1, pp. 51–59, 2020.

[23] M. O. Kim, Y. S. Kim, S. W. Chun, and S. K. Shin, "Effects of low intensity dance sports exercise for 16 weeks on senior fitness test and Fullerton advanced balance in elderly man," *The Korean Journal of Growth and Development*, vol. 27, no. 4, pp. 321–327, 2019.

[24] Wookyungkim and C. Park, "Casual relation between the partner confidence, exercise immersion and performance ability in the college dance sports athletes," *The Journal of Korean Alliance of Martial Arts*, vol. 21, no. 1, pp. 89–99, 2019.

[25] I. Lee and J. S. Ham, "Role performance difficulties and overcome strategies experienced by dance sports female instructors," *Journal of Korean Society for the Study of Physical Education*, vol. 23, no. 3, pp. 175–190, 2018.

[26] R. Xuebing, "81.Application of data mining for Investigating the cognition of how square dance promote community sports culture construction," *Boletin Tecnico/technical Bulletin*, vol. 55, no. 13, pp. 594–600, 2017.

[27] L. Chen, H. Sun, W. Zhao, and T. Yu, "Robotic arm control system based on AI wearable acceleration sensor," *Mathematical Problems in Engineering*, vol. 2021, Article ID 5544375, 13 pages, 2021.

[28] Z. Liqiu, Z. Yuexi, and W. Xiaodong, "Athlete's physical fitness prediction model algorithm and index optimization analysis under the environment of AI," *Mathematical Problems in Engineering*, vol. 2021, Article ID 6680629, 10 pages, 2021.

Research Article

Network Traffic Statistics Method for Resource-Constrained Industrial Project Group Scheduling under Big Data

Zongjie Huo,[1] **Wei Zhu** [2] **and Pei Pei**[1]

[1]*School of Economics and Management, Lanzhou University of Technology, Lanzhou, 730050 Gansu, China*
[2]*School of Economics, Lanzhou University, Lanzhou, 730000 Gansu, China*

Correspondence should be addressed to Wei Zhu; weizhu@lzu.edu.cn

With the advent of the Internet era, the demand for network in various fields is growing, and network applications are increasingly rich, which brings new challenges to network traffic statistics. How to carry out network traffic statistics efficiently and accurately has become the focus of research. Although the current research results are many, they are not very ideal. Based on the era background of big data and machine learning algorithm, this paper uses the ant colony algorithm to solve the typical resource-constrained project scheduling problem and finds the optimal solution of network traffic resource allocation problem. Firstly, the objective function and mathematical model of the resource-constrained project scheduling problem are established, and the ant colony algorithm is used for optimization. Then, the project scheduling problem in PSPLIB is introduced, which contains 10 tasks and 1 renewable resource. The mathematical model and ant colony algorithm are used to solve the resource-constrained project scheduling problem. Finally, the data quantity and frequency of a PCU with a busy hour IP of 112.58.14.66 are analyzed and counted. The experimental results show that the algorithm can get the unique optimal solution after the 94th generation, which shows that the parameters set in the solution method are appropriate and the optimal solution can be obtained. The schedule of each task in the optimal scheduling scheme is very compact and reasonable. The peak time of network traffic is usually between $9:00$ and $19:00\text{-}21:00$. We can reasonably schedule the network resources according to these time periods. Therefore, the network traffic statistics method based on the solution of resource constrained industrial project group scheduling problem under big data can effectively carry out network traffic statistics and trend analysis.

1. Introduction

1.1. Background Significance. With the increasing coverage of the Internet, the Internet has been widely used in various fields, and the demand for network construction is also growing. A network connection is becoming more and more complex, and the cost of network interconnection is also gradually increasing [1]. The statistical analysis of network traffic is very important, so it is imperative to explore a new efficient and convenient network traffic statistics method. In the era of big data, there is a new solution to the resource-constrained project scheduling problem. On this basis, it is innovative to take network traffic as a renewable resource to solve the optimal solution of project scheduling, which can provide new ideas for the statistics and analysis of network traffic.

1.2. Related Work. With the increasing importance of network traffic statistics, there are many research results. Rocha proposed some statistical and model multiplier equations for scaling coefficients in order to develop a new algorithm for network traffic statistics [2]. Solomon takes the network traffic of Botswana International University of Science and Technology (BIUST) as an example and proposes a mathematical model [3] for modeling the real-world problem. Their algorithm is not stable enough to calculate the peak value effectively. Resource-constrained project scheduling problem has always been the focus of attention, and its research has never stopped. Kreter studied the RCPSP problem with general time constraints and calendar constraints. It not only developed six different constraint programming (CP) models to solve the problem but also developed a special propagator to consider the cumulative resource constraints

of calendar constraints [4]. In order to optimize the production period and total delay time, Xiao tried to extend electromagnetic (EM) and integrate it into three well-known advanced multiobjective evolutionary algorithms (MOEA), namely, nondominated sorting based multiobjective evolutionary algorithm (NSGA-II), intensity Pareto evolution algorithm (SPEA2), and decomposition-based multiobjective evolutionary algorithm (MOEA/D) [5]. Both of them have a large amount of calculation in the calculation process, which is not suitable for big data calculation.

1.3. Innovative Points in This Paper. In order to explore a new efficient and convenient statistical method of network traffic, this study, based on the ant colony algorithm solving process of resource-constrained project scheduling problem, takes network traffic as a renewable resource and solves the optimal solution of project resource balance problem. The innovation points of this paper are (1) the objective function and mathematical model of resource-constrained project scheduling problem are successfully established; (2) the mathematical model of resource-constrained project scheduling problem is optimized by using ant colony algorithm; (3) the optimal scheduling scheme for a project is formulated successfully, and the peak value of network traffic is counted.

2. Statistical Method for Resource-Constrained Industrial Project Group Scheduling Network Flow

2.1. Resource-Constrained Project Scheduling Problem

2.1.1. Classification of Resource-Constrained Project Scheduling Problems. When the project resources are limited, the project scheduling problem is based on the job sequence in the project and the optimal solution is obtained.

According to the properties of resources, they can be divided into renewable resources, nonrenewable resources, and dual constraint resources. The available quantity of renewable resources is restricted in each period of the total project duration. Resources are obtained and used on the basis of time periods. The resources in each time period are limited, and they will be automatically updated in the next period after use, such as ordinary machinery and equipment and human resources. The available quantity of nonrenewable resources is limited within the total project duration, but it is not limited in each time period. If the resources are obtained and used based on the total construction period, they cannot be updated once they are used up [6]. The availability of dual constrained resources will be limited in the total project duration and each time period, such as funds.

According to the different project scheduling objectives, it can be divided into project duration minimization problem, resource balance problem, and maximum net present value problem. Project duration minimization is a common basic problem, and it is also the most common goal in project management. This problem is a combinatorial optimization problem under the constraints of time and resources. It needs to arrange the start and end time of all work reasonably, and the total project duration can reach the minimum. Resource

balance is also a very important research objective [7]. If the resources are limited, the progress of the whole project will be affected. Therefore, in the process of project implementation, we must reasonably arrange the work schedule so that the resources can be used in a balanced way. Otherwise, there will be fluctuations in the demand for resources, resulting in resource squeeze or conflict between supply and demand. The problem of maximum net present value (MNPV) is to establish a mathematical model with a discount rate to solve the problem. Because it is not only the main measurement index of production and R&D but also the embodiment of enterprise vitality and competitiveness.

According to the mode of project execution, it can be divided into project hypothesis of unique execution mode and project hypothesis of multiexecution mode. Unique execution mode means that all jobs in the project have only one mode that can be executed. Resources are only constrained by renewable resources, and the shortest construction period needs to be found [8]. Multiexecution mode means that there are multiple execution modes in the project, and resources are not limited to renewable resources. Each execution mode corresponds to a different resource combination mode and execution time, and multiple optimal solutions can be found. In practical projects, multiexecution mode is usually used.

2.1.2. Resource-Constrained Project Scheduling Problem Model. Single execution mode resource-constrained project scheduling problem is also a classical resource-constrained project scheduling problem, which needs to meet the following conditions: the minimum total project duration is the optimization goal. Once started, all operations must be completed continuously, and the number of operations is fixed. Each job corresponds to an execution mode, and the mode has no preemption. There is no delay start and feedback in the logical relationship between each job. The task execution process is only constrained by renewable resources, and each resource is a certain value in any time period of the project [9].

The solution of multimode resource-constrained project scheduling problem is to generate the most objective scheduling scheme under the tight relationship of work and resource constraints. It is a complex production scheduling problem, which needs to meet the following conditions: the project is composed of a limited number of jobs, and each job has a time sequence relationship. Once started, each job cannot be interrupted, and the corresponding execution mode cannot be changed. After the execution mode is selected, the duration is fixed and the resource demand is fixed. Resource types include updatable and nonupdatable.

2.1.3. Solution Method. At present, the algorithms for solving resource-constrained project scheduling problem mainly include accurate algorithm, heuristic algorithm, and intelligent optimization algorithm.

The exact algorithm includes many methods, such as exhaustive method, branch and bound method, and dynamic programming method [10]. The algorithm is practical and effective, which is suitable for small-scale problems. The exhaustive method can determine the approximate range of

feasible solutions according to the conditions of the problem to be solved and verify all feasible solutions. The verified ones are the solutions, and all feasible solutions need to be obtained. Therefore, although the accuracy of this method is high, the efficiency is very low. The dynamic programming method transforms the multistage into multiple single-stage and solves one by one, which can obtain the global optimal solution and improve the efficiency. However, it lacks a unified standard model and has a large amount of calculation. The branch and bound method will select different subproblems and branch variables to branch, exclude the impossible, narrow the search scope, close to the optimal solution, high efficiency, and effectiveness, but cannot solve large-scale complex problems.

The heuristic algorithm is composed of a schedule generation mechanism and priority rule [11]. The core of the algorithm is the schedule generation mechanism, which can expand the local plan from zero to generate a complete project schedule gradually. It can be divided into serial schedule generation mechanism with the task as variable and parallel schedule generation mechanism with time as the variable. Compared with the exact algorithm, the heuristic algorithm has great advantages in performance and efficiency and can obtain an ideal realizable scheme in a short time. However, this algorithm needs specific analysis based on specific problems and depends on the characteristics of the problem itself. In addition, it is easy to obtain only locally optimal solutions.

The intelligent optimization algorithm is the focus of this paper, and its content will be detailed in the next section.

2.2. The Intelligent Optimization Algorithm

2.2.1. The Ant Colony Algorithm.
The ant colony algorithm simulates the behavior of ant colony foraging to find the shortest path and uses the characteristics of ant colony foraging. For example, the ant colony can recognize the pheromone concentration in the neighborhood and can release pheromone continuously, but the pheromone will volatilize over time. After the double bridge experiment, artificial ants were designed to simulate moving in the double bridge system and find the shortest path [12]. Artificial ants have an effective pheromone renewal mechanism and pheromone volatilization mechanism and have the ability to evaluate and compare. Moreover, by using ants' pathfinding ability, repeated search and premature convergence can be avoided. Artificial ants, like real ants, can cooperate with each other to complete tasks. They use pheromones as communication media, and there is the phenomenon of pheromone volatilization. They complete tasks through local behaviors based on probability decision-making, and all of them are self-organized.

The ant colony algorithm is based on ant system, and its earliest application problem is traveling salesman problem (TSP) [13]. The TSP problem of n cities is to find the shortest path through n cities once. The parameters and their meanings of the basic ant colony algorithm are as follows: Q is the number of ants in the ant colony; $C_i(T)$ is the number of ants in city i at time t; Dij is the distance between city i and city j; H_{ij} is the visibility of edge (i, j), which remains unchanged; R_{ij} is the pheromone track intensity on edge (i, j), ΔR_{ij} is the

amount of pheromone per unit length left by ants on edge (i, j); $P_{ij}^s(t)$ is the transfer probability of ants s, i is the current city of ants, and j is the city that has not been visited. Therefore, at time t, the transfer probability of ant s in city i and city j is calculated as follows:

$$P_{ij}^s(t) = \begin{cases} \dfrac{R_{ij}^a(t)H_{ij}^b(t)}{\sum_{e \in \text{allowed}_s} R_{ie}^a(t)H_{ie}^b(t)}, & j \in \text{allowed}_s \\ 0, & \text{otherwise} \end{cases}. \tag{1}$$

Among them, $\text{allowed}_s = \{0, 1, 2, \cdots, n-1\}$ indicates that the cities allowed to be selected by ants s in the next step will change with the process of ants s [14]. a and b, respectively, reflect the relative importance of information accumulated and heuristic information in the process of ant's path selection.

The advantages of ant colony algorithm include the following: as a population-based evolutionary algorithm, it can be easier to achieve parallel computing; the algorithm has high reliability and stability, is not easy to be disturbed, and has a wide range of applications; and the algorithm has strong adaptability and can be combined with other heuristic algorithms to further improve the performance of the algorithm. In a word, the ability of the ant colony algorithm in finding the best solution is really good.

2.2.2. The Bacterial Foraging Algorithm.
The bacterial foraging algorithm imitates the foraging behavior of E. coli in the human intestinal tract. In the search process, the nutritional distribution function is used to judge the advantages and disadvantages of the algorithm, and the optimal value is found through chemotaxis, aggregation, replication, and dispersion calculation. In the implementation of the algorithm, the foraging behavior of bacteria is first realized through chemotaxis and aggregation operations [15]. Chemotaxis and aggregation of bacteria are defined as the life cycle of bacteria. At the end of the cycle, the bacteria enter the reproduction stage, and the reproduction of bacteria is completed by replication. In order to simulate the actual situation of bacteria in the environment, the algorithm requires bacteria to move to other places in the search area with a certain probability after reproduction.

The bacterial foraging algorithm needs to encode bacteria, then designs fitness function to generate initial population, and finally uses information communication between groups to optimize. The specific operation steps are as follows: initialize the parameters of the algorithm, including the execution times of chemotaxis, replication, and dispersal operations; the size of the bacterial population; and the dispersal probability in the dispersal operation. The initial position of bacteria is initialized, and the initial fitness value of bacteria is calculated, and then, it is modified by aggregation operation. The bacterial community was rotated, the bacterial position was updated, and the adaptive value was calculated. For the reproduction operation of bacterial flora, the health degree of bacteria is calculated first, and half of the bacteria with low health degree are eliminated, and then, the remaining healthy bacteria are regenerated [16]. After the dispersal operation, the population is updated according to

the dispersal probability, and the final judgment is whether it reaches the maximum iteration. If yes, it ends; otherwise, it returns to the circulation operation.

There are many factors that affect the efficiency of the bacterial foraging algorithm, especially in the selection of population size, the number of chemotaxis, replication and dispersal operations, the parameters, and dispersion probability in aggregation operation, because these parameters will directly affect the ability of the bacterial foraging algorithm. Large population size can increase population diversity and help to find the optimal solution, but it will make the calculation more complex and reduce the convergence rate. When the number of chemotaxis is less, the algorithm is more prone to the local optimal solution. Increasing the number of chemotaxis can enhance the search ability of the algorithm, but at the same time, it will increase the complexity of the algorithm. The more the number of replication and dispersal operations, the more bacteria have the chance to search in the eutrophic area, which can improve the convergence speed of the algorithm, but too many will lead to the algorithm is too complex.

2.2.3. The Genetic Algorithm.
The genetic algorithm is based on the probability search of biological natural selection and natural genetic mechanism. It does not rely on function gradient information but uses some coding technology to act on string, simulates the evolution process of string formation, exchanges and reorganizes information in an organized and random way, and finally generates the optimal solution.

The search process of the genetic algorithm starts from a series of initial solutions. Each individual in the population is an optimal solution called a chromosome. In the genetic algorithm, chromosome is usually a series of data as the code of solution [17]. The quality of chromosomes is determined by iterating through various operations. In the iteration process, the new chromosome produced by the change of genetic operator is called offspring. Some individuals were selected as the offspring of the new generation population. The size of the population is a specific constant because the chromosomes with low fitness are excluded. The genetic algorithm is a probability transformation, so it is more likely to select the chromosome with high fitness. After several iterations, the algorithm will converge to the best chromosome or better chromosome.

In the basic genetic algorithm, some individuals are copied according to the fitness ratio of the current generation. After crossover and mutation, a new generation of individuals will be formed. Individuals with high fitness are likely to be copied, and the best individuals are selected from the previous generation and, then, directly enter the next generation. This not only ensures that the coding of the optimal individual will not be destroyed but also promotes the propagation of excellent individual characteristics and the guidance of offspring.

2.3. Statistical Methods of Network Traffic

2.3.1. Network Traffic Identification and Classification.
Network traffic identification and classification technology is the basis of network traffic statistics. According to the characteristics of data samples, samples are found and extracted, and they are divided into the identified categories. At present, the commonly used network traffic identification and classification methods include well-known port number, signature, and flow statistical characteristics [18].

Well-known port number is a public service port predefined in the registry of service name and transport layer protocol port number published by the Internet Digital Distribution Agency (IANA), and its port number is generally between 0 and 1023 [19]. This method has high recognition accuracy, simple operation, and low complexity. However, its limitations are also obvious. The port number assignment of IANA is not oriented to all applications, and it cannot correspond with applications one by one. Sometimes some common protocols do not use the default port number for data transmission.

Signature is unique to some application protocol. In the actual application interaction environment, the attribute with the highest frequency can be used to distinguish different network applications. Signature based on application layer is identified and classified by analyzing whether the payload of data group is consistent with the signature database. By analyzing whether the payload contains regular expressions consistent with the function recognition rules, it is necessary to establish the network traffic application layer signature database in advance. Otherwise, the application will be marked as a match if it is successful. Although this method has a high classification accuracy rate, its system storage and processing costs are high, and it cannot parse the traffic of encrypted applications and may even violate the security risks of user privacy.

Identification and classification methods based on statistical characteristics of application flows are generated by various network applications, such as transport layer protocol, duration of network flow, and average number of data packets in network flow [20]. Because the classification method based on traffic statistical characteristics needs to deal with many complex big data problems, the machine learning algorithm is introduced to solve the tenfold sum classification of network traffic. The machine learning algorithm can realize the calculation and learning of large-scale data and mine the relationship and rules between data.

2.3.2. Data Mining.
Association rule mining is a classical method and an important research direction in data mining. Its essence is to find a meaningful association between data items in data set. The first step is to find frequent itemsets. Frequent itemsets are itemsets whose support is not less than the minimum support. This step is very important, because the basis of forming association rules is frequent itemsets. The second step is to generate association rules. All strong association rules are generated based on frequent itemsets with minimum confidence.

When mining frequent itemset, the Apriori algorithm is a classic algorithm, which is based on the iterative idea of layer by layer search [21]. Firstly, scan the database, count and record the number of times of an itemset, and compare it with the minimum support. If the minimum support is
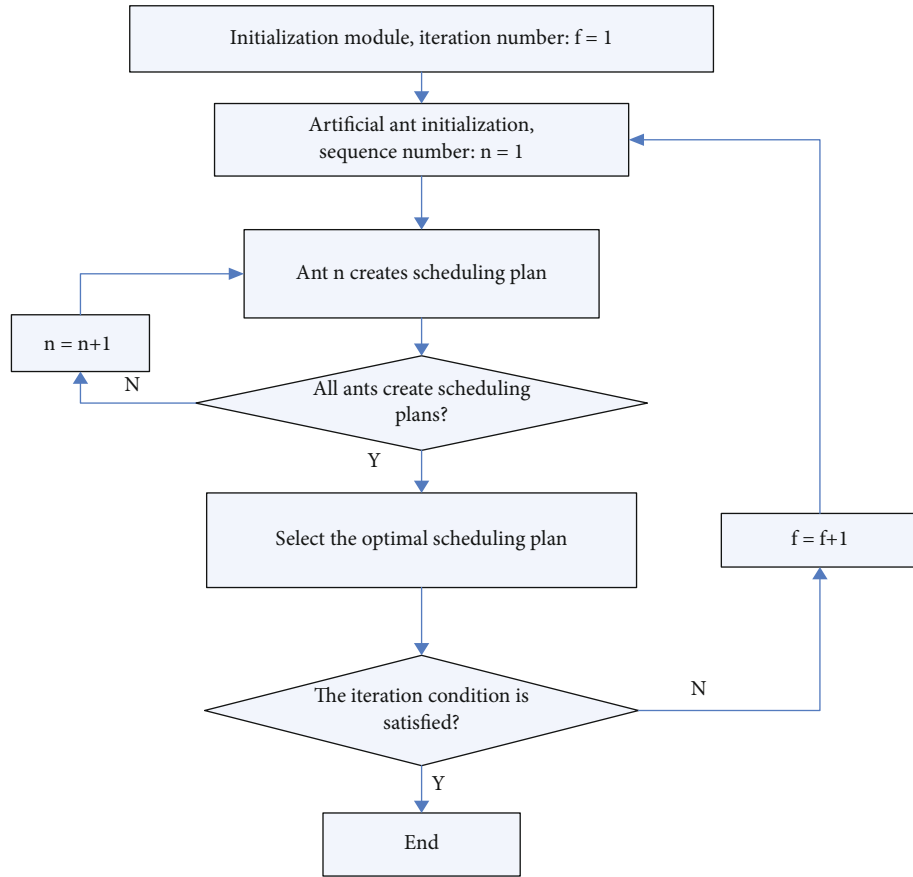
FIGURE 1: Algorithm flow chart.

greater than or equal to the minimum support, it is classified as one frequent itemset, and then, two frequent sets are used to find two frequent itemsets, and two frequent sets are used to find three frequent itemsets. The algorithm needs to scan the database for many times to generate a large number of candidate item sets, which greatly increases the storage cost.

Therefore, based on the Apriori algorithm, there are some improved algorithms. The AprioriTid algorithm reduces the amount of scanned data, thus reducing the candidate itemset and improving the efficiency of the algorithm [22]. The FP-Tree algorithm uses the prefix tree to improve the search speed, does not need to produce a large number of candidate sets, and has advantages in space and time [23]. The DHP algorithm uses Hash technology to reduce the number of candidate sets, thus improving the algorithm. The partition algorithm divides the database into disjoint partitions, thus reducing the number of database scans [24].

2.3.3. Demand Analysis of Network Traffic Statistics. Demand analysis is a very important link in the system design and implementation. The functions of the system must be defined according to the business objectives, and the business problems should be converted into technical problems. Therefore, before designing and implementing the network traffic statistical analysis system, it is necessary to analyze its requirements and define the functions and indicators required by the system.
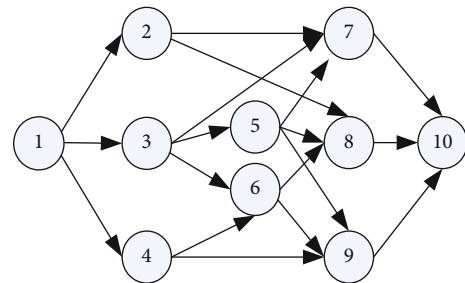
FIGURE 2: Project network structure.

The management system is divided into the acquisition layer, analysis layer, and presentation layer [25]. The acquisition layer is used to collect the corresponding data of different devices. The data must be comprehensive and accurate, and it must have a corresponding database to store the data. The analysis layer is to analyze the flow data, process the corresponding data in an orderly manner, and put forward sensitive information, total price, and store information. The presentation layer feeds back the statistical results to users. The platform and interface must be friendly and can handle abnormal operations in time.

Performance is reflected in response time, stability, and friendliness. In order to improve the efficiency of the system, it is necessary to respond and feedback every request of users in time when interacting with users. The excellence of the
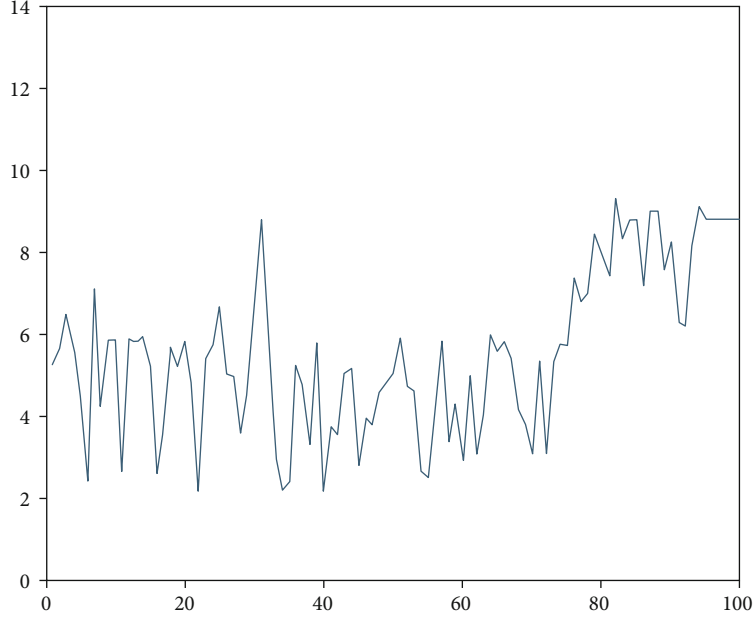
FIGURE 3: Number of occurrences of optimal solution.

program must be based on the stability. Once there is an unpredictable error, it must be able to ensure a certain stability. Good application interface is very important, always keep friendly interaction with users.

3. Experiments on Model Building and Algorithm Optimization

3.1. Modeling

3.1.1. Objective Function. The objective function of the project is mainly divided into time class, resource class, financial class, and quality class. In this paper, based on the resource of network traffic, the objective function of resource class is considered. In the project plan, if the arrangement is unreasonable, the resource demand will be unequal during the planned construction period. At this time, the resource restriction will lead to the delay of tasks or the overstock of resources. Therefore, this paper mainly studies the objective function of resource balance. The objective function of resource balance problem is not unique but is determined by the evaluation index of resource balance. When there is only one resource z in the project, the objective function can be expressed as Formula (2):

$$\min \sum_{t=1}^{f_n} \left(Rz(t) - \bar{R}_z \right)^2. \tag{2}$$

Among them, $R_z(t) = \sum R_i(t)$ represents the total demand for resource z in period t of the project, and $\bar{R}_z = 1/T\sum_{t=1}^{T} e_{iz}$ represents the average resource demand level of resource z in the whole project duration. Therefore, the optimization goal of resource-constrained project scheduling is to minimize the total project duration and resource balance.
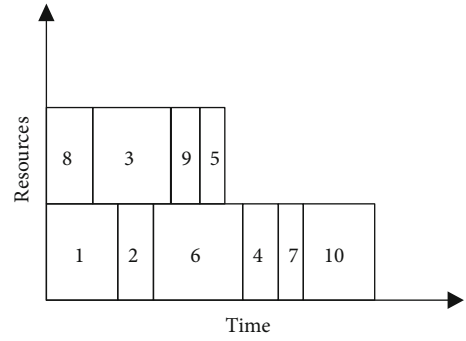
FIGURE 4: Project optimal scheduling scheme.

TABLE 1: Project scheduling schedule.

Number	1	2	3	4	5	6	7	8	9	10
Start T	1	6	4	18	14	10	22	1	12	26
End T	6	10	12	22	16	18	24	4	14	32

3.1.2. Mathematical Model. Suppose that there are m tasks and z kinds of renewable resources in the project, for task i, e_{iz} represents the demand for resources in the z, and n_z represents the weight of the zth resource. The mathematical model of resource-constrained target scheduling is as follows:

$$R_z(t) = \sum R_i(t), \tag{3}$$

$$\bar{R}_z = \frac{1}{T} \sum_{t=1}^{T} e_{iz}, \tag{4}$$

$$M_1 = 0, \tag{5}$$
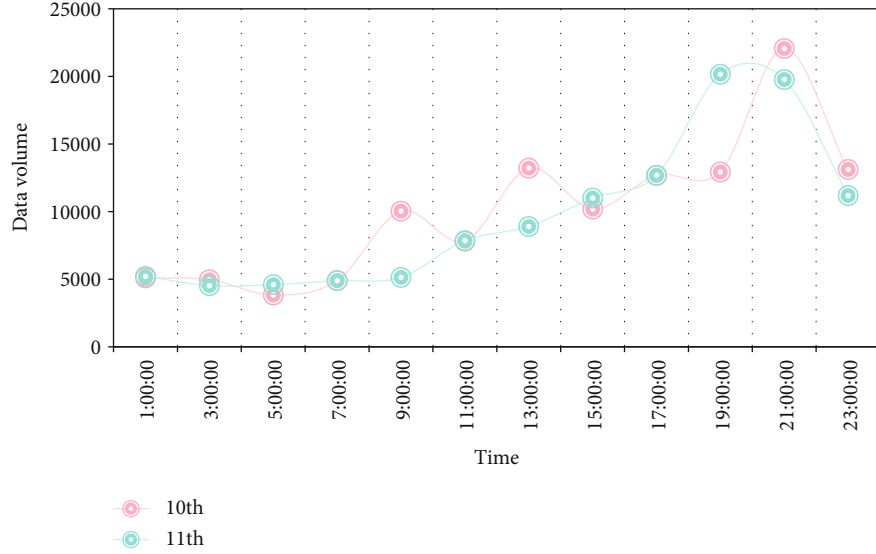
Figure 5: Trend of PCU data volume.

$$f_i - f_j \geq g_i, i = 1, 2, \cdots, n. \tag{6}$$

Among them, Formula (3) represents the total demand for resource z at time t, Formula (4) represents the average resource demand level of resource z within the project duration, Formula (5) represents the start time of the project, and Formula (6) represents the logical constraint of task objects.

3.2. Ant Colony Optimization. In order to solve the optimization problem by the ant colony algorithm, it is necessary to build a suitable algorithm, which not only reflects the characteristics of the problem but also selects the appropriate pheromone and heuristic information decision. In order to construct the path, it is necessary to choose a comfortable execution task that satisfies the immediate relationship and set a planned start time to meet the resource constraints for the work. Therefore, the ant's March should start from the same starting point and end at the same end point. The expression object of pheromone is the construction period, which is initialized and updated, while heuristic information considers that the work with a smaller latest start time and more follow-up work is more important and should be implemented earlier.

Artificial ants start from the same starting point and schedule the next task in the earliest time period that meets the resource constraints by repeatedly applying the state transition rules until the end of the project. During the search process, pheromone is updated twice. The specific workflow chart of the algorithm is shown in Figure 1:

3.3. Simulation Analysis. The benchmark problem in PSPLIB is introduced, and the mathematical model of resource-constrained project scheduling problem and the ant colony algorithm are used to solve the problem. The data source is a project scheduling problem with 10 tasks and 1 renewable resource in PSPLIB. The network diagram of each project is shown in Figure 2:

4. Discussion of Optimization Model Algorithm

4.1. Algorithm Performance Test. After counting all the solutions and calculating the number of optimal solutions, we can get the relationship between the number of iterations and the number of optimal solutions. The results were as follows:

As shown in Figure 3, there is a peak value of the number of optimal solutions around the 30th generation, but it is not stable afterwards but continues to fluctuate, indicating that the algorithm has certain randomness. The convergence is obvious after the 75th generation, and the unique optimal solution is obtained after the 94th generation, which indicates that the optimal solution can be obtained by setting appropriate parameters in the solution method.

4.2. Project Scheduling Results. The algorithm parameters are set as follows: the initial population size is 10, and the number of iterations is 30. The optimal scheduling scheme is shown in Figure 4:

Based on the above plan, the starting time and completion time of each task are planned, and the specific arrangement is as follows.

As shown in Table 1, the total construction period of the project is 32 days, and the schedule of each task is very compact, and in the first half of the construction period, both tasks are carried out at the same time. First of all, projects No.1 and No.8 were carried out at the same time. After the completion of project No.8 on day 4, task No.2 was started after task No.1 was completed on day 6, task No.6 was started after task No.2 was completed on day 10, task No.3 was completed on day 12, and task No.9 and task No.5 were started simultaneously with task No.6. On the 16th day, after the end of task No.5, the whole project entered the operation stage of single task, and the tasks of No.4, No.7, and No.10 were carried out according to the time sequence until the whole project was completed.

4.3. Flow Statistics. The system can analyze and count the amount and frequency of sending and receiving data of PCU IP in a busy hour and, then, analyze the change trend of PCU's received and received data in a period of time through the results. The PCU with IP 112.58.14.66 in December 10 and 11, 2019, is statistically analyzed, and the change trend chart of the PCU is obtained as follows:

As shown in Figure 5, the change trend of data volume of PCU with IP of 112.58.14.66 on December 10 and December 12 is roughly the same, but the peak time is different. The data volume at 9 : 00, 13 : 00, and 21 : 00 on December 10 is relatively large, while the data volume on 11 : 00 has been gradually rising after 9 : 00, and the peak value appears from 19 : 00 to 21 : 00. This shows that there are more users using data services in these time periods. We can pay attention to these time periods and reasonably schedule the network resources to prevent the occurrence of network failures.

5. Conclusions

With the development of mobile Internet, the statistical analysis of network traffic becomes more and more important. The effective and accurate network traffic statistics method can determine whether the equipment is likely to fail and can plan the market according to the distribution and type of data traffic. The advent of big data era makes the statistical data of network traffic more complicated. The application of the ant colony algorithm in the resource-constrained project scheduling problem can effectively obtain the optimal scheduling scheme, based on which the optimal solution of network traffic scheduling problem can be calculated.

The ant colony algorithm is established to optimize the resource-constrained project scheduling problem, which can count the usage trend of CPU network traffic of specific IP in a certain period of time, and obtain the time period of peak value, so as to carry out reasonable resource scheduling, avoid network failure, analyze the distribution of network traffic according to IP, and make overall planning for the market.

Due to the limited time and knowledge, although the ant colony algorithm is optimized for the mathematical model of resource-constrained project scheduling problem, its performance test is far from enough, and there may be some hidden dangers that have not been detected. In the next research work, we need to test it more comprehensively in order to improve the algorithm.

Data Availability

No data were used to support this study.

Conflicts of Interest

The authors declare that they have no conflicts of interest.

Acknowledgments

References

[1] N. R. O. Pimiento and F. J. D. Serna, "An optimization model to solve the resource constrained project scheduling problem RCPSP in new product development projects," *Dyna*, vol. 87, no. 212, pp. 179–188, 2020.

[2] F. G. C. Rocha and F. H. T. Vieira, "Adaptive estimation of parameters of multiplicative cascade-based network traffic model in wavelet domain," *Electronics Letters*, vol. 52, no. 9, pp. 708–710, 2016.

[3] T. Solomon, A. M. Zungeru, R. Selvaraj, M. Mangwala, and J. Chuma, "Network traffic model: a case of BIUST network," *Journal of Computer Science*, vol. 13, no. 7, pp. 218–227, 2017.

[4] S. Kreter, A. Schutt, and P. J. Stuckey, "Using constraint programming for solving RCPSP/max-cal," *Constraints*, vol. 22, no. 3, pp. 1–31, 2017.

[5] J. Xiao, Z. Wu, X.-X. Hong, J.-C. Tang, and Y. Tang, "Integration of electromagnetism with multi-objective evolutionary algorithms for RCPSP," *European Journal of Operational Research*, vol. 251, no. 1, pp. 22–35, 2016.

[6] J. Poppenborg and S. Knust, "A flow-based tabu search algorithm for the RCPSP with transfer times," *OR Spectrum*, vol. 38, no. 2, pp. 305–334, 2016.

[7] H. Mogaadi and B. F. Chaar, "Robust optimization for RCPSP under uncertainty," *International Journal of Software Engineering & Applications*, vol. 7, no. 2, pp. 45–55, 2016.

[8] Z. Chu, Z. Xu, and H. Li, "New heuristics for the RCPSP with multiple overlapping modes," *Computers & Industrial Engineering*, vol. 131, pp. 146–156, 2019.

[9] P. Jędrzejowicz and E. Ratajczak-Ropel, "PLA based strategy for solving RCPSP by a team of agents," *Smart Innovation*, vol. 22, no. 6, pp. 856–873, 2016.

[10] P. Fouilhoux, A. R. Mahjoub, A. Quilliot, and H. Toussaint, "Branch-and-Cut-and-Price algorithms for the preemptive RCPSP," *RAIRO - Operations Research*, vol. 52, no. 2, pp. 513–528, 2018.

[11] A. H. Hosseinian, V. Baradaran, and M. Bashiri, "Modeling of the time-dependent multi-skilled RCPSP considering learning effect," *Journal of Modelling in Management*, vol. 14, no. 2, pp. 521–558, 2019.

[12] S. S. Chaudhari and R. C. Biradar, "Traffic and mobility aware resource prediction using cognitive agent in mobile ad-hoc networks," *Journal of Network & Computer Applications*, vol. 72, pp. 87–103, 2016.

[13] D. Jankowski and M. Amanowicz, "On efficiency of selected machine learning algorithms for intrusion detection in software defined networks," *International Journal of Electronics and Telecommunications*, vol. 62, no. 3, pp. 247–252, 2016.

[14] Z. Trabelsi, S. Zeidan, and M. M. Masud, "Hybrid mechanism towards network packet early acceptance and rejection for unified threat management," *IET Information Security*, vol. 11, no. 2, pp. 104–113, 2017.

[15] P. Wang, Y. Qi, J. C. S. Lui, D. Towsley, J. Zhao, and J. Tao, "Inferring higher-order structure statistics of large networks from sampled edges," *IEEE Transactions on Knowledge and Data Engineering*, vol. 31, no. 1, pp. 61–74, 2019.

[16] A. Jaziri, R. Nasri, and T. Chahed, "Tracking traffic peaks in mobile networks using statistics of performance metrics," *International Journal of Wireless Information Networks*, vol. 24, no. 4, pp. 389–403, 2017.

[17] M. Siekkinen, M. A. Hoque, and J. K. Nurminen, "Using viewing statistics to control energy and traffic overhead in mobile video streaming," *IEEE/ACM Transactions on Networking*, vol. 24, no. 3, pp. 1489–1503, 2016.

[18] Z. Liang, J. Sun, Q. Lin, Z. du, J. Chen, and Z. Ming, "A novel multiple rule sets data classification algorithm based on ant colony algorithm," *Applied Soft Computing*, vol. 38, no. C, pp. 1000–1011, 2016.

[19] F. E. B. Otero and A. A. Freitas, "Improving the interpretability of classification rules discovered by an ant colony algorithm: extended results," *Evolutionary Computation*, vol. 24, no. 3, pp. 385–409, 2016.

[20] M. Liu, F. Zhang, Y. Ma, H. R. Pota, and W. Shen, "Evacuation path optimization based on quantum ant colony algorithm," *Advanced Engineering Informatics*, vol. 30, no. 3, pp. 259–267, 2016.

[21] J. Cao, "Robot global path planning based on an improved ant colony algorithm," *Journal of Computer and Communications*, vol. 4, no. 2, pp. 11–19, 2016.

[22] D. S. Chivilikhin, V. I. Ulyantsev, and A. A. Shalyto, "Modified ant colony algorithm for constructing finite state machines from execution scenarios and temporal formulas," *Automation and Remote Control*, vol. 77, no. 3, pp. 473–484, 2016.

[23] H. A. Ghani, M. H. Hamzah, S. Syahali, and N. H. A. Aziz, "Ant-colony algorithm with interference cancellation for cooperative transmission," *IET Signal Processing*, vol. 10, no. 6, pp. 603–610, 2016.

[24] L. Xiaojie, Z. Hongjin, F. Honghui, and Z. Min, "Design of vision measurement device for seeding robot based on ant colony algorithm and nonlinear circuit system," *International Journal of Information Technology and Web Engineering*, vol. 12, no. 3, pp. 42–50, 2018.

[25] S. Khudair and T. Younis, "Energy efficient routing protocol for maximizing the lifetime in Wsns using ant colony algorithm and artificial immune system," *International Journal of Advanced Computer Science and Applications*, vol. 7, no. 3, pp. 19–25, 2016.

WILEY | Hindawi

Research Article

Research on the Effect of Knowledge Network Embedding on the Dynamic Capabilities of Small and Micro Enterprises

Shuli Zheng (ID)

College of Economics & Management, Zhejiang University of Water Resource and Electric Power, Hangzhou 310018, China

Correspondence should be addressed to Shuli Zheng; zhengshl@zjweu.edu.cn

In the complex and dynamic economic environment, the growing pain of small and micro enterprises is long-standing. It is urgent to strengthen the research on the endogenous growth mechanism of small and micro enterprises. Based on the background of the era of knowledge-driven economy, this paper explores the relationship between knowledge network embeddedness and dynamic capabilities of small and micro enterprises with environmental munificence as the regulating variable. We have the structural equation empirical research with the data from 260 questionnaires of small and micro enterprises. The results show that structural embeddedness and relational embeddedness have a positive driving effect on the dynamic capability of small and micro enterprises, and environmental munificence plays a positive regulatory role in the positive impact of knowledge network embedding on the dynamic capability. The research conclusion is helpful for the small and micro enterprise to develop dynamic capacity and for the supportive policy making as well.

1. Introduction

With the continuous deepening of social division of labor and the fragmentation of production, the new ecology of "small and beautiful" enterprises is showing a trend of prosperity [1]. Small and micro enterprises (SMEs) have become the main body of market economic activities in many developing countries and play an irreplaceable role in increasing employment and promoting economic growth and technological innovation [2–4]. However, there are natural disadvantages such as lack of resources, small knowledge stock, limited human resources, and high cost. At present, the development of small and micro enterprises is faced with many difficulties. Weak operation foundation and financing difficulties are the fundamental problems, resulting in the lack of talent, vision, innovation ability, resource integration ability, and other aspects. Therefore, it is characterized by short life span and high failure rate, which make the SMEs' high failure rate [5]. For this reason, many people realize that it is important to solve the external policy support for small and micro enterprises, but it is more important for enter-

prises to build their own ability to transform knowledge into adaptability in a specific environment.

The update speed of knowledge and technology is constantly accelerating now, the life cycle of products, technologies, and enterprises becomes shorter, speed economy will replace economies of scale [6], and environmental uncertainty is greatly strengthened [7]. It is necessary to build a market-sensitive cognition ability, resource integration ability, and adaptability, that is, dynamic ability as the advantages brought by heterogeneous resources are no longer sustainable. Previous studies showed the prevariables of dynamic capabilities, including environmental uncertainty, organizational social capital, social networks, organizational learning, organizational resources, entrepreneurial orientation, and leadership style [8]. In fact, under the dual pressure of speed economy and knowledge creation cost, organizations attach more and more importance to acquiring knowledge through knowledge network embedding and creating new knowledge together with network partners [9], so as to build their dynamic capabilities and adapt to the needs of environmental changes. Small and micro enterprises are

considered to embed in alliances and operating networks due to their scale, resources, and capacity constraints and acquire universal knowledge in the network to narrow the knowledge gap with other businesses and keep the competitive advantages [10]. Research on startups, incubators, and small and micro enterprises supports the positive effects of dynamic capabilities on the competitiveness and performance [4, 11] and also explores the connotation of dynamic capabilities of SMEs. The government has been aware of the issue of high quality development of SMEs, while the academic research paid attention to the sustainable competitiveness and growth of small and micro enterprises [12]. The current research on dynamic capability is generally focused on high-tech enterprises, Internet companies, and manufacturing industries. It seems that dynamic capability is only an issue of large enterprises and has nothing to do with small and micro enterprises [13, 14]. According to the theory of Prahalad and Hamel [15], the dynamic capabilities of enterprises can only be accumulated gradually with a long period of time. Therefore, there are still doubts about the connotation of dynamic capabilities of SMEs [16] and whether small and micro enterprises can build their dynamic capabilities.

Based on this, we design the research framework of "knowledge network embeddedness-dynamic capabilities" for SMEs, introduce environmental munificence as a moderating variable, and raise the following research questions. What are the embedded connotations and dimensions of the dynamic capabilities of SMEs and knowledge networks? How do the dimensions of the embeddedness of knowledge networks affect the dimensions of dynamic capabilities? How does the environmental munificence regulate this process? Starting from the above questions, we explore the role of the embedded knowledge network of SMEs in the construction of dynamic capabilities and the regulating effect of environmental munificence and provide theoretical support for enterprises to learn external knowledge to realize the transformation of dynamic capabilities and also provide a reference for formulating incentive support policies.

2. Concept Description

2.1. Small and Micro Enterprises.
The World Bank defines micro and small enterprises as those with fewer than 50 employees and less than \$10 million in sales. Because of the vast territory and a large population, the enterprises' classification standards are different with other countries. According to the "Notice on Printing and Distributing the Standards for the Classification of Small and Medium-Sized Enterprises" issued by the National Bureau of Statistics (Gongxinbulianqi [2011] No. 300), we define the SME as enterprises with less than RMB 20 million operating revenue and less than 200 employees.

2.2. Dynamic Capabilities.
Dynamic capabilities are "the ability of an enterprise to construct, adjust, integrate, and reconstruct internal and external resources and capabilities." After that, many scholars gave different understandings of the dynamic capabilities of enterprises from different angles. The most representative ones are Winter, Eisenhardt, and Martin and domestic scholar Jiao Hao. Yan [17] divided the definition of dynamic capabilities in the literature into "gorgeous understanding" and "plain understanding." Huamei's understanding is easy to cause confusion with other concepts, and the connotation is too broad to lose its guiding significance. The naive understanding firstly understands the dynamic capability as an organizational capability that is routine. However, Teece [16] in an article questioned the view that dynamic capabilities are simply recognized as company-specific practices in 2012, especially that small and micro enterprises may lack organizational and technical redundant resources to repeatedly evaluate potential opportunities. Feng and Wei [18] classified dynamic capabilities into two categories: the ability to complete abstract organization and management processes and the ability to complete specific strategies and organizational processes. On the basis of absorbing literature viewpoints, this article believes that dynamic capabilities are the ability of an enterprise to perceive and identify opportunities and threats and the ability of an enterprise to construct, integrate, and reconstruct internal and external resources and capabilities to adapt to dynamic environmental changes. Existing literature believes that dynamic capabilities include market-oriented perception capabilities, absorptive capabilities, social network relationship capabilities, integration capabilities, organizational flexibility capabilities, innovation and transformation capabilities, and learning and utilization capabilities [19–23]. Based on the review of the above literature, combined with the characteristics of small and micro enterprises, this article divides the dynamic capabilities into opportunity perception capabilities, organizational flexibility capabilities, and resource integration capabilities.

2.3. Embeddedness of Knowledge Network.
Knowledge network is a system which is composed of a collection of nodes and connections between nodes, and a company is the node of the knowledge network [24]. Drawing lessons from the viewpoint of Granovetter [25], the embeddedness of knowledge network is divided into structural embeddedness and relational embeddedness. Tasi pointed out through investigation that in the knowledge transfer within an organization, network structure, relationship, and location affect the absorptive capacity of new knowledge and the innovation and performance of business units [26]. Li et al. empirically analyzed the impact of relational embedding and structural embedding on the effectiveness of knowledge acquisition by investigating the characteristics of four different stages of knowledge search, recognition, reception, and innovation [27]. Structural embeddedness features in overall network structure described the position of network nodes, which is described by network scale, network centrality, and network position difference; the embeddedness characteristics of the relationship are used to describe the nature of the communication relationship between the enterprise and its network members, and it is described by the mutual trust, information sharing, and joint problem solving between the enterprise and various partners.

2.4. Environmental Munificence. Environmental munificence refers to the abundance of resources required by the enterprise in the environment and the difficulty of obtaining the required resources by the enterprise [28]. The stronger the environmental munificence, the easier it is for companies to obtain the resources they need from the environment, while the weaker the environmental munificence, the more difficult it will be for companies to obtain the resources they need from the outside world, and the higher the cost will be. In terms of the measurement of environmental munificence, the objective succedaneous indicators adopted at the very beginning include industrial growth rate, sales growth, price and cost difference, and the total number of employment. Therefore, more emphasis is placed on the difficulty for enterprises to obtain resources from the macro environment.

3. Literature Review and Research Hypotheses

3.1. Embeddedness of Knowledge Network and Dynamic Capabilities of SME. After the 1980s, the relationship between social networks and social resources and how companies obtain resources through social networks began to receive academic attention. The relationship between enterprises and external organizations has also developed from a single binary relationship to an interdependent network relationship between multiple organizations [29]. Network members can quickly fill up their own knowledge gaps through the flow, transfer, and integration of knowledge [30]. And it is conducive to improve the core competence of enterprises [31, 32], which can directly or indirectly bring survival opportunities for startup small and micro enterprises [33]. Regarding the source of dynamic capabilities, the evolutionary economics perspective emphasizes the synergy and coevolution between the organization and the environment, the technological perspective emphasizes the capability transformation mechanism, and the knowledge-based research perspective believes that "dynamic capabilities come from organizational learning" [34, 35]. For small, medium, and micro enterprises, acquiring knowledge from outside the organization has become an important strategy to make up for their own shortcomings [36], which affirms the positive effect of knowledge network embedding on the dynamic capabilities of small and micro enterprises.

Structural embeddedness focuses on the structure of the network and the quality of social connections between network nodes and mainly analyzes the relationship between the position of the research target company in the network and its performance. Companies that occupy the central position of the network have more opportunities for contact with cooperative companies [37], and exchanges and cooperation with other companies are more active. Owning even more key information channels in the network can be controlled, and it is easier to obtain the required technology and knowledge than other enterprises, which directly reduces the cost of searching for information by the focus enterprise, which is conducive to improving the enterprise's opportunity perception ability [38]. From the perspective of resource theory, companies in the center of the network can coordinate resources more easily because of their advantageous network

locations, good relationships between companies, and strong bargaining power, and they can also control and guide the flow of innovative resources to projects that are beneficial to their competitive position [38, 39]. It can even control and coordinate the trajectory and direction of new knowledge generated in the network, so the structural embeddedness has a positive impact on the organization's flexibility. The closer the position of an enterprise in the network is to the network center, the faster it can obtain resources and information, especially the knowledge required for technological innovation, which provides conditions for its control of resources and integration of resources [40].

Relationship embeddedness is the transaction and interaction between the two parties based on good expectations of future interests. Its connotation includes trust, information sharing, and joint problem solving [41]. The trust relationship between enterprises is a prerequisite for tacit knowledge sharing. The relationship capital based on this trust can promote the transfer of knowledge and information between organizations. Both the quantity and quality of transfers are improved with the improvement of interorganizational trust [42], and they are completed in the process of solving problems together. The deepening of information sharing among enterprises can improve the timeliness, accuracy, and extensiveness of information exchange in the process of cooperation. It is conducive for companies to prioritize market dynamics, seize market opportunities [43], become the industry's first mover, and gain first-mover advantage. The better the foundation of the trust relationship between the enterprise and other enterprises, the more helpful it is to quickly obtain more scarce and effective resources and avoid excessive redundant and invalid processes. At the same time, in order to obtain more heterogeneous resources, enterprises will strengthen their openness and cooperation arrangements with external parties [42, 44]. The resources acquired from the outside and the resources owned by the enterprise may be complementary or reinforcing. Therefore, the enterprise can also perceive how the resources are integrated and utilized.

Because of their own resource constraints and growth needs, small and micro enterprises generally take the initiative to strengthen the relationship with their partners when the network location is not dominant, so as to enhance the trust between the two parties, in order to deepen cooperation, strive to produce and strengthen the lock-in effect, and strengthen its own role in the value network, to reduce the impact of the turbulent environment and continuously improve its own adaptability.

In summary, the following research hypotheses are proposed:

H1: the embeddedness of knowledge network has a positive impact on the dynamic capabilities of small and micro enterprises

H1-1: structural embeddedness has a positive impact on opportunity perception of small and micro enterprises

H1-2: structural embeddedness has a positive impact on the organizational flexibility of small and micro enterprises

H1-3: structural embeddedness has a positive impact on the ability of small and micro enterprises to integrate resources
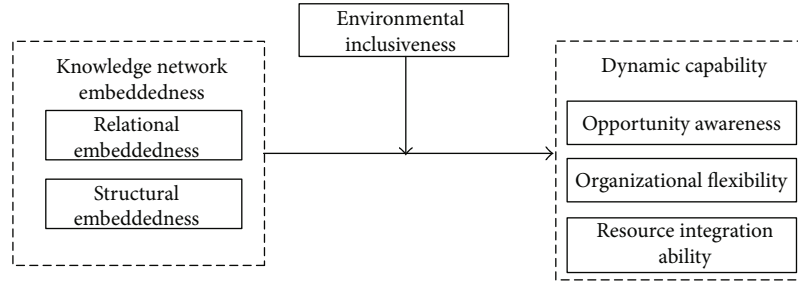
FIGURE 1: Theoretical model.

H1-4: relationship embeddedness has a positive impact on opportunity perception of small and micro enterprises

H1-5: relationship embeddedness has a positive impact on the organizational flexibility of small and micro enterprises

H1-6: relationship embeddedness has a positive impact on the ability of small and micro enterprises to integrate resources

3.2. Environmental Inclusive Moderating Effect. Environmental tolerance refers to the abundance of resources needed by the enterprise in the business environment of the enterprise and the degree of difficulty for the enterprise to obtain these resources [28]. Obviously, the more inclusive the environment is, the better living conditions can be created for enterprises. This is especially important for small and micro enterprises in the startup and growth stages. The initial policy support can bring easy access, market opportunities, and lower costs for enterprises. On the one hand, this rapid return can bring room for small and micro enterprises to survive, and on the other hand, it will strengthen enterprises' enthusiasm for policy dependence. Studies have shown that when environmental resources are sufficient and easy to obtain, the cost of resource acquisition is low, and the enterprise's survival pressure is small. It will also breed double organizational inertia at the structural and cultural levels and weaken the willingness of enterprises to obtain knowledge resources from the network [45, 46], resulting in the rigidity of the organization's core competence, but it is not conducive to improve organizational capabilities.

From the perspective of regional economic development results, my country's southeast coastal areas have the characteristics of a high degree of openness, a high degree of marketization, and a strong commercial and cultural atmosphere. At the same time, these characteristics derive a higher quality of government systems. The changes in the incentive structure brought about by the system can guide the competitive consciousness and innovative behavior of enterprises, and this is also one of the fundamental reasons for the differences in regional economic development [47, 48]. Macrolevel tolerance and microlevel corporate behavior form a mutually reinforcing coupling relationship. Therefore, there is a certain controversy in the current literature on the moderating effect of environmental munificence, which may be due to different research objects and perspectives or different definitions of the connotation of environmental munificence. Based on the differences in economic

development and the findings of the interviews at the beginning of the research, this paper proposes the following research hypotheses:

H2: environmental munificence positively regulates the relationship between the embeddedness of knowledge network and the dynamic capabilities of small and micro enterprises, that is, the stronger the environmental munificence, the more obvious the effect of embeddedness of knowledge network on the construction of dynamic capabilities of small and micro enterprises.

Based on the above theoretical analysis, the theoretical model construction is shown in Figure 1.

4. Research Design

4.1. Samples and Data Collection. The research object of this article is small and micro enterprises, which use questionnaire survey to complete data collection. The survey scope covered Zhejiang Province, Jiangsu Province, Henan Province, Hubei Province, Shanghai, Beijing, and other regions. Respondents must be middle-level or above managers with a college degree or above and have worked in the company for more than 3 years to ensure the correctness of their understanding of the questionnaire and the depth of their understanding of the company. A total of 350 questionnaires were issued and 306 were retrieved. Questionnaires that did not meet the requirements of the scale of the enterprise, the consistent response of the options, and the missing answers were excluded. There were 260 valid questionnaires, and the effective recovery rate was 74.3%. The specific situation of the sample is shown in Table 1.

4.2. Variable Measurement. The main variables in this study are measured using mature scales in existing literature at home and abroad to ensure the reliability and validity of the measurement tools. Using the Likert 7-point scale, "1" is very nonconforming, and "7" is very consistent.

(1) Structural Embeddedness. Refer to Fan et al. [39], Acemoglu et al. [48], Wu et al. [47], and other scholars to compile a scale. There are 5 measurement items in total. Typical items include "Your company has connections with many government agencies/universities/scientific research institutions/financial and investment institutions."

(2) Relationship Embeddedness. Refer to Uzzi [41], Balland et al. [49], and other scholars to compile a scale. There are 5

TABLE 1: Basic structural characteristics of the sample.

Enterprise attributes	Sample characteristics	Number of samples	Percent	Enterprise attributes	Sample characteristics	Number of samples	Percent
	1-2 years	47	17.97%		Electromechanical	24	9.15%
	3-5 years	59	22.55%		Construction industry	16	6.21%
Years of establishment	6-10 years	49	18.95%		Auto parts	9	3.5%
	11-15 years	39	15.03%		Food and drink	9	3.5%
	More than 15 years	66	25.49%		Other manufacturing	49	18.8%
	20 people or less	53	20.38%		Business	19	7.3%
Enterprise size	20 people–100 people	108	41.54%	Industry field of the company	Trading	17	6.5%
	101–199 people	99	38.08%		Financial	18	6.9%
	Below 500,000	39	15.00%		Advisory	9	3.5%
	500,000–1,000,000	50	19.23%		Software	13	5.0%
Total annual sales	1 million–5 million	66	25.38%		Catering	8	3.1%
	5 million–10 million	53	20.38%		Real estate	9	3.5%
	10 million–20 million	52	20.00%		Other service industries	60	23.1%

measurement items in total. Typical items include "Cooperative enterprise/institution and your company are willing to provide each other with the information each other needs."

(3) Chance Perception Ability. With reference to Jiao [22], Chen and Wang [50], and other scholars that compiled a scale, there are 5 measurement items for the measurement of opportunity perception ability. Typical items include "Your company can quickly obtain and analyze changes in consumer demand and preference."

(4) Organizational Flexibility. Refer to the scale compiled by Pavlou and El Sawy [51], Jiao [22], etc. There are 5 measurement items for organizational flexibility. Typical items include "Your company has unblocked communication channels, and information transmission between department members is accurate and fast."

(5) Ability to Integrate Resources. Refer to the scale compiled by Chen and Wang [50], Zhao et al. [52], etc. There are 5 measurement items for resource integration ability. Typical items include "Your company can centrally manage cross-departmental business to ensure work efficiency."

(6) Environmental Tolerance. Referring to the scale compiled by Tsai et al. [44] and Pavlou and El Sawy [51], there are 4 measurement items for environmental munificence. Typical topics include "The government's development plan provides strong support for enterprises."

(7) Control Variables. Judging from the research results of the enterprise life cycle theory and dynamic capability theory, the company's years, scale, and industry all have an impact on its position in the knowledge network, its ability to obtain resources, and its competitiveness. Therefore, age, scale, and industry are selected as control variables.

4.3. Reliability and Validity Test of Scale. In order to ensure that the scale has good content validity, the measurement

items used in this study are all from the mature scale of authoritative journals. Before the survey, we first conducted semistructured interviews with more than ten senior managers or entrepreneurs from six companies to verify whether the preliminary research ideas obtained through literature review are consistent with the corporate reality. The questionnaire was revised to improve the validity of the questionnaire. This paper uses SPSS19.0 software and internal consistency test to test the reliability of the scale of this study. The Cronbach's α values of the two variables in the embeddedness dimension of knowledge network are 0.890 and 0.902, respectively. The Cronbach's α values of the three variables of the dynamic capability dimension, opportunity perception capability, organizational flexibility capability, and resource integration capability are 0.851, 0.909, and 0.883, respectively. The Cronbach's α value of environmental tolerance is 0.872, indicating that the internal consistency of the measurement scale is good.

The validity test of the measurement scale is completed by exploratory factor analysis and confirmatory factor analysis. In the KMO suitability test and the Bartlett sphere test, the KMO values of knowledge network embeddedness, dynamic capabilities, and environmental tolerance are 0.810, 0.763, and 0.749, which are all greater than 0.7. And p is less than 0.05, indicating that the three variables are suitable for factor analysis, and then, use the principal component analysis method to perform factor component analysis on each item of the variable. The factor loads of all items of the three variables are greater than 0.5, and the cumulative variance contribution rates are 77.27%, 82.19%, and 73.13%, respectively. The analysis results are shown in Table 2. The factor loading and cumulative interpretation of each index meet the requirements, and the measurement scale has good convergence validity.

By establishing a structural equation model, this paper conducts confirmatory factor analysis on the dimensional variables of the embeddedness and dynamic capabilities of the knowledge network to verify whether the construct validity of each item in the scale is valid. The measurement model

TABLE 2: Exploratory factor analysis results ($N = 260$).

Variable	Item	Factor loading			Cumulative variance contribution rate	KMO value
		$F1$	$F2$	$F3$		
Structural embeddedness	AS1	0.878				
	AS2	0.876				
	AS3	0.810			43.009	
	AS4	0.806				
	AS5	0.849				
	AS6	0.791				0.810
Relational embeddedness	AR1		0.860			
	AR2		0.666			
	AR3		0.824		77.270	
	AR4		0.701			
	AR5		0.861			
	AR6		0.833			
Opportunity perception	CC1		0.849			
	CC2		0.754			
	CC3		0.871		28.048	
	CC4		0.837			
	CC5		0.698			
Organizational flexibility	CO1			0.938		
	CO2			0.894		
	CO3			0.943	55.417	0.763
	CO4			0.809		
	CO5			0.837		
Resource integration	CR1	0.736				
	CR2	0.807				
	CR3	0.868			82.188	
	CR4	0.850				
	CR5	0.813				
Environmental munificence	DE1	0.850				
	DE2	0.861			73.133	0.749
	DE3	0.782				
	DE4	0.922				

TABLE 3: Fitting of the measurement model.

Variable	Dimension	χ^2/df	CFI	RMSEA
Knowledge network embeddedness	Structural embeddedness Relational embeddedness	1.976	0.965	0.049
Dynamic capability	Opportunity awareness Organizational flexibility Resource integration ability	2.427	0.912	0.081

and the fit are shown in Table 3. The fitting result of the knowledge network embeddedness measurement model is χ^2/df = 1.976, CFI = 0.965, and RMSEA = 0.049, which is less than 0.1. The significance of each path coefficient is $p < 0.001$; the fitting result of the dynamic capability dimension measurement model is χ^2/df = 2.427, CFI = 0.912, RMSEA = 0.081, and the significance of each path coefficient is $p < 0.001$. The fitting results of the measurement model of each variable are good, indicating that the dimensional division of the two variables and the validity of item construction are good [53, 54].

5. Empirical Results

5.1. Main Effect Test. In this paper, a structural equation model is constructed to test the relevant research hypotheses,
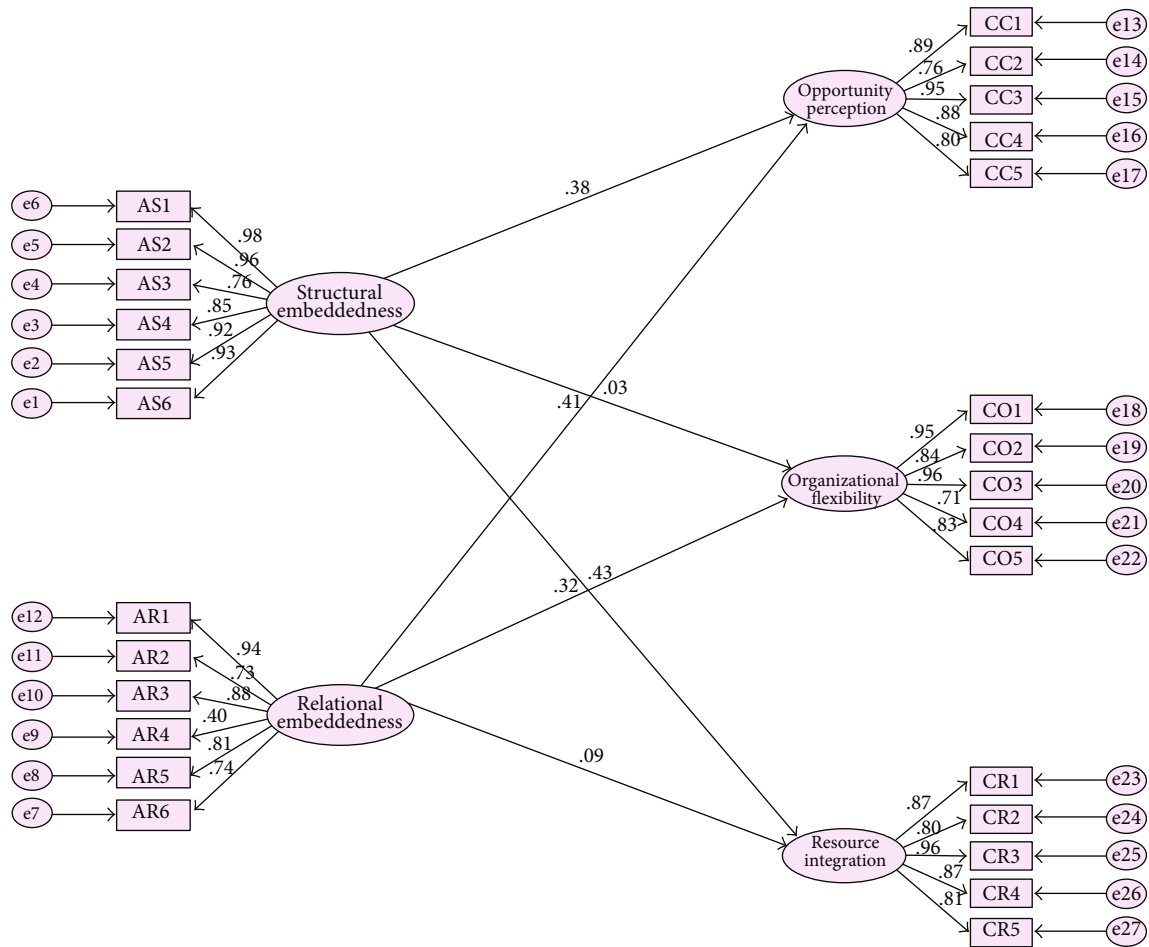
FIGURE 2: Structural equation model fitting diagram of the relationship between network embeddedness and dynamic capabilities.

and the model is revised through AMOS20.0. Firstly, establish the structural equation model between the independent variable and the dependent variable according to the theoretical basis, and test the relationship of each variable under the two dimensions of embeddedness of the knowledge network of small and micro enterprises and the three dimensions of dynamic capabilities. This article will use the maximum likelihood method to test the parameters of the structural equation model. The model fitting result will be evaluated from the significance of the model fit index and the hypothesis path. Choose χ^2/df, RMSEA, CFI, and TLI as the fitness index. The significance of the hypothesis path will be used to determine whether each hypothesis holds. Import the sample data into the AMOS20.0 software and test the initial model. The fitting results are shown in Figure 2. The fitting results of the structural equation model of the relationship between the embeddedness of the knowledge network and the dynamic capabilities are shown in Table 4.

It can be seen from Table 4 that the chi-square degree of freedom ratio of the main index of model adaptation is 3.393 > 3, and the other indicators do not fully meet the requirements of reasonable adaptation of the model. Therefore, on the premise of satisfying the theoretical basis, the fitting model needs to be revised according to the structural

equation model verification requirements. In the test summary of the path hypothesis, the significance of structural embeddedness to organizational flexibility and relationship embeddedness to resource integration $p > 0.05$ indicates that the relationship between variables is not significant and the hypothesis is invalid. Since the ratio of the chi-square degree of freedom of the initial model is greater than 3, it indicates that the model is not well adapted and needs to be further modified. After the correction, when the overall chi-square value of the model decreases, it indicates that the correction steps have produced an effect.

In the initial model, it was originally assumed that there is no correlation between the error terms of each measurement variable. However, the MI value from the fitting situation shows that the correlation between the error items of each variable is relatively high, indicating that there is a certain similarity between the items, leading to errors in the empirical data. Therefore, the fit of the model is affected, and the path between the error terms needs to be taken into account. So the correlation between e1, e3, e4, e5; e7, e8, e11, e12; e14, e15, e16; e18, e20, e21, e22; and e25, e26 is established to eliminate its impact on model adaptation. The modified structural equation model fitting diagram is shown in Figure 3, and the fitting results are shown in Table 5.

Table 4: Structural equation model fitting results of the relationship between embeddedness of knowledge network and dynamic capabilities ($N = 260$).

Path	Standardization factor	Nonstandardized coefficient	Critical ratio	p
Opportunity perception ← structure embeddedness	0.383	0.301	3.724	***
Organizational flexibility ← structure embeddedness	0.031	0.054	0.322	0.812
Resource integration ← structure embeddedness	0.234	0.203	2.328	**
Opportunity perception ← relationship embeddedness	0.407	0.395	4.215	***
Organizational flexibility ← relationship embeddedness	0.324	0.403	3.353	***
Resource integration ← relationship embeddedness	0.092	0.136	0.986	0.445
Chi-square degree of freedom ratio (χ^2/df)		3.393		
RMSEA		0.079		
CFI		0.908		
TLI		0.917		
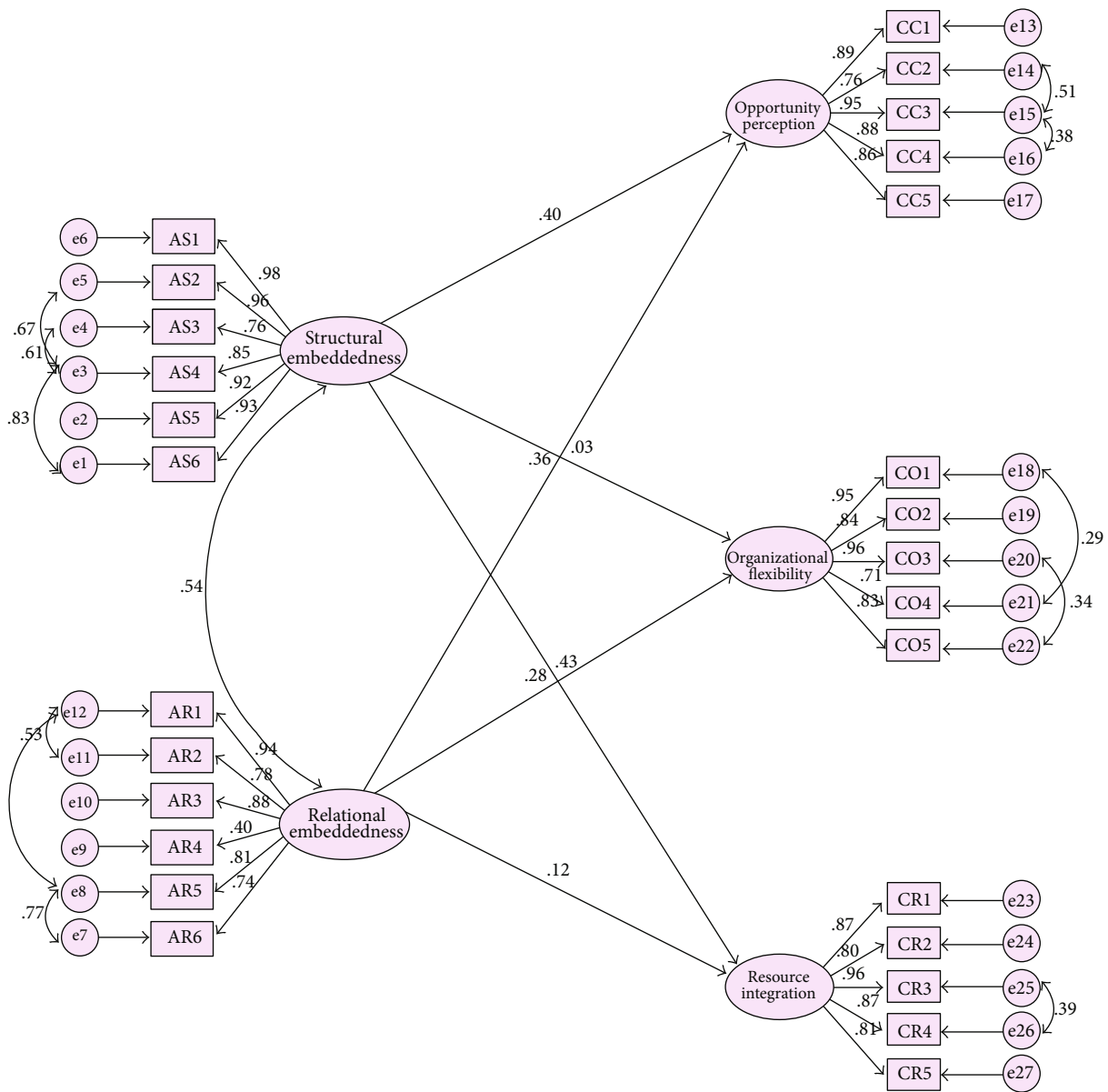
Figure 3: Structural equation model fitting diagram of the relationship between embeddedness of knowledge network and dynamic capabilities (corrected).

TABLE 5: Fitting results of structural equation model of the relationship between network embeddedness and dynamic capabilities (corrected) ($N = 260$).

Path	Standardization factor	Nonstandardized coefficient	Critical ratio (C.R.)	p	Hypothesis
Opportunity perception ← structure embeddedness	0.403	0.482	4.029	***	H1-1 supported
Organizational flexibility ← structure embeddedness	0.029	0.041	0.217	0.792	H1-2 not supported
Resource integration ← structure embeddedness	0.231	0.277	2.408	**	H1-3 supported
Opportunity perception ← relationship embeddedness	0.356	0.364	4.012	***	H1-4 supported
Organizational flexibility ← relationship embeddedness	0.282	0.343	3.813	***	H1-5 supported
Resource integration ← relationship embeddedness	0.117	0.167	0.784	0.416	H1-6 not supported
χ^2/df		2.813			
RMSEA		0.071			
CFI		0.916			
TLI		0.922			

Note: *** indicates significance $p < 0.001$; ** indicates significance $p < 0.01$; * indicates significance $p < 0.05$.

TABLE 6: Hierarchical regression analysis results of environmental munificence on the embeddedness and dynamic capabilities of knowledge networks.

		Model one		Model two		
		Coefficient	p value	Coefficient	p value	VIF
Main effect	Knowledge network embeddedness	0.057	0.027*	0.125	0.046*	1.445
	Environmental munificence	0.274	0.004**	0.337	0.001***	1.812
Moderating effect	Knowledge network embeddedness*environmental munificence			0.413	0.001	1.280
R^2		0.471		0.549		DW 2.036
Adjusted R^2		0.449		0.518		

The main effect equation is dynamic capability = $a + b$ knowledge network embeddedness + c environmental tolerance + e; the moderating effect equation is dynamic capability = $a1 + b$ knowledge network embeddedness + $c1$ environmental munificence + c' knowledge network embeddedness * environmental munificence + e.

After revision, the model's fitness indicators basically meet the good standards, and the ratio of chi-square degree of freedom after correction drops to 2.813, indicating that the correction idea is correct, which helps to improve the model's fitness. The revised fitting results show that at the significance level of 0.001, structural embeddedness has a significant positive impact on opportunity perception ability and relationship embeddedness has a significant positive influence on opportunity perception ability and organizational flexibility ability (C.R.>2), assuming that H1-1, H1-4, and H1-5 are verified, respectively. At the significance level of 0.01, structural embeddedness has a significant positive impact on the ability to integrate resources (C.R.>2); hypothesis H1-3 is verified. Structural embeddedness has no significant impact on organizational flexibility ($p = 0.792$, C.R. = 0.217 < 2); H1-2 is not supported. Relationship embeddedness has no significant effect on resource integration ability ($p = 0.416$, C.R. = 0.784 < 2); H1-6 is not supported.

5.2. Regulation Effect Test. This article uses hierarchical regression analysis to test the moderating effect of variables. Hierarchical regression analysis is a step-by-step test by add-ing the interaction term formed by the independent variable and the moderating variable to the regression equation and then obtaining the degree of influence and significance of the moderating variable on the relationship of the variables.

It can be seen from Table 6 that in the hierarchical regression of the moderating effect of environmental munificence on network embeddedness and dynamic capabilities, the overall R^2 value is greater than 0.5, indicating that the regression model has a certain degree of interpretation. In the collinearity test, the embeddedness of the knowledge network, the inclusiveness of the environment, and the variance inflation factor (VIF) of the two interaction terms are all between 1 and 2, which meets the critical standard of less than 10. It shows that the regression equation does not have the problem of multicollinearity; in the autocorrelation test, the DW value is close to 2, indicating that the equation does not have the autocorrelation problem, and the above indicators are within a reasonable range, indicating that the regression equation model is effective.

In the interaction term model composed of independent variables and moderating variables, the significance of moderating effect coefficient $p = 0.001$ is less than 0.05, indicating that environmental tolerance has moderating effects on

network embeddedness and dynamic capabilities. And the lower slope coefficient $(b + c' * \text{environmental tolerance})$ of the adjustment effect is greater than the lower slope coefficient b of the main effect, so it is a positive adjustment effect. Hypothesis 2 is verified.

6. Research Conclusions and Management Inspiration

After theoretical analysis and empirical research, based on the current situation of my country's small and micro enterprises, this paper discusses the logical relationship between the embeddedness, dynamic capabilities, and environmental tolerance of the knowledge network of small and micro enterprises. Explore the driving effect of the embeddedness of knowledge network on the production of dynamic capabilities of small and micro enterprises, and construct a corresponding theoretical model. In the context of the era of knowledge economy, the acquisition of resources through the knowledge network of small and micro enterprises is a necessary condition for creating a "small and sophisticated, small and beautiful" business model and achieving sustainable development of small and micro enterprises.

6.1. Research Conclusion. (1) The embeddedness of the knowledge network has a significant positive impact on the dynamic capabilities of small and micro enterprises. The embeddedness of the relationship has a significant impact on the company's opportunity perception and organizational flexibility, while the structural embeddedness has a significant impact on the opportunity perception and resource integration capabilities. Knowledge network embedding has become an important source for small and micro enterprises to obtain information and knowledge at low cost and improve their ability to adapt to the environment. At the same time, it shows that small and micro enterprises build a good relationship of trust with partner companies and complete work tasks together. It is conducive to obtain more direct information and tacit knowledge, so as to maintain the sensitivity to the market and the ability to respond to the market in a timely manner. Occupying the central position of the network is also conducive to improving small and micro enterprises to maintain relatively smooth information channels, obtain market and technical information in a timely manner, and eliminate the drawbacks caused by information asymmetry. At the same time, it is helpful for them to take advantage of existing resources and effectively realize resource allocation and resource sharing. But in fact, it is difficult for small and micro enterprises to be at the center of the knowledge network, so they pay more attention to the strength of the relationship with the cooperative enterprise, by increasing the number of partners, maintaining the density and depth of cooperation between the two parties, building trust, and making up for the lack of position in the network structure

Zahra et al. believe that the process of resource integration is very complex, including the activities of allocating, selecting, and reorganizing resources [55]. Trust relationship, information sharing, and joint problem solving cannot

directly promote the complex resource integration ability of the SME. At the same time, small and micro enterprises have a weak ability to occupy structural holes, so they do not have the ability to control and coordinate the flow of new knowledge generated within the network, so there is no significant positive correlation between the two.

(2) Environmental munificence has a positive moderating effect on the relationship between knowledge network embeddedness and dynamic capabilities of small and micro enterprises. The stronger the environmental munificence, the more obvious the effect of knowledge network embeddedness on dynamic capabilities. The existing literature's measurement of environmental tolerance includes factors such as government development plans, financial policies, industry development space, and resource support from the market. These factors are inexorably related to local economic development and regional culture. In areas with a more developed economy and a higher degree of openness, the business culture is often mature, the local government has a strong sense of service for small and micro enterprises, and the environment is more tolerant. The crisis awareness, competition awareness, and growth awareness of local small and micro enterprises are stronger than similar enterprises in other regions, and they pay more attention to being embedded in the knowledge network and acquire knowledge and skills from network members to strengthen their resilience and competitiveness. Therefore, as the degree of environmental munificence increases, the role of knowledge network embedding in the dynamic capabilities of small and micro enterprises has been further strengthened, which is also consistent with the conclusions of the previous interviews in this study

6.2. Management Enlightenment and Suggestion. Faced with the external environment and the internal dilemma of lack of resources, small and micro enterprises have become a life-and-death issue for small and micro enterprises to build their own dynamic capabilities. The empirical conclusions of this article provide certain practical suggestions for managers of small and micro enterprises.

(1) Small and micro enterprises should actively embed knowledge networks and pay attention to the construction of network relationships. The current competition is no longer a competition between individual enterprises, especially small and micro enterprises, especially when facing the impact of external crises. Research shows that striving for a favorable network location and maintaining good network relationships have a positive effect on small and micro enterprises' ability to maintain opportunity perception, organizational flexibility, and resource integration. Although it is difficult for small and micro enterprises to occupy the central position of the network, they should actively connect with the focal enterprises in the process of embedding and building social networks and try to be as close to the central position as possible. In addition, it is recommended that small and micro enterprises conduct stakeholder management. Under the condition of certain network maintenance costs, they should classify stakeholders according to their interest relationships, sort them according to their importance, and

adopt different methods to maintain relationships, by actively participating in the project, increasing the common language, promoting a common problem-solving framework, enhancing trust, and acquiring more valuable knowledge and skills in communication

(2) The government needs to adopt a combination of support and incentives to improve the environment for small and micro enterprises. Our country has a vast territory, and the level of economic development varies significantly between regions. Local governments have formulated many policies related to small and micro enterprises in accordance with local conditions to regulate and support the development of local small and micro enterprises. Therefore, this research found in the interview stage at the initial stage of the research that, for small and micro enterprises, there must be supportive policies to protect the living space of local small and micro enterprises, but they cannot be simply supported. The later empirical results also support this view. Environmental munificence has a positive regulatory effect on the relationship of "knowledge network embeddedness-dynamic capabilities." First of all, higher environmental munificence objectively provides better operating conditions for small and micro enterprises. For small and micro enterprises with scarce resources, the compensation effect brought by external knowledge and resources is more obvious. The dependence of small and micro enterprises on external resources has been further strengthened. Second, from the perspective of the formation of environmental tolerance and enterprise initiative, factors such as the degree of regional economic development, government guidance, and regional culture all have an inherent and lasting relationship with it. In general economically developed areas, the government has a strong sense of service to enterprises, many encouraging policies, and a high degree of environmental tolerance. At the same time, the degree of marketization in this area is also higher, and the competitiveness of enterprises is also stronger. Companies that grow up in this business environment are also paying more and more attention to acquiring knowledge and skills through network embedding to improve their competitiveness. Therefore, environmental munificence strengthens the relationship between the embeddedness of knowledge networks and dynamic capabilities. Based on the above analysis, on the one hand, the government supports small and micro enterprises by implementing supportive policies in finance, taxation, information, technology, and other aspects, integrating regional resources and alleviating resource bottlenecks and external crisis impacts. On the other hand, it is more important to improve the business conditions, strengthen the construction of business culture, and form a good business environment in the region. Third, increase economic interaction with surrounding areas, cultivate the strategic pattern and competitive awareness of entrepreneurs of small and micro enterprises, and avoid the breeding of innovation inertia. Fourth, it is recommended that the government provide incentive support to companies that have outstanding capabilities in technological innovation, energy conservation, emission reduction, and employment absorption, especially those that have substantively explored the transformation from factor-driven to innovation-driven.

Finally, small and micro enterprises should be supported in terms of talent policies. After all, the staff is the carrier of knowledge. Only by solving the problem of talent can enterprises cultivate their sustainable learning ability and the sustainable competitiveness

6.3. Limitations and Prospects. Although this article follows the logic of scientific research, it still has certain shortcomings. First, there is still room for improvement in the measurement and scoring process of the scale. Although the measurements of all variables are formed on the basis of literature collation and interviews with enterprises, they have passed reliability and validity tests. However, due to the limited research results on the dynamic capabilities of small and micro enterprises, it is inevitable that the scale reference in the article is not sufficiently targeted. Second, it did not conduct further subdivision research based on industry characteristics and regional differences. In the survey of this research, small and micro enterprises are the research objects, and the industries involved include mechanical and electrical, chemical, materials, textile, construction, trade, finance, software, catering, and other industries. The surveyed companies come from several provinces and municipalities across the country. In fact, different industries in different regions are in different life cycle stages, and their competition in the industry and the driving force for industry development are different. These factors all cause different sources of enterprise dynamic capabilities, and the mechanism of knowledge network embedding for the construction of dynamic capabilities of enterprises is also different. The above two deficiencies can also be referred to as the future direction of further research on small and micro enterprises.

Data Availability

The data used to support the finding are available upon the author's reasonable request.

Conflicts of Interest

The author declared no potential conflicts of interest with respect to the research, authorship, and/or publication of this article.

Acknowledgments

References

[1] R. Pearson, "E. F. Schumacher, Small is Beautiful: a study of economics as if people mattered," *Institute of Development Studies Bulletin*, vol. 7, no. 1, pp. 34-35, 1975.

[2] M. ZHANG, "Relying on the relationship between government and business or embedded in the innovation network? Research on the dynamic mechanism of innovation and

transformation of small and micro enterprises," *Chinese Administration*, vol. 35, no. 3, pp. 140–147, 2019.

[3] C. SWARNALATHA, "Micro small and medium enterprise sector in Indian context," *Innovative Construction Techniques and Ecological Development*, vol. 12, no. 1, pp. 377–386, 2016.

[4] S. S. BHATTACHARYYA and S. JHA, "Mapping micro small and medium enterprises from the resource-based view and dynamic capability theory perspectives and innovation classification," *International Journal of Entrepreneurship & Small Business*, vol. 25, no. 3, 2015.

[5] Y. T. Mu, "Analysis of market rational choice in small and micro enterprise financing," *Economic Research Guide*, vol. 11, pp. 17–20, 2018.

[6] D. Z. Sun, J. Z. Xu, and L. L. Jing, "The cultivation model of enterprise core competitiveness based on the 'centaur' configuration of speed economy," *Science and Technology Progress and Policy*, vol. 26, no. 3, pp. 49–51, 2009.

[7] Y. J. Jiang, "How to build dynamic capabilities for Chinese private manufacturing companies: a case study based on Geely automobile," *Foreign Economics and Management*, vol. 41, no. 6, 2019.

[8] X. J. Wu, Y. L. Shen, and X. Q. Wang, "A review of domestic dynamic capability research based on Abc integration framework," *Journal of Management*, vol. 13, no. 6, pp. 938–946, 2016.

[9] B. NIELSEN, "Synergies in strategic alliances: motivation and outcomes of complementary synergistic knowledge networks," *Journal of Knowledge Management Practice*, vol. 2, no. 2, pp. 1–15, 2002.

[10] M. STERBERG and J. FRISHAMMAR, "Inbound open innovation activities in high-tech SMEs: the impact on innovation performance," *Journal of Small Business Management*, vol. 50, no. 2, pp. 283–309, 2012.

[11] X. M. Tian, Q. F. Jiang, and C. M. Wang, "An empirical study on the relationship between dynamic capability and entrepreneurial performance of enterprises-a case study of 270 incubators," *Scientific Research*, vol. 4, pp. 812–819, 2008.

[12] M. NAJIB, F. R. DEWI, and H. Widyastuti, "Collaborative networks as a source of innovation and sustainable competitiveness for small and medium food processing enterprises in Indonesia," *International Journal of Business & Management*, vol. 9, no. 9, pp. 147–160, 2014.

[13] M. Chen, Z. Yang, W. Dou, and F. Wang, "Flying or dying? Organizational change, customer participation, and innovation ambidexterity in emerging economies," *Asia Pacific Journal of Management*, vol. 35, no. 1, pp. 97–119, 2018.

[14] NGUYEN THI NHU NGUYET, *Social Network, Dynamic Ability and Growth of Smes*, University, East China Normal, 2019.

[15] C. PRAHALAD and G. HAMEL, "The core competence of the corporation," *Harvard Business Review*, vol. 68, no. 3, pp. 275–292, 1990.

[16] D. J. Teece, "Dynamic capabilities: routines versus entrepreneurial action," *Journal of Management Studies*, vol. 49, no. 8, pp. 1395–1401, 2012.

[17] D. H. Yan, "Are the concepts and theories of dynamic capabilities valuable?," *Journal of Scientific Research*, vol. 25, no. 3, pp. 478–481, 2007.

[18] J. Z. Feng and J. Wei, "Review and prospect of foreign dynamic capability dimension division and measurement," *Research Foreign Economics and Management*, vol. 7, pp. 26–33, 2011.

[19] D. J. Teece, "Explicating dynamic capabilities: the nature and microfoundations of (sustainable) enterprise performance," *Strategic Management Journal*, vol. 28, no. 13, pp. 1319–1350, 2007.

[20] K. M. Eisenhardt, J. A. Martin, and J. A. MARTIN, "Dynamic capabilities: what are they?," *Tuck Conference on the Evolution of Firm Capabilities*, pp. 1105–1121, 2000.

[21] M. ZOLLO and S. G. WINTER, "Deliberate learning and the evolution of dynamic capabilities," *Organization Science*, vol. 13, no. 3, pp. 339–351, 2002.

[22] H. Jiao, "The construction path of the competitive advantage of bipartite organizations: an empirical study based on the dynamic capability theory," *Management World*, vol. 11, 2011.

[23] R. J. Arend, "Social and environmental performance at SMEs: considering motivations, capabilities, and instrumentalism," *Journal of Business Ethics*, vol. 125, no. 4, pp. 541–561, 2014.

[24] K. KOBAYASHI, *Knowledge Network and Market Structure: An Analytical Perspective*, Springer, Berlin Heidelberg, 1995.

[25] M. Granovetter, "The strength of weak ties: a network theory revisited," *Sociological Theory*, vol. 1, no. 6, pp. 201–233, 1983.

[26] W. Tasi, "Knowledge transfer in intraorganizational networks: effects of network postion and absoptive capaciy on business unit innovation and performance," *Academy of Management Journal*, vol. 44, no. 5, pp. 996–1004, 2001.

[27] L. Li, X. H. Dang, and W. F. Jia, "The influence of network embeddedness on the effective acquisition of knowledge," *Science of Science and Management of S.& T*, vol. 29, no. 12, pp. 97–100, 2008.

[28] G. J. Castrogiovanni, "Environmental munificence: a theoretical assessment," *Academy of Management Review*, vol. 16, no. 3, pp. 542–565, 1991.

[29] H. YANG, Z. J. LIN, and Y. L. LIN, "A multilevel framework of firm boundaries: firm characteristics, dyadic differences, and network attributes," *Strategic Management Journal*, vol. 31, no. 3, pp. 237–261, 2010.

[30] C. Y. Tang and D. L. HUANG, "In Chinese research review of knowledge network and creativity at home and abroad," *Science of science and management of science and technology*, vol. 37, no. 3, pp. 43–49, 2016.

[31] A. SEUFERT, G. VON KROGH, and A. BACH, "Towards knowledge networking," *Journal of Knowledge Management*, vol. 3, no. 3, pp. 180–190, 1999.

[32] L. N. Xiao and Y. F. Wang, "Study on countermeasures of internationalization of Chinese enterprises from the perspective of knowledge network," *International Trade*, vol. 4, pp. 26–29, 2012.

[33] O. N. Rank, "The effect of structural embeddedness on start-up survival: a case study in the German biotech industry," *Journal of Small Business & Entrepreneurship*, vol. 27, no. 3, pp. 275–299, 2014.

[34] S. G. Winter, "Understanding dynamic capabilities," *Strategic Management Journal*, vol. 24, no. 10, pp. 991–995, 2003.

[35] C. L. Wang and P. K. Ahmed, "Dynamic capabilities: a review and research agenda," *International Journal of Management Reviews*, vol. 9, no. 1, pp. 31–51, 2007.

[36] J. Xue, "Organizational learning research of small and micro science and technology enterprises – the antecedent role of system composition and strategic orientation," *Scientific Research Management*, vol. 40, no. 5, pp. 222–232, 2019.

[37] C. Y. Zhang, T. GUO, and H. D. Liu, "Influence of network embedding on business model innovation of technology

start-ups," *Research in Science of Science*, vol. 36, no. 1, pp. 167–175, 2008.

[38] L. ALINAGHIAN and K. RAZMDOOST, "How do network resources affect firms' network-oriented dynamic capabilities?," *Industrial Marketing Management*, vol. 71, pp. 79–94, 2017.

[39] Z. G. Fan, Y. Liu, and X. B. Wu, "Research on the influence of network embedding and organizational learning collaboration on strategic flexibility," *Scientific Research Management*, vol. 12, pp. 112–119, 2014.

[40] K. Muhammad, S. Khan, M. Elhoseny, S. H. Ahmed, and S. W. Baik, "Efficient fire detection for uncertain surveillance environment," *IEEE Transactions on Industrial Informatics*, vol. 15, no. 5, pp. 3113–3122, 2019.

[41] B. Uzzi, "Social structure and competition in interim networks," *Administrative ence Quarterly*, vol. 42, no. 1, pp. 37–69, 1997.

[42] J. GALLEGO, L. RUBALCABA, and C. Suarez, "Knowledge for innovation in Europe: the role of external knowledge on firms' cooperation strategies," *Journal of Business Research*, vol. 66, no. 10, pp. 2034–2041, 2013.

[43] D. L. Du, T. C. Jiang, and X. H. Zeng, "Research on the influence of corporate social capital on the growth of small and micro science and technology enterprises – taking dynamic capability as intermediary variable," *East China Economic Management*, vol. 2015, no. 6, pp. 148–156, 2015.

[44] S.-B. Tsai, Y.-Z. Xue, P.-Y. Huang et al., "Establishing a criteria system for green production," *Proceedings of the Institution of Mechanical Engineers, Part B: Journal of Engineering Manufacture*, vol. 229, no. 8, pp. 1395–1406, 2014.

[45] W. Wei, P. Peng, and J. K. Li, "Network embeddedness, external learning and enterprise performance of small and micro enterprises," *Scientific Decision-making*, vol. 3, pp. 38–55, 2016.

[46] X. Wang, *Case Study on the Relationship between AB Group's Policy Dependence and Enterprise Growth*, Jilin University of Finance and Economics, 2019.

[47] W. Wu, S. An, C. H. Wu, S. B. Tsai, and K. Yang, "An empirical study on green environmental system certification affects financing cost of high energy consumption enterprises-taking metallurgical enterprises as an example," *Journal of Cleaner Production*, vol. 244, p. 118848, 2020.

[48] D. ACEMOGLU, S. JOHNSON, and J. A. Robinson, "Institutions as the fundamental cause of long-run growth," *Nanjing Business Review*, vol. 1, no. 5, pp. 385–472, 2006.

[49] P.-A. Balland, J. A. Belso-Martínez, and A. Morrison, "The dynamics of technical and business knowledge networks in industrial clusters: embeddedness, status, or proximity?," *Economic Geography*, vol. 92, no. 1, pp. 35–60, 2016.

[50] X. S. Chen and Z. W. Wang, "Embedded enterprise external knowledge network, design learning and meaningful innovation ability," *Science and technology progress and countermeasures*, vol. 33, no. 20, pp. 140–146, 2016.

[51] P. A. Pavlou and O. A. El Sawy, "Understanding the elusive black box of dynamic capabilities," *Decision ences*, vol. 42, no. 1, pp. 239–273, 2011.

[52] Z. Zhao, R. Li, and B. Zhu, "A research on the influence of organizational flexibility on the growth of high-tech SMEs," *Science Research Management*, vol. 40, no. 7, pp. 247–256, 2019.

[53] H. Guo and R. Shen, "How to transform entrepreneurial opportunities into enterprise performance-the mediating role of business model innovation and the regulating role of market environment," *Economic Theory and Economic Management*, vol. 2014, no. 3, pp. 70–83, 2014.

[54] W. Wu, Y. Liu, C. H. Wu, and S. B. Tsai, "An empirical study on government direct environmental regulation and heterogeneous innovation investment," *Journal of Cleaner Production*, vol. 254, p. 120079, 2020.

[55] S. A. Zahra, H. J. Sapienza, and P. Davidsson, "Entrepreneurship and dynamic capabilities: a review, model and research agenda," *Journal of Management Studies*, vol. 43, no. 4, pp. 917–955, 2006.

WILEY | Hindawi

Research Article

Statistical Tracking Behavior Analysis for the Affine Projection Algorithm Based on Direction Error

Yongfeng Zhi [ID] **and Wenyan Guo** [ID]

Research & Development Institute in Shenzhen, Northwestern Polytechnical University, Shenzen 518057, Guangdong, China

Correspondence should be addressed to Yongfeng Zhi; yongfeng@nwpu.edu.cn

Under the condition that the step size is less than one, a statistical tracking behavior analysis for the affine projection algorithm based on direction error is discussed. When the unknown true weight vector is modeled by the stochastic walk model, the mean weight error is derived under the four assumptions based on the deterministic recursive equation. Furthermore, the statistical tracking behavior of the steady state is analyzed for the affine projection algorithm based on direction error. Simulation analysis is shown to suppniort the mathematical results.

1. Introduction

Since the normalized least mean square Wen algorithm is computational simplicity, this algorithm is widely put into use by the adaptation algorithm. And the normalized least mean square algorithm is also robust to the length of the finite word effects and ease of implementation in the signal processing. However, the highly colored input signals will cause the normalized least mean square algorithm converge slowly [1]. Compared to the normalized least mean square algorithm, the affine projection (AP) algorithm is a better alternative. The AP algorithm was firstly given by Ozeki and Umeda, and it improves the convergence speed by reusing the input signal [2]. Based on the idea that the successive vectors of the input signal are orthogonal with each other, the best improvement convergence will be obtained; the normalized least mean square based on orthogonal correction factors (NLMS-OCF) was shown in [3]. When we set the step size to be equal one, according to the input direction vectors of the input signal, a novel definition was given for the affine projection algorithm [4]. A pseudo-AP (PAP) algorithm is a simplified definition form to the affine projection algorithm, and this algorithm is ease of implementation [5]. Since the weights update direction and the direction that is caused by the adap-

tive error are not the same for the PAP algorithm, an AP algorithm based on direction error (AP-DE) was given to resolve the nonconformity problem [6]. Fast AP algorithms have been given as well [7]. These algorithms, including the AP, PAP, and NLMS-OCF, can be considered a class of the AP algorithms, which updates the adaptive weights according to the multiple vectors of the input signal. Some recent studies are as follows. A new class of AP algorithm is proposed based on the high-order error power criterion [8] and can achieve reliable performance under Gaussian interference. The effect of the noise vector on the weight-error vector is considered. The edified filtered-x affine projection algorithm is effective for active noise control owing to its good convergence behavior and medium computational burden [9]. The proposed method of sparsity aware affine-projection-like robust set membership M-estimate (SAPL-RSM) filtering has been utilized for alleviating the impact of impulsive noise on the adaptation of feedback canceler's weights [10]. A time-varying parameter PAPLM (TV-PAPLM) algorithm is proposed, which uses a modified exponential function to adjust the time-varying parameter according to the ratio of the mean square score function to the system noise variance [11].

There are lots of work that has been done to analyze the statistical convergence and tracking behavior of the AP and

NLMS-OCF algorithms. Based on the assumption that the input signal is the identically and independent distributed form, the statistical analysis of the class of the AP algorithms was shown, in which the mean weight error (MWE) and the mean-square error (MSE) were shown to study the convergence behavior for the NLMS-OCF algorithm [12, 13]. When we set the step size to be one, the closed-form expression is given for the convergence behavior of the MWE and MSE, appropriate for autoregressive-moving average (ARMA) input signal models of the AP algorithm, as in [14]. In the adaptive direction of the weight update, when we set each weight error to be zero, the optimal step size for the PAP algorithm was given; then using this model, the MWE and MSE were derived based on the deterministic recursive equations [15]. The statistical analysis of convergence model for the AP algorithm has been shown by using the (AR) input model [16–18]. Under the assumption given by [12, 13], the convergence model was shown for the kind of AP-DE algorithm in [19]. When the step size was equal to one, the statistical tracking behavior was given for the AP-DE algorithm [20], in which the MWE and MSE behaviors are analyzed.

In this paper, four assumptions are made for the input vectors and the direction vectors. When the unknown true weight vector is modeled by the stochastic walk model, the tracking MWE and MSE are obtained for the AP-DE algorithm. At last, the simulation analysis is given to show the proposed statistical tracking behavior.

2. AP-DE Algorithm

An affine projection algorithm with direction error (AP-DE) is presented to solve the nonconformity between the iterated direction of the adaptive filter and the direction caused by the iteration error. In the adaptive filtering system identification model, the colored input signal is transformed into the successive input vector $\mathbf{x}_n$, and then, we have obtained

$$\mathbf{x}_n = [x_n \, x_{n-1} \, \cdots \, x_{n-N+1}]^T. \tag{1}$$

According to the most recent successive m input vectors for the input signal, we can obtain the input matrix $\mathbf{X}_{n-1,m}$ as

$$\mathbf{X}_{n-1,m} = [\mathbf{x}_{n-1} \quad \mathbf{x}_{n-2} \quad \cdots \quad \mathbf{x}_{n-m}]. \tag{2}$$

The AP-DE algorithm updates of the weight vector are implemented by the adaptive filter [6], as follows:

$$e_n = d_n - \sum_{k=1}^{m} \hat{a}_{n,k} d_{n-k} - \mathbf{w}_n^H \boldsymbol{\varphi}_n, \tag{3a}$$

$$\mathbf{w}_{n+1} = \mathbf{w}_n + \mu \frac{e_n^*}{\boldsymbol{\varphi}_n^H \boldsymbol{\varphi}_n} \boldsymbol{\varphi}_n, \tag{3b}$$

where H denotes a transposed matrix or vector and the direction vector $\boldsymbol{\varphi}_n$ of the input signal is estimated based on

$$\boldsymbol{\varphi}_n = \mathbf{x}_n - \mathbf{X}_{n-1,m} \hat{\boldsymbol{\alpha}}_n. \tag{3c}$$

And from the least-squares formulation, the vector $\hat{\boldsymbol{\alpha}}_n = \begin{bmatrix} a\wedge_{n,1} & a\wedge_{n,2} & \cdots & a\wedge_{n,m} \end{bmatrix}^T$ is found as

$$\hat{\boldsymbol{\alpha}}_n = \left(\mathbf{X}_{n-1,m}^H \mathbf{X}_{n-1,m}\right)^{-1} \mathbf{X}_{n-1,m}^H \mathbf{x}_n. \tag{3d}$$

The iterated direction of AP is the input vector $\mathbf{x}_n$, which causes the iteration error. Compared with AP algorithms, if the measurement noise is absent, the iteration error of the AP-DE algorithm is caused only by the direction vector $\boldsymbol{\varphi}_n$, which is also the iterated direction of the adaptive filter. Thus, the AP-DE algorithm improves the convergence rate compared with the PAP and AP algorithms.

3. Statistical Properties of the Direction and Input Vectors

In order to study the tracking performance of the AP-DE algorithm, the four assumptions are as follows:

(A1) The successive input vector $\mathbf{x}_n$ is zero mean, identically and independent distributed, and then the covariance matrix can be obtained as [12, 13]

$$\mathbf{R} = E\left[\mathbf{x}_n \mathbf{x}_n^H\right] = \mathbf{V}\boldsymbol{\Lambda}\mathbf{V}^H, \tag{4}$$

where $\boldsymbol{\Lambda} = \text{diag} \begin{bmatrix} \lambda_1 & \lambda_2 & \cdots & \lambda_N \end{bmatrix}$ are the eigenvalues of $\mathbf{R}$ and the corresponding eigenvectors $\mathbf{V} = \begin{bmatrix} \boldsymbol{v}_1 & \boldsymbol{v}_2 & \cdots & \boldsymbol{v}_N \end{bmatrix}$ are orthonormal to each other, i.e., $\mathbf{V}^H \mathbf{V} = \mathbf{I}$

(A2) Using assumption A1 and assuming three different independent stochastic variables constitute the direction vector $\mathbf{x}_n$. That is,

$$\mathbf{x}_n = s_n r_n \mathbf{v}_n, \tag{5}$$

$$\begin{cases} P(s_n = \pm 1) = \dfrac{1}{2}, \\ r_n \sim \|\mathbf{x}_n\| \\ P(\mathbf{v}_n = \boldsymbol{v}_i) = \dfrac{\lambda_i}{\mathbf{tr}(\mathbf{R})}, \quad 1 \le i \le N, \end{cases} \tag{6}$$

where the matrix trace is denoted by the expression $\mathbf{tr}(\bullet)$, $r_n \sim \|\mathbf{x}_n\|$ means that the stochastic variable r_n, and the input vectors have the same distribution. Similar assumption has also been given in [12, 13]

(A3) Based on assumption A2, make the following assumption. The direction vectors $\boldsymbol{\varphi}_n$ of the successive input signal are independent on the weight vector $\mathbf{w}_n$, and they are the Gaussian stochastic vectors with variance $\sigma_{\boldsymbol{\varphi}}^2$ and zero mean. Therefore, the direction vectors are also three independent stochastic variables [20], i.e.,

$$\boldsymbol{\varphi}_n = \hat{s}_n \hat{r}_n \hat{\mathbf{v}}_n, \tag{7}$$

$$\begin{cases} P(\hat{s}_n = \pm 1) = \dfrac{1}{2}, \\ \hat{r}_n \sim \|\boldsymbol{\varphi}_n\| \\ P(\hat{\mathbf{v}}_n = \mathbf{v}_i) = \dfrac{1}{N}, \quad 1 \le i \le N, \end{cases} \tag{8}$$

where the stochastic variable $\hat{r}_n \sim \|\boldsymbol{\varphi}_n\|$ means that $\hat{r}_n$ has the same distribution as the direction vectors of the input signal, and then, the square of the stochastic variable is denoted by $r\wedge^2 = N\sigma_\varphi^2$

(A4) Based on assumption A3, make assumption about the vector $\boldsymbol{\omega}_n$. The desire output signal d_n is given by the mathematical model as follows:

$$d_n = \mathbf{w}_n^{oH} \mathbf{x}_n + \varepsilon_n, \tag{9}$$

where the measurement noise ε_n is identically distributed, independent, and stationary with variance σ_ε^2 and zero mean and the time-variant vectors $\mathbf{w}_n^o$ are the system model parameters. The unknown weight vector $\mathbf{w}_n^o$ is modeled by the stochastic walk model given,

$$\mathbf{w}_n^o = \mathbf{w}_{n-1}^o + \boldsymbol{\omega}_{n-1}, \tag{10}$$

where the vector $\boldsymbol{\omega}_{n-1}$ is an independent, stationary zero mean vector process with the variance σ_ω^2 and it is also the three independent stochastic variables that are identically and independent distributed. That is,

$$\boldsymbol{\omega}_n = \tilde{s}_n \tilde{r}_n \tilde{\mathbf{v}}_n, \tag{11}$$

$$\begin{cases} P(\tilde{s}_n = \pm 1) = \dfrac{1}{2}, \\ \tilde{r}_n \sim \|\boldsymbol{\omega}_n\|, \\ P(\tilde{\mathbf{v}}_n = \mathbf{v}_i) = \dfrac{1}{N}, \quad 1 \le i \le N, \end{cases} \tag{12}$$

where the independent stochastic variable $\tilde{r}_n \sim \|\boldsymbol{\omega}_n\|$ means that it has the same distribution as the vector $\boldsymbol{\omega}_n$ and the square of the independent stochastic variable is denoted by $\tilde{r}^2 = N\sigma_\omega^2$

Therefore, based on (3a) and (9), the iteration error e_n of the adaptive filtering can be obtained as

$$e_n = \mathbf{w}_n^{oH} \mathbf{x}_n - \sum_{k=1}^{m} \hat{a}_{n,k} \mathbf{w}_{n-k}^{oH} \mathbf{x}_{n-k} - \mathbf{w}_n^H \boldsymbol{\varphi}_n + \varepsilon_n - \sum_{k=1}^{m} \hat{a}_{n,k} \varepsilon_{n-k}. \tag{13}$$

From (10) and (13), we have

$$e_n = \mathbf{w}_n^{oH} \mathbf{x}_n - \sum_{k=1}^{m} \hat{a}_{n,k} \mathbf{w}_n^{oH} \mathbf{x}_{n-k} + \sum_{k=1}^{m} \hat{a}_{n,k} \left(\sum_{j=1}^{k} \boldsymbol{\omega}_{n-j}^H \right) \mathbf{x}_{n-k}$$
$$- \mathbf{w}_n^H \boldsymbol{\varphi}_n + \varepsilon_n - \sum_{k=1}^{m} \hat{a}_{n,k} \varepsilon_{n-k}. \tag{14}$$

From (3c) and (14), it yields

$$e_n = \tilde{\mathbf{w}}_n^H \boldsymbol{\varphi}_n + \sum_{k=1}^{m} \hat{a}_{n,k} \left(\sum_{j=1}^{k} \boldsymbol{\omega}_{n-j}^H \right) \mathbf{x}_{n-k} + \varepsilon_n - \sum_{k=1}^{m} \hat{a}_{n,k} \varepsilon_{n-k}, \tag{15}$$

where

$$\tilde{\mathbf{w}}_n = \mathbf{w}_n^o - \mathbf{w}_n. \tag{16}$$

4. Behavior of Mean Weight Error

In order to study the tracking performance of (3b), according to (15), we have

$$\mathbf{w}_{n+1} = \mathbf{w}_n + \mu \frac{\boldsymbol{\varphi}_n \boldsymbol{\varphi}_n^H}{\boldsymbol{\varphi}_n^H \boldsymbol{\varphi}_n} \tilde{\mathbf{w}}_n + \mu \frac{\boldsymbol{\varphi}_n}{\boldsymbol{\varphi}_n^H \boldsymbol{\varphi}_n} \sum_{k=1}^{m} \hat{a}_{n,k}^* \mathbf{x}_{n-k}^H \left(\sum_{j=1}^{k} \boldsymbol{\omega}_{n-j} \right)$$
$$+ \mu \frac{\boldsymbol{\varphi}_n}{\boldsymbol{\varphi}_n^H \boldsymbol{\varphi}_n} \left(\varepsilon_n^* - \sum_{k=1}^{m} \hat{a}_{n,k}^* \varepsilon_{n-k}^* \right). \tag{17}$$

Combining (10), (16), and (17), the adaptation equation is shown as

$$\tilde{\mathbf{w}}_{n+1} = \left(\mathbf{I} - \mu \frac{\boldsymbol{\varphi}_n \boldsymbol{\varphi}_n^H}{\boldsymbol{\varphi}_n^H \boldsymbol{\varphi}_n} \right) \tilde{\mathbf{w}}_n - \mu \frac{\boldsymbol{\varphi}_n}{\boldsymbol{\varphi}_n^H \boldsymbol{\varphi}_n} \sum_{k=1}^{m} \hat{a}_{n,k}^* \mathbf{x}_{n-k}^H \left(\sum_{j=1}^{k} \boldsymbol{\omega}_{n-j} \right)$$
$$- \mu \frac{\boldsymbol{\varphi}_n}{\boldsymbol{\varphi}_n^H \boldsymbol{\varphi}_n} \left(\varepsilon_n^* - \sum_{k=1}^{m} \hat{a}_{n,k}^* \varepsilon_{n-k}^* \right) + \boldsymbol{\omega}_n. \tag{18}$$

Since the parameter ε_n and the stochastic vector $\boldsymbol{\omega}_n$ are both white noise with zero mean, we can take expectation on both sides of (18), and the last three terms in (18) becomes zero, so they can be obtained as

$$E[\tilde{\mathbf{w}}_{n+1}] = E\left[\left(\mathbf{I} - \mu \frac{\boldsymbol{\varphi}_n \boldsymbol{\varphi}_n^H}{\boldsymbol{\varphi}_n^H \boldsymbol{\varphi}_n} \right) \tilde{\mathbf{w}}_n \right]. \tag{19}$$

Based on the vectors $\{\mathbf{v}_1, \mathbf{v}_2, \cdots, \mathbf{v}_N\}$ which are orthonormal to each other, the representation of $E[\tilde{\mathbf{w}}_n]$ can be defined as the vector $\boldsymbol{\rho}_n$. That is,

$$\boldsymbol{\rho}_n \equiv \mathbf{V}^H E[\tilde{\mathbf{w}}_n]. \tag{20}$$

Therefore,

$$\rho_{n,i} = \mathbf{v}_i^H E[\tilde{\mathbf{w}}_n] = E[\mathbf{v}_i^H \tilde{\mathbf{w}}_n]. \qquad (21)$$

Using this result, according to (7), premultiplication on both sides of (19) by $\mathbf{v}_i^H$, we have

$$\rho_{n+1,i} = E[\mathbf{v}_i^H (\mathbf{I} - \mu \hat{\mathbf{v}}_n \hat{\mathbf{v}}_n^H) \tilde{\mathbf{w}}_n]. \qquad (22)$$

For the orthonormality of the vector $\mathbf{v}_i$. That is,

$$\mathbf{v}_i^H \mathbf{v}_j \mathbf{v}_j^H = \begin{cases} \mathbf{v}_i^H, & \text{if } i = j, \\ 0, & \text{if } i \neq j. \end{cases} \qquad (23)$$

Based on (23), (22) becomes

$$\rho_{n+1,i} = \left(1 - \frac{\mu}{N}\right)\rho_{n,i}. \qquad (24)$$

5. Statistical MSE Behavior

Under assumption A3 where the direction vectors φ_n of the input signal are independent on the vector $\mathbf{w}_n$, according to (18), the covariance of the weight error is proposed as

$$
\begin{aligned}
\mathrm{cov}\,(\tilde{\mathbf{w}}_{n+1}) = {}& E\left[\left(\mathbf{I} - \mu\frac{\varphi_n\varphi_n^H}{\varphi_n^H\varphi_n}\right)\mathrm{cov}\,(\tilde{\mathbf{w}}_n)\left(\mathbf{I} - \mu\frac{\varphi_n\varphi_n^H}{\varphi_n^H\varphi_n}\right)\right] - \mu E\left[\left(I - \mu\frac{\varphi_n\varphi_n^H}{\varphi_n^H\varphi_n}\right)\tilde{\mathbf{w}}_n\left\{\sum_{k=1}^m \hat{a}_{n,k}\left(\sum_{j=1}^k \omega_{n-j}^H\right)\mathbf{x}_{n-k}\frac{\varphi_n^H}{\varphi_n^H\varphi_n}\right\}\right] \\
& - \mu E\left[\left\{\frac{\varphi_n}{\varphi_n^H\varphi_n}\sum_{k=1}^m \hat{a}_{n,k}^*\mathbf{x}_{n-k}^H\left(\sum_{j=1}^k \omega_{n-j}\right)\right\}\tilde{\mathbf{w}}_n^H\left(I - \mu\frac{\varphi_n\varphi_n^H}{\varphi_n^H\varphi_n}\right)\right] - E\left[\left(I - \mu\frac{\varphi_n\varphi_n^H}{\varphi_n^H\varphi_n}\right)\tilde{\mathbf{w}}_n\left\{\left(\varepsilon_n - \sum_{k=1}^m \hat{a}_{n,k}\varepsilon_{n-k}\right)\mu\frac{\varphi_n^H}{\varphi_n^H\varphi_n} - \omega_n^H\right\}\right] \\
& - E\left[\left\{\left(\varepsilon_n^* - \sum_{k=1}^m \hat{a}_{n,k}^*\varepsilon_{n-k}^*\right)\mu\frac{\varphi_n}{\varphi_n^H\varphi_n} - \omega_n\right\}\tilde{\mathbf{w}}_n^H\left(I - \mu\frac{\varphi_n\varphi_n^H}{\varphi_n^H\varphi_n}\right)\right] + \mu^2 E\left[\left\{\frac{\varphi_n}{\varphi_n^H\varphi_n}\sum_{k=1}^m \hat{a}_{n,k}^*\mathbf{x}_{n-k}^H\left(\sum_{j=1}^k \omega_{n-j}\right)\right\}\left\{\sum_{k=1}^m \hat{a}_{n,k}\left(\sum_{j=1}^k \omega_{n-j}^H\right)\mathbf{x}_{n-k}\frac{\varphi_n^H}{\varphi_n^H\varphi_n}\right\}\right] \\
& + \mu E\left[\left\{\frac{\varphi_n}{\varphi_n^H\varphi_n}\sum_{k=1}^m \hat{a}_{n,k}^*\mathbf{x}_{n-k}^H\left(\sum_{j=1}^k \omega_{n-j}\right)\right\}\left\{\left(\varepsilon_n - \sum_{k=1}^m \hat{a}_{n,k}\varepsilon_{n-k}\right)\mu\frac{\varphi_n^H}{\varphi_n^H\varphi_n} - \omega_n^H\right\}\right] + \mu E\left[\left\{\left(\varepsilon_n^* - \sum_{k=1}^m \hat{a}_{n,k}^*\varepsilon_{n-k}^*\right)\mu\frac{\varphi_n}{\varphi_n^H\varphi_n} - \omega_n\right\}\left\{\sum_{k=1}^m \hat{a}_{n,k}\left(\sum_{j=1}^k \omega_{n-j}^H\right)\mathbf{x}_{n-k}\frac{\varphi_n^H}{\varphi_n^H\varphi_n}\right\}\right] \\
& + E\left[\left\{\left(\varepsilon_n^* - \sum_{k=1}^m \hat{a}_{n,k}^*\varepsilon_{n-k}^*\right)\frac{\mu\varphi_n}{\varphi_n^H\varphi_n} - \omega_n\right\}\left\{\left(\varepsilon_n - \sum_{k=1}^m \hat{a}_{n,k}\varepsilon_{n-k}\right)\mu\frac{\varphi_n^H}{\varphi_n^H\varphi_n} - \omega_n^H\right\}\right].
\end{aligned}
$$

$$(25)$$

Under the assumption that ε_n is white noise with zero mean and the vector ω_n is an independent, stationary, zero mean white noise vector, so the six different polynomials, including the second, third, fourth, fifth, seventh, and eighth items, all turn into zero. Because the direction vector φ_n of the input signal is independent of the vector $\mathbf{w}_n$, so we obtain the following:

$$
\begin{aligned}
\mathrm{cov}\,(\tilde{\mathbf{w}}_{n+1}) = {}& E\left[\left(\mathbf{I} - \mu\frac{\varphi_n\varphi_n^H}{\varphi_n^H\varphi_n}\right)\mathrm{cov}\,(\tilde{\mathbf{w}}_n)\left(\mathbf{I} - \mu\frac{\varphi_n\varphi_n^H}{\varphi_n^H\varphi_n}\right)\right] + \mu^2\mathbf{tr}\left\{\sum_{k=1}^m \left(E\left[\hat{a}_{n,k}\hat{a}_{n,k}^*\right]E\left[\mathbf{x}_{n-k}\mathbf{x}_{n-k}^H\right]E\left[\sum_{j=1}^k \omega_{n-j}\omega_{n-j}^H\right]\right)\right\}E\left[\frac{\varphi_n\varphi_n^H}{(\varphi_n^H\varphi_n)^2}\right] \\
& + \mu^2 E\left[\left(\varepsilon_n - \sum_{k=1}^m a\wedge_{n,k}\varepsilon_{n-k}\right)^*\left(\varepsilon_n - \sum_{k=1}^m \hat{a}_{n,k}\varepsilon_{n-k}\right)\right]E\left[\frac{\varphi_n\varphi_n^H}{(\varphi_n^H\varphi_n)^2}\right] + E\left[\omega_n\omega_n^H\right].
\end{aligned}
$$

$$(26)$$

Since ε_n is identically distributed, independent with variance σ_ε^2 and zero mean, under assumptions A2, A3, and A4, using (5), (7), and (11), (26) becomes as follows:

$$
\begin{aligned}
\text{cov}\,(\tilde{\mathbf{w}}_{n+1}) &= E\left[\left(\mathbf{I} - \mu\hat{\mathbf{v}}_n\hat{\mathbf{v}}_n^H\right)\text{cov}\,(\tilde{\mathbf{w}}_n)\left(\mathbf{I} - \mu\hat{\mathbf{v}}_n\hat{\mathbf{v}}_n^H\right)\right] \\
&\quad + \mu^2\frac{r_n^2\sigma_\omega^2}{\hat{r}_n^2}\sum_{k=1}^m kE\left[\hat{a}_{n,k}\hat{a}_{n,k}^*\right]E\left[\hat{\mathbf{v}}_n\hat{\mathbf{v}}_n^H\right] \\
&\quad + \frac{\mu^2\sigma_\varepsilon^2}{\hat{r}_n^2}\left(1 + \sum_{k=1}^m E\left[\hat{a}_{n,k}\hat{a}_{n,k}^*\right]\right)E\left[\hat{\mathbf{v}}_n\hat{\mathbf{v}}_n^H\right] \\
&\quad + \tilde{r}_n^2 E\left[\tilde{\mathbf{v}}_n\tilde{\mathbf{v}}_n^H\right].
\end{aligned}
\tag{27}
$$

For the covariance matrix, we define the diagonal elements as $\tilde{\lambda}_{n+1,i}$. So we have

$$
\tilde{\lambda}_{n+1,i} \equiv \left[\mathbf{V}^H\,\text{cov}\,(\tilde{\mathbf{w}}_{n+1})\mathbf{V}\right]_{ii} \equiv \mathbf{v}_i^H\,\text{cov}\,(\tilde{\mathbf{w}}_{n+1})\mathbf{v}_i.
\tag{28}
$$

We premultiply and postmultiply on both sides of (27) by $\mathbf{v}_i^H$ and $\mathbf{v}_i$, respectively; under assumption A3, using (29), we can obtain

$$
E\left[\mathbf{v}_i^H\left(\mathbf{I} - \mu\hat{\mathbf{v}}_n\hat{\mathbf{v}}_n^H\right)\mathbf{A}\left(\mathbf{I} - \mu\hat{\mathbf{v}}_n\hat{\mathbf{v}}_n^H\right)\mathbf{v}_i\right] = \left(1 + \frac{\mu^2 - 2\mu}{N}\right)\mathbf{v}_i^H\mathbf{A}\mathbf{v}_i,
\tag{29}
$$

where $\mathbf{A}$ is a $N \times N$ dimension matrix; we can obtain

$$
\begin{aligned}
\tilde{\lambda}_{n+1,i} &= \left(1 + \frac{\mu^2 - 2\mu}{N}\right)\tilde{\lambda}_{n,i} + \mu^2\frac{r_n^2\sigma_\omega^2}{\hat{r}_n^2}\sum_{k=1}^m kE\left[\hat{a}_{n,k}\hat{a}_{n,k}^*\right]E\left[\mathbf{v}_i^H\hat{\mathbf{v}}_n\hat{\mathbf{v}}_n^H\mathbf{v}_i\right] \\
&\quad + \frac{\mu^2\sigma_\varepsilon^2}{\hat{r}_n^2}\left(1 + \sum_{k=1}^m E\left[\hat{a}_{n,k}\hat{a}_{n,k}^*\right]\right)E\left[\mathbf{v}_i^H\hat{\mathbf{v}}_n\hat{\mathbf{v}}_n^H\mathbf{v}_i\right] + \tilde{r}_n^2 E\left[\mathbf{v}_i^H\tilde{\mathbf{v}}_n\tilde{\mathbf{v}}_n^H\mathbf{v}_i\right].
\end{aligned}
\tag{30}
$$

Based on assumptions A3 and A4, we can obtain that the vectors $\hat{\mathbf{v}}_n$ and $\tilde{\mathbf{v}}_n$ both have the probability of $1/N$ to be $\mathbf{v}_i$, respectively. From (30), we can obtain

$$
\begin{aligned}
\tilde{\lambda}_{n+1,i} &= \left(1 + \frac{\mu^2 - 2\mu}{N}\right)\tilde{\lambda}_{n,i} + \mu^2\frac{r_n^2\sigma_\omega^2}{N\hat{r}_n^2}\sum_{k=1}^m kE\left[\hat{a}_{n,k}\hat{a}_{n,k}^*\right] \\
&\quad + \frac{\mu^2\sigma_\varepsilon^2}{N\hat{r}_n^2}\left(1 + \sum_{k=1}^m E\left[\hat{a}_{n,k}\hat{a}_{n,k}^*\right]\right) + \frac{\tilde{r}_n^2}{N}.
\end{aligned}
\tag{31}
$$

According to (15), we have the statistical MSE of tracking performance for the AP-DE algorithm as

$$
\begin{aligned}
E[e_n e_n^*] &= E\left[\tilde{\mathbf{w}}_n^H\boldsymbol{\varphi}_n\boldsymbol{\varphi}_n^H\tilde{\mathbf{w}}_n\right] + E\left[\tilde{\mathbf{w}}_n^H\boldsymbol{\varphi}_n\sum_{k=1}^m \hat{a}_{n,k}^*\mathbf{x}_{n-k}^H\left(\sum_{j=1}^k \boldsymbol{\omega}_{n-j}\right)\right] + E\left[\left\{\sum_{k=1}^m \hat{a}_{n,k}\left(\sum_{j=1}^k \boldsymbol{\omega}_{n-j}^H\right)\mathbf{x}_{n-k}\right\}\boldsymbol{\varphi}_n^H\tilde{\mathbf{w}}_n\right] \\
&\quad + E\left[\tilde{\mathbf{w}}_n^H\boldsymbol{\varphi}_n\left(\varepsilon_n^* - \sum_{k=1}^m \hat{a}_{n,k}^*\varepsilon_{n-k}^*\right)\right] + E\left[\left(\varepsilon_n - \sum_{k=1}^m \hat{a}_{n,k}\varepsilon_{n-k}\right)\boldsymbol{\varphi}_n^H\tilde{\mathbf{w}}_n\right] + E\left[\left\{\sum_{k=1}^m \hat{a}_{n,k}\left(\sum_{j=1}^k \boldsymbol{\omega}_{n-j}^H\right)\mathbf{x}_{n-k}\right\}\left\{\sum_{k=1}^m \hat{a}_{n,k}^*\mathbf{x}_{n-k}^H\left(\sum_{j=1}^k \boldsymbol{\omega}_{n-j}\right)\right\}\right] \\
&\quad + E\left[\left\{\sum_{k=1}^m \hat{a}_{n,k}\left(\sum_{j=1}^k \boldsymbol{\omega}_{n-j}^H\right)\mathbf{x}_{n-k}\right\}\left(\varepsilon_n^* - \sum_{k=1}^m \hat{a}_{n,k}^*\varepsilon_{n-k}^*\right)\right] + E\left[\left(\varepsilon_n - \sum_{k=1}^m \hat{a}_{n,k}\varepsilon_{n-k}\right)\left\{\sum_{k=1}^m \hat{a}_{n,k}^*\mathbf{x}_{n-k}^H\left(\sum_{j=1}^k \boldsymbol{\omega}_{n-j}\right)\right\}\right] + E\left[\left(\varepsilon_n - \sum_{k=1}^m \hat{a}_{n,k}\varepsilon_{n-k}\right)\left(\varepsilon_n^* - \sum_{k=1}^m \hat{a}_{n,k}^*\varepsilon_{n-k}^*\right)\right].
\end{aligned}
\tag{32}
$$

For ε_n and $\boldsymbol{\omega}_n$ which are independent, stationary white noise vectors with zero mean, so the second, third, fourth, fifth, seventh, and eighth terms all become zero. According to assumption A3 that the direction vector $\boldsymbol{\varphi}_n$ is independent on the weight vector $\mathbf{w}_n$, we can obtain

$$
\begin{aligned}
E[e_n e_n^*] &= \mathbf{tr}\left\{E\left[\tilde{\mathbf{w}}_n\tilde{\mathbf{w}}_n^H\right]E\left[\boldsymbol{\varphi}_n\boldsymbol{\varphi}_n^H\right]\right\} \\
&\quad + \sum_{k=1}^m E\left[\hat{a}_{n,k}\hat{a}_{n,k}^*\right]\mathbf{tr}\left\{E\left[\mathbf{x}_{n-k}\mathbf{x}_{n-k}^H\right]\left(\sum_{j=1}^k E\left[\boldsymbol{\omega}_{n-j}\boldsymbol{\omega}_{n-j}^H\right]\right)\right\} \\
&\quad + \sigma_\varepsilon^2\left\{1 + \sum_{k=1}^m E\left[\hat{a}_{n,k}\hat{a}_{n,k}^*\right]\right\}.
\end{aligned}
\tag{33}
$$

Under assumptions A3 and A4, based on the definition of $\tilde{\lambda}_{n,i}$, from (33), the statistical MSE of the tracking performance for the AP-DE algorithm can be rewritten as

$$
E[e_n e_n^*] = \sigma_\varphi^2\sum_{i=1}^N \tilde{\lambda}_{n,i} + r_n^2\sigma_\omega^2\sum_{k=1}^m kE\left[\hat{a}_{n,k}\hat{a}_{n,k}^*\right] + \sigma_\varepsilon^2\left(1 + \sum_{k=1}^m E\left[\hat{a}_{n,k}\hat{a}_{n,k}^*\right]\right).
\tag{34}
$$

6. Steady-State Behavior

Assuming convergence, as $n \longrightarrow \infty$, (31) can be transformed into

$$
\tilde{\lambda}_{\infty,i} = \frac{1}{2\mu - \mu^2}\left\{\mu^2\frac{r_n^2\sigma_\omega^2}{\hat{r}_n^2}\sum_{k=1}^m kE\left[\hat{a}_{n,k}\hat{a}_{n,k}^*\right] + \frac{\mu^2\sigma_\varepsilon^2}{\hat{r}_n^2}\left(1 + \sum_{k=1}^m E\left[\hat{a}_{n,k}\hat{a}_{n,k}^*\right]\right) + \tilde{r}_n^2\right\}.
\tag{35}
$$
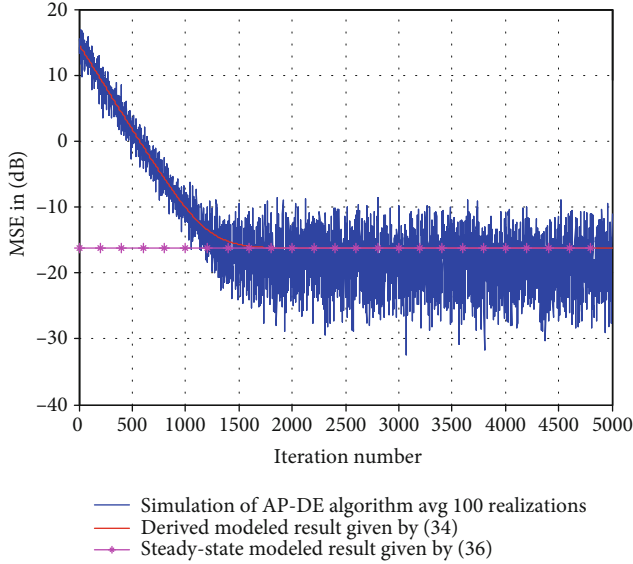
FIGURE 1: Learning MSE curves of the statistical tracking performance for AR (1) input.

Simulation of AP-DE algorithm avg 100 realizations
Derived modeled result given by (32)
Steady-state modeled result given by (36)

FIGURE 2: Learning MSE curves of the statistical tracking performance for ARMA (2, 1) input.

Combining with (34) and (35), based on $r\wedge^2 = N\sigma_\varphi^2$, the mean square error of the steady-state tracking performance can be written as

$$E[e_n e_n^*] = \frac{1}{2\mu - \mu^2} \left\{ \mu^2 r_n^2 \sigma_\omega^2 \sum_{k=1}^{m} kE\left[\hat{a}_{n,k}\hat{a}_{n,k}^*\right] + \mu^2 \sigma_\varepsilon^2 \left(1 + \sum_{k=1}^{m} E\left[\hat{a}_{n,k}\hat{a}_{n,k}^*\right]\right) + \hat{r}_n^2 \tilde{r}_n^2 \right\} + r_n^2 \sigma_\omega^2 \sum_{k=1}^{m} kE\left[\hat{a}_{n,k}\hat{a}_{n,k}^*\right] + \sigma_\varepsilon^2 \left(1 + \sum_{k=1}^{m} E\left[\hat{a}_{n,k}\hat{a}_{n,k}^*\right]\right).$$

(36)

7. Simulation

We give the statistical MSE of the tracking performance learning curves from the simulations in this section, and the derived models are given by (34) and (36). The initial system true weight $\mathbf{w}_0^o$ is stochastic produced by 32 taps. The length of the adaptive filtering is given with the same as the derived model. The weight of the initial estimated values is given as $\mathbf{w}_0 = 0$. The 100 independent simulations are averaged for each experiment, and each step size is equal to 0.1. The variance of the measurement noise and the vector ω_n are set to be $\sigma_\varepsilon^2 = 0.01$ and 2.5×10^{-5}, respectively.

Case 1. Consider that the input signal model defined by $x_n = -0.95x_{n-1} + z_n$ is an AR (1) model and the parameter z_n is the white Gaussian noise with the zero mean. The parameter m is set to be one. The statistical MSE for tracking behavior predicted by the model given by (34) and (36) are shown in Figure 1, together with the simulation results. We observe

that the derived models are almost the same simulation results in this case.

Case 2. When the parameter z_n is assumed to be the white Gaussian noise with the zero mean, the input signal is an ARMA (2, 1) model defined by $x_n = (0.7 - 0.3i)x_{n-1} - (0.4 - 0.6i)x_{n-2} + z_n + 0.5z_{n-1}$. The parameter is set to be $m = 3$. The mean square error of the tracking behavior predicted by the derived model given with (34) and (36) is shown in Figure 2. We find that the derived model cooperates with the simulation results well for the input ARMA (2, 1) model.

8. Conclusion

Under the condition that the unknown true weight vector is given by the stochastic walk model, a statistical tracking model for the AP-DE algorithm is analyzed. We give four assumptions that show the properties for both the input

and direction vectors. A statistical tracking model of the MWE and the MSE is derived based on these four assumptions. A prediction tracking model of the statistical steady-state MSE of the AP-DE algorithm is also proposed. According to the derived models in this paper, the simulation results for the input given by AR (1) and ARMA (2, 1) show the affine projection algorithm based on direction error, the better statistical tracking behavior.

Data Availability

The data used to support the findings of this study are available from the corresponding author upon request.

Conflicts of Interest

The authors declare that they have no conflicts of interest.

Acknowledgments

References

[1] S. Haykin, *Adaptive Filter Theory*, Prentice-Hall, Englewood Cliffs, NJ, 1991.

[2] K. Ozeki and T. Umeda, "An adaptive filtering algorithm using an orthogonal projection to an affine subspace and its properties," *Electronics and Communications in Japan (Part I: Communications)*, vol. 67, no. 5, pp. 19–27, 1984.

[3] S. G. Sankaran and A. A. Beex, "Normalized LMS algorithm with orthogonal correction factors," in *Conference Record of the Thirty-First Asilomar Conference on Signals, Systems and Computers (Cat. No.97CB36136)*, Pacific Grove, CA, USA, 1997.

[4] M. Rupp, "A family of adaptive filter algorithms with decorrelating properties," *IEEE Transactions on Signal Processing*, vol. 46, no. 3, pp. 771–775, 1998.

[5] F. Bouteille, P. Scalart, and M. Corazza, "Pseudo affine projection algorithm new solution for adaptive identification," *Proceedings Eurospeech*, vol. 1, pp. 427–430, 1999.

[6] Y. F. Zhi, R. Li, and H. X. Li, "A new affine projection algorithm and its statistical behavior," *Chinese Journal of Electronics*, vol. 22, no. 3, pp. 537–542, 2013.

[7] S. G. Sankaran and A. A. . L. Beex, "Fast generalized affine projection algorithm," *International Journal of Adaptive Control and Signal Processing*, vol. 14, no. 6, pp. 623–641, 2000.

[8] L. Lu, G. Zhu, X. Yang, K. Zhou, Z. Liu, and W. Wu, "Affine projection algorithm-based high-order error power for partial discharge denoising in power cables," *IEEE Transactions on Instrumentation and Measurement*, vol. 69, no. 4, pp. 1821–1832, 2020.

[9] J. Guo, F. Yang, and J. Yang, "Mean-square performance of the modified filtered-x affine projection algorithm," *Circuits Systems and Signal Processing*, vol. 39, no. 8, pp. 4243–4257, 2020.

[10] Vasundhara, "Sparsity aware affine-projection-like filtering integrated with robust set membership and M-estimate approach for acoustic feedback cancellation in hearing aids," *Applied Acoustics*, vol. 175, no. 2, article 107778, 2021.

[11] P. Song, H. Zhao, X. Zeng, W. Quan, and L. Zhao, "Robust time-varying parameter proportionate affine-projection-like algorithm for sparse system identification," *Circuits Systems and Signal Processing*, vol. 1, pp. 1–22, 2021.

[12] S. G. Sankaran and A. A. L. Beex, "Convergence behavior of affine projection algorithms," *IEEE Transactions on Signal Processing*, vol. 48, no. 4, pp. 1086–1096, 2000.

[13] T. K. Paul and T. Ogunfunmi, "On the convergence behavior of the affine projection algorithm for adaptive filters," *IEEE Transactions on Circuits and Systems*, vol. 58, no. 8, pp. 1813–1826, 2011.

[14] Y. F. Zhi, J. L. Li, J. Zhang, and Z. Wang, "Statistical convergence behavior of affine projection algorithms," *Applied Mathematics and Computation*, vol. 270, no. 1, pp. 511–526, 2015.

[15] Y. F. Zhi, F. F. Shang, J. Zhang, and Z. Wang, "Optimal step-size of pseudo affine projection algorithm," *Applied Mathematics and Computation*, vol. 273, no. 15, pp. 82–88, 2016.

[16] S. J. M. de Almeida, J. C. M. Bermudez, N. J. Bershad, and M. H. Costa, "A statistical analysis of the affine projection algorithm for unity step size and autoregressive inputs," *IEEE Transactions on Circuits and Systems*, vol. 52, no. 7, pp. 1394–1405, 2005.

[17] S. I. M. de Almeida, J. C. M. Bermudez, N. J. Bershad, and M. H. Costa, "A stochastic model for the convergence behavior of the affine projection algorithm for Gaussian inputs," in *2003 IEEE International Conference on Acoustics, Speech, and Signal Processing, 2003. Proceedings. (ICASSP '03)*, pp. 313–316, Hong Kong, China, 2003.

[18] S. J. M. de Almeida, J. C. M. Bermudez, and N. J. Bershad, "A stochastic model for a pseudo affine projection algorithm," *IEEE Transactions on Signal Processing*, vol. 57, no. 1, pp. 107–118, 2009.

[19] Y. F. Zhi, X. Zheng, and R. Li, "On the convergence behavior of affine projection algorithm with direction error," *Asian Journal of Control*, vol. 16, no. 2, pp. 530–538, 2014.

[20] Y. F. Zhi, Y. Y. Yang, X. Zheng, J. Zhang, and Z. Wang, "Statistical tracking behavior of affine projection algorithm for unity step size," *Applied Mathematics and Computation*, vol. 283, no. 20, pp. 22–28, 2016.

WILEY | Hindawi

Research Article
Fintech Index Prediction Based on RF-GA-DNN Algorithm

Chao Liu [ID]**, Yixin Fan** [ID]**, and Xiangyu Zhu** [ID]

School of Economics and Management, Beijing University of Technology, Beijing 100124, China

Correspondence should be addressed to Xiangyu Zhu; zhuxiangyubjut@126.com

The Fintech index has been more active in the stock market with the Fintech industry expanding. The prediction of the Fintech index is significant as it is capable of instructing investors to avoid risks and provide guidance for financial regulators. Traditional prediction methods adopt the deep neural network (DNN) or the combination of genetic algorithm (GA) and DNN mostly. However, heavy computational load is required by these algorithms. In this paper, we propose an integrated artificial intelligence-based algorithm, consisting of the random frog algorithm (RF), GA, and DNN, to predict the Fintech index. The proposed RF-GA-DNN prediction algorithm filters the key input variables and optimizes the hyperparameters of DNN. We compare the proposed RF-GA-DNN with the traditional GA-DNN in terms of convergence time and prediction accuracy. Results show that the convergence time of GA-DNN is up to 20 hours and its prediction accuracy is 97.4%. In comparison, the convergence time of our RF-GA-DNN is only about 1.5 hours and the prediction accuracy reaches 97.0%. These results demonstrate that the proposed RF-GA-DNN prediction algorithm significantly reduces the convergence time with the promise of competitive prediction accuracy. Thus, the proposed algorithm deserves to be widely recommended for predicting the Fintech index.

1. Introduction

The financial industry is reshaped by Fintech with the development of a new round of scientific and industrial revolution. Fintech provides an infinite space for innovative financial products and services [1]. At present, the market scale of the Fintech industry is in the forefront of the world [2]. The rapid expansion of the Fintech industry has drawn the attention of stock market investors to the Fintech index, which consists of 55 publicly listed Fintech companies. However, the Fintech index is subject to many factors, including financial and monetary policy and investor expectations [3, 4]. This may not only bring risk for investors but also affect financial regulation. Therefore, it is of great significance to predict the Fintech index in the stock market accurately and effectively.

Various researches have been conducted to predict indexes in the stock market. As an important stock price index in the stock market, the Fintech index is nonlinear and nonstationary [5]. The Fintech index is volatile and difficult to be predicted by the traditional time series methods. Machine learning algorithms, such as support vector regression (SVR) [6], genetic algorithm (GA) [7], and deep neural network (DNN) [8], have been widely used recently [9, 10]. SVR was introduced by Vapnik originally [11], which has a global optimum, while its hyperparameter selection needs to be determined by the experience of practitioners [5], which has strong subjectivity and may lead to poor performance in prediction [12]. GA is established on the concepts of natural selection and heredity, which can find the parameters of the algorithms that need to be optimized from a global perspective [13]. In recent years, DNN has attracted intense research interest. It has been widely adopted in many fields, such as computer vision, language processing, and speech recognition [14–17]. DNN is an algorithm of deep learning branch, which has a large number of layers and neurons. Therefore, it has a strong fitting ability and high prediction accuracy. However, overfitting is prone to occur because of the large number of layers and neurons [18].

For better prediction, some scholars have improved and integrated the algorithms for their advantages and disadvantages. Xin et al. [19] put forward the GA-SVR due to the good performance of the GA in seeking the parameters of the algorithms that need to be optimized. Similarly, the GA-DNN has recently been proposed for using in the fields of robotics

and speech separation [20, 21]. Although the GA-DNN algorithm's prediction accuracy has been greatly improved, its convergence time needs to be improved furtherly.

From the literature review mentioned above, to date, GA-DNN has not been used in the stock index forecasting research, and its convergence time is long. This study is aimed at filling the gap by proposing an integrated artificial intelligence-based algorithm, consisting of random frog algorithm (RF), GA, and DNN (RF-GA-DNN) to predict the Fintech index. In this new algorithm, RF is adopted to filter all technical variables that affect the Fintech index and some variables that have no contribution or little influence are removed firstly. Then, GA is employed to seek the parameters of DNN. Finally, DNN is used to predict the Fintech index by four times cross-validation.

he remainder of this paper is arranged as follows. Section 2 introduces the steps of RF, GA, and DNN in detail. Section 3 defines the principle of the proposed RF-GA-DNN prediction algorithm. The sample and prediction results are detailed in Section 4. The conclusions are presented in Section 5.

2. Methods

2.1. Random Frog (RF). The random frog algorithm was proposed by Li et al. [22] based on the framework of reversible jump Markov Chain Monte Carlo (MCMC). In this section, the partial least squares linear discriminant analysis (PLS-LDA) is employed to build a classifier [22]. The steps of the random frog algorithm are as follows:

Step 1. Hyperparameter initialization.

(1) N represents the number of iterations of the random frog algorithm Theoretically, the larger the N is, the model works better, whereas it takes more time to compute. Hence, N is set to 10000 according to experience

(2) Q is the number of variables in the initial variable set. Q variables make up the initial variable set V_0

(3) θ refers to a controlling factor for the variance of a normal distribution and a positive real number less than 1 in general. It is set to 0.3 by default

(4) ω is a scaling factor, which is employed to control the number of candidate variables and should be greater than 1. By default, ω is set to 3

(5) η refers to the upper bound of the probability of accepting the new variable set V^*, whose result is lower than V_0. The value ranges from 0 to 1, and the default value of η is 0.1 [22]

Step 2. The initial variable set is randomly selected as V_0, which contains Q variables. Define the set of all variables to be V.

Step 3. Q^* is the nearest rounded random number from the normal distribution with mean Q and standard deviation θQ. Then, a candidate variable subset V^* is constructed, which contains Q^* variables.

(1) If $Q^* = Q$, then $V^* = V$

(2) If $Q^* < Q$, construct a PLS-LDA method by the variable set V_0 firstly, and the regression coefficients for each variable are obtained. Then, $Q - Q^*$ variables with the smallest absolute value of the regression coefficient are removed from V_0, and V^* is composed of the remaining Q^* variables

(3) If $Q^* > Q$, $\omega(Q^* - Q)$ variables are randomly selected from $V - V_0$ to form a new variable set T. Then, T and V_0 are combined to establish the PLS-LDA, and the regression coefficients of each variable are capable of obtaining. V^* is composed of Q^* variables with the largest absolute value of the regression coefficient

Step 4. Determine whether V^* is acceptable or not. The prediction errors of the PLS-LDA established by V_0 and V^* are recorded as e_0 and e^* correspondingly.

(1) If $e^* \leq e_0$, then V^* can be accepted and $V_1 = V^*$

(2) If $e^* \geq e_0$, accept V^* with $\eta e_0/e^*$ and $V_1 = V^*$. Replace V_0 with V_1, and return to Step 2 for the next iteration until N iterations are completed

Step 5. Nvariable subsets can be obtained after N iterations. The frequency of selecting variable i is N_i; then, the selection probability of i is P_i:

$$P_i = \frac{N_i}{N}. \tag{1}$$

The variables can be selected according to their probabilities because the higher the probability of the selected variable, the more important it is.

2.2. Genetic Algorithm (GA). Holland [23] has proposed a random search intelligent algorithm, namely, genetic algorithm (GA), which simulates the evolution process of nature. It should be noted that the hyperparameters of the algorithms, which need to be optimized, can be searched by the GA [13]. The basic steps of GA are as follows:

Step 1. Initializing the population. The initial population is made up of randomly generated individuals. The application of fitness function is employed to analyze fitness factors.

Step 2. Calculating the fitness of individuals and ranking them.

Step 3. Selecting two individuals with high fitness and dealing with crossover and mutation to produce offspring individuals.

Step 4. Return to step 2 and keep optimizing the hyperparameters until the set evolutionary algebra is reached. Then, the model terminates.

2.3. Deep Neural Network (DNN). There are various structures for DNN, but the DNN structure is fixed in this paper. Based on the sample data dimension in this paper and
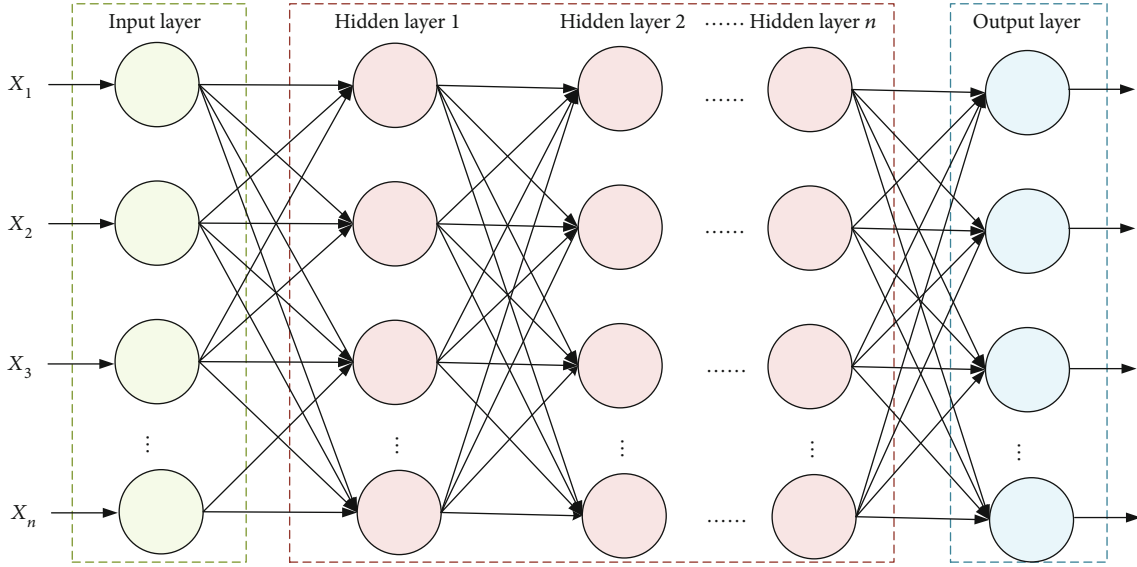
FIGURE 1: Deep neural network structure.

experience, the structure of DNN is determined as one input layer, three hidden layers, and one output layer. The output of the previous layer can be capable of using as the input of the next layer. The training strategy of DNN is to minimize the value of RMSE, and the samples have been divided randomly according to the rule of 80% training samples and 20% test samples. The prediction accuracy of the DNN model is also affected by some core hyperparameters, such as activation function, training times, number of monolayer neurons, learning rate, and batch size, which will be determined in Section 4.2. The input data of DNN is the 20 technical variables that affect the Fintech index, while the output data is the predicted value of the previous day's closing price of the Fintech Index. The operation steps of DNN are shown as follows.

Step 1. Supposing that $v^l = [v_i^l]$ is the hidden layer vector of layer l. The visible layer vector is $h^l = [h_i^l]$. The connection weight matrix of the hidden layer is $W^l = [w_{ij}^l]$. $a^l = [a_i^l]$ and $b^l = [b_i^l]$ are the bias vectors of the hidden layer and visible layer, respectively.

Step 2. Assigning values to W and a randomly in the range of (0,1).

Step 3. Calculating the probability that a hidden layer unit can be activated.

$$p\left(h_j^l = 1 \mid v^l\right) = \sigma\left(b_j^l + \sum_{i=1}^{I} w_{ij}^l v_i^l\right), \tag{2}$$

where $\sigma(\bullet)$ is set to ReLU function because of its better performance than other functions in this experiment. It can be described as follows:

$$\sigma(x) = \begin{cases} x & \text{if } x > 0, \\ 0 & \text{if } x \le 0. \end{cases} \tag{3}$$

Step 4. The value of the hidden layer unit is determined by Gibbs sampling.

$$h_j^l = \begin{cases} 1, & p\left(h_j^l = 1 \mid v^l\right) > r_j, \\ 0, & p\left(h_j^l = 1 \mid v^l\right) \le r_j, \end{cases} \tag{4}$$

where r_j is the random number generated on [0,1].

Step 5. Calculating the activation probability of the reconstructed visible layer unit and reconstructing the visible layer by Gibbs sampling.

$$p\left(v^{l*} = 1 \mid h^l\right) = \sigma\left(a_i^l + \sum_{j=1}^{n} w_{ji}^l h_j^l\right), \tag{5}$$

where $v^{l*} = [v_i^*]$ is the unit vector of the reconstructed visible layer.

Step 6. Calculating the activation probability of the hidden layer element and updating the parameter values according to the visible layer element vector v^{l*}.

$$\begin{cases} w_{ij}^{l*} = w_{ij}^l + \lambda\left[v_i^l p\left(h_j^l = 1 \mid v^l\right) - v_i^{l*} p\left(h_j^{l*} = 1 \mid v^{l*}\right)\right], \\ b_j^{l*} = b_j^l + \lambda^l\left[p\left(h_j^l = 1 \mid v^l\right) - p\left(h_j^{l*} = 1 \mid v^{l*}\right)\right], \\ a_i^{l*} = a_i^l + \lambda^l\left(v_i^l - v_i^*\right), \end{cases} \tag{6}$$

where w_{ij}^{l*}, b_j^{l*}, and a_i^{l*} are the updated values of w_{ij}^l, b_j^l, and a_i^l, respectively.
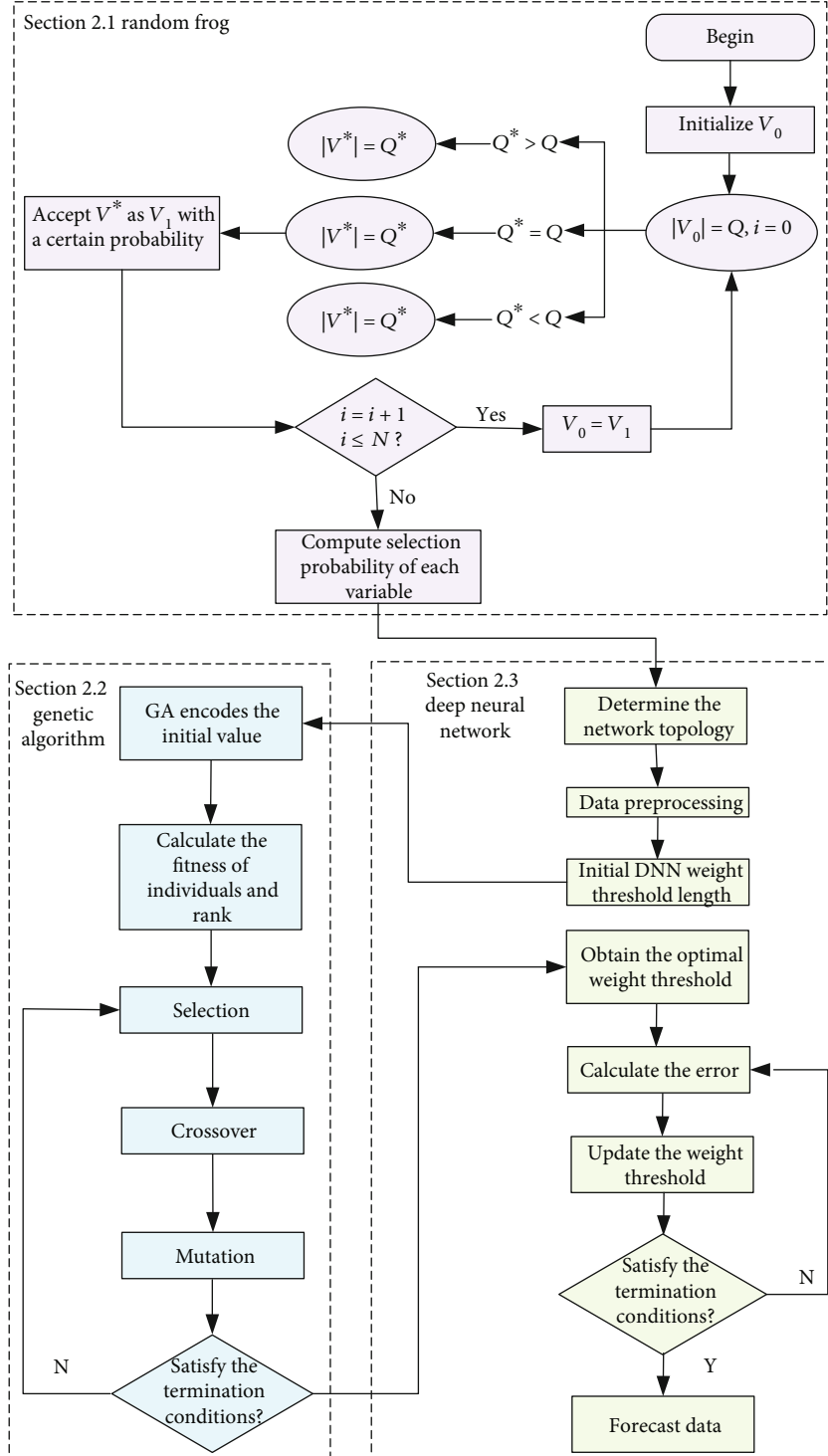
Figure 2: The proposed RF-GA-DNN algorithm workflow.

The input vector y^l of the next neural layer can be expressed as follows:

$$y^l = \sigma\left(W^l a^l + b^l\right). \tag{7}$$

Step 7. Steps 3–6 are looped until the number of iterations is finished. Then, the model terminates.

Table 1: The RMSE of different activation functions.

Activation function	RMSE
Sigmoid	1199.16
Softmax	1315.71
Tanh	1196.33
ReLU	113.74

(a)

(b)

(c)
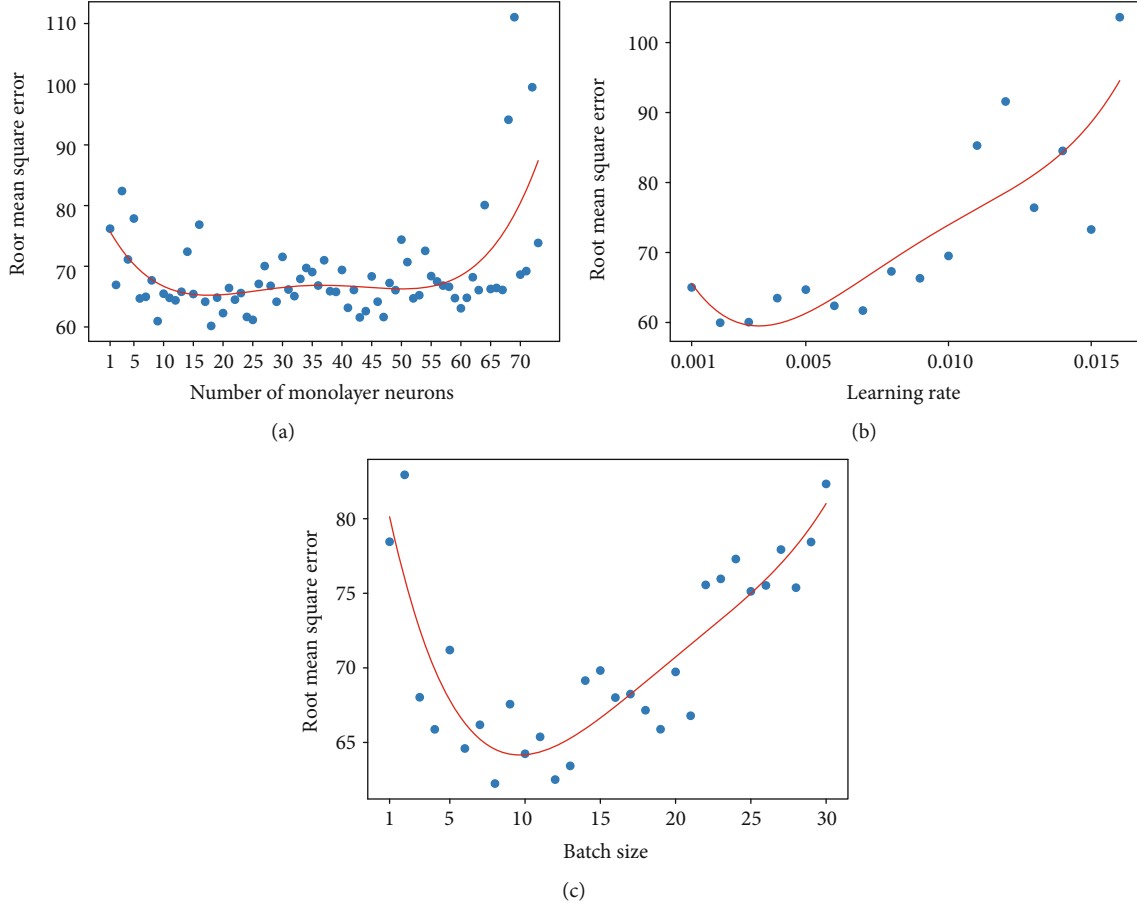
FIGURE 3: The RMSE of monolayer neurons, learning rate, and batch size (the red line represents a polynomial curve for fitting the change trend of the three hyperparameters).

Step 8. Reversing the fine-tuning of parameters by a gradient descent method, which adjusts the weights of interconnections and minimizes the output error.

$$
\begin{cases}
W^{l*} = W^l - \eta \dfrac{\partial E}{\partial W^l}, \\
b^{l*} = b^l - \eta \dfrac{\partial E}{\partial b^l},
\end{cases}
\tag{8}
$$

where η is the learning rate and E is the cost function, and it can be expressed as

$$
E = \frac{1}{2N} \sum_{n=1}^{N} \| y^n - o^n \|,
\tag{9}
$$

where y^n and o^n are the predicted and actual values obtained from the nth training sample in one training time, respectively. N is the size of the training sample. The specific DNN network structure is shown in Figure 1.

3. The Proposed RF-GA-DNN Prediction Algorithm

In this section, an integrated artificial intelligence-based algorithm, consisting of random frog algorithm (RF), GA, and DNN, is proposed to predict the Fintech index.

The core hyperparameters of DNN have a significant influence on its prediction accuracy, but the value of the core hyperparameters cannot be determined by calculation directly at present. GA is capable of searching for the optimal hyperparameters of DNN from a global scope. The principle of GA-DNN is to find the optimal hyperparameters through the GA firstly, and then, DNN is employed to predict. However, the convergence time will be increased for too many variables. The random frog algorithm is able to filter the key variables and reduce the convergence time. Therefore, the random frog algorithm has been added to GA-DNN, and we have proposed a hybrid RF-GA-DNN prediction algorithm to reduce the convergence time.

The workflow of this new algorithm is shown in Figure 2. As can be seen from Figure 2, firstly, the random frog algorithm was adopted to screen out input variables for obtaining variables related to the Fintech index. Secondly, the screened variables were imported into DNN with different
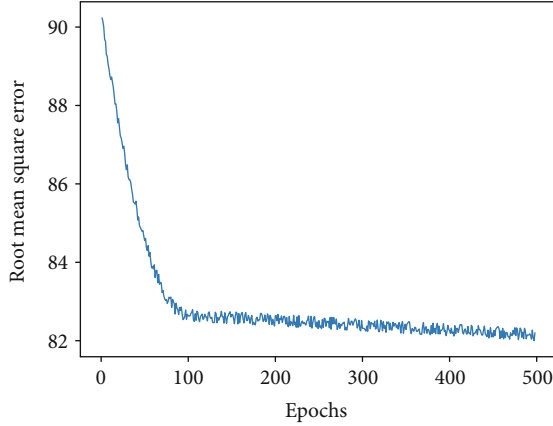
FIGURE 4: Effect of training times on RMSE.

FIGURE 5: The degree of deviation between the actual and predicted values of DNN (the red line represents the true value equal to the predicted value).

hyperparameter values to get the predicted values of the test samples. Then, to determine the value range of GA searching for hyperparameters, RMSE of predicted and true values was calculated. And then, within the value range obtained by the GA, take RMSE returned by each DNN model as a fitness function to get the optimal hyperparameter combination of DNN. Finally, the selected variables were imported into the DNN model with the optimal hyperparameter setting from the GA. Then, the predicted values are obtained, and the root mean square error can be gotten by using the predicted and the true values. Specific steps of RF-GA-DNN have been listed in Section 2.1, Section 2.2, and Section 2.3.

4. Experiment and Analysis

4.1. Sample and Variable Selection. The sample interval of this paper is from March 8, 2015, to April 9, 2021, with 1488 daily data totally. The next day's closing price of the Fintech index is selected as the output variable. The input variables include 20 technical variables (MACD, BBI, DDI, DMA, MTM, TRIX, RSI, ROC, B3612, BIAS, CCI, OSC, W&R, MASS, WVAD, CR, PSY, VR, BOLL, turnover rate). 80% of the data are the training samples, and 20% of the data are selected as the test samples. All data comes from the Wind database.

4.2. Core Hyperparameter Selection and Value Range Determination. Common hyperparameters in DNN include activation function, monolayer neurons, learning rate, batch size, and training times [18]. All of them are highly related to the prediction accuracy and convergence time. Therefore, their value range is investigated.

For the activation function, Sigmoid, Softmax, Tanh, and ReLU are the common activation functions. Table 1 tabulates the root mean square error (RMSE) of these activation functions. The root mean square error of the previous day's closing price and forecast price of the Fintech Index is presented by RMSE. Through the analysis of Table 1, the RMSE of ReLU is smaller than Sigmoid, Softmax, and Tanh. Therefore, ReLU is selected as the activation function of the method.
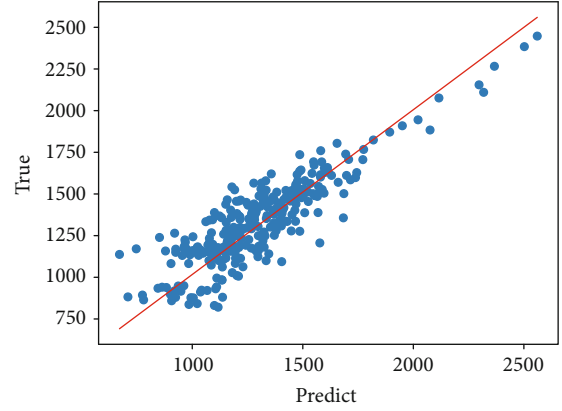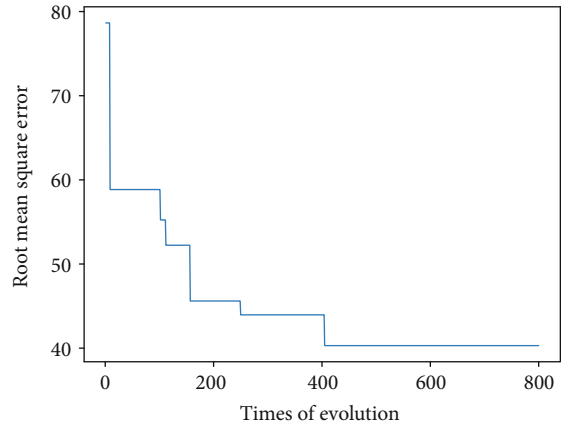
FIGURE 6: Effect of evolution times on RMSE of GA-DNN.
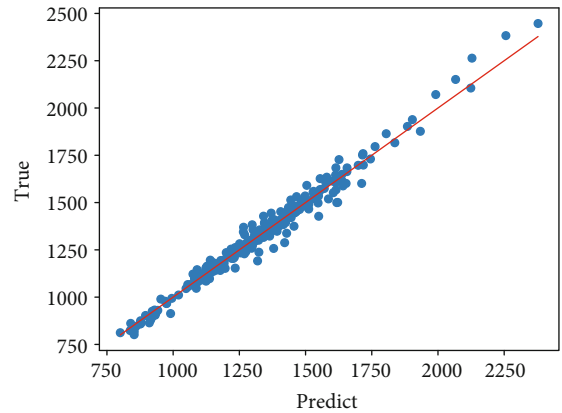
FIGURE 7: The degree of deviation between the actual and predicted values of GA-DNN (the red line represents the true value equal to the predicted value).

A trial parameter method is employed to obtain the optimization range. The RMSE of the number of monolayer neurons, learning rate, and batch size are shown in Figure 3. Figure 3(a) illustrates that the RMSE of the number of monolayer neurons is smaller in [10, 65]. Figure 3(b) reveals that the learning rate error can be fixed in [0.001, 0.015].
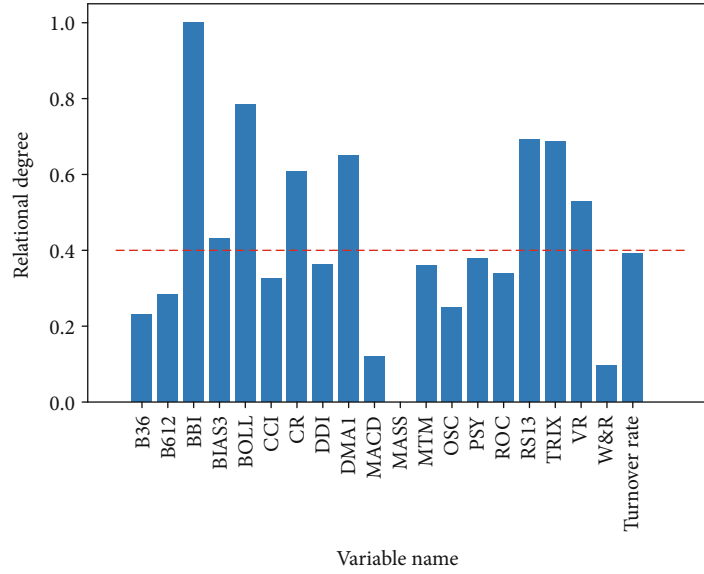
FIGURE 8: Correlation of different variables.
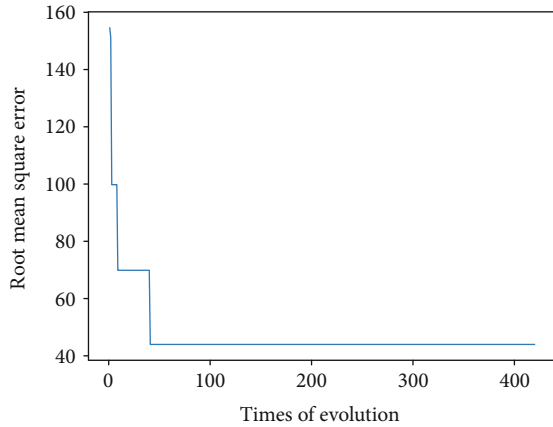
FIGURE 9: Effect of evolution times on RMSE of RF-GA-DNN.
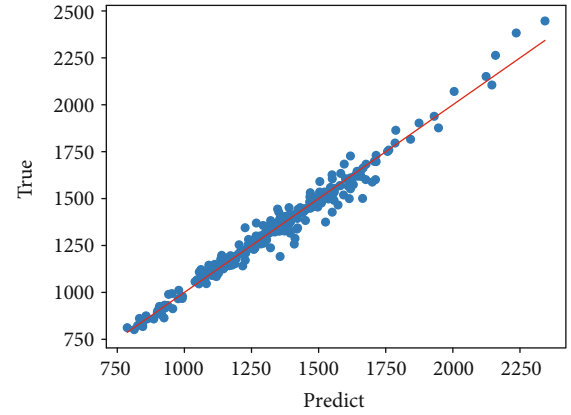
FIGURE 10: The degree of deviation between the actual and predicted values of RF-GA-DNN (the red line represents the true value equal to the predicted).

According to the analysis in Figure 3(c), [2, 20] is a better range for batch size due to its smallest RMSE in this interval.

To determinate the training times, based on the experience of deep learning, the number of monolayer neurons is set to 10 preliminarily, the learning rate is 0.001, and the batch size is random gradient descent by default. The RMSE has been obtained through four-time cross-validation, which is shown in Figure 4. Figure 4 reveals that the RMSE is significantly reduced between 0 and 100 training times, while there is almost no difference between 100 and 500 training times. Then, 100 is regarded as the number of training times for DNN, and the degree of deviation between the actual and predicted values of DNN is shown in Figure 5. We see that the prediction effect can be further optimized. However, it is not advisable to increase the training times. Therefore, the following models (including DNN, GA-DNN, and RF-GA-DNN) were completed under the condition of running a single DNN training of 100 times.

In summary, we select ReLU as the activation function. The range of number of monolayer neurons, learning rate,

TABLE 2: The RMSE of different activation functions.

Algorithm	Convergence time	Prediction accuracy
GA-DNN	20 h	97.4%
RF-GA-DNN	1.5 h	97.0%

and batch size is [10, 65], [0.001, 0.015], and [2, 20], respectively. 100 is set to the training times. The values of monolayer neurons, learning rate, and batch size can only be determined in a range by a trial parameter method, and then, the optimal combination of the hyperparameters can be found by the GA. In addition, the experiment shows that the single operation time of DNN is about 10 s when a specific hyperparameter combination is given. However, an enumeration method is needed to determine the optimal hyperparameter combination. By calculation, it will take years and be difficult to achieve.

4.3. Prediction of GA-DNN Algorithm. Based on the analysis of Section 4.2, GA is introduced in DNN due to its excellent performance in searching for the optimal hyperparameters' combination. According to the sample data dimension and experience, the number of hidden layers in DNN is set to 3. The optimal hyperparameter combination searched by the GA is as follows: the number of neurons in the three hidden layers is 35, 6, and 12; the learning rate is 0.002; and the batch size is 8. Input the optimal hyperparameter combination into DNN, train 100 times, and iterate 800 generations (each generation has 20 individuals). The optimal RMSE and forecast renderings can be gained, as shown in Figures 6 and 7.

Figure 6 shows the effect of the evolutionary times on the RMSE of GA-DNN. It can be seen from Figure 6 that GA-DNN converges from generation 405, and the RMSE is 40.49 after convergence. Figure 7 shows the degree of deviation between the actual and predicted values of GA-DNN. The prediction accuracy of GA-DNN is 97.4%. However, it is worth noting that the convergence time of GA-DNN is 73694 s (about 20 hours). From this, we know that the convergence time of GA-DNN is still too long and it could be optimized furtherly.

4.4. Prediction of RF-GA-DNN Algorithm. Random frog is an efficient approach for variable selection [22], which can move between fixed-dimensional and transdimensional in different methods to realize a search. We introduced the random frog algorithm into GA-DNN to screen out key variables. Variables filtered by the random frog algorithm are shown in Figure 8. We take 0.4 as the boundary to filter variables based on the characteristics of our variables. The optimal hyperparameter combination of RF-GA-DNN is as follows: the number of neurons in the three hidden layers is 23, 17, and 13; the learning rate is 0.001; and the batch size is 12.

Figure 9 illustrates the effect of the evolutionary times on the RMSE of RF-GA-DNN. It can be concluded that RF-GA-DNN converges from generation 41, and the RMSE is 43.15 after convergence. The convergence time is 5462 s (about 1.5 hours), which is much less than GA-DNN. Figure 10 shows the degree of deviation between the actual and predicted values of RF-GA-DNN. The prediction accuracy of RF-GA-DNN is 97.0%, which is very close to GA-DNN.

In summary, the comparison results of GA-DNN and RF-GA-DNN are shown in Table 2. As seen in Table 2, it can be concluded that the convergence time of RF-GA-DNN is only 1/13 of GA-DNN with the promise of a competitive prediction accuracy. Hence, RF-GA-DNN has an excellent performance in convergence time.

5. Conclusions

Predicting the Fintech index benefits various stakeholders, e.g., assisting investors to design profitable short, medium, and long-term strategies for investing and guiding financial regulators to make precise and effective regulatory policies. However, the convergence time of current prediction algorithms is far from eligible bearing this in mind. In this paper, we have proposed a hybrid RF-GA-DNN algorithm and employed this algorithm to predict the Fintech index.

We have examined the performance of the proposed RF-GA-DNN on predicting the Fintech index. The samples come from the Wind database with a time period from March 8, 2015, to April 9, 2021. Through the analysis of samples, the proposed hybrid RF-GA-DNN has endowed with excellent superiority compared with the traditional GA-DNN. More importantly, the convergence time of RF-GA-DNN is only 1/13 of that of GA-DNN. These results demonstrate that the proposed hybrid RF-GA-DNN prediction algorithm can be employed as a more effective tool to predict the Fintech index. In practical applications, the hybrid RF-GA-DNN prediction algorithm can be expected to not only provide a reference for investors to formulate investment strategies but also support financial regulators to supervise the market.

On the whole, this paper has proposed an efficient algorithm to predict the Fintech index. However, it still remains an open issue to determine a reasonable evolutionary algebra range to guarantee the convergence of the algorithm. For future work, it is worthwhile to provide a convergence analysis for the proposed algorithm. In addition, the proposed hybrid RF-GA-DNN prediction algorithm can be further utilized as an efficient tool to deal with other indexes in the stock market.

Data Availability

No data were used to support this study.

Conflicts of Interest

The authors declare that there is no conflict of interest.

Acknowledgments

References

[1] A. Alexandrov, R. Bergmann, S. Ewen et al., "The stratosphere platform for big data analytics," *The VLDB Journal*, vol. 23, no. 6, pp. 939–964, 2014.

[2] McKinsey, "What's next for China's booming fintech sector?," 2016, https://www.mckinsey.com/industries/financial-services/our-insights/whats-next-for-chinas-booming-fintech-sector.

[3] J. S. Chou and T. K. Nguyen, "Forward forecast of stock price using sliding-window metaheuristic-optimized machine-learning regression," *IEEE Transactions on Industrial Informatics*, vol. 14, no. 7, pp. 3132–3142, 2018.

[4] S. Chen, Y. Sun, and Y. Liu, "Forecast of stock price fluctuation based on the perspective of volume information in stock and exchange market," *China Finance Review International*, vol. 8, no. 3, pp. 297–314, 2018.

[5] A. Kazem, E. Sharifi, F. K. Hussain, O. K. Hussain, and M. Saberi, "Support vector regression with chaos-based firefly algorithm for stock market price forecasting," *Applied Soft Computing*, vol. 13, no. 2, pp. 947–958, 2013.

[6] V. V. Gavrishchaka and S. Banerjee, "Support vector machine as an efficient framework for stock market volatility forecasting," *Computational Management Science*, vol. 3, no. 2, pp. 147–160, 2006.

[7] K. Dasgupta, B. Mandal, P. Dutta, S. Dam, and J. K. Mandal, "A genetic algorithm (GA) based load balancing strategy for cloud computing," *Procedia Technology*, vol. 10, pp. 340–347, 2013.

[8] J. Duan, "Financial system modeling using deep neural networks (DNNs) for effective risk assessment and prediction," *Journal of the Franklin Institute*, vol. 356, no. 8, pp. 4716–4731, 2019.

[9] A. Dingli and K. S. Fournier, "Financial time series forecasting – a deep learning approach," *International Journal of Machine Learning and Computing*, vol. 7, no. 5, pp. 118–122, 2017.

[10] H. Cao, T. Lin, Y. Li, and H. Zhang, "Stock price pattern prediction based on complex network and machine learning," *Complexity*, vol. 2019, Article ID 4132485, 12 pages, 2019.

[11] V. Vapnik, *The Nature of Statistical Learning Theory*, Springer, New York, 1995.

[12] C. Y. Yeh, C. W. Huang, and S. J. Lee, "A multiple-kernel support vector regression approach for stock market price forecasting," *Expert Systems with Applications*, vol. 38, no. 3, pp. 2177–2186, 2011.

[13] A. Lambora, K. Gupta, and K. Chopra, "Genetic algorithm-a literature review," in *2019 International Conference on Machine Learning, Big Data, Cloud and Parallel Computing (COMITCon)*, pp. 380–384, Faridabad, India, 2019.

[14] W. Liu, Z. Wang, X. Liu, Y. Liu, F. E. Alsaadi, and N. Zeng, "A survey of deep neural network architectures and their applications," *Neurocomputing*, vol. 234, pp. 11–26, 2017.

[15] D. Yu and L. Deng, "Deep learning and its applications to signal and information processing [exploratory dsp]," *IEEE Signal Processing Magazine*, vol. 28, no. 1, pp. 145–154, 2011.

[16] A. Graves, A.-r. Mohamed, and G. Hinton, "Speech recognition with deep recurrent neural networks," in *2013 IEEE International Conference on Acoustics, Speech and Signal Processing*, pp. 6645–6649, Vancouver, BC, Canada, 2013.

[17] T. Young, D. Hazarika, S. Poria, and E. Cambria, "Recent trends in deep learning based natural language processing [review article]," *IEEE Computational Intelligence Magazine*, vol. 13, no. 3, pp. 55–75, 2018.

[18] S. Zhong, J. Hu, X. Fan, X. Yu, and H. Zhang, "A deep neural network combined with molecular fingerprints (DNN-MF) to develop predictive models for hydroxyl radical rate constants of water contaminants," *Journal of Hazardous Materials*, vol. 383, article 121141, 2020.

[19] N. Xin, X. Gu, H. Wu, Y. Hu, and Z. Yang, "Application of genetic algorithm-support vector regression (GA-SVR) for quantitative analysis of herbal medicines," *Journal of Chemometrics*, vol. 26, no. 7, pp. 353–360, 2012.

[20] S. Sivapatham, R. Ramadoss, A. Kar, and B. Majhi, "Monaural speech separation using GA-DNN integration scheme," *Applied Acoustics*, vol. 160, no. 3, article 107140, 2020.

[21] X. Chen, Q. Zhang, and Y. Sun, "Evolutionary robot calibration and nonlinear compensation methodology based on GA-DNN and an extra compliance error model," *Mathematical Problems in Engineering*, vol. 2020, Article ID 3981081, 15 pages, 2020.

[22] H. D. Li, Q. S. Xu, and Y. Z. Liang, "Random frog: an efficient reversible jump Markov Chain Monte Carlo-like approach for variable selection with applications to gene selection and disease classification," *Analytica Chimica Acta*, vol. 740, no. 8, pp. 20–26, 2012.

[23] J. H. Holland, *Adaptation in natural and artificial systems*, University of Michigan Press, Ann Arbor, Ml, 1975.

WILEY | Hindawi

Research Article

Classification of Tennis Video Types Based on Machine Learning Technology

Xun Gong[1] and Fucheng Wang [2]

[1]*Physical Education Department, Heilongjiang Bayi Agricultural University, Daqing, 163319 Heilongjiang, China*
[2]*Engineering College, Heilongjiang Bayi Agricultural University, Daqing, 163319 Heilongjiang, China*

Correspondence should be addressed to Fucheng Wang; wangfucheng@byau.edu.cn

With the rapid development of online video data, how to find the required information has become an urgent problem to be solved. This article focuses on sports videos and studies video classification and content-based retrieval techniques. Its purpose is to establish a mark and index of video content and to promote user acquisition through computer processing, analysis, and understanding of video content. Video tennis classification has high research and application value. This article focuses on video tennis based on the selection of the basic frame of each shot and proposes an algorithm for classification of shots based on average grouping. Based on this, we use a color-coded spatial detection method to detect the type of tennis match. Then, it integrates the results of audiovisual analysis to identify and classify exciting events in tennis matches. According to statistics, although the number of people participating in tennis cannot enter the top ten, the number of spectators ranks fourth. Four tennis tournaments, masters, and crown tournaments are held every year around the world. Watching large-scale international tennis matches has become a pillar of leisure and vacation for many people. Tennis matches last from two hours to four hours or more, and there are countless large and small tennis matches around the world every year, so the number of tennis records created is staggering. And artificial intelligence technology is rarely used in tennis in the sports world (5%), but football has reached 50%. Therefore, when dealing with such a large amount of data, we urgently need to find a fast and effective video retrieval classification method to find the required information. The experiment of tennis video classification research based on machine learning technology proves that the accuracy of tennis video classification reaches 98%, so this system has high feasibility.

1. Introduction

1.1. Background. Tennis video data contains a lot of information, such as characters, scenes, objects, actions, and stories. According to statistics, 80% of the information received by humans is received visually, while tennis video information is intuitive and vivid, making it the most effective way of communication in human life. In today's fast-changing, complex information age, the development of computer and network technology, and the promotion and application of multimedia, various tennis video materials are constantly being created, and more and more tennis videos and digital databases are emerging: on-demand tennis video, mobile, web TV, and many other new and tennis video streaming media. In the face of a large number of tennis videos, how

to quickly obtain the required information from them is very important. Machine learning has a wide range of applications in human behavior recognition, mainly focusing on smart video surveillance, patient monitoring systems, human-computer interaction, virtual reality, smart home, smart security, athlete-assisted training, and content-based video retrieval and smart image compression. It has broad application prospects and potential economic and social value, and many methods of behavior identification are also used. So machine learning provides technical support for tennis video classification.

1.2. Significance. Sports tennis video content analysis technology is individually evaluated by researchers due to its wide application prospects and significant academic value. The

basic technology of sports tennis video content analysis is actually the analysis of events and their relationships. By highlighting and organizing these events, the query needs of most users can be met. From an academic point of view, event detection and recognition are typical problems of computer vision and pattern recognition. On the one hand, content-based tennis video search technology creates an effective semantic index of tennis video information, allowing users to quickly and easily view and retrieve tennis video content. At the same time, the development of content-based tennis video search technology provides more user-friendly and personalized functions. New tennis video services have changed the way users watch tennis videos from passive acceptance to more active choices. It can be said that related technologies such as content analysis have changed the consumption of information. Users can not only view differentiated high-resolution professional tennis video data but also capture a large amount of effective information. Therefore, finding a way to solve these problems and successfully creating a sport tennis video content analysis system will provide important insights into other similar target semantic analysis problems and ultimately video analysis and search, thereby promoting the development of various fields.

1.3. Related Work. Rovithakis et al. proposed a hybrid neural network/genetic algorithm technology to design feature extractors to achieve highly separable classes in the feature space. The purpose of this system is to identify the condition of human tissues in the surrounding blood vessels (i.e., normal, fibrous, and calcified). In order to distinguish normal levels from normal cells and cells affected by acute lymphoblastic leukemia, the system was further tested and classified by the range of blood sample nucleus measurement. As an advantage of the proposed technique, you may encounter the fact that the algorithmic nature of the design process, the result of optimized classification, and the performance of the system are less dependent on the type of classifier used [1]. However, due to the uncertainty of the experimental process, there are still gaps in the experimental results. Zupanc and Bosnic believe that essays are considered to be the most useful tool for evaluating student learning outcomes, guiding the learning process, and measuring progress. Grading students manually is a time-consuming process, but it is still necessary. Automatic composition evaluation is a practical solution to this task, but its main disadvantage is that it mainly focuses on vocabulary and text grammar, while semantic testing is very limited. They suggested extending the existing automated paper evaluation system by incorporating consistency and other semantic features of consistency [2]. However, their experimental process is not closed, so there is a certain deviation in the experimental results. Jenke et al. use EEG signals for emotion recognition, which can directly assess the user's "internal" state, which is considered an important factor in human-computer interaction. Many feature extraction methods have been studied, and appropriate features and electrode positions are usually selected based on neuroscience findings. However, a small number of different feature sets have been used and their suitability for emotion recognition has been tested on different data sets that are usually small. One major limitation is the comparison of systems with no features. Therefore, they reviewed the feature extraction methods for emotion recognition in EEG signals based on 33 studies. An experiment was conducted to compare these features using machine learning techniques to perform feature selection on self-recorded data sets. The performance of different feature selection methods, the usage of selected feature types, and the results of electrode position selection are given [3]. However, the factors selected by their multivariate method are slightly inferior to that of the univariate method, resulting in inaccurate results.

1.4. Innovation Points/Main Content. The innovation of this paper is (1) the use of video stream semantic analysis methods, which mainly include shot classification, player detection, and player tracking. On the basis of the existing lens classification algorithm, the characteristics of the lens in the tennis match video are fully studied, and a lens classification scheme based on Hough transform and SVM is proposed, which divides the shots into match shots and nonmatch shots. Then, use the frame difference method to achieve player detection and player tracking and give the experimental results. (2) Through the audio and video feature fusion technology, the detection of ACE balls, bottom line matches, and tennis balls in tennis matches is realized. (3) Introduce a continuous hidden Markov model (CHMM). The sounds that appear in a tennis match are divided into five categories, namely, batting, cheering, enthusiastic commentary by the narrator, ordinary commentary by the narrator, and noise. Calculate the audio feature values, and then train the sample parameters to obtain the continuous hidden Markov model of the five types of sounds, and then calculate the output probability of the sound to the various CHMM models, and use the maximum output probability to realize the automatic classification of the audio stream in the tennis match.

2. Tennis Video Field Lens Detection

The traditional video structure analysis method is to edit the segmentation in the video stream, basic frame extraction, and scene segmentation to obtain structured video information [4, 5]. The structure of the tennis video is very good. Shot changes usually occur after the end of the round, usually with the player's close-up (maybe the audience's shot) and the beginning of the next round. Due to the large amount of tennis video data, the method of the first one detecting the download limit, then selecting the basic frame, and then downloading the game download content by shooting classification contains a lot of unnecessary content, which must be [6, 7]. Therefore, it is more effective to extract court shots directly from the tennis video stream. Figure 1 shows a common video structured block diagram. It can be seen from the figure that the video structure is mainly composed of video key frames, video shots, video groups, and video scenes. We know that video is composed of out-frame images, so the video frame is the most basic element of the video structure [8, 9]. A continuous video frame constitutes a video shot. In a video frame, one or more frames of video that can
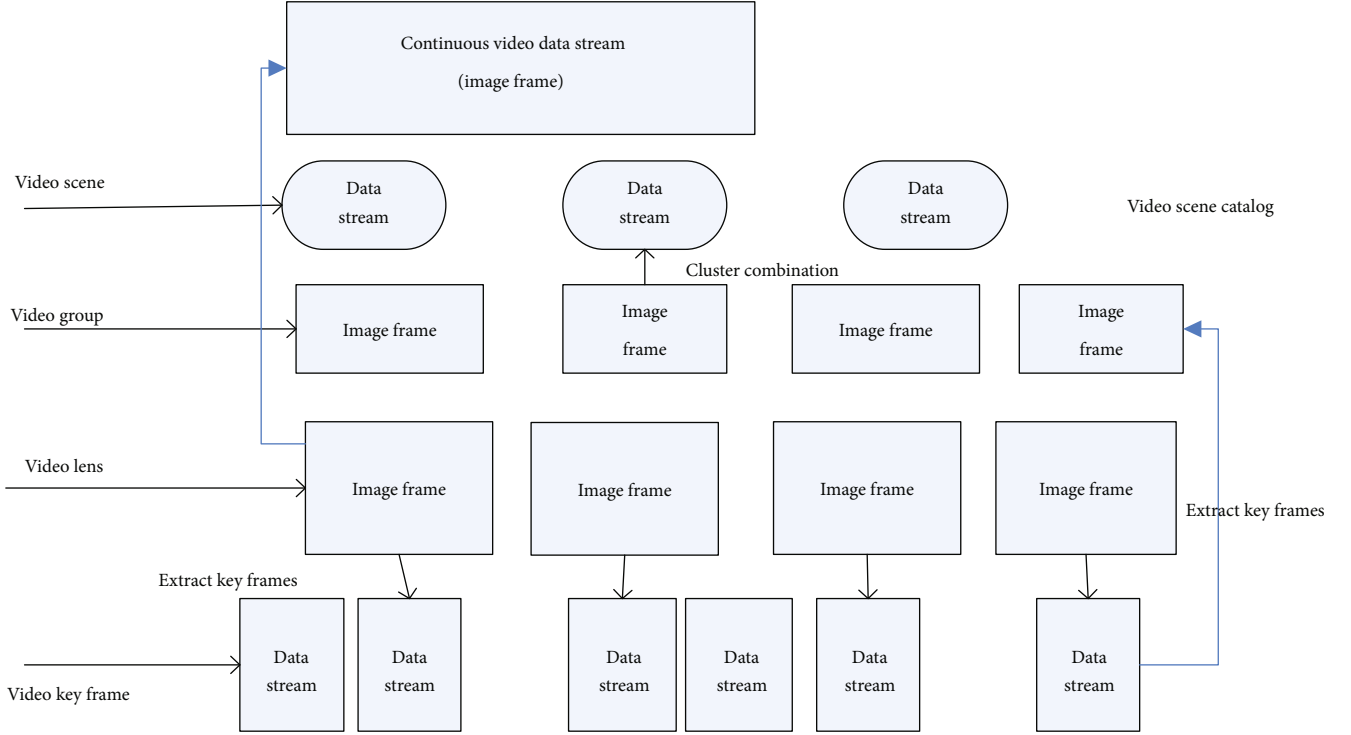
FIGURE 1: Structured block diagram of video stream.

represent the characteristics of a video shot constitute a key frame. Extracting key frames and segmenting video shots are the basis and key step of video structuring, which directly affects the efficiency of subsequent video detection [10]. Several video shots can constitute a video scene, and these shots are either semantically related or adjacent in time. The structure between the video scene and the video shot is defined as a group. The shots in the same group usually have similarity in content, similarity in background, and continuity in time [11], as shown in Figure 1.

2.1. Common Lens Detection Methods for Tennis Courts. The following briefly introduces several methods for detecting shots of tennis courts. The tennis match field shot referred to here is defined as a global shot containing the field [12, 13], because tennis video first needs to detect whether it is a tennis match, which is divided according to the color-coded spatial detection method of the tennis court.

(1) Detection method based on the statistical characteristics of the main color: there are four main types of tennis courts: clay courts, synthetic plastic courts, hard courts, and grass courts. These types can be distinguished by their color attributes [14]. Through the statistical analysis of some typical frames of tennis courts, Xu summarized the standard color attribute characteristics of four types of venues, as shown in Table 1.

This method first calculates the main color of the current frame image in the prescribed rectangular window and then calculates the Euclidean distance between the main color and the mean color value of various venue types (as shown in

TABLE 1: Color statistical characteristics of tennis courts.

Class of count	Mean (R : G : B) colors	Class threshold	Fraction threshold
Carpet	111 : 154 : 123 68 : 69 : 71 59 : 53 : 52 135 : 112 : 152	25	40
Clay	125 : 56 : 54 167 : 56 : 68	25	25
Hard	46 : 56 : 25	25	25
Grass	95 : 152 : 65 68 : 54 : 152	25	40

Table 1.1) and obtains the minimum Euclidean distance [15]. Which venue type has the smallest Euclidean distance, then court_class is recorded as the venue type, and court_color is recorded as the main color value corresponding to the venue type. The formula for calculating the Euclidean distance between pixel point (m, n) and point (j, k) is as follows:

$$d_e[(m, n), (j, k)] = \left[(m - j)^2 + (n - k)^2\right]^{1/2}. \quad (1)$$

For the color image of the color model, the formula for calculating the Euclidean distance is as follows:

$$d_e[(m, n), (j, k)] = \left[\left(B_{(x,y)} - B_{(j,k)}\right)^2 + \left(R_{(x,y)} - R_{(j,k)}\right)^2 \right. $$
$$\left. + \left(G_{(x,y)} - G_{(j,k)}\right)^2\right]^{1/2}.$$

$$(2)$$

If the minimum Euclidean distance obtained is not less than the marked field type threshold (Class Threshold), then, the frame image is considered to be not a frame containing a tennis court [16]. Otherwise, do the following for each pixel in the rectangular window area: calculate the Euclidean distance between the color of each pixel and the field color marked by count_color, if the distance is greater than the Fraction_Threshold threshold of the field type marked by count_class, then

$$\text{Court} = \text{court} + 1, \tag{3}$$

$$\text{Total} = \text{total} + 1. \tag{4}$$

Finally, the formula is used to calculate the proportion of pixels belonging to the court. If court_fraction is greater than 0.6 (determined as the set empirical value), the frame of image is considered to be a tennis court frame belonging to the current court type. Otherwise, the frame does not belong to the frame containing the playing field [17]. This method is more convenient and simple, easy to implement, and low computational complexity. However, there are two shortcomings. First, when calculating the Euclidean distance between a specific type of field frame and the color of the current frame, a fixed threshold is used to determine whether the current frame is a game scene frame. The problem is that the fixed closed value has certain limitations. If the selection is unreasonable, it will greatly affect the detection effect [18, 19]. Second, using color features alone cannot obtain good detection results. If the color of the clothing worn by the player is very close to the color of the field, the close-up shot of the player will also be considered a field shot [20].

(2) Detection method based on white pixels: Pan and Weijun observed that no matter what type of court, the boundary line of the tennis court is always white. In addition, the number of white pixels composing the boundary line of the field is a relatively constant [9]. Using these two characteristics, the algorithm is proposed.

   (i) Detection of white pixels: normally, the boundary line of any tennis court is white. However, in actual situations, there is not only the field line, which is the only white object in an image [21]. Advertising icons, parts of the stadium, spectators, and sometimes even the clothes worn by the players are more or less white. Therefore, it is assumed in the literature that the width of the field line will not be wider than one pixel. It is set in the literature to select a candidate pixel and compare whether the brightness value of the pixel in the four directions of the pixel distance is greater than the brightness value of the candidate pixel. If the brightness value of the surrounding pixels is less than the brightness value of the candidate pixel, the candidate pixel is marked as a white pixel [22].

(ii) Detection of the playing field frame: set a rectangular window; the length is the length of the image, the width is one-half of the width of the image, and the center of the rectangle is the center of the image. The selection of the threshold of this method is based on experience, so it greatly affects the accuracy and effectiveness of the detection [23]. In addition, for the clay field, the white field line is not complete, and the accuracy of detection is low by relying solely on the number of white pixels on the field line [24].

3. Audio Stream Analysis and Recognition in Tennis Video

In recent years, the semantic analysis of audio streams has attracted the attention of researchers in related technical fields such as content-based video analysis and retrieval, speech recognition, and audio retrieval. By comparing and analyzing several representative audio recognition and classification algorithms, we found that the algorithm based on the HMM Hidden Markov Model has better recognition efficiency. In this paper, the HMM classification algorithm is used to divide the tennis game audio stream into five categories: batting sound, cheering sound, passionate commentary by the narrator, gentle definition by the narrator, and background noise [23].

3.1. Implementation of Audio Classifier. Currently, the implementation of audio classifiers is mainly based on the following methods:

(1) Rule-based audio classification: the basic idea of this method is you can select a feature that can be distinguished from other audio categories, then set a threshold for the function, and compare the calculated actual function value with the threshold according to the default rule to specify the audio category. This method is easy to use, but due to its simplicity, it is only suitable for audio types that have simple identification functions such as mute. This method has the following disadvantages:

   (i) Decision rules and classification order are not necessarily optimal

   (ii) Decision errors at higher levels will accumulate to the next level, forming a "snowball" effect

   (iii) The classification error is large and requires prior human knowledge and experimental analysis, especially the threshold determination. Therefore, the classification accuracy of the rule classification method is low, and it is only suitable for simple voice classification that can be clearly distinguished, and it is difficult to support complex and multifunctional voice classification applications
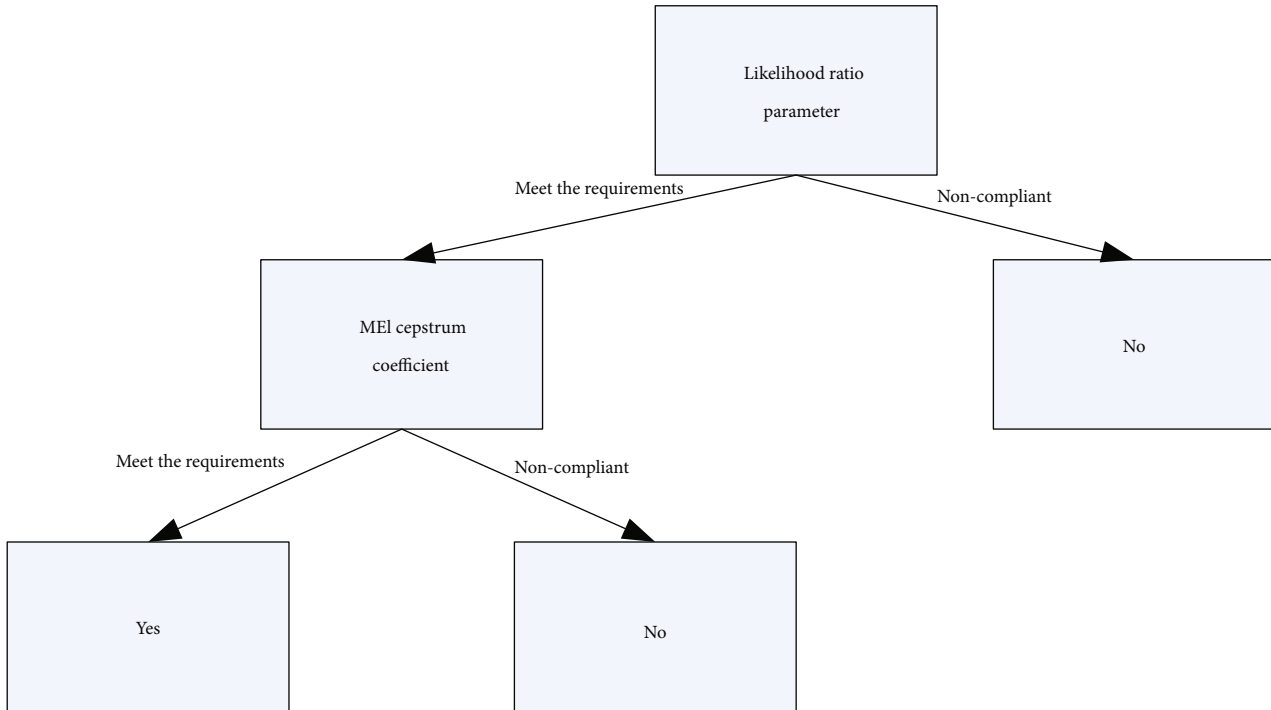
FIGURE 2: Schematic diagram of decision number.

(2) Minimum distance audio classification: this method uses the idea of matching templates to create a template for each audio type and then calculates the feature vector of the actual audio frame and uses the feature vector to match the template vector (usually calculating their distance from the vector space) to determine the type of sound.

(3) Audio classification based on statistical learning algorithm: this method requires specifying a batch of preclassified training samples, creating a classifier with guided learning and training and measuring the samples to be classified in the test set to measure the classification performance. Speech classification based on statistical learning algorithms is the focus of speech classification research. It provides an effective way to perform automatic and self-learning classification. This is the main research direction in this field now and in the future.

3.2. Typical Audio Classification Method. Typical audio classification methods include decision tree-based classification methods, KNN (nearest neighbor method) classification methods, Bayesian classification methods, neural network classification methods, SVM (support vector machine) classification methods, and hidden Markov model methods.

(1) Classification method based on decision tree: the so-called decision tree is a tree structure similar to a flowchart. Each node of the tree represents a test of an attribute (value), its branches represent the test results, and each node of the leaves of the tree represents a category. The highest node of the tree is the root node. The decision tree in Figure 2 describes whether the audio track is a speech signal and has been classified and predicted, as shown in Figure 2.

In order to sort and identify unknown data objects, the attribute values in the data set can be checked according to the structure of the decision tree. The path from the root node to the leaf node of the decision tree forms the class prediction of the corresponding object. Decision trees can be easily transformed into sorting rules. When building a decision tree, there are many branches in the data set that will generate noise or abnormal data. Pruning a tree is a method of locating and eliminating such branches to improve the classification accuracy of unknown objects.

(2) KNN (k-nearest neighbor method) classification method: KNN classification is a classification method that minimizes distance. KNN classifier is a classification calculation method based on learning rate. The training samples have n digital features, and each sample represents a node in a n-dimensional space, so all samples are stored in a n-dimensional space. When inputting an unknown data object (type), the KNN classifier will search the dimensionless space and find the k training samples closest to the unknown data object. When inputting an unknown data object (category), the KNN classifier will search the dimensionless space and find the k training samples closest to the unknown data object. These training samples k are the "k" of the unknown data object. The concept of "nearest" refers to the Euclidean shortest distance between two points in the e-dimensional space, and the two points in the n-dimensional

space $\quad X = \{x_1, x_2, \cdots, x_n\} \quad$ and $\quad Y = \{y_1, y_2,$ the Euclidean distance between, $\cdots, y_n)$ are defined as

$$d(X, Y) = \sqrt{\sum_{i=1}^{n}(X_i - Y_i)}. \tag{5}$$

Data objects of unknown categories are classified as the category with the highest occurrence among the "k-nearest neighbors". When $k = 1$, the data object of the unknown category will be attributed to the category of the training sample closest to its target. The nearest neighbor classifier is a classification technique based on instance learning or lazy leaning.

(3) Bayesian classification method: Bayesian classification is a very mature statistical classification, mainly used to predict the possibility of relationships between class members. For example, the probability that a particular observation belongs to a particular category can be determined by the associated characteristics. The Bayesian classifier is based on Bayes' theorem. The basic Bayesian classifier assumes that the value of each attribute in the specified category is independent of each other. When using large databases, Bayesian classifiers can provide higher classification accuracy and computational performance.

(4) Neural network classification method: as an advanced artificial intelligence technology, a neural network is very suitable for processing nonlinear and those processing problems characterized by fuzzy, incomplete, and imprecise knowledge or data due to its own processing, distributed storage, and high fault tolerance. This feature of it is very suitable to solve the problem of data mining.

Similar methods to classify tennis videos using machine learning include the following:

(1) Use ConvNet to divide frames one by one

(2) Use a time-distributed ConvNet in a network and pass such features to RNN

(3) Use a 3D convolutional network

(4) Use ConvNet to extract features from each frame and pass this feature sequence to another RNN

(5) Use ConvNet to extract features from each frame and pass this feature sequence to another MLP

In summary, the HMM has a unique advantage if the research problem is based on sequence, such as time sequence or state sequence. There are two types of data in the research question. One type of sequence data is observable, that is, the observation sequence, while the other type of data cannot be observed, that is, the hidden state sequence, referred to as the state sequence.

4. Audio Stream Analysis of Tennis Match

4.1. Basic Principles of Hidden Markov. Audio classification is an important means to extract audio structure and content semantics and has great application value in content-based audio retrieval. Because the hidden Markov model (HMM) can well describe the temporal statistical characteristics of audio signals and many audios, it is often classified into multiple classes. This paper proposes an audio multilabel classification algorithm based on a hidden Markov model. The classification algorithm is used to classify so that an audio has multiple labels. HMM has a double random process. A Markov chain is a meditation process with a finite state. Another stochastic process describes the statistical correspondence based on observations and statements.

The parameters included in an HMM are as follows:

(1) E: the number of states is included in the Markov chain. Let $a_1, \cdots, a$ be e states, then $n, n(a_1 \cdots a_n)$ are the states of the Markov chain at time t

(2) F: the number of observations is corresponding to N states. Let $b_1, \cdots, b_f$ be F observation values, then o, $o \in (b_1, \cdots b_f)$ are the observation values at time t

(3) Q: the probability of the initial state is $Q = (Q_1, \cdots, Q)$, and

$$Q_1 = P(n_1 = a_i), \quad 1 \leq i \leq n. \tag{6}$$

Equation (6) describes the probability that any state in the HMM is taken as the initial state

(4) N: state transition probability matrix is $A = (C_{ij})_{n \times n}$, and

$$C_{ij}P(n_{t+1} = a_j), \quad 1 \leq i, j \leq N. \tag{7}$$

Equation (7) describes the probability of the state at time $t + 1$ and takes the state at time t as the condition

(5) B: observation probability matrix is $M = (a_{jk})_{n \times m}$, and

$$a_{jk} = P(o_t = b_k), \quad 1 \leq j \leq N, 1 \leq k \leq M. \tag{8}$$

Equation (8) describes the probability that the observed value is b_k when the state is a_j at time t.

Therefore, according to the description of each parameter above, one HMM can be denoted as

$$\lambda = (E, F, Q, N, B) \tag{9}$$
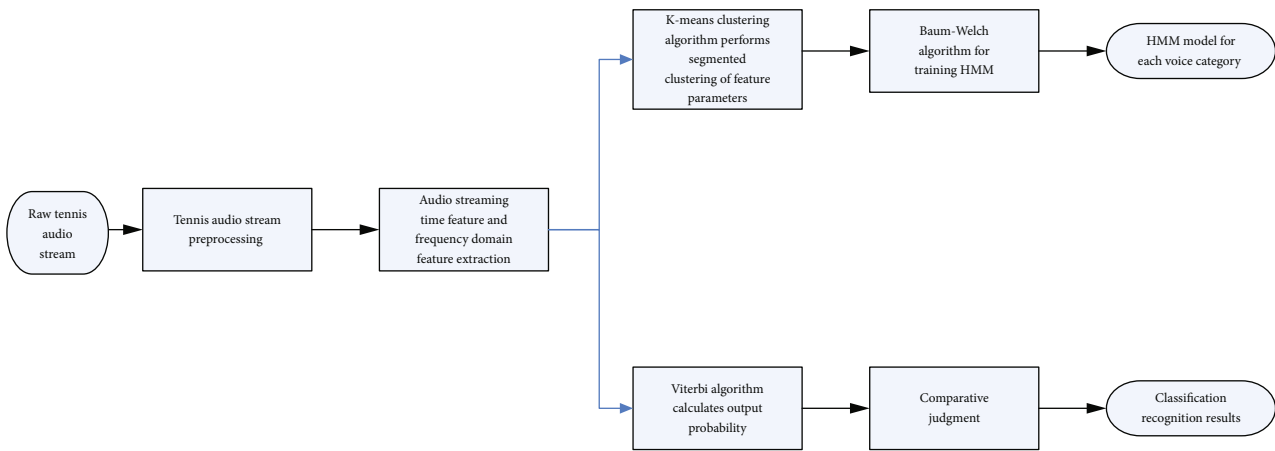
FIGURE 3: The flow diagram of the classification of I give you the ball audio stream based on HMM.
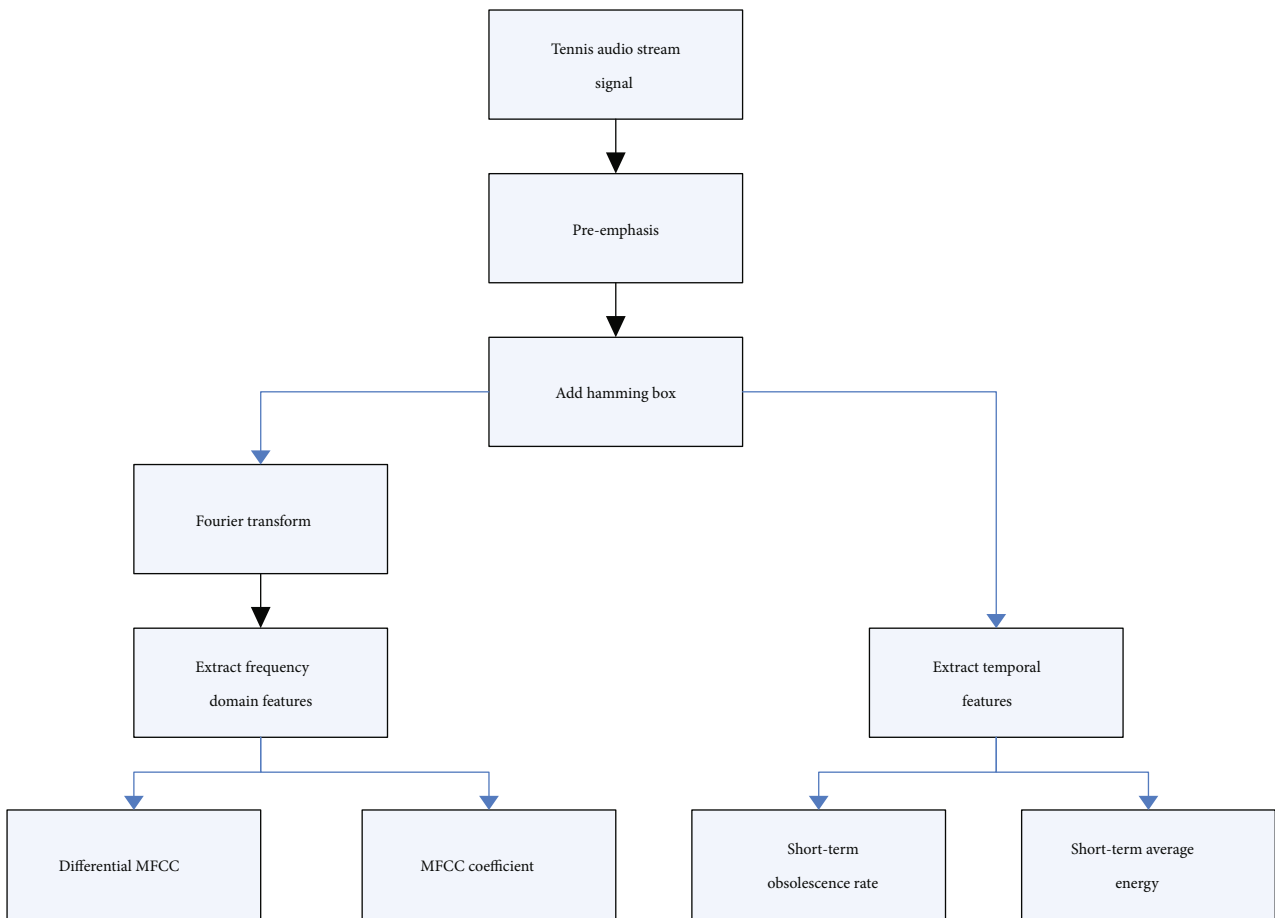
FIGURE 4: Block diagram of the extraction process of time domain feature and frequency domain feature parameter of tennis audio stream.

4.2. Overall Framework of Tennis Audio Stream Analysis

(1) First, preprocess the original audio stream, and extract the time-domain and frequency-domain features of the audio

(2) Second, analyze the extracted feature parameters using K-means clustering algorithm. And model the analysis results

(3) Finally, the Baum-Welch algorithm is used to train the HMM parameters. After the model is trained,
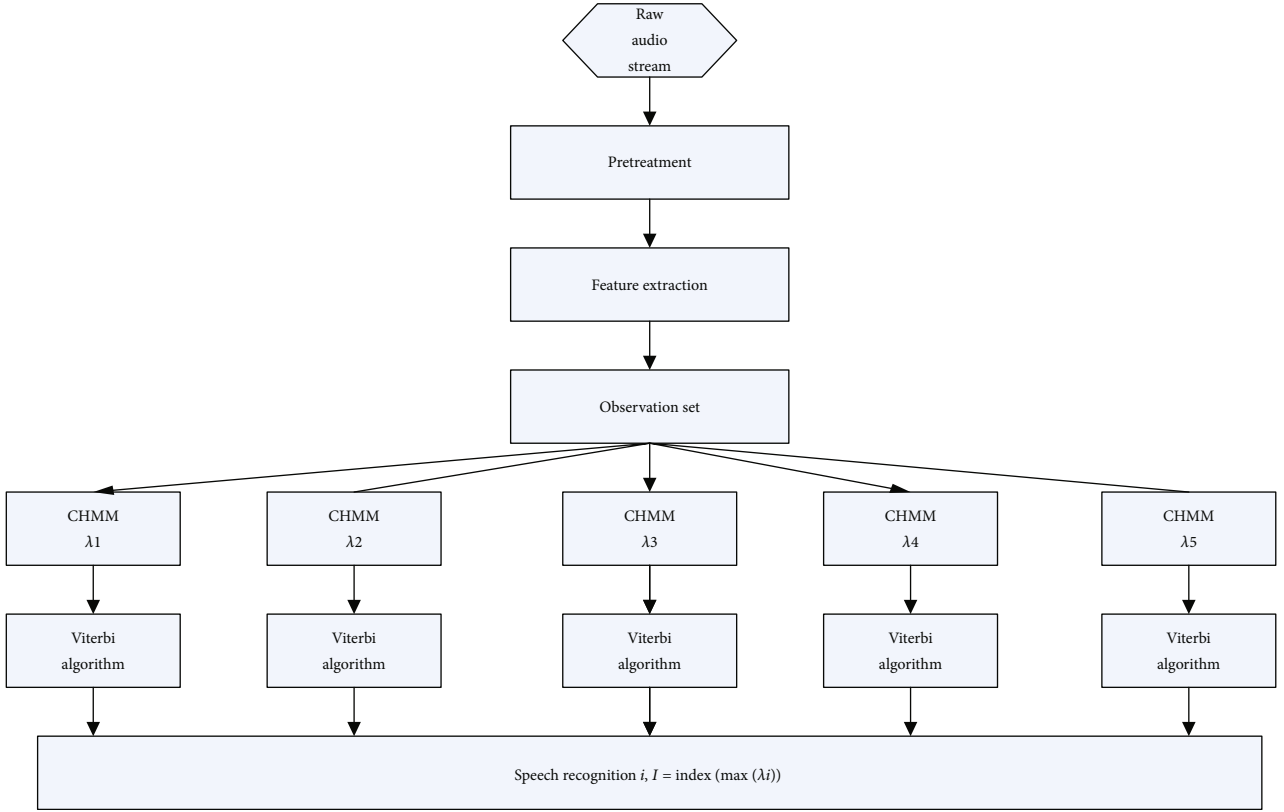
FIGURE 5: Flow chart of audio recognition and classification method based on CHMM.

load the tennis audio to be classified, and use the Viterbi algorithm to classify and recognize the audio to obtain the final result. The specific audio classification process block diagram is shown in Figure 3

4.3. Tennis Audio Feature Analysis and Extraction.
The extraction process of the time-domain feature parameters of the tennis audio stream in this paper is shown in Figure 4.

4.4. Parameters of Training Audio Model.
The core idea of parameter training is based on a specific sequence of observations $A = A_1, A_2, \cdots, A_t$ and the initial model parameters $\lambda = (E, F, Q, N, B)$; the model parameters are repeatedly adjusted to form a new model $\bar{\lambda}$, so that $C(O/\bar{\lambda}) > P(O/\lambda)$ will converge until the $C(O/\bar{\lambda})$ is converged. In the process, try to maximize the probability $C(O/\bar{\lambda})$, and finally get the best $\lambda = (Q, N, B)$. It can be seen from the reevaluation formula shown in Section 3.1.2 that the appropriate model structure and the corresponding initialization parameters π_i, a_{ij}, and b_{jk} should be selected before the model parameter training [9].

The continuous hidden Markov (CHMM) observation sequence is generated by simulating the Gaussian probability density function. Moreover, many linear combinations of Gaussian probability density functions are often used in simulations, and each Gaussian probability density function has its own mean and covariance. Since the HMM model can be

represented by triple $\lambda = (Q, N, B)$, the CHMM can be represented by a similar structure $\lambda = (E, F, W_{jt}, \mu_{jt}, \delta_{jt}^2)$, where W_{jt} is the weight of the l-th mixed Gaussian element in state j, μ_{jt} is the mean value of the l-th mixed Gaussian element in state j, and δ_{jt}^2 is the covariance of the l-th mixed Gaussian element in state j [22].

The most important step in CHMM model training is the selection of initial values. Choosing the correct initial value means that the number of iterations required to reach the convergence state is the least, and the calculation efficiency is significantly improved accordingly.

4.5. Audio Classification and Recognition.
After training the CHMM model of five types of tennis audio using the method introduced in the above section, we use the Viterbi algorithm to classify and recognize the five type of tennis audio that have been trained. The specific classification steps are [23, 24] as follows:

(1) In preprocessing the input tennis audio stream, firstly, the tennis audio stream is divided into a sequence of audio segments of length ls, and then a Hamming window is added to each audio segment to obtain a total of nFrame audio frames and each audio frame extraction feature parameters:

$$W_i = \gamma_{i1}, \gamma_{i2}, \cdots, \gamma_{i26}, \quad 1 \le i \le \text{nFrame}, \quad (10)$$
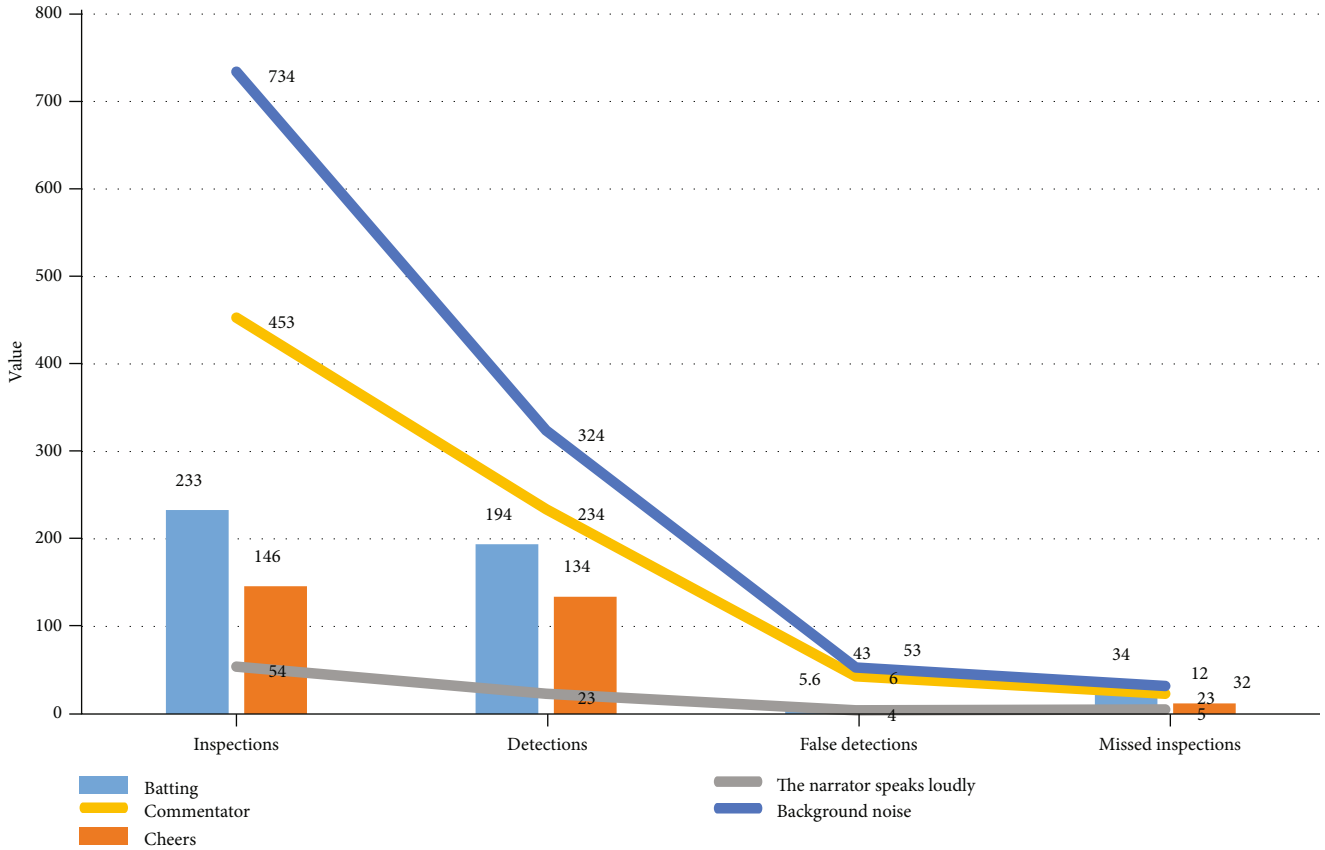
FIGURE 6: Experimental results of classification, recognition, and detection of audio segments in tennis matches.

where F_i represents the feature vector of the i-th frame and γ_{ij} represents the j-th feature value of the i-th frame.

(2) Obtain the feature vector $W = W_1, W_2, \cdots, W_{nFrame}$ of the audio segment from the feature parameters of the audio frame

(3) Calculate the output probability of five types of models: the sound of hitting a tennis ball, the excited cheers of the audience, the impassioned voice of the narrator, the gentle narration of the narrator, and the background noise contained in the tennis court. And these five types of models correspond to the observation sequence $W = W_1, W_2, \cdots, W_{nFrame}$ in step (2)

(4) Select the largest output probability $P(O/A)$ from the output probability group. The CHMM model corresponding to its subscript i is the category of the audio segment

(5) All audio segments are processed in steps (1)–(4), and finally, the classification and recognition of the tennis audio stream are completed. The whole process is shown in Figure 5

In order to verify the effectiveness of the algorithm, this article selects two tennis match audios for experimental analysis.

(1) The first segment contains 256 shots. Each of the five audio categories selects 20 samples as training data, and the audio test segment is composed of the remaining samples. The experimental results are shown in Figure 6

From the experimental results in Figure 6, it can be seen that the detection and recognition efficiency of background noise, impassioned commentary by the narrator, gentle commentary by the narrator, and cheers are relatively high. The recall rate of batting sound is only 82.3%, which is relatively low, and the number of false detection is relatively high. Analyzing the reasons, it is known that the sound of hitting a tennis ball is easily affected by the background noise of the playing field. For example, the referee's yelling when the player is unsuccessful in serving the ball or the sound of some hits in the game is relatively small and the sound is not obvious; these will increase the number of false detection and reduce the detection efficiency.

(2) This article selects a video of the US Open with 72 shots and 56 exciting events as the experimental material of the algorithm. The experimental results are shown in Figure 7

It can be seen from Figure 7 that the detection rate of the bottom line hit event has reached 92% and 88%, which are
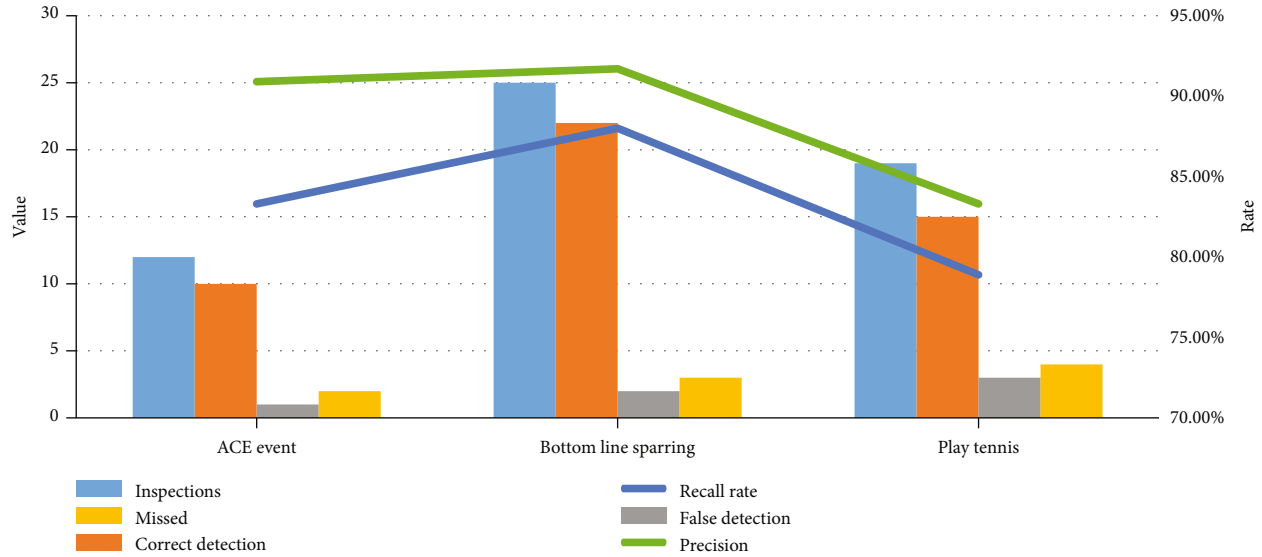
FIGURE 7: Detection results of exciting events in tennis video.

relatively high, while the detection efficiency of 84% and 80% of the ACE ball event and the tennis event is not very good. The main reasons are as follows:

(1) The duration of the successful ACE ball through the second serve is relatively long, and it is easy to miss the test

(2) It is easy to confuse the batting sound and the referee's shouting when the player fails to serve the ball, which reduces the detection rate of the batting sound

(3) The logo-based slow motion detection method needs to be further strengthened to reduce the missed detection rate and false detection rate of slow motion

In summary, the multimodal fusion-based tennis video event detection method constructed in this paper still has some areas to be improved and improved. However, compared with methods that rely solely on video features, audio features, and text features to detect exciting events, the detection efficiency is much improved. Therefore, the overall detection effect is satisfactory.

5. Conclusions

Applying the audio information of the lens to the lens class can better assist in the detection of some wonderful events in tennis. This article extracts audio signals from the game shots in the shot classification table and identifies the cheers and batting sounds in the audio signal of each game shot. Support vector machine (SVM) is a new machine learning method developed based on statistical learning theory. Through experiments, we found that the radial basis function has better classification performance and calculation speed in speech classification. In order to overcome the limitation that SVM can only handle two classification problems, this paper uses the method of combining SVM and decision tree-SVM decision method to deal with audio multiclassification

problems. And according to this method, a SVM classifier is constructed to identify three audio categories: Silence/Non-Silence, Cheer/Non-Cheer, and Rally/Non-Rally. These three SVM classifiers are integrated to realize the recognition of the audio segment type of the tennis match. The experimental results show that it is feasible to use the SVM decision tree multilevel classifier to identify the audio segment type in the tennis match. The disadvantage of HMM is that it only depends on each state and its corresponding observation object: the sequence labeling problem is not only related to a single word but also related to the length of the observation sequence, the context of the word, and so on. The objective function and the prediction objective function do not match: what HMM learns is the joint distribution $P(Y, X)$ of the state and the observation sequence, and in the prediction problem, what we need is the conditional probability $P(Y \mid X)$.

Data Availability

Data sharing is not applicable to this article as no datasets were generated or analyzed during the current study.

Disclosure

We confirm that the content of the manuscript has not been published or submitted for publication elsewhere.

Conflicts of Interest

There are no potential competing interests in our paper.

References

[1] G. A. Rovithakis, M. Maniadakis, and M. Zervakis, "A hybrid neural network/genetic algorithm approach to optimizing feature extraction for signal classification," *IEEE Transactions on Systems, Man and Cybernetics, Part B (Cybernetics)*, vol. 34, no. 1, pp. 695–703, 2004.

[2] K. Zupanc and Z. Bosnic, "Automated essay evaluation with semantic analysis," *Knowledge-Based Systems*, vol. 120, pp. 118–132, 2017.

[3] R. Jenke, A. Peer, and M. Buss, "Feature extraction and selection for emotion recognition from EEG," *IEEE Transactions on Affective Computing*, vol. 5, no. 3, pp. 327–339, 2017.

[4] S. Ding, S. Qu, Y. Xi, and S. Wan, "A long video caption generation algorithm for big video data retrieval," *Future Generation Computer Systems*, vol. 93, pp. 583–595, 2019.

[5] N. N. Hurrah, S. A. Parah, N. A. Loan, J. A. Sheikh, M. Elhoseny, and K. Muhammad, "Dual watermarking framework for privacy protection and content authentication of multimedia," *Future Generation Computer Systems*, vol. 94, pp. 654–673, 2019.

[6] N. Krishnaraj, M. Elhoseny, E. L. Lydia, K. Shankar, and O. ALDabbas, "An efficient radix trie-based semantic visual indexing model for large-scale image retrieval in cloud environment," *Software: Practice and Experience*, vol. 51, no. 3, pp. 489–502, 2021.

[7] J. Korpela, R. Miyaji, T. Maekawa, K. Nozaki, and H. Tamagawa, "Toothbrushing performance evaluation using smartphone audio based on hybrid HMM-recognition/SVM-regression model," *Journal of Information Processing*, vol. 24, no. 2, pp. 302–313, 2016.

[8] D. Lijuan, X. Tao, W. Chunpeng, M. Wei, M. Jun, and Q. Honggang, "Integration of spatial and temporal characteristics of the video image visual significant degree detection method," 2016.

[9] D. Pan and G. Weijun, "Sports video classification method based on hidden Markov model," *Journal of Natural Science of Xiangtan University*, vol. 39, no. 1, pp. 73–77, 2017.

[10] S. Xinyi, R. Wang, and Z. Hongxiang, "An improved K-means clustering algorithm," *Computer and Digital Engineering*, vol. 46, no. 4, pp. 682–685, 2018.

[11] Z. Jin and C. Zemao, "Anomaly detection algorithm based on improved K-means clustering," *Computer Science*, vol. 43, no. 8, pp. 258–261, 2016.

[12] Z. Rongjuan, C. Xie, and H. Fenghua, "Player detection and tracking in tennis video," *Journal of Yanbian University (Natural Science Edition)*, vol. 45, no. 2, pp. 161–165, 2019.

[13] Q. Datong, Z. Sen, Q. Zhenggang, and C. Shujiang, "Driving condition construction method based on K-means clustering algorithm," *Journal of Jilin University (Engineering and Technology Edition)*, vol. 46, no. 2, pp. 383–389, 2016.

[14] C. Xu, "Semantic analysis of tennis audio based on hidden Markov model," *Information Technology*, vol. 8, pp. 103–106, 2019.

[15] V. N. Phu, V. T. N. Tran, V. T. N. Chau, N. D. Dat, and K. L. D. Duy, "A decision tree using ID3 algorithm for English semantic analysis," *International Journal of Speech Technology*, vol. 20, no. 3, pp. 593–613, 2017.

[16] J. John and C. K. Raju, "Design and comparative analysis of mobile computing software framework," in *2018 Second International Conference on Inventive Communication and Computational Technologies (ICICCT)*, Coimbatore, India, 2018.

[17] J. E. Bibault, P. Giraud, and A. Burgun, "Big data and machine learning in radiation oncology: state of the art and future prospects," *Cancer Letters*, vol. 382, no. 1, pp. 110–117, 2016.

[18] A. Buczak and E. Guven, "A survey of data mining and machine learning methods for cyber security intrusion detection," *IEEE Communications Surveys& Tutorials*, vol. 18, no. 2, pp. 1153–1176, 2017.

[19] C. Helma, T. Cramer, S. Kramer, and L. De Raedt, "Data mining and machine learning techniques for the identification of mutagenicity inducing substructures and structure activity relationships of noncongeneric compounds," *Journal of Chemical Information and Computer Sciences*, vol. 44, no. 4, pp. 1402–1411, 2018.

[20] X. Yuan, Z. Ge, L. Ye, and Z. Song, "Supervised neighborhood preserving embedding for feature extraction and its application for soft sensor modeling," *Journal of Chemometrics*, vol. 30, no. 8, pp. 430–441, 2016.

[21] S. Rabie, S. Aridhi, E. M. Nguifo, and M. Maddouri, "Feature extraction in protein sequences classification: a new stability measure," *Medical Physics*, vol. 37, no. 6, pp. 683–689, 2018.

[22] H. Zhao, Z. Wang, and F. Nie, "Orthogonal least squares regression for feature extraction," *Neurocomputing*, vol. 216, no. DEC.5, pp. 200–207, 2016.

[23] V. A. Nugroho, D. P. Adi, A. T. Wibowo, M. Y. T. Sulistyono, and A. B. Gumelar, "Klasifikasi jenis pemeliharaan dan perawatan container crane menggunakan algoritma machine learning," *MATICS*, vol. 13, no. 1, pp. 21–27, 2021.

[24] L. Pitak, K. Laloon, S. Wongpichet, P. Sirisomboon, and J. Posom, "Machine learning-based prediction of selected parameters of commercial biomass pellets using line scan near infrared-hyperspectral image," *Processes*, vol. 9, no. 2, pp. 316–320, 2021.

WILEY | Hindawi

Research Article

An Improved Image Segmentation Algorithm CT Superpixel Grid Using Active Contour

Yuntao Wei and Xiaojuan Wang (ID)

College of Electronic Information Technology, Jiamusi University, Jiamusi 154007, China

Correspondence should be addressed to Xiaojuan Wang; wangxiaojuan@jmsu.edu.cn

The traditional CT image segmentation algorithm is easy to ignore image contour initialization, which leads to the problem of long time consuming and low accuracy. A superpixel mesh CT image improved segmentation algorithm using active contour was proposed. CT image superpixel gridding was carried out first; secondly, on the basis of gridding, the region growth criterion was improved by superpixel processing, the region growth graph was established, the image edge salient graph was calculated based on the growth graph, and the target edge was obtained as the initial contour; finally, the Mumford-Shah model in the active contour model was improved; the energy functional was constructed based on the improved model and transformed into the symbol distance function. The results show that the proposed algorithm takes less time to mesh superpixels, the accuracy of image edge calculation is high, the correct classification coefficient is as high as 0.9, and the accuracy of CT image segmentation is always higher than 90%, which has superiority.

1. Introduction

Computed tomography (CT) has the advantages of fast imaging and high image resolution. It is an important electronic imaging technology [1, 2]. As an important detection method in routine clinical examinations, it has become a computer-assisted human organ examination, and follow-up an important basis for medical treatment is currently widely used in clinical medicine [3, 4]. In the computer-aided diagnosis medical system, segmentation of the region of interest in the CT image is an important step in diagnosis and the key technical support for subsequent 3D image reconstruction. It plays an important role in the precise diagnosis and treatment of diseases and can also reduce calculations to a certain extent [5]. Human CT scan images include multiple organs such as the chest, abdomen, and blood vessels. In view of the complexity, irregularity, and uncertainty of human organs [6], it brings certain difficulties to image segmentation, and ordinary image segmentation techniques are difficult to obtain more accurate. As a result, the limitations are strong, so there is an urgent need to find an effective CT image segmentation algorithm, which is of

great significance for clinical auxiliary diagnosis and quantitative analysis with the help of CT images [7].

Traditional image segmentation algorithms mostly use pixels as the basic unit and represent the pixels by forming a matrix, but it is often easy to ignore the internal connection between pixels and cannot comprehensively consider pixel characteristics. Segmentation will occur when there is occlusion or low texture [8]. The basic principle of the concept of superpixel is to judge the similarity according to the texture features and brightness of the pixels. Therefore, the pixels can be divided into different subregions, which is convenient for subsequent calculation, improves the efficiency of image segmentation, and makes up for the shortcomings of traditional image segmentation algorithms [9]. Taha and Hanbury propose an efficient evaluation tool implementing the 20 selected metrics. The tool is optimized to perform efficiently in terms of speed and required memory, also if the image size is extremely large as in the case of whole body MRI or CT volume segmentation [10]. Chengcheng et al. [11] used convolutional neural network to extract image features, retrieved the image set, and used Gaussian kernel density estimation to weight the superpixels of the image,

thereby improving the pixel matching accuracy and completing high-precision image segmentation; Jiarui et al. [12] perform clustering analysis based on the results of superpixel segmentation and perform superpixel segmentation on the image area to obtain matching areas containing feature points. Based on this, effective feature points can be obtained to help subsequent analysis. Superpixel segmentation is used in this algorithm. Miao et al. [13] improved and analyzed the current superpixel method. First, iteratively clustered images based on local information performed the first superpixel segmentation on the clustered images and then performed iterative segmentation again based on the color standard deviation and merge to obtain an effective superpixel segmentation algorithm.

With the help of the concept of superpixel segmentation, this paper proposes an improved segmentation algorithm for superpixel grid CT images using active contours. The main contributions are as follows: (1) Using superpixels to improve the region growth criterion, the determination of the initial contour is more accurate. (2) The paper improves the Mumford-Shah model, fully considers the pixel texture characteristics, and increases the accuracy of CT image segmentation. (3)Various types of CT image data are used for experimental analysis, and the selection of experimental indicators is abundant, which greatly increases the validity of the experimental results.

2. Related Work

For CT image segmentation, many studies have been carried out at home and abroad. Literature [14] combines convolutional neural network and superpixel analysis for CT image segmentation, uses the superpixel method to grid the CT image while labeling the label, and uses the convolutional neural network to train the superpixel edge to complete the rough image segmentation. The segmented edge is used as the initial contour to be segmented again to obtain accurate segmentation results, but the algorithm has certain shortcomings in terms of running time; literature [15] also uses the superpixel method for image gridding and convolutional neural network for image edge extraction. The extracted edge pixels are formed as the initial contour and then combined with the integrated energy function to complete the image segmentation. The accuracy of the algorithm needs to be improved; the literature [16] combines superpixel segmentation and fuzzy C-means clustering to perform image segmentation. Use spatial neighborhood information to enhance image grayscale, use morphological knowledge to remove image peripheral influencing factors, and then perform superpixel classification on the grayscale and texture features of the image to obtain a more accurate image segmentation result, but for image pixel blocks underutilized.

In foreign studies, the literature [17] proposed a new three-dimensional adaptive active contour method for CT lung image segmentation. The method starts from a sphere in the lung. The force acting on the sphere is divided into the lung. This process is performed iteratively in order to minimize the energy function related to the 3D deformation model. The experimental results show the superiority of this

algorithm in CT image segmentation, but the use of active contours needs to be improved; the literature [18] that proposed an image segmentation algorithm based on superpixel clustering is proposed. First, the algorithm uses superpixel preprocessing technology to quickly divide the image into a certain number of superpixel regions with specific information and then uses the similarity matrix to provide input to the spectral clustering algorithm information. The superpixel area is clustered, and the final image segmentation result is obtained, but the segmentation accuracy is not high. Literature [19] focuses on simple linear iterative clustering superpixels and fast and automatically adjustable Gaussian path The image segmentation technology combined with the basis function kernel fuzzy C-means combines superpixels and image segmentation as a preprocessing step for image classification and then provides better results for image classification, but the accuracy of the algorithm is not high [20].

In order to obtain more accurate CT image segmentation results, this paper proposes an improved segmentation algorithm for CT images based on active contour superpixel grid. First, the CT image is processed with superpixel grids, and then based on the concept of superpixels, the region growth criterion is improved, and the concept of center-surround contrast is introduced to calculate the prominent area of the image edge, and the initial contour is obtained. The contour initialization problem of image segmentation is well completed. The active contour model is used to complete the segmentation of superpixel grid CT images. The experiment selects two data sets, TCIA and DeepLesion, as data sources and uses lung CT images, brain CT images, and vertebra CT images for analysis. The results show that the proposed algorithm is excellent in time-consuming, correct classification, and segmentation accuracy. Compared with other algorithms, it provides data support for further research on CT images.

3. CT Image Superpixel Gridding

In order to effectively complete the CT image segmentation, it is first necessary to perform the CT image superpixel gridding process, so that the pixels of the same pixel block in the image have a high degree of similarity in terms of color, texture, and intensity [21].

First, initialize the CT image pixels. The random collection of pixel seed points is represented as $D = \{d_{1n}, d_{2n}, \cdots, d_{kn}\}$ a grid with 2×2 units, the seed points are evenly distributed in the grid, and the pixels in the neighborhood of the seed points are marked. Expression:

$$\begin{cases} d(q) = \left(x_q, y_q\right) = 1, \\ d_k(q) = \left(x_{kq}, y_{kq}\right) = \infty, \end{cases} \quad (1)$$

where $\left(x_q, y_q\right)$ represents a certain gray pixel in the neighborhood.

The original grayscale D pixel of the seed point is expressed as (x_n, y_n); in the grid area, all the pixels D in the neighborhood of the seed point are counted, and the distance

between the seed point D and the pixel point is calculated separately, and the calculation is based on the grayscale feature. The formula is as follows:

$$s(p, q) = \sqrt{\left(x_p - x_q\right)^2 + \left(y_p - y_q\right)^2}, \tag{2}$$

where $s(p, q)$ represents the spatial distance of grayscale features between two pixels.

Calculated the straight D line distance between the seed point and the pixel point, expressed as:

$$s'(p, q) = \sqrt{\left(x_p - x_q\right)^2}. \tag{3}$$

The linear distance and the spatial distance are combined to synthesize a single unit of measure G. The formula is as

$$G = \sqrt{\left(\frac{s'}{\partial}\right)^2 + \left(\frac{s}{B}\right)^2}, \tag{4}$$

where ∂ represents the balance coefficient of the pixel gray feature in the straight line and B represents the step length between different seed points, which can be calculated by the following formula:

$$B = \sqrt{\frac{N}{L}}, \tag{5}$$

where N means that the CT image contains the number of L pixels and the number of pixel blocks to be divided.

4. Target Edge Calculation in CT Image Using Superpixel Region Growth

On the basis of CT image superpixel gridding, based on the superpixel processing to improve the region growth criterion, the target edge of CT image is obtained and used as the initial contour to lay the foundation for accurate image segmentation [22, 23].

This section introduces the production criteria to calculate the CT image saliency map to obtain the image target edge. Although the region growth criterion only considers the pixel brightness, there is a problem that the shadow image segmentation effect is not good [24]. This section is based on superpixels to make up for the deficiency of the region growth criterion and incorporates the texture features of superpixels to improve the accuracy of region growth.

The energy feature, entropy E feature, inertia H feature, and correlation K feature are, respectively, C used as edge superpixel texture features, combined with gray level features to calculate the similarity of superpixels; the formula is as follows:

$$T = \sqrt{\left(E_i - E_j\right)^2 + \left(H_i - H_j\right)^2 + \left(K_i - K_j\right)^2 + \left(C_i - C_j\right)^2 + \left(F_i - F_j\right)^2}, \tag{6}$$

where T represents the similarity between i the first pixel and j the first pixel at the edge of the image, that is, the characteristic distance. F indicates the average gray scale of the pixel.

According to the above formula, the feature distance between the organ pixel block and the background pixel block in the edge of the CT image is obtained, and the average feature distance is obtained by the statistical analysis principle, which can be used as the region growth criterion based on superpixels. Select a pixel block from the edge area of the image, take this pixel block as the center, determine whether the characteristic distance of its neighboring pixel blocks meets the growth criterion; if it meets, merge it, traverse all the pixel blocks according to the above method, and complete the growth. Get the growth map of the edge area of the CT image.

On the growth map of the edge area of the CT image, using the center-surround contrast idea [25] to calculate the edge salient area, the target edge can be obtained. The center-surround contrast idea is based on regional texture features and average gray levels. The texture feature distance of the edge region of the image is calculated according to the following formula, that is, the similarity of regional texture features:

$$T' = \sqrt{\left(E_i - E_j\right)^2 + \left(H_i - H_j\right)^2 + \left(K_i - K_j\right)^2 + \left(C_i - C_j\right)^2}. \tag{7}$$

Calculated the similarity weight of regional texture features according to the above β formula:

$$\beta = \frac{255}{'T_{max}}, \tag{8}$$

where $'T_{max}$ is the maximum difference of the T' distance of the regional texture feature.

Calculate the texture feature distance between the current area and other areas. If the distance value of the current area is large, the area will be integrated into the current area. If the distance value is less than this area, the distance value of the current area will be used to subtract the distance value of the area [26, 27]. Thus, get the global surround contrast of the current M area:

$$M = F' + \chi \sum_{i=1} \beta T'_i. \tag{9}$$

F' represents the gray value χ of the current area and the compensation coefficient. Under the condition of comparing the current area with different areas, it will change accordingly. The values are as follows:

$$\chi = \begin{cases} 1 & F' > F_{out}, \\ -1 & F' \le F_{out}. \end{cases} \tag{10}$$

F_{out} represents the gray value of other areas.

Considering that there will be organs of a certain area in the actual CT image and may exist as edge locations, in order

to clearly express the organ area, the global surround contrast weight should be set δ to calculate the image salience value. The calculation method is as follows:

$$\delta = \frac{Z_{\text{back}}}{Z_{\text{org}}}. \tag{11}$$

Z_{back} is the area of the background. Z_{org} is the area of the organ area.

Combined with δ the weights, the final significance value can M' be calculated:

$$M' = \delta M. \tag{12}$$

According to the above formula, the salience values of all the edge regions are calculated, and the most salience region is selected; then, the target edge of the CT image can be obtained, which is used as the initial contour.

5. The Proposed Algorithm

Active contour model is the mainstream algorithm used in image segmentation in recent years. It combines level set and energy functional, while considering features such as image edges and regions, and has better performance than single feature segmentation algorithms [28, 29]. Active contour models include many types. The Mumford-Shah model (the best approximation of the original image is found by piecewise smoothing function) is selected in this paper to improve CT image segmentation. Proceed as follows:

Input: CT image initial contour and superpixel information

Output: CT image improves segmentation results

Initialize the image superpixel and contour problem and use the Mumford-Shah model for final image segmentation, as follows:

(1) On the basis of the classic Mumford-Shah model, the level set method is used to solve the Mumford-Shah model and optimize it. This process is similar to curve evolution, transforming the energy function into a level set function, and the function solution value is obtained after continuous iteration. First, simplify the function of the Mumford-Shah model to obtain the energy functional:

$$W(A, r_{\text{org}}, r_{\text{back}}) = M' + \lambda \int_{\text{inside}(A)} (Q - r_{\text{org}})^2 + \lambda \int_{\text{outside}(A)} (Q - r_{\text{back}})^2, \tag{13}$$

where $V_{CCR} = K'/K_{total}$ is the contour line, is the λ edge level coefficient, is the r_{org} target area feature, and is the r_{back} background area feature and Q is the image domain.

(2) Introduce the level $J(x, y, t)$ set function, solve the model, and obtain a new energy functional:

$$W' = J(x, y, t) + M' + \lambda \int_{\text{inside}(J)} (Q - r_{\text{org}})^2 J(x, y, t) dx dy$$
$$+ \lambda \int_{\text{outside}(J)} (Q - r_{\text{back}})^2 J(x, y, t) dx dy. \tag{14}$$

(3) In order to make the segmentation result smoother, a Gaussian function convolution method is added to the energy function to convert the energy function into a signed distance function

(4) CT image segmentation is essentially the process of solving the target contour. In the Mumford-Shah model, it can also be regarded as the process of solving the minimum value of the energy functional (signed distance function), and the sign distance function of each pixel in the CT image is iterated. Use the initial contour obtained in the previous section to obtain the initial value of the U_0 symbolic distance function. Starting from the initialization of the symbolic distance function, the minimum value of the function is solved by traversal operation:

$$U = U_0 + \arg\min\left(W'\right). \tag{15}$$

(5) In this way, the superpixel grid segmentation of the CT image can be completed, and the final contour can be obtained

(6) End

Based on the above analysis, the flow of improved segmentation algorithm for superpixel grid CT image is given as shown in Figure 1.

6. Experimental Results

6.1. Experimental Environment and Data Set. In order to verify the effectiveness of the algorithm proposed in this paper, a comparative experiment was designed to highlight the performance of this algorithm. This experiment is run in the same environment, with 3.2 GHz CPU, Intel i7-6700 as the central processing unit, Windows 10 as the computer operating system, and running in the experimental platform MATLAB.

The experimental data comes from the TCIA data set and DeepLesion data set.

TCIA data set. This data set is a large-scale medical. The medical data set contains various image data such as CT and MRI, with abundant clinical medical information

DeepLesion data set. It includes more than 32,000 lesion labels from more than 10,000 case studies, including image data of lesions in the lung, kidney, bone, lymph, and
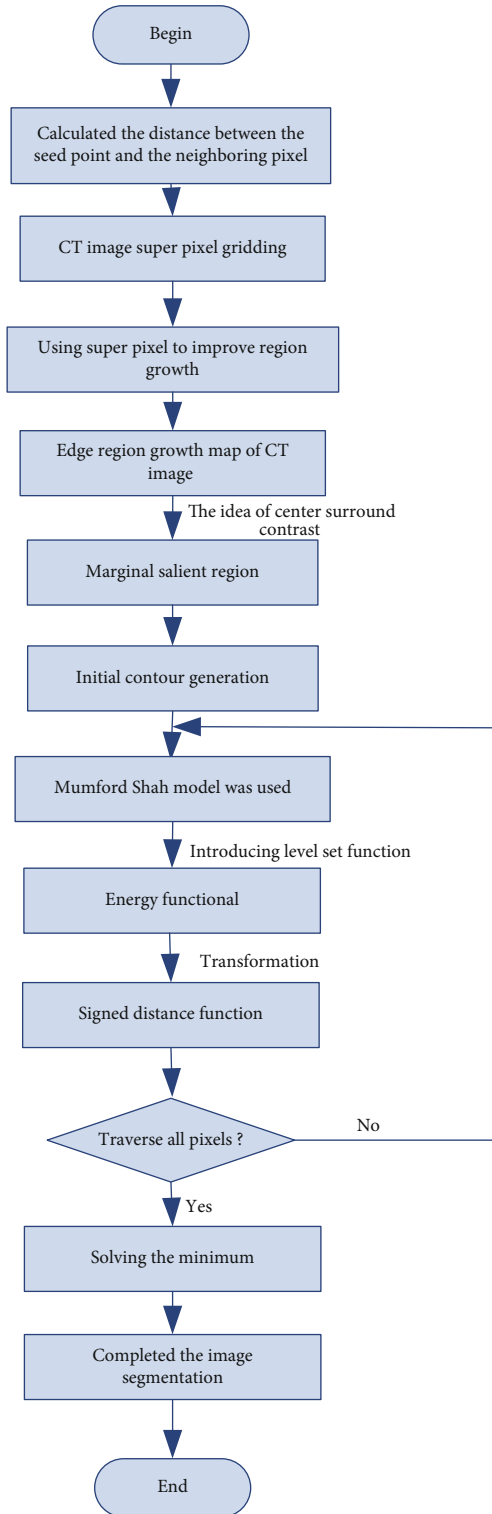
Figure 1: Flow of improved segmentation algorithm for superpixel grid CT image.

abdomen, a relatively comprehensive medical image data set currently released

The lung CT images, brain CT images, and vertebra CT images are selected from the above two data sets; 30 million

are selected for each data set, for a total of 60 million data. Half of them are used as training data sets, and half are used as test data sets.

The 2×2 grid was used to input images, and lung CT images, brain CT images, and vertebral CT images were selected from TCIA data set and deep vision data set. Each data set selected 30 million, a total of 60 million data, of which 40 million were used as training data set, 10 million as verification data set, 10 million as validation data set, and 1000 as test data set.

6.2. Experimental Steps

(1) First installed basic operating software, including CPU acceleration software, combined with the experimental environment parameters set above, and run in the experimental platform MATLAB

(2) Select the superpixel gridding parameter by multiple experiments, that is, the number of pixel blocks L to be divided. In this experiment, the final value of L is selected within [1000-3000]

(3) Construct an improved Mumford-Shah model for training, input the test data set after the training is completed, and run the algorithm in the set experimental environment

(4) Repeat experiments to verify the effectiveness of the proposed algorithm

6.3. Experimental Indicators

(1) *CT Image Segmentation Results and Manual Segmentation Results.*

Taking the lung CT images, brain CT images, and vertebra CT images as the objects, respectively, the segmentation maps are drawn by computer, and at the same time, to verify the segmentation effect of the algorithm in this paper, compare the results with manual segmentation.

(2) *Superpixel Grid Time-Consuming: Superpixel Grid.*

Transformation is the prerequisite of image segmentation in this paper. This process requires constant iteration to find the clustering center, so time-consuming can be used as an important indicator to measure the performance of the algorithm.

(3) *Image Target Edge Calculation Effect: According to the Public.*

Equation (12) shows that δ the weight has an important influence on the accuracy of solving the saliency value. δ If the weight is selected properly, the image edge saliency can be calculated accurately. Therefore, the adaptability of δ the weight is selected to judge the accuracy of the algorithm image target edge calculation in this paper.

(4) *Correct Classification Coefficient: Select the Correct Classification System.*

(a) CT image of the lung

(b) CT image of the brain

(c) CT images of the vertebrae
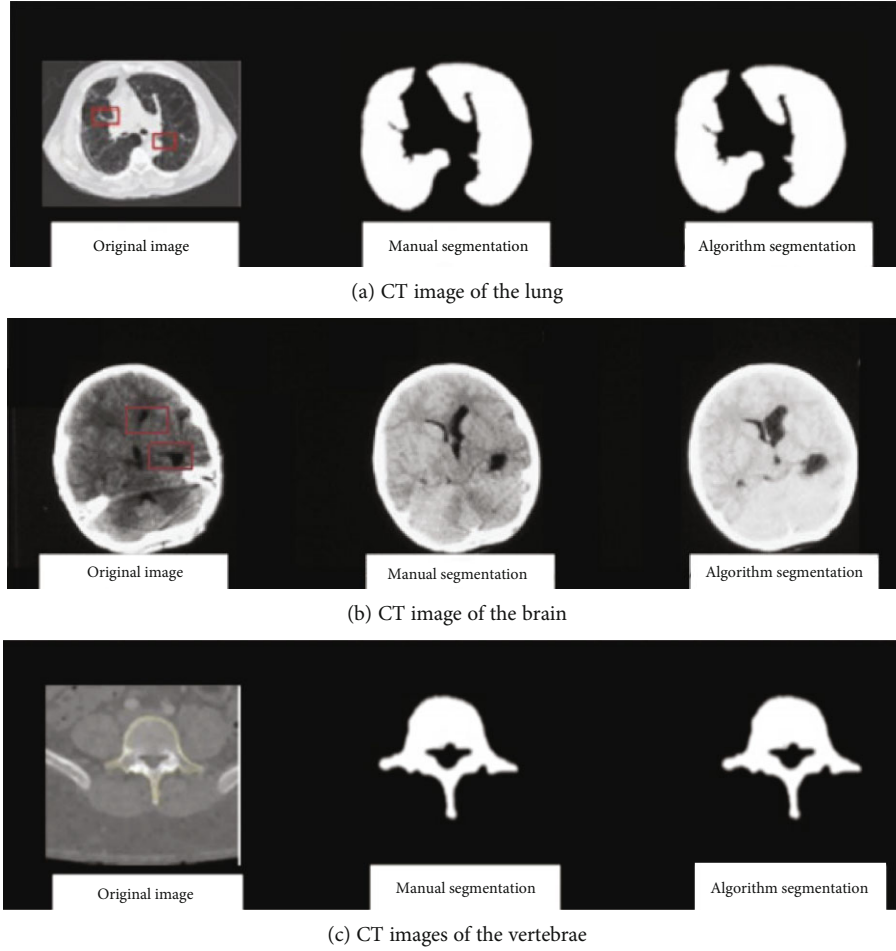
FIGURE 2: CT image segmentation results.

The V_{CCR} number is used as an indicator to judge the effect of algorithm segmentation, and the calculation formula is as follows:

$$V_{\text{CCR}} = \frac{K'}{K_{\text{total}}}, \tag{16}$$

where K' represents the number of superpixels that are correctly K_{total} segmented and represents the total number of image superpixels.

(5) *Image Segmentation Accuracy: Segmented by CT Image*.

The accuracy is the index to verify the performance of the algorithm, and the formula is as follows:

$$\text{SE}_{\text{accu}} = \frac{L_1}{L_{\text{tot}}} \times 100\%, \tag{17}$$

where L_{tot} represents the number of pixel blocks L_1 actually divided and it represents the number of pixel blocks obtained by algorithmic division.

6.4. Results and Discussion. In the environment set in this experiment, the computer is used to draw the lung CT image, brain CT image, and vertebra CT image segmentation of the algorithm in this paper, as shown in the following Figure 2.

It can be seen from Figure 2 that the segmentation of lung CT images, brain CT images, and vertebra CT images using the algorithm in this paper is basically consistent with the manual segmentation results, and the segmentation effect is significant, and the accuracy is high, indicating that the algorithm in this paper has a good performance.

6.4.1. Experiment 2. Taking the time consumption of superpixel gridding as an indicator, compare the algorithm in this paper with the algorithm in literature [15–19]. To ensure the efficiency of the algorithm in this paper, the comparison results are shown in Table 1.

Analyzing the time-consuming of superpixel gridding of different algorithms in Table 1, it can be seen that as the number of pixel blocks increases, the time-consuming gridding increases, but the algorithm in this paper has a faster overall speed, with the highest time-consuming 0.8 s, literature [19]. The algorithm has the highest time-consuming 2.5 s when the number of pixel blocks is 4000, the highest time-consuming of the algorithm in literature [16] and literature [17] reaches 2.0 s, and the algorithm in literature [15]

Table 1: Time-consuming comparison of superpixel gridding(s).

Algorithm	Pixel block/piece			
	1000	2000	3000	4000
Literature [15] algorithm	0.5	0.8	1.2	1.6
Literature [16] algorithm	0.9	1.2	1.5	2.0
Literature [17] algorithm	1.2	1.6	1.8	2.0
Literature [18] algorithm	1.3	1.5	1.5	1.9
Literature [19] algorithm	0.8	1.5	1.9	2.5
The proposed algorithm	0.3	0.5	0.6	0.8

Table 2: Fitness of weight δ.

Experiment times/time	Fitness factor
50	0.66
100	0.69
150	0.75
200	0.78
250	0.80

Figure 3: Comparison of correct classification coefficients.

Figure 4: Comparison of segmentation accuracy.

takes a short time when there are fewer pixel blocks. But with the increase in the number of pixel blocks, the time-consuming increases rapidly, which is much higher than the algorithm in this paper. According to the data comparison, the CT image gridding effect of the algorithm in this paper is better, which is inseparable from the use of superpixels for analysis.

6.4.2. Experiment 3. Use the δ fitness of the weights for analysis. Usually, the fitness factor is higher than 0.5, which means the fitness is good. The fitness of the weights δ used in the algorithm in this paper is shown in Table 2.

Analysis of Table 2 shows that the weights used in the algorithm of this paper have a fitness higher δ than 0.5 in the course of many experiments, which proves that this paper has a good calculation effect on the salience value and can accurately complete the image edge acquisition, that is, the initial. The determination of the contour has certain accuracy, which lays the foundation for the determination of the final segmentation contour of the subsequent image. At the same time, it is proved that this paper uses the center-surround contrast idea to calculate the significant area of the image edge with a certain degree of reliability.

6.4.3. Experiment 4. The value range of V_{CCR} the correct classification coefficient is usually between [0, 1].

The higher the value, the better the algorithm performance. In order to verify the superior segmentation performance of the proposed algorithm, the proposed algorithm is compared with the literature [15–19]. It is shown in Figure 3.

According to the comparison chart of correct classification coefficient in Figure 2, it can be clearly found that the overall curve of the algorithm in this paper is higher than that of other literature algorithms, and the correct classification coefficient is as high as 0.9, followed by the literature [16]
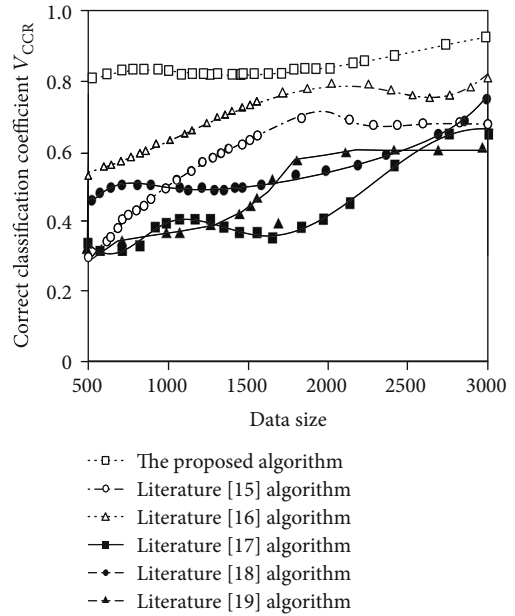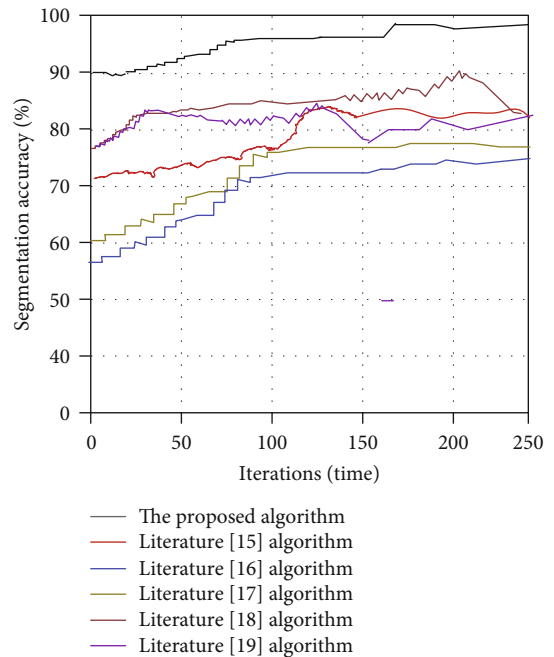
algorithm. The correct classification coefficient is [0.5, 0.8]. The algorithm of literature [17] has a maximum value of 0.7, literature [15] has a rapid growth trend, but the maximum does not exceed 0.7, and the maximum value of the remaining literature algorithms is below 0.7. The reason is that the algorithm in this paper first uses superpixels to improve the region growth criteria, calculates the salience value of the edge region of the image, and obtains the initial contour, which provides a basis for obtaining the final segmentation contour and improves the accuracy of pixel classification.

6.4.4. Experiment Five. The comparison results of algorithm segmentation accuracy for CT images are shown in Figure 4.

According to the segmentation accuracy curve in Figure 4, it can be found that the algorithm in this paper has very obvious advantages, and the segmentation accuracy is always higher than 90%. Among other documents, the average accuracy of literature [18] and literature [19] is above 80%, followed by literature [15]. In comparison, literature [16] and literature [17] have lower image segmentation accuracy. The average level is around 70%. Based on the initial contours obtained, this paper uses the level set method to improve the Mumford-Shah model in the active contour model. The improved active contour model is used for image segmentation, and the segmentation accuracy is higher.

7. Conclusions

The use of CT image detection to assist in clinical medical diagnosis has become the current mainstream. Image segmentation is an important step in image processing, and the results of segmentation play a cornerstone role in image three-dimensional reconstruction and other processing. At present, CT images are still a hot issue in medical image research. In order to obtain more accurate image segmentation results, this paper improves the active contour model and completes the superpixel grid CT image segmentation using the improved model. In the process of algorithm research, the problem of initial contour of the image is mainly considered, superpixels are used to improve the region growth criterion, the significant edge area is calculated, the initial contour is obtained, and the problem is solved by calculating the function based on the initial contour, and the final CT image segmentation is successfully completed. The results show that the proposed algorithm has high segmentation accuracy and short time-consuming, which provides a basis for CT image research.

However, this research still has certain shortcomings. The edge salient area obtained by using the region growth criterion and center-surround contrast can only get the largest salient area. In the future, a global saliency calculation method needs to be found to provide more efficient CT image segmentation. In addition, the processing of different types of medical images is also a direction that needs to be studied in the future to provide more useful help for medical diagnosis.

Data Availability

The data used to support the findings of this study are included within TCIA data set and DeepLesion data set.

Conflicts of Interest

The authors declare that they have no conflicts of interest.

Acknowledgments

References

[1] G. Ting, W. Weixing, L. Wei, and Y. Dandan, "Rock particle image segmentation based on improved normalized cut," *International Journal of Control and Automation*, vol. 10, no. 4, pp. 271–286, 2017.

[2] J. Xi, "Automatic spiking pulse-coupled neural network for image segmentation," *International Journal of Future Generation Communication and Networking*, vol. 10, no. 2, pp. 21–32, 2017.

[3] K. Srinivasa Rao, K. V. Satyanarayana, and P. Srinivasa Rao, "Segmentation of images using two parameter logistic type distribution and K-means clustering," *International Journal of Grid and Distributed Computing*, vol. 11, no. 12, pp. 1–20, 2018.

[4] G. L. F. da Silva, P. S. Diniz, J. L. Ferreira et al., "Superpixel-based deep convolutional neural networks and active contour model for automatic prostate segmentation on 3D MRI scans," *Medical & Biological Engineering & Computing*, vol. 58, no. 9, pp. 1947–1964, 2020.

[5] P. M. Gordaliza, A. Muñoz-Barrutia, M. Abella, M. Desco, S. Sharpe, and J. J. Vaquero, "Unsupervised CT lung image segmentation of a mycobacterium tuberculosis infection model," *Scientific Reports*, vol. 8, no. 1, pp. 9802–9808, 2018.

[6] X. Li, J. Sui, and Y. Wang, "Three-dimensional reconstruction of fuzzy medical images using quantum algorithm," *IEEE Access*, vol. 8, pp. 218279–218288, 2020.

[7] R. B. Holmes, I. S. Negus, S. J. Wiltshire, G. C. Thorne, P. Young, and The Alzheimer's Disease Neuroimaging Initiative, "Creation of an anthropomorphic CT head phantom for verification of image segmentation," *Medical Physics*, vol. 47, no. 6, pp. 2380–2391, 2020.

[8] M. Hamghalam and A. Ayatollahi, "White blood cell segmentation in Giemsa-stained images of blood smears," *International Journal of Advanced Science and Technology*, vol. 140, pp. 1–10, 2020.

[9] H. Transformation, V.-J. Algorithm, Indriyani, and I. M. Sudarma, "Automatic segmentation of U-zone area on facial images using fuzzy edge detection," *International Journal of Advanced Science and Technology*, vol. 133, pp. 19–30, 2019.

[10] A. A. Taha and A. Hanbury, "Metrics for evaluating 3D medical image segmentation: analysis, selection, and tool," *BMC Medical Imaging*, vol. 15, no. 29, pp. 1–28, 2015.

[11] G. Chengcheng, Y. Fengqin, and C. Ying, "Image semantic segmentation based on convolutional neural network features and improved superpixel matching," *Progress in Laser and Optoelectronics*, vol. 55, no. 8, pp. 229–235, 2018.

[12] L. Jiarui, L. Cong, L. Xianjin, L. Wei, L. Ke, and H. Xinchao, "Image copy-paste tampering detection based on superpixel segmentation," *Journal of Applied Sciences*, vol. 37, no. 3, pp. 419–426, 2019.

[13] L. Miao, L. Yang, Z. Yuqian, and L. Yizhi, "A new method of image superpixel segmentation," *Journal of Electronics and Information Technology*, vol. 42, no. 2, pp. 83–89, 2020.

[14] T. Yongpeng, J. Yu, and X. Cong, "CT image segmentation method combining superpixels and CNN," *Computer Engineering and Applications*, vol. 56, no. 5, pp. 1–8, 2019.

[15] L. Xia, G. Quan, L. Xiao, and W. Bo, "Joint energy active contour CT image segmentation method based on superpixels," *Optoelectronic Engineering*, vol. 47, no. 1, pp. 10–19, 2020.

[16] Q. Yan, W. Benzheng, Y. Yilong, C. Peipei, and C. Jinyu, "Lung parenchymal CT image refinement segmentation," *Journal of Image and Graphics*, vol. 22, no. 1, pp. 137–145, 2017.

[17] P. P. Rebouças Filho, P. C. Cortez, A. C. da Silva Barros, V. H. Albuquerque, and J. M. Tavares, "Novel and powerful 3D adaptive crisp active contour method applied in the segmentation of CT lung images," *Medical Image Analysis*, vol. 35, no. 2, pp. 503–516, 2017.

[18] L. Cong, S. Ding, L. Wang, A. Zhang, and W. Jia, "Image segmentation algorithm based on superpixel clustering," *IET Image Processing*, vol. 12, no. 11, pp. 2030–2035, 2018.

[19] N. Kishorjit Singh, N. Johny Singh, and W. Kanan Kumar, "Image classification using SLIC superpixel and FAAGKFCM image segmentation," *IET Image Processing*, vol. 14, no. 3, pp. 487–494, 2020.

[20] A. Ray, I. K. Maitra, and D. Bhattacharyya, "Detection of cervical cancer at an early stage using hybrid segmentation techniques from PAP smear images," *International Journal of Advanced Science and Technology*, vol. 112, pp. 23–32, 2018.

[21] M. V. Eijnatten, R. V. Dijk, J. Dobbe, G. Streekstra, J. Koivisto, and J. Wolff, "CT image segmentation methods for bone used in medical additive manufacturing," *Medical Engineering & Physics*, vol. 10, no. 2, pp. 24-25, 2017.

[22] Y. Yin, Q. Huang, H. Gao, and Y. Xu, "Personalized APIs recommendation with cognitive knowledge mining for industrial systems," *IEEE Transactions on Industrial Informatics*, p. 1, 2020.

[23] Y. Yin, Z. Cao, Y. Xu, H. Gao, R. Li, and Z. Mai, "QoS prediction for service recommendation with features learning in mobile edge computing environment," *IEEE Transactions on Cognitive Communications and Networking*, vol. 6, no. 4, pp. 1136–1145, 2020.

[24] Y. Li, G. Cao, Q. Yu, and X. Li, "Active contours driven by non-local Gaussian distribution fitting energy for image segmentation," *Applied Intelligence*, vol. 48, no. 12, pp. 4855–4870, 2018.

[25] K. Zhang, L. Zhang, K.-M. Lam, and D. Zhang, "A level set approach to image segmentation with intensity inhomogeneity," *IEEE Transactions on Cybernetics*, vol. 46, no. 2, pp. 546–557, 2016.

[26] Z. Zhou, M. M. R. Siddiquee, N. Tajbakhsh, and J. Liang, "UNet++: redesigning skip connections to exploit multiscale features in image segmentation," *IEEE Transactions on Medical Imaging*, vol. 39, no. 6, pp. 1856–1867, 2020.

[27] X. Liu, S. Guo, B. Yang et al., "Automatic organ segmentation for CT scans based on super-pixel and convolutional neural networks," *Journal of Digital Imaging*, vol. 31, no. 5, pp. 748–760, 2018.

[28] M. F. Bobo, S. Bao, Y. Huo et al., "Fully convolutional neural networks improve abdominal organ segmentation," in *Proceedings of SPIE-The International Society for Optical Engineering*, pp. 100–121, United States, March 2018.

[29] W. Y. Sun, E. Q. Dong, Z. L. Cao, and Q. Zheng, "A robust local segmentation method based on fuzzy-energy based active contour," *Acta Automatica Sinica*, vol. 43, no. 4, pp. 611–621, 2017.

WILEY | Hindawi

Research Article

Innovation Trend of Edge Computing Technology Based on Patent Perspective

Hualei Ju[1] and Lihua Liu [iD] [2]

[1]*School of Economics, Northwest University of Political Science and Law, Xi'an, 710122 Shaanxi, China*
[2]*College of Innovation & Entrepreneurship, Shanghai Jianqiao University, Shanghai 201306, China*

Correspondence should be addressed to Lihua Liu; 13075@gench.edu.cn

Edge computing is an important foundation for building 5G networks, but in my country, there are few applications or inventions based on edge computing. In order to improve the application of edge computing, this article innovatively designs a human behavior recognition system based on a patent perspective, which provides a reference for other researchers. This paper discusses and designs the software and hardware schemes and related communication methods of a new edge computing framework that combines edge devices and cloud computing centers. After processing the collected human behavior data, the behaviors of the corresponding monitoring objects are classified and modeled, and then the distributed computing of edge devices is used to modify these models. These systems are characterized by low energy consumption and fast response. The experimental results prove. The recognition efficiency of edge computing technology from the patent perspective has been greatly improved. Its recognition speed is more than 30% faster than other algorithm calculations, and the accuracy of recognition reaches 0.852, which is about 20% higher than traditional recognition. The authors show that edge computing technology based on a patent perspective can play an important role in our lives.

1. Introduction

With the rapid development of electronic, information, and communication technologies such as the Internet of Things, 5G, blockchain, and sensors, the growth of various types of data has shown an exponential trend, and the requirements of massive data on computing power and speed are also increasing [1, 2]. Cloud computing technology provides users with almost unlimited computing power through a large number of high-performance servers in the data center. It is one of the important solutions for big data analysis and processing. However, cloud computing also has a set of issues such as high network latency, high cost, security and privacy, and cannot adapt to all big data analytics and processing requirements. For example, in industrial production, operation, and other scenarios, real-time response to accidents, failures, and emergencies is very important; in network data capture scenarios, data transmission costs are more sensitive [3].

For this reason, edge data processing technology with edge computing as the core has been produced and widely promoted [4]. Edge computing is defined as a distributed open platform that integrates core capabilities of network, computing, storage, and application on the edge of the network close to the source of things or data [5, 6]. In fact, edge computing is a new ecological model. By converging five types of resources, including network, computing, storage, application, and intelligence, at the edge of the network, it can improve network service performance and open network control capabilities, thereby inspiring something similar to the mobile Internet [5].

For machine learning edge computing clone node recognition, experts at home and abroad also have many studies [7]. In foreign countries, TangX and ChansonST proposed an optimal task download allocation strategy based on the study of cloud and fog combination. Through experimental simulation, under the condition of service delay constraint, by sacrificing a small amount of computing resources, it is

possible to save communication bandwidth and reduce network delay, so that the energy consumption of the cloud can be reduced to a minimum [8]. DimokasN proposes a PCICC cache strategy according to the characteristics of cache nodes [9]. RabinovichM has studied the difficulties and challenges facing cloud and fog fusion services, sensor network technology, and network virtualization technology of cloud computing and fog computing [10]. Due to the late start of computers in China, there is little research on edge computing. Xue Heyu believes that with the popularization of artificial intelligence applications, traditional identification systems are vulnerable to unique infringements [11]. He believes that edge computing can be used in traditional cloud server systems. Introducing edge computing in this paper reduces the number of communications between the server and the user and improves the security performance of the system [12]. Jie believes that edge computing is close to computing nodes, which makes it face great challenges. In particular, cloned nodes are difficult to identify because other legitimate nodes have the same information. Therefore, they believe that they must be judged by cloning nodes based on channel information. The edge computing of the network improves the recognition accuracy [13]. These studies have a certain reference value for this article, but due to the narrow data cited in the research, the data industry is basically limited to individual industries, and it is difficult to play a universal role.

Based on edge computing innovation from the perspective of patents, this paper conducts research and analysis on cloud computing and big data and proposes a data acquisition and processing system architecture based on edge computing, which uses edge computing close to users to provide low latency and high processing capabilities. Data acquisition, processing, and analysis plan. The distributed computing of edge devices is used to modify these models, thereby realizing a human behavior recognition system with high efficiency, low energy consumption, and fast response, which verifies the applicability of the current computing framework to physical data processing.

2. Innovative Methods of Edge Computing Technology

2.1. Patent. The new century is the era of the knowledge economy. Whether an enterprise can survive and stand out in the fierce market competition depends more on its scientific and technological innovation capabilities and effective management and application of independent intellectual property rights [14]. Innovation is the driving force for the development of an enterprise, and only an enterprise that continues to innovate can remain invincible in the competition. With the increase of the complexity of innovation and the limitation of resources and corporate capabilities, corporate innovation has become more demanding for capital investment and accumulation [15]. How to consolidate and leverage existing resources, transform them into innovation results and corporate economic benefits, and form a company's competitive advantage to adapt to an era of accelerating product upgrades are especially important [16].

The ability of an enterprise to create and apply intellectual property rights is the key to enhancing the core competitiveness of an enterprise, and it is also an inevitable choice for an enterprise to adapt to the ever-changing market environment. Enterprises, especially high-tech enterprises, are the main force in the creation of intellectual property rights. Enterprises have produced a large number of patent achievements in the process of actively participating in scientific research and market activities. Only by combining patents and the market environment and maximizing the results of these patents will we continuously stimulate the creative enthusiasm of stakeholders and continuously improve the technical level and market competitiveness of the company [17].

Patent represents intellectual property and is the main source of technical information, containing 90%-95% of the world's scientific and technological information. Patent is a common indicator to measure the output of enterprise innovation activities. The patent data of various enterprises is relatively easy to obtain, which can more objectively reflect the innovation activities of enterprises [18].

Patent portfolio theory uses patent activity and patent quality as an evaluation index for corporate patents. Taking the number of patent applications as an indicator of patent activity in a company's patent portfolio, it is believed that companies with a large number of patent applications are more innovative and pioneering, and their corporate value is also higher. The number of patent applications not only reflects the number of patents of a company but also reflects the degree of activity of the company's innovation. The more the company's annual patent applications, the stronger the innovation activities of the company [19]. There is a certain degree of difference between patent quality and patent value, and the two cannot be equated. The difference is mainly reflected in the following two aspects: (1) The difference in subjectivity and objectivity: the quality of patents depends on the advancement and importance of patents in the same field, which mainly reflects the creativity and novelty of patents, and the judgment results are more objective. (2) Value manifestation process: the quality of patents reflects the practical problems solved by patents, and whether they are implemented or not does not affect the objective facts of whether they can solve practical problems, while the value of patents is the economics embodied after implementation. Benefit [20].

Generally, we can use the interactive items of innovation ability and patent quantity and patent quality to examine the role of patent quantity and patent quality in the process of affecting enterprise performance. Construct the following measurement model:

$$L = C + a_1 L + a_2 L + a_3 L + a_4 L + \varepsilon_1. \tag{1}$$

Among them, C is a constant term; a represents the regression coefficient of the respective variable and the control variable, which is used to express the influence of the independent variable and the control variable on the company's performance. The industry selection function can be used to calculate the value corresponding to each observation value, which is used λ to represent:

$$\lambda = \frac{\phi(\gamma)}{\psi(\gamma)}, \tag{2}$$

where $\phi(\gamma)$ and $\psi(\gamma)$ are, respectively, the probability density function and probability cumulative distribution function corresponding to the model. The following model is used to estimate the factors affecting corporate performance, namely,

$$L = c_0 + c_1 x_1 + c_2 x_2 + \cdots \cdots + c_i x_i + \delta\lambda + \gamma. \tag{3}$$

Among them, x_i represents a series of explanatory variables and control variables that affect corporate performance; δ is the estimated value of the coefficient of variable x_i; λ is the value obtained in the first stage. Explore the role of patent quantity and patent quality in the process of impacting a company's performance using interactive items of innovation capacity, patent quantity, and patent quality. Construct the following measurement model:

$$L = C + \sum_1^4 a_j L + d_2 RDCS_{it} + \sum_5^9 a_k C + \delta_i. \tag{4}$$

Among them, d is the coefficient of the adjustment variable. In order to avoid the influence of inconsistent dimensions on the statistical results, the data was standardized in the preresearch:

$$Y_i = \frac{(x_i - x_i)}{S_i}. \tag{5}$$

Among them, Y_i represents the normalized observation value; X_i represents the original data observation value; x_i is the average value of the original data X_i; S_i represents the sample standard deviation.

2.2. Edge Computing. Edge computing may have the richer and more complex characteristics of other systems. Its theoretical research models and methods have their own applicable scopes. The part and the whole are no longer unified, and they do not satisfy the superposition principle of linear systems. Even for other known systems, it is quite difficult to model and control them. When the structure of the controlled object is completely unknown, system research will become more complicated. This also makes edge computing system model identification and control become a hot topic in the current control field [21, 22]. In recent years, artificial intelligence has been widely used in the identification of black-box systems. Among them, the regional economy has attracted much attention. Its unique edge computing capabilities have brought vitality to the modeling of nonlinear systems.

In the process of researching real-time data services, it is not difficult to find that data communication is inseparable from real-time data collection, real-time data control, or real-time data transmission. Improper selection of communication methods can cause data delay or loss. Therefore, the choice of communication mode and communication protocol is particularly important. For network data, the edge device itself needs to access the target webpage through the network module, download the required data, and complete the data collection task [23]. The edge devices connected to the Internet and the cloud computing center complete data exchange through wireless transmission, so other devices are not needed for data collection [24]. The frame diagram of the system is shown in Figure 1.

Edge computing provides services to users locally. On the one hand, it can reduce service processing delays and improve work efficiency. On the other hand, it can reduce network and bandwidth requirements and save system overhead. Compared with other computing, edge computing has great advantages in response time and service quality, and it meets the requirements of low latency, high reliability, and security [25]. In addition, as a complement to other calculations, edge computing reduces pressure on the data center, reduces bandwidth requirements, balances data processing, and improves overall system efficiency. In recent years, with the rapid development of the Internet of Things, edge computing has been widely used in various fields, such as the Internet of Vehicles, wireless sensors and actuators, smart homes, and software-defined networks [26]. In the future development, edge computing will complement and integrate with other computing and be widely used in more industries and fields, providing an ideal software and hardware support platform for information processing in the Internet of Things era [27].

The real-time data service architecture of edge computing divides real-time data services into edge computing services and cloud application services. Edge computing services undertake the main work of real-time data services. Cloud application services, as the data receiver of edge computing services, mainly provide web services. There are two services with database services. The development of edge computing has promoted the development of big data, cloud computing, and informatization. Now, it has involved many fields such as medical care, agriculture, geological survey, astronomy, and the Internet of Things. It has even developed into the fields of news and e-government. The huge value contained in massive data brings new development opportunities for each field [28]. However, the generation of massive data also brings huge challenges to data processing. It not only requires strong computing and analysis capabilities but also requires a large storage space to store the data. This will undoubtedly cause excessive pressure on the computing center. Edge computing solves this problem well. Generally speaking, the algorithm of edge computing is as follows:

$$G(x, y) = \exp\left(-\frac{x^2 + y^2}{2\sigma^2}\right), \tag{6}$$

where σ is the mean square error. It is achieved by convolution of smoothing kernels with different σ values with the image. The resulting expression formula is as follows:

$$L(x, y) = -\frac{1}{\pi\sigma^4}\left(1 - \frac{x^2 + y^2}{2\sigma^2}\right)\exp\left(-\frac{x^2 + y^2}{2\sigma^2}\right). \tag{7}$$
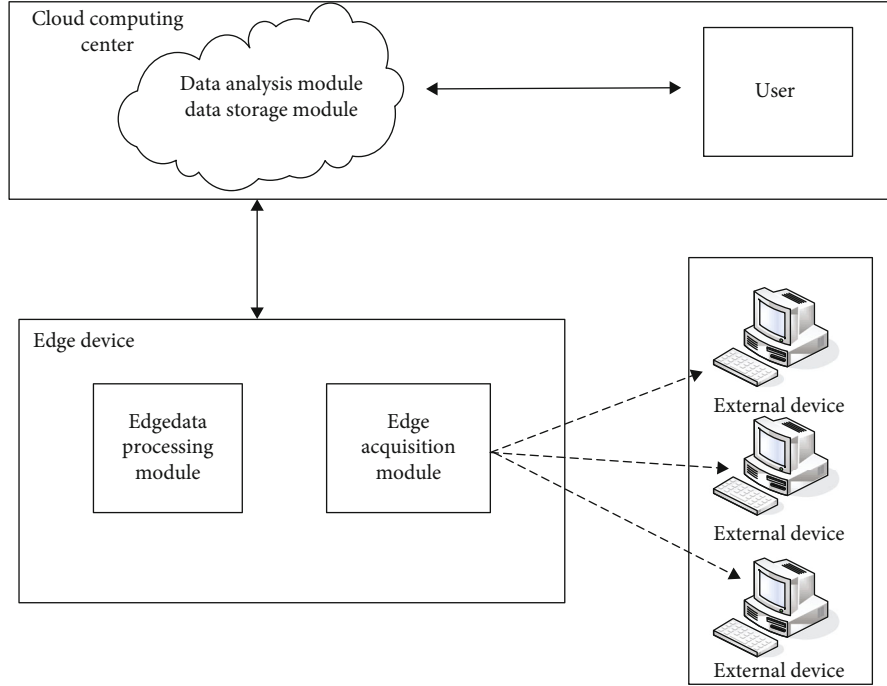
FIGURE 1: System framework diagram.
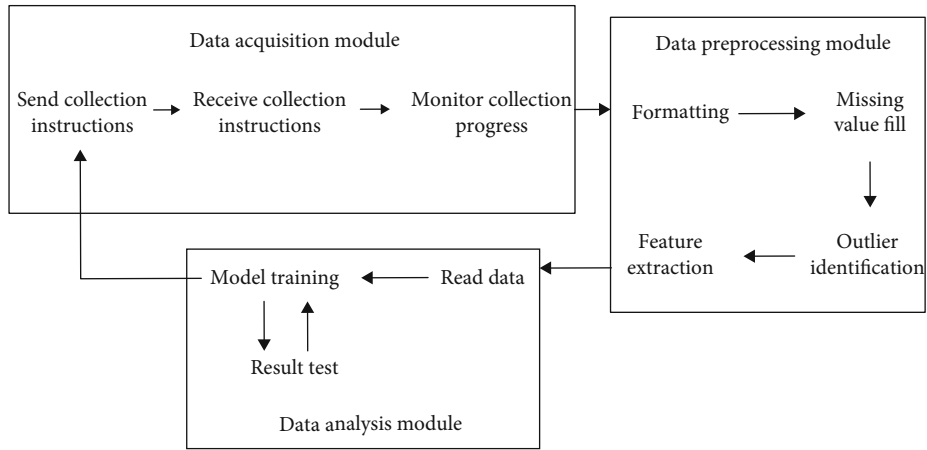
FIGURE 2: Workflow of data acquisition and processing based on edge computing.

The effect of edge detection is related to the value of σ; the smaller the σ, the smaller the smoothing effect, and the more noise.

$$Q = \frac{1}{2a^2 r^{-1}} \left(\frac{2b^2}{a^2 r^{-1}} p - t \right)^{-1} \left[a^2 r^{-1} t^2 + 2(1 - b^2)t \right], \quad (8)$$

$a \in [-1, 0] \cup [0, 1]$:

$$K = \frac{a}{2br} t, \quad (9)$$
$$\lambda_x (ct_n - t) > 0.$$

So

$$Q = \frac{1}{2a^2 r^{-1}} \left(\frac{2b^2}{a^2 r^{-1}} t - L \right)^{-1} \left[a^2 r^{-1} L^2 + 2(1 - a^2)L \right]. \quad (10)$$

The mathematical morphology method uses set algebra theory to analyze and process based on geometric characteristics. Mathematical morphology methods mainly use corrosion and expansion operations to extract morphological boundaries. Through the contraction effect of calculation and the expansion effect of expansion calculation, combined with certain logical calculations, a more precise boundary can be obtained. In order to obtain better edge computing nodes, the fitness function is determined according to the idea of the

TABLE 1: Equipment parameters.

Model	RPi B+	RPi2	Arduino UNO
CPU	ARM11 CPU	ARM Cortex-47 900 MHz	ATmega328 20 MHz
Operating system	Raspbian	Raspbian	Single Chip Microcomputer System
Interface	USB-host, RJ45	USB-host, RJ45	External interface board
RAM	512 MB	1 GB	32 KB

FIGURE 3: The data collector collects human body data.

TABLE 2: Computing patents.

	2016	2017	2018	2019	2020
Cloud computing	18	15	25	33	28
Fog computing	11	8	14	18	15
Big data	12	7	13	9	10
Edge computing	9	5	12	17	21

maximum between-class variance method, and the formula is as follows:

$$f(t) = \sigma(t)^2 = w_1(t) * w_2(t) * (u_1(t)) - u_1(t)^2. \quad (11)$$

Among them, t is the threshold, $f(x)$ is the fitness function, $w_1(t)$ is the number of nodes less than the threshold, and $w_2(t)$ is the number of nodes greater than the threshold. Generate a random number in the interval, and select the individual corresponding to the area where the random number belongs.

2.3. Data Collection. Complete data analysis and collect data through algorithms such as machine learning and artificial intelligence; minimize the deviation of the original data; correct the data to obtain more accurate data; establish a distributed edge computing and cloud computing collaborative big data analysis and mining platform to achieve data construction, the ability of the module [29]; the interaction between the functional modules is relatively simple, usually a unified software system completes the commands and scheduling, establishes long-term stable communication, and ensures the reasonable operation of the entire system [30, 31].

Aiming at the scene of human behavior recognition, a human behavior data collection, processing, and analysis system based on edge computing is designed and implemented. Using the distributed computing of edge devices to modify these models, a human behavior recognition system with high efficiency, low energy consumption, and fast response is realized. After data collection and data preprocessing, a model that can be directly modeled is obtained. According

to the mining target and data form, models such as classification and prediction, cluster analysis, and association rules can be established to help system users extract the value contained in the data. In order to be able to complete the support of the above-mentioned hardware overall design and achieve the corresponding computing capabilities, it is necessary to select a suitable microprocessor as the core part of the overall system-edge computing equipment [4].

The model is sent to the edge device, and the edge device combines the data received in real time to verify the basic model. When the user or the edge device itself determines that the results produced during the use of the model do not conform to the actual situation, the model will be returned to the cloud computing center. The cloud computing center uses the newly received data and feedback results to modify the model, then sends the retrained model to the edge device for another test, and loops until the test result of the model meets the requirements of the edge device, and the final generated. The model will be used normally on edge devices [32].

Finally, the overall functional architecture of the system can be obtained, which consists of three parts: data acquisition module, data preprocessing module, and data analysis module. The overall operation process is shown in Figure 2. This approach of putting the analysis model on the edge device can reduce the computing pressure on the cloud on the one hand, and on the other hand, for the delay-sensitive scenarios, the edge device to complete the data analysis work can effectively reduce the time for result generation. The real-time analysis results are presented to the system users in time.

The relevant sensors connected to the edge device are used to complete the real-time collection of data required for human body recognition, and then, the data is correspondingly preprocessed and sent to the cloud. The cloud computing center uses related machine learning algorithms to complete the modeling work and send the model back to the edge device. The edge device uses the trained model to predict the posture behavior of the currently monitored object [33]. When the predicted result of the model does
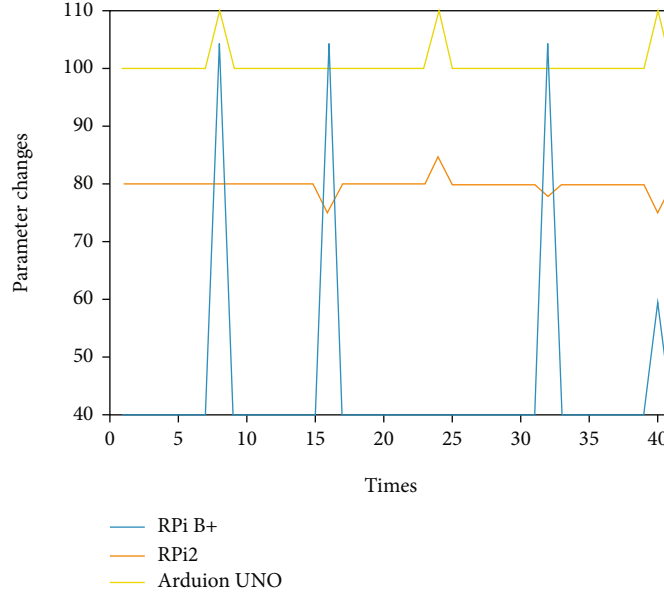
Figure 4: The fluctuation range of different devices.

not match the current status quo, it can also inform the cloud computing center of the data and the correct result to correct the relevant model.

3. Innovation Experiment of Edge Computing Technology

3.1. Data Sources. The collection of physical data in this system will be completed by edge devices controlling several sensors. In the scene of human behavior recognition, the sensors that can be used as data sources for model training include numerical data collection sensors such as gyroscopes, IMUs, and heart rate measuring machines, and image data collectors including infrared and thermal image data collectors. In this scenario, IMU equipment is used to collect human behavior data, depending on system requirements 1and model characteristics.

3.2. Edge Computing Equipment. The receiving and sending of the collected data are the current data processing module and the human behavior recognition module that will be designed later, and an edge device that meets the system requirements is required to support the realization of the above functions. The most popular and developed device is the most mature. There are mainly series of products under platforms such as RaspbeerPi and Arduino. Commonly used devices are RPi B+, RPi2, and Arduino UNO. The device parameters are shown in Table 1.

3.3. Human Behavior Data Collection. In order to ensure that the collected data is more suitable for model testing, this experiment requires the monitored object to complete corresponding actions in accordance with predetermined instructions for the behavior tags required by the experiment, including a series of daily behavior actions and some behaviors under special circumstances, such as Falling, by providing

Table 3: Data variable names and types.

Serial number	Name	Types
1	Acquisition time	Numerical
2	Behavior type	Categorical
3	Hand three-dimensional accelerometer	Numerical
4	Hand three-dimensional gyroscope	Numerical
5	Three-dimensional accelerometer of chest	Numerical
6	Three-dimensional gyroscope on chest	Numerical
7	Foot 3D accelerometer	Numerical
8	Foot 3D gyroscope	Numerical
9	Acquisition time	Numerical

Table 4: Data differences in operation.

	F-measure	Accuracy	Operation hours
Decision tree	0.933	0.932	28.73
Naive Bayes	0.944	0.946	35.21
MDD	0.923	0.936	43.51
Random forest	0.932	0.948	36.25
Edge computing	0.964	0.984	18.62

devices including built-in mobile power, serial port, and Bluetooth interface. When the sensor is turned on, the data collector will automatically start working and will continuously transmit the collected physical data to the serial port at the set frequency. The collection equipment is shown in Figure 3.

3.4. Statistics. All data analysis in this article uses SPSS19.0, the statistical test uses a two-sided test, significance is defined
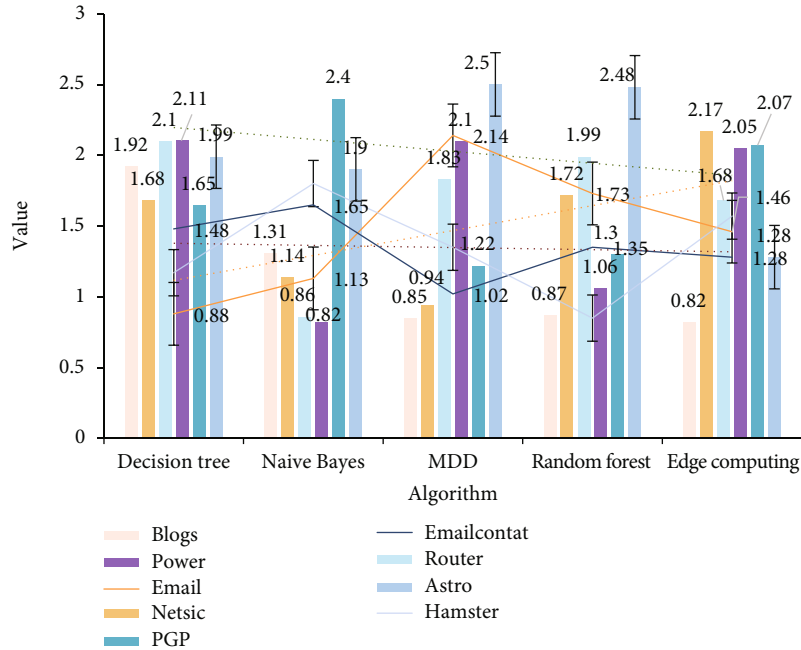
FIGURE 5: Calculation time of an algorithm.
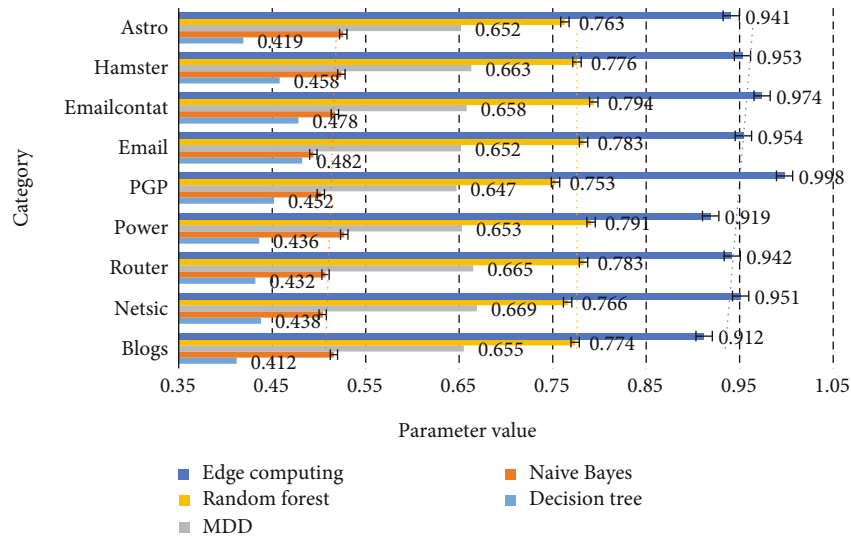
FIGURE 6: Ranking monotonicity of different algorithms.

as 0.05, and $p < 0.05$ is considered significant. The statistical results are displayed as mean ± standard deviation ($x ±$ SD). When the test data obeys the normal distribution, the double T test is used for comparison within the group, and the independent sample T test is used for comparison between the groups.

4. Experimental Analysis of Edge Computing Technology Innovation

4.1. Edge Computing Patent Changes. Through literature surveys and data from the patent office, we have made statistics on the changes in edge computing patents in recent years, as shown in Table 2.

From the table, we can see that with the development of time, the technology is constantly improving, and the patents of edge computing are increasing. In 2016, the patents of edge computing were only about half of that of cloud computing, but after 5 years with the development of edge computing, the patent of edge computing has approached cloud computing and has shown a trend beyond cloud computing, which shows that edge computing has great potential for development. In the experiment in this article, we need to collect human motion data through equipment. In order to ensure the effective stability of the data, we first test the collection capabilities of different equipment, as shown in Figure 4.

As shown in Figure 4, the three devices have different performances in data collection. RPi B+ has the largest
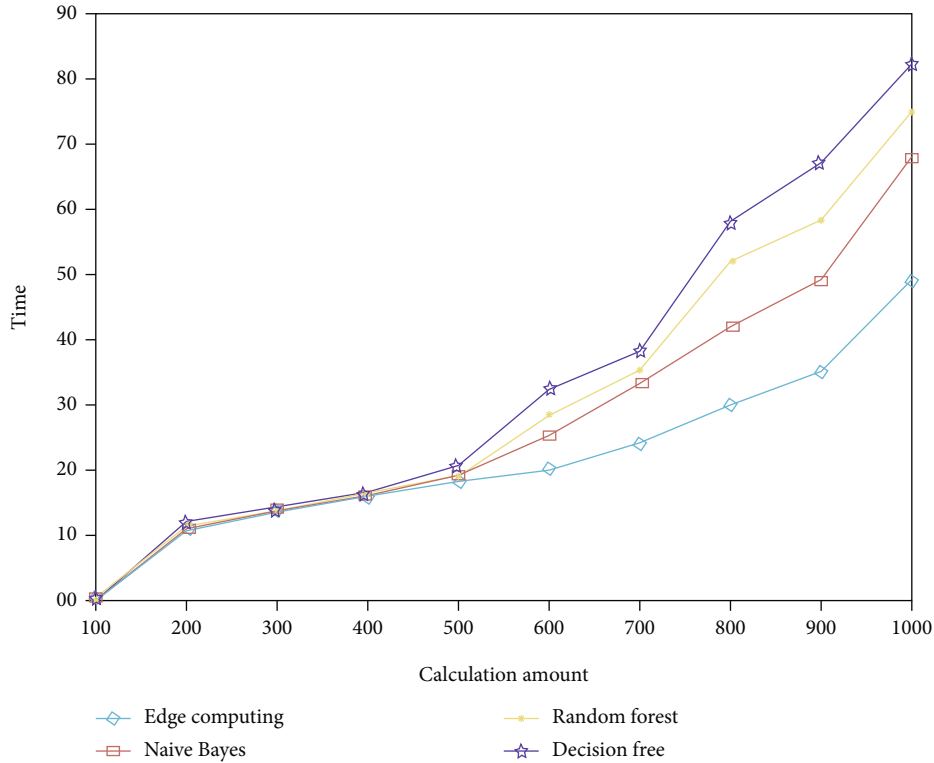
FIGURE 7: Running time under different algorithm unit tasks.

acquisition range, and its optimal value is also the largest; the data collected by RPi2 is the most stable among the three devices, with the smallest fluctuations, large memory, and a large amount of data collection; the data collected by Arduino UNO is the best, and the fluctuations are also only slightly larger than RPi2, but its memory is minimal and the amount of data collected is minimal. Under comprehensive consideration, we decided to use RPi2 equipment for collection.

As shown in Table 3, we interpret the names and types of variables, and after sorting out the collected data, we obtain experimental data, which, respectively, contain the relevant data of a total of 8 men and women monitoring subjects.

4.2. Effects of Different Algorithms. We collected the data under different algorithms and compared the differences in the values during their operation, as shown in Table 4.

Through analysis, it can be seen that compared with other basic algorithms, edge computing runs faster and has greater advantages in precision and recall. Compared with weak classifiers such as decision tree, it integrates learning. The advantages of the algorithm are more obvious. Because edge computing has more regularization of the self-model than other models, making this type of model has a stronger generalization ability. In actual work, as the amount of data continues to increase, the accuracy of edge computing will be more obvious.

In order to illustrate the cost of running different algorithms, we let different algorithms run separately and count the consumption. Due to differences in hardware configuration, different computer execution results may have deviations, but the relative differences between the running times of different algorithms should be comparable. The specific data is shown in Figure 5.

From Figure 5, we can see that in terms of computational cost, the advantages of edge-based computing are not very obvious. Two indicators are higher than other calculation methods, but the cost in other indicators is much lower than other algorithms. Particularly in terms of Blogs and Astro, it is about 40% lower than other algorithms.

From Figure 6, we can see the monotonicity of the ranking of different algorithms in the real network. It can be seen that the edge-based algorithm has obvious advantages in this regard. Its ranking monotonicity is higher than Naive Bayes, MDD, etc., and its algorithm ranking monotonicity is more than 30% higher than other algorithms. We calculate the calculation period of different algorithms per unit time and get Figure 7.

From Figure 7, we can see that at the beginning of different algorithms, there is little difference in operating efficiency between them, but after running more than 600 times, the efficiency between the algorithms begins to increase, and the speed of edge computing is compared with other algorithms. The speed is getting bigger and bigger, and the time after 1000 transportation is more than 20% less than other algorithms.

5. Conclusion

In recent years, society has gradually entered the era of "big data," and with the advent of cloud computing, the demand for big data processing and application functions is

increasing. Cloud computing has been vigorously promoted due to its advantages such as low operating costs, dynamic scalability, and simplified operation and maintenance. Cloud computing-related industries have also developed rapidly in my country. From the perspective of patents, this paper implements a data collection and processing system based on edge computing. Through the coordination and interaction of edge devices and cloud computing centers, it solves the problems of the original system such as slow computing speed and high energy consumption. Corresponding designs and implementations are made for the specific applications of the system in different scenarios. Due to time and technical reasons, this article also has some shortcomings. When designing the transmission of human behavior data, the frequency of data transmission can be improved according to the on-site situation. For example, when the edge device detects that the human behavior has not changed for a long time, the transmission frequency can be slowed down. In order to better reduce the energy consumption of the equipment, when storing document data, because the collected data is in the form of key-value pairs, the more popular databases in recent years can be used, which can improve the efficiency of transmission and storage. These tasks need to be improved in future research.

Data Availability

No data were used to support this study.

Conflicts of Interest

The authors declare that they have no conflicts of interest.

Acknowledgments

References

[1] W. Shi, J. Cao, Q. Zhang, Y. Li, and L. Xu, "Edge computing: vision and challenges," *Internet of Things Journal, IEEE*, vol. 3, no. 5, pp. 637–646, 2016.

[2] M. Zhou, Y. Wang, Z. Tian, Y. Lian, Y. Wang, and B. Wang, "Calibrated data simplification for energy-efficient location sensing in internet of things," *IEEE Internet of Things Journal*, vol. 6, no. 4, pp. 6125–6133, 2019.

[3] Y. Liu, C. Xu, Y. Zhan, Z. Liu, J. Guan, and H. Zhang, "Incentive mechanism for computation offloading using edge computing: a Stackelberg game approach," *Computer Networks*, vol. 129, no. DEC.24, pp. 399–409, 2017.

[4] Z. Lv, D. Chen, R. Lou, and Q. Wang, "Intelligent edge computing based on machine learning for smart city," *Future Generation Computer Systems*, vol. 115, pp. 90–99, 2021.

[5] A. Gumaei, M. al-Rakhami, M. M. Hassan et al., "Deep learning and blockchain with edge computing for 5G-enabled drone identification and flight mode detection," *IEEE Network*, vol. 35, no. 1, pp. 94–100, 2021.

[6] R. Olaniyan, O. Fadahunsi, M. Maheswaran, and M. F. Zhani, "Opportunistic edge computing: concepts, opportunities and research challenges," *Future Generation Computer Systems*, vol. 89, no. DEC, pp. 633–645, 2018.

[7] Z. Lv, L. Qiao, D. Chen, R. Lou, J. Li, and Y. Li, "Machine learning for proactive defense for critical infrastructure systems," *IEEE Communications Magazine*, 2020.

[8] W. J. Chang, L. B. Chen, C. Y. Sie, and C. H. Yang, "An artificial intelligence edge computing-based assistive system for visually impaired pedestrian safety at zebra crossings," *IEEE Transactions on Consumer Electronics*, vol. 67, no. 1, pp. 3–11, 2021.

[9] R. Li, Q. Ma, J. Gong, Z. Zhou, and X. Chen, "Age of processing: age-driven status sampling and processing offloading for edge computing-enabled real-time IoT applications," *IEEE Internet of Things Journal*, no. 99, pp. 1–7, 2021.

[10] Z. Lv, Y. Han, A. K. Singh, G. Manogaran, and H. Lv, "Trustworthiness in industrial IoT systems based on artificial intelligence," *IEEE Transactions on Industrial Informatics*, vol. 17, no. 2, pp. 1496–1504, 2021.

[11] G. Liu, X. Chen, R. Zhou, S. Xu, Y. C. Chen, and G. Chen, "Social learning discrete particle swarm optimization based two-stage X-routing for IC design under intelligent edge computing architecture," *Applied Soft Computing*, vol. 104, no. 6, p. 107215, 2021.

[12] S. Moon and Y. Lim, "Service migration based on reinforcement learning in vehicular edge computing," *Journal of KIISE*, vol. 48, no. 2, pp. 243–248, 2021.

[13] S. M. Kumar and D. Majumder, "Healthcare solution based on machine learning applications in IOT and edge computing," *International Journal of Pure and Applied Mathematics*, vol. 119, no. 16, pp. 1473–1784, 2020.

[14] Y. Lu, S. Cuiying, C. Hongwei, and Y. Hongwei, "Foreign body detection method for power transmission equipment based on edge computing and deep learning," *China Electric Power*, vol. 53, no. 6, pp. 27–33, 2020.

[15] W. Wu, S. An, C. H. Wu, S. B. Tsai, and K. Yang, "An empirical study on green environmental system certification affects financing cost of high energy consumption enterprises-taking metallurgical enterprises as an example," *Journal of Cleaner Production*, vol. 244, p. 118848, 2020.

[16] L. Zheng, "Application of smart new energy——solar electric bicycle power pile system based on edge computing," *Information Construction*, vol. 263, no. 8, pp. 58–61, 2020.

[17] S. Yueru and L. Jun, "Mobile edge computing offload strategy for multi-base station and multi-user scenarios," *Frontiers of Data and Computing Development*, vol. 5, no. 3, pp. 130–140, 2020.

[18] Y. Shen and L. Chang, "Visual analysis of enterprise electricity consumption behavior based on edge computing gateway," *Electrical Appliances and Energy Efficiency Management Technology*, vol. 592, no. 7, pp. 89–94, 2020.

[19] H. Haochen, L. Yutong, T. Wang, Q. Zhaoming, and C. Junwei, "A control strategy for energy Internet edge computing system based on mixed stochastic H_2/H_∞ method," *Proceedings of the Chinese Society of Electrical Engineering*, vol. 656, no. 21, pp. 115–125, 2020.

[20] Z. Jianmin, F. Yang, Z. Wu, Z. Zhengkun, and W. Yuwei, "Multi-access edge computing (MEC) and key technologies," *Telecommunications Science*, vol. 35, no. 3, pp. 160–160, 2019.

[21] J. Ma, X. Jia, Y. Shou, and C. Yang, "Industrial data collection based on edge computing," *Microcomputer Applications*, vol. 37, no. 4, pp. 91–93, 2018.

[22] F. Zhu, P. Lu, L. Jilong, L. Ke, and H. Bingtao, "The surreal experience of home intelligence——distributed real-time rendering at the edge," *Artificial Intelligence*, vol. 18, no. 5, pp. 41–48, 2020.

[23] I. Fajjari and F. Tobagi, "Cloud edge computing in the IoT," *Annals of Telecommunications*, vol. 73, no. 7-8, pp. 413-414, 2018.

[24] S. Namasudra and P. Roy, "PpBAC," *Journal of Organizational and End User Computing*, vol. 30, no. 4, pp. 14–31, 2018.

[25] X. Li and J. Wan, "Proactive caching for edge computing-enabled industrial mobile wireless networks," *Future Generation Computer Systems*, vol. 89, pp. 89–97, 2018.

[26] Z. Lv and L. Qiao, "Optimization of collaborative resource allocation for mobile edge computing," *Computer Communications*, vol. 161, pp. 19–27, 2020.

[27] B. Gu, Y. Chen, H. Liao, Z. Zhou, and D. Zhang, "A distributed and context-aware task assignment mechanism for collaborative mobile edge computing," *Sensors*, vol. 18, no. 8, pp. 2423–2427, 2018.

[28] H. Sun, F. Zhou, and R. Q. Hu, "Joint offloading and computation energy efficiency maximization in a mobile edge computing system," *IEEE Transactions on Vehicular Technology*, vol. 68, no. 3, pp. 3052–3056, 2019.

[29] Z. Lv and W. Xiu, "Interaction of edge-cloud computing based on SDN and NFV for next generation IoT," *IEEE Internet of Things Journal*, vol. 7, no. 7, pp. 5706–5712, 2020.

[30] X. Ma, J. Liang, R. Liu et al., "A survey on data storage and information discovery in the WSANs-based edge computing systems," *Sensors*, vol. 18, no. 2, pp. 546–548, 2018.

[31] B. Shrestha and H. Lin, "Data-centric edge computing to defend power grids against IoT-based attacks," *Computer*, vol. 53, no. 5, pp. 35–43, 2020.

[32] H. Wang, M. Zeng, Z. Xiong, and F. Yang, "Finding main causes of elevator accidents via multi-dimensional association rule in edge computing environment," *China Communications (English Edition)*, vol. 14, no. 11, pp. 39–47, 2017.

[33] M. Elhoseny, "Multi-object detection and tracking (MODT) machine learning model for real-time video surveillance systems," *Circuits, Systems, and Signal Processing, First Online*, vol. 39, pp. 611–630, 2019.

WILEY | Hindawi

Research Article
Using Machine Learning Algorithms to Recognize Shuttlecock Movements

Wei Wang (ID)

Department of Physical Education, Chongqing University of Technology, 400054 Chongqing, China

Correspondence should be addressed to Wei Wang; ww0206@cqut.edu.cn

Shuttlecock is an excellent traditional national sport in China. Because of its simplicity, convenience, and fun, it is loved by the broad masses of people, especially teenagers and children. The development of shuttlecock sports into a confrontational event is not long, and it takes a period of research to master the tactics and strategies of shuttlecock sports. Based on this, this article proposes the use of machine learning algorithms to recognize the movement of shuttlecock movements, aiming to provide more theoretical and technical support for shuttlecock competitions by identifying features through actions with the assistance of technical algorithms. This paper uses literature research methods, model methods, comparative analysis methods, and other methods to deeply study the motion characteristics of shuttlecock motion, the key algorithms of machine learning algorithms, and other theories and construct the shuttlecock motion recognition based on multiview clustering algorithm. The model analyzes the robustness and accuracy of the machine learning algorithm and other algorithms, such as a variety of performance comparisons, and the results of the shuttlecock motion recognition image. For the key movements of shuttlecock movement, disk, stretch, hook, wipe, knock, and abduction, the algorithm proposed in this paper has a good movement recognition rate, which can reach 91.2%. Although several similar actions can be recognized well, the average recognition accuracy rate can exceed 75%, and even through continuous image capture, the number of occurrences of the action can be automatically analyzed, which is beneficial to athletes. And the coach can better analyze tactics and research strategies.

1. Introduction

Shuttlecock is developed from the ancient shuttlecock game with a history of more than 2000 years in my country. It combines scientific ability, wide publicity, excellent skills, and rich entertainment. It is a relatively new sport in modern society. The technical difficulty is medium, the exercise intensity is low, and the requirements for gender, age, location, and equipment status are low. The development of shuttlecock has played a decisive role in promoting the implementation of nationwide fitness programs. The development of shuttlecock sports provides people with good sports and entertainment methods, promotes social stability, promotes people's physical and mental health, and delays the process of social aging [1].

Computer vision and machine learning technologies are widely used in data mining, information security, remote sensing image processing, bioinformatics, intelligent transportation, intelligent security, and medical services. As one of the important branches in the field of computer vision, moving target detection technology has been widely used in real scenes. Existing moving target detection methods have problems such as long calculation time and high complexity. How to meet the real-time performance in real scene problem is becoming more and more important. With the rapid development of deep learning, the recognition accuracy of another important branch in the field of computer vision-target recognition technology has been greatly improved. However, due to the complex network structure and high computational complexity of the deep learning, how to quickly complete the training process of deep learning

networks has become an urgent problem in the field of deep learning.

It is a challenge for Lin to track players and shuttlecocks in broadcast badminton videos, especially for small-sized and fast-moving shuttlecocks. There are many situations that may cause occlusion or misjudgment. A method for tracking athletes and badminton in broadcast badminton video is proposed. They use adaptive Kalman filtering, trajectory confidence estimation, and confidence update (position similarity and relative motion relationship, RMR) to improve the accuracy of the target trajectory. Experimental results show that this method significantly improves the tracking success rate of athletes and shuttlecocks. However, this method also has a shortcoming, that is, there are too many influencing factors to be considered when the accuracy test is carried out, and there is a certain degree of difficulty in practical application [2]. Aiming at the problem of action recognition in still images, Zhichen proposed a method to arrange the features of different semantic parts in spatial order. Their method consists of three parts: (1) a semantic learning algorithm, which collects a set of partial detectors, (2) an effective detection method, which uses the same grid to divide multiple images and computes them in parallel, and (3) a top-down spatial arrangement increases the variance between classes. The proposed semantic part learning algorithm can not only capture interactive objects but also capture distinguishing gestures. Their spatial layout can be seen as a kind of adaptive pyramid, which highlights the spatial distribution of body parts in different movements and provides a more distinctive representation. Experimental results show that their method significantly outperforms existing methods on two challenging benchmarks. However, their method has limitations in that it is only for the processing of static pictures. However, in reality, more needs are the processing and application of dynamic pictures [3]. Jean et al. reviewed and commented on the past, present, and future of numerical optimization algorithms in machine learning applications. Through case studies of text classification and deep neural network training, they discussed how optimization problems in machine learning arise and what makes them challenging. A major theme of their research is that large-scale machine learning represents a unique environment in which stochastic gradient (SG) methods traditionally play a central role, while traditional gradient-based nonlinear optimization techniques usually faltering. Based on this point of view, they proposed a simple and general SG algorithm comprehensive theory, discussed its actual behavior, and emphasized the opportunity to design algorithms with improved performance. This led to the discussion of the next generation of large-scale machine learning optimization methods, including the investigation of two mainstream research directions, techniques, and methods to reduce noise in random directions. However, their algorithm cannot fundamentally solve the difficulties in the application of machine learning [4].

The innovations of this paper are (1) combine qualitative research with quantitative research and fully analyze the research data and (2) combine theoretical research with empirical research and combine shuttlecock sports on the basis of machine learning algorithm theory.

2. Using Machine Learning Algorithms to Recognize Research Methods of Shuttlecock Movements

2.1. Shuttlecock. Shuttlecock is a traditional Chinese national sports event. The institutionalized event has a history of 26 years. It has now become the official event of my country's five large-scale comprehensive sports games [5]. Shuttlecock's good project participation makes it rank in the forefront of all ethnic traditional sports in China, and it has been well promoted worldwide [6]. The World Shuttlecock Federation was formally established this year, and shuttlecock sports have been developed in many countries including Asia and Europe. The international development of shuttlecock has greatly promoted the improvement of the level of competition.

(1) The research significance of shuttlecock

Shuttlecock is an excellent national traditional sport in our country. Shuttlecock has a history of more than 2,000 years. It not only inherits the national spirit of self-improvement in traditional Chinese culture but also integrates the spirit of modern culture and sports competition [7]. Enriching people's cultural life, if it can be widely promoted, can promote the construction of socialist spiritual culture, and contribute to the construction of a harmonious society. Shuttlecock is very valuable as well as entertainment value. It has a broad collective foundation, which is not only pleasing to the eyes but also popular with the audience. Through practice, the shuttlecock can improve a great level and has a unique charm [8]. We should dig, organize, inherit, and develop. With the development of national fitness exercises, key ball sports do not require high participants, and there are not many requirements for venues, and the equipment is cheap. Therefore, many squares, parks, schools, residential areas, and other open spaces and other shuttlecock sports are everywhere.

Scientific fitness, rich entertainment, and diverse skills have a good role in promoting the physical and intellectual development of the broad masses of people. In order to promote the inheritance and development of the current shuttlecock sport in our country, the action recognition is carried out to better learn the laws of the shuttlecock sport [9]. It also provides useful enlightenment for the development of the national fitness program and provides a theoretical basis for the national traditional sports to better integrate into the mass fitness activities. Using machine learning algorithms to conduct motion recognition research on shuttlecock sports can effectively promote the development of shuttle cock sports, carefully study the characteristics of shuttlecock sports, and win impressive results on the court.

(2) The characteristics of shuttlecock

At this stage, the shuttlecock sport is an emerging national sport that integrates fitness, entertainment, mass, popularity, high skill, strict collective, fierce confrontation, technical duality, and appreciation. The reason why the

shuttlecock sport is loved by people [10] is also because the shuttlecock itself also shows the characteristics of simplicity, small size, light weight, slow speed, low difficulty, simple control, and very interesting. Shuttlecock integrates football skills, badminton courts, and volleyball rules. It is easy to learn and understand. In addition, it is not affected by various indoor and outdoor spaces, equipment, and climatic conditions and can autonomously control the amount of exercise with strong adaptability. Athletes can practice regardless of age, gender, or level [11]. Therefore, the shuttlecock can not only move the body but also has a beautiful artistic performance. It is displayed on various occasions and plays a unique role in the audience.

(3) The value and function of shuttlecock

Viewing function: The viewing function of traditional national sports is a collection of natural beauty and social beauty. The main content includes physical beauty, sports beauty, spiritual beauty, and clothing beauty. National traditional sports are a kind of comprehensive overall beauty. The perfect movement skills are fascinating and indescribable. In basic sports, not only the body is exercised, but the artistic performance is also beautiful [12]. Therefore, the shuttlecock has both the beauty of the human body and the unique sports characteristics of the country. The movement of the button ball reflects the physique of the human body and can also improve the strength, speed, endurance, and flexibility of the human body [13].

Educational function: In this way, we can take advantage of the fitness function, aesthetic value, and ideological and educational significance of the shuttlecock sport itself to carry out educational activities, which can not only promote the traditional national sports culture of our country but also enrich the people's amateur life and at the same time enhance the cultivation of people's good thinking. Moral quality lays a solid foundation for lifelong sports [14]. Carrying forward traditional national sports in the process of developing mass sports will undoubtedly have certain positive significance for carrying out extensive traditional moral education.

Economic value: Shuttlecock, as a traditional cultural carrier, carries the unique cultural knowledge of the nation, can make people deeply feel the value of national sports, guide consumers to buy related sports goods, books, audio, and video products, and create the company's products. R&D, mass production, and large-scale business conditions improve the economic benefits of society [15]. Make full use of the cultural advantages of the shuttlecock project to carry out multiform cultural industry research and development to increase publicity and attract more tourists to participate in the entertainment of the shuttlecock. National aerobics attracts tourists from all over the world with its unique style, thereby driving the local economic development. Analyzed from multiple angles, the exhibition of the shuttlecock project has a positive effect on driving the development of various industries [16].

2.2. Feature Selection and Extraction of Moving Targets. Feature extraction section selects senior stage is the body motion

recognition. It is hot and difficult to study. Human feature selection and extraction refers to selecting appropriate features from related videos or images to effectively describe the human movement.

The feature extraction link is an indispensable part of a complete motion recognition system. It is not only related to the accuracy and speed of subsequent motion recognition but also affects the performance of motion classification and discrimination [17]. There are many kinds of human body features. Among the many features, only a few are effective. Therefore, how to extract features that are unique to the target itself and have low sensitivity to environmental changes is the main task of feature extraction, and it is also the focus of human action recognition research [18].

At present, the features used in human action recognition mainly include motion features, shape features, and the fusion of the two features. The extraction based on motion features is based on the information shown by the human body's motion state, such as motion displacement, motion speed, motion direction, and angle information. Motion characteristics have the advantages of relative invariance and periodicity [19]. The extraction based on the shape feature uses the static feature of the moving human body to describe the action. Commonly used shape features mainly include contour features, perimeter, area, compactness, and circumscribed rectangle features. Compared with motion features, shape features have the advantages of distance from the camera and insensitivity to the surrounding environment. Based on the extraction of contour features of human actions from multiple perspectives, excellent recognition results are obtained [20]. Extract the width feature of the circumscribed rectangle of the moving target as a feature vector to identify human gait changes.

2.3. Machine Learning. Machine learning is a discipline dedicated to the study of how to use computational methods and use the acquired knowledge to improve the performance of the system itself. In computer systems, the so-called "experience" usually exists in the form of "data," so the content of machine learning research is to use the characteristics of the data to generate the algorithm of the model [21]. From the core perspective of machine learning, optimization and statistics are the two core supporting technologies (as shown in Figure 1).

Machine learning can not only be regarded as a method but also can be used for pattern recognition or data mining. There are four main types of problems (applications) in the field of machine learning: (1) prediction-can be solved by regression algorithm; (2) clustering-such as K-means method and hierarchical clustering algorithm; (3) classification-such as support vector machine method and decision tree algorithm; (4) dimension reduction-such as principal component analysis (PCA) [22]. At present, in many fields of computing science, including graphics and image processing, software engineering, computer vision, and natural language processing, machine learning can serve them. At the same time, machine learning is also performing well in interdisciplinary subjects, especially in the field of bioinformatics, where a large amount of data needs to be processed
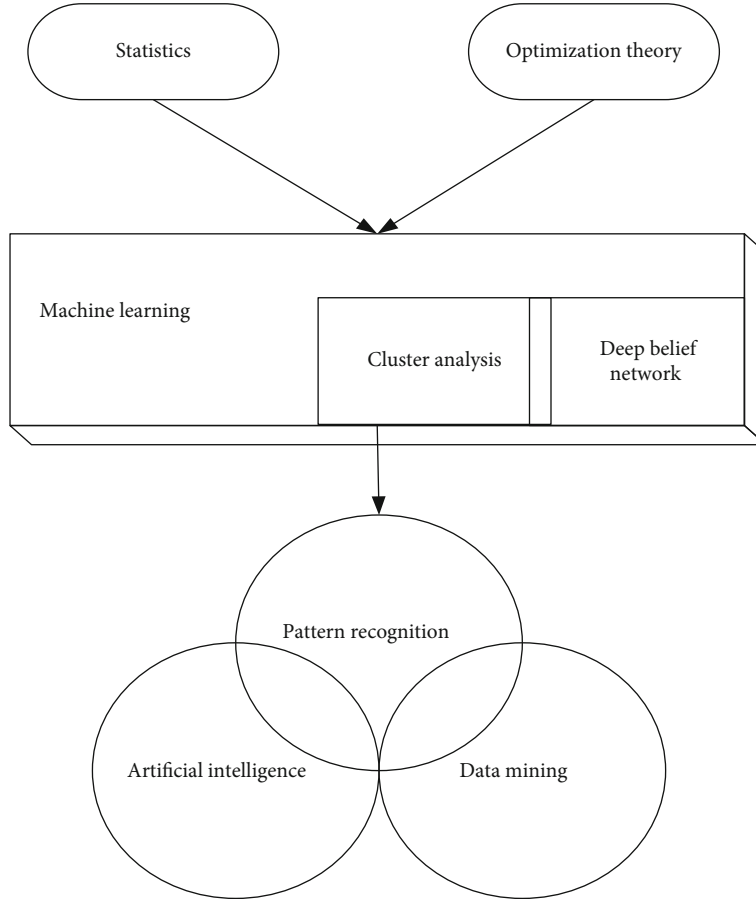
FIGURE 1: Application level of machine learning and pattern recognition.

and analyzed, and machine learning just meets its requirements.

2.4. Deep Belief Network. A deep belief network model can be regarded as the superposition of multiple RBM models, and the output of the hidden layer in each layer is used as the input of the visible layer in the next layer, so that a layered training model can be generated [23]. The training process of multiple RBM superimposed DBN. The restricted Boltzmann machine RBM is a bipartite undirected graph based on the energy model. RBM contains m visible layer nodes and n hidden layer nodes, and the connection between the visible layer and the hidden layer is obtained through the weight matrix W [24]. In addition, both the visible layer and the hidden layer contain the corresponding offset values $v$bias and $h$bias.

In a given state, the energy function of the visible layer and the hidden layer is defined as

$$R(b, l) = -\sum_{i=1}^{n}\sum_{j=1}^{m} e_{ij}l_i b_j - \sum_{j=1}^{m} a_j b_j - \sum_{i=1}^{n} c_i l_i. \quad (1)$$

This energy function indicates that in a certain state, each node of the visible layer and each node of the hidden layer

have a capability value, and then, the energy value in this state is obtained [25, 26]. According to the energy function, the joint probability of the visible layer node and the hidden layer node is defined as

$$o(b, l) = \frac{e^{-R(b,l)}}{\sum_{b,l} e^{-R(b,l)}}. \quad (2)$$

So, we get the conditional probability of the visible layer and the hidden layer, where the conditional probability of the visible layer is

$$o(b) = \sum_{l} 0(b, l) = \frac{1}{X}\sum_{l} e^{-R(b,l)}. \quad (3)$$

The conditional probability of the hidden layer is

$$o(l) = \sum_{b} o(b, l) = \frac{1}{X}\sum_{b} e^{-R(b,l)}. \quad (4)$$

Among them, $X = \sum_{b,l} e^{-R(b,l)}$, the maximum likelihood is used to solve the energy function, and the corresponding parameters (including the weight matrix, the visible layer offset value, and the hidden layer offset value) are obtained to

make the RBM energy function value the lowest [27]. The solution formula is as follows:

$$\frac{\partial \ln o(b, \vartheta)}{\partial} = \frac{\partial}{\partial \vartheta}\left(\ln \sum_l e^{-R(b,l)}\right) - \frac{\partial}{\partial \vartheta}\left(\ln \sum_{b,l} e^{-R(b,l)}\right),$$ (5)

$$\frac{\partial \ln o(b, \vartheta)}{\partial \vartheta} = -\sum_l o(b, l)\frac{\partial R(b, l)}{\partial \vartheta} + \sum_{b,l} o(b, l)\frac{\partial R(b, l)}{\partial \vartheta}.$$ (6)

By solving the W in the model by maximum likelihood estimation, we can get

$$\frac{\partial \ln o(b)}{\partial w_{ij}} = p(l_i = 1 \mid b)b_j - \sum_b o(b)o(l_i = 1 \mid b)b_j.$$ (7)

Among them, the solution of the first term is

$$o(l_i = 1 \mid b) = \tau\left(\sum_{j=1}^m w_{ij}b_j + v_i\right).$$ (8)

Among them, $\tau(x) = 1/(1 + e^{-x})$. The solution of the second term needs to traverse all possible values. The commonly used method is based on Monte Carlo's Gibbs sampling method.

3. Using Machine Learning Algorithms to Recognize the Research Model of Shuttlecock Movements

This article mainly uses multiview clustering algorithm based on multicore learning for the shuttlecock movement recognition model, which recognizes information through the state of human movement and movement. The basic movements of the shuttlecock sport include panning, turning, knocking, jumping, and step. Through experimental research, data collection, preprocessing, and feature extraction of these actions are carried out, and the key steps are continuously improved and optimized, so as to improve the accuracy of motion recognition as a whole.

(1) Multiview clustering algorithm based on multicore learning

In many machine learning, computer vision, and image processing applications, because the data comes from different data sources and reflects the different characteristics of the data itself, the data can often have multiple views. For example, the same image can contain multiple feature representations: color, shape, and texture. Compared with the traditional single-view clustering algorithm, the multiview clustering algorithm can make full use of the complementary information from different views in the same sample, thereby ultimately improving the performance of the clustering algorithm.

The existing multiview algorithms can be divided into three main categories: multiview clustering algorithms based on collaborative training, multiview clustering algorithms based on subspace, and multiview clustering algorithms based on multicore learning. Among these algorithms, our work mainly focuses on the multiview clustering algorithm based on multicore learning. This algorithm has been widely researched and applied in recent years and has achieved the best results among the current multiview clustering algorithms. In more detail, the multiview clustering algorithm based on multicore learning can be divided into two methods: the combined kernel function method and the public kernel function method. The combined kernel function method learns a linear or nonlinear kernel function combination as the input of the final clustering algorithm. This method has received a lot of attention in recent years. However, in a real environment, we often introduce noise information when we collect data, because it does not have a mechanism to deal with noise, so the combined kernel function method may not get better performance. Another method is the public kernel function method, which learns a public kernel function from the basic kernel function composed of multiple views. Compared with the combined kernel function method, this method has great advantages in noise processing.

Assuming that the same input data sample has the information of n views, we use the information of n views to construct n kernel functions F1, F2, …, Fn, and we use the method of multicore learning to learn from these basic kernels from different views. The function learns an optimal common kernel function B as the input of the final clustering algorithm to classify data from different categories into their respective categories. In order to better obtain the correct structure information implicit in the data and at the same time remove the noise information that may affect the performance of the final clustering algorithm from the learned public kernel function; we consider the following aspects of the problem: (1) we that learned public kernel function has low-rank characteristics and tends to block diagonal matrix structure and has less noise information; (2) since noise may be introduced when data is obtained, we construct multiple basic kernel functions There will be a certain amount of noise information.

Based on the above considerations, we define the model of joint optimization as follows:

$$\left| \min_{B, R_p} \text{rank}(B) + \gamma \sum_{p=1}^n \|R_p\|_l, \quad s.t. \forall p, F_p = B + R_p.\right.$$ (9)

Among them, the model or distribution of the error $\|\cdot\|_l$ is obtained a priori for the norm on the error matrix R, which γ is a parameter to weigh the two optimization items. In actual application scenarios, it $\|\cdot\|_l$ represents the noise associated with random elements. In order to solve the above optimization model more generally, we

adopt $\|\cdot\|_1$ the constraint of our error matrix R. Thus, the optimized model we retrieved is as follows:

$$\min_{B,R_p} \text{rank}\,(B) + \gamma \sum_{p=1}^{n} \|R_p\|_1, \quad s.t. \forall p, F_p = B + R_p. \quad (10)$$

The optimization problem becomes difficult to solve because the problem includes the solution of the rank function. We convert the rank function into a kernel norm to solve the problem. Since the kernel norm is a good approximation of the rank function, we can turn the problem into the following form:

$$\min_{B,R_p} \|B\|_* + \gamma \sum_{p=1}^{n} \|R_p\|_1, \quad s.t. \forall p, F_p = B + R_p. \quad (11)$$

We use the nondeterministic augmented Lagrangian method to solve the problem, so we can get the following form:

$$L\big(B, R_p, U_p, v\big) = \|B\|_* + \gamma \sum_{p=1}^{n} \|R_p\|_1 + \sum_{p=1}^{n} \langle U_p, F_p, -B - R_p \rangle$$
$$+ \frac{v}{2} \sum_{p=1}^{n} \|F_p - B - R_p\|_G^2. \quad (12)$$

Among them v, the convergence rate of the nondeterministic augmented Lagrangian method will be penalized, and Up is the Lagrangian multiplier constraint of Fp = B + Rp. $\langle \cdot \rangle$ represented inner product operation, and $\|\cdot\|_G$ represented G-norm.

(2) Optimization algorithm

Fix other parameters, optimization B: When other parameters are fixed, the subproblem of optimization is

$$B^{(k+1)} = \arg\,\min_{B} L\left(B, R_p^{(k)}, U_p^{(k)}, v^{(k)}\right). \quad (13)$$

The singular value threshold method can be used to solve the problem. Among them,

$$(I, M, V) = svd\left(\frac{1}{n}\sum_{p=1}^{n} F_p - \frac{1}{n}\sum_{p=1}^{n} R_p^{(k)} + \frac{1}{nv^{(k)}}\sum_{p=1}^{n} U_p^{(k)}\right). \quad (14)$$

After solving, we can get the result of B as

$$B^{(k+1)} = ID_{1/\left(v^{(k)}\right)}[\text{M}]V^T. \quad (15)$$

Among them, D is a shrink operation, which is defined as

$$D_\phi(x) = \begin{cases} x - \phi, & \text{if } x > \phi, \\ x + \phi, & \text{if } x < -\phi, \\ 0, & \text{otherwise.} \end{cases} \quad (16)$$

(3) Fix other parameters and optimize R

The subproblem obtained by optimizing R is

$$R_p^{(k+1)} = \arg\,\min_{R_p} L\left(B^{(k+1)}, R_p^{(k)}, U_p^{(k)}, v^{(k)}\right). \quad (17)$$

Its solution formula is

$$R_p^{k+1} = D_{\gamma/\left(v^{(k)}\right)}\left[F_p - B^{(k+1)} + \frac{1}{v^{(k)}} U_p^{(k)}\right]. \quad (18)$$

The optimization of the Lagrange multiplier can be defined as

$$U_p^{(k+1)} = U_p^{(k)} + v^{(k)}\left(F - B^{(k+1)} - R_p^{(k+1)}\right), \quad (19)$$

where $B\,(k+1)$ and $R_p^{(k+1)}$ are the result of the $k+1$ iteration above.

In feature extraction before extracting the characteristics of human motion state, data preprocessing needs to segment the data. The feature data extracted from the sensor data in a short time is called a window, which contains all the features of each human motion state. The duration of each cycle of each state determines the size of the window. Smaller windows may not accurately contain all the characteristics of each human motion state, but larger windows will bring more noise and affect the actual feature extraction. Usually, the time signal is sampled in a sliding window of 2.56 seconds with a fixed width, with an overlap rate of 50% and a sampling rate of 50 Hz, for data collection of human motion status.

4. Use Machine Learning Algorithms to Recognize Shuttlecock Movements

4.1. Image Result of Shuttlecock Motion Recognition. Shown in Figure 2 is the use of machine learning algorithms to identify the effect of shuttlecock movement. Figure 2(a) is a schematic diagram of the six key actions of shuttlecock (Figure 2(a), the original picture is borrowed from Baidu Gallery: https://wenku.baidu.com/view), and Figure 2(b) is binarized. After the image, Figure 2(c) is the effect image after recognition. It can be clearly seen from the picture that the red box outlines the key movements demonstrated by the shuttlecock player, namely, panning, stretching, hooking, wiping, knocking, and abduction. This shows that the research algorithm in this article is very effective, it can capture the actions of shuttlecock players very well, which is

(a)
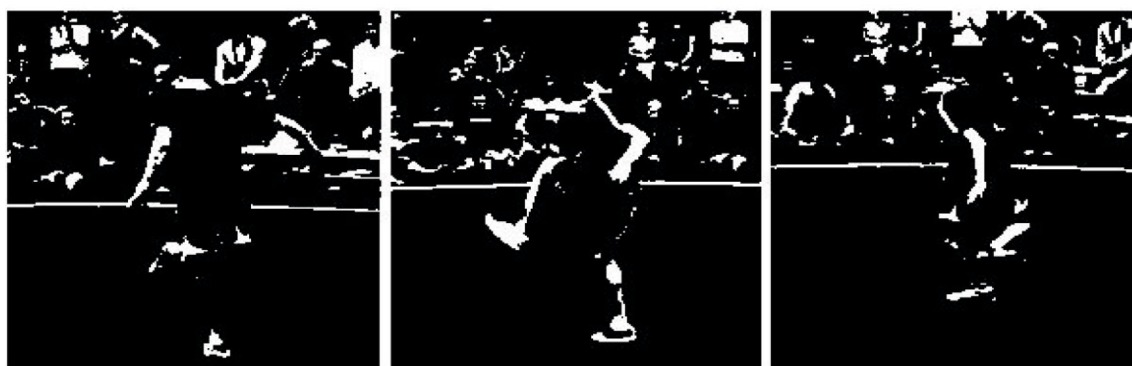
(b)

FIGURE 2: Continued.

(c)
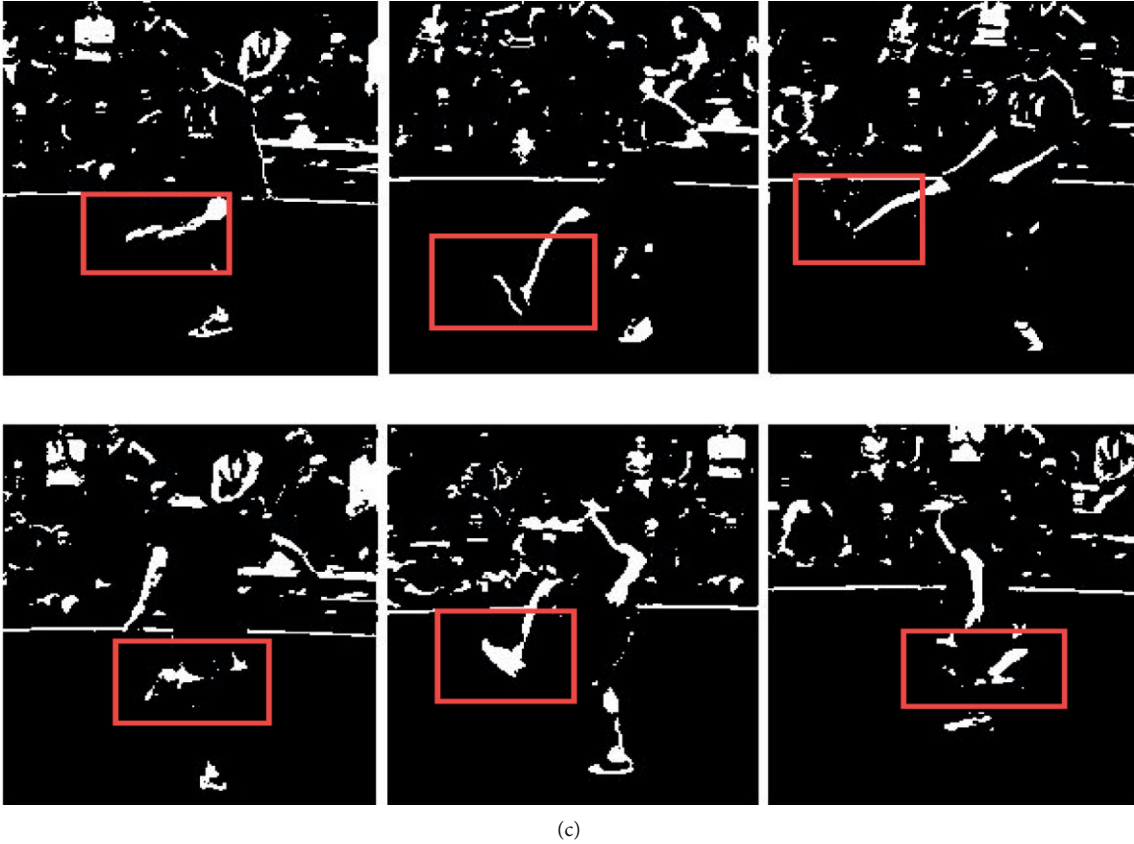
Figure 2: Using machine learning algorithm to recognize the effect of shuttlecock movement.

Table 1: Clustering algorithm confusion matrix result.

Classify		Predicted class						
		WK	WU	WD	SI	ST	LY	Recall
True class	WK	522	29	11	0	3	0	0.926
	WU	4	523	11	0	2	0	0.968
	WD	0	1	428	0	3	8	0.975
	SI	0	2	0	292	115	55	0.634
	ST	2	1	2	35	422	26	0.867
	LY	0	0	0	28	60	381	0.820
—	F1	0.956	0.955	0.961	0.725	0.775	0.822	—
	Precision	0.988	0.945	0.947	0.823	0.699	0.812	0.866

conducive to better application in shuttlecock competitions, analysis of opponents' game movements and habits, etc., and prepare for prevention in advance.

4.2. Comparison of Machine Learning Algorithm Performance. Table 1 is the confusion matrix of the experimental classification results. The confusion matrix can be used to calculate the accuracy rate, recall rate, and the value of *F*. Among them, the final accuracy rate of classification is 0.866. From the specific data, the clustering algorithm has a better recognition effect on WK, WU, and WD, while the recognition effect on SI, ST, and LY is poor. The main reason is dynamic action and static state. The difference in actions and the

similarity of actions have always been the difficulty of action recognition.

It can be seen from Table 2 that the recognition efficiency is evaluated by running time. In contrast, the algorithm in this paper can effectively improve the efficiency of motion recognition, and as the time complexity increases, the feature dimension increases, and the dimensionality reduction time is extremely high. And the algorithm in this paper effectively improves the recognition efficiency of feature dimensionality reduction.

As can be seen from Figure 3, after we fine-tuned the machine learning algorithm, the GPU platform value gradually increased, but its performance speedup ratio achieved the

TABLE 2: Image dimensionality reduction time of shuttlecock motion method.

Action type	30 dimensions			60 dimensions		
	RMSC	LMKKM	Method of this article	RMSC	LMKKM	Method of this article
Plate	5.11	5.23	4.51	22.36	15.87	8.53
Stretch	5.34	5.69	3.47	24.24	16.98	8.78
Abduction	6.18	7.18	4.78	22.16	17.22	9.45
Knock	5.92	7.24	3.96	20.11	20.13	8.73
Wipe	6.64	6.68	3.04	23.75	20.16	8.92
Rear	5.13	9.18	4.57	23.13	18.22	9.91
Hook	6.21	4.58	4.34	22.98	19.23	9.38
Kick	8.89	6.32	3.32	21.56	16.29	8.22
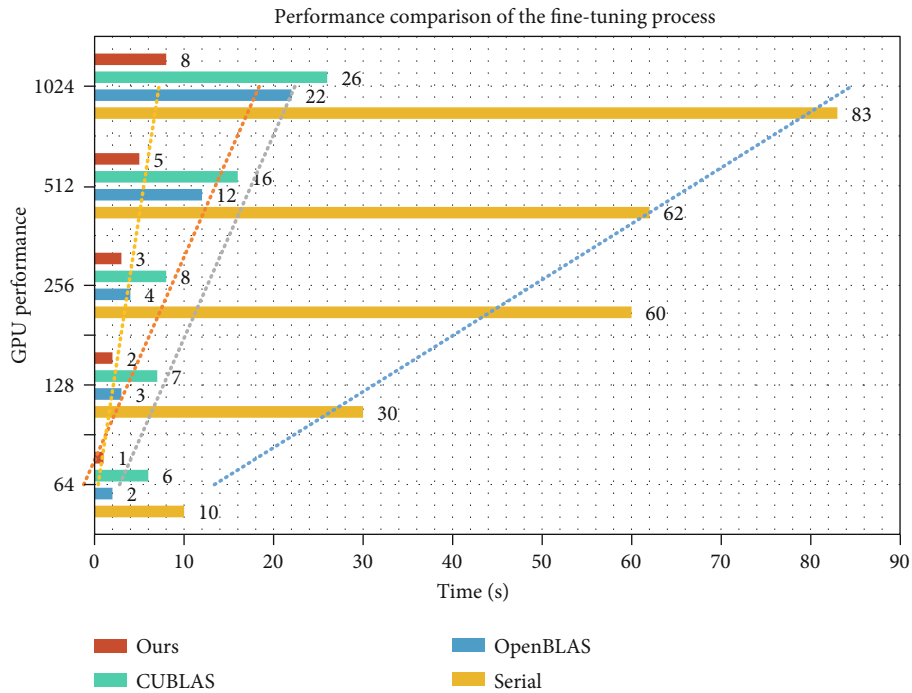
FIGURE 3: Performance comparison of the fine-tuning process.

ultimate effect. Compared with traditional algorithms, our method better verifies the effectiveness of the algorithm.

4.3. Experimental Results of Shuttlecock Motion Recognition Based on Machine Learning Algorithms. Figure 4 lists the experimental results of our method and other methods on the OxfordFlower17 dataset. From the table, we can see that the results obtained by all multiview-based methods optimize the experimental results of the optimal single view, thereby verifying the effectiveness of the multiview clustering algorithm; our proposed method is significantly better than the existing multiview Clustering Algorithm.

It can be seen from Figure 5 that when the proportion of damage gradually increases from 10% to 60%, the experimental results obtained by our method are better than the other two clustering performance indicators in accuracy, cross-correlation information, and purity. The multicore learning method of the public kernel function proves that

our method can deal with the noise information related to randomly generated elements. When the damage ratio is greater than 60%, the performance of the three methods is severely reduced due to the damage of the key information in the data. It is worth noting that when the proportion of damage is greater than 40%, the RMKC-SC method has been significantly reduced.

Figure 6 shows the classification accuracy obtained by the six algorithms of SVM, SPL, CSVM, CSPL, MV_SVM, and MV_SPL under the data set. It can be seen from the figure that under the same dictionary length and perspective, the classification effect of SPL is better than that of SVM. For the UTKinect-Action data set, the classification accuracy of SPL is about 6% higher than that of SVM on average. For the Florence3D-Action dataset, the classification accuracy of SPL is about 3% higher than that of SVM on average. Under the same dictionary length, the classification effect of MV_SPL is better than that of MV_SVM. For the
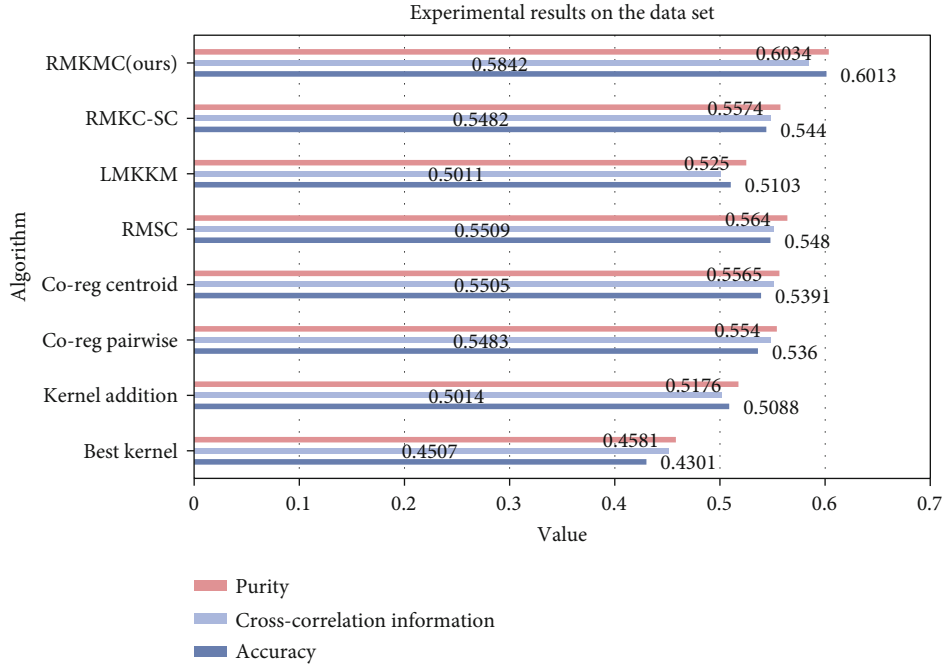
FIGURE 4: Experimental results on the data set.
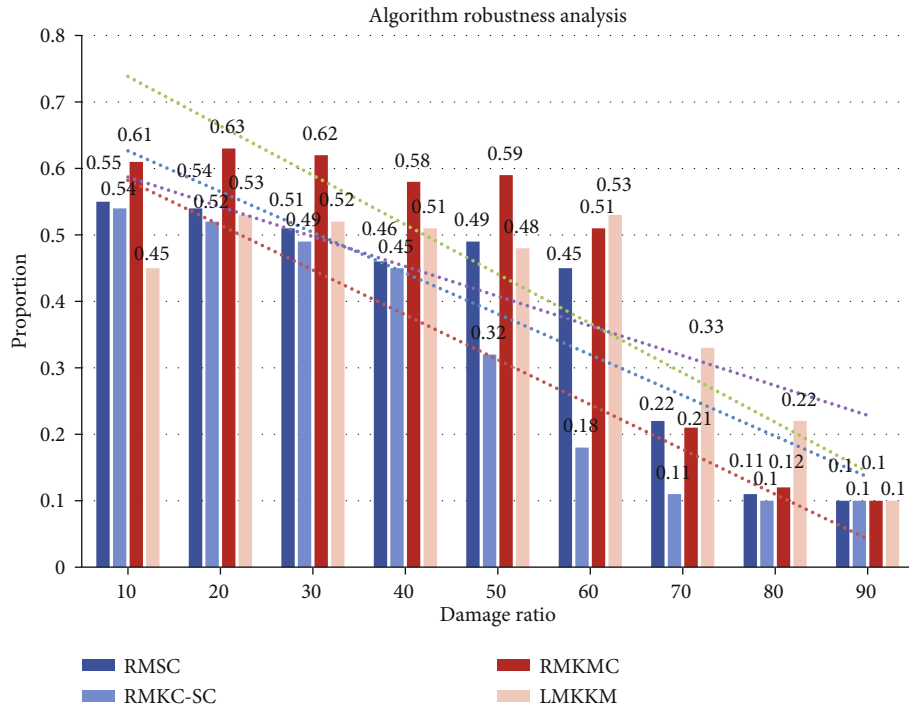
FIGURE 5: Algorithm robustness analysis.

UTKinect-Action dataset, the classification accuracy of MV_SPL is about 5.7% higher than that of MV_SVM. For the Florence3D-Action dataset, the classification accuracy of MV_SPL is 5.9% higher than that of MV_SVM on average. All of the above verify the effectiveness of the algorithm in this article.

Figure 7 shows the comparison of the recognition performance of the two classifiers. From the data in the table, it can be seen that in the case of the same dictionary length, the recognition performance of the shuttlecock action, taking the 500 dictionary length as an example, the recognition performance of SVM is generally worse than that of SPL, but under
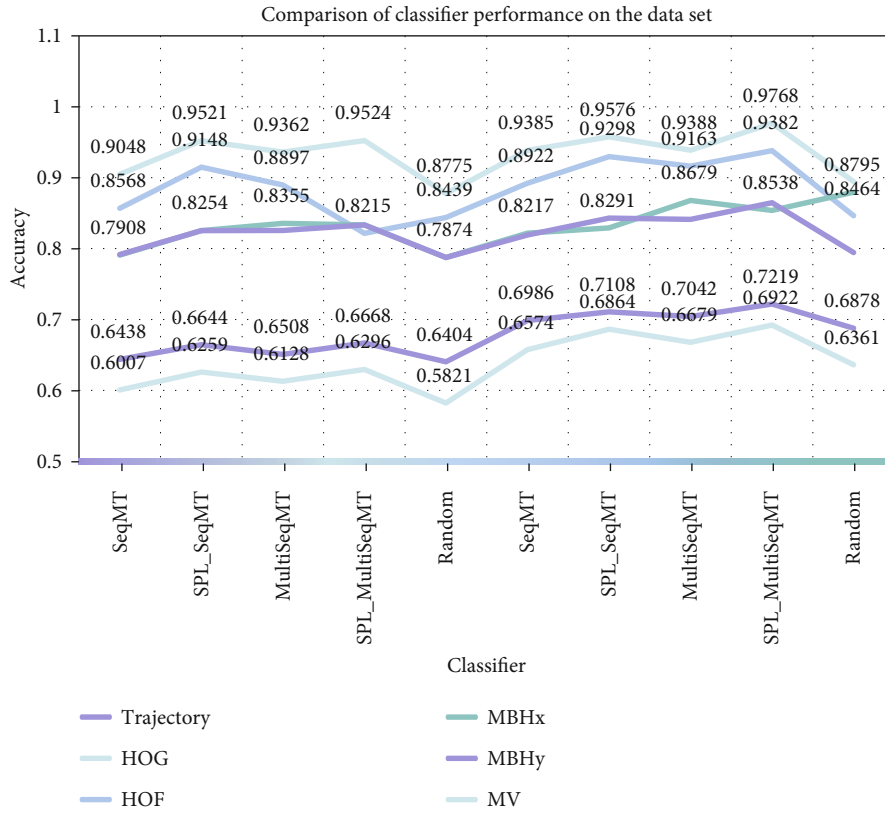
FIGURE 6: Comparison of classifier performance on the data set.
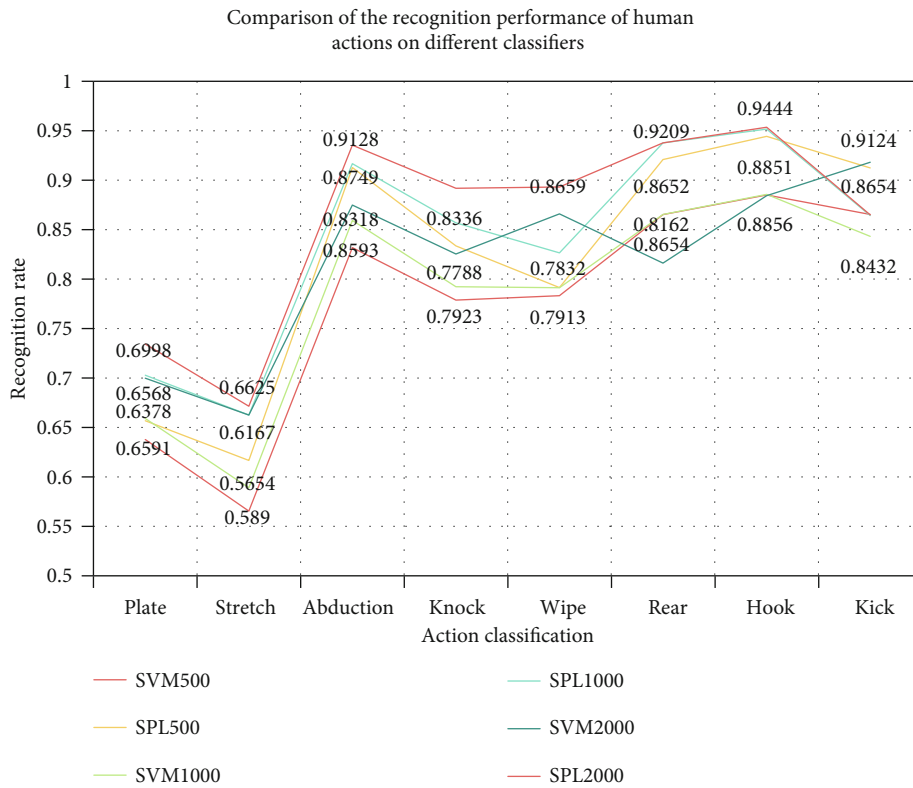
FIGURE 7: Comparison of the recognition performance of human actions on different classifiers.

Table 3: Experimental results of recognition of shuttlecock movements.

Action classification	Number of actions	Recall rate	Accuracy	Recognition rate
Plate	41	87.6	85.3	87.6
Stretch	156	85.3	91.4	91.2
Abduction	158	89.4	92.5	84.2
Knock	255	87.4	89.7	75.9
Wipe	136	57.3	62.5	76.3
Rear	170	64.8	75.1	72.3
Hook	224	59.6	66.8	75.4
Kick	207	58.4	68.9	71.8

the fusion algorithm, the multiview fusion algorithm is more effective. Especially in the two actions of hook and kick, SPL's action recognition rate exceeds 95%.

Table 3 shows the number of actions that occurred in a shuttlecock match, as well as the recall rate, precision rate and accuracy, and other indicators. For the shuttlecock game, the algorithm proposed in this paper has a good action recognition rate, up to 91.2%. Although several similar actions can be recognized well, the average recognition accuracy rate can exceed 75%, and even through continuous image capture, the number of occurrences of the action can be automatically analyzed, which is beneficial to athletes. And the coach can better analyze tactics and research strategies.

5. Conclusion

This paper mainly uses machine learning algorithms to recognize the shuttlecock movement. Through the multiview clustering algorithm and deep belief network algorithm, the shuttlecock movement is recognized and processed, and the shuttlecock movement recognition model is constructed, and various data sets are used. Perform performance testing. The algorithm in this paper can greatly improve the efficiency of motion recognition in shuttlecock motion and shows good performance in human motion detection, motion feature selection, and extraction. The innovation of this paper is to strengthen the accuracy and precision of action recognition through the application of machine learning algorithms and improve the application efficiency of the algorithm. The disadvantage of this article is that the research model of this article is not perfect, and it needs more experimental research data support. In the future, the algorithm in this article will be more widely used in motion recognition, but there are still more difficulties, and we need more in-depth research.

Data Availability

The data underlying the results presented in the study are available within the manuscript.

Conflicts of Interest

The author declares that there are no conflicts of interest.

References

[1] C. Yang and Z. Lv, "Gender based face aging with cycle-consistent adversarial networks," *Image and Vision Computing*, vol. 100, article 103945, 2020.

[2] Y. J. Lin and S. K. Weng, "Trajectory estimation of the players and shuttlecock for the broadcast badminton videos," *IEICE Transactions on Fundamentals of Electronics Communications and Computer Sciences*, vol. E101.A, no. 10, pp. 1730–1734, 2018.

[3] Z. Zhao, H. Ma, and X. Chen, "Semantic parts based top-down pyramid for action recognition," *Pattern Recognition Letters*, vol. 84, no. Dec.1, pp. 134–141, 2016.

[4] N. Jean, M. Burke, M. Xie, W. M. Davis, D. B. Lobell, and S. Ermon, "Combining satellite imagery and machine learning to predict poverty," *Science*, vol. 353, no. 6301, pp. 790–794, 2016.

[5] C. J. Hammerlind, "Patent eligibility used as the Federal Circuit's shuttlecock in weekly badminton match," *Intellectual Property & Technology Law Journal*, vol. 31, no. 6, pp. 8–13, 2019.

[6] S. Dalgleish, L. Reissig, Y. Shuku, C. Gourlaouen, S. Vela, and K. Awaga, "Controlling the crystallinity and crystalline orientation of "shuttlecock" naphthalocyanine films for near-infrared optoelectronic applications," *Journal of Materials Chemistry C*, vol. 6, no. 8, pp. 1959–1970, 2018.

[7] W. Chen, T. Liao, Z. Li et al., "Using FTOC to track shuttlecock for the badminton robot," *Neurocomputing*, vol. 334, no. MAR.21, pp. 182–196, 2019.

[8] C. Dally, S. Haddow, and E. Kershaw, "A shuttlecock for the visually impaired," *Electronics Education*, vol. 1996, no. 1, pp. 28–30, 2017.

[9] A. Abdulmunem, Y.-K. Lai, and X. Sun, "Saliency guided local and global descriptors for effective action recognition," *Computational Visual Media*, vol. 2, no. 1, pp. 97–106, 2016.

[10] P. Wang, W. Li, Z. Gao, J. Zhang, C. Tang, and P. O. Ogunbona, "Action recognition from depth maps using deep convolutional neural networks," *IEEE Transactions on Human-Machine Systems*, vol. 46, no. 4, pp. 498–509, 2016.

[11] M. Yu, L. Li, and S. Ling, "Structure-preserving binary representations for RGB-D action recognition," *IEEE Transactions on Pattern Analysis and Machine Intelligence*, vol. 38, no. 8, pp. 1651–1664, 2016.

[12] W. Du, Y. Wang, and Q. Yu, "Recurrent spatial-temporal attention network for action recognition in videos," *IEEE Transactions on Image Processing*, vol. 27, no. 99, pp. 1347–1360, 2017.

[13] D. Stephan, E. Mina, and H. H. Bülthoff, "Action recognition and movement direction discrimination tasks are associated with different adaptation patterns," *Frontiers in Human Neuroscience*, vol. 10, no. 752, pp. 1–6, 2016.

[14] M. Buonamente, H. Dindo, and M. Johnsson, "Hierarchies of self-organizing maps for action recognition," *Cognitive Systems Research*, vol. 39, pp. 33–41, 2016.

[15] J. Wang, H. Zheng, J. Gao, and J. Cen, "Cross-view action recognition based on a statistical translation framework," *IEEE Transactions on Circuits and Systems for Video Technology*, vol. 26, no. 8, pp. 1461–1475, 2016.

[16] C. Jia, M. Shao, S. Li, H. Zhao, and Y. Fu, "Stacked denoising tensor auto-encoder for action recognition with spatiotemporal

corruptions," *IEEE Transactions on Image Processing*, vol. 27, no. 4, pp. 1878–1887, 2018.

[17] S. Lv, Y. Lu, M. Dong, X. Wang, Y. Dou, and W. Zhuang, "Qualitative action recognition by wireless radio signals in human-machine systems," *IEEE Transactions on Human-Machine Systems*, vol. 47, no. 6, pp. 789–800, 2017.

[18] T. V. Nguyen and B. Mirza, "Dual-layer kernel extreme learning machine for action recognition," *Neurocomputing*, vol. 260, pp. 123–130, 2017.

[19] Z. Gao, S. H. Li, Y. J. Zhu, C. Wang, and H. Zhang, "Collaborative sparse representation leaning model for RGBD action recognition," *Journal of Visual Communication and Image Representation*, vol. 48, pp. 442–452, 2017.

[20] S. Yu, Y. Cheng, L. Xie, and S. Z. Li, "Fully convolutional networks for action recognition," *IET Computer Vision*, vol. 11, no. 8, pp. 744–749, 2017.

[21] S. Wilson and C. K. Mohan, "Coherent and noncoherent dictionaries for action recognition," *IEEE Signal Processing Letters*, vol. 24, no. 5, pp. 698–702, 2017.

[22] N. D. Sidiropoulos, L. De Lathauwer, X. Fu, K. Huang, E. E. Papalexakis, and C. Faloutsos, "Tensor decomposition for signal processing and machine learning," *IEEE Transactions on Signal Processing*, vol. 65, no. 13, pp. 3551–3582, 2017.

[23] C. Helma, T. Cramer, S. Kramer, and L. De Raedt, "Data mining and machine learning techniques for the identification of mutagenicity inducing substructures and structure activity relationships of noncongeneric compounds," *Journal of Chemical Information and Computer Sciences*, vol. 44, no. 4, pp. 1402–1411, 2004.

[24] Z. Obermeyer and E. J. Emanuel, "Predicting the future—big data, machine learning, and clinical medicine," *The New England Journal of Medicine*, vol. 375, no. 13, pp. 1216–1219, 2016.

[25] S. Ying, P. Babu, and D. P. Palomar, "Majorization-minimization algorithms in signal processing, communications, and machine learning," *IEEE Transactions on Signal Processing*, vol. 65, no. 3, pp. 794–816, 2016.

[26] M. Wang, Y. Cui, X. Wang, S. Xiao, and J. Jiang, "Machine learning for networking: workflow, advances and opportunities," *IEEE Network*, vol. 32, pp. 92–99, 2018.

[27] D. Assouline, N. Mohajeri, and J. L. Scartezzini, "Quantifying rooftop photovoltaic solar energy potential: a machine learning approach," *Solar Energy*, vol. 141, pp. 278–296, 2017.

WILEY | Hindawi

Research Article

Optimization Analysis of Tennis Players' Physical Fitness Index Based on Data Mining and Mobile Computing

Shoudong Zhang[1] and Huaqing Mao [iD] **[2]**

[1]*Sports Department, Jiangnan University, Wuxi, 214122 Jiangsu, China*
[2]*School of Computer Engineering, Hubei University of Arts and Science, Xiangyang, 441053 Hubei, China*

Correspondence should be addressed to Huaqing Mao; mr.maohuaqing@hbuas.edu.cn

Tennis is a very explosive, continuous, and intense sport, including many continuous short-term explosive actions. It has the characteristics of short-term, high-intensity, high-density training, and it belongs to the category of purely competitive skills. In the competition, athletes must maintain good physical condition, physical fitness, and long-term endurance in order to demonstrate outstanding technical and tactical skills. Therefore, this paper proposes a mobile processor performance data mining framework MobilePerfMiner, which uses hardware counters and iteratively uses the XGBoost algorithm to build a performance model, ranks the importance of the microarchitecture events of the big data task, and reduces the performance big data dimension, so as to optimize the big data algorithm according to the performance characteristics described. Undoubtedly, the comprehensive monitoring of the sports training process is complex system engineering. The main monitoring includes three aspects: physical condition, technical and tactical skills, and intelligence. Sports technology is reflected in the ultimate load. According to the convenience and actual needs of the research, this article will discuss the methods of evaluating tennis training load and the actual technical and tactical parameter characteristics that can be obtained by studying the characteristics of tennis, namely, kinematics. Parameters for noncontact testing, the next step is to discuss the appropriateness and necessity of the load, as well as the technical and routine monitoring of tennis training ability. The final experimental results show that it can improve the physical energy of tennis players by more than 17%.

1. Introduction

The rapid development of big data is profoundly changing people's production and life and changing the world. In recent years, with the increasing number of mobile devices and the increasingly powerful computing power of mobile processors, it has become more common to run big data tasks on mobile platforms. Running big data applications on mobile platforms helps developers quickly apply new big data algorithms to mobile platforms, enabling people to obtain big data services anytime and anywhere, improving people's production and life, and promoting industrial transformation [1].

Since Chinese tennis started late on the international stage, its relative level is low, and its growth rate is slow; one of the main reasons for this result is the lack of popularity of tennis. Many athletes are slow in contact with tennis, so

they miss the fast-growing fitness time, which hinders the development of tennis in the later period. New tennis players are the hope and new strength of the development of tennis in our country. Slowly they only start with basic knowledge. There will be many top tennis players. Therefore, tennis training for young people is the top priority, and the country has begun to pay attention to it. This has helped to carry out in-depth youth tennis training, and won many competitions and opportunities, and provided young tennis players with more opportunities.

Yang established a volleyball fitness model based on data mining, used mathematical statistics to analyze the five main components of volleyball players, and obtained volleyball representative volleyball indicators based on the five fitness characteristics. Based on the adaptability of various indicators, the ratio of the quality factor and the characteristic value

of the rotated index to the total characteristic value of the various factors can be used to obtain the weight coefficient of a healthy athlete representing the weight index of the physical index. Through the weighting factor, the physical fitness model of volleyball players based on data mining can be obtained. Using this model can effectively evaluate the athlete's training, competition, and health status. The factor analysis method is used to test the planned health evaluation model of volleyball player data mining, and the results show that the evaluation model is reliable. However, the experimental data is too few and not convincing enough [2]. In order to study and test the success factors of women's tennis matches, Yulin established bibliographic data methods, mathematical statistical methods, and decision tree prediction models to conduct statistical analysis on the data of 198 unemployed women from four continents. Research shows that the accuracy of the decision tree prediction standard model is 91.4%, and the new decision tree model is feasible. The main factor that determines a woman's chance of winning a tennis match is the percentage of receiving and scoring. The result of 41% shows that the rate of receiving and scoring is the lifeline for women to play tennis; 41% of service scores and 61% of first service scores are lower than 28 non-Mandatory errors which have the highest win rate, 96.7%. The conclusion is that technology sending and receiving is the link between current tennis technology and the key factors of the game result. Now, women playing tennis must pay attention to efficiency and reduce nonmandatory errors. The main ways are to improve the winning rate of women's tennis matches, provide appropriate countermeasures and suggestions to check the quantitative indicators of tennis match winners, and provide specific and effective implementation methods for tennis training. However, the data model he selected is not complete, and the data should be randomly selected for experiments [3]. Yang and Yan believe that diagnosing the scientific state of the tennis training process is the key link to improve the training level and competitive performance of tennis players. It is necessary to receive physical education through the reference index of the ability test of the university graduate school, train outstanding tennis players in the sports college, and carry out effective game monitoring. And method conclusions determine the physical condition and composition of excellent tennis players and other physiological indicators. The Graduate School of the School of Physical Education is aimed at understanding the physical functions of outstanding tennis players in the School of Physical Education, at providing scientific support for the tennis level and athletic performance of students across the country, at training their tennis enthusiasts, and at improving the overall improvement of ordinary tennis players. However, the amount of data is too large, and the data statistics process is very difficult [4].

The research goal of this work is to monitor mobile processor microarchitecture events when running big data tasks and use data mining methods to analyze event values and then characterize the performance characteristics of big data tasks on mobile processors. The final research goal of this work is to improve the performance of mobile processors from the perspective of characterizing the performance char-

acteristics of big data tasks and propose a plan for improving the physical fitness of tennis players. The computing power of modern mobile processors is getting stronger and stronger, and more and more applications are deployed on mobile platforms. How to measure and understand the performance characteristics of applications on mobile platforms is the main content of this research. This work structured event features and merged events as features. Structured means that the original data obtained by monitoring needs to be cleaned and corresponds to the feature names one to one; the reason for using events as features is that we hope to find events that affect system performance, that is, a factor that affects system performance, so events are taken as characteristics of system performance; merging refers to merging the event values obtained from each monitoring and making full use of the event values of each monitoring. Finally, the relationship between microarchitecture events and performance is established, and the event characteristics are sorted, so that we can find events that affect system performance.

2. Optimization Method of Tennis Player's Physical Fitness Index

This article takes the core elements of the long-term training model of tennis players as the research object, namely, the "ten-year phenomenon," "specialized timing," and "window of training opportunity" [5]. It demonstrates its rationality from two levels of theory and practice and its impact on my country's tennis talents, the guiding significance of training [6].

2.1. Literature Data Method. During the research process, more than 200 related documents were reviewed using a bibliographic search engine, collected, localized, and classified, including related documents about their current status [7]: 39 articles about the training of domestic and foreign athletes, 56 articles about the LTAD model, 8 articles about the LTAD tennis model, 18 articles about the retention of sports at home and abroad, 23 articles about the "decade phenomenon," and about the 20 of the 26 articles of "Century Phenomenon" related to the topic of specialization time and 19 related studies on "windows of training opportunities" [8]. Since there are relatively few studies on the LTAD model in China, it was carried out in the early stage of this study. A lot of foreign language reading work combined with knowledge of sports coaching, teaching methods, sports psychology, sports anatomy, etc., summarized the literature and knowledge points related to this article, and created a knowledge system and preliminary information for this article [9].

2.2. Empirical Research Method. Taking elite athletes as the research object and as their talents develop, collect information and data consistent with this article [10]. For example, when we investigated the elucidation of the "ten-year phenomenon" in the training of tennis talents in my country, we collected some data, such as the age of participation of famous tennis players and the performance age of the National Games to support the "ten-year phenomenon" [11]. When we investigated the clarification of the "timing of specialization" for training tennis talents in our country,

we checked a lot of historical data about talent training and found that the phenomenon of "early specialization" existed in the early stage. During the training process, while studying the inspiration of "Window of Opportunity" in cultivating excellent tennis talents in our country, we conducted retrospective interviews with coaches on various key characteristics of the training process of excellent tennis players and highlighted the sensitive time the paragraphs are relatively consistent, and a certain number of references have been found [12, 13].

2.3. Expert Interview Method. This research conducted a survey in the form of face-to-face interviews. First, the interviewed experts were introduced to the background, purpose, and significance of the interview, and then the experts were asked to answer and discuss the questions in the interview [14]. Time after time, summarize and clarify the main content of each question in the interview, use a tape recorder to record the interview process of the interviewed experts, and organize the data set [15]. The main content of the interview is based on the main part of the article: the basic elements of the long-term coaching model of tennis players, namely, "decade phenomenon," "special period," "window of training opportunities," three aspects, and years of athlete training and information experience and experts' interview [16, 17].

2.4. Data Mining Process

(1) Defining the problem according to the problems and needs of the enterprise: select the data mining target, through the precise positioning of the enterprise problem; select the data type and prediction model, so as to design a targeted marketing strategy; the main steps include business needs analysis, data relationship selection, business model association, and prediction model selection. Figure 1 shows a picture of a tennis player hitting the ball [18]

FIGURE 1: Tennis player hitting the ball (the picture comes from https://image.baidu.com/).

(2) Preparing the data [19]: the data set plays a decisive role in the mining model. Because the data format in the original data set is complex and diverse, there are often incorrect data, outliers, or dirty data, which cannot meet the data requirements of modeling [20]. Therefore, in order to improve the data quality, match the data requirements of the model and preprocess the data. The specific steps include data cleaning, data integration, data reduction, data transformation, and data dimensionality reduction, so as to extract structured data indicators related to the topic [21]. A follow-up analysis work provides effective data support

(3) Exploring data: exploring data is a key part of the data mining process. Data exploration is generally divided into classification and clustering [22]. The classification process is to train the data set by using the classification algorithm and then use the test data set to evaluate the accuracy of the selected classification rules. Clustering is to select a partition method to classify the data according to a certain standard and then test the accuracy of the method [23]

(4) The mining modeling (classification, clustering, association, and prediction): models are diverse, and analysis models are established according to specific needs, and the data content is researched and explored [24]. In addition, the model creation should match the data of the mining structure columns and link the data structure to the data set. And the data set that conforms to the mining structure will be matched to the database and become valuable data [24, 25]

(5) Model verification and evaluation: the ultimate goal of the model is to have commercial value [26]. Before the model is put into practical application, the performance of the model should be tested and evaluated in many aspects, and the test results should be understood and analyzed in combination with the practical application, and the results should be discovered [27]. Valuable business models can be compared and analyzed on multiple similar models to determine which model best meets the data requirements of the problem, to determine the feasibility of the model [28].

3. Correlation Experiment of Data Mining and Mobile Computing

3.1. Introduction to XGBoost Algorithm. The XGBoost algorithm is a tree-based lifting algorithm. It is a new tree learning algorithm for processing sparse data based on the gradient boosting tree method (GBM or GBRT (gradient boosting machine or gradient boosted regression tree)), a theoretically reasonable weighted quantile calculation program The instance weight can be handled in the approximation tree learning. Use scaling and column sampling to improve the model's ability to fit data.

For a given data set of n samples and m features, $D = (x, y)$:

$$\hat{y} = \Phi(x_i) = \sum_{k=1}^{k} f(x_i), \tag{1}$$

q represents each tree structure and maps a sample to the corresponding page index. T is the number of leaves in the tree. Each f corresponds to an independent tree structure q and leaf weight w. Unlike decision trees, each regression tree contains a continuous score on each leaf node, and w represents i-th leaf score.

$$\wedge(\varphi) = \sum_i L(y_i, x_i) + \sum k(f_k),$$
$$\prod(f) = \sum_i l\left(\hat{y}^{t-1} + f_t(x_i)\right) + f_k. \tag{2}$$

Among them, L is a differentiable convex loss function, used to measure the distance between the predicted value y and the true value. The second term of the formula is the penalty term for model complexity (such as the number of functions of the regression tree) [29]. The specific process of data mining is shown in Figure 2.

The accumulation rule is to help adjust the final learning rate to avoid overfitting. Instead, the model uses an accumulation operation for training.

$$\Delta(\varphi) = \sum_i l\left(\hat{y}, y_i^{t-1} + f_t(x)\right). \tag{3}$$

This means that we greedily accumulate t according to formula (3) to improve our model the most, and the second-order approximation of the objective function can be quickly optimized.

$$\Pi^t = \sum_{i=1}^{n}\left[l\left(y_i, \hat{y}\right) + g_i f(x) + \frac{1}{2} h_i f^2(x)\right] \tag{4}$$

Among them,

$$g_i = \partial(t-1) l\left(y_i, y^{t-1}\right). \tag{5}$$

It is the first-order and second-order statistics of the loss function; after deleting the constant term, we get

$$\lambda^t = \sum_{i=1}^{n}\left[g_i f(x_i) + \frac{1}{n} h_i + \gamma T\right] + \frac{1}{2}\lambda. \tag{6}$$

The above formula can be used as a scoring function to measure the quality of the tree structure q. This score is similar to the purity score of the evaluation decision tree, except that it is derived for a broader objective function [30].

3.2. XGBoost Algorithm and Feature Selection. Performance counters provide information about the state of the processor and can be used to detect the execution and performance of
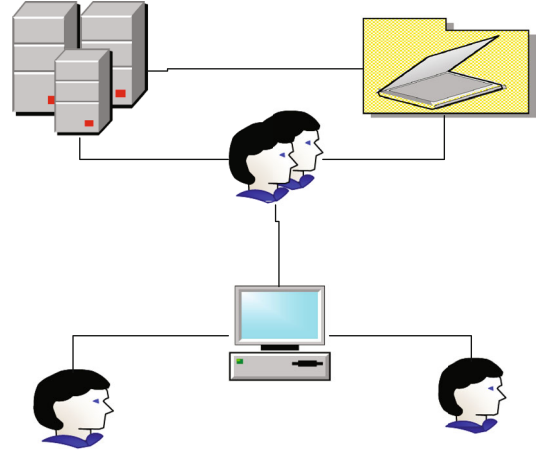
FIGURE 2: The specific process of data mining.

the workload. However, the link between the counter value and the observed performance is difficult to capture. On the one hand, the complexity of the processor makes it an arduous task to interpret the measured microarchitecture events and performance. On the other hand, the microarchitecture events supported by the processor are numerous and complicated. How to choose fewer microarchitecture events? And how to establish the connection between microarchitecture events and performance is the research goal of the MEE module.

$$IPC = \text{perf}(e_1, e_2, \cdots, e_n), \tag{7}$$

e is a certain microarchitectural event and IPC is how many instructions are executed in each cycle, which is an important indicator of performance and n is the number of microarchitectural events. Through the establishment of XGBoost algorithm model for events and performance, XGBoost is good at processing sparse data and high-dimensional data and characterizes the processor performance characteristics of running big data tasks on ARM processors. And use the feature importance obtained by the XGBoost modeling process to sort the events.

$$\prod_l^2(T) = \sum_{t=1}^{l-1} l_t^2 I(v(t) = l). \tag{8}$$

This importance metric can easily be extended to additive tree expansion, which simply averages the tree.

$$\prod_l^2 = \frac{1}{M} \sum_{m=1}^{M} T_m. \tag{9}$$

For each J in the hidden layer or output layer, the net input and input of the calculation unit J are relative to the previous layer I:

$$I_j = \sum_i w_{ij} O_i + \theta. \tag{10}$$

TABLE 1: Descriptive statistics of male athletes of different ages.

	Age	Number of cases	Average value	Standard deviation
Seat body forward bending performance	16-18 years old	39	-12.938	7.5906
Throwing a solid ball (2 kg) with both hands	16-18 years old	30	11.3213	2.13373
1 minute double-flying rope skipping results	16-18 years old	35	73.50	35.675
Fan running results	16-18 years old	40	16.6015	1.05556
800 m score	16-18 years old	43	27.85	19.780

Because the BP neural network has the advantages of nonlinear mapping ability, self-learning and adaptive ability, generalization ability, fault tolerance, etc., it has a wide range of applications in the fields of function approximation, pattern recognition, data prediction, etc. Each unit of the calculation output layer error selects the sigmoid function as the excitation function:

$$\text{Err}_i = O_i\left(1 - w_j\right)\left(T - m_i\right). \tag{11}$$

Aiming at the problems of BP neural network algorithms that are easy to fall into local extremes, slow convergence speed, and low optimization accuracy, there are many improvement methods at present. This paper uses the BP neural network model based on the improved PSO algorithm and the GA algorithm to predict mobile user behavior. The improved BP neural network model training has a faster convergence speed and a more accurate algorithm. The improved BP neural network algorithm is used to predict the behavior of mobile users, and the accuracy and stability are significantly improved.

4. Optimization Analysis of Tennis Player's Physical Fitness Index

4.1. Specific Physical Fitness of Young Tennis Players. Flexibility refers to the movement ability of human joints in different directions and the stretching ability of soft tissues such as muscles and ligaments. Flexibility is expressed through the range of joint motion, which is also reflected in the range of motion generated by a certain axis of motion.

Table 1 shows the descriptive statistics of various physical qualities of male athletes in different age groups. The table mainly lists the number of male athletes of each age group, the average value, and the standard deviation. The left and right hand solid balls improve with age. The 1-minute double-flying rope jumps better with age. The fan-shaped run and the 800-meter run also increase with age; the faster the running speed, the shorter the time. Under normal circumstances, specific physical fitness improves with age and conforms to the physiological laws of the human body, except for sitting forward bending.

It can be seen from Table 2 that in the intragroup comparison of the physical flexibility of male group A tennis players, the P values in the same group are all greater than 0.05, which indicates that the top eight male players in group A are compared with the non-top eight players. The difference in physical flexibility of famous athletes is not obvious.

TABLE 2: Comparison of the difference between men's group competition performance and seat bending performance.

Whether the top eight	Number of cases	Average value	Standard deviation	t value
Yes	8	-15.563	6.6586	-1.100
No	32	-12.261	7.7670	n.s.

From Figure 3, the 16-18-year-old male athletes in Group A are among the top eight in the seat body who bend forward and throw a solid ball with both left and right hands, 1-minute double-flying rope skipping, fan-shaped running, and 800-meter performance difference comparison table found. The top eight male athletes in the 16-18-year-old group have achieved a significant level in the t-statistics of each performance test of throwing a solid ball with both left and right hands, a 1-minute double flying skipping rope, and 800 meters. The significant probability value P is all less than 0.05, which means 16. Whether the top eight male athletes in the 18-year-old group have a solid ball with their right hands, a 1-minute double-flying rope, and 800 meters are significantly different.

It can be seen from Figure 4 that, first of all, experts particularly emphasize the cultivation of athletes' will and quality in training. Long-term professional sports training must be boring, and it is a great test for athletes' physiology and psychology. Because young athletes are in the developmental stage, their minds are also showing relatively immature characteristics. Most athletes love to "play" and can persist with the support of hobbies at the beginning of training. As the training content deepens and the amount of training increases, the training process inevitably tends to be repetitive and boring. If there is not enough mental motivation and will quality, it is difficult to persist. This requires coaches and parents to need more encouragement and support in training and conveys to them the basic concept of "training for oneself," so that they can generate independent restraint, so that the effect of training can be improved.

As shown in Figure 5, the overall curve describes the growth process of the body in terms of height and weight. It includes the growth of various systems of the body, such as the muscles, bones, lungs, heart, ligaments, and tendons. The shape of the curve indicates the slow and steady development of body structure or figure between the ages of 5 and 12. Simply put, this period is the best period for the development of basic motor skills. Neural curves describe the development of the brain and nervous system. At about 7 years old, 95% of
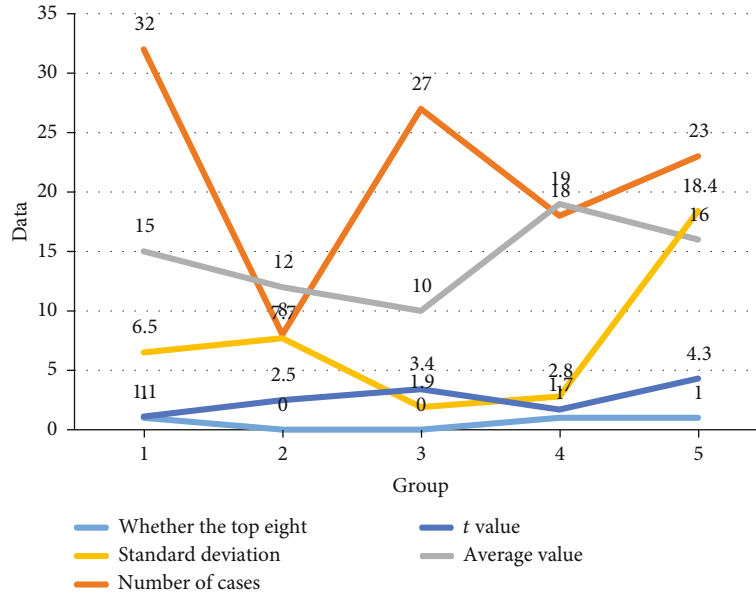
FIGURE 3: Comparison of the difference between male A group competition results and specific physical fitness results.

Group	A	B	C	D	E	F
Initial training age	6	8	9	8	7	6
Age of maturity	18	18	22	20	21	19
Time (years)	12	10	13	12	14	13
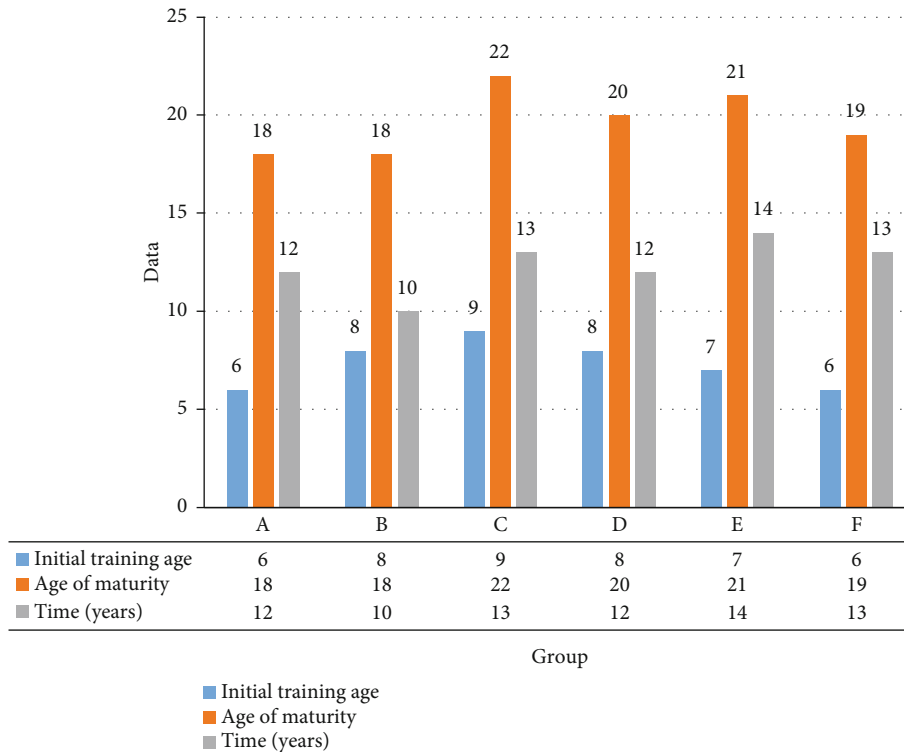
FIGURE 4: Table of the age of excellent tennis players at the beginning of training and the age of outstanding results.

the central nervous system has been developed. The shape of the nerve curve indicates that children should be trained early on motor skills such as agility, balance, coordination, and speed. The reproductive curve shows the growth pattern of the first and second sexual characteristics. The growth of reproductive tissues is slow, there is an incubation period in childhood, and it is extremely rapid before the growth spurt in adolescence. This curve shows that hormone maturation

has a significant increase in physical development and ability improvement.

4.2. Feature Extraction of Tennis Microarchitecture Events. By observing the importance ranking of the microarchitecture events of Spark-bench benchmarks, we have obtained the characteristics of four types of programs, which are common and individual characteristics, memory characteristics,
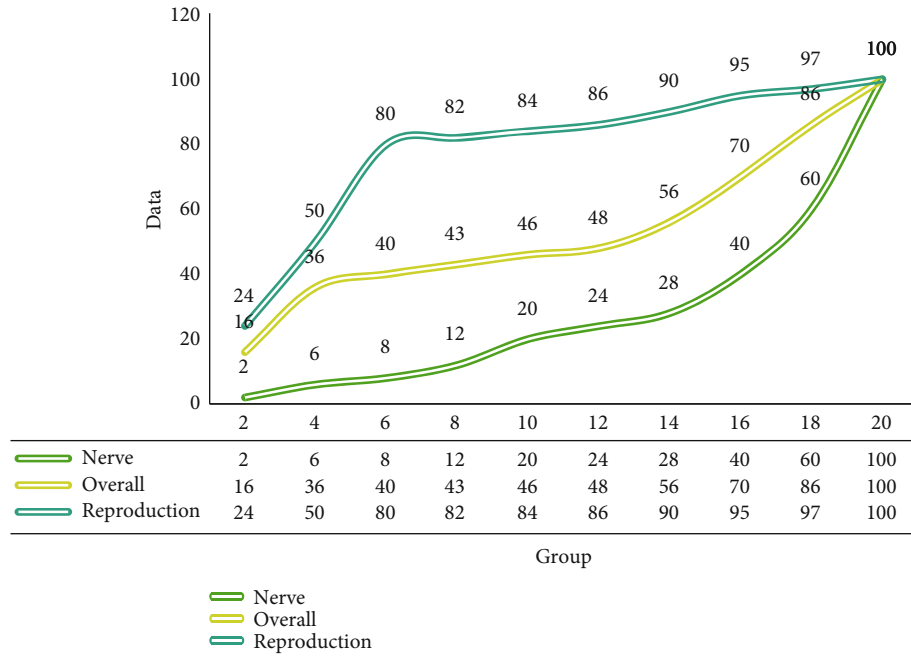
Figure 5: The curve of the human body's overall, neurological, and reproductive development trajectory.

Table 3: Event name and description.

Abbreviation	Event name	Description
BIR	BR_IMMED_RETIRED	Immediate branch instruction
BMP	BR_MIS_PRED	Prediction errors or unpredictable branch guess execution
BRP	BR_PRED	Predictable branch of guess execution
CDE	CLK_DE_EN	PLE request is programmed

Table 4: Partial Spark configuration parameters.

Parameter name	Defaults	Description
spark.driver.cores	1	Number of cores used for the driver process only in cluster mode
spark.driver.memory	1 g	The amount of memory used for the driver process
spark.executor.memory	1 g	The amount of memory used for the executor process
spark.executor.cores	All	Number of cores per executor
spark.reducer.maxSizeInFlight	48 m	The maximum size of the map output obtained from each reduce task at the same time
spark.shuffle.compress	True	Whether to compress the mapping output file

and instruction characteristics. The characterization of these events reflects the performance characteristics of the Spark program running on the mobile processor. It is helpful to analyze the execution characteristics of big data tasks on mobile devices and improve the execution efficiency of big data tasks on mobile devices.

As shown in Table 3, it is introduced that the MEE module of MobilePerfMiner uses the XGBoost algorithm to establish a performance model for microarchitecture events and performance and obtains the importance ranking of the event characteristics of performance. In the process of feature extraction, according to the change of the error curve, we found three data features and explained the relationship

between these three data features and the program and algorithm.

As shown in Table 4, Spark has been established as an attractive platform for big data analysis because it can hide most of the complexities related to parallelism, fault tolerance, and cluster settings from developers. However, this comes at the cost of having more than 150 configurable parameters, as shown in Table 4, which are some of the Spark configuration parameters. Due to the number of combinations of these parameters, it is not possible to fully examine the impact of these parameters. The default setting is to allow developers to quickly deploy their applications, but there is still the question of whether performance can be improved.
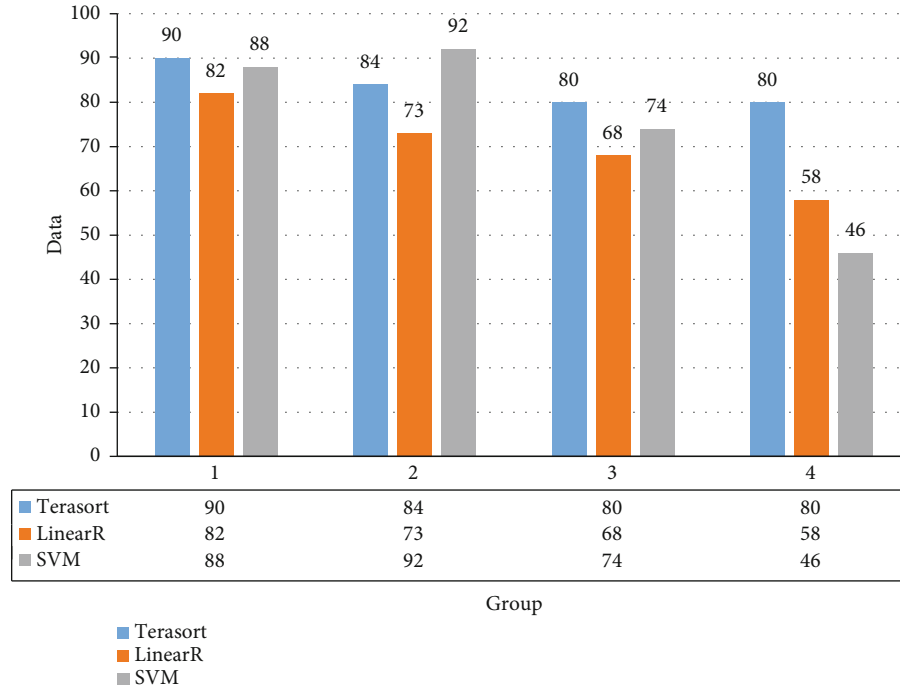
FIGURE 6: Runtime percentage diagram from different execution number parameters.

From the instruction characteristics of the Spark Bench program in Figure 6, we can see that branch instructions and floating-point instructions are key events in many programs. The number of CPU cores (spark.executor.cores) attribute of each executor controls the number of concurrent tasks that the executor can run. –spark.executor.cores 4 means that each executor can run up to 4 tasks at the same time. The number of cores affects the total number of instructions that the program can execute. The ARM Cortex-A9 mobile processor contains 4 processing cores (ARM Corporation, 2016). The picture shows the relationship between the running time ratio of Terasort, Linear Regression, and SVM programs with significant instruction characteristics and the number of execution cores. It can be seen that as the number of execution cores increases, the running time of the program decreases. When the number of execution cores increases to 4, the execution time of Linear Regression and SVM programs is reduced by 50% compared with the number of execution cores, indicating branching and floating for Spark programs with point instruction features; the configuration parameter execution core number can improve program execution efficiency. The use of tuned configuration parameters saves an average of 36% of program execution time.

As shown in Figure 7, we can see the memory characteristics of the Spark program. On the one hand, the data memory barrier instruction is the performance bottleneck of the program. On the other hand, the on-chip multilevel cache system hinders memory access. Therefore, we appropriately adjust the proportion of storage and execution to memory and allocate memory reasonably. Shown in Figure 7 is a comparison of program execution time obtained with different memory configurations. For strongly connected component program

and Terasort programs, the program execution time gradually increases from 0.3, while for SVDPlusPlus, the program execution time gradually decreases, showing that tuning the memory ratio can improve the efficiency of program execution. For example, for strongly connected component program, the optimal memory ratio can save 54% of program execution time. After tuning the parameters, an average of 37% of the program execution time was saved.

This article proposes a spark program parameter tuning method based on event sequencing based on microarchitecture events. Generally speaking, due to Spark's RDD data structure, data shuffling behavior, compression, and serialization parameters have a greater impact on performance. The serialization method has the greatest impact on CPU performance. Take Terasort as an example. The important events in the Terasort program are IFR (INS_FP_RR, the number of floating-point instructions through the register renaming phase) and ITA (INS_TLB_ALLOC, the number of TLB applications for instruction requests), indicating that the floating-point instructions of the program are an important event that affects performance, and the program optimizes the dependency of floating-point instructions during execution, so that it can be executed more efficiently in the out-of-order pipeline, so the structure of the optimized program can be Better reduce the blockage of the assembly line. The number of applications for TLB indicates that there are many instructions in the program that affect the performance of the virtual address translation physical address. Therefore, the capacity of the TLB table entry and the locality of page table access can be used to optimize the locality of the program. To reduce the number of TLB applications.

From Figure 8, we can see that the results of the above optimization we have reached the conclusion that the
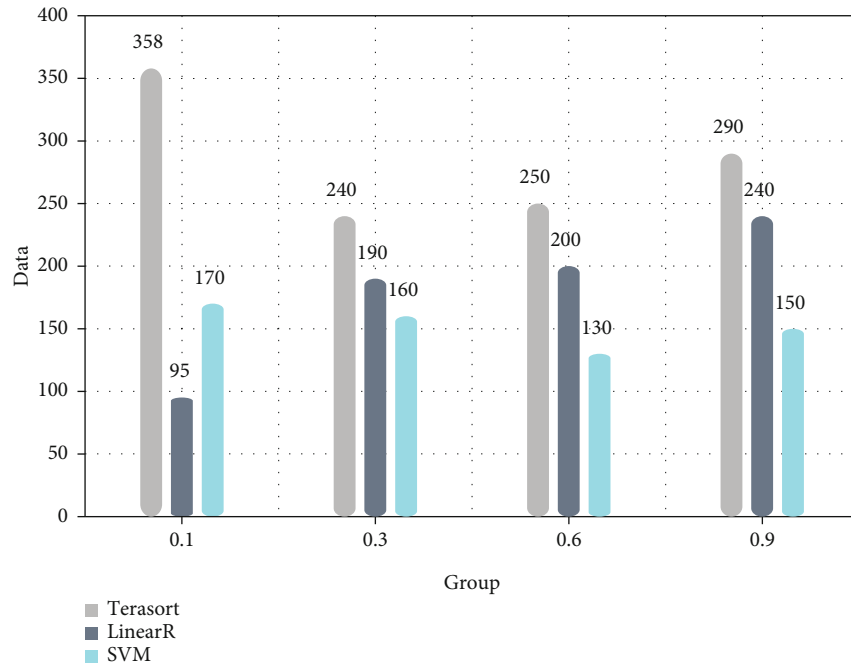
Figure 7: Runtime percentage diagram from different rate of memory.

	LogisicsR	Terasort	Shortest paths	lINEARr
JAVAS	300	160	500	190
KeyroS	220	170	460	280
CVS	350	240	480	230

Group

- JAVAS
- KeyroS
- CVS
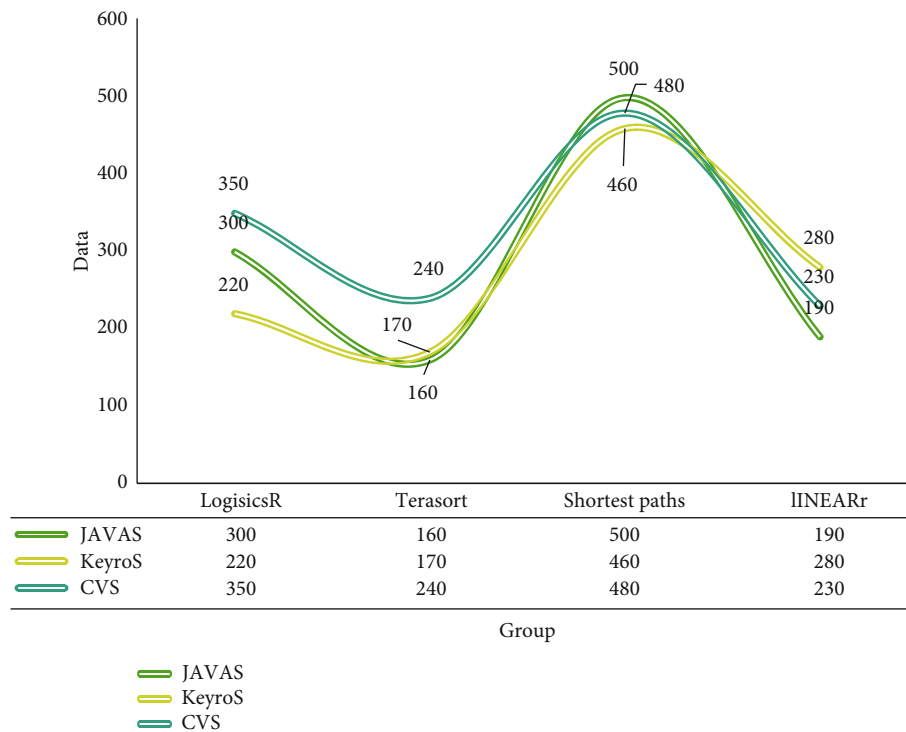
Figure 8: The optimization effect of serialization parameters is not obvious when the data set is small.

performance characteristics obtained by executing the program monitoring event and the configuration parameters correspond to the performance bottleneck. When the content of the table shows which event is the most important event, tuning the corresponding Spark parameters can reduce the execution time of the program and achieve the objective function shown in the formula. Executor core parameter

can reduce the program execution time. How to use the performance characteristics obtained through MobilePerfMiner to tune Spark programs was introduced. According to the program performance characteristics obtained in Chapter 4, we start to optimize Spark configuration parameters from two aspects: instruction characteristics and memory system characteristics. For programs whose instruction feature is a

key event, we optimized the configuration parameters of the number of execution cores, saving 36% of the average execution time. For programs with memory system characteristics, we optimized the memory weight configuration parameters, saving 37% of the program execution time on average. In addition, the data serialization parameter tuning has saved 21% of the program execution time.

5. Conclusions

This research investigated the characteristics and applications of ARM processor performance monitoring unit, hardware counter, and microarchitecture events and found that when running spark big data tasks on mobile platforms, hardware counters were used to measure events and performance characterization from the perspective of microarchitecture, of inadequacy. In order to understand the club's comprehensive ability, guide the club to develop its strengths and avoid weaknesses, and manage the athletes' athletic ability; this paper uses data mining technology to build a mining model to analyze the club's offensive and defensive balance ability, offensive combination ability, defensive ability, and psychological quality. This article firstly deals with the collected club technical statistics data and builds a mining model with the club's win or loss as the target attribute and the score as a decision attribute and analyzes the relationship between scores and wins. In order to study the comprehensive ability of the athletes and guide the club to manage the athletes' athletic ability more effectively, this article takes the core athletes of the club as the research object, uses data mining technology to construct a mining model, and analyzes the key ability and stability ability of the athletes. The disadvantage of this article is that the data studied are based on the original data obtained from the existing technical statistics database of the Tennis League. These data items are relatively fixed and cannot fully reflect the overall technical capabilities of the club or athletes; at the same time, some of the data is subject to the subjective judgment of the statistician. Impact, there are situations that are not objective enough, and the above problems will lead to incomplete or incomplete analysis results. Therefore, tennis coaches should strengthen the special physical fitness training of tennis players, improve the training plan, and learn from provinces and cities with higher levels of tennis, absorb advanced and excellent concepts, and improve the overall competitive level of national tennis. I will continue to work hard in the future, hoping to make my own contribution to the national tennis industry.

Data Availability

No data were used to support this study.

Conflicts of Interest

None of the authors have any conflicts of interest.

References

[1] Y. Chen, W. Zheng, W. Li, and Y. Huang, "Large group activity security risk assessment and risk early warning based on random forest algorithm," *Pattern Recognition Letters*, vol. 144, pp. 1–5, 2021.

[2] S. Yang, "Volleyball player physical fitness evaluation model based on data mining," *Modern Electronic Technology*, vol. 40, no. 11, pp. 119–122, 2017.

[3] X. Yulin, "Research on the construction of special physical fitness indexes for professional tennis players," *Diet Science*, vol. 416, no. 24, p. 258, 2018.

[4] Z. Yang and Z. Yan, "Diagnosis and assessment of physical function status of excellent tennis players in the Graduate School of Wuhan Institute of Physical Education," *West China Leather*, vol. 40, no. 8, pp. 89-90, 2018.

[5] C. Zhuoheng, "Analysis of the principles and methods of physical fitness test based on association rules mining," *China and Foreign Exchange*, no. 30, pp. 30-31, 2017.

[6] Y. Hu, "The development and significance analysis of physical training in tennis training," *Times Agricultural Machinery*, vol. 45, no. 11, pp. 118–118, 2018.

[7] K. Yong and P. Jianjun, "Research on the evaluation index system of specialized physical fitness training for excellent tennis players in my country," *Journal of Wuhan Institute of Physical Education*, vol. 52, no. 11, pp. 88–94, 2018.

[8] X. Ao, L. Baiyan, and F. Wang, "Analysis of acupoint application in the treatment of tennis elbow based on modern literature," *Jilin Journal of Traditional Chinese Medicine*, vol. 38, no. 1, pp. 1–5, 2018.

[9] H. Fei, "Research on the optimization of the physical training of canoeists: taking the youth rowing team of the Chongming District Sports School in Shanghai as an example," *Sports Fashion*, vol. 2, pp. 33-34, 2020.

[10] Z. Luo, "Thinking of functional training on physical training of tennis players in colleges and universities——taking the shoulder joint as an example," *Stationery & Sports Supplies & Technology*, vol. 13, no. 13, pp. 247-248, 2019.

[11] Z. Shuhua, "Design of college students' score data mining and physical fitness analysis system based on ID3 algorithm," *Modern Electronic Technology*, vol. 42, no. 5, pp. 104–106, 2019.

[12] L. Yichen, "Research on the body shape index of tennis players in Xi'an Institute of Physical Education," *Sports Fashion*, no. 3, pp. 210–210, 2018.

[13] Z. Dongbing, "Research on the evaluation model of volleyball mobilization training based on data mining," *Computer Knowledge and Technology*, vol. 16, no. 4, pp. 280-281, 2020.

[14] L. Zhongqing, "Research on the disability mutual aid insurance compensation of my country's elite athletes based on data mining," *Financial Theory and Practice*, no. 11, pp. 96–99, 2017.

[15] H. Zhengying, "Research on the characteristics of tennis players' body shape and physical function," *Sports Fashion*, no. 4, pp. 142–142, 2020.

[16] H. Wang, "Evaluation method of athlete's physical training effect based on Markov model," *Journal of Chifeng University (Natural Science Edition)*, vol. 36, no. 3, pp. 96–99, 2020.

[17] X. Yani, "The effect of functional training on the physical fitness of college tennis students," *Stationery, Sports & Technology*, vol. 444, no. 11, pp. 228-229, 2020.

[18] B. Liao, "Research on the characteristics of tennis players' body shape and physical function," *Journal of Jiamusi Education College*, no. 12, pp. 228-229, 2019.

[19] H. Rui and J. Yu, "Visual analysis of the research on "Tennis physical training" in my country," *Sports Fashion*, no. 11, pp. 68–68, 2019.

[20] B. Liao, "Research on the characteristics of tennis players' body shape and physical function," *Journal of Jiamusi Vocational College*, no. 12, pp. 219-220, 2019.

[21] Y. Qi, "Strategies and practice of optimizing physical fitness of elite athletes," *China Sports Coaches*, vol. 27, no. 1, pp. 21–25, 2019.

[22] Q. Jiaojiao, "Construction and simulation of athlete's multi-attribute training data mining model based on improved Apriori algorithm," *Microcomputer Applications*, vol. 34, no. 12, pp. 140–142, 2018.

[23] W. Mofei, "Application of physical training in tennis training in colleges and universities," *Science & Technology Information*, vol. 16, no. 22, pp. 226-227, 2018.

[24] C. Chen, "The impact of innovation in training methods on the improvement of tennis players' competitive ability——taking the national soft net team as an example," *Journal of Gansu Lianhe University (Natural Science Edition)*, vol. 32, no. 2, pp. 107–110, 2018.

[25] H. Luo, "Research on arc circle technology based on data mining algorithm," *Journal of Fuyang Vocational and Technical College*, vol. 29, no. 3, pp. 51–54, 2018.

[26] P. Yang, "Development and design based on the physical fitness test database system for table tennis players," *Automation and Instrumentation*, no. 1, pp. 50-51, 2017.

[27] Z. Shuyang, "Research on the training characteristics of tennis events," *Tomorrow Fashion*, no. 10, pp. 293–293, 2017.

[28] J. Yu and C. Jianyi, "Training and enlightenment of American junior tennis players," *Journal of Shenyang Institute of Physical Education*, vol. 36, no. 4, pp. 121–127, 2017.

[29] L. Lei and F. Yanhui, "Discussion on physical training of young tennis players," *Journal of Hebei University of Engineering (Social Science Edition)*, vol. 34, no. 2, pp. 111-112, 2017.

[30] J. Cheng, "Research on the guiding ideology of physical training for young tennis players in my country," *Exam Weekly*, no. 24, pp. 139–139, 2018.

WILEY | Hindawi

Research Article

Application of Mobile Edge Computing Technology in Civil Aviation Express Marketing

Ying Yu [ID]

Loughborough University (Bachelor in Shanghai Lixin University of Accounting and Finance), Zhaotong, 657000 Yunnan, China

Correspondence should be addressed to Ying Yu; 21027043@zju.edu.cn

With the popularization of mobile terminals and the rapid development of mobile communication technology, many PC-based services have placed high demands on data processing and storage functions. Cloud laptops that transfer data processing tasks to the cloud cannot meet the needs of users due to low latency and high-quality services. In view of this, some researchers have proposed the concept of mobile edge computing. Mobile edge computing (MEC) is based on the 5G evolution architecture. By deploying multiple service servers on the base station side near the edge of the user's mobile core network, it provides nearby computing and processing services for user business. This article is aimed at studying the use of caching and MEC processing functions to design an effective caching and distribution mechanism across the network edge and apply it to civil aviation express marketing. This paper proposes to focus on mobile edge computing technology, combining it with data warehouse technology, clustering algorithm, and other methods to build an experimental model of MEC-based caching mechanism applied to civil aviation express marketing. The experimental results in this paper show that when the cache space and the number of service contents are constant, the LECC mechanism among the five cache mechanisms is more effective than LENC, LRU, and RR in cache hit rate, average content transmission delay, and transmission overhead. For example, with the same cache space, ATC under the LECC mechanism is about 4%~9%, 8%~13%, and 18%~22% lower than that of LENC, LRU, and RR, respectively.

1. Introduction

In recent years, the ability of humans to use computer technology to generate and collect information has been greatly improved. Large-scale database systems have been widely used in the management of research companies, and their development momentum is very strong. This raises a new question for managers, how can we effectively manage and apply a large amount of data? In particular, in today's highly competitive society, data should be "used" effectively and has been put on the agenda.

With the in-depth development of domestic and foreign markets, the direction of civil aviation express marketing has gradually shifted from "product driven" to "market driven" and "customer driven," which requires civil aviation express to adopt a marketing strategy centered on market demand. After gradually realizing the role of historical data resources in improving the competitiveness of enterprises and increasing economic benefits, they tried to obtain their own sales data and sales data of competing companies to assist in the formulation of sales decision information and timely adjustment of sales strategies and focus on sales and improve the level of revenue. How to obtain useful data faster to help companies analyze the actual needs of customers? By providing a variety of layered and personalized service solutions, the civil aviation industry must give priority to increasing sales revenue and profits and improving customer satisfaction and loyalty. In the marketing process, in order to make accurate and timely business decisions, relevant information must be fully obtained and used to assist the decision-making process.

Mobile edge computing can provide cloud and IT services near mobile subscribers and allow cloud servers to be used inside or near base stations. Therefore, using the MEC platform can reduce the terminal delay perceived by mobile users; application developers can use real-time wireless access network information from MEC to provide context-aware services; MEC can also implement the execution of

computationally intensive applications. Yu introduced the MEC platform's architecture and described and realized the key functions of the above-mentioned functions, then investigated the relevant latest research results, and finally discussed and determined the MEC open research challenges [1]. The downside is that the detailed analysis of this article around MEC just stays at the technology itself, without extending it. Tran and Pompili consider an MEC-enabled multicell wireless network, where each base station (BS) is equipped with an MEC server, which can help mobile users perform computationally intensive tasks through task offloading. In order to maximize the user's task offloading revenue, the problem of joint task offloading and resource allocation is studied [2]. However, the problem under consideration involves joint optimization of task offloading decisions. Due to the combined nature of this problem, it is difficult and impractical to find the best solution for large-scale networks. Ahmed and Rehmani introduced and discussed the definition of MEC given by researchers, the opportunities that MEC brings, and the research challenges in the MEC environment. In addition, the motivation of MEC was highlighted by discussing various applications [3]. However, the discussions conducted by the institute are all theoretical knowledge, not combined with practice, and are rather vague.

The innovation of this article is (1) the introduction of big data technology into mobile edge caching, and by bringing cloud computing and cloud storage closer to the edge of the network, it can better cope with the impact of the rapid growth of data traffic on the network and provide a high-quality network service and user experience. (2) This paper proposes a collaborative caching mechanism based on machine learning under the distributed MEC service system. The mechanism uses the local caches of several MEC servers to form a cooperative cache domain as the overall structure and uses the migration learning method to predict the popularity of the content. Based on this prediction, an MEC with an optimization goal of minimizing the average content transmission cost is established.

2. Application Methods in Civil Aviation Express Marketing

2.1. Mobile Edge Computing Technology. As a new architecture to improve the efficiency of computing offload, mobile edge computing provides computing resources in the access network close to smart mobile devices [4, 5]. Mobile edge computing is the foundation of cloud computing. The quasi-cloud computing is located close to the local network where the data source is located, and the data will not be sent to the cloud as much as possible, so as to reduce transmission delay and network bandwidth costs as much as possible. Currently, mobile edge computing is widely used in various fields. In the communications field, network operators combine telecommunications network services with edge computing and provide services to users by arranging MEC servers (MEC servers) at access points (access point (AP)) or base stations (base station (BS)).

Mobile edge computing allows mobile terminals to transfer computing tasks to network edge nodes, such as wireless access points and base stations. The basic framework diagram of the mobile edge computing system is shown in Figure 1. Its design idea meets the needs of mobile terminals to expand computer functions and at the same time compensates for the long-term transmission delay of the platform [6].

It can be seen from Figure 1 that on the MEC platform, the edge computing server is installed on the side of the wireless access network, which greatly shortens the distance between it and the user equipment. In traditional cloud computing, data must pass through the wireless access network and the main network to reach the remote cloud server. After the cloud server processes the data, it returns the result to the user through a long and visible link [7]. It takes a lot of time to use the cloud platform to process this task. Due to the shorter transmission distance, MEC no longer needs to pass through large mobile links and the main network, thereby reducing delay costs. On the other hand, because the processing power of the server edge is much higher than that of the mobile device, the processing time of the task is greatly reduced.

The MEC technology and hierarchical microcloud (Cloudlet) technology that provide services such as computing and caching for users within the access range are both considered to be the natural evolution of mobile cloud technology. The MEC server can provide cloud services to mobile users within the coverage of its Wi-Fi access points. Currently, applications deployed on terminal devices have increasing demands for computing resources and storage resources; making offloading workloads deployed on mobile terminals to the cloud has become the most effective solution to the insufficient performance of terminal devices [8]. The MEC server brings traditional core cloud-centric computing closer to the edge of the network on the user side, accelerating content, services, and applications, thereby improving responsiveness from the edge. While providing users with a highly distributed computing environment, the MEC server can also perform special tasks that cannot be completed in the traditional Internet architecture, such as real-time big data analysis, perception performance optimization, and distributed cloud computing. For many emerging applications, such as intensive video coding and local streaming services, mobile operators can use MEC servers to work with core cloud systems. When the local MEC server cannot meet the needs of users or the computing power of the MEC server is insufficient to support when computing intensive tasks are performed by the mobile terminal, the MEC server can request computing resources from the core cloud and collaborate to complete the work [9, 10]. This MEC server and the core cloud data center cooperate to complete tasks, which can make up for the core cloud's long distance to users, long transmission delay, and small cloud Wi-Fi coverage. The MEC server is used to complete seamless task offloading and execution.

At present, the MEC technology has been recognized by the 5G PPP organization as one of the three key emerging technologies for 5G networks, including network
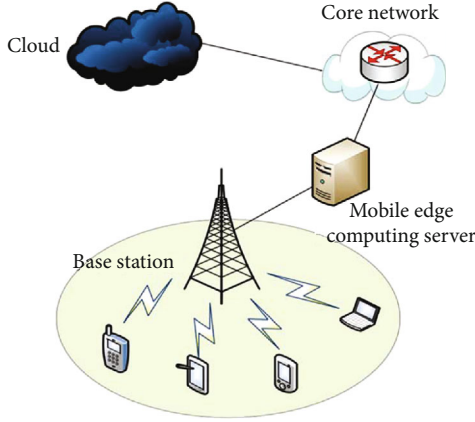
Figure 1: The basic framework of mobile edge computing system. (This picture is borrowed from Baidu Encyclopedia.)

function virtualization (NFV) and software-defined networking (SDN).

2.2. Data Warehouse Technology. Data warehouse is a new data processing architecture based on relational database technology to solve integrated data problems. The currently accepted concept of a data warehouse is the definition of the creator's data warehouse: a data warehouse is centralized, integrated, time-changing, and continuous data collection, supporting the execution of the decision-making process [11]. Regarding data warehouse, although domestic and foreign experts do not have a unified definition, their views all point out that data warehouse has the characteristics of subject-oriented, integrated, relatively stable, and historical.

2.2.1. Theme. Each topic corresponds to an analysis question raised by managers, which is an analysis field at the macro level. The theme refers to the abstract concept that aggregates and categorizes data in the macro field for mining, analysis, and utilization [12]. Since the data in the data warehouse is subject-oriented, there are two processes for the organization of the data: determining the subject and determining the content of the data that needs to be included in each subject. In a data warehouse, each topic corresponds to a relationship, that is, a data table, so the expression of the topic can be realized by using a data table in a relational database. Subject-oriented data organization has two characteristics: independence and completeness.

2.2.2. Granularity. Granularity refers to the level of detail and the level of the data warehouse in the data warehouse and is a very important concept in the data warehouse. The more detailed the description in the data warehouse, the lower the level of data analysis. On the other hand, the wider the description of the information, the higher the resolution. The data in the data warehouse usually has various resolution levels, including resolution level, resolution, openness, and advanced analysis. Analysis classification directly affects the amount of data in the repository and the adjustable data tables and numbers associated with the analysis process [13] as shown in Figure 2.

The data granularity of a data warehouse is related to the level of data collection organized in a specific topic. Data warehouse analysis must meet certain design principles to meet all levels of questionnaires and analysis requirements. Granular design principles are as follows: optimized storage structure, high query performance, space saving, and strive to eliminate data loss in the existing structure.

2.2.3. Metadata. Metadata is "data information" used to describe and identify the source of data elements, the activities of data elements in the process, the data warehouse, and the description of data and operations (input, calculation, and output). In order to effectively organize a data warehouse, metadata with clear description capabilities and rich content must be designed.

2.2.4. Data Segmentation. Data segmentation refers to a way to reasonably separate all data into small physical units suitable for independent storage management [14]. The main purpose of data segmentation is to improve the efficiency of organization and data analysis. There are many standards for data segmentation such as date, characteristics, region, and business area, or it can be a combination of two or more reference standards. Under normal circumstances, the date item should be regarded as the basic segmentation standard in the segmentation process. It can naturally segment the data according to people's understanding, and the segmentation is even. Data segmentation can be divided into two types: system level and application level [15]. System-level segmentation is done by most systems, such as database management and operating systems. Application-level segmentation is performed directly by password repository administrators or developers, and this level of segmentation is relatively more flexible.

2.3. Clustering Algorithm. Clustering algorithm is the most studied and widely used algorithm in unsupervised learning. Its basic function is to divide a specified data set into multiple subsets through a certain algorithm, that is, clusters [16, 17]. It can be said that clustering is a process of dividing samples in a data set into disjoint subsets through algorithms. The purpose of the clustering algorithm is to classify a group of data to form data clusters, and meet the following two conditions. (1) The tasks after the same cluster are as similar as possible. (2) The difference between tasks in different clusters is as large as possible.

The most commonly used criterion to determine the degree of similarity between points in the clustering algorithm is to use the Euclidean distance and Mahalanobis distance between two points [18, 19]. Generally, the Euclidean distance in the r-dimensional feature space can be expressed as

$$D_{m,n} = \sqrt{\sum_{i=1}^{r} (m_i - n_i)^2}. \tag{1}$$
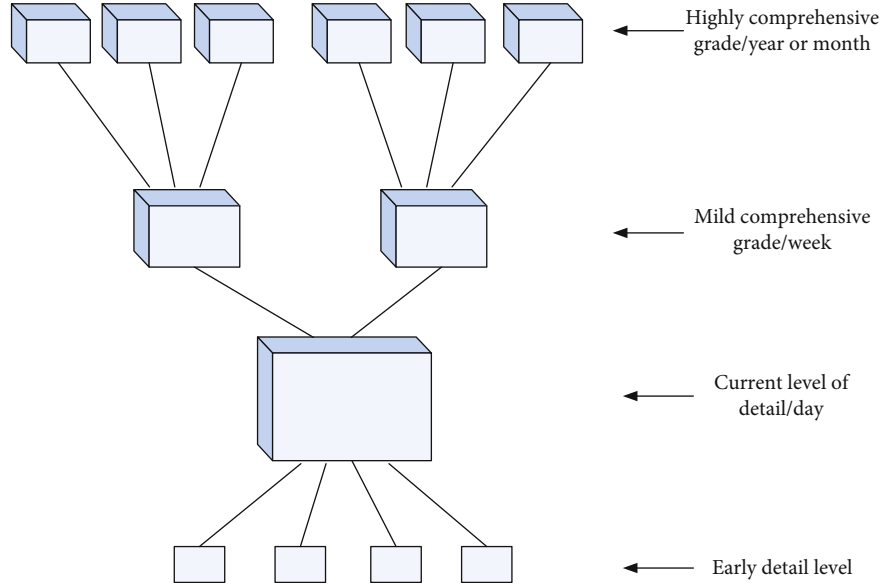
FIGURE 2: Data granularity in the data warehouse.

TABLE 1: Cache hit rate of MEC server mechanism in each cache space.

Cache space size	Caching mechanism	Cache hit rate (%)
20	GT	21.6
	LECC	20.3
	LENC	18.6
	LRU	11.8
	RR	7.5
40	GT	33.1
	LECC	31.5
	LENC	27.8
	LRU	21.7
	RR	15.1
60	GT	43.3
	LECC	39.8
	LENC	34.2
	LRU	28.1
	RR	21.9
80	GT	50.8
	LECC	47.6
	LENC	40.0
	LRU	36.7
	RR	28.8
100	GT	57.5
	LECC	54.8
	LENC	44.3
	LRU	42.1
	RR	34.9

The Mahalanobis distance can be expressed as

$$D_{(m,n)} = \sum_{i=1}^{r} |m_i - n_i|. \tag{2}$$

Ming's distance is a generalization of Mahalanobis distance, which can be expressed as

$$D_{(m,n)} = \left(\sum_{i=1}^{r} |m_i - n_i|^{\lambda} \right)^{1/\lambda}. \tag{3}$$

It can be seen that for Ming's distance, when $\lambda = 1$, it corresponds to the Mahalanobis distance, and when $\lambda = 2$, it corresponds to the Euclidean distance.

For the clustering problem in the MEC system, we need to determine the similarity metric before classification. Suppose there are currently X tasks, numbered $\{A_1, A_2, A_3, \cdots, A_X\}$, and the total amount of calculation required to complete each task is $\{B_1, B_2, B_3, \cdots, B_X\}$, respectively. Assuming that the sensitivity of all tasks to delay can be divided into Y categories, numbered $\{1, 2, 3, \cdots, Y\}$, when there are X tasks. The extension sensitivity can be expressed as $\{E_1, E_2, E_3, \cdots, E_X\}$, where $E_i \in \{1, 2, 3, \cdots, X\}$, $i = \{A_1, A_2, A_3, \cdots, A_X\}$. We define the classified cluster as $\{C_1, C_2, C_3, \cdots, C_j\}$ and hope that the maximum value of the standard deviation of all clusters obtained after classification is as small as possible.

Assume that at a certain moment the task in the controller is $\{A_1^*, A_2^*, \cdots, A_x^*\}$, and the corresponding delay sensitivity is $\{E_1', E_2', \cdots, E_x'\}$. After normalizing the delay sensitivity, the delay sensitivity obtained is $\{E_1^*, E_2^*, \cdots, E_x^*\}$, where

$$E_i^* = \frac{E_i'}{\sum_k^x E_k'}. \tag{4}$$
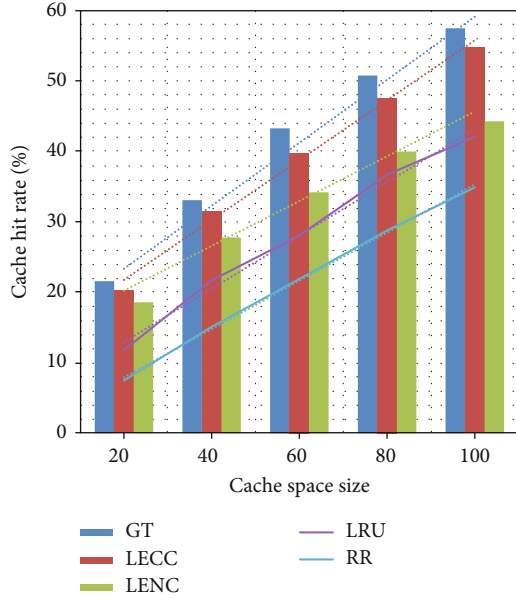
FIGURE 3: The trend of the cache hit rate with the size of the MEC cache space under each cache mechanism.

TABLE 2: The average content transmission delay of the MEC server mechanism in each cache space.

Cache space size	Caching mechanism	Average content transmission delay
20	GT	78.1
	LECC	79.7
	LENC	81.5
	LRU	88.6
	RR	92.2
40	GT	66.7
	LECC	69.3
	LENC	73.2
	LRU	79.1
	RR	85.2
60	GT	57.0
	LECC	60.8
	LENC	66.8
	LRU	72.1
	RR	79.2
80	GT	49.3
	LECC	53.9
	LENC	60.0
	LRU	64.1
	RR	72.2
100	GT	42.8
	LECC	45.7
	LENC	56.4
	LRU	58.9
	RR	66.7

The total amount of calculation required to complete the task is $\{B_1', B_2', \cdots, B_x'\}$, respectively, and the total calculation amount obtained after normalizing the calculation amount is $\{B_1^*, B_2^*, \cdots, B_x^*\}$, where

$$B_i^* = \frac{B_i'}{\sum_{k=1}^{x} B_k'}. \tag{5}$$

We define that the Euclidean distance between tasks A_i^* and A_k^* in the same cluster can be expressed as

$$D_{i,k} = \sqrt{(E_i^* - E_k^*) + (B_i^* - B_k^*)^2}. \tag{6}$$

The average of the distances in the same cluster can be expressed as

$$\bar{D} = \frac{\sum_{i=1}^{x} \sum_{k=1, k \neq i}^{x} D_{i,k}}{C_x^2}. \tag{7}$$

Define the standard deviation corresponding to tasks in the same cluster as W, when there is task $\{A_1^*, A_2^*, \cdots, A_x^*\}$ in cluster C_i; the corresponding standard deviation is

$$W_i = \sqrt{\frac{\sum_{i=1}^{x'} \sum_{k=1, k \neq i}^{x'} (D_{i,k} - \bar{D})^2}{C_{x'}^2}}. \tag{8}$$

We believe that in the same cluster, the smaller the standard deviation of all tasks, the higher the similarity of the tasks. Therefore, we hope that in the results obtained by clustering, the maximum value of the standard deviations in all

clusters is as small as possible. That is, when all tasks can be divided into j clusters, we hope to get

$$\min \{\max W_i\}, \quad i = 1, 2, 3, \cdots, j. \tag{9}$$

Assuming that there are a total of f' tasks in the current i-th cluster, then the average of the distances of all tasks in this cluster is

$$\bar{D_i} = \frac{\sum_{i=1}^{f'} \sum_{k=i}^{f'} D_{i,k}}{C_{f'}^2}, \tag{10}$$

where $C_{f'}^2$ means

$$C_{f'}^2 = \frac{f'!}{f'! \cdot (f' - 2)!}. \tag{11}$$

The weight vector w_i of the currently selected sample i, where $w_k = (w_{k,1}, w_{k,2})$ and w_k represent the weight vector between the current input sample in the output layer.
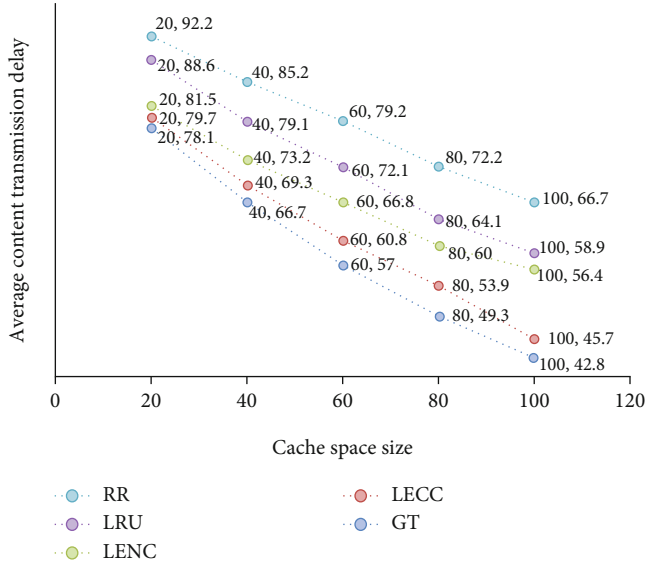
FIGURE 4: The average content transmission delay under each caching mechanism varies with the size of the MEC cache space.

TABLE 3: The average content transmission overhead of the MEC server mechanism in each cache space.

Cache space size	Caching mechanism	Average content transfer overhead
20	GT	376
	LECC	392
	LENC	409
	LRU	442
	RR	467
40	GT	334
	LECC	347
	LENC	365
	LRU	387
	RR	425
60	GT	281
	LECC	302
	LENC	327
	LRU	359
	RR	390
80	GT	244
	LECC	261
	LENC	301
	LRU	322
	RR	358
100	GT	213
	LECC	236
	LENC	278
	LRU	290
	RR	327
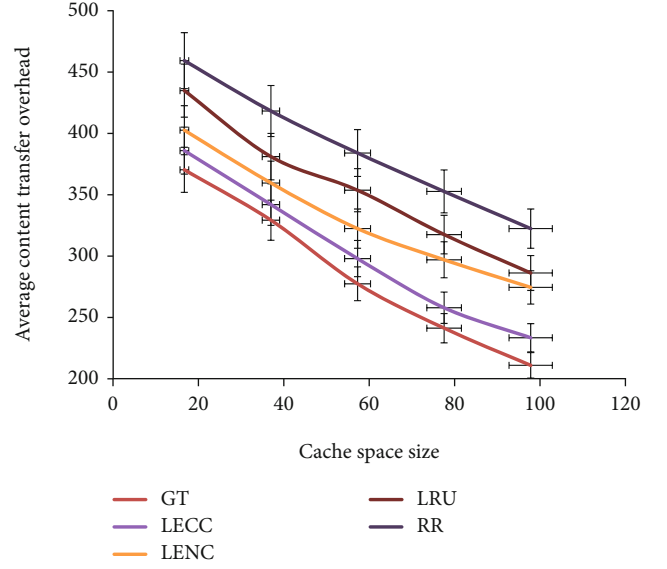
FIGURE 5: The trend of cache hit rate with the size of MEC cache space under each cache mechanism.

Therefore, the Euclidean distance vector D_i between the weight vector and the input M_i can be obtained by the following formula:

$$D_{i,k} = \|M_i - w_k\| = \left[\sum_{\lambda=1}^{2} (m_{i,\lambda} - w_{k,\lambda})^2 \right]^{1/2}, \quad k = 1, 2, \cdots, j. \tag{12}$$

Determine the winning neuron h by the smallest distance between the output layer neuron and the task sample i:

$$D_{i,h} = \min \{D_{i,k}\}, \quad k = 1, 2, \cdots, j. \tag{13}$$

Adjust the connection weight: for the winning neuron h and all the neurons in the output layer and input layer in its neighborhood $N_h(n)$, the connection weight vector of the algorithm executed at the $n + 1$th time is in accordance with the formula shown below, make corrections

$$w_{i,k}(n+1) = w_{i,k}(n) + \eta(n) \times (M_i - w_{i,k}(n)), \quad k = h, \tag{14}$$

$$w_{i,k}(n+1) = w_{i,k}(n) + \frac{\eta(n)}{2} \times (M_i - w_{i,k}(n)), \quad k \in N_h(n), \tag{15}$$

$$w_{i,k}(n+1) = w_{i,k}(n), \quad k \notin N_h(n). \tag{16}$$

The connection weight of the input neuron i and the output neuron k is also a two-dimensional vector, and h represents the winning neuron.

Update the learning rate $\eta(n)$ and the neighborhood function $N_h(n)$: the general learning rate and neighborhood

TABLE 4: Cache hit rate of MEC server mechanism under different service contents.

Number of service contents Cache hit rate (%) Caching mechanism	GT	LECC	LENC	LRU	RR
1000	37.2	35.6	30.4	24.9	19.3
2000	26.3	24.8	19.8	14.9	9.8
3000	21.2	18.7	16.2	10.5	7.2
4000	18.5	15.8	12.1	7.9	5.1

function will gradually decrease with the increase of the number of iterations, which can be expressed as

$$\eta(n+1) = \eta(0) \times \left(1 - \frac{n}{N}\right), \tag{17}$$

$$N_h(n+1) = N_h(0) \times \left(1 - \frac{n}{N}\right). \tag{18}$$

The clustering algorithm is a strategy for clustering mobile terminal tasks in the MEC system. For the results obtained after clustering, it is hoped that the maximum distance standard deviation in all clusters is as small as possible [20]. It can not only ensure the quality of service and improve the user experience but also reduce the queuing delay of subsequent tasks, which is conducive to reducing system overhead.

3. Application Experiment Based on Mobile Edge Computing Technology in Civil Aviation Express Marketing

3.1. Experimental Program Based on MEC Architecture. In order to verify the effectiveness of the prediction of content popularity to design the collaborative caching mechanism under the MEC architecture, this article compares the caching scheme with some known content caching schemes, including the least recently used (LRU) strategy and randomized cache strategy (randomized replacement (RR)). The least recently used (LRU) replacement strategy is a caching strategy for estimating future requested content by observing the content being accessed by users in the near future. When the amount of cached data exceeds the threshold, the least recently accessed content is deleted [21, 22]. The RR caching strategy randomly selects data content for caching.

In addition, in order to more intuitively and effectively illustrate the advantages of the content popularity prediction scheme based on migration learning proposed in this paper and the improvement of network performance by the MEC collaborative caching mechanism, this research also combines the caching scheme with LENC (noncooperative learning). Based caching scheme and GT (popularity-aware greedy strategy) scheme are compared. Specifically, the LENC scheme means that each MEC directly caches content with high popularity based on the prediction results of the content popularity based on the migration learning method in this article, until the cache space is full, that is, no collabo-

rative caching is performed between MEC servers; the GT scheme is when the true value of content popularity is known in advance; the MEC collaborative greedy algorithm proposed in this paper is used for cache deployment [23]. In fact, the GT algorithm provides the performance upper limit (not the real performance upper limit) under the greedy cooperative caching mechanism of this article for the other four algorithms (LECC, LENC, LRU, and RR).

3.2. Performance Indicators. The comparison is made from three performance index parameters, namely, the cache hit rate (hit rate (HR)), the average content transmission delay (average delivery latency (ADL)), and the average content transmission cost (average transmission cost (ATC)).

3.2.1. Cache Hit Rate (HR). In the MEC service system, the processing methods of user requests can be divided into the following two situations: one is that if the requested content has a backup in the MEC cooperative cache domain; the content is sent to the user, which we call a cache hit. The other is that if the content requested by the user is not cached in the local cooperative cache domain; the content needs to be obtained from the remote central server and then pushed to the user. This is called a miss [24–26].

3.2.2. Average Content Transmission Delay (ADL). In the MEC service system, the average delay for users to obtain content is an important performance indicator to measure the quality of user experience. The smaller the average content delivery delay, the more user requests can be satisfied by the local MEC, and the higher the quality of user experience [27, 28].

3.2.3. Average Content Transmission Cost (ATC). The average content transmission cost (ATC) index is the value of the objective function of the optimization problem. In addition, in the definition of the objective function of the optimization problem, we set the unit data content to be transmitted from C_m to $C_n(m \neq n)$, and the transmission cost through single-hop routing is γ. The unit data content is transmitted from the remote cache server to C_m, and the transmission cost of the single-hop route is γ_0. Since the exact values of γ and γ_0 cannot be known in the simulation of real test scenarios, we use simulation to illustrate the impact of γ and γ_0 value settings on performance. We define the cost factor μ:

$$\mu \stackrel{\text{def}}{=} \frac{\gamma_0}{\gamma}. \tag{19}$$

3.3. Experimental Parameter Settings. Consider the scenario where video content services are dominant in mobile Internet applications. The simulation parameters are as follows. There are 3 randomly distributed BSs in the cooperative buffer domain, and the number of mobile users in each cell is 400. Assume that the content provider publishes a total of 800 video files whose popularity obeys the ZipF distribution model, and the skewness coefficient is $\alpha = 0.52$. This parameter describes the degree of skewness of the content popularity distribution. For the cooperative cache domain model, we consider 3 MEC servers in a domain, and each server receives

TABLE 5: The average content transmission delay of the MEC server mechanism under different service content quantities.

Number of service contents Average content transmission delay Caching mechanism	GT	LECC	LENC	LRU	RR
1000	61.8	64.9	69.8	75.7	82.1
2000	74.8	77.2	80.6	85.6	90.3
3000	79.7	82.8	85.1	89.1	94.0
4000	82.3	84.9	88.7	92.5	95.1

TABLE 6: The average content transmission overhead of the MEC server mechanism under different service content quantities.

Number of service contents Average content transfer overhead Caching mechanism	GT	LECC	LENC	LRU	RR
1000	312	325	349	375	413
2000	371	383	402	425	451
3000	398	412	422	445	470
4000	415	423	440	462	476

an average of 9000 content requests per day. It is assumed that the MEC server in the domain has a uniform size of cache space. The update period Δt is 3 h. In addition, the transmission delay in the access network and core network refers to the 3GPP LTE standard. In the simulation experiment, we study the impact of system parameters on cache performance, including the size of cache space, the number of service contents, the skewness coefficient of the popularity distribution, and the cost coefficient [29, 30].

4. Application Experiment Analysis Based on Mobile Edge Computing Technology in Civil Aviation Express Marketing

4.1. Performance Comparison of Five Mechanisms in a Certain Cache Space. First, the five caching mechanisms under the change of the MEC cache space are described and the performance comparison in three aspects: cache hit rate, average content transmission delay, and transmission overhead. The value of each MEC buffer space size ranges from 10 to 100, the overhead coefficient γ is 10, the skew coefficient α is 0.52, and the number of service contents in the system is 800. Table 1 records the variation of the cache hit rate with the size of the MEC cache space under each cache mechanism.

According to the variation of the cache hit rate with the size of the MEC cache space under each cache mechanism recorded in Table 1, the trend change graph of the cache hit rate with the size of the MEC cache space under each cache mechanism in Figure 3 can be obtained.

It can be seen from Figure 3 that the cache hit rate under all strategies increases as the cache space increases. Experimental data shows that the LECC mechanism proposed in this paper is superior to LENC, LRU, and RR. Specifically, when the cache space is 60, the cache hit rate under the LECC mechanism is about 6%, 11%, and 18% higher than that of
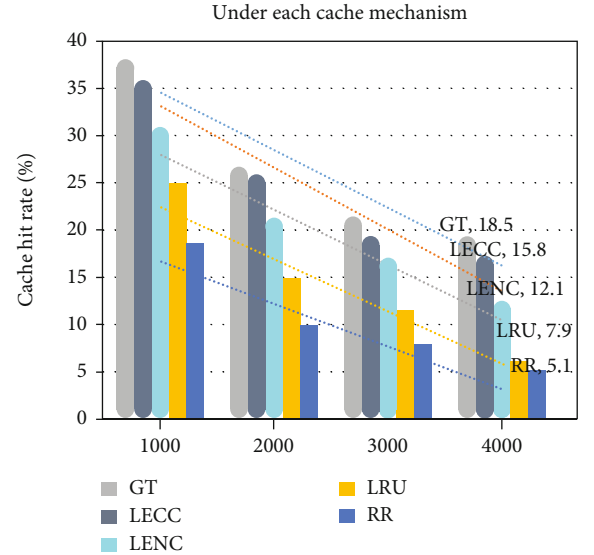
FIGURE 6: Cache hit rate of MEC server mechanism under different service contents.

LENC, LRU, and RR, respectively. In addition, when the size of the cache space changes from 20 to 100, the cache hit rate under the LECC mechanism differs from the upper limit of the cache hit rate obtained by GT by only 3%-5%. This proves the effectiveness of the caching mechanism based on intelligent prediction of content popularity in this paper.

Table 2 records the variation of the average content transmission delay with the size of the MEC cache space under each caching mechanism.

According to the variation of the average content transmission delay under each cache mechanism with the size of the MEC cache space recorded in Table 2, the trend change graph of the cache hit rate under each cache mechanism with the size of the MEC cache space can be obtained.
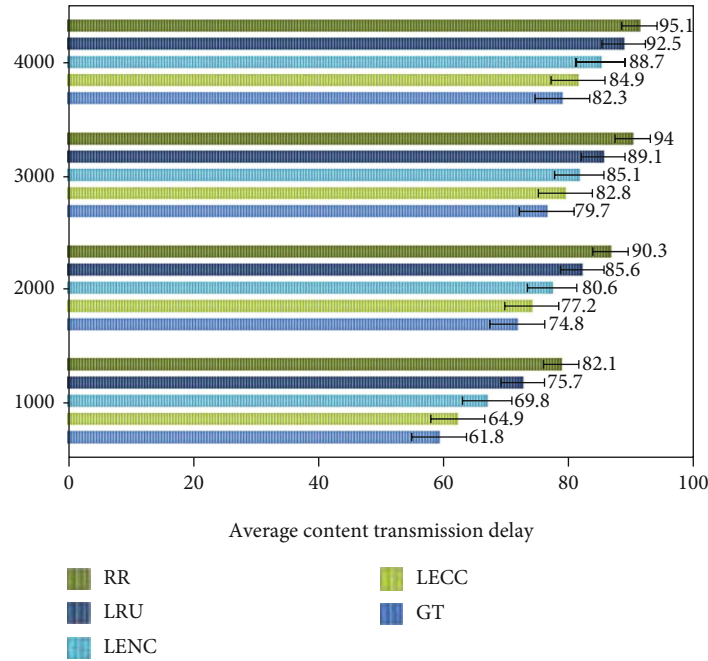
FIGURE 7: The average content transmission delay of the MEC server mechanism under different service content quantities.
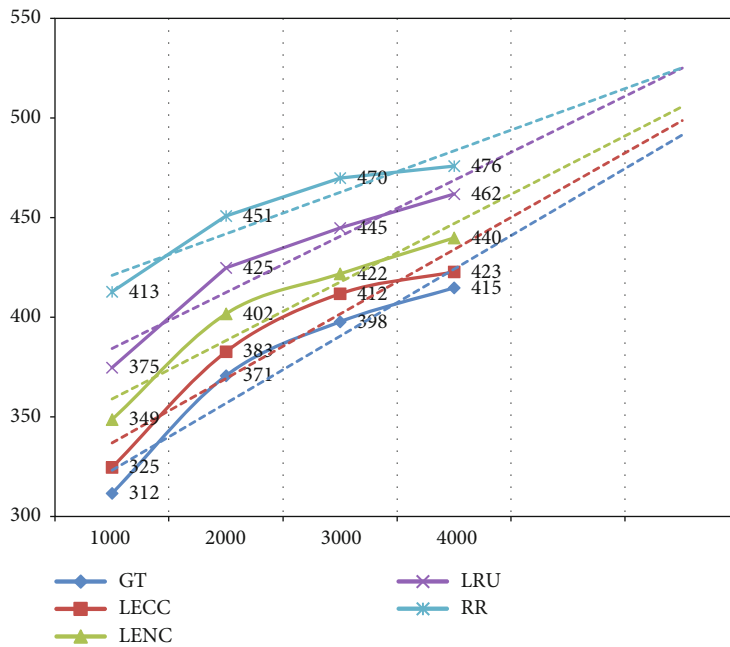
FIGURE 8: The average content transmission overhead of the MEC server mechanism under different service content quantities.

It can be seen from Figure 4 that the average content transmission delay under all strategies decreases as the cache space increases. This is because as the cache space increases, more content can be cached locally so that more user requests can be directly served by the local cooperative cache domain. Experimental data shows that the LECC mechanism has the lowest ADL. For example, when the storage space ranges from 60 to 100, the ADL under the LECC mechanism is about 6% to 10%, 10% to 15%, and 18% to 22% lower than that of LENC, LRU, and RR, respectively.

Table 3 records the variation of the average content transmission overhead with the size of the MEC cache space under each caching mechanism [31, 32].

According to the changes in the average content transmission overhead of each cache mechanism with the size of the MEC cache space recorded in Table 3, the trend graph of the cache hit rate with the size of the MEC cache space under each cache mechanism in Figure 5 can be obtained.

It can be seen from Figure 5 that the average content transmission overhead under all strategies decreases as the

cache space increases. Experimental data shows that the LECC mechanism has the lowest ATC. For example, when the storage space ranges from 60 to 100, the ATC under the LECC mechanism is about 4%-9%, 8%-13%, and 18%-22% lower than that of LENC, LRU, and RR, respectively. The significant improvement in cache performance brought about by the LECC mechanism mainly comes from the content popularity prediction based on migration learning proposed in this paper and the MEC collaborative cache [33].

4.2. Performance Comparison of Five Mechanisms under a Certain Amount of Service Content. Tables 4–6 record the cache hit rate, average content transmission delay, and transmission overhead under the five caching mechanisms as the number of different service contents changes. The value range of the number of service contents is 500 to 4000, the cost coefficient γ is fixed at 10, the skew coefficient α is taken at 0.52, and the size of the cache space of each MEC server is fixed at 60.

According to the changes in the cache hit rate of each cache mechanism with the number of different MEC service contents recorded in Table 4, the trend change graph of the cache hit rate with the size of the MEC cache space under each cache mechanism in Figure 6 can be obtained.

According to the variation of the average content transmission delay under each caching mechanism with the amount of different MEC service content recorded in Table 5, the trend change graph of the average content transmission delay under each caching mechanism in Figure 7 with the size of the MEC cache space can be obtained.

According to the variation of the average content transmission cost under each caching mechanism with the number of different MEC service contents recorded in Table 6, the trend graph of the average content transmission cost under each caching mechanism in Figure 8 with the size of the MEC cache space can be obtained.

Figures 6–8 describe the changes in the cache hit rate, average content transmission delay, and transmission overhead with the number of different service contents under the five caching mechanisms. Experimental data shows that the LECC mechanism proposed in this paper is superior to LENC, LRU, and RR in terms of HR, ADL, and ATC. It can be seen from Figure 6 that the cache hit rate under all strategies decreases as the number of service contents increases. The average content transmission delay and transmission overhead increase with the increase in the number of service contents. This is due to the limited cache space of the MEC server. With the continuous increase of service content, more and more user requests cannot be satisfied from the local cache. From the numerical results in Figure 6, when the number of service content changes from 1000 to 3000, the HR under the LECC mechanism is about 5%~9%, 11%~14%, and 16%~21% higher than that in LENC, LRU, and RR, respectively.

5. Conclusions

With the rapid development of the mobile Internet and the Internet of Things, mankind is about to usher in the 5G

era. 5G technology demands "large capacity, large bandwidth, low latency, and low power consumption," and mobile edge computing is precisely the 5G network that improves user experience. The key technology is deployed at the edge of the network, close to the data source, and has rapid feedback. It can sink the computing content and capabilities and localize the business. This paper proposes a collaborative caching mechanism based on machine learning under the 5G MEC architecture. The mechanism uses the local caches of several MEC servers to form a cooperative cache domain as the overall structure and uses the migration learning method to predict the popularity of the content. Based on this prediction, an MEC is established that optimizes the average content transmission cost. The content cache model further proves the above optimization problem. We use algorithms to solve the content caching scheme and perform simulation verification. Experimental results show that the proposed LECC caching strategy can effectively improve the cache hit rate and reduce transmission overhead and content transmission delay.

The proposed mobile edge computing architecture provides storage and computing and network services for mobile terminal users and provides a good platform for task migration. Task migration is to transfer all or part of large-capacity PC applications to mobile devices with a large amount of resources on the platform to deal with insufficient processing problems and limited power. The short-term capabilities of mobile edge computing provide users with powerful computing capabilities and ultra-high-speed networks, which can be accessed anytime, anywhere, shorter migration path and lower power consumption.

Data Availability

No data were used to support this study.

Conflicts of Interest

The author declares no conflicts of interest.

References

[1] Y. Yu, "Mobile edge computing towards 5G: vision, recent progress, and open challenges," *China Communications*, vol. 13, Supplement2, pp. 89–99, 2016.

[2] T. X. Tran and D. Pompili, "Joint task offloading and resource allocation for multi-server mobile-edge computing networks," *IEEE Transactions on Vehicular Technology*, vol. 68, no. 1, pp. 856–868, 2019.

[3] E. Ahmed and M. H. Rehmani, "Mobile edge computing: opportunities, solutions, and challenges," *Future Generation Computer Systems*, vol. 70, pp. 59–63, 2016.

[4] N. Ansari and X. Sun, "Mobile edge computing empowers Internet of things," *IEICE Transactions on Communications*, vol. 101, no. 3, pp. 604–619, 2018.

[5] W. Li, Z. Chen, X. Gao, W. Liu, and J. Wang, "Multimodel framework for indoor localization under mobile edge computing environment," *IEEE Internet of Things Journal*, vol. 6, no. 3, pp. 4844–4853, 2019.

[6] S. Wang, Y. Zhao, L. Huang, J. Xu, and C. H. Hsu, "QoS prediction for service recommendations in mobile edge computing," *Journal of Parallel & Distributed Computing*, vol. 127, pp. 134–144, 2017.

[7] J. Zeng, J. Sun, B. Wu, and X. Su, "Mobile edge communications, computing, and caching (MEC3) technology in the maritime communication network," *China Communications*, vol. 17, no. 5, pp. 223–234, 2020.

[8] K. Zhang, Y. Mao, S. Leng, Y. He, and Y. ZHANG, "Mobile-edge computing for vehicular networks: a promising network paradigm with predictive off-loading," *IEEE Vehicular Technology Magazine*, vol. 12, no. 2, pp. 36–44, 2017.

[9] T. Wang, H. Luo, X. Zheng, and M. Xie, "Crowdsourcing mechanism for trust evaluation in CPCS based on intelligent mobile edge computing," *ACM Transactions on Intelligent Systems and Technology*, vol. 10, no. 6, pp. 1–19, 2019.

[10] Q. V. Pham, L. B. Le, S. H. Chung, and W. J. Hwang, "Mobile edge computing with wireless backhaul: joint task offloading and resource allocation," *IEEE Access*, vol. 7, no. 99, pp. 16444–16459, 2019.

[11] J. C. Yim, S. H. Kim, and C. S. Keum, "Personalized service recommendation for mobile edge computing environment," *The Journal of Korean Institute of Communications and Information Sciences*, vol. 42, no. 5, pp. 1009–1019, 2017.

[12] Y. Mao, J. Zhang, S. H. Song, and K. B. Letaief, "Stochastic joint radio and computational resource management for multi-user mobile-edge computing systems," *IEEE Transactions on Wireless Communications*, vol. 16, no. 9, pp. 5994–6009, 2017.

[13] Y. Jararweh, M. Al-Ayyoub, M. Al-Quraan, A. T. Lo'ai, and E. Benkhelifa, "Delay-aware power optimization model for mobile edge computing systems," *Personal & Ubiquitous Computing*, vol. 21, no. 6, pp. 1–11, 2017.

[14] M. Zeng and V. Fodor, "Energy minimization for delay constrained mobile edge computing with orthogonal and non-orthogonal multiple access," *Ad Hoc Networks*, vol. 98, pp. 102060.1–102060.13, 2020.

[15] Y. Zhai, T. Bao, L. Zhu, M. Shen, X. du, and M. Guizani, "Toward reinforcement-learning-based service deployment of 5G mobile edge computing with request-aware scheduling," *IEEE Wireless Communications*, vol. 27, no. 1, pp. 84–91, 2020.

[16] Q. Zhang, L. Gui, F. Hou, J. Chen, S. Zhu, and F. Tian, "Dynamic task offloading and resource allocation for mobile edge computing in dense cloud RAN," *IEEE Internet of Things Journal*, vol. 7, no. 4, pp. 3282–3299, 2020.

[17] J. Zhang, H. Guo, and J. Liu, "Adaptive task offloading in vehicular edge computing networks: a reinforcement learning based scheme," *Mobile Networks and Applications*, vol. 25, no. 4, pp. 1–10, 2020.

[18] R. Fantacci and B. Picano, "Federated learning framework for mobile edge computing networks," *CAAI Transactions on Intelligence Technology*, vol. 5, no. 1, pp. 15–21, 2020.

[19] N. Saranya, K. Geetha, and C. Rajan, "Data replication in mobile edge computing systems to reduce latency in Internet of things," *Wireless Personal Communications*, vol. 112, no. 4, pp. 2643–2662, 2020.

[20] W. Wen, Y. Cui, T. Q. S. Quek, F. C. Zheng, and S. Jin, "Joint optimal software caching, computation offloading and communications resource allocation for mobile edge computing," *IEEE Transactions on Vehicular Technology*, vol. 69, no. 7, pp. 7879–7894, 2020.

[21] Y. Liu, Y. Li, Y. Niu, and D. Jin, "Joint optimization of path planning and resource allocation in mobile edge computing," *IEEE Transactions on Mobile Computing*, vol. 19, no. 9, pp. 2129–2144, 2020.

[22] J. Zhang, H. Guo, J. Liu, and Y. Zhang, "Task offloading in vehicular edge computing networks: a load-balancing solution," *IEEE Transactions on Vehicular Technology*, vol. 69, no. 2, pp. 2092–2104, 2020.

[23] J. Shen, Y. Ren, J. Wan, and Y. Lan, "Hard disk drive failure prediction for mobile edge computing based on an LSTM recurrent neural network," *Mobile Information Systems*, vol. 2021, Article ID 8878364, 12 pages, 2021.

[24] J. Ahn, J. Lee, S. Park, and H. S. Park, "Power efficient clustering scheme for 5G mobile edge computing environment," *Mobile Networks and Applications*, vol. 24, no. 2, pp. 643–652, 2019.

[25] X. Meng, W. Wang, Y. Wang, V. K. N. Lau, and Z. Zhang, "Closed-form delay-optimal computation offloading in mobile edge computing systems," *IEEE Transactions on Wireless Communications*, vol. 18, no. 10, pp. 4653–4667, 2019.

[26] Z. Lv and Q. Liang, "Optimization of collaborative resource allocation for mobile edge computing," *Computer Communications*, vol. 161, pp. 19–27, 2020.

[27] J. Xue, Z. Wang, Y. Zhang, and L. Wang, "Task allocation optimization scheme based on queuing theory for mobile edge computing in 5G heterogeneous networks," *Mobile Information Systems*, vol. 2020, Article ID 1501403, 12 pages, 2020.

[28] C. H. Wu and S. B. Tsai, "Using DEMATEL-based ANP model to measure the successful factors of E-commerce," *Journal of Global Information Management*, vol. 26, no. 1, pp. 120–135, 2018.

[29] S. Wang, Q. Li, J. Hou, S. Meng, B. Zhang, and C. Zhou, "Active defense by mimic association transmission in edge computing," *Mobile networks & applications*, vol. 25, no. 2, pp. 725–742, 2020.

[30] H. Sun, F. Zhou, and R. Q. Hu, "Joint offloading and computation energy efficiency maximization in a mobile edge computing system," *IEEE Transactions on Vehicular Technology*, vol. 68, no. 3, pp. 3052–3056, 2019.

[31] S. Li, D. Zhai, P. Du, and T. Han, "Energy-efficient task offloading, load balancing, and resource allocation in mobile edge computing enabled IoT networks," *Science China Information Sciences*, vol. 62, no. 2, pp. 1–3, 2019.

[32] M. Abdel-Basset, G. Manogaran, and M. Mohamed, "A neutrosophic theory based security approach for fog and mobile-edge computing," *Computer Networks*, vol. 157, pp. 122–132, 2019.

[33] B. Zhu, S. Ma, R. Xie, J. Chevallier, and Y. Wei, "Hilbert spectra and empirical mode decomposition: a multiscale event analysis method to detect the impact of economic crises on the European carbon market," *Computational Economics*, vol. 52, no. 1, pp. 105–121, 2018.

WILEY | Hindawi

Research Article

Decision-Making Optimization Design of Enterprise Standardization Management Planning Based on Mobile Network System

Qiao Wang [iD],[1] Jianjun Wang,[2,3] and Shenlin Ye[4]

[1]*School of Humanities and Arts, Xingzhi College of Xi'an University of Finance and Economics, Xi'an, 710038 Shaanxi, China*
[2]*Administration Office, Safety Supervision Station of Agricultural Machinery in Qindu District, Xianyang, 712099 Shaanxi, China*
[3]*Auditing Practices Department, China Quality Mark Certification Group Shaanxi Co., Ltd., Xi'an, 710048 Shaanxi, China*
[4]*Research and Development Department, Pinduoduo Inc., Shanghai 200050, China*

Correspondence should be addressed to Qiao Wang; wangqiao26708@163.com

With the continuous deepening of enterprise management and market competition, the pressure of production and operation of enterprises is increasing, and it is urgent to improve the management level of enterprises. This paper mainly studies the decision optimization design of enterprise standardization management planning based on mobile network system. In this paper, the idea of clustering is used to integrate the customers into a customer clustering mode, which will greatly reduce the number of customers studied in the model and simplify the optimization process of the model. Through online and offline processes, these can achieve dynamic and rapid processing of data flow and can well meet the needs of users for data flow analysis. In the construction of enterprise standardization strategic performance evaluation index system, it is necessary to decompose, combine, and converge the index system. According to the construction principles and methods discussed above, the influencing factors of standardized strategic performance evaluation indicators of construction enterprises are preliminarily stratified by using the expert survey method and cluster analysis method, so as to construct the initial evaluation system. For the mobile network system testing, we use the black box test and white box test. The test content mainly includes two modules: area calculation and label calculation. Experimental data show that when the time threshold Ts is set to 1 hour, the prediction accuracy of TBM increases from 46.9% to 47.7%. The results show that the mobile network system realizes the whole life cycle management of enterprise standards and improves the management level of enterprise standardization work.

1. Introduction

Only through the improvement of standardized management level of enterprises, through standardization to guide production, improves product quality and service quality, in order to stand out in such fierce competition, to achieve long-term development of enterprises. However, at present, because many enterprises have not realized the importance of standard informatization, or have not seen the needs of enterprises in this respect, the application examples of enterprise standardized information management system are not many, which can only learn from the experience of other information management systems for system development.

The research in this article enables decision makers to better use scientific decision-making methods to participate in the coordination activities between enterprises in the future, to maximize the profits of the supply chain, and to enhance the overall competitiveness of the supply chain. With the gradual development of the application of the performance analysis system and the full utilization of its functions, it will surely create important value for the enterprise and enhance its core competitiveness. For core enterprises, by helping small- and medium-sized enterprises in the supply chain to solve financing problems, it is conducive to maintaining sustained and stable trade relations and promoting the healthy development of the supply chain.

The mobile network plays a role in promoting the optimization of the enterprise's standardized management system. Choi proposed a millimeter wave- (MMW-) based mobile hotspot network (MHN) system for high-speed railways, which can support a peak backhaul link throughput of 1 Gbps per train at a speed of 400 km/h. The MHN system can be implemented in subways and high-speed trains to support passengers and provide access to the Internet through smart devices. The system he proposed can overcome the inherent high path loss of MMW through system design and high antenna gain. He also demonstrated the feasibility of using the test bed deployed in Seoul Metro Line 8 for the MHN system. There are some subtle loopholes in his research [1]. Jao believes that as the demand for new-generation mobile networks continues to grow, the ITU radiocommunication sector (ITU-R) has proposed key technical performance requirements for the development of IMT-2020 systems and has begun to invite submissions for IMT-2020 candidates radio interface technology. System-level simulation is used as the main tool to evaluate the performance of various application scenarios. Unlike link-level simulation, in link-level simulation, only the link between a base station (BS) and user equipment (UE) is evaluated, while system-level simulation simulates a large number of BSs and UEs in a wide service area. There is no clear direction for his research [2]. Bifulco believes that the service function chain is expected to simplify the process of introducing new services into the mobile network by enabling the dynamic combination of virtualized network functions. However, the current implementation relies on new tunneling protocols and changes in network infrastructure, which makes deployment in traditional networks difficult. He proposed a system for service function chains that can be easily deployed in mobile networks without any protocol or network modification. In addition, he proposed the design of a hybrid hardware-software software-defined network switch to implement a scalable network traffic classifier, which CATENAE uses to allocate network flows to corresponding functional chains. His research lacks necessary experimental data [3].

This paper mainly discusses the optimal design of enterprise standardized management planning decision-making under mobile network system and adopts the visual way to support the collaborative modeling process of value model and evaluation system. The evaluation results are displayed in a variety of graphical forms, and the local or global view can be viewed by zooming the view. The system makes full use of factory mode and multithread control technology to make the overall structure of the module clear and concise, and ensure the subsequent maintainability and scalability of the module.

2. Mobile Network System and Enterprise Standardized Management

2.1. Mobile Network System. The Manhattan distance function follows a grid-like path to calculate the distance from one data point to another. The Manhattan distance between two data points is the sum of the grid paths [4]. The formula

for the distance between point $X = (X_1, X_2, \cdots, X_n)$ and point $Y = (Y_1, Y_2, \cdots, Y_n)$ is as follows:

$$d = \sum_{i=1}^{n} |X_i - Y_i|. \tag{1}$$

The Euclidean distance function measures the straight line distance between two points. The formula for the distance between point $X = (X_1, X_2, \cdots, X_n)$ and point $Y = (Y_1, Y_2, \cdots, Y_n)$ is as follows:

$$d = \sqrt{\sum_{i=1}^{n} (X_j - Y_j)^2}. \tag{2}$$

The overall architecture design of the mobile network system is shown in Figure 1.

The objective function is defined as follows:

$$J = \sum_{k=1}^{K} \sum_{x_i \in D_k} \|x_i - c_k\|^2. \tag{3}$$

If the sample has the smallest distance from the center c_k of the k-th category, the sample belongs to the cluster D_k, which can be described as follows:

$$D_k = \left\{ x_i \in X | k = \underset{j \in \{1,2,\cdots,k\}}{\arg \min} \|x_i - c_j\|^2 \right\}, \tag{4}$$

$$c_k = \frac{\sum_{x_i \in D_k} x_i}{|D_k|}. \tag{5}$$

The weight calculation formula is defined as follows:

$$W_{A_i} = \frac{N_{A_i}}{\sum_{j=1}^{n} N_{A_j}}. \tag{6}$$

The calculation formula of the clustering coefficient of node $v2$ is as follows:

$$cc = \frac{n}{\binom{k}{2}} = \frac{2n}{k(k-1)}. \tag{7}$$

In the formula, k represents the number of all adjacent nodes of node $v2$ [5]. The calculation method of the cosine similarity between node i and node j is as follows:

$$\cos = \frac{a_i \cdot a_j}{\|a_i\| \cdot \|a_j\|}. \tag{8}$$

Among them, $\|\cdot\|$ means two norms. The similarity of network nodes is widely used in the clustering of networks and networked data. For example, the similarity between social network nodes can be used to recommend friends [6].
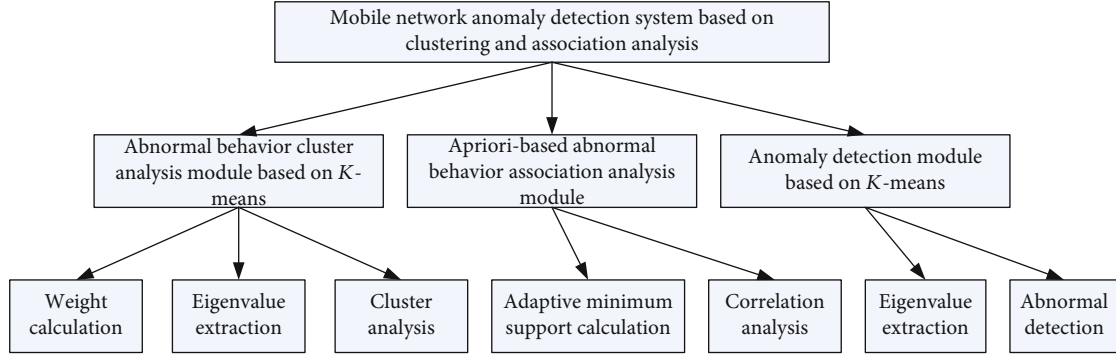
FIGURE 1: The overall architecture design of the mobile network system.

The probability of a network with n nodes and m edges obeys the binomial distribution shown in the following formula:

$$P(m) = \begin{pmatrix} \dfrac{n(n-1)}{2} \\ m \end{pmatrix} p^m (1-p)^{n(n-1)/2-m}. \tag{9}$$

The expected value of m is as follows:

$$\langle m \rangle = \sum_{m=0}^{n(n-1)/2} mP(m) = p \cdot \frac{n(n-1)}{2}. \tag{10}$$

The average degree of random network $\langle k \rangle$ is calculated as follows:

$$\langle k \rangle = \frac{2\langle m \rangle}{n} = \frac{2p \cdot n(n-1)/2}{n} = p \cdot (n-1). \tag{11}$$

The calculation method of the degree distribution of a random network is as follows:

$$P(k) = \begin{pmatrix} n \\ k \end{pmatrix} p^k (1-p)^{n-k} \approx e^{\langle k \rangle} \cdot \frac{\langle k \rangle^k}{k!}. \tag{12}$$

The platform monitors Internet traffic data through the self-developed traffic monitoring system TMS, which is deployed between the access network and the core network. Whenever a user uses the device to go online, TMS can collect all the upstream and downstream data packets and generate streams through collection recording. These stream records are distributed to the data processing module through the data distribution system [7]. The calculation results of batch processing and real-time processing can be stored in a relational database. The platform provides a friendly interface module to display these results. In addition, the cluster monitoring module is used to monitor the abnormality of the platform. It can collect the performance indicators of the hardware and software in the cluster. When errors and alarms occur, the cluster manager will notify the cluster manager through emails and text messages for processing [8].

2.2. Enterprise Standardization Management. Enterprise standardization information management system is based on the relevant information of enterprise standardization. After the full analysis and investigation of enterprise standardization management, the system of standardized information network is established based on the development goal of the enterprise, and the actions of various departments of the enterprise are connected in series, so as to enjoy the effective influence brought by standardization and maximize the benefits of the enterprise. A number of standards are organically combined and complemented to form a relatively perfect logistics standard system [9].

The logistics standard unit formed in the process of logistics enterprise management standardization can provide factual support and experience reference for logistics industry standardization, and logistics industry standardization, as a verified standard reference, can be applied to logistics enterprise standard unit, thus indirectly promoting logistics enterprise standardization management. But at the same time, the concept of logistics standardization can also be applied to the standardization management of enterprises based on nonlogistics business standards, playing a reference significance [10, 11].

In addition, with the development of computer monitoring technology and the improvement of automation degree of enterprise management information system, hydropower enterprises must timely adjust the original equipment management organization form and build a flat, cross-departmental matrix equipment management mechanism as soon as possible. In fact, when people really get a sense of accomplishment and satisfaction from their heart, that kind of enthusiasm will promote better completion of tasks. Therefore, hydropower enterprises should improve the living and working environment of employees, quantify objectives and tasks, and set up effective commendation methods, so that enterprises can make full use of their talents and employees can obtain a certain sense of achievement through work [12, 13].

The stronger the competitiveness of an enterprise, the higher its status, the higher its market visibility, and the higher the probability of establishing a corresponding relationship. The strong competitiveness and high status of an enterprise reflect the company's ability to solve problems and the current good operating conditions of the enterprise.

This also means that the knowledge and experience that the enterprise has stored in the market operation is quite rich. With the deepening of the degree of interaction between the core enterprise and the related organizations in the relationship network, it will help the core enterprise to lock the organization in the relationship network [14].

When the two parties to establish a relationship have a deeper understanding of each other, the two parties will carry out more in-depth cooperation around technology standardization, and there will be a certain degree of path dependence between each other. Therefore, relevant organizations such as intermediary, business, scientific research, and administration will be locked in the relationship network established by the core enterprises. An important prerequisite for the stable operation and development of relational network is that all the member organizations in the network can get the return corresponding to their efforts. When a member gains noncorresponding benefits, it will harm the interests of other members, thus causing other members to have reservations in the cooperation [15].

2.3. Decision Optimization System. The decomposition of engineering product design objects is actually the decomposition of complex product multidisciplinary design decision problems into multiple relatively simple disciplines or subsystems, and each discipline or subsystem can be analyzed and optimized in a relatively independent environment at the same time. This paper uses the fuzzy clustering method to divide the strategy set of each game party [16].

Single objective optimization is performed on n objective functions separately, so as to obtain the optimization vector of each objective function when the optimal value is obtained:

$$X_j^* = \left\{ x_{1j}^*, x_{2j}^*, \cdots, x_{mj}^* \right\}, \quad j = 1, 2, \cdots, n. \tag{13}$$

In the formula, X_j^* is the set of design variables corresponding to the j-th design goal when the optimal value is obtained.

DPI is defined as the expected value of the design performance preference function within the design solution range, namely,

$$\text{DPI} = E[P(y)] = \int_{\bar{y}-\Delta y}^{\bar{y}+\Delta y} P(y) f(y) dy. \tag{14}$$

The decision support system uses local branch and delimitation, tabu search, and neural network algorithms according to different underground roadway environment and inspection area status and other information to calculate the path planning of underground security personnel in different scenarios and different scales, and calculates the parking of each person and vehicle. Points need to arrange the number of security personnel, and the safety inspection system generates a safety inspection route for each security personnel, and can observe the entire downhole situation in real time through the personnel positioning module, and can conduct two-way early warning up and down [17, 18].

According to this platform, it can quickly and accurately calculate the inspection path planning of mine security personnel, and carry out positioning and early warning, so as to improve the mine safety and personnel work efficiency and reduce enterprise costs. The fitness function requires the planning scheme to make the objective optimal under the constraint conditions. In the fitness function, it is required to reflect both the expected factors of the solution and the undesirable factors of the solution, and reward the former and punish the latter [19]. Generally, the fitness function adopts the maximum principle; that is, the greater the fitness value, the better the variety. After the main grid positions are initially determined, the power flow of the network is calculated with the minimum line loss as the optimization objective, meeting the constraints of power supply radius and voltage loss, and the line loss of different grid structures is compared and analyzed, and finally, a new grid structure is obtained [20, 21].

3. Mobile Network System Simulation Experiment

3.1. Test Environment. Considering the common hardware environment in current practical application, we use IBM System x3650 M2 server as web server and database server, and select two smart phones for mobile terminal equipment. We use Windows Server 2008 as the operating system of the server, Tomcat as the web server, and MySQL database as the most common database [22]. The system simulation parameter settings are shown in Table 1.

3.2. Data Preprocessing. This paper adopts the idea of clustering, integrates customers into a customer clustering model, and gathers multiple small customers into one big customer, which will greatly reduce the number of customers studied in the model, thereby simplifying the optimization solution process of the model. Based on the principle of minimizing logistics costs, the distribution of production locations to customers often follows the principle of nearby distribution, and because the capacity of each production location is limited, it can only meet the needs of some nearby customers, so in order to reduce the scale of the problem, it can be based on the production location. Geographic location and historical data of distribution, the production area, and customers are divided into regions, the production area in each area mainly supplies the needs of customers in the area, and the remaining production is used for external supply. Through this division of the main supply area, the large-scale resource allocation problem is divided into several smaller-scale resource allocation problems [20, 23].

3.3. Data Stream Clustering. The data stream clustering of the mobile network system is divided into two parts: an online process that records the current data stream clustering characteristics and an offline process for users to perform offline queries. The online process quickly receives the input data stream, and saves the clustering results it produces as the intermediate results of mining for users to query offline. Through online and offline processes, dynamic and fast data

TABLE 1: System simulation parameter settings.

Simulation parameters	Simulation value
Number of SDP sites M	3
Number of functional modules per SDP site N	10
IoT business category K	6
IoT aggregation length L	10
IoT aggregation delay threshold T	ls

flow processing is realized, and users' needs for data flow analysis can be well met [24].

(1) Initialize the data stream. At the beginning, several data are read in at one time, and divided to form an initial grid, and calculate the feature vector of each grid unit

(2) Add new data objects. With the inflow of new data objects, each data point will be located in the corresponding spatial grid according to its own information, and the feature vector of the grid unit will be updated in real time. Due to the large amount of data flow and unpredictability, if you store all the grids, a lot of storage space is required. In order to save storage space, in this algorithm, we only store grid cells with data points [25]

(3) Mobile nonintensive units. Due to the complementary and overlapping division of the grid, some of the influence of the data points on the surrounding space is lost, and at the same time, the data points that originally belong to a certain category may be unevenly distributed into different grids. This effect has on the grid unit. The edge data is particularly obvious. After the grid unit is moved, a new grid unit is generated, and the grid unit vector and its density are calculated. At this time, it is not necessary to scan the entire data set, as long as the data unit adjacent to the grid unit is viewed [26]

(4) Update the feature vector of the grid unit. Under the condition of continuous data flow, after moving the entire data space, the data space is composed of the original dense unit and the newly added unit

(5) Identify clusters. After moving the nondense grid cells, the data space is composed of the original dense grid cells and newly added grid cells. According to the depth-first traversal algorithm to find the related dense units, find all the dense units associated with the unit and merge these units to generate a cluster [27]

3.4. Construction of Evaluation Indicators. In the construction of enterprise standardization strategic performance evaluation index system, it is necessary to decompose, combine, and converge the index system. In the performance of standardization strategy of construction enterprises, process and result are equally emphasized; that is, in the design of

index system, on the one hand, the final result of strategy implementation is emphasized; on the other hand, the process of strategic evaluation, selection, and implementation is also emphasized. According to the construction principles and methods discussed above, the influencing factors of standardized strategic performance evaluation indicators of construction enterprises are preliminarily stratified by using the expert survey method and cluster analysis method, so as to construct the initial evaluation system [28].

(1) Select 9 experts to score the 5 elements in the selected evaluation system and quantitatively score them according to their contribution to the evaluation target. The scores are, respectively, 5, 4, 3, 2, 1

(2) Analyze several elements with a small total score of the expert's score, and when it is determined that its contribution to the evaluation target is small or that it can be merged into other indicators, remove the indicator and perform cluster analysis on the remaining indicators

(3) Use SPSS software to perform cluster analysis, connect factors with similar properties in a step-by-step connection method, and cluster all influencing factors

(4) After the cluster analysis is completed and experts' opinions are consulted again, the preliminary index system of performance evaluation for standardization strategy of construction enterprises can be obtained. Finally, six parts are selected in the initial system indicators of construction industry standardization strategy evaluation, including standardization strategy planning and implementation, customer focus, internal management improvement, learning and growth, project management improvement, and economic benefit promotion [29]

4. System Simulation Analysis

4.1. Application Analysis of Enterprise Standard Management. The training set and test set data are sequentially input into the support vector regression machine, decision tree, and random forest for training. The training effect of the proxy model obtained after tuning the parameters is shown in Table 2 and Figure 2. It can be seen that the coefficient of R^2 when GA is used as an independent variable is 0.98, which is significantly positive at the 1% level. It proves that assuming H1 remains unchanged in other influencing factors, the improvement of business innovation ability in the new economic era indicates that the more effective the enterprise is to help the new economic era through innovative internal control. In addition, the effectiveness of external capital market supervision factors is significantly related to the audit effectiveness, indicating that the quality of the audit system of internal control audit reports has an effect on the effectiveness of corporate internal control, and confirms that further strengthening of internal control audits can promote the role of enterprises in helping the new economic era.

Table 2: Model training effect.

Model used	R^2		RMSE	
	Training set	Test set	Training set	Test set
Support vector regression machine	0.9774	0.971	0.9531	1.1184
Decision tree	0.9813	0.9673	0.867	1.187
Random forest	0.9873	0.9732	0.7135	1.0748
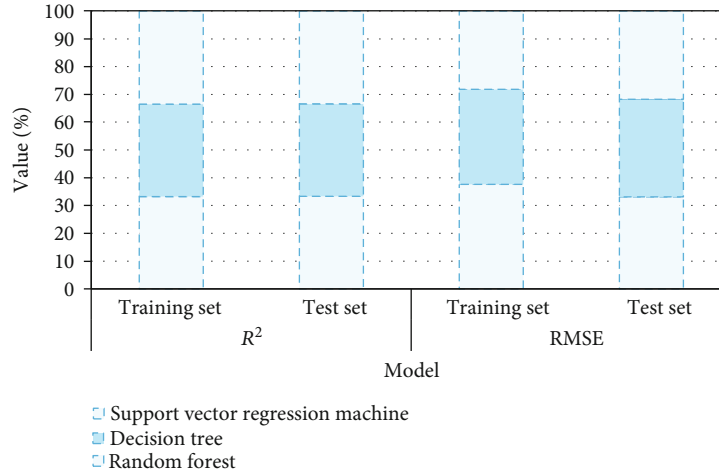
Figure 2: Model training effect.

Table 3: Movement characteristics at different times.

	Working hours	Nonworking hours	Weekend
Location entropy	1.71	1.81	1.97
Radius of gyration	0.58	0.59	0.72

Table 4: Experimental results.

Forecast accuracy	All users	Mobile users
Markov	34.3%	46.9%
TBM (Ts = 1 h)	36.2%	47.7%
TBM (Ts = 2 h)	37.2%	48.6%

The generation of decision support systems is based on the theoretical development of management information systems and other related disciplines. Although traditional MIS can organize and manage information on the surface, it cannot dig out the internal laws of information to serve decision-making. The help of managers is limited, and the expected socioeconomic effects have not been achieved. The movement characteristics at different times are shown in Table 3. It can be seen from the table that people are more inclined to move during nonworking hours, especially on weekends. Both the entropy and the radius of gyration increase significantly, indicating that people are more mobile at this time. This also illustrates the necessity of proposing time-based mobility algorithms.

We use Markov and TBM to experiment on the prediction accuracy, respectively, and the Ts parameter of TBM is set to 1 hour and 2 hours, respectively. At the same time, the algorithm was tested separately for mobile users and all users. The final experimental results are shown in Table 4 and Figure 3. It is known from the table that TBM can achieve a better prediction effect for mobile users than basic Markov. When the time threshold Ts is set to 1 hour, the prediction accuracy of TBM rises from 46.9% to 47.7%; when the time threshold Ts is set to 2 hours, higher prediction accuracy can be obtained. In a sense, it is "using the skills of others to do a good job." It is a collaborative activity that gathers people with different personalities, specialties, and preferences under the same organizational goal. The uniqueness of corporate goals determines that corporate standardization managers cannot seek common ground while reserving differences can only give up or change personal views, compromise, and compromise with each other for the common goals of the enterprise. On the other hand, in scientific research, scholars, as knowledge disseminators and research direction masters, generally adopt a condescending, authoritative, and paternalistic management mode for their disciples and students. Enterprise employees have professional skills and have been on the front line of research and development for a long time. They are the creators and specific implementers of innovative activities. Authoritative and too rigid management methods are not conducive to activating employees' thinking and maintaining creativity. Therefore, companies often use incentives: management mode.

4.2. Performance Analysis of Decision Optimization System. Normalized throughput is an important index to measure
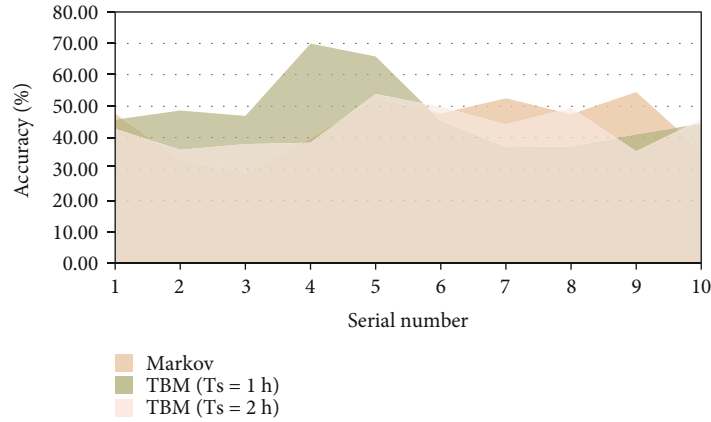
FIGURE 3: Experimental results.
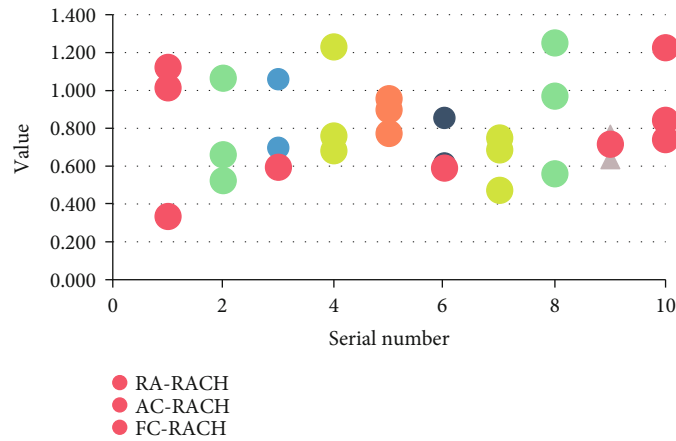
FIGURE 4: Normalized throughput rate under different access methods.

random access, which directly shows the quality of random access process. The high normalized throughput indicates that the system has strong access ability and can drive more devices under the limited time-frequency resources. When the number of RA-RACH users increases to a certain number, serious collision conflicts will occur, resulting in poor access ability. However, AC-RACH and FC-RACH will not have this problem. The normalized throughput under different access modes is shown in Figure 4. It can be seen from the figure that the normalized throughput of the random access mode with AC-RACH and FC-RACH is higher than that of RA-RACH. Especially when the arrival rate of user request is higher and higher, the throughput of RA-RACH access will decrease with collision until it approaches zero. AC-RACH and FC-RACH keep the normalized throughput near the maximum by restraining the real-time demand of some users, so as to realize the system optimization. Compared with AC-RACH, FC-RACH has more feedback to adjust the input and compensate the estimated value of access load to a position closer to the real load.

The comparison of throughput rate between genetic algorithm and assisted call admission algorithm is shown in Figure 5. It can be seen from the figure that the throughput rate of the system increases first as the number of users increases, and then stabilizes. When the number of users is

less than 1,000, there is little difference in throughput between GA and MACA. This is because when the number of users is small, the base station has enough resources to serve all users. Although the throughput rate is equal, the resource utilization rate of the base station is different. When the number of users increases again, MACA's system throughput rate will soon reach the upper limit and GA can continue to increase until the number of users is about 2,000. The final stable system throughput rate of GA is higher than that of MACA. Therefore, laboratory scientific research and enterprise innovation are two completely different fields, and there are many differences in communication management mode, thinking mode, innovation goal, implementation conditions, and so on. These differences make scholars have conflicts of roles in the process of transforming into executives. As a result, scholars with rich scientific research achievements and outstanding scientific research capabilities may not be able to successfully transform into outstanding corporate standardization managers.

The change of recognition accuracy with distance is shown in Figure 6. As can be seen from the figure, when the distance between devices increases, the accuracy of device selection gradually decreases. When the distance between devices is fixed and the angle increases, the accuracy of device selection also increases. Moreover, in the Spartacus system,
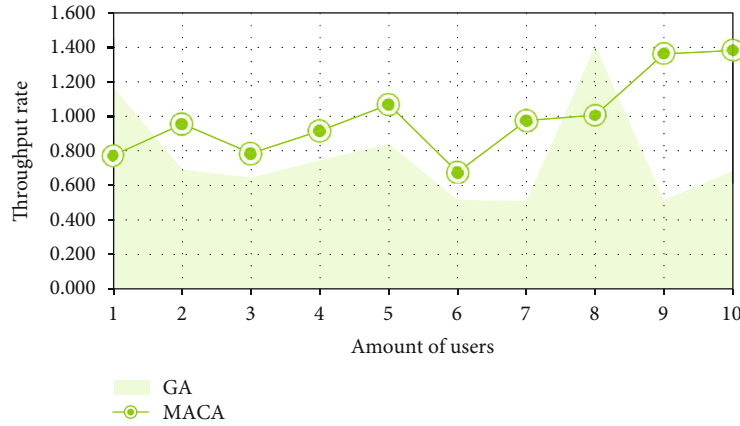
FIGURE 5: Comparison of throughput rate between genetic algorithm and assisted call admission algorithm.
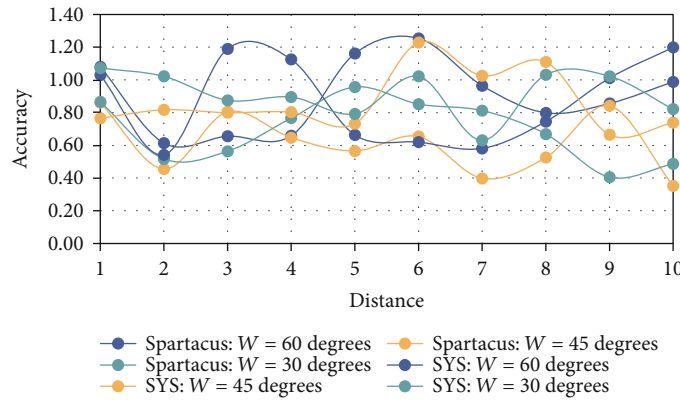
FIGURE 6: Variation of recognition accuracy with distance.

when the angle was 45 degrees and the distance between the source device and the receiving device was less than 4 meters, the accuracy rate could reach 95%. In this system, the same angle and distance, accuracy can be up to 100 percent. When the angle was 30 degrees and the distance was 3 meters, the device selection accuracy of Spartacus could reach 90%, while in the same environment of this system, the accuracy could reach 95%. When the distance between the source device and the receiving device is less than 3 meters, the accuracy of device identification is relatively stable. This is consistent with the phenomenon of sound energy depletion. Because SYS uses energy contrast to detect audio, the energy difference between audio and other bands decreases with distance. Moreover, due to the improved performance generated by arm extension, SYS was able to achieve 95% accuracy within 3 meters, 90% accuracy within 4 meters, and 85% accuracy within 5 meters for all device tests. For enterprise standardization management, there are obvious differences between this management and academic activities in many aspects such as communication methods, thinking modes, innovation goals, and restrictive conditions. This has led to a certain degree of a role conflict between scholars in the process of transforming into corporate executives. The innovation effect of a decisive position such as chairman or CEO is lower than that of other senior management positions, indicating that

TABLE 5: The recognition accuracy of the system in different environments.

	Distance (m)					
	0.5	1	1.5	2	2.5	3
Hall	94.5%	85.1%	82.4%	86.7%	90.1%	92.3%
Laboratory	97.1%	89.5%	87.4%	88.2%	92.1%	93.2%
Corridor	94.8%	92.4%	97.4%	85.2%	83.8%	86.4%

the innovation promotion effect of academic senior management is closely related to the position of the company.

The recognition accuracy of the system in different environments is shown in Table 5. For a distance range of 0.5 meters, 100% equipment selection accuracy can be achieved in all three scenarios. When the distance increases, the performance of the hall is basically stable, and the accuracy rate is close to 100%, but the performance of the laboratory and the corridor decreases slightly with the increase of the distance, but the laboratory environment can still guarantee an accuracy of more than 90%, and the corridor environment can still guarantee an accuracy of over 85%. Comparing these two scenes with the lobby, this is mainly due to the powerful multichannel effect. Before training activities, the actual needs of employees should be understood through

TABLE 6: Descriptive statistics of core corporate capabilities.

	H11	H12	H13	H21	H22	H23	H31	H32	H33	H41	H42
Mean	3.28	3.97	4.36	3.69	3.77	3.69	3.61	3.89	4.23	3.45	3.77
Median	3.00	4.00	5.00	4.00	4.00	4.00	4.00	4.00	4.00	3.00	4.00
Standard deviation	0.90	0.74	0.79	0.91	0.84	1.00	0.86	0.83	0.93	0.84	0.78

questionnaires, interviews, etc., and the needs of employees should be combined with the needs of the company, so that training can be as close as possible to standardized management and job requirements. Establish scientific and standardized employee training procedures, set up targeted training courses, and help employees improve their work skills and quality in the most efficient manner through the supervision of the training process and the assessment and feedback of the training results.

4.3. Role of Mobile Networks in Corporate Management. The descriptive statistics of core enterprise capabilities are shown in Table 6. In terms of scale, it is considered that 5 billion is an enterprise with certain regulations, with the highest average, reaching 4.36; the smallest degree of dispersion is that one billion is an enterprise with a certain scale, reaching 0.743; in terms of development capacity, the average number of high growth enterprises is higher, reaching 3.77, with a large degree of dispersion, reaching 0.849; in terms of leading ability, the average number of high growth enterprises is higher, reaching 3.77, with a large degree of dispersion, reaching 0.849. It is considered that the leading power of enterprises with 500 suppliers is strong, with the highest average value of 4.23. The smallest degree of dispersion is that the core enterprises with more than 200 suppliers have a strong leading ability in the supply chain, reaching 0.843.

The comparison between the predicted value and the real value of the test set is shown in Figure 7. The critical values of robustness of regular network and scale-free network are both 0, which means that the robustness of these two types of networks is almost the same. However, the essence of scale-free network is a sparse network; that is, the number of edges of the network is not too many, and the number of edges of regular network is too much; even some regular networks, the network is not sparse enough. When $k = 2$, the clustering criterion function value of the improved algorithm is significantly higher than that of the MinMax k-means algorithm, but from $k = 3$, the clustering criterion function value of the improved algorithm decreases obviously. With the increase of clustering number k, the clustering criterion function values of MinMax k-means algorithm and improved algorithm tend to be parallel to each other and always maintain a certain gap. Explain that the heterogeneity of enterprises (enterprise establishment time, enterprise profitability, business complexity, asset scale, and actual controller) has a significant impact on the empirical results, and different types of enterprises show the existence of effectiveness of the new era of internal control application economy significant differences. Finally, the three control variables PR, PETIC, and IDR related to the respondent failed to pass the test, indicating that the professional relevance, internal
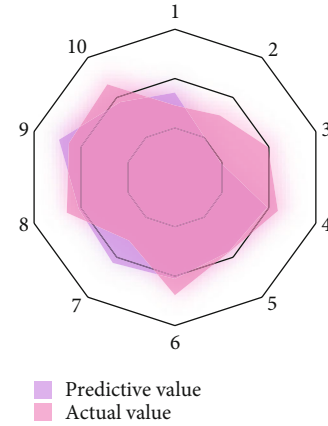
FIGURE 7: Comparison of the predicted value and the true value of the test set.

control experience, and regional differences of different respondents contribute to the business innovation ability and internal control innovation. The relationship between the effectiveness of the new economic era has no impact.

The traffic consumption comparison between MP2P-VPN and OpenVPN is shown in Figure 8. The average daily traffic consumed by MP2P-VPN and OpenVPN is 407 kB and 1508 kB, respectively. It can be seen that the traffic required to maintain the MP2P-VPN network is only about a quarter of that of OpenVPN, saving a lot of network traffic. The core task of the enterprise standardization strategy that is leading in terms of technical standards is to make its own standards the dominant or de facto standard in the industry. For this reason, it is necessary to find a strategy to make the network effect beneficial to itself and to establish its own installation foundation as soon as possible. Clever use of positive feedback loops attracts consumers to bear the switching costs and ultimately lock the market on its own technology. In the new economic era, the stronger the company's ability to stimulate new power, the more effective it is to help the new economic era through innovative internal control.

5. Conclusions

The mobile network automatic drive test system is implemented by C/S structure; the interface layer is based on the user-defined control implemented by the third party control and is completely separated from the data based on the event message mechanism; the business logic layer integrates the protocol analysis, signaling process judgment, namely, the use of event finite state machine, and the implementation of network optimization engineering algorithm. The optimized hierarchical structure, the most reasonable modular
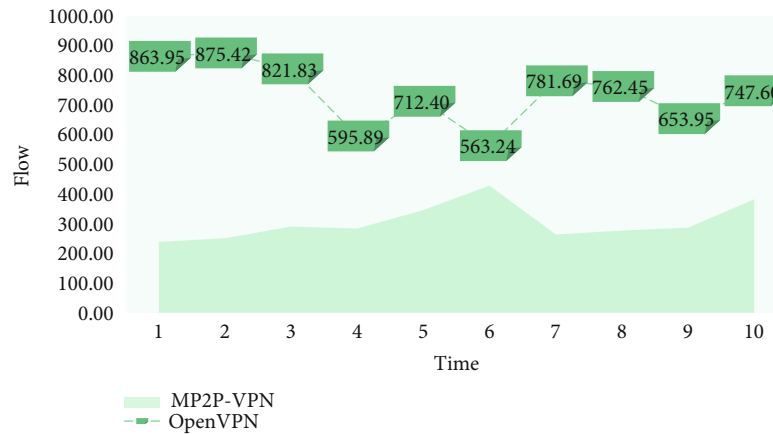
Figure 8: Traffic consumption comparison between MP2P-VPN and OpenVPN.

logic design, and the most rigorous code implementation make the mobile network automatic drive test system have powerful and perfect functions, which can easily and accurately realize the test scheme, analyze the network status, and generate test result reports. It provides comprehensive and accurate data support for network optimization and effectively improves the convenience of system use. The deployment of the whole network optimization system has gone through the process of demand collection, system development, and test acceptance, and most of the test results basically achieve the expected objectives, and the system runs normally.

This paper analyzes the existing research on the coordination and optimization of enterprise production and distribution and the application of decision support system in logistics distribution and production. According to the characteristics of multiorigin, multicustomer, and multiproduct logistics resource allocation problem, combined with the characteristics of decision support system, the framework of decision support system for logistics resource allocation is designed. The coordination and optimization model is established for the logistics resource allocation problem of multiorigin, multicustomer, and multiproduct types, and the DSS system is designed and developed. This paper establishes the general idea, main contents, and development principles of enterprise standardization management system. Through the establishment of the principle of standardization management mode, it specifically expounds the methods for functional departments, grass-roots units, and grass-roots teams to carry out the construction of standard system. The practical tools for functional departments to carry out the construction of standard system are given, which provides guidance and basis for enterprises to carry out standardization management.

The innovation effect of academic executives when they occupy decisive positions in enterprises is not significant when they hold other nondeterministic positions. The increase in the proportion of academic executives does not simultaneously bring about an increase in innovation effects. The above findings help to understand the role of academic executives in corporate innovation activities more rationally and objectively; that is, scientific and technological person-

nel's "breaking fence" entrepreneurship and participatory entrepreneurship may be better than dominant entrepreneurship. Therefore, it is recommended that companies do not seek intellectual support from scholars as much as possible. Instead, they should appropriately control the proportion of academic executives, so that they can not only give full play to the professional and resource advantages brought by academic experience but also avoid the "shortcomings" of scholars. The adverse impact is on innovation and entrepreneurship. In addition, enterprises should choose appropriate methods and methods, adopt various forms of "flexibility" to attract talents, make the best use of their talents, and realize the real purpose of hiring academic executives.

Data Availability

No data were used to support this study.

Conflicts of Interest

The authors declare that they have no conflicts of interest.

References

[1] S. Choi, H. Chung, J. Kim, J. Ahn, and I. Kim, "Mobile hotspot network system for high-speed railway communications using millimeter waves," *ETRI Journal*, vol. 38, no. 6, pp. 1052–1063, 2016.

[2] C.-K. Jao, C.-Y. Wang, T.-Y. Yeh et al., "WiSE: a system-level simulator for 5G mobile networks," *IEEE Wireless Communications*, vol. 25, no. 2, pp. 4–7, 2018.

[3] R. Bifulco, A. Matsiuk, and A. Silvestro, "CATENAE: a scalable service function chaining system for legacy mobile networks," *International Journal of Network Management*, vol. 27, no. 2, pp. 1–14, 2017.

[4] J. Kim, M. Sung, S. H. Cho et al., "MIMO-supporting radio-over-fiber system and its application in mmWave-based indoor 5G mobile network," *Journal of Lightwave Technology*, vol. 38, no. 1, pp. 101–111, 2020.

[5] F. Liu, Y. Liu, Y. Liu, and H. Wang, "A novel construction paradigm of multimedia awareness system for mobile network," *Cluster Computing*, vol. 22, Supplement 4, pp. 9697–9713, 2019.

[6] J. Kim, M. Schmieder, M. Peter et al., "A comprehensive study on mmWave-based mobile hotspot network system for high-speed train communications," *IEEE Transactions on Vehicular Technology*, vol. 68, no. 3, pp. 2087–2101, 2019.

[7] H. Jarrah, N. I. Sarkar, and J. Gutierrez, "Comparison-based system-level fault diagnosis protocols for mobile ad-hoc networks: a survey," *Journal of Network & Computer Applications*, vol. 60, no. 1, pp. 68–81, 2016.

[8] T. J. Gerpott and P. Meinert, "Correlates of using the billing system of a mobile network operator to pay for digital goods and services," *Information Systems Frontiers*, vol. 18, no. 6, pp. 1265–1283, 2016.

[9] B. Clerckx, A. Costanzo, A. Georgiadis, and N. B. Carvalho, "Toward 1G mobile power networks: RF, signal, and system designs to make smart objects autonomous," *IEEE Microwave Magazine*, vol. 19, no. 6, pp. 69–82, 2017.

[10] F. A. Khan, M. Imran, H. Abbas, and M. H. Durad, "A detection and prevention system against collaborative attacks in mobile ad hoc networks," *Future Generation Computer Systems*, vol. 68, no. 3, pp. 416–427, 2017.

[11] H. Al Moussawi, F. Fardoun, and H. Louahlia-Gualous, "Review of tri-generation technologies: design evaluation, optimization, decision-making, and selection approach," *Energy Conversion and Management*, vol. 120, no. 7, pp. 157–196, 2016.

[12] Z. Liang, J. Zang, X. Yang, X. Dong, and H. Song, "Integration interval determination and decision threshold optimization for improved TRPC-UWB communication systems," *China Communications*, vol. 14, no. 5, pp. 185–192, 2017.

[13] Q. Zhang, R. Wang, J. Yang, K. Ding, Y. Li, and J. Hu, "Collective decision optimization algorithm: a new heuristic optimization method," *Neurocomputing*, vol. 221, no. 1, pp. 123–137, 2016.

[14] S. Sekizaki, T. Yamasaki, I. Nishizaki, T. Hayashida, H. Ishikawa, and H. Uenishi, "A development of evolutionary many-objective optimization method for decision aid on distribution system reconfiguration," *IEEJ Transactions on Power and Energy*, vol. 138, no. 12, pp. 925–938, 2018.

[15] D. Plets, K. Chemmangat, D. Deschrijver et al., "Surrogate modeling based cognitive decision engine for optimization of WLAN performance," *Wireless Networks*, vol. 23, no. 8, pp. 2347–2359, 2017.

[16] X. Gu, S. Li, H. Liang, and K. Li, "Optimization decision-making method for looped network restoration to eliminate transmission line overload in network reconfiguration," *Proceedings of the CSEE*, vol. 37, no. 5, pp. 1379–1388, 2017.

[17] M. Pouraminian and S. Pourbakhshian, "Multi-criteria shape optimization of open-spandrel concrete arch bridges: Pareto front development and decision-making," *Military Operations Research*, vol. 16, no. 5, pp. 670–680, 2019.

[18] S.-B. Tsai, "Using the DEMATEL model to explore the job satisfaction of research and development professionals in China's photovoltaic cell industry," *Renewable and Sustainable Energy Reviews*, vol. 2018, no. 81, pp. 62–68, 2018.

[19] H. Wang, Y. Huang, A. Khajepour, D. Cao, and C. Lv, "Ethical decision-making platform in autonomous vehicles with lexicographic optimization based model predictive controller," *IEEE Transactions on Vehicular Technology*, vol. 69, no. 8, pp. 8164–8175, 2020.

[20] Z. Nedělková, P. Lindroth, M. Patriksson, and A.-B. Strömberg, "Efficient solution of many instances of a simulation-based optimization problem utilizing a partition of the decision space," *Annals of Operations Research*, vol. 265, no. 1, pp. 93–118, 2018.

[21] S.-B. Tsai, Y.-C. Lee, C.-H. Wu, and J.-J. Guo, "Examining how manufacturing corporations win orders," *South African Journal of Industrial Engineering*, vol. 24, no. 3, pp. 112–124, 2013.

[22] J. Li, S. Fong, S. Mohammed, J. Fiaidhi, Q. Chen, and Z. Tan, "Solving the under-fitting problem for decision tree algorithms by incremental swarm optimization in rare-event healthcare classification," *Journal of Medical Imaging and Health Informatics*, vol. 6, no. 4, pp. 1102–1110, 2016.

[23] W. Wu, Y. Liu, C. H. Wu, and S. B. Tsai, "An empirical study on government direct environmental regulation and heterogeneous innovation investment," *Journal of Cleaner Production*, vol. 254, article 120079, 2020.

[24] C. B. Xiao, D. Z. Feng, and M. D. Yuan, "Soft decision optimization method for robust fundamental matrix estimation," *Machine Vision and Applications*, vol. 30, no. 4, pp. 657–669, 2019.

[25] K. Meng, P. Lou, X. Peng, and V. Prybutok, "Multi-objective optimization decision-making of quality dependent product recovery for sustainability," *International Journal of Production Economics*, vol. 188, no. 6, pp. 72–85, 2017.

[26] M. Baldan, A. Nikanorov, and B. Nacke, "A novel multi-surrogate multi-objective decision-making optimization algorithm in induction heating," *COMPEL*, vol. 39, no. 1, pp. 144–157, 2020.

[27] X. Li, J. Wen, and A. Malkawi, "An operation optimization and decision framework for a building cluster with distributed energy systems," *Applied Energy*, vol. 178, no. 9, pp. 98–109, 2016.

[28] A. Jafari and V. Valentin, "Selection of optimization objectives for decision-making in building energy retrofits," *Building and Environment*, vol. 130, no. 2, pp. 94–103, 2018.

[29] K. S. Bhattacharjee, H. K. Singh, M. Ryan, and T. Ray, "Bridging the gap: many-objective optimization and informed decision-making," *IEEE Transactions on Evolutionary Computation*, vol. 21, no. 5, pp. 813–820, 2017.

WILEY | Hindawi

Retraction

Retracted: Monitoring System of Key Technical Features of Male Tennis Players Based on Internet of Things Security Technology

Wireless Communications and Mobile Computing

This article has been retracted by Hindawi following an investigation undertaken by the publisher [1]. This investigation has uncovered evidence of one or more of the following indicators of systematic manipulation of the publication process:

(1) Discrepancies in scope

(2) Discrepancies in the description of the research reported

(3) Discrepancies between the availability of data and the research described

(4) Inappropriate citations

(5) Incoherent, meaningless and/or irrelevant content included in the article

(6) Peer-review manipulation

The presence of these indicators undermines our confidence in the integrity of the article's content and we cannot, therefore, vouch for its reliability. Please note that this notice is intended solely to alert readers that the content of this article is unreliable. We have not investigated whether authors were aware of or involved in the systematic manipulation of the publication process.

Wiley and Hindawi regrets that the usual quality checks did not identify these issues before publication and have since put additional measures in place to safeguard research integrity.

We wish to credit our own Research Integrity and Research Publishing teams and anonymous and named external researchers and research integrity experts for contributing to this investigation.

The corresponding author, as the representative of all authors, has been given the opportunity to register their agreement or disagreement to this retraction. We have kept a record of any response received.

References

[1] G. Wu, "Monitoring System of Key Technical Features of Male Tennis Players Based on Internet of Things Security Technology," *Wireless Communications and Mobile Computing*, vol. 2021, Article ID 4076863, 6 pages, 2021.

WILEY | Hindawi

Research Article

Monitoring System of Key Technical Features of Male Tennis Players Based on Internet of Things Security Technology

Guodong Wu [ORCID]

Faculty of Arts and Sciences, Science and Technology College of Nanchang Hangkong University, Jiujiang, 332020 Jiangxi, China

Correspondence should be addressed to Guodong Wu; tennis0528@163.com

Nowadays, the development and innovation of tennis have basically been integrated with the Internet, and the penetration of big data is accelerating the development of tennis. Collect data and statistics about tennis matches, analyze the key winning factors of the game, assign players' gains and losses, and assign points. Fully understand the game's tactics and various key technical functions of the player and enhance the influence of the game's attention. Therefore, as the era of the Internet of Things is about to come, the development of sports events in my country should seize the opportunity of innovation in the application of Internet of Things technology, accelerate the process of upgrading informatization and intelligence, and achieve leapfrog development. This article is aimed at studying the use of the Internet of Things security technology, research, and design a monitoring system for the key technical characteristics of male tennis players. This paper proposes to develop a novel real-time video semantic analysis prototype system for tennis matches, taking the video from the monitoring perspective of tennis matches as the analysis object. The experimental results in this article show that from Wimbledon to the Australian Open, the Australian Open is very slow, and finally, to the French Open, the speed of the ball slows down and improves the accuracy of the tennis crisis system. The average level and the correct answer rate are 61.37%. Eventually, it rose from the highest 86.13% to 86.92%, and the highest was the lowest. It seems that a monitoring system for the basic technical characteristics of male tennis players is more feasible.

1. Introduction

1.1. Background. With the holding of large-scale sports events such as the Olympic Games and the World Cup, people are becoming more and more obsessed with sports. Tennis is a very popular ball sport, and every tennis enthusiast will pay attention to the four major open tennis tournaments. As well as business forms, there is still a lot of room for improvement and transformation. The Internet of Things industry is an emerging strategic industry that my country is focusing on developing. Based on this environment, the application of the Internet of Things has great potential and space. In recent years, the Internet of Things technology has gradually matured, focusing on sensors, software, etc., and at the same time, in terms of supporting equipment for the Internet of Things, especially the rapid development of basic equipment such as smart circuits and transmission networks. As far as the current situation is concerned, my country's Internet of Things has a relatively wide range of

applications, involving my country's industry, commerce, agriculture, and service industries [1, 2]. It plays an extremely important role in urban construction, environmental protection, urban safety, and intelligent transportation. This has also brought new development opportunities and challenges to various fields, especially in the sports industry. The use of advanced technologies of the Internet of Things can bring huge technological innovations to the research and development of sports events and comprehensively promote the development of sports events.

1.2. Significance. In a modern tennis game, key points are of the utmost importance to every player. Athletes often face great psychological pressure during key points. Losing key points means losing a game, a set, or even the entire game. In 2018, the global Internet of Things market will exceed 100 billion U.S. dollars, and 26 billion devices will be connected to the Internet of Things by 2020. This huge number will bring huge growth space for the development of the

sports industry. As an important part of the sports industry, sports events also show that people have the spirit of continuous innovation and challenge. Modern sports events are one of the important signs of current social progress, civilized develop, and economic strength. In today's social life, the process of economic integration and the rapid development of information technology make the combination of the Internet of Things and sport an important development direction for the development of the sports industry. "Internet +" sports continue to ferment, big data, VR, artificial intelligence, etc. [3] and will be deeply integrated with sports. Making full use of the Internet of Things technology in the operation of large-scale sports events is an important reality for further improving the level of sports events in Japan and promoting progress in game management, information management, and venue management. Promote the construction of industry and sports culture. There are relatively few researches on the application of the Internet of Things technology in the management of sports events, and the application of the Internet of Things in this field is still blank. This time, the research on the application of the Internet of Things technology in sports events has brought theoretical results and has special theoretical importance, filling the gaps in our research in this area.

1.3. Related Work. Zhang proposed a table tennis human body recognition scheme based on commercial smart watches. We have developed a data acquisition system based on the Internet of Things architecture to obtain data on the acceleration, angular velocity, and magnetic induction of the watch. According to the characteristics of the extracted data, experiments were carried out using main machine learning classification algorithms such as *k*-nearest neighbors, support vector machines, Naive Bayes, logistic regression, decision trees, and random forests. The results show that the random forest has the highest recognition rate, reaching 97.80%. In addition, Zhang designed a simple convolutional neural network to compare its performance on this issue. The network consists of two convolutional layers, two pooling layers, and two fully connected layers and uses data without extracted features. The results show that the accuracy of this method is 87.55%. This research can provide training aids for amateur table tennis players [4]. Although the recognition rate of random forest is very high, reaching 97.80%, there is still a certain gap. Wang uses a wireless wearable sensor device (WSD) based on MEMS (MicroElectro-Mechanical System) motion sensors to identify the different strokes of different badminton players and classify their technical level. The system includes custom sensor nodes for data collection, mobile applications, and cloud-based data processing units. Compared with the video-based badminton shot analysis method, the WSD method has the advantages of low cost, convenient use, and high computational efficiency. It provides the advantage of dynamically monitoring multiple players in indoor and outdoor environments [5]. Although WSD has many advantages, there are still certain errors. Fu recently discovered that following a consensus statement in 2009 requiring standardized literature and tennis-related injury analysis, several studies have been published describing the incidence of longitudinal injuries in the Grand Slam and Davis Cup. Recent research by ATP has further clarified the pattern of damage in tourism. Recently, there have also been some high-quality studies on the injury trend of college students and outstanding young tennis players, drawing attention to the musculoskeletal injuries and systemic diseases that young tennis players may be vulnerable to. Recent ATP and junior and junior level injury monitoring work has highlighted injury trends, which will help guide injury prevention strategies in different levels of competition [6]. Although certain results have been achieved, there is still room for improvement.

1.4. Innovation. The innovations of this paper include the following: (1) introduced the design and implementation of a prototype system for real-time semantic analysis of tennis match video and conducted a comprehensive analysis of various performance indicators of the entire system through experiments. (2) The semantic analysis part of tennis player's motion. First of all, because in the tennis match video frame from the monitoring perspective, both people and tennis belong to for small targets, and we propose a video small target detection algorithm based on the YOLO v3 algorithm. (3) A real-time semantic analysis algorithm for tennis match video based on deep learning is proposed.

2. Introduction to Related Technologies

The key to the world's outstanding male tennis players is to distribute the ball, whether they are leading or lagging, through a wide angle outside corner serve and a short flat and fast inside corner serve. The scoring rate is high, the loss rate is low, and the serve effect is significant. The score is high, and the serving effect is poor. Real-time video semantic analysis of tennis matches includes many specific technologies. This article mainly focuses on target tracking, target tracking, 2D human pose estimation, and lightweight MobileNet network. At the same time, due to the background of the special application of this article, the realization of related technologies is also inseparable from tennis. The preliminary knowledge of sports is also introduced here. In the research process, combined with prior knowledge, each technique was improved for various challenges, and so the original algorithm is more suitable for the specific sports scene of the tennis match. This article mainly focuses on the semantic analysis of the two major sports objects in the tennis match—athletes and tennis. The output semantic information includes the athlete's movement type, movement distance, movement speed, and tennis landing area.

2.1. Target Monitoring Technology. The Faster-RCNN algorithm is one of the main representatives of the deep learning target detection algorithm. This method combines the CNN classification of the candidate regions that have been separated to form an end-to-end target detection network, which is good in terms of speed and accuracy effect. However, Faster R-CNN obtains the candidate regions in advance, and then the strategy of classifying each candidate region leads to a large amount of calculation and cannot achieve real-

time results [7, 8]. The emergence of the YOLO series of algorithms has improved the speed of the target detection method. It regards the detection task as a regression problem, which greatly accelerates the speed of the algorithm [9, 10].

2.2. Target Tracking Technology. Target tracking, as the name implies, is the continuous tracking of the target. It is an indispensable link in our tennis match video semantic analysis system, because we need to continuously track the target athlete to facilitate the semantic analysis of the athlete's movement [11, 12]. The degree of motion matching refers to the use of the Mahalanobis distance between the detection result and the tracking result at the position predicted by the Kalman filter to describe the degree of motion matching [13, 14].

$$d^{(1)}(i, j) = \left(d_j - y_i\right)^T s_i^{-1} \left(d_j - y_i\right). \quad (1)$$

Among them, y_i is the predicted observation of the trajectory at the current moment, d_j is the state of the jth detection result, and s_i is the covariance matrix of the observation space at the current moment predicted by the trajectory by the Kalman filter [15, 16].

Apparent matching degree refers to serious situations such as ID deformation caused by using Mahalanobis distance alone as a matching degree metric. Especially when the camera is moving, the Mahalanobis distance measurement may be invalid; so, at this time, the apparent matching degree should be used to remedy [17, 18]. The system only calculates the minimum cosine distance of the detection result within the latest $L = 100$ of the trajectory [19, 20].

$$d_{i,j}^{(2)} = \min \left(1 - r_j^T r_k^{(i)} \mid r_k^{(i)} \in R_i\right). \quad (2)$$

The fusion of the two metrics refers to the weighted average $c_{i,j} = \gamma d^{(1)}(i, j) + (1 - \gamma) d^{(2)}(i, j)$, where γ is hyperparameters that are used to adjust the weights of different items [21].

2.3. Two-Dimensional Human Posture Recognition. From the perspective of computer vision, the best way to recognize an action gesture is to find out its action characteristics. These characteristics can include many aspects, such as the human body's stride frequency, stride length, facial features, gestures, body posture, walking trajectory, and shaking degree. Relying only on computer vision algorithms is often not good, usually combined with some hardware devices [22, 23]. In addition to the combination with hardware, it is a good method to perform human body action recognition and human body posture estimation by obtaining the skeleton and key points of the human body [24, 25].

3. Real-Time Video Semantic Analysis for Tennis Matches

In the research process of real-time video semantic analysis for tennis matches, the semantics we need to analyze are divided into two aspects from the perspective of the target object. One is the semantics of the athlete's action type and sports information, and the other is the semantics of the tennis landing area. YOLO-V3 uses a single network structure to predict the category and location of the object while generating the candidate area and does not need to be divided into two stages to complete the detection task [26, 27].

3.1. Monitoring for Small Target Athletes. In the tennis game video scene, target detection is mainly to find some targets on the sports field, namely, people and tennis. Since our application is in the video surveillance scene of a tennis court, the distance between the camera and the sports field is very long, resulting in relatively small players and tennis balls in the video, which brings challenges to our detection algorithm. We have compared and analyzed a series of mature target detections that currently exist and concluded that the YOLO v3 algorithm is superior to other algorithms in the detection accuracy of small targets under the premise of ensuring the detection speed. In response to the above challenges and conclusions, we have made corresponding improvements to the YOLO v3 algorithm to make it more suitable for small target detection tasks in our specific scenarios. Calculate the parameters according to formula (1), obtain the width conversion parameter θ_{i1} and the height conversion parameter θ_{j1}, and finally convert the original w_0, h_0 to w_1, and h_1.

$$\theta_{i1} = \frac{1}{2} \sum_{n=1}^{n} \left(\frac{2w_0}{w_{n1} + w_{n2}}\right), \theta_{j1} = \frac{1}{2} \sum_{n=1}^{n} \left(\frac{2h_0}{h_{n1} + h_{n2}}\right)(n = 2).$$
$$w_1 = \theta_{i1} \times w_0, h_1 = \theta_{j1} \times h_0, \quad (3)$$

According to the above theoretical method, we obtained the conversion coefficient of the original bounding box size width and height after performing statistics through experiments. The experimental results include three groups, corresponding to three different levels of size, and each group contains the width conversion parameter θ_{i1} and the height conversion parameter θ_{j1}. The results are shown in Table 1:

Combined with the conclusion of the conversion coefficient in Table 1, we modified the corresponding model configuration file of the detection algorithm YOLO v3 and put the original convolutional neural network model of YOLO v3 disclosed by the original author on the professional graphics processing server 24G of the M40 model, and the purpose of retraining under GPU is to make the trained model more suitable for the detection of small targets in our tennis match scene. In this training process, we have conducted more than 70,000 trainings on the end-to-end target detection network model YOLOv3. The experiment is mainly based on the tensor flow of mainstream deep learning frameworks and can be easily monitored through the training process that supports tensor tools. The figure below shows that the model was lost during training. Here, you can see that the loss has been reduced to 0.7, and the test mapping has reached 95% [28, 29].

3.2. Prediction of Tennis Movement and Impact Area Based on Prior Knowledge. Because the high-speed tennis ball is almost invisible to the naked eye in some video frames, in

TABLE 1: Result statistic table of width conversion parameter θ_{i1} and height conversion parameter θ_{j1}.

	Transform coefficient	Corresponding value
First group	θ_{i1}	0.813
	θ_{j1}	0.742
Second group	θ_{i2}	0.968
	θ_{j2}	0.683
Third group	θ_{i3}	0.353
	θ_{j3}	0.478

fact, we can only detect it in a few discrete video frames, and we need to restore it from being thrown to landing. The entire movement process requires a certain prior knowledge. As we all know, tennis is an oblique throwing motion, and its trajectory satisfies the quadratic parabolic equation, but we cannot know the third dimension of its height, but we know that tennis moves at a uniform speed in the horizontal direction; so, we need to find the tennis ball detecting the projected coordinate relationship between the coordinates and the real position on the horizontal plane, and then calculating, we can analyze the moving speed and direction of the tennis ball in the horizontal direction.

Knowing the occurrence time t_0 and location (x_0, y_0) of the first dashed ball, and the occurrence time t_1 and location (x_1, y_1) of the dashed ball in a later frame, the tennis ball can be calculated according to the following formula to get the horizontal plane the movement speed on the x-axis direction v_x and the y-axis direction movement speed v_y.

$$v_x = \frac{x_1 - x_0}{t_1 - t_0},$$
$$v_y = \frac{y_1 - y_0}{t_1 - t_0}, \tag{4}$$

According to the time stamp t, the horizontal movement distance is x_t, the vertical movement distance is y_t, and the horizontal plane movement trajectory is shown in the figure. The calculation result is as follows:

$$x_t = x_0 + v_x \times t,$$
$$y_t = y_0 + v_y \times t, \tag{5}$$

After obtaining x_t and y_t in this way, it is necessary to further determine the area of the tennis ball according to the real resolution of the tennis match video frame.

4. System Performance Evaluation

In order to verify the performance of the tennis match video semantic analysis system proposed in this article, experiments are carried out in the abovementioned data set and experimental environment introduced in this section, and the experimental results are analyzed and evaluated in terms of real-time and accuracy, and at the end, a comprehensive analysis of the influencing factors of the system is given in this section.

4.1. System Real-Time Analysis. From the perspective of system speed, the following content tests the real-time system performance under four conditions. The performance of the real-time system is affected by many factors, such as the game scene environment, the complexity of the server algorithm, the operating environment of the system, and the running time. In this experiment, we will test four tennis scenes separately to see if the control algorithm can achieve the system's processing frame rate (fps) in real time while maintaining the same operating time.

Perform comprehensive statistics on the test results of these 20 videos and draw a columnar line chart, as shown in Figure 1.

It can be seen from Figure 1 that although the speed of each operation is slightly different, the operating speed of the system is roughly maintained at a constant level. It shows that the running speed of the system is not affected by different game scenes and has universality in different scenes. The experimental results also prove that the system meets the real-time requirements.

4.2. System Accuracy Analysis. In testing the accuracy of the server-side algorithm of the test system, we conducted 6 sets of experiments. In each set of experiments, we randomly selected 1 video from each of the 4 game scenes in the database. In this experiment, 24 videos were shared, and the distribution in the control videos was even. Because the output result of the system includes the semantic part of the athlete's action discrimination, the accuracy test also needs to be carried out from this aspect.

Figure 2 shows the results of six sets of experiments used to distinguish action types in the system. You can see that the accuracy of system action recognition varies greatly between 50% and 100%, but it is not affected by scene changes. At the same time, experiments show that the system is less accurate in the crisis of swing sports. The reason is that in some video frames, the main point of the backrest and the point of the target player's arm to the camera are severely blocked, and the main point cannot be detected, which affects the judgment of the swing action.

4.3. Comprehensive Performance Index Evaluation. We further carried out a comparative experiment, adjusted the resolution of the video frame to different sizes under the same GPU environment, and evaluated the speed and intensive reading. The results are shown in Table 2.

According to the results in Table 2, in the same GPU server environment, the higher the image resolution, the higher the detection accuracy mAP, but the slower the processing speed, that is, the lower the frame rate.

5. Conclusions

The application of Internet of Things technology has greatly improved the management level and efficiency of sports events in my country. The application of IoT technology in sports management, event information management, and
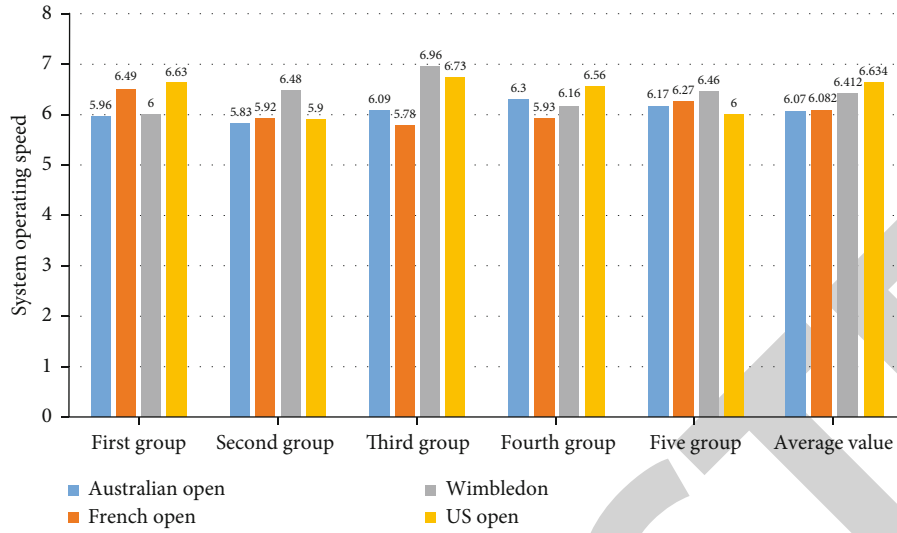
FIGURE 1: The operating speed of the system in four tennis scenarios.
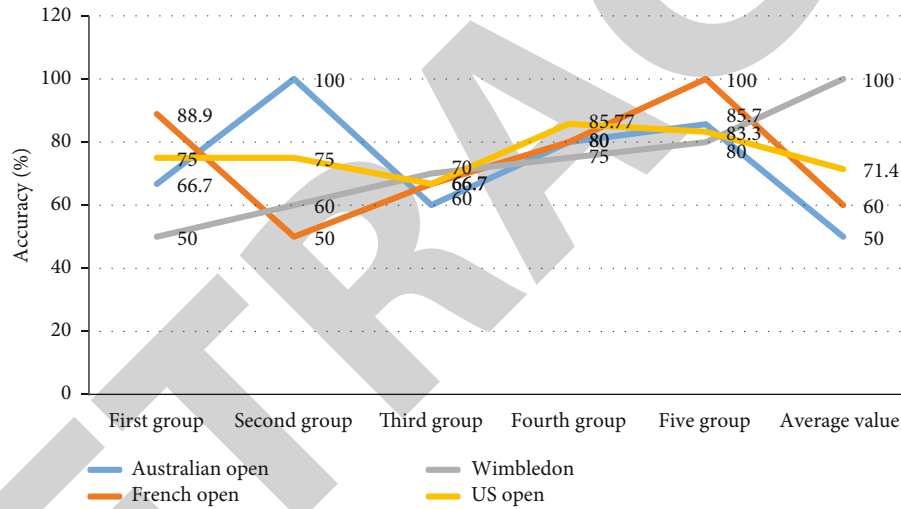
FIGURE 2: A statistical chart of the accuracy rate of the system for discriminating athletes' actions.

TABLE 2: The speed and accuracy test results of the YOLOv3 detection model at different image resolutions.

Lab environment	Image resolution	mAP	Frame rate
P100	640 × 360	85%	22 fps
P100	1280 × 720	88%	16 fps
P100	1920 × 1080	90%	13 fps

venue management has created digital management systems and organizations. It improves the management level of sports events, meets the needs of sports spectators, and provides athletes and coaches with more accurate information and data to achieve a higher level of stadium performance. The Internet of Things technology is a revolutionary change in the management of sports events in my country and is of great significance to the management and modernization of sports events in my country.

Data Availability

The data underlying the results presented in the study are available within the manuscript.

Conflicts of Interest

There is no potential conflict of interest in our paper, and all authors have seen the manuscript and approved to submit to your journal. We confirm that the content of the manuscript has not been published or submitted for publication elsewhere.

References

[1] S. Wan, L. Qi, X. Xu, C. Tong, and Z. Gu, "Deep learning models for real-time human activity recognition with smart-phones," *Mobile Networks and Applications*, vol. 1-13, 2019.

Research Article

Volleyball Data Analysis System and Method Based on Machine Learning

Xianyan Dai[1] and Shangbin Li [2]

[1]*School of Physical Education, Harbin University, Harbin 150086, China*
[2]*Physical Education Department, Harbin Engineering University, Harbin 150001, China*

Correspondence should be addressed to Shangbin Li; sports@hrbeu.edu.cn

After the reform and the opening up, the economy of my country has grown rapidly and people's lives have become better and better. As a result, there is a lot of time to pay attention to their health, which has promoted the rapid development of my country's sports industry. Since the 2008 Beijing Olympics, the successful hosting of the Beijing Olympics has been further strengthened. With the rise of the development of sports in our country, the use of machine learning in a large amount of information can process this data and analyze it well. Based on this, this article is aimed at making volleyball players and coaches better understand the technical structure of hiking and the technique of hiking. The paper understands the characteristics of muscle activity over time and uses machine learning methods to analyze a large number of volleyball sports data. In this experiment, 12 volleyball players from a college of physical education were selected. According to the actual situation of the students' physical fitness and skills, it is more reasonable to divide them into two arms with preswing technology (A type) group and two-arms without preswing technology (B type) group. Mainly study the volleyball spiking action, select the representative front-row 4th position strong attack and the back-row 6th position for comparison and analysis, and analyze the process from the take-off stage to the aerial shot stage in the four stages of the smash through the kinematics, dynamics, and surface electromyography parameters. Experiments have shown that for type A, the left gluteus maximus integral EMG sum value is significantly different between the front and rear rows ($P < 0.05$). The discharge volume of the left gluteus maximus during the front-row spiking process is greater than that of the back-row spiking. This difference is mainly reflected in the kicking stage and the air attack stage. It shows that volleyball data analysis has a very broad prospect of exploration and application, which can create huge social and economic benefits. How to analyze kinematics is also a very demanding research project and is also part of the future analysis of sports data. Academic value and broad practical significance are important.

1. Introduction

In a large amount of text and image information, if manual methods are used to extract useful information for volley data analysis, the enormous workload and slow speed are undoubtedly unrealistic. If you can use the excellent performance of the computer to complete the task, it is definitely the most effective solution; then, you can use machine learning to analyze volleyball data and use it in sports and other directions [1]. Regardless of the aspect, the key to volleyball data analysis is kinematics analysis and industrial analysis.

At present, the most mature industrial analysis is the complete analysis of surface electromyography.

With the application of the scoring method for each ball, the volleyball game is more intense than the previous game, the pace is faster, and the projection is stronger, more exciting, and exciting, attracting a large number of loyal fans. As the intensity of the competition increases, the requirements for the physical fitness, skills, and tactics of volleyball players are getting higher and higher. In a volleyball game, both sides of the game engage in fierce offensive and defensive confrontations on the Internet. Because the direction of the ball is

| Approach stage | Take-off phase | Smash phase | Landing stage |
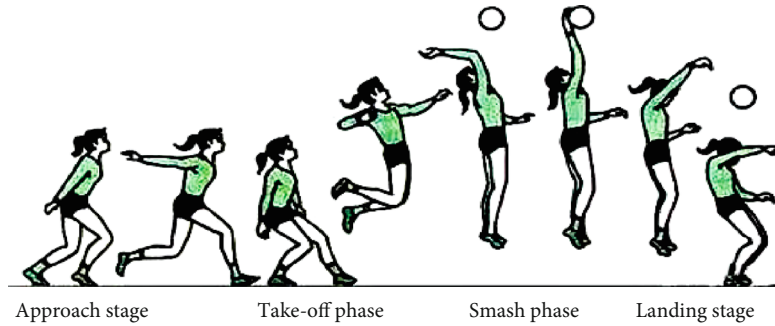
Figure 1: A series of action diagrams of volleyball spiking.

uncertain, volleyball players have different movement skills in the game. In volleyball games, smashing is the most ornamental and interesting technique.

Machine learning is playing an increasingly important role in data analysis [2]. There have been many cases of applying machine learning to solve practical problems at home and abroad. Zhao et al. pointed out that the rapid development of DNA microarray technology provides a wide range of data sources, which is expected to pave the way for better prediction and diagnosis of cancer and the determination of key targets for drug development. DNA microarray data analysis has been carried out using statistical analysis as well as machine learning and data mining methods. He conducted a comprehensive review of the machine learning methods that have been used on the acute lymphoblastic leukemia chip data. Following research conducted by the Leukemia Research Group in Child Biology and Medicine, machine learning has been used to enhance the diagnosis and subtype classification of cancer, develop new treatments, and accurately identify the risk stratification of patients. These methods have been used in the four main areas of microarray data analysis: gene selection, clustering, classification, and pathway analysis. However, their research did not explain the advantages and disadvantages of each machine learning algorithm [3]. Charlton et al. proposed that the support vector machine classification algorithm is the latest development in the machine learning community, proving its potential in structure-activity relationship analysis. In the benchmark test, the support vector machine was compared with several machine learning techniques currently used in the field. The classification task involves using data obtained from the UCI machine learning repository to predict the inhibitory effect of pyrimidine on dihydrofolate reductase. The performance of support vector machine is better than three artificial neural networks, radial basis function network, and C5.0 decision tree. SVM is significantly better than all of these. There is only a neural network controlled by artificial capacity, and the training time is much longer. However, the experimental results lack more data support so that the machine learning mechanism can predict pyrimidine pair two; the inhibitory effect of hydrofolate reductase remains doubtful [4]. Astuti continues to expand the current Internet by providing connectivity and interaction between the physical world and the network world. In addition to increasing capacity, the IoT also produces big data with speed characteristics, which depend on time and

location and have a variety of standards and different data quality [5]. Intelligent big data processing and analysis is the key to developing intelligent IoT applications. This article uses smart cities as the main use case for evaluating various machine learning methods to address the data challenges of the Internet of Things. However, his research does not clearly raise the issue of how to evaluate different machine learning methods and the overall research lacks data support [6].

This article uses a combination of kinematics analysis and biomechanical analysis to analyze volleyball data from kinematics, dynamics, and electromyography. This article is aimed at giving volleyball players and coaches a more in-depth understanding of the technical structure of some movements in volleyball and the activity characteristics of related muscles when doing these movements. At the same time, to provide more targeted guidance data for athletes in physical training and technical training. Select volleyball before and after the row of spikes to conduct a series of comprehensive analysis, from the perspective of biomechanics, preliminary discussion of some more in-depth action description.

2. Application of Machine Learning in Volleyball Data Analysis System

2.1. Technical Structure of Volleyball Spike in Volleyball. The purpose of the approach is to bring the athlete closer to the ball in the horizontal dimension, to choose a suitable take-off position, and to play a role in increasing the height of the jump. The purpose of the jump is to bring the athlete closer to the ball in the spatial dimension, and the ultimate goal is to get a proper spiking position. The two parts of the approach and the jump are related to each other, effectively making the athlete closer to the ball [7, 8]. In a volleyball game, the athlete's posture directly affects the spiker's speed, making full use of both run-up and take-off sections to prepare for a quick shot. After completing the spike, the athlete falls from the air. The athlete must have good landing skills without being injured. Good landing skills can reduce the impact on the knee and ankle joints. Figure 1 shows a series of action diagrams of volleyball spiking in volleyball.

2.2. Machine Learning-Related Algorithms. Machine learning solves the problem of how to construct a learning algorithm so that it can automatically improve with the acquisition of experience or information and perform tasks such as
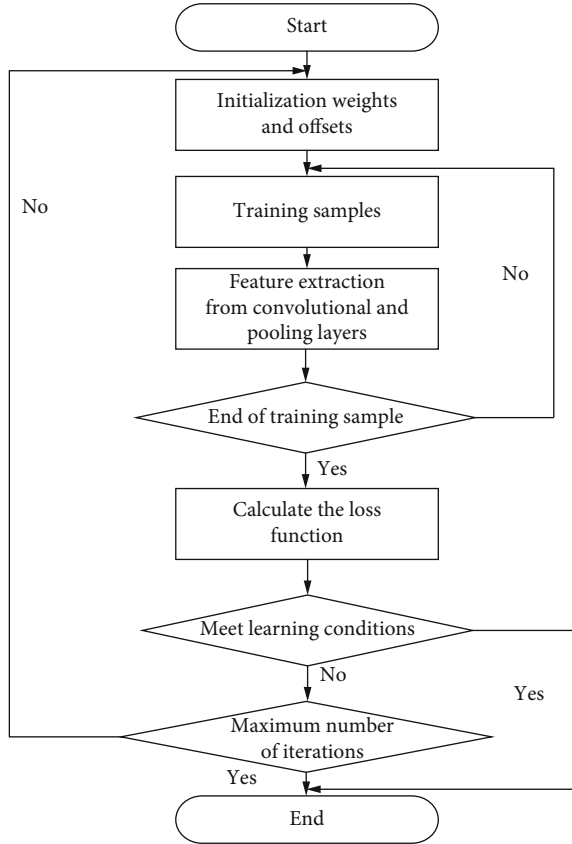
FIGURE 2: Machine learning flowchart.

acquiring knowledge, making predictions, making decisions, or building models based on given input data [9, 10]. Data can be viewed as a collection of information containing the relationships between related variables. The complete set of all possible patterns may be too large to be covered by the information in the training data. Therefore, the difficulty of machine learning lies in how to get a good generalization from the observed data set in order to be able to generate useful models for new data [11, 12]. Many machine learning algorithms have been successfully applied to a wide range of scientific and engineering problems. In typical scenarios, the output results of machine learning algorithms can be quantitative results [13].

Figure 2 is a flowchart of machine learning. In supervised learning, variables are divided into two groups: explanatory variables and dependent variables. The goal of supervised learning is to determine the relationship between the explanatory variable (input) and the dependent variable (output) and generate a function that maps the input to the output [14, 15]. Some supervised algorithms can be used for classification and prediction tasks. In these cases, the paired labeled training samples are represented as follows:

$$\{(x_i, y_i), i = 1, 2, \cdots, n\}, \tag{1}$$

Among them, x_i is the input and y_i is the output. Supervised learning needs to learn a prediction function f that maps from x_i to y_i and compare $f(x_i)$ and y_i to cal-

culate the error rate of the prediction function [16, 17]. Two types of machine learning methods are introduced below, matrix factorization algorithms and subspace segmentation algorithms.

(1) Matrix factorization algorithm

Matrix factorization has been successfully applied in many fields, and there are many kinds of decomposition methods. For any matrix $A \in R^{m \times n}$, there is

$$A = UDV^T. \tag{2}$$

Among them, $D = \mathrm{diag}\,(\sigma_1, \sigma_2, \cdots, \sigma_r), \sigma_i > 0 (i = 1, 2, \cdots, r)$ is the singularity of matrix A, and $r = \mathrm{rank}\,(A)$ is the rank of matrix A. For the data matrix $A \in R^{m \times n}$, including n samples and m features, the total covariance matrix of the samples is as follows:

$$S = \frac{1}{n}\sum_{i=1}^{n}(x_i - \bar{x})(x_i - \bar{x})^T. \tag{3}$$

The purpose of the principal component analysis algorithm is to maximize the covariance after projection, and its objective function can be expressed as follows:

$$\max_{W} W^T S W \quad s.t.\, W^T W = I. \tag{4}$$

Among them, the constraint condition $W^T W = I$ is used to prevent the covariance from increasing indefinitely. Assuming that the rank of S is r, there is

$$S = rW. \tag{5}$$

Given that $\lambda_1, \lambda_2, \cdots, \lambda_d$ is the first a largest eigenvalues of Equation (5), its eigenvector is $W_1, W_2, \cdots, W_d$. Therefore, the low-dimensional space feature Z for any data X can be expressed as follows:

$$Z = (W_1, W_2, \cdots, W_d)^T X = W^T X. \tag{6}$$

(2) Subspace segmentation algorithm

Realistic data can be viewed as approximate samples drawn from multiple mixed low-dimensional subspaces [18, 19]. Given a data matrix $A \in R^{m \times n}$, including n samples and m features, its objective function can be expressed as follows:

$$\min_{A,E} \mathrm{rank}\,(A) + \lambda\|E\|_0 \quad s.t.\, X = A + E. \tag{7}$$

Among them, $B\lambda > 0$ is an adjustable parameter. The above formula can be optimized by using kernel norm or $L1$ norm, namely,

$$\min_{A,E} \|A\|_* + \lambda\|E\|_1 \quad s.t.\, X = A + E. \tag{8}$$
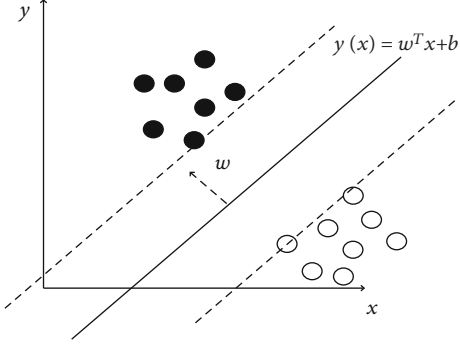
FIGURE 3: Support vector machines.

Among them, $\|A\|_* = \sum_i \sigma_i(A)$ is the kernel norm of matrix A, and $\|E\|_1 = \sum_{ij} |E_{ij}|$ is the $L1$ norm of matrix E. Assuming that the data is noise-free, the subspace clustering method can express the data matrix X as a dictionary D multiplied by the low-rank representation matrix A through dictionary learning; then, the objective function of the subspace clustering method can be expressed as [20, 21] follows:

$$\min_A \text{rank}(A) \quad s.t. X = DA, \tag{9}$$

where rank (A) is the rank of A. Equation (9) can use the kernel norm to constrain A to get

$$\min_A \|A\|_* \quad s.t. X = DA. \tag{10}$$

There is a lot of noise in the real data set, so the subspace clustering method can be extended to a robust form.

$$\min_{A,E} \|A\|_* + \lambda \|E\|_{2,1} \quad s.t. X = DA + E. \tag{11}$$

Among them, $\lambda > 0$ is a balance parameter, and $\|E\|_{2,1} = \sum_{j=1}^n \sqrt{\sum_{i=1}^m E_{ij}^2}$ is the $L2, 1$ norm of E.

(1) Support vector machines

This is the perfect one among the countless straight lines that can be classified, because it is exactly in the middle of the two classes and is the same distance from the points of the two classes. The so-called support vector is the point with the closest vertical distance to the dividing line [22, 23], as shown in Figure 3.

Regarding this line, it is at the same distance from both sides. The distance from any point x_0 to the line is

$$\frac{1}{\|w\|} \left(w^T x_0 + b \right). \tag{12}$$

Then, normalize it so that the linearly separable training set (x_i, y_i), $I = 1, 2, \cdots, n$, $x \in R^m$ satisfies the following formula:

$$y_i \left(w^T x_i + b \right) - 1 \geq 0, \cdots, n. \tag{13}$$

At this time, the distance between the dividing line and the two sides is equal to $2/\|w^2\|$. The ultimate goal is to maximize the distance between the dividing line and the two sides, which is equivalent to minimizing $\|w^2\|$. At this time, the classification surface is the optimal classification surface [24, 25]. For the information (x_i, y_i) of N training points, it can also be written as shown in Equation (14).

$$\arg \max \left\{ \frac{1}{\|w^2\|} \min_n \left[y_i \left(w^T x_i + b \right) \right] \right\}. \tag{14}$$

Although the objective function is clearly expressed but difficult to calculate, a series of mathematical operations such as the Lagrangian multiplier method are used here to finally obtain the objective function [26].

$$\max_{\text{all} a_n} L(a) = \sum_{n=1}^N a_n - \frac{1}{2} \sum_{n=1}^N \sum_{m=1}^N a_n a_m y_n y_m x_n^T x_m. \tag{15}$$

The constraints are $a_n \geq 0, \forall n, \sum_{n=1}^N a_n y_n = 0$.

Ideally, all classifications should be straight lines, but in actual situations, it may be curves, planes, curved surfaces, or higher-dimensional surfaces [27, 28]. The input of the radial basis kernel function is a vector, and finally, a scalar is obtained according to the input based on the vector distance operation. The specific formula is shown in Equation (16).

$$k(x, y) = \exp \left[\frac{-\|x - y\|^2}{2\sigma^2} \right]. \tag{16}$$

Here is the Gaussian version of the radial basis kernel function. The σ in the formula is the speed parameter whose function value is reduced to 0. The kernel function maps the input data to an infinite dimensional space. The radial basis kernel function is very dependent on the parameters, and the training is very time-consuming [29, 30].

3. Experimental Design of Volleyball Data Analysis System

3.1. Test Subject. Here, we select 12 volleyball players from a physical education college. According to the students' real circumstances, such as physical abilities and skills, they are logically divided into type A and type B groups, with 6 people in each group. These 12 individuals did not suffer serious sports injuries before and after the experiment, and their basic physical condition was essentially the same at the beginning of the experiment. The basic conditions of the subjects are shown in Table 1. All subjects had no history of injury or smoking. Before the test, the subjects have explained the whole test process and precautions in detail and agreed to participate in this study voluntarily. This experiment mainly studies the volleyball spiking action. This experiment selects representative front-row four-position strong attack and back-row six-position strong attack for comparison and analysis. The research mainly analyzes the

TABLE 1: General information of the two groups of patients.

Group	Number of cases		Years	Average weight	Average height
	Male	Female			
Both arms have preswing technology (A type) group	3	3	19.27 ± 1.33	74.6 ± 9.3	182.4 ± 4.7
Double arms without preswing technology (B type) group	3	3	19.98 ± 1.09	75.7 ± 9.9	183.1 ± 5.2
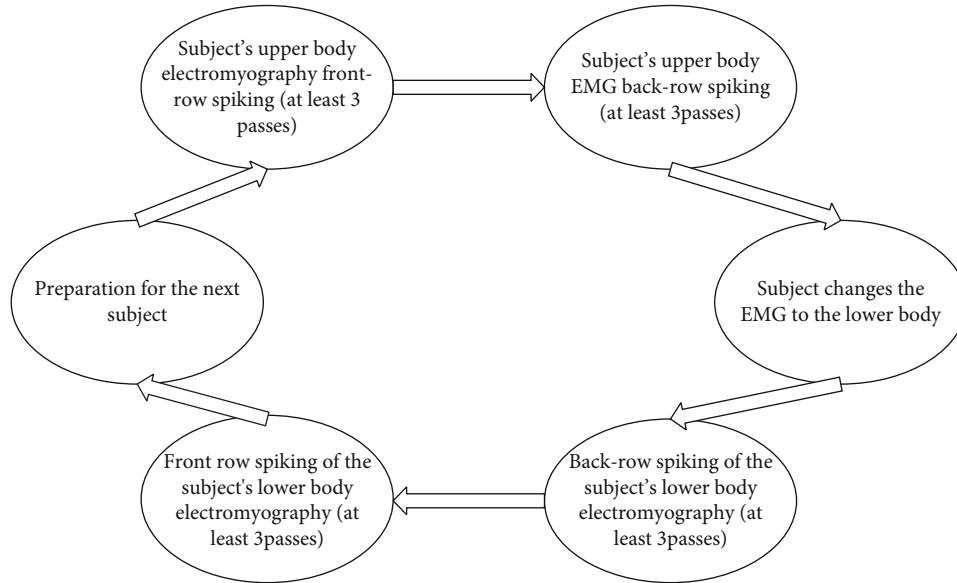
FIGURE 4: Experimental flowchart.

four stages of smashing in the take-off phase to the air. The hitting stage mainly includes kinematics, dynamics, and surface electromyography parameters.

3.2. Testing Process. This experiment was performed indoors, and the experiment was completed in one day. The test equipment is arranged according to the layout of the test site of the experimental design, and the test officially begins after the debugging is completed. The experiment requires people to be naked in the upper body and to wear tight shorts in the lower body. This is done to facilitate the bonding of the electrode sheets during the electromyography test and the analysis of the 3D image after the experiment. Under the responsibility of a dedicated experimenter, in accordance with the EMG test plan, help the subject to paste the electrode sheet, wire it, and fix it with a bandage. After completion, remind the subject whether the subject is uncomfortable due to too tight bandage or whether it affects normal limb activity amplitude, and when everything is normal, let the subject try to smash the ball in the test field and become familiar with the action. When the subject takes off, both feet must land on a platform composed of four force plates, and the shot does not fall off the net or out of bounds; then, the action is considered a qualified action. A volleyball expert was specially invited to evaluate the pros and cons of each subject's 3 qualified smashes. The quality of the 3 qualified smashes was recorded as excellent, medium, and poor. This study selects the best movement for analysis. Finally, put away the instrument and check for damage or omissions,

clean the experimental site, and copy out the measured data, and the experimental process is shown in Figure 4.

3.3. Test Site. The experimental site layout is shown in Figure 4. In the picture, you can see that the 4 force plates in the center of the site are laid flat in the trough, which are fixed and cannot be moved, so other instruments and equipment need to be arranged with the force plate as the center. The direction the subject faces is the positive direction, which is the direction of the spike and approach. We will explain from the subject's left, right, front, and back. The subject's left is the force plate and the EMG operation area, as well as a fill light. The light is aimed at the force plate; the subject's right is the three-dimensional high-speed camera operation area, two high-speed cameras are located at the back right and front right when the subject is spiking, the main optical axis of the two machines are connected the angle is about 90°, and there are one fill light in front and one back in the vicinity of the force plate. The light is directed at the force plate. The position of the fill light is adjusted so that it will not block the high-speed camera shooting; There is a volleyball net directly in the front, which can be moved to facilitate the adjustment of the distance between the front and rear smashes; the subject is empty, which is convenient for the subject to choose a suitable distance for the smash approach. Since the domestic high-speed camera cannot be synchronized with the force plate and the EMG, this experiment only uses the force plate and the
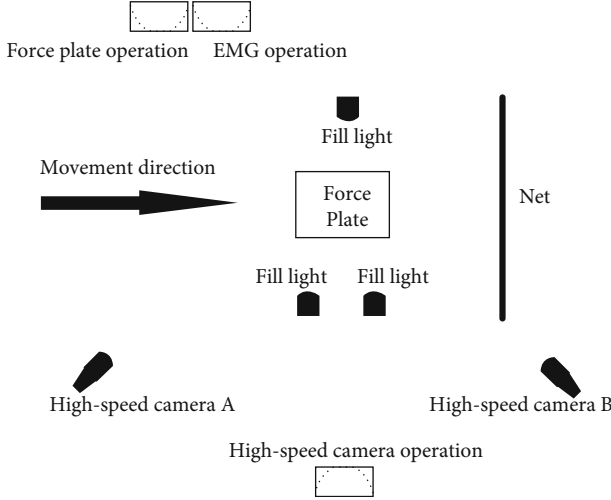
Figure 5: Schematic diagram of experimental site layout.

Table 2: The angle of the lower limbs at the maximum buffer moment in the take-off phase.

Parameter	Type A front row	Type A rear row	P	Type B front row	Type B rear row
Right hip	129.06	125.76	0.39	117.37	109.42
Left hip	117.22	116.16	0.81	117.49	106.95
Right knee	106.96	106.47	0.93	83.30	73.49
Left knee	122.12	127.87	0.15	117.10	110.78
Right ankle	59.49	62.03	0.38	51.36	41.77
Left ankle	88.73	91.36	0.46	86.36	80.66

EMG to synchronize, and the two sets of instruments are synchronized through the synchronization device, and the force plate triggers the synchronization signal for synchronous measurement. The two high-speed cameras were tested synchronously by artificial arm movements. After the standby device is connected and warmed up, the subject is placed in the test area to simulate the test process, during which the camera angle is adjusted to ensure that the subject is within the test range, and the images from the take-off stage to the air shot stage can be completely recorded. And finally, carry out the three-dimensional frame calibration and wait for the formal entry into the test process. The layout of the experimental site is shown in Figure 5.

3.4. Statistical Processing. Kinematics data processing: export high-speed video, use video synthesis software to synchronize the video of the two machines [31], edit the synchronized synthesis video from the take-off stage to the air shot stage, analyze the synthesized video with video analysis software, and export the TSV files. Then, use the QTOOLS software and EXCEL office software to calculate and process the exported raw data to obtain parameters such as time, joint angle, link speed, and displacement.

Kinetic data processing: use the Kistler software to screen and export the test results, use the EXCEL software for calculation and statistical processing, and obtain parameter indexes such as force value, impulse, and power.

EMG data processing: the test results are processed with the Mega software, and the ASCCI file of each muscle integrated EMG is exported, and then, the EXCEL software is used for calculation and statistical processing, and the integrated EMG sum value, contribution rate, and other parameter indexes are obtained.

4. Experimental Volleyball Data Analysis System

4.1. Kinematics Results and Analysis

(1) Results and analysis of the take-off phase

First, perform a kinematics analysis on the take-off phase. Table 2 shows the joint angle of the lower limbs at the maximum buffer time in the take-off phase.

It can be seen from Table 2 that whether it is type A or type B, they have the same law at the moment of maximum take-off buffer for the front and rear spiking: there is no significant difference between the left and right side related angles, but the right hip angle > left hip angle, right knee angle < left knee angle, and right ankle angle < left ankle angle, which means that the right leg has a large degree of cushioning, and the right leg plays a major role in the cushioning process. The paired-sample t-test is used to obtain type A left and right hip angles and left and right knees; there was no significant difference between the angle and the left and right ankle angles ($P > 0.05$); for type B, the angle of the right joint was mainly seen. The hip, knee, and ankle angles of the front-row spiking were all greater than the hip, knee, and ankle angles of the back-row spiking. In other words, the degree of flexion of the lower limb joints in the back row is greater than that of the front-row spiking. Regardless of whether it is a front-row smash or a back-row smash, the corresponding joint angles of type B and type A are as follows: type B < type A, indicating that type B has a larger cushioning range. As mentioned earlier, the buffering time of type B technology is much longer than that of type A technology. This shows that type B technology has sufficient time for buffering. Since there is no double-arm preswing coordination, the buffering process is completely dependent on the lower limbs, so the lower limb joints must have more sufficient flexion can store enough energy to prepare for stretching.

(2) Results and analysis of the air shot stage

Kinematics analysis is carried out on the flying shot stage. The relevant indexes of the center of gravity at the moment of take-off include the angle of the center of gravity at the moment of take-off, the vertical speed of the center of gravity, the horizontal speed, and the speed of the center of gravity. The results are shown in Table 3.

It can be seen from Table 3 that from the comparison of the front and back spikes, the type A technique is obtained through the paired-sample t-test. At the moment of take-off, the center of gravity rise angle, the center of gravity horizontal speed, and the center of gravity closing speed are all

TABLE 3: Center of gravity-related indicators at take-off time.

Parameter	Type A front row	Type A rear row	P	Type B front row	Type B rear row
Center of gravity (°)	66.67	53.39	0.03	65.71	67.32
Vertical speed of center of gravity (m/s)	3.15	3.17	0.76	3.19	3.33
Horizontal speed (m/s)	1.52	2.55	0.03	1.37	1.39
Center of gravity speed (m/s)	3.13	3.35	0.02	3.66	3.59
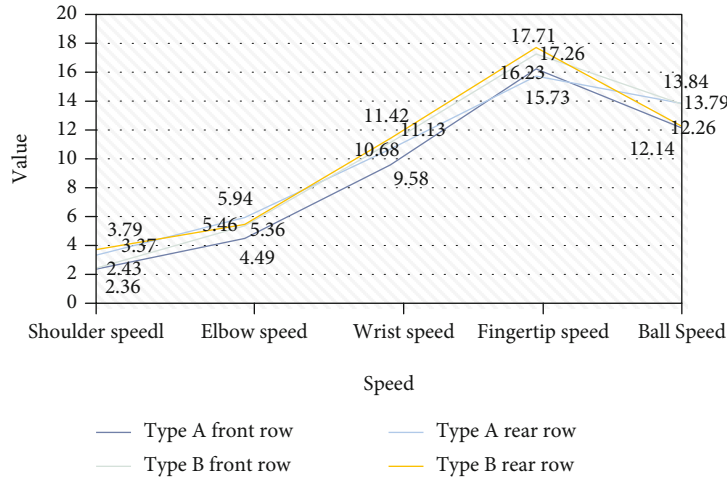
FIGURE 6: Speed of each link at the moment of hitting, ball speed.

significantly different ($P < 0.05$), and there is no difference in the vertical speed of the center of gravity ($P > 0.05$). At the center of gravity, the angle of type A front-row smash is about 67 degrees, which is much larger than the back row of 53 degrees. It can be seen that the front-row smashes jump upwards, and the back-row smashes jump forwards. Yes, this can also be seen from the horizontal speed of the center of gravity. The front row is about 1.52 m/s less than the back row 2.55 m/s. The high horizontal speed indicates that the approach speed is high. This shows that in the game, when the front-row smash is closer to the net, in order to avoid touching the net, the smasher will control the approach speed, jump up as much as possible when jumping, strive to get the height in front of the net, and have more options for smashing. Spikes are more threatening.

(3) Results and analysis at the moment of hitting

The quality of the shot determines the success or failure of the attack. Regarding the shot, leaving aside various additional factors on the field, the most important indicator in this technique is speed. The results are shown in Figure 6.

It can be seen from Figure 6 that from the comparison of front and rear smashes, for type A, through the paired sample t-test, there is a significant new difference in shoulder speed between the back smash and the front smash ($P < 0.05$). There is no difference in elbow speed, wrist speed, fingertip speed, and ball speed. The shoulder speed at the moment of impact can represent the speed of the trunk movement. The back row (3.60 m/s) is greater than the front row (2.48 m/s).

For type B, the shoulder speed of the back row is also significantly greater than the front row. From the technical type according to the above comparative analysis, there is no difference between the two types A and B in the front and rear index correspondence, but the difference is in the back-row spiking speed. The type A back-row spiking speed is higher than the type B back-row spiking speed, which may be the center of gravity.

4.2. Kinetic Results and Analysis

(1) Comparative analysis of force-related parameters

The force value statistics of the take-off link include the vertical force value and the horizontal plane force value. The results are shown in Table 4.

It can be seen from Table 4 that for type A technology, there is no significant difference between the absolute force peak and the relative force peak in the front and rear spiking force peaks ($P > 0.05$), but the rear spiking peak thrust force is greater than the tendency of front-row spiking. For the type B technique, there is little difference in the peak extension force of the front and rear spikes, and the back row is larger than the front row. Looking at the comparison between A and B, whether it is the relative value or absolute value of the front-row smash or the relative value or absolute value of the back-row smash, the type B is smaller than the type A. The reason for this result is the type A take-off the swing of the arms in the stage greatly increases the reaction force of the ground against the human body.

TABLE 4: The angle of the lower limbs at the maximum buffer moment in the take-off phase.

Parameter	Type A front row	Type A rear row	P	Type B front row	Type B rear row
Fz absolute force peak (N)	3529.08	3626.44	0.26	2623.39	2969.56
Fz peak normalized force (N/BW)	3.27	4.27	0.26	2.87	3.22
Fxy absolute force peak (N)	1281.15	1371.20	0.87	628.51	485.64
Fxy peak normalized force(N/BW)	1.32	1.21	0.74	0.74	0.66
Fz absolute value (N)	1609.18	1688.94	0.31	1174.88	1598.49
Fz normalized value (N/BW)	2.66	1.18	0.33	1.26	1.79
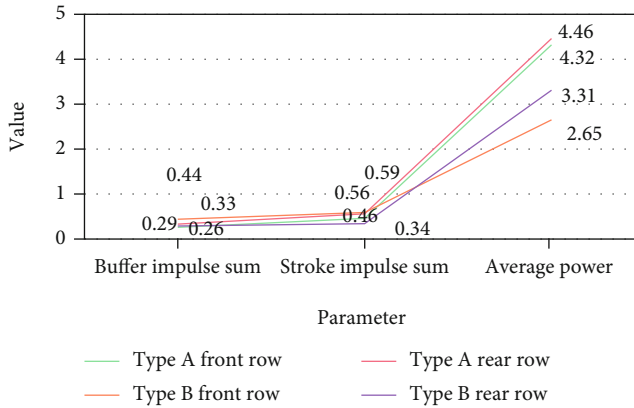
FIGURE 7: Standardized impulse and pedaling power statistics table.

(2) Result analysis of impulse and pedaling power

Combining the characteristics of the volleyball spiking technique, three indicators of buffer impulse sum, thrust impulse sum, and thrust average power are selected for analysis, and the results are shown in Figure 7.

It can be seen from Figure 7 that for the type A technique, there is a significant difference between the buffer impulse during the take-off phase and the front and rear smashes ($P < 0.05$). The back-row smash and the front-row smash have sufficient buffer brakings during the take-off, so as to control the forward speed of the body, and at the same time, the lower limb muscles stretch and store energy and finally complete the upward jump. The time is short, so the buffer is not sufficient and the braking is not obvious. This can reduce the loss of approach horizontal speed and momentum, so that it can jump forward during the take-off and maintain a large horizontal speed.

4.3. EMG Results and Analysis

(1) Integral EMG and results and analysis

Figure 8 shows the integrated EMG and value of each muscle during the whole action stage from jumping to flying.

It can be seen from Figure 8 that for type A, the left gluteus maximus integral EMG sum value is significantly different between the front and rear rows ($P < 0.05$), and the discharge of the left gluteus maximus during the front-row spiking is greater than the back-row spiking. This difference

is mainly reflected in the kick-stroke stage and the air-strike stage, the right rectus abdominis integrated EMG and the value of the front and rear rows are significantly different ($P < 0.05$), and the right rectus abdominis discharge during the back-row spiking process is significantly larger than the front-row smash; this shows that the right rectus abdominis has a more obvious role in the back-row smash during this process, which is determined by the characteristics of the type A technique between the front and rear smashes. On the whole, the discharge of the upper and lower limbs and trunk muscles during the front and rear smashes of type A technique is relatively balanced, the difference between the front and rear smash is not big, and the discharge of the left and right limbs is also relatively balanced. Compared with type A and type B, as a whole, type B technology has a larger discharge volume of the muscles of the front-row and back-row spiking than type A technology; type B technology is inferior to type A in the balance of overall muscle discharge technology; type B technology has a clearer primary and secondary role of each muscle, while type A reflects a clear balance.

(2) Contribution rate of myoelectric activity during the flight shot stage

The contribution rate of each muscle's integrated EMG activity during the flight shot stage is shown in Figure 9.

It can be seen from Figure 9 that in the comparison of the front and rear spiking, there is a significant difference between the left gluteus maximus and the right rectus abdominis ($P < 0.05$), and there is no significant difference in other muscles. From the perspective of the right gluteus maximus, at this stage, the contribution rate of the left and right gluteus maximus is relatively balanced when the front row smashes. When the front row smashes into the air, the body back arch is greatly twisted, and the back row smashes the body back arch. The degree of torsion is comparable; for the right rectus abdominis, the back-row spiking is significantly greater than the front-row spiking, which means that the muscle has a greater role in the back-row spiking than the front-row spiking during the front bow of the spiking. On the whole, the contribution rate of the upper limbs and trunk muscles is greater than that of the lower limbs. They dominate, and the lower limbs are inferior. But this does not mean that the lower limbs are not important. In the process of flying shots, the back bow of the trunk is clockwise. Twisting and smashing the back
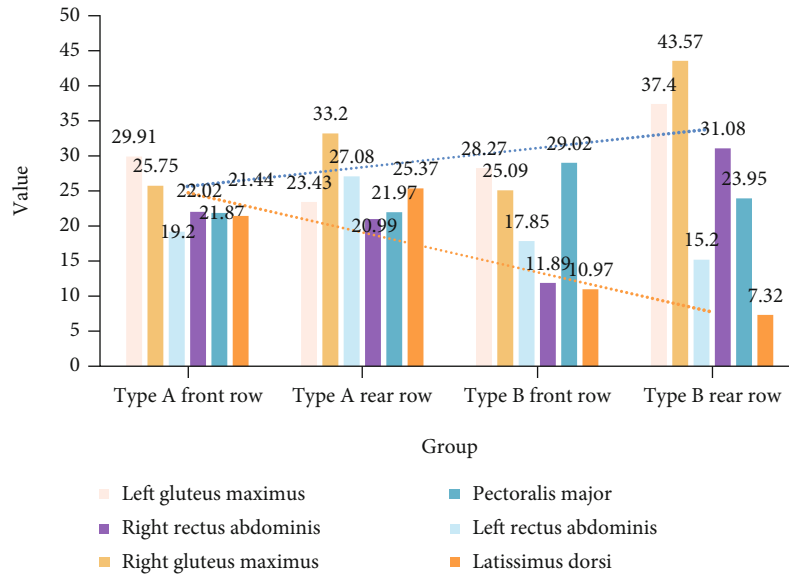
FIGURE 8: Comparison of standardized integrated EMG and value of each muscle in the whole stage of the ball.
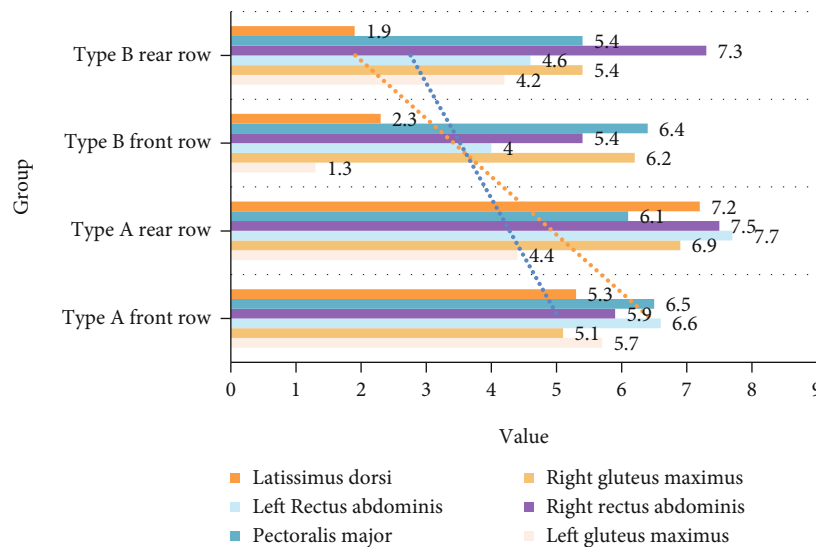
FIGURE 9: Comparison of the contribution rate of each muscle in the front and back row of spikes.

swing of the spiking arm to the front bow of the torso counterclockwise twisting the spiking arm whipping action to hit the ball are inseparable from the force of the lower limb muscles to drive the active coordination of each link of the movement.

5. Conclusions

The vertical force curves of spiking and jumping for the front and rear players are all single-peak curves. The peak force appears at a certain moment in the stretch phase, and the curve appears like a platform curve in the buffer phase. Through comparative analysis, this article finds that type B athletes must have strong muscle power, lower limbs, and good waist and abdomen strength. However, type B has

shortcomings and cannot perfectly combine technology with physical fitness. Therefore, this article recommends type B athletes to improve their skills. Transition to type A, so combined with its own conditions, in the future competitions can release their potential and maximize energy. This article comprehensively analyzes and compares the two types of techniques from the three aspects of kinematics, dynamics, and electromyography: the characteristics of front and rear spikes summarize some rules and find out some differences. However, these rules and these differences are all established in the group, and due to the large individual differences in the technique of spiking, this article suggests that in training, we still need to carry out targeted exercises according to different athletes to improve technical ability and special strength.

Data Availability

No data were used to support this study.

Conflicts of Interest

The authors declare that they have no conflicts of interest.

Acknowledgments

References

[1] Z. Lv, Q. Liang, and A. K. Singh, "Advanced machine learning on cognitive computing for human behavior analysis," *IEEE Transactions on Computational Social Systems*, 2020.

[2] G. Dartmann, H. Song, and A. Schmeink, *Big Data Analytics for Cyber-Physical Systems: Machine Learning for the Internet of Things*, Elsevier, Germany, 2019.

[3] K. Zhao, W. Jiang, X. Jin, and X. Xiao, "Artificial intelligence system based on the layout effect of both sides in volleyball matches," *Journal of Intelligent & Fuzzy Systems*, vol. 40, no. 2, pp. 3075–3084, 2021.

[4] P. C. Charlton, C. Kenneally-Dabrowski, J. Sheppard, and W. Spratford, "A simple method for quantifying jump loads in volleyball athletes," *Journal of Science and Medicine in Sport*, vol. 20, no. 3, pp. 241–245, 2017.

[5] Z. Lv, Y. Han, A. K. Singh, G. Manogaran, and H. Lv, "Trustworthiness in industrial IoT systems based on artificial intelligence," *IEEE Transactions on Industrial Informatics*, vol. 17, 2021.

[6] Y. Astuti, "The effect of circuit training methods, circuit series and learning motivation on students' volleyball basic skill," *Journal of Education Research and Evaluation*, vol. 2, no. 3, pp. 120–131, 2019.

[7] G. D. C. T. Costa, M. P. Maia, J. Capuzzo et al., "Offensive structuring in men's high-level volleyball: analysis of: the attack zone," *Brazilian Journal of Kinanthropometry and Human Performance*, vol. 18, no. 5, pp. 611–619, 2016.

[8] J. Haiyan and F. Jianqiang, "Application of data mining in technical and tactical analysis of volleyball match," *Boletin Tecnico/Technical Bulletin*, vol. 55, no. 20, pp. 327–332, 2017.

[9] Z. Wang, "D. Chen. An optimized data mining algorithm application in volleyball match technique and competition tactics analysis," *Boletin Tecnico/Technical Bulletin*, vol. 55, no. 17, pp. 782–787, 2017.

[10] Y. Chen, W. Zheng, W. Li, and Y. Huang, "Large group activity security risk assessment and risk early warning based on random forest algorithm," *Pattern Recognition Letters*, vol. 144, pp. 1–5, 2021.

[11] M. Conejero, F. Claver, J. González-Silva, C. Fernández-Echeverría, and P. Moreno, "Analysis of performance in game actions in volleyball, according to the classification," *Revista Portuguesa de Ciências do Desporto*, vol. 2017, no. S1A, pp. 196–204, 2017.

[12] X. Cheng, Y. Liu, and T. Ikenaga, "3D global and multi-view local features combination based qualitative action recognition for volleyball game analysis," *IEICE Transactions on Fundamentals of Electronics, Communications and Computer Sciences*, vol. E102.A, no. 12, pp. 1891–1899, 2019.

[13] Z. Lv, L. Qiao, D. Chen, R. Lou, J. Li, and Y. Li, "Machine learning for proactive defense for critical infrastructure systems," *IEEE Communications Magazine*, vol. 6, no. 1, 2020.

[14] M. C. Lopes, R. T. Magalhães, L. B. F. Diniz, J. P. A. Moreira, and M. R. Albuquerque, "RT Magalhães, Diniz L, et al. The influence of technical skills on decision making of novice volleyball players," *Revista Brasileira de Cineantropometria e Desempenho Humano*, vol. 18, no. 3, pp. 362–370, 2016.

[15] S. Sugemi, "Upaya Meningkatkan Teknik Dasar Pasing Atas Bola Voli Mini melalui Bantuan Tutor Sebaya Siswa kelas IV SD Negeri Balongwono Kecamatan Trowulan Kabupaten Mojokerto Tahun 2018/2019," *Progressa Journal of Islamic Religious Instruction*, vol. 4, no. 1, pp. 93–108, 2020.

[16] K. Treethong, C. Chatpunyakul, and T. Gulthawatvichai, "Effects of social interaction and transformational leadership on sport event volunteers' perception of team member exchange," *Test Engineering and Management*, vol. 2021, no. 83, pp. 30348–30356, 2020.

[17] S. Wenninger, D. Link, and M. Lames, "Performance of machine learning models in application to beach volleyball data," *International Journal of Computer Science in Sport*, vol. 19, no. 1, pp. 24–36, 2020.

[18] M. Sharshouh, "The effectiveness of the system methodology to teach some basic skills in volleyball," *International Journal of Sports Science and Arts*, vol. 6, no. 6, pp. 50–72, 2018.

[19] M. Boehm, M. W. Dusenberry, D. Eriksson et al., "System ML: declarative machine learning on spark," *Proceedings of the VLDB Endowment*, vol. 9, no. 13, pp. 1425–1436, 2016.

[20] A. L. Buczak and E. Guven, "A survey of data mining and machine learning methods for cyber security intrusion detection," *IEEE Communications Surveys & Tutorials*, vol. 18, no. 2, pp. 1153–1176, 2016.

[21] C. Helma, T. Cramer, S. Kramer, and L. De Raedt, "Data mining and machine learning techniques for the identification of mutagenicity inducing substructures and structure activity relationships of noncongeneric compounds," *Journal of Chemical Information and Computer Sciences*, vol. 44, no. 4, pp. 1402–1411, 2004.

[22] S. Mullainathan and Z. Obermeyer, "Does machine learning automate moral hazard and error?," *The American Economic Review*, vol. 107, no. 5, pp. 476–480, 2017.

[23] A. Muscoloni, J. M. Thomas, S. Ciucci, G. Bianconi, and C. V. Cannistraci, "Machine learning meets complex networks via coalescent embedding in the hyperbolic space," *Nature Communications*, vol. 8, no. 1, pp. 1615–1630, 2017.

[24] M.-D. Yu, M. Hiller, J. Delvaux, R. Sowell, S. Devadas, and I. Verbauwhede, "A lockdown technique to prevent machine learning on PUFs for lightweight authentication," *IEEE Transactions on Multi-Scale Computing Systems*, vol. 2, no. 3, pp. 146–159, 2017.

[25] Y. Chen, T. Chen, Z. Xu, N. Sun, and O. Temam, "DianNao family: energy-efficient hardware accelerators for machine learning," *Communications of the ACM*, vol. 59, no. 11, pp. 105–112, 2016.

[26] C. Austin, S. Yang, and C. James, "Detection of urban damage using remote sensing and machine learning algorithms: revisiting the 2010 Haiti earthquake," *Remote Sensing*, vol. 8, no. 10, pp. 868–910, 2016.

[27] D. Sacha, M. Sedlmair, L. Zhang et al., "What you see is what you can change: human-centered machine learning by interactive visualization," *Neurocomputing*, vol. 268, pp. 164–175, 2017.

[28] J. Lemley, S. Bazrafkan, and P. Corcoran, "Deep learning for consumer devices and services: pushing the limits for machine learning, artificial intelligence, and computer vision," *IEEE Consumer Electronics Magazine*, vol. 6, no. 2, pp. 48–56, 2017.

[29] S. Saeb, L. Lonini, A. Jayaraman, D. C. Mohr, and K. P. Kording, "The need to approximate the use-case in clinical machine learning," *Gigascience*, vol. 6, no. 5, pp. 1–9, 2017.

[30] B. van Ginneken, "Fifty years of computer analysis in chest imaging: rule-based, machine learning, deep learning," *Radiological Physics and Technology*, vol. 10, no. 1, pp. 23–32, 2017.

[31] B. S. Murugan, M. Elhoseny, K. Shankar, and J. Uthayakumar, "Region-based scalable smart system for anomaly detection in pedestrian walkways," *Computers & Electrical Engineering*, vol. 75, pp. 146–160, 2019.

WILEY | Hindawi

Research Article

Intelligent Monitoring Method of Short-Distance Swimming Physical Function Fatigue Limit Mobile Calculation

Jianxia Yin,[1] **Shimeng Huang** ,[2] **Lei Lei** ,[3] **and Jing Yao**[4]

[1]*Swimming Teaching and Research Office, Xi'an Physical Education University, Xi'an, 710068 Shaanxi, China*
[2]*Swimming Teaching and Research Office, Guangzhou Sport University, Guangzhou, 510500 Guangdong, China*
[3]*Department of Physical Education, Northwest A&F University, Yangling, 712100 Shaanxi, China*
[4]*P.E Department, Xi'an University of Technology, Xi'an, 710048 Shaanxi, China*

Correspondence should be addressed to Shimeng Huang; 101067@tea.xaipe.edu.cn

The detection and classification of moving targets have always been a key technology in intelligent video surveillance. Current detection and classification algorithms for moving targets still face many difficulties, mainly because of the complexity of the monitoring environment and the limitations of target characteristics. Therefore, this article conducts corresponding research on moving target detection and classification in intelligent video surveillance. According to the Gaussian Mixture Background Model and Frame Difference Method, this paper proposes a moving target detection method based on GMM (Gaussians Mixture Model) and Frame Difference Method. This method first proposes a new image combination algorithm that combines GMM and frame difference method, which solves the problems of noise and voids inside the target caused by the fusion of traditional GMM and frame difference method. The moving target detection method can effectively solve the problems of incomplete moving target detection, target internal gap, and noise, and it plays a vital role in the subsequent moving target classification process. Then, the method adds image inpainting technology to compensate the moving target in space and obtain a better target shape. The innovation of this paper is that in order to solve the multiobject classification problem, a binary tree decision support vector machine based on statistical learning is constructed as a classifier for moving object classification. Improve the learning efficiency of the classifier, solve the competitive classification problem of the traditional SVM, and increase the efficiency of the mobile computing intelligent monitoring method by more than 70%.

1. Introduction

The rapid development of computer science and multimedia technology has driven more and more image and video applications to gradually extend to every corner of daily life. However, because the amount of information carried in images and videos is often very huge, human energy is limited after all. In some special scenes, complex and changeable harsh environments may make it difficult for humans to directly operate or cause vision due to huge workload. Fatigue, reduced work efficiency, and even operational errors lead to various unexpected and undesirable consequences. The intelligent development of society and the continuous expansion of application requirements, moving target detection and tracking algorithms with good real-time performance, high

accuracy, and strong stability have become urgent needs in various fields [1]. On the basis of detailed research on the principles of various algorithms in the field of moving target detection and tracking, this article improves these two algorithms to make them have better real-time performance, thereby further improving the performance of the algorithm and improving the algorithm. Improving practicality in the field of intelligence and video survillance.

Liu Xiayu believes that based on the fusion analysis of the human body's functional characteristics, he proposed a method to monitor the natural limit of fatigue during short-distance swimming. First, a physiological indicator system was developed to monitor the natural fatigue limit of short-distance swimming, and then, feature extraction was performed to construct the natural limit of short-term

swimmer fatigue. According to the characteristic analysis method of human physiological indicators, the monitoring characteristics of the dynamic analysis model were carried out. Monitor and, finally, monitor the functional fatigue limit of the human body in short-distance swimming. Perform machine learning and pattern recognition methods, perform short-term floating function fatigue limit monitoring, and perform data fusion analysis. However, the experiment did not carry out actual testing and lacked convincing [2]. Wang Shaohong believes that as an important part of the scientific training of competitive athletes, monitoring the physical condition of athletes is the key to supporting the scientific training of coaches. Currently, the indicators used to monitor the physical function of athletes are invasive (invasive) and noninvasive (noninvasive). The latter are mainly simple and easy-to-use noninvasive indicators, such as heart rate and weight and blood oxygen saturation. With the continuous improvement of the degree, these indicators are becoming less and less able to meet the needs of sports training. However, the algorithm is not perfect and needs to be improved [3]. Zhao Xuyang proposed a detection algorithm to determine the fatigue state of eye features and proposed a pattern recognition system based on the boundary structure learning machine to complete the tracking. When editing the facial features in this document, first, use grayscale and binary image processing, then use the KLT algorithm for face detection and positioning of the image eyes, and finally use an extreme learning machine to detect fatigue. But the system is too slow to be put into actual use [4].

Since the mobile computing intelligent monitoring method has many advantages, such as economy, convenience, and safety, compared with the traditional detection method, if it is confirmed that the mobile computing intelligent monitoring method can significantly improve the swimming ability of the swimming athletes and improve the training and competition performance, then this monitoring method will. It is a good choice for endurance sports to improve athletic ability. The influence on the athletic ability of swimmers is the most important indicator for evaluating this training method [5, 6]. This article attempts to reveal the influence of short-distance swimming physical function fatigue limit on swimmers' athletic ability through comparative experiments, analyze the mechanism of its effect on the body, evaluate the training effects, and propose scientific training methods [1].

2. Mobile Computing Intelligent Monitoring Method

2.1. Interframe Difference Method. When a foreground target appears in a video sequence, the images of the two frames before and after it will change significantly. The frame difference method uses this function to subtract the video sequence frame by frame to obtain the brightness difference [2, 7]. To determine whether the current frame contains foreground objects, you need to compare the difference with the set threshold. The frame difference method has low algorithm complexity, good real-time performance, and strong robustness for image sequences with relatively clear fore-

ground target contours. However, this algorithm cannot accurately identify a complete foreground target and can only extract the approximate outline of the target, thereby forming a large number of holes in the foreground area. And for images with blurred target contours, it is often impossible to achieve better detection results [8, 9].

2.2. Background Subtraction. In order to solve the problem of the frame difference method, Glober et al. used a prospect extraction method combined with mathematical statistics. First, the median method is used to construct a background sample set for the image, that is, the median value of the pixel in the adjacent frames is obtained for sampling. Then, the newly arrived image and the sample set are subjected to a different operation to extract the foreground pixels. Although this algorithm can overcome the problem that the frame difference method can only detect the target contour, its time efficiency and space efficiency are not high, and large detection errors are often prone to occur in video sequences with unstable lighting conditions [10, 11]. In order to overcome this problem, Wren et al. introduced the Gaussian model to improve the sample modeling and set a threshold to classify the pixels.

2.3. Other Target Detection Methods. The development of background subtraction has gone through a process from simple to complex and, then, from complex to simplification [12, 13]. While the background subtraction method continues to improve, other target detection algorithms with different principles have gradually entered people's sight, such as target detection algorithm combined with fuzzy theory, target detection algorithm combined with motion estimation, and target detection algorithm combined with neural network. In order to solve the problem of low accuracy and poor stability in the detection process of some background subtraction methods [14, 15], some researchers have proposed a method that combines target detection algorithms with fuzzy theory. The experimental results do verify that this type of algorithm has high accuracy and stability, but its time and space efficiency do not have good real-time performance under current hardware conditions [16].

3. Correlation Experiment of Moving Target Detection and Classification Algorithm

In computer image processing and analysis, moving target detection technology has always been a research hotspot in video sequence analysis. The so-called moving object detection is the process of separating moving objects from the background image of the video. Due to the complex background, illumination changes, and severe weather in the real scene, the detection of moving objects still faces huge challenges [17, 18].

3.1. Optical Flow Method. Assume that in the case of n dimensions (the same applies to 3D and higher dimensions) after time t and time t, the gray value of the pixel (x, y) of the video frame is $f(x, y)$, and the pixel is at move $x1$ in x direction and $y1$ in y direction. The pixel value corresponding to

the pixel at this moment is $f(x + x1, y + y1)$ [19]. Assuming that t is small, the gray value of the pixel will remain unchanged in a very short time, so formula (1) can be used to express that the pixel values of the two points are equal.

$$f(x, y, t) = f(x + x1, y + y1, t + t1). \qquad (1)$$

Since the displacement is very small, the Taylor expansion of equation (1) is performed to obtain the equation [20, 21]:

$$f(x + x1, y + y1, t + t1) = f(x, y, t) + \sigma^2. \qquad (2)$$

Among them, ∂ is the partial derivative of $f(x, y, t)$ with respect to x, y, t of the second order and above, which can be ignored, so formula (3) can be obtained:

$$\frac{df}{dx}x + \frac{df}{dy}y + \frac{df}{dt}t = 0. \qquad (3)$$

Divide both sides of the equation by t to obtain equation (4):

$$\frac{df}{dx}\frac{dx}{dt} + \frac{df}{dy}\frac{dy}{dt} + \frac{df}{dt}\frac{dt}{dt} = 0. \qquad (4)$$

When t approaches 0, there are [22, 23]:

$$\frac{df}{dx}W_x + \frac{df}{dy}V_y + \frac{df}{dt} = 0. \qquad (5)$$

The vector sum of W and V is the luminous flux of a certain pixel in the video image. Equation (5) is called the optical flow constraint equation.

3.2. Frame Difference Method. The frame difference method uses the difference operation of two or three consecutive frames in the video sequence and uses the time difference to extract the moving area in the image, thereby obtaining the moving target. Figure 1 shows the effect of the frame difference method on moving target detection.

$f(x, y, t)$, $f(x, y, t - 1)$ represent the current frame and the previous frame of the current frame, respectively, assuming $D(x, y, t)$ is the difference between the current frame and the previous frame. The result can be expressed by equation (6) [23, 24]:

$$D(x, y, t) = f(x, y, t) - f(x, y, t - 1), \qquad (6)$$

where (x, y) represents the position of the pixel $R(x, y)$, $Rxyk$ represents the image after binarization processing, $R(x, y)$ takes 1 to indicate that the current pixel is a moving target, $R(x, y)$ takes 0, which indicates that the current pixel is the background, and T represents the threshold [25, 26].

$$R(x, y) = \begin{cases} 1 & D(x, y) \geq T \\ 0 & D(x, y) \leq T \end{cases}. \qquad (7)$$

FIGURE 1: Examples of moving target detection pictures.

TABLE 1: The dynamic changes of intermittent hypoxia training on athletes' RBC.

	Test group	Control group
Before the experiment	4.54	4.52
Day 4	4.66	4.50
Day 8	4.80	4.52
Day 11	4.86	4.57
Day 15	4.79	4.48
Day 18	4.68	4.42
Day 21	5.10	4.65

The frame difference method is simple to implement, does not require background modeling and updating, the algorithm is fast, is not sensitive to changes in lighting, and can adapt to complex and changeable environments, and is suitable for scenes with high real-time requirements. However, the frame difference method cannot completely extract the moving target; only the contour information can be extracted, so the target information is incomplete. If the target feature is subsequently extracted, the feature information will be incomplete [27].

4. Short-Distance Swimming Physical Function Fatigue Limit Analysis

4.1. Effect of Intermittent Hypoxia Training on Swimmers. In this study, the serum ferritin of the athletes in the experimental group and the control group was in the normal range before and after the experiment, and there was no significant difference, indicating that the two groups did not decrease serum ferritin due to a lot of training. Iron is the raw material for red blood cell production, and serum ferritin is an indicator for detecting human iron reserves.

It can be seen from Table 1 that before the start of the experiment, there was no significant difference in the red blood cell counts of the athletes in the experimental group and the control group, and the two groups were comparable; in the simulated hypoxic environment caused by living high and training low, the red blood cell counts of the athletes in the experimental group were short-term. Although there was an increase in internal, it did not reach statistical significance. Until the end of the experiment, the number of red

	Test group	Control group
■ Before the experiment	41.54	45.2
■ Day 4	49.66	50.51
■ Day 8	48.24	47.52
■ Day 11	44.86	46.57
■ Day 15	41.79	44.48
■ Day 18	45.68	39.42
■ Day 21	38.16	34.65
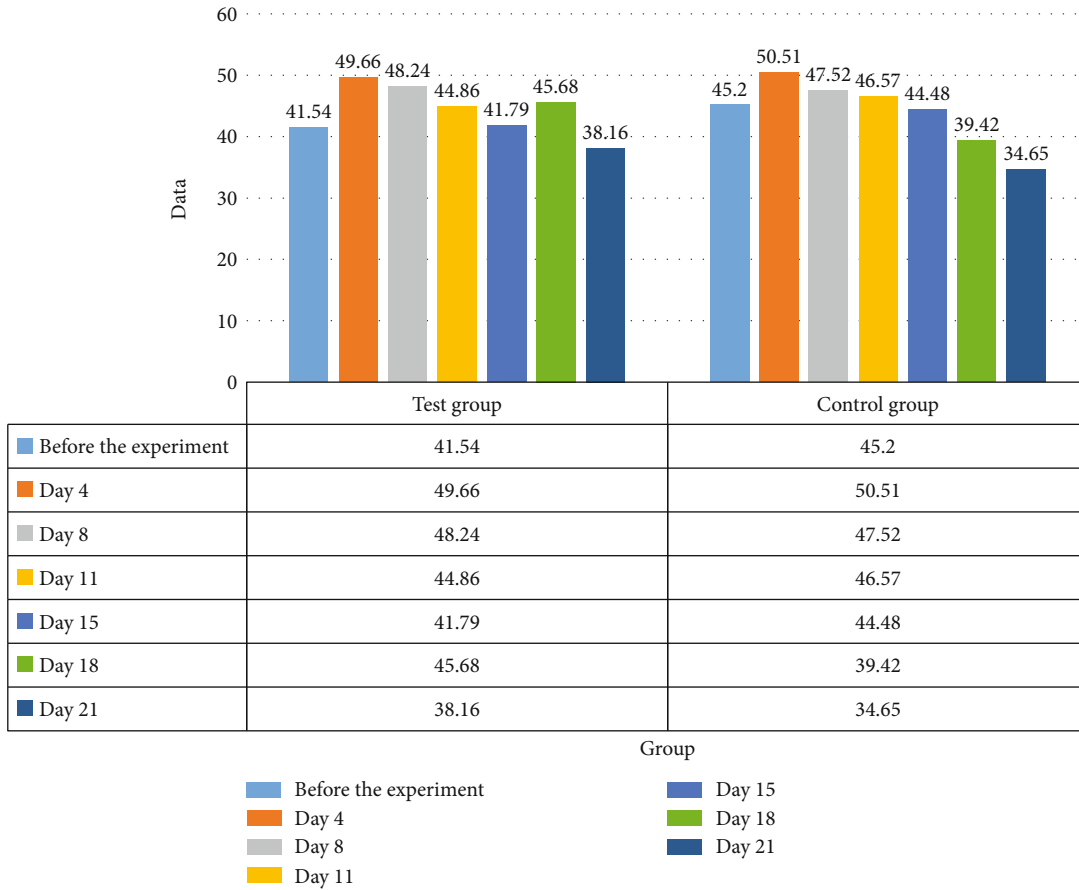
FIGURE 2: The dynamic changes of HCT of athletes during intermittent hypoxia training.

blood cells increased significantly compared to before the experiment. There was no significant change in the number of red blood cells of the athletes in the control group before and after the experiment. It shows that the training method of intermittent hypoxic training can significantly increase the red blood cell count and enhance the body's oxygen-carrying capacity, but this effect must be displayed after about 3 weeks of training, so pay attention to intermittent hypoxic training time control. Since the life span of normal red blood cells in the human body is 120 days, after the athlete returns to normal training after the intermittent hypoxic training, the high level of RBC will remain for a period of time.

As shown in Figure 2, before the start of the experiment, there was no significant difference in hematocrit between the test group and the control group, and the two groups were comparable. In the simulated hypoxic environment caused by living high and training low, the hematocrit of the experimental group had a significant increase on the 8th day, and it continued to reach the highest value at the end of the experiment. There was no significant change in the hematocrit of the control group athletes before and after the experiment. Within a certain range, the hematocrit is directly proportional to the blood's oxygen-carrying capacity, that is, the larger the HCT, the stronger the blood's oxygen-carrying capacity; however, when the HCT exceeds a certain range (generally considered to be more than 50%), the blood is

TABLE 2: Weight measurement values before and after intermittent hypoxia training.

	Test group	Control group	Experimental group compared with control
Before the experiment 1	67.08	63.38	$P > 0.05$
Before the experiment 2	66.37	63.42	$P > 0.05$
In experiment 1	66.39	63.33	$P > 0.05$
In experiment 2	66.20	63.17	$P > 0.05$
After the experiment	65.29	63.43	$P > 0.05$

sticky. Sexual enhancement affects blood rheology. Experiments show that the HCT of all athletes is in the best range, indicating that the effective oxygen uptake of the athletes' "red blood cells" is in the best state.

4.2. Effect of Intermittent Hypoxia Training on the Body Water of Swimmers. The stable state of human physiological processes relies on the close coordination of nerves and body fluids. Generally speaking, nerve regulation is rapid and short-lived, while body fluid regulation is slow and long. The two complement each other and are in harmony.

	Day 4	Day 8	Day 11	Day 15	Day 18	Day 21
Test group	13966	14824	15486	11709	12568	13816
Control group	15051	13752	12657	14448	15942	13465

Group

— Test group
— Control group
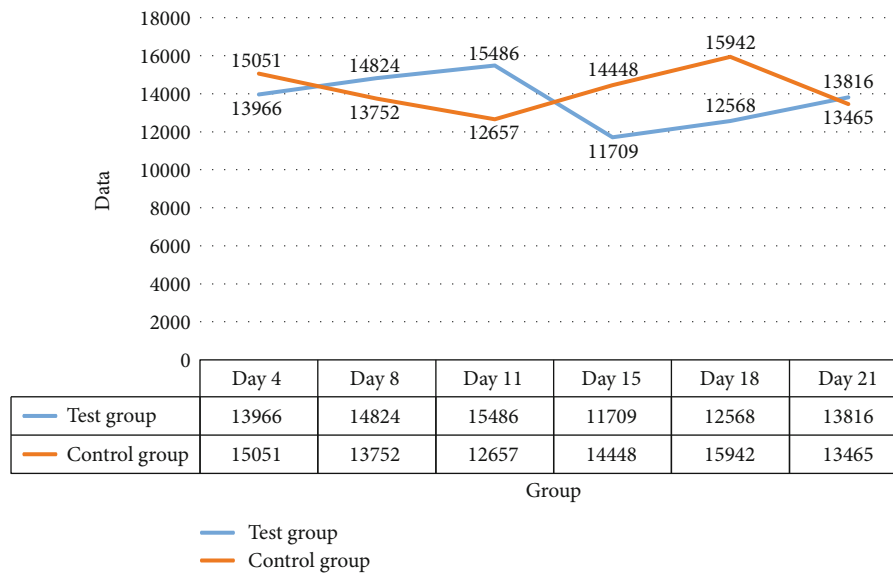
FIGURE 3: Control of exercise load of swimmers during intermittent hypoxic training.

It can be seen from Table 2 that the weight of athletes in the experimental group before intermittent hypoxic training is not significantly different from that of the control group ($P > 0.05$), indicating that the two groups are comparable; tested in the experiment and after the experiment, the experimental group had no significant difference between the athletes' weight and the control group ($P > 0.05$). There was no significant difference in weight before and after the experiment in the control group athletes. The weight of the athletes in the experimental group decreased significantly after the experiment compared with before the experiment ($P < 0.05$), indicating that the athletes' weight decreased significantly after the intermittent hypoxic training.

As can be seen from Figure 3, the amount of exercise curve goes from low to high and, then, from high to low. The exercise volume in the first two weeks is higher, which is to adapt to the exercise load stimulation and hypoxic stimulation to make the athlete's body produce and improve the exercise adaptability. At 15 days, the red blood cell count and hemoglobin showed a downward trend, indicating that the athletes had accumulated a certain degree of fatigue after two weeks of training. Therefore, in the third week, the amount of exercise decreased and the exercise intensity increased moderately.

5. Conclusions

This paper combines the idea of background difference in the target detection algorithm to realize the automatic initialization of the search box. Aiming at the problem that the Camshift algorithm is easy to lose the target when the lighting conditions change drastically, a judgment strategy of the average value and the actual value of the Hue component is introduced to realize the real-time update of the color probability model. Aiming at the problem of tracking failure of the Camshift algorithm after the target moves at a high speed or is temporarily occluded, this paper combines the Kalman filter algorithm to introduce a motion prediction mechanism, which predicts the possible position of the target in the next frame during the tracking process. Experimental results show that the improved Camshift algorithm can maintain a good tracking effect even under sudden changes in lighting. In addition, when the target moves at a high speed or is temporarily occluded, the improved algorithm can still maintain a stable recognition rate. This paper proposes an improved strategy for the deficiencies of the ViBe target detection algorithm and the Camshift target tracking algorithm, and the effectiveness of the improvement is verified through experiments. However, there are still some unresolved problems in the research process. Therefore, the realization of adaptive sharpening of the target area will be the focus of future research. It is also in the future to extend the improved Camshift algorithm to the application of multitarget tracking, a new direction of work.

Data Availability

The data that support the findings of this study are available from the corresponding author upon reasonable request.

Conflicts of Interest

The authors declare that they have no conflicts of interest.

References

[1] L. Xiayu and N. Zhebin, "Research on the limit monitoring method of physical function fatigue in short-distance swimming," *Journal of Chifeng University (Natural Science Edition)*, vol. 35, no. 300, pp. 107–110, 2019.

[2] W. Shaohong, L. Weiguo, N. Yuhua, and W. Chunjian, "Exercise load monitoring and fatigue evaluation, recovery and nutritional supplementation of middle and short distance swimmers," *Contemporary Sports Science and Technology*, vol. 9, no. 21, pp. 28-29, 2019.

[3] Z. Xuyang and Y. Wang, "Research on fatigue driving monitoring method based on extreme learning machine face recognition," *China Equipment Engineering*, no. 9, pp. 85-86, 2018.

[4] Y. Liang, X. Hu, and Q. Yang, "Research on intelligent recommendation algorithm for mobile services based on group intelligence computing," *Digital Technology and Application*, vol. 38, no. 358, pp. 119-120, 2020.

[5] B. Yuanyuan, "Analysis and research on fatigue characteristics of swimming training," *Stationery & Sports Supplies & Technology*, no. 21, pp. 214-215, 2019.

[6] L. Qing and Y. Qiang, "Short-distance swimming squatting start technical characteristics and special training," *Journal of Capital Institute of Physical Education*, vol. 29, no. 6, pp. 549–553, 2017.

[7] Z. Qixiang, "Research on the structure and level of the special ability of short-distance swimmers," *Sports Time and Space*, no. 23, pp. 96-97, 2017.

[8] J. Chengping, S. Yunyun, and H. Xinzhong, "The control of Yu Hexin's multi-year training arrangements for outstanding short-distance swimmers," *Journal of Beijing Sport University*, vol. 41, no. 11, pp. 109–115, 2018.

[9] L. Jianxun, "A preliminary study on the short-distance special ability training of swimmers aged 6-12 years," *Leisure*, no. 7, pp. 89–89, 2019.

[10] Z. Jie, L. Yijun, Z. Xiaodong, and K. Dejia, "Study on stroke frequency, stroke width and speed of excellent female 200m swimmers during competition," *Journal of Xi'an Institute of Physical Education*, vol. 33, no. 1, pp. 124–128, 2016.

[11] Y. Tian, L. Zhang, H. Wang et al., "Intelligent detection platform for simultaneous detection of multiple MiRNAs based on smartphone," *ACS Sensors*, vol. 4, no. 7, pp. 1873–1880, 2019.

[12] S. Yang and L. Ying, "Research on winning factors of 50m short-distance swimming competition," *Contemporary Sports Science and Technology*, vol. 7, no. 32, pp. 160-161, 2017.

[13] L. Mingguang, "The importance and methods of strength training for short-distance swimmers," *Journal of Science Education (Electronic Edition)*, no. 2, pp. 103–103, 2017.

[14] Z. Yong, "Monitoring and analysis of biochemical indicators of outstanding long and short distance female swimmers," *Chinese Sports Coaches*, vol. 26, no. 4, pp. 74-75, 2018.

[15] W. Youhuai, "Discussion on the pre-match training of short-distance high-level swimmers in Guangdong Province," *Sports Fashion*, no. 11, pp. 36-37, 2019.

[16] J. Zhixiang, "Research on the methods of strength training for short-distance swimming athletes," *Contemporary Sports Science and Technology*, vol. 6, no. 28, pp. 57-58, 2016.

[17] S. Wen and C. Jingjing, "Analysis of the stroke time of men's short-distance freestyle swimmers of Guangdong swimming team," *Contemporary Sports Science and Technology*, vol. 6, no. 10, pp. 138–140, 2016.

[18] G. Lei, "Research on the stroke technique of men's short-distance freestyle swimmers," *Knowledge Library*, no. 6, pp. 196-197, 2019.

[19] Б. П. Yakovlev, Г. Д. Babshikin, P. E. Lou Bin, E. Г. Babshikin, И. Б. Taraschenko, and Y. Songping, "Special training research on swimmers in the pre-competition and mid-cycle period," *Journal of Capital Institute of Physical Education*, vol. 30, no. 4, pp. 289–291, 2018.

[20] M. Xiaochen, H. Yu, and R. Chen, "Research on effective land-based intensity exercise methods for 100m swimming events," *Contemporary Sports Science and Technology*, vol. 7, no. 2, pp. 249–252, 2017, 254.

[21] Z. Wenxiu, "Research on physical training methods and characteristics of short, middle and long distance swimming events," *Contemporary Sports Science and Technology*, vol. 9, no. 35, pp. 27-28, 2019, 30.

[22] L. Dongyu and Z. Deshan, "Bivariate analysis of Chinese and foreign outstanding men's 50m breaststroke," *Contemporary Sports Science and Technology*, vol. 8, no. 20, pp. 235-236, 2018.

[23] L. Dongyu and L. Wenmin, "Using Pearson correlation to analyze the effect of stroke frequency on the performance of 50-meter breaststroke," *Guizhou Sports Science and Technology*, no. 2, pp. 46–48, 2018.

[24] Y.-S. Choi, J.-H. Hong, and J.-M. Woo, "Design of Antenna for intelligent detection sensor," *The Journal of The Korea Institute of Intelligent Transport Systems*, vol. 19, no. 2, pp. 104–109, 2020.

[25] Z. Xiaofeng, "Discussion on the explosive training methods of upper limbs of swimmers," *Contemporary Sports Science and Technology*, vol. 8, no. 5, pp. 38-39, 2018.

[26] L. Taibo, "Research on the swimming training mode of the seamen's skill competition," *Sports Boutique (Academic Edition)*, vol. 36, no. 11, pp. 83-84, 2017.

[27] L. Hai, W. Yongxue, Q. Jinjin et al., "Niche and interspecies encounter probability of main swimming animals in Yiwan Bay, Taizhou," *Chinese Journal of Fishery Sciences*, vol. 26, no. 2, pp. 136–144, 2019.

WILEY | Hindawi

Research Article

Information Security Terminal Architecture of Power Transportation Mobile Internet of Things Based on Big Data Analysis

Xianzhi Tang[1] and Chunyan Ding [iD][2]

[1]College of Civil Engineering, Chongqing Vocational Institute of Engineering, Chongqing 402260, China
[2]Department of Mechanical Engineering, Yantai Engineering & Technology College, Yantai, 264006 Shandong, China

Correspondence should be addressed to Chunyan Ding; dingchunyan@ytetc.edu.cn

The progress of the social economy and the rapid development of the power field have created more favorable conditions for the construction of my country's power grid. In this network age, how to further realize the connection between the power system and the Internet of Things is the key content of many scholars' research. In the Internet of Things environment, there have been many excellent results in the collection, storage, and management of electric power big data, but the problem of information security has not been completely solved. Based on big data analysis and Internet of Things technology, this paper studies the architecture design of power information security terminals. In view of the diverse types of power grid mobile information and the large amount of data, this paper designs a power transportation mobile information security management system structure, which improves the effective management of power data by the system through big data, smart sensors, and wireless communication technology. According to the experiment, the power information security terminal constructed in this paper can effectively reduce communication resources and save communication costs in the process of aggregating multidimensional data. In the user satisfaction survey, residents' satisfaction with the convenience and safety of the intelligent power system is also as high as 9.312 and 9.233. On the whole, the application of big data and Internet of Things technology to the construction of power information security terminals can indeed improve the service efficiency of power companies under the premise of ensuring safety and allow users to have a better experience.

1. Introduction

Electricity plays a very important role in the country's economic development and people's daily life. Only by ensuring the stable operation of the power grid can the normal development of the entire society be guaranteed. The IoT is a network concept that realizes a wide range of connections between things and things, and between people and things through various information sensing devices such as radio frequency identification (RFID), infrared sensors, and global positioning systems (GPS). Its core technology is the identification and management of object information. In the field of power transportation, the most widely used value of Internet of Things technology is the collection, analysis, and management

of power data in the power acquisition and control system. The main work of the power grid is to regulate and control the voltage and scientifically complete the transmission and distribution of electrical energy. Only by continuously improving the security of power information can the risks in the power communication process be effectively reduced.

In recent years, people have carried out a lot of research on the information security of the mobile Internet of Things, and the Internet of Things has become more and more widely used in various fields of life. Kok et al. has conducted research on smart grids embedded with renewable energy and distributed power generation. He believes that the development of public grids from the centralized control structure to decentralized control structure has changed rapidly. The

use of multiagent structure can help people further optimize the power control system. From the research results, further efforts are needed to improve the data islands in the smart grid [1]. Fadel et al. proposed a power system called smart grid (SG), which is used as an evolutionary system for power transformation, transmission, and distribution. SG uses renewable energy to generate electricity and manages the power system through smart meters and sensing and communication technologies. On the whole, this system has a good effect on improving performance, but there is still room for improvement in data security management [2]. Ejaz et al. analyzed the efficient energy management of the Internet of Things in smart cities. He believes that the Internet of Things provides many complex and diverse smart services for smart cities, and electric traffic management is a key example of implementing complex energy systems in smart cities. His team provided a unified framework for energy efficiency optimization and dispatching for IoT smart cities. However, this framework still lacks sufficient practicality for complex and changeable grid data [3].

My country's research on power information has been carried out earlier, and many good results have been achieved so far. Jia et al. conducted an analysis and research on the security of the power system. He believes that the successful development of smart grids is inseparable from the security of the system. He proposed a new and efficient safety analysis method, which includes a cascaded fault simulation module (CFSM) for postmortem analysis and a risk assessment module based on correlation neural network integration (DNNE). Although this method overcomes the problem of high computational cost in the traditional N-k algorithm, its stability needs long-term practice to be guaranteed [4]. Tu analyzed the interface design of the control and protection system based on the multiterminal HVDC flexible project. He took the control and protection system interface scheme of the multiterminal HVDC flexible project as an example and proved through research that the interface between the valve group controls satisfies the control protection system requirements. From the research report, the application of this scheme in power stations has a good protection effect on data security, but there is room for improvement in operating speed [5].

This article combines big data thinking and analyzes how to reasonably develop secure terminals for power transportation mobile information and form an Internet of Things system in the power industry. At the same time, this article introduces the Internet of Things information security technology and applies encryption algorithms to the development of Internet of Things security systems for power use. Smart grid is an inevitable trend of the development of the times, and the mobile Internet of Things security system for electric power transportation can effectively monitor the entire process of power transmission and distribution and conduct a more comprehensive management of power transportation [6].

2. Information Security Technology for Power Transportation Mobile Internet of Things

2.1. Basic Structure of Power Transportation Mobile Terminal.
Electric power traffic data usually has the characteristics of many types, large data volume, and fast transmission speed. To realize the processing of electric power big data more effectively, the information security system must be improved [7]. In the construction of power information terminal, this article takes big data as the core concept to establish the connection between power data and users. To put it simply, you can refer to the operating idea of the Internet of Things, that is, using smart sensors to realize the mining, storage, and analysis of electric power data and finally realize the safe sharing of network information in the field of electric transportation and mobility [8]. Figure 1 is a schematic diagram of the power information security platform structure based on big data analysis.

It can be seen from Figure 1 that the power transportation mobile terminal system can be basically divided into a user layer, a big data analysis layer, and a terminal big data collection layer. There are three common service models for cloud computing, namely, infrastructure as a service, platform as a service, and software as a service [9, 10]. In this system, platform services and software services are mainly used to help users achieve various power data analysis requirements. The terminal collection layer uniformly collects the data generated during power operation through handheld or monitoring terminals. Generally speaking, the data involved in the power transportation mobile system includes but is not limited to power transformation, transmission, distribution data, line distribution data, and line operation data [11].

The big data analysis layer is the most complicated part of the system, and the data of the terminal collection layer will be stored here and received for further processing and scheduling [12]. Compared with the traditional data storage mode, big data storage has higher real-time performance, because the analysis layer will update the historical data in real time during data scheduling to ensure the dynamic allocation of data and ensure the smooth operation of the system.

2.2. Power Information Security Storage System Based on Big Data.
According to the specific needs of data storage and analysis in electric transportation, this paper combines the basic structure of the cloud computing system to design a power information security storage system. This system consists of three parts, namely, storage, application, and management. In the safe storage system, a large amount of data information will be generated in the process of power transformation, transmission, and distribution, including static data, dynamic time series data, picture, and video data [13]. In order to ensure the smooth operation of transmission and distribution lines in complex environments, it is necessary to improve some of the problems in data storage and create more favorable conditions for data analysis and calculation [14].

2.3. Security Mechanism of the IoT Terminal System.
The security architecture of the Internet of Things is usually divided into a perception layer, a network layer, and an application layer. The key difference between the security of the Internet of Things and the traditional network security lies in the perception of the security of the terminal system [15]. The Internet of Things terminal system is the forefront of the entire Internet of Things data perception and processing.
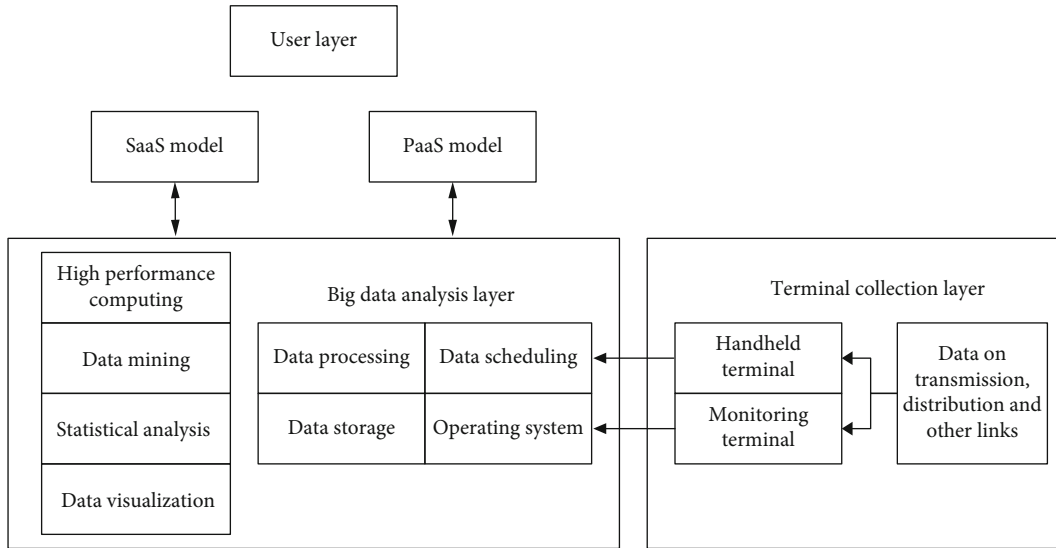
Figure 1: Structure diagram of power information security platform based on big data analysis.

Its biggest feature is limited resources. If you want to ensure the security of the Internet of Things, you must design a security mechanism that can adapt to the characteristics of the Internet of Things terminal system [16]. Generally speaking, RFID technology and wireless sensor network (WSN) technology are the most important technologies in the sensing layer.

2.3.1. RFID Technology. Radio frequency identification (RFID) is a kind of automatic identification technology. It carries out noncontact two-way data communication through radio frequency and uses radio frequency to read and write the recording media (electronic tags or radio frequency cards), so as to achieve the purpose of identifying targets and data exchange.

Radio frequency identification technology (RFID) is a noncontact two-way automatic data identification technology, because it has a strong data storage capacity, high accuracy and adaptability, and can simultaneously identify and process objects and tags. Its often used in the field of Internet of Things [17]. However, the openness of the RFID system will still cause it to have certain security problems. Although the existing security authentication protocols can detect the presence of false tags, these security authentication protocols are generally based on the single-proof interaction mode. Although this authentication mode is highly reliable, it cannot meet the actual needs of large-scale RFID systems in terms of efficiency [18].

2.3.2. Wireless Sensor Network (WSN) Technology. Wireless sensor network (WSN) is a distributed sensor network, combined with data fusion technology, and it has the effects of reducing node energy consumption, enhancing data perception capabilities, reducing network delay, and optimizing network resource allocation [19, 20]. Therefore, reasonable and efficient data fusion technology is very important for wireless sensor networks.

The data collected by a single node is limited, and the perception ability is limited. Therefore, it is necessary to deploy a large number of nodes in the wireless sensor network to improve the accuracy of the data and enhance the robustness of the network. However, nodes in the same detection area will have the phenomenon of communication crossing, resulting in data redundancy. If the node transmits redundant data directly to the sink, it will not only increase the amount of communication and calculation but also reduce the user's data decision-making ability [21]. Therefore, designing a reasonable and efficient data fusion technology, eliminating redundant data, and reducing computational complexity and node energy consumption, not only can improve the life cycle of the network but also improve the user's decision-making ability.

2.4. Mobile IoT Information Security Encryption Algorithm. The sensing layer lacks sufficient security protection barriers. If someone tries to attack the sensing nodes of the wireless sensor network, they will often start from the sensing layer. In addition, the sensing nodes in the sensing layer are distributed in various different complex environments, which further increase the probability of being attacked and causing information data damage and loss [22]. In order to ensure the confidentiality and integrity of the power, transportation, and mobile Internet of Things information, appropriate encryption algorithms must be used.

2.4.1. Byte Substitution. The round function of each round of the AES algorithm must go through the process of byte substitution, row shift, column mixing transformation, and round key addition operation. Compared with other algorithms, the AES algorithm is more symmetrical, and the expression is simple and easy to understand [23]. Byte substitution is the only nonlinear transformation in the algorithm. It is a bricker's replacement. The replacement contains an $s-$ box that acts on the state byte, denoted by SRD. Box $s-$ is a matrix of 16×16; so, there are 256 possible transformations. Among them, the algebra of byte substitution is

expressed as $bi, j = S[ai, j]$, and then the structure of SRD satisfies the formula:

$$SRD[a] = f(g(a)). \tag{1}$$

If $g(a)$ represents transformation $a \rightarrow b$, then

$$a \rightarrow a^{-1} \text{inGF}(2^8). \tag{2}$$

Among them, $f(a)$ is an affine transformation, and this change has no effect on nonlinearity, but it can make the algebraic expression very complicated.

2.4.2. Row Shift. The essence of the row shift is only one byte transformed; that is, the row in the state is cyclically shifted according to a different offset. For a $128bits$ component, the state offset is 0, 1, 2, and 3, and the offset used by each row can be any one of them [24]. The inverse operation of row shift is called InvShiftRows, which can make the rows of the state matrix cyclically shift. In the $AES - 128$ decryption algorithm, the first row moves three bytes to the right, and the second row moves two bytes to the right. The third row moves two bytes to the right, and the last row remains unchanged.

2.4.3. Column Confusion. Column confusion operation is a kind of linear transformation, which only performs mixing on each column included in the state. Column confusion transformation helps the state matrix to further provide higher diffusibility after row shifting and diffusion, which confuses each column of the state matrix [25]. This kind of replacement is to separately treat each column as a polynomial whose coefficients are in a finite field, then multiply with another intrinsic polynomial, and finally perform a modular operation on the formula $(x^4 + 1)$, where the mathematical formula of the polynomial $c(x)$ satisfies

$$c(x) = 0.3 \cdot x^3 + 0.1 \cdot x^2 + 0.1 \cdot x + 0.2. \tag{3}$$

When the inverse nematic hybrid transformation is expressed by matrix multiplication, the corresponding polynomial satisfies the formula:

$$(0.3 \cdot x^3 + 0.1 \cdot x^2 + 0.1 \cdot x + 0.2) \cdot d(x) = 0.1 (\text{mod } x^4 + 1). \tag{4}$$

Among them, $d(x)$ satisfies

$$d(x) = 0B \cdot x^3 + 0D \cdot x^2 + 09 \cdot x + 0E. \tag{5}$$

2.4.4. Add Round Key. In the round key addition transformation, each round of the round transformation will have a round key, and the round key is expanded by the key, where ki, j is the round key, and the mathematical expression of round key addition is

$$bi, j = ai, j \oplus ki, j. \tag{6}$$

3. Construction Experiment of the Power Information Security System Based on Big Data Analysis

3.1. Experimental Background. The Internet of Things is the application of the Internet of Things in the smart grid. It is the result of the development of information and communication technology to a certain stage. It will effectively integrate the communication infrastructure resources and the power system infrastructure resources, improve the information level of the power system, and improve the current situation of the power system. With infrastructure utilization efficiency, it provides important technical support for power grid generation, transmission, transformation, distribution, and power consumption. A huge intelligent complex network integrates electrical equipment and facilities for unified management. Power information is not only diverse in types, large in data volume, and extremely fast in updating, it is difficult for traditional management methods to fully control power big data. During the preanalysis of the experiment, this article believes that the difficulty of the experiment will appear in the construction of the big data platform and the efficiency of part of the real-time information return. Therefore, this article focuses on information security and constructs the Internet of Things information system framework in the power field. In this way, the effect of comprehensive management of electric power big data can be improved.

3.2. Experiment Process. This article combines the characteristics of the power industry with big data and uses the radio frequency identification technology and intelligent information sensors in the Internet of Things to try to combine big data and the Internet of Things technology to construct a power information security terminal. The entire system is composed of the user layer, the big data analysis layer, and the terminal collection layer. The three are connected and complementary to each other, converging various data in the power industry into the power Internet of Things. After the completion of the terminal construction, this article will start with the big data-based IoT power acquisition and control and power marketing information security, as well as the big data-based power traffic management system security, and elaborate on the big data and the IoT model for the power industry.

3.3. Experimental Platform Development. The power transportation mobile Internet of Things information security platform constructed in this article takes the Hapoop MapReduceV2 framework as the core and establishes a distributed computing cluster through the Map-Reduce programming model to complete the operation and management of the power big data in the system. In the big data storage system, this article uses the manager to manage the system content and serves as an excuse for users to use the client to access data. At the same time, Hadoop is used to complete the construction of distributed clusters, and various data generated by the lines during daily power transmission and distribution are stored in a large number of data nodes to achieve distributed storage. The application layer consists of the Map-Reduce programming model and the distributed

TABLE 1: Basic protocol format of configuration information data in power transmission node.

Byte	0	1	2-3	4-5	6-10	11-14	15-18	19-20
Description	Data header	Logo	Local address	Target address	Server address	Time stamps	CRC	Data tail
Byte length	1	2	2	2	6	6	4	2

open source database HBase, so that data storage and management can be implemented according to parallel programming and storage excuses.

In the development of terminal collection systems, advanced information technologies such as mobile Internet technology, global positioning system, radio frequency identification technology, mobile communication technology, and intelligent information sensing technology need to be comprehensively utilized. Specifically, it includes a lan communication module for communication maintenance, an identity recognition module for personal information recognition, and a beidou module for precise positioning. In addition, video modules, infrared communication modules, and expansion modules also play important values in the system.

4. Based on Big Data and Internet of Things Technology Research on Electric Traffic Information Security Terminal Architecture

4.1. Big Data-Based Internet of Things Power Acquisition and Control and Power Marketing Information Security Analysis

4.1.1. Security Analysis of Electric Transportation Terminal Based on Big Data. Electricity is an indispensable resource for the normal operation of the country. Therefore, grid operation companies bear heavy responsibilities. They must not only provide high-quality electric energy to all users and ensure the stable operation of users' electrical equipment but also ensure the stability of the entire power grid system and carry out special regulation on power transmission at key nodes. In order to better realize grid management, it is a very correct decision to connect the power industry with big data of the Internet of Things. The transmission system of the power transportation mobile Internet of Things includes three parts: monitoring equipment, application software, and transmission network. In order to ensure the normal operation of the system, its safety must be guaranteed from the system architecture and functions. Table 1 is the basic protocol format of the configuration information data in the power transmission node.

Regardless of the collection node or the transmission node, configuration information is written to the node through the RS485 bus. The configuration information is used to write the local physical address, target physical address, server IP address, time base reference, and other parameters into the node. It can be seen from Table 1 that when a node is identified as a sending node, the target address is the address of the relay node corresponding to the sending; when the node is identified as a relay node, the target address is the address of the standby relay node; when the current relay node is used as a sending node, or the relay forwarding function of the current relay node cannot be used

normally, the node forwards information through the standby relay node of the wireless communication module box. In order to further test the transmission delay and correctness of power transmission, this paper evaluates the wireless transmission effect under different distances. Figure 2 is a statistical diagram of the test results of wireless transmission.

It can be seen from Figure 2 that when the transmission distance is within 300 meters, the accuracy of wireless transmission is 100%, and the transmission delay is less than 0.2 milliseconds. But with the expansion of the transmission distance, the transmission delay will continue to increase, and the transmission accuracy rate will continue to decrease. On the whole, the transmission performance of wireless communication within 450 meters is still relatively good. It can be seen that the power transportation mobile Internet of Things information security terminal constructed in this article can realize normal applications in the power field while ensuring the secure transmission of information.

4.1.2. Security Analysis of Internet of Things Power Marketing Information Based on Big Data. The so-called power marketing refers to the power services provided by enterprises in order to meet the power consumption needs of the masses in the power market. The essence of power marketing is to achieve a balance between supply and demand in the power market. With the indepth development of power marketing information, the development of marketing acquisition and control business has become more and more mature in recent years, and the application of automated electrical energy measurement collection devices has become increasingly widespread. The pressure of a large number of automated electric energy metering devices on their uplink databases during operation is also increasing. In addition, there are also certain problems in the storage of acquisition and control systems and power big data. Figure 3 is a statistical diagram of the causes of various equipment failures in the power transportation mobile Internet of Things.

As can be seen from Figure 3, among the causes of various equipment failures in the power transportation mobile Internet of Things, the most frequent occurrence is the integrated access equipment (PCM). In addition, power failures caused by optical cables, cables, and other accessory equipment also have a higher frequency. This paper uses the fuzzy logic toolbox in MATLAB to obtain the support of the fuzzy C-means clustering method to achieve the effect of discretion index. Before clustering the attribute values, first analyze the clustering validity of the number of clustering points.

From the calculation results, the five indicators of optical fiber, PCM equipment, microwave equipment, dispatching switch, and auxiliary equipment occupy a relatively important position in the entire indicator system. Among the index weights, the weight of optical fiber is 0.4697, which is the

Statistics of wireless transmission test results
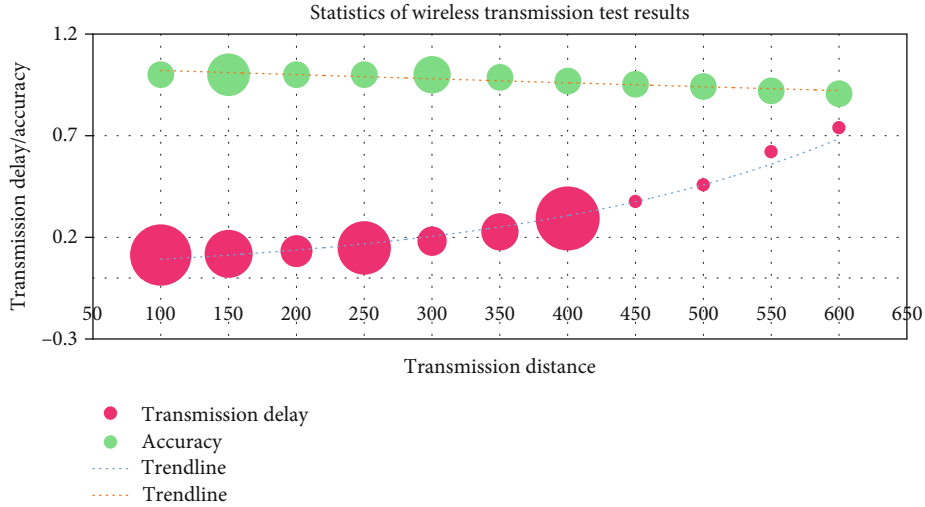
FIGURE 2: Classification of user resource sharing in agricultural information exchange platform.

Statistics of equipment failure causes
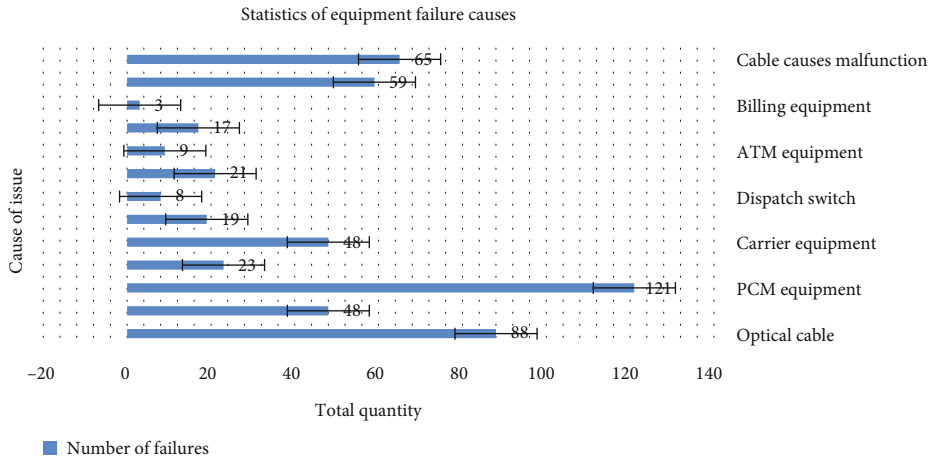
FIGURE 3: Statistical diagrams of the causes of various equipment failures in the power Internet of Things.

highest among the five indicators. This shows that the safety of optical fiber plays a very important role in the information security of the power, transportation, and mobile Internet of Things.

4.2. Safety Analysis of the Electric Traffic Management System Based on Big Data

4.2.1. Security Analysis of Intelligent Power Monitoring Terminal Based on Big Data. When constructing the information security terminal framework of the electric transportation mobile network, this article adds a monitoring terminal to the terminal collection layer, and the monitoring terminal system includes real-time data collection, data display, data statistical analysis, platform resource management, and predictive warning information. The basic characteristics of the Internet of Things technology include a wide variety of collection terminals, a large number of collected data, a wide range of transmission networks, and intelligent data processing. Therefore, power monitoring terminals developed based on big data and the Internet of Things can better

improve the intelligence of the power grid under the premise of ensuring information security. The monitoring system of the mobile power grid is a very important part of the information security framework. The effective visual processing in the monitoring system is precisely because of the auxiliary effect of wireless sensor network technology.

The smart grid is an extremely large system. It is responsible for coordinating the load balance between the user end and the power system. Therefore, it is necessary to monitor the operating status of the equipment in real time to ensure that the equipment maintains normal operation. As the number of users and devices added to the smart grid continues to grow, the amount of data that needs to be monitored in the grid system also multiplies. Therefore, this article starts with improving the control efficiency of smart monitoring terminals and reducing operating costs and improves the monitoring system. Figure 4 is a statistical diagram of power communication consumption.

The improved secret signature scheme in this paper can collect mostly data at the same time and send it to the corresponding recipient. The user can obtain the corresponding
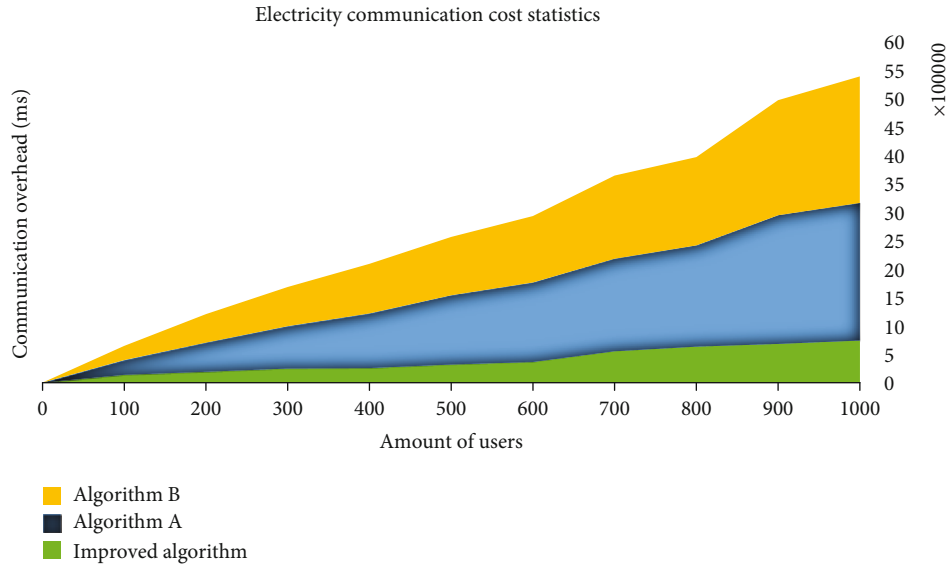
FIGURE 4: Statistic chart of user power communication overhead with different algorithms.
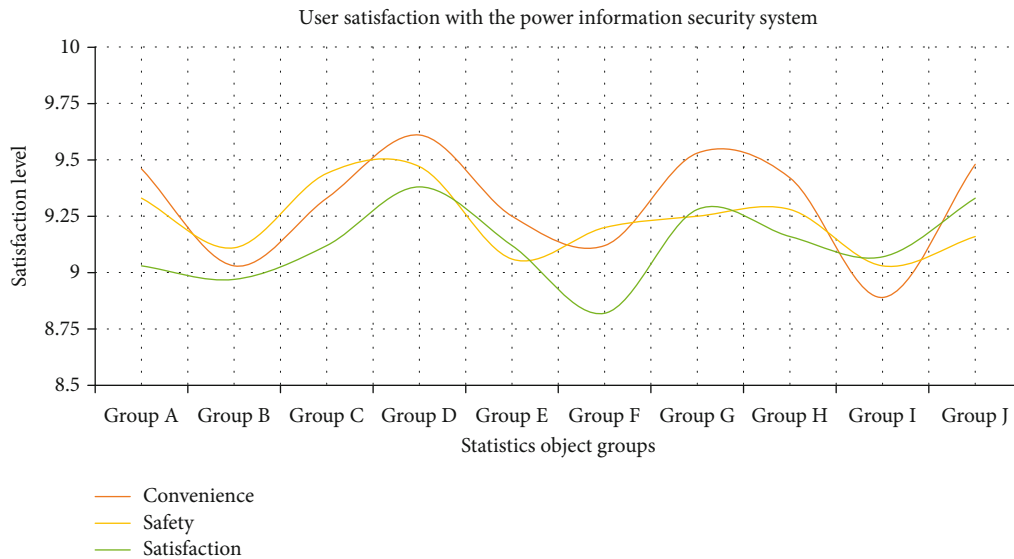
FIGURE 5: Statistics of user satisfaction with the power information security system.

plaintext information after entering the key. Compared with the two types of traditional algorithm solutions that can only aggregate one-dimensional data, the improved power data monitoring system is obviously more competitive. It can be seen from Figure 4 that comparing the communication resources consumed by the three schemes in the process of aggregating multidimensional data, the improved secret signature scheme significantly saves more communication costs. From a practical application point of view, this solution is used in an intelligent power information security system, which can effectively reduce communication resources and reduce the complexity of system calculations while ensuring information security.

4.2.2. Smart Power Privacy and Security Protection Based on Big Data. When constructing the intelligent power informa-

tion security terminal based on big data, this article strengthens the data protection function in the information system based on the principle of ensuring data confidentiality, integrity, and nonrepudiation. Even if someone tries to monitor the power communication information, they cannot decrypt it and get the corresponding plaintext. The use of irreversible hashing to achieve data encapsulation can effectively guarantee the confidentiality of data, and the combination of big data and blockchain technology can further ensure the integrity of the data. In addition, since each sensing node has a unique ID as a token when publishing and receiving information, the signed information has nonrepudiation. Figure 5 is the statistical data of users' satisfaction with the intelligent power system. The survey objects are from 10 different communities. The survey method is a questionnaire in the system, and the scoring mechanism is a ten-point system.

It can be seen from Figure 5 that the average scores of users for the convenience, safety. and overall satisfaction of the power system are 9.312, 9.233, and 9.128, respectively. Among the districts B, F, and I with lower scores, the proportion of middle-aged and elderly people living is higher; so, the understanding of the intelligent power security system is also insufficient, while the higher scores in the districts D and G have a significantly higher proportion of young people. In their view, the intelligent power security platform only needs to use the Internet to easily understand the power consumption and complete the electricity bill payment, which improves the convenience of power security services.

5. Conclusions

This paper analyzes the security of power transportation transmission terminal based on big data. This article introduces the power acquisition, control, and transmission terminal based on the Internet of Things technology, analyzes the basic protocol format of the configuration information data in the power transmission node, and tests the core functions of the power transmission system. The experimental results show that the system can indeed meet in engineering practice, and smart grids have high requirements for real-time and reliability of power transmission. This article analyzes the Internet of Things power marketing information security based on big data. The extensive promotion of marketing acquisition and control systems and intelligent acquisition and control terminals has effectively reduced the work pressure of grassroots personnel in the power industry and improved the efficiency of various services in the power system. In order to solve the deficiencies in the traditional information service system, this article analyzes the causes of failures of various devices in the power transportation mobile Internet of Things, improves the problems in the system architecture, and optimizes the existing business service processes.

This article analyzes the safety of the electric traffic management system based on big data. The improved scheme in this paper uses the designed sign cryption algorithm to collect the multidimensional data of the user's power and send it to multiple receivers. In the regulation stage, after the control center analyzes and processes the multidimensional data, it is stored in an immutable and permanent blockchain to achieve efficient management of power data; grid operators can achieve smart contracts for individual consumer power consumption regulation; equipment suppliers can also implement equipment operating status monitoring to ensure that grid equipment operates as usual. This article investigates users' satisfaction with using smart power systems. From the results, most users hold a positive attitude towards the convenience and safety of power information security systems.

This article has carried out research on the construction of power information security terminal based on big data analysis and Internet of Things technology. In order to ensure the safety of power information, it is necessary to take security measures for the entire power information transmission process. Only when the power smart equipment can complete the work smoothly and can the construction and development of the smart grid be further promoted. When looking forward to the future development direction, we believe that the structure and operation mode of the power grid will undergo major changes with the widespread application of new energy and new materials. Therefore, we believe that the focus of future work can be placed on the following aspects: (1) realize more precise control of the smart grid through the Internet of Things technology, (2) combine the big data analysis function to realize real-time grid operation status and carry out fault warning, and (3) realize power of the high degree of integration of industry and information system that provides users with more convenient power services.

Data Availability

The data underlying the results presented in the study are available within the manuscript.

Conflicts of Interest

The author(s) declare(s) that they have no conflicts of interest.

Acknowledgments

References

[1] J. K. Kok, M. J. J. Scheepers, and I. G. Kamphuis, "Intelligence in electricity networks for embedding renewables and distributed generation," *Journal of Renewable & Sustainable Energy*, vol. 103, no. 2, pp. 179–209, 2015.

[2] E. Fadel, V. C. Gungor, L. Nassef et al., "A survey on wireless sensor networks for smart grid," *Computer Communications*, vol. 71, pp. 22–33, 2015.

[3] W. Ejaz, M. Naeem, A. Shahid, A. Anpalagan, and M. Jo, "Efficient energy management for the Internet of things in smart cities," *IEEE Communications Magazine*, vol. 55, no. 1, pp. 84–91, 2017.

[4] Y. Jia, Z. Xu, L. Lai, and K. P. Wong, "Risk-based power system security analysis considering cascading outages," *IEEE Transactions on Industrial Informatics*, vol. 12, no. 2, pp. 872–882, 2016.

[5] T. Xiaogang, L. Haiyun, and C. Xiaoxuan, "Control and protection system interface design for multi-terminal HVDC flexible project," *Power System Protection & Control*, vol. 43, no. 9, pp. 124–128, 2015.

[6] S. F. Chang, C. F. Chen, J. H. Wen, J. H. Liu, J. H. Weng, and J. L. Dong, "Application and development of Zigbee technology for smart grid environment," *Journal of Power and Energy Engineering*, vol. 3, no. 4, pp. 356–361, 2015.

[7] S. Hong, S. Park, L. W. Park, M. Jeon, and H. Chang, "An analysis of security systems for electronic information for establishing secure internet of things environments: Focusing on

research trends in the security field in South Korea," *Future Generation Computer Systems*, vol. 82, pp. 769–782, 2018.

[8] X. Lu, Z. Qu, Q. Li, and P. Hui, "Privacy information security classification for Internet of Things based on internet data," *International Journal of Distributed Sensor Networks*, vol. 11, no. 8, Article ID 932941, 2015.

[9] J. M. Alcaraz Calero and J. Aguado, "MonPaaS: an adaptive monitoring platformas a service for cloud computing infrastructures and services," *IEEE Transactions on Services Computing*, vol. 8, no. 1, pp. 65–78, 2015.

[10] M. B. Alotaibi, "Antecedents of software-as-a-service (SaaS) adoption: a structural equation model," *International Journal of Advanced Computer Research*, vol. 6, no. 25, pp. 114–129, 2016.

[11] S. Costache, D. Dib, N. Parlavantzas, and C. Morin, "Resource management in cloud platform as a service systems: analysis and opportunities," *Journal of Systems and Software*, vol. 132, pp. 98–118, 2017.

[12] Y. Zhu, L. Li, Y. Song, and L. Wang, "Storage and parallel processing of big data of power equipment condition monitoring on ODPS platform," *Diangong Jishu Xuebao/Transactions of China Electrotechnical Society*, vol. 32, no. 9, pp. 199–210, 2017.

[13] H. Cai, B. Xu, L. Jiang, and A. V. Vasilakos, "IoT-based big data storage systems in cloud computing: perspectives and challenges," *IEEE Internet of Things Journal*, vol. 4, no. 1, pp. 75–87, 2017.

[14] Kaitai Liang, W. Susilo, and J. Liu, "Privacy-preserving ciphertext multi-sharing control for big data storage," *IEEE Transactions on Information Forensics and Security*, vol. 10, no. 8, pp. 1578–1589, 2015.

[15] A. da Veiga and N. Martins, "Information security culture and information protection culture: a validated assessment instrument," *Computer Law & Security Review*, vol. 31, no. 2, pp. 243–256, 2015.

[16] C. Hamon, M. Perninge, and L. Söder, "A computational framework for risk-based power system operations under uncertainty. Part II: case studies," *Electric Power Systems Research*, vol. 119, pp. 66–75, 2015.

[17] J.-S. Cho, Y.-S. Jeong, and S. O. Park, "Consideration on the brute-force attack cost and retrieval cost: a hash-based radio-frequency identification (RFID) tag mutual authentication protocol," *Computers & Mathematics with Applications*, vol. 69, no. 1, pp. 58–65, 2015.

[18] G. Yimin, L. Shundong, D. Jiawei, and Z. Sufang, "Deterministic cloned tag detection protocol for anonymous radio-frequency identification systems," *IET Information Security*, vol. 10, no. 1, pp. 28–32, 2016.

[19] Y. Zhang, W. Liu, W. Lou, and Y. Fang, "Location-based compromise-tolerant security mechanisms for wireless sensor networks," *IEEE Journal on Selected Areas in Communications*, vol. 24, no. 2, pp. 247–260, 2006.

[20] J. Plata-Chaves, N. Bogdanovic, and K. Berberidis, "Distributed diffusion-based LMS for node-specific adaptive parameter estimation," *IEEE Transactions on Signal Processing*, vol. 63, no. 13, pp. 3448–3460, 2015.

[21] M. Jiang, Y. Li, Y. Ge, K. Lou, and W. Gao, "An advanced DV-hop localization algorithm in wireless sensor network," *International Journal of Control and Automation*, vol. 8, no. 3, pp. 405–422, 2015.

[22] S. Fan and H. Zhao, "Delay-based cross-layer QoS scheme for video streaming in wireless ad hoc networks," *China Communications*, vol. 15, no. 9, pp. 215–234, 2018.

[23] K. M. Abdellatif, R. Chotin-Avot, and H. Mehrez, "AES-GCM and AEGIS: efficient and high speed hardware implementations," *Journal of Signal Processing Systems*, vol. 88, no. 1, pp. 1–12, 2017.

[24] A. H. Al-Wattar, R. Mahmod, Z. A. Zukarnain, and N. I. Udzir, "A new DNA-based approach of generating key-dependent ShiftRows transformation," *International Journal of Network Security & Its Applications*, vol. 7, no. 2, pp. 93–102, 2015.

[25] H. K. Kim and M. H. Sunwoo, "Low power AES using 8-bit and 32-bit datapath optimization for small Internet-of-Things (IoT)," *Journal of Signal Processing Systems*, vol. 91, no. 11-12, pp. 1283–1289, 2019.

WILEY | Hindawi

Research Article

Modeling of Badminton Intelligent Teaching System Based on Neural Network

Ping Wang (iD)

Institute of Physical Education, North Minzu University, Yinchuan, 750021 Ningxia, China

Correspondence should be addressed to Ping Wang; 2009031@nmu.edu.cn

With the popularity of neural networks and the maturity of network technology, fully functional intelligent terminals have become indispensable devices for people's lives, research, and entertainment. However, in the badminton teaching of people's daily exercise, the old traditional teaching mode is still used, which cannot achieve good teaching effects. In order to study the best of badminton teaching, this article is based on the previous research, by introducing neural network, using literature data method, questionnaire survey method, interview method, experimental method, and other research methods to conduct research. The intelligent learning of the network is connected, experiments are designed to be applied, and then, data analysis is conducted. The research results show that with the use of smartphone mobile learning teaching methods, the experimental group students' technical movements, theoretical knowledge, learning interest, and learning enthusiasm are about 20% higher than those of the control group, and the badminton intelligent teaching system based on neural network is better than the control group's traditional teaching methods. The satisfaction of the students in the experimental group was also higher than that of the students in the control group. Based on what network, the satisfaction of badminton teaching can reach more than 90%. This student recognizes and accepts the teaching methods of intelligent teaching.

1. Introduction

Badminton sports were introduced to China in 1920 and gradually evolved into popular sports as the times evolved. In college physical education, badminton instruction is generally faced by ordinary college students, and the foundation of badminton technology is very weak or poor. Zero foundation: first, they face more complex badminton skills; after the normal teaching process from easy to difficult, from part to the whole, students tend to easily forget and master the technical essentials inaccurately; second, they have to face relatively boring explanations; when explaining difficult techniques, students are easily distracted and have low interest in learning.

In the process of badminton teaching in colleges and universities, it is generally faced with ordinary college students. The foundation of badminton technology is very weak or zero, first of all, facing more complex badminton skills, normal education from part to whole, from easy to difficult. After the process, students tend to forget and master the technical essentials inaccurately; secondly, when faced with relatively boring and incomprehensible technical explanations, students are easily distracted and have a low interest in learning; finally, college badminton technical teaching needs. Faced with the large number of students, it is impossible for the teacher to take into account the acceptance of each student in a short time of teaching. Many colleges and universities have relatively few badminton teaching hours, and most colleges and universities only offer badminton teaching for one semester. It takes a relatively long time to teach complex and diverse badminton. Educational progress is relatively tight, and students with relatively low receptivity cannot take care of it. Therefore, it is particularly necessary to construct a badminton intelligent education system based on a neural network [1].

For the intelligent teaching of badminton, experts at home and abroad also have a lot of research. In foreign countries, the most active research on intelligent teaching is in the United States, European countries, Japan, Canada, and so on. American universities such as Stanford, MIT, Memphis,

Carnegie Mellon, and California have developed some intelligent prototype systems. For example, the National Science Foundation of the United States has invested US$22.50 million in the research and development of learning and intelligent systems for human learning and creation. The Tutor system developed by Memphis University over 25 years can be used by computers to give prompts and hints to students' problems. In response, Tutor can make decisions based on typing and oral responses to the question without multiple choices and give corresponding explanations for possible grammatical or semantically incorrect language [2]. However, domestic badminton teaching started relatively late. Liu [3] pointed out in the article "Discussion on the Development Trend of Badminton in Colleges and Universities" that with the improvement of the country's comprehensive strength, quality education has become the basis for talent training; it has become more and more important to promote the overall development of school physical and psychological qualities. At the same time, the physical quality of college students has been declining year by year. With the gradual popularization of badminton, college badminton teaching also appears to be particularly important. While improving the quality of teaching, teachers should improve their own technical level and innovate teaching methods. Li [4] pointed out in the article "Study on the Practice of Multilevel Cooperative Teaching Method in Badminton Teaching" that badminton is an antagonistic sport across the net, especially doubles, which requires the tacit cooperation of two people. Therefore, it should be used in the process of badminton teaching in colleges and universities. Try more new teaching methods, and do more teaching practice in cultivating students' sense of unity and cooperation and learning interest. In his article, I tried to apply the hierarchical cooperative teaching method in the process of college badminton teaching. After experimental comparative research, the cooperative consciousness of experimental class students and the interest, initiative and enthusiasm of students in learning. These studies have provided some references for the research of this article, but due to the lack of samples in previous experiments, the experimental results are difficult to reproduce and are not operable.

This article briefly summarizes and analyzes existing intelligent education systems and neural network technologies. Aiming at the problems of learner modeling and selection of teaching strategies, based on repeated discussions in the study group, it is based on relevant educational objective theories and multiple intelligent theory, project reflection theory, and error backpropagation algorithm technology, designing and describing the theoretical model structure of intelligent guided badminton system based on neural network technology, which lays the foundation for the research of badminton intelligent teaching system and the realization of intelligent goals.

2. Intelligent Teaching Methods of Badminton

2.1. Neural Network. A neural network is composed of a large number of artificial neurons. Humans use computer technology to simulate and realize the functional connection of biological neurons [5]. The weight of the connections between each neuron is determined by a particular learning algorithm, and the structure has a particular function. Network system: each neuron of the neural network is nonlinear, interacts and affects during operation, and has the properties of a nonlinear (dynamic) system [6]. At the same time, the neural network has the characteristics of high-dimensionality (composed of many neurons, multiple input-multiple output), parallelism, distribution, self-adaptation, self-organization, and self-learning capabilities [7]. A single neuron is not complex, but a neural network of many neurons can produce very complex and very rich phenomena and consequences.

In a neural network, each neuron is an independent information unit, and the entire network system performs parallel and distributed processing [8]; its operations not only follow logical rules but can also operate in accordance with the rules of different disciplines such as physics, mathematics, neurobiology, and psychology [9]. The data acquisition module, control module, and data processing module are the three major components of the neural network-based control system [10]. The control system of the neural network is shown in Figure 1.

Neural controllers already have huge applications in the field of automation. In recent years, great results have been achieved in the application of control systems in the fields of industry, aviation, and robotics [11]. However, few people have set foot in the field of intelligent badminton teaching, which is closely related to people's lives. Intelligent badminton teaching is only a controller and does not have thinking, that is, it cannot think and decide the control scheme of the system according to the environment [12]. The self-learning and self-adaptive characteristics of the neural network provide a solution for it [13].

Generally speaking, the algorithm of neural network is as follows:

$$G(x, y) = \exp\left(-\frac{x^2 + y^2}{2\sigma^2}\right), \tag{1}$$

where σ is the mean square error. It is achieved by convolution of smoothing kernels with different σ values with the image. The resulting expression formula is as follows:

$$L(x, y) = -\frac{1}{\pi\sigma^4}\left(1 - \frac{x^2 + y^2}{2\sigma^2}\right)\exp\left(-\frac{x^2 + y^2}{2\sigma^2}\right). \tag{2}$$

The effect is related to the value of σ; the smaller the σ, the smaller the smoothing effect, and the more noise

$$Q = \frac{1}{2a^2 r^{-1}}\left(\frac{2b^2}{a^2 r^{-1}}p - t\right)^{-1}\left[a^2 r^{-1} t^2 + 2(1 - b^2)t\right]. \tag{3}$$

In case $a \in [-1, 0] \cup [0, 1]$,

$$K = \frac{a}{2br}t, \tag{4}$$
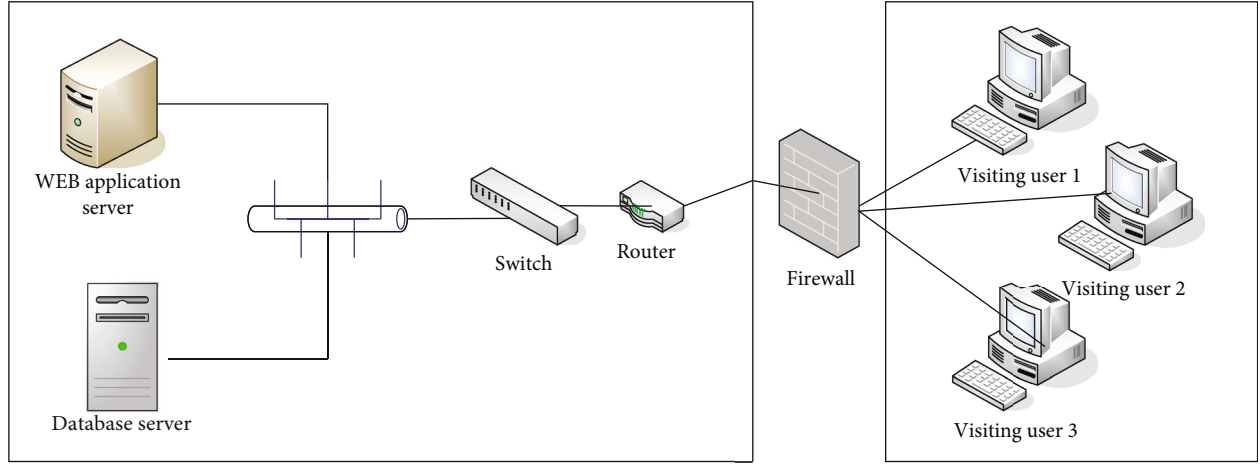
FIGURE 1: Basic framework diagram of a neural network.

$$\lambda_x(ct_n - t) > 0. \tag{5}$$

And so

$$Q = \frac{1}{2a^2r^{-1}} \left(\frac{2b^2}{a^2r^{-1}} t - L \right)^{-1} \left[a^2r^{-1}L^2 + 2(1 - a^2)L \right]. \tag{6}$$

Mathematical morphology method is to use set algebra theory to analyze and process based on geometric characteristics. Mathematical morphology methods mainly use corrosion and expansion operations to extract morphological boundaries [14]. You can get more accurate boundaries by combining the contraction effect of a calculation and the extension effect of an extension calculation with a specific logical operation. According to the idea of the maximum between-class variance method to determine the fitness function, the formula is as follows:

$$f(t) = \sigma(t)^2 = w_1(t) * w_2(t) * (u_1(t)) - u_1(t)^2. \tag{7}$$

Among them, t is the threshold, $f(x)$ is the fitness function, $w_1(t)$ is the number of nodes less than the threshold, and $w_2(t)$ is the number of nodes greater than the threshold [15]. Generate a random number in the interval, and select the individual corresponding to the area where the random number belongs. It can be seen that the greater the fitness of an individual, the higher the probability of being selected. The probability of an individual being selected is

$$P_i = \frac{f_i}{\sum_{i=1}^{n} f_i}. \tag{8}$$

In this badminton intelligent teaching system, the system extracts user data from a database as input to train a neural network. That is, it uses the self-learning and self-adaptive properties of neural networks to learn the user's lifestyle. Then, according to the real-time training data, a control scheme close to the user's life habits is obtained [16]. Therefore, the intelligent badminton teaching system after the introduction of neural network can formulate badminton

teaching strategies for the user's living habits according to the user's habits. Give the teaching system a "brain," and finally free users from the cumbersome traditional teaching [17]. Since this system is to learn the user's living habits in real time and then to formulate a control plan, the system can quickly adjust to this situation when the user changes or the user's habits change. The above advantages fully reflect the improvement of the intelligence of the badminton intelligent teaching system after the introduction of the neural network [18].

2.2. Smart Teaching. With the continuous promotion of intelligent learning, people's intelligent learning exchanges continue to deepen, and a large amount of semistructured data has also been accumulated in various learning platforms [19]. There are various types of data, and people organize and sort out the hidden value behind it. Educational data mining refers to mining the unique data of the education system so that the chaotic educational data becomes useful information, which can better understand students, make educational decisions for us, and optimize our badminton teaching [20].

Intelligent teaching generally refers to a digital learning support system that adaptively organizes knowledge resources, implements teaching strategies, provides teaching process services, and conducts teaching evaluation with the help of artificial intelligence and computer technology in a distributed network environment [21]. The ultimate importance of research is to give intelligence to computer systems. Computer systems replace human education to some extent to achieve the best education, reduce the workload of human teachers, improve the quality of education, enhance human understanding of the process of self-awareness, and relate. Promote the development of subjects.

Teaching not only has important value for the development of individual students but also has irreplaceable value for the development of society [22]. This is because the continuation and development of society mainly refer to the continuation and development of politics, economy, culture, and technology. The cultivation of people who develop social politics, economy, culture, and technology must be achieved

through education, more precisely through school education. Teaching is the basic form of school education [23]. With its basic educational form, schools promote students to receive a planned, purposeful, and systematic education. Through teaching activities, students can acquire the necessary knowledge, skills, emotional attitudes and values, etc., and can promote the progress of social politics, economy, culture, and technology, thereby promoting social development. This kind of value that takes social development as the main body and serves the real life of society and the future development of society is the social value of teaching, which is based on the individual value of teaching [24].

Smart education has changed the way students acquire knowledge and has an intangible impact on traditional teaching models. Online teaching is the trend of future teaching development. Each teacher has their own advantages and disadvantages [25]. For example, some teachers are experienced but lack energy physically or due to other reasons. Some teachers are energetic but lack experience; some teachers are quick-thinking but jumping. They are more sexual; some teachers are careful and patient but not flexible enough. Online teaching is not only helpful for students to find their own learning level but also for teachers to find their own teaching level, so as to better utilize their own advantages.

University courses are independent subjects, related courses require scientific placement and research, and much energy can be spent on research to place the corresponding courses in a scientific and rational way. In order to teach courses in colleges and universities, science and correct guiding ideology are indispensable. From a long-term perspective, the arrangement of courses in colleges and universities must adhere to the concept of being "reasonable and practical" and integrate sports teaching in the context of the new era. Relevant trends of thought promote the development of students' sports awareness, so as to achieve the realization of students' self-worth, and make badminton teaching an indispensable part in the true sense.

Intelligent teaching is generally carried out in groups, and only reasonable grouping can ensure the efficiency of learning. Through analysis, we can conclude that the learning effect of students in different groups will be different. First of all, the original group leader recruitment and the free grouping of students have changed to free grouping under the guidance of teachers. Completely free grouping. Students who are more familiar in a class will get together in a group. Because each student is too familiar with each other in the group, when studying, you cannot concentrate on learning, and there are too many small chat topics. Teachers can group students reasonably on the basis of students' willingness so that everyone can have a good learning atmosphere and learn more effectively. Secondly, teachers should understand the students' personality, preferences, learning ability, and learning foundation through pretests before grouping, and grouping different students can achieve the effect of learning from each other's strengths and weaknesses. Finally, teachers should select students with organizational skills and high levels of activity as the group leader, because the activity and sense of responsibility of the group leader play a vital role in the learning of the students in the group.
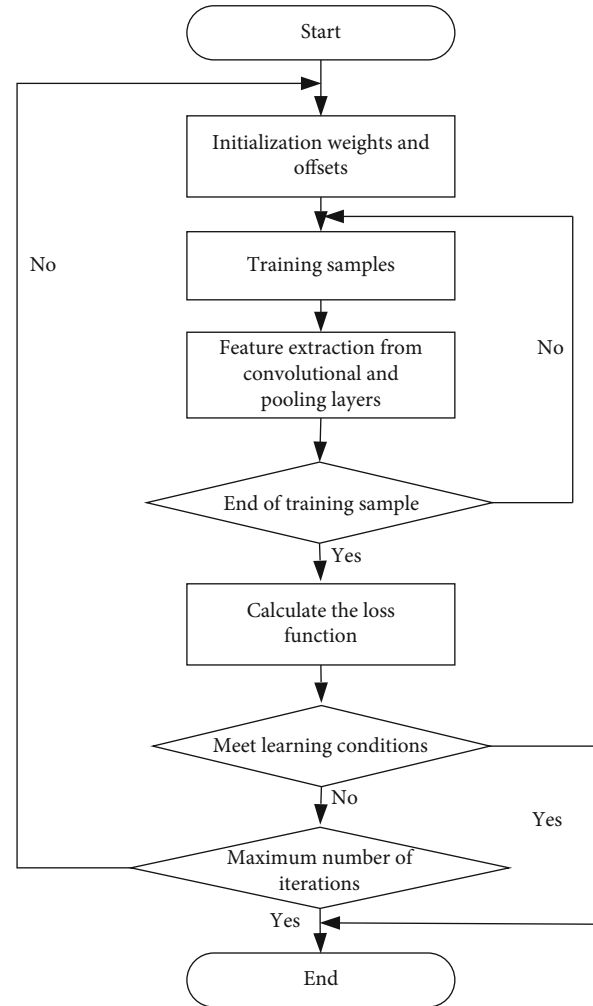
FIGURE 2: Intelligent teaching process.

2.3. Badminton Teaching. Badminton is a kind of mass sports event. Basically everyone can play, but the movements are not very standardized. Due to the lack of class hours in college badminton teaching, usually after the basic skills of badminton are taught, systematic learning and training will not be carried out. The direct badminton sparring practice did not correct some of the students' irregular movements, nor did they have time to guide and systematically complete the movement learning. Without being able to connect the courses, students find learning in class boring and boring. After completing the instruction, the teacher must prepare for the test and exam to complete the instruction progress, and the student will not practice again after the exam. In the process of badminton teaching in colleges and universities, due to the limitation of class time and insufficient time, most students are required to be taught in technology while ignoring the explanation of badminton theory.

Badminton teaching is also a sports subject with both technical and theoretical aspects, but in college badminton teaching, technical teaching still occupies the dominant position. In the process of technical teaching, it is first necessary to have venues and equipment [26]. Although currently compared to football, basketball, and volleyball courts, the football, blue,

TABLE 1: Student level statistics.

	Forehand	High forehand	Forehand lob	Forehand	Forehand rubbing	Backhand rubbing	P
Class 1	2.11	2.44	1.81	1.92	2.28	2.45	$0.046 < 0.05$
Class 2	2.18	2.09	2.44	1.89	1.96	1.99	$0.014 < 0.05$
Class 3	2.21	2	2.15	2.48	1.96	2.44	$0.012 < 0.05$
Class 4	2.29	2.05	2.19	2.21	2.01	2.11	$0.023 < 0.05$
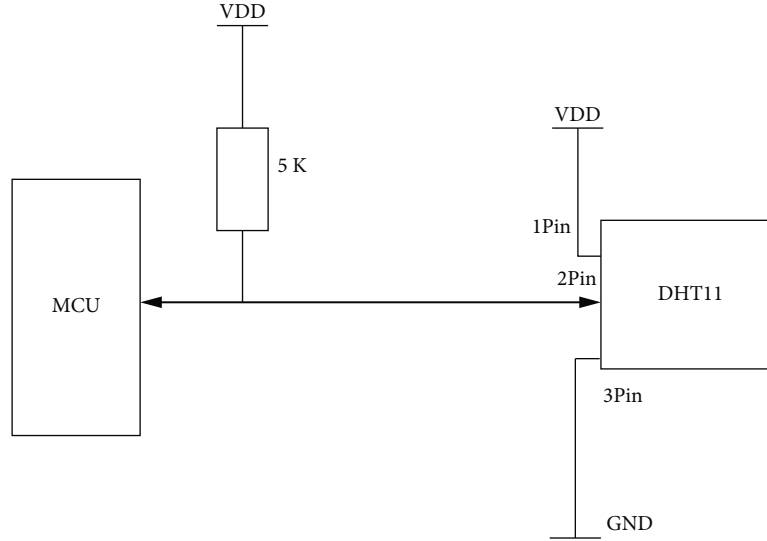
FIGURE 3: Typical application circuit.

and volleyball stadiums of many colleges and universities still occupy most of the college's sports grounds, although for badminton, the requirements for venues and other hardware facilities are relatively low. The area of badminton sports venues is generally far less than that of the three major sports venues. Therefore, many universities have to control the number of participants in badminton activities without reducing the number of classes. Badminton courts and badminton equipment are also two major obstacles.

For badminton, the purpose of students' learning is more practical, direct, and purposeful. The knowledge goal is to learn the basic knowledge of badminton, as well as badminton technology, tactics, and basic refereeing knowledge through a stage of learning. The goal of the skill is to be able to master basic badminton techniques and tactics, badminton training methods, and physical training with badminton training in class. Emotional attitude is to combine the characteristics of badminton sports [27], cultivate good physical exercise habits, and cultivate lifelong sports ideas for college students. Cultivate students to actively participate in physical exercises, and cultivate the students' hard-working spirit and the tenacious quality of persevering in hard work. The teaching process is shown in Figure 2.

3. Experiments on Badminton Intelligent Teaching Methods

3.1. Subjects. This paper conducts group experiments on the badminton teaching of a middle school student in this city.

One group uses traditional badminton teaching, and the other uses intelligent robot teaching based on neural network. Make full use of the research results in the field of college badminton education and teaching, construct a system for the optimization of college badminton teaching, and put forward feasibility and scientific opinions on the badminton teaching reform, so as to help colleges and universities build a badminton teaching system that is more suitable for students.

3.2. Construction of Teaching System

3.2.1. Neural Network Construction. We have built a machine that can perform intelligent teaching through neural network, which can teach according to the personal characteristics of students, and its operation mode is as follows.

For each input $X(k)$, calculate the output $Y(k)$ of each layer

$$Y(k) = [y_1(k), y_n(k)],$$
$$y_j^i(k) = \phi\left(s_j^k(k)\right) = \frac{1}{1 + e^{-s_j^i(k)}}, \tag{9}$$

$$s_j^i(k) = \sum_{i=0}^{N_{i-1}} W_{ji}^i y_i^{i-1}(k) = \left(W_j^i\right)^t Y^{i1}(k), \tag{10}$$

$$\left(W_J^I\right)^T = \left[w_{j0}^i, w_{j1}^i, \cdots, w_{jN-1}^i\right], \quad w_{j0}^i = -\theta_j^1,$$
$$\left(Y^l(k)\right)^t = \left[1 \cdot y_1^i(k), \cdots, y_{N1}^i(k)\right]. \tag{11}$$
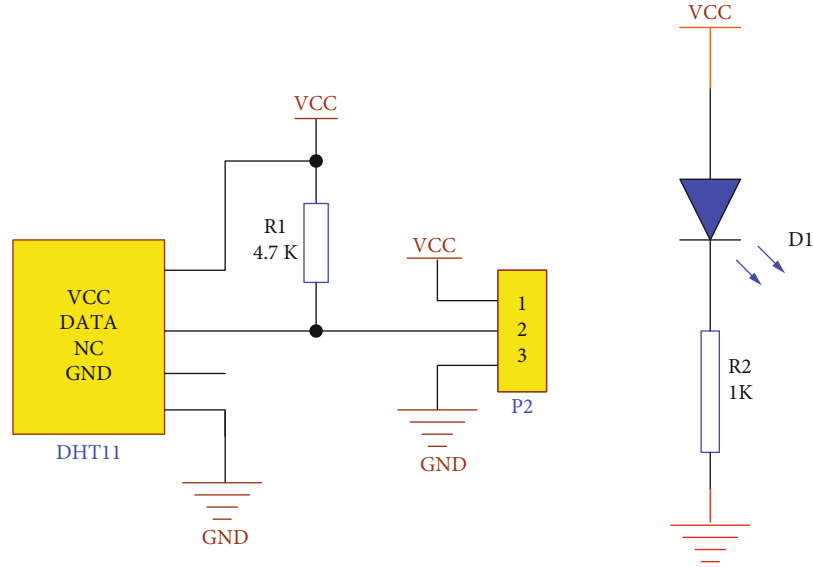
FIGURE 4: DHT11 schematic diagram.

From this, we can get the general situation, that is, for any i-th layer, there is

$$\Delta w_{ji}^l(k) = \delta_j^l(k)y_i^{l-1}(k). \tag{12}$$

Among them,

$$\delta_j^l(k) = \begin{cases} y_j^l(k)\left(1 - y_j^l(k)\right)\left(d_j(k) - y_j^l(k)\right), & \text{to the output layer, } y_j^l(k) = y_j(k), \\ y_j^l(k)\left(1 - y_j^l(k)\right)\sum_q \delta_q^{l+1}(k)w_{qj}^{l+1}(k), & l \le L - 1, \text{ to layer 1, } y_j^0(k) = x_i(k). \end{cases} \tag{13}$$

3.2.2. Student Parameter Statistics. We make statistics on the badminton level of 4 classes in a middle school so that we can compare the level changes after different teaching, as shown in Table 1.

3.3. Determine the Evaluation Weight. The index weight is a numerical index indicating the importance and function of the index. In the indicator system of the evaluation plan, the weight of each indicator is different. Even if the indicator level is the same, the weight is different. Index weight is also called weight and is usually represented by a. It is a number greater than zero but less than 1, and the sum of the weights of all first-level indicators must be equal to 1, that is, satisfy the conditions $0 < a < 1$ and $\sum a - 1$.

3.4. Comprehensive Evaluation Model. At present, there are two main evaluation models: one is the main factor highlight model, and the other is the weighted average model. If the weight of a single factor is significant and the evaluator has a predominant factor, you can choose a major key factor model. If the weight of the evaluation factors is relatively average, you can choose the weighted average model. These two models have their own characteristics. In the specific implementation process, the two methods can be imple-

FIGURE 5: Intelligent badminton teaching machine model (from http://image.baidu.com/).

mented separately. Finally, compare the results of the two models.

4. Badminton Intelligent Teaching Methods

4.1. Intelligent Machine Model. In order to complete intelligent badminton teaching, our system decision-making model based on the production rules of "cause and effect" has indeed improved the level of intelligence of the system in the early application, but there are also difficulties that cannot be overcome in practice. First, teaching strategies are difficult to obtain and express. Second, the expression format of production rules is fixed, and it is difficult to maintain an educational strategy model. For this reason, we have designed an intelligent model that is more suitable for teaching. The design concept is shown in Figures 3 and 4.

TABLE 2: Basic situation of students.

Physical fitness	Group	Mean	T	P
Height	Test group	176.33 ± 7.102	1.6003	0.184 > 0.05
	Control group	174.33 ± 6.783		
Body weight	Test group	65.6667 ± 7.652	1.4005	0.622 > 0.05
	Control group	64.6667 ± 8.015		
Badminton	Test group	5.266 ± 0.125	0.5645	0.602 > 0.05
	Control group	5.233 ± 0.359		
Standing long jump	Test group	2.37 ± 0.382	0.2031	0.848 > 005
	Control group	2.34 ± 0.295		

TABLE 3: Technical level of students.

	Experimental class	Control class	T	P
Forehand	81.6	80.0	1.789	0.077
Forehand backcourt	77.4	75.8	1.444	0.153
Forehand to pick the backcourt high ball	80.0	79.2	0.99	0.325

As shown in the figure, based on the neural network model, this paper redesigns the system structure on the basis of retaining the traditional machine functions, enhances and enriches the self-organization, self-learning, and self-adaptive functions of the system decision-making model, and comprehensively improves the guidance of the system the ability to organize, make decisions, and plan for the environment and process. The final intelligent badminton teaching machine is shown in Figure 5.

Through this intelligent machine [28], we have established a direct connection between the data management model and the student model, making the entire teaching process a multivariable control state of a single-input multiple-output system and a multiple-input multiple-output system. Teaching strategy resources include a wealth of experience-level teaching strategy resources, all of which can be continuously filled, organized, scheduled, and real-time data processed. With the network-style parallelism, intersection, and storage under the variable structure of the three major data modules of teachers, students, and data management, the teaching strategy of system decision-making will no longer be "solidified" and must be dynamic, diverse, and selectable.

4.2. Basic Situation of Students. Before the implementation of the teaching, we conducted a basic situation test on the two groups of students in the experimental group and the control group. The test content included physical fitness, degree of preference for badminton, learning interest, and learning enthusiasm. The data source is in the form of experimental method and questionnaire survey as shown in Table 2.

After an independent sample t-test ($P > 0.05$), data were measured by the physical shape and badminton-specific quality of the experimental and control classes ($P > 0.05$) and the physical shape and badminton in the experimental and control groups. You can see that there is no specific qual-

TABLE 4: Students' interest in badminton.

	Very interested	Interested	General	Not interested
Experimental class 1	7	18	9	6
Experimental class 2	9	12	11	5
Control class 1	6	15	8	7
Control class 2	7	16	12	6

ity before the experiment. We have made relevant statistics on the existing badminton skills of the students in the experimental class and the control class, as shown in Table 3.

As shown in the table, the data were obtained after the test, using the analysis of variance to get the experimental class and the control class in the badminton technique of the forehand backcourt high ball, forehand hit the backcourt high ball, and forehand to pick the backcourt high ball. The P values are all greater than 0.05, which shows that there is no significant difference in the badminton skill level between the experimental class and the control class. We make statistics on the badminton interests of the two groups of people, as shown in Table 4.

From the recovery of the questionnaires sent to the students and analysis according to the display of the statistical graph, 46 students in the experimental class are interested in badminton, accounting for 59.7% of the total number. The students in the control class are interested in badminton. The number is 42, accounting for 56% of the total; 11 people in the experimental class are not interested in badminton, accounting for 14.3% of the total number of people, and 13 people in the control class are not interested in badminton, accounting for 17.3% of the total number of people. In
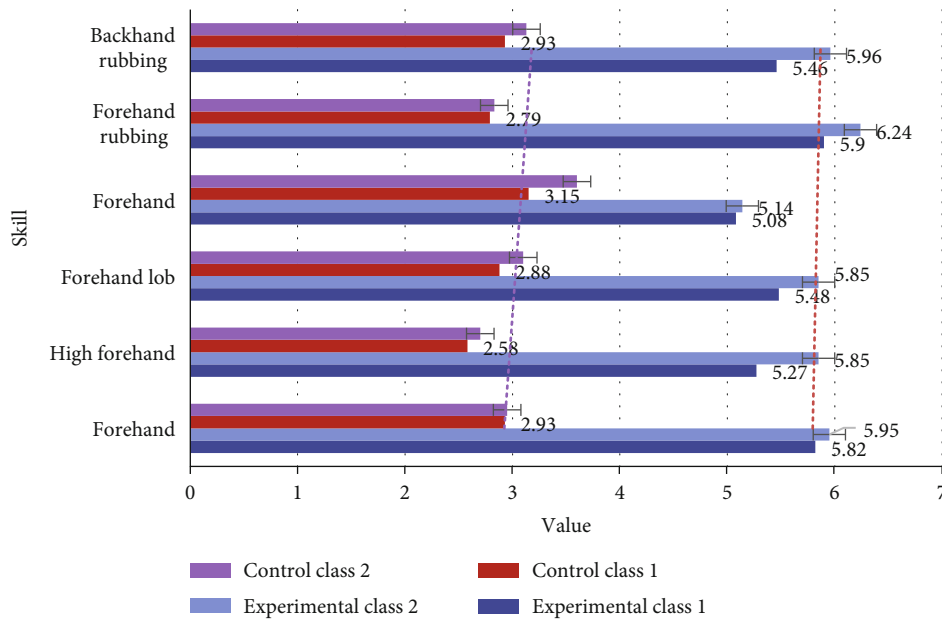
FIGURE 6: The difference between students' skills after training.
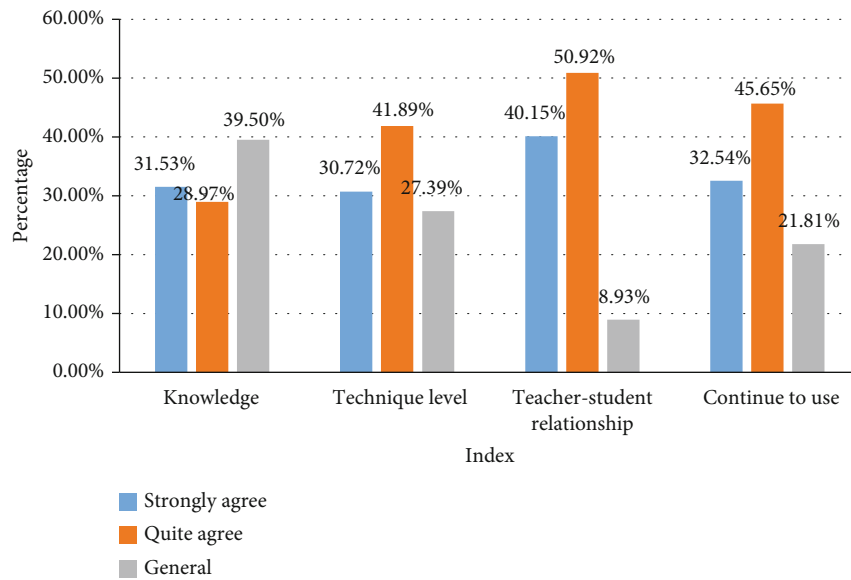
FIGURE 7: Student evaluation effect.

general, the percentages of the number of people interested and not interested in badminton in the experimental class and the control class are not much different. From the results of data analysis, before the teaching experiment, the students in the experimental class and the control class are interested in badminton. There is no obvious difference in the degree.

4.3. Changes before and after Training.
After three weeks of training in different teaching methods, we have made statistics on the changes in the badminton level of the students in the class. The changes in badminton level are shown in Figure 6.

From the figure, we can see that after training with different teaching methods, there is a big difference in the badmin-

ton level of the students. After the students in the experimental class are taught, their badminton skills have increased significantly. However, the score increase and knowledge reproduction badminton technique test results of the control class students in the second test are not very important. This result proves that there is a certain difference between the intelligent badminton teaching method under the neural network and the traditional teaching method. The intelligent teaching method has a greater advantage in consolidating and allowing students to firmly grasp the knowledge. After the teaching, we made a survey on the students' understanding of badminton, as shown in Figure 7.

From the figure, we can see that 31.53% and 28.97% of the students who understand badminton knowledge very much agree and quite agree, and 39.5% of the average students think it is important to improve the level of badminton skills and change the relationship between teachers and students. And in the question survey that needs to continue to be used in teaching, the total proportions expressing strong agreement and relatively agree are 72.61%, 91.07%, and 78.19%, respectively; the number of disapproval is 0. It can be seen from this that most students believe that the intelligent teaching model has advantages in improving interpersonal relationships and improving abilities. In terms of continued use of satisfaction, this teaching method can be considered acceptable and recognized.

5. Conclusion

By using an intelligent education system based on a neural network, students' technical movements, theoretical knowledge, interest in learning, and learning motivation are higher than those in conventional education, and student satisfaction is also higher than that in conventional teaching. It will be higher than the law. Students are more concerned about intelligent teaching. The way of learning and teaching is recognized. Smartphone mobile teaching makes the relationship between teachers and students more harmonious and intimate and improves students' enthusiasm and initiative to participate in badminton learning, and their academic performance is improved. The effect is better than traditional teaching methods. It can be passed to students positively and promote students' development of technology and knowledge capabilities. This article also has certain shortcomings. Due to my limited time and ability, the sample size of the experimental subjects is small, the implementation content of the intelligent badminton teaching method design using neural network in this article is still imperfect, and the scope of the experiment should be expanded, with further scientific and comprehensive research to increase its effectiveness. In the future, it can be studied whether it can be applied to the teaching of other subjects and whether it is more practical for girls.

Data Availability

The data underlying the results presented in the study are available within the manuscript.

Conflicts of Interest

The author declares no conflict of interest regarding the publication of the research article.

Acknowledgments

References

[1] D. Shen, "An experimental research on layered teaching in badminton optional course teaching," *Sports Boutique (Academic Edition)*, vol. 35, no. 8, pp. 56-57, 2016.

[2] M. Ali, L. T. Jung, A.-H. Abdel-Aty, M. Y. Abubakar, M. Elhoseny, and I. Ali, "Semantic-k-NN algorithm: an enhanced version of traditional k-NN algorithm," *Expert Systems with Applications*, vol. 151, article 113374, 2020.

[3] M. Segler, M. Preuss, and M. P. Waller, "Planning chemical syntheses with deep neural networks and symbolic AI," *Nature*, vol. 555, no. 7698, pp. 604–610, 2018.

[4] D. Holden, T. Komura, and J. Saito, "Phase-functioned neural networks for character control," *ACM Transactions on Graphics*, vol. 36, no. 4, pp. 1–13, 2017.

[5] Y. Ganin, E. Ustinova, H. Ajakan et al., "Domain-adversarial training of neural networks," *Journal of Machine Learning Research*, vol. 17, no. 1, 2017.

[6] H. Lu, R. Setiono, and H. Liu, "Effective data mining using neural networks," *IEEE Transactions on Knowledge and Data Engineering*, vol. 8, no. 6, pp. 957–961, 2016.

[7] Y. Han, J. Kim, and K. Lee, "Deep convolutional neural networks for predominant instrument recognition in polyphonic music," *IEEE/ACM Transactions on Audio Speech & Language Processing*, vol. 25, no. 1, pp. 208–221, 2017.

[8] B. Han, J. Li, S. Jinshu, M. Guo, and B. Zhao, "Secrecy capacity optimization via cooperative relaying and jamming for WANETs," *IEEE Transactions on Parallel and Distributed Systems*, vol. 26, no. 4, pp. 1117–1128, 2014.

[9] B.-K. Kim, J. Roh, S. -Y. Dong, and S.-Y. Lee, "Hierarchical committee of deep convolutional neural networks for robust facial expression recognition," *Journal on Multimodal User Interfaces*, vol. 10, no. 2, pp. 173–189, 2016.

[10] F. Dernoncourt, J. Y. Lee, O. Uzuner, and P. Szolovits, "De-identification of patient notes with recurrent neural networks," *Journal of the American Medical Informatics Association*, vol. 24, no. 3, pp. 596–606, 2017.

[11] Z. Lv and L. Qiao, "Deep belief network and linear perceptron based cognitive computing for collaborative robots," *Applied Soft Computing*, vol. 20, article 106300, 2020.

[12] G. Suddrey, C. Lehnert, M. Eich, F. Maire, and J. Roberts, "Teaching robots generalisable hierarchical tasks through natural language instruction," *IEEE Robotics and Automation Letters*, vol. 2, no. 1, pp. 201–208, 2016.

[13] L. Zhou, H. Li, and K. Sun, "Teaching performance evaluation by means of a hierarchical multifactorial evaluation model based on type-2 fuzzy sets," *Applied Intelligence*, vol. 46, no. 1, pp. 34–44, 2016.

[14] L. Yang, "Discussion on physical education teaching reform in colleges and universities," *Science & Technology Information*, vol. 16, no. 5, pp. 159-160, 2018.

[15] Z. Zhentao, "Discussion on the reform and development of physical education in primary and middle schools," *Contemporary Sports Science & Technology*, vol. 6, no. 28, pp. 115-116, 2016.

[16] Y. Liang, "The enlightenment of the "people-oriented" education view on the reform of college physical education,"

Teaching Management and Education Research, vol. 2, no. 8, pp. 30–32, 2017.

[17] Y. Wang, "Rethinking the current reform of college physical education," *Sports World (Academic Edition)*, vol. 751, no. 1, pp. 125-126, 2016.

[18] R. Yu, "On the innovation education and the reform of middle school physical education," *Xue Weekly*, vol. 283, no. 7, pp. 186–189, 2016.

[19] X. Shenglong, "Research on influencing factors and development countermeasures of physical education reform in Chinese universities," *Journal of Jiamusi Vocational College*, vol. 159, no. 2, p. 345, 2016.

[20] J. Bin, "College physical education teaching reform from the perspective of general education," *Contemporary Sports Science & Technology*, vol. 7, no. 4, pp. 7-8, 2017.

[21] L. Yang, "Employment-oriented reform of physical education in higher vocational colleges," *Quality Education in West China*, vol. 3, no. 14, pp. 76–78, 2017.

[22] X. Chen, "Employment-oriented reform of physical education in higher vocational colleges," *Stationery & Sports Supplies & Technology*, vol. 20, no. 381, pp. 101-102, 2017.

[23] X. Ma, "Employment-oriented reform of physical education in higher vocational colleges," *New West*, vol. 438, no. 11, pp. 162-163, 2018.

[24] X. Wan, "Employment-oriented reform of physical education in higher vocational colleges," *Nongjia Staff*, vol. 16, no. 556, pp. 205–207, 2017.

[25] H. Wang, "Research on higher vocational physical education teaching reform oriented by teaching innovation," *Journal of Hubei Correspondence University*, vol. 29, no. 8, pp. 129-130, 2016.

[26] Z. Lv, A. Halawani, S. Feng, H. Li, and S. U. Réhman, "Multimodal hand and foot gesture interaction for handheld devices," *ACM Transactions on Multimedia Computing, Communications, and Applications (TOMM)*, vol. 11, no. 1s, pp. 1–19, 2014.

[27] M. Abdel-Basset, M. Mohamed, M. Elhoseny, L. H. Son, F. Chiclana, and A. E.-N. H. Zaied, "Cosine similarity measures of bipolar neutrosophic set for diagnosis of bipolar disorder diseases," *Artificial Intelligence in Medicine*, vol. 101, p. 101735, 2019.

[28] G. Dartmann, H. Song, and A. Schmeink, *Big Data Analytics for Cyber-Physical Systems: Machine Learning for the Internet of Things*, Elsevier, 2019.

WILEY | Hindawi

Retraction

Retracted: Holographic Projection Technology in the Field of Digital Media Art

Wireless Communications and Mobile Computing

This article has been retracted by Hindawi following an investigation undertaken by the publisher [1]. This investigation has uncovered evidence of one or more of the following indicators of systematic manipulation of the publication process:

1. Discrepancies in scope
2. Discrepancies in the description of the research reported
3. Discrepancies between the availability of data and the research described
4. Inappropriate citations
5. Incoherent, meaningless and/or irrelevant content included in the article
6. Peer-review manipulation

The presence of these indicators undermines our confidence in the integrity of the article's content and we cannot, therefore, vouch for its reliability. Please note that this notice is intended solely to alert readers that the content of this article is unreliable. We have not investigated whether authors were aware of or involved in the systematic manipulation of the publication process.

Wiley and Hindawi regrets that the usual quality checks did not identify these issues before publication and have since put additional measures in place to safeguard research integrity.

We wish to credit our own Research Integrity and Research Publishing teams and anonymous and named external researchers and research integrity experts for contributing to this investigation.

The corresponding author, as the representative of all authors, has been given the opportunity to register their agreement or disagreement to this retraction. We have kept a record of any response received.

References

[1] Y. Liu, S. Wu, Q. Xu, and H. Liu, "Holographic Projection Technology in the Field of Digital Media Art," *Wireless Communications and Mobile Computing*, vol. 2021, Article ID 9997037, 12 pages, 2021.

Research Article

Holographic Projection Technology in the Field of Digital Media Art

Yulong Liu, Shan Wu [iD], Qi Xu, and Hubin Liu

Graduate School, Sejong University, Seoul 05006, Republic of Korea

Correspondence should be addressed to Shan Wu; s.wu@baiyunu.edu.cn

The advent of the digital age has given new forms and new connotations to artistic creation, and more and more digital media technologies have entered the stage of artistic creation and exhibitions. At present, holographic projection technology has become a hot application technology in the field of digital media art. The purpose of this paper is to explore the technical principles of holographic projection technology and its application in the field of digital media art, so as to provide suggestions for the application and promotion of holographic projection technology and the development and innovation of digital media art. First of all, this article understands the technical principles of holographic projection and its application status in various fields, especially in the field of digital media art, through relevant literature research. Then, this article introduces the digital holographic technology, virtual imaging technology, and computer simulation technology used in the realization of holographic projection technology. Then, based on the advantages of holographic projection technology in three-dimensional image recording and reproduction, this paper proposes to introduce holographic projection technology to digital art museums, digital art exhibitions, and other digital media art applications and to study the effect of holographic projection technology on art through simulation experiments, the effect of recording and reproducing the image of the work. Finally, the three-dimensional reconstruction image of the digital holographic projection experiment on the artwork is compared with the simulated image of the Contour GT profiler to verify the feasibility of applying the holographic projection technology to art exhibitions and the effect of three-dimensional image recording and reproduction. Research shows that the holographic projection technology can achieve 93.34% of the simulation effect of recording and reproducing 3D images of artworks. It is also found that 59.86% of the audience who pay attention to the art experience strongly support the application of holographic projection technology in digital media art fields such as digital art gallery. This fully proves the feasibility of applying holographic projection technology to digital art exhibitions and provides a full range of artistic experience for audiences who cannot be present.

1. Introduction

1.1. Background and Significance. With the continuous development of material living standards, people's love and pursuit of art are also increasing. However, traditional forms of artistic creation and communication can no longer meet the needs of art pursuers who are restricted by time and space and cannot be present in person. The development of digital media technology provides a new perspective for artistic creation and communication. Digital media art is not a short-lived emerging art form. As early as the 19th century, scholars have put forward the concept of the interactive integration of technology and art through computers [1]. With

the development of digital technology, this art form plays an increasingly important role in the development of the art field. The most significant example of the development of digital media art is the application of digital technology in film and television animation, such as the magnificent shipwreck scene in "Titanic," the reproduction of extinct species in "Jurassic Park," and the scene production of today's 3D animation. [2]. Unlike digital media art with a long history of development, holographic projection technology is a novel digital virtual technology [3]. Holographic projection technology breaks the traditional image recording and presentation form, combining 3D technology and holographic technology, not only can record and reproduce three-dimensional

images with higher precision, but also can realize the correction through digital holographic microscopy technology and three-dimensional image traceability reconstruction, microscopic observation of objects and replay of missing images [4]. Therefore, holographic projection technology has important applications in holographic microscopic observation of biology, chemistry, and other fields such as image processing in physics and mathematics [5]. However, because the art field pays more attention to immersive art experience and specific and subtle artistic representations and the application of holographic projection technology in some fields is not yet mature, the application of holographic projection technology in the art field has not been deepened.

1.2. Related Research at Home and Abroad. Since the introduction of holographic projection technology, scholars from all walks of life have paid constant attention to and research on holographic projection. Makey et al. obtains Fourier holography by preshaping the wavefront to locally reduce the Fresnel diffraction, which combines complex images with complete depth control, allowing random phases to be included at each depth without changing the specific depth projection of the image at [6]. However, true 3D holographic technology also requires complete depth control and dynamic projection functions, which will be affected by high string interference. Makowski et al. proposed a phase-free random method to make hologram reconstruction with very low noise, so that fine projection can be performed without time integration of subholograms [7]. Research shows that through experiments comparing the depth of focus and imaging resolution of various defocus parameters, it can be concluded that the phase-free random method can effectively improve the extended depth of clear imaging. Jamerson discussed the application of digital media art in mental health treatment through examples of using digital media art and technology in group mental health treatment meetings [8]. Research shows that story art plays an important role in people's perception and interaction of the world. Therefore, narrative therapy and art therapy combined with digital media art have a significant effect on the research and treatment of people's mental health. Heydon et al. integrated digital media technology into public art courses, collected data through case studies, and conducted a qualitative thematic analysis of multimodal elements in people's transferable understanding of digitally enhanced multimodal courses throughout the life cycle [9]. The study found that digital media is mainly used to create digital portfolios, and the corresponding nondigital media text production and text production led by teachers and participants are used as references.

In China, holographic projection technology is also a research hotspot in various digital media technology applications. Qu proposed a holographic projection with higher image quality that has a reconstructed image that has twice the spatial resolution of existing holographic projections and can well suppress speckles. Experiments show that this holographic projection can effectively improve the spatial resolution of the projected image without being restricted by the size of the spatial light modulator. Chang et al. proposed an implementation method of speckle reduction based

on phase-only computer-generated hologram and lensless holographic projection. Virtual convergent light is applied to the image to ensure that its wavefront is focused on the virtual plane established between the image and the hologram plane [10]. Experiments show that in a compact lensless holographic projection system, this method is effective for simultaneously improving the image quality and image size and the size of the projected image can reach the maximum diffraction bandwidth of the spatial light modulator at a given distance. Wu and Krewer reexamined the process of digital practice in the University of Houston library through digital media technology using data-driven methods and put forward strategic recommendations for library digital practice in terms of workflow, digital resources, and infrastructure [11]. Research has shown that the data-driven strategy of digital media technology can effectively improve the quality and efficiency of digital operations. Liang and Kim combined the theory of expression psychology in the field of art, and studied the application of projection mapping technology and digital media technology in the field of new media art design [12]. It was found that the advanced projection mapping technology can not only show the realistic image reproduction effect of the artwork, but even combine the image reconstruction transformation and color adjustment of the digital media technology to show the artistic effect beyond the original artwork.

1.3. Innovations in This Article. This article puts forward the new application research directions of holographic projection technology in digital art museums, digital art exhibitions, and other digital media art fields. This paper uses the holographic image recording method based on Fresnel diffraction and lensless Fourier transform in the holographic projection technology to record the holographic image of the artworks allowed to be displayed in art places such as art museums and galleries [13]; then, through Fresnel approximation reconstruction, convolution reconstruction, and angular spectrum reconstruction, holographic projection reproduction of artworks is realized [14]. For paintings, sculptures, and other specific and microspace artworks, this article uses holographic projection technology combined with holographic microscopy to accurately record the optical wavefront and phase distribution of the images of these works and then uses wavefront reconstruction and holographic microscopy to include tiny features in the image of the artwork inside which is reproduced [15]. The application of holographic projection technology in digital art galleries, digital galleries, and art exhibitions in this article can not only satisfy the immersive art experience of audiences who cannot be present but also present three-dimensional images of artworks including tiny features such as lines and brushstrokes. For art lovers who are concerned about artistic creation, it is an innovative research in the application of holographic projection technology in the field of digital media art.

2. Digital Holographic Projection Technology

2.1. Holographic Image Recording and Reproduction of Artworks. For object image recording methods, such as

traditional camera shooting and projector projection, most of them are recorded according to the coordinates and pixel distribution of the physical object, and then, the object image is presented to the audience through the corresponding projection magnification equipment [16, 17]. The digital holographic projection uses the principle of virtual imaging to record the wavefront information of the light wave emitted by the object in the holographic projection device through the optical light wave phase and amplitude and then converts the recorded wavefront phase information into light wave intensity information and passes optical the principle of the process of reproduction. At present, the holographic image recording methods used in holographic projection technology mainly include three digital holographic image recording methods: Fresnel diffraction holographic recording, lensless Fourier transform holographic recording, and image surface digital holographic recording [18, 19]. Their main principle is to record based on the optical wavefront information reflected by the object, but the recording methods used are different. The process of wavefront recording is to convert the spatial phase information of the reflected light waves of the recorded object into spatial intensity information through light wave interference, which is also the core principle of optical holography technology. During the wavefront recording process, the information of the object light wave $O(x, y)$ and the reference light wave $R(x, y)$ will be recorded. They can be recorded in the following formats:

$$
\begin{aligned}
O(x, y) &= o(x, y) \cdot e^{j\varphi(x,y)}, \\
R(x, y) &= r(x, y) \cdot e^{j\phi(x,y)}.
\end{aligned}
\tag{1}
$$

Equation (1) records the object light wave and reference light wave information of the artwork. Where $o(x, y)$ represents the amplitude distribution of the object light wave, and $\varphi(x, y)$ represents the phase distribution of the object light wave. Similarly, $r(x, y)$ represents the amplitude distribution of the reference light wave and $\phi(x, y)$ represents the phase distribution of the reference light wave. Then the total light wave $T(x, y)$ of the digital holographic image of the artwork can be obtained by superposing the real functions of the amplitude and phase of the two light waves, and its distribution form is as follows:

$$
T(x, y) = O(x, y) + R(x, y).
\tag{2}
$$

Equation (2) records the phase and amplitude information of the total light wave of the artwork, but this information can only record the phase distribution of the light wave of the artwork in the holographic projection, which is not conducive to image reproduction and processing, so it needs to be converted into the total light wave of the artwork intensity distribution information. The distribution form of the total light wave intensity $I(x, y)$ is as follows:

$$
\begin{aligned}
I(x, y) &= |O(x, y) + R(x, y)|^2 \\
&= |O(x, y)|^2 + |R(x, y)|^2 \\
&\quad + 2o(x, y)r(x, y)\cos\left(\varphi(x, y) - \phi(x, y)\right).
\end{aligned}
\tag{3}
$$

Equation (3) records the total light wave intensity information of the artwork in the holographic projection, where $|O(x, y)|^2$ represents the intensity distribution of the object light wave of the artwork and $|R(x, y)|^2$ represents the intensity distribution of the reference light wave of the artwork. Fresnel diffraction holographic recording is to record the complex amplitude distribution of the object light wave and the reference light wave of the artwork on the basis of the wavefront recording to obtain the spatial frequency of the interference fringes in the holographic projection of the work to record the information of the holographic image of the work. The form of the complex amplitude distribution of the object light wave and the reference light wave is as follows:

$$
\begin{aligned}
O\left(x', y'\right) &= o\left(x', y'\right) e^{j\varphi(x'y')} = \frac{e^{jdk}}{\lambda j d} \iint O(x_0, y_0) e^{jk\left[(x'-x_0)^2 + (y'-y_0)^2\right]/2d} dx_0 dy_0, \\
R\left(x', y'\right) &= r\left(x', y'\right) e^{j\phi(x'y')} = e^{-jk(x' \sin \alpha + y' \sin \beta)}.
\end{aligned}
\tag{4}
$$

In equation (4), (x_0, y_0) and (x', y') represent the two-dimensional coordinates of the work of art on the object plane and the projection plane, respectively, and represent the distance between the two planes. According to the complex amplitude distribution of the object light wave and the reference light wave, the spatial frequency distribution of the interference fringes in the projection direction of the digital holographic projection image in Fresnel diffraction can be obtained as follows:

$$
\begin{aligned}
f_x &= \frac{\partial \varphi}{2\pi \partial x'} = \frac{x' - x_0 + d \sin \alpha}{\lambda d}, \\
f_y &= \frac{\partial \phi}{2\pi \partial y'} = \frac{y' - y_0 + d \sin \beta}{\lambda d}.
\end{aligned}
\tag{5}
$$

Equation (5) records the spatial frequency of the interference fringes of the artwork according to the diffraction angle of Fresnel diffraction in the x and y directions and is similar to the lensless Fourier transform holographic recording method. The lensless Fourier transform does not use the reflection angle to record the spatial frequency but instead limits the bias conditions of the reference light wave to record the spatial frequency according to the Quist sampling principle. The conditions for the interference fringes to reach the highest spatial frequency in lensless Fourier transform holographic recording are as follows:

$$
\begin{aligned}
f_{x \max} &= \frac{X + 2x_0}{2\lambda d} \le \frac{1}{2\Delta x}, \quad x_0 \ge 3X/2, \\
f_{y \max} &= \frac{Y + 2y_0}{2\lambda d} \le \frac{1}{2\Delta y}, \quad y_0 \ge 3Y/2.
\end{aligned}
\tag{6}
$$

The image surface digital holographic recording method is mainly the process of imaging through the lens under the interference of the object light wave and the reference light wave through the principle of lens magnification. When studying image digital holographic recording, the influence

of the lens' numerical aperture on the imaging system is generally not considered. The frequency of the object light wave of the artwork recorded by the digital holographic image is as follows:

$$\eta_x = \frac{1}{2\pi} \cdot \frac{\partial \varphi}{\partial x} = \frac{f_{x_0}}{2\pi m} + \frac{x}{\lambda m f},$$

$$\eta_y = \frac{1}{2\pi} \cdot \frac{\partial \phi}{\partial x} = \frac{f_{y_0}}{2\pi m} + \frac{y}{\lambda m f}. \tag{7}$$

Equation (7) records the frequency of the object light wave in the x and y directions of the work of art, where the sum represents the spatial frequency of the initial object light wave emitted by the light source in the holographic projection shooting of the work of art, which is the magnification of the lens.

2.2. Digital Holographic Image Reconstruction Algorithm. According to the above research on digital holographic image recording methods, there are three holographic image reconstruction algorithms for digital holographic image reproduction of works of art: Fresnel diffraction integral, convolution algorithm, and angular spectrum algorithm [20, 21]. According to the approximate conditions of Fresnel diffraction, the form of the object light wave recorded in the hologram of the artwork can be obtained by the Fresnel diffraction integral formula as follows:

$$U(x_i, y_i) = \frac{e^{idk + ik\left(\left(x_i^2 + y_i^2\right)/\lambda d\right)}}{\lambda id} \cdot \mathfrak{F}\left\{I(x_i, y_i)R(x_i, y_i)e^{\left(\pi i\left(x_i^2 + y_i^2\right)\right)/\lambda d}\right\}. \tag{8}$$

In equation (8), $I(x, y)$ represents the light wave intensity of the hologram recorded by Fresnel diffraction and $R(x, y)$ represents the reproduction mode of the reference light wave recorded by the hologram. The Fourier transform method converts the recorded light wave information of the hologram into a discrete numerical recording form through photoelectric coupling. The object light wave reproduction form of the hologram of the artwork is as follows:

$$U(x_i, y_i) = \frac{e^{idk + (\pi \lambda id/MN)\left(\left(x_i^2/\Delta x^2\right) + \left(y_i^2/\Delta y^2\right)\right)}}{\lambda id}$$
$$\times D\mathfrak{F}\left\{I(x_i, y_i)R(x_i, y_i)e^{(\pi i/\lambda d)\left(x_i^2 \Delta x^2 + y_i^2 \Delta y^2\right)}\right\}. \tag{9}$$

In equation (9), Δx and Δy are the pixel dimensions of the digital hologram recording tool, M and N represent the number of pixels of the recording tool, and $D\mathfrak{F}$ represents the discrete Fourier transform operation. The convolution algorithm is based on the impulse response function of the digital holographic projection system and the discrete Fourier transform to obtain the object light wave distribution of the reproduced hologram. The form of the object light wave reproduced by the hologram is as follows:

$$g(x_i, y_i) = \frac{d_i}{\lambda i} \cdot \frac{e^{jk\sqrt{d_i^2 + (x-x_i)^2 + (y-y_i)^2}}}{d_i^2 + (x-x_i)^2 + (y-y_i)^2},$$

$$U(x_i, y_i) = \mathfrak{F}^{-1}\left\{\mathfrak{F}(I(x_i, y_i) \cdot R(x_i, y_i)) \bullet \mathfrak{F}(g(x_i, y_i))\right\}. \tag{10}$$

In equation (10), $\mathfrak{F}$ and $\mathfrak{F}^{-1}$ represent the forward and inverse transform of the discrete Fourier transform and $g(x_i, y_i)$ represents the impulse response function of the holographic projection system. The hologram reconstruction principle of the angular spectrum algorithm is to obtain the object light wave information reconstructed by the hologram through the transfer function of the holographic projection optical system and Fourier transform. The angular spectrum distribution of the holographic projection plane and the reproduction plane of the artwork is as follows:

$$u(x, y) = \iint A\left(\frac{\cos \alpha}{\lambda}, \frac{\cos \beta}{\lambda}\right) e^{2\pi i((\cos \alpha/\lambda)x + (\cos \beta/\lambda)y)} df_x df_y,$$

$$h(f_x, f_y) = e^{jdk\sqrt{1 - (\lambda f_x)^2 - (\lambda f_y)^2}}, \quad f_x = \frac{\cos \alpha}{\lambda}, f_y = \frac{\cos \beta}{\lambda}. \tag{11}$$

In equation (11), $u(x, y)$ represents the light field distribution of the projection plane and the reproduction plane and $h(f_x, f_y)$ represents the optical transfer function of the holographic projection system. According to the angular spectrum distribution, the light field intensity of the holographic projection reconstruction plane can be obtained as follows:

$$U(x_i, y_i) = \mathfrak{F}^{-1}\left\{\mathfrak{F}(u(x_i, y_i)) \cdot h(f_x, f_y)\right\}. \tag{12}$$

According to the principle of the above digital holographic image reconstruction algorithm, it can be seen that the three reconstruction algorithms all use the Fourier transform method. For the difference and comparison of the three algorithms, this article discusses their calculation formula, transformation space, and pixel size of the reconstructed image. The reproduction speed is compared and analyzed, and the comparison of the three algorithms is shown in Table 1. It can be seen from the research results that the reconstruction speed of Fresnel diffraction is the fastest because Fourier image transformation is only carried out in the spatial domain, while convolution algorithm and angular spectrum reconstruction algorithm have more transformation process in the frequency domain, so the reconstruction speed is slower.

2.3. Digital Holographic Image Processing Technology. In the process of holographic projection display of digital artworks such as digital art galleries, galleries, and art exhibitions, in addition to the steps of recording and reproducing the images taken by the holographic projection of the works of art, it is also necessary to combine some image processing technologies to process the holographic projection images. A digital holographic image with a more realistic image and richer colors is obtained [22, 23]. According to the principle of transform space in the process of hologram recording and

TABLE 1: Comparison of digital hologram reconstruction algorithms.

Reproduction algorithm	Transform space	Reproduction pixel	Reproduction speed
Fresnel diffraction	Space to frequency	$\Delta x_i = \lambda d/N_x \Delta x, \Delta y_i = \lambda d/N_y \Delta y$	Fastest
Convolution	Airspace to frequency to airspace	$\Delta x_i = \Delta x, \Delta y_i = \Delta y$	Medium speed
Angular spectrum	Airspace to frequency to airspace	$\Delta x_i = \Delta x, \Delta y_i = \Delta y$	Slowest

reproduction, the filter method is used to filter the spectrum of the hologram in the frequency domain and the space domain where the Fourier transform is performed [24]. The frequency spectrum of the virtual image reconstructed by the digital hologram is filtered out by setting the diaphragm, and then, the Fourier transform is performed to obtain a clear and realistic image of the real object. The spectrum of the hologram obtained after spectral filtering by filtering method is as follows:

$$U\left(f_x, f_y\right) = \mathfrak{F}\left\{|O(x,y)|^2\right\} + \mathfrak{F}\left\{|R(x,y)|^2\right\} + \mathfrak{F}\left\{O(x,y)R'(x,y)\right\} + \mathfrak{F}\left\{O'(x,y)R(x,y)\right\}. \tag{13}$$

Filtering out the zero-order spectrum and conjugate virtual image in equation (13) and then performing Fourier transform, a relatively clear digital hologram can be obtained. Then, the light intensity method can be used to add and subtract the light intensity of the object light wave and the reference light wave of the obtained hologram. First, the light intensity distribution record of the original hologram is stored in the computer, and then, the intensity of the object light wave and the reference light wave are controlled until the light spot in the hologram is invisible or disappears, and then, the light intensity distribution of the hologram at this time is recorded [25]. Through the addition and subtraction of the light intensity, the digital hologram with the light spot removed can be obtained. In addition, the phase and amplitude distribution of the hologram can also be recorded and adjusted by the phase shift method. The phase shift method transforms the spatial phase of the reference light wave by shifting the phase of the projection plane and the reproduction plane of the holographic projection system to achieve interference with the light wave. The complex amplitude distribution of the object light wave on the projection plane obtained by the phase shift method is shown in equation (14), where $I(x, y, \theta)$ represents the light intensity distribution of the hologram under different angular phase shifts.

$$O(x,y) = \frac{I_1(x,y,0) - I_3(x,y,\pi) + j[I_2(x,y,\pi/2) - I_4(x,y,3\pi/2)]}{\lambda R'}. \tag{14}$$

2.4. Digital Holographic Imaging and Reconstruction Simulation. In the process of holographic projection of artworks, it is necessary to go through the process of hologram imaging enlargement and reduction. It is one of the key technologies in holographic projection to ensure that

there will be no blur and distortion in the process of hologram enlargement and imaging [26]. The magnification and imaging of the hologram are generally achieved by using a lens, so the diffracted light wave is usually a spherical wave, and the complex amplitude of the spherical wave of the reference light on the projection plane is as follows:

$$C(x,y) = \frac{C}{|d|} e^{-jdk - (jk/\lambda d)\left[(x-x_0)^2 + (y-y_0)^2\right]}. \tag{15}$$

According to the principle of optical imaging, digital holographic magnification imaging mainly involves object light waves, reference light waves, recording light waves, and reproduced imaging light waves. Through the above study of object light waves and reference light waves, the horizontal magnification M_x and longitudinal magnification M_y of the digital hologram can be obtained. The calculation formula is as follows:

$$M_x = \pm \frac{\lambda d_i}{\lambda_0 d_0} = \left(1 - \frac{d_0}{d_i} \pm \frac{\lambda_0 d_0}{\lambda d_i}\right)^{-1},$$
$$M_y = \pm \frac{\lambda d_i^2}{\lambda_0 d_0^2} = \frac{\lambda_0}{\lambda} M_x^2. \tag{16}$$

λ_0 and λ represent the wavelength of the recording light wave and the reproduced light wave, respectively, in the holographic projection imaging and d_0 and d_i represent the object distance and the image distance, respectively, of the hologram of the artwork in the holographic projection. The horizontal and vertical magnification ratio of the image can be adjusted by adjusting the wavelengths of the recording light wave and the reproducing light wave, and combined with the above-mentioned Fourier transform method, a desired magnification and distortion-free holographic image can be obtained.

3. Application Examples of the Holographic Projection Technology in the Digital Media Art

3.1. Research Object and Experimental Environment. The experimental objects of this research are artworks in art museums, galleries, and other art exhibitions that are exhibited to the public. In this paper, some artworks with complex structures and the consent of the creator are selected for holographic projection simulation experiments and the holographic projection technology is studied accordingly. This article first learns the knowledge of holographic projection and optical imaging and asks professionals for help and

builds a simple holographic projection optical physical environment through purchase and lease. The main equipment includes adjustable light source, beam splitter, LCD lightwave recording board, CCD light wave reproduction board, and digital computer. According to the development of holographic technology, this paper proposes a digital holographic projection method combined with digital technology for complex physical image processing such as complex exposure, bleaching, denoising, and pixel difference removal in the early traditional optical holography and computed holographic imaging process. The holographic projection reproduction of artworks is transformed into a digital processing process. In order to study the application effect of holographic projection technology in the field of digital media art, this article sets up a control experiment to compare the quality and fidelity of the artwork obtained by various optical virtual imaging methods, and then, this article simulates the artwork obtained from the holographic projection experiment. The holographic images are uploaded to the media, and an online questionnaire on the "views and suggestions on the application of holographic projection technology to digital art museums and other digital media art fields" is randomly distributed. After experimental investigation and statistics, a total of 80 valid questionnaires were received.

3.2. Design of the Holographic Projection Simulation Experiment. According to the digital holographic recording and reproduction method of holographic projection technology in the second part, this article sets up multiple control experiments to discuss the advantages and disadvantages of digital holographic projection technology compared with other holographic technologies and image processing methods. The experimental group used analog digital holography technology to perform holographic image recording and reproduction steps on selected artwork samples, while the control group used traditional optical holography and computer holography technology for holographic image processing. This experiment is mainly divided into the following steps. First, build a holographic projection simulation test environment by collecting data and seeking help from holographic projection research professionals to understand the principles and main processes of holographic projection technology. Then, select artworks exhibited in art museums or galleries with the consent of the creator as the experimental objects and set up the experimental group and the control group to conduct holographic projection simulation experiments through different shooting and hologram recording and reproduction methods. In order to ensure the accuracy and reliability of the experiment, this article invites professional holographic projection film shooting workers who volunteer to participate in the experiment to provide guidance and suggestions. Through the light wave reflection and multiangle diffraction of the artwork by the adjustable light source, the phase and amplitude of the object light wave and the reference light wave of the artwork are recorded in the LCD light wave recording board and then uploaded to the digital computer for processing, and then, the artwork is reproduced by the CCD light wave reproduction board. Finally, upload the holographic projection image of the

artwork obtained from the experiment to digital media and issue an online questionnaire to investigate the quality and experience effect of the holographic projection image of the experimental artwork and the audience's application of the holographic projection technology to digital art museums and other digital media art fields. The basic principle of holographic projection imaging is shown in Figure 1.

3.3. Data Processing and Error Analysis. The survey data in this article is mainly divided into two parts, namely, the application of holographic projection technology for the holographic image recording and reproduction of artworks and the simulation experiment data and the opinions and suggestions on the application of holographic projection technology to digital art museums, galleries, and art exhibitions. The data processing and error analysis of this experiment are processed by SPSS20.0 software. For the statistical data of the experimental results, the analyses of variance and nonhomogeneity of variance are used to test the accuracy and error of the results. This method uses parameter α to represent all significant levels of experimental data between 0 and 1. The test level of this experimental data can reach $\alpha = 0.05$. In the data of the entire experimental group, excluding the influence of other factors, analyze the data under the change of a single factor and compare it with the average value and then perform error testing. For a set of experimental data, the number of data under a factor level that needs to be studied is denoted as n and the error is MSE; then, the analysis and test formula for the homogeneity of variance are shown in equation (17) as follows:

$$L = \sqrt{\text{MSE}\left(\frac{1}{n_i} + \frac{1}{n_j}\right)}. \tag{17}$$

In the experiment, according to the different degrees of freedom of the variables, if the difference between the experimental group and the control group in group k is to be tested, the variance and nonhomogeneity analysis method is generally used to test as shown in the following:

$$S^2 = \text{MSe}\left(\frac{1}{n_i} + \frac{1}{n_j}\right),$$
$$D = \left(\bar{X}_k - \bar{X}_0\right)/S^2. \tag{18}$$

In the above formula, $\bar{X}_k$ represents the data mean of the experimental group of group k, $\bar{X}_0$ represents the mean of the experimental data of its control group, and MSe represents the mean error variance. This test method can make the difference between the mean of multiple experimental groups and a control group. Multiple comparisons are used in this study to verify the conclusions drawn from the experimental results.
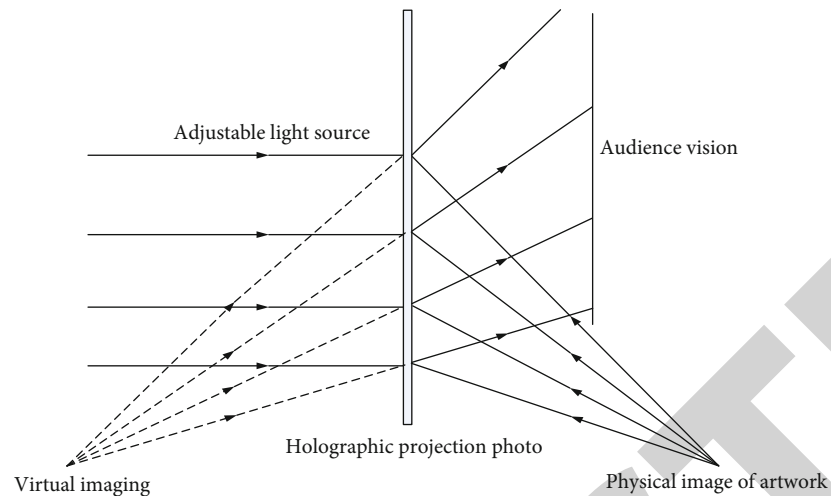
FIGURE 1: Holographic projection imaging process of artwork.

4. Discussion on the Application of the Holographic Projection Technology in the Digital Media Art

4.1. Development History of the Holographic Projection Technology. According to related literature research, this article investigates the four stages of development of holographic projection technology. This article divides holographic projection technology into four development stages: budding, development, maturity, and prosperity. As shown in Table 2, this article briefly introduces the recording media, reproduction methods, and representative applications of the various stages of holographic projection. In the development process from budding to prosperity, holographic projection technology has mainly experienced mercury lamp light source recording, white light recording, laser recording, and digital light source recording. The corresponding reproduction methods also range from light source reproduction to laser reproduction and finally to digital reproduction. The principle is to record and reproduce based on optical holography. The difference is that with the development of digital media, holographic projection gradually combines computer image processing and other digital technologies to make holographic projection images clearer and richer in colors. The representative applications of holographic projection in these periods are in-line holograms, off-axis holograms, rainbow holograms, and digital holograms.

The application of holographic projection technology and 3D technology is most closely related. In order to study the application of holographic projection technology, this article investigates and understands the 3D technology related to holographic projection. The survey results are shown in Figure 2. At present, the main holographic technologies are divided into optical holography, computational holography, and digital holography. These holographic technologies are mainly put into practical application by combining five 3D technologies including air projection and interaction, laser projection of solid 3D images, 360 holographic display screen, and edge blanking technology.

4.2. Analysis of Simulation Experiment of Holographic Projection. Through the in-depth study of holographic projection technology, this article conducts a simulated holographic projection experiment on artworks. The holographic projection image obtained in the experiment is shown in Table 3. This article mainly analyzes the image reproduction effect of holographic projection from the image quality and the similarity of the actual comparison with the artwork.

According to the experimental data in Table 3, the error accuracy and inspection level of the experimental data shown in Figure 3 are obtained by processing statistics. It can be seen from the figure that the maximum standard deviation of the error mean of the experimental data in this paper is 2.267, and it is obvious that this is a set of abnormal data by comparing with other sets of data. Therefore, the highest accuracy of the data in this paper should be 1.918, which belongs to higher accuracy.

According to the experimental data, this article records the phase, amplitude, diffraction angle, light wave intensity, and simulation effect changes of several experimental groups and control groups during the holographic projection simulation experiment of artworks. As shown in Table 4, the best simulation effect can be achieved when the light intensity is 50.64 and the simulation accuracy of the hologram at this time reaches 93.34%.

According to the Fresnel diffraction recording research of holographic projection technology, this paper records the simulation accuracy of holographic images of artworks recorded under different diffraction angles. As shown in Figure 4, under the diffraction angle of −80 degrees to 80 degrees, the error accuracy of the quality and similarity of the holographic image has been controlled below the level of 0.6.

4.3. Validation of Holographic Projection Image Effect of the Artwork. According to the image quality evaluation standard, this article evaluates the quality of the holographic image of the artwork obtained from the experiment, mainly from the signal-to-noise ratio of the hologram PSNR, structural similarity SSIM, mean square error MSE, normalized mean

TABLE 2: Development period of holographic projection technology.

Phase	Development period	Recording medium	Reproduction method	Representative
First	Bud	Mercury lamp	Light reproduction	Coaxial holography
Second	Development	White light	Light reproduction	Off-axis holography
Third	Mature	Laser	Laser reproduction	Rainbow hologram
Fourth	Peak	Digital light source	Digital reproduction	Digital holography
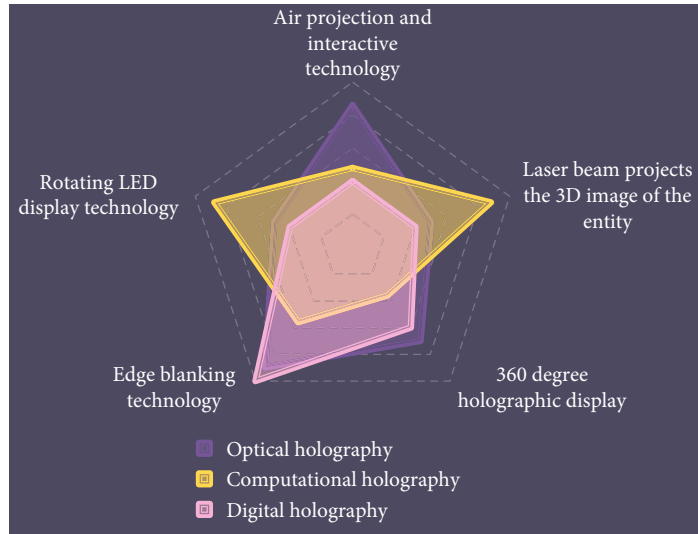
FIGURE 2: Holographic technology and related 3D technology applications.

TABLE 3: Comparison results of holographic projection simulation experiment.

Item	Class	Number	Mean	SD	T	P
Image quality	Experimental	20	12.667	1.796	0.256	0.216
	Control	20	11.825	1.574	2.235	0.007
Image similarity	Experimental	20	15.468	1.918	-0.223	0.825
	Control	20	12.176	2.267	0.312	0.754
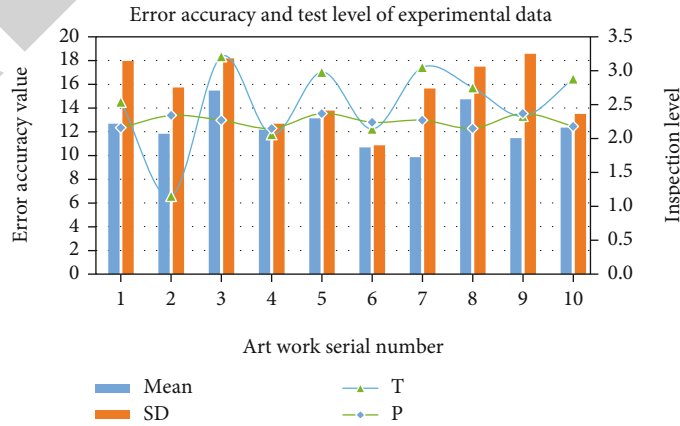
FIGURE 3: Error accuracy and test level of experimental data.

TABLE 4: Light wave phase and amplitude and simulation accuracy changes in the simulation experiment.

Sample number	Phase	Amplitude	Diffraction angle	Light intensity	Simulation effect
E1	0	1.876	0	43.76	91.06%
C1	$0.25^*\pi$	2.564	60	54.35	79.86%
E2	$0.5^*\pi$	3.951	120	44.69	83.25%
C2	π	5.467	180	38.76	76.89%
E3	$1.5^*\pi$	7.984	240	49.86	87.65%
C3	$2^*\pi$	9.897	360	50.64	93.34%
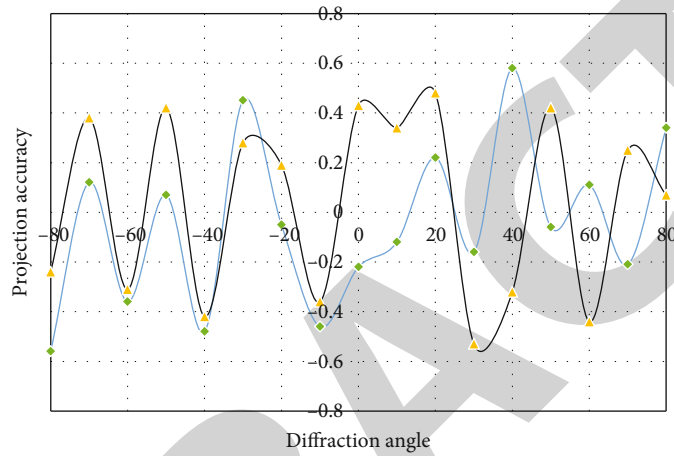
FIGURE 4: The accuracy of holographic projection images under different diffraction angles.

TABLE 5: Image quality of artworks by different shooting techniques.

Type	Technology	PSNR	SSIM	MSE	d	r
Ordinary shooting	Camera shot	25.32	0.8237	0.3526	0.1873	0.1436
	3D shooting	27.43	0.8946	0.3273	0.2036	0.1563
Holographic projection	Optical holography	28.14	0.8973	0.2461	0.1472	0.0958
	Computational holography	28.96	0.9025	0.4025	0.2365	0.1847
	Digital holography	29.67	0.9164	0.2364	0.1437	0.0975

square distance d. The average absolute distance r is analyzed. In addition, this article also compares the quality of the images obtained by several holographic techniques and ordinary photography techniques that do not use holography. The results are shown in Table 5.

According to the experimental test results in Table 5, this paper draws a line chart of the comparative analysis of image quality of several artwork image shooting techniques, as shown in Figure 5. This experiment mainly researches and discusses the image capturing technology including the nonholographic technology, optical holography, computerized holography, and digital holography technology in 3D photography and holographic technology. It can be seen from the figure that the holographic image obtained by digital holographic projection has the lowest mean square error, normalized mean square distance, or normalized average absolute distance.

4.4. Audience's Attitude towards Application of Holographic Projection to the Exhibition of Digital Artworks. This article analyzes the audience's awareness and acceptance of holographic projection from the results of online questionnaires and experimental data, mainly from the audience's evaluation of the image quality and experience effects of holographic projection of artworks and the application of holographic projection technology to the digital art. The attitude of the museum is discussed and analyzed. As shown in Table 6, according to the audience's attitude, it is divided into five levels: A, B, C, D, and E to reflect the audience's attitude of strongly welcoming, supporting, indifferent, undesirable, and strongly opposed to the application of holographic projection technology in the field of the digital media art.

The audience's perception of the holographic projection technology and its application in digital media art fields such

Image quality of art works by different shooting techniques
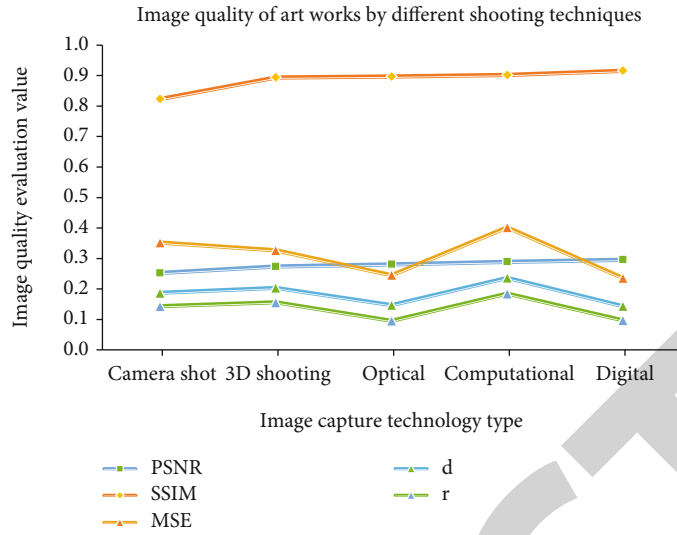
Figure 5: Image quality of artworks by different shooting techniques.

Table 6: The audience's evaluation and attitude towards the effect of holographic projection.

Investors	Number	Proportion	Total	Evaluation	Sort
A	45	56.25%	59.86%	8.98	2
B	51	63.75%	61.59%	7.59	1
C	37	46.25%	50.24%	6.16	4
D	39	48.75%	46.37%	5.94	3
E	21	26.25%	34.76%	4.73	5

Audience's perception and attitude towards
holographic projection technology
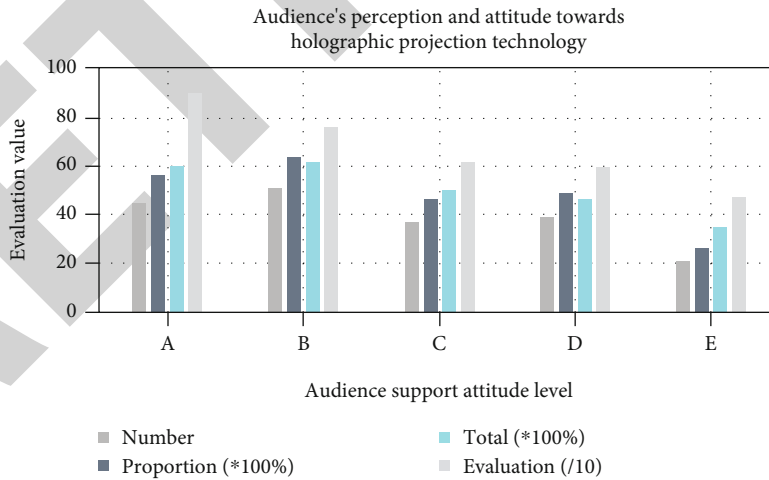
Figure 6: Audience's perception and attitude towards holographic projection technology.

as digital art galleries, digital galleries, digital art exhibitions, and other art exhibitions are shown in Figure 6. It can be seen from the figure that most audiences have a high evaluation of the multisensory virtual experience of holographic projection and up to 59.86% of the audience strongly support the application of holographic projection in the field of the digital media art.

5. Conclusions

Since its introduction, holographic technology has been welcomed by various industries and paid attention to from all walks of life and has broad development prospects. Some of these holographic technologies still remain in theoretical research and have not been truly realized. Among the

holographic technologies that have been realized, digital holographic projection is undoubtedly the best. Holographic projection technology has important applications in various fields. For example, 3D animation production, VR virtual technology, and 3D virtual game development all use the method of virtual imaging in holographic projection to bring people a multisensory three-dimensional virtual experience. This paper discusses the current application status of holographic projection technology in the field of digital media art and finds that the main application of holographic projection technology is in the production of film and game in digital media art. Based on this, this article proposes to apply holographic projection technology to the construction of digital art museums and digital media art exhibitions.

This paper sets up the holographic projection simulation experiment of the artwork, using the Fresnel diffraction method and Fourier transform to record the phase and amplitude information of the diffracted light wave of the holographic projection image of the artwork under the adjustable light source, and through the Fresnel integration Algorithm, inverse Fourier transform, convolution reconstruction algorithm, and angular spectrum reconstruction algorithm are the processes of projection and reconstruction of the recorded hologram. In this paper, a computer digital holographic projection system is used to drive the process of recording and reproducing the holographic image of the artwork and the computer image processing technology is used to collect the experimental simulation holographic projection image and output the processed image after digital image transformation, so as to realize the holographic recording and reproduction of the artwork. The study found that after the holographic projection and computer image processing, the holographic image of the artwork obtained can still maintain the original quality and the degree of simulation is high, indicating that it is feasible to apply the holographic projection technology to digital art fields such as digital art galleries, this will be of great significance to the development of digital media art.

Since the holographic projection technology is a novel digital holographic technology and researchers in some fields have not yet realized and put it into application at the theoretical stage and the understanding of the holographic projection technology in this article is not deep enough, there are still some shortcomings in this article. For example, the construction of the optical physical environment for holographic projection is limited by economic conditions and knowledge reserves, so it is relatively crude, which causes large errors in the experimental results, and the immature operation of the holographic projection process may also cause the accuracy of the experimental results to decrease. I hope that in the future, we can improve and continue to in-depth study the holographic projection technology in the field of digital media art more in-depth and broader applications. The research in this article is the author's own discussion on the application of the holographic projection technology in the field of digital media art, and there is no plagiarism and interest competition. The manuscripts of all the contents of this article have been reviewed by relevant personnel and have not been published or submitted for publication elsewhere and agree to submit them to your journal.

Data Availability

The data that support the findings of this study are available from the corresponding author upon reasonable request.

Conflicts of Interest

The authors declare that they have no conflicts of interest.

References

[1] F. L. F. Lee and J. M. Chan, "Digital media activities and mode of participation in a protest campaign: a study of the umbrella movement," *Information Communication and Society*, vol. 19, no. 2, pp. 4–22, 2016.

[2] G. Caggianese, L. Gallo, and P. Neroni, "Evaluation of spatial interaction techniques for virtual heritage applications: a case study of an interactive holographic projection," *Future Generation Computer Systems*, vol. 81, no. 4, pp. 516–527, 2017.

[3] Z. Yan and Z. Lv, "The influence of immersive virtual reality systems on online social application," *Applied Sciences*, vol. 10, no. 15, article 5058, 2020.

[4] M. Gansner, E. Belfort, C. Leahy, D. Mirda, and N. Carson, "An assessment of digital media-related admissions in psychiatrically hospitalized adolescents," *Adolescent Psychiatry*, vol. 9, no. 3, pp. 220–231, 2020.

[5] D. A. E. Silva and S. V. D. Camargogrillo, "New paths for science: a contrastive discourse analysis of modifications in popularizing science through digital media," *Bakhtiniana Revista de Estudos do Discurso*, vol. 14, no. 1, pp. 54–81, 2019.

[6] G. Makey, Ö. Yavuz, D. K. Kesim et al., "Breaking crosstalk limits to dynamic holography using orthogonality of high-dimensional random vectors," *Nature Photonics*, vol. 13, no. 4, pp. 251–256, 2019.

[7] M. M. M. Makowski, T. S. T. Shimobaba, T. Ito, and T. Ito, "Increased depth of focus in random-phase-free holographic projection," *Chinese Optics Letters*, vol. 12, pp. 60–64, 2016.

[8] J. Jamerson, "Expressive remix therapy: using digital media art in therapeutic group sessions with children and adolescents," *Creative Nursing*, vol. 24, no. 1, pp. 159–165, 2018.

[9] R. Heydon, L. Mckee, and B. Daly, "iPads and paintbrushes: integrating digital media into an intergenerational art class," *Language and Education*, vol. 31, no. 4, pp. 351–373, 2017.

[10] C. Chang, Y. Qi, J. Wu, J. Xia, and S. Nie, "Speckle reduced lensless holographic projection from phase-only computer-generated hologram," *Optics Express*, vol. 24, no. 6, pp. 6568–6580, 2017.

[11] A. Wu and D. Krewer, "Maximising efficiency and standardisation in digitisation at University of Houston Libraries: a programme-based vs project-based approach," *Journal of Digital Media Management*, vol. 5, no. 3, pp. 248–258, 2017.

[12] K. Liang and H. Kim, "The application of projection mapping in the field of new media art in combination with expression psychology," *TECHART: Journal of Arts and Imaging Science*, vol. 5, no. 1, pp. 23-24, 2018.

[13] M. Olesen, "Media evolution and 'epi-technic' digital media: media as cultural selection mechanisms," *Explorations in Media Ecology*, vol. 14, no. 1, pp. 141–160, 2016.

Research Article

Comprehensive Medical System for Early Diagnosis of Rheumatoid Arthritis Based on Autoimmune Antibodies

Sha Liu [1,2]

[1]*Department of Rheumatology and Immunology, The First Hospital of Qiqihar, Qiqihar, 161000 Heilongjiang, China*
[2]*Affiliated Qiqihar Hospital Southern Medical University, Qiqihar, 161000 Heilongjiang, China*

Correspondence should be addressed to Sha Liu; 02238@qqhru.edu.cn

With the development of understanding of the pathogenesis of rheumatoid arthritis, it has led to the development of new treatment targets and new treatment guidelines. In the past 10 years, the treatment effect of RA patients has improved significantly. Due to the special clinical symptoms of RA, it is very important to have a clear assessment of the overall activity of the patient's disease and timely adjustment of treatment through joint monitoring of symptoms and laboratory indicators. Clinicians have always relied on clinical manifestations and imaging progress as the key basis for diagnosis. In addition, some markers that reflect disease activity are used to aid the diagnosis of RA, but in other autoimmune diseases, these markers are usually increased. The emergence of specific autoantibodies makes it easier for clinicians to distinguish RA from other autoimmune diseases and osteoarthritis. This study collected a large number of medical records through retrospective analysis, analyzed the epidemiological data, clinical characteristics, and laboratory indicators of RA patients, and analyzed the characteristics and laboratory indicators of patients in the stable disease group and active disease group. In order to further understand the clinical features, disease activity and related factors of RA in our country, and some new biomarkers for early rheumatoid arthritis, for example, the study found that the specificity of RF for the diagnosis of RA was 71.1%, the sensitivity was 73.3%, the combined detection of anti-CCP antibody + RF increased the specificity to 97.8%, and anti-CCP the combined diagnosis of antibody+RF + GPI antigen increases the specificity of diagnosis to 100%, which significantly reduces the sensitivity compared with all tests. These autoimmune antibodies can more effectively prevent the progression of the disease in the early diagnosis and treatment of rheumatoid arthritis, achieve long-term remission, and obtain very effective therapeutic effects.

1. Introduction

1.1. Background and Significance. In the early stage of rheumatoid arthritis, there is a "curing period" during which reasonable and effective treatment of the disease can prevent the progression of the disease, keep the patient in a state of asymptomatic for a long time, and effectively prevent joints. Therefore, early diagnosis of rheumatoid arthritis has become a prerequisite for early treatment and intervention to avoid poor prognosis. In recent years, many studies have been conducted on the early diagnosis of rheumatoid arthritis [1]. The application of magnetic resonance imaging is to see the pathological changes of early rheumatoid arthritis, and bone marrow edema is a special imaging of rheumatoid arthritis, which is very useful for the diagnosis of early rheumatoid arthritis. At the same time, people have been trying to find specific markers of early rheumatoid arthritis, such as the widely used anticyclic citrullinated peptide antibody (CCP). Someone used protein chip technology to select early rheumatoid arthritis proteins for patients with early rheumatoid arthritis and control groups (normal healthy people and other patients who cause rheumatoid arthritis). As an objective and easy-to-use indicator, biological indicators have always attracted people's attention and are also a hot research topic [2]. In recent years, people have adopted a variety of methods to discover some new biomarkers in the early stages of rheumatoid arthritis, which provides a basis for the early diagnosis and treatment of RA, thereby improving joint function, improving work ability, and improving life. Quality provides a new method to diagnose early rheumatoid

arthritis. Therefore, a comprehensive medical system designed to reduce the early diagnosis of autoimmune antibodies is very important for the treatment of rheumatoid arthritis by reducing doses, reducing toxic side effects, and improving curative effects [3].

1.2. Related Work Research. Vojdanian believes that although the current treatment prospects for rheumatoid arthritis have shown great improvement, many side effects have been reported. Within 12 weeks of M2000 treatment, RA index includes disease activity score (DAS28), simple disease activity index (SDAI) and C-reactive protein (CRP), erythrocyte sedimentation rate (ESR), rheumatoid factor (RF)), and anticirculation citrulline measured peptide antibodies against CCP and blood determinants. After 12 weeks of treatment with M2000, rheumatoid arthritis and migraine, which are considered inflammatory diseases, have been significantly improved. Therefore, it can be concluded that M2000, as a new type of nonsteroidal anti-inflammatory drug (NSAID) with immunosuppressive properties, can not only effectively treat rheumatoid arthritis but also treat migraine [4, 5].

Orsolini found that anticitrullinated protein antibody (ACPA) directly induces the differentiation and activation of osteoclasts, thus leading to bone loss around the joints. To analyze the effect of ACPA on the body bone mineral density (BMD) of established RA patients, 127 RA patients were recruited. In univariate analysis, ACPA-positive patients had lower BMD Z scores at the femoral site (SD was lower than the average reference value for age and gender matching) ($p < 0.01$). A negative correlation between ACPA titer and BMD Z score was observed at all sites ($p < 0.01$). Multivariate analysis adjusted for the main confounding variables confirmed the adverse effects of ACPA on the femoral site ($p < 0.05$), but no effect on lumbar spine BMD. ACPA has a negative potency dependence on the BMD of the femur, which is mainly composed of the cortical bone. ACPA-positive patients, especially those with high titers, should undergo bone examination and receive treatment with bone protectants. Antirheumatic drugs that reduce the ACPA titers that can change the disease may have a positive impact on systemic bone mass [6, 7].

1.3. Innovation

(1) This paper studies the detection of serum anti-PDI4 antibody levels and found that the level and positive rate of anti-PLD4 antibodies in the PA group are higher than those in the non-RA group and healthy controls, indicating that the antibody RAD4 is an autoantibody for rheumatoid arthritis and can be used for serology The new effective markers detected are used for the diagnosis and differential diagnosis of RA

(2) This paper found that in the detection of RA autoantibodies, RF is a diagnostic marker with lower specificity and sensitivity than anti-CCP antibodies. The combination of RF, anti-CCP antibody, AKA, and anti-PADI4 antibody can provide a lot of clinical diagnostic information

(3) In this article, by detecting the level of DKK-1 in the serum of patients with rheumatoid arthritis and healthy individuals, and analyzing its correlation with the results of clinical trials, bone density determination, and other related tests, the expression level of DKK-1 in the serum of RA patient preliminary exploration and related clinical significance provides clinical evidence for the clinical application of DKK-1

2. Early Diagnosis of Autoimmune Antibodies

2.1. Autoimmune Antibody. The autoantibodies produced by humoral immunity are not only related to the onset and severity of the disease. Compared with the diagnosis of RA, the importance of its research is irreplaceable. The new guidelines for the diagnosis and treatment of rheumatoid arthritis indicate that the goal of RA treatment is to achieve clinical relief and control the destruction of cartilage and subchondral bone after early joint hyperplasia. Therefore, rheumatoid arthritis is mainly based on timely and accurate diagnosis and treatment to effectively prevent irreversible joint damage [7]. In 1987, the American College of Rheumatology (ACR) diagnostic RA classification criteria were widely used in the diagnosis of RA, mainly focusing on clinical manifestations. However, early patients with RA do not have specific symptoms; so, its criteria are not suitable for early diagnosis of RA [8].

Searching for sensitive and specific indicators in the serum of patients with early rheumatoid arthritis has always been a hot spot for researchers at home and abroad. Previous indicators include rheumatoid factor, C-reactive protein (CRP), and red blood cell sedimentation rate. In recent years, anticyclic yellow peptide (CCP) antibodies have become the subject of extensive research. In 2009, the new diagnostic criteria of rheumatology in the United States for RA included the above four serological indicators into the diagnostic criteria [9]. The detection of autoantibodies in rheumatoid arthritis has always been a hot spot for researchers, and its research progress mainly includes the following aspects.

(1) Rheumatoid factor (RF). RF was first discovered in 1927 and was one of the first important serological markers for the diagnosis of RA. RF is synthesized in the plasma cells of the synovium and is mainly an autoantibody against epitopes in the Fc fragment of Ig molecules in serum

(2) Antiperinuclear factor (APF). This substance is a protein in the form of IgG in human serum. APF is related to the condition of RA patients. Its appearance suggests a poor prognosis, but many reasons limit its clinical application

(3) Antikeratin antibody (AKA). The study found that there is no difference between AKA and RF and can be detected in the early serum of patients. Therefore, AKA provides a powerful indication for the diagnosis of early RA patients who are negative for RF and has been widely used clinically

TABLE 1: Calculation formulas for sensitivity, specificity, positive predictive value, and negative predictive value.

Test	Case	Noncase	Total
Positive	w (true positive)	x (false positive)	$w + x$
Negative	y (false negative)	z (true negative)	$y + z$
Total	$w + y$	$x + z$	$w + x + y + z$

(4) Antifilaggrin antibody (AFA). Experiments have shown that AFA appears in the serum of patients with early RA, even earlier than anti-CCP antibodies, and is related to disease activity

(5) Anti-RA33 antibody. It can appear in the serum of early RA patients and is a good indicator of serological diagnosis. It has nothing to do with rheumatoid factor. Detection of anti-PA33 in early RA patients with negative atypical rheumatoid factor can help improve diagnosis and achieve early diagnosis and treatment

(6) Anticyclic citrullinated peptide (CCP) antibody. Internal and external comparisons show that the diagnostic specificity of anti-CCP antibodies is relatively certain, but there are some differences in sensitivity. Due to its high diagnostic value, anti-CCP antibodies have been a hot spot for scholars in recent years

(7) Peptidyl arginine deiminase 4 (PADI4). The specificity is 99%, which is the most specific serological diagnostic index of RA, which can occur before the onset of RA; so, it can be used for the early diagnosis of RA

(8) Comprehensive detection of rheumatoid arthritis. Many researchers have conducted a lot of research on the combined detection of RF and anti-CCP antibodies, seeking a logical combination of diagnostic experiments to provide a rich and accurate scientific experimental basis for the diagnosis of clinical diseases [10], so as to achieve accurate diagnosis and reasonable treatment

2.2. Rheumatoid Arthritis. Rheumatoid arthritis (RA) is a common clinical autoimmune disease that occurs in the joints of the limbs. It mainly manifests as repeated chronic inflammation of the joints. In advanced patients, joint deformities and disabilities can even lead to serious complications of the heart, skin, and other tissues and organs. In my country, the incidence of RA is about 0.35%, and the incidence of women is still very high, with about 4 million patients. The etiology of RA is complex, and the high incidence may be related to many factors, such as infection stimulation, genetic factors, internal and external environmental changes, immune diseases, and smoking [11, 12].

Rheumatoid arthritis is a systemic disease of chronic immune system disease. Worldwide, the incidence of rheumatoid arthritis is about 1%, and the ratio of men to women is 2.5/1. The high incidence of this disease is between 40 and 70 years old. With age, there is an upward trend. The disease is characterized by joint pain, swelling, stiffness and destruction of bone and cartilage tissue, and in severe cases even loss of mobility, resulting in a severe reduction in the quality of life of the patient and a reduction in the life expectancy of the patient. The pathological changes of rheumatoid arthritis are mainly the proliferation of joint cells in the joint cavity, inflammatory cells that erode inflammatory joints, and the formation of new blood vessels in the joint joint cavity, leading to joint damage and deformity [13, 14].

Most patients with rheumatoid arthritis have chronic relapsing episodes, and some patients develop rapidly within 1-2 years. The etiology of rheumatoid arthritis is not fully understood. Many studies have been conducted on the pathogenesis of rheumatoid arthritis, but it is still unclear. Current research has found that rheumatoid arthritis is related to genetic factors, infectious factors, sex hormones, and the environment. The pathogenesis of rheumatoid arthritis is based on susceptibility genes and immune disorders caused by pathogens such as the environment and infection. These diseases can cause autoimmune reactions and cause inflammatory damage to joint tissues [15].

Early diagnosis and treatment of rheumatoid arthritis are very important, because the damage to the joint structure of patients with rheumatoid arthritis is irreversible [16]. It is important to be able to detect the disease as soon as possible and treat it with standard therapies so that the disease can be well controlled. Delay or even prevent the progression of the disease, prevent joint damage, avoid the poor prognosis of patients with disability or death, and strive to enable patients to enjoy a higher quality of life [17].

2.3. Diagnostic Criteria for RA. The diagnosis of RA refers to the classification standard and scoring system proposed by ACR (American Association of Rheumatology) and EULAR (European Alliance against Rheumatism). That is to say, there is at least 1 joint swelling and pain, there is evidence of arthritis (clinical or ultrasound or magnetic resonance imaging), arthritis caused by other diseases is excluded, and there is a typical routine RA radiological change or meet the RA classification criteria. According to the scoring system, a total score of 6 is diagnosed as RA [18, 19], as shown in Table 1.

Sensitivity refers to the percentage of confirmed cases that are also judged positive through evaluation [20]. The ideal value is 100%. The calculation formula is

$$w/(w + y) \times 100\%. \qquad (1)$$

Specificity refers to the percentage of confirmed noncases that are also judged negative by the evaluation test, and the ideal value is 100%. The calculation formula is

$$z/(x + z) \times 100\%. \qquad (2)$$

The positive prognostic value refers to the ratio of true positive individuals to the number of positive test results. The calculation formula of the measured value is

$$w/(w + x) \times 100\%. \qquad (3)$$

TABLE 2: Comparison of antibody, antigen, and concentration of each group.

Detection Indicator	RA group	Non-RA group	Control group
Anti-MCV antibody (U/mL)	268.9 ± 125.36	12.44 ± 3.89	10.01 ± 3.08
GPI antigen (mg/L)	1.211 ± 0.528	0.13 ± 0.06	0.087 ± 0.033
Anti-CCP antibody (RU/mL)	719.43 ± 477.15	13.66 ± 4.41	11.2 ± 3.55
RF (IU/mL)	144.20 ± 81.68	13.72 ± 5.23	8.16 ± 2.96
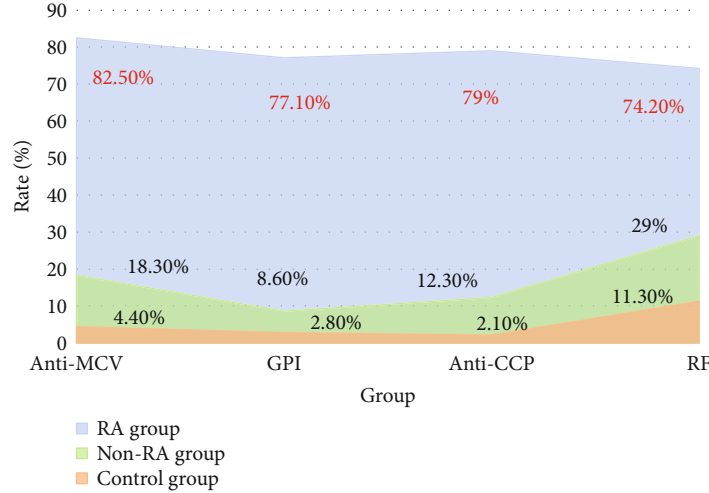
FIGURE 1: Comparison of antibody, antigen, and positive rate of each group.

TABLE 3: Comparison of antibody, antigen and positive rate of each group.

Detection indicator	RA group	Non-RA group	Control group
Anti-MCV antibody (U/mL)	82.5%	18.3%	4.4%
GPI antigen (mg/L)	77.1%	8.6%	2.8%
Anti-CCP antibody (RU/mL)	79%	12.3%	2.1%
RF (IU/mL)	74.2%	29%	11.3%

Negative predictive value refers to the percentage of true negative individuals whose test results are negative. The formula for calculating the predicted value is

$$z/(y + z) \times 100\%. \tag{4}$$

The DAS28 scoring standard widely used in clinical practice is used to determine the degree of RA activity [21]. DAS28 rating refers to the PREVOO calculation method, which is based on the DAS28 rating calculation formula for 28 joints:

$$DAS28 = [0.56 \times \mathrm{sqrt}(t28) + 0.28 \times \mathrm{sqrt}(sw28) + 0.70 \times Ln(\mathrm{SER})] \times 1.08 + 0.16. \tag{5}$$

2.4. Peak Admission for Rheumatoid Arthritis. Collect the clinical data of 2500 RA patients admitted to the rheumatology department in the last 3 years, carry out periodic statistical analysis, calculate the peak period of admission for rheumatoid arthritis, and summarize the seasonality of admission for rheumatoid arthritis. It not only provides an epidemiological basis for the clinical prevention and treatment of RA, but also improves the ability of traditional Chinese medicine to cure the disease. At the same time, it also provides scientific statistical methods for time medicine and provides a scientific basis for our country to understand the relationship between time and disease [22, 23]. According to the season, patients with rheumatoid arthritis were divided into four groups, namely, the spring group (631 people), the summer group (572 people), the autumn group (628 people), and the winter group (669 people). The statistical method uses the periodic distribution method to first determine the average cumulative number of days in each season, convert it to an angle, take the sine and cosine values, and then multiply by the group frequency (number of patients). Then, use the formula

$$x = \sum f \cos \alpha/n, \tag{6}$$

$$y = y \sum f \sin \alpha/n, \tag{7}$$

$$r = \sqrt{x^2 + y^2}, \tag{8}$$

$$\alpha = \mathrm{arctg} y/x. \tag{9}$$
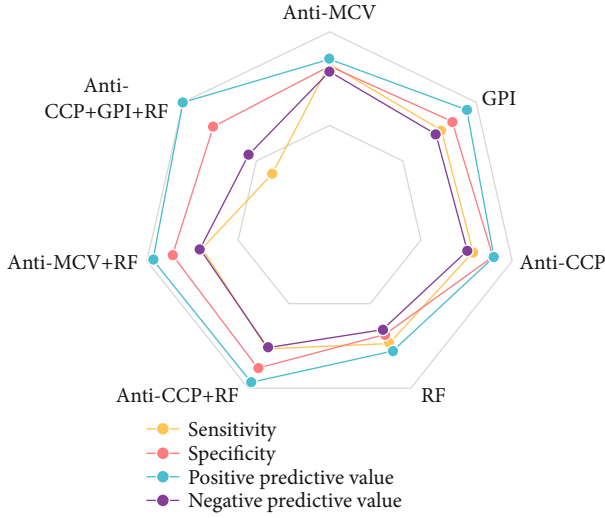
FIGURE 2: Sensitivity and specificity of serum markers in RA.

Simplified conversion is available:

$$\alpha = \text{arctg} \sum \sin\alpha / \sum \cos\alpha, \tag{10}$$

$$s = (180/\pi)\sqrt{-2\ln r}. \tag{11}$$

Look up the table, calculate the angle mean α and standard deviation s, convert them to the corresponding time, perform a significant test on the concentration vector r, and get the peak of the introduction of rheumatoid arthritis [24, 25].

2.5. Slice Image Feature Extraction. First, we observed a large number of neural slice images. The shapes of different types of neural function packages in the nerve slice images do not show specific feature rules. However, in actual situations, according to the doctor's professional introduction, it shows different types of nerve function keys. Shape cannot be used as a feature evaluation parameter, and nerve bundles of the same type can also have different shapes. Therefore, this article does not take the form of graph as the evaluation parameter, but chooses internal features to represent it [26]. Since the color feature difference between different types of nerve function bundles is very small, it cannot be used as an effective evaluation parameter. In this way, we choose local texture as the internal feature of the neural slice image, and the choice of texture feature will directly affect the result of subsequent recognition. Based on the following evaluation parameters, the texture features of the image stained by neurofetus are calculated [27, 28].

The average gray value reflects the average gray value of the image

$$m = \sum_{i=0}^{L-1} ip(i). \tag{12}$$

Variance reflects the discrete distribution of image gray levels.

$$\beta = \sqrt{\sum_{i=0}^{L-1} (i-m)^2 p(i)}. \tag{13}$$

Kurtosis reflects the approximate state of the gray image distribution when it is close to the mean. It is used to judge whether the grayscale distribution of the image is too concentrated near the middle grayscale. The smaller the kurtosis, the more concentrated it is.

$$\omega = \frac{1}{\beta^4} \sum_{i=0}^{L-1} (i-m)^2 p(i) - 3. \tag{14}$$

Smoothness is a measure of the relative smoothness of brightness in an area. For areas with constant brightness, the change is small, and so T is equal to zero. For areas with large deviations in grayscale values, if the change is large, T is close to 1.

$$T = 1 - \frac{1}{1+\beta^2}. \tag{15}$$

The principle of average filtering is to select a template composed of several adjacent pixels, find the average value of all pixels in the template, and then match the average value of the current pixel with the gray level of the processed image, which is

$$g(x,y) = \frac{1}{m} \sum f(x,y). \tag{16}$$

The basic design idea of the median filter is to replace the value of a point in the digital image or sequence with the average value of each point near the point and then change the pixels with a large difference in the gray value of the surrounding pixels to be close to the surrounding pixels. Therefore, a single noise point can be eliminated.

$$Y(n) = \text{med}[X(n-N) \cdots X(n) \cdots X(n+N)]. \tag{17}$$

3. Comprehensive Medical System for Early Diagnosis of Autoimmune Antibodies

3.1. Test Subject. From March 2019 to September 2019, select RA patients, non-RA patients, and health examiners in orthopedic hospitals and record the clinical and laboratory data of the patients, such as gender, age, course of disease, joint performance, erythrocyte sedimentation rate, and C-reactive protein etc. The fasting venous blood of the patient was collected. The above data and samples were collected under the informed consent of the patient and the approval of the competent committee.

3.2. Test Design

TABLE 4: Sensitivity and specificity of serum markers in RA.

Index	Sensitivity	Specificity	Positive predictive value	Negative predictive value
Anti-MCV antibody	82.9%	81.8%	85.5%	78.8%
GPI antigen	76.3%	95.7%	93.7%	72.7%
Anti-CCP antibody	78.6%	89.5%	90.1%	75.5%
RF	73.5%	68.2%	78%	65.3%
Anti-CCP antibody+RF	76.7%	88.1%	96.5%	76%
Anti-MCV antibody+RF	69.8%	86%	96.6%	70.9%
Anti-CCP antibody+GPI antigen+RF	39%	79.3%	100%	55.2%
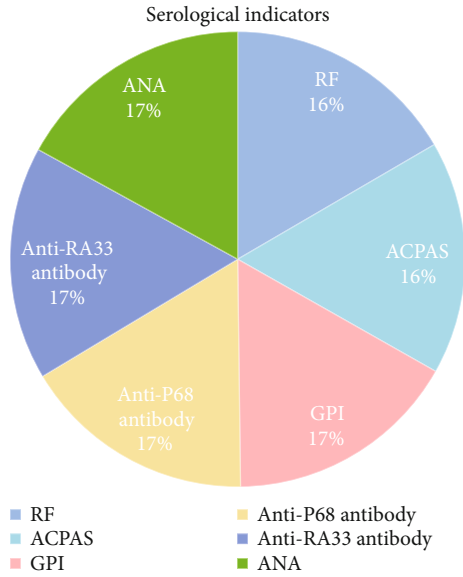
FIGURE 3: Related serological indicators.

(1) Sample collection. All subjects in the study collect 3-5 mL of venous blood on an empty stomach, centrifuge at 3000 r/min for 5-10 minutes, and collect the supernatant. Store in a low-temperature refrigerator at -70°C and determine the batch after the freeze-thaw cycle

(2) ELISA test. Anti-CCP antibody, anti-MCV antibody, and serum GPI antigen concentration were all measured by the double antibody ELISA sandwich method

(3) Take out the 96-well plate coated with different antibodies purchased from the reagent company from the refrigerator and place it at room temperature. Add 100 μl of diluted test serum, negative control, positive control, and reference standard to 96-well wells

(4) Incubate for 30 or 60 minutes in a water bath at room temperature or 37°C. Empty the 96-well plate, wash it 5 times with the predetermined washing solution, and then dry it with clean absorbent paper

(5) Add 100 μl of enzyme-labeled antibody solution to each well. Incubate for 15 or 60 minutes in a water

bath at room temperature or 37°C. The 96-well plate is washed, washed again, and dried

(6) Add 100 μl of substrate solution to each well, incubate at room temperature for 15 minutes, and add 100 μl of reaction stop solution to each well

(7) Rate nephelometry detection. The turbidimetric method is used for automatic RF detection in serum

Use SPSS13.0 statistical software for statistical analysis. Use a four grid table to calculate the sensitivity, specificity, positive predictive value, and negative predictive value of each test index. For comparison between groups or between groups, the enumeration data uses the second test, the normal distribution measurement data uses the t-test to compare the two groups, and the distortion distribution uses the nonparametric test. Spearman correlation analysis was used to compare the correlation between serum markers and the DAS28 score of RA disease activity. $p < 0.05$ was regarded as a statistically significant standard.

3.3. Experimental Results. The anti-MCV antibody, GPI antigen, and anti-CCP serum levels of the three groups of subjects were calculated by ELISA technology. Rate nephelometry was used to determine the serum RF concentration of three groups of individuals. The results showed that compared with the other two groups, the concentrations of anti-MCV antibody, GPI antigen, anti-CCP antibody, and RF in the RA group were significantly higher ($p < 0.05$). Comparing the non-RA group and the normal group, there was no significant difference in the concentration of the four serum markers ($p > 0.05$), as shown in Table 2.

4. Effect of the Early Diagnosis System of Autoimmune Antibodies

4.1. Comparison of Positive Rates of Serum Markers. There are relatively few reports on the combination of anticitrulline antibody and GPI antigen for the diagnosis of RA. This article analyzes and compares the four sera by measuring the concentration of anti-MCV antibody, anti-CCP antibody, GPI antigen, and RF in the serum of patients diagnosed with RA. The sensitivity, specificity, and relevance of markers are in the clinical diagnosis of RA. The positive crisis standard of each serum marker is the positive standard of anti-MCV antibody which is >20 U/mL. The positive standard for CPI

TABLE 5: Related serological indicators.

Serum index	Application					
RF	RF is the earliest and most common test index used in clinical practice. The test results are fast, stable, reliable, cheap, and the most widely used.					
ACPAS	Anti-MCV antibody	Anti-CCP antibody	Anti-APF antibody	Anti-AKA antibody	Anti-AFA antibody	Anti-ACF antibody
	ACPAS is a large class of autoantibodies that have similar chemical structures and directly fight against epitopes of citrulline. They are highly specific for the diagnosis of RA.					
GPI	GPI antigen level may become an independent new indicator for diagnosing RA patients and combined inspection with other indicators can effectively reduce missed diagnosis.					
Anti-P68 antibody	Combined detection with other indicators can effectively reduce missed diagnosis and has important value for the patient's disease activity, bone erosion degree, and prognosis judgment.					
Anti-RA33 antibody	Positives also have early diagnostic value and predictive value, and joint detection can significantly improve diagnostic efficiency and reduce missed diagnosis.					
ANA	The general term for a large class of autoantibodies that extends from the original antinuclear antigen to all antigen components in the cell is an effective method for detecting various autoimmune diseases.					
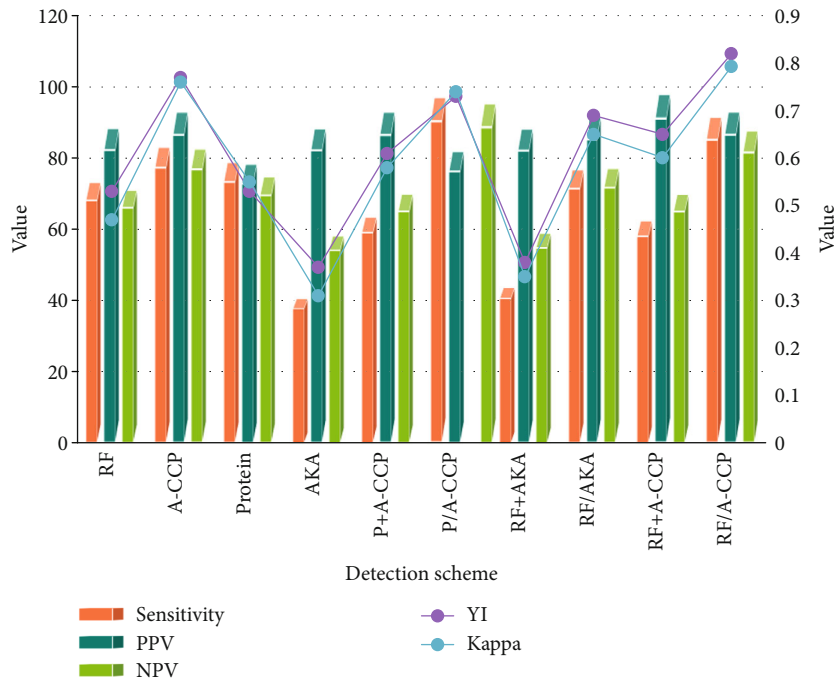
FIGURE 4: Comparison of single and combined testing schemes for 4 indicators.

Table 6: Comparison of single and combined testing schemes for 4 indicators.

Test items	Sensitivity	Specificity	PPV	NPV	Accuracy	YI	Kappa
RF	73.4	89.8	88.6	71.2	75.03	0.53	0.47
Anti-CCP antibody	83.3	92.5	93.2	82.8	88	0.77	0.76
14-3-3η	79	74.1	78.5	75	76.9	0.53	0.55
AKA	40.7	94.2	88.5	58.3	65	0.37	0.31
14-3-3η+anti-CCP antibody	63.65	95.64	93.18	70.14	78.56	0.61	0.58
14-3-3η/anti-CCP antibody	97.3	72.61	82.16	95.77	86	0.73	0.74
RF + AKA	43.85	94.35	88.42	59.07	66.22	0.38	0.35
RF/AKA	76.91	93	91.86	77.32	86.12	0.69	0.65
RF + anti-CCP antibody	62.59	99	98.16	70.07	79.36	0.65	0.601
RF/anti-CCP antibody	91.78	90.39	93.23	87.92	90.08	0.82	0.793

Table 7: Serum concentration of each group.

Group	ZNF706	WIBG	GABAPAPL2
ERA	86.35 + 2.96	1539.12 ± 116.42	39.47 ± 2.86
NERA	60.37 + 2.19	1233.67 ± 99.34	28.63 ± 1.76
CTD	52.64 ± 3.91	993.14 ± 85.91	20.68 ± 0.94
Healthy	47.35 ± 2.64	424.52 ± 30.96	15.03 ± 0.55

antigen is >0.20 mg/L. The positive standard for CCP antibody is >25 RU/mL. The positive RF standard is >15 IU/mL. The positive rate of the four serum markers in the RA group was significantly higher than that of the non-RA group and the control group, and the difference was statistically significant ($p < 0.05$), as shown in Figure 1, Table 3.

4.2. Comparison of Sensitivity and Specificity of Serum Markers in RA.
The sensitivity of the four detection markers from high to low is anti $-$ MCV antibody (82.9%) > anti $-$ CCP antibody (78.6%) > GPI antigen (76.3%) > RF (73.5%), of which anti-MCV antibody is (82.9%). The sensitivity is the highest, significantly higher than RF ($p < 0.05$), and there is no significant difference between other indicators ($p > 0.05$). The specificity of the four detection markers from high to low is GPI antigen (95.7%) > anti $-$ CCP antibody (89.5%) > anti $-$ MCV antibody (81.8%) > RF (68.2%), among which is GPI antigen and anti-CCP antibody. The specificity of RF was significantly higher than that of RF ($p < 0.01$ and < 0.05), and the specificity among other markers was not statistically significant ($p > 0.05$). The positive predictive value of the four test markers was GPI antigen (93.7%) > anti $-$ CCP antibody (90.1%) > anti $-$ MCV antibody (85.5%) > RF (78%). The negative predictive value from high to low is anti $-$ MCV antibody (78.8%) > anti $-$ CCP antibody (75.5%) > GPI antigen (72.7%) > RF (65.3%). In the comparison of the positive predictive value, the value of GPI antigen was significantly higher than that of RF ($p < 0.05$), and there was no statistical significance among other indicators (P >0.05). There was no statistical difference in the negative prognostic value of each index ($p > 0.05$), as shown in Figure 2 and Table 4.

4.3. Serological Indicators Related to Rheumatoid Arthritis.
RA cannot be cured, but early diagnosis can control RA patients as soon as possible and use drugs in a timely and reasonable manner, thereby significantly improving the quality of life of patients. ACR and the European Union Against Rheumatism (EULAR) jointly proposed a new RA diagnostic model in 2009, including a new laboratory-labeled anticyclic citrullinated peptide (CCP) antibody. The combined detection of the two can improve the efficiency of early diagnosis of rheumatoid arthritis. With the deepening of research, domestic and foreign researchers gradually discovered some new indicators and detection methods. Some of them have higher sensitivity, some have stronger specificity, some are closely related to the development and prognosis of the disease, and some can be found in the early stages of the disease or even long before clinical diagnosis. With the continuous emergence of new detection markers, understanding the pros and cons of different markers in diagnosis and complementarity is what clinicians need in clinical practice. ACPAS is a large class of autoantibodies important for the diagnosis of RA, including anti-MCV antibodies, anti-cyclic citrullinated peptide antibodies (CCP) antibodies, anti-perinuclear factor antibodies (APF), and anti-keratin antibodies (AKA), anti-keratin-filaggrin antibody (AFA), and anti-citrullinated fibrinogen antibody (ACF), as shown in Figure 3 and Table 5.

4.4. Comparison of RF, Anti-CCP Antibody, 14-3-3η, and AKA Detection Protocols.
Finding high-sensitivity and high-specificity laboratory diagnostic methods [29], especially early diagnostic indicators, has always been the focus of laboratory diagnosis. In the research of RA autoantibodies, we have experienced RF, AKA, anti-CCP antibodies, and so on. The accuracy and value of YI and Kappa are comprehensive statistical parameters of sensitivity and specificity. Generally, the higher the YI, the better the authenticity of the measurement. The higher the accuracy, the better the consistency between the test result and the actual value. Kappa analysis examined the influence of random factors on cohesion. The higher the Kappa value, the better the reliability of the diagnostic test [30]. The four indicators were combined in two projects in parallel, and the parameters of a total of twelve combinations were analyzed. When the dual target detection is parallel, the highest sensitivity of the combined
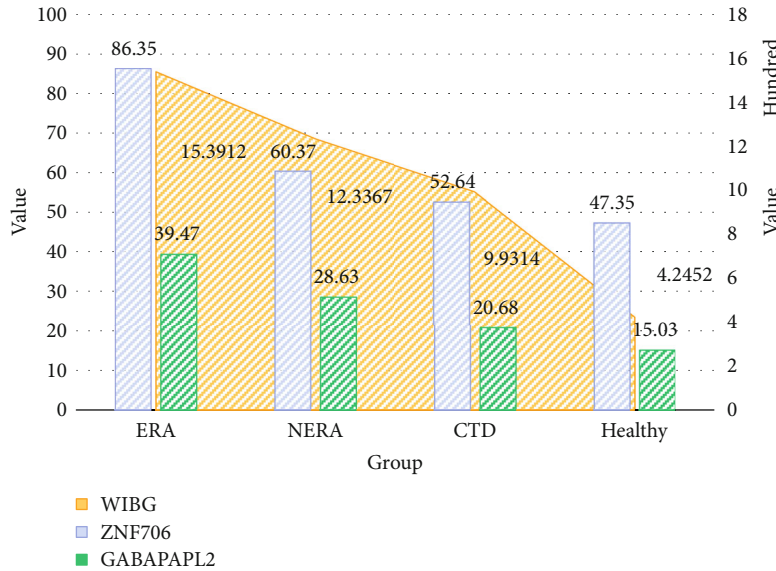
Figure 5: Serum concentration of each group.
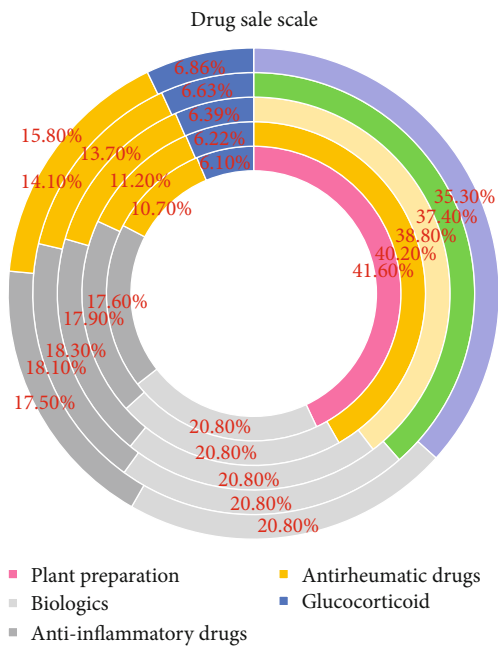
Figure 6: Proportion of drugs in recent years.

14-3-3 protein detection (shown as protein in the figure) and anti-CCP antibody is 96.81%, but the specificity of this combination is only 73.75%, positive predictive value. The negative predictive value is 81.25%, the negative predictive value is 95.16%, the accuracy is 86.21%, the YI is 0.71, and the Kappa value is 0.718. When the two are combined in series, the sensitivity, specificity, positive predictive value, negative predictive value, accuracy, and YI and Kappa values are 63.65%, 95.54%, 93.18%, 70.14%, 78.56%, 0.61, and 0.58, respectively, as shown in Figure 4 and Table 6.

4.5. Comparison of Four Groups of Serum Concentrations.
The levels of serum WIBG, ZNF706, and GABARAPL2 in the four groups are shown in Table 7. In this experiment, they were compared. The serum ZNF706 levels of the four groups were compared. The serum ZNF706 levels of the ERA group, the NERA group, the CTD group, and the healthy group were [(86.35 ± 2.96), (60.37 ± 2.19), (52.64 ± 3.91), and (47.35 ± 2.64) ng/L], the ZNF706 level in the serum of the ERA group was the highest, which was significantly higher than that of the NERA group, CTD group, and healthy group, and the difference was statistically significant ($p < 0.05$). The levels of WIBG in the four groups were [(1539.12 ± 116.42), (1233.67 ± 99.34), (993.14 ± 85.91), and (424.52 ± 30.96) ng/L]. The serum WIBG level in the ERA group was the highest, which was significantly higher than that in the NERA group, CTD group, and healthy group, and the difference was statistically significant ($p < 0.05$). The levels of GABARAPL2 in the four groups were [(39.47 ± 2.86), (28.63 ± 1.76), (20.68 ± 0.94), and (15.03 ± 0.55) ng/ml]. The level of GABARAPL2 in the serum of the ERA group was the highest, which was significantly higher than that of the NERA group, CTD group, and healthy group, and the difference was statistically significant ($p < 0.05$), as shown in Figure 5 and Table 7.

4.6. Rheumatoid Arthritis-Related Drugs. With the rapid development of economy and society, people's lives and eating habits have changed. According to the monitoring data of Zhongkang CMH, among the five major rheumatoid arthritis drugs, Chinese herbal preparations have the largest market share. The market size reached 22.3 billion yuan in 2019, accounting for 37.4%, and it is expected to reach 25.6 billion yuan by 2020. The estimated compound annual growth rate (2016-2019) is 6.1%. As rheumatoid arthritis is a chronic disease, antirheumatic drugs (DMARD) to improve this condition are also getting more and more attention, and the market performance of DMARD also shows this. The market size of DMARD has expanded from RMB 9 billion in 2016 to 2019. From 11.7 billion yuan (18.1%), it will reach 12.9

TABLE 8: Proportion of drugs in recent years.

Drugs	2016	2017	2018	2019	2020 (E)
Plant preparation	41.60%	40.20%	38.80%	37.40%	35.30%
Biologics	20.80%	20.80%	20.80%	20.80%	20.80%
Anti-inflammatory drugs	17.60%	17.90%	18.30%	18.10%	17.50%
Antirheumatic drugs	10.70%	11.20%	13.70%	14.10%	15.80%
Glucocorticoid	6.10%	6.22%	6.39%	6.63%	6.86%

billion yuan by 2020. Among the five main categories of therapeutic drugs, the compound annual growth rate (2016-2020) is the highest, reaching 11.8%, as shown in Figure 6 and Table 8.

5. Conclusion

New disease research methods are helping the experiment find new evidence for the diagnosis of diseases. Protein chip technology and the combination of computer technology and biomedicine will have more applications and developments. Autoantibodies ZNF706, GABARAPL2, and WIBG can identify early RA and provide a new direction for understanding the mechanism of early disease and the mechanism of disease development. At the same time, the experiment showed that the expression of certain markers in the early and early stages of rheumatoid arthritis is quite different. The discovery of these markers enables the experiment to show that the pathological process of rheumatoid arthritis is different in the early and late stages. At the same time, their application will inevitably improve the accuracy of rheumatoid arthritis and will also play an important role and improve the early diagnosis of rheumatoid arthritis. Some of these indicators will also provide more clues and guidance for the development of new drugs.

At present, there is consensus on the treatment of rheumatoid arthritis at home and abroad. Once a patient is diagnosed with rheumatoid arthritis, effective disease-improving drugs should be used as soon as possible to control disease progression and prevent or reduce bone damage. This is conducive to improving the prognosis of the disease, and early diagnosis is the basis for early treatment. The diagnostic criteria currently revised by the American Academy of Rheumatology in 1987 are mainly based on clinical manifestations, X-ray examinations, and serum rheumatoid factor (RF) tests. When the diagnostic criteria for imaging are met, the patient will experience bone destruction. RF has low sensitivity and specificity in other autoimmune diseases (such as systemic lupus erythematosus and healthy elderly) and also has a certain positive rate. There are some shortcomings in clinical application, which delays the optimal treatment time and increase the disability rate. The above criteria are not helpful for the early diagnosis of RA. Therefore, in recent years, research has become a research hotspot in finding simple and easy-to-detect laboratory detection methods with high sensitivity or specificity to improve the early diagnosis rate.

Early diagnosis of rheumatoid arthritis is a hot spot in recent years, because early diagnosis and treatment of rheumatoid arthritis can effectively prevent the progression of the disease and delay or even prevent the process of bone destruction. The current ACR/EULAU 2010 RA diagnostic criteria for early diagnosis of rheumatoid arthritis have been significantly improved. Among them, RF and CCP antibodies are used for diagnosis. However, in clinical practice, there are some difficulties in diagnosing patients with negative RF and CCP antibodies. For some patients who are highly suspected but have not yet reached the diagnostic criteria, more information is needed to support the diagnosis. At the same time, the current ACR/EULAU2010 RA diagnostic criteria still has a certain false positive rate for the early diagnosis of rheumatoid arthritis, which also requires more data to help diagnosis.

Data Availability

The data that support the findings of this study are available from the corresponding author upon reasonable request.

Conflicts of Interest

The author(s) declare(s) that they have no conflicts of interest.

References

[1] L. Buisman, J. Luime, M. Oppe, J. M. W. Hazes, and M. P. M. H. Rutten-van Mölken, "A five-year model to assess the early cost-effectiveness of new diagnostic tests in the early diagnosis of rheumatoid arthritis," *Arthritis Research & Therapy*, vol. 18, no. 1, article 1020, pp. 135–A359, 2016.

[2] H. Y. Wu, A. Filer, I. Styles, and H. Dehghani, "Development of a multi-wavelength diffuse optical tomography system for early diagnosis of rheumatoid arthritis: simulation, phantoms and healthy human studies," *Biomedical Optics Express*, vol. 7, no. 11, pp. 4769–4786, 2016.

[3] Y. H. Cheon and S. I. Lee, "Impact of early diagnosis on functional preservation in patients with rheumatoid arthritis: the early bird catches the worm," *Korean Journal of Internal Medicine*, vol. 32, no. 4, pp. 634-635, 2017.

[4] M. Vojdanian, H. Ahmadi, A. R. Jamshidi et al., "The anti-migraine effects of M2000 (β-D-mannuronic acid) on a patient with rheumatoid arthritis: case report," *Current Clinical Pharmacology*, vol. 12, no. 2, pp. 127–130, 2017.

[5] Q. Feng, Y. Li, N. Wang et al., "A biomimetic nanogenerator of reactive nitrogen species based on battlefield transfer strategy for enhanced immunotherapy," *Small (Weinheim an der Bergstrasse, Germany)*, vol. 16, no. 25, article e2002138, 2020.

[6] G. Orsolini, C. Caimmi, O. Viapiana et al., "Titer-dependent effect of anti-citrullinated protein antibodies on systemic bone mass in rheumatoid arthritis patients," *Calcified Tissue International*, vol. 101, no. 1, pp. 17–23, 2017.

[7] V. F. A. M. Derksen, S. Ajeganova, L. A. Trouw et al., "Rheumatoid arthritis phenotype at presentation differs depending on the number of autoantibodies present," *Annals of the Rheumatic Diseases*, vol. 76, no. 4, pp. 716–720, 2017.

[8] L. Mayordomo, M. L. Velloso, C. Almeida, L. M. Jimenez-Liñan, C. Gomez-Cano, and J. L. Marenco, "AB0221 Predictive value of power Doppler ultrasonography (PDUS) in the diagnosis of very early rheumatoid arthritis," *Annals of the Rheumatic Diseases*, vol. 75, Supplement 2, pp. 973.3–97973, 2016.

[9] S. M. Al-Shaer, "Role of CT scan in early diagnosis of temporomandibular joint injury in patients with rheumatoid arthritis," *The Journal of Contemporary Dental Practice*, vol. 21, no. 7, pp. 769–775, 2020.

[10] M. Elhoseny, K. Shankar, and J. Uthayakumar, "Intelligent diagnostic prediction and classification system for chronic kidney disease," *Scientific Reports*, vol. 9, no. 1, article 46074, p. 9583, 2019.

[11] M. Peña and F. Rondón, "AB0224 Role of anti-RA33 as a biomarker for diagnosis in Colombian patients with rheumatoid arthritis," *Annals of the Rheumatic Diseases*, vol. 75, Supplement 2, pp. 974.3–97974, 2016.

[12] H. Song and M. Brandt-Pearce, "Range of influence and impact of physical impairments in long-haul DWDM systems," *Journal of Lightwave Technology*, vol. 31, no. 6, pp. 846–854, 2013.

[13] P. R. Lage-Hansen, H. Lindegaard, S. Chrysidis, and L. Terslev, "The role of ultrasound in diagnosing rheumatoid arthritis, what do we know? An updated review," *Rheumatology International*, vol. 37, no. 2, article 3587, pp. 179–187, 2017.

[14] L. B. Solnes, K. M. Jones, S. P. Rowe et al., "Diagnostic value of 18F-FDG PET/CT versus MRI in the setting of antibody-specific autoimmune encephalitis," *Journal of Nuclear Medicine*, vol. 58, no. 8, pp. 1307–1313, 2017.

[15] L. Ji, X. Deng, Y. Geng, Z. Song, and Z. Zhang, "The additional benefit of ultrasonography to 2010 ACR/EULAR classification criteria when diagnosing rheumatoid arthritis in the absence of anti-cyclic citrullinated peptide antibodies," *Clinical Rheumatology*, vol. 36, no. 2, article 3465, pp. 261–267, 2017.

[16] L. Ji, G. Li, Y. Xu, W. Zhou, and Z. Zhang, "Early prediction of rheumatoid arthritis by magnetic resonance imaging in the absence of anti-cyclic citrullinated peptide antibodies and radiographic erosions in undifferentiated inflammatory arthritis patients: a prospective study," *International Journal of Rheumatic Diseases*, vol. 18, no. 8, pp. 859–865, 2015.

[17] S. Chaudhary, D. Dutta, M. Kumar et al., "Vitamin D supplementation reduces thyroid peroxidase antibody levels in patients with autoimmune thyroid disease: an open-labeled randomized controlled trial," *Indian Journal of Endocrinology & Metabolism*, vol. 20, no. 3, article 179997, pp. 391–398, 2016.

[18] S. Arora, A. Rafiq, and M. Jolly, "Management of rheumatoid arthritis: review of current guidelines," *Journal of Arthroscopy & Joint Surgery*, vol. 3, no. 2, pp. 45–50, 2016.

[19] Z. C. Ozdemir, O. Bor, E. C. Dinleyici, and E. Kiral, "Plasmapheresis in a child with cold antibody autoimmune hemolytic anemia: case report," *Turkish Archives of Pediatrics/Türk Pediatri Arşivi*, vol. 52, no. 3, pp. 169–172, 2017.

[20] J. Y. Mao, X. H. Zhao, H. Dai, X. J. Gao, and L. L. Lu, "Rheumatoid arthritis involving tibialis posterior tendon: study on the early diagnostic value of power Doppler ultrasonography and comparison with surgery," *Zhonghua Yi Xue Za Zhi*, vol. 96, no. 41, pp. 3311–3314, 2016.

[21] E. L. Nasonov, Y. A. Olyunin, and A. M. Lila, "Rheumatoid arthritis: the problems of remission and therapy resistance," *Scientific and practical rheumatology*, vol. 56, no. 3, pp. 263–271, 2018.

[22] C. Strehl, L. Maurizi, S. Hermann et al., "AB0014 nanoparticles as MRI contrast agent for early diagnosis of RA: effects of amino-PVA-coated SPIONS on CD4+ T cell activity," *Annals of the Rheumatic Diseases*, vol. 75, Supplement 2, pp. 901–901, 2016.

[23] J. A. Schwartz, I. Prado, J. Misamore et al., "An HIV gp120-CD4 immunogen does not elicit autoimmune antibody responses in cynomolgus macaques," *Clinical & Vaccine Immunology*, vol. 23, no. 7, pp. 618–627, 2016.

[24] V. Hamuryudan, H. Direskeneli, I. Ertenli et al., "Direct and indirect healthcare costs of rheumatoid arthritis patients in Turkey," *Clinical & Experimental Rheumatology*, vol. 34, no. 6, pp. 1033–1037, 2016.

[25] M. P. Brown, P. Hissaria, A. H. Hsieh, C. Kneebone, and W. Vallat, "Autoimmune limbic encephalitis with anti-contactin-associated protein-like 2 antibody secondary to pembrolizumab therapy," *Journal of Neuroimmunology*, vol. 305, pp. 16–18, 2017.

[26] N. M. Mcgrath and C. P. Turner, "Isolated gluteal and paravertebral muscle weakness due to anti-3-hydroxy-3-methylglutaryl-coenzyme a reductase antibody-associated necrotizing autoimmune myopathy," *Muscle & Nerve*, vol. 54, no. 1, pp. 150–152, 2016.

[27] B. I. Gavrilă, C. Ciofu, and V. Stoica, "Biomarkers in rheumatoid arthritis, what is new?," *Journal of Medicine & Life*, vol. 9, no. 2, pp. 144–148, 2016.

[28] J. A. Lansita, K. M. Mease, H. Qiu, T. Yednock, S. Sankaranarayanan, and S. Kramer, "Nonclinical development of ANX005: a humanized anti-C1q antibody for treatment of autoimmune and neurodegenerative diseases," *International Journal of Toxicology*, vol. 36, no. 6, pp. 449–462, 2017.

[29] S.-B. Tsai, Y.-Z. Xue, P.-Y. Huang et al., "Establishing a criteria system for green production," *Proceedings of the Institution of Mechanical Engineers, Part B: Journal of Engineering Manufacture*, vol. 229, no. 8, pp. 1395–1406, 2015.

[30] X. Xu, D. Cao, Y. Zhou, and J. Gao, "Application of neural network algorithm in fault diagnosis of mechanical intelligence," *Mechanical Systems and Signal Processing*, vol. 141, article 106625, 2020.

Retraction

Retracted: Student Physical Fitness Test System and Test Data Analysis System Based on Computer Vision

Wireless Communications and Mobile Computing

This article has been retracted by Hindawi following an investigation undertaken by the publisher [1]. This investigation has uncovered evidence of one or more of the following indicators of systematic manipulation of the publication process:

(1) Discrepancies in scope

(2) Discrepancies in the description of the research reported

(3) Discrepancies between the availability of data and the research described

(4) Inappropriate citations

(5) Incoherent, meaningless and/or irrelevant content included in the article

(6) Peer-review manipulation

The presence of these indicators undermines our confidence in the integrity of the article's content and we cannot, therefore, vouch for its reliability. Please note that this notice is intended solely to alert readers that the content of this article is unreliable. We have not investigated whether authors were aware of or involved in the systematic manipulation of the publication process.

In addition, our investigation has also shown that one or more of the following human-subject reporting requirements has not been met in this article: ethical approval by an Institutional Review Board (IRB) committee or equivalent, patient/participant consent to participate, and/or agreement to publish patient/participant details (where relevant).

Wiley and Hindawi regrets that the usual quality checks did not identify these issues before publication and have since put additional measures in place to safeguard research integrity.

We wish to credit our own Research Integrity and Research Publishing teams and anonymous and named external researchers and research integrity experts for contributing to this investigation.

The corresponding author, as the representative of all authors, has been given the opportunity to register their agreement or disagreement to this retraction. We have kept a record of any response received.

References

[1] L. Wang and S. Chen, "Student Physical Fitness Test System and Test Data Analysis System Based on Computer Vision," *Wireless Communications and Mobile Computing*, vol. 2021, Article ID 5589065, 8 pages, 2021.

Research Article

Student Physical Fitness Test System and Test Data Analysis System Based on Computer Vision

Ling Wang[1] and Sitong Chen [2]

[1]*School of Physical Education, Shenyang University, Shenyang, 110044 Liaoning, China*
[2]*School of Mechanical Engineering and Automation, Northeastern University, Shenyang, 110819 Liaoning, China*

Correspondence should be addressed to Sitong Chen; 1510112@stu.neu.edu.cn

Computer vision technology is one of the main research directions of artificial intelligence. With the rapid growth of image or video data scale and the improvement of computing power, computer vision technology has achieved unprecedented development in recent years and is widely used in a variety of scenes. This study mainly discusses the design of student physical fitness test system and test data analysis system based on computer vision. This study is mainly based on the motion attitude determination algorithm to identify the motion. In hardware configuration, the key is CPU and GPU. The model realizes large-scale matrix computation based on the parallel computing power provided by GPU and uses CPU to realize data reading and preprocessing. The assessment controller is responsible for the transmission of instructions and status information and controls the operation of the entire pitch assessment system. It is the control center of the entire system. ZigBee wireless communication technology is adopted as the communication method of human posture measurement terminal and assessment controller. The input image is preprocessed through scaling and standardization. The image is scaled to the resolution of 224×224 when input, which is performed to realize data parallel training. The image was changed by means of random horizontal flip, random rotation, and color change to achieve the effect of expanding the dataset. Then, the test evaluation module was used to evaluate various test indexes of the body. During the sit-up test, nine out of 10 sit-ups can be accurately counted and the recognition rate reaches 90 percent. The results show that the system designed in this study has high accuracy and good performance, which can be used for the physical fitness test and test data analysis of students.

1. Introduction

In the early days, due to the backwardness of the economy, our people's physical requirements only stayed on the basis of food and clothing. Later, with the development of the economy and the improvement of living standards, people paid more and more attention to the improvement of their overall physical fitness. With the improvement of the quality of life of our people and since the reform and opening up, China has strengthened the communication with the United States and many other countries in the aspects of economy, culture, science and technology, and political system and directly introduced many foreign advanced ideas and practices in the aspect of physical improvement.

Our country has gradually launched a physical fitness test program combined with physical examination during the compulsory education stage. So far, basic schools in our country have organized students to conduct physical examinations in school hospitals and physical fitness tests in sports venues. The health of students has been regarded as an important guarantee for the country's new force. In recent years, the term "health records" has become popular in my country's medical circles. Although many difficulties have been encountered in implementation, now basically only large hospitals have established electronic medical records instead of national unified health records. As for physical fitness testing, information technology has not been fully promoted. Only independent systems equipped with physical fitness testing equipment cannot comprehensively reflect

health conditions. Due to the lack of information technology and integrated system for physical fitness testing in China, this has brought great challenges to the research of this subject [1].

Computer vision methods have been applied to cell segmentation and feature extraction, while machine learning methods have been developed to help phenotype classification and clustering of data obtained from biological images [2]. Grys et al. believe that with the latest developments in high-throughput automated microscopes, there is an increasing demand for effective computing strategies for analyzing large-scale image-based data. Here, they outline the common computer vision and machine learning methods used to generate and classify phenotypic profiles, focusing on the general biological uses of each method. Their research lacks data [3]. Yeung et al. introduced VideoSET, which is a method for evaluating video summaries through text. It can evaluate the extent to which the video summary can retain the semantic information contained in the original video [4]. They observed that semantics are most easily expressed in words and developed a text-based evaluation method. Their research has no practical significance [5]. Chang proposed a pixel-based cost calculation method that uses weighted distance information for cross-scale stereo matching. The method he proposed uses a hierarchical structure to accurately estimate the disparity value in a uniform area. He also uses distance information to supplement the pixel-based cost function. His research sample data is insufficient [6]. Zaki introduced a novel method for binary classification of two-wheeled road users at dense mixed traffic intersections. Classification is a monitoring procedure used to distinguish electric and nonelectric (manpowered) bicycles. First, use object recognition methods to detect and track road users. Then, select classification features from the collected trajectories. Functions include maximum speed, rhythm frequency, and acceleration-based parameters. Experiments were conducted on a video dataset from Shanghai, China, where cyclists and motorcycles tend to share major road facilities. A sensitivity analysis was performed to evaluate the quality of selected features to improve the accuracy of classification. His research is not novel enough [7]. Meireles proposes an automatic and direct method to classify tooth wear in the oral cavity. The eight extracted teeth were etched with acid for different times to produce abrasion and scanned with an intraoral optical scanner. Computer vision algorithms are used for alignment and comparison between models. He estimated the amount of wear and determined the reliability through visual scoring. His research has no practical significance [8]. Wang proposed an automatic flexible printed circuit (FPC) defect detection method based on computer vision, which provides a method for calculating dimensionality increment matrix and image segmentation combined with fuzzy clustering algorithm. The visibility of the segmented image and the segmentation accuracy of the defective image are guaranteed. The method he proposed is not accurate [9].

This research mainly discusses the design of student physical test system and test data analysis system based on computer vision. This research is mainly based on the

motion recognition algorithm for motion recognition. In the hardware configuration, the key is CPU and GPU. The model realizes large-scale matrix calculation based on the parallel computing capability provided by GPU and uses CPU to realize data reading and preprocessing. The assessment controller is responsible for the transmission of instructions and status information and controls the operation of the entire pitch assessment system. It is the center of the entire system control. ZigBee wireless communication technology is used as the communication method between the human body posture measurement terminal and the assessment controller [10]. The input image is subject to preprocessing steps of scaling and standardization. The image is scaled to a resolution of 224×224 during input. This step is performed to achieve data parallel training. Three methods of random horizontal flip, random rotation, and color change are used to change the image to achieve the effect of expanding the dataset, and then, the test evaluation module is used to evaluate various test indicators of the body.

2. Student Physical Fitness Test System

2.1. Computer Vision.
In recent years, due to the wide application of computer vision in intelligent surveillance and surveillance, health and medicine, sports and entertainment, robotics, drones, and driverless cars, it has become more and more important and effective [11–13]. Depth information is one of the most important elements for generating three-dimensional (3D) content [14]. The stereo matching method uses binocular characteristics to estimate depth information [15, 16]. The estimated depth information is usually represented by the disparity value [17]. Therefore, two slightly different viewpoints are used to find the disparity value. However, in a uniform area, since the area is untextured, the corresponding point finding is problematic [18].

Many computer vision and imaging problems are learned from large-scale datasets, which have millions of observations and features. A novel effective learning scheme tightens the sparsity constraint by gradually deleting variables based on criteria and schedules [19, 20]. The fascinating fact that the size of the problem continues to decrease throughout the iteration process makes it particularly suitable for big data learning [21], generally applicable to the optimization of any differential loss function and find applications in regression, classification, and ranking. The resulting algorithm incorporates variable screening into the estimation and is very simple to implement [22], providing theoretical guarantees of convergence and selection consistency. In addition, one-dimensional piecewise linear response functions are used to solve nonlinear problems, and second-order priors are applied to these functions to avoid overfitting [23, 24].

2.2. Motion Attitude Determination Algorithm.
This algorithm does not record all the angle values and then analyzes and processes, but uses a mobile real-time determination method to obtain the effective number of cycles, collect and record key information, and use a possible cycle as the

algorithm execution cycle to extract the effective cycle [14]. The core idea of the algorithm is to take the maximum value of a certain number of accumulated records as the peak and the minimum value of the accumulated record of a certain number of times as the trough. If it is greater than the set evaluation standard, it will be recorded as a valid period [5, 16]. The execution cycle of the algorithm is the execution cycle of the entire program; each time the current angle value is obtained as an input variable for judgment [25].

The algorithm can be obviously divided into three parts. The first part is to judge the angle accumulation and accumulation. Each time it is executed, the current value and the recorded maximum and minimum values are used for judgment; the second part is to identify the number of accumulation and subtraction. The peaks and troughs are accumulated to 20 times, and it is considered that there is a trough. Similarly, there is a trough after the accumulation of 20 times. The identification of the peak is a condition for trough identification. The identification process of the two is similar; the third part is after obtaining the peak and peak value. To determine whether it is a qualified period, use a pair of recorded peak and valley values as the key variable to accurately obtain the possible effective period. In actual applications, time judgment is added, that is, the limit time for the human body to complete a pitching action is 300 ms. If the cycle is lower than this time, it is considered to be an abnormal fluctuation and is not adopted [18, 26]. The execution stage refers to the process in which the neural network processes the input information and generates the corresponding output [19]. In the execution stage, the connection structure and weight coefficients of the network have been determined and will not change. At this time

$$U(t+1) = \sum_{j=1}^{n} W_{ij}(t+1)X_j(t) - \theta(t+1). \tag{1}$$

Among them, W_{ij} is the weight coefficient of the connection between the i neuron and the former j level neuron. The motion attitude determination optimization algorithm has faster convergence speed and better optimization effect, which is very suitable for large-scale data or large-scale model problems.

$$m_t = \beta_1 m_{t-1} + (1-\beta_1)g_t,$$

$$v_t = \beta_1 v_{t-1} + (1-\beta_1)g_t^2,$$

$$\theta_{t+1} = \theta - \frac{\eta}{\sqrt{v+\varepsilon}}m. \tag{2}$$

Among them, m_t and v_t calculate the first and second moments of the gradient [6].

2.3. Network Input Layer. For the BP network, the input layer acts as a buffer memory and can add data to the network. The number of nodes depends on the dimensionality of the data source. The output layer outputs the processing results of the network, and the number of nodes can be designed

according to the requirements of use. For sports events, the physical status of students is affected by many factors; among which gender, age, height, weight, and the 14 physical fitness test indicators mentioned above have a greater impact on determining the physical status of students. We must evaluate a student's overall physical fitness status or individual physical fitness status in terms of running, jumping, and shooting based on these influencing factors. Taking the evaluation of students' comprehensive physical fitness status as an example, we set the dimension of the network input layer to 18, and each node represents the student's gender, age, height, weight, and 14 physical fitness test indicators; in actual training, the current physical state of students is divided into three states: poor, normal, and good. Therefore, the dimension of the network output layer is set to 3, representing these three states, respectively.

3. Student Physical Fitness Test System Experiment

3.1. Experimental Environment. The operating system configuration is shown in Table 1. In the hardware configuration, the key is CPU and GPU. Although the model is based on the parallel computing capabilities provided by GPU to achieve large-scale matrix calculation, CPU is still needed to achieve data reading and preprocessing. Therefore, when building a deep learning platform, the CPU performance should also be taken into consideration. The CPU of the deep learning platform is Intel 7700k, the GPU is Nvidia Gtx 1080, and the GPU memory capacity is 8 GB. The key software platform components are parallel computing framework, deep learning framework, and programming language. The experiment in this study uses the CUDA 9.0 parallel computing framework and the PyTorch deep learning framework. The experiment is mainly implemented by the Python 3.6 programming language. The deep learning platform chose the Ubuntu 16.04 operating system because it has good support for deep learning-related software and hardware. Many open source frameworks are implemented based on the Ubuntu 16.04 operating system and then ported to other operating systems.

3.2. Communication Technology between the Assessment Controller and the Host Computer. The assessment controller is responsible for the transmission of instructions and status information and controls the operation of the entire pitch assessment system. It is the center of the entire system control. The main task of the assessment controller is data transmission. There are three main parts: RS232 serial port and upper computer wired communication, ZigBee and anthropometric terminal wireless communication, and RS485 serial port and LCD display terminal wired communication. This design selects the widely used RS232 serial communication method.

3.3. Communication Technology between the Assessment Controller and the Human Body Posture Measurement Terminal. The human body posture measuring terminal is installed on the human body to measure the human body's

TABLE 1: Operating system configuration.

Operating system	Ubuntu 16.04
CPU	Intel 7700k
GPU	Nvidia Gtx 1080
Parallel computing framework	CUDA 9.0
Deep learning framework	PyTorch
Programming language	Python 3.6

movement posture. In order not to affect the actions of the reference personnel and the reliability of communication, this design uses wireless communication as the means of communication between the assessment controller and the human body posture measurement terminal. During the sit-up assessment, the distance between the two reference personnel is relatively large, the maximum is 2 m, and the entire assessment site is up to 5 m × 8 m, which belongs to the short-distance category. Considering all aspects, the Zig-Bee wireless communication technology suitable for short-range wireless communication is selected.

3.4. "Handshake" between Upper and Lower Computers. The lower computer receives the test data of muscle strength transmitted by the measuring device and stores it in the external memory of the single-chip microcomputer. Then, the lower computer sends a handshake request to the upper computer. If the handshake is unsuccessful, it will send the request repeatedly. If it exceeds three times, the system will prompt an error to exit. If the handshake is successful, it will start to enter the next stage, and the host computer will begin to receive test data.

3.5. Test Data Receiving and Storage. After the successful handshake between the upper and lower computer, the upper computer initializes the serial port, configures the serial port parameters, and is ready to receive data. Then, the upper computer sends signals to the lower computer and receives data through the serial port. The upper computer simultaneously checks whether the received data is complete according to the agreement between the upper and lower computers. If the received data is incomplete, it will be resent. If the received data is complete, it will undergo corresponding format conversion and store the data in the designated database.

3.6. Microcontroller Module Design. This design intends to use ZigBee wireless communication technology as the communication method of the human body posture measurement terminal and the assessment controller, and it is necessary to select a suitable wireless transceiver chip. This design uses the CC2430 chip introduced by TI. It combines an industrial-grade enhanced 8051 controller and a high-performance 2.4 GHz ZigBee RF transceiver chip, which meets the needs of control and communication and is a small measurement terminal. It provides great convenience.

3.7. Preprocessing and Data Enhancement. The input image is subject to preprocessing steps of scaling and normalization (normalization). The image is scaled to a resolution of 224

× 224 during input. This step is performed to achieve data parallel training and reduce the time consumption of neural network training. Data standardization can speed up training. In the actual implementation process, the mean and variance of each channel of RGB of the Image-Net dataset are used. The mean vector is $\mu = [0.485, 0.456, 0.406]$, and the variance vector is $\delta = [0.229, 0.224, 0.225]$.

The parameter of deep neural network is very large, and the model with high training complexity will need massive data. Data augmentation can effectively expand the data diversity of the training set through flip, translation, rotation, and other methods. Three methods of random horizontal flip, random rotation, and color change are used to change the image to achieve the effect of expanding the dataset. For each input image, determine whether to flip horizontally according to the probability of 0.5. This data enhancement method is used because the static image data used uses different camera settings in the historical acquisition process, some of which are camera settings. The images taken by the left and right cameras are flipped horizontally. At the same time, each image is randomly rotated within the range of $[-10, 10]$ according to the image center, which is in line with the characteristic that different cameras cannot guarantee the same angle during the placement process. Brightness, contrast, and saturation are randomly changed in the range of $[0.5, 1.5]$ according to a uniform distribution, and the hue (hue) is randomly changed in the range of $[-0.2, 0.2]$ according to a uniform distribution.

3.8. Information Management Module Design. The information management module refers to the management of some basic information that students, physical fitness test teachers, and counselors need to use during the test. This basic information is collected by the administrator before the physical fitness test and input in advance. The system, in this way, can assign the user name and password of the student, the physical test teacher, and the counselor. With the user name and password, the teacher and student can log in to the system to perform the physical test appointment operation. Whether it is a teacher or a student, their login accounts are all only one, and the input, maintenance, and update of this basic information are all operated by the system administrator.

The use of barcode scanners is mainly used for candidates who failed to take the exam due to special circumstances. When the barcode scanner scans the barcode of the candidate's admission ticket, the focus will automatically focus on the candidate's name. Recheck the candidates' names in the entire data sheet to find them. After the barcode scanner scans the barcode, the admission ticket number is automatically entered into the text box focused by the mouse, which is equivalent to manual input and pressing the enter key.

3.9. Test and Evaluation Module Design. This module is to evaluate various test indicators of healthy physical fitness. The test indicators included in the central lung fitness item include resting heart rhythm, vital capacity, 3-minute step test, systolic blood pressure, and diastolic blood pressure, and the test indicator of muscle strength is grip strength.

And muscular endurance is measured by sit-ups within 1 minute. The flexibility of the body is measured by the degree of flexion in the sitting position. The body composition items are height, weight, BMI value, waist circumference, and hip circumference to measure.

In addition, there are extended indicators, including reaction time, standing time on one foot with closed eyes, blood lipid indicators, and blood glucose indicators. According to the measurement values of each index in different reference ranges, the evaluation can be divided into several standards: excellent, good, fair, acceptable, and poor. If it is a blood pressure index, the evaluation criteria can be normal blood pressure, normal blood pressure, mild hypertension, moderate hypertension, and severe hypertension. If it is blood lipid and blood sugar index, the evaluation criteria can be divided into low, normal, and high. If it is body weight, the evaluation criteria are underweight, normal, and overweight.

3.10. Design of Performance Management Module. The physical fitness test score management module is used by physical fitness teachers and students or counselors after the corresponding physical fitness test is over, in order to enter and query the students' scores after completing the physical fitness test. The physical fitness test teacher logs in to the system through the teacher to summarize the physical fitness and the test scores are entered into the corresponding student information in the system. After the scores are entered, the teacher can also view them at any time, as well as query the analysis of the data. The students or counselors can log in to the system on the interface to query their (the class) physical test scores.

3.11. Test Evaluation Function Module. Test purpose: check whether the link of each test item is correct and whether each test index is wrong. After the test data is entered for each index item, whether it can be correctly evaluated, whether the evaluation result is displayed in the form of graphics and text, and whether there is a comprehensive evaluation after the completion of the test of each index item. Check whether the data can be saved and printed correctly after user testing.

4. Student Physical Fitness Test System

4.1. Recognition Results. The accuracy rate and average accuracy rate of the designed behavior recognition model in each category are compared with the baseline model MSN. The identification analysis results are shown in Table 2. The average accuracy of MSN in the five categories is 80.31%, and the behavior recognition model achieved by the dual-stream neural network and gesture recognition model in this study reached 83.2%. This study did not compare its operating speed in this part, because the model implemented in this study uses the optical flow algorithm FlowNet2, which is faster than the EpicFlow used by MSN, and the dual-stream neural network is much simplified than MSN, so there must be some operating speed. As mentioned earlier, the behavior recognition model implemented in this study is better than the MSN model in terms of speed and accuracy. Because this

Table 2: Identify analysis results.

Result Model	Two stream+FlowNet2	MSN
REACH	93.1%	89.74%
RETRACT	94.3%	90.47%
HAND IN SHELF	68.66%	65.56%
INSPECT PRODUCT	83.9%	82.7%
INSPECT SHEIF	76%	73.09%
MEAN	83.2%	80.31

research can capture fine-grained behaviors very well and accurately, this research can achieve performance that exceeds that of complex MSN only through dual-stream neural networks.

4.2. Algorithm Performance Test Analysis. The attitude process changes smoothly, the cycle is relatively unchanged, and the peak angle is about 5 degrees to 50 degrees. The algorithm performance test result is shown in Figure 1. The overall shape of Figure 1 is similar to the analysis, but there is a big difference in the local area. There is a large jitter in the extreme part, and the cycle change is large; the peak-to-peak value of the first half of Figure 1 is large, and the peak value is gradually in the second half due to physical consumption. Reduce, there is greater jitter at large angles. It can be seen from the above angle curve that the actual situation is more complicated, and the algorithm should be able to avoid any problems in the actual situation and accurately record the number of effective motion cycles. Taking sit-ups as an example, the human body posture measurement terminal is installed on the tester's head as a training cap. The tester does sit-ups normally, and the measurement terminal performs angle capture and counting operations. Here, the standard angle is set to 90°. Use the serial port to output the real-time angle measured by the measuring terminal and the current count result, use the serial debugging assistant to record these two values, and then import EXCEL to draw the corresponding chart. In order to read the graph clearly and conveniently, the count value is multiplied by 10. The ordinate corresponding to the horizontal line in Figure 1 is 10 times the count value. It can be seen that the human body posture measurement terminal has performed the correct count. The initial angle of the tester when lying down is 90°, and the angle when sitting up is 0°, at the moment of lying down, the tester did 10 sit-ups, but the seventh one was not standard and did not reach 90°, the measuring terminal did not count, and the final count was 9.

4.3. Muscle Strength Test Analysis. Use different colors to show the strength curves of the four tested individuals on different graphs. The four tested individuals can choose any specified conditions. The color of the curve can be changed. Click any graph to display its detailed information. The muscle strength test results are shown in Figure 2. It can be seen from Figure 2 that the same figure is more obvious, and it can be seen that the grip strength curves caused by the differences between the two test individuals are significantly different.
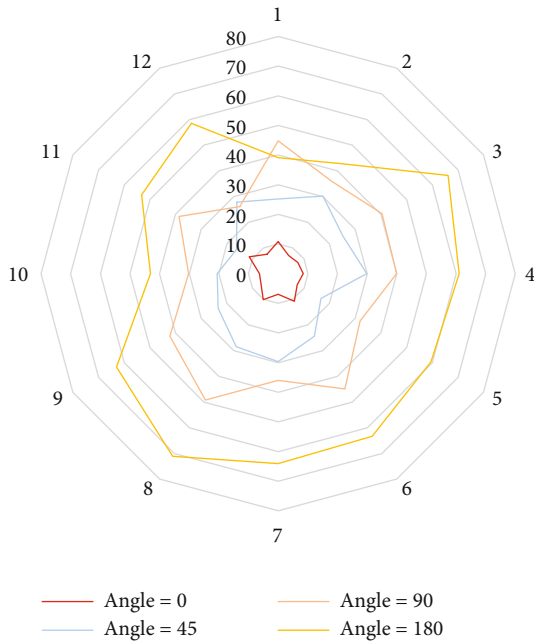
FIGURE 1: Algorithm performance test results.
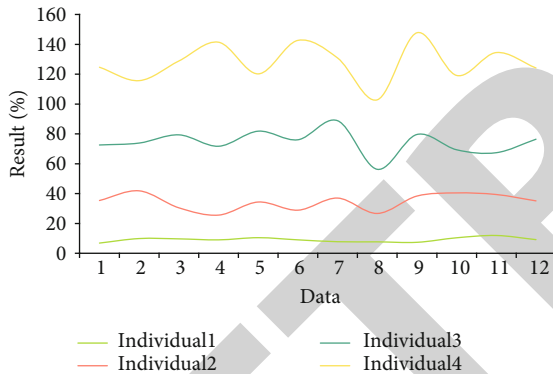
FIGURE 2: Muscle strength test results.

The dynamic data model of this sample set is obtained through statistical calculation steps on the data of 35 individuals participating in the test using statistical principles. Because the selected experimenters are all students of the same age, there is no need to redivide the two fields of age and work nature. First, use the system function to select gender: male, test item: right grip strength, search in the database and find that meets the conditions, and then, count the searched data, store the data obtained from the test data table into an array, and then, take the next testee's data and add them to the data group in the corresponding order of time until all matches conditional data are all superimposed, and finally, each number in the array is averaged to get a dynamic data model. It can be seen that under the same time setting, the man's curve is short and the peak is prominent, the woman's curve is long and the trend is relaxed, and the man is in the comparison of the absolute strength, explosive power, rapid reaction coefficient, and other human parameters, having an advantage over women, and women have an advantage over men in endurance.

4.4. System Performance Test. In order to facilitate user operation and achieve good human-computer interaction, the interface design of the system adopts an all-Chinese graphic frame structure, with friendly interface design and simple operation. The interface item side is the traditional drop-down menu and toolbar; the left side of the interface adopts the popular tree-like menu structure, and clicking can produce the same effect as the drop-down menu, making the human-computer interaction faster and more practical, and the interface is more beautiful; the right side is the interface. The main display area can display graphics, data, tables, etc. The system performance test result is shown in Figure 3. All functions can be automatically completed by clicking the menu or button with the mouse. The main menu of the system includes data acquisition, data query, graph display, data analysis, comparison, and data output. This research is based on the theory of serial communication between the computer and the single-chip computer and makes full use of the powerful data storage and processing ability of the PC and the communication technology, as well as the data acquisition, keyboard input, and display functions of the single-chip computer to develop a basketball special comprehensive test system. The system has been debugged and developed, and various functions have been basically realized and have been used in physical fitness tests. Through continuous debugging and trial and error in the process of system development and development and with the changes in sports college entrance examination requirements, the function is further improved. System is reasonable in design, advanced in technology, accurate in data transmission, data processing, and score recording, and has reached expectations. The effect also played a powerful role in practical applications, which greatly improved the efficiency and accuracy of sports testing.

The student physical test data analysis system can change that the students taking the test are no longer passively tested, but can choose the appropriate test time and subjects according to their own personal situation. At the same time, for physical fitness test teachers, after the on-site test is completed and recorded, there is no need to pass it layer by layer. It is first handed over to the Sports Basic Department, then distributed to the departments, and finally transmitted to the students by the instructor. It is also prone to errors. The data analysis result of the student's physical fitness test is shown in Figure 4. The system can directly enter the scores by the physical fitness test teacher. After the entry is completed, the students can log in and view by themselves. It is also convenient for students to compare their physical fitness test with other students, changing the phenomenon that students only care about whether their physical fitness test scores have passed. The system greatly improves the accuracy and timeliness of data, reducing the workload of the Sports Basic Department and the instructors and department staff. It has a huge positive effect on the management of students' physical fitness test. It receives a segment as input, and the time series flow part of the model receives motion information. A segment is composed of 6 frames of images, and two successive images calculate 5 sets of optical flow results from each other, that is, 10 frames of optical flow information
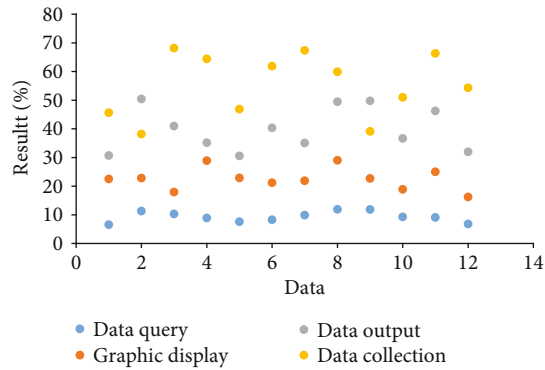
FIGURE 3: System performance test results.

FIGURE 4: Data analysis results of student physical fitness test.

(x direction and y direction). Correspondingly, the timing stream receives 10 channels of data. In order to change the original VGG network from receiving 3 channels of RGB images to receiving 10 channels of optical flow information, the author calculated the input layer along the dimension of the input channel, the weight of the convolution kernel, and copy the weight average to 10 channels. The size of the optical flow data is 256×256 dimensions, and the $8 \times 8 \times 512$ dimension feature map is obtained after the calculation of the convolutional layer. Immediately after that, there are two fully connected layers with dimensions of 32768×4096 and 4096×5. The spatial stream receives an ordinary RGB image, and it randomly selects a frame of image from the input segment as input. After the calculation of the convolutional layer, it obtains a feature map of $7 \times 7 \times 512$ dimensions. Similarly, it connects two layers of fully connected layers. The dimensions are 25088×4096 and 4096×5.

5. Conclusion

The parameter of deep neural network is very large, and the model with high training complexity will need massive data. Data augmentation can effectively expand the data diversity of the training set through flip, translation, rotation, and other methods. Three methods of random horizontal flip, random rotation, and color change are used to change the image to achieve the effect of expanding the dataset. For each

input image, it is determined whether to flip horizontally according to a certain probability. This data enhancement method is used because the static image data used uses different camera settings in the historical acquisition process, some of which are camera settings. The images taken by the left and right cameras are flipped horizontally.

The physical fitness test score management module is used by physical fitness teachers and students or counselors after the corresponding physical fitness test is over, in order to enter and query the students' scores after completing the physical fitness test. The physical fitness test teacher logs in to the system through the teacher to summarize the physical fitness and the test scores are entered into the corresponding student information in the system. After the scores are entered, the teacher can also view them at any time, as well as query the analysis of the data. The students or counselors can log in to the system on the interface to query their (the class) physical test scores.

This research mainly discusses the design of student physical test system and test data analysis system based on computer vision. This research is mainly based on the motion recognition algorithm for motion recognition. In the hardware configuration, the key is CPU and GPU. The model realizes large-scale matrix calculation based on the parallel computing capability provided by GPU and uses CPU to realize data reading and preprocessing. The assessment controller is responsible for the transmission of instructions and status information and controls the operation of the entire pitch assessment system. It is the center of the entire system control. ZigBee wireless communication technology is used as the communication method between the human body posture measurement terminal and the assessment controller. The input image is subject to preprocessing steps of scaling and standardization. Three methods of random horizontal flip, random rotation, and color change are used to change the image to achieve the effect of expanding the dataset, and then, the test evaluation module is used to evaluate various test indicators of the body.

Data Availability

The data that support the findings of this study are available from the corresponding author upon reasonable request.

Conflicts of Interest

There are no potential competing interests in our paper. And all authors have seen the manuscript and approved to submit to your journal.

Acknowledgments

Research Article

Semantic Matching Efficiency of Supply and Demand Text on Cross-Border E-Commerce Online Technology Trading Platforms

Xuhua Chen [ID]

College of E-Commerce, Yiwu Industrial and Commercial College, Yiwu, 322000 Zhejiang, China

Correspondence should be addressed to Xuhua Chen; cxh@ywicc.edu.cn

With the innovation of global trade business models, more and more foreign trade companies are transforming and developing in the direction of cross-border e-commerce. However, due to the limitation of platform language processing and analysis technology, foreign trade companies encounter many bottlenecks in the process of transformation and upgrading. From the perspective of the semantic matching efficiency of e-commerce platforms, this paper improves the logical and technical problems of cross-border e-commerce in the operation process and uses semantic matching efficiency as the research object to conduct experiments on the QQP dataset. We propose a graph network text semantic analysis model TextSGN based on semantic dependency analysis for the problem that the existing text semantic matching method does not consider the semantic dependency information between words in the text and requires a large amount of training data. The model first analyzes the semantic dependence of the text and performs word embedding and one-hot encoding on the nodes (single words) and edges (dependencies) in the semantic dependence graph. On this basis, in order to quickly mine semantic dependencies, an SGN network block is proposed. The network block defines the way of information transmission from the structural level to update the nodes and edges in the graph, thereby quickly mining semantics dependent information allows the network to converge faster, train classification models on multiple public datasets, and perform classification tests. The experimental results show that the accuracy rate of TextSGN model in short text classification reaches 95.2%, which is 3.6% higher than the suboptimal classification method; the accuracy rate is 86.16%, the $F1$ value is 88.77%, and the result is better than other methods.

1. Introduction

Traditional text similarity research methods mainly use one-hot, bag-of-words model, N-gram, and TF-IDF as the feature vector of the text and use methods such as cosine similarity as an index to quantify the degree of text similarity. However, these methods simply use the statistical information of the text as the feature vector of the text [1] and fail to consider the context information of the word. At the same time, there are problems of feature sparseness and dimensional explosion in feature extraction. With the development of deep learning [2], the use of deep learning methods to study text similarity tasks has become the mainstream method today.

Yang et al. proposed the word2vec word vector embedding method in the article; as a neural network language model, this method converts words into multidimensional

vector representation, which greatly facilitates the follow-up work [3]. Radionova-Girsa and Lahiža proposed the GloVe word vector embedding method in the article. The word vector embedding considers the context information, more accurately expresses the context information of the text, and has good performance in multiple natural language processing tasks [4]. Li et al. proposed the TextCNN model in a paper published in 2019 and applied CNN to the field of natural language processing for text classification tasks [5]. Tenyakov and Mamon save more information in the form of vectors and at the same time train the capsule network with a dynamic routing mechanism [6], which reduces the parameters of the network and has a good effect on the handwritten digit recognition dataset [7]. Sun et al. introduce the capsule network into natural language processing to do the task of text classification. The capsule network can effectively

encode the text information and save the multilevel features of the text, and the extracted feature vector can more accurately express the text obtained [8].

Guo et al. use CNN to complete the entity relationship extraction task in the article. The convolutional network with multiple granularities used in this model has good performance [9]. Wang et al. introduced the recurrent neural network into the field of natural language processing, traversed the entire text using a recurrent structure, and obtained the global characteristics of the text [10]. Zhang et al. applied LSTM to the field of natural language processing in the literature. LSTM solves the problem of traditional recurrent neural network's dependence on long-distance information of the input sequence [11, 12]. Jin et al. proposed a bidirectional long- and short-term memory neural network based on the twin network structure for text similarity. The network traverses the entire text through two LSTM networks, comprehensively considers the context information of each word, extracts the characteristics of the sentence, and completes the text similarity [13]. Lu et al. applied the weighting mechanism to the field of network text processing. Through the weighting mechanism, the neural network has the ability to focus on certain features and assigns more weights to important features [14].

Aiming at the characteristics of the supply and demand text network structure on the cross-border e-commerce online technology trading platform [15], this paper proposes a text semantic similarity matching method based on capsule-BiGRU. This method uses two texts through two neural network structures to obtain text feature vectors. Perform similarity analysis to obtain the local similarity matrix and the global similarity matrix, and merge the two levels of similarity matrix to complete the text similarity analysis. The method proposed in this paper first uses the mutual attention mechanism to assign different weights to words. For two texts, the word vector distance of the two texts is calculated, and the words closer to the other text are given higher weights. Secondly, the capsule network and BiGRU network are combined to construct an integrated model, the local features of the text extracted by the capsule network and the global features of the text extracted by the BiGRU network are, respectively, analyzed for similarity, and the two levels of similarity matrices are merged. Finally, judge whether the text is similar according to the similarity vector of the two sentences.

2. Online Trading Platform Text Semantic Matching Analysis Technology

2.1. Characteristics of Cross-Border E-Commerce Platforms. The new format of foreign trade is an important driving force for China's trade development, driven by market changes and government regulation [16]. The three types of new business types are cross-border e-commerce, market procurement, and external comprehensive services. They have different structures, origins, characteristics, principles, and regulatory service systems [17]. It can be seen from comparison that the new business format is the result of the recombination process of foreign trade and domestic trade and the

change of the division of labor by various agents, and it has multiple development possibilities [18]. The current new business formats have problems and risks such as erosion and crowding, short-term profit-seeking, and lack of systems [19]. The next development strategy should be appropriate to the overall score and promote the comprehensive management of various business types, the innovation of cross-border e-commerce models, the iteration of market procurement mechanisms, the transformation and development of external comprehensive services, and the rapid development of information technology combined with wide-area interconnection. According to different participants, it can be divided into three types: enterprise-enterprise (B-B), enterprise-consumer individual (B-C), and individual seller-individual buyer (C-C). Among them, under the B-C type, there are three modes: retail import and export, "haitao," "purchasing," and "overseas warehouse" export [20]. The retail import and export model can be subdivided into four specific models according to its flow and whether it is bonded or not [21]. It can be seen that the model classification of cross-border e-commerce is extremely complicated, and the regulatory codes and flow identifications of various models are completely different [22].

2.2. Semantic Matching Methods and Channels of Supply and Demand Text

2.2.1. Text Similarity Analysis Algorithm Based on Capsule-BiGRU. The text semantic matching model mainly includes word vector embedding module, feature matrix extraction module, feature matrix analysis, and judgment module. Secondly, the capsule network (capsule) and the bidirectional gated recurrent unit network (BiGRU) are combined, and the capsule network is used to extract the local features of the text [23]. At the same time, the traditional capsule network is improved, words that have nothing to do with text semantics are regarded as noise capsules, and smaller weights are assigned to reduce the impact on subsequent tasks [24].

The text semantic matching method first uses the pretrained GloVe model to map the two texts into a 300-dimensional word vector matrix [25]. The word vector matrix is used as the input of the model, and weights are given by the attention mechanism module, and then, the results are input into the BiGRU network and the capsule network model, respectively. In the capsule network, the convolution operation is first performed, and the capsule convolution operation is performed through the main capsule layer. After the squeeze function operation, it is used as the output of the main capsule layer. After the dynamic routing protocol mechanism is calculated, it is connected to the classification capsule layer to classify the capsule [26]. The output result of the layer is expanded as a local feature vector of the text. In the BiGRU network, a bidirectional GRU network is used to extract text information from two directions to obtain the global feature vector of the text. At the same time, in the feature vector extraction stage, a twin neural network structure is used, that is, two word vector matrices are processed using the same network structure so that the two word vector matrices are encoded into the same vector space.

Finally, the respective local features and global features of the two texts are, respectively, analyzed for similarity, and the similarity matrix of the two texts is obtained. The similarity matrix is used as the input of the big data network. The last layer of the big data network uses the SGD function as the classifier to determine whether the two texts are similar [27].

(1) Word Vector Embedding Module. The word vector embedding module first preprocesses the text, including removing stop words and special symbols [28]. Through analysis of all texts, this experiment chooses a maximum sentence length of 25 characters and completes sentences with less than 25 characters. For sentences with more than 25 characters, the first 25 characters are cut off as the sentence. The GVe model pretrained by the Natural Language Processing Group of Stanford University was used to convert each text in the text into a 250-dimensional word vector:

$$X_j = \sum_{j=1}^{N} X_{ij},$$

$$P_{ij} = \frac{X_{ij}}{X_j}. \tag{1}$$

P represents the number of times the word appears in the corpus, and represents the probability of the word appearing in the context of the word [29]. Assuming that the word vector of the word sum is known, the similarity is calculated [30]. When the difference is small, it is proved that the word vector and the cooccurrence matrix are more consistent, and the word vector can accurately grasp the context information:

$$J = \sum_{i,j}^{N} f(X_{ij}) \left(v_i^T v_j + b_i + b_j - \log(X_{ij})\right)^2. \tag{2}$$

Use cost value to represent the difference between two items, and is the deviation item. By iteratively changing the word vectors of all words, the cost value is the smallest in the entire corpus, that is, the optimal word vector of all words in the corpus is obtained so that the word vector of the word is calculated through the context information [31]. The dataset contains a large amount of English text, and the word vector obtained by pretraining contains more accurate context information. The training results of 50-dimensional, 100-dimensional, 200-dimensional, and 300-dimensional word vectors are released. This paper uses the 300-dimensional word vector issued by the Natural Language Processing Group of Stanford University as the word vector representation.

(2) Feature Matrix Extraction Module. With attention in natural language processing, the traditional attention model mainly analyzes the words in the text that are more relevant to the task, so as to give higher attention. Such an attention model will be better in processing a single sentence task

which performed. But for the task of this article-text similarity, the main concern is whether the two texts are similar. For the two input text t_1 and t_2, more attention should be paid to the similar part of t_1 and t_2, and more attention should be paid to the similar part. Calculate and sum the similarity between any word in t_1 and all words in t_2. The similarity calculation method uses cosine similarity, and the sum of cosine similarity is used as the value of the weight to describe the word. Suppose that the word vector matrix obtained by text t_1 and t_2 through the word vector embedding layer is

$$v_{t1} = \left(w_1^1, w_2^1, w_3^1, w_4^1, w_5^1\right),$$

$$v_{t2} = \left(w_1^2, w_2^2, w_3^2, w_4^2, w_5^2\right). \tag{3}$$

According to the above matrix, the semantic analyzer combines the matching degree algorithm to obtain the matching degree:

$$\cos(a, b) = \frac{a \cdot b}{|a| * |b|}. \tag{4}$$

According to the word vector matrix of the previous texts 1t and 2t, the cosine similarity calculation formula is used to calculate the degree of similarity between all words of the two input texts and the other text.

$$k_{t1}[i] = \sum_j \cos\left(w_i^1, w_j^2\right),$$

$$k_{t2}[i] = \sum_j \cos\left(w_j^1, w_i^2\right), \tag{5}$$

where k is the sum of the cosine similarity between the *i*th word in the text t_1 and the text t_2 each word and the cosine similarity of each word in the text t_1 and t_2 is calculated and used as the value for calculating the weight of each word. Use k_{t1}, k_{t2} and SoftMax functions to complete the calculation of word weights.

$$A_{t1} = \text{SoftMax}(k_{t1}),$$

$$A_{t2} = \text{SoftMax}(k_{t2}). \tag{6}$$

A_{t1}, A_{t2} are the weight corresponding to each word of the text; multiply the word vector of the word and the corresponding weight to obtain the feature matrix of the text, which is used as the input of the subsequent network.

The capsule network has a large number of articles, conjunctions, interjections, and other words unrelated to the semantics of the text in the text. These words have a high probability of coexisting in the two texts. These words can be high after the attention module is calculated. However, these words do not significantly affect the semantics of the text. Assigning a greater weight will have a certain impact on the final result. These unrelated words are called noise capsules in the capsule network module. Use the NLTK tool to tag the words in the sentence. In the capsule

network, the qualifiers, conjunctions, interjections, and pronouns are first assigned lower weights according to the word parts to reduce the impact of the noise capsule on the subsequent tasks and solve the above problems. Input the characteristic matrix of the attention mechanism into the capsule network, and use the dynamic routing algorithm to calculate the output of the upper layer capsule. The calculation steps are as follows:

$$A_i = \text{attention}(u^i),$$

$$\lambda(A_i, A_j) = \left[\log\left(\frac{\left|x_{A_i} - a_{A_j}\right|}{w_{A_j}}\right), \log\left(\frac{\left|y_{A_i} - y_{A_j}\right|}{h_{A_j}}\right), \log \\ \cdot \left(\frac{w_{A_i}}{w_{A_j}}\right), \log\left(\frac{h_{A_i}}{h_{A_j}}\right) \right].$$

$$(7)$$

Iterate r times:

$$c_{ij} = \frac{e^{b_{ij}}}{\sum_k e^{b_{ik}}},$$

$$u_{(j|i)} = w_{ij} A_i,$$

$$s_j = \sum_i c_{ij} u_{(j|i)},$$

$$\text{squash}(k) = \frac{\|k\|^2}{1 + \|k\|^2} \frac{k}{\|k\|},$$

$$v_j = \text{squash}(s_j),$$

$$b_{ij} = b_{ij} + u_{(j|i)} v_j. \tag{8}$$

Return v_j:

$$\sigma_{ikjl} = \begin{cases} \dfrac{n}{\Delta_{ikjl}} \sqrt{\sum_{s=1}^{n} \left(x_{ik}(\varepsilon) - x_{jl}(\varepsilon)\right)^2 \Delta_{ikjl}(\varepsilon)}, & \Delta_{ikjl} > 0, \\ 0, & \Delta_{ikjl} < 0, \end{cases}$$

$$\Delta_{ikjl} = \sum_{\delta=1}^{n} \Delta_{ikjl}(\varepsilon), \tag{9}$$

where u_i is the feature vector obtained by the mutual attention module, A_i is the feature vector after reducing the weight of the noise capsule, r is the number of iterations of the dynamic routing algorithm, w_{ij} is the weight matrix between the two layers of capsules, is the coupling coefficient, c_{ij} is the lower layer capsule i activates the possibility of the upper capsule j, $(j \mid i)u$ is the input of the upper capsule, squash is the activation function, and v_j is the output of the upper capsule. The dynamic routing algorithm sets the initial value to 0. Such an initial value is the mean value

Table 1: Experimental parameter settings of semantic matching efficiency.

Parameter name	Parameter value	Adam optimization	Keras
Epoch	25	60	0.3
Batch size	512	75	0.5
Dropout	0.3	75	0.5
Capsule dimension	64	60	0.6
Dynamic routing iteration times	3	60	0.2
BiGRU neuron	100	60	0.8

Table 2: Comparison of mainstream models in the field of deep learning.

Model	Accuracy (%)	Accuracy-J (%)	Recall rate (%)	F1 value (%)
LSTM	80.08	82.41	86.24	84.28
BiLSTM	81.95	81.97	88.12	84.93
GRU	80.11	83.81	84.58	84.19
BiGRU	81.95	83.08	87.71	85.33
Siamese-BiGRU	84.47	86.07	89.02	87.52
Capsule	81.91	84.74	86.38	85.55
Siamese-capsule	83.79	88.37	86.31	87.33
Capsule-BiGRU	86.16	86.56	91.11	88.77

of b_{ij}, which is updated through iteration to update the value of c_{ij}. For the neural network model $u_{(j|i)}$ parameters, the model learns values through a large amount of training data.

The capsule network proposed by Sabour in the article includes a three-layer structure, namely, convolutional layer, primaryCaps layer, and DigitCaps layer. In the method proposed in this paper, the output of the DigitCaps layer is used as the local feature matrix of the text. Bidirectional gated recurrent unit network (BiGRU) is a bidirectional gated-based recurrent neural network, which is composed of forward GRU and backward GRU. The text is traversed over the network in two directions to get information, including the text context. This solves the problem that the GRU model can only contain the above information. The GRU model is a variant of the long short-term memory network (LSTM). Compared with LSTM, the GRU model has a simpler network structure, but the effect is basically the same as that of LSTM, which greatly reduces the time required for network training. The output of the current time step of the cyclic neural network is related to the output of the previous time step, which makes the cyclic neural network memorable and suitable for processing sequence data. The GRU network merges the input gate and the forget gate in LSTM, called
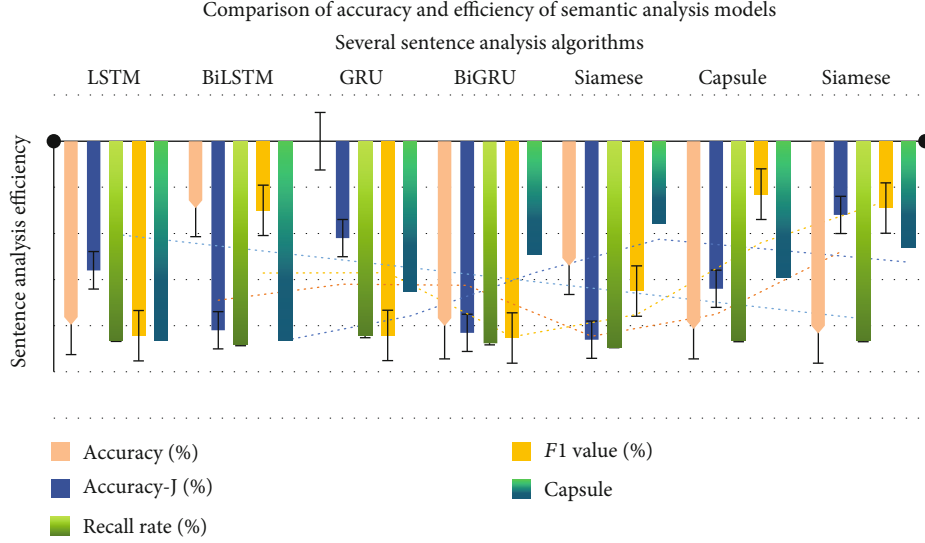
Figure 1: Comparison of accuracy and efficiency of semantic analysis models.

the update gate, which greatly reduces the time required to train the network:

$$z_t = \sigma(w_z x_t + u_z h_{t-1} + b_z),$$

$$r_t = \sigma(w_r x_t + u_r h_{t-1} + b_r),$$

$$h_t = \tanh\left(w_c x_t + u_c(r_t \Theta h_{t-1}) + b_c\right),$$

$$h_t = z_t \Theta h_{t-1} + (1 - z_t)\Theta h_t,$$

$$y_t = \sigma(W_0 \cdot h_t). \tag{10}$$

x is the next input, h_{t-1} is the suspension of the previous import, h_t is the candidate state at the current moment, W_0 is the hidden state at the current moment, and y_t is the output at the current moment. In the GRU network, information can only be transmitted in one direction, but in practice, each word may have a dependency relationship with the word in the context. Using the BiGRU network to train text through the network in two directions makes the model more effective. The method proposed in this paper uses the output of the BiGRU network as the global feature matrix of the text. The local feature matrix and the global feature matrix of the two texts are, respectively, calculated for similarity, and the similarity matrix 1E of the local features and the global similarity matrix 2E are obtained. The calculation method of 1E and 2E is the same; here is the calculation method of 1E. Assuming that the local features of the two texts are 1S and 2S, respectively, the calculation formula of 1E is as follows:

$$E_1^{ij} = \cos\left(S_1^i, S_2^j\right). \tag{11}$$

E_1^{ij} is the element in the ith row and jth column of the similarity matrix, S_1^i is the ith row of S_1, and S_2^j is the jth row of S_2. After the similarity matrix is obtained, the two similarity

matrices are flattened and connected. The fused similarity vector is used as the input of the fully connected layer, and the output of the fully connected network is connected with the sigmoid classifier. Use the sigmoid classifier to determine whether two texts are similar.

2.3. Evaluation Model of Semantic Matching Efficiency of Supply and Demand Text. The text classification methods currently proposed are mainly divided into two categories: traditional classification algorithms and classification algorithms based on deep learning. Traditional classification methods use feature engineering and feature selection to extract features from original documents and then input the extracted features into classifiers such as SVM and KNN for training and prediction. More classic feature extraction methods include frequency method and mutual information method (PMI), inverse text frequency index (TF-IDF), and N-gram. With the popularity of deep learning, more and more people use deep learning methods to classify text, mainly as convolutional neural network (CNN) and its improved version of the application, such as TextCNN training word vectors to represent text, and CNN local relevance feature is applied to text classification problems; the method proposed on the basis of TextCNN does not dig out the potential semantic relationship between words in the text from the semantic level when processing the text [32] and directly represents the internal meaning of the text. In recent years, graph convolutional neural network (GCN) has attracted widespread attention in the academic community as an emerging research direction. GCN is an extension of CNN in the irregular domain and is mainly used to process irregular graph structure data.

The CRF classifier model and the neural network classifier model have their own advantages and disadvantages [27]. The CRF model needs to manually annotate the corpus information in advance and manually design the features such as the part of speech and degree of the word, while the neural network model can learn the training data to
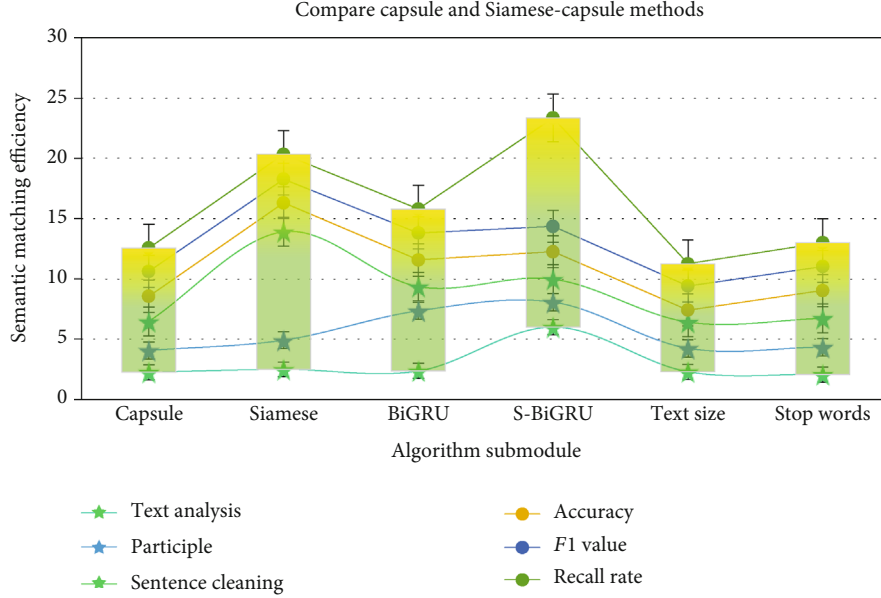
Figure 2: Comparison of capsule and Siamese-capsule methods.

automatically generate feature vectors to achieve better results. However, neural network models often require longer training time, and some outputs of neural network models are illegal in named entity recognition. Therefore, it is necessary to use CRF to subsequently add the rules of named entities to the sequence labeling process. This paper combines the characteristics of CRF and neural network models to obtain a joint model with more advantages in performance. The learning and prediction of the CRF model is performed on multiple features of the sample. The CRF model itself can generate feature vectors and perform classification. This article uses the features extracted by the hybrid neural network as the intermediate quantity to replace the vector value in the original formula. The emission probability in the CRF classifier model refers to the probability that the words in the sequence belong to each sentiment category [33]. The transition probability is the probability from a label class to an adjacent label class. The emission probability of the conventional CRF classifier is generated based on the feature template, but the features automatically collected by the hybrid neural network are used as the emission probability to get better context information.

3. Online Text Semantic Analysis Research Model Construction

3.1. Semantic Matching Text Data Source. In order to evaluate the performance of the model on the text similarity task, this paper uses the Quora Question Pairs dataset and the MRPC dataset for experiments. The Quora Question Pairs dataset contains 404000 sentence pairs, and the label of similar sentence pairs is 1; otherwise, it is 0. In the experiment of this article, the dataset is divided: 80% as the training set, 10% as the test set, and 10% as the verification set. The MRPC

dataset includes 4076 training samples and 1725 test samples. The label of similar sentence pairs is 1; otherwise, it is 0.

3.2. Steps of Semantic Matching Efficiency. The experiment carried out in this paper is implemented based on the Keras framework, using the Adam optimizer, and the experimental model parameter settings performed on the Quora Question Pairs dataset are shown in Table 1.

The performance evaluation indexes of this experiment mainly include accuracy rate, precision rate, recall rate, and $F1$ value. Let TP be the number of correct classes predicted as correct classes. The calculation formula of the evaluation index is as follows:

$$\text{Accuracy} = \frac{\text{TP} + \text{TN}}{\text{TP} + \text{TN} + \text{FP} + \text{FN}},$$

$$\text{Precision} = \frac{\text{TP}}{\text{TP} + \text{FP}},$$

$$\text{Recall} = \frac{\text{TP}}{\text{TP} + \text{FN}},$$

$$F1 = 2 \times \frac{\text{Precision} \times \text{Recall}}{\text{Precision} + \text{Recall}}. \tag{12}$$

To verify the effectiveness of the method proposed in this article, three experiments are carried out in this article.

Experiment 1: conduct comparative experiments with mainstream models in the deep learning field.

Experiment 2: conduct comparative experiments with the methods proposed in other papers.

Experiment 3: change the number of iterations of the capsule network to conduct a comparative experiment.

Experiment 4: test model performance on two datasets.

Comparison with traditional neural network structure

FIGURE 3: Comparison with traditional neural network structure.
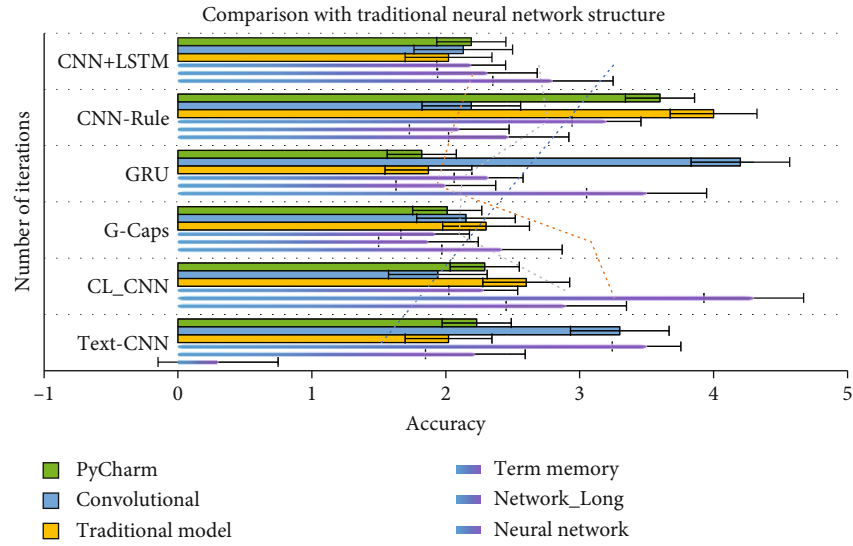
Comparison of improved accuracy of G-caps model
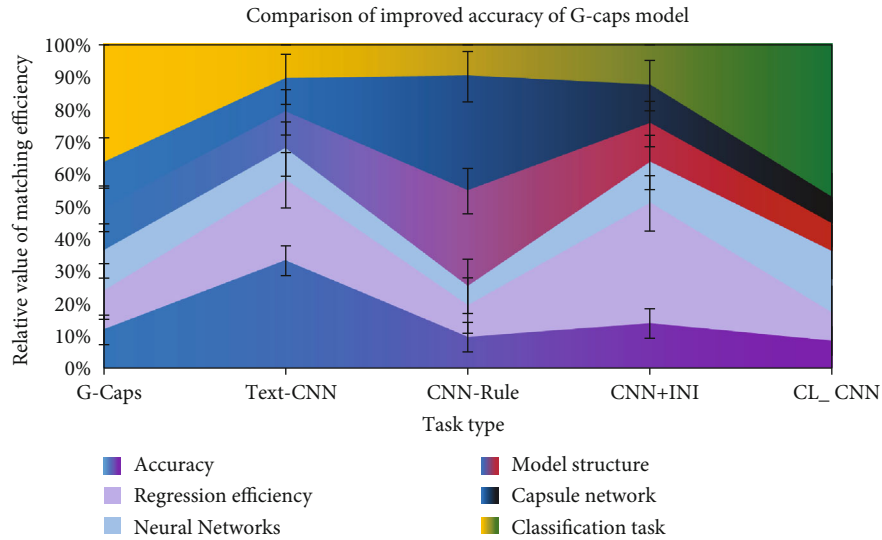
FIGURE 4: Comparison of improved accuracy of G-Caps model.

4. Experimental Analysis of Online Text Semantic Analysis Model

In experiment (1), the mainstream models in the deep learning field are selected for comparison experiments, including LSTM, BiLSTM, capsule, GRU, BiGRU, Siamese-capsule, Siamese-BiGRU, capsule-BiGRU, and use the above models to perform experiments. The experimental results are shown in Table 2.

As shown in Figure 1, compared with traditional CNN and LSTM networks, the model proposed in this paper performs better in text similarity tasks. The performance of the GRU network and the LSTM network in the task is basically the same, but at the same network scale, the time required to train the GRU network is much less than training the LSTM network.

As shown in Figure 2, by comparing the performance of capsule and Siamese-capsule, BiGRU and Siamese-BiGRU, it is found that compared with BiGRU network, the accuracy of Siamese-BiGRU network has increased by 2.52%, the accuracy rate has increased by 2.99%, the recall rate has increased by 1.31%, and the $F1$ value increased by 2.19%. Compared with the capsule network, the Siamese-capsule network has an accuracy rate of 1.88%, an accuracy rate of 3.63%, a recall rate of 1.93%, and an $F1$ value of 1.78%. It can be found that the twin neural network structure can effectively improve the performance of the model.

As shown in Figure 3, when comparing this paper with the traditional neural network structure, the settings of the same parameters, such as Batch_size and Epoch, are consistent. Changes in these parameters have a specific effect on the experimental results. Although the effect of this model
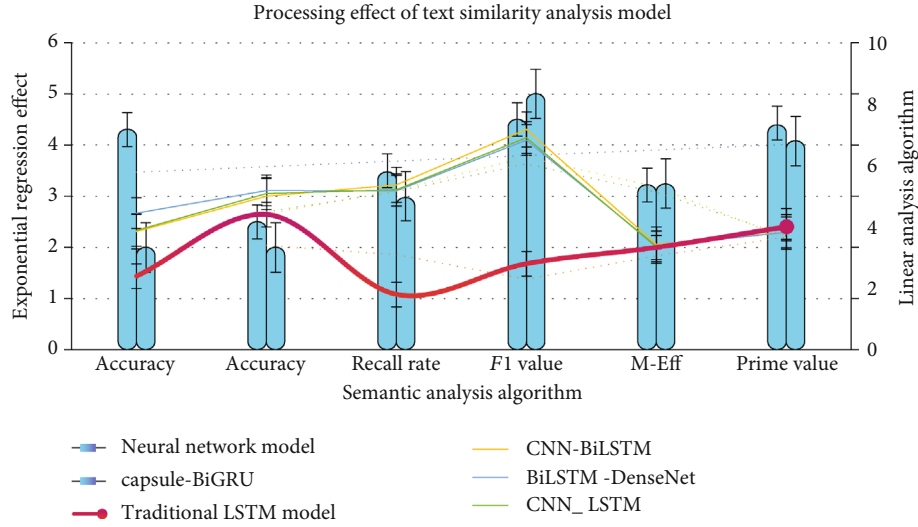
FIGURE 5: Processing effect of text similarity analysis model.

TABLE 3: Comparison with the methods proposed in other papers.

Model	Accuracy (%)	F1 value (%)
Capsule-BiGRU	86.16	88.77
CNN-BiLSTM	84.58	85.02
BiLSTM-DenseNet	85.50	87.10

at the beginning of the iteration is worse than that of the CNN_LSTM and BiLSTM models, the effect of this model gradually surpassed the traditional models and surpassed them stably in the middle of the day.

As shown in Figure 4, compared with CNN_LSTM and BiLSTM, the accuracy of the G-Caps model is increased by 5.3% and 7.6%, respectively. The model in this paper extracts vector features as effective information and has achieved good classification results compared with traditional network structure models.

The processing effect of the text similarity analysis model based on capsule-BiGRU is shown in Figure 5. Compared with the traditional LSTM model, the accuracy rate has increased by 6.08%, and the $F1$ value has increased by 4.49%. In experiment (2), the method proposed in this paper is compared with the methods proposed in other papers, and the comparison results are shown in Table 3.

Through comparison, it can be found that compared with the original model, the accuracy of the proposed method is increased by 1.58%, and the $F1$ value is increased by 3.75%. Compared with the direct comparison model, the accuracy rate is increased by 0.66%, and the $F1$ value is increased by 1.67%. This model uses a 6-layer stacked BiLSTM network, the model is more complex, and the training takes longer.

Due to the small number of samples in the MRPC dataset, the dropout parameter is adjusted to 0.1, and other model parameters are not adjusted. As can be seen in Figure 6, the model performs better on the QQP dataset because the QQP dataset has a larger number of samples and the model training is more complete, indicating that the performance of the model proposed in this article is
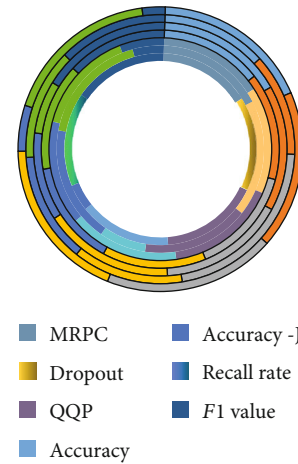
FIGURE 6: The model performs better on the QQP dataset.

TABLE 4: Comparison of iteration times of dynamic routing algorithms.

Number of iterations	Accuracy (%)	Accuracy-J (%)	Recall rate (%)	F1 value (%)
1	83.37	87.60	86.30	86.94
2	83.68	86.09	87.85	86.96
3	83.79	88.37	86.31	87.33
4	83.58	85.72	87.38	86.54
5	82.34	87.97	84.69	86.30
6	79.85	85.58	83.25	84.30
7	78.57	86.31	81.02	83.58
8	77.97	83.08	82.24	82.26

more dependent on the number of samples in the dataset. In experiment (3), the number of iterations of the dynamic routing algorithm in the capsule network was
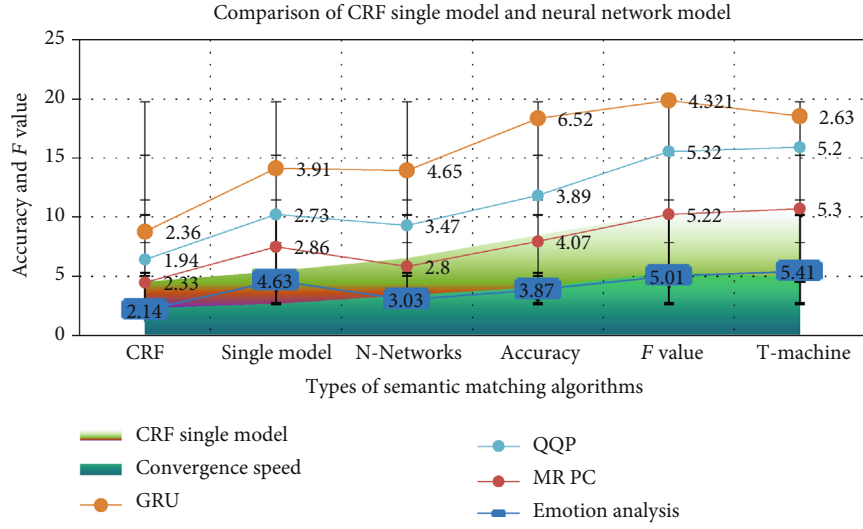
Figure 7: Comparison of CRF single model and neural network model.
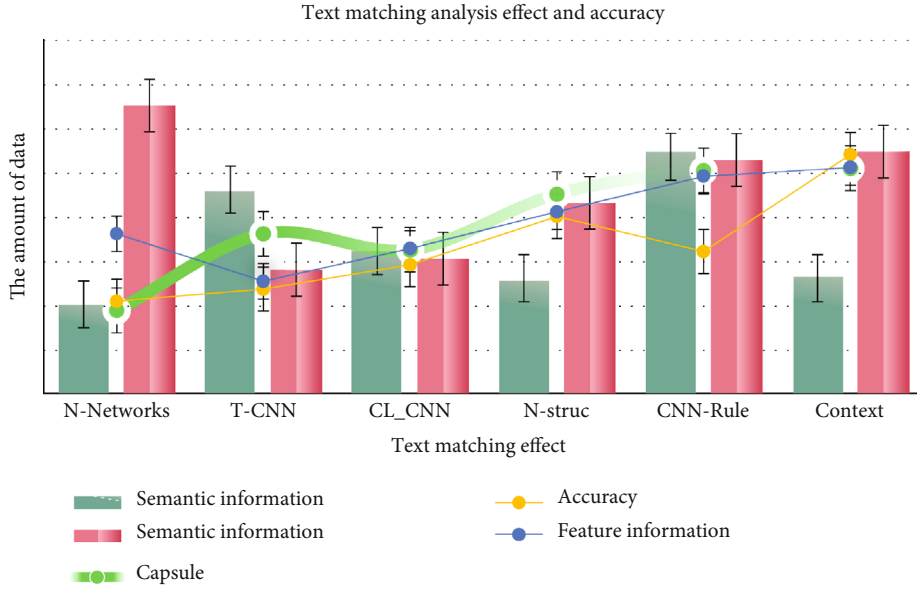
Figure 8: Text matching analysis effect and accuracy.

Table 5: The model depends on the number of samples in the dataset.

Dataset	Accuracy (%)	Accuracy (%)	Recall rate (%)	F1 value (%)
Quora Question Pairs	86.16	86.56	91.11	88.77
MRPC	87.88	83.04	81.21	82.12

changed to do a comparative experiment. The experimental results are shown in Table 4.

Based on the above experimental results, it can be seen that the number of iterations of the dynamic routing algorithm has a certain impact on the capsule network. As the number of iterations increases, the time required to train

the model continues to increase. When the number of iterations of the dynamic routing algorithm is set to 3, the model has good performance and the training time is 198 min. After the number of iterations exceeds 3, the performance of the model gradually decreases. In other experiments in this article, the number of dynamic routing iterations of the capsule network is set to 3 to obtain better performance.

As shown in Figure 7, compared with the neural network model, the CRF single model has lower classification accuracy and F value, which proves that there is a real gap between the performance of traditional machine learning methods in sentiment analysis and deep learning. The convergence speed of this model is not much different from that of the CRF single model, and it is better than other models in terms of accuracy and F value, which proves the effectiveness

FIGURE 9: Comparison of this model with other models.

of this model. The test results of the comparative experiment are shown in Table 4.

As shown in Figure 8, compared with the improved neural network Text-CNN and CL_CNN, the model in this paper has a simpler network structure; compared with the rule-based network model CNN-Rule, the model in this paper has no artificial rules when the rules are defined. As shown in Table 5, except for the model in this paper, the accuracy of CL_CNN with the best classification effect is 84.3%. G-Caps is still 0.5% higher than this, which proves that the GRU model proposed in this paper is used to capture the overall contextual semantic information, and then, the feature information model is extracted from the semantic information through the capsule.

As shown in Figure 9, TextSGN has shown good superiority in indicators such as accuracy, recall, and F value and indeed has better results in semantic analysis tasks. The model in this paper has improved classification effect compared to the CNN+BiGRU model. Because the model in this paper uses CRF as the classifier instead of the SoftMax function, it has better accuracy in the processing of abnormal tags, which can effectively promote the performance of the sentiment classifier. Compared with the BiGRU+CRF model, the F value of the model in this paper is improved, and the convergence speed is accelerated. The characteristics obtained by the two kinds of neural networks are more sufficient than a single network, and the accuracy is improved. Experiments show that compared with the fusion model, the model in this paper does have a better effect on sentiment analysis tasks.

5. Conclusions

In recent years, with the development of deep learning, deep learning has been widely used in the task of text similarity. Because convolutional neural networks and recurrent neural networks have shown good performance in tasks in various fields, they have become the main two neural network model structures. The convolutional neural network can effectively extract the local features of the text by processing the word vector matrix, but the disadvantage is that it cannot consider the context information of the text and sometimes cannot express the true meaning of the text. Therefore, this network structure is memorable. The cyclic neural network is used to complete the text feature vector extraction. The sequence information of the words can be considered, and the text context information can be used to extract the global features of the text. However, for long-distance dependence, the cyclic neural network cannot extract text features well.

Aiming at the task of text similarity, this paper proposes a text similarity analysis method based on capsule-BiGRU. The capsule network can effectively extract the local feature vector of the text. The BiGRU network uses a two-way cyclic network structure to traverse the entire text from two directions, thereby effectively extracting context information to obtain the global feature matrix of the text and make similar the feature matrix of the two texts. Degree analysis is used to determine whether the text is similar. Experiments show that the method proposed in this paper has a better effect on text similarity tasks.

Aiming at the problem that traditional neural network models cannot extract text features well, a text similarity analysis method based on capsule-BiGRU is proposed. This method combines the local feature matrix of the text extracted by the capsule network and the bidirectional gated recurrent unit network. The global feature matrix of the text extracted by BiGRU is analyzed, respectively, to obtain the similarity matrix of the text, and the similarity matrix is merged to obtain the multilevel similarity vector of the two texts, so as to determine the text similarity. The existing capsule network is improved, words that are not related to textual meaning are considered noise capsules, and smaller weights are assigned to reduce their impact on subsequent work. For the task of text similarity, a mutual attention mechanism is added before the text feature matrix extraction. For

the two texts to be analyzed, the word vector is weighted by calculating the similarity between words in one text and all words in the other text, which can more accurately determine the similarity of the text.

Data Availability

This article is not supported by data.

Conflicts of Interest

The author declares no conflicts of interest.

Acknowledgments

References

[1] J. Yang, Y. Zhao, J. Liu et al., "No reference quality assessment for screen content images using stacked auto-encoders in pictorial and textual regions," *IEEE Transactions on Cybernetics*, pp. 1–13, 2020.

[2] L. Wu, C.-H. Chen, and Q. Zhang, "A mobile positioning method based on deep learning techniques," *Electronics*, vol. 8, no. 1, 2019.

[3] H. Yang, K. Zhu, and M. Zhang, "Analysis and building of trading platform of construction 3D printing technology and products," *Mathematical Problems in Engineering*, vol. 2019, Article ID 9507192, 11 pages, 2019.

[4] E. Radionova-Girsa and A. Lahiža, "Comparison of E-trust and trust concepts in online and offline dimensions," *Economics and Business*, vol. 30, no. 1, pp. 126–133, 2017.

[5] Y.-N. Li, X. Feng, J. Xie, H. Feng, Z. Guan, and Q. Wu, "A decentralized and secure blockchain platform for open fair data trading," *Concurrency and Computation Practice and Experience*, vol. 32, no. 7, pp. 4–9, 2020.

[6] A. Tenyakov and R. Mamon, "A computing platform for pairs-trading online implementation via a blended Kalman-HMM filtering approach," *Journal of Big Data*, vol. 4, no. 1, pp. 46–52, 2017.

[7] S. Wan, "Topology hiding routing based on learning with errors," *Concurrency and Computation: Practice and Experience*, no. article e5740, 2020.

[8] K. X. Sun, M. Valles, H. Valencia, and R. O. Nelson, "Gallium nitride (GaN) devices as a platform technology for radiation hard inertial confinement fusion diagnostics," *Review of Scientific Instruments*, vol. 89, no. 10, 2018.

[9] J. Guo, Y. Fan, Q. Ai, and W. B. Croft, "Semantic matching by non-linear word transportation for information retrieval," in *CIKM'16: ACM Conference on Information and Knowledge Management*, pp. 701–710, Indianapolis Indiana USA, 2016.

[10] C. Wang, H. Zhang, L. Yang, X. Cao, and H. Xiong, "Multiple semantic matching on augmented N -partite graph for object co-segmentation," *IEEE Transactions on Image Processing*, vol. 26, no. 12, pp. 5825–5839, 2017.

[11] X. Zhang, W. Lu, F. Li, X. Peng, and R. Zhang, "Deep feature fusion model for sentence semantic matching," *Computers, Materials & Continua*, vol. 61, no. 2, pp. 601–616, 2019.

[12] X. Liu, Y. Li, and Q. Wang, "Multi-view hierarchical bidirectional recurrent neural network for depth video sequence based action recognition," *International Journal of Pattern Recognition and Artificial Intelligence*, vol. 32, no. 10, article 1850033, 2018.

[13] H. Jin, Y. Luo, C. Gao, X. Tang, and P. Yuan, "ComQA: question answering over knowledge base via semantic matching," *IEEE Access*, vol. 7, no. 9, pp. 75235–75246, 2019.

[14] W. Lu, P. Wang, X. Ma, W. Xu, and C. Chen, "Enrich cross-lingual entity links for online wikis via multi-modal semantic matching," *Information Processing & Management*, vol. 57, no. 5, article 102271, 2020.

[15] C. H. Wu and S. B. Tsai, "Using DEMATEL-based ANP model to measure the successful factors of E-commerce," *Journal of Global Information Management*, vol. 26, no. 1, pp. 120–135, 2018.

[16] A. Gupta and Z. Zhang, "Swings and roundabouts: attention-structure interaction effect in deep semantic matching," *IEEE/ACM Transactions on Audio, Speech, and Language Processing*, vol. 28, no. 2, pp. 2295–2307, 2020.

[17] M. Gyssens and G. Simari, Eds., "Semantic matching strategies for job recruitment: a comparison of new and known approaches," in *Foundations of Information and Knowledge Systems*, vol. 9616 of Lecture Notes in Computer Science, , pp. 149–168, Springer, 2016.

[18] M. Grbovic, N. Djuric, V. Radosavljevic et al., "Scalable semantic matching of queries to ads in sponsored search advertising," in *SIGIR '16: The 39th International ACM SIGIR conference on research and development in Information Retrieval*, pp. 375–384, Pisa Italy, 2016.

[19] B. Sheng, C. Zhang, X. Yin et al., "Common intelligent semantic matching engines of cloud manufacturing service based on OWL-S," *The International Journal of Advanced Manufacturing Technology*, vol. 84, no. 1-4, pp. 103–118, 2016.

[20] X. Ma, Q. Zhu, Y. Zhou, and X. Li, "Improving question generation with sentence-level semantic matching and answer position inferring," *Proceedings of the AAAI Conference on Artificial Intelligence*, vol. 34, no. 5, pp. 8464–8471, 2020.

[21] Z. Tang and J. Li, "Jointly considering Siamese network and MatchPyramid network for text semantic matching," *IOP Conference Series: Materials Science and Engineering*, vol. 490, no. 4, pp. 42-43, 2019.

[22] Y. C. Chen, Y. Y. Lin, M. H. Yang, and J. B. Huang, "Show, match and segment: joint weakly supervised learning of semantic matching and object co-segmentation," *IEEE Transactions on Pattern Analysis and Machine Intelligence*, vol. 12, no. 9, pp. 1–5, 2020.

[23] R. Zhang, J. Cheng, F. Li, W. Lu, and X. Zhang, "A deep neural architecture for sentence semantic matching," *International Journal of Computational Science and Engineering*, vol. 21, no. 4, pp. 574–579, 2020.

[24] K. Zhang, G. Lv, L. Wang et al., "DRr-net: dynamic re-read network for sentence semantic matching," *Proceedings of the AAAI Conference on Artificial Intelligence*, vol. 33, no. 5, pp. 7442–7449, 2019.

[25] A. Abid, M. Rouached, N. Messai, M. Abid, and T. Devogele, "A semantic matching engine for web service composition," *International Journal of Business Information Systems*, vol. 30, no. 1, pp. 92–95, 2019.

[26] C. Li, Z. Zhou, and W. Zhang, "An image retrieval method based on semantic matching with multiple positional representations," *Multimedia Tools and Applications*, vol. 78, no. 24, pp. 35607–35631, 2019.

[27] G. Xiao, Q. Cheng, and C. Zhang, "Detecting travel modes using rule-based classification system and Gaussian process classifier," *IEEE Access*, vol. 7, pp. 116741–116752, 2019.

[28] H. Wang, Z. Ji, Z. Lin, Y. Pang, and X. Li, "Stacked squeeze-and-excitation recurrent residual network for visual-semantic matching," *Pattern Recognition*, vol. 105, no. 41, pp. 107359–107359, 2020.

[29] J. Wang, M. Pan, T. He, X. Huang, X. Wang, and X. Tu, "A pseudo-relevance feedback framework combining relevance matching and semantic matching for information retrieval," *Information Processing & Management*, vol. 57, no. 6, pp. 102342–102342, 2020.

[30] J. Bernabé-Moreno, Á. Tejeda-Lorente, J. Herce-Zelaya, C. Porcel, and E. Herrera-Viedma, "An automatic skills standardization method based on subject expert knowledge extraction and semantic matching," *Procedia Computer Science*, vol. 162, no. 45, pp. 857–864, 2019.

[31] G. Xu, L. Xu, M. Zhang, and X. Li, "Two-stage semantic matching for cross-media retrieval," *International Journal of Performability Engineering*, vol. 14, no. 4, pp. 795–804, 2018.

[32] N. Krishnaraj, M. Elhoseny, E. L. Lydia, K. Shankar, and O. ALDabbas, "An efficientradix trie-based semantic visual indexing model forlarge-scaleimage retrieval in cloud environment," *Software Practice and Experience*, vol. 51, no. 3, pp. 489–502, 2021.

[33] S. Biswas, D. Devi, and M. Chakraborty, "A hybrid case based reasoning model for classification in Internet of things (IoT) environment," *Journal of Organizational and End User Computing*, vol. 30, no. 4, pp. 104–122, 2018.

WILEY | Hindawi

Research Article

How Government Regulations and Consumer Behavior Influence Manufacturers' Product Green Degree Decision-Making: An Agent-Based Model

Pengwei Yuan [ID],[1] **Xiaoqing Dong** [ID],[1] **Jia Xu** [ID],[2] **and Xiaofei Lin** [ID][3]

[1]*School of Business, University of Jinan, Jinan, 250022 Shandong, China*
[2]*School of Urban Rail Transportation, Shanghai University of Engineering Science, Shanghai 201700, China*
[3]*Civil Engineering and Agriculture School, Anhui University of Technology, Maanshan, 243032 Anhui, China*

Correspondence should be addressed to Xiaoqing Dong; sm_dongxq@ujn.edu.cn

In recent years, green product issues have received increasing attention. Both government regulations and consumer behaviors have a strong influence on the product green degree decisions of manufacturers' products. In order to find how government regulations and individual's green product purchase behavior affect manufacturers' green degree decisions and the market evolution characteristics, this paper proposes a multiagent model that considers the interaction among government, consumers, and manufacturers. The simulation results show that, firstly, the product green degree decision-making of manufacturers needs the guidance and regulation of the government. Secondly, product price subsidies are the most effective way to affect the manufacturers' product green degree decisions. In contrast to giving green cost subsidies to manufacturers, the government employs various publicity means to improve the environmental awareness of consumers is also an effective way to enhance the green degree of manufacturers' products. Thirdly, there is a "Crowding Out Effect" on the other qualities of manufacturers' products when manufacturers focus on the green degree of their products.

1. Introduction

As the global economy develops and the population increases, the consumption of natural resources around the world is growing at a high-speed rate [1, 2]. In consequence, air pollution, water pollution, and other environmental problems are becoming extremely serious [3]. The production and consumption of green products are becoming the consensus of all countries in the world [4]. Consequently, manufacturers are motivated and encouraged to produce green products by government [1, 5, 6]. The concept of product green degree, which indicates the environmental friendliness of the product, was used to identify nongreen products and competitive products [7]. Consumers in the market have different demands for the green degree of products [8]. In order to better meet the requirements of government and consumers, manufacturers have to consider an appropriate green degree of products to enhance market competitiveness. So,

what level of green degree is both popular with consumers and profitable for a manufacturer? It is a question worth looking into.

There are three main stakeholders related to the green degree decision-making of products, namely, manufacturers, consumers, and government [9]. As the supplier of green products, manufacturers need to weigh various factors when making decisions on the green degree of products to adapt to the fierce market competition. First of all, manufacturers have to clearly understand their resources, such as the green degree of products, market share, profits, and whether there are extra resources and capabilities to enhance their products' green degree [10]. Secondly, the profitability of a manufacturer is closely related to its competitors [11, 12]. Therefore, manufacturers often need to consider the situation of their competitors when deciding on the green degree of products, with the aim of learning and surpassing them. As the demander of green products, consumers' preference for

the green degree of products directly affects the decision-making behavior of manufacturers [9]. Consumers' purchasing behaviors are influenced not only by the product's characteristics (such as price and quality) [5, 6] but also by the people around them [13]. In recent years, with the development of mobile Internet, the prosperity of social media represented by Twitter and microblog provides a more convenient and efficient platform for the spread of word-of-mouth products. A growing number of people are willing to buy products recommended by others on social media, which shows that more and more people recognize the shopping information and have trust in this information on social media [14]. Thus, we put consumers' mutual learning behavior in online social network into the purchase decision model in this study.

Besides, the price of green products is usually higher than that of ordinary products, which will reduce consumers' purchase desire to some degree [15]. Therefore, the government needs to take corresponding measures to stimulate green product consumption, and of course, it also needs the government to formulate related environmental standards and punishment measures to restrain manufacturers [16], which are all aimed at reducing carbon emissions and protecting the environment. Therefore, the interactions of manufacture, consumers, and the government make the decision-making of product green degree very complicated. And the evolutionary mechanism of manufacturers' green decision-making is unclear. Therefore, we find that the following problems are worth to in depth study: How does the manufacturer make decisions of products' green degree under government regulation? How does the manufacturer make decisions of products' green degree in the face of consumers' demand, preference, and interaction? What are the evolutionary tendencies of green products in the market for manufacturer groups under different scenarios?

To solve these three problems, we use the agent-based modeling approach to study the mechanism of manufacturers' green degree decisions and analyze the trend of the evolving choices of manufacturers with different green degrees, which is rare in the study of manufacturers' green decision problems. These are very important for clarifying the macro behavior mechanism of manufacturers' green degree decision and the market evolution characteristics of green products in different situations. The originalities and features of this work are described below. Firstly, this work focuses on the influences and interactions among consumers, manufacturers, and government on the micro green degree decision of manufacture, which is different from the previous studies concentrating on the relationship between manufacturers and government or manufacturers and consumers. Secondly, apart from considering the impact of a product's multiple attributes (price, green degree, quality, etc.), this work also considers the characteristics of agent purchasing behavior, like the customers' purchasing power, their environmental preference differentiation, the influence of interaction on customers' purchase decisions in online social networks, the government's subsidies and penalties, and the competition and learning behaviors among manufacturers. Consequently, the model we develop in this work is closer to the real market. Thirdly, this study gives an observable

evolution of the product's green degree in different scenarios like different consumers' environmental awareness and analyzes various market indicators such as the average product green degree, average product green degree, and average manufacturer profits.

2. Literature Review

2.1. Manufacture's Decisions on Green Product. The studies of manufacture's decision on green products could be classified into two aspects: the influence of market and consumer attributes and how to decide in the supply chain environment. On the subject of the market and consumer attributes, Liu et al. [17] analyzed the impacts of competition and consumers' environmental awareness on the profiting ability of manufacturers having various eco-friendly products. Swami and Shah [18] indicated that manufacturers' and retailers' green efforts result in increased market demand, and their optimal green efforts depend on their green sensitivity and green costs. Nouira et al. [19] suggested that when a company faces a market with both regular and green customers, offering different types of products to each market segment can significantly increase the company's profits. Moser [20] suggested that companies need to maintain a specific pricing strategy as well as conduct appropriate promotions to promote the benefits of green products to consumers. Chen and Sheu [21] analyzed the impact of market uncertainty and consumer rationality on firms' green strategies and found that it is not always advantageous to adopt a differentiation strategy to produce products with different green degrees; in some cases, it is more beneficial for firms to adopt a follow strategy to produce products with the same green degree as their competitors. Hong et al. [22] studied the green product pricing problem by considering consumers' environmental awareness and the reference of non-green products and found that firms should adopt different pricing strategies based on their green production costs in an asymmetric information scenario. Du et al. [5, 6] found that traditional enterprises tend to reduce the price of products in order to maintain market share, resulting in green products only sold to some green consumers in the competitive environment. Li et al. [11, 12] showed that the product green degree of manufacturers shows a "convergence" effect if manufacturers learn the benchmark manufacture that gets the best profits in the market.

With reference to how to make decisions on green products in a supply chain environment, Ghosh and Shah [23] studied that how greening levels, prices, and profits of green apparels supply chain are influenced by channel structures, greening costs, and consumer sensitivity. Xie [24] studied the Chinese automobile supply chain and found the market competition intensity has an impact on the energy-saving level of green products. Li et al. [11, 12] revealed that the revenue-sharing contract and cost-sharing contract between manufacturers and retailers have different effects on emission reduction efforts and corporate profitability. Yang and Xiao [25] investigated the way in which prices, greenness, and expected profits of green supply chains are influenced by the channel leadership and government subsidies in an

environment where production costs and consumer demand are ambiguous. Shen et al. [26] discussed the product lines of supply chain and product quality for green and nongreen products. They found that improving product quality can enhance consumer welfare and lessen environmental impact. Saha et al. [27] discussed the important role of intermediaries in coordinating green supply chains under price and green level sensitive demand. Fang et al. [28] investigated price and order strategies for innovative green products using demand forecasting and sharing. Xin et al. [29] studied the problem of coordinating two levels of green product supply chains in the presence of uncertain demand from environmentally conscious consumers and found that two-part tariff contracts can always coordinate the supply chain. Zhang et al. [30] found that if manufacturers distributed brown and green products separately through different retailers, they could achieve higher profits through strategic pricing without changing their product portfolios.

2.2. Consumers' Green Product Purchasing Behavior.

Consumers' green product purchasing behaviors have mainly been studied in consumer demands, preferences, purchasing power, etc. Olson [31] found that because green products usually have higher prices and lower quality, consumers tend to buy products with lower green degrees. Zhao et al. [32] found that consumer attitude is the most critical indicator to predict consumers' green purchasing behavior. When consumers' attitude is more positive, and they pay more attention to the environment, consumers are more likely to buy green products. Du et al. [5, 6] suggested that consumers with green preferences are willing to pay higher prices for products with low-carbon emissions. Yadav and Pathak [33] found that the green purchasing behavior of young Indian consumers can be predicted by their attitudes, subjective norms, and environmental concerns. Suki [34] revealed that consumers' knowledge of green brands is the most critical factor in the formation of their green purchase intention, and green brand knowledge can effectively enhance consumers' green awareness and promote their purchase of green products. Zhu et al. [35] found that the purchasing power of consumers' families often determines whether the consumers' purchase intention of green food can be transformed into real green food purchasing behavior. Yang and Zhao [36] analyzed 526 Chinese consumers about their purchase behavior of household energy-saving and renewable energy equipment. They found that consumer purchasing power had a positive moderating effect on the relationship between equipment purchase attitude and behavior intention. Jo and Shin [37] showed that age and purchasing power would evidently influence consumers' preference for green product attributes. Kowalska-Pyzalska [38] revealed that the willingness of Polish residents to pay for renewable energy was positively correlated with their purchasing power and education.

In addition, many studies have identified consumer interaction as an important factor in influencing consumer purchases of green products. Lin et al. [39] built a consumer choice model by adding social influence attributes. They took hybrid electric vehicles as an instance to explore the impact of consumer interaction networks on the promotion of hybrid charged vehicles. McCoy and Lyons [40] found that although the overall purchase rate of electric cars is low, the slight peer effect brought by the network will promote consumers to purchase actively and form a higher purchase rate in some regions. Khare [41] found that peer influence, previous green purchasing behavior, and green self-identity enhance Indian consumers' purchase intention of green products. Using green hotels as an example, Wang et al. [13] showed that the green image of a green product strongly influences consumers' green satisfaction and green trust, which in turn positively drives word-of-mouth interactions in order to recommend the product to other consumers. Chen et al. [42] used empirical research on the green purchasing behavior of consumers in the "Belt and Road" country and showed that consumer interactions have a positive influence on consumers' green purchasing behavior.

2.3. The Influence of Government Regulation on Green Product Decision.

The Porter hypothesis first proposed that environmental supervision can promote green innovation in manufacturers under appropriate conditions [43]. In recent years, many scholars have shown that government environmental regulation can provide incentives for manufacturers to carry out green innovation when they do not choose to do so themselves. Sheu and Chen [44] suggested that the government should adopt taxation and subsidy policies to ensure that the green profits from the production of green products by firms are nonnegative. van Leeuwen and Mohnen [45] demonstrate the positive impact of environmental regulation on corporate green innovation through an empirical study of Dutch manufacturing firms. Wang et al. [46] compared and analyzed the incentive effects of different subsidy policies, such as product subsidies and R&D subsidies, in different stages of green efforts in the remanufacturing industry. Madani et al. [47] pointed out that an increase in government subsidy rates will lead to increased product green degree, supply chain profits, and government revenues, which will be better than an increase in tax rates. Yang et al. [25] found that in an ambiguous environment, the green degree of products increases when government subsidies rise, but government subsidies do not always favor the green supply chains and can even lead to action disadvantages for first movers. Huang et al. [48] analyzed the influence of green loan size and government's green subsidies on enterprise green innovation, and they confirmed the effectiveness of government subsidies in facilitating green innovation and environmental sustainability. Saha et al. [27] discussed the impact of government subsidies to consumers and subsidies to manufacturers on supply chain profits from the perspective of supply chain cooperation contracts. Nielsen et al. [49, 50] studied the impacts of government's per-unit product cost subsidies and R&D investment subsidies on supply chain members under different circumstances. Xu et al. [51] found that government regulations can promote green decision-making behavior, and the regulations on manufacturers are more effective than those on suppliers.

To sum up, the existing literature has conducted a lot of studies on the manufacture's decision on green products,

which has laid a good foundation for this paper. However, most of the studies focus on the decision problems in a single enterprise or a single supply chain under the influence of different factors and less on the group behavior of green product decisions. In fact, when manufacturers are competing in the market, they are not only influenced by partners in the supply chain, but also by their competitors in the market. Furthermore, consumers' green purchasing behavior is not only related to their characteristics but also influenced by their interactions. In fact, consumers are in social networks, and their purchasing behavior will be affected by other consumers in the social network. So, the market demand of consumers cannot be portrayed as a result of a linear function of attributes such as product price and quality. Finally, facing the interaction between manufacturers and consumers, the influence of consumer interactions, imitation, and learning among manufacturers, how the government implements their regulatory measures to improve the green degree of products in the market as a whole has not been well explained.

3. Agent-Based Modeling

3.1. The System Design. Manufacturers, customers, and the government make up the market system. And it is a complex adaptive system with the characteristics of complex, dynamic, and nonlinear. In this study, we used an agent-based modeling method to build our model. ABM can clarify the evolution law of the nonlinear behavior of the complex system in the real world by setting interaction rules of agents [52]. Agent-based models are widely used to model dynamical behaviors of systems in a variety of fields, such as economics, social science, organizational science, behavioral ecology, and physics [53].

Our goal is to find how government regulation and individuals' green product purchasing behavior affect manufacturers' green degree decision and market evolution characteristics. Therefore, we developed an ABM simulation model of the green product market, which including government, consumers, and manufacturers. The government, consumers, and manufacturers are connected through products in the market. A schematic illustration of agents' decision-making and interaction mechanism is shown in Figure 1.

As shown in Figure 1, in order to increase environmental benefits and reduce pollution, the government will set green standards for products and subsidize the manufacturers and consumers who produce and purchase corresponding green products and punish enterprises that are lower than the related standards. The consumer agents in the model are connected to each other through social links. The social links connect one consumer to another works as a channel that can transmit information and knowledge of products. In the process of market transactions, consumers will make purchase decisions that are affected by one's purchasing power, the expectation and sensitivity of the product's price, quality, etc. Besides, communications among consumers like recommendations, criticism, and complaints, can influence consumers' purchase decisions, and it may create a herd effect during the interaction. In the process of market transactions,

manufacturers will modify the product green degree and other quality on the basis of competitors' information nearby and their own historical experience.

3.2. The Government Agent. The government implements some interventions for social welfare [2, 54]. It is supposed that the government sets a product green degree standard g_l for the manufacturers' product to enter the market. The government dynamically supervises the manufacturer by the mean of random sampling according to the probability $\theta(0 \leq \theta \leq 1)$. Then, if the green degree g_j of manufacturer j's product fails to meet the standard $g_l(g_j < g_l)$, the government will punish the manufacturer in the form of a fine, which is related to the green degree of the products. The lower the products' green degree g_j is, the greater the punishment is. It is assumed that $sm_j = 1$ denotes the manufacturer j is sampled; otherwise, $sm_j = 0$. The punishment function PF_j is defined as follows:

$$PF_j = \begin{cases} \rho\left(g_l - g_j\right) & \text{if } sm_j = 1 \text{ and } g_j < g_l, \\ 0 & \text{if } sm_j = 1 \text{ and } g_j \geq g_l, \\ 0 & \text{if } sm_j = 0, \end{cases} \tag{1}$$

where ρ is the penalty coefficient and $\rho > 0$.

Similarly, it is assumed that the government develops the product green degree standard g_h of product, and the manufacturer can apply for subsidies of product's cost when its product is higher than the standard g_h. The subsidy function is as follows:

$$SF_j = \begin{cases} \dfrac{1}{2} \alpha u_j\left(g_j - g_h\right)^2 & \text{if } g_j \geq g_h, \\ 0 & \text{if } g_j \leq g_h, \end{cases} \tag{2}$$

where u_j represents the cost factor associating with the green degree g_j, and $\alpha \ (0 < \alpha < 1)$ denotes the subsidy proportion of the green production cost of manufacturer j.

Moreover, the price subsidy is an effective means for the government to guide consumers to buy green products [55]. It is supposed that p_{sj} denotes the subsidy for green product of manufacturer j whose green degree is higher than the specified standard g_h; and it can be expressed as follows:

$$p_{sj} = \begin{cases} p_j \gamma\left(g_j - g_h\right) & \text{if } g_j \geq g_s, \\ 0 & \text{if } g_j \leq g_s. \end{cases} \tag{3}$$

3.3. Consumer Agents

3.3.1. Consumers' Social Network. Consumers' social networks in the real world are different from those formed by Internet users [56]. Many empirical analyses show that social networks in the real world are mainly represented by small-world networks, and most of the social networks in the internet world are scale-free networks [40, 57]. In recent years,
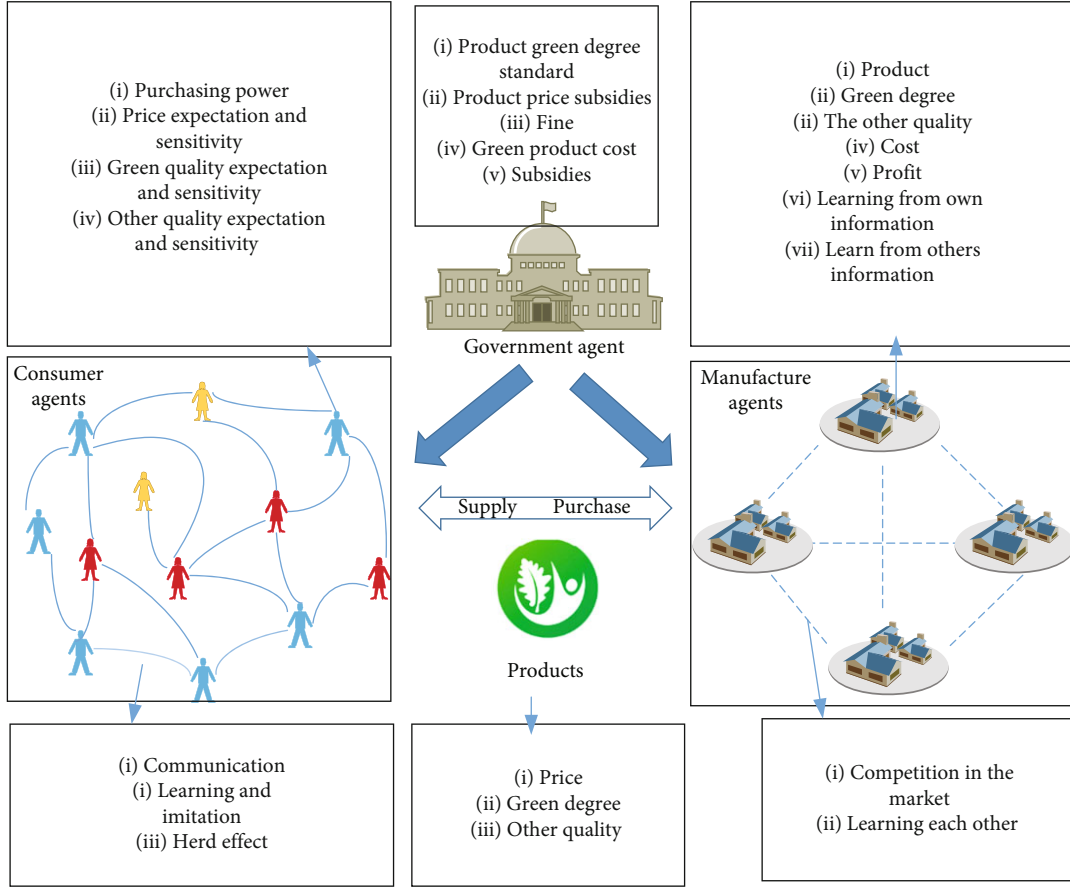
FIGURE 1: Agents' decision and interaction mechanism.

with the popularity of online social platforms, more and more consumers spontaneously share product purchase experience and evaluation information on social media (like Twitter, Weibo, and WeChat), so we use a scale-free network to describe the network relationship of consumers. The scale-free network refers to the network whose node degree satisfies "power law distribution", and it can describe both the small-world property and large variations of node degrees in a network [58]. In a scale-free network, most "ordinary" nodes have few connections, while a few "hot" nodes have extremely many connections. The scale-free network starts from m_0 nodes (m_0 is a positive integer), which are connected, and each evolution produces a new node. The probability of the new node connecting with the original nodes is directly proportional to the degree of the original nodes and finally evolves into the state that the degree distribution does not change with the network size and obeys the power-law distribution [58].

3.3.2. Consumer Choice Behavior. It is assumed that a consumer only makes one purchase decision and only chooses one product of a manufacturer in a simulation tick. The comprehensive utility function of consumers is developed on the ground of the information collected on the product and the interactions with his friends in the social network. According to the researches of Zhang T. and Zhang D. [59] and Čavoški

and Marković [60], we can formulate the function as follows:

$$U_{ij} = C_{ij} \times p_j + \beta_i \times G_{ij} \times g_j + Q_{ij} \times q_j + \text{FE}_{ij}, \quad (4)$$

where U_{ij} is the utility that consumer i ($i = 1$ to M) purchases a product of manufacturer j ($j = 1$ to N); C_{ij} is a consumer agent assessing the j-th manufacturer's price, and P_j is the price of manufacturer j's product; G_{ij} is the effect of j-th manufacturer's green degree on consumer agent i, g_j is j-th manufacturer's green degree, and $\beta_i (0 < \beta_i < 1)$ denotes the consumer agent's green preference and environmental awareness; Q_{ij} is other quality utility (like perform and life) except green degree, and q_j is the product other quality of manufacturer j; FE_{ij} reflect the "WOM" effect of the consumer agent following his friends' opinion about manufacturer j's products in the social network.

The coefficient C_{ij} expresses the effect of manufacturer's price on consumer agent's attitude to purchasing the product of manufacturer j. In general, a higher price tends to reduce the consumers' purchasing motivation of the product. Kim et al.'s research suggested that the lower price a product is, the less sensitivity of the consumer towards the product is [61]. So, sensitivity to price can be expressed as follows:

$$C_{ij} = -\varepsilon_i^{p_j - p_{sj} - p_e}, \quad (5)$$

TABLE 1: The parameters and variables' initial value in the model.

Parameters	Explanation	Range	Distribution
M	Number of consumers	30,000	Constant
N	Number of manufacturers	40	Constant
g_j	Green degree of manufacturer j's product	[0, 100]	The initial value follows a uniform distribution
g_l	Standard for manufacturers' product entering the market.	30	Constant
g_h	Green degree requirement for subsidy application	70	Constant
θ	Government sampling rate	0.3	Constant
ρ	Government's penalty coefficient	2000	Constant
α	Government's cost subsidy coefficient	0.5	Constant
γ	Government's price subsidy coefficient	0.08	Constant
q_j	The other quality of manufacturer j's product	[20, 100]	The initial value follows a uniform distribution
β_i	Environmental awareness	[0.5, 2]	Uniform distribution
ε_i	Consumer's price-sensitive parameters	[1, 20]	Uniform distribution
δ_i	Consumer's green degree sensitive parameters	[0.4, 0.6]	Uniform distribution
τ_i	Consumer's other quality sensitive parameters	[0.4, 0.6]	Uniform distribution
k_i	Consumer's purchasing power	N (55, 15)	Normal distribution
a_1, a_2	Regression coefficient of purchasing power	0.75	Constant
a_3, a_4	Consumers' cost coefficient of product green degree and the other quality	1.5	Constant
b_1, b_2	Consumer's fixed expectation of product green degree and the other quality	-13.54	Constant
f_i	Consumer's sensitivity parameter to his friends' influence	(0, 1.5)	Uniform distribution
c_j	Regular unit cost of manufacture	[3, 10]	Uniform distribution
u_j	The cost coefficient associating with the green degree g_j	0.03	Constant
z_j	The cost coefficient associating with the other quality	0.03	Constant
e_j	Manufacture's profit margins	[0.1, 0.3]	Uniform distribution
v	Random number	[0, 1]	Uniform distribution
lea1_j	Manufacture's leaning ability of green degree	[0.1, 0.5]	Uniform distribution
lea2_j	Manufacture's leaning ability of the other quality	[0.1, 0.5]	Uniform distribution
d	Distance threshold	15	Constant

TABLE 2: The parameters' change of different scenarios.

Scenarios	Parameters change
Scenario 1	$\theta = 0.3, \rho = 2000, \alpha = 0.5, \gamma = 0.08 \longrightarrow s = 0, \rho = 0, \alpha = 0, \gamma = 0$
Scenario 2	$\theta = 0.3, \rho = 2000, \alpha = 0.5, \gamma = 0.08, \beta_i \in [0.5, 2] \longrightarrow s = 0, \rho = 0, \alpha = 0, \gamma = 0, \beta_i \in [1.5, 3]$
Scenario 3	$\gamma = 0.08 \longrightarrow \gamma = 0$
Scenario 4	$\theta = 0.3, \rho = 2000, \alpha = 0.5 \longrightarrow s = 0, \rho = 0, \alpha = 0$

where ε_i is a parameter $\varepsilon_i > 1$ and p_{sj} is the subsidy for the green product of manufacturer j whose green degree is higher than the specified standard which is shown in Equation (3), and p_e is the consumer expected price of the product.

In the utility function, we assume that the quality of the product consists of green quality and the other quality. The green quality is defined as the overall impact of the multiple green attributes of a manufacturer's product, which is

TABLE 3: The definitions of indicators.

Indicators	Definitions
Number of LGDM in the market	Number of manufacturers whose product green degree is lower than government enter standard g_l
Number of MGDM in the market	Number of manufacturers whose product green degree is between g_l and g_h
Number of HGDM in the market	Number of manufacturers whose product green degree is larger than g_h
Average product green degree of all manufacturers	$\dfrac{1}{N}\sum_N g_j$
Market share of LGDM	$\sum_{LGDM}\sum_i^N s_{ij}$
Market share of MGDM	$\sum_{MGDM}\sum_i^N s_{ij}$
Market share of HGDM	$\sum_{HGDM}\sum_i^N s_{ij}$
Average product other quality of manufacturers	$\dfrac{1}{N}\sum_N q_j$
Average profit of manufacturers	$\dfrac{1}{N}\sum_N \pi_j$

supposed to represent by green degree g_j. The other quality refers to the qualities in other aspects except for green degree which is denoted by q_j. According to the outlier avoidance consumer psychological theory [62], when a consumer chooses a manufacturer's product, the nearer the quality of a manufacturer's product is to the quality expected by the consumer, the more sensitive the consumer is to the quality of the product. Therefore, the consumer's sensitivity to green degree and the other quality can be, respectively, expressed as follows:

$$G_{ij} = \delta_i^{\left|g_j - g_e\right|},$$
$$Q_{ij} = \tau_i^{\left|q_j - q_e\right|}, \tag{6}$$

where δ_i is a parameter and $0 < \delta_i < 1$, g_e denotes the costumer agent i's expected green degree to the j-th manufacturer's product, δ_i is a parameter and $0 < \tau_i < 1$, and q_e is the customer agent i's expected other quality for the j-th manufacturer's product. According to the studies of [11, 12, 63], g_e and q_e are positively correlated with consumers purchasing power, that is, the higher the consumers' purchasing power status is, the more attention they attach to the quality of products. Therefore, they can be defined as follows:

$$g_e = a_1 \times k_i + b_1 + \varphi_{1i},$$
$$q_e = a_2 \times k_i + b_2 + \varphi_{2i}, \tag{7}$$

where k_i is the purchasing power of consumer i, $a_1(a_1 > 0)$ is the regression coefficient between the expected green degree of the consumer and his/her purchasing power, b_1 represents the consumer's fixed expectation of product green degree

when his/her purchasing power is 0, and φ_{1i} is a random number sampled from the uniform distribution, which indicates the random influence of other factors on the expected green degree of consumers. Similarly, $a_2(a_1 > 0)$ denotes the regression coefficient between the expected other quality of the consumer and his/her purchasing power, b_2 is the consumer's fixed expectation of the product when his/her purchasing power is 0, and φ_{2i} is a random number drawn from the uniform distribution denoting the random influence of other factors on expected other quality of consumers. In order to obtain the value of a_1, a_2, b_1, b_2, we have made an investigation and got the value of them by two linear regressions ($R_1 = 0.31$ and $R_2 = 0.29$).

Furthermore, we assume that consumers can estimate their expected price based on their expectations of green degrees and other qualities of products. Therefore, p_e in Equation (5) can be as shown in Equation (8), where a_3 is the cost coefficient of the expected green degree for consumers, a_4 denotes consumers' cost coefficient of the expected other quality, and φ_{3i} is a random number sampled from the uniform distribution that represents the variety of a consumer's expect price of a product.

$$p_e = a_3 \times g_e + a_4 \times q_e + \varphi_{3i}. \tag{8}$$

The next parameter of the utility function is about the consumer agent sensitivity to the "WOM" effect and herd effect [64]. When a consumer i keeps in touch with his/her friend about the product in the social network, his/her utility of the product will be modified correspondingly. The changing rules of utility FE_{ij} for consumer are defined as follows:

$$\text{FE}_{ij} = f_i \times sf_{ij}, \tag{9}$$
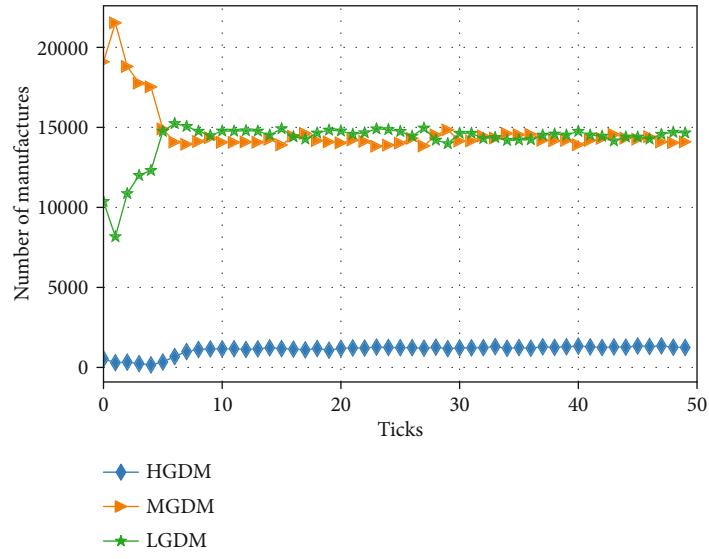
(a) Scenario 1
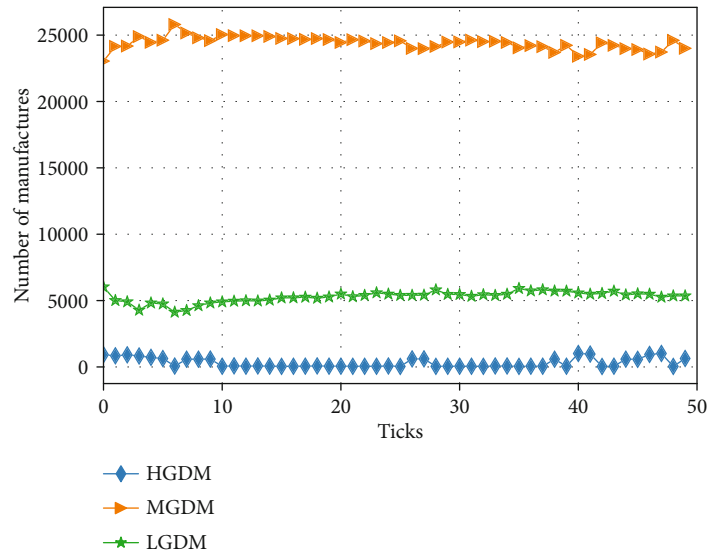
(b) Scenario 2

Figure 2: Continued.

(c) Scenario 3
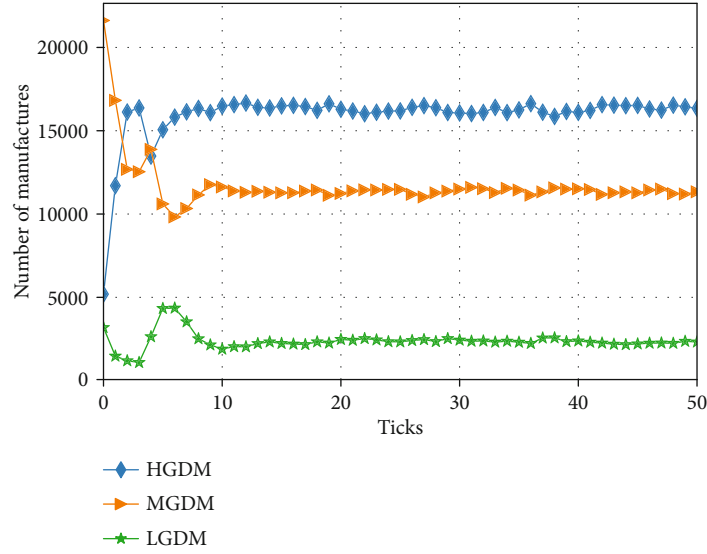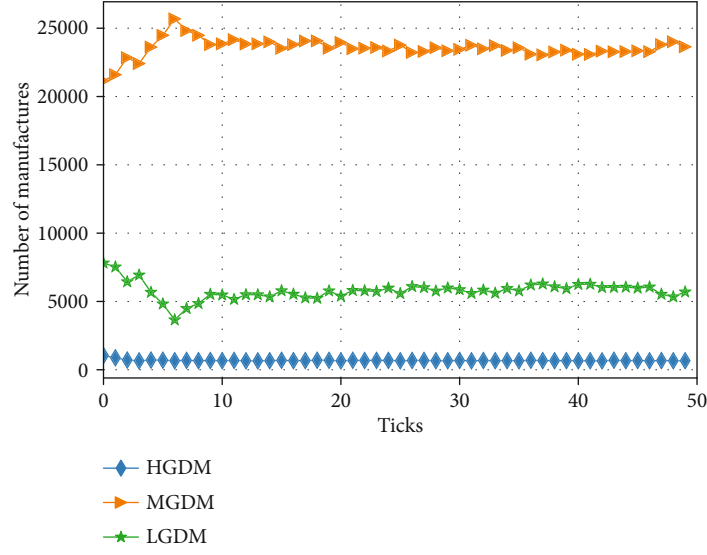
(d) Scenario 4

FIGURE 2: Evolutions of the three kinds of manufacturers' numbers under four scenarios.

where f_i is the sensitivity parameter of consumer i to his friends' influence, and we supposed that f_i follows an uniform distribution on (0,1.5). The smaller the value of f_i is, the less possible consumer i is to be affected by others around him/her and vice versa. sf_j stands for the impact of other consumers in the social network, which is got by consumer i; it is measured as the average utility of manufacturer j's product for his/her neighbors who have purchased the product j in the social network. We set parameter $sl_{lj} = 1$ denotes that a consumer i's neighbor l buys a product of manufacturer j and $sl_{lj} = 0$ stands for a neighbor who does not purchase the product, and the number of consumer i's friends who have purchased manufacturer j's product in the social network can be calculated by $\sum_{\text{neighbors}} sl_{lj}$. The coefficient

sf_{ij} is shown in Equation (10).

$$sf_{ij} = \frac{\sum_{\text{neighbors}} U_{lj} \times sl_{lj}}{\sum_{\text{neighbors}} sl_j}, \quad (10)$$

where U_{lj} is the neighbor l's utility of manufacturer j's products.

Furthermore, it is considered that consumers do not only compare the total utility of the product to decide whether to buy or not but to have irrational behavior. A common way to describe consumers' bounded rationality is to use a logit model [65] in which the bigger utility value means that consumers have a higher probability of purchasing the product, while the less utility value indicates lower purchasing
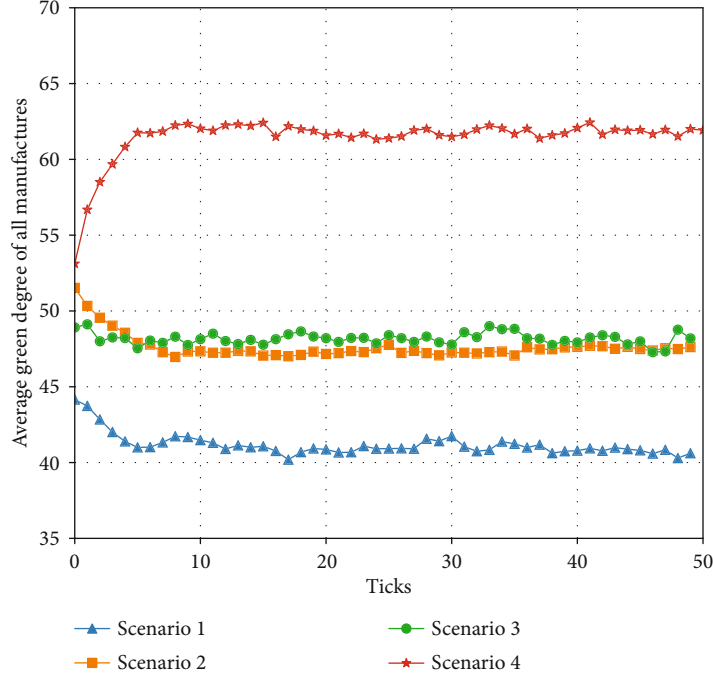
FIGURE 3: Evolutions of average products' green degree of the three types of manufacturers.

probability. According to the research of Xuanming [66], the probability of consumer i with bound irrationality buying a product j is shown as follows:

$$\text{Prob}_{ij} = \frac{e^{U_{ij}}}{1 + e^{U_{ij}}}, \tag{11}$$

where U_{ij} is the utility that consumer i perceives a product of manufacturer j.

According to Equations (10) and (11), the order in which consumer i enters the market will affect the probability of purchasing a product. We assume that the consumer with the maximum degree, which means this consumer has the most friends in the network, firstly makes the decision. The rest of consumers randomly do the decision-making of purchasing products.

3.4. The Manufacturer Agents. We suppose that there are N manufacturers with different locations in a specific industry. And the manufacturer processes raw materials and sells its products to consumers. It is supposed that products from manufacturers have differences in price, green degree, and the other quality. And the rest attributes are all the same. Consequently, manufacturers will compete on the price, green degrees, and other quality of their products.

It is well known that when a manufacturer produces a product that is greener or of higher other quality, the production process should be more complex and more demanding in terms of technology or materials, so the manufacturer will inevitably have to invest additional costs for these. We divide the cost of per unit product into three parts: the first part is the fixed unit cost; the second part is the extra margin cost caused by green degree, and the third is the additional margin

cost caused by the other quality. Then, the cost function of manufacturer j is defined as follows:

$$C_j = c_j + \frac{1}{2} u_j g_j^2 + \frac{1}{2} z_j q_j^2, \tag{12}$$

where c_j is the regular unit cost and follows a uniform distribution for the manufacturer j's product, u_j represents the cost coefficient associating with the green degree g_j, and z_j stands for the cost factor related to the other quality q_j. According to previous studies of ([3, 30]), $1/2 u_j g_j^2$ and $1/2 z_j q_j^2$ are quadratic function of g_j and q_j, because it is well known that environmental performance and quality improvement have an increasing marginal cost.

We assume that the manufacturer employs the cost-plus pricing method to decide the price of their products. Hence, the product's price of the j-th manufacturer is given as $p_j = C_j(1 + e_j)$, where e_j symbolizes the profit margins. As a result, the expression of p_j is shown as follows:

$$p_j = \left(C_j + \frac{1}{2} u_j g_j^2 + \frac{1}{2} z_j q_j^2 \right)(1 + e_j). \tag{13}$$

In addition, if we set parameter $s_{ij} = 1$, it denotes that a consumer i buys a product of manufacturer j, and $s_{ij} = 0$ stands for a consumer i who does not purchase the product. Then, the sale amount of manufacturer j in a simulation cycle can be calculated by $\sum_{i=1}^{N} s_{ij}$. And the profit function of
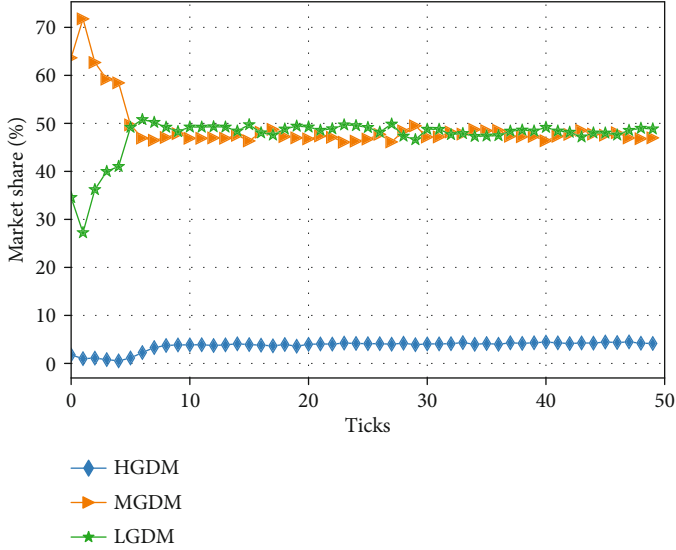
(a) Scenario 1
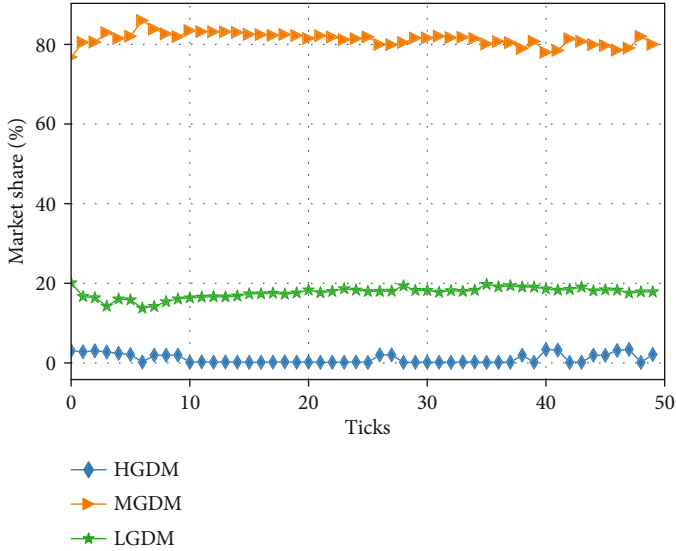
(b) Scenario 2

Figure 4: Continued.
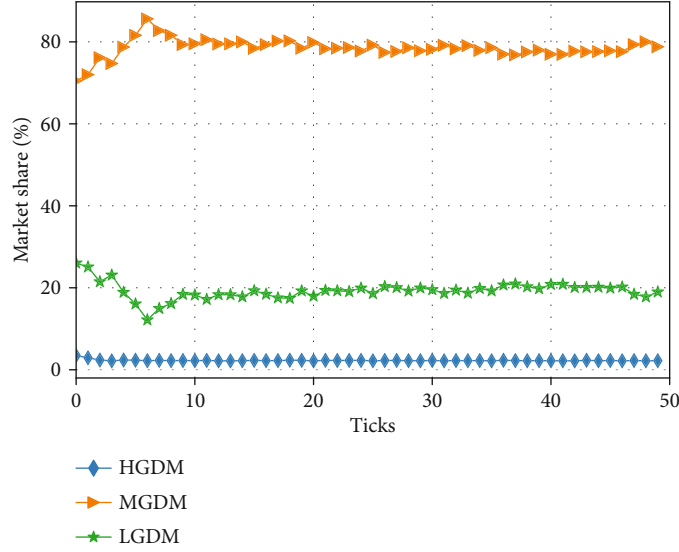
(c) Scenario 3
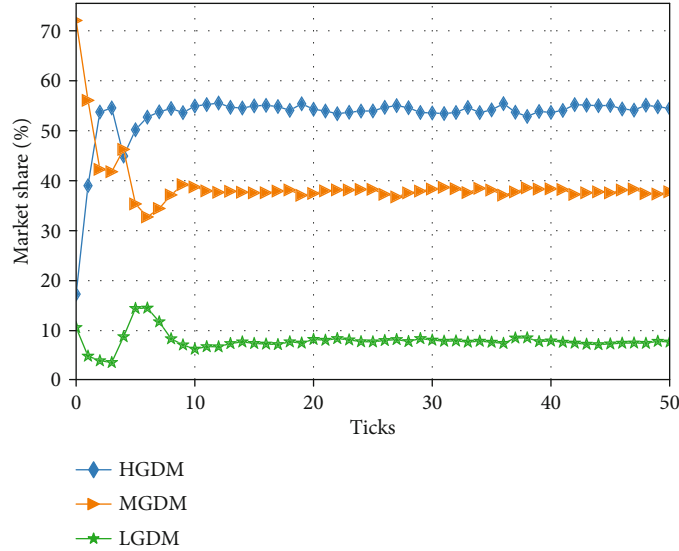
(d) Scenario 4

Figure 4: Evolutions of the market share of three types of manufacturers in four scenarios.

manufacturer j is shown as follows:

$$\pi_j = \left(p_j - C_j\right) \sum_{i=1}^{M} s_{ij}. \tag{14}$$

Moreover, if a manufacturer's product green degree is higher than the government's stipulated standards g_h, it will apply for subsidies from the government. When a manufacture's product's green degree is lower than the g_l, it could be punished by the government. Based on Equations (1) and (2), the profit function of manufacturer j can be shown as follows:

$$\pi_j = \left(p_j - C_j\right) \sum_{i=1}^{M} s_{ij} + SF_j \sum_{i=1}^{M} s_{ij} - PF_j. \tag{15}$$

Each manufacturer in the market has intelligence and adaptability, and they are learning from each other in the process of competition, especially the manufacturer with the highest profits in their neighborhood. It is supposed that manufacturers do not have technical barriers and production capacity constraints. So, the manufacturer can modify the green degree and the other quality according to their profits without additional costs of production adjustment.

The manufacturer j decides the successive green degree $(g_j(t+1))$ and the other quality $(q_j(t+1))$ of its products according to its current product green degree $(g_j(t))$ and the other quality $(q_j(t))$, the historical product green degree $(g_{j\text{best}})$ and the other quality $(q_{j\text{best}})$ which led to the best profit in its history, and the current product green degree and the other quality of its best neighbor who has the maximum profits among all its neighbors within a specific range.
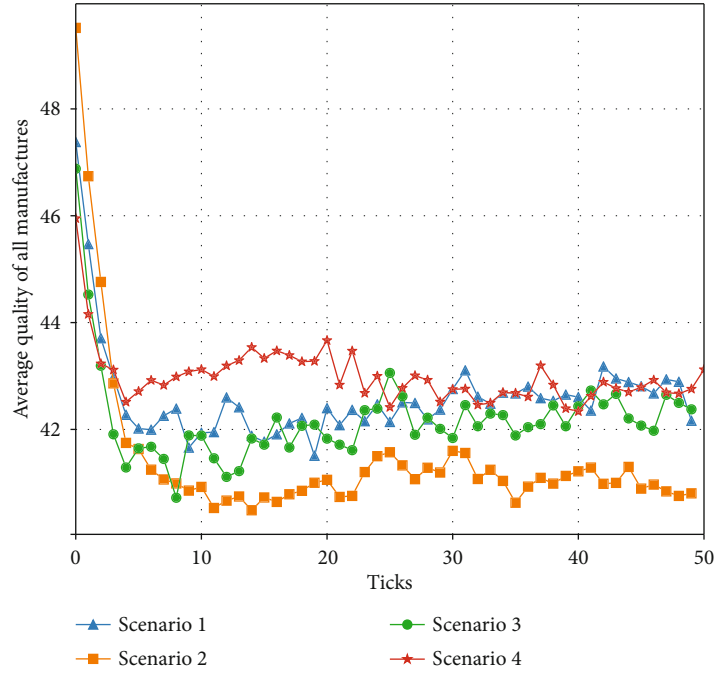
FIGURE 5: Evolutions of average products' other quality of the three types of manufacturers.
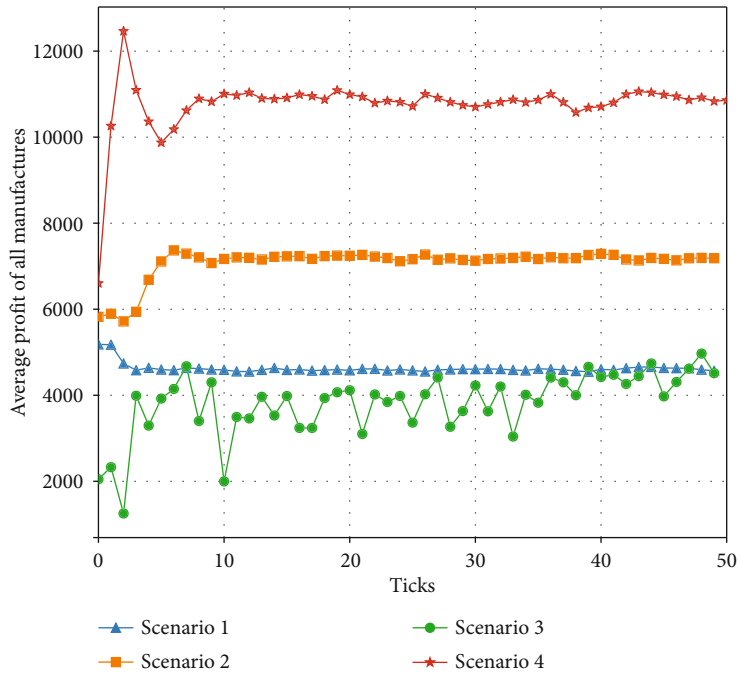
FIGURE 6: Evolutions of the average profits of the three types of manufacturers.

There are five steps for a manufacturers' updating its green degree and the other quality. The five steps are described as follows:

Step 1. There are M manufacturers in a 2-D space. And generate their positions X and Y, the initial green degree g_j, and other quality q_j at random.

Step 2. Calculating manufacturer j's profit $\pi_j(t)$ according to Equation (15).

Step 3. When the current manufacture's profits $\pi_j(t)$ is higher than its historical π_{jbest}, then we replace the values of π_{jbest}, g_{jbest}, and q_{jbest} with the values of $\pi_j(t)$, $g_j(t)$. and $q_j(t)$.

Step 4. Setting a distance threshold d and finding out all the neighbors within the distance d. The best neighbor who has the maximum profit among all its neighbors is identified, and its profit, green degree, and other quality are defined as π_{best}, g_{best}, and q_{best}. If $\pi_{\text{best}} > \pi_{j\text{best}}$, then the manufacturer will learn the best neighbor's strategies in green degree and other quality with a certain probability. In order to represent the noise and irrational behavior of the learning process, we use the Fermi function [67] to calculate the learning probability, which is expressed in Equation (16)

$$\text{Prob}\left(j \xrightarrow{\text{learning}} \text{best neighbor}\right) = \frac{1}{1 + \exp\left[\left(\pi_{\text{best}} - \pi_{j\text{best}}\right)/\omega\right]}. \tag{16}$$

where ω denotes the noise in the updating process of strategy and $\omega > 0$. A random variable $v(v \in [0, 1])$ is generated by computer to determine how the manufacturer ultimately changes its green degree and other quality. The update rules are shown in Equations (17) and (18).

$$g_j(t+1) = \begin{cases} g_j(t) + \text{lea1}_j\left(g_{\text{best}} - g_{j\text{best}}\right) & \text{if } v < \text{Prob}, g_{\text{best}} > g_{j\text{best}}, \\ g_j(t) - \text{lea1}_j\left(g_{j\text{best}} - g_{\text{best}}\right) & \text{if } v < \text{Prob}, g_{\text{best}} < g_{j\text{best}}, \\ g_j(t) & \text{if } v > \text{Prob}, \end{cases} \tag{17}$$

$$p_j(t+1) = \begin{cases} p_j(t) + \text{lea2}_j\left(p_{\text{best}} - p_{j\text{best}}\right) & \text{if } v < \text{Prob}, p_{\text{best}} > p_{j\text{best}}, \\ p_j(t) - \text{lea2}_j\left(p_{j\text{best}} - p_{\text{best}}\right) & \text{if } v < \text{Prob}, p_{\text{best}} < p_{j\text{best}}, \\ p_j(t) & \text{if } v > \text{Prob} \end{cases} \tag{18}$$

where $\text{lea1}_j(0 < \text{lea1}_j \leq 1)$ and $\text{lea2}_j(0 < \text{lea2}_j \leq 1)$ are the learning ability coefficient of manufacturer j.

If $\pi_{j\text{best}}$ is larger than $\pi_j(t)$, we update $g_j(t+1)$ and $q_j(t+1)$ as Equations (19) and (20).

$$g_j(t+1) = g_{j\text{best}}, \tag{19}$$

$$q_j(t+1) = q_{j\text{best}}, \tag{20}$$

Step 5. Return to step 2, when every manufacturer has been updated.

4. Simulation Scenario Design

We suppose that there are 40 manufacturer agents and 30,000 consumer agents in a particular market. To obtain the simulation results, we set the used parameters' initial values that are shown in Table 1.

On the basis of additional guidance and regulation strategies of the government, four different scenarios are constructed. Scenario 1 assumes that the government does not interfere with manufacturers' production and consumer's purchasing price. Scenario 2 supposes that consumer envi-

ronmental awareness is increased. Scenario 3 supposes that the government subsidizes the costs of manufacturers whose products are greener than the subsidized standard and penalizes the manufacturers whose products are lower than the market entry standard in the form of sampling. Scenario 4 assumes that the government subsidizes the price of products above the specified standard. The four scenarios' parameters' changes are shown in Tables 2.

To facilitate the analysis, we classify manufacturers into three categories: those whose products' green degree is lower than government enter standard g_l (we call them low green degree manufacturer (LGDM)), those whose product green degree is between g_l and g_h (we call them medium green degree manufacturer (MGDM)), and those whose products are greener than subsidy standard g_h (we call them high green degree manufacturer (HGDM)). Several indicators are designed to discover the relationships among government regulation, consumers' product choice and manufacturers' production decisions, and the whole market characteristics and evolutionary trend. The numbers of LGDM, MGDM, and HGDM, the average green degree of manufacture's product, the market share, the average other quality, and profits of three types of manufacturers are analyzed in the four scenarios. The details of the indicators are present in Table 3.

We executed the ABM model in Python 3.7.1 and carried out the experiments in four scenarios. Then, we compute the value of the indicators and analyze them in the next section.

5. Result Analysis

5.1. Numbers of LGDM, MGDM, and HGDM. The quantity change of three kinds of manufacturers' numbers can directly show the modifications of manufacturers' production behavior. The numbers of LGDM, MGDM, and HGDM in the four scenarios are shown in Figure 2. The number of MGDM manufacturers increases to a stable level, and the number of LGDM and HGDM both gradually decrease to a specific value in scenarios 1, 2, and 3, while in scenario 4, the number of MGDM manufacturers first rises and then reduces to stable status, and the number of HGDM manufacturers gradually increases to the stable level, and the number of LGDM manufacturers gradually decreases to a stable value. Comparing the four scenarios, the number of HGDM manufacturers in different scenarios follows the descending order of scenario 4, scenario 2, scenario 3, and scenario 1; the number of MGDM follows the order of scenario 2, scenario 3, scenario 1, and scenario 4; the number of LGDM follows the order of scenario 1, scenario 2, scenario 3, and scenario 4.

In analyzing the number of LGDM, MGDM, and HGDM, we get two observations. Firstly, manufacturers' green production behavior needs government guidance and regulation, and appropriate policies and measures have effective impacts on the manufacturers' decisions of green degree. Secondly, the government's green cost subsidy and low green degree punishment and increasing consumer awareness of the environment could increase the number of MGDN, but they could not have a significant impact on HGDM

manufacturer, while the government's product price subsidy has an essential impact on the number of HGDM manufacturers.

In Figure 3, we describe the evolution of the average green degree of all manufacturers in four scenarios. It can be seen from Figure 3 that the average green degree of all manufacturers is the highest in scenario 4, and there is no significant difference between scenario 2 and scenario 3. Thus, price subsidies are the most effective means to affect the green degree of the products; compared to green cost subsidies to manufacturers, the government takes various publicity means to improve the environmental awareness of consumers are also an effective way to increase the green degree of manufacturers' products in the whole market.

5.2. Market Share of Three Kinds of Manufacturers.

Consumers are the focus of market competition. Consumers' preferences are heterogeneous (this study shows the heterogeneity of consumer price preference, environmental awareness, and quality preference). Some manufacturers win a large number of consumers and occupy a high market share by positioning their product appropriately on price, green degree, and the other quality. Figure 4 shows the market share of three types of manufacturers in four scenarios. In scenario 1, the market share of MGDM manufacturers first increases and then decreases and stabilizes at about 48%. The market share of LGDM first falls and then rises and remains stable at about 48%. Without intervention, the market share is occupied by LGDM and MGDM manufacturers, while HGDM manufacturers have a small market share (about 3%). The market share distribution of scenario 2 and scenario 3 is similar. MGDM manufacturers occupy about 80% of the market share, while LGDM manufacturers have about 17% of the market share, and HGDM firms have about 3% of the market share. In scenario 4, the market share of HGDM manufacturer increases first and then decreases and gradually stabilizes at about 54%. The market share of MGDM manufacturers decreases from 72% to 38%. The market share of LGDM manufacturers fall first, then increased and then decreased, and finally stabilized at about 8%.

Through the above analysis, it can be concluded that the distribution of the market share of the three types of manufacturers is different with different guidance and regulation strategies of the government. When consumers' environmental awareness is enhanced, and the government punishes LGDM enterprises, gives green cost subsidies to manufacturers with a high green degree, most of the market share is obtained by MGDM manufacturers. When the government subsidizes the price of products, the market share is occupied by HGDM manufacture.

5.3. Average Other Quality of Manufacturers.

In Figure 5, we depict the evolutionary trend of the average other quality of the manufacturer's products in the four scenarios. As can be seen in Figure 5, as competition in the market proceeds, the average other quality of the products in the market shows a tendency first to decline and then fluctuate within a small range. On the whole, the average quality of the products in

scenario 4 and scenario 1 is highest, followed by scenario 3 and the lowest in scenario 2.

Therefore, it can be concluded that manufacturers would learn to modify the other quality of their products to increase the profits in a competitive market. Second, there may be a "Crowding Out Effect" on the other qualities of manufacturers' products when they focus on the green degree of its products. This "Crowding Out Effect" is significant when consumers are more environmentally conscious in the four scenarios. When the government subsidizes the green cost of a manufacturer whose green degree is larger than a stander and punishes the manufacturer whose green degree is smaller than the environmental access standards, it is less significant; subsidizing the price of the product basically does not have this effect.

5.4. Average Profit of Manufacturers.

The three types of manufacturers' average profits of the four scenarios are presented in Figure 6, and the evolution of it shows different characteristics. In scenario 1, the average profits of the manufacturers fluctuate in a small range. In scenario 2, the average profits of the manufacturer are bigger than that of scenario 1, and it rises initially and gradually stabilizes at a stable level. This is due to the enhancement of consumers' environmental awareness, and consumers with high environmental preferences tend to buy high green products and pay higher prices for them. In scenario 3, the average profit of the manufacturers fluctuates in a wide range and shows an upward trend. The main reason for this phenomenon is when manufacturers with a low green degree are investigated and punished, and they bear high fines, which affects the average profit of manufacturers in the market. The punished manufacturers improve the product green degrees to avoid the fine. Besides, government subsidies also stimulate manufacturer to enhance the green degree of products, and because the manufacturer adopts the cost-plus pricing method to decide the product's price, the higher the green degree of the product, the higher the cost, and the larger the profit of a product, so the average profit of the manufacturers is gradually increasing. In scenario 4, the average profits of the manufacturer are always kept at a high level and progressively stabilized after a wide fluctuation. This duo to the market is occupied by the manufacturers of HGDM according to Figure 4, and the manufacturers with the high green degree products have gained decent profits.

The above analysis indicates that government green cost subsidies and punishment of low green degree manufacturers can produce good results, but they will affect the stability of manufacturers' profit and the market. The government's price subsidies and increasing consumers' environmental awareness can improve the average profit level of the manufacturers while maintaining market stability.

6. Conclusions

It is crucial to clear up the evolving trends of product green degree in the market and its influence upon the manufacturers' competitive performance in different scenarios. To help the government and manufacturers make reasonable

decisions, we construct an agent-based model to study the green production behavior of manufacture, which considers the interactions of government, consumer, and government.

The results of the simulations provide three conclusions, which could be summarized as follows: firstly, the green product production behavior of the manufacturer needs the guidance and regulation of the government. Secondly, product price subsidies are the most effective means to affect the green degree of the products; comparing with giving green cost subsidies to manufacturers, the government employs various publicity means to improve the environmental awareness of consumers is also an effective way to improve the green degree of manufacturers' products. Thirdly, there is a "Crowding Out Effect" on the other qualities of manufacturers' products when manufacturers focus on the green degree of their products.

In light of the above findings, we suggest the as following insights for the government when developing policies about facilitating the production of green products. Firstly, the government can improve the environmental awareness of consumers and cultivate their green consumption habits by enhancing environmental protection publicity or subsidizing green products. In this way, firms have an incentive to produce green products, because market demand preference will stimulate manufacturers to make green production and increase their market share. Secondly, when the government subsidizes green products, it can choose to subsidize the price of products to consumers as a more efficient way than subsidizing the cost of manufacturers. In addition, the government should also pay active attention to other qualities of green products. When the government conducts green product subsidies, it will cause "Crowding Out Effect" on other qualities, which will cause a loss of consumer welfare.

In addition, to facilitate the study, this work only considers the government and consumers who have a more significant effect on the manufacturers' product green degree decisions. In reality, investors and nongovernmental environmental organizations will also affect the green product production behavior of enterprises. In further research, we can add the above subjects to the model, enrich, and improve the model, so that it can reflect the complex reality.

Data Availability

The simulation model and experimental data used to support the findings of this study are available from the corresponding author upon request.

Conflicts of Interest

The authors declare that they have no conflicts of interest.

Acknowledgments

References

[1] V. Albino, A. Balice, and R. M. Dangelico, "Environmental strategies and green product development: an overview on sustainability-driven companies," *Business Strategy and the Environment*, vol. 18, no. 2, pp. 83–96, 2009.

[2] J. Gao, Z. Xiao, H. Wei, and G. Zhou, "Active or passive? Sustainable manufacturing in the direct-channel green supply chain: a perspective of two types of green product designs," *Transportation Research Part D: Transport and Environment*, vol. 65, pp. 332–354, 2018.

[3] Q. Meng, M. Li, Z. Li, and J. Zhu, "How different government subsidy objects impact on green supply chain decision considering consumer group complexity," *Mathematical Problems in Engineering*, vol. 2020, Article ID 5387867, 12 pages, 2020.

[4] R. M. Dangelico, "What drives green product development and how do different antecedents affect market performance? A survey of Italian companies with eco-labels," *Business Strategy and the Environment*, vol. 26, no. 8, pp. 1144–1161, 2017.

[5] S. Du, W. Tang, J. Zhao, and T. Nie, "Sell to whom? Firm's green production in competition facing market segmentation," *Annals of Operations Research*, vol. 270, no. 1-2, pp. 125–154, 2018.

[6] S. Du, J. Zhu, H. Jiao, and W. Ye, "Game-theoretical analysis for supply chain with consumer preference to low carbon," *International Journal of Production Research*, vol. 53, no. 12, pp. 3753–3768, 2015.

[7] P. Liu and S.-p. Yi, "Pricing policies of green supply chain considering targeted advertising and product green degree in the big data environment," *Journal of Cleaner Production*, vol. 164, pp. 1614–1622, 2017.

[8] M. A. Ülkü and J. Hsuan, "Towards sustainable consumption and production: competitive pricing of modular products for green consumers," *Journal of Cleaner Production*, vol. 142, pp. 4230–4242, 2017.

[9] Y. Yu, X. Han, and G. Hu, "Optimal production for manufacturers considering consumer environmental awareness and green subsidies," *International Journal of Production Economics*, vol. 182, pp. 397–408, 2016.

[10] E. Moser, A. Seidl, and G. Feichtinger, "History-dependence in production-pollution-trade-off models: a multi-stage approach," *Annals of Operations Research*, vol. 222, no. 1, pp. 457–481, 2014.

[11] Z. Li, H. Zhu, Q. Meng, C. Wu, and J. Du, "Manufacturers' green decision evolution based on multi-agent modeling," *Complexity*, vol. 2019, Article ID 3512142, 14 pages, 2019.

[12] T. Li, R. Zhang, S. Zhao, and B. Liu, "Low carbon strategy analysis under revenue-sharing and cost-sharing contracts," *Journal of Cleaner Production*, vol. 212, pp. 1462–1477, 2019.

[13] J. Wang, S. Wang, H. Xue, W. Yu, and J. Li, "Green image and consumers' word-of-mouth intention in the green hotel industry: the moderating effect of Millennials," *Journal of Cleaner Production*, vol. 181, pp. 426–436, 2018.

[14] E. J. Seo, J.-W. Park, and Y. J. Choi, "The effect of social media usage characteristics on e-WOM, trust, and brand equity: focusing on users of airline social media," *Sustainability*, vol. 12, no. 4, p. 1691, 2020.

[15] S. Hendershot, "Is green enough to lure clients," *Crain's Chicago Business*, vol. 32, no. 28, p. 16, 2009.

[16] T. Stucki, M. Woerter, S. Arvanitis, M. Peneder, and C. Rammer, "How different policy instruments affect green

product innovation: a differentiated perspective," *Energy Policy*, vol. 114, pp. 245–261, 2018.

[17] Z. Liu, T. D. Anderson, and J. M. Cruz, "Consumer environmental awareness and competition in two-stage supply chains," *European Journal of Operational Research*, vol. 218, no. 3, pp. 602–613, 2012.

[18] S. Swami and J. Shah, "Channel coordination in green supply chain management," *Journal of the Operational Research Society*, vol. 64, no. 3, pp. 336–351, 2013.

[19] I. Nouira, Y. Frein, and A. B. Hadj-Alouane, "Optimization of manufacturing systems under environmental considerations for a greenness-dependent demand," *International Journal of Production Economics*, vol. 150, pp. 188–198, 2014.

[20] A. K. Moser, "Thinking green, buying green? Drivers of pro-environmental purchasing behavior," *Journal of Consumer Marketing*, vol. 32, no. 3, pp. 167–175, 2015.

[21] Y. J. Chen and J.-B. Sheu, "Non-differentiated green product positioning: roles of uncertainty and rationality," *Transportation Research Part E: Logistics and Transportation Review*, vol. 103, pp. 248–260, 2017.

[22] Z. Hong, H. Wang, and Y. Yu, "Green product pricing with non-green product reference," *Transportation Research Part E: Logistics and Transportation Review*, vol. 115, pp. 1–15, 2018.

[23] D. Ghosh and J. Shah, "A comparative analysis of greening policies across supply chain structures," *International Journal of Production Economics*, vol. 135, no. 2, pp. 568–583, 2012.

[24] G. Xie, "Cooperative strategies for sustainability in a decentralized supply chain with competing suppliers," *Journal of Cleaner Production*, vol. 113, pp. 807–821, 2016.

[25] D. Yang and T. Xiao, "Pricing and green level decisions of a green supply chain with governmental interventions under fuzzy uncertainties," *Journal of Cleaner Production*, vol. 149, pp. 1174–1187, 2017.

[26] B. Shen, Y. Cao, and X. Xu, "Product line design and quality differentiation for green and non-green products in a supply chain," *International Journal of Production Research*, vol. 58, no. 1, pp. 148–164, 2020.

[27] S. Saha, S. Majumder, and I. E. Nielsen, "Is it a strategic move to subsidized consumers instead of the manufacturer?," *IEEE access*, vol. 7, pp. 169807–169824, 2019.

[28] Y. Fang, X. Wang, and J. Yan, "Green product pricing and order strategies in a supply chain under demand forecasting," *Sustainability*, vol. 12, no. 2, p. 713, 2020.

[29] C. Xin, X. Chen, H. Chen, S. Chen, and M. Zhang, "Green product supply chain coordination under demand uncertainty," *IEEE Access*, vol. 8, pp. 25877–25891, 2020.

[30] S. Zhang, Y. Yu, Q. Zhu, C. M. Qiu, and A. Tian, "Green innovation mode under carbon tax and innovation subsidy: an evolutionary game analysis for portfolio policies," *Sustainability*, vol. 12, no. 4, p. 1385, 2020.

[31] E. L. Olson, "It's not easy being green: the effects of attribute tradeoffs on green product preference and choice," *Journal of the Academy of Marketing Science*, vol. 41, no. 2, pp. 171–184, 2013.

[32] H.-h. Zhao, Q. Gao, Y.-p. Wu, Y. Wang, and X.-d. Zhu, "What affects green consumer behavior in China? A case study from Qingdao," *Journal of Cleaner Production*, vol. 63, pp. 143–151, 2014.

[33] R. Yadav and G. S. Pathak, "Young consumers' intention towards buying green products in a developing nation: extend-

ing the theory of planned behavior," *Journal of Cleaner Production*, vol. 135, pp. 732–739, 2016.

[34] N. M. Suki, "Green product purchase intention: impact of green brands, attitude, and knowledge," *British Food Journal*, vol. 118, no. 12, pp. 2893–2910, 2016.

[35] Q. Zhu, Y. Li, Y. Geng, and Y. Qi, "Green food consumption intention, behaviors and influencing factors among Chinese consumers," *Food Quality and Preference*, vol. 28, no. 1, pp. 279–286, 2013.

[36] S. Yang and D. Zhao, "Do subsidies work better in low-income than in high-income families? Survey on domestic energy-efficient and renewable energy equipment purchase in China," *Journal of Cleaner Production*, vol. 108, pp. 841–851, 2015.

[37] M. Jo and J. Shin, "Market strategy for promoting green consumption: consumer preference and policy implications for laundry detergent," *International Journal of Consumer Studies*, vol. 41, no. 3, pp. 283–290, 2017.

[38] A. Kowalska-Pyzalska, "An empirical analysis of green electricity adoption among residential consumers in Poland," *Sustainability*, vol. 10, no. 7, p. 2281, 2018.

[39] H. Lin, M. Wang, W. Chen, and G. Conzelmann, "Incorporating social impact on new product adoption in choice modeling: a case study in green vehicles," *Transportation Research Part D: Transport and Environment*, vol. 32, pp. 421–434, 2014.

[40] D. McCoy and S. Lyons, "Consumer preferences and the influence of networks in electric vehicle diffusion: an agent-based microsimulation in Ireland," *Energy Research & Social Science*, vol. 3, pp. 89–101, 2014.

[41] A. Khare, "Antecedents to green buying behaviour: a study on consumers in an emerging economy," *Marketing Intelligence & Planning*, vol. 33, no. 3, pp. 309–329, 2015.

[42] C.-C. Chen, C.-W. Chen, and Y.-C. Tung, "Exploring the consumer behavior of intention to purchase green products in belt and road countries: an empirical analysis," *Sustainability*, vol. 10, no. 3, p. 854, 2018.

[43] M. Porter and C. Van der Linde, "Green and competitive: ending the stalemate," *Harvard Business Review*, vol. 73, no. 5, pp. 120–134, 1995.

[44] J.-B. Sheu and Y. J. Chen, "Impact of government financial intervention on competition among green supply chains," *International Journal of Production Economics*, vol. 138, no. 1, pp. 201–213, 2012.

[45] G. van Leeuwen and P. Mohnen, "Revisiting the Porter hypothesis: an empirical analysis of green innovation for the Netherlands," *Economics of Innovation and New Technology*, vol. 26, no. 1-2, pp. 63–77, 2017.

[46] Y. Wang, X. Chang, Z. Chen, Y. Zhong, and T. Fan, "Impact of subsidy policies on recycling and remanufacturing using system dynamics methodology: a case of auto parts in China," *Journal of Cleaner Production*, vol. 74, pp. 161–171, 2014.

[47] S. R. Madani and M. Rasti-Barzoki, "Sustainable supply chain management with pricing, greening and governmental tariffs determining strategies: a game-theoretic approach," *Computers & Industrial Engineering*, vol. 105, pp. 287–298, 2017.

[48] Z. Huang, G. Liao, and Z. Li, "Loaning scale and government subsidy for promoting green innovation," *Technological Forecasting and Social Change*, vol. 144, pp. 148–156, 2019.

[49] I. E. Nielsen, S. Majumder, and S. Saha, "Exploring the intervention of intermediary in a green supply chain," *Journal of Cleaner Production*, vol. 233, pp. 1525–1544, 2019.

[50] I. E. Nielsen, S. Majumder, S. S. Sana, and S. Saha, "Comparative analysis of government incentives and game structures on single and two-period green supply chain," *Journal of Cleaner Production*, vol. 235, pp. 1371–1398, 2019.

[51] J. Xu, J. Cao, Y. Wang, X. Shi, and J. Zeng, "Evolutionary game on government regulation and green supply chain decision-making," *Energies*, vol. 13, no. 3, p. 620, 2020.

[52] R. Dominguez and S. Cannella, "Insights on multi-agent systems applications for supply chain management," *Sustainability*, vol. 12, no. 5, p. 1935, 2020.

[53] M. P. Wellman, "Putting the agent in agent-based modeling," *Autonomous Agents and Multi-Agent Systems*, vol. 30, no. 6, pp. 1175–1189, 2016.

[54] A. Hafezalkotob, "Competition, cooperation, and coopetition of green supply chains under regulations on energy saving levels," *Transportation Research Part E: Logistics and Transportation Review*, vol. 97, pp. 228–250, 2017.

[55] C. Luo, M. Leng, J. Huang, and L. Liang, "Supply chain analysis under a price-discount incentive scheme for electric vehicles," *European Journal of Operational Research*, vol. 235, no. 1, pp. 329–333, 2014.

[56] C. Kiss and M. Bichler, "Identification of influencers — measuring influence in customer networks," *Decision Support Systems*, vol. 46, no. 1, pp. 233–253, 2008.

[57] Q. Yan, L. Wu, and L. Zheng, "Social network based microblog user behavior analysis," *Physica A: Statistical Mechanics and its Applications*, vol. 392, no. 7, pp. 1712–1723, 2013.

[58] A.-L. Barabási and E. Bonabeau, "Scale-free networks," *Scientific American*, vol. 288, no. 5, pp. 60–69, 2003.

[59] T. Zhang and D. Zhang, "Agent-based simulation of consumer purchase decision-making and the decoy effect," *Journal of Business Research*, vol. 60, no. 8, pp. 912–922, 2007.

[60] S. Čavoški and A. Marković, "Agent-based modelling and simulation in the analysis of customer behaviour on B2C e-commerce sites," *Journal of Simulation*, vol. 11, no. 4, pp. 335–345, 2017.

[61] B.-D. Kim, R. C. Blattberg, and P. E. Rossi, "Modeling the distribution of price sensitivity and implications for optimal retail pricing," *Journal of Business & Economic Statistics*, vol. 13, no. 3, pp. 291–303, 2010.

[62] S. Patel and A. Schlijper, "Models of consumer behaviour," in *49th European Study Group with Industry*, Oxford, UK, 2004.

[63] A. Adepetu, S. Keshav, and V. Arya, "An agent-based electric vehicle ecosystem model: San Francisco case study," *Transport Policy*, vol. 46, pp. 109–122, 2016.

[64] D. Godes and D. Mayzlin, "Using online conversations to study word-of-mouth communication," *Marketing Science*, vol. 23, no. 4, pp. 545–560, 2004.

[65] D. G. Fiebig, M. P. Keane, J. Louviere, and N. Wasi, "The generalized multinomial logit model: accounting for scale and coefficient heterogeneity," *Marketing Science*, vol. 29, no. 3, pp. 393–421, 2010.

[66] S. Xuanming, "Bounded rationality in newsvendor models," *Manufacturing & Service Operations Management*, vol. 10, no. 4, pp. 566–589, 2008.

[67] G. Szabó and G. Fáth, "Evolutionary games on graphs," *Physics Reports*, vol. 446, no. 4-6, pp. 97–216, 2007.

WILEY | Hindawi

Research Article

Design, Implementation, and Evaluation of Online English Learning Platforms

Jie Li (ORCID)

School of International Studies, Zhengzhou University, Zhengzhou, 450001 Henan, China

Correspondence should be addressed to Jie Li; karenli@zzu.edu.cn

With the rapid development of internet technology, various online learning platforms have emerged. The combination of the internet and education is an inevitable trend, and smart online learning platforms based on neural network become popular. This paper introduces how to design online English learning platforms through a neural network. It proposes the construction of a universally designed online English learning platform and the design of an online English learning platform server development architecture. Then, the implementation of online English learning platforms is discussed. Evaluation of the platforms is also very important, which is conducted through two questionnaire surveys. The first survey is general and the second one is more specific. Results of both surveys show that the learners' demand for online English learning platforms is still growing, especially among the young learners. In addition, this paper reports the results of the feasibility analysis and performance test of online English learning platforms: (1) The well-designed online English learning platform has relatively complete functions and meets the needs of both students and teachers. It includes a series of functional modules such as students' registration, analysis of students' profile, courseware and learning resources management, test management, test score analysis, interactive discussion, online monitor and feedback. (2) There are no major defects in the implementation of the online English learning platform in this experiment. (3) The reliability and security of the online English learning platform are relatively high.

1. Introduction

Online learning platform is also known as E-learning platform, online teaching platform, or learning management system. An online learning platform is a web-based access and a software system that provides comprehensive services for distance teaching and learning through two-way multimedia communication networks. It greatly facilitates course preparation, information transmission, and teacher-student interaction. As a supplement to the traditional teaching model, the online learning platform should be open, intelligent, and interactive, which is convenient for teachers to "teach" and students to "learn." At the same time, it should be able to provide a quick and effective feedback to both teachers and students.

The traditional English learning model in China mainly has 3 problems. First, it focuses on the process of "teachers' teaching" and ignores "students' learning." Second, due to the lack of English language environment, English learning is not effective after class. Thirdly, large amount of tedious homework makes students lose interest in English learning. In the past two decades, internet technology developed quickly in China and brought a lot of changes to education. One obvious change is adaptive learning. Online learning platforms can better meet the needs of learners of different ages and different learning goals. The smartly designed platforms pay attention to the individual differences of learners and develop learning materials that conform to their cognition and proficiency. During the COVID-19 pandemic, teachers can share teaching content and teaching procedures through public online learning platforms, so as to achieve the effect of teaching without going out. Compared with the conventional teaching model, online learning platforms can improve students' ability to use resources, thereby enhancing their learning autonomy.

Effective English teaching depends on good teaching design, and the design of an English learning platform is not merely the matter of IT professionals. English teachers' teaching design concepts are important factors to be counted. Tseng et al. made a research on how 6 English teachers formulate various forms of English teaching design concepts, while considering the impact of online platform teaching within 14 weeks. Through the quantitative analysis of the 6 teachers' discussion and the interview, it was found that the discussion obviously represented their different preferences of the teaching content. In addition, two factors that affect teachers' online platform teaching were discovered: technical issues related to the quality of online lessons and students' role [1]. Bollegala believes that scaling feature value is an important step in the construction of many network learning platforms. Different features have different value ranges, and some form of feature scaling is often required to ensure that accurate classifiers are learned. However, feature scaling is a preprocessing task before learning. If only a few training examples are observed, it may not be possible to accurately determine the value range of the feature in the initial stage of learning platform construction. Next, the distribution of data will change over time, which makes any feature scaling performed in the preprocessing step seem not enough to keep up with the times. Bollegala proposes a simple but effective method to dynamically scale features during training, so as to quickly adapt to any changes in the data stream, and compares the proposed dynamic feature scaling method with a more complex method that uses several benchmark data sets for classification. This method is more complicated and has many processes, which may lead to a high error rate [2]. Anshari et al. propose that the use of online learning resources from multiple channels in learning activities is expected to transform from traditional learning-centric content expansion to a collaborative learning center that emphasizes universal learning anytime and anywhere. When compiling big data, cloud computing and Semantic Web can be integrated into online learning resources, thus providing a wide range of knowledge acquisition and enriching users' learning experience. In traditional learning practices, students are regarded as recipients of information and knowledge. However, nowadays, students participate in the learning process, which plays an active role in the creation, extraction, and improvement of collaborative learning platforms for online learning resources and knowledge sharing and distribution. Anshari et al. believe that popularized knowledge can meet the needs of integrating cloud computing, big data, Web 2.0, and Semantic Web. Popularized knowledge redefines the added value, type, quantity, and speed of online learning resources and network learning platforms. There is considerable flexibility in adoption, knowledge acquisition, and technology implementation. This research has strong operability but high cost, which is not conducive to popularization [3].

The innovations of this paper are as follows: (1) it proposes the use of neural networks to construct an online English learning platform, (2) it proposes the construction of a universally designed online English learning platform,

and (3) it proposes the design of an online English learning platform server development architecture.

2. Design of Online English Learning Platforms

2.1. Constructing Online English Learning Platforms through Neural Network. As far as English teaching is concerned, instructional design is extremely important. The online leaning platform is based on artificial intelligence technology, knowledge mining technology, and neuron network technology. After learning all kinds of information about students, the platform is designed according to a comprehensive analysis of students' interests, knowledge structure, preferences, learning status, and adaptability of courseware resources, and then, the purposeful step-by-step training is conducted according to the students' level and learning ability [4, 5]. At the same time, the platform provides a step-by-step interactive teaching mode through the machine memory function, to track and evaluate students' learning [6]. For teachers, such a platform not only provides the functions of the traditional online English teaching system such as course arrangement, courseware production, examination arrangement, question answering, and homework guidance, but also provides the feedback of students' adaptability and learning progress. Tracking and evaluation have achieved the purpose of humanization, intelligence, and personalization [7].

A neural network is a complex network system formed by the extensive connection of many simple neurons. It maps a large number of basic characteristics of human brain functions and is an extremely complex network system [8, 9]. Neural networks have distributed storage, large-scale parallelism and processing, self-adaptation, self-organization, and self-learning capabilities and are especially suitable for dealing with fuzzy and inaccurate information processing-related problems that need to consider many factors and conditions at the same time [10]. A neural network is composed of neuron models, and this information processing network composed of many neurons has a parallel distributed structure [11]. Each neuron has a single output and can also be connected to other neurons. It has many output connection methods, and one connection method has a connection right [12]. The meridian cell is the basic unit of the neural network, which imitates the biological neuron. The characteristics of the neuron determine the overall characteristics of the neural network in a certain program [13]. The interconnections between many simple neurons form a neural network. Input $x_1, x_2, \cdots, x_n$ represents the n inputs of the neuron, expressed as a vector X in column $n \times 1$ as

$$X = [x_1, x_2, \cdots, x_n]^T. \tag{1}$$

Using the first relevant neuron to process the input signal, the summing unit can complete the weighted summation of the input signal. The following relationship exists:

$$net = \sum_{k-1}^{n} x_k w_{i,k} + b. \tag{2}$$

Neural network algorithms are usually divided into convolutional neural networks, recurrent neural networks, and multilayer feedforward neural networks. Here, only the use of multilayer feedforward neural networks or BP neural networks for English network learning platform design is explained [14]. Suppose the number of input neural units in the BP neural network is n, the number of hidden layer neural units is q, the number of output layer neural units is m, the nth neural unit of the input layer is A_n, and the qth neural unit of the hidden layer is C_q, The mth neural unit of the output layer is B_m, $A = A_1, \cdots, A_i, \cdots A_n$ is the output vector, $C = C_1, \cdots, C_i, \cdots C_n$ is the output vector of the hidden layer, $B = B_1, \cdots, B_i, \cdots B_n$ is the output vector of the output layer, R is the weight matrix from the input layer to the hidden layer, and S is the hidden layer to the output of the weight matrix of the layer [15, 16].

The hidden layer formula is

$$C_k = f(\text{net}_k), \quad k = 1, 2, \cdots, q, \tag{3}$$

$$\text{net}_k = \sum_{i=1}^{q} R_{ki} A_i, \quad k = 1, 2, \cdots, q. \tag{4}$$

The output layer formula is

$$B_j = f(\text{net}_j), \quad j = 1, 2, \cdots, m, \tag{5}$$

$$\text{net}_j = \sum_{k=1}^{q} S_{kj} C_k, \quad j = 12 = 1, 2, \cdots, m. \tag{6}$$

The actual output of the network is

$$B(n) = \left[S_m^1, S_m^2, \cdots, S_m^m \right]. \tag{7}$$

The expected output of the network is

$$d(n) = [d_1, d_1, \cdots, d_m]. \tag{8}$$

The error of repeating the process for the nth time is

$$e_m(n) = d_m(n) - B_m(n). \tag{9}$$

Define the error energy as

$$e(n) = \frac{1}{2} \sum_{m=1}^{m} e_m^2(n). \tag{10}$$

Randomly connect weights ω_{ji} and v_{ij}, threshold θ_i, and assignment γ_i to the BP neural network in $[-1, 1]$, provide network input, and divide a set of random sample data into input sample $P_k = (a_1^k, a_2^k, \cdots, a_n^k)$ and target sample $T_k = (s_1^k, s_2^k, \cdots, s_m^k)$, where n is the number of input layer nodes, and m is the number of nodes in the output layer [17]. After setting the initial weights, thresholds, training samples, and target samples of the neural network, the training can be carried out. During this process, the BP neural network will calculate the input s_j of each hidden layer unit and calculate the output

of each hidden layer unit b_j; the formula is expressed as

$$s_j = \sum \omega_{ji} a_i - \theta_i, \quad j = 1, 2, \cdots, m, \tag{11}$$

$$s_j = f(s_i), \quad j = 1, 2, \cdots, m. \tag{12}$$

2.2. RBF Algorithm in Neural Network. The neural network corresponding to the radial basis function (RBF) is composed of an input layer and a hidden layer plus an output layer, a total of three layers. The transformation function of the hidden layer is a kind of locally distributed nonnegative linear function with radial symmetric attenuation about the center point, which is usually a Gaussian function:

$$\zeta_j(x) = \exp\left(-\frac{\|X - C_j\|}{2\zeta_j^2}\right)(j = 1, 2 \cdots, h). \tag{13}$$

In the formula, ζ_j is the output of the jth unit of the hidden layer, X is the input vector, $\|\bullet\|$ is the normal form, C_j is the center of the jth Gaussian unit of the hidden layer, ζ_j is the width of the Gaussian function of the jth hidden layer borrowed point, in addition,

$$\|X - C_j\| = (X - C_j)^T (X - C_j). \tag{14}$$

The output of the network can be expressed as

$$y_k = \sum_{j=1}^{h} w_{kj} \zeta_j(x)(k = 1, 2, \cdots, m). \tag{15}$$

Written in matrix form:

$$Y = W\theta, \tag{16}$$

$$Y = [y_1, y_2, \cdots, y_m]^T, \tag{17}$$

$$W = [w_1, w_2, \cdots, w_m]^T, \tag{18}$$

$$w_k = [w_{k1}, w_{k2}, \cdots, w_{kn}]^T, \tag{19}$$

$$\zeta = [\zeta_1(x), \zeta_2(x), \cdots, \zeta_3(x)]^T. \tag{20}$$

In the formula, Y is the output vector, W is the weight matrix from the hidden layer to the output layer, and ζ is the output of the hidden layer.

2.3. Universally Designed Online English Learning Platforms

(1) Universal design

The concept of universal design comes from manufacturing, which emphasizes the uniqueness of each individual, and proposes that when designing and producing products, it is possible to consider the various problems that various users may face, while trying to prevent individuals from feeling unfairly treated [18]. Among the seven basic principles of universal design, equal usability is the most critical principle. The other six principles are all supplementary explanations

for equal usability, which means that products based on the universal design concept must adapt to users who have different knowledge background, technical levels, physical conditions, and different levels of proficiency [19]. The concept of "universal" broadens the designer's thinking and vision, lets the designer consider expanding the design applicability of the product as much as possible to meet the needs of more people, helps the product reach a higher utilization rate, and extends the use time limit of the product. At the same time, it can reduce the waste of resources and bring more far-reaching significance [20].

(2) Application of universal design in building online English learning platforms

According to the purpose of English teaching, applying the concept of universal design to construct an online English learning platform should meet the following goals: operability—the platform should be user-friendly and can meet the physiological characteristics and operating habits of various learners at the same time; recognizablility—the information conveyed by the platform is easy for learners to understand and can accurately provide feedback information in various ways; correctability—the platform can correct or avoid user misoperation and assist learners when they are in doubt of operation; safety and comfort—learners should have a smooth and comfortable experience when using the product, which allows them to use the product for a long time without excessive eye fatigue; pleasure—learners enjoy both physical and mental pleasure when using the platform, and they are willing to use for a long time. Dylan Sung once investigated Taiwanese university students' perceptions and feedbacks regarding an online English learning platform. Results show that when the user interface is not intuitive and the experience is not smooth, students hold a fairly negative attitude toward the use of the online platform. Therefore, the design of online English learning platforms is crucial, which requires close cooperation between technicians and teachers who understand students' needs, collect their response to the platform from time to time, and give objective feedback to technicians to perfect the interface and functions of the learning platform.

2.4. The Server-Side Development Architecture of Online English Learning Platforms. The advantage of the three-tier architecture is that its clients are unified as browsers, and there is no need to install the client, and the client's request will be sent through the browser. After receiving the request, the web server performs corresponding data processing. During this period, the web server also exchanges data with the background server. Finally, the web server sends the processed data result back to the browser. In this structure, all user interfaces are implemented through the browser, and only a relatively small amount of transaction logic will be implemented in the front stage, and most of the transaction logic will be implemented on the server side, thus turning the client/server model into three parts: the database system, application server, and client browser. In the choice of database server software, you can choose the currently popular MySQL database server. It is an open source software and provides powerful database service support functions, following standard SQL syntax. Compared with commercial server software such as Oracle and SQL server, using MySQL saves software development costs while the system performance is not affected. At the application server level, developers may choose common components provided by various vendors and free software developers to save development time and, at the same time, modify and upgrade certain component functions according to their specific needs. The development of all application function components follows and supports standard network protocols such as the TCP/IP protocol, HTTP protocol, and SSL protocol. Under the premise of ensuring system performance, it saves a lot of development time, and the application scope and compatibility of the system are obtained. It is fully guaranteed. In this way, after the system development is completed, the user only needs to access the system for work or use the functions provided by the system on a computer with ordinary browser software installed. The development cost can be controlled as far as possible under the premise of ensuring system performance. There are also many choices in system development languages and development tools. For example, development languages include Java, PHP, JavaScript, Ajax, and HTML; development tools that can be used include Dreamweaver, Eclipse, and Flash; database management tools include MyAdmin.

In summary, the technical elements in the design of online English learning platforms are shown in Figure 1.

3. Implementation of Online English Learning Platforms

The subject of self-study is the learner, so after logging in as a learner, he/she can enter the system. The learner's information is initialized by the administrator in the early stage, but it can be modified after logging in. Before formally starting independent learning, the learner should first select a class. The learning module will adapt to learners who are at different levels and with different schedules, and the teachers will be different on each level of learning. Therefore, for most autonomous online English learning platforms, learners should first proceed to the class. After entering the class, learners make a choice of learning resources and courses. The online system will help the teacher track each learner's learning status and learning process. Since this system is a self-learning platform, the learning resources should be diversified and can be provided to students of different levels for self-learning. Learning resources consist of English reading, writing, listening, speaking and translation, so that learners can strengthen their English proficiency in a targeted manner. The courses in the platform are generally maintained by the administrator, and teachers also have certain permissions to add, delete, and update course content. After completing the course selection, learners can start learning independently. In the process of independent learning, when one part of the learning content is completed, learners' learning condition will be uploaded to the database, so through this platform teachers get students' learning data in time.
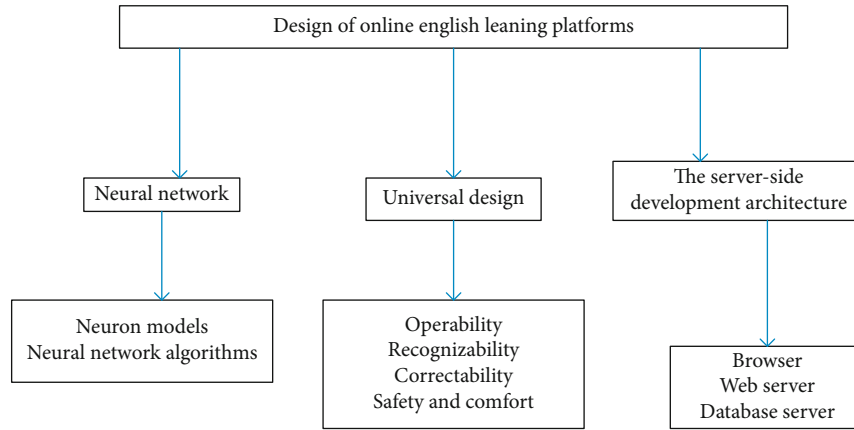
FIGURE 1: Technical elements in the design of online English learning platforms.

TABLE 1: Questionnaire composition.

Item		Quantity	Percentage
Total number of questionnaires		200	100%
Total number of valid questionnaires		187	93.5%
Total invalid questionnaires		13	6.5%
Male questionnaire	Effective	90	92.8%
	Invalid	7	7.2%
Female questionnaire	Effective	97	94.2%
	Invalid	6	5.8%

After completing the self-study, learners can take a self-test to make a self-judgment of the learning effect. The system will continue to store and update each learner's data, so that the teacher can make corresponding responses. In order to adjust the content of learning, the administrator retains the highest authority for the maintenance of the most tested content. After the completion of the self-test, learners may choose whether to enter the community for further study and discussion or not according to their own interests. They can ask questions in the community, and other learners or teachers online will discuss and answer them accordingly. Finally, learners exit the self-learning platform. This is the operation process of an English online learning platform.

4. Evaluation of Online English Learning Platforms

4.1. Learners' Response to Online English Learning Platforms. In order to know learners' response to the online English learning platform, questionnaire survey should be conducted. A questionnaire is a set of questions for obtaining statistically useful or personal information from individuals, which is a very useful tool in social science and empirical studies. In this research, first an online questionnaire (20 questions) is distributed to students of different kinds of schools (middle school, high school, college, and university) and adult learners who like to learn English in 15 provinces of China. The questionnaire is divided into two parts. The

first part includes questions about the conditions of students' use of mobile terminal equipment, students' English learning preferences, and online uploads and downloads of learning resources. The second part of the questionnaire is mainly about the teaching and learning effects of online learning platforms. Participants' satisfaction of online learning is measured by a 5-point Likert scale, and their written feedback is also collected. After the survey, the reliability of the questionnaire is tested. That is to say, 6 weeks later, the same questionnaire survey is conducted again, and the correlation coefficients of the results of the two surveys are calculated by SPSS 22.0 statistical software [21]. Results show that 73% of participants accept the way of learning English through online learning platforms, and they give positive comments on the online platforms they have used. As to learning effects, 57% of participants show satisfaction.

Then, another questionnaire survey is made among 200 university students (97 boys and 103 girls) who are required to use online English learning platforms in their study. There are 200 questionnaires in total.

(1) The composition of the questionnaire is statistically analyzed and drawn into statistical charts, as shown in Table 1 and Figure 2

It can be seen from the chart that 187 valid questionnaires and 13 invalid questionnaires are collected, and the questionnaire validity rate is 93.5%. Regardless of the effectiveness of the overall questionnaire or the effectiveness of the male and female questionnaires, the questionnaire is highly effective and can be used for reference.

(2) The questionnaire covers five aspects: listening, speaking, reading, writing, and teaching design. The questions are related to students' specific expectation and demand for the online English learning platform when they get access to it. The results of the survey are shown in Table 2

Among the 187 valid questionnaires, students pay most attention to the improvement of oral English, which really reflects the students' demand and the present condition of
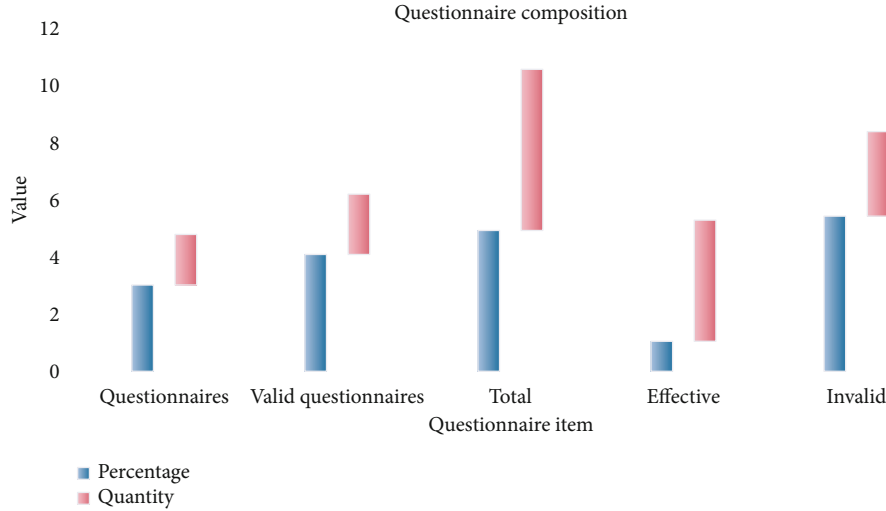
Figure 2: Questionnaire composition.

Table 2: Learners' demand for the platform.

Item	Number of students	Percentage
English listening	36	19.25%
Oral English	41	21.93%
English reading	39	20.86%
English writing	37	19.79%
English teaching design	34	18.17%

Table 3: Learners' interest in English online learning platforms.

Not accept	Male	4
	Female	9
Does not care	Male	17
	Female	15
Interested	Male	26
	Female	37
Very interested	Male	38
	Female	41

college English teaching—limited time and opportunity for students to practice oral English on class, so they want to get more practice through online learning platforms. Dylan Sung's investigation showed that if the online English learning platform did not have the functionality for users to improve speaking skills, this is a major weakness. Several newly designed platforms have virtual communities where learners may talk to each other or talk to their teachers with the help of the audio facilities on their computers or mobile phones. With the development of artificial intelligence, an intelligent oral English robot coach can be designed and embedded into the network learning platform. They can have dialogues with learners and correct their mistakes from time to time. Virtual reality technology makes online learning

environment as natural as the offline classroom setting, and even more interesting and attractive.

(3) Next is a statistical analysis of learners' interest in the English online learning platforms. As is known, the learners' interest in learning materials, teaching methods, and learning facilities will directly affect their initiative and enthusiasm in learning. Male and female students obviously have different attitudes toward English online learning platforms. Results are shown in Table 3 and Figure 3

It can be seen from the chart that the number of students who expressed "very interested" in the English online learning platform accounted for the largest proportion, followed by the proportion of more female learners than male learners in the four levels of interest. Usually, females enjoy learning English from childhood, so they may want to try different ways of English learning including using online platforms. The adaptive learning technology makes it possible for learners to learn different contents according to their preferences. Therefore, platform administrators should update the latest English learning materials in time and those materials should cover a wide range of topics so as to satisfy different learners' tastes.

(4) The frequency of learners using the online English learning platforms is also investigated, and the results are shown in Table 4 and Figure 4

As can be seen clearly from the figure, female students use online English learning platforms more frequently than male students. 55 female students use it more than three times a day, which is really a high percentage of using the platform. If the learning resources in the platform are abundant and they keep practice listening, speaking, reading and writing through the platform, they will make progress quickly. The reason why male students use less can still be explained by learning interest, since interest is one important
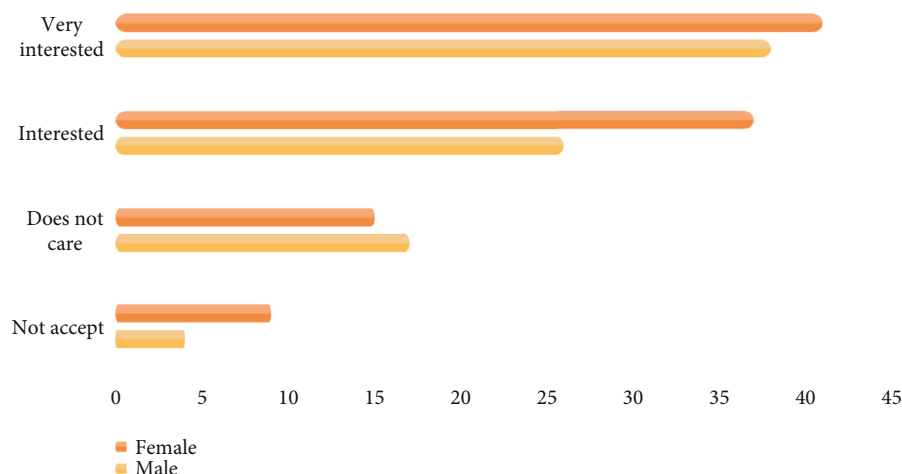
FIGURE 3: Learners' interest in English online learning platforms.

TABLE 4: The frequency of learners' use of online English learning platforms.

Frequency of usage	Number of male users	Number of female users
Three times a day or more	43	55
Once or twice a day	26	38
Four to six times a week	17	11
One to three times a week	4	3

learning motive. The design of online English learning platforms should better serve users and provide users with a convenient and complete learning environment.

4.2. Feasibility Analysis of Designing and Implementing Online English Learning Platforms. The purpose of the feasibility study is to determine whether a platform has development value and can be completed within a limited time with existing resources and technology. This paper discusses the design and development of an online English learning platform that is supported by the mobile phone and computer. The time for development (excluding prerequirement analysis and system testing work) is limited to two months. Such an English learning platform mainly provides users with a channel to learn daily English vocabulary and practice listening, reading, writing skills, and oral English. At present, the learners' demand for online English learning platforms or apps is still growing, especially among the young learners.

The online learning platform provides a good many network connection interfaces and tools and can easily filter the content of HTML files. In addition, a variety of additional development kits are provided for developers to use. By obtaining the HTML file content of a specific webpage and then using the document tool or string tool to filter and intercept the text content, the desired content can be obtained. In such a system, the function that needs to use web crawling content is mainly to pull the podcast list and get the podcast tags, complete original texts, and audios. The SQLite database provided by the platform is a lightweight and powerful database. The database operation process is roughly the same as that of the SQL server, so there is basically no difficulty. The content that needs to use data interaction in this system includes managing favorites and downloading tasks and thesaurus. At present, the development skills of the English network learning platform have become mature, and the development-related technical reference materials have been completed. The experience sharing of many developers has also provided instructive answers to the problems that may be encountered in the development process. Therefore, it is completely feasible to develop an English learning platform based on the system's own development capabilities.

This kind of English learning platform is oriented to computer and mobile phone users, with a friendly interface and clear prompts. It provides users with multiple personalized operations, and users can quickly understand how to use the application. Each module of the application supports touch screen operation, and users can conveniently use all the functions. Developers also try to fully consider the needs of users, solicit opinions during the needs analysis, and obtain suggestions for improvement through feedback during the testing phase.

This kind of English online learning platform does not violate national laws and regulations and will not infringe the rights and interests of others. It is developed under an open source system, and its development tools, reference materials, and launching do not contain any infringement.

In addition, this paper collects the information of some popular online English learning platforms among English learners in China, such as Youdao, Do not recite words, Baicizhan, and Scallop English. The details are shown in Table 5 and Figure 5.

Among the four well-known online English learning platforms/apps on the market, Youdao is the earliest one, and the number of downloads is significantly more than others. Youdao has complete functions, beautiful interface, and convenient design, which is very friendly to users. Once users like
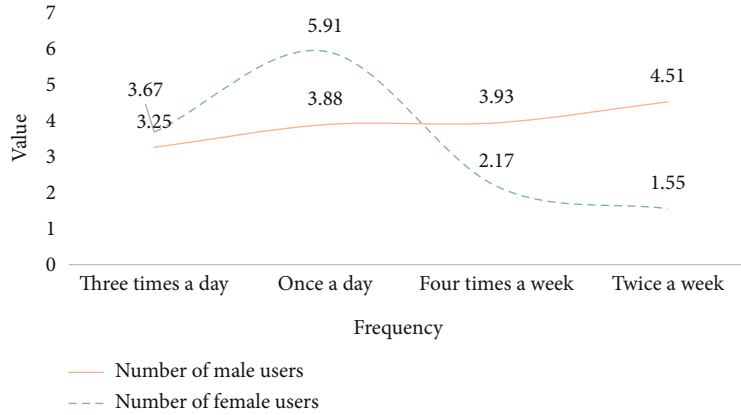
FIGURE 4: The frequency of learners' use of online English learning platforms.

TABLE 5: Popular online English learning platforms.

Name of the platform or app		Youdao	Do not recite words	Baicizhan	Scallop English
Time to market (year)		2007	2016	2014	2014
Downloads (unit: ten million)	Android	46.4	3.9	27.3	21.4
	iOS	39.5	4.7	22.6	15.2
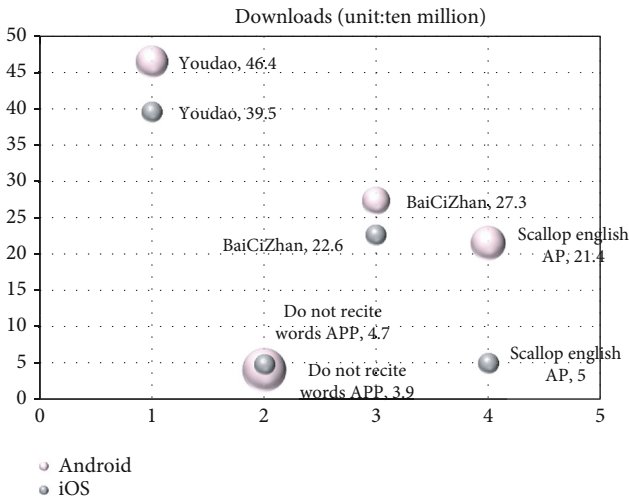
FIGURE 5: Popular online English learning platforms.

one platform/app, they will keep using it for a long time and share it with friends. As a result, more users will download it and this platform/app will take up a large market share. Baicizhan is very popular among college students who want to have a large vocabulary. Baicizhan contains different types of learning activities that are designed to help learners remember English words actively, so this app is much more interesting than the traditional way of reciting English words. At present, Scallop English seems to be less known than Youdao and Baicizhan. However, its adaptive system is more trendy and will have greater influence in the near future.

4.3. Performance Test of Online English Learning Platforms. The concurrency, fault tolerance, real-time performance,

instantaneous peak value of the server, and the load of the system of the network learning platform should be tested. When testing the performance, you must choose a suitable place. The detailed information of the pressure situation in this scenario is shown in Table 6.

With the pressure in the testing process and on the basis of recording various information, the performance of an online English learning platform can be obtained and shown in Figures 6 and 7.

The buffer delay test is to test the data transmission speed in 4G environment. The previous functional test has proved that the system can play video files normally. In the text buffer experiment, a total of six smartphones with similar configurations is used. To perform video on demand, we record the different buffer delay time (in seconds) of each mobile phone for each on-demand. The experiment is carried out 10 times. The results are shown in Table 7 and Figure 8.

It can be seen from the results of function test and performance test that each performance index has reached the target requirements set by the school, and the online learning platform can be widely used to replace the existing teaching management system. According to the above analysis, the following conclusions can be drawn:

(1) The well-designed online English learning platform has relatively complete functions and meets the needs of both students and teachers. It includes a series of functional modules such as students' registration, analysis of students' profile, courseware and learning resources management, test management, test score analysis, interactive discussion, online monitor, and feedback

TABLE 6: Performance test.

Serial number	1	2	3	4	5	6
Item	Total duration	Maximum number of runs	Total throughput	Average throughput	Total clicks	Average hits per second
Value	1 h 8 min 35 s	2,489	155,854,354	38,546,	15,634	3.878
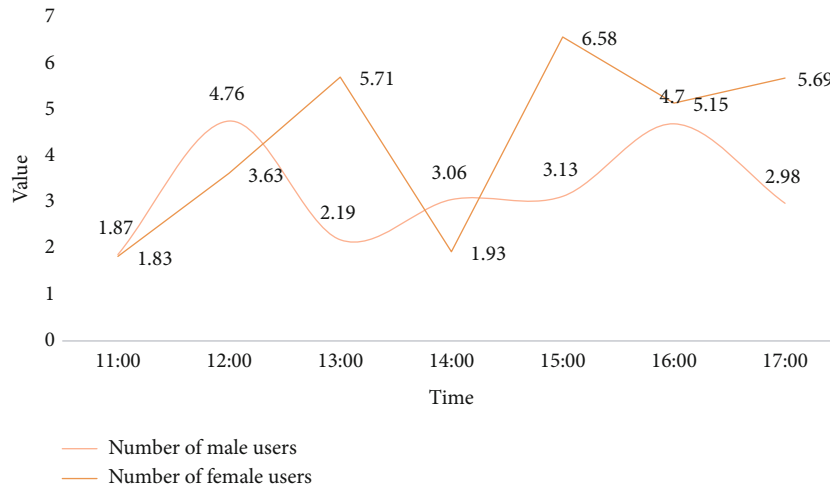
FIGURE 6: Online population test.
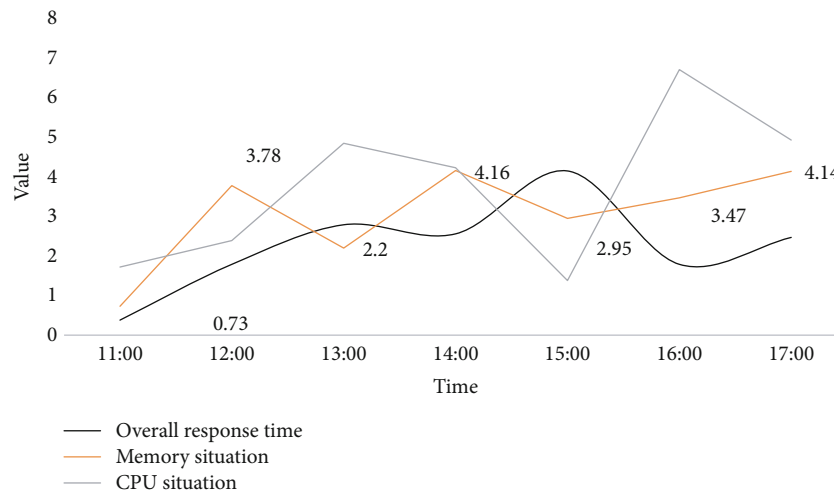
FIGURE 7: Overall response time, memory, and CUP test.

TABLE 7: Statistics of buffer delay test.

Number of experiments	1	2	3	4	5	6	7	8	9	10
User 1	1	0.9	1	0.9	0.85	1.2	1.1	1.1	0.85	1
User 2	1.2	0.8	1.1	1	0.7	1.1	1.5	1	0.85	1
User 3	1.1	0.85	1	0.9	0.8	1.3	1.1	0.9	0.85	1
User 4	1.2	0.85	1.1	1	0.9	0.7	0.75	0.8	0.85	1
User 5	1.1	1.2	1.1	1	0.95	0.9	0.8	0.7	0.05	1
User 6	1	1.1	1.05	1.2	1.25	1	0.85	0.8	0.85	1

(2) There are no major defects in the implementation of the present online English learning platform

(3) The reliability and security of the online English learning platform are relatively high

4.4. Impact of Online English Learning Platforms on Learner Performance. In order to know whether online English learning platforms are effective or not, a simple empirical research was made in a college. 60 students were selected randomly as participants from the freshmen who major in engineering. They were divided into the treatment group and control group randomly. There was no significant difference in English proficiency between the two groups, as a proficiency
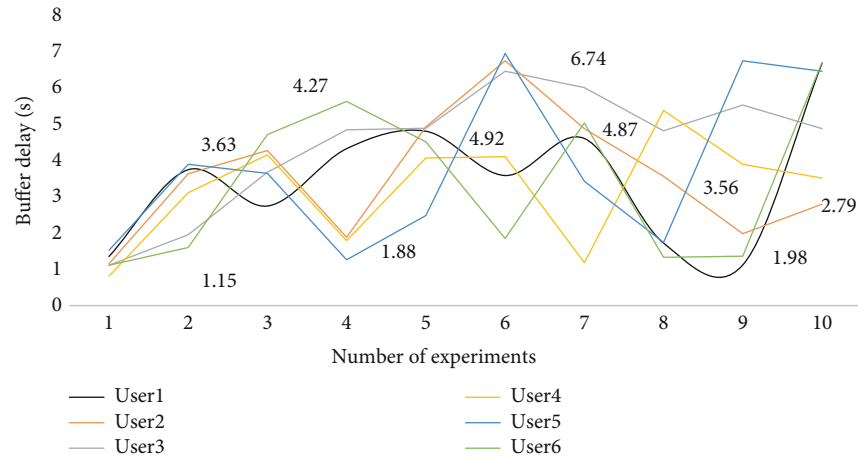
FIGURE 8: Results of the buffer delay test.

test of English was made shortly after they entered college. Participants were asked to fill in the blanks of 10 sentences after self-study, and the missing words for the blanks were in the text of their textbooks. For the treatment group, participants learned the text through the online learning platform, and for the control group, participants learned by themselves. After learning for 20 minutes, they began to fill in the blanks. The result showed that there was significant difference between the two groups. 21 participants of the treatment group got 10 correct answers, which accounted for 70% of the group number, while only 6 participants of the control group got 10 correct answers, which accounted for 20% of the group number. Furthermore, the average correct answers of the treatment group and control group were 7 and 4, respectively. Therefore, an online English learning platform is very effective for learners' self-study, which makes a good supplement for class teaching.

According to interviews among the participants, most of them like to learn online and can adapt to online learning. They find that online learning through platforms is sometimes more interesting and flexible, especially during the pandemic when schools are closed. Meanwhile, the resources provided by the online English learning platforms are much more abundant than those on class. Online learning is favored by students who have a strong learner autonomy.

5. Conclusion

Modern advancement is becoming prominent these days, and it also affects the way people studies. Online learning platforms transform the traditional learning model into the process of active knowledge construction. With the help of these platforms, learning becomes more flexible, and it is available for individual learners wherever they have computers, mobile phones, and internet access. Online learning platforms can better meet the needs of learners of different ages and different learning goals. The smartly designed platforms pay attention to the individual differences of learners and assign learning materials that conform to their interests, cognition, and level of learning. Teachers may share the excellent teaching content and teaching design through

online learning platforms to truly enjoy quality teaching without going out of the home. Compared with the conventional teaching model, online learning platforms can improve students' ability to use resources, thereby enhancing their learning autonomy.

This paper discusses the design, implementation, and evaluation of online English learning platforms. In the stage of design, neural network, universal design, and the server-side development architecture may be employed. Of course, there are still other types of technology to be applied. The implementation of online learning platforms is related to easy usability and operability. A good platform should be user-friendly, bringing convenience to both students and teachers. The evaluation of online learning platforms is made empirically and technically. Through questionnaire, data analysis, and case study, students' responses to online English learning platforms are shown clearly—most of them believe online English learning platforms are beneficial to their study. In addition, performance test of this study shows that the reliability and security of the online English learning platform are relatively high. However, this paper has limitations due to the number of participants and conditions of tests. More and more attention is paid to the inquiry of online learning platforms, and future research will be directed towards this aspect.

Data Availability

No data were used to support this study.

Conflicts of Interest

There are no potential competing interests in our paper.

Acknowledgments

References

[1] J. J. Tseng, Y. S. Cheng, and H. N. Yeh, "How pre-service English teachers enact TPACK in the context of web-conferencing teaching: a design thinking approach," *Computers & Education*, vol. 128, pp. 171–182, 2019.

[2] D. Bollegala, "Dynamic feature scaling for online learning of binary classifiers," *Knowledge Based Systems*, vol. 2012, no. 1, pp. 53–58, 2017.

[3] M. Anshari, Y. Alas, and L. S. Guan, "Developing online learning resources: big data, social networks, and cloud computing to support pervasive knowledge," *Education & Information Technologies*, vol. 21, no. 6, pp. 1663–1677, 2016.

[4] A. M. Korhonen, S. Ruhalahti, and M. Veermans, "The online learning process and scaffolding in student teachers' personal learning environments," *Education and Information Technologies*, vol. 24, no. 1, pp. 755–779, 2019.

[5] Z. Q. Tang, H. L. Heung, K. Y. Tong, and Z. Li, "A probabilistic model-based online learning optimal control algorithm for soft pneumatic actuators," *IEEE Robotics and Automation Letters*, vol. 5, no. 2, pp. 1437–1444, 2020.

[6] A. J. Prunuske, L. Henn, A. M. Brearley, and J. Prunuske, "A randomized crossover design to assess learning impact and student preference for active and passive online learning modules," *Medical Science Educator*, vol. 26, no. 1, pp. 135–141, 2016.

[7] J. Djan and B. George, "Standardization or localization: a study of online learning Programmes by tertiary institutions in Ghana," *European Journal of Contemporary Education*, vol. 4, no. 184, pp. 430–437, 2016.

[8] A. Bellocchi, K. A. Mills, and S. M. Ritchie, "Emotional experiences of preservice science teachers in online learning: the formation, disruption and maintenance of social bonds," *Cultural Studies of Science Education*, vol. 11, no. 3, pp. 629–652, 2016.

[9] N. W. Tsai, "Assessment of students' learning behavior and academic misconduct in a student-pulled online learning and student-governed testing environment: a case study," *Journal of Education for Business*, vol. 91, no. 7, pp. 1–6, 2016.

[10] M. King, M. Forsey, and M. Pegrum, "Southern agency and digital education: an ethnography of open online learning in Dili Timor-Leste," *Learning Media and Technology*, vol. 44, no. 3, pp. 1–16, 2019.

[11] R. Vanoostveen, F. Desjardins, and S. Bullock, "Professional development learning environments (PDLEs) embedded in a collaborative online learning environment (COLE): moving towards a new conception of online professional learning," *Education and Information Technologies*, vol. 24, no. 2, pp. 1863–1900, 2019.

[12] F. Silva, L. Correia, and A. L. Christensen, "Evolutionary online learning in multirobot systems," *Ai Matters*, vol. 3, no. 1, pp. 23-24, 2016.

[13] R. Dixit and U. S. Bedi, "Online learning with inexact proximal online gradient descent algorithms," *IEEE Transactions on Signal Processing*, vol. 67, no. 5, pp. 1338–1352, 2019.

[14] R. A. Perkins, "Assessment and evaluation in online learning," *Library Technology Reports*, vol. 55, no. 4, pp. 31–34, 2019.

[15] S. Kim and S. K. Moon, "Sustainable platform identification for product family design," *Journal of Cleaner Production*, vol. 143, pp. 567–581, 2017.

[16] C. Xie, C. Schimpf, J. Chao, S. Nourian, and J. Massicotte, "Learning and teaching engineering design through modeling and simulation on a CAD platform," *Computer Applications in Engineering Education*, vol. 26, no. 4, pp. 824–840, 2018.

[17] J. Laakkonen and J. Parkkila, "Incorporating privacy into digital game platform design: the what, why, and how," *IEEE Security & Privacy*, vol. 14, no. 4, pp. 22–32, 2016.

[18] C. Bing-Er and X. Jian-Ning, "The platform design of space-based optical observations of space debris," *Chinese Astronomy and Astrophysics*, vol. 41, no. 1, pp. 109–124, 2016.

[19] H. Gürsoy, "Control system implementation on an FPGA platform," *IFAC-Papers OnLine*, vol. 49, no. 25, pp. 425–430, 2016.

[20] C. Yang, T. Wang, and Y. Chen, "Design and analysis of an omnidirectional and positioning tolerant AUV charging platform," *IET Power Electronics*, vol. 12, no. 8, pp. 2108–2117, 2019.

[21] M. M. Chingos, R. J. Griffiths, C. Mulhern, and R. R. Spies, "Interactive online learning on campus: comparing students' outcomes in hybrid and traditional courses in the university system of Maryland," *The Journal of Higher Education*, vol. 88, no. 2, pp. 210–233, 2017.

Research Article

Analysis and Optimization of Low-Speed Road Noise in Electric Vehicles

Wentao Yu (ID)

School of Automotive Engineering, Tianjin Vocational Institute, Tianjin 300000, China

Correspondence should be addressed to Wentao Yu; 000855@th.tjtc.edu.cn

When a certain electric vehicle is driving at a constant speed of 40 km/h on the rough asphalt road, the rear passenger can obviously feel the ear pressure, which seriously affects the comfort. Through the analysis of objective data, it was found that the problem was caused by the road excitation, which leads to the coupling between the mode of the backup door and the mode of the acoustic cavity, and causes the resonance of the car cavity, thus causing the ear pressure sensation. To solve this problem, this paper optimizes the backup door by means of experiment and simulation, increases the dynamic vibration absorber, makes its modal frequency avoid the acoustic cavity modal frequency, and achieves the purpose of reducing the interior noise. After optimization, the vehicle noise is reduced by 8 dBA at 42 Hz under 40 km/h working condition of rough road surface, and the ear pressure sensation is reduced at the same time, thus improving the NVH (noise, vibration, and harshness) performance of the vehicle.

1. Introduction

In the automotive industry, noise, vibration, and harshness is referred to as the NVH problem of automobile, which is a comprehensive problem to measure the manufacturing quality and core technology of automobile. It gives the automobile users and consumers the most superficial and direct feeling. Excessive vehicle noise will reduce the sound quality in the car and negatively affect the psychology and physiology of passengers. Therefore, reducing the noise and vibration in the car has attracted widespread attention. Vehicle noise, vibration, and harshness performance have become design standards. In terms of NVH performance, new-energy models do not have the noise masking effect of engine and other components, but the noise of road noise, wind noise, and electronic and electrical accessories is more prominent.

Noise control usually requires reducing the sound by changing the sound source, increasing the transmission path, or removing objects or subjects exposed to the noise. Therefore, the vehicle noise level can be improved from the following three aspects: noise source, transmission path, and receiver [1, 2].

Only by accurately identifying and characterizing noise and vibration sources can new design improvements and solutions be verified, thereby improving the sound comfort of the vehicle interior. The internal noise of the vehicle mainly comes from the engine and gearbox, intake and exhaust system, road noise, and high-speed wind noise, which are closely related to the structure and working state of the vehicle and have the characteristics of time-varying and randomness [3]. According to the mechanism of noise generation, noise sources can be divided into two types. Structural noise source: the noise generated by the vibration of vehicle structural components, which can excite the vibration of the vehicle compartment and cause structural noise. Air noise source: the noise generated by the mutual excitation of various subsystems and aerodynamics of the vehicle, which is transmitted through the body and is perceived by passengers [4]. Structure noise is mainly low frequency of main frequency, and air noise is mainly main frequency intermediate frequency and high frequency. Related research and analysis show that the contribution of air noise to vehicle internal noise is less than structural noise [1]. When the vehicle is running at a relatively low speed, especially on rough roads and cruising or partial throttle conditions, no obvious
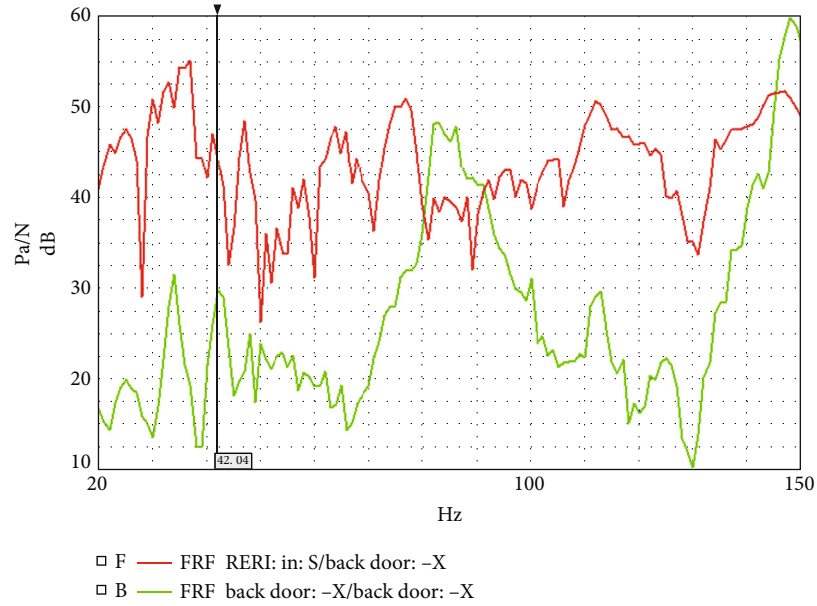
FIGURE 1: Backup door NTF.
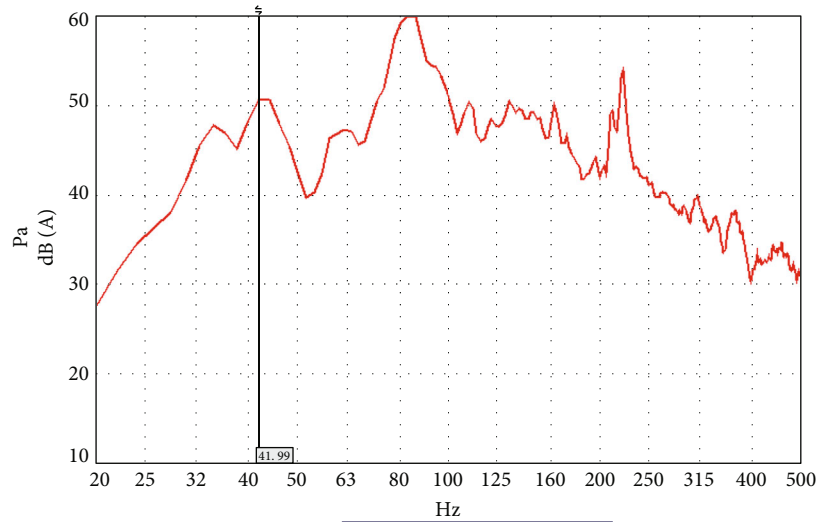
FIGURE 2: Noise in the vehicle.

aerodynamic noise will be produced [5]. The noise generated by the front structure, the noise and power generated by the rear structure, and the noise generated by the system air are the main noise source below 500 Hz [6, 7].

At present, the control of road noise is mainly divided into active and passive noise control technology. The principle of active noise control (ANC) is to effectively reduce the road noise problem by collecting noise samples according to the characteristics of noise sound waves and after systematic analysis and processing, and a noise sound wave with the same amplitude and opposite phase is designed to offset the noise, thus effectively reducing the road noise problem. This control technology is a potential supplementary technology for passive noise control of light vehicles [8]. The advantage of the control technology is that the sound device is arranged

conveniently, and the noise suppression effect of low-frequency structure is good. Its disadvantages are poor stability, high technical requirements, and high cost.

Passive noise control technology has been widely used to control noise, vibration, and harsh sounds in the cabin [9]. Passive noise control technology is the stage of engineering sample vehicle, and the main noise reduction method is often adopted to solve the road noise problem of real vehicle, which is mainly to take measures from the response point and structure transfer path of the body structure. The control methods include the following: the muffler is used in the key parts of the vehicle to weaken the noise source, the local stiffness mode is improved by increasing damping or strengthening the SMT material, and the vibration of the structure is weakened. Or by improving the sound

Mode 1 : 24. 5386 Hz, 2.77%
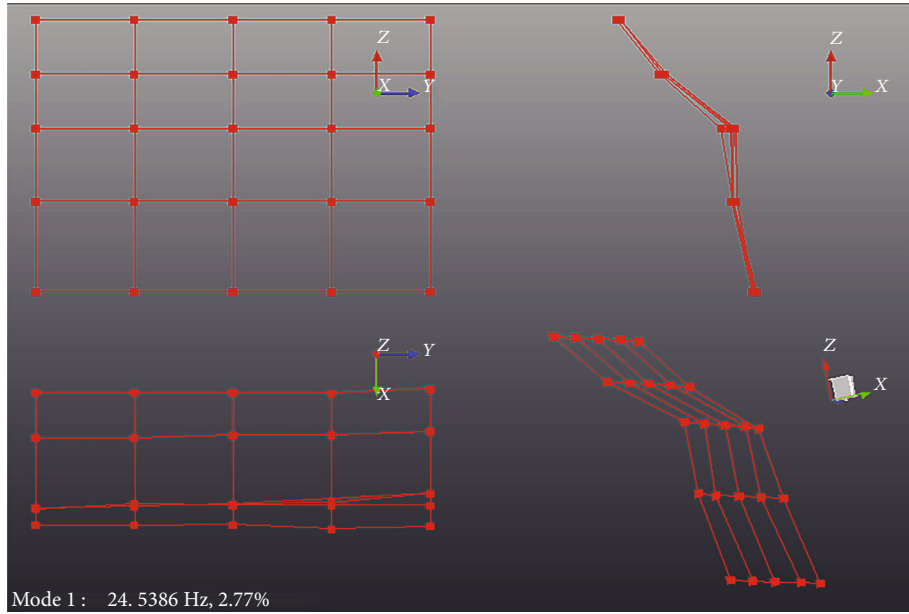
(a) Results of the experiment 24.5 Hz

0:Trucklid. op2 : Scalar: Strain energy, energy density : : Scale factor 6.000E+000 : Subcase 1 ::Mode 1
,Frequency 2.572220E+001 ,Eigenvalue 2.612018E+004 ::Subcase 1 Subcase 1

- >0.05
- 0.045
- 0.04
- 0.035
- 0.03
- 0.025
- 0.02
- 0.015
- 0.01
- 0.005
- <−1.60111e^-010

No value
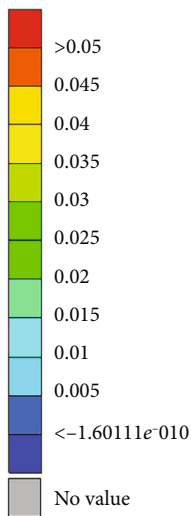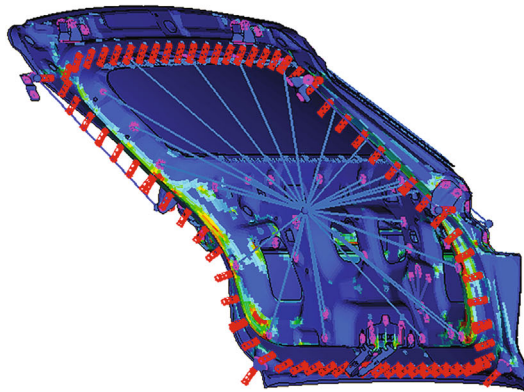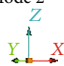
(b) Simulation results 25.7 Hz

FIGURE 3: The first-order bending mode of the backup door.

Mode 2: 40.3160 Hz,   3.76 %
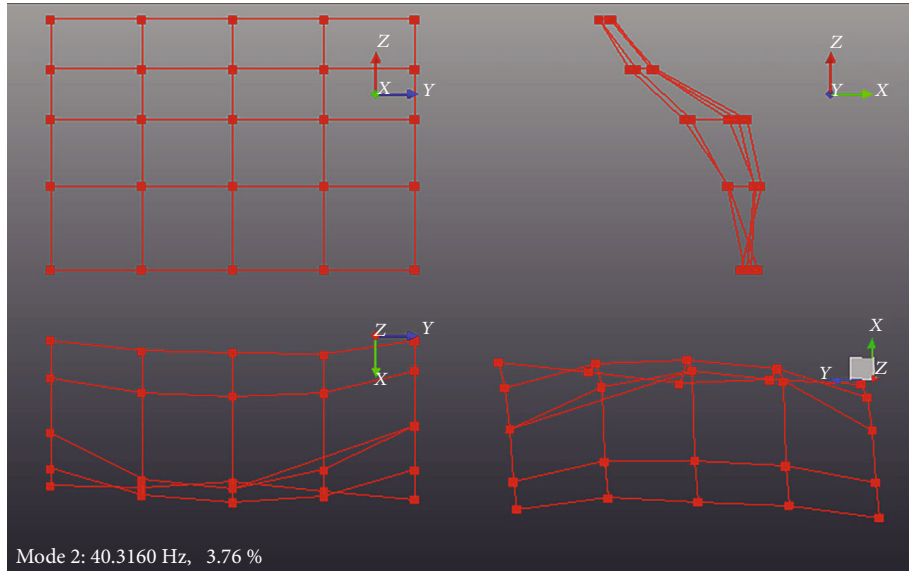
(a) Results of the experiment 40.3 Hz

0:Trucklid. op2   : Scalar: Strain energy, energy density   :   : scale factor   6.000E+000 : Subcase 1   ::Mode 2
,Frequency 4.306652E+001   ,Eigenvalue 7.322161E+004   ::Subcase 1 Subcase 1
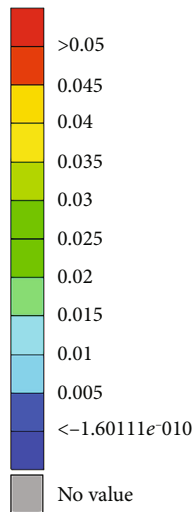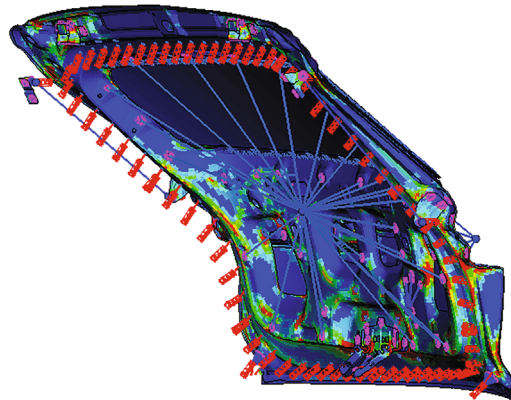
(b) Simulation results43.1 Hz

FIGURE 4: The first-order torsional mode of the backup door.

Mode 3: 59.4111 Hz, 1.40%
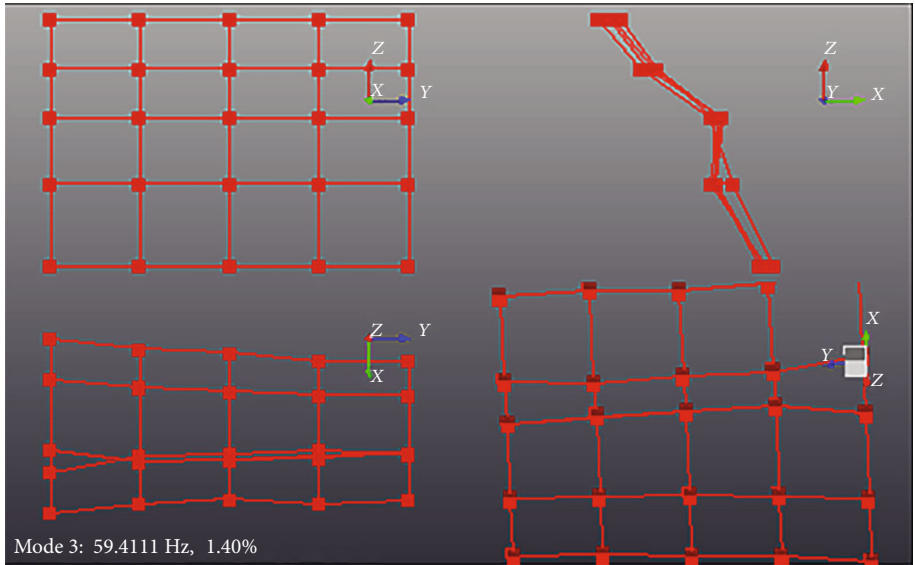
(a) Results of the experiment 59.4 Hz

0:Trucklid. op2 : Scalar: Strain energy, energy density : : Scale factor 6.000E+000 : Subcase 1 ::Mode 3
,Frequency 5.866864E+001 ,Eigenvalue 1.358851E+005 ::Subcase 1 Subcase 1

>0.05
0.045
0.04
0.035
0.03
0.025
0.02
0.015
0.01
0.005
<−1.60111e^-010

No value
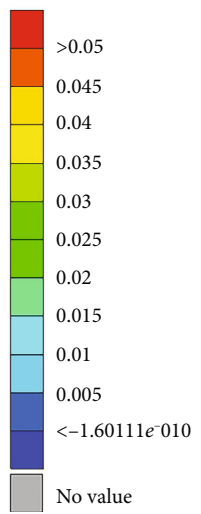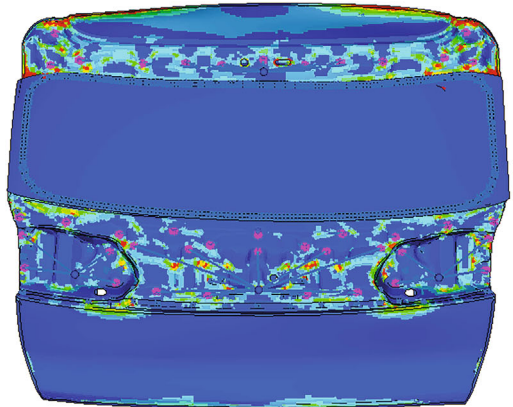
(b) Simulation results 58.7 Hz

FIGURE 5: Second-order bending modes of the backup gate.

Mode 4:   66.0196 Hz,   3.42%

(a) Results of the experiment 66.0 Hz

0:Trucklid. op2   : Scalar: Strain energy, energy density   :   : Scale factor   6.000E+000 : SUBCASE 1   ::Mode 4
    ,Frequency 6.295791E+001   ,Eigenvalue 1.564805E+005   ::Subcase 1 Subcase 1

	>0.05
	0.045
	0.04
	0.035
	0.03
	0.025
	0.02
	0.015
	0.01
	0.005
	<−1.60111e^-010
	No value
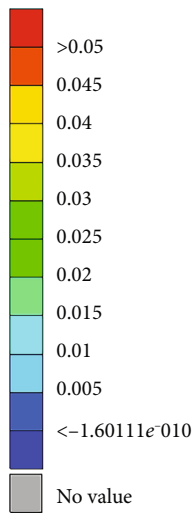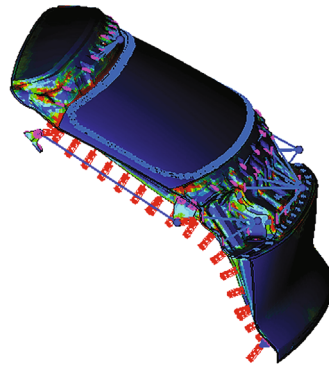
(b) Simulation results 63.0 Hz

FIGURE 6: Second-order torsional modes of the backup gate.

absorption and insulation performance of the acoustic package to reduce the car noise set the format: font color: red set the format: red set the format: highlight set the format: highlight radiation, through the above means to reduce the vibration of the body structure. Local stiffness, modal, and acoustic transfer indicators are improved by optimizing the body structure. Based on the above analysis, the test vehicle in this paper is still in the stage of engineering sample vehicle, so passive noise control technology is adopted.

The research on the performance of road noise will go on and on. This paper takes the road noise problem of a new energy vehicle as the research object and introduces in detail the finite element modeling, benchmarking, road noise simulation analysis process, road noise simulation analysis, and benchmarking in the engineering design stage. On this basis, the validity and accuracy of the analysis results are confirmed. Aiming at the road noise problem in real cars, the real cause of the problem is found by using the transfer path analysis. After the improvement scheme is proposed, the improvement effect is verified by the real car test.

2. Problem Analysis

2.1. Problem Description. When the pure electric SUV is driving at a constant speed of 40 km/h on the rough asphalt road, the passengers in the back can feel a very obvious feeling of ear pressure. Through experimental verification, it is found that the ear pressure problem of this SUV mainly occurs in the engine idle speed and low-speed condition. The low rotation speed is mainly shown in 1500 rpm-3000 rpm, but the subjective feeling in the car was not obvious in the low-speed condition. In contrast, the subjective feeling of the ear pressure in the car was more obvious in the idle condition, which was unacceptable.

2.2. Problem Analysis. In order to reduce the noise in the car more scientifically, the first step is to identify the noise source. Generally speaking, simulation methods and experimental methods can be used to determine the noise source of the vehicle. Simulation methods usually use numerical analysis methods to predict the noise characteristics of products in the design stage of automotive products. The experimental method is usually based on the real environment, and the adjustment plan can be verified in the mass production stage of the car. In actual automobile production, the two methods are indispensable and complement each other [1]. Through experiments and simulation analysis, it is found that the cause of the low-frequency aural sense problem of the SUV is the first-order torsional mode of the backup door is coupled with the acoustic mode of the vehicle, thus causing a series of NVH problems.

After testing, the first-order longitudinal acoustic mode of the SUV is about 43 Hz, and it is along the x-direction of the vehicle (that is, the axis direction from the front to the rear of the vehicle). As a result, sheet metal and panel mounted in the x-direction can easily push the acoustic cavity modes to move. When these sheet metal and panel modes are close to the acoustic cavity modes, the acoustic cavity modes will be excited by them, causing the acoustic cavity

TABLE 1: Comparison of the natural frequencies of the front four modes.

Formation	Finite metacalculation frequency/Hz	Modal test frequency/Hz
First-order bending	25.7	24.5
First-order twist	43.1	40.3
Second-order bending	58.7	59.4
Second-order twist	63.0	66.0

modes to move in accordance with their original modal formation, thus generating noise.

The first-order torsion mode of the SUV's backup door is about 42 Hz, which is close to the acoustic cavity mode. Therefore, the acoustic cavity mode is excited and low-frequency noise is generated, resulting in low-frequency ear pressing sensation. It leads to worse subjective feelings.

The structure of the vehicle is complicated. Some assumptions have been introduced into the numerical analysis of the dynamic characteristics of the vibration-acoustic system and have led to a significant simplification of the simulation model. However, the reliability of the simulation results is very consistent with the accuracy of the model. Experimental measurement and testing can provide better solutions [1].

The structure and installation method of the car backup door is relatively simple and is generally connected with the body through two hinges, and through the limit block and door lock, it is fixed on the car body, thereby limiting its displacement. In order to better investigate the causes of the 42 Hz peak in the car, NTF (noise transfer function) test was carried out on the backup door, after testing and analysis. The results are shown in Figures 1 and 2.

Figure 1 shows the NTF test data of the backup door. Figure 2 shows the spectrum diagram of the inner ear noise of the rear right rear passenger under 40 km/h condition. The peak value problem of 42 Hz mainly exists in ultralow frequency. Moreover, the peak value of 42 Hz makes a great contribution to the vehicle and occupies a dominant position in the ultralow frequency. Meanwhile, the vibration amplitude of 42 Hz is larger. Moreover, the peak value of vibration coincides with the peak value of interior noise. Therefore, simulation analysis and modal analysis are needed for the backup door to understand its structural characteristics and determine the cause of noise generation.

3. Simulation Analysis

3.1. Simulation Results of Backup Door. Simulation analysis methods are fast and efficient in the prediction and identification of noise sources. Common methods include statistical energy analysis method, boundary element method, and finite element method [10].

Modal analysis is a common method to study the dynamic characteristics of structures. It has been widely used in engineering field. By analyzing the modes, you can get a lot of information, such as system mass, dynamic stiffness, natural frequency, and the main formation parameters. At the
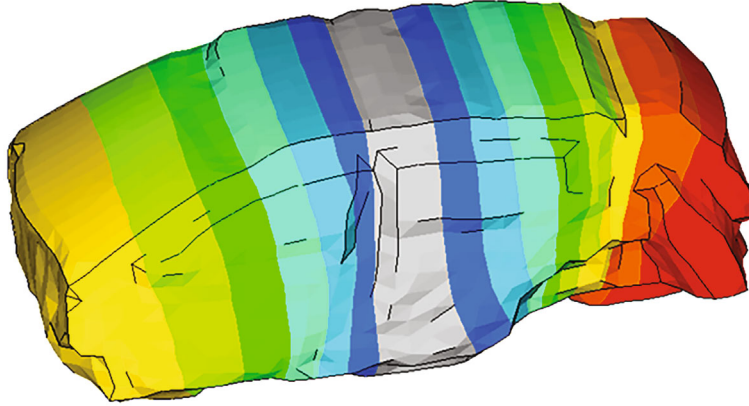
FIGURE 7: First-order longitudinal mode 43 Hz.
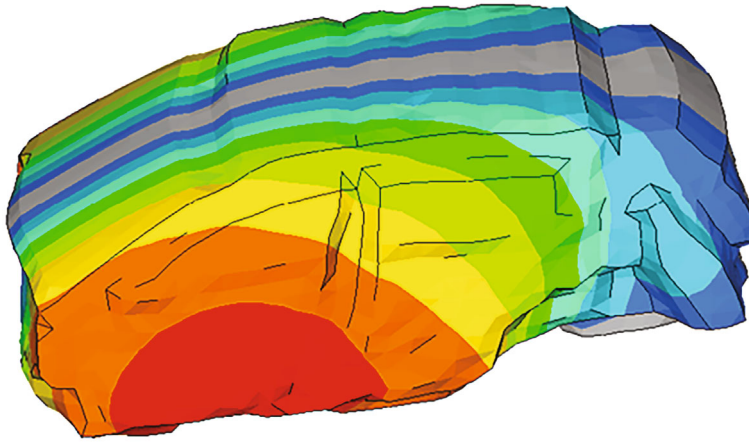
FIGURE 8: First-order transverse mode 90.5 Hz.

same time, modal analysis can more truly reflect the structural characteristics of the object. But the only drawback is that modal analysis is not clear about the division of measurement points. The finite element method includes all possible methods. These methods connect many simple equations on a small area called finite element and use it to estimate complex equations on a larger area. It regards the solution domain as composed of many small interconnected subdomains called finite elements, assumes an appropriate (simpler) approximate solution for each element, and then derives the solution to this domain to satisfy the conditions (such as structure the equilibrium condition), so as to get the solution of the problem [10]. The finite element simulation can reflect all the details of the object. Therefore, in this paper, comprehensive tests are combined with tests and simulations on the backup gate. Conduct modal analysis. In the actual test, in order to better reflect the movement formation of the backup door, 25 measuring points are arranged for the backup door. Test the mode state of the backup door by LMS Test.Lab/Impact testing module. Artificial excitation test is a quick and simple method to find out which resonance frequencies radiate more noise. Measure the sound pressure generated by the force input by hitting the system with a hammer at one position and measuring the sound pressure

generated at the receiver position [11]. The experiment was carried out under the constraint of the whole vehicle, and the power hammer was used to stimulate the backup door. In order to make the formation more accurate, the mode test is carried out by using single excitation point and moving sensor. Figures 3–6, respectively, show the experimental and simulation results of the first-order bending mode, first-order torque mode, second-order bending mode, and second-order torque mode of the backup door. The statistics are shown in the comparison of the natural frequencies of the fourth-order mode in the backup front door in Table 1. It can be seen that the error between the simulation and the test is less than 5%, which indicates that the results obtained by the simulation method are very close to the reality. The simulation method will be used to analyze the optimized scheme below.

3.2. Simulation Results of Acoustic Cavity Mode. During vehicle development, a finite element model (FEM) was used to analyze the fully trimmed car body. The accuracy of this coupled structure-acoustic system model depends on the accuracy of the dynamic characteristics expressed on the input, output, and structural acoustic coupling surfaces. In the digital development stage, the mode shape and frequency

0:Trucklid. op2   : Scalar: Strain energy, energy density   :   : Scale factor   6.000E+000   : Subcase 1   ::Mode 1
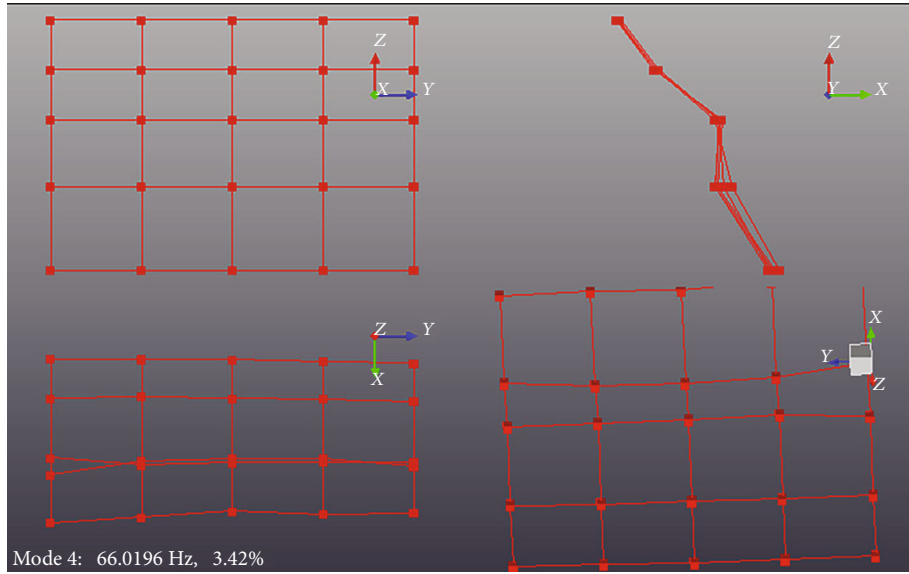,Frequency 2.572220E+001   ,Eigenvalue 2.612018E+004   ::Subcase 1 Subcase 1

>0.05
0.045
0.04
0.035
0.03
0.025
0.02
0.015
0.01
0.005
<−1.60111e⁻010

No value

(a) Before optimization 25.7 Hz

0:Trucklid. op2   : Scalar: Strain energy, energy density   :   : Scale factor   5.000E+000   : Subcase 1   ::Mode 1
,Frequency 2.508302E+001   ,Eigenvalue 2.483817E+004   ::Subcase 1 Subcase 1

>1
0.9
0.8
0.7
0.6
0.5
0.4
0.3
0.2
0.1
<−6.13321e⁻009

No value

(b) After optimization 25.0 Hz

FIGURE 9: Comparison before and after optimization of the first-order bending mode of the backup door.

0:Trucklid. op2   : Scalar: Strain energy, energy density   :   : Scale factor   6.000E+000 : Subcase 1   ::Mode 2
,Frequency 4.306652E+001   ,Elgenvalue 7.322161E+004   ::Subcase 1 Subcase 1

(a) Before optimization 43.1 Hz

0:Trucklid. op2   : Scalar: Strain energy, energy density   :   : Scale factor   5.000E+000 : Subcase 1   ::Mode 2
,Frequency 3.723165E+001   ,Eigenvalue 5.472481E+004   ::Subcase 1 Subcase 1
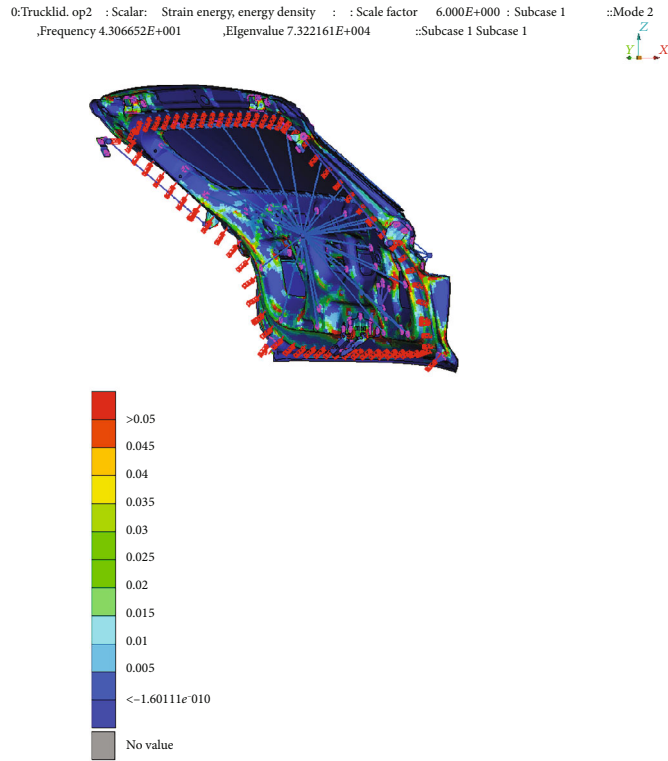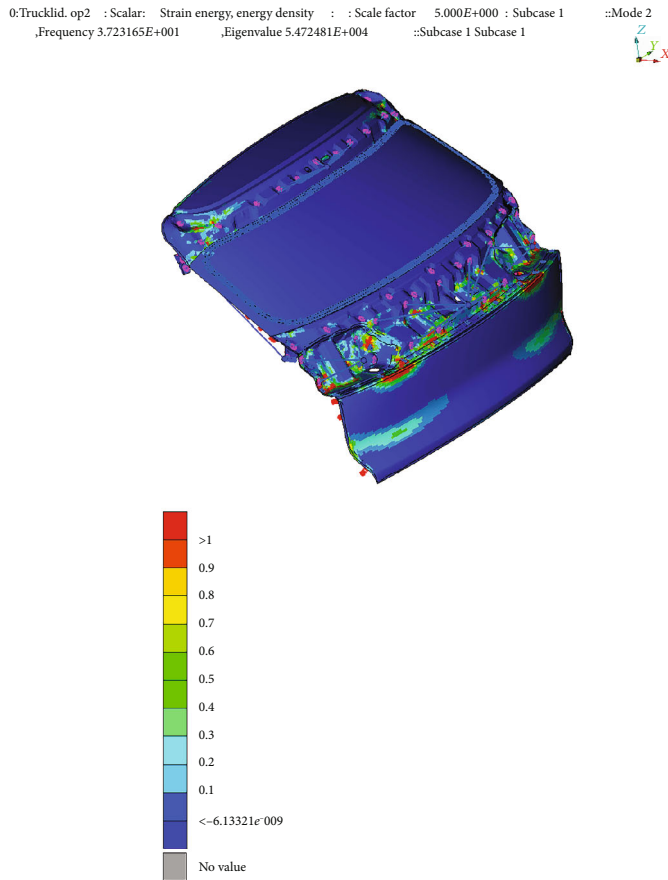
(b) After optimization 37.2 Hz

FIGURE 10: Comparison before and after optimization of the first-order torsional mode of the backup door.

0:Trucklid. op2 : Scalar: Strain energy, energy density : : Scale factor 6.000E+000 : Subcase 1 ::Mode 3
,Frequency 5.866864E+001 ,Eigenvalue 1.358851E+005 ::Subcase 1 Subcase 1

>0.05
0.045
0.04
0.035
0.03
0.025
0.02
0.015
0.01
0.005
<−1.60111e^-010

No value
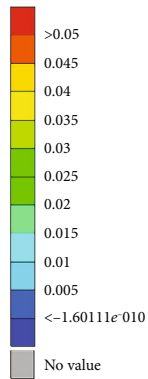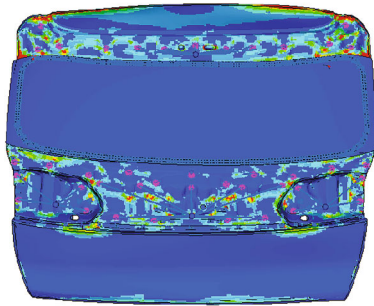
(a) Before optimization 58.7 Hz

0:Trucklid. op2 : Scalar: Strain energy, energy density : : Scale factor 5.000E+000 : Subcase 1 ::Mode 3
,Frequency 5.217122E+001 ,Eigenvalue 1.074538E+005 ::Subcase 1 Subcase 1

>1
0.9
0.8
0.7
0.6
0.5
0.4
0.3
0.2
0.1
<−6.13321e^-009

No value
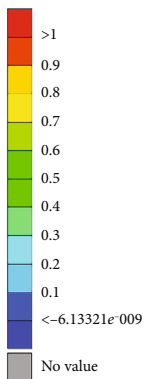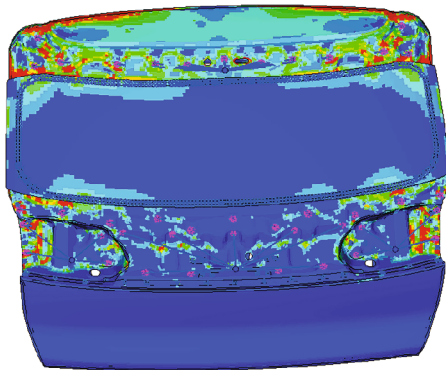
(b) After optimization 52.2 Hz

FIGURE 11: Comparison before and after optimization of second-order bending modes of the backup door.

0:Trucklid. op2   : Scalar: Strain energy, energy density   :   : Scale factor   6.000E+000   : Subcase 1   ::Mode 4
                ,Frequency 6.295791E+001   ,Eigenvalue 1.564805E+005   ::Subcase 1 Subcase 1
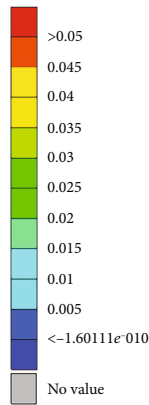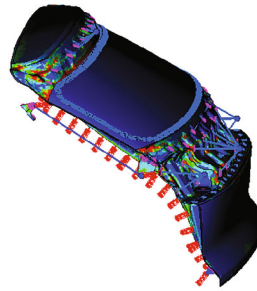
(a) Before optimization 63.0 Hz

0:Trucklid. op2   : Scalar: Strain energy, energy density   :   : Scale factor   5.000E+000   : Subcase 1   ::Mode 4
                ,Frequency 5.619062E+001   ,Eigenvalue 1.246486E+005   ::Subcase 1 Subcase 1
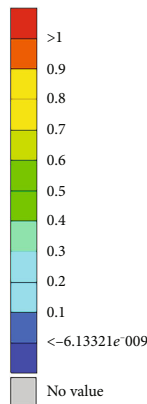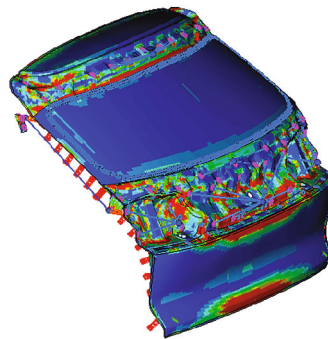
(b) After optimization 56.2 Hz

FIGURE 12: Before and after optimization of the torsional bending mode of the backup door.

TABLE 2: Frequency comparison before and after optimization of the backup door.

Formation	Frequency before optimization	Frequency after optimization	Difference
First-order bending	25.7 Hz	25.0 Hz	0.7 Hz
First-order twist	43.1 Hz	37.2 Hz	5.9 Hz
Second-order bending	58.7 Hz	52.2 Hz	6.5 Hz
Second-order twist	63.0 Hz	56.2 Hz	6.8 Hz

of the body structure and panels (i.e., panels) are designed to not cause noise and vibration problems. In order to optimize the modal shape of the plate and reduce vibration, it is very important to understand the acoustic mode shape on the coupling surface. Acoustic modal analysis is a method used to verify noise and vibration characteristics through experiments [12].

Acoustic cavity modal analysis can better grasp the frequency and formation of the vehicle's acoustic cavity modal. Therefore, in the later design process, all kinds of system excitation and acoustic cavity modes are matched to avoid a series of resonance problems caused by the vibration of body structure. Figures 7 and 8 show the first-order longitudinal and transverse acoustic cavity modes of the SUV, which are 43 Hz and 90.5 Hz, respectively.

Through the analysis of the mode data of the backup door, the simulation and cavity mode data of the backup door, the peak value of the 42 Hz channel noise response is close to the natural frequency of the first-order torsional mode of the backup door in the system. The first-order cavity mode is close to the backup door mode, but it has some test error. According to the principle of modal superposition, the structural modes of the two frequency points contribute greatly to the amplitude of the response of the whole system. The results show that the cause of ear-pressing sensation in the back row is the resonance between the mode of the backup door and the mode of the acoustic cavity.

4. Optimization Scheme

Generally speaking, the air noise frequency of vehicles is mainly high frequency, and the noise reduction method is mainly to use sound insulation materials and sound absorption materials. The frequency of structure noise is mainly low frequency, and the noise reduction method is mainly achieved by suppressing structural vibration [13–15].

At the same time, the acoustic cavity mode has been finalized in the design of the vehicle, and it is difficult to change it in the later stage. Therefore, the general solution to the problem caused by the modal resonance between the acoustic cavity mode and the body plate structure is to change the modal resonance of the body plate structure to prevent its modal coupling and thus generate resonance.

Commonly used methods to solve resonance in engineering can be roughly divided into three categories:

(1) *Increase Quality*. Adding mass reduces the overall mode.

(2) *Increase Stiffness*. By supporting the backup door, the stiffness of the whole or part can be increased; thus, the mode can be slightly increased.

(3) *Increase the Power Vibration Absorber*. The dynamic vibration absorber can absorb the energy generated by the original system and reduce the single peak value of the system, thus reducing the vibration generated by a single frequency.

4.1. Scheme Verification. Dynamic vibration absorber (DVA) is one of the vibration control methods to solve the vibration problem. DVA was first submitted by Frahm, also known as tuned vibration absorber (TVA). It consists of a single degree of freedom (SDOF) oscillation system, which can be placed on any structure or machine. This kind of DVA can most effectively offset the vibration of the main structure by adjusting the natural frequency of the main structure to make it consistent with the natural frequency of the structure. Passively tune the DVA and manually adjust the natural frequency of the DVA to match the modal frequency of the main structure. In order to obtain the required natural frequency, the stiffness is usually changed instead of the mass [16–20].

In order to solve the problem of in-car ear pressure caused by modal coupling, the natural frequency of the backup door needs to be changed, thus achieving frequency avoidance. Because this peak value is more prominent, and the amplitude is relatively large. Therefore, the damping dynamic vibration absorber with the backup door is verified. Figures 9–12 are the simulation calculation results of adding the damping dynamic vibration absorber to the backup door. The modal frequencies before and after optimization are shown in Table 2. In the optimized idle speed condition, it can be seen that the mode of the backup door is reduced by about 7 Hz, and the frequency is avoided by the mode of the excitation source sound. Meanwhile, the original modal formation is also greatly changed, which solves the problem of ear pressure in the car caused by the modal coupling.

4.2. Test Verification. In order to further verify the vibration absorption effect of the dynamic vibration absorber, the vehicle with and without the installed dynamic vibration absorber is verified by road test. It is verified that the operating condition is a rough road with a uniform speed of 40 km/h. At the same time, use LMS Test.Lab/Test. Lab-Signature module for data collection.

Figures 13 and 14, respectively, show the in-car noise spectrum of the uninstalled and installed power vibration
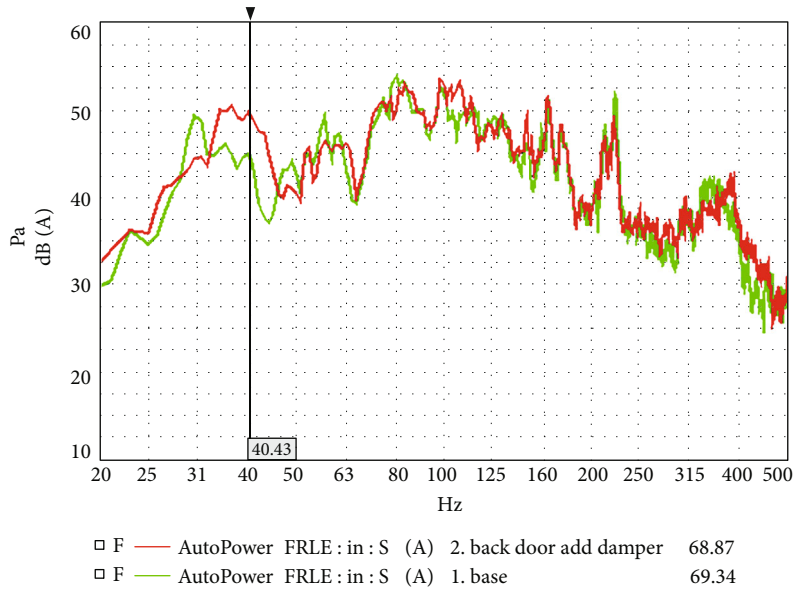
FIGURE 13: Comparison of front-row noise before and after modification.
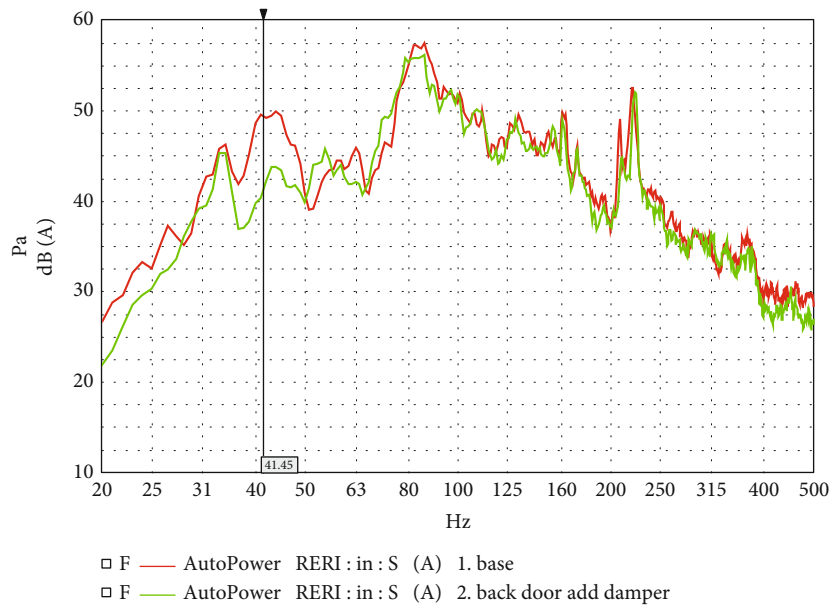
FIGURE 14: Comparison of back-row noise before and after changes.

absorber. From the comparison of the red and green decibel lines in the figure, it can be seen that the dynamic shock absorber has a significant effect. The peak value of 42 Hz in the driver's inner ear was reduced by about 5 dB, and the peak value of 42 Hz in the rear passenger's inner ear was reduced by 8 dB. At the same time, after installing the power vibration absorber, the in-car ear pressure sensation is improved significantly, which is acceptable and has practical application value.

5. Conclusion

A series of NVH problems caused by modal coupling are very common in engineering. The general solution in engineering is to change its natural frequency by changing its original mass, damping, and local or global dynamic stiffness. For the backup door such as large sheet metal parts, the natural frequency is lower and the mode is lower. Therefore, it is easier to cause modal coupling and thus emit low-frequency noise.

This paper is aimed at the engineering problem that when a pure electric SUV is driving at a constant speed of 40 km/h on a rough asphalt road, the rear passengers in the car can clearly feel the ear pressure. In this paper, the finite element method is first used to model the backup door, and the experimental calibration is carried out at the same time to establish the accuracy of the simulation method to obtain the modal natural frequency data. Reserve on this basis, the

selection of door type of dynamic vibration absorber which is used to increase damping scheme, the method of using the simulation contrast optimization before and after optimization scheme, see backup door modal reduced about 7 Hz, and incentive source acoustic mode state from the set format: font colors: red frequency, and at the same time, the original modal formation have significant changes, which were solved due to the modal coupling pressure inside the ear problems, finally carries on the real vehicle tests to verify the improvement effect, but also to verify the effectiveness of the method in vehicle engineering design phase.

Through this method, significant results have been achieved, and the same working conditions: rough road, 40 km/h, at a constant speed, vehicle drivers' ear 42 Hz peak decreases about 5 dB, rear passengers' inner ear noise reduces 8 dB, and 42 Hz peak has practical application value. At the same time, this solution also has a certain reference for the low-speed road noise problem of electric vehicles.

Data Availability

No data were used to support this study.

Conflicts of Interest

The author declares that he has no conflicts of interest.

Acknowledgments

References

[1] H. B. Huang, X. R. Huang, M. L. Yang, T. C. Lim, and W. P. Ding, "Identification of vehicle interior noise sources based on wavelet transform and partial coherence analysis," *Mechanical Systems and Signal Processing*, vol. 109, pp. 247–267, 2018.

[2] D. A. Bies, C. H. Hansen, and C. Q. Howard, *Engineering Noise Control: Theory and Practice*, CRC Press, London, 2009.

[3] S. Zhang, Y. S. Wang, H. Guo, C. Yang, X. L. Wang, and N. N. Liu, "A normalized frequency-domain block filtered-x LMS algorithm for active vehicle interior noise control," *Mechanical Systems and Signal Processing*, vol. 120, pp. 150–165, 2019.

[4] M. H. Fouladi, M. J. M. Nor, and A. K. Ariffin, "Spectral analysis methods for vehicle interior vibro-acoustics identification," *Mechanical Systems & Signal Processing*, vol. 23, no. 2, pp. 489–500, 2009.

[5] M. S. Qatu, "Recent research on vehicle noise and vibration," *International Journal of Vehicle Noise and Vibration*, vol. 8, no. 4, pp. 289–301, 2012.

[6] W. Jung, S. J. Elliott, and J. Cheer, "Local active control of road noise inside a vehicle," *Mechanical Systems and Signal Processing*, vol. 121, pp. 144–157, 2018.

[7] N. Lalor and H. H. Priebsch, "The prediction of low- and mid-frequency internal road vehicle noise: a literature survey," *Proceedings of the Institution of Mechanical Engineers Part D Journal of Automobile Engineering*, vol. 221, no. 3, pp. 245–269, 2007.

[8] M. A. Panza, "A review of experimental techniques for NVH analysis on a commercial vehicle," *Energy Procedia*, vol. 82, pp. 1017–1023, 2015.

[9] J. Cheer and S. J. Elliott, "Multichannel control systems for the attenuation of interior road noise in vehicles," *Mechanical Systems & Signal Processing*, vol. 60-61, pp. 753–769, 2015.

[10] X. Sheng, C. J. C. Jones, and D. J. Thompson, "Prediction of ground vibration from trains using the wavenumber finite and boundary element methods," *Journal of Sound & Vibration*, vol. 293, no. 3-5, pp. 575–586, 2006.

[11] G. Cerrato and P. Goodes, "Practical approaches to solving noise and vibration problems," *Sound & vibration*, vol. 45, no. 4, pp. 18–23, 2011.

[12] H. Tsuji, T. Enomoto, S. Maruyama, and T. Yoshimura, "A study of experimental acoustic modal analysis of automotive interior acoustic field coupled with the body structure," in Sae World Congress & Exhibition, Detroit, USA, 2012.

[13] P. P. Narang, "Material parameter selection in polyester fibre insulation for sound transmission and absorption," *Applied Acoustics*, vol. 45, no. 4, pp. 335–358, 1995.

[14] W. Ding and H. Chen, "Research on the interior noise contributed from a local panel's vibration of an elastic thin-walled cavity," *Applied Acoustics*, vol. 63, no. 1, pp. 95–102, 2002.

[15] A. R. Mohanty, B. D. S. Pierre, and P. Suruli-Narayanasami, "Structure-borne noise reduction in a truck cab interior using numerical techniques," *Applied Acoustics*, vol. 59, no. 1, pp. 1–17, 2000.

[16] T. Pais and D. Boote, "Developments of Tuned Mass Damper for yacht structures," *Ocean Engineering*, vol. 141, pp. 249–264, 2017.

[17] W. Gafsi, R. Chaari, N. Masmoudi, M. T. Khabou, F. Chaari, and M. Haddar, "Modeling of a passive absorber in milling tool machine," *Applied Acoustics*, vol. 128, pp. 94–110, 2017.

[18] H. B. Huang, R. X. Li, M. L. Yang, T. C. Lim, and W. P. Ding, "Evaluation of vehicle interior sound quality using a continuous restricted Boltzmann machine-based DBN," *Mechanical Systems and Signal Processing*, vol. 88, Part A, pp. 245–267, 2017.

[19] R. I. Wright and M. R. F. Kidner, "Vibration absorbers: a review of applications in interior noise control of propeller aircraft," *Journal of Vibration and Control*, vol. 10, no. 8, pp. 1221–1237, 2004.

[20] M. J. Brennan, "Some recent developments in adaptive tuned vibration absorbers/neutralisers," *Shock & Vibration*, vol. 13, pp. 531–543, 2006.

WILEY | Hindawi

Research Article

Choice of Environmental and Economic Path for Building a Supply Chain Financial Cloud Ecosystem under the Background of "Internet +"

Dongchang Zhao 🆔

School of Economics, Lanzhou University, Lanzhou, 710000 Gansu, China

Correspondence should be addressed to Dongchang Zhao; 1169233446@nefu.edu.cn

With the development of the Internet age, the gradual deepening of reforms, and the continuous improvement of marketization, the financial ecological environment is directly related to the risk of financial institutions' loans and the enthusiasm to support local economic development. Capital is accompanied by the physical development and evolution of the production and circulation of goods. After thousands of years of historical development and evolution, it has formulated its own development law and internal logic. In view of the unclear environmental and social evaluation indicators in supply chain research and the model's failure to accurately describe the real supply chain network, an adaptive dynamic relaxation approximation algorithm model is proposed. This model introduces upstream and downstream transit stations as distributors and as a hub between customers, the transportation mode is improved to horizontal and vertical coordinated transportation, and multiple transportation methods are used for transportation. In this paper, the experimental group adopts a new model based on the approximate algorithm of dynamic relaxation factors, and the control group adopts the original old model. The two groups conduct comprehensive data analysis on social indicators, self-indicators, initial indicators, economic indicators, and environmental indicators in each year. Starting from the dimension, comprehensively consider the selection of indicators to measure the level of enterprise performance. The experiment proves that the transportation loss in the green supply chain is between the new model and the old model. When the number of partners is small, the degree of the optimal solution between the new and old models is not obvious, and the degree of optimization of the new model relative to the old model is increasing. It has a significant statistical difference ($P < 0.05$). This shows that efforts to build a good financial ecological environment and an honest and reliable and healthy economic ecological environment are of great importance for promoting the continuous and rapid growth of the social economy.

1. Introduction

Driven by the new era, the traditional supply chain is slowly transforming into a green supply chain [1]. Traditional enterprise supply chain coordination and management have many shortcomings, such as incomplete communication methods and low utilization efficiency; procurement interaction and tracking methods are performed offline without real-time performance; enterprises and suppliers are not connected. While understanding the development of our country's software and information technology service industry, there is a research on the impact of supply chain integration on the performance of enterprises in the industry. According

to the concept and characteristics of supply chain integration, the relevant factors that influence the methods of evaluation and evaluation of business performance determine the supply chain integration and the indicators of measuring the performance of companies and define relevant models. This document uses existing data from listed companies in the software services and information technology industry to separate supply chain integration into customer integration and supplier integration, exploring the relationship between customer integration, vendor integration, and corporate performance.

There have been research results in many aspects of green supply chains abroad. In terms of green supply chain model

collaboration models, although the design models are very different, the overall direction remains the same. The supply chain collaboration model of green supply chain is an efficient collaboration. The mode is to meet customer order needs through good materials and commodities. Azzi et al. proposed a new type of supply chain network collaboration planning model and found that the total profit level of supply chain nodes is positively correlated, and the two-way collaborative green supply chain is optional [2]. Lin CS and Lin CY use a multistage Stackelberg game method to study the green procurement relationship between manufacturers and suppliers in the supply chain and effectively reduce suppliers' carbon emissions [3]. Lin CS and Lin CY studied the asymmetric duopoly model of two competing supply chains under different carbon emission technologies and encouraged the use of clean energy technologies to reduce carbon emissions [3, 4]. Papert and Pflaum study the production and emission reduction decision-making problems of an order-based supply chain composed of manufacturers and retailers under the constraints of the capital market and trade market [5].

In recent years, there have been more and more researches on the green supply chain in China. The logistics technology in the green supply chain is also the focus of the supply chain research. The ultimate goal of the green logistics technology is the sustainable development of the ecological environment [6]. Development is not only for economic benefits, but also environmental benefits and social benefits, and it is the unity of these benefits. Papert and Pflaum's research focuses on carbon dioxide emissions in the supply chain, from freight energy use to inventory storage, and establishes a supply chain model based on discrete event simulation [5]. Stolze et al. studied the dual-objective, multistage, multi-commodity mixed integer nonlinear programming model considering the impact of different vehicle and raw material quality on the total cost and carbon dioxide emissions of the green supply chain and finally explained and solved the method through constraint numerical examples [7]. Christensen et al. use a hybrid life cycle assessment method to generate the carbon emissions of a monocrystalline silicon photovoltaic system and use a multiregion input-output model to ensure the integrity of the system boundary [8]. Souza et al. studied the decision-making of low-carbon supply chain and coordinated low-carbon manufacturers to produce a product and approved investment in green technology to reduce carbon emissions in production applications [9, 10].

This article mainly focuses on the optimization design of the multilayer structure of the green supply chain of small and medium manufacturing enterprises at the economic, social, and environmental levels. When studying the impact of supply chain integration on corporate performance, we comprehensively consider the selection of indicators to measure corporate performance from multiple dimensions, breaking through the limitation that most scholars in the past only use financial indicators to represent the impact of supply chain integration on corporate performance. Explore the impact of supply chain integration on corporate performance and drawing conclusions, judge the relationship between supply chain management and corporate perfor-

mance in our country's software and information technology services sector, and strengthen corporate governance and improve corporate performance [11].

2. Choice of Environmental Economic Path for Constructing a Supply Chain Financial Cloud Ecosystem

2.1. Financial Ecological Environment Index and Factor Analysis Method. Since each principal factor rotates the original variables by the data transformation matrix to make them independent of each other, then the comprehensive evaluation value of the principal factors is calculated, thereby eliminating the correlation images between the indicators [12, 13]. In factor analysis, the weight of each major factor is not determined and is determined by the percentage of the major factor that determines uterine change. This overcomes the shortcomings of certain evaluation methods that define the entire book and makes the evaluation results more objective and logical [14, 15]. Steps of factor analysis evaluation method are as follows:

(1) Build the original data matrix

Set n samples, and each sample has p indicators, so the original data matrix is obtained:

$$X = \begin{bmatrix} X_{11} & X_{12} & \cdots & X_{1p} \\ X_{21} & X_{22} & \cdots & X_{2p} \\ \cdots & \cdots & \cdots & \cdots \\ X_{n1} & X_{n2} & \cdots & X_{np} \end{bmatrix}. \tag{1}$$

(2) Standardize the transformation of the original data

In order to avoid the influence of differences and the order of the measured values and variables, it is necessary to standardize the data first to make the indicators comparable [16]. The specific standardized formula is as follows:

$$Y_{ij} = \frac{\left(X_{ij} - EX_j\right)}{\sqrt{DX_j}}. \tag{2}$$

Among them,

$$EX_j = \frac{1}{n} \sum_{i=1}^{n} X_{ij}, \tag{3}$$

$$DX_j = \frac{1}{n-1} \sum_{i=1}^{n} \left(X_{ij} - EX_j\right)^2. \tag{4}$$

In the above formula, $i = 1, 2, 3, \cdots, n$, $j = 1, 2, 3, \cdots, 18$, and X_{ij} are the index values before standardization, and Y_{ij} is the index value after standardization. With certain performance improvements, there are new requirements for general adaptability and specific adaptability. The main problem with basketball gymnastics in Japan is that there are too many regular gymnastics, special gymnastics are not covered, and the obtained physical condition cannot be used for special gymnastics.

(3) Calculate the correlation coefficient matrix R

Let r_{ij} be the correlation coefficient between index i and index j after standardization; then,

$$r_{ij} = \frac{COV(Y_i, Y_j)}{\sqrt{DY_i DY_j}} = EY_i Y_j, \tag{5}$$

$$R = \begin{bmatrix} r_{11} & r_{12} & \cdots & r_{1p} \\ r_{21} & r_{22} & \cdots & r_{2p} \\ \cdots & \cdots & \cdots & \cdots \\ r_{n1} & r_{n2} & \cdots & r_{np} \end{bmatrix}. \tag{6}$$

(4) Find the characteristic root, characteristic vector, and contribution rate of the correlation matrix R

Human motion tracking based on template matching currently primarily uses error metrics between two matching pixel blocks. There are three main error metrics based on block matching, an error metric based on a cross-correlation function and a normalized mean square. According to characteristic equation $|R - \lambda I| = 0$, $|R - \lambda I| = 0$ characteristic roots $\lambda_j (j = 1, 2, \cdots, p)$ are obtained, and Formula (7) can be obtained.

$$(R - \lambda_j I)\mu_j = 0. \tag{7}$$

Find the feature vector $\mu_j (j = 1, 2, \cdots, p)$ corresponding to the feature root λ_j.

(5) Determine the cumulative variance contribution rate of the main factor

The contribution rate of the i factor is $d_i = \lambda_i / \sum_{i=1} \lambda_i$, that is, the variation degree of each factor accounts for the percentage of the overall matrix variation degree.

(6) Calculate factor score and total score

$$F(a) = \lambda_1 f_{a1} + \lambda_2 f_{a2} + \cdots + \lambda_m f_{am}. \tag{8}$$

Among them,

$$f_i = A^T R^{-1} X_a. \tag{9}$$

2.2. Dynamic Relaxation Approximation Algorithm

2.2.1. Traditional Particle Swarm Algorithm. The maximum communication delay that the user can tolerate under the cloud and fog architecture is guaranteed, and the user's request is processed within the acceptable communication delay [17]. The initial settings of the particle swarm algorithm will affect the search performance of the particle swarm algorithm. The more individual particles, the larger the search range of the particle swarm, the easier it is to get the best approximate solution close to the optimal solution, and the search speed of the particles is too fast. It is easy to fall into the local optimal solution [18, 19]. Therefore, it is of theoretical and practical importance for the application of the particle swarm algorithm to generate the initial particle swarm in an appropriate manner. The single-particle tree structure coding design emphasizes the connection between upstream and downstream in the supply chain network. The initial position encoding method of individual particles is as Formula (10), and the initial velocity encoding method is as Formula (11).

$$X_{in}^t = (X_{i1}^t, X_{i2}^t, \cdots, X_{iD}^t), i \in I, n \in D, t \in T, \tag{10}$$

$$V_{in}^t = (V_{i1}^t, V_{i2}^t, \cdots, V_{iD}^t), i \in I, n \in D, t \in T. \tag{11}$$

In constructing the initial particle swarm, let D be the spatial dimension of individual particles in the particle swarm, the value of D will affect the search ability of the particle swarm, let T be the maximum number of iterations of the algorithm, and T is the number of search particles in each individual particle [20, 21].

For all search speeds that exceed the speed range area, change all cross-border speeds to the maximum or minimum search speeds. The particle value range and speed range are shown in Formulas (12) and (13).

$$\begin{cases} X_{in}^t (X_{in}^t \geq X_{\max\_n}) = X_{\max\_n}, n \in D, \\ X_{in}^t (X_{in}^t \leq X_{\min\_n}) = X_{\min\_n}, n \in D, \end{cases} \tag{12}$$

$$\begin{cases} V_{in}^t (V_{in}^t \geq V_{\max\_n}) = V_{\max\_n}, n \in D, \\ V_{in}^t (V_{in}^t \leq V_{\min\_n}) = V_{\min\_n}, n \in D. \end{cases} \tag{13}$$

The initial speed of the particle swarm has a great influence on the convergence speed of the algorithm. If the speed is set too fast, the optimal solution of the algorithm will easily exceed the optimal solution, and if the initial speed is set too slow, it will easily fall into the local optimum.

2.2.2. Lagrangian Relaxation Algorithm. The complex constraints that make the final problem difficult are added to the objective function as penalty conditions, so that the objective function is easy to solve, and the constrained optimization problem can be transformed into an unconstrained optimization problem [22]. In the process of solving the throat relaxation of the objective function, the objective function can always remain linear. The model description of the original problem is shown in Formula (14):

$$Z_{IP} = \min C^T X, s.t. AX \geq b, CX \geq d, X \in Z_n^+. \tag{14}$$

Lagrangian relaxation transformation is performed on the original problem to obtain a Lagrangian linear model, as shown in Formula (15):

$$Z_{LP} = \min C^T X + \mu^T \times (b - AX), s.t. CX \geq d, X \in Z_n^+. \tag{15}$$

In the above formula, μ is the Lagrangian relaxation factor, and the initial value cannot be defaulted to 0. The calculation is shown in Formula (16):

$$\mu^{i+1} = \max \left\{ \mu^{i+1} + \text{step}^i \times \text{sub}^i, 0 \right\}. \tag{16}$$

The solution of the subgradient of Lagrangian relaxation is shown in Formula (17):

$$\text{sub}^i = \partial Z_{UP}(X^i). \tag{17}$$

In the formula, Z_{UP} is the boundary value of Z_{LP}, which is generally the maximum or minimum value of the current iteration. Select the step size. The step size affects the convergence of the relaxation algorithm iteration. If the step size is too short, the algorithm will not be able to get the optimal solution. If the step size is too long, the calculation will exceed the extreme value and the settlement result will diverge. Therefore, the relaxation algorithm of the step length needs to take a gradually reduced value. The calculation of the step length step is shown in Formula (18):

$$\text{step}^i = \frac{Z_{UP}(X^i) - Z_{LP}(X^i)}{\left\| \text{sub}^i \right\|_2^2}. \tag{18}$$

2.2.3. Dynamic Relaxation Approximation Algorithm. According to the initial distribution of individual particles X, it is necessary to determine whether each supplier and manufacturer has joined the production operation in the current distribution plan [23]. The constraints of suppliers and manufacturers determine the corresponding supply of individual particles whether the company and the manufacturer are operating [24, 25], and the corresponding location decision formula for the company is shown in Formulas (19) and (20):

$$OS_i = \begin{cases} 0, \text{if} \cdot \sum_{j=1}^{J} \sum_{m=1}^{M} Adcp_{ijm} = 0, \\ \\ 1, \text{if} \cdot \sum_{j=1}^{J} \sum_{m=1}^{M} Adcp_{ijm} > 0, \end{cases} \tag{19}$$

$$OP_i = \begin{cases} 0, \text{if} \cdot \sum_{k=1}^{K} \sum_{n=1}^{N} Adcp_{jkn} = 0, \\ \\ 1, \text{if} \cdot \sum_{k=1}^{K} \sum_{n=1}^{N} Adcp_{jkn} > 0. \end{cases} \tag{20}$$

Every time the particle swarm is updated, the location decisions of suppliers and manufacturers need to be updated as the particle swarm changes.

2.3. Financial Ecology and Financial Ecological Environment

2.3.1. Ecological and Ecological Characteristics. The economic environment is the most basic environment. It is the basis for the survival of the financial system and determines the degree of development of the financial system. The financial system was created after economic growth reached a certain level and developed simultaneously with economic growth [26]. Traditional financial theory understands financing as a tool and understands financing as the external and dependent elements of the economy and essentially separates the inevitable internal links between the financial system and the economic
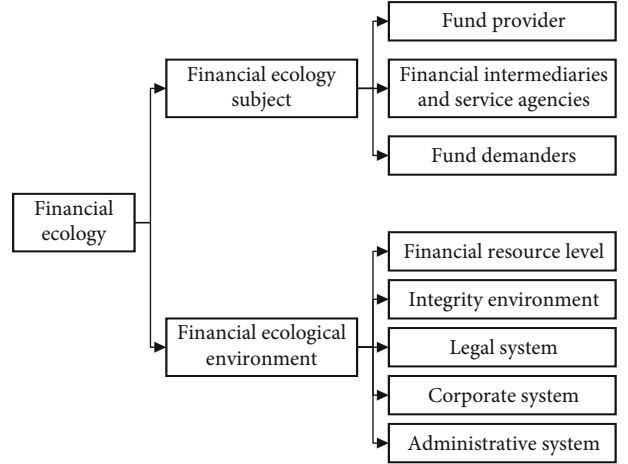
Figure 1: Relationship between financial ecology and financial ecology environment.

environment [27, 28]. Modern financial theory believes that finance is inherent in the economy, and the economy is increasingly globalized and spread to the overall economy. Finance has become the economy itself and the core of the modern economy. The relationship between the financial system and the economic environment is that the economic environment determines the financial growth and the limits of financial growth or promotes economic growth. Laws and regulations are relatively stable, authoritative, and coercive. At this point, policies cannot be compared with them. However, the flexibility and timeliness of policies are stronger than those of laws and regulations. The characteristics of the policy determine that when judging the policy environment, it is necessary to adopt different standards from judging the legal environment [23, 29, 30].

2.3.2. The Connotation of Financial Ecological Environment. The law must be able to effectively protect the interests of investors and creditors, to contribute to the establishment and maintenance of good economic order, and thus to ensure the smooth and efficient operation of the financial system. A well-developed credit system can not only effectively reduce the cost of information collection, but also reduce the negative choice and moral hazard caused by information asymmetry and reduce the occurrence of financial gaps and financial crises. At present, in order to improve the regional financial ecological environment, many regions are actively preparing to build financial security zones [31, 32]. However, improving the financial ecological environment cannot simply be equated with building a financial safety zone, and these two concepts cannot be confused with each other. Therefore, the construction of a financial security zone cannot be equated with improving the financial ecological environment.

2.3.3. Financial Ecology and Financial Ecological Environment. The financial ecosystem includes financial institutions and financial markets that provide direct financial products and financial services, as well as individuals, enterprises, and government agencies that consume various financial products and financial services, as well as those who formulate policies

TABLE 1: Data sheet of evaluation index system for index reliability testing.

	Very clear	Clear	General	Not clear	Chaotic	Alpha
Social indicators	0.307	0.388	0.174	0.083	0.048	0.9064
Self index	0.191	0.241	0.253	0.189	0.146	0.8433
Initial index	0.224	0.284	0.229	0.177	0.086	0.8169
Economic indicators	0.192	0.176	0.312	0.184	0.136	0.7672
Environmental indicators	0.217	0.208	0.244	0.194	0.137	0.7394
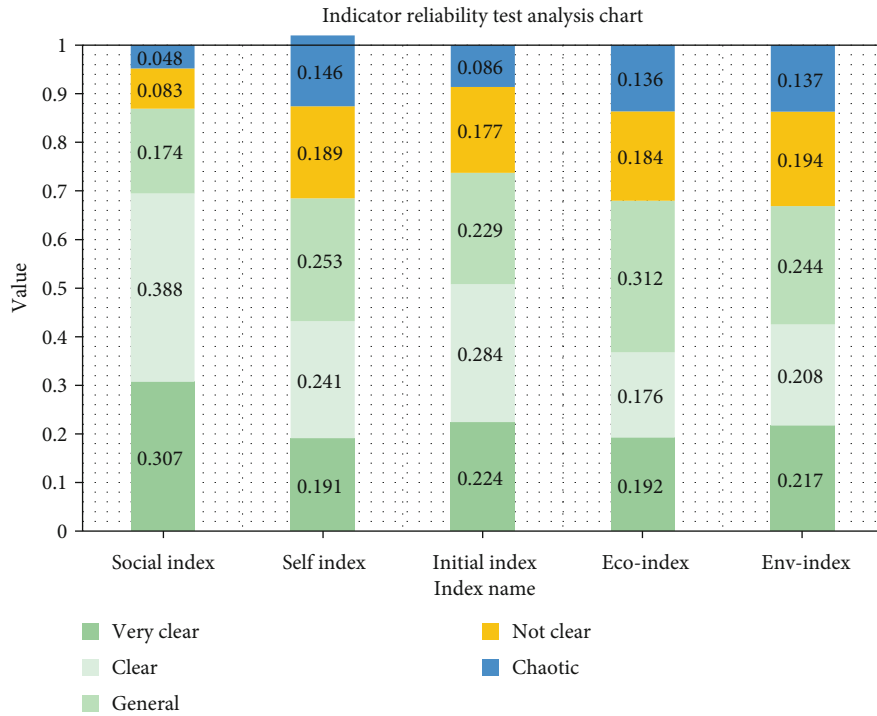
FIGURE 2: Indicator reliability test analysis chart.

and regulate financial services. The implementation of supervision is a function that directly affects the operation of financial institutions and financial markets. It is also a financial decision-making agency and financial regulatory agency that directly affect the type, price, and quality of financial products and services [33]. Figure 1 can clearly show the relationship between the financial ecology and the financial ecological environment.

A comprehensive survey of the survival and development status of the elements of financial entities is important, and without any of these elements, it is difficult to achieve realistic financial transactions. Therefore, it is difficult to fully understand the connotation of financial ecology only from the perspective of financial organization, ignoring the living conditions of other financial entities. Like the natural ecosystem, financial ecology is deeply influenced by people. However, the economic transactions and social interactions brought about by people, as well as the spillover effects produced in this process, make the financial ecological environment more complicated than the natural ecological environment [34, 35]. Human activities not only involve producers, consumers, and decomposers, but also strongly affect economic systems, social systems, laws and regulations, and culture. The relationship

TABLE 2: Social indicator preprocessing data table.

Year	Old model	New model	Optimal solution	P
2016	1.92	1.28	1.14	0.032
2017	2.57	2.23	2.03	0.027
2018	4.72	4.26	3.97	0.019
2019	6.33	5.86	5.59	0.010
2020	14.95	13.18	12.76	0.012

between them is frequent, diverse, and complex. Therefore, it is very difficult and unnecessary to absolutely distinguish between financial ecology and financial ecology.

3. Experimental Design of Environmental Economic Path Selection for Constructing Supply Chain Financial Cloud Ecosystem

3.1. Data Sources. In terms of data selection, to ensure the authenticity and authority of the data, this article mostly uses official data or authoritative research results. The data mainly come from 2016-2020 China Statistical Yearbook, China
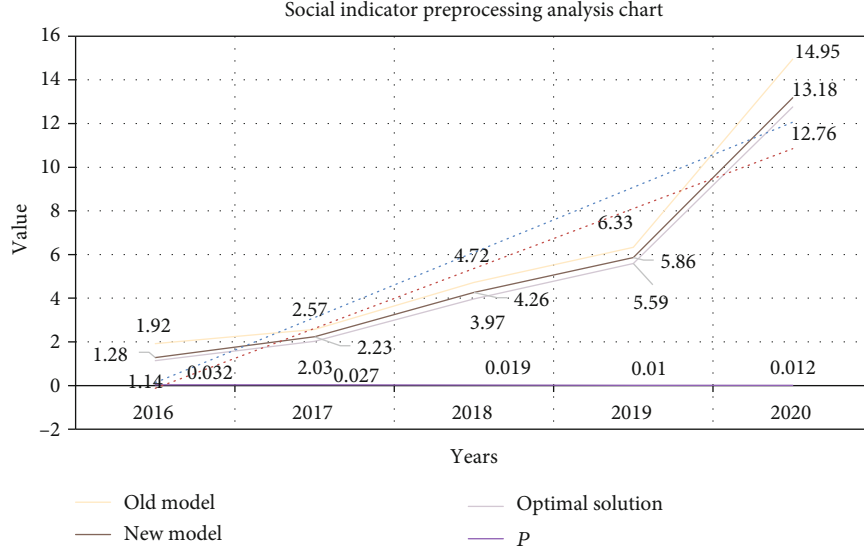
FIGURE 3: Social indicator preprocessing analysis chart.

Regional Economic Statistical Yearbook, financial operation report, and other relevant statistical data. Combining multiparty statistical data from financial institutions and their regulatory agencies, the evaluation index data is collected through multiple channels, and considering that price factors have a greater impact on the fitting results, all selected indicators are processed at constant prices. The experimental group adopts a new model based on the approximate algorithm of dynamic relaxation factors, and the control group adopts the original old model. The two groups conduct comprehensive data analysis on social indicators, self indicators, initial indicators, economic indicators, and environmental indicators for each year. Set out to comprehensively consider the selection of indicators to measure the level of corporate performance, explore the impact of supply chain integration on corporate performance, and summarize conclusions.

3.2. Experimental Method.
The green supply chain model of manufacturing companies is more complex in terms of the spatial complexity of the model. The cooperation between the partners is not only the initial horizontal cooperation, but also the vertical cooperation relationship. For different numbers of partners, transit stations, customers, and different customer order numbers, the approximate dynamic relaxation factor algorithm is used to calculate the weight values of various indicators in the construction company's supply chain, and then, cplex is used to solve the problem.

3.3. Data Preprocessing.
A benchmark value is anchored for each index collected, and the standardized score obtained by each year's index on this index depends on the proportional relationship between the original value of the city index and the anchored benchmark value.

Regarding positive indicators (the higher the value, the better the indicator), the standardized score = the original value of the indicator/anchored reference value.

TABLE 3: Environmental index preprocessing data sheet.

Year	Water pollution	Air pollution	Noise pollution	Total pollution	P
2016	2.56	3.08	3.66	3.41	0.017
2017	2.72	2.90	3.69	3.37	0.014
2018	2.69	2.92	3.35	3.48	0.011
2019	2.42	3.25	3.15	3.50	0.008
2020	2.43	2.92	3.16	3.55	0.005

Regarding the inverse index (the smaller the value, the better the index), the standardized score = anchored benchmark value/the original value of the index.

3.4. Statistical Data Processing Method.
The SPSS23.0 software was used for data processing, and the count data was expressed in percentage (%), k is the number of data in this experiment, σ^2 is the variance of all survey results, and $P < 0.05$ indicates that the difference is statistically significant. The formula for calculating reliability is shown in Formula (21).

$$a = \frac{k}{k-1}\left(1 - \frac{\sum \sigma_i^2}{\sigma^2}\right).$$ (21)

4. Experimental Choice of Environmental Economic Paths for Constructing Supply Chain Financial Cloud Ecosystem

4.1. Evaluation Index System Based on Index Reliability Testing.
Reliability refers to the stability and reliability of the questionnaire. This article adopts the α coefficient method created by L.J. Cronbach. The α coefficient can be obtained by Reliability Analysis in SPSS software. It is generally believed that the α coefficient above 0.8 indicates that the effect of the index setting is very good, and above 0.7 is also
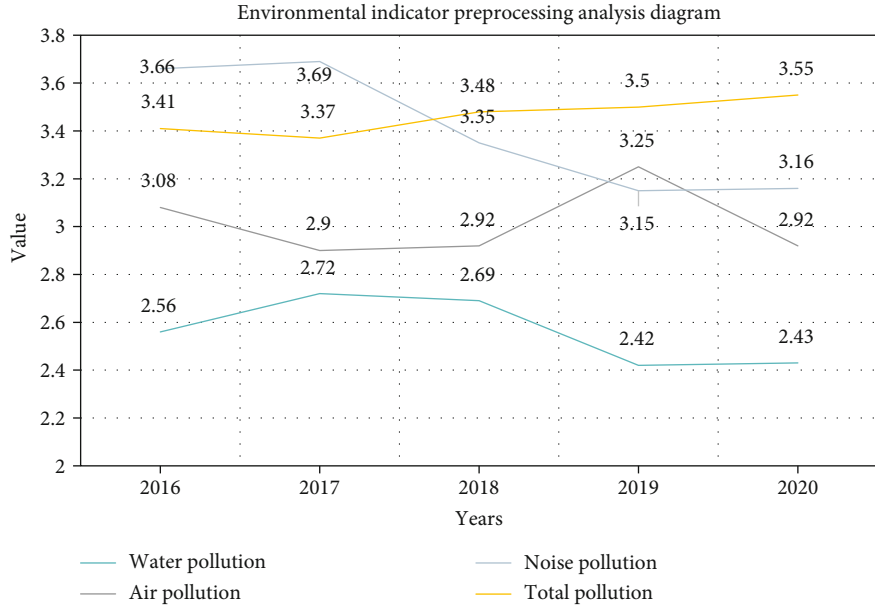
FIGURE 4: Environmental indicator preprocessing analysis diagram.

acceptable. Here, we analyze the reliability of each type of object, and the reliability index we choose for each type of object is slightly different. The results are shown in Table 1.

It can be seen from Figure 2 that the data obtained from social indicators, own indicators, initial indicators, economic indicators, and environmental indicators have an acceptable impact on this experiment ($\alpha > 0.7$), which can be analyzed from the side in the comparative analysis of the subitem evaluation indicators of the financial ecological environment of the supply chain of various cities in our country, and the regional economic development and financial foundation are not balanced.

4.2. Based on a Single Indicator

4.2.1. Analysis Based on Social Indicators. Starting from multiple dimensions, comprehensively consider the selection of indicators to measure the level of corporate performance, explore the impact of supply chain integration on corporate performance, and summarize conclusions. Here, we have collected social indicator data through various channels from 2016 to 2020. After preprocessing these data, we analyze the preprocessed data. The results are shown in Table 2.

Figure 3 uses a line chart to describe the social indicators in the economic aspects of the green supply chain of manufacturing companies and compares the social indicators between the new model and the old model with the optimal solution. At first, the optimization effect of the new model is not obvious. As the degree of marketization continues to increase, the approximate algorithm of dynamic relaxation factors is used to deal with partners, and the model optimization effect with transit stations becomes more and more obvious, and it is close to the value obtained from the optimal solution ($P < 0.05$).

4.2.2. Analysis Based on Environmental Indicators. For the environmental aspects of the green supply chain, including

water pollution, carbon emissions, and noise pollution, multiply the corresponding weight values to calculate the governance cost indicators of the old model and the new model. Here, we have collected environmental indicator data through multiple channels from 2016 to 2020. After preprocessing these data, we analyze the preprocessed data. The results are shown in Table 3.

Figure 4 linearly describes the data of transportation losses in the green supply chain between the new model and the old model. When the number of partners is small, the degree of new and old model in relation to the optimal solution is not obvious. When the number of partners is large, the new model's model optimization effect is slightly reduced. As the number of partners gradually increased, the degree of optimization of the new model compared to the old model became more and more evident ($P < 0.05$).

4.2.3. Analysis Based on Initial Indicators. Starting from multiple dimensions, comprehensively consider the selection of indicators to measure the level of corporate performance, explore the impact of supply chain integration on corporate performance, and summarize conclusions. Here, we have collected the initial indicator data through various channels from 2016 to 2020. After preprocessing these data, we analyze the preprocessed data. The results are shown in Table 4.

TABLE 4: Initial index preprocessing data table.

Year	Rail transport	Road transport	Number of partners	Customer order	P
2016	2.65	3.05	3.27	3.41	0.005
2017	2.56	3.30	3.17	3.76	0.005
2018	2.91	3.21	3.64	3.64	0.005
2019	2.92	3.01	3.51	3.35	0.005
2020	2.97	3.03	3.05	3.56	0.005
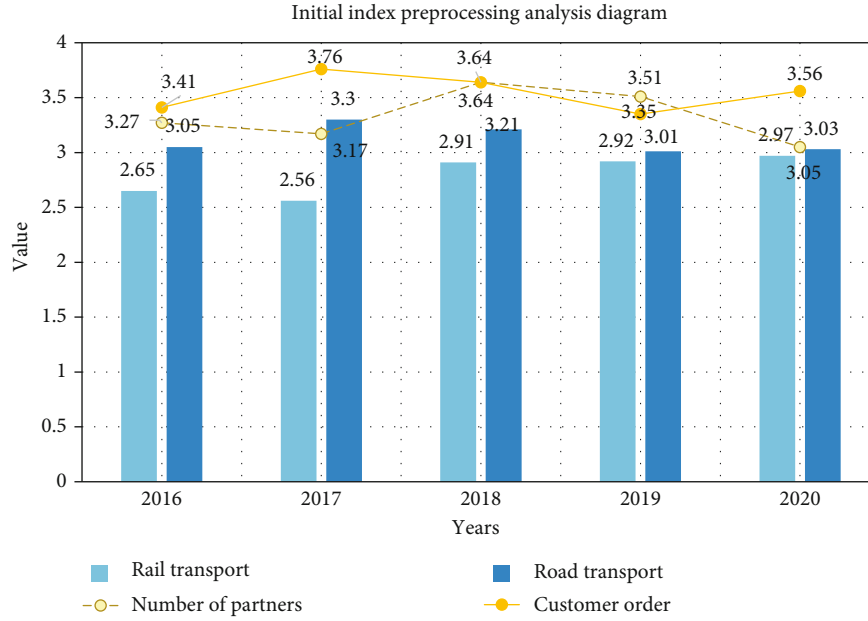
FIGURE 5: Initial index preprocessing analysis diagram.

TABLE 5: Economic index preprocessing data table.

Year	Transportation cost	Other expenses	Transportation time	Transport distance	Breakdown cost	P
2016	2.01	2.88	3.29	3.57	3.31	0.024
2017	2.46	2.69	2.99	3.16	3.56	0.029
2018	2.11	2.64	2.95	3.50	3.67	0.032
2019	2.26	2.65	2.94	3.52	3.34	0.017
2020	2.33	2.38	3.19	3.51	3.31	0.021

Figure 5 depicts the comparison of the accident rate in the green supply chain between the new model and the old model, because the introduction of rail transport in the new model has generally reduced the accident rate of road transport. With the gradual increase in the number of partners and customer orders, the optimization degree of the new model relative to the old model has become more and more obvious ($P < 0.05$).

4.2.4. Analysis Based on Economic Indicators. Starting from multiple dimensions, comprehensively consider the selection of indicators to measure the level of corporate performance, explore the impact of supply chain integration on corporate performance, and summarize conclusions. Here, we have collected economic indicator data through various channels from 2016 to 2020. After preprocessing these data, we analyze the preprocessed data. The results are shown in Table 5.

It can be seen from Figure 6 that in terms of economic indicators, the comparison between the new model using the approximate algorithm of the dynamic relaxation factor and the old model shows that the processing effect of the new model is better, even better than the optimal solution ($P < 0.05$), which shows that the integration of suppliers as a whole has a significant moderating effect on improving

the performance of enterprises. The obvious reasons for the results may be caused by the characteristics of the industry and the high degree of dependence on suppliers by enterprises in the industry.

4.2.5. Analysis Based on Own Indicators. Starting from multiple dimensions, comprehensively consider the selection of indicators to measure the level of corporate performance, explore the impact of supply chain integration on corporate performance, and summarize conclusions. Here, we have collected our own indicator data through multiple channels from 2016 to 2020. After preprocessing these data, we analyze the preprocessed data. The results are shown in Table 6.

It can be seen from Figure 7 that for its own indicators, the comparison between the new model using the dynamic relaxation factor approximation algorithm and the old model shows that the processing effect of the new model is better ($P < 0.05$), which shows that the method is not only useful, and the next algorithm reduces the complexity of the space, reduces the operating time, and improves the efficiency of the supply chain to solve the partners. And as the number of partners increases, the faster the improvement algorithm runs, the more obvious the benefits.
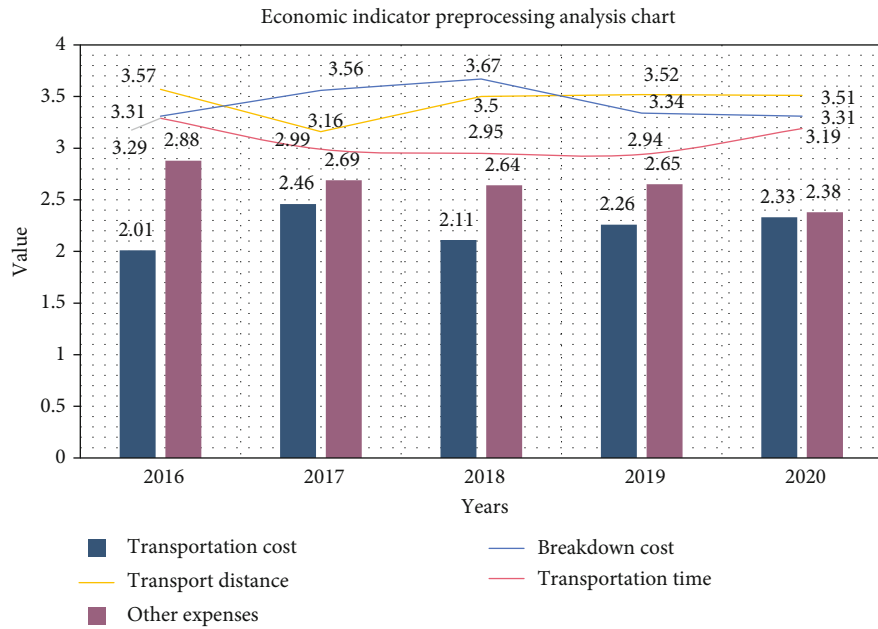
Figure 6: Economic indicator preprocessing analysis chart.

Table 6: Self index preprocessing data table.

Year	Operating cost	Operating loss	Raw material cost	Operational pollution cost	Carbon allowance	P
2016	2.12	2.31	3.15	3.17	3.49	0.001
2017	2.54	2.55	3.10	3.20	3.78	0.002
2018	2.29	2.31	3.01	3.22	3.76	0.002
2019	2.43	2.59	3.20	3.58	3.77	0.001
2020	2.06	2.73	3.20	3.65	3.94	0.001
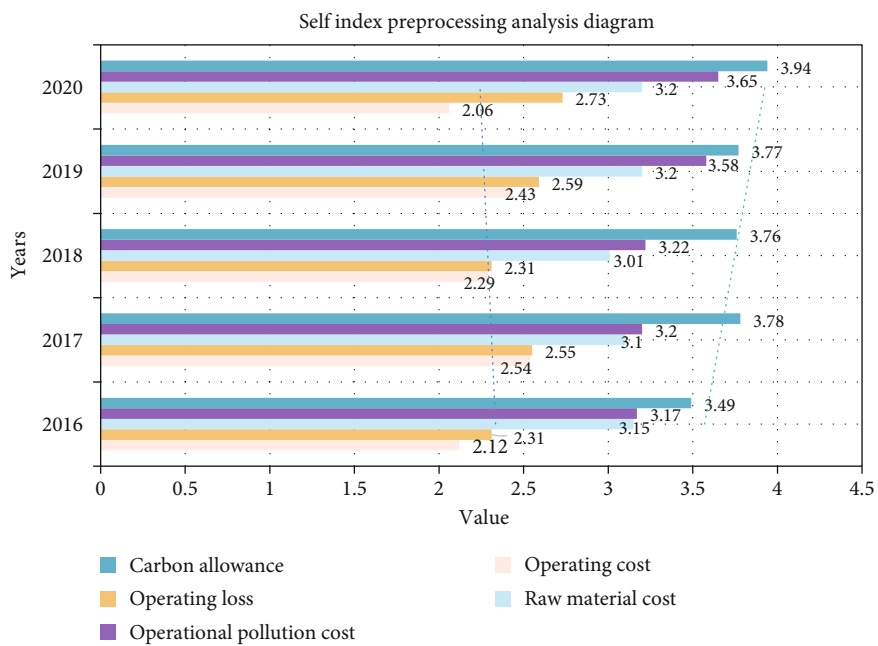
Figure 7: Self index preprocessing analysis diagram.

5. Conclusions

On the basis of studying the optimization methods of various green supply chain mathematical models at home and abroad, this paper designs a new green supply chain model for small and medium manufacturing enterprises based on the compound weight method. The newly introduced coordinated transportation method improves transportation efficiency, reduces transportation time, and reduces transportation accident rate. In the four-level network architecture of the traditional supply chain, upstream and downstream transfer stations are newly introduced to integrate the volume of vehicles that are not fully loaded. The upstream transfer station to the downstream transfer station is railway transportation, which reduces transportation costs and increases the supply chain. The complexity of the model effectively innovates the structure of the model. The improved supply chain model with transit can effectively deal with the problem of green supply chain network optimization. In the study of small and medium-sized green supply chain examples, the improved index solution quality of the transit supply chain model is significantly better than that of the nontransit supply chain model. And as the scale of the calculation example increases, the optimization effect of each index becomes more obvious.

The government should be the leader in the construction of financial ecological environment. When formulating economic plans, it should start with improving the regional economic environment, based on resource advantages, adapt measures to local conditions, and formulate economic development plans around market reforms, so as to create a harmonious economic environment for financial development. One is to establish a financial ecological environment evaluation and assessment mechanism. The main indicators are the default rate of loan customers, the rate of nonperforming financial assets, the completion rate of financial disputes, and the level of credit intermediary services to establish evaluation standards. The improvement of the financial ecological environment will be included in the assessment scope of government performance. The second is to combat untrustworthy behaviors in the eyes of enterprises and legal representatives who maliciously evade bank debts and strengthen the role of news media. The government must further strengthen financial opening up based on the principles of building nests and attracting phoenixes, mutual benefit, and common development, so as to encourage foreign capital to expand business and form a trend of interaction between financial and economic development.

This work uses an approximate algorithm based on dynamic relaxation factors to solve this model. The particle structure adopts tree coding. In order to avoid the phenomenon that the particle algorithm accumulates prematurely or falls to the local optimum, a dynamic relaxation approach algorithm based on the current physical condition is proposed. The fitness function is combined with the dynamic relaxation factor to perform corrective functions to optimize particle search. Optimize speed, enhance the local search ability of each particle, and improve the convergence of the particle. After assessing the impact of a sustainable supply chain on economic, environmental, and social factors, the experiment looked at the best cooperation options for a sustainable supply chain, effectively reducing environmental pollution and avoiding overcapacity in the supply chain.

Data Availability

The data that support the findings of this study are available from the corresponding author upon reasonable request.

Conflicts of Interest

The authors declare that they have no conflicts of interest.

References

[1] C. Bals, "Toward a supply chain finance (SCF) ecosystem – proposing a framework and agenda for future research," *Journal of Purchasing and Supply Management*, vol. 25, no. 2, pp. 105–117, 2019.

[2] R. Azzi, R. K. Chamoun, and M. Sokhn, "The power of a blockchain-based supply chain," *Computers & Industrial Engineering*, vol. 135, pp. 582–592, 2019.

[3] C. S. Lin and C. Y. Lin, "Constructing a network evaluation framework for improving the financial ecosystem in small-medium size firms," *Technological and Economic Development of Economy*, vol. 24, no. 3, pp. 893–913, 2018.

[4] V. Puri, S. Jha, R. Kumar et al., "A hybrid artificial intelligence and internet of things model for generation of renewable resource of energy," *IEEE Access*, vol. 7, no. 1, pp. 111181–111191, 2019.

[5] M. Papert and A. Pflaum, "Development of an ecosystem model for the realization of Internet of Things (IoT) services in supply chain management," *Electronic Markets*, vol. 27, no. 2, pp. 175–189, 2017.

[6] Y. Chen, W. Zheng, W. Li, and Y. Huang, "The robustness and sustainability of port logistics systems for emergency supplies from overseas," *Journal of Advanced Transportation*, vol. 2020, Article ID 8868533, 10 pages, 2020.

[7] H. J. Stolze, D. A. Mollenkopf, and D. J. Flint, "What is the right supply chain for your shopper? Exploring the shopper service ecosystem," *Journal of Business Logistics*, vol. 37, no. 2, pp. 185–197, 2016.

[8] V. Christensen, J. Steenbeek, and P. Failler, "A combined ecosystem and value chain modeling approach for evaluating societal cost and benefit of fishing," *Ecological Modelling*, vol. 222, no. 3, pp. 857–864, 2011.

[9] V. De Souza, J. Bloemhof-Ruwaard, and M. Borsato, "Exploring ecosystem network analysis to balance resilience and performance in sustainable supply chain design," *International Journal of Advanced Operations Management*, vol. 11, no. 1/2, pp. 26–45, 2019.

[10] D. Weimer, B. Scholz-Reiter, and M. Shpitalni, "Design of deep convolutional neural network architectures for automated feature extraction in industrial inspection," *Cirp Annals Manufacturing Technology*, vol. 65, no. 1, pp. 417–420, 2016.

[11] W. Wu, S. An, C. H. Wu, S. B. Tsai, and K. Yang, "An empirical study on green environmental system certification affects financing cost of high energy consumption enterprises-taking metallurgical enterprises as an example," *Journal of Cleaner Production*, vol. 244, p. 118848, 2020.

[12] B. C. Boehmke and B. T. Hazen, "The future of supply chain information systems: the open source ecosystem," *Global Journal of Flexible Systems Management*, vol. 18, no. 2, pp. 163–168, 2017.

[13] W. Scacchi and T. A. Alspaugh, "Securing software ecosystem architectures: challenges and opportunities," *IEEE Software*, vol. 36, no. 3, pp. 33–38, 2019.

[14] P. Hu, F. Wu, J. Peng, Y. Bao, F. Chen, and D. Kong, "Automatic abdominal multi-organ segmentation using deep convolutional neural network and time-implicit level sets," *International Journal of Computer Assisted Radiology and Surgery*, vol. 12, no. 3, pp. 399–411, 2017.

[15] S. B. Larsen, D. Masi, D. C. Feibert, and P. Jacobsen, "How the reverse supply chain impacts the firm's financial performance: a manufacturer's perspective," *International Journal of Physical Distribution and Logistics Management*, vol. 48, no. 3, pp. 284–307, 2018.

[16] E. Kopanaki, P. Karvela, and N. Georgopoulos, "From traditional interorganisational systems to cloud-based solutions: the impact on supply chain flexibility," *Journal of Organizational Computing and Electronic Commerce*, vol. 28, no. 4, pp. 334–353, 2018.

[17] M. A. El Aziz, A. M. Hemdan, A. A. Ewees et al., "Prediction of biochar yield using adaptive neuro-fuzzy inference system with particle swarm optimization," in *2017 IEEE PES PowerAfrica*, pp. 115–120, Accra, Ghana, June 2017.

[18] I. D. Blackman, C. P. Holland, and T. Westcott, "Motorola's global financial supply chain strategy," *IEEE Engineering Management Review*, vol. 45, no. 1, pp. 137–137, 2017.

[19] M. Abdel-Basset, G. Manogaran, and M. Mohamed, "Internet of Things (IoT) and its impact on supply chain: a framework for building smart, secure and efficient systems," *Future Generation Computer Systems*, vol. 86, pp. 614–628, 2018.

[20] G. K. Mweshi and K. Sakyi, "Building sustainable supply chain investment decisions through financial analysis -case study of Lusaka SMEs," *American Scientific Research Journal for Engineering, Technology, and Sciences*, vol. 59, no. 1, pp. 81–92, 2019.

[21] K. Kok, S. Pedde, M. Gramberger, P. A. Harrison, and I. P. Holman, "New European socio-economic scenarios for climate change research: operationalising concepts to extend the shared socio-economic pathways," *Regional Environmental Change*, vol. 19, no. 3, pp. 643–654, 2019.

[22] N. Harring, S. C. Jagers, and S. Matti, "The significance of political culture, economic context and instrument type for climate policy support: a cross-national study," *Climate Policy*, vol. 19, no. 5, pp. 636–650, 2019.

[23] S.-B. Tsai, R. Saito, Y.-C. Lin, Q. Chen, and J. Zhou, "Discussing measurement criteria and competitive strategies of green suppliers from a green law perspective," *Proceedings of the Institution of Mechanical Engineers, Part B: Journal of Engineering Manufacture*, vol. 229, Supplement 1, pp. 135–145, 2015.

[24] G. I. Bischi, U. Merlone, and E. Pruscini, "Evolutionary dynamics in club goods binary games," *Journal of Economic Dynamics and Control*, vol. 91, pp. 104–119, 2018.

[25] A. C. C. Lu, D. Gursoy, and G. del Chiappa, "The influence of materialism on ecotourism attitudes and behaviors," *Journal of Travel Research*, vol. 55, no. 2, pp. 176–189, 2016.

[26] J.-Y. Yeh and C.-H. Chen, "A machine learning approach to predict the success of crowdfunding fintech project," *Journal of Enterprise Information Management*, 2020.

[27] C. Liston-Heyes and D. A. Vazquez Brust, "Environmental protection in environmentally reactive firms: lessons from corporate Argentina," *Journal of Business Ethics*, vol. 135, no. 2, pp. 361–379, 2016.

[28] A. McMullan and A. Majumdar, "Assessing the impact of travel path choice on London's rail network using an automatic fare collection system," *Transportation Research Record*, vol. 2274, no. 1, pp. 154–163, 2018.

[29] N. Tajbakhsh, J. Y. Shin, S. R. Gurudu et al., "Convolutional neural networks for medical image analysis: full training or fine tuning?," *IEEE Transactions on Medical Imaging*, vol. 35, no. 5, pp. 1299–1312, 2016.

[30] M. Leroy, "Delivering on environmental commitments? Guidelines and evaluation framework for an "On-board" approach," *Sécheresse*, vol. 23, no. 3, pp. 185–195, 2016.

[31] A. Veipa, V. Kirsanovs, and A. Barisa, "Techno-economic analysis of biofuel production plants producing biofuels using Fisher Tropsch synthesis," *Environmental and Climate Technologies*, vol. 24, no. 2, pp. 373–387, 2020.

[32] Y. Bai and X. Yang, "The research on the economic effect of market-based environmental policy instruments," *Open Journal of Social Sciences*, vol. 4, no. 4, pp. 38–47, 2016.

[33] I. Bouwma, D. Liefferink, R. Van Apeldoorn, and B. Arts, "Following old paths or shaping new ones in Natura 2000 Implementation? Mapping path dependency in instrument choice," *Journal of Environmental Policy & Planning*, vol. 18, no. 2, pp. 214–233, 2016.

[34] P. R. Croes and W. J. V. Vermeulen, "In search of income reference points for SLCA using a country level sustainability benchmark (part 2): fair minimum wage. A contribution to the Oiconomy project," *International Journal of Life Cycle Assessment*, vol. 21, no. 3, pp. 363–377, 2016.

[35] M. K. M. Singh, "Socio-economic, environmental and personal factors in the choice of country and higher education institution for studying abroad among international students in Malaysia," *International Journal of Educational Management*, vol. 30, no. 4, pp. 505–519, 2016.

WILEY | Hindawi

Research Article

A Road Environment Prediction System for Intelligent Vehicle

Chao Ma,[1] **Zhao Sun** ,[1] **Shanshan Pei,**[1] **Chao Liu,**[2] **and Feng Cui** [3]

¹Faculty of Information Technology, Macau University of Science and Technology, Macau 999078, China
²Research Base of Beijing Modern Manufacturing Development, Beijing University of Technology, Beijing 100124, China
³Beijing Smarter Eye Technology Co.Ltd, Beijing 100023, China

Correspondence should be addressed to Feng Cui; feng.cui@smartereye.com

The road environment prediction is an essential task for intelligent vehicle. In this study, we provide a flexible system that focuses on freespace detection and road environment prediction to host vehicle. The hardware of this system includes two parts: a binocular camera and a low-power mobile platform, which is flexible and portable for a variety of intelligent vehicle. We put forward a multiscale stereo matching algorithm to reduce the computing cost of the hardware unit. Based on disparity space and points cloud, we propose a weighted probability grid map to detect freespace region and a state model to describe the road environment. The experiments show that the proposed system is accurate and robust, which indicates that this technique is fully competent for road environment prediction for intelligent vehicle.

1. Introduction

The road environment prediction is an essential task for intelligent vehicle and robotic applications. As the basis of path planning [1], motion strategy [2], and collision avoidance [3], the road environment prediction focuses on whether the host vehicle or robot will pass through without collision [4].

In recent years, light detection and ranging (LiDAR) [5], cameras [6], and multisensor fusion technique are adopted to perceive the road environment. In literatures, LiDAR and cameras are devoted to the odometry method, in which the relative motion is estimated by matched points in continuous frames. The multisensors fusion technique includes visual sensors, inertial sensors, and precision map. The inertial sensors are used to estimate the relative pose based on laws of classical mechanics. Those methods are considered as passive sensing that has only detected road information when a vehicle drives into it. The precision map method relies on a global positioning system (GPS) signal that can predict the road path; however, it is not robust in tunnel or underground parking.

In this paper, we propose a flexible and robust road environment perception system. This system consists of a binoc-ular camera and a low-power mobile platform. Because that software functions run in the terminal device rather than transmitting a large amount of data to the cloud [7], the proposed system is suitable for the Internet of Things (IoT) [8]. For the sake of real-time system in the low-power platform, we propose a multiscale stereo matching algorithm, weight probability grid map, and state model to describe road environment.

The traditional stereo matching algorithms, such as [9, 10], provide dense disparity map by predefined matching measures and semiglobal optimization, which consumes a lot of computing sources and takes a large of electric power. In this study, we propose a new stereo matching framework to adapt to the field-programmable gate array (FPGA) implement environment. The focus of the improvement is to reduce the computational cost, maintain the matching accuracy, and effectively perceive the target in different scales.

The traditional road environment perception methods, such as [11, 12], focus on the detection of freespace, which estimates the boundary of freespace region by geometric constraints in u-disparity or v-disparity space. The traditional position estimate methods, such as [13, 14], put forward motion estimation method based on the Bundle Adjustment

(BA) algorithm with feature points. It is necessary to select the points which are motionless relative to world coordinate system from the feature points. In this paper, we propose a weighted probability grid map to freespace detection. It is a robust and flexible strategy because we avoid the motion estimate that is different to match the feature point on static objects. In addition, we define a state model to describe the road environment, which describes the road status in the front of the host vehicle.

The main contributions of this work are summarized as follows.

(i) A multiscale stereo matching algorithm is presented to reduce the computing cost and improve the accuracy

(ii) Based on the disparity map, a weight probability grid map is proposed to detection the freespace region

(iii) A state model is proposed to describe the road environment in the front of the host vehicle

(iv) An efficient deployment programme is put forward to process our system at the low-power mobile platform in realtime

2. Related Work

2.1. Stereo Matching. Humenberger et al. [15] have presented a large spare Census mask for the fast stereo matching algorithm. In this literature, authors compare the large sparse masks and small dense masks, which the experiment shows that the former has better performance.

Yang [16] has presented a new matching cost aggregation method to preserve depth edges and reduce the computing complexity. In this literature, the author suggests an adaptive cost aggregation technique based on pixel similarity. A bilateral filter is used to compute the aggregation cost with the spatial similarity and the range (intensity/color) similarity, respectively.

Zhang et al. [17] have presented a cross-scale cost aggregation framework to allow multiscale interaction in cost aggregation. In this literature, the authors consider the cost aggregation as a weighted least square optimization problem. Therefore, multiscale cost aggregation methods come from different similarity kernels in the optimization objective.

Mao et al. [18] have presented a robust deep learning solution for semidense stereo matching. In this literature, two CNN models are utilized for computing stereo matching cost and performing confidence-based filtering. Due to that the global information is provided, the model is suitable for dealing with the challenging cases, such as lighting changes and lack of textures.

However, the above algorithms cost a large number of computing resources, which is a risk to process in realtime. In this paper, we propose a multiscale stereo matching fusion algorithm. This algorithm is designed to reduce the computing cost of FPGA and process stereo matching in realtime.

2.2. Road Environment Perception. Qu et al. [19] have presented an improved V-disparity space algorithm to generate the confidence map to estimate the freespace. In this literature, the authors discuss a sub-V-disparity space method to avoid the assumption that the road is locally planar and the variance in the latitudinal slope is small. Based on the v-disparity space, road confidence map and obstacle confidence map are calculated for freespace estimation by dynamic programming.

Deilamsalehy and Havens [20] have presented a multi-sensor fusion method to improve the accuracy of the estimation and to compensate for individual sensor deficiencies. In this literature, the three sensors, inertial measurement unit (IMU), camera, and LiDAR, form a rigid body, where position estimates from the camera and LiDAR are used in the EKF as a measurement to correct the IMU pose estimation.

Xiao et al. [21] have presented a Bayesian framework and conditional random field to fuse the multiple features that includes 2D image and 3D point cloud geometric information. Besides, a Gaussian process regression is employed to enhance performance. In this literature, the results are outstanding compared to some relevant LiDAR-based methods when a conditional random field with color and geometry constraints is applied to make the result more robust.

Zheng et al. [22] have presented a low-cost GPS-assisted LiDAR state estimation system for autonomous vehicle. In this literature, a LiDAR is employed to obtain highly precise 3D geometry data and an IMU is used to correct point cloud misalignment. A low-cost GPS is used to refine the estimated LiDAR inertial odometry.

Cong et al. [23] have presented LiDAR-based simultaneous localization and mapping (SLAM) system embedding dynamic objects removal module to improve the pose estimation. In this literature, the authors remove the point clouds of moving objects to relieve their influence on the odometry, so that the precision relative pose is estimated.

In this paper, we propose a weighted probability grid map to freespace detection and a state model to describe the road environment. By describing of road state in front of the host vehicle, we predict the future road environment information and vehicle's estimation direction.

3. Proposed Method

3.1. Multiscale Stereo Matching Algorithm. In binocular stereo matching algorithm, feature similarity is an unsupervised matching method, such as census feature [15], structural similarity (SSIM) [10], and convolutional neural network (CNN) model [24]. In this study, our binocular system is set to synchronous exposure and same image signal processing (ISP) parameters. In order to tolerate the small grey difference between the two sensors in the imaging process, the SSIM method is adopted for stereo matching.

The SSIM method [25, 26] is proposed to perceive image quality, because this index considers the luminance ($l(\varphi, \phi)$), contrast ($c(\varphi, \phi)$), and structure ($s(\varphi, \phi)$) as shown in

Equation. (1), where φ is the index of row and ϕ is the index of column.

$$l(\varphi, \phi) = \frac{2\mu_\varphi \mu_\phi + C_1}{\mu_\varphi^2 + \mu_\phi^2 + C_1}$$

$$c(\varphi, \phi) = \frac{2\sigma_\varphi \sigma_\phi + C_2}{\sigma_\varphi^2 \sigma_\phi^2 + C_2}, \qquad (1)$$

$$s(\varphi, \phi) = \frac{\sigma_\varphi \sigma_\phi + C_3}{\sigma_{\varphi\phi} + C_3}$$

where μ, σ^2, and σ denote the mean, variance, and covariance, respectively. Approximately, μ and σ^2 are viewed as the estimated luminance and contrast, respectively, and σ measures the tendency. C1, C2, and C3 are constants. The general form of the SSIM index between u (disparity) and p (pixel coordinate in image) is defined as Equation (2):

$$\text{SSIM}(p, u) = l^\alpha(\varphi, \phi) c^\beta(\varphi, \phi) s^\gamma(\varphi, \phi). \qquad (2)$$

In engineering practice, α, β, and γ are set as 1 and $C_1 = 0.01$, $C_2 = 0.03$, and $C_3 = C_2/2$. Therefore, the matching similarity value is simplified as Equation (3):

$$\text{SSIM}(p, u) = \frac{\left(2\mu_\phi \mu_\psi + C_1\right)\left(2\sigma_{\phi\psi} + C_2\right)}{\left(\mu_\phi^2 + \mu_\psi^2 + C_1\right)\left(\sigma_\phi^2 + \sigma_\psi^2 + C_2\right)}, \qquad (3)$$

which satisfies the following conditions to be a matching cost:

  (i) *Boundedness.* $0 < \text{SSIM} \leq 1$, which indicates that the more similar the patch, the higher the value

  (ii) *Unique Extremum.* $\text{SSIM} = 1$ if and only if the two patches are the same

In order to adapt to the high dynamic matching cost aggregation method, we define the matching cost based on SSIM as Equation (4):

$$\text{cost}(p, u) = L(1 - \text{SSIM}(p, u)), \qquad (4)$$

where $L = 255$ is the dynamic range of the pixel values for 8 bits/pixel greyscale images. Therefore, the maximum aggregation cost is less than 512 without penalty item by the semiglobal matching method. The purpose of transforming matching cost into integer type is to be more suitable for FPGA implementation. In this study, we limited the single matching cost to 255, which is represented by 8 bits. Therefore, the maximum matching cost is within a reasonable range in the semiglobal cost aggregation process, in which the maximum cost is limited to 10 binary digits in this system.

We set the penalty item to $P1 = 30$ and $P2 = 100$ in this system, which indicates an assumption that the disparity of adjacent pixels is smooth. In fact, the depth change is discontinuous in automatic driving, which leads to that the disparity fluctuates greatly and the precision decreases in the depth discontinue pixel. In order to improve this problem, we propose to build a guide map to show where depth changes are possible [27]. Compared with the literature [27], we assume that the depth charge always occurs at the edge of objects. In addition, the structure is obvious at the edge region, which makes it easier to get the real and accurate disparity.

First, we provide a one-dimensional Gaussian edge feature map (setting to $\mu = 0$ and $\sigma = 3$ in the system) to indicate where the obvious edge is and where is the stereo matching result is more credible. Then, the first derivative in the same direction is calculated to obtain the gradient response. Next, the same process is implemented in the tangent direction. Finally, the sum of the square root of two gradient responses is considered as a feature map, as shown in Figure 1.

Based on the feature map, the larger the response value is, the stronger the edge characteristics are, and the greater the possibility of depth change. According to the above method, we infer that the maximum aggregation cost between adjacent pixels is 610 (255 + 100 + 255) in one path. The sum cost in eight paths is less than 4880 (610 × 8), which is represented by 13 binary digits. Therefore, the maximum memory cost of a single pixel is limited within 16 binary digits (2 Bytes) by eight aggregation paths. To reduce the computing cost, we propose a stereo matching optimization method, which focuses on reducing the disparity search range. We construct the multiscale images by the image pyramid method. In this study, we propose three layers pyramid method. As shown in Figure 2, the large-scale layer images have the original resolution of 1280 × 720. The middle-scale layer images are downsampled from the large-scale layer images, and the small-scale layer images are downsampled from the middle-scale layer images.

The structure features are obvious in the large-scale layer. Correspondingly, the remote details are completely preserved in the small-scale layer. At first, we propose to set the disparity search range as 16 pixels in the small-scale layer, which is equal to the search range of 64 pixels in the large-scale layer. Based on that, we calculate the small-scale disparity map by the SSIM algorithm in the small-scale layer. Then, we initialize the middle-scale disparity map by upsampling from the small-scale disparity map by the linear interpolation method. Because the small-scale disparity map has the same size as the small-scale layer, 320 × 180, the size of initialized middle-scale disparity map is the same as that of the middle-scale layer, 640 × 360. Next, we refine the middle-scale disparity map. Based on the initialized disparity map, we set the same search range as 16 pixels. However, the beginning of the search depends on the initialized disparity, in which the search range with 16 pixels is a symmetric interval centered on the initialized disparity. Finally, we repeat the above processes to obtain the large-scale disparity map.

At the calculation process of the multiscale stereo matching algorithm, the feature map is only adopted in the large-scale layer. The proposed stereo matching method is suitable for the FPGA to process:

  (i) There are many reusable operation modules because the rules and parameters are the same

(a)

(b)

FIGURE 1: An example of the feature map in stereo matching. Left: grey image. Right: feature map.
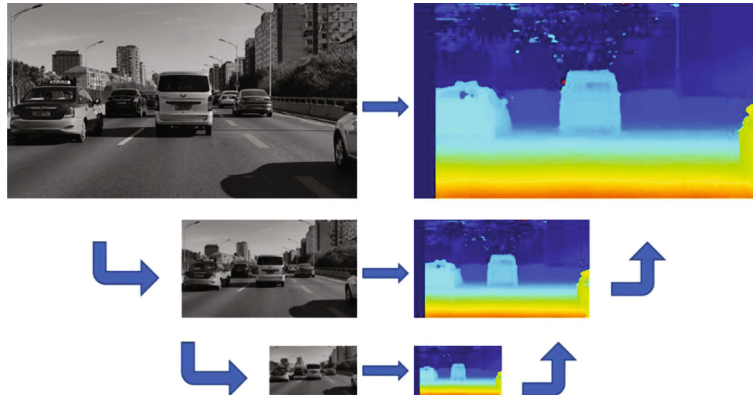
FIGURE 2: Multiscale images pyramid and disparity map. Top: the large-scale layer. Middle: the middle-scale layer. Bottom: the small-scale layer.

(a)

(b)

(c)
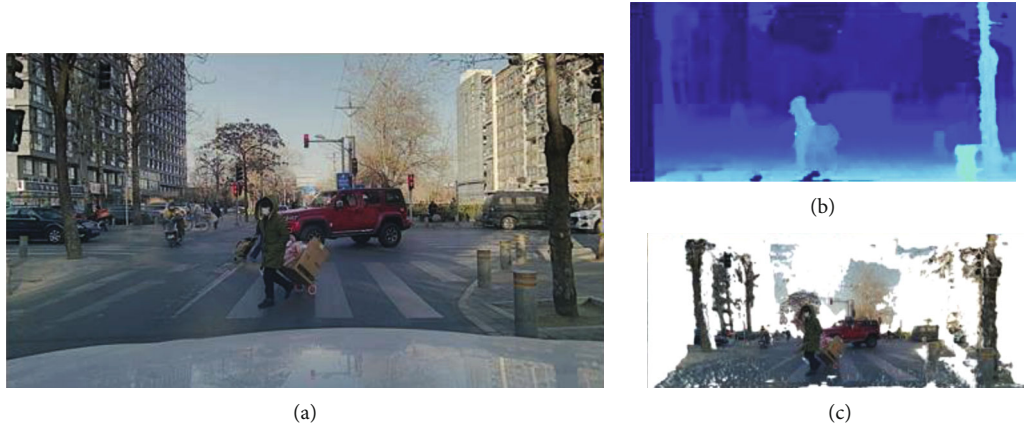
FIGURE 3: Disparity and 3D point cloud. (a) The left image. (b) Disparity map. (c) 3D point cloud.

(ii) There is no need to cache all image data in memory at the same time, so the calculation process can be consistent with the data transmission process

(iii) The algorithm is designed to process numerical multiplication and addition by a large number of fixed-point data

3.2. Road Prediction. In practice, we focus on two issues: (1) where is the obstacle and (2) what is the trend of road. We propose the grid projection method to predict the trend of

road. When obstacles occupy the road, the trend prediction will be hindered, but the freespace region should be correctly described. In this study, our method consists of three stages: grid projection, boundary search, and shape detection.

3.2.1. Grid Projection. Based on the disparity map, we calculate the 3D point cloud coordinate by Equation (5):

$$x = \frac{b(u - u_0)}{\text{disp}}, y = \frac{b(v - v_0)}{\text{disp}}, z = \frac{bf_{\text{eq}}}{\text{disp}} \qquad (5)$$

(a)   (b)

(c)   (d)
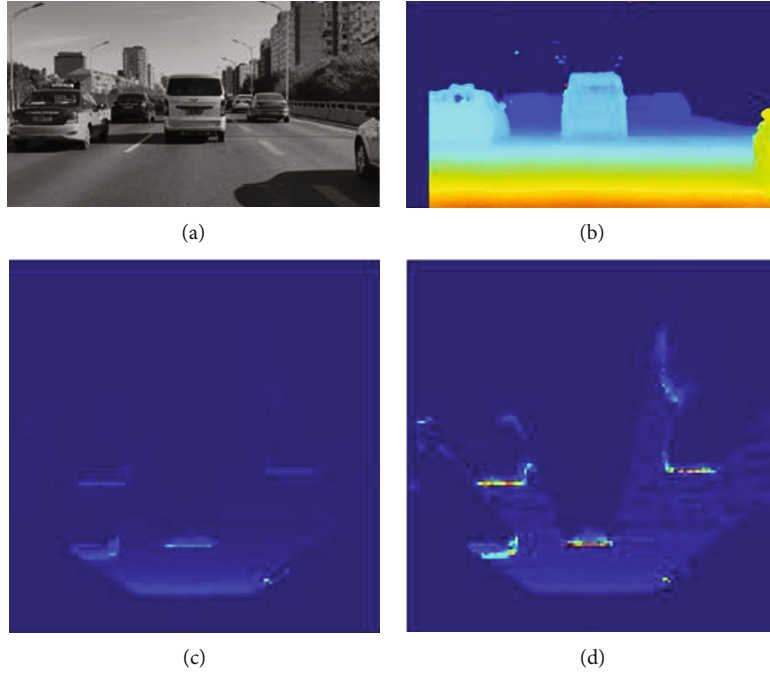
Figure 4: The process of probability grid map. (a) Left grey image. (b) Disparity map. (c) Grid projection. (d) Probability grid map.
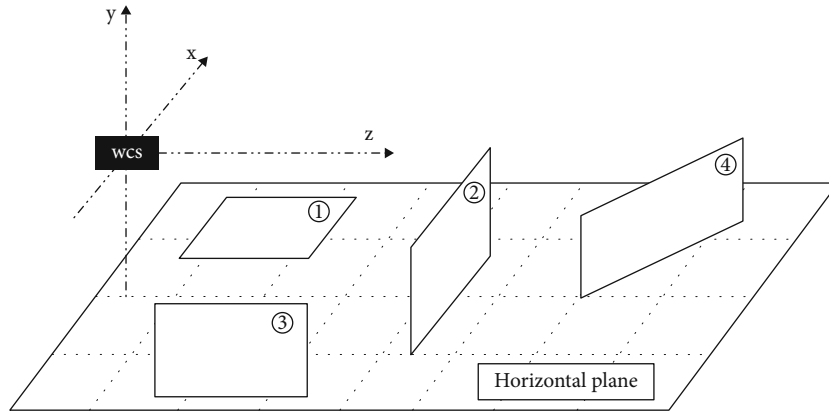
Figure 5: Road plane and three obstacle plane models in wcs.

where (x, y, z) is the 3D coordinate in the world coordinate system (wcs), (u, v) is pixel coordinate in image coordinate system (ics), (u_0, v_0) is the camera central point, disp is the disparity, b is the baseline of binocular camera, and f_{eq} is equivalent focal length. The disparity map and 3D pints cloud are shown in Figure 3.

Inspired by pseudolidar data from visual [28], we build a projection space from bird eye view (BEV) in wcs. At BEV, the x-axis, which is parallel to the baseline of the binocular camera, represents the horizontal direction, and the y-axis, which is parallel to the optical axis of the camera and is positive horizontally to the front, represents the depth direction. In the projection space, the fixed size grid is divided as the basic projection unit, which the grid is a rectangle by setting $10\,cm \times 50\,cm$ in x-direction and z-direction. First, we divide point cloud data by grid mesh and drop out the outliers that points do not belong to the detection space $\Pi = \{(x, y, z) \mid y \in (-0.5, 2.5), z \in (0, 60)\}$. This constraint represents a priori
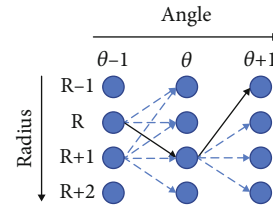
Figure 6: Directed acyclic graph with dynamic programming method. The black arrow indicates the best path.

assumption that the maximum height of the obstacles on road will not exceed 3 m, and the farthest observation distance is 60 m. Then, we count the number of points in each grid and set this value as the feature value of this grid. In this way, grids with lots of points cloud data have a larger accumulated number. As shown in Figure 4(c), we use color to represent the accumulated number, where the dark blue

(a)   (b)
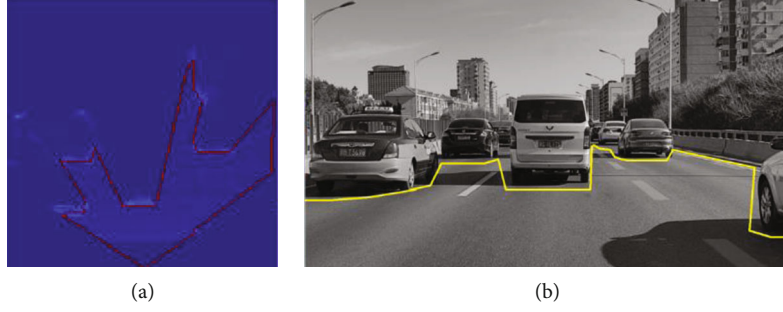
Figure 7: Freespace boundary. (a) Optimal path by DP. (b) Boundary in ics.

(a)   (b)   (c)

(d1)   (d2)   (d3)

(d)   (e)
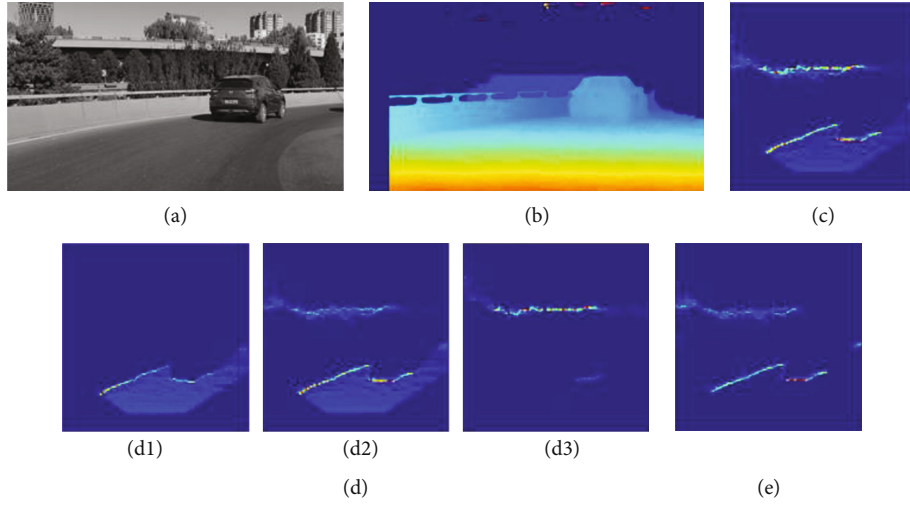
Figure 8: Multilayers grid projection. (a) Left image. (b) Disparity map. (c) PGM in Π. (d1) PGM in Π_1. (d2) PGM in Π_2. (d3) PGM in Π_3. (d) WPGM in Π.

indicates zero and the brighter the color, the greater the accumulated number.

3.2.2. Boundary Search. Inspired by the stochastic occupancy grids method [29], grids with larger feature values represent that there is a greater possibility of an obstacle. On the contrary, grids with smaller feature values are more likely to represent the road region. In addition, grids with zero feature value indicate that it is occluded and cannot be observed.

By transferring the ics (disparity map) to vcs (grid projection), a unified physical scale is helpful to build a more robust mathematical model to solve the problem. In detection space Π, we consider the ground as a plane parallel to the xoz and obstacles as a plane vertical to the horizontal plane. As shown in Figure 5, obstacles can be approximated by three plane models in the detection space Π: perpendicular to the optical axis (marked ②), parallel to the optical axis and perpendicular to the horizontal plane (marked ③), and perpendicular to the horizontal plane and intersecting with the optical axis (marked ④). In addition, the road plane is another plane (marked ①) that parallel to the horizontal plane or intersecting at a smaller angle.

These plane models describe obstacles in different states. The plane ② represents obstacles perpendicular to the optical axis on the driving route, such as a vehicle in the same lane, which only the vehicle rear is visible. The plane ③ represents

obstacles parallel to the optical axis adjacent to the driving route, such as fences and barriers, which only the side is visible. The plane ④ represents obstacles that intersect the optical axis on the driving route, such as guardrails and walls in the curve road. In addition, plane ② and plane ③ are combined to describe adjacent discontinuous obstacles, such as cut-in vehicles, the vehicle side and rear are visible. Based on the above model, obstacles generate a large number of 3D point cloud data on its plane. Therefore, there are many accumulated points in the projection area of the obstacle plane in the grid projection.

Suppose that the basic detection unit on planes is a square, which represents that the obstacle is divided into many square units. In practice, the side length of the unit is consistent with the gird projection size in *x*-direction. At different distances, the number of point clouds generated by the detection unit conforms to the Equation (6):

$$N_{\text{unit}} = \left(\frac{a \times f}{z \times \mu}\right)^2, \tag{6}$$

where N_{unit} represents the number of 3D points in unit, a is the side length of unit ($a = 10$ cm in this study), f is the focal length of lens, μ is the pixel size of sensor, and z is distance in wcs (0 m $< z \leq 60$ m in this study).
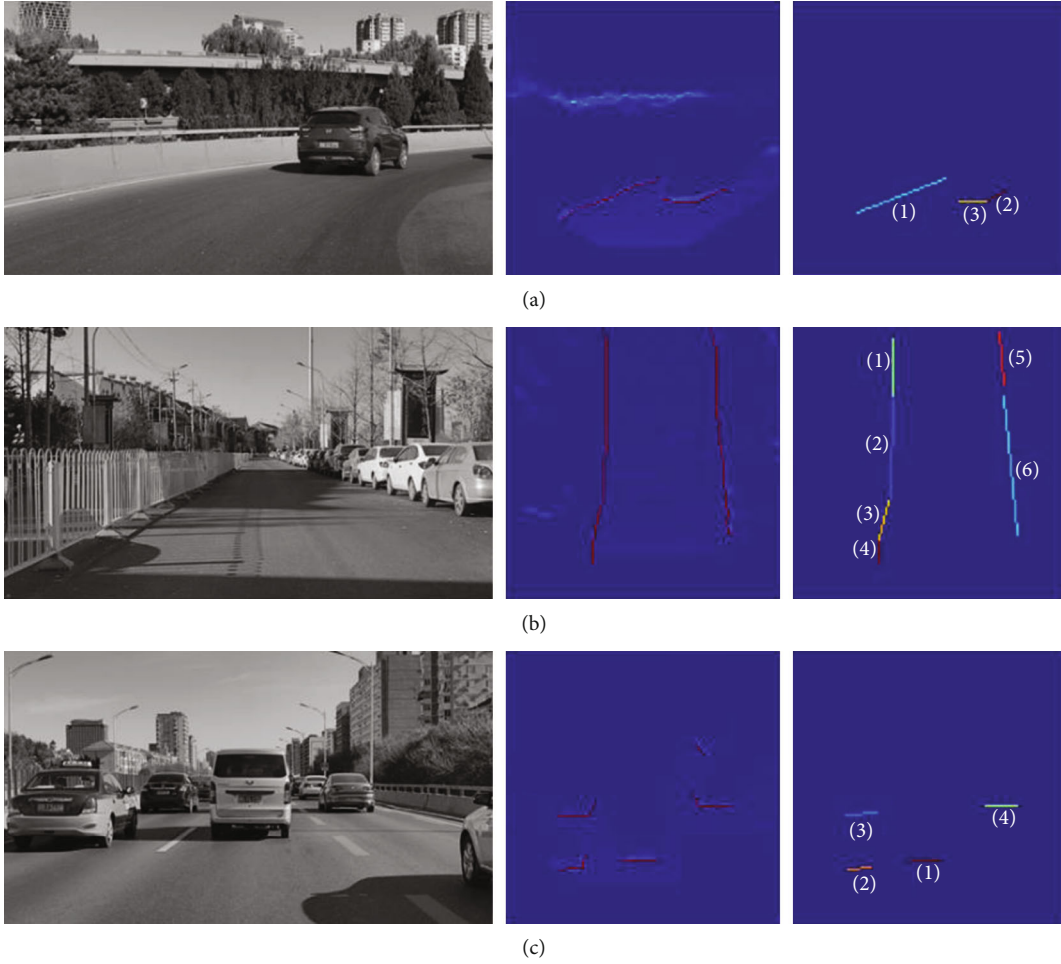
FIGURE 9: The process of shape detection. (a) In curved road. (b) In straight road. (c) With obstacles.

In the detection space Π, the height constraint is less than $h\,m$. Therefore, the maximum of 3D points is $h \times N_{\text{unit}}/a$ in a grid. Furthermore, we construct a probabilistic occupancy grid, where we divide the accumulated number by the maximum. As shown in Figure 4(d), we use the color to indicate the probability. The dark blue represents low probability and red represents high probability. In polar coordinates, we transform the probability grid map (PGM) into a graph model, where the nodes represent elements in PGM with fixed angle resolution and radius resolution. The value of the node is the probability of the grid, the column index is angle, and the row index is radius. Therefore, the road boundary search problem is transformed into a dynamic programming problem to find the path with maximum probability. We consider the graph as a directed acyclic graph (DAG) that the direction is from left to right or opposite. In theory, the two directions have the same path. In this study, we propose a semiglobal optimization method to solve the dynamic programming problem.

As shown in Figure 6, the node represents the probability of the grid. The horizontal axis is the angle of the field of view, where the resolution is 1 degree. The vertical axis is the radius, where the resolution is the same as that of the grid

in z direction. The FOV and grid projection space Π are not completely coincident, so the number of nodes in each column is not consistent. We propose a semiglobal energy function in Equation (7).

$$E(p \mid p \in N) = P_{p-1}(\theta, R) + T(p - 1, p) + P_p(\theta, R), \qquad (7)$$

where N is the best path that the summary of probability is maximum. $P_p(\theta, R)$ represents the probability of $p(\theta, R)$, and this point belongs to the best path $(p \in N)$. $T(p - 1, p)$ represents the penalty term between adjacent column nodes, in which the $p - 1$ is previous nodes and p is current nodes. The penalty term is defined as Equation (8).

$$T(p - 1, p) = \begin{cases} 0 & |R(p - 1) - R(p)| = 0 \\ T_1 & |R(p - 1) - R(p)| \leq 1 \\ T_2 & \text{otherwise} \end{cases} \qquad (8)$$

The penalty term represents an assumption that the path between adjacent columns is smooth in DAG. $R(p - 1)$ is the radius index of node in the previous column and $R(p)$ is in

current column. Obviously, the penalty term is constrained to $-1 \leq T2 < T1 < 0$. Finally, the optimization function is defined as Equation (9).

$$N(p) = \arg \min \sum E(p). \tag{9}$$

The purpose of parameter setting is that the row coordinate changes of adjacent column nodes should be smooth. In this study, we set the $T_1 = -0.1$ and $T_2 = -0.3$. As a result, we obtain an optimal path in DAG, where the sum of probability exists maximum. We convert the node index into the coordinate of PGM, where grids are considered as boundary points of freespace in wcs. In addition, the boundary points in wcs are back projected into ics through Equation (6). As shown in Figure 7, the red line in the probability grad map is the optimal path and the yellow line is the freespace boundary in ics.

In practice, we employ the multilayer grid projection to overcome that case where the near obstacle is lower than the far obstacles. Three layers are divided by height with -0.5 m ~ 0.5 m (subspace Π_1), 0.5 m ~ 1.5 m (subspace Π_2), and 1.5 m ~ 2.5 m (subspace Π_3). As shown in Figure 8(a), the height of the near barrier is lower than the far greenbelt, so that the probability of barrier is smaller than the probability of greenbelt in Figure 8(c). We propose a weight energy function as Equation (10).

$$E(p \mid p \in N) = \omega_{p-1} P_{p-1}(\theta, R) + T(p-1, p) + \omega_p P_p(\theta, R), \tag{10}$$

where ω_p is the weight of node p that the coordinate of this point is (θ, R) and $0 < \omega \leq 1$. The $p - 1$ indicates the previous node. The capital P indicates the penalty item. The ω in Π_1 is greater than ω in Π_2, and ω in Π_2 is greater than ω in Π_3. In this study, we set weight as $\omega = 1$ in Π_1, $\omega = 0.6$ in Π_2, and $\omega = 0.3$ in Π_3. As a result, the Figure 8(e) shows the weight probability grid map (WPGM) that the best path corresponds to our expectations, where the high brightness represents a large probability.

3.2.3. Shape Detection. Based on the three obstacle models, we detect geometric constraints on the multilayer grid projection. In practice, we propose to identify the geometry feature by prior. The plane ②, in Figure 5, is a segment parallel to the x-axis in the WPGM, the plane ③ is another segment parallel to the z-axis, and the plane ④ is an oblique line or curve. Therefore, we detect these geometry features on the boundary to identify if there any obstacle exists and road environment, for example, vehicle is going to drive into straight road or curved road.

To reduce the noise, we discard the grid whose probability is less than 0.1. The result is shown in Figure 9. The left column is the grey images, the middle column is the feature points in WPGM, and the right column is the result of shape detection.

In the middle column of Figure 9, the red points are feature points that make up the shape feature map (SFM). These feature points are used to progressive probabilistic Hough

TABLE 1: Describe the road environment by state model.

	Curve road	Straight road	Obstacles
(a)	1	0	1
(b)	0	6	0
(c)	0	0	4
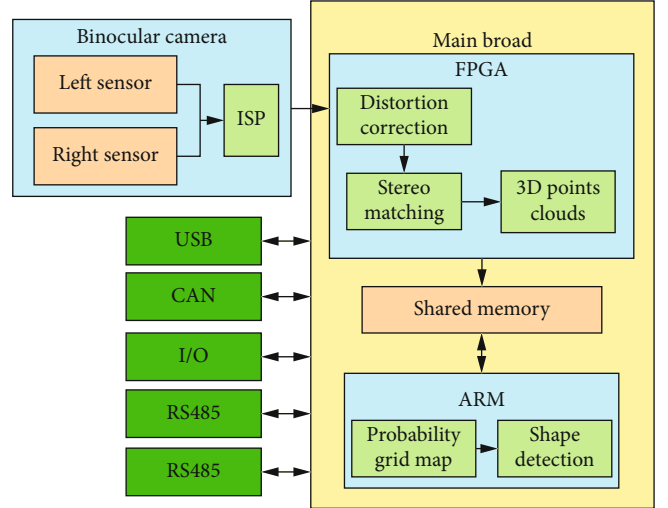
FIGURE 10: System hardware platform.

TABLE 2: System hardware parameters.

Items	Parameters	Items	Parameters
Baseline	120 mm	Focal length	8.26 mm
Pixel size	4.2×10^{-3} mm	Resolution	1280×720
Horizontal FOV	$30°$	Vertical FOV	$22°$

transform, in which the coordinates use pixel dimensions in the SFM. For example, in the right column of Figure 9(a), the different color line represents different slopes: the slope of line (1) is 0.3862, the slope of line (2) is 0.5062, and the slope of line (3) is 0.0082. We consider the line (3) is modelled as the plane ②, while the line (1) and line (3) are modelled as plane ④. However, the plane ② is usually considered to be an independent obstacle, such as a vehicle. Because line (2) and line (3) are connected, they are regarded as independent obstacle in the wcs. In addition, plane ④ is usually considered continue obstacle, such as guardrails and walls in the curve road. The line (1) is regarded as a guardrails or walls in the curve road.

We describe the shape feature by different plane models so that the complex road environment is classified into finite-state models. Table 1 describes Figure 9. The (a) scene is described as 1 curve road model and 1 obstacle model, the (b) scene is described as 6 straight road models, and the (c) scene is described as 4 obstacle models. Therefore, the (a) scene is predicted to be going to drive into curve road and there is an obstacle. The (b) scene is predicted to drive on a straight road without obstacle. The (c) scene is predicted to
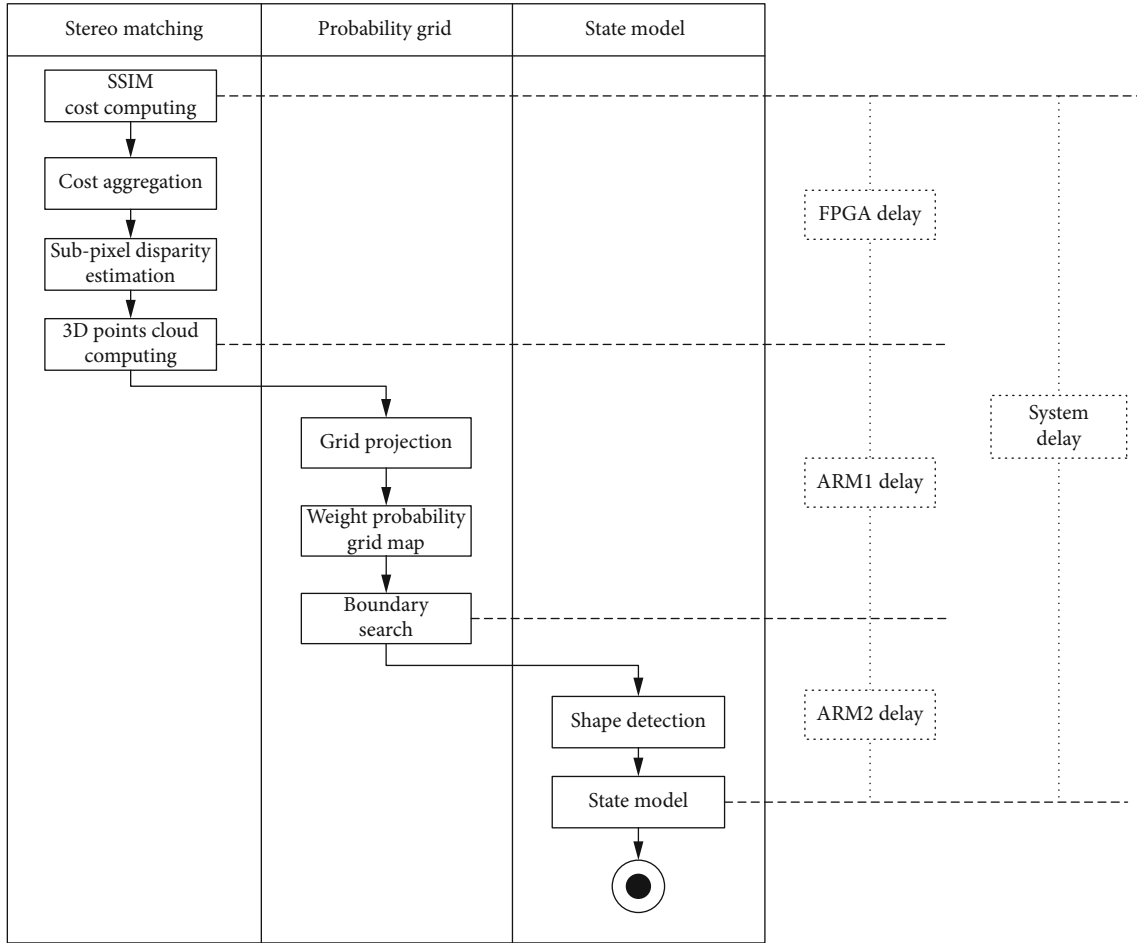
FIGURE 11: System software flow framework.

that there are many obstacles in front of the vehicle and other road information is invalid.

4. System Design

4.1. Hardware Architecture. The proposed system is used for forward sensing of automatic driving or advanced driver assistance system (ADAS). In practice, the system is generally installed in the narrow space between the windshield and the inside rearview mirror. It requires that the space volume of the hardware system must be small. The system hardware design architecture is shown in Figure 10.

The lens focal length is 8.26 mm and the image resolution is 1280×720. The embedded computing core is a Xilinx Z-7020 system on chip (SoC) that includes an Artix-7 field-programmable gate array (FPGA) and two A9 advanced RISC machines (ARM). Based on this hardware platform, the system's full load power is 6 W without any cooling system. In addition, its volume is only $17\,cm \times 8\,cm \times 4\,cm$. Other system parameters are shown in Table 2.

4.2. Software Architecture. In the algorithm function, we divide three parts: stereo matching, probability grid, and state model, as shown in Figure 11. The stereo matching module

TABLE 3: Evaluation of stereo matching in KITTI.

Method	Accuracy (%)	Efficiency
Our proposed	93.22	1.00
Origin MPV	94.43	3.05
SGBM	92.36	—
ELAS	91.76	—

includes SSIM cost computing, cost aggregation, subpixel disparity estimation, and 3D point cloud computing. The probability grid module includes grid projection, weight probability grid map, and boundary search. The state model module includes shape detection and state module.

The three modules are processed by parallel computing on three processing units. The frequency of data processing depends on the slowest one of the three modules, and the system delay is equal to the sum of the three modules. In the proposed system, the FPGA delay is 66 ms, the ARM1 delay is 16 ms, and the ARM2 delay is 21 ms. Therefore, the frequency of the system is 15 fps and the system delay is 103 ms.

TABLE 4: Evaluation of stereo matching in private dataset.

Test case	Sunny	Cloudy	Night	Backlight
Accuracy (1.0)	78.94%	80.06%	58.68%	78.49%
Accuracy (0.5)	51.00%	51.33%	32.47%	50.11%
Accuracy (0.3)	33.84%	32.42%	19.54%	31.62%
Accuracy (0.1)	11.97%	11.13%	6.66%	10.84%
Convergence (pixel)	4.66	4.15	5.73	5.37
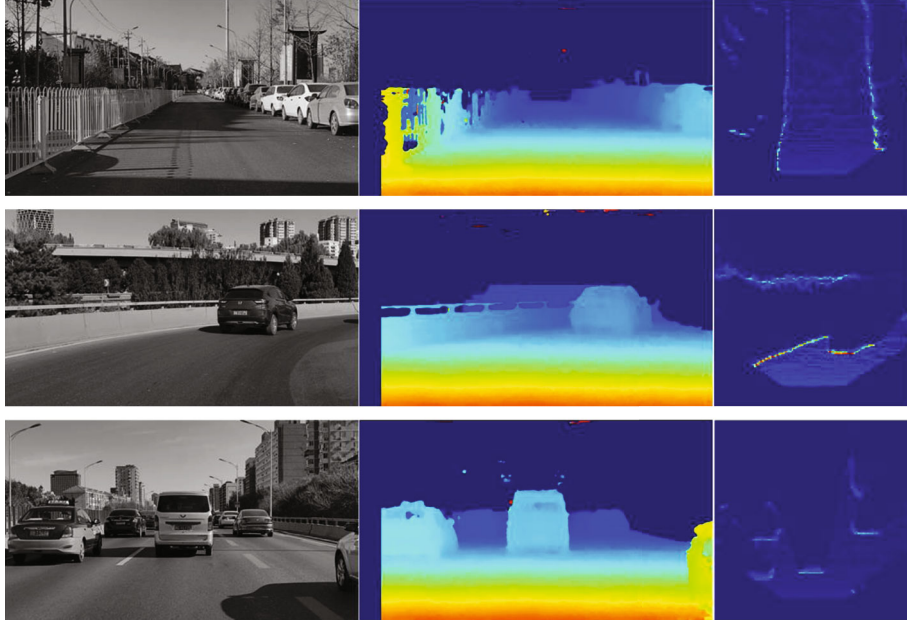
FIGURE 12: The WPGM in different road environment. Grey images, disparity space, and weight probability grid map.

5. Experiment and Analysis

5.1. Stereo Matching. We evaluate our stereo matching method by two comparative experiments: efficiency and accuracy. By compared on KITTI dataset [30] as benchmark data set, our multiscale stereo matching algorithm (93.22%) is lower average error rate than classical unsupervised stereo matching algorithm, such as SGMB [9] (92.36%), ELAS [31] (91.76%), and origin MPV algorithm [10] (94.43%). The accuracy of our method is higher than SGBM and ELAS. Although our method is lower than the origin MPV algorithm in accuracy, its computing efficiency is higher than the origin MPV algorithm. The detail is shown in Table 3. Based on the running times of our proposed algorithm as the benchmark, the efficiency is defined as the running time of the comparison algorithm divided by the benchmark. Therefore, the efficiency of our algorithm is 1.

In addition, we test the multiscale stereo matching method in the private dataset, where we focus following items: subpixel disparity accuracy, light condition, and point cloud distribution.

(i) *Subpixel Disparity Accuracy.* When the absolute value of disparity error is less than 1.0 (0.5, 0.3, 0.1) pixel, the matching disparity is correct. The

TABLE 5: Evaluation of freespace detection in private dataset.

Method	Running time (ms)	Recall (%)
Hautiere et al. [33]	30	95.0
Xin et al. [32]	18360	91.7
Ours	16	93.5

index is defined as the corrected number divided by the total pixels

(ii) *Light Condition.* The disparity accuracy is evaluated by the different light condition, such as sunny, cloudy, night, and backlight

(iii) *Convergence.* Assuming the distribution of point clouds being Gaussian model, disparity's variance represents the convergence degree of the point clouds

The result is shown in Table 4. The subpixel disparity accuracy represents a more precise ability of the stereo matching algorithm, which the large proportion in high precision range indicates the disparity estimation algorithm is close to ground truth (GT). The proposed multiscale stereo matching method has the highest precision in sunny and
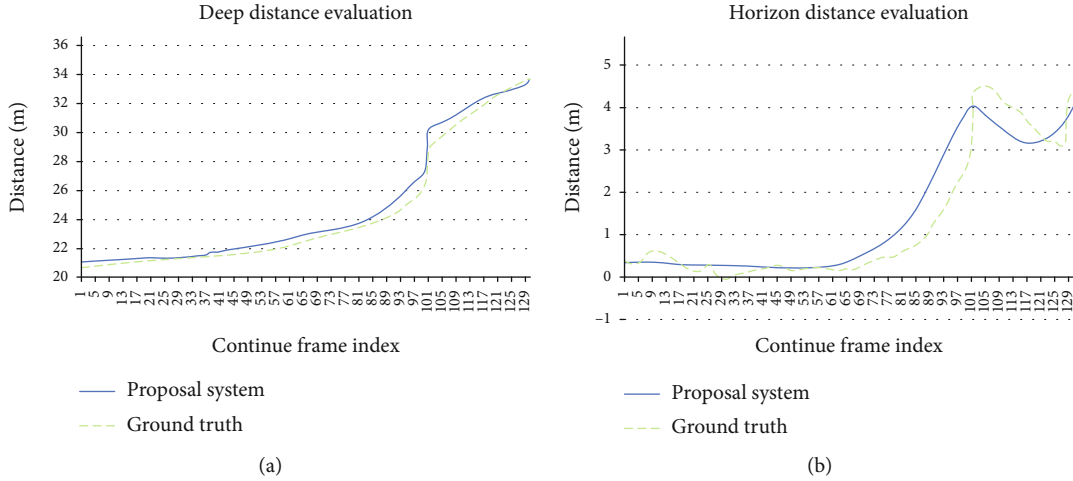
FIGURE 13: Obstacle prediction in deep and horizon distance.

TABLE 6: Evaluation of state model prediction in private dataset.

	Curve road	Straight road	Obstacle	Precision
Curve road	293	7	4	96.38%
Straight road	1	591	0	99.83%
Obstacle	5	2	96	93.20%
Recall	97.67%	98.50%	96.00%	—

cloudy, because the imaging quality is best in this weather. The edge will become unclear due to overexposure in back-light, and the texture features will be blurred in dark environment, such as at night. Therefore, the subpixel disparity accuracy decreases slightly in the backlight, but significantly at night. In addition, the variance indicates the aggregation degree of disparity on the same obstacle plane. The small variance represents that the disparity estimation is stable and the point clouds converge in space. The experimental results show that the proposed method is stable and robust under good light conditions.

Figure 12 shows middle processing to explain our multi-scale stereo matching algorithm and weight probability grid map. The left column is grey images, the middle column is a disparity map corresponding to points cloud space, and the right column is a weighted probability grid map corresponding to points cloud space.

5.2. Road Prediction. We evaluate the proposed system by following experiments: freespace detection, obstacle prediction, road environment prediction, and system performance.

Based on the private dataset, we label the GT of freespace on images. We evaluate the freespace by recall method, in which the index represents the similarity between the detection result and GT. Recall = 100% indicates that the detection result is completely consistent with the true value, while IoU = 0 indicates completely inconsistent. The result is shown in Table 5, where our system is compared by two classic methods to shows that our method is advanced in efficiency and result. Our system is more efficient than Xin et al. [32] method in running time and recall. Compared to

Hautiere et al. [33] method, we have halved our running time but lost only 1.5% of recall. The experiment shows that our system is robust and stable in freespace detection.

The obstacle prediction is one of the tasks based on the state model. We evaluate the results of obstacle prediction by the number and location of obstacles based on our private dataset. The GT of obstacles is labelled manually, where we focus on independent objects such as vehicles and pedestrians. We count the number of obstacles in the state model to compare with GT, so the average recall rate of obstacle detection of obstacles is 98.3% in private dataset. As shown in Figure 13, the left shows the deep distance and the right shows the horizon distance, where the deep distance is represented by the vertical axis and horizon distance is represented by the horizontal axis on WPGM. We employ the root mean squared error (RMSE) to evaluate the error of relative distance by Equation (11):

$$\text{RMSE} = \frac{1}{n} \sqrt{\sum_{i=1}^{n} (\text{data}_i - \text{GT}_i)^2}, \tag{11}$$

where data_i is observations and n is the total number of test dataset. The RMSE in the deep distance is 0.42 m and 0.46 m in the horizon distance. The experiment shows that our method is robust and stable in obstacle prediction.

We evaluate the state model by precision and recall as Table 6, where the first row represents the GT, and the first column represents the observations. We provide 1000 images including 600 straight road state, 300 curve road state, and 100 obstacle state. Precision and recall index are employed

TABLE 7: Running time of modules.

Hardware unit	FPGA			ARM1	ARM2	
Module	Stereo matching	Point cloud	WPGM	Path planning	Shape detection	State model
Running time	55 ms	11 ms	12 ms	4 ms	20 ms	1 ms
Delay time	66 ms			16 ms	21 ms	

TABLE 8: Chip temperature test.

Ambient temp ($^\circ$C)	Chip temp ($^\circ$C)	Load power (W)
-15	40~50	6
15	50~60	6
45	60~75	6
65	75~90	6

to evaluate state model prediction. The experiment shows that our system is sensitive to road environment prediction.

In addition, we test the system performance by running time and power cost. As shown in Table 7, we record the running time of three hardware units. The largest time cost is stereo matching and point cloud in FPGA, where its running time is 66 ms. The frame rate of the system is decided by this module to 15 fps. The system delay time is a summary of three modules, which is 103 ms.

Finally, we test the power cost and the chip temperature. Our system is installed between the front windshield and the rear-view mirror, so it must meet the requirements of GB/T 28046.4, which stipulates that the maximum operating temperature of the system shall not exceed 90°C. Table 8 shows that the maximum temperature in full load power meets the standard requirement.

6. Conclusions

In this study, we propose a low-power road environment prediction system, which the proposed system consists of a binocular camera and a low-power computing unit. Our contribution includes three points as follows. Firstly, a multiscale stereo matching algorithm is proposed for hardware computing. Next, we propose a weighted probability grid map-based points cloud. Finally, the plane model and state model are proposed to describe the road environment. Our work proves that the existing technology achieves the function requirement under the low-power constraint. Experiments show that the proposed system is robust and sensitive to road environment prediction and the performance meets the mandatory standards in practice. In future work, our study provides a benchmark for obstacles recognition and path planning.

Data Availability

No data were used to support this study.

Conflicts of Interest

The authors declare that there is no conflict of interest regarding the publication of this paper.

Acknowledgments

References

[1] Y. Shi, Q. Li, S. Bu, J. Yang, and L. Zhu, "Research on intelligent vehicle path planning based on rapidly-exploring random tree," *Mathematical Problems in Engineering*, vol. 2020, 14 pages, 2020.

[2] M. Shahjalal, M. Hossan, M. Hasan, M. Z. Chowdhury, and J. Y. M. Le NT, "An implementation approach and performance analysis of image sensor based multilateral indoor localization and navigation system," *Wireless Communications and Mobile Computing*, vol. 2018, 13 pages, 2018.

[3] L. Claussmann, M. Revilloud, D. Gruyer, and S. Glaser, "A review of motion planning for highway autonomous driving," *IEEE Transactions on Intelligent Transportation Systems*, vol. 21, no. 5, pp. 1826–1848, 2019.

[4] Z. Wang and H. Zhang, "A novel approach for free space detection using u-disparity and dynamic programming," in *2016 5th International Conference on Computer Science and Network Technology (ICCSNT)*, pp. 391–395, Changchun, 2016.

[5] X. Zhang, J. Lai, D. Xu, H. Li, and M. Fu, "2d lidar-based slam and path planning for indoor rescue using mobile robots," *Journal of Advanced Transportation*, vol. 2020, 14 pages, 2020.

[6] K. Zhou, X. Meng, and B. Cheng, "Review of stereo matching algorithms based on deep learning," *Computational Intelligence and Neuroscience*, vol. 2020, 12 pages, 2020.

[7] C.-H. Hsu, S. Wang, Y. Zhang, and A. Kobusinska, "Mobile edge computing," *Wireless Communications and Mobile Computing*, vol. 2018, 3 pages, 2018.

[8] S. Raza, S. Wang, M. Ahmed, and M. R. Anwar, "A survey on vehicular edge computing: architecture, applications, technical issues, and future directions," *Wireless Communications and Mobile Computing*, vol. 2019, 19 pages, 2019.

[9] H. Hirschmuller, "Stereo processing by semiglobal matching and mutual information," *IEEE Transactions on Pattern Analysis and Machine Intelligence*, vol. 30, no. 2, pp. 328–341, 2007.

[10] Q. Xie, Q. Long, and S. Mita, "Integration of optical flow and multi-path-viterbi algorithm for stereo vision," *International Journal of Wavelets, Multiresolution and Information Processing*, vol. 15, no. 3, article 1750022, 2017.

[11] Z. Hu and K. Uchimura, "Uv-disparity: an efficient algorithm for stereovision based scene analysis," in *IEEE Proceedings. Intelligent Vehicles Symposium*, pp. 48–54, Las Vegas, NV, USA, 2005.

[12] A. Harakeh, D. Asmar, and E. Shammas, "Ground segmentation and occupancy grid generation using probability fields," in *2015 IEEE/RSJ International Conference on Intelligent Robots and Systems (IROS)*, pp. 695–702, Hamburg, Germany, 2015.

[13] R. Mur-Artal and J. D. Tardós, "ORB-SLAM2: an open-source slam system for monocular, stereo, and rgb-d cameras," *IEEE Transactions on Robotics*, vol. 33, no. 5, pp. 1255–1262, 2017.

[14] K. Tateno, F. Tombari, I. Laina, and N. Navab, "Cnn-slam: real-time dense monocular slam with learned depth prediction," in *Proceedings of the IEEE Conference on Computer Vision and Pattern Recognition*, pp. 6243–6252, Honolulu, HI, USA, 2017.

[15] M. Humenberger, C. Zinner, M. Weber, W. Kubinger, and M. Vincze, "A fast stereo matching algorithm suitable for embedded real-time systems," *Computer Vision and Image Understanding*, vol. 114, no. 11, pp. 1180–1202, 2010.

[16] Q. Yang, "A non-local cost aggregation method for stereo matching," in *2012 IEEE Conference on Computer Vision and Pattern Recognition*, pp. 1402–1409, Providence, RI, USA, 2012.

[17] K. Zhang, Y. Fang, D. Min et al., "Cross-scale cost aggregation for stereo matching," in *Proceedings of the IEEE Conference on Computer Vision and Pattern Recognition*, pp. 1590–1597, Columbus, OH, USA, 2014.

[18] W. Mao, M. Wang, J. Zhou, and M. Gong, "Semi-dense stereo matching using dual cnns," in *2019 IEEE Winter Conference on Applications of Computer Vision (WACV)*, pp. 1588–1597, Waikoloa, HI, USA, 2019.

[19] L. Qu, K. Wang, L. Chen, Y. Gu, and X. Zhang, "Free space estimation on nonflat plane based on v-disparity," *IEEE Signal Processing Letters*, vol. 23, no. 11, pp. 1617–1621, 2016.

[20] H. Deilamsalehy and T. C. Havens, "Sensor fused three-dimensional localization using imu, camera and lidar," in *2016 IEEE Sensors*, pp. 1–3, Orlando, FL, USA, 2016.

[21] Z. Xiao, B. Dai, H. Li et al., "Gaussian process regression-based robust free space detection for autonomous vehicle by 3-d point cloud and 2-d appearance information fusion," *International Journal of Advanced Robotic Systems*, vol. 14, no. 4, article 1729881417717058, 2017.

[22] L. Zheng, Y. Zhu, B. Xue, M. Liu, and R. Fan, "Low-cost gps-aided lidar state estimation and map building," in *2019 IEEE International Conference on Imaging Systems and Techniques (IST)*, pp. 1–6, Abu Dhabi, United Arab Emirates, 2019.

[23] Y. Cong, C. Chen, J. Li, W. Wu, S. Li, and B. Yang, "Mapping without dynamic: robust lidar-slam for ugv mobile mapping in dynamic environments," *The International Archives of Photogrammetry, Remote Sensing and Spatial Information Sciences*, vol. 43, pp. 515–520, 2020.

[24] J. Zbontar and Y. LeCun, "Stereo matching by training a convolutional neural network to compare image patches," *The journal of Machine Learning Research*, vol. 17, no. 1, pp. 2287–2318, 2016.

[25] Z. Wang, E. P. Simoncelli, and A. C. Bovik, "Multiscale structural similarity for image quality assessment," in *The Thrity-Seventh Asilomar Conference on Signals, Systems & Computers, 2003*, vol. 2, pp. 1398–1402, Pacific Grove, CA, USA, 2003.

[26] W. Lai, J. Huang, Z. Hu, N. Ahuja, and M.-H. Yang, "A comparative study for single image blind deblurring," in *Proceedings of the IEEE Conference on Computer Vision and Pattern Recognition*, pp. 1701–1709, Las Vegas, NV, USA, 2016.

[27] M. Park and K. Yoon, "Learning and selecting confidence measures for robust stereo matching," *IEEE Transactions on Pattern Analysis and Machine Intelligence*, vol. 41, no. 6, pp. 1397–1411, 2018.

[28] Y. Wang, W.-L. Chao, D. Garg, B. Hariharan, M. Campbell, and K. Q. Weinberger, "Pseudo-lidar from visual depth estimation: bridging the gap in 3d object detection for autonomous driving," in *Proceedings of the IEEE Conference on Computer Vision and Pattern Recognition*, pp. 8445–8453, Long Beach, CA, USA, 2019.

[29] H. Badino, U. Franke, and R. Mester, "Free space computation using stochastic occupancy grids and dynamic programming," in *Workshop on Dynamical Vision, ICCV*, vol. 20, Rio de Janeiro, Brazil, 2007.

[30] A. Geiger, P. Lenz, and R. Urtasun, "Are we ready for autonomous driving? the kitti vision benchmark suite," in *2012 IEEE Conference on Computer Vision and Pattern Recognition*, pp. 3354–3361, Providence, RI, USA, 2012.

[31] A. Geiger, M. Roser, and R. Urtasun, "Efficient large-scale stereo matching," in *Asian Conference on Computer Vision*, pp. 25–38, Berlin, Heidelberg, 2010.

[32] L. Xin, J. Song, Y. Chen, and J. Hu, "Robust free-space detection in urban roads based on mser extraction using gradient images," in *2018 37th Chinese Control Conference (CCC)*, pp. 4141–4146, Wuhan, 2018.

[33] N. Hautière, J. P. Tarel, H. Halmaoui, R. Brémond, and D. Aubert, "Enhanced fog detection and free-space segmentation for car navigation," *Machine Vision and Applications*, vol. 25, no. 3, pp. 667–679, 2014.

WILEY | Hindawi

Research Article

An Improved Empirical Mode Decomposition Method for Vibration Signal

Xiaohan Liu,[1,2] **Guangfeng Shi** [1] **and Weina Liu**[1,2]

[1]*College of Electromechanical Engineering, Changchun University of Science and Technology, Changchun, 130022 Jilin, China*
[2]*Department of Electromechanical Engineering, College of Optical and Electronical Information Changchun University of Science and Technology, Changchun, 130114 Jilin, China*

Correspondence should be addressed to Guangfeng Shi; 2017200046@mails.cust.edu.cn

With the development of electronic measurement and signal processing technology, nonstationary and nonlinear signal characteristics are widely used in the fields of error diagnosis, system recognition, and biomedical instruments. Whether these features can be extracted effectively usually affects the performance of the entire system. Based on the above background, the research purpose of this paper is an improved vibration empirical mode decomposition method. This article introduces a method of blasting vibration signal processing—Differential Empirical Mode Decomposition (DEMD), combined with phosphate rock engineering blasting vibration monitoring test, and Empirical Mode Decomposition (EMD) to compare and analyze the frequency screening of blasting vibration signals, the aliasing distortion, and the power spectrum characteristics of the decomposed signal. The results show that compared with EMD, DEMD effectively suppresses signal aliasing and distortion, and from the characteristics of signal power spectrum changes, DEMD extracts different dominant frequency components, and the frequency screening effect of blasting vibration signals is superior to EMD. It can bring about an obvious improvement in accuracy, and the calculation time is about 4 times that of the EMD method. Based on the ground analysis of ground motion signals, this paper uses the EMD algorithm to analyze measured ground blast motion signals and study its velocity characteristics and differential time, which provides a new way of studying motion signals.

1. Introduction

With the development of the information age, signal processing plays an important role in industry and scientific research. Signal is defined as the physical quantity that transmits and carries information, that is, the specific form or carrier of information. Signal analysis is an important means of identifying, detecting, and diagnosing system status. Its main goal is to find a simple and effective signal conversion method to display the important information contained in the signal and finally achieve the purpose of extracting effective signal features. Therefore, it is necessary to identify useful information, such as physical characteristics and statistical characteristics. This process is called signal feature extraction. The signal attribute extraction method can be sorted by selected domain, real-time domain, frequency domain, or time frequency domain. Decomposition of the empirical mode is a new adaptive

method of signal processing. The signal is no longer considered the combination of the signature weight value and the cosine total, the base function is not predetermined, and the signal is not used for decomposition according to the signal characteristics. Because it is a dictionary knowledge, it has good adaptability and is particularly suitable for the analysis and processing of nonlinear and abnormal signals.

Although there are many algorithms to analyze these data, a signal processing theory (similar to detection and estimation in the classical Euclidean environment) for evaluating these technologies still needs to be developed. Hassan AR uses an example: detecting embedded signatures in the background graph, which illustrates the conceptual advantages gained by constructing graph analysis problems in the signal processing framework. Hassan AR describes a method based on detection theory, which shows that the proposed test statistics have reasonable detection capabilities for dense

signatures on large random graphs [1]. Inspired by the continuous development of wireless body area networks (WBANs), Ren Y introduced the conceptual and exploratory research of wireless electroencephalogram (EEG) sensor networks (WESNs), with a focus on distributed signal processing. WESN is considered as a modular neural monitoring platform for high-density EEG recording, where each node is equipped with electrode arrays, signal processing units, and wireless communication facilities [2]. Valles-Novo et al. introduced a random signal processing method. Valles-Novo et al. introduced various high-dimensional Markov Chain Monte Carlo (MCMC) methods and deterministic agent methods, such as variational Bayes method, Bethe method, belief and expectation propagation, and approximate message passing algorithms. A series of optimization methods for solving stochastic problems and stochastic methods for deterministic optimization are also discussed. Subsequently, the overlap area between simulation and optimization is discussed, especially the optimization within MCMC and the optimization driven by MCMC [3].

Integrated Empirical Mode Decomposition (EEMD) and its complete variant (CEEMDAN) are an adaptive, noise-assisted data analysis method that improves the traditional Empirical Mode Decomposition (EMD). Chambers DP proposed a free software implementation of EMD, EEMD, and CEEMDAN and gave an overview of the EMD method and the algorithms used in the decomposition. Chambers DP released their implementation, libeemd, with the goal of providing a user-friendly, fast, stable, well-documented, and easily extensible EEMD library for anyone interested in using (E) EMD in time series data analysis [4]. Pachori et al. proposed a hybrid time series adaptive network fuzzy inference system (ANFIS) model with Empirical Mode Decomposition (EMD) as the core to predict the stocks of Taiwan Stock Exchange Weighted Stock Index (TAIEX) and Hang Seng Index (HSI) price. In order to measure its predictive performance, the model is compared with Chen's model, Yu's model, autoregressive (AR) model, ANFIS model, and support vector regression (SVR) model [5]. Van and Kang proposed a wind speed prediction method that combines empirical mode decomposition (EMD) and support vector regression (SVR). The empirical mode decomposition method is used to decompose the wind speed time series into several intrinsic mode functions and a residual. Then, a vector is generated, and a historical data of each IMF is combined with the residual to train the SVR. The EMD-SVR model was evaluated using wind speed data [6].

The EMD algorithm is an empirical method and its theoretical basic research remains insufficient. Therefore, this study intends to explain the screening process from a systematic perspective and to analyze in depth the characteristics of cubic spine insertion. Innovations in this research:

(1) In order to achieve the final result, it is planned to improve the EMD algorithm to achieve the suppression effect

(2) Analyze the analysis of ground motion signals with EMD algorithm

2. Empirical Mode Decomposition

2.1. Empirical Mode Decomposition.
The empirical mode decomposition (EMD) algorithm has three limitations when processing the original nonstationary signal: (1) the signal has at least one maximum value and one minimum value; (2) the characteristic time scale of the signal is determined by the time interval between adjacent extreme values; (3) there is no extreme point in the data, but there is a defect. The extreme minute can be obtained by one or more micro-values [7, 8].

2.1.1. Stationary Signal and Nonstationary Signal.
Any signal that can be uniquely described by an explicit mathematical expression, data, or definite rule is called a deterministic signal [9] provided for sure. This type of signal is called a random signal, and the random signal can be divided into stationary signal and nonstationary signal. Random signals can be described by statistical methods, and the most commonly used are probability density function or power density spectrum [10, 11].

Stationary random signal is a kind of important random signal. In engineering practice, random signal is often regarded as stationary, so that the problem can be simplified [12].

For a stationary random signal of finite length, its mean value can be expressed as

$$E[X(n)] = \frac{1}{N} \sum_{n=0}^{N} x(n). \tag{1}$$

The autocorrelation function is

$$\varphi_x(n_1, n_2) = E[X^*(n)X(n + m)], \quad m = n_1 - n_2. \tag{2}$$

Signals whose statistical characteristics change over time are called collectively unstable signals, also called time-varying signals. Due to its statistical characteristics they change over time, although the traditional Fourier analysis can show all the frequency data of the whole process, it cannot accurately describe the relationship between the frequency components [13, 14]. The biggest advantage of the EMD algorithm is that it can process adaptive nonstatic signals.

2.1.2. Instantaneous Frequency.
In the Fourier transform, each frequency component corresponds to a certain frequency w_j that does not change with time, but the frequency of nonstationary signals changes with time, that is, $w_j(t)$, so it is necessary to establish the concept of instantaneous frequency [15, 16]. Instantaneous frequency is an important concept of the EMD method. Proposing and applying it to signal time-frequency analysis is an innovative point of the EMD algorithm. In the EMD algorithm, the instantaneous frequency comes from the Hilbert transform.

For the continuous time function $X(t)$, its Hilbert transform $Y(t)$ is defined as

$$Y(t) = \frac{1}{\pi} P \int_{-\infty}^{+\infty} \frac{X(t')}{t - t'} dt'. \tag{3}$$

Among them, P is the main value of Cauchy. This change exists for all L^P level functions. Mathematical formula (3) expresses the convolution of $X(t)$ and $1/t$, so the Hilbert transform emphasizes the locality of $X(t)$ [17]. It can be seen from the definition formula (3) that the Hilbert transform is a transformation from the time domain to the time domain, and the Fourier transform is a transformation from the time domain to the frequency domain.

According to formula (3), an analytical signal $Z(t)$ can be constructed:

$$Z(t) = X(t) + iY(t) = a(t)e^{i\theta(t)}. \tag{4}$$

Among them,

$$\alpha(t) = \left[X^2(t) + Y^2(t) \right]^{1/2}, \tag{5}$$

$$\theta(t) = \arctan \left(\frac{Y(t)}{X(t)} \right). \tag{6}$$

Use the time derivative of the argument to define the instantaneous frequency:

$$\omega(t) = \frac{d\theta(t)}{dt}. \tag{7}$$

Equation (7) shows that the instantaneous frequency is a single-valued function of time, and at a given moment, there is only one frequency value. The instantaneous frequency limits the signal to a "narrow band," that is, the number of maximum points (minimum points) is equal to the number of zero crossing points.

2.1.3. Screening Process. The basic foundation of EMD is that the signal is composed of high-frequency components and low-frequency components, so it can be generalized [18, 19]. This algorithm is a process of continuously separating the high-frequency components of the signal and using the remaining low-frequency components as a new signal [20]. The separated high-frequency components are called eigenmode functions [21, 22]. IMF must meet two conditions. In the entire data area, the total value of the maximum value and the minimum value and the number of zero intervals must be the same, and the maximum value must also differ by 1. The average value of the upper envelope of the maximum value and the lower envelope of the minimum value is zero. For a given discrete signal $x(n)$, to find the IMF that meets the definition, the detailed screening process is as follows:

(1) Order $x_{i,j}(n) = x(n), i = 1, l = 1$

(2) Find all local extreme points of $x_{i,j}(n)$

(3) Calculate the envelope mean value $m_{i,l}(n) = (e_u(n) + e_d(n))/2$

(4) Take out component $h_{i,l}(n) = x_{i,l}(n) - m_{i,l}(n)$

(5) If the screening stop criterion is met, it is considered that $c_i(n) = h_{i,j}(n)$ is an IMF, $i = i + 1$, $l = 1$; if not, then, $x_{i,j}(n) = h_{i,j}(n)$, $l = l + 1$, repeat steps (2) to (5)

(6) Record the residual value $r_i(n) = x(n) - \sum c_i(n)$, and let $x_{i,j}(n) = r_i(n)$ repeat steps (2) to (6) to get the next IMF

(7) When $r_i(n)$ is a trend component, the algorithm stops. Otherwise, repeat the above steps until the end conditions are met

From the above process, the original signal can be expressed as the sum of IMF components and a trend component, and its expression is shown in the following formula:

$$x(n) = \sum_{i=I}^{I} c_i(n) + r_I(n). \tag{8}$$

The top and bottom envelopes defined by the local point end contain the low-frequency element of the signal, but not the high-frequency element. In this way, the filtering process is to continuously delete the average value of the envelope representing the low-frequency components from the original signal and finally to extract the high-frequency components of the signal. Throughout the screening process, the low-frequency carrier and the signal waveform have two effects on eliminating the gradual symmetry [23].

2.2. Properties of EMD. EMD algorithm is a signal processing method based on time domain. This is only based on the assumption that the signal consists of different modes of natural vibration. The purpose of EMD method is to decompose the complex signal function into the sum of finite intrinsic mode functions (IMF). After EMD decomposition, the instantaneous frequency also has physical significance [24, 25]. Through the Hilbert transform of the eigenmode functions, the instantaneous frequency and amplitude of each eigenmode function with time variation can be obtained, and the complete time-frequency distribution of the unsteady signal can be obtained. EMD method is not limited by Heisenberg's uncertainty principle and can obtain high-frequency resolution. In addition, the method is decomposed according to the characteristics of the signal itself. The basis function is not defined in advance, and the prior knowledge of the signal is not used. The attributes of EMD mainly include adaptability, integrity, orthogonality, and filtering characteristics.

2.2.1. Adaptability. Adaptability is the biggest characteristic of EMD algorithm. The adaptability of EMD algorithm is summarized in two aspects: one is that the composition of IMF subband signal can be adjusted automatically according

to the signal; the other is that the frequency resolution of IMF is adaptive and has adaptive filtering characteristics.

From the point of view of signal analysis, the decomposition quantity obtained by EMD decomposition of signal decomposition is the adaptive generalization basis of a series of IMF with variable frequency and variable amplitude. The signal can be fully adapted in the process of decomposition.

The adaptive resolution of the eigenmode function is that the characteristic time scales of the eigenmode functions obtained by EMD decomposition are different. The instantaneous frequency resolution of the ith eigenmode function is as follows:

$$\Delta f_i = \frac{f_{i\,\max}}{N},\tag{9}$$

where $f_{i\,\max}$ represents the highest frequency contained in the ith eigenmode function and N is the number of signal samples. It can be seen from Equation (9) that the frequency resolution of each eigenmode function is different, and the frequency resolution of components including low-frequency components is high, and the frequency resolution of components including high-frequency components is low. For each eigenmode function, the corresponding frequency resolution is adaptive, independent of the time resolution. At this point, the mutual influence between time and frequency resolution in wavelet analysis is completely different, and the principle of uncertainty is not limited.

The characteristic of adaptive filtering is that some IMF components decomposed by EMD have different bandwidths from different frequency components. At the same time, these frequency components and bandwidths are different according to the decomposed signal and are included in the decomposition process. The high-frequency component IMF component is always decomposed first. Therefore, the EMD decomposition method can be regarded as a set of band-pass filters with adaptive characteristics, the cut-off frequency, and bandwidth of which differ depending on the decomposed signal. Compared with wavelet and wavelet group decomposition, EMD is corresponding, but wavelet analysis is not like this. If the decomposition ratio of wavelet is selected, the time-domain waveform obtained by decomposition is a fixed frequency range, the frequency range is only related to the analysis, and the frequency has nothing to do with the signal itself.

2.2.2. Completeness and Orthogonality.
For any signal decomposition method, completeness is necessary. Completeness means that the decomposed signal can completely recover the original signal through reconstruction. The IMF and residual components of the original signal obtained by EMD decomposition can be accumulated and recovered by the formula.

Orthogonality refers to the orthogonality between the decomposed signal components. There is no theory to prove that the IMF is orthogonal to each other.

2.2.3. Filtering Characteristics.
Looking back on the screening process, the upper envelope and the lower envelope are obtained by interpolating the maximum and minimum points, respectively, so the frequency of the local upper envelope or lower envelope is less than the local frequency of the signal. The mean signal is the arithmetic mean of the upper envelope and the lower envelope, so the frequency of the mean signal is less than that of the upper envelope or the lower envelope. To sum up, the frequency of the mean signal is less than the highest local frequency of the original signal. This process can be regarded as a special filtering process, that is, the signal continuously subtracts a low-frequency component from itself. The process can be equivalent to an iterative high pass filter (where the mean value is a low-frequency component), and the IMF can be regarded as a locally narrow-band high-frequency signal component at the end of the iteration.

3. Experimental Design of Blasting Vibration Signal Analysis

3.1. Background of Experimental Data.
In this study, the EMD method is used to decompose the monitored blast vibration signals and analyzes the frequency sorting, pseudonym deformation, and power spectrum of the decomposed signals. The geomorphic type of this experiment belongs to the low tectonic mountain. The overall trend of the mountains and the distribution of gullies are consistent with the main structural line, showing the NNE direction. The highest point of the ore block is Niujing, with an elevation of 1502.5 m; the lowest point is Yingpingxi near line 7, with an elevation of 1170 m. The relative height difference is 100~300 meters. The ore section is located in a nearly north-south valley, the elevation of the east-west watershed is 1440-1450 meters, the valley bottom elevation is 1150-1254 meters, the west side is the forward slope, the slope is 15-28 degrees, the east side is the reverse slope, and the slope is 20-24 degrees.

3.2. Experimental Instruments and Methods.
The system consists of a and D vibration transducer, which is shown in Figure 1. The vibration recorder shall meet the requirements of negative delay recording, reliable self-touch setting, multi-channel, portable, and durable.

This monitoring adopts tc-4850 vibration meter produced by Chengdu Zhongke measurement and Control Co., Ltd.

3.2.1. Test Method

(1) According to the blasting situation on site, it is important to monitor the buildings and structures that are relatively affected in the blasting area. The measuring points are arranged on the foundation of the building, and some important measuring points should be arranged repeatedly

(2) Three sensors with different directions (tangential, radial, and vertical) are arranged at each measuring point
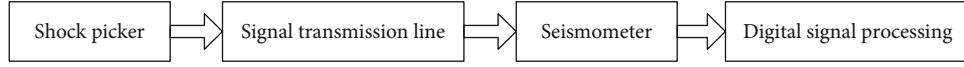
FIGURE 1: The block diagram of the seismic collection analysis system.

(3) Set the range, sampling rate, delay, and trigger of the vibration recording instrument, and modify the instrument setting items according to the actual situation of the measuring point each time

(4) During the test, gypsum is used to adhere the sensor and the base stone to ensure the firm connection between the sensor and the surface of the measuring point

The Tc-4850 has the auto save function. It only needs to extract the blast vibration data from the instrument blast recording log using the analysis software provided by the instrument. The instrument software provides the text data output function, which can store the data in a decimal text file.

However, since the three-channel data recorded by the instrument are voltage quantities, it is necessary to convert them to obtain the speed time history file of our data analysis:

$$M = \frac{U}{K + B}. \qquad (10)$$

Among them, M is the physical quantity; U is the voltage quantity; K is the channel sensitivity; B is the channel offset.

According to the instrument monitoring settings, k is 28 and B is 0, so that the speed time history file can be obtained, and the data can be analyzed by programming with MATLAB software.

3.3. Calculation of Experimental Speed Peak. The propagation of blasting seismic waves in the ground is a complicated mechanical process. Therefore, in actual engineering, the Sadowski empirical formula is generally used to describe the propagation law of blasting seismic waves. According to relevant regulations, the empirical formula describing the propagation law of blasting seismic waves takes the following form:

$$V = K \left(\frac{\sqrt[3]{Q}}{R} \right)^{\alpha} = K\rho^{\alpha}, \qquad (11)$$

where V: peak vibration velocity of the particle, cm/s

K: field constant

α: decay index

ρ: proportional dose,$\rho = \sqrt[3]{Q}/RQ$: maximum single-stage charge, kg

R: distance of burst center from measuring point, m.

As long as the site constant K value and the attenuation index α value are determined, the blasting seismic wave propagation law can be found, which can also provide a scientific basis for the future blasting construction design. Use the computer to sort out all the measured data (including the ore body observation data) and then perform regression analysis and variance analysis to get the K value, α value, and variance analysis results of No. II pit explosion area (as shown in Table 1).

It is known from the measured empirical formula (11) that the peak vibration velocity of the particle is proportional to the cubic root of the maximum charge amount. When the explosion center is at a certain distance from the protected object, the smaller the maximum charge, the smaller the peak vibration velocity of the particle. Deformation of the actual measured empirical formula, the calculation formula for the maximum allowable charge in the No. 2 pit blast area of Deyingping Mine:

$$Q_{\text{allow}} = R^3 \left(\frac{V_{\text{allow}}}{588.4721} \right)^{1.61481}. \qquad (12)$$

In the formula, V_{allow}: the control standard of the particle vibration speed of each protected object, cm/s

Q_{allow}: the maximum allowable single-stage charge, kg.

4. Analysis of Blasting Vibration Signal Based on EMD

4.1. Blasting Vibration Signal Analysis. In this study, the blasting vibration monitoring signal of phosphate rock engineering is adopted. The total charge of blasting is 54 kg, which is divided into 9 sections, and the maximum charge is about 13 kg. Three measuring points were selected for the project. In order to ensure the safety and stability of the surrounding workshops, 5×10 measuring points were arranged on the screening belt corridor in the northwest of the blasting area, 6×10 measuring points were arranged in the medium and fine crushing workshop in the south of the blasting area, and 2×10 measuring points were arranged near the highway in the north of the blasting area. Specific arrangement method: firstly, the position of the point to be measured is cleaned, then plaster is applied to the measuring point, and finally, the sensor is tightly attached to the measuring point. And make the sensor x point to the explosion source direction, y point to the horizontal tangential direction, and Z point to the vertical direction. The monitoring data are shown in Table 2.

The sampling frequency is 2 kHz, the signal length is 1 s, and the signal is shown in Figure 2. Now, use EMD method to analyze the signal.

The original signal is decomposed by the EMD method, and the components of the decomposition result and their frequency spectrum are shown in Figure 3.

(1) The original signal decomposes into 7 IMF components and a voltage component, and the high-frequency to low-frequency components are decomposed sequentially according to the inherent time scale, i.e., the frequency of c1 is the highest. As the EMD decomposes, the frequency of the received component gradually decreases until the last voltage

TABLE 1: Measured blasting vibration velocity regression equation.

Radial vibration velocity regression equation	Tangential vibration velocity regression equation	Vertical vibration velocity regression equation
$V = 169.4274 \left(\dfrac{Q^{1/3}}{R} \right)^{1.6178}$	$V = 27.9884 \left(Q^{1/3}/R \right)^{1.2206}$	$V = 588.4721 \left(Q^{1/3}/R \right)^{1.8578}$

TABLE 2: Blasting monitoring data.

Measuring point number	Peak measuring point vibration velocity/(cm/s)			Burst/m	Initiating charge/kg
	Horizontal speed	Radial velocity	Vertical speed		
2#	0.010	0.008	0.008	74.5	10
5#	0.020	0.014	0.025	46.8	10
6#	0.012	0.009	0.020	26.0	10
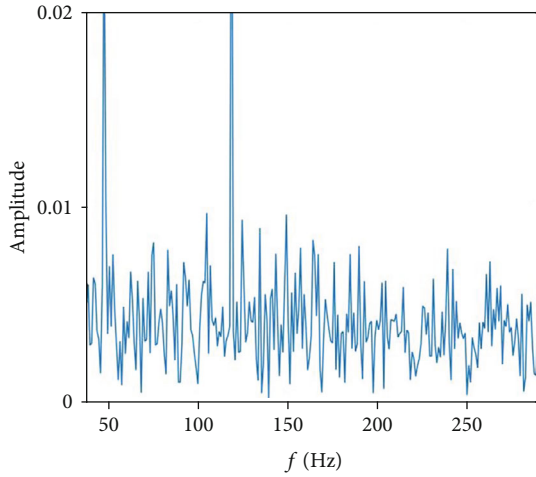
FIGURE 2: Waveform of blasting ground motion signal.
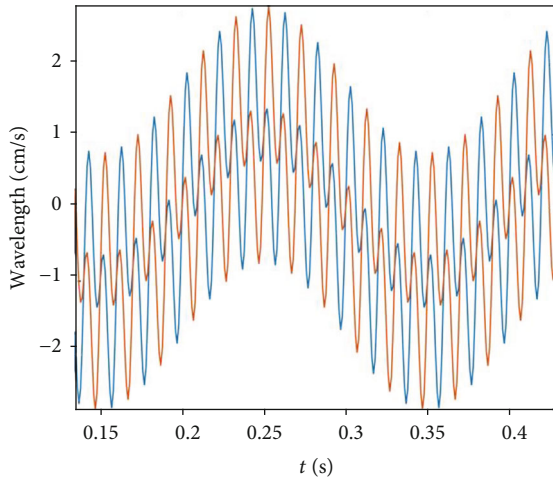
FIGURE 3: EMD decomposition result and corresponding frequency spectrum of blasting ground motion signal.

element is resolved. The output of each IMF component is determined by the inherent time scale, which is adaptive. Compared to the analysis methods that define the base function in advance, such as wave transform, the EMD analysis method is more flexible and variable and also eliminates the choice of the base function, which is simpler

(2) The IMF component has physical meaning. The component c1 has the highest frequency and the widest frequency band, but it occupies the smallest energy. It is the high-frequency noise introduced by the monitoring equipment and should be eliminated during analysis. The components c2~c5, mainly concentrated in 10 Hz~100 Hz, concentrate most of the energy of the original signal. The building is affected by vibration mainly due to these frequency components. The frequency spectrum of the original signal and the frequency spectrum of c2, c3, c4, and c5 are given. It can be seen that the frequency spectrum of these four components is almost the same as that of the original signal. C6 is the lower frequency component obtained by decomposition, and the energy is also very low. This may be inherent to the signal or caused by other reasons. The trend component indicates the weak trend of the signal or the zero drift of the measuring instrument. The decomposition results show that the EMD algorithm can extract the eigenmode function of the signal in the order of frequency from high to low, and several of the IMFs reflect the most significant features of the original signal

(3) The decomposed IMF subbands are transformed by Hilbert, and the Hilbert energy spectrum is shown in Figure 4

It can be seen from Figure 4 that the energy is mainly distributed within 100 Hz and mainly in the low-frequency region below 40 Hz. It can be seen in time that the vibration mainly occurs in 0.2 s~0.8 s. Integrate the Hilbert energy spectrum with frequency to get the edge spectrum. The concentration of signal energy can be seen from the boundary spectrum, and its energy is distributed in the main frequency range of 0~30 Hz.

4.2. Precision Analysis. The resolution accuracy of the two-tone signal is selected for investigation, and the performance of EMD, second-generation wavelet interpolation, and the method in this paper are compared. The configuration of the experiment in this section is similar to the previous demonstration experiment, considering the input signal $x(t) = \cos(2\pi \times 10t) + \cos(2\pi \times 10\text{ft})$. Perform the EMD decomposition of $x(t)$ at different sampling rates, and calculate
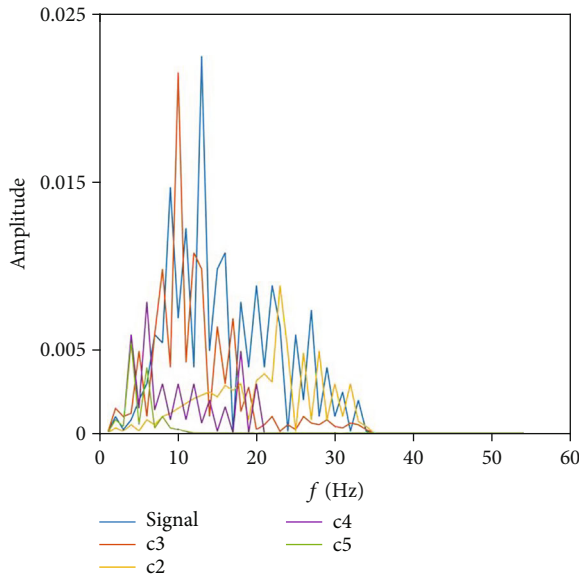
FIGURE 4: The spectrum of c2, c3, c4, c5, and the original signal.
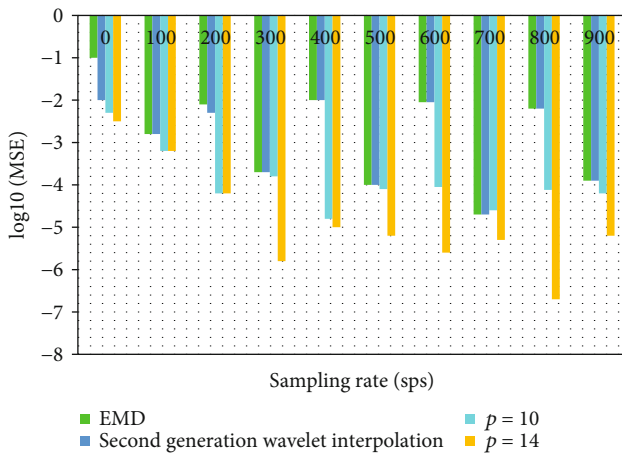
FIGURE 5: Comparison of decomposition accuracy under different sampling rates.

the mean square error between the primary IMF of the decomposition result and the actual result. In the experiment, f is 0.1 to 0.4, and the sampling rate range is set to 25 to 1000 sps. The arithmetic means and logarithm of the results obtained from the decomposition of different two-tone signals; the experimental results are shown in Figure 5.

First, compare the resolution performance of sampling rates from 25 sps to 100 sps. Compared with EMD, the decomposition accuracy of the second-generation wavelet interpolation method in this field is greatly improved, and the accuracy is increased by one digit when the sampling rate is 25 sps. The accuracy improvement obtained by using this white paper method is even more obvious. When the sampling rate is 25 sps, the accuracy will increase by about 1.5 bits. The following is a comparison of the accuracy of l00 sps and l000 sps resolution. Although the accuracy cannot be improved by interpolation in this field, it is because the improvement of the interpolation extreme value position prediction is very

small. On the other hand, the improvement of accuracy by interpolation is limited by the accuracy of EMD's own decomposition. In order to compare the influence of the B-spline order p on the decomposition accuracy, the method in this paper uses $p = 14$ and 2 orders for decomposition and comparison. It is found that the method in this paper can improve the decomposition performance in the entire sampling rate range. On the other hand, the greater the order of the B-spline, the higher the resolution accuracy. This is because the greater the value of p, the greater the roll-off of the B-spline filter (indicating the attenuation of the filter's stopband), and the closer it is to an ideal low-pass filter. However, if the value is too large, the solution becomes more complicated. Therefore, an increase in p leads to an increase in performance, which is sacrificed with an increase in calculation time. When $p = 14$, the accuracy is obviously improved, and the calculation time is about 4 times that of the EMD method.

5. Conclusions

Since the theoretical basis of the EMD method is not enough, it is still an experience-based signal decomposition method. Although EMD has been widely used, there are still many problems that limit its performance. In this article, three main problems in EMD are discussed and improved, namely, frequency analysis, pseudonym mode, and sampling rate. By establishing a logical theoretical model and exploring reasonable signal characteristics, the EMD theoretical system is improved and supplemented. On this basis, an improved algorithm is proposed. Finally, an experimental analysis is performed to verify the effectiveness and superiority of the method.

In this study, the screening process is explained from the perspective of system. The EMD algorithm is regarded as a multistage series grey box system, and the characteristics of cubic spline interpolation determine the system function. Therefore, in this paper, the characteristics of cubic spline interpolation are analyzed in depth. The matrix analysis method is used to split the coefficient matrix in the calculation process of cubic spline interpolation function, and the mean square deviation expression of cubic spline interpolation results with different number of extreme points is obtained.

In this study, an improved EMD algorithm for suppressing the final result is proposed. This method is based on the data expansion method. It is concluded that when the extremity points increase to a certain number, the increase of the unnecessary extremity points does not affect the interference results. The original method is changed to extend the entire signal to four endpoints at the endpoints, which can significantly improve operating efficiency while maintaining the adaptability of the original method. On this basis, the EMD algorithm is applied to the analysis of the measured ground motion signals, and its velocity characteristics and millisecond time are studied, providing a report on the fine-grained analysis of future ground signals.

Data Availability

No data were used to support this study.

Conflicts of Interest

Acknowledgments

References

[1] A. R. Hassan and M. I. H. Bhuiyan, "Computer-aided sleep staging using complete ensemble empirical mode decomposition with adaptive noise and bootstrap aggregating," *Biomedical Signal Processing & Control*, vol. 24, pp. 1–10, 2016.

[2] Y. Ren, P. N. Suganthan, and N. Srikanth, "A comparative study of empirical mode decomposition-based short-term wind speed forecasting methods," *IEEE Transactions on Sustainable Energy*, vol. 6, no. 1, pp. 236–244, 2015.

[3] R. Valles-Novo, J. de Jesus Rangel-Magdaleno, J. M. Ramirez-Cortes, H. Peregrina-Barreto, and R. Morales-Caporal, "Empirical mode decomposition analysis for broken-bar detection on squirrel cage induction motors," *IEEE Transactions on Instrumentation & Measurement*, vol. 64, no. 5, pp. 1118–1128, 2015.

[4] D. P. Chambers, "Evaluation of empirical mode decomposition for quantifying multi-decadal variations and acceleration in sea level records," *Nonlinear Processes in Geophysics*, vol. 22, no. 2, pp. 157–166, 2015.

[5] R. B. Pachori, P. Avinash, K. Shashank, R. Sharma, and U. R. Acharya, "Application of empirical mode decomposition for analysis of normal and diabetic RR-interval signals," *Expert Systems with Applications*, vol. 42, no. 9, pp. 4567–4581, 2015.

[6] M. Van and H. J. Kang, "Bearing-fault diagnosis using non-local means algorithm and empirical mode decomposition-based feature extraction and two-stage feature selection," *IET Science, Measurement & Technology*, vol. 9, no. 6, pp. 671–680, 2015.

[7] P. J. J. Luukko, J. Helske, and E. Räsänen, "Introducing libeemd: a program package for performing the ensemble empirical mode decomposition," *Computational Stats*, vol. 31, no. 2, pp. 545–557, 2016.

[8] B. Zhu, D. Han, P. Wang, Z. Wu, T. Zhang, and Y.-M. Wei, "Forecasting carbon price using empirical mode decomposition and evolutionary least squares support vector regression," *Applied Energy*, vol. 191, pp. 521–530, 2017.

[9] K. Zhao, W. Jiang, X. Jin, and X. Xiao, "Artificial intelligence system based on the layout effect of both sides in volleyball matches," *Journal of Intelligent and Fuzzy Systems*, vol. 40, no. 2, pp. 3075–3084, 2021.

[10] C. Damour, M. Benne, B. Grondin-Perez, M. Bessafi, D. Hissel, and J.-P. Chabriat, "Polymer electrolyte membrane fuel cell fault diagnosis based on empirical mode decomposition," *Journal of Power Sources*, vol. 299, pp. 596–603, 2015.

[11] V. K. Mishra, V. Bajaj, A. Kumar, and G. K. Singh, "Analysis of ALS and normal EMG signals based on empirical mode decomposition," *Iet ence Measurement & Technology*, vol. 10, no. 8, pp. 963–971, 2016.

[12] A. Humeau-Heurtier, G. Mahe, and P. Abraham, "Multi-dimensional complete ensemble empirical mode decomposition with adaptive noise applied to laser speckle contrast images," *IEEE Transactions on Medical Imaging*, vol. 34, no. 10, pp. 2103–2117, 2015.

[13] W. Chen, J. Xie, S. Zu, S. Gan, and Y. Chen, "Multiple-reflection noise attenuation using adaptive randomized-order empirical mode decomposition," *IEEE Geoence & Remote Sensing Letters*, vol. 14, no. 1, pp. 18–22, 2017.

[14] S. V. Tavildar, "The application of multivariate empirical mode decomposition with canonical correlation for EEG artifact removal," *Dissertations & Theses-Gradworks*, vol. 12, no. 1, pp. 47–54, 2015.

[15] Z. Liu, F. Huang, and B. Li, "Analysis on characteristics and influential factors of grain yield fluctuation in China based on empirical mode decomposition," *Nongye Gongcheng Xuebao/Transactions of the Chinese Society of Agricultural Engineering*, vol. 31, no. 2, pp. 7–13(7), 2015.

[16] W. Yang, Z. Peng, K. Wei, P. Shi, and W. Tian, "Superiorities of variational mode decomposition over empirical mode decomposition particularly in time–frequency feature extraction and wind turbine condition monitoring," *IET Renewable Power Generation*, vol. 11, no. 4, pp. 443–452, 2017.

[17] R. Pilkar, E. Bollt, and C. Robinson, "Empirical mode decomposition/Hilbert transform analysis of postural responses to small amplitude anterior-posterior sinusoidal translations of varying frequencies," *Mathematical Bioences & Engineering*, vol. 8, no. 4, pp. 1085–1097, 2017.

[18] S. K. Subhani, B. Suresh, and V. S. Ghali, "Empirical mode decomposition approach for defect detection in non-stationary thermal wave imaging," *Ndt & E International*, vol. 81, no. Jul., pp. 39–45, 2016.

[19] F. Zhou, L. Yang, H. Zhou, and L. Yang, "Optimal averages for nonlinear signal decompositions–another alternative for empirical mode decomposition," *Signal Processing*, vol. 121, no. Apr., pp. 17–29, 2016.

[20] Y. Kim and K. Cho, "Sea level rise around Korea: analysis of tide gauge station data with the ensemble empirical mode decomposition method," *Journal of Hydro-environment Research*, vol. 11, pp. 138–145, 2016.

[21] W. H. Wu, C. C. Chen, J. W. Jhou, and G. Lai, "A rapidly convergent empirical mode decomposition method for analyzing the environmental temperature effects on stay cable force," *Computer-Aided Civil and Infrastructure Engineering*, vol. 33, no. 8, pp. 672–690, 2018.

[22] X. Yang, G. Cheng, and H. Liu, "Improved empirical mode decomposition algorithm of processing complex signal for IoT application," *International Journal of Distributed Sensor Networks*, vol. 2015, no. 3, 2015.

[23] S. Jin, J. S. Kim, and S. K. Lee, "Sensitive method for detecting tooth faults in gearboxes based on wavelet denoising and empirical mode decomposition," *Journal of Mechanical ence & Technology*, vol. 29, no. 8, pp. 3165–3173, 2015.

[24] P. C. Charlton, C. Kenneally-Dabrowski, J. Sheppard, and W. Spratford, "A simple method for quantifying jump loads in volleyball athletes," *Journal of Science & Medicine in Sport*, vol. 20, no. 3, pp. 241–245, 2017.

[25] W. Huang, X. Liu, and E. W. Gill, "An empirical mode decomposition method for sea surface wind measurements from X-band nautical radar data," *IEEE Transactions on Geoence and Remote Sensing*, vol. 55, no. 11, pp. 6218–6227, 2017.

WILEY | Hindawi

Research Article

Image Recognition of Crop Diseases and Insect Pests Based on Deep Learning

Mingyuan Xin [iD][1] **and Yong Wang**[2]

[1]*School of Computer and Information Engineering, Heihe University, Heihe, China*
[2]*Institute of International Education, Heihe University, Heihe, China*

Correspondence should be addressed to Mingyuan Xin; xinmy0817@126.com

Deep learning algorithms have the advantages of clear structure and high accuracy in image recognition. Accurate identification of pests and diseases in crops can improve the pertinence of pest control in farmland, which is beneficial to agricultural production. This paper proposes a DCNN-G model based on deep learning and fusion of Google data analysis, using this model to train 640 data samples, and then using 5000 test samples for testing, selecting 80% as the training set and 20% as the test set, and compare the accuracy of the model with the conventional recognition model. Research results show that after degrading a quality level 1 image using the degradation parameters above, 9 quality level images are obtained. Use YOLO's improved network, YOLO-V4, to test and validate images after quality level classification. Images of different quality levels, especially images of adjacent levels, are subjectively observed by human eyes, and it is difficult to distinguish the quality of the images. Using the algorithm model proposed in this article, the recognition accuracy is 95%, which is much higher than the basic 84% of the DCNN model. The quality level classification of crop disease and insect pest images can provide important prior information for the understanding of crop disease and insect pest images and can also provide a scientific basis for testing the imaging capabilities of sensors and objectively evaluating the image quality of crop diseases and pests. The use of convolutional neural networks to realize the classification of crop pest and disease image quality not only expands the application field of deep learning but also provides a new method for crop pest and disease image quality assessment.

1. Introduction

The correct diagnosis and prevention of various crop diseases and insect pests can create a bumper harvest in agricultural production and thus meet the daily needs of the people. Deep learning technology has great advantages in image recognition, but the basic recognition algorithm requires a large number of parameters and requires a large sample database as a comparison library. For crop diseases and insect pests, deep learning technology needs a lot of optimization in sample training.

After the rise of artificial intelligence, deep learning technology has also been widely used in saliency detection. Han proposed SRNet; the model is composed of four parts of convolutional layer modules with different functions. The BN layer and residual network are effectively used, and channel selection is added to improve the accuracy of the model's detection of steganographic algorithms [1]. Chen et al. proposed Zhu-Net, using 3&3 cores instead of traditional 5&5 cores, and optimizing the convolutional layer in the preprocessing layer to improve the detection accuracy of spatial steganography [2]. Chen et al. proposed that different spatial locations obtain saliency through competition and then obtain saliency regions through saliency map fusion and designed a winner-take-all activation network at the back end of the model to simulate the location of human visual dynamic updates [2]. Chui et al. proposed to control the two-way transfer of shallow and deep features to obtain accurate predictions. Using HED iteratively refines its output by using a reverse attention model [3]. Based on the parameter assumptions of the outdoor illumination map, Zhao and Liu use CNN to predict the sun position parameters,

atmospheric condition parameters, and camera parameters in the input image and then use the predicted parameters to synthesize the corresponding HDR environmental illumination map [4].

Zhao et al. add the residual items of local illumination on the basis of global illumination and restore the global illumination information and local illumination information through cascaded CNN through staged prediction and obtain more detailed illumination information [5]. Wu and An predict the pixel-level attention map through the context attention network and combine it with the U-Net network structure to detect the saliency area [6]. Zhai et al. proposed a saliency detection model BASNet based on boundary perception. This model integrates BCE, SSIM, and IoU three loss functions to guide the network to pay more attention to boundary quality, accurately segment saliency regions, and make the boundaries of saliency regions more clear [7]. Miao et al. use the skylight model to predict good outdoor lighting information with only a few parameters and realize the rerendering application of virtual object insertion [8]. Tao et al. use CNN to complete the prediction of outdoor HDR environmental lighting images. The method used can correctly estimate the illuminators in the scene, but the lack of illuminators in the scene can lead to incorrect predictions [9]. Although these methods have improved the standard of saliency detection, there is still much room for improvement in the quality of fine structure segments and the accuracy of the boundary. The illumination information predicted by the above method is very detailed but contains a large number of parameters. For this reason, this paper proposes a deep network model fused with Google data analysis.

Based on the existing objective quality evaluation and quality level classification of crop pests and diseases, this paper uses the classification function of deep learning to construct a deep convolutional neural network model for the classification of crop pest and disease image quality. The model realizes the classification of crop disease and insect pest images with multiple quality levels, which is more detailed and accurate than the comparison literature method. The images after the quality level classification are tested and verified by the improved network YOLO-V3 of YOLO (you only look once), and the detection accuracy is significantly improved.

2. Image Recognition of Deep Learning Convolutional Network

2.1. Three-Dimensional Image Recognition Technology. At present, a small number of studies have established projection models with different aspect ratios and sizes in advance and then use radar to sense the depth information of the surrounding environment of the object, select the projection model that best fits the current scene, and project the 3D objects close to itself to the wall of the model. In space rather than on a two-dimensional plane, the display distortion of three-dimensional objects is reduced [10]. However, this method can only roughly estimate the surrounding environment of the object. When there are multiple three-dimensional objects in the environment, it cannot optimize the display of each three-dimensional object [11]. Combining the radar information and the binocular ranging principle, after jointly estimating the accurate three-dimensional information of the environment, a specific projection model conforming to the current scene is established and then projected [12]. This method can more accurately solve the display distortion problem of each large three-dimensional object, but the real-time performance is reduced due to the need to dynamically change the shape of the projection model, and the projection model with a special shape may also cause projection distortion to other scenes [13]. In the above two methods, the variable projection model is used to solve the problem of projection distortion, and the radar sensor is used to measure the depth of field, which not only causes the increase in system cost but also complicates the processing process [14]. Through analysis, it can be seen that the three-dimensional objects that workers are most concerned about in the process of field work are only other crops and pedestrians (the two are collectively referred to as objects of interest below), so this article combines the characteristics of the application scene and proposes an enhanced three-dimensional method. The synthesis method of panoramic images, combined with object detection and coordinate ascending and inverse mapping, renders the preprepared three-dimensional model of the object of interest on the estimated position, thereby solving the above problem [15].

With the widespread application of deep learning in the field of digital image processing, the use of deep convolutional neural network (DCNN) methods to restore and reconstruct digital images, feature extraction, target detection, and semantic segmentation has become the mainstream research direction of many scholars [16]. Digital image processing based on DCNN employs a data-driven learning and training mode, and the accuracy and effectiveness of the processing are highly dependent on the quality and category of the training set images [17]. For crop disease and insect pest images, due to the impact of the imaging environment, it is difficult to ensure that the acquired image data sets are at the same quality level. This will not only affect the processing effects of crop disease and insect pest images of other quality levels but also affect the processing of the overall business system effect [18]. The root cause of such problems is the imbalance of data quality [19]. The problem of data imbalance is also an important issue that deep learning algorithms pay attention to [20]. Aiming at the problem of unbalanced data quality, the existing methods generally deal with the problem of massively expanding the image data set, increasing the training time and the number of iterations [21]. This method finally obtains only an average value of the processing effect and does not improve the overall effect; the other way is to restore or superresolve the image of crop diseases and insect pests and then perform top-level processing after improving the image quality, although it has a certain effect. However, the reconstruction effect will still be affected by the amount of image data of heterogeneous crop diseases and insect pests [22].

2.2. Image Quality Classification Model of Crop Diseases and Insect Pests. The classification of image quality levels belongs to the category of objective image quality evaluation and is a complicated scientific problem [23]. Automatic evaluation using NIIRS standards is mainly accomplished through the following quality equations:

$$H_{nb} = \sum_{j=2}^{k} \sum_{h=1}^{j-1} G_{jh} \left(p_j s_h + p_h s_j \right) D_{jh},$$

$$D_{jh} = \frac{d_{jh} - P_{jh}}{d_{jh} + P_{jh}}, \tag{1}$$

$$\text{RER}_{jh} = \int_0^{\infty} dF_j(y) \int_0^y (y - x) dF_h(x),$$

where D represents the coefficient of the equation; there are different assignment versions: RER (relative edge response) represents the relative edge response; G (Convolved Gain) represents the noise gain of the imaging system postprocessing; H (Edge Overshoot) represents the edge after the system postprocessing overshoot factor [24]. Since it is difficult for general researchers to obtain GSD-related parameters of crop disease and insect pest images, the calculation of RER also requires the image to have appropriate edge shape characteristics, and the calculation method of SNR is not unique. The image quality equation is used to quality crop disease and insect pest images. Hierarchical classification has great limitations:

$$f(x) = \frac{1}{Nh} \sum_{i=1}^{N} k \left(\frac{X_i - x}{h} \right),$$

$$k(x) = \frac{1}{\sqrt{2\pi}} \exp \left(-\frac{x^2}{2} \right), \tag{2}$$

$$h_t = \tanh \left(w_c x_t + u_c (r_t \Theta h_{t-1}) + b_c \right),$$

$$h_t = z_t \Theta h_{t-1} + (1 - z_t) \Theta h_t.$$

There are relatively few research results on the use of deep learning to achieve image quality classification. From the perspective of blind image restoration, the literature divides close-up images into two simple types, clear and blurred, due to the lack of batch normalization (BN) layer, greatly reducing the generalization ability of the network:

$$\sigma t = \frac{\sqrt{1/n \sum_{i=1}^{n} (FI_{it} - FI_{it})^2}}{FI_{it}},$$

$$u_{(j|i)} = w_{ij} A_i, \tag{3}$$

$$s_j = \sum_i c_{ij} u_{(j|i)}.$$

From the perspective of quality evaluation, a multitask quality grade prediction DCNN method is proposed. This method uses NIIRS as the subjective quality label, con-

structs a quality grade classification and regression network, and realizes 10 quality grade classifications. The feature extraction network structure of this method is deep, and the calculation efficiency is too low for the problem of coarse quality level classification; due to the lack of random loss of connections, it is also prone to overfitting:

$$\ln \left(\frac{FI_{it}}{FI_{it} - 1} \right) = \alpha + \beta \ln FI_{it} - 1 + v_i + \mathfrak{I}_t. \tag{4}$$

At the same time, there are considerable errors and difficulties in the calculation of subjective quality labels. The image quality classification of crop diseases and insect pests is a qualitative study of images, which is a typical mathematical classification problem. The feedforward convolutional neural network structure based on supervised learning has a powerful classification function, which is very suitable for quality level classification using this type of network structure:

$$c_{ij} = \frac{e^{b_{ij}}}{\sum_k e^{b_{ik}}},$$

$$r = \frac{\alpha}{1 - \beta},$$

$$\theta = -\frac{1}{T} \ln (1 + \beta), \tag{5}$$

$$\tau = \frac{\ln (2)}{\theta}.$$

2.3. Basic Convolutional Neural Network Structure for Image Quality Classification. Our goal is to train a classifier through DCNN to classify images of crop diseases and insect pests into different levels according to their quality. The classification network takes the image of crop diseases and insect pests as input and outputs a label value representing the quality level of the image. Therefore, the entire network is a frame from large to small, from coarse to fine. Since the quality of the image of crop diseases and insect pests is not necessarily related to the size of the image, the input image can be taken into a relatively fixed size. First, the input sample image is preprocessed by zero score standardization. The purpose is to adjust the pixel value distribution of crop pest images to a nearly normal distribution and improve the ability to activate network training. Secondly, in order to alleviate the overfitting problem and reduce additional connection parameters, multiple BN layers are added to the middle layer, and the global average pooling layer is replaced with a fully connected layer commonly used in classifiers. In order to maintain the detailed characteristics of the image from large to small, the maximum pooling (MaxPooling) method is used for data scale compression; in order to improve the convergence speed while avoiding the disappearance of the gradient, a linear correction is added after the convolution (convolution, Conv) layer

unit ReLU function:

$$\ln\left(\frac{FI_{it}}{FI_{it}-1}\right) = \alpha + \beta \ln FI_{it} - 1 + \phi X_{it} - 1 + \nu_i + \tau_t,$$

$$k_{t1}[i] = \sum_j \cos\left(w_i^1, w_j^2\right),$$

$$BCRM_{jh} = \frac{\sum_{Z=1}^{h_j}\sum_{r=1}^{n_h}\left|y_{ji} - y_{hr}\right|}{n_j n_h (u_j + u_h)},$$

$$DCNN_t = \sum_{j=2}^{k}\sum_{h=1}^{j-1} G_{jh}\left(p_j s_h + p_h s_j\right) D_{jh}\left(1 - D_{jh}\right). \tag{6}$$

The above formula shows the DCNN architecture of quality classification, in which K is the number of BCRM, and BCRM is the abbreviation of BN layer, Conv layer, ReLU layer, and max-pooling layer. After conversion, it can be expressed by the following formula:

$$Gjj = \frac{1/2 u_j \sum_{i=1}^{n_j}\sum_{r=1}^{n_j}\left|y_{ji} - y_{jr}\right|}{n_j^2},$$

$$Gw = \sum_{j=1}^{k} G_{jj} p_j s_j. \tag{7}$$

Convolution neural networks need to choose an appropriate loss function to transform the convolution parameter acquisition problem into an optimization problem. The label of data classification problem is often understood as a probability value, so its loss function is mainly set for this probability value. The most common loss function is the cross-entropy function, which has the advantage of faster weight update than the variance loss function. Assuming that X represents the input image and the network parameters to be trained, the DCNN quality classification network can be understood as a probability function for predicting the X quality index:

$$d_{jh} = \int_0^\infty dF_h(y) \int_0^y (y - x) dF_j(y),$$

$$G = G_w + G_{nb} + G_t. \tag{8}$$

In the formula, G is the number of samples in each batch, and the optimal classification level value of the segment quality level classification network is preset. Once it exceeds the preset level value, the convergence speed will be slow and the classification accuracy will be low.

2.4. Multistage Quality Classification. Multisegment hierarchical classification is to use a shallow convolutional neural network, through adjusting the label, similar to the shape of the pyramid, from coarse to fine layer by layer classification,

can achieve fixed network depth, but not fixed number of levels of quality classification. Since any integer greater than 1 can be regarded as a linear combination of positive integers less than 1, any level of quality classification can be achieved by using a 2-level, 3-level, and 4-level quality classification network with less feature extraction layer. During the training process, the input for each segment of the network is the original training data and only a simple classification network is used to achieve the classification. In the process of testing, we need to use the judgment method to select the appropriate network structure path to achieve classification, but the judgment method is a convolutional network. The advantage of multistage network structure quality level classification is that the classification level can be set freely, the network structure is fixed, and the classification is realized layer by layer through internal circulation, so the training process is relatively simple.

The generalized camera internal parameters include the camera internal parameter matrix and the camera distortion parameters, which reflect the internal optical structure of the camera and are related to the characteristics of the camera itself. They are mainly responsible for the mapping process from the camera coordinate system to the pixel coordinate system. They are the mapping process from three-dimensional to two-dimensional, and also the conversion process from the physical length unit to the pixel length unit. The transformation of internal parameters of insect camera is as follows:

$$G = \frac{\sum_{j=1}^{k}\sum_{h=1}^{k}\sum_{t=1}^{n_j}\sum_{r=1}^{n_h}\left|y_{ij} - y_{hr}\right|}{2n^2 u}, \tag{9}$$

where the subscript g is the camera coordinate system, K is the distortion parameter of the insect camera, and H is the coordinate point in the pixel coordinate system, which is generally half of the image length and width. Based on the above conversion principle, with the help of camera calibration chessboard, the internal parameter, external parameter matrix, and distortion parameters of four insect cameras are calibrated, respectively. The mapping projection model establishes a virtual object surrounding the environment, and the points on it are taken as the points in the world coordinate system. Through the above mapping relationship, the corresponding pixel coordinates (i.e., the points in the four images) are obtained, and the RGB information of the corresponding image points is rendered on the projection model to complete the synthesis of the basic three-dimensional panoramic image. Using this kind of projection model, the road surface can be projected to the model ground and the three-dimensional objects such as crops can be projected to the model wall in most cases, so as to ensure the correct projection relationship of the objects and avoid distortion.

It is difficult to optimize these two kinds of distortions at the same time simply by changing the size of the projection model. When the projection model is enlarged, the line bending distortion can be alleviated, but more crops, pedestrians, and other three-dimensional objects will fall into the ground area of the projection model, thus aggravating the object

The four evaluation indicators of MEMA-T classification
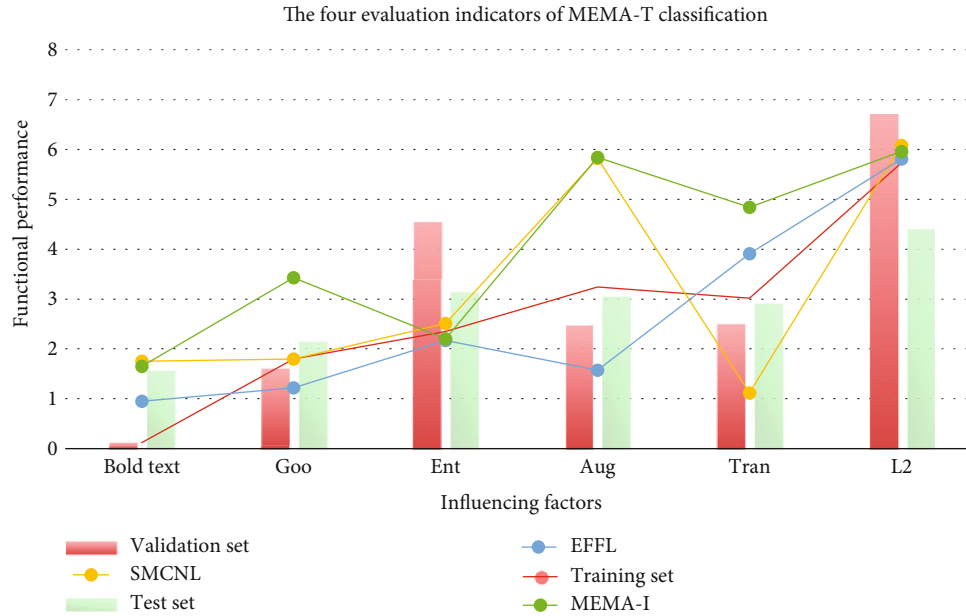
Figure 1: The four evaluation indicators of MEMA-T classification.

stretching distortion; on the contrary, although reducing the projection model can ensure the accuracy of most three-dimensional objects projected on the wall, it can not guarantee the straightness of the ground line. And in the process of dynamic adjustment of the model, the display screen is prone to jump, which affects the display effect.

3. Image Recognition Design of Crop Diseases and Insect Pests

3.1. Objects. In this paper, a DCNN-G model based on deep learning and Google data analysis is proposed. 640 data samples are trained by this model, and then, 5000 test samples are tested. The accuracy of this model is compared with the conventional recognition model. The 5000 images are cut into 256 pixel × 256 pixel images, and 80% of the training set and 20% of the data are selected as the test set. After one image of quality level 1 is degraded by using the above degradation parameters, nine quality level images are obtained. The images classified by quality level are tested by using the improved network YOLO-V4 of YOLO (you only look once).

3.2. Steps. A high-performance computing platform (TSMC server) and nvidi card are used for model training. The training parameters were set as batch size of 32, learning rate of 0.001, and turn of 1500. Use Adam network optimizer to update the weight parameters. The model training needs about 23,400 s, and the image preprocessing uses the MATLAB r2018b platform and Python 3.7. The classification results of SMCNL, EFFL, MEMA-I, and MEMA-T in the test data set containing 640 data samples are compared. It is difficult to distinguish the quality of images with different quality levels, especially those with adjacent levels, by subjective

observation with human eyes. The results show that both one segment and multiple segments can achieve a 10-grade image quality classification of crop diseases and pests. For the three models designed by the one-stage quality classification method, accuracy, recall, and precision of n-type are significantly improved compared with S-type, and the evaluation index of n-type is basically unchanged compared with C-type. The Gaussian blur and Gaussian noise of different scales added to the original data are artificially degraded, and they are marked as 2-10 levels, respectively, with a total of 5000 images. The 5000 images are then cut into 256 pixel × 256 pixel images, and 80% of the training set and 20% of the data are selected as the test set.

(1) Image preprocessing

Color normalization in the process of staining and scanning of aortic wall tissue samples, due to the different laboratory conditions of staining, parameter settings of a digital scanner, and illumination, the color differences of digital pest images are often caused. Color normalization can not only ensure the color consistency of the image but also preserve the biological information in the pest image, so as to improve the classification performance of the model. A normalization method based on staining separation is used to reduce the color difference of histopathological images, and the structure information in the images is saved as much as possible by generating the staining density map.

(2) 3D panorama of crop enhanced image

The adaptive projection model method is easy to take one thing into account and lose the other when solving the distortion problem. In view of the problem of display distortion and the shortage of current solutions, this paper proposes

TABLE 1: The GoogLeNet model achieved classification performance comparable.

Item	Training set	Validation set	Test set	SMCNL	EFFL	MEMA-I
Bold text	0.12	0.15	1.59	1.75	0.95	1.65
Goo	1.8	1.63	2.17	1.8	1.22	3.43
Ent	2.35	4.56	3.15	2.51	2.17	2.2
Aug	3.24	2.48	3.05	5.82	1.57	5.84
Tran	3.02	2.51	2.91	1.12	3.91	4.84
L2	5.73	6.71	4.4	6.08	5.81	5.96
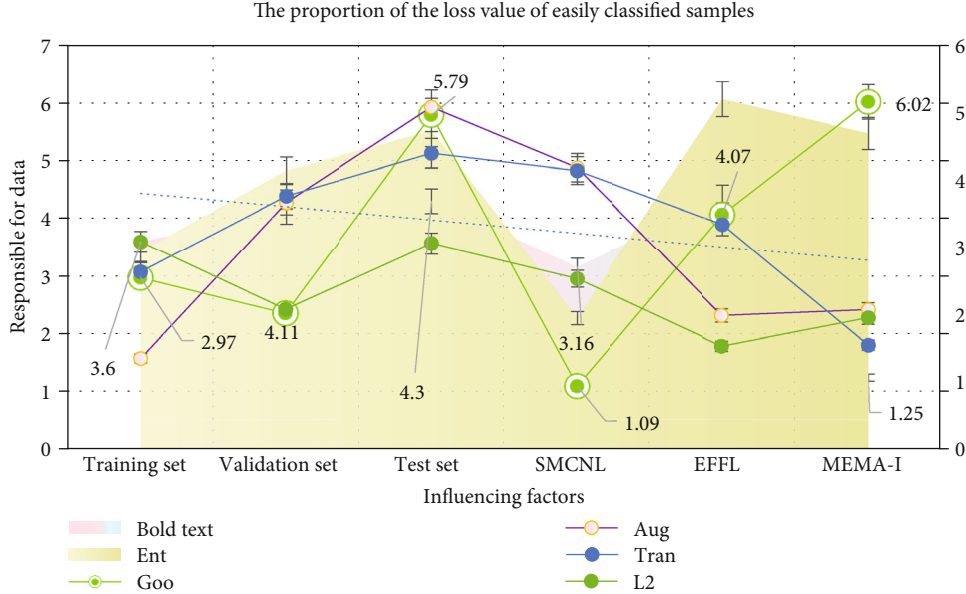
FIGURE 2: The proportion of the loss value of easily classified samples.

an enhanced 3D panoramic image synthesis method. With the help of the YOLO detection network and the coordinate dimension elevation inverse mapping method proposed in this paper, the 3D objects around the agricultural objects are represented in the way of virtual synthesis without dynamically changing the projection model. This paper will focus on how to detect the object of interest and estimate its accurate world space position through the image. The steps are as follows: firstly, the original image captured by four cameras is taken as the input of the object detection network, and all the interested objects are identified and selected; secondly, the object's position in the world coordinate system is estimated by using the object's pixel coordinates through the coordinate dimension ascending inverse mapping method proposed in this paper; and then, after a series of data processing for the estimated position, the accurate object is obtained. Finally, the general model of crops and pedestrians built in advance is placed and rendered on the estimated position, which will overlay and display the three-dimensional objects that are wrongly mapped on the ground. This method can reduce the line bending distortion as much as possible while solving the object stretching distortion and make the display more natural while providing accurate object position information.

TABLE 2: GoogLeNet model improves training efficiency.

Item	Bold text	Goo	Ent	Aug	Tran	L2
Training set	3.6	2.97	2.94	1.58	3.08	3.6
Validation set	4.11	2.35	4.14	4.28	4.39	2.42
Test set	4.3	5.79	4.73	5.93	5.13	3.57
SMCNL	3.16	1.09	1.95	4.88	4.83	2.96
EFFL	4.36	4.07	5.2	2.32	3.9	1.79
MEMA-I	1.25	6.02	4.69	2.42	1.81	2.28

4. Image Recognition and Analysis of Crop Diseases and Pests Based on Deep Learning

4.1. Improvement of Data Imbalance by Deep Learning. As shown in Figure 1, it is found that the four evaluation indexes of MEMA-T classification have been effectively improved, which indicates that data enhancement helps to improve the classification performance of pest images with data imbalance. L2 regularization is used to eliminate the overfitting phenomenon in the training process. This paper uses focal loss instead of cross-entropy loss function to solve the problem of data imbalance. To assess the effectiveness of
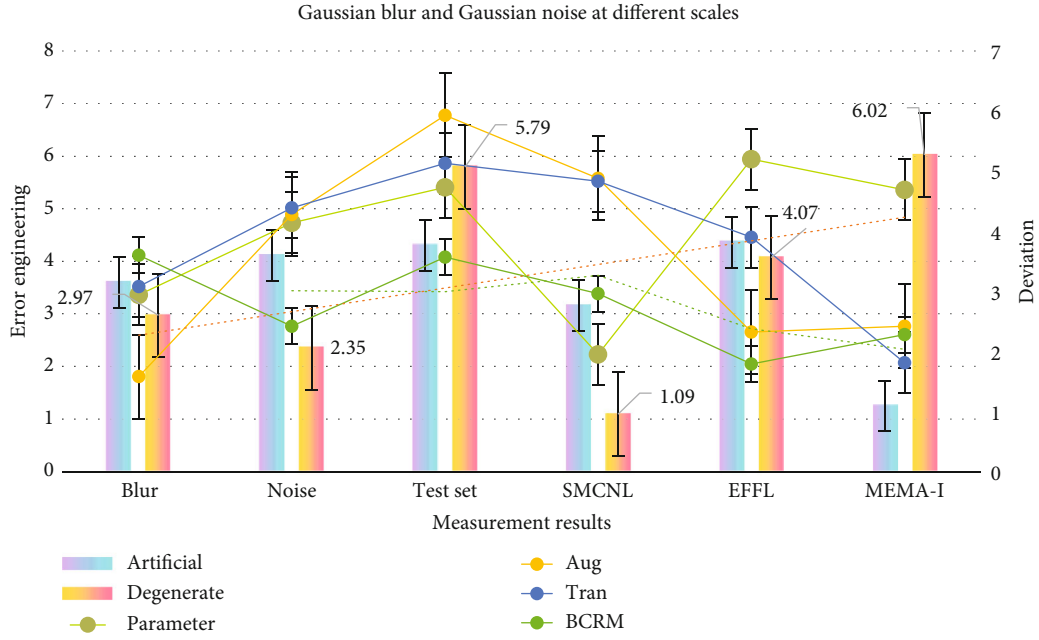
Figure 3: Gaussian blur and Gaussian noise at different scales.

Table 3: Use image information entropy as standard.

Item	Artificial	Degenerate	Parameter	Aug	Tran	BCRM
Gaussian blur	3.6	2.97	2.94	1.58	3.08	3.6
Gaussian noise	4.11	2.35	4.14	4.28	4.39	2.42
Test set	4.3	5.79	4.73	5.93	5.13	3.57
SMCNL	3.16	1.09	1.95	4.88	4.83	2.96
EFFL	4.36	4.07	5.2	2.32	3.9	1.79
MEMA-I	1.25	6.02	4.69	2.42	1.81	2.28

Table 4: For multistage quality classification.

Item	ResNet	MnasNet	SMCNL	EFFL	MEMA-I	AlexNet	GoogLeNet
MD	0.62	1.56	0.12	0.15	1.59	1.75	0.95
EFFL	1.03	1.04	1.8	1.63	2.17	1.8	1.22
MEMA-I	3.06	4.38	2.35	4.56	3.15	2.51	2.17
MEMA-T	5.18	3	3.24	2.48	3.05	5.82	1.57
VGG16	2.16	3.77	3.02	2.51	2.91	1.12	3.91
AlexNet	5.25	5.02	5.73	6.71	4.4	6.08	5.81

the different methods in the model, we used the mean classification accuracy of the four types of lesions, the training set, the validation set, and the test set, as metrics.

The simplified GoogLeNet model achieves the same classification performance as the original model, as shown in Table 1. Among them, bold text, Goo, Ent, Aug, Tran, L2, and FOC represent the best performance, respectively. The simplified GoogLeNet model has cross-entropy loss function, data enhancement, transfer learning, L2 regularization, and focal loss function. Both data enhancement and transfer learning can improve the classification performance of the

model, and the combination of the two methods can obtain higher classification accuracy than using them alone. The use of L2 regularization can restrain overfitting to a certain extent and enhance the stability of model fitting function.

As shown in Figure 2, focal loss can further improve the multiclassification performance by reducing the proportion of loss values of easy to classify samples and forcing training for difficult to classify samples. In the pathological data of this paper, MEMA-I and MEMA-T are two similar types of lesions, which are difficult to distinguish. Compared with the original GoogLeNet model, the classification accuracy
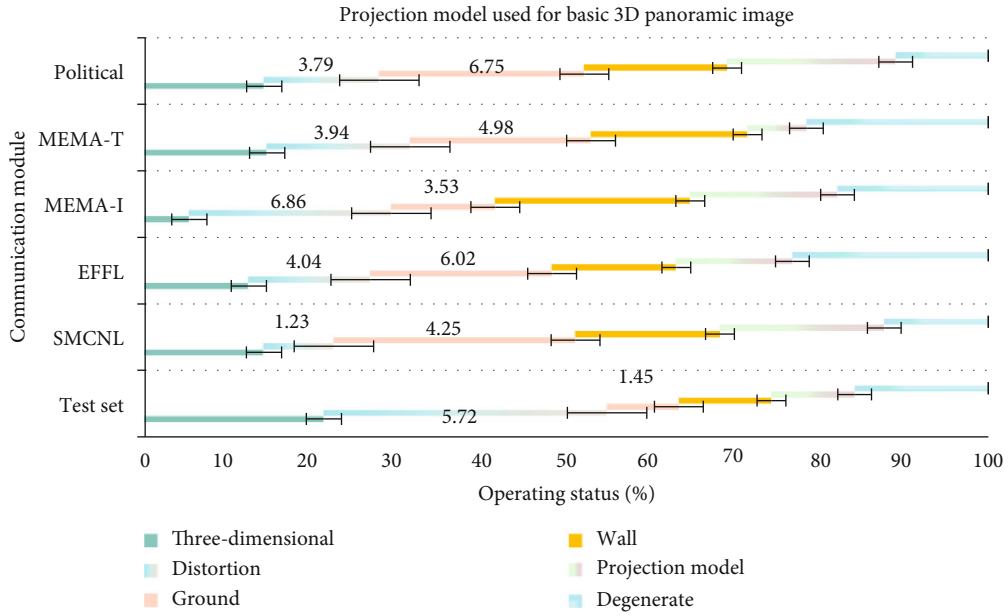
Figure 4: Projection model used for basic 3D panoramic image.

Table 5: The parameter combination is set according to the results of previous work.

Item	Test set	SMCNL	EFFL	MEMA-I	MEMA-T	Political
Three-dimensional	3.61	2.09	3.44	1.5	3.36	3.92
Distortion	5.72	1.23	4.04	6.86	3.94	3.79
Ground	1.45	4.25	6.02	3.53	4.98	6.75
Wall	1.87	2.54	4.12	6.62	4.31	4.7
Projection model	1.68	2.89	3.85	5	1.62	5.55
Degenerate	2.7	1.83	6.5	5.12	5.01	3.05
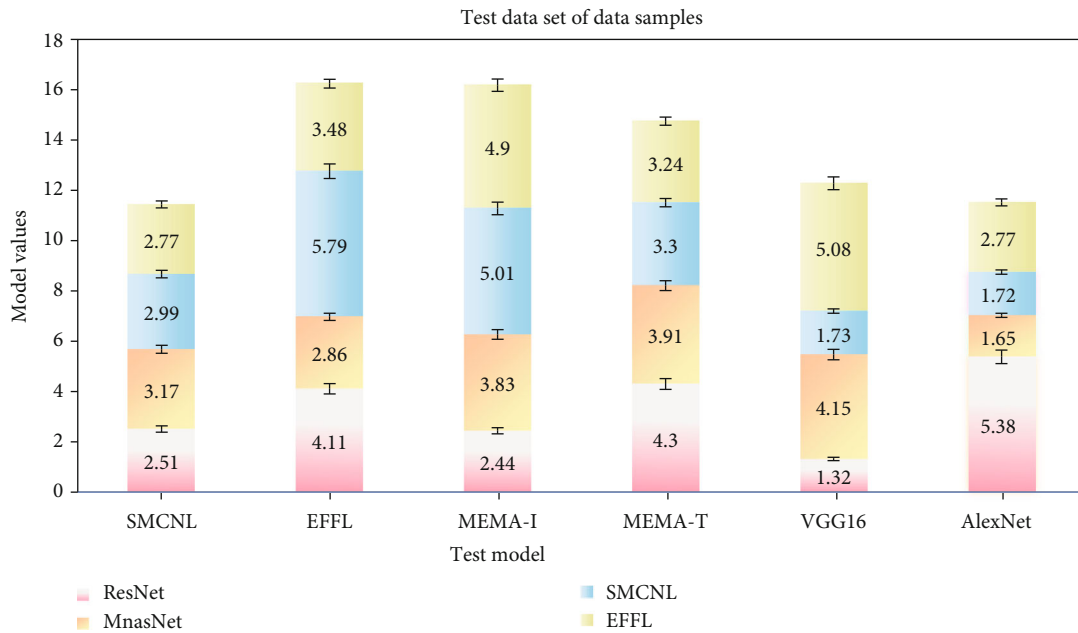
Figure 5: Test data set of data samples.
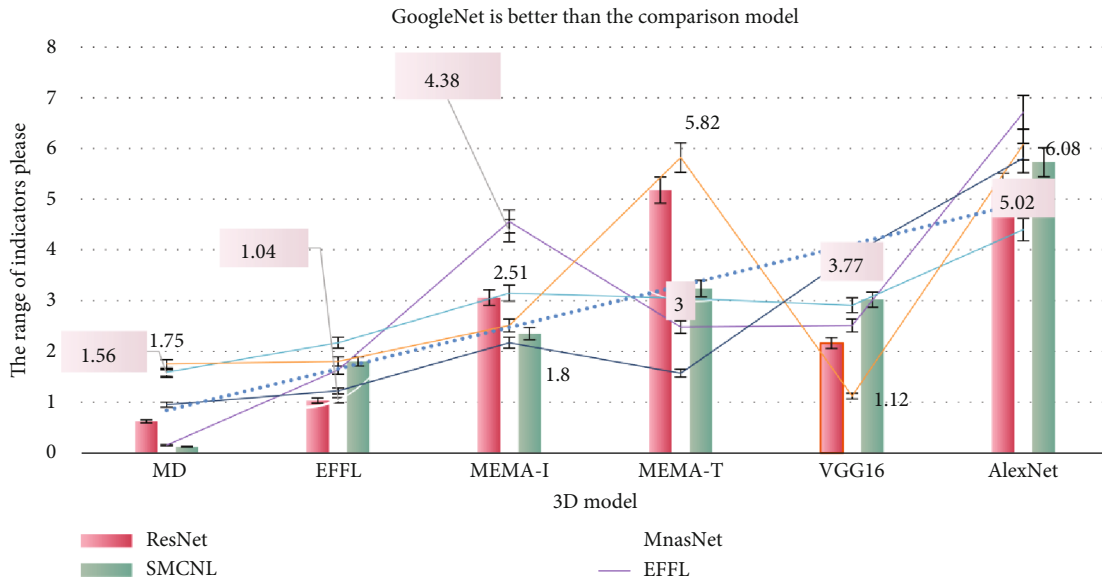
Figure 6: GoogLeNet is better than the comparison model.

Table 6: Residual learning to improve the classification performance of the model.

Item	ResNet	MnasNet	SMCNL	EFFL	MEMA-I	MEMA-T
SMCNL	2.51	3.17	2.99	2.77	2.78	3.12
EFFL	4.11	2.86	5.79	3.48	5.47	2.53
MEMA-I	2.44	3.83	5.01	4.9	5.73	5.32
MEMA-T	4.3	3.91	3.3	3.24	4.5	2.34
VGG16	1.32	4.15	1.73	5.08	1.47	1.88
AlexNet	5.38	1.65	1.72	2.77	2.22	6.43
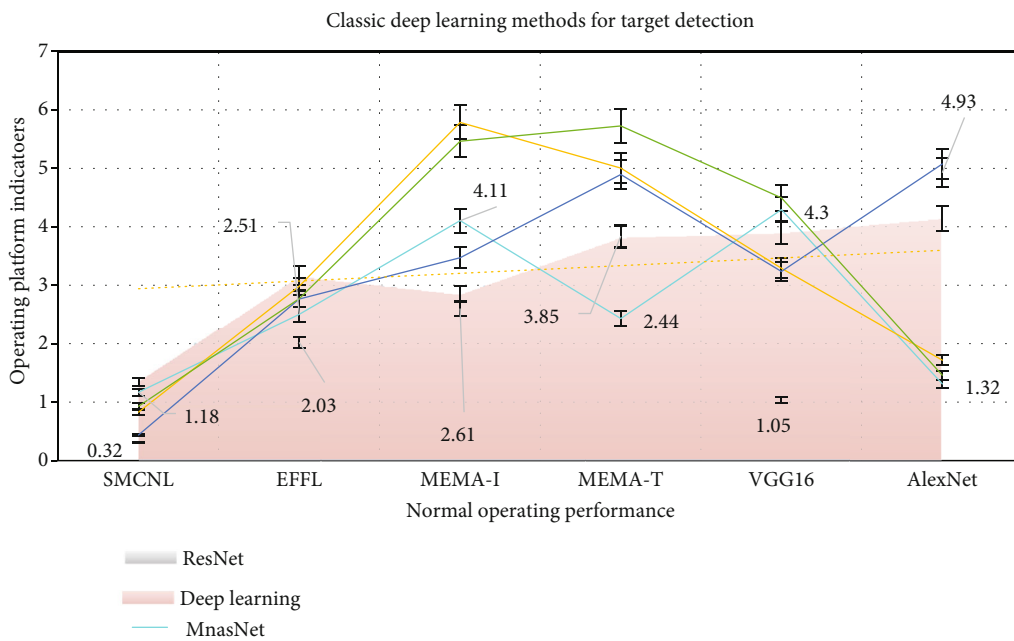
Figure 7: Classic deep learning methods for target detection.

of simplified GoogLeNet for MEMA-I and MEMA-T is improved by about 4%.

As shown in Table 2, the simplified GoogLeNet model is used to improve the training efficiency, and the data enhancement, migration learning, and L2 regularization are effectively used to further improve the network performance. Focal loss is used to solve the problem of image data imbalances in mesomorphic diseases and pests. The experimental results show that the simplified GoogLeNet model is superior to the commonly used deep learning model in MD classification performance. This study provides a new idea for deep learning technology to classify noninflammatory aortic media lesions based on pest images. In the future work, we will get more and more kinds of pest images to further improve the generalization ability of the model.

The Gaussian blur and Gaussian noise of different scales added to the original data are artificially degraded, which are, respectively, marked as 2-10 levels, with a total of 5000 pieces. The artificial degradation parameters are shown in Figure 3. The 5000 images are then cut into $256\,\mathrm{pixel} \times 256$ pixel images, and 80% of the training set and 20% of the data are selected as the test set. After one image of quality level 1 is degraded by using the above degradation parameters, nine quality level images are obtained. It is difficult to distinguish the quality of images with different quality levels, especially the images with adjacent levels, by subjective observation with human eyes. Using the algorithm model proposed in this paper, the recognition accuracy is 95%, which is much higher than 84% of the basic DCNN model.

Because the imaging parameters of the above images can not be obtained, the NIIRS quality equation can not be used for classification. The image information entropy is used as the standard for classification and evaluation. It is also difficult to distinguish the quality level of 30 images selected from the test set with the quality level labels of 1, 5, and 10 through the value of information entropy and curve, as shown in Table 3.

In the DCNN architecture of quality classification, there are three kinds of network models. The first one is called normal type (referred to as n-type). There are three BCRM layers in the middle of the network; the second one is called simple type (referred to as S-type). Compared with n-type, there is only one BCRM layer in the middle of the network. The third type is called complex type (C-type for short). Compared with n-type, there are five BCRM layers in the middle of the network. For the multistage quality classification, the 2-fork structure is adopted in all layers, and the n-type network structure is adopted in all layers. The input image size of crop diseases and insect pests is 256×256, the number of iterations is set to 200, and the network parameters are shown in Table 4.

4.2. Image Recognition Effect Analysis of Training DCNN-G. As shown in Figure 4, because the projection model used in the basic three-dimensional panoramic image is established in advance according to experience, it is impossible to adapt to all scenes, so when the real three-dimensional environment of the crop does not match the projection

Table 7: Method is limited to certain types of resolution data.

Item	ResNet	MnasNet	Deep learning	Remote sensing	Crop	Pests and diseases
SMCNL	0.32	1.18	1.35	0.84	0.45	0.94
EFFL	2.03	2.51	3.17	2.99	2.77	2.78
MEMA-I	2.61	4.11	2.86	5.79	3.48	5.47
MEMA-T	3.85	2.44	3.83	5.01	4.9	5.73
VGG16	1.05	4.3	3.91	3.3	3.24	4.5
AlexNet	4.93	1.32	4.15	1.73	5.08	1.47

model created by the simulation, the display will be distorted.

As shown in Table 5, the best training effect can be obtained by manually adjusting the parameters of L2 regularization ($\lambda = 0.001$). Two key parameters involved in focal loss are $\alpha = 0.25$ and $\gamma = 2$. The parameter combination is set according to the results of previous work to ensure the best classification performance of the model.

As shown in Figure 5, the classification results of SMCNL, EFFL, MEMA-I, and MEMA-T in the test data set contain 640 data samples, in which the bold text represents the best result. Two samples of SMCNL and EFFL were misclassified into other types. The model has good recognition and resolution ability for SMCNL and EFFL. Compared with SMCNL and EFFL, MEMA-I and MEMA-T have more misclassification samples, especially about 16% of them are identified as MEMA-I. The reason is that the two types of lesions show similar pathological features. In addition, due to the serious imbalance of data, MEMA-T data samples are less, resulting in poor classification results.

As shown in Figure 6, all models adopt the same data enhancement, migration learning, L2 regularization, and focal loss. Through observation, it is found that the improved GoogLeNet is better than the comparison model in MD classification performance. EFFL got the best results among all the classification indexes. MEMA-I achieves the best results in accuracy, accuracy, and F value. SMCNL has the highest accuracy and precision. Due to the imbalance of data and the small number of MEMA-T samples in the test data set, the MEMA-T classification results are inadequate.

As shown in Table 6, the ResNet model also performs well. It has an 18 layer network structure, which is close to the network depth of the GoogLeNet model used in this paper. In addition, it introduces residual learning to improve the classification performance of the model. However, due to the large difference of lesion size among different lesion types of MD, GoogLeNet introduces convolution kernels of different sizes, which can better extract the context information of MD, so its performance is better than ResNet. Compared with other networks, the performance of AlexNet is poor. The main reason is that AlexNet is a shallow network with an eight-layer network structure, which reduces the accuracy of MD classification tasks due to its limited ability to capture
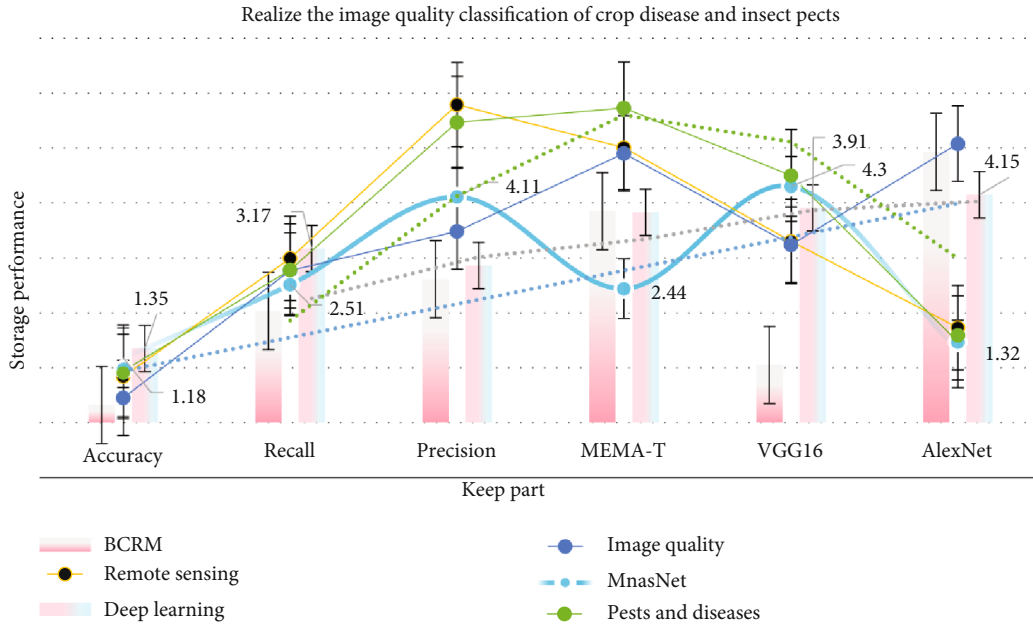
FIGURE 8: Realize the image quality classification of crop diseases and insect pests.

TABLE 8: Training and detection of crop disease and insect pest image data.

Item	BCRM	MnasNet	Deep learning	Remote sensing	Image quality	Pests and diseases
Accuracy	0.32	1.18	1.35	0.84	0.45	0.94
Recall	2.03	2.51	3.17	2.99	2.77	2.78
Precision	2.61	4.11	2.86	5.79	3.48	5.47
MEMA-T	3.85	2.44	3.83	5.01	4.9	5.73
VGG16	1.05	4.3	3.91	3.3	3.24	4.5
AlexNet	4.93	1.32	4.15	1.73	5.08	1.47

TABLE 9: The average value of mAP detected by 3 types of different data targets.

Item	Epoch	YOLO-V3	Precision	MEMA-T	VGG16	AlexNet
YOLO-V4	0.03	1.82	0.28	0	1.09	1.89
OpenGL	3.76	2	1.94	3.9	1.05	1.1
Deep learning	3.46	3.64	2.68	3.22	5.24	3.15
Remote sensing	5.44	3.26	3.94	4.01	3.1	5.82
OpenCV	2.16	2.35	4.16	1.65	3.18	3.82
OpenGL	5.89	6.34	2.22	6.89	2.57	6.38
SMCNL	1.01	3.3	3	6.43	6.87	1.62

image features of diseases and pests. The comparison results show that the improved GoogLeNet model can recognize specific histopathological changes from the images of diseases and insect pests and help to improve the automatic classification of four types of MD lesions. The results show that the classification results of MEMA-T are poor, mainly due to the small number of samples and serious data imbalance.

4.3. Use YOLO-V4 to Test and Analyze the Model after Training. As shown in Figure 7, the model tested by

YOLO-V4 can not only realize the classification of fixed number of grades but also realize the classification of non-fixed number of grades, and the classification results are more detailed and accurate. After the preprocessing of quality level classification, the classical deep learning method is used for target detection, and the detection accuracy is significantly improved, which can effectively solve the problem of imbalanced data quality in the training set. A convolution neural network is used to classify the image quality of crop diseases and insect pests, which not only expands the

The display effect of the basic 3D panoramic imaging system
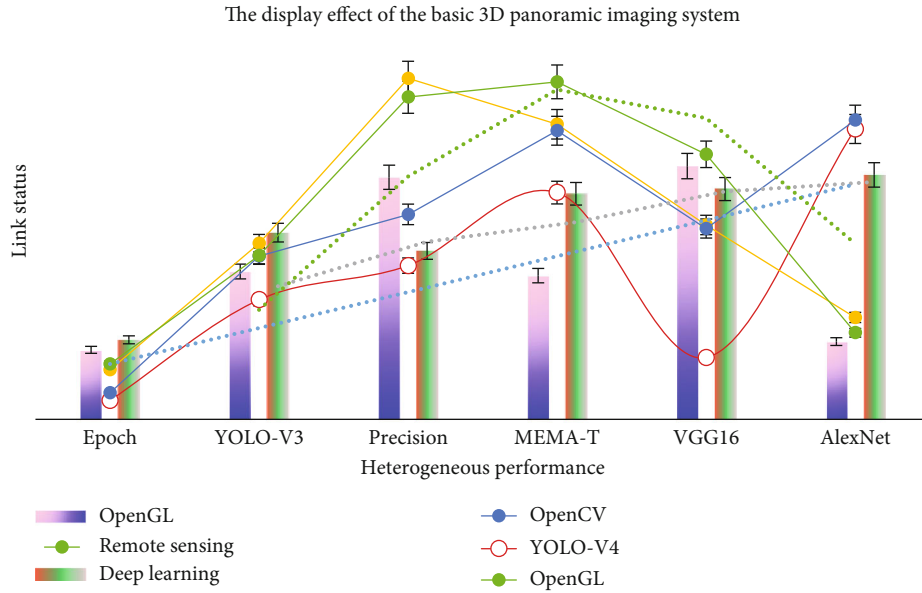
FIGURE 9: The display effect of the basic 3D panoramic imaging system.
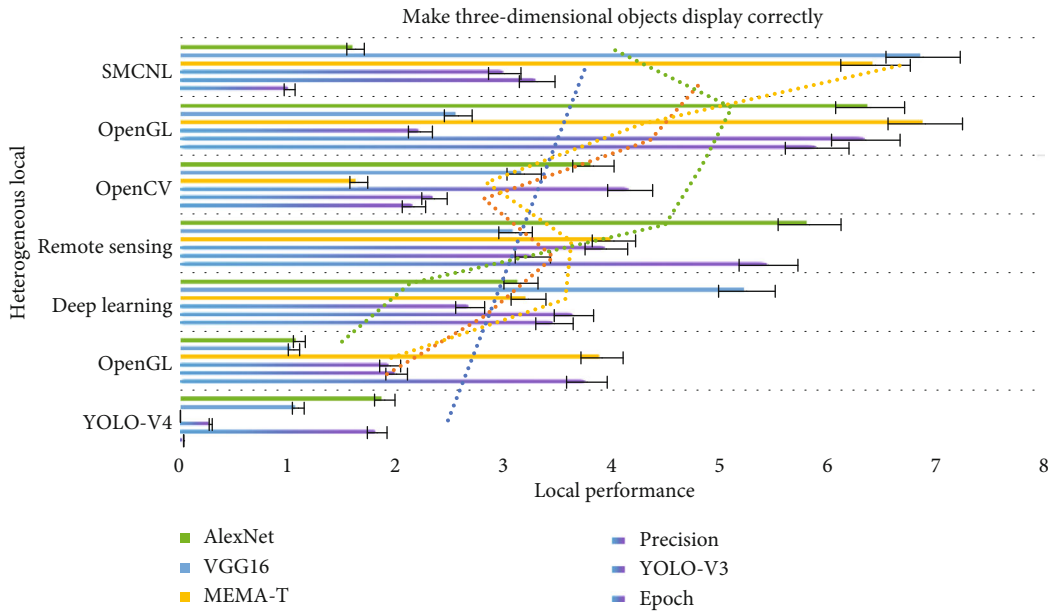
FIGURE 10: Make three-dimensional objects display correctly.

application field of deep learning but also provides a new method for image quality evaluation of crop diseases and insect pests.

As shown in Table 7, many image processing methods of crop diseases and insect pests are based on the same image quality level, such as crop disease and insect pest image registration, landmark detection, and target recognition; generally, different data sources, different spatial resolution, and different spectral resolution data are distinguished, and different technical means are used for processing, and even some methods are used. The method is limited to some kind of resolution data. Another example is image restoration; many methods are known that the image is degraded under

the premise of restoration processing. This makes people have to design different methods or adjust the corresponding parameters for different quality levels of images in order to obtain the corresponding processing effect, which is obviously inconsistent with the technical requirements of the fully automated intelligent era. The quality classification of crop disease and insect pest images can not only provide important prior information for understanding crop disease and insect pest images but also provide scientific basis for testing the imaging ability of sensors and objectively evaluating the image quality of crop diseases and insect pests.

As shown in Figure 8, both one segment and multisegment can well achieve 10 levels of image quality classification

(a) (b)
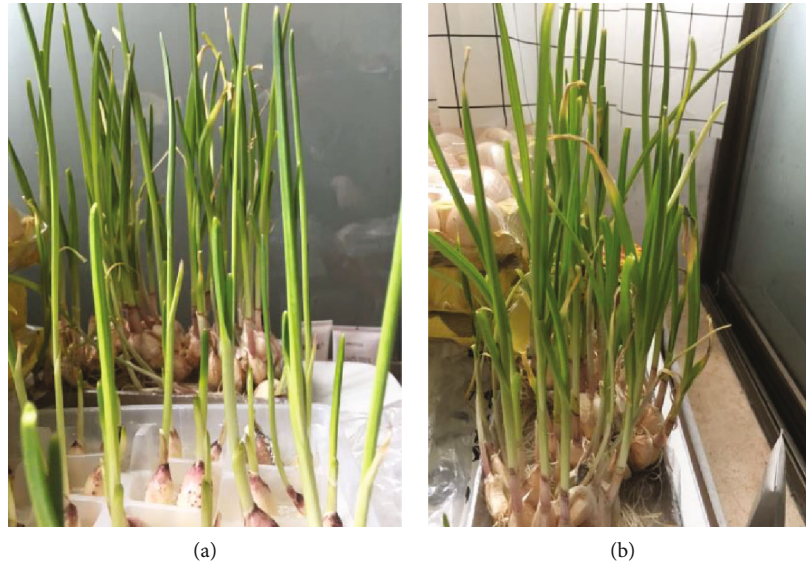
Figure 11: Sample image of processing sample (camera live shooting, left (a), right (b)).

of crop diseases and insect pests. For the three models of one-stage quality classification, accuracy, recall, and precision of n-type are significantly improved compared with S-type, and the evaluation indexes of n-type are basically unchanged compared with C-type, which indicates that BCRM has an impact on the results, and it also means that n-type can fully meet the application requirements for 10 quality classification. For the multistage quality level classification, it also achieves the effect of one-stage classification and does not need to estimate the number of BCRM. Each stage adopts the n-type classification structure of 10 quality levels, which can fully ensure the accuracy of two quality levels in each stage and further reduce the error accumulation. However, the training time and detection time are relatively long, which is the reason, that closely related to the number of parameters and the complexity of intermediate computation.

The original 610 image data of agricultural crop diseases and pests are directly trained and detected, as shown in Table 8. Quality classification refers to training and testing according to different quality classes. That is, the training set and the test set belong to the same quality class. The number ratio of the training set data and test set data is 4 : 1, and the test set data is not in the training set. Because the similar quality level has little influence on the target detection, the images of crop diseases and insect pests of levels 1-4, levels 5-8, and levels 9-10 are classified into the same quality class in the experiment, and the final map value is the average value of map of these three types of different data target detection, and the results are shown in Table 9.

As shown in Figure 9, the display effect in the same perspective and scene is compared when the method is used and not used. It shows the display effect of the basic three-dimensional panoramic image system. When the pests and diseases are in the ground area of the projection model, the system will cause projection distortion to these objects, so that the workers can not accurately obtain the position information of the objects around the objects, or even can not see

the objects clearly. Using the enhanced three-dimensional panoramic image synthesis method in this paper, the images of diseases and pests are clearly presented in the scene through the three-dimensional model, which can greatly facilitate workers to observe.

As shown in Figure 10, compared with the existing solutions, this method does not need to reduce the projection model to make the three-dimensional object display correctly, so it can maximize the ground part of the model, so it can better weaken the line bending distortion, that is, to maintain the flatness of the road as far as possible.

As shown in Figure 11, (a) shows the display effect of this method. The projection model size is set to 3000 mm, and the light is basically straight by observing the vertical line. However, the existing solution (adaptive model method) can only make 3D objects mapped on the wall by reducing the projection model, as shown in (b). At this time, the size of the projection model is 700 mm; although the lateral pests are well displayed, the image obviously causes great bending to the road.

5. Conclusions

This paper first introduces the basic three-dimensional panoramic image synthesis algorithm and analyzes the causes of its display distortion, then proposes the enhanced three-dimensional panoramic image synthesis method, and finally verifies the performance indicators of this method through experiments. Based on the existing algorithms of 3D panoramic image synthesis of pests and diseases, this paper proposes an enhanced 3D panoramic image synthesis method of pests and diseases based on coordinate ascending inverse mapping, which is used to solve the display distortion problem of 3D objects in the original system. Firstly, the position of the object of interest in each image is detected by using the YOLO-V4 network, and then, the inverse mapping method of coordinate elevation from the pixel coordinate system to

the world coordinate system is derived by using the insect camera calibration parameters combined with the supplementary conditions, so as to preliminarily estimate the position of the object of interest in the world coordinate system. Then, by merging and filtering the estimated positions, you get the final estimated position, place the preset model in the corresponding position, and render it to complete the highlighting. Compared with the existing solutions, this method has many advantages, such as low cost, less computation, and good display effect. At the same time, the generation speed meets the real-time requirements, and the position estimation also meets the accuracy requirements. It can further improve the display quality and use value of panoramic images of diseases and pests. In the future, the experiment can be extended to real pests to test the display performance of the system on real roads.

Due to the need to display the surrounding conditions of diseases and pests in real time in the process of field work, it is required that the screen should not appear the phenomenon of jam, so it puts forward high requirements for the real-time performance of the image generation method in this paper, so the real-time performance of this method will be verified first. Then, the accuracy of object detection and position estimation in this method is quantitatively tested. The scene generation is divided into two parts: using OpenCV to generate the ground part and using OpenGL to render the scene part. When OpenCV is used to generate the ground point by point, the LUT look-up table method is used in the former. The calculation of the mapping relationship is completed and saved when the program is initialized, and only look-up table is needed in real-time rendering, thus reducing the processing time of a single frame.

Compared with the existing solutions, this method has many advantages, which can intuitively and prominently display the position of other crops and pedestrians around the object. When the object of interest is displayed, it will not cause projection distortion to other scenes, and the overall view is comfortable. In addition, this model does not need other depth sensors. Because a fixed projection model can be used, LUT can be used to ensure real-time performance. The algorithm in this paper can keep the straightness of the ground lines to the maximum in the display. In conclusion, this method has a high application value.

Data Availability

No data were used to support this study.

Conflicts of Interest

The authors declare that they have no conflicts of interest.

Acknowledgments

References

[1] T. Han, "Design and application of multicolor image identification in soil pollution component detection," *Arabian Journal of Geosciences*, vol. 13, no. 18, 2020.

[2] B. Chen, H. Li, W. Luo, and J. Huang, "Image processing operations identification via convolutional neural network," *SCIENCE CHINA Information Sciences*, vol. 63, no. 3, 2020.

[3] T.-K. Chui, J. Tan, Y. Li, and H. A. Raynor, "Validating an automated image identification process of a passive image-assisted dietary assessment method: proof of concept," *Public Health Nutrition*, vol. 23, no. 15, pp. 2700–2710, 2020.

[4] Z. Zhao and N. Liu, "the recognition and localization of insulators adopting SURF and IFS based on correlation coefficient," *Optik*, vol. 125, no. 20, pp. 6049–6052, 2020.

[5] Z. Zhao, N. Liu, and L. Wang, "Localization of multiple insulators by orientation angle detection and binary shape prior knowledge," *IEEE Transactions on Dielectrics and Electrical Insulation*, vol. 22, no. 6, pp. 3421–3428, 2019.

[6] Q. Wu and J. An, "an active contour model based on texture distribution for extracting inhomo geneous insulators from aerial images," *IEEE Transactions on Geoscience & Remote Sensing*, vol. 52, no. 6, pp. 3613–3626, 2019.

[7] Y. Zhai, R. Chen, Q. Yang, X. Li, and Z. Zhao, "Insulator fault detection based on spatial morphological features of aerial images," *IEEE Access*, vol. 122, no. 6, pp. 35316–35326, 2019.

[8] X. Miao, X. Liu, J. Chen, S. Zhuang, J. Fan, and H. Jiang, "Insulator detection in aerial images for transmission line inspection using single shot multibox detector," *IEEE Access*, vol. 125, no. 7, pp. 9945–9956, 2019.

[9] X. Tao, D. Zhang, Z. Wang, X. Liu, H. Zhang, and D. Xu, "Detection of power line insulator defects using aerial images analyzed with convolutional neural networks," *IEEE Transactions on Systems Man & Cybernetics Systems*, vol. 50, no. 4, pp. 1486–1498, 2018.

[10] Y. W. Tian, I. Cheng, and X. Q. Wang, *Feature vectors determination for pest detection on apples based on hyperspectral imaging*, Transactions of the Chinese Society of Agricultural, 2014.

[11] *Engineering (Transactions of the CSAE)*, vol. 30, no. 12, pp. 132–139, 2019.

[12] R. P. Haff, S. Saranwong, W. Thanapase, A. Janhiran, S. Kasemsumran, and S. Kawano, "Automatic image analysis and spot classification for detection of fruit fly infestation in hyperspectral images of mangoes," *Postharvest Biology and Technology*, vol. 86, no. 1, pp. 23–28, 2013.

[13] D. E. Purcell, M. G. O'Shea, R. A. Johnson, and S. Kokot, "Near-infrared spectroscopy for the prediction of disease ratings for leaf gall in sugarcane clones," *Applied Spectroscopy*, vol. 63, no. 4, pp. 450–457, 2009.

[14] R. Teixeira, J. I. R. Fernandéz, J. Pereira, and L. B. Monteiro, "Identification of grapholita molesta (Busk) (Lepidoptera: Tortricidae) biotypes using infrared spectroscopy," *Neotropical Entomology*, vol. 44, no. 2, pp. 129–133, 2019.

[15] L. Z. Cheng, X. C. Zhu, and L. L. Gao, "Hyperspectral estimation of phosphorus content for apple leaves based on the random forest model," *Journal of Fruit Science*, vol. 33, no. 10, pp. 1219–1229, 2019.

[16] S. J. Liu, Y. W. Tian, and D. Feng, "Nondestructive detection method of hyperspectral imaging for apple disease," *Journal*

of Shenyang Agricultural University, vol. 47, no. 5, pp. 634–640, 2016.

[17] R. Van Beers, B. Aernouts, L. L. Gutiérrez et al., "Optimal illumination-detection distance and detector size for predicting Braeburn apple maturity from Vis/NIR laser reflectance measurements," *Food and Bioprocess Technology*, vol. 8, no. 10, pp. 2123–2136, 2019.

[18] X. L. Wang, "Extraction and modeling of physical and chemical properties of fruit trees flowers and leaves based on spectral analysis technique," *Beijing Forestry University,2017WU Fei, LU Xinyan, SONG Jun. Learning of multimodal representations with random walks on the click graph, IEEE Trans. Image Process*, vol. 25, no. 2, pp. 630–642, 2019.

[19] L. U. Xiaoqiang, W. A. N. G. Binqiang, and Z. H. E. N. G. Xiangtao, "Exploring models and data for remote sensing image caption generation," *IEEE Transactions on Geoscience and Remote Sensing*, vol. 56, no. 4, pp. 2183–2195, 2018.

[20] N. MERKLE, S. AUER, R. MULLER, and P. REINARTZ, "Exploring the potential of conditional adversarial networks for optical and SAR image matching," *IEEE Journal of Selected Topics in Applied Earth Observations and Remote Sensing*, vol. 11, no. 6, pp. 1811–1820, 2018.

[21] J. T. Barron and J. Malik, "Shape, illumination, and reflectance from shading," *IEEE Transactions on Pattern Analysis and Machine Intelligence*, vol. 37, no. 8, pp. 1670–1687, 2019.

[22] Y. LeCun, Y. Bengio, and G. Hinton, "Deep learning," *Nature*, vol. 521, no. 7553, pp. 436–444, 2018.

[23] X. Li, Y. Dong, P. Peers, and X. Tong, "Modeling surface appearance from a single photograph using self-augmented convolutional neural networks," *ACM Transactions on Graphics (TOG)*, vol. 36, no. 4, pp. 1–11, 2017.

[24] D. Guarnera, G. C. Guarnera, A. Ghosh, C. Denk, and M. Glencross, "BRDF representation and acquisition [C]//computer graphics," *Forum*, vol. 35, no. 2, pp. 625–650, 2019.

WILEY | Hindawi

Research Article

Open Relation Extraction in Patent Claims with a Hybrid Network

Boting Geng (ID)

School of Computer Science and Computing, Zhejiang University, 310063, China

Correspondence should be addressed to Boting Geng; 11321030@zju.edu.cn

Research on relation extraction from patent documents, a high-priority topic of natural language process in recent years, is of great significance to a series of patent downstream applications, such as patent content mining, patent retrieval, and patent knowledge base constructions. Due to lengthy sentences, crossdomain technical terms, and complex structure of patent claims, it is extremely difficult to extract open triples with traditional methods of Natural Language Processing (NLP) parsers. In this paper, we propose an Open Relation Extraction (ORE) approach with transforming relation extraction problem into sequence labeling problem in patent claims, which extract none predefined relationship triples from patent claims with a hybrid neural network architecture based on multihead attention mechanism. The hybrid neural network framework combined with Bi-LSTM and CNN is proposed to extract argument phrase features and relation phrase features simultaneously. The Bi-LSTM network gains long distance dependency features, and the CNN obtains local content feature; then, multihead attention mechanism is applied to get potential dependency relationship for time series of RNN model; the result of neural network proposed above applied to our constructed open patent relation dataset shows that our method outperforms both traditional classification algorithms of machine learning and the-state-of-art neural network classification models in the measures of Precision, Recall, and F1.

1. Introduction

With the development of economy, patent documents, being an extremely important knowledge carrier, record a large number of valuable inventions, creative ideas, and excellent design concepts. Automatically extracting none predefined relation triples from patent claims, which contains a series of rights granted by a government for a given limited period, is a vital basic research application for some upper level applications of patent document analysis, such as patent information retrieval [1, 2], patent classification [3], patent categorization [4], and patent knowledge graph construction [5].

However, relation extraction from patent document is not an easy task. On one hand, specification requirements for patent writing leads to lengthy and complex sentence, which results in its difficulties to parse with normal NLP tools; on the other hand, traditional approaches, NLP-based linguistic method, statistics-based machine learning method, and multimethod hybrid method [6] cannot catch temporal information and long sentence-level global dependency features.

In this paper, we propose an open relation extraction model of hybrid neural network to extract relation triples from patent claims, where Bi-LSTM network can obtain temporal information from the whole sentence, and CNN pooling can gain local content information; at the same time, multihead attention is incorporated into extracting content dependency feature in order to better serve for sequence label classification problems. Our main contributions are summarized as follows:

(1) A hybrid neural network (Bi-LSTM+CNN+CRF) of open relation extraction (ORE) model is firstly proposed to extract none predefined triples from patent document

(2) Multihead attention technique serves for better sequence label dependency classification

(3) We constructed an open patent relation corpus in favor of adopting supervised approaches to ORE task in patent analysis, including 1309 annotated claims with about 29850 sentences

(4) We systematically compare the performance of a series of exiting neural model in the context of the ORE in patent claims. Meanwhile, a variety of experiments help readers to better understand reliability of our hybrid model

2. Related Work

As for the traditional semantic relation extraction from patent documents, there are mainly four methods, which are NLP-based linguistic method, statistics-based machine learning method, and multimethod hybrid method.

On one hand, in the early period of semantic relation extraction from patent documents, NLP-based linguistic methods are dominant. Most of the existing methods made use of linguistic analysis. Regular expression pattern matching techniques is proposed to parse, annotate, and extract target semantic information for knowledge sharing in machine readable format OWL [7]; extracting hyponymy lexical relations is conducted on patent documents using lexico-syntactic patterns [8] and extracting knowledge combined with domain ontology from patent unstructured data [9]. Data-intensive methods are incorporating into patent claim analysis for enhancing analysis robustness combined with symbolic grammar formalisms [10]. Conceptual graphs are extracted from patent claims for comparing patent similarity analysis or any domain of interest [5]. A patent processing system named PATExpert is designed for summarizing patent claims, where deep strategies of syntactic dependency relationship analysis operate on deep-syntactic structures of the claims for improving its readability [11]. Gabriela et al. [12] proposed an extraction of verbal content relations from patent claims using deep syntactic structures. Fantoni et al. [13] proposed a method of automatically detecting and extracting information about functions, the physical behaviours, and states of the system from patent text with a large knowledge base and a series of NLP tools. Lee et al. [14] proposed a hierarchical keyword vector for representing the dependency relationships among claim elements and a tree matching algorithm for comparing claim elements of parents to assess patent infringement risks. Taeyeoun Roh et al. [15] proposed a series of rules to structure and layer technological information in patent claims through NLP tools.

On the other hand, statistical-based machine learning is frequently applied for processing patent analysis in recent years. Gabriela [16] proposed a two-stage method of rule-based claim paragraph segmentation and machine learning-based of conditional random field (CRF) lengthy sentence segmentation which will help automatically detect division phrases for forming meaningful shorter sentences. Wang et al. [17] present an approach to extracting principle knowledge from process patents classifying with contraction matrix. Okamoto et al. [18] proposed an information-based technique to grasp the patent claim structure through entity mention extraction and the relation extraction method with DeepDive [19] platform which using Markov logic network-based inference [20] and distant supervision-based labeling [21] to extract relations from unstructured text. Deng et al. [22] proposed to construct knowledge graph for

facilitating technology transfer where common knowledge base can reveal the technical details of technical documents and assist with the identification of suitable technologies.

Besides, with the rise of deep learning technology, especially its wide application in natural language processing, hybrid technologies as above have emerged for patent mining, such as patent information extraction, patent relations extraction, and construction of patent semantic knowledge base. Yang and Soo [5] proposed a method to convert a patent claim into a formally defined conceptual graph with hybrid techniques of part-of-speech tags, conceptual graphs, domain ontology, and dependency tree. Korobkin et al. [23] proposed a hybrid methodology of LDA-based statistical and semantic text analysis to extract a physical knowledge in the form of physical effects and their practical applications. Carvalho et al. [24] present a hybrid method of extracting semantic information from patent claims by using semantic annotations phrasal structures, abstracting domain ontology information, and outputting ontology-friendly structures to achieve generalization. Lv et al. [25] proposed a hybrid method of patent terminology relation extraction combined with attention mechanism and Bi-LSTM [26] model to construct the patent knowledge graph.

Different from traditional relation extraction, where categories of relationships are classified at advance, open relation extraction (ORE) extract none predefined triples from unstructured text. ORE is firstly defined by Banko et al. [27] who proposed to extract none predefined relations from web, attracting extensive attention and follow-up researches in various fields. Del Corro and Gemulla [28] then proposed dependency parsing-based clause IE framework to detect and extract "useful" pieces of information clauses. Neural network are also incorporated into ORE [29, 30] with end-to-end sequence model or encoder-decoder model.

Our work is similar with Lv et al. [25] and [29–31], but Bi-LSTM and attention mechanism, together with open relation extraction, are firstly proposed to extract the none predefined relationship from the patent documents forming Subject-Relation-Object triples. As we believe that NLP-based parsing tools cannot catch long dependency relationship of lengthy patent sentences, different phased attention would improve the end-to-end sequence labeling classifications. We propose a hybrid neural network framework of extracting open relations from patent claims with multihead attention. Although Bidirectional Encoder Representation from Transformers (BERT) [32–35], another neural network model based on bidirectional transformer, performs excellent in a series of natural language processing tasks including sequence tagging, we would leave it for the future work.

3. Our Hybrid ORE Neural Framework

The paper proposes a supervised neural network of extracting open relations from patent claims without predefined relation categories, which enables a supervised machine learning approach to ORE in patent claims. We define the task as a sequence tagging problem, and we develop an
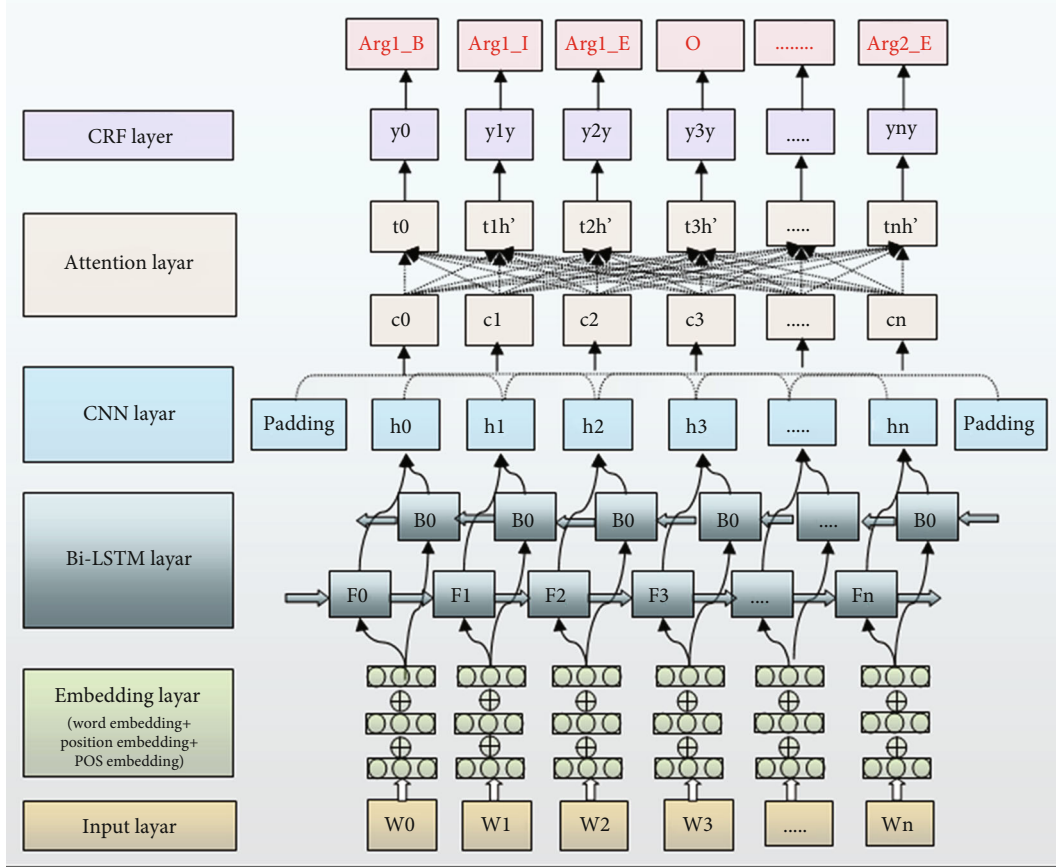
FIGURE 1: Our hybrid network architecture.

end-to-end neural mode with Bi-LSTM and CNN with multihead attention to classify labels above. At first stage, as for the lengthy and complex structure, a machine learning-based method is used to detect segmentation word or phrases for splitting meaningful pieces of short sentences. And then word features and part-of-speech features are incorporated into the Bi-LSTM network. At then, multihead attention mechanism is applied to Bi-LSTM features for help dependency relationship label classification. Postprocessing operation is done for getting Argument1-relation-Argument2-like triples. Our neural ORE architecture is shown in Figure 1.

3.1. Task Formulation. In this paper, we define our neural ORE model as extracting triples from patent claims, where a triple often consists of a predicate and two arguments with contiguous spans from the sentence. As we show in the follow table, the formulation is defined with a more expressive BIEOS tagging scheme as shown the dashed lines, which can better capture dependency relationships from content than BIO tagging scheme. The relation phrase labels are encoded as Verb, Prep, or Noun labels type, while arguments are represented as Arg labels, where Arg1 stands for the first argument and Arg2 acts as the second argument. Several examples are shown in Table 1.

3.2. Feature Embedding. Word embedding is an operation of transforming a word token into a real-valued vector to represent syntactic and semantic information from content. Given a sentence consisting of n words $S = \{x_1, x_2, x_3 \cdots \cdots x_n\}$, every word x_i is converted into a real-valued vector e_i by looking up the embedding matrix $W^{\text{word}} \in \mathbb{R}^{d^w |V|}$, where V stands for the whole vocabulary and d^w represents as the size of word embedding. We use Glove [26] as our word embedding model. Part of speech embedding is transforming POS of each word x_i in sentence S into a one-hot vector p_i, which comes from annotated brown corpus with 36 types. Finally, the concatenation of word embedding e_i and POS embedding p_i is input feature of our neural model.

3.3. Bi-LSTM Network. As deep learning technology and natural language processing combine more and more closely, long short-term memory (LSTM) network, which is firstly proposed by Hochreiter and Schmidhuber in 1997 to solve gradient vanishing problem, shows its good merit on capturing long distance relationship in different NLP subtasks. The transfer diagram of adjacent units in LSTM neural network is shown in Figure 2.

The core design philosophy of LSTM is an adaptive gating mechanism, which decides the degree to which LSTM units keep the previous state and memorize the

TABLE 1: Our neural open relation extraction model.

Neural open relation extraction model
(a) A mono-block engine having a cylinder head structure according to claim 2.
(A mono-block engine; having; a cylinder head structure)
AB_Arg1 mono-blockI_Arg1 engineE_Arg1 havingS_Verb aB_Arg2 cylinderI_Arg2 headI_Arg2 structureE_Arg2 accordingO toO claimO 2O .O
(b) A ported housing having at least one housing port, said housing having an inside diameter and an outside diameter
(a ported housing; having; at least one housing port)
(said housing; having; an inside diameter and an outside diameter)
AB_Arg1 portedI_Arg1 housingE_Arg1 havingS_Verb atB_Arg2 leastI_Arg2 oneI_Arg2 housingI_Arg2 portE_Arg2,O saidB_Arg1 housingE_Arg1 havingS_Verb anB_Arg2 insideI_Arg2 diameterI_Arg2 and I_Arg2 an I_Arg2 outsideI_Arg2 diameterE_Arg2 ;O
(c) Wherein a flexible press plate, anchored in the counterpart at one of the edges running in the longitudinal direction of the counterpart, is arranged on the surface of the counterpart located in the press zone
(a flexible press plate; anchored in; the counterpart)
(a flexible press plate; running; in the longitudinal direction of the counterpart)
(a flexible press plate; is arranged on; the surface of the counterpart)
whereinO aB_Arg1 flexibleI_Arg1 pressI_Arg1 plateE_Arg1,O anchoredB_Verb inE_Verb theB_Arg2 counterpartI_Arg2 atO oneO ofO theO edgesO runningS_Verb inB_Arg2 theI_Arg2 longitudinal I_Arg2 directionI_Arg2 ofI_Arg2 theI_Arg2 counterpartE_Arg2, isB_Verb arrangedI_Verb onE_Verb theB_Arg2 surfaceI_Arg2 ofI_Arg2 theI_Arg2 counterpartE_Arg2 locatedO inO theO pressO zone O .O
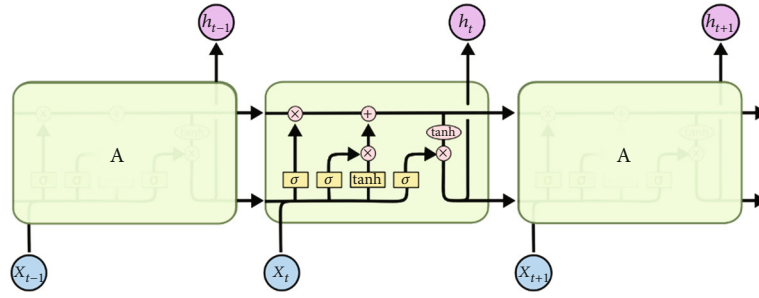
FIGURE 2: Basic neural LSTM unit.

extracted features of current data input [36]. The calculation process is as follows:

$$f_t = \sigma\left(W_f * [h_{t-1}, x_t] + b_f\right), \tag{1}$$

$$i_t = \sigma\left(W_i * [h_{t-1}, x_t] + b_i\right), \tag{2}$$

$$\tilde{C}t = \tanh\left(W_c * [h_{t-1}, x_t] + b_C\right), \tag{3}$$

$$C_t = f_t * C_{t-1} + i_t * \tilde{C}t, \tag{4}$$

$$O_t = \sigma\left(W_o[h_{t-1}, x_t] + b_O\right), \tag{5}$$

$$h_t = O_t * \tanh\left(C_t\right). \tag{6}$$

A typical LSTM network consists of four parts: one forget gate f_t, one input gate i_t, one current cell state C_t, and one output gate O_t. Through four parts of the iterative calculation above, cell units decide whether to take the inputs, forget the memory stored before, and output the state generated later. Bidirectional LSTM network is the combination of forward LSTM networks and backward LSTM networks, where the hidden layer of the latter network flows in opposite position as that of the former, which can cap-

ture the future information as well as the past one. Thus, the Bi-LSTM model is able to exploit information both from the past and the future, more suitable for the sequence tagging model tasks. In this paper, we use the Bi-LSTM model to obtain the semantic and syntactic information from the sentence, and we get the combined hidden information h_i with element-wise sum operation as the following equation from two subnetworks of the forward hidden state $\overrightarrow{h_i}$ and backward hidden state $\overleftarrow{h_i}$.

$$h_i = \left[\overrightarrow{h_i} \oplus \overleftarrow{h_i}\right]. \tag{7}$$

3.4. Multihead Attention. Attention mechanism has now become a predominant concept in neural network literature in recent years and has received varying degrees of attention and research within the artificial intelligence (AI) community in a large number of applications, such as speech recognition, computer vision, natural language processing, and statistical learning. In this paper, we adopt the multihead attention, which has shown excellent performance in many tasks, such as reading comprehension [36] (Cheng et al., 2016), text inheritance [37] (textual ailment/Parikh

et al., 2016), and automatic text summary [38] (Paulus et al., 2017). The essence of multihead attention is to do multiple calculations of self-attention, which can enable sequence-to-sequence neural model to obtain more features from different representation subspaces, so that the model can capture more context information of sentences. The relevant attention equations are described as below:

$$\text{Attention}(Q, K, V) = \text{softmax}\left(\frac{QK^T}{\sqrt{d_k}}\right) * V,$$

$$\text{head}_i = \text{Attention}\left(QW_i^Q, KW_i^K, VW_i^V\right),$$

$$\text{MultiHead}(Q, K, V) = \text{concat}(\text{head}_1, \text{head}_2 \cdots \cdots \text{head}_h),$$

$$(8)$$

where Q, K, and V represent query matrix, key matrix, and value matrix of the multihead attention mechanism, and in the above equations, $Q = n * d_k$, $K = n * d_k$, $V = n * d_k$, and $i \in h$. For each head attention, we compute the attention weight by Equation (2), and finally, we concatenate each head as output results of attention layer.

3.5. CNN Network. Convolutional neural networks (CNN) is a good means of capturing salient local features from whole sequence as for its capability of learning local semantic patterns by its flexible convolutional structure in multidimensional feature extraction [39]. Convolution is often thought of as the product of a weight vector and a sequence vector. The weights matrix is regarded as the filter for the convolution [40]. Given various convolution window length, different outputs are fed to a max-pooling layer, where we can get a feature vector of fixed length.

3.6. CRF Layer. The output of the softmax layer does not affect each other and is independent of each other, while Bi-LSTM can learn semantic and syntactic information about the content. But as for some tasks, such as Noun chunking and Named Entity Recognition (NER), output labels are mutually restrictive. Taking " aB_Arg1 flexibleI_ Arg1 pressI_Arg1 plateE_Arg1" for an example, label B_ Arg1 must be in front of I_Arg1, and label E_Arg1 must come after label B_Arg1 and I_Arg1, and other sequence is illegal. And the result label calculation of the CRF layer is realized by dynamic programming optimization, which would obviously outperform the model without the CRF layer int the time series estimation problem.

4. Experiments

4.1. Dataset. We extract 1309 claims from patent documents form USPTO and annotate the claims with thirty undergraduates for about 2 months. The constructed dataset finally contains 29850 sentences, where 60% for training, 20% for verification, and 20% for test. For argument1 and argument2, we use BIEOS label mechanism, which is also suitable for relation phrase labels. There are three relationships in the whole labeled dataset, and each relationship contains a single tag "S" or two more tags "BE" or "BIE."

TABLE 2: Annotation statistics of our constructed dataset.

	S	B	I	E
Verb	16994	13707	10921	13689
Prep	2624	902	752	874
Adj	409	1712	1186	1693

TABLE 3: Hyperparameter setting of the framework.

Layer	Hyperparameter	
	Word embedding size	300
Embedding	POS embedding size	26
	Entity embedding size	12
CNN	Kernel size	3
	Number of filters	100
Bi-LSTM	State size	300
Dropout	Dropout rate	0.5
	Batch size	50
	Initial learning rate	0.01
	Sequence length	50

TABLE 4: Results of ORE dataset experiments on models.

	P (%)	R (%)	F1-score (%)
Bi-LSTM[1]	89.1542%	90.2017%	89.6749%
Bi-LSTM+CNN+CRF[2]	93.9204%	93.1501%	93.5337%
Bi-LSTM+CNN+CRF (label embedding)[3]	97.0457%	96.1206%	96.5809%
Bi-LSTM+CNN+CRF (label embedding+attention)[4]	97.3074%	97.7388%	97.5226%

The statistics of all labels are shown in Table 1. Finally, we evaluate our patent ORE mode on above dataset. The results are measured by Precision (P), Recall (R), and F1-score, which is defined in Table 2.

$$P = \frac{TP}{TP + FP},$$

$$R = \frac{TP}{TP + FN}, \quad (9)$$

$$F1_{\text{score}} = \frac{2 * P * R}{P + R}.$$

4.2. Hyperparameters Setting. We implement our model with python 3.5 in Keras on NVIDIA Quadro P2000. Adam method is used to optimize our model, learning rate is set to 0.01, and batch size is 50. For multihead attention, we set the number of attention heads is 4, and we use Glove as word embedding model, and the dimension of word vectors is set as 300. Part of speech embedding size is one-hot vector and is set as 26, and relation label embedding size is also set as 12. The dropout rate is set to 0.1 to prevent overfitting, and L2 regularization is also employed in training to

prevent overfitting. The max length of the sentence is set as 100. The detailed parameters of the framework are shown in the following Table 3.

4.3. Experiments and Discussion. In our model, label embedding of our hybrid neural network model consists of word embedding, part-of-speech embedding, and relation tagging embedding. More information feature would be incorporated into the embedding layer though the concatenation by the last dimension for each word. The attention mechanism used in our model is multihead attention, which layer is followed by CNN layer. From a series of experiments in Table 4 above, we obviously conclude that hybrid neural network model performs better than traditional neural network model like Bi-LSTM, such as model 1and model 2 in Table 4, and neural network models with the help of label embedding obviously perform better than the models without the label embedding, such as model 3 and the model 1, in the evaluation measures of Precision, Recall, and F1 score. Through the comparison with the other neural models, our model with multihead attention outperforms other model as well.

4.4. Conclusion and Future Work. In this paper, we propose a Patent Open Relation Extraction neural model. Instead of employing feature engineering, we use a hybrid Bi-LSTM +CNN+CRF neural model with multihead attention mechanism. The hybrid model outperforms the single other model obviously on our self-constructed patent sequence tagging dataset. In the future, we consider incorporating the transform model into our model, such as Bidirectional Encoder Representation from Transformers (BERT), and we also consider patent domain word embedding, which we think would potentially improve the performance.

Data Availability

The dataset used to support the findings of this study have not been made available as the dataset also forms part of an ongoing study.

Conflicts of Interest

The author declares that they have no conflicts of interest.

References

[1] L. Chen, N. Tokuda, and H. Adachi, "A patent document retrieval system addressing both semantic and syntactic properties," in *Proceedings of ACL Workshop on Patent Corpus Processing*, pp. 1–6, Sapporo Convention Center, Sapporo, Japan, 2003.

[2] M. Iwayama, A. Fujii, N. Kando, and Y. Marukawa, "Evaluating patent retrieval in the third NTCIR workshop," *Information Processing & Management*, vol. 42, no. 1, pp. 207–221, 2006.

[3] C. J. Fall, A. Törcsvári, K. Benzineb, and G. Karetka, "Automatedcategorizationin the international patent classification," *ACM SIGIR Forum*, vol. 37, no. 1, pp. 10–25, 2003.

[4] J. H. Kim and K. S. Choi, "Patent document categorization based on semantic structural information," *Information Processing & Management*, vol. 43, no. 5, pp. 1200–1215, 2007.

[5] S.-Y. Yang and V.-W. Soo, "Extract conceptual graphs from plain texts in patent claims," *Engineering Applications of Artificial Intelligence*, vol. 25, no. 4, pp. 874–887, 2012.

[6] X. Lv, X. Lv, X. You, Z. Dong, and J. Han, "Relation extraction toward patent domain based on keyword strategy and attention+BiLSTM model," in *Collaborative Computing: Networking, Applications and Worksharing. CollaborateCom 2019*, vol. 292 of Lecture Notes of the Institute for Computer Sciences, Social Informatics and Telecommunications Engineering, , pp. 408–416, Springer, 2019.

[7] S.-Y. L. Shi-Yao, S.-N. Lin, C.-F. Lee, S.-L. Cheng, and V.-W. Soo, "Automatic extraction of semantic relations from patent claims," *International Journal of Electronic Business Management*, vol. 6, no. 1, pp. 45–54, 2008.

[8] L. Andersson, M. L. J. Pallotti, F. Piroi, A. Hanbury, and A. Rauber, *Insight to hyponymy lexical relation extraction in the patent genre versus other text genresProceedings of the First International Workshop on Patent Mining and Its Applications (IPAMIN)*, Hildesheim, Germany, 2014.

[9] A. Souili, D. Cavallucci, and F. Rousselot, "Natural language processing (NLP) - a solution for knowledge extraction from patent unstructured data," *Procedia Engineering*, vol. 131, pp. 635–643, 2015.

[10] S. Sheremetyeva, "Natural language analysis of patent claims," in *Proceedings of the ACL-2003 workshop on Patent corpus processing*, pp. 66–73, Sapporo Convention Center, Sapporo, Japan, 2003.

[11] N. Bouayad-Agha, G. Casamayor, G. Ferraro, S. Mille, V. Vidal, and L. Wanner, *Improving the Comprehension of Legal Documentation: The Case of Patent Claims*, ICAIL, Barcelona, Spain., 2009.

[12] T. Roh, Y. Jeong, and B. Yoon, "Developing a methodology of structuring and layering technological information in patent documents through natural language processing," *Sustainability*, vol. 9, no. 11, p. 2117, 2017.

[13] G. Fantoni, R. Apreda, F. Dell'Orletta, and M. Monge, "Automatic extraction of function-behaviour-state information from patents," *Advanced Engineering Informatics*, vol. 27, no. 3, pp. 317–334, 2013.

[14] C. Lee, B. Song, and Y. Park, "How to assess patent infringement risks: a semantic patent claim analysis using dependency relationships," *Technology Analysis & Strategic Management*, vol. 25, no. 1, pp. 23–38, 2013.

[15] G. Ferraro and L. Wanner, "Labeling semantically motivated clusters of verbal relations," *Procesamiento del Lenguaje Natural*, vol. 49, pp. 129–138, 2012.

[16] G. Ferraro, H. Suominen, and J. Nualart, "Segmentation of patent claims for improving their readability," in *Proceedings of the 3rd Workshop on Predicting and Improving Text Readability for Target Reader Populations (PITR)*, pp. 66–73, Gothenburg, Sweden, 2014.

[17] G. Wang, X. Tian, J. Geng, R. Evans, and S. Che, "Extraction of principle knowledge from process patents for manufacturing process innovation," *Procedia CIRP*, vol. 56, pp. 193–198, 2016.

[18] M. Okamoto, Z. Shan, and R. Orihara, "Applying information extraction for patent structure analysis," in *Proceedings of the 40th International ACM SIGIR Conference on Research and*

Development in Information Retrieval, pp. 989–992, Tokyo, Japan, 2017.

[19] J. Shin, F. W. SenWu, C. De Sa, C. Zhang, and C. Ré, "Incremental knowledge base construction using DeepDive," *Proceedings of the VLDB Endowment*, vol. 8, no. 11, 2015.

[20] P. Domingos and D. Lowd, "Markov logic: an interface layer for artificial intelligence," *Synthesis Lectures on Artificial Intelligence and Machine Learning*, vol. 3, no. 1, 2009.

[21] M. Mintz, S. Bills, R. Snow, and D. Jurafsky, "Distant supervision for relation extraction without labeled data," in *Proceedings of the Joint Conference of the 47th Annual Meeting of the ACL and the 4th International Joint Conference on Natural Language Processing of the AFNLP: Volume 2 - ACL-IJCNLP '09*, pp. 1003–1011, Singapore, 2009.

[22] W. Deng, X. Huang, and P. Zhu, "Facilitating technology transfer by patent knowledge graph," in *Proceedings of the 52nd Hawaii International Conference on System Sciences*, Grand Wailea, United States, 2019.

[23] D. M. Korobkin, S. A. Fomenkov, and A. G. Kravets, "Extraction of physical effects practical applications from patent database," in *2017 8th International Conference on Information, Intelligence, Systems & Applications (IISA)*, pp. 1–5, Larnaca, Cyprus, 2017.

[24] D. S. Carvalho, F. M. G. Franca, and P. M. V. Lima, "Extracting semantic information from patent claims using phrasal structure annotations," in *2014 Brazilian Conference on Intelligent Systems*, pp. 31–36, Sao Paulo, Brazil, December 2014.

[25] X. Lv, X. Lv, X. You, Z. Dong, and J. Han, "Relation extraction toward patent domain based on keyword strategy and attention+BiLSTM model (short paper)," Springer, 2019.

[26] D. Zhang and D. Wang, "Relation classification via recurrent neural network [EB/OL]," http://arxiv.org/abs/1508.01006.

[27] M. Banko, M. J. Cafarella, S. Soderland, M. Broadhead, and O. Etzioni, "IJCAI," in *Proceedings of the 20th international joint conference on artificial intelligence*, pp. 355–366, Hyderabad, India, 2007.

[28] L. Del Corro and R. Gemulla, *ClausIE: Clause-Based Open Information Extraction*, ACM, Rio de Janeiro, Brazil, 2013.

[29] G. Stanovsky, J. Michael, L. Zettlemoyer, and I. Dagan, "Supervised open information extraction," in *Proceedings of the 2018 Conference of the North American Chapter of the Association for Computational Linguistics: Human Language Technologies, Volume 1 (Long Papers)*, pp. 885–895, Melbourne, Australia ACL, 2018.

[30] L. Cui, F. Wei, and M. Zhou, "Neural open information extraction," http://arxiv.org/abs/1805.04270.

[31] G. Ferraro and L. Wanner, "Towards the derivation of verbal content relations from patent claims using deep syntactic structures," *Knowledge-Based Systems*, vol. 24, no. 8, pp. 1233–1244, 2011.

[32] J. Devlin, M.-W. Chang, K. Lee, and K. Toutanova, "BERT: pre-training of deep bidirectional transformers for language understanding," 2019, http://arxiv.org/abs/1810.04805.

[33] A. Vaswani, N. Shazeer, N. Parmar et al., "Attention is all you need," *Advances in Neural Information Processing Systems.*, pp. 5998–6008, 2017.

[34] E. H. Huang, R. Socher, C. D. Manning, and A. Y. Ng, "Improving word representations via global context and multiple word prototypes," in *Proceedings of the 50th Annual Meeting of the Association for Computational Linguistics*, pp. 873–882, Minneapolis, MIN, USA, 2012.

[35] D. Zeng, K. Liu, S. Lai, G. Zhou, and J. Zhao, "Relation classification via convolutional deep neural network," in *25th International Conference on Computational Linguistics COLING 2014*, pp. 2335–2344, Long Beach City, CA, USA, 2014.

[36] P. Zhou, W. Shi, J. Tian et al., "Attention-based bidirectional long short-term memory networks for relation classification," in *Proceedings of the 54th Annual Meeting of the Association for Computational Linguistics (Volume 2: Short Papers)*, pp. 207–212, Berlin, Germany, 2016.

[37] J. Cheng, L. Dong, and M. Lapata, "Long short-term memory-networks for machine reading," *EMNLP*, vol. 2016, pp. 551–561, 2016.

[38] A. P. Parikh, O. Täckström, D. Das, and J. Uszkoreit, "A decomposable attention model for natural language inference," in *Proceedings of the 2016 Conference on Empirical Methods in Natural Language Processing*, Kunming, China, 2016.

[39] R. Paulus, C. Xiong, and R. Socher, "A deep reinforced model for abstractive summarization," 2017, http://arxiv.org/abs/1705.04304.

[40] D. Zhang and W. Dong, "Relation classification: CNN or RNN? NLPCC-ICCPOL 2016," *LNAI*, vol. 10102, pp. 665–675, 2016.

WILEY | Hindawi

Research Article
Expert Control of Mine Hoist Control System

Xiuzhi Liu and Tao Sui

College of Electrical Engineering and Automation, Shandong University of Science and Technology, Qingdao, China

Correspondence should be addressed to Tao Sui; suitao@sdust.edu.cn

This paper presents a kind of intelligence control algorithm for the mine hoist control system. Firstly, the desired output of the system is described by a speed curve of hoisting process. Then, the structure diagram of the hoist system is constructed, and the expert PID controller is designed based on the model of this control system; the expert knowledge base was established according to the analysis of characteristics in different periods of the hoist process. Finally, the control effect was verified by SIMULINK simulation; by comparing with the result of conventional PID control, expert PID control is improved more safe and suitable for the mine hoist control system.

1. Introduction

Mine hoist is mainly used in coal and other mining enterprises. It is the key equipment in production and is the only channel to transport person and material in the mines. Its performance directly affects the reliability and safety of production; once it fails, not only will it seriously damage the device but also cause server casualties [1–3]. In this paper, we are concerned on the designing expert control algorithm for the mine hoist control system.

Expert control is a cross-subject of artificial intelligence and control theory. It can simulate expert intelligence in an unknown environment and realize effective control. It has been widely used in many industries and provides a new approach to solve the industrial control problem and realizes industrial process control. Chen et al. designed a supervisory expert controller for ball mill grinding circuits [4]. Shi et al. combined fuzzy PID control and the expert decision to regulate the temperature and an expert fuzzy PID controller is designed [5]. Bergh et al. used expert control in the tuning of an industrial thickener [6]. An intelligent energy-efficient outdoor lighting control system using an expert system was developed by Atis and Ekren that could be used in green buildings [7]. Bergh et al. designed a predictive expert control system for a hybrid pilot rougher flotation circuit [8]. Belle et al. designed and realized a distributed expert system on a

control strategy to manage the execution flow of rule activation [9]. Di Maioa et al. designed a regional sensitivity analysis-based expert system for safety margin control [10]. Ye et al. used the expert PID to control the valve positioner [11].

Many researchers have been carrying out the research on the control of the mine hoist system and other DC speed control system; they have obtained some achievements. Hamed et al. designed a fuzzy PID controllers for real-time DC motor speed control [12, 13]. Liu et al. and Gundogdu et al. used fuzzy PID control and self-tuning PID control in the brushless DC motor system separately [14, 15]. Ma et al. designed a parameter self-tuning fuzzy PID control for DC motor [16]. Zdrozis worked on the analysis of abnormal modes of the hoisting DC electric drive system [17]. Gupta et al. analyzed the applications of artificial intelligence in permanent magnet brushless DC motor drives [18]. Emhemed and Mamat presented an overview of proportional integral control (PI) and artificial intelligent control (AI) algorithms for industrial DC motor [19]. Chang et al. modeled the nonlinear DC motor system as Takagi-Sugeno (T-S) fuzzy model [20]. Ulasyar et al. designed an intelligent speed controller for brushless DC motor (2018) [21].

All these achievements listed above will bring great help in the research in this paper. This paper adopts expert PID control in the mine hoist system, by analyzing hoisting

process in different periods. Based on experiences, expert rules are designed to regulate controller parameters to achieve desired hoist process. Compared with the simulation results of conventional PID control, it is indicated that expert PID is more suitable for mine hoisting control.

2. Description of Mine Hoist Control System

2.1. Analysis of Hoisting Process. The mine hoist system is to transport workers and materials up and down the well; both safety and comfort should be considered in the designing of the hoist control system. The hoisting process of the mine hoist system is shown in Figure 1, where n represent the rotate speed of the DC motor which is used in the hoist system. In some cases with large load and special hoisting control requirements, the acceleration stage can be further subdivided into three stages (as shown in t_0-t_3).

The whole hoisting process divides into five stages, namely, the acceleration stage, constant stage, deceleration stage, crawling stage, and parking stage, respectively. In the acceleration stage, the speed of the DC motor accelerates from standstill to maximum speed. In the constant stage, the machine keeps running at maximum steady speed, and the constant stage is the main operational stage. The speed slows down from steady to creeping period in the deceleration stage. In the crawling stage, the container, such as cage or elevator car, is ready to locate and to brake. In parking stage, the cage reaches to the target position and then stops. The detail of each period is describes as the following paragraph.

The acceleration stage happens between moment 0 and t_3 as described in Figure 1; in this stage, underground workers transfer the signal that the cage has been filled of materials to surface workers, the hoist begins to work. Due to mechanical inertia, speed increase slowly during moment 0 and t_1 and then at a rapid rate during t_1 and t_2, when the speed approximate to maximum, the increase rate slows down during t_2 and t_3.

The constant stage happens between moment t_3 and t_4; in this stage, hoist operates at maximum speed so that the cage can steadily upgrade; it is the main stages of the process because it occupies the longest time in the hoisting process.

The deceleration stage happens between moment t_4 and t_5; when the cage is near the wellhead, hoist starts to slow down, and its deceleration rate is from slow to fast and then to slow; this is shown in Figure 1.

The crawling stage happens between moment t_5 and t_6; in this stage, the cage gets into the dump rail, and it operates slowly to eliminate the impact when parked at target location.

The parking stage happens between moment t_6 and t_7, the hoist brake along with its speed decreasing from creeping speed to zero in this stage, which indicates the end of the whole process.

Of course, the operation safety should be taken into consideration while the size of speed and acceleration are determined in different stages.

2.2. The Structure of Mine Hoist Control System. In order to implement the hoist function described in the previous para-
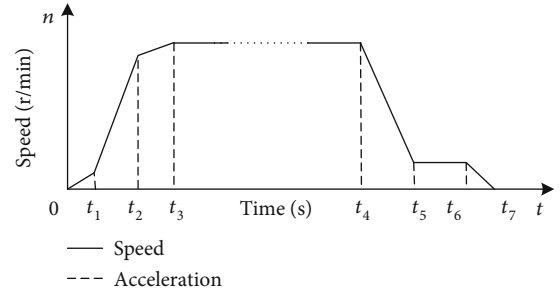
FIGURE 1: The desired hoisting process curve.

graph, we construct the control system shown as Figure 2. The closed-loop system uses a tachogenerator to measure the speed; this signal is taken as a feedback signal to compare with the reference input and the error signal is gained. The speed controller utilizes error signal as input and its output signal is taken as the control signal of the controlled object. Its task is to make the hoister work at expected speed and low overshoot. It is important for us to design a suitable control algorithm to achieve the functions mentioned above.

3. Design of Control Algorithm for Mine Hoist System

In the process speed regulation, the speed controller plays a leading role. The expert control algorithm can adjust the control parameters adaptively, so we use this control algorithm to decrease speed overshoot and to make the acceleration meet requirement when the mine hoist system starts working, and the expert PID algorithm is adopted finally. The input of the expert controller is the error signal between the reference and feedback signal, which is shown in Figure 2. Based on the practical situation and expert rules, control variable $U_n{}^*$ and U_c are used to regulate the mine hoisting process.

3.1. Description of Expert Control. The expert system is a system with a large amount of expertise and experience. It makes inference and judgment according to the knowledge and experience provided by experts in a certain field and simulates the decision-making process of human experts; its main framework consists of knowledge base and reasoning mechanism. Based on the knowledge (prior experience, dynamic information, target, etc.) of control domain, it outputs appropriate control signal according to reasoning rules in a certain strategy and realizes the control function of the controlled object. The structure of expert control is shown in Figure 3.

According to the role and function that expert control plays in the control system, expert control can divide into two types: direct and indirect expert controller. In the direct expert control system, the expert system gives the control signal directly to control the working process of control object. The direct expert control system gives the control signal at each sampling time according to the measured process information and the rules in knowledge base. The indirect expert controller is an intelligent control system which is the combination of expert control and the conventional controller. The bottom layer of the system may be simple PID, fuzzy, and
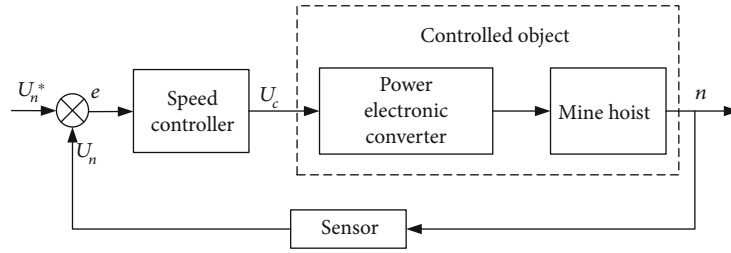
FIGURE 2: The structure diagram of the mine hoist control system.
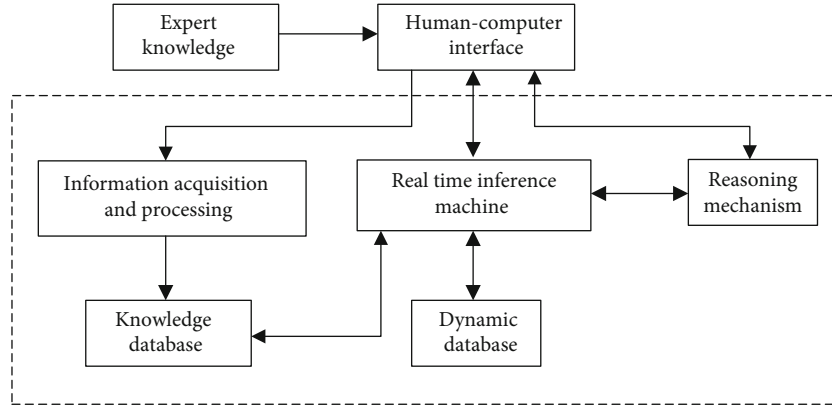
FIGURE 3: The basic structure of the expert control system.
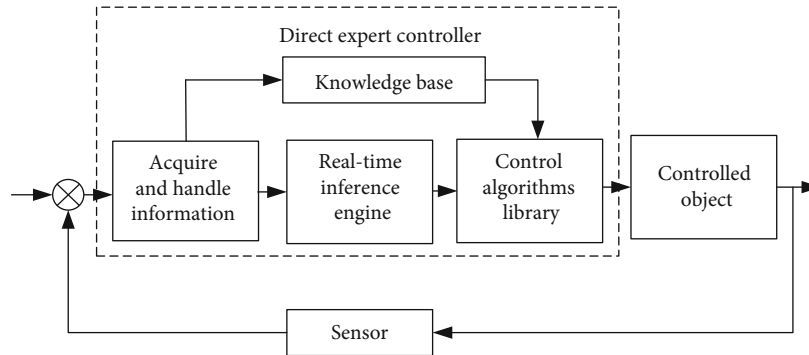
FIGURE 4: The direct expert controller.
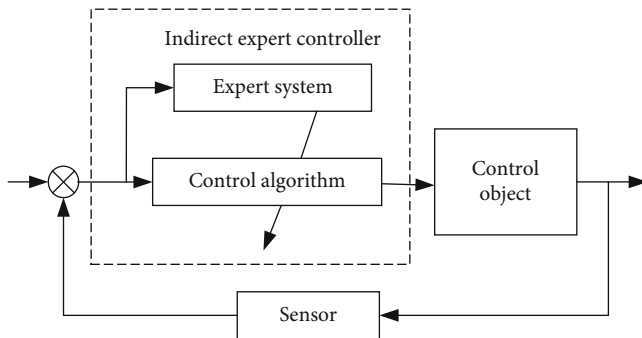
FIGURE 5: The indirect expert controller.

TABLE 1: Parameters of the system.

Parameter	Value
Nominal voltage UN (V)	750
Nominal current IN (A)	760
Nominal speed IN (r/min)	375
Electromotive force coefficient (V·r/min)	1.82
Magnification factor of the thyristor device K_s	75
Resistance of armature circuit R (Ω)	0.14
Time constants T_1 (s)	0.031
Time constants T_m (s)	0.112
Feedback coefficient of speed α	0.027
Maximum given input $U_{nm}{}^*$ (V)	10

*Corresponds to the nominal speed.

(a)

(b)
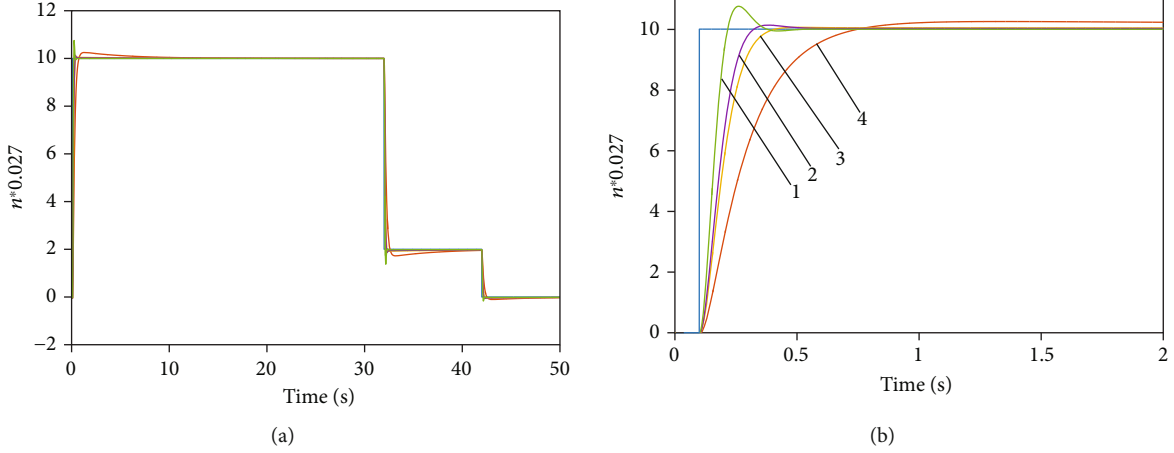
FIGURE 6: Output curve with conventional PID control ($k_i = 0.1$).

(a)

(b)
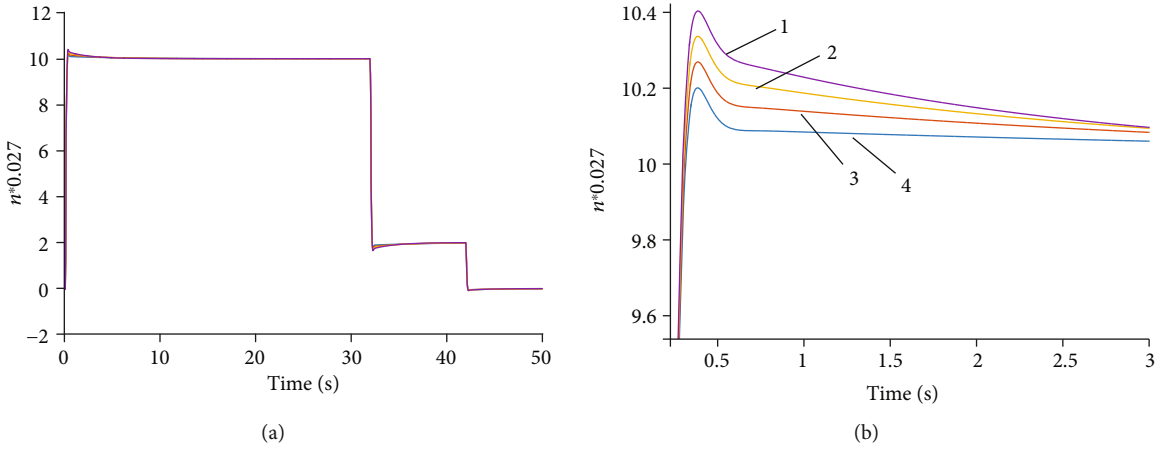
FIGURE 7: Output curve with conventional PID control ($k_p = 1.2$).

other algorithms, and expert control is used to adjust the parameters of the bottom layer algorithm. The structure of direct expert control system and indirect expert control system is shown as shown in Figures 4 and 5, respectively.

This paper chooses an expert PID controller to replace the conventional PID controller as the outer controller to control the hoist process. This controller is one kind of indirect controller. Expert control can adjust the parameters of PID controller adaptively according to the size of system deviation. The key problem of the outer controller design is to design expert control rules to improve the dynamic performance of the system at startup.

3.2. The Design of Expert Controller.
The function of the expert controller is to make the hoisting process as shown in Figure 1. The acceleration during the start and stop process is neither too large nor too small, which will ensure both comfort and safety. The integral separation algorithm is adopted when expert rules are designed. When the error is large, open loop control is adopted, and the output of control is fixed to reduce the error quickly. When the error reduces to a certain range, PID control is adopted, and the parameters of the

TABLE 2: Response parameter of the system.

k_i	k_p	$V_{\max}$	$t_{\max}$ (s)	No. of curve
	2.0	10.75	0.262	1st in Figure 6
	1.2	10.13	0.037	2st in Figure 6
0.1	1.0	10.05	0.496	3rd in Figure 6
	0.5	10.25	1.232	4th in Figure 6
0.2		10.4	0.388	1st in Figure 7
0.3		10.34	0.386	2st in Figure 7
0.4	0.12	10.27	0.384	3rd in Figure 7
0.5		10.2	0.386	4th in Figure 7

$^*V_{\max}$ is the maximum speed feedback signal.

PID controller are adjusted accordingly with the size of the error. Several related parameters need to be defined before designing rules as that is shown in the following paragraph.

Error bound M_1 and M_2, $M_1 > M_2 > 0$. When the error is bigger than M_1, several error threshold are defined as $a_i(i = 1, 2, \cdots, n)$, $a_1 > a_2 > \cdots > a_n$, the value of n is determined by the characteristics of control objectives, The output of the controller is $b_i(i = 1, 2, \cdots, n)$ corresponding to a_i, When the
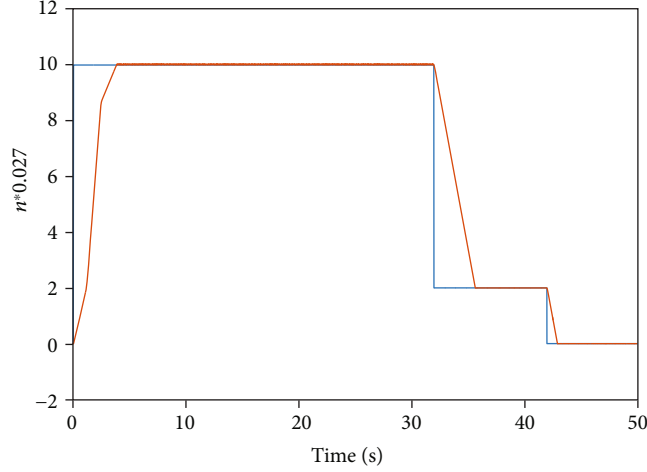
FIGURE 8: Output curve with expert PID.

(a)

(b)
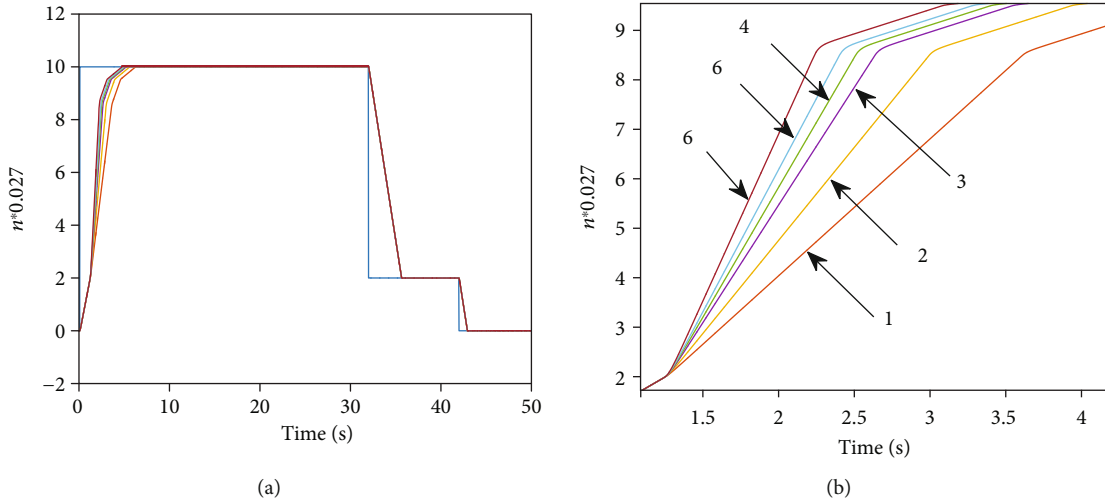
FIGURE 9: Output curves with variable parameters of expert PID. (a) Six output curves of the whole working process correspond to six different values of b_2 shown in line 1 to line 6. (b) Corresponding starting processes.

absolute value of error is greater than a_i, b_i is a constant value, and the control mode of the system is open loop control. When the error is smaller than M_1, the PID controller works, and several parameters are defined as follows: proportional parameter k_p, integral parameter k_i, differential parameter k_d, amplification gain coefficient $k_1 > 1$, Inhibition coefficient $0 < k_2 < 1$, at k and k-1 times, error is $e(k)$ and $e(k-1)$, controller output is $u(k)$ and $u(k-1)$.

Expert control rules of mine hoisting system are designed as follows:

When $|e(k)| \geq M_1$, $n = 4$, in order to get the desired starting process, the value of b_i ($i = 1, 2, 3, 4$) is as $b_1 < b_2$, $b_2 > b_3$, $b_3 > b_4$, accurate values adjust according to the control needs.

If $|e(k)| > a_1$, then $u(k) = b_1$.
If $|e(k)| > a_2$, then $u(k) = b_2$.
If $|e(k)| > a_3$, then $u(k) = b_3$.
If $|e(k)| > a_4$, then $u(k) = b_4$.

When $|e(k)| < M_1$, PI control works; if the error is higher and its absolute value gradually increases, the regulator

TABLE 3: The value of the acceleration.

b_2	Sl	No. of curve
0.3	6.740	1st in Figure 9
0.4	5.746	2st in Figure 9
0.5	5.250	3rd in Figure 9
0.55	4.753	4th in Figure 9
0.6	3.760	5th in Figure 9
0.7	2.767	6th in Figure 9

should implement stronger control; if the error is lower and its absolute value increase, then implement general control to correct the tendency. If the absolute value decreases or the system are in the state of balance, the regulator implement according to conventional PID parameters.

If $e(k)\Delta e(k) > 0$ and $|e(k)| \geq M_2$, then $u(k) = u(k-1) + k_1 k_p e(k)$.
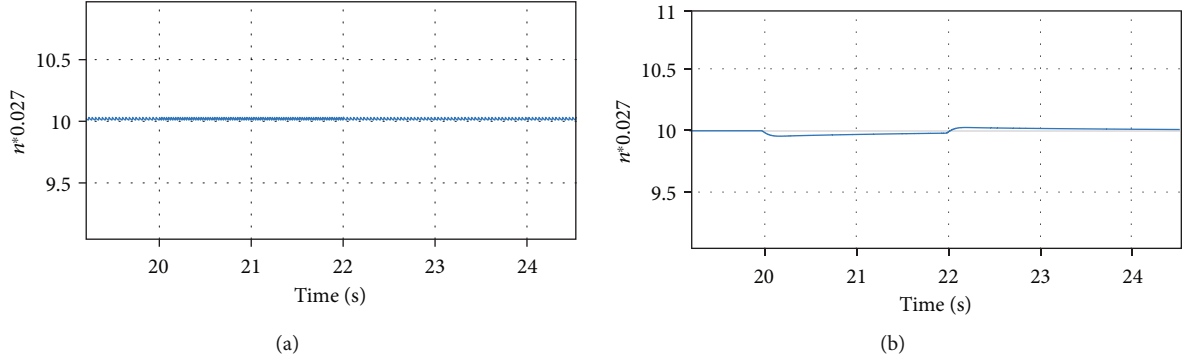
FIGURE 10: Impact of sudden load increase.
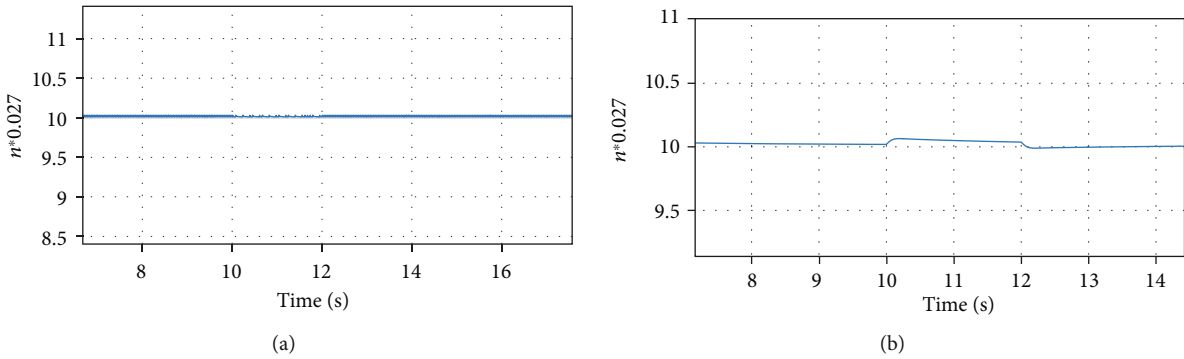
FIGURE 11: Impact of sudden load drop.

If $e(k)\Delta e(k) > 0$ and $|e(k)| < M_2$, then $u(k) = u(k-1) + k_2 k_p e(k)$.

If $e(k)\Delta e(k) < 0$ and $\Delta e(k)\Delta e(k-1) < 0$ or $|e(k)| = 0$, then $u(k) = u(k-1)$.

If $e(k)\Delta e(k) < 0$ and $\Delta e(k)\Delta e(k-1) < 0$ and $|e(k)| \geq M_2$, then $u(k) = u(k-1) + k_1 k_p e(k)$.

If $e(k)\Delta e(k) < 0$ and $\Delta e(k)\Delta e(k-1) < 0$ and $|e(k)| < M_2$, then $u(k) = u(k-1) + k_2 k_p e(k)$.

If the absolute value of error is small enough, in order to decrease final error, conventional PI control is needed.

If $|e(k)| \leq \varepsilon$, then $u(k) = k_p e(k) + k_i(e(k) + e(k-1)t_s)$.

4. Simulation Analysis

The simulation model is established based on a speed regulation circuit of the SCR-D system. The basic parameters are shown in Table 1.

4.1. Control by the Conventional PID Algorithm. From the given parameters mentioned above, we can get the error range is (0, 10), and output range of controller is (0, 1). Now, two kinds of control methods are used to the motor control system, one is an ordinary PID controller and another is an expert PID controller, and their control effects will be compared.

The given input signal curve and the corresponding output response curve of the system when the PI controller is used is shown in Figures 6 and 7, (a) is the output curve of the whole working process and (b) describes starting process.

In order to show the control effect, we unify the input and output signals into the same dimension. There are four output curves of the system both in Figures 6 and 7.

From the result get from Figures 6 and 7, we can find the acceleration in the starting process is large and overweight and weightlessness can be greater and the strain on the cable will be large. Although we can reduce acceleration and overshoot by reducing k_p or k_i, this will increase the error.

The respond parameter to different controller parameters is listed in Table 2.

4.2. Control by the Expert PID Algorithm. When expert PID algorithm is adopted, according to the expert rules, parameters are selected as follows:

$$a_1 = 8.0, a_2 = 1.5, a_3 = 0.5, a_4 = 0.01;$$
$$b_1 = 0.2, b_2 = 0.55, b_3 = 0.12, b_4 = 0.05;$$
$$k_1 = 2, k_2 = 0.4;$$
$$k_p = 60, k_i = 11.5, k_d = 0.01.$$

(1)

When a given signal is descending for deceleration, the parameters a and b are turned into negative values of the response. The system response curve and the given input curve are shown as Figure 8.

Apparently, the curve in Figure 8 close to the ideal hoist process shown in Figure 1, that is, expert control is suitable for mine hoist control system.

If we want to change the acceleration of the startup process, we can change b_2, it plays a major role in the starting process. Increasing b_2 can increase the starting acceleration, it can be shown by Figure 9.

The relationship between the performance index in the system startup process in Figure 9 and the value of b_2 is shown in Table 3.

In Table 3, sl represent the slope of the of output curve when the output of expert controller is b_2.

In the designing of the expert controller of the mine hoist control system, the value of b_2 is determined by the object to be transported. For example, for the system of transporting people, comfort is more important, the value of b_2 should be smaller, and for system of transporting cargo, speed is more important, the value of b_2 should be larger.

4.3. Effect of Load Mutation. Since the hoist is generally hoisted by a steel wire rope, which has certain elasticity, and load fluctuation may occur during operation, so this study adds the interference of load mutation.

In the period of constant speed operation (10 s, 12 s) and (20 s, 22 s), when the torque is increased by 30 or dropped by 30, the system will fluctuate slightly. The results are shown in Figures 10 and 11.

It can be seen from the figures that whether the load suddenly increases or decreases, both of these methods can effectively inhibit the effect of load mutation. Both of these methods can inhibit the effect of load mutation. However, the output curve of the system with expert PID algorithm fluctuates less (as shown in Figures 10 and 11(a)), while the curve of the system with PID algorithm fluctuates more (as shown in Figures 10 and 11(b)).

5. Conclusions

This paper is concerned with the research on the application of expert control on the DC speed control system, and the mine hoist control system which uses a DC motor is taken as the control object. By comparing the control result of conventional PID control the expert control, we can find that expert control is more suitable for the hoist control system. Firstly, the hoisting and stopping acceleration of the hoist system by expert control is less than the system which is controlled by conventional PI controller, and this will greatly improve comfort level of the people; this will also improve the safety of the system for smaller acceleration can reduce the strain on the cable. Secondly, the expert control mine hoist control system can be designed as having no overshot, although conventional PID control can also make the system having no overshot, but on this situation, the acceleration will be much larger and the system may be not safe. When designing an expert controller for a mine hoist control system, both the comfort and the safety should be considered, which are determined by the sense of overweight and weightlessness and the strain of the cable separately, and these are all determined by the acceleration during the starting and stopping period, the rules of expert controller and the control parameters are all determined by the facts mentioned above. It is need to be said that the expert rules in this paper is not

necessarily suitable other motor control system, especially the system that need positive and negative rotation and need changing frequently. Of course, this method could be extended to other applications, such as the elevators, the hoisting machines.

Data Availability

The data that support the findings of this study are available from the corresponding author upon reasonable request.

Conflicts of Interest

The authors declare that they have no conflicts of interest.

Acknowledgments

References

[1] S. Xue, J. Tan, L. Shi, and J. Deng, "Rope tension fault diagnosis in hoisting systems based on vibration signals using EEMD, improved permutation entropy, and PSO-SVM," *Entropy*, vol. 22, no. 2, p. 209, 2020.

[2] N. Vayenas and S. Peng, "Reliability analysis of underground mining equipment using genetic algorithms," *Journal of Quality in Maintenance Engineering*, vol. 20, no. 1, pp. 32–50, 2014.

[3] X. Li, Q. Pan, and K. He, "Modeling and analysis of harmonic in the mine hoist cnverter based on double closed-loop control," *Journal of Computers*, vol. 7, no. 6, pp. 1353–1360, 2012.

[4] X. Chen, Q. Li, and S. Fei, "Supervisory expert control for ball mill grinding circuits," *Expert Systems with Applications*, vol. 34, no. 3, pp. 1877–1885, 2008.

[5] D. Shi, G. Gao, Z. Gao, and P. Xiao, "Application of expert fuzzy PID method for temperature control of heating furnace," *Procedia Engineering*, vol. 29, pp. 257–261, 2012.

[6] L. Bergh, P. Ojeda, and L. Torres, "Expert control tuning of an industrial thickener," *IFAC-Papers OnLine*, vol. 48, no. 17, pp. 86–91, 2015.

[7] S. Atis and N. Ekren, "Development of an outdoor lighting control system using expert system," *Energy and Buildings*, vol. 130, pp. 773–786, 2016.

[8] L. Bergh, J. Yianatos, J. Olivares, and J. Durán, "Predictive expert control system of a hybrid pilot rougher flotation circuit," *IFAC-PapersOnLine*, vol. 49-20, pp. 155–160, 2016.

[9] A. Boaye Belle, T. C. Lethbridge, M. Garzón, and O. O. Adesina, "Design and implementation of distributed expert systems: on a control strategy to manage the execution flow of rule activation," *Expert Systems with Applications*, vol. 96, pp. 129–148, 2018.

[10] F. di Maio, A. Bandini, M. Damato, and E. Zio, "A regional sensitivity analysis-based expert system for safety margins control," *Nuclear Engineering and Design*, vol. 330, pp. 400–408, 2018.

[11] L. Ye, X.-b. Wang, and W. Xin, "A type of control method based on expert PID for intelligent valve positioner," *Control Engineering of China*, vol. 26, no. 1, pp. 87–91, 2019.

[12] B. Hamed and M. Almobaied, "Fuzzy PID controllers using FPGA technique for real time DC motor speed control," *Intelligent Control & Automation*, vol. 2, no. 3, pp. 233–240, 2011.

[13] S. Abel, G. Erdem, M. Amanullah, M. Morari, M. Mazzotti, and M. Morbidelli, "Optimizing control of simulated moving beds–experimental implementation," *Journal of Chromatography A*, vol. 1092, no. 1, pp. 2–16, 2005.

[14] G. Liu, J. Min, and Q. Sheng, "Brushless DC motor fuzzy PID control system and simulation," *Sensors & Transducers Journal*, vol. 181, no. 10, pp. 111–116, 2014.

[15] T. Gundogdu and G. Komurgoz, "Self-tuning PID control of a brushless DC motor by adaptive interaction," *Ieej Transactions on Electrical & Electronic Engineering*, vol. 9, no. 4, pp. 384–390, 2014.

[16] Y. Ma, Y. Liu, and C. Wang, "Design of parameters self-tuning fuzzy PID control for DC motor," in *International Conference on Industrial Mechatronics and Automation*, pp. 345–348, Wuhan, China, 2010.

[17] K. Zdrozis, "Analysis of abnormal modes of hoisting DC electric drive System," *American Journal of Applied Sciences*, vol. 7, no. 4, pp. 527–534, 2010.

[18] R. A. Gupta, R. Kumar, and A. K. Bansal, "Artificial intelligence applications in permanent magnet brushless DC motor drives," *Artificial Intelligence Review*, vol. 33, no. 3, pp. 175–186, 2010.

[19] A. A. A. Emhemed and R. B. Mamat, "Modelling and simulation for industrial DC motor using intelligent control," *Procedia Engineering*, vol. 41, pp. 420–425, 2012.

[20] X. Chang, Y. Wang, X. H. Chang, and Y. M. Wang, "Peak-to-peak filtering for networked nonlinear DC motor systems with quantization," *IEEE Transactions on Industrial Informatics*, vol. 14, no. 12, pp. 5378–5388, 2018.

[21] A. Ulasyar, H. S. Zad, and A. Zohaib, "Intelligent speed controller design for brushless DC motor," *International Conference on Frontiers of Information Technology*, pp. 19–23, Islamabad, Pakistan, December 2018.

Research Article

Key Technologies of Steel Plate Surface Defect Detection System Based on Artificial Intelligence Machine Vision

Bin Xue[1,2] **and Zhisheng Wu** [1]

[1]*School of Materials Science and Engineering, Taiyuan University of Science and Technology, Taiyuan, 030024 Shanxi, China*
[2]*School of Mechanical and Electrical Engineering, Qingdao Binhai University, Qingdao 266555, Shandong, China*

Correspondence should be addressed to Zhisheng Wu; zswu1963@tyust.edu.cn

With the rapid development of visual inspection technology, computer technology, and image processing technology, machine vision technology has become more and more mature, and the role of quality inspection and control in the steel industry is becoming more and more obvious and important. Defects on the surface of the strip are a key factor affecting the quality inspection process. Its inspection plays an extremely important role in improving the final quality. For a long time, traditional manual inspection methods cannot meet actual production needs, so in-depth research on steel surface defect inspection systems has become the consensus of today's steel companies. The accuracy and low performance of traditional detection methods can no longer meet the needs of people and society. The surface defect detection method based on machine vision has the characteristics of high accuracy, fast processing speed, and intelligent processing, which is the main trend of surface defect detection. We select a steel plate; take the invariant moment features of the cracks, holes, scratches, oil stains, and other images on it; extract the data results; and analyze them. Then, we read the texture features of these defect images again, extract the data results, and analyze them. The experimental results prove that after the mean value filter and Gaussian filter process the image, the mean variance value MSE is relatively large ($46.276 > 31.2271$), and as the concentration of salt and pepper noise increases, the rate of increase of MSE increases obviously, and as the peak signal-to-noise ratio and the mean variance value MSE increase continuously ($32.2271 < 33.3695$), the image distortion is more serious. The method designed in this paper is extremely effective. Improving the surface quality of steel is of great significance to improving market competitiveness.

1. Introduction

Ophthalmic diseases have more complex causes, more different diseases, and more variable conditions and belong to clinical ophthalmic diseases [1]. It will seriously affect the vision of the patient and may even cause blindness. Therefore, in order to effectively improve the vision of patients, the above-mentioned various consequences must be effectively prevented. Due to the introduction of advanced technology and production technology, product quality and standard production technology have been significantly improved in recent decades. However, due to the extensive influence of many complex reasons, such as initial production habits and inspection methods, it is used as steel. A large part of the surface quality has not changed much. As an important

raw material for modernization [2], steel plates are used in all aspects of social development, from bridge construction to aerospace machinery and many other essential fields. The quality of the metal plate is directly related to the reliability of public use and the safety of society and public industries [3]. Detecting and inspecting the surface defects of steel plates are currently the primary task of steel companies. The development of a cost-effective surface quality inspection system suitable for Chinese steel companies has become a top priority.

Defects on the surface of the strip are a key indicator for evaluating the quality of the film. The effective method of detecting defects has attracted people's attention for a long time. Researchers at home and abroad have done a lot of work for this and achieved some results. Ohkubo et al.
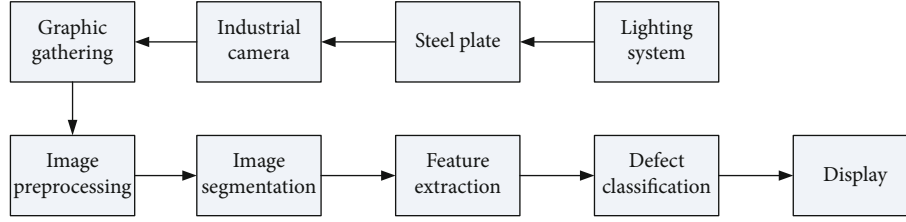
FIGURE 1: System flow chart.

proposed a detection system that uses a laser as a scanning light source, a 12-sided reflective prism and a cylindrical mirror as an optical system, and a photomultiplier tube to receive the detection system [4, 5]. Liu et al. proposed the theory of eddy current testing and successfully used eddy current testing technology to detect metal barium, which opened up the research boom of eddy current testing in the application of metal surface defect detection [6]. Choudhary et al. have developed an online automatic detection system for surface defects of continuous casting billets, which has set off a research boom in infrared detection of surface defects [7]. Dombrowski et al. chose a fully programmable image digitizer and a fully programmable high-speed digital signal processor to process digital image signals and used the system for cold-rolled strip steel surface, edge cracks, and other edge tests [8]. Shu et al. conducted the research on the strip steel surface detection system which analyzes the CCD detection method and proposes some effective algorithms [9]. Hossam et al. use computer image processing technology and pattern recognition technology to perform image processing and defect classification algorithms and perform effective surface defect detection [10]. Therefore, the research on the key technology of the steel plate surface defect detection system based on artificial intelligence machine vision is of great significance.

The existing extraction methods are mainly aimed at normal retinal images, which are not universal; this paper adopts an improved maximum classification algorithm based on constant torque to solve the inefficient ground-to-ground detection problem, using gray scale and texture feature extraction methods, feature selection methods based on principal component analysis, and defect classification algorithms based on support carrier machines. Research on key technologies such as image processing and detection system classification and recognition has solved the problem of steel surface defect detection system. Defect segmentation takes a long time, there are many feature sizes, and the classification result is low.

2. Key Technologies of Steel Plate Surface Defect Detection System Based on Artificial Intelligence Machine Vision

2.1. Defect Image Preprocessing and Segmentation Technology

2.1.1. Image Denoising Analysis. Generally, we hope that the image captured by the camera is clear and noise-free [11]. Since optoelectronic noise will hinder the conversion of images from optical to electronic forms and electronic signal

TABLE 1: Summary table of reliability test results.

Category	Index combination	Alpha coefficient (α)
Crack	The crack itself	
	Crack right	0.8227
	Crack left	
	Crack transpose	
Hole	The hole itself	
	Hole moves right	0.8742
	Hole moves left	
	Hole transposition	
Bruise	Bruise itself	
	Bruise shifts right	0.7663
	Bruise shifts left	
	Bruise transposition	
Inclusion	Inclusion itself	
	Inclusion shifts right	0.7414
	Inclusion shifts left	
	Inclusion transposition	

processing amplifiers will cause thermal noise interference, images will inevitably produce noise during this series of complex processing processes [12, 13]. After that, the method of comparative treatment was adopted, and the experimental group and the control group were compared with two different treatment methods. According to the relationship between noise and signal, it can be divided into additional noise and amplified noise [14].

(1) Types of Noise. The probability density function obeys a kind of noise with Gaussian distribution, and the one-dimensional probability density function is shown in the following formula:

$$P(x) = \frac{1}{\sqrt{2\prod}} \exp\left[-\frac{(x-\mu)^2}{2\sigma^2}\right]. \tag{1}$$

Among them, x is the gray value, μ is the mean value, and σ^2 is the variance. Suppose a useful signal is $f(x, y)$ and noise is $m(x, y)$ and the output signal is $g(x, y)$ under the influence of the noise signal, then

$$g(x, y) = f(x, y) + n(x, y) = f(x, y) + \mu + \sigma X. \tag{2}$$

TABLE 2: Invariant moment feature extraction data table.

Sample defect type	IM1	IM2	IM3	IM4	IM5	IM6	IM7
The crack itself	3.9843	17.7438	7.6313	2.6201	4.3140	5.4762	12.6321
Crack right	3.3242	10.8950	7.3796	2.3861	4.6513	1.3793	7.2141
Crack left	3.5124	11.3472	9.3724	2.3912	2.6724	1.6742	6.3241
Crack transpose	3.9843	17.7438	9.1313	2.1201	3.8140	0.4762	12.6321
The hole itself	5.7260	31.5000	27.8151	27.1595	15.6138	19.4741	9.6081
Hole moves right	5.7260	31.5000	27.8151	27.1595	15.6138	19.4741	9.6081
Hole moves left	5.7260	31.5000	27.8151	27.1595	15.6138	19.4741	9.6081
Hole transposition	5.7260	31.5000	27.8151	27.1595	15.6138	0.8770	9.6081
Bruise itself	2.7234	4.7278	7.5965	6.4868	8.2521	9.7417	9.6433
Bruise shifts right	2.5343	2.9342	1.2417	7.5237	3.8921	5.8660	5.4276
Bruise shifts left	2.5621	3.1137	1.2887	45181	2.7710	2.7770	0.3873
Bruise transposition	2.7234	4.7278	0.5965	2.4868	0.2521	2.7417	0.6433
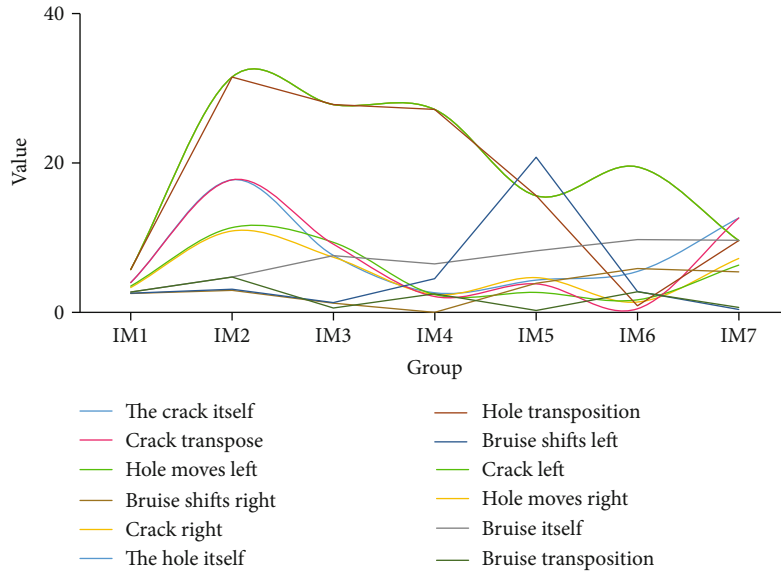
FIGURE 2: Moment invariant feature extraction data analysis diagram.

In multiplicative noise, the relationship is as follows:

$$g(x, y) = f(x, y)[1 + n(x, y)] = f(x, y) + f(x, y)n(x, y). \quad (3)$$

Some infection spots with small gray values (close to black) or large gray values (close to white) appear in the image, and dark and bright spots similar to pepper and salt particles appear in the image, calculated as follows:

$$g(x, y) = \begin{cases} 0, & f(x, y) < \dfrac{2}{d}, \\ 255, & \dfrac{2}{d} \leq f(x, y) \leq d, \\ f(x, y), & \text{otherwise.} \end{cases} \quad (4)$$

(2) Mean Filter. The filtering process of the mean is to make the window slide in the image, then find the average value of each pixel in its neighborhood, and finally replace the value of the center position of the window with the average value of each point in the window [15–17]. Assuming an image $f(x, y)$ of $n \times n$, an image $g(x, y)$ is obtained after the mean filtering process is as shown in the following equation:

$$g(x, y) = \frac{1}{M} \sum_{(m,n) \in S} f(x - m, y - n). \quad (5)$$

In the formula, S is the predetermined neighborhood and M is the total number of pixels contained in the neighborhood. The gray value of each pixel in the image $g(x, y)$ is determined by the average value of the gray values of several pixels of $f(x, y)$ contained in the predetermined neighborhood of (x, y). The area with a radius of 1 is expressed as

$$S_1 = \{(x, y + 1), (x, y - 1), (x + 1, y), (x - 1, y)\}. \quad (6)$$
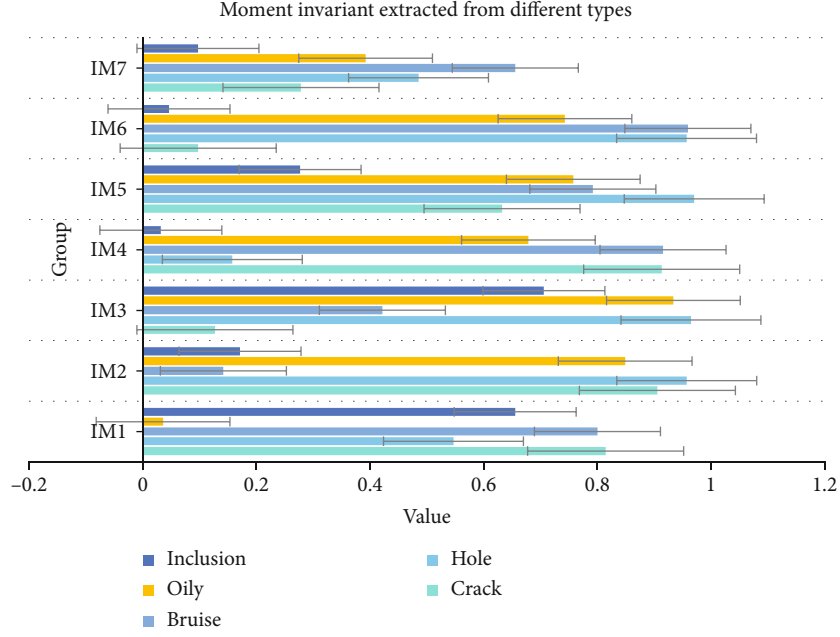
Figure 3: Moment invariant feature maps extracted from different types of defects.

Table 3: Defect image texture feature extraction table.

Defect sample	Crack	Hole	Bruise	Oily	Inclusion
Energy	0.9547	0.9491	0.8798	0.9736	0.8473
Mean gray value	0.0278	0.0121	0.0372	0.0232	0.1422
Gray mean square error	0.3312	0.0378	0.6208	0.3564	1.0381
Gradient mean	0.1639	0.0761	0.3942	0.1536	0.2010
Gradient mean square error	2.6790	0.9712	4.0097	2.7180	4.9014
Gray entropy	0.0540	0.0166	0.0719	0.0794	0.0359
Gradient entropy	0.0534	0.0154	0.0565	0.0670	0.1673
Mixed entropy	0.0796	0.0165	0.1185	0.1786	0.1451

Formula (5) is expressed by convolution.

$$g(x, y) = h(x, y) * f(x, y) = \sum_{(m,n) \in S} \sum h(m, n) f(x - m, y - n). \tag{7}$$

(3) Wiener Filter. Wiener filtering is an adaptive filter that minimizes the average square error between the original image and the restored image. The smaller the mean square error, the better the filtering effect of filtering noise [18, 19]. The mean and variance are

$$\mu = \frac{1}{MN} \sum_{(i,j) \in S} F(i, j),$$

$$\sigma^2 = \frac{1}{MN} \sum_{(i,j) \in S} F^2(i, j). \tag{8}$$

In the formula, S is the $M \times N$ field of each pixel, and its estimated formula is

$$G[i, j] = \mu + \frac{\sigma^2 - v^2}{\sigma^2} [F(i, j) - \mu]. \tag{9}$$

In nanomaterials, when the particle size reaches a certain physical characteristic size, the energy levels of electrons adjacent to the metal Fermi plane change from an almost continuous state to a discrete state, while the nanoparticles have discontinuous, higher-occupancy molecules.

2.1.2. Filter Effect Evaluation and Result Analysis. After filtering the image, we must also evaluate the image quality [20]. Image quality mainly includes two aspects: one is the degree of difference between the image and the original standard image; the other is the ability of the image to provide information to individuals or machines from subjective and

Texture feature extraction map of defect images
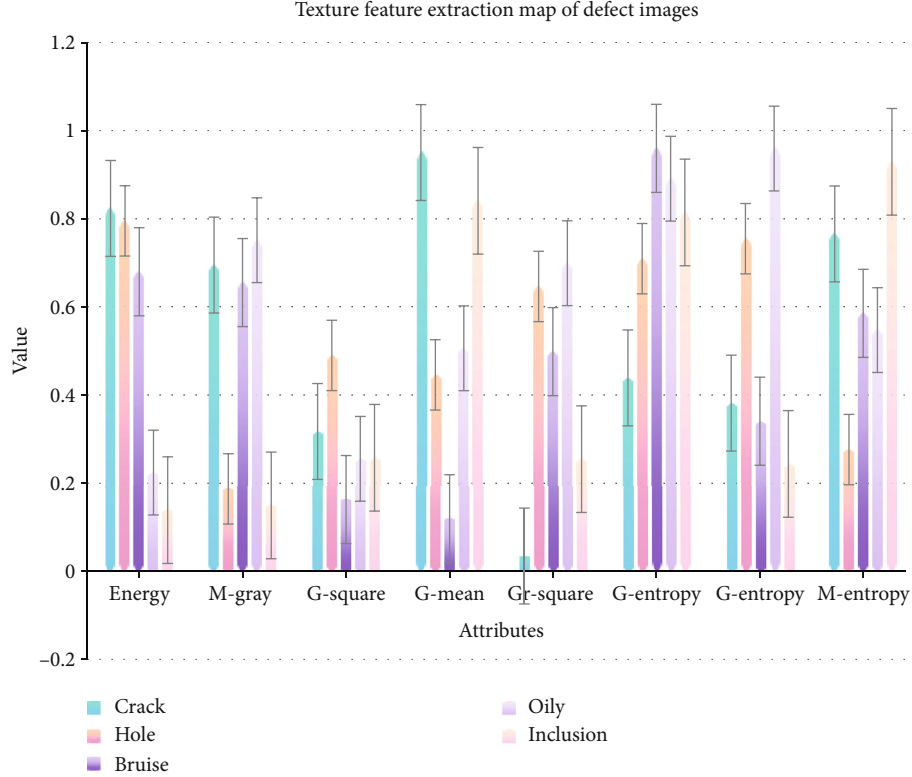
Figure 4: Texture feature extraction map of defect images.

objective aspects. Commonly used indicators are the signal-to-noise ratio of PSNR and the normalized mean square error NMSE [21, 22]. They are expressed as follows:

$$\text{PSNR} = 10 \log \frac{255^2}{1/MN \sum_{j=0}^{M-1} \sum_{i=0}^{N-1} \left(f_{ij} - e_{ij}\right)^2},$$

$$\text{NMSE} = \sum_{i=1}^{N} \sum_{j=1}^{N} \frac{\left|f(i,j) - f'(i,j)\right|^2}{f(i,j)^2}. \tag{10}$$

2.1.3. Two-Dimensional Maximum Entropy Threshold.

Assuming that the A region and the B region have different probability distributions, the posterior probability p_{ij} of the A region and the B region is used to normalize the probability of each region to make the partition entropy have additivity, and the threshold is set at (s, t), then

$$H = -\sum_{i=0}^{L=1} \sum_{j=0}^{L=1} p_{ij} \ln p_{ij}. \tag{11}$$

Then, the two-dimensional entropy of zone A and zone B is

$$H(A) = -\sum_{i=0}^{s} \sum_{j=0}^{t} \left(\frac{p_{ij}}{p_A}\right) \ln \left(\frac{p_{ij}}{p_A}\right) = \ln p_A + \frac{H_A}{p_A},$$

$$H(B) = -\sum_{i=s+1}^{L=1} \sum_{j=t+1}^{L=1} \left(\frac{p_{ij}}{p_B}\right) \ln \left(\frac{p_{ij}}{p_B}\right) = \ln p_B + \frac{H_B}{p_B}. \tag{12}$$

The discriminant function that defines entropy is

$$\phi(s, t) = H_{(A)} + H_{(B)}. \tag{13}$$

2.2. Traditional Threshold Segmentation Technology.

The so-called threshold segmentation technology is to use a threshold in the picture to divide the entire picture into two parts, a black part and a white part, with one part as the target object and the other part as the background object [23–25]. Throughout the scientific frontier literature and books on nanoelectrocatalysts, the most mentioned word is energy. Energy is no longer a problem of a certain country but has become a problem of global concern. When a crisis occurs, there is no one. The country can take care of itself. The vast number of scientific researchers is working against clean energy. Based on Otsu threshold segmentation, an iterative threshold segmentation was proposed.

2.2.1. Otsu Threshold Segmentation Method.

In the process of detecting data image defects, if you want to request the

Table 4: Depression data analysis table.

Sample number	$\bar{m}$	σ^2	m_η	m_k	E	H
1	-0.6666	-0.6961	0.2436	1.9268	-0.3848	-0.5962
2	-0.7104	-0.7108	0.5538	1.7370	-0.3880	-0.6295
3	-0.6335	-0.6378	0.4459	1.8837	-0.3642	-0.6141
4	-0.8493	-0.8457	1.3670	0.9165	0.1147	-0.7533
5	-0.7154	-0.7567	0.8430	1.6722	-0.2849	-0.6791
6	-0.7378	-0.7761	0.6645	1.7827	-0.2274	-0.6609
7	-0.5272	-0.5786	0.1737	1.9857	-0.4264	-0.5432
8	-0.7264	-0.7565	0.7528	1.6483	-0.2781	-0.6341
9	-0.8715	-0.8262	0.9458	1.4934	-0.1535	-0.6670

optimal threshold, you must cross all pixel values in the gray-scale range and calculate the amount of change. When the amount of calculation is large, the output will be very low [26, 27]. At the same time, due to the influence of factors such as the gray level of the image itself and the noise interference that has not been eliminated, the best limit cannot be reached by using only the gray histogram, which will lead to very unsatisfactory processing results [28].

2.2.2. Iterative Threshold Segmentation Method. Compared with the Otsu threshold segmentation, it is not necessary to determine an optimal threshold for each picture, which has a certain degree of adaptability [29, 30]. The specific steps are as follows. First, determine a parameter T0 based on pictures and experience, and select a preliminary estimated threshold T1. Then, use T1 to divide the image into two parts.

2.3. Improved Threshold Segmentation Algorithm Based on Pixel Search. In the detection process of steel plate surface defects [31], some defects occupy fewer pixels and have a low signal-to-noise ratio. Due to the reflective characteristics of the steel plate surface, the background light is uneven, and the defect characteristics and the background gray value are not obvious. After the research of the previous section, it is found that the processing effect of traditional edge detection and threshold segmentation algorithms is not ideal [29, 32]. In order to improve the segmentation of weak steel plate surface defect features, this section explores the use of pixel search methods. Defect threshold segmentation is carried out, and the method of segmentation of weak defect images is combined in the segmentation process. As a result, it is found that the segmentation effect has certain advantages, which is of great help to the later feature extraction of steel plate defects [33].

Integrate the various small areas so that the steel plate defect target and background can be separated as a whole [34, 35]. Uveitis is a chronic inflammation. At present, glucocorticoids, nonsteroidal anti-inflammatory drugs, and immunosuppressive agents can effectively treat uveitis, but these drugs have difficulty reaching the retina to achieve a complete therapeutic effect. Therefore, treating uveitis remains a challenge. Recent studies have shown that nanocells can improve the solubility of drugs and increase the per-
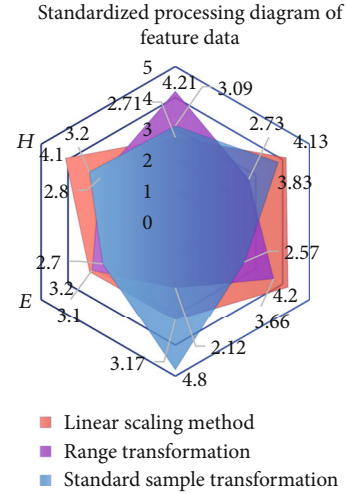
Figure 5: Standardized processing diagram of feature data.

meability of conjunctival epithelial cells through good hydrophilicity and high drug encapsulation potential. Finally, each defect target will not exist in the form of a pixel, and it must meet the gray level of the same area. Uniformity and connectivity must be achieved, so that the segmented defect images can better meet the needs of defect feature extraction.

In view of the small defect segmentation problem where the contrast between the defect target and the background is not obvious due to uneven illumination of the steel plate surface image and the reflection of the steel plate itself, the steel plate defect target segmentation algorithm proposed in this section fully considers the similarity of the defect target and the background pixel in the same area. Therefore, in the process of target segmentation, first, divide a small area; then, discharge whether there are defective targets in the small area; and finally, confirm whether the small defective target is a target [36, 37]. The specific implementation process of the target segmentation algorithm based on pixel search in the entire segmentation process is as follows:

(1) The preprocessed steel plate surface image is divided into different small areas. In the small areas, each small area can be a background image or a combination of a background image and a defect target. It is better not to be all defective images

(2) Calculate the variance of each small area, and arrange them in an ordered sequence in the order of variance

(3) Set an initial threshold. If the variance change range is less than the initial threshold, the small area is determined to be a background image; if the variance change range is greater than the initial threshold, the small area is determined to have a defective target

(4) If it is determined that there is a defective target in a small area, the threshold within the variance is determined adaptively; if it is greater than the threshold within the variance, it is determined as the defective

TABLE 5: Analysis table based on the experimental results of image denoising.

Assignment variable		Proportion
Mean filter	No salt and pepper added	
	15% salt and pepper	
	30% salt and pepper	93.33%
	50% salt and pepper	
Gaussian filtering	No salt and pepper added	
	15% salt and pepper	
	30% salt and pepper	94.44%
	50% salt and pepper	
Median filter	No salt and pepper added	
	15% salt and pepper	
	30% salt and pepper	91.43%
	50% salt and pepper	
Median filtering based on partial differentiation	No salt and pepper added	
	15% salt and pepper	
	30% salt and pepper	94.12%
	50% salt and pepper	

target; and if it is less than the threshold within the variance, it is determined as the background image

(5) After traversing each small area, each small area is divided into two parts: the defect target and the background. During the whole process, some backgrounds will be mistaken for the surface defect target of the steel plate, so it must be eliminated. The defect target has a certain path. Connected domains exist. This article takes the current pixel as the center and sets a $3 * 3$ window. If more than half of the pixels in this window are defective pixels, it is confirmed that the pixel is a defective point

3. Key Technologies of Steel Plate Surface Defect Inspection System

3.1. System Composition. The steel plate surface defect detection system based on machine vision is mainly composed of optical lighting system, industrial camera, image acquisition system, image processing system, terminal computer, and data management system [38]. The system consists of two parts: hardware system and software system. The system flow chart is shown as in Figure 1.

3.2. Test Subject. The three doctors with rich work experience in this hospital are comprehensively judged for judging the degree of treatment. If there is a dispute, the result can be selected through discussion. We can regard the gray level of an image as a two-dimensional gray density function; then, a gray matrix can be used to describe the image moment features. We select a steel plate; take the invariant moment features of the cracks, holes, scratches, oil stains, and other images on it; extract the data results; and analyze them. Then, we read the texture features of these defect images again,

extract the data results, and analyze them. Taking the image of steel plate without bonding defects and adding different concentrations of salt and pepper noise as the research object, 4 kinds of filtering methods are used to denoise mixed experiments.

3.3. Experimental Method. There are many ways of data standard processing, but different data standardization methods will have a certain impact on the evaluation results of the system. For the positive index standardization method,

$$y_{ij} = \frac{x_{ij} - \min\left\{x_{ij}\right\}}{\max\left\{x_{ij}\right\} - \min\left\{x_{ij}\right\}}. \tag{14}$$

For the negative index standardization method,

$$y_{ij} = \frac{\max\left\{x_{ij}\right\} - x_{ij}}{\max\left\{x_{ij}\right\} - \min\left\{x_{ij}\right\}}. \tag{15}$$

After standardizing the data, using the principal component analysis of nonlinear logarithmic centering, the processing steps of logarithmic transformation and row vector centering are

$$z_{ij} = \ln y_{ij} - \frac{\sum_{i=1}^{m} \ln y_{ij}}{m}. \tag{16}$$

3.4. Statistical Data Processing Method. SPSS23.0 software was used for data processing, and the count data was expressed as a percentage (%), k is the number of data in this experiment, σ^2 is the variance of all survey results, and $P < 0.05$ indicates that the difference is statistically significant. The formula for calculating reliability is shown in the following equation:

$$a = \frac{k}{k-1}\left(1 - \frac{\sum \sigma_i^2}{\sigma^2}\right). \tag{17}$$

4. Key Technology Research on Steel Plate Surface Defect Detection System

4.1. Evaluation Index System Based on Index Reliability Testing. Reliability refers to the stability and reliability of the questionnaire [39]. This article adopts the α coefficient method created by L.J. Cronbach. The α coefficient can be obtained by Reliability Analysis in SPSS software. It is generally believed that the α coefficient above 0.8 indicates that the effect of the index setting is very good, and above 0.7 is also acceptable. Here, we analyze the reliability of each type of object, and the reliability index we choose for each type of object is slightly different. The results are shown in Table 1.

It can be seen from Table 1 that the data obtained from the surface defects of various steel plates has an acceptable influence on this experiment ($\alpha > 0.7$), and the influence of the data around the defects on the surface of various steel plates is acceptable. Within the scope, meet the prerequisites for the start of the experiment.
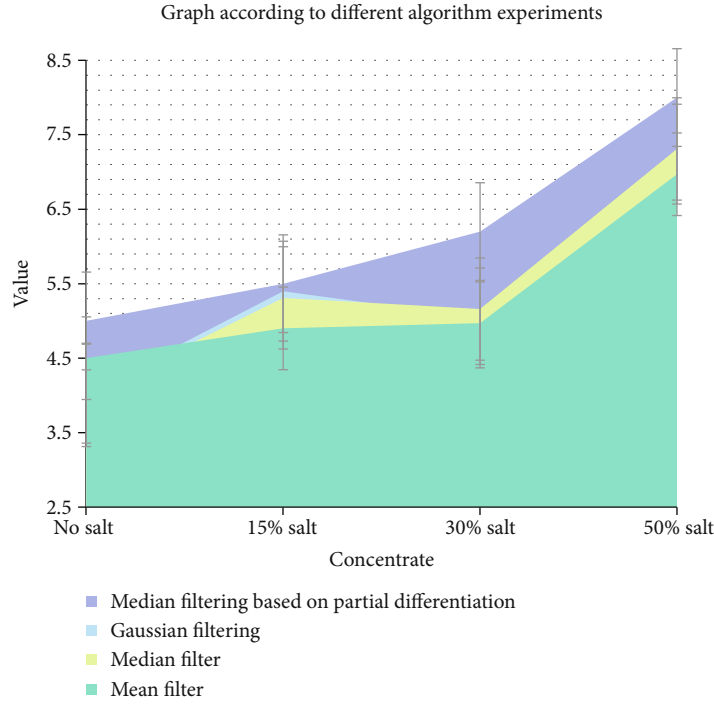
FIGURE 6: Analyze the graph according to different algorithm experiments.
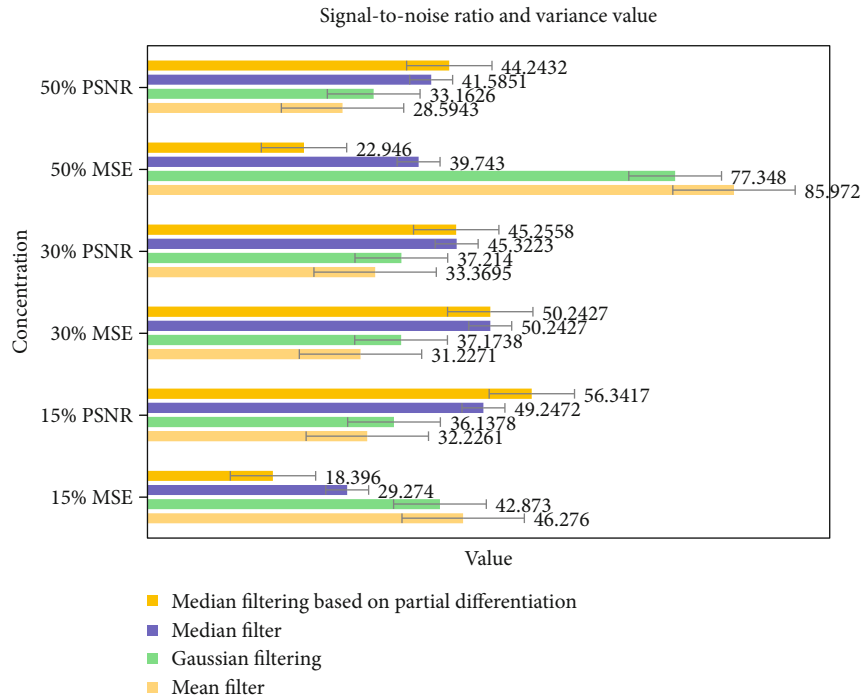
FIGURE 7: Analyze the graph according to the signal-to-noise ratio and variance value.

4.2. Sample Feature Extraction Data Analysis

4.2.1. Invariant Moment Feature Extraction Data Analysis. Feature extraction, as a key link in the image processing process in the system, is an important process to ensure the practicability of the system and the accuracy of defect recognition

[38]. We separately analyze the cracks, holes, scratches, and inclusion defects in the samples and their own, right shift. The left-shifted and transposed image extracts moment-invariant features. The extraction results are shown in Table 2. We make a line graph based on this result, as shown in Figure 2.

TABLE 6: Analysis table based on the experimental results of image denoising.

Filtering algorithm	15% salt and pepper noise		30% salt and pepper noise		50% salt and pepper noise	
	MSE	PSNR	MSE	PSNR	MSE	PSNR
Mean filter	46.276	32. 2271	31. 2271	33.3695	85.972	28. 5943
Gaussian filtering	42.873	36.1378	37.1738	37.2514	77.348	33. 1626
Median filter	29.274	49.2472	50.2427	45.3223	39.734	41.5851
Median filtering based on partial differentiation	18.396	56. 3471	57. 4317	45.2558	22.946	44.2432.

It can be seen from Figure 2 that the invariant moments of the same type of defects are not much different after they are themselves shifted left, shifted right, or transposed. The two groups of patients were compared at the end of the first course of treatment and at the end of the second course of treatment. The anxiety level of the experimental group is lower than that of the control group during half of the treatment. This conclusion is reliable, and there is no significant difference.

Feature extraction, as a key link in the image processing process in the system, is an important process to ensure the practicability of the system and the accuracy of defect recognition. We gather the moment invariant features extracted from different types of defects according to Table 2, and the results are shown in Figure 3.

It can be seen from Figure 3 that the invariant moments of different types of defects themselves, after shifting to the left, shifting right, or rotating, are quite different, which also verifies that the invariant moments have translation and rotation invariance. This also proves the accuracy of the median filtering algorithm system based on partial differentiation selected in this paper from the side. The new gray median value obtained by the algorithm can more accurately restore the original pixel value when there is no noise [40], and using the new gray the median degree value replaces the original noise points so that the algorithm can better retain the texture details of the image while filtering the noise.

4.2.2. Texture Feature Extraction of Defect Images. As a global feature, texture is a ubiquitous but difficult to describe possibility in images. The texture attribute refers to the law of change from pixel level to gray level in an image, which is an irregular but normal feature in the macroscopic view. We extracted the texture features of the cracks, holes, scratches, and inclusion defects in the samples, and the extraction results are shown in Table 3. We make a histogram based on this result, as shown in Figure 4.

It can be seen from Figure 4 that from the feature data extracted above, the difference between different features of different types or the same type is also very large. Because there is a unique sample, using this data for defect classification will cause the classifier to converge too late or even fail to converge, resulting in low classification accuracy or classification failure. Therefore, before classification, different methods should be selected according to needs. The exported attribute data has been standardized.

4.2.3. Standardized Processing of Characteristic Data. Here, our method is to standardize the extracted feature data. We

choose the linear scale transformation method, the range transformation method, and the standard sample transformation method. These three methods are different. The standard values of the data after linear transformation are all in (within the range of 0, 1); when the positive and negative indicators are equalized to positive indicators, the optimal value is 1, the worst value is 0, and the larger the value, the better. When the maximum value of a positive indicator is 0, this method cannot be used to standardize the indicator; when the value of a reverse indicator is 0, this method cannot be used to standardize the indicator. The results are shown in Table 4. We make a radar chart based on this result, as shown in Figure 5.

It can be seen from Figure 5 that the values of the four indicators of the hole are all equal, so the standard sample transformation method and the range transformation method cannot be used, but the linear proportional transformation method can only be used; the values of the four indicators of the crack are all close to 0, so the range transformation method cannot be used and the linear scale transformation method can only use the standard sample transformation method; the values of the four indicators of abrasion are all close to 1; and you can choose to use the range transformation method and the linear proportional transformation method; the values are close to 1; you can choose to use the range transformation method and the linear scale transformation method.

4.3. Experimental Results Based on Image Denoising

4.3.1. Analyze according to Different Algorithm Experiments. Through four different strip steel surface defect detection system designs, work in the same environment at the same time to analyze the changes in detection accuracy. Data-type factors adopt independent sample t-test, and the experimental results are shown in Table 5. We make an area map based on this result, as shown in Figure 6.

Figure 6 shows that the median filter and Gaussian filter have a particularly poor effect on salt and pepper noise. The middle filter can remove the salt and pepper noise in the middle, but it is not effective at the edges of the salt and pepper noise. The intermediate filter based on partial differentiation has the effect of salt and pepper noise, which is better. As the concentration of salt and pepper noise increases, the average Gaussian filter and filter are less capable of handling salt and pepper noise. Medium filtering still does not perform well in terms of edge noise. The medium filter based on partial differential has the best effect on the noise of salt and pepper.

4.3.2. Analyze according to the Signal-to-Noise Ratio and Variance Value. In order to compare different filtering effects more intuitively, this article uses signal-to-noise ratio and variance to evaluate the image quality after skipping. Comparing the maximum signal-to-noise ratio and image fluctuation after denaturation under different salt and pepper noise concentrations, it can be compared that the filtering effect studied in this paper is the best. Through experiments, the maximum signal-to-noise ratio and change value of each filter under different salt and pepper noise concentrations are obtained, as shown in Figure 6. We make a line chart based on this result, as shown in Figure 7.

It can be seen from Figure 7 that after processing the mean filter and Gaussian filter images, the average MSE fluctuation value is relatively large, and as the salt and pepper noise concentration increases, the growth rate of MSE increases significantly, and the signal-to-noise ratio also increases with the average fluctuation value. The increase in MSE continues to decrease, and image distortion becomes more serious. After performing intermediate filtering and adaptive filtering on the image, compared with the first two images, the image distortion is reduced, but the distortion is also more serious. After filtering the image, the image repayment effect is better.

5. Conclusions

An effective threshold segmentation algorithm for coefficient of variation is proposed. This algorithm overcomes the disadvantage of using only one threshold per iteration in repeated threshold segmentation. It also utilizes the sliding window used in adaptive threshold segmentation, which reduces the amount of calculation and improves detection efficiency. The system structure of the whole system is designed, and the system is divided into imaging module, fault detection software module, and storage management module. According to different principles of detection methods, different image capturing methods are given. The overall process of defect detection software is designed, and the design and implementation of basic software units are introduced in detail. This paper analyzes the design of the steel strip surface defect detection system based on machine vision. According to the application requirements of machine vision technology, based on the surface quality of strip steel, the detection of surface defects is adjusted and optimized for the design of this article. Experiments prove that the method designed in this paper is very effective. We hope that the research in this article can provide a theoretical basis for the design method of steel surface defect detection system based on machine vision.

At present, most retinal blood vessel extraction methods are mainly used for normal retinal images. Therefore, when applied to a large range of lesion images, it is difficult to accurately extract blood vessels due to the interference of lesions and other nonvascular structures, and a large number of nonvascular structures cannot be filtered. In addition, this article focuses on vascular bone extraction and vascular structure segmentation methods suitable for retinal imaging. Analyze the characteristics of defects, and find the entry point for

detecting defects. According to the edge feature, uneven texture feature, and uneven defect feature, the defect detection method based on edge feature, the defect detection method based on unequal texture feature, and the defect detection method based on irregular feature are proposed. The techniques and theories on which this method relies are introduced and discussed.

The steel industry occupies an important position in China's economic industry. It can be regarded as the main core of manufacturing. This is an intensive industry that has accumulated a lot of capital and energy. Although China produces a large amount of steel every year, the quality of various steel products in China is obviously not as good as that of developed countries. In the quality of steel products, the importance of surface quality is self-evident, but improving quality is always difficult. Improving the surface quality of steel is of great significance to improving market competitiveness. Accurate detection of steel plate surface defects and the establishment of a steel plate surface defect evaluation system are important conditions for improving the quality of steel plates. This article makes full use of the image data of steel surface defects and introduces artificial intelligence methods to classify and identify steel defects and target detection. It solves the problem of long iteration time of ant colony optimization algorithm and particle optimization algorithm. The algorithm is easy to fall into local optimization, improves the classification accuracy of the support machine, optimizes the optimization process, and is made of steel.

Data Availability

The data underlying the results presented in the study are available within the manuscript.

Conflicts of Interest

The authors declare that they have no conflicts of interest.

References

[1] K. Shankar, Y. Zhang, Y. Liu, L. Wu, and C.-H. Chen, "Hyperparameter tuning deep learning for diabetic retinopathy fundus image classification," *IEEE Access*, vol. 8, pp. 118164–118173, 2020.

[2] Y. Tang, S. Fang, J. Chen, L. Ma, L. Li, and X. Wu, "Axial compression behavior of recycled-aggregate-concrete-filled GFRP-steel composite tube columns," *Engineering Structures*, vol. 216, article 110676, 2020.

[3] N. Gao and Y. Zhang, "A low frequency underwater metastructure composed by helix metal and viscoelastic damping rubber," *Journal of Vibration and Control*, vol. 25, no. 3, pp. 538–548, 2019.

[4] T. Ohkubo, N. Terada, and Y. Yoshida, "Preliminary scanning fluorescence detection of a minute particle running along a waveguide implemented microfluidic channel using a light switching mechanism," *Microsystem Technologies*, vol. 22, no. 6, pp. 1227–1240, 2016.

[5] J. Zhao, J. Huang, R. Wang, H. R. Peng, and S. Ji, "Investigation of the optimal parameters for the surface finish of k9 optical

glass using a soft abrasive rotary flow polishing process," *Journal of Manufacturing Processes*, vol. 49, pp. 26–34, 2020.

[6] S. Liu, Y. Sun, M. Gu, C. Liu, L. He, and Y. Kang, "Review and analysis of three representative electromagnetic NDT methods," *Insight-Non-Destructive Testing and Condition Monitoring*, vol. 59, no. 4, pp. 176–183, 2017.

[7] S. K. Choudhary, A. Kumar, S. Ganguly, M. Laru, and E. Z. Chacko, "Application of thermodynamics in mitigating wire rod chipping during hot rolling of continuously cast steel billets," *ISIJ International*, vol. 58, no. 10, pp. 1811–1819, 2018.

[8] M. P. Dombrowski, J. Labelle, D. G. McGaw, and M. C. Broughton, "An autonomous receiver/digital signal processor applied to ground-based and rocket-borne wave experiments," *Journal of Geophysical Research: Space Physics*, vol. 121, no. 7, pp. 7334–7343, 2016.

[9] S. B. Shu, C. M. Yu, C. Liu, M.-W. Chen, Y.-Z. Zhang, and X. Li, "Improved plasma position detection method in EAST Tokamak using fast CCD camera," *Nuclear Science and Techniques*, vol. 30, no. 2, pp. 67–76, 2019.

[10] M. A. Hossam, H. M. Ebied, M. H. Abdel-Aziz, and M. F. Tolba, "Accelerated hyperspectral image recursive hierarchical segmentation using GPUs, multicore CPUs, and hybrid CPU/GPU cluster," *Journal of Real-Time Image Processing*, vol. 14, no. 2, pp. 413–432, 2018.

[11] X. Q. Zhang and S. G. Zhao, "Cervical image classification based on image segmentation preprocessing and a CapsNet network model," *International Journal of Imaging Systems and Technology*, vol. 29, no. 1, pp. 19–28, 2019.

[12] C. Zuo, L. Jovanov, B. Goossens et al., "Image denoising using quadtree-based nonlocal means with locally adaptive principal component analysis," *IEEE Signal Processing Letters*, vol. 23, no. 4, pp. 434–438, 2016.

[13] L. Feng and L. Lin, "Comparative analysis of image denoising methods based on wavelet transform and threshold functions," *International Journal of Engineering Transactions B Applications*, vol. 30, no. 2, pp. 199–206, 2017.

[14] C. Yang, Z. Yang, and Z. Deng, "Robust weighted state fusion Kalman estimators for networked systems with mixed uncertainties," *Information Fusion*, vol. 45, pp. 246–265, 2019.

[15] K. J. H. Law, H. Tembine, and R. Tempone, "Deterministic mean-field ensemble Kalman filtering," *SIAM Journal on Scientific Computing*, vol. 38, no. 3, pp. A1251–A1279, 2016.

[16] M. V. Basin, "Root-mean-square filtering of the state of polynomial stochastic systems with multiplicative noise," *Automation & Remote Control*, vol. 77, no. 2, pp. 242–260, 2016.

[17] M. Elhoseny and K. Shankar, "Optimal bilateral filter and convolutional neural network based denoising method of medical image measurements," *Measurement*, vol. 143, pp. 125–135, 2019.

[18] R. K. Wang, C. R. Chatwin, and R. C. D. Young, "Assessment of a Wiener filter synthetic discriminant function for optical correlation," *Optics & Lasers in Engineering*, vol. 22, no. 1, pp. 33–51, 2016.

[19] M. L. Honig and J. S. Goldstein, "Adaptive reduced-rank interference suppression based on the multistage Wiener filter," *IEEE Transactions on Communications*, vol. 50, no. 6, pp. 986–994, 2016.

[20] J. Yang, Z. Yang, J. Liu, B. Jiang, W. Lu, and X. Gao, "No reference quality assessment for screen content images using stacked auto-encoders in pictorial and textual regions," *IEEE Transactions on Cybernetics*, pp. 1–13, 2020.

[21] Y. Li, J. Liu, and Y. Wang, "Railway wheel flat detection based on improved empirical mode decomposition," *Shock and Vibration*, vol. 2016, Article ID 4879283, 14 pages, 2016.

[22] E. Cauda, A. Miller, and P. Drake, "Promoting early exposure monitoring for respirable crystalline silica: taking the laboratory to the mine site," *Journal of Occupational & Environmental Hygiene*, vol. 13, no. 3, pp. D39–D45, 2016.

[23] S. Ren and F. Liu, "The optimal thresholding technique for image segmentation using fuzzy Otsu method," *Advances in Computational Sciences and Technology*, vol. 11, no. 6, pp. 445–454, 2018.

[24] Z. Luo, T. Wu, Z. He, and X. Chen, "Extraction of sea-clutter and RFI regions based on image segmentation for high-frequency sky-wave radar," *IET Radar, Sonar & Navigation*, vol. 13, no. 1, pp. 58–64, 2019.

[25] Y. Liu, C. Yang, and Q. Sun, "Thresholds based image extraction schemes in big data environment in intelligent traffic management," *IEEE Transactions on Intelligent Transportation Systems*, pp. 1–9, 2020.

[26] T. Sathiya and B. Sathiyabhama, "Fuzzy relevance vector machine based classification of lung nodules in computed tomography images," *International Journal of Imaging Systems and Technology*, vol. 29, no. 3, pp. 360–373, 2019.

[27] X. Wang, X. Zhao, Y. Zhu, and X. Su, "NSST and vector-valued C–V model based image segmentation algorithm," *IET Image Processing*, vol. 14, no. 8, pp. 1614–1620, 2020.

[28] S. Wan, Y. Xia, L. Qi, Y. H. Yang, and M. Atiquzzaman, "Automated colorization of a grayscale image with seed points propagation," *IEEE Transactions on Multimedia*, vol. 22, no. 7, pp. 1756–1768, 2020.

[29] J. Qin, X. Shen, F. Mei, and Z. Fang, "An Otsu multi-thresholds segmentation algorithm based on improved ACO," *The Journal of Supercomputing*, vol. 75, no. 2, pp. 955–967, 2019.

[30] Y. Liu, Y. Chen, B. Han, Y. Zhang, X. Zhang, and Y. Su, "Fully automatic breast ultrasound image segmentation based on fuzzy cellular automata framework," *Biomedical Signal Processing & Control*, vol. 40, pp. 433–442, 2018.

[31] H. Chen, D. Fan, J. Huang, W. Huang, G. Zhang, and L. Huang, "Finite element analysis model on ultrasonic phased array technique for material defect time of flight diffraction detection," *Science of Advanced Materials*, vol. 12, no. 5, pp. 665–675, 2020.

[32] X. Deng, Y. Du, C. Wang, and X. Wang, "An adaptive threshold corner detection algorithm based on auto-correlation matrix of image pixel," *Transactions of the Chinese Society of Agricultural Engineering*, vol. 33, no. 18, pp. 134–140, 2017.

[33] Y. Sun, "Analysis for center deviation of circular target under perspective projection," *Engineering Computations*, vol. 36, no. 7, pp. 2403–2413, 2019.

[34] C.-y. Han, "Improved SLIC imagine segmentation algorithm based on K-means," *Cluster Computing*, vol. 20, no. 2, pp. 1–7, 2017.

[35] Z. Wang, Y. Wang, L. Jiang, C. Zhang, and P. Wang, "An image segmentation method using automatic threshold based on improved genetic selecting algorithm," *Automatic Control and Computer Sciences*, vol. 50, no. 6, pp. 432–440, 2016.

[36] L. Sun, Y. Li, Y. Zou, and Y. Li, "Pig image segmentation method based on improved graph cut algorithm," *Transactions of the Chinese Society of Agricultural Engineering*, vol. 33, no. 16, pp. 196–202, 2017.

[37] F. Argüello, D. L. Vilariño, D. B. Heras, and A. Nieto, "GPU-based segmentation of retinal blood vessels," *Journal of Real-Time Image Processing*, vol. 14, no. 4, pp. 773–782, 2018.

[38] N. Krishnaraj, M. Elhoseny, M. Thenmozhi, M. M. Selim, and K. Shankar, "Deep learning model for real-time image compression in Internet of Underwater Things (IoUT)," *Journal of Real-Time Image Processing*, vol. 17, no. 6, pp. 2097–2111, 2020.

[39] F. Xiao, "Multi-sensor data fusion based on the belief divergence measure of evidences and the belief entropy," *Information Fusion*, vol. 46, pp. 23–32, 2019.

[40] L. Zhang, H.-M. Shi, X.-H. Zeng, and Z. Zhuang, "Theoretical and experimental study on the transmission loss of a side outlet muffler," *Shock and Vibration*, vol. 2020, Article ID 6927574, 8 pages, 2020.

WILEY | Hindawi

Research Article

National Sports AI Health Management Service System Based on Edge Computing

Huali Yang[1] and Xiaowei Han [2]

[1]*School of Physical Education, Hebei Normal University for Nationalities, Chengde, 067000 Hebei, China*
[2]*School of Basic Medicine, Weifang Medical University, Weifang, 261053 Shandong, China*

Correspondence should be addressed to Xiaowei Han; hanxw@wfmc.edu.cn

With the development of the economy, people's living standards continue to improve, and the management awareness of their own health and safety has gradually increased. The human body usually has a long process of transition from being healthy to the appearance of disease, and people's lifestyle and daily behavior will affect the health of the body to a large extent. This paper studies the national sports AI health management service system based on edge computing. This paper organically combines edge computing, artificial intelligence, and health management service systems. Through detection devices with smart sensors and smart health systems, a comprehensive health management service platform for the masses is constructed to promote the development of sports health management services. Upgrade and transform to make it more in line with the modern intelligent environment. The advancement of modern technology has gradually transformed my country's traditional health record management service to an intelligent electronic health record management system. From the experimental data, it can be seen that the filing rate and pass rate of residents' electronic files have reached 88.275% and 87.435%, but the utilization rate of health files is only 31.685%. The establishment of a supporting health management service system is precisely to effectively increase the utilization rate of health files, so that users can truly enjoy intelligent, professional, and real-time health services.

1. Introduction

In the context of modern social culture and economic development, technologies such as the Internet, cloud platforms, fog computing, big data, and artificial intelligence. continue to impact and influence various industries. The health industry is also being reintroduced in this era. With the increase of people's health awareness, the cognitive demand for health and consumer demand is constantly evolving and growing. Under this general background, health management, as a new health service model, has received more and more attention from people. However, there are still many difficulties in development. If we continue to follow the current service models, it is difficult to make health management implementation and promotion, whether it is the lack of industry norms and technical standards; the prominent contradiction between human resource supply and demand; the lagging of information standardization and network construction; or

the lack of commercial sustainability of existing management service organizations, more research, and practice to promote the solution. As an important part of health management, community health service is a primary health service system that takes human health as the center, family as the unit, and community as the service scope. It has certain research value to allow communities, families, and individuals to better enjoy health services and conduct health management more scientifically.

Research on health management service system abroad has been going on for many years, and many results have been obtained. Iamsumang conducted research on the application of dynamic hybrid Bayesian network in online system health management. In the article, he introduced a new modeling method and analyzed the application examples of the algorithm in health monitoring and learning in online system health management. By modeling theoretical or empirical degradation models with continuous variables, a

hybrid dynamic Bayesian network (DBN) is introduced to represent complex engineering systems with potentially faulty physics. This method can be flexibly and intuitively extended from small localization functions to large complex dynamic systems. If more data analysis can be conducted in the research, the accuracy of computational reasoning can be better improved [1]. Thorat has conducted research on patient health management systems based on wireless sensor networks. He believes that the scattered relationship between various units in the health care field has affected the development of health management systems. If close cooperation in the medical field can be achieved based on the Internet of Things and wireless sensors, the current deficiencies in health management services can be resolved to a large extent. From the system simulation experiment, the health management system he established still has room for optimization in database selection [2].

In recent years, China has actively advocated the organic integration of advanced science and technology with sports health management and other fields. Pan has conducted research on the application of big data in medical and health management and services. In his research, he discussed the background of medical information and summarized the current situation, market analysis, and construction process of medical information health management. The big data application of medical health management and services in daily life include clinical decision-making, remote treatment, and personalized medicine. After analyzing the current challenges of medical big data, he put forward suggestions to improve the status quo. From a practical point of view, these suggestions can indeed help to improve medical and health management services. If the advanced edge computing and artificial intelligence in Internet technology can be further combined, the intelligence and scientificity of the service system can be further improved [3].

Based on edge computing and artificial intelligence, this article has launched an in-depth study on the health management service system. The research is mainly carried out from the following aspects: this article describes the technologies and methods involved in the health management service system, including edge computing, artificial intelligence, query optimization algorithms for distributed heterogeneous databases, and decision-making in the data transmission scheduling method. This article introduces the structural framework and database design of the health management service system, and the experimental data confirms the superiority of the system in increasing the utilization rate of user health files and improving the user's health management service experience.

2. Technology Used in the Health Management Service System Based on Edge Computing

2.1. Edge Computing.
Edge computing refers to the use of an open platform that integrates network, computing, storage, and application core capabilities on the side close to the source of things or data and provides the nearest services nearby. Its applications are initiated on the edge side to generate faster network service responses and meet the indus-

try's basic needs in real-time business, application intelligence, security, and privacy protection [4]. Compared with cloud computing, edge computing can achieve user response faster and improve processing efficiency. At present, relevant research on edge computing technology at home and abroad is mainly aimed at the connection between mobile devices and cloud platforms, which mainly depends on the rapid development of mobile devices in contemporary society and its important position in modern society [5]. In order to effectively solve the high network load, high bandwidth, low latency, and other requirements brought about by the rapid development of the mobile Internet and the Internet of Things, the concept of mobile edge computing (MEC) was proposed and has received extensive attention from academia and industry [6].

As a hot technology, edge computing has been widely used in the business field. Among them, Internet companies hope to extend their existing cloud service capabilities to the edge network by taking advantage of their own service industry-related advantages [7]. The main difficulty in the current system lies in the integration of heterogeneous data and the collaboration between various platforms. As the data belongs to different subsystems, a unified data model needs to be established at the edge nodes [8]. Although the various attributes of edge devices continue to improve, in order to make the overall performance more efficient, it is necessary to strategically migrate cloud services under the premise of considering the operating capabilities of edge devices and future scalability [9].

2.2. Artificial Intelligence-Based Health Management System.
Artificial intelligence is a branch of computer science, and its essence lies in the simulation and expansion of human intelligence through machines [10]. Judging from the current health service provision, the development of artificial intelligence mobile communication technology can provide a more convenient way to meet the diverse health needs of residents [11]. When analyzing the needs of the health management service system, this article believes that the system should have the functions of collecting user health information, storing and transmitting user health data, and analyzing and counting user health data. Therefore, in the system design, this paper combines the edge computing concept to divide the system into five levels [12]. Figure 1 shows the structural design of the health management service system.

As can be seen from Figure 1, the system includes user layer, business layer, service layer, data layer, and hardware facility layer. A complete structural framework design can improve the scientific nature of system intelligent services while ensuring data security [13]. The user layer is oriented to the end users of the system, including ordinary residents, medical personnel, and medical institutions. Business layer involves data collection, storage, query, and statistics. The application service layer is mainly the related technology used when the system realizes the business function. The data support layer contains system data and computing framework based on distributed computing.

2.3. Query Optimization Algorithm for the Distributed Heterogeneous Database.
The distributed heterogeneous

User layer

| Ordinary residents | Medical staff | Medical institutions |

Business layer

| Data collection | Data storage | Data query | Statistics |

Application service layer

| Application server | WEB framework | Data access service | Data exchange protocol |

Data support layer

| Distributed file system | Distributed computing framework | Distributed database |

Hardware facility layer

| Universal server | Storage | Internet equipment | Routing |

FIGURE 1: Structure design of the health management service system.

database system is a kind of database system based on computer network, physically dispersed and logically unified, with site autonomy and different data models [14]. The most basic operation in a database is query operation, and query cost is an important criterion for measuring a database system. Query operations often involve multiple tables. For distributed heterogeneous databases, these tables may be stored on different sites; so, the choice of join operation is very important [15]. In distributed heterogeneous databases, there are two goals for query optimization: one is to minimize the total cost of the query; the other is to minimize the local response time of the query. The total cost of distributed query is different from that of centralized query. In addition to the total CPU cost and the total I/O cost of the query, the cost of data communication between sites is also added.

Assuming that the relationship R, S is located at site 1 and site 2, A is an attribute of R, and its corresponding attribute in S is B. The connection operation on it satisfies the formula:

$$R \infty A = BS = (R \propto A = BS) \infty A = BS, \qquad (1)$$

$$T = C0 + C1 \times X. \qquad (2)$$

Through the semiconnection step, the communication cost required to complete the entire board connection opera-

tion can be calculated as

$$T = 2C0 + C1 \times \left(\text{Size}(B) \right) \times \text{Val}(B[S]) + \text{Size}(R) \times \text{Card}(R)' \right). \qquad (3)$$

The SDD-1 algorithm is based on the semiconnected algorithm, which is a multirelational semiconnected algorithm [16]. Assuming that R and S are two relations to be semiconnected, the semiconnected selection factor, semiconnected cost, and semiconnected revenue of the algorithm satisfy the formula

$$SFsj(R \propto S) = \text{card}\ (\pi a(S))/\text{card}\ (S), \qquad (4)$$

$$\text{cost}(R \propto S) = \text{size}(\pi a(S)) = \text{card}\ (\pi a(S)) \times \text{length}(a), \qquad (5)$$

$$\text{benefit}(R \propto S) = (1 - SFsj(R \propto S))/\text{size}(R). \qquad (6)$$

At the same time, the effective semijoin and the most beneficial semijoin satisfy

$$\text{benefit}(R \propto S) > \text{cost}(R \propto S). \qquad (7)$$

The basic idea of the SDD-1 algorithm is to use the greedy algorithm to repeatedly search for the most beneficial semijoins until the query is completed and then transmit all the data to the site with the largest amount of data for final assembly [17]. The basic steps are as follows: (1) generate a

set of beneficial semiconnections from all semiconnections of relations. (2) Find the most beneficial semiconnection from the set of beneficial semiconnections, add it to the execution strategy, delete it from the set of beneficial semiconnections, and modify all affected statistical values. (3) Repeat the first two steps until all beneficial semiconnections have been added to the execution strategy. (4) Choose the site with the largest amount of data as the assembly site and execute the semijoin operation in the order in the execution strategy [18].

When performing multijoin query optimization, in order to measure the degree of similarity between two antibodies, the concept of similarity can be introduced [19]. Assume that i, j are two antibodies, and $i[k], j[k]$, respectively, express the genes of their kth locus. Then, the similarity formula design meets

$$S(i, j) = \sum_{k=1}^{k=2N-1} \text{Round}\left(\frac{(2N - 1 - K)(N - 1)}{2N - 1}\right). \quad (8)$$

The antibody concentration is a measure of the proportion of antibodies similar to the antibody in the entire immune system [20]. It is known that X is an antibody, and $C(k)$ is the size of the intermediate relationship. Then, in a nonempty immune system composed of M antibodies, the antibody concentration and fitness function can be set as

$$\rho(i) = \sum_{j=1}^{j=M} S(i, j), \quad (9)$$

$$F(x) = \sum_{K=1}^{K=N-1} C(k). \quad (10)$$

2.4. Decision Method in Data Transmission Scheduling. In intelligent systems based on edge computing, data transmission scheduling is a very important research content. Cross-layer data transmission scheduling issues involve buffer storage, modulation methods, available channels, and so on. The system state will shift to different states with different transmission strategies [21].

The dynamic programming method is a method of solving the decision-making process in operations research. It is mainly aimed at multistage decision-making problems and transforms multistage decision-making problems into single-stage decision-making. In order to obtain the optimal strategy with long-term benefits, it is necessary to consider the immediate benefits in the current state and the average benefit value of each step [22]. The edge device receives the data transmitted by the sensor, and after data preprocessing, it needs to send the data to the cloud computing center. The following formula is used to express the average benefit of each behavior in the decision-making process:

$$\rho\pi(s0) = \lim_{n \to \infty} \frac{1}{n} E\pi \left[\sum_{i=0}^{n-1} R(Si, \pi(Si))\right], \quad (11)$$

Where $\rho\pi(s0)$ is the average benefit obtained when exe-

cuting the strategy π in the initial state. Considering the optimal strategy under future benefits, the equation can be expressed as

$$\rho^* + h^*(s) = \max_{a \in A}\left[R(s, a) + \sum_{s}^{\prime=1} |s|ps\right]. \quad (12)$$

When using the strategy iteration method to solve the MDP problem, starting from a strategy and continuously improving until there is no change, the number of linear equations and the number of states in the solution process are equal. First, evaluate the strategy, choose a strategy rule, and solve the equation system containing l linear equations in the same form as formula (13).

$$r(i, a(i)) + \beta \sum_{j \in S} P(j|i, a(i)) V(j) = V(i), \quad (13)$$

where $\beta(\in [0, 1))$ is the discount factor. When performing strategy improvement operations, a new decision function can be obtained through calculation to satisfy

$$\max_{a \in A(i)} = r(i, g(i)) + \beta \sum_{j \in S} P(j|i, g(i)). \quad (14)$$

When the rule is terminated, if the above formula is true for all states $i \in S$, then the operation will be terminated for a long time; otherwise, it is necessary to replace f with g and jump to the first step to perform the operation again. When the strategy iteration method solves the MDP problem, it is necessary to know all the state information of the system, and there will be a linear equation system for each state; so, it is more difficult to solve the calculation. Therefore, if the state space of the system is not very large, it can be solved directly by this method [23]. When the system scale is large, it is more troublesome to calculate.

The Q learning algorithm is a kind of reinforcement learning method, which has a relatively wide range of references in artificial intelligence. The idea of reinforcement learning is the constant interaction between the agent and the environment, seeking to maximize benefits in the decision-making process]. Set $Qi(si, ai)$ to represent the maximum discount cumulative benefit value obtained when selecting the strategy from the initial state, then there is

$$Qi(si, ai) = r(si, ai) + \gamma V_i^*(si, ai), \quad (15)$$

$$Qi(si, ai) \leftarrow Q(si, ai) + \partial[ri = 1 + \gamma Q(si + 1, ai + 1) - Q(si, ai)]. \quad (16)$$

The W learning algorithm is a self-organizing behavioral selection scheme applied to multiple parallel task target systems, which is developed on the basis of Q learning [24]. W learning can well realize the distributed learning function of multiagents, which overcomes the shortcomings of insufficient environmental information in complex heterogeneous networks. When the system selects and executes the strategy

TABLE 1: Health data statistics.

Sign	Name	Definition
A101	File creation date	Time to create health file
A102	Event name	Basic information about health events
A103	Event location	Location of health incident
A104	Message number	Serial number of the information file
A201	User name	Name of health service recipient
A202	Emergency contact	Emergency contact for health service recipients

TABLE 2: Maternal and child health management service data.

Index (%)	A	B	C	D	E	F
Newborn visit	80.5	90.23	97.81	88.63	83.27	92.44
Child health management	90.64	92.68	93.73	85.54	91.76	88.82
Child system management	61.48	58.59	83.46	78.67	76.78	80.21
Early pregnancy test	86.61	87.53	72.59	90.54	70.64	81.29
Maternal health management	60.43	91.85	99.34	85.89	89.63	93.26
Postpartum visit	80.28	95.36	98.05	95.15	90.87	92.23

	Newborn visit	Child health management	Child system management	Early pregnancy test	Maternal health management	Postpartum visit
A	80.5	90.64	61.48	86.61	60.43	80.28
B	90.23	92.68	58.59	87.53	91.85	95.36
C	97.81	93.73	83.46	72.59	99.34	98.05
D	88.63	85.54	78.67	90.54	85.89	95.15
E	83.27	91.76	76.78	70.64	89.63	90.87
F	92.44	88.82	80.21	81.29	93.26	92.23
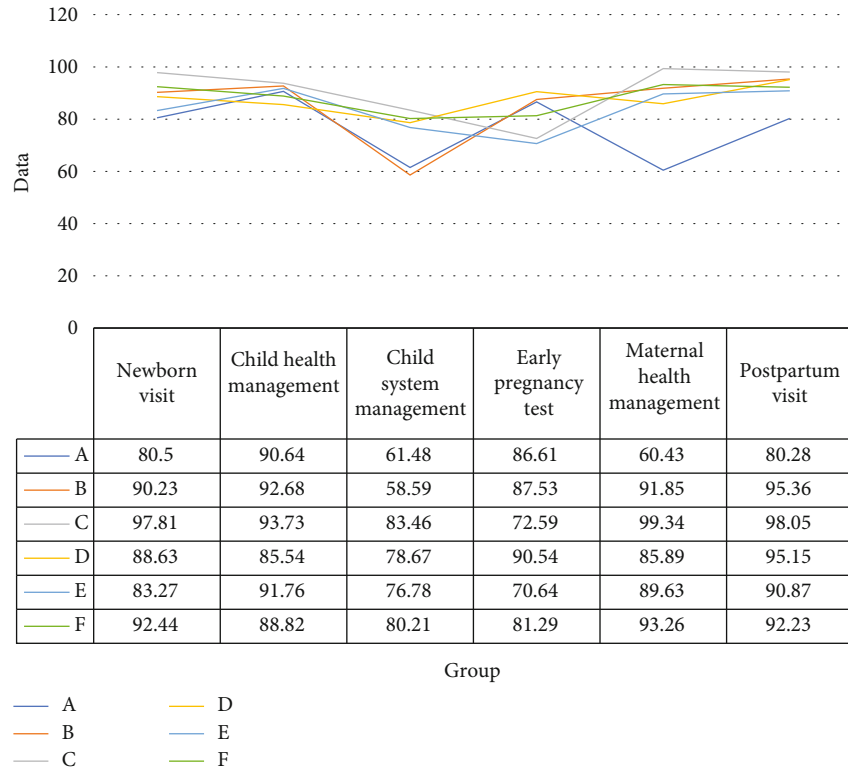
FIGURE 2: Maternal and child health management service data.

$ak(x)$ with the largest W value, it satisfies

$$Wk(x) = \max_{i \in 1,2,\cdots,n} Wi(x). \qquad (17)$$

The W value represents the importance of implementing the recommended behavior and is the difference between the predicted benefit and the actual benefit. In this algorithm, a single agent does not need to know the information of other agents participating in the competition, and at the same time, it no longer needs to obtain the state transition probability of the system, but only needs to know the local environmental

TABLE 3: Elderly health management service data.

Index (%)	A	B	C	D	E	F
Elderly health management	60.93	70.26	57.89	75.35	64.37	68.21
Examination table	87.13	75.67	64.28	81.39	72.28	85.68
Common disease detection	73.21	63.84	80.36	75.92	83.23	69.42
Health advisory	70.21	79.18	81.43	82.75	75.36	65.36
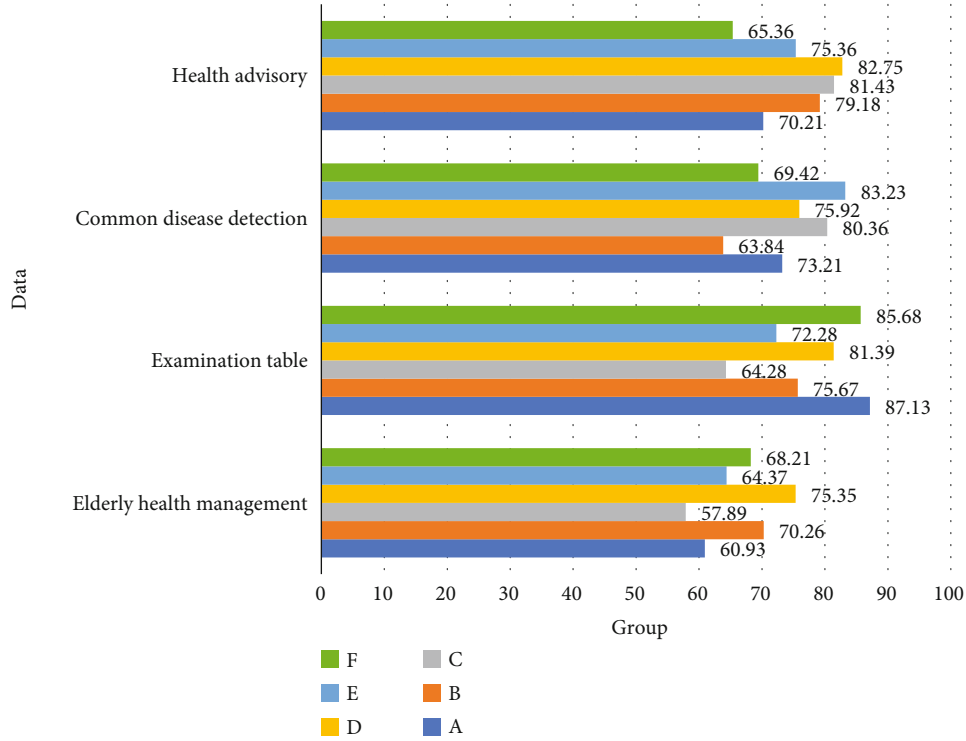
FIGURE 3: Elderly health management service data.

TABLE 4: Health management service data for patients with hypertension and diabetes.

Index (%)	A	B	C	D	E	F
Health management of patients with hypertension	94.53	81.82	84.86	90.21	87.28	82.36
Standardized management of hypertension patients	81.27	68.27	94.92	89.13	82.68	78.53
Manage crowd blood pressure control	42.19	36.58	51.23	60.82	59.63	48.35
Diabetes patient health management	90.18	86.57	85.32	84.18	91.63	82.15
Standardized management of diabetic patients	60.38	73.15	76.74	85.28	79.34	82.55
Manage crowd blood sugar control	38.15	45.43	50.28	49.63	54.15	40.28

knowledge [25]. The update method of the W value is

$$W(x) = Q(x, a) - \min_{a \in A} Q(x, a), \qquad (18)$$

$$Wi(si) = (1 - \partial)wi(si) + \partial(Qi(xi, ai)). \qquad (19)$$

3. Simulation Experiment of the Health Management Service System Based on Edge Computing

3.1. Experimental Background. As an important part of health management, community health service is a primary health service system that takes human health as the center, family as the unit, and community as the service scope. At

	Health management of patients with hypertension	Standardized management of hypertension patients	Manage crowd blood pressure control	Diabetes patient health management	Standardized management of diabetic patients	Manage crowd blood sugar control
A	94.53	81.27	42.19	90.18	60.38	38.15
B	81.82	68.27	36.58	86.57	73.15	45.43
C	84.86	94.92	51.23	85.32	76.74	50.28
D	90.21	89.13	60.82	84.18	85.28	49.63
E	87.28	82.68	59.63	91.63	79.34	54.15
F	82.36	78.53	48.35	82.15	82.55	40.28

Group

- A
- B
- C
- D
- E
- F
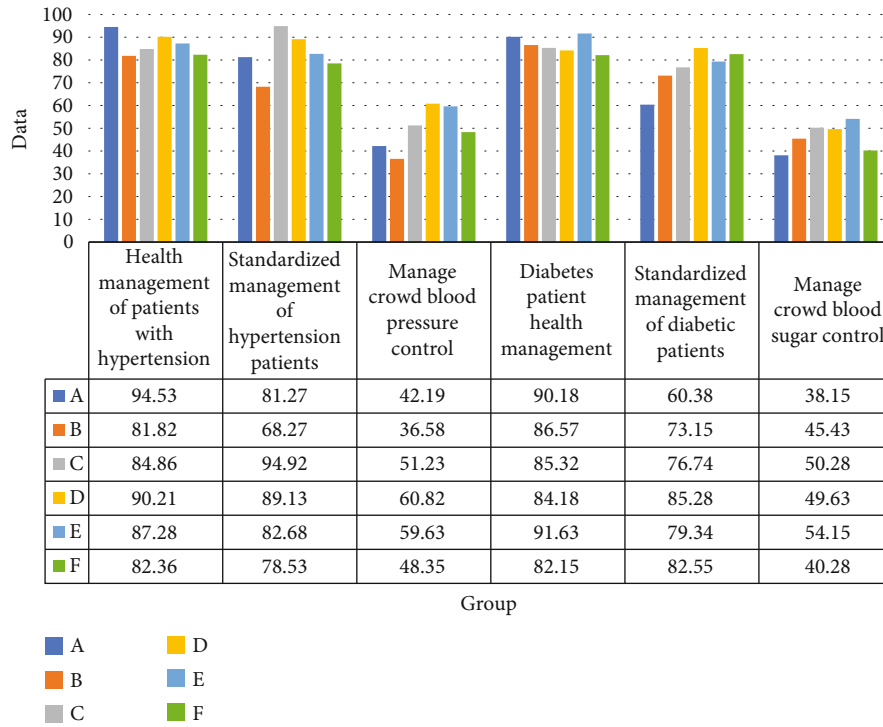
FIGURE 4: Health management service data for patients with hypertension and diabetes.

the same time, as a focus of health management issues, how to better play the role of community health services so that communities, families, and individuals can better enjoy health services and conduct health management more scientifically has certain research value. Based on the above background, this article explores how to develop a family-applicable health management service system through the investigation of community hospitals, with the help of service design tools and artificial intelligence technology, combined with existing health management problems and people's health needs.

3.2. Experimental System Structure Design. In the system structure, the goal of this article is to allow users to participate in the establishment of health records through health management, so that community medical treatment, prevention, and health care can move toward a scientific, systematic, and sustainable medical service path, trying to use the existing community health service institutions which a closer link is formed between the resource system and community residents, and an attempt is made to break the status quo of information islands. Secondly, through the establishment of family-based health files with individuals as the core, and using technologies such as big data and cloud platforms as a supplement to traditional epidemiology and medical statistics, it provides more comprehensive theoretical assistance to the medical service system.

The system designed in this paper includes five parts: user layer, business layer, service layer, data layer, and hardware facility layer. The user layer faces the end users of the system, including ordinary residents, medical personnel, and medical institutions. The business layer involves data

collection, storage, query, and statistics. The application service layer is mainly related technologies used when the system realizes business functions. The data support layer contains system data and computing framework based on the concept of distributed computing.

3.3. Experimental System Database Design. In the era of big data, we need to consider the impact of data growth on database stability before system development. When selecting a database, it is necessary to comprehensively consider its data storage capacity and stability when facing a large number of users. The health management service system contains a lot of user data; so, this article finally chose the nonrelational database HBase for the system. In order to distinguish various data indicators in the database, this article divides the data types into string, date, integer, byte, and other types. Table 1 is a statistical table of some health data.

4. AI Health Management Service System Based on Edge Computing

4.1. Service Effect of the Health Management Service System for Different Groups. Health management refers to the user's health needs as the orientation, through medical means to check, evaluate, analyze, and predict their health status and risk index and provide health guidance and health plans, so as to coordinate the interaction between individuals, organizations, and society. This article will focus on multiple groups such as mothers and infants, the elderly, hypertension, and diabetes and explore how the health management service system can help them. In order to improve the credibility of the research, this paper investigates the health service

TABLE 5: Completion of public health file management services.

Index (%)	A	B	C	D	E	F
Health file creation rate	95.53	98.31	80.67	85.89	93.72	89.11
Electronic file creation rate	95.53	86.92	80.12	85.89	92.08	89.11
Health record pass rate	85.31	82.18	84.33	93.16	90.28	89.35
Health file utilization rate	30.52	26.49	35.71	29.36	36.15	31.88
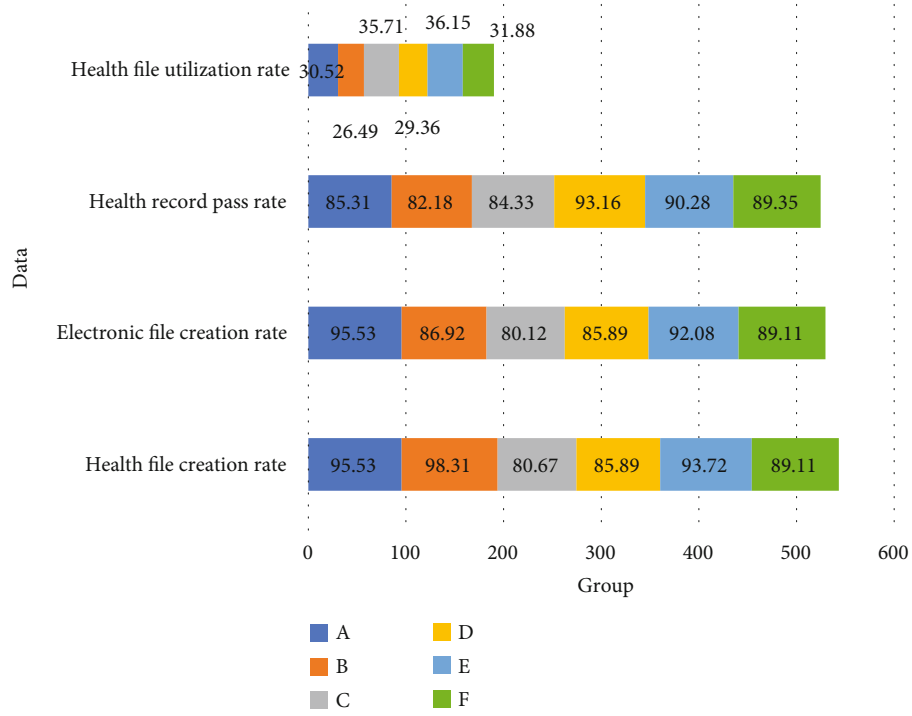
FIGURE 5: Completion of public health file management services.

TABLE 6: Health management service coverage of each unit.

Index (%)	A	B	C	D	E	F
Government agencies	71.83	67.28	69.35	72.16	63.85	75.32
Private enterprise	75.12	70.31	59.21	63.28	58.45	68.31
Primary and secondary school	100	99.42	99.57	100	98.63	100
University	100	100	100	100	99.85	100
Rural towns	68.15	60.28	55.21	63.21	48.63	61.34

data in six different areas of the city, and the difference in the data reflects the service effect of the system to different groups.

Compared with other groups, people tend to pay more attention to the health and safety management of newborns and pregnant women. This article focuses on newborn visits, child health management, child system management in child health management services, and early pregnancy in pregnant women's health management. Testing, maternal health management, and the probability of postpartum visits were investigated. A-F are the six areas of this survey. Table 2 and Figure 2 are the data of pregnant women and children's health management services.

It can be seen from Table 2 and Figure 2 that in the child health management service, the average newborn visit rate is 88.81%, and the average child health management rate is 90.53%, and the indicators exceed the expected 80% target value. At the same time, the average management rate of the children's system is only 73.2%, and only two of the six regions barely reach the target value, and the management rate of the children's system in the B region is only 58.59%. In maternal health management services, the average values of early pregnancy detection rate, maternal health management rate, and postpartum visit rate are 81.54%, 86.73%, and 91.99%, respectively. The postpartum visit rates in the six regions all reached the target value, but the performance

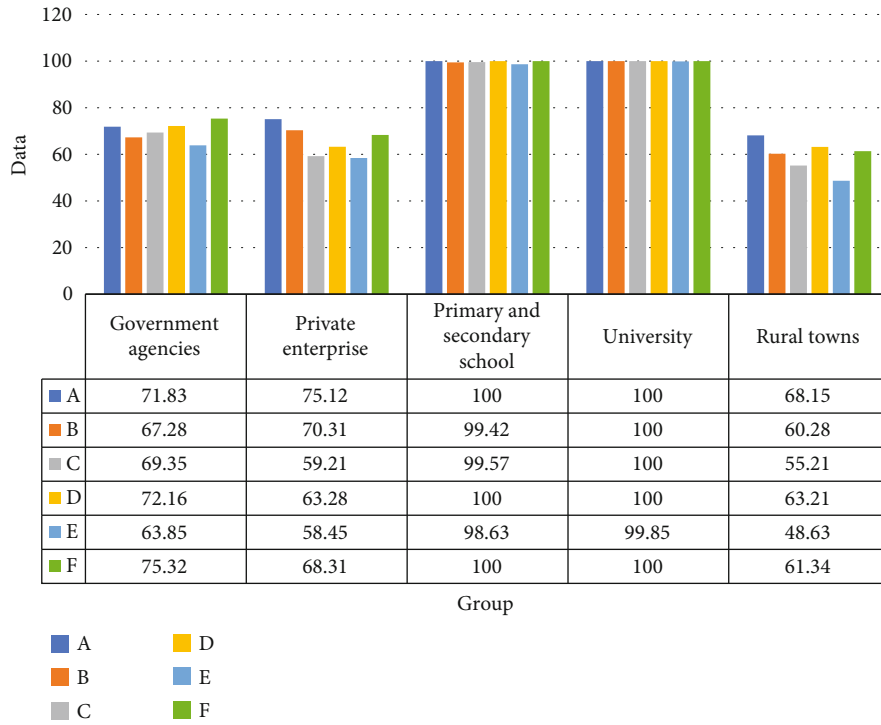|	Government agencies	Private enterprise	Primary and secondary school	University	Rural towns
A	71.83	75.12	100	100	68.15
B	67.28	70.31	99.42	100	60.28
C	69.35	59.21	99.57	100	55.21
D	72.16	63.28	100	100	63.21
E	63.85	58.45	98.63	99.85	48.63
F	75.32	68.31	100	100	61.34

FIGURE 6: Health management service coverage of each unit.

TABLE 7: Survey data of residents' physical exercise and eating habits.

Index (%)	A	B	C	D	E	F
Exercise days per week	2.53	2.65	3.21	2.87	2.41	2.72
Daily exercise time (minutes)	35.15	39.28	43.37	42.51	38.76	40.85
Exercise intensity	1.58	1.71	1.63	1.74	1.47	1.68
Standard salt intake	46.15	70.38	70.26	45.62	53.15	66.37
Salt intake awareness	75.28	76.13	69.35	72.68	74.13	68.21
Awareness of edible oil intake	72.15	68.95	69.34	71.03	73.28	70.05

in the early pregnancy detection rate was relatively poor. Table 3 and Figure 3 are the elderly health management service data.

It can be seen from Table 3 and Figure 3 that among the elderly health management services, the average value of elderly health management services is only 66.17%. Except for area D, which has a value of 75.35%, the performance in other areas is relatively average. The average completion rate of the elderly physical examination table is 77.74%, but there is still a certain distance from the target value of 85%. In addition, the frequency of detection of common diseases in the elderly and the frequency of health consultation were 74.33% and 75.715%, respectively. On the whole, there is still a lot of room for improvement in health management services for the elderly. Table 4 and Figure 4 are the health management service data for patients with hypertension and diabetes. The indicators 1-6 in the legend correspond to the indicators in the chart.

It can be seen from Table 4 and Figure 4 that in the health management services for patients with hypertension, the average health management rate and standardized management rate are 86.84% and 82.47%, respectively, far exceeding the target value of 60%. The blood pressure control rate of the management population is 49.8%, which is a small gap from the 50% target value. In the health management services for diabetic patients, the average health management rate and standardized management rate were 86.67% and 76.24%, respectively, but the population blood glucose control rate was only 46.32%. On the whole, the health management service system is more scientific in the management of hypertension and diabetes patients, but the control effect of various indicators is not good enough.

4.2. Social Coverage Rate of the Health Management Service System Based on Edge Computing. In this paper, starting from four aspects: health file establishment rate, electronic file
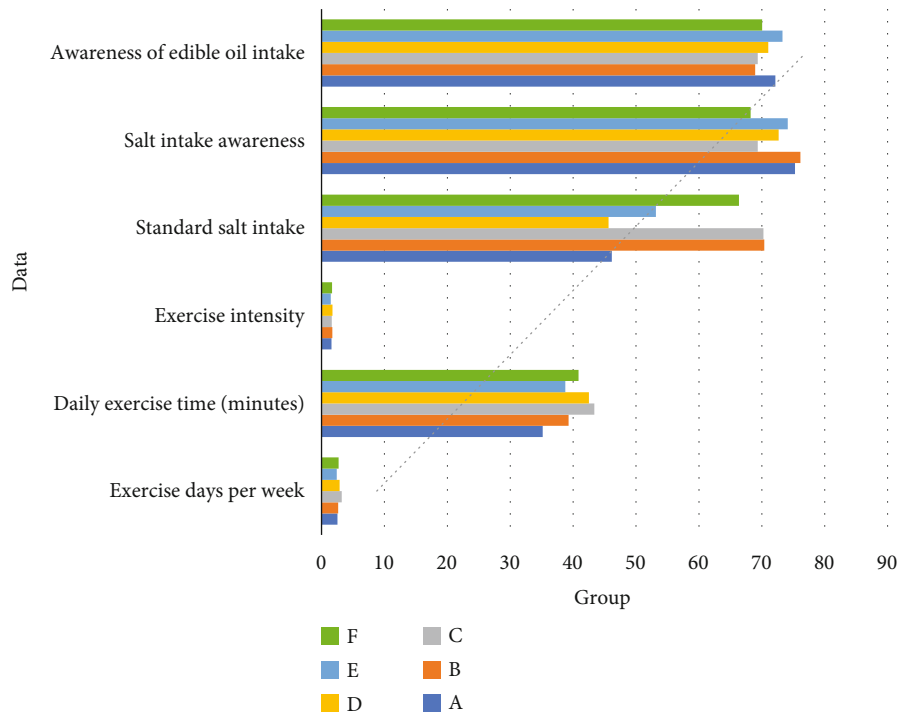
Figure 7: Survey data of residents' physical exercise and eating habits.

establishment rate, health file qualification rate, and health file utilization rate, the coverage rate of health management service transformation from traditional mode to electronic system is investigated. Table 5 and Figure 5 show the completion status of residents' health file management services.

It can be seen from Table 5 and Figure 5 that among the 6 surveyed areas, the health record establishment rate B is the highest, at 98.31%; the electronic health record establishment rate in area A is the highest, 95.53%; the health record qualification rate is the highest district D that is 93.16%; district E has the highest utilization rate of health files, which is 36.15%. Among the four indicators surveyed, overall, the index of the health file creation rate is the best completed, followed by the rate of electronic file creation, and the health file utilization rate is the worst indicator, none of the 6 regions. Table 6 and Figure 6 show the health management service coverage of each unit.

It can be seen from Table 6 and Figure 6 that in the 6 regions surveyed, the health management coverage rates of primary, secondary, and university are basically close to 100%, and the health probability coverage rates of government agencies and private enterprises are 69.965% and 65.78%, respectively, estimated 60% of the target. In contrast, the health management coverage rate in rural towns is only 59.47%, and the worst performing area E coverage rate is only 48.63%. It can be seen that the health relationship service in rural areas needs to be promoted, because many residents have not formed a correct understanding of their own health management. Table 7 and Figure 7 are survey data of residents' physical exercise and eating habits.

It can be seen from Table 7 and Figure 7 that the results of the one-way analysis of variance showed that the differences

in the number of days of exercise per week, average daily exercise duration, and exercise intensity of residents from different functional areas were statistically significant ($P < 0.05$). In terms of the number of days of exercise per week, the residents in area C have the most days at 3.21 days; in terms of the average daily exercise time, the residents in area C also spend the longest time at 43.37 minutes; in terms of exercise intensity, the intensity of residents in urban agricultural areas, the highest is moderate exercise intensity. From a comprehensive point of view, the average daily exercise time of residents is 2.73 days, and the average daily exercise time is 39.98 minutes.

Maintaining good eating habits and reducing the intake of fat and salt can play a very good role in promoting people's health. According to the results of the one-way analysis of variance, the differences in the salt intake compliance rate and salt intake awareness rate of residents from different functional areas were statistically significant ($P < 0.05$). Among them, the salt intake compliance rate and salt intake awareness rate are both in zone B, and the indicators are 70.38% and 76.13%, respectively; in terms of the awareness rate of edible oil intake, residents in zone E have the highest awareness rate. It is 73.28%.

5. Conclusions

This article's research on the service status of the health care management system mainly involves the following aspects: (1) the status of key population health management services, including child health management services, maternal health management services, and elderly health management services. (2) Health management services for people with

chronic diseases, including health management services for patients with hypertension, and health management services for diabetic patients. (3) Social coverage of health management services, including residents' health record management, the coverage rate of health management services in enterprises and institutions, the coverage rate of health management services in primary and middle schools, and the coverage rate of health management in rural towns. Through the survey data, it can be found that the health management service system based on edge computing and artificial intelligence has made more and more people aware of the importance of health management through professional and convenient service effects and promoted the standardization of community medical management services.

The AI health management service system based on edge computing gradually affects people's perception of their own health. At this stage, our country is gradually transforming from traditional health record management services to intelligent electronic health records management. From the survey data, the filing rate and pass rate of residents' electronic files have reached 88.275% and 87.435%,respectively, but the utilization rate of health files is only 31.685%. The establishment of a supporting health management service system is to effectively improve the utilization rate of health records, so that users can really enjoy intelligent, professional, and real-time health services. The artificial intelligence-based health management service system narrows the distance between ordinary residents and medical institutions through big data sharing. The health management service system will provide professional and targeted health care strategies based on the user's physical data, encouraging users to actively use physical exercise, healthy diet, and regular physical fitness to achieve disease prevention and have a healthier body.

Taken together, the research in this article has yielded certain results, but limited by various conditions, and the research still has the following areas worthy of improvement: (1) there are many institutions and services involved in the health management service system, but taking into account the operability of the research, this article only selects some representative indicators for analysis, which will lead to a lack of comprehensiveness in the final results. (2) Most health management service systems need to be paid before they can be used. Due to the different research directions, this article does not describe the payment mechanism of medical health management services and social medical insurance reimbursement too much. (3) How to ensure the security of user health data in the system in the era of big data is an important direction in subsequent research.

Data Availability

No data were used to support this article.

Conflicts of Interest

The author(s) declare(s) that they have no conflicts of interest.

References

[1] C. Iamsumang, A. Mosleh, and M. Modarres, "Monitoring and learning algorithms for dynamic hybrid Bayesian network in on- line system health management applications," *Reliability Engineering & System Safety*, vol. 178, pp. 118–129, 2018.

[2] C. G. Thorat, V. R. Salve, P. P. Thorat et al., "Patient health management system using E-health monitoring architecture using WSN," *IJARCCE*, vol. 6, no. 3, pp. 783-784, 2017.

[3] M. Pan, W. Xue, and S. Xu, "Research on big data application of medical health management and service," *Medical Health Management Big Data Analysis*, vol. 1, no. 1, pp. 24–30, 2018.

[4] R. Dautov, S. Distefano, D. Bruneo et al., "metropolitan intelligent surveillance systems for urban areas by harnessing IoT and edge computing paradigms," *Software: Practice and experience*, vol. 48, no. 8, pp. 1475–1492, 2018.

[5] Y. Shu and F. Zhu, "An edge computing offloading mechanism for mobile peer sensing and network load weak balancing in 5G network," *Journal of Ambient Intelligence and Humanized Computing*, vol. 11, no. 2, pp. 503–510, 2020.

[6] M. Satyanarayanan, "Edge computing," *Computer*, vol. 50, no. 10, pp. 36–38, 2017.

[7] S. M. Kumar and D. Majumder, "Healthcare solution based on machine learning applications in IOT and edge computing," *International Journal of Pure and Applied Mathematics*, vol. 119, no. 16, pp. 1473–1784, 2020.

[8] Y. Liu, C. Xu, Y. Zhan, Z. Liu, J. Guan, and H. Zhang, "Incentive mechanism for computation offloading using edge computing: A Stackelberg game approach," *Computer Networks*, vol. 129, pp. 399–409, 2017.

[9] D. Kashkarov and A. Koucheryavy, "The multi-access edge computing applications and development analysis for telecommunication networks," *Telecom IT*, vol. 8, no. 1, pp. 28–33, 2020.

[10] K. Kumar, "Design and development of travel and tourism recommendation system using web-scraped data positioned on artificial intelligence and machine learning," *International Journal of Advanced Trends in Computer ence and Engineering*, vol. 9, no. 4, pp. 5670 −−565679, 2020.

[11] F. Goyache, J. J. del Coz, J. R. Quevedo et al., "Using artificial intelligence to design and implement a morphological assessment system in beef cattle," *Animal Science*, vol. 73, no. 1, pp. 49–60, 2001.

[12] R. Bhandari and J. Gill, "An artificial intelligence ATM forecasting system for hybrid neural networks," *International Journal of Computer Applications*, vol. 133, no. 3, pp. 13–16, 2016.

[13] L. Vanneschi, D. M. Horn, M. Castelli, and A. Popovič, "An artificial intelligence system for predicting customer default in e-commerce," *Expert Systems with Applications*, vol. 104, pp. 1–21, 2018.

[14] G. Slivinskas, C. S. Jensen, and R. T. Snodgrass, "A foundation for conventional and temporal query optimization addressing duplicates and ordering," *IEEE Transactions on Knowledge & Data Engineering*, vol. 13, no. 1, pp. 21–49, 2001.

[15] R. Sahal, M. H. Khafagy, and F. A. Omara, "Exploiting coarse-grained reused-based opportunities in big data multi-query optimization," *Journal of computational science*, vol. 26, pp. 432–452, 2018.

[16] K. Chakravarthi and V. Bhushan, "Modern query optimization technique (nature inspired) for improving energy efficient data

gathering and processing in wireless sensor networks," *International Journal of Computer Applications*, vol. 132, no. 2, pp. 24–30, 2015.

[17] S. L. Liao, G. Li, Q. Y. Sun, and Z. F. Li, "Real-time correction of antecedent precipitation for the Xinanjiang model using the genetic algorithm," *Journal of Hydroinformatics*, vol. 18, no. 5, pp. 803–815, 2016.

[18] M. Jafarinejad and M. Amini, "Multi-join query optimization in bucket-based encrypted databases using an enhanced ant colony optimization algorithm," *Distributed and Parallel Databases*, vol. 36, no. 2, pp. 399–441, 2018.

[19] N. Bradai, L. Chaari Fourati, and L. Kamoun, "WBAN data scheduling and aggregation under WBAN/WLAN healthcare network," *Ad Hoc Networks*, vol. 25, pp. 251–262, 2015.

[20] N. Bradai, E. Charfi, L. C. Fourati, and L. Kamoun, "priority consideration in inter-WBAN data scheduling and aggregation for monitoring systems," *Transactions on Emerging Telecommunications Technologies*, vol. 27, no. 4, pp. 589–600, 2016.

[21] School of Electronics Science and Engineering, National University of Defense Technology, Changsha 410073, China, C. Hao, W. Jiangjiang, S. Wenyuan, and First Engineers Scientific Research Institute of General Armaments Department, People's Liberation Army, Wuxi 214035, China, "Coordinate scheduling approach for EDS observation tasks and data transmission jobs," *Journal of Systems Engineering and Electronics*, vol. 27, no. 4, pp. 822–835, 2016.

[22] C. Joo and S. Kang, "Joint scheduling of data transmission and wireless power transfer in multi-channel device-to-device networks," *Journal of Communications & Networks*, vol. 19, no. 2, pp. 180–188, 2017.

[23] A. Calhan, "A non-preemptive priority scheduling algorithm for improving priority data transmission delay in wireless body area networks," *Ad Hoc & Sensor Wireless Networks*, vol. 34, no. 1-4, pp. 59–75, 2016.

[24] H. Chen, B. Zhai, J. Wu, C. du, and J. Li, "A satellite observation data transmission scheduling algorithm oriented to data topics," *International Journal of Aerospace Engineering*, vol. 2020, no. 11, Article ID 2180674, p. 16, 2020.

[25] K. M. Dogan, T. Yucelen, and J. A. Muse, "Hedging approach for scheduling actuator data transmission in networked adaptive control systems," *IFAC-PapersOnLine*, vol. 52, no. 29, pp. 110–115, 2019.

WILEY | Hindawi

Research Article

Management Model on Electronic Commerce Data Based on Cloud Computing

Hailan Pan [1,2] **and Xiaohuan Yang** [3]

[1]Research Center of Resource Recycling Science and Engineering, Shanghai Polytechnic University, Shanghai 201209, China
[2]School of Economics and Management, Shanghai Polytechnic University, Shanghai 201209, China
[3]Cosco Shipping Technology Co., Ltd., Shanghai, China

Correspondence should be addressed to Hailan Pan; panhailan@sspu.edu.cn

Judging from the current situation, China's e-commerce companies are developing more and more rapidly, and the sales records of e-commerce platforms continue to break through. However, in this rapid development, many problems have been exposed. Because B2C e-commerce business management methods are different from traditional business management methods, there are many fundamental differences between the risks faced by traditional e-commerce companies and traditional enterprises. Compared with traditional enterprises, the risks faced by e-commerce enterprises have greater uncertainty and complexity, and the related risk management measures have not fully kept up with the development speed of B2C e-commerce and are still in the stage of continuous exploration. With the popularity of e-commerce and higher applicability, the research on e-commerce data management model is urgent. In order to study the e-commerce data management model, theoretical research and commercial application of cloud computing are discussed in depth from literature analysis, comparative analysis, graphical analysis, and case analysis. I hope to expand the application research of cloud computing platform in e-commerce. Finally, it proves that e-commerce has a good development advantage in the future development.

1. Introduction

With the advancement of the times, the application, popularization, and development of Internet technology, as one of the most basic activities of human activities, has undergone tremendous changes. On the one hand, because online shopping is not limited by time and space, it does not require face-to-face communication and communication between buyers and sellers, so that consumers can purchase goods without leaving home, and the transaction method is relatively free; on the other hand, due to online shopping, the product categories are diverse and the types are relatively complete. The price is also quite advantageous compared to offline stores. Therefore, more and more consumers are attracted to online shopping, and e-commerce is born. E-commerce has now entered people's lives and infiltrated into people's lives. Therefore, in every big environment where B2C e-commerce [1–3] enterprises want to stand out from the fierce

market competition, the quality of enterprise risk management will undoubtedly become a direct factor affecting the competitiveness of enterprises, affecting the survival and development of enterprises. How to strengthen the risk management of B2C e-commerce enterprises has become a very practical issue.

It can be seen from the introduction of the research background that China's e-commerce has great development potential and good development prospects. From the perspective of long-term development, traditional enterprises are bound to develop into e-commerce enterprises or combine with e-commerce enterprises. Although the competition in the industry is very cruel, only a small number of companies can stand out from the competition and succeed. However, the rapid development of the industry and the rapid changes in the environment have caused many risks and opportunities for enterprises. Whether it is a large-scale enterprise or a small family-owned enterprise, there are plans

to enter the industry more or less. Therefore, conducting risk management research on the mainstream B2C model in e-commerce is not only conducive to the development of existing enterprises. Its entry is conducive to the future development of the enterprise and provides valuable experience for it, thereby reducing the risk of new entrants.

On December 18, 2015, General Secretary Xi Jinping said at the second "World Internet Conference - Wuzhen Summit" to accelerate the construction of Internet infrastructure and increase research and innovation and interoperability of network technology and application development. Sichuan has also increased its time and funding investment in other areas of data such as the Internet of Things, big data and cloud computing. This will lower the digital divide and reduce the imbalance of information flow. If it develops well, it may spread network technology in third world countries. As a new business model in today's society, e-commerce is changing the development of the world in its unique way and integrating into people's daily life. With the development of e-commerce, it can be divided into many different modes according to different transaction objects, mainly including B2B [4], B2C, C2C [5], and O20.

Business-to-business (B2B model) is the first e-commerce model to emerge. This model is mainly used for business activities between merchants and businessmen. Through this model, merchants can improve business activity efficiency and reduce costs through network resource management, collaborative work, and information sharing. China's Alibaba, trade network, and other companies are typical B2B models. Business-to-customer (B2C model) is a business-to-consumer model in which business and consumer teams conduct business activities directly. The C2C model (customer-to-customer) is a consumer-to-consumer model in which consumers use the network for business activities. Consumers promote products they plan to sell on specific e-commerce platforms. Consumers in need can obtain product information through the platform. After the two parties reach an agreement, the transaction is completed. The role of network mediation can be clearly seen from the C2C model. The O2O mode (online-to-offline) is an online transaction offline consumption experience mode. This model is to use the advantages of the smooth flow of the Internet to launch their own characteristics and create their own brand, and after completing online transactions with consumers, consumers can personally come to the offline experience center to experience and then carry out a real experience.

E-commerce is a new way of trading that is different from traditional business activities. First, on the trading platform, there is no fixed sales location and sales time for e-commerce. E-commerce can provide services according to the needs of consumers, regardless of time and space, and can improve transaction efficiency. Second, through e-commerce, transaction costs can be saved very well, and the cost savings will benefit consumers, and consumers are more willing to choose a network to form a virtuous circle. The e-commerce platform can display products to consumers more comprehensively from the aspects of use, application scope, functional structure, material technology, etc., so that con-

sumers can choose a more reasonable purchase method. Third, compared with traditional commerce, e-commerce reduces the intermediate links, allowing direct transactions between producers and consumers, while strengthening communication between producers and consumers, and gradually forming a close cooperative relationship. Based on the advantages of e-commerce, in order to study the e-commerce data management model, the theoretical research and commercial application of cloud computing are discussed in depth from literature analysis, comparative analysis, graphical analysis, and case analysis. I hope to expand the application research of cloud computing platform in e-commerce. Finally, it proves that e-commerce has a good development advantage in the future development.

2. Cloud Computing and E-Commerce

2.1. Cloud Computing Overview. Cloud computing [6, 7], the core of which, is to implement distributed computing methods through the network. This technology allows centralized management of shared hardware and software resources as well as informational materials and provides them to computers and other devices as needed. Cloud computing is a distributed computing technology. The most basic concept is to automatically split a large computational processor into a myriad of smaller subroutines over a network and then transfer it to a large system of multiple servers. After searching, calculating, and analyzing, the processing results are returned to the user.

In fact, many of the everyday applications used today are based on cloud computing technology, for example, the commonly used Baidu search engine, 163 network mailbox, and so on. The large-scale distributed computing technology studied by early technologists can be called the origin of "cloud computing." Cloud computing connects distributed technologies to the network and scales to provide more services. The basic principles of cloud computing can be similar. This is like switching from the old single-generator mode to the centralized power supply mode of the plant. This means that computing power can also be circulated as commodities, just like natural gas and hydropower. Again, it is easy to use, low cost, and of course, the biggest difference is that it is transmitted over the Internet. In fact, the cloud of cloud computing represents the entire Internet. Instead of using the software originally installed on your computer, or replacing the original operation of storing data on your own hard disk, you will use the network. This kind of work, and storing the files on the network, is a huge virtual space. We use web services to store data in servers on the network, browse the pages of these services through a browser, and perform various calculations and work using the above interface.

Cloud computing has had a profound impact on the entire IT industry, including three cloud computing builders, server vendors, software developers and cloud terminal providers, and cloud providers as cloud operators. The frame diagram is shown in Figure 1.

Currently, cloud computing includes the following levels of services: infrastructure as a service (IaaS),
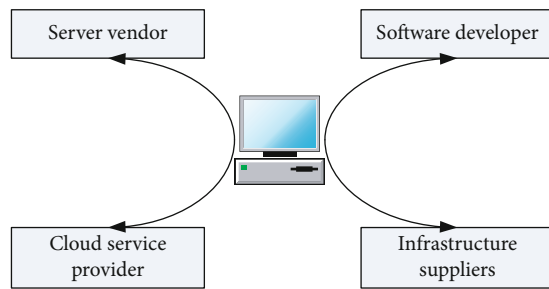
Figure 1: Cloud computing area network.

platform as a service (PaaS), and software as a service (SaaS). The three-tier service architecture is shown in Figure 2.

In terms of services, the main focus is on providing users with a variety of cloud-based services. There are three levels: one is software as a service, called SaaS. The role of this layer is to provide the web to customers. The second is the platform as a service platform service called PaaS. The role of this layer is to provide users with application development and deployment platform as a service: the third layer is the infrastructure as a service infrastructure. The service is abbreviated as IaaS and is used to provide users with various basic computing (such as virtual machines) and storage resources as services. From the user's point of view, the relationship between these three layers of services is independent and different, because the services they provide are completely different and the users are different. But, from a technical point of view, the relationship between the three layers of cloud services is not independent but has a certain dependence. For example, the SaaS layer of products and services not only need to use the technology of the SaaS layer itself but also rely on it. The development and deployment platform provided by the PaaS layer is directly deployed on the computing resources provided by the IaaS layer, and the products and services of the PaaS layer may also be established on the IaaS layer service.

2.2. Advantages and Characteristics of E-Commerce. E-commerce has unparalleled advantages compared with traditional enterprise management, which is mainly reflected in the six aspects shown in Table 1.

(1) Establish corporate image and brand

In the market competition, the company's good image will directly affect its survival. In the traditional business model, it takes a long time to get a good corporate image or product brand name. The business model of e-commerce can obtain corporate image and brand in a relatively short period of time

(2) Shorten the production cycle

E-commerce uses the Internet to synchronize product production information and customer demand information,

expand the scope of corporate electronic contacts, share product specifications and drawings, or work with other companies to shorten product life cycles. E-commerce enables suppliers and customers to connect and establish business contacts over the Internet, reducing the time between sending and receiving orders, invoices, and delivery notifications between suppliers and customers

(3) Create new sales opportunities

Because the e-commerce sales model allows products to be sold (24 hours a day, 7 days a week), in some ways, the company has found new markets that can attract more customers

(4) Change the internal structure of the enterprise

E-commerce reduces the cost of communication between vertical organizational structures through the Internet. Companies must adapt to this change and restructure to increase efficiency. Therefore, Internet-based e-commerce is changing the internal structure of the enterprise

(5) Changing the way companies compete

E-commerce provides businesses and consumers with more opportunities to explore consumer markets and consumer choices. At the same time, it also provides a smoother and faster place for information exchange, thus improving the company's macrounderstanding of market demand and consumer understanding. The ability to market information also speeds up the company's ability to develop new products and deliver new services. E-commerce enables companies to quickly understand consumer demand information and quickly feed it back to the decision-making level, making it easier for companies to conduct R&D activities that target consumer needs. E-commerce has changed the cost structure between the upstream and downstream companies and established strategic alliances between the upstream and downstream companies. E-commerce extends the competition among enterprises to the competition of the entire supply chain, enabling enterprises to compete from the competition of enterprises to the virtual alliance formed among enterprises in various fields such as advertising competition, promotion means, product design, and packaging, mainly reflected in the significant increase in the initial cost of the new company entering the competitive market

(6) Change the basis of enterprise competition

E-commerce has changed the foundation of corporate competition. On this basis, e-commerce has changed the transaction costs of buyers and sellers. E-commerce can make enterprises with large annual transaction volume relatively smaller than transactions, and enterprises with insufficient financial resources are more profitable and have competitive advantages, because e-commerce has the characteristics of high one-time input cost and low variable cost.

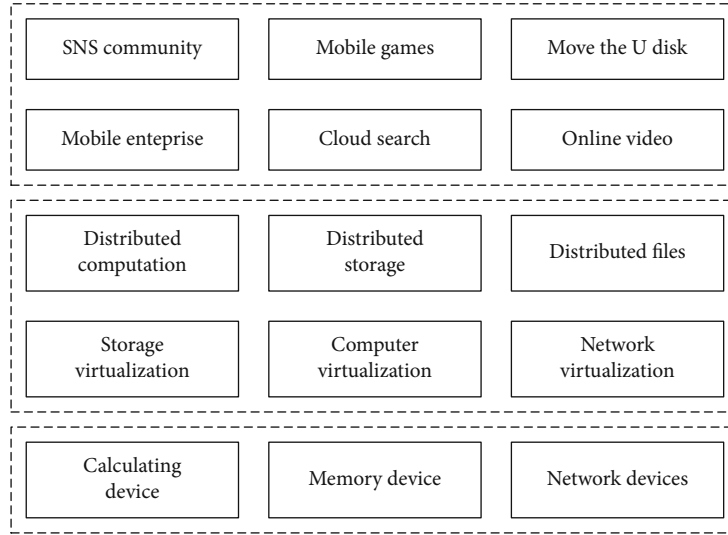The characteristics of e-commerce can be summarized as follows:

FIGURE 2: Three-tier service architecture diagram.

TABLE 1: Characteristics of e-commerce.

	Basic characteristics
1	Establish corporate image and brand
2	Shorten the production cycle
3	Create new sales opportunities
4	Change the internal structure of the enterprise
5	Change the way companies compete
6	Change the basis of corporate competition

(1) Business: this is the most basic feature of e-commerce, namely, the services, means, and opportunities for buying and selling transactions. It is based on the Internet and provides a powerful and comprehensive trading and feedback platform for suppliers, sellers, and customers. It expands the market, increases the number of customers, and provides convenient service to every customer in the supply chain. Therefore, e-commerce is an opportunity for any large enterprise

(2) Serviceability: in an e-commerce environment, customers are not subject to geographical conditions. The focus of buying goods is no longer just low prices. Today's customers also regard service quality as one of the considerations. Therefore, in a sense, service quality has become a key point of business activities, and one of the characteristics of services is convenience. Not only the customer benefits but also the company benefits

(3) Integration: the real business value of e-commerce is to coordinate old and new technologies, enabling users to more effectively use their existing resources and technologies to accomplish tasks more efficiently. The integration of e-commerce lies in the integrity and uniformity of transaction processing. It standardizes the workflow of transaction processing and integrates manual operations and electronic information processing into an inseparable whole. This not only improves the utilization of manpower and material resources but also improves the rigor of the system operation

(4) Coordination: business activities are a process of coordinating business cooperation among customers, manufacturing, suppliers, and business partners. Efficiency is generally based on an interactive protocol as the basis for e-commerce activities

(5) Low cost: e-commerce has obvious low cost

(6) Security: for customers, if there is any doubt about the security of electronic transactions, they will not buy or sell on the Internet at all, and the transactions between enterprises will be the same. Therefore, the security of e-commerce is one of the core issues that must be considered

(7) Electronification and its scalability: one is electronic writing and data transmission of e-commerce; the other is that payment methods are highly electronic. In order for e-commerce to function properly for a long time, it must be ensured that it is scalable because the scalable system is a stable system

Analysis of the seven-point characteristics of e-commerce helps to understand the impact of e-commerce environment on supply chain management. To implement the e-commerce strategy, we must face the coordination of various production factors inside and outside the enterprise, face the market, emphasize customer service and management, pay attention to the integration of various systems, and establish a sound and effective information management system, enabling them to more effectively accomplish their business management goals.

E-commerce does not completely replace the traditional business model, because traditional businesses also have the advantages that e-commerce does not have. Traditional business allows consumers to experience goods first and then buy them after they are satisfied. Many consumers are more inclined to accept actual goods and enjoy shopping. However, fast and efficient e-commerce is unmatched by traditional companies. With the development of e-commerce, more complex trading methods in traditional businesses will also be optimized, and some traditional businesses may undergo subversive changes. The future will be an era of traditional business and e-commerce convergence. By summarizing, it is found that there is a big difference between traditional business and e-commerce. Therefore, the e-commerce background discussed in this paper is still very different from the previous traditional business background and has certain research value.

3. Key Technology of Data Management Based on Cloud Computing

As one of the core functions of cloud computing, cloud storage has received extensive attention. Metadata management plays a key role in cloud storage. Wikipedia introduces metadata in detail: metadata, also known as metadata, and mediation data, is data describing data (data about data), mainly information describing data attributes, such as storage location, historical data, resource search, and file recording. Metadata primarily describes data about file system structures, such as heterogeneous namespaces, file and directory attributes, and file-to-block mappings. Although the size of the metadata is relatively small throughout the file system, operations on metadata account for more than 75% of the overall file system operation. Therefore, the management of metadata is critical to the performance of the file system.

Today's large-scale cloud computing systems typically have thousands to tens of thousands of node devices, and the CPU cores are numerous. As system processing power and user demands continue to increase, the demand for high-performance distributed file systems is also increasing. According to the statistics of 13 file systems, the files and directories in each file system are hundreds of millions. In addition, the I/O of each CPU core is independent, which results in a large amount of parallel access to the file system. Therefore, the file system in the cloud computing environment needs to process thousands and tens of thousands of operations for metadata every second. This situation shows that it is unrealistic to rely on a centralized server for metadata processing. Only a set of servers can be used for distributed processing of metadata to meet actual needs.

Since the cloud computing system is in the same LAN in most cases, it is very rare that the message is tampered with. Even if the message is incomplete due to the hardware and network of the system, it only needs to be verified by simple verification. The complete message is fine. Therefore, it can be assumed that the cloud computing system does not have a Byzantine general problem. Based on HDFS, this paper proposes a distributed metadata management mechanism in a new cloud computing environment, which provides good scalability and usability for the system while improving metadata operation performance. The metadata mentioned in this article contains catalog metadata as well as file metadata. Directory metadata includes hierarchical namespaces and directory attributes; file metadata includes file attributes and file-to-block mappings.

GLOBLE_ID is a unique global identifier that cannot be changed after the path is created. USER_ID is the identifier of the user who created the path. PARENT_GLOBAL_ID represents the GLOBLE_ID of the path's parent directory. BLOCK_PTR is a pointer to a data block of the file, which is used only for files. Other information such as permissions, last access time, and update time are saved in OTHER_META. Through this metadata format, the structured name space is changed to a flat data structure and can be stored in the database and name nodes. Figure 3 shows the architecture of the metadata management system.

The system consists of four main parts: the client, multiple name nodes, name node manager, and database. The system exposes the metadata access interface to the client. To improve system performance, some of the most recently used metadata can be cached on the client. The name node is responsible for managing the metadata and processing metadata access requests from the client. The updated metadata in the name node is periodically persisted to the database. The name node manager provides routing for the client to obtain the target name node. In addition, it manages the distribution of metadata between many name nodes and load balancing by periodically receiving heartbeat signals from name nodes.

4. E-Commerce Data Management Model

The logical model of e-commerce data [8–10] is a division of e-commerce data from the user's perspective. It classifies the various information involved in the entire e-commerce and divides the different levels of utilization according to the method of network information organization. According to this model, we can make a good division of the data types of the entire e-commerce according to functions and expressions. From the perspective of network information organization, network information is divided into three levels: micro, meso, and macro.

The mesoorganizational model of network information resources is related to the micromodel, which includes the secondary organization of network information resources and three organizations. Secondary information organization is the reorganization of information organized by various microorganizational models. These three information organizations are the reorganization of secondary information. Online secondary information resource organization mode was used. This mode is very common, including the search engine methods we usually use, the directory guide method (topic tree mode), and the database method. Then, there are three organizations; the reorganization of the secondary information organization, to help users find the right search engine, directory guide, or instruction database faster. This is the organization and management mode of the three information resources of "directory and directory" which represents a search engine directory in multiple search engines.
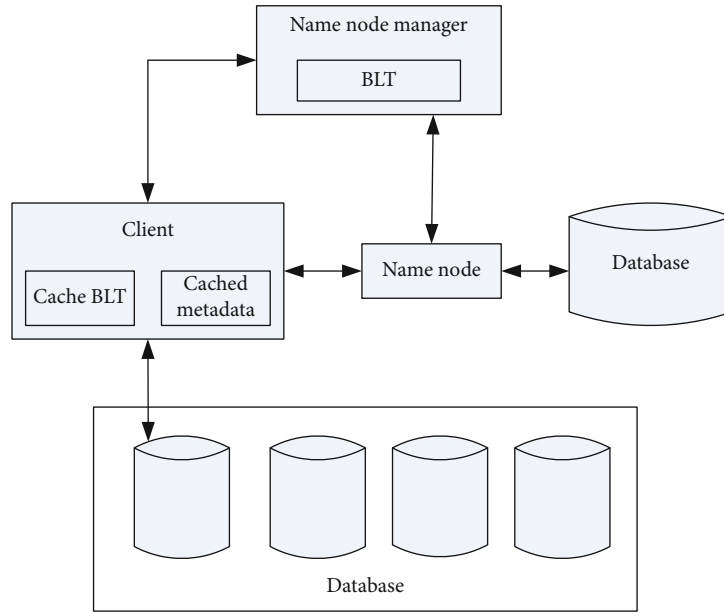
FIGURE 3: Metadata management system architecture.

The model proposed in this paper adopts a multilevel structure, using front-end page cache squid [11], multiple web servers, page fragment cache, Hadoop storage system, DAL data interface layer, memcache distributed cache, and sublibrary strategy. It is roughly divided into four layers, as shown in Figure 4.

After the user's access request is submitted, the front-end page cache is first reached. If the webpage data cached here cannot satisfy the user's request, the Squid server will submit the user request information to the web server. The web server we use here is Apache, which is widely used based on open source servers. The web server then accesses the page fragment cache ESI to see if there is a user request, and if not, what type of user's request is being resolved. If the unstructured data request such as a web page is read, the request is sent to the Hadoop system; if the user logs in, the structured data request such as the user information needs to be viewed, and the request is sent to the database. Then, the two parts get a result and return it to the user.

5. Performance Analysis

5.1. The Cost Advantage of E-Commerce under Cloud Computing. Cloud services pay for users based on their needs and also get users based on their own needs. In this way, there is no risk, which can save the cost of the e-commerce enterprise, and enable the e-commerce enterprise to select the cloud computing platform provided by the cloud provider according to its own wishes and enterprise needs. Cloud computing integrates a computer cluster into a virtual resource pool. All information on the e-commerce website, including the enterprise itself and users, is stored in the virtual resource pool. Specific data management is implemented by cloud computing platforms and enterprises, which means you need to choose the right system software and data platform for you. All other content has cloud computing man-

agement capabilities, which greatly reduces the company's investment in data management and reduces business costs. At present, large, medium, and small e-commerce enterprises at all levels are equipped with a large number of computers and network equipment, but with the upgrade of the machine, enterprises must spend a lot of money to buy new PCs. As a result, the computer before the enterprise was eliminated. But, with cloud computing, companies do not have to give up these computers that should be eliminated, which can greatly reduce hardware investment costs. Since the user only needs to have a terminal device that can be connected to the network, the terminal device can be connected to the cloud computing platform, and the cloud computing issues performance of the terminal device that does not care about the user. Cloud computing can build a virtualized data storage center for users. It has real-world computing power. It integrates all the hardware and software functions distributed across a large number of different computers into a virtual resource pool that connects users over the network. Go to the resource pool and get the information you need from the resource pool. Cloud computing has provided many basic applications, such as office software and email systems. These applications are cheap, and some are free. And, at the other end of the cloud, there is a very professional IT team that can manage hardware and update and upgrade software for users, so users do not have to worry about whether the application is up to date. The cost savings histogram of cloud computing in different aspects is shown in Figure 5. It can be seen that in almost all aspects, the cost of cloud computing is almost more capital saving than traditional business data processing.

5.2. Data Security Advantages of E-Commerce under Cloud Computing. The cloud computing data management platform is responsible for saving data on e-commerce websites, including data backup, system maintenance, data security,
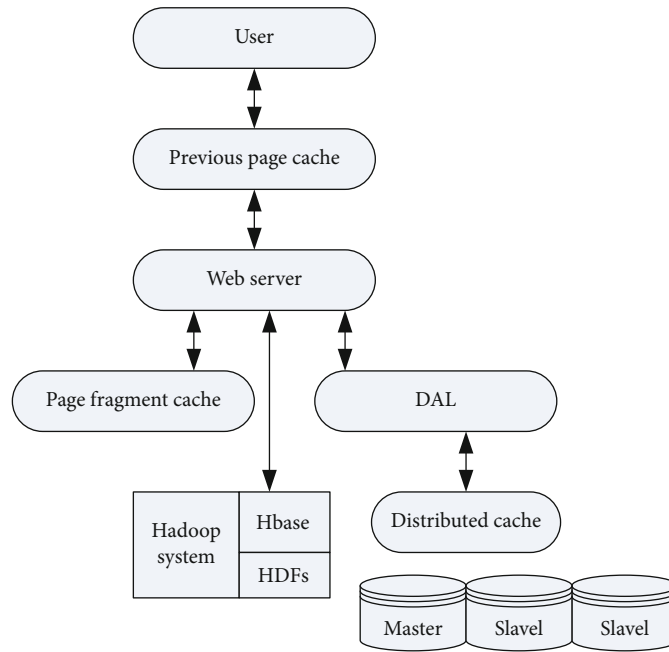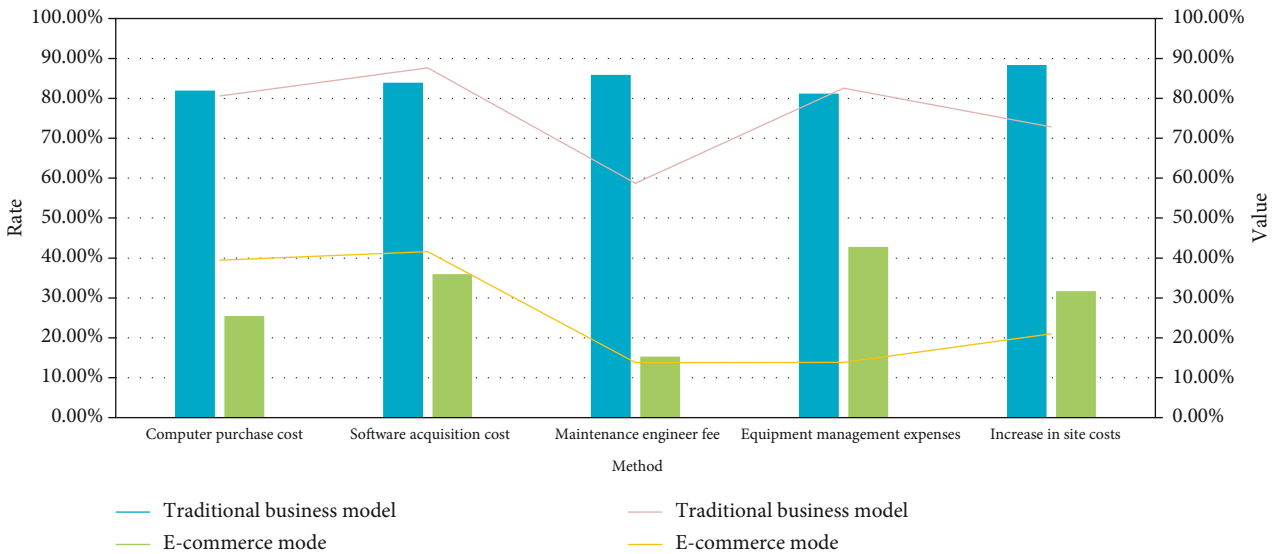
FIGURE 4: E-commerce data management model.

FIGURE 5: E-commerce cost advantages in different aspects.

and platform system upgrade. The cloud computing data management platform will ensure the security of these data, equipped with the most powerful computer administrator. And the most secure data management technology ensures the security of e-commerce enterprise data. The main task of the cloud computing data management platform is to manage the user's storage information, access information, basic information, upgrade the platform system, and virus protection, so that the entire data management platform runs normally. The user's computer, U disk, etc. are particularly susceptible to poisoning, which causes a lot of trouble. A large amount of transaction information on the e-commerce website will be lost, and data related to the com-

pany's life and death may be destroyed. Cloud computing can provide a secure data storage center for enterprise e-commerce sites. Cloud computing storage technology stores enterprise data in a unified cloud data management platform, and cloud computing service providers are responsible for the security of data storage. Therefore, using cloud computing data management technology to build e-commerce websites, e-commerce companies do not have to worry about data damage caused by virus damage, hacking, and computer hardware problems, which greatly enhances data security. E-commerce sites no longer need to worry about data loss caused by viruses and hackers and hardware damage. More-over, the emergence of these problems will increase the
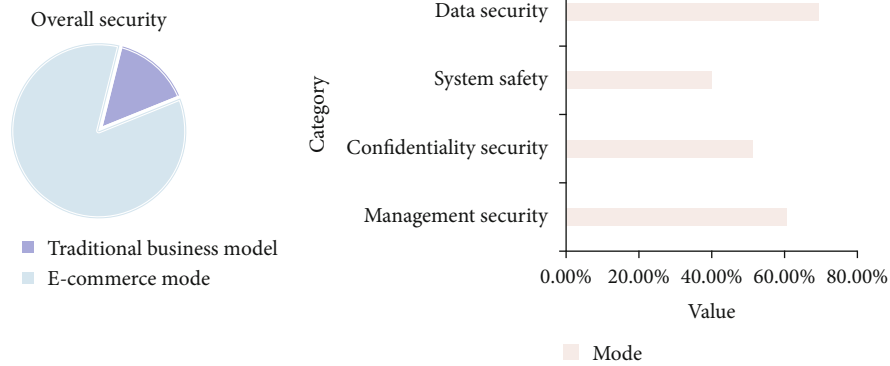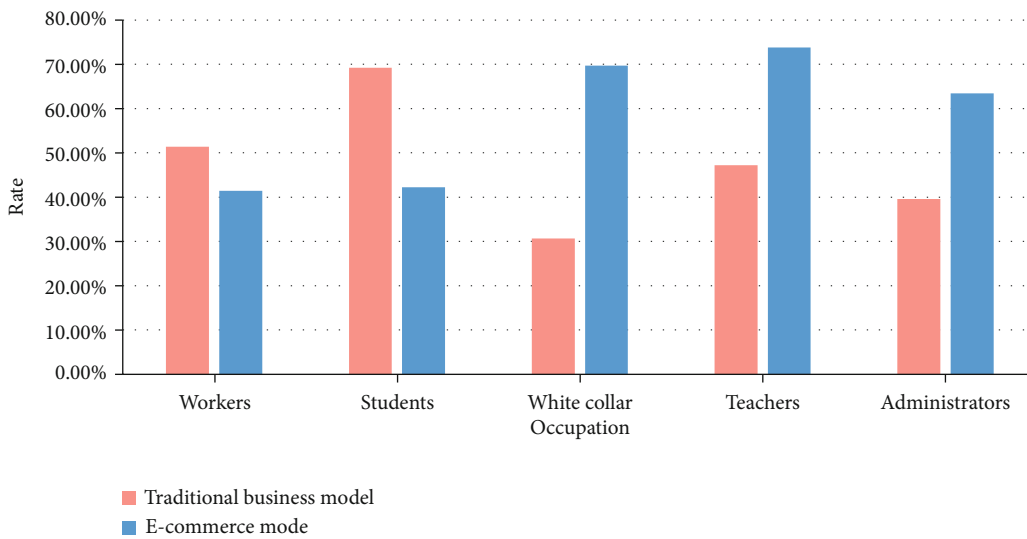
FIGURE 6: E-commerce security comparison.

FIGURE 7: Satisfaction of different people in the information sharing advantage of e-commerce.

capital investment in e-commerce enterprise data management operations. To ensure the security of product information on the site, companies must upgrade existing systems or adopt new data management technologies, but the number of e-commerce users is increasing. It also brings a lot of data, and the cost of the business will increase. With cloud computing, these issues have been resolved. It can be seen from the above that the cloud computing data management technology for e-commerce data management can ensure the security and reliability of user data. E-commerce companies and users do not have to worry about their information being leaked or destroyed because information is the most important resource for the business. Only when the information is protected can the company carry out its activities smoothly without having to concentrate. Focusing on the secure storage of data, it can be said that cloud computing storage technology solves the worries of e-commerce enterprises. In order to prove the security advantages of e-commerce, here is a comparison of the e-commerce model and the traditional e-commerce model in this paper. Figure 6 shows the comparative analysis of the security advantages of e-commerce and traditional commerce.

5.3. *Information Sharing Advantages of E-Commerce under Cloud Computing.* The construction of cloud computing data management platform can enable e-commerce enterprises to share information resources to a large extent. Due to the different geographical distributions, the processing time and content of information resources of different e-commerce enterprises are different. Some enterprises cannot quickly obtain the information on the website for various reasons, which leads to the closure of enterprise information and even affects the development of the enterprise. With the cloud computing data management platform, enterprises can synchronize the business activity information of the enterprise, the resources of the enterprise, and the resources of other enterprises on the platform, which is from the external aspect. As far as the internal enterprise is concerned, it is possible to share information of the same enterprise in different places and at different times. Some enterprises have business all over the country. If the information of each branch of the enterprise cannot be communicated with each other in time, the information flow of the whole enterprise will be poor, which will affect the business activities of the enterprise. For example, a company forms an information chain from
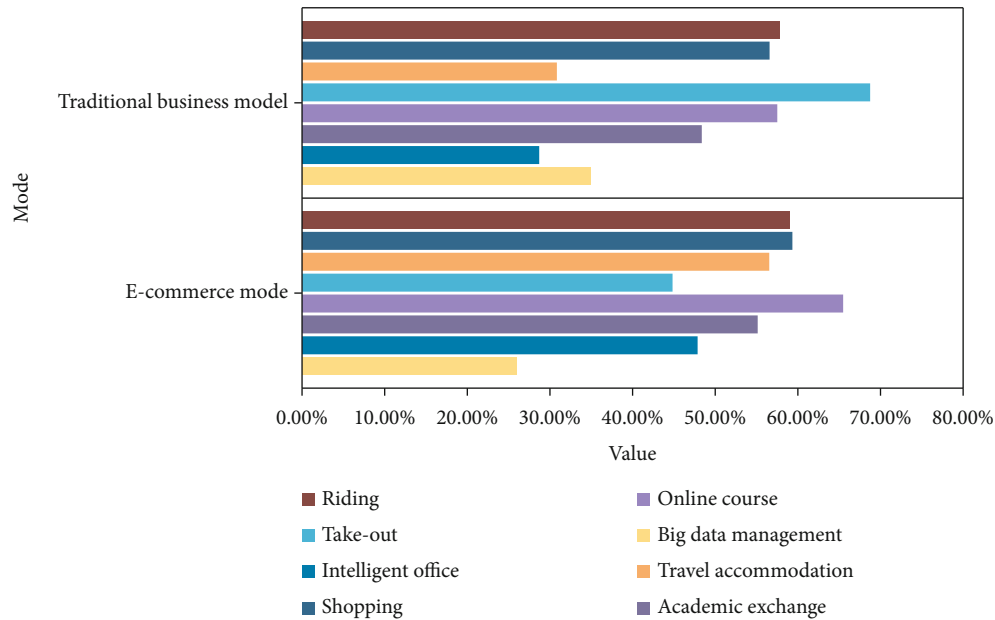
FIGURE 8: E-commerce convenience in life.

the development, production, sale, after-sales, price, market demand, logistics, etc. of the goods. In the overall market environment, not only does the company better track and understand the goods but also makes it different. The exchange and intercommunication between enterprises in the information, the sharing of information in the true sense, breaking the limits of the region and time is one advantage. At present, China's major e-commerce websites have built a large amount of commodity data. The use of cloud computing in e-commerce can share product information in the cloud and truly achieve interoperability of network resources. All e-commerce websites or business executives are able to create network resources with the powerful interoperability of computers. Cloud computing has a strong expansion, and all the data resources contained in all e-commerce websites are included in the cloud computing platform, which can greatly reduce the investment in cost and time of an e-commerce website and truly realize resource sharing. Figure 7 shows the statistics of different people's information sharing advantages in e-commerce. This survey has a total of 254 people in five categories and gives their comparison of traditional business and e-commerce advantages.

5.4. Convenient Advantage. All the data information of the e-commerce enterprise is stored on the cloud computing data management platform, and the manual management is removed, so that the user can more conveniently obtain the information he needs in any way anytime, anywhere. Since the cloud computing data management platform itself has the advantage of being efficient and fast, users will not encounter any resistance when accessing and can quickly access the platform. The customer accesses the website, processes the information, and accepts the service by connecting to the Internet, using a terminal device such as a computer, and the process is very fast and convenient. The mobile

transaction is based on the wireless mobile communication network technology and related communication equipment, etc. and is obtained from the transaction of the e-commerce activity. It is not limited by time and place and can be traded as long as the terminal device can access the Internet. The emergence of cloud computing has brought greater convenience to e-commerce activities, users can conduct transactions and inquiries without restrictions, and all information about products is well known. When users want to conduct commodity transactions, they can use mobile devices to query all the information they need on the e-commerce website. E-commerce enterprise staff can even bring merchandise transactions to any place, as long as there is a computer with Internet access. Because their data is stored in the cloud, users can use this data at any time. Figure 8 shows that e-commerce is a convenience to people's lives. E-commerce has brought a lot of convenience to our lives. As you can see from Figure 8, travel expenses and online courses provide little convenience for our lives. But, in general, e-commerce has brought great convenience to people's daily lives.

In Figure 8, it can be seen that by comparing traditional business and e-commerce, e-commerce has brought a lot of convenience to people in the current social life, which also proves that the current social e-commerce has become an indispensable form of existence in people's lives. In general, e-commerce is superior to traditional business forms in the above seven aspects.

6. Conclusions

Cloud computing is a new form of business model and business. The advanced technology it brings can fully promote the development of future data management technology, and it also represents its development direction. As far as the development of cloud computing is concerned, it has

strong development potential, which can reduce the time required for e-commerce enterprises to manage data, provide more convenient services for enterprises, solve problems faster, and operate more easily. More importantly, it reduces the cost of the entire operation of e-commerce data management, greatly reducing costs. As far as the development of cloud computing is concerned, cloud computing brings an opportunity for data management of e-commerce enterprises and enhances the ability of e-commerce data management from the technical level, making e-commerce enter a new stage of development. In this paper, the e-commerce data management model is mainly used as the main research object. This proves that e-commerce has great advantages in future development, and it also proves that e-commerce as a new business model will play a decisive role in future development.

Data Availability

No data were used to support this study.

Conflicts of Interest

The authors declare that they have no conflicts of interest.

Acknowledgments

References

[1] F. Arnold, I. Cardenas, K. Sörensen, and W. Dewulf, "Simulation of B2C e-commerce distribution in Antwerp using cargo bikes and delivery points," *European Transport Research Review*, vol. 10, no. 1, 2018.

[2] H. Zhang, C. Beltran-Royo, B. Wang, and Z. Zhang, "Two-phase semi-Lagrangian relaxation for solving the uncapacitated distribution centers location problem for B2C E-commerce," *Computational Optimization and Applications*, vol. 72, no. 3, pp. 827–848, 2019.

[3] W. Lin, A. Xu, Q. Zheng, L. Ke, and J. Lin, "Influence of customer perceived value on the online shopping intention of aquatic products under B2C E-commerce," *Journal of Discrete Mathematical Sciences and Cryptography*, vol. 21, no. 6, pp. 1189–1192, 2018.

[4] S. X. Xu and G. Q. Huang, "Efficient multi-attribute multi-unit auctions for B2B E-commerce logistics," *Production & Operations Management*, vol. 26, no. 2, pp. 292–304, 2017.

[5] F. M. Yang, A. Y. Wang, J. Wu, and L. Tang, "Designing credit supervision mechanism in C2B2C e-commerce based on game theory," *Systems Engineering-Theory & Practice*, vol. 37, no. 8, pp. 2102–2110, 2017.

[6] Y. Al-Dhuraibi, F. Paraiso, N. Djarallah, and P. Merle, "Elasticity in cloud computing: state of the art and research challenges," *IEEE Transactions on Services Computing*, vol. 11, no. 2, pp. 430–447, 2018.

[7] S. Sagnika, S. Bilgaiyan, and B. S. Mishra, "Workflow scheduling in cloud computing environment using bat algorithm," *International Journal of Computer Applications*, vol. 89, no. 2, pp. 11–18, 2018.

[8] M. Zhang, Y. Yao, Y. Jiang, B. Li, and C. Tang, "Accountable mobile E-commerce scheme in intelligent cloud system transactions," *Journal of Ambient Intelligence & Humanized Computing*, vol. 9, no. 6, pp. 1889–1899, 2018.

[9] R. Gubela, A. Bequé, S. Lessmann, and F. Gebert, "Conversion uplift in E-commerce: a systematic benchmark of modeling strategies," *International Journal of Information Technology & Decision Making*, vol. 18, no. 3, pp. 747–791, 2019.

[10] J. Xue and S. Jarvis, "Mining association rules for admission control and service differentiation in e-commerce applications," *Wiley Interdisciplinary Reviews Data Mining & Knowledge Discovery*, vol. 8, no. 3, article e1241, 2018.

[11] H. J. M. Ter Brake, J. Flokstra, E. P. Houwman et al., "Design and construction of a 19-channel DC-SQUID neurokagnetometer," *Physica B: Condensed Matter*, vol. 165-166, Part 1, pp. 95-96, 1990.

WILEY | Hindawi

Research Article

Application of Motion Sensor Based on Neural Network in Basketball Technology and Physical Fitness Evaluation System

Bin Yuan,[1] M. M. Kamruzzaman [ID],[2] and Shaonan Shan [ID][3,4]

[1]*School of Physical Education, Chengdu Normal University, Chengdu, 611130 Sichuan, China*
[2]*Department of Computer and Information Science, Jouf University, Sakaka, Al Jouf 72311, Saudi Arabia*
[3]*School of Urban Economics and Public Administration, Capital University of Economics and Business, Beijing 100070, China*
[4]*School of Business Management, Liaoning Vocation Technical College of Modern Service, Shenyang, 110000 Liaoning, China*

Correspondence should be addressed to Shaonan Shan; rose_1844100@cueb.edu.cn

Basketball is a sport that requires high athletes' skills and physical fitness and is deeply loved by the people in our country. This paper studies the application of neural network-based motion sensors in basketball technology and physical fitness evaluation system. The ideal effect of the system is to scientifically analyze relevant data through intelligent algorithms and provide more accurate diagnosis suggestions. Recognizing human movements requires collecting various data of the human body through motion sensors. The data acquisition components of this system are based on considerations of portability and power consumption and are equipped with equipment with strong computing power to realize the functions of data preprocessing, training, and recognition of the recognition model. The system only needs to send the data in the data collector to the computing device; it can effectively realize the action recognition and judge whether the athlete's technical action and physical fitness level meet the standard. From the experimental data, the pass rate of the subjects in the 1000-meter run was 83.3%, and the excellent rate was 10%; the pass rate in the 1-mile run was 90%, and the excellent rate was 6.7%; and the pass rate in the 20-meter round trip was only at 56.67%; it can be seen that there is still room for improvement in the reaction speed and agility of most subjects. According to intelligent data analysis, athletes can better understand where they have shortcomings and improve their physical fitness and basketball skills through targeted training.

1. Introduction

With the advancement of science and technology, intelligent systems have been rapidly developed in various fields, and the availability and use speed of wearable sensor technology have also grown rapidly. The aspects that need to be considered when acquiring athlete information outside the laboratory environment are severely affected and dependent on currently available technologies. Through technological innovation and development, new sensor equipment and systems will provide the possibility for them. Wearable sensor technology is gradually popular in the sports field, which can provide data safely and effectively, promote the development of sports, and meet the needs of coaches and athletes for equipment. Basketball is a sport that requires a constantly changing rhythm, requiring speed, acceleration, and explo-

sive power, such as rebounds, layups, jump shots, and fast breaks. There is a big gap between our country's basketball skills and the United States and European basketball powers. Therefore, it is particularly important to strive to improve the technical and physical level of basketball players and to train excellent basketball players.

The application of mobile sensors in various fields in foreign countries started early, and many good results have been achieved in the research of intelligent sports systems. Conte conducted research on the physical and technical requirements of young basketball players' training. In order to examine the physiological and technical requirements of No Game Training (NDGD) and Conventional Training (RD), he tested 19 young basketball players and used Wilcoxon symbols to test and evaluate the relationship between NDGD and RD conditions for each dependent variable.

From the experimental results, this research has played a role in optimizing the training program of young athletes, but due to the small number of research objects, it has affected the credibility of the final conclusion [1]. Santos conducted an in-depth study on the changing laws of basketball technical indicators. He conducted a survey on the data of the Brazilian basketball championship from 2005 to 2015 and analyzed the changes in 13 standard indicators in the basketball game. For basketball players, good physical fitness and accurate grasp of technical standards are essential. If the basketball technical indicators and physical fitness evaluation standards can be analyzed through the intelligent system, the scientific nature of basketball training can be further improved [2].

Although domestic research on artificial neural networks and sports intelligence started relatively late, they have developed rapidly. Yuzhou carried out research on basketball multidirectional training and technical analysis based on BP neural network model. Artificial neural networks can acquire various abilities through learning. If the characteristics of the brain neural network can be used reasonably, an intelligent system with similar functions to the human brain can be designed to process various information. He and his team analyzed the multidirectional training and technical analysis of basketball based on the BP neural network model. Through the analysis of the data, the basketball players' training and team strategy are optimized. Taking the smallest error and the highest accuracy as the standard, the best method was selected as the predictive model for each performance. From the experimental test results, the model can be helpful to improve basketball training, but more experimental data is needed to improve the accuracy of the model [3].

Based on artificial neural networks and mobile smart sensors, this paper conducts in-depth research on physical fitness assessment and technical improvement training in basketball training. The research is mainly carried out from the following aspects. This article introduces the technologies and methods involved in the basketball training system, including neural network-based mobile sensors, decision tree classification algorithms, wavelet transform, and system data acquisition technology. Based on the analysis of product requirements, this article has completed the development of the intelligent basketball training system and introduced the overall structure and data modules of the system in detail. Finally, this article starts from the two directions of basketball technical statistical indicators and physical fitness evaluation, combined with experimental data to verify the positive impact of the system in improving the effect of basketball training.

2. Application of Technology in Basketball Test and Evaluation System Based on Neural Network

2.1. Mobile Sensor Based on Neural Network. Artificial neural network is a technology that simulates the neurons of the human brain for abstract processing and realizes information processing by establishing models [4]. With the continuous deepening of neural network research, it has become more and more widely used in the fields of intelligent machines, intelligent recognition, intelligent prediction, and automatic control. Real-time recognition of human body data based on neural networks using mobile sensors can provide data support for intelligent evaluation systems to make scientific decisions [5, 6].

Radio frequency identification technology (RFID) is a kind of communication technology, also called radio frequency identification or electronic tag [7]. It recognizes specific targets and reads data mainly through radio signals. Commonly used technologies mainly include passive, low frequency, ultrahigh frequency, and high frequency. This technology is mainly used for data function positioning in basketball training [8]. The sensor is a kind of signal conversion device, which is mainly composed of a conversion original and a sensitive element. The sensor has the function of sensing external signals and detecting, including heat, light, and humidity, and at the same time transmitting the acquired signals to other organs and devices [9].

2.2. Decision Tree Classification Algorithm. The human motion data collected by sensors is based on the reference system of each sensor [10]. Since human movement cannot be described in accordance with the sensor's reference system, such source data cannot be used directly, so it is necessary to classify and process the data through related technologies. Decision tree algorithm is a common machine learning algorithm. When doing machine learning, the decision tree uses a tree structure to resolve the problem one by one [11]. Decision trees make selection judgments at each node, which is similar to the process of human selection when facing some decision problems [12].

Information entropy, information gain, conditional entropy, and information gain ratio are commonly used in decision trees as the basis for division. Information entropy indicates whether the sample subset is single, that is, the smaller the value, the single the type of data in the set, which means that the division is more ideal [13]. Information entropy is defined as

$$\mathrm{Eet}(D) = -\sum_{k=1}^{|v|} pk \log 2pk. \tag{1}$$

Assuming that there are V possible values for the discrete attribute a, the information gain can be calculated according to the weights assigned to the branch nodes according to the number of samples:

$$\mathrm{Gain}(D, a) = \mathrm{Ent}(D) - \sum_{v=1}^{V} \frac{|D^V|}{|D|} \mathrm{Ent}(D^V). \tag{2}$$

According to the definition of information gain, attributes that account for the majority of numbers have inherent advantages and therefore make the division effect worse. The decision tree algorithm is different from the above; it uses the gain rate as the partition index to minimize the impact [14]. Its definition is

$$\text{Gain\_ratio}(D, a) = \frac{\text{Gain}(D, a)}{IV(a)}. \tag{3}$$

Among them

$$IV(a) = -\sum_{v=1}^{V} \frac{|D^V|}{|D|} \log 2 \frac{|D^V|}{|D|}. \tag{4}$$

This is called the "intrinsic value" of the attribute. At the same time, the decision tree is divided by the Gini index. The Gini value can represent the unity of data, and its definition satisfies

$$\text{Gini\_index}(D, a) = \sum_{v=1}^{V} \frac{|D^v|}{|D|} \text{Gini}(D^V), \tag{5}$$

$$\text{Gini}(D, a) = \sum_{k=1}^{|v|} \sum_{k \neq k} pkpk = 1 - \sum_{k=1}^{|y|} p_k^2. \tag{6}$$

When the decision tree is divided, it will not only encounter discrete values but also divide continuous values. When conducting experiments, sampling is often used to discretize continuous values for continuous variables. For continuous variables, discrete values are essentially processed [15]. Therefore, dealing with the division of continuous variables is essentially dealing with the problem of a large number of possible discrete values of attributes. As samples are sampled, there will be some missing attributes in some samples. If only the samples with values on these attributes are divided, it will lead to a waste of sample sets.

Set each sample x to be given a weight wx and define

$$\rho = \frac{\sum x \in \tilde{D}^{Wx}}{\sum x \in D^{Wx}}, \tag{7}$$

$$\tilde{P}k = \frac{\sum x \in Dk^{Wx}}{\sum x \in \tilde{D}^{Wx}} (1 \leq k \leq |y|), \tag{8}$$

$$\tilde{r}k = \frac{\sum x \in \tilde{D}v^{Wx}}{\sum x \in \tilde{D}^{Wx}} (1 \leq v \leq |V|). \tag{9}$$

According to formulas (7)–(9), the promotion of information gain can be defined to satisfy

$$\begin{aligned}
\text{Gain}(D, a) &= \rho \times \text{Gain}(\tilde{D}, a) \\
&= \rho \times \left(\text{Ent}(\tilde{D}) - \sum_{v=1}^{V} \tilde{r}v\text{Ent}(\tilde{D}^v) \right),
\end{aligned} \tag{10}$$

$$\text{Ent}(\tilde{D}) = -\sum_{k=1}^{|y|} \tilde{p}k \log 2\tilde{p}k. \tag{11}$$

Since the classification boundary formed by the decision tree is characterized by being parallel to the coordinate axis, when the boundary of the attribute value to be classified is more complicated, the decision tree must be divided into multiple segments due to the axis-parallel attribute to achieve a good fitting effect. It will increase the number of decision tree layers, which will undoubtedly lead to increased training and prediction costs [16]. Therefore, if the function combination value of multiple attributes can be used for division, it will not only be parallel to the coordinate axis in the multidimensional division plane, which is to find a suitable linear classifier for the node.

2.3. Wavelet Transform. When identifying the specific pattern of data, it is necessary to understand the detailed characteristics of the data, such as the order and quantity of various frequencies, in order to better extract the signal characteristics and construct the recognition model. It is necessary to conduct a comprehensive time-frequency analysis of the signal, so it is necessary to introduce wavelet analysis [17].

Wavelet analysis decomposes the signal through wavelet transform and analyzes the signal according to the prominent local features of the signal by analyzing the local time domain or frequency domain. This solves the problem that the traditional Fourier transform cannot be analyzed from the global shortcomings of capturing the detailed characteristics of the signal, while solving the problem that the signal cannot be adaptively changed with the change of the signal after the fixed window size decomposition [18].

Let the expression of a basic function be $\psi(t)$, and let

$$\psi ab(t) = \frac{1}{\sqrt{a}} \psi \left(\frac{t - b}{a} \right). \tag{12}$$

Among them, a, b are constants, and $\psi ab(t)$ is the basic function obtained through translation and expansion. Given a square-integrable signal $x(t) \in L^2(R)$, the wavelet transform of $x(t)$ is defined as

$$ETx(a, b) = \frac{1}{\sqrt{a}} \int_{-\infty}^{+\infty} x(t)\psi^* \left(\frac{t - b}{a} \right) dt. \tag{13}$$

Among them, a, b represents the scale factor and time shift, respectively, and $\psi(t)$ is the basic wavelet. Let the Fourier transform of $x(t)$ be $X(\Omega)$, and then, the frequency domain expression of wavelet transform is

$$WTx(a, b) = \frac{1}{2\pi} (X(\Omega), \psi a, b(\Omega)). \tag{14}$$

A low-pass filter can filter out high-frequency noise to achieve denoising of human body motion data. However, this method cannot filter out the sensor jitter noise that is similar to the human body motion frequency, because the human body motion frequency is not fixed at a certain low frequency, but has a different frequency in each motion [19]. Figure 1 shows the steps of wavelet threshold denoising.

It can be seen from Figure 1 that the basic steps are as follows: wavelet transforms the signal, uses the threshold function to process each layer of wavelet separately, and gets the signal after wavelet reconstruction to remove noise. In the denoising process, by using the threshold function, the noise
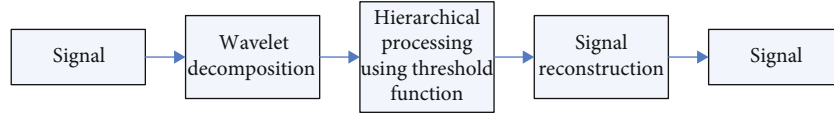
FIGURE 1: Wavelet threshold denoising steps.

below the threshold can be effectively filtered out [20]. If the selected threshold is too large, part of the effective information of the signal will be filtered out, resulting in serious signal distortion; if the selected threshold is too small, the denoising will be incomplete. Therefore, the choice of the threshold is related to the quality of the filtering effect.

For the joint distribution of multidimensional independent normal random variables, when the data tends to infinite dimensionality, the optimal threshold is calculated according to the maximum and minimum limits of the estimated data [21]. The constraints are

$$\lambda = \sigma_k \sqrt{2 \ln k}, \tag{15}$$

where σ_k represents the standard deviation of noise and k represents the signal length. ω_i represents the square value of the wavelet coefficient, and assuming that the risk vector is $\vec{R}$, the element r_i in it satisfies

$$r_i = \frac{\left[n - 2i - (n - i)\omega_i + \sum_{k=1}^{i}\omega_k\right]}{n}, \quad i = 1, 2, \cdots, n. \tag{16}$$

Find the minimum value from r_i as the risk value, and then, the corresponding $\omega_{\min}$ can be obtained according to the above formula.

$$\lambda = \sigma_k \sqrt{\omega_{\min}}. \tag{17}$$

The basic idea of the extreme value criterion is to estimate the threshold value by producing the extreme value of the smallest mean square error. The threshold estimation formula is

$$\sigma_k = \frac{\mathrm{mid}\left(W_1, k, 0 \le k \le 2^{j-1} - 1\right)}{0.6745}. \tag{18}$$

On the whole, different threshold estimation methods have different denoising effects. Therefore, in actual application, it is necessary to consider the thresholds obtained by different threshold estimation methods to compare the signal denoising effects [22].

2.4. System Data Acquisition Technology. The collection of basketball technology and data belongs to the process of automatically collecting information, and the sources of data collection are mainly other equipment under test and sensors [23]. The system has user-defined and flexible functions, with 8 slots and 4 slots as commonly used, but based on sensors and technical physical fitness tests, there are obstacles in data fusion, and further development is needed to realize the com-

bination of network computers and sensors. To ensure the feasibility and accuracy of signal detection and then form a complete detection system [24], in this system, the sensor is a device that outputs signals and senses the measured size. Data is the main transmission content. When the above functional systems exist as independent individuals, the data transmission must be transmitted step by step. The data processing is mainly the conversion processing of the sensor output signal. The measurement results are displayed in analog or digital and recorded by an automatic recording device [25].

3. Simulation Experiment of Basketball Technique and Physical Fitness Evaluation System Based on Neural Network

3.1. Experimental Background. The country has always attached great importance to the improvement of the overall quality of the masses, hoping to promote the overall development of the masses' moral, intellectual, and physical capabilities. However, due to the impact of exam-oriented education, the lack of physical education teachers in grassroots schools has resulted in relatively low quality of physical education in grassroots schools. Basketball is one of the most popular sports in our country, but even professional basketball players cannot always keep one-on-one accompany training when they are training. At this stage, our country has also done a lot of research on basketball training, mainly from the perspective of analyzing common training problems and changing classroom teaching methods. However, the current problems in various physical education have not been well resolved. To this end, this article will use neural network-based mobile sensors to try to combine basketball technical training and physical fitness assessment with an intelligent system to improve the efficiency of basketball teaching. Participants in this experiment include 3 senior basketball coaches, 3 professional basketball players, and 30 basketball enthusiasts with varying technical levels. In this article, 30 subjects were divided into 6 groups (5 people in each group) of similar levels, and they were asked to wear mobile sensors to complete the required basketball technical action and physical fitness assessment items.

3.2. Experimental System Structure Design. Before proceeding with the system structure design, this article conducted a research and analysis of the basic functions of the product and determined that the main task of the system is to improve the scientific nature of the athlete's physical fitness assessment and provide targeted training and guidance programs for athletes to improve their basketball skills. With a detailed understanding and comprehensive analysis of the
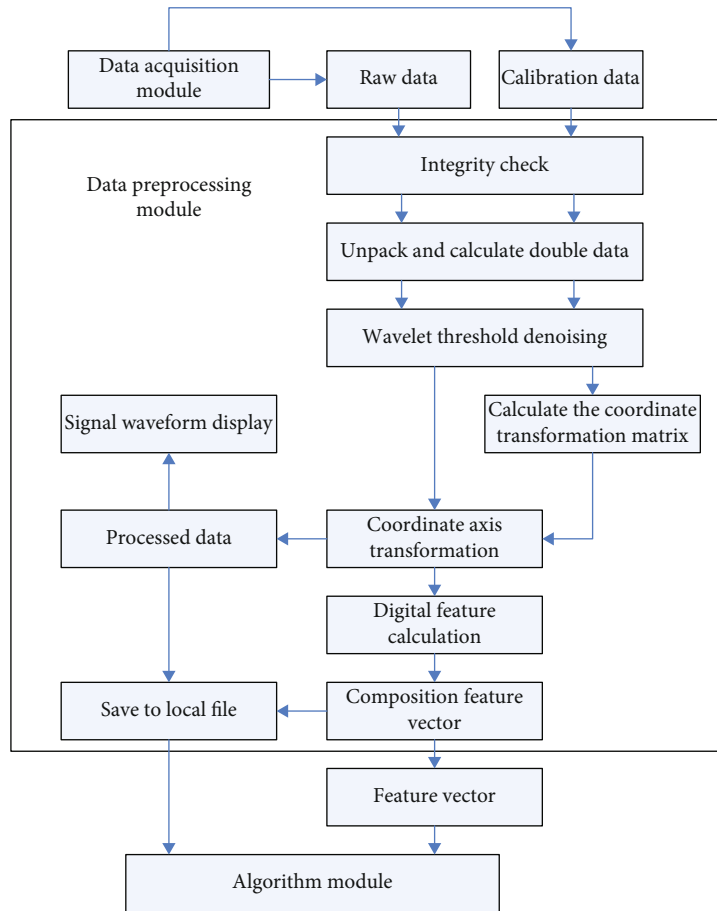
FIGURE 2: System data preprocessing process.

physical fitness characteristics and competition rules of basketball sports, the evaluation system of basketball physical fitness and technology is constructed by modern technology.

For intelligent systems, a reliable source of information and data is the basic prerequisite for intelligent analysis. When an athlete wears a smart device with a built-in mobile sensor, the instrument can detect the athlete anytime and anywhere and it can also achieve rapid multiparameter detection and feedback in terms of test data. The intelligent system uses a microcomputer as the data processing software monitoring processor, which can effectively complete the conversion of electronic signals to digital signals and has the characteristics of automation in scoring processing. The data analysis software also has the characteristics of networking and intelligence. It is the main reference basis for the analysis of technical actions.

The system mainly includes the following components: data analysis and performance recording software, basketball technical index database, and basketball special tester. The selected core control device is a single-chip microprocessor, the processing and analysis modes mainly include B/S mode and C/S mode, and the front end of collecting intelligent data mainly includes a single-chip microprocessor, sensor, and corresponding interface circuit.

3.3. Data Module Design of Experimental System. The overall system is divided into three parts, namely, the data acquisition part, the data transmission part, and the data processing part. The data processing part to complete the functions including data preprocessing, training, and recognition of the recognition model is the key to the entire system. Considering that if an embedded device is used for algorithm implementation, it is necessary to select the device and the system architecture for this problem. The overall implementation cost and complexity are relatively high. At the same time, the PC also has certain portability. At the same time, it has PC equipment and development cost. And the complexity is low, so the PC is used to implement the algorithm here. Figure 2 shows the system data preprocessing process.

It can be seen from Figure 2 that the process of data preprocessing is as follows: firstly, pass data verification to determine the correctness of the data packet, then parse the data packet to obtain the decimal value of the original data, and finally filter the signal. After filtering the data, the data is transformed with coordinate axes to obtain the coordinates of the human body travel reference system. Finally, the digital features are calculated for these coordinates, and finally, the feature vector is obtained, and the feature vector is given to the algorithm module as input.

4. Motion Sensor Based on Neural Network in Basketball Technology and Physical Fitness Evaluation System

4.1. Motion Sensor Based on Neural Network in Improving Basketball Technical Training. Basketball technical statistics is one of the methods used by sports researchers to organize, analyze, and research basketball game data. It has been widely used in basketball games today. It can intuitively and scientifically analyze some basketball game-related data. Coaches use data analysis to better study its own advantages and disadvantages, in order to finally win the game, help the team to formulate reasonable countermeasures, and implement the formulation plan; and the postgame summary needs to combine data statistics, field performance, etc. to make the game summary reach more accurate and targeted purpose. It is helpful to summarize the reasons for the failure and find out the winning method and avoid the same mistakes in the next game; through the accumulation and dataization of basketball game statistics, the establishment of a game database for the team and players can better understand the growth of the team and players to understand the player's training effect and the completion of tactics; at the same time, it also sets the task of playing technical and tactical indicators for the basketball team and players.

The only way to score in a basketball game is through the technical action of shooting, so the technical action of shooting is the most critical in basketball technology. The field goal percentage is an important indicator for evaluating the offensive team's shots. It is classified as two-pointers, three-pointers, and free throws. The calculation formula is field goal percentage = total field goal attempts/full field goal attempts. If the scoring is only supported by the number of shots, then the total field goal percentage does not reflect the shooting efficiency, and the coach may lose the right to know the team's offensive effect and affect the next tactical arrangement. Table 1 and Figure 3 are the statistics of shooting angle and distance.

From Table 1 and Figure 3, it can be seen that the common shooting strategies of different groups are determined by the players' technical preferences. For example, the probability of left shots in Group A is 43.0%, and the probability of close shots and midrange shots is as high as 86.1%. In subsequent matches, the opposing coach can make strategic deployments to this point to make their players pay more attention to the left side infield defense. Table 2 and Figure 4 are the analysis of players' shooting scores.

From Table 2 and Figure 4, it can be seen that there is also a big difference in the players' shooting scores. For example, the fast break scores organized by the D players have 29 points, while Group E has only 13 points, which shows the fast break of the D players. Ability is much stronger than that in Group E. In addition, players in different groups have different shooting percentages for three-pointers, two-pointers, and free throws. In this case, the coach can analyze the technical indicators of the shooting area, not only make tactical arrangements but also clearly see the number of two-pointers, three-pointers, free throws, and hits of the team

TABLE 1: Statistics of shooting angle and distance.

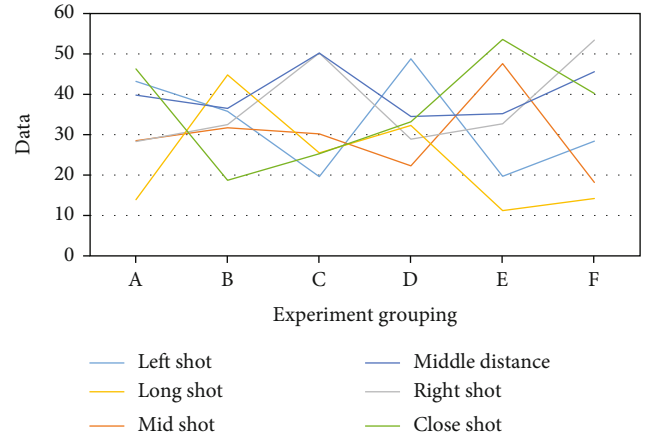| Group	Left shot	Mid shot	Right shot	Long shot	Middle distance	Close shot
A	43.2	28.5	28.3	13.9	39.8	46.3
B	35.8	31.7	32.5	44.8	36.5	18.7
C	19.6	30.2	50.2	25.5	50.2	25.3
D	48.8	22.3	28.9	32.3	34.5	33.2
E	19.7	47.6	32.7	11.2	35.2	53.6
F	28.4	18.2	53.4	14.2	45.6	40.2

FIGURE 3: Statistics of shooting angle and distance.

TABLE 2: Analysis of players' shot scores.

Group	Fast break score	Second attack	Three-pointer	Two-pointer	Penalty
A	15	21	54	34	10
B	27	16	45	46	7
C	21	20	51	26	8
D	29	15	57	36	11
E	13	19	48	28	9
F	16	14	54	32	12

and each player through the data. Calculate the shooting percentage of players. Collect shooting hot zone data to make targeted defensive tactics in order to win the game. Figure 5 shows the number of dribbling rolls of the player during the dribble.

In basketball, even seemingly ordinary actions have relatively strict technical standards. For example, the most common is dribbling. Many players are prone to dribbling and turning their wrists, which leads to the violation of "carrying the ball." In the course of the experiment, this article sets a stricter index for the dribbling wrist roll, taking 90 degrees and 0 seconds as the "critical value of the X-axis angle of the motion sensor" and "the duration of exceeding the critical value" as the initial values. It can be seen from Figure 5 that while adjusting the parameter self-convergence, the effective monitoring ratio of the sensor is also constantly changing. From the recognition of professional coaches,
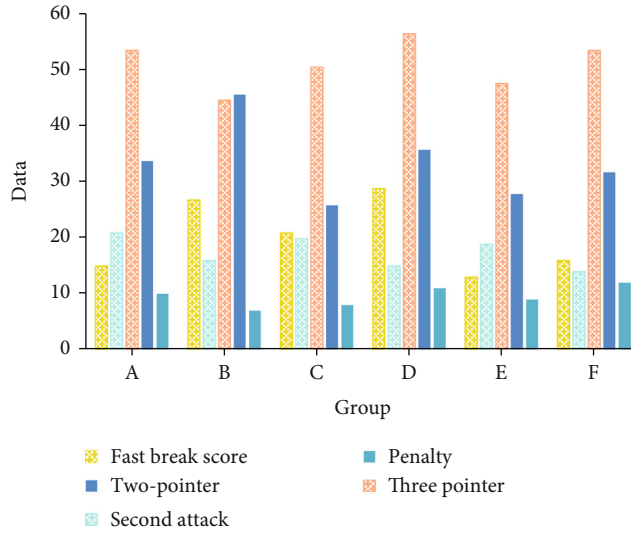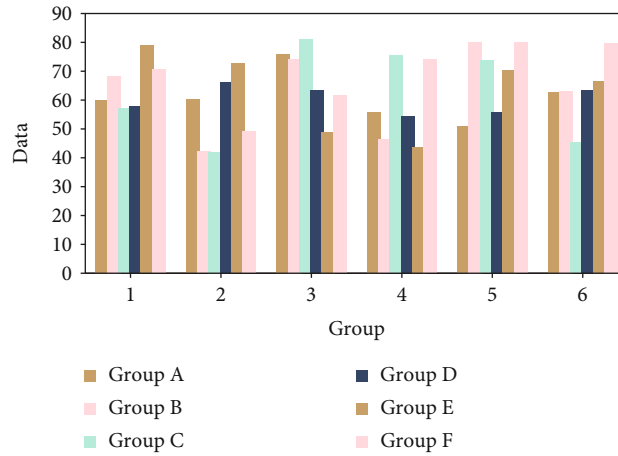
Figure 4: Analysis of players' shot scores.

Figure 5: Number of dribbling rolls of player during the dribble.

Table 3: Statistics of player technical errors.

Group	Dribble error	Missed shot	Rebound turnover	Pass error	Foul
A	5	12	8	4	8
B	7	18	14	6	12
C	6	11	9	11	9
D	9	19	11	8	13
E	13	15	13	10	10
F	10	13	10	12	11

when the X-axis angle value of the motion sensor is at a critical value of 105°, the system has the best effect on correcting the wrong posture of the dribble turning wrist. Table 3 and Figure 6 are the statistics of the number of players' technical errors.

Except for some minor posture errors, players may make varying degrees of errors during dribbling, shooting, rebounding, and passing. If the offensive efficiency represents the points obtained by each offensive and defensive conversion in a team game, the defensive efficiency represents the points obtained by the opponent for each offensive and defensive transition during the team competition. Offensive efficiency and defensive efficiency are added to the number of team offensive and defensive conversions, allowing this indicator to evaluate the offensive and defensive capabilities of each team based on a scientific and equal principle.

From Table 3 and Figure 6, it can be seen that Group A made fewer mistakes in dribbling and passing, but made more mistakes in shooting and rebounding. Group F had a higher number of mistakes in all aspects, which means that players need to be stronger. The coach can also set the corresponding target based on the team's average turnover rate. The coach can evaluate the performance of the team and the opponent in terms of ball control through the indicator of the turnover rate.

4.2. Motion Sensor Based on Neural Network in Physical Fitness Evaluation. For basketball players, good physical
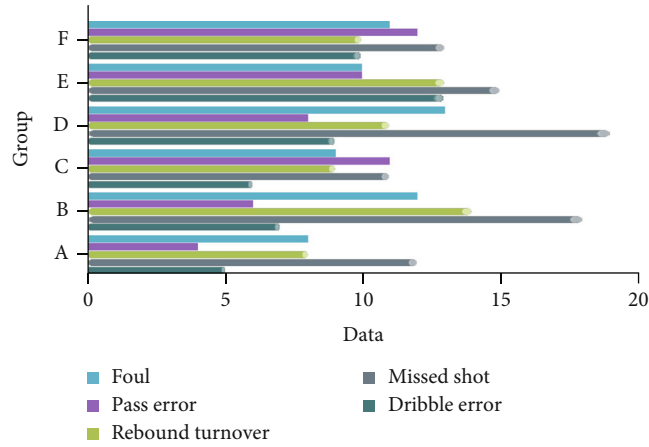
Figure 6: Statistics of player technical errors.

Table 4: Athlete's endurance test results.

Group	20mSRT	12 min	1-mile run	1000 m
A	63.5 ± 14.6	2413.8 ± 192.5	475.6 ± 43.8	253.3 ± 20.8
B	69.8 ± 13.2	2369.5 ± 188.2	486.3 ± 45.5	249.5 ± 21.3
C	67.7 ± 11.6	2436.7 ± 190.3	473.3 ± 44.2	251.6 ± 22.5
D	71.7 ± 13.5	2515.6 ± 184.4	478.5 ± 45.8	243.3 ± 20.5
E	72.8 ± 14.2	2452.5 ± 193.8	496.2 ± 47.3	261.7 ± 21.9
F	74.2 ± 12.8	2508.3 ± 192.7	458.9 ± 42.7	255.5 ± 21.5
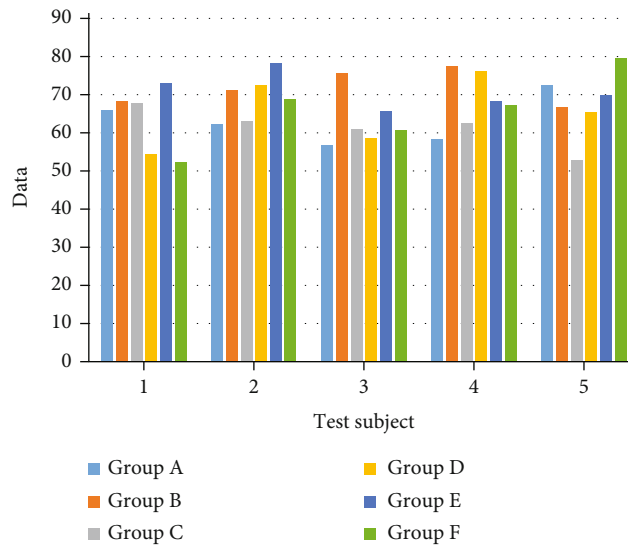
Figure 7: Athletes' 20-meter round-trip test data statistics.

fitness is a necessary condition for sports competition. A large amount of data information is usually involved in physical fitness assessment. These physical data not only change rapidly but also have no obvious symbolic meaning. In this case, the use of wireless sensors and intelligent analysis systems can help coaches better understand the physical fitness of athletes.

In the experiment in this article, the physical fitness of basketball players will be tested through four items: 1000-meter running, 1-mile running, 20-meter round-trip running, and 12-minute long-distance running. Table 4 is the test result table of the athletes' endurance item.

It can be seen from Table 4 that the average score of the subjects in the 20-meter round-trip run was 71.95 laps, the

FIGURE 8: Athletes' 1000-meter test data.

FIGURE 9: Athletes' 1-mile test data.

score in the 12-minute run was 2448.8 meters, the score in the 1-mile run was 478.13 seconds, and the score in the 1000-meter run was 252.48 seconds. Figure 7 shows the statistics of the athletes' 20-meter round-trip test data.

According to the physical fitness evaluation standard, this article believes that the data of an adult male in a 20-meter round trip should reach 70 laps to be considered qualified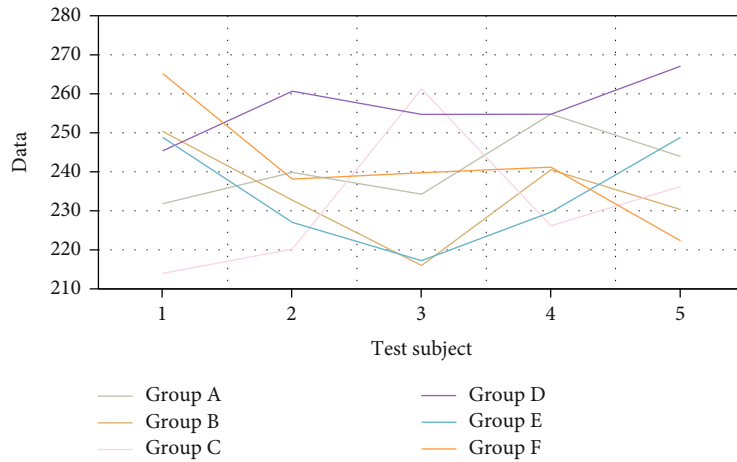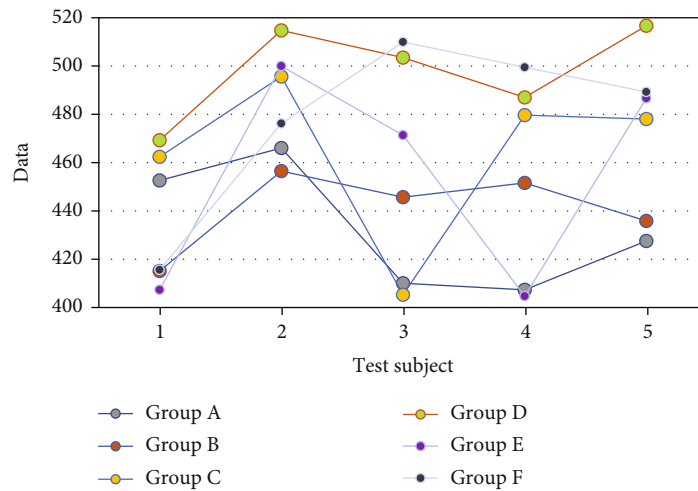. It can be seen from Figure 7 that only 17 of the test subjects in this article have reached the eligibility standard. Although the overall average score is 71.95 laps, there is still room for improvement in physical fitness for some people. Figure 8 is the athletes' 1000-meter test data.

According to the physical fitness evaluation standard, this article believes that the data of adult males in the 1000-meter run should be at least 272 s to be considered qualified. From the data in Figure 8, the average score of the 30 subjects was 252.48 s, of which 2 did not meet the pass standard and 3 reached the excellent standard. Figure 9 is the athletes' 1-mile test data.

According to the physical fitness evaluation standard, this article believes that the qualified data for an adult male in a 1-mile run is 7:00-8:30 (min/s). From the data in

Figure 9, the average score of the 30 subjects was 478.13 s, of which 1 did not meet the eligibility standard and 2 reached the excellent standard.

Taken together, it can be found that most of the subjects' data in various physical fitness tests are only at the qualified level, and the number of excellent ones is still small. For basketball, endurance, explosiveness, and agility are all very important physical indicators. If you want to further improve your own basketball level, you can use the intelligent evaluation system to understand your shortcomings more clearly and perform targeted physical fitness work out.

5. Conclusions

In this paper, through the study of basketball technical statistical index system, according to the basketball technical statistical index system in professional competitions, the representative technical indicators are selected, and these indicators are analyzed, and their significance and function are explained. To build a complete and scientific technical statistical indicator system, "make contributions." This article conducts in-depth exploration and research on technical

indicators such as scoring, rebounds, assists, turnovers, and hit rate and obtains effective hit rate, true hit rate, rebound efficiency, offensive and defensive conversions, offensive and defensive efficiency, assist rate, turnover rate, shooting area, scoring composition and other technical indicators which can be more intuitive, scientific, and comprehensive analysis of the substantive issues of the game. The technical indicators of rebounding are the analysis of offensive and defensive rebounding efficiency, combining the offensive and defensive conversion times of both sides to study the team's offensive and defensive efficiency; in the assist and turnover technical indicators, the offensive and defensive conversion times are added to analyze the assist efficiency and turnover efficiency.

This article uses mobile sensors and intelligent systems to evaluate the physical fitness of the subjects. The test items include four kinds, namely, 1000-meter running, 1-mile running, 20-meter round-trip running, and 12-minute long-distance running. From the test data, there is still room for improvement in the physical fitness of most subjects. Among them, the pass rate for the 1000-meter run was 83.3%, and the excellent rate was 10%; the pass rate for the 1-mile run was 90%, and the excellent rate was 6.7%; and the pass rate for the 20-meter round-trip run was only 56.67%. Compared with long-distance running, round-trip running is more a test of athletes' short-term explosiveness and agility. In the follow-up exercise, subjects can start from this aspect to improve their overall physical fitness and lay the foundation for improving comprehensive basketball skills.

On the whole, the research of this article has achieved certain results. Due to the limitations of various aspects, the research still has certain deficiencies. In the future, this article suggests that the research can be improved from the following aspects: (1) starting from the changes in basketball technical indicators, further discuss the scientific nature of the technical indicators; (2) on the shooting area, assist rate, and offensive and defensive conversion times, carry out more detailed analysis; and (3) optimize intelligent algorithms to improve system data analysis and processing capabilities.

Data Availability

No data were used to support this study.

Conflicts of Interest

The authors declare that they have no conflicts of interest.

Acknowledgments

References

[1] D. Conte, T. G. Favero, M. Niederhausen, L. Capranica, and A. Tessitore, "Physiological and technical demands of no dribble game drill in young basketball players," *Journal of Strength & Conditioning Research*, vol. 29, no. 12, pp. 3375–3379, 2015.

[2] Y. Y. S. D. Santos, L. A. Monezi, M. S. Misuta, and L. A. Mercadante, "Technical indicators registered as a function of the playing time in Brazilian basketball," *Revista Brasilra de Cineantropometria e Desempenho Humano*, vol. 20, no. 2, pp. 172–181, 2018.

[3] G. Yuzhou and H. Qi, "Research on multi direction training and technical analysis of basketball based on BP neural network model," *International Journal for Engineering Modelling*, vol. 31, no. 1, pp. 54–60, 2018.

[4] M. Song and Y. Wang, "A study of granular computing in the agenda of growth of artificial neural networks," *Granular Computing*, vol. 1, no. 4, pp. 247–257, 2016.

[5] M. T. B. Florentino, E. G. da Costa, T. V. Ferreira, and A. D. Germano, "Spectral subband centroid energy vectors algorithm and artificial neural networks for acoustic emission pattern classification," *Advances in Electrical and Computer Engineering*, vol. 19, no. 3, pp. 49–56, 2019.

[6] T. J. Choi, J. H. Lee, H. Y. Youn, and C. W. Ahn, "Adaptive differential evolution with elite opposition-based learning and its application to training artificial neural networks," *Fundamenta Informaticae*, vol. 164, no. 2-3, pp. 227–242, 2019.

[7] C. H. Ko, "Accessibility of radio frequency identification technology in facilities maintenance," *Journal of Engineering, Project, and Production Management*, vol. 7, no. 1, pp. 45–53, 2017.

[8] W. Wang, "Digital logistics warehouse management system based on radio frequency identification technology," *Science, Technology and Engineering*, vol. 19, no. 2, pp. 170–174, 2019.

[9] F. Adamo, F. Attivissimo, C. Guarnieri Calo Carducci, and A. M. L. Lanzolla, "A smart sensor network for sea water quality monitoring," *IEEE Sensors Journal*, vol. 15, no. 5, pp. 2514–2522, 2015.

[10] M. Jaradat, M. Jarrah, A. Bousselham, Y. Jararweh, and M. al-Ayyoub, "The internet of energy: smart sensor networks and big data management for smart grid," *Procedia Computer Science*, vol. 56, no. 1, pp. 592–597, 2015.

[11] Z. Jiang, S. Shekhar, X. Zhou, J. Knight, and J. Corcoran, "Focal-test-based spatial decision tree learning," *IEEE Transactions on Knowledge and Data Engineering*, vol. 27, no. 6, pp. 1547–1559, 2015.

[12] R. Pandya and J. Pandya, "C5. 0 algorithm to improved decision tree with feature selection and reduced error pruning," *International Journal of Computer Applications*, vol. 117, no. 16, pp. 18–21, 2015.

[13] Y. Zhang, S. Lu, X. Zhou et al., "Comparison of machine learning methods for stationary wavelet entropy-based multiple sclerosis detection: decision tree, k-nearest neighbors, and support vector machine," *SIMULATION*, vol. 92, no. 9, pp. 861–871, 2016.

[14] M. Konishi, S. Okubo, T. Nishino, and M. Wakatsuki, "A decision tree analysis of a multi-player card game with imperfect information," *International Journal of Software Innovation*, vol. 6, no. 3, pp. 1–17, 2018.

[15] P. Rajesh, M. Karthikeyan, B. Santhosh Kumar, and M. Y. Mohamed Parvees, "Comparative study of decision tree approaches in data mining using chronic disease indicators (CDI) data," *Journal of Computational and Theoretical Nanoscience*, vol. 16, no. 4, pp. 1472–1477, 2019.

[16] P. Sai Diwakar Nutheti, N. Hasyagar, R. Shettar, and S. Guggari, "Ferrer diagram based partitioning technique to decision tree using genetic algorithm," *International Journal*

of Mathematical Sciences and Computing, vol. 6, no. 1, pp. 25–32, 2020.

[17] D. K. Chaturvedi, A. P. Sinha, and O. P. Malik, "Short term load forecast using fuzzy logic and wavelet transform integrated generalized neural network," *International Journal of Electrical Power & Energy Systems*, vol. 67, pp. 230–237, 2015.

[18] E. Bassey, J. Whalley, P. Sallis, and K. Prasad, "Wavelet transform smoothing filters for metal oxide gas sensor signal cleaning," *International Journal on Smart Sensing and Intelligent Systems*, vol. 7, no. 5, pp. 1–5, 2020.

[19] A. A. Shah, B. S. Chowdhry, T. D. Memon, I. H. Kalwar, and J. A. Ware, "Real time identification of railway track surface faults using canny edge detector and 2D discrete wavelet transform," *Annals of Emerging Technologies in Computing*, vol. 4, no. 2, pp. 53–60, 2020.

[20] A. Khmag, A. R. Ramli, S. A. R. al-haddad, S. Yusoff, and N. H. Kamarudin, "Denoising of natural images through robust wavelet thresholding and genetic programming," *The Visual Computer*, vol. 33, no. 9, pp. 1141–1154, 2017.

[21] D. C. Jeronymo, Y. C. C. Borges, and L. . S. Coelho, "Image forgery detection by semi-automatic wavelet soft-thresholding with error level analysis," *Expert Systems with Applications*, vol. 85, pp. 348–356, 2017.

[22] X. Zhang, "A modified artificial bee colony algorithm for image denoising using parametric wavelet thresholding method," *Pattern Recognition and Image Analysis*, vol. 28, no. 3, pp. 557–568, 2018.

[23] P. O'Donovan, D. Coburn, E. Jones et al., "A cloud-based distributed data collection system for decentralised wastewater treatment plants," *Procedia Engineering*, vol. 119, no. 1, pp. 464–469, 2015.

[24] W. Yu, D. Griffith, L. Ge, S. Bhattarai, and N. Golmie, "An integrated detection system against false data injection attacks in the smart grid," *Security & Communication Networks*, vol. 8, no. 2, pp. 91–109, 2015.

[25] Y. Masuda, A. Noda, and H. Shinoda, "A low power and high speed data transmission system based on 2D communication," *IEICE Communications Express*, vol. 5, no. 9, pp. 322–328, 2016.

Research Article

Design and Implementation of Home Health System Based on ID Card Identification and Multidevice Access

Chao Gao[1] **and Xiaobing Hu** [2]

[1]*Graduate School, Jingdezhen Ceramic Institute, Jingdezhen, 333000 Jiangxi, China*
[2]*School of Fine Art, Anqing Normal University, Anqing, 246001 Anhui, China*

Correspondence should be addressed to Xiaobing Hu; 1976hxb@aqnu.edu.cn

With the development of society and the gradual arrival of an ageing society, various diseases threaten human health. If you use the software that comes with your medical device to understand and analyze your health, not only the user is in trouble but also a variety of health data can not be linked, giving users a more three-dimensional health analysis. In this case, this article will design and implement a mobile client for a home health system. The user's information is hosted by the remote data center. It is necessary to collect the user's information to facilitate management and analysis of health conditions. The manual input method is easy to input errors due to the long address and ID number, so the system will collect user information based on ID card identification. Train ID information to achieve accurate identification. For the multidevice access function, the key parts of the IEEE 11073 standard are used for communication. The mobile phone client that implements the home health system runs on the Android platform. According to the user information management, the user physiological data management, the user physiological data collection, and the user information synchronization are divided into four modules. The ID card identification module is called in the user management module, and the IEEE11073 communication plug-in is called by JNI in the health data measurement module. The health data can be presented intuitively to the user, or the information can be synchronized to the remote data center for further analysis.

1. Introduction

With advances in science and technology, social, and economic development, people's standard of living has improved. In daily life, they also pay more attention to their health. [1–4] At the same time, the global social demographic structure is rapidly entering the aging stage, and the demand for health monitoring and inspection is becoming more and more obvious [5]. It is difficult to meet the normal monitoring needs of the large population in the physical condition. It is difficult to achieve the requirement only by the resource allocation of the existing hospitals. Therefore, it is necessary to establish a simple and effective home health monitoring system [6]. With the development of portable computer technology, the home health system will gradually be developed, which we hope will meet the needs of daily physical examination and telemedicine of humans [7]. The home health monitoring system includes various health intelligent devices, such as sphygmomanometer, ECG monitoring device, blood oxygen monitor, environment temperature and humidity sensor, lighting regulator, and other [8–10]. Some of these devices are carried by users in wearable form, while others are fixed in the home environment. Although functions are different, they are generally considered as sensor devices to collect physiological data or environmental data of users [11]. After the completion of the acquisition, these devices will send data to the host in the home health network, and the host will gather data and analyze the [12].

The existing health system at home has some obvious shortcomings. On the one hand, the central computers in existing systems are mainly computers, and usually, there is only one central computer in a system. Users can view the device data via this central computer and receive the remote service [13, 14]. Then, with the rapid development of

intelligent devices, the popularity of smart phones and tablet computers has been greatly increased in the home environment. Users hope to directly check their own blood pressure, ECG, and other information through mobile phones, tablet computers, or other portable devices, instead of restricting the use of PC [15–17]. This requires that the new home health system includes PC, health set-top boxes, tablet computers, smart phones, and other hosts, and support blood pressure meters, oximeter, and other health devices can be linked to Windows, Linux, Android, and other operating system cross platform [18]. On the other hand, different communication interfaces adopted by different companies and organizations adopt different communication interfaces. Different communication protocols are used, which makes the existing system more closed. One device can only use [19] in one system. For example, using the terminal equipment of a company to measure the data of the user's vital capacity can only be transmitted through a company's own communication interface [20]. If the user uses the equipment of the company's blood pressure measurement, it needs to use another set of communication systems to transmit data. This undoubtedly increases the complexity of the use of equipment and increases the user's use cost. If the home health system can include a host platform running multiple operating systems and support the communication connection between devices and different platforms [21] and solve the problem of relative closure between different systems, there is no need to design special terminal equipment for different system platforms, which will greatly save costs, improve people's efficiency in life and work, and bring more convenience to real life [22–25].

In the country, there are many experts and scholars who do research on healthy home systems. Deng Yu proposed the concept of healthy home system through the analysis of the elements of healthy home system such as living population, lifestyle, and system design in modern cities. The theoretical preliminary construction, module construction, and related service construction of the healthy home system were carried out and further clarify the development trend and design direction of healthy home systems [26]. Sun Lei studied the national physique health management software based on SSH framework technology [27]. Combining database technology with Java language, we designed and implemented a personal health management system that provides comprehensive, comprehensive and effective tools, and means in the three processes of investigation, evaluation, and intervention with the health as the observation point [28]. Zou and other scholars have studied the physiological parameters acquisition system and wireless transmission mode of the elderly, analyzed the significance of blood oxygen saturation and long-term monitoring of body temperature, combined with sensor technology and embedded technology, using Bluetooth wireless transmission technology, and the Android system platform has established an elderly health monitoring system. The system platform can collect the oxygen saturation and body temperature information of the elderly and has the function of falling to the detection. The system design uses a portable design, and the sensor adopts wearable type, which is more practical [29]. In foreign countries, Maeng

et al. designed a social network-based care delivery framework (CDF) for the elderly home telehealth system, transforming the family telehealth system into a relationship between the elderly and family members. The system connects to existing social networking sites, such as Facebook, to encourage interpersonal communication between seniors and young family members. The home telehealth system is implemented as an application on a personal mobile device [30]. The research described above has certain deficiencies, not the low efficiency of data collection or the single use of equipment.

In this paper, the system will collect user information based on ID card identification and train ID card information to achieve accurate identification purposes. For multidevice access operations, the essential parts of IEEE 11073 shall be used for communication. The mobile phone client applying the home health system operates on the Android platform according to user information management, the management of normal user data, the collection of normal user data, and the synchronization of user information are divided into four modules. The ID card identification module is called in the user management module, and the IEEE11073 communication plug-in is called by JNI in the health data measurement module. The health data can be presented intuitively to the user, or the information can be synchronized to the remote data center for further analysis.

2. Proposed Method

2.1. ID Card Processing

2.1.1. Preprocessing of ID Card Images. In order to detect the destination file in relation to the area where the whole image is located, the image must first be preprocessed. Image preprocessing is the use of image processing technology to obtain the functions required for the current job, suppressing unwanted functions. In other words, reducing image noise and improving image quality so that subsequent work is not interfered with by unnecessary functions [31]. Typical image preparation techniques include grayscale, binarization, expansion, and corrosion. Image processing will improve the quality of the original image or reduce it to the best quality for our next operation. The effect of the processing directly affects whether the area where the target file is located can be extracted without problems, which further affects the progress of the follow-up work.

(1) Gaussian Blur. Gaussian blur, also known as Gaussian filtering, is essentially a process of smoothing data. This process smoothes the data, because it can remove noise, so it is widely used in the process of image processing noise. The calculation of Gaussian blur is to calculate the weighted average of each pixel and specifically obtain the value of Gaussian blur for a specific pixel. The pixel values themselves and near the specified range are the result of a weighted average under the weight matrix obtained after calculation with the Gaussian function. The formula of the Gaussian function is as follows.

$$G(x, y) = \frac{1}{2\pi\sigma^2} e^{-\left(x^2 + y^2\right)/2\sigma^2}. \tag{1}$$

Taking the $3 * 3$ matrix as an example, the specific calculation of Gaussian blur with a blur radius of 1 and a standard deviation of 1.5 is as follows:

The first step, the application formula (1), is based on the coordinates of each point to obtain its weight:

In the second step, the weight matrix obtained above is normalized: each weight is divided by the sum of the ownership values. After this step, a new weight matrix will be obtained, and the sum of the weights is 1.

In the third step, the original image and the new weight matrix are multiplied correspondingly.

In the fourth step, all the pixel values of the new matrix obtained in the third step are added and reaveraged, and the obtained value is the value of the center point after the Gaussian blur with the blur radius of 1.

(2) Grayscale. Each pixel of a color picture needs to be represented by three color components of *R*, *G*, and *B*. For example, RGB (29, 70, 180) represents a color pixel. The color pixel needs 3 components to represent, that is to say, 24 bit storage space is needed, so the color image requires a large storage space, and for the computer, a picture is a three-dimensional matrix, and the calculation of the three-dimensional matrix of the color image is processed. The amount is very complicated and is a serious test for efficiency. In fact, the three components of the color are only the reaction color matching information, and it has nothing to do with the image morphological features, and our extraction of the document image is to use the edge information of the document image and does not need color information to assist. For more convenient calculation and storage, we grayscale the color image for subsequent calculations. A specific variation of grayscale is to normalize the three components of the color pixel points to the same value according to the rules [32]. For example, if the pixel point (29, 70, 180) is grayed out using the maximum rule, it is normalized to a point (180, 180, 180). In this way, a pixel needs only one value to represent, the storage space is also reduced from 24 bits to 8 bits, and the amount of calculation is also reduced accordingly, so that the subsequent use of the edge processing algorithm sobel operator, the Canny operator can be processed faster.

There are usually several common grayscale rules:

(1) Component method

The value of any one of the three color components is selected as the grayscale image value according to the objective needs of the application.

$$\mathrm{Gray}(i, j) = R(i, j)/G(i, j)/B(i, j). \tag{2}$$

(2) Maximum method

The method compares the three component values by numerical value and uses the maximum value as the value of the grayscale image.

$$\mathrm{Gray}(i, j) = \max\{R(i, j), G(i, j), B(i, j)\}. \tag{3}$$

(3) Average method

The values of the three components of the color are averaged to obtain the gray value of the grayscale image.

$$\mathrm{Gray}(i, j) = \frac{(R(i, j) + G(i, j) + B(i, j))}{3}. \tag{4}$$

(4) Weighted averaging method

According to formula (5), the gray image obtained by weighted averaging of three-component color is more natural, and the gray image is more in line with human visual perception.

$$\mathrm{Gray}(i, j) = k_1 \times R(i, j) + k_2 \times G(i, j) + k_3 G(i, j),$$
$$k_1 = 0.298, k_2 = 0.567, k_3 = 0.124. \tag{5}$$

(1) Image Noise Reduction. In reality, images obtained with camera equipment are definitely affected by light, and images are often affected by external environmental noise during transmission. Such images are called noise images. In the process of binarizing certain images, many granular unidentified objects appear on the image. These unidentified objects are called noise. The process of reducing noise in digital images is called image denoising [33]. There are a lot of noises in the ID card image due to various factors, and these noises will cause some interference to the ID card identification. Filtering effectively removes noise from the image. After the image is filtered, the unknown objects μ can be removed, and the original binarized image contour can be kept unchanged. Filtering mainly includes mean filtering, median filtering, Wiener filtering and image wavelet domain filtering [34]. Mean filtering is a kind of filtering algorithm. It refers to giving a template to the target pixel on the image. This template includes the pixels around it. The principle of the template is to form a template with 8 pixels around the target pixel, remove the target pixel itself, and then replace the original pixel value with the average of all the pixels in the template.

2.1.2. Edge Detection

(1) Canny Edge Detection. Canny is a point optimization operator with filtering, enhancement, and detection. Compared to other edge operators, Canny edge performs noise processing when exporting image characteristics [35], effectively suppressing noise, and has more advantages in anti-interference, and the edge processing effect is clearer, and the Canny operator can accurately determine the position of the edge. By measuring the signal-to-noise ratio and the positioning product, the Canny operator can quickly and

accurately obtain the edge extraction map. The Canny operator smoothes the image after extracting the feature. The threshold is extracted in such a way that the resulting image features are more coherent. Before the edge feature extraction, the Canny operator performs Gaussian smoothing on the image to clear the image features, which is beneficial to the feature extraction of the image. After processing the color image into a grayscale image, edge feature extraction is performed on the two grayscale images by feature edge matching.

In order to evaluate the effectiveness of the edge detection method, Canny proposed three edge detection criteria: (1) good detection performance. The true edge is not missed, and the nonedge point is not detected as the edge point so that the output signal-to-noise ratio is maximized. (2) Good positioning performance. The detected edge point is closest to the actual edge point location. (3) Uniqueness. There is only one response for a single edge point. Under the guidance of the above three standards, Canny proposed the Canny edge detection algorithm as follows:

(1) Select a Gaussian filter to smooth the image

(2) Calculate the gradient of the smoothed image using the finite difference of the first-order partial derivative

(3) The nonmaximum suppression of the gradient, the pixel that retains the local gradient maxima, and the largest gradient mutation at this point, in order to refine the ridgeband in the amplitude image

(4) Detect and join edges with a double threshold algorithm [36]

The key to detecting the edge of the image using Canny is to select the appropriate threshold and C. A high and low level logical adjustment can detect more actual peaks and remove as many false peaks as possible. If the high threshold is set too small, the detected edge will be mixed with a lot of noise. If the setting is too large, the real edge will be missed. For the low threshold, if the setting is too large, the edge with a small change in the gray value will be caused. It is also missed. In addition, the reasonable σ size is also very important. The larger σ is, the more smooth the image will be, which will cause the image details to disappear, the gray level mutation will be far away from the original edge position, and the Gaussian filter length will be longer. To increase the amount of calculation, conversely, the smaller the σ is, the more the image is smoothed, so that there is a lot of noise mixed in the edge of the detection.

In general, the result of the Canny operator detection is better; it can reduce the interruption of the edge in the detection, which is beneficial to get a more complete edge. And in the case of noise, the Canny operator can effectively remove noise, so it is widely used to compare with other algorithms to evaluate the performance of other algorithms.

(2) Roberts Operator. The Roberts operator determines the gradient value by calculating the difference between two adjacent pixels in the diagonal direction of the point to be mea-

sured, so Roberts is also called the local difference operator. This method can effectively determine the edge points. Therefore, Roberts also called the gradient crossover operator; the Roberts operator uses a $2 * 2$ template with the difference:

$$\begin{cases} G_x = f(x, y) - f(x - 1, y - 1), \\ G_y = f(x - 1, y) - f(x, y - 1). \end{cases} \quad (6)$$

Roberts' gradient is centered on $(x - 1/2, y - 1/2)$, and the metric is the change in pixel gray value in the 45 and 135 directions at the center point. The threshold is taken as T, and when $G(x, y) > T$, the (x, y) point is the edge point.

(3) Sobel Edge Detection Operator. Sobel operator is another common first-order edge detection operator, but unlike Roberts edge detection operator, Sobel edge detection operator uses a $3 * 3$ template. Sobel operator takes the template as the core and then convolutes and calculates with each pixel in the image to be processed. The difference between the longitudinal brightness and the transverse brightness can be obtained.

The characteristic of Sobel operator is that it can effectively eliminate the noise of the image to be processed and locate the edge direction of each edge point accurately. Although Sobel operator can find the edge direction better, the effect of Sobel operator in locating the edge is not ideal. This is mainly because when Sobel operator locates the edge, it can get 4 of a single pixel point by calculating [37]. The weighted difference of neighboring pixels is used to find the extreme points of edges as edges. Therefore, in the application or experiment, the operator can be considered when the accuracy of the test results is not strict.

(4) Log Operator. The Log operator is also called the Laplace Gauss algorithm. Its principle is to combine the Gauss filter with Laplacian. The main reason is that the two-order derivative is more sensitive to noise. The Laplace transform of the two variable function $f(x, y)$ is defined as:

$$\nabla^2 f = \left(\frac{\partial}{\partial x^2} + \frac{\partial}{\partial y^2} \right) f(x, y). \quad (7)$$

The Gauss filtering function is as follows:

$$G(x, y) = \frac{1}{2\pi\sigma^2} \exp \left(-\frac{x^2 + y^2}{2\sigma^2} \right). \quad (8)$$

The Log operator uses two filtering methods to process images, namely, Gauss filter and pull Blass operator.

These two filtering methods are applied to low pass filtering and high pass filtering, respectively, and image edge detection is performed after filtering.
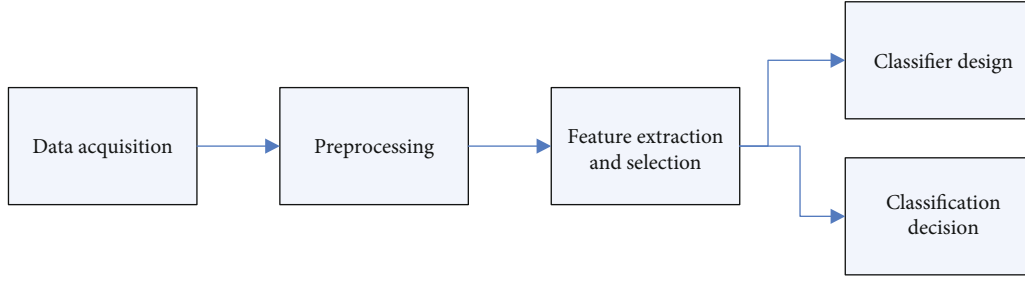
FIGURE 1: A schematic diagram of a pattern recognition system.

Log filter is as follows:

$$\nabla^2 G(x, y) = \frac{1}{\pi\sigma^2} \left(\frac{x^2 + y^2}{2\sigma^2} - 1 \right) \exp \left(-\frac{x^2 + y^2}{2\sigma^2} \right). \quad (9)$$

Compared with other edge detection operators, Log edge detection operator has the advantage that template can be calculated ahead of time, so when computing, it can directly call the calculated template to convolution the image.

2.2. Identity Card Recognition

2.2.1. Identity Card Character Feature Extraction

(1) Character Normalization. Typically, image extraction is not directly applicable to the export of features, because the quality of the image extracted from the preprocessed image directly poses the risk of identity card differences. Image size, attribute distribution, and so on will affect image output. Therefore, the character image obtained after character segmentation needs to be normalized before feature extraction.

Assuming that the size of the characters after segmentation is $M * N$, the position of the center of gravity can be expressed by formula (10):

$$\begin{cases} x = \dfrac{\sum_{j=1}^{N} \sum_{i=1}^{M} i \times C(j, i)}{\sum_{j=1}^{N} \sum_{i=1}^{M} C(j, i)}, \\[3mm] y = \dfrac{\sum_{j=1}^{N} \sum_{i=1}^{M} j \times C(j, i)}{\sum_{j=1}^{N} \sum_{i=1}^{M} C(j, i)}. \end{cases} \quad (10)$$

After obtaining the center of gravity of the image from formula (10), the center of gravity of the image is then transferred to the center of the image to normalize the position of the character image.

There are two ways to achieve normalization of image size: one is to enlarge or shrink the image to the specified scale through the border of the image. This method is simple in operation and relatively small in calculation. Another method is to incorporate the distribution characteristics of images into consideration. A relatively simple method is the distribution variance of images. The distribution variance of

the image can be calculated by formula (11).

$$\begin{cases} \sigma_x^2 = \dfrac{\sum_{j=1}^{N} \left(\sum_{i=1}^{M} C(j, i) \times (i - x) \right)^2}{\sum_{j=1}^{N} \sum_{i=1}^{M} C(j, i)}, \\[5mm] \sigma_x^2 = \dfrac{\sum_{j=1}^{N} \left(\sum_{i=1}^{M} C(j, i) \times (j - y) \right)^2}{\sum_{j=1}^{N} \sum_{i=1}^{M} C(j, i)}. \end{cases} \quad (11)$$

(2) Character Feature Statistics. The global characteristics of character images are essentially the processing of character images as a common image, and characters are only objects with certain characteristics. Therefore, the global feature extraction method of character image is similar to the general image feature extraction method. The global feature extraction methods of character images are mainly as follows:

Invariant moments (*moment feature*): invariant moments are important methods for object detection and recognition in optical image processing. The central moment and the origin moment of the image can distinguish the geometric information of the projection of the target in the imaging plane, but the geometry of the projection surface does not have scale, rotation, or affine invariance

Global projection features: the images are projected to several reference directions, respectively, and only the strokes that are perpendicular to the reference direction are projected to the reference direction. Compared with the stroke extraction method based on structural features, the method is simple and fast. The global projection features can reflect to some extent the complexity of the whole Chinese character, the main direction of strokes, and the possible connection between strokes

Background features: the background part of the ID card, the image, and the stroke of Chinese characters can also be used as a global feature of Chinese character and image. We usually select the blank points (nonstroke points) located on the two diagonal lines of the image to count the stroke density in each direction of the characters as the global background features of the images

2.2.2. Identity Card Identification

(1) Pattern Recognition Theory. Character recognition technology belongs to the category of pattern recognition and is also a very important application area. In short, pattern
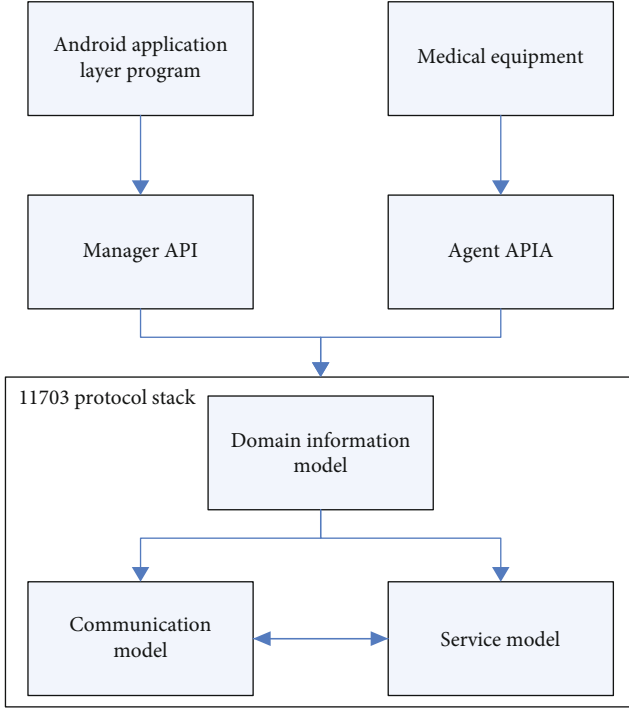
FIGURE 2: 11073 standard overall design.

recognition is the identification of the category of a given object. It is an important branch of signal processing and artificial intelligence. Computers are used to describe and classify physical quantities and their changing processes. They are usually used to process, classify, and recognize information such as images, words, photographs, and sounds. In our daily life and work, we can not do without pattern recognition, such as recognition, discrimination, and discrimination. In general, we call information that is spatially and spatially distributed through observation of specific individual objects as patterns and refer to the category of patterns or the general pattern of the same category as mode classes. A pattern recognition system consists of 4 parts: data acquisition, preprocessing, feature extraction and selection, and classification decision. Its basic function is to identify which category the system has to deal with, as shown in Figure 1.

(2) Pattern Recognition Method and Classification. Pattern recognition technology can be generalized into two categories: statistical pattern recognition based on decision theory and syntactic pattern recognition based on formal language. They can be complementary in many cases. If the structural information of a schema is not important, the identification problem is mainly classified, rather than descriptive; then, the statistical method is enough; if the structure information of the pattern is very rich and the identification problem requires classification and description, then the syntax method is needed.

    (1) Statistical decision-making is a theoretical aspect which is relatively mature and has more methods.

Its main idea is to classify decisions based on various posterior probabilities and probability density functions and minimize the error rate of decision-making. However, this method has its shortcomings, that is, it is very difficult to extract the pattern features in complex environment, and it is difficult to accurately reflect the structural characteristics of patterns. When using statistical decision method to classify and discriminate, the commonly used criteria are distance D and similarity degree R, which is the basis of classification and recognition. For example, the Minkowski distance of order S:

$$D(X, G) = \left[\sum_{i=1}^{m} |x_i - g_i|^s \right]^{1/S}. \tag{12}$$

When $S = 1$, it is the absolute distance:

$$D(X, G) = \sum_{i=1}^{m} |x_i - g_i|. \tag{13}$$

When $s = 2$, the Euclidean distance is obtained.

$$D(X, G) = \left[\sum_{i=1}^{m} (x_i - g_i)^2 \right]^{1/2} = [(x_i - g_i) T (x_i - g_i)]^{1/2}. \tag{14}$$

    (2) *Artificial Neural Network Method.* Artificial neural network is a nonlinear dynamic system composed of a large number of simple basic units and neurons. The structure and function of each neuron are relatively simple, but the system composed of them can be very complex. It has some characteristics of human brain and can be used for association, recognition, and decision-making. Neural network is a "model independent" machine. It shows the performance of a classifier without tutor learning conditions, and it has the characteristics of training to make the output approximate any target in the type space, especially when the dimension of the training set is smaller than the dimension of the problem to be solved. In pattern recognition, noise interference or partial loss of input patterns often exist, while neural networks store the information distribution in the full coefficients of the links, making the network highly fault-tolerant and robust. This feature is also one of the reasons why it successfully solves the problem of pattern recognition. In addition, the self-organizing and adaptive learning function of neural network have shown great superiority in identifying problems. The distinguishing feature of this method is that the neural network after training can complete the extraction and classification of pattern features in parallel
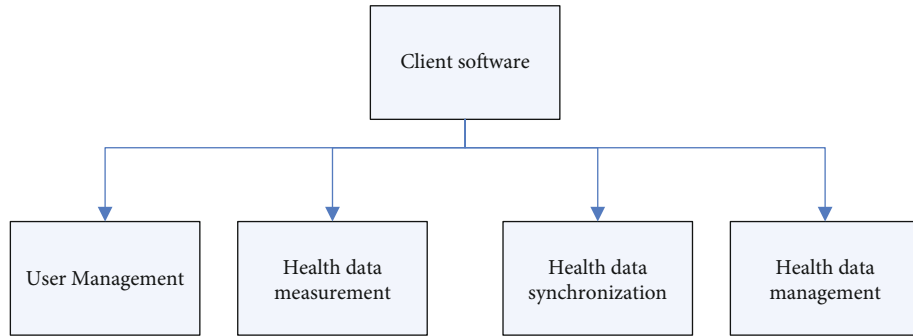
FIGURE 3: Client module partition diagram.

(a) Original image	(b) Edge detection image

FIGURE 4: Edge detection diagram.

3. Experiments

3.1. Design of the Core Part of the IEEE 11073 Standard. The IEEE11073 standard is made up of many models, including communication model, domain information model, and service model. This paper focuses on the design and implementation of the three key models in the optimal exchange protocol of IEEE11073 standard. The administrator and agent in the protocol correspond to terminal devices (such as mobile phone terminals and computers) and medical devices (such as temperature apparatus and blood fat apparatus). The overall design of the IEEE11073 standard is shown in Figure 2.

3.2. Client Design. The home health system server is primarily responsible for connecting the user, registering users, measuring normal data, loading normal data, the question of normal data, and the management of normal data. Based on the above functions, the customer service terminal can be divided into the following modules: health data measurement module, antidata management module, user manage-

TABLE 1: Comparison of recognition results by different methods.

Method	Comprehensive accuracy
PCA + SVM	87.1%
PCA + RF	85.4%
PCA + CNN (this article)	96.8%

ment module, and health data synchronization module four parts. The division of client software is shown in Figure 3 below.

(1) *The Health Data Measurement Module.* The module obtains the user's physiological data by calling the IEEE11073 standard communication plug-in and various health devices to create connections

(2) *Health Data Management.* Statistical analysis of user health data and draw a data graph, allowing users to observe their health trends directly
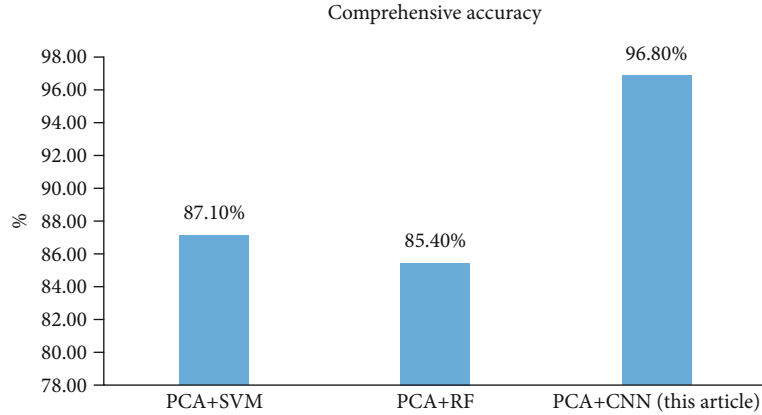
Comprehensive accuracy

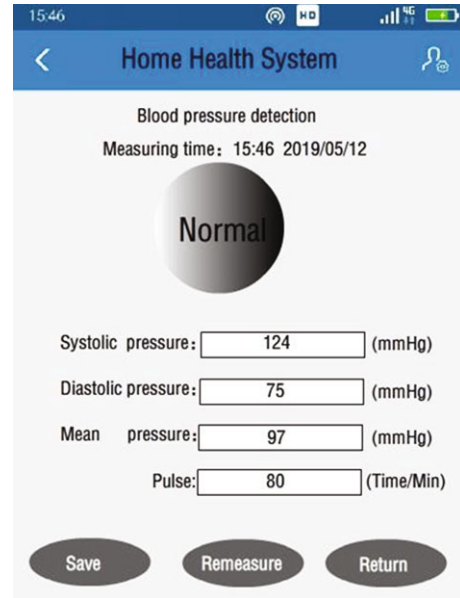Figure 5: Comparison of recognition results of different methods.
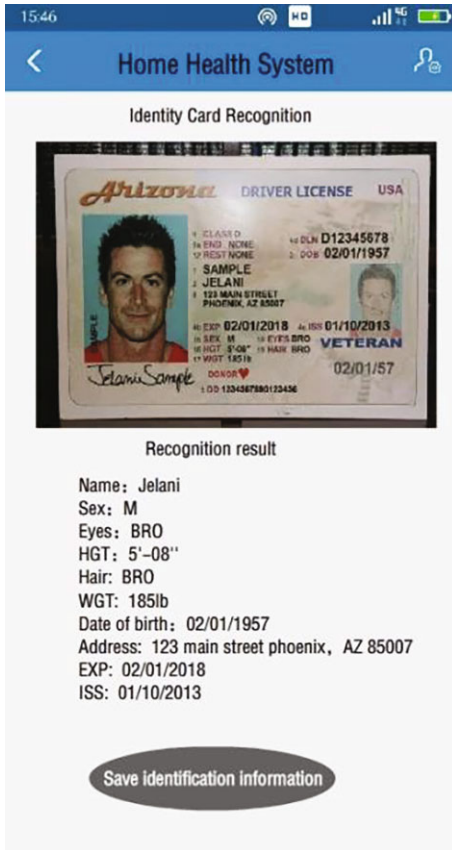
Figure 6: Recognition result diagram.

(3) *Synchronization of Health Data*. Home health system client and remote data center connect through the network, upload, or download health data

(4) *User Management Module*. Manage user's personal information, call the user when landing, if you have not saved the account password, you can register new users, use ID card identification module to collect user information, users can also register and modify their own information

Figure 7: Health monitoring result chart.

4. Discussion

4.1. Identity Card Image Preprocessing and Recognition Analysis

4.1.1. Image Processing of Identity Card. In order to have a more intuitive understanding of the edge detection algorithm proposed in this paper, we carry out two groups of experiments: the first group is to experiment with the algorithm in the case of no noise, and the second group is to experiment with the algorithm in the case of noise. The way of adding noise is to add 5% Gauss noise and 2% salt and pepper noise at the same time. The experimental results are shown in Figure 4.

Because Laplacian operator has good positioning performance, the gradient of real edge pixels can be increased by multiplying with Sobel operator, while the gradient of other pixels is weakened. Therefore, the edge detection algorithm based on gradient multiplication will have better accuracy
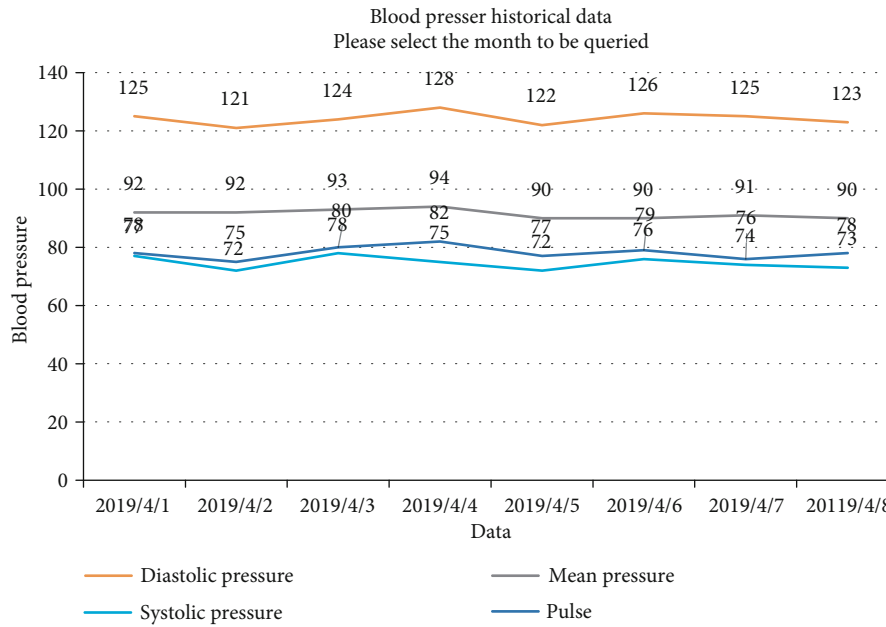
Figure 8: Trend chart of historic blood pressure change.

than the edge detection based on first derivative, and the edge extracted by this algorithm is generally better than the edge detection based on first derivative. The result of edge detection based on derivative is finer and more complete. Compared with the edge detection algorithm based on second derivative, this algorithm has obvious advantages in antinoise.

4.1.2. Identity Card Image Recognition and Analysis. The recognition results of the algorithms and comparison algorithms used in this paper are shown in Table 1 and Figure 5. Random forest is a forest built randomly by multiple decision trees, and there is no correlation between each decision tree. For the recognition problem that can be solved by a single decision tree, it undoubtedly causes serious waste of resources without improving the results. Therefore, the design of this experiment is more reasonable for the resource overhead in smartphone environment. In conclusion, compared with the existing research methods and applications, the proposed method has been improved, and the recognition accuracy of basic behavior has also been improved. In a word, this method improves the accuracy and reduces the complexity, achieves the desired purpose, and proves the effectiveness of the proposed method. The recognition accuracy and resource utilization are good, and the identification of identity cards can be achieved.

4.2. Implementation of Main Functions of the System. The user can choose photos saved on the phone or use the camera on the phone to take photos. After shooting, you can automatically enter the photo clipping interface. Here, you can choose different proportions to tailor, cut out the background outside the frame of the ID card, cut out the photos on the identity card, and choose the tailoring. First of all, the system does the preprocessing and denoising of the ID card image and then identifies the text on the image. First, use the font

library of the system to identify it, then recognize it with the font library that you have trained, and the result is shown in Figure 6.

After the mobile client connects with the health testing instrument, the data of the uploaded blood pressure is received. After analyzing the data of the XML format, the values of systolic blood pressure, diastolic pressure, average pressure, pulse, and measurement time are obtained. The blood pressure is calculated and compared and shown in the app measurement interface as shown in Figure 7.

In the main interface selection and cloud synchronization function, will download the recent eight measurement data or upload the new data collected by the mobile client. If the user chooses the function of healthy change trend at the main interface, it will synchronize data from the cloud and draw the trend line chart, for example, select the history blood pressure trend chart and display the result as shown in Figure 8.

5. Conclusions

(1) In order to better address the areas of text and portrait in the image of identity, image preprocessing is carried out, such as greying, duplication, improving image, and filtering to effectively separate useful areas of identity information

(2) In the aspect of ID card character recognition, we design the function modules of image preprocessing, character segmentation, feature extraction, and character recognition. In this paper, we use uniform grid feature, rough periphery feature, and hog feature to describe character image and use CNN to classify character image. In view of the characteristics of carrying information on ID card, we design different character recognition methods. Classifier classifies

and recognizes different information on ID card, which greatly improves the speed of character recognition

(3) Design and implement the development of client and server under Android platform. The client program calls the core part of IEEE11073 standard implemented in this paper through JNI, receives and parses the health data of medical equipment, stores the data into the local database of mobile phone, and displays the health data of users in the way of graph statistics. At the same time, users can synchronize the data of local to remote centers to better realize the cross-device use of the client system

Data Availability

There is no data available to support this article.

Conflicts of Interest

The authors declare that they have no conflicts of interest.

References

[1] M. Chen, Y. Ma, J. Song, C. F. Lai, and B. Hu, "Smart clothing: connecting human with clouds and big data for sustainable health monitoring," *Mobile Networks and Applications*, vol. 21, no. 5, pp. 825–845, 2016.

[2] W. Honda, S. Harada, T. Arie, S. Akita, and K. Takei, "Wearable, human-interactive, health-monitoring, wireless devices fabricated by macroscale printing techniques," *Advanced Functional Materials*, vol. 24, no. 22, pp. 3299–3304, 2014.

[3] N. Wu, X. Cheng, Q. Zhong et al., "Cellular polypropylene piezoelectret for human body energy harvesting and health monitoring," *Advanced Functional Materials*, vol. 25, no. 30, pp. 4788–4794, 2015.

[4] H. F. Nweke, Y. W. Teh, G. Mujtaba, and M. A. al-garadi, "Data fusion and multiple classifier systems for human activity detection and health monitoring: review and open research directions," *Information Fusion*, vol. 46, pp. 147–170, 2019.

[5] S. Maity, D. Das, and S. Sen, "Wearable health monitoring using capacitive voltage-mode human body communication," in *2017 39th Annual International Conference of the IEEE Engineering in Medicine and Biology Society (EMBC)*, pp. 1–4, Jeju, South Korea, 2017.

[6] S. Chen, S. Liu, P. Wang, H. Liu, and L. Liu, "Highly stretchable fiber-shaped e-textiles for strain/pressure sensing, full-range human motions detection, health monitoring, and 2D force mapping," *Journal of Materials Science*, vol. 53, no. 4, pp. 2995–3005, 2018.

[7] S. Thakur, A. K. Singh, S. P. Ghrera, and M. Elhoseny, "Multilayer security of medical data through watermarking and chaotic encryption for tele-health applications," *Multimedia Tools and Applications*, vol. 78, no. 3, pp. 3457–3470, 2019.

[8] A. M. Humadi and A. K. Hamoud, "Online real time fuzzy inference system based human health monitoring and medical decision making," *International Journal of Computer Science and Information Security*, vol. 15, no. 4, p. 197, 2017.

[9] Y. Jiao, C. W. Young, S. Yang et al., "Wearable graphene sensors with microfluidic liquid metal wiring for structural health monitoring and human body motion sensing," *IEEE Sensors Journal*, vol. 16, no. 22, pp. 7870–7875, 2016.

[10] D. Mascareñas, C. Plont, C. Brown et al., "A vibro-haptic human-machine interface for structural health monitoring," *Structural Health Monitoring*, vol. 13, no. 6, pp. 671–685, 2014.

[11] S. N. Mohanty, E. L. Lydia, M. Elhoseny, M. M. G. al Otaibi, and K. Shankar, "Deep learning with LSTM based distributed data mining model for energy efficient wireless sensor networks," *Physical Communication*, vol. 40, article 101097, 2020.

[12] S. A. Lowe and G. Ólaighin, "Monitoring human health behaviour in one's living environment: a technological review," *Medical Engineering & Physics*, vol. 36, no. 2, pp. 147–168, 2014.

[13] Y. C. Huang and Y. L. Hsu, "Social networking-based personal home telehealth system: a pilot study," *Journal of Clinical Gerontology & Geriatrics*, vol. 5, no. 4, pp. 132–139, 2014.

[14] T. Tsukiyama, "In-home health monitoring system for solitary elderly," *Procedia Computer Science*, vol. 63, pp. 229–235, 2015.

[15] P. J. Huckfeldt, N. Sood, J. J. Escarce, D. C. Grabowski, and J. P. Newhouse, "Effects of Medicare payment reform: evidence from the home health interim and prospective payment systems," *Journal of Health Economics*, vol. 34, no. 1, pp. 1–18, 2014.

[16] J. M. Beer, S. E. McBride, T. L. Mitzner, and W. A. Rogers, "Understanding challenges in the front lines of home health care: a human- systems approach," *Applied Ergonomics*, vol. 45, no. 6, pp. 1687–1699, 2014.

[17] A. Alaiad and L. Zhou, "Patients' adoption of WSN-based smart home healthcare systems: an integrated model of facilitators and barriers," *IEEE Transactions on Professional Communication*, vol. 60, no. 1, pp. 4–23, 2017.

[18] T. Tamura, S. Maeno, T. Hattori et al., "Assessment of participant compliance with a web-based home healthcare system for promoting specific health checkups," *Biocybernetics & Biomedical Engineering*, vol. 34, no. 1, pp. 63–69, 2014.

[19] J. J. Rissi, S. Gelmon, E. Saulino, R. Baker, P. Hatcher, and N. Merrithew, "Building the foundation for health system transformation: Oregon's patient-centered primary care home program," *Journal of Public Health Management & Practice*, vol. 21, no. 1, pp. 34–41, 2015.

[20] Z. Lv, W. Kong, X. Zhang, D. Jiang, H. Lv, and X. Lu, "Intelligent security planning for regional distributed energy internet," *IEEE Transactions on Industrial Informatics*, vol. 16, no. 5, pp. 3540–3547, 2020.

[21] Z. Lv, A. Halawani, S. Feng, H. Li, and S. U. Réhman, "Multimodal hand and foot gesture interaction for handheld devices," *ACM Transactions on Multimedia Computing, Communications, and Applications (TOMM)*, vol. 11, no. 1s, pp. 1–19, 2014.

[22] R. SujiPramila and A. Shajin Nargunam, "A survey on effective in-home health monitoring system," *International Journal of Computer Applications*, vol. 68, no. 7, pp. 15–19, 2013.

[23] D. De and A. Mukherjee, "Femto-cloud based secure and economic distributed diagnosis and home health care system," *Journal of Medical Imaging & Health Informatics*, vol. 5, no. 3, pp. 435–447, 2015.

[24] A. E. Rose, E. N. Robinson, J. A. Premo, L. J. Hauschild, P. J. Trapskin, and A. M. McBride, "Improving warfarin management within the medical home: a health-system approach," *American Journal of Medicine*, vol. 130, no. 3, pp. 365.e7–365.e12, 2017.

[25] H. Ko and M. Song, "A study on the secure user profiling structure and procedure for home healthcare systems," *Journal of Medical Systems*, vol. 40, no. 1, p. 1, 2016.

[26] R. Deng, "Design of healthy home system," *Design*, vol. 12, pp. 17–19, 2017.

[27] N. N. Hurrah, S. A. Parah, N. A. Loan, J. A. Sheikh, M. Elhoseny, and K. Muhammad, "Dual watermarking framework for privacy protection and content authentication of multimedia," *Future Generation Computer Systems*, vol. 94, pp. 654–673, 2019.

[28] L. Sun, "Design and implementation of personal health management system based on SSH," *Journal of University of Electronic Science and Technology.*, vol. 23, no. 4, pp. 71-72, 2016.

[29] S. B. Zou and C. X. Xie, "Development of family-based telehealth monitoring system," *Computer Engineering and Application*, vol. 41, no. 10, pp. 30–34, 2015.

[30] D. D. Maeng, N. Khan, J. Tomcavage, T. R. Graf, D. E. Davis, and G. D. Steele, "Reduced acute inpatient care was largest savings component of Geisinger Health System's patient-centered medical home," *Health Affairs*, vol. 34, no. 4, pp. 636–644, 2015.

[31] C. Yang, Z. Yang, and Z. Deng, "Robust weighted state fusion Kalman estimators for networked systems with mixed uncertainties," *Information Fusion*, vol. 45, pp. 246–265, 2019.

[32] S. Wan, Y. Xia, L. Qi, Y. H. Yang, and M. Atiquzzaman, "Automated colorization of a grayscale image with seed points propagation," *IEEE Transactions on Multimedia*, vol. 22, no. 7, pp. 1756–1768, 2020.

[33] L. Zhang, H. Shi, X. Zeng, and Z. Zhuang, "Theoretical and experimental study on the transmission loss of a side outlet muffler," *Shock and Vibration*, vol. 2020, Article ID 6927574, 8 pages, 2020.

[34] M. Elhoseny and K. Shankar, "Optimal bilateral filter and convolutional neural network based denoising method of medical image measurements," *Measurement*, vol. 143, pp. 125–135, 2019.

[35] S. Yu, "Analysis for center deviation of circular target under perspective projection," *Engineering Computations*, vol. -ahead-of-print, pp. 2403–2413, 2019.

[36] Y. Liu, C. Yang, and Q. Sun, "Thresholds based image extraction schemes in big data environment in intelligent traffic management," *IEEE transactions on intelligent transportation systems*, pp. 1–9, 2020.

[37] M. Zhou, Y. Wang, Y. Liu, and Z. Tian, "An information-theoretic view of WLAN localization error bound in GPS-denied environment," *IEEE Transactions on Vehicular Technology*, vol. 68, no. 4, pp. 4089–4093, 2019.

WILEY | Hindawi

Research Article

Research on Prediction of Investment Fund's Performance before and after Investment Based on Improved Neural Network Algorithm

Cong Gu [ID]

College of Science, Zhongyuan University of Technology, Zhengzhou, 450007 Henan, China

Correspondence should be addressed to Cong Gu; gucong@zut.edu.cn

There are more and more popular investment fund projects in the continuous economic development; the prediction and performance continuity become hot topics in the financial field. Scholars' enthusiasm for this also reflects the domestic fund primary stage progress, and there is a huge application demand in China. The prediction of fund performance can help investors to avoid risks and improve returns and help managers to learn more unknown information from the prediction for the sake of guide market well and manage the market orderly. In the past research, the traditional way is to use the advantages of neural network to build a model to predict the continuous trend foundation performance, but the author found that the traditional single neural network (NN) algorithm has a large error value in the research. With the discussion, the particle swarm optimization (PSO) algorithm is added to the radial basis function (BRF) neural network, and PSO is conditioned to optimize and improve the RBF NN combining the advantages of both sides; a new set of PSO-RBF neural network security fund performance prediction method is summed up, which optimizes the structure and workflow of the algorithm. In the research, the author takes the real data as the reference and compares the prediction results with the traditional method RBF and the improved PSO-RBF. In the prediction results of the continuous trend, the highest value, and the lowest value in the period of the security fund performance, the new PSO-RBF has a good prediction in the fund performance prediction, and its accuracy rate is greatly improved compared with the traditional method Sheng, with good application value, and is worth popularizing.

1. Introduction

Since the establishment of investment fund, the fund industry has developed rapidly. The scale is getting bigger and bigger and more and more varieties; it has greatly improved the structure of investors and played an increasingly stable and healthy evolution historical securities. Although domestic fund has made considerable progress in the past eight years, compared with the mature western market, the scale is still small. At present, there are more than 8000 kinds of funds in the US financial market, far higher than the number of listed company, while there are 642 in China. Investment funds have great potential in China [1].

The sustainability of fund performance refers to the phenomenon that a better fund will perform relatively well earlier in the future, while a worse fund will perform relatively poorly in the future, which is often called "strong often strong, weak often weak." By concept, suppose the investor can identify early excellent performance of the fund and continuous performance, can be purchased these capital and holdings them after a period, so as to obtain the above average excess return. Similarly, poor performance can be avoided if investors are able to identify funds with poor early and sustained performance and avoid investing in them. From this point of view, performance sustainability characteristics are undoubtedly as important as fund performance itself.

Final performance of security forecast is very central link to promote sustainable development of security fund. In a mature market, it means a lot for buyer, manage company, and function supervision to predict fund performance scientifically and objectively. Helping the buyer, through the

analysis of security market, we can get the accurate information of fund investment effect, adjust the investment strategy in time, and make the right investment choice. For fund management companies, scientific evaluation of their fund performance can not only give a quantitative evaluation of specific performance to each fund manager but also determine the advantages and disadvantages of investment strategies, summarize successful experience, improve the deficiencies, and improve the management level of the company. For regulators, they can formulate various relevant policies and regulations based on scientific security performance and management effect. Since the 1990s, the in-depth research on the prediction, optimization, and control of the financial system, as well as the extensive application of information and control theory and technology in the current financial problems, have brought challenges to the development of financial engineering. Financial forecast is an important part of financial engineering. For financial investors, it is difficult to explain the inherent laws of stock price, return, and risk of financial derivatives by using the traditional time series prediction technology. In recent ten years, neural network theory has gradually become a powerful tool for nonlinear dynamic system prediction and modeling. From the origin to now, the research and application of artificial neural network have entered a mature stage, and the application field is also expanding. At present, NN is mainly used for price prediction, trend, and rise of the stock market, with relatively high prediction accuracy [2, 3].

By simulating the structure of human neurons, neural network has a strong ability of self-learning, self-organization, and memory. It can predict the future development trend of stock price according to the historical data and relevant information of stock market. RBF NN is an infinite approximation and outstanding goodness of fit. Hence, RBF NN can be used as stock price prediction with high complexity. In this article, the basic principle of RBF NN is described in detail, and the gradient descent for RBF NN algorithm is analyzed. In the initial stage of global search, PSO is proved to be fast and effective. Based on the advantages and disadvantages of the two algorithms, this mentioned in the article hybrid computing method combines PSO calculation method and RBF algorithm exercise of front NN weight, which is called PSO-RBF computing method. Mixed calculation method not only uses the powerful global search power PSO algorithm but also uses the powerful search ability in the range of RBF calculation method. Case study of security performance of PSO-RBF NN, in this paper, discusses the basic concepts and structural characteristics of RBF and PSO. For different optimization algorithms, an optimization algorithm based on RBF neural network and particle swarm optimization algorithm is proposed. The working process and principle are introduced in detail, and the actual data are compared. In the comparative study, we find that the new calculation method is better than the traditional one security fund performance prediction, and its accuracy has been greatly improved. Experimental best results show that improved algorithm for PSO-RBF NN has rich value in fund performance research, and the model has a good application prospect [4–6].

2. The Development and Research of Security Fund Performance Prediction

2.1. The Concept and Characteristics of Security Investment Fund. Fund refers to a method of collective investment sharing benefits and risks. The funds of investors are centralized through the funds of public issuance of shares, which are entrusted by the fund custodian, management use, and control, and invested the remaining, other helpful market tools of the fund holders.

Different countries have different names for fund, considered as "shared fund" in the United States; Britain and Hong Kong are called "unit trust fund"; Japan and Taiwan are called "Investment fund."

Fund can rapidly develop into popular investment tools, which is closely related to its own characteristics:

(1) Security investment funds are widely invested in different securities, which can fully disperse risks

Due to the limited funds, small- and medium-sized investors generally cannot reduce the risk through fully diversified investment. And fund not only has the abundant capital strength but also can fully disperse the investment in various securities and realize the diversification of the asset portfolio. This diversification reduces the risk faced by each investor. Even if some securities have poor performance or even loss, they can be made up by other securities with excellent performance to achieve the purpose of dispersing investment risk.

(2) Security investment funds are managed by experts, professional financial management, and collective investment

The fund collects the funds of many investors, which are handed over to professional institutions and invested in various financial instruments by professionals with solid professional knowledge and rich investment experience. At the same time, investors can also decide the amount of investment according to their own economic situation. Although each investor does not invest much capital, because the fund can collect a lot of investors' funds, it rarely enters, controls costs, and gives play to the advantage of capital scale.

(3) Security investment funds have good supervision system and reasonable operation mode

The regulatory authorities strictly regulate fund industry and require the fund to disclose sufficient, timely standard message. In operation, foundation custodian keeps foundation assets independently, which is conducive to the safety of the fund assets. The principal supervises the purchase and operation activities of the investment manager and conduct accounting and performance calculation for the fund assets, which is conducive to protecting the interests of shareholders [7, 8].

2.2. The Development Course and Current Situation of Security Investment Fund in China. The fund established before 1997 is called "old fund," which mainly invests in

industry, but actually is a direct investment fund. In the real sense, security investment fund has experienced the development stages of closed-end fund and open-end fund since 1998.

The second stage (from September 2001 to now): the fund has entered an open development stage.

After 2001, China's fund scale expanded rapidly, the innovative varieties began to accelerate, and the supervision of the fund industry continued to strengthen. By the end of 2007, 59 fund management companies had been established in China, 9 of which had assets under management of more than 100 billion yuan. The number of funds reached 345, including 310 unrestricted form funds and 35 restricted form funds. Open-end funds account for 90% of the total funds. The total value of the fund is 3.28 trillion yuan. The asset performance of the unrestricted fund is 3.04 RMB 100 million, accounting for 92% total fund performance. Unrestricted fund has become the mainstream of market evolution instead of closed-end fund.

Despite China's portfolio investment fund industry has developed rapidly current stage, it is an emerging market after all. Compared with the development of the history of financial power more than 100 years, there is still a significant gap. In order to ensure the further sustainable development of financial market, many problems need to be solved to coordinate the expansion of fund scale and asset management level: to prevent the moral hazard number of fund managers; to further improve the internal governance structure of fund management companies; to implement incentive mechanism to weaken the frequent change of fund managers; to increase financial innovation and change the fund portfolio to be the same [9, 10].

2.3. Research on Fund Performance Forecast and Its Influencing Factors. At present, there are few studies speaking of performance prediction of direct domestic fund. Only the prediction method based on Markov chain proposed by Liu Tie thinks that according to the previous data of the fund, the probability of fund performance falling in each interval and the probability of fund performance falling in each interval can be predicted. However, when the fund managers' strength of stock selection is constantly studied, the impact of fund and fund managers on fund performance changes, such as some niche studies: to study the strength of fund managers to choose stocks, although the basic T-M and H-M models are adopted, but because the selected research scope is different, there are great differences in the conclusions. In recent years, continuous fund performance discussion is very popular, but the results are different. Tang Zhenyu made data analysis on the merger of small- and medium-sized enterprises in China, June 1008, 2003, and think the performance of domestic fund managers is sustainable. By analyzing the performance and risk sustainability of equity funds and from 2004 to 2008, the mixed fund in domestic unrestricted fund are in different performance markets; Yang found that only in 2004-2005, the risk-adjusted fund performance can be sustained. When the market enters the period of shock adjustment from bull market, the fund performance appears reversal phenomenon, and the risk

has obvious continuity. With regard to the change of fund managers, studies by domestic scholars such as Xiong Shengjun, Yang Chaojun, and Xu Xiaolei show that the change of fund managers in China has no impact on fund performance [11, 12].

2.4. Application of Neural Network in Fund Performance Prediction. The development of artificial intelligence provides a new method for fund performance prediction. Among them, NN has a strong nonlinear property data processing ability, which is very suitable for fund performance prediction. BP NN is used to establish the fund performance and guess the model. The data shows that the prediction accuracy of BP NN is high and is better than that of traditional linear prediction model. But BP NN is easy to fall into local optimum minimization and slow convergence, so BP neural network is not the best fund prediction method. Compared with BP NN, RBF NN is a better choice to predict the performance changes of nonlinear funds. However, RBF neural network itself has some disadvantages, such as slow convergence speed and no global search ability [13, 14]. Therefore, RBF neural network is not the best method to predict fund performance. Sample data, the author of this paper, a reasonably constructed index system for fund performance change, is trained and tested by using the nonlinear processing ability and PSO RBF NN has better overall search capability and sample data set. The BP NN and RBF NN are fully avoided from slow speed and easy access to local minimum dilemma in the process of predicting fund performance, and the accuracy of fund sale performance prediction is greatly improved [15–17].

3. Research and Methods

3.1. Particle Swarm Optimization Algorithm. PSO is a kind of evolutionary computing technology, which originated from the study of bird feeding. Now, it has been proved to be a good optimization method. PSO calculation method can be similar to an abstract scene. There is a piece of food in an area, and many birds look for that piece of food randomly in different areas. Where is the food? Birds do not know; they only know the approximate distance of the food and how the information is transmitted from one population to another, so the problem of finding food has become that each bird looks for food nearby. PSO has inspiration through the model and uses optimization solved problems. The result of every optimization problem in PSO can be understood as a bird in search space, which is called "particle." Particles can fly in search space according to a certain trajectory and speed, which is dynamically adjusted by their own speed and flight information. Birds imagine a point without mass and volume and develop it into n-dimensional space. The position of the i th particle in space can be displayed by vector $x = (x_{i1}, x_{i2}, \cdots, x_{iN})$. The speed of flight can be displayed by vector $v_i = (v_{i1}, v_{i2}, \cdots, v_{iN})$. The best place in history is called personal extremum. So far, all particles are in the most suitable position; whole population is called global extreme value gbest. In particle swarm optimization, all particles have corresponding fitting the value is optimization function, and the

individual extremum pbest and global extremum gbest are determined by the minimum fitting value of each particle [18–20].

3.2. Application Research Status.

For the first time, the PSO calculation method is applied to the optimization of nonlinear continuous functions and the training of neural networks. Eberhart uses particle swarm optimization to analyze tremors, such as Parkinson's disease. Yoshida et al. optimized various discrete continuous variables through PSO to control the output stable voltage of nuclear power unit. Robinson et al. use PSO calculation method optimization of profile wave horn antenna, compared the optimization effect with genetic algorithm, and studied the feasibility of their hybrid application. Ciuprina proposes intelligent PSO (intelligent PSO) to optimize the size of the solenoid coil. Abido uses PSO calculation method to solve the most typical problems. In China, more and more scholars also pay attention to the application of the algorithm, which shows a good application prospect of multiobjective optimization, data classification, data gathering, pattern identification, telecom service quality management, process planning, signal processing, intelligent machine control, decision reference, and true and false identification system identification [21–23].

3.3. RBF Neural Network

(1) Introduction to the structure of RBF NN

RBF NN consists of three parts. The nonlinear mapping is completed as shown below.

$$f_n(Y) = s_0 + \sum_{q=1}^{n} s_q \varphi\left(\|y\text{-}u_q\|\right), \tag{1}$$

where $Y \in K_n$ is the write in vector and $\varphi(\bullet)$ is a nonlinear ability of $K^+ \to K$. Generally, Gaussian function is adopted:

$$\varphi\left(\|Y\text{-}U_q\|\right) = eyp\left(-\frac{\|y\text{-}u_q\|^2}{\sigma_q^2}\right). \tag{2}$$

w_i is the weight, c_i and σ_i are the data sets and base ability, and h is the coding of centers.

RBF neural network needs to determine two kinds of parameters: unique center c_i and width σ_i basic function and intermediate value h, one remaining connection weight between write in time and bury time. Here, c_i and width σ_i basic functions and number of centers h are determined; the internet weight value output is linear when it is written in, but obtained by the least square method. Therefore, the determination of c_i, width σ_i, and number of centers h is the construction of the core of RBF NN [24–26].

(2) The determination of the number of centers of basic functions

The kernel subtraction clustering method is kind the optimal calculation method of confirming the number of basic function centers. In this paper, we consider normalizing

the data into P numerical value $(Y_1, Y_2, \cdots, Y_p)$ in the n-dimensional space of the unit hypercube. First, we give the degree value of numerical concentration point Y_q by formula (1) [27, 28]:

$$D = \sum_{q=1}^{p} eyp\left[-\frac{\|y_q\text{-}y_j\|^2}{(\gamma_a/2)^2}\right]. \tag{3}$$

After calculating the degree of aggregation each data point, the point with the highest degree of aggregation selected becomes a hub, and its density index is recorded as D_{c1}. Update the aggregation degree formula of each numerical point (2):

$$D_q = D_q\text{-}\sum_{q=1}^{p} eyp\left[-\frac{\|y_q\text{-}y_{um}\|^2}{(\gamma_b/2)^2}\right]. \tag{4}$$

After updating each aggregation level, select another cluster center and modify the aggregation level again. Repeat this to solve the maximum density index D_{max} of the current very small relative to the initial maximum density index, that is,

$$\frac{D_{max}}{D_{c1}} < \lambda. \tag{5}$$

The number of aggregation cores is the number of basic function cores.

3.4. PSO Algorithm Principle.

PSO calculation method was proposed by Eberhart and Kennedy in 1995. It is an evolutionary computing technology that simulates the flight and foraging behavior of birds and seeks the optimal solution through cooperation among individuals. Suppose the search space is n dimension. The number of particles is y, and the orientation of the ith particle in y-dimensional space is $y = (y_{q1}, y_{q2}, \cdots, y_{qh})$, and the speed is indicated as $v_q = (v_{q1}, v_{q2}, \cdots, v_{qh})$. All particles contain an adaptive value determined using update function to master the best position pbest and current position y_q it finds at present. Each particle masters the best position the entire population found successfully. Post of each particle is changed according to formulas (3) and (4) [29–31].

$$\begin{aligned} v_{qd}^{k+1} = w \times v_{qd}^k + \eta_1 \times \text{rand}\,() \times \left(p_{qd}\text{-}y_{qd}^k\right) \\ + \eta_2 \times \text{rand}\,() \times \left(p_{gd}\text{-}y_{qd}^k\right), \end{aligned} \tag{6}$$

$$y_{qd}^{k+1} = y_{qd}^k + v_{yd}^{k+1}, \tag{7}$$

where v_{qd}^k are d-dimensional flight components speed in the kth iteration ith particle; y_{qd}^k is the d-dimensional composite member ith in the particle orientation in the kth iteration; p_{gd} best position is the component of D group; p_{id} is the dth

FIGURE 1: Comparative analysis of RBF neural network algorithm and fund actual performance.

TABLE 1: Relative error value of average value of RBF neural network for fund performance prediction.

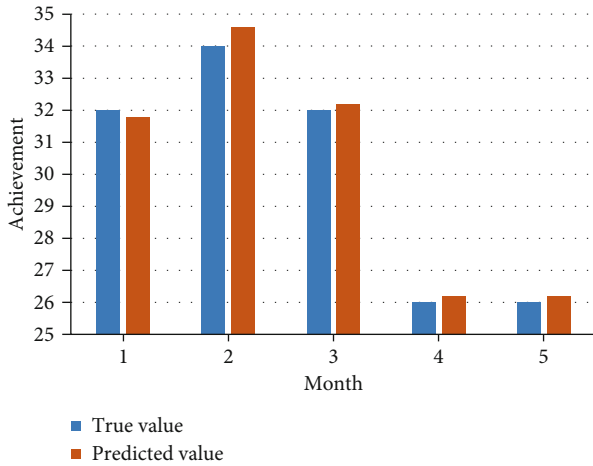| Frequency	1	2	3	4	5	Mean value
Average relative error of test	0.0921	0.0921	0.1069	0.0753	0.0780	0.0953

FIGURE 2: Comparison analysis of PSO-RBF neural network prediction and real fund performance results.

dimension best position member particle I; rand () is the random number of randomly generated [0,1]; η_1, η_2 is the specific gravity factor; S for weight. The solution of S is (5):

$$s = s_{\max} - \frac{s_{\max} - s_{\min}}{Num_{\max}} \times Num, \qquad (8)$$

where $s_{\max}$ and $s_{\min}$ are larger and smaller values of s; $Num_{\max}$ and Num are the maximum and current iterations, respectively.

3.5. Learning Algorithm of RBF Neural Network Based on PSO

(1) Encoding and function of PSO calculation method

In particle swarm optimization, particles correspond to dissolvable, so the particle value includes the core value and width of the basic function, particle speed, and sensitivity. If there are m centers, each m is K, then the particle's position is $m \times (T + 1)$ dimension, and the corresponding particle velocity should also be $m \times (T + 1)$ dimension. In addition, there is another fitness [32, 33]. The coding structure of particles is as follows:

$J_{11} J_{12} \cdots J_{1T} \sigma_1 \cdots J_{21} J_{22} \cdots$
$f(y)$
$V_1 V_2 \cdots V_m \times (T + 1)$
$J_{1T} \sigma_1 \cdots J_{m1} J_{m2} \cdots J_{mT} \sigma_m$

The goal of NN exercise is to find the parameters that make the mean square error the minimum, so the reciprocal of the error chosen becomes a fitness ability. Comfort ith individual is:

$$f_i = \frac{1}{R_i}, \qquad (9)$$

$$R_i = \frac{1}{N} \sum_{k=1}^{N} (y_k - y\wedge_k)^2. \qquad (10)$$

(2) Calculation method steps

Step 1. Collect exercise members.

Step 2. The kernel number of the basic function is determined by clustering the members with kernel subtraction.

Step 3. Initialize the number of particles swarm.

TABLE 2: Relative error value of average value of PSO-RBF neural network for fund performance prediction.

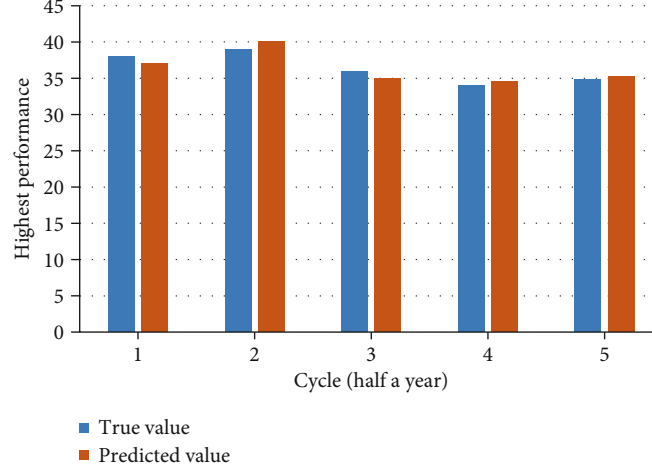| Frequency	1	2	3	4	5	Mean value
Average relative error of test	0.0162	0.0246	0.0248	0.0231	0.0176	0.0215

FIGURE 3: Comparison analysis of the real results of PSO-RBF neural network prediction and the highest fund performance.

TABLE 3: Relative error value of the average value predicted by PSO-RBF neural network for the highest value of fund performance.

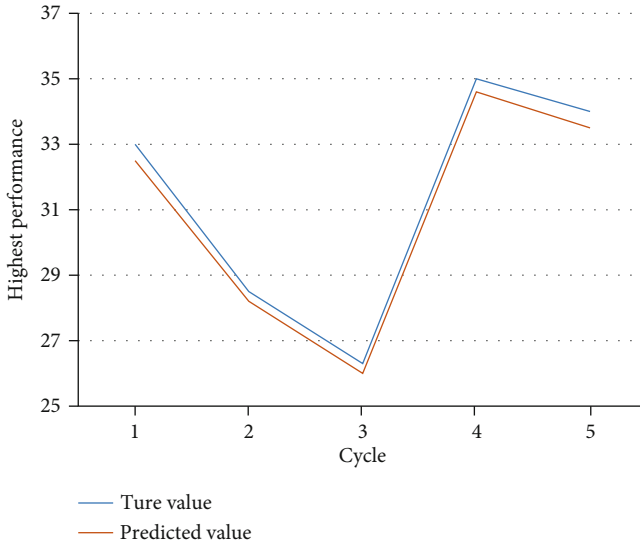| Frequency	1	2	3	4	5	Mean value
Average relative error of test	0.0158	0.0176	0.0169	0.0183	0.0265	0.0196

FIGURE 4: Comparison analysis of real results of PSO-RBF neural network prediction and minimum fund performance.

Step 4. For each particle, compare its fitness with that of the best position it experiences, and update p_{id} if it is better.

Step 5. Compare the comfort of each particle of the best position experienced by the population; if better, update p_{gd}.

Step 6. Adjust the speed and position of particles.

Step 7. Repeat steps 4 to 6 until the calculation requirements are met.

Step 8. Take the decoding value of the best position experienced by the packet as the structural the value of RBF NN, and then, learn.

Step 9. Stop the operation.

4. Experiment and Analysis

In order to further verify that the neural network based on PSO has a good ability fund income estimate, this experiment selects performance of a fund for 5 months as a case study. In this paper, RBF and PSO-RBF are used to predict the performance of a fund in five months, and PSO-RBF algorithm is used to predict the trend of the highest and lowest performance of the fund, so as to study the reliability and accuracy of this research method.

4.1. RBF Algorithm Prediction. The input value is a single vector, which is taking the closing performance of a fund as the input variable exercise radial basis function-based NN and then using the trained network to predict the next time's fund performance. The results are shown in Figure 1.

TABLE 4: Relative error value of average value predicted by PSO-RBF neural network for the lowest value of fund performance.

Frequency	1	2	3	4	5	Mean value
Average relative error of test	0.0169	0.0175	0.0163	0.0229	0.0187	0.0191

Through the analysis of Table 1, it can be concluded that the RBF neural network algorithm is feasible in theory, but there are some errors in the example analysis. The experiment according to evaluation error is 9.53% five times, and the highest and lowest values are 10.69% and 7.8%. The error is relatively large, which obviously does not meet the requirements in practical application and does not reach the accuracy required in this paper. Because there are such problems in the prediction only by RBF neural network, we need to improve and optimize the algorithm on this basis.

4.2. Prediction of Improved POS-RBF Algorithm. Figure 2 shows the optimization calculation method in PSO-RBF NN. According to the prediction data, we get the consistency between the prediction results and the real data storage trend. In addition, we can see from the relative error table of the average value of the performance forecast in Table 2 that in the five experiments, the error values of 1.62%, 2.46%, 2.48%, 2.31%, and 1.76% are, respectively, obtained, and the error average value is 2.15%. This result is very accurate compared with most of the current prediction methods, and it is a big research difficulty to reduce the error value within 3 percentage points. Especially for the above-mentioned RBF neural network single algorithm want to compare has made obvious progress, its accuracy is worthy of promotion and use.

4.3. Prediction of the Highest Value of Fund Performance by Improved POS-RBF Algorithm. Through the analysis of Figure 3, we have seen the comparison results of PSO-RBF NN and simple RBF NN algorithm for the prediction of the continuous performance of security funds. Obviously, the optimized and improved algorithm has greater advantages and greatly improves the accuracy. For the sake of further verifying program effect of PSO-RBF NN algorithm in fund performance, we take half a year as a cycle to predict the highest value of fund performance.

According to the data in Table 3, the optimization algorithm using PSO-RBF neural network can predict the trend of the highest value of fund performance, with small error with the actual results. The lowest relative error value of the five tests is 1.58%, and the average relative error is also kept within 2%. The error is small and can be widely used.

4.4. Prediction of the Highest Value of Fund Performance by Improved POS-RBF Algorithm. Different from the prediction of the highest value of fund performance, the change of the decline and the lowest value of fund is often more complicated, which also involves more influencing factors. To verify PSO-RBF NN in the most unfavorable environment of fund performance prediction, based on an example, we also predict the minimum performance of a fund in a half-year cycle for five cycles. Figure 4 is a comparative analysis of the predicted results and the actual performance. Through Table 4, we calculated the relative error value and the average value of the five tests, which are the same as the results of the above tests. The optimization algorithm using PSO-RBF also achieved good results in the prediction of the lowest value, and the average value was also controlled within 2%, which fully proves the feasibility and superiority of this research method in the prediction of fund performance.

5. Conclusions

The trend of security fund performance is generally restricted by many factors, such as politics, market environment, and business strategy. But in disorder, it can also find the hidden rules, and with the help of neural network, it can predict the sustainable trend of fund performance. For example, the RBF neural network introduced at the beginning of this paper is widely used in the financial field and has a good research method for the performance and sustainability of the fund. In this paper, after exploring the structure and workflow of the traditional algorithm, PSO is improved on its basis, and a new PSO algorithm based on RBF is obtained. In the specific study of PSO-RBF, we find that although the prediction solution of RBF is consistent with the actual numerical trend, there is a large error value, and the latest PSO-RBF algorithm can improve this point very well; no matter in accuracy and stability, there is a big breakthrough. In the prediction of the sustainable performance of security funds, the accuracy of the prediction results of the highest value and the lowest value is controlled within 2%. Generally speaking, the performance estimation PSO-RBF NN model in this paper is good, but the current research is still in its infancy. I believe that in the next in-depth research, this method will also improve its application value, which is worth popularizing security fund performance prediction model.

Data Availability

No data were used to support this study.

Conflicts of Interest

The author declares that there is no conflict of interest.

Acknowledgments

References

[1] S. G. Hanson, D. S. Scharfstein, and A. Sunderam, "An evaluation of money market fund reform proposals," *IMF Economic Review*, vol. 63, no. 4, pp. 984–1023, 2015.

[2] T. J. Walker, K. Lopatta, and T. Kaspereit, "Corporate sustainability in asset pricing models and mutual funds performance measurement," *Financial Markets & Portfolio Management*, vol. 28, no. 4, pp. 1–45, 2015.

[3] L. Novickyte, V. Rabikauskaite, and G. Pedroja, "Social security issues: II pillar pension funds' performance in Lithuania," *Journal of security & sustainability issues*, vol. 5, no. 3, pp. 329–354, 2016.

[4] K. Gregor, I. Danihelka, A. Graves, D. Rezende, and D. Wierstra, "Draw: a recurrent neural network for image generation," in *International Conference on Machine Learning*, pp. 1462–1471, Lile, France, 2015.

[5] W. He, Y. Chen, and Z. Yin, "Adaptive neural network control of an uncertain robot with full-state constraints," *IEEE Transactions on Cybernetics*, vol. 46, no. 3, pp. 620–629, 2016.

[6] A. Graves, G. Wayne, M. Reynolds et al., "Hybrid computing using a neural network with dynamic external memory," *Nature*, vol. 538, no. 7626, pp. 471–476, 2016.

[7] M. Buszko and D. Krupa, "Discussion about developing securitisation in Poland with participation of securitisation investment funds," *Ekonomia I Prawo*, vol. 15, no. 3, pp. 279–294, 2016.

[8] D. P. Stowell and S. Carlson, "A tale of two hedge funds: magnetar and peloton. An introduction to investment banks hedge funds & private equity," 2017.

[9] T. T. L. Chong, Y. Ding, and T. Pang, "Extreme risk value and dependence structure of the China securities index," *Economics Bulletin*, vol. 37, no. 1, pp. 520–529, 2017.

[10] Y. S. Huang, J. Yao, and Y. Zhu, "Thriving in a disrupted market: a study of Chinese hedge fund performance," *Pacific Basin Finance Journal*, vol. 48, pp. 210–223, 2018.

[11] J. A. Haslem, "Mutual fund portfolio manager structures: attributes, implications, and performance," *Journal of Wealth Management*, vol. 19, no. 4, pp. 115–127, 2017.

[12] K. Root, "The rising sun: Keiron Root meets David Mitchinson, a fund manager generating impressive returns from the Japanese market.(Fund Manager Profile)," *studia commercialia bratislavensia*, vol. 8,(no. 30, pp. 266–274, 2015.

[13] P. M. Watson, K. C. Gupta, and R. L. Mahajan, "Applications of knowledge-based artificial neural network modeling to microwave components," *International Journal of Rf & Microwave Computer Aided Engineering*, vol. 9, no. 3, pp. 254–260, 1999.

[14] E. Hodo, X. Bellekens, A. Hamilton et al., "Threat analysis of IoT networks using artificial neural network intrusion detection system," in *2016 International Symposium on Networks, Computers and Communications (ISNCC)*, pp. 1–6, Yasmine Hammamet, Tunisia, 2016.

[15] X. Chen, W. Shen, M. Dai, Z. Cao, J. Jin, and A. Kapoor, "Robust adaptive sliding-mode observer using RBF neural network for lithium-ion battery state of charge estimation in electric vehicles," *IEEE Transactions on Vehicular Technology*, vol. 65, no. 4, pp. 1936–1947, 2016.

[16] Z. Chen, J. Ding, H. Zhou, X. Cheng, and X. Zhu, "A model of very short-term photovoltaic power forecasting based on ground-based cloud images and RBF neural network," *Zhongguo Dianji Gongcheng Xuebao/Proceedings of the Chinese Society of Electrical Engineering*, vol. 35, no. 3, pp. 561–567, 2015.

[17] B. Wu, S. Han, J. Xiao, J. Fan, and X. Hu, "Error compensation based on BP neural network for airborne laser ranging," *Optik International Journal for Light & Electron Optics*, vol. 127, no. 8, pp. 4083–4088, 2016.

[18] H. Huang, Y. Lei, C. Xiong, and D. Yang, "An improved particle swarm optimization algorithm," *Basic sciences journal of textile universities*, vol. 11, no. 11, pp. 868–874, 2015.

[19] X. I. Maolong, W. U. Xiaojun, and W. Fang, "Quantum-behaved particle swarm optimization algorithm with self-renewal mechanism," *Computer engineering & applications*, vol. 2, no. 10, pp. 100–114, 2015.

[20] X. Lirong, L. Runxue, L. Qiyu, and G. Zhiqiang, "An adaptive multi-objective particle swarm optimization algorithm based on dynamic AHP and its application% adaptive multi-objective particle swarm optimization algorithm based on dynamic analytic hierarchy process and its application," *Control and Decision*, vol. 2, pp. 215–221, 2015.

[21] F. Wang, V. K. Devabhaktuni, C. Xi, and Q. J. Zhang, "Neural network structures and training algorithms for RF and microwave applications," *International Journal of Rf & Microwave Computer Aided Engineering*, vol. 9, no. 3, pp. 216–240, 2015.

[22] L. Wang, Y. Yang, R. Min, and S. Chakradhar, "Accelerating deep neural network training with inconsistent stochastic gradient descent," *Neural Networks the Official Journal of the International Neural Network Society*, vol. 93, pp. 219–229, 2017.

[23] G. Kang, J. Li, and D. Tao, "Shakeout: a new approach to regularized deep neural network training," *IEEE Transactions on Pattern Analysis & Machine Intelligence*, vol. 40, 2018.

[24] P. Zhang, X. Zhou, P. Pelliccione, and H. Leung, "RBF-MLMR: a multi-label metamorphic relation prediction approach using RBF neural network," *IEEE Access*, vol. 5, pp. 21791–21805, 2017.

[25] M. Rajendra and K. Shankar, "Damage identification of multi-member structure using improved neural networks," *International Journal of Manufacturing*, vol. 3, no. 3, pp. 57–75, 2015.

[26] R. Zhang, J. Tao, R. Lu, and Q. Jin, "Decoupled ARX and RBF neural network modeling using PCA and GA optimization for nonlinear distributed parameter systems," *IEEE Transactions on Neural Networks and Learning Systems*, vol. 29, no. 2, pp. 457–469, 2018.

[27] A. Alexandridis, E. Chondrodima, and H. Sarimveis, "Cooperative learning for radial basis function networks using particle swarm optimization," *Applied Soft Computing*, vol. 49, pp. 485–497, 2016.

[28] Y. Wang, N. Qin, and N. Zhao, "Delaunay graph and radial basis function for fast quality mesh deformation," *Journal of Computational Physics*, vol. 294, pp. 149–172, 2015.

[29] J. F. Chen, Q. Do, and H. N. Hsieh, "Training artificial neural networks by a hybrid PSO-CS algorithm," *Algorithms*, vol. 8, no. 2, pp. 292–308, 2015.

[30] N. B. Guedria, "Improved accelerated PSO algorithm for mechanical engineering optimization problems," *Applied Soft Computing*, vol. 53, no. 40, pp. 455–467, 2016.

[31] P. K. Das, H. S. Behera, S. Das, H. K. Tripathy, B. K. Panigrahi, and S. K. Pradhan, "A hybrid improved PSO-DV algorithm for multi-robot path planning in a clutter environment," *Neurocomputing*, vol. 207, pp. 735–753, 2016.

[32] Y. Hou, S. Huang, and X. Liang, "Ship hull optimization based on PSO training FRBF neural network," *Harbin Gongcheng Daxue Xuebao/journal of Harbin Engineering University*, vol. 38, no. 2, pp. 175–180, 2017.

[33] H. G. Han, W. Lu, Y. Hou, and J. F. Qiao, "An adaptive-PSO-based self-organizing RBF neural network," *IEEE Transactions on Neural Networks and Learning Systems*, vol. 29, no. 99, pp. 1–14, 2016.

WILEY | Hindawi

Research Article
Synesthetic Design of Digital Elderly Products Based on Big Data

Shan Li [ID]

College of Landscape Architecture and Art, Henan Agricultural University, Zhengzhou, 450002 Henan, China

Correspondence should be addressed to Shan Li; lishan@henau.edu.cn

With the development of digital information technology, digital products have been integrated into people's lives. The advent of the era of big data and the application of artificial intelligence have greatly accelerated this process. However, the increasingly high-end technology of these digital products brings more and more complex operations. The use and operation of these digital products have become a huge problem for the elderly who have a low level of acceptance of digital products or even a little out of touch. The purpose of this article is to study the influence of synesthetic design of digital senior products based on big data on the development of digital senior products. This article first understands the current problems in the development of digital elderly products and the design concepts and design processes of these digital elderly products through questionnaire surveys and market research. Then, this article analyzes the importance of synesthesia design for digital product design for the elderly through literature research and related product design cases. Then, this article combines the application of big data technology and complex intelligent system to carry out the synesthesia design of digital elderly products, the most important of which is to use the image recognition technology of complex intelligent system and intelligent voice interaction technology to achieve the synesthesia effect of these product designs. Finally, this paper uses the mathematical model of maximum utility and some statistical methods to analyze the effect of the product synesthesia design experiment in this research. Studies have shown that synesthesia design can maximize the utility of digital products for the elderly. This result is more than 95% confident in statistical analysis. Therefore, synesthesia design plays an important role in the popularization and development of digital elderly products in the elderly consumer groups.

1. Introduction

1.1. Background and Significance. Today's society is rapidly entering the stage of population aging. The food, clothing, housing, and transportation of the elderly have become a social issue that cannot be ignored. Digital products and services for the elderly have also entered a new stage of development. In the era of big data, digital products are popular among young consumers. With the application and development of big data and artificial intelligence, digital products have begun to take new steps towards the elderly. Different from the traditional digital products for the broad masses of young people, digital products for the elderly need to take into account the different sensory experiences of the elderly and the special psychological emotions of the elderly. The five senses of vision, hearing, touch, smell, and taste of the elderly are weakened with age and decline in body organ

functions. Therefore, the synesthesia design of digital products for the elderly has become an important factor in the development of digital products for the elderly.

The application of big data and complex intelligent systems can better realize the synesthesia design of digital elderly products. At present, the development of digital elderly products is encountering huge difficulties [1, 2]. The most important reason is that these digital elderly products are still difficult to use and operate for the elderly and cannot meet the real needs of the elderly. Studies have proposed that interactive, personalized, and emotional design of digital products for the elderly should be based on the physical and psychological characteristics of the elderly, and digital product design should be carried out from the perspective of emotional care for the elderly. This design concept and method fully consider the emotional appeal of the elderly and provide caring and warm services for the elderly [3, 4].

However, due to the complex and profound psychological emotions of the elderly, and lack of a large amount of data support, the accuracy of emotional analysis and grasping for the elderly is not high, so the application is not wide.

1.2. Related Research at Home and Abroad. For digital product design in the era of big data, a lot of research and discussions have been conducted at home and abroad, and considerable achievements have been made. Lin et al. conduct empirical research on the concept of sustainable development product design from the perspective of big data through experiments on designing digital products combined with big data and market sales surveys. Studies have shown that sustainable development is an important scientific and reasonable product design concept in today's era [5]. However, due to the single product of experimental design, it cannot represent all digital product design situations. Li et al. studied digital products and service models in the era of big data and optimized the design of some free digital product samples. Experiments have proved that consumers have a higher degree of acceptance for free digital products [6]. This is the psychological function of consumers, but consumers simply use them and do not trust these free products. Kong carried out digital media product design based on human-computer interaction technology, which is an important application of artificial intelligence in digital product design [7]. This research is of great significance for the realization of human-computer interaction. But for some special consumer groups such as young children and the elderly, there are limitations such as difficulty in truly realizing human-computer interaction. Su et al. proposed a model for automatically interpreting synthetic metaphors, which can learn the semantic knowledge of features and simulate cross-modal semantic similarity to achieve cross-type synesthetic connections between the same perceptual methods [8]. However, although this model can consider semantic knowledge and reflect cross-modal relationships, it cannot further classify and apply these cross-modal relationships.

In foreign countries, the research on big data and synesthesia has penetrated various fields. Hagtvedt and Brasel conducted three eye movement experimental studies on the comprehensive cross-modal correspondence between sound frequency and color brightness. Studies have shown that this comprehensive cross-modal correspondence between sound frequency and color brightness can automatically guide visual attention [9]. It is a pity that the research results have not been applied to product design. Nagaraj et al. introduce new digital and physical tools to identify internal and even team internal patterns of the design process. These digital tool products can evolve into multiple forms to meet the needs of different designs in the design process [10]. However, because these digital tool products are highly targeted, it is difficult to popularize the majority of user groups. Through experiments, Neckar and Bop found that word color associations are closely related to psychopathological symptoms such as anxiety, depression, mental retardation, and traumatic stress symptoms. Experiments have shown that this is caused by an abnormal experience in another unstimulated way caused by stimulation of one sensory or

cognitive pathway [11]. To put it simply, it is a neuropsychological disease caused by synesthesia, just like what people call "the wrong line of nerves." Lipscomb proposed the product synesthesia design based on the perception process, especially the cross-mode experience, and evolved from the discussion of cross-mode influence to a higher-level product design cognitive process [12]. The flaw in the digital product design for the elderly is less applications.

1.3. Related Work and Innovations in This Article. This paper proposes a synesthetic design concept for digital elderly products based on big data, using the parallelism of the five senses of the elderly to synesthesia design for digital elderly products [13, 14]. In the design process, this research uses the data mining technology in big data and the image recognition and intelligent voice interaction technology of complex intelligent systems to realize the synesthesia effect of the product and bring convenience to the elderly to use digital products [15, 16]. In the market analysis of synesthesia design for digital products for the elderly, this article also conducts market research and statistical analysis. Through the utility maximization model in product economics and mathematics, the utility of the synesthetic design of digital elderly products and the popularity of elderly consumers are analyzed. The synesthesia design of digital products for the elderly is to design the product functions in parallel through the synesthesia of some senses. For example, for old people with poor eyesight, they try to transform the visualization into the form of sound, and for the forgetful elderly, they are reminded to take medicine on time through the combination of auditory and visual sensory perception.

2. Research Method of Synesthetic Design of Digital Products for Elderly

2.1. Utility Maximization Model of Digital Product Design for Elderly. Whether it is a physical product or a virtual digital product, the concept and goal of its product design are inseparable from the realization of maximum utility. In the synesthesia design of digital elderly products, in order to maximize utility, it is necessary to understand the relationship between the quality and demand of digital elderly products. The so-called utility maximization is the process by which consumers meet part of their needs to the maximum extent through the purchased products under their existing conditions [17]. This is the basic means for the product to attract consumers to buy, and it is also the use value that the product must have. In the utility maximization model of digital elderly products, it is assumed that elderly consumers buy digital products at the selling price and the quantity purchased, respectively, as N and S. Before purchasing the product, the disposable income of the elderly is P; after purchasing the product, the remaining asset is D. According to the theory of utility maximization model, the income constraint conditions of elderly consumers can be obtained as shown in

$$D = pn + s. \tag{1}$$

According to the abovementioned constraints and the

knowledge of utility maximization, the utility function ω of the digital products purchased by the elderly consumers can be obtained, where f represents the use value of the digital elderly products:

$$\omega = \omega(f, n, s). \qquad (2)$$

Therefore, starting from the economic conditions of the elderly consumers and the use value of the digital products purchased, we can see that the utility maximization model of digital elderly products is shown in

$$\begin{cases} \max \omega(f, fn, s), \\ pn + s = D. \end{cases} \qquad (3)$$

In the synesthesia design process of digital products for the elderly, the above constraints need to be lifted according to the actual situation and the needs and interests of the elderly. That is, the income restriction conditions of the elderly are substituted into the utility function of digital products. According to Cobb Douglas's utility number theory, a reference coordinate system that is easy to analyze can be selected. The utility function of digital products can be written in the form of equation (4), where μ is the A4 reference coordinate system and λ, α, and β are all parameters greater than 0 in the reference coordinate system [18, 19]:

$$\begin{cases} \omega(f, n, s) = \omega(f, n, D - pn) = \mu f^{\alpha} n^{\beta} + \lambda(D - pn), \\ \mu > 0, \lambda > 0, 0 < \alpha < y, 0 < \beta < 1. \end{cases} \qquad (4)$$

After obtaining the utility function of digital elderly products, since the quality, product price, and product quantity of similar products on the market are single, elderly consumers can only purchase one of these products to obtain its use value. Therefore, in order to maximize the utility of digital products purchased by elderly consumers, the number of products must meet the first-order condition in

$$\frac{\partial \omega}{\partial n} = \mu \beta f^{\alpha} n^{\beta - 1} - \lambda p = 0. \qquad (5)$$

According to the first-order constraint conditions in (5),

the optimal purchase quantity n and the actual expenditure pn of digital products for the elderly consumers under the optimal purchase quantity can be obtained:

$$\begin{cases} n = \left(\dfrac{\mu\beta}{\lambda p}\right)^{1/1-\beta} f^{\alpha/1-\beta}, \\ pn = \left(\dfrac{\mu\beta}{\lambda}\right)^{1/1-\beta} f^{\alpha/1-\beta} p^{-\alpha/1-\beta}. \end{cases} \qquad (6)$$

Substituting formula (6) into formula (4), the utility function in the utility maximization model of digital elderly products can be obtained as shown in

$$\omega(f, n, D - pn) = \mu(1 - \beta)\left(\frac{\mu\beta}{\lambda}\right)^{1/1-\beta} f^{\alpha/1-\beta} n^{\alpha/1-\beta} + \lambda D. \quad (7)$$

When the disposable income D of the elderly consumers is constant, according to the utility function and the partial derivative of the multivariate function, formula (7) can be obtained:

$$-\frac{\partial \omega}{\partial n} = \mu \alpha \left(\frac{\mu\beta}{\lambda}\right)^{\beta/1-\beta} f^{\alpha+\beta-1/1-\beta} n^{\alpha/1-\beta}. \qquad (8)$$

Utility reflects the extent to which elderly people meet their needs and interests by consuming digital products or services. It most directly reflects the use value of the product. Therefore, the utility of consumers buying products is closely related to the use value of the products. The use value of a product is actually the ratio of product quality to price. According to the relationship between product use value and quality and price and the partial derivative knowledge of multivariate function, the constraints that need to be met to maximize utility can be obtained:

$$f = \frac{m}{n}, \frac{\partial f}{\partial m} = 1. \qquad (9)$$

According to the constraint condition of formula (9), the partial derivatives of the utility function ω of digital elderly products with respect to product quality m and sales quantity n are calculated to reflect the correlation between them:

$$\begin{cases} \dfrac{\partial \omega}{\partial m} = \dfrac{\partial \omega}{\partial f} * \dfrac{\partial f}{\partial m} = \mu\partial\left(\dfrac{\mu\beta}{\lambda}\right)^{\beta/1-\beta} f^{\alpha+\beta-1/1-\beta} n^{\alpha/1-\beta} > 0, \\ \dfrac{\partial \omega}{\partial n} = \dfrac{\partial \omega}{\partial f} * \dfrac{\partial f}{\partial n} + \dfrac{\partial \omega}{\partial n} = -\mu\left(\dfrac{\beta - 1}{\lambda}\right)^{\beta/1-\beta} * \left(\alpha f^{\alpha+\beta-1/1-\beta} n^{-1/1-\beta} + \beta f^{\alpha/1-\beta} n^{-\alpha/1-\beta}\right) < 0. \end{cases} \qquad (10)$$

It can be obtained $\partial \omega/\partial m > 0$, $\partial \omega/\partial n < 0$ through the calculation and verification of the above formula. Therefore, when the disposable income of elderly consumers is certain,

the utility function of elderly consumers is positively correlated with the quality of digital products they buy and negatively correlated with the price of digital products. In other

words, the improvement of the quality of digital products can promote the demand for digital products of the elderly. The main content of this article is to improve the quality of products through synesthesia design of digital products for senior citizens combined with big data.

2.2. Data Mining of Synesthetic Design of Digital Elderly Products. Because most of the elderly have a very vague understanding of digital products, such as the use of smart phones, when the elderly use digital products brought by electronic devices such as smart phones, they do not know how to obtain the products and services they need or are interested in through operations. The application of big data and artificial intelligence has brought new opportunities to solve this problem. In this paper, the Apriori algorithm of big data is used to realize the data mining of synesthetic design of digital elderly products, and based on this, the association interest degree model is established. The core idea of the Apriori algorithm is to filter the collected data iteratively according to Boolean association rules. It is a data mining algorithm based on recursive thinking. The specific workflow of the Apriori algorithm is to first scan the database and count the occurrence times of each data set or item in the database, generate a frequent itemset from these data sets, and then generate a candidate itemset through a Boolean operation. Then, repeat the above steps to generate a new frequent itemset and candidate itemset each time, and search until candidate itemsets cannot be generated [20, 21]. The Apriori algorithm generates a large number of frequent itemsets and candidate itemsets during data mining, and the generation of Boolean association rules for screening does not involve the participation of elderly consumers. Therefore, this method of digital product data mining not only consumes huge resources but also has low efficiency in data mining, making it more difficult to meet the real needs and hobbies of elderly users. The interest degree association model improves the way of generating Boolean association rules in the Apriori algorithm. The interest association rule is to use the Boolean association rules generated by existing data mining and use mathematical statistics to screen the association interest degree to obtain the value of the association interest degree. Its calculation formula is as follows:

$$\operatorname{corr}(x, y) = \frac{p(x, y)}{p(x)p(y)} = \frac{p(y \mid x)}{p(y)}. \tag{11}$$

The numerator and denominator in the above formula are the probability of the corresponding data set, where $p(y \mid x)$ represents the probability of data set y appearing in the case of data set x and $\operatorname{corr}(x, y)$ reflects the degree of correlation between data set x and data set y; the larger the value of corr (x, y), the closer the connection between the data sets, and the strong association rules of the interest degree $\operatorname{corr}(x, y) \leq 1$ that can be removed accordingly, which can better cater to the needs and interests of users.

2.3. Application of Image Recognition Technology in Synesthesia Design of Digital Products for Elderly. For the elderly, the biggest obstacle to the use of digital products is the understanding and operation of product functions. Even with

today's highly intelligent mobile phones, computers, and other digital product devices that have implemented graphical operation interfaces, it is still not possible for the elderly to quickly learn to operate and use them. Therefore, combined with complex intelligent system technology, this paper uses image recognition technology, especially face recognition technology, to facilitate the elderly to use digital elderly products. For example, with the design of a sticky note phone, the elderly only need to click on the corresponding face avatar to make a call when making a call, without having to enter a lengthy phone number.

In order to recognize images, especially human faces, to realize the synesthesia design of senses such as vision and hearing of elderly products, this paper adopts the commonly used Haar-like feature extraction method in face recognition and improves on this basis. This feature extraction method is to find out the three-dimensional position coordinates of similar gray-level distribution in the image based on the principle of gray-level similarity, so as to determine the data feature points of the selected image [22, 23]. But this method is more suitable for feature extraction of static pictures, and the running time and resources consumed in the process of selecting images are too much, so this article uses the method of an integral graph in mathematics to improve it. In the selected image, this paper uses T to represent the sample of feature learning, and the integral graph of similar gray distribution position (x, y) is as follows:

$$tt(x, y) = \sum_{x' \leq x, y' \leq y} t\left(x', y'\right), \tag{12}$$

where $tt(x, y)$ represents the sum of pixels in a similar gray-scale distribution area, and its specific calculation formula is shown in equation (13), where $l(x, y)$ represents the gray-scale sum of the similar gray-scale distribution position (x, y) on the ordinate:

$$tt(x, y) = tt(x - 1, y) + l(x, y). \tag{13}$$

Initialize the sum of gray levels $l(x, y)$ and the sum of pixels $tt(x, y)$ of the similar gray-level distribution area, respectively, and then perform feature extraction on the extracted image once to obtain the integral image of the similar gray-level distribution and then obtain the feature data information of the picture. The improvement of the integral map to the Haar-like feature extraction method reduces the computational complexity of feature extraction and effectively reduces the running time and resources consumed by the algorithm. The calculation formula of the gray sum is shown in

$$l(x, y) = \sum_{y' \leq y} t\left(x, y'\right) = l(x, y - 1) + t(x, y). \tag{14}$$

2.4. Application of Intelligent Voice Interaction Technology in Synesthesia Design of Digital Products for Elderly. In the past digital product design for the elderly, it is still difficult to popularize and promote electronic equipment products such as mobile phones and computers that are already very intelligent

for young people. Although the digital products and services brought by these devices have simple voice communication functions, such as voice assistants, the elderly still have greater difficulties in using them. For example, a mobile phone voice assistant is more like a one-way communication between a machine and the elderly for the elderly, and the language of the elderly is often not recognized correctly due to factors such as confusing accents and illegible words, thus providing the real needs of the elderly.

The intelligent voice interaction technology used in this paper is similar to the image recognition technology, which uses feature extraction to identify the real demands of the elderly [24, 25]. On this basis, this article further introduces the concept of synesthesia design and the application of complex intelligent systems, through the study of visual images and even the psychological and emotional research of the elderly and the synesthesia design combined with the voice assistant to solve the traditional voice assistant's difficulty in identifying the real demands of the elderly problem.

3. Experiment on Synesthetic Design of Digital Products for Elderly

3.1. Research Object. This research experiment is mainly aimed at the synesthetic design of digital elderly products. In this experiment, this article carried out digital products for the elderly such as mobile phones, radios, televisions, computers for the elderly, electronic notebooks, medication aids, electronic alarm clocks, and other digital products for the elderly in leisure and entertainment, communication, medical care, and daily assistance.

For example, in view of the difficulty of dialing on mobile phones of the elderly, synesthesia can be designed through the face and voice. The elderly only need to follow the avatar and voice prompts to make a call without entering a number. This study sets up a controlled experiment to investigate and analyze the market sales of digital products of universal design and digital products for the elderly through synesthesia design and the use of the elderly. This article uses a questionnaire survey to study the opinions of the elderly on these digital products. In this experiment, the elderly volunteers who volunteer to participate in the study are required to have the experience of purchasing digital products and also pay attention to the protection of the privacy of these elderly volunteers and the safety of the use of digital products. In this questionnaire survey, a total of 120 questionnaires were distributed, of which 100 were valid questionnaires, and the effective response rate of the questionnaire reached 83.3%. In order to exclude the influence of other factors, this controlled experiment requires that the basic functions of the designed digital elderly products be consistent. Except for the synesthesia design of the product, the quality of the product and other indicators are at the same level.

3.2. Experimental Design. After understanding the current problems in the design and development of digital elderly products and related research results through literature research and questionnaire surveys, this study conducted a synesthesia design experiment of digital elderly products

Table 1: Factors influencing the elderly not buying digital products.

Influencing factors	Number	Proportion	Average	IL
No entity	43	35.83%	36.43%	0.4437
Not safe	65	54.17%	53.55%	0.5438
Inconvenient operation	72	60.83%	61.22%	0.8375
Like to buy in store	37	30.83%	31.62%	0.3564
Others	19	15.83%	16.33%	0.2133

based on big data. This experiment is divided into four steps. First, collect information and ask the designers of digital elderly products about the design concepts and basic processes of these products. Then, select companies that voluntarily participate in the experiment and research in the design and production of digital elderly products, and set up a synesthesia design group and a control design group to design digital elderly products. Among them, the synesthesia design group adopts the latest big data and complex intelligent systems and other technologies for synesthesia design of digital products, while the control design group is based on general digital product design for all consumer groups. Then, this study takes six months' sales as a cycle to understand the impact of synesthesia design of digital products for the elderly on the market, and the relevant experimental personnel investigate and analyze the sales situation and market popularity of these products. Finally, through the utility maximization model and statistical knowledge, the market research situation is statistically analyzed.

3.3. Market Research Data Statistics. In this experiment, SPSS 22.0 is used for data analysis. For the experimental results, the LSD method and Dunnett's method are used for variance analysis. The accuracy and error of the test results are up to $\alpha = 0.05$. α can represent all significant levels between 0 and 1. In the data of the whole experimental group, excluding the influence of other factors, analyze the data under the change of single factor and compare with the average value, and then conduct an error test. For a group of experimental data, the number of data at a factor level to be studied is recorded as m, and the error is MS_E; then, the LSD test formula is as follows:

$$W = \sqrt{MS_E \left(\frac{1}{m_i} + \frac{1}{m_j} \right)}. \tag{15}$$

In the experiment, according to the different degrees of freedom of the variables, if you want to test the difference between the experimental combination of the group k and the control group, Dunnett's method is generally used for the test. It is a special form of the LSD method, and the formula is as follows:

$$\text{Dunnett} = \frac{\bar{X}_k - \bar{X}_0}{s_E^2}, s_E^2 = MS_e \left(\frac{1}{m_i} + \frac{1}{m_j} \right). \tag{16}$$

Among them, $\bar{X}_k$ represents the data mean of the experimental group in group k, $\bar{X}_0$ represents the mean of the experimental data of its control group, and MS_e represents the mean
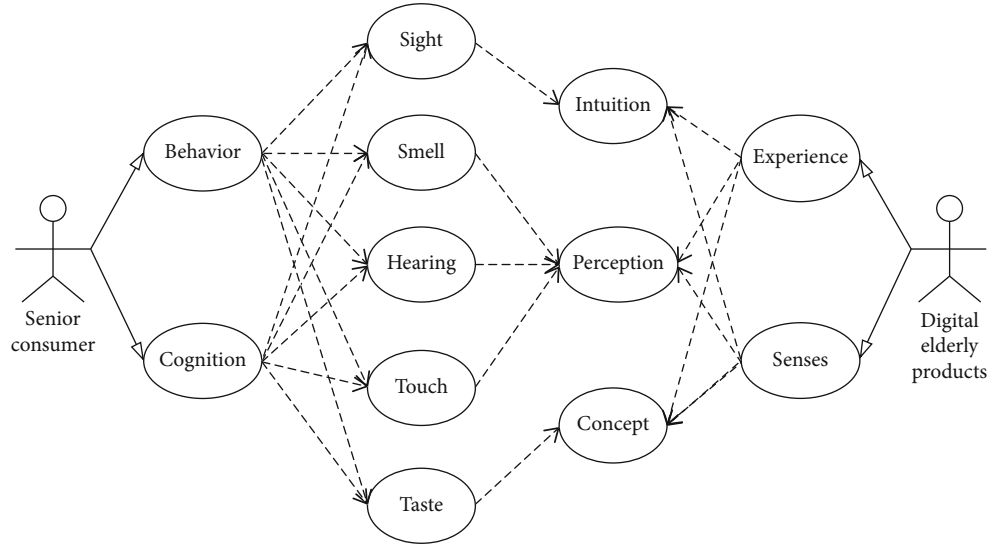
FIGURE 1: The interaction process between the five senses of the elderly and digital elderly products.

square error. This test method allows multiple comparisons of the mean differences between multiple experimental groups and a control group, used in this study to verify the conclusions drawn from the experimental results.

4. Discussion on Synesthetic Design Experiments of Digital Products for Elderly

4.1. The Reasons Why the Elderly Do Not Choose to Buy Digital Products. In order to understand the purchase of digital products by the elderly, this article uses a questionnaire to analyze some of their basic consumption and the reasons why they do not choose to buy digital products. The specific situation of this survey is shown in Table 1. In the survey of the reasons why 120 elderly consumers are unwilling to buy digital products, 72 elderly consumers indicated that they are unwilling to buy digital products because of difficulty in operation 60.83% of the survey group. This is mainly due to the fact that the operation of traditional digital products relies on a certain cognitive basis for digitization and the ability to read related texts. It can be seen that the synesthesia design of digital elderly products can effectively improve and solve this problem. In Table 1, IL represents the influence of no physical products, low safety, difficult operation, like to buy products in physical stores, and other reasons on the purchase mode and products of the elderly.

According to the survey in Table 1, this article studies and understands the specific process of how elderly users use digital elderly products to obtain the required service experience. As shown in Figure 1, the interaction process between digital products and the elderly is mainly realized through the perception of the five senses. The behaviors and cognition of the elderly are conveyed through sight, smell, hearing, touch, and taste and obtain digital products and services that they need or are interested in through various electronic devices. In the past, digital products are generally designed to provide digital products and services for elderly users

and therefore rely on the active perception and operation of elderly users.

4.2. The Influence of Digital Elderly Products under Different Designs on the Purchasing Desire of the Elderly. This paper studies the influence of synesthetic design and traditional universal design of digital products for the elderly on the purchase desire of the elderly through comparative experiments. Here, we mainly introduce the logo design and audio-visual function design of digital products. As shown in Figure 2, this article compares and analyzes the influence of synesthetic design on the purchase desire of the elderly from the color, form, three-dimensional texture of the logo of digital elderly products, and the use of audio-visual equipment, sound, and material. As can be seen from the figure, digital products for the elderly with synesthesia design are obviously more popular with the elderly. As shown in the figure, among the factors that affect the purchase desire of the elderly, the texture and operation of the product, which account for 95.6% and 92.5%, respectively, are the most important factors.

4.3. Sensual Weakening Disability Ratio of the Elderly and the Utility of Digital Elderly Products under Different Designs. In order to study the sales and development of digital products for the elderly, this article first investigates the types of products that elderly consumers mainly buy and the ways and designs of these products. As shown in Table 2, for food, clothing, electronic products, phone bills, water and electricity recharges, and other products, elderly consumers tend to go to physical stores to buy instead of buying digital products or obtaining digital services such as online shopping and recharging through digital products.

According to the survey in Table 2, this article further investigates the sensory weakness of elderly people of different ages and genders and the utility of using digital elderly products. As shown in Figure 3, with the increase of age, both elderly men and elderly women have different degrees of disability. This has created more and more serious obstacles to
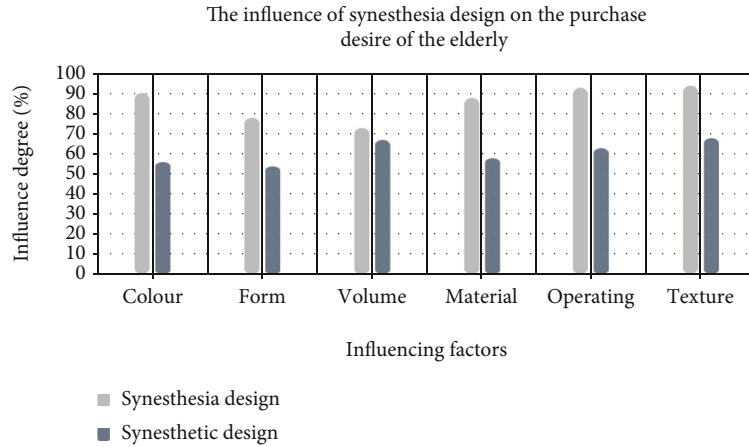
FIGURE 2: The influence of synesthesia design on the purchase desire of the elderly.

TABLE 2: Types of products purchased by seniors.

| Product type		Number	Proportion	Average	Utility
Foods	Digital product	8	6.67%	7.12%	33.6%
	Physical product	25	20.83%	22.65%	54.2%
Clothes	Digital product	11	9.17%	10.13%	25.4%
	Physical product	49	40.83%	41.25%	62.5%
Electronic product	Digital product	26	21.67%	20.87%	42.5%
	Physical product	35	29.17%	30.12%	68.7%
Recharge	Digital product	39	32.5%	31.26%	66.9%
	Physical product	33	27.5%	28.09%	56.6%
Others	Digital product	37	30.33%	29.97%	44.3%
	Physical product	22	18.33%	19.98%	37.6%
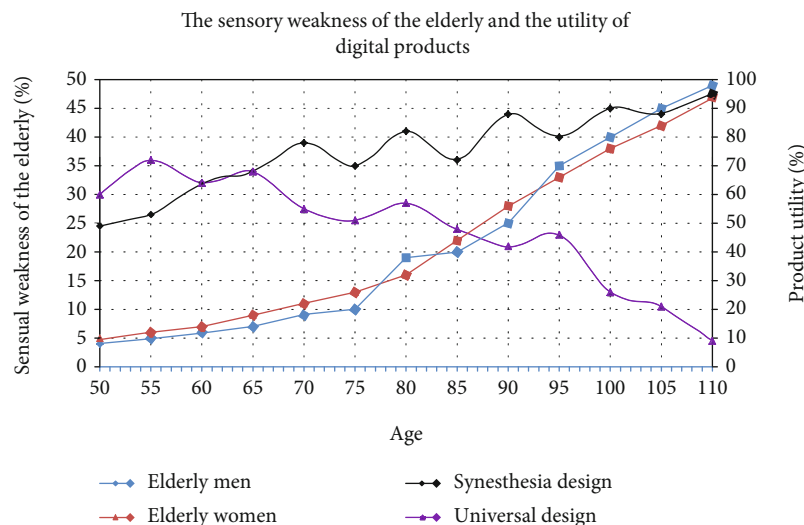
FIGURE 3: The sensory weakness of the elderly and the utility of digital products.

the use of digital elderly products and also restricted the development of digital elderly products. It can be seen from Figure 3 that before the age of 60, the utility of products designed by the middle-aged and the elderly for whether there is synesthesia design is between 25% and 35%. After

the age of 60, the utility of digital products for the elderly with synesthesia design is rapidly improving, reaching more than 95% for the centenarians, which is of great help to them. Under this circumstance, it can be seen that the utility of synesthesia-designed digital products for the elderly is
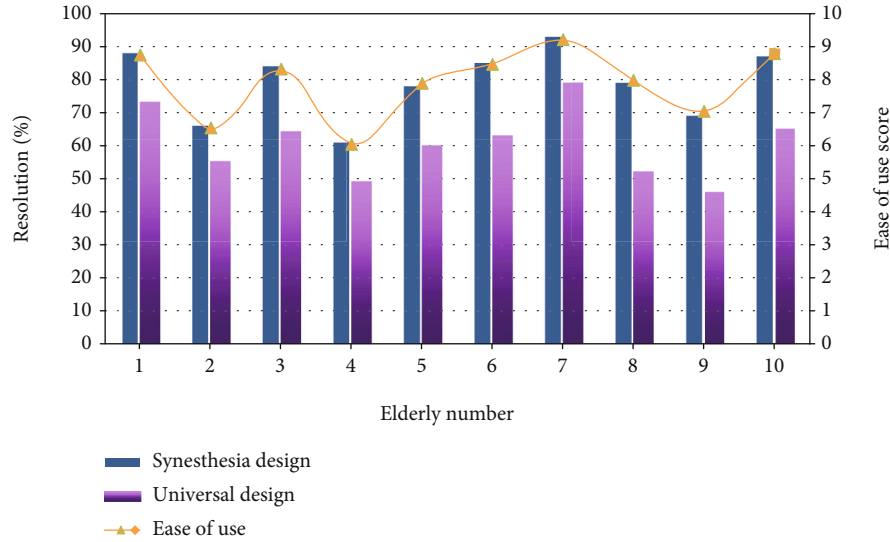
FIGURE 4: Senior citizens' recognition and ease of use of digital products under different designs.

continuously improving for the elderly with increasing age, while the utility of traditional digital products in these elderly people is rapidly decreasing with age.

4.4. The Recognition and Ease of Use of Digital Elderly Products under Different Designs by the Elderly. Regarding the convenience brought by the synesthetic design of digital products for the elderly, this article mainly analyzes the recognition of these products by the elderly, especially the sound and color. As shown in Figure 4, this article intercepted the survey results of 10 elderly people in the questionnaire for analysis. Among these 10 elderly users, their perception of digital products with synesthesia design is significantly higher than that of digital products without synesthesia design, and the ease of use of digital products with synesthesia design is also higher. It can be seen from Figure 4 that the digital products for the elderly after synesthesia design are obviously more popular with the elderly, and with the growth of age, synesthesia design plays an increasingly prominent role in the market of digital elderly products.

5. Conclusions

This paper investigates the current domestic digital product design and sales for the elderly, discovers some problems in the development of digital products for the elderly, and proposes the concept of applying big data and complex intelligent systems for synesthetic product design. For the sales of digital elderly products, this article adopts the method of quantitative model analysis to compare and analyze the sales data of digital elderly products in the past ten years. Find out the factors affecting the development of digital elderly products from the changes in the sales volume of digital elderly products and the questionnaire survey of elderly consumers. In the survey results, this article found the following problems in the development of digital elderly products. First, the elderly are deeply affected by the development of information technology, such as network fraud, and are more con-

cerned about the safety of digital products. Second, in the process of using these digital products, it is difficult for the elderly to learn how to use and operate these products. Third, in the past, digital products for the elderly were designed according to a certain aspect of the needs of the elderly, and it is difficult to popularize all elderly consumer groups. Fourth, there are still obstacles to the interaction between digital elderly products and elderly consumers. Even smart voice assistants and various image operation interfaces cannot truly realize the human-computer interaction between elderly consumers and digital products.

In response to the above problems, a research on synesthesia design of digital elderly products based on big data is proposed. Through synesthesia design, it can effectively solve the obstacles to the use of digital products and the inconvenience in daily life caused by the weakened senses of the elderly. For example, compared to the traditional string and semigraphical interface of DOS and Windows, the elderly computer stores the main functions in the module through the synesthetic design, so that the elderly originally need to go through visual and brain operations. Transformed into tactile operation, there are also automatic medicine boxes, etc., which can prompt the forgetful elderly to take medicine on time. This is the convenience brought by synesthesia design to the elderly consumer groups.

To sum up, the research on synesthesia design of digital elderly products based on big data has brought great convenience for the elderly to use digital products, which has far-reaching research significance and important market application value. Due to the lack of in-depth knowledge of product synesthesia design and the complicated application of artificial intelligence technology, this research still has major limitations. For example, in addition to the five senses of the elderly, the synesthetic design of digital elderly products can also take into account the emotional and psychological state of the elderly. However, because the psychology and emotion of the elderly are deep and complex, and there is no large amount of experimental data to prove, this article does not consider

the emotional care design of digital elderly products. I hope that the future can extend the "mind" synesthesia on the basis of this research on digital product design for senior citizens.

Data Availability

No data were used.

Conflicts of Interest

The author declares that they have no conflicts of interest.

References

[1] N. Rothen, K. Jünemann, A. D. Mealor, V. Burckhardt, and J. Ward, "The sensitivity and specificity of a diagnostic test of sequence-space synesthesia," *Behavior Research Methods*, vol. 48, no. 4, pp. 1476–1481, 2016.

[2] L. Fang, "Application of digital simulation technology in agricultural products park architecture design," *Advance Journal of Food ence & Technology*, vol. 10, no. 2, pp. 115–118, 2016.

[3] A. Sengupta, "Design flow of a digital ic: the role of digital ic/soc design in ce products," *IEEE Consumer Electronics Magazine*, vol. 5, no. 2, pp. 58–62, 2016.

[4] V. Salehi, "Development of an agile concept for MBSE for future digital products through the entire life cycle management called Munich agile MBSE concept (MAGIC)," *Computer-Aided Design and Applications*, vol. 17, no. 1, pp. 147–166, 2019.

[5] L. Feng, B. Sun, K. Wang, and S.-B. Tsai, "An empirical study on the design of digital content products from a big data perspective," *Sustainability*, vol. 10, no. 9, pp. 3092–3098, 2018.

[6] H. Li, S. Jain, and P. K. Kannan, "Optimal design of free samples for digital products and services," *Journal of Marketing Research*, vol. 56, no. 3, pp. 419–438, 2019.

[7] W. Kong, "Digital media art design based on human-computer interaction technology in the background of big data," *Revista de la Facultad de Ingenieria*, vol. 32, no. 14, pp. 485–489, 2017.

[8] C. Su, X. Wang, Z. Wang, and Y. Chen, "A model of synesthetic metaphor interpretation based on cross-modality similarity," *Computer Speech & Language*, vol. 58, no. 11, pp. 1–16, 2019.

[9] H. Hagtvedt and S. A. Brasel, "Crossmodal communication: sound frequency influences consumer responses to color lightness," *Journal of Marketing Research*, vol. 53, no. 4, pp. 551–562, 2016.

[10] V. Nagaraj, N. Berente, J. Gaskin, and K. Lyytinen, "How does design thinking impact the market success of digital products?," *Academy of Management Annual Meeting Proceedings*, vol. 2018, no. 1, pp. 15737–15742, 2018.

[11] M. Neckar and P. Bob, "Synesthetic associations and psychopathological symptoms: preliminary evidence in young women," *Activitas Nervosa Superior*, vol. 58, no. 3-4, pp. 78–83, 2016.

[12] S. D. Lipscomb, "Review of synesthetic design: handbook for a multisensory approach," *Psychomusicology*, vol. 26, no. 2, pp. 196–198, 2016.

[13] N. Zhang, J. Jiao, H. Liu, and Z. Yao, "Research on complex products based on digital layout design and simulation modeling," *International Journal of Security & Its Applications*, vol. 10, no. 8, pp. 303–314, 2016.

[14] C. P. Alonso, "Tectonics of perception," *Journal of Architectural Education*, vol. 73, no. 1, pp. 128–135, 2019.

[15] K. Uno, M. Asano, H. Kadowaki, and K. Yokosawa, "Grapheme-color associations can transfer to novel graphemes when synesthetic colors function as grapheme "discriminating markers"," *Psychonomic Bulletin & Review*, vol. 27, no. 4, pp. 700–706, 2020.

[16] M. Ross, "Virtual reality's new synesthetic possibilities," *Television & new media*, vol. 21, no. 3, pp. 297–314, 2020.

[17] D. Dyck, "Writing wisdom: George Herberts synesthetic poetics," *Christianity & Literature*, vol. 66, no. 1, pp. 39–56, 2016.

[18] M. A. Zawisawska, "Synamet - a microcorpus of synesthetic metaphors. Preliminary premises of the description of metaphor in discourse," *Cognitive Studies|tudes cognitives*, vol. 2016, no. 16, pp. 107–118, 2016.

[19] B. Brogaard, K. Marlow, and K. Rice, "Do synesthetic colors grab attention in visual search?," *Review of Philosophy & Psychology*, vol. 7, no. 4, pp. 701–714, 2016.

[20] D. Hamada, H. Yamamoto, and J. Saiki, "Database of synesthetic color associations for Japanese kanji," *Behavior Research Methods*, vol. 49, no. 1, pp. 1–16, 2016.

[21] A. B. J. Mcerlean and M. J. Banissy, "Color processing in synesthesia: what synesthesia can and cannot tell us about mechanisms of color processing," *Topics in Cognitive Science*, vol. 9, no. 1, pp. 215–227, 2016.

[22] I. Zykova, "Synesthesia in the process of phraseologismformation: a new approach," *Yearbook of Phraseology*, vol. 9, no. 1, pp. 85–110, 2018.

[23] M. Miozzo and B. Laeng, "Why Saturday could be both green and red in synesthesia," *Cognitive Processing*, vol. 17, no. 4, pp. 337–355, 2016.

[24] M. Bae and S. Kim, "Implementation of muscular sense into both color and sound conversion system based on wearable device," *Journal of Korea Multimedia Society*, vol. 19, no. 3, pp. 642–649, 2016.

[25] K. R. Bankieris and R. N. Aslin, "Implicit associative learning in synesthetes and nonsynesthetes," *Psychonomic Bulletin & Review*, vol. 24, no. 3, pp. 935–943, 2017.

WILEY | Hindawi

Research Article

System Dynamic Simulation of Online Customers for Cruise Travel: Based on the Customer Life Cycle Perspective

Hou Jian and Jiang Yuantao [ID]

School of Economics and Management, Shanghai Maritime University, Shanghai 201306, China

Correspondence should be addressed to Jiang Yuantao; ytjiang@shmtu.edu.cn

Cruise tourism is an emerging tourism industry. Under the current online consumer market, expanding the number of online customers is an important consideration for the sound development of cruise tourism, starting from the reality of cruise travel, integrating life cycle theory, demand theory, and network consumption behavior theory, defining the evolution model of customer life cycle, using system dynamics for simulation analysis to discover the dynamic changes in the number of cruise travel online customers in different life periods. The analysis of the simulation results found that at different stages of the life cycle evolution of cruise travel network customers, travel demand is comprehensively affected by various factors such as basic needs, novelty, offline experience, Internet word-of-mouth, and information quality. The number of potential customers first accelerates and then declines. The trend is flat, the number of waiting customers is normally distributed over time, and the number of existing customers and lost customers tends to stabilize after an accelerated increase. The simulation results with word-of-mouth factor as the test function show that the model has good robustness and sensitivity. The number of waiting customers is sensitive to changes in word-of-mouth impact factors, and the number of existing customers has not increased significantly. Finally, summarize the development strategies of cruise tourism from the perspective of life cycle: increase the promotion of cruise tourism network and expand the range of potential customers, highlight the characteristic orientation of cruise tourism differentiation, induce waiting for customers to pay online, improve the quality of cruise tourism experience and maintain existing customer loyalty, and optimize the quality of travel information on the online platform to attract lost customers to turn back.

1. Introduction

Cruise ships in foreign countries can be traced back to the beginning of the 19th century and have a history of more than a hundred years, but they are new things in China and belong to the field of emerging industries [1]. Previous studies believe that the market for innovative products is mainly driven by supply and demand, and the latter is obviously a more effective way of emerging industries to diffuse in the face of consumer demand [2]. As a capital and technology-intensive innovative product, cruise ships have a large initial purchase investment and high subsequent operation and maintenance costs. The sustainable development of cruise tourism is full of high risks. Only after a period of rapid development with a certain scale of customer groups and the formation of scale effects in the cruise tourism market can the uncertainty of the future development of cruise tourism be effectively reduced. Consumers face the new form of cruise tourism, from understanding to acceptance, familiarity, and then exit, presenting a phased life cycle evolution process. Customers in different life cycle stages have different levels of understanding of cruise ships and different travel

experiences, which will generate different travel needs accordingly. At different stages of the life cycle, it provides customers with cruise travel services corresponding to their needs, that is, on the basis of meeting the basic travel needs of first-time customers, and then providing higher-level travel services, can we attract as many loyal customers as possible to participate in cruise travel.

An international market survey of cruise travel shows that customers participating in cruise travel are satisfied with the overall product as high as 98%. Among them, the satisfaction of travel intermediary channels is 89%. Cruise travel has the highest satisfaction among all types of tourism projects. Both the customer satisfaction rate and the revisit rate get the highest scores [3]. Cruise travel has such a high satisfaction rate and return rate, which has a lot to do with the cruise ship's ability to provide different levels of travel services. Cruise travel has such factors as leisure atmosphere, exotic destinations, entertainment and food on board, status symbols, and cruise appearance. It can meet the travel needs of customers at different levels.

Emerging industries cater to the trend of individualization and diversification of consumer demand and become the inevitable choice for major countries in the world to cultivate new kinetic energy for economic growth [4]. Under the macrobackground of China's "Strategy for a Powerful Maritime Power" and the "Maritime Silk Road Strategy" of the 21st century, the cruise tourism industry has shown rapid development. The number of tourists has shown exponential growth for many years, which has become a driving force for China's economic development and tourism industry expansion. By 2016, after a decade or so of rapid development, the number of Chinese cruise travel customers surpassed Germany to rank second in the world. However, compared with the national population base, the market penetration rate has not exceeded 0.2%, which is much lower than the global average of 3.03%. The Chinese cruise tourism market still has huge potential and room for growth. How to make full use of various cruise tourism promotion channels, provide cruise tourism products that meet customer needs, and continue to cultivate loyal customers is the direction of future efforts. The current cruise travel market promotion includes traditional channels and online channels. According to relevant statistics, the current penetration rate of cruise travel Internet channels is close to 60%. It will continue to grow in the future [5]. Therefore, in the process of expanding the scale of the cruise travel market through online channels, relevant companies must consider the changes in the needs of online customers in different life cycles and take reasonable countermeasures according to the stages of the evolution of the life cycle of online customers [6, 7]. This article selects online customers as the research object, uses demand theory and life cycle theory, combines the differences between online consumption and traditional consumption, and constructs demand-led system dynamics for the life cycle evolution process of cruise travel online customers from initial stage to maturity to exit Model, and perform simulation analysis to evaluate the demand and quantity change characteristics of online customers in the life cycle evolution process, so as to provide enlightenment for the maintenance of cruise travel online customers.

2. Literature Review

2.1. Current Status of Cruise Tourism. In the beginning, cruise ships were mainly high-end social venues involving the social elites and the wealthy. They met both leisure and social needs. After more than 40 years of rapid development, the customer structure of the cruise industry has undergone significant changes, and it has become a tourism project widely participated by the general public for the purpose of satisfying leisure. It is one of the fastest growing and most effective tourism projects in the modern tourism industry [8]. Cruise tourism is positioned as a new tourism industry in China, and national and regional incentive policies for cruise tourism and cruise construction have been introduced one after another. The number of cruise travel trips has continued to grow rapidly. From a total of 100,000 trips in 2006, the number of trips increased rapidly to more than 2 million in 2016, an annual increase of about 70%. Since 2015, the State Council has issued a number of policy documents on promoting the development of cruise tourism, encouraging companies to develop and build cruise ships, and granting 15-day visa exemption to international passengers entering the country via cruise ships. In 2017, six departments including the Ministry of Transport and the National Tourism Administration jointly issued the "Several Opinions on Promoting the Integrated Development of Transportation and Tourism," proposing to promote the construction of cruise ports and increase cruise travel routes. China has continuously introduced cruise tourism development policies, strengthened support for the cruise industry, and provided guidance from ports, infrastructure, and visa concessions for inbound tourists [9]. China cruise tourism ushered in a policy dividend period.

Faced with the rapid development of cruise tourism, cities such as Shanghai, Xiamen, and Shenzhen regard cruise tourism as a key emerging industry and take cruise homeports as their urban development positioning. The mainland city of Wuhan plans to build a homeport for inland cruises based mainly on the Yangtze River mainline tourism. However, as a new form of tourism, there are still many problems in China cruise tourism [10]. First of all, as an emerging industry, the number of cruise travel customers, the participation structure of business entities, and the degree of competition are all undergoing dynamic changes. There are risks such as technological uncertainty, strategic uncertainty, and rapid cost changes from high to low. The characteristic is that only by closely tracking the changes in customer demand and quantity and ensuring that the number of cruise travel customers maintain a certain scale can various risks be effectively reduced [11]. Secondly, the current Chinese cruise travel is completely occupied by international cruise companies, and local cruise companies are still in the embryonic stage. They need to accumulate experience in cooperative agency, ticket sales, ship management, and customer management, especially around the dynamic changes in customer demand. Travel customer discovery, cultivation, and value mining are all facing knowledge gaps. Finally, China's cruise tourism promotion and sales model is dominated by "chartered ships," which is different from the "one-to-one" service

model of European and American cruise markets that meets individual needs. The charter model with Chinese characteristics shows price competition and low-end services. Problems such as unclear rights and responsibilities have seriously damaged the brands of charter parties and cruise companies. Customers cannot experience the "high-end image" of cruise travel, which has a negative impact on the growth of cruise travel customers. Under the influence of various unfavorable factors, for a certain period of time in the future, the number of international cruise ships and the number of cruise tourists will experience negative growth, and in the long term, it will show a slow growth trend [12, 13].

2.2. Demand Theory in the Life Cycle. The life cycle theory was first proposed by Hill and Hansen at the end of the 1930s. Taking the life cycle of life as a reference, the evolution process of things is divided into different stages such as birth, growth, maturity, and decline. Later scholars combined with specific objects to propose customer life cycles, product life cycles, and enterprise and industrial life cycles [14]. The customer life cycle is based on the business relationship established by the enterprise and the customer and is divided into four evolutionary periods according to the characteristics of the business relationship in different periods: relationship establishment period, relationship growth period, relationship maturity period, and relationship degradation period. During the development of the customer life cycle, customer needs and customer value will also change dynamically due to changes in business relationships. In the process of continuous transformation from the customer's first purchase to short-term customers to loyal customers, customers' judgment criteria for products and services are becoming more and more objective and rational. Customer needs develop from curiosity and cost to a solid relationship of dependence, and customer value will also occur from appearance, peak to disappearance [15]. When companies implement important decisions such as strategic planning, major policies, and performance appraisal, if they only use traditional customer value evaluation indicators such as market size and maintenance costs and ignore the dynamic value of customers based on life cycle and demand changes, then the company's operations countermeasures will have a short-term tendency, thus deviating from the company's long-term value maximization goal.

The hierarchy of needs theory believes that all human behaviors are to meet certain needs, and after satisfying the lowest-level needs, human behaviors will begin to shift to higher-level needs. Therefore, in the dynamic evolution process of the customer life cycle, demand plays an important guiding role. After the first stage needs are met, more advanced needs will guide consumers into the next stage of the life cycle. In the mature period, customer needs are relatively stable and can bring the greatest value to the enterprise, but every stage of the customer's life cycle is indispensable. With the dynamic evolution of the customer's life cycle, with changes in customer demand as the core, the relationship between the enterprise and the customer follows a certain evolutionary law under the comprehensive influence of various factors, and the form of external development manifests

as the development from one state to another [16]. The relationship establishment period is the first stage of the evolution of the customer's life cycle. Customers and companies begin to tentatively contact each other and do not know each other well. Driven by the customer's curiosity for products or services, they have a desire to buy and become potential customers, and they begin to collect information and data, comparing and selecting the products or services of enterprises. The relationship growth period is the second stage of the life cycle. The relationship between the company and the customer develops rapidly. After the first stage of comparison, the customer makes a decision whether to purchase, thereby realizing customer value. For customers in the growth period, companies should continue to increase marketing investment and guide customers to make purchase decisions through price factors and brand factors. The maturity period marks the development of the relationship between the customer and the enterprise to the highest level. Customers have continuous consumer demand for the products or services provided by the enterprise and show a certain degree of loyalty.

2.3. The Theory of Customer Consumption Behavior under the Network Environment. The round-the-clock convenience and easy accessibility of online channels make it a trend for consumers to inquire, compare, and select cruise tours and complete online bookings through website platforms. Compared with traditional channels, the characteristics and influencing factors of Internet channels have both commonalities and differences. The commonality is that the customer needs of the two channels have an experienced process from unfamiliar to familiar to emerging products and, then, to exit, showing the characteristics of the phased evolution of the life cycle; the difference is that customer needs in online channel to purchase products through online platforms are not only affected by website popularity and word-of-mouth but also by user reviews and cost-effectiveness. Traditional marketing theory believes that customer consumption behavior is mainly divided into goal-oriented and shopping experience. Goal-oriented is task-driven, characterized by focusing on efficiency, rationality, and caution. Consumers hope to buy what they want as soon as possible and do not care about the amusement and pleasure of the purchase process. The shopping experience type is just the opposite. Customers focus on the various experiences of the purchase process, such as surprise, participation, and the meaning of the product. Therefore, buyers often make purchase decisions based on intuition rather than rational and rational consumption behavior.

Online consumption behavior can also be divided into goal-oriented and shopping experience. Compared with traditional customers, goal-oriented online customers spend more time thinking and do not make purchase decisions as quickly as traditional customers; experiential online customers visit websites with different characteristics according to their hobbies, like to interact with people who have common hobbies through social media, and actively participate in online shopping evaluation [17]. In China's online consumer market, young and middle-aged rational consumers

occupy an absolute proportion. Online customers have a process of thinking about online product search. Since there is no face-to-face communication, online consumers have enough time to compare product performance, price, and quality. Therefore, whether it is a target customer or an experiential customer, in the online environment, the rational motive occupies a larger proportion. Related studies have found that compared with traditional consumption models, online customers have a very high churn rate. If they can reduce the exit rate of online customers and extend their life cycle, it will significantly increase corporate profits [18]. Previous models for predicting customer purchasing behavior include probabilistic model groups based on past transaction behaviors and optimization models based on data mining and structural risk minimization [19].

3. Construction of Online Customer Life Cycle Evolution Model

Previous studies have suggested that China's cruise tourism has entered a period of slow development after rapid development, but there is a lack of systematic research on solutions, and there are relatively few studies that predict the development of cruise tourism from the combination of life cycle, demand theory, and network customer characteristics. It provides space for this research. System Dynamics (System Dynamics abbreviated as SD) is a method system for studying the dynamic behavior of information feedback systems, which is based on feedback control theory and computer simulation technology [20]. According to the stage division of the customer life cycle theory, combined with the needs of cruise travel online customers and consumption behavior characteristics, the cruise travel online customer life cycle is divided into four periods: potential customers, waiting for customers, existing customers, and lost customers, constructing the evolution model of the online customer life cycle and conducting system dynamics simulation analysis.

There is a big difference between the online customers of cruise travel and traditional customers. The former has the inherent advantages of obtaining information and can easily obtain abundant travel information. Its purchase decision is a process of repeated comparison. Each stage has a long-time span, and there is sufficient time to consider the pros and cons of each tourism format. The first is the evolution process from potential customers to waiting customers. Affected by the gradual improvement of living standards, people with a certain stable income, who like leisure travel and have the ability to purchase online become potential customers of cruise travel, whether they decide to buy and become waiting customers, are affected by the comprehensive influence of service reputation, service value, competitors, product performance, and the number of existing customers, as well as the word-of-mouth communication of experienced customers. Although the life cycle evolution of the first stage is comprehensively affected by various factors, potential customers are choosing cruise travel for the first time. Whether they decide to purchase becomes a waiting customer is mainly affected by basic travel needs. Therefore, once a certain factor reaches a degree of satisfaction, they will take the

next step. The evolution of waiting customers to existing customers is the most critical transformation process in the life cycle. Waiting for customers to make a payment decision after deciding whether to approve cruise travel after deciding whether to purchase on the cruise travel network is mainly to see whether they compare different travel products. The more travel products you are prepared to pay for, the more unique the cruise travel can be found. Finally, there is the evolution process from existing customers to lost customers. This is not only affected by the offline experience of cruise travel but also by the branding and information quality improvement brought by the investment of cruise travel websites. This stage is about whether customers can maintain their loyalty. On the basis of satisfying basic travel needs, they need to provide customers with higher-level and more complex needs, including social needs, respectful needs, and quality needs. Since online customers rely more on website information, the return of lost customers is closely related to website satisfaction. During the evolution of the cruise travel online customer life cycle stages, from potential customers to the evolution of existing customers, companies can only evolve to the next stage after satisfying the specific needs of customers. If the needs at this stage are not met, the evolution of the customer life cycle will end. Therefore, cruise companies need to take distinctive service measures for customers in different life cycle stages and constantly promote potential customers to develop into waiting customers and, then, develop into existing customers, in order to form a certain scale of cruise travel customer groups.

The system dynamics simulation model is established based on the causality analysis. The main variables include state variables, rate variables, auxiliary variables, and constants. State variables include potential customers, waiting customers, existing customers, lost customers, revenue, and products in use; the rate variable is a quantity of differential nature, indicating how fast the accumulation effect changes, including purchase rate, completion rate, churn rate, and order rate. Auxiliary variables are diversified in form and are the amount of information in the system dynamic model. In this model, it is the most variable; constants are important parameters that determine the system structure [21]. The system dynamics model of the evolution process is shown in Figure 1. The settings and key variable values are in Table 1.

4. Results and Countermeasures

4.1. Potential Customers and Wait Customers. The system dynamics software, Vensim PLE, is used to construct a simulation model. The data used comes from cruise travel customer data on a travel network platform, and other data comes from empirical data or industry standards [22]. Since it mainly analyzes the evolution of the life cycle of online customers, it selects landmark variables such as potential customers, waiting customers, existing customers, and lost customers and analyzes the simulation results of their number changes. In the initial stage of the simulation, all consumers who are interested in traveling are considered potential customers, so it is assumed that the number of
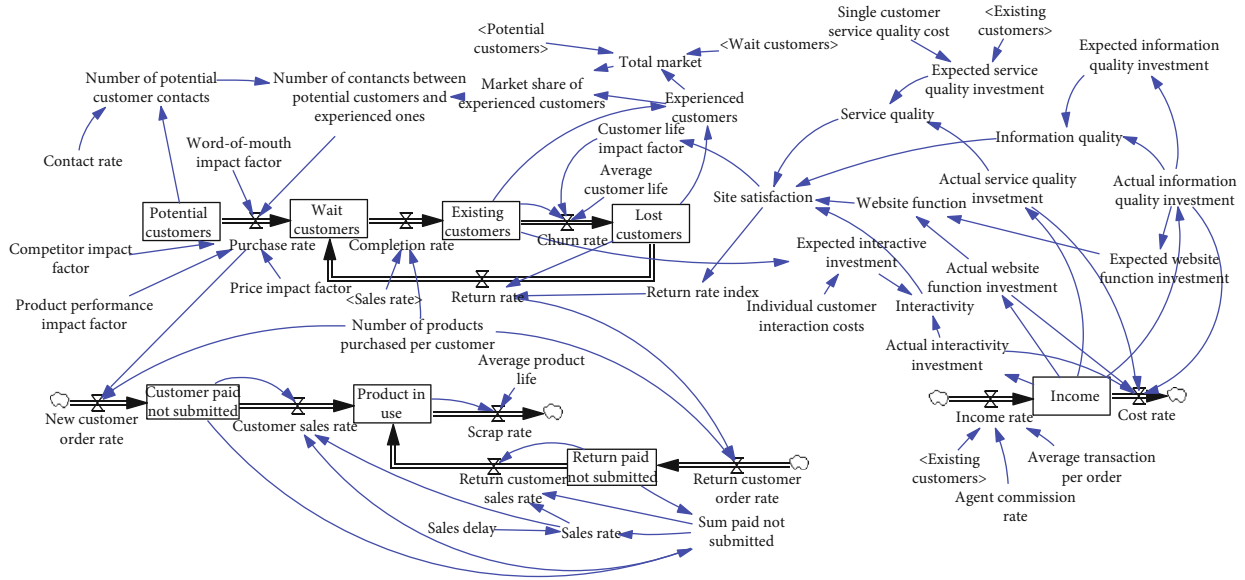
FIGURE 1: System dynamics model of cruise travel online customers.

TABLE 1: Settings and key variable values.

Settings and variables	Value	Settings and variables	Value
Initial time	0	Price impact factor	0.6
Final time	200	Sales delay	1
Time step	0.25	Single customer service quality cost	0.9
Contact rate	50	Individual customer interaction costs	1.5
Competitor impact factor	0.5	Agent commission rate	0.2

potential customers in the initial stage is the maximum. With the evolution and development of the customer life cycle, changes in the number of different types of customers show unique characteristics. As potential customers of cruise travel turn to waiting customers and then to existing customers, the number of potential customers has always been in a downward trend, experiencing an accelerated decline to a gentle process, and the evolutionary trajectory presents a steep exponential decline, as shown in Figure 2.

The evolutionary dynamics of waiting customers are more complicated. It can be seen from Figure 3 that waiting customers are characterized by smooth growth before the first wave peak. After reaching the maximum value, they will show a wave-like decline and will stabilize after an accelerated decline. The direct influencing factors of waiting for customers include purchase rate, return rate, completion rate, the number of products purchased per customer, and the total number of unpaid orders, among which the purchase rate, return rate, and the number of products purchased per customer increase the number of waiting customers, while the completion rate led to a reduction in waiting customers. The direct reason for the change in the waiting customer curve is caused by the difference between the purchase rate and return rate and the completion rate. If the difference is positive, the number of waiting customers increases, and the curve shows an upward trend; if the difference is negative, the number of waiting customers decreases, and the curve

shows a downward trend, resulting in complex changes in the waiting customer curve.

4.2. Existing Customers and Lost Customers. Existing customers are important customers of cruise travel, and the relationship between customers and the company is in the best condition. The goal of cruise travel companies is to maintain a certain number of scale stability through the rapid increase of existing customers. Figure 4 shows the overall growth of existing customers, from the initial slow increase to exponential growth, and, finally, stabilized the rapid growth period from the 20th to the 140th month, about a 10-year cycle. The simulation results are consistent with the judgment of the cruise industry news. Although existing customers have maintained a slow growth, they have gradually stabilized. The direct influencing factors of the existing customers are the churn rate and the completion rate. The completion rate changes from large to small and, finally, approaches the churn rate gradually, making the difference between the two from large to small, and finally to zero, so existing customers show an S-shaped growth.

In-depth analysis of the three curves in Figure 4, it is found that the difference between the completion rate curve and the churn rate curve is exactly in line with the slope of the existing customer curve. The completion rate is from greater than the churn rate to equal, and the current customer's quantity has stabilized after S-shaped growth.
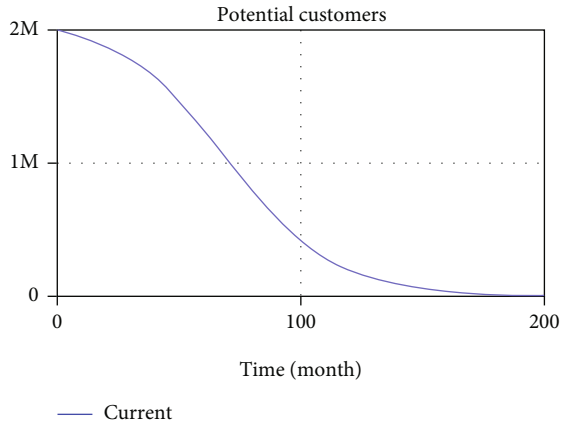
Figure 2: Potential customer simulation results.

Figure 3: Wait customers simulation results.

Figure 5 shows that the evolution trajectory of lost customers presents an elongated S-shaped curve, and the final state also tends to be stable. Return rate and lost rate directly affect the rate of change of lost customers, and others are indirect factors. The curves of the lost rate and the return rate are similar to the shape of the lost customers, all of which are elongated S-shaped, but the lost rate is always greater than the return rate and tends to be equivalent in the later stage of the simulation. The difference between the lost rate and the return rate is always greater than zero, and the rule that the difference changes from large to small determines that the number of lost customers continues to increase, and it shows an elongated S-shaped growth. The simulation results show that lost customers always exist. While the rapid growth of wait customers and existing customers, if cruise travel and website service quality cannot keep up with the substantial increase in the number of customers, lost customers will show an accelerated growth trend. Therefore, online sales platforms, cruise tourism companies, and travel agencies need to work closely together to provide high-quality services to meet the needs of existing customers, while increasing the number of waiting customers and existing customers, while reducing the number of lost customers [23].

5. The Impact of Word-of-Mouth Test Function

In order to obtain more information from the simulation model and the feedback system described by it, especially to discover the different guiding effects of requirements, the test function is used to conduct different types of perturbation experiments on the model and analyze the response characteristics of the model parameters in different periods. The influencing factors of the evolution of the customer life cycle of cruise travel network include competitors, product performance, services, prices, sales rates, and average customer life. Various factors are inherently manifested in the satisfaction of different needs, and affecting the purchase rate, completion rate, the lost rate, and return rate led to the dynamic evolution of the customer life cycle. Website competitors, website product performance, and network product prices have a positive impact on the purchase rate. Perturbation experiments on the model can select one or a few of the key
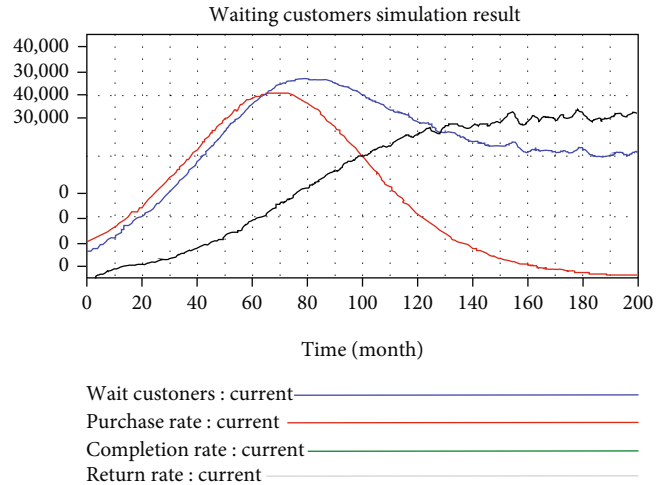
variables to achieve the goal. Word of mouth and investment costs affect both the lost rate and return rate and play a vital role in the life cycle evolution system. Therefore, it selects word-of-mouth influence factors for model testing and analyzes the implications of countermeasures.

5.1. The Impact of Word-of-Mouth on Waiting Customers. First, it uses the step function to output the word-of-mouth impact factor. Assuming that the word-of-mouth impact factor = 0.005, the output of the step function is 0.005 + STEP (0.001, 20). The meaning of the word-of-mouth factor step output is that the customer life cycle of the cruise travel network at the 20th month of evolution, the website platform began to improve its reputation, and it will continue. The main methods of improving word-of-mouth include general competitive strategies such as product price reduction and preferential activities, or high-quality competitive strategies such as improving the quality of tourism information, choosing international excellent cruise ships, and cooperating with authoritative media. It can be seen from Figure 6 that the peak of waiting customers starts from the 20th week and immediately increases due to the influence of the word-of-mouth influence factor. The peak appearance time is advanced from $t = 110$ to $t = 80$, and the later impact is counterproductive, which shows that the word-of-mouth factor cannot always affect the increase in the number of waiting customers. This phenomenon shows that waiting customers to cruise travel is the basic travel demand and changes in potential or direct influencing factors will immediately lead to customers purchase decisions. The word-of-mouth factor is more sensitive to the impact of each stage of the life cycle, but the role played by each stage of the life cycle is different. With the rapid increase in the number of potential customers converted into waiting customers, the order processing capacity of the website platform and the reception capacity of cruise travel are facing challenges. Therefore, for the website platform and cruise companies, they need to make countermeasures before improving the word-of-mouth factor. Otherwise, even if a large number of potential customers are converted into waiting customers, the expected goals will
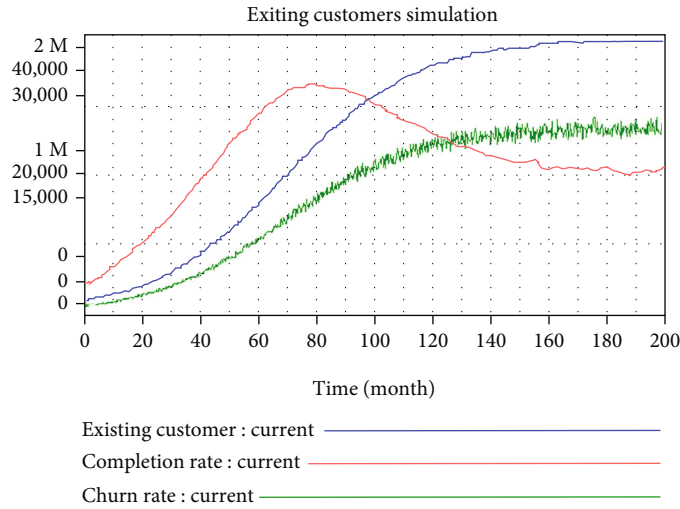
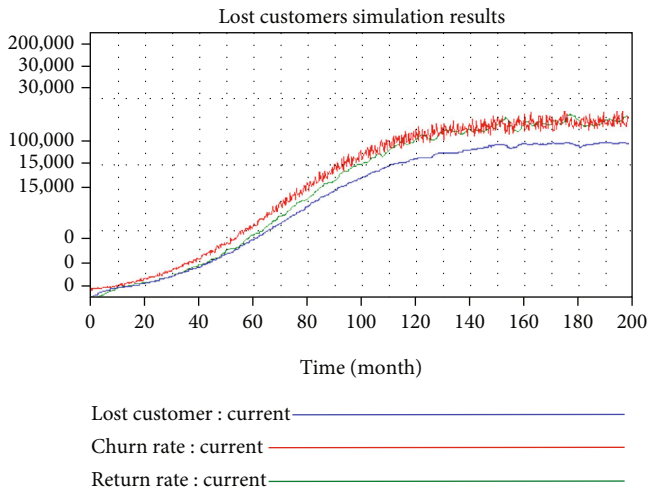Figure 4: Existing customers simulation results.

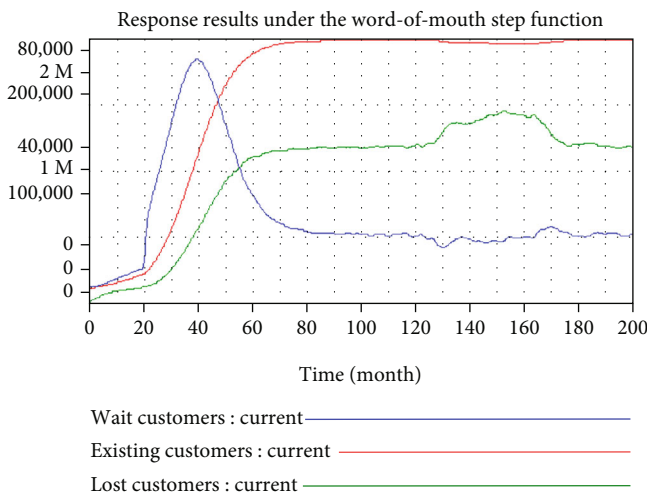Figure 5: Lost customers simulation results.

Figure 6: Response results under the word-of-mouth step function.

not be achieved due to insufficient order processing capacity and cruise ship passenger capacity.

5.2. The Impact of Word-of-Mouth Step Function. From Figures 4 and 6, it can be seen that, compared to the word-of-mouth impact factor = 0.005, on the same life cycle time axis, if the word-of-mouth impact factor is increased, the evolutionary trajectories of existing customers and lost customers will move upward. It is above the original trajectory, but the upward movement of the curve has not waited for the increase of customers. The waiting customers of the cruise travel network increase, and the existing customers may not increase by the same amount, and there is a time delay. First of all, potential customers choosing cruise travel includes curiosity needs and basic travel needs, but waiting customers have a wealth of information about cruise travel, there is a higher level of service needs, and at the same time, as the number of existing customers increases, the volume of lost customers will increase accordingly. Therefore, it is particularly important to maintain the quality of service and even improve the quality of service when the existing customers increase. Secondly, although waiting customer substantially increase, the order processing capacity and cruise reception capacity have not been improved accordingly. Therefore, for website companies and cruise companies, when a large number of potential customers became waiting customers, the existing customers did not increase by the same magnitude or even greater increase. In this case, we must carefully analyze the reasons and, then, develop a targeted strategy. If it is the result of insufficient order processing capacity, it is relatively easy to solve, as long as the website system is upgraded and the cruise number is increased. However, if it is because the higher service needs are not met, it will be more complicated, because whether it is a website platform or a cruise tour, the service level is the performance of the enterprise gradually fixed after long-term operation, and the service quality is easy to decline. It can be difficult to maintain or improve. The reasons for service quality may come from different aspects for different customers.
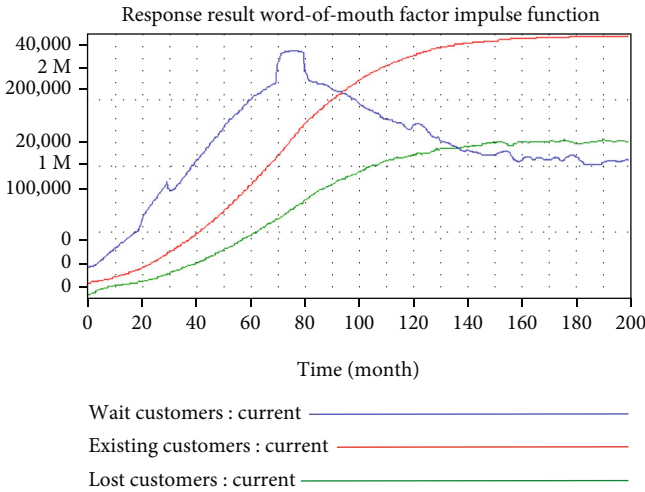
Figure 7: Response result of word-of-mouth factor impulse function.

This requires detailed and comprehensive research and interviews for lost customers and classification solutions. Obviously, this is a systematic and long-term process.

5.3. The Impact of Word-of-Mouth Pulse Function. The pulse function is an interval jump output, which can test the influence of a sudden change of a factor on the system. Assuming the word-of-mouth influence factor = 0.005, the pulse output of the word-of-mouth influence factor is $0.005 + 0.001^*$ PULSE TRAIN (20, 10, 50, 200); its management meaning is as follows. The cruise travel network platform improves word-of-mouth in various ways, and the 20th month lasts for 10 months. After 50 months, the value of word-of-mouth impact factor increases again and lasts for 10 months. This means that the operator will organize a similar activity every 40 months to improve word-of-mouth until the end of the 200th month, and each time the word-of-mouth impact factor is increased to 0.006. The specific situation is shown in Figure 7, which shows that every time the organization's word of mouth is improved through various activities, there will be a peak in booking behavior, leading to a surge in the number of waiting customers, but the peak of waiting customers lacks continuity and will fall as the word-of-mouth value drops. Further analysis of Figure 7 found that by repeatedly and intermittently using various methods to improve word-of-mouth, existing customers will not have peak fluctuations like waiting customers. The number development trajectory is only a slight smooth upward shift and loss. The development trajectory of the number of lost customers has basically remained unchanged, indicating that the indirect improvement of word-of-mouth has a slight positive effect on the increase of cruise customer visits.

The enlightenment is that website platforms and cruise companies take intermittent measures to improve the organization's reputation, waiting customers reach peak accordingly, existing customers have a slight smooth upward movement, and the lost customers are basically unchanged. The impact of word of mouth on cruise travel customers is effectiveness and timeliness at the beginning of the cycle,

and the intermittent effects that appear in the later period will gradually decrease until it no longer affects. Therefore, only in the initial stage can we establish and maintain the continuity of online reputation and service reputation in order to have a profound impact on increasing the number of cruise tourists. Whether it is a website platform or a cruise company, it should pay attention to the importance of the continuation of the initial reputation and ensure the continuity of service quality in all links of website service, image display, and cruise travel [24].

6. Conclusion

This paper uses the system dynamics method to construct the life cycle evolution process of cruise travel network customers and has passed the model test and rationality test of simulation software. Under extreme conditions and sudden changes in word-of-mouth variables, the changes produced by the model and the actual system behavior are consistent, and the reason for the change can be found, indicating that the simulation model established in this paper can simulate the life cycle process of cruise travel network customers. The simulation results of the model and the response analysis of the test function found that the cruise travel online customers showed different quantitative characteristics in the potential stage, waiting stage, current stage, and lost stage of the life cycle, and the evolutionary development of potential customers, waiting customers, and lost customers is significantly affected by online travel information, while existing customers are mainly affected by the real experience of cruise travel. In order to increase the number of existing customers of cruise travel, cruise travel-related companies should promote the evolution of potential customers, waiting customers and lost customers, and adopt different countermeasures for customers in different life cycle stages: potential customers adopt promotional strategies and waiting customers to adopt Motivation strategies, existing customers to maintain strategies, and lost customers to take back strategies.

(1) Potential customers are people who are potentially interested in cruise travel. The simulation model finds that the size of the potential group has a direct impact on the number of existing customers. Judging from the experience of international market development, young and middle-aged people are the backbone of cruise tourism consumption. The future development of China's cruise tourism customer base should focus on the active cultivation of young and middle-aged groups. This requires that in the process of cruise tourism promotion, attention should be paid to the advantages of strong penetration of online channels and rich tourism information, especially the role of online channels in attracting young and middle-aged groups. Relevant business entities can conduct in-depth cooperation with well-known comprehensive websites and brand-based tourism professional websites and maximize the scale of potential customers by expanding the scope of publicity, increasing the intensity and accuracy of promotion

(2) Cruise tourism has a long history of development abroad, but it is a new thing in China. The evolution from potential customers to waiting customers, in addition to considering consumption level, online shopping experience, and customer reputation, more attention should be paid to stimulating customer curiosity and basic tourism needs. After a ten-year period of rapid growth in cruise tourism, the next step in its development is not only to attract new customer groups through service quality improvement but also to improve the quality of website platform information and continue to increase the scope of publicity that reflects the new characteristics of cruise tourism, attracting lost customers look back

(3) From the model's response to the test function, it can be seen that waiting customers are more sensitive to changes in the word-of-mouth impact factor, but frequent and intermittent use of the word-of-mouth factor can only bring about a short-term increase in the number of orders, no fundamental change in the number of existing customers. What really attracts existing customers to stay and lost customers to return is the reputation of the website and the quality of cruise travel services. Continuous website investment is the foundation for maintaining the high-quality operation of online channels. Therefore, the selection of network partners is the key to ensuring high-quality online reputation

(4) After more than ten consecutive years of rapid development, China's cruise tourism has entered a period of stable development, and the number of trips and the number of cruise ships calling at has stagnated or even declined. The simulation results confirmed that under the existing countermeasures, the rapid development period of China's cruise tourism market is about 10 years, which is consistent with the actual situation. However, China has a huge population base, and the annual number of trips of millions of people is still low compared with developed countries. The resident penetration rate of cruise tourism is only a fraction of that of developed countries. Therefore, it should take differentiated countermeasures for online customers in different life cycles: the publicity strategy of potential customers, the incentive strategy of waiting customers, the retaining strategy of existing customers, and the returning strategy of lost customers, China's cruise tourism market will usher in a new round of development climax

From the perspective of life cycle, the cruise travel network customer development process is essentially a time-varying system. The driving mechanism of the same individual customer in different life cycle stages may change, and further analysis is needed. Moreover, the development process of cruise travel network customers is in a dynamic process. When conducting simulation research on it, some variables and parameters should be paid attention to. Subsequent research should improve the predictive effectiveness of the model and need to adjust model variables and parameters appropriately.

Data Availability

The data that support the findings of this study are available from the corresponding author upon reasonable request.

Conflicts of Interest

The authors declare that they have no conflicts of interest.

Acknowledgments

References

[1] E. Stefanidaki and M. Lekakou, "Cruise carrying capacity: a conceptual approach," *Research in Transportation Business Management*, vol. 13, pp. 43–52, 2014.

[2] M. Hannibal and G. Knight, "Additive manufacturing and the global factory: disruptive technologies and the location of international business," *International Business Review*, vol. 27, no. 6, pp. 1116–1127, 2018.

[3] A. Papathanassis and I. Beckmann, "Assessing the 'poverty of cruise theory' hypothesis," *Annals of Tourism Research*, vol. 38, no. 1, pp. 153–174, 2011.

[4] P. C. Thakur, D. D. Cabrera, N. DeCarolis, and A. A. Boni, "Innovation and commercialization strategies for three-dimensional-bioprinting technology: a lean business model perspective," *Journal of Commercial Biotechnology*, vol. 24, no. 1, pp. 78–87, 2018.

[5] Y. Ha and S. J. Lennon, "Online visual merchandising (VMD) cues and consumer pleasure and arousal: purchasing versus browsing situation," *Psychology & Marketing*, vol. 27, no. 2, pp. 141–165, 2010.

[6] D. Weathers, S. Sharma, and S. L. Wood, "Effects of online communication practices on consumer perceptions of performance uncertainty for search and experience goods," *Journal of Retailing*, vol. 83, no. 4, pp. 393–401, 2007.

[7] J. Lee, D. H. Park, and I. Han, "The different effects of online consumers' reviews on consumers' purchase intentions depending on trust in online shopping malls: an advertising perspective," *Internet Research*, vol. 21, no. 2, pp. 187–206, 2011.

[8] P. F. Wilkinson, "Ocean travel and cruising: a cultural analysis," *Annals of Tourism Research*, vol. 32, no. 2, pp. 503–505, 2005.

[9] K. Hung, S. Wang, B. Denizci Guillet, and Z. Liu, "An overview of cruise tourism research through comparison of cruise studies published in English and Chinese," *International Journal of Hospitality Management*, vol. 77, pp. 207–216, 2019.

[10] K. Hung, H. Huang, and J. Lyu, "The means and ends of luxury value creation in cruise tourism: the case of Chinese tourists," *Journal of Hospitality and Tourism Management*, vol. 44, pp. 143–151, 2020.

[11] A. Bonaccorsi, "On the relationship between firm size and export intensity," *Journal of International Business Studies*, vol. 23, no. 4, pp. 605–635, 1992.

[12] G. Xie, Y. Qian, and S. Wang, "Forecasting Chinese cruise tourism demand with big data: an optimized machine learning approach," *Tourism Management*, vol. 82, p. 104208, 2021.

[13] X. D. Sun, X. Feng, and D. K. Gauri, "The cruise industry in China: efforts, progress and challenges," *International Journal of Hospitality Management*, vol. 42, pp. 71–84, 2014.

[14] P. Hribar and N. Yehuda, "The mispricing of cash flows and accruals at different life-cycle stages," *Contemporary Accounting Research*, vol. 32, no. 3, pp. 1053–1072, 2014.

[15] D. C. Schmittlein, D. G. Morrison, and R. Colombo, "Counting your customers: who-are they and what will they do next?," *Management Science*, vol. 33, no. 1, pp. 1–24, 1987.

[16] D. C. Schmittlein and R. A. Peterson, "Customer base analysis: an industrial purchase process application," *Marketing Science*, vol. 13, no. 1, pp. 41–67, 1994.

[17] P. Huang, N. H. Lurie, and S. Mitra, "Searching for experience on the web: an empirical examination of consumer behavior for search and experience goods," *Journal of Marketing*, vol. 73, no. 2, pp. 55–69, 2009.

[18] J. I. Castillo-Manzano and L. López-Valpuesta, "What does cruise passengers' satisfaction depend on? Does size really matter?," *International Journal of Hospitality Management*, vol. 75, pp. 116–118, 2018.

[19] W. Z. Reinartz and V. Kumar, "On the profitability of long-life customers in a noncontractual setting: an empirical investigation and implications for marketing," *Journal of Marketing*, vol. 64, no. 4, pp. 17–35, 2000.

[20] R. Hegselmann and U. Krause, "Opinion dynamics and bounded confidence models, analysis and simulation," *Journal of Artificial Societies & Social Simulation*, vol. 5, no. 3, pp. 2–34, 2002.

[21] A. Tukulis, I. Pakere, A. Gravelsins, and D. Blumberga, "Methodology of system dynamic approach for solar energy integration in district heating," *Energy Procedia*, vol. 147, pp. 130–136, 2018.

[22] P. D. Berger and N. I. Nasr, "Customer lifetime value: marketing models and applications," *Journal of Interactive Marketing*, vol. 12, no. 1, pp. 17–30, 1998.

[23] Z. U. Ahmed, J. P. Johnson, C. Pei Ling, T. Wai Fang, and A. Kah Hui, "Country-of-origin and brand effects on consumers' evaluations of cruise lines," *International Marketing Review*, vol. 19, no. 3, pp. 279–302, 2002.

[24] B. Yoo and N. Donthu, "Developing and validating a multidimensional consumer-based brand equity scale," *Journal of Business Research*, vol. 52, no. 1, pp. 1–14, 2001.

WILEY | Hindawi

Research Article

Development of Art and Culture Creative Industry Using FPGA and Dynamic Image Sampling

Yi Li [ID] and Jialin Gang

School of Digital Art and Design, Dalian Neusoft University of Information, Dalian, 116023 Liaoning, China

Correspondence should be addressed to Yi Li; liyi@neusoft.edu.cn

The TVPS146's digital video processor is used for digital video processing and image output on digital signal processing (DSP) ports. The following is a summary of the field programmable gate array (FPGA) features and programming principles. FPGA is designed by the ping-pong operation, including serial to parallel conversion design, pipeline operation, and data interface synchronization. A dance video screenshot analysis microsystem is composed of it and video dynamic image processing. Finally, according to the number of dance culture performance institutions based on the internet from 2014 to 2018, the development strategy of dance culture and creativity based on the internet is put forward. The results show that the image sharpness of the video screenshots processed by the system is improved, and the effect of enhanced processing is achieved compared to the unprocessed video screenshots. In addition, after the video screenshot processed by the system is compressed, some details are lost and the outline of the image is blurred. The combination of internet immediacy, mass, grassroots, and interactivity can accelerate the development of China's dance culture and creative industry and provide an effective practical foundation for innovation in the development of art and culture.

1. Introduction

With the rapid development of China's economic level, people's demands for spiritual levels are increasing, and the manifestation of spiritual levels is undoubtedly the creative development of art and culture. Since China's Beijing Olympic Games shows the art stage with national characteristics to the world, electronic technology of different scientific and technological levels has been added to the stage design of the Spring Festival Gala every year, which perfectly combines sound effect and equipment [1, 2].

Since the conference on the reform of the cultural system, the state has demanded to improve the process of socialist cultural construction [3]. After the implementation of the spirit of the plenary session of the Central Committee, Chinese culture comes to a valuable golden period of development. In the east of the world, there is a cultural China with standardized market, scientific management, vigorous creation, and consumption [4]. Since then, various places in China have carried out the reconstruction of cultural facilities and the development of art and culture creative industries.

The development of dance art is an important part of it. All kinds of high and new technologies are applied to the construction of dance industry, thus promoting the rapid development of China's dance culture and creative industry [5, 6]. At the same time, the development of world cultural industry becomes intenser and intenser. As a part of dance art, drama develops rapidly in its industrialization process. The Broadway drama industry has developed into a core American art and culture creative industry that can keep pace with the Hollywood film industry and American record industry. The drama industry in the west end of London has made London the "capital of drama" and the cultural and creative center of the world [7–9]. The prosperity and development of the drama industry shows that dance art can form a creative industrialization road and lays the foundation for the creative development of Chinese dance industry.

When dancers constantly summarize their own road experience and carry out practical exploration on dance creative industrialization, it is particularly important to vigorously study the technology and equipment related to the creative development of Chinese dance industry [10]. Since

the 16th National Congress of the Communist Party of China decided to prosper the cultural industry, it has become a social consensus to develop the cultural industry creatively and rapidly. Dance is one of the oldest arts in human society. To make dance develop well in the world pattern of economic globalization, and continuously give play to its artistic creativity and charm, it is inevitable to take the road of industrialization [11, 12]. However, the late start of domestic cultural industry mode and the lack of outstanding talents and cutting-edge art and technology level hinder the development of domestic dance culture and creative industry.

Based on this, this exploration focuses on the research of cutting-edge technology in the dance culture and creative industry. Based on the field programmable gate array (FPGA) and dynamic image acquisition technology, a dance video image real-time processing system is proposed to analyze dance video in real time [13]. This system is flexible, convenient, and universal and belongs to the high-performance digital image acquisition and processing system. At the same time, constructive proposals for the future development of dance culture and creative industry are proposed based on the ideal height of establishing a high standard of the dance industry and the practical development of the dance culture and creative industry. I am. It provides a theoretical basis for the development of the dance culture and creative industries, which have certain leadership and practical importance.

2. Method

2.1. Dance Video Dynamic Image Processing Technology.
First, the input and acquisition of video dynamic image are performed. Analog processing and A/D conversion are used. In this exploration, Phase Alteration Line (PAL) video is used. After the switch selection of the input video is implemented, the signal is processed by simulation, automatic gain control, and A/D conversion. The resolution of the converted data is 10 bit, and the A/D conversion channel can receive the unified phase-locked loop (PLL) clock (in (25 MHz-30 MHz)). Figure 1 shows analog processing and A/D conversion. In factor analysis, the weight of each major factor is not determined and is determined by the percentage of the major factor that determines uterine change.

Then, digital video processing is performed. In this exploration, the digital video processor of TVPS146 is used. The processor can process many kinds of video formats and analyze the processing flow of the dance video processing circuit. In the video processing circuit, the output of A/D receives the digital dance video, performs Y/C separation, completes the chroma demodulation of the National Television Systems Committee (NTSC)/PAL, and enhances the luminance-bandwidth-chrominance (YUV) signal. The 10-bit dance video signal is multiplied by the subcarriers in the integral regulator to form a color difference signal. The U and V signals enter the low-pass filter to generate bandwidth that can be utilized [14]. Five adaptive comb filters [15] separate the U and V signals from Y and derive them. Then, the chroma and brightness are debugged to generate signal W. Furthermore, the output format of the chip can be 20-bit 4:2:2 W or 10-bit 4:2:2 W. Figure 2 shows the flow. With

certain performance improvements, there are new requirements for general adaptability and specific adaptability. The main problem with basketball gymnastics in Japan is that there are too many regular gymnastics, special gymnastics are not covered, and the obtained physical condition cannot be used for special gymnastics.

Human motion tracking based on template matching currently primarily uses error metrics between two matching pixel blocks. There are three main error metrics based on block matching: an error metric based on a cross-correlation function and a normalized mean square and finally, the image output. When the image is output through DSP port, the output interface of the video terminal is needed. The output interface consists of an online video display processor and a video encoder [16]. An online video display processor can display not only two different video windows and two different on-screen display (OSD) windows but also one video window, one OSD window, and one other attribute window. The frequency of video decoder in D/A conversion is 55 MHz, which can output video and audio in many formats such as NTSC/PAL. The output video signal can be directly transmitted to the monitor after D/A conversion to complete the output display. The maximum communication delay that the user can tolerate under the cloud and fog architecture is guaranteed, and the user's request is processed within the acceptable communication delay.

2.2. Function Analysis of FPGA.
The maximum communication delay that the user can tolerate under the cloud and fog architecture is guaranteed, and the user's request is processed within the acceptable communication delay. FPGA is the core part of the system control and image processing and plays an important role. FPGA needs to carry out logic control, image preanalysis, image data storage control, and communication with DSP for image acquisition.

After the system is powered on, FPGA automatically loads the program through external electrically erasable programmable read-only memory (EEPROM). After receiving the instruction from DSP, FPGA starts to work, receives the imported image data signal, and separates the effective data according to its own working principle, to realize the control of image acquisition. The collected data are denoised, corrected, and enhanced, and the image data is converted to the YUV format. The processed data are exported to the external synchronous dynamic random access memory (SDRAM) through the SDRAM read-write control. SDRAM needs to be initialized before normal reading and writing. SDRAM can be initialized after being powered on for a period of time. The time required for this process cannot be determined, which is determined by the equipment used, usually 100 μs; then, the Precharge command is transmitted to SDRAM. After Precharge is carried out in all pages, the SDRAM is refreshed. The purpose of refresh is to enable SDRAM to be configured normally. In this configuration, SDRAM can perform automatic Precharge, and the clock delay value depends on the dataset of SDRAM. The number of clock delays in this exploration is 3. The initialization process needs to comply with the parameters of the dataset of the
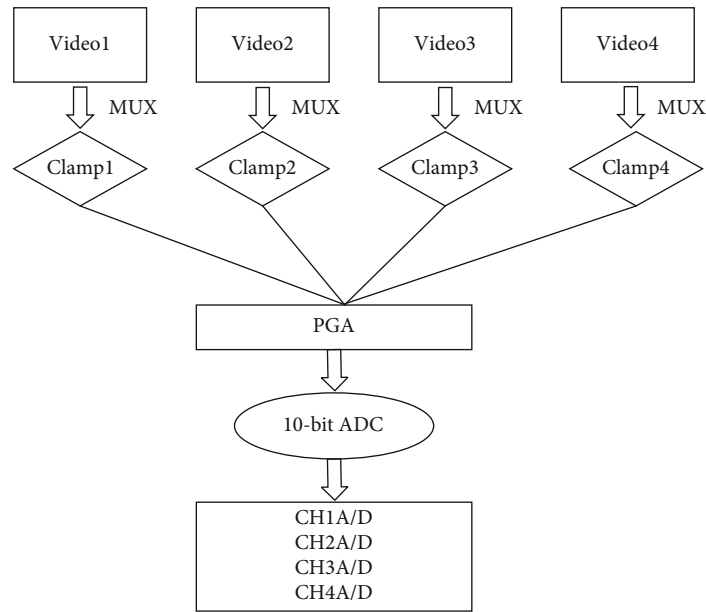
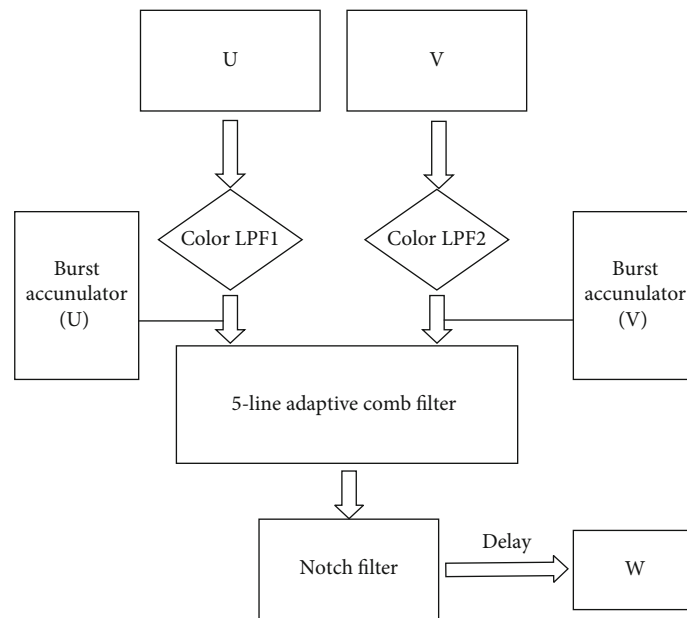Figure 1: Video dynamic image simulation processing and A/D conversion.

Figure 2: Digital video processing flow.

SDRAM chip. Otherwise, the normal initialization cannot be completed, which will directly make the subsequent SDRAM unable to read and write normally [17].

The decisive factors of SDRAM reading and writing content are DSP and image acquisition control module [18]. Its read-write control module mainly transmits the collected image data to SDRAM and reads the upper computer parameters written into SDRAM by DSP. To make the read-write speed reach the fastest level, SDRAM controller is equipped with two 256×2 bit random access memory (RAM), both of which are in the FPGA. Its working speed is very fast. At the same time, the ping-pong operation is used to greatly improve the data transmission rate in FPGA. The law must be able to

effectively protect the interests of investors and creditors, to contribute to the establishment and maintenance of good economic order, and thus to ensure the smooth and efficient operation of the financial system. A well-developed credit system can not only effectively reduce the cost of information collection but also reduces the negative choice and moral hazard caused by information asymmetry and reduces the occurrence of financial gaps and financial crises.

2.3. FPGA Programming Principles. In this study, the principle of designing a system is that the system belongs to a hardware system. However, the FPGA design must consider how a single board completes module task assignments, the type of

algorithm suitable for use with the FPGA, and the capabilities it provides. This indicates that the system must have the proper placement of global macros such as clock domain and execution speed.

In general, the functional modules with high real-time requirement and high frequency can be realized by the FPGA/complex programmable logic device (CPLD). Compared with CPLD, FPGA is more suitable for the design of wide scale, high frequency, and large number of registers. Compared with PLD's rich combinational logic, FPGA's triggers are very rich. In terms of FPGA design ideas, the use of four common design ideas can maximize the use efficiency [19].

(1) Ping-pong operation

The ping-pong operation can be often applied to data stream control and processing. Figure 3 shows the classic ping-pong operation mode [20].

The ping-pong operation processing steps are as follows.

First, input the data stream. The input data selection module divides the data stream into two different data buffer areas. The data buffer area can hold any storage module and commonly used storage unit such as dual-port RAM, single-port RAM, and first input first output (FIFO).

Second, in the first buffer cycle, the imported data stream is cached to the first data buffer module. In the second buffer cycle, the input data selection unit is switched to cache the input data stream to the second data buffer module. At the same time, the data of the first cycle cached by the first data buffer module is transferred to the data stream operation and processing module after specific selection.

Third, in the third buffer cycle, the imported data stream is cached to the first data buffer module by switching the data again, and the cache data of the second data buffer module is switched through the "input data selection unit" to reach the "data stream operation processing module" to complete the operation and processing. From the first step to the third step, the cycle is carried out.

The core feature of the ping-pong operation is to switch through "input data selection unit" and "output data selection unit" according to a certain rhythm and send the buffered data stream to the "data stream operation processing module" at a stable speed to complete the operation and processing. The ping-pong operation module belongs to a whole, and the module's input data stream and output data stream will not produce any pause, so it is very suitable for pipeline processing of data stream. Therefore, the ping-pong operation is usually applied to the pipeline algorithm to realize seamless buffering and processing of data. Another characteristic of the ping-pong operation is that it can save buffer interval. Using the ping-pong operation, only two RAM which can buffer one time slot data need to be defined. If data are read from another RAM while data is written to one RAM and sent to the processing unit for processing, the capacity of each RAM is only 256 bits.

(2) Design of series to parallel conversion

Serial to parallel conversion is an important skill in the FPGA design, a common way of data stream processing,

and a direct embodiment of the idea of area and speed exchange. There are many ways to realize serial to parallel conversion. The selected registers and RAM can complete the sorting and quantity requirements according to the data. In the ping-pong operation diagram, DPRAM is used to complete the serial to parallel conversion of the data stream. Because of the use of DPRAM, the data buffer area can be opened very large. For a small number of designs, the register can be used to complete the serial to parallel conversion. If there is no special requirement, a synchronous timing design can be used for the conversion between serial and parallel.

(3) Pipeline operation

The pipeline proposed in this exploration refers to a design idea of processing flow and sequential operation [21], which is not the design idea used to optimize timing in application-specific integrated circuit (ASIC) design. Pipeline processing is a common design method in high-speed design. If the processing flow of a design is divided into several steps, and the whole data processing is "single flow," there is no feedback and iterative operation. Moreover, the output of the previous step is the import of the next step, so it is necessary to consider using the pipeline design method to improve the working frequency of the system. Its basic structure is as follows. All the operation steps divided properly are connected in a single flow direction. The biggest characteristic and requirement of pipeline operation is that the processing of data stream in each step is continuous in time. If each operation step is simplified and assumed to start with a trigger, the pipeline operation can be regarded as a shift register group, and the data stream flows through the trigger in sequence. Finally, the work of each step is completed. The key point of the pipeline design is the proper arrangement of the whole design sequence and the reasonable division of each operation step [22, 23].

(4) Data interface synchronization

First, if the beat of the input data and the processing clock of the current chip have the same frequency, the master clock of the current chip can be used to complete the register sampling and the synchronization of the input data. Second, if the input data is not synchronized with the processing clock of the current chip, especially when the frequency does not match, the synchronization of the input data can be realized only by using the processing clock to carry out register sampling for the input data twice. The register is used to sample the data in the asynchronous clock domain twice, which can effectively prevent the unstable propagation of the data state and make the data processed by the later stage circuit effective. However, this method cannot guarantee that the data sampled by two-stage registers is correct, and there will be a certain amount of wrong data. Therefore, it is only applicable to functional units that are not sensitive to a small number of errors [24, 25]. In order to avoid wrong sampling in the asynchronous clock domain, RAM and FIFO are usually used to realize data conversion in the asynchronous clock domain. The buffer unit used most is DPRAM. In the input port, the upper clock is used to write data, and the current level clock
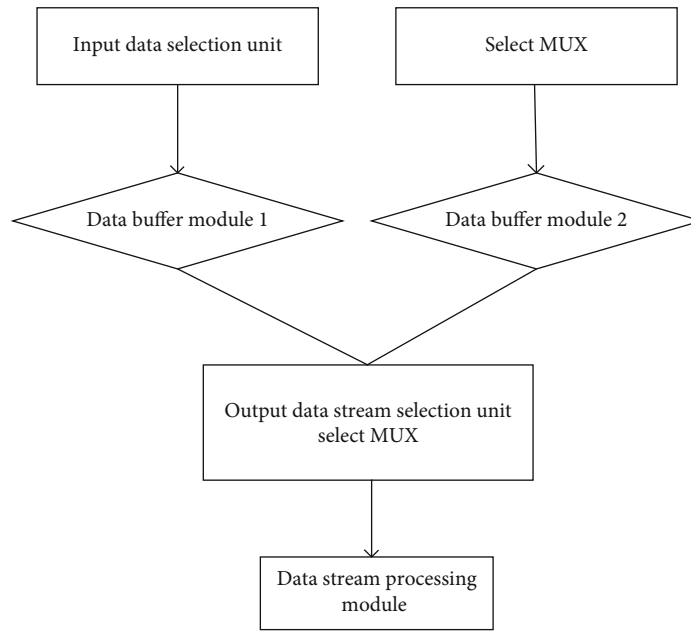
FIGURE 3: Ping-pong operation steps.

is used to read data at the output port. Thus, it is very convenient to implement the data exchange between asynchronous clock domains.

Finally, data exchange is carried out. The video data transmission methods between FIFO and DSP in FPGA are usually software query, interrupt data, and enhanced direct memory access (EDMA). Software query consumes too much central processing unit (CPU) resources, while interrupt data transmission can save a lot of CPU time, but it cannot play an appropriate EDMA resource. The development foundation of EDMA is direct memory access (DMA), which can convert data between different storage spaces without CPU. DM6437 in this exploration can provide 64 independent EDMA channels. The priority of the channel can be programmed. Without the participation of CPU, high-speed data transfer between on-chip memory, on-chip peripherals, and external storage space is realized. Therefore, in order to reduce the burden of CPU and exert the powerful external data transmission ability of DM6437, the video image acquisition unit sends out a EDMA transmission request and establishes an EDMA channel to complete the transmission of video data from FIFO to LZSRAM and SDRAM.

3. Results and Discussion

3.1. System Image Analysis Results. The system proposed in this exploration captures the image of dance video. After debugging, the outputs are shown in Figures 4–6.

Figure 4 is the original video screenshot without any processing, Figure 5 is the image processed by the system, and Figure 6 is the image after 10 times compression after the system processing. Compared with Figure 4, the sharpness of the image in Figure 5 is improved, and the effect of the enhancement process is obtained. Compared to Figures 4

and 5, some details are lost in Figure 6 and the outline of the image is quite blurry.

Image compression will cause loss to the file, so some details will be lost. According to the results of image output, the system proposed in this exploration can achieve the optimization of video image and achieve the ideal level.

3.2. The Number of Dance Culture and Creative Performance Institutions Based on Internet. According to the data of the State Statistical Bureau, the number of internet-based dance culture and creative performance institutions is shown in Figure 7.

Figure 7 shows that from 2014 to 2018, the number of state-owned and collective dance performance institutions remains at a certain number, basically unchanged, while the dance performance institutions based on the internet show a growing trend. Especially after 2016, the growth rate increases significantly. The internet is characterized by immediacy, massiveness, grassroots, and interactivity. The dissemination of dance content and dance resources on the internet platform not only enhances the vitality of dance art but also provides materials for dance content producers, which helps to stimulate the creative inspiration and creative power of producers.

For consumers of dance products, the internet platform provides them with convenient channels for retrieval, comparison, selection, payment, and sharing. In terms of retrieval, comparison, and selection, the network platform enables them to quickly obtain all-round dance product information and lock in the required products according to their own needs; the payment function saves time and cost for consumers' purchase and payment, and it is more convenient to obtain dance products or dance experience at the most favorable price through "shop around." By sharing an internet platform, consumers often gather in specific

FIGURE 4: Original video screenshot.

FIGURE 5: Video screenshot after system processing.

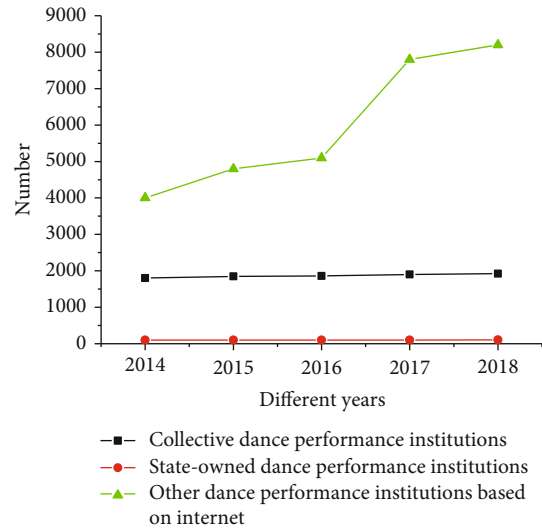

FIGURE 6: Compressed image.

FIGURE 7: Number of dance performance institutions.

internet-based development strategy for dance culture and creativity [26].

4. Conclusion

This study uses the main processor DM6437, which is suitable for single-channel video processing systems, as the main chip. First, stage video dynamic image processing is performed. Then, use the ping-pong operation to design the FPGA. This includes serial to parallel conversion design, pipeline operations, and data interface synchronization. You can complete fast external data exchange and data manipulation. The proposed architecture is flexible and has strong generality. It can be modularized to improve the efficiency of the algorithm. In addition, the short development cycle makes it convenient for system maintenance and upgrades. The system can capture and process dynamic images of video. The sharpness of the obtained image is improved, the image quality is greatly improved, and the internet can be widely used.

At the same time, according to the increasing number of dance culture performance institutions based on the internet from 2014 to 2018, the development strategy of dance culture and creativity is put forward. The dance content and dance resources are spread on the internet platform, providing consumers with convenient retrieval, comparison, selection, payment, and sharing channels, so that they can gather in a certain community or site for communication, and quickly obtain all-round dance product information, and lock in the required products according to their own needs. Consumers can get dance products or dance experience at the most favorable price. Moreover, the internet platform provides a low-cost, convenient, and efficient promotion platform for promoters. It not only enhances the vitality of dance art but also provides materials for dance content producers, which helps to stimulate the creative inspiration and creative power of producers. Compared with manual promotion, the internet platform eliminates the complex intermediate links, saves the cost, and thus speeds up the

communities or sites for communication. This is also the spread of dance products. For dance product promoters, the internet platform is a cheap, convenient, and efficient promotion platform. Compared to manual promotions, internet platforms help eliminate complex intermediate links, save costs, and accelerate promotions. It is also an

promotion speed. Due to personal and time reasons, there are still some deficiencies in this exploration. The dynamic acquisition speed and image output quality of the dance video are not well controlled, which is the focus of the follow-up study and needs to be further improved.

Data Availability

No data were used to support this study.

Conflicts of Interest

The authors declare that they have no conflicts of interest.

References

[1] W. Yao, "Approaching Chineseness: investigating the cultural transfer of behavioural factors in and through Chinese industrial design," *Journal of Information Science*, vol. 36, no. 4, pp. 517–529, 2015.

[2] Y. Yuan, "Casting an 'Outsider' in the ritual centre: two decades of performances of 'Rural Migrants' in CCTV's Spring Festival Gala," *Global Media & China*, vol. 2, no. 2, article 205943641770732, 2017.

[3] Y. Zhang, L. Guan, and Q. Liu, "Liu Tungsheng: a geologist from a traditional Chinese cultural background who became an international star of science," *Journal of Asian Earth Sciences*, vol. 155, pp. 8–20, 2018.

[4] X. G. Zhao and L. Z. Ren, "Focus on the development of offshore wind power in China: has the golden period come?," *Renewable Energy*, vol. 81, pp. 644–657, 2015.

[5] J. A. Tai, "A study of cultural and creative industries on dance in Taiwan," *The Korean Journal of Dance Studies*, vol. 59, no. 2, pp. 117–128, 2016.

[6] S. B. Tsai, "Using the DEMATEL model to explore the job satisfaction of research and development professionals in China's photovoltaic cell industry," *Renewable and Sustainable Energy Reviews*, vol. 81, pp. 62–68, 2018.

[7] M. Frisch, "Blue collar Broadway: the craft and industry of American theater, by Timothy R. White," *Journal of Urban Affairs*, vol. 39, no. 5, pp. 732–734, 2017.

[8] K. L. Record and S. B. Austin, ""Paris thin": a call to regulate life-threatening starvation of runway models in the US fashion industry," *American Journal of Public Health*, vol. 106, no. 2, pp. 205-206, 2016.

[9] R. M. Smeke Cassorla, "From bastion to enactment: the 'non-dream' in the theatre of analysis," *The International Journal of Psychoanalysis*, vol. 86, no. 3, pp. 699–719, 2017.

[10] D. Weimer, B. Scholz-Reiter, and M. Shpitalni, "Design of deep convolutional neural network architectures for automated feature extraction in industrial inspection," *CIRP Annals*, vol. 65, no. 1, pp. 417–420, 2016.

[11] H. Bungay, S. Hughes, C. Jacobs, and J. Zhang, "Dance for health: the impact of creative dance sessions on older people in an acute hospital setting," *Arts & Health*, vol. 4, pp. 1–13, 2020.

[12] P. Hu, F. Wu, J. Peng, Y. Bao, F. Chen, and D. Kong, "Automatic abdominal multi-organ segmentation using deep convolutional neural network and time-implicit level sets," *International Journal of Computer Assisted Radiology & Surgery*, vol. 12, no. 3, pp. 1–13, 2017.

[13] Q. Wang, Y. Li, and X. Liu, "The influence of photo elements on EEG signal recognition," *EURASIP Journal on Image and Video Processing*, vol. 2018, no. 1, 2018.

[14] M. Elhoseny and K. Shankar, "Optimal bilateral filter and convolutional neural network based denoising method of medical image measurements," *Measurement*, vol. 143, pp. 125–135, 2019.

[15] J. Pei, M. Zou, and Y. Zhao, "Adaptive comb-type filtering method for stripe noise removal in infrared images," *Journal of Electronic Imaging*, vol. 28, no. 1, pp. 013037.1–013037.17, 2019.

[16] C. Li, S. Zhang, P. Liu, F. Sun, J. M. Cioffi, and L. Yang, "Overhearing protocol design exploiting intercell interference in cooperative green networks," *IEEE Transactions on Vehicular Technology*, vol. 65, no. 1, pp. 441–446, 2016.

[17] I. Pomeranz, "An initialization process to support on-line testing based on output comparison for identical finite-state machines," *IEEE Transactions on Computer-Aided Design of Integrated Circuits and Systems*, vol. 37, no. 7, pp. 1494–1504, 2017.

[18] W. C. Lee, M. K. Chae, K. J. Soh et al., "Parallel branching of two 2-DIMM sections with write-direction impedance matching for an 8-drop 6.4-Gb/s SDRAM Interface," *IEEE Transactions on Components, Packaging and Manufacturing Technology*, vol. 9, no. 2, pp. 336–342, 2019.

[19] Y. Guo, X. Wang, and Z. Zeng, "A compact Memristor-CMOS hybrid look-up-table design and potential application in FPGA," *IEEE Transactions on Computer-Aided Design of Integrated Circuits and Systems*, vol. 36, no. 12, pp. 2144–2148, 2017.

[20] F. Z. Teng and L. I. Xuxin, "A control strategy for smooth switching between island operation mode and grid-connection operation mode of microgrid containing photovoltaic generations," *Power System Technology*, vol. 39, pp. 904–910, 2015.

[21] F. E. Sanchez, M. Naylor, M. Lucquiaud et al., "Impacts of geological store uncertainties on the design and operation of flexible CCS offshore pipeline infrastructure," *International Journal of Greenhouse Gas Control*, vol. 52, pp. 139–154, 2016.

[22] K. Yasueda, D. Shinjo, and A. Kataoka, "Arrangement of control points for sound spot generation in the multi-point control method," *Journal of the Acoustical Society of America*, vol. 140, no. 4, pp. 3140–3140, 2016.

[23] C. Ji, C. Li, B. Wang, M. Liu, and L. Wang, "Multi-stage dynamic programming method for short-term cascade reservoirs optimal operation with flow attenuation," *Water Resources Management*, vol. 31, no. 14, pp. 4571–4586, 2017.

[24] T. Donker, M. Blankers, E. Hedman, B. Ljótsson, K. Petrie, and H. Christensen, "Economic evaluations of internet interventions for mental health: a systematic review," *Psychological Medicine*, vol. 45, no. 16, pp. 3357–3376, 2015.

[25] J. Feller, R. Gleasure, and S. Treacy, "Information sharing and user behavior in internet-enabled peer-to-peer lending systems: an empirical study," *Journal of Information Technology*, vol. 32, no. 2, pp. 127–146, 2017.

[26] N. Tajbakhsh, J. Y. Shin, S. R. Gurudu et al., "Convolutional neural networks for medical image analysis: full training or fine tuning?," *IEEE Transactions on Medical Imaging*, vol. 35, no. 5, pp. 1299–1312, 2016.

WILEY | Hindawi

Research Article

Application of Nonarbitrage Pricing Model and Finite Element Numerical Solution in the Value of Convertible Bonds in the Stock Market

Xiaoxiao Guo [iD]

College of Commercial, Wuxi Taihu University, Wuxi, 214064 Jiangsu, China

Correspondence should be addressed to Xiaoxiao Guo; guoxx@wxu.edu.cn

Because of its creditor's rights, equity, and options, convertible bonds have been developed rapidly since its emergence and have become one of the main tools in the financial market. One of the core problems of convertible bonds is pricing. The research on the pricing model of convertible bonds in China is relatively late. Most of them use foreign technologies, but they are quite different from the actual situation in China, and most of the models are characterized by a single factor. Therefore, this paper puts forward the nonarbitrage pricing model in the stock market and the application of the finite element numerical solution in the value of convertible bonds. The biggest innovation of this paper is to design a combined pricing model by using the model of nonarbitrage pricing theory and finite element numerical solution. The model combines the advantages of the nonarbitrage pricing theory and finite element numerical solution, and through the design of this paper, the model effectively improves the calculation accuracy and is suitable for most of the current market environment. While improving the comprehensive performance of the pricing model, it also simplifies the calculation methods and steps. In order to further verify the actual effect of the pricing model in this paper, the traditional binary tree model is taken as the experimental contrast object, including the comparative analysis of the market price and the theoretical price of the convertible bond, the comparative experiment of the prediction effect between the model and the binary tree model, and the analysis of the relative price error of the convertible bond. The results show that the comprehensive performance of the pricing model in this paper is significantly better than the traditional binary tree model. This study has achieved ideal results and can be widely recommended.

1. Introduction

A convertible bond is a kind of corporate bond. The holder has the right to convert the bond into a certain number of common shares of the issuing company within a certain period of time. With the nature of creditor's rights, stock rights, and options, it is a kind of financial derivative investment product with ingenious design and strong vitality, which is often called a convertible bond. Convertible bonds were first issued in the United States in the mid-19th century and have experienced a long process of development. In the 1970s, convertible bonds began to develop rapidly. At present, it has become one of the main financing and investment tools in the world stock market. In Asia, the financing amount of convertible bonds has exceeded that of stock

financing, and in Europe, the financing amount of convertible bonds has been close to half of that of stocks. China's convertible bond market began in the early 1990s. After a period of downturn, especially in 2002, the issuance of convertible bonds fluctuated, and the situation deteriorated further. In a short period of half a year, the sales of convertible bonds reversed significantly. In 2003, the issuance of convertible bonds was sluggish. A total of 16 convertible bonds were issued in the whole year, raising an accumulated amount of 18.15 billion yuan, which exceeded the financing scale of allotment shares in that year, and became one of the main means of refinancing for listed companies. The unique charm of convertible bonds is gradually recognized by more investors, and the convertible bond market is generally bullish.

Before the mid-1970s, the theoretical research of convertible bonds mainly focused on the establishment of the basic concept of a convertible bond, the determination of conversion price, and the adjustment method. Due to the backwardness of theoretical methods and research tools, most of the work is limited to the characterization of the value characteristics of convertible bonds, which cannot be discussed in depth. Since the mid-1970s, the research on convertible bonds has entered a stage of rapid development. In modern research, option pricing theory and technology have been greatly expanded, mainly reflected in the pricing model, research object, and numerical simulation. In the pricing model, the restrictive assumptions in the derivation of the original option pricing formula are relaxed. In modern option pricing, the interest rate can be stochastic, the stock price process cannot be a geometric Brownian motion, and the price process can include jump, transaction cost, and dividend payment. Almost all financial products can be included in the option pricing framework. In terms of numerical simulation, the rapid development of the computer provides material guarantee for the numerical simulation of financial product pricing, and the development of some computing technologies provides technical support for numerical simulation. Finite difference method, grid method, and finite element method have been widely used in the pricing of financial products. In this process, the pricing of convertible claims is no exception. But at the same time, the pricing models of convertible bonds are mostly single factor models, and there are many deficiencies. Therefore, this paper puts forward the nonarbitrage pricing model in the stock market and the application of the finite element numerical solution in the value of convertible bonds.

First of all, this paper studies the basic theory and core concepts of the convertible bond and pricing model. Through the research, this paper believes that the convertible bond is one of the most important financial instruments, which plays an important role in China's financial market and economic development. Then, in view of the shortcomings of the existing convertible bond pricing model, this paper innovatively proposes a combined pricing model which combines the nonarbitrage pricing theory and the finite element numerical solution. Based on the theory of nonarbitrage pricing, the model defines the market as a one-dimensional standard Brownian motion and recalculates the value of the company. According to the characteristics of the existing market, this model also fully considers the control of credit risk and makes a detailed and clear division of the upper limit and lower limit of arbitrage. According to the preliminary calculation results, the finite element numerical method is used to optimize and calculate the total value of bonds. Through a series of optimization operations, the model can effectively improve the calculation accuracy. In order to further verify the actual effect of the pricing model in this paper, a number of practical examples including the comparative analysis of the market price and theoretical price of convertible bonds, comparative experiment of the prediction effect between this model and the binary tree model, and analysis of the relative price error of convertible bonds are given. Through the analysis of experimental data,

we can see that the calculation results of this pricing model are more accurate than the traditional binary tree model, and the calculated results are more in line with the actual market value [1–3].

The second part of this paper introduces the related research, the third part gives the basic concept and theory of the article, the fourth part discusses and gives the pricing model based on nonarbitrage and the finite element method, the fifth part explains the effect of the method proposed in this paper, and the sixth part summarizes the full text.

2. Related Works

The pricing model of foreign convertible bonds first appeared in the 1960s. In this period, the theory holds that the price of convertible bonds is equal to the larger value between the value of convertible bonds as ordinary bonds and the discounted value of convertible bonds at a certain time in the future. The emergence of the Black-Scholes' option pricing theory and the rapid development of computer technology in 1973 have fundamentally changed the development of convertible bond pricing theory. The convertible bond pricing theory has been mature after more than 30 years of development.

Due to the development of the pricing theory of convertible bonds in foreign countries, the research of convertible bonds in China is based on the reference of foreign models, combined with the actual situation of China, such as the design of various terms or numerical methods. Zhang [4] used Monte Carlo simulation and the finite difference numerical method to price the redemption terms and redemption terms of domestic convertible bonds and analyzed the impact of these two terms on convertible bonds. Zhao et al. [5] use the finite difference method and binary tree method to solve this problem. Based on the pricing model of convertible bonds, this paper analyzes the impact of these two terms on convertible bonds under random interest rates. This paper discusses five factors that affect the pricing of convertible bonds, establishes a two factor pricing model based on the stock price and interest rate, and makes an empirical test of airport convertible bonds. It is found that the convertible bonds in China are not sensitive to the change of interest rate, which leads to some technical problems such as large calculation error and inaccurate trend prediction and analysis. Therefore, this paper proposes a combination of nonarbitrage theory and finite element method to improve the pricing accuracy of the model.

3. Basic Theory and Core Concepts of This Paper

3.1. Definition of Convertible Bonds. On March 25, 1997, the Securities Commission of the State Council issued the Interim Measures for the administration of convertible company bonds. Among them, Article 3 defines convertible bonds as follows: convertible corporate bonds refer to corporate bonds issued by issuers in accordance with legal procedures and can be converted into stocks within a certain period of time in accordance with agreed conditions. The

issuers here include domestic listed companies and joint stock limited companies established after the overall or partial restructuring of key state-owned enterprises.

Like ordinary bonds, convertible bonds have several elements, such as face value, coupon rate, and maturity. The coupon rate of convertible bonds is mainly determined by the market interest rate level, enterprise credit rating, and issuing conditions. Generally speaking, the higher the market interest rate, the higher the coupon rate, and the lower the enterprise credit rating, the higher the coupon rate. Other issuing conditions will also affect the coupon rate, for example, the redemption clause limits the upper limit of investors' income, and the coupon rate can be appropriately increased. The repurchase clause protects the investors' income, increases the financial burden and risk of the issuing company, and can appropriately reduce the coupon rate. At the same time, it should be noted that the coupon rate of convertible bonds is lower than that of ordinary bonds with the same maturity and credit rating and sometimes even lower than the bank deposit interest rate of the same period. Due to the existence of convertible options, convertible bonds have the characteristics of bonds, stocks, and options. These options include equity conversion, that is, the right of investors to convert convertible bonds into common shares of the company at a certain price within a certain period of time according to the agreement. Put back right refers to the right of investors to sell convertible bonds back to the company at a certain price under certain conditions. Redemption right refers to the company's right to redeem convertible bonds in accordance with the agreement under certain conditions. The right to reduce the conversion price refers to the right of the company to reduce the conversion price under certain conditions [6, 7].

3.2. Value Analysis of Convertible Bond. A convertible bond is a kind of hybrid bond; the coupon rate is generally lower than the corresponding period bond. Investors are willing to accept lower interest rates because they attach more importance to the option of converting bonds into corporate shares. When the stock market of the issuing enterprise performs well and the stock price continues to rise, the convertible bond holder can convert the convertible bond into the common stock of the company at the conversion price lower than the current stock price and obtain the conversion income. If the stock price of the enterprise is low, investors will choose to hold the bond to obtain stable interest income or recover the investment principal on schedule. It not only has the characteristics of ordinary bonds but also has the characteristics of equity. For standard convertible bonds, it gives investors the lowest return in the form of value, that is, the value of ordinary interest-bearing bonds composed of bond coupon payment and principal repayment at maturity. At the same time, when the stock rises to a certain level, that is, when the stock value reaches a certain level, investors also have the right to convert to the common stock of the issuer.

The option value of convertible bonds refers to the right of a convertible bond holder to purchase corresponding stock at any time before the maturity of the convertible bond. If he/she is willing and meets the conditions, he/she can convert the convertible bond into stock. Due to the value of options, the actual value of convertible bonds is always higher than the bottom line before maturity. The difference between the market value of convertible bonds and the bottom-line value is the call right value and option value of stocks [8, 9].

3.3. Nonarbitrage Pricing. In the process of pricing financial assets, the nonarbitrage pricing method is not only a common pricing method but also one of the most basic principles in pricing theory.

Strictly speaking, arbitrage means that in the process of trading financial assets, traders can obtain risk-free returns without initial investment. However, if the market is effective, the market price must be adjusted according to arbitrage behavior and return to equilibrium. This is the nonarbitrage pricing principle. We can apply the nonarbitrage pricing method to term pricing from another perspective. The idea is as follows: in an efficient market, without arbitrage opportunities, investors can build a risk-free portfolio, including derivative positions and underlying asset positions. By adjusting the investment ratio of the underlying asset and the derivative asset, the long-term profit (or loss) of the underlying asset can offset the short-term loss (or profit) of the derivative. This principle actually represents an equilibrium condition between the expected yield of the derivative securities, the expected yield rate of the underlying security, and the risk-free interest rate. The binary tree pricing model of convertible bonds is a successful application of this principle [10–12].

3.4. Brief Introduction of Finite Element Method. The uniform finite element method is a numerical approximation method combined with the variational method or weak formulation method. The following structure is the same in any d dimensional space: for example, for a weak formula formed in an infinite dimensional function space V, the following structure is the same:

$$V = H^1(\Omega) = \left\{ w \in L^2(\Omega): \nabla w \in L^2(\Omega)^d \right\}. \tag{1}$$

It consists of finite dimensional subspace V_h of V, such as continuous piecewise affine function space on some triangles, and problem test function space when V_h replaces V. In the simple finite element method, the space V is established as follows:

(1) The region is divided into nonoverlapping elements with simple fixed shape. Examples include one-dimensional spacing, two-dimensional triangles or quadrangles, three-dimensional tetrahedrons, prisms, or hexahedrons. Usually, the element set is an unstructured mesh, called triangulation

(2) The maximum dimension k of the polynomial approximation of the selected element

(3) V_h consists of functions in V and is restricted by the highest degree of polynomials less than k

The programming of this method has certain similarity in each dimension, but the grid generation of different latitudes is very independent [13–15].

4. Pricing Model Based on No Arbitrage and Finite Element Method

4.1. Establishment of Nonarbitrage Pricing Model. Suppose $(\Omega, F, \{F_t\}, P)$ is a complete probability space with flow. One dimensional standard Brownian $W = (W_t, 0 \le t \le T)$ motion is defined on it. It is assumed that the flow $\{F_t, 0 \le t \le T\}$ is generated by Brownian motion and satisfies the general conditions.

4.1.1. Hypothesis

(1) There are three types of financial instruments continuously traded in the market. These three financial instruments are stocks, convertible bonds, and cash market accounts. Risk free rate $r > 0$

(2) Determine the time periods T and $0 < T < \infty$

(3) Assuming that the asset value of the company at t is X_t, the asset value of the company consists of the equity value and the convertible bond value, where D_t is the market value of a single convertible bond at time t, assuming that the convertible bond is a single bond, only to ensure that all debts are immediately convertible, and S_t is the total value of the stock at t

(4) Convertible bonds are not callable

(5) Shareholders receive δS_t and $\delta \ge 0$ dividends continuously

(6) The bondholder pays interest continuously at the interest rate $\alpha > 0$

(7) If the bondholder does not choose to convert before T, then T and $\min(X_T, L)$ are obtained, where L is the face value of the convertible bond

Since the market is complete, we know that there is an equivalent martingale measure $Q \sim P$ from the nonarbitrage pricing principle. Under the equivalent martingale measure Q, the stock price discount + cumulative dividend discount and convertible bond price discount + accumulated interest discount are all local martingales. Under the risk neutral probability Q, the value of the company satisfies the following stochastic differential equation:

$$dX_t = rX_t dt - \alpha dt - \delta S_t dt + \sigma X_t dw_t^*. \tag{2}$$

σ is the constant volatility and $\{W_t^*, 0 \le t \le T\}$ is the Brownian motion with medium risk Q.

4.2. Credit Risks. Now consider a convertible bond with credit risk. This paper uses the default risk model to deal with the credit risk of convertible bonds. Suppose the default risk rate $[t_{i-1}, t_i]$ and λ_i for a period of time; when the company defaults, the bondholder can only get a surface part and finally assumes the recovery rate i, that is, the ratio of the bond price to book value ξ_i.

If there are risk-free zero-coupon bonds with different maturities in the financial market, the price is called $\{p(1), p(2), p(3), \cdots, p(n)\}$, while the price of risk-free zero-coupon corporate bonds with different maturities is $\{D(1), D(2), D(3), \cdots, D(n)\}$; thus, the term structure of the risk-free interest rate can be obtained. If the recovery rate ξ_i is known, the default risk rate λ_i of the bond can be obtained from it. The specific analysis process is as follows:

If the one-year risk-free interest rate is r_0 and the risk interest rate is r_1^*, then there are

$$e^{-r_1^*} = [1 \cdot (1 - \lambda_1) + \xi_1 \cdot \lambda_1]e^{-r_0}. \tag{3}$$

When calculating λ_1, we can get λ_2 from the above formula. By analogy, we can get the default rate $\{\lambda_1, i \ge 1\}$ of each bond.

4.3. Arbitrage Cap. When the price of the CSI 300 stock index futures is overestimated to a certain extent, arbitrageurs in the market can carry out arbitrage by selling futures contracts and buying a stock portfolio. Arbitrageurs will adopt this strategy: first, sell the price of the CSI 300 stock index futures contract for the next month or quarter F_t and t and purchase the stock portfolio based on the sample weight of the CSI 300 index in the Shanghai and Shenzhen stock markets; t is the current air ticket purchase of a package of stocks S_t. Then, funds and investors need to borrow money from banks to transfer the trading cost μF_t of the stock index futures contract, the margin ηF_t, and the price t of the CSI300 futures contract. The transaction cost θS_t of the stock portfolio is separately calculated at time t on time S_t to obtain the risk-free loan interest rate.

When the contract of CSI 300 index futures matures, it will be delivered in cash. On the expiration date of the contract, the arbitrage operator will deliver the stock portfolio in the futures exchange, sell it in the stock market, and carry out arbitrage by using the unreasonable price at the t moment. This strategy allows investors to receive cash delivery from futures at any time, return margin sell stock portfolios and complete transactions, and obtain stock interest and the final value of the fund at any time. At the same time, they need to repay the principal and interest on the bank loans.

4.4. Lower Limit of Arbitrage. If the price of the Shenzhen Shanghai 300 stock index futures contract is obviously undervalued, we can use the method of buying a stock index futures contract and selling a stock portfolio to carry out reverse arbitrage. Investors first buy the CSI300 Stock Index Futures t according to the price F_t and then short the stock index futures contract t of the stock portfolio, income S_t, and cash payment. The stock portfolio includes the

transaction cost μF_t of the futures market, the margin ηF_t, and the transaction cost S_t of the futures contract. The stock portfolio will receive the bank deposit income at time t according to the risk-free interest rate and withdraw the deposit interest and principal on the maturity date θS_t of the CSI 300 contract.

Similar to the arbitrage strategy mentioned above, assets $F_t - S_T$ are paid when they are due and delivered in the stock index futures market T, and the margin ηF_t is returned from the stock index futures market. On the T maturity date, the investor receives S_t from 300 shares purchased from the Shanghai and Shenzhen stock markets in the amount of $(1 + \theta)S_T$, during which the investor does not hold shares. Therefore, in contrast, after losing the cycle, his stock portfolio should receive dividends, subtracting the final value of opportunity cost D_T in calculating the final cash flow.

4.5. Finite Element Numerical Solution of the Model. In this paper, we use the finite difference method to estimate the price of convertible bonds, that is, to solve the governing equation of the pricing model of convertible bonds. Therefore, the pricing problem of convertible bonds must be limited in a limited region. In this paper, the infinite region of the pricing problem is divided into a bounded region: take sufficiently large s and R values and assume that they are the upper bounds of the stock price and interest rate, respectively. Obviously, this assumption is reasonable. The areas of pricing problems are truncated, such as

$$(s, r, t) = [0, S] \times [0, R] \times [0, T]. \tag{4}$$

If $\Omega = [0, S] \times [0, R]$, then the region is $\Omega \times [0, T]$.

The governing equation of the pricing model is derived as follows:

$$\frac{\partial V}{\partial t} + rs\frac{\partial V}{\partial s} + \frac{1}{2}\left(\frac{\partial^2 V}{\partial s^2}\sigma_1^2 s^2 + \frac{\partial^2 V}{\partial r^2}w^2 + 2\frac{\partial^2 V}{\partial s \partial r}\rho\sigma_1 sw\right)$$
$$- rV + p\left(\max\left(ns(1-\eta^*), R^*B\right) + \eta^* s\frac{\partial V}{\partial s} - V\right)$$
$$= (w\lambda - u + p\lambda_1)\frac{\partial V}{\partial r}. \tag{5}$$

The conditions of the equation on domain $(s, r, t) = [0, S] \times [0, R] \times [0, T]$ are as follows:

(1) At the expiration of the contract, the value shall be the greater of the face value and the exchange value

(2) When the company's share price is high enough, investors will definitely consider converting bonds into stocks

(3) When the stock price of the company is very low, the value of the bond can be equal to the value of the ordinary bond regardless of the repurchase conditions

Table 1: Sample information of convertible bonds.

Name and research number of convertible bonds	Listing date
Brother convertible bond (A)	2017-12-27
Guozhen convertible bonds (B)	2017-12-25
Shengyi convertible bonds (C)	2017-12-11
Crystal bonds (D)	2017-12-12
Jichuan convertible bonds (E)	2017-11-29

(4) When the market interest rate is large enough, bond investors will consider selling. Therefore, the value of bonds can be considered as zero without considering the conditions of redemption and repurchase. If the bonds meet the conditions for redemption or resale, the value shall be the redemption or resale price

(5) When the interest rate tends to zero, the value of the bond is difficult to determine. Only when the interest rate tends to zero, the partial derivative of the bond value to interest rate will be limited

4.6. Total Value of Convertible Bonds. According to the above value calculation method, the option price including the value of each period of convertible bond can be obtained. According to the nonarbitrage pricing algorithm, the following model can be established to price the convertible bond.

(1) On the terminal node, the value of bonds is as follows:

$$\max\left(V_o, V_B\right), \tag{6}$$

where the stock price V_O is the conversion value of the bond at maturity, expressed as the stock price multiplied by the conversion ratio at maturity. V_B is the net value of the bond at maturity, equal to the sum of the face value of the bond and the final interest.

(2) At the intermediate node, the value of the bond is

$$\max\left(V_B, V_c, V_p, V_r, V_o\right), \tag{7}$$

where V_B is the value of the basic terms of the bond, V_c is the value of the bond's redemption period, V_p the value of the bond's repurchase clause, and V_r is the value of the bond's modification clause, that is, the value of the bond without considering other additional terms. All the values here need to be converted into the corresponding value of the whole bond according to the face value and conversion price of the bond. According to the reverse calculation algorithm, the value of each node is calculated in turn, and the theoretical value of each bond is finally obtained.
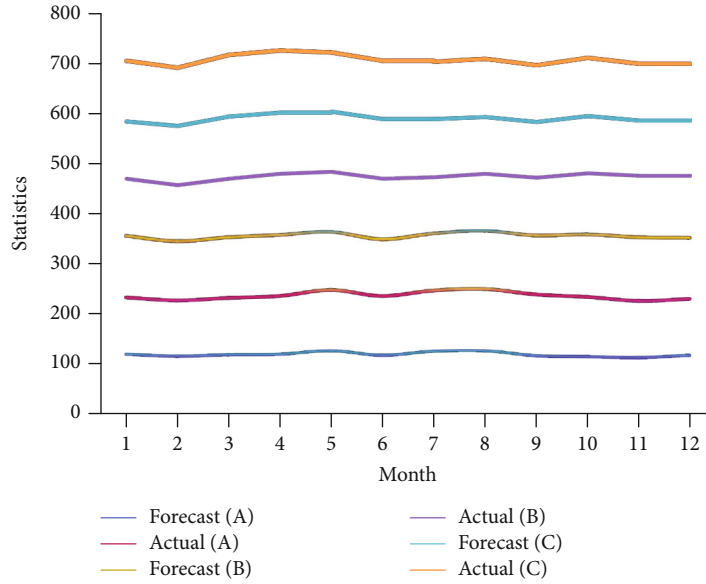
FIGURE 1: Comparative analysis of market price and theoretical price of convertible bond.
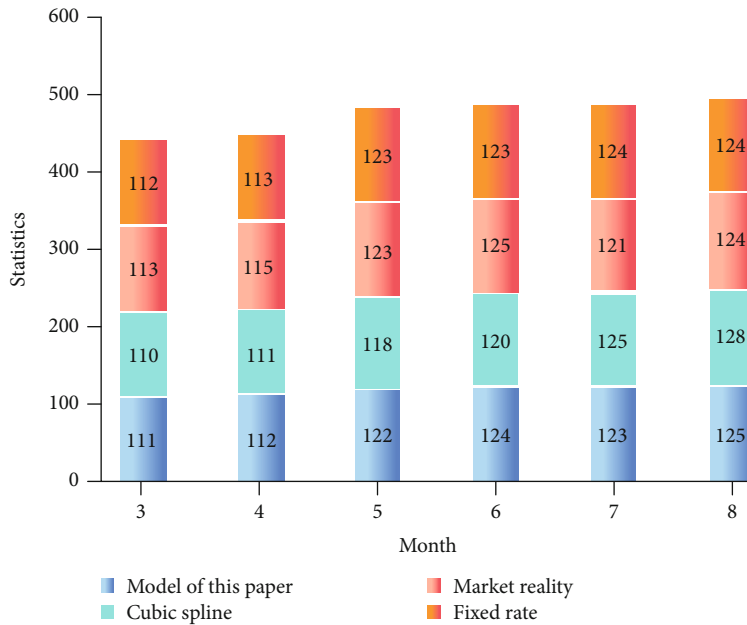

FIGURE 2: Comparative analysis of the impact of term structure of interest rate on convertible bond pricing.

5. Case Analysis

5.1. Sample Selection. This part of the research sample is composed of five convertible bonds listed in 2017 and still in trading, and the research range is from January 2, 2018, to November 30, 2018, excluding 2118 sample points after statutory holidays, closing date of convertible bonds, and closing date of benchmark stocks. The selected convertible bonds are shown in Table 1.

5.2. Comparative Analysis of Market Price and Theoretical Price of Bonds. It can be seen from the comparison results in Figure 1 that, in general, the theoretical value of convertible bonds in China is overestimated, but the gap between the theoretical value and the market price is small, and the model fitting is good. Although the value of some convertible bonds has been underestimated for some time, the theoretical value of convertible bonds has been underestimated. Take Guozhen convertible bonds as an example. Before the suspension of Guozhen convertible bonds in July 2018, the company's operating performance was not good. In mid-August, the stock price suddenly fell, leading to the theoretical value of the Guozhen convertible bond falling below the market price since mid-August. Among them, Brother convertible bonds and Shengyi convertible bonds are closer to the theoretical price, and the model fitting effect is better. Overall analysis shows that the market price trend predicted by the model is similar to the theoretical price.
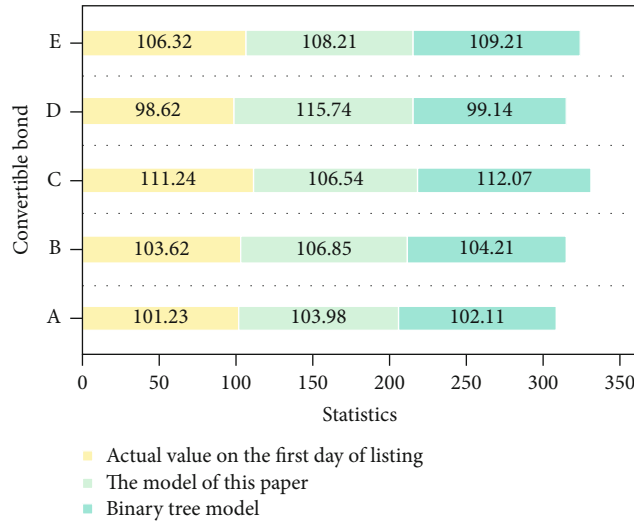
FIGURE 3: Comparison of the prediction results between the model of this paper and the binary tree model.

TABLE 2: Statistical results of relative error calculation.

Name and research number of convertible bonds	Maximum value	Minimum value	Average value
Brother convertible bond (A)	-0.1625	-0.0472	-0.1041
Guozhen convertible bonds (B)	0.0714	-0.0011	0.012
Shengyi convertible bonds (C)	-0.1118	-0.0014	-0.0614
Crystal bonds (D)	0.1251	0.0007	0.0974
Jichuan convertible bonds (E)	-0.0852	0.0048	-0.0214
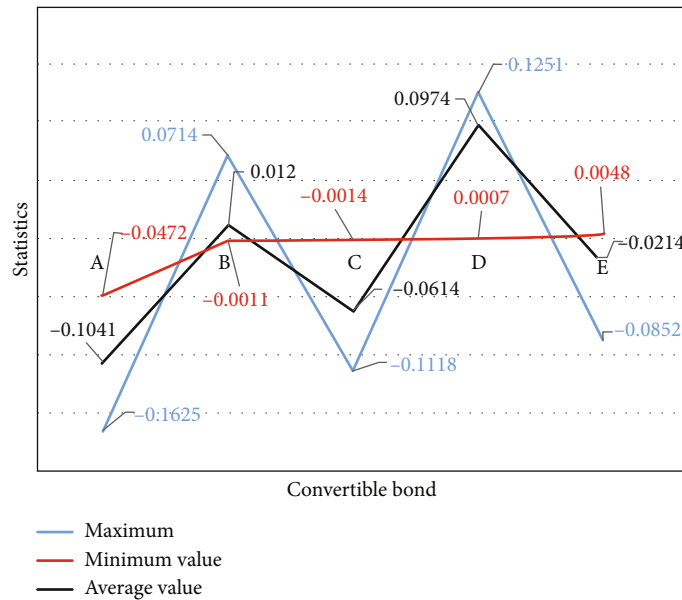
FIGURE 4: Analysis of experimental results of relative price error of convertible bonds.

5.3. Influence of Term Structure of Interest Rate on Convertible Bond Pricing. On the basis of the pricing model in this paper, we use the model and cubic spline to estimate the theoretical value of the convertible bond and compare it with the market price and fixed interest rate results, as shown in Figure 2. It can be seen from the analysis results in Figure 2 that the theoretical value of convertible bonds estimated by the model is slightly higher than that estimated by the cubic

polynomial spline model and is closer to the market price than that estimated by the cubic polynomial spline model. The main reason is that the risk-free interest rate calculated by the index model is greater than the risk-free interest rate calculated by the spline function model in the short term. In addition, it can be seen that the estimation results of the fixed interest rate and the estimation trend of the model are very stable. Because the change of the risk-free interest rate is very small in a short time, the static risk-free interest rate can be used to replace the dynamic risk-free interest rate. The results show that the pricing model in this paper has higher accuracy.

5.4. A Comparative Experiment on the Prediction Effect of the Model and the Binary Tree Model. In order to test the prediction effect of the model, it is compared with the traditional binary tree model. The simulation results of five kinds of convertible bonds are shown in Figure 3.

According to the result analysis in Figure 3, except for Jichuan convertible bonds, the error values of the other four convertible bonds are smaller than the traditional binary tree model, and the error values of Jichuan convertible bonds are all within 3%. Generally speaking, the combination pricing model in this paper is closer to the actual market value than the traditional binary tree model. Therefore, this paper considers that the combination pricing model studied in this paper is superior to the traditional binary tree model in forecasting ability and can replace the traditional binary tree model.

5.5. Analysis of Relative Price Error of Convertible Bonds. It can be seen from the statistical results in Table 2 and Figure 4 that the volatility significantly reduces the relative price error of pricing after the model is modified. From the maximum value of the relative price error, except for the Guozhen convertible bonds which did not decline, the rest fell. From the minimum value of the relative price error, except for the Brother convertible bonds, the other relative price errors are decreasing. From the average value of the relative price error, the Guozhen convertible bonds increased and the rest decreased. The average relative price error of the five convertible bonds is -0.0113, that is, the simulated price is 1.32% lower than the market price. But the relative price error of the five convertible bonds is -0.0213, that is, the simulated price is 2.15% lower than the market price. From the overall results, the calculation error is relatively small, and the effect of error improvement is obvious.

6. Conclusions

The financial market is an important part of economic development, which plays an important strategic role in national development. Because of its own advantages, convertible bonds play an important role in the economic activities of various countries. The research on convertible bonds in China is relatively late. In the late 1970s, convertible bonds developed rapidly in China. Although the scale of convertible bond trading in China is very large and the development trend is good, there is little research on the pricing model of convertible bonds. At present, most of the domestic pricing technology is used abroad, but due to the different market conditions, the calculation accuracy is not high. The research on the application of the nonarbitrage pricing model and the finite element numerical solution in the value of convertible bonds proposed in this paper, to a certain extent, makes up for the lack of research in this field. The pricing model studied in this paper is based on the nonarbitrage pricing theory and finite element numerical solution. These two methods are one of the mainstream pricing theories at present, and their combination design is the biggest innovation of this paper. The combination design improves the traditional pricing model of single factor deficiencies, but also further enhances the accuracy of the pricing model. In the final comparative experiment, the traditional binary tree model is taken as the main contrast experimental object. Through the analysis of experimental data, the pricing model based on the nonarbitrage pricing theory and finite element numerical solution is significantly better than the traditional binary tree model in the calculation error value and market development trend prediction analysis, and the comprehensive performance has been significantly improved.

Data Availability

No data were used to support this study.

Conflicts of Interest

The author declares that she has no conflicts of interest.

Acknowledgments

References

[1] J. R. Hoffmeister, P. A. Hays, and G. D. Kelley, "Conditions affecting the timing of convertible bond sales," *Journal of Business Research*, vol. 15, no. 1, pp. 101–106, 1987.

[2] Z. Zhang, Q. Qi, and J. Deng, "Building intelligent transportation cloud data center based on SOA," *Journal of Ambient Intelligence and Humanized Computing*, vol. 8, no. 2, pp. 1–11, 2017.

[3] H. Yan, S. Yang, and zhao, "Research on convertible bond pricing efficiency based on nonparametric fixed effect panel data model," *China Finance Review International*, vol. 6, no. 1, pp. 32–55, 2016.

[4] S. Zhang, "Finite difference method for barrier option pricing under stochastic volatility," *Liaoning Gongcheng Jishu Daxue Xuebao (Ziran Kexue Ban)/Journal of Liaoning Technical University (Natural Science Edition)*, vol. 36, no. 10, pp. 1111–1115, 2017.

[5] Z. Jing, F. Zhaoben, and J. Zhu, "The prediction of corporate bond credit spreads on output and inflation: a study based on the BMA model," *Mathematical Statistics and Management*, vol. 37, no. 1, pp. 183–194, 2018.

[6] D. Yaman, "Industry effects and convertible bond sequence," *Global Journal of Business Research*, vol. 10, no. 3, pp. 9–20, 2017.

[7] M. J. Wang, Y. W. Lin, and T. S. Lee, "A study of the causality between convertible bond prices and stock prices in conversion-price reset periods—time-series and cross-section analyses," *Asia-Pacific Journal of Financial Studies*, vol. 44, no. 3, pp. 447–474, 2015.

[8] Z. Zhang, W. Liu, and X. Zhang, "Valuation of convertible bond under uncertain mean-reverting stock model," *Journal of Ambient Intelligence & Humanized Computing*, vol. 8, no. 5, pp. 641–650, 2017.

[9] L. Wang and H. Jiang, "Directors from bank and convertible bond issuing: Chinese evidence," *Finance and Economics Theory and Practice*, vol. 38, no. 1, pp. 88–94, 2017.

[10] A. Amerjee, "The foreign currency convertible bond crisis: counting chickens before they hatched," *International Journal of Public Law and Policy*, vol. 4, no. 3, pp. 279–292, 2014.

[11] T. R. Bielecki, I. Cialenco, and R. Rodriguez, "No-arbitrage pricing for dividend-paying securities in discrete-time markets with transaction costs," *Mathematical Finance*, vol. 25, no. 4, pp. 673–701, 2015.

[12] S. Hendriks and C. Martini, "The extended SSVI volatility surface," *The Journal of Computational Finance*, vol. 22, no. 5, pp. 25–39, 2019.

[13] K. Boukir, "A high-order characteristic/finite element method for the incompressible Navier-Stokes equations," *International Journal for Numerical Methods in Fluids*, vol. 25, no. 12, pp. 1421–1454, 2015.

[14] F. Tornabene, N. Fantuzzi, F. Ubertini, and E. Viola, "Strong formulation finite element method based on differential quadrature: a survey," *Applied Mechanics Reviews*, vol. 67, no. 2, pp. 145–175, 2015.

[15] M. E. Mabsout, L. C. Reese, and J. L. Tassoulas, "Study of pile driving by finite-element method," *Journal of Geotechnical Engineering*, vol. 121, no. 7, pp. 535–543, 2016.

Retraction

Retracted: Dynamic Index Optimal Investment Strategy Based on Stochastic Differential Equations in Financial Market Options

Wireless Communications and Mobile Computing

This article has been retracted by Hindawi following an investigation undertaken by the publisher [1]. This investigation has uncovered evidence of one or more of the following indicators of systematic manipulation of the publication process:

(1) Discrepancies in scope

(2) Discrepancies in the description of the research reported

(3) Discrepancies between the availability of data and the research described

(4) Inappropriate citations

(5) Incoherent, meaningless and/or irrelevant content included in the article

(6) Peer-review manipulation

The presence of these indicators undermines our confidence in the integrity of the article's content and we cannot, therefore, vouch for its reliability. Please note that this notice is intended solely to alert readers that the content of this article is unreliable. We have not investigated whether authors were aware of or involved in the systematic manipulation of the publication process.

Wiley and Hindawi regrets that the usual quality checks did not identify these issues before publication and have since put additional measures in place to safeguard research integrity.

We wish to credit our own Research Integrity and Research Publishing teams and anonymous and named external researchers and research integrity experts for contributing to this investigation.

The corresponding author, as the representative of all authors, has been given the opportunity to register their agreement or disagreement to this retraction. We have kept a record of any response received.

References

[1] J. Zhang, "Dynamic Index Optimal Investment Strategy Based on Stochastic Differential Equations in Financial Market Options," *Wireless Communications and Mobile Computing*, vol. 2021, Article ID 5545956, 9 pages, 2021.

WILEY | Hindawi

Research Article

Dynamic Index Optimal Investment Strategy Based on Stochastic Differential Equations in Financial Market Options

Jun Zhang [ID]

College of Commercial, Wuxi Taihu University, Wuxi, 214064 Jiangsu, China

Correspondence should be addressed to Jun Zhang; zhangj3@wxu.edu.cn

With the gradual development and improvement of the financial market, financial derivatives such as futures and options have also become the objects of competition in the financial market. Therefore, how to make the most favorable and optimized investment and consumption when options are included? It has become a problem facing investors. Aiming at the optimal investment problem of investors, this paper studies the calculation of an optimal investment strategy in stochastic differential equations in financial market options on the basis of fuzzy theory. Now, stochastic calculus has become an important branch of stochastic analysis, finance, control, and other fields. The study of introducing stochastic differential equations is mainly to solve the stochastic control problem, which is the principle of the stochastic maximum. In finance, some hedging or pricing problems of contingent rights can eventually be transformed into a series of stochastic differential equations. Based on the historical data of five aspects of bank deposits, bonds, funds, stocks, and real estate of four listed insurance companies, the paper analyzes the optimization strategy of the capital investment of listed insurance companies based on the investment yield of the domestic investment market. According to the final results, the historical proportion of bank deposits of the superior company is 27%, and the optimal proportion given by the model is 25%; the total proportion of funds and stocks is 15%, and the optimal proportion of funds analyzed in the model is 20% and the optimal proportion of stocks is 10%. Therefore, the final results show that the investment efficiency of listed insurance companies can actually increase investment in stocks and funds and reduce the proportion of bank deposits to obtain greater investment returns.

1. Introduction

1.1. Background Meaning. In the era of economic globalization, the important position of finance in the economy has been further highlighted. The issue of optimal investment and consumption of financial derivatives in the financial market has always been a hot issue in the current financial investment market, as well as a problem that investors have been paying attention to. The main problem of finance is resource allocation. Time and random uncertainty are the key factors that affect investors' financial and economic behavior in the financial market. Scholars across multiple disciplines and policy makers from multiple institutions have been looking for economic, political, and institutional foundations to improve the strength of the financial market [1]. Therefore, in random financial markets, there is research on how market participants (individuals or institutions) treat

limited wealth or resources which will be allocated to various (financial) assets, such as stocks, cash accounts, bonds, and capital market consumption, so as to achieve timely optimal allocation of resources to achieve reasonable cash flow and risk/return characteristics to meet the financial needs of market participants. Its main content is to maximize the use of investors' interests as the decision criterion to obtain the optimal investment portfolio and optimal consumption plan for the wealth distribution of participants. Econometrics, financial econometrics, mathematical finance, and empirical financial methods have made significant contributions to the study of financial econometrics. Derivatives include market-based stochastic volatility model estimation, the fine structure of equity index option dynamics, and multifactor Wishart option pricing based on stochastic volatility, etc. [2]. Option, as one of the derivative securities in the financial market, is the same as any other derivative product. Its value

depends on the underlying securities. For example, the value of stock options depends on the stock price, which has always been at the forefront of research in financial mathematics. The stochastic differential equation has become a very practical tool in the financial field, especially in the problem of optimal investment in options.

The purpose of this paper is to consider the optimal investment strategy of options in the financial investment market under the premise of an incomplete market closer to the actual situation, so that investors can maximize their investment benefits. Therefore, on the basis of previous studies, this paper uses stochastic differential equations to calculate the dynamic index of financial market options on the basis of fuzzy theory, gives the expression of the optimal investment strategy in an incomplete market, and studies the optimal investment solution in the case of options.

2. Proposed Method

2.1. Related Work. Wang et al. studied several linear quadratic optimal control problems of the forward and backward stochastic differential equations of the mean field [3]; this control problem is different from the existing literature on the optimal control of the mean field stochastic system, and it has more applications; a closed-form optimal solution can be obtained under detailed conditions. Yang and Zhao applied it to the special type of forward and backward stochastic differential equations (FB-SDE) that appeared in finance and stochastic control and provided convergence analysis for the recently proposed multistep scheme [4], but this method is more difficult to solve. Tardelli uses reverse stochastic differential equations (BSDE) and filtering techniques to study stochastic control problems [5], but this method has certain limitations; it requires a sequence of functions that converge to a value function. Wang et al. use the method and Monte Carlo method to study the optimal investment problem of DC pension under inflation and loss avoidance [6], but this method has a large amount of calculation and slower improvement in accuracy. Li et al. studied the optimal investment strategy based on derivatives based on the asset-liability management (ALM) problem of the mean-variance criterion in the presence of random volatility [7]. Xu et al. use the dynamic programming method to discuss the best investment and reinsurance policies of an insurance company with a classic earnings process [8], but this method has prominent spatial contradictions and difficult data storage. Kim and Lee used the Black–Scholes–Merton model to study the best investment using real option valuation and fuzzy logic [9], but the derivation process of this model is unacceptable. Ibrahim studied the three-stage investment ratio and the impact of key factors on the real option investment threshold [10]. Wang and Huang use a multiple jump-diffusion (MJD) model to provide an optimal asset allocation strategy that can improve risk management performance in the face of financial crises [11]; this model requires careful analysis of the optimization process.

This article applies theoretical research and experimental research, adopts a combination of quantitative and qualitative theoretical and numerical calculation methods, and uses a variety of calculation methods, such as theoretical analysis, mathematical modeling, analytical subtraction, and numerical calculation. Based on the dynamic optimal investment strategy, we conduct more systematic and in-depth research and discussion. Moreover, this article contains basic theories such as financial economics, financial mathematics, financial stochastic analysis, modern securities investment, and stochastic differential equations, which can analyze the problems of this article in a more comprehensive and detailed manner. In the research of this article, the only information that investors can obtain is the information generated by asset prices, and the unobservable process will be modeled by stochastic differential equation models [12].

2.2. Stochastic Differential Equation. Stochastic differential equation (SDE) is now an important branch of mathematics. Since its development, it has been gradually improved after many scholars' research and discussion. Stochastic differential equation theory inherits many ideas and methods in deterministic theory. Its research content includes existence and uniqueness, constraints, solution evaluation, solution stability and branching, and martingale and Markov properties in stochastic analysis. Stochastic differential equations can be used to obtain the autocorrelation function of the output noise voltage and other solution statistics such as the mean and variance [13]. In recent years, due to the profound mathematical and physical background of stochastic stability and the stochastic branch, many researchers have paid great attention to it, and it has become an important part of the theoretical research of stochastic dynamical systems. At present, although stochastic stability has obtained more theoretical results, it is still very small compared with the stability theory of deterministic equations, and there are still many unsolved problems. The theoretical system needs to be further improved and perfected. The research on stochastic separation theory is based on stochastic stability and is still in its infancy, especially for high-dimensional and time-delay differential systems.

Stochastic differential equations are usually ordinary differential equations, whose coefficients are random variables and differential equations driven by random processes. Stochastic differential equations can be used to describe various natural phenomena, economic phenomena, financial phenomena, etc. These phenomena have a similarity, that is, reducing the input to continuous, very fast random operations, that is, using a Brown as the system driving force. The formula of stochastic differential equation is generally

$$d\xi_t = A(t, \xi_t)dt + B(t, \xi_t)dB_t, \quad (1)$$

where $A(t, \xi_t)B(t, \xi_t)$ is a given function, with more specific and normal characteristics; this stochastic differential equation can be integrated to get its integral formula:

$$\xi_t = \xi_0 + \int_0^t A(t, \xi_t)dt + \int_0^t B(t, \xi_t)dB_t. \quad (2)$$

So it is also called a stochastic integral equation, where the first integral is the integral using the time parameter as

a regular function, and the second integral is the Ito integral, and ξ_0 is a random initial value independent of Brownian motion $\{B_t : t \geq 0\}$.

Stochastic differential equations can be divided into many types, of which backward stochastic differential equations are widely used in finance. In option pricing, the backward stochastic differential equation (BSDE) has a wide range of applications, and the Black-Scholes model is one of the classic pricing models [14]. First, consider simple deterministic systems and ordinary differential equations. In order to solve specific results, first give a definite solution condition for the solution within a period of time. When $0 \leq t \leq T$, there is a positive condition that gives the definite solution condition at the initial time $t = 0$. To ordinary differential equations,

$$\begin{cases} dx(t) = f(x(t))dt, \\ x(0) = x_0. \end{cases} \tag{3}$$

Then, we consider the backward ordinary differential equation and still give the definite solution condition. The backward ordinary differential equation based on the fixed solution condition at the end time $t = T$ is as follows:

$$\begin{cases} dW(t) = g(W(t))dt, \\ W(T) = W_T. \end{cases} \tag{4}$$

Then, we consider the complex nondeterministic system, use $B(t)$ to represent Brownian motion, and assume that there are d mutually independent interference sources, that is, we use d to represent the dimension and still give the initial conditions when $t = 0$ and get the positive Stochastic differential equation:

$$\begin{cases} dx(t) = f(x(t))dt + \sigma(x(t))dB(t), \\ x(0) = x_0. \end{cases} \tag{5}$$

We use η to denote the fixed value at T, and $W(t)$ and $H(t)$ are two adaptation processes that represent the backward stochastic differential equations that can be obtained in the initial state according to the law of motion of the differential equation:

$$\begin{cases} -dW(t) = g(W(t), H(t))dt - H(t)dB(T), \\ W(T) = \eta. \end{cases} \tag{6}$$

2.3. Fuzzy Logic. Fuzzy logic is developed on the mathematical basis of fuzzy set theory founded by Professor L.A. Zadeh of the Electrical Engineering Department of the University of California, Berwick. Fuzzy theory refers to the application of the basic concepts of imprecise sets or adhesion functions, which are mainly divided into five branches: fuzzy mathematics, fuzzy logic and artificial intelligence, fuzzy systems, uncertain information and theory, and fuzzy decision-making.

In the real world, many uncertain technical rules are expressed through physical rules (such as uncertain words and languages), and the recent fuzzy reasoning mechanism can solve this problem well. Uncertain finance is a new field in which the risk process is described by the uncertain process. Good uncertainty predicts that future economic activities, such as consumption, output, and investment, will increase and are positively correlated with the valuation ratio, while bad uncertainty predicts that economic growth will decline and depress asset prices [15]. Uncertainty and competition will have an important impact on the value of investment projects [16]. The existence of inevitable uncertainty brings some difficulties to the numerical processing of optimization tasks [17]. In finance, the current technical analysis using fuzzy theory is mainly through assigning different input variables and parameters to the fuzzy system. For example, T. Chavarnakul and D. Enke constructed a neuro-fuzzy inference system with trading volume as input variables and then used genetic algorithms to adjust the membership functions of the input variables in the inference system, thereby building a multi-intelligent algorithm for securities trading system; T. Anbalagan and S.U. Maheswari used technical indicators Simple Moving Average (SMA), Moving Average Convergence/Divergence (MACD), and Relative Strength Index (RSI) as input variables of the fuzzy decision-making system for decision-making; for A.D. Ijegwa et al., MACD, RSI, Stochastic Oscillator (SO), and Balance Volume (OBV) indicators are used as the input variables of the fuzzy decision system to determine the trading time; and G. Rubell Marion Lincy and C. Jessy John use less used earnings per share (EPS) information, as well as closing prices, profit fluctuations, and investor risk behavior, as input variables. Finally, three different fuzzy systems of buying, selling, and holding are established, and decisions are made based on the fuzzy decision values obtained by the three fuzzy systems. However, if a large number of secondary indicators are selected as input variables, duplication of information and calculation troubles may occur.

2.4. Option. Options are financial products derived from underlying securities, which refer to the right to buy or sell financial products or futures contracts at an agreed price within a specified time limit. Options are important financial derivatives, and their risk management characteristics have been widely accepted by investors [18]. The first batch of option transactions in history was only used for physical commodities and precious metals, and they were all spot options. Subsequently, the emergence of the world's first option house caused a huge change in the option trading market, which brought trading options into a new stage of fully integrated and standardized management. Standardized functions make the transaction process simple, and the exchange also guarantees the final performance. The emergence of exchanges introduced optional transactions from over-the-counter trading to on-exchange trading, which led to a sharp increase in the trading volume at the bottom of the transaction; the standardization of option contracts increased market liquidity, improved transaction efficiency, and reduced transaction costs. Options are the right of the

buyer and the obligation of the seller. Options have the following characteristics: (1) the buyer must pay the seller corresponding fees to obtain the right, (2) the buyer obtains the right on a specific date or within a specific time period in the future, (3) the purchase or sale of the item in the future is specific, and (4) the price of the basic material purchased or sold by the option buyer in the future is predetermined. The buyer can choose whether to implement it and can flexibly choose according to the price of the expired asset.

The most important feature of option trading is to allow the holders of expected rights to have a certain degree of flexibility in decision-making so that they can flexibly use the possibility of various changes in the financial market and control market risks such as interest rates and exchange rates to maximize the percentage, without losing potential profit opportunities. A call option is the right to purchase an asset at the current fixed price at a specific time in the future, not a burden. A put option is the right to sell an asset at a predetermined price at a specific time in the future, but if the trading option shows an asymmetric ability, it is impossible to predict the analyst's suggestion to modify the underlying stock [19]. From a different perspective, options are divided into many types, such as European options and American options. European options are delivered at a specified future time T, and American options are delivered at any time before time T. The European call parity condition is used to estimate the preexercise premium for US currency options traded on the Philadelphia Stock Exchange [20]. For European stock purchase options, the holder has the power, but is not obliged, to sell the stock at a specific price in the future T time, for example, sell the stock for 10 yuan. If the stock price rises by more than 10 yuan at time T, the holder of the call option will buy the stock for 10 yuan. If the price is less than 10 yuan, then it will obviously give up the implementation of the agreement (no obligation to pay for damages), then the price of the right is zero.

Option pricing is an important field of financial research [21]. At present, there are mainly the following methods for option pricing:

(1) Black-Scholes Option Pricing Method. At time 0, the values c and p of European call and European put options that do not pay dividends are

$$c = SN(d_1) - Ke^{-rT}N(d_2), \tag{7}$$

$$p = Ke^{-rT}N(-d_2) - SN(-d_1), \tag{8}$$

$$d_1 = \frac{\ln (S/K) + (r + \sigma^2/2) T}{\sigma\sqrt{T}}, d_2 = d_1 - \sigma\sqrt{T}. \tag{9}$$

Among them, $N(x)$ is the distribution function of the standard normal distribution; S and K are the current stock price and execution price, respectively; r is the risk-free interest rate; and σ is the asset volatility rate. When the number of options to be calculated is small, this method is more convenient, but it can only calculate the analytical solution of European options and cannot be applied to American options.

(2) Binomial Tree Option Pricing Method. In this model, the effective period of the option is divided into several equal cell intervals, and the duration of each small period is $\Delta t = T/n$. Taking European call options as an example, the option value is

$$f = \frac{\sum_{i=0}^{n}(n!/(n-i)!i!)p^i(1-p)^{n-i} \max \left(Su^i d^{n-i} - X, 0\right)}{(1+r)^n}. \tag{10}$$

If other factors (such as transaction taxes) are not taken into account, then if a lucrative option is not redeemed before the expiry date, it will definitely be redeemed on the expiry date. For an option, we can set its intrinsic value. Assuming that A represents the strike price and X_T represents the price of the underlying asset at the expiry date, the intrinsic value of the long call option is defined as

$$\max (X_T - A, 0). \tag{11}$$

This means that if $X_T > A$, the option will be executed; otherwise, the option will not be executed. Similarly, the intrinsic value of a put option is defined as

$$\max (A - X_T, 0). \tag{12}$$

This means that if $X_T < A$, the option will be executed; otherwise, the option will not be executed. But no matter what, the intrinsic value of options is nonnegative.

For an option, whether it is profitable, in addition to considering the intrinsic value of the option, the purchase period of the option should also be considered. For call options, suppose the price of each option is Y, and by the intrinsic value of the call option, the buyer's income per share of the call option is

$$\max (X_T - A, 0) - Y = \begin{cases} -Y, & X_T \leq A, \\ X_T - A - Y, & X_T > A. \end{cases} \tag{13}$$

The seller's return per call option is

$$Y - \max (X_T - A, 0) = \begin{cases} Y, & X_T \leq A, \\ -X_T + A + Y, & X_T > A. \end{cases} \tag{14}$$

Similarly, the corresponding formula can be obtained for put options.

2.5. Optimal Investment Strategy. The research on the optimal investment strategy was first mentioned in Markowitz's "Securities Portfolio Theory." He used the mean variance model to describe the risk of insurance companies. Samuelson extended his model and used the principle of stochastic dynamic programming to obtain an optimal investment strategy. Later, after the research and promotion of many researchers, the optimal investment strategy model was

gradually improved and widely used in the financial investment market. In addition, according to whether the investment portfolio changes dynamically over time, the investment portfolio can be divided into a one-period portfolio model and a multiperiod portfolio model. The one-year portfolio model means that investors keep their portfolio unchanged from the beginning to the end of the period. If it is believed that the one-period portfolio model cannot cope with the rapidly changing market, then a dynamic multiperiod model is needed to simulate the portfolio problem. Martingale theory is also a powerful tool for studying optimal investment problems. Previous scholars used the martingale method and duality theory to conduct detailed research on the investment problem of maximizing the utility function. Using the martingale method, they studied the option pricing problem in underdeveloped financial markets and discussed the optimal investment with options. The problem of high-dimensional optimal investment and consumption is difficult to deal with, especially because it is difficult to characterize the value function [22].

To study the optimal investment problem, the decision-making between investors also influences each other. Therefore, when considering this problem, we should start from two aspects: the optimal investment choice of a single investor and the optimal investment choice of multiple investors. The research of a single investor's dynamic portfolio model has produced a lot of research results. The collection of investment opportunities determines the investment market environment of the financial market facing investors and therefore further determines the stochastic economic model faced by investors and determines the type and quantity of financial assets that investors can choose. Existing research on the potential optimal consumption and investment portfolio of two or more economic entities still has the following problems to be solved: First, when defining investment criteria, most models only consider the relative distance between the investors' respective wealth levels. Mathematically speaking, they usually directly target the relative distance between two levels of wealth. In addition, participants mainly involve investors and virtual opponents of the "market."

3. Experiment Setup

3.1. Test Subject. This article uses stochastic differential equations and Markowitz's model to calculate and analyze the optimal investment strategies of listed insurance companies in terms of fixed deposits, bonds, funds, stocks, and other factors of four listed insurance companies from 2015 to 2019. The research mainly focuses on risk-free investment and risk investment and establishes six variables: bank deposit yield, treasury bond yield, fund yield, stock yield, and real estate investment yield to solve the company's optimal investment strategy.

3.2. Experimental Data

3.2.1. Bond Investment. The investment in bonds of listed insurance companies mainly includes government bonds,

Table 1: Bond investment proportion table.

Year	Company A	Company B	Company C	Company D	Average value
2015	0.69	0.59	0.59	0.53	0.6
2016	0.66	0.57	0.46	0.52	0.55
2017	0.55	0.57	0.43	0.52	0.52
2018	0.47	0.50	0.51	0.50	0.495
2019	0.41	0.45	0.46	0.47	0.45

Table 2: Proportion of stock investment.

Year	Company A	Company B	Company C	Company D	Average value
2015	0.045	0.047	0.014	0.01	0.029
2016	0.084	0.076	0.06	0.073	0.073
2017	0.063	0.055	0.043	0.051	0.053
2018	0.074	0.08	0.037	0.06	0.063
2019	0.08	0.085	0.04	0.047	0.063

Table 3: Fund investment proportion table.

Year	Company A	Company B	Company C	Company D	Average value
2015	0.0561	0.0341	0.0641	0.0297	0.046
2016	0.0423	0.0297	0.0415	0.0531	0.042
2017	0.0416	0.0258	0.0721	0.0251	0.041
2018	0.0347	0.0372	0.0591	0.0463	0.044
2019	0.0619	0.0395	0.0362	0.0347	0.043

financial bonds, and corporate bonds. The yield of bond investment is higher than that of bank deposits, and its risk is lower than that of stock investment. Regardless of whether it is government bonds, financial bonds, or corporate bonds, there are corresponding credit entities. As a guarantee, under certain risk control, insurance companies can obtain stable investment income satisfactorily, maintain insurance funds, and increase value. It is to an insurance company the best investment option. The bond investment proportions of the four listed insurance companies from 2015 to 2019 are shown in Table 1.

According to the data in Table 1, the bond investment proportion of listed insurance companies has a downward trend, but it is basically stable at about 50%. Bond investment has become the preferred investment channel for insurance companies to maintain and increase their value.

3.2.2. Stock Investment. Since the China Insurance Regulatory Commission clearly stated that insurance funds can be directly invested in the stock market, investors in many insurance companies have rushed because of the high rate of return that stocks can obtain. Table 2 shows the proportion of the four companies' investment in stocks.

It can be seen from the data in the table that the share of stock investment of the four companies fluctuates and fluctuates greatly each year. But in the end, the company's average
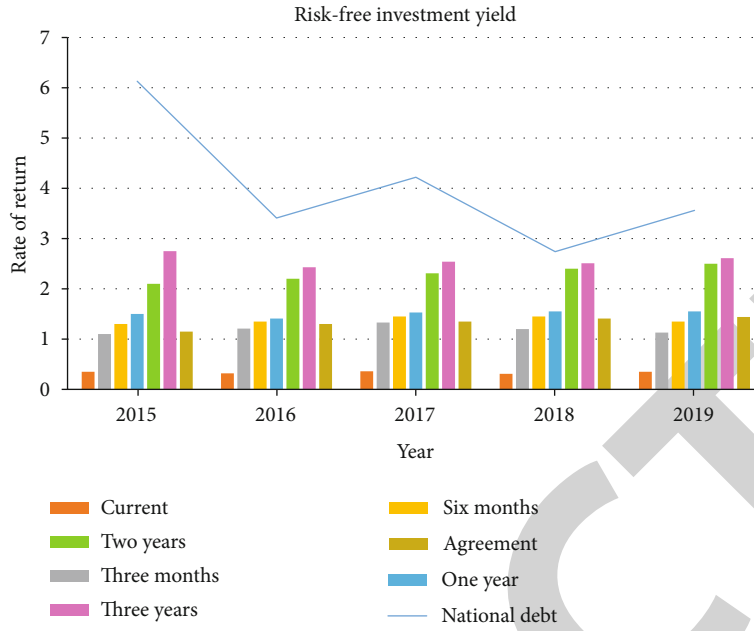
FIGURE 1: Risk-free investment yield chart.

investment ratio was basically stable at around 0.063. Although the share of listed insurance companies is small, they have a greater impact on investment returns and investment robustness. In addition, the incomplete development of the author's country's capital market has made the guesses of insurance companies more serious. In the past two years, the capital market has fluctuated frequently, and frequent reports of insurance funds have undoubtedly become the hottest topic in the capital market recently.

3.2.3. Fund Investment. As an important part of the financial market, funds have become an important participant in asset allocation. They are matched with a large amount of insurance funds, with a long term and continuous stability. They have optimized the asset allocation of listed insurance companies and improved the long-term stability of investment returns, playing an active role in diversifying investment risks. Table 3 shows the proportion of the investment of the four listed insurance companies in the fund.

According to the fund investment proportion data in Table 3, it can be seen that the average investment proportion of insurance companies in funds is basically around 0.04. The proportion of investment funds of listed insurance companies is relatively low and needs to be improved. Mutual funds can bring higher return on investment for listed insurance companies. The rate of return on investment and the rate of return on the market are positively correlated: when stocks are expected to grow, listed insurance companies can choose funds with higher risk factors to obtain higher rates of return. When the stock market is expected to fall, you can choose a mutual fund with a lower risk factor to reduce risk. The listed insurance company chooses the appropriate amount of capital investment according to the risk tolerance and market risk level.
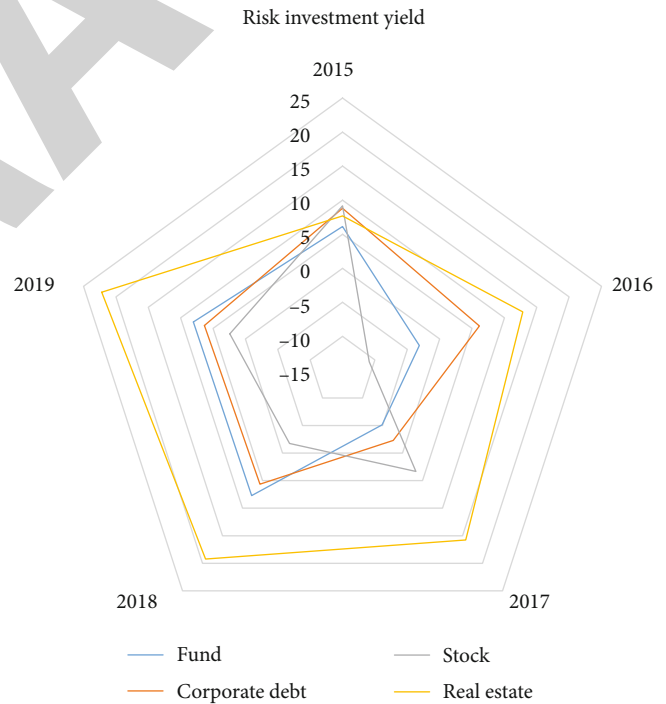

FIGURE 2: Risk investment yield chart.

4. Discussion of Result

4.1. Risk-Free Investment Income. This article regards bank deposits and government bonds as investment risk returns of listed insurance companies. The value of treasury bonds is determined by the stock market based on the weighted value of treasury bonds issued by listed companies, which can reflect the overall fluctuations in the bond market; bank
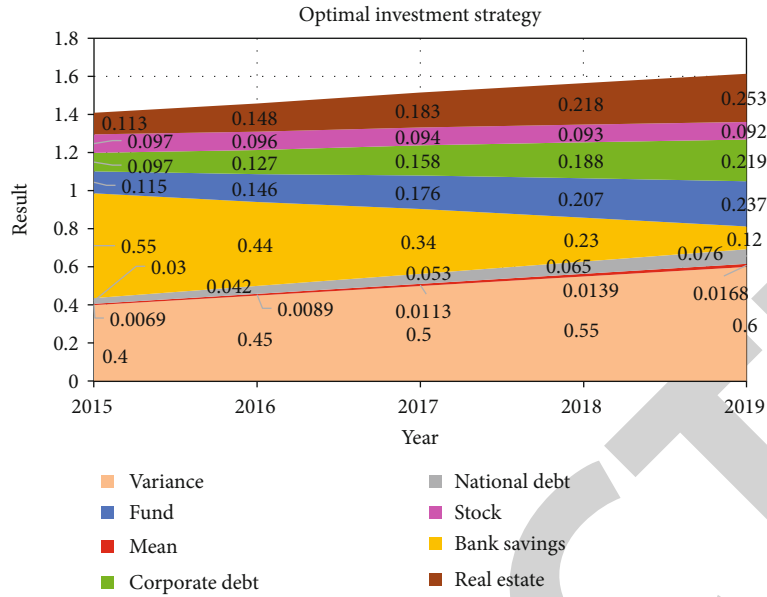
Figure 3: Diagram of optimal investment strategy.

deposits are based on the current deposit interest rate on the official website of the Bank of China from 2015 to 2019, 3 months, 6. The sum of monthly, 1-year, 2-year, and 3-year fixed interest rates and agreed deposit rates finds the average return on deposit rates for each year. The upper and lower limits of interest rates are popular interest rate derivatives in financial markets [23]. Finally, the data of treasury bonds and bank deposits are sorted and calculated to get a risk-free investment income chart as shown in Figure 1.

According to the graphical trend in Figure 1, it can be seen that the yield of government bonds is much higher than the yield of bank deposits, and the demand yield of bank deposits is the lowest; the three-year yield from 2015 to 2019 is higher than the two-year yield and the one-year yield. The annual yield of bank deposits is basically stable. The order of high and low is as follows: three-year yield > two-year yield > one-year yield > six-month yield > agreement yield > three-month yield > demand deposits.

4.2. Risk Investment Yield. The venture capital in this article mainly includes corporate bonds, capital, stocks, and real estate. Select corporate bonds are based on the weighted Shanghai Stock Exchange bond issuance ratio. The selected fund is the Shanghai Stock Exchange Mutual Fund Index, which reflects the price change index of the capital market; the stock is the Shanghai Composite Index, and its stock samples are all listed stocks, including A shares and B shares. According to the data of the opening and closing prices of each index in 2015-2019, the annual average return rate of each risk asset is calculated as shown in Figure 2.

It can be seen from the trend of risk investment yield in Figure 2 that the investment yield of real estate is rising year by year, and it is predicted that there will be an upward trend in the next few years; the investment yield of stocks fluctuates the most, with the highest risk, reaching below -10% at the lowest. The yield of funds and corporate bonds has gradually stabilized in 2018, basically stabilizing between 5% and 10%. The investment yield of the fund is higher than the corporate bond yield and stock yield after 2018.

4.3. Optimal Investment under Different Risks and Returns. Due to the restrictions of the China Insurance Regulatory Commission, insurance companies have established a major asset supervision ratio for their insurance funds. The bank deposit limit ratio is 5% or more, the total investment ratio of funds and stocks is limited to 30% or less, the real estate investment ratio is limited to 30% or less, and the investment ratio of government bonds and corporate bonds is unlimited. Using the above data, we calculate the mean and variance of each investment through the Solver function and get the optimal investment strategy of listed insurance companies. The specific data trend is shown in Figure 3.

From the empirical results of the effective investment portfolio of listed insurance companies in Figure 3, it can be seen that as the rate of return continues to increase, the risks faced have also increased, which is more in line with the principle of negative correlation between risk and rate of return. As the yield increases, the percentage of bank deposits in the portfolio gradually decreases, while the percentage of capital and corporate bonds gradually increases as the yield increases. Since the total investment limit of funds and stocks cannot exceed 30%, the best combination can be achieved when the rate of return is 5.5% and the fluctuation is 0.0139. At present, the bank deposit investment ratio is 23%, government bond investment ratio is 6.5%, funds account for 20.7%, corporate bonds account for 18.8%, stocks account for 9.3%, and real estate investment account for 21.8%. It can be concluded from empirical analysis that bank deposits are a necessary and important investment field for listed insurance companies in the game of risk control and returns. In addition, they can increase their investment in corporate bonds and funds.
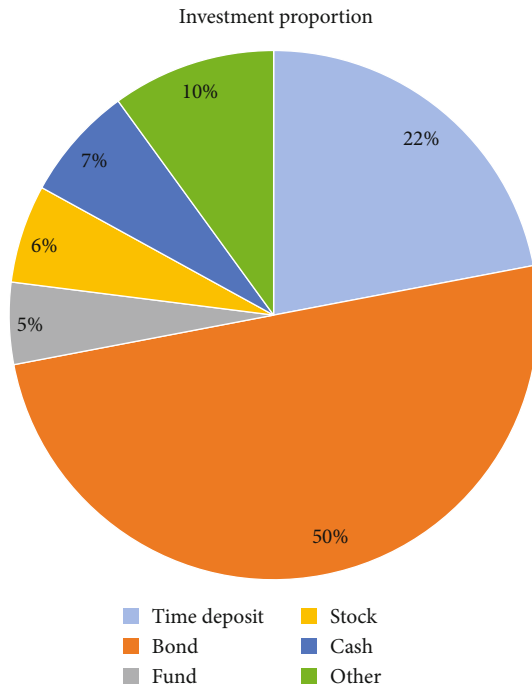
Investment proportion

Figure 4: Historical investment ratio chart.

4.4. Analysis of Optimal Investment Strategy. In the actual situation, the investment channels of listed insurance companies are not limited to these six categories, and the risk asset investment rate of return in this article is determined based on the average value of each risk index of the Shanghai Stock Exchange. The investment yields of risk assets selected in the application of insurance capital investment are different, and the deviation between theory and reality will bring errors to the accuracy of the empirical results. The historical investment ratio of listed insurance companies is shown in Figure 4.

According to the historical investment proportion data of listed insurance companies in Figure 4, it can be seen that the total investment proportion of funds and stocks is 11%, but the optimal investment proportion of funds obtained by the analysis of the model results is 20.7%; the optimal investment of stocks accounted for 9.3%. This shows that in fact, the investment efficiency of listed insurance companies can be improved by increasing the allocation of capital and stock investment, but since the control of the regulatory ratio reduces the actual investment income, under certain risk control, listed insurance companies can appropriately increase the allocation equity in order to obtain a higher return on investment.

5. Conclusions

In recent years, due to the development and improvement of the financial market, people are full of great interest and enthusiasm in financial investment, financial transactions, and other businesses, especially the transactions of financial derivatives. People have invested a lot of assets and energy in the transactions of financial derivatives, especially in

financial transactions with options. However, investment transactions in this area have great benefits and also have great risks. Therefore, how to make investors obtain greater benefits with less risk is a problem that everyone has been discussing all the time.

This paper calculates the optimal investment strategy based on the historical investment yields of the four listed insurance companies in various aspects and the function of the data. The investment efficiency of listed insurance companies can be improved by increasing capital allocation and stock investment. The China Insurance Regulatory Commission's control of the investment regulatory index actually reduces the assessment of the actual investment efficiency of insurance companies. As a leader in the insurance industry, listed insurance companies need to hedge risks. The stability of investment in the insurance industry requires listed insurance companies to invest to cover costs and achieve surpluses. This requires listed insurance companies to have a strong market crisis and investment opportunities. Under specific risk management and control, they can increase owners' equity. The distribution of assets is expected to have a higher return on investment. The two Brownian motions in the investor's surplus process and the risky asset price process are related, and they describe the correlation or dependence between the insurance market and the financial market [24].

In today's world of continuous financial fluctuations [25], financial markets are developing rapidly, financial innovations are constantly emerging, financial services have entered the era of big data, digital financial decision-making has become a trend, and quantitative investment and data-based algorithmic transactions have been widely implemented abroad. The research is biased towards theoretical research, and the conclusions drawn are consistent with economic intuition. In the next step, we will conduct more in-depth theoretical and empirical research on the best high-frequency trading strategies and asset pricing based on high-frequency data in the financial market.

Data Availability

No data were used to support this study.

Conflicts of Interest

There are no potential competing interests in our paper. And all authors have seen the manuscript and approved to submit to your journal.

Acknowledgments

WILEY | Hindawi

Research Article

Joint Strategy of Dynamic Ordering and Pricing for Competing Perishables with Q-Learning Algorithm

Jiangbo Zheng,[1] **Yanhong Gan,**[2] **Ying Liang** (ID),[3] **Qingqing Jiang** (ID),[1] **and Jiatai Chang**[1]

[1]*School of Management, Jinan University, Guangzhou, 510632 Guangdong, China*
[2]*School of Business Administration, South China University of Technology, 510640 Guangzhou, China*
[3]*School of Economics and Management, South China Normal University, Guangzhou, 510006 Guangdong, China*

Correspondence should be addressed to Ying Liang; 20131196@m.scnu.edu.cn

We use Machine Learning (ML) to study firms' joint pricing and ordering decisions for perishables in a dynamic loop. The research assumption is as follows: at the beginning of each period, the retailer prices both the new and old products and determines how many new products to order, while at the end of each period, the retailer decides how much remaining inventory should be carried over to the next period. The objective is to determine a joint pricing, ordering, and disposal strategy to maximize the total expected discounted profit. We establish a decision model based on Markov processes and use the Q-learning algorithm to obtain a near-optimal policy. From numerical analysis, we find that (i) the optimal number of old products carried over to the next period depends on the upper quantitative bound for old inventory; (ii) the optimal prices for new products are positively related to potential demand but negatively related to the decay rate, while the optimal prices for old products have a positive relationship with both; and (iii) ordering decisions are unrelated to the quantity of old products. When the decay rate is low or the variable ordering cost is high, the optimal orders exhibit a trapezoidal decline as the quantity of new products increases.

1. Introduction

Due to the scarcity of resources and the advance of technology, both academia and practice have highlighted the significance of value deterioration, focusing on perishables as a central issue. Many previous studies on perishable products focused on food items (e.g., meat, poultry, produce, dairy, and bakery products), pharmaceuticals (e.g., drugs and vitamins), and cut flowers; this paper studies perishables caused by the replacement of high-tech products, such as laptop computers and telephones, have an increasingly short life cycle due to rapid advances in science and technology and thus exhibit perishable characteristics. It is more convincing to study the joint dynamic ordering and pricing of high-tech products in multiperiods than traditional static pricing. According to a survey conducted by *China Youth Daily* in April 2018, 71.8% of respondents changed their mobile phones at least once every two years and 42% said that their still in use digital products should be updated in a higher frequency.

Managing perishables remains a significant but open issue for industry and academia. A key feature of perishable inventory systems is that each product has its own finite shelf-life; retailers may even have an inventory of a single product with a wide variety of ages on the same shelf. Therefore, the biggest challenge may stem from matching the supply of variously aged perishable goods with the diversity of customers' demand. For instance, some customers like high-quality products while others prefer low prices. Retailers could thus do more to ensure that the quantity of new products meet the demands of consumers with quality sensitivity while discounting older products to attract consumers with price sensitivity when considering the dynamic demand competition between different ages' products, with the purpose of maximizing their profits. For example, when Apple introduces new mobile phones, it will continue to sell old phones at low prices; when the car launches a new model, the old model will continue to sell at a reduced price. How should these retailers dynamically develop joint ordering and pricing strategies when considering the purchase

behavior of heterogeneous consumers and dynamic demand substitution between different ages' products in a multiperiod? However, many studies have neglected the impact of the number of old products carried into the next period on joint strategy with assuming that all remaining valuable old products are entered to the next period or all are discarded. This paper will verify the optimal dynamic data of old products carried into next period as well as the optimal dynamic ordering and pricing strategy in a multiperiod when different ages' products sale simultaneously. Further, this paper is aimed at answering the complicated questions as follows. How should retailers make a trade-off between decreasing order quantity to reduce ordering costs and increasing quantity to accrue a greater share of profit? How should retailers make a trade-off between discarding valuable old products and swallowing new products' profits?

Specifically, we consider two different types of products, new and old, each with its own set of qualities, being sold simultaneously in a given period. The retailer must vary the quantity and price of the two products to maximize long-term revenue when considering dynamic demand competition, positive lead time, fixed ordering cost, and inventory holding cost. In addition, we introduce a consumer utility function to develop a demand model that considers customer purchase behaviors and build our Markov decision model to obtain an optimal strategy, including the decision actions selected for each state that can maximize the total expected discounted profit over an infinite horizon. Then, we originally develop a reinforcement learning algorithm, Q learning, which can solve optimal strategies more effectively without the state transition probability. Finally, we analyze changes to the optimal strategy under different parameters and then present management implications corresponding to our numerical experiments. We find that by incorporating the number of old products carried into the next period in the decision-making, retailers have greater flexibility and more decision options. Although each strategy presents complex features, the Markov decision-making model has a more comprehensive reference value.

The remainder of the article is structured as follows. In Section 2, we review the related literature. Section 3 describes the cost and demand models (the latter based on the vertical differentiation model in Moorthy, 1988) and develops the final model based on Markov decision processes. In Section 4, we use the Q-learning algorithm to analyze the model's optimal strategy; the characteristics of which are illustrated through numerical analyses. Finally, Section 5 presents managerial implications and offers directions for future research.

2. Literature Review

The literature on ordering and pricing strategies for perishable inventories is substantial, while very few studies combine ordering, pricing, and disposal policies in a single model validating different ages' products sold in the same period. Hence, the literature streams most relevant to our research concerns involve (i) inventory control for perishables, (ii) dynamic pricing for perishable inventories, and

(iii) customer behavior modeling for ordering, pricing, and other controls.

The research on inventory control for perishables involves two types of perishability: random and fixed lifetime. Fixed lifetime models were pioneered by Nahmias and Pierskalla, who considered inventory control for perishables with a two-period lifetime and discussed the optimal ordering strategy within a finite period without a detailed solution [1]. When a product's lifetime is longer than two periods, ordering strategies involving old products have complex, nonlinear structures. This approach was developed by Fries and Nahmias, but both of these studies involve trade-offs: lost sales in the former and delayed deliveries in the latter [2, 3]. Researchers therefore sought more effective heuristic strategies to solve these problems. Nandakumar and Morton studied a heuristic ordering strategy for multilifetime perishables based on a discrete time-inventory model. He proposed and verified a heuristic strategy for retailers to determine the upper and lower bounds of order quantity [4]. Li et al. studied joint replenishment and clearance sales for perishables under a general finite lifetime and a last-in-first-out (LIFO) issuing rule. They found that optimal strategies can be characterized by two product-inventory thresholds and proposed that products with different lifetime remainders be sold at clearance sales [5]. When considering fixed ordering costs and lead time constraints, inventory strategies are likely to have to be adaptable, as retailers face a trade-off between the frequency and quantity of orders based on cost. Coelho and Laporte introduced the joint replenishment and inventory control of perishable product, while considering inventory holding costs, disposal costs, they modeled the problem under general assumptions as a MILP and solved it exactly by branch and cut [6]. Berk and Gürler used the Markov decision process to develop their model and evaluated it using the (Q, r) strategy. In this way, they were able to study ordering strategies' various parameters for multilifetime perishable products with positive lead time, allowing for lost sales [7]. Chao et al. developed an approximation algorithm for perishable inventory systems with positive lead times and finite ordering capacities, showing that their model admits a theoretical worst-case performance under positively correlated demand processes [8]. Our study builds on this work to focus on perishable inventory systems with a fixed lifetime, positive lead time, and fixed ordering costs. However, it is insufficient to study only the inventory control problem for perishables. Ordering and pricing strategies influence each other, and it is necessary to incorporate both into the decision-making process to maximize the retailer's revenue.

There is a rapidly growing stream of literature on dynamic pricing and inventory control for perishables. Feng studied an optimal replenishment model with dynamic pricing and quality investment for perishable products, and the dynamic optimization model is proposed to maximize the total profit per unit time and solved on the basis of Pontryagin's maximum principle [9]. Kaya and Polat investigated the problem of jointly determining the optimal pricing and inventory replenishment strategy for a deterministic perishable inventory system, in which demand is both time and

price dependent. Their model also determined the optimal point to adjust prices in relation to the optimal price and the optimal order quantity [10]. Rabbani et al. discussed optimal dynamic pricing and replenishment policies for items that exhibit deterioration in both quality and physical quantity, where the selling price was defined as a time-dependent function of the initial price and discount rate [11]. When the decision cycle involves more than two periods, the joint pricing and inventory control solutions become extremely difficult. Only a few studies limitedly address this issue. Li et al. considered a dynamic joint pricing and inventory control problem for a perishable product over an infinite horizon, assuming a linear price-response demand model with backlogging and zero lead time. They characterized the optimal strategy's structure as having a two-period lifetime and developed a base-stock/list-price heuristic for stationary systems with multiperiod lifetimes [12]. Li et al. proposed a stationary structural policy consisting of an inventory order-up-to level, state-dependent price, and inventory-clearing decisions and developed a fractional programming algorithm to compute the optimal policy in an infinite-horizon lost-sales case, in which the retailer does not sell new and old inventory at the same time [13]. Chen et al. analyzed joint pricing and inventory control problem for a perishable product with a fixed lifetime over a finite period when different ages' perishables sale simultaneously, but they uniformly priced them [14]. All these papers still have not developed model validation of consumer behaviors and the competition between new and old products.

Finally, our study relates to research that models customer behaviors in the context of ordering, pricing, and other controls. The consumer utility function in Smith et al. provides a reference for dealing with vertical differentiation between different ages' perishables [15]. Ferguson and Koenigsberg studied a two-period joint pricing and inventory control problem, addressing the impact of competition between new and old inventory in a secondary period [16]. Akçay et al. considered a dynamic pricing problem over a finite selling horizon, in which the firm has an initial inventory of multiple substitutable and perishable products. They modeled the multiproduct dynamic pricing problem as a stochastic dynamic program, analyzing its optimal prices with an integrative model of consumer choice that was based on linear random consumer utilities [17]. Sainathan cited consumer utility functions to describe the utility evaluations among different ages' products. He determined the retailer's optimal procurement and pricing strategies for different ages' perishable products over an infinite horizon using a Markov decision problem [18]. Chew et al. determined order quantities and prices for a perishable with a multiple period lifetime, allowing substitution between different ages' products. Specifically, they modeled demand for different ages' products as dependent on both their own prices and the prices of substitutable products, i.e., products of "neighboring ages." They used a stochastic dynamic programming model to obtain the optimal joint policy for a two-period lifetime; however, they failed to provide a specific method for products that have lifetimes longer than two periods [19].

In summary, although there are many studies on perishable inventories, there is a research gap that addresses both dynamic demand substitution and joint ordering, pricing, and disposal strategy for different ages' products in a multiperiod, also lacking of precise algorithms to gain the optimal strategy. On this basis, our contribution to bridge the existing research gap involves the following: (i) we incorporate the number of old products carried to the next period into the joint strategy to better cope with consumer preferences and dynamic demand substitution, with the purpose of maximizing the retailers' profits when considering fixed order cost and inventory holding cost, which is not included in Sainathan [18]; (ii) we develop the Q-learning algorithm rather than dynamic programming or value iteration to solve the Markov model and gain the multiperiod optimal strategy. This algorithm can obtain a stable optimal policy effectively, including the actions of all states, after being trained without the state-transition probability and current expected return. Some results from multiple numerical experiments can provide theoretical guidance to retailers' daily decisions.

3. Model

We consider a retailer who sells a perishable product with a two-period lifetime over an infinite horizon. The retailer has a chance to order in each period, and the lead time is one period. At the beginning of each period, the retailer observes the initial inventory, which includes both old products from the previous period and new products, and decides how many new products to order for the next period. The total number of old and new products on the shelves at any given time cannot exceed the retailer's capacity. The retailer then decides the prices for the new and old products. There are N customers in each period, whose arrival follows a Poisson distribution. Each customer purchases up to one product to maximize utility based on price and quality sensitivity, which follows 0-1 uniform distribution. Because the two products are vertically differentiated, the retailer loses more from trying to sell old products due to their lower price. Hence, the retailer faces a trade-off between product spoilage and demand substitution and thus must take into account the optimal number of old products carried into the next period. The objective of the retailer is to maximize the total expected discounted profit over an infinite horizon. The notations and decisions defining the model are provided in the next sections.

3.1. Notations. λ: average number of arrivals,

N: total number of arrivals in each period following a Poisson distribution,

I: the capacity on shelf,

c_f: fixed ordering cost,

c_v: ordering cost per unit,

c_I: inventory holding cost per unit,

τ_n: the new product quality,

τ_o: the old product quality,

θ: customer's quality sensitivity following 0-1 uniform distribution,

o_r^t: the number of old products remaining at the beginning of period t,

n^t: the number of new products available at the beginning of period t,

g^t: $g^t \in \{0, 1\}$, $g^t = 1$ if the retailer ordered in period t, otherwise $g^t = 0$,

U_{mn}^t: the m customer's utility for new products in period t,

U_{mo}^t: the m customer's utility for old products in period t,

x_{mn}^t: the m customer's purchase of new product in period t,

x_{mo}^t: the m customer's purchase of old product in period t,

d_n^t: the demand of new product in period t,

d_o^t: the demand of old product in period t,

C^t: total cost in period t,

R^t: net profits in period t.

3.2. Decisions. q^t: the order quantity in period t,

o_s^t: the number of products unsold in period t and carried over to period $t + 1$,

p_n^t: the price of new product in period t,

p_o^t: the price of old product in period t.

3.3. Demand Model. Any customer who visits the retailer has three choices—buy one old product, buy one new product, or buy nothing. All customers make their decisions based on utility and preference. Similar to Sainathan utility function [18], let $U_{mn}^t = \theta_m^t \tau_n - p_n^t$ be the utility of a new product for customer m, and $U_{mo}^t = \theta_m^t \tau_o - p_o^t$ be the utility of the old product.

If it meets two conditions, customer m will choose product i:

$$\begin{cases} U_{mi}^t = \max_{j=n,o} U_{mj}^t, \\ U_{mi}^t > 0. \end{cases} \quad (1)$$

According to the above two conditions and granted that the old product will be priced lower than the new product, we can obtain the upper and lower bounds for each product's price:

$$0 < p_o^t < \min \left(\tau_o, p_n^t \right), 0 < p_n^t < \tau_n. \quad (2)$$

There are six situations, and we discuss them independently.

(1) When $U_{mn}^t > 0 \geq U_{mo}^t$ or $U_{mo}^t > 0 \geq U_{mn}^t$, customer m will only purchase new products (or old products) and buy nothing if they are out of stock

(2) When $U_{mn}^t \geq U_{mo}^t > 0$, customers prefer to purchase new products and buy old products if the new products are out of stock; otherwise, they buy nothing. When $U_{mo}^t > U_{mn}^t > 0$, customers prefer to buy old products and purchase new products when old products are out of stock; otherwise, they buy nothing

(3) When $0 \geq U_{mn}^t \geq U_{mo}^t$ or $0 \geq U_{mo}^t > U_{mn}^t$, customers buy nothing

TABLE 1: Parameter setting.

Parameter	Value
Average number of arrivals	$\lambda = 12$
Capacity on the shelf	$I = 15$
Fixed ordering cost	$c_f = 3$
Ordering cost per unit	$c_v = 3$
Inventory holding cost per unit	$c_I = 1$
Discount factor	$\gamma = 0.9$
New product quality	$\tau_1 = 20$
Old product quality	$\tau_2 = 12$

Then, after customer m makes a choice, there are three cases:

(1) A new product was purchased ($x_{mn}^t = 1$, $x_{mo}^t = 0$)

(2) An old product was purchased ($x_{mn}^t = 0$, $x_{mo}^t = 1$)

(3) Nothing was purchased ($x_{mn}^t = 0$, $x_{mo}^t = 0$)

After all of the customers have made their decisions, the demand for each product in the current period is $D^t(d_n^t, d_o^t)$ ($d_n^t = \sum_{i=1}^{N^t} x_{in}^t$, $d_o^t = \sum_{i=1}^{N^t} x_{io}^t$).

3.4. Cost Model. At the beginning of period t, the retailer decides how many new products to order, q^t. If the quantity is 0, then $g^t = 0$; otherwise, $g^t = 1$. The product has a two-period shelf-life, and its salvage value is zero at the end of second period. The procurement lead time is assumed to be one, such that units ordered in period t will be available for sale as a "new" product in period $t + 1$. The retailer will also have to decide the number of old products to be carried into the next period, o_s^t, and these products will generate inventory holding costs $c_h^t = o_s^t c_I$. The total cost of the period is

$$C^t = g^t c_f + q^t c_v + c_h^t. \quad (3)$$

The current net profit for the period is

$$R^t = d_n^t p_n^t + d_o^t p_o^t - C^t. \quad (4)$$

3.5. Decision Model. Based on the previous two sections, we used the Markov decision process to model the sales process over an infinite horizon. At the beginning of period t, the retailer's states are $S^t(o_r^t, n^t)$ and actions are $a^t(q^t; o_s^t; p_n^t, p_o^t)$ ($o_s^t \leq \min (I - n^t, o_r^t)$, $q^t \leq I$). After all consumers make their purchase decisions in that period, the remaining old products are discarded directly because they have reached their lifetime threshold and the remaining new products become old products in the next period. The number of old products remaining at the beginning of period $t + 1$ is therefore $o_r^{t+1} = n^t - d_n^t$, and the number of new products in period $t + 1$ is the same as the previous order
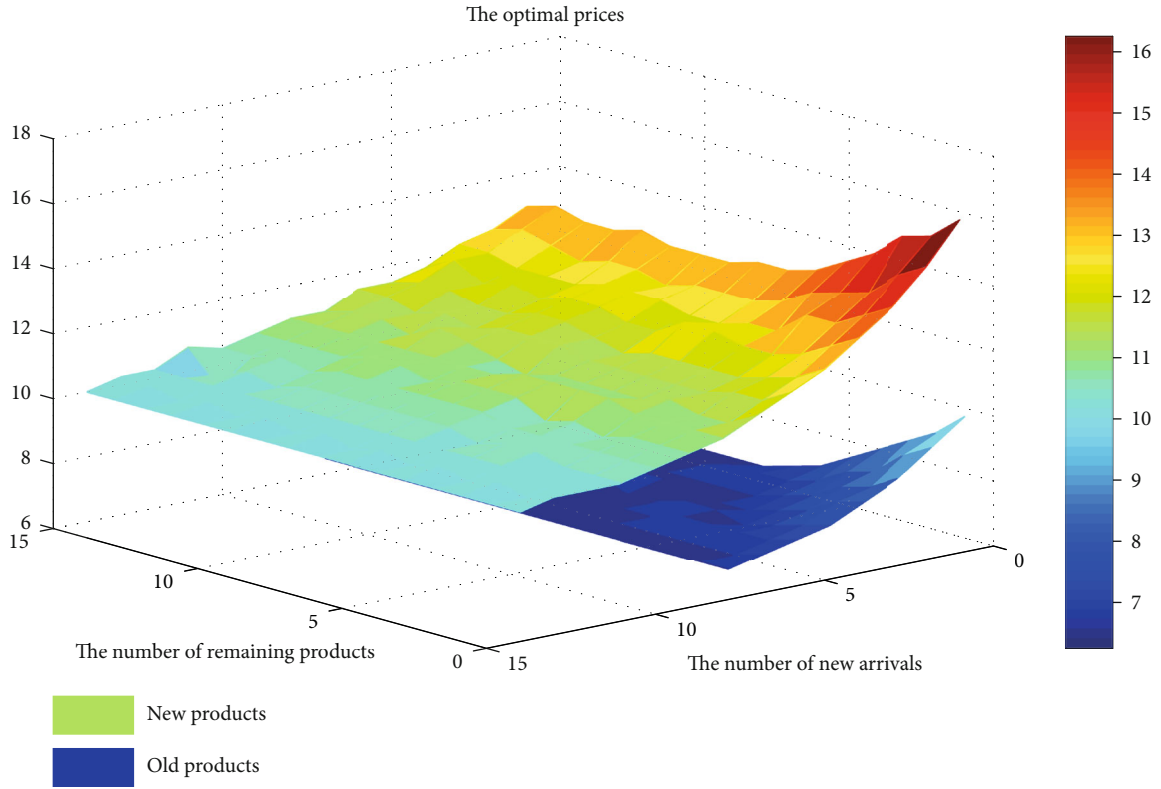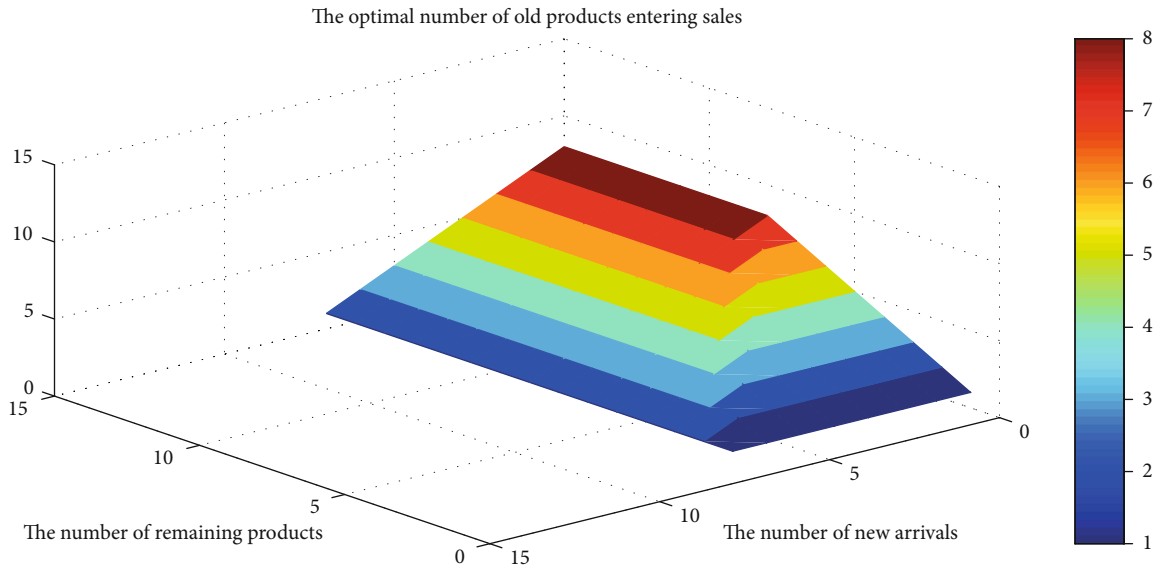
FIGURE 1: Basic model: optimal pricing.

FIGURE 2: Basic model: the optimal number of old products carried into the next period.

quantity q^t. Therefore, the retailer's state in period $t+1$ will be $S^{t+1}(o_r^{t+1} = n^t - d_n^t, n^{t+1} = q^t)$.

Let π be a strategy that involves the actions taken in each state and Π the set of all strategies, i.e., $\pi \in \Pi$. Let V be the total discounted expected return when a certain strategy π_j

is taken from a certain state S^t. Therefrom, we developed the following result:

$$V\left(S^t, \pi_j\right) = E\left[R^t\right] + \gamma E\left[R^{t+1}\right] + \gamma^2 E\left[R^{t+2}\right] + \cdots = \sum_{i=t}^{\infty} \gamma^{i-t} E\left[R^i\right]. \quad (5)$$
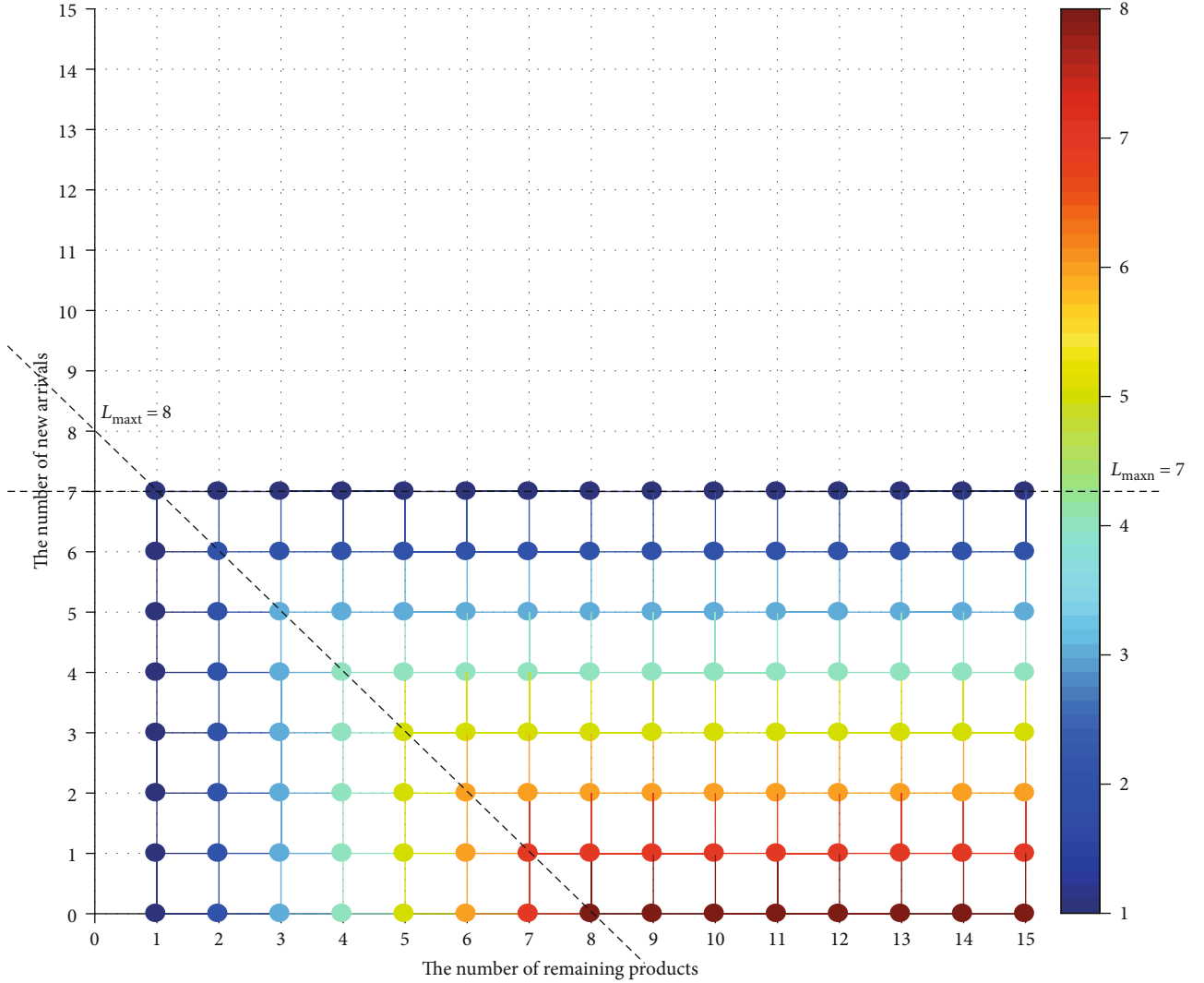
FIGURE 3: Basic model: the line represents the number of old products carried into the next period.

Equation (5) also has an equivalent expression, namely, the Bellman equation:

$$V\left(S^t, \pi_j\right) = E\left[R^t\right] + \gamma \cdot \sum_{S^{t+1} \in \Phi} \left[P_{S^t \to S^{t+1}, \pi_j} \cdot V\left(S^{t+1}, \pi_j\right)\right]. \quad (6)$$

The optimal strategy $\pi_{S^t}^*$ maximizes the value of state S^t, which is

$$V\left(S^t, \pi_{S^t}^*\right) = \max_{\pi \in \Pi} V\left(S^t, \pi\right). \quad (7)$$

If the policy $\pi *$ holds for all states $S \in \Phi$, then $\pi *$ is the optimal strategy for this model.

3.6. Solution Approach: Q-Learning Algorithm. In this paper, the new product orders, the number of old products carried into the next period, and pricing decisions are considered an infinite discount Markov decision model consisting of four main components: state set, action set, current expected return, and state transition probability. The states and
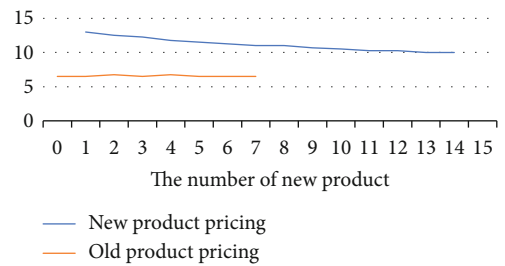
FIGURE 4: Optimal pricing for 2 products with 10 remaining products.

actions of this model are $S^t\left(o_r^t, n^t\right)$ and $a^t\left(q^t; o_s^t; p_n^t, p_o^t\right)$, respectively. The states and actions for q^t and o_s^t are discrete and finite due to shelf-life constraints; furthermore, actions related to pricing can also be regarded as discrete with a price step. According to Puterman, when the state set and the action set are finite and discrete and the discount factor satisfies $0 < \gamma < 1$, the infinite discount model has an optimal
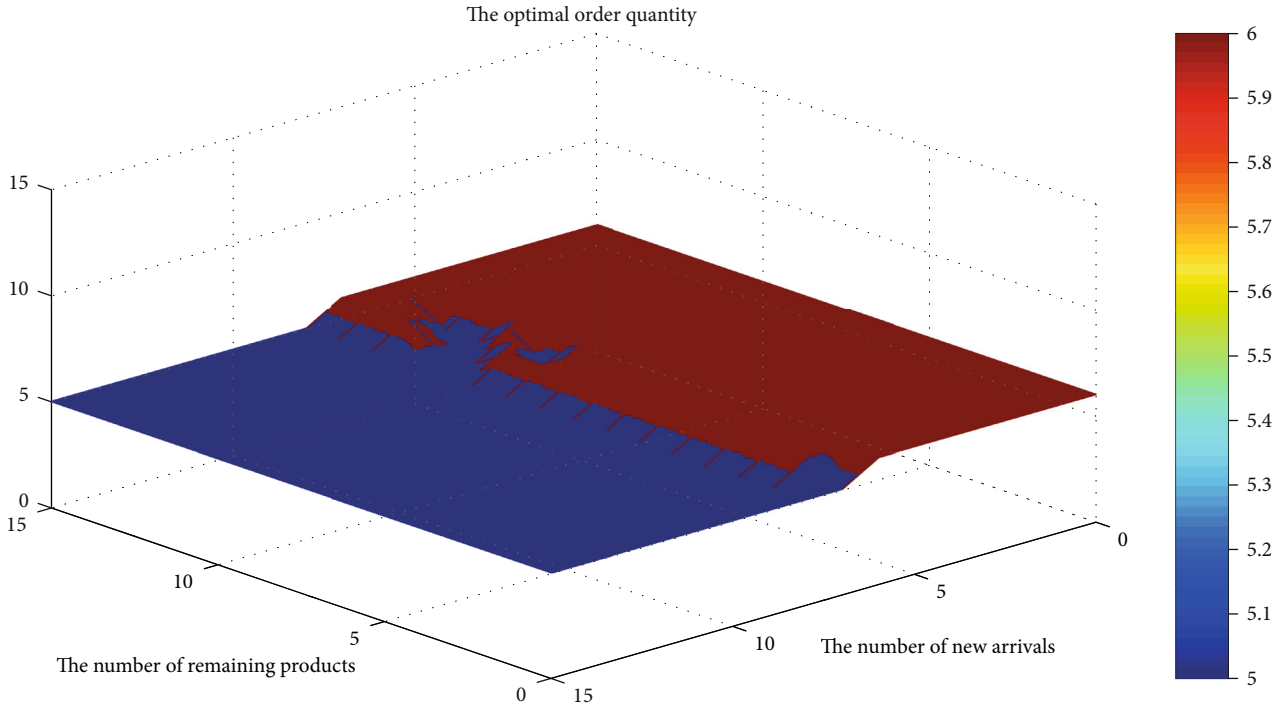
Figure 5: Basic model: optimal product order quantity.

stationary strategy [20]; in other words, the optimal strategy is only related to the states.

DP provides a number of methods for determining the optimal strategy by calculating $V*$ and one $\pi*$, assuming that R^t and $P_{S^t \to S^{t+1}, \pi_j}$ are known. One example is the value-iterative solution that Sainathan uses [18]. Although this method is intuitive, when the state action set is particularly large (for example, there are a total of 256 states in the basic model of this paper, and the largest number of possible actions exceeds 400,000), this method is very complex and unstable. Watkins and Dayan first proposed a Q-learning algorithm, which does not require knowledge of the current return and state transition probability and can determine the optimal strategy more quickly when the states and action spaces are large [21]. More recently, scholars have further optimized the Q-learning algorithm to provide precise solutions to more complex problems. Liang et al. used the deep Q-learning (DQN) algorithm to generate the watermarked positions adaptively and make some inspiration on the copyright protection issue of intellectual property (IP) circuit resources of the electronic devices in IoT environment [22]. Zhou et al. proposed an improved anisotropic Q-learning routing algorithm which can provide stable and dynamic solutions for AGV routing [23]. In recent years, Q-learning algorithm also has a good application in the field of operations management. Dittrich and Fohlmeister based on deep Q learning developed a self-optimizing inventory control, in which input is modeled as a state vector that describes the current stocks and orders within the process chain, and the output represents a control vector that controls orders for each individual station [24]. In this study, we will develop
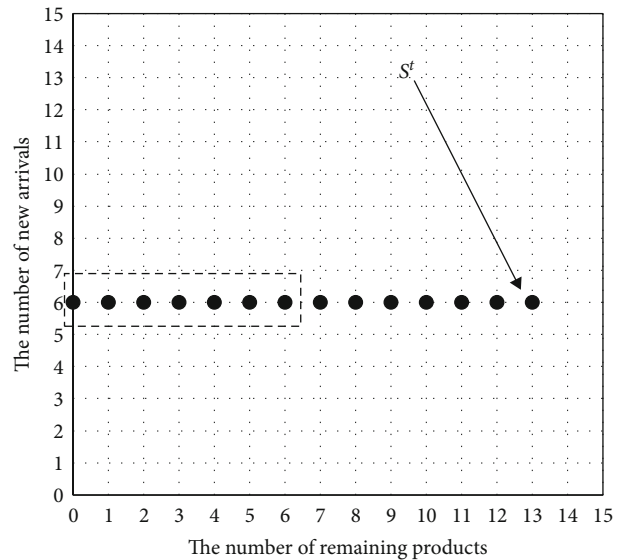

Figure 6: State transition.

the Q-learning algorithm to find a joint optimal strategy for perishable products.

Reinforcement learning methods evolved from animal learning and parameter perturbation adaptive control theory. The fundamental premise is that if an agent's actions lead to a positive environmental reward (enhanced signal), then the agent will be more likely to take this action again in the future. Q learning is an important algorithm in reinforcement learning. It combines dynamic programming with learning psychology to make the sequential optimization
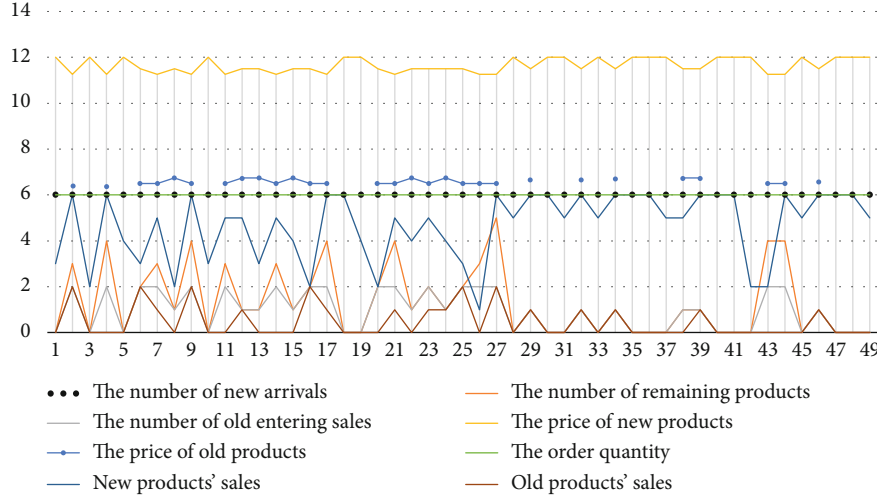
FIGURE 7: Parameters of the optimal strategy.

decision with delayed returns. The purpose of the reinforcement learning system is to obtain a strategy π, such that the total discount returns $\sum_{i=0}^{\infty} \gamma^i r_{t+i}$ will be maximized ($0 < \gamma < 1$ is a discount factor, γ indicates the degree of hyperopia of the system; if the value is small, then the system pays more attention to the recent actions; otherwise, it prioritizes future actions). When the state transition probability and current expected return function are unknown, the learning system can gain the optimal strategy by only using information contained in the training data for the immediate reward R^t. The learning system usually does not estimate the environment model; rather, it directly optimizes an iteratively calculated Q function. Given a strategy π, Watkins and Dayan defined the Q function as the mathematical expectation of the total discount reward when the state is s_t, the action is a_t, and the subsequent strategy is π [21].

$$Q^{\pi}(s_t, a_t) = R(s_t, a_t) + \gamma \sum_{s_t' \in S} P_{s_t s_t'} [\pi(s_t)] V^{\pi}(s_t'). \quad (8)$$

The Q value is the expected discounted reward for executing action a_t at state s_t and following policy π thereafter. The object in Q learning is to estimate the Q values for an optimal policy. It is straightforward to show that $V^*(s) = \max_{a \in A} Q^*(s, a)$ and that if $a*$ is an action at which the maximum is attained, then an optimal policy can be defined as $\pi^*(s) = a^*$. In Q learning, the agent's experience consists of a sequence of distinct stages or episodes. In the tth episode, the agent observes its current state s_t, selects and performs an action a_t, observes the subsequent state s_t', receives an immediate reward r_t, and adjusts its Q_{t-1} values using a learning factor β_t according to the following.

$$Q_t(s, a)$$
$$= \begin{cases} (1 - \beta_t) Q_{t-1}(s, a) + \beta_t \left[r_t + \gamma V_{t-1}(s_t') \right] & \text{if } s = s_t \text{ and } a = a_t, \\ Q_{t-1}(s, a), & \text{otherwise,} \end{cases}$$
$$(9)$$

where

$$V_{t-1}(s') = \max_b \left\{ Q_{t-1}(s', b) \right\} \quad (10)$$

is the best the agent thinks it can do from state s'. The initial Q values, $Q_0(s, a)$, for all states and actions are assumed to be given. In Equation (9), β_t is the learning factor, which controls the speed of learning. Larger β_t indicate faster convergence. However, excessively large β_t may lead to nonconvergence. Watkins and Dayan showed that if a pair (s, a) can perform infinite iterations using Equation (9) under certain conditions, then when $t \to \infty$, $Q_t(s, a)$ has probability 1 of convergence to $Q^*(s, a)$ [21].

4. Numerical Studies and Observations

In this section, we provide an initial set of basic parameters for the simulation and then adjust parameters to analyze select features of the optimal policy. Through many numerical experiments, it is found that there are some regular patterns that can reflect the intrinsic mechanism of the model. Due to the limited space, only a set of representative parameters are selected for specific analysis and discussion. It is worth noting that the parameter settings in different situations are determined by combining the actual and the previous analysis principles to ensure the scientific results. The simulation calculation is based on the VC program and runs on the Windows platform.

4.1. Experiment Design. Table 1 shows the basic parameters used in the simulation. To ensure the accuracy of our results, we set the price step to 0.25. Finally, the average number of Q function iterations per model reached 1.5 billion and was eventually stabilized.

Through the computer simulation calculation, the optimal pricing strategy, the optimal number of old products carried into the next period, and the optimal ordering strategy of the basic model are given as Figures 1 and 2.
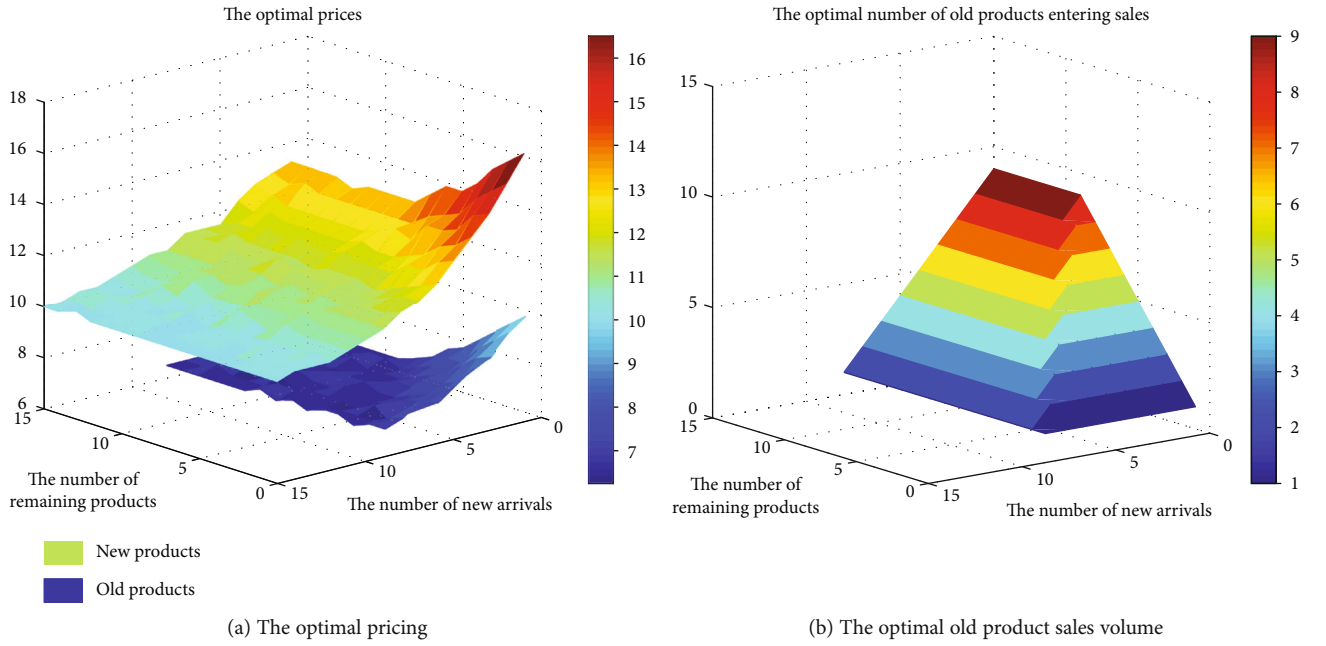
(a) The optimal pricing

(b) The optimal old product sales volume

FIGURE 8: The optimal pricing and old product sales volume with an average arrival rate of 14.

(a) The optimal pricing

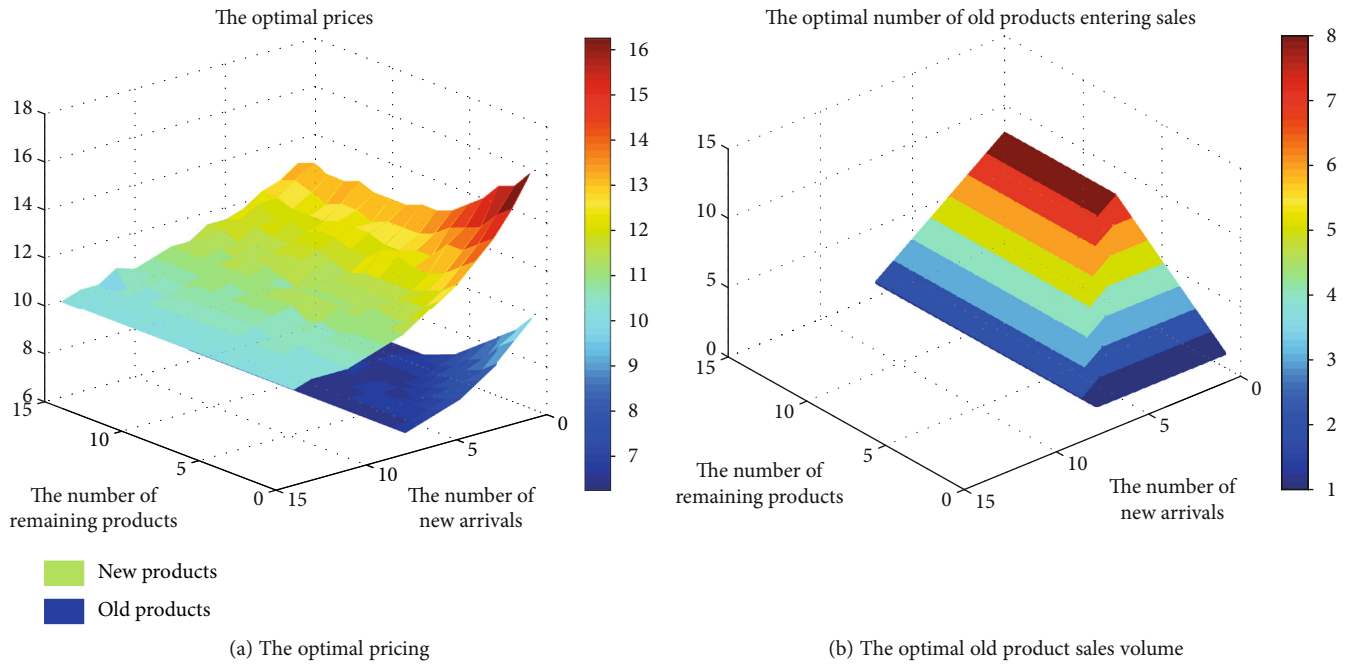(b) The optimal old product sales volume

FIGURE 9: The optimal pricing and old product sales volume with an average arrival rate of 12.

Both figures' characteristics suggest that there is an association between the optimal pricing and the number of old products carried into the next period.

As shown in Figure 3, in the region where {new + old ≤ $(L_{\max t} = 8)$} (new represents the number of new arrivals and old represents the number of remaining products), the number of old products carried into the next period is not affected by the number of new products; as such, the remaining old products all carry into the next period. In the area where {new + old > $(L_{\max t} = 8)$, new ≤ $(L_{\max n} = 7)$},

the number of old products carried into the next period increases as the number of new products decreases until the number of new products exceeds eight, after which no old products are sold. Therefore, the more intuitive conclusion is that there is a product bound $(L_{\max t})$. The retailer can yield greater profit by adding the remaining old products to the shelf when the number of new products does not exceed $L_{\max t}$. The findings also show that new products will be sold preferentially before old products when the potential demand is limited. Moreover, the sizes of $L_{\max t}$ and $L_{\max n}$
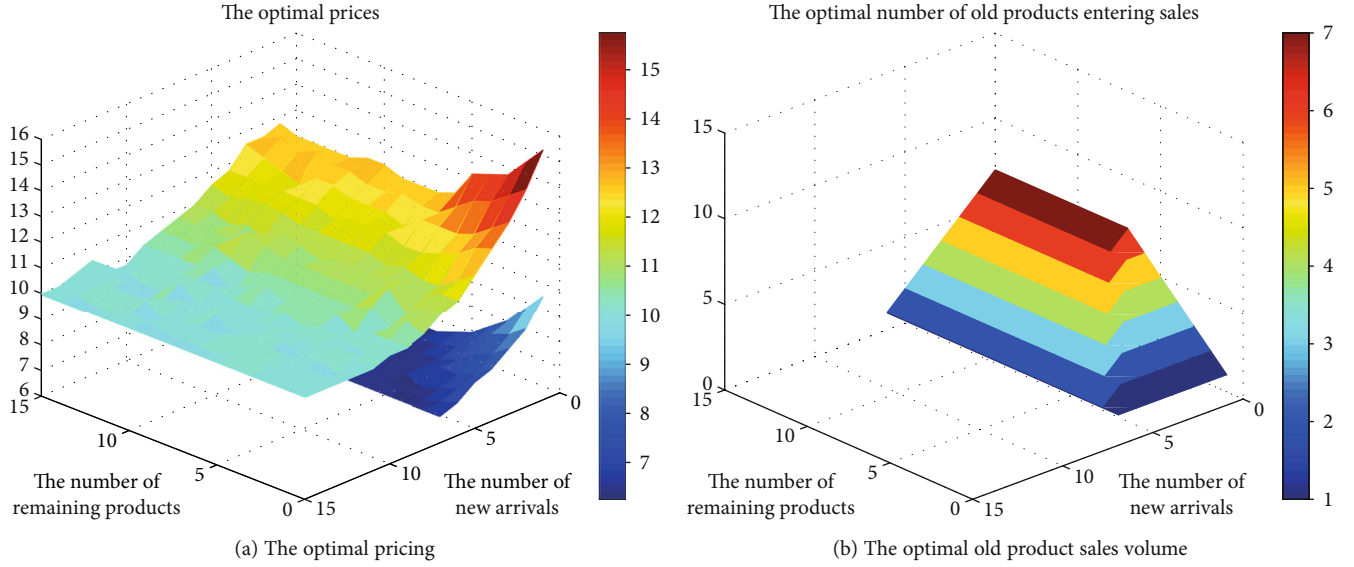
(a) The optimal pricing

(b) The optimal old product sales volume

FIGURE 10: The optimal pricing and old product sales volume with an average arrival rate of 10.

(a) The optimal pricing
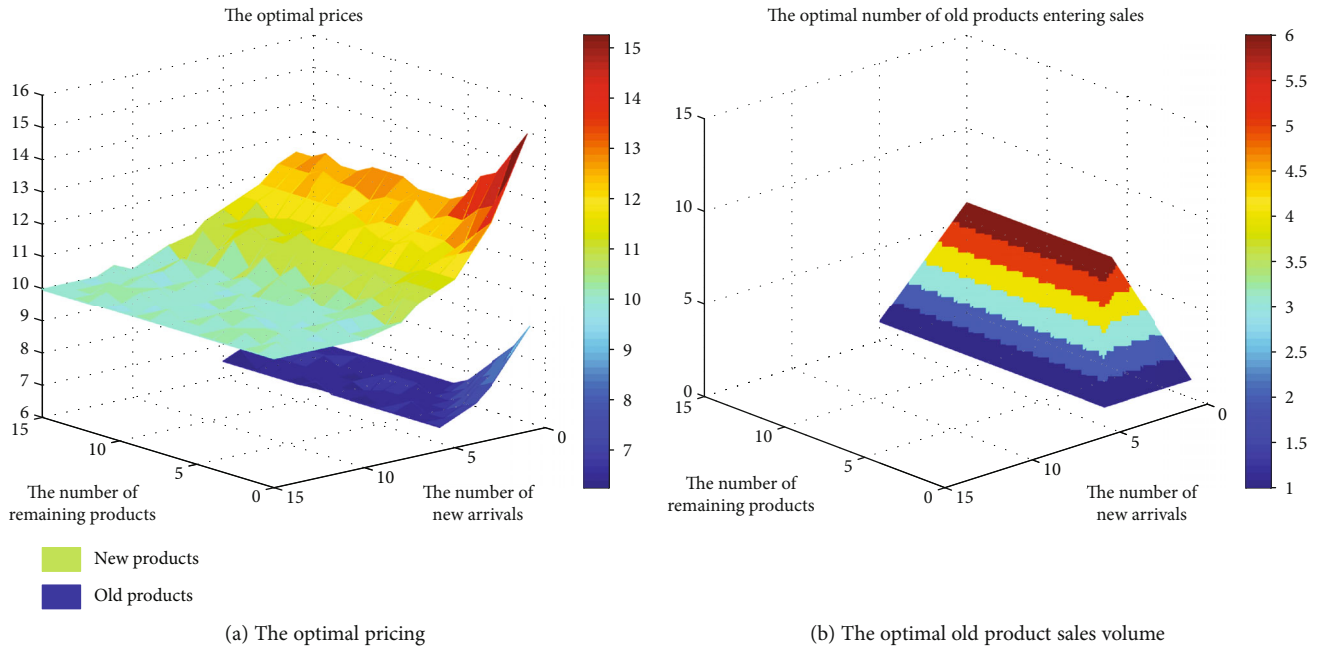
(b) The optimal old product sales volume

FIGURE 11: The optimal pricing and old product sales volume with an average arrival rate of 8.

affect performance across contexts (system parameters), as we explain in greater detail in the following sections.

Based on our analysis of correlations between the optimal pricing and the optimal number of old products carried into the next period, we were able to draw some initial conclusions about the optimal pricing of both new and old products.

(1) For new products, there are four conditions affecting optimization:

First, when $\{\text{new} + \text{old} \leq (L_{\max\,t} = 8)\}$, the relationship between the new product's optimal price and the number of new and old products is negative.

Second, when $\{\text{new} + \text{old} > (L_{\max\,t} = 8)\}$, the new product's optimal price only decreases slightly as new arrivals increase, but there is no relationship to the number of old products remaining. In this region, the number of old products that get carried into the next period remains the same, even as the number of old products changes. In general, a reduction in substitute products will cause the product's price to rise, but we find that the product's price declines as the number of substitute products decreases; this indicates that increases to the number of new products have a greater impact on the price than the number of old products carried into the next period.
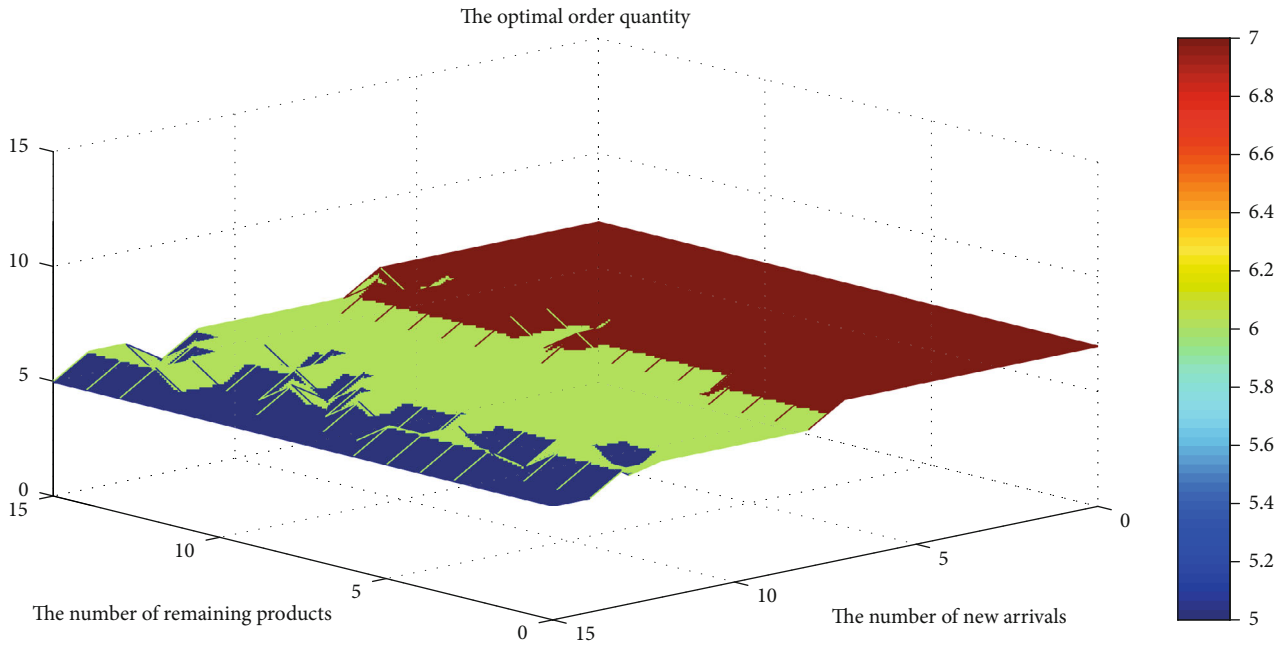
FIGURE 12: The optimal order quantity with an average arrival rate of 14.
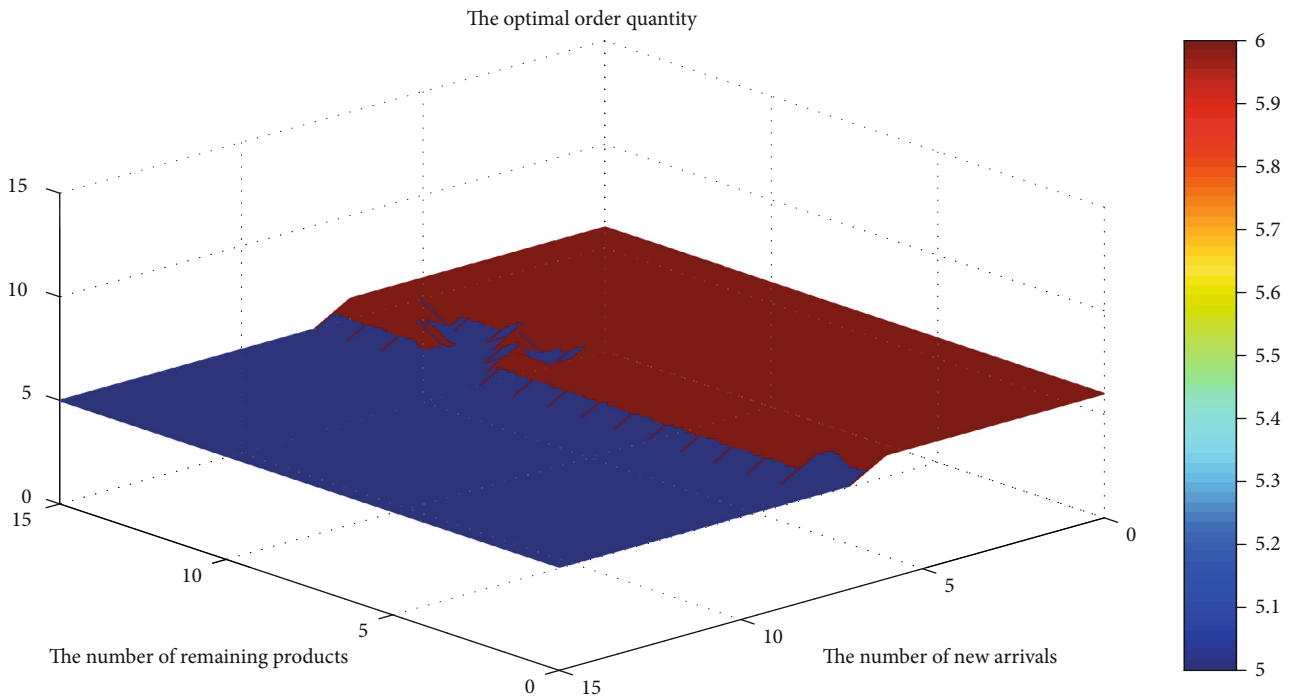

FIGURE 13: The optimal order quantity with an average arrival rate of 12.

Third, when (new > 8), only new products are sold. Therefore, the new product price will decrease as the number of new products increases.

Finally, when (new > 12), the optimal price of new products remains basically unchanged. When the sales volume approaches or exceeds the potential average number of arrivals, no more benefits can be accrued. As such, we can discern that discounts are not always beneficial.

(2) For old products, when {new + old ≤ ($L_{\max t} = 8$)}, there is a negative relationship between the optimal price, the number of products carried over into the next period, and new product arrivals. But outside of this region, there are no obvious relationships: the old product pricing curve is generally smooth. As with new products, the pricing of old products will be affected both by the quantity of old products and
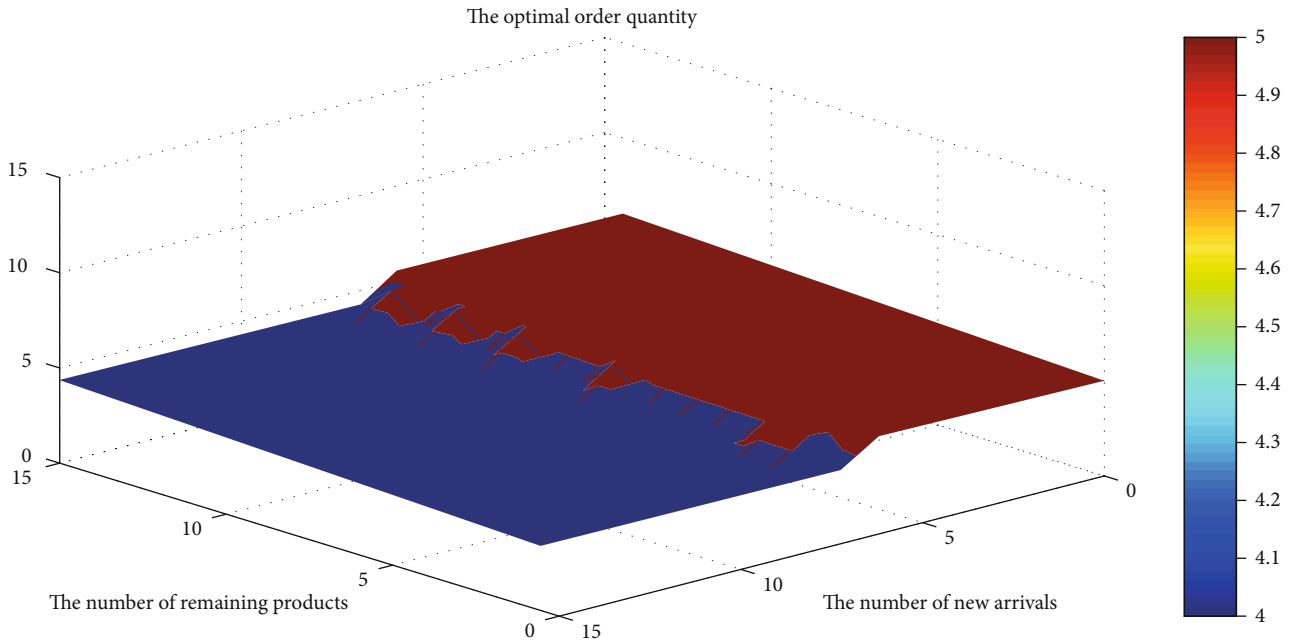
The optimal order quantity

FIGURE 14: The optimal order quantity with an average arrival rate of 10.

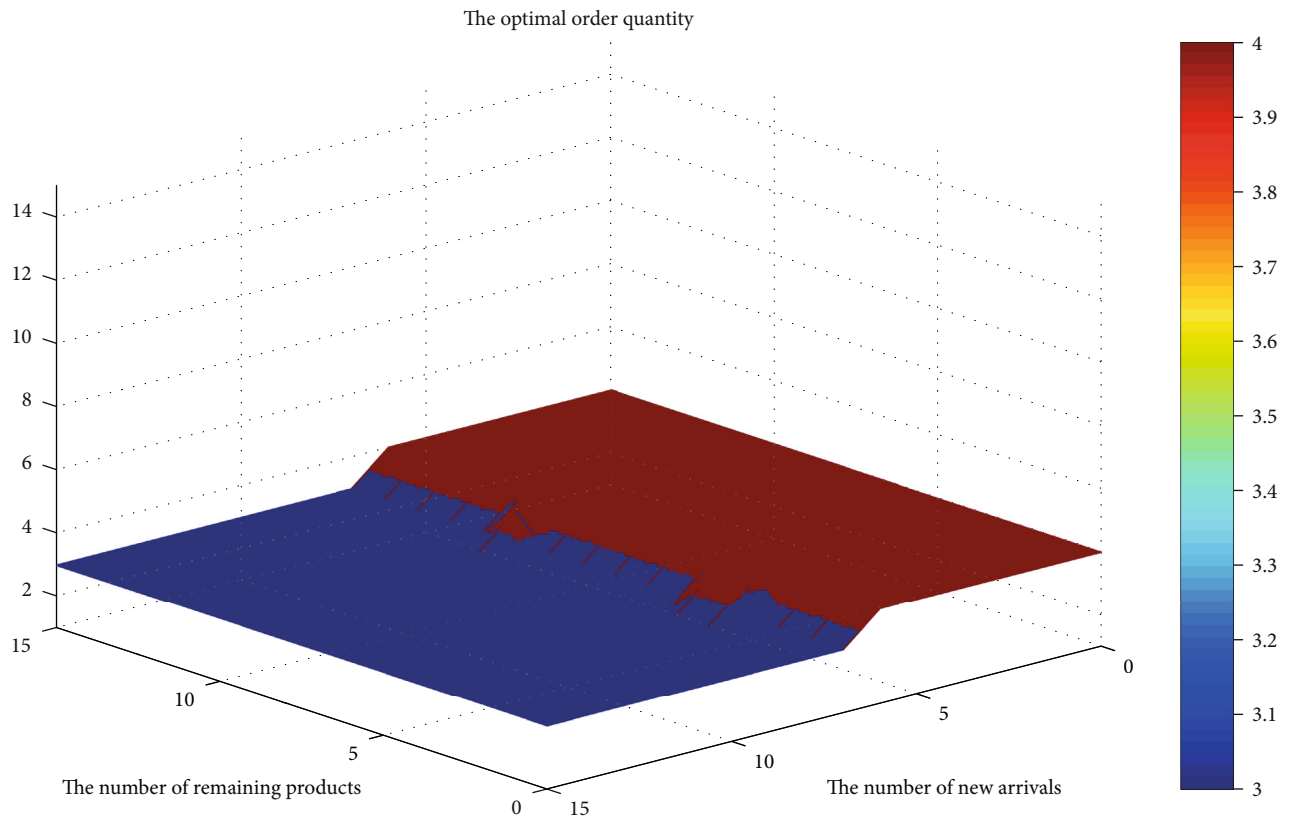The optimal order quantity

FIGURE 15: The optimal order quantity with an average arrival rate of 8.

by the number of substitute products. As such, the result for this parametric setting suggests that the impacts of quantity and pricing are the same. We

can therefore infer that new product quantity has a greater effect on the price of new products than on the price of old products, as shown in Figure 4

(a) The optimal pricing

(b) The optimal old product sales volume
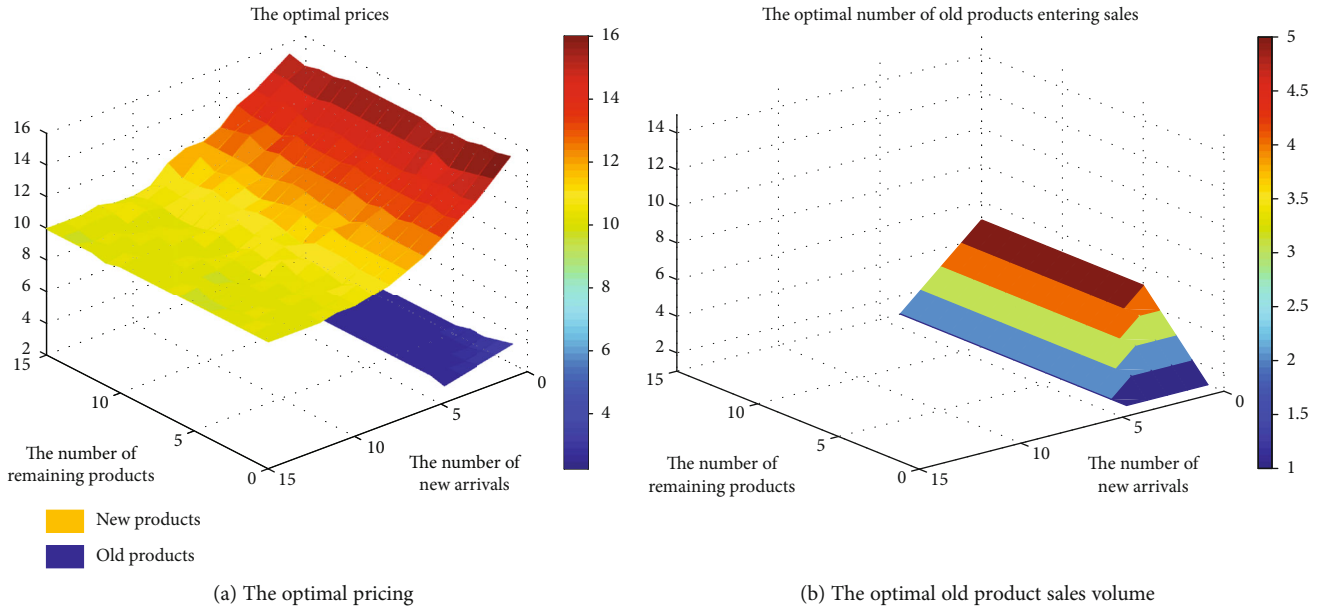
FIGURE 16: The optimal pricing and old product sales volume with an 80% decay.

(a) The optimal pricing
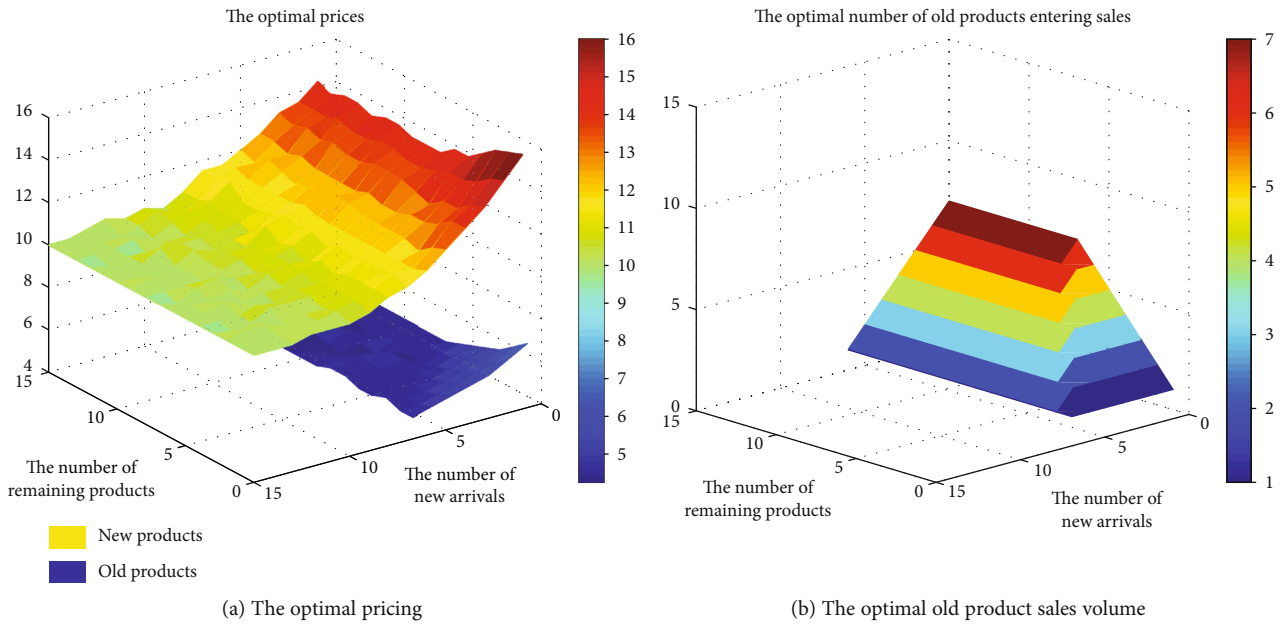
(b) The optimal old product sales volume

FIGURE 17: The optimal pricing and old product sales volume with a 60% decay.

Figure 5 shows the optimal order quantity and reveals that new product order quantity has no relationship to the quantity of remaining products. In the (new ≤ 7) area, the optimal order quantity is 6, and in the (new > 8) region, the optimal order quantity is 5, indicating that the expected number of old products carried into the next period will increase when there are too many new products.

Combined with the optimal number of old products carried into the next period, the retailer faces a trade-off between decreasing order quantity to reduce ordering costs and increasing quantity to accrue a greater share of profit.

Through derivation, we find that within a certain range, the probability distribution for different combinations of products can vary significantly, while the long-term expected return for different combinations may also differ. If the total number of products remains the same, the retailer can determine an appropriate ordering strategy by comparing the marginal long-term expected return between old and new product sales. However, it should be noted that long-term expected return must be considered because product combinations affect the state of the later period, which affects the long-term discounted total value of the current period.
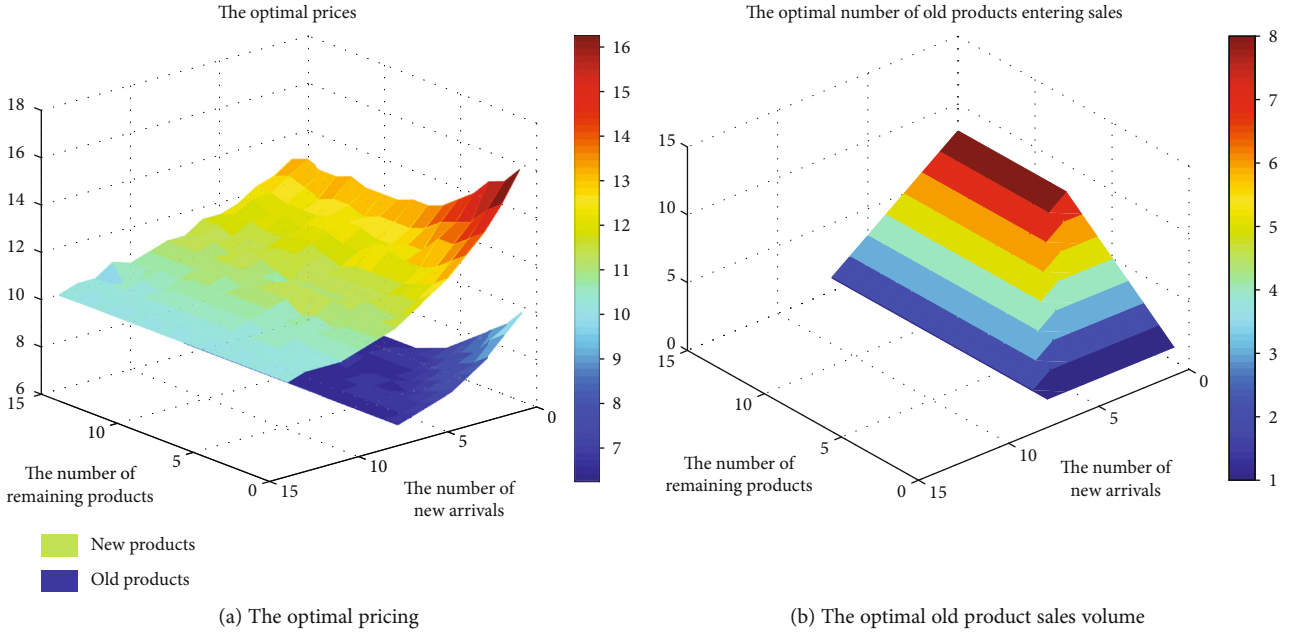
(a) The optimal pricing

(b) The optimal old product sales volume

FIGURE 18: The optimal pricing and old product sales volume with a 40% decay.

(a) The optimal pricing
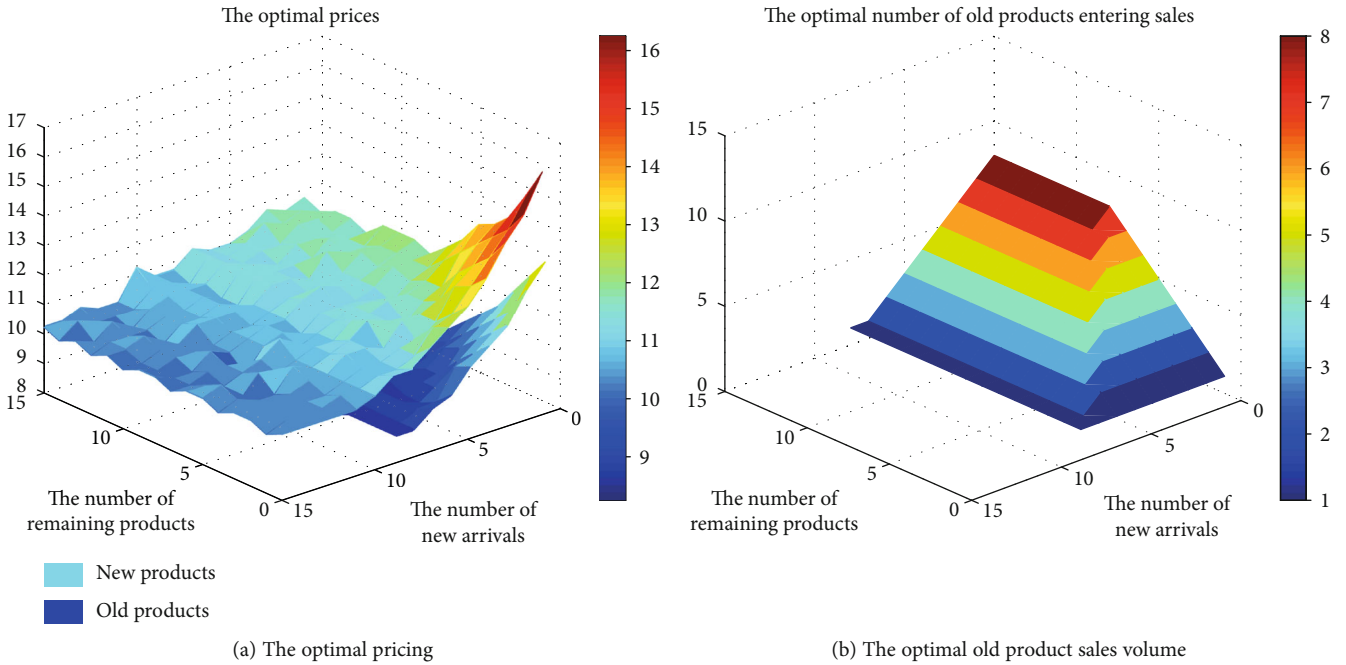
(b) The optimal old product sales volume

FIGURE 19: The optimal pricing and old product sales volume with a 20% decay.

Similarly, there is a relationship between order quantity, new product quantity, and remaining product quantity:

$$q^t = n^{t+1} \geq o_r^{t+2}. \tag{11}$$

We conducted further analysis based on this relationship. As shown in Figures 4–6, assuming that the state is S^t (new = 13, old = 9), the possible locations of the next state are shown as solid circles according to the relation-

ship (11). After a finite number of periods, the system state is only transferred within the dashed box in the figure; further, we find that any initial state has this property.

To better understand the characteristics of optimal strategy, we simulated an optimal strategy for each period under various parameters.

As Figure 7 shows, we found the order quantity to be stable at six, but the price of new products changes within a relatively limited range, and the old product's price is

(a) 80% decay

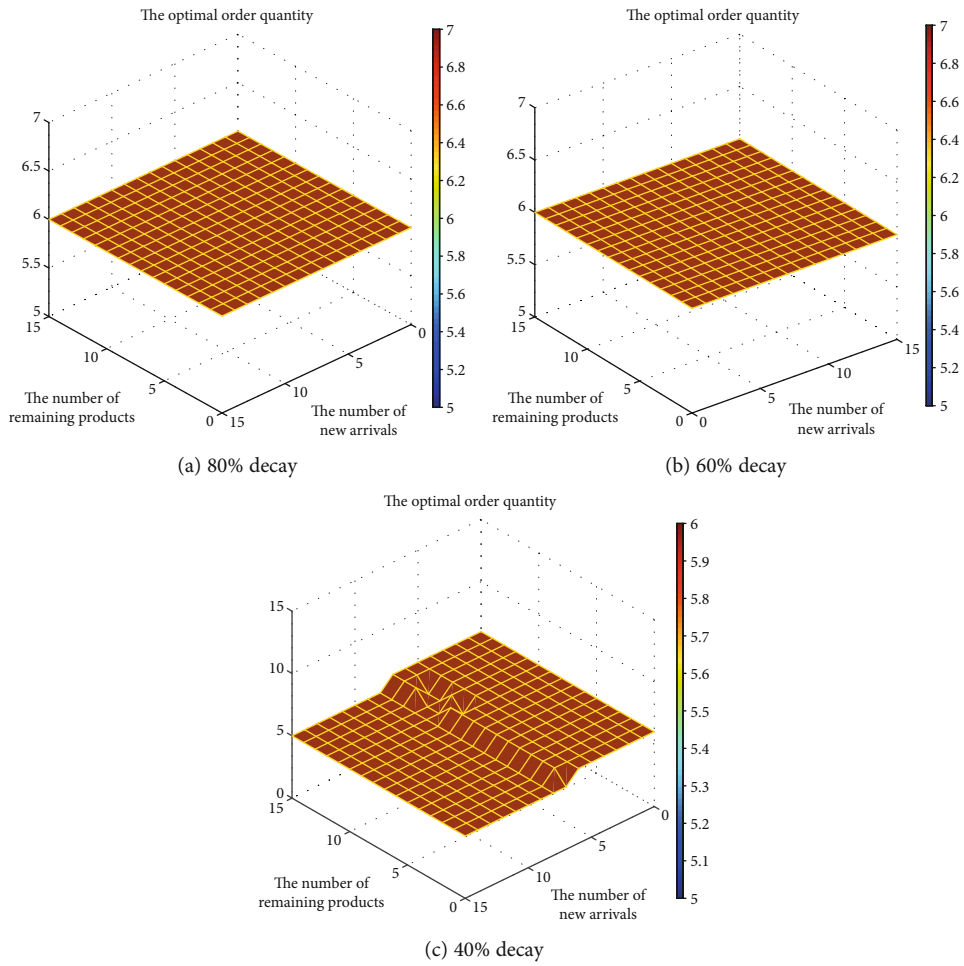
(b) 60% decay

(c) 40% decay

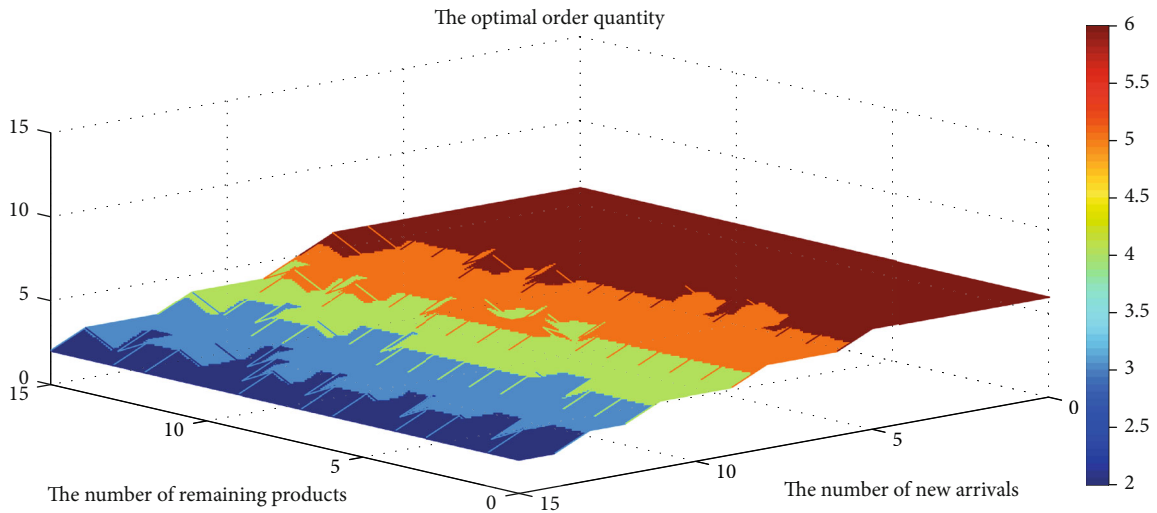Figure 20: The optimal order quantity with 80%, 60%, and 40% decay.

Figure 21: The optimal order quantity with a 20% decay.

also limited when sold. This suggests that (i) changes to the states and strategies are limited, which provides a basis for the retailer to enact some heuristic strategies (or fixed strategies), and (ii) even if the scope of the state transition is small, the retailer's joint strategy still presents complex features.
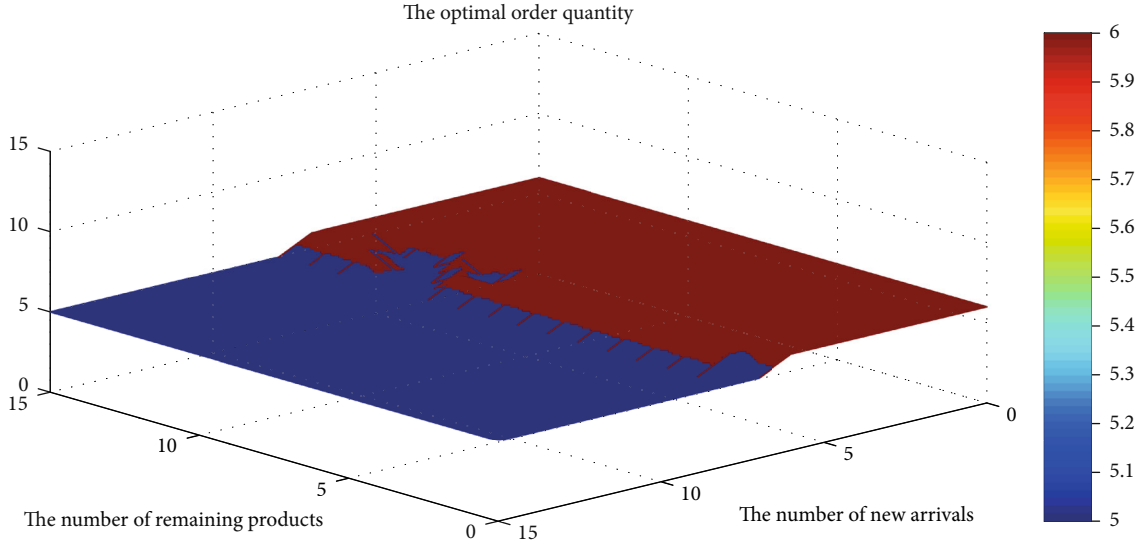
The optimal order quantity

FIGURE 22: The optimal order quantity with an ordering cost of 3 per unit.
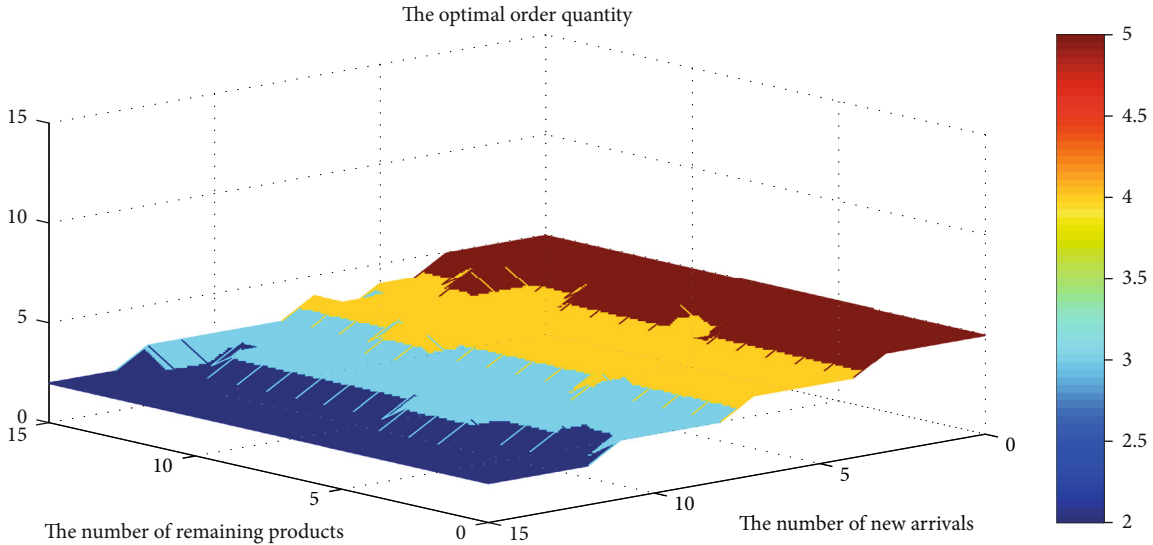
The optimal order quantity

FIGURE 23: The optimal order quantity with an ordering cost of 5 per unit.

4.2. Expected Customer Arrivals. This section discusses the different characteristics of the optimal strategy for different expected customer arrival rates.

As shown in Figures 8–11, the price of new or old products declines as the number of customer arrivals decreases.

Likewise, the optimal order quantity decreases with the expected number of customers, as shown in Figures 12–15.

In summary, there is a positive correlation between the optimal price of both new and old products and the expected rate of customer arrivals, in addition to the optimal order quantity. For the number of old products carried into the next period, $L_{\max t}$ and $L_{\max n}$ decrease with the expected customer rate, indicating that the retailer should give the old product more shelf capacity to avoid losses when demand is adequate but prioritize new product sales if the demand is insufficient.

4.3. Product Quality Decay. Let β be the rate of perishable decay when the period is over:

$$\beta = \frac{\tau_n - \tau_o}{\tau_n}. \tag{12}$$

We can draw the following conclusion from Figures 16–19.

First, given the optimal number of old products carried into the next period in the above four figures, $L_{\max t}$ and $L_{\max n}$ increase as the decay rate decreases. A decrease in the decay rate correlates with a relative increase in the value of old products' quality such that old products have more opportunities to be sold.

Second, the optimal pricing strategy exhibits the same trend with the decay rate such that the area of the optimal price (new + old $\leq L_{\max t}$) and (new $\leq L_{\max n}$) expands. In this

The optimal order quantity
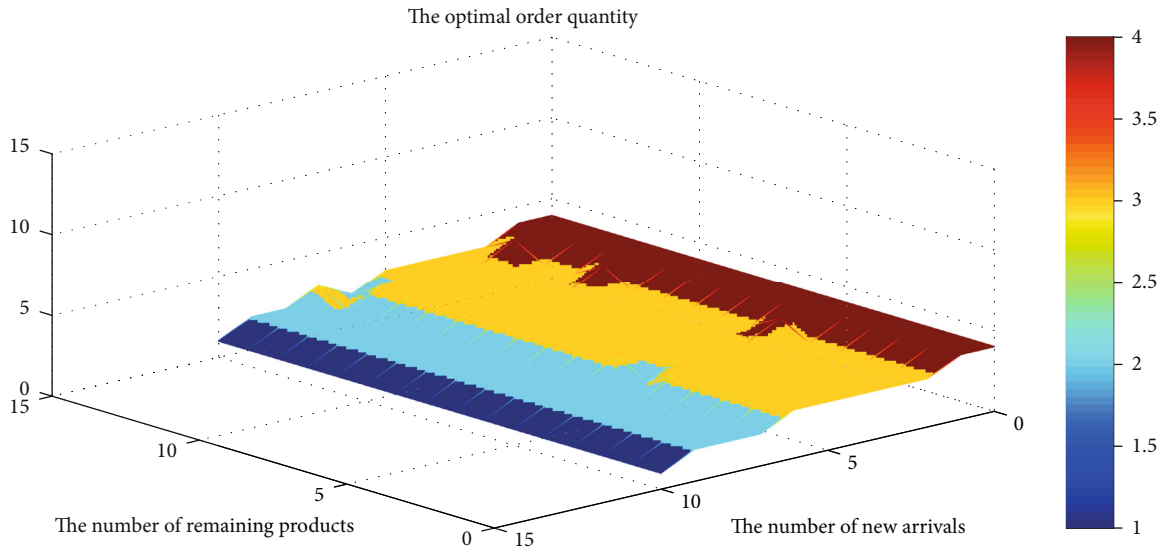

FIGURE 24: The optimal order quantity with an ordering cost of 7 per unit.
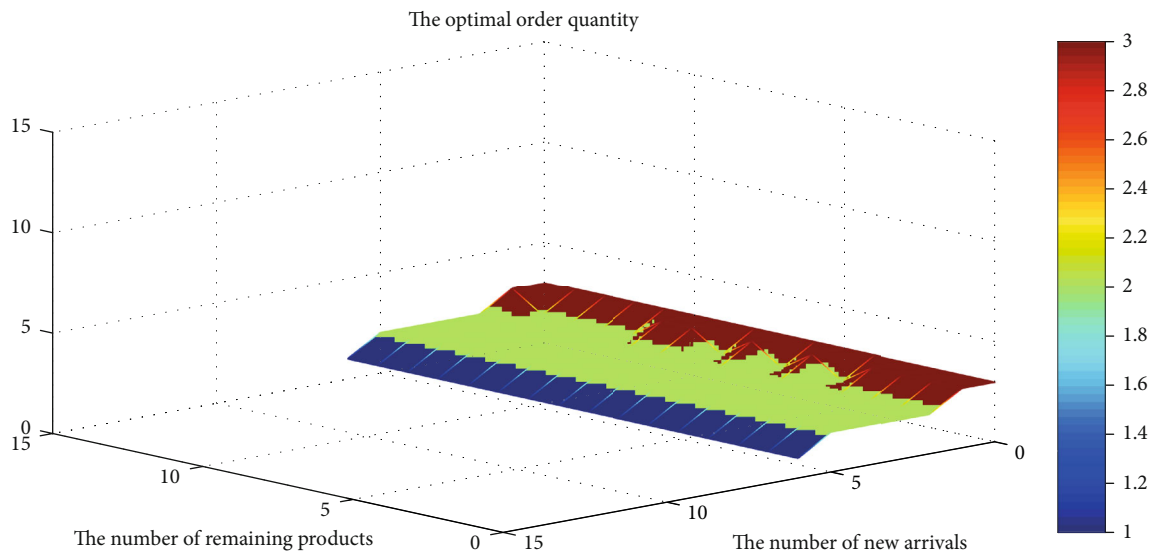
The optimal order quantity

FIGURE 25: The optimal order quantity with an ordering cost of 9 per unit.

area, the optimal prices (for both new and old products) decrease as the number of products increases. Outside of this region, product pricing will only be affected by the number of new products because the number of old products carried into the next period decreases when the decay rate is high. In addition, the lower value of the old product has a negative effect on its own price, namely, the lower the value, the lower the price.

Figure 20 shows the optimal ordering strategy when the decay rates are 80%, 60%, and 40%, respectively. When the decay rate is either 80% or 60%, the optimal ordering strategy remains at six. However, when we decrease the rate to 40%, the characteristics are different (a detailed description accompanies Figure 5).

When we reduced the decay rate to 20%, as shown in Figure 21, the optimal ordering quantities in the (new ≥ 6)

region decrease as the number of newly arrived products increases. This suggests that retailers will reduce current ordering when the number of new products in the current period is high and the decay rate is low.

4.4. Variable Ordering Cost per Unit. Variable ordering costs include the purchase price of the new products, the shipping costs, and other costs that are linearly related to the number of new products. This section focuses on the relationship between ordering strategies and adjustable ordering costs.

Figures 22–25 show the optimal ordering strategies when the variable costs are 3, 5, 7, and 9, respectively. First, we found the optimal ordering quantity to be unrelated to the quantity of remaining products. Second, the optimal ordering quantity decreases, exhibiting a trapezoidal decline as the variable unit cost increases. However, when the unit

order cost is too high, the possible waste due to product perishability also increases. In Figures 24 and 25, we found a case in which the ordering is 0; this indicates that when the unit order cost is too high, the retailer will try to sell the remaining old products to avoid new orders.

5. Conclusion and Future Research

Given that few works researched on pricing and inventory optimization for perishables considering multiperiod joint strategies and consumer choice behaviors, this paper conducts a simulation study centered on optimal joint strategy especially when different ages' products are sold simultaneously. In essence, this paper addresses such a problem when retailers sale a single perishable with a two-period lifetime, they should dynamically determine the joint ordering, pricing, and disposal strategy considering dynamic demand substitution, in which customers substitute between the two products when either new or old products are out of stock. In particular, the retailer sets the prices for both the new and old products and determines how many new products to order and how many remaining products to carry into the next period given demand uncertainty and diverse quality preferences among customers in each period.

We used the Markov decision process to construct the model, and the approach to seek the optimal strategy used an up-to-date version of the Q-learning algorithm. The main contribution of this paper is to utilize an accurate algorithm, Q learning, to help the retailers make their joint ordering, pricing, and disposal strategy in a time horizon allowing theoretically infinite periods. We initially apply a reinforcement learning algorithm to the inventory field, and our results also prove the efficiency of the Q learning through a large number of numerical experiments.

We further summarize the key results and insights based on our analysis as follows.

(1) We found that joint strategies of competing perishables based on dynamic ordering and pricing can yield more precise and targeted guidance for retailers. Although each strategy presents complex features, the decision-making model based on Markov decision processes has a general reference value. At the same time, determining the number of old products carried into the next period provides retailers more decision options comparing to they only decide disposal strategy, whether discard all valuable old products or enter all into the next period

(2) The optimal number of old products carried into the next period is affected by $L_{\max t}$, the total quantity of old products on shelves. All old products should be carried into the next period until the total amount of products reaches $L_{\max t}$. We found these determinations to be positively related to the potential demand and negatively related to the decay rate

(3) The pricing strategy involves several considerations: (i) optimal pricing for both new and old products is negatively related to the quantity of new and old products given that the total quantity does not exceed $L_{\max t}$; otherwise, the optimal price is only negatively related to the number of new products; (ii) the optimal pricing of both new and old products is positively correlated with the expected demand; and (iii) the optimal pricing of new products is positively related to the decay rate, but the optimal price of old products is negatively related to the decay rate

(4) Ordering decisions have complex characteristics: (i) the order size is unrelated to the quantity of remaining products but does have a positive correlation with the number of potential consumers; (ii) order quantities are not related to the number of new products when the decay rate is high or the variable ordering cost is low; however, the optimal ordering quantities exhibit a trapezoidal decline as the number of new products increases and the decay rate is low or the variable ordering cost is high

(5) In essence, our contribution to bridge the existing research gap involved both dynamic demand substitution and joint ordering, pricing, and disposal strategy for different ages' products within a multiperiod. We analyzed the optimal strategy under different parameters, by developing the Q-learning algorithm rather than dynamic programming or value iteration to solve the Markov model and gain the multiperiod optimal strategy. This provides a basis for exploring heuristic strategies and practical guidance for both academia and practice

Possible extensions of this research involve relaxing some of our assumptions, for example, by considering multiple replenishments and price changes within a period or a shelf-life of more than two periods. However, optimal solution still might be distorted due to any slight changes; as such, a more balanced measure will be expected when weighing between the model's practicality and tractability.

Data Availability

We adopted digital simulation in this paper, so the basic parameter setting is according to qualitative research of real business; there is no underlying data in this study.

Conflicts of Interest

The authors declare that they have no conflicts of interest.

Authors' Contributions

Jiangbo Zheng put forward the research topic, completed the construction of the logical framework of the paper, and finished the primary writing. Yanhong Gan wrote the program and got experimental data and finished conclusion analysis. Ying Liang gave advice and guidance on the design of the experiment and the framework of the paper and provided administrative, technical, or managerial support. Qingqing

Jiang analyzed experimental data and explored valuable experimental conclusions. Jiatai Chang had participated in paper revision and polishing.

References

[1] S. Nahmias and W. P. Pierskalla, "Optimal ordering policies for a product that perishes in two periods subject to stochastic demand," *Naval Research Logistics*, vol. 20, no. 2, pp. 207–229, 1973.

[2] B. E. Fries, "Optimal ordering policy for a perishable commodity with fixed lifetime," *Operations Research*, vol. 23, no. 1, pp. 46–61, 1975.

[3] S. Nahmias, "Optimal ordering policies for perishable inventory—II," *Operations Research*, vol. 23, no. 4, pp. 735–749, 1975.

[4] N. T. E. Morton, "Near myopic heuristics for the fixed-life perishability problem," *Management Science*, vol. 39, no. 12, pp. 1490–1498, 1993.

[5] Q. Li, P. Yu, and X. Wu, "Managing perishable inventories in retailing: replenishment, clearance sales, and segregation," *Operations Research*, vol. 64, no. 6, pp. 1270–1284, 2016.

[6] L. C. Coelho and G. Laporte, "Optimal joint replenishment, delivery and inventory management policies for perishable products," *Computers & Operations Research*, vol. 47, pp. 42–52, 2014.

[7] E. Berk and Ü. Gürler, "Analysis of the (Q, r) inventory model for perishables with positive lead times and lost sales," *Operations Research*, vol. 56, no. 5, pp. 1238–1246, 2008.

[8] X. Chao, X. Gong, C. Shi, C. Yang, H. Zhang, and S. X. Zhou, "Approximation algorithms for capacitated perishable inventory systems with positive lead times," *Management Science*, vol. 64, no. 11, pp. 5038–5061, 2018.

[9] L. Feng, "Dynamic pricing, quality investment, and replenishment model for perishable items," *International Transactions in Operational Research*, vol. 26, no. 4, pp. 1558–1575, 2019.

[10] O. Kaya and A. L. Polat, "Coordinated pricing and inventory decisions for perishable products," *OR Spectrum*, vol. 39, no. 2, pp. 1–18, 2017.

[11] M. Rabbani, N. P. Zia, and H. Rafiei, "Joint optimal dynamic pricing and replenishment policies for items with simultaneous quality and physical quantity deterioration," *Applied Mathematics and Computation*, vol. 287-288, pp. 149–160, 2016.

[12] Y. Li, A. Lim, and B. Rodrigues, "Note—pricing and inventory control for a perishable product," *Manufacturing & Service Operations Management*, vol. 11, no. 3, pp. 538–542, 2009.

[13] Y. Li, B. Cheang, and A. Lim, "Grocery perishables management," *Production and Operations Management*, vol. 21, no. 3, pp. 504–517, 2012.

[14] X. Chen, Z. Pang, and L. Pan, "Coordinating inventory control and pricing strategies for perishable products," *Operations Research*, vol. 62, no. 2, pp. 284–300, 2014.

[15] S. A. Smith and N. Agrawal, "Management of multi-item retail inventory systems with demand substitution," *Operations Research*, vol. 48, no. 1, pp. 50–64, 2000.

[16] M. E. Ferguson and O. Koenigsberg, "How should a firm manage deteriorating inventory?," *Production and Operations Management*, vol. 16, no. 3, pp. 306–321, 2007.

[17] Y. Akçay, H. P. Natarajan, and S. H. Xu, "Joint dynamic pricing of multiple perishable products under consumer choice," *Management Science*, vol. 56, no. 8, pp. 1345–1361, 2010.

[18] A. Sainathan, "Pricing and replenishment of competing perishable product variants under dynamic demand substitution," *Production & Operations Management*, vol. 22, no. 5, pp. 1157–1181, 2013.

[19] E. P. Chew, C. Lee, R. Liu, K. S. Hong, and A. Zhang, "Optimal dynamic pricing and ordering decisions for perishable products," *International Journal of Production Economics*, vol. 157, pp. 39–48, 2014.

[20] M. L. Puterman, *Markov Decision Problems*, John Wiley & Sons, 1994.

[21] C. J. C. H. Watkins and P. Dayan, "Q-learning," *Machine Learning*, vol. 8, no. 3-4, pp. 279–292, 1992.

[22] W. Liang, W. Huang, J. Long, K. Zhang, K. C. Li, and D. Zhang, "Deep reinforcement learning for resource protection and real-time detection in IoT environment," *IEEE Internet of Things Journal*, vol. 7, no. 7, pp. 6392–6401, 2020.

[23] P. Zhou, L. Lin, and K. H. Kim, "Anisotropic Q-learning and waiting estimation based real-time routing for automated guided vehicles at container terminals," *Journal of Heuristics*, vol. 4, pp. 1–22, 2021.

[24] M.-A. Dittrich and S. Fohlmeister, "A deep q-learning-based optimization of the inventory control in a linear process chain," *Production Engineering*, vol. 15, no. 1, pp. 35–43, 2021.